Virchows Arch (2011) 458:1–19
DOI 10.1007/s00428-010-0977-6

REVIEW AND PERSPECTIVE

Quality assurance in pathology in colorectal cancer screening and diagnosis—European recommendations

Phil Quirke · Mauro Risio · René Lambert · Lawrence von Karsa · Michael Vieth

Received: 6 August 2010 / Revised: 29 August 2010 / Accepted: 5 September 2010 / Published online: 9 November 2010
© The Author(s) 2010. This article is published with open access at Springerlink.com

Abstract In Europe, colorectal cancer is the most common newly diagnosed cancer and the second most common cause of cancer deaths, accounting for approximately 436,000 incident cases and 212,000 deaths in 2008. The potential of high-quality screening to improve control of the disease has been recognized by the Council of the European Union who issued a recommendation on cancer screening in 2003. Multidisciplinary, evidence-based European Guidelines for quality assurance in colorectal cancer screening and diagnosis have recently been developed by experts in a pan-European project coordinated by the International Agency for Research on Cancer. The full guideline document consists of ten chapters and an extensive evidence base. The content of the chapter dealing with pathology in colorectal cancer screening and diagnosis is presented here in order to promote international discussion and collaboration leading to improvements in colorectal cancer screening and diagnosis by making the principles and standards recommended in the new EU Guidelines known to a wider scientific community.

Keywords Colorectal cancer screening · Multidisciplinary evidence-based guidelines · Quality assurance · Histopathology · Classification · Precursor lesions

P. Quirke
Pathology and Tumour Biology,
Leeds Institute of Molecular Medicine, University of Leeds,
Leeds, UK

M. Risio
Pathology Department, Institute for Cancer Research and Treatment,
Turin, Italy

R. Lambert
Screening Group, Early Detection and Prevention
Section, International Agency for Research on Cancer,
Lyon, France

L. von Karsa
Quality Assurance Group, Early Detection and Prevention
Section, International Agency for Research on Cancer,
Lyon, France

M. Vieth (✉)
Institute of Pathology, Klinikum Bayreuth,
Preuschwitzerstr. 101,
95445 Bayreuth, Germany
e-mail: vieth.lkpathol@uni-bayreuth.de

Introduction

Colorectal cancer is a significant health problem, the importance of which will increase substantially in the coming years [1]. In Europe, colorectal cancer is the most common newly diagnosed cancer and the second most common cause of cancer deaths, accounting for approximately 436,000 incident cases and 212,000 deaths in 2008 [2]. Randomized trials have shown that systematic screening of a target population of suitable age can reduce colorectal cancer (CRC) by detecting asymptomatic lesions [3–5]. Early treatment is more effective and has a lower morbidity and mortality. Moreover, the endoscopic removal of adenomas reduces the incidence of CRC by stopping the progression of precursor lesions to cancer. The potential of high-quality screening to improve control of CRC has been recognized by the Council of the European Union who issued a recommendation on cancer screening in 2003 [6]. The recommendation encourages the EU Member States to implement population-based screening programmes using evidence-based tests for breast, cervical and colorectal cancer, according to European Quality Assurance Guidelines where they exist. Comprehensive European Guidelines for quality

assurance of breast and cervical cancer screening have been prepared by experts and published by the European Commission [7, 8]. Multidisciplinary, evidence-based European Guidelines for quality assurance in colorectal cancer screening and diagnosis have recently been developed by experts in a pan-European project coordinated by the International Agency for Research on Cancer. The comprehensive guidelines cover the entire screening process including clinical aspects, public health, organization and communication. The full guideline document consists of ten chapters and an extensive evidence base [9]. The content of the chapter dealing with pathology in colorectal cancer screening and diagnosis [10] is presented here in a slightly modified format in order to promote international collaboration in improvement of colorectal cancer screening and diagnosis by making the principles and standards recommended in the new EU Guidelines known to a wider scientific community. This area is rapidly developing and future evidence-based revisions will be required.

The pathology service plays a very important role in colorectal cancer screening since the management of participants in the programme depends on the quality and accuracy of the diagnosis. Pathology affects the decision to undergo further local and/or a major resection as well as surveillance after screening. The adoption of formal screening programmes leads to improvement not only in the management of early but also advanced disease by the introduction of guidelines, quality standards, external quality assurance and audit. In screening programmes, the performance of individuals and programmes must be assessed and it is advantageous if common diagnostic standards are developed to ensure quality, recognise areas where sufficient evidence is still lacking, and initiate high-quality studies to answer these questions. The present chapter suggests practical guidelines for pathology within a colorectal screening programme. We have concentrated on the areas of clinical importance in the hope of standardising these across the European Union. In the associated annex [11], we deal with some of the more difficult areas and suggest topics for future research. We have included guidelines for the reporting and management of resected specimens in an attempt to move towards agreed minimum European standards of pathology in these areas as well. This is the first edition of what will be a continuing process of revision as new data emerge on the pathology, screening and management of colorectal cancer. We hope to set minimum standards that will be followed in all programmes and to encourage the development of higher standards amongst the pathology community and screening programmes.

Many lesions are found within a screening programme some of which are of little or no relevance to the aim of lowering the burden of colorectal cancer in the population. The range of pathology differs between the different approaches, with faecal occult blood programmes yielding later, more advanced disease than flexible sigmoidoscopy and colonoscopy screening. Programme activities must focus on the identification and appropriate management of invasive colorectal cancer and its precursors. The management of pre-invasive lesions involves surveillance to allow the prevention of future disease, whereas management of adenocarcinoma focuses on immediate treatment and decisions on local removal, or radical surgery with the potential for operative mortality. Overuse of radical surgery must be avoided and recommendations for its use must be balanced with the risks to the patient.

There are a number of lesions, especially in the serrated pathway leading from hyperplastic polyps to other serrated lesions and in some cases to adenocarcinoma, that may be difficult to diagnose and for which knowledge of their natural history and clinical implications is limited [12]. Further work is required in this area, but until we understand these lesions better it is recommended that all serrated lesions, with the exception of hyperplastic polyps, be fully removed.

Few data were present in the literature on this issue. This paucity of data is caused in part by a lack of standardisation in terminology and limited observer agreement. Furthermore, a lack of prospective studies precludes a clear indication of the optimal treatment and surveillance strategy for lesions in the serrated pathway. For more information, see Ref. [11]. The screening programme will also identify other non-serrated neoplastic and non-neoplastic lesions and provide important data on such conditions.

Methods

The process of evidence-based guideline development is reported elsewhere in detail [13]. Briefly, scientific and editorial management was performed by an editorial board with experience in development of best practice guidelines, in programme management and in evaluation of strategies for CRC screening. The editorial board drafted an initial comprehensive outline of the Guidelines and recruited a multidisciplinary group of 50 experts across the European Union to collaborate in revising the outline and drafting the chapters according to an agreed methodology. An expert Literature Group consisting of epidemiologists with special expertise in the field of CRC and in critical appraisal of clinical studies provided technical and scientific support to the authors and editors in searching the relevant literature, assessing the methodological quality of retrieved studies and defining a grading system of the level of evidence and strength of the recommendations.

The subgroup of authors responsible for the presently reported chapter defined key clinical questions (modified Patient-Intervention-Comparison-Outcome-Study method) [14–16] for sensitive and specific bibliographic searches

(Medline, Embase, Cochrane library) for the calendar years 2000–2008; articles suggested by authors were also considered. A study design hierarchy and inclusion/exclusion criteria were developed for each type of question (effectiveness, diagnostic accuracy, acceptability, etc.). The methodological quality of the studies retrieved for the clinical questions was assessed using validated checklists for systematic reviews [17], randomized controlled trials [18], observational studies [19] and diagnostic accuracy studies [20]. Evidence tables and summary documents with a synthesis of results and the level of evidence were produced for each question by the literature group.

The subgroup of authors responsible for the presently reported chapter received all the evidence tables and summary documents relating to the formulated clinical questions dealing with quality assurance in pathology of CRC screening and diagnosis. The authors elaborated the chapter draft describing the relevant issues and including issues deemed to be relevant for a comprehensive multidisciplinary guideline, but not covered by the key clinical questions. The authors summarized the available evidence, and included recommendations and conclusions, as well as a proposal for the strength of the evidence and the level of each of the recommendations based on the evidence collected by the literature group, their clinical experience, and any additional relevant references collected by the authors, including publications after December 2008. The manuscript draft was repeatedly reviewed and revised in workshops attended by the authors of all of the guideline chapters as well as the editors and the literature group to develop consensus on the final recommendations and other content. A preliminary and a nearly final draft of the present chapter was also reviewed and discussed in multidisciplinary, pan-European meetings on colorectal cancer screening conducted in 2008 and 2009 in which experts from the 27 EU member states participated.

For each recommendation the strength of evidence was indicated according to the following grading:

I. Multiple randomized controlled trials (RCTs) of reasonable sample size, or systematic reviews (SRs) of RCTs
II. One RCT of reasonable sample size, or three or less RCTs with small sample size
III. Prospective or retrospective cohort studies or SRs of cohort studies; diagnostic cross-sectional accuracy studies
IV. Retrospective case–control studies or SRs of case–controls studies, time series analysis
V. Case series; before/after studies without control group, cross-sectional surveys
VI. Expert opinion

If applicable, the lack of sufficient evidence to make a recommendation was explicitly mentioned in the guideline text. The consensus of the authors and editors on the strength of a given recommendation was indicated according to the following grading:

A. Intervention strongly recommended for all patients
B. Intervention recommended
C. Intervention to be considered but with uncertainty about its impact
D. Intervention not recommended
E. Intervention strongly not recommended

Statements of advisory character that the authors considered to be good practice but not of sufficient importance to warrant formal grading were included in the chapter text.

In the final editing, the consistency and coherence of recommendations was checked by the editorial board. Strong recommendations, e.g. with grading A or E, but with comparatively low levels of evidence, e.g. levels III–VI, were accepted if an appropriate explanation was provided by the authors.

Classification of lesions in the adenoma–carcinoma sequence

A colorectal adenoma is defined as a lesion in the colon or rectum containing unequivocal epithelial neoplasia. Classification of adenomas should include grading of neoplasia according to the revised Vienna classification that has been modified for the European Guidelines to obtain a two-tiered system of low-grade and high-grade neoplasia (Table 1); see also Ref. [21]. This modified grading system aims to minimise intra- and inter-observer variation and facilitate management of endoscopically detected lesions by improving correlation between histopathology of biopsies and resection specimens [22]. Classically, adenomas are divided into tubular, tubulo-villous or villous types and demarcation between the three is based on the relative proportions of tubular and villous components, according to the "20% rule" described in the WHO classification of tumours in the digestive tract [23]. At least 20% of the estimated volume of an adenoma should be villous to be classified as a tubulo-villous adenoma and 80% villous to be defined as a villous adenoma. All other lesions are classified as tubular [23] (VI-A). The reproducibility of villousness increases when collapsing the categories into only two: tubular vs. any villous component (i.e. anything >20% villous). Adenomas can be endoscopically polypoid, flat or depressed. Due to the increased risk of colorectal cancer associated with flat and/or depressed lesions (III) they should be reported as non-polypoid lesions (see: "Non-polypoid adenomas"). The Paris endoscopic classification of superficial neoplastic lesions should be used to describe the gross appearance of colorectal adenomas (V-B). Key features to report in a programme are size, villousness, the

Table 1 Adaptation of the revised Vienna classification for colorectal cancer screening

1. No neoplasia[a]
Vienna category 1 (negative for neoplasia)
2. Mucosal low-grade neoplasia
Vienna category 3
Mucosal low-grade neoplasia
Low-grade adenoma
Low-grade dysplasia
Other common terminology
Mild and moderate dysplasia
WHO: low-grade intraepithelial neoplasia
3. Mucosal high-grade neoplasia
Vienna: category 4.1–4.4
Mucosal high-grade neoplasia
High-grade adenoma/dysplasia
Non-invasive carcinoma (carcinoma in situ)
Suspicious for invasive carcinoma
Intramucosal carcinoma
Other common terminology
Severe dysplasia
High-grade intraepithelial neoplasia
WHO: high-grade intraepithelial neoplasia
TNM: pTis
4. CARCINOMA invading the submucosa or beyond
4a. Carcinoma confined to submucosa
Vienna: category 5 (Submucosal invasion by carcinoma)
TNM: pT1
4b. Carcinoma beyond submucosa
TNM: pT2-T4

For revised Vienna classification, see Ref. [26]; for WHO classification, see Ref. [23]; and for TNM, see [40–42]

[a] Category 2 of the Vienna Classification (indefinite) is not recommended for screening

grading of neoplasia, the recognition of invasion and features suggesting the need for further intervention either local or radical. The size of adenomas is important for their risk of containing an adenocarcinoma but it is also related to the need for subsequent surveillance, or colonoscopy.

The two-tiered grading of mucosal colorectal neoplasia recommended in the European Guidelines (see Table 1) is based on the revised Vienna Classification that has improved diagnostic reproducibility, particularly for non-polypoid lesions [24–28] (IV-B). The recommended two-tiered grading system also permits translation of histopathology findings of Western and Japanese pathologists into a uniform system for classification of colorectal neoplastic lesions.

In screening programmes the use of the term advanced adenoma has developed and is sometimes used to categorise adenomas for management. In this context an advanced adenoma is one that is either ≥10 mm or contains high-grade mucosal neoplasia or a villous component.

The hyperplastic polyp must be distinguished from other serrated lesions due to its extremely low malignant potential. The significance of other lesions in the serrated spectrum is controversial and our knowledge is still developing; traditional-serrated adenomas and mixed polyps with neoplasia should be considered as adenomas for the purpose of follow-up (surveillance). More details are provided in Ref. [11].

Measurement of size of adenomas

Size (largest diameter) is an important objective measurement best performed by the pathologist [29] from the slide, as is recommended in the EU guidelines for breast cancer screening [30]. Endoscopy measurements are less accurate and should only be used when strictly necessary (III-B). Pathology measurements are auditable, accurate, simple to perform and able to assess the size of the adenomatous component of mixed lesions. Although the quality of evidence is low, there are some indications that different modalities of advanced adenoma measurement (endoscopic measurement vs. pathologist's measurement before and after fixation, on slide preparation) can affect diagnostic reproducibility and the detection rate of advanced adenomas. An overestimation or underestimation of a large or a small polyp is important when the misjudgement crosses the 10-mm threshold. It seems that the use of the pathologist's measurement is currently the most accurate. If the lesion is too large for the maximum dimension to be measured by this method, because it cannot be represented on a single slide, the measurements taken at the time of specimen dissection should be used. If a biopsy is received or the specimen is fragmented it should be stated that it cannot be accurately assessed for size by the pathologist and the endoscopy measurements should be used. Measurements should exclude the stalk if it is composed of normal mucosa however the distance to the excision margin should be noted. The size of adenomas is used to determine the need for surveillance and therefore must be measured accurately to the nearest millimetre (and not rounded-up to the nearest 5 or 10 mm). Where the lesion is mixed or only part of a lesion is adenomatous, measurement should be performed on the adenomatous component. Programmes should have a policy on the methodology of, and should regularly monitor the accuracy of size measurements of endoscopically removed lesions. Deviation between the actual size and the measurements of pathologists and endoscopists should be minimised. Management decisions that depend on lesion size should take into account potential inaccuracy in the size measurement. The multidisciplinary team should consider deviating from the recommended size categories

in treatment and surveillance algorithms, if the review of a case indicates that there is sufficient reason to doubt the accuracy of the measurement. Such cases should be captured as an auditable outcome (VI-B).

Tubular, tubulo-villous and villous adenomas: the typing of villousness

The 20% rule only applies to wholly excised polyps and to intact sections of lesions large enough to provide reliable proportions. For small fragmented lesions or superficial polyp biopsies, the presence of at least one clearly identifiable villus merits classification as "at least tubulo-villous". Definitions of the types of villousness are presented in Ref [11].

Non-polypoid adenomas

The role of the pathologist in the evaluation of non-polypoid adenomas is to confirm the adenomatous nature of the lesion, and to determine the grade of neoplasia as well as the depth of depression in the case of a depressed non-polypoid lesion (see below). Since the expression "flat adenoma" is not well defined, it is recommended to group together all adenomatous lesions other than polypoid into the category of "non-polypoid adenomas" and avoid the term "flat". Non-polypoid adenomas correspond to an endoscopical diagnosis of neoplasia in the subtypes IIa, IIb and IIc according to the Paris classification. Completely flat adenomas (type IIb) and depressed lesions (type IIc) are rarely found in the colon and rectum, while slightly elevated lesions (type IIa) are frequent. In the literature, the height of non-polypoid adenomas has been described histologically as not exceeding twice the height of normal mucosa, thus measuring less than 3 mm in height. This definition may be difficult to apply due to fixation artefacts and in slightly depressed lesions since the adjacent mucosa may be thinner than the normal epithelium. The endoscopic diagnosis of a non-polypoid lesion should be reported according to the Paris classification [21, 28, 31, 32] (III-B). We were unable to retrieve studies that specifically address the topic of the differences in the detection rates of non-polypoid colorectal neoplasms among the different types of screening programmes (FOBT vs. flexible sigmoidoscopy vs. total colonoscopy), although a prevalence of 9–10% of non-polypoid colorectal neoplasm (flat and depressed) was recently reported by Western pathologists in a large cross-sectional study [32]. Depressed lesions (type IIc) should be mentioned in the histological report for clinico-pathological correlation. Special care should be taken for centrally depressed lesions, especially when the depression is deeper than half of the adjacent lesion. These are reported to have a higher frequency of high-grade neoplasia and invasion at a smaller size than other flat or depressed lesions [21]. Non-polypoid adenomas can show so-called lateral spread with poor delineation of the margins thus making endoscopic removal difficult.

Serrated lesions

Terminology

These lesions have in common a serrated morphology, but depending on other characteristics, the potential to develop into invasive adenocarcinoma differs considerably. Serrated lesions vary from the *hyperplastic polyp*, which although relatively common, has no implications for the screening programme unless very numerous, proximally located or of a large size (>10 mm), to *sessile-serrated lesions* (sometimes referred to as *sessile-serrated polyps/sessile-serrated adenomas*), *traditional-serrated adenomas*, or *mixed lesions/mixed polyps*. Serrated lesions are infrequent, the evidence base is poor and recommendations are not well established, but until further evidence is forthcoming we recommend the following:

Hyperplastic (metaplastic) polyp

Hyperplastic polyps are often small lesions (<5 mm in diameter), frequently found in the left (distal) colon. They are composed of simple elongated crypts with a serrated structure in the upper half. These polyps usually show some proliferation in the basal (non-serrated) part of the crypts (regular proliferation). Nuclei are small, regular and basally orientated. There is no hyperchromasia, and stratification of the upper half of the crypts has a serrated appearance without cytological atypia.

Hyperplastic polyposis should be excluded in cases with giant hyperplastic polyps (>10 mm), or multiple hyperplastic polyps in the right colon, or in first-degree relatives of individuals with hyperplastic polyposis.

Sessile-serrated lesions

We recommend the use of the term sessile-serrated lesion for serrated lesions with structural alterations that do not show mucosal neoplasia. This term should replace the use of sessile-serrated polyp and sessile-serrated adenomas until better definitions are created.[1] It is not recommended to use the latter terms in screening programmes because it would

[1] The term *sessile-serrated polyp* has been proposed elsewhere for serrated lesions that cannot be definitely classified into the category of *hyperplastic polyps* or *serrated adenomas* [12], especially in cases with technical inconsistencies such as tangential cuts or superficial biopsies. The same terminology has been propsed for lesions with minimal and focal structural alterations in the absence of cytological atypia [86].

add additional ill-defined categories that may confuse practitioners.

Traditional-serrated adenomas

If the lesion shows a serrated morphology as well as mucosal neoplasia (cytological abnormalities), it is considered to be a traditional-serrated adenoma (TSA) [33]. It should be reported as such (TSA) and treatment and surveillance should be the same as for adenomas. For details see Ref. [11] as well as Chapter 9 of the EU guidelines (*Colonoscopic surveillance after adenoma removal*) [34]. This pragmatic recommendation recognises the neoplastic nature of these lesions. The non-serrated features found in such lesions (e.g. size and grade of neoplasia) and any co-existing pathology (e.g. number of neoplastic lesions) should be taken into account in selecting an appropriate surveillance protocol (VI-C).

Mixed polyp

These are lesions with combinations of more than one histopathologic type in the serrated spectrum (hyperplastic polyps, sessile-serrated lesions, traditional-serrated adenomas) or at least one type in combination with adenoma [35]. The important feature to recognise for the screening programme is the presence of neoplasia. The respective types of lesion in a mixed polyp should be reported and the term "mixed polyp" should only be used in brackets after the diagnosis of the individual components (e.g. adenoma and hyperplastic polyp, or traditional-serrated adenoma plus adenoma). Mixed polyps should be completely removed. If there is an adenomatous component, the lesion should be followed up (surveillance) in the same manner as for adenomas, taking into account the size and the grade of the adenomatous component (VI-C).

Grading of neoplasia

The revised Vienna classification has been adopted here, but in a simplified form suitable for screening and diagnosis, by removing the indefinite category between "negative for neoplasia" and "low-grade neoplasia". This category has no clinical value and unlike inflammatory bowel disease is likely to be chosen very infrequently. Excluding it reduces the number of categories and simplifies the subsequent management choices. The advantages of the revised Vienna Classification on which the European screening classification is based are that it improves diagnostic reproducibility [24, 26–28] (IV-B). The modified format with a two-tiered grading of mucosal colorectal neoplasia aims to further reduce inter-observer variation [36] (IV-B). It encompasses the diagnostic categories used in the Eastern and the Western schools and each level has a clinical consequence. In the revised Vienna classification, the term neoplasia is used which is synonymous with the formerly used term "dysplasia". In the two-tiered grading system recommended in the European Guidelines, mucosal low-grade neoplasia corresponds to neoplasia of the same grade in the revised Vienna classification; mucosal high-grade neoplasia likewise corresponds to neoplasia of the same grade in the revised Vienna classification. Invasive submucosal neoplasia in the European classification corresponds to carcinoma invading the submucosa or beyond in the Vienna classification (see Table 1).

Low-grade neoplasia

Low-grade neoplasia is an unequivocal neoplastic condition confined to the epithelial glands. It should not be mistaken for inflammatory or regenerative changes. Alterations characteristic for low-grade neoplasia start from one gland and develop into a microadenoma that then grows to become macroscopically visible. Caution should be exercised in patients with chronic inflammatory bowel disease where the diagnosis of a neoplastic sporadic adenoma has implications different from that of neoplasia in colitic mucosa.

High-grade neoplasia

The changes of high-grade neoplasia should involve more than just one or two glands (except in tiny biopsies of polyps), and should therefore be identifiable at low-power examination. Caution should be exercised in over-interpreting isolated surface changes that may be due to trauma, erosion or prolapse.

High-grade neoplasia is diagnosed on structure, supplemented by an appropriate cytology. Hence, its presence is nearly always suspected by the low-power appearances where complex structural abnormalities are present in structures whose epithelium looks thick, blue, disorganised and with focal cell debris and necrosis.[2] The structural features are:

- Complex glandular crowding and irregularity (note that the word "complex" is important and excludes simple crowding of regular tubules that might result from crushing);
- Prominent glandular budding;
- A cribriform appearance and "back to back" glands; and
- Prominent intraluminal papillary tufting.

[2] High-grade neoplasia also contains the subgroup of intramucosal carcinoma used by some pathologists but not recommended here. For details see Ref. [11].

While many of these features often coexist in high-grade neoplasia, individually they are neither necessary nor usually sufficient. Indeed they may occasionally occur in lower grades of neoplasia, and that is why it is necessary to further scrutinise the cytological features for signs of high-grade neoplasia. The cytological features of high-grade neoplasia are:

- Loss of cell polarity or nuclear stratification. High-grade neoplasia should show at least 2–5 nuclear rows and preferably a variable number of rows within individual glands. The nuclei are haphazardly distributed within all three thirds of the height of the epithelium. No maturation of the epithelium is seen towards the luminal surface;
- Neoplastic goblet cells (retronuclear/dystrophic goblet cells);
- Cytology includes vesicular or/and irregular round nuclei with loss of polarity whereas spindle-like palisading nuclei are a sign of low-grade intraepithelial neoplasia;
- Markedly enlarged nuclei, often with a dispersed chromatin pattern and a prominent nucleolus;
- Atypical mitotic figures; and
- Prominent apoptosis, focal cell debris and necrosis.

Again, these features usually coexist in high-grade neoplasia, and caution must be exercised in using just one. It should be emphasised again that they should occur in a background of complex structural abnormality. Marked loss of polarity and nuclear stratification sometimes occurs on the surface of small, structurally regular, tubular adenomas that otherwise have a lower grade of neoplasia, probably as a result of trauma, and must not be used to classify a lesion as high grade. The only exception to the rule is when the specimen consists of just a small biopsy from a polyp, when there is insufficient tissue to assess the architecture properly. In this situation it is permissible to label florid cytological abnormalities alone as high-grade neoplasia, but this will usually lead to re-excision of the whole polyp, when it will be possible to assess the whole lesion properly.

Also included within high-grade neoplasia is the presence of definite invasion into the lamina propria of the mucosa but not invasion through the mucscularis mucosae.

Other lesions

Inflammatory polyps

Experience from UK pilot sites has shown that inflammatory-type polyps are relatively common. Whilst they are most usually seen as a complication of chronic inflammatory bowel disease, particularly ulcerative colitis, they are also seen in association with diverticulosis, mucosal prolapse and at the site of ureterosigmoidostomy. Furthermore, sporadic, single inflammatory-type polyps (inflammatory cap polyp, cloacogenic inflammatory polyp, myoglandular polyp, granulation tissue polyp etc.) are well described in the colorectum. As the reporting pathologist may not know the true context of such polyps, we recommend that all such polyps be classified as "post inflammatory polyp". The term inflammatory pseudopolyp (or even just "pseudopolyp") should be avoided. Biopsies with mucosal prolapse syndrome should be identified and reported as such and not as neoplastic conditions.

Juvenile polyps

Juvenile polyps are spherical in shape, show an excess of lamina propria, and have cystically dilated glands. The expanded lamina propria shows oedema and mixed inflammatory cells. Experience from the UK faecal occult blood pilot sites suggests that occasional juvenile-type polyps are identified, even in the screening age group [37]. Juvenile polyps are most common in children but occasional examples are seen in adults. We advise that any polyp showing juvenile polyp-type features should be classified as "juvenile polyp" for the purposes of diagnostic reporting in a screening programme. Juvenile polyps often show epithelial hyperplasia but neoplasia is very rare. Single sporadic juvenile polyps have a smooth surface, can be found in all age groups and often are eroded. So-called atypical juvenile polyps show different morphological features, with a multilobated architecture, intact surface mucosa and (usually) a much more pronounced epithelial component. They are a characteristic feature of juvenile polyposis.

Peutz–Jeghers polyps

Whilst these polyps are usually seen in the Peutz–Jeghers syndrome, occasional examples are demonstrated as single, sporadic polyps in the colon. There remains uncertainty as to whether "inflammatory myoglandular polyp" represents a similar entity. As with juvenile polyposis, it would seem most unlikely, given the rarity of the syndrome and the age of the screening population, that Peutz–Jeghers syndrome would be diagnosed as part of a screening programme. Although Peutz–Jeghers polyps are classified as hamartomas, they have a very organised structure. They have a central core of smooth muscle with conspicuous branching, each branch being covered by colorectal-type mucosa that appears hyperplastic but not neoplastic. As with sporadic juvenile polyps, solitary Peutz–Jeghers-type polyps are most unlikely to demonstrate foci of neoplasia.

Serrated (hyperplastic) polyposis

This condition is characterised by one or more of the following conditions [38]:

- At least five histologically diagnosed serrated polyps proximal to the sigmoid colon, of which two are >10 mm;
- Any number of serrated polyps occurring proximal to the sigmoid colon in an individual who has a first-degree relative with hyperplastic polyposis; and/or
- More than 30 serrated polyps of any size, but distributed throughout the colon.

As mentioned above (see: "Hyperplastic (metaplastic) polyp"), hyperplastic polyposis should be excluded in cases with giant hyperplastic polyps (>10 mm, hyperplastic polyps in the right colon or in first-degree relatives of individuals with hyperplastic polyposis).

Cronkhite–Canada syndrome

We believe it is most unlikely that such cases will present via a screening programme and the true diagnosis may not be recognised by pathological assessment. However, if Cronkhite–Canada syndrome is suspected, the pathologist should contact the endoscopist and ask for clinical details to ensure the diagnosis.

Neuroendocrine tumour

It is recommended to use the term "neuroendocrine tumour" rather than carcinoid in accordance with the WHO classification. These lesions are usually benign, small lesions and do not give rise to diagnostic difficulty.

Colorectal intramucosal tumours with epithelial entrapment and surface serration

Entrapment and pseudoinvasion of glands into the submucosal layer must be distinguished from invasive carcinoma. If in doubt, the relevant findings should be stated in the written report. If evaluation is problematic, step sections, a second opinion and further biopsies from the polypectomy ulcer should be considered.

Non epithelial polyps

- Lipoma
- Leiomyoma of the muscularis mucosae
- Ganglioneuroma
- Gastrointestinal schwannoma
- Neurofibroma
- GIST
- Various forms of vascular tumour
- Perineurioma
- Fibroblastic polyp
- Epithelioid nerve sheath tumour
- Inflammatory fibroid polyp

Assessment of the degree of invasion of pT1 colorectal cancer

pT1 cancers are those showing invasion through the muscularis mucosae into the submucosa but not into the muscularis propria.

Definition of invasion

We recommend the use of the WHO definition [23, 39] of an adenocarcinoma as an invasion of neoplastic cells through the muscularis mucosae into the submucosa (VI-A). The term intramucosal carcinoma should be substituted by mucosal high-grade neoplasia according to the WHO classification and the modified classification of neoplasia recommended in the European Guidelines based on the revised Vienna classification (see Table 1). We recognise that this will not allow detailed comparison with Japanese series where, contrary to the previous US and European literature, a diagnosis of carcinoma can be made on cases of neoplasia without submucosal invasion, or even on the basis of marked intraepithelial atypia. The TNM classification [40–42] allows carcinoma in situ (Tis) but this does not improve on the revised Vienna classification and should not be used. Please see Ref. [11] for details (VI-B).

Careful consideration should be given to the potential for surgical overtreatment of misclassified early T1 cancers. Screening programmes require explicit criteria for the diagnosis and staging of early adenocarcinoma because unnecessary radical resection will raise the morbidity and mortality in colorectal cancer screening programmes. Please see annex [11] for further discussion of this point. Post-operative mortality (within 30 days) ranges between 0.6% and 4.4% in T1 cancers depending on the population, age of patient and quality of services available. Achieving the optimum balance between removing all disease by resection and minimising harm is very important.

Epithelial misplacement

Epithelial misplacement of adenomatous epithelium into the submucosa of a polyp is a well-recognised phenomenon [43]. It is commonly seen in prolapsing polyps in the sigmoid colon. Experience suggests that this will be one of the most difficult areas of pathological diagnostic practice in FOBT screening. Sigmoid colonic polyps are particularly

prone to inflammation, a feature that tends to enhance the neoplastic changes present. When associated with epithelial misplacement, the potential for misdiagnosis of these lesions as early carcinoma become much greater. In cases of epithelial misplacement, surrounding lamina propria and haemosiderin-laden macrophages are found. Submucosal mucinous lakes may be seen. These do not warrant an immediate diagnosis of invasion and must be interpreted in association with the surrounding features.

High-risk pT1 adenocarcinoma

pT1 tumours provide many difficulties in a screening programme and the current evidence base for management of these lesions is poor and based on symptomatic patients [44–48] (V-B). With regard to the correlation between clinical outcomes and tumour pathology, a clear indication of an increased risk of residual disease, lymph-node metastasis, haematogenous metastasis, and mortality was observed after endoscopic polypectomy and subsequent surgical resection of poorly differentiated tumours (i.e. tumours with incomplete excision, poor grade of histological differentiation, venous and lymphatic invasion, tumour budding). Some pathology features, such as tumour budding and lymphatic and venous invasion appeared as possible prognostic factors for increased risk of lymph node metastasis but a clear guideline cannot be drawn as this correlation was not statistically significant in all studies. The available methods for substaging and differentiation grading are shown below. The most appropriate method depends on the morphology of the lesion and depth of invasion, e.g. non-polypoid-Kikuchi levels, and polypoid-Haggitt levels. In the future, more quantitative measurements should be investigated as suggested by the Japanese.

Substaging pT1

In pT1 tumours the frequency of lymph node metastasis in tumours that involve the superficial, middle and deep thirds of the submucosa, i.e. so-called Kikuchi levels sm1, sm2, and sm3 (Fig. 1) [49, 50] has been reported to be 2%, 8% and 23%, respectively [51].

In pedunculated polypoid lesions, Haggitt identified the level of invasion into the stalk of the polyp (Fig. 2) as being important in predicting outcome and found that level 4 invasion, in which the tumour extended beyond the stalk of the polyp into the submucosa, but did not invade the muscularis propria, was an adverse factor [52].

However, both the Kikuchi (for non-polypoid tumours) and the Haggitt (for pedunculated tumours) systems may be difficult to use in practice, especially if there is fragmentation or suboptimal orientation of the tissue, and one study found lymph node metastases in six of 24 Haggitt level 3 lesions. More recently Ueno et al. [53] have proposed use of the depth (>2,000 μm) and width (>4,000 μm) of invasion measured in microns beyond the muscularis mucosae provides a more objective assessment of lymph node metastatic potential 2.5% vs. 18.2% when submucosal invasion width is < or ≥4,000 μm, respectively; and 3.9% vs. 17.1%, when submucosal invasion depth is < or ≥2,000 μm, respectively; and this approach has been adopted in Japan. Each classification has advantages and disadvantages.

Kikuchi cannot be used in the absence of muscularis propria; Haggitt is not applicable in non-polypoid lesions, and measurement depends on a recognisable submucosa from which to measure. In view of the uncertainty and lack of consensus, a firm evidence-based recommendation for one method of assessing local invasion cannot yet be made. At present we recommend the Kikuchi stage for non-polypoid lesions and Haggitt for pedunculated lesions (VI-C). All three approaches must be evaluated in further large series from multiple programmes to derive adequately evidence-based recommendations.

Tumour grade in pT1 lesions

Poorly differentiated carcinomas are identified by the presence of either irregularly folded, distorted and often small tubules or the lack of any tubular formation and showing marked cytological pleomorphism. In the absence of good evidence we recommend that a grade of poor differentiation should be applied in a polyp cancer when ANY area of the lesion is considered to show poor differentiation. Poor differentiation should equate to the WHO categories of poor and undifferentiated tumours [54]. The frequency should not exceed 20%. According to the WHO classification [39], budding of the tumour cells at the front of invasion should not influence grading of the tumour. Please see Ref. [11] for details.

Lymphovascular invasion in pT1 adenocarcinomas

Definite invasion of endothelium-lined vascular spaces in the submucosa is generally regarded as a significant risk for lymph node or distant metastasis. Sometimes retraction artefact around tumour aggregates can make assessment uncertain, in which case this uncertainty should be recorded and the observation should be interpreted in a multidisciplinary conference in the light of any other adverse histological features. At the moment there are no consistent data available on the additional use of immunohistochemistry, but this might be helpful in distinguishing retraction artefacts from lymphatic (e.g. LEM D 2–40) or capillary spread (e.g. CD 34).

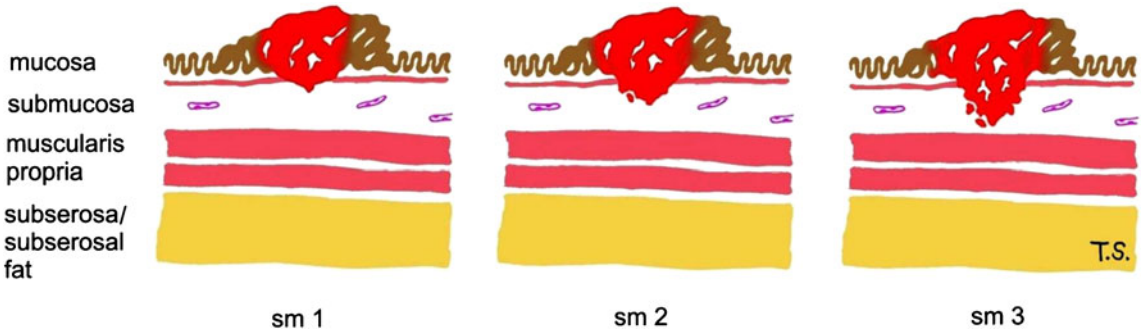

Fig. 1 Kikuchi levels of submucosal infiltration modified from Ref. [51]

Margin involvement in pT1 adenocarcinomas

It is important to record whether the deep (basal) resection margin is involved by invasive tumour (that may be a reason for further surgery) and whether the lateral mucosal resection margin is involved by carcinoma or the pre-existing mucosal neoplasia (in which case a further local excision may be attempted) (VI-B).

There has been considerable discussion and controversy in the literature over what degree of clearance might be regarded as acceptable in tumours that extend close to the deep submucosal margin [55]. It is important that clearance be measured and recorded in the report. All would agree that a clearance of 0 mm, and most would agree that a clearance of <1 mm is an indication for further therapy, others would use <2 mm. Currently, we recommend that clearance of 1 mm or less indicates margin involvement (VI-B). However, this may be handled by removal of any residual polyp endoscopically.

Tumour cell budding in pT1 adenocarcinomas

Tumour cell budding, i.e. the presence of small islands or single infiltrating tumour cells at the front of tumour invasion, has been described in the Japanese literature as an unfavourable prognostic factor if present in a marked degree [53, 56, 57]. Budding has been assessed either as slight, moderate or marked; or as present/absent [58, 59]. However, its reproducibility has been criticised, the diagnostic criteria vary [60] and the ability to predict metastasis compared to the previously discussed factors is unproven. Further research is needed in this area to identify the optimum method and its reproducibility before tumour cell budding can be recommended for routine use as an indicator of metastasis. Please see Ref [11] for details.

Site

The site of origin of each specimen should be individually identified by the clinician and provided to the pathologist on the request form (VI-B). This should preferably include both the segment of the bowel and the distance in cm from the anus. The pathologist should record this information on the proforma. This is important as the risk of lymph node metastases from a T1 adenocarcinoma has been reported to vary depending on the site of the lesion [61].

Specimen handling

Specimen handling is an important issue, as poor handling and dissection procedures can impair diagnostic accuracy.

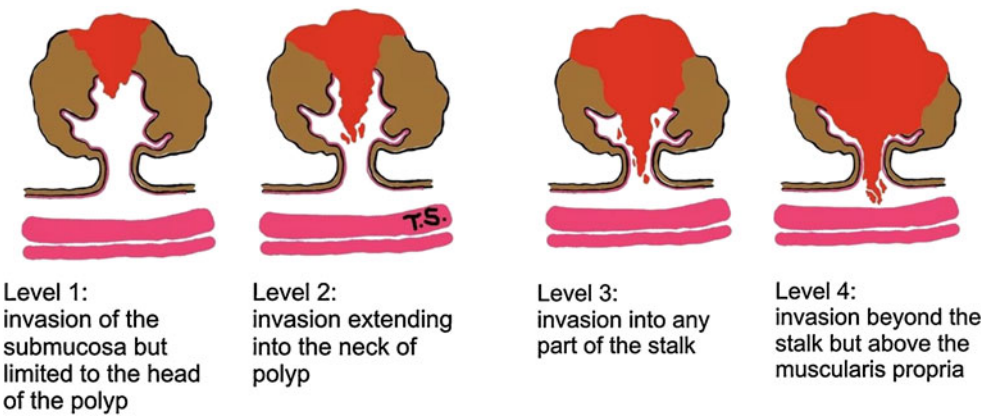

Fig. 2 Haggitt levels of invasion in polypoid carcinomas

Specimen handling starts with the endoscopic removal of the specimen and ends with the histopathological diagnosis and report. The need for a close relationship between endoscopists and histopathologists is stressed.

Submission of specimens

It is recommended to place specimens in separate containers, one for each lesion, to avoid confusion about exact location; if lesions are small, individual cassettes or multicassettes can be used. Biopsies from the same lesion can be placed in the same container. For endoscopic resections it is helpful to pin out specimens by inserting pins through the periphery of the specimen onto cork or thick paper. Too much tension on the specimen could result in artificially thinned lesions. Needles should not be placed directly through a lesion but at the margin. Besides patient data, an exact description on location should be provided (e.g. cms from anocutanous line), as well as size and morphology (stalked polyp, non-polypoid—Paris classification, etc.). Additional information about central depression or focal erosion or ulceration or coexistent chronic inflammatory bowel disease can be useful. Endoscopic pictures can also be submitted with the specimen(s).

Fixation

Fixation should be by buffered 10% formalin; this equals a roughly 4% paraformaldehyde concentration, as formalin is 30–40% paraformaldehyde. Specimen(s) can shrink due to formalin fixation, therefore measurements taken after fixation can differ from those prior to fixation. Fixation in alcohol is not recommended and if any other fixatives are used a comparative study of size of adenomas after fixation should be performed prior to use to avoid excessive shrinkage of adenomas to avoid under treatment.

Dissection

The pathologist should verify the complete removal of neoplastic lesions (clear margins) and the absence of submucosal invasion in biopsy specimens. Currently, we recommend that clearance of 1 mm or less indicates margin involvement (VI-B). Cases of incomplete removal or uncertainty about submucosal invasion should be highlighted in the pathology report (VI-B). Lesion size should be given in millimetres. Size should be carefully measured identifying the maximum diameter of the adenomatous component as well as the distance to the margin of excision(s) to within a millimeter (V-B).

Given the small dimensions of the submucosal layer, infiltration into the submucosal level should be measured in microns from the bottom line of the muscularis mucosae (VI-B).

Polypoid lesions

Polyps must be sliced and totally embedded. Special attention should be paid to the resection margin, which should be identified and described (dot-like, broad, stalked etc.) and either dissected tangentially into an extra cassette or sliced in a way that allows complete assessment.

Mucosal excisions

Mucosal excisions need to be pinned out on a cork board or on another suitable type of material, fixed, described and dissected allowing the identification of involvement of the deep and lateral surgical margins. Particular attention should be paid to any areas of ulceration or induration for signs of invasion. Inking margins is recommended.

Piecemeal removal

If it is possible to reconstruct a lesion removed piecemeal it may be helpful but this is not commonly the case. It is good practice to embed the entire lesion to allow exclusion of invasive malignancy. Occasionally, whole embedding will not be possible.

Sectioning and levels

Three or more levels should be cut through each block and stained with haematoxylin and eosin.

Surgically removed lesions

Classification

The staging of colorectal cancer can be undertaken by a number of different systems. The two used in Europe are TNM and the older Dukes classification. Originally the Dukes classification system placed patients into one of three categories (stages A, B, C) (see Table 2). This system

Table 2 Modified Dukes stage

Dukes A	Tumour penetrates into but not through the muscularis propria (the muscular layer) of the bowel wall
Dukes B	Tumour penetrates into and through the muscularis propria of the bowel wall but does not involve lymph nodes
Dukes C	C1: There is pathological evidence of adenocarcinoma in one or more lymph nodes but not the highest node
	C2: There is pathological evidence of adenocarcinoma in the lymph node at the high surgical tie
Stage D	Tumour has spread to other organs (such as the liver, lung or bone)

was subsequently modified by dividing stage C into stage C1 and C2 and the addition of a fourth stage (D). More recently, the Union Internationale Contra le Cancer (UICC) and the American Joint Committee on Cancer (AJCC) has introduced the TNM staging system, that places patients into one of four stages (stages I–IV). TNM is superior to Dukes because of the greater information it yields, but there are currently major issues due to the periodic reclassification of this system that can lead to stage migration. TNM has a number of versions, so the version used should be noted in brackets (e.g. v5, v6, v7). Tables 3, 4 and 5 permit comparison of the most recent versions, 5, 6 and 7 [40–42]. However, there are differences between the versions, particularly regarding the notes on T and N classification. There is also variation between countries as to the TNM classification used. For example, TNM 5 is recommended in the UK, Holland, Belgium and Denmark and is growing in popularity in other countries.

In the USA, version 7 is used. TNM 7 appears to be more subjective than TNM 5 due to the notes on N classification and the category N1c, promoting stage migration from II to III [62–64]. National results should be reported with the version of TNM used in a given country (VI-B).

Practical issues

High-quality reporting of colorectal cancer is very important both to the clinicians treating the patients and to the cancer registry. The introduction of a 'minimum' data proforma template allows more complete reporting compared with interpretation of free text reports by medical staff [65–72]. All biopsies and lesions identified in the screening programme and the subsequent resection specimens should be reported on a paper or electronic proforma (II-B) in a timely manner and in a minimum of 90% of all cases. The proforma should be sent to the referring physician, the relevant cancer registry and the screening programme (VI-B).

Dissection should be according to national guidelines such as those for the UK; Royal College of Pathologists

Table 3 TNM classification of tumours of the colon and rectum

	Clinical classification	5th edition (1997)	6th edition (2002)	7th edition (2009)
T—primary tumour				
TX	Primary tumour cannot be assessed	+	+	+
T0	No evidence of primary tumour	+	+	+
Tis[1]	Carcinoma in situ: intraepithelial or invasion of lamina propria	+	+	+
T1	Tumour invades submucosa	+	+	+
T2	Tumour invades muscularis propria	+	+	+
T3	Tumour invades through muscularis propria into subserosa or into non-peritonealised pericolic or perirectal tissues	+	+	+
T4[2,3]	Tumour directly invades into other organs or structures and/or perforates visceral peritoneum	+	+	+
T4a	Perforates visceral peritoneum	–	–	+
T4b	Directly invades other organ or structures	–	–	+
N—regional lymph nodes				
NX	Regional lymph nodes cannot be assessed	+	+	+
N0	No regional lymph node metastasis	+	+	+
N1	Metastasis in 1 to 3 regional lymph nodes	+	+	+
N1a	1 node	–	–	+
N1b	2–3 nodes	–	–	+
N1c	Satellites[4] in subserosa, without regional nodes	–	–	+
N2	Metastasis in 4 or more regional lymph nodes	+	+	+
N2a	4–6 nodes	–	–	+
N2b	7 or more nodes	–	–	+
M—distant metastasis				
MX	Distant metastasis cannot be assessed	+	+	–
M0	No distant metastasis	+	+	+
M1	Distant metastasis	+	+	+
M1a	Metastasis confined to one organ (liver, lung, ovary, non-regional lymph node(s))	–	–	+
M1b	Metastasis in more than one organ or the peritoneum	–	–	+

Table 4 TNM stage grouping of tumors

Stage	Stage grouping			5th Edition (1997)	6th Edition (2002)	7th Edition (2009)
	T	N	M			
Stage 0	Tis	N0	M0	+	+	+
Stage I	T1,T2	N0	M0	+	+	+
Stage II	T3,T4	N0	M0	–	–	+
Stage IIA	T3	N0	M0	+	+	+
Stage IIB	T4	N0	M0	+	+	–
Stage IIB	T4a	N0	M0	–	–	+
Stage IIC	T4b	N0	M0	–	–	+
Stage III	Any T	N1, N2	M0	–	–	+
Stage IIIA	T1,T2	N1	M0	+	+	+
Stage IIIA	T1,T2	N1c	M0	–	–	+
Stage IIIA	T1	N2a	M0	–	–	+
Stage IIIB	T3,T4	N1	M0	+	+	–
Stage IIIB	T3,T4a	N1/N1c	M0	–	–	+
Stage IIIB	T2,T3	N2a	M0	–	–	+
Stage IIIB	T1,T2	N2b	M0	–	–	+
Stage IIIC	Any T	N2	M0	+	+	–
Stage IIIC	T4a	N2a	M0	–	–	+
Stage IIIC	T3,T4a	N2b	M0	–	–	+
Stage IIIC	T4b	N1, N2	M0	–	–	+
Stage IV	Any T	Any N	M1	+	+	–
Stage IVA	Any T	Any N	M1a	–	–	+
Stage IVB	Any T	Any N	M1b	–	–	+

T tumour, *N* node, *M* metastasis

[73–75] and the NHS Bowel Cancer Screening publication [76], the Scottish clinical guidelines [77], the Dutch guidelines [78, 79], the German guidelines [80] or the Italian guidelines [81]. For examples of these guidelines see the list of websites in Appendix 4 of the full guideline document [9]. If national guidelines do not exist they should be created or adopted from elsewhere (VI-B). An additional free text written report is optional, but needs to include all of the data required in the proforma (VI-B).

Pathologists need access to a high-quality, binocular microscope with at least the following objectives: 5×, 10×, 20× and 40× and that fulfils national guidelines such as those of the Sector Committee for Pathology and Neuropathology of the German Accreditation Body [82]

A computer is required for identifying previous material from a given patient and for filling in proformas electronically and online if secure online services are available. Adequate time must be available for dissection, reporting, and attendance at meetings of the screening team and the colorectal cancer multidisciplinary team (VI-B). Time and funding are required for pathologists to attend national meetings on the screening programme and continued training in histopathology of colorectal neoplasia. Pathologists should attend one refresher training course every year on the pathology of colorectal neoplasia to maintain quality (VI-B).

Standards and quality indicators

There should be good communication between members of the screening team with agreed terminology, regular meetings and clinical discussions (VI-B).

An external quality assurance programme should be put in place, specifying a minimum of two slide circulations per year of an adequate number of slides (VI-B). This may be via clusters or cells of pathologists using glass slides, or can be electronic using images or virtual slides [83] distributed via DVD or the web (see http://www.virtualpathology.leeds.ac.uk). There should be external oversight of such programmes. In the absence of evidence-based guidelines we recommend that pathologists reporting in a colonoscopy programme should not report high-grade neoplasia in more than 5% of lesions and those in an FOBT programme in not more than 10% of lesions (VI-B).

The pathologists reporting in the programme must meet their national criteria for safety in reporting colorectal cancer (VI-B). Departments and pathologists taking part in screening programmes should audit their own reporting practices for key features, including the number of lymph nodes retrieved, the frequency of circumferential resection margin involvement (CRM) and the frequency of high-risk features such as extramural vascular invasion and peritoneal

Table 5 Notes

No.	Notes		
	5th edition	6th edition	7th edition
1	Tis includes cancer cells confined within the glandular basement membrane (intraepithelial) or lamina propria (intramucosal) with no extension through muscularis mucosae into the submucosa. Note: the authors of the European Guidelines for quality assurance in pathology in CRC screening and diagnosis recommend not using this category. Respective lesions should be reported as mucosal high-grade neoplasia, see above ("Grading of neoplasia")		
2	Direct invasion in T4 includes invasion of other segments of the colon or rectum by way of the serosa, e.g. invasion of sigmoid colon by a carcinoma of the cecum		Direct invasion in T4b includes invasion of other organs or segments of the colon or rectum by way of the serosa, as confirmed on microscopic examination, or for tumours in a retroperitoneal or subperitoneal location, direct invasion of other organs or structures by virtue of extension beyond the muscularis propria
3		Tumour that is adherent to other organs or structures, macroscopically, is classified T4. However, if no tumour is present in the adhesion, microscopically, the classification should be pT3	Tumour that is adherent to other organs or structures, macroscopically, is classified cT4b. However, if no tumour is present in the adhesion, microscopically, the classification should be pT1–T3, depending on the anatomical depth of wall invasion
4	A tumour nodule greater than 3 mm in diameter in perirectal or pericolic adipose tissue without histological evidence of a residual lymph node in the nodule is classified as regional lymph node metastasis. However, a tumour nodule up to 3 mm in diameter is classified in the T category as discontinuous extension i.e. T3.	A tumour nodule in the pericolic/perirectal adipose tissue without histological evidence of a residual lymph node in the nodule is classified in the pN category as a regional lymph node metastasis if the nodule has the form and smooth contour of a lymph node. If the nodule has an irregular contour it should be classified in the T category and also coded as V1 (microscopic venous invasion) or V2, if it was grossly evident, because there is a strong likelihood that it represents venous invasion	Tumour deposits (satellites), i.e. macroscopic or microscopic nests or nodules, in the pericolorectal adipose tissue's lymph drainage area of a primary carcinoma without histological evidence of residual lymph node in the nodule, may represent discontinuous spread, venous invasion with extra-vascular spread (V1/2) or a totally replaced lymph node (N1/2). If such deposits are observed with lesions that would otherwise be classified as T1 or T2, then the T classification is not changed, but the nodule is recorded as N1c. If a nodule is considered by the pathologist to be a totally replaced lymph node (generally having a smooth contour), it should be recorded as a positive lymph node and not as a satellite, and each nodule should be counted separately as a lymph node in the final pN determination. (Note of the authors of the European Guidelines for quality assurance in pathology in CRC screening and diagnosis: introduction of N1c category leads to stage shift from II to III for some tumours)

invasion reported (VI-B). In the UK, national standards suggest that the number of nodes retrieved should be above a median of 12, CRM positivity in rectal cancer should be below 15%, extramural vascular invasion reported in more than 25%, and peritoneal invasion in more than 20%. The laboratory must be able to demonstrate participation in a laboratory technical external quality assurance programme, such as Clinical Pathology Accreditation UK (http://www.cpa-uk.co.uk/), the ISO/IEC accreditation developed by the Sector Committee for Pathology and Neuropathology of the German Accreditation Body (http://www.dakks.de/, see also Ref. [84]), or other national standards (VI-C).

Data collection and monitoring

Lesions reported in the screening programme should be reported by proforma (II-B) or structured reporting, and the

data returned to the screening programme or national tumour registries. This will include all lesions identified and the subsequent resection specimen. This should occur in a minimum of 90% of all cases (VI-B).

Studies have shown discrepancy between the histopathology of biopsies and total removal by polypectomy, EMR and surgical specimens. Colorectal cancer was detected in surgical specimens in over 20% of biopsies diagnosed with high-grade neoplasia [85]. Sub-mucosal invasion was detected in surgical specimens in over 25% of cases with mucosal neoplasia [22]. Therefore, the correlation between histological diagnosis of biopsies and resections should be reported. Any lack of correlation should be discussed by the multidisciplinary team and the results of this discussion should be documented (III-B).

Pathologists must ensure that their proformas are received by the screening programme coordinators or a cancer registry for the purposes of clinical management, audit and quality assurance (VI-B).

Results from the key indicators of quality should be returned for analysis to the funding body: either the Health Authority or the national screening programme's offices (VI-B).

Statistics should include the frequency of colorectal cancer and the distribution of TNM stages and version used; as well as the distribution of the type of lesion, size, location, frequency of grades of dysplasia and villousness (villous, tubulo-villous or tubular) and presence of non-neoplastic lesions (VI-B).

Images

A selection of images and digital slides showing the histopathology of lesions commonly detected in screening programmes, as well as some images illustrating pitfalls in histopathologic interpretation is provided in the internet at http://www.virtualpathology.leeds.ac.uk (go to: "European Guidelines for quality assurance in pathology in colorectal cancer screening and diagnosis—Imaging library"). The site has been created to establish an initial, quality-assured repository for images illustrating the chapter on pathology in the first guideline edition [10]. The images are provided here for reference and have been reviewed by pathologists from at least three European countries. We encourage colleagues to submit further images which they feel could be instructive or otherwise useful in illustrating or further developing the European Guidelines.

We also aim to extend the scope of this site in the future to promote pan-European and international collaboration in training and in expanding the evidence base for further advances in colorectal cancer screening and diagnosis.

Conclusions and recommendations

In a state-of-the-art process, wide consensus has been achieved on the following evidence-based recommendations for quality assurance of pathology in colorectal cancer screening and diagnosis. In light of the experience with similar guidelines for breast and cervical cancer screening in the EU, the future availability of this reference document has the potential to improve multidisciplinary management of colorectal cancer detected within and outside the setting of screening programmes. The availability of a uniform classification for reporting lesions detected in screening programmes across Europe also has the potential to improve international collaboration and exchange of experience in improving the quality and effectiveness of colorectal cancer care.

1. Due to the improved diagnostic reproducibility of the revised Vienna classification use of this classification in a format modified for lesions detected in screening is recommended to ensure consistent international communication and comparison of histopathology of biopsies and resection specimens (IV-B). Only two grades of colorectal neoplasia (low grade and high grade) should be used, to minimise intraobserver and interobserver error (V-B). The terms intramucosal adenocarcinoma or in-situ carcinoma should not be used (VI-B).
2. The World Health Organisation (WHO) definition of colorectal adenocarcinoma should be used: "an invasion of neoplastic cells through the muscularis mucosae into the submucosa" (VI-A).
3. Adenocarcinomas should be reported according to the tumour, node, metastasis (TNM) classification. The version of TNM to be used should be decided nationally and should be stated e.g. pT1 pN0 pMX (Version 5) or pT4 pN2 pM1 (Version 7). These can be further abbreviated to pT1N0MX (v5) or to pT4N2M1 (v7) (VI-B).
4. The WHO classification of adenomas into tubular, tubulo-villous and villous should be used (VI-A).
5. Due to the increased risk of colorectal cancer associated with flat and/or depressed lesions they should be reported as non-polypoid lesions (III) and further classified by the Paris classification (V-B).
6. The pathologist should verify the complete removal of neoplastic lesions (clear margins) and the absence of submucosal invasion in biopsy specimens. Currently we recommend that clearance of 1 mm or less indicates margin involvement (VI-B). Cases of incomplete removal or uncertainty about submucosal invasion should be highlighted in the pathology report (VI-B).
7. Substaging of T1 cancers should be performed to determine the risk of residual disease. Consideration

should be given to the appropriate method, which may vary depending on the morphology of the lesion (Kikuchi/Haggitt or measurement). For non-polypoid lesions the Kikuchi stage and for pedunculated lesions Haggitt are currently recommended (VI-C). High-risk features for residual disease such as lack of margin clearance (≤1 mm), poor differentiation and lymphatic and vascular invasion should be reported (V-B). The multidisciplinary team should be consulted on whether or not surgical resection of pT1 adenocarcinoma is recommended; if surgical resection is recommended, consideration should be given to obtaining an opinion from a second histopathologist as variation exists in evaluating high-risk features (VI-A).

8. The size of lesions should be carefully measured by the pathologist to the nearest mm on the haematoxylin and eosin slide, or on the fixed specimen when the largest dimension of the lesion cannot be reliably measured on the slide. Endoscopy measurements are less accurate and should only be used when strictly necessary, e.g. if the lesion is fragmented (III-B). Given the small dimensions of the submucosal layer, infiltration into the submucosal level should be measured in microns from the bottom line of the muscularis mucosae (VI-B).
9. Programmes should have a policy on the methodology of, and should regularly monitor the accuracy of size measurements of endoscopically removed lesions. Deviation between the actual size and the measurements of pathologists and endoscopists should be minimised. Management decisions which depend on lesion size should take into account potential inaccuracy in the size measurement. The multidisciplinary team should consider deviating from the recommended size categories in treatment and surveillance algorithms, if the review of a case indicates that there is sufficient reason to doubt the accuracy of the measurement. Such cases should be captured as an auditable outcome (VI-B).
10. Hyperplastic polyps are non-neoplastic and their complete removal is optional. All other lesions in the serrated pathway should be excised and serrated lesions with neoplasia should be followed up (surveillance) as if they were adenomas (VI-C).
11. All biopsies and lesions identified in the screening programme and the subsequent resection specimen should be reported on a proforma (IV-B) in a timely manner and in a minimum of 90% of all cases. The proforma should be sent to the referring physician, the relevant cancer registry and the screening programme (VI-B).
12. Dissection of all specimens should be according to national guidelines. If national guidelines do not exist they should be created or adopted from elsewhere. An additional free text written report is optional, but must include all of the data required in the proforma (VI-B).
13. The correlation between histological diagnosis of biopsy and surgical specimens should be reported. Any lack of correlation should be discussed by the multidisciplinary team, and the results of this discussion should be documented (III-B).
14. Pathologists must ensure that their proformas are received by the screening programme coordinators or a cancer registry for the purposes of clinical management, audit and quality assurance. Results from the key indicators of quality should be returned to the funding body: either the Health Authority or the national screening programmes' offices for analysis (VI-B).
15. Statistics should include the frequency of colorectal cancer and the distribution of TNM stages and version used, as well as the distribution of the type of lesion, size, location, frequency of grades of neoplasia and villousness (villous, tubulo-villous or tubular) and presence of non-neoplastic lesions (VI-B).
16. There should be good communication between the members of the screening team with agreed terminology, regular meetings and clinical discussions (VI-B).
17. Pathologists taking part in a colorectal cancer screening programme must participate regularly in multidisciplinary team meetings, and twice a year in an external quality assurance programme that has external oversight of the results (VI-B).
18. Departments and individual pathologists should audit their own reporting practices for key features (VI-B).
19. Pathologists reporting in a colorectal cancer screening programme must meet their national criteria for safety in reporting colorectal cancer (VI-B).
20. Departments and pathologists taking part in screening programmes should audit the number of lymph nodes retrieved, the frequency of circumferential resection margin involvement and the frequency of high-risk features such as extramural vascular invasion, tumour perforation and peritoneal invasion reported (VI-B).
21. Pathologists reporting in a colonoscopy screening programme should not report high-grade neoplasia in more than 5% of lesions and those in an Faecal Occult Blood Test programme in not more than 10% of lesions (VI-B).
22. Pathologists should attend one refresher training course every year on the pathology of colorectal neoplasia to maintain quality (VI-B).
23. Laboratories participating in a screening programme must be able to demonstrate participation in a laboratory technical external quality assurance programme and hold external accreditation for their services (VI-C).

Further detailed information can be found in Ref. [11].

Acknowledgements Some of the materials contained in these guidelines is reproduced with permission of the UK bowel cancer screening programme pathology screening committee (Carey F, Mapstone N, Quirke P (Chair), Shepherd N, Warren B, Williams G) and the Royal College of Pathologists minimum dataset for colorectal cancer reporting (Williams G, Quirke P, Shepherd N).

We thank the following external reviewers for reading and providing helpful comments and suggestions on the draft chapter and annex on *Quality assurance in pathology in colorectal cancer screening and diagnosis* during the preparation of the full guidelines document: Robert Riddell, Toronto, Canada; Hiroshi Saito, Tokyo and Hidenobu Watanabe, Niigata, Japan.

The comments and suggestions received from consultation of the European Cancer Network are gratefully acknowledged.

Phil Quirke is supported by Yorkshire Cancer Research and the Department of Health/Cancer Research UK Experimental Cancer Medicine Centre Initiative

Financial support of the European Communities through the EU Public Health Programme (Development of European Guidelines for Quality Assurance of Colorectal Cancer Screening lCRC), grant agreement No. 2005317), of the Public Affairs Committee of the United European Gastroenterology Federation, and from a cooperative agreement between the American Cancer Society and the Division of Cancer Prevention and Control at the Centers for Disease Control and Prevention is gratefully acknowledged.

The technical support of Tracy Lignini, Krittika Guinot and Simon Ducarroz at the International Agency for Research on Cancer, Lyon, France, in the preparation of the manuscript and the assistance of Dr. Tilman Schulz, Bayreuth, Germany, in the creation of illustrations is gratefully acknowledged.

Conflicts of interest Pathology and Tumour Biology at the Leeds Institute of Molecular Medicine, led by Phil Quirke, at the University of Leeds has received funding from the EU Public Health Programme (Development of European Guidelines for Quality Assurance of Colorectal Cancer Screening (CRC), grant agreement No. 2005317) to develop a prototype web-based training tool for pathology in colorectal cancer screening. Phil Quirke has also received funding from the National Health Service Bowel Cancer Screening Programme and Yorkshire Cancer Research.

The International Agency for Research on Cancer, where Lawrence von Karsa is employed, is a recipient of research grants from the EU Public Health Programme.

Open Access This article is distributed under the terms of the Creative Commons Attribution Noncommercial License which permits any noncommercial use, distribution, and reproduction in any medium, provided the original author(s) and source are credited.

References

1. von Karsa L, Anttila A, Ronco G, Ponti A, Malila N, Arbyn M, Segnan N, Castillo-Beltran M, Boniol M, Ferlay J, Hery C, Sauvaget C, Voti L, Autier P (2008) Cancer screening in the European Union—Report on the implementation of the Council Recommendation on cancer screening, First Report. European Commission, Luxembourg
2. Ferlay J, Shin HR, Bray F, Forman D, Mathers C, Parkin DM (2010) GLOBOCAN 2008, Cancer Incidence and Mortality Worldwide: IARC CancerBase No. 10 [Internet]. International Agency for Research on Cancer, Lyon
3. Hardcastle JD, Chamberlain JO, Robinson MH, Moss SM, Amar SS, Balfour TW, James PD, Mangham CM (1996) Randomised controlled trial of faecal-occult-blood screening for colorectal cancer. Lancet 348(9040):1472–1477
4. Kronborg O, Fenger C, Olsen J, Jorgensen OD, Sondergaard O (1996) Randomised study of screening for colorectal cancer with faecal-occult-blood test. Lancet 348(9040):1467–1471
5. Mandel JS, Bond JH, Church TR, Snover DC, Bradley GM, Schuman LM, Ederer F (1993) Reducing mortality from colorectal cancer by screening for fecal occult blood. Minnesota colon cancer control study. N Engl J Med 328(19):1365–1371
6. Council of the European Union (2003) Council recommendation of 2 December 2003 on cancer screening (2003/878/EC). Off J Eur Union (L 327):34–38
7. Perry N, Broeders M, de Wolf C, Tornberg S, Holland R, von Karsa L (eds) (2006) European guidelines for quality assurance in breast cancer screening and diagnosis. European guidelines for quality assurance in breast cancer screening and diagnosis, 4th edn. Office for Official Publications of the European Communities, Luxembourg
8. European guidelines for quality assurance in cervical cancer screening - Second Edition. Arbyn M, Anttila A, Jordan J, Schenck U, Ronco G, Segnan N, Wiener H, Herbert A, Daniel J, von Karsa L (eds) (2008) European Guidelines for Quality Assurance in Cervical Cancer Screening—Second Edition. Office for Official Publications of the European Communities, Luxembourg
9. European guidelines for quality assurance in colorectal cancer screening and diagnosis. Segnan N, Patnick J, von Karsa L (eds) (2010) European guidelines for quality assurance in colorectal cancer screening and diagnosis - First edition (in press)
10. Quirke P, Risio M, Lambert R, Vieth M (2010) Quality assurance in pathology in colorectal cancer screening and diagnosis. In: Segnan N, Patnick J, von Karsa L (eds) European Guidelines for Quality Assurance in Colorectal Cancer Screening and Diagnosis - First edition (in press)
11. Vieth M, Quirke P, Lambert R, von Karsa L, Risio M (2010) Annotations of colorectal lesions. In: Segnan N, Patnick J, von Karsa L (eds) European guidelines for quality assurance in colorectal cancer screening and diagnosis - First edition (in press)
12. Snover DC, Jass JR, Fenoglio-Preiser C, Batts KP (2005) Serrated polyps of the large intestine: a morphologic and molecular review of an evolving concept. Am J Clin Pathol 124(3):380–391
13. Minozzi S, Armaroli P, Segnan N (2010) Principles of evidence assessment and methods for reaching recommendations. In: Segnan N, Patnick J, von Karsa L (eds) European guidelines for quality assurance in colorectal cancer screening and diagnosis - First Edition, pp LIII–LXI (in press)
14. Greenhalgh T (1997) Why read papers at all? In: How to read a paper. The basics of evidence-based medicine. BMJ Books, London. pp 1–14
15. O'Connor D, Green S, Higgins JPT (2008) Defining the review question and developing criteria for including studies. In: Higgins JPT, Green S (eds) Cochrane handbook for systematic reviews of interventions (Wiley Cochrane Series) (Hardcover). Wiley-Blackwell, UK
16. Richardson WS, Wilson MC, Nishikawa J, Hayward RS (1995) The well-built clinical question: a key to evidence-based decisions. ACP J Club 123(3):A12–A13
17. Shea BJ, Grimshaw JM, Wells GA, Boers M, Andersson N, Hamel C, Porter AC, Tugwell P, Moher D, Bouter LM (2007) Development of AMSTAR: a measurement tool to assess the methodological quality of systematic reviews. BMC Med Res Methodol 7:10
18. Higgins JPT, Altman DG (2008) Assessing risk of bias in included studies. In: Higgins JPT, Green S (eds) Cochrane handbook for systematic reviews of interventions. Wiley-Blackwell, UK
19. Wells GA, Shea B, O'Connell D, Peterson J, Welch V, Losos M, Tugwell P (2010) The Newcastle-Ottawa Scale (NOS) for

assessing the quality of nonrandomised studies in meta-analyses. Available at: http://www.ohri.ca/programs/clinical_epidemiology/oxford.htm. Accessed 16 Sept 2010
20. Whiting P, Rutjes AW, Reitsma JB, Bossuyt PM, Kleijnen J (2003) The development of QUADAS: a tool for the quality assessment of studies of diagnostic accuracy included in systematic reviews. BMC Med Res Methodol 3:25
21. Kudo S, Lambert R, Allen JI, Fujii H, Fujii T, Kashida H, Matsuda T, Mori M, Saito H, Shimoda T, Tanaka S, Watanabe H, Sung JJ, Feld AD, Inadomi JM, O'Brien MJ, Lieberman DA, Ransohoff DF, Soetikno RM, Triadafilopoulos G, Zauber A, Teixeira CR, Rey JF, Jaramillo E, Rubio CA, Van GA, Jung M, Vieth M, Jass JR, Hurlstone PD (2008) Nonpolypoid neoplastic lesions of the colorectal mucosa. Gastrointest Endosc 68(4 Suppl): S3–S47
22. Tominaga K, Fujinuma S, Endo T, Saida Y, Takahashi K, Maetani I (2009) Efficacy of the revised Vienna classification for diagnosing colorectal epithelial neoplasias. World J Gastroenterol 15(19):2351–2356
23. WHO (2000) Pathology and genetics of tumours in the digestive system. Carcinoma of the colon and rectum. In: Hamilton SR, Aaltonen LA (eds) World health organization international histological classification of tumours. IARC, Lyon, pp 105–119
24. Schlemper RJ, Riddell RH, Kato Y, Borchard F, Cooper HS, Dawsey SM, Dixon MF, Fenoglio-Preiser CM, Flejou JF, Geboes K, Hattori T, Hirota T, Itabashi M, Iwafuchi M, Iwashita A, Kim YI, Kirchner T, Klimpfinger M, Koike M, Lauwers GY, Lewin KJ, Oberhuber G, Offner F, Price AB, Rubio CA, Shimizu M, Shimoda T, Sipponen P, Solcia E, Stolte M, Watanabe H, Yamabe H (2000) The Vienna classification of gastrointestinal epithelial neoplasia. Gut 47(2):251–255
25. Schlemper RJ, Kato Y, Stolte M (2001) Review of histological classifications of gastrointestinal epithelial neoplasia: differences in diagnosis of early carcinomas between Japanese and Western pathologists. J Gastroenterol 36(7):445–456
26. Dixon MF (2002) Gastrointestinal epithelial neoplasia: Vienna revisited. Gut 51(1):130–131
27. Stolte M (2003) The new Vienna classification of epithelial neoplasia of the gastrointestinal tract: advantages and disadvantages. Virchows Arch 442(2):99–106
28. Suzuki N, Price AB, Talbot IC, Wakasa K, Arakawa T, Ishiguro S, Fraser C, Saunders BP (2006) Flat colorectal neoplasms and the impact of the revised Vienna Classification on their reporting: a case-control study in UK and Japanese patients. Scand. J Gastroenterol 41(7):812–819
29. Schoen RE, Gerber LD, Margulies C (1997) The pathologic measurement of polyp size is preferable to the endoscopic estimate. Gastrointest Endosc 46(6):492–496
30. EC Working Group on Breast Screening Pathology (2006) Quality assurance guidelines for pathology. Open biopsy and resection specimens. In: Perry N, Broeders M, de Wolf C, Tornberg S, Holland R, von Karsa L (eds) European guidelines for quality assurance in breast cancer screening and diagnosis, 4th edn. Office for Official Publications of the European Communities, Luxembourg
31. The Paris Classification (2003) The Paris endoscopic classification of superficial neoplastic lesions: esophagus, stomach, and colon: November 30 to December 1, 2002. Gastrointest Endosc 58 (6 Suppl):S3–S43
32. Soetikno RM, Kaltenbach T, Rouse RV, Park W, Maheshwari A, Sato T, Matsui S, Friedland S (2008) Prevalence of nonpolypoid (flat and depressed) colorectal neoplasms in asymptomatic and symptomatic adults. JAMA 299(9):1027–1035
33. Longacre TA, Fenoglio-Preiser CM (1990) Mixed hyperplastic adenomatous polyps/serrated adenomas. A distinct form of colorectal neoplasia. Am J Surg Pathol 14(6):524–537
34. Atkin W, Valori R, Kuipers EJ, Hoff G, Senore C, Segnan N, Jover R, Schmiegel W, Lambert R, Pox C (2010) Colonoscopic surveillance after adenoma removal. In: Segnan N, Patnick J, von Karsa L (eds) European Guidelines for Quality Assurance in Colorectal Cancer Screening and Diagnosis - First edition (in press)
35. Jass JR, Baker K, Zlobec I, Higuchi T, Barker M, Buchanan D, Young J (2006) Advanced colorectal polyps with the molecular and morphological features of serrated polyps and adenomas: concept of a 'fusion' pathway to colorectal cancer. Histopathology 49(2):121–131
36. Fenger C, Bak M, Kronborg O, Svanholm H (1990) Observer reproducibility in grading dysplasia in colorectal adenomas: comparison between two different grading systems. J Clin Pathol 43(4):320–324
37. Jass JR, Williams CB, Bussey HJ, Morson BC (1988) Juvenile polyposis—a precancerous condition. Histopathology 13(6):619–630
38. Burt R, Jass J (2000) Hyperplastic polyposis. World health organisation classification of tumours: pathology and genetics of tumours of the digestive system. IARC, Lyon, pp 135–136
39. WHO (1989) Histological typing of intestinal tumours. In: Jass JR, Sobin LH (eds) World health organisation international histological classification of tumours, 2nd edn. Springer-Verlag, Berlin, p 30
40. Sobin LH, Wittekind C (eds) (1997) TNM classification of malignant tumours, 5th edn. Wiley, New York
41. Sobin LH, Wittekind C (eds) (2002) TNM Classification of malignant tumours, 6th edn. Wiley, New Jersey
42. TNM Classification of Malignant Tumours, 7th Edition Sobin LH, Gospodarowicz MK, Wittekind C (eds) (2009) TNM Classification of Malignant Tumours, 7th Edition. Wiley-Blackwell, New York
43. Muto T, Bussey HJ, Morson BC (1973) Pseudo-carcinomatous invasion in adenomatous polyps of the colon and rectum. J Clin Pathol 26(1):25–31
44. Cooper HS, Deppisch LM, Gourley WK, Kahn EI, Lev R, Manley PN, Pascal RR, Qizilbash AH, Rickert RR, Silverman JF (1995) Endoscopically removed malignant colorectal polyps: clinicopathologic correlations. Gastroenterology 108(6):1657–1665
45. Coverlizza S, Risio M, Ferrari A, Fenoglio-Preiser CM, Rossini FP (1989) Colorectal adenomas containing invasive carcinoma. Pathologic assessment of lymph node metastatic potential. Cancer 64(9):1937–1947
46. Hassan C, Zullo A, Risio M, Rossini FP, Morini S (2005) Histologic risk factors and clinical outcome in colorectal malignant polyp: a pooled-data analysis. Dis Colon Rectum 48 (8):1588–1596
47. Volk EE, Goldblum JR, Petras RE, Carey WD, Fazio VW (1995) Management and outcome of patients with invasive carcinoma arising in colorectal polyps. Gastroenterology 109(6):1801–1807
48. Blumberg D, Paty PB, Guillem JG, Picon AI, Minsky BD, Wong WD, Cohen AM (1999) All patients with small intramural rectal cancers are at risk for lymph node metastasis. Dis Colon Rectum 42(7):881–885
49. Kikuchi R, Takano M, Takagi K, Fujimoto N, Nozaki R, Fujiyoshi T, Uchida Y (1995) Management of early invasive colorectal cancer. Risk of recurrence and clinical guidelines. Dis Colon Rectum 38(12):1286–1295
50. Kudo S (1993) Endoscopic mucosal resection of flat and depressed types of early colorectal cancer. Endoscopy 25 (7):455–461
51. Nascimbeni R, Burgart LJ, Nivatvongs S, Larson DR (2002) Risk of lymph node metastasis in T1 carcinoma of the colon and rectum. Dis Colon Rectum 45(2):200–206
52. Haggitt RC, Glotzbach RE, Soffer EE, Wruble LD (1985) Prognostic factors in colorectal carcinomas arising in adenomas:

implications for lesions removed by endoscopic polypectomy. Gastroenterology 89(2):328–336
53. Ueno H, Mochizuki H, Hashiguchi Y, Shimazaki H, Aida S, Hase K, Matsukuma S, Kanai T, Kurihara H, Ozawa K, Yoshimura K, Bekku S (2004) Risk factors for an adverse outcome in early invasive colorectal carcinoma. Gastroenterology 127(2):385–394
54. Washington MK, Berlin J, Branton P, Burgart LJ, Carter DK, Fitzgibbons PL, Halling K, Frankel W, Jessup J, Kakar S, Minsky B, Nakhleh R, Compton CC (2009) Protocol for the examination of specimens from patients with primary carcinoma of the colon and rectum. Arch Pathol Lab Med 133(10):1539–1551
55. Cooper HS, Deppisch LM, Kahn EI, Lev R, Manley PN, Pascal RR, Qizilbash AH, Rickert RR, Silverman JF, Wirman JA (1998) Pathology of the malignant colorectal polyp. Hum Pathol 29 (1):15–26
56. Masaki T, Matsuoka H, Sugiyama M, Abe N, Sakamoto A, Atomi Y (2006) Actual number of tumor budding as a new tool for the individualization of treatment of T1 colorectal carcinomas. J Gastroenterol Hepatol 21(7):1115–1121
57. Sakuragi M, Togashi K, Konishi F, Koinuma K, Kawamura Y, Okada M, Nagai H (2003) Predictive factors for lymph node metastasis in T1 stage colorectal carcinomas. Dis Colon Rectum 46(12):1626–1632
58. Deinlein P, Reulbach U, Stolte M, Vieth M (2003) Risk factors for lymphatic metastasis from pT1 colorectal adenocarcinoma. Pathologe 24(5):387–393
59. Wang HS, Liang WY, Lin TC, Chen WS, Jiang JK, Yang SH, Chang SC, Lin JK (2005) Curative resection of T1 colorectal carcinoma: risk of lymph node metastasis and long-term prognosis. Dis Colon Rectum 48(6):1182–1192
60. Prall F (2007) Tumour budding in colorectal carcinoma. Histopathology 50(1):151–162
61. Okuyama T, Oya M, Ishikawa H (2002) Budding as a risk factor for lymph node metastasis in pT1 or pT2 well-differentiated colorectal adenocarcinoma. Dis Colon Rectum 45(5):628–634
62. Jass JR, O'Brien J, Riddell RH, Snover DC (2008) Recommendations for the reporting of surgically resected specimens of colorectal carcinoma: association of directors of anatomic and surgical pathology. Am J Clin Pathol 129(1):13–23
63. Quirke P, Cuvelier C, Ensari A, Glimelius B, Laurberg S, Ortiz H, Piard F, Punt CJA, Glenthoj A, Pennickx F, Seymour M, Valentini V, Williams G, Nagtegaal I (2010) Evidence-based medicine: the time has come to set standards for staging. J Pathol 221(4):357–360
64. Quirke P, Williams GT, Ectors N, Ensari A, Piard F, Nagtegaal I (2007) The future of the TNM staging system in colorectal cancer: time for a debate? Lancet Oncol 8(7):651–657
65. Beattie GC, McAdam TK, Elliott S, Sloan JM, Irwin ST (2003) Improvement in quality of colorectal cancer pathology reporting with a standardized proforma—a comparative study. Colorectal Dis 5(6):558–562
66. Branston LK, Greening S, Newcombe RG, Daoud R, Abraham JM, Wood F, Dallimore NS, Steward J, Rogers C, Williams GT (2002) The implementation of guidelines and computerised forms improves the completeness of cancer pathology reporting. The CROPS project: a randomised controlled trial in pathology. Eur J Cancer 38(6):764–772
67. Eon Y, Le Douy JY, Lamer B, Battini J, Bretagne JF (2006) Quality and completeness of histopathology reports of rectal cancer resections. Results of an audit in Brittany. Gastroentérol Clin Biol 30(2):235–240
68. Oppong C, Robertson N, Sherwood A, Brodribb J (2002) The use of a proforma improves colorectal cancer pathology reporting. Ann R Coll Surg Engl 84(4):290
69. Quirke P, Williams GT (1998) Minimum dataset for colorectal cancer histopathology reports. Royal College of Pathologists, London
70. Rigby K, Brown SR, Lakin G, Balsitis M, Hosie KB (1999) The use of a proforma improves colorectal cancer pathology reporting. Ann R Coll Surg Engl 81(6):401–403
71. Wei JT, Miller EA, Woosley JT, Martin CF, Sandler RS (2004) Quality of colon carcinoma pathology reporting: a process of care study. Cancer 100(6):1262–1267
72. Cross SS, Feeley KM, Angel CA (1998) The effect of four interventions on the informational content of histopathology reports of resected colorectal carcinomas. J Clin Pathol 51 (6):481-482
73. Williams GT, Quirke P, Shepherd NA (2007) Dataset for colorectal cancer (2nd edition) - Appendix D: Proforma for local excision specimens. Available at: http://www.rcpath.org/resources/worddocs/G049ColorectalDatasetAppendixD-Sep07.doc. Accessed 16 Sept 2010
74. Williams GT, Quirke P, Shepherd NA (2007) Dataset for colorectal cancer (2nd edition) - Appendix C: Proforma for colorectal cancer resections. Available at: http://www.rcpath.org/resources/worddocs/G049ColorectalDatasetAppendixC-Sep07.doc. Accessed 16 Sept 2010
75. Williams GT, Quirke P, Shepherd NA (2007) Dataset for colorectal cancer (2nd edition). Available at: http://www.rcpath.org/resources/pdf/G049-ColorectalDataset-Sep07.pdf. Accessed 16 Sept 2010
76. NHS Bowel Cancer Screening Programme (2007) Reporting lesions in the NHS bowel cancer screening programme - guidelines from the bowel cancer screening programme pathology group. Available at: http://www.cancerscreening.nhs.uk/bowel/publications/nhsbcsp01.pdf. Accessed 16 Sept 2010
77. SIGN (2003) Scottish intercollegiate guidelines network—guidelines for the management of colorectal cancer. Available at: http://www.sign.ac.uk/pdf/sign67.pdf. Accessed 16 Sept 2010
78. Vereniging integrale kankercentra (2008) Rectal cancer. Nationwide guideline, Version: 2.0. Available at: http://www.oncoline.nl/richtlijn/doc/index.php?type=save&richtlijn_id=615. Accessed 16 Sept 2010
79. Vereniging integrale kankercentra (2008) Colon cancer. Nationwide guideline, Version: 2.0. Available at: http://www.oncoline.nl/richtlijn/doc/index.php?type=save&richtlijn_id=598. Accessed 16 Sept 2010
80. Schmiegel W, Reinacher-Schick A, Arnold D, Graeven U, Heinemann V, Porschen R, Riemann J, Rodel C, Sauer R, Wieser M, Schmitt W, Schmoll HJ, Seufferlein T, Kopp I, Pox C (2008) [Update S3-guideline "colorectal cancer" 2008]. Z Gastroenterol 46(8):799–840
81. Risio M, Baccarini P, Casson P, Clemente C, Ederle A, Fiocca R, Senore C, Sonzogno A, Tomezzoli A, Zamboni G (2006) Histopathologic diagnosis in colorectal cancer screening: guidelines. Pathologica 98(3):171–174
82. DAP-TM-30 (2007) Leitfaden zur Interpretation der Anforderungen der DIN EN ISO/IEC 17020 : 2004 und technische Kriterien fuer deren Anwendung zur Akkreditierung in der Pathologie/Neuropathologie. Available at: http://www.dap.de/95doc/DAP-TM-30.pdf :11. Accessed 16 Sept 2010
83. Risio M, Bussolati G, Senore C, Vigna S, Frangipane E, Segnan N, Cassoni P (2010) Virtual microscopy for histology quality assurance of screen-detected polyps. J Clin Pathol 63(10):916-920
84. Roecken C, Manke H (2010) Akkreditierung in der Pathologie. Systemdarstellung und Dokumentation der Taetigkeiten in der Pathologie. Pathologe 31:268–278
85. Gondal G, Grotmol T, Hofstad B, Bretthauer M, Eide TJ, Hoff G (2005) Biopsy of colorectal polyps is not adequate for grading of neoplasia. Endoscopy 37(12):1193–1197
86. Torlakovic EE, Gomez JD, Driman DK, Parfitt JR, Wang C, Benerjee T, Snover DC (2008) Sessile serrated adenoma (SSA) vs. traditional serrated adenoma (TSA). Am J Surg Pathol 32(1):21–29

Virchows Arch (2011) 458:21–30
DOI 10.1007/s00428-010-0997-2

REVIEW AND PERSPECTIVE

Annex to Quirke et al. Quality assurance in pathology in colorectal cancer screening and diagnosis: annotations of colorectal lesions

Michael Vieth · Phil Quirke · René Lambert · Lawrence von Karsa · Mauro Risio

Received: 6 August 2010 / Accepted: 24 August 2010 / Published online: 9 November 2010
© The Author(s) 2010. This article is published with open access at Springerlink.com

Abstract Multidisciplinary, evidence-based European Guidelines for quality assurance in colorectal cancer screening and diagnosis have recently been developed by experts in a pan-European project coordinated by the International Agency for Research on Cancer. The full guideline document includes a chapter on pathology with pan-European recommendations which take into account the diversity and heterogeneity of health care systems across the EU. The present paper is based on the annex to the pathology chapter which attempts to describe in greater depth some of the issues raised in the chapter in greater depth, particularly details of special interest to pathologists. It is presented here to make the relevant discussion known to a wider scientific audience.

M. Vieth (✉)
Institute of Pathology, Klinikum Bayreuth,
Preuschwitzerstr. 101,
95445 Bayreuth, Germany
e-mail: vieth.lkpathol@uni-bayreuth.de

P. Quirke
Pathology and Tumour Biology,
Leeds Institute of Molecular Medicine, Leeds University,
Leeds, UK

R. Lambert
Screening Group, Early Detection and Prevention Section,
International Agency for Research on Cancer,
Lyon, France

L. von Karsa
Quality Assurance Group, Early Detection and Prevention Section,
International Agency for Research on Cancer,
Lyon, France

M. Risio
Pathology Department,
Institute for Cancer Research and Treatment,
Turin, Italy

Keywords Colorectal cancer screening · Multidisciplinary evidence-based guidelines · Quality assurance · Histopathology · Classification · Precursor lesions

Introduction

In 2004 and 2006 the European Union (EU) was expanded to include 12 new Member States. This has added greater diversity and heterogeneity in health care systems, including professional and technical standards and capacities. The authors and editors of the European guidelines for quality assurance in colorectal cancer screening and diagnosis have been conscious of the importance of raising and maintaining standards across the EU. While recommending standards and procedures that are of prime importance for mortality reduction, an equitable balance of best practice and ease of service delivery that can be achieved across a wide spectrum of cultural and economic healthcare settings has been sought. Care was taken to avoid promotion of recent research findings before their putative benefit has been demonstrated in clinical practice.

In preparing the guidelines chapter with pan-European recommendations dealing with pathology [1], the authors were aware that the rapid pace of developments in the field and the diversity in the EU would not permit a discussion of some of the issues in greater depth, even though a more detailed discussion would be welcomed by a number of readers, particularly regarding items of special interest to pathologists. All of the guideline recommendations for quality assurance in pathology are therefore presented in the preceding paper and in the pathology chapter in the full guidelines document [1], on which the preceding paper is based.

The present paper is based on the annex to the chapter on pathology in the full guidelines document [2]. It attempts to address the limitations of the discussion in the

chapter, but for the abovementioned reasons, none of the statements in the following text should be understood as guideline recommendations. The authors and editors also felt that an annex would be the appropriate place to point out new insights not yet widely adopted in Europe that may be relevant to future updates of the guidelines.

Grading of neoplasia

In the present European Guidelines [1], a classification system for colorectal neoplasia has been recommended based on a modified version of the revised Vienna classification (see *Grading of Neoplasia* in main publication). For readers not yet familiar with the Vienna classification, it may be helpful to note that it is the first classification to include a clinical recommendation for each neoplastic category. Furthermore, the system was developed to improve diagnostic reproducibility in the interpretation of biopsy specimens and subsequent resection specimens [3–5]. Strictly speaking, the Vienna classification is only valid for biopsy specimens, since a clinical recommendation should follow. However, to avoid diagnostic inconsistencies, the Vienna classification can be used for resection specimens as well.

In the Vienna classification and hence in the European Guidelines, the term *neoplasia* rather than *dysplasia* is used to refer to epithelial tumours associated with and without chronic inflammatory diseases. Whereas the Vienna classification differentiates between strictly intraepithelial lesions and those involving the lamina propria, the European Guidelines only refer to *mucosal neoplasia* that may or may not involve the lamina propria (see *Grading of Neoplasia* in main publication). More importantly, the EU Guidelines recommend a two-tiered grading of mucosal neoplasia. The pathologist must decide whether a neoplastic mucosal lesion can be categorised as low or as high grade; for criteria see Table 1.

As always in neoplasia, the lesion should reach the mucosal surface (no epithelial maturation). Undermining edges of an adjacent carcinoma should be excluded.

The criteria in Table 1 can be weighted. The most important criteria for the diagnosis of carcinoma are the lateral expansion and the number of nuclear rows. In carcinoma, the number of nuclear rows should change within a single gland. High-grade neoplasia is diagnosed when the nuclear rows do not exceed two to five nuclei, and the glands do not show lateral expansion. Low-grade neoplasia is diagnosed when the nuclear rows do not exceed two to three nuclei [6–8].

In histopathology, the entity of carcinoma in situ is generally defined as carcinoma confined to the epithelial layer. In squamous epithelium such an entity can be readily diagnosed. In columnar epithelium, an analogous entity should theoretically also exist. However, to date there are no exact criteria that would permit diagnosis and that would enable the histopathologist to distinguish high-grade intraepithelial neoplasia from carcinoma limited to the epithelial layer that is not invasive in the lamina propria. Therefore, throughout the gastrointestinal tract, use of the term *carcinoma* in situ is not recommended for respective lesions in columnar epithelium. The term *intramucosal carcinoma* is widely introduced in the upper GI tract but not yet in the lower GI tract (see also below: *Definition of invasion*). We prefer the term "mucosal neoplasia" to intraepithelial neoplasia as high-grade dysplasia can contain epithelial neoplasia and invasion into the lamina propria according to the TNM classification.

Classification of serrated lesions

Terminology

The terminology is still under discussion. Serrated lesions can be regarded as a continuous spectrum of colorectal lesions

Table 1 Grading of gastrointestinal neoplasia

	Normal	Low-grade mucosal/intraepithelial neoplasia (LGMN)	High-grade mucosal/intraepithelial neoplasia (HGMN)	Invasive cancer
Glands	Non-branching	Villous	Branching, cribriform, irregular, solid	Branching, cribriform, irregular, solid
Expansion	Up/down	Till surface	Till surface	Lateral expansion
Epithelial differentation	Up/down	Top–down and exceptional down–top	No maturation towards surface	
Goblet cells	+ +	+	−/+ Retronuclear, atypic	
Nuclear rows	1	2–3	2–5	Changing
Nuclear size	Small, basal	Palisading	Enlarged	Vesicular
Chromatin	Few	+	+ +	+ +/+ + +
Nucleoli	None	None	Few small	Several/prominent

Source: modified from [67–69]

with increasingly more pronounced serrated morphology starting with a *hyperplastic polyp* (HP) and progressing to *sessile serrated lesions* (SSLs, sometimes referred to as *sessile serrated adenomas* or *sessile serrated polyps*), *traditional serrated adenomas* (TSA) and leading, finally, to *adenocarcinoma*. Not only the adenomatous component but also other alterations associated with more pronounced serrated morphology may potentially progress to cancer (see Table 2).

The situation involving *sessile serrated lesion*s is complicated as these lesions only reveal complex structural abnormalities, not adenomatous changes. Therefore, these lesions are neither adenomatous nor are they neoplastic. This is why Kudo et al. [9] and Lambert et al. [10] recommended that these lesions no longer be called adenomas; instead they should be referred to as SSLs. Few of these lesions are reported to rapidly progress to invasive carcinoma, [11]. Those few cases that do progress rapidly, particularly in the right colon, may be expected to appear more frequently as interval cancers. TSAs, unlike SSLs, do contain adenomatous alterations, albeit sometimes quite subtle [12]; they are therefore termed correctly and treatment and surveillance should correspond to that of adenomas (see Chapters 8 and 9 in the full guideline document [13, 14]).

Due to the continuous spectrum in the serrated pathway to colorectal cancer, lesions with combinations of serrated morphology and adenomatous cytology can be observed. If more than one histopathologic type in the serrated spectrum (HP, SSL, TSA) is discernible in a given lesion, or at least one type in combination with adenomatous tissue, such lesions are referred to as *mixed polyps*.

The different histopathologic types (e.g. HP and SSL, SSL and TSA, adenoma and SSL, etc.) must be stated in the diagnosis.

Hyperplastic polyp

Hyperplastic polyps (HPs) are composed of elongated crypts (no complex architecture) with serrated architecture in the upper half of the crypt. These polyps usually show some proliferation in the basal (non-serrated) part of the crypts (regular proliferation). Nuclei are small, regular, basal-orientated and lacking hyperchromasia, but with stratification of the upper (serrated) half of the crypts, and without cytological or structural signs of neoplasia.

Differences in the appearance of the cytoplasma permit recognition of three types:

- Microvesicular type
- Goblet-cell-rich type
- Mucin-poor type.

The microvesicular variant greatly predominates, but distinction between types is subject to wide interobserver variation, especially in small lesions, and is not always possible. Currently, routine subclassification is therefore neither feasible, nor has it been shown to be beneficial.

At the molecular level the microvesicular variant of HP may be the precursor lesion for sessile serrated lesion, and a goblet-cell-rich HP may be the precursor lesion for a traditional serrated adenoma [15–17]. Routine distinction of these types is not necessary.

Sessile serrated lesion

Sessile serrated lesions are described in the literature as "sessile serrated adenoma" and are often found in the right colon. This is a misnomer since sessile serrated lesions do not contain adenomatous changes [9, 10, 18].

To date, four synonymously used terms exist for these lesions: sessile serrated adenoma [19], superficial serrated adenoma [20], type 1 serrated adenoma [21] and serrated polyp with abnormal proliferation [17].

We recommend using only the term *sessile serrated lesion* and avoiding use of any other terms for this entity. This recommendation is given in full awareness that sessile serrated lesions do not show histological signs of an adenoma, but, like adenomas, they should be excised if detected during an endoscopic examination. Currently, even in the hands of expert GI pathologists, the agreement on the sub-types of serrated lesions is only moderate [22].

The vast majority of SSLs will not progress to adenocarcinoma. Histological criteria of these sessile,

Table 2 Continuous spectrum of serrated lesions and possible combinations of histopathologic types

Lesion	Neoplasia	Risk of malignant transformation
Hyperplastic polyp	No	Minimal
Sessile serrated lesion	No	Slightly increased but exact data are missing (rapid transformation may be possible in a short time)
Traditional serrated adenoma	Yes	Increased and suggested worse prognosis than carcinomas arising in sessile serrated lesions
Mixed polyp	Yes	Increased, but exact data are not available
Adenoma (tubular, villous)	Yes	Increased, 17 years on average

Every lesion can give rise to adenocarcinoma

Most of the adenocarcinomas are believed to derive from adenomatous components

usually larger lesions include an abnormal proliferation zone with structural distortion, usually most pronounced in dilatation of the crypts, particularly near the base. Abundant mucus production is usually also observed as pools of mucin in the lumen of the crypts and on the surface of the mucosa. SSLs are found mainly in the right colon and may be misdiagnosed as hyperplastic polyps. Clues to the correct diagnosis include location and large size. As discussed above, cytological signs of "neoplasia" are lacking, but structural abnormalities are present, i.e. glandular branching [18].

Sessile serrated lesions have an elevated serration index and serration in the basal half of crypts with basal dilation of crypts. The epithelium/stroma-ratio is believed to be >50% in SSL. There is crypt branching with horizontal growth (above muscularis mucosae; e.g. T- and L-shaped glands) and often pseudoinvasion into the submucosal layer, rectangular dilation of whole crypts with and without presence of mucus, increased number of goblet cells at the base of the crypts, vesicular nuclei with prominent nucleoli and proliferation zone in the middle of the crypts. Currently there is insufficient evidence available in the literature for weighting of these criteria.

A well-oriented polypectomy is mandatory for the identification of such histological features. Correct assessment of the deepest portions of the mucosa is impossible in superficial or tangentially cut lesions [15, 16].

Further criteria include an often asymmetrical expansion of the proliferation zone into the middle third of crypts. Often mild cytological atypia (slightly enlarged vesicular nuclei, nucleoli) is found without clear signs of neoplasia (dysplasia).

BRAF mutations depend on the type and location of lesion (see Table 3).

Other abnormalities include:

- The majority of SSL and TSA show CpG island methylator phenotype (CIMP) and promoter methylation of hMLH1
- BRAF mutations in 8–10% of all colorectal cancer (CRC; 27–76% of CIMP and sporadic MSI-H CRC)
- BRAF mutations in the majority of SSL and TSA (also microvesicular variant of HP, especially proximal), but rarely (0–5%) in adenoma [23–34].

The frequency of sessile serrated lesions in small retrospective series is estimated at 2–11% of all mucosal lesions in the colon [35, 36]; between 8% and 23% are misdiagnosed as hyperplastic polyps with an interobserver variation of up to 40% [17, 37–39].

The histological features separating HPs from SSLs constitute a continuous spectrum, and intermingled features can often be seen. This could explain the moderate interobserver concordance (k=0.47) and the overlapping proliferative activity, and may justify establishing semi-quantitative criteria for diagnosis (e.g. >30% of undifferentiated cells) [40, 41]. Only a few immunohistochemical markers (Ki67, Ki67+CK20, MUC6) have been tested for differentiating HPs and SSAs, and their usefulness in colorectal screening and diagnosis remains to be validated [42, 43]. At present, such an additional immunohistochemical analysis cannot be recommended (see Table 4).

In all likelihood, lesions formerly interpreted as *mixed hyperplastic* and *adenomatous polyp* are, in fact, SSLs complicated by conventional neoplasia, [44]. Special care must be taken in such cases to document the respective histopathologic components in such mixed polyps. Sometimes the conventional neoplastic part shows features other than in classical adenomas. The nuclei are prominent, less palisading and smaller than in classical adenomas. It is not clear whether this type of morphology is distinct for serrated lesions and whether any clinical implications can be drawn.

Prospective studies with risk stratification are needed to develop more precise methods of diagnosis and recommendations for classification. Sessile serrated lesions appear to take a long time (average 17 years) to develop into an invasive carcinoma. In contrast, an ill-defined, small subsample of SSLs seems to rapidly progress [11, 44]. Therefore, SSLs should be completely excised, particularly if they are located on the right side of the colon [16, 45].

Diagnosis on a biopsy is not adequate to exclude SSL since the most severe histologic changes might only appear

Table 3 Prevalence of serrated lesions with BRAF Mutation—a prospective study of patients undergoing colonoscopy

Lesion	Number (n=414) (% of all lesions)	Proximal location (% of BRAF mutations)	Distal location (% of BRAF mutations)
Hyperplastic polyp	120 (29)	35 (29)	85 (71)
Sessile serrated lesion	36 (9)	27 (75)	9 (25)
Trad. serrated adenoma	3 (1)	2 (66)	1 (33)
Mixed polyp	7 (2)	4 (57)	3 (43)
Tubular adenoma	237 (57)	176 (74)	61 (26)
Villous adenoma	11 (3)	6 (55)	5 (45)

Source: modified from [54]

Table 4 Comparison of proliferative activity in adenoma, hyperplastic polyps, sessile serrated lesion and traditional serrated adenoma

Ki-67	Adenoma (%)	Hyperplastic polyps (%)	Sessile serrated lesion (%)	Traditional serrated adenoma (%)
Upper 1/3	68.8	0.1	1.6	27.9
Middle 1/3	48.7	9.1	20.3	30.6
Lower 1/3	29.6	60.3	64.9	38.2

Source: modified from [38, 44]

focally within a lesion that otherwise appears to be a hyperplastic polyp [46].

The German guidelines for colorectal cancer [47] recommend complete removal and follow-up of SSL similar to adenomas. An intensive surveillance protocol is recommended for sessile serrated lesions (surveillance colonoscopy after 3–5 years subsequent to complete excision of non-neoplastic SSL, after 1 year after excision of SSL HGIEN [47]).

The UK Guidelines [48–51] recommend complete excision but classify these lesions in the same risk category as hyperplastic polyps. The existing evidence base is not definitive as to the level of risk, and follow-up decisions should be made locally until more evidence is forthcoming.

Traditional serrated adenoma

Traditional serrated adenomas show neoplastic crypts with a serrated structure [52]. Compared to hyperplastic polyps, the most striking diagnostic feature of traditional serrated adenomas are the complex serrated morphology and the eosinophilic, "dysplastic" cytoplasm that still can be identified in cases with invasive adenocarcinoma. These lesions also frequently show *BRAF* mutations and CIMP with *hMLH1* promoter methylation. Additionally, so-called intraepithelial microacini can be observed in the upper half of the mucosa (ectopic crypt formation). Often, these lesions are located in the distal colon and can be found more frequently in elderly female individuals [12, 18, 43].

Mixed polyp

A mixed polyp may contain partially hyperplastic, classical adenomatous or traditional serrated adenoma or sessile serrated lesion components. Rather than a continuous spectrum such lesions most probably represent several evolutionary lines, depending on the order of certain abnormalities in genes such as *APC*, *BRAF* and *KRAS* [15, 16]. It has to be determined whether mixed polyps represent serrated lesions complicated by conventional neoplasia [53].

Focal, hyperplastic-like narrowing of the basal region of a few crypts in SSL and the findings of flat sectors or *ectopic crypt formation* in SSL/TSA [43] are examples of combinations of serrated and adenomatous components. However, these features add no information of further diagnostic value; they probably result from the continuous developing nature of serrated lesions. We therefore recommend that the diagnosis of mixed polyp should be restricted to the definition given above under Terminology (i.e. lesions with—*...more than one histopathologic type in the serrated spectrum (*HP, SSL, TSA*) ... or at least one type in combination with adenomatous tissue…*). Mixed polyps are serrated lesions in which more than one histopathologic type in the serrated spectrum (HP, SSL, TSA) is discernible in a given lesion or at least one type in combination with classical (unserrated) adenomatous tissue. The different histopathological types must be mentioned in the diagnosis, e.g. mixed polyp (HP and SSL, adenoma and SSL).

Risk of progression

The vast majority of hyperplastic polyps and serrated lesions will not undergo malignant transformation. Only a fraction, especially in the group of sessile serrated lesions, may progress to rapidly aggressive carcinoma [35, 54].

Hyperplastic polyps rarely progress to carcinoma. A single case report can be found in the literature [55] and a second (unpublished) case has been reported in southern Germany. Interestingly, these carcinomas show features of gastric differentiation.

Little evidence is available on which the risk of colorectal cancer associated with serrated lesions other than hyperplastic polyps could be reliably judged. The risk assessment for sessile serrated lesions is not yet defined, but a subset of these lesions appears to give rise to carcinoma often less than a few millimeters in size. In a series of 110 traditional serrated adenomas, 37% exhibited foci of significant neoplasia and 11% contained areas of intramucosal carcinoma [12]. Mixed polyps (e.g., HP/TSA/SSL or HP/adenoma) seem to have at least the same rate of progression to colorectal carcinoma as adenomas, and the risk might be higher [56, 57].

Assessment of T1 adenocarcinoma

Careful assessment in T1 adenocarcinoma is mandatory because a decision is required on local excision or a major operation.

Size

Firstly, accurate measurement is very important, and measurement must be to the nearest millimeter (and not rounded-up to the nearest 5 or 10 mm). The maximum size of the lesion should be measured from the histological slide and if the lesion is disrupted or too large, from the formalin-fixed macroscopic specimen. If a biopsy is received it should be stated that size cannot be assessed.

Tumour grade

Poorly differentiated carcinomas are identified by the presence of either irregularly folded, distorted and often small tubules, or the lack of any tubular formation and showing marked cytological pleomorphism. In the absence of good evidence, we recommend that a grade of poor differentiation should be applied in a pT1 cancer when ANY area of the lesion is considered to show poor differentiation. It should be noted that this is not in accordance with the WHO classification that recommends a certain proportion of lesion showing poor differentiation before diagnosing a lesion as G3. Poor differentiation includes undifferentiated and poorly differentiated as defined by the WHO classification [58].

Budding

Budding describes the biological behaviour of the tumour at the front of invasion [59]. Budding or tumour cell dissociation [60] can be divided into slight, moderate and marked and is known from the Japanese literature of the 1950s [61] and 1990s [62].

At this time, evidence is lacking concerning reproducibility of the numerous methods for tumour budding measurement (see Table 5). It is good practice but not mandatory to document the presence or absence of single tumour cells at the front of invasion and we therefore

Table 5 Measurement of tumour budding

Author	Year	pT	Count	Magnification	Objective	Area (mm^2)	Classification	Cut-off	Notes
Ueno	2004		H&E		×20	0, 785	Negative/positive	5	
Ueno	2002		H&E		×25	0, 385	<10/>10	10	Degree of grading agreement
Ueno	2004		H&E	250	×25	0, 385	Low (<10)/high (>10)	10	
Shinto	2005		IHC:MNF 116		×20		Low (<10)/high (>10) moderate (10–19), severe (>20)		Identification of cytoplasmic fragments
Shinto	2006	3	IHC:MNF 116		×20		Low (<10)/high (>10) moderate (10–19), severe (>20)		Scoring of cytoplasmic fragments called now podia
Okuyama	2002	1 and 2	H&E	n.a.	n.a.	n.a.	Present/absent	1	Endoscopically resected tumours were excluded
Okuyama	2003	3	H&E	n.a.	n.a.	n.a.	Present/absent	1	
Okuyama	2003	3	H&E	n.a.	n.a.	n.a.	Present/absent	1	
Prall	2005		IHC:MNF 116	250		0, 785	Low/high	25	ROC metastatic progression; 0–120 buds range; 14 median 20,46 mean
Kazama	2006	1	IHC: CAM5.2 and AE1/AE3	n.a.	n.a.	n.a.	Present/absent	1	
Kanazawa	2007		H&E	n.a.	n.a.	n.a.	None/mild/moderate/ marked		
Nakamura	2008		H&E	n.a.	n.a.	n.a.	None/mild/low moderate/ marked=high		
Choi	2007	2 or more	H&E		×20		(0–3)/(4–5)/(6–10)/(11–38)		
Park	2005	2 or more	H&E		×20		(0–3)/(4–5)/(6–9)/(10–38)		Mean intesity: (+/−SD) 6,6+/−5,6
Hori	2005		H&E	200	×40			0,05	5% of the horizontal length of the invasive front
Yasuda	2007		H&E				Present/absent		
Ishikawa	2008		IHC:MNFIIb	400			Negative/positive	5	

Source: modified from [65, 74–79]

recommend providing this additional information in the written report with an explanatory comment as budding has been suggested as a prognostic factor in colorectal cancer [63–65].

Site

The site of origin of each specimen should be individually identified by the clinician and reported to the pathologist on the histopathology request form. The pathologist should record this on the proforma. This is important information because the risk of lymph node metastasis from a T1 adenocarcinoma varies depending on the site and size of the lesion (rectum vs. other locations) [66].

Definition of invasion

In columnar epithelium it is difficult to define the onset of invasive carcinoma and reliably distinguish it from high-grade intraepithelial neoplasia. Criteria such as single tumour cells are more likely to be seen in more advanced carcinomas, but not in early carcinomas. Desmoplastic stromal reactions are also seldom seen in very early carcinomas. However, basal membrane structures are frequently discernible in well-differentiated early carcinomas [67–69], so that definitions using "invasion through the basement membrane" are incorrect.

The WHO definition of adenocarcinoma in use when the EU guidelines were developed excluded diagnosis of intramucosal carcinoma in the colon or rectum, in contrast to the accepted WHO definitions for the stomach, oesophagus and small bowel. In the latter cases, a decision on surgical versus local therapy is made based on respective protocols. Comparable lesions in the colon and rectum are reported as high-grade mucosal neoplasia, because a carcinoma in the colon is defined by infiltration of the submucosa, according to the WHO classification.

The discussion on this issue among the authors of the pathology chapter in the EU Guidelines reflects, among other things, concern about potential overtreatment of early T1 carcinomas which are detected much more frequently in a screening setting. The clinical management of a lesion where invasion of the lamina propria has occurred is no different from that where high-grade changes are confined to the glands. This legitimate concern as to increased morbidity and mortality due to miscommunication of diagnostic criteria may be dealt with more effectively in the future, as multidisciplinary management of lesions detected in and outside of screening programmes advances. The authors hope that such advances and their effective dissemination will be stimulated by the publication of the new EU guidelines. This, in turn, may lead to revision of the current WHO definition of colorectal adenocarcinoma in a future revision of the WHO classification of gastrointestinal tumours. Pathologists should report on what version of the WHO and TNM classifications their diagnosis is based.

In those cases in which intramucosal colorectal cancer is suspected, and particularly in countries in which this diagnosis is documented in addition to the WHO terminology, explicit comments by the pathologist are recommended. Based on the cytological characteristics of the case, the pathologist should indicate whether local endoscopic or surgical removal is recommended, and the basis for this recommendation should be indicated. This recommendation should be discussed in a multidisciplinary conference prior to surgery. The Japanese criteria for such stratification have been published [55]. The updated Paris classification based on a workshop in Feb 2008 in Kyoto [9] permits such subclassification based on improved grouping and explains in detail the grading criteria [10].

The use of the term *carcinoma* in situ introduced by the TNM system is inadequate because the criteria are too vague and cannot be used for columnar epithelium.

A subclassification of all carcinomas into low-risk and high-risk based on risk of lymph node involvement should always be undertaken. For exact criteria please see main text of the present publication and Chapter 7 of the full GL document [1] and the updated Paris classification [9, 10].

Perineural invasion

Perineural invasion (PNI) was recently described as an independent risk factor for colorectal cancer [66, 70]. PNI is significantly associated with high tumour stage, grade and metastases. Furthermore, PNI serves as an independent predictor of disease-free and cancer survival [66, 70]. Recently, an association with other criteria indicating an aggressive course of disease such as lymphatic vessel permeation, venous invasion, tumour growth pattern, budding [71] were described by Poeschl et al. [66]. Also, it was described that PNI-positive tumours are more likely to be incompletely resected, and more likely to progress after Mayo regimen chemotherapy than PNI-negative tumours. Lately, Poeschl et al. were able to show that PNI is an additional independent factor for local tumour relapse.

It is recommended to record PNI in routine sections of colorectal cancer. According to recent studies [66, 70, 72, 73], immunohistochemistry or special stains are not necessary to detect PNI. Prospective studies are needed to show the clinical relevance of PNI, its relationship to other features such as lymphatic and vascular invasion and the benefit of alternative treatment for such more aggressive tumours that are PNI positive.

Conclusions

The rapid pace of developments in screening, diagnosis and treatment of colorectal cancer is likely to continue unabated in the coming years. Pathologists interested in colorectal cancer should be aware of the topics likely to be of future relevance to quality assurance. This may help to recognise opportunities to continuously improve the quality and performance of current screening and diagnostic activities.

Acknowledgements We thank the following external reviewers for reading and providing helpful comments and suggestions on the draft chapter and annex on quality assurance in pathology in colorectal cancer screening and diagnosis during the preparation of the full guidelines document: Robert Riddell, Toronto, Canada; Hiroshi Saito, Tokyo and Hidenobu Watanabe, Niigata, Japan.

The comments and suggestions received from consultation of the European Cancer Network are gratefully acknowledged.

Phil Quirke is supported by Yorkshire Cancer Research and the Department of Health/Cancer Research UK Experimental Cancer Medicine Centre Initiative

Financial support of the European Communities through the EU Public Health Programme (Development of European Guidelines for Quality Assurance of Colorectal Cancer Screening (CRC), grant agreement No. 2005317), of the Public Affairs Committee of the United European Gastroenterology Federation, and from a cooperative agreement between the American Cancer Society and the Division of Cancer Prevention and Control at the Centers for Disease Control and Prevention is gratefully acknowledged.

The technical support of Tracy Lignini, Krittika Guinot and Simon Ducarroz at the International Agency for Research on Cancer in the preparation of the manuscript is gratefully acknowledged.

Conflict of interest Pathology and tumour biology at the Leeds Institute of Molecular Medicine, led by Philip Quirke, at the University of Leeds has received funding from the EU Public Health Programme (Development of European Guidelines for Quality Assurance of Colorectal Cancer Screening (CRC), grant agreement No. 2005317) to develop a prototype web-based training tool for pathology in colorectal cancer screening.

The International Agency for Research on Cancer, where Lawrence von Karsa is employed, is a recipient of research grants from the EU Public Health Programme.

Open Access This article is distributed under the terms of the Creative Commons Attribution Noncommercial License which permits any noncommercial use, distribution, and reproduction in any medium, provided the original author(s) and source are credited.

References

1. Quirke P, Risio M, Lambert R, Vieth M (2010) Quality assurance in pathology in colorectal cancer screening and diagnosis. In: Segnan N, Patnick J, von Karsa L (eds) European Guidelines for Quality Assurance in Colorectal Cancer Screening and Diagnosis - First Edition (In press)
2. Vieth M, Quirke P, Lambert R, von Karsa L, Risio M (2010) Annotations of colorectal lesions. In: Segnan N, Patnick J, von Karsa L (eds) European Guidelines for Quality Assurance in Colorectal Cancer Screening and Diagnosis - First Edition, (In press)
3. Schlemper RJ, Riddell RH, Kato Y, Borchard F, Cooper HS, Dawsey SM, Dixon MF, Fenoglio-Preiser CM, Flejou JF, Geboes K, Hattori T, Hirota T, Itabashi M, Iwafuchi M, Iwashita A, Kim YI, Kirchner T, Klimpfinger M, Koike M, Lauwers GY, Lewin KJ, Oberhuber G, Offner F, Price AB, Rubio CA, Shimizu M, Shimoda T, Sipponen P, Solcia E, Stolte M, Watanabe H, Yamabe H (2000) The Vienna classification of gastrointestinal epithelial neoplasia. Gut 47(2):251–255
4. Schlemper RJ, Kato Y, Stolte M (2001) Review of histological classifications of gastrointestinal epithelial neoplasia: differences in diagnosis of early carcinomas between Japanese and Western pathologists. J Gastroenterol 36(7):445–456
5. Schlemper RJ, Kato Y, Stolte M (2000) Diagnostic criteria for gastrointestinal carcinomas in Japan and Western countries: proposal for a new classification system of gastrointestinal epithelial neoplasia. J Gastroenterol Hepatol 15(Suppl):G49–G57
6. Wolber RA, Owen DA (1991) Flat adenomas of the colon. Hum Pathol 22(1):70–74
7. Ajioka Y, Watanabe H, Kobayashi M, Maeo S, Yoshida M (1994) Macroscopic classification of colorectal (minute) neoplasia. I to Cho 29:89
8. Ajioka Y, Watanabe H, Kazama S, Hashidate H, Yokoyama J, Yamada S, Takaku H, Nishikura K (2000) Early colorectal cancer with special reference to the superficial nonpolypoid type from a histopathologic point of view. World J Surg 24(9):1075–1080
9. Kudo S, Lambert R, Allen JI, Fujii H, Fujii T, Kashida H, Matsuda T, Mori M, Saito H, Shimoda T, Tanaka S, Watanabe H, Sung JJ, Feld AD, Inadomi JM, O'Brien MJ, Lieberman DA, Ransohoff DF, Soetikno RM, Triadafilopoulos G, Zauber A, Teixeira CR, Rey JF, Jaramillo E, Rubio CA, Van GA, Jung M, Vieth M, Jass JR, Hurlstone PD (2008) Nonpolypoid neoplastic lesions of the colorectal mucosa. Gastrointest Endosc 68(4 Suppl):S3–S47
10. Lambert R, O'Brien MJ, Jaramillo E, Vieth M (2009) The serrated pathway to colorectal cancer. World Gastroenterology News 14 (2):5–10
11. Oono Y, Fu K, Nakamura H, Iriguchi Y, Yamamura A, Tomino Y, Oda J, Mizutani M, Takayanagi S, Kishi D, Shinohara T, Yamada K, Matumoto J, Imamura K (2009) Progression of a sessile serrated adenoma to an early invasive cancer within 8 months. Dig Dis Sci 54(4):906–909
12. Longacre TA, Fenoglio-Preiser CM (1990) Mixed hyperplastic adenomatous polyps/serrated adenomas. A distinct form of colorectal neoplasia. Am J Surg Pathol 14(6):524–537
13. Atkin W, Valori R, Kuipers EJ, Hoff G, Senore C, Segnan N, Jover R, Schmiegel W, Lambert R, Pox C (2010) Colonoscopic surveillance after adenoma removal. In: Segnan N, Patnick J, von Karsa L (eds) European Guidelines for Quality Assurance in Colorectal Cancer Screening and Diagnosis - First Edition, (In press)
14. Steele RJC, Pox C, Kuipers EJ, Minoli G, Lambert R (2010) Management of screen-detected lesions. In: Segnan N, Patnick J, von Karsa L (eds) European Guidelines for Quality Assurance in Colorectal Cancer Screening and Diagnosis - First Edition, (In press)
15. O'Brien MJ (2007) Hyperplastic and serrated polyps of the colorectum. Gastroenterol Clin North Am 36(4):947–968, viii
16. O'Brien MJ, Yang S, Huang CS, Shepherd C, Cerda S, Farraye F (2008) The serrated polyp pathway to colorectal carcinoma. Diagn Histopathol 14(2):78–93
17. Torlakovic E, Skovlund E, Snover DC, Torlakovic G, Nesland JM (2003) Morphologic reappraisal of serrated colorectal polyps. Am J Surg Pathol 27(1):65–81

18. Higuchi T, Jass JR (2004) My approach to serrated polyps of the colorectum. J Clin Pathol 57(7):682–686
19. Torlakovic E, Snover DC (1996) Serrated adenomatous polyposis in humans. Gastroenterology 110(3):748–755
20. Oka S, Tanaka S, Hiyama T, Ito M, Kitadai Y, Yoshihara M, Haruma K, Chayama K (2004) Clinicopathologic and endoscopic features of colorectal serrated adenoma: differences between polypoid and superficial types. Gastrointest Endosc 59(2):213–219
21. Jaramillo E, Tamura S, Mitomi H (2005) Endoscopic appearance of serrated adenomas in the colon. Endoscopy 37(3):254–260
22. Wong NA, Hunt LP, Novelli MR, Shepherd NA, Warren BF (2009) Observer agreement in the diagnosis of serrated polyps of the large bowel. Histopathology 55(1):63–66
23. Jass JR (2007) Classification of colorectal cancer based on correlation of clinical, morphological and molecular features. Histopathology 50(1):113–130
24. Grady WM, Carethers JM (2008) Genomic and epigenetic instability in colorectal cancer pathogenesis. Gastroenterology 135(4):1079–1099
25. Samowitz WS, Slattery ML, Sweeney C, Herrick J, Wolff RK, Albertsen H (2007) APC mutations and other genetic and epigenetic changes in colon cancer. Mol Cancer Res 5(2):165–170
26. Kawasaki T, Ohnishi M, Nosho K, Suemoto Y, Kirkner GJ, Meyerhardt JA, Fuchs CS, Ogino S (2008) CpG island methylator phenotype-low (CIMP-low) colorectal cancer shows not only few methylated CIMP-high-specific CpG islands, but also low-level methylation at individual loci. Mod Pathol 21(3):245–255
27. Ogino S, Goel A (2008) Molecular classification and correlates in colorectal cancer. J Mol Diagn 10(1):13–27
28. Ogino S, Kawasaki T, Kirkner GJ, Loda M, Fuchs CS (2006) CpG island methylator phenotype-low (CIMP-low) in colorectal cancer: possible associations with male sex and KRAS mutations. J Mol Diagn 8(5):582–588
29. Ogino S, Kawasaki T, Kirkner GJ, Kraft P, Loda M, Fuchs CS (2007) Evaluation of markers for CpG island methylator phenotype (CIMP) in colorectal cancer by a large population-based sample. J Mol Diagn 9(3):305–314
30. Shen L, Toyota M, Kondo Y, Lin E, Zhang L, Guo Y, Hernandez NS, Chen X, Ahmed S, Konishi K, Hamilton SR, Issa JP (2007) Integrated genetic and epigenetic analysis identifies three different subclasses of colon cancer. Proc Natl Acad Sci USA 104 (47):18654–18659
31. Suehiro Y, Wong CW, Chirieac LR, Kondo Y, Shen L, Webb CR, Chan YW, Chan AS, Chan TL, Wu TT, Rashid A, Hamanaka Y, Hinoda Y, Shannon RL, Wang X, Morris J, Issa JP, Yuen ST, Leung SY, Hamilton SR (2008) Epigenetic-genetic interactions in the APC/WNT, RAS/RAF, and P53 pathways in colorectal carcinoma. Clin Cancer Res 14(9):2560–2569
32. Toyota M, Ohe-Toyota M, Ahuja N, Issa JP (2000) Distinct genetic profiles in colorectal tumors with or without the CpG island methylator phenotype. Proc Natl Acad Sci USA 97(2):710–715
33. Toyota M, Ahuja N, Ohe-Toyota M, Herman JG, Baylin SB, Issa JP (1999) CpG island methylator phenotype in colorectal cancer. Proc Natl Acad Sci USA 96(15):8681–8686
34. Ogino S, Nosho K, Kirkner GJ, Kawasaki T, Meyerhardt JA, Loda M, Giovannucci EL, Fuchs CS (2009) CpG island methylator phenotype, microsatellite instability, BRAF mutation and clinical outcome in colon cancer. Gut 58(1):90–96
35. Carr NJ, Mahajan H, Tan KL, Hawkins NJ, Ward RL (2009) Serrated and non-serrated polyps of the colorectum: their prevalence in an unselected case series and correlation of BRAF mutation analysis with the diagnosis of sessile serrated adenoma. J Clin Pathol 62(6):516–518
36. Jass JR, Baker K, Zlobec I, Higuchi T, Barker M, Buchanan D, Young J (2006) Advanced colorectal polyps with the molecular and morphological features of serrated polyps and adenomas: concept of a 'fusion' pathway to colorectal cancer. Histopathology 49(2):121–131
37. Goldstein NS, Bhanot P, Odish E, Hunter S (2003) Hyperplastic-like colon polyps that preceded microsatellite-unstable adenocarcinomas. Am J Clin Pathol 119(6):778–796
38. Higuchi T, Sugihara K, Jass JR (2005) Demographic and pathological characteristics of serrated polyps of colorectum. Histopathology 47(1):32–40
39. Montgomery E (2004) Serrated colorectal polyps: emerging evidence suggests the need for a reappraisal. Adv Anat Pathol 11(3):143–149
40. Farris AB, Misdraji J, Srivastava A, Muzikansky A, Deshpande V, Lauwers GY, Mino-Kenudson M (2008) Sessile serrated adenoma: challenging discrimination from other serrated colonic polyps. Am J Surg Pathol 32(1):30–35
41. Sandmeier D, Seelentag W, Bouzourene H (2007) Serrated polyps of the colorectum: is sessile serrated adenoma distinguishable from hyperplastic polyp in a daily practice? Virchows Arch 450 (6):613–618
42. Owens SR, Chiosea SI, Kuan SF (2008) Selective expression of gastric mucin MUC6 in colonic sessile serrated adenoma but not in hyperplastic polyp aids in morphological diagnosis of serrated polyps. Mod Pathol 21(6):660–669
43. Torlakovic EE, Gomez JD, Driman DK, Parfitt JR, Wang C, Benerjee T, Snover DC (2008) Sessile serrated adenoma (SSA) vs. traditional serrated adenoma (TSA). Am J Surg Pathol 32(1):21–29
44. Sheridan TB, Fenton H, Lewin MR, Burkart AL, Iacobuzio-Donahue CA, Frankel WL, Montgomery E (2006) Sessile serrated adenomas with low- and high-grade dysplasia and early carcinomas: an immunohistochemical study of serrated lesions "caught in the act". Am J Clin Pathol 126(4):564–571
45. Noffsinger AE (2009) Serrated polyps and colorectal cancer: new pathway to malignancy. Annu Rev Pathol 4:343–364
46. Schreiner MA, Weiss DG, Lieberman DA (2010) Proximal and large hyperplastic and nondysplastic serrated polyps detected by colonoscopy are associated with neoplasia. Gastroenterology 139 (5):1497–1502
47. Schmiegel W, Reinacher-Schick A, Arnold D, Graeven U, Heinemann V, Porschen R, Riemann J, Rodel C, Sauer R, Wieser M, Schmitt W, Schmoll HJ, Seufferlein T, Kopp I, Pox C (2008) Update S3-guideline "colorectal cancer". Z Gastroenterol 46 (8):799–840
48. Williams GT, Quirke P, Shepherd NA (2007) Dataset for colorectal cancer, 2nd edn - Appendix D: Proforma for local excision specimens. http://www.rcpath.org/resources/worddocs/G049ColorectalDatasetAppendixD-Sep07.doc
49. Williams GT, Quirke P, Shepherd NA (2007) Dataset for colorectal cancer, 2nd edn - Appendix C: Proforma for colorectal cancer resections. http://www.rcpath.org/resources/worddocs/G049ColorectalDatasetAppendixC-Sep07.doc
50. Williams GT, Quirke P, Shepherd NA (2007) Dataset for colorectal cancer, 2nd edn. http://www.rcpath.org/resources/pdf/G049-ColorectalDataset-Sep07.pdf
51. NHS Bowel Cancer Screening Programme (2007) Reporting lesions in the NHS Bowel Cancer Screening Programme - guidelines from the Bowel Cancer Screening Programme Pathology Group. http://www.cancerscreening.nhs.uk/bowel/publications/nhsbcsp01.pdf
52. WHO (2000) Pathology and genetics of tumours in the digestive system. Carcinoma of the colon and rectum. In: Hamilton SR, Aaltonen LA (eds) World Health Organization International Histological Classification of Tumours. IARC, Lyon, pp 105–119
53. Snover DC, Jass JR, Fenoglio-Preiser C, Batts KP (2005) Serrated polyps of the large intestine: a morphologic and molecular review of an evolving concept. Am J Clin Pathol 124(3):380–391

54. Spring KJ, Zhao ZZ, Karamatic R, Walsh MD, Whitehall VL, Pike T, Simms LA, Young J, James M, Montgomery GW, Appleyard M, Hewett D, Togashi K, Jass JR, Leggett BA (2006) High prevalence of sessile serrated adenomas with BRAF mutations: a prospective study of patients undergoing colonoscopy. Gastroenterology 131(5):1400–1407
55. Watanabe H, Suda T (1984) Precancerous lesions of the colon and rectum. Gan To Kagaku Ryoho 11(1):1–9
56. Hyman NH, Anderson P, Blasyk H (2004) Hyperplastic polyposis and the risk of colorectal cancer. Dis Colon Rectum 47(12):2101–2104
57. Leggett BA, Devereaux B, Biden K, Searle J, Young J, Jass J (2001) Hyperplastic polyposis: association with colorectal cancer. Am J Surg Pathol 25(2):177–184
58. Washington MK, Berlin J, Branton P, Burgart LJ, Carter DK, Fitzgibbons PL, Halling K, Frankel W, Jessup J, Kakar S, Minsky B, Nakhleh R, Compton CC (2009) Protocol for the examination of specimens from patients with primary carcinoma of the colon and rectum. Arch Pathol Lab Med 133(10):1539–1551
59. Deinlein P, Reulbach U, Stolte M, Vieth M (2003) Risk factors for lymphatic metastasis from pT1 colorectal adenocarcinoma. Pathologe 24(5):387–393
60. Gabbert HE, Meier S, Gerharz CD, Hommel G (1992) Tumor-cell dissociation at the invasion front: a new prognostic parameter in gastric cancer patients. Int J Cancer 50(2):202–207
61. Imai T (1954) The growth of human carcinoma: a morphological analysis. Fukuoka Igaku Zasshi 45:13–43
62. Kobayashi M, Watanabe H, Maeo S, Ajioka Y, Yoshida M (1994) Correlation of histological atypia and cancer-sprouting with vascular permeation and lymph nodal metastasis by our new histological classification of submucosal invasion by colorectal carcinomas. Stomach Intest 29:1151–1156
63. Ogawa T, Yoshida T, Tsuruta T, Tokuyama W, Adachi S, Kikuchi M, Mikami T, Saigenji K, Okayasu I (2009) Tumor budding is predictive of lymphatic involvement and lymph node metastases in submucosal invasive colorectal adenocarcinomas and in non-polypoid compared with polypoid growths. Scand J Gastroenterol 44(5):605–614
64. Sy J, Fung CL, Dent OF, Chapuis PH, Bokey L, Chan C (2010) Tumor budding and survival after potentially curative resection of node-positive colon cancer. Dis Colon Rectum 53(3):301–307
65. Nakamura T, Mitomi H, Kanazawa H, Ohkura Y, Watanabe M (2008) Tumor budding as an index to identify high-risk patients with stage II colon cancer. Dis Colon Rectum 51(5):568–572
66. Poeschl EM, Pollheimer MJ, Kornprat P, Lindtner RA, Schlemmer A, Rehak P, Vieth M, Langner C (2010) Perineural invasion: correlation with aggressive phenotype and independent prognostic variable in both colon and rectum cancer. J Clin Oncol 28(21):e358–e360
67. Borchard F (2000) Forms and nomenclature of gastrointestinal epithelial expansion: what is invasion? Verh Dtsch Ges Pathol 84:50–61
68. Borchard F, Heilmann KL, Hermanek P, Gebbers JO, Heitz PU, Stolte M, Pfeifer U, Schaefer HE, Wiebecke B, Schlake W (1991) Definition and clinical significance of dysplasia in the digestive tract$ Results of a meeting of the Society of Gastroenterologic Pathology of the German Society of Pathology 25 November 1989 in Kronberg. Pathologe 12(1):50–56
69. Vieth M, Stolte M (2005) Distinction of high-grade intraepithelial neoplasia and tubular gastric adenocarcinoma. In: Kaminishi M, Takubo K, Mafune K (eds) The diversity of gastric carcinoma: pathogenesis, diagnosis and therapy. Springer, Tokyo, pp 109–116
70. Liebig C, Ayala G, Wilks J, Verstovsek G, Liu H, Agarwal N, Berger DH, Albo D (2009) Perineural invasion is an independent predictor of outcome in colorectal cancer. J Clin Oncol 27(31):5131–5137
71. Jass JR, Love SB, Northover JM (1987) A new prognostic classification of rectal cancer. Lancet 1(8545):1303–1306
72. Liebig C, Ayala G, Wilks JA, Berger DH, Albo D (2009) Perineural invasion in cancer: a review of the literature. Cancer 115(15):3379–3391
73. Marshall CL, Liebig C, Wilks J, Agarwal N, Berger DH, Albo D, Ayala G, Verstovsek G, Liu H (2010) Reply to E.M. Poeschl et al. J Clin Oncol 28(21):e361–e363
74. Cooper HS, Deppisch LM, Gourley WK, Kahn EI, Lev R, Manley PN, Pascal RR, Qizilbash AH, Rickert RR, Silverman JF (1995) Endoscopically removed malignant colorectal polyps: clinicopathologic correlations. Gastroenterology 108(6):1657–1665
75. Haggitt RC, Glotzbach RE, Soffer EE, Wruble LD (1985) Prognostic factors in colorectal carcinomas arising in adenomas: implications for lesions removed by endoscopic polypectomy. Gastroenterology 89(2):328–336
76. Konishi F, Morson BC (1982) Pathology of colorectal adenomas: a colonoscopic survey. J Clin Pathol 35(8):830–841
77. Nascimbeni R, Burgart LJ, Nivatvongs S, Larson DR (2002) Risk of lymph node metastasis in T1 carcinoma of the colon and rectum. Dis Colon Rectum 45(2):200–206
78. Ueno H, Mochizuki H, Hashiguchi Y, Shimazaki H, Aida S, Hase K, Matsukuma S, Kanai T, Kurihara H, Ozawa K, Yoshimura K, Bekku S (2004) Risk factors for an adverse outcome in early invasive colorectal carcinoma. Gastroenterology 127(2):385–394
79. Volk EE, Goldblum JR, Petras RE, Carey WD, Fazio VW (1995) Management and outcome of patients with invasive carcinoma arising in colorectal polyps. Gastroenterology 109(6):1801–1807

Virchows Arch (2011) 458:31–38
DOI 10.1007/s00428-010-0989-2

REVIEW ARTICLE

Philadelphia: cradle of American pathology

Carol Starr · William A. Gardner

Received: 9 September 2010 / Accepted: 23 September 2010 / Published online: 6 November 2010
© The Author(s) 2010. This article is published with open access at Springerlink.com

Keywords Philadelphia · American Pathology · Pathology

The city of Philadelphia led the political, commercial, educational, and cultural development of the American nation. As the new nation began, Philadelphia was the largest English-speaking city in the world next to London and both the center of the government and the center of commerce. Not as widely recognized is Philadelphia's contribution to transforming America's stature from nineteenth century European apprentice to that of twentieth century worldwide leader in experimental scientific medical research and practice.

Nursery of American medicine

The nation's first medical community developed in Philadelphia. The first recognized hospital in the colonies, the Blockley Almshouse, opened in Philadelphia in 1742. The goal of the Almshouse was to provide medical care for the indigent. Benjamin Franklin (1706–1770) and Thomas Bond subsequently opened Pennsylvania Hospital in 1751 to improve on Blockley's services (Fig. 1). Medical leaders also recognized the need for formal medical education. John Bard, John Morgan, and William Shippen, Jr. established the first medical school in the colonies by persuading the trustees of the College, Academy, and Charitable School of Philadelphia (as the University of Pennsylvania was known at that time) to create a department of medicine. In 1779 a new board of trustees named the College the University of the State of Pennsylvania and organized a medical faculty modeled on the University of Edinburgh Medical School.

Franklin felt there was a need to support forums that could investigate, discuss, and develop ideas and issues of importance. He established the American Philosophical Society in 1743 to pursue equally "all philosophical Experiments that let Light into the Nature of Things, tend to increase the Power of Man over Matter, and multiply the Conveniences or Pleasures of Life" [1]. It was in this spirit that in 1787 the medical community established The College of Physicians of Philadelphia, the nation's oldest professional medical organization. The College held regular meetings and formal discussions about provocative topics of importance to medicine and published its "Transactions" as the documentation of findings.

By the end of the eighteenth century, graduates and professors of Philadelphia medical schools began leaving Philadelphia to start new medical schools in universities throughout the new nation. In 1791, David Hosack began teaching medical courses at Columbia University. Nathaniel Potter and John Shaw, also Pennsylvania medical school graduates, founded the medical school at the University of Maryland in 1807. George McClellan graduated from the University of Pennsylvania in 1819 and founded a new medical college in Philadelphia, Jefferson Medical College. Thomas Hunt started the Medical College of Louisiana in 1834. David Brainard, Jefferson graduate, established Rush Medical College of Chicago in 1834 [2]. During these years, the Philadelphia community continued to serve as the national center and forum for medical education, practice,

C. Starr · W. A. Gardner (✉)
American Registry of Pathology,
8605 Cameron Street, Suite 202,
Silver Spring, MD 20910, USA
e-mail: pathprof@aol.com

Fig. 1 Dr. Henry Fisher, Pathologist, examines a specimen in the pathology lab of Pennsylvania Hospital, c. 1890s. (Courtesy of Pennsylvania Hospital historic collections, Philadelphia)

Fig. 2 The Pennsylvania Hospital Surgical Amphitheater, which was the first of its kind in the Philadelphia area, was in use as an operating room from 1804 to 1868. Seating around the room provided a place for medical students to observe and learn, as well as a place for paying spectators to be entertained. (Courtesy of Pennsylvania Hospital historic collections, Philadelphia)

publication, and the exchange and discussion of the nature of disease and its treatment.

Philadelphia's role as cradle of modern pathology in America

Philadelphia's success in nurturing the development of the discipline of pathology can be attributed to those who worked, both individually and in concert, to find and apply scientific advances to medical practice throughout the nineteenth century. These developments required ongoing communication, both verbal and written, between scientists and professors.

Postmortem examinations contribute to the differentiation of diseases

From its founding, lectures at the Pennsylvania Hospital by University of Pennsylvania medical school professors included postmortem examinations and demonstrations for medical students (Fig. 2). One of these professors, an anatomist named Samuel Jackson, assisted Nathaniel Chapman, who founded the American Medical Association, as professor of the Institutes of Medicine at the School of Medicine of the University of Pennsylvania in 1832. In his text, "The Principles of Medicine Founded on the Structure and Functions of the Animal Organism" (1832), Jackson used dissections and the study of pathological anatomy as a means to determine the cause and course of diseases. William Wood Gerhard (1809–1872), who operated his own medical school in Philadelphia, joined a group of American medical doctors, including Alfred Stillé and Caspar Pennock of Philadelphia to take a private course from Pierre Charles Alexandre Louis in Paris in 1831.

When an epidemic disease with characteristics of typhoid fever broke out in Philadelphia in 1836, Gerhard and Pennock used the approaches they had learned from Louis to distinguish between typhus and typhoid fever to prevent the spread of the contagious typhus. Gerhard went on to publish an article in the *American Journal of the Medical Sciences* in 1836 which became one of the earliest and most significant published distinctions between the two diseases and he is credited with the first accurate study of tuberculosis meningitis [3]. His book on *Diseases of the Chest* ran through four editions.

In Philadelphia, Gerhard's pupil, Alfred Stillé, collaborated with the Bostonian, George Shattuck, Jr. at Harvard to categorize the distinctions among the numerous highly contagious "fevers." Stillé continued to differentiate typhus and typhoid fever and taught in the School of Medicine. In addition to this research, he contributed to the organization of the American Medical Association in 1847, later served as its president, published "Elements of Pathology" in 1848 and contributed a monograph of Cerebrospinal Meningitis and Cholera.

Horner develops pathological anatomy

William Edmonds Horner (1793–1853) (Fig. 3) had studied at Caspar Wistar's museum before being appointed Dean of

Fig. 3 William Edmonds Horner, images from Historical Medicine of the National Library of Medicine

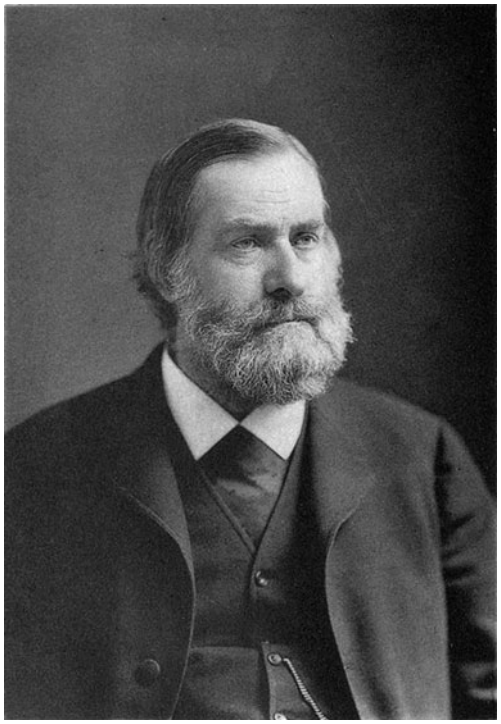

Fig. 4 Joseph Leidy

the University of Pennsylvania medical faculty in 1822. His "Treatise on Pathological Anatomy," published in 1829, was considered to be a compendium of pathology, guide to post-mortem examinations, and America's first pathology text [4]. He continued as curator of the Anatomical Museum of the University of Pennsylvania, which had been established in 1809 by Caspar Wistar. Horner traveled to France early in his career where he worked with Bichat, Louis, and Andral and revisited Europe in 1848 with Joseph Leidy, where they met with leading scientists in England, France, Austria, and Germany.

Leidy pioneers natural and medical sciences

Seldom recognized are the contributions made by Joseph Leidy (1823–1891) (Fig. 4) to the Philadelphia medical and scientific community. From 1844 when he graduated from the University of Pennsylvania medical school, Leidy introduced the utility and versatility of the microscope to examine a wide range of subjects, including fossils, gems, parasites, and forensic medicine and human tissues. When presented with a dinner of terrapin at the Biological Club, instead of eating the creatures, he dissected them and discovered three new intestinal parasites. "Never give Leidy anything that is edible and worth dissecting," S. Weir Mitchell observed, "We all know where it will go" [5].

Leidy's examination of parasite cysts in cooked ham led him to advocate the thorough cooking of meat to prevent infection by harmful parasites. He found houseflies to be carriers of disease and worked to eliminate their presence in hospitals.

Leidy may even have been the first to use the microscope in forensic medicine when he examined blood on the shirt of an accused murderer. He demonstrated that, since the red blood cells were not nucleated, the blood was definitely not that of a chicken as claimed but, instead, that of a human.

He published the *Elementary Treatise on Human Anatomy* in 1861, the standard medical school textbook widely used by generations of students and practitioners. With this publication, Leidy was the preeminent human anatomist in the United States. He is also known as the father of American vertebrate paleontology by having connected the relationships among fossil skeletons, evolution, and Darwin's theory of natural selection for which he is known as the father of American vertebrate paleontology. Leidy became the first chair of the Department of Biology at the University of Pennsylvania and, in 1882, served as Dean of the University of Pennsylvania Medical School. His 800 published articles provided the groundwork for much scientific investigation throughout the country [6].

Advances in surgery contribute to the development of surgical pathology

Advances in surgical practices contributed to the emergence of surgical pathology. Samuel D. Gross (1805–1884) (Fig. 5), a 1827 graduate from Jefferson Medical College, published the *Elements of Pathological Anatomy* in 1839. It remained the most comprehensive American pathology text of its kind for over 40 years. After teaching in Kentucky, Ohio, and New York, Gross became professor of Surgery at Jefferson Medical College. His two volume work, *A System of Surgery: Pathological, Diagnostic, Therapeutic, and Operative* went through six editions. As a member of the Royal Medical Society of Vienna and the Royal Medico-Surgical Society of London, he presided over the 1876 International Medical Congress in Philadelphia. Although not formally trained in pathology, he made critical innovations to surgical techniques and publicized elaborate reflections about the diseases he encountered surgically. Gross advocated for more attention to the study of pathology, noting "It is certainly an anomaly in the history of our profession that a science (pathology) which admits of such extensive application as the present, and which may be regarded as constituting the very foundation of the grand edifice of medicine should be so neglected as a branch of elementary study in the United States" [7].

Samuel Gross shared with David Hayes Agnew (1818–1892) his approaches and insights to making continuous improvements in surgical practice. Agnew led surgical practice and instruction at the University of Pennsylvania Medical School and gained the reputation as one of America's leading surgeons. After James Garfield was shot in 1881, Agnew was the chief consultant during the months of illness before Garfield's death.

Fig. 5 Samuel Gross and the Gross clinic

As was the case in many European medical centers, the Philadelphia Hospital, Blockley Hospital, Pennsylvania Hospital, and the College of Physicians of Pennsylvania each developed its own extensive museum that served as foundation for the study of pathology.

Improvements in surgical practice contributed to the quality of anatomic pathology and forensic pathology. Moreton Stillé, graduate of University of Pennsylvania and brother of Alfred and Charles Stillé, was well recognized as an expert in legal aspects of medicine. With Francis Wharton, he published *Treatise on Medical Jurisprudence* in 1855 which included precise instructions on post-mortem examination.

Pepper leads university reorganization and modernization

Efforts were also beginning to reform and change the nature of upper level education. As Charles Eliot was introducing major reforms at Harvard, Charles Janeway Stillé, Alfred Stillé's brother, took steps to modernize and expand the University when he became Provost in 1868. Stillé successfully increased funding to guarantee the university's growth and financial stability and convinced the trustees and faculty to support improvements in scientific education. The campus moved and expanded to include the University Hospital and a new scientific department.

William Pepper, Jr. (1843–1898) (Fig. 6) assumed the office of Provost of the University of Pennsylvania in 1881 and provided both the visionary and practical leadership to make sweeping changes to increase the quality of University and Medical School educational instruction, research, and publications.

Pepper had served as Medical School professor and curator of the hospital museum. This title was synonymous with being the pathologist and director of the hospital's laboratory [2, p. 124]. His contributions to medicine included descriptions of perforative appendicitis and peritonitis, malarial parasites, the role of bone marrow in pernicious anemia, the treatment of tuberculosis, and numerous publications, including the *Textbook of the Theory and Practice of Medicine*.

Along with Horatio C. Wood, he organized the University of Pennsylvania with its various graduate schools and programs with sequenced courses and extensive curricula. A fourth year was added to the medical school curriculum. His efforts resulted in a remarkable number of American firsts for the University of Pennsylvania Medical College;

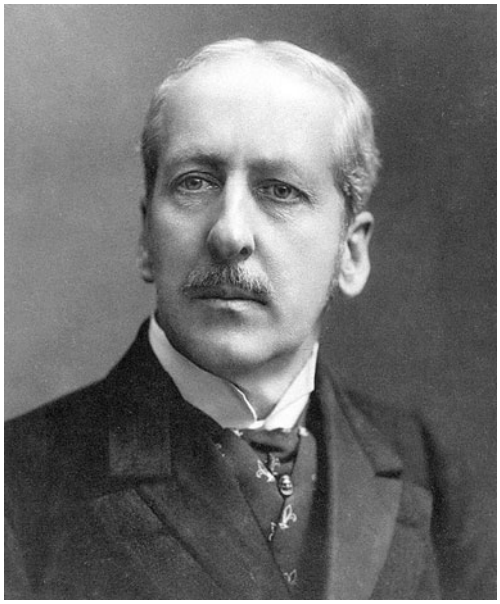

Fig. 6 William Pepper, Jr.

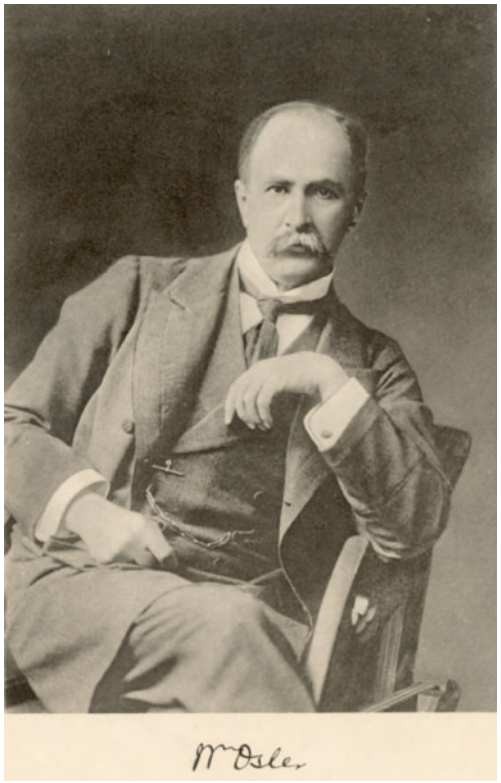

Fig. 7 William Osler. (Courtesy of the University of Pennsylvania Archives)

the first teaching hospital affiliated with a university medical school (1874), the first nurse's training school (1887), and the first laboratory of clinical medicine (1894) [8]. Pathology was designated to be a department in 1877 and James Tyson appointed as chair.

William Osler invigorates the Philadelphia community

During this period of reform and transformation, the trustees of the University of Pennsylvania medical school appointed William Osler (1849–1919) (Fig. 7) to follow Pepper as professor of clinical medicine in 1884. In its first 120 years, the medical school had appointed only one faculty member who was not a Pennsylvanian or an alumnus. Most professors were both. "Inbreeding of a faculty could hardly go farther," the official history notes [9]. "Quality had not necessarily suffered. Philadelphia arguably remained America's leading medical center" [10].

At the time, Osler was professor of the Institutes of Medicine at McGill University and pathologist at Montreal General Hospital. He had studied with leading British, German, and Austrian physicians and researchers, including Virchow. Osler attended the Seventh International Medical Congress in 1881 and was elected fellow in the Royal College of Physicians of London. Pepper's vacant chair presented trustees of the Pennsylvania Medical School with the opportunity to invigorate the medical school faculty.

He did not disappoint. Osler immediately set up a small clinical laboratory under the hospital amphitheater and there he is said to have produced an atmosphere so encouraging and helpful that young fellows trooped to his side [11]. This was a new experience to the senior students who had previously been fed more graceful generalizations and personal anecdotes than scientific study.

"In Philadelphia Osler was the doctor's pathologist" [2, p.160]. He immediately joined dining clubs in the University community, including the Pathological Society, Club of 19, whose members had positions of influence in the medical school, and the Biological Club, led by Joseph Leidy and S. Weir Mitchell (1829–1914). Mitchell was a neurologist and future president of the American Association of Physicians. Osler shared observations on blood platelets, the malaria parasite, cardiovascular lesions, especially aneurysms within these various groups.

What was remarkable about Osler's experience in Philadelphia was his success at bringing together a community of scientists and physicians to share, discuss, and refine their understandings of medical science and practice. He had Sunday dinners at the home of Samuel D. Gross where he met with the "Jefferson men," as he referred to the staff at the Jefferson College of Medicine. While he delighted in the company of high performing, inquisitive colleagues, he had little patience for staff whose practices were outdated. Concerned that the American Medical Association and related societies were rewarding such practices, he, James Tyson, and William Pepper, Jr., along with a number of prominent physicians, most of whom were pathologists, organized the

Association of American Physicians in 1885 to encourage the pursuit of medical knowledge through experimentation and the application of basic and clinical science to clinical medicine.

Osler both contributed to, and grew from, his Philadelphia experiences by practicing, instructing, writing about, and sharing insights as part of that community. The stimulating and provocative experiences in Philadelphia foreshadowed more significant contributions to medical and pathology practice at Johns Hopkins University. Osler left behind a group of colleagues at the University of Pennsylvania who were able to implement reforms that raised the quality of instruction with respect to medical practice and produced investigative research of the highest quality.

The new pathology emerges as Hopkins' cornerstone

Baltimore millionaire Johns Hopkins donated his fortune to create the most scientifically progressive of universities and hospitals. When Hopkins died in 1873 he left US $3.5 million to finance America's premier hospital, and Daniel Colt Gilman and John Shaw Billings (1838–1913) convinced the trustees to make pathology the cornerstone of Johns Hopkins Medical Institutions [12]. William H. Welch (1850–1934) was designated to direct the department of pathology and its laboratory in 1884 based upon recommendations of Julius Cohnheim in Germany and his own work at New York's Bellevue pathological laboratory. Welch tapped three physicians who had contributed significantly to the Philadelphia community to support and develop the new medical center. By 1888 Billings and Welch had recruited William Osler as physician-in-chief of the hospital and professor of the Theory and Practice of Medicine. Osler chose Howard A. Kelly, University of Pennsylvania graduate, physician, and surgeon from the Kensington neighborhood in Philadelphia, to organize the gynecological service at the Hospital. Kelly, along with Welch, was instrumental in founding the first experimental pathology laboratory at Hopkins and in the United States devoted to the study of specimens removed during surgery. Welch named William Halsted, his former colleague at Bellvue as professor of surgery. Halsted, in turn, selected another Osler assistant and Pennsylvania graduate, Joseph Colt Bloodgood, as his primary first assistant. Bloodgood graduated from the University of Pennsylvania Medical School and had worked with Osler there. Welch, Halsted, and Bloodgood established and developed the surgical pathology laboratory at Hopkins. Bloodgood made significant contributions to the development of surgical pathology as he and Thomas Cullen developed procedures for biopsy and frozen sections for intraoperative diagnoses.

Osler, Kelly, and Bloodgood replicated and extended on practices from Philadelphia, including regular cross-disciplinary meetings, publications, discussions, and reviews of ongoing practices and findings. "The Pathological Department at Hopkins was to revolutionize not only the teaching of pathology in this country, but in large measure that of every branch of medicine as well. From then on pathology was an independent science in America, but it was a science that made use of all other biological and medical sciences as well" [2, p.147].

Philadelphia plays key role as pathology takes full stage

By the time Johns Hopkins graduated its first class of medical students, pathology had won its place there and at the University of Pennsylvania, Jefferson Medical College, Harvard, and Columbia. The University of Pennsylvania had supplied Hopkins with three outstanding professors to create the University with the new pathology as its cornerstone. In turn, Pennsylvania pathologists now valued and selected Hopkins' leaders and graduates of the Hopkins medical and pathology program as prime candidates for teaching and leadership positions at the University of Pennsylvania.

Pepper launches first clinical research lab associated with medical clinic and hospital

William Pepper had invited John Shaw Billings to create, design, construct, and staff a Laboratory of Hygiene in 1892. Billings had served as curator of the Army Medical Museum for 10 years and Gilman's personal advisor as he planned and developed Johns Hopkins. Although he only stayed a year, Billings was able to staff the laboratory with researchers who pioneered frontiers in bacterial research such as D.H. Bergey whose work, *Bergey's Manual*, currently in its ninth edition as the reference text for bacterial classification. When Billings left the directorship, Pepper decided that it should be a robust clinical laboratory whose staff would perform applied research but with this critical distinction they would also "concern themselves with many problems which apparently have no immediate and direct bearing upon practical medicine" [13]. He became its first director, having both secured outside funding and made a US $50,000 personal contribution to finance its development.

This was the first laboratory in the United States associated directly with a medical clinic and a university. George Dock, graduate of the University of Pennsylvania, had studied in the Leipzig Institute and Laboratory and collaborated closely with Pepper on its design. Alfred Stengel succeeded Pepper and

during his tenure as director, published the *Textbook of Pathology* which correlated anatomic and physiological changes in patients with their clinical status. Herbert Fox, the laboratory's third director in 1911, expanded its responsibility to include all chemical, serological, bacteriological, and electrocardiographic studies of hospital patients. The laboratory pioneered numerous breakthrough innovations, including molecular pathology testing on a routine basis and inspired even discoveries and innovations throughout the United States and the rest of the world.

Philadelphia leaders influence subsequent developments in pathology

As the nineteenth century ended, the Department of Pathology at the University of Pennsylvania was providing high caliber instruction as well as leading innovative clinical research. Simon Flexner was a protégé of William Welch at Hopkins. Flexner came to the department in 1899 and soon became chair. He isolated the dysentery *Bacillus* that causes a prevalent form of the disease, now known as the Flexner's bacillus. His skills in both the laboratory and in management were so well recognized that John D. Rockefeller, Jr. asked him to head his Rockefeller Institute for Medical Research in 1903. Flexner's younger brother, Abraham, a researcher at the Rockefeller Foundation, published the famous "Flexner Report" in 1910 which served to reform medical education in the United States. Hideyo Noguchi who had worked with Flexner at the University of Pennsylvania studying bacteriology and diseases of the blood joined him at the Rockefeller Institute. Noguchi went on to discover *Treponema pallidum*, the agent of syphilis.

The medical community in Philadelphia continued to progress and transform throughout the twentieth century. The Wistar Institute of Anatomy and Biology, which developed from the Wistar Anatomy Museum, has exerted a leading influence as a center for vaccine, cancer, and most recently generics and immunology research. In 1904, the first cancer hospital in the United States, the American Oncologic Hospital, opened in Philadelphia and later became the Fox Chase Center when it merged with the Institute for Cancer Research. Numerous significant discoveries have been made by and Nobel prizes awarded to Fox Chase scientists.

As the practice of pathology transformed, key professional associations emerged to support pathology and products or members of the Philadelphia community, such as Howard T. Karsner and R. M. Pearce, provided outstanding leadership for them. Karsner graduated from and served as demonstrator at the University of Pennsylvania, School of Medicine and resident physician at Philadelphia Hospital, taught at Harvard, and chaired and oversaw the development of the Institute of Pathology at Case Western Reserve School of Medicine. Dr. Karsner contributed directly to the organization and work of the American Association of Pathologists and Bacteriologists, the National Research Council, National Board of Pathology, the Armed Forces Institute of Pathology, and other associations related to pathology. R. M. Pearce chaired the Department of Research Medicine and Department of Pathology at the University Of Pennsylvania School of Medicine and became director of the Division of Medical Education of the Rockefeller Foundation and founded the American Society for Experimental Pathology.

The contributions of the Philadelphia medical community provided a cradle for pathology, helping it enter the twentieth century as the discipline that provided the foundation of medical science in America throughout the twentieth century. The field itself has expanded and transformed continuously as a result of the revolution begun by Virchow's *omnis cellula e cellula*, "every cell stems from another cell" [14]. Changes include distinction between bacterial and viral infections, malignant and non-malignant tumors, and the molecular structure of DNA. Notably, the discovery in 1960 of the first genetic abnormality associated with a human cancer, by David Hungerford of the Fox Chase Cancer Center and Peter Nowell (52 University of Pennsylvania School of Medicine) (Fig. 8) of the University of Pennsylvania, was recognized as the "Philadelphia Chromosome" in recognition of this medical community that nurtured the development of modern pathology in America.

Fig. 8 Peter Nowell. (Courtesy of Peter C. Nowell, MD)

Conflict of interest We declare that there is no conflict of interest.

Open Access This article is distributed under the terms of the Creative Commons Attribution Noncommercial License which permits any noncommercial use, distribution, and reproduction in any medium, provided the original author(s) and source are credited.

References

1. American Philosophical Society (2010) About the APS. http://www.amphilsoc.org/about. Accessed 28 July 2010
2. Long ER (1962) A history of American pathology. Charles C Thomas, Springfield
3. Osler W (1926) An Alabama student. Oxford University Press, London, p 207
4. Rosai J (ed) (1997) Guiding the surgeon's hand: the history of American pathology. American Registry of Pathology, Washington DC
5. Earnest E (1950) S. Weir Mitchell, novelist and physician. University of Pennsylvania Press, Pennsylvania, p 91
6. Warren J (1998) The last man who knew everything. Yale University Press, New Haven, p 130
7. Gross SD (1839) Elements of pathological anatomy. March, Capen, Lyon, and Webb, Boston
8. Penn University Archives & Records Center (2010) Office of the Provost, William Pepper Jr 1881–1894. http://www.archives.upenn.edu/faids/upa/upa6/upa6_2pep.html
9. Corner GW (1965) Two centuries of medicine: history of the School of Medicine. The University of Pennsylvania, Lippincott
10. Bliss M (1999) William Osler: a life in medicine. Oxford University Press, New York, p 128
11. Cushing H (1925) The Life of Sir William Osler, vol 2. Clarendon Press, Oxford, pp 235–236
12. Carter D (1997) Surgical pathology at Johns Hopkins. In: Rosai J (ed) Guiding the surgeon's hand: the history of American pathology. American Registry of Pathology, Washington, DC, p 23
13. Young DS, Berwick MC, Jarett L (1994) The William Pepper laboratory and department of pathology and laboratory medicine of the University of Pennsylvania: an integrated history. The University of Pennsylvania, Philadelphia, p 27
14. Rather LJ (1966) Rudolph Virchow's views on pathology, pathological anatomy, and cellular pathology. Arch Pathol 82:197–204

Virchows Arch (2011) 458:39–45
DOI 10.1007/s00428-010-1001-x

ORIGINAL ARTICLE

Chromosome 3p alterations in pancreatic endocrine neoplasia

Eliana Amato · Stefano Barbi · Giorgio Malpeli · Samantha Bersani · Giuseppe Pelosi · Paola Capelli · Aldo Scarpa

Received: 23 August 2010 / Revised: 28 September 2010 / Accepted: 10 October 2010 / Published online: 28 October 2010
© The Author(s) 2010. This article is published with open access at Springerlink.com

Abstract Pancreatic endocrine tumors (PET) are rare neoplasms classified as functioning (F-PET) or non-functioning (NF-PET) according to the presence of a clinical syndrome due to hormonal hypersecretion. PETs show variable degrees of clinical aggressiveness and loss of chromosome 3p has been suggested to be associated with an advanced stage of disease. We assessed chromosome 3p copy number in 113 primary PETs and 32 metastases by fluorescence in situ hybridization (FISH) using tissue microarrays. The series included 56 well-differentiated endocrine tumors (WDET), 62 well-differentiated endocrine carcinomas (WDEC), and 6 poorly differentiated endocrine carcinomas (PDEC). Chromosome 3p alterations were found in 23/113 (20%) primary tumors, with losses being predominant over gains (14% vs. 6%). Loss of 3p was found in 5/55 (9%) WDET, 11/52 (21%) WDEC, and never in PDEC. Gains of 3p were detected in 4/55 (7%) WDET, no WDEC, but notably in 3/6 (50%) PDEC (OR 23.6; P=0.003). Metastases were more frequently monosomic for 3p compared to primary tumors (OR 3.6; P=0.005). Monosomy was significantly associated with larger tumor size, more advanced tumor stage, and metastasis. No association was found with survival. Chromosome 3p copy number alterations are frequent events in advanced stage PET, with gains prevailing in PDEC while losses are more frequent in WDEC, supporting the view that a specific pattern of alterations are involved in these diverse disease subtypes.

Keywords FISH · Pancreatic endocrine tumors · Metastasis · 3p · Chromosomal aberrations

E. Amato · A. Scarpa
ARC-NET Center for Applied Research on Cancer,
Hospital Concern and University School of Medicine,
Verona, Italy

S. Barbi · G. Malpeli · S. Bersani · P. Capelli · A. Scarpa (✉)
Department of Pathology, University Hospital of Verona,
Policlinico G.B. Rossi, piazzale L.A. Scuro 10,
37134 Verona, Italy
e-mail: aldo.scarpa@univr.it

G. Malpeli
Department of Surgical and Gastroenterological Sciences,
University of Verona,
Verona, Italy

G. Pelosi
Department of Pathology and Laboratory Medicine, National
Cancer Institute and University of Milan School of Medicine,
Milan, Italy

Introduction

Pancreatic endocrine tumors (PET) are rare neoplasms whose molecular pathogenesis is being unraveled but is still largely unknown [1–4]. PET are classified clinically as functioning (F-PET) or non-functioning (NF-PET) according to the presence of a syndrome due to hormonal hypersecretion. NF-PET and F-PET other than insulinoma are malignant in up to 70% of cases. The WHO classification distinguishes three categories: well-differentiated endocrine tumor having an indolent clinical course; well-differentiated endocrine carcinoma (WDEC) that is diagnosed based on the presence of invasion or metastasis; poorly differentiated endocrine carcinoma (PDEC) with a survival as poor as that of pancreatic adenocarcinoma [5]. However, the malignant potential of WDEC varies greatly and cannot be predicted by histological appearance alone. Although the recently proposed TNM staging and the proliferation rate of the neoplasia

are valuable predictors of clinical outcome, additional prognostic parameters are warranted [6, 7].

Chromosomal alterations have been suggested to be prognostic parameters for tumor progression, recurrence, and tumor-specific death in these tumors. In PETs, alterations of 3p were investigated using two approaches: by LOH microsatellite analysis, allelic imbalance at 3p was observed in an average of 47% of cases [8–13] whereas by means of comparative genomic hybridization (CGH), loss of 3p was found in 21% of PETs [14–16]. Moreover, in almost all studies investigating this subject, these alterations were associated with an advanced stage of disease.

Potential candidate genes at this locus include *VHL* and *RASSF1A*, that have been recently associated with PET pathogenesis [12, 17–19]. Interestingly, recent data from Schmitt et al. suggest that *VHL* inactivation and consecutive hypoxia signals may be a mechanism for the development of sporadic PET with an adverse outcome [17]. Moreover, inactivation of the tumor suppressor gene *RASSF1A* by hypermethylation and 3p LOH has been proposed as a major event in PET tumorigenesis [12, 18, 19].

A large amount of evidences support the association of 3p alterations with prognosis, however the methods previously employed to detect this association are not easily applicable to clinical practice. Fluorescence in situ hybridization (FISH) is commonly used as a diagnostic device in cancer. Here, we explore the possibility to use FISH on chromosome 3p as a prognostic tool for PET by screening a large series composed of 113 PET and 32 metastases and correlating the results with clinical–pathological features of patients.

Materials and methods

Samples

The series comprises 113 primitive neoplasms and 32 metastases obtained from 124 PET patients operated on at the University Hospital of Verona, Italy. Of the metastases, 21 had a matched primary tumor in the series. Clinical–pathological features of the present series are shown in Table 1. Informed consent for the analysis of normal and neoplastic tissues was obtained from patients, in accordance with the approval of the Verona University and Hospital Trust's Ethical Committee.

Tissue microarrays

Six tissue microarrays (TMAs) containing the 113 primary PETs and 32 metastases were constructed, using a tissue arrayer (Beecher Instruments, Silver Spring, MD) and including at least three cores of 1 mm diameter per sample [3].

Fluorescence in situ hybridization

FISH assay for chromosome 3p was performed on 4-μm-thick sections from TMAs, using a home-made SpectrumOrange

Table 1 Clinical–pathological features of 124 PETs consisting of 113 primitive samples and 11 unmatched metastases

Parameter	Category[a]	Frequency (percent)
Gender	F	67 (54%)
	M	57 (46%)
Age	mean (1st quartile to 3rd quartile)	56 (44–65)
PT	T1	34 (27%)
	T2	33 (27%)
	T3	21 (17%)
	T4	36 (29%)
PN	N0	74 (60%)
	N1	50 (40%)
PM	M0	85 (69%)
	M1	39 (32%)
WHO	PDEC	6 (5%)
	WDEC	62 (50%)
	WDET	56 (45%)
Hormone secretion	Functioning	26 (21%)
	Non-functioning	98 (79%)
Proliferative index	Ki67>5%	28 (23%)
	Ki67<5%	96 (77%)
Tumor size	Mean (1st quartile to 3rd quartile)	30 (15–45)

[a] *PDEC* poorly differentiated endocrine carcinoma, *WDEC* well-differentiated endocrine carcinoma, *WDET* well-differentiated tumor

labeled DNA probe for the relevant region (Abbott-Vysis, Downer Grove, IL, USA). Briefly, BAC clone specific for chromosome 3p (RP11-894C9) mapping at 3p21.31 and belonging to the Roswell Park Cancer Institute libraries (Peter J. de Jong at http://bacpac.chori.org/) was selected. Paraffin sections were hybridized with the probe labeled by nick translation [20], using 500 ng of probe labeled with Fluorolink Cy3-dUTP or Fluor-X-dCTP (Amersham, Buckinghamshire, UK). For each sample, at least 110 nuclei were analyzed for presence of 3p signals.

Statistical analysis

k-means algorithm using Hartigan–Wong method was used to classify PET samples into three classes, with no a priori centroid definition, based on the distribution of FISH counts. For sample assignation, 1,000 iterations were used. For association of samples locus status with clinical–pathological features, Fisher's test was used. For correlation of percent of PET cells showing monosomy with clinical–pathological features, Kruskal–Wallis' test was used for categorical covariates and Spearman's correlation for numeric variables. Survival estimates were calculated with Kaplan–Meier's method and compared by the log-rank test. *P* values less than 0.05 were considered significant. Where applicable, the tests were two-tailed. For all the calculations, the *R* statistical software package was used (http://www.r-project.org).

Results

FISH was performed on six TMAs containing 113 primary PETs and 32 metastases. For each sample, we counted neoplastic cells having one, two or more than two signals per nucleus, for at least 110 cells per sample. Therefore, we used the cell counts to assign samples to three unsupervised classes, by the k-means algorithm. The centroids obtained and distributions of the three classes are shown in Fig. 1. The three classes were composed of 28 samples (19%) with an excess of monosomic signals, 108 samples (75%) with a predominant disomic state and 9 samples (6%) with evidence of gains (Table 2).

Using such classification, we also found a high frequency of samples showing gains among PDEC (3/6; OR 23.6; 95% CI 2.4–243.4; Fisher's test $P=0.003$). In addition, we found that monosomic samples were significantly more represented in metastases (OR 3.6; 95% CI 1.3–9.6; Fisher's test $P=0.005$).

In order to investigate possible 3p alterations de novo acquired in metastases, we compared the 3p status of 21 metastases with their matched primary samples (Table 3). Thirteen patients had the same 3p copy number whereas in three samples, the copy number increased and five showed de novo losses.

As 3p loss was the most represented event, we then focused on the correlation between losses and other clinical–pathological covariates. In addition, to avoid potential misclassification, the percent of monosomic cells was directly used in the analysis instead of the categorization introduced above. The results of this analysis are summarized in Table 4. Percent of monosomic cells was higher in metastases and positively correlated with larger size, more advanced tumor invasion, carcinoma of the well-differentiated type and absence of hormone secretions. Although correlated with worse patients' outcome, we did not find a significant association between monosomy and survival, even when considering only the WDEC group. Similarly, we did not find any significant association between gains of 3p and survival.

Discussion

Several studies employing two main molecular approaches (LOH by microsatellites and CGH) have suggested a role

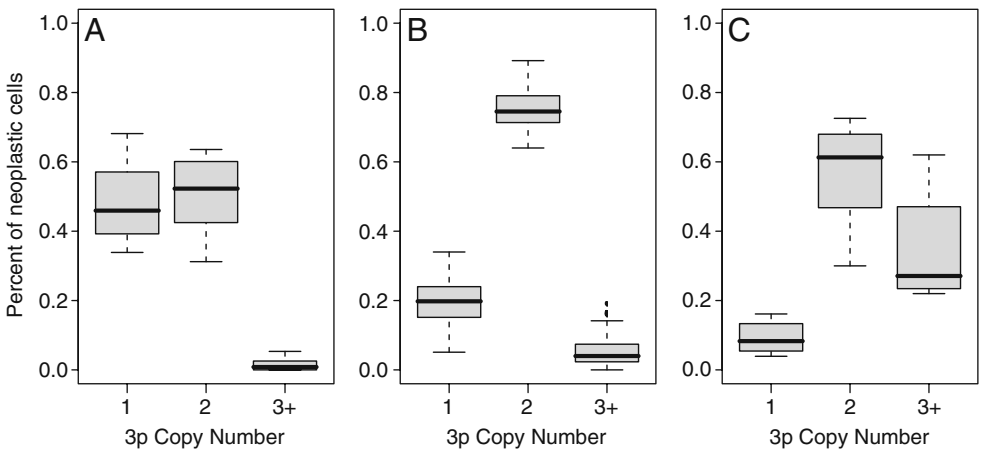

Fig. 1 Distribution of frequency of neoplastic nuclei with one, two or at least three FISH signals of PET cases belonging to the classes of monosomic (**a**), disomic (**b**), gains (**c**), based on the frequency of signals per nucleus. The samples were assigned to the three classes using k-means algorithm

Table 2 Frequency of DNA copy number status among 113 primitive PETs and 32 metastases

Sample type	WHO classification[a]	DNA copy number		
		1	2	3+
Primitive	PDEC	0	3 (50%)	3 (50%)
	WDEC	11 (21%)	41 (79%)	0
	WDET	5 (9%)	46 (84%)	4 (7%)
	Functioning	2 (9%)	18 (82%)	2 (9%)
	Non-functioning	14 (15%)	72 (79%)	5 (6%)
	Total	16 (14%)	90 (80%)	7 (6%)
Metastasis	PDEC	0	2 (67%)	1 (33%)
	WDEC	12 (41%)	16 (55%)	1 (3%)
	Functioning	2 (40%)	3 (60%)	0
	Non-functioning	10 (37%)	15 (56%)	2 (7%)
	Total	12 (38%)	18 (56%)	2 (6%)

[a] *PDEC* poorly differentiated endocrine carcinomas, *WDEC* well-differentiated endocrine carcinomas, *WDET*, well-differentiated tumors

for alterations of chromosome 3p in PET. A detailed survey of the relevant literature has been collected in Table 5. In particular, a relationship between LOH at 3p and locally advanced or metastatic PETs was found in all previous works. Of the two techniques used, LOH detected consistently a higher number of alterations [8–13] compared to CGH [14–16] (47% vs. 21%). This apparent discrepancy can be accounted for by the intrinsic features of the two methods. In fact, although LOH by microsatellites provides the ability to finely map the region where the alterations occur, it sums up gains and losses that are difficult to tell apart as both are seen as allelic imbalances. On the other hand, with CGH only true losses are reported.

Our study showed that a consistent number of chromosomal alterations, detected by FISH, involved the 3p locus with losses predominant over gains (14% vs. 6%). The use of FISH allows the characterization of chromosomal alterations at specific loci with a small cost per sample and avoids artifacts deriving from analysis with other molecular techniques such as LOH microsatellite analysis. Our results are more in line with previous CGH reports, probably due to the ability of both techniques to discern losses and gains.

In our series, we found that monosomic samples were significantly more represented in metastases than in primitive samples, in agreement with all previous studies reporting a higher frequency of 3p loss in association with metastatic event (see Table 5). Furthermore, in pair-wise analysis of 21 matched primaries and metastases, we observed that 3p copy number was conserved from primitive to metastasis in 13 samples. However, five metastases showed a decrease in 3p copy number; in two patients, primitive samples were monosomic and metastasis showed a disomic state, and one patient had a gain in metastasis. This suggests the occurrence of tumor heterogeneity in PET and as such a role in their metastasis formation mechanism.

Table 3 DNA copy number of 3p in 21 primitive samples and their matched metastases

Primitive copy number	Metastases copy number		
	1	2	3+
1	3	2	0
2	5	9	1
3+	0	0	1

In addition, we found that the proportion of monosomic cells was positively correlated with non-functioning status, larger size, a diagnosis of carcinoma of the well-differentiated type and a more advanced pT stage. The higher percent of monosomy found in non-functioning PET was already suggested by previous studies describing this class of PET as having both larger size and higher rate of chromosomal aberrations compared to the functioning ones [8, 10, 16]. These data suggest that 3p monosomy may occur later during the development of disease and may contribute to the progression of malignancy of PET. Although correlated with worse patient features, we did not find a significant association between monosomy and survival, also when considering only the WDEC group, probably due to the general high survival rate of PET.

Interestingly, several data support the role of genes mapping on 3p in PET pathogenesis and malignancy. Among these genes, *VHL* is a major candidate as patients with Von-Hippel Lindau syndrome may develop pancreatic endocrine tumors. Schmitt and colleagues have investigated the presence of genetic and epigenetic alterations at *VHL* locus in PETs [17]. By using FISH, they detected a frequency of 3p loss of 18%, a number that is very close to that found in our series. They suggest that *VHL* inactivation and consecutive hypoxia signals may be a mechanism for the development of sporadic PET with an adverse outcome. However, another study identified LOH

Table 4 Distribution of percent of monosomy according to clinical–pathological features of 113 primary pancreatic endocrine tumors

Parameter	Class	Median (1st quartile to 3rd quartile)	*P* value
	Primitives	0.19 (0.14–0.25)	<0.001
	Metastases	0.26 (0.22–0.41)	
pT	T1	0.15 (0.13–0.23)	0.027
	T2	0.18 (0.15–0.22)	
	T3	0.22 (0.16–0.27)	
	T4	0.23 (0.17–0.32)	
pN	N0	0.19 (0.14–0.25)	0.704
	N1	0.20 (0.14–0.24)	
pM	M0	0.19 (0.14–0.24)	0.095
	M1	0.22 (0.16–0.28)	
WHO	PDEC	0.11 (0.08–0.13)	<0.001
	WDEC	0.18 (0.13–0.21)	
	WDET	0.16 (0.14–0.24)	
Hormone secretion	Functioning	0.15 (0.11–0.21)	0.029
	Non-functioning	0.20 (0.15–0.27)	
Tumor size		0.30 (Spearman's rho)	0.002
Ki67		0.05 (Spearman's rho)	0.596

PDEC poorly differentiated endocrine carcinoma, *WDEC* well-differentiated endocrine carcinoma, *WDET* well-differentiated tumor

in an area outside the *VHL* gene (3p14.2–3p21), in 83% of malignant insulinomas compared with 53% of benign insulinomas [11], suggesting that other candidates are also likely to be involved in PET onset and progression. Another hypothesis suggests the presence of a novel pancreatic endocrine tumor suppressor gene at 3p25, being the frequency of 3p loss about 33% in the region flanking the *VHL* gene. Allelic loss of this chromosomal region has been

Table 5 Summary of 3p LOH data available in literature for PET

No. of Cases	3p LOH (*total*)	WHO[a]		Tumor type[b]		Metastasis		Method[c]	Reference
		WDET	WDEC	F	NF	No	Yes		
10	3/10	0/5	3/5	nr	nr	0/5	3/5	ms	[12]
	30%	0%	60%	–	–	0%	60%		
82	47/82	7/25	40/57	24/47	23/35	17/41	28/38	ms	[8]
	57%	28%	70%	51%	65%	41.5%	74%		
20	9/20	1/8	8/12	0/11	9/9	0/6	9/12	ms	[10]
	45%	12.5%	67%	0%	100%	0%	75%		
43	14/43	2/22	12/21	11/29	3/14	2/22	12/21	ms	[9]
	33%	9%	57%	38%	21%	9%	57%		
21	13/21	8/15	5/6	13/21	none	8/15	5/6	ms	[11]
	62%	53%	83%	62%	–	53%	83%		
16	5/16	2/8	3/8	none	5/16	2/9	3/7	ms	[13]
	31%	25%	37.5%	–	31%	22%	30%		
192	91/192	20/83	71/109	48/108	40/74	29/98	60/89	Total LOH by ms	
	47%	24%	65%	44%	54%	30%	67%		
44	13/44	6/9	7/35	nr	nr	2/22	10/18	CGH	[15]
	30%	67%	20%	–	–	9%	56%		
45	9/45	3/28	6/17	5/31	4/14	3/28	6/17	CGH	[16]
	20%	11%	35%	16%	29%	11%	35%		
20	1/20	0/8	1/12	none	1/20	0/9	1/11	CGH	[14]
	5%	0%	8%	–	5%	0%	9%		
109	23/109	9/45	14/64	5/31	5/34	5/59	17/46	Total LOH by CGH	
	21%	20%	22%	16%	15%	8%	37%		

[a] *WDEC* well-differentiated endocrine carcinoma, *WDET* well-differentiated endocrine tumor

[b] *F* functioning, *NF* non-functioning

[c] *ms* LOH by microsatellite analysis

nr not reported

proposed to serve as a molecular marker discriminating benign from clinically malignant disease [9].

Also, Barghorn et al. identified a common deleted region (3p25-p24.2) in PETs that does not include *VHL* and propose a new member of the nuclear receptor superfamily, the peroxisome proliferator-activated receptor gamma (*PPARγ*), as a possible candidate tumor suppressor [8]. Indeed, this gene has been demonstrated to act as a regulator of differentiation and/or growth of many different cell types [21, 22] and loss-of-function of mutations in *PPARγ* have already been identified in human colon cancer [23]. Another candidate gene on chromosome 3p is the tumor suppressor gene *RASSF1A* that has been suggested to be inactivated by 3p LOH and hypermethylation in 30% of malignant well-differentiated carcinomas of the pancreas [12]. In light of the association of 3p loss with malignancy, we can underline the relevance of the pattern of 3p allelic losses during progression of PET. However, the specific targets of such alterations and their functional meaning in PET tumorigenesis remain to be further investigated.

Notably, we found a higher proportion of gains in PDEC with respect to WDEC, suggesting that this feature is characteristic of poorly differentiated tumors. We did not find any significant association between gains of 3p and survival, although it is worth noting that none of the seven patients showing gains (including the three PDECs) died of disease, suggesting that gain of 3p could be a positive prognostic factor.

Previous papers have demonstrated the presence of gain of 3p in different types of cancer such as hepatocarcinoma [24] and ductal carcinoma of the breast [25], but this feature has never been observed in pancreatic endocrine tumors. The reason may be probably due to the fact that poorly differentiated carcinomas are rarely included in PET studies. Therefore, based on our evidences, we cannot hypothesize any potential oncogene that could be a target for this kind of alteration.

As a methodological remark, we found that percent of monosomic cells showed more power in detecting association with clinical–pathological features, compared to a discrete classification based on 3p copy number. The reason for such a greater power may be due to the inherent higher precision of a quantitative measure as it can more finely reflect intermediate *status*, along the tumor development path, in which the neoplastic population is composed of genetically different clones with different selective advantages.

In conclusion, our data showed that alterations in 3p copy number may play an important role in tumor progression, malignant behavior and metastasis and may occur as a later event in cancer development. In addition, we found that losses and gains of 3p locus are associated with different forms of the disease: namely, gains with poorly differentiated endocrine carcinoma, losses with well-differentiated endocrine carcinoma. These data together confirm that 3p may contain genes important for metastatic development of PETs, but the specific targets as well as the prognostic potential of these alterations need to be further investigated.

Acknowledgments This work was supported by grants from: Associazione Italiana Ricerca Cancro (AIRC, http://www.airc.it/), Fondazione CariParo (www.fondazionecariparo.it), Fondazione Cariverona (http://www.fondazionecariverona.org/); Italian Ministry of Health, Rome, Italy (http://www.salute.gov.it/).

Conflict of interest statement We declare that we have no conflict of interest.

Open Access This article is distributed under the terms of the Creative Commons Attribution Noncommercial License which permits any noncommercial use, distribution, and reproduction in any medium, provided the original author(s) and source are credited.

References

1. Roldo C, Missiaglia E, Hagan JP, Falconi M, Capelli P, Bersani S, Calin GA, Volinia S, Liu CG, Scarpa A, Croce CM (2006) MicroRNA expression abnormalities in pancreatic endocrine and acinar tumors are associated with distinctive pathologic features and clinical behavior. J Clin Oncol 24(29):4677–4684
2. Capelli P, Martignoni G, Pedica F, Falconi M, Antonello D, Malpeli G, Scarpa A (2009) Endocrine neoplasms of the pancreas: pathologic and genetic features. Arch Pathol Lab Med 133 (3):350–364
3. Missiaglia E, Dalai I, Barbi S, Beghelli S, Falconi M, della Peruta M, Piemonti L, Capurso G, Di Florio A, delle Fave G, Pederzoli P, Croce CM, Scarpa A (2010) Pancreatic endocrine tumors: expression profiling evidences a role for AKT-mTOR pathway. J Clin Oncol 28(2):245–255
4. Corbo V, Dalai I, Scardoni M, Barbi S, Beghelli S, Bersani S, Albarello L, Doglioni C, Schott C, Capelli P, Chilosi M, Boninsegna L, Becker KF, Falconi M, Scarpa A (2010) MEN1 in pancreatic endocrine tumors: analysis of gene and protein status in 169 sporadic neoplasms reveals alterations in the vast majority of cases. Endocr Relat Cancer 17:771–783
5. Kloppel G, Perren A, Heitz P (2004) The gastroenteropancreatic neuroendocrine cell system and its tumors: the WHO classification. Ann NY Acad Sci 1014:13–27
6. Rindi G, Kloppel G, Alhman H, Caplin M, Couvelard A, de Herder WW, Erikssson B, Falchetti A, Falconi M, Komminoth P, Korner M, Lopes JM, McNicol AM, Nilsson O, Perren A, Scarpa A, Scoazec JY, Wiedenmann B (2006) TNM staging of foregut (neuro)endocrine tumors: a consensus proposal including a grading system. Virchows Arch 449(4):395–401
7. Scarpa A, Mantovani W, Capelli P, Beghelli S, Boninsegna L, Bettini R, Panzuto F, Pederzoli P, Fave GD, Falconi M (2010) Pancreatic endocrine tumors: improved TNM staging and histopathological grading permit a clinically efficient prognostic stratification of patients. Mod Pathol 23:824–833
8. Barghorn A, Komminoth P, Bachmann D, Rutimann K, Saremaslani P, Muletta-Feurer S, Perren A, Roth J, Heitz PU, Speel EJ (2001)

Deletion at 3p25.3-p23 is frequently encountered in endocrine pancreatic tumours and is associated with metastatic progression. J Pathol 194(4):451–458
9. Chung DC, Smith AP, Louis DN, Graeme-Cook F, Warshaw AL, Arnold A (1997) A novel pancreatic endocrine tumor suppressor gene locus on chromosome 3p with clinical prognostic implications. J Clin Invest 100(2):404–410
10. Hessman O, Lindberg D, Einarsson A, Lillhager P, Carling T, Grimelius L, Eriksson B, Akerstrom G, Westin G, Skogseid B (1999) Genetic alterations on 3p, 11q13, and 18q in nonfamilial and MEN 1-associated pancreatic endocrine tumors. Genes Chromosom Cancer 26(3):258–264
11. Nikiforova MN, Nikiforov YE, Biddinger P, Gnepp DR, Grosembacher LA, Wajchenberg BL, Fagin JA, Cohen RM (1999) Frequent loss of heterozygosity at chromosome 3p14.2-3p21 in human pancreatic islet cell tumours. Clin Endocrinol (Oxf) 51 (1):27–33
12. Pizzi S, Azzoni C, Bottarelli L, Campanini N, D'Adda T, Pasquali C, Rossi G, Rindi G, Bordi C (2005) Rassf1a promoter methylation and 3p21.3 loss of heterozygosity are features of foregut, but not midgut and hindgut, malignant endocrine tumours. J Pathol 206(4):409–416
13. Rigaud G, Missiaglia E, Moore PS, Zamboni G, Falconi M, Talamini G, Pesci A, Baron A, Lissandrini D, Rindi G, Grigolato P, Pederzoli P, Scarpa A (2001) High resolution allelotype of nonfunctional pancreatic endocrine tumors: identification of two molecular subgroups with clinical implications. Cancer Res 61 (1):285–292
14. Floridia M, Bucciardini R, Fragola V, Galluzzo CM, Giannini G, Pirillo MF, Amici R, Andreotti M, Ricciardulli D, Tomino C, Vella S (2004) Risk factors and occurrence of rash in HIV-positive patients not receiving nonnucleoside reverse transcriptase inhibitor: data from a randomized study evaluating use of protease inhibitors in nucleoside-experienced patients with very low cd4 levels (<50 cells/microl). HIV Med 5(1):1–10
15. Speel EJ, Richter J, Moch H, Egenter C, Saremaslani P, Rutimann K, Zhao J, Barghorn A, Roth J, Heitz PU, Komminoth P (1999) Genetic differences in endocrine pancreatic tumor subtypes detected by comparative genomic hybridization. Am J Pathol 155(6):1787–1794
16. Zhao J, Moch H, Scheidweiler AF, Baer A, Schaffer AA, Speel EJ, Roth J, Heitz PU, Komminoth P (2001) Genomic imbalances in the progression of endocrine pancreatic tumors. Genes Chromosom Cancer 32(4):364–372
17. Schmitt AM, Schmid S, Rudolph T, Anlauf M, Prinz C, Kloppel G, Moch H, Heitz PU, Komminoth P, Perren A (2009) VHL inactivation is an important pathway for the development of malignant sporadic pancreatic endocrine tumors. Endocr Relat Cancer 16(4):1219–1227
18. Liu L, Broaddus RR, Yao JC, Xie S, White JA, Wu TT, Hamilton SR, Rashid A (2005) Epigenetic alterations in neuroendocrine tumors: methylation of RAS-association domain family 1, isoform a and p16 genes are associated with metastasis. Mod Pathol 18(12):1632–1640
19. Dammann R, Schagdarsurengin U, Strunnikova M, Rastetter M, Seidel C, Liu L, Tommasi S, Pfeifer GP (2003) Epigenetic inactivation of the Ras-association domain family 1 (RASSF1A) gene and its function in human carcinogenesis. Histol Histopathol 18(2):665–677
20. Lichter P, Jauch A, Cremer T, Ward DC (1990) Detection of Down syndrome by in situ hybridization with chromosome 21 specific DNA probes. Prog Clin Biol Res 360:69–78
21. Elstner E, Muller C, Koshizuka K, Williamson EA, Park D, Asou H, Shintaku P, Said JW, Heber D, Koeffler HP (1998) Ligands for peroxisome proliferator-activated receptorgamma and retinoic acid receptor inhibit growth and induce apoptosis of human breast cancer cells in vitro and in BNX mice. Proc Natl Acad Sci USA 95(15):8806–8811
22. Sarraf P, Mueller E, Jones D, King FJ, DeAngelo DJ, Partridge JB, Holden SA, Chen LB, Singer S, Fletcher C, Spiegelman BM (1998) Differentiation and reversal of malignant changes in colon cancer through PPARgamma. Nat Med 4(9):1046–1052
23. Sarraf P, Mueller E, Smith WM, Wright HM, Kum JB, Aaltonen LA, de la Chapelle A, Spiegelman BM, Eng C (1999) Loss-of-function mutations in PPAR gamma associated with human colon cancer. Mol Cell 3(6):799–804
24. Qin LX, Tang ZY, Sham JS, Ma ZC, Ye SL, Zhou XD, Wu ZQ, Trent JM, Guan XY (1999) The association of chromosome 8p deletion and tumor metastasis in human hepatocellular carcinoma. Cancer Res 59(22):5662–5665
25. Aubele M, Mattis A, Zitzelsberger H, Walch A, Kremer M, Hutzler P, Hofler H, Werner M (1999) Intratumoral heterogeneity in breast carcinoma revealed by laser-microdissection and comparative genomic hybridization. Cancer Genet Cytogenet 110 (2):94–102

Virchows Arch (2011) 458:47–53
DOI 10.1007/s00428-010-0985-6

ORIGINAL ARTICLE

Glucagon expression in cystic pancreatic neuroendocrine neoplasms: an immunohistochemical analysis

Björn Konukiewitz · Tetsuji Enosawa · Günter Klöppel

Received: 30 August 2010 / Revised: 15 September 2010 / Accepted: 16 September 2010 / Published online: 5 October 2010
© Springer-Verlag 2010

Abstract Pancreatic neuroendocrine neoplasms (P-NENs) are usually solid and only rarely cystic. Glucagon expression and the association with multiple endocrine neoplasia type 1 (MEN1) seem to be common in cystic P-NENs. In this study, we analyzed 404 P-NENs to gain information about the relative frequency of grossly cystic P-NENs and their association with glucagon production by the tumor cells. Three hundred forty-six solitary P-NENs and 58 P-NENs (>1 cm in diameter) from 35 patients with an MEN1 syndrome were studied. Immunostaining was performed for the four pancreatic hormones; 5.5% (19/346) of the sporadic P-NENs showed unilocular or multilocular cystic changes that were macroscopically detectable. Sixty-three percent of the solitary cystic P-NENs (versus 7% of the solitary non-cystic P-NENs) expressed predominantly glucagon. In MEN1-associated P-NENs, the relative frequency of cystic tumors was 10.3%, and all of them expressed glucagon. None of the glucagon-positive cystic P-NENs were associated with a glucagonoma syndrome. Solitary non-MEN1-associated and MEN1-associated cystic P-NENs are predominantly non-syndromic glucagon-expressing tumors. However, cystic insulinomas may also occur. Cyst formation seems to be related to hormone production.

Keywords Pancreatic neoplasms · Neuroendocrine · Cystic tumors · Glucagon · Insulin

B. Konukiewitz · T. Enosawa · G. Klöppel
Department of Pathology, University of Kiel,
Kiel, Germany

T. Enosawa
First Department of Pathology, Faculty of Medicine,
Showa University,
Tokyo, Japan

G. Klöppel (✉)
Department of Pathology, Technical University of München,
Ismaningerstr. 22,
81675 Munich, Germany
e-mail: guenter.kloeppel@alumni.uni-kiel.de

Introduction

Pancreatic neuroendocrine neoplasms (P-NENs) usually present as solid tumors. However, in a small percentage of cases, they may show cystic changes and need to be considered in the differential diagnosis of cystic neoplasms and lesions in the pancreas [1, 2]. In a series of 418 cystic neoplasms and lesions of the pancreas, they accounted for 4.3% of the cases [3]. In another recent series, cystic P-NENs comprised 5.4% of all resected cystic tumors of the pancreas [4]. When only the cystic variants among all P-NENs were considered, the latter retrospective review found 17% of the P-NENs to show grossly cystic changes [4]. However, this series also included tumors from patients with multiple endocrine neoplasia type 1 (MEN1), who are known to have a high rate of cystic neoplasms among their P-NENs. In two French studies [1, 5], the rate ranged from 13% to 20%.

Only few case reports and one study including 13 cystic P-NENs from ten patients examined the cellular composition and hormonal content of the cystic tumors [1, 6, 7]. They found a predominance of glucagon, while insulin, pancreatic polypeptide, and somatostatin were less frequently expressed [1, 2, 6, 7]. Again, these reports mixed MEN1 and non-MEN1 cases.

In this retrospective study, we reviewed 346 functioning and non-functioning solitary P-NENs from non-MEN1 patients. Our aim was to determine the relative frequency

of macroscopically cystic P-NENs in a well-characterized series of neuroendocrine tumors of the pancreas and to clarify whether glucagon is indeed the hormone that predominates in cystic P-NENs. In addition, we also analyzed P-NENs larger than 1 cm resected from patients with known MEN1 for cystic changes combined with glucagon positivity and compared these data with those from the solitary sporadic P-NENs. Our results show that cystic changes most frequently develop in glucagon-expressing P-NENs.

Materials and methods

A total of 404 P-NENs were analyzed. The neoplastic tissue, which was collected between 1971 and 2007, was retrieved from the surgical pathology files and consultation files of the Department of Pathology of the University of Kiel. All P-NENs had been surgically removed. Three hundred forty-six P-NENs were solitary and non-MEN1 associated. Fifty-eight P-NENs were from 35 patients suffering from MEN1. Twenty-eight of these patients were included in an earlier study investigating the histopathology of duodenal gastrinomas and pancreatic neoplasms in MEN1 [8]. All 58 MEN1 associated P-NENs were larger than 1 cm. The multiple tumors smaller than 1 cm that were also seen in most MEN1 patients [8] were not considered in this study. Clinical data (age, sex, and hormonal syndrome) and data on tumor size, metastasis, and gross local invasion at the time of diagnosis were obtained from the patients' records. Detailed histopathological data, including histological pattern, angioinvasion, and perineural invasion, were obtained by reviewing the slides from the available blocks. The tissue had been fixed in formaldehyde and embedded in paraffin.

The P-NENs were identified using the diagnostic standard procedure of the European Neuroendocrine Tumor Society [9] and classified according to the WHO 2004 classification [10]. We also distinguished between well-differentiated neoplasms with probably benign behavior (including those with uncertain behavior) and neoplasms showing malignant behavior [10, 11].

Immunohistochemistry

Three-micrometer sections were cut from the blocks. They were immunostained for synaptophysin (polyclonal antibody, DakoCytomation, Glostrup, Denmark, 1:50), chromogranin A (monoclonal antibody Ventana medical systems, Tucson, AZ, USA, 1:2), insulin (monoclonal antibody, Biogenex, Dan Ramon, CA, USA, 1:40), glucagon (polyclonal antibody, Biogenex, 1:60), somatostatin (polyclonal antibody, DakoCytomation, 1:200), pancreatic polypeptide (PP, polyclonal antibody, DakoCytomation, 1:5000), CD31 (DakoCytomation, 1:50), and D2-40 (DakoCytomation 1:50). MIB1 staining was performed using a mouse monoclonal antibody (M0722 DAKO, Hamburg, Germany 1:100). Staining for gastrin (polyclonal, Paesel, Frankfurt, Germany, 1:3,000), vasoactive intestinal polypeptide (polyclonal, Zymed, San Francisco, CA, USA 1:10), and adrenocorticotropic hormone (ACTH, monoclonal, Dako Cytomation, 1:500) was performed only in the P-NENs showing the respective hormonal syndrome. Immunostaining was carried out using the avidin–biotin peroxidase complex method. Before synaptophysin staining, the slides were subjected to pressure cooker treatment for 3.5 min.

Positive immumostaining was recorded as 1+, 2+, and 3+ if the percentage of positive tumor cells were between 1% and 10%, 10% and 50%, and more than 50%, respectively. All non-functioning glucagon-expressing P-NENs included in the group of glucagon-producing P-NENs scored 2+ and 3+. All P-NENs associated with a glucagonoma syndrome were included in the glucagon-positive P-NEN group, even if they scored <2+ (two cases).

Results

Solitary (non-MEN1-associated) P-NENs

Of the 346 solitary well-differentiated P-NENs in our series, 60% were classified as tumors that showed the criteria of benign (and uncertain) behavior and 40% as tumors with criteria associated with malignant behavior. There were 193 female (56%) and 153 male (44%) patients with ages ranging from 3 to 88 years (mean, 54). In 124 patients (36%), the P-NENs caused a hormonal syndrome [including 93 insulinomas (75%), 16 gastrinomas (13%), 7 glucagonomas (5.6%), 5 vipomas (4%), and 3 ACTHomas (2.4%)]. In 222 patients (64%), the P-NENs were non-functioning.

Among the 346 solitary P-NENs, there were 19 cystic tumors (5.5%; Fig. 1). Table 1 summarizes the clinicopathological details of these tumors. The cysts, which were more frequently multilocular (60%) than unilocular (Fig. 2), contained jelly-like, occasionally slightly hemorrhagic fluid. The cyst lumina showed a smooth inner surface, sometimes with protruding solid tissue nodules. The size of the cystic tumors ranged from 1.0 to 12.0 cm (mean, 5.2 cm). The cystic cavities within the tumors were all macroscopically easily recognizable but varied considerably in size (0.8–9.0 cm). In one case, the entire tumor tissue showed a microcystic pattern (Fig. 3). In the other cases, single microcystic structures were occasionally seen in the tissue surrounding the macroscopic cysts. In a few cases, only a small capsule-like rim of peripheral tumor tissue remained between the cyst lumen and the tumor surface. Histologically, all of the unilocular cystic P-NENs and most of the

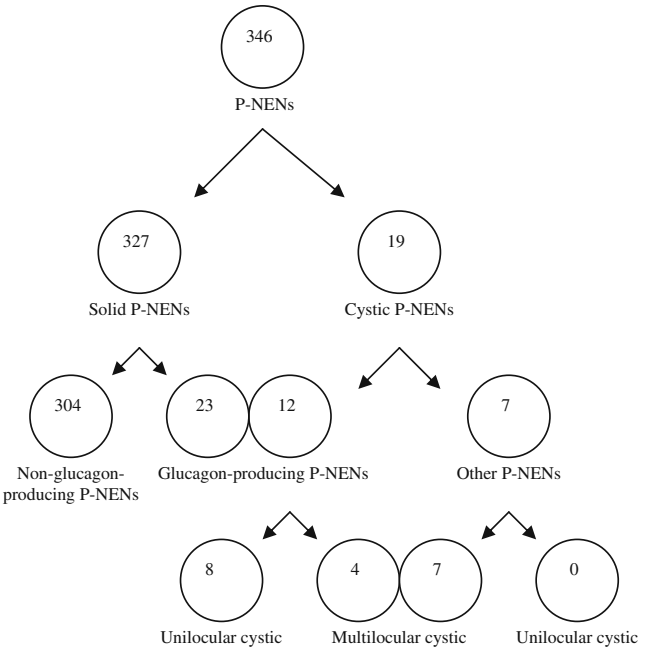

Fig. 1 Distribution of sporadic solid and (uni- or multi-) cystic P-NENs and glucagon expression in a series of 346 sporadic solitary P-NENs

multilocular cystic P-NENs displayed a trabecular arrangement of the uniform tumor cells (Fig. 4a). The cyst lumen was entirely or partly lined by tumor cells. Occasionally, there was loosely arranged fibrocytic stroma with a small fibrin layer between the tumor cells and the cyst lumen. Using the WHO criteria, seven of 19 cystic tumors were classified as benign and 12 of 19 (63%) as malignant. All tumors considered to be benign had a size below 2 cm and a Ki67/MIB1 index of ≤2% (Table 1). All the tumors considered to be malignant were either 2 cm in size or greater. In addition, six of 12 tumors had a proliferative activity between 5% and 10% (G2), and two of 19 showed lymph node metastases. Angioinvasion was not found in these tumors.

Immunohistochemical analysis revealed that 12 of 19 (63%) cystic P-NENs expressed glucagon (2+ or 3+; Fig. 4b) and three of 19 (15%) insulin (Table 1). Glucagon positivity was associated with PP positivity in four of 12 cases. The remaining cystic P-NENs were either weakly positive for glucagon (1+) and other hormones (3/19) or strongly positive for PP (1/19). Of the 346 solitary P-NENs, 72 (20.8%) tumors expressed glucagon, including seven glucagonomas (10%). Of the glucagon positive P-NENs, 35 were 2+ or 3+ positive, and of these, 19 (54%) were classified as malignant. Twelve of 35 (34.3%) of the 2+ or

Table 1 Histopathological and immunohistochemical features of sporadic cystic P-NENs

Case no.	Age (years)	Sex	Site	Size (cm)	Histology	GLU	INS	PP	SOM	MIB1	WHO
Unilocular cystic											
1	68	M	Tail	2	trab	++	−	−	−	<2%	wdet
2	57	M	Body	3.6	trab	++	−	−	−	<2%	wdec
3	26	F	Tail	2	solid	+++	−	+	−	<2%	wdet
4	75	M	Tail	10	trab	++	+	++	−	6%	wdec
5	41	F	Body	1.1	trab/gland	+++	−	+	−	<2%	wdet
6	21	F	Head	6	trab	++	−	+	−	<2%	wdec
7	24	F	Head	9.5	trab	++	−	+	+	<2%	wdec
8	68	M	Tail	1.9	trab	+++	-	++	−	<2%	wdet
Multilocular cystic											
9	75	F	Tail	2	trab	++	−	+++	−	5%	wdec
10	42	F	Head	1	trab	++	−	+	−	<2%	wdet
11	54	F	Tail	7.5	solid/trab	−	+	++	−	7%	wdec
12	57	M	Tail	2	trab	−	+++	−	−	<2%	wdet
13	60	M	Body	1.8	trab/solid	+++	−	++	−	<2%	wdet
14	65	F	Tail	12	trab	+	−	−	+	9%	wdec
15	80	F	Tail	6.5	trab	+	−	+	−	10%	wdec
16	34	F	Body	3.7	solid/trab	−	−	+	−	<2%	wdec
17	63	F	Body	5	trab/gland	−	+++	−	−	<2%	wdec
18	73	F	Body	4.5	solid/trab	−	+++	−	−	<2%	wdec
19	65	F	Tail	11	solid/trab	++	−	−	−	10%	wdec

GLU glucagon, *INS* insulin, *PP* pancreatic polypeptide, *SOM* somatostatin, *MIB1* Ki67 index; WHO classification in well-differentiated endocrine tumor (wdet) or carcinoma (wdec)

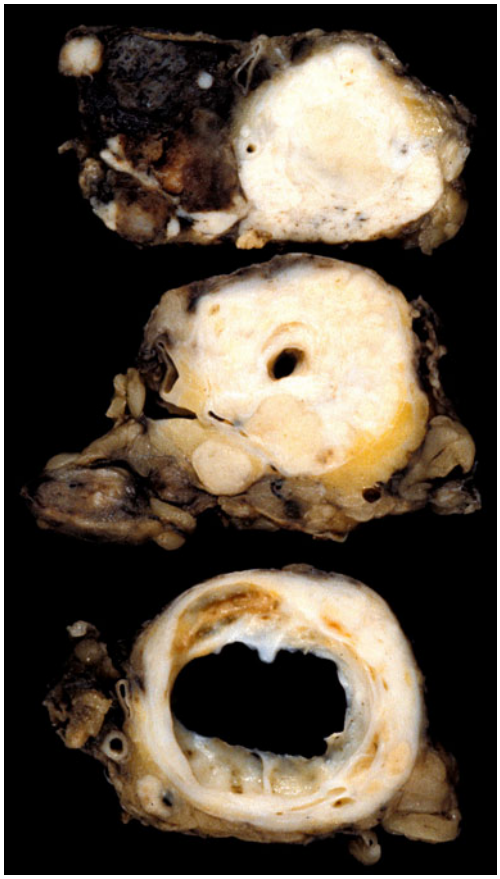

Fig. 2 Serial cut sections of a unilocular cystic pancreatic neuroendocrine carcinoma with lymph node metastases (case no. 2)

3+ positive glucagon P-NENs (none of them syndromatic) belonged to the group of cystic P-NENs. In contrast, only three of 93 (3.2%) predominantly insulin-producing P-NENs (all of them insulinomas) were cystic.

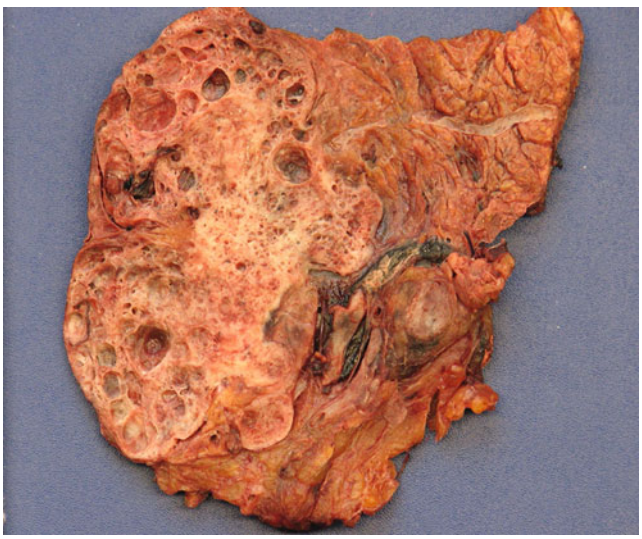

Fig. 3 Cut section of a cystic pancreatic neuroendocrine carcinoma with a microcystic pattern (case no. 19)

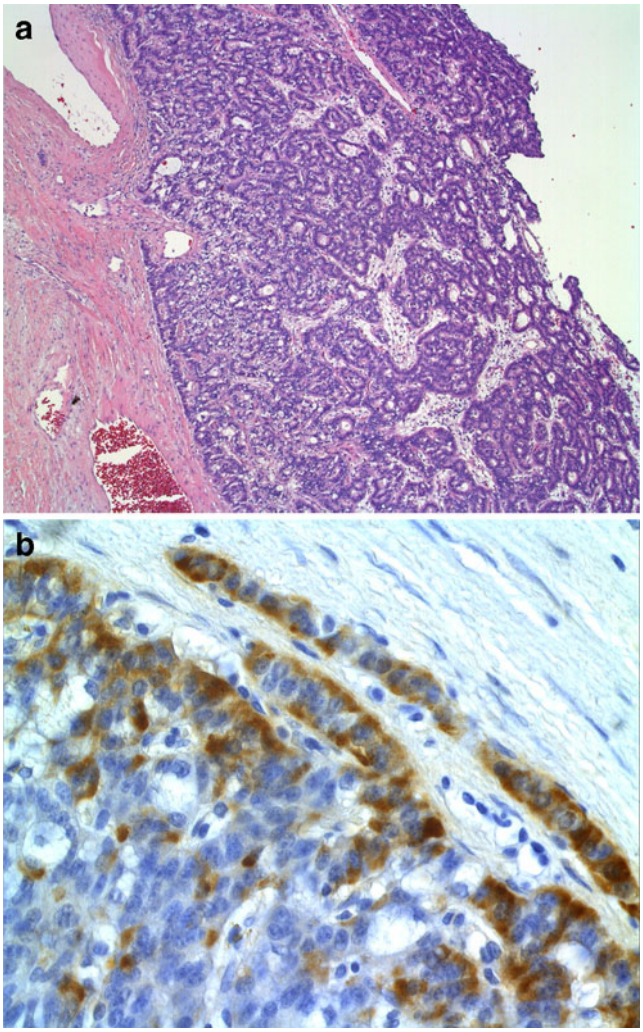

Fig. 4 **a** Cystic pancreatic neuroendocrine neoplasm with a trabecular pattern: The wall of the cyst is lined by well differentiated cells (H&E). **b** The tumor cells show an immunostaining for glucagon

MEN1- associated P-NENs

From 35 patients (20 women and 15 men; age range, 19–72 years; mean, 42) with a MEN1 syndrome, we studied 58 resected P-NENs whose diameter ranged from 1 to 5.5 cm (Table 2). All these P-NENs were well-differentiated, lacked angioinvasion, had a low proliferative activity (Ki67/MIB1 <2%), and showed no metastases. Multiple (up to five tumors) were observed in 15 of 35 patients. In total, six of 58 P-NENs were cystic (10.3%). No patient had more than one cystic tumor. The macroscopic and microscopic features of the cystic tumors were identical to those described in the solitary tumor group. The solid part of one cystic tumor contained microcystic structures (Fig. 5).

Immunohistochemically, 2+ or 3+ positive glucagon P-NENs comprised 22 of 58 (38%) P-NENs, including the six cystic tumors (6/22; 27.3%; Table 2). None of these P-NENs were associated with a glucagonoma syndrome.

Table 2 Histopathological and immunohistochemical features of cystic P-NENs associated with MEN1

Case no.	Age (years)	Sex	Site	Size (cm)	Histology	GLU	INS	PP	SOM	MIB1	WHO
Unilocular cystic											
1	27	F	Head	4	trab	++	−	+	−	<2%	wdec
2	43	F	Body	6	trab	+++	−	−	−	<2%	wdec
3	44	F	Head	1.7	trab	++	−	−	−	<2%	wdet
4	36	F	Tail	5.5	trab	++	−	++	−	<2%	wdec
5	38	F	Tail	3.5	trab	+++	−	−	−	<2%	wdec
Multilocular cystic											
6	27	F	Body	1.7	trab	++	−	+	+	<2%	wdet

GLU glucagon, *INS* insulin, *PP* pancreatic polypeptide, *SOM* somatostatin; *MIB1* Ki67 index, WHO classification in well differentiated endocrine tumor (wdet) or carcinoma (wdnec)

Expression of CD31, D2-40, E-cadherin, and β-catenin

A limited number of solitary cystic P-NENs (n=3) were tested for the expression of CD31 (blood vessels), D2-40 (lymphatic vessels), E-cadherin (adhesion molecules), and β-catenin (adhesion molecules). None of the cystic cavities were lined by endothelium that was recognized by CD31 or D2-40. All cells of the tested tumors, regardless of whether they lined the cysts or not, showed a regular membranous expression pattern for E-cadherin and β-catenin.

Discussion

Cystic P-NENs of the pancreas were recently reported in a frequency of 17% [4]. This is a surprisingly high figure compared with data from older studies, which reported a frequency of 1.9% [12] and 3.9% [13]. The explanation is that the study by Bordeianou includes cystic P-NENs from both MEN1 and non-MEN1 patients and that the frequency of cystic P-NENs in MEN1 patients exceeds that in non-MEN1 patients [5]. In our study of a large cohort of 404 P-NENs, we therefore separated solitary (and most likely sporadic) tumors from MEN1-associated tumors. Our results revealed that 5.5% of 346 solitary P-NENs presented with cystic changes that were grossly detectable (> 0.5 cm). Tumors with a completely multilocular microcystic pattern [14] were only once encountered in this series. In contrast and confirming earlier notions, MEN1-associated P-NENs larger than 1 cm in size showed almost twice as many cystic changes as their non-MEN1 associated counterparts, namely, 10.3% versus 5.5%. Using the prognostic stratification of the WHO classification [10], 63% of the solitary cystic P-NENs and 66% of the MEN1-associated cystic P-NENs revealed criteria of malignancy. When size was analyzed separately, however, it became obvious that the MEN1-associated P-NENs were on the average smaller than the non-MEN1-associated cystic P-NENs (3.7 versus 5.2 cm). Moreover, none of the MEN1-associated P-NENs, including the cystic tumors, had evidence of metastases. This suggests that either the P-NENs in MEN1 patients have a lower malignant potential than the sporadic P-NENs or are detected earlier because of the better surveillance of these patients. The question whether the entire group of cystic P-NENs has a better outcome than the comparable solid P-NENs, as it seems to be the case [15], cannot be clearly answered by this study, since follow-up data are yet only available in a small number of cases.

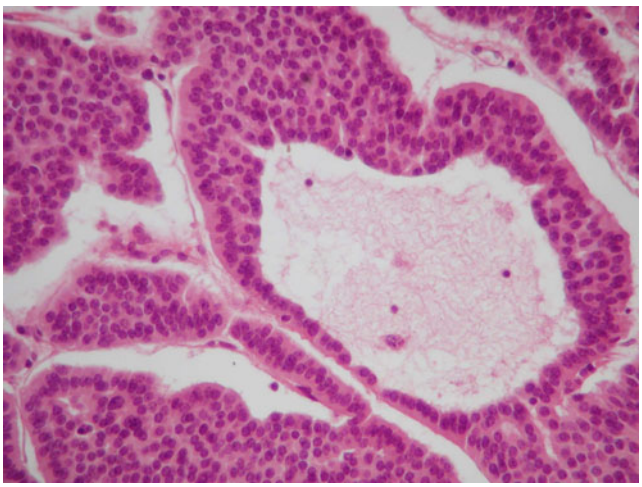

Fig. 5 Cystic pancreatic neuroendocrine neoplasm showing a microcystic structure (H&E)

Our data indicate that glucagon expression is common in cystic P-NENs. In their study of 16 cystic P-NENs, which included MEN1 and non-MEN1 patients, Ligneau et al. [1] reported that the immunohistochemical expression of glucagon dominated in the tumors of nine of ten patients. In our series of solitary cystic P-NENs, 63% of the tumors were predominantly glucagon-positive (versus 7% of solitary non-cystic P-NENs). Two other cystic P-NENs showed a low degree of glucagon positivity in association with other hormones. Although more than half of the

glucagon-expressing tumors, both cystic and non-cystic, were strongly positive for this hormone, there was no association with a glucagonoma syndrome [16]. Of the remaining cystic P-NENs, three of 19 (15%) were insulinomas and one of 19 exhibited predominantly PP. These findings in solitary cystic P-NENs suggest that glucagon-producing P-NENs have a much stronger propensity to develop cystic changes, namely, in approximately 32% of the cases, than non-glucagon-producing P-NENs. The reason for this peculiar feature of glucagon-producing P-NENs is not known.

In the group of MEN1-associated P-NENs all cystic tumors (100%) strongly expressed glucagon, while this was only the case in 30% of the non-cystic MEN1 tumors. This again underlines the close relationship between glucagon expression in P-NENs and cyst formation. The reason that, in MEN1 glucagon, expression is seen in 100% of cystic P-NENs and vastly exceeds that in sporadic tumors may be that most of the P-NENs in MEN1-patients are glucagon positive, a well-known finding that so far has no ready explanation [8].

The cause of the cystic changes in P-NENs may be related to ischemic necrosis, hemorrhage, angioectatic changes, or secretion of serous fluid by the tumor cells. Cystic degeneration due to ischemic necrosis of or heavy bleeding into the tumor tissue is highly unlikely in these tumors because evidence, such as granulation tissue with macrophages containing iron pigment, is lacking. The negative staining for the endothelial markers CD31 or D2-40 also excludes any angioectatic formations. Instead, it appears that the tumor cells are directly involved in the formation of the cysts. The ultrastructure [1, 7] and the histopathology of the cystic cavities reveal that at least at the beginning when the cyst is still small, the cyst lumen is directly lined by neoplastic endocrine cells. This composition of the cyst wall suggests that the tumor cells along the cyst lumen may release their hormones into the cyst cavity and contribute to its enlargement. This assumption is supported by analyses of the cyst content that was performed in a case of cystic insulinoma [6] and a cystic glucagon-producing P-NEN [7], which revealed high concentrations of insulin and glucagon, respectively. It is therefore very likely that in the cystic P-NENs with glucagon or insulin positivity, the cyst fluid contains large amounts of the respective hormones. In addition, the serous cyst fluid may also contain amylase and some serum-bound proteins [6], although it is unclear how these proteins may reach the cyst lumen, since neither are blood vessels found in direct contact with the cysts nor are defects of the membranous expression of the adhesion molecules E-cadherin and β-catenin detectable in the tumor cell layers adjacent to the cysts.

In summary, most cystic P-NENs present as a distinct tumor type characterized in more than half of the cases by the expression of glucagon, followed by insulin and other pancreatic hormones, such as PP. The cystic P-NENs are usually large tumors (average, 5.2 cm) whose unilocular or multilocular cystic cavities probably contain large amounts of glucagon or insulin if the tumor tissue is predominantly composed of tumor cells producing these hormones. A hormonal syndrome was only encountered in the few insulin-producing cystic P-NENs, and a number of such cases have been described in the literature [17]. When we studied the frequently cited literature on cystic glucagonomas, it turned out that the reported tumors were not glucagonomas (i.e., glucagon-producing tumors with a glucagonoma syndrome) but non-functioning glucagon-producing P-NENs [7]. We were also unable to identify cystic gastrinomas or other functioning tumors.

Acknowledgments We are gratful to Maike Pacena for excellent technical assistance and Katherine Dege for editing the manuscript. We also thank all colleagues who provided consultation cases, which were included in the study. Special thanks are due to Prof. Wierich and Dr. Schmitz, Institute of Pathology, Recklinghausen, Germany, for providing macroscopic illustrations. This work was supported by Ipsen GmbH, Ettlingen, Germany in association with the German NET bank.

Conflict of interest We declare that we have no conflict of interest.

References

1. Ligneau B, Lombard-Bohas C, Partensky C, Valette PJ, Calender A, Dumortier J, Gouysse G, Boulez J, Napoleon B, Berger F, Chayvialle JA, Scoazec JY (2001) Cystic endocrine tumors of the pancreas: clinical, radiologic, and histopathologic features in 13 cases. Am J Surg Pathol 25:760
2. Nojima T, Kojima T, Kato H, Inoue K, Nagashima K (1991) Cystic endocrine tumor of the pancreas. Int J Pancreatol 10:65–72
3. Kosmahl M, Pauser U, Peters K, Sipos B, Lüttges J, Kremer B, Klöppel G (2004) Cystic neoplasms of the pancreas and tumor-like lesions with cystic features: a review of 418 cases and a classification proposal. Virchows Arch 445:168–178
4. Bordeianou L, Vagefi PA, Sahani D, Deshpande V, Rakhlin E, Warshaw AL, Fernandez-del Castillo C (2008) Cystic pancreatic endocrine neoplasms: a distinct tumor type? J Am Coll Surg 206:1154–1158
5. Heymann MF, Moreau A, Chetritt J, Murat A, Leborgne J, Le Neel JC, Visset J, Le Bodic MF (1996) Pathologic study with immunohistochemistry of 61 pancreatic endocrine tumors in 16 patients suffering from multiple endocrine neoplasia type I (MEN I). Review of the literature. Ann Pathol 16:167–173
6. Weissmann D, Lewandrowski K, Godine J, Centeno B, Warshaw A (1994) Pancreatic cystic islet-cell tumors. Clinical and pathologic features in two cases with cyst fluid analysis. Int J Pancreatol 15:75–79
7. Yagihashi S, Yagihashi N, Nagai K (1992) Cystic pancreatic glucagonoma in contact with insulinoma found in a hypoglycemic patient. Pathol Res Pract 188:751–756

8. Anlauf M, Schlenger R, Perren A, Bauersfeld J, Koch CA, Dralle H, Raffel A, Knoefel WT, Weihe E, Ruszniewski P, Couvelard A, Komminoth P, Heitz PU, Klöppel G (2006) Microadenomatosis of the endocrine pancreas in patients with and without the multiple endocrine neoplasia type 1 syndrome. Am J Surg Pathol 30:560–574
9. Klöppel G, Couvelard A, Perren A, Komminoth P, McNicol AM, Nilsson O, Scarpa A, Scoazec JY, Wiedenmann B, Papotti M, Rindi G, Plöckinger U (2009) ENETS Consensus Guidelines for the Standards of Care in Neuroendocrine Tumors: towards a standardized approach to the diagnosis of gastroenteropancreatic neuroendocrine tumors and their prognostic stratification. Neuroendocrinology 90:162–166
10. Heitz PU, Perren A, Klimstra DS, Dayal Y, Bordi C, LeChago J, Centeno B, Klöppel G (1994) WHO histological classification of tumours of the endocrine pancreas. IARC Press, Lyon
11. Schmitt AM, Anlauf M, Rousson V, Schmid S, Kofler A, Riniker F, Bauersfeld J, Barghorn A, Probst-Hensch NM, Moch H, Heitz PU, Kloeppel G, Komminoth P, Perren A (2007) WHO 2004 criteria and CK19 are reliable prognostic markers in pancreatic endocrine tumors. Am J Surg Pathol 31:1677–1682
12. le Borgne J (1998) Cystic tumours of the pancreas. Br J Surg 85:577–579
13. Iacono C, Serio G, Fugazzola C, Zamboni G, Bergamo-Andreis IA, Jannucci A, Zicari M, Dagradi A (1992) Cystic islet cell tumors of the pancreas. A clinico-pathological report of two nonfunctioning cases and review of the literature. Int J Pancreatol 11:199–208
14. Gerke H, Byrne MF, Xie HB, Paulson EK, Tyler DS, Baillie J, Jowell PS (2004) A wolf in sheep's clothing: a non-functioning islet cell tumor of the pancreas masquerading as a microcystic (serous cystic) adenoma. JOP 5:225–230
15. Boninsegna L, Partelli S, D'Innocenzio MM, Capelli P, Scarpa A, Bassi C, Perderzoli P, Falconi M (2010) Pancreatic cystic endocrine tumors: a different morphological entity associated with less aggressive behavior. Neuroendocrinology. doi:10.1159/000318771
16. Ruttmann E, Klöppel G, Bommer G, Kiehn M, Heitz PU (1980) Pancreatic glucagonoma with and without syndrome. Immunocytochemical study of 5 tumour cases and review of the literature. Virchows Arch [A] Pathol Anat 388:51–67
17. Adsay NV, Klimstra DS (2000) Cystic forms of typically solid pancreatic tumors. Semin Diagn Pathol 17:81–88

Virchows Arch (2011) 458:55–64
DOI 10.1007/s00428-010-0988-3

ORIGINAL ARTICLE

Immunophenotypic predictive profiling of *BRCA1*-associated breast cancer

Pawel Domagala · Tomasz Huzarski · Jan Lubinski · Karol Gugala · Wenancjusz Domagala

Received: 31 July 2010 / Revised: 23 September 2010 / Accepted: 27 September 2010 / Published online: 13 October 2010
© The Author(s) 2010. This article is published with open access at Springerlink.com

Abstract The immunophenotypic predictive profile of *BRCA1*-associated cancers including major predictive markers, i.e., PARP-1, EGFR, c-kit, HER-2, and steroid hormones (ER/PR) that may have therapeutic relevance has not yet been reported in a comprehensive study. Using immunohistochemistry, we examined the expression of these proteins in a large cohort of *BRCA1*-associated breast cancers. PARP-1 immunoreactivity was found in 81.9%, EGFR in 43.6%, ER/PR in 17.9%, c-kit in 14.7%, and overexpression of HER-2 in 3.6% of cancers. For all markers studied, 8.2% of tumors were negative. Expression of only one predictive marker was found in 29.7% of cancers, and most frequently, it was PARP-1 (20.8%). In 62.1% of tumors, more than one predictive marker was expressed: PARP-1 and EGFR in 30.4%, PARP-1, and hormone receptors in 13.3% and PARP-1 with c-kit in 7.5% of all tumors. Coexpression of two or more other predictive markers was rare. There were significant differences in the median age at diagnosis of *BRCA1*-associated cancer between patients with ER+ vs. ER− and grades 1–2 vs. grade 3 tumors. These results demonstrate that *BRCA1*-associated cancers differ with respect to expression of proteins that are regarded as targets for specific therapies and that 92% of patients with *BRCA1*-associated cancers may benefit from one or several options for specific therapy (in addition to DNA damaging agents, e.g., cisplatin). About 8% of cancers which do not express therapeutic target proteins may not respond to such therapies. Knowledge of the immunophenotypic predictive profile may help with the recruitment of patients for trials of targeted therapies.

Keywords Breast cancer · *BRCA1* · Estrogen receptor · PARP-1 · EGFR · c-kit

P. Domagala · T. Huzarski · J. Lubinski
Department of Genetics and Pathology, International Hereditary Cancer Center, Pomeranian Medical University,
Polabska 4,
70-115 Szczecin, Poland

K. Gugala
Department of Pathology, Regional Oncology Hospital,
Zolnierska 18,
10-561 Olsztyn, Poland

W. Domagala (✉)
Department of Pathology, Pomeranian Medical University,
Unii Lubelskiej 1,
71-242 Szczecin, Poland
e-mail: sekrpato@ams.edu.pl

Introduction

Mutations in either of the two breast cancer susceptibility genes *BRCA1* and *BRCA2* account for 2–3% of all breast cancers, and they confer a lifetime risk of breast cancer of 60–85% [1]. *BRCA1* is essential for the repair of DNA double-strand breaks through the process of homologous recombination. In the absence of functional *BRCA1,* DNA defects may either be repaired by other mechanisms that are error-prone or may remain unrepaired. Such *BRCA* dysfunction constitutes the basis of some new targeted therapeutic strategies [2, 3].

With a better understanding of the molecular pathways that control cancer development and progression, new therapeutic agents designed to target specific breast cancer populations, such as poly(ADP-ribose)polymerase-1 (PARP-1) inhibitors, epidermal growth factor receptor (EGFR) antagonists, or transmembrane tyrosine kinase c-kit (CD117) inhibitors, are being tested in patients with

breast cancer and, in particular, in patients with *BRCA1*-associated cancer [3, 4]. However, despite the significant progress that has been made, a variable percentage of patients have been resistant to such therapies. One possible reason may be that resistant tumors lack the expression of proteins that serve as targets for such specific therapies. In this context, we studied in this report immunohistochemical expression of PARP-1, EGFR, estrogen receptor (ER), progesterone receptor (PR), c-kit, and HER-2 in tissue microarrays of a large series of *BRCA1*-associated breast carcinomas in order to reveal subpopulations of *BRCA1*-associated cancers that exhibit predictive immunophenotypes, i.e., cancers that could respond to specific targeted therapies. The expression of common predictive markers such as ER, PR, HER-2, and EGFR has been reported in series of *BRCA1*-associated breast carcinomas [5–9]; however, a comprehensive study including these proteins with PARP-1 and c-kit has not been published.

Materials and methods

Patients This study included 140 consecutive breast cancer patients with *BRCA1* mutations (median age, 46.0 years; range, 23–71 years) diagnosed at the West Pomeranian Oncology Center in Szczecin (from 1996 to 2009) and at the Regional Oncology Hospital in Olsztyn (from 1997 to 2007). Patients did not receive endocrine therapy, chemotherapy, or radiotherapy before surgery. All cases were unselected for family history. The study was approved by the local ethics committee.

Genotyping Patients were invited to participate either during hospital stays or through mailed invitations. During the interview, the goals of the study were explained, informed consent was obtained, genetic counseling was given, and a blood sample was taken for DNA analysis. *BRCA1* genetic testing was conducted at the Department of Genetics and Pathology, Pomeranian Medical University, Szczecin. Genomic DNA was prepared from 5–10 ml of peripheral blood. Mutation analysis for the common Polish mutations was performed as described previously [10]. In brief, there are three common founder mutations in *BRCA1* in Poland. The 4153delA and 5382insC mutations were detected using a multiplex-specific polymerase chain reaction (PCR) assay. The third mutation (C61G) generates a novel restriction enzyme site in exon 5. This mutation is detected after digesting amplified DNA with AvaII restriction enzyme. To visualize the different *BRCA1* alleles, the PCR products were subjected to electrophoresis in a 1.5% agarose gel and stained with ethidium bromide. To avoid false results in all reactions, positive and negative controls (without DNA) were used. DNA testing results indicating the presence of mutations were confirmed by sequencing of material from a second blood sample obtained on a different day.

Tumor pathology Pathology review was conducted at the Department of Pathology, Pomeranian Medical University in Szczecin by two pathologists (PD and TH) associated with the study. In cases where there was disagreement, consensus was reached by consultation with a third reviewer (WD). Only first primary invasive breast cancers were included. Representative histological slides organized according to an assigned random number were evaluated to confirm the diagnosis of breast cancer type and classified according to the Elston–Ellis histological grade [11].

Tissue microarray construction We collected all available paraffin blocks containing enough tumor tissue from primary breast cancers. Two different regions of tumors in the area of the outer invasive margin of cancer were identified and marked on hematoxylin and eosin-stained sections. Sections were matched to their corresponding wax blocks (the donor blocks), and two 0.6-mm-diameter cores of the tumor were removed from these donor blocks and inserted into the recipient master block using a tissue microarrayer (Beecher Instruments, Silver Spring, MD). The recipient block was cut, and sections were transferred onto adhesive slides.

Immunohistochemistry and fluorescent in situ hybridization Slides were deparaffinized, rehydrated, and immersed in antigen retrieval buffer at pH 6.0 (PARP-1 and c-kit) or pH 9.0 (ER and PR). Heat-induced antigen retrieval was performed in a water bath at 98°C for 20 min (PARP-1) or a pressure cooker at 120°C for 3 min (ER, PR, and c-kit). The following monoclonal antibodies were used: anti-PARP-1 (clone F-2, dilution 1:500; Santa Cruz Biotechnology, Santa Cruz, CA), anti-estrogen receptor (clone 1D5, dilution 1:50; Dako, Glostrup, Denmark), and anti-progesterone receptor (clone PgR 636, dilution 1:50; Dako). We performed preliminary experiments with breast cancer tissue microarray to determine the optimal PARP-1 antibody dilutions which would give the strongest nuclear-specific staining with minimal background. Of several dilutions tested, the dilution 1:500 proved to be the best. Expression of HER-2 and c-kit was tested using the HercepTest kit (Dako) and c-kit pharmDx kit (Dako), respectively, according to the manufacturer's instructions**.** EGFR staining was performed using the EGFR pharmDx kit (Dako) with incubation with proteinase K for 5 min for enzymatic antigen retrieval. Slides were incubated with the primary antibodies for 30 min at room temperature and immunostained using the EnVision+ kit (Dako). The reaction was developed with a diaminobenzidine substrate–chromogen solution, and slides were counter-

stained with hematoxylin. Appropriate positive and negative controls were included. Normal mouse immunoglobulins were substituted for primary antibody as negative controls. Sections of pharyngeal tonsil served as external positive controls for PARP-1. Strong PARP-1 immunostaining was seen in the tonsil's lymphocytes. PARP-1-positive stromal lymphocytes in breast cancers served as additional built-in positive control. Cases with HER-2 staining of 2+ were further evaluated by fluorescent in situ hybridization for *HER-2* gene amplification. In this assay, slides were hybridized with probes to LSI HER-2/neu and CEP17 with the PathVysion HER-2 DNA Probe Kit (Abbott Laboratories, Abbott Park, IL) according to the manufacturer's instructions. Fluorescent in situ hybridization with an amplification ratio >2.2 was considered positive.

Immunohistochemistry scoring Tumor cores were independently assessed by two observers (PD and WD) who were blinded to mutation status and clinicopathological data. In cases of disagreement, the result was reached by consensus. Tumors with lost cores or insufficient tumor tissue in the cores were excluded from the analysis. Of the three most frequently applied scoring systems (intensity score, pattern score, or both combined), we used the multiplicative quickscore method because it seemed to be the most reliable and proved to be useful and reproducible [12]. This system accounts for both the intensity and the extent of cell staining. Briefly, the proportion of positive cells was estimated and given a score on a scale from 1 to 6 (1=1% to 4%, 2=5% to 19%, 3=20% to 39%, 4=40% to 59%, 5=60% to 79%, and 6=80% to 100%). The average intensity of the positively staining of cells was given a score from 0 to 3 (0=no staining, 1=weak, 2=intermediate, and 3=strong staining). A final score was then calculated by multiplying the percentage score by the intensity score, to yield a minimum value of zero and a maximum value of 18. Based on the final score, nuclear PARP-1 expression was graded as low (0–9, further referred as negative) or high (10–18, further referred as positive). Tumors were considered as HER-2 positive if scored as 3+ or 2+ with amplification tested by FISH [13]. ER and PR were considered positive if staining was detected in ≥1% of nuclei [14]. There are no commonly accepted cut-off points reported for EGFR and c-kit. For scoring of samples stained with EGFR, only unequivocally membranous staining in ≥1% of tumor cells was applied to define protein positivity according to the Dako criteria in the pharmDx kit instructions. For c-kit cytoplasmic and/or membranous staining, ≥10% of tumor cells was counted as positive [15].

Statistics Analysis of differences in distributions of study markers expression between the two groups of patients was performed using the Mann–Whitney *U* test, and differences between more than two groups were evaluated by the Kruskal–Wallis test. The chi-square contingency test for categorical variables was used to determine differences between groups. Spearman's nonparametric correlation test was used for correlative analysis. All reported p values were two sided. For all statistical analyses, a p value <0.05 was considered significant. Statistical analyses were performed using GraphPad Prism 5.0 software (San Diego, CA).

Results

Table 1 lists the clinicopathological details of 140 tumors and patients with *BRCA1* mutations. PARP-1 immunoreactivity (Fig. 1a, b) was found in 81.9% of cancers, EGFR overexpression (Fig. 1e, f) in 43.6%, hormone receptor (ER/PR) immunoreactivity in 17.9%, c-kit (Fig. 1g, h) in 14.7%, and overexpression of HER-2 in only 3.6% of cancers (Table 2). Eleven (8.2%) tumors were negative for all predictive markers studied (pentanegative). Five of the latter were atypical medullary, four were ductal grade 3, one was medullary, and one was metaplastic carcinoma. It is worth noting that 18.1% of *BRCA1*-associated cancers were PARP-1 negative (Fig. 1c, d; 20.7% in the triple-negative subgroup). Of these, 44% were pentanegative. Expression of only one predictive marker was found in 29.7% of *BRCA1*-associated cancers, and most frequently, it was the expression of PARP-1 (20.8%) followed by EGFR (6.7%). In 62.1% of tumors, more than one predictive marker was expressed, and a coexpression of PARP-1 and EGFR constituted 30.4% of all tumors (Table 3). Coexpression of PARP-1 and hormone receptors was found in 13.3% of all cancers and PARP-1 with c-kit in 7.5%. Coexpression of two or more other predictive markers was a rare event. In one tumor, a coexpression was seen of all markers studied with the exception of EGFR (Table 3). There were no statistically significant differences between the frequencies of *BRCA1*-associated breast cancers expressing only one marker, two markers, or more than two markers in the group of young patients (<50 years of age) vs. older patients (p=0.89). A cumulative frequency distribution of PARP-1, EGFR, ER, PR, and c-kit showed that PARP-1 was the marker with the highest frequency of tumors with very high score (Fig. 2). A statistically significant positive correlation between the expression of ER and PR (r=0.81, p<0.0001) and negative correlation between the expression of ER and EGFR (r=−0.26, p=0.002) as well as PR and EGFR (r=−0.24, p<0.005) were found. There were significant differences in the median age at the diagnosis of *BRCA1*-associated cancers between patients with ER+ vs. ER− (p=0.01) as well as grades 1–2 vs. grade 3 tumors (p=0.02, Fig. 3). No statistically

Table 1 Clinicopathological characteristics of 140 *BRCA1*-associated breast carcinomas

	Number	Percentage
Age		
<50	98	70.0
≥50	42	30.0
Histological type		
Ductal	83	59.3
Atypical medullary	32	22.8
Medullary	17	12.1
Metaplastic	4	2.9
Other	4	2.9
Histological grade		
1	2	1.5
2	11	7.8
3	127	90.7
Nodal status (n=136)		
Positive	44	32.4
Negative	92	67.6
Tumor size (n=131)		
≤2	58	44.3
>2	73	55.7
Bilateral		
Yes	29	20.7
No	111	79.3
Triple negative		
Yes	112	80.0
No	28	20.0
Mutation		
5382insC	90	64.3
C61G	34	24.3
4153delA	16	11.4

significant differences were noted for PR (p=0.14) or the other markers studied.

Discussion

In the present study, we report a five marker immunophenotypic predictive profile of *BRCA1*-associated cancers including PARP-1, EGFR, c-kit, HER-2, and steroid hormones (ER/PR). ER and PR are considered one predictive marker because expression of either one predicts response to hormonal therapy. Recently, it has become obvious that classical pathologic features used to predict a treatment response are insufficient as a predictive tool. Patients with *BRCA1*-associated cancers in the same stage of the disease may exhibit variable responses to therapy, hence the need to explain these differences and reveal the underlying molecular mechanisms. Although there are several ongoing clinical trials aimed at demonstrating the value of targeted therapies in patients with *BRCA1*-associated breast cancers [2, 3], no comprehensive study has been published examining the expression in tumor cells of major proteins against which those therapies are directed.

Our results indicate that *BRCA1*-associated cancers differ with respect to expression of major proteins that are regarded as targets for specific therapies. A variable percentage of *BRCA1*-associated cancers expressed each one of the five major predictive markers, ranging from 82% of PARP-1 positive cancers to only 3.6% of HER-2 positive tumors. These findings have potential therapeutic implications. It has been recognized that cisplatin compounds may effectively target *BRCA1*-associated cancers [16] because *BRCA1*-deficient cells have an impaired ability to repair DNA damage via homologous recombination [17]. Our results indicate that in addition to cisplatin, roughly 30% of *BRCA1*-associated patients may have one option of specific targeted therapy while the remaining 62% of patients with tumors which expressed two or more predictive markers may have several options that should be judiciously considered by their physicians in order to apply the most effective treatment. Furthermore, it seems that about 82% of patients with *BRCA1*-associated cancers that express PARP-1 protein will most likely respond to PARP-1 inhibitor therapy, 44% expressing EGFR may respond to EGFR antagonists, approximately 18% may respond to hormone therapy, and 15% may respond to c-kit inhibitors (e.g., imatinib), but only about 4% may respond to anti-HER-2 therapy (e.g., trastuzumab). However, about 8% may not respond to any of the abovementioned targeted therapies because their tumors do not express proteins that are therapeutic targets (pentanegative, i.e., PARP-1, HER-2, EGFR, c-kit, and steroid hormone receptor negative tumors).

In this report, we identified a subpopulation of *BRCA1*-associated breast cancers characterized by low or null expression of PARP-1 protein. This subpopulation has two pathways of DNA repair inactive or severely compromised, i.e., base excision repair pathway and homologous recombination pathway. PARP-1 is a nuclear enzyme that plays an important role in DNA damage repair through the base excision single-strand repair pathway [18]. When PARP-1 is inhibited, homologous recombination repair is used in response to DNA damage. However, *BRCA*-associated cancers cannot use the homologous recombination pathway; hence, PARP inhibition leads to tumor cells death. This novel concept of treating *BRCA*-associated cancer by causing so-called “synthetic lethality” [19, 20] led to clinical trials of PARP-1 inhibitors in breast cancer [3]. Several active clinical trials involve *BRCA*-associated or triple-negative (ER−, PR−, HER-2−) breast carcinomas.

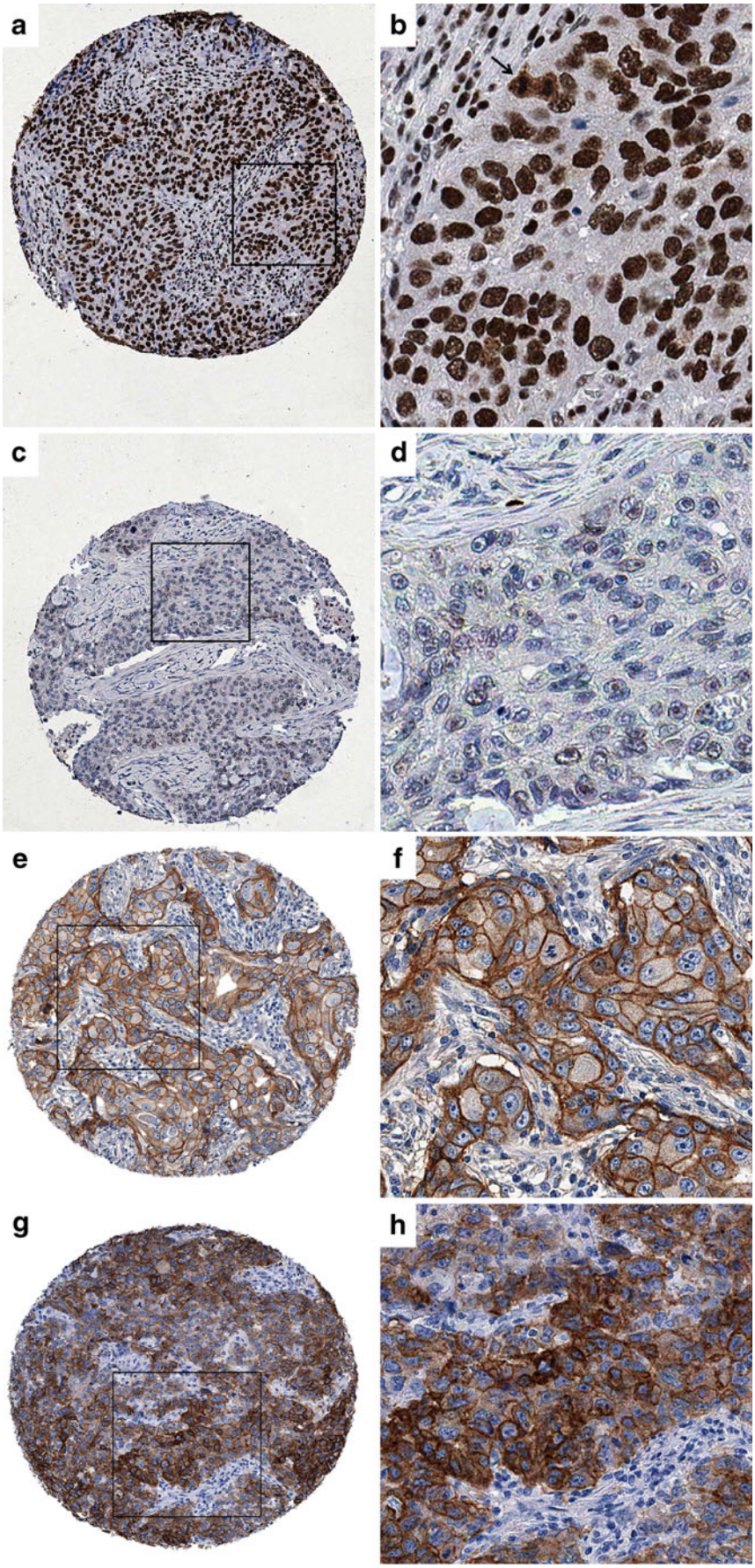

Fig. 1 Expression of PARP-1, EGFR, and c-kit in representative cores of *BRCA1*-associated breast carcinoma. **a**, **c** Fragment of a tissue microarray with a two neighboring cores from different cancers. **a** PARP-1 expression in the nuclei of cancer cells. **b** Marked fragment of the core from **a** at high magnification showing PARP-1-positive (*brown*) nuclei of cancer cells and some lymphocytes. Mitosis (*arrow*) with cytoplasmic PARP-1 immunoreactivity. **c** PARP-1 negative cancer. **d** Marked fragment of the core from **c** at high magnification showing lack of PARP-1 immunoreactivity. **e** EGFR expression. **f** Marked fragment of the core from **e** showing membranous EGFR staining. **g** c-kit expression. **h** Marked fragment of the core from **g** showing cytoplasmic and membranous expression of c-kit

Table 2 Expression of ER/PR, HER-2, EGFR, PARP-1, and c-kit in *BRCA1*-associated breast carcinomas

	Number[a]	Positive (%)	Negative (%)
PARP-1	138	113 (81.9)	25 (18.1)
EGFR	140	61 (43.6)	79 (56.4)
ER and/or PR[b]	140	25 (17.9)	115 (82.1)
c-kit	136	20 (14.7)	116 (85.3)
HER-2	140	5 (3.6)	135 (96.4)

[a] Tumors with lost cores or insufficient tumor tissue in cores were excluded from the analysis

[b] Only one case was PR positive and ER negative

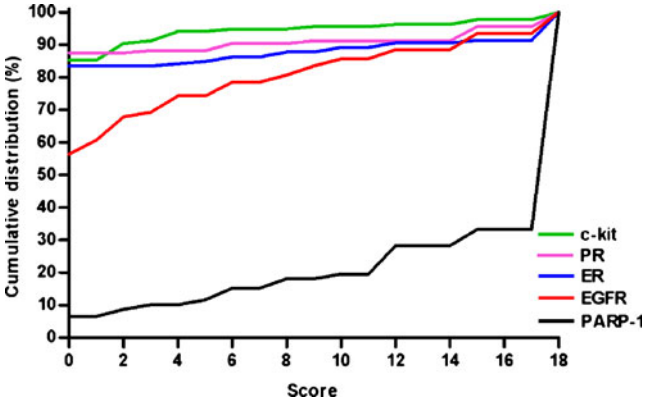

Fig. 2 Cumulative frequency distribution of EGFR, c-kit, PARP-1, ER, and PR in the whole cohort. PARP-1 shows the highest frequency of cases with very high scores

However, the success of PARP inhibitor therapy may depend not only on the constitutional genetic background (responsible for impairment of DNA repair mechanisms) but also on the level of PARP-1 protein expression in tumor cells. A dose-dependent clinical response to PARP inhibitor therapy in phase 1 [21] and phase 2 [22] studies and less abundant PARP-1 in MCF-7 cells that are resistant to mitoxantrone and etoposide than in cells susceptible to these drugs [23] suggest the therapeutic importance of the level of PARP-1 expression in tumor cells. Our results indicate that approximately 18% of *BRCA1*-associated breast cancers may be refractory to PARP-1 inhibitor therapy because of lack or low expression of PARP-1.

Table 3 Number (%) of *BRCA1*-associated cancers with the expression of one or more or null predictive markers

	Number	Percentage
5-Negative	11	8.2
One marker		
PARP-1+	28	20.8
EGFR+	9	6.7
c-kit+	2	1.5
ER/PR+	1	0.7
Coexpression of two markers		
PARP-1+, EGFR+	41	30.4
PARP-1+, ER/PR+	18	13.3
PARP-1+, c-kit+	10	7.5
PARP-1+, HER-2+	3	2.2
EGFR+, ER/PR+	1	0.7
EGFR+, c-kit+	1	0.7
Coexpression of more than two markers		
PARP-1+, EGFR+, c-kit+	6	4.4
PARP-1+, EGFR+, ER/PR+	2	1.5
PARP-1+, ER/PR+, HER-2+	1	0.7
PARP-1+, ER/PR+, c-kit+, HER-2+	1	0.7
Total	135	100

The results of studies on PARP$^{-/-}$ mice and cell lines indicate that they may be extremely sensitive to genotoxic agents such as alkylating agents and γ-rays [24, 25]. This may be especially important in treatment of pentanegative tumors (44% of all tumors with lack or low expression of PARP-1) because they lack protein targets for major targeted therapies.

Our data suggest that about 55% of *BRCA1*-associated cancers may not respond to anti-EGFR therapy because they show null or very low expression of this protein. Equally important seems to be the result indicating that the vast majority of *BRCA1*-associated cancers may be relatively resistant to hormonal therapy as well as to anti-c-kit and anti-HER-2 therapies. Although one has to take into

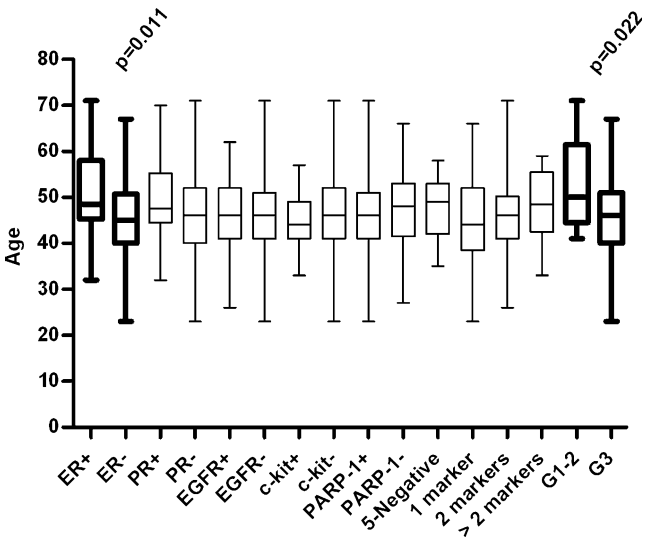

Fig. 3 Differences in age at diagnosis of *BRCA1*-associated breast cancer patients with respect to the expression of predictive markers and tumor grade. The differences of median age between patients with ER+ vs. ER− as well as grades 1–2 vs. 3 are significant

account the fact that immunohistochemical detection of these proteins does not necessarily reflect functional competence, lack of their presence suggests ineffectiveness of a particular targeted therapy, for example, ER—the target of the first targeted therapy in breast cancer—is regarded as one of the most important predictive markers for breast cancers [26]. For ER-positive cancers tamoxifen is an effective treatment regardless of the patient's genotype [27]. Hence, adjuvant anti-estrogen therapy will likely be ineffective in the treatment of breast cancer patients with

Table 4 ER, PR, HER-2, EGFR, c-kit, and PARP-1 immunohistochemical studies in *BRCA1*-associated breast carcinomas reported in the literature and in the current study

References	ER+ % (*n*+/*n*)	PR+ % (*n*+/*n*)	HER-2+ % (*n*+/*n*)	EGFR+ % (*n*+/*n*)	c-kit+ % (*n*+/*n*)	PARP-1+ % (*n*+/*n*)
Johannsson et al. 1997 [32]	8 (3/38)	0 (0/21)	25 (9/36)[a]	–	–	–
Lynch et al. 1998 [33]	23 (5/22)	23 (5/22)	5 (1/22)[a]	–	–	–
Osin et al. 1998 [34]	12 (3/25)	4 (1/25)	–	–	–	–
Eisinger et al. 1999 [35]	11 (3/28)	18 (5/28)	7 (2/28)[a]	–	–	–
Vaziri et al. 2001 [36]	41.4 (12/29)	41.4 (12/29)	9.7 (3/31)[a]	–	–	–
Grushko et al. 2002 [37]	31 (8/26)	–	13 (5/39)	–	–	–
Lakhani et al. 2002, 2005 [5, 6]	10[b]	21[b]	3[b]	67.3[b]	–	–[b]
Quenneville et al. 2002 [38]	15.4 (4/26)[c]	30.8 (8/26)[c]	3.1 (1/32)[a]	–	–	–
Goffin et al. 2003 [39]	23 (7/30)	–	–	–	–	–
Foulkes et al. 2004 [40]	23.6 (49/208)[c]	–	–	–	–	–
Brekelmans et al. 2006 [7]	26.4 (37/140)	30.3 (36/119)	–	–	–	–
Lubiński et al. 2006 [41]	15.5 (18/116)[d]	–	–	–	–	–
Oldenburg et al. 2006 [42]	14.3[e]	21.4[e]	3.9[e]	–	–	–
van der Groep et al. 2006 [43]	–	–	19 (4/21)	67 (14/21)	–	–
Hagen et al. 2007 [44]	20 (8/40)	–	–[f]	–	–	–
Honrado et al. 2007 [45]	28.1 (9/32)	21.2 (7/33)	–	46.4 (13/28)	–	–
Atchley et al. 2008 [46]	30.9 (17/56)	28.9 (15/52)	2.6 (1/38)[g]	–	–	–
Aaltonen et al. 2008 [47]	28.6 (14/49)	20.4 (10/49)	0 (0/35)	–	–	–
Litwiniuk et al. 2008 [48]	14.5 (7/48)	12.5 (6/48)	6.2 (3/48)	–	–	–
Collins et al. 2009 [49]	–	–	–	75 (15/20)[h]	–	–
Evans et al. 2009 [50]	24 (22/87)	–	0 (0/51)	–	–	–
Graeser et al. 2009 [8]	26.9 (158/587)	27 (159/587)	–	–	–	–
Kwong et al. 2009 [51]	48.4 (15/31)[i]	36.7 (11/30)[i]	31.0 (9/29)[i]	–	–	–
Manié et al. 2009 [52]	35 (19/54)	32 (18/57)	0 (0/53)	62 (24/39)	–	–
Joosse et al. 2009 [53]	5.9 (2/34)[a]	5.9 (2/34)[a]	2.9 (1/34)	–	–	–
Lim et al. 2009 [31]	–	–	–	–	48.1 (13/27)	–
Tung et al. 2010 [9]	33.7 (58/172)[j]	34.1 (40/117)[j]	3.4 (4/117)	–	–	–
Domagala et al. (current study)	17.1 (24/140)	13.6 (19/140)	3.6 (5/140)	43.6 (61/140)	14.7 (20/136)	81.9 (113/138)

Only reports based on more than 20 *BRCA1*-associated cancers are included

[a] Different than generally used scoring system

[b] The percentage is based on numbers of scores assigned by two pathologists and not on the number of tumors examined. There were 165 tumors examined for ER/PR and 158 for EGFR

[c] Using both biochemical methods and immunohistochemistry

[d] Early onset breast cancers only

[e] Only percentage given

[f] 15% (six of 40) by FISH

[g] 12% (three of 25) by FISH

[h] Triple-negative *BRCA1*-associated cancers

[i] Includes nine bilateral cancers

[j] 16.3% measured using biochemical methods

ERα deficiency [28]. Targeting HER-2 protein in HER-2-overexpressing breast cancers has resulted in significant clinical benefit for those patients [29]. In a similar manner, patients with *BRCA1*-associated tumors that overexpress EGFR could potentially benefit from EGFR-targeted therapy. However, the relationship of EGFR expression to therapeutic response is not straightforward and has yet to be fully investigated in breast cancer. This is due to various mechanisms of EGFR dysregulation and several compensatory pathways present in tumor cells [30].

We found that 14.7% of *BRCA1*-associated breast carcinomas expressed c-kit. In the only published report, 48.1% of *BRCA1*-associated tumors were c-kit positive [31]. The difference may be explained by a low number of cases (n=27), different cut-off level applied to distinguish positive vs. negative cases (authors did not specify it) and different antibody used. Imatinib has proven to be an efficient anti-c-kit-targeted therapy for gastrointestinal stromal tumors; however, little is known about the results of such therapy in breast cancer, and nothing is known about it in *BRCA1*-associated breast cancer, so the clinical value of c-kit therapy in patients with c-kit positive *BRCA1*-associated carcinomas has yet to be established. Our finding that about 15% of *BRCA1*-associated breast cancers express c-kit may help in the proper recruitment of patients for future prospective clinical trials because only those cancers may serve as a target for therapy with imatinib.

In Table 4, the results of our study are compared with major reports in the literature on the immunohistochemical assessment of ER/PR, HER-2, EGFR, and c-kit in *BRCA1*-associated breast carcinomas. The results concerning the expression of steroid receptors and HER-2 confirm previous reports showing that the vast majority of *BRCA1*-associated cancers are steroid receptor and HER-2 negative. However, there are some differences, and they may be attributed to limitations of the previous studies. The majority of published reports (1) were based on a low number of cancers (e.g., only two reports on HER-2 immunohistochemical expression are based on more than 100 cancers [5, 9]); (2) used data concerning ER/PR and HER-2 only from pathology reports; (3) analyzed highly selected cases, i.e., only familial *BRCA1*-associated cancers, or early onset breast cancers, or triple-negative *BRCA1*-associated cancers; (4) applied various criteria for scoring and various immunohistochemical techniques which underwent refinements over the years; and (5) included patients whose cancers were diagnosed before *BRCA1* testing era and this might have selected patients with longer survival, e.g., with ER+ tumors. Our study is the first that is not restricted to familial *BRCA1*-associated cancers but is based on a large group of consecutive *BRCA1*-associated breast cancer patients.

In conclusion, the current treatment recommendations are similar for all patients with *BRCA1*-related cancers. However, we have shown here that these cancers differ with respect to their expression of the proteins that are regarded as targets for specific therapies. Thus, *BRCA1* mutation carriers may have various therapeutic options available. Therefore, we suggest that in order to reveal all therapeutic options accessible to a particular patient, the tumor should be tested for the expression of all five major predictive markers. We believe that in the era of targeted therapy, treatment regimens may become more tumor specific (i.e., more personalized) if the expression of major predictive proteins in tumor cells is taken into account when making treatment decisions about patients with *BRCA1*-associated breast cancers. This data may also be useful when recruiting patients for trials of specific targeted therapy, for example, it seems probable that overall response rate of patients with advanced breast cancer and germline *BRCA1* or *BRCA2* mutations in the phase 2 study of olaparib [22] might have been better if tumors were tested for PARP-1 expression and only patients with PARP-1-positive cancer were enrolled and treated. However, full screening of *BRCA1* may not be readily available in some countries what may hamper recruitment of patients for such trials. Clearly, further prospective studies are needed to reveal the clinical utility of the immunophenotypic predictive profile proposed in this report. Finally, because the majority of *BRCA1*-associated breast cancers are thought to represent the basal-like subtype, such predictive immunophenotype may also be applicable to that subset of breast cancers.

Acknowledgments This study was supported by the Pomeranian Medical University Research Program, grant no. WL-125-01/S/10.

Conflict of interest The authors declare that they have no conflict of interest.

Open Access This article is distributed under the terms of the Creative Commons Attribution Noncommercial License which permits any noncommercial use, distribution, and reproduction in any medium, provided the original author(s) and source are credited.

References

1. Wooster R, Weber BL (2003) Breast and ovarian cancer. N Engl J Med 348:2339–2347
2. Fasano J, Muggia F (2009) Breast cancer arising in a BRCA-mutated background: therapeutic implications from an animal model and drug development. Ann Oncol 20:609–614
3. Comen EA, Robson M (2010) Inhibition of poly(ADP)-ribose polymerase as a therapeutic strategy for breast cancer. Oncology (Williston Park) 24:55–62
4. Bosch A, Eroles P, Zaragoza R, Vina JR, Lluch A (2010) Triple-negative breast cancer: molecular features, pathogenesis, treatment and current lines of research. Cancer Treat Rev 36:206–215

5. Lakhani SR, Van De Vijver MJ, Jacquemier J, Anderson TJ, Osin PP, McGuffog L, Easton DF (2002) The pathology of familial breast cancer: predictive value of immunohistochemical markers estrogen receptor, progesterone receptor, HER-2, and p53 in patients with mutations in BRCA1 and BRCA2. J Clin Oncol 20:2310–2318
6. Lakhani SR, Reis-Filho JS, Fulford L, Penault-Llorca F, van der Vijver M, Parry S, Bishop T, Benitez J, Rivas C, Bignon YJ, Chang-Claude J, Hamann U, Cornelisse CJ, Devilee P, Beckmann MW, Nestle-Kramling C, Daly PA, Haites N, Varley J, Lalloo F, Evans G, Maugard C, Meijers-Heijboer H, Klijn JG, Olah E, Gusterson BA, Pilotti S, Radice P, Scherneck S, Sobol H, Jacquemier J, Wagner T, Peto J, Stratton MR, McGuffog L, Easton DF, Breast Cancer Linkage Consortium (2005) Prediction of BRCA1 status in patients with breast cancer using estrogen receptor and basal phenotype. Clin Cancer Res 11:5175–5180
7. Brekelmans CT, Seynaeve C, Menke-Pluymers M, Bruggenwirth HT, Tilanus-Linthorst MM, Bartels CC, Kriege M, van Geel AN, Crepin CM, Blom JC, Meijers-Heijboer H, Klijn JG (2006) Survival and prognostic factors in BRCA1-associated breast cancer. Ann Oncol 17:391–400
8. Graeser M, Bosse K, Brosig M, Engel C, Schmutzler RK, German Consortium for Hereditary Breast and Ovarian Cancer (2009) Association of hormone receptor status with grading, age of onset, and tumor size in BRCA1-associated breast cancer. Virchows Arch 454:519–524
9. Tung N, Wang Y, Collins LC, Kaplan J, Li H, Gelman R, Comander AH, Gallagher B, Fetten K, Krag K, Stoeckert KA, Legare RD, Sgroi D, Ryan PD, Garber JE, Schnitt SJ (2010) Estrogen receptor positive breast cancers in BRCA1 mutation carriers: clinical risk factors and pathologic features. Breast Cancer Res 12:R12
10. Gorski B, Cybulski C, Huzarski T, Byrski T, Gronwald J, Jakubowska A, Stawicka M, Gozdecka-Grodecka S, Szwiec M, Urbanski K, Mitus J, Marczyk E, Dziuba J, Wandzel P, Surdyka D, Haus O, Janiszewska H, Debniak T, Toloczko-Grabarek A, Medrek K, Masojc B, Mierzejewski M, Kowalska E, Narod SA, Lubinski J (2005) Breast cancer predisposing alleles in Poland. Breast Cancer Res Treat 92:19–24
11. Elston CW, Ellis IO (1991) Pathological prognostic factors in breast cancer. I. The value of histological grade in breast cancer: experience from a large study with long-term follow-up. Histopathology 19:403–410
12. Detre S, Saclani Jotti G, Dowsett M (1995) A "quickscore" method for immunohistochemical semiquantitation: validation for oestrogen receptor in breast carcinomas. J Clin Pathol 48:876–878
13. Wolff AC, Hammond ME, Schwartz JN, Hagerty KL, Allred DC, Cote RJ, Dowsett M, Fitzgibbons PL, Hanna WM, Langer A, McShane LM, Paik S, Pegram MD, Perez EA, Press MF, Rhodes A, Sturgeon C, Taube SE, Tubbs R, Vance GH, van de Vijver M, Wheeler TM, Hayes DF, American Society of Clinical Oncology/College of American Pathologists (2007) American Society of Clinical Oncology/College of American Pathologists guideline recommendations for human epidermal growth factor receptor 2 testing in breast cancer. Arch Pathol Lab Med 131:18–43
14. Hammond ME, Hayes DF, Dowsett M, Allred DC, Hagerty KL, Badve S, Fitzgibbons PL, Francis G, Goldstein NS, Hayes M, Hicks DG, Lester S, Love R, Mangu PB, McShane L, Miller K, Osborne CK, Paik S, Perlmutter J, Rhodes A, Sasano H, Schwartz JN, Sweep FC, Taube S, Torlakovic EE, Valenstein P, Viale G, Visscher D, Wheeler T, Williams RB, Wittliff JL, Wolff AC (2010) American Society of Clinical Oncology/College of American Pathologists guideline recommendations for immunohistochemical testing of estrogen and progesterone receptors in breast cancer. Arch Pathol Lab Med 134:907–922
15. Ulivi P, Zoli W, Medri L, Amadori D, Saragoni L, Barbanti F, Calistri D, Silvestrini R (2004) c-kit and SCF expression in normal and tumor breast tissue. Breast Cancer Res Treat 83:33–42
16. Byrski T, Huzarski T, Dent R, Gronwald J, Zuziak D, Cybulski C, Kladny J, Gorski B, Lubinski J, Narod SA (2009) Response to neoadjuvant therapy with cisplatin in BRCA1-positive breast cancer patients. Breast Cancer Res Treat 115:359–363
17. Bhattacharyya A, Ear US, Koller BH, Weichselbaum RR, Bishop DK (2000) The breast cancer susceptibility gene BRCA1 is required for subnuclear assembly of Rad51 and survival following treatment with the DNA cross-linking agent cisplatin. J Biol Chem 275:23899–23903
18. Schreiber V, Dantzer F, Ame JC, de Murcia G (2006) Poly (ADP-ribose): novel functions for an old molecule. Nat Rev Mol Cell Biol 7:517–528
19. Farmer H, McCabe N, Lord CJ, Tutt AN, Johnson DA, Richardson TB, Santarosa M, Dillon KJ, Hickson I, Knights C, Martin NM, Jackson SP, Smith GC, Ashworth A (2005) Targeting the DNA repair defect in BRCA mutant cells as a therapeutic strategy. Nature 434:917–921
20. Bryant HE, Schultz N, Thomas HD, Parker KM, Flower D, Lopez E, Kyle S, Meuth M, Curtin NJ, Helleday T (2005) Specific killing of BRCA2-deficient tumours with inhibitors of poly(ADP-ribose) polymerase. Nature 434:913–917
21. Fong PC, Boss DS, Yap TA, Tutt A, Wu P, Mergui-Roelvink M, Mortimer P, Swaisland H, Lau A, O'Connor MJ, Ashworth A, Carmichael J, Kaye SB, Schellens JH, de Bono JS (2009) Inhibition of poly(ADP-ribose) polymerase in tumors from BRCA mutation carriers. N Engl J Med 361:123–134
22. Tutt A, Robson M, Garber JE, Domchek SM, Audeh MW, Weitzel JN, Friedlander M, Arun B, Loman N, Schmutzler RK, Wardley A, Mitchell G, Earl H, Wickens M, Carmichael J (2010) Oral poly (ADP-ribose) polymerase inhibitor olaparib in patients with BRCA1 or BRCA2 mutations and advanced breast cancer: a proof-of-concept trial. Lancet 376:235–244
23. Fu Z, Fenselau C (2005) Proteomic evidence for roles for nucleolin and poly[ADP-ribosyl] transferase in drug resistance. J Proteome Res 4:1583–1591
24. de Murcia JM, Niedergang C, Trucco C, Ricoul M, Dutrillaux B, Mark M, Oliver FJ, Masson M, Dierich A, LeMeur M, Walztinger C, Chambon P, de Murcia G (1997) Requirement of poly(ADP-ribose) polymerase in recovery from DNA damage in mice and in cells. Proc Natl Acad Sci U S A 94:7303–7307
25. Trucco C, Oliver FJ, de Murcia G, Menissier-de Murcia J (1998) DNA repair defect in poly(ADP-ribose) polymerase-deficient cell lines. Nucleic Acids Res 26:2644–2649
26. Osborne CK (1998) Steroid hormone receptors in breast cancer management. Breast Cancer Res Treat 51:227–238
27. King MC, Wieand S, Hale K, Lee M, Walsh T, Owens K, Tait J, Ford L, Dunn BK, Costantino J, Wickerham L, Wolmark N, Fisher B, National Surgical Adjuvant Breast and Bowel Project (2001) Tamoxifen and breast cancer incidence among women with inherited mutations in BRCA1 and BRCA2: National Surgical Adjuvant Breast and Bowel Project (NSABP-P1) Breast Cancer Prevention Trial. JAMA 286:2251–2256
28. Hosey AM, Gorski JJ, Murray MM, Quinn JE, Chung WY, Stewart GE, James CR, Farragher SM, Mulligan JM, Scott AN, Dervan PA, Johnston PG, Couch FJ, Daly PA, Kay E, McCann A, Mullan PB, Harkin DP (2007) Molecular basis for estrogen receptor alpha deficiency in BRCA1-linked breast cancer. J Natl Cancer Inst 99:1683–1694
29. Ross JS, Slodkowska EA, Symmans WF, Pusztai L, Ravdin PM, Hortobagyi GN (2009) The HER-2 receptor and breast cancer: ten years of targeted anti-HER-2 therapy and personalized medicine. Oncologist 14:320–368
30. Milanezi F, Carvalho S, Schmitt FC (2008) EGFR/HER2 in breast cancer: a biological approach for molecular diagnosis and therapy. Expert Rev Mol Diagn 8:417–434

31. Lim E, Vaillant F, Wu D, Forrest NC, Pal B, Hart AH, Asselin-Labat ML, Gyorki DE, Ward T, Partanen A, Feleppa F, Huschtscha LI, Thorne HJ, kConFab, Fox SB, Yan M, French JD, Brown MA, Smyth GK, Visvader JE, Lindeman GJ (2009) Aberrant luminal progenitors as the candidate target population for basal tumor development in BRCA1 mutation carriers. Nat Med 15:907–913
32. Johannsson OT, Idvall I, Anderson C, Borg A, Barkardottir RB, Egilsson V, Olsson H (1997) Tumour biological features of BRCA1-induced breast and ovarian cancer. Eur J Cancer 33:362–371
33. Lynch BJ, Holden JA, Buys SS, Neuhausen SL, Gaffney DK (1998) Pathobiologic characteristics of hereditary breast cancer. Hum Pathol 29:1140–1144
34. Osin P, Gusterson BA, Philp E, Waller J, Bartek J, Peto J, Crook T (1998) Predicted anti-oestrogen resistance in BRCA-associated familial breast cancers. Eur J Cancer 34:1683–1686
35. Eisinger F, Nogues C, Guinebretiere JM, Peyrat JP, Bardou VJ, Noguchi T, Vennin P, Sauvan R, Lidereau R, Birnbaum D, Jacquemier J, Sobol H (1999) Novel indications for BRCA1 screening using individual clinical and morphological features. Int J Cancer 84:263–267
36. Vaziri SA, Krumroy LM, Elson P, Budd GT, Darlington G, Myles J, Tubbs RR, Casey G (2001) Breast tumor immunophenotype of BRCA1-mutation carriers is influenced by age at diagnosis. Clin Cancer Res 7:1937–1945
37. Grushko TA, Blackwood MA, Schumm PL, Hagos FG, Adeyanju MO, Feldman MD, Sanders MO, Weber BL, Olopade OI (2002) Molecular-cytogenetic analysis of HER-2/neu gene in BRCA1-associated breast cancers. Cancer Res 62:1481–1488
38. Quenneville LA, Phillips KA, Ozcelik H, Parkes RK, Knight JA, Goodwin PJ, Andrulis IL, O'Malley FP (2002) HER-2/neu status and tumor morphology of invasive breast carcinomas in Ashkenazi women with known BRCA1 mutation status in the Ontario Familial Breast Cancer Registry. Cancer 95:2068–2075
39. Goffin JR, Chappuis PO, Begin LR, Wong N, Brunet JS, Hamel N, Paradis AJ, Boyd J, Foulkes WD (2003) Impact of germline BRCA1 mutations and overexpression of p53 on prognosis and response to treatment following breast carcinoma: 10-year follow up data. Cancer 97:527–536
40. Foulkes WD, Metcalfe K, Sun P, Hanna WM, Lynch HT, Ghadirian P, Tung N, Olopade OI, Weber BL, McLennan J, Olivotto IA, Begin LR, Narod SA (2004) Estrogen receptor status in BRCA1- and BRCA2-related breast cancer: the influence of age, grade, and histological type. Clin Cancer Res 10:2029–2034
41. Lubinski J, Gorski B, Huzarski T, Byrski T, Gronwald J, Serrano-Fernandez P, Domagala W, Chosia M, Ucinski M, Grzybowska E, Lange D, Maka B, Mackiewicz A, Karczewska A, Breborowicz J, Lamperska K, Stawicka M, Gozdecka-Grodecka S, Bebenek M, Sorokin D, Wojnar A, Haus O, Sir J, Mierzwa T, Niepsuj S, Gugala K, Gozdz S, Sygut J, Kozak-Klonowska B, Musiatowicz B, Posmyk M, Kordek R, Morawiec M, Zambrano O, Wasko B, Fudali L, Skret J, Surdyka D, Urbanski K, Mitus J, Rys J, Szwiec M, Rozmiarek A, Dziuba I, Wandzel P, Wisniowski R, Szczylik C, Kozak A, Kozlowski W, Narod SA (2006) BRCA1-positive breast cancers in young women from Poland. Breast Cancer Res Treat 99:71–76
42. Oldenburg RA, Kroeze-Jansema K, Meijers-Heijboer H, van Asperen CJ, Hoogerbrugge N, van Leeuwen I, Vasen HF, Cleton-Jansen AM, Kraan J, Houwing-Duistermaat JJ, Morreau H, Cornelisse CJ, Devilee P (2006) Characterization of familial non-BRCA1/2 breast tumors by loss of heterozygosity and immunophenotyping. Clin Cancer Res 12:1693–1700
43. van der Groep P, Bouter A, van der Zanden R, Siccama I, Menko FH, Gille JJ, van Kalken C, van der Wall E, Verheijen RH, van Diest PJ (2006) Distinction between hereditary and sporadic breast cancer on the basis of clinicopathological data. J Clin Pathol 59:611–617
44. Hagen AI, Bofin AM, Ytterhus B, Maehle LO, Kjellevold KH, Myhre HO, Moller P, Lonning PE (2007) Amplification of TOP2A and HER-2 genes in breast cancers occurring in patients harbouring BRCA1 germline mutations. Acta Oncol 46:199–203
45. Honrado E, Osorio A, Milne RL, Paz MF, Melchor L, Cascon A, Urioste M, Cazorla A, Diez O, Lerma E, Esteller M, Palacios J, Benitez J (2007) Immunohistochemical classification of non-BRCA1/2 tumors identifies different groups that demonstrate the heterogeneity of BRCAX families. Mod Pathol 20:1298–1306
46. Atchley DP, Albarracin CT, Lopez A, Valero V, Amos CI, Gonzalez-Angulo AM, Hortobagyi GN, Arun BK (2008) Clinical and pathologic characteristics of patients with BRCA-positive and BRCA-negative breast cancer. J Clin Oncol 26:4282–4288
47. Aaltonen K, Blomqvist C, Amini RM, Eerola H, Aittomaki K, Heikkila P, Nevanlinna H (2008) Familial breast cancers without mutations in BRCA1 or BRCA2 have low cyclin E and high cyclin D1 in contrast to cancers in BRCA mutation carriers. Clin Cancer Res 14:1976–1983
48. Litwiniuk MM, Roznowski K, Filas V, Godlewski DD, Stawicka M, Kaleta R, Breborowicz J (2008) Expression of estrogen receptor beta in the breast carcinoma of BRCA1 mutation carriers. BMC Cancer 8:100
49. Collins LC, Martyniak A, Kandel MJ, Stadler ZK, Masciari S, Miron A, Richardson AL, Schnitt SJ, Garber JE (2009) Basal cytokeratin and epidermal growth factor receptor expression are not predictive of BRCA1 mutation status in women with triple-negative breast cancers. Am J Surg Pathol 33:1093–1097
50. Evans DG, Lalloo F, Cramer A, Jones EA, Knox F, Amir E, Howell A (2009) Addition of pathology and biomarker information significantly improves the performance of the Manchester scoring system for BRCA1 and BRCA2 testing. J Med Genet 46:811–817
51. Kwong A, Wong LP, Wong HN, Law FB, Ng EK, Tang YH, Chan WK, Suen DT, Choi C, Ho LS, Kwan KH, Poon M, Wong TT, Chan K, Chan SW, Ying MW, Chan WC, Ma ES, Ford JM, West DW (2009) Clinical and pathological characteristics of Chinese patients with BRCA related breast cancer. Hugo J 3:63–76
52. Manie E, Vincent-Salomon A, Lehmann-Che J, Pierron G, Turpin E, Warcoin M, Gruel N, Lebigot I, Sastre-Garau X, Lidereau R, Remenieras A, Feunteun J, Delattre O, de The H, Stoppa-Lyonnet D, Stern MH (2009) High frequency of TP53 mutation in BRCA1 and sporadic basal-like carcinomas but not in BRCA1 luminal breast tumors. Cancer Res 69:663–671
53. Joosse SA, van Beers EH, Tielen IH, Horlings H, Peterse JL, Hoogerbrugge N, Ligtenberg MJ, Wessels LF, Axwijk P, Verhoef S, Hogervorst FB, Nederlof PM (2009) Prediction of BRCA1-association in hereditary non-BRCA1/2 breast carcinomas with array-CGH. Breast Cancer Res Treat 116:479–489

Virchows Arch (2011) 458:65–72
DOI 10.1007/s00428-010-1009-2

ORIGINAL ARTICLE

Histopathological subclassification of triple negative breast cancer using prognostic scoring system: five variables as candidates

Minoru Miyashita · Takanori Ishida · Kazuyuki Ishida · Kentaro Tamaki · Masakazu Amari · Mika Watanabe · Noriaki Ohuchi · Hironobu Sasano

Received: 23 August 2010 / Revised: 11 October 2010 / Accepted: 4 November 2010 / Published online: 21 November 2010
© Springer-Verlag 2010

Abstract We attempted to subclassify triple negative breast cancer (TNBC) cases into subgroups according to clinical outcome or prognosis of TNBC patients using archival specimens. We analyzed 102 Japanese cases of invasive TNBC who underwent surgery between January 1998 and December 2007. The clinicopathological factors and clinical information were retrospectively retrieved from reviewing the charts of the patients. Immunohistochemical staining was performed for estrogen receptor (ER), progesterone receptor (PR), human epidermal growth factor receptor 2 (HER2), epidermal growth factor receptor 1 (EGFR1), CK5/6, CK14, Ki-67, and CD31 for microvessel density (MVD). Median follow-up time of the patients was 68.5 months. Multivariable analysis demonstrated that pathologic node status was the most significantly associated with relapse-free survival (RFS) and breast cancer-specific survival (BCSS) of these patients. Pathological tumor size, basal-like type, Ki-67 labeling index (LI) and MVD were also independently associated with RFS and BCSS. Based on these results, we devised the risk score system reflecting hazard ratios of these prognostic factors above. With this system, TNBC patients in this study were classified into three subgroups (low-risk group: score 0–3, intermediate-risk group: score 4–7 and high-risk group: score 8–10). The significant difference of RFS and BCSS was detected among these three different subgroups of the patients ($p < 0.05$). We propose the risk score system, which incorporated pathologic nodal status, size of the primary tumor, the presence or absence of basal-like features, Ki-67 LI, and MVD in order to predict postoperative clinical course of the Japanese TNBC patients.

Keywords Triple negative breast cancer · Histopathology · Prognosis · MVD · Ki-67 · Basal-like

M. Miyashita · T. Ishida · K. Tamaki · M. Amari · N. Ohuchi
Department of Surgical Oncology,
Tohoku University Graduate School of Medicine,
1-1 Seiryo-machi, Aoba-ku, Sendai 980-8574, Japan

M. Miyashita · K. Ishida · M. Watanabe · H. Sasano (✉)
Department of Pathology, Tohoku University Hospital,
1-1 Seiryo-machi, Aoba-ku, Sendai 980-8574, Japan
e-mail: hsasano@patholo2.med.tohoku.ac.jp

Introduction

Breast cancer is a heterogeneous disease and has been recently proposed to be further classified into five different subtypes according to the results of gene expression profiling using DNA microarrays (luminal A, luminal B, human epidermal growth factor receptor 2 (HER2) over-expressing, basal-like and normal-like) [1, 2]. This analysis has been generally considered to be of clinical value because individual subtypes were associated with different clinical course or prognosis. Basal-like type has been reported to be associated with more unfavorable clinical course or outcome compared to luminal types and to be characterized by expression of myoepitherial/basal cytokeratins (CK5/6, CK14, and CK17) and epidermal growth factor receptor 1 (EGFR1) [3]. In addition, this type principally lacks the expression of estrogen receptor (ER), progesterone receptor (PR), and HER2 and has been also frequently termed triple negative breast cancer (TNBC) in routine clinical practice [3–5]. These two basal-like type and TNBC have a similar feature but the overlap is not

necessarily complete [6]. Basal-like type breast carcinoma is currently considered not a synonym, but rather one of the prognostic factors for TNBC [6–9].

TNBC account for approximately 10–20% of the whole breast cancer cases and are associated with relatively early clinical relapses within 3 years, with frequent progression to distant metastasis, particularly, visceral metastasis and poor prognosis, although it is also true that they are sensitive to chemotherapy [10–13]. TNBC is generally considered the most difficult subtype to treat among these newly proposed subtypes of breast cancer because of the aggressive clinical behavior and the lack of current availability of specific targeted therapy such as selective ER modulators, aromatase inhibitors, trastuzumab, and lapatinib.

In addition, TNBC cases are also considered to be subclassified into different prognostic groups, because the patients associated with worse prognosis should be selected to receive the novel developing therapy. TNBC has been divided into subgroups based on the single prognostic biomarker, but further subclassification according to combination of valid biomarkers have not been reported in the literature at least in Asian patients of TNBC to the best of our knowledge. Therefore, in this study, we focused on tumor angiogenesis and proliferation that are major determinations of potential biological or clinical behavior of human breast cancer patients. We assessed Ki-67 labeling index (LI) and microvessel density (MVD) using CD31 staining, in addition to reported basal markers (CK5/6, CK14, and EGFR) and conventional clinicopathologic factors in TNBC. We also selected these markers from the standpoint that assessment tool should be used widely in clinical settings. We subsequently attempted to devise a scoring system which could reflect clinical outcome of the Japanese patients with TNBC patients in routine clinical practice.

Materials and methods

Patients

We identified 841 patients with primary operable breast cancer who underwent surgery at the Department of Surgery, Tohoku University Hospital (Sendai, Japan) between January 1998 and December 2007 and collected information through the breast cancer management database of the hospital. Among these 841 Japanese patients, 642 (76.3%) had hormone receptor positive, 138 (16.4%) had HER2-positive, 118 (14.0%) had triple receptor-negative tumors, and 6 (0.7%) lacked the receptor information. Of 118 TNBC above, patients with ductal carcinoma in situ apocrine carcinoma, medullary carcinoma were excluded from the present analysis, because these tumors have different biological and clinical features from those of invasive ductal TNBC [14–16], and we also excluded the cases that were not treated with adjuvant chemotherapy after the surgery in order to standardize backgrounds of the patients.

Characteristics of 102 triple negative patients examined in this study were summarized in Table 1. The median age of the patients was 56 years (range: 30–81 years). A number of 54 cases (53%) were classified as pT1, 36 (35%) pT2, and the others pT3/4. The median of pathological tumor size was 18 mm (range: 3–90 mm). Axillary node dissection was carried out in all the patients examined in this study. A total of 55 cases (54%) had a node-negative and 47 (46%) had a node-positive breast cancer. A number of 51 patients underwent breast conserving surgery who subsequently received postoperative radiotherapy against remaining breast tissue. Systemic adjuvant chemotherapy was administered to all the patients, and none of them was treated by hormonal therapy and HER2 targeting therapy.

Histopathology and immunohistochemistry

Hematoxylin–eosin (H&E)-stained glass slides were retrieved from surgical pathology files of Tohoku University Hospital,

Table 1 Characteristics of TNBC patients (n=102)

Characteristics	
Age, years	
Median (range)	56 (30–81)
≤50	39 (38%)
>50	63 (62%)
Pathological tumor size (mm)	
0–20	54 (53%)
21–30	18 (18%)
31–50	21 (20%)
51–	9 (9%)
Pathological node status	
0	55 (54%)
1–3	29 (28%)
4–9	8 (8%)
10–	10 (10%)
Distant metastasis	
Negative	102 (100%)
Positive	0 (0%)
Operation	
Mastectomy	51 (50%)
BCS	51 (50%)
Adjuvant systemic therapy	
Chemotherapy	102 (100%)
Endcrine therapy	0 (0%)
Anti-HER2 therapy	0 (0%)

BCS breast conserving surgery

Sendai, Japan, and reviewed in all of these 102 triple negative cases. The specimens were cut into 4-μm-thick sections and placed on glue-coated glass slides for immunohistochemistry (IHC). Tumor staging was based *on TNM Classification of Malignant Tumors*, 6th edn. by the International Union Against Cancer (UICC) [17]. Histological grades were assessed according to the criteria of Elston and Ellis [18]. We also identified the presence or absence of peritumoral vascular invasion (PVI), according to the report of Rosen and Obermann [19]. ER and PR status were immunostained by using monoclonal antibodies (codes 107925 and 102333, Roche Diagnostics, Basel, Switzerland), and nuclear staining of more than 1% was considered positive. HER2 status was evaluated by IHC (HercepTest, code K5204, Dako, Glostrup, Denmark) or by fluorescence in situ hybridization (FISH) that was used to calculate the gene copy ratio of HER2-to-CEP17 (the PathVysion HER2 DNA Probe Kit; Abbott, Chicago, IL). HER2 positivity was defined as 3+ receptor overexpression by IHC and/or as 2.2 or greater of a HER2-to-CEP17 ratio by FISH according to the American Society of Clinical Oncology/College of American Pathologists Guideline [20]. We performed IHC for Ki-67, CD31, EGFR, CK5/6, and CK14. Ki-67 LI was determined with MIB-1 monoclonal antibody (code M7240, Dako) through counting 1,000 tumor cells at the hot spots [21–24]. Microvessels were identified as the lumen lined by endothelial cells, complemented by IHC of endothelial cells with CD31 (code M0823, Dako). We counted microvessels at one high-power field (×200) as MVD after the areas with the greatest number of microvessels were selected at low magnification (×40 and×100) [25, 26]. EGFR was positive if the membrane of 10% or more carcinoma cells were stained by using representative monoclonal antibody (code K1492, Dako). CK5/6 and CK14 were interpreted positive if 10% or more carcinoma cells were positive in the cytoplasm with monoclonal antibodies (code M7237, Dako for CK5/6 and code NCL-LL002, Leica, Newcastle, UK for CK14) [5, 7, 8]. All of pathological diagnosis and staining assessments of individual cases were performed by two pathologists (Fig. 1).

Statistical methods

Breast cancer-specific survival (BCSS) was evaluated from the date of definitive surgery to that of the last follow-up or death due to breast cancer. Relapse-free survival (RFS) was defined as the length of time from the date of definitive surgery to the last follow-up or first event. Both BCSS and RFS were estimated by using the Kaplan–Meier methods, and the differences in survival curve between these two groups of the patients were assessed by the log–rank test. Cox proportional hazard model was used for univariate and multivariate analyses to evaluate each factor including pathological tumor size, pathological node status, PVI, histological grade, basal-like type, Ki-67 LI, and MVD. The hazard ratios (HRs) calculated for each significant factor in the multivariable model were defined as scores representing the risks of relapse and breast cancer specific death, and totaled or summated value of scores was subsequently defined as the risk score of TNBC patients. All analyses were performed using StatMate III® for Windows ver. 3.18 (ATMS, Tokyo, Japan). The results were considered significant with p value of <0.05. All statistical tests were two-sided.

Results

Table 2 shows the results of histopathological factors and biomarkers of TNBC patients. A number of 65 tumors (64%) had high-grade characteristics corresponding to histological grade III, and 39 tumors (38%) were associated with PVI. EGFR, CK5/6, and CK14 immunoreactivity was detected in 36 (35%), 60 (59%), and 42 cases (41%), respectively. TNBC was subsequently subdivided into the following groups: 67 (66%) basal-like cases which expressed one or more of the specific basal markers, EGFR, CK5/6, and CK14, and 35 (34%) nonbasal-like cases which did not express any of these markers above. The median value of Ki-67 LI was 37%, and 48 cases (47%) were assessed that cancer cells of more than 40% were stained. A number of 48 (47%) cases were positive for MVD at the cutoff point set at 20 as the optimal cutoff value near the median 19. During the median follow-up time of 68.5 months (range: 7–146 months), 37 patients experienced disease relapse and 28 patients died due to breast cancer. In univariate analysis, pathological tumor size with two cutoff points, i.e., 20 and 30 mm, pathological node status, PVI, the basal-like features, Ki-67 LI with two cutoff points, 30% and 40%, and the amount of microvessels were significantly correlated with poor prognosis or adverse clinical outcome of the patients.

Multivariate analysis and the subsequent risk score for TNBC

Age (≤50 vs. >50 years), pathological tumor size (≤20 vs. >20 mm or≤30 vs. >30 mm), pathological node status (negative vs. positive), PVI (negative vs. positive), histological grade (I, II vs. III), basal-like type (basal-like vs. nonbasal-like), Ki-67 LI (≤30% vs. >30% or≤40% vs. >40%), and MVD (≤20 vs. >20) were all assessed in multivariate analysis for RFS and BCSS. Among the factors evaluated above, the pathological nodal status was strongly associated with RFS (HR=2.99, 95% CI=1.45–6.19; p=0.003) and BCSS (HR=2.71, 95% CI=1.18–6.21;

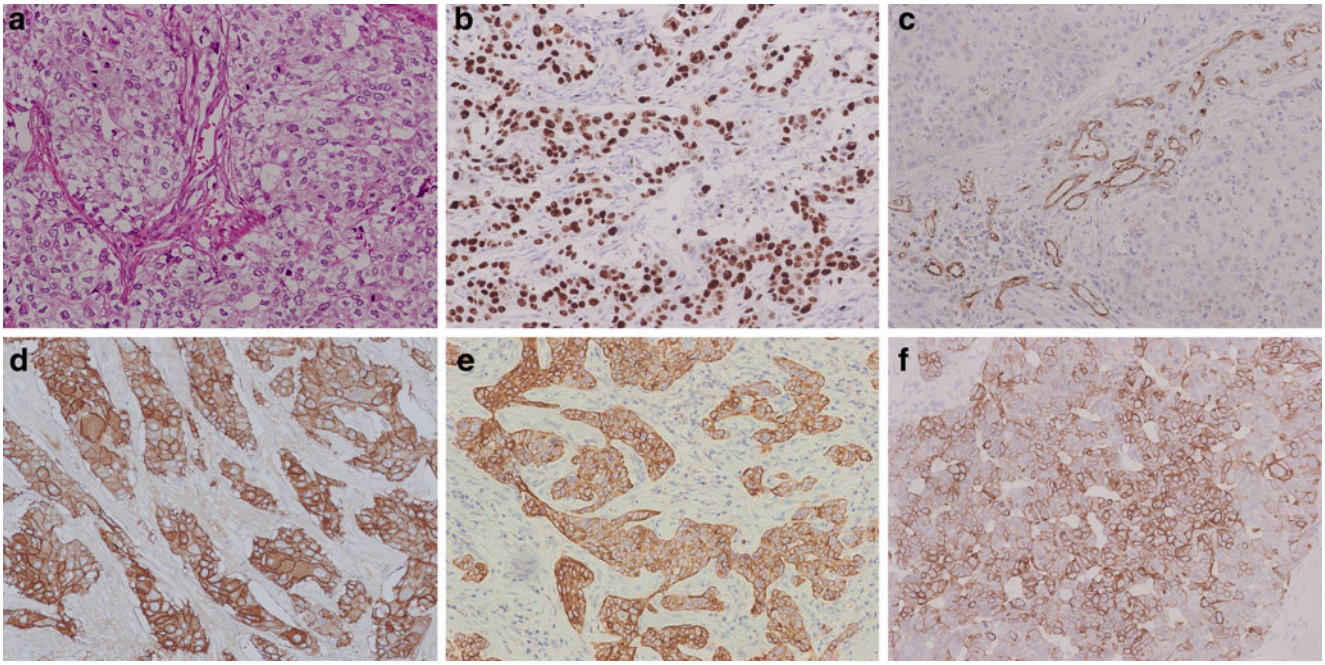

Fig. 1 Presentitative illustrations of H&E and immunohistochemical staining. **a** H&E, **b** high LI of Ki-67 staining, **c** high microvessel density by CD31 staining, **d** overexpression of epidermal growth factor receptor 1 (EGFR), **e** positive immunoreactivity of cytokeratin 5/6, and **f** positive staining of cytokeratin 14 (original magnification, ×200)

p=0.019). Pathological tumor size (≤30 vs. >30 mm) was also significantly associated with RFS (HR=2.23, 95% CI=1.06–4.70; p=0.035) and BCSS (HR=2.63, 95% CI=1.13–6.12; p=0.025). Basal-like type was also significantly associated with RFS (HR=2.76, 95% CI=1.14–6.66; p=0.024) and BCSS (HR=3.02, 95% CI=1.05–8.67; p=0.040). Ki-67 LI (tentatively classified into two groups: ≤40% vs. >40%) was also significantly associated with RFS (HR=2.44, 95% CI=1.20–4.96; p=0.014) and BCSS (HR=2.68, 95% CI=1.15–6.26; p=0.023). MVD was also significantly associated with RFS (HR=2.32, 95% CI=1.09–4.94; p=0.029) and BCSS (HR=2.44, 95% CI=1.02–5.86; p=0.046). Age, pathological tumor size (≤20 vs. >20 mm), PVI, histological grade, Ki-67 LI (≤30% vs. >30%) were not independently associated with RFS and BCSS (Table 3).

After these statistical analyses, we identified the following five significant factors which were significantly correlated with prognosis or clinical outcome of TNBC patients in multivariate analysis (pathological tumor size, pathological node status, basal-like type, Ki-67 LI, and MVD). We then further subclassified TNBC according to the five statistically significant risk factors described above. We applied scores reflecting HR points to each risk factor using a method that was presented for the prognostic models in cardiovascular disease as well as preoperative endocrine prognostic index (PEPI) for breast cancer cases built by this approach with some modifications [27, 28]. The procedure of scoring was summarized in Table 4. TNBC patients were classified into three groups by the risk score representing totaled value or summed score of each risk factor. Patients with score 0–3 are in low-risk group (A), score 4–7 in intermediate-risk group (B), and score 8–10 in high-risk group (C). These three groups had statistically different risks of relapse and breast cancer specific death, respectively (RFS: A vs. B, p<0.001; A vs. C, p < 0.001; B vs. C, p=0.013; BCSS: A vs. B, p = 0.025; A vs. C, p<0.001; B vs. C, p=0.005; Figs. 2 and 3).

Discussion

TNBC is generally considered to be associated with aggressive clinical behavior partly due to the limitations of the specific therapies currently available in clinical practice. However, it is also true that a marked heterogeneity exists in terms of clinical outcome or prognosis and response to various chemotherapeutic agents among TNBC patients [6, 10–13]. For instance, in putative low-risk patients of TNBC, the current standard chemotherapy regimens including anthracycline and taxanes have been usually considered somewhat effective [29–31]. However, it is also true that the new therapeutic strategy is being required to improve the prognosis of high-risk patients with TNBC. BRCA1 dysfunction and deficiency of DNA double-strand break repair were also reported to be detected in triple negative tumors, and these tumors may be more sensitive to poly(ADP-ribose) polymerase (PARP) inhib-

Table 2 Histopathological factors and biomarkers of TNBC patients (n=102)

Histopathological factors and biomarkers	
Histological grade	
I	5 (5%)
II	32 (31%)
III	65 (64%)
PVI	
Negative	63 (62%)
Positive	39 (38%)
EGFR	
Negative	66 (65%)
Positive	36 (35%)
CK5/6	
Negative	42 (41%)
Positive	60 (59%)
CK14	
Negative	60 (59%)
Positive	42 (41%)
Ki-67 labeling index	
0–15%	18 (18%)
16–30%	25 (24%)
31–40%	11 (11%)
41–100%	48 (47%)
Microvessel density	
≤20	54 (53%)
>20	48 (47%)

PVI:peritumoral vascular invasion, EGFR:epidermal growth factor receptor 1

itors [32, 33]. Ongoing phase III trial for PARP inhibitor is particularly expected to contribute to the treatment of TNBC. In addition, vascular endothelial growth factor (VEGF), recognized as the major angiogenic factor, was also abundantly detected in TNBC, and its levels have been demonstrated to be correlated with the survival time in TNBC [34–37]. In addition, several ongoing clinical trials suggest that bevacizumab could demonstrate the activity in patients with ER- and PR-negative cancer, most of them were also HER2-negative at subset analysis [31, 38, 39]. Therefore, considering these recent development of target-specific therapy in the patients with breast cancer, TNBC is currently being required to be classified pluralistically by the several prognostic factors in order to provide the most appropriate therapy to the patients, and these factors should be available in routine clinical settings considering the increment of breast cancer incidence in many parts of the world including the countries of Asia.

Therefore, in this study, we first examined the possible value of Ki-67 LI as the tool to evaluate cell proliferation because this has been proven to be one of the most useful and widely used prognostic markers in breast cancer despite some problems in procedures, interpretation, and reproducibility [21–24]. However, the analysis between Ki-67 LI in carcinoma cells and clinical outcome or behavior has not been reported in details in TNBC patients. The results of our study demonstrated that RFS and BCSS were categorized at two cutoff points of 30% and 40% and the patients whose LI was more than 40% were significantly associated with aggressive clinical behavior. High Ki-67 expression in carcinoma cells has been reported a prognostic factor for

Table 3 Multivariate analysis of clinicopathological factors and biomarkers for Relapse-free survival and Breast cancer-specific survival

Clinicopathological factors and biomarkers	Relapse-free survival				Breast cancer-specific survival			
	HR	95%CI		P value	HR	95%CI		P value
		Lower	Upper			Lower	Upper	
Age (>50 vs≤50)	0.93	0.46	1.91	0.85	0.62	0.27	1.43	0.260
Pathological tumor size								
≤20 vs >20 (mm)	1.64	0.81	3.32	0.17	2.05	0.89	4.72	0.091
≤30 vs >30 (mm)	2.23	1.06	4.70	0.04	2.63	1.13	6.12	0.025
Pathological node status (negative vs positive)	2.99	1.45	6.19	<0.01	2.71	1.18	6.21	0.019
PVI (negative vs positive)	1.43	0.71	2.90	0.32	1.05	0.46	2.38	0.905
Histological grade (I,II vs III)	1.01	0.65	1.52	0.97	1.17	0.48	2.83	0.728
Basal type (non basal-like vs basal-like)	2.76	1.14	6.66	0.02	3.02	1.05	8.67	0.040
Ki-67 labeling index								
≤30% vs >30%	1.82	0.84	3.91	0.13	2.34	0.91	6.05	0.079
≤40% vs >40%	2.44	1.20	4.96	0.01	2.68	1.15	6.26	0.023
Microvessel density (≤20 vs >20)	2.32	1.09	4.94	0.03	2.44	1.02	5.86	0.046

PVI peritumoral vascular invasion, *HR* hazard ratio, *CI* confidence interval

Table 4 The risk score for TNBC patients

Clinicopathological factors and biomarkers	Relapse-free survival		Breast cancer-specific survival	
	HR	Score	HR	Score
Pathological tumor size				
≤30 mm	–	0	–	0
>30 mm	2.23	2	2.63	3
Pathological node status				
Negative	–	0	–	0
Positive	2.99	3	2.71	3
Basal type				
Non basal-like	–	0	–	0
Basal-like	2.76	3	3.02	3
Ki-67 labeling index				
≤ 40%	–	0	–	0
> 40%	2.44	2	2.68	3
Microvessel density				
≤ 20	–	0	–	0
> 20	2.32	2	2.44	2

Hazard Ratio (HR) in the range of 1–2 receives 1 risk score, HR in the 2–2.5 range receives 2 risk scores, HR greater than 2.5 receives 3 risk scores. The Risk Score for each patient is the sum of all the risk scores accumulated from the five prognostic factors

breast cancer in many studies, but standard threshold in daily practice has not been established yet, partly due to various inert problems described above. In meta-analysis of Ki-67 LI in breast carcinoma patients reported in the literature, some studies used 10% as the cutoff (arbitrary value), whereas others have selected mean, median, and the optimal cutoff values [24]. The choice of cutoff points was also reported to depend on the various clinical objectives [24]. In our present studies of Ki-67 LI of TNBC, the cutoff point corresponding to high proliferation group was set at 40% as the optimal cutoff value near the median (Ki-67 LI: median; 37%) [22, 24], and Ki-67 LI determined in this manner turned out to be significant prognostic factor of the patients with TNBC.

We then evaluated the status of neovascularization in these TNBC cases using MVD. The analysis of MVD in resected tissue specimens has been generally reported to be a useful marker of tumor angiogenesis [40–45]. Meta-analysis of angiogenesis has been reported previously in 87 studies in the patients with breast cancer. Among these reported studies, 25 studies demonstrated the significant association between MVD and eventual survival of the patients. It is true, however, that the patients characteristics, antibodies, staining techniques, counting procedures, and

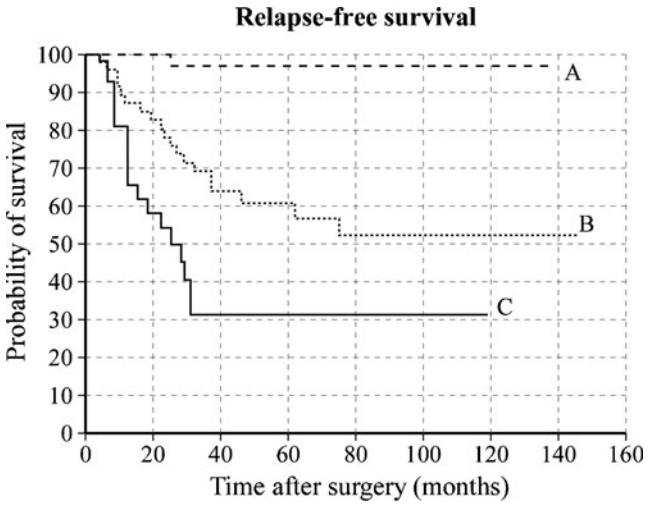

Fig. 2 Relapse-free survival in **a** low-risk group (score: 0–3, n=29), **b** intermediate-risk group (score: 4–7, n=48), and **c** high-risk group (score: 8–10, n=25) by the risk score system for TNBC (log–rank test: **a** vs. **b**, p<0.001; **A** vs. **C,** p < 0.001; **b** vs. **c**, p=0.013)

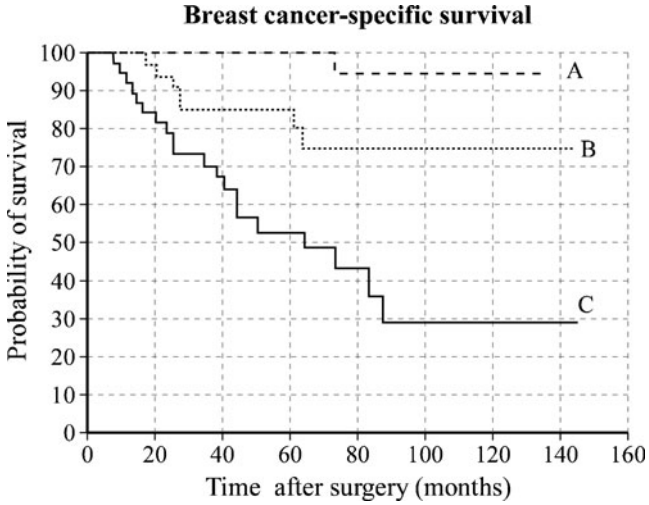

Fig. 3 Breast cancer-specific survival in **a** low-risk group (score: 0–3, n=29), **b** intermediate-risk group (score: 4–7, n=34), and **C** high-risk group (score: 8–10, n = 39) by the risk score system for TNBC (log–rank test: **a** vs. **b**, p=0.025; **a** vs. **c**, p<0.001; **b** vs. **c**, p=0.005)

selection of the cutoff levels of MVD assessment enormously varied among these reported studies, and it is very difficult to compare the results among individual studies [41]. In our present study, the statistically significant association was detected between high MVD and RFS, BCSS in TNBC patients using CD31, one of the gold standard markers of analyzing vascularity, with the optimal cutoff value near the median. However, standardization of assessment technique for MVD is required to obtain the vascularity in a more reproducible manner [46], and it requires further investigations to consolidate the clinical value of MVD analysis as a prognostic marker of the patients with TNBC.

EGFR, CK5/6, and CK14 were reported as more specific biomarkers to define the basal-like subtype and to reflect the cancer survival as a result of surrogating gene expression profiles analysis [3–9]. The results of our present study also demonstrated that the basal-like subtype was correlated with worse RFS and BCSS as well as reported in the previous studies [7–9]. Not all of the special histological types present triple negative features, but in our present study, typical medullary and apocrine carcinomas were excluded from the analysis because these two special subtypes were usually associated with the better clinical outcome than invasive ductal TNBC, despite the fact that they shared triple negative features [14–16].

The results of our present study also clearly suggest which subgroup should be indicated and received benefit by the optional strategy, novel agents including PARP inhibitors, bevacizumab, cetuximab, platinum drugs, and others [31, 47]. The risk score is generally considered a useful index when clinicians make a decision to treat patients of any condition including cancer. In our presently proposed risk score model for patients categorized in the low-risk group, the additional therapy may not provide additional clinical benefits because of the potentially intrinsic better clinical outcome or of the not aggressive clinical course of the patients. However, a more aggressive treatment should be served to the intermediate and high-risk group at an early phase as possible for adjuvant settings. As an annotation, the number of patients in the indeterminate and high-risk group was different at the assessment of RFS from that of BCSS, because HR points and risk scores were variable between RFS and BCSS in some of prognostic factors.

In addition, it is also important to note that this scoring system which we proposed in this report can be performed only by immunohistochemical techniques available for the great majority of diagnostic pathology laboratories. Therefore, an assessment of the risk score for TNBC can be reasonably postulated to be incorporated in any surgical pathology. The limitations of this study, however, include the retrospective nature of analysis, the strength of relatively short follow-up time for the patients with breast cancer (median: 68.5 months), and the availability of only one ethnic group, Japanese. Further studies with prospective validation, larger sample size, and longer follow-up are required to confirm this scoring system and to improve the model as a tool of classification of TNBC.

In conclusion, the results of our present study firstly demonstrated that TNBC could be further subclassified into three different groups according to the risk score system evaluating the following five prognostic variables (pathological tumor size, pathological node status, basal-like type, Ki67 LI, and MVD). Such a classification, which can be performed in diagnostic pathology laboratory, can be useful as a decision-making tool for triple negative patients.

Acknowledgments We wish to thank Yayoi Takahashi, MT, for her excellent technical assistance. This work was partly supported by a grant-in-aid for researches on biological feature and therapeutic strategy of TNBC (no. 22591421) from the Japanese Ministry of Education, Culture, Sports Science and Technology.

Conflicts of interest None

References

1. Perou CM, Sorlie T, Eisen MB et al (2000) Molecular portraits of human breast tumors. Nature 406:747–752
2. Sorlie T, Perou C, Tibshirani R et al (2001) Gene expression patterns of breast carcinomas distinguish tumor subclasses with clinical implications. Proc Natl Acad Sci USA 98(19):10869–10874
3. Nielsen TO, Hsu FD, Jensen K et al (2004) Immunohistochemical and clinical characterization of the basal-like subtype of invasive breast carcinoma. Clin Cancer Res 10(16):5367–5374
4. Livasy CA, Karaca G, Nanda R et al (2006) Phenotypic evaluation of the basal-like subtype of invasive breast carcinoma. Mod Pathol 19(2):264–271
5. Lerma E, Peiro G, Ramo'n T et al (2007) Immunohistochemical heterogeneity of breast carcinomas negative for estrogen receptors, progesterone receptors and Her2//neu (basal-like breast carcinomas). Mod Pathol 20(11):1200–1207
6. Reis-Filho JS, Tutt ANJ (2008) Triple negative tumours: a critical review. Histopathology 52:108–118
7. Rakha EA, El-Sayed ME, Green AR et al (2007) Prognostic markers in triple-negative breast cancer. Cancer 109(1):25–32
8. Rakha EA, Reis-Filho JS, Ian OE (2008) Basal-like breast cancer: a critical review. J Clin Oncol 26:2568–2581
9. Maggie CU-C, David V, Chris B et al (2008) Basal-like breast cancer defined by five biomarkers has superior prognostic value than triple-negative phenotype. Clin Cancer Res 14(5):1368–1376
10. Bauer KR, Brown M, Cress RD et al (2007) Descriptive analysis of estrogen receptor (ER)-negative, progesterone receptor (PR)-negative, and HER2-negative invasive breast cancer, the socalled triple-negative phenotype: a population-based study from the California cancer registry. Cancer 109(9):1721–1728
11. Carey LA, Dees EC, Sawyer L et al (2007) The triple negative paradox: primary tumor chemosensitivity of breast cancer subtypes. Clin Cancer Res 13(8):2329–2334
12. Rhee J, Han SW, Oh DY et al (2008) The clinicopathologic characteristics and prognostic significance of triple-negativity in node-negative breast cancer. BMC Cancer 8(1):307

13. Cornelia L, Chafika M, Kenneth RH et al (2008) Response to neoadjuvant therapy and long-term survival in patients with triple-negative breast cancer. J Clin Oncol 26:1275–1281
14. Anne VS, Nadège G, Carlo L et al (2007) Identification of typical medullary breast carcinoma as a genomic sub-group of basal-like carcinomas, a heterogeneous new molecular entity. Breast Cancer Res 9(2):1–15
15. Jocelyne J, Laetitia P, Laetitia R et al (2005) Typical medullary breast carcinomas have a basal/myoepithelial phenotype. J Pathol 207(3):260–268
16. Francois B, Pascal F, Nathalie C et al (2006) Gene expression profiling shows medullary breast cancer is a subgroup of basal breast cancers. Cancer Res 66(9):4636–4644
17. Sobin LH, Wittekind C (eds) (2002) TNM classification of malignant tumours, 6th edn. Wiley-Liss, New York, pp 131–141
18. Elston CW, Ellis IO (1991) Pathological prognostic factors in breast cancer: I. The value of histological grade in breast cancer: experience from a larger study with long-term follow-up. Histopathology 19:403–410
19. Rosen PP, Oberman H (1993) Tumors of the mammary gland. Armed Forces Institute of Pathology, Washington, DC
20. Wolff AC, Hammond MH, Schwartz JN et al (2007) American society of clinical oncology/college of American pathologists guideline recommendations for human epidermal growth factor receptor 2 testing in breast cancer. J Clin Oncol 25:118–145
21. Spyratos F, Ferrero-PM TM et al (2002) Correlation between MIB-1 and other proliferation marker clinical implications of the MIB-1 cutoff value. Cancer 94(8):2151–2159
22. Attiqa N, Nadeem Q, Georges V et al (2002) Prognostic factors in node-negative breast cancer a review of studies with sample size more than 200 and follow-up more than 5 years. Ann Surg 235:10–26
23. Ander U, Ian ES, Mitch D (2005) Proliferation marker Ki-67 in early breast cancer. J Clin Oncol 23:7212–7220
24. Azambuja E, Cardoso F, Castro G et al (2007) Ki-67 as prognostic marker in early breast cancer: a meta-analysis of published studies involving 12 155 patients. Br J Cancer 96:1504–1513
25. Weidner N, Semple JP, Welch WR et al (1991) Tumor angiogenesis and metastasis correlation in invasive breast carcinoma. N Engl J Med 324:1–8
26. Weidner N, Folkman J, Pozza F et al (1992) Tumor angiogenesis: a new significant and independent prognostic indicator in early-stage breast carcinoma. J Natl Cancer Inst 84:1875–1887
27. Morrow DA, Antman EM, Charlesworth A et al (2000) TIMI risk score for ST-elevation myocardial infarction: a convenient, bedside, clinical score for risk assessment at presentation: an intravenous nPA for treatment of infarcting myocardium early II trial substudy. Circulation 102(17):2031–2037
28. Matthew JE, Yu T, Jingqin L et al (2008) Outcome prediction for estrogen receptor-positive breast cancer based on postneoadjuvant endocrine therapy tumor characteristics. J Natl Cancer Inst 100:1380–1388
29. Wang S, Yang H, Tong F et al (2009) Response to neoadjuvant therapy and disease free survival in patients with triple-negative breast cancer. Gan To Kagaku Ryoho 36(2):255–258
30. Hugh J, Hanson J, Cheang MC et al (2009) Breast cancer subtypes and response to docetaxel in node-positive breast cancer: use of an immunohistochemical definition in the BCIRG 001 trial. J Clin Oncol 27(8):1168–1176
31. Edith A, Perez A, Aubrey T et al (2010) Adjuvant therapy of triple negative breast cancer. Breast Cancer Res Treat 120:285–291
32. Bryant HE, Schultz N, Thomas HD et al (2005) Specific killing of BRCA2-deficient tumours with inhibitors of poly (ADP-ribose) polymerase. Nature 434(7035):913–917
33. Ratnam K, Low JA (2007) Current development of clinical inhibitors of poly(ADP-ribose) polymerase in oncology. Clin Cancer Res 13(5):1383–1388
34. Yamamoto Y, Toi M, Kondo S et al (1996) Concentrations of vascular endothelial growth factor in the sera of normal controls and cancer patients. Clin Cancer Res 2:821–826
35. Adams J, Carder PJ, Downey S et al (2000) Vascular endothelial growth factor (VEGF) in breast cancer: comparison of plasma, serum, and tissue VEGF and microvessel density and effects of tamoxifen. Cancer Res 60:2898–2905
36. Foekens JA, Peters HA, Grebenchtchikov N et al (2001) High tumor levels of vascular endothelial growth factor predict poor response to systemic therapy in advanced breast cancer. Cancer Res 61:5407–5414
37. Linderholm BK, Hellborg H, Johansson U et al (2009) Significantly higher levels of vascular endothelial growth factor (VEGF) and shorter survival times for patients with primary operable triple-negative breast cancer. Ann Oncol 20(10):1639–1646
38. Miller K, Wang M, Gralow J et al (2007) Paclitaxel plus bevacizumab versus paclitaxel alone for metastatic breast cancer. N Engl J Med 357:2666–2676
39. Ryan PD, Tung NM, Isakoff SJ et al (2009) Neoadjuvant cisplatin and bevacizumab in triple negative breast cancer (TNBC): safety and efficacy. J Clin Oncol 27 (Suppl). (Abstr 551)
40. Steinbjørn H, Dorthe AG, Flemming BS et al (2000) The prognostic value of angiogenesis by Chalkley counting in a confirmatory study design on 836 breast cancer patients. Clin Cancer Res 6:139–146
41. Bernard U, Patrick N, Michel C et al (2004) Microvessel density as a prognostic factor in women with breast cancer: a systematic review of the literature and meta-analysis. Cancer Res 64:2941–2955
42. Mohammed RAA, Green A, El-Shikh S et al (2007) Prognostic significance of vascular endothelial cell growth factors-A, -C and -D in breast cancer and their relationship with angio- and lymphangiogenesis. Br J Cancer 96:1092–1100
43. Rabab A, Ian O, Somaia E et al (2009) Lymphatic and angiogenic characteristics in breast cancer: morphometric analysis and prognostic implications. Breast Cancer Res Treat 113:261–273
44. Nair L, Barbara S, Daniella V et al (2009) Vessel density assessed by endoglin expression in breast carcinomas with different expression profiles. Histopathology 55:594–599
45. Nieto Y, Woods J, Nawaz F et al (2007) Prognostic analysis of tumour angiogenesis, determined by microvessel density and expression of vascular endothelial growth factor, in high-risk primary breast cancer patients treated with high-dose chemotherapy. Br J Cancer 97:391–397
46. Acenero MJ, Gonzalez JF, Gallego MG et al (1998) Vascular enumeration as a significant prognosticator for invasive breast carcinoma. J Clin Oncol 16:1684–1688
47. Ana B, Pilar E, Rosa Z et al (2010) Triple-negative breast cancer: molecular features, pathogenesis, treatment and current lines of research. Cancer Treat Rev 36:206–215

Virchows Arch (2011) 458:73–84
DOI 10.1007/s00428-010-1013-6

ORIGINAL ARTICLE

Promoter CpG island hypermethylation during breast cancer progression

So Yeon Park · Hyeong Ju Kwon · Hee Eun Lee · Han Suk Ryu · Sung-Won Kim · Jee Hyun Kim · In Ah Kim · Namhee Jung · Nam-Yun Cho · Gyeong Hoon Kang

Received: 14 August 2010 / Revised: 11 November 2010 / Accepted: 12 November 2010 / Published online: 1 December 2010
© Springer-Verlag 2010

Abstract This study was designed to evaluate the changes in promoter CpG islands hypermethylation during breast cancer progression from pre-invasive lesions [flat epithelial atypia (FEA), atypical ductal hyperplasia (ADH), and ductal carcinoma in situ (DCIS)] to invasive ductal carcinoma (IDC). We performed MethyLight analysis for the methylation status of 57 promoter CpG island loci in 20 IDCs and their paired normal breast tissues. After selecting 15 CpG island loci showing breast cancer-specific DNA methylation, another set of normal breast tissue (n=10), ADH/FEA (n=30), DCIS (n=35), and IDC (n=30) of the breast were analyzed for these loci. We found six new methylation markers of breast cancer, namely *DLEC1*, *GRIN2B*, *HOXA1*, *MT1G*, *SFRP4*, and *TMEFF2*, in addition to *APC*, *GSTP1*, *HOXA10*, *IGF2*, *RARB*, *RASSF1A*, *RUNX3*, *SCGB3A1 (HIN-1)*, and *SFRP1*. The number of methylated genes increased stepwise from normal breast to ADH/FEA and DCIS, while IDC did not differ from DCIS. Methylation levels and frequencies of *APC*, *DLEC1*, *HOXA1*, and *RASSF1A* promoter CpG islands were significantly higher in ADH/FEA than in normal breast tissue. *GRIN2B*, *GSTP1*, *HOXA1*, *RARB*, *RUNX3*, *SFRP1*, and *TMEFF2* showed higher methylation levels and frequencies in DCIS than in ADH/FEA. DICS and IDC did not differ in the methylation levels or frequencies for most CpG island loci except *SFRP1* and *HOXA10*. Our findings showed that promoter CpG island methylation changed significantly in pre-invasive lesions, and was similar in IDC and DCIS, suggesting that CpG island methylation of tumor-related genes is an early event in breast cancer progression.

Keywords Breast cancer · Tumor progression · CpG islands · Methylation

S. Y. Park · H. J. Kwon · H. E. Lee · G. H. Kang (✉)
Department of Pathology,
Seoul National University College of Medicine,
28 Yongon-dong, Chongno-gu,
Seoul 110-744, South Korea
e-mail: ghkang@snu.ac.kr

S. Y. Park · H. S. Ryu
Department of Pathology,
Seoul National University Bundang Hospital,
Seongnam, Gyeonggi, South Korea

S. Y. Park · S.-W. Kim · J. H. Kim · I. A. Kim
Breast Care Center, Seoul National University Bundang Hospital,
Seongnam, Gyeonggi, South Korea

N. Jung · N.-Y. Cho · G. H. Kang
Laboratory of Epigenetics, Cancer Research Institute,
Seoul National University,
Seoul, South Korea

Introduction

Breast cancer is the most common malignancy in women in the Western world. It is generally accepted that breast cancers arise by a multistep process from normal epithelium to invasive cancer via the potential precursor lesions, atypical ductal hyperplasia, and in situ carcinoma, although it may not necessarily occur in a linear fashion [1,2]. Atypical ductal hyperplasia (ADH) is a neoplastic intraductal proliferative lesion with some but not all the characteristics of in situ carcinoma [3]. Ductal carcinoma in situ (DCIS) is a pre-invasive malignancy with diverse histologic features and molecular alterations [3]. Flat epithelial atypia (FEA), another pre-invasive atypical proliferative lesion of cuboidal to columnar epithelial cells with low grade cytologic atypia, is increasingly detected in breast core biopsy and commonly coexists with ADH or

low grade DCIS [4]. Clinical follow-up studies have shown that these pre-invasive lesions are associated with different levels of risk to develop invasive breast cancer that ranges from 1.3- to 2-fold of the reference population for FEA, 4–5-fold for ADH, and to 8–10-fold for DCIS [2–4].

Genetic analyses of cancer have demonstrated that tumor development involves the accumulation of a variety of genetic alterations including amplification of oncogenes and mutation or loss of tumor suppressor genes [1]. However, epigenetic changes as well as genetic changes are known to accumulate with tumor progression in multistep carcinogenesis [5–7]. Hypermethylation of promoter CpG islands represents an alternative mechanism for inactivating tumor suppressor genes and is known to be an early molecular event in carcinogenesis. Moreover, promoter CpG island hypermethylation is being investigated as an indicator of the risk of progression or development of cancer [5–7]. In breast cancer, promoter CpG island hypermethylation has been described for various genes controlling all aspects of cellular function [7]. However, most studies have focused on the methylation status of tumor-related genes in invasive breast cancer compared to normal breast tissue, and studies of the methylation in potential precursor lesions of breast cancer were rare.

Promoter methylation of *14-3-3 sigma* [8,9], *RASSF1A* [9–11], *GSTP1* [10,12], *APC1* [11], *HIN-1* [11], and *p16 (INK4a)* [13] has been reported in ductal hyperplasia. However, some studies have reported an increase of methylation levels or frequencies with progression to DCIS, while other analyses of the same tumor-related genes detected no difference between ductal hyperplasia and DCIS. Methylation studies of FEA was even rare, and only *p16 (INK4a)* promoter methylation has been reported in FEA [13]. Moreover, most of the studies focused on a single specific gene, or at most a few genes. With regard to epigenetic changes in DICS and IDC, it has been reported that promoter methylation in DCIS and IDC was not significantly different for the genes studied, except for a few genes including *CCND2*, *CDH1*, and *FOXC1* [9,12,14–17]. Lehmann et al. [9] reported that CCND2 showed variable patterns of methylation during tumor progression, while there were no changes in promoter methylation levels for *p16*, *RASSF1A*, and *14-3-3 sigma* in synchronous DCIS-IDCs. Hoque et al. [15] examined the methylation status of nine genes (*APC*, *CDH1*, *CTNNB1*, *TIMP3*, *ESR1*, *GSTP1*, *MGMT*, *THBS1*, and *TMS1*) in pre-invasive lesions (ADH and DCIS) and IDC, and found that only *CDH1* had higher methylation levels in invasive tumors than in ADH or DCIS. Recently, Muggerud et al. [17] reported that only *FOXC1* had significantly lower methylation levels in DCIS than in IDC based on quantitative DNA methylation analysis of 11 genes (*ABCB1*, *CDKN2A/p16^{INK4a}*, *ESR1*, *FOXC1*, *GSTP1*, *IGF2*, *MGMT*, *MLH1*, *PPP2R2B*, *PTEN*, and *RASSF1A*). However, these studies used different sets of methylation markers and different kind of samples, making it difficult to compare them.

In this study, we investigated promoter CpG islands hypermethylation during progression from FEA, ADH, and DCIS to invasive ductal carcinoma (IDC) of the breast, using a large number of CpG islands, and tried to identify specific changes in each step of tumorigenesis. For this purpose, we screened the methylation status of 57 CpG island loci in IDCs and paired normal breast tissue by MethyLight analysis. After selecting 15 CpG island loci showing breast cancer-specific DNA methylation, we analyzed the methylation status of another set of normal breast tissues, pre-invasive lesions (FEA, ADH, and DCIS) and IDCs of the breast, at these loci.

Materials and methods

Patients and tissue specimens

Formalin-fixed, paraffin-embedded archival tissue samples of 125 patients who underwent surgical resection of breast between 2007 and 2009 were obtained from the files of the Department of Pathology, Seoul National University Bundang Hospital. CpG island methylation status was initially determined on 20 IDCs and matched normal breast tissues adjacent to the IDCs as a tester set. Additional 30 IDCs, 35 pure DCISs, 20 ADHs (12 ADHs were associated with FEA), 10 FEAs, and 10 normal breast tissues from reduction mammoplasty specimens were examined as a validation set. All patients were female, with a median age of 48 (range, 27–80 years). Clinicopathologic information was obtained by reviewing pathology reports and hematoxylin- and eosin-stained sections. The following histopathologic variables were determined in the IDCs: histologic subtype, tumor size, T stage, N stage, Nottingham combined histologic grade, lymphovascular invasion, tumor border, and presence or absence of DCIS component. For pure DCIS cases, we recorded tumor size, nuclear grade (low, intermediate, or high), presence or absence of necrosis, and architectural pattern. All cases were independently reviewed by two breast pathologists (SYP and HEL). This study was approved by the institutional review board of Seoul National University Bundang Hospital (protocol # B-1005-100-302).

MethyLight analysis

Three to five serial sections (4-μm thick) from each representative paraffin block of the selected cases were stained with hematoxylin and eosin. Tumor areas with more

than 70% neoplastic cells and histologically normal breast tissue were marked and manually dissected under microscope. Dissected tissues were subjected to tissue lysis using proteinase K lysis buffer at 55°C for 24 h to 48 h. Bisulfite modification of the digested samples was performed using an EZ DNA methylation kit according to the manufacturer's specifications (Zymo Research, Orange, CA, USA). DNA methylation analyses were performed with the MethyLight assay [18]. From the 170 DNA methylation markers that had been tested previously [19,20], we selected 57 CpG DNA methylation markers that had been found to be hypermethylated in various cancers. First, we performed MethyLight analyses for the selected 57 DNA methylation markers in a tester set. After selecting the 15 CpG island loci showing breast cancer-specific DNA methylation, subsequent DNA methylation analysis were performed on another set of breast tissues. The DNA sequences of the MethyLight reaction primers and probes for these 15 CpG island loci are shown in Table 1. MethyLight PCR was performed as described previously. Briefly, PCR was performed in 30-μl volumes containing 0.2 mM deoxyribonucleotide triphosphates, 0.3 μM forward and reverse primers, 0.05 μM probe, 3.5 mM $MgCl_2$, 0.05% gelatin, 0.01% Tween-20, 1× PCR buffer, and 0.5 U of AmpliTaq Gold polymerase. The amplification conditions for all primers consisted of 95°C for 10 min, followed by 50 cycles of 95°C for 20 s and 59°C for 40 s. *ALU* repeats were used as an internal reference to normalize input DNA and to generate a standard curve. Bisulfite-modified placental genomic DNA treated with M.*Sss*I was used as a control reaction for the *ALU* repeat and selected promoter CpG loci. The percentage of methylated reference (PMR) for each genetic locus was calculated as 100 times the *GENE*/*ALU* methylation ratio of each sample divided by the *GENE*/*ALU* methylation ratio of reference DNA treated with M.*Sss*I. The methylation status of each sample was determined as positive when PMR >4, a cutoff value based on validated data [21].

Immunohistochemical analyses

Immunohistochemical analyses of standard prognostic biomarkers were performed on IDCs and DCIS. Four-micrometer-thick tissue sections were cut, dried, deparaffinized, and rehydrated following standard procedures. All the sections were subjected to heat-induced antigen retrieval in citrate (pH 6.0) buffer. Immunohistochemical staining was carried out in a DAKO Autostainer Plus (DakoCytomation, Glostrup, Denmark) using an LSAB detection kit (DakoCytomation). The following mouse monoclonal antibodies were used: estrogen receptor (ER, clone SP1, 1:100; Labvision, Fremont, CA, USA), progesterone receptor (PR, clone PgR 636, 1:70; Dako, Carpinteria, CA), p53 (clone DO-7, 1:600; Dako), and Ki-67 (clone MIB-1, 1:250; Dako). ER and PR were scored using the Allred scoring system [22], and a total score of three or more was regarded as positive. For p53 and Ki-67, cases with 10% or more positive staining were grouped as positive.

Fluorescence in situ hybridization (FISH) assays for HER2 gene amplification

To assess HER2 gene amplification in DCIS and IDC, PathVysion (Vysis, Downers Grove, IL, USA) assays were carried out and evaluated as previously described [23]. At least 50 cells were evaluated for each case, and the HER2 gene was considered to be amplified in tumors with ratio of HER-2 to CEP17 ≥2.2.

Statistical analysis

Statistical analysis was performed with SPSS software (version 12.0; SPSS Inc., Chicago, IL, USA). The chi-square test or Fisher's exact test was used when comparing frequencies between groups. For the 20 IDCs with matched normal breast tissue in the tester set, Wilcoxon signed-ranks tests were used to see if the (paired) difference between the PMR levels in the invasive tumor and normal breast tissue was significantly different from random. For the extended data set, differences in PMR values were evaluated with the Kruskal–Wallis and Mann–Whitney tests. *P* values less than 0.05 were considered statistically significant. All *p* values reported were two-sided.

Results

Identification of 15 CpG island loci showing breast cancer-specific DNA methylation

We prescreened the 57 CpG island loci on a tester set of 20 breast IDCs and their matched, cancer-associated normal breast (NBC) tissues to identify those markers that differentiate breast cancer from normal breast tissue. First, we removed five markers exhibiting PMR >4 or PMC ≤4 in all IDC and NBC samples. Second, we selected 15 CpG island loci that were methylated at a higher level or frequency in IDC than in NBC. Fourteen CpG island loci were more methylated in IDC than in NBC: *HOXA1*, *TMEFF2*, *MT1G*, *DLEC1*, *GSTP1*, *RARB*, *RASSF1A*, *GRIN2B*, *SFRP1*, *SFRP4*, *SCGB3A1 (HIN-1)*, *APC*, *HOXA10*, and *RUNX3* (in descending order of statistical significance). Eleven CpG island loci were more frequently hypermethylated (PMR >4) in IDC than in NBC: *GSTP1*, *HOXA1*, *MT1G*, *DLEC1*,

Table 1 MethyLight primers and probes

Genes	Primer and probe sequences	Size (bp)	Annealing temperature (°C)
APC	Forward: GAACCAAAACGCTCCCCAT Reverse: TTATATGTCGGTTACGTGCGTTTATAT	74	59
	Probe: 6FAM-CCCGTCGAAAACCCGCCGATTA-TAMRA		
DLEC1	Forward: TCGTTGCGTATTTAAGATATTTCGTATT Reverse: CGTAACGCTCATTCTCGCTACC	130	59
	Probe: 6FAM-TAATCAAACTTACGCTCACTTCGTCGCCG-TAMRA		
GRIN2B	Forward: GTCGGATTTACGCGTCGAGT Reverse: CTACCGCCGCGCTAAAATAC	83	59
	Probe: 6FAM-ACGCACGAAACTTCACCTACAACGTATCG-TAMRA		
GSTP1	Forward: GTCGGCGTCGTGATTTAGTATTG Reverse: AAACTACGACGACGAAACTCCAA	100	59
	Probe: 6FAM-AAACCTCGCGACCTCCGAACCTTATAAAA-TAMRA		
HOXA1	Forward: TTGTTTATTAGGAAGCGGTCGTC Reverse: TCGAACCATAAAATTACAACTTTCCA	83	59
	Probe: 6FAM-TCGTACGCGATCAACGCCAACAATTA-TAMRA		
HOXA10	Forward: ATCGGAAGTGCGTTATTTCGTG Reverse: TTCCGTCTCTCGACTCGAAACT	76	59
	Probe: 6FAM-CTCCGACCCAACCTAAACGCGCA-TAMRA		
IGF2	Forward: GAGCGGTTTCGGTGTCGTTA Reverse: CCAACTCGATTTAAACCGACG	88	59
	Probe: 6FAM-CCCTCTACCGTCGCGAACCCGA-TAMRA		
MT1G	Forward: CGTTTAAGGGATTTTGTATTTGGTTTAT Reverse: CCGCTAAATCCGCACCG	77	59
	Probe: 6FAM-CGCGATCCCGACCTAAACTATACGCA-TAMRA		
RARB	Forward: TTTATGCGAGTTGTTTGAGGATTG Reverse: CGAATCCTACCCCGACGATAC	86	59
	Probe: 6FAM-CTCGAATCGCTCGCGTTCTCGACAT-TAMRA		
RASSF1A	Forward: ATTGAGTTGCGGGAGTTGGT Reverse: ACACGCTCCAACCGAATACG	65	59
	Probe: 6FAM-CCCTTCCCAACGCGCCCA-TAMRA		
RUNX3	Forward: CGTTCGATGGTGGACGTGT Reverse: GACGAACAACGTCTTATTACAACGC	117	59
	Probe: 6FAM-CGCACGAACTCGCCTACGTAATCCG-TAMRA		
SCGB3A1 (HIN-1)	Forward: GGCGTAGCGGGCGTC Reverse: CTACGTAACCCTATCCTACAACTCCG	87	59
	Probe: 6FAM-CGAACTCCTAACGCGCACGATAAAACCTAA-TAMRA		
SFRP1	Forward: GAATTCGTTCGCGAGGGA Reverse: AAACGAACCGCACTCGTTACC	70	59
	Probe: 6FAM-CCGTCACCGACGCGAAAACCAAT-TAMRA		
SFRP4	Forward: GTTGTTCGGGCGGGTTC Reverse: GCGAAACTCCGCCGTCTA	79	59
	Probe: 6FAM-AAACACGAACAACGCCAACTCTCAACCT-TAMRA		
TMEFF	Forward: CGACGAGGAGGTGTAAGGATG Reverse: CAACGCCTAACGAACGAACC	73	59
	Probe: 6FAM-TATAACTTCCGCGACCGCCTCCTCCT-TAMRA		

GRIN2B, *SCGB3A1 (HIN-1)*, *SFRP1*, *TMEFF2*, *RARB*, *IGF2*, and *RUNX3* (in descending order of statistical significance). Altogether 15 CpG island loci showing cancer-specific methylation in terms of level or frequency were identified and used for further study: *APC*, *DLEC1*, *GRIN2B*, *GSTP1*, *HOXA1*, *HOXA10*, *IGF2*, *MT1G*, *RARB*, *RASSF1A*, *RUNX3*, *SCGB3A1 (HIN-1)*, *SFRP1*, *SFRP4*, and *TMEFF2*. Using this approach, we thus identified six novel methylation markers for the breast: *DLEC1*, *GRIN2B*, *HOXA1*, *MT1G*, *SFRP4*, and *TMEFF2*.

MethyLight analysis of the 15 CpG islands in normal breast, ADH/FEA, DCIS, and IDC

We performed MethyLight analysis of the15 selected CpG island loci on another set of normal breast from non-cancer patients (NBNC) (n=10), FEA (n=10), ADH (n=20), DCIS (n=35), and IDC (n=30), and we combined the results with those obtained with the tester set. The baseline characteristics of each group, including immunohistochemical data, are summarized in Table 2. The age distribution was similar in each group and the expression of ER, PR, HER-2, p53, and Ki-67 did not differ between DCIS and IDC.

According to the MethyLight analysis, the methylation levels and frequencies for 14 of the CpG islands were the same in NBC and NBNC; the exception was *TMEFF2,* whose methylation levels and frequency were higher in NBC [4.24 (3.41–6.99) vs. 2.53 (0.52–3.13), median (inter-quartile range, IQR), p=0.005 for levels; 55% vs.10%, p=0.024 for frequency]. Thus, NBC and NBNC were grouped together as normal breast (NB) for further analysis, except for the comparison of number of methylated genes. In addition, ADH and FEA did not show a difference in the methylation levels or frequencies for the 15 CpG islands tested and were grouped as ADH/FEA for further analysis.

The number of CpG island loci methylated (PMR >4) varied from 0 to 3 in the NBNC samples, 0 to 5 in the NBC samples, 0 to 8 in ADH/FEA samples, 2 to 11 in the DCIS samples, and 1 to 13 in the IDC samples. There was no difference between NBNC and NBC in the distribution of number of CpG island loci methylated. The number of CpG island loci methylated was significantly higher in ADH/FEA than in NB [2.5 (1.0–4.0) vs. 1.0 (0–2.0), median (IQR), p=0.006]. The median number of CpG island loci methylated in DCIS was 5.0 (IQR, 3.5–6.5), significantly higher than in NB and ADH/FEA (DCIS vs. NB, p<0.001; DCIS vs. ADH/FEA, p<0.001), and the median number of methylated CpG islands in IDC was 5.5 (IQR, 3.0–9.0), significantly higher than in both NB and ADH/FEA (IDC vs. NB, p<0.001; IDC vs. ADH/FEA, p<0.001), but not different from that in DCIS (Fig. 1).

Comparison of methylation of the 15 CpG islands in normal breast, ADH/FEA, DCIS, and IDC

Multiple comparisons among NB, ADH/FEA, DCIS, and IDC revealed differences in methylation frequency for all 15 CpG island loci, and in methylation level for 13 loci except *HOXA10* and *IGF2* (Tables 3 and 4; Fig. 2). All the CpG island loci except *IGF2* and *SFRP4* had methylation frequencies >20% in IDC, with the highest methylation frequency of 76% in *HOXA1*, *RASSF1A*, and *TMEFF2* (Table 4). The methylation frequencies for *APC*, *DLEC1*, *GRIN2B*, *GSTP1*, *HOXA1*, *IGF2*, *MT1G*, *RUNX3*, *SCGB3A1 (HIN-1)*, and *SFRP4* in IDC were more than five times higher than those for the respective genes in NB (Table 4).

Comparing NB with ADH/FEA, methylation levels of *APC* (p=0.026), *DLEC1* (p=0.005), *HOXA1* (p<0.001), *RASSF1A* (p<0.001), *SCGB3A1 (HIN-1)* (p=0.004), and *SFRP4* (p=0.021) were significantly higher in ADH/FEA than in NB and methylation frequencies were significantly higher for *APC* (p=0.038), *DLEC1* (p=0.010), *HOXA1* (p=0.010), and *RASSF1A* (p=0.015) (Tables 3 and 4; Fig. 3). Methylation of *APC*, *DLEC1*, *HOXA1*, *HOXA10*, *RARB*, *RASSF1A*, *SCGB3A1 (HIN-1)*, *SFRP1*, and *TMEFF2* was already detectible in NB tissue, but methylation of *GRIN2B*, *GSTP1*, *IGF2*, *MT1G*, *RUNX3*, and *SFRP4* was not (Table 4; Fig. 2). Methylation of *IGF2* and *RUNX3* was not found in ADH/FEA tissue either (Table 4; Fig. 2).

When ADH/FEA and DCIS were compared, CpG islands of *GRIN2B*, *GSTP1*, *HOXA1*, *RARB*, *RUNX3*, *SFRP1*, and *TMEFF2* showed significantly higher methylation levels and frequency in DCIS than in ADH/FEA (Tables 3 and 4; Fig. 4). *MT1G* showed higher methylation in DCIS than in ADH/FEA, only in the methylation levels (Table 3; Fig. 4). Comparing ADH/FEA and low grade DCIS, none of the CpG island loci showed difference in the methylation levels or frequencies.

Methylation levels and frequencies were the same in DCIS and IDC for most CpG island loci except *SFRP1* for levels and *HOXA10* for frequencies (Tables 3 and 4). *HOXA10* (p=0.056), *MT1G* (p=0.062), and *SFRP1* (p=0.057) had a tendency to display higher methylation levels or frequencies in IDC, compared to DCIS (Tables 3 and 4).

Association of CpG island methylation with histopathologic features of tumors

GRIN2B, *MT1G*, and *RARB* showed significantly higher methylation frequencies in grade III IDCs than in grade I and II IDCs (p=0.026, p=0.026, p=0.012, respectively), whereas *RASSF1A* revealed higher methylation frequency in grade I and II tumors (p=0.044). *DLEC1*, *RASSF1A*, and *SFRP1* displayed significant differences in methylation between ER-negative and ER-positive IDCs, with ER-positive tumors having higher methylation frequencies than ER-negative IDCs (p=0.037, p=0.007, p=0.014, respectively). *MT1G* and *RARB* methylation was significantly associated with a high Ki-67 proliferation index (p=0.026, p=0.006, respectively) (Table 5) and *RARB* methylation was also associated with high T stage [3/25 (12%) vs. 10/25 (40%), T1 vs. T2 and T3, p=0.024]. Other clinicopathologic factors including patients' age, N stage, and p53 overexpression were not associated with CpG island methylation.

Table 2 Baseline characteristics of specimens

		IDC (n=50)	DCIS (n=35)	ADH/FEA (n=30)	Normal (n=30)
Age	Mean (SD)	52.2 (10.1)	50.7 (11.2)	47.7 (8.1)	51.3 (10.0)
	Range	34–72	33–75	41–72	37–72
T stage	T1	25 (50)	NA	NA	NA
	T2 and T3	25 (50)	NA	NA	NA
N stage	N0	34 (68)	NA	NA	NA
	N1–N3	16 (32)	NA	NA	NA
Grade	1	12 (24)	8 (23)	NA	NA
	2	18 (36)	13 (37)	NA	NA
	3	20 (40)	14 (40)	NA	NA
Estrogen receptor	Negative	10 (20)	7 (20)	NA	NA
	Positive	40 (80)	28 (80)	NA	NA
Progesterone receptor	Negative	14 (28)	11 (31)	NA	NA
	Positive	36 (72)	24 (69)	NA	NA
HER-2[a]	Negative	43 (86)	27 (77)	NA	NA
	Positive	7 (14)	8 (23)	NA	NA
P53 overexpression	Absent	43 (86)	28 (80)	NA	NA
	Present	7 (14)	7 (20)	NA	NA
Ki-67 proliferation index	<10%	24 (48)	21 (60)	NA	NA
	≥10%	26 (52)	14 (40)	NA	NA

Numbers in parentheses indicate row percentage

IDC invasive ductal carcinoma, *DCIS* ductal carcinoma in situ, *ADH* atypical ductal hyperplasia, *FEA* flat epithelial atypia

[a] Determined by fluorescence in situ hybridization

APC and *RARB* showed significantly higher methylation frequencies in high grade DCIS than in low/intermediate grade DCIS (60% vs. 15%, p=0.006; 53% vs. 15%, p=0.027, respectively). DCIS showed an association between *DLEC1* methylation and HER-2 gene amplification, with HER-2 amplified DCIS having a higher frequency of *DLEC1* methylation than HER-2 non-amplified cases (75% vs. 26%, p=0.032). There were no associations between other clinicopathologic variables and CpG island methylation in DCIS.

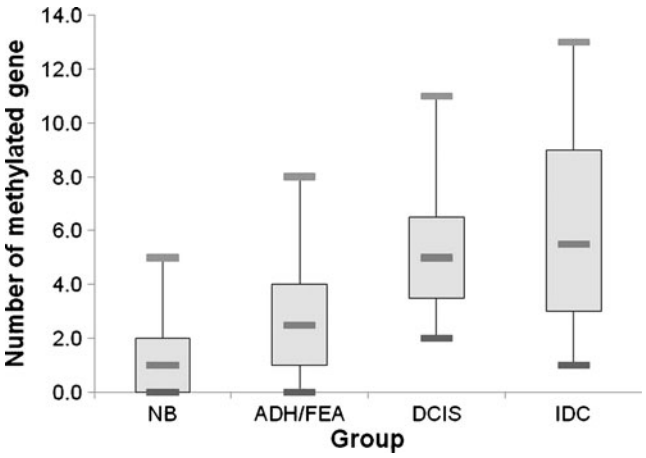

Fig. 1 Box plot depicting the number of methylated genes of the 15 CpG island loci tested in normal breast (*NB*), atypical ductal hyperplasia (*ADH*)/flat epithelial atypia (*FEA*), ductal carcinoma in situ (*DCIS*), and invasive ductal carcinoma (*IDC*). The *box* shows the 25th to 75th percentile, the *horizontal line* inside the box represents the median, and the *whiskers* extend to the minimum and maximum

Discussion

Although many studies have demonstrated that CpG island methylation plays an important role in breast cancer development, the results were quite variable. The different outcomes may be related to the use of different DNA methylation markers and methods of analysis. Moreover, although promoter CpG island methylation is well documented in invasive breast cancers, studies of methylation in the putative precursor lesions of breast cancer are rare. In the present study, we identified 15 breast cancer-specific methylation markers among 57 CpG island loci tested and analyzed the 15 selected CpG island loci in FEA, ADH, and DCIS as well as IDC. This approach revealed six new methylation markers for breast cancer, namely *DLEC1*, *GRIN2B*, *HOXA1*, *MT1G*, *SFRP4*, and *TMEFF2* in addition to others whose promoters were already known to be methylated in breast cancers [7,9–12,14–17,24–27].

Table 3 Comparison of the PMR values of the 15 analyzed genes in normal breast, atypical ductal hyperplasia/flat epithelial atypia, ductal carcinoma in situ, and invasive ductal carcinoma in the extended data samples

Gene	PMR value [median (inter-quartile range)]				*p* value[a]			
	NB (*n*=30)	ADH/FEA (*n*=30)	DCIS (*n*=35)	IDC (*n*=50)	All groups	NB vs. ADH/FEA	ADH/FEA vs. DCIS	DCIS vs. IDC
APC	0 (0)	0 (0–4.14)	0.07 (0–7.28)	0 (0–24.77)	0.011	0.026	0.374	0.772
DLEC1	0.03 (0–0.77)	1.11 (0.02–6.62)	0.51 (0–11.45)	2.05 (0–16.93)	0.018	0.005	0.869	0.574
GRIN2B	0 (0)	0 (0)	0 (0–3.53)	0.13 (0–9.76)	<0.001	0.363	0.002	0.313
GSTP1	0 (0)	0 (0)	0 (0–5.22)	0 (0–4.87)	0.001	0.936	0.004	0.801
HOXA1	0 (0–0.43)	2.37 (0.25–8.14)	13.72 (6.85–25.61)	22.87 (3.73–39.35)	<0.001	<0.001	<0.001.	0.173
HOXA10	0.01 (0–2.00)	0 (0–0.43)	0.02 (0–1.17)	0.69 (0–7.21)	0.057	0.502	0.551	0.056
IGF2	0 (0)	0 (0)	0 (0–0.19)	0 (0–0.22)	0.224	0.940	0.129	0.986
MT1G	0 (0–0.04)	0 (0–0.58)	0.44 (0–1.61)	0.42 (0–6.98)	0.001	0.380	0.012	0.749
RARB	0 (0–0.05)	0 (0–1.08)	1.48 (0–6.90)	0.42 (0–5.84)	<0.001	0.332	0.003	0.506
RASSF1A	0.59 (0–7.78)	11.62 (4.46–18.87)	12.96 (7.87–29.55)	18.23 (4.15–35.47)	<0.001	<0.001	0.234	0.538
RUNX3	0 (0)	0 (0)	0 (0–2.80)	0 (0–2.62)	0.003	0.044	0.029	0.472
SCGB3A1 (HIN-1)	0 (0)	0 (0–3.52)	0 (0–6.40)	0 (0–11.09)	0.003	0.004	0.422	0.706
SFRP1	0 (0–1.52)	0.01 (0–1.39)	0.92 (0–4.25)	3.44 (0–13.43)	<0.001	0.994	0.041	0.035
SFRP4	0 (0)	0 (0)	0 (0–0.33)	0 (0–2.72)	0.001	0.021	0.289	0.222
TMEFF2	3.54 (2.24–5.90)	3.88 (2.34–7.56)	11.49 (6.04–20.41)	14.60 (4.55–29.81)	<0.001	0.315	<0.001	0.509

NB normal breast, *ADH* atypical ductal hyperplasia, *FEA* flat epithelial atypia, *DCIS* ductal carcinoma in situ, *IDC* invasive ductal carcinoma, *PMR* percentage of methylated reference

[a] *p* values were calculated using Kruskal–Wallis and Mann–Whitney tests

Table 4 Comparison of methylation frequencies (PMR value >4) of the 15 analyzed genes in normal breast, atypical ductal hyperplasia/flat epithelial atypia, ductal carcinoma in situ, and invasive ductal carcinoma samples in the extended data samples

Gene	Methylation frequency (%)				*p* value[a]			
	NB (*n*=30)	ADH/FEA (*n*=30)	DCIS (*n*=35)	IDC (*n*=50)	All groups	NB vs. ADH/FEA	ADH/FEA vs. DCIS	DCIS vs. IDC
APC	7	27	34	38	0.019	0.038	0.507	0.726
DLEC1	7	33	37	40	0.012	0.010	0.749	0.790
GRIN2B	0	3	23	32	<0.001	1.000	0.031	0.357
GSTP1	0	3	31	28	<0.001	1.000	0.004	0.733
HOXA1	13	43	80	76	<0.001	0.010	0.002	0.663
HOXA10	10	3	9	34	0.001	0.612	0.618	0.007
IGF2	0	0	11	14	0.035	–	0.118	1.000
MT1G	0	7	14	32	0.001	0.492	0.437	0.062
RARB	7	7	31	26	0.012	1.000	0.013	0.584
RASSF1A	40	77	89	76	<0.001	0.004	0.202	0.144
RUNX3	0	0	17	24	0.002	–	0.027	0.446
SCGB3A1 (HIN-1)	3	23	34	36	0.008	0.052	0.416	0.871
SFRP1	13	3	26	46	<0.001	0.353	0.016	0.057
SFRP4	0	7	6	18	0.035	0.492	1.000	0.115
TMEFF2	40	47	86	76	<0.001	0.602	0.001	0.270

NB normal breast, *ADH* atypical ductal hyperplasia, *FEA* flat epithelial atypia, *DCIS* ductal carcinoma in situ, *IDC* invasive ductal carcinoma

[a] *p* values were calculated using chi-square test or Fisher's exact tests

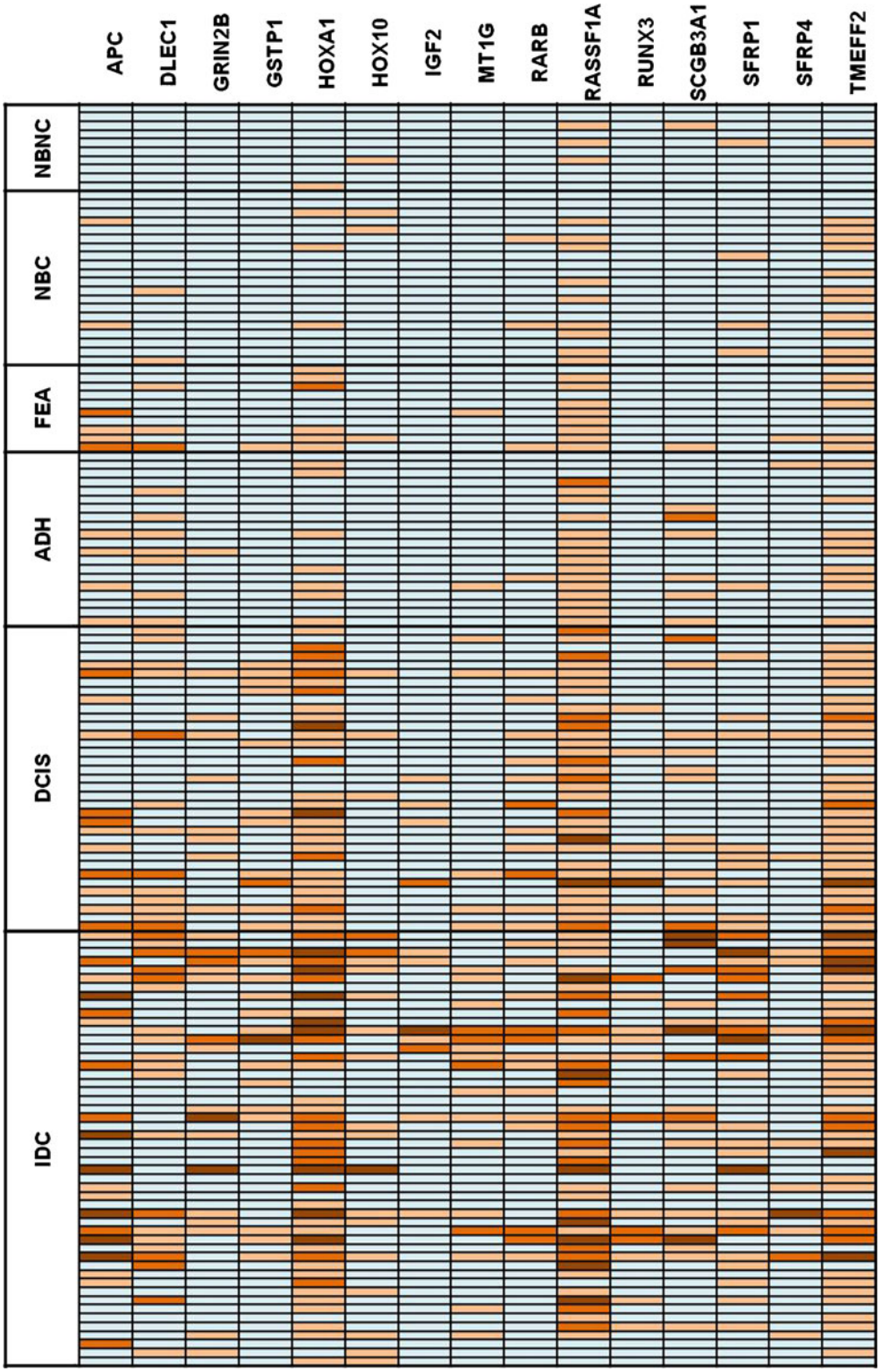

Fig. 2 Methylation map of the PMR values obtained for each CpG island locus in normal breast from non-cancer patients (NBNC), cancer-associated normal breast (NBC), flat epithelial atypia (FEA), atypical ductal hyperplasia (ADH), ductal carcinoma in situ (DCIS), and invasive ductal carcinoma (IDC). Colored boxed represent four classes of methylation levels [0<PMR<4 (light blue), 4≤PMR<20 (light orange), 20≤PMR<50 (orange), PMR≥50 (brown)]

We found that the number of methylated CpG island loci increased progressively from NB, ADH/FEA to DCIS, suggesting that epigenetic changes accumulate with the progression of breast cancer, as in the multistep carcinogenesis of other tissue type [28–30]. Based on our data of methylation levels and frequencies of the 15 CpG island loci in four disease groups (NB, ADH/FEA, DCIS, IDC), biologic role of promoter CpG island methylation of these genes during multistep carcinogenesis of breast cancer can be grouped as follows: (1) genes involved in the development of ADH/FEA, including *APC*, *DLEC1*, *HOXA1*, and *RASSF1A*; (2) genes involved in the progression of ADH/

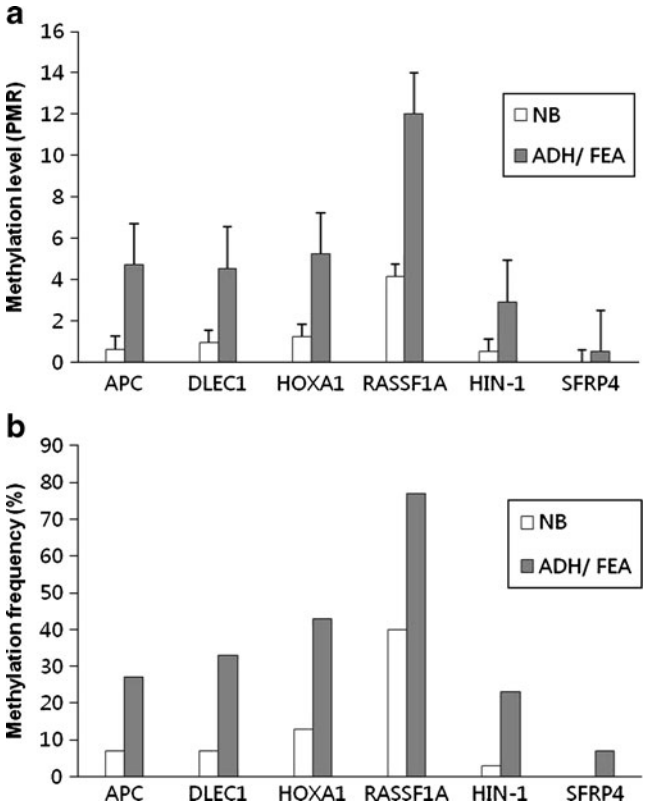

Fig. 3 Comparison of methylation levels (A) and frequencies (B) of CpG island loci between normal breast (NB) and atypical ductal hyperplasia (ADH)/flat epithelial atypia (FEA). Methylation levels are indicated as mean and SE (error bar). (A) Methylation levels of *APC*, *DLEC1*, *HOXA1*, *RASSF1A*, *SCGB3A1 (HIN-1)*, and *SFRP4* are significantly higher in ADH/FEA than in NB. (B) Methylation frequencies are significantly higher in ADH/FEA than in NB for *APC*, *DLEC1*, *HOXA1*, and *RASSF1A*, but not for *SCGB3A1 (HIN-1)* and *SFRP4*

FEA to DCIS, including *GRIN2B*, *GSTP1*, *HOXA1*, *RARB*, *RUNX3*, *SFRP1*, and *TMEFF2*; and (3) genes involved in the progression of DCIS to IDC, including *HOXA10* and *SFRP1*. Of the various stages of breast cancer progression, promoter CpG island methylation changed significantly during the progression of ADH/FEA to DCIS in this study. Considering that the only difference between ADH and low grade DCIS in histology is a quantitative one [3] and that ADH is generally regarded as the non-obligate precursor of low grade DCIS [31], our data seems to show much difference between ADH/FEA and DCIS. However, in this study, DCIS cases included large portion of high grade DCIS, which has been known to have different genetic alterations and gene expression patterns from low grade DCIS [32,33]. When ADH/FEA and low grade DCIS were compared, none of the CpG island loci showed significant difference in methylation, indicating that promoter CpG island methylation is an early event occurring in ADH/FEA stage during progression of low grade breast cancers. Ductal carcinoma in situ (DCIS) shows variations in the degree of differentiation and molecular alterations [3]. Allred et al. reported that multiple histologic grades, biomarker phenotypes, and intrinsic subtypes often coexist even in the same DCIS, suggesting that high grade DCIS gradually evolve from low grade DCIS by randomly acquiring additional genetic and epigenetic alterations [31]. We also showed that CpG islands methylation of *APC* and *RARB* was different according to the grade of DCIS, suggesting that DCIS is heterogeneous in epigenetic as well as genetic alterations.

DCIS is a well-established precursor lesion of IDC. It is frequently found adjacent to invasive breast cancers and exhibits gene expression patterns similar to those found in IDCs [33,34]. The present study demonstrated that most of the genes methylated in IDC were already methylated in DCIS, suggesting that DCIS and IDC share similar epigenetic as well as genetic alterations. This result is consistent with the previous study of Muggerud et al. [17] who preformed a quantitative DNA methylation analysis of 11 genes (*ABCB1*, *CDKN2A/p16*^{INK4a}, *ESR1*, *FOXC1*, *GSTP1*, *IGF2*, *MGMT*, *MLH1*, *PPP2R2B*, *PTEN*, and *RASSF1A*) in a series of DCIS and IDCs and found the

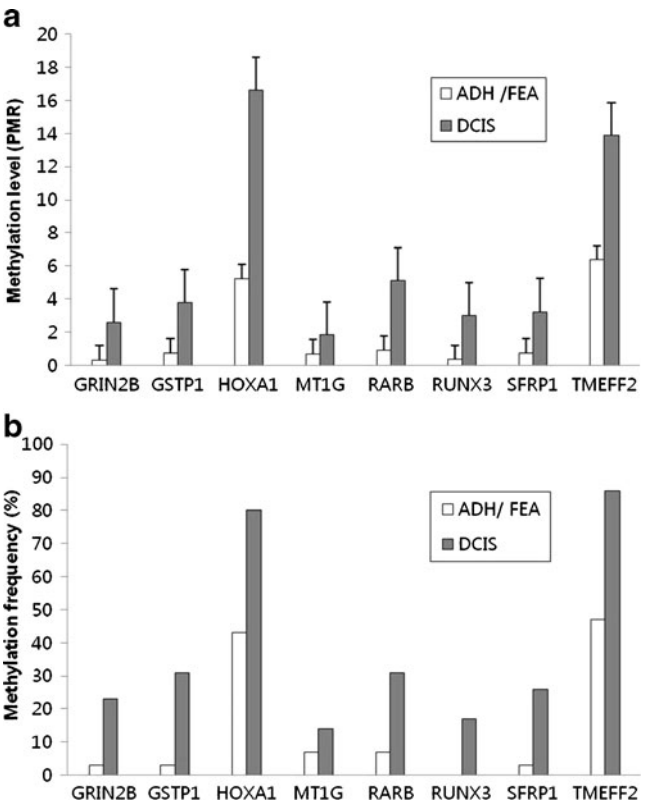

Fig. 4 Comparison of methylation levels (**a**) and frequencies (**b**) of CpG island loci between atypical ductal hyperplasia (*ADH*)/flat epithelial atypia (*FEA*) and ductal carcinoma in situ (*DCIS*). Methylation levels are indicated as mean and SE (*error bar*). Methylation levels and frequencies of *GRIN2B*, *GSTP1*, *HOXA1*, *RARB*, *RUNX3*, *SFRP1*, and *TMEFF2* are significantly higher in DCIS than in ADH/FEA. *MT1G* show higher methylation in DCIS compared to ADH/FEA, only for the methylation levels

Table 5 Methylation frequency (%) of CpG island loci in relation to clinicopathologic features of invasive ductal carcinoma of breast

Gene	Histologic grade			ER status			Ki-67 proliferation index		
	Grade I and II (n=30)	Grade III (n=20)	p value[a]	Negative (n=10)	Positive (n=40)	p value[a]	<10% (n=24)	≥10% (n=26)	p value[a]
APC	43	30	0.341	20	43	0.282	38	39	0.944
DLEC1	43	35	0.556	10	48	0.037	38	42	0.779
GRIN2B	20	50	0.026	50	28	0.256	21	42	0.104
GSTP1	20	40	0.123	20	30	0.704	17	39	0.086
HOXA1	77	75	1.000	60	80	0.225	71	81	0.411
HOXA10	27	45	0.180	40	33	0.717	29	39	0.488
IGF2	7	25	0.100	20	13	0.616	8	19	0.420
MT1G	20	50	0.026	40	30	0.707	17	46	0.026
RARB	13	45	0.012	30	25	0.707	8	42	0.006
RASSF1A	87	60	0.044	40	85	0.007	83	69	0.243
RUNX3	23	25	1.000	10	28	0.416	21	27	0.614
SCGB3A1 (HIN-1)	37	35	0.904	30	38	0.730	33	39	0.706
SFRP1	50	40	0.487	10	55	0.014	46	46	1.000
SFRP4	17	20	1.000	10	20	0.655	13	23	0.467
TMEFF2	80	70	0.506	60	80	0.225	79	73	0.614

ER estrogen receptor

[a] p values were calculated using the chi-square test or Fisher's exact tests

same frequency of methylation in DCIS as in IDC for all the genes except *FOXC1*. In the present study, 13 CpG island loci showed the same frequencies and levels of methylation in DCIS as in IDC, only *HOXA10* and *SFRP1* displaying higher methylation frequencies or levels in IDC than in DCIS. HOX genes are evolutionarily well conserved and act as regulators of embryonic development and differentiation [35], and a growing body of evidence points to their involvement in the pathogenesis of cancer. It has been reported that *HOXA10* expression is modulated by estradiol and tamoxifen in ER-positive breast cancer cell lines, and that its constitutive expression results in decreased breast cancer cell invasiveness, suggesting a regulatory role in breast cancer cell function [36]. Recently, Bloushtain-Qimron et al. [26] reported that methylation of *HOXA10* was higher in distant metastases than in primary tumors, implying a role in the progression of breast cancer. *SFRP1*, a tumor suppressor gene encoding a negative regulator of Wnt signaling pathway, has been reported to be frequently down-regulated in breast cancers by promoter hypermethylation, and its loss of expression was found to be associated with tumor stage and poor prognosis in early stage breast cancers [14,37]. Further studies are needed of the role of *HOXA10* and *SFRP1* in the progression of DCIS to IDC and the functional consequence of their methylations in breast cancers.

A novel finding of our study was the identification of promoter CpG island methylation of *DLEC1*, *GRIN2B*, *HOXA1*, *MT1G*, *SFRP4*, and *TMEFF2* in pre-invasive lesions of breast and in invasive breast cancers. Methylation frequencies were similar in DCIS and IDC for *DLEC1*, *GRIN2B*, *HOXA1*, *SFRP4*, and *TMEFF2*. *DLEC1* is a major 3p22.3 tumor suppressor gene and is reported to be frequently down-regulated by methylation in multiple cancers, including ovarian, lung, colorectal, and gastric cancers [20,38–40]. These findings, together with our results on *DLEC1* methylation in breast cancers and their precursor lesions, suggest that inactivation of *DLEC1* by promoter methylation plays an important role in the development of many types of tumor. The methalothionein gene family encodes a group of metal-binding proteins involved in several cellular processes, and whose expression is often deregulated in human cancers [41]. *MT1G* is reported to be down-regulated by promoter methylation in papillary thyroid carcinoma, prostate cancer, renal cell carcinoma, and gastric cancer [20,42–44]. In the present study, promoter CpG islands of *MT1G* tended to show a higher methylation frequency in IDC than in DCIS and was associated with IDCs of high histologic grade and high Ki-67 proliferation index, suggesting an association with tumor aggressiveness. Recent studies have demonstrated that CpG island hypermethylation of specific genes can be used as biomarkers of clinical outcome [5–7]. However, in the present study, the follow-up period was too short to reveal associations with clinical outcome. Thus, further extended studies are needed to investigate the potential value of *MT1G* as a prognostic marker of breast cancer.

We also detected a significant difference in the methylation frequencies of *DLEC1*, *RASSF1A*, and *SFRP1* in ER-positive and ER-negative IDCs, indicating that ER status may have an effect on epigenetic changes of certain genes. The association of *RASSF1A* methylation and ER positivity was reported in previous studies [17,45,46]. However, *APC*, *GSTP1*, and *SCGB3A1 (HIN-1)*, whose promoter methylation have been reported to be associated with ER positivity of breast cancer [45,46], failed to show any correlation with ER status in our study. This discrepancy may be due to differences in sample size and methylation analysis. Although we used the sensitive MethyLight assay for methylation analysis, our study is limited by the rarity of ER-negative cases (10 only). Recently, Lee et al. [47] reported that breast cancers shows different patterns of promoter methylation depending on their immunohistochemical subtypes. Thus, additional study would be desirable to evaluate the correlation of ER, HER-2, and subtype status of breast cancer with the 15 CpG island loci used in this study.

In summary, we studied the CpG island methylation of 15 tumor-related genes including six novel methylation markers of breast cancer and compared the methylation events during breast cancer progression. CpG island methylation was significantly changed in ADH/FEA and DCIS, and DCIS showed similar CpG island methylation to IDC. Our results suggest that CpG island methylation of tumor-related genes is an early event, predominantly occurring in pre-invasive stage of breast cancer and accumulates with breast cancer progression.

Acknowledgments This study was supported by a grant from the National R&D Program for Cancer Control, Ministry of Health & Welfare, Republic of Korea (0720540), and by a Priority Research Centers Program through the National Research Foundation of Korea (NRF), funded by the Ministry of Education, Science and Technology (2009-0093820).

Disclosure/conflict of interest The authors declare no conflict of interest.

References

1. Beckmann MW, Niederacher D, Schnürch HG, Gusterson BA, Bender HG (1997) Multistep carcinogenesis of breast cancer and tumour heterogeneity. J Mol Med 75:429–439
2. Dupont WD, Page DL (1985) Risk factors for breast cancer in women with proliferative breast disease. N Engl J Med 312:146–151
3. Tavassoli FA, Hoefler H, Rosai J, Holland R, Ellis IO, Schnitt SJ, Boecker W, Heywang-Köbrunner SH, Moinfar F, Lakhani SR (2003) Intraductal proliferative lesions. In: Tavassoli FA, Delvilee P (eds) World Health Organization classification of tumors: pathology and genetics of tumours of the breast and female genital organs. IARC, Lyon, pp 63–73
4. Schnitt SJ, Collins LC (2009) Columnar cell lesions and flat epithelial atypia. In: Biopsy interpretation of the breast. Lippincott Williams & Wilkins, Philadelphia, pp 96–122
5. Esteller M, Corn PG, Baylin SB, Herman JG (2001) A gene hypermethylation profile of human cancer. Cancer Res 61:3225–3229
6. Costello JF, Frühwald MC, Smiraglia DJ, Rush LJ, Robertson GP, Gao X, Wright FA, Feramisco JD, Peltomäki P, Lang JC, Schuller DE, Yu L, Bloomfield CD, Caligiuri MA, Yates A, Nishikawa R, Su Huang H, Petrelli NJ, Zhang X, O'Dorisio MS, Held WA, Cavenee WK, Plass C (2000) Aberrant CpG-island methylation has non-random and tumour-type-specific patterns. Nat Genet 24:132–138
7. Widschwendter M, Jones PA (2002) DNA methylation and breast carcinogenesis. Oncogene 21:5462–5482
8. Umbricht CB, Evron E, Gabrielson E, Ferguson A, Marks J, Sukumar S (2001) Hypermethylation of 14-3-3 sigma (stratifin) is an early event in breast cancer. Oncogene 20:3348–3353
9. Lehmann U, Länger F, Feist H, Glöckner S, Hasemeier B, Kreipe H (2002) Quantitative assessment of promoter hypermethylation during breast cancer development. Am J Pathol 160:605–612
10. Pasquali L, Bedeir A, Ringquist S, Styche A, Bhargava R, Trucco G (2007) Quantification of CpG island methylation in progressive breast lesions from normal to invasive carcinoma. Cancer Lett 257:136–144
11. Lee JS, Fackler MJ, Teo WW, Lee JH, Choi C, Park MH, Yoon JH, Zhang Z, Argani P, Sukumar S (2008) Quantitative promoter hypermethylation profiles of ductal carcinoma in situ in North American and Korean women: potential applications for diagnosis. Cancer Biol Ther 7:1398–1406
12. Lee JS (2007) GSTP1 promoter hypermethylation is an early event in breast carcinogenesis. Virchows Arch 450:637–642
13. Liu T, Niu Y, Feng Y, Niu R, Yu Y, Lv A, Yang Y (2008) Methylation of CpG islands of p16(INK4a) and cyclinD1 overexpression associated with progression of intraductal proliferative lesions of the breast. Hum Pathol 39:1637–1646
14. Lo P, Mehrotra J, D'Costa A, Fackler MJ, Garrett-Mayer E, Argani P, Sukumar S (2006) Epigenetic suppression of secreted frizzled related protein 1 (SFRP1) expression in human breast cancer. Cancer Biol Ther 5:281–286
15. Hoque MO, Prencipe M, Poeta ML, Barbano R, Valori VM, Copetti M, Gallo AP, Brait M, Maiello E, Apicella A, Rossiello R, Zito F, Stefania T, Paradiso A, Carella M, Dallapiccola B, Murgo R, Carosi I, Bisceglia M, Fazio VM, Sidransky D, Parrella P (2009) Changes in CpG islands promoter methylation patterns during ductal breast carcinoma progression. Cancer Epidemiol Biomark Prev 18:2694–2700
16. Subramaniam MM, Chan JY, Soong R, Ito K, Ito Y, Yeoh KG, Salto-Tellez M, Putti TC (2009) RUNX3 inactivation by frequent promoter hypermethylation and protein mislocalization constitute an early event in breast cancer progression. Breast Cancer Res Treat 113:113–121
17. Muggerud AA, Rønneberg JA, Wärnberg F, Botling J, Busato F, Jovanovic J, Solvang H, Bukholm I, Børresen-Dale A, Kristensen VN, Sørlie T, Tost J (2010) Frequent aberrant DNA methylation of ABCB1, FOXC1, PPP2R2B and PTEN in ductal carcinoma in situ and early invasive breast cancer. Breast Cancer Res 12:R3
18. Weisenberger DJ, Campan M, Long TI, Kim M, Woods C, Fiala E, Ehrlich M, Laird PW (2005) Analysis of repetitive element DNA methylation by MethyLight. Nucleic Acids Res 33:6823–6836
19. Weisenberger DJ, Siegmund KD, Campan M, Young J, Long TI, Faasse MA, Kang GH, Widschwendter M, Weener D, Buchanan D, Koh H, Simms L, Barker M, Leggett B, Levine J, Kim M, French AJ, Thibodeau SN, Jass J, Haile R, Laird PW (2006) CpG island methylator phenotype underlies sporadic microsatellite

instability and is tightly associated with BRAF mutation in colorectal cancer. Nat Genet 38:787–793
20. Kang GH, Lee S, Cho N, Gandamihardja T, Long TI, Weisenberger DJ, Campan M, Laird PW (2008) DNA methylation profiles of gastric carcinoma characterized by quantitative DNA methylation analysis. Lab Invest 88:161–170
21. Ogino S, Kawasaki T, Brahmandam M, Cantor M, Kirkner GJ, Spiegelman D, Makrigiorgos GM, Weisenberger DJ, Laird PW, Loda M, Fuchs CS (2006) Precision and performance characteristics of bisulfite conversion and real-time PCR (MethyLight) for quantitative DNA methylation analysis. J Mol Diagn 8:209–217
22. Harvey JM, Clark GM, Osborne CK, Allred DC (1999) Estrogen receptor status by immunohistochemistry is superior to the ligand-binding assay for predicting response to adjuvant endocrine therapy in breast cancer. J Clin Oncol 17:1474–1481
23. Hyun CL, Lee HE, Kim KS, Kim S, Kim JH, Choe G, Park SY (2008) The effect of chromosome 17 polysomy on HER-2/neu status in breast cancer. J Clin Pathol 61:317–321
24. Lee JS, Lo P, Fackler MJ, Argani P, Zhang Z, Garrett-Meyer E, Sukumar S (2007) A comparative study of Korean with Caucasian breast cancer reveals frequency of methylation in multiple genes correlates with breast cancer in young, ER, PR-negative breast cancer in Korean women. Cancer Biol Ther 6:1114–1120
25. Shigematsu H, Suzuki M, Takahashi T, Miyajima K, Toyooka S, Shivapurkar N, Tomlinson GE, Mastrangelo D, Pass HI, Brambilla E, Sathyanarayana UG, Czerniak B, Fujisawa T, Shimizu N, Gazdar A (2005) Aberrant methylation of HIN-1 (high in normal-1) is a frequent event in many human malignancies. Int J Cancer 113:600–604
26. Bloushtain-Qimron N, Yao J, Snyder EL, Shipitsin M, Campbell LL, Mani SA, Hu M, Chen H, Ustyansky V, Antosiewicz JE, Argani P, Halushka MK, Thomson JA, Pharoah P, Porgador A, Sukumar S, Parsons R, Richardson AL, Stampfer MR, Gelman RS, Nikolskaya T, Nikolsky Y, Polyak K (2008) Cell type-specific DNA methylation patterns in the human breast. Proc Natl Acad Sci USA 105:14076–14081
27. Krop IE, Sgroi D, Porter DA, Lunetta KL, LeVangie R, Seth P, Kaelin CM, Rhei E, Bosenberg M, Schnitt S, Marks JR, Pagon Z, Belina D, Razumovic J, Polyak K (2001) HIN-1, a putative cytokine highly expressed in normal but not cancerous mammary epithelial cells. Proc Natl Acad Sci USA 98:9796–9801
28. Kang GH, Lee S, Kim J, Jung H (2003) Profile of aberrant CpG island methylation along multistep gastric carcinogenesis. Lab Invest 83:519–526
29. Kang GH, Lee S, Lee HJ, Hwang K (2004) Aberrant CpG island hypermethylation of multiple genes in prostate cancer and prostatic intraepithelial neoplasia. J Pathol 202:233–240
30. Lee S, Lee HJ, Kim J, Lee H, Jang JJ, Kang GH (2003) Aberrant CpG island hypermethylation along multistep hepatocarcinogenesis. Am J Pathol 163:1371–1378
31. Allred DC, Wu Y, Mao S, Nagtegaal ID, Lee S, Perou CM, Mohsin SK, O'Connell P, Tsimelzon A, Medina D (2008) Ductal carcinoma in situ and the emergence of diversity during breast cancer evolution. Clin Cancer Res 14:370–378
32. Hwang ES, DeVries S, Chew KL, Moore DH 2nd, Kerlikowske K, Thor A, Ljung BM, Waldman FM (2004) Patterns of chromosomal alterations in breast ductal carcinoma in situ. Clin Cancer Res 10:5160–5167
33. Adeyinka A, Emberley E, Niu Y, Snell L, Murphy LC, Sowter H, Wykoff CC, Harris AL, Watson PH (2002) Analysis of gene expression in ductal carcinoma in situ of the breast. Clin Cancer Res 8:3788–3795
34. Ma XJ, Salunga R, Tuggle JT, Gaudet J, Enright E, McQuary P, Payette T, Pistone M, Stecker K, Zhang BM, Zhou YX, Varnholt H, Smith B, Gadd M, Chatfield E, Kessler J, Baer TM, Erlander MG, Sgroi DC (2003) Gene expression profiles of human breast cancer progression. Proc Natl Acad Sci USA 100:5974–5979
35. McGinnis W, Krumlauf R (1992) Homeobox genes and axial patterning. Cell 68:283–302
36. Chu MC, Selam FB, Taylor HS (2004) HOXA10 regulates p53 expression and matrigel invasion in human breast cancer cells. Cancer Biol Ther 3:568–572
37. Klopocki E, Kristiansen G, Wild PJ, Klaman I, Castanos-Velez E, Singer G, Stöhr R, Simon R, Sauter G, Leibiger H, Essers L, Weber B, Hermann K, Rosenthal A, Hartmann A, Dahl E (2004) Loss of SFRP1 is associated with breast cancer progression and poor prognosis in early stage tumors. Int J Oncol 25:641–649
38. Kwong J, Lee J, Wong K, Zhou X, Wong DTW, Lo K, Welch WR, Berkowitz RS, Mok SC (2006) Candidate tumor-suppressor gene DLEC1 is frequently downregulated by promoter hypermethylation and histone hypoacetylation in human epithelial ovarian cancer. Neoplasia 8:268–278
39. Seng TJ, Currey N, Cooper WA, Lee C, Chan C, Horvath L, Sutherland RL, Kennedy C, McCaughan B, Kohonen-Corish MRJ (2008) DLEC1 and MLH1 promoter methylation are associated with poor prognosis in non-small cell lung carcinoma. Br J Cancer 99:375–382
40. Ying J, Poon FF, Yu J, Geng H, Wong AHY, Qiu G, Goh HK, Rha SY, Tian L, Chan ATC, Sung JJY, Tao Q (2009) DLEC1 is a functional 3p22.3 tumour suppressor silenced by promoter CpG methylation in colon and gastric cancers. Br J Cancer 100:663–669
41. Ferrario C, Lavagni P, Gariboldi M, Miranda C, Losa M, Cleris L, Formelli F, Pilotti S, Pierotti MA, Greco A (2008) Metallothionein 1G acts as an oncosupressor in papillary thyroid carcinoma. Lab Invest 88:474–481
42. Huang Y, de la Chapelle A, Pellegata NS (2003) Hypermethylation, but not LOH, is associated with the low expression of MT1G and CRABP1 in papillary thyroid carcinoma. Int J Cancer 104:735–744
43. Henrique R, Jerónimo C, Hoque MO, Nomoto S, Carvalho AL, Costa VL, Oliveira J, Teixeira MR, Lopes C, Sidransky D (2005) MT1G hypermethylation is associated with higher tumor stage in prostate cancer. Cancer Epidemiol Biomark Prev 14:1274–1278
44. Dalgin GS, Drever M, Williams T, King T, DeLisi C, Liou LS (2008) Identification of novel epigenetic markers for clear cell renal cell carcinoma. J Urol 180:1126–1130
45. Feng W, Shen L, Wen S, Rosen DG, Jelinek J, Hu X, Huan S, Huang M, Liu J, Sahin AA, Hunt KK, Bast RC, Shen Y, Issa JJ, Yu Y (2007) Correlation between CpG methylation profiles and hormone receptor status in breast cancers. Breast Cancer Res 9:R57
46. Sunami E, Shinozaki M, Sim M, Nguyen SL, Vu A, Giuliano AE, Hoon DSB (2008) Estrogen receptor and HER2/neu status affect epigenetic differences of tumor-related genes in primary breast tumors. Breast Cancer Res 10:R46
47. Lee JS, Fackler MJ, Lee JH, Choi C, Park MH, Yoon JH, Zhang Z, Sukumar S (2010) Basal-like breast cancer displays distinct patterns of promoter methylation. Cancer Biol Ther 9:1017–1024

Virchows Arch (2011) 458:85–94
DOI 10.1007/s00428-010-1002-9

ORIGINAL ARTICLE

Expression and localization of E-cadherin and β-catenin in uterine carcinosarcoma

Izumi Nishimura · Yoshihiro Ohishi · Yoshinao Oda · Junji Kishimoto · Masafumi Yasunaga · Emi Okuma · Hiroaki Kobayashi · Norio Wake · Masazumi Tsuneyoshi

Received: 8 May 2010 / Revised: 10 October 2010 / Accepted: 14 October 2010 / Published online: 3 November 2010
© Springer-Verlag 2010

Abstract This study was designed to analyze the subcellular localization of E-cadherin and β-catenin both of which play a critical role in cell–cell adhesion in uterine carcinosarcoma (UCS). We performed an immunohistochemical reaction analysis of the subcellular localization of E-cadherin and β-catenin proteins in 46 cases of UCSs consisting of 28 UCSs with heterologous sarcoma and 18 UCSs with homologous sarcoma and compared their clinicopathological features. In most UCSs, membranous expression of E-cadherin and β-catenin was completely lost in sarcomatous components, but it was preserved in carcinomatous components. Nuclear β-catenin expression was observed significantly more frequently in sarcomatous components (31/46, 67.4%) than in carcinomatous components (22/46, 47.8%; P=0.0025). In sarcomatous components, nuclear β-catenin expression was found significantly more frequently in heterologous sarcoma (23/28, 82.1%) than in homologous sarcoma (8/18, 44.4%; P=0.0279). The stage was the only independent prognostic significant factor. These results suggest that reduced membranous expression of E-cadherin and β-catenin may contribute to the biphasic morphology of UCS. Furthermore, although the precise mechanism is unclear, nuclear β-catenin expression in sarcomatous components may also be associated with biphasic morphology and heterologous sarcomatous differentiation.

Keywords Carcinosarcoma · β-catenin · E-cadherin · Cyclin D1 · Immunohistochemistry · Morphology

I. Nishimura · Y. Ohishi (✉) · Y. Oda · M. Yasunaga · E. Okuma · M. Tsuneyoshi
Department of Anatomic Pathology,
Graduate School of Medical Sciences,
Kyushu University,
Maidashi 3-1-1, Higashi-ku,
Fukuoka 812-8582, Japan
e-mail: yohishi@surgpath.med.kyushu-u.ac.jp

Y. Ohishi
Department of Diagnostic Laboratory,
Kyushu University Hospital at Beppu,
Beppu, Japan

J. Kishimoto
Digital Medicine Initiative, Kyushu University,
Fukuoka, Japan

H. Kobayashi · N. Wake
Department of Gynecology and Obstetrics,
Graduate School of Medical Sciences, Kyushu University,
Fukuoka, Japan

Introduction

Uterine carcinosarcoma (UCS) is a rare, highly aggressive neoplasm that accounts for no more than 5% of all malignancies of the uterus [1, 2]. Despite their relatively low incidence, this aggressive tumor represents a significant clinical problem. Histologically, UCS is a biphasic tumor characterized by an admixture of carcinomatous and sarcomatous components, and both components are usually high grade. In addition, sarcomatous components may be either homologous or heterologous, with approximately half being of one type and half being of the other [1].

Clinical, pathological, and molecular evidences indicate that most UCSs are monoclonal in origin and undergo differentiation in separate epithelial and mesenchymal directions [1–4]. McCluggage proposed that UCSs were actually metaplastic carcinomas, carcinomas with sarcomatous metaplasia, in which the sarcomatous components were derived as a result of dedifferentiation [2, 4–7]. In this context, it has been reported that epithelial–mesenchymal

Table 1 E-cadherin and β-catenin membranous expression

		Reduced expression				Preserved expression			*P* value[a]
	Score	0	2	3	4	5	6	7	
E-cadherin	Carcinomatous components	1	1	3	9	20	8	4	<0.01
	Sarcomatous components	44	0	2	0	0	0	0	
β-catenin	Carcinomatous components	1	1	4	6	14	9	11	<0.01
	Sarcomatous components	36	3	5	2	0	0	0	

[a] *P* value by the Wilcoxon signed-rank test

transition (EMT) could best describe the origin of the sarcoma-like components of sarcomatoid carcinoma [8, 9].

The loss of E-cadherin expression seems to play an important role in EMT, and E-cadherin is therefore emerging as one of the caretakers of the epithelial phenotype [10]. Reduced E-cadherin expression has also been shown to cause morphological changes in epithelial cells, altering their phenotype from more epithelial features to more fibroblastic [11, 12]. β-catenin is involved in the control of cell–cell adhesion and binds directly to the cytoplasmic tail of E-cadherin [13]. Reduced expression of β-catenin as well as E-cadherin is associated with the characteristics of invasiveness and loss of differentiation [11, 12, 14, 15].

In addition to its adhesive functions, β-catenin is also a multifunctional protein that is involved in the Wnt signaling pathway [16]. Intracellular β-catenin accumulation eventually results in its nuclear translocation. Nuclear β-catenin accumulation could serve as a transcription factor activator, followed by increased expression of conventional Wnt target genes such as cyclin D1 [17]. In the Wnt signaling pathway, accumulated β-catenin in the nucleus behaves as an oncoprotein. In fact, nuclear accumulation of β-catenin has been observed in various cancers, and the deregulation of β-catenin may be associated with the development and progression of a wide range of many human malignancies [18–21].

Several studies have shown a significant correlation between β-catenin gene mutation and its nuclear protein accumulation, but tumors without mutation also showed nuclear accumulation [19, 22, 23]. Additional alterations may be required for the nuclear accumulation of β-catenin, as well as the altered expression of genes that interact with β-catenin, such as E-cadherin, which has been shown to influence the intracellular localization of β-catenin [24]. In addition, Saegusa et al. reported that immunohistochemical analysis was more accurate than PCR-based assays for assessing actual levels of β-catenin protein in endometrial carcinoma, even if PCR-based assays were more sensitive [20].

The relationships between the expression profiles of adhesion molecules (E-cadherin and β-catenin) and both clinicopathological features and the occurrence of nuclear β-catenin accumulation in UCS have not been fully clarified. Accordingly, we have investigated the subcellular localization of E-cadherin and β-catenin in UCS, and compared the results with the associated clinicopathological features. Furthermore, cyclin D1, which is known as a target of the Wnt/β-catenin signal [17], was also investigated.

Materials and methods

Patients

Forty-six cases of primary carcinosarcoma of the uterus were selected from the files of the Department of Anatomic Pathology and the Department of Gynecology and Obstetrics, the Graduate School of Medical Sciences, Kyushu University. Epithelioid variants of leiomyosarcoma and endometrial stromal sarcoma, uterine tumor resembling ovarian sex cord tumor, low-grade endometrioid adenocarcinoma with biphasic appearance (corded and hyalinized variant or spindle cell change of endometrioid adenocarcinoma), adenosarcoma, and atypical polypoid adenomyoma were carefully excluded from this study. All cases were staged according to the International Federation of Gyne-

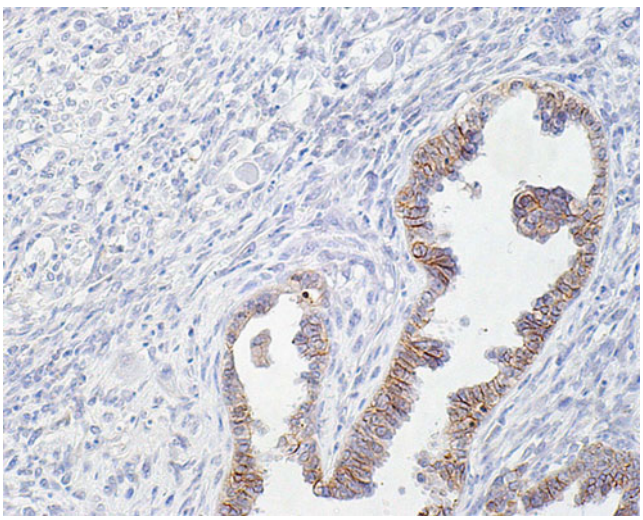

Fig. 1 Membranous expression of E-cadherin. Membranous E-cadherin expression was well preserved in carcinomatous components. In contrast, E-cadherin staining was not observed in sarcomatous components

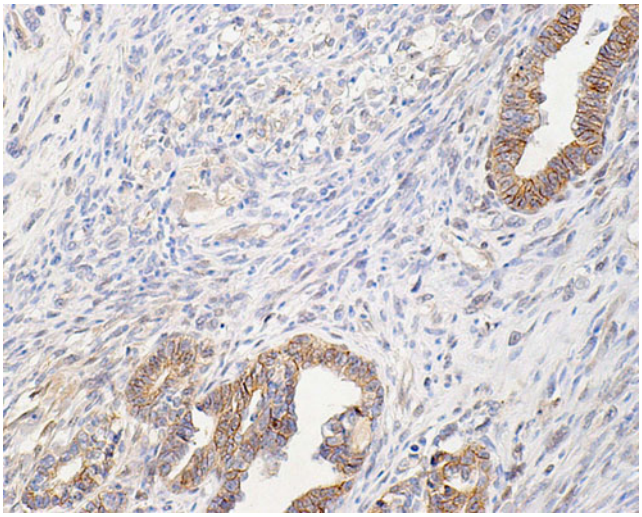

Fig. 2 Membranous expression of β-catenin. Membranous β-catenin expression was also well preserved in carcinomatous components. In sarcomatous components, membranous β-catenin expression was lost, although cytoplasmic β-catenin expression was focally observed

cology and Obstetrics (FIGO) staging system. All samples were obtained by surgery between 1982 and 2006 and were fixed in 10% phosphate-buffered formalin and embedded in paraffin. Serial sections of 3 μm thickness were made for hematoxylin and eosin staining and for immunohistochemistry. With respect to the categorization of a tissue sample as being a "predominantly glandular but cytologically high-grade adenocarcinoma," in analyses of the carcinomatous component of each tumor, we utilized the following policy: Adenocarcinomatous glands with gaping structure, undulating luminal margin, and marked nuclear pleomorphism were deemed to be serous type. Adenocarcinomatous glands with relatively tall columnar epithelium, sharp luminal margin, nuclear stratification, and hyperchromatic and enlarged but not markedly pleomorphic nuclei (mid-range pleomorphism) were identified upgraded endometrioid type.

Immunohistochemistry

Immunohistochemical study was performed using mouse IgG monoclonal antibodies against E-cadherin (clone 36, BD Transduction Laboratories, San Jose, CA, USA, 1:1,000) and β-catenin (clone 14, BD Transduction Laboratories, 1:200), and cyclin D1 (clone SP4, Thermo Scientific, CA, USA, 1:50). After antigen was retrieved by a microwave oven technique, the sections were incubated with primary antibodies at 4°C overnight, followed by the use of a streptavidin–biotin–peroxidase kit (Nichirei, Tokyo, Japan) and hematoxylin counterstaining.

Evaluation of expression

Immunohistochemical reaction was evaluated independently by two pathologists (IN and YO). Membranous expression of β-catenin and E-cadherin was semiquantitatively estimated using a scoring protocol as previously reported [25, 26]; briefly, an expression intensity score (on a scale of 0 to 3) and the percentage of positive cells (on a scale of 0 to 4). Scoring categories were defined with composite scores ranging from 0 to 4 (reduced expression) and from 5 to 7 (preserved expression). In accordance with a previous study [20, 21], nuclear expression was considered positive if at least 1% of the cells showed nuclear immunopositivity. If more than 25% of cells were stained, this was considered "diffuse positive"; less than 25% staining was considered "focal positive." The percentage of cyclin D1-immunoreactive cells was evaluated, and its

Table 2 Correlation between clinicopathological parameters and nuclear β-catenin expression

		Carcinomatous components			Sarcomatous components			
	Negative	Focal positive	Diffuse positive	*P* value[a]	Negative	Focal positive	Diffuse positive	*P* value[a]
Age (*n*=46)								
65 (years) >	14	6	3	N.S.	9	5	9	N.S.
65 (years) ≤	10	12	1		6	8	9	
Size (*n*=44)								
50 (mm) >	9	5	0	N.S.	5	5	4	N.S.
50 (mm) ≤	14	12	4		9	7	14	
Stage (*n*=44)								
I, II	9	7	1	N.S.	5	8	4	N.S.
III, IV	15	9	3		10	4	13	
Sarcoma subtype (*n*=46)								
Homologous	8	6	4	0.0331	10	3	5	0.0279
Heterologous	16	12	0		5	10	12	

[a] *P* value by the Fisher's exact probability test

Table 3 Nuclear β-catenin expression

β-catenin	Negative (<1%)	Focal positive (1~24%)	Diffuse positive (≥25%)	*P* value[a]
Carcinomatous components	24	18	4	0.0025
Sarcomatous components	15	13	18	

[a] *P* value by the Fisher's exact probability test

overexpression was determined to be positive if more than 5% of the tumor cells exhibited positive nuclear expression [27].

Statistical analysis

The survival curves were analyzed by the Kaplan–Meier method, and the outcomes of the different patient groups were compared by the log-rank test. The Cox proportional hazards regression with the nonstepwise procedure was used in multivariate analysis of the survival data. The correlations between β-catenin and E-cadherin expression and carcinomatous/sarcomatous components were evaluated using the Wilcoxon signed-rank test. The correlations between β-catenin and E-cadherin or cyclin D1 expression and each parameter were evaluated using Fisher's exact probability test or Mann–Whitney *U* test. Statistical correlations between immunostaining counts were assessed by the Spearman rank correlation test. The significance level was defined as a *P* value <0.05.

Results

Clinical features

Patient ages ranged from 45 to 83 years (mean, 64.6 years). A total abdominal hysterectomy with bilateral salpingo-oophorectomy was performed in 36 patients. One patient underwent a supravaginal hysterectomy with bilateral salpingo-oophorectomy. Seven patients underwent radical abdominal hysterectomy. Lymph node dissection was performed in 35 patients. Nine cases underwent operation without lymphadenectomy and therefore were staged clinically. Detailed operative records were not available in two patients. After surgery, a total of 18 patients had received chemotherapy. One patient had neoadjuvant chemotherapy, seven had external radiation treatment to the pelvis, one received chemotherapy and radiation, and 11 received no treatment after surgery. One patient had undergone pelvic irradiation for uterine cervical carcinoma 18 years before presentation, and therefore, she had received supravaginal hysterectomy. The tumors ranged in greatest diameter from 0.8 to 15 cm in 44 patients, tumor diameter was not recorded for the remaining two patients. Seventeen patients had stage I tumors, 15 stage III, and 12 stage IV tumors. The surgical stage was not recorded for the remaining two patients. There were 16 patients with pelvic lymph node metastasis. Survival data were available for 42 cases, with follow-up periods ranging from 0.5 to 136 months (mean 27.1 months, median 17.5 months). Twenty-three patients died of disease following surgery. One patient died of other causes 21 months after surgery. Five patients were alive with disease and 14 were alive with no evidence of disease following surgery. Follow-up information could not be obtained in four patients. The median progression-free survival of 42 patients was 10.5 months (range, 0.5–136 months), whereas the median overall survival was 17.5 months (range, 0.5–136 months). The median follow-up of those patients who are currently progression-free is 53.0 months (range, 1.5–136 months).

Microscopic findings

Histologically, all tumors were composed of carcinomatous and sarcomatous components and showed biphasic appearance.

When the carcinomatous component of each tumor was analyzed separately, the majority of cases were FIGO grade 2 or 3 carcinoma (43 cases, 93%). The most common histologic subtype was endometrioid adenocarcinoma (26 cases; G1 3, G2 13, G3 10 cases). The second most

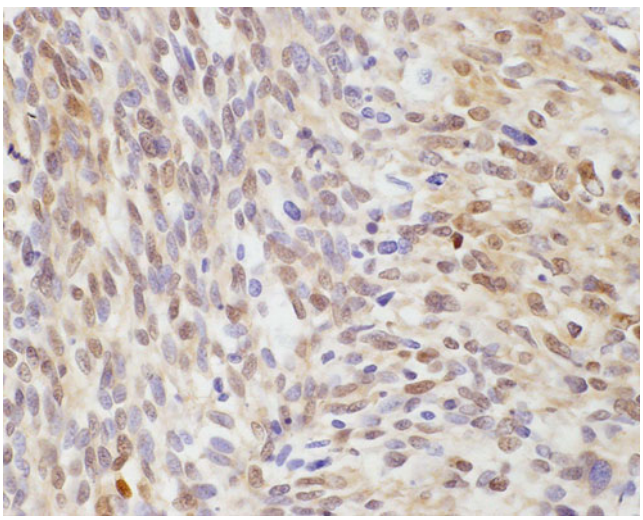

Fig. 3 Representative immunohistochemical analyses of nuclear β-catenin accumulation in UCSs. Diffuse nuclear β-catenin expression was observed in relatively less pleomorphic rounded sarcomatous cells in UCSs with both homologous and heterologous sarcoma

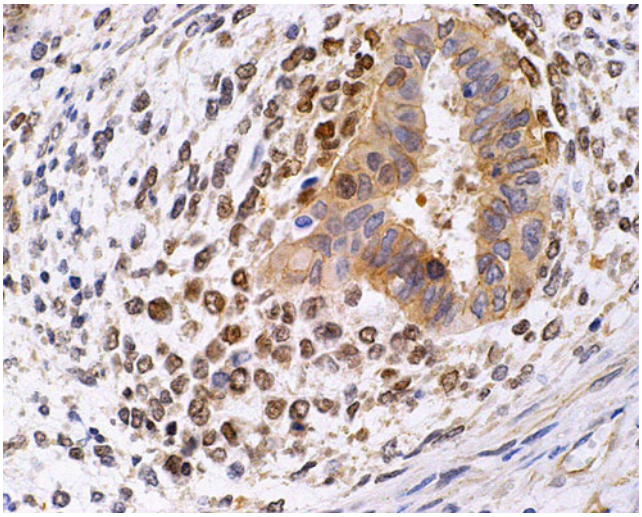

Fig. 4 Representative immunohistochemical analyses of nuclear β-catenin accumulation in UCSs. Focal nuclear β-catenin expression was conspicuous in rounded sarcomatous cells surrounding the carcinomatous glands in UCSs with both homologous and heterologous sarcoma

common histologic subtypes were serous and mixed epithelial carcinomas (nine cases each). Samples from all of the nine mixed epithelial carcinoma components showed either an endometrioid type (eight cases), a serous type (eight cases), a clear cell type (three cases), or some combination thereof. Squamous differentiation was observed in ten cases. In two cases, the determination of adenocarcinoma subtype was difficult, since the size of the adenocarcinomatous components was exceedingly small. The adenocarcinomatous components of the two cases were judged as "high-grade" simply due to the presence of high-grade nuclear atypia.

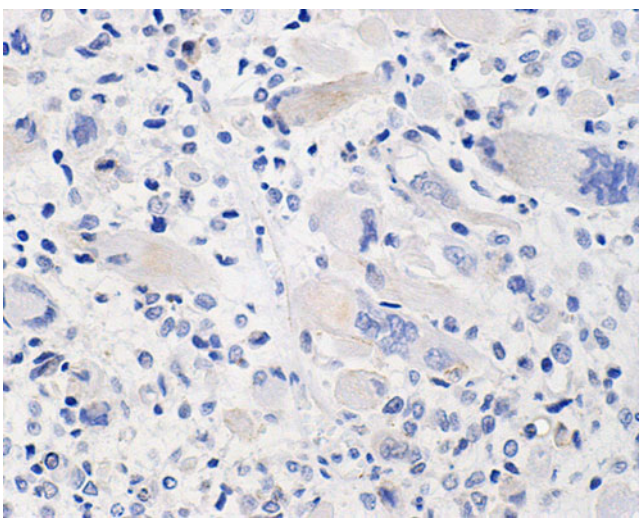

Fig. 5 Representative immunohistochemical analyses of nuclear β-catenin accumulation in UCSs. Nuclear β-catenin expression was lost in rhabdomyosarcoma

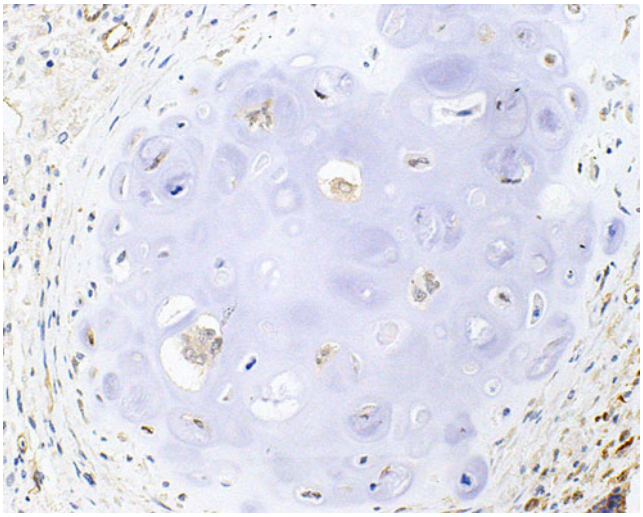

Fig. 6 Representative immunohistochemical analyses of nuclear β-catenin accumulation in UCSs. Nuclear β-catenin expression was lost also in chondrosarcoma

In all 46 cases, sarcomatous components were mainly composed of high-grade spindle to polygonal mesenchymal cells with pleomorphic nuclei. Oval to rounded mesenchymal cells with high-grade atypia were also observed in 33 UCSs. Heterologous sarcomatous components were identified in 28 UCSs; rhabdomyosarcoma was observed in 20 cases, chondrosarcoma in three cases, osteosarcoma in one case, a combination of rhabdomyosarcoma and chondrosarcoma in three cases, and a combination of rhabdomyosarcoma, chondrosarcoma, and osteosarcoma in one case. Liposarcomatous differentiation was not observed. None of the cases contained typical leiomyosarcoma or endometrial stromal sarcoma.

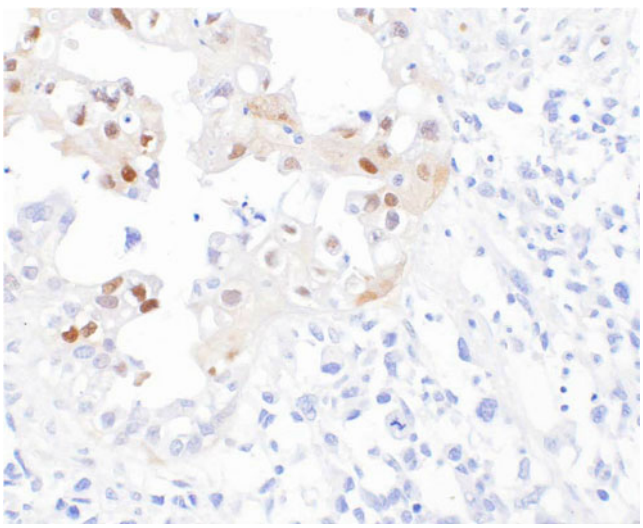

Fig. 7 Representative immunohistochemical analyses of cyclin D1 expression in UCSs. Diffuse cyclin D1 expression was observed in carcinoma cells. Surrounding sarcoma cells were not immunoreactive

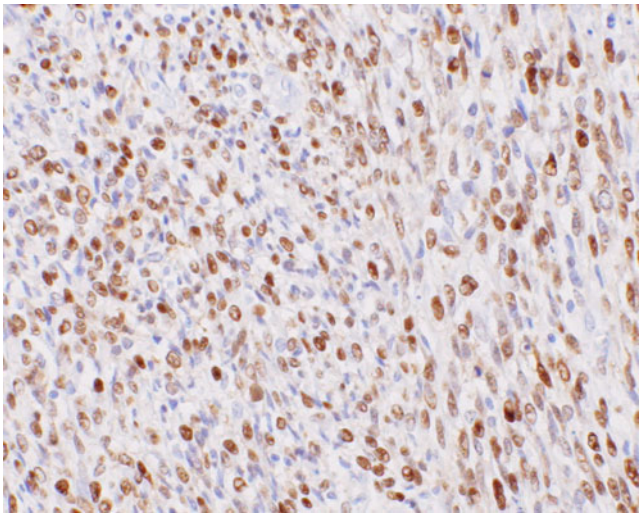

Fig. 8 Representative immunohistochemical analyses of cyclin D1 expression in UCSs. Diffuse cyclin D1 expression was observed in homologous sarcoma cells

Membranous expression of E-cadherin and β-catenin in UCSs

The immunohistochemical results regarding the membranous expression of adhesion molecules (E-cadherin and β-catenin) are summarized in Table 1. Membranous E-cadherin expression was completely lost in the sarcomatous components of 44 cases (95.7%; Fig. 1). The remaining two cases demonstrated only focal and weak E-cadherin immunoreactivity in their sarcomatous components. In the carcinomatous components, membranous E-cadherin expression was well preserved in 32 cases and reduced in 14. Meanwhile, membranous β-catenin expression in the sarcomatous components was reduced in all 46 cases and was completely lost in 36 cases (78.3%; Fig. 2). In the carcinomatous components, membranous β-catenin expression was well preserved in 34 cases (73.9%) and reduced in 12 cases (26.1%).

Membranous expressions of E-cadherin and β-catenin were significantly preserved in the carcinomatous components, when compared with the sarcomatous components ($P<0.01$, respectively; Table 1). Membranous expression of E-cadherin was significantly correlated with that of β-catenin in the carcinomatous components ($P<0.0001$, $\rho=0.626$ by the Spearman rank correlation test), while no such correlation was detectable in the sarcomatous components ($P=0.3129$, $\rho=0.150$ by the Spearman rank correlation test). There was no significant correlation in any of the data sets between the membranous expression of adhesion molecules (E-cadherin and β-catenin) and clinicopathological parameters (age, tumor size, stage, and carcinoma or sarcoma subtypes).

Nuclear expression of β-catenin in UCSs

Nuclear β-catenin expression was found in sarcomatous and/or carcinomatous components in 35 UCSs. In most areas that contained both carcinomatous and sarcomatous components, the tumor cells with nuclear β-catenin expression were also positive for cytoplasmic β-catenin staining, but lost their membranous expression of β-catenin and E-cadherin. There was no significant correlation in any of the data sets between nuclear β-catenin expression and other clinicopathological parameters (age, tumor size, and stage) except for sarcoma subtypes (Table 2).

(a) Sarcomatous components vs carcinomatous components

The frequency of nuclear β-catenin expression was significantly higher in the sarcomatous components (31/46, 67.4%) than in the carcinomatous components (22/46, 47.8%; $P=0.0025$; Table 3).

Table 4 The immunohistochemical results of β-catenin and cyclin D1 nuclear expression in UCSs with cyclin D1 overexpression

Cases	Sarcoma type	Carcinomatous components		Sarcomatous components	
		β-catenin (%)	Cyclin D1 (%)	β-catenin (%)	Cyclin D1 (%)
1	Homologous	10	30	10	0
2	Homologous	1	15	0	5
3	Homologous	10	0	30	35
4	Homologous	10	25	70	5
5	Homologous	50	20	25	0
6	Homologous	25	40	25	75
7	Heterologous	0	15	1	0
8	Heterologous	1	30	25	0
9	Heterologous	1	20	5	2
10	Heterologous	0	30	1	3

With regard to the sarcomatous components, diffuse nuclear β-catenin expression was observed in relatively oval to rounded and less pleomorphic sarcomatous cells rather than in markedly pleomorphic spindle cells (Fig. 3). Nuclear β-catenin expression was mainly pronounced in sarcomatous cells adjacent to carcinomatous glands (Fig. 4).

With regard to the carcinomatous components, nuclear β-catenin expression was mainly observed in carcinomatous glands that were surrounded by sarcomatous cells with β-catenin nuclear expression (Fig. 4). All four UCSs with diffuse nuclear β-catenin expression in their carcinomatous components also showed diffuse nuclear β-catenin expression in their sarcomatous components. There was no significant correlation between nuclear β-catenin expression and carcinoma subtype (serous vs endometrioid).

(b) Homologous sarcoma vs heterologous sarcoma

Nuclear β-catenin expression in the sarcomatous components was observed with significantly greater frequency in heterologous (23/28, 82.1%) than in homologous sarcomas (8/18, 44.4%; P=0.0279; Table 2). Diffuse nuclear expression of β-catenin in sarcomatous components was observed in 18 cases (13 cases with heterologous and five cases with homologous sarcomas). In heterologous sarcoma, nuclear β-catenin expression tended to disappear gradually in conjunction with the transformation into specifically differentiated sarcoma types (rhabdomyosarcoma, chondrosarcoma; Figs. 5 and 6).

(c) Relationship between nuclear β-catenin expression and cyclin D1 overexpression

With regard to the carcinomatous components, the percentage of cyclin D1-immunoreactive cells in tumors with nuclear β-catenin was significantly higher than that in tumors without nuclear β-catenin (p= 0.0029, Mann–Whitney U test). With regard to the sarcomatous components, however, such correlation was not observed.

Cyclin D1 overexpression was observed in only ten UCSs (the overexpression was observed in both carcinomatous and sarcomatous components in three cases, only in carcinomatous components in six cases, only in sarcomatous components in one case; Figs. 7 and 8). There were no heterologous sarcomas with cyclin D1 overexpression. The immunohistochemical results of the ten cases are summarized in Table 4.

Statistical analysis for prognosis

The results of survival analyses are summarized in Table 5. In univariate analysis, large tumor size (≥50 mm) and advanced stage were significantly correlated with a short period of overall survival (P=0.0447 and P<0.0001, respectively). Multivariate analyses revealed that only the advanced stage was an independent poor prognostic factor (P=0.015). There was no statistically significant relationship between expression of adhesion molecules (E-cadherin and β-catenin) and overall survival.

Discussion

Reduced expressions of E-cadherin and β-catenin are associated with the characteristics of invasiveness and loss of differentiation [11, 12]. It has been reported that E-

Table 5 Univariate and multivariate analyses of various parameters for overall survival in UCSs

Variables	P value	
	Univariate[a]	Multivariate[b]
Clinicopathological		
Age (<65 vs ≥65 years)	0.0532	0.1732
Size (<5 vs ≥5 cm)	0.0447	0.4298
Stage (I, II vs III, IV)	<0.0001	0.0015
Sarcoma subtype (homologous vs heterologous)	0.9814	0.6417
Immunohistochemical		
Nuclear β-catenin (cut-off 25%)		
Carcinomatous components	0.9029	0.5918
Sarcomatous components	0.7627	0.1391
Membranous β-catenin (preserved vs reduced)		
Carcinomatous components	0.7719	0.7968
Membranous E-cadherin (preserved vs reduced)		
Carcinomatous components	0.7821	0.1599

[a] P value by the log-rank test

[b] P value by the Cox proportional hazards regression test

cadherin dysfunction is associated with biphasic morphology in malignant tumors [11, 12]. Furthermore, it is considered that E-cadherin dysregulation through Akt/β-catenin pathway responsible for triggering EMT may occur during development of UCS [28]. In this study, we demonstrated the complete loss of membranous expression of E-cadherin and β-catenin in sarcomatous components of most UCSs, whereas membranous expression of these proteins was preserved in carcinomatous components. It may suggest that the presence or absence of membranous expression of E-cadherin and β-catenin contribute to the biphasic morphology of UCS.

In the present study, nuclear β-catenin expression was also observed in both carcinomatous and sarcomatous components, though it was more diffuse and frequent in the sarcomatous components. Kirchner et al. reported that cells displaying nuclear β-catenin accumulation undergo a mesenchymal-like transdifferentiation, or possibly dedifferentiation, as changes in morphology and gene expression profiles suggested [29]. Experimental studies have provided several pieces of evidence that β-catenin accumulation plays a role in the occurrence of the epithelial–mesenchymal transition during embryogenesis and in tumorigenesis [30]. In this context, it may be possible that nuclear β-catenin expression may also play some role in the biphasic appearance of UCS.

Experimental studies have shown that the Wnt/β-catenin signaling pathway is involved in several biological processes associated with differentiation, suggesting important roles for the pathway during embryogenesis and stem cell differentiation [29, 31]. Additionally, the Wnt signaling pathway, acting via β-catenin, has been found to be necessary and sufficient for skeletal myogenesis in vitro [32].

Sato et al. demonstrated that Wnt signaling is a common pathway for maintenance of the undifferentiated state in both mouse and human embryonic stem cells [33]. The authors found that Wnt pathway activation by 6-bromoindirubin-3′-oxime (BIO), a specific pharmacological inhibitor of glycogen synthase kinase-3, maintained the undifferentiated phenotype in embryonic stem cells and sustained expression of the pluripotent state-specific transcription factors Oct-3/4, Rex-1, and Nanog [33]. In addition, inhibition of Wnt activation by withdrawal of BIO led to normal multidifferentiation in embryonic stem cells [33].

In our study, nuclear β-catenin expression was frequently detected in relatively rounded and less pleomorphic sarcomatous cells immediately adjacent to neoplastic glands, and in rhabdomyosarcoma or chondrosarcoma components, nuclear β-catenin expression gradually decreased. If the undifferentiated sarcomatous cells near the epithelial–mesenchymal interface are hypothesized to have cancer stem cell phenotype, our observation is consistent with Sato's basic data in that Wnt pathway activation maintains the undifferentiated phenotype in stem cells and sustains expression of the pluripotent state-specific transcription factors. In this context, the finding that nuclear β-catenin expression was more frequently detected in heterologous than in homologous sarcomas strengthens this possibility (Fig. 9a).

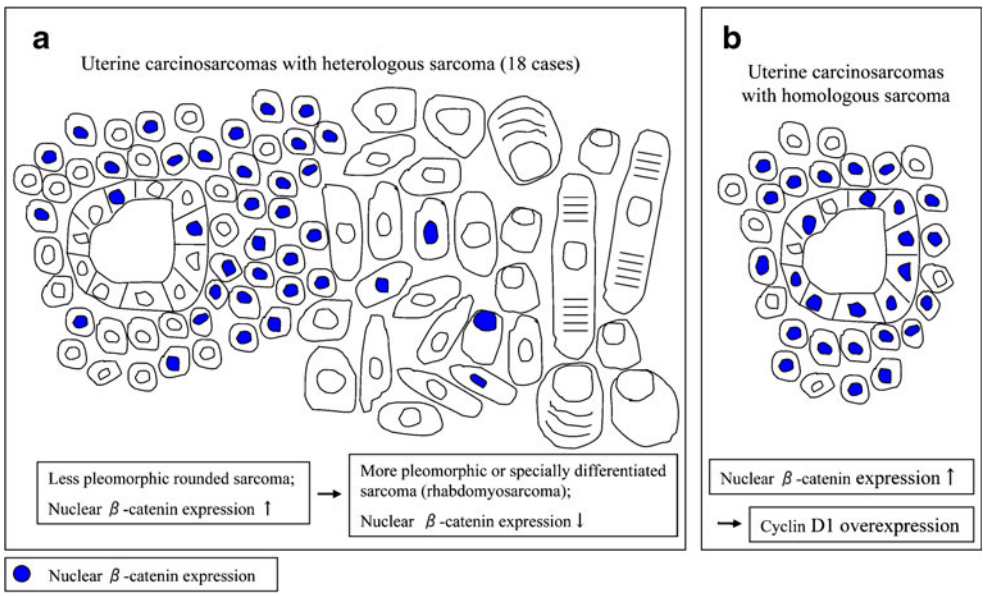

Fig. 9 Schematic diagram showing the role of nuclear β-catenin expression in UCS. Its possible contribution to **a** heterologous sarcomatous differentiation and **b** increased proliferative activity via cyclin D1 overexpression. **a** Diffuse nuclear β-catenin expression was observed in less pleomorphic rounded sarcoma cells in UCSs with heterologous sarcoma. Nuclear β-catenin expression tended to disappear gradually in conjunction with the transformation into more pleomorphic or specifically differentiated sarcoma types. **b** In some UCSs, nuclear β-catenin expression may contribute to cyclin D1 overexpression in carcinomatous or homologous sarcomatous components

Table 6 Immunohistochemical results of E-cadherin, β-catenin, and cyclin D1 in adenosarcoma and endometrioid carcinoma variants

	E-cadherin				β-catenin				Cyclin D1			
	Epithelial	Sarcoma	EC	Sp/CH component	Epithelial	Sarcoma	EC	Sp/CH component	Epithelial	Sarcoma	EC	Sp/CH component
Adenosarcoma												
Case 1	40% (M)	0%			40% (M)	0%			0%	70% (N)		
Case 2	10% (M)	0%			10% (M)	0%			10% (N)	0%		
Case 3	20% (M)	0%			20% (M)	5% (N)			0%	15% (N)		
Endometrioid ca. variant												
Case 4 (spindle change)			5% (M)	0%			5% (M)	60% (N)			3% (N)	0%
Case 5 (CHEC)			40% (M)	50% (M)			30% (M)	40% (M)			3% (N)	0%

M membranous immunohistochemical reaction, *N* nuclear immunohistochemical reaction, *EC* endometrioid carcinoma, *Sp/CH* spindle change/corded and hyalinized, *CHEC* corded and hyalinized endometrioid carcinoma

It is interesting that immunoreactive carcinomatous cells for nuclear β-catenin are located closely adjacent to areas of the immunopositive sarcomatous cells. Transient nuclear β-catenin expression in these cells may contribute to the formation of UCS's multiple phenotypic diversity (Fig. 9a).

However, further studies are warranted to provide additional evidence for the direct role of the Wnt signaling pathway in promoting EMT and/or direction of differentiation in UCS cells by focusing on transcription factors such as MyoD and Sox9.

Cyclin D1 is a cell cycle regulator and is associated with progression in the G1 phase of the cell cycle [34] and is a target of accumulated β-catenin in some types of malignancies [17, 35]. In this study, nuclear expression of cyclin D1 and β-catenin were correlated in carcinomatous components but not in sarcomatous components. Furthermore, cyclin D1 overexpression was observed in only ten UCSs, and the sarcoma components with cyclin D1 overexpression were all homologous. These findings suggest that aberrant Wnt signal promotes proliferation activity of carcinoma or homologous sarcoma cells by overexpression of cyclin D1 in a small number of UCS cases (Fig. 9b).

Taking into consideration the fact that (1) nuclear β-catenin expression is frequently observed in sarcomatous components, especially heterologous type and (2) nuclear expression of cyclin D1 and β-catenin were not correlated in sarcomatous components, aberrant Wnt signal in sarcomatous cells may play more variety of roles such as contribution to the maintenance of undifferentiated phenotype, multidirectional differentiation, and/or cyclin D1 overexpression.

We have also analyzed five cases with different type of biphasic uterine tumors; three adenosarcomas, one endometrioid carcinoma with spindle change (ECSp), and one corded and hyalinized endometrioid carcinoma (CHEC), and the results are summarized in Table 6. Similar to UCSs, in all adenosarcomas and ECSp, membranous expression of E-cadherin and β-catenin was lost in sarcoma or spindle cell components. On the other hand, membranous expression of E-cadherin and β-catenin was preserved in corded and hyalinized components. Diffuse nuclear β-catenin expression in spindle cell components of ECSp may support the general concept that spindle cell components represent abortive squamous cells as is true with morular component (immature squamous cells), which is well-known to show diffuse nuclear β-catenin expression. Two of the three adenosarcomas showed cyclin D1 overexpression in sarcomatous components, but its relationship with aberrant Wnt signal was unclear. It is difficult to conclude the differences of E-cadherin, β-catenin, and cyclin D1 expression between UCSs and other biphasic uterine tumors since the number of cases with adenosarcomas and endometrioid carcinoma variants we could evaluate was extremely small.

It is generally considered that the most important prognostic factor for UCS is the clinical stage at the initial treatment [36]. Similar to such previous studies, our data confirmed that the patients with early stage disease had significantly more favorable survival rates than the patients at more advanced stages (P=0.0015). Although several reports have correlated poor prognosis with altered profiles in adhesion molecule expression [14, 15], there was no prognostic relevance in this study.

In conclusion, reduced membranous expression of E-cadherin and β-catenin may contribute to the biphasic morphology of UCS. Furthermore, it may also be possible that nuclear β-catenin expression contribute to biphasic morphology, direction of differentiation, or cell proliferation at least in some UCS cases.

Acknowledgments We are grateful to Yoko Kamitani for her excellent technical assistance. We thank KN International for revising the English used in this article.

Conflict of interest statement The authors have no conflicts of interest to declare.

References

1. Silverberg SG, Major FJ, Blessing JA et al (1990) Carcinosarcoma (malignant mixed mesodernal tumor) of the uterus. A gynecologic oncology group pathologic study of 203 cases. Int J Gynecol Pathol 9:1–19
2. Wada H, Enomoto T, Fujita M et al (1997) Molecular evidence that most but not all carcinosarcomas of the uterus are combination tumors. Cancer Res 57:5379–5385
3. Emoto M, Iwasaki H, Kikuchi M, Shirakawa K (1993) Characteristics of cloned cells of mixed mullerian tumor of the human uterus. Carcinoma cells showing myogenic differentiation in vitro. Cancer 71:3065–3075
4. Fujii H, Yoshida M, Gong ZX et al (2000) Frequent genetic heterogeneity in the clonal evolution of gynecological carcinosarcoma and its influence on phenotypic diversity. Cancer Res 60:114–120
5. McCluggage WG (2002) Uterine carcinosarcomas (malignant mixed mullerian tumors) are metaplastic carcinomas. Int J Gynecol Cancer 12:687–690
6. Sreenan JJ, Hart WR (1995) Carcinosarcomas of the female genital tract. A pathologic study of 29 metastatic tumors: further evidence for the dominant role of the epithelial component and the conversion theory of histogenesis. Am J Surg Pathol 19:666–674
7. Ferguson SE, Tornos C, Hummer A, Barakat RR, Soslow RA (2007) Prognostic features of surgical stage I uterine carcinosarcoma. Am J Surg Pathol 31:1653–1661
8. Goltzmann J, Mikula M, Eger A et al (2004) Molecular aspects of epithelial cell plasticity: implications for local tumor invasion and metastasis. Mutat Res 566:9–20
9. Sarrió D, Rodriguez-Pinilla SM, Hardisson D, Cano A, Moreno-Bueno G, Palacios J (2006) Epithelial–mesenchymal transition in breast cancer relates to the basal-like phenotype. Cancer Res 68:989–997
10. Thiery JP (2002) Epithelial–mesenchymal transitions in tumour progression. Nat Rev Cancer 2:442–454
11. Mayer B, Johnson JP, Leitl F et al (1993) E-cadherin expression in primary and metastatic gastric cancer: down-regulation correlates with cellular dedifferentiation and glandular disintegration. Cancer Res 53:1690–1695
12. Saito T, Oda Y, Sugimachi K et al (2001) E-cadherin gene mutations frequently occur in synovial sarcoma as a determinant of histological features. Am J Pathol 159:2117–2124
13. Gumbiner BM (2000) Regulation of cadherin adhesive activity. J Cell Biol 148:399–404
14. Saito T, Oda Y, Sakamoto A et al (2000) Prognostic value of the preserved expression of the E-cadherin and catenin families of adhesion molecules and of β-catenin mutations in synovial sarcoma. J Pathol 192:342–350
15. Shimazui T, Schalken JA, Giroldi LA et al (1996) Prognostic value of cadherin-associated molecules (α-, β-, and γ-catenins and $p120^{cas}$) in bladder tumors. Cancer Res 56:4154–4158
16. Ilyas M (2005) Wnt signalling and the mechanistic basis of tumour development. J Pathol 205:130–144
17. Tetsu O, McCormick F (1999) β-catenin regulates expression of cyclin D1 in colon carcinoma cells. Nature 398:422–426
18. Chen G, Shukeir N, Potti A et al (2004) Up-regulation of Wnt-1 and β-catenin production in patients with advanced metastatic prostate carcinoma. Potential pathologenetic and prognostic implications. Cancer 101:1345–1356
19. Fukuchi T, Sakamoto M, Tsuda H, Maruyama K, Nozawa S, Hirohashi S (1998) β-catenin mutation in carcinoma of the uterine endometrium. Cancer Res 58:3526–3528
20. Saegusa M, Hashimura T, Yoshida T, Okayasu I (2001) β-catenin mutations and aberrant nuclear expression during endometrial tumorigenesis. Br J Cancer 84:209–217
21. Scholten AN, Creutzberg CL, van den Broek LJCM, Noordijk EM, Smit VTHBM (2003) Nuclear β-catenin is a molecular feature of type I endometrial carcinoma. J Pathol 201:460–465
22. Kondo Y, Kanai Y, Sakamoto M et al (1999) β-catenin accumulation and mutation of exon 3 of the β-catenin gene in hepatocellular carcinoma. Jpn J Cancer Res 90:1301–1309
23. Van Nhieu JT, Renard CA, Wei Y, Cherqui D, Zafrani ES, Buendia MA (1999) Nuclear accumulation of mutated β-catenin in hepatocellular carcinoma is associated with increased cell proliferation. Am J Pathol 155:703–710
24. Eger A, Stockinger A, Park J et al (2004) β-catenin and TGFβ signalling cooperate to maintain a mesenchymal phenotype after FosER-induced epithelial to mesenchymal transition. Oncogene 23:2672–2680
25. Moreno-Bueno G, Hardisson D, Sarrio D et al (2003) Abnormalities of E- and P-cadherin and catenin (β-, γ-catenin, and $p120^{ctn}$) expression in endometrial cancer and endometrial atypical hyperplasia. J Pathol 199:471–478
26. Scholten AN, Aliredjo R, Creutzberg CL, Smit VTHBM (2006) Combined E-cadherin, α-catenin, and β-catenin expression is a favorable prognostic factor in endometrial carcinoma. Int J Gynecol Cancer 16:1379–1385
27. Nikaido T, Li SF, Shiozawa T, Fujii S (1996) Coabnormal expression of cyclin D1 and p53 protein in human uterine endometrial carcinomas. Cancer 78:1248–1253
28. Saegusa M, Hashimura M, Kuwata T, Okayasu I (2009) Requirement of the Akt/β-catenin pathway for uterine carcinosarcoma genesis, modulating E-cadherin expression through the transactivation of Slug. Am J Pathol 174:2107–2115
29. Kirchner T, Brabletz T (2000) Patterning and nuclear beta-catenin expression in the colonic adenoma-carcinoma sequence. Analogies with embryonic gastrulation. Am J Pathol 157:1113–1121
30. Fodde R, Brabletz T (2007) Wnt/β-catenin signaling in cancer stemness and malignant behavior. Cur Op Cell Biol 19:150–158
31. Van Es JH, Barker N, Clevers H (2003) You Wnt some, you lose some: oncogenes in the Wnt signaling pathway. Curr Opin Genet Dev 13:28–33
32. Petropoulos H, Skerjanc IS (2002) β-catenin is essential and sufficient for skeletal myogenesis in P19 cells. J Biol Chem 277:15393–15399
33. Sato N, Meijer L, Skaltsounis L, Greengard P, Brivanlou AH (2004) Maintenance of pluripotency in human and mouse embryonic stem cells through activation of Wnt signaling by a pharmacological GSK-3-specific inhibitor. Nat Med 10:55–63
34. Matsushime H, Ewen ME, Strom DK et al (1992) Identification and properties of an atypical catalytic subunit (p34psk-j3/CDK4) for mammalian D type G1 cyclins. Cell 71:323–334
35. Ozaki S, Ikeda S, Ishizaki Y et al (2005) Alterations and correlations of the components in the Wnt signaling pathway and its target genes in breast cancer. Oncol Rep 14:1437–1443
36. Iwasa Y, Haga H, Konishi I et al (1998) Prognostic factors in uterine carcinosarcoma. A clinicopathologic study of 25 patients. Cancer 82:512–519

Virchows Arch (2011) 458:95–98
DOI 10.1007/s00428-010-1000-y

ORIGINAL ARTICLE

EGFR mutation detection in NSCLC—assessment of diagnostic application and recommendations of the German Panel for Mutation Testing in NSCLC

Roland Penzel · Christine Sers · Yuan Chen · Ulrich Lehmann-Mühlenhoff · Sabine Merkelbach-Bruse · Andreas Jung · Thomas Kirchner · Reinhard Büttner · Hans H. Kreipe · Iver Petersen · Manfred Dietel · Peter Schirmacher

Received: 9 July 2010 / Revised: 1 October 2010 / Accepted: 5 October 2010 / Published online: 6 November 2010
© Springer-Verlag 2010

Abstract *EGFR* mutation testing in non-small cell lung cancer (NSCLC) is a novel and important molecular pathological diagnostic assay that is predictive of response to anti-epidermal growth factor receptor (EGFR) therapy. A comprehensive compilation of a large number of *EGFR* mutation analyses of the German Panel for Mutation Analyses in NSCLC demonstrates (a) a higher than previously reported mutation frequency outside the conventionally tested exons 19 and 21 and (b) an overall superiority of sequencing based assays over mutation-specific PCR. The implications for future diagnostic EGFR mutation testing are discussed.

Keywords *EGFR* mutations · NSCLC · Gefitinib · Targeted detection · Sequencing

Introduction

Epidermal growth factor receptor (EGFR)-targeted therapy has been shown to significantly improve progression-free and overall survival in a subgroup of non-small cell lung cancer (NSCLC) patients carrying "activating" mutations of the *EGFR* gene in their tumors, predominantly representing those NSCLC with adenocarcinoma differentiation. Targeted therapy against EGFR using gefitinib has obtained approval by the European Medicines Agency as first-line therapy in non-resectable NSCLC under the premise that the presence of an "activating" (presumably gefitinib-sensitive) mutation has been demonstrated prior to treatment [1]. Thus, the detection and correct reporting of "activating" mutations in

R. Penzel, C. Sers, Y. Chen, U. Lehmann-Mühlenhoff, S. Merkelbach-Bruse, A. Jung, T. Kirchner, R. Büttner, H.H. Kreipe, I. Petersen, M. Dietel, P. Schirmacher are members of the German Panel for Mutation Testing in NSCLC.

Electronic supplementary material The online version of this article (doi:10.1007/s00428-010-1000-y) contains supplementary material, which is available to authorized users.

R. Penzel · P. Schirmacher (✉)
Institute of Pathology, University Hospital Heidelberg,
Im Neuenheimer Feld 220,
69120 Heidelberg, Germany
e-mail: peter.schirmacher@med.uni-heidelberg.de

C. Sers · M. Dietel
Institute of Pathology, Charité-Universitätsmedizin Berlin,
Charitéplatz 1,
10117 Berlin, Germany

Y. Chen · I. Petersen
Institute of Pathology, Universitätsklinikum Jena,
Ziegenmühlenweg,
07743 Jena, Germany

U. Lehmann-Mühlenhoff · H. H. Kreipe
Institute of Pathology, Hannover Medical School,
Carl-Neuberg-Str. 1,
30625 Hannover, Germany

S. Merkelbach-Bruse · R. Büttner
Department of Pathology, University of Bonn Medical School,
Sigmund-Freud-Str. 25,
53127 Bonn, Germany

A. Jung · T. Kirchner
Department of Pathology,
Ludwig-Maximilians Universität München,
Thalkirchner Strasse 36,
80337 Munich, Germany

the tumor tissue is essential for gefitinib therapy and has gained significant impact in diagnostic molecular pathology. In order to initiate and supervise large-scale and nationwide quality-controlled testing for *EGFR* mutations in NSCLC in Germany, a steering panel consisting of six institutions was implemented. Besides quality management, central questions addressed by the panel were the frequency and potential therapeutic relevance of *EGFR* mutations as well as the critical evaluation of testing modalities. The latter aspect concentrated on the evaluation of the two methodologies available for diagnostic testing, i.e., sequencing of the exons in question (18–21) and mutation-specific PCR.

Methodology

All panel institutions performed mutation analyses by bidirectional Sanger sequencing of exons 18–21 of the *EGFR* gene from formalin-fixed paraffin-embedded tissues obtained by biopsy or resection. A complete compilation of the applied technical procedures of all panel institutes including DNA extraction methods, primer sequences, and PCR conditions is available online (www.dgp-berlin.de/downloads/public/protocols/EGFR_Mutations_Protocols_engl.pdf). Internal quality assessment of the panel institutes was carried out as following: A series of 40 NSCLC (20 mutated, 20 non-mutated) were initially analyzed by two panel institutes (20 cases contributed by each institute). All 40 cases were cross-tested in a blinded manner by the respective other institutes; there was no disagreement on the analysis results between the two institutes. From this collective, a test set of ten cases (five mutation-positive) was composed and circulated among the four other panel institutes. Positive quality assessments were given to those institutes which correctly analyzed nine of ten cases within a turnaround time of ten working days. All panel institutes participating in this analysis identified all test cases correctly.

Mutation data derived exclusively from routine diagnosis (n=1,047) from the six panel institutes were collected and analyzed for the distribution of mutations among the different exons. The compiled collective consisted of biopsies (between 25% and 40% of the cases, depending on the respective center) and resection specimen; cytology specimens were not among the analyzed cases. Microscopically guided dissection (by an experienced morphologist, no laser microdissection) was performed in almost all cases in order to increase tumor content above 50% and was only omitted in those resection cases that contained almost exclusively tumor in the analyzed material. Cases without tumor in the preanalytical HE section (~4%) were not analyzed and not included in the compilation. Cases with <50% tumor content after dissection were analyzed and counted valid when mutations were detected; the non-mutated cases (~5%) among them were reported with the necessary precautions and were included in the compilation. All new mutations (n=14; not present in the Catalogue of Somatic Mutations in Cancer Database, www.sanger.ac.uk/genetics/CGP/cosmic/) were confirmed by a second independent diagnostic analysis of the same DNA source. Furthermore, all mutations reported were carefully reviewed in regard to sequence pattern potentially resulting from formalin fixation artifacts [2]. The detectability of these mutations by the commercially available mutation-specific PCR detection kit (TheraScreen® EGFR29 Mutation Kit; DXS Ltd., Manchester, UK) was assessed based on the detailed description of its composition by the supplier. Evaluation of "activation" status (presumed gefitinib responsiveness) was based on the data published by Sharma et al. [3] and, if not addressed in this publication, by the Somatic Mutation-EGFR database [4]. Additional relevant parameters (costs, turnaround time, aspects of quality management and sensitivity, and innovative potential) affecting the choice of assay were addressed.

Results

Compilation of all reported mutation data (Supplementary Table) resulted in 163 mutation-positive tumors among 1,047 analyses representing a mutation rate of 15.6% (status 1st December 2009). This frequency is unlikely to reflect exactly the true mutation frequency in German NSCLC since clinical practice of ordering the diagnostic assay preselected patient populations with higher prevalence of *EGFR* mutations (adenocarcinoma/non-smoker or light smokers) to various extents. Nevertheless, it is likely to reflect the relative distribution of the mutations in regard to the different exons. The overall frequency of exon 20 mutations in this collective may be slightly underestimated since two of the six institutions did not perform bidirectional sequencing of exon 20 in all cases. Mutation frequency in exon 18 (10.4%) was significantly higher compared to Sharma et al. [3], at the relative expense of exon 21 mutations (Table 1). Frequencies of exon 18 and exon 20 mutations were remarkably different between some of the panel centers.

Next, the panel addressed the question which mutations detected by the sequencing approach would have been identified by the commercially available mutation-specific PCR test. Compilation of the data (Table 2) demonstrated that 67 of the 169 mutations (40%) would have been missed by the mutation-specific PCR analysis. For the different exons, the results were as follows: exon 18, 17/21 (81%); exon 19, 33/82 (40%); exon 20, 9/9 (100%); exon 21, 8/57 (14%). Based on Sharma et al. [3] and the Somatic Mutation-EGFR-Database [4], 47 of the 67 mutations

Table 1 Exon distribution of *EGFR* mutations in NSCLC

Institute (analyzed cases)	Mutated (cases)	Exon 18	Exon 19	Exon 20	Exon 21
A (169)	24 (14.3%)	1 (4.2%)	18 (75%)	0	5 (20.8%)
B (130)	16 (12.3%)	2 (12.5%)	8 (50%)	0[a]	6 (37.5%)
C (248)	24 (9.7%)	2 (7.7%)	13 (50%)	0[b]	11 (42.3%)
D (201)	52 (25.9%)	2 (3.8%)	28 (53.8%)	7 (13.5%)	15 (28.9%)
E (73)	5 (6.8%)	0	3 (60%)	0	2 (40%)
F (226)	42 (18.6%)	10 (23.8%)	12 (28.6%)	2 (4.8%)	18 (42.8%)
Total	163/1,047 (15.6%)	17 (10.4%)	81 (49.7%)	9 (5.5%)	56 (34.4%)
Sharma SV et al. Nature Rev Cancer (2007)		5%	45%	5%	40–45%

[a] Thirty cases analyzed

[b] One hundred ten cases analyzed

(70%) missed by mutation-specific PCR represented "activating" mutations. Evaluating the different exons, the distribution of these mutations was as follows: exon 18, 11/17 (65%); exon 19, 30/33 (91%); exon 20, 3/9 (33%); exon 21, 3/8 (38%). In summary, 47 of all 149 activating mutations (32%) detected by routine diagnostic sequencing of exons 18–21 by the panel institutes would have been missed by sole application of mutation-specific PCR testing.

Discussion

The panel evaluation represents the first assessment of daily routine diagnostic application of *EGFR* mutation testing in NSCLC on a quality-controlled multicenter and on a nationwide basis. All panel centers had agreed to perform bidirectional sequencing of exons 18–21 and had previously submitted their diagnostic testing to standardized internal quality control (round-robin testing). Compilation of the data obtained between 01 January 2009 and 1 December 2009 provided a sufficient basis for combined analyses and generated several unexpected results with significant impact on diagnostic testing.

Interestingly, the panel evaluation demonstrated that the distribution of mutations between the different exons varied from published data. Especially, the frequency of mutations in exons 18 and 20 that were not uniformly addressed in general and by several previous trials was found to represent 16% of all detected *EGFR* mutations, which was a higher rate compared to previous reports. Based on the available information, 69% (18/26) of these mutations were judged as activating (gefitinib-responsive). This result suggests the reevaluation of recommendations and studies that were based only on the analysis of exons 19 and 21. Thus, based on these findings, the panel recommends including exons 18 and 20 into routine diagnostic testing. Importantly, frequencies of exon 18 and exon 20 mutations varied remarkably between the different centers. The most likely explanation are differences in patient collectives, e.g., due to patient background or exposure bias. Etiology-specific mutation pattern are a well-documented phenomenon in other solid

Table 2 Sequencing-based detected mutations vs. targeted detection

Institutes	Mutations	Exon 18	Exon 19	Exon 20	Exon 21
A	24	1	18	0	5
B	17[a]	3	8	0	6
C	26[b]	2	13	0	11
D	55[c]	5	28	7	15
E	5	0	3	0	2
F	42	10	12	2	18
Total	169	21	82	9	57
Not detectable by ARMS PCR	67 (40%)	17 (81%)	33 (40%)	9 (100%)	8 (14%)
Missed activating mutations	47/149 (32%)	11/15 (73%)	30/79 (38%)	3/3 (100%)	3/52 (6%)

[a] One patient carried two mutations

[b] Two patients carried two mutations

[c] One patient carried two mutations and one patient three mutations

adulthood malignancies [5] and are likely to be present also in NSCLC, as suggested by the correlation of smoking habits and *EGFR* mutation frequency [6]. Thus, comprehensive analyses of mutation distribution may provide an important source for molecular epidemiology and unraveling of so far undetected etiological factors of NSCLC. This will be addressed by future studies and further comprehensive compilation of *EGFR* mutations by the panel.

An important aspect of the evaluation was the question which assay(s) should be implemented in diagnostic settings. All panel institutes used bidirectional sequencing of exons 18–21. Exact central reporting of all mutation data allowed their evaluation in regard to detectability by mutation-specific PCR. Overall, 32% of tumors carrying "activating" mutations as detected by sequencing would have been missed by the commercially available PCR test; notably, 38% of the complex exon 19 mutations would have been missed. This is especially relevant since there is some indication that tumors carrying exon 19 mutations may respond especially favorably to gefitinib treatment [7]. Overall, the percentage of missed mutations is too high to recommend the use of mutation-specific PCR for diagnostic application. It should be mentioned that none of the 38 institutions that had passed the first nationwide quality assessment in Germany for *EGFR* mutation testing in NSCLC had performed mutation-specific PCR testing as the sole diagnostic test. In all institutes, final reporting was based on sequencing analyses. Furthermore, among the 169 mutations detected by the panel institutes in this study, 14 had not been reported before, underscoring that only sequencing-based assays will further enhance our knowledge about *EGFR* mutations. Considering the fact that well over 200 different *EGFR* mutations are reported meanwhile (and the vast majority being considered "activating"), a mutation-specific approach appears to be unsuited for diagnostic *EGFR* mutation analyses for technological reasons. Further evaluation by the panel of other aspects, such as costs, turnaround time, and quality management, failed to demonstrate favorable aspects of the current mutation-specific PCR testing. In conclusion, the panel emphasizes the disadvantages of the current mutation-specific PCR assays for the detection of *EGFR* mutations in NSCLC. Instead, the use of sequencing-based detection is recommended. Currently, the analysis of exons 19 and 21 is considered mandatory, but the compiled results of the panel institutes strongly suggest including the analysis of exons 18 and 20 into the diagnostic setting.

Conflict of interest Round-robin testing of the panel institutes was supported by Astra Zeneca.

References

1. Mok TS, Wu YL, Thongprasert S, Yang CH, Chu DT, Saijo N, Sunpaweravong P, Han B, Margono B, Ichinose Y, Nishiwaki Y, Ohe Y, Yang JJ, Chewaskulyong B, Jiang H, Duffield EL, Watkins CL, Armour AA, Fukuoka M (2009) Gefitinib or carboplatin–paclitaxel in pulmonary adenocarcinoma. N Engl J Med 361:947–957
2. Marchetti A, Felicioni L, Buttitta F, Tsao MS, Kamel-Reid S, Shepherd FA (2006) Assessing EGFR mutations. N Engl J Med 354:526–528
3. Sharma SV, Bell DW, Settleman J, Haber DA (2007) Epidermal growth factor receptor mutations in lung cancer. Nat Rev Cancer 7:169–1681
4. Somatic Mutations in Epidermal Growth Factor Receptor DataBase (2008) Department of Molecular Pathology and Translational Oncology at Metropolitan Hospital, Athens, Greece. www.somaticmutations-egfr.info/index.html
5. Bressac B, Kew M, Wands J, Ozturk M (1991) Selective G to T mutations of p53 gene in hepatocellular carcinoma from southern Africa. Nature 350:429–431
6. Rosell R, Moran T, Queralt C et al (2009) Screening for epidermal growth factor receptor mutations in lung cancer. N Engl J Med 361:958–967
7. Jackman DM, Miller VA, Cioffredi LA, Yeap BY, Jänne PA, Riely GJ, Ruiz MG, Giaccone G, Sequist LV, Johnson BE (2009) Impact of epidermal growth factor receptor and KRAS mutations on clinical outcomes in previously untreated non-small cell lung cancer patients: results of an online tumor registry of clinical trials. Clin Cancer Res 15:5267–5273

Virchows Arch (2011) 458:99–107
DOI 10.1007/s00428-010-1016-3

ORIGINAL ARTICLE

Expression of integrin-linked kinase in lung squamous cell carcinoma and adenocarcinoma: correlation with E-cadherin expression, tumor microvessel density and clinical outcome

Juanhan Yu · Rui Shi · Daorong Zhang · Enhua Wang · Xueshan Qiu

Received: 9 September 2010 / Revised: 14 November 2010 / Accepted: 20 November 2010 / Published online: 7 December 2010
© Springer-Verlag 2010

Abstract Integrin-linked kinase (ILK) plays a role in integrin signaling-mediated cell-extracellular matrix interactions and is involved in signal transduction pathways to control cell survival, differentiation, and proliferation in mammalian cells. ILK has been implicated in the progression of several human malignancies. However, its function in malignant tumors is not fully enunciated. Previous in vitro studies also implicated ILK in the regulation of E-cadherin expression and vascular endothelial growth factor expression. In the current study, we investigated the protein expression of ILK and its correlation with clinicopathological profiles, E-cadherin expression, microvessel density (MVD) and clinical outcome in 57 lung squamous cell carcinoma and 44 adenocarcinoma, using immunohistochemistry. No ILK was detected in normal bronchial epithelium, while it was positively expressed in 39 (68.42%) squamous cell carcinoma cases and 27 (61.36%) adenocarcinoma cases. Positive ILK expression was significantly associated with advanced TNM stage (P=0.022) in adenocarcinoma, and associated with high MVD in lung squamous cell carcinoma (P<0.001) and adenocarcinoma (P=0.049). The Spearman's correlation test revealed that increased ILK expression was correlated with reduced E-cadherin expression in lung squamous cell carcinoma (correlation coefficient=0.364, P=0.005). Moreover, the Kaplan–Meier survival analysis showed that ILK, E-cadherin, and MVD were all statistically significant prognostic factors in patients with lung squamous cell carcinoma and adenocarcinoma. Measuring ILK and E-cadherin expression, and MVD may contribute to a better understanding of the prognosis of patients with lung squamous cell carcinoma and adenocarcinoma.

Keywords E-cadherin · Integrin-linked kinase · Microvessel density · Lung squamous cell carcinoma–lung adenocarcinoma · Prognosis

J. Yu · D. Zhang (✉) · E. Wang · X. Qiu
Department of Pathology, First Affiliated Hospital and College of Basic Medical Sciences of China Medical University, Shenyang 110001, China
e-mail: zhangdr46@yahoo.cn

J. Yu
e-mail: yjh_109@yahoo.com.cn

E. Wang
e-mail: wangeh@hotmail.com

X. Qiu
e-mail: qiuxues@hotmail.com

R. Shi
Department of General Surgery, First Affiliated Hospital, China Medical University, Shenyang 110001, China
e-mail: sr04422@yahoo.com.cn

Introduction

Cell-extracellular matrix (ECM) interactions play an important role in cell survival, growth, differentiation, and migration [1]. As a key component of cell-ECM structures, integrin-linked kinase (ILK) associates with cytoplasmic domains of β1 and β3 integrins and couples them to the actin cytoskeleton [2]. In addition, ILK has been shown to act as a serine/threonine kinase originally, but there is an ongoing controversy if ILK is a kinase or not.

There is mounting experimental evidence indicating that ILK plays a pivotal role in many processes associated with oncogenesis. Overexpression and constitutive activation of ILK in epithelial cells suppresses anoikis and elicits anchorage-independent cell cycle progression, cell migration, and invasion [2–4]. Moreover, overexpression of ILK in epithelial cells also induces tumor formation in vivo [5]. Increased expression of ILK has also been reported in several malignancies, such as gastric carcinoma, prostate tumor, colon tumor, ovary carcinoma, melanoma, and non-small cell lung cancer [6–11]. However, inconsistent results with regard to ILK expression exist for lymphoma, retinoblastoma, and renal carcinoma [12]. Up to the current time, these discrepancies remain unsolved, and the function of ILK in tumor biology is still under debate.

E-cadherin is an important epithelial cell adhesion molecule mediating cell–cell interactions. Research revealed that overexpression of ILK leads to the loss of cell–cell adhesion because of downregulation of E-cadherin [13, 14]. Further evidence has indicated that ILK might play a key role in vascular endothelial growth factor (VEGF)-mediated endothelial activation and angiogenesis [15, 16]. However, currently, there is little evidence of the relationship between ILK expression and E-cadherin expression and microvessel density (MVD). Thus, we investigated the expression of ILK in lung squamous cell carcinoma and adenocarcinoma, and analyzed the relationship between ILK expression and some clinical pathological factors, E-cadherin expression, MVD, and clinical outcome.

Materials and methods

Tissue samples

One hundred one samples were collected for histological and immunohistochemical analysis. They included 57 lung squamous cell carcinomas and 44 lung adenocarcinomas with neighboring noncancerous tissues, which were obtained from patients who had surgery in the Liaoning Province Tumor Hospital and the First Affiliated Hospital of China Medical University between 1998 and 2002. All patients had no radiotherapy or chemotherapy before the operation, and median follow-up of the patients was 22.87 months (range 1–80 months), and their outcomes were known.

The histologic diagnosis was evaluated by examination of hematoxylin and eosin-stained sections according to the classification system of the World Health Organization (2004). All tumors were staged according to the 7th edition of TNM staging system for lung cancer of International Union Against Cancer (2010). There were 21 patients with stage I, 21 with stage II, 54 with stage III, and 5 with stage IV. Also, there were lymph node metastases in 58 cases.

Immunohistochemistry

Tissue sections (4-μm thick) of formalin-fixed, paraffin-embedded specimens were deparaffinized in xylene, rehydrated in graded alcohol, and transferred to phosphate buffered saline (PBS). The slides were rinsed three times with PBS, and antigen retrieval was performed with a pressure cooker for 90 s. Endogenous peroxidase was blocked by the use of 3% hydrogen peroxide in PBS for 20 min. The samples were washed three times with PBS and incubated for 30 min at room temperature with a protein blocking solution. Excess blocking solution was drained, and the samples were incubated overnight at 4°C with anti-ILK antibody (1:400) (Millipore, Billerica, MA, USA), anti-E-cadherin antibody (1:200) (Santa Cruz Biotechnology, CA, USA), and anti-CD34 antibody (ready-to-use) (MaiXin, Fuzhou, China). Bound primary antibodies were detected with biotin–streptavidin–peroxidase method. Immunodetection was performed with diaminobenzidine as the chromogen, and counterstained with hematoxylin and dehydrated in alcohol before mounting.

The results of immunohistochemical staining were evaluated independently by three observers with no prior knowledge of patients' clinical data. The smooth muscle cells, fibroblasts, and endothelial cells of blood vessels, all known to be abundant in ILK, were used as positive controls. For a negative control, PBS was used for the primary antibody. Cytoplasmic and nuclear expression of ILK was scored based on two parameters: the proportion of immunopositive cells and their intensity of immunoreactivity. The proportion of immunopositive cells was categorized as follows: 0: <10%; 1: ≥10% to <25%; 2: ≥25% to <50%; 3: ≥50% to <75%; and 4: ≥75%. The staining intensity was categorized by relative intensity as follows: 0, no positivity; 1, weak; 2, moderate; and 3, strong. A final immunoreactivity score of each section was obtained by multiplying the two individual scores. Cases with scores <2 were considered as negative expression, while cases with scores ≥2 were considered as positive expression. Membranous expression of E-cadherin showed no significant variations in intensity of staining, and the scoring system was applied based on the percentage of positive cells: 0: <10%; 1: ≥10% to <25%; 2: ≥25% to <50%; 3: ≥50% to <75%, and 4: ≥75%. Since the adjacent non-neoplastic bronchial epithelium had a score of 4 for membranous localization of E-cadherin, cases with scores <4 was defined as decreased E-cadherin expression, while cases with a score of 4 were defined as preserved E-cadherin expression.

Quantification of MVD

MVD was assessed by immunohistochemical analysis with antibodies to the endothelial marker CD34 and determined according to the method of Weidner [17]. Briefly, the

immunostained sections were initially screened at low magnifications (×40 and ×100) to identify hot spots, which are the areas of highest neovascularization. Any yellow brown-stained endothelial cell or endothelial cell cluster that was clearly separate from adjacent microvessels, tumor cells, and other stromal cells was considered a single, countable microvessel. Within the hot spot area, the stained microvessels were counted in a single high-power (×200) field, and the average vessel count in three hot spots was considered the value of MVD.

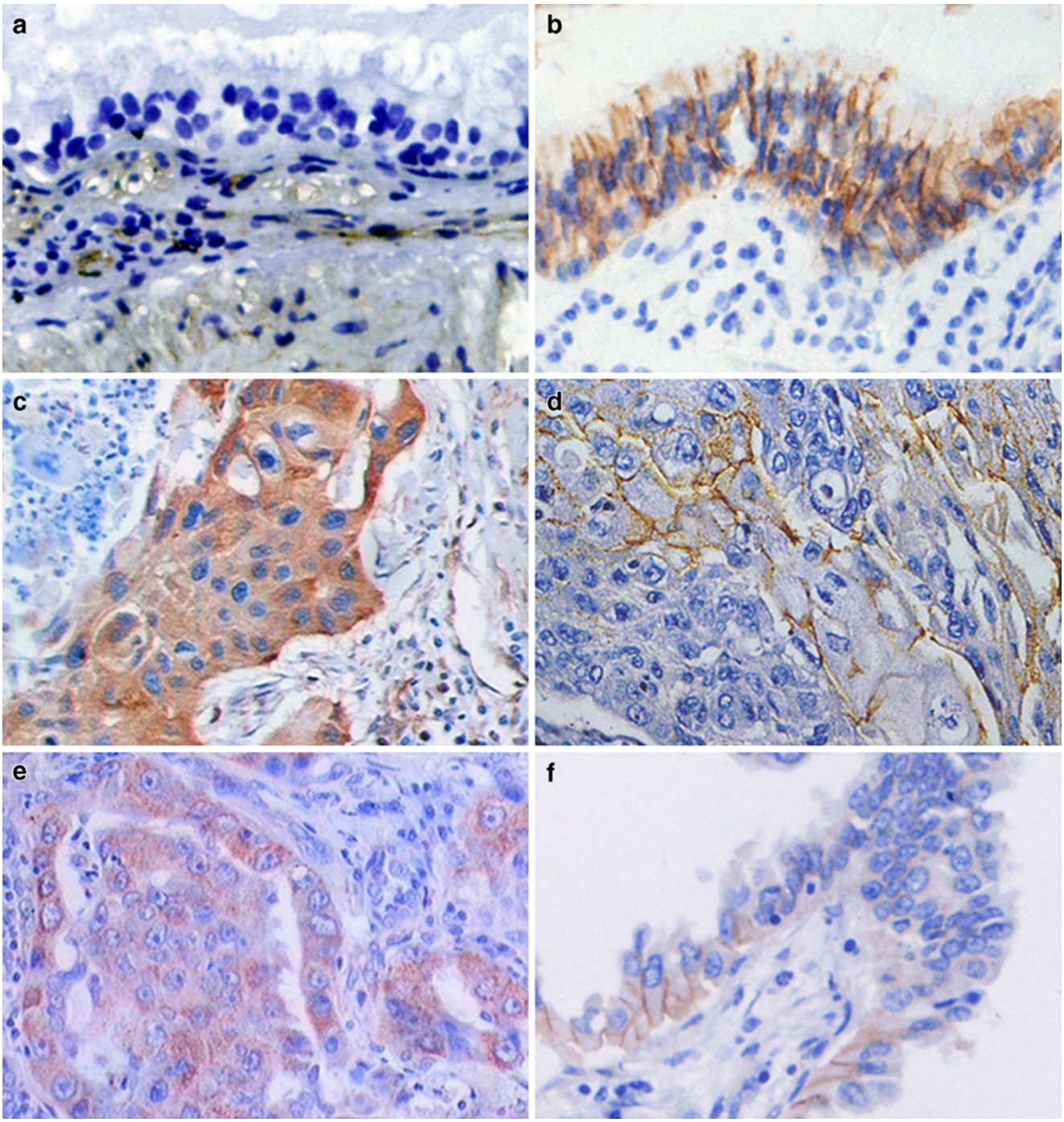

Fig. 1 ILK and E-cadherin expression in bronchial mucosa epithelial cells and lung cancer tissues. Negative immunostaining for ILK in bronchial mucosa epithelial cells (**a**), cytoplasmic staining for ILK in squamous cell carcinoma (**c**), and adenocarcinoma (**e**). Membranous staining of E-cadherin in bronchial mucosa epithelial cells (**b**), decreased expression of E-cadherin in squamous cell carcinoma (**d**), and adenocarcinoma (**f**). (×400)

Statistical analysis

All the data were analyzed with SPSS for Windows, version 13.0. The Pearson's chi-square test was used to analyze the relationship between ILK or E-cadherin expression and the clinicopathologic characteristics. The Spearman's correlation test was used to examine the correlation between the expression levels of ILK and E-cadherin. Correlations of MVD with clinicopathological factors and ILK expression were analyzed by *T*- test. Postoperative survival periods were calculated by the Kaplan–Meier method and compared by the log-rank test. The significance level was defined as $P<0.05$.

Results

Expression of ILK and E-cadherin in normal lung tissues and lung squamous cell carcinoma, and adenocarcinoma

Immunohistochemistry of normal bronchial epithelium showed expression of E-cadherin primarily in the cell membrane, but the expression of ILK was not detected (Fig. 1a, b). Of the 57 squamous cell carcinoma samples stained, 34 (59.65%) cases showing decreased expression of E-cadherin (Fig. 1d), and 39 (68.42%) cases showing positive expression of ILK (Fig. 1c), including 11 (19.30%) cases showing both cytoplasmic and nuclear expressions of ILK (Fig. 2a). In 44 adenocarcinoma cases, there were 25 (56.82%) cases showing decreased expression of E-cadherin (Fig. 1f), and 27 (61.36%) cases showing positive ILK expression (Fig. 1e), including 6 (13.64%) cases showing both cytoplasmic and nuclear expressions of ILK (Fig. 2b). There was no case showing sole nuclear staining for ILK in squamous cell carcinoma and adenocarcinoma.

Relationship between ILK or E-cadherin expression and clinicopathological factors

As shown in Table 1, there was no statistically significant correlation between ILK expression and any clinicopathological parameters in squamous cell carcinoma ($P>0.05$). The positive ILK expression was directly related to advanced TNM stage in adenocarcinoma ($P=0.022$). There was no statistically significant correlation between nuclear ILK expression and any clinicopathological parameters in squamous cell carcinoma and adenocarcinoma ($P>0.05$).

Decreased expression of E-cadherin was correlated with lymph node metastasis in squamous cell carcinoma ($P=0.033$). In adenocarcinoma, decreased E-cadherin expression was correlated with advanced TNM stage ($P=0.020$) and lymph node metastasis ($P=0.009$; Table 2).

In addition, the Spearman's correlation test revealed that increased ILK expression was correlated with reduced E-cadherin expression in squamous cell carcinoma (correlation coefficient=0.364, $P=0.005$). In adenocarcinoma, ILK expression was not correlated with E-cadherin expression ($P=0.101$).

Correlation of MVD with clinicopathological factors and ILK expression

Distribution of microvessels in sections of squamous cell carcinoma and adenocarcinoma is illustrated in Fig. 3. The average MVD in squamous cell carcinoma and adenocarcinoma cases were 43.19±9.71 and 44.09±8.19, respectively. The correlation of MVD with clinicopathological factors and ILK expression is shown in Table 3. In squamous cell carcinoma and adenocarcinoma, the MVD in positive ILK-staining cases was much higher than that in negative ILK-staining cases (squamous cell carcinoma

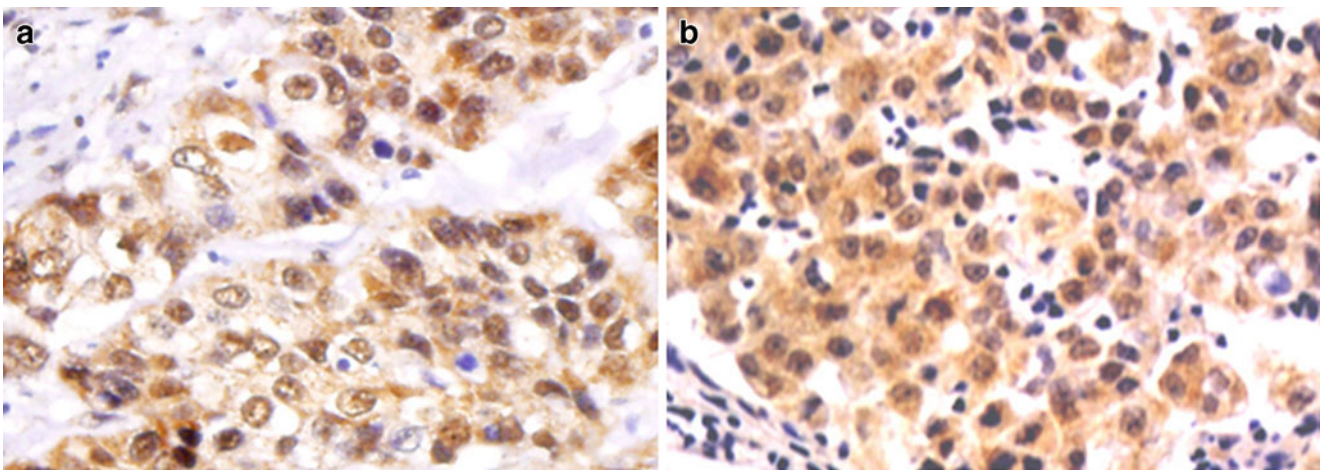

Fig. 2 Cytoplasmic and nuclear staining for ILK in squamous cell carcinoma (**a**) and adenocarcinoma (**b**). (×400)

Table 1 Expression of ILK in lung squamous cell carcinomas and adenocarcinomas and correlation with clinicopathological parameters

	Lung squamous cell carcinomas					Adenocarcinomas				
	Samples	Cytoplasm	*P* values	Nucleus	*P* values	Samples	Cytoplasm	*P* values	Nucleus	*P* values
Gender			1.000		1.000			0.757		0.664
Male	42	29		8		22	13		4	
Female	15	10		3		22	14		2	
Age			0.652		0.493			0.977		0.375
≤55	31	22		7		18	11		1	
>55	26	17		4		26	16		5	
TNM stage			0.313		1.000			0.022		0.684
I and II	23	14		4		19	8		2	
III and IV	34	25		7		25	19		4	
Lymph node metastasis			0.075		1.000			0.055		0.375
Negative	25	14		5		18	8		1	
Positive	32	25		6		26	19		5	

47.72±7.10 vs.33.39±7.03, T=7.106, P<0.001; adenocarcinoma 46.04±7.83 vs 41.06±8.09, T=2.028, P=0.049).

Cumulative Kaplan–Meier survival analysis

In squamous cell carcinoma, the 5-year survival rate for the patients with positive and negative ILK expression was 3% and 38%, respectively; the difference was statistically significant (P<0.001; Fig. 4a). Furthermore, the 5-year survival rate for the patients with decreased E-cadherin expression was 9%, and that with preserved E-cadherin expression was 21% (P=0.009; Fig. 4b). The Kaplan–Meier survival analysis also showed that TNM stage (P<0.001), lymph node metastasis (P<0.001), and MVD (P<0.001) were all statistically significant prognostic factors.

In adenocarcinoma, the 5-year survival rate for the patients with positive and negative ILK expression was 4% and 18%, respectively; the difference was statistically significant (P<0.001; Fig. 4c). The 5-year survival rate for the patients with decreased E-cadherin expression was 4%, and that with preserved E-cadherin expression was 16% (P=0.046; Fig. 4d). The Kaplan–Meier survival analysis also showed that TNM stage (P<0.001), lymph node metastasis (P=0.002), and MVD (P<0.001) were all statistically significant prognostic factors.

Table 2 Expression of E-cadherin in lung squamous cell carcinomas and adenocarcinomas and correlation with clinicopathological parameters

	Lung squamous cell carcinomas			Adenocarcinomas		
	Samples	Decreased E-cadherin expression	*P* values	Samples	Decreased E-cadherin expression	*P* values
Gender			0.208			0.361
Male	42	23		22	11	
Female	15	11		22	14	
Age			0.419			0.632
≤55	31	17		18	11	
>55	26	17		26	14	
TNM stage			0.344			0.020
I and II	23	12		19	7	
III and IV	34	22		25	18	
Lymph node metastasis			0.033			0.009
Negative	25	11		18	6	
Positive	32	23		26	19	

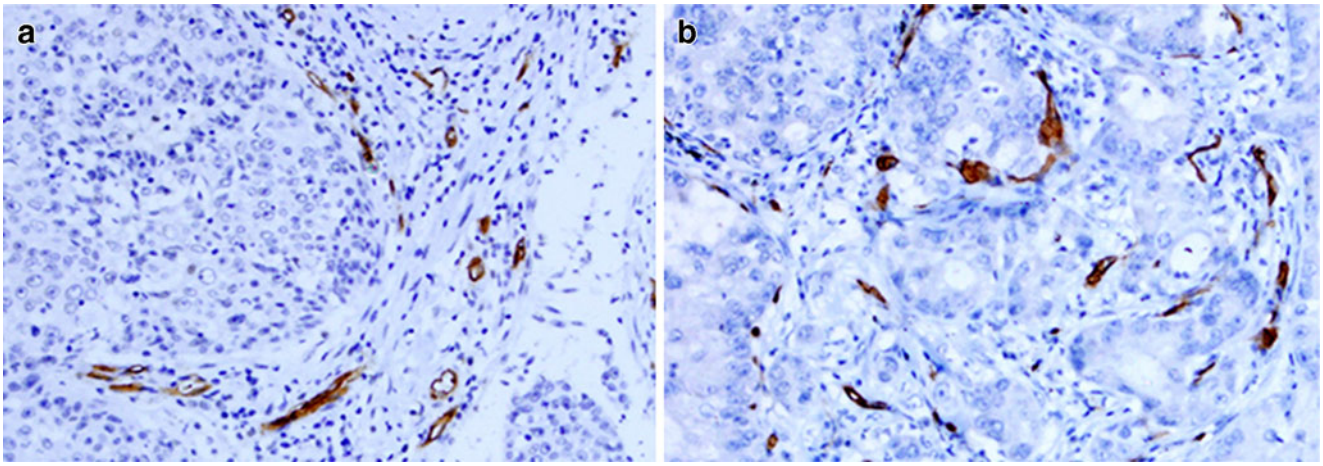

Fig. 3 Distribution of microvessels in fields of two hot spots in sections of squamous cell carcinoma (**a**) and adenocarcinoma (**b**). (×200)

However, gender and age were not statistically significant prognostic factors in patients with squamous cell carcinoma and adenocarcinoma ($P>0.05$).

Discussion

Cell-ECM interactions play an important role in cell survival, growth, differentiation, and migration [1]. As a key component of cell-ECM structures, ILK associates with cytoplasmic domains of β1 and β3 integrins, and apart from its unconventional kinase activity, it also functions as a scaffolding protein which mediates linkage of integrins to the actin cytoskeleton [2, 18]. As a scaffolding protein, the N-terminal domain of ILK associates with adapter proteins PINCH1 and PINCH2, while its C-terminal domain interacts with α/β-Parvin. This ternary PINCH/ILK/Parvin complex not only serves as a platform for structurally linking integrins with the actin cytoskeleton, but also interacts with specific additional partners and positively regulates PKB/Akt, MMP activity and negatively regulates GSK-3β activity, thus, implicating ILK in the pathologic processes of tumor invasion, progression, and metastasis [18–21].

In the current study, we detected ILK expression using immunohistochemistry in 57 lung squamous cell carcinomas and 44 lung adenocarcinomas. ILK was positively expressed in 39 (68.42%) squamous cell carcinoma cases

Table 3 Correlation of MVD with clinicopathological factors and ILK expression in lung squamous cell carcinomas and adenocarcinomas

	Squamous cell carcinoma				Adenocarcinoma			
	Samples	MVD	*T*-test	*P* values	Samples	MVD	*T*-test	*P* values
Gender			0.249	0.804			2.555	0.014
Male	42	43.00±10.03			22	41.14±8.72		
Female	15	43.73±9.06			22	47.09±6.59		
Age			0.326	0.745			0.334	0.740
≤55	31	43.58±9.98			18	43.61±8.77		
>55	26	42.73±9.56			26	44.46±7.96		
TNM stage			2.845	0.006			4.323	<0.001
I and II	23	39.00±10.20			19	38.95±8.50		
III and IV	34	46.03±8.38			25	48.04±5.40		
Lymph node metastasis			3.059	0.003			3.320	0.002
Negative	25	39.04±11.39			18	39.67±8.92		
Positive	32	46.44±6.72			26	47.19±6.14		
ILK expression			7.106	<0.001			2.028	0.049
Negative	18	33.39±7.03			17	41.06±8.09		
Positive	39	47.72±7.10			27	46.04±7.83		

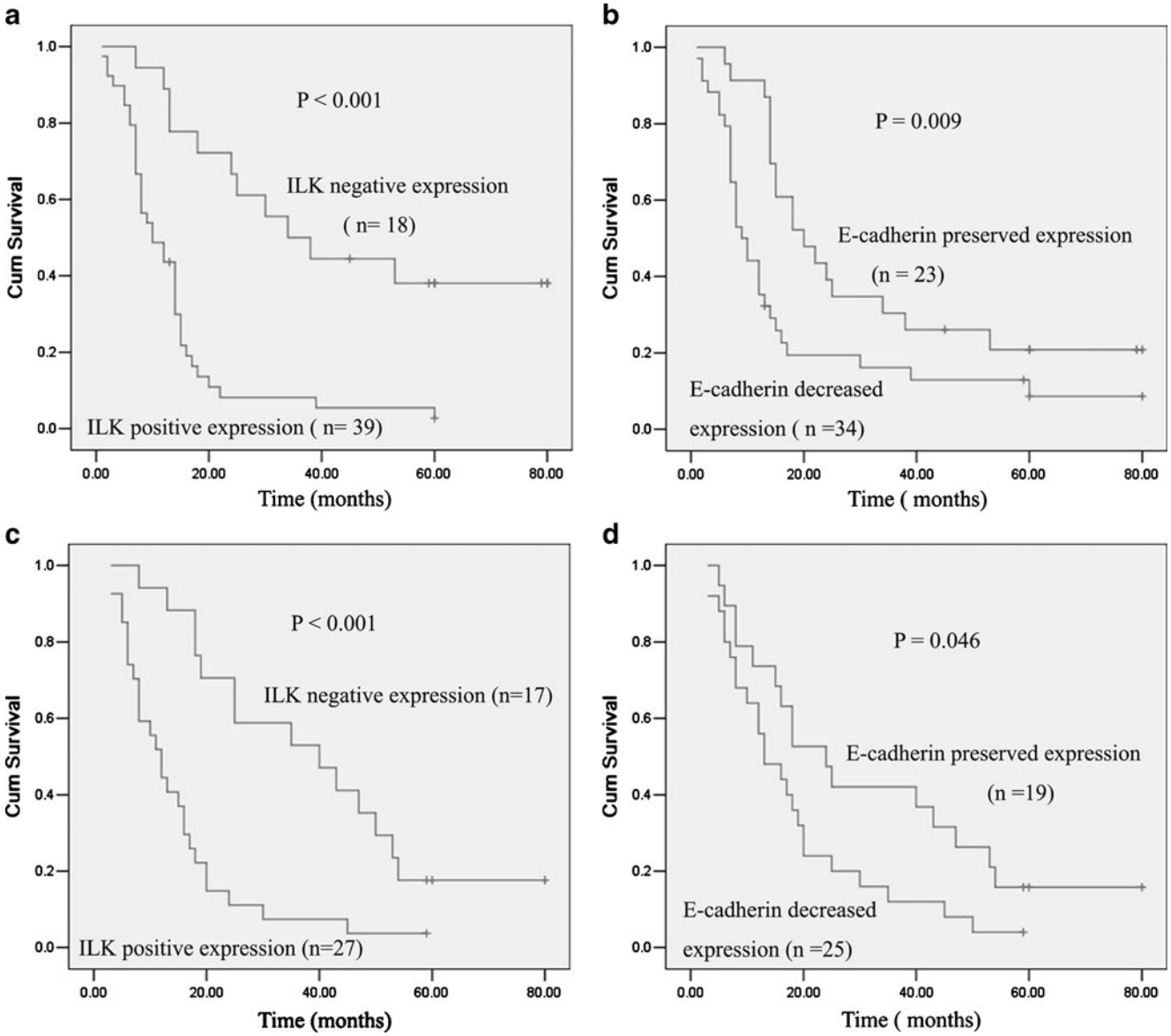

Fig. 4 Kaplan–Meier survival curve according to ILK and E-cadherin expression in lung squamous cell carcinoma and adenocarcinoma. Patients with negative ILK expression have a significantly better survival than those with positive ILK expression in squamous cell carcinoma (**a**) and adenocarcinoma (**c**), respectively. Patients with decreased E-cadherin expression have a significantly poorer survival than those with preserved E-cadherin expression in squamous cell carcinoma (**b**) and adenocarcinoma (**d**), respectively

and 27 (61.36%) adenocarcinoma cases, whereas there was no ILK expression in normal bronchial epithelium cells. Furthermore, our results showed that positive expression of ILK was correlated with advanced TNM stage in adenocarcinoma. In squamous cell carcinoma and adenocarcinoma, we also found that the cases with lymph node metastasis had higher ILK expression, though the differences were not significant (P=0.075 and P=0.055, respectively). These results are similar to the studies in gastric carcinoma, prostate tumor, colon cancer, ovary carcinoma, melanoma, and lung cancer [6–11]. The data indicate that increased ILK expression is associated with progression of lung squamous cell carcinoma and adenocarcinoma. In contrast, renal cell carcinoma and several non-epithelial tumors, such as lymphoma, retinoblastoma, mesenchymal chondrosarcomas, and sarcomas of bone and soft tissue have been reported to have decreased or no ILK expression [22, 23], which suggest that ILK may have different functions in tumors of different origins.

Interestingly, of the 66 cases with positive ILK expression, 17 cases showed both cytoplasm and nuclear staining of ILK, including 11 squamous cell carcinomas and 6 adenocarcinomas. However, there was no statistically significant correlation between nuclear ILK expression and any clinicopathological factors. Consistent with our findings, nuclear localization of ILK has been reported in

non-small cell lung cancer and laryngeal carcinoma [11, 24]. Takanami did not investigate the correlation between nuclear ILK expression and clinicopathological parameters in non-small cell lung cancer [11]. There were no significant differences between nuclear ILK expression and clinicopathological parameters in laryngeal carcinoma [24]. It has been demonstrated that nuclear localization of ILK in breast cancer cell lines was attributed to a mechanism involving activation of PAK-1 [25]. Additionally, ILK has been shown to regulate the organization of the mitotic spindle [26]. Taken together, the nuclear function of ILK in lung squamous cell carcinoma and adenocarcinoma requires further study.

E-cadherin is an important epithelial cell adhesion molecule mediating cell–cell interactions. In epithelial derived tumors, loss of cell–cell adhesion is correlated with downregulation of E-cadherin, as well as increases proliferation, invasiveness, and metastasis. Consistent with these, we found that the expression of E-cadherin was downregulated in lung squamous cell carcinoma and adenocarcinoma, and reduced expression of E-cadherin was correlated with lymph node metastasis. In adenocarcinoma, decreased E-cadherin expression was also correlated with advanced TNM stage. Importantly, our data showed that increased ILK expression was correlated with reduced E-cadherin expression in squamous cell carcinoma. However, ILK expression was not correlated with E-cadherin expression in adenocarcinoma. Research revealed that overexpression of ILK leads to the loss of cell–cell adhesion because of the downregulation of E-cadherin, possibly by ILK-mediated activation of the E-cadherin repressor Snail [13, 14], or nuclear β-catenin stabilization by ILK-mediated inhibition on GSK-3 activity [21]. Our findings indicate that increased expression of ILK may be involved in the loss of E-cadherin expression in squamous cell carcinoma.

Tumor angiogenesis is critical to the growth and invasion of tumor cells, and MVD is accepted as a standard indicator of angiogenesis. In agreement with the published data, our study showed that high MVD was correlated with advanced TNM stage and lymph node metastasis in squamous cell carcinoma and adenocarcinoma. Previous studies indicate that ILK could positively regulate Akt activity, and, activation of Akt could also upregulate VEGF expression, thus, stimulating tumor angiogenesis [19, 27]. Inhibition of ILK expression or activity results in the inhibition of VEGF-mediated endothelial cell migration, capillary formation in vitro, and angiogenesis in vivo [15, 16]. For the first time, we demonstrated that MVD in positive ILK-staining cases was much higher than that in negative ILK-staining cases in squamous cell carcinoma and adenocarcinoma. These data probably indicate that ILK may be involved in angiogenesis, and thus, enhance tumor progression of lung squamous cell carcinoma and adenocarcinoma.

The overall prognosis of patients with positive ILK expression was poorer than those with negative ILK expression in squamous cell carcinoma and adenocarcinoma. The univariate survival analysis revealed that ILK was a significant prognostic factor in patients with lung squamous cell carcinoma and adenocarcinoma, as well as E-cadherin, TNM stage, lymph node metastasis, and MVD, which are consistent with previous studies [10, 11]. These data further support the notion that enhanced ILK expression may be involved in the malignant progression of lung squamous cell carcinoma and adenocarcinoma.

In conclusion, we found that overexpression of ILK is a common abnormality and correlates with high MVD in lung squamous cell carcinoma and adenocarcinoma. The findings also indicate a causative relation between loss of E-cadherin and overexpression of ILK in lung squamous cell carcinoma. The ILK, E-cadherin proteins and tumor angiogenesis appear to play important roles in the progression of lung squamous cell carcinoma and adenocarcinoma. Measuring ILK and E-cadherin expression, and MVD may contribute to a better understanding of the prognosis of patients with lung squamous cell carcinoma and adenocarcinoma.

Conflict of interest statement We declare that we have no conflict of interest.

References

1. Dedhar S (2000) Cell-substrate interactions and signaling through ILK. Curr Opin Cell Biol 12:250–256
2. Hannigan GE, Leung-Hagesteijn C, Fitz-Gibbon L et al (1996) Regulation of cell adhesion and anchorage-dependent growth by a new beta 1-integrin-linked protein kinase. Nature 379:91–96
3. Attwell S, Roskelley C, Dedhar S (2000) The integrin-linked kinase (ILK) suppresses anoikis. Oncogene 19:3811–3815
4. Radeva G, Petrocelli T, Behrend E et al (1997) Overexpression of the integrin-linked kinase promotes anchorage-independent cell cycle progression. J Biol Chem 272:13937–13944
5. Wu C, Keightley SY, Leung-Hagesteijn C et al (1998) Integrin-linked protein kinase regulates fibronectin matrix assembly, E-cadherin expression, and tumorigenicity. J Biol Chem 273:528–536
6. Ito R, Oue N, Zhu X et al (2003) Expression of integrin-linked kinase is closely correlated with invasion and metastasis of gastric carcinoma. Virchows Arch 442:118–123
7. Graff JR, Deddens JA, Konicek BW et al (2001) Integrin-linked kinase expression increases with prostate tumor grade. Clin Cancer Res 7:1987–1991
8. Bravou V, Klironomos G, Papadaki E et al (2003) Integrin-linked kinase (ILK) expression in human colon cancer. Br J Cancer 89:2340–2341
9. Ahmed N, Riley C, Oliva K et al (2003) Integrin-linked kinase expression increases with ovarian tumour grade and is sustained by peritoneal tumour fluid. J Pathol 201:229–237

10. Dai DL, Makretsov N, Campos EI et al (2003) Increased expression of integrin-linked kinase is correlated with melanoma progression and poor patient survival. Clin Cancer Res 9:4409–4414
11. Takanami I (2005) Increased expression of integrin-linked kinase is associated with shorter survival in non-small cell lung cancer. BMC Cancer 5:1
12. Eke I, Hehlgans S, Cordes N (2009) There's something about ILK. Int J Radiat Biol 85:929–936
13. Tan C, Costello P, Sanghera J et al (2001) Inhibition of integrin linked kinase (ILK) suppresses beta-catenin-Lef/Tcf-dependent transcription and expression of the E-cadherin repressor, snail, in APC-/- human colon carcinoma cells. Oncogene 20:133–140
14. McPhee TR, McDonald PC, Oloumi A et al (2008) Integrin-linked kinase regulates E-cadherin expression through PARP-1. Dev Dyn 237:2737–2747
15. Tan C, Cruet-Hennequart S, Troussard A et al (2004) Regulation of tumor angiogenesis by integrin-linked kinase (ILK). Cancer Cell 5:79–90
16. Edwards LA, Woo J, Huxham LA et al (2008) Suppression of VEGF secretion and changes in glioblastoma multiforme microenvironment by inhibition of integrin-linked kinase (ILK). Mol Cancer Ther 7:59–70
17. Weidner N (1995) Current pathologic methods for measuring intratumoral microvessel density within breast carcinoma and other solid tumors. Breast Cancer Res Treat 36:169–180
18. McDonald PC, Fielding AB, Dedhar S (2008) Integrin-linked kinase–essential roles in physiology and cancer biology. J Cell Sci 121:3121–3132
19. McDonald PC, Oloumi A, Mills J et al (2008) Rictor and integrin-linked kinase interact and regulate Akt phosphorylation and cancer cell survival. Cancer Res 68:1618–1624
20. Troussard AA, Costello P, Yoganathan TN et al (2000) The integrin linked kinase (ILK) induces an invasive phenotype via AP-1 transcription factor-dependent upregulation of matrix metalloproteinase 9 (MMP-9). Oncogene 19:5444–5452
21. Delcommenne M, Tan C, Gray V et al (1998) Phosphoinositide-3-OH kinase-dependent regulation of glycogen synthase kinase 3 and protein kinase B/AKT by the integrin-linked kinase. Proc Natl Acad Sci USA 95:11211–11216
22. Haase M, Gmach CC, Eke I et al (2008) Expression of integrin-linked kinase is increased in differentiated cells. J Histochem Cytochem 56:819–829
23. Chung DH, Lee JI, Kook MC et al (1998) ILK (beta1-integrin-linked protein kinase): a novel immunohistochemical marker for Ewing's sarcoma and primitive neuroectodermal tumour. Virchows Arch 433:113–117
24. Goulioumis AK, Bravou V, Varakis J et al (2008) Integrin-linked kinase cytoplasmic and nuclear expression in laryngeal carcinomas. Virchows Arch 453:511–519
25. Acconcia F, Barnes CJ, Singh RR et al (2007) Phosphorylation-dependent regulation of nuclear localization and functions of integrin-linked kinase. Proc Natl Acad Sci USA 104:6782–6787
26. Fielding AB, Dobreva I, McDonald PC et al (2008) Integrin-linked kinase localizes to the centrosome and regulates mitotic spindle organization. J Cell Biol 180:681–689
27. Banerjee S, Saxena N, Sengupta K et al (2003) 17alpha-estradiol-induced VEGF-A expression in rat pituitary tumor cells is mediated through ER independent but PI3K-Akt dependent signaling pathway. Biochem Biophys Res Commun 300:209–215

Virchows Arch (2011) 458:109–113
DOI 10.1007/s00428-010-0995-4

ORIGINAL ARTICLE

Paratesticular fibrous pseudotumor—an IgG4-related disorder?

Hans Bösmüller · Claus Hann von Weyhern · Patrick Adam · Vedat Alibegovic · Gregor Mikuz · Falko Fend

Received: 8 September 2010 / Accepted: 4 October 2010 / Published online: 19 October 2010
© Springer-Verlag 2010

Abstract Paratesticular fibrous pseudotumor (nodular periorchitis, inflammatory pseudotumor of the spermatic cord) is a rare, benign condition of unknown etiology characterized by solitary or multiple intrascrotal nodules composed of dense fibrous tissue with a variable, sometimes sparse inflammatory infiltrate. Based on certain similarities to other fibroinflammatory disorders characterized by infiltrates of IgG4-expressing plasma cells and recently subsumed under the heading of IgG4-mediated diseases, we investigated the plasma cell distribution and immunoglobulin isotypes in three cases of paratesticular fibrous and inflammatory pseudotumor. All three cases showed a high number of IgG4-positive plasma cells with an IgG4 to IgG ratio of 44–48%. This finding indicates that paratesticular fibrous pseudotumor might belong to the growing list of IgG4-related diseases, which by now includes such diverse entities as retroperitoneal fibrosis, sclerosing pancreatitis and cholangitis, Riedel's thyroiditis, or sclerosing sialadenitis.

Keywords Inflammatory pseudotumor · Paratesticular fibrous pseudotumor · Testis · IgG4

H. Bösmüller (✉) · V. Alibegovic
Department of Pathology, Krankenhaus Barmherzige Schwestern, Seilerstätte 4,
4020 Linz, Austria
e-mail: hans-christian.boesmueller@bhs.at

C. H. von Weyhern · P. Adam · F. Fend
Department of Pathology, University of Tübingen, Tübingen, Germany

G. Mikuz
Department of Pathology, University of Innsbruck, Innsbruck, Austria

Introduction

Paratesticular fibrous pseudotumors (PFPT) are rare, benign fibrous proliferations in the tunica vaginalis testis or along the spermatic cord and the epididymis. Due to their variable presentation and histology, these lesions have received different designations such as fibromatous periorchitis or nodular periorchitis [1–4]. The first description goes back to 1830 [5]. PFPT does not show an age predilection and is usually characterized by multiple, sometimes solitary paratesticular nodules or plaques, and only a minority of cases are adherent to the spermatic cord or epididymis [6–8]. Paratesticular inflammatory pseudotumors, also described as pseudosarcomatous myofibroblastic proliferation or proliferative funiculitis [9, 10], are solitary lesions of the spermatic cord and very rarely occur in a testicular or epididymal location [11, 12]. They are characterized by a densely arranged myofibroblastic proliferation with heterogeneous inflammatory components like plasma cells, lymphocytes, histiocytes and granulocytes, and hyalinized areas and hypercellular areas are intermixed [13]. Inflammatory pseudotumors may clinically mimic malignancy [14–16]. Some of these cases may correspond to other entities such as solitary fibrous tumor [17] or inflammatory myofibroblastic tumor; however, the majority of paratesticular inflammatory pseudotumors and PFPT nowadays are thought to represent the same lesion in various stages of development, with predominance of inflammation and myofibroblastic proliferation in early lesions, to heavily collagenized, paucicellular fibrous nodules in more advanced stages [18].

Based on similarities to fibrous pseudotumors and chronic fibroinflammatory processes in other localizations, which have recently been summarized under the term IgG4-related sclerosing disease due to the abundance of IgG4-

expressing plasma cells in affected tissues and high serum concentration of IgG4, we investigated the plasma cell content and isotype distribution in three cases of PFPT and demonstrate that PFPT may represent another localized manifestation of IgG4-related disease [13, 19–24].

Material and methods

Case selection

Two patients with PFPT were identified in the files of the Department of Pathology, University Hospital Tübingen, Germany (case 1 and 2); a case of inflammatory pseudotumor of the spermatic cord was found in St. Vincent Hospital of Linz, Austria (case 3).

Case one The 23-year-old patient felt multiple indolent floating masses up to 2 cm in diameter in the paratesticular region and along both spermatic cords. There was no history of associated trauma or infection. A total of 13 nodules, some of them corpora libera, some adherent to the tunica albuginea, were removed with preservation of both testicles, epididymis, and spermatic cords.

Case two The 52-year-old patient presented with right-sided, palpable paratesticular nodules suspicious for malignancy. There was no history of trauma or infection. Four nodules up to 1.7 cm in diameter adherent to the tunica albuginea testis were removed.

Case three The 25-year-old patient noted an initially indolent swelling of the right testicle for several weeks, but increasing pain prompted hospitalization. Clinical investigation revealed a suspected testicular mass, corresponding to a hyperdense lesion of about 5 cm by ultrasound examination. No enlarged lymph nodes or other pathological lesions were identified by CT of the abdomen. The patient underwent semicastration. On gross examination, the testis was partially necrotic, the epididymis was grossly normal. A sharply demarcated, yellow-gray mass of 5 cm in diameter occupied the space between the testis and epididymis, displacing the spermatic cord and the neighboring necrotic testicular area.

Histology and immunohistochemistry

Based on examination of conventional hematoxylin and eosin-stained sections, tumor areas rich in plasma cells were selected for immunohistochemistry. Serial 3 μm paraffin sections were used for immunostaining on a Ventana BenchMark XT automated immunostainer (Ventana Medical Systems, Tucson, AZ, 85755 USA). The following primary antibodies were used: IgA (rabbit polyclonal 1:80.000; DAKO, Glostrup, Denmark), IgD (rabbit polyclonal 1:500, DAKO), IgM (rabbit polyclonal 1:10.000, DAKO), IgG (rabbit polyclonal 1:3.000, DAKO), IgG4 (clone HP6025 1:500; The Binding Site, Birmingham, UK), CD138 (clone MI15 1:200, DAKO), kappa and lambda light chains (rabbit polyclonal 1:10.000; CYTOMED, Baden-Baden, Germany), CD3 (rabbit clone SP7 1:100, DCS Diagnostics 22397 Hamburg, Germany), and CD20 (clone L26 1:800, DCS Diagnostics), ALK-1 (mouse clone ALK1, ready to use, DAKO).

The scoring system for plasma cells and the IgG4 to IgG ratio proposed by Zen [24] was used for quantification. We counted total plasma cells stained with CD138, as well as IgG- and IgG4-expressing plasma cells in absolute numbers per 10 HPF and considered an IgG4 to IgG ratio of ≥30% as positive for IgG4-related disease.

Results

The fibrous paratesticular fibrous pseudotumors of patients 1 and 2 showed very similar histological findings. All nodules had a similar appearance with hyalinized collagenous stroma, sparse residual mesothelial cell nests and an unequal infiltrate of plasma cells and lymphocytes (Fig. 1). The distribution of plasma cells had little relationship to the size of the lesions, only a few smaller nodules revealed a more distinct inflammation. Staining for CD 138 and IgG revealed significant numbers of plasma cells, whereas IgA, IgD, and IgM highlighted only rare cells. Kappa and lambda light chains confirmed a polyclonal plasma cell population. Congo red staining and ALK-1 immunohistochemistry was negative, CD20 or CD3 lymphocytes were virtually absent, and there was no evidence of phlebitis.

The lesion of patient 3 diagnosed as paratesticular inflammatory pseudotumor was characterized by a dense myofibroblastic proliferation with sparse mitoses. Inflammatory areas with plasma cells, lymphocytes, and eosinophils alternated with hyalinized regions, especially around blood vessels. Small areas of inflammatory necrosis were present and showed partial organization. The spermatic duct and the epididymis were involved by the proliferation. Within the fibroinflammatory lesion, numerous venous blood vessels with obliterative phlebitis were present (Fig. 2). At the specimen's margin, neighboring fat was organized by granulation tissue. The testicular parenchyma exhibited extensive ischemic necrosis, probably due to local tumor compression. Immunohistochemistry revealed numerous plasma cells positive for CD138, but both T and B lymphocytes, eosinophilic

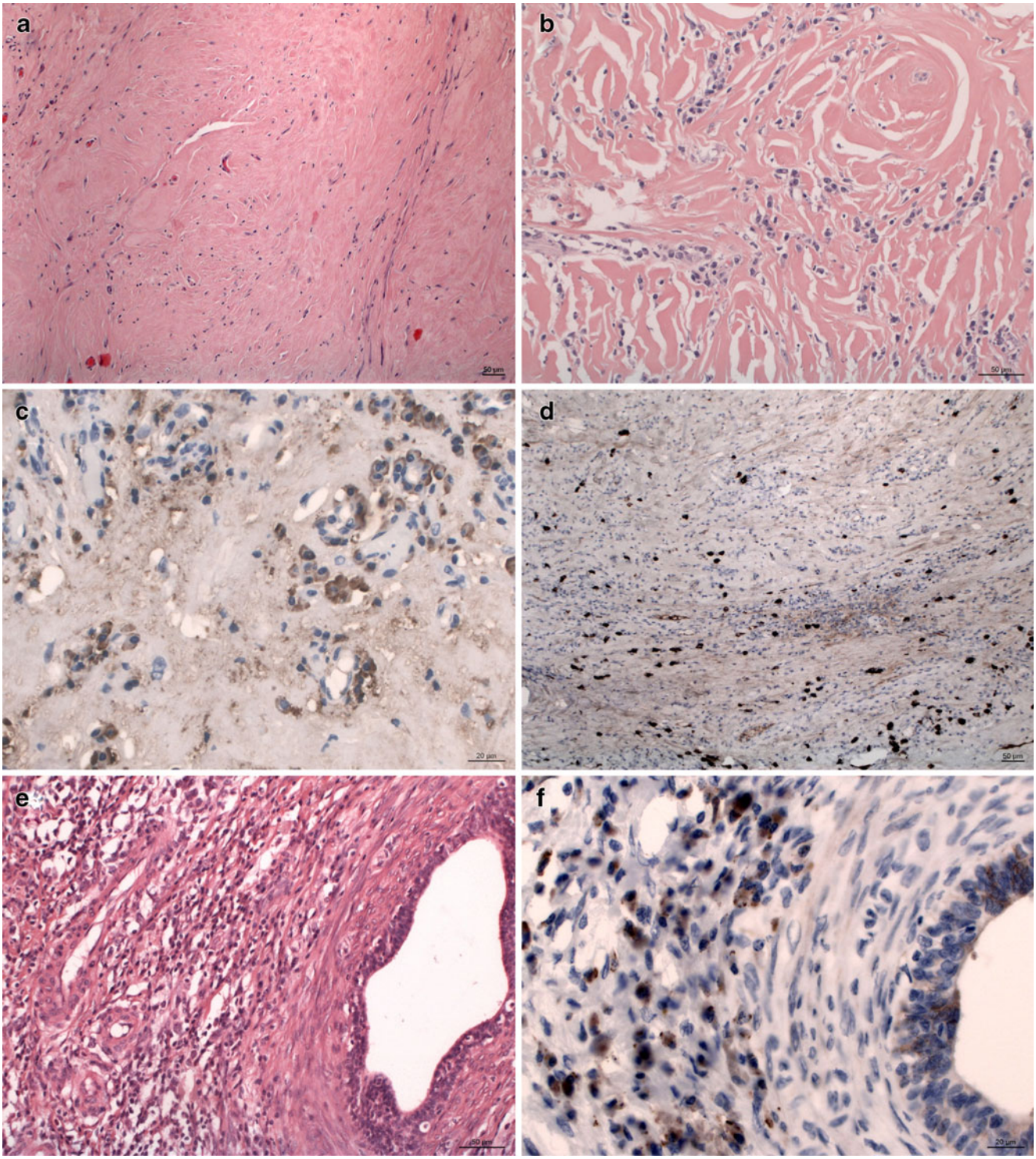

Fig. 1 Hyalinized area of PFPT (**a**) and area rich in plasma cells (**b**). Immunostaining for IgG in PFPT (**c**) in comparison to IgG4 expression pattern (**d**). Mixed periepididymal inflammatory infiltrates in the inflammatory pseudotumor of patient 3 (**e**) and CD138 immunostaining (**f**)

granulocytes, and histiocytes were likewise increased; ALK-1 immunostaining was negative. The plasma cell counts and IgG4 to IgG ratios of the three cases are summarized in Table 1.

Discussion

In the present study, we investigated the composition of the inflammatory infiltrate in paratesticular fibrous pseudotu-

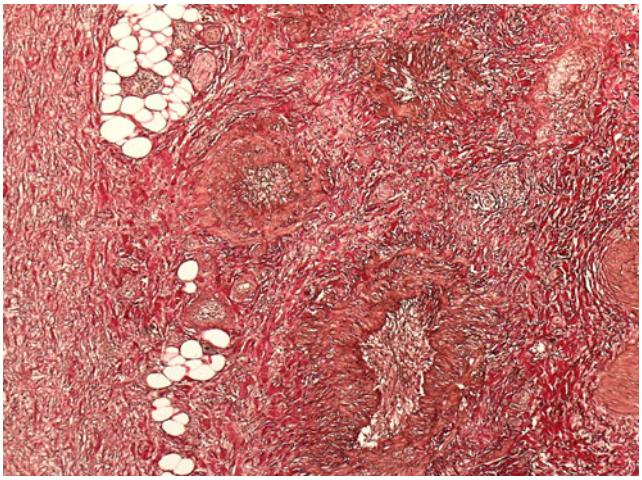

Fig. 2 Venous blood vessels with obliterative phlebitis in patient 3. Elastica van Gieson stain, ×100

mor (PFPT), a rare benign lesion of the scrotal region of unknown etiology. The notable increase in IgG4-positive plasma cells, in addition to other features of the studied lesions, indicates that PFPT might represent another localized manifestation of an IgG4-related disease. Although lesions like inflammatory or fibrous pseudotumors of the tunica vaginalis testis and testicular adnexal structures have already been known for a long time and were generally regarded as reactive proliferations, hypotheses to explain their origin are sparse in the literature. Usually, there is no evidence for antecedent trauma or inflammation. A study of two cases by Chan et al. failed to demonstrate evidence for Epstein-Barr virus infection in contrast to inflammatory pseudotumors in other locations [25]. In addition, the lack of an age predilection or a relationship to other diseases failed to give clues towards the etiology of this disorder [7].

Based on the different amounts of inflammatory cells, active myofibroblasts and hyalinisation or regression, respectively, two categories of paratesticular pseudoneoplastic proliferations were proposed, namely inflammatory and fibrous pseudotumors [4, 26, 27]. Inflammatory pseudotumors may be mistaken for inflammatory variants

Table 1 Random count of plasma cells in absolute numbers per 10 HPF, range per HPF in parentheses

	Patient 1	Patient 2	Patient 3
Diagnosis	PFPT	PFPT	PIPT
PC/10 HPF	393 (19–71)	141 (7–25)	232 (9–45)
IgG/10 HPF	248 (7–82)	103 (6–17)	149 (5–59)
IgG4/10 HPF	111 (2–17)	48 (2–9)	72 (4–10)
IgG4 ratio	44%	46%	48%

PC plasma cell, *HPF* high-power field, *PIPT* paratesticular inflammatory pseudotumor

of sarcoma, such as inflammatory fibrosarcoma, leiomyosarcoma, or liposarcoma [28], but malignant mesenchymal tumors in this site are very rare. Some cases, however, may indeed represent inflammatory myofibroblastic tumors observed at other sites [9, 10, 12, 15]. Fibrous pseudotumors, due to their close connection to the tunica albuginea, might be interpreted as fibroma, fibromatosis, or solitary fibrous tumor; however, multiplicity, paucicellularity, and hyalinisation as well as the presence of residual inflammatory infiltrates, including plasma cells sets these lesions apart from fibromatoses and related lesions [29]. For the reasons mentioned above, Bégin considered the latter entity to be a burnt out variant of inflammatory pseudotumor [30], and recently Miyamoto et al. reviewed 13 cases of paratesticular fibrous pseudotumors and proposed a plaque-like type, an inflammatory/sclerotic type, and a myofibroblastic type, based on differences in their amount of collagen, capillaries, and inflammatory component [18].

The morphological spectrum of PFPT and related lesions are reminiscent of a group of diseases associated with chronic fibroinflammatory processes at various sites, which have recently been integrated into the common pathogenetic concept of IgG4-related disorders [31]. Diseases like sclerosing pancreatitis, sclerosing sialadenitis, possibly Riedel's thyroiditis, and retroperitoneal fibrosis as well as other rare variants and organ manifestations have been demonstrated to show convincing evidence of IgG4 involvement [11, 31, 32]. The same hypothesis has been extended to include inflammatory pseudotumors or plasma cell granulomas of the lung, liver, mesentery, breast, orbit, and pancreas [23]. Some of these lesions show different appearances in different stages of development, as discussed by Zen et al. [24] for retroperitoneal fibrosis. He hypothesized that IgG4-depleted lesions were mature variants of the same entity. Of note, in all of our cases of PFPT, a high amount of IgG4-positive plasma cells and a mean IgG4 to IgG ratio of 46% were present, despite the pronounced fibrosis in two of the three specimens. This fact, in addition to the morphological similarities such as the presence of obliterative phlebitic changes in case 3 and the lack of a known etiology, support the hypothesis that PFPT might represent an IgG4-related disorder. Very sparse reports exist about retroperitoneal fibrosis with scrotal involvement [33, 34]. The only case known to us of metachronous retroperitoneal fibrosis with succeeding paratesticular fibrosis was reported by Nistal et al; however, these authors attributed paratesticular fibrosis to interrupted lymphatic drainage [35].

In summary, despite the small number of cases, the markedly increased number of intralesional IgG4-expressing plasma cells, together with the clinical and morphological features, provides evidence that paratesticular fibrous pseudotumor and related lesions might represent

yet another localized organ manifestation of IgG4-related sclerosing disease. Further studies including serological data, which unfortunately were not available in our cases, will be needed to confirm these findings.

Conflict of interest statement We declare that we have no conflict of interest.

References

1. Goodwin WE (1946) Multiple, benign, fibrous tumors of tunica vaginalis testis. J Urol 56:438–447
2. Meyer AW (1928) Corpora libera in the tunica vaginalis testis. Am J Pathol 4:445–455
3. Mikuz G, Damjanov I (1982) Inflammation of the testis, epididymis, paratesticular membranes and scrotum. Pathol Annu Part 1:101–128
4. White WM, Hilsenbeck J, Waters WB (2006) Fibromatous periorchitis of testis. Urology 67(623):e15–e16
5. Cooper A (1830) Observations on the structure and diseases of the testis. Longmans, London
6. Gilchrist KW, Benson RC Jr (1979) Multifocal fibrous pseudotumor of testicular tunics. Possible clinical dilemma. Urology 14:285–287
7. Vates TS, Ruemmler-Fisch C, Smilow PC, Fleisher MH (1993) Benign fibrous testicular pseudotumors in children. J Urol 150:1886–1888
8. Zenker I, Schütz A, Sorge I, Tröbs RB (2006) Nodular periorchitis masquerading as a malignant parafunicular tumor in an adolescent. J Pediatr Surg 41:e33–e35
9. Hollowood K, Fletcher CD (1992) Pseudosarcomatous myofibroblastic proliferation of the spermatic cord ("proliferative funiculitis"). Histologic and immunohistochemical analysis of a distinctive entity. Am J Surg Pathol 16:448–454
10. Milanezi MF, Schmitt F (1997) Pseudosarcomatous myofibroblastic proliferation of the spermatic cord (proliferative funiculitis). Histopathology 31:387–388
11. Kamisawa T (2004) IgG4-positive plasma cells specially infiltrate various organs in autoimmune pancreatitis. Pancreas 29:167–168
12. Lam KY, Chan KW, Ho MH (1995) Inflammatory pseudotumor of the epididymis. Br J Urol 75:255–257
13. Zen Y, Kasahara Y, Horita K, Miyayama S, Miura S, Kitagawa S, Nakanuma Y (2005) Inflammatory pseudotumor of the breast in a patient with high serum IgG4 level: histologic similarity to sclerosing pancreatitis. Am J Surg Pathol 29:275–278
14. Lai FM, Allen PW, Chan LW, Chan PS, Cooper JE, Mackenzie TM (1995) Aggressive fibromatosis of the spermatic cord. A typical lesion in a "new" location. Am J Clin Pathol 104:403–407
15. Morgan AD (1964) Inflammatory lesions simulating malignancy. Br J Urol 36(Suppl):95–102
16. Yamashima M, Honma T, Uchijima Y (1992) Myofibroblastic pseudotumor mimicking epididymal sarcoma. A clinicopathologic study of three cases. Pathol Res Pract 188:1054–1059
17. Jones MA, Young RH, Scully RE (1997) Benign fibromatous tumors of the testis and paratesticular region: a report of 9 cases with a proposed classification of fibromatous tumors and tumor-like lesions. Am J Surg Pathol 21:296–305
18. Miyamoto H, Montgomery E, Epstein J (2010) Paratesticular fibrous pseudotumor: a morphologic and immunohistochemical study of 13 cases. Am J Surg Pathol 34:569–574
19. Comings DE, Skubi KB, Van Eyes J, Motulsky AG (1967) Familial multifocal fibrosclerosis. Findings suggesting that retroperitoneal fibrosis, mediastinal fibrosis, sclerosing cholangitis, Riedel's thyroiditis, and pseudotumor of the orbit may be different manifestations of a single disease. Ann Intern Med 66:884–892
20. Geyer JT, Ferry JA, Harris NL, Stone JH et al (2010) Chronic sclerosing sialadenitis (Küttner tumor) is an IgG4-associated disease. Am J Surg Pathol 34:202–210
21. Kitagawa S, Zen Y, Harada K, Sasaki M, Sato Y, Minato H, Watanabe K, Kurumaya H, Katayanagi K, Masuda S et al (2005) Abundant IgG4-positive plasma cell infiltration characterizes chronic sclerosing sialadenitis (Kuttner's tumor). Am J Surg Pathol 29:783–791
22. Khalil KH, Ball RY, Eardley I, Ashken MH (1996) Inflammatory pseudotumor of the rete testis. J Urol Pathol 5:39–43
23. Nield GH, Rodriguez-Justo M, Wall C, O'Conolly J (2006) Hyper-IgG4 disease: report and characterisation of a new disease. BMC Med 4:23
24. Zen Y, Onodera M, Kitao A, Matsui O, Nohara T, Namiki M et al (2009) Retroperitoneal fibrosis: a clinicopathologic study with respect to immunoglobulin G4. Am J Surg Pathol 33:1833–1939
25. Chan KW, Chan KL, Lam KY (1997) Inflammatory pseudotumor of epididymis and Epstein-Barr virus: a study of two cases. Pathology 29:100–101
26. Sen S, Patterson D, Sandoval O Jr, Wold L (1984) Testicular adnexal fibrous pseudotumors. Urology 23:594–597
27. Thompson JE, Van Der Walt JD (1986) Nodular proliferation (fibrous pseudotumor) of the tunica vaginalis testis. A light, electron microscopic and immunocytochemical study of a case and review of the literature. Histopathology 10:741–748
28. Kraus MD, Guillou L, Fletcher CD (1997) Well-differentiated inflammatory liposarcoma: an uncommon and easily overlooked variant of a common sarcoma. Am J Surg Pathol 21:518–527
29. Ulbright T, Amin M, Young R (1999) Tumors of the testis, adnexa, spermatic cord, and scrotum. In: Atlas of tumor pathology 3rd series, vol 25. ARP, Washington, pp 315–319
30. Bégin LR, Frail D, Brezezinsky A (1990) Myofibroblastoma of the tunica testis: evolving phase of so-called fibrous pseudotumor? Hum Pathol 21:866–868
31. Bateman AC, Deheragoda M (2009) IgG4-related systemic sclerosing disease—an emerging and under-diagnosed condition. Histopathology 55:373–383
32. Acenero MJ, Vorwald PW, Yamauchi SC (2010) Calcifying fibrous pseudotumor affecting the retroperitoneum: could it be a new entity within the spectrum of IgG-4 sclerosing disease? Virchows Arch 456:719–721
33. Debruyne FM, Bogman MJ, Ypma AF (1982) Retroperitoneal fibrosis in the scrotum. Eur Urol 8:45–48
34. Schulte-Baukloh H, Knispel HH, Dallenbach F, Miller K (1999) Scrotal involvement with idiopathic retroperitoneal fibrosis. J Urol 162:1692–1693
35. Nistal M, Paniagua R, Torres A, Hidalgo L, Regadera J (1986) Idiopathic peritesticular fibrosis associated with retroperitoneal fibrosis. Eur Urol 12:64–68

Virchows Arch (2011) 458:115–116
DOI 10.1007/s00428-010-1019-0

LETTER TO THE EDITOR

Use of alginate gel in the pathological work-up of the endoscopically resected mucosal lesions

Shu Ichihara · Masaki Hasegawa · Akari Iwakoshi · Tomoko Sato · Suzuko Moritani

Received: 30 October 2010 / Accepted: 23 November 2010 / Published online: 14 December 2010
© The Author(s) 2010. This article is published with open access at Springerlink.com

Dear Sir,

Endoscopic resection of mucosal lesions has become a common practice for early stage gastrointestinal neoplasms [1, 2]. Consequently, endoscopically resected mucosal lesions are increasingly examined in pathology laboratories. The success of the endoscopic management of such neoplasms heavily depends on the precise and complete histological examination of the resected specimen regarding the margin status, tumor depth, histological type, and lymphovascular invasion.

Most Japanese guidelines recommend that all endoscopically resected mucosal lesions are sliced into parallel sections, each measuring 2–3 mm in thickness. However, the endoscopically resected mucosa is often so fragile, distorted, and irregular in thickness and consistency that the specimens easily get broken apart during slicing. Furthermore, there may be originally defects in the specimen due to technical reasons. To protect the specimen from breaking and misplacing during pathology work-up and to obtain correctly oriented sequential slices, some authors have proposed embedding the whole specimen in paraffin or agar before slicing [3, 4]. These are reasonable proposals but the problems with the use of paraffin and agar prior to slicing is that they need the control of temperature to melt and solidify and they are consequently laborious.

Here, we suggest that sodium alginate, a polysaccharide distributed widely in the cell walls of brown algae, may be an ideal material to generate a gel containing the delicate and fragile specimens. The advantage of sodium alginate is its simple gelation with divalent cations such as Ca^{2+} in room temperature, its cheapness, and its harmlessness. Sodium alginate sol has been used as a submucosal injection material at endoscopic submucosal resection in animal experiments [5] and at bedside in some countries.

We have found that embedding endoscopically resected mucosa in its entirety within sodium alginate gel is an efficient treatment to obtain slices of even thickness (Fig. 1). After inking the margins, we put the specimen in a plastic container filled with 2% sodium alginate liquid and add 1 M calcium chloride to solidify. Gelation begins from the surface to the core of the alginate gel. When the thickness of the alginate sol is 6 mm, it takes about 1 h for the transparent alginate gel to become gel in its entirety.

When the lesion is a polyp, the procedure is simpler. After inking the margin, we dip the entire polyp into 2% sodium alginate liquid and then drop it into 1 M calcium chloride, resulting in a polyp coated with a layer of sodium alginate after a few minutes. The encapsulated polyp is tough enough to be cut into parallel sections by trimming knife, each measuring 2–3 mm in thickness to show the relationship between the neoplasm and the inked margins.

S. Ichihara (✉) · M. Hasegawa · S. Moritani
Department of Pathology, Nagoya Medical Center,
Sannomaru 4-1-1 Naka-ku,
Nagoya, Aichi 460-0001, Japan
e-mail: shu-kkr@umin.ac.jp

A. Iwakoshi
Department of Pathology,
Nagoya University Graduate School of Medicine,
65 Tsuruma-Cho, Showa-Ku,
Nagoya, Aichi 466-8550, Japan

T. Sato
Department of Pathology, Social Insurance Chukyo Hospital,
1-1-10, Sanjo, Minami-ku,
Nagoya, Aichi 457-8510, Japan

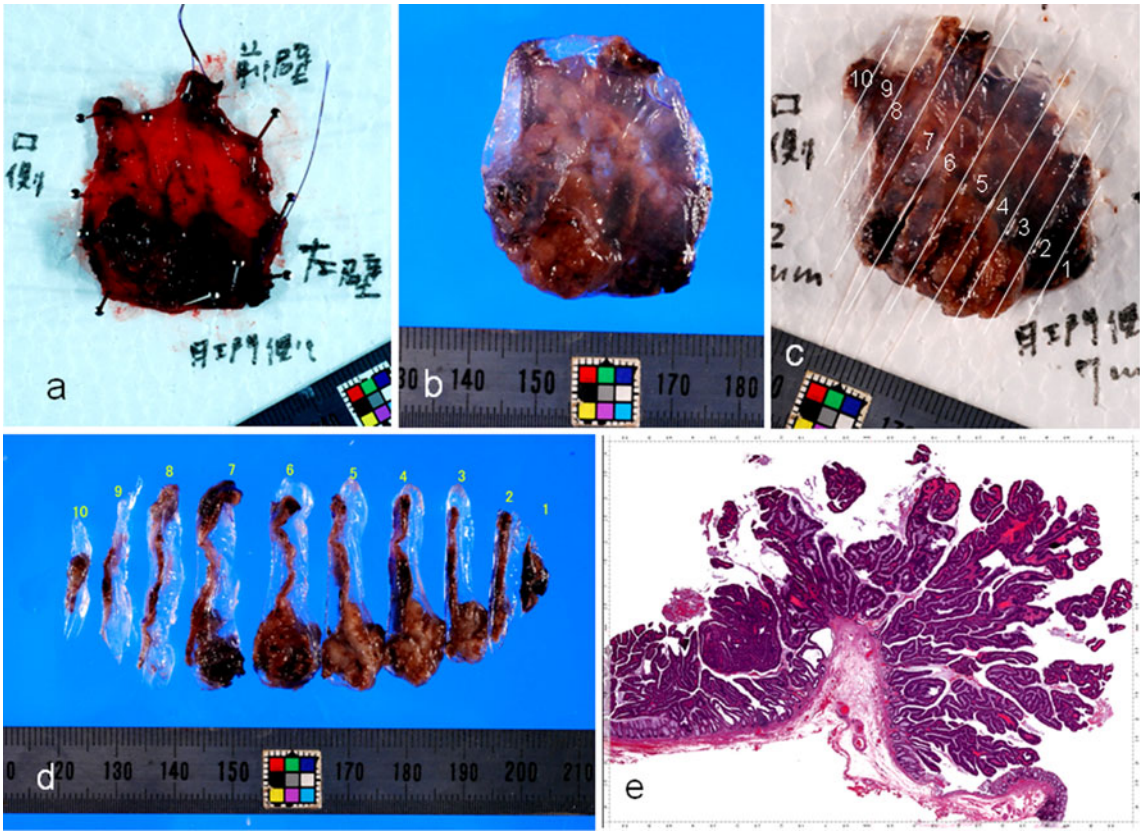

Fig. 1 Tubulovillous adenoma of the rectum treated by endoscopic mucosal resection and examined by the method described in the text. **a** A piece of mucosa with villous tumor obtained by endoscopic mucosal resection. The specimen was pinned on the expanded polystyrene board and fixed with 10% formalin. **b** Endoscopically resected mucosa coated with alginate gel. **c** The mucosa coated with alginate gel was easily sliced into even parallel sections, each measuring about 3 mm in thickness. **d** Ten slices were numbered consecutively. Note that the mucosa is irregular in thickness and villous structures are kept in the alginate gel. **e** Histological section of the slice no. 4 showed villotubular adenoma. The nearest margin width was 3 mm. The mucus-like substance over the polyp was gelled alginate

Embedding the mucosal lesions in alginate gel prior to slicing has several advantages: (1) villous structures are kept in situ after slicing, (2) the fragile portions are protected from breaking into pieces, and (3) the specimen is given relatively monotonous hard consistency making it easy to get sliced into pieces of even thickness.

This technique is also applicable to the shaved margin evaluation in the breast conservative surgery since the peripheral margins are often irregular and may have crevasses. Sodium alginate itself is structureless material, with faintly purple color in hematoxylin and eosin stain reminiscent of mucin, and does not affect immunostains.

Open Access This article is distributed under the terms of the Creative Commons Attribution Noncommercial License which permits any noncommercial use, distribution, and reproduction in any medium, provided the original author(s) and source are credited.

References

1. Ohashi K, Momma K, Yamada Y, Yoshida M, Horiguchi S, Matsubayashi J, Shimizu S, Moriyama S, Hishima T, Funata N, Takizawa T, Koike M (2002) Vertical and horizontal growth features of superficial esophageal squamous cell carcinomas: histopathological evaluation of endoscopically resected specimens. Virchows Arch 441:350–357
2. Shiotani A, Haruma K, Uedo N, Iishi H, Ishihara R, Tatsuta M, Kumamoto M, Nakae Y, Ishiguro S, Graham DY (2006) Histological risk markers for non-cardia early gastric cancer. Pattern of mucin expression and gastric cancer. Virchows Arch 449:652–659
3. Ishigami K, Wakasa T, Osawa M, Obatake H, Shiba I, Tanaka S, Nagami Y, Wakasa K (2010) Slicing endoscopically resected mucosa after paraffin embeding (in Japanese). Pathol Clin Med 28:339–342
4. Omori Y, Morichi H, Moriyasu T, Nishimura T, Yamashita K, Zouga O (2008) Specimen preparation for endoscopically resected mucosa using agar (in Japanese). Pathol Clin Med 26:1313–1316
5. Eun SH, Cho JY, Jung IS, Ko BM, Hong SJ, Ryu CB, Kim JO, Jin SY, Lee JS, Lee MS, Shim CS, Kim BS (2007) Effectiveness of sodium alginate as a submucosal injection material for endoscopic mucosal resection in animal. Gut liver 1:27–32

Virchows Arch (2011) 458:117–123
DOI 10.1007/s00428-010-1006-5

REVIEW AND PERSPECTIVE

Current advances in understanding of immunopathology of atherosclerosis

Colin-John Perrins · Yuri V. Bobryshev

Received: 20 June 2010 / Revised: 5 October 2010 / Accepted: 20 October 2010 / Published online: 11 November 2010
© Springer-Verlag 2010

Abstract The importance of the involvement of the immune system in the development and progression of atherosclerosis was first suggested after the discovery of T cells in atherosclerotic lesions in 1990s. In order to be activated, T cell needs to be presented with an antigen but how this occurs in atherosclerosis has been unclear until recently. Current research has recognised dendritic cells as key initiators and regulators of immune processes in atherosclerosis. Accumulating evidence has revealed novel functions of several subsets of regulatory T cells, which have been shown to maintain immunological tolerance to self-antigens and to inhibit atherosclerosis development by suppressing the inflammatory response of effector T cells. Recent studies have also revealed the importance of natural killer T cells and their interaction with dendritic cells in atherogenesis. This review briefly summarises recent advances in the understanding of immune mechanisms in atherosclerosis and highlights the perspective of immunisation as an approach against this disease.

Keywords Atherogenesis · Arteries · Dendritic cells · Natural killer T cells · Immune inflammation

Introduction

The importance of the immune system's involvement in the development and progression of atherosclerosis was first suggested after the discovery of T cells in atherosclerotic lesions in 1990s [1–3]. Further studies utilising human tissue specimens and experimental animal models have shown that T cells are present within plaques from the initial stages of the disease and that the adaptive transfer of CD4(+) T cells is potentially proatherogenic [4, 5]. Accumulating evidence has revealed novel functions of several subsets of regulatory T cells, which have been shown to maintain immunological tolerance to self-antigens and to inhibit atherosclerosis development by suppressing the inflammatory response of effector T cells [4, 6]. These studies have provided insights into the immunopathogenetic mechanisms of atherosclerosis and indicate that the promotion of regulatory immune responses may have therapeutic potential for the suppression of atherosclerotic disease [4]. Both naturally occurring CD4(+) CD25(+) Foxp3(+) regulatory T cells and IL-10-producing regulatory T cells have been shown to inhibit atherosclerosis in mouse models [4–8]. Recent studies have revealed that natural killer T (NKT) cells play an important role in atherogenesis [9].

It is known that in order to be activated, T cells need to acquire antigen [4]. However, how this might occur in atherosclerosis remained unknown until the demonstration of direct contacts of dendritic cells (DCs) with T cells in atherogenesis [10, 11]. Recent research findings have shown that the regulation of immune processes by DCs is a key event in a cascade of processes, occurring during the development and progression of atherosclerosis [12].

Immune mechanisms are involved in all stages of the development and progression of atherosclerotic lesions [4, 13]. The formation of atherosclerotic plaques can be broadly summarised into several stages [14, 15]. The first macroscopically identifiable atherosclerotic alteration of the arterial wall is presented by so-called ‘fatty streaks’ which form as a result of excessive focal accumulation of lipids in the tunica intima. Most of these lipids originate from plasma-derived lipoproteins [14]. After crossing the endo-

C.-J. Perrins · Y. V. Bobryshev (✉)
Faculty of Medicine, SOMS, University of New South Wales, Kensington 2052 NSW, Australia
e-mail: y.bobryshev@unsw.edu.au

thelial barrier, plasma-derived lipoproteins enter the subendothelial space where direct contact of lipoproteins with networks formed by resident immunocompetent cells occurs [12, 16, 17]. These networks of resident immune cell populations survey the tissue microenvironment, continuously testing components entering into the intima from the blood for the presence of 'danger signals' [16, 17].

Lipoproteins, especially low-density lipoproteins (LDL), entering the intima might become oxidised or otherwise modified [14]. Interactions of modified LDL with the luminal endothelium, as well as with resident cells located in the subendothelial space, initiate the formation of chemotactic gradients that attract monocytes, immune cells and circulating stem cells into the arterial wall from the blood [12, 14–17]. A complex cascade of processes, which include the penetration of blood cells through the inflamed endothelium in atherosclerosis-predisposed regions of the intima, as well as receptor-dependent accumulation of excessive lipids within intimal cells in these sites, lead to the formation of foam cells and, eventually, to the appearance of 'fatty streaks' in arteries [14, 18].

The adhesion of foam cells to each other in regions of the altered intima eventually results in the formation of a lipid core [14, 15, 18]. This is followed by the development of an atherosclerotic 'fibrous plaque', in which the lipid/necrotic core becomes separated from the arterial lumen by a 'fibrous cap'. The plaque then develops into a 'complicated lesion' with a lipid/necrotic core at the centre and large numbers of lymphocytes and macrophages at the shoulders of the lesion, which also contain capillaries of neovascularisation that originate from the adventitial vasa vasorum [14, 15]. As a complicated plaque 'matures', there is an increased possibility of a breakdown of the plaque, which is ultimately accompanied by the formation of thrombi in zones of the plaque's damaged surface [14]. As the plague damage occurs, there is an increased risk of thrombi breaking off the plaque and travelling to the lung, heart or brain [13, 14, 19].

This review briefly summarises recent advances in the understanding of immune processes in the development and progression of atherosclerotic lesions, focusing on the roles of DCs and NKT cells. The review also highlights the emerging perspective of immunisation as an approach for atherosclerosis immunotherapy.

DCs and their emergence in atherosclerosis

In a 1973 publication, Steinman et al. [20] launched a new scientific discipline with their discovery of the dendritic cell, a key antigen-presenting cell in the immune system. Since then, DCs have proved to be critical sentinels on the lookout for 'danger signals' [21].

A possible role of DCs in the activation of immune reactions in atherosclerosis was suggested for the first time in 1995 when the presence of DCs was recognised in healthy human arteries [10]. However, in the intervening years the potential importance of DCs in atherosclerosis has received little attention and, until recently, the impact of DCs in atherosclerosis was not known [22]. Utilising various mouse models of atherosclerosis, recent experimental works have proved the crucial importance of DCs as regulators of immune reactions in atherogenesis [23–25].

Antigen presentation as a major property of DCs

Antigen-presenting cells are an essential part of the immune system because they provide surveillance of body tissues for foreign antigens and danger signals as well as delivering antigen to localised populations of lymphocytes to produce a coordinated immune response [21, 26–29]. Responses by both the adaptive and the innate immune systems require DC participation [26–30]. DCs act as professional antigen-presenting cells that recognise foreign and potentially dangerous antigens and display them bound to major histocompatibility complex (MHC) molecules on the cell surface [21, 25–28, 30].

As key players in the adaptive immune system, most DCs that acquire antigens are thought to migrate to lymph nodes where they form direct contacts with naive and memory T cells, thus causing a primary or secondary immune response and the differentiation of T cells into Th1 or Th2 effector cells [21, 26–28]. DCs also have a unique role in the innate immune system, as they secrete cytokines in response to foreign antigens which have non antigen-specific protective effects [21, 26–29]. These cytokines have a role in the activation of T cells, NKT cells and natural killer (NK) cells [9, 30].

A recent study has shown that DCs isolated from the mouse aorta are just as effective at presenting foreign substances and stimulating the immune system's killer cells as those in immune organs such as the spleen and lymph nodes [24], proving earlier speculation that DCs in the arterial wall possess the same antigen-presenting properties as well studied DCs from the skin and the lymphoid organs [10, 11].

DC distribution in tissues and location in arteries

It is now well known that DCs are present in small numbers in their so-called 'immature' form in almost all peripheral tissues, where they function as an alarm system and are capable of activating a response to perceived danger signals and foreign antigens [21, 26–29]. In the walls of healthy arteries, DCs reside in the subendothelial space of the

tunica intima and the tunica adventitia [10, 16, 17, 22, 31], where they play a crucial role in the early recognition of blood-borne danger signals, which is of great importance for immunity [17, 31]. Ample evidence now exists of the presence of DCs in the aorta, carotid arteries and coronary arteries, where the development of atherosclerosis most commonly takes place and is most dangerous [10, 11, 16, 17, 22, 31]. DCs have been identified also in the aortic root, arch and descending aorta of experimental animals, in particular, in the areas that are prone to the disease [23–25, 32, 33] and these findings facilitated studies of the functional significance of DCs in atherosclerosis and other vascular disorders [23–25].

Dendritic cells in the body are presented structurally and functionally as highly heterogeneous populations [21, 34–39]. DCs are structurally and functionally heterogeneous in their differentiation pathways as well, although a full classification of the different branches of the cell family has yet to be completed [34–39]. Existing classifications take into account location, morphology, antigen expression, migratory routes and trafficking between organs, T cell activation or inhibition [34–39]. In the healthy arterial wall, different DC phenotypes have been identified based on their ultrastructural characteristics [10, 22], but whether the structurally different vascular-associated DC phenotypes have different predispositions and differ in functions is not yet known.

Most commonly, the grouping of different subpopulations in the DC family is based on their function and two major types are commonly considered [34–39]. Myeloid DCs (mDCs) include Langerhans cells of the skin and interstitial DCs, present in the stroma of the peripheral tissues, and these express CD1c, CD11c and CD33 marker proteins [34–39]. Myeloid DCs are considered to have a primary role in T cell activation [31, 34–39]. In contrast, plasmacytoid DCs (pDCs) are involved in T cell tolerance of autoantigens by silencing T cells [31, 34–39]. This function is thought to be important in avoiding the over-activation of the immune response which can lead to autoimmune reactions [21, 31, 34–39]. Accumulating evidence suggests that both mDCs and pDCs not only contribute in the progression of atherosclerosis but also might be present in the arteries at the pre-atherosclerotic stage [12, 31].

Interaction of DCs with atherogenic lipoproteins

There is an important connection to be noted between DC-mediated inflammation of large arteries due to DC activation and recruitment, and atherosclerosis induced by high cholesterol levels [40–44]. The increased accumulation of DCs in arterial lesions has been associated with plaque growth and the development of atherosclerosis, due to the pro-inflammatory affect that the presence of DC implies [40, 41].

Modified low-density lipoproteins, in particular, oxidised low-density lipoproteins (oxLDL) associated with dyslipidemia in atherosclerosis, have the effect of demonstrably altering DC function [42–49] even though, in spite of the hypercholesterolemic conditions, DCs retain their ability to activate T cells [45]. In mouse models of atherosclerosis DCs have been shown to prime T cells specific to modified LDL, which resulted in the production of oxLDL-specific antibodies to reduce atherosclerotic lesion size [42–48].

DC activation and DC function in atherosclerosis

Atherosclerotic arteries display a marked increase in the number of DCs present [11, 12, 17]. This might be accounted for by the migration of circulating DCs into the arterial wall through the luminal endothelium and they might also invade atherosclerotic plaques from the adventitia through neovascularisation (Figs. 1, 2a, b).

As part of the innate immune system, DCs are known to become activated in response to damage-associated molecular patterns, endogenous alarm signals and pathogen-associated molecular patters [50–52]. The most studied receptors for danger signals on DCs are Toll-like receptors (TLRs) [50, 51]. TLRs recognise lipopolysaccarides, oxLDL and heat shock proteins, all of which are signals that promote a signalling cascade for both the innate and adaptive immune systems, rendering DCs as immune regulators [31, 50, 51]. TLRs have been proved to play an important role in the activation of DCs in atherosclerotic lesions [51, 53].

Activated DCs then act under two different pathways. In the same way as this usually occurs in the peripheral tissues, DCs migrate to regional lymph nodes to present antigen to T cells, initiating a response of the adaptive immune system [21]. T cell activation might also occur within the atherosclerotic plaques as the clustering of DCs with T cells has been consistently observed (Fig. 2c, d). More than 90% of the increased population of DCs in atherosclerotic plaques have been reported to cluster in plaque shoulders which represent rupture-prone zones [11, 54]. Clustering of T cells with DCs has been associated with clonal expansion of the T cells in situ in the arterial wall [4, 12, 54].

The clustering of DCs with T cells has been suggested to contribute to plaque destabilisation [11, 54]. It is well known that plaque destabilisation is a complex process in which a variety factors, including the expression of metalloproteinases, alterations of the extracellular matrix are critically important and spatial cell distribution [13, 14]. T cells have been implicated in plaque destabilisation as well because activated T cells might ‘kill’ plaque-resident cells

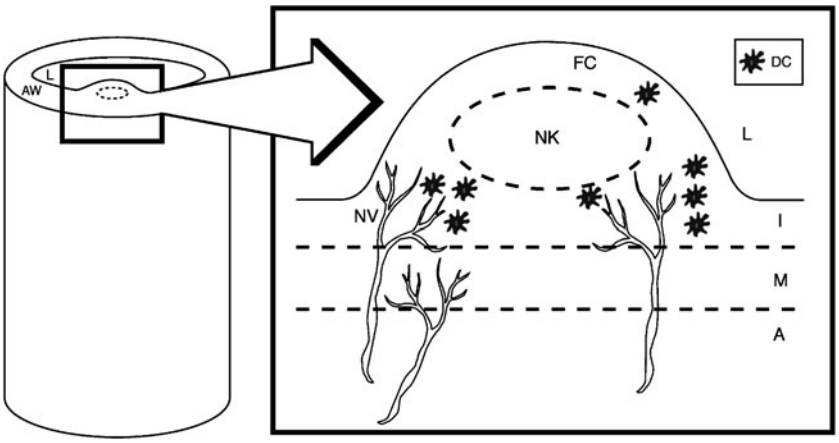

Fig. 1 Scheme showing the distribution of dendritic cells (DCs) in atherosclerotic plaque. *AW*, arterial wall; *L*, arterial lumen; *I*, intima; *M*, media; *A*, adventitia; *NV*, neovascularisation; *NK*, necrotic core; *FC*, fibrous cap; *DC*, dendritic cell

by releasing cytotoxic enzymes perforin and granzyme B which in turn activate caspaces in the cells to induce apoptosis [4, 7]; in this respect, clustering T cells with DCs is of importance for the regulation of these T cell functions [21, 27–29, 54–56].

It is documented that pDCs play a special role in plaque destabilisation [54, 57]; these DCs have a different array of receptors to mDCs, with TLR7, TLR8 and TLR9 being abundantly expressed [51]. pDCs are activated by viral RNA, DNA and nucleotides from necrotic cells, which present abundantly in plague, with the effect of producing large amounts of type 1 interferon (IFN) [55, 56]. This response upregulates T cells to kill plaque-resident cells, as well as sensitising mDCs. The effect of these two distinct

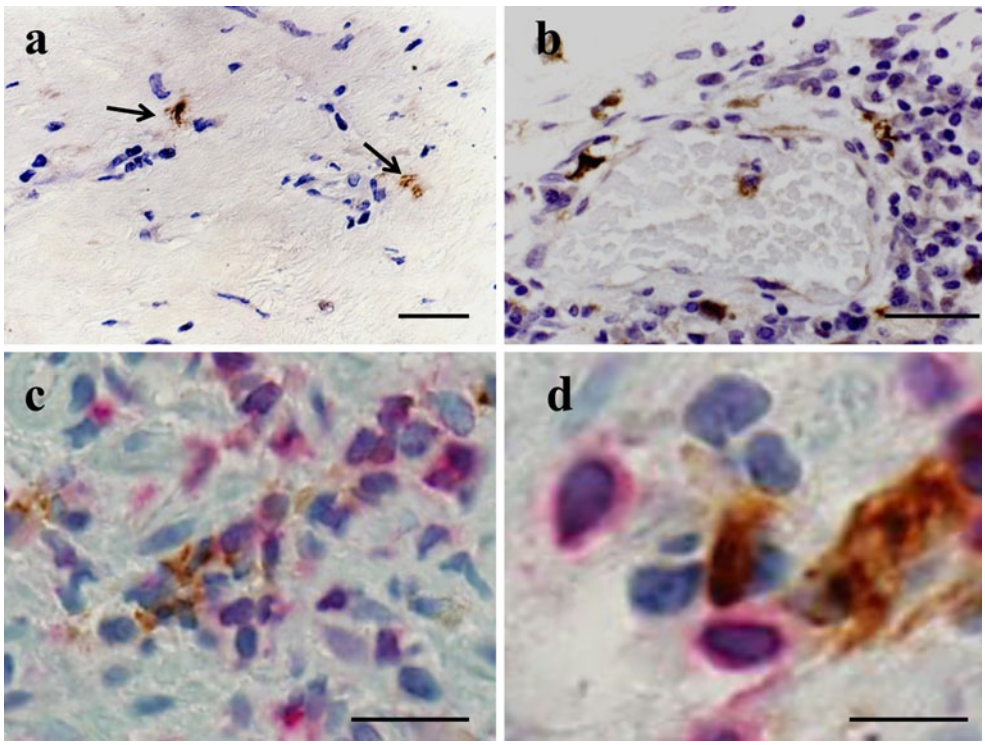

Fig. 2 Immunohistochemical identification of dendritic cells (DCs) (**a**-**d**) and their direct contacts with T lymphocytes (**c, d**) in atherosclerotic lesions. Figures (**a**) and (**b**) demonstrate DCs which locate in the deep layer of the intima (**a**), as shown by *arrows*, and around and within a microvessel, formed in the intima as result of neovascularisation (**b**). In **a** and **b** DCs were visualised by using anti-S100 (S100A1+S100B) (Dako) and immunoperoxidise reaction followed by treatment with 3-3′diaminobenzidine. Figures **c** and **d** represent double immunostained sections which show the formation of cell clusters consisting of DCs (*brown*) and T cells (*rose*) in shoulder regions of advanced atherosclerotic plaque. In figures **c** and **d,** DCs were visualised using anti-CD83 (Immunotech) and immunoperoxidise reaction followed by treatment with 3-3′diaminobenzidine while T cells were visualised using anti-CD3 (Dako) and fast red substrate. *Bars*=100 μm (**a**, **b**), 50 μm (**c**) and 10 μm (**d**)

activation pathways is to produce a strong inflammatory response to varied signals [50, 55–57].

NKT cells and their role in atherogenesis

Recent research into atherogenesis has further elucidated the role of NKT cells [9]. NKT cells are an intermediary of the innate and immune systems and were named thus because they share characteristics with both NK cells and T lymphocytes [9, 58]. NKT cells are 'sensitive' to CD1d, a molecule with antigen-presenting properties similar to MHC molecules [10, 39–41, 52]. NKT cells express the NK1.1 marker protein characteristic of NK cells in mice and CD161 in humans, which are characteristic of NK cells [9, 52]. They also may express CD4 which is characteristic of helper T cells [9, 52].

NKT cells are found in atherosclerotic plaques, although in smaller numbers than other lymphocytes, macrophages or DCs [9, 58]. In plaque, NKT cells are activated by signals such as oxLDLs and can release cytokines characteristic of both Th1 and Th2 cells as well as being able to activate NK cells [9, 58]. Th1 cytokines interleukin (IL)-12 and IFN-γ are known as proatherogenic cytokines and contribute to the formation of atherosclerotic lesions, while Th2 cytokines IL-4 and IL-10 are known as anti-atherogenic [9, 59–64]. In light of these features, several research groups have described NKT cells as proatherogenic [9, 63, 64]. Such a view is supported well by studies in which NKT cell-deficient mice had fewer and smaller atherosclerotic lesions after 4 weeks on an atherosclerotic diet compared to mice with of NKT cells [9, 64]. It is currently thought that while NKT cells do not cause atherosclerosis, this cell type might play a role in the progression of atherosclerotic lesions [9, 63–68].

In human atherosclerotic plaques, NKT cells have been identified in close apposition to DCs, with DC/NKT cell clusters being most prominent in the plaque shoulder regions [58]. As revealed by recent studies, DCs play a crucial role in the activation of NKT cells [65–67]. In mouse models, the presentation of α-galactosylceramide (α-GalCer) antigen by DCs resulted in a much greater NKT cell response than that when the antigen was presented by B cells or other antigen-presenting cells [52, 66–68]. These studies have revealed a unique ability of DCs to efficiently activate NKT cells [66–68]. The mechanism for this specificity has been shown to reside in the sensitivity of NKT cells to CD1d lipoprotein presentation, with CD1d being expressed exclusively by DCs [52, 66, 68]. An experiment involving the treatment of CD1d deficient mice with α-GalCer resulted in no atherosclerosis progression and with no NKT cell recruitment, thus confirming the importance of DCs in the activation of NKT cells [63].

Perspective for immunisation against atherosclerosis

Current therapeutic approaches to atherosclerosis may be revolutionised by the results of recent studies into the use of lipoproteins for immunisation [69–74]. Ongoing research indicates that priming the adaptive immune system against oxLDL presents a possible mode of vaccination against atherosclerosis [69–74]. Oxidised phospholipids and phosphorylcholine within oxLDL have also been identified as major epitopes responsible for immune reactions [69–74].

As professional antigen-presenting cells, DCs may represent an exciting new field for research into cell vaccination [75]. Mature DCs obtained from a patient can be 'pulsed' ex vivo by cultivating them in media containing atherogenic antigens [75]. Antigen-pulsed DCs have been proved as a treatment against some cancers [76–79]. Perhaps the vaccination of a patient with their own DCs, pulsed ex vivo with oxLDL or with oxLDL components, might result in the regulation of immune reactions that promote an anti-atherogenic Th2 response and down-regulates a proatherogenic Th1 response. Such a cell vaccination might have fewer side effects than immunisation using oxLDL or lipoproteins components. Recent results of experiments performed using mouse models [46–48] support a possibility that DC cell vaccination might become an effective immunotherapy approach in atherosclerosis.

Concluding remarks

Current research into the mechanisms of atherogenesis recognises that DCs are key players in the immune processes involved in atherosclerosis. Recent studies have also revealed the importance of DC interaction with NKT cells in the regulation of NKT cell-dependent immune responses in atherogenesis. With research into the applicability of DCs in immunotherapy underway, cell vaccination against atherosclerosis might become a valuable therapeutic option.

Acknowledgements We thank the Faculty of Medicine, University of New South Wales, Sydney, Australia, for support.

Conflict of interest statement We have no commercial associations (i.e. pharmaceutical stock ownership, consultancy, advisory board membership or relevant patents) that might pose a conflict of interest. We declare that we have no conflict of interest.

References

1. Jonasson L, Holm J, Skalli O, Bondjers G, Hansson GK (1986) Regional accumulations of T cells, macrophages, and smooth muscle cells in the human atherosclerotic plaque. Arteriosclerosis 6:131–138

2. Hansson GK, Holm J, Jonasson L (1989) Detection of activated T lymphocytes in the human atherosclerotic plaque. Am J Pathol 135:169–175
3. Hansson GK, Jonasson L (2009) The discovery of cellular immunity in the atherosclerotic plaque. Arterioscler Thromb Vasc Biol 29:1714–1717
4. Hansson GK (2009) Atherosclerosis—an immune disease: the Anitschkov Lecture 2007. Atherosclerosis 202:2–10
5. Zhou X, Nicoletti A, Elhage R, Hansson GK (2000) Transfer of CD4(+) T cells aggravates atherosclerosis in immunodeficient apolipoprotein E knockout mice. Circulation 102:2919–2922
6. Ait-Oufella H, Salomon BL, Potteaux S, Robertson AK, Gourdy P, Zoll J, Merval R, Esposito B, Cohen JL, Fisson S, Flavell RA, Hansson GK, Klatzmann D, Tedgui A, Mallat Z (2006) Natural regulatory T cells control the development of atherosclerosis in mice. Nat Med 12:178–180
7. Mallat Z, Gojova A, Brun V, Esposito B, Fournier N, Cottrez F, Tedgui A, Groux H (2003) Induction of a regulatory T cell type 1 response reduces the development of atherosclerosis in apolipoprotein E-knockout mice. Circulation 108:1232–1237
8. Mor A, Planer D, Luboshits G, Afek A, Metzger S, Chajek-Shaul T, Keren G, George J (2007) Role of naturally occurring CD4+ CD25+ regulatory T cells in experimental atherosclerosis. Arterioscler Thromb Vasc Biol 27:893–900, 2007
9. Whitham S, Ramsamy T (2006) articipatory role of natural killer and natural killer T cells in atherosclerosis: lessons learned from in vivo mouse studies. Canad J Physiol Pharmacol 84:67–75
10. Bobryshev YV, Lord RS (1995) Ultrastructural recognition of cells with dendritic cell morphology in human aortic intima. Contacting interactions of vascular dendritic cells in athero-resistant and athero-prone areas of the normal aorta. Arch Histol Cytol 58:307–322
11. Bobryshev YV, Lord RS (1998) Mapping of vascular dendritic cells in atherosclerotic arteries suggests their involvement in local immune-inflammatory reactions. Cardiovasc Res 37:799–810
12. Bobryshev YV (2010) Dendritic cells and their role in atherogenesis. Lab Invest 90:970–984
13. Stoll G, Bendszus M (2006) Inflammation and atherosclerosis: novel insights into plaque formation and destabilization. Stroke 37:1923–1932
14. Ross R (1993) The pathogenesis of atherosclerosis: a perspective for the 1990s. Nature 362:801–809
15. Lord RS, Bobryshev YV (2002) Hallmarks of atherosclerotic lesion development with special reference to immune inflammatory mechanisms. Cardiovasc Surg 10:405–414
16. Millonig G, Schwentner C, Mueller P, Mayerl C, Wick G (2001) The vascular-associated lymphoid tissue: a new site of local immunity. Curr Opin Lipidol 12:547–553
17. Wick G, Knoflach M, Xu Q (2004) Autoimmune and inflammatory mechanisms in atherosclerosis. Annu Rev Immunol 22:361–403
18. Bobryshev YV (2006) Monocyte recruitment and foam cell formation in atherosclerosis. Micron 37:208–222
19. Niessner A, Goronzy JJ, Weyand CM (2007) Immune-mediated mechanisms in atherosclerosis: prevention and treatment of clinical manifestations. Curr Pharm Des 13:3701–3710
20. Steinman R, Adams J, Cohn Z (1973) Identification of a novel cell type in peripheral lymphoid organs of mice, morphology, quantitation, tissue distribution. J Exp Med 137:1142–1162
21. Lotze M, Thomson A (2001) Dendritic cells: biology and clinical applications, Ed 2nd edn. Academic, San Diego, California, USA
22. Bobryshev YV (2005) Dendritic cells in atherosclerosis: current status of the problem and clinical relevance. Eur Heart J 26:1700–1704
23. Jongstra-Bilen J, Haidari M, Zhu SN, Chen M, Guha D, Cybulsky MI (2006) Low-grade chronic inflammation in regions of the normal mouse arterial intima predisposed to atherosclerosis. J Exp Med 203:2073–2083
24. Choi JH, Do Y, Cheong C, Koh H, Boscardin SB, Oh YS, Bozzacco L, Trumpfheller C, Park CG, Steinman RM (2009) Identification of antigen-presenting dendritic cells in mouse aorta and cardiac valves. J Exp Med 206:479–505
25. Randolph GJ, Potteaux S (2010) Vascular dendritic cells as gatekeepers of lipid accumulation within nascent atherosclerotic plaques. Circ Res 106:227–229
26. Lipscomb M, Masten B (2002) Dendritic cells: immune regulators in health and disease. Physiol Rev 82:97–130
27. Steinman R, Hawiger D, Nussenzweig M (2003) Tolerogenic dendritic cells. Ann Rev Immunol 21:685–711
28. Heath W, Belz G, Behrens G (2004) Cross-presentation, dendritic cell subsets and the generation of immunity to cellular agents. Immunol Rev 199:9–26
29. de Jong E, Smits H, Kapsenberg M (2005) Dendritic cell-mediated T cell polarization. Springer Semin Immunopathol 26:289–307
30. Gelin C, Sloma I, Charron D, Mooney N (2006) Regulation of MHC II and CD1 antigen presentation: from ubiquity to security. J Leukoc Biol 85:215–224, 2009
31. Niessner A, Weyland C (2009) Dendritic cells in atherosclerotic disease. Clin Immunol 134:25–32
32. Bobryshev YV, Taksir T, Lord RS, Freeman MW (2001) Evidence that dendritic cells infiltrate atherosclerotic lesions in apolipoprotein E-deficient mice. Histol Histopathol 16:801–808
33. Ozmen J, Bobryshev YV, Lord RS, Ashwell KW (2002) Identification of dendritic cells in aortic atherosclerotic lesions in rats with diet-induced hypercholesterolaemia. Histol Histopathol 17:223–237
34. Steinman RM, Hawiger D, Liu K, Bonifaz L, Bonnyay D, Mahnke K, Iyoda T, Ravetch J, Dhodapkar M, Inaba K, Nussenzweig M (2003) Dendritic cell function in vivo during the steady state: a role in peripheral tolerance. Ann NY Acad Sci 987:15–25
35. Naik SH, Metcalf D, van Nieuwenhuijze A, Wicks I, Wu L, O'Keeffe M, Shortman K (2006) Intrasplenic steady-state dendritic cell precursors that are distinct from monocytes. Nat Immunol 7:663–671
36. Shortman K, Naik S (2007) Steady-state and inflammatory dendritic cell development. Nat Rev Immunol 7:19
37. Ueno H, Klechevsky E, Morita R, Aspord C, Cao T, Matsui T, Di Pucchio T, Connolly J, Fay JW, Pascual V, Palucka AK, Banchereau J (2007) Dendritic cell subsets in health and disease. Immunol Rev 219:118–142
38. Wilson NS, El-Sukkari D, Belz GT, Smith CM, Steptoe RJ, Heath WR, Shortman K, Villadangos JA (2003) Most lymphoid organ dendritic cell types are phenotypically and functionally immature. Blood 102:2187–2194
39. Auffray C, Sieweke M, Geissmann F (2003) Blood monocytes: development, heterogeneity, and relationship with dendritic cells. Ann Rev Immunol 27:669–692
40. Gautier EL, Huby T, Saint-Charles F, Ouzilleau B, Pirault J, Deswaerte V, Ginhoux F, Miller ER, Witztum JL, Chapman MJ, Lesnik P (2009) Conventional dendritic cells at the crossroads between immunity and cholesterol homeostasis in atherosclerosis. Circulation 119:2367–2375
41. Wang L, Li D, Yang K, Hu Y, Zeng Q (2008) Toll-like receptor 4 and mitogen-activated protein kinase signal system are involved in activation of dendritic cells in patients with acute coronary syndrome. Immunology 125:122–130
42. Paulson KE, Zhu SN, Chen M, Nurmohamed S, Jongstra-Bilen J, Cybulsky MI (2010) Resident intimal dendritic cells accumulate lipid and contribute to the initiation of atherosclerosis. Circ Res 106:383–390

43. Ludewig B, Freigang S, Jäggi M, Kurrer MO, Pei YC, Vlk L, Odermatt B, Zinkernagel RM, Hengartner H (2000) Linking immune-mediated arterial inflammation and cholesterol-induced atherosclerosis in a transgenic mouse model. Proc Natl Acad Sci USA 97:12752–12757
44. Angeli V, Llodrá J, Rong JX, Satoh K, Ishii S, Shimizu T, Fisher EA, Randolph GJ (2004) Dyslipidemia associated with atherosclerotic disease systemically alters dendritic cell mobilisation. Immunity 21:561–574
45. Packard RR, Maganto-García E, Gotsman I, Tabas I, Libby P, Lichtman AH (2008) CD11c(+) dendritic cells maintain antigen processing presentation capabilities and CD4(+) T-cell priming efficacy under hypercholesterolemia conditions. Circ Res 103:965–973
46. Habets KL, van Puijvelde GH, van Duivenvoorde LM, van Wanrooij EJ, de Vos P, Tervaert JW, van Berkel TJ, Toes RE, Kuiper J (2010) Vaccination using oxidised low-density lipoproteins-pulsed dendritic cells reduces atherosclerosis in LDL receptor-deficient mice. Cardiovasc Res 85:622–630
47. Hjerpe C, Johansson D, Hermansson A, Hansson GK, Zhou X (2010) Dendritic cells pulsed with melondialdehyde modified low density lipoprotein aggravate atherosclerosis in ApoE (−/−) mice. Atherosclerosis 209:436–441
48. van Es T, van Puijvelde GH, Foks AC, Habets KL, Bot I, Gilboa E, Van Berkel TJ, Kuiper J (2010) Vaccination against Foxp3(+) regulatory T cells aggravates atherosclerosis. Atherosclerosis 209:74–80
49. Alderman CJ, Bunyard PR, Chain BM, Foreman JC, Leake DS, Katz DR (2002) Effects of oxidised low density lipoprotein on dendritic cells: a possible immunoregulatory component of the atherogenic micro-environment? Cardiovasc Res 55:806–819
50. Matzinger P (2007) Friendly and dangerous signals: is the tissue in control? Nat Immunol 8:11–13
51. Doherty TM, Fisher EA, Arditi M (2006) TLR signaling and trapped vascular dendritic cells in the development of atherosclerosis. Trends Immunol 27:222–227
52. Bendelac A, Savage PB, Teyton L (2007) The biology of NKT cells. Annu Rev Immunol 25:297–336, 2007
53. Erbel C, Sato K, Meyer FB, Kopecky SL, Frye RL, Goronzy JJ, Weyand CM (2007) Functional profile of activated dendritic cells in unstable atherosclerotic plaque. Basic Res Cardiol 102:123–132
54. Yilmaz A, Lochno M, Traeg F, Cicha I, Reiss C, Stumpf C, Raaz D, Anger T, Amann K, Probst T, Ludwig J, Daniel WG, Garlichs CD (2004) Emergence of dendritic cells in rupture-prone regions of vulnerable carotid plaques. Atherosclerosis 176:85–93
55. Asselin-Paturel C, Trinchieri G (2005) Production of type I interferons: plasmacytoid dendritic cells and beyond. J Exp Med 202:461–465
56. Decker T, Muller M, Stockinger S (2005) The yin and yang of type I interferon activity in bacterial infection. Nat Rev Immunol 5:675–687
57. Van Vré EA, Hoymans VY, Bult H, Lenjou M, Van Bockstaele DR, Vrints CJ, Bosmans JM (2006) Decreased number of circulating plasmacytoid dendritic cells in patients with atherosclerotic coronary artery disease. Coron Artery Dis 17:243–248
58. Bobryshev YV, Lord RS (2005) Co-accumulation of dendritic cells and natural killer T cells within rupture-prone regions in human atherosclerotic plaques. J Histochem Cytochem 53:781–785
59. Lee T, Yen H, Pan C, Chau L (1999) The role of interleukin 12 in the development of atherosclerosis in ApoE-deficient mice. Atheroscler Thromb Vasc Biol 19:734–742
60. Davenport P, Tipping P (2003) The role of interleukin-4 and interleukin-12 in the progression of atherosclerosis in apolipoprotein E-deficient mice. Am J Pathol 163:1117–1125
61. Caligiuri G, Rudling M, Ollivier V, Jacob MP, Michel JB, Hansson GK, Nicoletti A (2003) Interleukin-10 deficiency increases atherosclerosis, thrombosis, and low-density lipoproteins in apolipoprotein E knockout mice. Mol Med 9:10–17
62. Pinderski L, Fyfe A, Hedrick C, Olvera T (1999) Interleukin-10 blocks atherosclerotic events in vitro and in vivo. Atheroscler ThrombVasc Biol 19:2847–2853
63. Aslanian A, Chapman H, Charo I (2005) Transient role for CD1d-restricted natural killer T cells in the formation of atherosclerotic lesions. Atheroscler ThrombVasc Biol 25:628–632
64. Whitman SC, Rateri DL, Szilvassy SJ, Yokoyama W, Daugherty A (2004) Depletion of natural killer cell function decreases atherosclerosis in low-density lipoprotein receptor null mice. Arterioscler Thromb Vasc Biol 24:1049–1054
65. Van Kaer L (2007) NKT cells: T lymphocytes with innate effector functions. Curr Opin Immunol 19:354–364
66. Bezbradica JS, Stanic AK, Matsuki N, Bour-Jordan H, Bluestone JA, Thomas JW, Unutmaz D, Van Kaer L, Joyce S (2005) Distinct roles of dendritic cells and B cells in Va14Ja18 natural T cell activation in vivo. J Immunol 174:4694–4705
67. Schmieg J, Yang G, Franck RW, Van Rooijen N, Tsuji M (2005) Glycolipid presentation to natural killer T cells differs in an organ-dependent fashion. Proc Natl Acad Sci USA 102:1127–1132
68. Van Kaer L (2004) Natural killer T cells as targets for immunotherapy of autoimmune diseases. Immunol Cell Biol 82:315–322
69. Hansson G, Nilsson J (2009) Vaccination against atherosclerosis? Induction of atheroprotective immunity. Semin Immunopathol 31:95–101
70. Palinski W, Millller E, Witztum J (1995) Immunisation of low density lipoprotein (LDL) receptor-deficient rabbits with homologous malondialdehyde-modified LDL reduces atherogenesis. Proc Natl Acad Sci USA 92:821–825
71. Binder CJ, Hartvigsen K, Witztum JL (2007) Promise of immune modulation to inhibit atherogenesis. J Am Coll Cardiol 50:547–550
72. Nilsson J, Nordin Fredrikson G, Schiopu A, Shah PK, Jansson B, Carlsson R (2007) Oxidized LDL antibodies in treatment and risk assessment of atherosclerosis and associated cardiovascular disease. Curr Pharm Des 13:1021–1030
73. Fredrikson GN, Björkbacka H, Söderberg I, Ljungcrantz I, Nilsson J (2008) Treatment with apo B peptide vaccines inhibits atherosclerosis in human apo B-100 transgenic mice without inducing an increase in peptide-specific antibodies. J Intern Med 264:563–570
74. van Leeuwen M, Damoiseaux J, Duijvestijn A, Tervaert JW (2009) The therapeutic potential of targeting B cells and anti-oxLDL antibodies in atherosclerosis. Autoimmun Rev 9:53–57
75. Bobryshev YV (2001) Can dendritic cells be exploited for therapeutic intervention in atherosclerosis? Atherosclerosis 154:511–512
76. Markiewicz M, Kast W (2004) Progress in the development of immunotherapy of cancer using ex vivo-generated dendritic cells expressing multiple tumor antigen epitopes. Cancer Investig 22:417–434
77. Dubsky P, Ueno H, Piqueras B, Connolly J, Banchereau J, Palucka AK (2005) Human dendritic cell subsets for vaccination. J Clin Immunol 25:551–572
78. Benko S, Magyarics Z, Szabó A, Rajnavölgyi E (2008) Dendritic cell subtypes as primary targets of vaccines: the emerging role and cross-talk of pattern recognition receptors. Biol Chem 389:469–485
79. Steinman RM (2008) Dendritic cells in vivo: a key target for a new vaccine science. Immunity 29:319–324

Virchows Arch (2011) 458:125–131
DOI 10.1007/s00428-010-1005-6

REVIEW AND PERSPECTIVE

The role of radiological–pathological correlation in diagnosing early breast cancer: the pathologist's perspective

Tibor Tot · László Tabár

Received: 19 September 2010 / Revised: 17 October 2010 / Accepted: 19 October 2010 / Published online: 3 November 2010
© Springer-Verlag 2010

Abstract Early breast carcinoma, defined as purely in situ cancer and invasive carcinomas<15 mm, represents the most frequent category of breast carcinomas in diagnostic routine in a regularly screened population. These tumors are usually detected with mammography screening and are preoperatively characterized with radiological imaging. The role of pathology in preoperative settings is to help understand the subgross morphology and to confirm malignancy in biopsy material. Postoperatively, the pathologist needs to verify the size of the cancer (defined as the largest dimension of the largest invasive focus), the extent of the disease (defined as the area or the volume of the breast tissue containing all the malignant foci), the distribution of the in situ and invasive lesions (as unifocal, multifocal, or diffuse), and intratumoral and intertumoral heterogeneity (in addition to determining margin status, histologic tumor type, hormone receptor status, and other parameters). Despite their small size, early breast carcinomas often exhibit complex morphology as they are multifocal/diffuse in about 60% and extensive (occupying an area≥4 cm) in 40% of the cases. Routine use of large-format histopathology technique is a prerequisite for detailed correlation of the radiologic and histopathologic findings and for the correct assessment of these parameters. Breast pathologists must be aware of the advantages and disadvantages of the different imaging modalities and have detailed information about the radiological findings before work-up of the operative specimen. Multidisciplinary preoperative and postoperative tumor board meetings are essential in guiding the pathologists and in confirming the radiological findings. Interdisciplinary diagnosis is inevitably becoming the new gold standard in the diagnosis and management of early breast carcinomas.

Keywords Breast · Breast cancer · Multifocality · Sick lobe theory · Radiological–pathological correlation · Large-format histology

T. Tot (✉)
Department of Pathology and Clinical Cytology,
Central Hospital Falun,
79182 Falun, Sweden
e-mail: tibor.tot@ltdalarna.se

L. Tabár
Department of Mammography, Central Hospital Falun,
Falun, Sweden

Introduction

The term "early breast carcinoma" or "minimal breast carcinoma" has been repeatedly used to designate tumors detected at the early phase of their natural history and having favorable prognosis [1–3]. In our view, this category of breast carcinoma comprises purely in situ tumors of any size and invasive carcinomas<15 mm in size with or without in situ component. Such tumors are most often nonpalpable and are detected by mammography screening; patients with such tumors have excellent (>90%) 20-year disease-specific survival [4, 5]. This category of the tumors accounts for about 50% of all breast cancer cases in a regularly screened population and about 70–80% of the cancers detected with mammography screening [6]. Thus, cancers belonging to this category represent the most frequent findings in modern breast pathology routine.

It seems to be a paradox that the work-up of a case of early breast carcinoma is much more laborious and time-consuming than the work-up of an advance cancer. These lesions are often nonpalpable, of small size, and hardly visible with the naked eye. Nevertheless, despite their small size, early breast carcinomas are often multifocal and extensive [7–11], and the multiple foci within the same

tumor may occupy a several centimeter large tissue volume. This indicates the need for using special nonfragmenting histology technique in these cases and also underlines the paramount importance of a detailed radiological–pathological correlation in diagnosing early breast cancer.

Theoretical background

According to our hypothesis, the theory of the sick lobe, breast carcinoma is a lobar disease in the meaning that the simultaneously or asynchronously appearing in situ or invasive tumor foci develop within a single sick lobe [12]. The sick lobe probably contains more or more sensitive committed progenitor cells than the other lobes of the same breast and is more sensitive to the endogenous or exogenous oncogenic stimuli. This theory is congruent with the concept of committed progenitor cells [13], as well as with the concept of mammary field cancerization [14]. The most important implication of these concepts is that a several centimeter large area of genetically altered tissue may exist in the breast, and breast cancer develops within this area. The time of complete malignant transformation of the committed progenitor cells is determined by the number of required additional genetic alterations, which are mostly acquired during the division of these cells. This transformation may appear in a single locus within the sick lobe, at more than one locus at the same time or with considerable time difference, or at a large number of loci leading to unifocal, multifocal, or diffuse malignant process. Although the variations in breast cancer morphology are practically unlimited, three patterns of cancer development seem to be the most frequent: the peripheral pattern (involving multiple individual terminal ductal–lobular units), the segmental pattern (involving a segmental duct together with its branches and terminal units), and the lobar pattern (involving the entire sick lobe or large parts of it).

Although the malignant cells may invade beyond the area of the sick lobe in more advanced cases, in early carcinomas, defined above, the lesions are regularly localized within this lobe. Therefore, the surgical intervention in early breast cancer must aim to excise the already developed and morphologically evident cancer foci together with the surrounding genetically altered but morphologically normal at-risk tissue; in other words, the aim is to remove the entire sick lobe together with the lesions within it. Sector resection, i.e., removing a lobe-like piece of breast tissue, represents the best effort to do so. On the other hand, as the lobes of the breast vary considerably in size and shape [15], it is difficult to delineate and excise an entire lobe. Partial excision of the sick lobe represents a risk for tumor recurrence, which may be reduced with postoperative irradiation or adjuvant therapy.

It is not sufficient to restrict the preoperative diagnosis on confirming the presence of malignancy. To properly guide the surgeon, the following parameters should be preoperatively assessed: (1) the tumor size (defined as the largest dimension of the largest invasive focus, most important for categorizing the case as "early," <15 mm, or more advanced); (2) extent of the disease (the area or the tissue volume of the breast containing all the malignant lesions, in situ as well as invasive foci); (3) distribution of the lesions within this area as unifocal, multifocal, and diffuse; (4) intratumoral or intertumoral heterogeneity; and (5) tumor localization. In addition, one should also take into account the possibility of the field of cancerization surrounding the detected lesions attempting to put the lesions into a virtual sick lobe. The localization of the individual lesions has to be recorded based on imaging findings.

The listed parameters are not only important for management decisions but also represent independent prognostic parameters in breast carcinoma. Multifocal/multicentric/diffuse distribution of the lesions is associated with increased propensity for metastatic tumor spreading and with shortened breast cancer-specific cumulative survival [16–18]. Extent of the disease≥4 cm also represent a survival related negative prognostic parameter [18].

Subgross morphology of early breast cancer

According to the results of our previous studies [9–11], approximately one-third of all breast carcinomas are unifocal, the rest are multifocal or diffuse due to distribution of the in situ or the invasive tumor foci, or both. In addition, in about one-half of cases, the malignant lesions occupy a space larger than or equal to 4 cm in the largest dimension (extensive tumors). These results are congruent with the findings of other studies that used a similar technique [7, 8, 19].

In our approach, the distributions of the invasive and in situ components of the same cancer are determined separately. Invasive lesions are considered to be "unifocal" if only one invasive focus is observed, which may or may not have contained an in situ component. "Multifocal" invasive lesions are characterized by the presence of multiple, well-delineated invasive tumor foci separated from each other by uninvolved breast tissue, regardless of the distance between the foci. Careful assessment at several tissue levels is necessary to verify the presence of uninvolved breast tissue in order to avoid overinterpretation of continuous invasive extensions as being separate foci. Tumors dispersed over a large area in the section, much like a spider's web, with no distinct tumor mass are classified as "diffuse," but they are usually large and are not represented

among early cancers. In situ carcinomas are regarded as unifocal if they appear to involve a single terminal ductal lobular unit (TDLU) or several neighboring TDLUs. In situ carcinomas are designated multifocal if they involve several distant TDLUs with uninvolved breast tissue in between and as diffuse if they involved mainly the larger ducts [6, 9–11]. After the initial separate assessment of the distribution of the invasive and in situ foci, we combine the findings so that diffuse distribution of the in situ or the invasive component qualifies the lesion for a tumor having diffuse combined lesion distribution. Multifocality of either in situ or invasive tumor component, or both, results in multifocal combined lesion distribution. We define extensive tumors as those occupying a tissue area larger than or equal to 40 mm in largest dimension in contrast to breast carcinomas of limited extent.

We compared the extent of the disease and the distribution of the lesions in a consecutive series of 120 purely in situ carcinomas, 332 early invasive carcinomas (<15 mm), and 340 more advanced invasive carcinomas (≥15 mm) and found that the proportion of extensive cases in these categories was 45%, 42.5%, and 42.4%, respectively [6]. In another study on carcinomas 1–14 mm in size, we found that 96 of 301 (31.9%) had a multifocal invasive component and none of them demonstrated diffuse invasive growth pattern [11]. Thus, early breast carcinomas are as often extensive and as often multifocal as their more advanced counterparts; they differ from the advanced carcinomas in smaller (<15 mm) size of the individual invasive lesion(s).

Capabilities and limitations of the currently used breast imaging methods

The imaging methods used to detect and diagnose breast carcinoma [mammography, breast ultrasound, and breast magnetic resonance imaging (MRI)] have a much lower resolution compared to microscopic examination. None of them is able to visualize changes at a cellular level like cellular atypia, absence of myoepithelial cell layer, or invasive cell growth, which are microscopic characteristics decisive for the diagnosis of malignancy. On the other hand, the current imaging methods give a good overview of the lesions and the normal tissue in the entire breast, which is extremely important during the preoperative assessment of disease extent and lesion distribution. Using different projections, the imaging methods give a three-dimensional (3-D) reconstruction of the lesion(s), showing their localization, interrelation to each other and their relation to the skin, pectoral muscle, or the nipple. Such reconstruction often reveals the lobar distribution of the detected lesions. The imaging methods can be repeated, which offers the opportunity of following the progression of the detected lesions and detection of additional newly developed lesions. All this information is essential in planning the type and the extent of the surgical intervention.

Most of the malignant tumors appear on the mammogram as mass lesions with or without microcalcifications (about 80%), the rest manifesting as microcalcifications only [20]. Mammography has an >80% accuracy in detecting mass lesions as reported in comparative studies [21, 22]. Detection of some subtypes of invasive lobular carcinoma with mammography represents a challenge even for experienced radiologists [22]. Although pure ductal carcinoma in situ (DCIS) may also manifest as mass lesion or architectural distortion on the mammogram, 75% of the DCIS cases are detected by finding microcalcifications [23]. It is, however, important to notice that pure DCIS and the in situ component of invasive carcinomas calcify in only 25% of low-grade DCIS cases and in 50% of high-grade DCIS cases [24]. Consequently, the in situ component and the extent of the disease are underestimated by mammography in a substantial proportion of cases, especially if the DCIS is of low grade. Micropapillary DCIS represents a problematic subtype of in situ cancer, which may manifest clinically with nipple discharge allowing proper characterization of the process with galactography. It also may produce typical snake skin-like microcalcifications, but it also may remain clinically and radiologically occult, even if extensive and of high grade [23]. Lobular carcinoma in situ and some borderline lesions (atypical hyperplasia, columnar cell change) are not visible on the mammogram if they are not calcified.

Breast ultrasound is the most useful adjunctive method in examining women with dense breasts or examining the dense portion of the breast. This imaging modality has the clear technical advantage in guiding preoperative needle biopsies and is the frequently used method for “second look” when lesions are detected by mammography or MRI. It is very efficient in discriminating solid and cystic lesions and in demonstrating intracystic papillary tumor growth. Further, ultrasound is excellent predictor of the true tumor size in invasive ductal carcinomas compared to clinical examination and mammography [25], but it is less reliable in determining the tumor size in invasive lobular carcinomas [26]. Multifocal, multicentric, and contralateral breast carcinomas are more frequently detected with ultrasound compared to the detection rate of mammography, especially if 3-D automated multislice ultrasound is used. However, MRI may still demonstrate additional tumor foci after ultrasound examination [27]. Microcalcifications are rarely seen on ultrasound and in situ carcinomas, or the in situ component of the invasive tumors may be missed on ultrasound examination.

MRI detects cancers by rapid contrast enhancement after injection of gadolinium because of tumor vascularization. MRI is characterized by higher sensitivity compared to ultrasound and mammography in detecting mass lesions, but benign lesions may give false positive enhancement, decreasing the specificity of this method. MRI is not dependent on density of the breast tissue. The sensitivity of MRI is less dependent on tumor type than the sensitivity of mammography and ultrasound. In some studies, MRI detected invasive ductal and lobular carcinomas with the same high sensitivity of 95% and 96%, respectively [21]. In our experience, however, invasive lobular carcinoma foci may be more frequently missed on MRI than ductal tumors. False negative MRI findings in cases of lobular invasive carcinoma have also been reported in the literature [28]. MRI is less sensitive in detecting DCIS than in detecting invasive cancer. The detection rate of DCIS is related to the grade of the in situ tumor: high-grade (grade 2 and grade 3 together) DCIS was detected by MRI in 92% of cases, low-grade DCIS in only 53% in one study [29]. In our experience, micropapillary in situ carcinoma may be occasionally occult on MRI even if extensive and high grade. The advantage of MRI, compared to mammography and breast ultrasound, is that it is a functional imaging tool, which combines the kinetic features of contrast enhancement within the tissue with the morphologic appearance of this enhancement on the image. This allows analysis of prognostic parameters as tumor grade or proliferation rate [30].

While mammography can effectively discriminate most in situ carcinomas from invasive lesions (microcalcifications from mass lesions) and ultrasound mainly verifies mass lesions, MRI demonstrates rather the extent of the malignant process than separately its invasive and in situ component. The radiologists are able to summarize the findings using the different imaging modalities. With this multimodality approach, they can efficiently compensate the limitations of the individual imaging methods and provide correct description of the findings in the majority of the cases [31].

Capabilities and limitations of the microscopic examination

Microscopic examination with its high-resolution capability detects cellular characteristics and histological changes which are decisive in confirming or ruling out malignancy with the highest achievable accuracy today. The conventional histopathology method used in most pathology laboratories today is, however, clearly insufficient in assessing the most important subgross morphological characteristics in early breast carcinoma listed above. The pathologist needs to examine the available breast tissue in greater length, width, and depth to achieve similar accuracy in assessing lesion distribution, disease extent, and tumor heterogeneity as in assessing malignancy itself. This can be reached if nonfragmented sufficiently large tissue slices are embedded and examined with the technique of large-format histopathology. Sectioning 4-μm-thick histology slides (two-dimensional method) gives the same resolution quality as the conventional histology method and the overview image in a single plane at the same time, giving the advantage of adequately assessing the relation of the lesions to each other and to normal structures. Sectioning 1- to 2-mm-thick slides (3-D method) and viewing them in stereoscopic microscope gives 3-D view limited to a slice, which is similar to that produced by radiology imaging.

Large-section histopathology represents the currently best histology method for determining tumor size, disease extent, and lesion distribution, with documented advantages compared to conventional standard technique. Conventional methods based on sampling small, representative tissue pieces, chosen by the naked eye or according to radiological markers, are adequate for assessing oncological parameters like tumor grade or receptor status but are insufficient for determining radiological–surgical parameters. Small or microscopic invasive and in situ tumor foci are missed regularly at macroscopy and are not sampled for histological evaluation, resulting in underestimation of tumor multifocality. Sampling fragments the specimen and destroys the relationships between the multiple tumor foci: the distances between the foci and their distances from the surgical margins are not preserved, prohibiting assessment of disease extent. Thus, the conventional methods used for pathological analysis of breast tissue actually underestimate multifocality and disease extent and do not document tumor size adequately in many cases [32, 33]. On the other hand, the advantages of large-format histopathology in this aspect have been repeatedly confirmed [31–37]. Using megacasettes (7.5×5.5 cm) or sampling an entire representative slice of the whole specimen into multiple adjacent conventional small blocks are another option, but still suboptimal, more laborious, and more expensive [37].

Diagnosing early breast cancer

After detecting the lesion(s) at mammography screening or based on clinical signs, the radiological work-up will provide a clinical and/or radiological diagnosis which is accurate in the majority of the cases, but according to the current guidelines, the diagnosis needs microscopic confirmation. This confirmation is only an initial step in the adequate preoperative diagnosis; more detailed information is needed for planning surgical and oncological manage-

ment. At the preoperative tumor board meeting, the radiological extent of the disease and the distribution of lesions have to be reviewed and registered. Microscopic methods (fine-needle aspiration cytology, core biopsy, and/or larger bore needle biopsy) are indicated to confirm the malignant character of additional lesions and/or the most distant ones to verify tumor multifocality and disease extent. This is necessary due to the risk of false positive findings. The pathologist has to be aware of the capabilities and limitations of the currently used breast imaging methods.

Detailed and systematic radiological–pathological correlation is also essential during the postoperative work-up of the specimen, during the analysis of the large-format histology sections as well as during the interpretation of the findings.

The specimen is received unfixed, oriented with help of sutures and contained metal wires marking the lesions. The radiologist marks the detected lesions on the specimen radiograph which is sent to the pathology department together with the specimen. Figure 1 illustrates a specimen radiograph with use of the EasyMarkSpecimen accessory. The specimen is color-marked to facilitate orientation. The specimen is sliced into 3- to 4-mm-thick slices, which are also radiographed and magnified in order to detect additional radiological abnormalities not seen on original specimen radiogram. The radiologist marks all the lesions seen on the radiograms of the slices. The pathologist decides which slice to embed based on all the preoperative information about the case and on the marks of the radiologist.

The produced large-format histology sections are analyzed in several steps. First of all, the orientation of the section has to be checked on the basis of color inking and the specimen radiogram (Fig. 1). The analysis of the large-format slides should begin with the specimen margins and continue toward the central parts with marking the most peripheral malignant structures in order to determine the histological extent of the disease. An attempt should be made to summarize the findings in large sections taken at different levels of the specimen. The histological extent must be compared to the radiological disease extent to determine whether sampling of additional slices for histological work-up is necessary (in case of the histological extent being substantially smaller than the radiological one). If the histological and radiological extents are similar and comparable, the distribution of the invasive and in situ tumor components within the marked area must be analyzed. Tumor size is determined by measuring the largest diameter of the largest invasive focus in the large-format histology slides. We advocate measuring the tumor body without any extensions; this diameter is most often comparable to the radiological size as measured on MRI

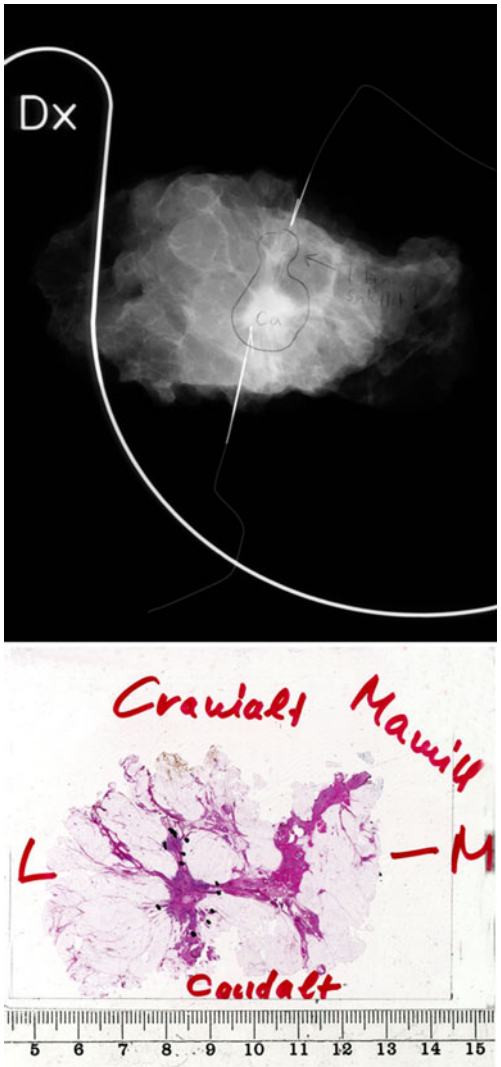

Fig. 1 *Upper image*: Radiograph of the specimen placed on the EasyMarkSpecimen accessory preserving the orientation of the specimen. Two individual lesions are marked with guide wires and the extent of the disease is outlined by the radiologist. (Courtesy of Dr. Mats Ingvarsson.). *Lower image*: Large-format histology image representing a non-fragmented cross-section of the entire specimen. The two radiologically marked lesions are outlined by the pathologist

and ultrasound examination and to the macroscopical tumor size. The analysis is then completed with histological typing and grading the lesions and assessing the hormone receptor status.

Figure 2 illustrates a case of early invasive breast carcinoma with mammographically occult in situ component and the advantage of the multimodality breast imaging. Intratumoral and intertumoral heterogeneity is the less studied parameter among the above listed ones. It is well known that the same tumor may contain components of different tumor types and grade, a phenomenon seen more often when large-format sections are routinely used. Radiological–pathological

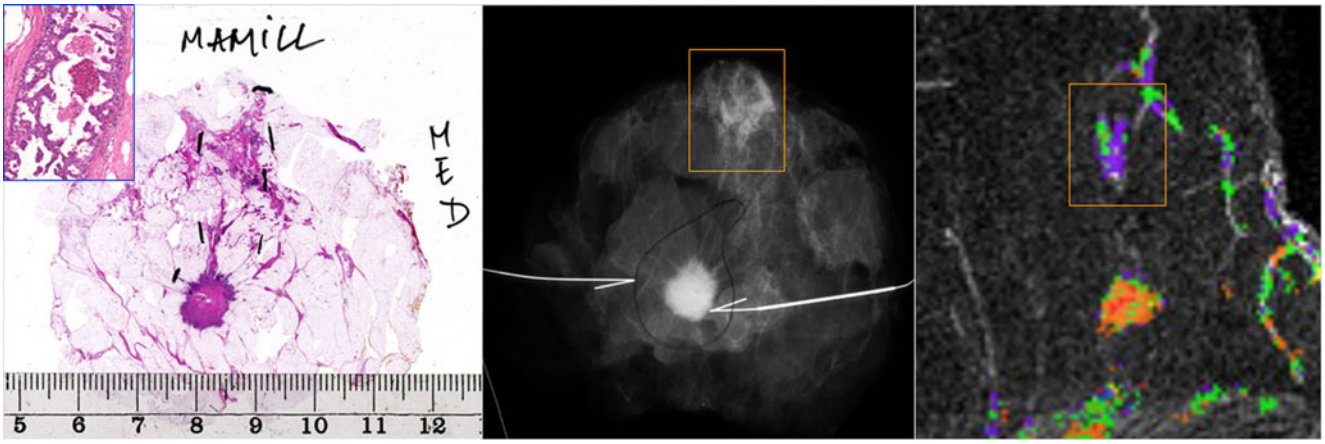

Fig. 2 Large section histology image (*left*), specimen radiograph (*central image*) and corresponding MRI (*right*) demonstrating an invasive carcinoma marked by the radiologist with guide wires. A large area of high-grade micropapillary DCIS (*insert* in the *left image*) was evidenced at histologic examination, not marked at mammography and corresponding to a nonspecific low-enhancement area on MRI. (Courtesy of Dr. Mats Ingvarsson.)

correlation facilitates recognition of tumoral heterogeneity (Fig. 3). Further studies are warranted for elucidating the biological significance of this phenomenon.

Every cancer case should be discussed by the postoperative tumor board to correlate radiological and pathological tumors size, disease extent, lesion distribution and localization as well as tumor heterogeneity. As a more sensitive method, pathology may reveal larger size and extent or more tumor foci than the radiology methods, but the opposite is only acceptable if the false positivity of the radiological finding can be proved. The postoperative tumor board is the last checkpoint in avoiding or correcting the eventual mistakes before they have influenced postoperative treatment decisions.

Practical points

- The pathologist has to receive detailed information about the radiological findings before starting the work-up of an early breast cancer specimen.
- Thorough knowledge of the capabilities and limitations of the individual imaging methods enables the pathologist to adequately use this information.
- Thorough histopathological–radiological correlation using large-format histology technique is the best way of correctly diagnosing and mapping early breast carcinomas.
- The most frequent cause of diagnostic failure is inadequate radiological–pathological correlation.

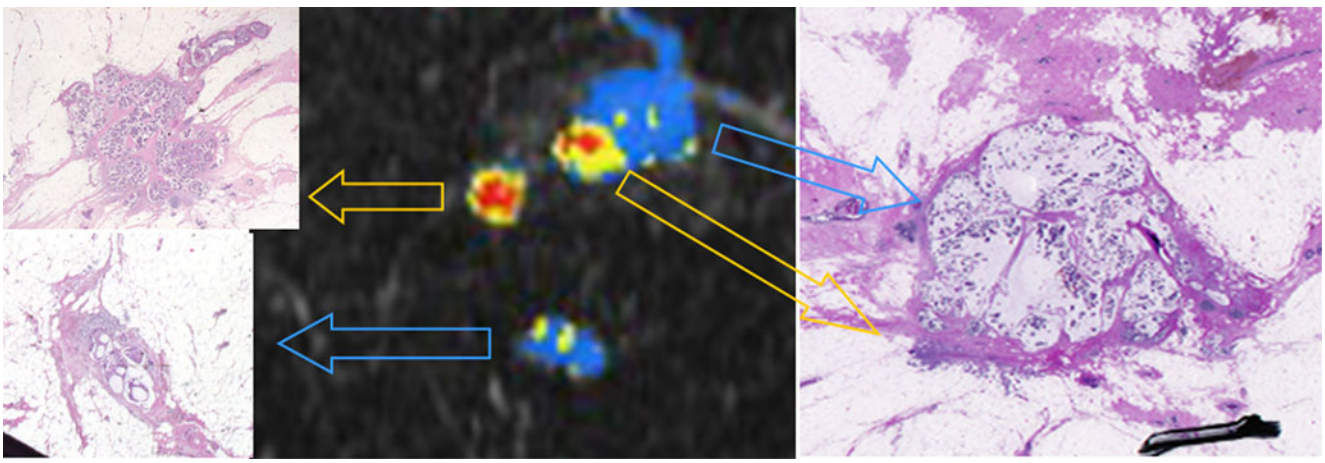

Fig. 3 A case of multifocal early invasive breast carcinoma with intratumoral and intertumoral heterogeneity. Low enhancement (coded with *blue color*) areas in MRI corresponded to mucinous tumor component, while the more intense enhancement (coded with *yellow and red colors*) to ductal component. The *central image* is a detail from MRI. (Courtesy of Dr. Mats Ingvarsson.)

- Low-grade in situ lesions, certain subtypes of micropapillary carcinoma in situ, and invasive lobular carcinoma are overrepresented among cases with discordant correlation parameters.

Acknowledgment The authors thank all the colleagues and the members of the technical staff on the Departments of Mammography and Pathology and all the members of the breast team of the Central Hospital in Falun, Sweden, for their high quality support.

Conflicts of Interest None

References

1. Gallager HS (1976) Treatment selection in primary breast cancer. Pathologic considerations. Am J Roentgenol 126:135–138
2. Nealon TF, Nkongho A, Grossi CE, Ward R, Nealon C, Gillooley JF (1981) Treatment of early cancer of the breast (T1N0M0 and T2N0M0) on the basis of histologic characteristics. Surgery 89:279–289
3. Hartmann WH (1984) Minimal breast cancer. An update. Cancer 53:681–684 (suppl)
4. Tabár L, Chen HH, Duffy SW et al (2000) A novel method for prediction of long-term outcome of women with T1a, T1b and 10–14 mm invasive breast cancers: a prospective study. Lancet 355:429–433
5. Tabár L, Chen HT, Yen MFA et al (2004) Mammographic tumor features can predict long-term outcomes reliably in women with 1–14 mm invasive carcinoma. Cancer 101:1745–1759
6. Tot T (2010) The origins of early breast carcinoma. Sem Diagn Pathol 27:62–68
7. Holland R, Veling SH, Mravunac M, Hendriks JH (1985) Histologic multifocality of Tis, T1–2 breast carcinomas. Cancer 56:979–990
8. Faverly DRG, Henricks JHCL, Holland R (2001) Breast carcinoma of limited extent. Frequency, radiologic–pathologic characteristics, and surgical margin requirements. Cancer 91:647–659
9. Tot T (2007) The clinical relevance of the distribution of the lesions in 500 consecutive breast cancer cases documented in large-format histological sections. Cancer 110:2551–2560
10. Tot T (2009) The metastastic capacity of multifocal breast carcinomas: extensive tumors versus tumors of limited extent. Hum Pathol 40:199–205
11. Tot T, Gy P, Hofmeyer S, Sollie T, Tarján M, Gere M (2009) The distribution of lesions in 1–14-mm invasive breast carcinomas and its relation to metastatic potential. Virchows Arch 455:109–115
12. Tot T (2005) DCIS, cytokeratins and the theory of the sick lobe. Virchows Arch 447:1–8
13. Agelopoulos K, Buerger H, Brandt B (2008) Allelic imbalance of the egfr gene as key event in breast cancer progression—the concept of committed progenitor cells. Curr Cancer Drug Targets 8:431–445
14. Heaphy CM, Griffith JK, Bisoffi M (2009) Mammary field cancerization: molecular evidence and clinical importance. Breast Cancer Res Treat 118(2):229–239
15. Going JJ, Mohun TJ (2006) Human breast duct anatomy, the 'sick lobe' hypothesis and intraductal approach to breast cancer. Breast Cancer Res Treat 97:285–291
16. Boyages J, Jayashinghe UW, Coombs N (2010) Multifocal breast cancer and survival: each focus does matter particularly for larger tumors. Eur J Cancer 46(11):1990–1996
17. Weissenbacher TM, Zschage M, Janni W, Jeschke U, Dimpfl T, Mayr D, Rack B, Schindlbeck C, Friese K, Dian D (2010) Multicentric and multifocal versus unifocal breast cancer: is the tumor-node-metastasis classification justified? Breast Cancer Res Treat 122(1):27–34
18. Tot T (2010) Towards a renaissance of subgross breast morphology. Editorial. Eur H Cancer 46(11):1946–1948
19. Fochsini MP, Tot T, Eusebi V (2002) Large section (macrosection) histologic slides. In: Silverstein MJ (ed) Ductal carcinoma in situ of the breast, 2nd edn. Lippincott Williams & Wilkins, Philadelphia, pp 249–254
20. Tabár L, Tot T, Dean PB (2005) Breast cancer: the art and science of early detection by mammography: perception, interpretation, histopathologic correlation. Thieme, Stuttgart, pp 405–438
21. Van Goethem M, Schelfout K, Dijkmans L et al (2004) MR mammography in the pre-operative staging of breast cancer in patients with dense breast tissue: comparison with mammography and ultrasound. Eur Radiol 14:809–816
22. Berg WA, Gutierrez L, NessAiver MS et al (2004) Diagnostic accuracy of mammography, clinical examination, US, and MRI imaging in preoperative assessment of breast cancer. Radiology 233:830–849
23. Tabár L, Tot T, Dean PB (2007) Breast cancer: early detection with mammography. Casting type calcifications: sign of a subtype with deceptive features. Thieme, Stuttgart
24. Tot T. unpublished data
25. Bosch AM, Kessels AG, Beets GL et al (2003) Preoperative estimation of the pathological breast tumor size by physical examination, mammography and ultrasound: a prospective study of 105 invasive tumors. Eur J Radiol 48:285–292
26. Skaane P, Skjorten F (1999) Ultrasonographic evaluation of invasive lobular carcinoma. Acta Radiol 40:369–375
27. Winstein SP, Orel SG, Heller R et al (2001) MR imaging of the breast in patients with invasive lobular carcinomas. Am J Roentgenol 176:399–406
28. Schelfout K, Van Goethem M, Kersschot E et al (2004) Preoperative breast MRI in patients with invasive lobular breast cancer. Eur Radiol 14:1209–1216
29. Neubauer H, Li M, Kuhne-Heid R, Schneider A, Kaiser WA (2003) High grade and non-high grade ductal carcinoma in situ on dynamic MR mammography: characteristic findings for signal increase and morphological pattern of enhancement. Br J Radiol 76:3–12
30. Szabó BK, Aspelin P, Kristoffersen Wiberg A et al (2003) Invasive breast cancer: correlation of dynamic MR features with prognostic factors. Eur Radiol 13:2425–2435
31. Tot T, Gere M (2008) Radiological–pathological correlation in diagnosing breast carcinoma: the role of pathology in the multimodality era. Pathol Oncol Res 14(2):173–178
32. Jackson PA, Merchant W, McCormick CJ, Cook MG (1994) A comparison of large block macrosectioning and conventional techniques in breast pathology. Virchows Arch 425:243–248
33. Tucker FL (2008) New era in pathologic techniques in diagnosing and reporting breast cancers. Semin Breast Dis 11:140–147
34. Tot T, Tabár L (2005) Radio-pathologic correlation of ductal carcinoma in situ of the breast using two- and three-dimensional large histologic sections. Semin Breast Dis 8:144–151
35. Biesemier KW, Alexander CM (2005) Enhancement of mammographic–pathologic correlation utilizing large format histology for malignant breast diseases. Semin Breast Dis 8:152–162
36. Tot T, Tabár L, Dean PB (2002) Practical breast pathology. Springer, Stuttgart, pp 115–123
37. Tot T (2010) Cost–benefit analysis of using large-format histology sections in routine diagnostic breast care. Breast 19 (4):284–288

Virchows Arch (2011) 458:133–140
DOI 10.1007/s00428-011-1040-y

ORIGINAL ARTICLE

Mucoepidermoid carcinoma: a five-decade journey

Jacinthe Chenevert · Leon E. Barnes · Simion I. Chiosea

Received: 8 October 2010 / Revised: 19 December 2010 / Accepted: 30 December 2010 / Published online: 18 January 2011
© Springer-Verlag 2011

Abstract Several decades after a comprehensive description of mucoepidermoid carcinoma (MEC), there is no uniformly accepted grading system. The most recent debate regarding the histologic grading of MECs, centers on the wide range of reported prevalence of cyclic AMP response element-binding protein (**C**REB)-regulated transcription coactivator (*CRTC1-MAML2*) rearrangement in high-grade (HG) MECs. We hypothesize that difficulties in morphologic classification may partially explain problems in grading MECs. We believe that HG MECs, as diagnosed over the last several decades, represent a blend of true MECs with unrelated clinicopathologic entities. To examine the historic aspects of this problem, and to identify neoplasms that most commonly mimic "high-grade" MEC, we reviewed 46 cases of alleged MEC diagnosed in our department from 1956 to 1974. The diagnosis of MEC was confirmed in 22 cases and was changed in 24 cases. Compared to cases of confirmed MEC, cases with changed diagnoses had higher incidence of lymph node metastases, perineural invasion, and shorter overall survival. Adenosquamous carcinoma, squamous cell carcinoma, and salivary duct carcinoma emerged as the most common mimics of HG MEC. The single most common diagnostic issue in these cases is the level of keratinization acceptable for MEC. Twenty cases of confirmed MEC were tested for *CRTC1-MAML2* rearrangement and 5 low-grade MECs, 7 intermediate grade MECs, and 2 cases of HG MEC were translocation-positive.

J. Chenevert · L. E. Barnes · S. I. Chiosea (✉)
Department of Pathology, Presbyterian Hospital,
University of Pittsburgh Medical Center,
PUH A616.2, 200 Lothrop Street,
Pittsburgh, PA 15213, USA
e-mail: chioseasi@upmc.edu

Keywords Mucoepidermoid carcinoma · *CRTC1-MAML2* · Adenosquamous · Archive

Introduction

Mucoepidermoid carcinoma (MEC) is the most common malignant salivary gland tumor. Sixty-five years after the first comprehensive description of MEC [1], there is still controversy surrounding the tumor, and there is no uniformly accepted grading system [2]. We now know that significant number of MECs are characterized by a cyclic AMP response element-binding protein (**C**REB)-regulated transcription coactivator (*CRTC1-MAML2) t(11;19)* gene fusion product [3, 4], which initially, was thought to be limited to low- and intermediate-grade MECs. More recent studies, however, have sparked the debate on its prevalence in high-grade MECs, where it is stated to range from 0% [5–7] to 52% [4, 8, 9].

We hypothesize that discrepancies in grading MEC are explained in part by problems in histologic classification. We believe that appropriate morphologic diagnosis of high-grade MEC is frequently complicated by its mimics. To examine the historic aspects of this problem, and to identify neoplasms, that most commonly mimic "high-grade" MEC, we reviewed all alleged MEC diagnosed in our department from 1956 to 1974.

Materials and methods

Tissue samples

The study was approved by the University of Pittsburgh Institutional Review Board (IRB# PRO10060222). Pathol-

Table 1 Demographic and clinicopathologic features of patients diagnosed with mucoepidermoid carcinoma (MEC) in 1956 to 1974 (n=46)

		Patients with confirmed MEC (n=22)	Patients with changed diagnosis (non-MEC) (n=24)
Mean age, years		39	62
Male:female ratio		1:2.7	2:1
Tumor site	Parotid	14	8
	Oral cavity (palate)	5 (3)	4 (1)
	Sinonasal	0	6
	Submandibular	0	3
	Larynx	0	3
	Mandible, intraosseous	1	0
	Sublingual gland	1	0
	Base of tongue	1	0
Mean size, cm		1.6[a]	2.5[b]
Positive lymph nodes		1/9 (lymph nodes sampled in nine cases)	6/10 (lymph nodes sampled in ten cases)
Perineural invasion		3/19	8/11
Differentiation, as determined by the original pathologist		8/9–well differentiated [c]	10/10– poorly differentiated (n=8), anaplastic (n=1), or "highly malignant" (n=1)

[a] In two cases, only biopsy material was available; therefore, true tumor size could not be determined

[b] Tumor size was not available in eight cases (due to fragmented nature of the specimen or availability of biopsy material only)

[c] These eight cases include two cases that were called "benign mucoepidermoid tumor" (signed out in 1958)

ogy reports from 1956 to 1974 were searched for mucoepidermoid carcinomas of head and neck [10]. During this time period, the Department of Pathology at the Presbyterian Hospital of Pittsburgh examined 6,000 to 10,000 general surgical pathology cases yearly. Only "in house" cases with available slides and/or blocks were included in this study. Overall, 57 cases diagnosed as MEC were identified. Blocks and slides were not available in 11 cases. The remaining 46 cases were included in this study.

We followed the diagnostic criteria of salivary tumors as described in WHO Classification of Head and Neck Tumors [11]. The group of cases, in which the original diagnosis was modified by us, was designated as "non-MEC". All studied cases were signed out by six different pathologists, some of whom had special interest in diagnostic pathology of salivary tumors [12]. Medical records from that time period have been destroyed—all clinical information was therefore extracted from pathology reports.

Table 2 In 24 cases, the diagnosis of MEC carcinoma was changed as follows

Adenosquamous carcinoma	8
Squamous cell carcinoma	8
Salivary duct carcinoma	4
Adenoid cystic carcinoma	1
Basal cell adenocarcinoma	1
Sinonasal adenocarcinoma with neuroendocrine differentiation	1
Polymorphous low grade adenocarcinoma	1

All pathology reports were reviewed (including microscopic description and diagnostic comments) along with glass slides. The following clinicopathologic features were indexed: age, gender, tumor site and size, and tumor differentiation as evaluated in original reports, perineural invasion, lymph node status, histologic grading [4] of confirmed cases of MEC, and overall survival.

To confirm the diagnosis, in some cases, hematoxylin and eosin (H&E) stained sections and immunohistochemical studies (p63, androgen receptor, S100, smooth muscle actin) were performed as previously described [13].

Cases with confirmed histologic diagnosis of MEC were also tested for *CRTC1-MAML2* translocation by fluores-

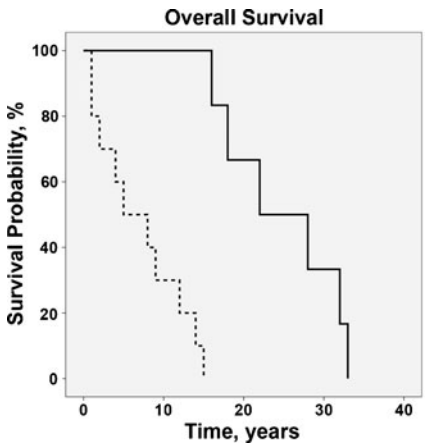

Fig. 1 Comparing overall survival in cases of confirmed mucoepidermoid carcinoma (MEC) and in non-MEC cases, Kaplan–Meier method

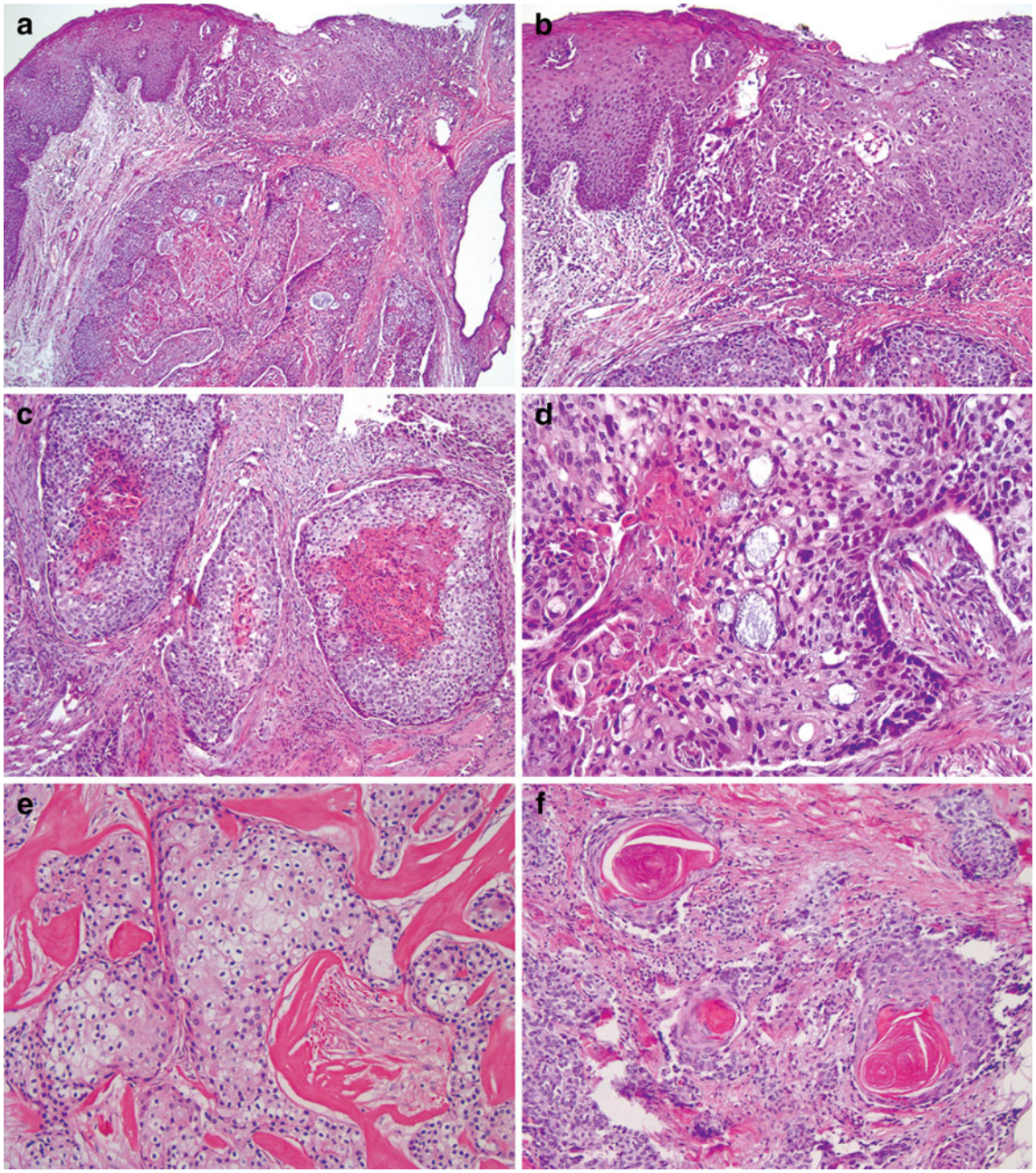

Fig. 2 Representative case diagnosed as MEC and re-categorized by us as ASC (**a**–**d**) and apparent historic trends in level of keratinization accepted in MEC (**e** and **f**). **a** Tumor is associated with overlying mucosa, H&E ×100, all images taken from original slides dating back to 1959. **b** Overlying mucosa with squamous carcinoma in situ, ×200 H&E. **c** Extensive keratinization and overlying mucosa with carcinoma in situ—two main reasons for re-classification of this case, H&E ×200. **d** Gland-like spaces and mucous cells are intermingled with squamous component. Based on this field alone, differentiation between MEC and ASC is very challenging. If mucoid substance in the lumen of glands fails to stain for mucin, adenoid SCC should be considered, H&E ×200. **e** Prototypical epidermoid component of *CRTC1-MAML2* translocated MEC -polygonal cells, three to four times larger than basal cells, without intercellular brides, squamous pearls, or keratohyaline granules, H&E ×200. **f** Representative field from a case diagnosed as MEC in early 1960s. "Epithelial pearls with cornification" were mentioned in microscopic description by the pathologist who signed out the case accepting this level of keratinization as part of MEC

cence in situ hybridization (FISH) as described previously [4]. Tissue blocks were not available in two cases of confirmed MEC and *CRTC1-MAML2* FISH could not be performed.

Overall survival analysis was performed using Kaplan–Meier method with a log-rank test using MedCalc software, Mariakerke, Belgium. Two-tailed Fisher's exact test was performed on http://www.graphpad.com/

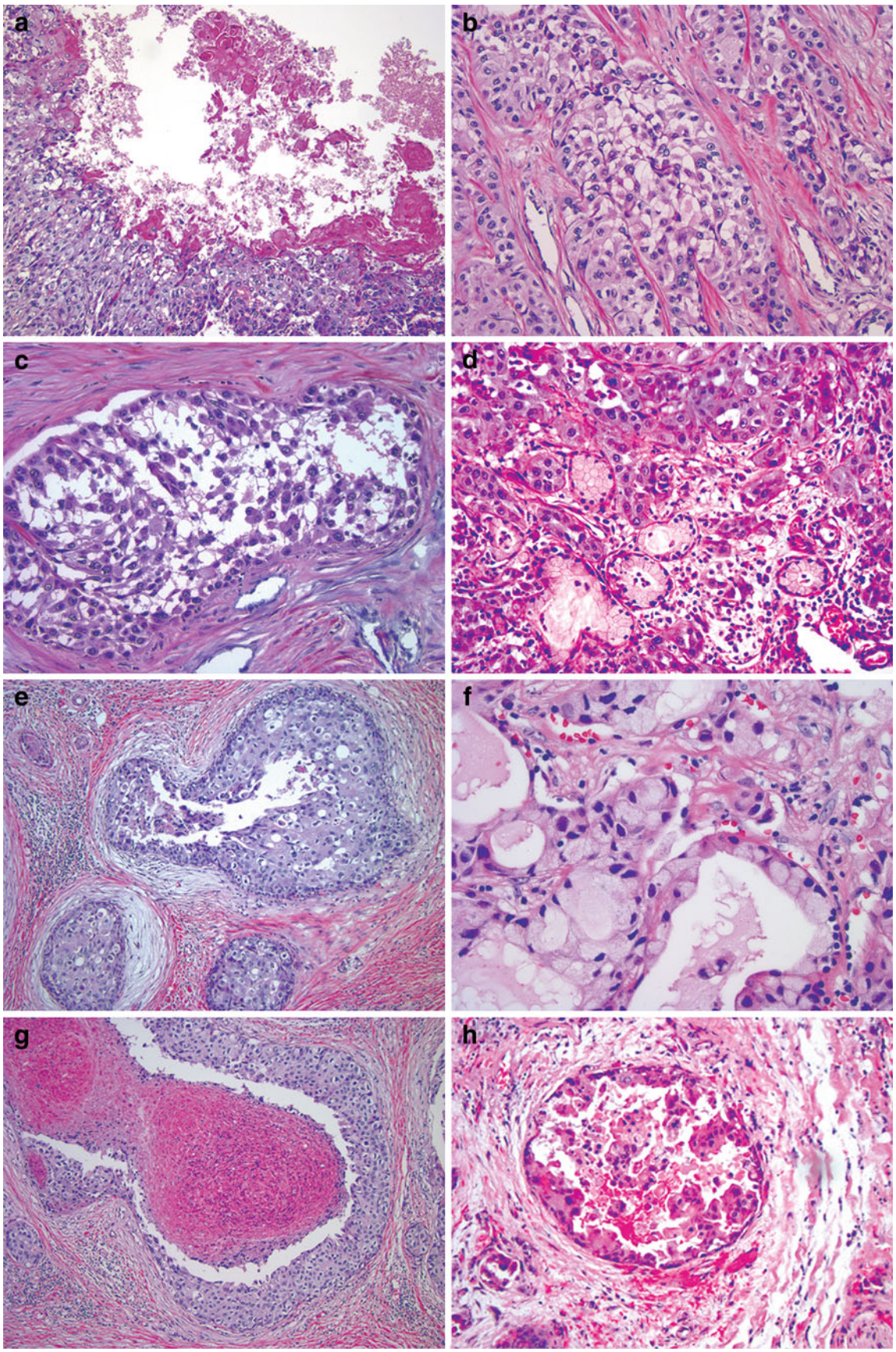
a
b
c
d
e
f
g
h

Fig. 3 SCC and SDC mimicking MEC **a** SCC with cystic change. Keratin debris and extensive keratinization argue against the diagnosis of MEC, H&E ×100. **b** Clear cell change mimicking mucocytes. Mucicarmine and/or periodic acid-Schiff stain with diastase stain may help in distinguishing clear cell change (due to glycogen accumulation) from true mucocytes, H&E ×200. **c** Acantholytic change mimicking mucocytes and lumena, H&E ×200. **d** SCC with acantholytic change (*upper ¼ of the image*) invading minor salivary glands. Entrapped mucinous acini mimic mucocytes of MEC, H&E original magnification ×100. **e** SDC, androgen receptor positive (not shown), mimicking MEC. SDC may present with significant areas of "epidermoid" appearance, H&E ×100. **f** Small areas of mucinous metaplasia can be identified, even in SDC metastatic to lymph nodes, H&E ×400. **g** However, lobular arrangement and comedo-type necrosis (along with other high-grade histologic features) are typical of SDC, H&E ×100. **h** Small papillary projections resembling intraductal carcinoma of the breast, H&E ×200

quickcalcs/contingency1.cfm. ANOVA was performed using Soper, D.S. (2010) "The Free Statistics Calculators Website", *Online Software*, http://www.danielsoper.com/statcalc/.

Results

Clinicopathologic features of confirmed MECs and re-classified cases

From 1956 to 1974, 46 cases diagnosed as MEC met inclusion criteria. On review, the diagnosis of MEC was confirmed in 22 cases and was changed to other malignant diagnoses in the remaining 24 cases. Clinicopathologic features of these two groups are summarized in Table 1. The age, gender, and anatomic distribution were significantly different in MEC and non-MEC groups ($p<0.05$). Overall, patients with confirmed MEC were on average 23 years younger. Remarkably, most of the 24 non-MEC cases were histologic entities that are generally more aggressive than MEC (Table 2). The tumors in the non-MEC group tended to be larger and presented more frequently with regional lymph node metastases and perineural invasion. The overall survival (OS) data were available for 16 patients. Six patients in the MEC group showed an average OS of 22 years, and for ten patients in the non-MEC group, the OS was 6.8 years ($p<0.05$) (Fig. 1).

In 19 cases, the original sign-out pathologists commented on tumor differentiation. Most of the cases of confirmed MEC were characterized as "well-differentiated" (8/9; 89%). Cases categorized by us as non-MEC were described as poorly differentiated and "as highly malignant MEC" (10/10) by the original pathologists at the time of sign out. Therefore, in at least 42% of cases (10/24), the original sign-out pathologist recognized that the histologic appearance was more aggressive than that accepted for the "usual" MEC.

Impact of immunohistochemical studies

Additional immunohistochemical studies were needed only in 3 of 46 cases. P63 immunostain was used in one case to highlight the biphasic nature of a small focus of adenoid cystic carcinoma. In the second case, p63 was used to confirm the lack of epidermoid cells in salivary duct carcinoma with a "squamoid" appearance (it was also shown to be positive for an androgen receptor) [14, 15]. Finally, p63 was helpful in confirming the lack of epidermoid cells in a case that was re-classified as polymorphous low-grade adenocarcinoma.

Mimics of high-grade MEC

Tumors in eight patients with the original diagnosis of MEC were re-classified by us as adenosquamous carcinoma (ASC) (8 of 24 re-classified cases). Review of the microscopic description revealed that in most cases the pathologists did identify two components of the tumor (i.e., squamous and adenocarcinomatous) and commented on spatial relationship between the two (e.g., well-demarcated). The main reason for our re-classification was the presence of dysplastic and/or in situ carcinoma in the mucosa overlying the tumor and extensive keratinization that is unacceptable in MEC by current standards (Fig. 2a–d) [16].

In eight cases, the diagnosis of squamous cell carcinoma (SCC) was more appropriate than that of MEC (8 of 24 re-classified cases). Six of eight cases were *keratinizing* SCCs, and the extent of keratinization was the main reason for our re-classification (Fig. 2e and f). Review of microscopic description showed that original sign-out pathologists were aware of extensive keratinization and believed that it was acceptable in MEC (see discussion). Other histologic features of SCC that mimic MEC are summarized in Fig. 3a–d. In two remaining *non-keratinizing* squamous cell carcinomas, re-classification was prompted by the lack of mucin on mucicarmine and Periodic acid-Schiff stain with diastase (PASD). In addition, these carcinomas were characterized by solid growth, nuclear pleomorphism,

Table 3 Histologic grading and status of *CRTC1-MAML2* translocation as determined by fluorescence in situ hybridization (FISH) in cases of confirmed mucoepidermoid carcinoma ($n=14$)[a]

	Translocation *CRTC1-MAML2* status	
Grade	Positive	Negative
Low	5	0
Intermediate	7	0
High	2	0

[a] FISH failed in six cases; tissue block was not available in two cases

Table 4 Selected salivary tumors described after mucoepidermoid carcinoma

Salivary tumor	Year of first comprehensive description	Reference
Salivary duct carcinoma	1968	[21]
Adenosquamous carcinoma	1968	[16, 24]
Epithelial-myoepithelial carcinoma	1972	[25]
Polymorphous low grade adenocarcinoma	1983	[26, 27]
Basal cell adenocarcinoma	1990	[28]

mitotic count of >5 per 10 HPF, and close association with the overlying mucosa.

In four cases, the diagnosis of MEC was changed to that of salivary duct carcinoma (SDC). The histologic features that are unique to SDC and features that may mimic MEC are illustrated in Fig. 3e–h. Three of these four cases presented with lymph node metastases. In one case, "epidermoid" appearance and focal mucinous metaplasia prompted us to perform p63 (it was negative) and androgen receptor immunostaining (it was positive).

CRTC1-MAML2 translocation in cases of confirmed MEC

The histologic grading for cases of confirmed MEC and the frequency of *CRTC1-MAML2* translocation are summarized in Table 3. The most common morphologic features that led to assigning intermediate or high grade were: <25% cystic area, microcystic/small nested appearance with infiltrative growth pattern, and presence of perineural invasion. Technically, FISH on tissue blocks dating back to 1956 was successful in 14 of 20 cases.

Discussion

Since the first comprehensive analysis of MEC [1, 17], new specific salivary malignancies have been recognized (Table 4). Applying modern diagnostic criteria [11] and the knowledge of salivary gland tumors discovered after MEC, we have re-classified 24 of 46 cases diagnosed as MEC from 1956 to 1974. In previous study of MECs diagnosed in our department from 1973 to 2004, we have shown that 22 of 100 alleged MECs were ASC [18]. Judging from our consult practice, the diagnostic challenges experienced by pathologists half a century ago still plague us today [19].

In the present study, almost all re-categorized cases belong to diagnostic entities that are generally more aggressive than MEC. The clinical significance of separating MEC from its mimics is apparent: as a group, non-MEC entities occur predominantly in elderly men and are characterized by higher rate of lymph node metastases, perineural invasion, and shorter overall survival.

The most common mimics of MEC are ASC and SCC. For a long time, MEC and ASC were considered to be the same [20]. In 14 of 24 non-MEC cases (8 ASC and 6 keratinizing SCC), the diagnostic challenge was most often related to a single issue: what level of keratinization is acceptable for MEC? Epidermoid cells illustrated in Fig. 2e would most likely be accepted by most pathologists now and half a century ago. The level of keratinization shown in Fig. 2f (epithelial pearls) was acceptable for MEC 50 years

Table 5 High-grade mucoepidermoid carcinoma—summary of differential diagnostic considerations

Feature	MEC, high grade	ASC	SCC	SDC
Extensive keratinization[a]	No	Yes	Yes	No
Mucosal dysplastic component[b]	No	Yes	Yes	N.A.
Adenocarcinomatous component	Intermingled with epidermoid and intermediate	Distinct, well demarcated	No	Dominant
Mucicarmine	Positive, intracytoplasmic mucin[c]	Positive, intraluminal mucin	Negative	Intraluminal
IHC: p63	Positive	Positive	Positive	Negative [d]
IHC: AR	Negative	Negative	Negative	Positive
CRTC1-MAML2 FISH	Positive	Negative	Negative	Negative

[a] Squamous pearls

[b] Overlying mucosa with squamous carcinoma in situ

[c] High-grade MECs are almost always characterized by the solid growth pattern and predominance of epidermoid cells—identification of rare mucus cells may require mucicarmine stain

[d] p63 may highlight residual basal cells (i.e., in situ component)

MEC mucoepidermoid carcinoma; *ASC* adenosquamous carcinoma; *SCC* squamous cell carcinoma; *SDC* salivary duct carcinoma; *N.A.* not applicable; *IHC* immunohistochemistry; *AR* androgen receptor; *FISH* fluorescence in situ hybridization

ago, and the historic reason for this may lie in the first thorough description of MEC [1]. In the description of the histology of 19 "malignant mucoepidermoid tumors", the authors stated that

> true squamous cells having intercellular bridges AND epithelial pearls were found in five cases. There were four other cases in which intercellular bridges alone were present [1].

Furthermore, Stewart et al. indicated that

> in all probability, a certain number of rather anaplastic and diffuse cancers of salivary glands are fundamentally mucoepidermoid in type but have become so overgrown that the mucous element is no longer discernible. This is perhaps especially true in that group of salivary gland tumors referred to by most observers as squamous or epidermoid carcinoma [1].

Fifty years ago, this paragraph alone might have justified the diagnosis of MEC in tumors that we now classified as ASC and keratinizing SCC. At present, it is known that primary SCCs of salivary glands are extremely rare. The essential clinical implication of diagnosing SCC of salivary gland is the necessity to rule out a metastasis.

The third most common mimic of MEC was SDC, first described in 1968 [21]. With the increased awareness, only two SDC were categorized as MEC in our department from 1974 to 2004 [4].

The data presented here may prompt a more critical review of larger and more frequently referenced studies of MEC [22, 23]. The implication of this study on incidence of MEC as diagnosed in 1950s through 1970s is uncertain. At first glance, one may assume that MEC was over-diagnosed and includes many salivary type tumors not described at that time. Although this may be true, our study was not designed to identify "under-diagnosed" cases of MEC.

Immunohistochemical studies may be helpful in highlighting a few of the more silent morphologic features of salivary gland tumors, such as biphasic cell population in adenoid cystic carcinomas or epithelial myoepithelial carcinomas and the lack of epidermoid cells in SDC. Immunohistochemistry, however, was necessary only in the minority of cases in this study (3/46 cases).

Identification of *t(11;19) CRTC1-MAML2* is the most recent discovery concerning MEC [3]. Whether its presence has direct favorable prognostic significance across all grades of MEC remains unclear. Both HG MECs in this study were translocation-positive. Our results indicate that most HG MECs represent other, more aggressive morphologic entities only mimicking MEC. In this setting, studies for *CRTC1-MAML2* translocation serve as an objective diagnostic feature of MEC rather than an independent favorable prognosticator. Routine clinical testing of MEC-like lesions may help to refine MEC as an entity. In practice, before diagnosing a translocation-negative high-grade MEC, it may be prudent to re-examine the gross specimen. If the tumor is located outside of major salivary glands, submission of additional sections of overlying mucosa in search for an in situ component may help to establish the diagnosis of ASC (Table 5).

In summary, 24 of 46 cases of MEC diagnosed from 1956 to 1974 were re-classified. We have shown that virtually all re-classified cases were histologically and clinically more aggressive than MEC. The two most common pathologic entities in the non-MEC group were ASC and SCC. The accurate diagnosis of high-grade MEC can be improved by "fine-tuning" the level of keratinization one accepts for this entity (no epithelial pearls), by thorough search for overlying dysplastic squamous mucosa and by increased awareness of SDC.

Acknowledgments Authors would like to thank Kimberly Fuhrer, Katherine Cieply, and Frank Fusca for excellent technical support.

Conflict of interest statement We declare that we have no conflict of interest.

References

1. Stewart FW, Foote FW, Becker WF (1945) Muco-epidermoid tumors of salivary glands. Ann Surg 122(5):820–844
2. Luna MA (2006) Salivary mucoepidermoid carcinoma: revisited. Adv Anat Pathol 13(6):293–307
3. Nordkvist A, Gustafsson H, Juberg-Ode M, Stenman G (1994) Recurrent rearrangements of 11q14-22 in mucoepidermoid carcinoma. Cancer Genet Cytogenet 74(2):77–83
4. Seethala RR, Dacic S, Cieply K, Kelly LM, Nikiforova MN (2010) A reappraisal of the MECT1/MAML2 translocation in salivary mucoepidermoid carcinomas. Am J Surg Pathol 34 (8):1106–1121
5. Okabe M, Miyabe S, Nagatsuka H, Terada A, Hanai N, Yokoi M, Shimozato K, Eimoto T, Nakamura S, Nagai N, Hasegawa Y, Inagaki H (2006) MECT1-MAML2 fusion transcript defines a favorable subset of mucoepidermoid carcinoma. Clin Cancer Res 12(13):3902–3907
6. Behboudi A, Enlund F, Winnes M, Andren Y, Nordkvist A, Leivo I, Flaberg E, Szekely L, Makitie A, Grenman R, Mark J, Stenman G (2006) Molecular classification of mucoepidermoid carcinomas-prognostic significance of the MECT1-MAML2 fusion oncogene. Genes Chromosomes Cancer 45(5):470–481
7. Martins C, Cavaco B, Tonon G, Kaye FJ, Soares J, Fonseca I (2004) A study of MECT1-MAML2 in mucoepidermoid carcinoma and Warthin's tumor of salivary glands. J Mol Diagn 6 (3):205–210
8. Tirado Y, Williams MD, Hanna EY, Kaye FJ, Batsakis JG, El-Naggar AK (2007) CRTC1/MAML2 fusion transcript in high grade mucoepidermoid carcinomas of salivary and thyroid glands and Warthin's tumors: implications for histogenesis and biologic behavior. Genes Chromosomes Cancer 46(7):708–715
9. Fehr A, Roser K, Belge G, Loning T, Bullerdiek J (2008) A closer look at Warthin tumors and the t(11;19). Cancer Genet Cytogenet 180(2):135–139

10. Smith MA, Barnes, L.E., Chiosea, S.I. Pathology archive: evaluation of integrity, regulatory compliance, and construction of searchable database from print reports. Am J Clinical Pathol (in press)
11. Barnes EL, Eveson JW, Reichart P, Sidransky D (eds) (2005) Pathology & genetics. Head and neck tumors. WHO classification of tumours. IARCPress, Lyon
12. Totten RS (1971) Tumors of the oral cavity, pharynx, and larynx. Pathologic aspects. JAMA 215(3):454–455
13. Seethala RR, Barnes EL, Hunt JL (2007) Epithelial-myoepithelial carcinoma: a review of the clinicopathologic spectrum and immunophenotypic characteristics in 61 tumors of the salivary glands and upper aerodigestive tract. Am J Surg Pathol 31(1):44–57
14. Fan CY, Wang J, Barnes EL (2000) Expression of androgen receptor and prostatic specific markers in salivary duct carcinoma: an immunohistochemical analysis of 13 cases and review of the literature. Am J Surg Pathol 24(4):579–586
15. Kapadia SB, Barnes L (1998) Expression of androgen receptor, gross cystic disease fluid protein, and CD44 in salivary duct carcinoma. Mod Pathol 11(11):1033–1038
16. Alos L, Castillo M, Nadal A, Caballero M, Mallofre C, Palacin A, Cardesa A (2004) Adenosquamous carcinoma of the head and neck: criteria for diagnosis in a study of 12 cases. Histopathology 44(6):570–579
17. Foote FW Jr, Frazell EL (1953) Tumors of the major salivary glands. Cancer 6(6):1065–1133
18. Chiosea SI, Barnes EL, Lai SY, Egloff AM, Sargent RL, Hunt JL, Seethala RR (2008) Mucoepidermoid carcinoma of upper aerodigestive tract: clinicopathologic study of 78 cases with immunohistochemical analysis of Dicer expression. Virchows Arch 452 (6):629–635
19. Chiosea SI, Peel R, Barnes EL, Seethala RR (2009) Salivary type tumors seen in consultation. Virchows Arch 454(4):457–466
20. Damiani JM, Damiani KK, Hauck K, Hyams VJ (1981) Mucoepidermoid-adenosquamous carcinoma of the larynx and hypopharynx: a report of 21 cases and a review of the literature. Otolaryngol Head Neck Surg 89(2):235–243
21. Kleinsasser O, Klein HJ, Hubner G (1968) Salivary duct carcinoma. A group of salivary gland tumors analogous to mammary duct carcinoma. Arch Klin Exp Ohren Nasen Kehlkopfheilkd 192(1):100–105
22. Spiro RH, Huvos AG, Berk R, Strong EW (1978) Mucoepidermoid carcinoma of salivary gland origin. A clinicopathologic study of 367 cases. Am J Surg 136(4):461–468
23. Eveson JW, Cawson RA (1985) Salivary gland tumours. A review of 2410 cases with particular reference to histological types, site, age and sex distribution. J Pathol 146(1):51–58
24. Gerughty RM, Hennigar GR, Brown FM (1968) Adenosquamous carcinoma of the nasal, oral and laryngeal cavities. A clinicopathologic survey of ten cases. Cancer 22(6):1140–1155
25. Donath K, Seifert G, Schmitz R (1972) Diagnosis and ultrastructure of the tubular carcinoma of salivary gland ducts. Epithelial-myoepithelial carcinoma of the intercalated ducts. Virchows Arch A Pathol Pathol Anat 356(1):16–31
26. Batsakis JG, Pinkston GR, Luna MA, Byers RM, Sciubba JJ, Tillery GW (1983) Adenocarcinomas of the oral cavity: a clinicopathologic study of terminal duct carcinomas. J Laryngol Otol 97(9):825–835
27. Freedman PD, Lumerman H (1983) Lobular carcinoma of intraoral minor salivary gland origin. Report of twelve cases. Oral Surg Oral Med Oral Pathol 56(2):157–166
28. Ellis GL, Wiscovitch JG (1990) Basal cell adenocarcinomas of the major salivary glands. Oral Surg Oral Med Oral Pathol 69(4):461–469

Virchows Arch (2011) 458:141–151
DOI 10.1007/s00428-010-1036-z

ORIGINAL ARTICLE

High corn oil and extra virgin olive oil diets and experimental mammary carcinogenesis: clinicopathological and immunohistochemical p21Ha-Ras expression study

Irmgard Costa · Raquel Moral · Montserrat Solanas · Francisco Javier Andreu · Maria Carmen Ruiz de Villa · Eduard Escrich

Received: 3 August 2010 / Revised: 25 November 2010 / Accepted: 13 December 2010 / Published online: 15 January 2011
© Springer-Verlag 2011

Abstract Dietary lipids have a role in the aetiology of breast cancer, acting at several cellular levels. We investigated the effects of a high corn oil and a high extra virgin olive oil diet on the clinical and histopathological characteristics of rat dimethylbenz(α)anthracene-induced mammary carcinogenesis and on the expression of p21Ha-Ras, detected by immunohistochemistry, in one experimental series including a low-fat corn oil diet (LFCO) and two high-fat diet groups: $HFCO_P$, rich in corn oil, and $HFOO_P$, rich in extra virgin olive oil. Whereas the high corn oil diet tended to reduce latency time, to raise tumour incidence and to increase total tumour yield, the high extra virgin olive oil diet led to a latency time similar to that of LFCO and to a lower tumour incidence than $HFCO_P$ and lower total tumour yield, even than LFCO. $HFCO_P$ tumours displayed a higher histological grade and profile than LFCO tumours, while adenocarcinomas in $HFOO_P$ were similar to LFCO ones. Although no significant differences in p21Ha-Ras expression among dietary groups was found, we detected a significant p21Ha-Ras decreasing expression as grade increased, in groups LFCO and $HFCO_P$. $HFOO_P$ tumours exhibited a higher staining in high-grade carcinomas compared to the similar malignant tumours of the two other dietary groups. These data suggest that dietary lipids influence the clinical behaviour and the morphological malignancy of the experimental mammary carcinogenesis, according to the type of fat, without altering p21Ha-Ras expression. Nevertheless, this expression could be affected by the malignancy of tumours, probably through a post-translational event.

Keywords Dietary lipids · Breast cancer · Experimental model · Histopathology · Immunohistochemistry · p21Ha-Ras

I. Costa · R. Moral · M. Solanas · E. Escrich (✉)
Department of Cell Biology, Physiology and Immunology,
Medical Physiology Unit, Medical School,
Universitat Autònoma de Barcelona,
08193 Bellaterra,
Barcelona, Spain
e-mail: Eduard.Escrich@uab.es

I. Costa · F. J. Andreu
Department of Pathology, Corporació Parc Taulí-UDIAT,
08208 Sabadell,
Barcelona, Spain

M. C. Ruiz de Villa
Department of Statistics, Universitat de Barcelona,
08028, Barcelona, Spain

Introduction

Breast cancer is the most common malignancy in Western country women [1]. Its association with dietary fat has been examined for a long time and it remains controversial [2, 3]. Although some epidemiological studies have generated conflicting data [4–6], animal studies have shown that dietary lipids constitute a remarkable breast cancer risk, the amount and type of fat being the key factors of this relationship. In general, the high dietary intake of n-6 polyunsaturated fatty acids (PUFAs), primarily linoleic acid (18:2 *n-6*), a main component of corn oil, has a strong stimulating effect on mammary carcinogenesis, whereas high levels of very long-chain *n-3* PUFAs, conjugated linoleic acid and γ-linolenic acid inhibit tumour growth. Concerning monounsaturated fatty acids (MUFAs), such as oleic acid (18:1 *n-9*), present in high levels in olive oil and the main source of fat in Mediterranean countries, although there is growing evidence of their protective role in breast

cancer, some experimental studies have yielded conflicting results [7–11]. Dietary lipids seem to influence breast cancer development at various stages in the tumourigenic process, but mainly at promotion, through specific mechanisms independent of the most general effect of a high caloric intake [11, 12].

Ras proteins include the three classical isoforms of p21Ras proteins, Ha-Ras, Ki-Ras and N-Ras. They function as molecular switches of many signalling pathways that regulate cell growth, differentiation and survival [13]. Mutational-activated Ras as well as the upregulation of normal Ras have been shown to play a role in mammary tumourigenesis and metastasis [14]. Specifically, enhanced levels of *Ha-ras* expression have been found in human and experimental mammary tumours, and induction of mammary carcinomas in rats by exposure to a carcinogen often involves malignant activation of *Ha-Ras* [15, 16]. Moreover, changes in Ras expression and activation seem to play a role in the molecular changes induced by dietary lipids on breast cancer, not completely understood and probably dependent on the type of fat evaluated [12, 17].

One of the most accepted experimental animal models for the study of breast cancer is that of the dimethylbenz(α) anthracene (DMBA)-induction in female Sprague–Dawley rats. In this model, we have previously demonstrated a tumour-enhancing effect of a high corn oil diet and a negative modulatory effect of a high extra virgin olive oil diet on clinical mammary carcinogenesis and on the histopathological features of the carcinomas [18, 19]. We have also investigated several molecular mechanisms to gain insight into the complex pathways underlying these modulatory effects [20–27]. In this sense, we recently showed that high extra virgin olive oil diet decreases Ras activity, while high corn oil diet stimulates breast cancer without affecting Ras-cell signalling pathways [28].

The present study was conducted to investigate the effects of a high corn oil and a high extra virgin olive oil diet on the promotion stage of DMBA-induced mammary carcinogenesis, and to compare them with those of a normolipidic control one, from three experimental approaches: the clinical behaviour of the tumours, by means of the analysis of some carcinogenesis parameters; their morphological degree of malignancy, through the study of the histopathological characteristics of the carcinomas; and the influence of the different diets on p21Ras expression, specifically on p21Ha-Ras, by immunohistochemistry. The aim was to analyse whether dietary lipids exert their influence on mammary tumour development by altering the p21Ha-Ras protein isoform expression and/or its cellular localisation and to evaluate the relationship of this expression with the histopathological aggressiveness of these experimental tumours.

Materials and methods

Experimental design and diets

The experimental series consisted of 60 Sprague–Dawley female rats (IFFA-CREDO-source ICO: OFA. SD [IOPS Caw]). On starting, the animals were 22 days of age, housed four per cage and maintained under environmentally controlled conditions with a 12-h light/dark cycle. They were fed fresh experimental diets and water ad libitum. At 53 days of age, the rats were treated with a single dose of 5 mg of 7, 12-DMBA (Sigma-Aldrich, Madrid, Spain) administered in corn oil by means of gastric gavage [29, 30]. All animals received humane care under an institutionally approved experimental animal protocol, following the legislation applicable in this country.

Animals were randomly distributed into three groups (n=20 for each group) depending on the provided diet throughout the study: a control group, low-fat corn oil (LFCO), fed throughout the study with the low-fat diet, and two promotion groups, the high-fat corn oil promotion (HFCO) and the high-fat olive oil promotion ($HFOO_P$), where rats were fed the control diet from weaning until induction with the carcinogen and then changed to HFCO or HFOO diet, respectively. Rats were inspected weekly for the detection of mammary tumours. The animals were sacrificed by decapitation at an average age of 261 days old and a complete post-mortem examination was carried out.

The definition, preparation and suitability of the semi-synthetic experimental diets used were previously described [31, 32]. Three diets were designed: the LFCO diet (3% corn oil), the HFCO diet (20% corn oil) and the HFOO diet (3% corn oil+17% extra virgin olive oil). Diets also contained 18% (LFCO) or 23% (HFCO and HFOO) casein, 67.9% (LFCO) or 45% (HFCO and HFOO) dextrose, and 5% cellulose, 5.9% salt mixture and 0.24% vitamin mixture. In order to maintain the normal lipidic metabolism, they were supplemented with methionine (0.51% in LFCO and 0.66% in the two high-fat diets), choline (1800 mg/Kg diet) and folic acid (5 mg/Kg diet). Diets were prepared weekly and stored under nitrogen in the dark at 4°C.

Tissue processing, histopathology and immunohistochemical analysis

Macroscopic mammary lesions were collected at sacrifice and fixed in 10% buffered formalin. Four-micron sections were cut from paraffin-embedded tissue and stained with haematoxylin and eosin for light microscopic study. The slides were analysed by a pathologist blinded to the dietary groups.

Epithelial lesions were classified by applying the morphological criteria delineated by Young and Hallowes

[33] on rat mammary tumours. Seven histopathological parameters were analysed in each carcinoma: structural pattern, pattern and nuclear grade, mitotic index, stromal reaction, lymphoplasmacytic infiltration and secretion. Some of these features have been previously adapted to the characteristics of rat mammary tumours [34]. Specifically, as these experimental carcinomas predominantly display cribiform and/or papillary differentiation rather than a tubular formation, structural pattern was evaluated according to the proportion of the cribriform/papillary areas. Regarding pattern grade, we applied the same proportion of tubular formation as it is done in human breast ductal carcinomas, but depending on the extent of the solid ones: grade 1, less than 25% solid areas; grade 2, 25–75% solid areas and grade 3, more than 75% of these areas. Tumour mitotic activity was defined as the number of mitoses in 10 high-power fields (HPF), at ×400 magnification, in the most mitotically areas, and distributed as≤3 mitoses, 4–6 mitoses, 7–9 mitoses, 10 to <20 mitoses, and ≥20 mitoses. The histopathological grading method for rat mammary carcinomas [19], which integrates the three parameters used in human breast pathology for morphological grading [35], was applied to each tumour. In order to obtain the overall grade, the scores for the degree of pattern differentiation, nuclear pleomorphism and mitotic index were added. Pattern and nuclear grades were scored with 1, 2 and 3 points and the mitotic index parameter accepted 5 scores. When adding the scores, the global histopathological grade in each carcinoma was determined as: 3–5 points corresponded to a grade I, 6–8 points to a grade II and 9–11 points to a grade III.

The immunohistochemical study was performed with a mouse monoclonal antibody against p21Ha-Ras (clone F235-1.7.1, Calbiochem; San Diego, CA, USA) which binds specifically to *c-* and *v-Ha-ras*, but not to *c-N-ras* or *c-K-ras*, encoded proteins. Briefly, unstained 4-μ sections were cut from paraffin-embedded blocks and deparaffinised by routine techniques before being placed in citrate ph 6.0 for 3 min at 95–99°C, for antigen retrieval. After cooling down for 20 min, slides were treated with pepsin and then quenched with 3% H_2O_2 for 5 min. The slides were then incubated with the primary antibody (1/40 dilution), for 8 h, using the Dakocytomation Autostainer. Labelling was detected with the peroxidase reaction EnVision™+Dual Link kit (Dako, Envision Plus Detection Kit; Carpinteria, CA, USA) as per the manufacturer's protocol. All sections were counterstained with Harris' haematoxylin.

The same positive control case was used in order to match the intensity of the staining; and a negative control staining was carried out by substituting the primary antibody with non-immunised serum in every working procedure. The results were evaluated quantitatively, using an image analysis software (NOESIS-VISILOG 5.1) which allows a measurement of the positive area from a self-defined ×400 magnification tumour field, in terms of percentage, and the degree of the intensity of this staining (G1–G3 as intensity increases). The slides were analysed by a pathologist blinded to the dietary groups.

Statistical evaluation

The statistical analysis of the qualitative data was carried out using the X^2 test (histopathological study and carcinogenesis at sacrifice). The quantitative data (% p21Ha-Ras expression) was analysed by an ANOVA test with multiple comparisons (Tukey's DHS test) when significant differences were obtained. When non-normality was found, the Arc Sin transformation was applied and the residual check for normality was carried out. In all cases, the level of significance was set at $P<0.05$.

Results

Parameters of the carcinogenesis

The results of the analysis of the carcinogenesis parameters are depicted in Table 1. Latency time, defined by means of the average time from carcinogen administration to first palpable malignant tumour, was shorter in group $HFCO_P$ than those recorded for the control and $HFOO_P$ groups (close to significance, $0.05<P<0.1$), whereas it was virtually identical between $HFOO_P$ and control groups. Tumour incidence, defined as the percentage of animals bearing at least one malignant mammary tumour at sacrifice, was increased in the high-fat corn oil group (90%) more than in the control (70%), while group $HFOO_P$

Table 1 Parameters of the carcinogenesis

	Experimental group[a]		
	LFCO	$HFCO_P$	$HFOO_P$
Latency time (days)[b]			
M±SD (M)	102.5±42.3 (103)	77.3±32.1 (73)	102.3±47.4 (109)
At sacrifice			
Incidence of animals with tumours (%)	70 (14/20)	90 (18/20)	80 (16/20)
Total tumour yield	72	95	69
Tumour yield per rat (m)	3	3.5	2.5

[a] *LFCO* low-fat corn oil group, *$HFCO_P$* high-fat corn oil group, *$HFOO_P$* high-fat olive oil group

M mean, *SD* standard deviation, *m* median

displayed intermediate values (80%). These differences were not statistically significant. Finally, the total tumour yield, defined as the cumulative total number of malignant mammary tumours in each dietary group at sacrifice, was higher in the group of animals fed the high corn oil diet (n= 95) than that in the control (n=72). The group $HFOO_P$ showed the lowest value (n=69), even lower than that of the control group, although the differences were not statistically significant. A similar non-statistical distribution was obtained when the tumour yield per rat was analysed, with higher values in group $HFCO_P$ (3.5), the lowest in group $HFOO_P$ (2.5) and intermediate in group LFCO (3).

Histopathology

The histopathological study was carried out on 227 mammary carcinomas (69 from LFCO, 91 from $HFCO_P$ and 67 from $HFOO_P$). Figure 1 depicts a characteristic image of each of the parameters studied and the results obtained, displayed as the percentage of tumours from each dietary group exhibiting the different categories of the histopathological feature analysed. No differences were observed among the dietary groups when structural pattern was analysed. Most carcinomas exhibited a pure or a prevailing cribriform pattern (100–70% of the tumour), although tumours from $HFOO_P$ displayed more papillary areas than those from $HFCO_P$ and LFCO groups. With regard to pattern and nuclear grade, we found that carcinomas from the high-fat corn oil group displayed a trend towards higher grades compared to the control situation, nearly significant when pattern grade was studied (P=0.056). Thus, while more than 50% of the carcinomas showed a pattern or a nuclear grade 1 in groups LFCO, the high-fat corn oil group displayed a greater distribution among the three scores for each parameter. Regarding group $HFOO_P$, the carcinomas exhibited a similar pattern and nuclear grades distribution to group LFCO. With respect to mitotic activity, a higher percentage of tumours exhibiting >3 mitosis/10 HPF was found in the high-fat diet groups than that in the control situation. More than 50% of carcinomas from $HFCO_P$ displayed >3 mitosis/10 HPF, while less than 30% of control group carcinomas exhibited that mitotic index, being these differences significant (P= 0.012). As for the high-fat olive oil group, although the tumours exhibited a higher mitotic index than in LFCO, the differences were not significant. Most of the tumours from the three dietary groups were well circumscribed, with slight invasion of neighbouring tissues, and only some of them presented an infiltrative pattern, clearly invasive and with an intense desmoplastic reaction. High-fat olive oil tumours exhibited the lowest high (+++) stromal response. Lymphocytic infiltration was similar among the three dietary groups, although the most prominent inflammation (+++) was seen in tumours from Group $HFCO_P$. Regarding secretion, carcinomas from high-fat groups exhibited lipid droplets more often than those from group LFCO, significantly when comparing groups $HFCO_P$ and LFCO (P= 0.011).

Applying the modified histopathological grading method adapted to rat tumours, we appreciated a higher percentage of histological grade II and III carcinomas in the high-fat corn oil group than in those from the control and the high extra virgin olive oil diet situation (Fig. 2). Specifically, a statistical tendency towards higher grade carcinomas in group $HFCO_P$, compared to those from the control (P= 0.078), was found. There were no differences in the rate distribution between groups LFCO and $HFOO_P$. Most of the carcinomas of each rat were morphologically similar and displayed the same or one less or more histopathological grade (79% (11/14) in group LFCO, 72% (13/18) in group $HFCO_P$ and in 81% (13/16) of the rats from group $HFOO_P$).

p21Ha-Ras immunohistochemical analysis

The immunohistochemical detection of p21Ha-Ras was performed on 220 carcinomas (68 LFCO, 87 $HFCO_P$ and 65 $HFOO_P$). Immunoreaction was not strictly confined to tumour cells, but it also was evident in benign tissue components of the section analysed, including myoepithelia, ductal and lobular epithelia, fibroblasts, muscle cells, skin and vessel walls. The staining reaction was always dominated by fine intracytoplasmic granules that exhibited a heterogeneous distribution and density among tumours. We did not find any variations in the localisation of the protein. A positive stain was found in all tumours, although differences in the quantitative evaluation of the slides were noted. Thus, some tumours exhibited a uniformly weak staining on tumour cells; others, a mixed mild to moderate staining intensity in the same tumour and others, a diffuse and strong expression of the protein (Fig. 3). No significant differences among dietary groups were appreciated, although expression of p21Ha-Ras was somehow higher in the two high-fat dietary groups than in the control situation (Table 2). In this sense, while the average percentage of the positive area was 50.34% (median of 46.05), in carcinomas of the low-fat diet, high-fat corn oil and olive oil groups showed a positive area staining of 54.92% and 53.96% (median of 56.43 and 54.26), respectively. When the relationship between p21Ha-Ras expression and the histological grade was evaluated, we detected that p21Ha-Ras expression tended to decrease as grade increased (Fig. 4). Analysing all the carcinomas irrespective of the dietary group, we found that grade I carcinomas showed a statistically significant higher expression (median 56.69% positive area) than did grade II (42.82%) and grade III carcinomas (43.13%; P=0.041 and

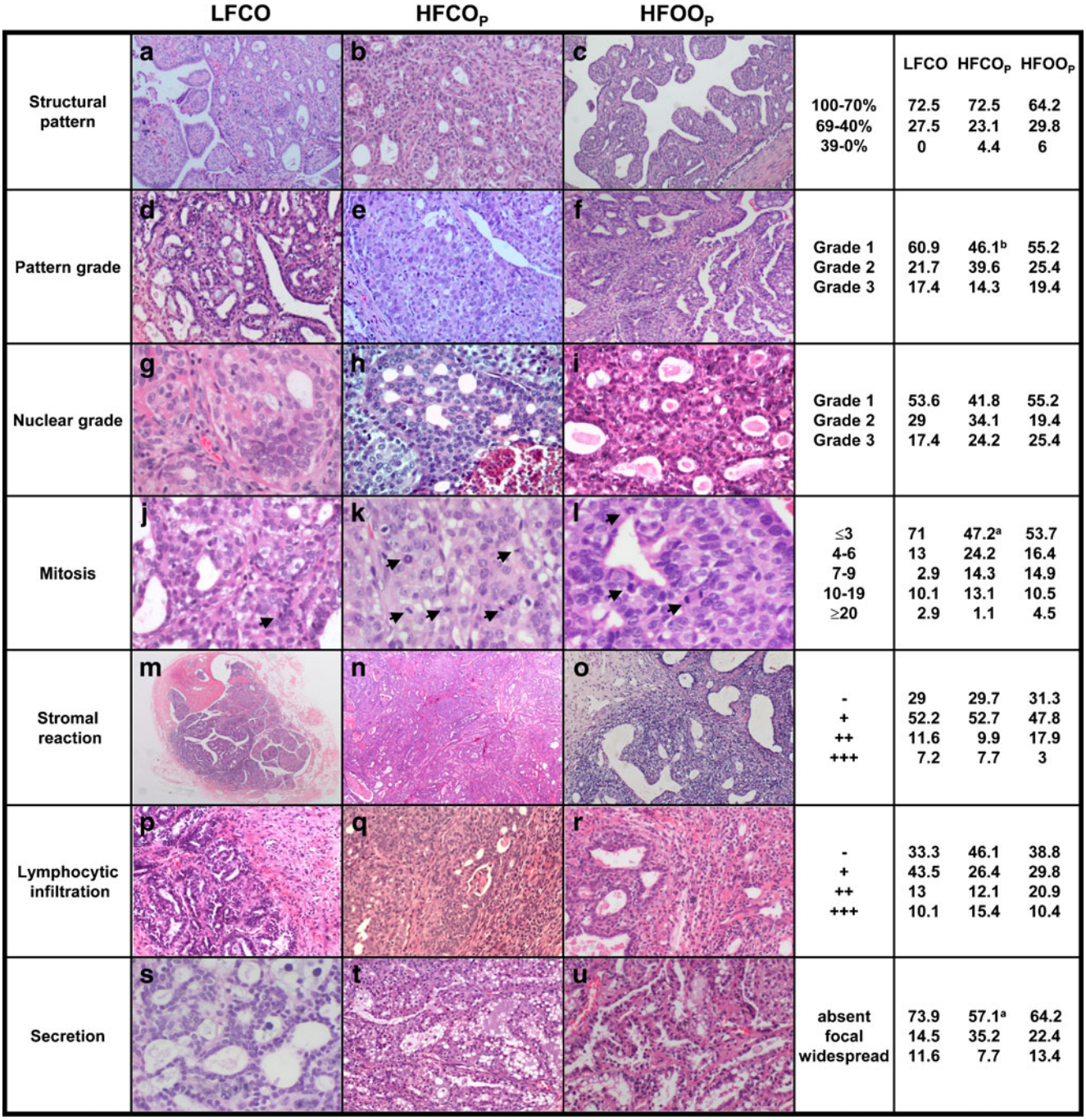

	LFCO	$HFCO_P$	$HFOO_P$
Structural pattern			
100-70%	72.5	72.5	64.2
69-40%	27.5	23.1	29.8
39-0%	0	4.4	6
Pattern grade			
Grade 1	60.9	46.1[b]	55.2
Grade 2	21.7	39.6	25.4
Grade 3	17.4	14.3	19.4
Nuclear grade			
Grade 1	53.6	41.8	55.2
Grade 2	29	34.1	19.4
Grade 3	17.4	24.2	25.4
Mitosis			
≤3	71	47.2[a]	53.7
4-6	13	24.2	16.4
7-9	2.9	14.3	14.9
10-19	10.1	13.1	10.5
≥20	2.9	1.1	4.5
Stromal reaction			
-	29	29.7	31.3
+	52.2	52.7	47.8
++	11.6	9.9	17.9
+++	7.2	7.7	3
Lymphocytic infiltration			
-	33.3	46.1	38.8
+	43.5	26.4	29.8
++	13	12.1	20.9
+++	10.1	15.4	10.4
Secretion			
absent	73.9	57.1[a]	64.2
focal	14.5	35.2	22.4
widespread	11.6	7.7	13.4

Fig. 1 Histopathological features and results of the morphological analysis of rat DMBA-induced mammary adenocarcinomas from the different dietary groups, displayed as the percentage of tumours from each dietary group exhibiting the different categories of the histopathological feature analysed. Adenocarcinomas from $HFOO_P$ exhibited more papillary areas (*c*) than LFCO (*a*) and $HFCO_P$ (*b*) tumours, while carcinomas from $HFCO_P$ displayed a higher pattern (*e*) and nuclear (*h*) grades and a higher mitotic activity (*k*) than those from LFCO (*d*, *g* and *j*) and $HFOO_P$ (*f*, *i* and *l*). No differences were found between the three dietary groups when stromal reaction was analysed. Most of the tumours were well circumscribed (*m*), with slight invasion of neighbouring tissues (*o*), and only some of them presented an infiltrative pattern, clearly invasive and with an intense desmoplastic reaction (*n*). Lymphocytic infiltration was similar among the three dietary groups, although a more prominent inflammation (++ and +++) was seen in tumours from group $HFCO_P$ (*q*) and $HFOO_P$ (*r*) than in LFCO (*p*). Secretion was present more often in tumours from HFCOP (*t*) and $HFOO_P$ (*u*) than in LFCO (*s*). Refer to the text and to [34] for detailed descriptions. *LFCO* low-fat corn oil group, *$HFCO_P$* high-fat corn oil group, *$HFOO_P$* high-fat olive oil group; *m*, *n* (H&E ×40); *a–f*, *o* (H&E ×100); *p–u* (H&E ×200); *g–l* (H&E ×400); *a* significantly different ($P<0.05$) from the values of the control group; *b* $0.1>P>0.05$ from the values of the control group

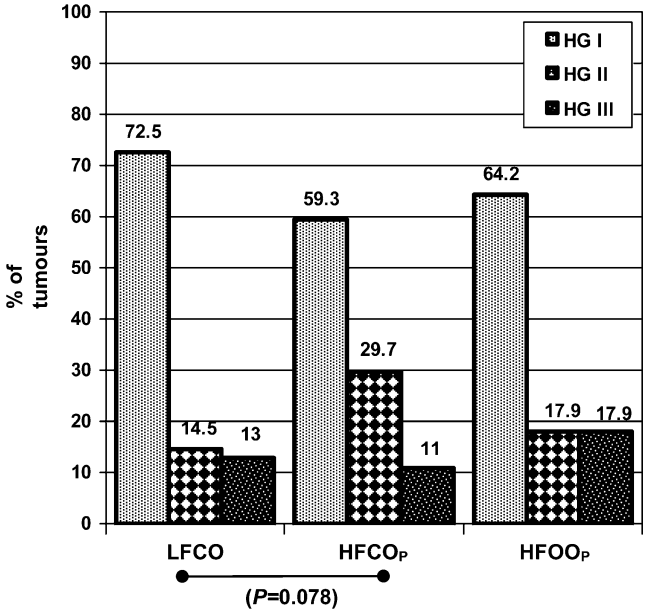

Fig. 2 Histopathological grading of rat DMBA-induced mammary carcinomas using the method previously adapted to rat tumours. *LFCO* low-fat corn oil group, *HFCO$_P$* high-fat corn oil group, *HFOO$_P$* high-fat olive oil group, *HG* histolopathological grade

P=0.009, respectively). Specifically, carcinomas from low-fat and high-fat corn oil groups exhibited the same tendency in the distribution of p21Ha-Ras expression according to histological grade. However, a different distribution of the staining in the high-fat olive oil group, as compared to the other dietary groups, was observed. In this group, the positive p21Ha-Ras staining area was very similar between low- (median of 56.02%) and high-grade carcinomas (median of 53.14%). Moreover, grade III carcinomas from this dietary group expressed a higher percentage of stained area than did the similar poorly differentiated tumours of LFCO and HFCO$_P$ groups (median of 25.5% and 35.31%, respectively).

Discussion

In the present study, we evaluated the clinical and histopathological effects of diets rich in corn oil and extra virgin olive oil on DMBA-induced mammary carcinogenesis, and the possible role of p21Ha-Ras expression as a mechanism of such effects. For the histopathological analysis, a modified grading system for rat mammary cancer previously developed by our group was applied [19]. This grading method has been shown to provide an integrated view of these experimental breast carcinomas and to be a useful tool to analyse the effects of an environmental factor on tumour morphological malignancy [36, 37]. Our results showed that the high-fat corn oil diet

Fig. 3 p21Ha-Ras expression by immunohistochemistry in rat DMBA-induced mammary carcinomas (**a**, **c** and **e**) and the image analysis measurement from the NOESIS-VISILOG 5.1 software (**b**, **d** and **f**): **a** and **b** low and weak staining (×200); **c** and **d** mild to moderate p21Ha-Ras expression (×200), and **e** and **f** diffuse and strong staining (×200)

has a stimulatory effect on mammary carcinogenesis: tumours appeared earlier, the percentage of affected animals was increased, and there were a higher number of tumours per group and per animal when compared with control and high-fat olive oil groups. Moreover, tumours from HFCO$_P$ group displayed higher pattern and nuclear grades, a higher mitotic count and a higher global histological grade than group LFCO. On the other hand, the high extra virgin olive oil diet, with the same amount of fat than the high corn oil diet, had a different effect on breast tumourigenesis, since most of the parameters in group HFOO$_P$ indicated a lower tumour malignancy in comparison to that of group HFCO$_P$. Thus, the high-fat extra virgin olive oil diet caused higher latency as well as lower incidence and tumour yield per group and per animal than the high-fat corn oil diet. Moreover, in group HFOO$_P$, tumour yields were lower even than those of the control group, although there were more affected animals and the tumours appeared at the same time. The histopathological analysis indicated that carcinomas from group HFOO$_P$ displayed lower nuclear and pattern grades and a lower histological grade as compared to those from the high-fat corn oil group, and no differences with the control situation. Furthermore, most carcinomas from the olive oil group were well circumscribed, exhibited the least infiltrative pattern and the most extensive papillary areas, according with a lower morphological aggressiveness. The results obtained in this work are in concordance with previous studies carried out in our laboratory where we analysed the clinical behaviour of tumours throughout the time. Such works clearly demonstrated the tumour-enhancing effect of the high-fat corn oil diet and a negative modulatory effect of the high extra virgin olive oil diet [18, 23]. In the present work, most of the clinical differences among groups were non-significant or close to significance, but this could be probably due to the fact that it was performed at one time point (the end of the assay) and not throughout the time, hence with a lower statistical power. In addition, in other two experimental series, we found significant higher pattern, nuclear and global histological grades in mammary carcinomas from high-fat corn oil groups than in those from their controls [19]. The significant higher mitotic activity observed in group HFCO$_P$ in the present study could be attributed to the proliferative effect of high corn oil diets and linoleic acid, as it has been already described in vivo and in vitro [19, 38–40]. On the other hand, the non-significant increase in the mitotic count as well as in the tumour incidence observed in group HFOO$_P$ as compared to the control may be related to

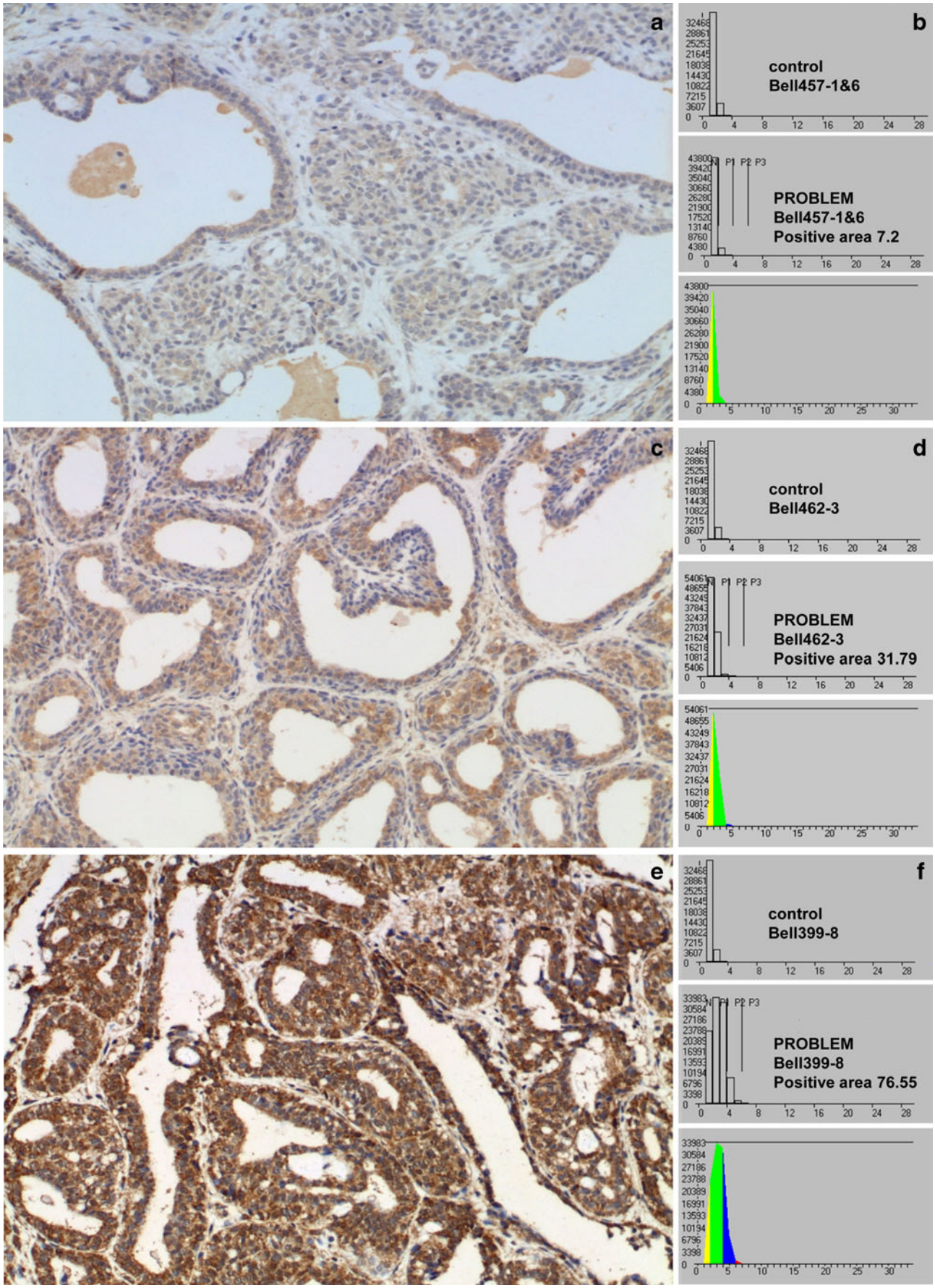
a
b
control
Bell457-1&6
PROBLEM
Bell457-1&6
Positive area 7.2
c
d
control
Bell462-3
PROBLEM
Bell462-3
Positive area 31.79
e
f
control
Bell399-8
PROBLEM
Bell399-8
Positive area 76.55

Table 2 Quantitative evaluation of the immumohistochemical expression of p21Ha-Ras among dietary groups

	Total p21Ha-Ras M±SD (m)	G1 M±SD (m)	G2 M±SD (m)	G3 M±SD (m)
LFCO	50.34±24.97 (46.05)	45.14±18.97 (45.63)	5.03±10.28 (0.26)	0.17±0.63 (0.00)
$HFCO_P$	54.92±19.75 (56.43)	50.40±15.02 (55.22)	4.41±6.43 (0.76)	0.11±0.58 (0.00)
$HFOO_P$	53.96±20.23 (54.26)	50.84±16.73 (52.90)	3.10±5.25 (0.48)	0.01±0.04 (0.00)

Results expressed as the percentage of the positive staining area from a defined tumour field

M mean, *SD* standard deviation, *m* median; *G1, G2 and G3* degree of the intensity of the staining, from low to high; *LFCO* low-fat corn oil group, $HFCO_P$ high-fat corn oil group, $HFOO_P$ high-fat olive oil group

the non-specific stimulatory effect of calories described for high-fat diets [41]. Finally, no differences regarding lymphocytic infiltration were found, whereas secretion was higher in carcinomas from the high-fat groups than in the control situation, being significant when comparing $HFCO_P$ and LFCO, probably because of the storage of intracytoplasmic lipid droplets in response to an excessive amount of fat [42, 43].

Interestingly, we observed that most of the mammary carcinomas developed in each rat were morphologically similar, what suggests a uniform morphological distribution of the carcinomas per animal. This fact was more evident in the control and the high-fat olive oil groups than in group $HFCO_P$. Further studies may be designed to investigate a possible effect of diets at this level.

The influence of dietary lipids on cancer has been proposed to be exerted at several cellular and physiological processes, probably in an integrated, simultaneous and/or sequential way [11, 17]. We have investigated whether Ras, in particular p21Ha-Ras, may be involved in the modulatory effects of dietary fat on breast cancer. The product of *c-Ha-ras* is a 21 kDa GTPase, being active in its GTP-bound form and inactive when it is bound to GDP, and acting as a critical regulator of cell function, including proliferation, differentiation and apoptosis [13, 16, 44]. The present study specifically evaluated the expression of p21Ha-Ras protein on carcinoma-tissue samples from the three dietary groups by immunohistochemistry. This methodology allows us to localise the protein in the cell and to detect and to select the suitable tumour areas for the quantitative analysis. To our knowledge, there are no published studies of the effects of dietary lipids on p21Ha-Ras expression with this experimental approach. The results showed that p21Ha-Ras was expressed in the non-tumour mammary gland associated with the carcinomas and in all tumours. The staining was diffusely cytoplasmic—we did not find any variations in the localisation of the protein—but it exhibited heterogeneity in its intensity. However, we did not observe any

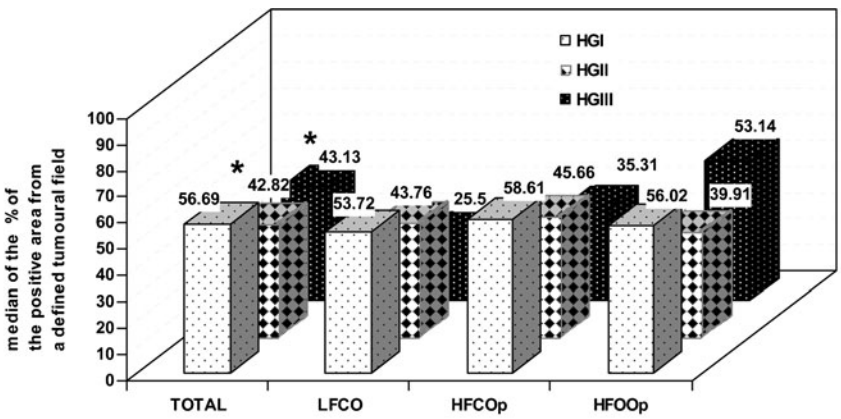

	LFCO			$HFCO_P$			$HFOO_P$			TOTAL		
	HGI	HGII	HGIII	HGI	HGII	HGIII	HGI	HGII	HGIII	HGI	HGII	HGIII
n	49	10	9	52	26	9	41	12	12	142	48	30

Fig. 4 Relationship between histopathological grade and p21Ha-Ras expression in the whole carcinomas from all dietary groups and in carcinomas from the different dietary groups. The results are expressed as the median of the percentage of positive p21Ha-Ras stained area from a defined ×400 magnification tumour field, for each histopathological grade, per total and per experimental group evaluated. *HG* histopathological grade, *TOTAL* total carcinomas from all dietary groups, *LFCO* low-fat corn oil group, $HFCO_P$ high-fat corn oil group, $HFOO_P$ high-fat olive oil group, *n* number of mammary carcinomas analysed; *$P<0.05$, significantly different from the values of low-grade (HGI) carcinomas

significant differences on p21Ha-Ras expression due to dietary lipids. In this sense, no differences between high-fat corn oil and low-fat diets were neither found when Ha-ras mRNA and protein expression by Western Blot were studied, nor when p21Ha-Ras activation was evaluated [21, 28, 45], that suggests that the HFCO diet stimulates mammary carcinogenesis through Ras-independent pathways. Concerning the high extra virgin olive oil diet, we previously found that it decreased the levels of the activated Ras and increased those of the total protein, probably by raising the relative levels of the non-activated form [28]. The lack of differences in total levels detected by immunohistochemistry would be related to methodological issues and to the small magnitude of the differences. In the literature, there are no other data about the influence of olive oil on Ras status in cancer. Studies performed in colon cancer models and cell lines have shown an effect of n-3 PUFA as compared to n-6 PUFA on Ras protein and that this could take place at a post-translational level, by changes in Ras localisation or activation [46–48].

Although several reports have evaluated the association between p21Ha-Ras expression and some clinical and histopathological parameters in human breast cancer, the results have been contradictory, probably due to the different methods and analyses used [49–58]. Our study was carried out with image analysis software, in order to obtain more objective values than with a simple semi-quantitative method. A significant decrease of p21Ha-Ras expression as histological grade increased was found when tumours were considered all together, irrespective to the dietary condition. Considering that there may be an inverse relationship between p21Ha-Ras total expression and activity, this result could indicate increased Ras activity levels with higher malignancy degrees. This association, however, was not observed in group $HFOO_P$ where, in addition, grade III carcinomas exhibited a higher staining than did the similar poorly differentiated tumours of the other two experimental groups. These results suggest that the relationship between tumour morphological malignancy and p21Ha-Ras is complex and it would be affected by factors such as dietary lipids, and that other molecular pathways could be playing an important role in tumour aggressiveness.

In summary, our study demonstrates that dietary lipids influence clinical and morphological characteristics of experimental mammary adenocarcinomas. However, p21Ha-Ras expression does not seem to play a direct role in the enhancing effect of the high-fat corn oil diet and the non-promoting effect of the high extra virgin olive oil diet. Moreover, we have found that tumour p21Ha-Ras expression depends on the histological grade and that olive oil may affect this relationship. Thus, carcinomas morphologically similar may have a different molecular context due to the influence of an environmental factor such as dietary lipids, what may have biological and behavioural consequences.

Acknowledgements This work was supported by grants from "Plan Nacional de I+D+I 2004-2007" (AGL2006-07691), "Fundación Patrimonio Comunal Olivarero 2008-1012" (FPCO2008-165.396), "Agencia para el Aceite de Oliva, Ministerio de Medio Ambiente y de Medio Rural y Marino 2008-2012" (AAO2008-165.471), "Organización Interprofesional del Aceite de Oliva Español" (OIP2009-165.646) and the "Departaments d'Agricultura, Alimentació i Acció Rural, i de Salut de la Generalitat de Catalunya" (GC2010-165.000). The sponsors had no role in the study design, data collection and analysis, interpretation of results, the preparation of the manuscript, the decision to submit the manuscript for publication and the writing of the manuscript.

Conflict of interest statement We declare that we have no conflict of interest.

References

1. Jemal A, Siegel R, Ward E, Hao Y, Xu J, Murray T, Thun MJ (2008) Cancer statistics. CA Cancer J Clin 58:71–96
2. World Cancer Research Foundation (WCRF) and American Institute for Cancer Research (AICR) (2007) Food, nutrition, physical activity and the prevention of cancer: a global perspective. American Institute for Cancer Research, Washington, DC
3. Lee MM, Lin SS (2000) Dietary fat and breast cancer. Annu Rev Nutr 20:221–248
4. Trichopoulou A, Lagiou P, Kuper H, Trichopoulos D (2000) Cancer and Mediterranean dietary traditions. Cancer Epidemiol Biomark Prev 9:869–873
5. Kushi L, Giovannucci E (2002) Dietary fat and cancer. Am Med 113 Suppl 9B:63S-70S
6. Freedman LS, Potischman N, Kipnis V, Midthune D, Schatzkin A, Thompson FE, Troiano RP, Prentice R, Patterson R, Carroll R, Subar AF (2006) A comparison of two dietary instruments for evaluating the fat–breast cancer relationship. Int J Epidemiol 35:1011–1021
7. Ip C (1997) Review of the effects of trans fatty acids, oleic acid, n-3 polyunsaturated fatty acid, and conjugated linoleic acid on mammary carcinogenesis in animals. Am J Clin Nutr 66:1523S–1529S
8. Rose DP (1997) Effects of dietary fatty acids on breast and prostate cancers: evidence from in vitro experiments and animal studies. Am J Clin Nutr 66:1513S–1522S
9. Zusman I, Gurevich P, Madar Z, Nyska A, Korol D, Timar B, Zuckerman A (1997) Tumor-promoting and tumor-protective effects of high-fat diets on chemically induced mammary cancer in rats. Anticancer Res 17:349–356
10. Bartsch H, Nair J, Owen RW (1999) Dietary polyunsaturated fatty acids and cancers of the breast and colorectum: emerging evidence for their role as risk modifiers. Carcinogenesis 20:2209–2218
11. Escrich E, Solanas M, Moral R (2006) Olive oil, and other lipids, in cancer: experimental approaches. In: Quiles JL, Ramírez-Tortosa MC, Yaqoob P (eds) Olive Oil and Health. CAB International Publishing, Oxfordshire, UK, pp 317–374
12. Escrich E, Solanas M, Moral R, Costa I, Grau L (2006) Are the olive oil and other dietary lipids related to cancer? Experimental evidence. Clin Transl Oncol 8:868–883
13. Karnoub AE, Weinberg RA (2008) Ras oncogenes: split personalities. Nat Rev Mol Cell Biol 9:517–531
14. Malaney S, Daly RJ (2001) The Ras signalling pathway in mammary tumorigenesis and metastasis. J Mammary Gland Biol Neoplasia 6:101–113

15. Miyakis S, Sourvinos G, Spandidos DA (1998) Differential expression and mutation of the Ras family genes in human breast cancer. Biochem Biophys Res Commun 251:609–612
16. Malumbres M, Barbacid M (2003) Ras oncogenes: the first 30 years. Nat Rev Cancer 3:459–465
17. Escrich E, Moral R, Grau L, Costa I, Solanas M (2007) Molecular mechanisms of the effects of olive oil and other dietary lipids on cancer. Mol Nutr Food Res 51:1279–1292
18. Solanas M, Hurtado A, Costa I, Moral R, Menendez JA, Colomer R, Escrich E (2002) Effects of a high olive oil diet on the clinical behavior and histopathological features of rat DMBA-induced mammary tumors compared with a high corn oil diet. Int J Oncol 21:745–753
19. Costa I, Moral R, Solanas M, Escrich E (2004) High-fat corn oil diet promotes the development of high histologic grade rat DMBA-induced mammary adenocarcinomas, while high olive oil does not. Breast Cancer Res Treat 86:225–235
20. Escrich E, Solanas M, Soler M, Ruiz de Villa MC, Sánchez JA, Segura R (2001) Dietary polyunsaturated n-6 lipids effects on the growth and fatty acid composition of rat mammary tumors. J Nutr Biochem 12:536–549
21. Solanas M, Moral R, Escrich E (2001) The stimulating effect of a high-fat n-6 polyunsaturated diet on rat DMBA-induced mammary tumors is not related to changes in *c-Ha-ras1* mRNA tumor expression. Nutr Res 21:1261–1273
22. Solanas M, Escrich E, Rouzaut A, Costa I, Martinez A, Notario V (2002) Deregulated expression of the PCPH proto-oncogene in rat mammary tumors induced with 7, 12-dimethylbenz[a]antracene. Mol Carcinog 33:219–227
23. Moral R, Solanas M, García G, Colomer R, Escrich E (2003) Modulation of EGFR and neu expression by n-6 and n-9 high-fat diets in experimental mammary adenocarcinomas. Oncol Rep 10:1417–1424
24. Escrich E, Moral R, García G, Costa I, Sánchez JA, Solanas M (2004) Identification of novel differentially expressed genes by the effect of a high-fat n-6 diet in experimental breast cancer. Mol Carcinog 40:73–78
25. Moral R, Solanas M, Manzanares EM, Haro D, Escrich E (2004) Influence of DMBA-induced mammary cancer on the liver *CPT1, mit HMG-CoA synthase* and *PPARα* mRNA expression in rats fed a low or high corn oil diet. Int J Mol Med 14:283–287
26. Moral R, Solanas M, Garcia G, Grau L, Vela E, Escrich R, Escrich E (2008) High corn oil and high extra virgin olive oil diets have different effects on the expression of differentiation-related genes in experimental mammary tumors. Oncol Rep 20:429–435
27. Solanas M, Moral R, García G, Grau L, Vela E, Escrich R, Costa I, Escrich E (2009) Differential expression of H19 and vitamin D3 upregulated protein 1 as a mechanism of the modulatory effects of high virgin olive oil and high corn oil diets on experimental mammary tumours. Eur J Cancer Prev 18:153–161
28. Solanas M, Grau L, Moral R, Vela E, Escrich R, Escrich E (2010) Dietary olive oil and corn oil differentially affect experimental breast cancer through distinct modulation of the p21Ras signalling and the proliferation-apoptosis balance. Carcinogenesis 31:871–879
29. Huggins C, Morii S, Grand LC (1961) Mammary cancer induced by a single dose of polynuclear hydrocarbons: routes of administration. Ann Surg 154:315–318
30. Escrich E (1987) Validity of the DMBA-induced mammary cancer model for the study of human breast cancer. Int J Biol Markers 2:197–206
31. Escrich E, Solanas M, Segura R (1994) Experimental diets for the study of lipid influence on the induced mammary carcinoma in rats: I-diet definition. In Vivo 8:1099–1106
32. Escrich E, Solanas M, Ruiz de Villa MC, Ribalta T, Muntané J, Segura R (1994) Experimental diets for the study of lipid influence on the induced mammary carcinoma in rats: II-suitability of the diets. In Vivo 8:1107–1112
33. Young S, Hallowes RC (1973) Tumours of the mammary gland. In: Turusov V (ed) Pathology of tumours in laboratory animals, vol I, Tumours of the rat. IARC Sci Publ, Lyon, pp 31–86
34. Costa I, Solanas M, Escrich E (2002) Histopathologic characterization of mammary neoplastic lesions induced with 7, 12 dimethylbenz (a)anthracene in the rat. A comparative analysis with human breast tumors. Arch Pathol Lab Med 126:915–927
35. Elston CW, Ellis IO (1991) Pathological prognostic factors in breast cancer. The value of histological grade in breast cancer: experience from a large study with long-term follow up. Histopathology 19:403–410
36. Shan L, Yu M, Snyderwine EG (2005) Gene expression profiling of chemically induced rat mammary gland cancer. Carcinogenesis 26:503–509
37. Qiu C, Shan L, Yu M, Snyderwine EG (2005) Steroid hormone receptor expression and proliferation in rat mammary gland carcinomas induced by 2-amino-1-methyl-6-phenylimidazo[4, 5-b]pyridine. Carcinogenesis 26:763–769
38. Snyderwine EG, Thorgeirsson UP, Venugopal M, Roberts-Thomson SJ (1998) Mammary gland carcinogenicity of 2-amino-1-methyl-6-phenylimidazol [4, 5-b]pyridine in Sprague–Dawley rats on high and low-fat diets. Nutr Cancer 31:160–167
39. Zhang L, Bird RP, Bruce WR (1987) Proliferative activity of murine mammary epithelium as affected by dietary fat and calcium. Cancer Res 47:4905–4908
40. Cunningham DC, Harrison LY, Shultz TD (1997) Proliferative responses of normal human mammary and MCF-7 breast cancer cells to linoleic acid, conjugated linoleic acid and eicosanoid synthesis inhibitors in culture. Anticancer Res 17:197–203
41. Guthrie N, Carroll KK (1999) Specific versus non-specific effects of dietary fats on carcinogenesis. Prog Lipid Res 38:261–271
42. Hubbard NE, Erickson KL (1987) Influence of dietary fats on cell populations of line 168 mouse mammary tumors: a morphometric and ultrastructural study. Cancer Lett 35:281–294
43. Kossoy G, Yarden G, Ben-Hur H, Kossoy N, Stark A, Madar Z, Zusm I (2001) Comparative effects of dimethylbenz(a)anthracene and a 15% olive oil diet on cellular components and expression of apoptosis-related proteins in the spleen and mammary gland tumors of rats. Oncol Rep 8:435–439
44. Ramos JW (2008) The regulation of extracellular signal-regulated kinase (ERK) in mammalian cells. Int J Biochem Cell Biol 40:2707–2719
45. Roberts-Thomson SJ, Snyderwine EG (1997) Effect of dietary fat on codon 12 and 13 *Ha-Ras* gene mutations in 2-amino-1methyl-6-phenylimidazo[4, 5b]pyridine-induced rat mammary gland tumors. Mol Carcinog 20:348–354
46. Singh J, Hamid R, Reddy BS (1997) Dietary fat and colon cancer: modulating effect of types and amount of dietary fat on Ras-p21 function during promotion and progression stages of colon cancer. Cancer Res 57:253–258
47. Davidson LA, Lupton JR, Jiang YH, Chapkin RS (1999) Carcinogen and dietary lipid regulate ras expression and localization in rat colon without affecting farnesylation kinetics. Carcinogenesis 20:785–791
48. Collet ED, Davidson LA, Fan YY, Lupton JR, Chapkin RS (2001) n-6 and n-3 polyunsaturated fatty acids differentially modulate oncogenic Ras activation in colonocytes. Am J Physiol Cell Physiol 280:C1066–C1075
49. Agnantis NJ, Parissi P, Anagnostakis D, Spandidos DA (1986) Comparative study of Harvey-ras oncogene expression with conventional clinicopathologic parameters of breast cancer. Oncology 43:36–39
50. Saccani Jotti G, Fontanesi M, Bombardieri E, Gabrielli M, Veronesi P, Bianchi M, Becchi G, Bogni A, Tardini A (1992) Preliminary

study on oncogene product immunohistochemistry (c-erbB2, c-myc, ras, p21, EGFR) in breast pathology. Int J Biol Markers 7:35–42
51. Agnantis NJ, Apostolikas NA, Zolotas VG, Spandidos DA (1994) Immunohistochemical detection of ras p21 oncoprotein in breast cancer imprints. Acta Cytol 38:335–340
52. Özer E, Sis B, Özen E, Sakizli M, Canda T, Sarioglu S (2000) BRCA1, c-erbB2, and H-ras gene expressions in young women with breast cancer. An immunohistochemical study. Appl Immunohistochem Mol Morphol 8:12–18
53. Watson DM, Elton RA, Jack WJ, Dixon JM, Chetty U, Miller WR (1991) The H-ras oncogene product p21 and prognosis in human breast cancer. Breast Cancer Res Treat 17:161–169
54. Göhring UJ, Schöndorf T, Kiecker VR, Becker M, Kurbacher C, Scharl A (1999) Immunohistochemical detection of H-ras proto-oncoprotein p21 indicates favorable prognosis in node-negative breast cancer patients. Tumour Biol 20:173–183
55. Schondorf T, Rutzel S, Andrack A, Becker M, Hoopmann M, Breidenbach M, Gohring UJ (2002) Immunohistochemical analysis reveals a protective effect of H-ras expression mediated via apoptosis in node-negative breast cancer patients. Int J Oncol 20:273–277
56. Walker RA, Wilkinson N (1988) p21 ras protein expression in benign and malignant human breast. J Pathol 156:147–153
57. Spaventi R, Kamenjicki E, Pecina N, Grazio S, Pavelic J, Kusic B, Curtila D, Danilovic Z, Spaventi S (1994) Immunohistochemical detection of TGF-alpha, EGF-R, c-erbB2, c-H-ras, c-myc, estrogen and progesterone in benign and malignant human breast lesions: a concomitant expression. In Vivo 8:183–189
58. Going JJ, Anderson TJ, Wyllie AH (1992) Ras p21 in breast tissue: associations with pathology and cellular localisation. Br J Cancer 65:45–50

Virchows Arch (2011) 458:153–158
DOI 10.1007/s00428-010-1025-2

ORIGINAL ARTICLE

Usefulness of liquid-based cytology in hormone receptor analysis of breast cancer specimens

Rieko Nishimura · Kenjiro Aogi · Tamami Yamamoto · Daisuke Takabatake · Seiki Takashima · Norihiro Teramoto · Akihiro Kagawa · Sachiko Morita

Received: 5 September 2010 / Revised: 30 November 2010 / Accepted: 3 December 2010 / Published online: 21 December 2010
© Springer-Verlag 2010

Abstract Immunohistochemical (IHC) analysis of the hormone receptor (HR) in breast cancer cytology is an important issue nowadays. Several studies have shown discrepancy in the HR status between the primary tumor and metastases. Cytology can be used for patients with metastatic disease. Although cytological assessment of HR is an excellent method, it has not been routinely used because of the difficulty in consistently preparing multiple good quality slides. Liquid-based cytology (LBC) preparation is considered as the key to resolving the aforementioned problem; however, few studies have reported the HR assessment in breast cancer using LBC. Therefore, the HR status of LBC slides from 82 breast cancers was compared with that of the corresponding surgical specimens. The HR assay in both the LBC slides and surgical specimens was conducted by IHC using an autostainer. For the IHC staining, the protocol recommended by the manufacturer for paraffin-embedded sections was used for both the cytology and histology specimens. The HR results of the cytology agreed with those of the histology in 80 of the 82 cases (accuracy rate, 98%) for estrogen receptor, and in 78 of the 82 cases (accuracy rate, 95%) for progesterone receptor. The overall accuracy of the HR status on the cytology and the histology was 99% in 81 of the 82 cases. In conclusion, in HR analysis of breast cancers, LBC followed by IHC using an autostainer was useful for the standard processing of cytological specimens and showed a good correlation with the results of analysis on the histology specimens.

Keywords Breast cancer · Hormone receptor · Immunohistochemistry · Fine needle aspirate · Liquid-based cytology

R. Nishimura (✉) · T. Yamamoto · A. Kagawa · S. Morita
Department of Clinical Laboratory,
National Hospital Organization Shikoku Cancer Center,
160 Kou, Minamiumemoto-machi,
Matsuyama, Ehime 791-0280, Japan
e-mail: rnishimu@shikoku-cc.go.jp

K. Aogi · D. Takabatake · S. Takashima
Department of Breast Oncology,
National Hospital Organization Shikoku Cancer Center,
160 Kou, Minamiumemoto-machi,
Matsuyama, Ehime 791-0280, Japan

N. Teramoto
Department of Pathology,
National Hospital Organization Shikoku Cancer Center,
160 Kou, Minamiumemoto-machi,
Matsuyama, Ehime 791-0280, Japan

Introduction

Immunohistochemical analysis of the hormone receptor (HR) status of breast cancer cytology specimens has become a very important diagnostic tool nowadays, because more and more studies are showing discrepancy in the HR status between the primary tumor and metastases [1–4]. The 2010 guideline of the American Society of Clinical Oncology (ASCO) and the College of American Pathologists (CAP) recommends determination of the HR status not only in the primary tumor, but also in the tumors at sites of recurrence [5]. Analysis of the HR status is also important for patients who need preoperative chemotherapy. Fine needle aspiration cytology is useful for patients with large tumors or in poor general condition. Thus, diagnostic cytology is a quick, inexpensive, and less-invasive tool for approaching these types of tumors and patients.

Several studies have reported on assessment of the HR status using cytological specimens [6–18]. All of the literature reports suggest a good correlation between the results of the HR status obtained on the cytological specimens and those obtained on the corresponding surgical specimens. However, this method has not been routinely used because of the difficulty in consistently preparing multiple good-quality slides from cytological specimens. Liquid-based cytology (LBC) is a useful tool for the

standardization of cytological specimens; however, few studies have reported assessment of the HR status in breast cancer using LBC specimens [11, 18].

Therefore, fine needle aspirate (FNA) specimens obtained from breast cancers were processed for LBC and the HR status was assessed by immunohistochemistry (IHC). The results were compared with those obtained by IHC on the corresponding paraffin-embedded histological sections.

Materials and methods

FNA specimens from breast cancer

From October 2008 to December 2009, 105 FNA specimens from breast cancers were collected. One specimen was collected for each lesion punched once by the 21-gauge needle. The needle was attached to a 20-ml syringe which was mounted on an aspiration gun. Sixty-six specimens were obtained from patients by the same surgeon (KA) and 39 from the surgically excised tumors by the same pathologist (RN). All the patients were scheduled to undergo tumor resection without preoperative chemotherapy.

The FNA specimens were directly rinsed into a cytopreservative solution containing fixative (PreserveCyt Solution, Hologic, Bedford, MA, USA). The vials were stored at room temperature for 3–7 days.

Histological types of breast cancer

The examined tumors included 95 invasive ductal carcinomas, not otherwise specified, five invasive lobular carcinomas, two mucinous carcinomas, and three noninvasive ductal carcinomas.

Preparation of FNA slides

Slides of the FNA specimens were prepared by LBC (ThinPrep System, Hologic), according to the directions in the operator's manual provided by the manufacturer. Silanized glass slides were used for better adhesion of the cells. Three slides were prepared from each specimen, and fixed in 95% ethanol for 24–48 h. One slide was used for Papanicolaou staining and the remaining two for IHC.

Preparation of the histological specimens for IHC

Representative sections were prepared from the cut surface of the resected breast cancers. The tissues were fixed in 10% buffered formalin for 24–48 h and embedded in paraffin according to routine procedures. Approximately 4-μm thick sections were prepared and placed on the silanized glass slides.

IHC

The IHC assay was performed with an autostainer (Ventana XT System, Benchmark, Roche Diagnostics, Basel, Switzerland) using the Ventana Medical Systems' Detection Kit. The staining procedure using this kit is based on the labeled streptavidin biotin method. For the IHC staining, the protocol involving heat antigen retrieval recommended by the manufacturer for paraffin-embedded sections was used for both the FNA and surgically resected specimens. The anti-estrogen receptor (ER) (mouse monoclonal antibody, clone 6 F11) and progesterone receptor (PR; mouse monoclonal antibody, clone 16) of Ventana I-VIEW CONFIRM primary antibody series (Roche Diagnostics) were used as the primary antibodies. The previously confirmed histological sections were used for positive and negative control.

Evaluation of the IHC results

Both in the cytological and histological slides, positive nuclear staining of the malignant cells was evaluated on the basis of the percentage of stained cells. The cutoff value was 1% based on the ASCO and the CAP guideline for HRs in breast cancer published in 2010 [5].

The final HR status considering both the ER and the PR status was called "over all HR status". If a case presents ER or PR positive, the case is assessed all over HR positive, and a case with both ER and PR negative is called all over HR negative.

Data management

The data obtained were analyzed to determine the sensitivity, specificity, accuracy, false positive rate, false negative rate, and positive and negative predictive values (PPV and NPV) of the diagnostic tests. The Cohen kappa test was used to assess the consistency between the cytological and the histological results. The consistency is "good" if the kappa value exceeds 0.6 and "excellent" if it exceeds 0.8.

Results

The results of IHC analysis of a total of 82 of the 105 FNA specimens obtained from breast cancers were compared with those of the corresponding histological sections. Of the 66 FNA specimens obtained from breast cancer patients, 58 were evaluated, as the remaining eight tumor-bearing patients did not undergo tumor resection at our institution. In all, 47 of 58 (81%) FNAs obtained from breast cancer patients and 35 of 39 (90%) FNAs obtained from the surgically excised breast cancer specimens were analyzed, because the remaining 11

from the former group and the remaining four from the latter group showed scant cellularity.

Tables 1 and 2 summarize the results on the HR status between the cytology specimens and the histological sections.

Estrogen receptor status

The results of assessment of the FNA specimens agreed with those of the histological sections in 80 of the 82 cases (accuracy rate, 98%; kappa=0.926). There were 64 positive results (Fig. 1) and 18 negative results (Fig. 2; sensitivity, 97%; specificity, 100%; PPV, 100%; NPV, 89%), and no discordant positive and two discordant negative results (false positive rate, 0%; false negative rate, 3%).

Progesterone receptor status

The results of assessment of the FNA specimens agreed with those of the histological sections in 78 of the 82 cases (accuracy rate, 95%; kappa=0.885). There were 56 positive results and 26 negative results (sensitivity, 95%; specificity, 96%; PPV, 98%; NPV, 88%), and one discordant positive and three discordant negative results (false positive rate, 4%; false negative rate, 5%).

Overall hormone receptor status

The results of assessment of the FNA specimens agreed with those of the histological sections in 81 of the 82 cases (accuracy rate, 99%; kappa=0.962). There were 65 positive results and 17 negative results (sensitivity, 98%; specificity, 100%; PPV, 100%; NPV, 94%), and one discordant negative result but no discordant positive result (false positive rate, 0%; false negative rate, 2%).

Discussion

Immunohistochemical analysis of the HR status in breast cancer cytology specimens is a very important diagnostic tool nowadays, because more and more studies are showing discrepancy in the HR status between the primary tumor and metastases [1–4]. Cytology can be used for the diagnosis of some metastatic lesions, such as pleural effusion, ascites, and liver metastases. Analysis of the HR status is also important in patients who need preoperative chemotherapy. In addition, fine needle aspiration cytology is useful for patients who have inoperable large tumors or are in poor general condition. Therefore, diagnostic cytology is a quick, inexpensive and less traumatic tool for approaching these types of tumors and patients.

Several studies have reported on assessment of the HR status using cytological specimens [6–18]. From the mid 1980s to the late 1990s, the HR status in cytological specimens was reported to show a good correlation with that of biochemical assays [9, 11, 12, 19]. More recently, several studies have reported comparison of the HR status by IHC in cytological specimens and frozen [8, 10] or paraffin-embedded [7, 11, 13, 15, 17, 18, 20] histological sections. All of the literature published until now indicates the existence of a good correlation between the HR status in cytological specimens and that in the corresponding surgical specimens. The concordance rate in previously reported literature for the ER status ranges from 82% to 99% and for the PR status ranges from 71% to 97%. Although assessment of the HR status in cytological specimens is an excellent method, with good correlation of the results with those of standard methods, it has not been routinely used, because of the difficulty in consistently preparing multiple good quality slides. Specimen fixation was also a problem that needed to be addressed. Until the early 2000s, mainly buffered formalin-fixed slides [6, 7, 9, 12, 19] were used. Some studies recommended special sequential fixation [14, 21]. After the early 2000s, it was reported that alcohol fixation can be used for new antibodies [8].

LBC preparation is considered as the key to resolving the aforementioned problems. In this study, we used LBC preparations for all the FNA specimens. It has been demonstrated that the processing of FNA breast specimens for LBC with ThinPrep is an accurate method and is useful for the standardization of cytological specimens [22, 23]. Moreover, it offers the potential advantage of preserving material for additional IHC and mRNA analyses [24]. Preservation of the HR antigenicity has been assured in mammary tumor cells stored in a cytopreservative solution (PreservCyt) over a 56-day storage period [25].

Table 1 Comparison of the results of assessment of the hormone receptor status on cytological and histological specimens

Histology	Cytology								
	Estrogen receptor			Progesterone receptor			Overall hormone receptor		
	Positive	Negative	Total	Positive	Negative	Total	Positive	Negative	Total
Positive	64	2	66	55	3	58	65	1	66
Negative	0	16	16	1	23	24	0	16	16
Total	64	18	82	56	26	82	65	17	82

Table 2 Comparison of the hormone receptor status of breast cancer as assessed in cytological and histological specimens

	Estrogen receptor (%)	Progesterone receptor (%)	Overall hormone receptor (%)
Sensitivity	64/66 (97)	55/58 (95)	65/66 (98)
Specificity	16/16 (100)	23/24 (96)	16/16 (100)
Accuracy	80/82 (98)	78/82 (95)	81/82 (99)
FPR	0/16 (0)	1/24 (4)	0/16 (0)
FNR	2/66 (3)	3/58 (5)	1/66 (2)
PPV	64/64 (100)	55/56(98)	65/65 (100)
NPV	16/18 (89)	23/26 (88)	16/17 (94)

FPR false positive rate, *FNR* false negative rate, *PPV* positive-predictive value, *NPV* negative-predictive value

Until date, there are two reports on HR assessment in breast cancer by IHC using ThinPrep [11, 18]. The differences between these two studies and our study are the post fixation method used in one [18], and the IHC method used in both. In all three studies, including our study, an alcohol-based fixative was used, but cold acetone was used for post fixation before IHC staining in one [18]. In regard to the IHC method, a manual procedure using Dako staining kit was used in one [11] and the Dako Autostainer was used in the other [18]. We used the Ventana Autostainer. The antibodies used were different in all three studies, but mouse monoclonal antibody and antigen retrieval with heat was used in all. All three studies showed excellent concordance rates for the ER (98–99%) and PR (89–97%) status. Our results showed excellent

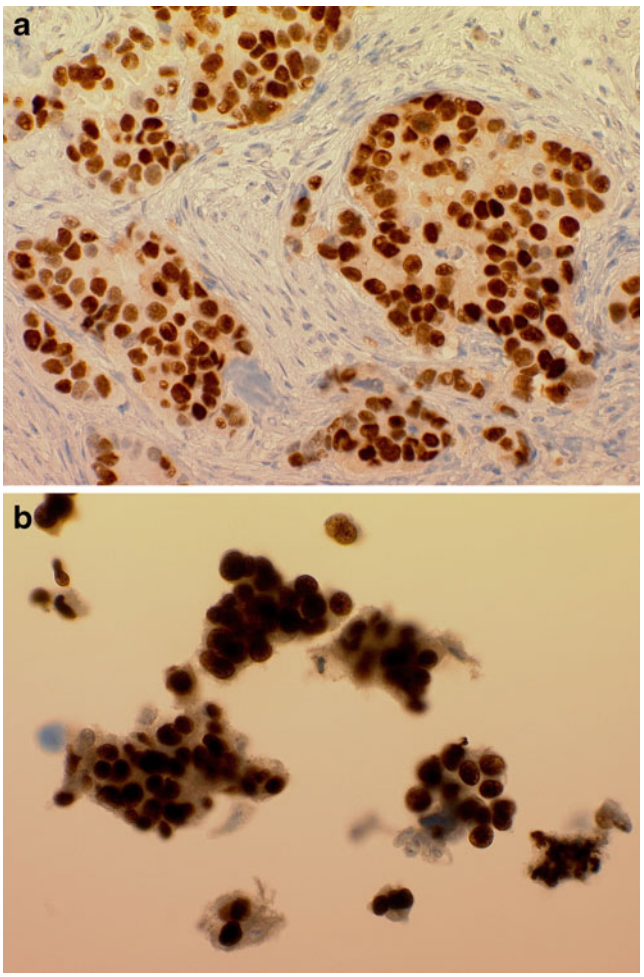

Fig. 1 An example of a hormone receptor-positive case showing concordant results in the histological and cytological specimens. Both the histological (**a**) and cytological (**b**) specimens show strong nuclear staining in all cancer cells

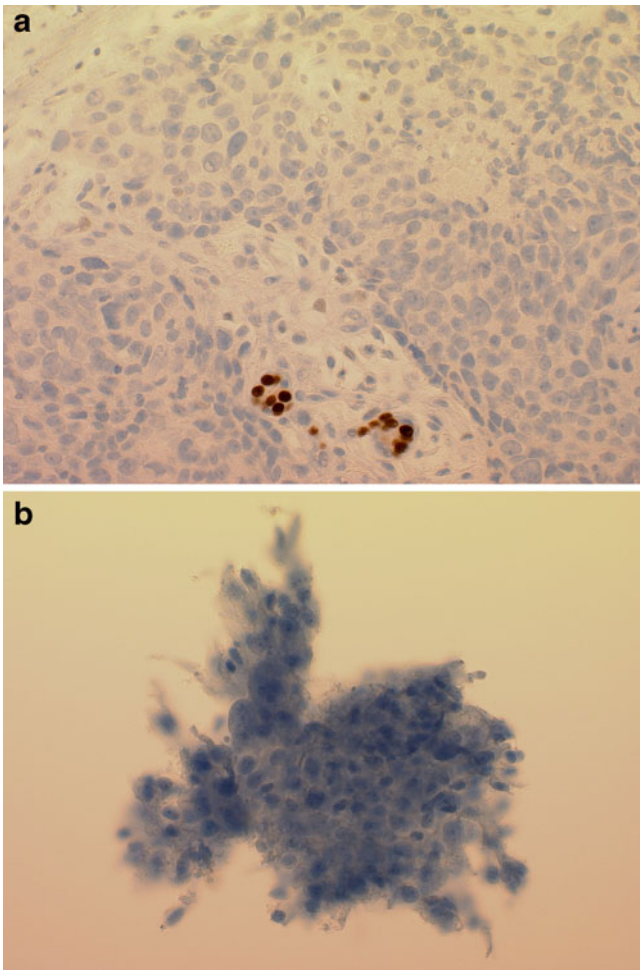

Fig. 2 An example of hormone receptor-negative case showing concordant results in the histological and cytological specimens. Both the histological (**a**) and cytological (**b**) specimens show negative nuclear staining in all cancer cells. The positively stained cells in the middle, at the bottom of the histology slide (**a**), are normal ductal cells

consistency by the Cohen kappa test in ER, PR, and over all HR status.

In our study, we obtained no discordant positive results for ER and one discordant positive result for PR, and two discordant negative results for ER and three discordant negative results for PR. The reason for the discordance in the one discordant negative case for ER and three discordant negative cases for PR was the difference in the distribution of the positive cells between the cytological specimens and histological sections. In one discordant positive case for PR, the invasive component was negative whereas the noninvasive component was positive in histological sections; therefore, the noninvasive component was thought to be aspirated by FNA. The reason for discordance in the one discordant negative case for ER was that the FNA specimen was of poor quality and nuclear staining was faint. In regard to the overall HR status, one case showed a discordant negative result, in which a few positive cells were found in the histological section. Previous studies have pointed out the intratumoral heterogeneity of positive cells as the main reason for discordant results between cytologic and histologic specimens [7, 9, 12, 14, 15] similar to the case in our results. One study suggested that the mucin over the mucinous carcinoma cells may have prevented proper immunostaining [15]. There were two cases of mucinous carcinoma in our study; however, both showed positive results for the HR status. In one study, it was not possible to evaluate the ER status on the cytological material in one case, because of the presence of abundant debris [8]. We did not encounter any such specimens. We expect that the cytopreservative solution for LBC washed out the mucin or the debris.

In summary, cytological assessment of the HR status of breast cancer using LBC prepared with ThinPrep followed by IHC using the Ventana Autostainer allowed easy preparation of the specimens and showed excellent concordance rates.

Acknowledgments This study was supported in part by Grants-in-Aid for Cancer Research from the Ministry of Health, Labour and Welfare of Japan, and Grants-in-Aid for Clinical Research from the National Hospital Organization.

We thank Dr. Takahiro Hasebe of the Center for Cancer Control and Information Services, National Cancer Center for his precious advice on this research.

Conflict of interest statement We have no conflict of interest.

References

1. Lower EE, Glass EL, Bradley DA, Blau R, Heffelfinger S (2005) Impact of metastatic estrogen receptor and progesterone receptor status on survival. Breast Cancer Res Treat 90:65–70
2. Guarneri V, Giovannelli S, Ficarra G et al (2008) Comparison of HER-2 and hormone receptor expression in primary breast cancers and asynchronous paired metastases: impact on patient management. Oncologist 13:838–844
3. Broom RJ, Tang PA, Simmons C et al (2009) Changes in estrogen receptor, progesterone receptor and Her-2/neu status with time: discordance rates between primary and metastatic breast cancer. Anticancer Res 29:1557–1562
4. Idirisinghe PK, Thike AA, Cheok PY et al (2010) Hormone receptor and c-ERBB2 status in distant metastatic and locally recurrent breast cancer: pathologic correlations and clinical significance. Am J Clin Pathol 133:416–429
5. Hammond MEH, Hayes DF, Dowsett M et al (2010) American Society of Clinical Oncology/College of American Pathologists guideline recommendations for immunohistochemical testing of estrogen and progesterone receptors in breast cancer. J Clin Oncol 28:2784–2795
6. Reiner A, Spona J, Reiner G et al (1986) Estrogen receptor analysis on biopsies and fine-needle aspirates from human breast carcinoma. Correlation of biochemical and immunohistochemical methods using monoclonal antireceptor antibodies. Am J Pathol 125:443–449
7. Nizzoli R, Bozzetti C, Naldi N et al (2000) Comparison of the results of immunocytochemical assays for biologic variables on preoperative fine-needle aspirates and on surgical specimens of primary breast carcinomas. Cancer Cytopathol 90:61–66
8. Schmitt FC, Bento MJ, Amendoeira I (1995) Estimation of estrogen receptor content in fine-needle aspirates from breast cancer using the monoclonal antibody 1D5 and microwave oven processing: correlation with paraffin embedded and frozen sections determinations. Diagn Cytopathol 13:347–351
9. Marrazzo A, Taormina P, Leonardi P, Lupo F, Filosto S (1995) Immunocytochemical determination of estrogen and progesterone receptors on 219 fine-needle aspirates of breast cancer. A prospective study. Anticancer Res 15:521–526
10. Railo M, Nordling S, Krogerus L, Sioris T, vonSmitten K (1996) Preoparative assessment of proliferative activity and hormonal receptor status in carcinoma of the breast: a comparison of needle aspiration and needle-core biopsies to the surgical specimen. Diagn Cytopathol 15:205–210
11. Leung SW, Bédard YC (1999) Estorogen and progesterone receptor contents in ThinPrep-processed fine-needle aspirates of breast. Am J Clin Pathol 112:50–56
12. Nizzoli R, Bozzetti C, Savoldi L et al (1994) Immunocytochemical assay of estrogen and progesterone receptors in fine needle aspirates from breast cancer patients. Acta Cytol 38:933–938
13. Cano G, Milanezi F, Leitão D, Ricardo S, Brito MJ, Schmitt FC (2003) Estimation of hormone receptor status in fine-needle aspirates and paraffin-embedded sections from breast cancer using the novel rabbit monoclonal antibodies SP1 and SP2. Dagn Cytopathol 29:207–211
14. Gong Y, Symmans WF, Krishnamurthy S, Patel S, Sneige N (2004) Optimal fixation conditions for immunocytochemical analysis of estrogen receptor in cytologic specimens of breast carcinoma. Cancer Cytopathol 102:34–40
15. Moriki T, Takahashi T, Ueta S, Mitani M, Ichien M (2004) Hormone receptor status and HER2/neu overexpression determined by automated immunostainer on routinely fixed cytologic specimens from breast carcinoma: correlation with histologic sections determinations and diagnostic pitfalls. Diagn Cytopathol 30:251–256
16. Fernando IN, Powles TJ, Dowsett M et al (1995) Determining factors which predict response to primary medical therapy in breast cancer using a single fine needle aspirate with immunocytochemical staining and flow cytometry. Virchows Arch 426:155–166
17. Zoppi JA, Rotundo AV, Sundblad AS (2002) Correlation of immunocytochemical and immunohistochemical determination of estrogen and progesterone receptors in breast cancer. Acta Cytol 46:337–340

18. Konofaos P, Kontzoglou K, Georgoulakis J et al (2006) The role of ThinPrep cytology in the evaluation of estrogen and progesterone receptor content of breast tumors. Surg Oncol 15:257–266
19. Sauer T, Beraki E, Jebsen PW et al (1998) Assessing estrogen and progestrone receptor status in fine needle aspirates from breast carcinomas. Results on six years of material and correlation with biochemical assay. Anal Quant Cytol Histol 20:122–126
20. Malaviya AA, Chinoy RF, Prabhundesai NM, Sawant MH, Parmar V, Badwe RA (2006) Immunohistochemistry on scrape cytology in breast cancer: will it unearth the weaker positives? Acta Cytol 50:284–290
21. Hudock JA, Hanau CA, Christen R, Bibbo M (1996) Expression of estrogen and progesterone receptors in cytologic specimens using various fixatives. Diagn Cytopathol 15:78–83
22. Bédard YC, Pollett AF (1999) Breast fine-needle aspiration: a comparison of ThinPrep and conventional smears. Am J Clin Pathol 111:523–527
23. Kontzoglou K, Moulakakis KG, Konofaos P, Kyriazi M, Kyroudes A, Karakitsos P (2005) The role of liquid-basd cytology in the investigation of breast lesions using fine-needle aspiration: a cytohistopathological evaluation. J Surg Oncol 89: 75–78
24. Komatsu K, Nakanishi Y, Seki T et al (2008) Application of liquid-based preparation to fine needle aspiration cytology in breast cancer. Acta Cytol 52:591–596
25. Tabbara SO, Sidawy MK, Frost AR et al (1998) The stability of estrogen and progesterone receptor expression on breast carcinoma cells stored PreservCyt suspensions and as ThinPrep slides. Cancer 84:355–360

Virchows Arch (2011) 458:159–169
DOI 10.1007/s00428-010-1033-2

ORIGINAL ARTICLE

Incomplete inside-out growth pattern in invasive breast carcinoma: association with lymph vessel invasion and recurrence-free survival

Sayaka Kuba · Hiroshi Ohtani · Junzo Yamaguchi · Hiroko Hayashi · Tatsuya Uga · Takashi Kanematsu · Isao Shimokawa

Received: 1 November 2010 / Revised: 16 December 2010 / Accepted: 20 December 2010 / Published online: 8 January 2011
© Springer-Verlag 2011

Abstract Invasive micropapillary carcinoma (IMPC) is a rare subtype of epithelial tumor of the breast listed in the 2003 World Health Organization histologic classification of tumors of the breast. It is characterized by inside-out micropapillary morphology, frequent lymph vessel invasion (LVI), and lymph node metastasis; however, its etiology remains unknown. This study investigated the incomplete inside-out growth pattern (IGP) in invasive ductal carcinoma, not otherwise specified (NOS), and examined the association between incomplete IGP and clinicopathologic features, including the presence of intratumoral lymph vessels (ILV), LVI, nodal metastasis, and prognosis. Tumor tissues from 166 invasive duct carcinomas NOS and 10 IMPCs were immunostained using an anti-epithelial membrane antigen antibody to detect IGP and with D2-40 antibody to determine the presence of ILV and LVI. Incomplete IGP was detected focally in 88 (53%) of 166 invasive duct carcinomas NOS. Transition areas between IMPC and invasive duct carcinoma NOS also showed prominent incomplete IGP in 9 (90%) of 10 IMPCs. Incomplete IGP in invasive duct carcinomas NOS was associated with larger tumor size, higher frequencies of ILV, LVI, nodal metastasis, and poorer recurrence-free survival by univariate analysis. Incomplete IGP, ILV, and tumor size independently affected LVI by multivariate analysis. These findings indicate that incomplete IGP of tumor cell clusters is not uncommon and is a useful tool for predicting LVI in invasive duct carcinoma NOS of the breast.

Keywords Breast cancer · Incomplete inside-out growth pattern · Lymph vessel invasion · Intratumoral lymph vessel · Invasive micropapillary carcinoma · Prognosis

S. Kuba · T. Uga · T. Kanematsu
Department of Surgery, Graduate School of Biomedical Science, Nagasaki University,
Nagasaki, Japan

H. Ohtani (✉)
Department of Pathology, Hakujyuji Hospital,
3-2-1 Ishimaru, Nishi-Ku,
Fukuoka 819-8511, Japan
e-mail: ohtani@hakujyujikai.or.jp

J. Yamaguchi
Department of Surgery, National Hospital Organization, Saga Hospital,
Saga, Japan

H. Hayashi · I. Shimokawa
Department of Investigative Pathology, Graduate School of Biomedical Science, Nagasaki University,
Nagasaki, Japan

Introduction

Several pathways mediate tumor dissemination, including local tissue invasion, direct seeding of body cavities or surface, and lymphatic or hematogenous spread [1]. Lymph node metastasis is known to be the most important independent prognostic factor in breast cancer. Invasion of tumor cells into lymphatic vessels is a critical step in metastasis, and lymph vessel invasion (LVI) is a predictor for axillary lymph node metastasis and a prognostic factor in node-negative cancer [2–8]. LVI can also be used to determine the appropriate indications for chemotherapy [7–9].

The mechanisms of lymphatic tumor spread have still not been clarified. Recent studies have indicated that lymphangiogenesis occurred in breast cancer and that specific lymphangiogenic factors, such as vascular endo-

thelial growth factors C and D, were expressed [2–4]. However, other immunohistochemical studies have found no evidence of proliferation in lymphatic vessels [10, 11]. Thus, the development of lymph vessels within breast tumors, and their relation to LVI and subsequent nodal metastasis, remains controversial [1, 12].

Invasive micropapillary carcinoma (IMPC) is a rare subtype of epithelial tumor of the breast listed in the 2003 World Health Organization (WHO) histologic classification of tumors of the breast [13]. It is characterized by aggregates of small clusters of tumor cells lying within clear stromal spaces resembling dilated vascular channels, reversed polarity, an "inside-out" micropapillary morphology, and frequent LVI and lymph node metastasis [13–17]. The term "inside-out growth pattern" and its clinicopathologic significance in breast cancer were first introduced by Peterse [18]. Further studies described the external surface of the tumor cell clusters as identical to a true luminal surface and characterized by the presence of microvilli on electron microscopy and immumoreactivity to epithelial membrane antigen (EMA) [19]. Gradual or abrupt transitions from typical invasive ductal carcinoma to the micropapillary components are observed in non-pure IMPC [13]. Routine pathologic examination has shown that these transition areas in IMPC frequently include tumor cell clusters with an incomplete inside-out growth pattern (IGP); "incomplete" IGP was defined in the present study as the presence of tumor cell clusters that were partly but not completely fringed with strong EMA immunostaining facing the stroma. Incomplete IGP was also noted in invasive ductal carcinoma, not otherwise specified (NOS), and we therefore hypothesized that invasive duct carcinoma NOS with incomplete IGP would tend to develop LVI and nodal metastasis, simulating IMPC.

The purpose of this study was to investigate the correlation between incomplete IGP and the presence of intratumoral lymph vessels (ILV), LVI, and nodal metastasis in invasive duct carcinoma NOS of the breast. We also evaluated the prognostic value of incomplete IGP and comment on a specific case that provides potential insight into the mechanisms of LVI.

Materials and methods

Patients

A total of 197 patients with invasive ductal carcinoma of the breast who underwent surgery from 2000 to 2004 were retrospectively analyzed. The study materials represented 67% (197/296) of all new breast carcinomas diagnosed in the same period. Complete axillary lymph node resection was performed in 98% (194/197), and no sentinel node biopsy was carried out in this period. Patients with bilateral breast cancer (synchronous, metachronous), clinically multifocal or multicentric tumors in the unilateral breast, distant metastasis, or malignancy at another site were excluded, together with patients who had received preoperative neoadjuvant chemotherapy. Special histologic types other than IMPC were excluded from the immunohistochemical analyses.

Clinicopathologic features

Tumor size was measured as the largest dimension of the microscopic invasive component in pathologic sections. All tumors were graded according to a modified version of the Bloom–Richardson grading system [20]. Immunohistochemistry for hormone receptors (estrogen and progesterone; Dako, Tokyo, Japan) and Her2/new status (Dako) were evaluated at the time of diagnosis. Tumors with staining of >10% of tumor cell nuclei were defined as positive for hormone receptors. Her2/neu immunostaining was classified according to the Dako-HercepTest scoring system. All those cancers scoring equivocal (2+) were subjected to Her2/neu gene amplification analysis using fluorescence in situ hybridization (FISH; Path Vysion; Abbott, USA) at the time of diagnosis in three cases and at the time of study in nine cases. When the fluorescent signal ratio of Her2/chromosome 17 exceeded 2.0, the sample was judged to be FISH-positive. Her2 status was divided into three categories: negative, 0/1+ and 2+ (FISH-negative); positive, 3+ and 2+ (FISH-positive); and not examined.

Immunohistochemical staining

Formalin-fixed, paraffin-embedded blocks from primary tumors were available for all patients. Three 4-μm-thick serial sections were prepared from one representative block for each tumor. Sections from all cases were stained with hematoxylin and eosin (H&E), anti-EMA antibody, and D2-40 antibody. The streptavidin–biotin–immunoperoxidase method (Histofine SAB-PO kit; Nichirei, Tokyo, Japan) was used for immunohistochemistry. The epitope for D2-40 was retrieved by autoclaving the sections at 120°C for 30 min. No antigen retrieval was used for EMA immunostaining. Endogenous peroxidase was inhibited by 3% hydrogen peroxidase in methanol for 15 min. The sections were incubated with anti-EMA (prediluted; Nichirei) or D2-40 (1:100 dilution; Dako) antibodies overnight at 4°C. After staining with 3,3′-diaminobenzidine, the sections were counterstained with hematoxylin for visualization of the nucleus. Interpretation of histologic and immunohistochemical specimens was made without knowledge of the other clinical or pathologic findings.

Criteria for IMPC and invasive duct carcinoma NOS with incomplete IGP

The luminal surface of invasive duct carcinomas NOS usually showed dense eosinophilic staining by H&E staining (Fig. 1a), and the surface consistently revealed strong membranous reactivity by EMA immunostaining (Fig. 1b). According to the WHO classification, we defined IMPC by H&E staining as a carcinoma consisting of small clusters of tumor cells lying within clear stromal spaces resembling dilated vascular channels (Fig. 1c) [13]. In addition, IMPC in the present study was also restricted to an aggregate of three or more micropapillary clusters that were entirely fringed with strong EMA immunostaining (complete IGP; Fig. 1d). An invasive carcinoma was classified as IMPC if it had at least one focal IMPC component.

Invasive duct carcinoma NOS with incomplete IGP was defined as the presence of tumor cell clusters that were partly but not completely fringed with strong EMA immunostaining (incomplete IGP) facing the stroma (Fig. 1e–h). Single cell or single file infiltration of tumor cells was excluded from incomplete IGP. Simultaneous D2-40 immunostaining was used to exclude lymphatic tumor embolism (Fig. 1g). Tumors were considered to be incomplete IGP-positive if at least one incomplete IGP was found.

Definition of ILV and LVI

Obliterated lymph vessels were frequently detected within and beside the breast tumor by immunostaining with D2-40 antibody (Fig. 2a), while these vessels were rarely found in non-neoplastic breast tissue far from the tumor. Since these obliterated vessels might not be involved in lymphogenous metastasis, only opened lymph vessels were used to evaluate the presence or absence of intratumoral lymph vessels by D2-40 immunostaining (Fig. 2b). The term "intratumoral" included the borderline zone between the tumor and the surrounding non-neoplastic tissue in the present study. Tumors were considered to be ILV-positive when the endothelial cells in at least one opened vessel were immunostained with D2-40 antibody in the primary invasive tumor area.

LVI was defined as the presence of tumor cells surrounded by lymphatic endothelial cells that were immunostained with D2-40 antibody.

Statistical analysis

Differences between groups were analyzed using χ^2 tests and Student's *t* tests. Multivariate analysis was conducted to investigate the factors influencing the presence of ILV, LVI, and nodal involvement. Survival curves for cancer-specific survival were constructed using the method of Kaplan and Meier, and the differences between the two groups were assessed using the log rank test. Disease-specific survival was calculated as the period from surgery to death of breast cancer. Probability (*p*) values were calculated using Stat View 5 software (SAS Institute, Cary, NC, USA). A *p* value of <0.05 was considered statistically significant.

Results

Clinicopathologic features

A total of 197 patients with invasive breast carcinoma were included in the present study. The median age at diagnosis was 54 years (range, 32–96 years). Tumors ranged in size from 0.1 to 5.0 cm (median, 1.6 cm). Of the patients with nodal resection (n=194), 61% (n=118) were node-negative and 39% (n=76) were node-positive. The frequencies of different histologic types were: invasive duct carcinoma NOS 84% (n=166), IMPC 5% (n=10), mucinous carcinoma 2% (n=4), invasive lobular carcinoma 4% (n=8), and others 5% (n=9). All IMPCs were of mixed (non-pure) type, with the percentage of IMPC ranging from 5" to 75%. Among the patients with invasive duct carcinoma NOS, 162 (98%) of 166 were followed up until October 31, 2009, with a median follow-up period of 72 months (range, 8–111 months). The pTNM0 stages of the 166 invasive duct carcinomas NOS/10 IMPCs were as follows: pT1N0, 86/4; pT2N0, 12/2; pT4N0, 3/1; pT1N+, 33/3; pT2N+, 23/0; pT4N+, 7/0; unknown, 2/0.

Detection of IGP

All of the breast carcinomas showed EMA immunostaining in the cytoplasm and cytoplasmic membrane of the neoplastic cells. Staining intensity varied among the tumors and occasionally differed within the same tumor. Since only the luminal surface of the ductal tumor cells consistently showed strong membranous EMA immunostaining at the cytoplasmic membrane, incomplete IGP could be detected even when typical micropapillary morphology was absent (Fig. 1h). Incomplete IGP was found focally in 88 (53%) of 166 invasive duct carcinomas NOS (Table 1). Each incomplete IGP was very limited and occupied <5% of the primary tumor area in the majority of cases (Fig. 1). The cluster with incomplete IGP was partly fringed with linear EMA immunostaining, which was partly surrounded by retraction cleft or completely surrounded by clear stromal spaces (Fig. 1e–h). Among ten IMPCs, one showed a nodular micropapillary component with abrupt transition to mucinous carcinoma. The remaining nine (90%) showed

gradual transitions from micropapillary carcinoma to conventional ductal carcinoma, or a mixture of these components (Fig. 3a). These nine IMPCs consistently showed prominent incomplete IGP at transition areas, which were sometimes accompanied by adjacent tiny clusters or isolated tumor cells with inflammatory infiltrate (Fig. 3a–d). Incomplete IGP was also detected by H&E staining alone, which identified the presence of clusters with a sharp, dense eosinophilic surface accompanied by the retraction clefts (Fig. 3c).

Detection of ILV

In contrast to non-neoplastic breast tissue, D2-40 immunostaining of the primary tumor area revealed a marked decrease or disappearance of preexisting lymph vessels, such as perivascular and periductal lymph vessels, in all patients. ILV was detected in only 73 patients with invasive duct carcinoma NOS (73/166, 44%) by D2-40 immunostaining (Table 1), and most of these were located at the periphery of the tumors (Fig. 2). Relatively abundant ILV, suggestive of lymphangiogenesis, was occasionally noted in granulation tissue after preoperative biopsy and in areas of inflammatory infiltration.

Relationship between incomplete IGP and clinicopathologic parameters

As shown in Table 1, patients with incomplete IGP-positive tumors had a high frequency of ILV (55/88, 63%) compared with incomplete IGP-negative patients (18/78, 23%; $p<0.0001$). Furthermore, incomplete IGP was significantly associated with higher frequencies of LVI (54/88, 61%; $p<0.0001$), and lymph node metastasis (46/87, 53%; $p<0.0001$). When pT1 tumors ($n=120$) were separately analyzed, incomplete IGP also influenced these factors; incomplete IGP-positive pT1 tumors showed higher frequencies of ILV (26/54, 48%; $p=0.006$), LVI (31/54, 57%; $p<0.0001$), and nodal metastasis (22/54, 41%; $p=0.001$) compared with incomplete IGP-negative pT1 tumors (not shown in Table 1). Pathologic tumor size was also related to the presence of incomplete IGP ($p<0.0001$). There were no significant correlations between incomplete IGP and patient age, histologic grade, hormone receptor status, or HER2 status (Table 1). The locations of incomplete IGP, ILV, and LVI were not always identical in the same tumor. However, one case revealed a close sequential association between incomplete IGP and LVI (Fig. 4a–d); a few tiny clusters with incomplete IGP were located in a clear stromal space. These clusters migrated via lymphatic drainage into an orifice of the narrow portion of a funnel-shaped lymph vessel, and a floating micropapillary cluster was formed in the dilated portion of the lymph vessel (Fig. 4a–d).

Fig. 1 **a** Invasive duct carcinoma NOS without IGP showing dense eosinophilic staining of the luminal surface (×400). **b** Immunostaining for EMA showing membranous reactivity in the same part of the invasive duct carcinoma NOS (×400). **c** IMPC consisting of aggregates of numerous micropapillary cell clusters within clear spaces (×100). **d** Immunostaining for EMA clearly showing encircled membranous reactivity (complete IGP) in the majority of clusters (×100). **e** Invasive duct carcinoma NOS with incomplete IGP showing isolated clusters surrounded by clear spaces (×100). **f** Two of the clusters seen in **e** showing focal membranous reactivity (*arrows*) on their surface by EMA immunostaining (×400). **g** Same area of **e** showing positive reactivity of the perivascular lymph vessel (*arrow*) but negative reactivity around the clusters by immunostaining with D2-40 (×100). **h** Invasive duct carcinoma NOS with IGP showing a tiny cluster with focal membranous EMA immunostaining facing retraction cleft (*arrow*, ×400)

Comparison between invasive duct carcinoma NOS with incomplete IGP and IMPC

As shown in Table 1, the clinicopathologic features of IMPC were similar to those of invasive duct carcinoma NOS with incomplete IGP. There were no significant differences in clinicopathologic features between the two groups (age, $p=0.23$; tumor size, $p=0.56$; histologic grade, $p=0.34$; estrogen receptor, $p=0.27$; progesterone receptor, $p=0.32$; Her2 status, $p=0.25$; ILV, $p=0.74$; LVI, $p=0.56$; nodal metastasis, $p=0.17$; not shown in Table 1).

Multivariate analysis of ILV, LVI, and nodal metastasis

Multivariate analysis of factors associated with the presence of ILV, LVI, and nodal metastasis are shown in Table 2. Pathologic tumor size ($p=0.002$) and incomplete IGP ($p<0.0001$) were significant independent factors influencing the presence of ILV. Tumor size ($p=0.049$), incomplete IGP ($p=0.0001$), and the presence of ILV ($p=0.0002$) were significantly associated with LVI. Furthermore, LVI ($p=0.004$) and pathologic tumor size ($p=0.005$) were independent predictors for nodal involvement (Table 2).

Survival data for invasive duct carcinoma NOS with incomplete IGP and IMPC

Follow-up data were available for a total of 162 patients with invasive duct carcinoma NOS and 10 patients with IMPC. The 5- and 8-year recurrence-free survival rates were 81% and 70% ($p=0.0356$), respectively, in patients with incomplete IGP-positive invasive duct carcinoma NOS and 91% and 89%, respectively, in patients with incomplete IGP-negative invasive duct carcinoma NOS (Fig. 5a). There was no significant difference in disease-specific survival between patients with or without incomplete IGP (Fig. 5b). Only one of ten patients with IMPC had recurrence and died of breast cancer; the remaining nine patients were alive and tumor-free at the end of follow-up.

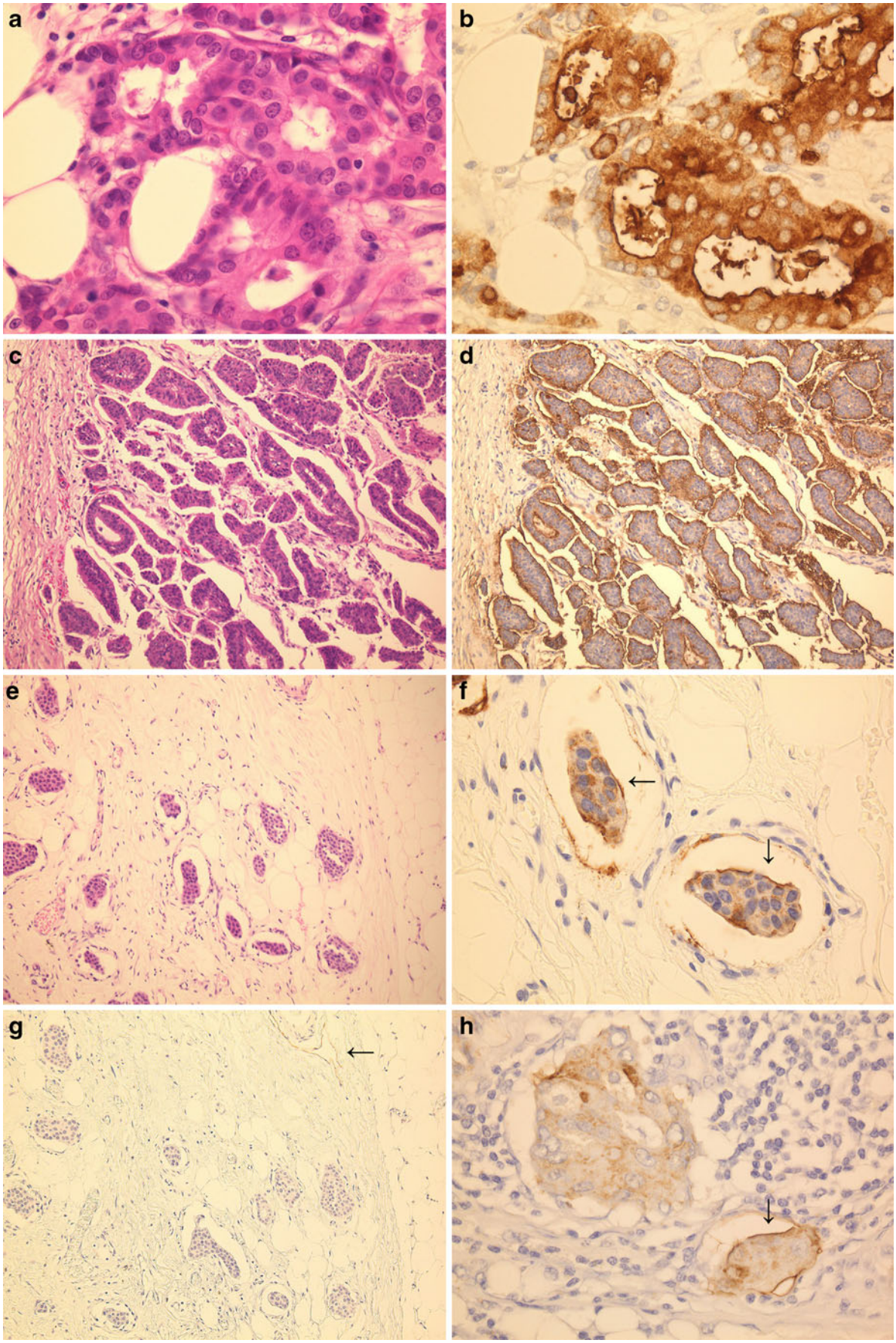
a
b
c
d
e
f
g
h

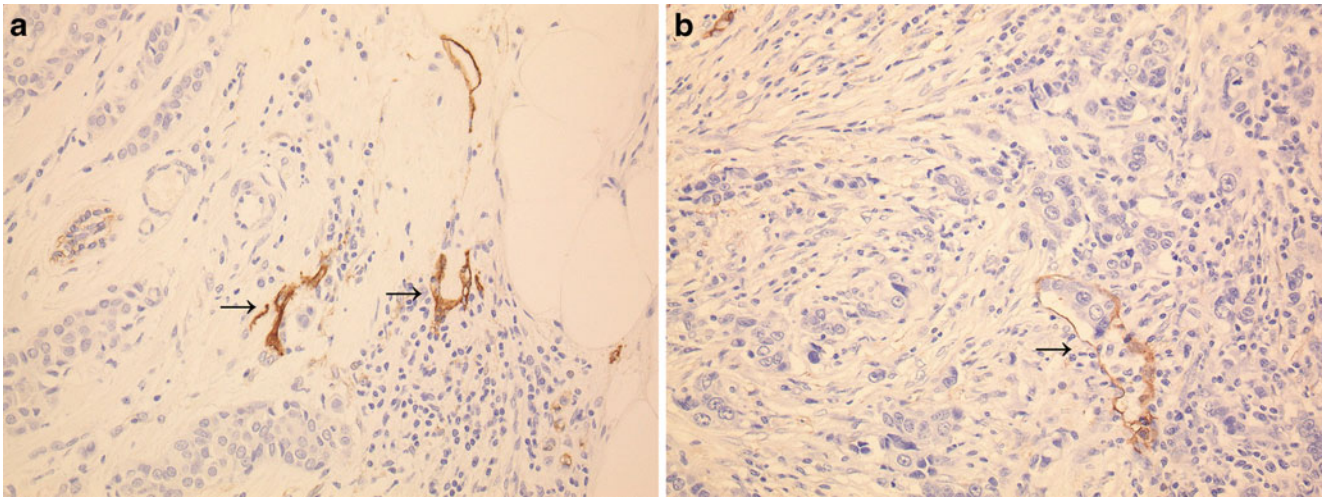

Fig. 2 **a** Absence of intratumoral lymph vessels. Immunostaining with D2-40 showing obliterated lymph vessels (*arrows*) in the borderline and peritumoral areas (×200). **b** Presence of intratumoral lymph vessels. D2-40 immunostaining shows an opened lymph vessel containing some tumor cells in the tumor (*arrow*, ×200)

Table 1 Clinicopathologic parameters of invasive duct carcinoma NOS with or without IGP (n=166) and IMPC (n=10)

Parameters	Invasive duct carcinoma NOS (n=166)			IMPC (n=10)
	Incomplete IGP(+) (n=88)	Incomplete IGP(−) (n=78)	p[a]	
Age (years)[b]	55.6±11.3	56.8±13.5	0.56	60.3±13.6
Tumor size (cm)[b]	1.9±0.7	1.4±0.8	<0.0001	1.8±0.5
Histologic grade				
I	23	29	0.22	4
II	38	28		4
III	27	21		2
Estrogen receptor				
Negative	23	24	0.51	1
Positive	65	54		9
Progesterone receptor				
Negative	30	33	0.28	5
Positive	58	45		5
Her2 status				
Negative	54	59	0.14	6
Positive	12	6		4
Not examined[c]	22	13		0
ILV				
Absent	33	60	<0.0001	4
Present	55	18		6
LVI				
Negative	34	64	<0.0001	5
Positive	54	14		5
Nodal metastasis				
Negative	41	60	<0.0001	7
Positive	46	17		3
Not resected	1	1		0

NOS not otherwise specified, *IMPC* invasive micropapillary carcinoma, *IGP* inside-out growth pattern, *ILV* intratumoral lymph vessel, *LVI* lymph vessel invasion

[a] p values show significant difference between incomplete IGP-positive and incomplete IGP-negative

[b] Mean ± standard deviation

[c] Not examined cases were excluded from the statistical analyses

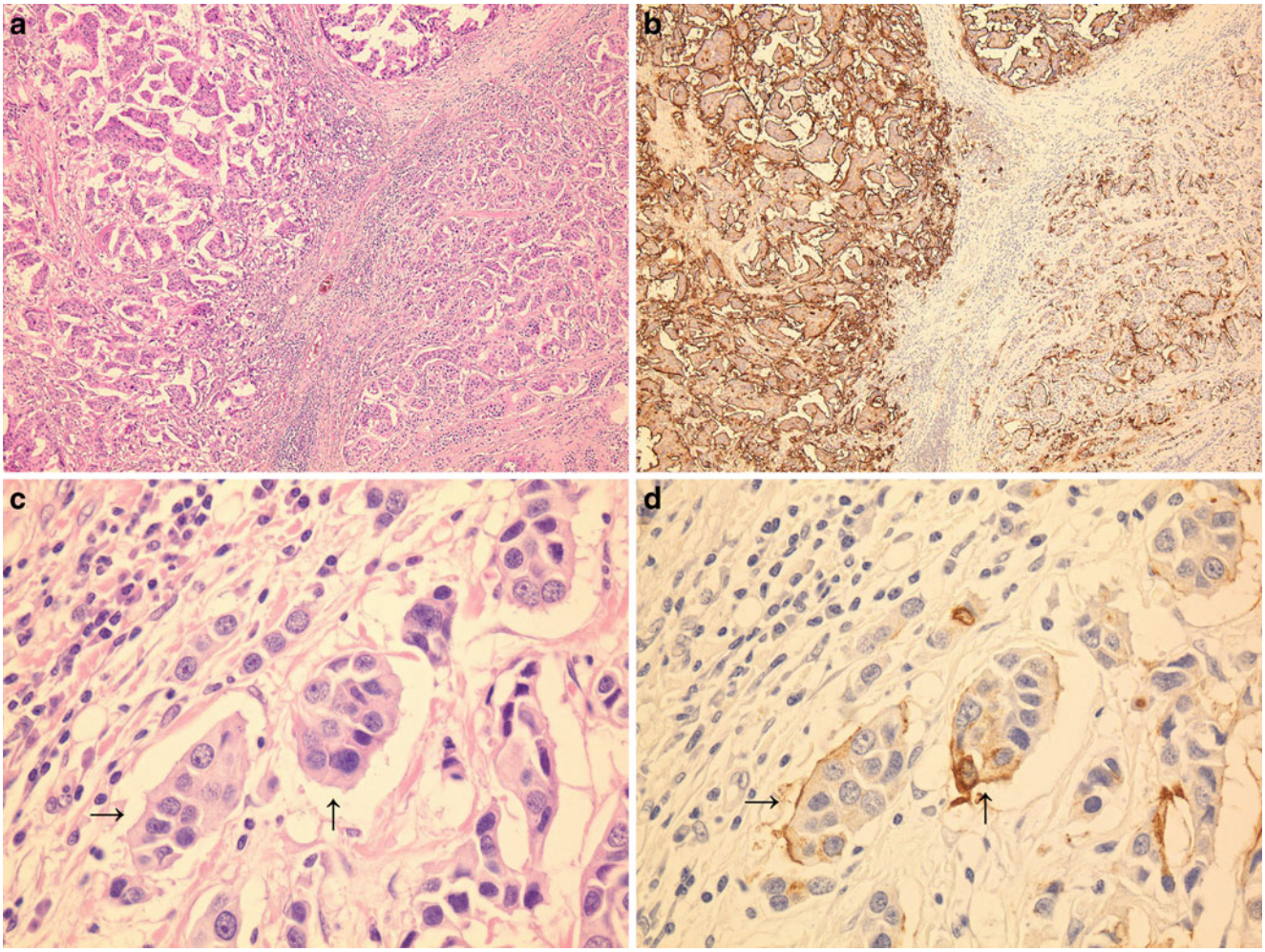

Fig. 3 IMPC of mixed type. **a** IMPC area (*left half*) and invasive duct carcinoma NOS with prominent incomplete IGP area (*right half*) are shown (×40). **b** In contrast to IMPC area, invasive duct carcinoma NOS with incomplete IGP area showing incomplete hemming of EMA immunoreactivity in each cluster (×40). **c** Incomplete IGP area containing tiny clusters and single tumor cells with inflammatory infiltration. Note a dense eosinophilic surface in part (*arrows*, ×400). **d** The same surface showing strong EMA immunoreactivity (*arrows*, ×400)

Discussion

IMPC is quite rare in its pure form, but focal micropapillary growth has been reported in 3–6% of more common types of invasive carcinomas [13]. Based on the strict morphologic and immunohistochemical definitions of IMPC used in this series, IMPC accounted for 5% of invasive breast carcinomas, while incomplete IGP was detected by immunostaining in 53% of invasive duct carcinomas NOS. The microscopic differential diagnosis of incomplete IGP includes tumor embolism of lymph vessels and retraction artifacts with no evidence of micropapillary carcinoma [21]. Serial sections immunostained with anti-EMA and D2-40 antibodies can distinguish incomplete IGP from lymphatic tumor embolism to simple retraction artifacts.

IMPC generally shows frequent LVI and lymph node metastasis [13–17]; however, our ten IMPC cases showed relatively low frequencies of LVI (50%) and nodal involvement (30%). The reason for this is unclear, but it may be related to the small number of cases and the histologic features [22]. Invasive duct carcinoma NOS with incomplete IGP, as expected, showed high frequencies of LVI (61%) and nodal metastasis (53%). This feature was retained even when only small tumors (pT1) were analyzed, resembling those of IMPC cases reported by Walsh and Bleiweiss [23]. Furthermore, nine of ten IMPCs showed gradual transitions from invasive duct carcinomas NOS to micropapillary carcinomas, and these nine IMPCs consistently showed prominent incomplete IGP in the transition areas. This close relationship between IMPC and invasive duct carcinoma NOS with incomplete IGP suggests that both morphologic entities form a histologic spectrum characterized by varying degrees of a common inside-out morphology.

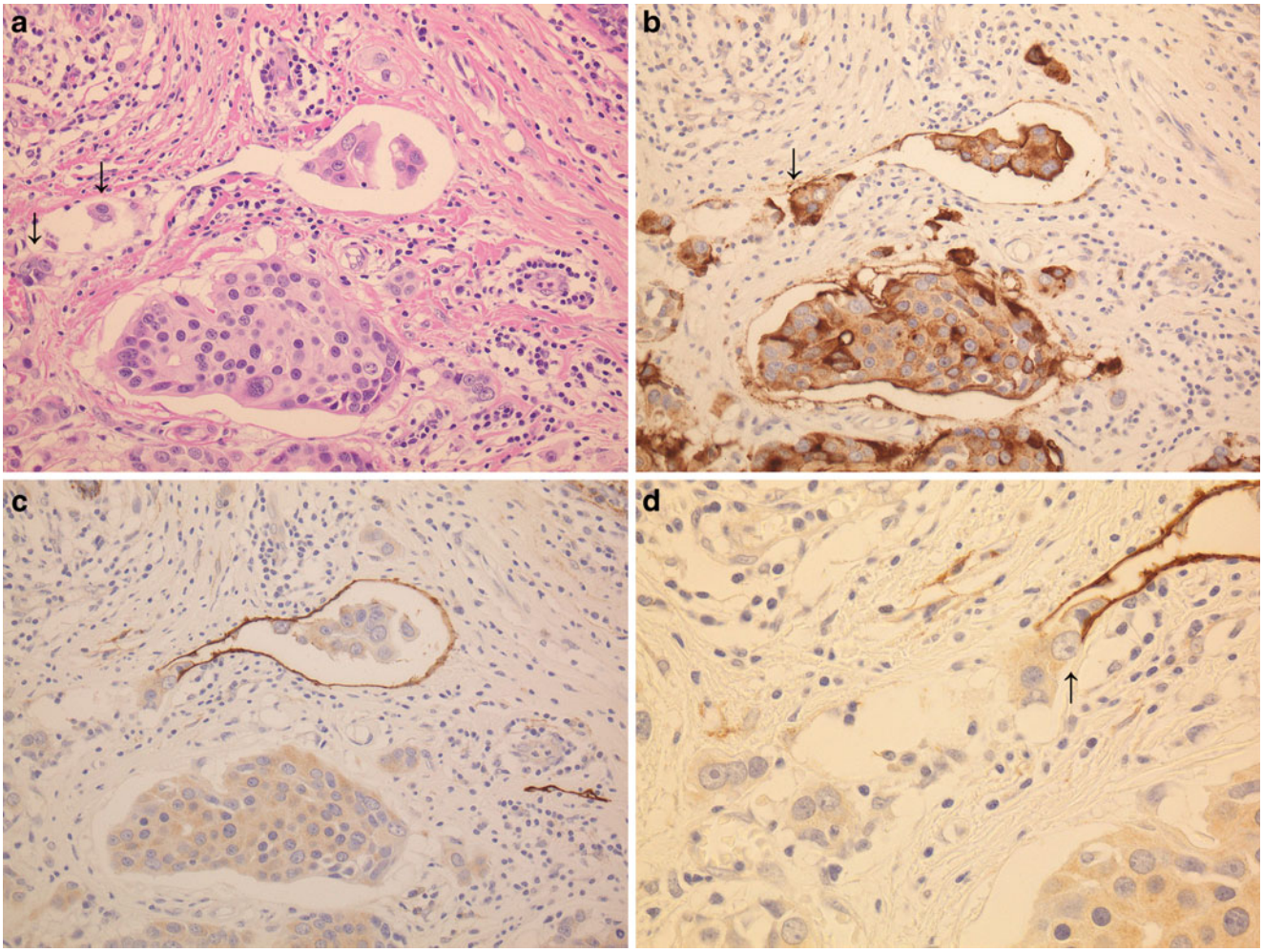

Fig. 4 Lymph vessel invasion in invasive duct carcinoma NOS with incomplete IGP. **a** A few tiny clusters (*arrows*) are present in a clear stromal cavity in front of the opening of a lymph vessel (see **c**) (×200). **b** One of the clusters (*arrow*) and an adjacent larger cluster showing incomplete IGP by EMA immunostaining. A micropapillary floating cluster is also noted within a dilated lymph vessel (see **c**) (×200). **c** Immunostaining with D2-40 clearly demonstrates the funnel-shaped lymph vessel containing the loosely arranged micropapillary cluster at the dilated portion (×200). **d** High-power view of D2-40 immunostaining highlights a tiny tumor cluster just entering into the narrow portion of the lymph vessel (*arrow*, ×400)

The biological significance and mechanisms of inside-out morphologic change have not been clarified. EMA is thought to include episialin (MUC-1), a glycoprotein normally located on the apical cell surface of normal glandular epithelium [24]. In vitro studies have shown that increased MUC-1 expression was associated with decreased adhesion between adjacent cells and between cells and the extracellular matrix [25–27]. The current study revealed that complete or incomplete IGP in either IMPC or invasive duct carcinoma NOS was consistently accompanied by clear spaces or retraction clefts between the cytoplasmic membrane and the surrounding stroma. This suggests that an inside-out morphologic change is at least partly responsible for the detachment of tumor cells from the stroma. As we identified an incidental case with a connection between a clear space and a D2-40 positive lymphatic vessel with draining tumor cells, it is possible that the clear spaces share the "pre-lymphatic channels" connecting to true lymphatics described by some investigators [28–30].

Although the reasons for the effects of incomplete IGP on the presence of ILV are unclear, tumor–stromal interactions appear to be involved. Invasive duct carcinoma NOS with incomplete IGP may potentially be less damaging to lymph vessels because of less remodeling of the extracellular matrix at the invasive front [31–33]. Reduced adhesiveness between the tumor cells and the stroma may contribute to the creation of this conservative microenvironment. The regulation of the expressions of cell–matrix adhesion molecules such as integrins may also be involved [32–34]. In contrast to IMPC and invasive duct carcinoma NOS with incomplete IGP, tubular carcinoma, a distinctive variant of ductal carcinoma, is characterized by well-formed neoplastic

Table 2 Multivariate analysis of factors associated with the presence of ILV, LVI, and nodal metastasis in invasive ductal carcinoma NOS (n=164)

ILV intratumoral lymph vessel, *LVI* lymph vessel invasion, *IGP* inside-out growth pattern, *na* not adopted for each multivariate analysis

Factors	p value (odds ratio)		
	ILV	LVI	Nodal metastasis
Tumor size	0.002 (2.35)	0.049 (1.76)	0.005 (2.27)
Incomplete IGP	<0.0001 (4.37)	0.0001 (4.58)	0.08 (2.03)
ILV	na	0.0002 (3.67)	0.19 (1.57)
LVI	na	na	0.004 (2.35)

glands with good polarity, altered collagenous stroma, and virtually no lymphatic tumor emboli [35].

LVI in breast cancer potentially represents the divergence from local to systemic disease, and at the St Gallen meeting in 2009, extensive peritumoral vascular invasion was listed as one of the useful factors for identifying patients who required chemotherapy in addition to endocrine therapy [9]. We have previously identified a possible characteristic of local disease, which is histologically recognized as early invasive breast carcinoma without marginal adipose tissue invasion or peritumoral LVI [8]. Several investigators have reported the occurrence of lymphangiogenesis in breast cancer and have suggested that it plays an important role in disease progression [2–4]. We speculated, however, that most lymph vessels within breast carcinoma tissue are preexisting entrapped vessels rather than newly formed ones [10, 11]. This is based on several facts: (1) We found no apparent increase in lymph vessel number within tumor tissues compared with normal breast tissue, except under special conditions, such as in granulation tissue after preoperative biopsy; (2) ILV were detected in only 44% of patients with invasive duct carcinoma NOS, and most of these were small in number and present at the periphery or border of the tumor, as shown by Mohammed et al. [4]; and (3) in contrast to normal breast tissue, occluded lymph vessels were frequently found within or beside the tumor, suggesting obliteration, destruction, and subsequent disappearance of lymph vessels by the growing tumor. This fragile nature of lymph vessels, compared with blood vessels, might be explained by their simple structure, with fenestrated or absent basement membranes and no covering pericytes [36]. Consequently, lymphatic endothelial cells are in direct contact with the extracellular matrix at least in part and are thus likely to be influenced by the microenvironment, such as the remodeling of the matrix accompanying the tumor invasion [31–33].

The majority of histologic LVI reported are tumor embolisms in lymph vessels, and the mechanism of LVI, including the entrance of tumor cells into the lymph vessels, has not been clearly demonstrated to date. In the current study, we incidentally observed an instantaneous picture of tumor cells entering a lymph vessel, which could help elucidate the process of LVI associated with incomplete or complete IGP occurring in breast carcinomas. The suggested process is summarized as follows: A tumor cell cluster with IGP detaches itself from the stroma and then decomposes into tiny clusters or isolated cells, simulating epithelial–mesenchymal transition [34, 37], in a clear stromal space beside an opened lymph vessel. The tumor clusters and cells then migrate via the lymphatic drainage into the narrow entrance of the lymph vessel, like immune cells homing to the lymphatics (drainage theory) [38–40]. Finally, they remain in the dilated lymph vessel in the peritumoral area to reconstruct a cluster with IGP. These intralymphatic tumor cells and clusters would provide a

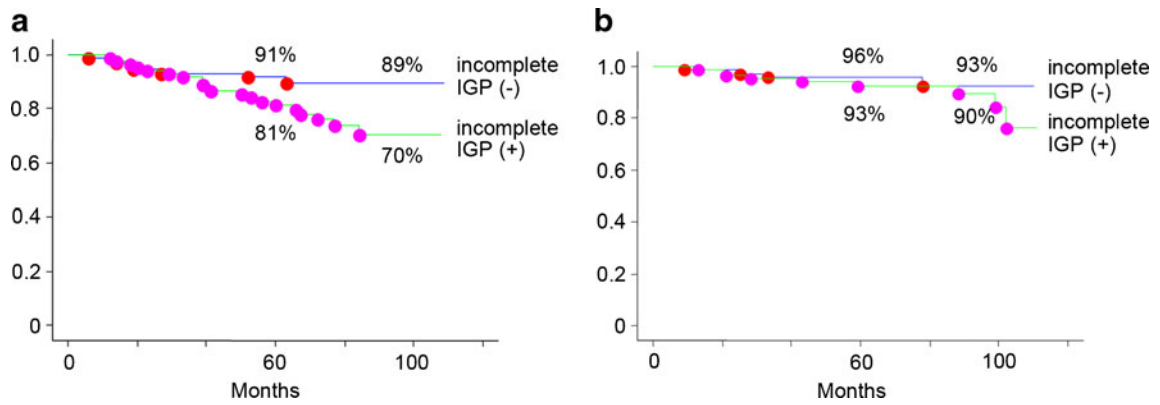

Fig. 5 Recurrence-free (**a**) and disease-specific (**b**) survival of 86 incomplete IGP-positive and 76 incomplete IGP-negative patients with invasive duct carcinoma NOS. The 5- and 8-year survivals (%) are shown: **a** p=0.0356; **b** p=0.3564

source of lymph node metastasis. The peritumoral LVI detected in conventional H&E specimens likely corresponded to this last event. The small clusters or isolated tumor cells with inflammatory infiltrate occasionally observed beside the clusters with incomplete IGP in invasive duct carcinoma NOS and IMPC also support this drainage theory. Interestingly, Guo et al. [22] described lymphocytic infiltration of IMPC as one of the key factors influencing lymph node metastasis.

In conclusion, incomplete IGP is common in invasive duct carcinoma NOS and frequently occurs in transitional areas of non-pure IMPC. Incomplete IGP is a useful tool for predicting LVI, and inside-out morphologic changes of tumor cell clusters may be an initial critical step in LVI in invasive ductal carcinomas. Further investigations, especially into the molecular mechanisms of LVI, are required to aid in the development of new therapeutic strategies.

Acknowledgments The authors are grateful to Ms. Yuko Moriyama, Ms. Yuko Koide, and Mr. Ken-ichi Mori for their kind technical support.

Conflict of interest statement We declare that we have no conflicts of interest.

References

1. Pepper MS (2001) Lymphangiogenesis and tumor metastasis: myth or reality? Clin Cancer Res 7:462–468
2. Schoppmann SF, Bayer G, Aumayr K et al (2004) Prognostic value of lymphangiogenesis and lymphovascular invasion in invasive breast cancer. Ann Surg 240:306–312
3. Schoppmann SF, Fenzl A, Nagy K et al (2006) VEGF-C expressing tumor-associated macrophages in lymph node positive breast cancer: impact on lymphangiogenesis and survival. Surgery 139:839–846
4. Mohammed RA, Ellis IO, Elsheikh S et al (2009) Lymphatic and angiogenic characteristics in breast cancer: morphometric analysis and prognostic implications. Breast Cancer Res Treat 113:261–273
5. Arnaout-Alkarain A, Kahn HJ, Narod SA et al (2007) Significance of lymph vessel invasion identified by the endothelial lymphatic marker D2-40 in node negative breast cancer. Mod Pathol 20:183–191
6. Mohammed RA, Martin SG, Gill MS et al (2007) Improved methods of detection of lymphovascular invasion demonstrate that it is the predominant method of vascular invasion in breast cancer and has important clinical consequences. Am J Surg Pathol 31:1825–1833
7. Colleoni M, Rotmensz N, Maisonneuve P et al (2007) Prognostic role of the extent of peritumoral vascular invasion in operable breast cancer. Ann Oncol 18:1632–1640
8. Yamaguchi J, Ohtani H, Nakamura K et al (2008) Prognostic impact of marginal adipose tissue invasion in ductal carcinoma of the breast. Am J Clin Pathol 130:382–388
9. Goldhirsch A, Ingle JN, Gelber RD et al (2009) Thresholds for therapies: highlights of the St Gallen International Expert Consensus on the Primary Therapy of Early Breast Cancer 2009. Ann Oncol 20:1319–1329
10. Agarwal B, Saxena R, Morimiya A et al (2005) Lymphangiogenesis does not occur in breast cancer. Am J Surg Pathol 29:1449–1455
11. van der Schaft DW, Pauwels P, Hulsmans S et al (2007) Absence of lymphangiogenesis in ductal breast cancer at the primary tumor site. Cancer Lett 254:128–136
12. Clarijs R, Ruiter DJ, de Waal RM (2001) Lymphangiogenesis in malignant tumours: does it occur? J Pathol 193:143–146
13. Ellis IO, Cornelisse CJ, Schnitt SJ et al (2003) Invasive breast carcinoma. In: Tavassoli FA, Devilee P (eds) Pathology and genetics of tumours of the breast and female genital organs. World Health Organization classification of tumours. IARC, Lyon, pp 13–59
14. Siriaunkgul S, Tavassoli FA (1993) Invasive micropapillary carcinoma of the breast. Mod Pathol 6:660–662
15. Nassar H, Wallis T, Andea A et al (2001) Clinicopathologic analysis of invasive micropapillary differentiation in breast carcinoma. Mod Pathol 14:836–841
16. Kuroda H, Sakamoto G, Ohnishi K et al (2004) Clinical and pathologic features of invasive micropapillary carcinoma. Breast Cancer 11:169–174
17. Pettinato G, Manivel CJ, Panico L et al (2004) Invasive micropapillary carcinoma of the breast. Clinicopathologic study of 62 cases of a poorly recognized variant with highly aggressive behavior. Am J Clin Pathol 121:857–866
18. Peterse JL (1993) Breast carcinomas with an unexpected inside out growth pattern. Rotation of polarization associated with angioinvasion (abstract). Pathol Res Pract 189:780
19. Luna-More S, Gonzalez B, Acedo C et al (1994) Invasive micropapillary carcinoma of the breast. A new special type of invasive mammary carcinoma. Pathol Res Pract 190:668–674
20. Robbins P, Pinder S, Klerk N et al (1995) Histological grading of breast carcinomas: a study of interobserver agreement. Hum Pathol 26:873–879
21. Acs G, Dumoff KL, Solin LJ et al (2007) Extensive retraction artifact correlates with lymphatic invasion and nodal metastasis and predicts poor outcome in early stage breast carcinoma. Am J Surg Pathol 31:129–140
22. Guo X, Chen L, Lang R et al (2006) Invasive micropapillary carcinoma of the breast. Am J Clin Pathol 126:740–746
23. Walsh MM, Bleiweiss IJ (2001) Invasive micropapillary carcinoma of the breast: eighty cases of an underrecognized entity. Hum Pathol 32:583–589
24. Nassar H, Pansare V, Zhang H et al (2004) Pathogenesis of invasive micropapillary carcinoma: role of MUC1 glycoprotein. Mod Pathol 17:1045–1050
25. Wesseling J, van der Valk SW, Vos HL et al (1995) Episialin (MUC-1) overexpression inhibits integrin-mediated cell adhesion to extracellular matrix components. J Cell Biol 129:255–265
26. Wesseling J, van der Valk SW, Hilkens J (1996) A mechanism for inhibition of E-cadherin-mediated cell–cell adhesion by the membrane-associated mucin episialin/MUC-1. Mol Biol Cell 7:565–577
27. McDermott KM, Crocker PR, Harris A et al (2001) Overexpression of MUC-1 reconfigures the binding properties of tumor cells. Int J Cancer 94:783–791
28. Hartveit E (1990) Attenuated cells in breast stroma: the missing lymphatic system of the breast. Histopathology 16:533–543
29. Damiani S, Peterse JL, Eusebi V (2002) Malignant neoplasms infiltrating 'pseudoangiomatous' stromal hyperplasia of the breast: an unrecognized pathway of tumor spread. Histopathology 41:208–215
30. Asioli S, Eusebi V, Gaetano L et al (2008) The pre-lymphatic pathway, the rooths of the lymphatic system in the breast tissue: a 3D study. Virchows Arch 453:401–406
31. Hugo H, Ackland ML, Blick T et al (2007) Epithelial-mesenchymal and mesenchymal–epithelial transitions in carcinoma progression. J Cell Physiol 213:374–383

32. Wipff PJ, Hinz B (2008) Integrins and the activation of latent transforming growth factor beta1—an intimate relationship. Eur J Cell Biol 87:601–615
33. Ingber DE (2003) Tensegrity II. How structural networks influence cellular information processing networks. J Cell Sci 116:1397–1408
34. Guarino M (2007) Epithelial–mesenchymal transition and tumour invasion. Int J Biochem Cell Biol 39:2153–2160
35. Rosen PP (2009) Tubular carcinoma. In: Rosen PP (ed) Rosen's breast pathology, 3rd edn. Lippincott Williams & Wilkins, Philadelphia, pp 405–422
36. Dua RS, Gui GP, Isacke CM (2005) Endothelial adhesion molecules in breast cancer invasion into the vascular and lymphatic systems. Eur J Surg Oncol 31:824–832
37. Guarino M, Rubino B, Ballabio G (2007) The role of epithelial–mesenchymal transition in cancer pathology. Pathology 39:305–318
38. Issa A, Le TX, Shoushtari AN et al (2009) Vascular endothelial growth factor-C and C-C chemokine receptor 7 in tumor cell-lymphatic cross-talk promote invasive phenotype. Cancer Res 69:349–357
39. Su JL, Yen CJ, Chen PS et al (2007) The role of the VEGF-C/VEGFR-3 axis in cancer progression. Br J Cancer 96:541–545
40. Shields JD, Fleury ME, Yong C et al (2007) Autologous chemotaxis as a mechanism of tumor cell homing to lymphatics via interstitial flow and autocrine CCR7 signaling. Cancer Cell 11:526–538

Virchows Arch (2011) 458:171–178
DOI 10.1007/s00428-010-0994-5

ORIGINAL ARTICLE

High expression of phosphorylated 4E-binding protein 1 is an adverse prognostic factor in esophageal squamous cell carcinoma

Chi-Ju Yeh · Wen-Yu Chuang · Yin-Kai Chao · Yun-Hen Liu · Yu-Sun Chang · Shao-Yun Kuo · Chen-Kan Tseng · Hsien-Kun Chang · Chuen Hsueh

Received: 6 August 2010 / Revised: 30 September 2010 / Accepted: 3 October 2010 / Published online: 3 November 2010
© Springer-Verlag 2010

Abstract Cell signaling pathways play important roles in oncogenesis. Among a large number of signaling regulators in different pathways, 4E-binding protein 1 (4E-BP1) was found to be a key factor, which converges several oncogenic signals, phosphorylates the molecules, and drives the downstream proliferative signals. Recent studies showed that high expression of phosphorylated 4E-BP-1 (p-4E-BP1) is associated with poor prognosis, tumor progression, or nodal metastasis in different human cancers, but its prognostic significance in esophageal cancer remains undefined. In this study, we investigated the expression levels of p-4E-BP1 with two different phosphorylation sites $Thr^{37/46}$ and Thr^{70} by immunohistochemistry and their prognostic significance in 78 cases of surgically resected esophageal squamous cell carcinoma (SCC) for the first time. We found no correlation of p-4E-BP1 expression with age, gender, preoperative concurrent chemoradiotherapy, tumor grade, pT classification, pN, pM, or pStage. Multivariate Cox regression analysis showed that high expression of p-4E-BP-1 $Thr^{37/46}$ was an independent adverse prognostic factor, with a hazard ratio of 1.73 (95% confidence interval=1.03–2.90) and a p value of 0.038. Stratifying the patients with other prognostic factors, we found that the effect of p-4E-BP1 $Thr^{37/46}$ on survival was significant only in patients with relatively early stage disease (pT1/pT2, pN0, or pStage I/II; p=0.0047, 0.012, and 0.011, respectively). Our data suggest that assessment of p-4E-BP1 expression could identify a subpopulation of earlier stage esophageal SCC patients with poor prognosis. These patients could be possible candidates for future studies on more aggressive treatment or target therapy.

Keywords Phosphorylated 4E-binding protein 1 (p-4E-BP1) · Esophagus · Cancer · Squamous cell carcinoma · Survival

C.-J. Yeh · W.-Y. Chuang · C. Hsueh (✉)
Department of Pathology, Chang Gung Memorial Hospital, Linko, Chang Gung University College of Medicine,
5 Fu-Hsing Street, Kwei-Shan,
Taoyuan 333, Taiwan
e-mail: ch9211@adm.cgmh.org.tw

Y.-K. Chao · Y.-H. Liu
Division of Thoracic and Cardiovascular Surgery, Department of Surgery, Chang Gung Memorial Hospital, Linko, Chang Gung University College of Medicine,
Taoyuan, Taiwan

Y.-S. Chang · S.-Y. Kuo · C. Hsueh
Chang Gung Molecular Medicine Research Center and Graduate Institute of Basic Medical Sciences,
Chang Gung University College of Medicine,
Taoyuan, Taiwan

C.-K. Tseng
Department of Radiation Oncology, Chang Gung Memorial Hospital, Linko, Chang Gung University College of Medicine,
Taoyuan, Taiwan

H.-K. Chang
Division of Hematology and Oncology, Department of Internal Medicine, Chang Gung Memorial Hospital, Linko, Chang Gung University College of Medicine,
Taoyuan, Taiwan

Introduction

4E-binding protein 1 (4E-BP1) is a protein which binds to eukaryotic translation initiation factor 4E (eIF-4E) and plays a critical role in controlling protein synthesis, cell survival, and growth [1–3]. Cell signaling pathways are essential in oncogenesis of human cancers, and complex cross-talk occurs

between the pathways. Thus, the concept of "funnel factors" has emerged because they could converge the oncogenic signals and drive the downstream proliferative signal regardless of the individual upstream oncogenic alteration [1]. In the majority of the tumors, specific molecular alterations are frequently detected in phosphatidylinositol 3-kinase (PI3K)/protein kinase B (AKT)/mammalian target of rapamycin (mTOR) pathway and mitogen-activated protein kinase (MAPK) pathway. A final effector of these signaling cascades is the cap-dependent mRNA translation initiation complex, which is negatively regulated by 4E-BP1 and favors the expression of potent growth and survival factors including c-myc, cyclin D1, vascular endothelial growth factor, and Bcl-2. When 4E-BP1 is non-phosphorylated, it binds tightly to the eIF-4E, blocking the formation of the cap-dependent mRNA translation initiation complex to suppress the translation. When 4E-BP1 is phosphorylated, eIF-4E is released, and the initiation complex can be formed to promote the translation [4]. Therefore, phosphorylated 4E-BP-1 (p-4E-BP1) could be one of funnel factors, and its expression in tumor cells could reflect their malignant potential. High expression of p-4E-BP1 was found to be associated with poor prognosis in several human cancers, including carcinomas of the breast, ovary, uterine cervix and endometrium [1,5–8], childhood rhabdomyosarcoma [9], and malignant melanoma [10]. As for esophageal squamous cell carcinoma (SCC), only one previous report showed increased expression of p-4E-BP1 in esophageal SCC cell lines at mRNA and protein levels [11]. Another report on esophageal SCC was regarding eIF-4E and 4E-BP-1 expression in tumor tissues using Western blot analysis [12]. Up to date, no correlation of p-4E-BP1 expression with disease outcome has been carried out in esophageal SCC patients. Our study is the first to investigate tumor expression of p-4E-BP1 in 78 cases of surgically resected esophageal SCC by immunohistochemistry, and to correlate the result with clinicopathologic features and patient survival to determine the prognostic significance of p-4E-BP1. Two different phosphorylation sites including $Thr^{37/46}$ and Thr^{70} were studied since both antibodies have been applied to various human cancers previously [1,5–10].

Materials and methods

Patients

A total of 78 cases of surgically resected esophageal SCC within a period of 4 years were recruited for this study. Fifty-

Table 1 Clinicopathologic characteristics and p-4E-BP1 $Thr^{37/46}$ expression of cases included in the study

Characteristic	p-4E-BP1 $Thr^{37/46}$ expression		Total (n=78)	p value
	Low (n=40)	High (n=38)		
Age at diagnosis				
Mean±SD	57±13	56±12	57±12	0.67
Median (min; max)	59 (37; 100)	57 (32; 85)	57 (32; 100)	
Gender (%)				
Female	2 (5)	1 (3)	3 (4)	0.96
Male	38 (95)	37 (97)	75 (96)	
Pre-operative CCRT				
Yes	28 (70)	26 (68)	54 (69)	0.88
No	12 (30)	12 (32)	24 (31)	
Tumor grade (%)				
Grade 1	2 (5)	3 (8)	5 (6)	0.99
Grade 2	28 (70)	27 (71)	55 (71)	
Grade 3	10 (25)	8 (21)	18 (23)	
pT (%)				
pT1/pT2	13 (33)	12 (32)	25 (32)	0.93
pT3/pT4	27 (67)	26 (68)	53 (68)	
pN (%)				
pN0	22 (55)	24 (63)	46 (59)	0.46
pN1	18 (45)	14 (37)	32 (41)	
pM (%)				
pM0	38 (95)	35 (92)	73 (94)	0.95
pM1	2 (5)	3 (8)	5 (6)	
Pathologic stage (%)				
I/II	21 (52)	25 (66)	46 (59)	0.23
III/IV	19 (48)	13 (34)	32 (41)	

SD standard deviation, *CCRT* concurrent chemoradiotherapy

four (69%) of them received preoperative concurrent chemo-radiotherapy (CCRT). The pathologic stage was evaluated by pathologic examination of resected esophagus and lymph nodes. The clinicopathologic characteristics are listed in Table 1.

Immunohistochemistry

Immunohistochemical detection of p-4E-BP1 was performed on formalin-fixed, paraffin-embedded 5-μm-thick sections using bond polymer detection system and bond-automated machine with polymer refine kit. The primary antibodies used were rabbit anti-phospho-4E-BP1 (Thr37/46) monoclonal antibody (clone 236B4, Cell Signaling Technology, Danvers, MA, USA) at a dilution of 1:400 and rabbit anti-phospho-4E-BP1 (Thr70) polyclonal antibody (Cell Signaling Technology, Danvers, MA, USA) at a dilution of 1:50. After deparaffinization, antigen retrieval was performed with ER1 buffer. Sections were incubated with the primary antibody at room temperature for 60 min, followed by poly-horseradish peroxidase anti-mouse/rabbit IgG reagent to localize the primary antibody, and the complex was visualized using diaminobenzidine. The sections were then counterstained with hematoxylin, dehydrated, cleared, and mounted.

The immunostaining patterns in normal esophageal squamous cells and tumor cells were similar using either primary antibody. Both the normal epithelium and tumor showed mainly cytoplasmic staining and focally nuclear staining. The normal squamous epithelium adjacent to the resected tumor was used as an internal positive control (Figs. 1a and 2a). We followed a previously published method to score the expression of p-4E-BP1 [5]. The immunostained slides were evaluated by two pathologists (C.-J. Y and W.-Y. C.) under a dual-head microscope without knowing the clinicopathologic information. A Histo-score (H-score; range=0–300) was calculated by multiplying the intensity score (0=negative; 1=weak; 2=intermediate; 3=strong; Figs. 1b–d and 2b–d) and the fraction score (percentage of positive tumor cells; range=0–100).

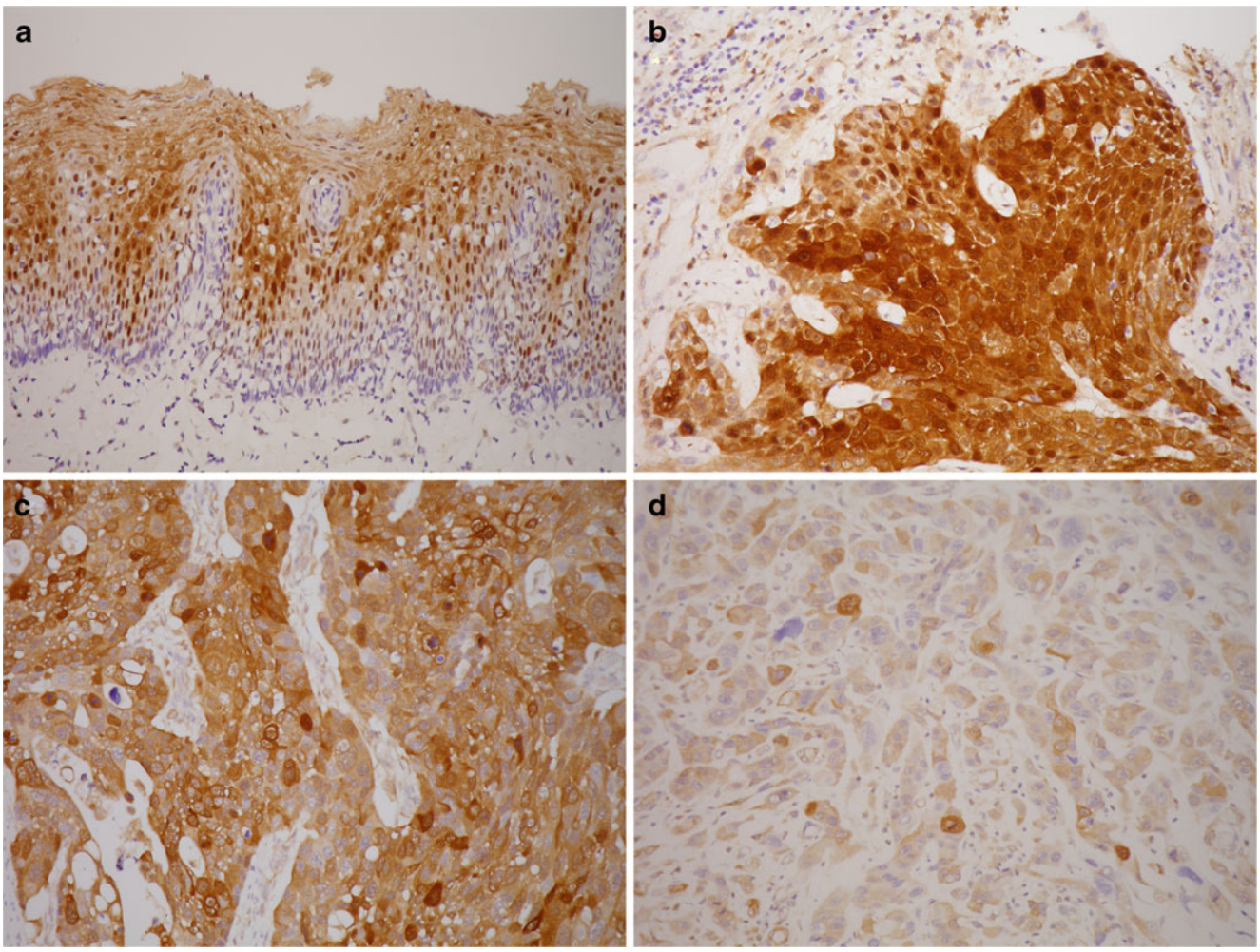

Fig. 1 Immunostaining of p-4E-BP1 $Thr^{37/46}$ in normal esophageal mucosa (**a**). The staining patterns were mainly cytoplasmic and focally nuclear both in normal mucosa and in tumor cells. The intensity scores of tumor cells were graded as 3 (strong; **b**), 2 (intermediate; **c**), 1 (weak; **d**), or 0 (negative)

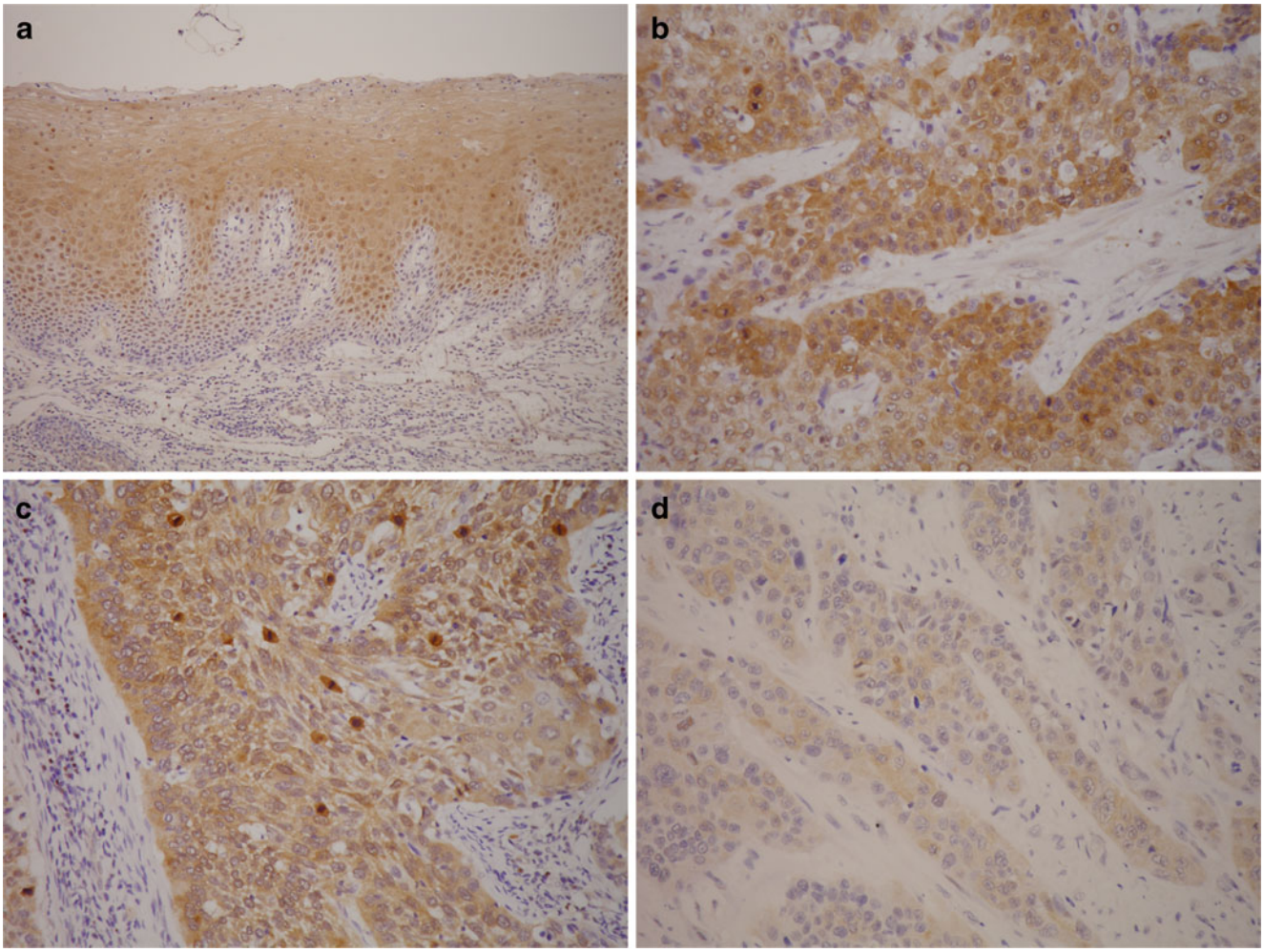

Fig. 2 Immunostaining of p-4E-BP1 Thr^{70} in normal esophageal mucosa (**a**). The intensity scores of tumor cells were graded as 3 (strong; **b**), 2 (intermediate; **c**), 1 (weak; **d**), or 0 (negative)

Statistical analysis

Difference in age between groups was assessed by the Mann–Whitney *U* test. Differences in categorical data were assessed by a chi-square test, and Yates' correction was performed if expected frequencies less than 5 were encountered. We used Pearson correlation to evaluate the relationship between the expression levels of p-4E-BP1 with different phosphorylation sites ($Thr^{37/46}$ and Thr^{70}). Overall survival was analyzed by the Kaplan–Meier method and compared by log-rank tests. The influence of parameters on survival was analyzed using multivariate Cox regression. A p value less than 0.05 was considered statistically significant. All statistical analyses were done using the WinSTAT® for Excel (R. Fitch Software, Bad Krozingen, Germany).

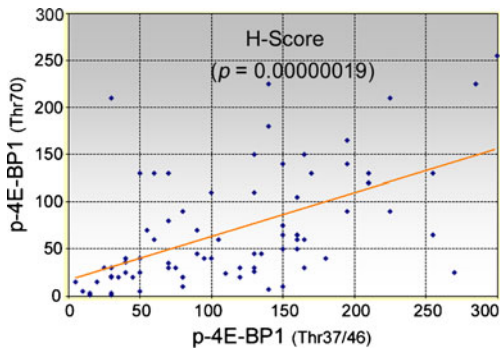

Fig. 3 There was a strong correlation between p-4E-BP1 $Thr^{37/46}$ and p-4E-BP1 Thr^{70} expressions

Results

p-4E-BP1 $Thr^{37/46}$ and p-4E-BP1 Thr^{70} expressions

For p-4E-BP1 $Thr^{37/46}$, the H-scores of the tumors ranged from 5 to 300, with a median of 107.5. Therefore, an H-score of 108 or larger was considered high p-4E-BP1 $Thr^{37/46}$ expression, whereas an H-score of 107 or lower was

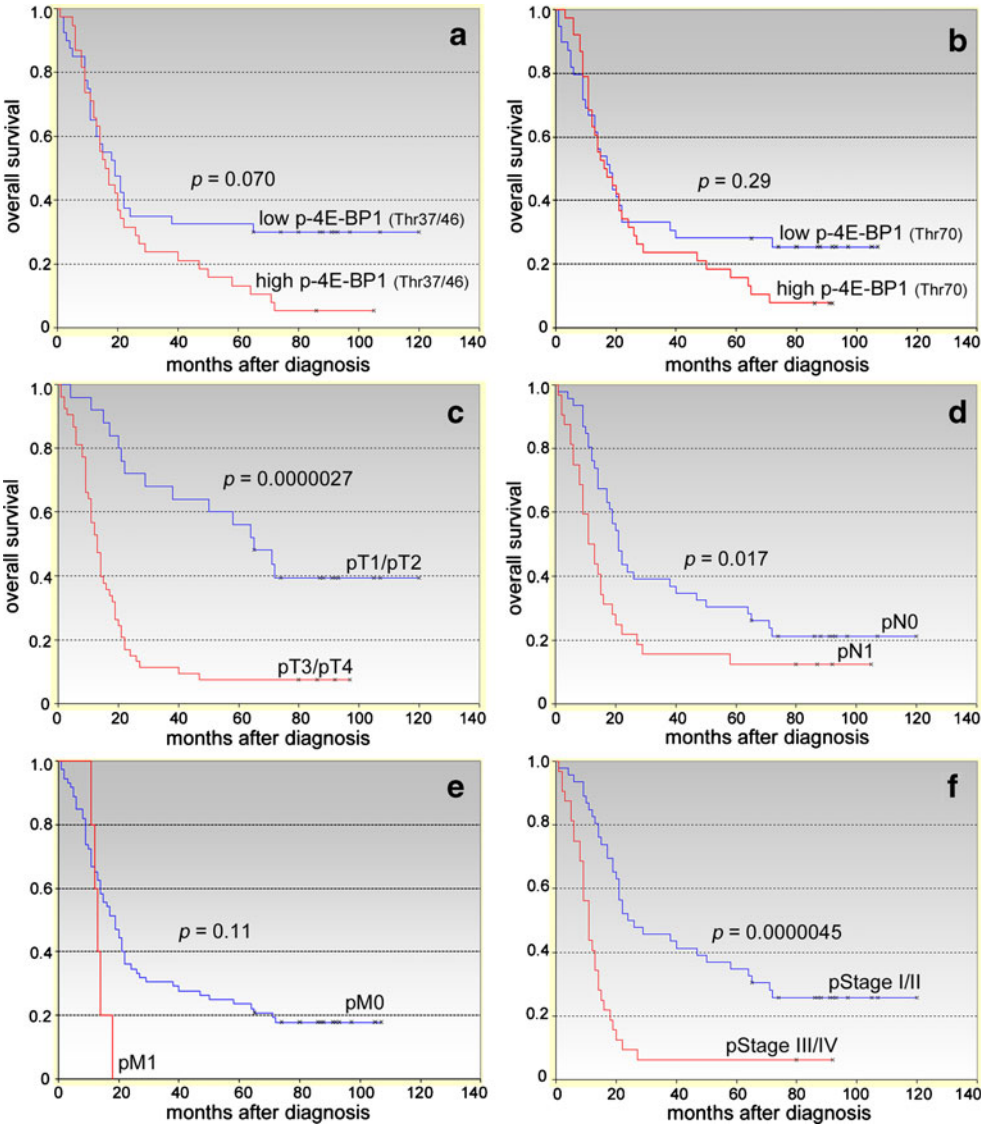

Fig. 4 Survival curves of patients grouped with p-4E-BP1 Thr$^{37/46}$ expression (**a**), p-4E-BP1 Thr^{70} expression (**b**), pT classification (**c**), pN (**d**), pM (**e**), or pathologic stage (**f**)

considered low expression. For p-4E-BP1 Thr^{70}, the H-scores of the tumors ranged from 1 to 255, with a median of 47.5. Hence, an H-score of 48 or larger was considered high p-4E-BP1 Thr^{70} expression, whereas an H-score of 47 or lower was considered low expression. There was a strong correlation between p-4E-BP1 Thr$^{37/46}$ and p-4E-BP1 Thr^{70} expressions (p=0.00000019; Fig. 3). We found a similar trend of short survival in patients with high expression of p-4E-BP1 Thr$^{37/46}$ and p-4E-BP1 Thr^{70}, but the trend was stronger in p-4E-BP1 Thr$^{37/46}$ (p=0.070 vs. 0.29; Fig. 4a, b). Therefore, further analysis of p-4E-BP1 expression was focused on the phosphorylation site Thr$^{37/46}$.

p-4E-BP1 Thr$^{37/46}$ expression and clinicopathologic features

Thirty-eight (49%) of the 78 cases had high p-4E-BP1 Thr$^{37/46}$ expression. The clinicopathologic features of patients grouped by p-4E-BP1 Thr$^{37/46}$ expression level are listed in Table 1. We found no correlation of p-4E-BP1 Thr$^{37/46}$ expression with age at diagnosis, gender, preoperative CCRT, tumor grade, pT classification, pN, pM, or pathologic stage (pStage).

p-4E-BP1 Thr$^{37/46}$ expression and survival

The hazard ratios (HRs) and p values of independent clinicopathologic parameters using multivariate Cox regression are listed in Table 2. The parameter with the strongest independent association with short overall survival was pT3/pT4 (HR=3.47; 95% confidence interval [CI]=1.87–6.42; p=0.000076). High p-4E-BP1 Thr$^{37/46}$ expression was another independent adverse prognostic factor (HR=1.73; 95% CI=1.03–2.90; p=0.038). There was also a clear trend of short survival in pN1 patients (HR=1.63; 95% CI=0.97–2.74; p=0.066). Age at diagnosis, pM classification,

Table 2 Hazard ratios and *p* values of independent clinicopathologic parameters using multivariate Cox regression

Parameter	Overall survival	
	HR (95% CI)	*p* value
p-4E-BP1 $Thr^{37/46}$ expression		
Low	1.00	
High	1.73 (1.03–2.90)	0.038
Primary tumor		
pT1/pT2	1.00	
pT3/pT4	3.47 (1.87–6.42)	0.000076
Regional lymph nodes		
N0	1.00	
N1	1.63 (0.97–2.74)	0.066
Distant metastasis		
M0	1.00	
M1	1.71 (0.65–4.54)	0.28
Histological grade		
Grade 1/Grade 2	1.00	
Grade 3	0.84 (0.46–1.56)	0.59
Age at diagnosis	1.00 (0.98–1.02)	0.94
Pre-operative CCRT		
Yes	1.00	
No	0.96 (0.56–1.66)	0.90

HR hazard ratio, *95% CI* 95% confidence interval, *CCRT* concurrent chemoradiotherapy

and tumor grade showed no significant influence on survival. Survival curves according to more important parameters are shown in Fig. 4.

We stratified the patients according to pT classification, pN, or pStage and analyzed the effect of p-4E-BP1 $Thr^{37/46}$ expression on survival. The adverse prognostic effect was even more significant in patients with relatively early stage disease, including pT1/pT2, N0, and pStageI/II (p=0.0047, 0.012, and 0.011, respectively; Fig. 5a, c, and e). In stark contrast, p-4E-BP-1 $Thr^{37/46}$ had no significant influence on survival in patients with more advanced disease, including pT3/pT4, pN1, and pStage III/IV (p=0.59, 0.97, and 0.47, respectively; Fig. 5b, d, and f).

Discussion

Our study showed high p-4E-BP1 expression independently correlated with short survival in esophageal SCC patients. Unlike previous studies on breast cancer [5] or colorectal cancer [1], no association of high p-4E-BP1 expression with tumor grade or nodal metastasis was found. Our result is consistent with two previous studies on esophageal SCC. The one on tumor cell lines showed increased expression of p-4E-BP1, and the other on tumor tissues regarding eIF-4E and 4E-BP-1 expression found higher eIF-4E expression and lower 4E-BP-1 expression levels significantly associated with advanced tumor stage [12]. These findings can all be explained by the fact that the phosphorylation of 4E-BP-1 releases eIF-4E and enhances cap-dependent translation in favor of tumor cell growth and survival. As evidenced by a previous study, transferring 4E-BP1 phosphorylation site mutants into breast carcinoma cells suppressed their tumorigenicity [13]. We also found that the prognostic effect of p-4E-BP1 expression was significant only in patients with earlier stage disease (pT1/pT2, pN0, or pStage I/II). It is not surprising that p-4E-BP1 expression showed no prognostic effect in patients with more advanced disease, since esophageal SCC is known to be an aggressive cancer with poor survival.

mTOR signaling pathway is frequently involved in human cancers and has been considered as an attractive therapeutic target for cancer therapy in recent years [14,15]. Its activation leads to the phosphorylation of two major targets including 4E-BP-1 and ribosomal S6 kinase 1 (S6K1), and thereby contributes to oncogenesis by inducing cell survival, proliferation, and angiogenesis in a diversity of cell types. The potential applications of mTOR inhibitors for treating a variety of cancers including renal, prostate, breast, pancreatic, and lung cancers have been extensively studied. mTOR pathway was also found to be activated in the above-mentioned study on esophageal SCC cell lines [11]. The mTOR inhibitor rapamycin and small interference RNA against mTOR were shown to inhibit the expression of mTOR, suppress the phosphorylation of its major downstream effectors S6K and 4E-BP1, and arrest the cells in the G0/G1 phase. In addition, an animal study confirmed that mTOR inhibitor rapamycin alone or combined with cisplatin can inhibit growth of esophageal SCC in nude mice [16].

We found a stronger association of short survival with high expression of p-4E-BP1 $Thr^{37/46}$ than with high expression of p-4E-BP1 Thr^{70}. The 4E-BP1 phosphorylation sites regulated via signaling pathways include $Thr^{37/46}$, Thr^{70}, and Ser^{65}. Previous studies on cultured cells found a hierarchical phosphorylation of 4E-BP-1, with sequential phosphorylation of $Thr^{37/46}$, Thr^{70}, and Ser^{65}. Final phosphorylation of Thr^{70} and Ser^{65} are essential for the release of eIF-4E, but phosphorylation of these two sites only is unable to dissociate 4E-BP-1 from eIF-4E unless $Thr^{37/46}$ is also phosphorylated [17]. In a study using antibodies against $Thr^{37/46}$, Thr^{70}, and Ser^{65} on pediatric rhabdomyosarcoma, the high expression of p-4E-BP-1 $Thr^{37/46}$ was found to have the strongest association with poor prognosis [9]. Interestingly, a recent study discovered a new hierarchical phosphorylation of 4E-BP-1 using an animal model of brain ischemia and reperfusion [18]. They found an ordered phosphorylation of Thr^{70}, $Thr^{37/46}$, and Ser^{65}. In this new hierarchy, phosphorylation of $Thr^{37/46}$ is

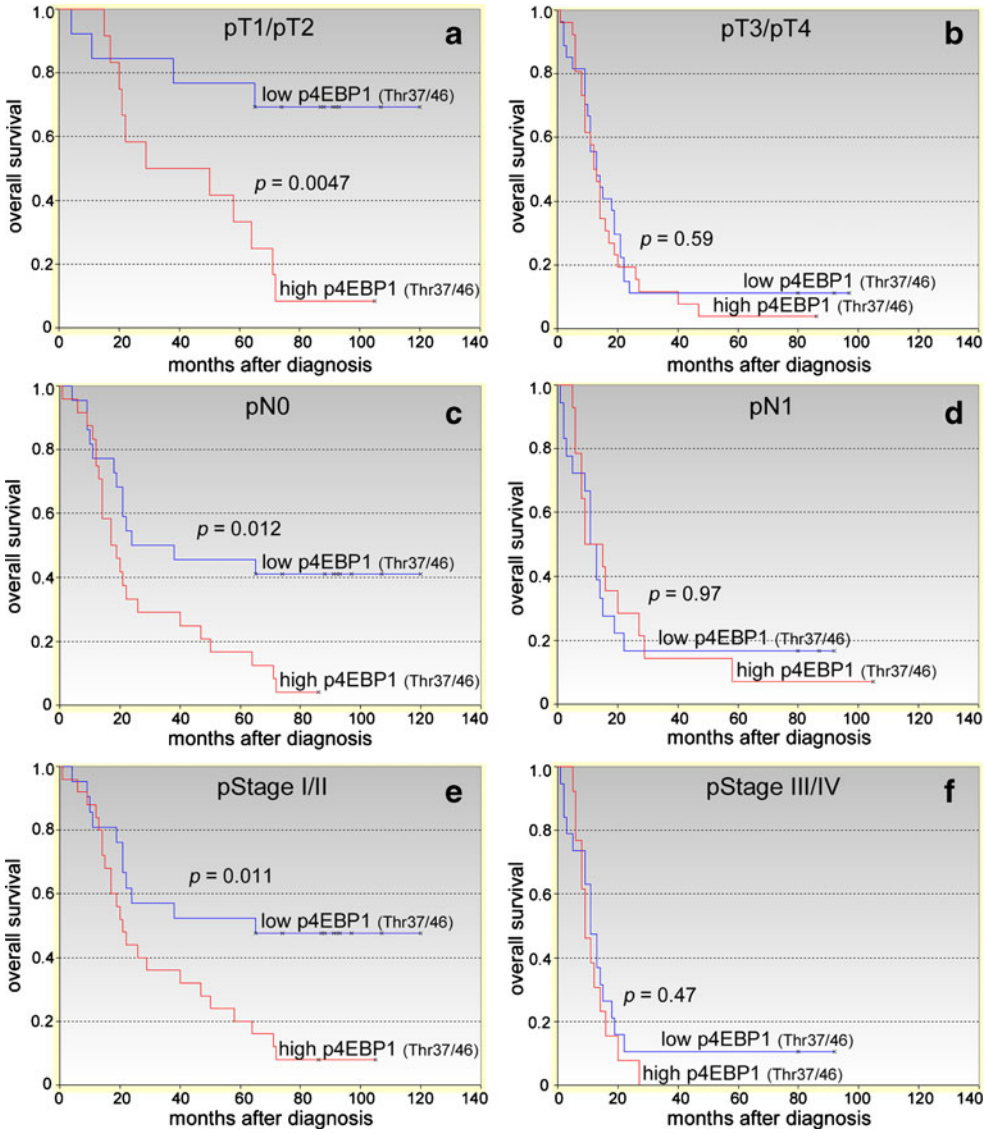

Fig. 5 The adverse prognostic effect of high p-4E-BP1 $Thr^{37/46}$ expression was only significant in patients with pT1/pT2 (**a**), pN0 (**c**), or pStage I/II (**e**) disease. No prognostic effect was found in pT3/pT4 (**b**), pN1 (**d**), or pStage III/IV (**f**) patients

the crucial step for the release eIF-4E. However, further studies are needed to clarify the exact mechanism of 4E-BP-1 phosphorylation in different tumor cells.

Of note, few other previous studies showed inconsistent correlation between phosphorylated mTOR (p-mTOR; activated mTOR) expression and prognosis in esophageal SCC [19–21]. High p-mTOR expression was found to be associated with either high tumor grade [19] or poor prognosis [21]. The remaining study found that activation of AKT but not mTOR had an adverse prognostic effect [20]. Since 4E-BP1 receives convergent signals from both AKT/mTOR to MAPK pathways [22], p-4E-BP1 could well be a better indicator of oncogenic signaling than p-mTOR or p-AKT.

The overall survival rate ranges from 10% to 20% in patients with esophageal SCC. Most patients who present with symptoms, such as dysphagia, have either locally advanced or metastatic disease [23]. At the time of diagnosis, two thirds of the patients had tumors considered inoperable due to patient comorbidities or tumor extension [24]. Therefore, it is important to find novel therapeutic strategy for esophageal SCC. Our study suggests that esophageal SCC patients may be a possible candidate for target therapy with mTOR inhibitors, although further studies are warranted to evaluate their effect.

In conclusion, this is the first study to show that high p-4E-BP1 expression is an independent adverse prognostic factor in esophageal SCC patients, especially in those with relatively early stage disease. Thus, p-4E-BP1 may serve as a potential prognostic indicator in esophageal SCC. In addition, by assessing p-4E-BP1 expression with immunohistochemistry, we could easily identify a subgroup of earlier stage patients with poor prognosis. These patients could then be possible candidates for more aggressive treatment or target therapy with mTOR inhibitors. However, further investigations and more studies with a larger number of patient samples are warranted.

Acknowledgements This study was supported by grants from the Ministry of Education, Taiwan, ROC (EMRPD190031, to C. H.) and the Chang Gung Medical Research Program (CMRPG370021, to W.-Y. C.).

Conflict of interest The authors declare that they have no conflict of interest.

References

1. Armengol G, Rojo F, Castellví J, Iglesias C, Cuatrecasas M, Pons B, Baselga J, Ramón y Cajal S (2007) 4E-binding protein 1: a key molecular "funnel factor" in human cancer with clinical implications. Cancer Res 67:7551–7555
2. Heesom KJ, Gampel A, Mellor H, Denton RM (2001) Cell cycle-dependent phosphorylation of the translational repressor eIF-4E binding protein-1 (4E-BP1). Curr Biol 11:1374–1379
3. Topisirovic I, Ruiz-Gutierrez M, Borden KL (2004) Phosphorylation of the eukaryotic translation initiation factor eIF4E contributes to its transformation and mRNA transport activities. Cancer Res 64:8639–8642
4. Averous J, Proud CG (2006) When translation meets transformation: the mTOR story. Oncogene 25:6423–6435
5. Rojo F, Najera L, Lirola J, Jiménez J, Guzmán M, Sabadell MD, Baselga J, Ramon y Cajal S (2007) 4E-binding protein 1, a cell signaling hallmark in breast cancer that correlates with pathologic grade and prognosis. Clin Cancer Res 13:81–89
6. Castellvi J, Garcia A, Rojo F, Ruiz-Marcellan C, Gil A, Baselga J, Ramon y Cajal S (2006) Phosphorylated 4E binding protein 1: a hallmark of cell signaling that correlates with survival in ovarian cancer. Cancer 107:1801–1811
7. Benavente S, Vergés R, Hermosilla E, Fumanal V, Casanova N, García A, Ramón Y Cajal S, Giralt J (2009) Overexpression of phosphorylated 4E-BP1 predicts for tumor recurrence and reduced survival in cervical carcinoma treated with postoperative radiotherapy. Int J Radiat Oncol Biol Phys 75:1316–1322
8. Castellvi J, Garcia A, Ruiz-Marcellan C, Hernández-Losa J, Peg V, Salcedo M, Gil-Moreno A, Ramon y Cajal S (2009) Cell signaling in endometrial carcinoma: phosphorylated 4E-binding protein-1 expression in endometrial cancer correlates with aggressive tumors and prognosis. Hum Pathol 40:1418–1426
9. Petricoin EF 3 rd, Espina V, Araujo RP, Midura B, Yeung C, Wan X, Eichler GS, Johann DJ Jr, Qualman S, Tsokos M, Krishnan K, Helman LJ, Liotta LA (2007) Phosphoprotein pathway mapping: akt/mammalian target of rapamycin activation is negatively associated with childhood rhabdomyosarcoma survival. Cancer Res 67:3431–3440
10. O'Reilly KE, Warycha M, Davies MA, Rodrik V, Zhou XK, Yee H, Polsky D, Pavlick AC, Rosen N, Bhardwaj N, Mills G, Osman I (2009) Phosphorylated 4E-BP1 is associated with poor survival in melanoma. Clin Cancer Res 15:2872–2878
11. Hou G, Xue L, Lu Z, Fan T, Tian F, Xue Y (2007) An activated mTOR/p70S6K signaling pathway in esophageal squamous cell carcinoma cell lines and inhibition of the pathway by rapamycin and siRNA against mTOR. Cancer Lett 253:236–248
12. Salehi Z, Mashayekhi F (2006) Expression of the eukaryotic translation initiation factor 4E (eIF4E) and 4E-BP1 in esophageal cancer. Clin Biochem 39:404–409
13. Avdulov S, Li S, Michalek V, Burrichter D, Peterson M, Perlman DM, Manivel JC, Sonenberg N, Yee D, Bitterman PB, Polunovsky VA (2004) Activation of translation complex eIF4F is essential for the genesis and maintenance of the malignant phenotype in human mammary epithelial cells. Cancer Cell 5:553–563
14. Huang S, Houghton PJ (2003) Targeting mTOR signaling for cancer therapy. Curr Opin Pharmacol 3:371–373
15. Meric-Bernstam F, Gonzalez-Angulo AM (2009) Targeting the mTOR signaling network for cancer therapy. J Clin Oncol 27:2278–2287
16. Hou G, Zhang Q, Wang L, Liu M, Wang J, Xue L (2010) mTOR inhibitor rapamycin alone or combined with cisplatin inhibits growth of esophageal squamous cell carcinoma in nude mice. Cancer Lett 289:248–254
17. Gingras AC, Raught B, Gygi SP, Niedzwiecka A, Miron M, Burley SK, Polakiewicz RD, Wyslouch-Cieszynska A, Aebersold R, Sonenberg N (2001) Hierarchical phosphorylation of the translation inhibitor 4E-BP1. Genes Dev 15:2852–2864
18. Ayuso MI, Hernández-Jiménez M, Martin ME, Salinas M, Alcázar A (2010) A new hierarchical phosphorylation pathway of the translational repressor eIF4E-binding protein 1 (4E-BP1) in ischemia-reperfusion stress. J Biol Chem. doi: 10.1074/jbc.M110.135103
19. Boone J, Ten Kate FJ, Offerhaus GJ, van Diest PJ, Rinkes IH, van Hillegersberg R (2008) mTOR in squamous cell carcinoma of the oesophagus: a potential target for molecular therapy? J Clin Pathol 61:909–913
20. Yoshioka A, Miyata H, Doki Y, Yasuda T, Yamasaki M, Motoori M, Okada K, Matsuyama J, Makari Y, Sohma I, Takiguchi S, Fujiwara Y, Monden M (2008) The activation of Akt during preoperative chemotherapy for esophageal cancer correlates with poor prognosis. Oncol Rep 19:1099–1107
21. Hirashima K, Baba Y, Watanabe M, Karashima RI, Sato N, Imamura Y, Hiyoshi Y, Nagai Y, Hayashi N, Iyama KI, Baba H (2010) Phosphorylated mTOR expression is associated with poor prognosis for patients with esophageal squamous cell carcinoma. Ann Surg Oncol. doi: 10.1245/s10434-010-1040-1
22. She QB, Halilovic E, Ye Q, Zhen W, Shirasawa S, Sasazuki T, Solit DB, Rosen N (2010) 4E-BP1 is a key effector of the oncogenic activation of the AKT and ERK signaling pathways that integrates their function in tumors. Cancer Cell 18:39–51
23. van Meerten E, van der Gaast A (2005) Systemic treatment for oesophageal cancer. Eur J Cancer 41:664–672
24. Mariette C, Piessen G, Triboulet JP (2007) Therapeutic strategies in oesophageal carcinoma: role of surgery and other modalities. Lancet Oncol 8:545–553

Virchows Arch (2011) 458:179–187
DOI 10.1007/s00428-010-1037-y

ORIGINAL ARTICLE

The role of high-risk human papillomavirus infection in oral and oropharyngeal squamous cell carcinoma in non-smoking and non-drinking patients: a clinicopathological and molecular study of 46 cases

Jan Laco · Hana Vosmikova · Vendula Novakova · Petr Celakovsky · Helena Dolezalova · Lubos Tucek · Jana Nekvindova · Milan Vosmik · Eva Cermakova · Ales Ryska

Received: 4 October 2010 / Revised: 29 November 2010 / Accepted: 12 December 2010 / Published online: 11 January 2011
© Springer-Verlag 2011

Abstract The aim of the study was to investigate the role of high-risk human papillomavirus (HR-HPV) infection in the etiopathogenesis of oral (OSCC) and oropharyngeal (OPSCC) squamous cell carcinoma in non-smoking and non-drinking patients (NSNDP). Twenty-four OSCCs and 22 OPSCCs were analyzed by immunohistochemistry for $p16^{INK4a}$ protein (p16) expression and by chromogene in situ hybridization (CISH) and polymerase chain reaction (PCR) for HR-HPV DNA presence. The series included 23 males and 23 females aged 35–93 years. p16 expression was seen in 7 out of 24 (29%) OSCCs and in 22 out of 22 (100%) OPSCCs. Using CISH, HR-HPV DNA was observed in 6 out of 24 (25%) OSCCs and in 21 out of 22 (95%) OPSCCs. HPV DNA was found in 3 out of 24 (13%) OSCCs and in 18 out of 22 (82%) OPSCCs using PCR. HPV 16 and 33 were detected in 16 and in two cases, respectively. Compared with OSCCs, OPSCCs more frequently showed basaloid morphology ($p<0.0001$), lymph node involvement ($p=0.0063$), diffuse p16 expression ($p<0.0001$), HR-HPV DNA presence using both CISH and PCR ($p<0.0001$; $p<0.0001$), and better outcome. The sensitivity and specificity of p16 expression for HR-HPV DNA presence detected by CISH were 0.89 and 0.95, respectively, and 0.95 and 0.85 for PCR detected HPV DNA. The sensitivity and specificity of CISH for PCR detected presence of HPV DNA were 1.00 and 0.73, respectively. Our study is the first larger study analyzing OSCC and OPSCC in NSNDP. Our results indicate that unlike OSCC, a vast majority of OPSCCs may be associated with HR-HPV infection.

Keywords Squamous cell carcinoma · Oral cavity · Tonsil · HPV · p16 · CISH

J. Laco (✉) · A. Ryska
The Fingerland Department of Pathology, Faculty of Medicine and Faculty Hospital in Hradec Kralove, Charles University, Sokolská 581, 500 05, Hradec Králové, Czech Republic
e-mail: lacoj@lfhk.cuni.cz

H. Vosmikova · J. Nekvindova
Institute of Clinical Biochemistry and Diagnostics, Faculty of Medicine and Faculty Hospital in Hradec Kralove, Charles University, Hradec Králové, Czech Republic

V. Novakova · H. Dolezalova · L. Tucek
Department of Dentistry, Faculty of Medicine and Faculty Hospital in Hradec Kralove, Charles University, Hradec Králové, Czech Republic

P. Celakovsky
Department of Otorhinolaryngology, Faculty of Medicine and Faculty Hospital in Hradec Kralove, Charles University, Hradec Králové, Czech Republic

M. Vosmik
Department of Oncology and Radiotherapy, Faculty of Medicine and Faculty Hospital in Hradec Kralove, Charles University, Hradec Králové, Czech Republic

E. Cermakova
Computer Technology Center, Faculty of Medicine in Hradec Kralove, Charles University, Hradec Králové, Czech Republic

Introduction

Squamous cell carcinomas (SCCs) are the most common malignancies in the head and neck area. Traditionally, they are associated with smoking and alcohol abuse, which still represent important risk factors. Since the 1980s, however, evidence has been emerging, suggesting that a subset of oropharyngeal SCCs (OPSCCs), in contrast to oral SCCs (OSCCs), is associated with oral high-risk human papillomavirus (HR-HPV) infection [1]. The prevalence of HPV-positive head and neck SCCs (HNSCCs) shows considerable regional variation. In the last decade, at least 20 studies on this topic were published, reporting a prevalence range of HPV-positive HNSCC as wide as 0% to 93% [2]. In a multicentre case–control study organized by the International Agency for Research on Cancer, a total of 70% of HNSCCs were shown to harbor HPV DNA, with HPV 16 being the most commonly observed type [3].

HPV-positive and HPV-negative HNSCCs seem to be separate clinicopathologic entities. The former occur in younger patients without sex predilection; show poorly differentiated and/or basaloid morphology; display minimal p53, cyclin D1, and epidermal growth factor receptor expression; and feature good prognosis despite frequent regional lymph node metastases. The reverse is true for HPV-negative HNSCCs in most cases [4].

The incidence of HPV-positive HNSCCs is increasing worldwide. A recent study from Sweden reports that 23% of tonsillar carcinomas were HPV positive in the 1970s whereas there was up to 93% positivity in 2006–2007 [5].

Because of the considerable regional prevalence differences and lack of large studies focused on patients without personal history of classic risk factors for HNSCC, we investigated HPV status and other clinicopathologic characteristics in a group of non-smoking and non-drinking patients with oral and oropharyngeal SCC in the Czech Republic using three different detection methods, with the aim to clarify the etiopathogenesis of HNSCCs in this patients' cohort. Furthermore, we compared selected clinicopathological parameters of the patients and/or tumors with particular regard to the anatomic localization and HPV status of the tumors.

Material and methods

An institutional computer search revealed a total of 289 OSCCs and 214 OPSCCs diagnosed between 2000 and 2009 at The Fingerland Department of Pathology, Faculty Hospital, Hradec Kralove, Czech Republic in patients who had undergone surgical resection of these lesions. To eliminate the role of actinic damage, SCCs of lips were excluded from the search.

Twenty-four out of 289 (8%) of the patients with OSCC and 22 out of 214 (10%) of the patients with OPSCC had no personal history of either smoking or chronic alcohol abuse. These cases were the subject of this study. Ethical approval was obtained from the Ethics Committee, Faculty Hospital Hradec Kralove.

For every patient, gender and age were recorded. Tumors occurring in the oral vestibulum, on the cheek, hard palate, floor of mouth, gingival/alveolar mucosa, and on the anterior tongue (the first 2/3 of the tongue) were classified as OSCCs, whereas OPSCCs included tumors of the root of tongue, palatine tonsils and arches, soft palate, and the posterior wall of the oropharynx [6]. In every case, tumor size ("pT" category), presence of microscopically confirmed regional lymph node metastases ("pN" category), and presence of distant metastases ("cM" category) were recorded. Histologic subtypes of SCC ("conventional", verrucous, basaloid, papillary, spindle cell, acantholytic, adenosquamous, and carcinoma cuniculatum) and differentiation grade in cases of "conventional" SCC were recorded according to the current WHO classification of head and neck tumors [6]. Pathologic staging was done from the material from radical tumor resection with neck lymph node dissection at the time of presentation according to current TNM classification [7]. As controls, we examined 10 fibromas from various parts of oral cavity covered by normal squamous epithelium and 10 tonsils with chronic tonsillitis. The control lesions were obtained from gender- and age-matched patients.

During the follow-up period, data on local, regional, and locoregional recurrence; on occurrence of distant metastases; on development of other metachronous malignant tumors; and on tumor-associated death were recorded. After resection, the specimens were immediately fixed in 10% formalin, routinely processed, embedded in paraffin, and stained with hematoxylin–eosin. Paraffin blocks for further analysis were available in all cases.

For immunohistochemical detection of $p16^{INK4a}$ protein (p16), the CINtec® Histology Kit (mtm laboratories AG, Heidelberg, Germany) was used according to the manufacturer's manual. Samples of cervical intraepithelial lesion grade III were used as positive controls. Control slides provided by the manufacturer were used as negative controls. Brown staining of tumor cell nuclei and/or cytoplasm was interpreted as positive. The p16 immunostaining was scored according to criteria set out in our previous study [8] as follows: 0 absent, + 1–5% tumor cells stained, ++ 6–20% tumor cells stained, +++ 21–50% tumor cells stained, and ++++ 51–100% tumor cells stained.

In addition, the samples were examined using molecular genetic methods. First, HR-HPV DNA detection was

performed by chromogene in situ hybridization (CISH) using the GenPoint™ HPV biotinylated DNA probe (Dako, Glostrup, Denmark), which detects 13 HR-HPV types, namely 16, 18, 31, 33, 35, 39, 45, 51, 52, 56, 58, 59, and 68, according to the manufacturer's manual. Briefly, after sample preparation, the DNA probe was added and denaturated by placing the slides on a heating block at 92°C for 5 min. Following denaturation, the slides were transferred to a humid chamber for hybridization at 37°C for 18 h. Then, detection of the hybridized probe was performed using the Genpoint™ Detection System (Dako) according to the kit instructions using primary streptavidin-horseradish peroxidase (HRP; dilution 1:100), biotinyl tyramide, and secondary streptavidin-HRP. Finally, DAB was used as chromogene. Samples of cervical intraepithelial lesion grade III were used as positive controls. The correct performance of the staining procedure was checked using Positive Control (Human DNA) Biotinylated DNA Probe and Negative Control (Plasmid DNA) Biotinylated DNA Probe (Dako) instead of GenPoint™ HPV Biotinylated DNA Probe. Only the brown signals from tumor cell nuclei were interpreted as positive. The CISH results were scored according to our previous study [8] as follows: 0 absent, + 1–5% epithelial cells stained, and ++ >5% epithelial cells stained.

HPV DNA detection was then performed by polymerase chain reaction (PCR) as follows: HPV DNA was extracted from paraffin-embedded tissue after deparaffinization in xylene and rehydration in ethanol using the commercial QIAamp DNA FFPE Tissue Kit (Qiagen GmBH, Hilden, Germany) according to the manufacturer's protocol. PCR amplification of β-globin sequences was performed to confirm sample fitness for PCR assay. All samples were screened for presence of HPV DNA by PCR amplification with primers GP5+/GP6+ located within the HPV L1 gene. The sequences of the forward and reverse primers used were 5′-TTTGTTACTGTGGTAGATACTAC-3′ (GP5+) and 5′-GAAAAATAAACTGTAAATCATATT-3′ (GP6+). PCR reaction was performed in a volume of 25 μL, containing 25 mM $MgCl_2$, 2.5 mM of each dNTP, 2.5 U of Takara Taq polymerase (Takara Bio Inc., Shiga, Japan), 100 pmol of each primer (GP5+/GP6+), and 2 μL of HPV DNA at various dilutions. The PCR protocol was then carried out with an initial denaturation at 95°C for 10 min, followed by 40 cycles of denaturation at 95°C for 30 s, annealing at 55°C for 60 s, and extension at 72°C for 45 s. Amplified products were run on 2% agarose gel and stained with ethidium bromide for size verification.

Samples showing HPV DNA presence by the above-mentioned procedure were subsequently analyzed by Linear Array HPV Genotyping Test (Roche, Basel, Switzerland). The manufacturer's protocol was modified to adapt the test for use on paraffin-embedded tissue according to Siriaunkgul et al. [9]. The test involves three steps: PCR amplification of target DNA, nucleic acid hybridization, and detection of 37 HPV types, specifically 6, 11, 16, 18, 26, 31, 33, 35, 39, 40, 42, 45, 51, 52, 53, 54, 55, 56, 58, 59, 61, 62, 64, 66, 67, 68, 69, 70, 71, 72, 73 (MM9), 81, 82 (MM4), 83 (MM7), 84 (MM8), IS39, and CP6108. PCR was performed in a total volume of 100 μL containing 50 μL of the manufacturer's master mix and 50 μL of GP5+/GP6+ PCR product. The amplification program consisted of 2 min at 50°C and 9 min at 95°C, followed by 40 cycles of 30 s at 50°C, of 1 min at 55°C, and of 1 min at 72°C, with a final extension at 72°C for 5 min. The PCR product was denaturated with denaturation solution and hybridized on to a strip containing specific probes for the 37 above-mentioned HPV types and β-globin reference lines. Detection was carried out using streptavidin-HRP and 0.1% tetramethylbenzidine as a chromogen. Positive reaction was visible as a blue line on the strip.

Statistical analysis using NCSS 2007 program, chi-squared test, Fisher's exact test, and two-sample *t* test was performed. Differences were considered statistically significant at $p<0.05$.

Results

The study sample consisted of 23 male and 23 female patients aged 35–93 years (mean 63±15 years; median 61 years). The clinicopathological data of the patients are shown in Table 1. None of the patients had a personal history of any precancerous disorder for OSCC or OPSCC, namely oral lichen planus, oral submucous fibrosis, and proliferative verrucous leukoplakia. The follow-up information was available in 44 out of 46 (96%) patients and ranged from 7 to 168 months (median 41 months). Twenty-eight patients underwent adjuvant radiotherapy only, 14 patients underwent adjuvant chemoradiotherapy, and two patients underwent adjuvant chemotherapy only. Among the OSCC patients, 9 out of 22 (41%) developed local, 10 out of 22 (46%) regional, and 12 out of 22 (55%) locoregional recurrences; 1 out of 22 (5%) patient developed distant metastases in skeleton; 5 out of 22 (23%) patients developed other metachronous malignancies (SCC of tongue, SCC of larynx, colonic adenocarcinoma, chronic B-lymphocytic leukemia/small cell lymphoma, and Langerhans cell histiocytosis each); and 16 out of 22 (73%) patients died due to OSCC. Among the OPSCC patients, 3 out of 22 (14%) developed local, 1 out of 22 (5%) regional, and 4 out of 22 (18%) locoregional recurrences; 2 out of 22 (9%) patients developed distant metastases in skeleton and in liver each; 3 out of 22 (14%) patients developed other metachronous malignancies (SCC of lung, neuroendocrine carcinoma of pancreas and chronic B-

Table 1 Clinicopathological data of patients and staging status of tumors

Tumor localization	Gender		Age (years; *M*=SD)	pT				pN			
	Male	Female		T1	T2	T3	T4	N0	N1	N2	N3
OSCC (*n*=24)	10	14	66±15	6	6	4	8	16	3	5	0
Anterior tongue	3	5		3	3	1	1	6	2	0	0
Cheek	3	3		2	0	1	3	2	0	4	0
Gingiva	1	4		1	3	0	1	4	0	1	0
Floor of mouth	3	0		0	0	2	1	2	1	0	0
Hard palate	0	2		0	0	0	2	2	0	0	0
OPSCC (*n*=22)	13	9	60±9	1	12	5	4	5	4	11	2
Tonsil	10	7		0	10	5	2	4	3	10	0
Root of tongue	3	2		1	2	0	2	1	1	1	2
Total (*n*=46)	23	23	63±15	7	18	9	12	21	7	16	2

M mean, *OSCC* oral squamous cell carcinoma, *OPSCC* oropharyngeal squamous cell carcinoma, *SD* standard deviation

lymphocytic leukemia/small cell lymphoma each); and 7 out of 22 (32%) patients died due to OPSCC.

The 24 OSCC cases included SCCs of the anterior tongue (4× left, 4× right), cheek (4× left, 2× right), gingival/alveolar mucosa (3× lower left, 1× upper left, 1× lower right), floor of mouth (1× left, 2× right), and the hard palate (2× left). The 22 OPSCC cases comprised SCCs of the tonsils (9× left, 8× right) and of the root of the tongue (3× left, 2× right).

The staging characteristics of the tumors are shown in Table 1. No tumor in the "pT4b" category was seen. Among the OSCCs, most tumors were advanced at presentation being classed as "pT4a" (8 out of 24), whereas the most common tumor size category of OPSCC was "pT2", seen in 12 out of 22 cases. Regional lymph node metastases were found in 17 out of 22 of OPSCCs while the majority of OSCCs displayed no dissemination (16 out of 24 cases). All tumors characterized as "pN2" were actually "pN2b" except for one tonsillar tumor which featured "pN2c" status. No "pN2a" carcinoma was found. Distant metastases were not detected in any of the cases using imaging methods ("cM0").

Microscopically, apart from one tumor of the floor of mouth which was classified as a spindle cell variant, all the cases of OSCCs were classified as "conventional" SCC. The "conventional" OSCCs were moderately differentiated in 17 out of 24 cases (Fig. 1a). Five of the tumors were graded as well differentiated and one as poorly differentiated. No tumor from the OSCC group featured basaloid morphology. Almost all OPSCCs showed basaloid morphology with pushing borders, frequent peripheral palisading of dark tumor cells, and common central comedo-like necroses (Fig. 2a). Only one tumor of right tonsil showed different morphological features and was classified as a moderately differentiated "conventional" SCC. The microscopic appearance of regional lymph node metastases followed that of the primary tumor in all cases.

The results of p16 expression and of HPV DNA presence, the latter detected using both CISH and PCR, are summarized in Table 2. p16 expression was detected in 7 out of 24 (29%) OSCCs and in 22 out of 22 (100%) OPSCCs. In OSCCs, the expression was usually weak and limited to less than 5% of tumor cells (four out of seven cases). Only one tumor of the anterior tongue was scored as +++, with 30% positive tumor cells (Fig. 1b). The p16-positive tumor cells appeared to be more frequently seen in the superficial portion of the tumors and at the periphery of the tumor nests. On the contrary, all the OPSCCs showed almost always strong diffuse p16 expression throughout the tumor tissue (Fig. 2b). Variable p16 expression was seen in dysplastic squamous epithelium adjacent to p16-positive invasive SCC in both groups. In the control group, isolated weakly p16-positive cells within non-dysplastic squamous epithelium were found in 3 out of 10 oral fibromas and in 2 out of 10 tonsils with chronic tonsillitis.

Using CISH, HR-HPV DNA was observed in 6 out of 24 (25%) OSCCs (Fig. 3) and in 21 out of 22 (95%) OPSCCs (Fig. 4). The distribution pattern of CISH positivity generally followed that of p16 expression in tumors in both groups. Positive CISH signals were seen as variably sized brown dots within the nuclei of neoplastic cells or as diffuse brown nuclear staining. All controls were uniformly CISH negative.

Using PCR, HPV DNA was found in 3 out of 24 (13%) OSCCs and in 18 out of 22 (82%) OPSCCs. Subsequent HPV typization was successful in 18 out of 21 cases. HPV 16 was the predominant type, detected in 16 cases (11× tonsil, 3× root of tongue, 1× anterior tongue, and 1× gingiva). Two tonsillar SCCs showed the presence of HPV

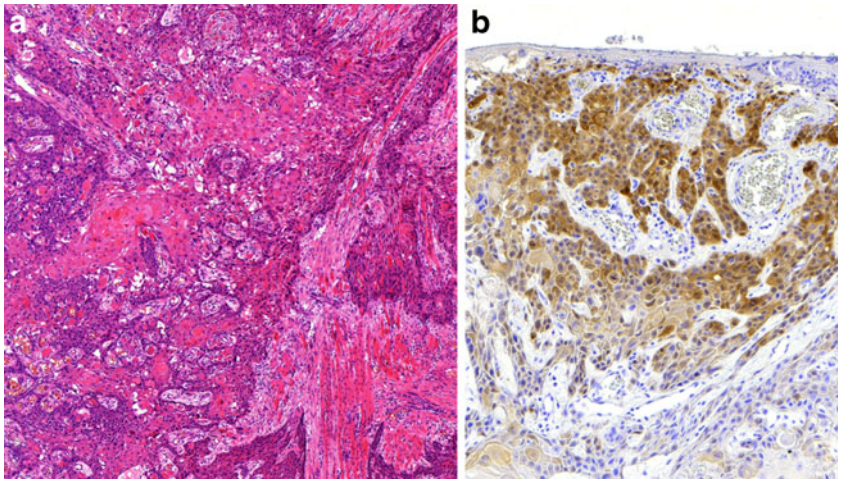

Fig. 1 **a** Moderately differentiated "conventional" squamous cell carcinoma of the anterior part of the tongue (HE, ×200). **b** Focal expression of p16 particularly in the superficial portion of the tumor (×200). This figure and Fig. 3 show identical case with HPV 16 subsequently detected by PCR

33. No low-risk HPV types were found. No HPV co-infection was observed.

There was no statistically significant difference regarding the gender and age of patients and the "pT" tumor status between OSCC and OPSCC groups. OSCCs frequently showed "conventional" morphology whereas the basaloid variant ($p<0.0001$) was the principal morphologic subtype of OPSCCs. Furthermore, OPSCCs showed more frequent regional lymph node involvement ($p=0.003$), more frequent p16 expression ($p<0.0001$), and more frequent HR-HPV DNA presence using both CISH and PCR ($p<0.0001$; $p<0.0001$), when compared to OSCCs. For the purpose of statistical analysis, "pN2b" and "pN2c" subcategories were regarded as one "pN2" category. Regarding the follow-up data, OPSCC patients experienced less frequent local ($p=0.042$), regional ($p=0.002$), and locoregional ($p=0.030$) tumor recurrences and tumor-associated death ($p=0.007$). There were no significant differences between OSCC and OPSCC patients regarding distant metastases development and occurrence of metachronous malignancies.

With regard to the HPV status assessed by PCR, the HPV-positive SCCs occurred more frequently in oropharynx ($p<0.0001$), displayed more frequently basaloid morphology ($p<0.0001$), showed more frequent lymph node dissemination ($p=0.006$), and more frequent p16 expression ($p<0.0001$), when compared to HPV-negative tumors. During the follow-up period, the patients with HPV-positive SCCs experienced less frequent regional recurrence ($p=0.005$), when compared to the patients with HPV-negative tumors. There were no significant differences between HPV-positive and HPV-negative SCCs regarding the gender and age of the patients, the "pT" tumor status, the frequency of both local and locoregional recurrences, the development of distant metastases, the occurrence of metachronous malignancies, and the frequency of tumor-associated death.

The optimal sensitivity, specificity, positive predictive value, and negative predictive value of p16 expression for HR-HPV DNA presence were detected at positivity threshold level "more than 20% positive tumor cells" and were calculated 0.89, 0.95, 0.96, and 0.86 when compared to CISH (CISH used as gold standard) and 0.95, 0.85, 0.83,

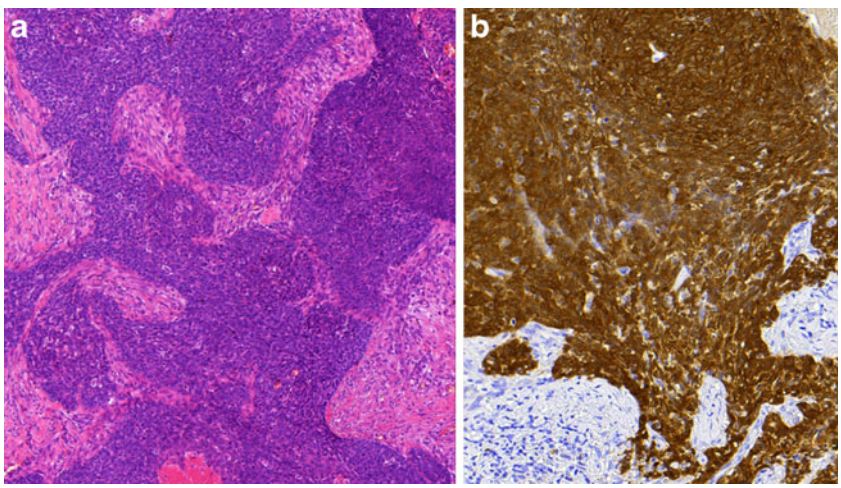

Fig. 2 **a** Basaloid squamous cell carcinoma of the tonsil (HE, ×200). **b** Diffuse expression of p16 in the deeper portion of the tumor (×200). This figure and Fig. 4 show identical case with HPV 16 subsequently detected by PCR

Table 2 Results of p16 expression and HPV DNA presence in tumors

Tumor localization	p16 protein					HPV DNA CISH			HPV DNA PCR	
	0	+	++	+++	++++	0	+	++	0	+
OSCC	17	4	2	1	0	18	4	2	21	3
Anterior tongue	6	1	0	1	0	6	1	1	7	1
Cheek	5	0	1	0	0	5	1	0	5	1
Gingiva	2	2	1	0	0	4	1	0	4	1
Floor of mouth	3	0	0	0	0	2	0	1	3	0
Hard palate	1	1	0	0	0	1	1	0	0	0
OPSCC	0	0	0	0	22	1	8	13	4	18
Tonsil	0	0	0	0	17	1	7	9	2	15
Root of tongue	0	0	0	0	5	0	1	4	2	3

CISH chromogene in situ hybridization, *OSCC* oral squamous cell carcinoma, *OPSCC* oropharyngeal squamous cell carcinoma, *PCR* polymerase chain reaction

and 0.96 when compared to PCR (PCR used as gold standard). The optimal sensitivity, specificity, positive predictive value, and negative predictive value of CISH for HR-HPV DNA presence compared to PCR (when PCR used as gold standard) were detected at positivity threshold level of "any positive tumor cell" and were calculated 1.00, 0.73, 0.74, and 1.00. Calculated at the above-mentioned levels of threshold, the correlation index between p16 expression and HR-HPV DNA presence detected by CISH and PCR was 0.82 and 0.80, respectively. The correlation index between CISH and PCR was 0.74.

Discussion

Nowadays, it is widely accepted that persistent HR-HPV infection is the major cause of uterine cervix carcinoma, HPV 16 and 18 being responsible for about 70% of these tumors [10]. In addition, HR-HPVs have been shown to be associated with a subset of vulvar, penile, and anal carcinomas, as well [11]. The first study analyzing HPV status in HNSCCs was published in 1983 by Syrjänen et al. who suggested that HPV infection may be involved in the development of a subset of these lesions [12]. Subsequently in 1985, two series were published by de Villiers et al. [13] and by Löning et al. [14] who both found HPV infection in their cases of oropharyngeal cancer. Since that time, at least 30 studies on this topic were published in the English literature providing good evidence that oral HPV infection is an independent risk factor for HNSCCs [2,15]. The precise proportion of HPV-positive HNSCCs, however, varies considerably, ranging from 0% up to 93% [2]. This discordance may be partially explained by true regional differences in oral HPV infection prevalence probably influenced by different sexual habits in particular cultures, by precise anatomic localization of the tumors, and by different detection methods used in the studies [16]. In a multicentre case–control study on HNSCCs, 70% of tumors harbor HPV DNA, with HPV 16 being most commonly observed [3].

HPV-positive oral and oropharyngeal SCCs seem constitute a distinct entity, different from HPV-negative tumors [17]. They tend to occur in younger patients without sex predilection. Up to 20% of these cancers develop in patients

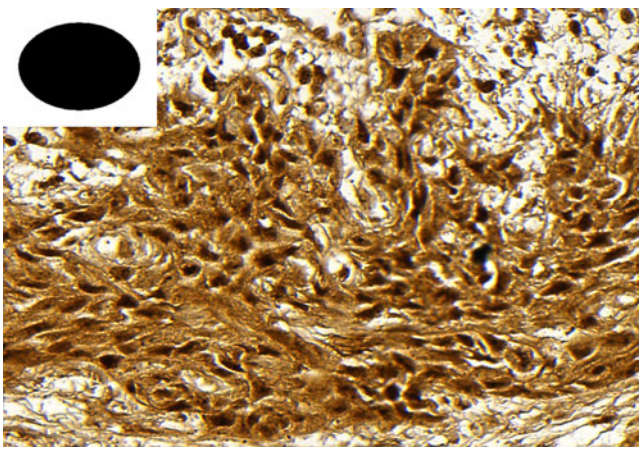

Fig. 3 Diffuse nuclear signals of HR-HPV DNA detected by CISH (×400). *Inset*: schematic drawing of diffuse nuclear CISH signal

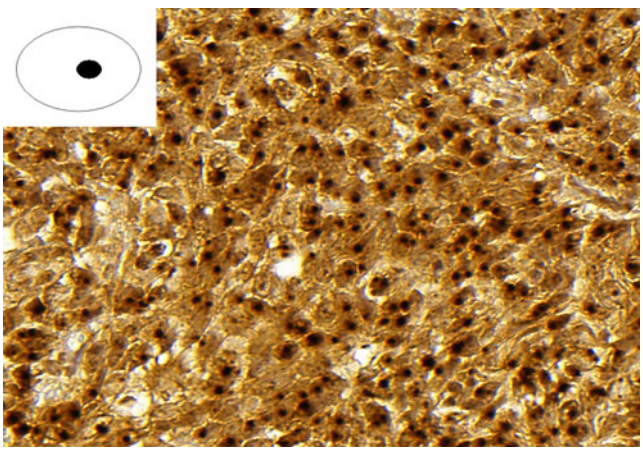

Fig. 4 Dot-like nuclear signals of HR-HPV DNA detected by CISH (×400). *Inset*: schematic drawing of dot-like nuclear CISH signal

without traditional risk factors, i.e., smoking and alcohol abuse. Conversely, their risk factors include young age at first intercourse, promiscuity, and history of genital warts in men and number of sexual partners in women [18]. As positive personal history of oral–genital and oral–anal sexual contact, during which the HPV infection may be transmitted to the oral cavity, increases the risk for HPV-positive HNSCCs, they may be regarded as sexually transmitted disease [2]. It is assumed that long-lasting oral HPV infection, which prevalence increases after the onset of sexual activity, precedes the development of HPV-positive HNSCC for about 10 years [3]. In addition, these tumors seem to be related to immunosuppression [17]. The influence of smoking on HPV-positive HNSCCs is yet unclear, suggesting either synergistic or additional effect [2].

Despite intensive research, larger studies analyzing selective cohorts of non-smoking and non-drinking patients with HNSCCs in detail are lacking. The results of previous studies with these patients included are summarized in Table 3 [19–32]. The number of examined cases is, however, low, not exceeding 20 patients in most studies. We found data on patients that were non-smokers and concurrently non-drinkers in only three studies [19–21]. All the other studies report either non-smokers or non-drinkers, making interpretation of the results and correlation even more difficult. The precise anatomic localization of the patients' tumors is also difficult to identify. The HPV DNA detection rate ranged as wide as from 20% to 100% in non-smokers and from 0% to 82% in non-drinkers. In our study, HPV DNA was found in 3 out of 24 (13%) of OSCCs and in 18 out of 22 (82%) of OPSCCs using PCR, which was the most common detection method used in previous studies. The result differences may be caused by several factors, namely (1) different prevalence of oral HPV infection in studied populations which may range from 0% to about 11% [16], (2) low numbers of non-smokers and non-drinkers, (3) precise anatomical localization of the tumors (oral cavity versus oropharynx, see below), and (4) variations in the detection methods. Our findings indicate that the vast majority of OPSCCs developing in this cohort of patients are caused by HR-HPV infection. On the contrary, as only 13% of OSCCs in our patients showed HR-HPV DNA presence, other yet unidentified risk factors must exist for SCCs arising in this anatomic area which need to be elucidated by further studies.

HPV-positive HNSCCs show tendency to occur in the oropharynx, particularly in palatine tonsils and at the root of the tongue, both areas rich on lymphoid tissue [1]. This phenomenon was observed in our selective cohort as HPV infection was detected in 82% of OPSCCs, in contrast with only 13% HPV-positive cases of OSCC. The affinity of HPV to these anatomic areas may be explained by production of currently unspecified cytokines by lymphoid tissue and/or by deep invagination of the tonsillar surface and incompact squamous epithelium at the base of the tonsillar crypts, the latter factors blocking simple mechanical clearing of the epithelium and making the epithelium more susceptible to HPV infection [14].

Microscopically, HPV-positive HNSCCs tend to display basaloid and/or poorly differentiated morphology. This

Table 3 Prevalence of HPV in non-smokers and non-drinkers

Authors [ref.]	Tumor localization	Method	NS/Tot (%), ND/Tot (%)	PosNS/NS (%), PosND/ND (%)	HPV type
Cruz [19][a]	OSCC	PCR	3/35 (9)	0/3	–
Smith [20][a]	OSCC/OPSCC	RT-PCR	34/193 (18)	5/34 (15)	16, 18, 33
Koppikar [21][a]	OSCC	PCR	6/102 (6)	3/6 (50)	16, 18
Tachezy [22]	OSCC/OPSCC	PCR	7/68 (10), 16/68 (24)	7/7 (100), 11/16 (69)	16, 33
Slebos [23]	OSCC/OPSCC	RT-PCR	4/36 (11), 14/36 (39)	2/4 (50), 4/14 (29)	16
Weinberger [24]	OPSCC	RT-PCR	21/107 (20), 39/107 (36)	15/21 (71), 32/39 (82)	16
Luo [25]	OSCC	PCR	3/51 (6), 3/51 (6)	2/3 (67), 1/3 (33)	16
Chuang [26]	OSCC/OPSCC	RT-PCR	19/59 (32), 10/59 (17)	7/19 (37), 2/10 (20)	16
Simonato [27]	OSCC	nested PCR	3/29 (10), 11/29 (38)	2/3 (67), 3/11 (27)	NT
Gudleviciene [28]	OSCC/OPSCC	PCR	6/48 (13), 1/48 (2)	1/6 (17), 0/1	16
Lohavanichbutr [29]	OSCC/OPSCC	PCR	25/119 (21), 11/119 (9)	5/25 (20), 3/11 (27)	16
Weinberger [30]	OPSCC	PCR/IHC	15/77 (19), 32/77 (42)	14/15 (93), 20/32 (63)	16
Luginbuhl [31]	OPSCC	ISH	8/44 (18), 21/44 (47)	4/8 (50), 7/21 (33)	NT
Straetmans [32]	OPSCC	ISH	16/81 (20), 38/81 (47)	11/16 (69), 22/38 (58)	16

IHC immunohistochemistry, *ISH* in situ hybridization, *ND* no. of non-drinkers, *NS* no. of non-smokers, *NT* not tested, *OPSCC* oropharyngeal squamous cell carcinoma, *OSCC* oral squamous cell carcinoma, *PCR* polymerase chain reaction, *PosND* no. of HPV-positive non-drinkers, *PosNS* no. of HPV-positive non-smokers, *RT-PCR* real-time PCR, *Tot* total no. of patients

[a] Indicates concurrent non-smokers and non-drinkers

finding was confirmed in our series as this growth pattern was observed in 17 out of 21 (81%) of HPV-positive SCCs whereas it was seen in only 4 out of 25 (16%) of HPV-negative tumors. Interestingly, all four of these tumors occurred in the tonsil and at the root of the tongue, but PCR assay failed to prove HPV DNA presence. Conversely, only 4 out of 21 (19%) of "conventional" SCCs, arising on the gingiva, cheek, anterior part of the tongue, and in the tonsil, were found to contain HPV DNA by PCR.

The immunohistochemical characteristics of HPV-positive HNSCCs seem to be different from those of HPV-negative tumors. The former display minimal p53, cyclin D1, and epidermal growth factor receptor expression whereas the reverse is mostly true for the HPV-negative tumors [4].

The HPV types detected in HNSCCs include most frequently HPV 16, 18, and 33 [2,17]. Less commonly, HPV 35, 38, 52, and 59 as well as low-risk types 6 and 11 were observed. In our study, the HPV types observed were HPV 16 and 33 only, detected in 16 and in two cases, respectively.

PCR assay and the FDA-approved Hybrid Capture 2 assay may serve as gold standard detection methods for HPV testing [33]. In routine biopsy practice, the immunohistochemical detection of $p16^{INK4a}$ protein (p16), which is regarded as a sensitive marker of active HPV replication, is widely used as a surrogate marker, particularly in cervical pathology [34]. However, little is known about the application of this marker in HNSCCs. The sensitivity and specificity of p16 expression for HR-HPV DNA presence when compared to PCR were in our study 0.95 and 0.85, confirming the use of this marker as an acceptable tool in testing the HPV status of head and neck tumors. As the specificity of the particular chromogene in situ hybridization method used in our study for HR-HPV DNA presence when compared to PCR was only 0.73, this appears to be of little additional diagnostic value.

Importantly, HPV-associated HNSCCs show better outcome and reduced risk of recurrence, compared to HPV-negative tumors [1,17], as they were shown to display enhanced radiochemosensitivity. This finding was in part confirmed in our study, as despite frequent initial lymph node dissemination, HPV-positive SCCs showed less frequent regional recurrence rate whereas the opposite was true for HPV-negative tumors. Furthermore, the nodal status of HPV-positive HNSCCs was reported to be of little prognostic value [35]. It seems that HPV-positive HNSCC represents a distinct clinicopathological entity, for which more effective treatment options may develop in the near future different from HPV-negative tumors. Thus, HPV testing in every case of HNSCC is of particular importance.

In summary, we report the first large study analyzing in detail a selective cohort of patients with oral and oropharyngeal squamous cell carcinoma without positive personal history of smoking and alcohol abuse, classic risk factors for this type of malignancy. Our results indicate that the majority of oropharyngeal tumors developing in these patients are related to oral HPV infection whereas the viral etiology is responsible for a substantially smaller subset of tumors occurring in oral cavity, stressing the need for identification of further, still unknown, risk factors playing role in the pathogenesis of squamous cell carcinoma of the oral cavity.

Acknowledgments The authors thank Mrs. M. Zakova for her excellent technical support and Dr. F.A. Sobande for English language correction. The experiments carried out in this study comply with the current laws of the Czech Republic. This study was supported by the Research Project of the Ministry of Health of the Czech Republic No. 00179906.

Conflict of interest statement The authors declare that they have no conflict of interest.

References

1. Mannarini L, Kratochvil V, Calabrese L et al (2009) Human papilloma virus (HPV) in head and neck region: review of literature. Acta Otorhinolaryngol Ital 29:119–126
2. Lajer CB, von Buchwald C (2010) The role of human papillomavirus in head and neck cancer. APMIS 118:510–519
3. D'Souza G (2007) Case–control study of human papillomavirus and oropharyngeal cancer. N Engl J Med 356:1125–1131
4. Nguyen NP, Chi A, Nquyen LM et al (2010) Human papillomavirus-associated oropharyngeal cancer: a new clinical entity. Q J Med 103:229–236
5. Nasman A, Attner P, Hammarstedt L et al (2009) Incidence of human papillomavirus (HPV) positive tonsillar carcinoma in Stockholm, Sweden: an epidemic of viral-induced carcinoma? Int J Cancer 125:362–366
6. Slootweg PJ, Eveson JW (2005) Tumours of the oral cavity and oropharynx. In: Barnes L, Eveson JW, Reichart P, Sidransky D (eds) World Health Organization classification of tumours. Pathology and genetics of head and neck tumours, 1st edn. IARC, Lyon, pp 166–175
7. Sobin LH, Gospodarowicz MK, Wittekind C (eds) (2009) TNM classification of malignant tumours, 7th edn. Wiley-Blackwell, Chichester, pp 25–38
8. Laco J, Slaninka I, Jirasek M et al (2008) High risk human papillomavirus infection and $p16^{INK4a}$ protein expression in laryngeal lesions. Pathol Res Pract 204:545–552
9. Siriaunkgul S, Suwiwat S, Settakorn J et al (2008) HPV genotyping in cervical cancer in northern Thailand: adapting the linear array HPV assay for use on paraffin-embedded tissue. Gynecol Oncol 108:555–560
10. zur Hausen H (2002) Papillomavirus and cancer: from basic studies to clinical application. Nat Rev Cancer 2:342–350
11. zur Hausen H (2009) Papillomaviruses in the causation of human cancers—a brief historical account. Virology 384:260–265
12. Syrjänen K, Syrjänen S, Lamberg M et al (1983) Morphological and immunohistochemical evidence suggesting human papillomavirus (HPV) involvement in oral squamous cell carcinogenesis. Int J Oral Surg 12:418–424
13. de Villiers E, Weiddauer H, Otto H et al (1985) Papillomavirus DNA in human tongue carcinomas. Int J Cancer 36:575–578

14. Löning T, Ikenberg H, Becker J et al (1985) Analysis of oral papillomas, leukoplakias, and invasive carcinomas for human papillomavirus type related DNA. J Invest Dermatol 84:417–420
15. Glombitza F, Guntinas-Lichius O, Petersen I (2010) HPV status in head and neck tumors. Pathol Res Pract 206:229–234
16. Novakova V, Laco J (2008) Role of human papillomavirus in carcinogenesis of head and neck cancer. Klin Onkol 21:141–148 [in Czech]
17. Gillison ML (2004) Human papillomavirus-associated head and neck cancer is a distinct epidemiologic, clinical, and molecular entity. Semin Oncol 31:744–754
18. Swartz SM, Daling JR, Doody DR et al (1998) Oral cancer risk in relation to sexual history and evidence of human papillomavirus infection. J Natl Cancer Inst 90:1626–1636
19. Cruz IB, Snijders PJ, Steenbergen RD et al (1996) Age-dependence of human papillomavirus DNA presence in oral squamous cell carcinomas. Eur J Cancer B Oral Oncol 32B:55–62
20. Smith EM, Ritchie JM, Summersgill KF et al (2004) Age, sexual behavior and human papillomavirus infection in oral cavity and oropharyngeal cancers. Int J Cancer 108:766–772
21. Koppikar P, de Villiers EM, Mulherkar R (2005) Identification of human papillomaviruses in tumors of the oral cavity in an Indian community. Int J Cancer 113:946–950
22. Tachezy R, Klozar J, Salakova M et al (2005) HPV and other risk factors of oral cavity/oropharyngeal cancer in the Czech Republic. Oral Dis 11:181–185
23. Slebos RJ, Yi Y, Ely K et al (2006) Gene expression differences associated with human papillomavirus status in head and neck squamous cell carcinomas. Clin Cancer Res 12(3Pt1):701–709
24. Weinberger PM, Yu Z, Haffty BG et al (2006) Molecular classification identifies a subset of human papillomavirus-associated oropharyngeal cancers with favourable prognosis. J Clin Oncol 24:736–747
25. Luo CW, Roan CH, Liu CJ (2007) Human papilloma viruses in oral squamous cell carcinoma and precancerous lesions detected by PCR-based gene-chip array. Int J Oral Maxillofac Surg 36:153–158
26. Chuang AY, Chuang TC, Chang S et al (2008) Presence of HPV DNA in convalescent salivary rinses is an adverse prognostic marker in head and neck squamous cell carcinoma. Oral Oncol 44:915–919
27. Simonato LE, Garcia JF, Sundefeld ML et al (2008) Detection of HPV in mouth floor squamous cell carcinoma and its correlation with clinicopathologic variables, risk factors and survival. J Oral Pathol Med 37:593–598
28. Gudleviciene Z, Smailyte G, Mickonas A et al (2009) Prevalence of human papillomavirus and other risk factors in Lithuanian patients with head and neck cancer. Oncology 76:205–208
29. Lohavanichbutr P, Houck J, Fan W et al (2009) Genomewide gene expression profiles of HPV-positive and HPV-negative oropharyngeal cancer: potential implications for treatment choices. Arch Otolaryngol Head Neck Surg 135:180–188
30. Weinberger PM, Yu Z, Kountourakis P et al (2009) Defining molecular phenotypes of human papillomavirus-associated oropharyngeal squamous cell carcinoma: validation of three class hypothesis. Otolaryngol Head Neck Surg 141:382–389
31. Luginbuhl A, Sanders M, Spiro JD (2009) Prevalence, morphology, and prognosis of human papillomavirus in tonsillar cancer. Ann Otol Rhinol Laryngol 118:742–749
32. Straetmans JM, Olthof N, Mooren JJ et al (2009) Human papillomavirus reduces the prognostic value of nodal involvement in tonsillar squamous cell carcinomas. Laryngoscope 119:1951–1957
33. Zaravinos A, Mammas IN, Sourvinos G et al (2009) Molecular detection methods of human papillomavirus (HPV). Int J Biol Markers 24:215–222
34. von Knebel Doeberitz M (2002) New markers for cervical dysplasia to visualise the genomic chaos created by aberrant oncogenic papillomavirus infection. Eur J Cancer 38:2229–2242
35. Klozar J, Kratochvil V, Salakova et al (2008) HPV status and regional metastasis in the prognosis of oral and oropharyngeal cancer. Eur Arch Otorhinolaryngol 265(Suppl 1):S75–S82

Virchows Arch (2011) 458:189–195
DOI 10.1007/s00428-010-1010-9

ORIGINAL ARTICLE

Stem cell-related proteins C-KIT, C-MYC and BMI-1 in juvenile nasopharyngeal angiofibroma—do they have a role?

Suvi Renkonen · Valtteri Häyry · Päivi Heikkilä · Ilmo Leivo · Caj Haglund · Antti A. Mäkitie · Jaana Hagström

Received: 1 October 2010 / Revised: 3 November 2010 / Accepted: 7 November 2010 / Published online: 27 November 2010
© Springer-Verlag 2010

Abstract Juvenile nasopharyngeal angiofibroma (JNA) is a highly vascular tumour, occuring almost exclusively in adolescent males. Histogenesis of JNA remains unclear, two optional theories proposing either fibrous or vascular tissue as the tissue of origin. Stem cell-related proteins have been discussed to possibly participate in the growth of these tumours. In our study, we reviewed retrospective clinicopathological data of 26 JNA patients. By immunohistochemistry, we investigated the cellular distribution and expression levels of stem cell-related proteins C-KIT, C-MYC and BMI-1 and their correlation with cell and vessel density of the tumour. Contrary to earlier reports, we detected C-KIT expression in addition to stromal cells also in endothelial cells. The C-KIT expression was more dominant in slit vessels than large vessels. A significant correlation was found between endothelial immunoexpression of C-KIT and cellular density of the tumour. C-MYC and BMI-1 expression was detected in stromal cells only. Due to our finding of C-KIT expression in both stromal and endothelial cells and the strong correlation between the endothelial C-KIT expression and cellular density, we suggest that, besides the stromal tissue, the vascular component might take part in the neoplastic growth of JNA.

Keywords Immunohistochemistry · Head and neck · Neoplasm

Mäkitie and Hagström equally contributed to this work

S. Renkonen · V. Häyry · A. A. Mäkitie
Department of Otorhinolaryngology, Head and Neck Surgery, Helsinki University Central Hospital, Helsinki, Finland

P. Heikkilä · I. Leivo · C. Haglund · J. Hagström
Department of Pathology, Haartman Institute and HusLab, University of Helsinki, Helsinki University Central Hospital, Helsinki, Finland

C. Haglund
Department of Surgery, Helsinki University Central Hospital, Helsinki, Finland

J. Hagström
Department of Oral Pathology, Helsinki University, Helsinki, Finland

J. Hagström (✉)
Department of Pathology, Haartman Institute, University of Helsinki, P.O. Box 21, FI-00041, Helsinki, Finland
e-mail: jaana.hagstrom@helsinki.fi

Introduction

Juvenile nasopharyngeal angiofibroma (JNA) is a rare, histologically benign, highly vascular tumour, originating in the nasopharynx and affecting almost exclusively male adolescents. It is approximated that JNA accounts for 0.5% of all head and neck neoplasms, and it is considered to be the most common benign neoplasm of the nasopharynx [1–5]. This nonencapsulated fibrous tumour has rich vasculature, and despite its benign nature, it is locally destructive. Surgical excision is the treatment of choice for these tumours. However, recurrence rates as high as 50% (range 6–50%) have been reported [5–9].

JNA is composed of a fibrous stroma, rich in collagen and fibroblasts, and numerous blood vessels of different calibres. Vessels are slit or dilated, and organized in clusters [10, 11], and the muscular lining normally seen in blood vessels is incomplete in larger vessels, and totally absent in smaller channels. Neither tumour initiation nor its development is well known, and it has even been suggested that JNA is not a true neoplasm [11, 12]. Efforts to determine

the pathogenesis of the tumour have been done by studying the expression of various growth factors, i.e. vascular endothelial growth factor (VEGF), transforming growth factor (TGF), insulin-like growth factor (IGF) and platelet-derived growth factor (PDGF) [11, 13–18]. Most of these are suggested to be related to stromal or vascular growth and to correlate with high vessel density [11, 14, 19]. Also, oncogenes C-KIT and C-MYC have been discussed to possibly participate in the growth and promotion of JNA [13, 18, 20]. However, their role remains unclear.

CD117, also known as C-KIT, is a type III receptor tyrosine kinase that belongs to the family of PDGF receptors (PDGFRs). Activation of C-KIT leads to the activation of numerous transcription factors regulating, e.g. apoptosis, cell differentiation, proliferation, chemotaxis and cell adhesion [21–24]. C-KIT is essential in regulating the developement of stem cells, germ cells, melanocytes, and peristalsis regulating Cajal cells in the gastrointestinal tract [22, 25–27]. Overexpression of C-KIT has been found in many malignant solid tumours [28–31], and interestingly, aberrant C-KIT overexpression is also found in the tumour vasculature of many types of malignancies [32]. C-KIT expression in benign tumours is less studied, and it is suggested to be mostly absent in benign neoplasms [33]. However, moderate to strong immunopositivity for C-KIT has been found in salivary gland adenomas and in angiomyofibroblastomas of male genital tract [28, 32, 34].

C-MYC is a proto-oncogene, taking part in many cellular processes, such as proliferation, differentiation and apoptosis by activating many other genes [35–38]. It has a central role in cell-cycle progression and also a potent angiogenic activity [38, 39]. Its overexpression is associated with many malignant neoplasms, such as breast and colon carcinomas, osteosarcomas and melanomas [36, 40, 41]. Numerous studies have shown that *C-MYC* gene amplification is associated with advanced stage of the disease [38, 39, 41]. The few studies trying to demonstrate C-MYC expression in benign tumours have been negative [42, 43].

BMI-1 is an epigenetic regulator required to maintain the transcriptionally repressed state of many genes through methylation and acetylation of chromatin and histones [44]. Thus, it maintains the primitive state of tissue stem cells and maintains stem cell self-renewal [45–48]. BMI-1 regulates genes involved in cell cycle and cell differentiation, notably Rb and p53, and therefore can function as a potent oncogene [49–51]. BMI-1 is overexpressed in many malignant neoplasms, and this overexpression is found to correlate with poor prognosis. On the other hand, in some tumours, lack of BMI-1 expression has been found to correlate with a high recurrence rate [50–53].

Both BMI-1 and C-MYC are capable of immortalising certain cells in vitro and these factors converge on the same pathways, since C-MYC signalling can influence BMI-1 activity and vice versa [54–56].

In this study, we analysed the expression and cellular distribution of C-KIT, C-MYC and BMI-1 in a series of JNAs, in order to investigate their potential role in the pathogenesis of this neoplasm.

Materials and methods

Patients

Retrospective clinicopathological data of 26 patients diagnosed with a histologically verified JNA between 1970 and 2008 at the Helsinki University Central Hospital (HUCH), Helsinki, Finland were reviewed. The referral area of this tertiary care academic institution currently covers an area of approximately 1.5 million people. Surgical and discharge registries of the hospital as well as the database of the Department of Pathology were used to identify the patients. All patients (n=26, 100%) had undergone surgical resection of the primary tumour. The overall recurrence rate was 38.4% (n=10) and the recurrence was discovered on average 10.5 months (range 3–19 months) after the first operation. The median follow-up time was 106 months (range 2–360 months). At the last follow-up visit, all patients remained either free of disease without evidence of recurrence (n=19, 73%) or were alive with minimal signs of persistent disease (n=6, 23%), but without evidence of malignant transformation. The management and outcome of these patients is described in detail in our previous work, where we found a statistically significant correlation between the vascular density of the tumour and the need of resurgery due to persistent and growing recurrence [57].

Tissue samples, cell and vascular density

We used 26 formalin-fixed and paraffin-embedded JNA samples obtained from the archives of Central Pathology Department of HUSLAB. Initially these samples were achieved from the surgical operation, when tumours were removed for the primary diagnosis. We scored the samples for cell number per mm^2 and from these calculated the mean cell density. For vessel density analysis, vessels marked by CD31 were counted per mm^2 and the mean counts were calculated (Table 1). All CD31 positive vessels were included in this counting, and at this point, no separation between smaller and larger vessels was made.

Immunohistochemistry

For immunohistochemistry, formalin-fixed and paraffin-embedded samples were cut into 4-μm-thick sections,

Table 1 Cellular and vascular densities of JNA samples

Patient	Cell number (×60)/mm^2	Vessels (×20)/mm^2
No. 1	443.0	148.0
No. 2	331.0	150.0
No. 3	470.0	174.0
No. 4	56.0	34.0
No. 5	284.0	75.0
No. 6	14.0	8.0
No. 7	307.0	54.0
No. 8	149.0	66.0
No. 9	214.0	264.0
No. 10	350.0	67.0
No. 11	347.0	193.0
No. 12	397.0	114.0
No. 13	383.0	39.0
No. 14	322.0	57.0
No. 15	387.0	32.0
No. 16	346.0	198.0
No. 17	252.0	202.0
No. 18	103.0	64.0
No. 19	656.0	182.0
No. 20	662.0	176.0
No. 21	318.0	55.0
No. 22	155.0	128.0
No. 23	264.0	174.0
No. 24	97.0	51.0
No. 25	261.0	310.0
No. 26	205.0	36.0

deparaffinized in xylene and rehydrated through a graded alcohol series. For antigen retrieval, slides were treated in a PT module (LabVision UK, UK) with Tris–HCl buffer (8.5) (for BMI-1 and C-MYC) or Tris-EDTA (for C-KIT) for 20 min at 98°C. Immunohistochemical stainings were performed in Autostainer 480 (LabVision) using Dako REAL EnVision Detection System, Peroxidase/DAB+, Rabbit/Mouse (Dako, Glostrup, Denmark). Slides were treated with 0.3% Dako REAL peroxidase-blocking solution to block endogenous peroxidase activity followed by primary antibody incubation with mouse monoclonal C-MYC (9E10) antibody (Santa Cruz, diluted 1:400 in Dako REAL Antibody Diluent, Biohit, Helsinki, Finland), mouse monoclonal BMI-1 (ab 14389) (Abcam, Cambridge, UK, 1:400) or polyclonal C-KIT (Dako A4502, 1.300) for 1 h, followed by a 30-min incubation with Dako REAL EnVision/HRP detection system, rabbit/mouse (ENV) reagent. Slides were finally visualized by Dako REAL DAB + Chromogen (Dako) for 10 min. PBS-0.04%-Tween20 washing was accomplished between each step. Slides were counterstained with Meyer's hematoxylin and mounted in mounting medium (Aquamount, BDH, Poole, UK). C-MYC and BMI-1 antibodies have been previously used in study by Hayry et al. [58] and the C-KIT antibody is commonly used in diagnostics in the HUSLAB.

Evaluation of immunostainings

All stained samples were evaluated (n=26) except for C-MYC and BMI-1 (n=25) because one biopsy sample was insufficient.

The evaluation of the immunostainings was done by two experienced pathologists (JH and PH) independently and without knowledge of the clinical data, by approximating the percentage of positive tumour cells within the tumour tissue. The whole tissue slide was evaluated. No positivity was scored as 0, up to 30% positive cells as 1 (very low), 30–50% as 2 (low), 50–80% as 3 (moderate) and over 80% as 4 (high). The scoring system is modified from Hayry et al. [58]. BMI-1 and C-MYC positivity was nuclear C-KIT was both nuclear and cytoplasmic. C-KIT was scored separately in stromal and endothelial cells.

Statistical analyses

Categorical variables were cross-tabulated and analysed using the Fisher's exact test or Spearmann correlation. We used SPSS version 15.0 software (SPSS, Chicago, IL, USA) for all statistical analyses.

Results

The cell densities varied notably between different tumour samples, from high to very low (ranged from 840 to 2,383,200 cells/mm^2; Table 1), and the amount of fibrous stroma varied as well. The vascular architecture of the samples showed vessels of different numbers, size and shape, as detected with the endothelial marker CD31 (Fig. 1). The number of blood vessels ranged between 160 and 6,200 vessels/mm^2 (median 2340; Table 1).

The expression fractions and cellular expression distribution of C-KIT, C-MYC and BMI-1 were as follows.

C-KIT

C-KIT expression was frequently present both in stromal (25/26, 96.0%) and endothelial cells (24/26, 92.3%) of JNA tissue samples. Interestingly, C-KIT expression seemed to be more dominant in slit vessels without muscular lining. Out of all 26 samples, C-KIT positivity of endothelial cells in slit vessels was seen in 23 samples (23/26, 88.5%, Fig. 1), whereas C-KIT positivity in large vessels was only seen in 14 samples (14/26, 53.8%). C-KIT expression, when present, ranged from very low to moderate frequency (Table 2, Fig. 1).

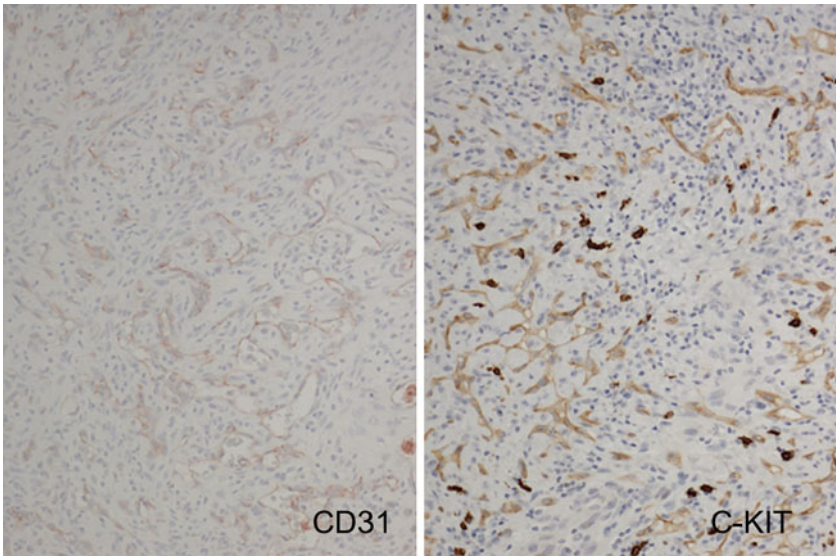

Fig. 1 CD31 and C-KIT immunostainings in slit-like vessels found in juvenile angiofibroma tissue

C-MYC

Nuclear C-MYC positivity was detected in most JNA tissue samples (21/25, 84.0%), in stromal cells (Table 2, Fig. 2). The level of C-MYC expression ranged from very low to high. Four cases (4/26, 16.0%) were totally negative for C-MYC.

BMI-1

Nuclear BMI-1 protein expression in stromal cells was detected in all JNA tissue samples analysed (25/25, 100%, Fig. 2). The frequency of BMI-1 expression levels varied from very low to high (Table 2).

Correlations to cell and vessel density

The protein expression levels of C-KIT, C-MYC and BMI-1 were compared with cell and vessel density. A significant correlation was found between the endothelial expression of C-KIT and the cell density (Spearman correlation $p=0.009$). Endothelial C-KIT protein expression was also found to correlate with stromal C-MYC protein expression (Fisher's exact test $p = 0.006$ and Spearman correlation $p = 0.005$), while there was no correlation between the C-MYC protein expression and cellular or vascular density. We found no correlation between the immunoexpression of BMI-1 and other parameters studied.

Discussion

In this study, we describe the expression of growth factor receptor C-KIT, proto-oncogene C-MYC and polycomb protein and oncogene BMI-1, in a series of 26 JNA tumours. Levels of immunoexpression are compared to cell and vascular density, within the tumours, in order to analyse their putative role in the growth and vascularisation of JNA.

The process of growth and angiogenesis of JNA still remains largely unclear, despite numerous studies trying to investigate the molecular mechanisms behind it. While most of these studies have examined the presence of growth factors [11, 14, 15, 17, 18, 20, 40, 59–61], only a few studies have discussed the role of stem cell-related proteins [13, 18, 20, 40]. In a series of 12 JNA samples, Zhang et al. [18] reported strong C-KIT expression in stromal cells only, suggested that C-KIT might have a role in the progression of JNA and concluded that stromal cells were likely to be the neoplastic component of the JNA. However, Pauli et al.

Table 2 Immunoexpression of C-KIT, C-MYC and BMI-1 in JNA samples

	Number of cases					
	Negative	Very low	Low	Moderate	High	Total
C-KIT (str)	1	3	14	8	0	26
C-KIT (en)	2	13	8	3	0	26
C-MYC	4	6	6	5	4	25[a]
BMI-1	0	5	7	5	8	25[a]

C-KIT (str) Stromal staining, *C-KIT (en)* endothelial staining

[a] For these stainings, less than 26 representative samples were available

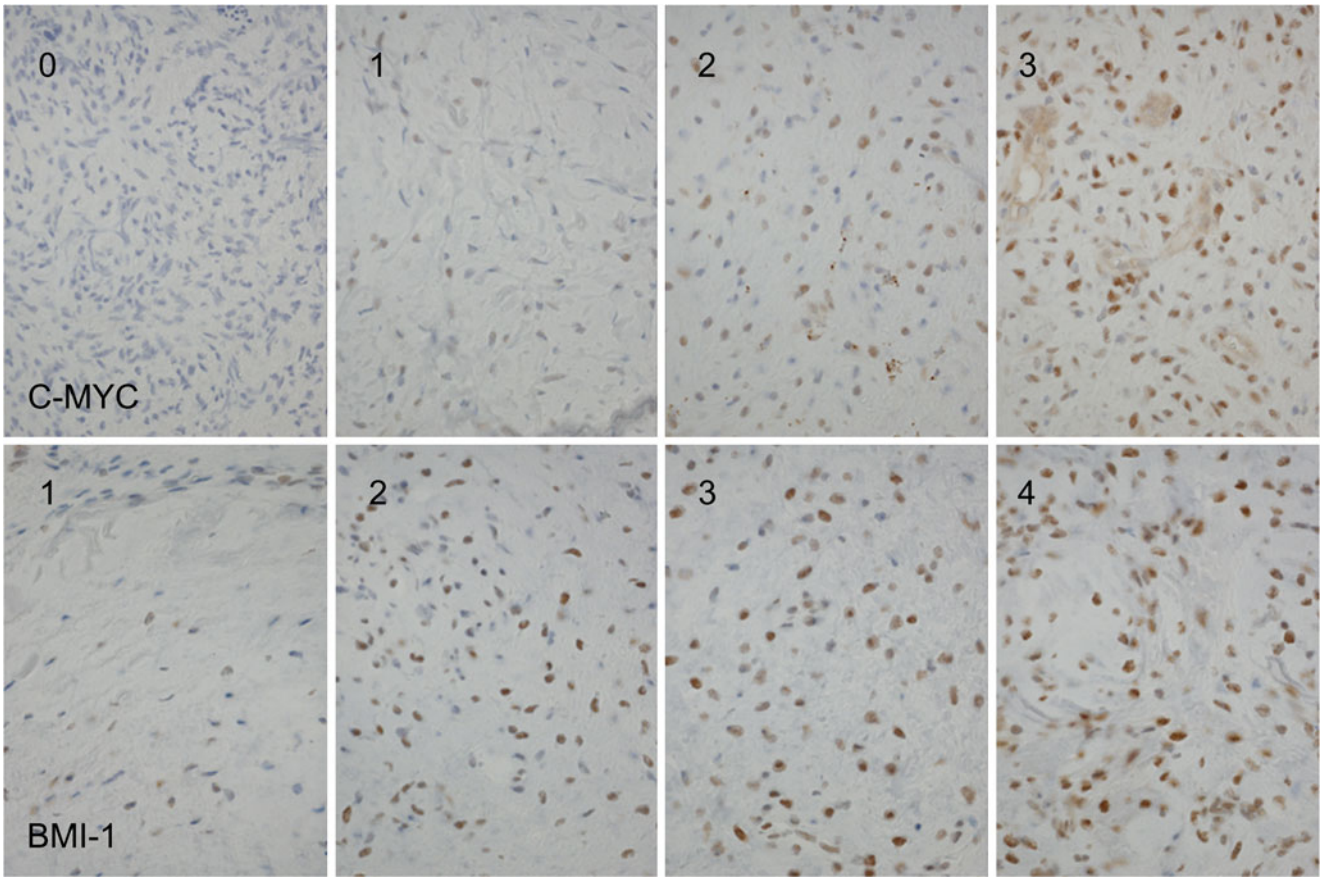

Fig. 2 C-MYC and BMI-1 immunoscoring in stroma of juvenile angiofibroma tissue. *0* No positivity, *1* very low positivity, *2* low positivity, *3* moderate positivity, and *4* high positivity

[20] evaluated the stromal cells in 52 samples of JNA and found all of them to be C-KIT negative. In our study, we found that C-KIT was expressed not only in 96% of JNA samples in stromal cells but also in 92% samples in endothelial cells, differing from earlier reports [18]. Interestingly, we also found that C-KIT expression was more dominant in slit-like vessels (23/26, 88.5%) than in larger vessels (14/26, 53.8%). A statistically significant correlation was found between the endothelial immunoexpression of C-KIT and cellular density. These results support the putative role of C-KIT in the JNA tumourigenesis and leave us with the question, if stromal cells truly are the only neoplastic component of this tumour.

In 1996, Nagai et al. [13] performed a Northern blot study on the expression of C-MYC mRNA in 25 cases of JNA but found no difference in expression compared to normal tissue. In three advanced cases of JNA, Schick et al. [40] succeeded to demonstrate that there were gains of *C-MYC*, associated with increases of C-MYC mRNA and protein expression levels, suggesting a probable role of C-MYC in the progression of JNA. C-MYC has also been thought to have a potential role in angiogenesis, inducing fibroblasts to build up an immature vascular network of leaky, unstable kind of blood vessels [62]. This observation is of great interest, because malformed, slit-like vessels are known to be a part of JNA histological architecture [10]. In the present study, C-MYC protein was expressed in 84% of stromal JNA cells, and no expression was detected in endothelial cells. Although C-MYC immunoexpression did not show any correlation to the vessel density, it had a correlation with endothelial C-KIT expression, suggesting a connection between these two markers.

Polycomb group proteins (PcGs) are epigenetic gene-silencing proteins, participating in embryonic developement and oncogenesis [46, 55, 56, 63]. *BMI-1* was the first mammalian PcG gene identified in 1991 as a C-MYC collaborator in oncogenesis [54]. Many studies have shown BMI-1 to be dysregulated in various cancer forms and to correlate with invasiveness and poor prognosis [50–53]. However, the role of BMI-1 in cancer invasion is poorly known. In our study, stromal cells frequently expressed BMI-1, which suggests that BMI-1 might be involved in the pathogenesis of JNA.

In conclusion, in our study, C-KIT immunoexpression was shown in both stromal and endothelial cells, differing from that of C-MYC and BMI-1. Endothelial cells in slit-like

vessels expressed C-KIT more abundantly than those in larger vessels. Furthermore, endothelial immunostaining of C-KIT was found to correlate with cell density, highlighting the putative role of C-KIT in JNA growth and progression. Despite the fact that the biphasic histological nature of JNA is still not understood in detail, a number of immunohistochemical studies examinining JNA growth mechanisms have suggested the stromal component to be the key neoplastic element [11, 14, 15, 17]. Based on our findings of C-KIT expression in both stromal and endothelial cells and the fact that C-KIT is known to be essential in regulating the development of stem cells and its overexpression is connected to neoplastic processes [28–31], we propose that both the stromal and the vascular component possibly take part in the neoplastic growth of JNA.

In addition, our finding that expression of endothelial C-KIT correlated with C-MYC expression, leads us to the hypothesis, that the presence of C-MYC might influence the growth of immature blood vessels via regulating the expression and effect of C-KIT on endothelial cells. Interestingly, mutations of the *C-KIT* gene and *C-MYC* amplification are known to be involved in the pathogenesis of gastrointestinal stromal tumour [64], but their role in JNA remains to be elucidated.

Acknowledgements The authors thank Päivi Peltokangas, Tuire Koski and Elina Aspiala for excellent technical assistance. This study was supported by the Sigrid Jusélius Foundation, Finska Läkaresällskapet, Medicinska Understödsföreningen Liv och Hälsa and the Helsinki University Central Hospital Research Fund, Helsinki, Finland.

Conflicts of Interest None

References

1. Doyle PJ, Riding K, Kahn K (1977) Management of nasopharyngeal angiofibroma. J Otolaryngol 6(3):224–232
2. Liang J, Yi Z, Lianq P (2000) The nature of juvenile nasopharyngeal angiofibroma. Otolaryngol Head Neck Surg 123(4):475–481
3. Mistry RC, Qureshi SS, Gupta S (2005) Juvenile nasopharyngeal angiofibroma: a single institution study. Indian J Cancer 42(1):35–39
4. Paris J, Guelfucci B, Moulin G, Zanaret M, Triglia JM (2001) Diagnosis and treatment of juvenile nasopharyngeal angiofibroma. Eur Arch Otorhinolaryngol 258(3):120–124
5. Scholtz AW, Appenroth E, Kammen-Jolly K, Scholtz LU, Thumfart WF (2001) Juvenile nasopharyngeal angiofibroma: management and therapy. Laryngoscope 111(4 Pt 1):681–687
6. Radkowski D, McGill T, Healy GB, Ohlms L, Jones DT (1996) Angiofibroma. Changes in staging and treatment. Arch Otolaryngol Head Neck Surg 122(2):122–129
7. Fagan JJ, Snyderman CH, Carrau RL, Janecka IP (1997) Nasopharyngeal angiofibromas: selecting a surgical approach. Head Neck 19(5):391–399
8. Howard DJ, Lloyd G, Lund V (2001) Recurrence and its avoidance in juvenile angiofibroma. Laryngoscope 111(9):1509–1511
9. Tyagi I, Syal R, Goyal A (2007) Recurrent and residual juvenile angiofibromas. J Laryngol Otol 121(5):460–467
10. Sennes LU, Fortes FS, Butugan O, Saldiva PH, Bernardi FC (2005) Tissue maturation correlating to clinical manifestations in juvenile angiofibroma. Ann Otol Rhinol Laryngol 114(9):705–708
11. Schuon R, Brieger J, Heinrich UR, Roth Y, Szyfter W, Mann WJ (2007) Immunohistochemical analysis of growth mechanisms in juvenile nasopharyngeal angiofibroma. Eur Arch Otorhinolaryngol 264(4):389–394
12. Hofmann T, Bernal-Sprekelsen M, Koele W, Reittner P, Klein E, Stammberger H (2005) Endoscopic resection of juvenile angiofibromas—long term results. Rhinology 43(4):282–289
13. Nagai MA, Butugan O, Logullo A, Brentani MM (1996) Expression of growth factors, proto-oncogenes, and p53 in nasopharyngeal angiofibromas. Laryngoscope 106(2 Pt 1):190–195
14. Saylam G, Yucel OT, Sungur A, Onerci M (2006) Proliferation, angiogenesis and hormonal markers in juvenile nasopharyngeal angiofibroma. Int J Pediatr Otorhinolaryngol 70(2):227–234
15. Brieger J, Wierzbicka M, Sokolov M, Roth Y, Szyfter W, Mann WJ (2004) Vessel density, proliferation, and immunolocalization of vascular endothelial growth factor in juvenile nasopharyngeal angiofibromas. Arch Otolaryngol Head Neck Surg 130(6):727–731
16. Ngan BY, Forte V, Campisi P (2008) Molecular angiogenic signaling in angiofibromas after embolization: Implications for therapy. Arch Otolaryngol Head Neck Surg 134(11):1170–1176
17. Dillard DG, Cohen C, Muller S, Del Gaudio J, Reichman O, Parrish B, Rackley D, Gal AA (2000) Immunolocalization of activated transforming growth factor beta1 in juvenile nasopharyngeal angiofibroma. Arch Otolaryngol Head Neck Surg 126 (6):723–725
18. Zhang PJ, Weber R, Liang HH, Pasha TL, LiVolsi VA (2003) Growth factors and receptors in juvenile nasopharyngeal angiofibroma and nasal polyps: an immunohistochemical study. Arch Pathol Lab Med 127(11):1480–1484
19. Coutinho-Camillo CM, Brentani MM, Nagai MA (2008) Genetic alterations in juvenile nasopharyngeal angiofibromas. Head Neck 30(3):390–400
20. Pauli J, Gundelach R, Vanelli-Rees A, Rees G, Campbell C, Dubey S, Perry C (2008) Juvenile nasopharyngeal angiofibroma: an immunohistochemical characterisation of the stromal cell. Pathology 40(4):396–400
21. Besmer P, Murphy JE, George PC, Qiu FH, Bergold PJ, Lederman L, Snyder HW Jr, Brodeur D, Zuckerman EE, Hardy WD (1986) A new acute transforming feline retrovirus and relationship of its oncogene v-kit with the protein kinase gene family. Nature 320 (6061):415–421
22. Miettinen M, Lasota J (2005) Kit (cd117): a review on expression in normal and neoplastic tissues, and mutations and their clinicopathologic correlation. Appl Immunohistochem Mol Morphol 13(3):205–220
23. Roskoski R Jr (2005) Structure and regulation of kit protein-tyrosine kinase—the stem cell factor receptor. Biochem Biophys Res Commun 338(3):1307–1315
24. Roskoski R Jr (2005) Signaling by kit protein-tyrosine kinase—the stem cell factor receptor. Biochem Biophys Res Commun 337(1):1–13
25. Al-Muhsen SZ, Shablovsky G, Olivenstein R, Mazer B, Hamid Q (2004) The expression of stem cell factor and c-kit receptor in human asthmatic airways. Clin Exp Allergy 34(6):911–916
26. Alexeev V, Yoon K (2006) Distinctive role of the ckit receptor tyrosine kinase signaling in mammalian melanocytes. J Invest Dermatol 126(5):1102–1110
27. Tsuura Y, Hiraki H, Watanabe K, Igarashi S, Shimamura K, Fukuda T, Suzuki T, Seito T (1994) Preferential localization of c-kit product in tissue mast cells, basal cells of skin, epithelial cells of breast, small cell lung carcinoma and seminoma/dysgerminoma in human: Immunohistochemical study on formalin-fixed, paraffin-embedded tissues. Virchows Arch 424 (2):135–141

28. Andreadis D, Epivatianos A, Poulopoulos A, Nomikos A, Papazoglou G, Antoniades D, Barbatis C (2006) Detection of c-kit (cd117) molecule in benign and malignant salivary gland tumours. Oral Oncol 42(1):57–65
29. Bociek RG (2005) Adult burkitt's lymphoma. Clin Lymphoma 6 (1):11–20
30. Chan JK (1999) Mesenchymal tumors of the gastrointestinal tract: a paradise for acronyms (stump, gist, gant, and now gipact), implication of c-kit in genesis, and yet another of the many emerging roles of the interstitial cell of cajal in the pathogenesis of gastrointestinal diseases? Adv Anat Pathol 6(1):19–40
31. Kitamura Y, Hirotab S (2004) Kit as a human oncogenic tyrosine kinase. Cell Mol Life Sci 61(23):2924–2931
32. Sihto H, Tynninen O, Butzow R, Saarialho-Kere U, Joensuu H (2007) Endothelial cell kit expression in human tumours. J Pathol 211(4):481–488
33. Huber AR, Shikle JF (2009) Benign fibroblastic polyps of the colon. Arch Pathol Lab Med 133(11):1872–1876
34. Chatelain D, Lazure T, Manaouil D, Homsi T, Ganansia R, Cordonnier C, Sevestre H (2005) angiomyofibroblastoma of the male genital tract. Pathological and immunohistochemical study of three cases. Ann Pathol 25(1):58–62
35. Cole MD, Cowling VH (2008) Transcription-independent functions of myc: regulation of translation and DNA replication. Nat Rev Mol Cell Biol 9(10):810–815
36. Guney I, Sedivy JM (2006) Cellular senescence, epigenetic switches and c-myc. Cell Cycle 5(20):2319–2323
37. Morrish F, Isern N, Sadilek M, Jeffrey M, Hockenbery DM (2009) C-myc activates multiple metabolic networks to generate substrates for cell-cycle entry. Oncogene 28(27):2485–2491
38. Pelengaris S, Khan M, Evan G (2002) C-myc: More than just a matter of life and death. Nat Rev Cancer 2(10):764–776
39. Vora HH, Shah NG, Trivedi TI, Goswami JV, Shukla SN, Shah PM (2007) Expression of c-myc mrna in squamous cell carcinoma of the tongue. J Surg Oncol 95(1):70–78
40. Schick B, Wemmert S, Jung V, Steudel WI, Montenarh M, Urbschat S (2006) Genetic heterogeneity of the myc oncogene in advanced juvenile angiofibromas. Cancer Genet Cytogenet 164(1):25–31
41. Gil J, Kerai P, Lleonart M, Bernard D, Cigudosa JC, Peters G, Carnero A, Beach D (2005) Immortalization of primary human prostate epithelial cells by c-myc. Cancer Res 65(6):2179–2185
42. Manjarrez ME, Ocadiz R, Valle L, Pacheco C, Marroquin A, De la Torre C, Selman M, Gariglio P (2006) Detection of human papillomavirus and relevant tumor suppressors and oncoproteins in laryngeal tumors. Clin Cancer Res 12 (23):6946–6951
43. Corzo C, Corominas JM, Tusquets I, Salido M, Bellet M, Fabregat X, Serrano S, Sole F (2006) The myc oncogene in breast cancer progression: from benign epithelium to invasive carcinoma. Cancer Genet Cytogenet 165(2):151–156
44. Spivakov M, Fisher AG (2007) Epigenetic signatures of stem-cell identity. Nat Rev Genet 8(4):263–271
45. Iwama A, Oguro H, Negishi M, Kato Y, Morita Y, Tsukui H, Ema H, Kamijo T, Katoh-Fukui Y, Koseki H, van Lohuizen M, Nakauchi H (2004) Enhanced self-renewal of hematopoietic stem cells mediated by the polycomb gene product BMI-1. Immunity 21(6):843–851
46. Lao TT, Chan BC, Leung WC, Ho LF (2004) Postpartum anemia unrelated to maternal prepregnancy bmi. Obes Res 12(11):1903–1904; author reply 1904–1905
47. van der Lugt NM, Domen J, Linders K, van Roon M, Robanus-Maandag E, te Riele H, van der Valk M, Deschamps J, Sofroniew M, van Lohuizen M et al (1994) Posterior transformation, neurological abnormalities, and severe hematopoietic defects in mice with a targeted deletion of the BMI-1 proto-oncogene. Genes Dev 8(7):757–769
48. Molofsky AV, Pardal R, Iwashita T, Park IK, Clarke MF, Morrison SJ (2003) BMI-1 dependence distinguishes neural stem cell self-renewal from progenitor proliferation. Nature 425 (6961):962–967
49. Dimri GP, Martinez JL, Jacobs JJ, Keblusek P, Itahana K, Van Lohuizen M, Campisi J, Wazer DE, Band V (2002) The BMI-1 oncogene induces telomerase activity and immortalizes human mammary epithelial cells. Cancer Res 62 (16):4736–4745
50. Song LB, Zeng MS, Liao WT, Zhang L, Mo HY, Liu WL, Shao JY, Wu QL, Li MZ, Xia YF, Fu LW, Huang WL, Dimri GP, Band V, Zeng YX (2006) BMI-1 is a novel molecular marker of nasopharyngeal carcinoma progression and immortalizes primary human nasopharyngeal epithelial cells. Cancer Res 66(12):6225–6232
51. Kim JH, Yoon SY, Kim CN, Joo JH, Moon SK, Choe IS, Choe YK, Kim JW (2004) The BMI-1 oncoprotein is overexpressed in human colorectal cancer and correlates with the reduced p16ink4a/p14arf proteins. Cancer Lett 203(2):217–224
52. Wang H, Pan K, Zhang HK, Weng DS, Zhou J, Li JJ, Huang W, Song HF, Chen MS, Xia JC (2008) Increased polycomb-group oncogene BMI-1 expression correlates with poor prognosis in hepatocellular carcinoma. J Cancer Res Clin Oncol 134(5):535–541
53. Hayry V, Tynninen O, Haapasalo HK, Wolfer J, Paulus W, Hasselblatt M, Sariola H, Paetau A, Sarna S, Niemela M, Wartiovaara K, Nupponen NN (2008) Stem cell protein BMI-1 is an independent marker for poor prognosis in oligodendroglial tumours. Neuropathol Appl Neurobiol 34(5):555–563
54. van Lohuizen M, Frasch M, Wientjens E, Berns A (1991) Sequence similarity between the mammalian BMI-1 proto-oncogene and the *Drosophila* regulatory genes psc and su(z)2. Nature 353(6342):353–355
55. Haupt Y, Bath ML, Harris AW, Adams JM (1993) BMI-1 transgene induces lymphomas and collaborates with myc in tumorigenesis. Oncogene 8(11):3161–3164
56. Levy LS, Lobelle-Rich PA, Overbaugh J (1993) Flvi-2, a target of retroviral insertional mutagenesis in feline thymic lymphosarcomas, encodes BMI-1. Oncogene 8(7):1833–1838
57. Renkonen S, Hagstrom J, Vuola J, Niemela M, Porras M, Kivivuori SM, Leivo I, Makitie AA (2010) The changing surgical management of juvenile nasopharyngeal angiofibroma. Eur Arch Otorhinolaryngol 22:172–175
58. Hayry V, Makinen LK, Atula T, Sariola H, Makitie A, Leivo I, Keski-Santti H, Lundin J, Haglund C, Hagstrom J (2010) BMI-1 expression predicts prognosis in squamous cell carcinoma of the tongue. Br J Cancer 102(5):892–897
59. Abraham SC, Montgomery EA, Giardiello FM, Wu TT (2001) Frequent beta-catenin mutations in juvenile nasopharyngeal angiofibromas. Am J Pathol 158(3):1073–1078
60. Duerr S, Wendler O, Aigner T, Karosi S, Schick B (2008) Metalloproteinases in juvenile angiofibroma—a collagen rich tumor. Hum Pathol 39(2):259–268
61. Ponti G, Losi L, Pellacani G, Rossi GB, Presutti L, Mattioli F, Villari D, Wannesson L, Alicandri Ciufelli M, Izzo P, De Rosa M, Marone P, Seidenari S (2008) Wnt pathway, angiogenetic and hormonal markers in sporadic and familial adenomatous polyposis-associated juvenile nasopharyngeal angiofibromas (JNA). Appl Immunohistochem Mol Morphol 16(2):173–178
62. Evan GI, Vousden KH (2001) Proliferation, cell cycle and apoptosis in cancer. Nature 411(6835):342–348
63. Martin EC, Adler PN (1993) The polycomb group gene posterior sex combs encodes a chromosomal protein. Development 117 (2):641–655
64. Yang J, Du X, Lazar AJ, Pollock R, Hunt K, Chen K, Hao X, Trent J, Zhang W (2008) Genetic aberrations of gastrointestinal stromal tumors. Cancer 113(7):1532–1543

Virchows Arch (2011) 458:197–203
DOI 10.1007/s00428-010-1012-7

ORIGINAL ARTICLE

MDM2 gene amplification and protein expressions in colon carcinoma: is targeting MDM2 a new therapeutic option?

Monirath Hav · Louis Libbrecht · Liesbeth Ferdinande · Piet Pattyn · Stephanie Laurent · Marc Peeters · Marleen Praet · Patrick Pauwels

Received: 14 May 2010 / Revised: 29 September 2010 / Accepted: 11 November 2010 / Published online: 27 November 2010
© Springer-Verlag 2010

Abstract The aim of this study was to investigate murine double minute-2 (MDM2) gene copy number changes in colon carcinoma and to correlate these findings with an immunohistochemical analysis of MDM2 protein expression and histopathologic prognostic indicators of the tumors. The study included 80 cases of sporadic colon carcinomas. MDM2 protein expression was assessed by immunohistochemistry, and MDM2 gene status by fluorescence in situ hybridization. MDM2 gene amplification was detected in 18% of the 80 cases examined. A strong correlation was found between MDM2 gene amplification and the presence, intensity, and staining proportion of cytoplasmic MDM2 protein expression ($p=0.01$). No correlation was found between MDM2 gene amplification and the well-established histopathologic prognostic factors. Given the correlation with gene amplification, we clearly demonstrated that cytoplasmic expression of MDM2 protein is true and relevant and that this finding has to be taken into account when immunohistochemistry would be used as a screening for MDM2 gene amplification in the near future. Targeting MDM2 could be a new approach in colon cancer therapy. The amplification status could be a predictive factor of the response to MDM2-targeted therapy.

Keywords MDM2 · MDM2 protein expression · MDM2 gene amplification · MDM2 in colon carcinoma · Colon carcinoma · Targeted treatment in colon carcinoma

M. Hav (✉) · L. Libbrecht · L. Ferdinande · M. Praet · P. Pauwels
Department of Pathology,
Ghent University Hospital,
De Pintelaan 185,
9000 Ghent, Belgium
e-mail: hav_monirath@yahoo.com

P. Pattyn
Department of Gastrointestinal Surgery,
Ghent University Hospital,
De Pintelaan 185,
9000 Ghent, Belgium

S. Laurent · M. Peeters
Department of Gastrointestinal Oncology,
Ghent University Hospital,
De Pintelaan 185,
9000 Ghent, Belgium

Introduction

The p53 tumor suppressor protein is a transcription factor that is activated in response to cellular stress. Depending on the severity of the threat to genome integrity, p53 then imposes cell-cycle arrest or apoptosis [1–4]. Because p53 has strong growth-suppressive activity, it must be tightly regulated to allow normal cells to function. This is achieved to a large extent by a protein known as murine double minute-2 (MDM2), it is so called because its gene function was first discovered in DNA associated with paired acentric chromatin bodies, termed double minutes, in spontaneously transformed mouse 3T3 fibroblasts. The functions of p53 are ablated in cancer to avoid apoptosis, which can be achieved through mutation or deletion of the TP53 gene, but also by alteration of the MDM2 function. One example of MDM2 alteration is overexpression, which is found in 7% of cancers. MDM2 overexpression due to gene amplification is especially frequent in sarcomas [5]. Reports in the literature on MDM2 gene status in colon cancer are controversial. Apart from one recent study, which was

mainly based on PCR/ligase detection of MDM2 gene status, most studies could not demonstrate amplification in colon carcinoma [5, 6]. In our fluorescence in situ hybridization (FISH) study, however, we found a significant proportion of cases with MDM2 amplification. Another interesting finding is the correlation of MDM2 amplification with cytoplasmic overexpression of MDM2 protein. These findings could change the therapeutic strategy in a certain subset of colon cancer patients. To our knowledge, this is the first study to examine MDM2 status by FISH in a large series of formalin-fixed, paraffin-embedded colon carcinomas.

Materials and methods

Tissue

Our study was conducted on 80 sporadic colon carcinomas which included 69 cases retrieved from the archives and 11 cases that were sent for K-ras mutation analyses, at Pathology department of Ghent University Hospital between 2006 and 2009. These latter 11 cases did not include information on the pathological stage and histopathologic features. The other 69 tumors were classified according to TNM sixth edition [7]. The patients' data and histopathologic characteristics of the tumors are summarized in Table 1.

Table 1 Patient data and tumor characteristics

	No. (%)
Sex	80
Male	45 (56%)
Female	35 (44%)
Median age (years) (range)	72 (29–90)
TNM stage	
T stage	69
T1	1 (1%)
T2	7 (10%)
T3	41 (59%)
T4	20 (30%)
N stage	69
N0	36 (52%)
N1	23 (33%)
N2	10 (15%)
Differentiation	69
Good	7 (10%)
Moderate	43 (62%)
Poor	19 (28%)
Lympho-vascular invasion	69
Present	29 (42%)
Absent	40 (58%)
Perineural invasion	69
Present	12 (17%)
Absent	57 (83%)

Immunohistochemistry

Immunohistochemical staining for MDM2 was performed on formalin-fixed, paraffin-embedded material using a standardized and automated immunostainer (Nexes; Ventana Medical Systems, Tucson, AZ). Four-micrometer-thick sections were deparaffinized in a series of graded alcohol and microwaved in EDTA buffer for 2×10 min at 450 W. After cooling to room temperature and rinsing with Tris buffer, endogenous peroxidase was blocked by preincubation of the slides with 0.3% H_2O_2, followed by incubation with anti-MDM2 antibody (Dilution, SMP-14; DAKO, Hamburg, Germany) in an immunostainer. IgG2b-stained sections were used as negative controls, and sections from dedifferentiated liposarcoma were used as positive controls. MDM2 protein expression was assessed by a single pathologist (MH). Nuclear staining was recorded separately from cytoplasmic staining. For each staining pattern, MDM2 expression was evaluated based on staining intensity and proportion of positive tumor cells, the latter by calculating the percentage of stained cells in 30 high-power fields. We classified MDM2 expression into three different staining intensities, namely weak, moderate, and strong. In cases where variable staining intensities were noticed, possibly due to tumor heterogeneity, the predominant staining intensity determined the overall intensity of MDM2 expression in the tumors.

MDM2 amplification

MDM2 gene amplification status was detected by dual-color FISH. The FISH assay was performed on all the 80 colon tumors according to established laboratory protocol by using Poseidon repeat-free fluorescent-labeled DNA probes specific for MDM2 (12q15) and probes specific for the centromeric region of chromosome 12 (KREATECH Diagnostics, Amsterdam, The Netherlands). The MDM2 FISH assays were scored blindly by counting a minimum of 20 nuclei per case at ×100 magnification with a DAPI/Green/Red triple band pass filter. Only nuclei with at least two CEP12 signals were evaluated to minimize nuclear truncation artifact, and overlapping tumor nuclei were excluded from evaluation to decrease false-positive scoring. The average number of MDM2 and CEP12 signals was then determined and a MDM2/CEP12 ratio was calculated for each case. A ratio of more than 2.0 was considered amplified for the MDM2 gene, whereas a ratio of less than 2.0 was considered nonamplified. A ratio of less than 2.0 with ≥2 signals of both probes was considered polysomic for chromosome 12.

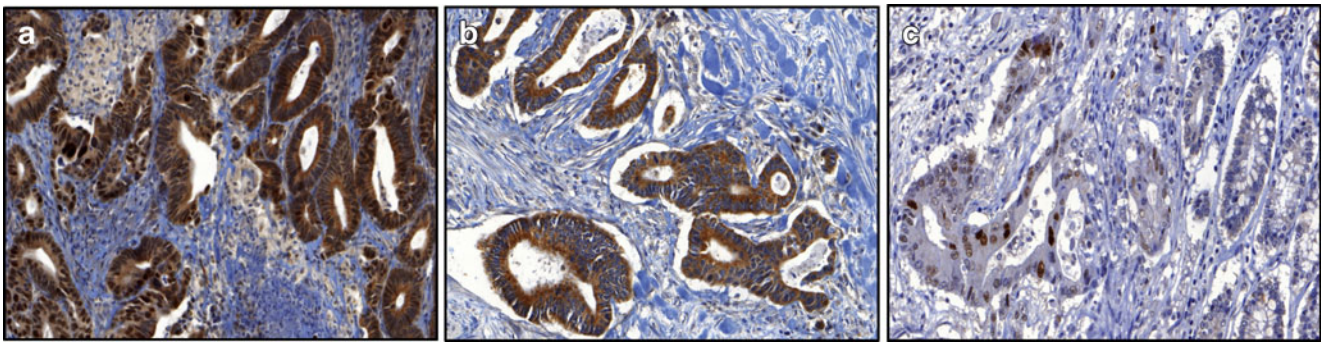

Fig. 1 **a** Case with both nuclear and cytoplasmic MDM2 expression (×10 magnification); **b** case with only cytoplasmic MDM2 expression (×20 magnification); **c** case with only nuclear MDM2 expression (×20 magnification)

Statistical evaluation

The significance of associations between MDM2 gene amplification status, protein expression, and histopathologic features was measured statistically with Chi-squared and Mann–Whitney test, when appropriate. Statview 5.0.1 statistical software system (SAS Institute, Inc., Cary, NC) was used. A probability value of less than 0.05 was considered significant.

Results

MDM2 protein expression

Of the 80 tumors, nuclear MDM2 expression was seen in 18 cases (23%), whereas cytoplasmic expression was present in 29 cases (36%). Only seven cases (11%) showed both nuclear and cytoplasmic MDM2 expression. The different patterns of MDM2 protein expression are illustrated in Fig. 1. We observed an inverse correlation between MDM2 nuclear expression and differentiation grade of the tumors (p=0.03). Tables 2 and 3 summarize the different expression patterns of MDM2 protein and their correlation with histopathologic prognostic factors.

MDM2 gene amplification

FISH analyses revealed that 14 (18%) out of 80 colon carcinomas showed MDM2 gene amplification (Fig. 2). This amplification significantly correlated with the presence, intensity and staining proportion of cytoplasmic expression of MDM2 protein (Table 4). No association was found between MDM2 gene amplification and any of the major histopathologic prognostic parameters (Table 5).

Discussion

Proper p53 control is critical for its tumor suppressive function. Under homeostatic conditions, p53 is maintained at low levels by MDM2, which catalyzes p53 ubiquitination, marking it for degradation by the proteasome [8, 9]. MDM2 also binds and inhibits the p53 transcriptional activation domain [10]. The importance of MDM2 in p53 regulation was shown in vivo by the lethality of MDM2−/− embryos at 3.5 days post coitum whereas p53−/−MDM2−/− mice develop without abnormalities [11, 12]. Deletion of MDM2 in vivo results in apoptosis. In cancer, inactivation of the tumor suppression function of p53 can be achieved by different mechanisms.

Table 2 MDM2 protein expressions in the 80 colon carcinoma

	MDM2 expression patterns			
	Number of cases	Nuclear (%)	Number of cases	Cytoplasmic (%)
MDM2 expression	80		80	
Positive		18 (23%)		29 (36%)
Negative		62 (77%)		51 (64%)
Mean proportion of tumor cells stained	(%)	4.87%		18.62%
	(range)	(0–70%)		(0–100%)
Staining intensity	18		30	
Weak		2 (11%)		17 (57%)
Moderate to strong		16 (89%)		13 (43%)

Table 3 Correlation between MDM2 protein expressions and histopathologic paramenters

	Number of cases	Nuclear expression			Cytoplasmic expression		
		Positive (%)	Negative (%)	*p* value	Positive (%)	Negative (%)	*p* value
TNM stage				0.55			0.27
I	7	3 (43%)	4 (57%)		1 (14%)	6 (86%)	
II	27	5 (19%)	22 (81%)		6 (22%)	21 (78%)	
III	25	5 (20%)	20 (80%)		9 (36%)	16 (64%)	
IV	10	2 (20%)	8 (80%)		5 (50%)	5 (50%)	
Differentiation				0.03[a]			0.23
Good	7	4 (57%)	3 (43%)		2 (29%)	5 (71%)	
Moderate	43	6 (14%)	37 (86%)		16 (37%)	27 (63%)	
Poor	19	5 (26%)	14 (74%)		3 (16%)	16 (84%)	
LV invasion				0.68			0.24
Present	29	7 (24%)	22 (76%)		11 (38%)	18 (62%)	
Absent	40	8 (20%)	32 (80%)		10 (25%)	30 (75%)	
PN invasion				0..21			0.10
Present	12	1 (8%)	11 (92%)		6 (50%)	6 (50%)	
Absent	57	14 (25%)	43 (75%)		15 (26%)	42 (74%)	

LV lympho-vascular; *PN* perineural

[a] Significance value

Mutational inactivation of p53 occurs frequently. Loss of p53 function also occurs by overexpression of MDM2. This can result from small nucleotide polymorphisms (SNPs) in the MDM2 gene. Bond et al. showed that, in cell culture, SNP309 in the promoter of the MDM2 gene increased the binding affinity of the transcriptional activator Sp1, resulting in high levels of MDM2 RNA and protein [13]. A novel role of the MDM2 SNP309 locus in regulating pancreatic ductal adenocarcinoma formation has recently been suggested and described by Grochola et al. [14]. MDM2 protein overexpression can also be due to gene amplification and the concomitant appearance of double minutes, hence the name murine double minute [15]. MDM2 gene amplification has been described in different tumors, such as well and dedifferentiated liposarcoma. In fact, more than 95% of these tumors show MDM2 amplification [16]. MDM2 gene amplification has also been reported in glioma, osteosarcoma, hematological malignancies, and carcinomas such as non-small cell lung cancer [5, 17].

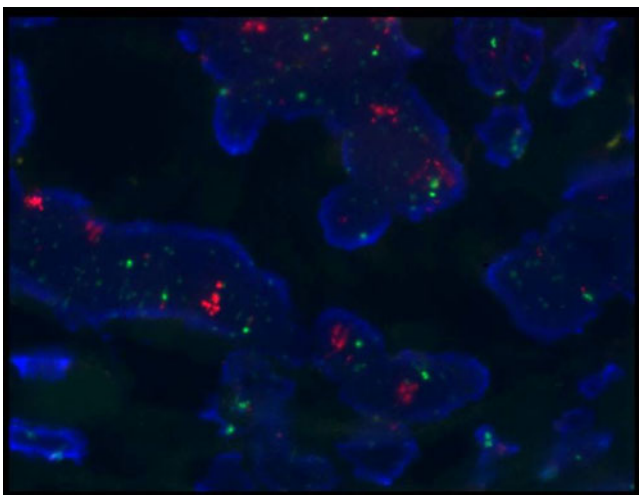

Fig. 2 Representative photomicrograph of the dual-color FISH analysis of MDM2 gene (*red*) and centromere 12 (*green*) in a paraffine section of one of our colon carcinoma cases, showing MDM2 amplifciation with clusters of MDM2 gene copies

In our study of colon carcinoma, we found MDM2 amplification in 18% of our cases, which is 9% higher than previously reported [6]. This might be explained by the use of different methodoligies (FISH vs qPCR). This has also been demonstrated in other studies. Vanden Bempt and colleagues conducted a study on polysomy 17 and HER-2 expression in breast cancer and also found discrepancies between HER-2 status shown by FISH and qPCR [18]. Our finding can be of therapeutic interest for several reasons. In most studies, MDM2 amplification occurred only in p53 wild-type tumors [17]. Indeed, a study of MDM2 gene amplification in tumors of 28 different types comprising more than 3,000 tumors supported this notion [5]. A recent study by Forslund et al., however, showed MDM2 amplification in 8% of p53-mutated cases, almost all of which were low-level amplified cases [6]. It seems that concurrent p53 mutation and MDM2 gene amplification is a rare event. A series of genetic studies in mouse models have shown that loss of wild-type p53 induces tumor formation, whereas restoration of p53 leads to a rapid and impressive tumor regression. This provides strong evidence for the benefits of designing anticancer drugs that restore p53 functions [2]. Inhibiting MDM2 activity in tumors with wild-type p53 and amplified MDM2 genes has been

Table 4 Correlation between MDM2 gene amplification and protein expression

	MDM2 gene amplification status			
	Number of cases	Amplified (%)	Non-amplified (%)	*p* value
All cases	80	14 (18%)	66 (82%)	–
Protein expression patterns				
Nuclear				0.91
Negative	62	11 (18%)	51 (82%)	
Positive	18	3 (17%)	15 (83%)	
Staining intensity				0.17
Weak	2	1 (33%)	1 (67%)	
Moderate to strong	16	2 (8%)	14 (92%)	
Staining proportion				0.93
Mean (range)		10% (0–70%)	3.78% (0–60%)	
Cytoplasmic				0.01[a]
Negative	51	5 (10%)	46 (90%)	
Positive	29	9 (31%)	20 (69%)	
Staining intensity				0.01[a]
Weak	17	2 (12%)	15 (88%)	
Moderate to strong	13	7 (54%)	6(46%)	
Staining proportion				0.01[a]
Mean (range)		43.21% (0–100%)	13.40% (0–100%)	

[a] Significance value

considered an attractive anticancer strategy for many years [19]. The aim is to reactivate wild-type p53 by regressing the inhibitory function of MDM2. One of the approaches is to find small molecules that target MDM2 in such a way that it can no longer bind to p53. In a screening to identify small-molecule inhibitors of MDM2-p53 interaction, Nutlin 3a, MI-219 and MI-319 were identified [20–24]. MI-219 and MI-319 have been shown to disrupt the MDM2-p53 interaction and activate the p53 pathway in cells with wild-type p53, thereby leading to cell-cycle arrest in both normal and tumor cells and selective apoptosis in the latter. In a recent study in pancreatic cancer, these two MDM2 small-molecule inhibitors synergistically augmented anti-tumor effects of therapeutic drug gemcitabine both in terms of cell-growth inhibition as well as apoptosis [25]. Similarly, mice bearing human tumor transplants that were orally administered with Nutlin 3a showed a decrease of 90% in tumor growth, without evident side effects. Treatment of

Table 5 Correlation between MDM2 gene amplification and histopathologic parameters

	Mdm2 gene amplification status			
	Number of cases	Amplified (%)	Non-amplified (%)	*P* value
TNM stage				0.22
I	7	1 (14%)	6 (86%)	
II	27	3 (11%)	24 (89%)	
III	25	4 (16%)	21 (84%)	
IV	10	4 (40%)	6 (60%)	
Differentiation				0.93
Good	7	1 (14%)	6 (86%)	
Moderate	43	8 (19%)	35 (81%)	
Poor	19	3 (16%)	16 (84%)	
Lymphovascular invasion				0.53
Present	29	6 (21%)	23 (79%)	
Absent	40	6 (15%)	34 (85%)	
Perineural invasion				0.10
Present	12	4 (30%)	8 (70%)	
Absent	57	8 (14%)	49 (86%)	

wild-type p53 containing HCT116 cells, a colon carcinoma cell line, with Nutlin 3a resulted in increased level of p53, MDM2 and p21, which is consistent with activation of the p53 pathway. Results confirmed that p53 accumulation is caused by a decrease in degradation rather than an increase in expression. How does MDM2 amplification influence the response to MDM2 antagonists such as Nutlin-3a? Tovar et al. tested the effects on cell-cycle arrest and apoptosis in several cancer cell lines and interestingly found that the degree of induction of apoptosis by Nutlin-3a varied among cancer cell lines. Osteosarcoma cell lines (SJSA-1 and MHM) with MDM2 gene amplification were the most sensitive, whereas HCT116 (colon cancer) and A549 (lung cancer cell lines) harboring no MDM2 gene amplification were the least sensitive to MDM2 antagonists [26]. Therefore, it appears that MDM2 amplification is a predictive marker for response to anti-MDM2 therapy [27, 28].

In contrast to Forslund et al. [6], we found no correlation between MDM2 amplification and the well-recognized histopathologic prognostic predictors including tumor stage. However, we observed a significant correlation between the presence, intensity, and staining proportion of cytoplasmic MDM2 protein expression and MDM2 gene amplification, implying that MDM2 gene amplification could have prognostic value in this specific subgroup of patients since cytoplasmic MDM2 proteins have been shown to play an important role in p53 inactivation [29]. There are conflicting data concerning whether cytoplasmic expression of MDM2 protein is true or false positive [30–33]. Given the correlation with gene amplification, we clearly demonstrated that cytoplasmic expression of MDM2 protein is true and relevant. Therefore, this finding has to be taken into account when immunohistochemistry would be used as a screening for MDM2 gene amplification in the near future, assuming that clinical studies validate the in vitro and animal findings regarding small-molecule inhibitors of MDM2.

Conclusion

Our study is the first MDM2 FISH study in colon carcinoma, correlating the amplification status with protein expression detected by immunohistochemistry. MDM2 amplification was demonstrated in 18% of cases and significantly correlated with presence, intensity, and staining proportion of cytoplasmic MDM2 protein expression. No correlation was found between MDM2 gene amplification and histopathologic prognostic factors. These findings suggest that targeting MDM2 could be a new approach in colon cancer therapy, and amplification status could be a predictive factor of response to MDM2-targeted therapy.

Acknowledgement The authors would like to thank Prof. Nadine Van Roy, Bart Matthys, Isabelle Rottiers, Anne Nuyts, Lyda Kea, and Horiyah Hilal Al-Azri for their technical assistance.

Disclosure/conflict of interest None of the authors has conflict of interests to declare.

References

1. Farnebo M, Bykov VJ, Wiman KG (2010) The p53 tumor suppressor: a master regulator of diverse cellular processes and therapeutic target in cancer. Biochem Biophys Res Commun 396(1):85–89
2. Ventura A, Kirsch DG, McLaughlin ME et al (2007) Restoration of p53 function leads to tumour regression in vivo. Nature 445:661–665
3. Qian Y, Chen X (2010) Tumor suppression by p53: making cells senescent. Histol Histopathol 25(4):515–526
4. Zuckerman V, Wolyniec K, Sionov RV, Haupt S, Haupt Y (2009) Tumour suppression by p53: the importance of apoptosis and cellular senescence. J Pathol 219(1):3–15
5. Momand J, Jung D, Wilczynski S, Niland J (1998) The MDM2 gene amplification database. Nucleic Acids Res 26(15):3453–3459
6. Forslund A, Zeng Z, Qin Li-Xuan et al (2008) MDM2 gene amplification is correlated to tumor progression but not to the presence of SNP309 or TP53 mutational status in primary colorectal cancers. Mol Cancer Res 6(2):205–211
7. Spiessl B, Beahrs OH, Hermanek P et al (1992) UICC—TNM atlas. 3rd ed. 2nd Rev. Springer-Verlag, Berlin
8. Haupt Y, Maya R, Kazaz A, Aron M (1997) MDM2 promotes the rapid degradation of p53. Nature 387:296–299
9. Honda R, Tanaka H, Yasuda H (1997) Oncoprotein MDM2 is a ubiquitin ligase E3 for tumour suppressor p53. FEBS Lett 420:25–27
10. Oliner JD, Pictonpol JA, Thiagalingam S, Gyeris J, Kinzler KW, Vogelstein B (1993) Oncoprotein MDM2 conceals the activation domain of tumour suppressor p53. Nature 362(6423):857–860
11. Jones SN, Roe AE, Donehower LA, Bradley A (1995) Rescue of embryonic lethality in MDM2-deficient mice by absence of p53. Nature 378:206–208
12. de Oca M, Luna R, Wagner DS, Lozano G (1995) Rescue of early embryonic lethality in MDM2-deficient mice by deletion of p53. Nature 378:203–206
13. Bond GL, Hu W, Bond EE et al (2004) A single nucleotide polymorphism in the MDM2 promoter attenuates the p53 tumor suppressor pathway and accelerates tumor formation in humans. Cell 119(5):591–602
14. Grochola LF, Müller TH, Bond GL et al (2010) MDM2 SNP309 associates with accelerated pancreatic adenocarcinoma formation. Pancreas 39(1):76–80
15. Onel K, Cordon-Cardo C (2004) MDM2 and prognosis. Mol Cancer Res 2(1):1–8
16. Weaver J, Downs-Kelly E, Goldblum JR et al (2008) Fluorescence in situ hybridization for MDM2 gene amplification as a diagnostic tool in lipomatous neoplasms. Mod Pathololgy 21(8):943–949
17. Schiebe M, Ohneseit P, Hoffmann W, Meyermann R, Rodemann HP, Bamberg M (2000) Analysis of MDM2 and p53 gene alterations in glioblastomas and its correlation with clinical factors. J Neurooncol 49:197–203
18. Vanden Bempt I, Van Loo P, Drijkoningen M et al (2008) Polysomy 17 in breast cancer: clinicopathologic significance and impact on HER-2 testing. J Clin Oncol 26(30):4869–4874
19. Vassilev LT (2007) MDM2 inhibitors for cancer therapy. Trens Mol Med 13:23–31

20. Vassilev LT, Vu BT, Graves B et al (2004) In vivo activation of the p53 pathway by the small molecule antagonists of MDM2. Science 303:844–848
21. Shangary S, Qin D, McEachern D et al (2008) Temporal activation of p53 by a specific MDM2 inhibitor is selectively toxic to tumors and leads to complete tumor growth inhibition. Proc Natl Acad Sci 105(10):3933–3938
22. Shangary S, Wang S (2009) Small-molecule inhibitors of the MDM2-p53 protein-protein interaction to reactivate p53 function: a novel approach for cancer therapy. Annu Rev Pharmacol Toxicol 49:223–241
23. Dickens MP, Fitzgerald R, Fischer PM (2010) Small-molecule inhibitors of MDM2 as new anticancer therapeutics. Semin Cancer Biol 20:10–18
24. Azmi AS, Aboukameel A, Banerjee S et al (2010) MDM2 inhibitor MI-319 in combination with cisplatin is an effective treatment for pancreatic cancer independent of p53 function. Eur J Cancer 46(6):1122–1131
25. Azmi AS, Philip PA, Aboukameel A et al (2010) Reactivation of p53 by novel MDM2 inhibitors: implications for pancreatic cancer therapy. Curr Cancer Drug Targets 10(3):319–331
26. Tovar C, Rosinski J, Filipovic Z et al (2006) Small-molecule MDM2 antagonists reveal aberrant p53 signaling in cancer: implications for therapy. Proc Natl Acad Sci USA 103:1888–1893
27. Bond GL, Menin C, Bertorelle R, Alhopuro P, Aaltonen LA, Levine AJ (2006) MDM2 SNP309 accelerates colorectal tumour formation in women. J Med Genet 43:950–952
28. Bond GL, Hirshfield KM, Kirchhoff T et al (2006) MDM2 SNP309 accelerates tumor formation in a gender-specific and hormone-dependent manner. Cancer Res 66:5104–5110
29. Ohtsubo C, Shiokawa D, Kodama M et al (2009) Cytoplasmic tethering is involved in synergistic inhibition of p53 by MDMX and MDM2. Cancer Sci 100(7):1291–1299
30. Broll R, Stark A, Windhovel U et al (1999) Expression of p53 and mdm2 mRNA and protein in colorectal carcinomas. Eur J Cancer 35(7):1083–1088
31. Lam KY, Lo CY, Wat NMS, Luk JM, Lam KSL (2001) The clinicopathological features and importance of p53, Rb, and mdm2 expression in phaeochromocytomas and paragangliomas. J Clin Pathol 54:443–448
32. Hori1 M, Shimazaki1 J, Inagawa1 S et al (2002) Over-expression of MDM2 oncoprotein correlates with possession of estrogen receptor alpha and lack of MDM2 mRNA splice variants in human breast cancer. Breast Cancer Res Treat 71:77–84
33. Hao X-P, Günther T, Roessner A, Price AB, Talbot IC (1998) Expression of mdm2 and p53 in epithelial neoplasms of the colorectum. J Clin Pathol Mol Pathol 51:26–29

Virchows Arch (2011) 458:205–211
DOI 10.1007/s00428-010-1038-x

ORIGINAL ARTICLE

Association between polymorphisms in the XRCC1 and GST genes, and CpG island methylation status in colonic mucosa in ulcerative colitis

Tomomitsu Tahara · Tomoyuki Shibata · Masakatsu Nakamura · Masaaki Okubo · Hiromi Yamashita · Daisuke Yoshioka · Joh Yonemura · Ichiro Hirata · Tomiyasu Arisawa

Received: 1 November 2010 / Revised: 22 December 2010 / Accepted: 29 December 2010 / Published online: 14 January 2011
© Springer-Verlag 2011

Abstract CpG island hypermethylation (CIHM) is frequently observed in the colonic mucosa in ulcerative colitis (UC) and is deeply involved in UC-associated colorectal carcinogenesis. We evaluated the influence of common polymorphisms related to DNA repair or xenobiotic pathway (XRCC1, GSTP1, GSTT1, and GSTM1) on the individual susceptibility to CIHM status in the non-neoplastic rectal mucosa in UC patients. XRCC1 Arg399Gln and Arg194Trp, GSTP1 Ile104Val, and GSTT1, GSTM1 null polymorphisms were genotyped in 84 UC patients without neoplastic lesions, in relation to CIHM in the rectal mucosa of three candidate CpG loci (p14, p16, and CDH1) assessed by methylation-specific polymerase chain reaction. XRCC1 codon 399 Arg/Gln genotype (odds ratio (OR)=0.31, 95% CI=0.12–0.81, p=0.017) and 399 Gln carrier (GlnGln+Arg/Gln: OR=0.30, 95%CI=0.12–0.76, p=0.01) were significantly associated with reduced susceptibility to CIHM of the CDH1 promoter. GSTP1 Val carrier (Ile Val+Val/Val) also held a significantly lower susceptibility to CIHM of the p16 promoter (OR=0.26, 95%CI=0.08–0.86, p=0.028). In contrast, GSTT1 present genotype (OR=3.16, 95%CI=1.27–7.89, p=0.01) was significantly associated with increased susceptibility to CIHM of the same gene. XRCC1 codon 399 Gln/Gln genotype was significantly associated with lower mean number of CIHM when compared to the Arg/Arg genotype (1.53±1.01 vs. 0.63±1.06, p=0.024). In addition, the GSTP1 Ile/Val carrier (Ile/Val+Val/Val) was also significantly associated with lower mean number of CIHM (1.43±1.03 vs. 0.84±1.07, p=0.03). XRCC1 Arg399Gln and GSTP1 Ile104Val polymorphisms may influence the CIHM status in the rectal mucosa of UC patients and may be substantially involved in UC-associated carcinogenesis.

Keywords Polymorphism · Ulcerative colitis · DNA methylation · XRCC1 · GSTP1 · GSTT1 · GSTM1

Abbreviation

UC	Ulcerative colitis
CIHM	CpG island hypermethylation
PCR	Polymerase chain reaction
RFLP	Restricted fragment length polymorphism
MSP	Methylation-specific polymerase chain reaction
XRCC	X-ray repair cross-complementing groups
GSTs	Glutathione S-transferases

Introduction

Patients with ulcerative colitis (UC) have a more increased risk of the development of colorectal cancers compared with the average-risk population [1, 2]. Important risk factors for developing colorectal cancer in UC are long-standing colitis [2], extensive colonic involvement [1], positive family history of colorectal cancers [3, 4], primary sclerosing cholangitis [5], and histologic evidence of active inflammation [6]; therefore, intensive CRC surveillance is strongly recommended for these patients. However, the

T. Tahara (✉) · T. Shibata · M. Nakamura · M. Okubo · H. Yamashita · D. Yoshioka · J. Yonemura · I. Hirata
Department of Gastroenterology, Fujita Health University School of Medicine,
1-98 Dengakugakubo, Kutsukake-cho,
Toyoake, Aichi 470-1192, Japan
e-mail: tomomiccyu@yahoo.co.jp

T. Arisawa
Department of Gastroenterology, Kanazawa Medical University,
1-1 Daigaku,
Uchinadamachi, Ishikawa 920-0293, Japan

accuracy of risk factors to predict neoplasias at an early stage is limited.

CpG island hypermethylation (CIHM) was shown as an important mechanism in gene silencing. In many kinds of cancer, some genes acquire aberrant methylation in their CpG islands. Some genes are also methylated in non-neoplastic tissues by aging, and this alteration is known as age-related methylation [7, 8]. In addition, it was shown that gene methylation is closely associated with the inflammatory state of digestive organs [9–13], suggesting that gene methylation is a result of chronic inflammation. In UC patients, a high degree of CIHM was reported in both the dysplastic and non-dysplastic colonic mucosa [10] and closely correlated with the risk of colorectal cancer [14]. It is possible that CIHM is one of the mediators of UC-associated neoplasias, and thus, this molecular abnormality may allow the identification of effective markers to stratify the risk of progression to cancer in UC.

As the mechanisms of CIHM, exogenous carcinogens, generated reactive oxygen, and host genetic differences may influence its status [15]. It is clear that continuous severe inflammation in the colonic mucosa would accelerate CIHM in UC patients. However, not all UC patients show the same CIHM status. This suggests that some genetic factors may contribute to this process.

X-ray repair cross-complementing groups (XRCCs) are important proteins of the DNA repair pathways. The XRCC1 gene is responsible for a scaffolding protein that directly associates with other proteins such as DNA polymerase β, PARP (ADP-ribose polymerase), and DNA ligase III in a complex to facilitate the processes of base excision repair (BER) or single-strand break repair [16]. The BER pathway repairs DNA damage caused by a variety of endogenous and exogenous factors, including oxidation, alkylating agents, and ionizing radiation [17, 18]. The XRCC1 protein can bind directly to both gapped and nicked DNA, as well as to gapped DNA associated with DNA polymerase β, suggesting that this protein might be independently involved in DNA damage recognition [19]. Two polymorphisms, more often found in XRCC1 conserved sites, lead to a C-to-T substitution at codon 194 in exon 6 and to a G-to-A substitution at codon 399 in exon 10 of the gene, leading to the amino acid alterations arginine (Arg) to tryptophan (Trp) and arginine (Arg) to glutamine (Gln), respectively. These changes in conserved protein sites may alter the BER capacity, increasing the chances of DNA damage [20]. Both the Arg399Gln and Arg194Trp variants have been associated mainly with various cancer susceptibility [21–26].

Glutathione S-transferases (GSTs) are also important enzymes of the xenobiotic pathway. These enzymes catalyze the conjugation of potentially mutagenic electrophilic compounds, with nucleophilic glutathione yielding less toxic and more water-soluble compounds, which are readily excreted via urine or bile [27]. Thus, GSTs protect our body from the harmful effects of carcinogens, and a reduction of their activity can render an individual more susceptible to various cancers [28]. Both GSTT1 and GSTM1 genes of the GST super gene family exhibit null or deletion polymorphism [28, 29]. Individuals homozygous for the null allele lack GST enzyme activity and hence have an increased risk of cancer [28]. GSTP1 also exhibits a polymorphism within its coding region, which leads to a A-to-G substitution at codon 104 of the gene, leading to the amino acid alterations isoleucine (Ile) to valine (Val), which reduces enzyme activity [30]. So far, GSTM1, GSTT1, and GSTP1 polymorphisms have been studied in several malignancies [30, 31].

Because of the important role of XRCCs, GSTs with respect to DNA repair or xenobiotic pathway, common polymorphisms of these genes related to their activities might modify the susceptibility to CIHM status in UC patients and may reflect the future risk of developing colorectal cancer. To clarify this concept, we evaluated the association between XRCC 1, GSTP1, GSTT1, and GSTM1 polymorphisms with the CIHM status of three tumor suppressor genes (p16, p14, and CDH1) in the rectal mucosa in UC.

Materials and methods

Patients and samples

Enrolled in the study were 84 patients with ulcerative colitis, including 49 cases of men and 35 cases of women. The average age was 41.0±13.4 years, and the median clinical duration was 10.2±10.1 years. Thirty-five patients had clinical history of hospitalization more than once to control the disease, while 43 patients had no clinical history of hospitalization. For the remaining six patients, information on hospitalization was not available. Rectal inflammatory mucosal specimens were obtained from all the patients during colonoscopic biopsy and preserved in −80°C until use. All UC were clinically in remission at endoscopy. The histopathological examinations showed mild or moderate inflammation, but no evidence of dysplasia or neoplasia in all the cases. According to the endoscopic appearance, 24 patients showed inflammatory mucosa only in the rectum, while the remaining 60 patients also showed extension of inflammatory mucosa in proximal sites (sigmoid, descending, transverse, and ascending colons, and cecum).

The Ethics Committee in Fujita Health University approved the specimen collection procedures.

Bisulfite modification and methylation-specific PCR

DNA was extracted from the specimens by protein precipitation methods, and bisulfite modification was performed according to the protocol recommended by the manufacture (BisulFast Kit Toyobo Co., Osaka, Japan). To detect CIHM, we chose three candidate promoter CpG islands, p16, p14, and CDH1. Methylation-specific PCR (MSP) chain reaction was carried out with the primers listed in Table 1. Annealing temperature and times were determined using DNA from the peripheral blood of a young individual, and DNA was methylated with SssI methylase (New England BioLabs Inc., Beverly, MA, USA). The MSP chain reaction was carried out in a volume of 20 μl containing 20 ng of bisulfite-modified DNA. The DNA was denatured at 95°C for 5 min, followed by 33–35 cycles at 95°C for 30 s, 57–69°C for 1 min, and 72°C for 1 min with a final extension at 72°C for 5 min. MSP reactions were done using EX Taq HS (Takara Bio, Inc., Shiga, Japan). PCR products (10 μl) were separated by electrophoresis in 2.5% agarose gels and visualized by UV illumination using ethidium bromide staining. CIHM was defined as the presence of a positive methylation band showing signals approximately equal to or greater than that of the size marker (10 ng/μl: 100-bp DNA Ladder, Takara Bio, Inc.) regardless of the presence of unmethylated bands (Fig. 1). Samples giving faint positive signals were analyzed another two times, and only samples with a consistent positive methylation band were considered CHIM. In addition, we measured the fluorescent intensities of methylated bands for randomly selected CHIM samples using a digital densitometer (Lane Analyzer, Atto, Tokyo, Japan) and confirmed that the fluorescent intensities of all methylated bands were approximately equal to or greater than that of the size marker (data not shown).

Genotyping for polymorphisms

Genomic DNA was extracted from the rectal mucosa or peripheral blood in all the patients. Genotyping for the XRCC1 gene codons 399 and 194 and GSTP1 polymorphisms were carried out by multiplex PCR-RFLP, as previously described [22, 34], while the GSTT1 and GSTM1 null polymorphisms were detected by PCR using exon 7 of the constitutional CYP1A1 gene as internal control, as previously described with slight modifications [35]. Instead of multiplex PCR, genotyping for GSTT1 and GSTM1 were done separately.

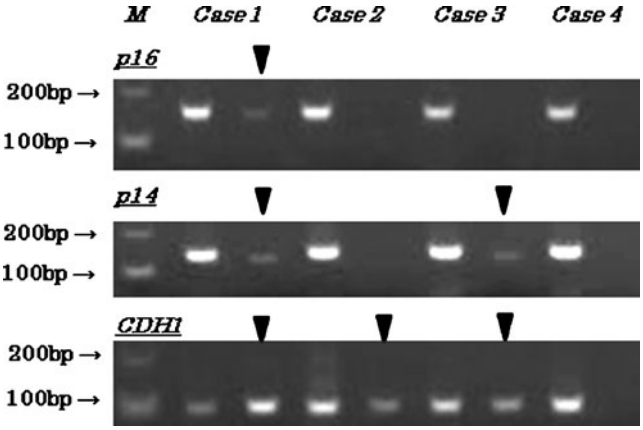

Fig. 1 MSP analysis of four promoters (p16, p14, and CDH1) in four cases. *Arrows* show positive methylated band. *U* unmethylated band, *M* methylated band, *(M)* size marker

Statistical analyses

CIHM and genotype frequencies were calculated by direct counting. Association between CIHM status and individual genotypes was determined by the chi-square test using a 2×2 contingency table, and the odds ratio (OR) with 95% confidence interval (CI) were calculated. Mean number of CIHM was assessed in different genotypes using Student's *t* test. A p value <0.05 was considered statistically significant.

Result

All 84 rectal mucosa samples were available for MSP. In all subjects, CIHM was found in 38 for p16 (45.2%), 29 for p14 (34.5%), and 45(53.6%) subjects for CDH1.

Table 1 Primer sequences for MSP

Primer name	Forward sequence	Reverse sequence	Product size (bp)	Reference
p14 Methylated	5′-gtgttaaagggcggcgtagc-3′	5′-aaaaccctcactcgcgacga-3′	122	[32]
p14 Unmethylated	5′-tttttggtgttaaagggtggtgtagt-3′	5′-cacaaaaaccctcactcacaacaa-3′	132	[32]
p16 Methylated	5′-ttattagagggtggggcggatcgc-3′	5′-gaccccgaaccgcgaccgtaa-3′	150	[33]
p16 Unmethylated	5′-ttattagagggtggggtggattgt-3′	5′-caaccccaaaccacaaccataa-3′	151	[33]
CDH1 Methylated	5′-ttaggttagagggttatcgcgt-3′	5′-taactaaaaattcacctaccgac-3′	115	[32]
CDH1 Unmethylated	5′-taattttaggttagagggttattgt-3′	5′-cacaaccaatcaacaacaca-3′	97	[32]

Compared to a UC cohort without neoplastic lesion in another recent study [14], our UC cohort showed higher methylation frequencies of the p16 and p14 promoters and lower methylation frequency of the CDH1 promoter. CHIM of all three genes were not significantly associated with age and gender (all $p>0.20$, data not shown). Table 2 shows the associations of CIHM status of the three promoter CpG islands and CIHM high and selected genotypes. XRCC1 codon 399 and 194 polymorphisms could not be genotyped for two subjects, respectively. The distributions of genotypes in the UC cohort were: 45 Arg/Arg (54.9%), 29 Arg/Gln (35.4%), and 8 Gln/Gln (9.7%) for XRCC1 codon 399; 33 Arg/Arg (40.2%), 29 Arg/Trp (51.2%), and 7 Trp/Trp (8.5%) for XRCC1 codon 194; and 65 Ile/Ile (77.3%), 18 Ile/Val (21.4%), and 1 Val/Val (1.2%) for GSTP1. The null genotypes in GSTT1 and GSTM1 were found in 49 (58.3%) and 48 (57.1%), respectively. When comparing these distributions with healthy Japanese [36–38] and Caucasian [39, 40], frequency of XRCC1 codon 399 Arg/Arg genotype was slightly higher than that of healthy Japanese and Caucasian, and frequency of XRCC1 codon 194 Arg/Arg genotype was slightly lower than that of healthy Japanese and much lower than that of Caucasian. The frequency of GSTP1 Ile/Ile genotype was slightly lower than that of healthy Japanese and much lower than that of Caucasian. Concerning GSTT1 and GSTM1, frequency of GSTM1 null genotype was almost the same, but the frequency of GSTT1 null genotype was about 10% higher in our UC cohort than in the healthy Japanese and much higher than that of Caucasian.

Table 2 Association between genetic polymorphisms and CIHM status of colonic mucosa in UC patients

Variables (*n*)	p16		p14		CDH1	
	UM	*M*	*UM*	*M*	*UM*	*M*
XRCC1 codon 399						
Arg/Arg	23	22	28	17	15	30
Arg/Gln	15	14	19	10	18	11
Gln/Gln	7	1	7	1	5	3
XRCC1 codon 194						
Arg/Arg	18	15	24	9	18	15
Arg/Trp	21	21	24	18	17	25
Trp/Trp	6	1	6	1	3	4
GSTP1						
Ile/Ile	32	33	42	23	28	37
Ile/Val	14	4	13	5	11	7
Val/Val	1	0	1	0	1	0
GSTT1						
GSTT1	21	14	20	15	11	24
Null	26	23	36	13	29	20
GSTM1						
Present	24	12	27	9	17	19
Null	23	15	29	19	23	25

All analysis was done by the chi-square test. XRCC1 codon 399 and 194 polymorphisms could not be genotyped for two subjects, respectively

p16 M—XRCC1 codon 399 Gln/Gln: OR=0.15, 95%CI=0.02–1.32, p=0.087; GSTP1 Val carrier (Ile Val+Val/Val): OR=0.26, 95%CI=0.08–0.86, p=0.028; GSTM1 present: OR=0.46, 95%CI=0.19–1.13, p=0.089

CDH1M—XRCC1 codon 399 Arg/Gln: OR=0.31, 95%CI=0.12–0.81, p=0.017; XRCC1 codon 399 Gln carrier (Arg/Gln+Gln/Gln): OR=0.30, 95%CI=0.12–0.76, p=0.01; GSTT1 present: OR=3.16, 95%CI=1.27–7.89, p=0.01

UM unmethylated, *M* methylated

Since age and gender were not associated with CIHM status, we assessed these associations by the chi-square test using a 2×2 contingency table. In the comparison of genotype frequencies, GSTP1 Val carrier (Ile Val+Val/Val) held a significantly lower susceptibility to CIHM of the p16 promoter (OR=0.26, 95%CI=0.08–0.86, p=0.028), while XRCC1 codon 399 Gln/Gln (OR=0.15, 95%CI=0.02–1.32, p=0.087) and GSTM1 present (OR=0.46, 95%CI=0.19–1.13, p=0.089) were also weakly associated with lower susceptibility to the p16 promoter. We also found that XRCC1 codon 399 Arg/Gln genotype (OR=0.31, 95%CI=0.12–0.81, p=0.017) and 399 Gln carrier (Arg/Gln+Gln/Gln: OR=0.30, 95%CI=0.12–0.76, p=0.01) were significantly associated with reduced susceptibility to CIHM of the CDH1 promoter. In contrast, the GSTT1 present genotype (OR=3.16, 95%CI=1.27–7.89, p=0.01) was significantly associated with increased susceptibility to CIHM of the same gene. Figure 2 shows the association between the mean number of CIHM in different genotypes. We found that XRCC1 codon 399 Gln/Gln genotype was significantly associated with lower mean number of CIHM when compared to the Arg/Arg genotype (1.53±1.01 vs. 0.63±1.06, p=0.024). In addition, GSTP1 Ile/Val carrier (Ile/Val+Val/Val) was also significantly associated with lower mean number of CIHM (1.43±1.03vs. 0.84±1.07, p= 0.03).

Discussion

In our study, some of the selected polymorphisms, related to DNA repair or xenobiotic pathway, showed a significant association with CIHM status of the rectal mucosa in UC patients. In UC patients, a high degree of CIHM was reported in both the dysplastic and non-dysplastic colonic mucosa [10], and the CIHM status of non-dysplastic colonic mucosa was closely correlated with the inflammatory state and risk of colorectal cancer development [14]. Our current result provided an evidence that the CIHM

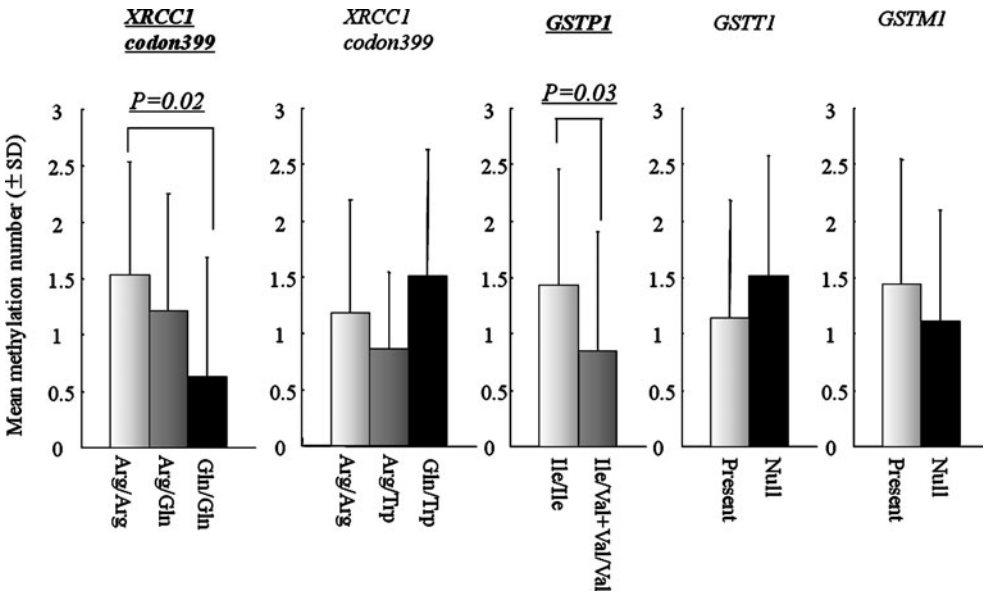

Fig. 2 Association between methylation number expressed as mean±SD and polymorphisms. Statistical analysis was performed using the Student's *t* test. Since the number of Val/Val genotype of GSTP1was low, it was considered as Val carriers (Le Val+Val/Val)

status in the rectal mucosa in UC patients, an important early step in UC-related tumorigenesis, may be modified by polymorphisms in DNA repair or xenobiotic pathway-related genes; thus, this inter-individual difference may substantially predict the future risk of developing colorectal cancer in UC patients.

In our study, XRCC1 codon 399 Arg/Gln genotype and 399 Gln carrier (GlnGln+Arg/Gln) were significantly associated with reduced susceptibility to CIHM of the CDH1 promoter. In addition, XRCC1 codon 399 Gln/Gln genotype was significantly associated with lower mean number of CIHM when compared to the Arg/Arg genotype. The same genotype was also weakly associated with lower susceptibility to the p16 promoter. XRCC are important proteins of the DNA repair through the processes of BER or single-strand break repair [16], which has an important protective role against DNA damage caused by a variety of endogenous and exogenous factors [17, 18]. The codon 399 polymorphism, a G-to-A substitution at exon 10 XRCC1 conserved site, leading to the amino acid alterations (Arg to Gln), may alter the BER capacity, increasing the chances of DNA damage [20]. Although both the common polymorphisms in the XRCC1 gene (Arg399Gln and Arg194Trp) have been associated mainly with various cancer susceptibility [21–26], our data suggest that XRCC1 codon 399 Gln allele, but not any genotype in codon 194, might confer protection against CIHM status in the colonic mucosa in UC through DNA repair pathways.

However, Wang et al. [41] showed that individuals with the 399 Gln/Gln homozygotes had higher mutagen sensitivity against bleomycin than those with other genotypes, suggesting that the Gln allele might be a rather risk allele for carcinogenesis. Furthermore, previous studies investigating the association between XRCC1 polymorphisms and colorectal cancer risk have provided inconsistent results, and the recent a meta-analysis has concluded that XRCC1 polymorphisms including both Arg399Gln and Arg194Trp are not associated with risk of colorectal cancer [42]. Therefore, our association needs to be treated carefully until it will be replicated.

We have shown that the GSTP1 Val carrier with lower activity (Ile Val+Val/Val) held a significantly lower susceptibility to CIHM of the p16 promoter and lower mean number of CIHM. In addition, wild-type GSTT1 present genotype was significantly associated with increased susceptibility to CIHM of the CDH1 promoter. When considering the functional perspective, Val allele and null genotypes might confer risk for carcinogenesis and thus may be associated with susceptibility to CIHM. Indeed, wild-type GSTM1 present genotype related to a lower susceptibility to CIHM of the p16 promoter. However, associations were rather striking for GSTT1 present genotype with increased risk of CIHM especially in the CDH1 promoter. Our result also suggests that the GSTP1 Val carrier has a rather protective effect against CIHM status. There are three potential speculations for these unexpected associations that we found. First, this polymorphism may be in linkage disequilibrium with other polymorphisms elsewhere in the GSTP1 and GSTT1 genes, demonstrating biologically relevant variability for influencing the CIHM status. Second, there exists the possibility that this polymorphism is in linkage disequilibrium with a genetic variation of another gene located near the GSTP1 and GSTT1 genes that might be related to susceptibility to CIHM. The third possible explanation is that GSTP1 and GSTT1 might also have roles in catalyzing some enzymes that might have protective roles against gene methylation. However, our data lack mechanistic evidence to interpret

our association, and detailed biological mechanisms remained to be unclear.

In our study cohort, CIHM are found in a relatively higher frequency in non-neoplastic colonic mucosa in UC patients (45.2%% for p16, 34.5% for p14, and 53.6% for CDH1).

In particular, our UC cohort showed higher methylation frequencies of p16 and p14 promoters compared to UC cohort without neoplastic lesion in another recent study [14].

It is possibly due to the longer median clinical duration (10.2±10.1 years), suggesting that they might be especially at high risk of developing colorectal cancer. In this context, our association indicates that genetic factor related to DNA repair or xenobiotic pathway may influence the CIHM status in the long-term outcome of UC and may substantially predict patients who may be at risk of developing colorectal cancer. However, whether our association directly contributes to risk prediction of colorectal cancer is unclear because our cohort did not include colorectal cancer patients; therefore, further well-designed study will be needed to confirm our result and evaluate the clinical utility in risk prediction of colorectal cancer in UC patients. Also, the same evaluation will be needed for the risk prediction of sporadic colorectal cancer. Furthermore, the distribution of polymorphisms would vary in different populations [39, 40]. A study using a diverse population will also be needed to apply our result to other ethnics.

Conflict of interest statement We declare that we have no conflict of interest.

References

1. Ekbom A, Helmick C, Zack M et al (1990) Ulcerative colitis and colorectal cancer. A population-based study. N Engl J Med 323:1228–1233
2. Eaden JA, Abrams KR, Mayberry JF (2001) The risk of colorectal cancer in ulcerative colitis: a meta-analysis. Gut 48:526–535
3. Askling J, Dickman PW, Karlen P et al (2001) Family history as a risk factor for colorectal cancer in inflammatory bowel disease. Gastroenterology 120:1356–1362
4. Nuako KW, Ahlquist DA, Mahoney DW et al (1998) Familial predisposition for colorectal cancer in chronic ulcerative colitis: a case–control study. Gastroenterology 115:1079–1083
5. Jayaram H, Satsangi J, Chapman RW (2001) Increased colorectal neoplasia in chronic ulcerative colitis complicated by primary sclerosing cholangitis: fact or fiction? Gut 48:430–434
6. Rutter MD, Saunders BP, Wilkinson KH et al (2004) Cancer surveillance in longstanding ulcerative colitis: endoscopic appearances help predict cancer risk. Gut 53:1813–1816
7. Issa JP, Ottaviano YL, Celano P et al (1994) Methylation of the oestrogen receptor CpG island links ageing and neoplasia in human colon. Nat Genet 4:536–540
8. Ahuja N, Li Q, Mohan AL, Baylin SB et al (1998) Aging and DNA methylation in colorectal mucosa and cancer. Cancer Res 23:5489–5494
9. Sato F, Harpaz N, Shibata D et al (2002) Hypermethylation of the p14 (ARF) gene in ulcerative colitis-associated colorectal carcinogenesis. Cancer Res 62:1148–1151
10. Issa JP, Ahuja N, Toyota M et al (2001) Accelerated age-related CpG island methylation in ulcerative colitis. Cancer Res 61:3537–3573
11. Bian YS, Osterheld MC, Fontolliet C et al (2002) p16 inactivation by methylation of the CDKN2A promoter occurs early during neoplastic progression in Barrett's esophagus. Gastroenterology 122:1113–1121
12. Wong DJ, Paulson TG, Prevo LJ et al (2001) p16 (INK4a) lesions are common, early abnormalities that undergo clonal expansion in Barrett's metaplastic epithelium. Cancer Res 61:8284–8289
13. Kaneto H, Sasaki S, Yamamoto H et al (2001) Detection of hypermethylation of the p16(INK4A) gene promoter in chronic hepatitis and cirrhosis associated with hepatitis B or C virus. Gut 48:372–377
14. Garrity-Park MM, Loftus EV Jr, Sandborn WJ et al (2010) Methylation status of genes in non-neoplastic mucosa from patients with ulcerative colitis-associated colorectal cancer. Am J Gastroenterol 105:1610–1619
15. Issa JP (2000) GpG-island methylation in aging and cancer. Curr Top Microbiol Immunol 249:101–118
16. Caldecott KW, Aoufouchi S, Johnson P et al (1996) XRCC1 polypeptide interacts with DNA polymerase beta and possibly poly(ADP-ribose) polymerase, and DNA ligase III is a novel molecular 'nick-sensor' in vitro. Nucleic Acids Res 24:4387–4394
17. Lindahl T (2000) Suppression of spontaneous mutagenesis in human cells by DNA base excision-repair. Mutat Res 462:129–135
18. Christmann M, Tomicic MT, Roos WP et al (2003) Mechanisms of human DNA repair: an update. Toxicology 193:3–34
19. Marintchev A, Mullen MA, Maciejewski MW et al (1999) Solution structure of the single-strand break repair protein XRCC1 N-terminal domain. Nat Struct Biol 6:884–893
20. Butkiewicz D, Rusin M, Harris CC et al (2000) Identification of four single nucleotide polymorphisms in DNA repair genes: XPA and XPB (ERCC3) in Polish population. Hum Mutat 15:558–577
21. Sturgis EM, Castillo EJ, Li L et al (1999) Polymorphisms of DNA repair gene XRCC1 in squamous cell carcinoma of the head and neck. Carcinogenesis 20:2125–2129
22. Abdel-Rahman SZ, Soliman AS, Bondy ML et al (2000) Inheritance f the 194Trp and the 399Gln variant alleles of the DNA repair gene XRCC1 are associated with increased risk of early-onset colorectal carcinoma in Egypt. Cancer Lett 159:79–86
23. Shen H, Xu Y, Qian Y et al (2000) Polymorphisms of the DNA repair gene XRCC1 and risk of gastric cancer in a Chinese population. Int J Cancer 88:601–606
24. Lee JM, Lee YC, Yang SY et al (2001) Genetic polymorphisms of XRCC1 and risk of the esophageal cancer. Int J Cancer 95:240–246
25. Duell EJ, Millikan RC, Pittman GS et al (2001) Polymorphisms in the DNA repair gene XRCC1 and breast cancer. Cancer Epidemiol Biomark Prev 10:217–222
26. Zhou W, Liu G, Miller DP et al (2003) Polymorphisms in the DNA repair genes XRCC1 and ERCC2, smoking, and lung cancer risk. Cancer Epidemiol Biomark Prev 12:359–365
27. Kettrer B (1988) Protective role of GSH and GST in mutagenesis and carcinogenesis. Mutat Res 202:343–361
28. Hayes JD, Pulford DJ (1995) The GST supergene family: regulation of GST and the contribution of the isoenzymes to cancer chemoprevention and drug resistance. Crit Rev Biochem Mol Biol 30:445–600
29. Ali-Osman F, Akande O, Antoun G et al (1997) Molecular cloning, characterization and expression in *E. coli* of full-length cDNAs of 3 human glutathione-S-transferase Pi gene variants. J Biol Chem 272:10004–100012
30. Nakazato H, Suzuki K, Matsui H et al (2003) Association of genetic polymorphisms of glutathione-S-transferase genes

(GSTM1, GSTT1 and GSTP1) with familial prostate cancer risk in a Japanese population. Anticancer Res 23:2897–2902
31. Wang J, Deng Y, Chang J et al (2003) GST genetic polymorphism and lung adenocarcinoma susceptibility in a Chinese population. Cancer Lett 203:185–193
32. Herman JG, Graff JR, Myöhänen S et al (1996) Methylation-specific PCR: a novel PCR assay for methylation status of CpG islands. Proc Natl Acad Sci USA 93:9821–9826
33. Esteller M, Tortola S, Toyota M et al (2000) Hypermethylation-associated inactivation of p14(ARF) is independent of p16 (INK4a) methylation and p53 mutational status. Cancer Res 60:129–133
34. Harries LW, Stubbins MJ, Forman D et al (1997) Identification of genetic polymorphisms at the glutathione-S-transferase Pi locus and association with susceptibility to bladder, testicular and prostate cancer. Carcinogenesis 18:641–644
35. Abdel-Rahaman SZ, El-Zein RA, Anwar WA et al (1996) A multiplex PCR procedure for genetic polymorphism of the GSTM1 and GSTT1 genes in human. Cancer Lett 107:229–233
36. Kawai S, Nishio K, Nakamura S et al (2005) Multiplex PCR with confronting two-pair primers for CYP1A1 Ile462Val, GSTM1, GSTT1, and NQO1 C609T. Asian Pac J Cancer Prev 6:346–352
37. Weng H, Weng Z, Lu Y et al (2009) Effects of cigarette smoking, XRCC1 genetic polymorphisms, and age on basal DNA damage in human blood mononuclear cells. Mutat Res 679:59–64
38. Kiyohara C, Miyake Y, Koyanagi M et al (2010) GST polymorphisms, interaction with smoking and pesticide use, and risk for Parkinson's disease in a Japanese population. Parkinsonism Relat Disord 16:447–452
39. Capellá G, Pera G, Sala N et al (2008) DNA repair polymorphisms and the risk of stomach adenocarcinoma and severe chronic gastritis in the EPIC-EURGAST Study. Int J Epidemiol 37:1316–1325
40. Zendehdel K, Bahmanyar S, McCarthy S et al (2009) Genetic polymorphisms of glutathione S-transferase genes GSTP1, GSTM1, and GSTT1 and risk of esophageal and gastric cardia cancers. Cancer Causes Control 20:2031–2038
41. Wang Y, Spitz MR, Zhu Y et al (2003) From genotype to phenotype: correlating XRCC1 polymorphisms with mutagen sensitivity. DNA Repair (Amst) 2:901–908
42. Wang B, Wang D, Huang G et al (2010) XRCC1 polymorphisms and risk of colorectal cancer: a meta-analysis. Int J Colorectal Dis 25:313–321

Virchows Arch (2011) 458:213–219
DOI 10.1007/s00428-010-1031-4

ORIGINAL ARTICLE

Downregulation of the hedgehog receptor PTCH1 in colorectal serrated adenocarcinomas is not caused by *PTCH1* mutations

Karoliina Stefanius · Tiina Kantola · Anne Tuomisto · Pia Vahteristo · Tuomo J. Karttunen · Lauri A. Aaltonen · Markus J. Mäkinen · Auli Karhu

Received: 1 October 2010 / Revised: 9 December 2010 / Accepted: 18 December 2010 / Published online: 14 January 2011
© Springer-Verlag 2011

Abstract Colorectal serrated adenocarcinoma forms about 15–20% of colorectal carcinomas. We have previously shown that downregulation of PTCH1 is distinctive for this type of colorectal cancer. In several other tumor types, somatic inactivating *PTCH1* mutations have been shown to lead to aberrant Hedgehog signaling, but in colorectal cancer the role of *PTCH1* mutations has not been thoroughly studied. Here, we have analyzed the mutation status of *PTCH1* in a series of 33 colorectal serrated adenocarcinomas by sequencing all 23 coding exons. We detected 11 previously known SNPs and eight new alterations. The latter included five synonymous changes and two previously unknown missense variations, somatic M319V, and germline V1231A. V1231A was also present in population controls and likely represents polymorphism. The somatic M319V variant does not appear to be an attractive candidate for a disease-associated mutation because in silico analyses did not support the pathogenic nature of the change. A somatic, intronic 1-bp deletion was detected in a short poly(T) stretch in two microsatellite unstable tumors. None of the three changes had predicted effect on splicing when analyzed in silico. Our results did not reveal any clearly deleterious inactivating *PTCH1* mutations in our collection of colorectal serrated adenocarcinomas. This suggests that other mechanisms are involved in the observed downregulation of the *PTCH1* gene. These might include, e.g., constantly active MAPK signaling by *KRAS* or *BRAF* mutations or silencing of *PTCH1* by hypermethylation, and further studies are needed to reveal these mechanisms.

Keywords Hedgehog signaling · PTCH1 · Mutation · Serrated adenocarcinoma · Colorectal cancer

Abbreviations

PTCH	Patched
Hh	Hedgehog
CRC	Colorectal cancer
MSI	Microsatellite instability
MAPK	Mitogen-activated protein kinase
CIM	CpG island hypermethylation
BCC	Basal cell carcinoma syndrome
LOH	Loss of heterozygosity

Introduction

Colorectal cancer (CRC) is among the three most common cancers with an annual global incidence of over one million new cases [1]. Around 80–85% of CRCs develop via the classical adenoma–carcinoma sequence, one of the best-described models in human cancer development. During the last 20 years, so-called serrated neoplasia pathway has emerged to explain most of the remaining 15–20% of

K. Stefanius · T. Kantola · A. Tuomisto · T. J. Karttunen · M. J. Mäkinen
Department of Pathology, Institute of Diagnostics, University of Oulu, FI-90014 Oulu, Finland

P. Vahteristo · L. A. Aaltonen · A. Karhu
Department of Medical Genetics, Genome-Scale Biology Research Program, University of Helsinki, FI-00014 Helsinki, Finland

P. Vahteristo · L. A. Aaltonen · A. Karhu (✉)
Department of Medical Genetics, Biomedicum Helsinki, University of Helsinki, (Haartmaninkatu 8), P.O. Box 63, FI-00014 Helsinki, Finland
e-mail: auli.karhu@helsinki.fi

sporadic CRCs [2, 3]. The serrated pathway precursor lesions include traditional serrated adenomas, sessile serrated adenomas, and admixed polyps. These lesions possess morphology and genetic features distinct from adenomatous polyps of the classical pathway. Characteristic, genetic, and pathologic alterations of the serrated pathway include DNA CpG island hypermethylation (CIM) and microsatellite instability (MSI), *BRAF* and *KRAS* mutations, and inhibition of apoptosis [2, 3]. A combination of MSI, *BRAF* mutations, and CIM is rarely if ever seen in CRC arising from conventional adenomas, nor in hereditary CRC, including familial adenomatous polyposis and hereditary non-polyposis colorectal cancer (reviewed in [2]).

Our earlier RNA expression microarray analysis showed that *PTCH1* (*patched homolog 1* (*Drosophila*)) is downregulated and the gene product is lost in serrated carcinomas when compared to conventional CRCs [4]. The *PTCH1* gene consists of 23 exons encoding a 1447-amino acid transmembrane glycoprotein with two large ligand-binding extracellular loops and an intracellular N- and C-termini [5]. *PTCH1* is a member of the Hedgehog (Hh) signaling pathway, in which its role is to act as a transmembrane receptor for secreted Hh ligands, Sonic-(SHH), Indian-(IHH), and Desert-(DHH) Hh. Hh signaling is involved in regulation of cell proliferation, differentiation, and growth during embryonic development and in a number of adult tissues, such as gastrointestinal (GI) tract [4, 6]. When Hh ligand binds to the PTCH1 protein, repression of smoothened is relieved. This causes activation of a transcription factor GLI-1, and upregulation of target genes, including *PTCH1*, *GLI-1*, *Cyclin D*, and *myc*, where PTCH1 offers negative feedback for Hh activation. Mutations or functional aberration of the Hh signaling pathway have been observed in several cancer types [7, 8].

Germline *PTCH1* mutations result in nevoid basal cell carcinoma syndrome, also known as Gorlin's syndrome, which is characterized by cutaneous basal cell carcinomas (BCC), jaw cysts, skeletal abnormalities, and occasional cerebellar medulloblastoma [5, 9, 10]. Somatic inactivating *PTCH1* mutations have been detected in various tumors, including BCC, medulloblastoma, meningeoma, and breast cancer [5, 9–14]. *PTCH1* mutations are mainly clustered into the two large extracellular loops and the large intracellular loop. Occurrence of loss of heterozygosity (LOH) in tumors suggests that *PTCH1* acts as a tumor suppressor gene [13].

Currently, the relevance of Hh pathway signaling in CRCs is controversial probably due to conflicting data provided by different models of CRC, human CRC-derived cell lines, mouse models, and sporadic tumor samples (review by Gulino et al. [15]). Kolterud et al. [16] and Van Dop et al. [17] showed Hh signaling from epithelium to mesenchymal cells in developing and adult mice GI tract. Paracrine signaling was further verified in xenografts with human cell lines and cancer biopsies in mice [18]. According to Chatel and co-workers, activation of Hh pathway is not a common event in cultured cells [19]. However, several other studies have addressed the essential role of epithelial Hh signaling in CRC development, growth, stem cell renewal, and metastatic behavior in advanced cancer [20–24]. In addition, oncogenic mitogen-activated protein kinase (MAPK) signaling activates Hh pathway ligand independently through upregulation of GLI-1, further justifying the analysis of Hh pathway component PTCH1 in serrated adenocarcinomas [7].

*PTCH1*mutations have earlier been studied in ten colorectal carcinomas with negative results [11]. In addition, one study has linked a subset of familial CRC to the 9q22.2–31.2.2 region, including *PTCH1*, DNA repair gene *XPA*, and tyrosine kinase *SYK* [25]. Our earlier study showed preserved *PTCH1* expression in conventional CRCs, whereas in the serrated CRCs, the expression was lost both in RNA and protein levels [4]. This supports the possible role of *PTCH1* defects in serrated tumors. To test this hypothesis, we performed a *PTCH1* mutation analyses in 33 colorectal serrated adenocarcinoma samples. To our knowledge, this is the first time the role *PTCH1* mutations have been studied in colorectal serrated adenocarcinomas.

Materials and methods

Sample selection

A series of serrated CRCs was extracted from three different, consecutively collected sets of colorectal cancer cases. A total of 33 serrated adenocarcinomas yielded sufficient quality DNA to enter the analyses. DNA was extracted from fresh-frozen or paraffin-embedded tissues according to standard procedures. Ten cases (fresh-frozen) were obtained from a previously described set of 1,042 samples [26, 27], 16 cases (paraffin-embedded) were obtained from a series of 466 CRC patients from the Oulu University Hospital District area between the years 1986 and 1996 [28], and seven cases (paraffin-embedded) were obtained from a series of 86 CRC patients from the Oulu University Hospital District area between the years 1997 and 1998. The diagnosis of serrated adenocarcinoma was based on validated histopathological criteria. In brief, serrated adenocarcinomas were characterized by apparent epithelial serrations composed of only epithelium, epithelium and basement membrane material, clear or eosinophilic and often abundant cytoplasm, vesicular nuclei, and in the mucinous tumors, the presence of serrations and

eosinophilic cell balls and rods floating in the mucus [2]. Examples of serrated adenocarcinoma and conventional adenocarcinoma are presented in Fig. 1 [2, 29]. Clinicopathological features are presented in Table 1.

DNA isolated from the blood samples of 118 anonymous blood donors obtained via Finnish Red Cross were used as controls for mutation validation analysis.

Mutation analysis of the *PTCH1* gene

Primers for all the coding exons of the *PTCH1* gene were designed using Primer3 v.0.4.0. program (http://frodo.wi.mit.edu/primer3/input.htm). Primer sequences and PCR conditions are available on request. PCR products were enzymatically purified with EXOSAPit® (USB, Cleveland, OH, USA) according to the manufacturer's instructions. All 23 coding exons (ENST00000375274) were analyzed by direct sequencing. Sequencing of a 1-μl aliquot of the product was performed on both directions using the BigDye 3.1 Termination chemistry on an ABI3730 DNA sequencer (Applied Biosystems, Foster City, CA, USA). The data was analyzed with Chromas 1.6 sequencing analysis software (Technelysium Pty Ltd, Halensvale, Australia) and Bioedit v7.0.9 sequence alignment editor (Ibis Biosciences, Carlsbad, CA, USA). Mutation analysis was initially performed on tumor samples, and the presence of other than silent changes was studied in the respective normal samples.

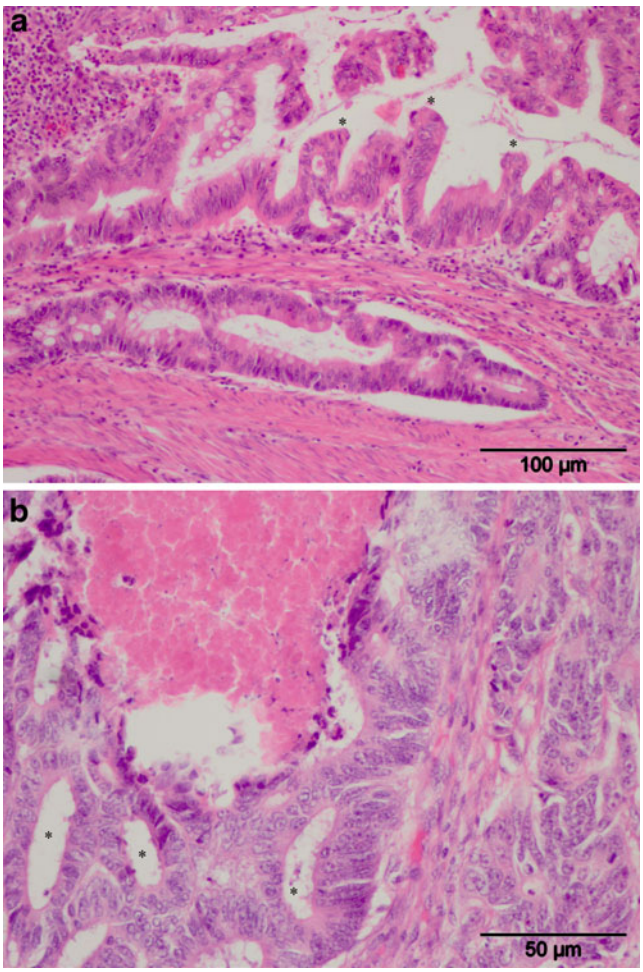

Fig. 1 **a** A case of serrated adenocarcinoma. The tumor consists of eosinophilic cells with vesicular nuclei, and form tufting serrated structures (*asterisks*). **b** A case of conventional adenocarcinoma. The tumor, which has developed from a tubular adenoma, consists of basophilic epithelium with irregular nuclei, and forms tubular structures (*asterisks*). There is prominent necrosis (*upper left quadrant*)

Table 1 The clinicopathological features of the colorectal tumor samples analyzed for *PTCH1* mutations

	Serrated carcinomas (n=33)	
	No.	%
Age at diagnosis (years)	68.5[a]	46–87 (range)
Gender		
Male	19	57.6
Female	14	42.4
Location		
Proximal	16	48.5
Distal	17	51.5
Grade		
I	4	12.1
II	24	69.7
III	5	15.2
Dukes' stage		
A	7	21.2
B	8	24.2
C	16	48.5
D	2	6.1
Mucinous		
Not mucinous	29	87.8
Mucinous components	2	6.1
Mucinous	2	6.1

[a] Mean age

In silico analysis

The potential effects on splicing of the unreported intronic and exonic changes were evaluated in silico using NetGene2 (http://www.cbs.dtu.dk/services/NetGene2/) and Alternative Splice Site Predictor, ASSP, (http://es.embnet.org/~mwang/assp.html). Two sequence homology-based softwares were used to predict the potential impact of the identified missense variants on protein function; PolyPhen (http://www.bork.embl-heidelberg.de/PolyPhen/) and SIFT (http://sift.jcvi.org/).

PTCH1 immunohistochemistry and *KRAS/BRAF* mutation statuses

PTCH1 (Santa Cruz, G-19) immunohistochemistry was performed on selected cases of 25 out of 33 serrated adenocarcinomas. The intensity of the immunoreaction was recorded negative or showing weak, moderate, or strong immunoreaction.

MSI analyses as well as *KRAS codon 12/13* and *BRAFV600E* mutation status were analyzed on 32 out of 33 cases, as previously described [30].

Ethical aspects

The protocol was approved by the Ethical Committees of Oulu University Hospital and patient information and samples from Helsinki were obtained after informed consent and Ethical Review Board approval.

Results

Our previous studies have shown that the *PTCH1* gene is downregulated in serrated adenocarcinomas. To evaluate whether the reduced expression results from gene mutations, we sequenced the coding region of *PTCH1* gene in 33 morphologically classified serrated adenocarcinomas. All the coding exons and exon–intron junctions were screened. Success rates were 90.4% and 100% in paraffin-embedded and fresh-frozen isolated DNA, respectively. To avoid false-positive PCR artifacts, each new variant detected in paraffin samples was confirmed by performing new PCR and sequencing reactions.

Sequencing analysis revealed both previously described exonic and intronic polymorphisms, as well as eight new variants. In cases with a new sequence alteration, corresponding normal tissue was also sequenced when available. All detected sequence changes are presented in Table 2. Sequencing analysis revealed altogether 19 different alterations. We observed five previously detected silent exonic and five intronic polymorphisms (Table 2). Two most common heterozygous SNPs, c.1686C>T (rs2066836) observed in 15 cases (45%), and c.1665C>T (rs1805155) observed in nine cases (27%) were both located in exon 12. Seven cases (21%) carried both of these polymorphisms. In addition, we detected one previously described germline nucleotide change c.3944C>T (rs357564) in exon 23, which has been suggested to associate with a decreased risk of breast cancer [12, 31]. Six cases heterozygous and three cases homozygous for an associated T allele were detected. This *PTCH1* SNP achieved the Hardy–Weinberg equilibrium (χ^2=2.9, p=0.09).

Table 2 Alterations of the *PTCH1* gene in a series of 33 serrated colorectal carcinomas

Exonic/intronic	Nucleotide change	Amino acid	No. of samples	Type of alteration	Mutation type	Protein location
Exon 2	c.258C>T	L106L	1	SNP (rs1805153)	Germline	Transmembrain domain 1
Exon 5	c.735A>G	T245T	4	SNP (rs1805154)	Germline	Extracellular loop 1
Intron 5–6	IVS6-55 A>G	–	1	SNP (rs2297087)	Germline	
Exon 6	c.885C>T	P295P	1	Silent variation[a]		Extracellular loop 1
Exon 7	c.955A>G	M319V	1	Missense[a]	Somatic	Extracellular loop 1
Exon 9	c.1308C>T	D436D	1	Silent variation[a]		Extracellular loop 1
Intron 10–11	IVS10 +99C>T	–	10	SNP (rs28448271)	Germline	
Intron10–11	IVS11-51C>G	–	5	SNP (rs574688)	Germline	
Exon 12	c.1665C>T	N555N	10	SNP (rs1805155)	Germline	Transmembraine domain 5
Exon 12	c.1686C>T	A562A	14	SNP (rs2066836)	Germline	Transmembraine domain 5
Intron 12–13	IVS13–18, T8-1del	–	2	Intronic repeat deletion**	Somatic	
Exon 14	c.2199A>G	S733S	1	SNP (rs2227970)	Germline	Intracellular loop 3
Intron 15–16	IVS15 +9G>C	–	4	SNP (rs2066829)	Germline	
Exon 16	c.2643C>T	V881V	1	Silent variation[a]		Extracellular loop 2
Exon 17	c.2763C>T	I921I	1	Silent variation[a]		Extracellular loop 2
Intron 17–18	IVS17 +21G>A	–	3	SNP (rs2236406)	Germline	
Exon 22	c.3692T>C	V1231A	2	Missense[a]	Germline	C-terminal
Exon 23	c.3944C>T	P1315L	9	Missense (rs357564)	Germline	C-terminal
Exon 23	c.4047T>A	P1349P	2	Silent variation[a]		C-terminal

[a] Novel sequence alterations detected in this study

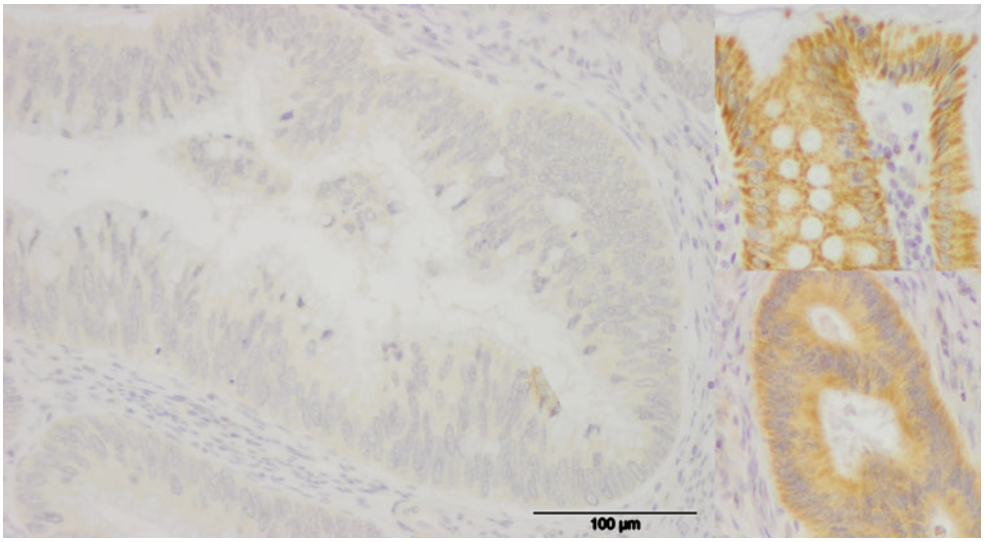

Fig. 2 Weak PTCH1 immunoreaction in a serrated adenocarcinoma, in contrast to normal mucosa of the colon (*upper insert*) and to an example of conventional colorectal carcinoma, where the epithelium shows a strong immunoreaction (*lower insert*)

Out of the eight previously unpublished sequence changes, five were silent exonic changes (Table 2). Their possible effects on splicing were analyzed in silico, and no evidence of a splicing defect was found. Therefore, they were not screened in the respective normal DNA samples or in healthy controls. Two previously unreported missense variations were also observed. Heterozygous V1231A variant in exon 22, proved to be germline and was present in two (2/33, 6.1%) serrated CRC cases. No LOH was detected in corresponding tumor samples (data not shown). This missense variant was also detected in population controls (5/118, 4.2%), and therefore, is likely to be a neutral polymorphism. The other new missense variant was a somatic heterozygous nucleotide change c.955A>G in exon 7, causing M319V amino acid alteration in the first extracellular loop of the protein, observed in a case presenting with microsatellite instability. The protein prediction programs, SIFT and PolyPhen, did not show any impact of the variant on the protein function. In addition, two cases harbored a previously unreported intronic deletion (Table 2). This 1-bp deletion IVS13-18, T8-1del was in a repetitive T track. In silico analyses did not revealed any effects on splicing. Both cases showed MSI.

We also tested the possible associations of the variants to clinicopathological characteristics (Table 1), but no association between these parameters and the variants were detected.

PTCH1 immunoreaction was negative in 48%, weak in 24%, moderate in 20%, and strong in only 8% of the cases (Fig. 2). This observed downregulation of *PTCH1* gene is well in accordance with our previous study, where 67% of the cases showed negative or weak PTCH1 staining pattern [4]. MSI, which is more common feature in serrated than conventional adenocarcinomas [29], was shown in 34% of the cases. No association was observed between PTCH1 staining pattern and MSI status.

MAPK pathway activation by either *KRAS* or *BRAF* mutation was present in 78% of the cases (Table 3). All specimens with mutant *BRAF* harbored wild-type *KRAS* and vice versa.

Discussion

The role of the tumor suppressor gene *PTCH1* in the pathogenesis of colorectal carcinoma has not been thoroughly examined. Here, we have analyzed *PTCH1* mutations in a set of 33 colorectal serrated adenocarcinomas, which unlike conventional CRCs, show downregulation of *PTCH1* in both RNA and protein levels [4]. The whole coding region, as well as exon–intron junctions, were sequenced. Altogether, 19 alterations were present in 82% (27/33) of serrated CRCs (Table 2). The great majority of the alterations (11) were previously known germline polymorphisms, including five silent, one missense, and five intronic SNPs. A dense cluster of coding and intronic SNPs was detected in exon 12 and between exons 9 and 13, respectively (Table 2). Similar kind of clustering of SNPs

Table 3 The prevalence of *BRAF* and *KRAS* mutations in relation to MSI status in serrated adenocarcinoma series

Mutation	Number of samples (%)	MSS tumors	MSI tumors
BRAF V600E mutation	14 (44%)	10	4
KRAS c12/13 mutation	11 (34%)	6	5
BRAF and *KRAS* wild type	7 (22%)	5	2

around this region, containing a putative sterol-sensing domain, has been reported previously, probably reflecting frequent normal variability of this region [13]. The previously described missense variant detected in our study, c.3944C>T (P1315L, rs357564), has been suggested to decrease breast cancer risk in association with the use of oral contraceptives [12]. We did not find any associations between the variant and clinicopathological parameters or MSI status.

In addition to the 11 previously described variants, we identified also eight new *PTCH1* variants, five silent, two missense, and one intronic. All five silent changes were classified as neutral variants, since they did not lead to amino acid change, and no effects on splicing were detected when analyzed in silico. Two new missense changes were identified: V1231A and M319V. The germline missense change V1231A was detected in two serrated CRC cases (2/33, 6.1%) and was found also among cancer-free controls (5/118, 4.2%). There was no significant difference in the frequency of the variant allele between cases and controls suggesting that the change is neutral. Absence of LOH in the respective tumor DNAs also argues against pathogenic nature.

The only detected somatic missense variant M319V locates in the extracellular loop 1 [5, 13]. Both methionine and valine are hydrophobic amino acids, and thus resemble each other for the chemical properties. In addition, when analyzed in silico, M319V was not predicted to have a damaging effect on the PTCH1 protein function. Therefore, it appears unlikely that this sequence variant has a strong effect on the function of the PTCH1 protein.

The only observed single nucleotide deletion, IVS13-18T8-1del, occurred in an intronic repetitive track of nucleotides (T_8). This somatic 1-bp deletion was detected in two MSI tumors and likely represents functionally neutral microsatellite slippage commonly seen in MSI CRCs.

In conclusion, our results indicate that *PTCH1* downregulation in serrated adenocarcinomas cannot be explained by simple inactivating DNA sequence alterations. The presence of large rearrangements and/or deletions cannot be excluded as they cannot be detected by direct sequencing, although the detected 32 heterozygous changes provide some evidence against frequent and large *PTCH1* deletions in the studied cancers. Alternative mechanisms for *PTCH1* downregulation could include, e.g., epigenetic silencing of *PTCH1* or constantly activated MAPK signaling [31, 32]. We have recently observed that serrated adenocarcinomas are characterized by *BRAF* and *KRAS* mutations [30], and also in this study, 78% of the analyzed tumors carried a mutation in either gene (Table 3). Hence, it is conceivable that the loss of PTCH1 protein expression may result from constant activation of MAPK pathway caused by either *KRAS* or *BRAF* mutations. Indeed, in pancreatic cancer, *KRAS* mutations have been reported to activate the Hh signaling pathway downstream of PTCH1 [7]. Further studies are warranted to unravel the mechanism(s) behind the observed downregulation of PTCH1 in serrated colorectal adenocarcinomas. This would increase our knowledge of the development and progression of this intriguing tumor type.

Acknowledgments The authors wish to express sincere gratitude to Mikko Aho, Mairi Kuiris, and Riitta Vuento for their skillful technical assistance and to Anna Vuolteenaho for the linguistic corrections. This study was supported by the Northern Ostrobothnia Hospital District, Oulu, Finland, and by grants from Emil Aaltonen Foundation, Finnish Cancer Society, the Northern Finland Cancer Foundation, the Finnish Cultural Foundation, Ida Montin Foundation, the Instrumentarium Science Foundation, the Research and Science Foundation of Farmos, Sigrid Juselius Foundation, and the Academy of Finland.

Conflict of interest statement We declare that we have no conflict of interest.

References

1. Jemal A, Siegel R, Ward E, Hao Y, Xu J, Murray T, Thun MJ (2008) Cancer statistics, 2008. CA Cancer J Clin 58:71–96
2. Mäkinen MJ (2007) Colorectal serrated adenocarcinoma. Histopathology 50:131–150
3. O'Brien MJ, Yang S, Huang CS, Shepher C, Cerda S, Farraye FA (2008) The serrated polyp pathway to colorectal carcinoma. Diagn Histopathol 14:78–93
4. Laiho P, Kokko A, Vanharanta S, Salovaara R, Sammalkorpi H, Jarvinen H, Mecklin JP, Karttunen TJ, Tuppurainen K, Davalos V, Schwartz S Jr, Arango D, Makinen MJ, Aaltonen LA (2007) Serrated carcinomas form a subclass of colorectal cancer with distinct molecular basis. Oncogene 26:312–320
5. Toftgard R (2000) Hedgehog signalling in cancer. Cell Mol Life Sci 57:1720–1731
6. Ramalho-Santos M, Melton DA, McMahon AP (2000) Hedgehog signals regulate multiple aspects of gastrointestinal development. Development 127:2763–2772
7. Ji Z, Mei FC, Xie J, Cheng X (2007) Oncogenic KRAS activates hedgehog signaling pathway in pancreatic cancer cells. J Biol Chem 282:14048–14055
8. Ma X, Chen K, Huang S, Zhang X, Adegboyega PA, Evers BM, Zhang H, Xie J (2005) Frequent activation of the hedgehog pathway in advanced gastric adenocarcinomas. Carcinogenesis 26:1698–1705
9. Gorlin RJ (2004) Nevoid basal cell carcinoma (Gorlin) syndrome. Genet Med 6:530–539
10. Hahn H, Wicking C, Zaphiropoulous PG, Gailani MR, Shanley S, Chidambaram A, Vorechovsky I, Holmberg E, Unden AB, Gillies S, Negus K, Smyth I, Pressman C, Leffell DJ, Gerrard B, Goldstein AM, Dean M, Toftgard R, Chenevix-Trench G, Wainwright B, Bale AE (1996) Mutations of the human homolog of *Drosophila* patched in the nevoid basal cell carcinoma syndrome. Cell 85:841–851
11. Xie J, Johnson RL, Zhang X, Bare JW, Waldman FM, Cogen PH, Menon AG, Warren RS, Chen LC, Scott MP, Epstein EH Jr (1997) Mutations of the PATCHED gene in several types of sporadic extracutaneous tumors. Cancer Res 57:2369–2372

12. Chang-Claude J, Dunning A, Schnitzbauer U, Galmbacher P, Tee L, Wjst M, Chalmers J, Zemzoum I, Harbeck N, Pharoah PD, Hahn H (2003) The patched polymorphism Pro1315Leu (C3944T) may modulate the association between use of oral contraceptives and breast cancer risk. Int J Cancer 103:779–783
13. Lindstrom E, Shimokawa T, Toftgard R, Zaphiropoulos PG (2006) PTCH mutations: distribution and analyses. Hum Mutat 27:215–219
14. Tanioka M, Takahashi K, Kawabata T, Kosugi S, Murakami K, Miyachi Y, Nishigori C, Iizuka T (2005) Germline mutations of the PTCH gene in Japanese patients with nevoid basal cell carcinoma syndrome. Arch Dermatol Res 296:303–308
15. Gulino A, Ferretti E, De Smaele E (2009) Hedgehog signalling in colon cancer and stem cells. EMBO Mol Med 1:300–302
16. Kolterud A, Grosse AS, Zacharias WJ, Walton KD, Kretovich KE, Madison BB, Waghray M, Ferris JE, Hu C, Merchant JL, Dlugosz AA, Kottmann AH, Gumucio DL (2009) Paracrine Hedgehog signaling in stomach and intestine: new roles for hedgehog in gastrointestinal patterning. Gastroenterology 137:618–628
17. van Dop WA, Uhmann A, Wijgerde M, Sleddens-Linkels E, Heijmans J, Offerhaus GJ, van den Bergh Weerman MA, Boeckxstaens GE, Hommes DW, Hardwick JC, Hahn H, van den Brink GR (2009) Depletion of the colonic epithelial precursor cell compartment upon conditional activation of the hedgehog pathway. Gastroenterology 136(7):2195–2203
18. Yauch RL, Gould SE, Scales SJ, Tang T, Tian H, Ahn CP, Marshall D, Fu L, Januario T, Kallop D, Nannini-Pepe M, Kotkow K, Marsters JC, Rubin LL, de Sauvage FJ (2008) A paracrine requirement for hedgehog signalling in cancer. Nature 455:406–410
19. Chatel G, Ganeff C, Boussif N, Delacroix L, Briquet A, Nolens G, Winkler R (2007) Hedgehog signaling pathway is inactive in colorectal cancer cell lines. Int J Cancer 121:2622–2627
20. Oniscu A, James RM, Morris RG, Bader S, Malcomson RD, Harrison DJ (2004) Expression of Sonic hedgehog pathway genes is altered in colonic neoplasia. J Pathol 203:909–917
21. Bian YH, Huang SH, Yang L, Ma XL, Xie JW, Zhang HW (2007) Sonic hedgehog-Gli1 pathway in colorectal adenocarcinomas. World J Gastroenterol 13:1659–1665
22. Parfitt JR, Driman DK (2007) Survivin and hedgehog protein expression in serrated colorectal polyps: an immunohistochemical study. Hum Pathol 38:710–717
23. Varnat F, Duquet A, Malerba M, Zbinden M, Mas C, Gervaz P, Ruiz i Altaba A (2009) Human colon cancer epithelial cells harbour active HEDGEHOG-GLI signalling that is essential for tumour growth, recurrence, metastasis and stem cell survival and expansion. EMBO Mol Med 1:338–351
24. Yoshikawa K, Shimada M, Miyamoto H, Higashijima J, Miyatani T, Nishioka M, Kurita N, Iwata T, Uehara H (2009) Sonic hedgehog relates to colorectal carcinogenesis. J Gastroenterol 44:1113–1117
25. Wiesner GL, Daley D, Lewis S, Ticknor C, Platzer P, Lutterbaugh J, MacMillen M, Baliner B, Willis J, Elston RC, Markowitz SD (2003) A subset of familial colorectal neoplasia kindreds linked to chromosome 9q22.2-31.2. Proc Natl Acad Sci U S A 100:12961–12965
26. Aaltonen LA, Salovaara R, Kristo P, Canzian F, Hemminki A, Peltomäki P, Chadwick RB, Kääriäinen H, Eskelinen M, Järvinen H, Mecklin JP, de la Chapelle A (1998) Incidence of hereditary nonpolyposis colorectal cancer and the feasibility of molecular screening for the disease. N Engl J Med 338:1481–1487
27. Salovaara R, Loukola A, Kristo P, Kääriäinen H, Ahtola H, Eskelinen M, Härkönen N, Julkunen R, Kangas E, Ojala S, Tulikoura J, Valkamo E, Järvinen H, Mecklin JP, Aaltonen LA, de la Chapelle A (2000) Population-based molecular detection of hereditary nonpolyposis colorectal cancer. J Clin Oncol 18:2193–2200
28. Mäkinen MJ, George SM, Jernvall P, Mäkelä J, Vihko P, Karttunen TJ (2001) Colorectal carcinoma associated with serrated adenoma—prevalence, histological features, and prognosis. J Pathol 193:286–294
29. Tuppurainen K, Mäkinen JM, Junttila O, Liakka A, Kyllönen AP, Tuominen H, Karttunen TJ, Mäkinen MJ (2005) Morphology and microsatellite instability in sporadic serrated and non-serrated colorectal cancer. J Pathol 207:285–294
30. Stefanius K, Ylitalo L, Tuomisto A, Kuivila R, Kantola T, Sirniö P, Karttunen TJ, Mäkinen MJ (2011) Frequent mutations of KRAS in addition to BRAF in colorectal serrated adenocarcinoma. Histopathology (in press)
31. Wolf I, Bose S, Desmond JC, Lin BT, Williamson EA, Karlan BY, Koeffler HP (2007) Unmasking of epigenetically silenced genes reveals DNA promoter methylation and reduced expression of PTCH in breast cancer. Breast Cancer Res Treat 105:139–155
32. Du P, Ye HR, Gao J, Chen W, Wang ZC, Jiang HH, Xu J, Zhang JW, Zhang JC, Cui L (2009) Methylation of PTCH1a gene in a subset of gastric cancers. World J Gastroenterol 15:3799–3806

Virchows Arch (2011) 458:221–229
DOI 10.1007/s00428-010-1007-4

ORIGINAL ARTICLE

Alterations in the tumor suppressor gene *p16*^{INK4A} are associated with aggressive behavior of penile carcinomas

Micaela Poetsch · Martin Hemmerich · Christoph Kakies · Britta Kleist · Eduard Wolf · Frank vom Dorp · Oliver W. Hakenberg · Chris Protzel

Received: 6 August 2010 / Revised: 25 October 2010 / Accepted: 2 November 2010 / Published online: 18 November 2010
© Springer-Verlag 2010

Abstract Alterations in the p16/cyclinD1/Rb and ARF/Mdm2/p53 pathways are frequent events in the pathogenesis of squamous cell carcinomas. Different mechanisms of p16 regulation have been described for penile carcinomas so far. Therefore, expression of p16 and p53 was immunohistochemically detected with monoclonal antibodies in 52 primary invasive penile squamous cell carcinomas. The carcinomas were analyzed for allelic loss (LOH) in *p16*^{INK4A} and *p53*, as well as for mutations in the *p16*^{INK4A} and the *p53* gene. In addition, we examined the promoter status of *p16*^{INK4A} by methylation-specific PCR. The presence of human papilloma virus (HPV) 6/11, HPV 16 and HPV 18 DNA was analyzed by PCR. Data were compared to clinical data. Concerning p16, 26 (50%) tumors showed positive immunohistochemistry, 32 (62%) tumors showed allelic loss and 22 tumors (42%) showed promoter hypermethylation. All tumors with negative p16 immunohistochemistry showed LOH near the *p16*^{INK4A} locus and/or hypermethylation of the *p16*^{INK4A} promoter. HPV 16 DNA was detected in 17 tumors, ten of them with positive p16 immunostaining. The remaining seven tumors with negative p16 staining showed allelic loss and/or promoter hypermethylation. Evidence of lymph node metastasis was significantly associated with negative p16 immunohistochemistry as well as with combined LOH and promoter hypermethylation (p=0.003 and p=0.018, respectively). Allelic loss around p53 was found in 22 tumors (42%), and seven mutations of the p53 gene could be demonstrated in our tumors. No correlations could be found between any p53 alteration and clinical parameters.

Keywords Penile carcinoma · Metastasis · p16 · HPV · LOH

M. Poetsch (✉) · M. Hemmerich
Institute of Legal Medicine, University Hospital Essen,
Hufelandstr. 55,
45122, Essen, Germany
e-mail: micaela.poetsch@uk-essen.de

C. Kakies
Institute of Pathology, University of Rostock,
Rostock, Germany

B. Kleist
Department of Pathology, Soerlandet sykehus Kristiansand,
Kristiansand, Norway

E. Wolf
Institute of Hematopathology and Osteopathology,
Hamburg, Germany

F. vom Dorp
Department of Urology, University Hospital Essen,
Essen, Germany

O. W. Hakenberg · C. Protzel
Department of Urology, University of Rostock,
Rostock, Germany

Introduction

The tumor suppressor genes *p16*^{INK4A} and *p53* play an essential role in prevention of malignant transformation of cells and of tumor progression. Especially the expression of p16 increases at an early stage of tumorigenesis. The tumor suppressor p16 induces cell cycle arrest and prevents cell division by inhibition of the cyclin-dependent kinases CDK4 and CDK6 and inhibition of CDK-mediated phosphorylation of the retinoblastoma (Rb) gene [1].

Expression of p16 increases in reaction to DNA damage including UV damage, oxygen radicals, ionizing radiation, and activating mutations of oncogenes (e.g. RAS) [1, 2]. A close association of oncogenic stress by human papilloma

virus (HPV) infection and increased p16 expression has been described for several tumor entities, including squamous cell carcinomas of the head and neck region and of the cervix uteri [3–5].

Since the presence of HPV DNA is found in 15–71% of penile carcinomas [6–8], depending on detection method and geographical location, a possible role of p16 alterations and HPV was discussed for the carcinogenesis of penile cancer. Due to the low incidence of penile carcinomas in North America and Western Europe, there is scant information about the oncogenesis and tumor progression of this tumor. The limited studies of *p16*^{INK4A} showed conflicting results so far. Overexpression as well as loss of *p16*^{INK4A} tumor suppressor gene has been described in penile carcinoma [9]. The prognostic implications of this phenomenon in patients with penile carcinoma as well as whether all HPV-related tumors show that alterations in the p16^{INK4a} pathway are pending issues that remain unclear. Solving these issues will also permit a better estimation of the putative benefits of HPV vaccination in men.

Besides positive and negative regulation of p16^{INK4A} expression, genetic and epigenetic alteration of the *p16*^{INK4A} gene has been described. Loss of heterozygosity (LOH) at chromosome 9p21, including the *p16* and *ARF* region, is a frequent event in several tumor entities and has been described before for penile carcinomas [10]. Point mutations of *p16*^{INK4A} and—more frequently—silencing of the *p16*^{INK4A} gene by hypermethylation of the promoter have been reported for many human cancers [11, 12]. Therefore, we examined the mechanisms of p16 regulation in penile squamous carcinoma (PSCC), including HPV analysis. Since regulation of the tumor suppressor gene *p53* is closely related to p16 (ARF and p21 pathways) and alterations of p53 have been described for penile cancer, we additionally investigated p53 expression and genetic alterations in the *p53* gene area.

Furthermore, we analyzed clinical data and examined the prognostic role of p16 and p53 alterations for lymph node metastases and prognosis in penile cancer.

Materials and methods

Patients

Fifty-two patients (median patient age, 59.8 years, range 22–89 years) with invasive PSCC treated at the University Hospital of Greifswald, Helios Hospital Schwerin and University Hospital of Essen were available for investigation. Follow-up data were available from all but three patients. Median follow-up was 44.2 months (range, 2–105). Patient data and tissues were obtained and used after advice from the Medical Ethics Committee of the University of Greifswald and University of Essen in accordance with the declaration of Helsinki and the International Conference of Harmonisation—Good Clinical Practice. The anonymity of the patients investigated was preserved corresponding to rules of data protection of the Human Medical Faculty Greifswald and the Human Medical Faculty Essen.

The samples from 52 patients comprised 15 pT1 (28.8%), 24 pT2 (46.2%), 12 pT3 (23.1%), and 1 pT4 (1.9%) tumors. Lymph node metastases were diagnosed in 32 patients (61.5%). Forty-one tumors were conventional squamous cell carcinoma (SCC). Moreover, four patients with basaloid variants of SCC, three patients with verrucous variants, and one patient each with a papillary, a condylomatous, and two sarcomatoid variants of SCC were included in this study. Lymphadenectomy was done within 2–4 weeks after operation of the primary tumor according to the recommendations of the EAU Guidelines. Dynamic sentinel lymph node dissection was done in three patients; all other patients underwent modified or radical lymphadenectomy depending on the extension of lymph node metastasis. Six elderly patients underwent radiotherapy for histologically confirmed inguinal lymph node metastases. Due to micrometastasis or pathological preparations, enough material for DNA extraction was available only in ten metastases.

Representative tumor tissue samples with adjacent non-neoplastic tissue allowing sufficient classification and grading were obtained during surgery and subjected to 4% buffered formalin. For each patient, DNA was extracted from tumor tissue samples as well as non-neoplastic tissue. Pathological classification was done on hematoxylin and eosin stained specimen. All specimens underwent additional independent histopathological review (CK, EW). Tumors were staged according to the 2002 TNM system, histological grading was classified as follows: grade 1 (G1), well-differentiated; grade 2 (G2), moderately differentiated; and grade 3 (G3), poorly differentiated [13]. The tumors were additionally histologically subtyped according WHO classification [14].

Immunohistochemistry

Immunohistochemistry was done on paraffin sections (4 μm). After blocking of endogenous peroxidase activity (Peroxydazed 1, Biocarta, Hamburg, Germany, 5 min 22°C), sections were subjected to heat antigen retrieval (microwave oven, 700 W, 20 min) using 10 mM citrate buffer (pH 6.0). After cooling in citrate buffer and subsequent washings in phosphate-buffered saline (PBS), immunohistochemistry was performed using a staining kit (Biocarta). Application of blocking solution (Biocarta, 10 min) was followed by overnight incubation with

monoclonal antibodies against p16 (Novocastra, UK) and p53 (Dako, Denmark) at 4°C. After two washes in PBS (2×5 min), antibody binding was achieved using the 4plus™ Universal Immunoperoxidase Detection System (Biocarta). Sections were incubated with secondary antibody (20 min, 22°C) and washed in PBS (2×5 min). Slides were subjected to streptavidin–horseradish peroxidase (HRP) solution (Biocarta, 10 min). Visualization was performed after washing in PBS (2×5 min) with 0.1% diamino-benzidine (Sigma) in PBS/0.01% H_2O_2 (3–8 min). Slides were counterstained with hematoxylin, dehydrated and mounted in Neo-mount (Merck, Darmstadt, Germany). Control reactions were done by (1) using PBS instead of primary antibody and (2) replacing the primary antibodies with a monoclonal antibody (β1-integrin, Biomol, Hamburg, Germany) not reactive in paraffin sections. Photographs were taken on an Olympus Bx50 microscope equipped with an Olympus DP 10 digital camera.

The percentage of p16- and p53-positive tumor cells was evaluated by three independent observers (CK, EW, and BK), and intensity was measured by percentage of stained tumor cells. According to previous studies, expression of p16 was classified as negative (<5% of the tumor cells positive) or positive (>5% of the tumor cells positive), while the expression of p53 was classified as weak expression (<20% of the tumor cells positive) or overexpression (>20% of tumor cells positive) [15–17].

DNA extraction

For DNA extraction, hematoxylin and eosin stained slides were carefully inspected by light microscopy to identify areas that carry a sufficient amount (at least 3 mm^2) of tumor tissue measured by a scaled optical adjustment. This same area was then identified on the unstained 10 μm dewaxed, rehydrated, and air-dried tissue section, which was fixed in an optical installation allowing the separate isolation of predominantly tumor tissue without adherent non-tumorous structures under microscopical control with a cannula (used for intravenous injections). DNA isolation from paraffin-embedded tissue was performed as previously described [18, 19] with the High Pure PCR Template Preparation Kit (Roche Molecular Biochemicals, Mannheim, Germany) and the innuPrep DNA Minikit (Analytik Jena, Jena, Germany). Quality of DNA was assessed by agarose gel electrophoresis.

Human papilloma virus DNA

The amplification of HPV6/11, HPV16, and HPV18 DNA was detected in a multiplex PCR with primer sequences as described by Sotlar et al. [20] with fluorescence-labeled primers. The products were analyzed on an ABIPrism310 Genetic Analyzer. To prove the presence of amplificable DNA in the extractions, all of them were amplified with primers for the human beta-globin gene.

LOH analysis

The following nine microsatellite loci were studied: D9S1604, D9S1748, D9S161, D9S286, D9S162, and D9S171 (9p21, covering the $p16^{INK4A}$ region) and D17S513 (17p13), D17S786, and D17S952 (17p, around *p53*). Primer sequences and cytogenetic locations were obtained from Ensembl Data Base (http://www.ensembl.org). PCR amplification was performed in multiplex assays with fluorochrome-labeled primers (6-FAM, JOE, or TAMRA) in 12.5-μl sample volumes with 2–5 ng of genomic tumor or nonneoplastic DNA as template in 15 mM Tris/HCl, 50 mM KCl, with 200 μM dNTPs, 1.5 mM $MgCl_2$, 0.1 nM primers, and 1 U HotStart Taq Polymerase (Applied Biosystems, Darmstadt, Germany). An initial denaturation and activation step of 8 min at 95°C was followed by 30–35 cycles of 1 min at 95°C, 1 min at 55–58°C, and 2 min at 72°C, and a 30 min final elongation step at 72°C. PCR products were analyzed on an ABI310 genetic analyzer (Applied Biosystems, Darmstadt, Germany) with ROX-labeled internal lane standard. All PCR assays were repeated at least once. LOH was scored if one allele was >90% decreased in tumor DNA when compared with the same allele in normal control DNA in both PCR assays.

Sequencing analysis

Mutation analysis of $p16^{INK4A}$ was carried out with primers as described before [21]. For mutation analysis of *p53*, the exons 5, 7, and 8 were amplified using primers as described by Yano et al. [22]; for exon 6, we designed new primers as follows: forward, 5′CCAGGCCTCTGATTCCTCA and reverse, 5′TTAACCCCTCCTCCCAGAGA.

PCR amplification was performed in 12.5-μl sample volumes with 2–5 ng of genomic tumor or nonneoplastic DNA as template in 15 mM Tris/HCl, 50 mM KCl, with 200 μM dNTPs, 1.5 mM $MgCl_2$, 0.1 nM primers, and 1 U HotStart Taq Polymerase (Applied Biosystems). An initial denaturation and activation step of 8 min at 95°C was followed by 30–35 cycles of 1 min at 95°C, 1 min at 55–62°C, and 2 min at 72°C, and a 30-min final elongation step at 72°C. Sequencing was always carried out in both directions with the BigDye sequencing kit (Applied Biosystems). Each polymorphism or mutation was verified by a second sequencing reaction of an independent amplification product.

Methylation analysis

Methylation analysis of $p16^{INK4A}$ promoter was performed on tumor DNA and nonneoplatic DNA as described by Liu et al. in a two-stage methylation specific PCR [23]. Bisulfite treatment was done with the EpiTect Biosulfite kit (Qiagen, Hilden, Germany) according to the manufacturer's instructions. PCR products were evaluated on silver-stained polyacrylamide gels.

Statistical analysis

Descriptive statistical data were reported in terms of mean values and standard deviation. The chi-square test was used to examine the association among p16 and p53 expression and genomic alteration and clinical parameters. A $p<0.05$ was considered statistically significant.

Results

All 52 primary tumors and ten metastases were investigated for expression of p16 and p53, presence of HPV DNA, LOH in microsatellite markers surrounding the genes $p16^{INK4A}$ and *p53*, as well as promoter methylation of the $p16^{INK4A}$ gene (Table 1).

$p16^{INK4A}$

Overexpression of p16 was found in 26 primary tumors (50%), including all four basaloid SCCs as well as two verrucous SCCs (Fig. 1a). In contrast, one half of conventional PSCCs, the condylomatous, papillar, and sarcomatoid variants expressed no p16 (Fig. 1b).

Promoter hypermethylation of the $p16^{INK4A}$ gene was observed in 22 primary penile carcinomas (42%) and seven metastases, and loss of heterozygosity in at least one microsatellite marker around this gene was detected in 32 primary tumors (62%) and eight metastases (Fig. 2a), while 16 tumors (31%) did not show loss of heterozygosity or promoter methylation. Mutations were evident in only five tumors. None of these genetic aberrations could be found in non-neoplastic DNA.

Negative p16 protein expression status was detected significantly more often in those penile carcinoma in which a methylation of the $p16^{INK4A}$ promoter or loss of heterozygosity in at least one microsatellite marker around the $p16^{INK4A}$ gene occurred ($p<0.0001$), independent of the detection of HPV DNA. All tumors with negative p16 immunohistochemistry showed LOH near the $p16^{INK4A}$ locus and/or hypermethylation of the $p16^{INK4A}$ promoter.

p53

Overexpression of p53 was found in 29 of 50 primary carcinomas (58%; in two primary carcinomas, no analysis of p53 was possible due to material shortage) and four metastases (Fig. 1c), whereas weak expression of p53 was detected in the remaining 21 carcinomas (Fig. 1d). LOH in at least one microsatellite marker surrounding the p53 gene was found in 22 primary tumors (44%), including the sarcomatoid, condylomatous, papillar, and one verrucous subtype as well as 46% of conventional SCCs, and four metastases (Fig. 2b). Four primary carcinomas displayed five missense mutations in the p53 gene (Fig. 3). An additional missense mutation was detected in a skin metastasis, one nonsense mutation in a lymph node metastasis. There was neither a significant association

Table 1 Analysis of p16 and p53 in penile cancer

Pathological data	p16-positive staining, *n* (%)	$p16^{INK4A}$ methylation, *n* (%)	$p16^{INK4A}$ LOH, *n* (%)	$p16^{INK4A}$ meth-/LOH-, *n* (%)	p53 overexpression, *n* (%)	*p53* LOH, *n* (%)	HPV6/11 DNA, *n* (%)	HPV16/18 DNA, *n* (%)	Any HPV DNA, *n* (%)
All carcinomas (*n*=52)	26 (50)	22 (42)	32 (61)	16 (31)	29/50 (58)	22 (42)	2 (4)	18 (35)	20 (38)
Conventional SCCs (*n*=39)	20 (49)	19 (46)	27 (66)	11 (27)	24/39 (62)	17 (41)	2 (5)	13 (31)	15 (38)
Basaloid SCCs (*n*=4)	4 (100)	0	1 (25)	3 (75)	1/4 (25)	0	1 (33)	3 (75)	4 (100)
Verrucous SCCs (*n*=3)	2 (67)	1 (33)	1 (33)	2 (67)	2 (67)	1 (33)	0	0	0
Condylomatous SCCs (*n*=1)	0	0	1 (100)	0	0	1 (100)	0	0	0
Papillary SCCs (*n*=1)	0	1 (100)	1 (100)	0	1 (100)	1 (100)	0	0	0
Sarcomatoid SCCs (*n*=2)	0	1 (50)	1 (50)	0	1 (50)	1 (50)	0	1 (50)	1 (50)

between genetic alteration of *p53* and p53 expression nor between p16 and p53 expression in tumors of our study. Moreover, we were not able to show a correlation between LOH in the 9p21 area (*ARF* region) and the expression of p53 in penile carcinomas of our study.

Human papilloma virus DNA

HPV DNA was detected in 20 tumors, in detail 17 HPV16 (33%), one HPV18 (2%), and two HPV6/11 (4%). Ten HPV 16 positive tumors showed a positive $p16^{INK4A}$ staining. The remaining seven tumors with negative staining showed allelic loss and/or promoter hypermethylation ($p=0.035$). The HPV 18 positive tumor was found to have negative $p16^{INK4A}$ staining and allelic loss and promoter hypermethylation. Positive $p16^{INK4A}$ staining and no allelic loss/promoter hypermethylation were observed in both HPV 6/11 positive tumors.

There was no association between the presence of HPV DNA and expression of p53 (eight p53 negative tumors with HPV16 vs. ten p53 positive tumors with HPV16; $p=0.77$), but 56% of the tumors with positive p16 staining and no HPV-DNA showed a p53 expression.

Correlation with clinical data

Negative p16 immunohistochemistry was significantly associated with the occurrence of lymph node metastasis ($p=0.003$). Loss of heterozygosity around $p16^{INK4A}$ and promoter hypermethylation could be found more frequently in carcinomas with metastasis (Table 2). A combination of LOH and promoter hypermethylation was also significantly associated with lymph node metastases. Patients with positive p16 immunohistochemistry showed a better prognosis, but the Kaplan–Meier analysis failed to show statistical significance ($p=0.381$). There was no significant association between p16 expression and local tumor stage (T stage).

Analyses of p53 expression, LOH, or mutations in the *p53* locus and clinical data failed to show a statistical significance (data not shown).

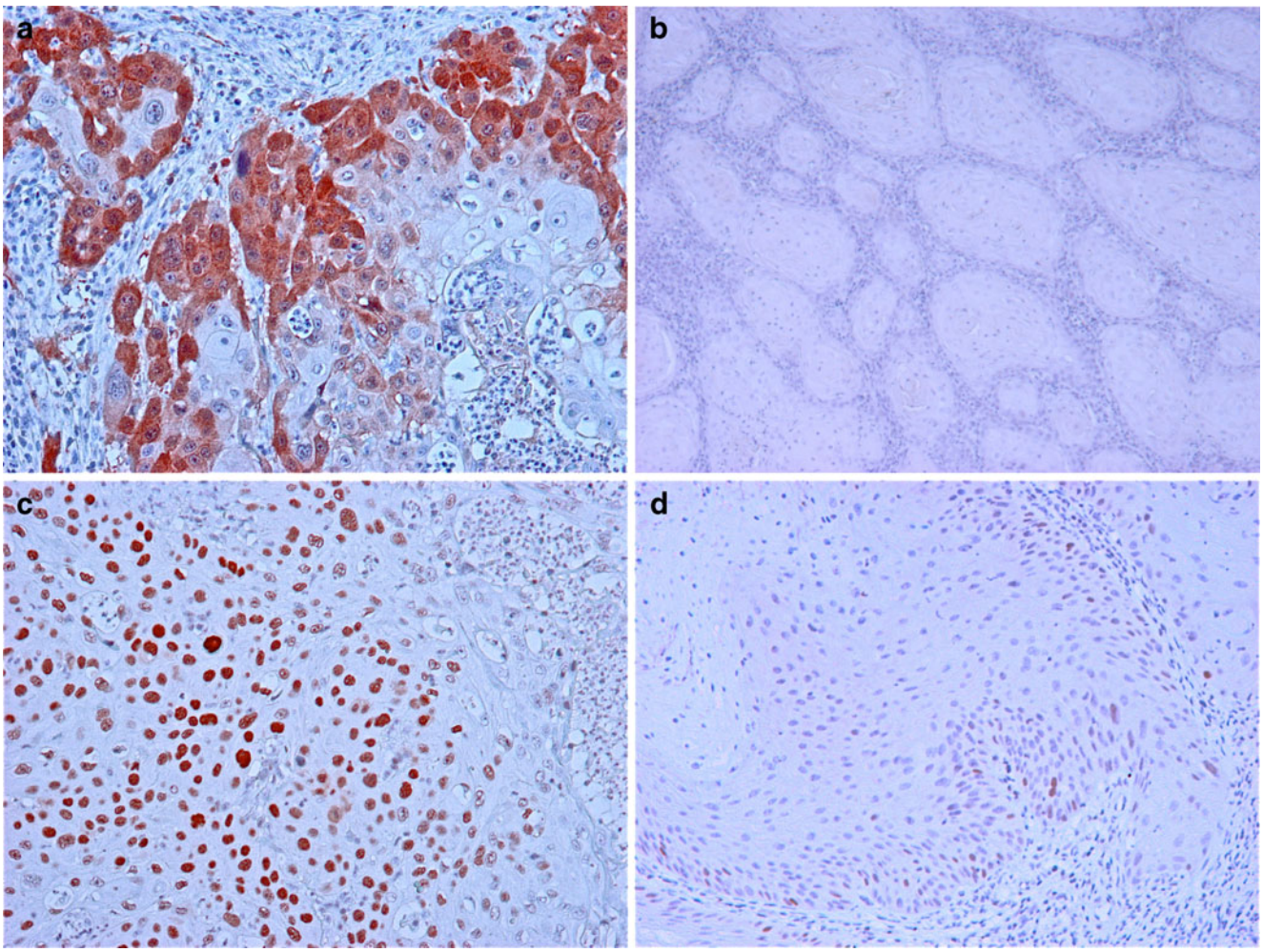

Fig. 1 Representative photomicrographs for p16 and p53 immunohistochemistry in squamous cell carcinomas of the penis: **a** positive p16 immunohistochemistry, **b** negative p16 immunohistochemistry, **c** strong expression of p53, and **d** weak expression of p53

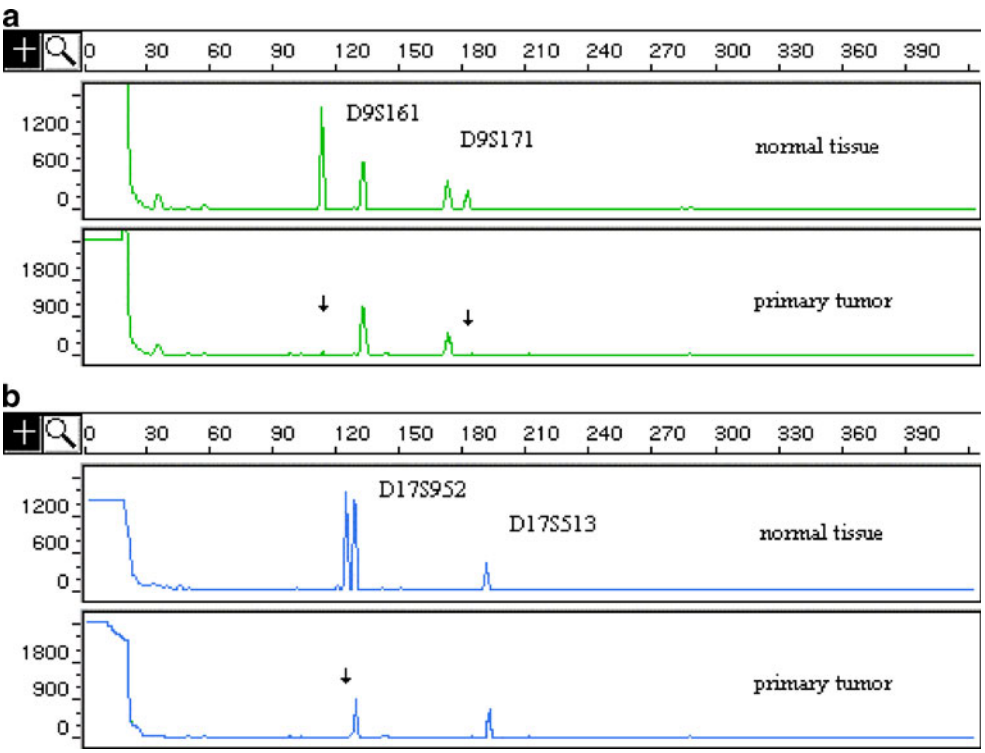

Fig. 2 Electropherogram of microsatellite loci in a penile primary tumor and the corresponding normal tissue. The *y*-axis represents the peak height in fluorescence units. The *arrows* mark the lost alleles. **a** D9S161 and D9S171 show LOH in the primary tumor. **b** D17S952 shows LOH, whereas D17S513 is not informative

Discussion

The overall HPV DNA detection rate in the primary tumors of this study is 35.8%, which is in line with results from other working groups regarding European countries [7, 9, 24, 25]. The HPV DNA detection rate depends on the sensitivity of the detection method and on the number of HPV subtypes investigated. Given that only four HPV genotypes were investigated in this study, we cannot rule out either an HPV infection by other genotypes or absence of viral infection in our HPV negative cases. In accordance with data from Stankiewicz et al. [26], none of the verrucous carcinomas displayed an HPV infection.

Overexpression of p16 was found in several squamous cell carcinomas of different origins. While p16 overexpression is essentially associated with the presence of HPV-DNA in nearly 100% of cervical carcinomas, a relevant part of head and neck carcinomas and vulvar

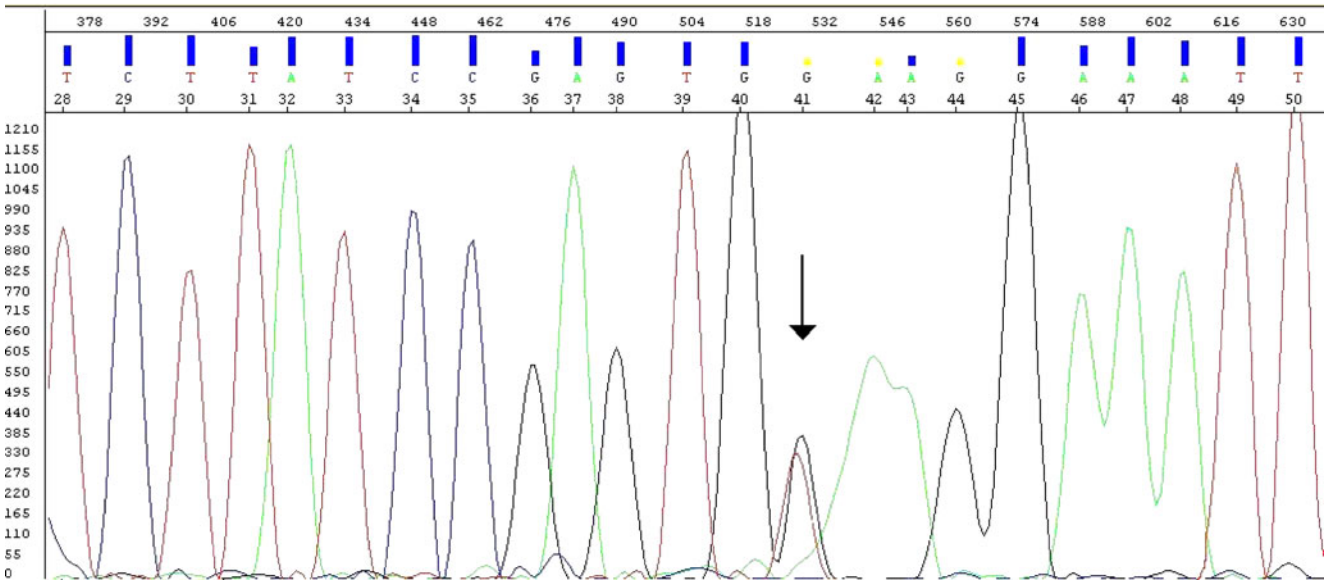

Fig. 3 Electropherogram of a sequencing reaction. Codon 198 of the *p53* gene (exon 6) in a conventional SCC; a heterozygous G/T is displayed at the first position of this codon (*arrow*), resulting in a nonsense mutation

Table 2 Statistical examination of p16 immunohistochemistry, methylation status, LOH, and HPV-DNA

	$p16^{INK4}$ staining pos. (n=26)	$p16^{INK4}$ staining neg. (n=26)	p value (chi-square)
Presence of HPV DNA	12 (46%)	8 (27%)	0.20
$p16^{INK4A}$ methylation	3 (12%)	19 (73%)	<0.0001
$p16^{INK4A}$ LOH	8 (31%)	24 (92%)	<0.0001
No $p16^{INK4A}$ methyl. and no $p16^{INK4A}$ LOH	16 (62%)	0	<0.0001

carcinomas shows p16 overexpression in the absence of HPV infection [27–29]. Our results show that overexpression of p16 is a frequent event also in penile carcinomas, although not necessarily associated with the presence of HPV DNA. Several other pathways have to be taken into consideration, since we found p16- and p53-positive carcinomas without the presence of HPV-DNA. Overexpression of p16 is also frequently seen in tumors, which are unrelated to HPV [30], and has even been described in HPV-independent squamous dysplasias [31].

Recently, a variety of studies focused on p16 alterations in penile cancer, but with different emphases. Ferreux found an overexpression of p16 in 29% of penile carcinomas, especially in connection with HPV infection [9]. Prowse et al. detected p16 overexpression in 46% of penile SCCs, which was significantly associated with HPV infection [24]. In contrast, Senba et al. described p16 overexpression in an equal amount of HPV-positive and HPV-negative penile carcinomas from Kenya [32].

Interestingly, all HPV16 positive tumors in our study showed a positive p16 immunoreaction, except those with allelic loss in the $p16^{INK4A}$ region and/or promoter hypermethylation. HPV DNA-positive but p16-negative tumors have been described for head and neck tumors, but the pathogenesis remains unclear so far [33].

Our results propose at least two important ways of p16 inactivation since all p16 negative tumors showed LOH in the $p16^{INK4A}$ gene locus and/or promoter hypermethylation. A significant role of LOH at chromosome 9p21 was reported for penile carcinomas in an earlier study [10]. Allelic loss in the $p16^{INK4A}$ region was found in over 60%, and promoter hypermethylation was evident in over 40% of the tumors of our study. Yanagawa et al. reported $p16^{INK4A}$ methylation in 26% of penile carcinomas, exclusively in those without HPV DNA [8]. Ferreux et al. found $p16^{INK4A}$ methylation in 17% of tumors, only in HPV negative ones with the exception of two tumors [9]. In agreement with data from Ferreux et al., 75% of penile carcinomas of this study with $p16^{INK4A}$ promoter methylation displayed no p16 staining. The crucial role of $p16^{INK4A}$ alterations is underlined by the significant association of LOH and promoter hypermethylation with the occurrence of lymph node metastasis.

Inactivation of the tumor suppressor $p16^{INK4A}$ seems to play an important role in tumor progression and dissemination [34]. In accordance to squamous cell carcinomas of other origins, we were able to demonstrate a more aggressive behavior of p16-negative tumors. Besides its impact in suppression of cell division, p16 seems to play a major role in suppression of lymphangiogenesis and lymphatic metastasis, since in vivo re-expression of p16 inhibited the process of lymphangiogenesis in pancreatic cancer [35].

The tumor suppressor gene *p53* is the second important key holder in the cell cycle that is, like p16, connected to the oncoproteins of HPV-DNA. Furthermore, a close connection of the ARF/MDM2/p53 and the $p16^{INK4}$/RB pathways is known. ARF, a part of the INK4a/ARF/INK4b locus at 9p21, acts "upstream" of p53 by antagonizing the p53-negative regulator MDM2 [2]. Expression of p53 is closely related to p16 expression (p21 pathway), and expression of both tumor suppressor genes is partly influenced by the same regulators [1, 2]. Since strong expression of p53 has been shown to be associated with metastasis and poor prognosis in penile carcinomas [36, 37], we additionally examined the expression of p53, searched for allelic losses and mutations in the *p53* gene, and compared p53 expression to HPV status, LOH in 9p21, and p16 expression.

There are slightly more data regarding the overexpression of p53 than the expression status of p16. However, the results vary greatly between 26% and 91% [8, 32, 36, 38, 39]. Moreover, correlations between p53 overexpression and HPV status or *p53* mutations also display a very heterogenous picture. Gentile et al. reported that all HPV-positive penile carcinomas had an overexpression of p53 [39], whereas Yanagawa found p53 staining in 67% of HPV-positive and 48% of HPV-negative tumors [8] and Levi et al. in a quarter of HPV-positive and HPV-negative carcinomas [38]. In this study, p53 overexpression was seen in about one third of penile tumors with and without HPV DNA. There was no significant difference in p53 expression in HPV-DNA positive or negative tumors. Regulation of p53 expression remains a multifactor process. We showed that *p53* mutations play a minor role in penile cancer, while LOH in the *p53* locus is frequently found.

Allelic loss and mutations are also only one possibility for p53 alteration in penile cancer, since we did not found a significant association between p53 expression status and genetic alterations.

There was no significant association between allelic loss in the *ARF* gene locus and expression of p53 in penile carcinomas, demonstrating once more that ARF-mediated activation is only one pathway in p53 regulation. On the other hand, there may be HPV-independent ways of coactivation of p53 and p16, since over 50% of HPV-negative tumors with positive p16 expression showed also p53 activation.

Surprisingly, we did not found a significant association of p53 expression and lymph node metastasis in the patients of our study. This may be a result of the limited number of patients, but it underlines the problems of the prognostic role of immunohistochemical detection in clinical praxis [40].

Our data underline the important role of alterations of tumor suppressor genes *p16* in carcinogenesis, invasion, and dissemination of penile carcinomas. We were able to demonstrate that promoter hypermethylation and allelic loss are the most important ways for p16 inactivation in penile cancer. Re-expression of p16 may be a future target in new anti-neoplastic treatment regimens. Due to the limited number of patients in the study, the preliminary results should be confirmed in a larger study.

Conflict of interest statement We declare that we have no conflict of interest.

References

1. Kim WY, Sharpless NE (2006) The regulation of INK4/ARF in cancer and aging. Cell 127:265–275
2. Sherr CJ (2000) The Pezcoller lecture: cancer cell cycles revisited. Cancer Res 60:3689–3695
3. zur Hausen H (2009) Papillomaviruses in the causation of human cancers—a brief historical account. Virology 384:260–265
4. Munoz N, Bosch FX, de Sanjose S, Tafur L, Izarzugaza I, Gili M, Viladiu P, Navarro C, Martos C, Ascunce N et al (1992) The causal link between human papillomavirus and invasive cervical cancer: a population-based case–control study in Colombia and Spain. Int J Cancer 52:743–749
5. Weinberger PM, Yu Z, Haffty BG, Kowalski D, Harigopal M, Brandsma J, Sasaki C, Joe J, Camp RL, Rimm DL, Psyrri A (2006) Molecular classification identifies a subset of human papillomavirus-associated oropharyngeal cancers with favorable prognosis. J Clin Oncol 24:736–747
6. Rubin MA, Kleter B, Zhou M, Ayala G, Cubilla AL, Quint WG, Pirog EC (2001) Detection and typing of human papillomavirus DNA in penile carcinoma: evidence for multiple independent pathways of penile carcinogenesis. Am J Pathol 159:1211–1218
7. Lont AP, Kroon BK, Horenblas S, Gallee MP, Berkhof J, Meijer CJ, Snijders PJ (2006) Presence of high-risk human papillomavirus DNA in penile carcinoma predicts favorable outcome in survival. Int J Cancer 119:1078–1081
8. Yanagawa N, Osakabe M, Hayashi M, Tamura G, Motoyama T (2008) Detection of HPV-DNA, p53 alterations, and methylation in penile squamous cell carcinoma in Japanese men. Pathol Int 58:477–482
9. Ferreux E, Lont AP, Horenblas S, Gallee MPW, Raaphorst FM, von Knebel DM, Meijer CJLM, Snijders PJF (2003) Evidence for at least three alternative mechanisms targeting the p16INK4A/Cyclin D/Rb pathway in penile carcinoma, one of which is mediated by high-risk human papillomavirus. J Pathol 201:109–118
10. Poetsch M, Schuart B-J, Schwesinger G, Kleist B, Protzel C (2007) Screening of microsatellite markers in penile cancer reveals differences between metastatic and non-metastatic carcinomas. Mod Pathol 20:1069–1077
11. Forbes S, Clements J, Dawson E, Bamford S, Webb T, Dogan A, Flanagan A, Teague J, Wooster R, Futreal PA, Stratton MR (2006) Cosmic 2005. Br J Cancer 94:318–322
12. Esteller M, Corn PF, Baylin SB, Herman JG (2001) A gene hypermethylation profile of human cancer. Cancer Res 61:3225–3229
13. Sobin LH, Wittekind C (2002) TNM classification of malignant tumours, 6th edn. Wiley-Liss, New York
14. Eble JN, Sauter G, Epstein JI, Sesterhenn IA (2004) World Health Organization classification of tumours. Pathology and genetics of tumours of the urinary system and male genital organs. IARC, Lyon, pp 280–290
15. Hendricksen K, Moonen PM, der Heijden AG, Witjes JA (2006) False-positive lesions detected by fluorescence cystoscopy: any association with p53 and p16 expression? World J Urol 24:597–601
16. Kong CS, Balzer BL, Troxell ML, Patterson BK, Longacre TA (2007) p16INK4A immunohistochemistry is superior to HPV in situ hybridization for the detection of high-risk HPV in atypical squamous metaplasia. Am J Surg Pathol 31:33–43
17. Stelow EB, Shaco-Levy R, Bao F, Garcia J, Klimstra DS (2010) Pancreatic acinar cell carcinomas with prominent ductal differentiation: mixed acinar ductal carcinoma and mixed acinar endocrine ductal carcinoma. Am J Surg Pathol 34:510–518
18. Poetsch M, Dittberner T, Woenckhaus C (2001) *PTEN/MMAC1* in malignant melanoma and its importance for tumour progression. Cancer Genet Cytogenet 125:21–26
19. Poetsch M, Zimmermann A, Wolf E, Kleist B (2005) Loss of heterozygosity occurs predominantly, but not exclusively in the epithelial compartment of pleomorphic adenoma. Neoplasia 7:688–695
20. Sotlar K, Diemer D, Dethleffs A, Hack Y, Stubner A, Vollmer N, Menton S, Menton M, Dietz K, Wallwiener D, Kandolf R, Bültmann B (2004) Detection and typing of human papillomavirus by E6 nested multiplex PCR. J Clin Microbiol 42:3176–3184
21. Poetsch M, Lorenz G, Kleist B (2002) Detection of new *PTEN/MMAC1* mutations in head and neck squamous cell carcinomas with loss of chromosomes 10. Cancer Genet Cytogenet 132:20–24
22. Yano M, Hamatani K, Eguchi H, Hirai Y, MacPhee DG, Sugino K, Dohi K, Itamoto T, Asahara T (2007) Prognosis in patients with hepatocellular carcinoma correlates to mutations of *p53* and/or *hMSH2* genes. Eur J Cancer 43:1092–1100
23. Liu Y, Lan Q, Siegfried JM, Luketich JD, Keohavong P (2006) Aberrant promoter methylation of p16 and MGMT genes in lung tumors from smoking and never-smoking lung cancer patients. Neoplasia 8:46–51
24. Prowse DM, Ktori EN, Chandrasekaran D, Prapa A, Baithun S (2008) Human papillomavirus-associated increase in p16INK4A expression in penile lichen sclerosus and squamous cell carcioma. Br J Dermatol 158:261–265

25. Pascual A, Pariente M, Godinez JM, Sánchez-Prieto R, Atienzar M, Segura M, Poblet E (2007) High prevalence of human papillomavirus 16 in penile carcinoma. Histol Histopathol 22:177–183
26. Stankiewicz E, Kudahette SC, Prowse DM, Ktori E, Cuzick J, Ambroisine L, Zhang X, Watkin N, Corbishley C, Berney DM (2009) HPV infection and immunochemical detection of cell-cycle markers in verrucous carcinoma of the penis. Mod Pathol 22:1160–1168
27. Walboomers JM, Jacobs MV, Manos MM, Bosch FX, Kummer JA, Shah KV, Snijders PF, Peto J, Meijer CJ, Munoz N (1999) Human papillomavirus is a necessary cause of invasive cervical cancer worldwide. J Pathol 189:12–19
28. Singhi AD, Westra WH (2010) Comparison of human papillomavirus in situ hybridization and p16 immunohistochemistry in the detection of human papillomavirus-associated head and neck cancer based on a prospective clinical experience. Cancer 116:2166–2173
29. van de Nieuwenhof HP, van Kempen LC, de Hullu JA, Bekkers RL, Bulten J, Melchers WJ, Massuger LF (2009) The etiologic role of HPV in vulvar squamous cell carcinoma fine tuned. Cancer Epidemiol Biomarkers Prev 18:2061–2067
30. Mulvany NJ, Allen DG, Wilson SM (2008) Diagnostic utility of $p16^{INK4a}$: a reappraisal of its use in cervical biopsies. Pathology 40:335–344
31. Galmiche L, Coste-Burel M, Lopez P, Phillippe HJ, Laboisse C (2006) The expression of $p16^{INK4a}$ is not correlated with HPV status in CIN 1. Histopathology 48:767
32. Senba M, Buziba N, Mori N, Wada A, Irie S, Toriyama K (2009) Detection of human papillomavirus and cellular regulators p16INK4a, p53, and NF.kappaB in penile cancer cases in Kenya. Acta Virol 53:43–48
33. Smith EM, Rubenstein LM, Hoffman H, Haugen TH, Turek LP (2010) Human papillomavirus, p16 and p53 expression associated with survival of head and neck cancer. Infect Agent Cancer 5:4
34. Karamitopoulou E, Zlober I, Koumarianou A, Patsouris ES, Peros G, Lugli A (2010) Expression of p16 in lymph node metastases of adjuvantly treated stage III colorectal cancer patients identifies poor prognostic subgroups: a retrospective analysis of biomarkers in matched primary tumor and lymph node metastases. Cancer 116:4474–4486
35. Schulz P, Scholz A, Rexin A, Hauff P, Schirner M, Wiedenmann B, Detjen K (2008) Inducible re-expression of p16 in an orthotopic mouse model of pancreatic cancer inhibits lymphangiogenesis and lymphatic metastasis. Br J Cancer 99:110–117
36. Lopes A, Bezerra AL, Pinto CA, Serrano SV, de Mello CA, Villa LL (2002) p53 as a new prognostic factor for lymph node metastasis in penile carcinoma: analysis of 82 patients treated with amputation and bilateral lymphadenectomy. J Urol 168:81–86
37. Martins AC, Faria SM, Cologna AJ, Suaid HJ, Tucci S Jr (2002) Immunoexpression of p53 protein and proliferating cell nuclear antigen in penile carcinoma. J Urol 167:89–93
38. Levi JE, Rahal P, Sarkis AS, Villa L (1998) Human papillomarvirus DNA and p53 status in penile carcinomas. Int J Cancer 76:779–783
39. Gentile V, Vicini P, Giacomelli L, Cardillo MR, Pierangeli A, Degener AM (2006) Detection of human papillomavirus DNA, p53 and ki67 expression in penile carcinomas. Int J Immunopathol Pharmacol 19:209–215
40. Goebell PJ, Groshen SG, Schmitz-Drager BJ (2010) p53 immunohistochemistry in bladder cancer—a new approach to an old question. Urol Oncol 28:377–388

Virchows Arch (2011) 458:231–235
DOI 10.1007/s00428-010-1004-7

ORIGINAL ARTICLE

The development of hepatoportal sclerosis and portal hypertension due to didanosine use in HIV

Thomas D. Schiano · Alison Uriel · Douglas T. Dieterich · M. Isabel Fiel

Received: 6 August 2010 / Revised: 16 October 2010 / Accepted: 19 October 2010 / Published online: 6 November 2010
© Springer-Verlag 2010

Abstract Hepatoportal sclerosis (HPS) is one of several entities known to cause noncirrhotic portal hypertension. To date, its etiology is unknown. There have been increasing reports of HPS occurring in patients with human immunodeficiency virus (HIV), and the US Food and Drug Administration (FDA) recently issued an advisory regarding the development of noncirrhotic portal hypertension in association with didanosine (ddI) use. We report on a patient with HIV who had taken ddI for 4 years and who developed portal hypertension. Histopathological review of paired liver biopsies showed an initial drug hepatotoxicity, microvascular liver injury, and the presence of HPS. Despite cessation of ddI, the latter biopsy showed resolution of the drug-induced injury, but it also showed progression of the HPS. The patient's portal hypertension also progressed suggestive of an unremitting vascular injury. This case demonstrates the development of HPS resulting from a drug-induced microvascular injury. The paired biopsies demonstrate that the initial vascular injury may disappear but that the portal hypertension and HPS progress.

Keywords HIV · Noncirrhotic portal hypertension · Hepatoportal sclerosis · Nodular regenerative hyperplasia · Didanosine · Antiretroviral therapy

T. D. Schiano · A. Uriel · D. T. Dieterich
Division of Liver Diseases, Department of Medicine,
The Mount Sinai Medical Center,
New York, NY, USA

M. I. Fiel (✉)
Department of Pathology, The Mount Sinai Medical Center,
Box 1194, One Gustave Levy Place,
New York, NY, USA
e-mail: Mariaisabel.fiel@mountsinai.org

Introduction

Hepatoportal sclerosis (HPS) and nodular regenerative hyperplasia (NRH) are two of several entities that are known to cause portal hypertension in the absence of cirrhosis [1, 2]. Unlike NRH which has several well-documented causes (medications such as azathioprine, collagen vascular, and myeloproliferative diseases, etc.) [3], HPS, to date, has no known etiology. In HPS, the primary hepatic lesions are found in the portal tracts which show varying degrees of fibrosis, sclerosis of portal vein radicles, and abnormally formed portal veins. There are increasing reports of both HPS and NRH as well as noncirrhotic portal hypertension occurring in patients having human immunodeficiency virus (HIV) [4–6]. Several investigators have suggested that the portal hypertension may be related to use of certain highly active anti retroviral therapy (HAART) medications [7–10]. After reviewing 42 such cases, on January 29, 2010, the FDA issued an advisory regarding the development of portal hypertension occurring in patients with HIV taking didanosine (ddI; http://www.fda.gov/Safety/MedWatch/SafetyInformation/SafetyAlertsforHumanMedicalProducts/ucm199343.htm).

NRH has been shown to develop after the use of 6-thioguanine in patients being treated for inflammatory bowel disease and acute lymphoblastic leukemia [11, 12]. 6-Thioguanine is an antimetabolite akin in structure to nucleoside reverse transcriptase inhibitors such as zidovudine (AZT), stavudine (d4T), and ddI. Such drugs may affect the hepatic microvasculature as other antimetabolite medications are known to do, such as azathioprine causing both veno-occlusive disease and NRH [13]. Herein, we report a case of HPS and NRH developing in a patient who was using ddI with the initial histologic findings suggestive

of drug hepatotoxicity and injury to the hepatic microvasculature. This thus suggests drug hepatotoxicity (possibly from ddI) as an etiology for HPS. Also of concern in this case is the progressive development of portal hypertension despite cessation of ddI, which suggests an unremitting hepatic vascular injury.

Material and methods

Clinical history

A 45-year-old man with HIV presented in 2003 with abnormal liver chemistry tests. His risk factor for HIV acquisition was men having sex with men. The HIV was initially diagnosed in 1992, and, to date, he has not had an AIDS-defining illness. The HIV RNA was 98 copies/ml and the CD4 count was 376/mm^3. There was no history of alcohol use or previous history of liver disease. Upon presentation, AST was 70 U/l, ALT 87 U/l, alkaline phosphatase 286 U/l, and GGTP 584 U/l with normal serum bilirubin, albumin, platelets, and INR. Liver tests 1 year previously were AST 59 U/l, ALT 46 U/l, alkaline phosphatase 151 U/l, and GGTP 300 U/l. Fasting glucose/insulin and lipid panel were normal with no clinical evidence of metabolic syndrome. Extensive serologic work-up for etiology of the abnormal liver chemistry tests as well as abdominal imaging was unremarkable except for mild hepatomegaly. The patient had been taking antiretroviral medications since 1994, starting with AZT and lamivudine which were subsequently changed to d4T, ddI, and saquinavir in 1998. In 1999, nelfinavir was substituted for saquinavir. Two liver biopsies were performed, and paired specimens were histopathologically analyzed.

Results

The first liver biopsy performed consisted of a 3.8-cm length of liver tissue with bland hepatocellular cholestasis and formation of rosettes as well as mild feathery degeneration of hepatocytes. There was no portal or lobular inflammation. Portal areas were densely fibrotic and portal vein radicles were either totally obliterated or had markedly diminished luminal caliber (phlebosclerosis). Hepatic arterioles had thickened walls and a decreased lumen (Fig. 1a). Patchy chronic inflammatory cells were present around the obliterated portal veins; foci of central venulitis were also present (Fig. 1b). Some densely fibrotic portal tracts were in close proximity to each other indicative of an abnormality of the hepatic architecture (Fig. 1c). Furthermore, although there was no cirrhosis, a distinctly nodular architecture was apparent and, when highlighted by a reticulin stain, consisted of hyperplastic hepatocytes bordered by condensed reticulin fibers with atrophic hepatocytes, consistent with NRH (Fig. 1d). There was no microvesicular or macrovesicular steatosis present in the biopsy. The constellation of findings was consistent with a drug-induced liver injury and concomitant HPS with NRH.

Based on the liver biopsy findings and concern for drug hepatotoxicity, the patient's antiretroviral regimen was changed to Trizivir (AZT/abacavir/lamivudine) and tenofovir (Viread). He subsequently followed up on a biannual basis and was asymptomatic until 2008, when a computerized tomography (CT) scan was performed as part of a work-up for anemia and thrombocytopenia. The platelet count had decreased from 179,000 mm^3 in July 2005 to 149,000 mm^3 in May 2006 to 104,000 mm^3 in November 2008. Other laboratory testing at this time included hemoglobin 11.2 g/dl, GGTP 333 U/l, albumin 4.0 g/dl, bilirubin 1.0 mg/dl, alkaline phosphatase 166 U/l, AST 44 U/l, ALT 43 U/l, total protein 7.5 g/dl, rapid plasma reagin (RPR) negative, testosterone 318 ng/dl, and CD4 count 370/mm^3. CT scan showed hepatosplenomegaly and varices; the portal vein was patent. Further extensive serologic work-up was negative for viral hepatitis and other etiologies of liver disease such as autoimmune hepatitis, Wilson disease or hemochromatosis, and alpha-1-anti-trypsin deficiency. He was not taking any other prescription or herbal medications.

The second needle liver biopsy that was performed consisted of a 2.1-cm length of liver tissue that showed small portal tracts with no fibrosis, markedly dilated and dystrophic portal vein branches, some of which herniated into the periportal zones consistent with HPS (Fig. 2). Bile ducts appeared normal; however, the accompanying hepatic arterioles were difficult to identify. Portal tracts were distant from each other with thickening of hepatocyte plates indicative of regeneration; mild condensation of reticulin fibers and subtle nodularity were also noted. Compared to the initial biopsy, the current liver histology showed a significant regression in portal fibrosis with dramatic changes in portal vein configuration (consistent with HPS), the cholestasis had resolved, and the hepatic venulitis had disappeared; the NRH was less defined.

Discussion

The development of noncirrhotic portal hypertension due to both NRH and HPS in patients with HIV is being increasingly recognized. Several investigators have also noted that patients with HIV may develop cryptogenic liver injury and cirrhosis, even in the pediatric population [6, 14]. In January 2010, the FDA issued an advisory regarding the potential causation of this hepatotoxicity as

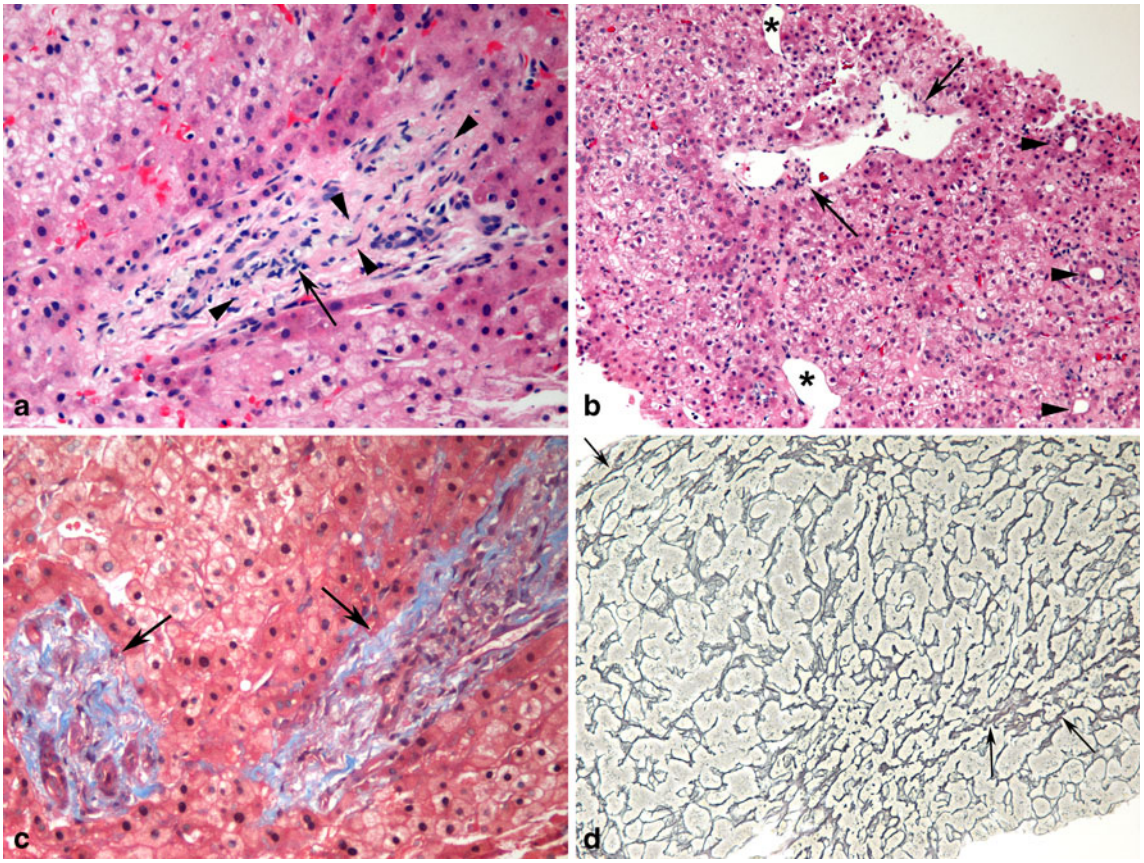

Fig. 1 **a** First liver biopsy. A densely fibrotic portal tract is shown with partial obliteration of the portal vein branch (*arrowheads*). A focus of inflammatory cells lifting the endothelial lining at the edge of the vein indicative of venulitis is also shown (*arrow*). The hepatic arteriole has a thickened wall. (H&E, original magnification ×400). **b** A representative centrilobular area showing central venulitis (*arrow*). The lobules show cholestasis with formation of rosettes (*arrowheads*). Note the presence of markedly dilated sinusoids (*asterisks*). (H&E, original magnification ×100). **c** Two portal tracts with dense fibrosis with no apparent portal vein branch identified (*phlebosclerosis*). (Trichrome stain, original magnification ×100). **d** Nodular regenerative hyperplasia showing condensation of reticulin fibers at the edge of a poorly defined nodule (*arrows*). (Reticulin stain, original magnification ×100)

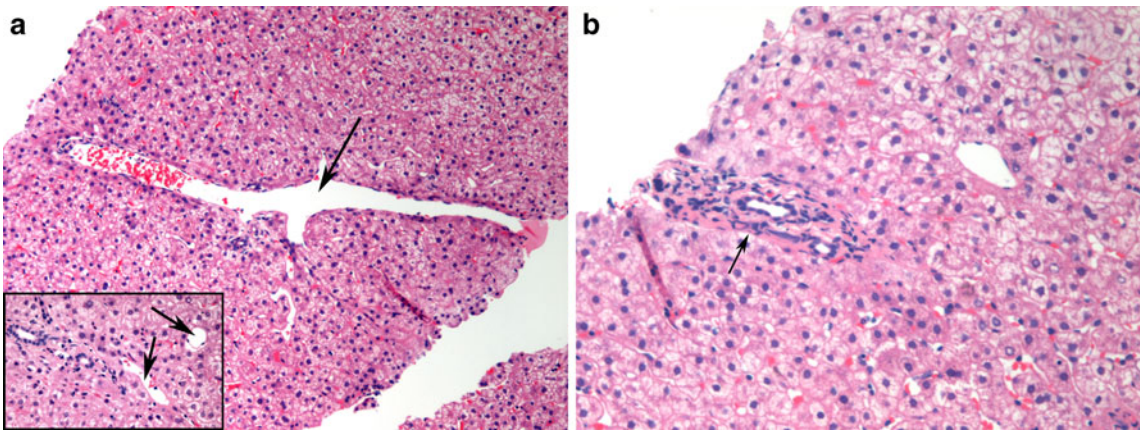

Fig. 2 **a** Second liver biopsy. A portal tract is shown with a disproportionately enlarged dystrophic portal vein that herniates into the surrounding parenchyma (*arrow*). *Inset* shows another portal tract with herniated portal veins creating megasinusoids (*arrows*). (H&E, original magnification ×100). **b** A portal tract with fibrosis is shown (*arrow*). A slightly damaged bile duct with the accompanying artery are present; however, the portal vein branch is missing

being due to ddI (http://www.fda.gov/Safety/MedWatch/SafetyInformation/SafetyAlertsforHumanMedicalProducts/ucm199343.htm). The FDA's decision to revise the drug label for ddI was based on 42 postmarketing reports of noncirrhotic portal hypertension occurring in patients using ddI. Twenty-six patients were male, ages ranging from 10 to 65 years, with a duration of ddI treatment ranging from months to years.

The current case demonstrates the initial development of histologic liver damage strongly suggestive of drug hepatotoxicity with hepatic microvascular injury in a patient taking ddI for 4 years. The initial changes were consistent with a cholestatic-type drug-induced liver injury and portal tracts showed changes of HPS. Endotheliitis of the portal vein branches and central venulitis were present. NRH was also noted at initial presentation. Subsequent liver biopsy showed the well-established portal venopathy of HPS and concomitant NRH with the resolution of the portal vein endotheliitis and central venulitis. These paired biopsies suggest that HPS stemmed from an endothelial injury most likely due to ddI. This is the first documentation that HPS is related to a drug-induced vascular injury and is the root cause for the cases of noncirrhotic portal hypertension being described in HIV.

HPS and NRH are known to be part of the same spectrum of conditions causing noncirrhotic portal hypertension that include incomplete septal cirrhosis, portal vein thrombosis, different vasculitides, and schistosomiasis [15–17]. NRH has been known to result from hepatic vascular injury so the current report now confirms a similar etiology for HPS. Although it has been long presumed that HPS results from hepatic vascular injury, the current report strongly suggests that direct drug hepatotoxicity can now be implicated.

Although it is possible that ddI is not the cause of hepatotoxicity in the current case, the increasing reports of liver disease and noncirrhotic portal hypertension occurring with ddI use strongly implicate it. What is most concerning about the progression of the histologic changes in the patient we describe is the rapid development of portal hypertension (as suggested by worsening thrombocytopenia) and persistence of HPS and NRH over 5 years despite cessation of ddI. This occurred despite minimal abnormalities in liver chemistry tests; clearly, a similar development might be otherwise masked in patients having concurrent viral hepatitis. Patients with HIV are often coinfected with viral hepatitides, such as hepatitis B and C, and can also have appreciable steatosis [18]. These heterogeneous histologic features may potentially confound the identification of HPS especially on needle liver biopsy in which it can be easily missed. Although HPS appears rarely associated with hepatic synthetic compromise and liver failure [19–21], it is now being increasingly recognized. At our own center, retrospective review of the liver explant of a patient with HIV transplanted in 1999 for presumed cryptogenic cirrhosis also showed HPS. This patient had taken ddI for several years.

It is well-established that patients with HIV and HCV coinfection have a more rapid progression in hepatic fibrosis [22]. The use of HAART including ddI has actually been shown to slow fibrosis progression in such patients [23, 24]. Several investigators have shown the development of HPS occurring in the absence of ddI use with the suggestion of there being an underlying hypercoagulable disorder or concurrent portal vein thrombosis [4, 8, 25]. However, it is difficult to definitively prove that these patients never previously used ddI as it was a major part of the early anti-HIV armamentarium. It appears from the current study and from others that even short-term use of ddI can result in hepatotoxicity.

It is clear that in some patients with HIV having used ddI even for short periods of time, the gradual development of biochemical and radiologic evidence of portal hypertension can occur in the presence of minimal liver chemistry test abnormalities. The current case strongly suggests that the development of noncirrhotic portal hypertension from ddI use is directly related to a drug hepatotoxicity and resultant hepatic vascular injury. Similar precedents exist with patients developing veno-occlusive disease and NRH after the short-term use of azathioprine and 6-thioguanine. In this case, the initial insult resulted in progressive and more chronic liver injury despite cessation of the inciting agent. The paired liver biopsies in this case showed resolution of cholestasis, absence of endotheliitis and central venulitis, consistent with the removal of a hepatotoxic agent. The fibrosis seen on the initial liver biopsy was also resolved, suggesting the removal of an inciting agent. HPS and NRH were seen on both liver biopsies with NRH being less defined on the latter biopsy. In addition, HPS was manifested by dystrophic veins without surrounding hepatocellular damage, suggesting that the increasing portal hypertension is ascribable to this vascular abnormality. Whether intervention at the initial detection of the hepatic vascular injury would prevent the development of HPS or NRH is not known.

In conclusion, the current case demonstrates the development of HPS and noncirrhotic portal hypertension in a patient initially developing drug hepatotoxicity and hepatic microvascular injury from ddI use. Thus, HPS should no longer be considered idiopathic, as this case suggests that it may share similar pathophysiologic origins as NRH. It appears that drug hepatotoxicity from

ddI may be the cause of this hepatic microvascular insult and supports the recent concerns regarding its use.

Conflicts of Interest None.

References

1. Bioulac-Sage P, Le Bail B, Bernard PH, Balabaud C (1995) Hepatoportal sclerosis. Semin Liver Dis 15:329–339
2. Sarin SK, Kumar A, Chawla YK et al (2007) Noncirrhotic portal fibrosis/idiopathic portal hypertension: APASL recommendations for diagnosis and treatment. Hepatol Int 1:398–413
3. Reshamwala PA, Kleiner DE, Heller T (2006) Nodular regenerative hyperplasia: not all nodules are created equal. Hepatology 44:7–14
4. Schiano TD, Kotler DP, Ferran E, Fiel MI (2007) Hepatoportal sclerosis as a cause of noncirrhotic portal hypertension in patients with HIV. Am J Gastroenterol 102:2536–2540
5. Mallet V, Blanchard P, Verkarre V et al (2007) Nodular regenerative hyperplasia is a new cause of chronic liver disease in HIV-infected patients. AIDS 21:187–192
6. Maida I, Nunez M, Rios MJ et al (2006) Severe liver disease associated with prolonged exposure to antiretroviral drugs. J Acquir Immune Defic Syndr 42:177–182
7. Maida I, Garcia-Gasco P, Sotgiu G et al (2008) Antiretroviral-associated portal hypertension: a new clinical condition? Prevalence, predictors and outcome. Antivir Ther 13:103–107
8. Saifee S, Joelson D, Braude J et al (2008) Noncirrhotic portal hypertension in patients with human immunodeficiency virus-1 infection. Clin Gastroenterol Hepatol 6:1167–1169
9. Chang PE, Miquel R, Blanco JL et al (2009) Idiopathic portal hypertension in patients with HIV infection treated with highly active antiretroviral therapy. Am J Gastroenterol 104:1707–1714
10. Kovari H, Ledergerber B, Peter U et al (2009) Association of noncirrhotic portal hypertension in HIV-infected persons and antiretroviral therapy with didanosine: a nested case-control study. Clin Infect Dis 49:626–635
11. Geller SA, Dubinsky MC, Poordad FF et al (2004) Early hepatic nodular hyperplasia and submicroscopic fibrosis associated with 6-thioguanine therapy in inflammatory bowel disease. Am J Surg Pathol 28:1204–1211
12. De Bruyne R, Portmann B, Samyn M et al (2006) Chronic liver disease related to 6-thioguanine in children with acute lymphoblastic leukaemia. J Hepatol 44:407–410
13. Katzka DA, Saul SH, Jorkasky D, Sigal H, Reynolds JC, Soloway RD (1986) Azathioprine and hepatic venocclusive disease in renal transplant patients. Gastroenterology 90:446–454
14. Kochin I, Magid M, Arnon R, Glasscock A, Kerkar N, Miloh T (2010) Variceal bleeding in an adolescent with HIV diagnosed with hepatoportal sclerosis and nodular regenerative hyperplasia. J Pediatr Gastroenterol Nutr 50:340–343
15. Ludwig J, Hashimoto E, Obata H, Baldus WP (1993) Idiopathic portal hypertension; a histopathological study of 26 Japanese cases. Histopathology 22:227–234
16. Hillaire S, Bonte E, Denninger MH et al (2002) Idiopathic non-cirrhotic intrahepatic portal hypertension in the West: a re-evaluation in 28 patients. Gut 51:275–280
17. Okudaira M, Ohbu M, Okuda K (2002) Idiopathic portal hypertension and its pathology. Semin Liver Dis 22:59–72
18. Crum-Cianflone N, Dilay A, Collins G et al (2009) Nonalcoholic fatty liver disease among HIV-infected persons. J Acquir Immune Defic Syndr 50:464–473
19. Geramizadeh B, Malek-Hosseini SA, Salahi H, Bahador A, Nikeghbalian S (2008) Liver failure and the need for transplantation in three patients with hepatoportal sclerosis. Transplant Proc 40:3526–3528
20. Isabel Fiel M, Thung SN, Hytiroglou P, Emre S, Schiano TD (2007) Liver failure and need for liver transplantation in patients with advanced hepatoportal sclerosis. Am J Surg Pathol 31:607–614
21. Krasinskas AM, Eghtesad B, Kamath PS, Demetris AJ, Abraham SC (2005) Liver transplantation for severe intrahepatic noncirrhotic portal hypertension. Liver Transpl 11:627–634
22. Gonzalez SA, Talal AH (2003) Hepatitis C virus in human immunodeficiency virus-infected individuals: an emerging comorbidity with significant implications. Semin Liver Dis 23:149–166
23. Marine-Barjoan E, Saint-Paul MC, Pradier C et al (2004) Impact of antiretroviral treatment on progression of hepatic fibrosis in HIV/hepatitis C virus co-infected patients. AIDS 18:2163–2170
24. Brau N, Salvatore M, Rios-Bedoya CF et al (2006) Slower fibrosis progression in HIV/HCV-coinfected patients with successful HIV suppression using antiretroviral therapy. J Hepatol 44:47–55
25. Mallet VO, Varthaman A, Lasne D et al (2009) Acquired protein S deficiency leads to obliterative portal venopathy and to compensatory nodular regenerative hyperplasia in HIV-infected patients. AIDS 23:1511–1518

Virchows Arch (2011) 458:237–245
DOI 10.1007/s00428-010-1008-3

ORIGINAL ARTICLE

JPEG2000 for automated quantification of immunohistochemically stained cell nuclei: a comparative study with standard JPEG format

Marylène Lejeune · Carlos López · Ramón Bosch · Anna Korzyńska · Maria-Teresa Salvadó · Marcial García-Rojo · Urszula Neuman · Łukasz Witkowski · Jordi Baucells · Joaquín Jaén

Received: 13 August 2010 / Revised: 14 October 2010 / Accepted: 2 November 2010 / Published online: 18 November 2010
© Springer-Verlag 2010

Abstract The Joint Photographic Experts Group (JPEG) standard format is one of the most widely used in image compression technologies. More recently, JPEG2000 format has emerged as a state-of-the-art technology that provides substantial improvements in picture quality at higher compression ratios. However, there has been no attempt to date to determine which of the two compression formats produces less variability in the automated evaluation of immunohistochemically stained digital images in agreement with their compression rates and complexity degrees. The evaluation of Ki67 and FOXP3 immunohistochemical nuclear markers was performed in a total of 329 digital images: 47 were captured in uncompressed Tagged Image File Format (TIFF), 141 were converted to three JPEG compressed formats (47 each with 1:3, 1:23 and 1:46 compression) and 141 were converted to three JPEG2000 compressed formats (47 each with 1:3, 1:23 and 1:46 compression). The count differences between images in TIFF versus JPEG formats were compared with those obtained between images in TIFF versus JPEG2000 formats at the three levels of compression. It was found that, using JPEG2000 compression, the results of the stained nuclei count are close enough to the results obtained with uncompressed images, especially in highly complex images at minimum and medium compression. Otherwise, in images of low complexity, JPEG and JPEG2000 had similar count efficiency to that of the original TIFF images at all compression levels. These data suggest that JPEG2000 could give rise to an efficient means of storage, reducing file size and storage capacity, without compromise on the immunohistochemical analytical quality.

Keywords Automated image analysis · immunohistochemistry · JPEG · JPEG2000

Marylène Lejeune and Carlos López have contributed equally to this work.

M. Lejeune (✉) · C. López
Molecular Biology and Research Section, Hospital de Tortosa Verge de la Cinta, IISPV, URV,
c/Esplanetes 14,
43500, Tortosa, Spain
e-mail: mlejeune.htvc.ics@gmail.com

R. Bosch · M.-T. Salvadó · J. Jaén
Department of Pathology, Hospital de Tortosa Verge de la Cinta, IISPV, URV,
Tortosa, Spain

A. Korzyńska · U. Neuman · Ł. Witkowski
Laboratory of Processing Systems of Microscopic Image Information, Nalecz Institute of Biocybernetics and Biomedical Engineering, Polish Academy of Sciences,
Warsaw, Poland

M. García-Rojo
Department of Pathology, Hospital General de Ciudad Real,
Ciudad Real, Spain

J. Baucells
Department of Informatics, Hospital de Tortosa Verge de la Cinta, IISPV, URV,
Tortosa, Spain

Introduction

Cell quantification and morphological measurement in the field of pathology have several clinical and research applications [1–7]. Non-automated immunohistochemical quantification has an inherent variability that produces various results, leading to intra- and inter-observer variability [8–11]. Intra-observer variability is defined as the

differences between repeated evaluations made by the same observer, and inter-observer variability arises from those between evaluations made by different observers. The use of digital image computer analysis to quantify and measure the different morphological parameters of cells or tissues reduces these variabilities [12].

Image quality is one of the most important features in digital image analysis and several factors, such as tissue processing, illumination and camera quality, are very important in ensuring good-definition images. The large number of digital images created in scientific studies and current clinical practice require a suitable image capture format since high-resolution images stored without compression needs very-high-volume devices. Image compression has been used in several fields of medicine to reduce the file size and data transmission time [13–17]. Although compression improves the ability to handle large numbers of photographs, the use of different compression techniques could produce variations in digital images that affect their medical interpretation. There are two types of image compression: lossless and lossy. Lossless compression enables the original file to be reconstructed without loss of data, but with the disadvantage of poor file-size reduction. Lossy compression allows greater file size reduction but with the disadvantage that some details may be lost. Two of the most widely used lossy formats in medicine are JPEG and JPEG2000 compression. The first uses the discrete cosine transform (DCT) technique and the latter the discrete wavelet transform (DWT) method. Despite all the advantages of JPEG compression schemes based on DCT—simplicity, satisfactory performance for human eyes and availability of special-purpose hardware for implementation—shortcomings exist. Since the input image needs to be "blocked", correlation across the block boundaries is not eliminated, causing noticeable artefacts well visible in high compression rates. Wavelet-based coding has emerged as a state-of-the-art technology within the field of image compression and appears to be more robust than other compression techniques with respect to transmission and decoding errors as well as facilitates the progressive transmission of images. Different studies that have compared the DCT technique to wavelet transformation in different kinds of radiological images with different compression ratios provided contradictory results [18–21]. In immunohistochemical digital images, there is no agreement about whether JPEG2000 is better than JPEG or if differences are indistinguishable at lower or higher compression ratios with the two formats.

Most of the studies in the field of pathology that use digital images of immunohistochemically stained tissue sections stored these in the uncompressed TIFF format [12, 22], but some studies have also employed JPEG compression [5, 23]. Our group has developed an automated computer-assisted method to quantify digital images with immunohistochemically stained nuclear markers that have been tested and validated resting digital image stored in TIFF format [12]. When this method was applied to images after JPEG compression, we found a distortion in the images that reduces the nuclear quantification efficiency with an increase in the compression rates and image complexity degrees [24]. To the best of our knowledge, no previous studies have evaluated the effects of JPEG2000 compression in computer-assisted immunohistochemical nuclear quantification. The method developed in our laboratory is based on colour and morphological segmentation methods and used to compare the results of images stored in TIFF and JPEG formats. The aim of this study is to evaluate the differences in images stored in TIFF and JPEG2000 formats using our method of automated quantification of stained nuclei. We also compare the count differences between JPEG and JPEG2000 with the same or similar degree of compression in order to determine which of the two techniques of compression is better for image storage taking into account the fidelity of further analysis.

Materials and methods

Sample selection and immunohistochemistry

The samples used in this study were selected from the archives of the Department of Pathology of the Hospital de Tortosa Verge de la Cinta, Catalonia, Spain. Sample pretreatment and staining procedures were standardized as previously described [25]. Briefly, 3-μm-thick sections were dried, deparaffinized in xylene, rehydrated in graded ethanol and washed in water and PBS. Staining was performed with monoclonal antibodies directed against the nuclear proteins Ki67 (clone MIB-1, Dako, Carpinteria, CA, USA) and FOXP3 (clone FOXP3-236A/E7, CNIO, Spain) using standard protocols as previously described [25]. This study receives an institutional review board approval.

Image capture and file compression

The photographs of each sample were taken with a Leica DFC320 digital camera at a resolution of 3.3 Mpixels CCD with a Bayer Array RGB filter for brilliant pictures and with exposure times from 320 μs to 20 s. The camera was connected to a Leica DM LB2 microscope (Leica Microsystems Wetzlar GmbH, Wetzlar, Germany) with ×40 magnification and 0.65 numeric aperture under the same range of illumination. The camera was controlled with the Leica IM50 v.4.0 software installed on a Compaq Professional Workstation computer (3.6 GHz Pentium IV CPU,

1.00 GB RAM). Forty-seven images marked with both immunohistochemical markers were saved as TIFF files of around 9.27 Mbytes. These images were selected according to the variety in the concentration and distribution of the stained nucleus. All images were converted to JPEG/JFIF (JPEG File Interchange Format), a format with the ACDSee 9.0 program that uses an adjustable compression factor, subsampling (colour compression scheme) and Huffman code optimization processes. The adjustable compression factor uses a 0–100 scale of compression (high quality/low compression—low quality/high compression). The ratio of the "chroma subsampling" was adjusted automatically at the standard of 4:2:2 (or 2:1 horizontal) for all compression rates. At the final process, TIFF format images were converted to JPEG images with the lowest compression and the highest quality that the software allows (1:3 compression, file size approximately 3.25 Mbytes), intermediate-quality images (1:23 compression, 400 kbytes) and images with maximum compression rate and poor quality (1:46 compression, 200 kbytes) [24]. We used the same software to convert the original TIFF files to JPEG2000 with the same degrees of compression as the JPEG files and similar file sizes.

Nuclear quantification

All of the images were quantified by a method developed in our centre and that had been previously tested and validated [12]. In this method, the images are processed in two steps. In the first step, the contrast of the image is modified in order to reduce the background and minimize variations in staining intensity. A colour and iterative morphological segmentation is applied to these modified images to select the positive-stained objects and all the information associated to these objects such as their number, the area and the roundness values of each of them. The second step of the method involves data management of all the extracted information using several algorithms in order to obtain the final number of nuclei in each image, including those of the clusters. We used this automatic procedure to analyse 329 images, 47 from original uncompressed TIFF digital images, 141 from JPEG compressed images (47 each with 1:3, 1:23 and 1:46 JPEG compression) and 141 from JPEG2000 compressed images (47 each with 1:3, 1:23 and 1:46 JPEG2000 compression).

Statistical analysis

Statistical analysis was carried out with SPSS 11.0. Bland–Altman and Kaplan–Meier analyses, with their corresponding graphical output, were used to determine the nuclear count differences between the original TIFF images and both types of compressed images and to measure in order to identify which of the two compression methods produced less variability in comparison to the results obtained with TIFF-format images. Bland–Altman graphs illustrate the difference of the TIFF/JPEG and TIFF/JPEG2000 count results obtained with respect to the mean of each paired count. Kaplan–Meier curves portray the conditional probability of observing count differences between the results obtained with the TIFF and compressed methods. The paired results were obtained for TIFF images versus each group of compressed JPEG images with 1:3, 1:23 and 1:46 compression and TIFF images versus each group of compressed JPEG2000 images with 1:3, 1:23 and 1:46 compression. Furthermore, nuclear count differences between JPEG and JPEG2000 were compared for the same compression degree.

Results

Nuclear counts based on images stored in TIFF formats are taken as reference in comparison with those obtained in different compression rates of JPEG and JPEG2000 image formats. Overall, Fig. 1 shows that the differences in nuclear counts between TIFF and the two compressed formats were lowest in JPEG2000 at the low (1:3) and medium (1:23) compression levels. This indicates that, at these compression rates, the JPEG2000 compression method does not damage the objects and the results of stained nuclei counts are more accurate than for the images compressed in JPEG format. The differences in the number of stained nuclei increase in both compressed formats as the compression level rises. The count differences between TIFF and JPEG 1:46 compression and between TIFF and JPEG2000 1:46 were very similar, indicating that the two methods had similar count variability at maximum compression.

As previously demonstrated, image complexity, relative to the number of positive-stained nuclei and the presence of clusters, may affect the automated nuclear quantification and lead to count variability in images compressed in JPEG format [12]. In the present study, the images were divided as before into a low-complexity group (Fig. 2a, b; images with fewer than 100 nuclei, no clusters or small-area clusters of less than 25 μm^2) and a high-complexity group (Fig. 2c, d; images with more than 100 nuclei or large clusters of more than 25 μm^2). The current results obtained with low-complexity images showed that the count differences in TIFF vs. JPEG compressed images and the count differences in TIFF vs. JPEG2000 compressed images were very similar at all compression levels. Figure 3 shows these small differences obtained in images with small-area clusters and Fig. 4 shows the results obtained from images of samples with fewer than 100 nuclei.

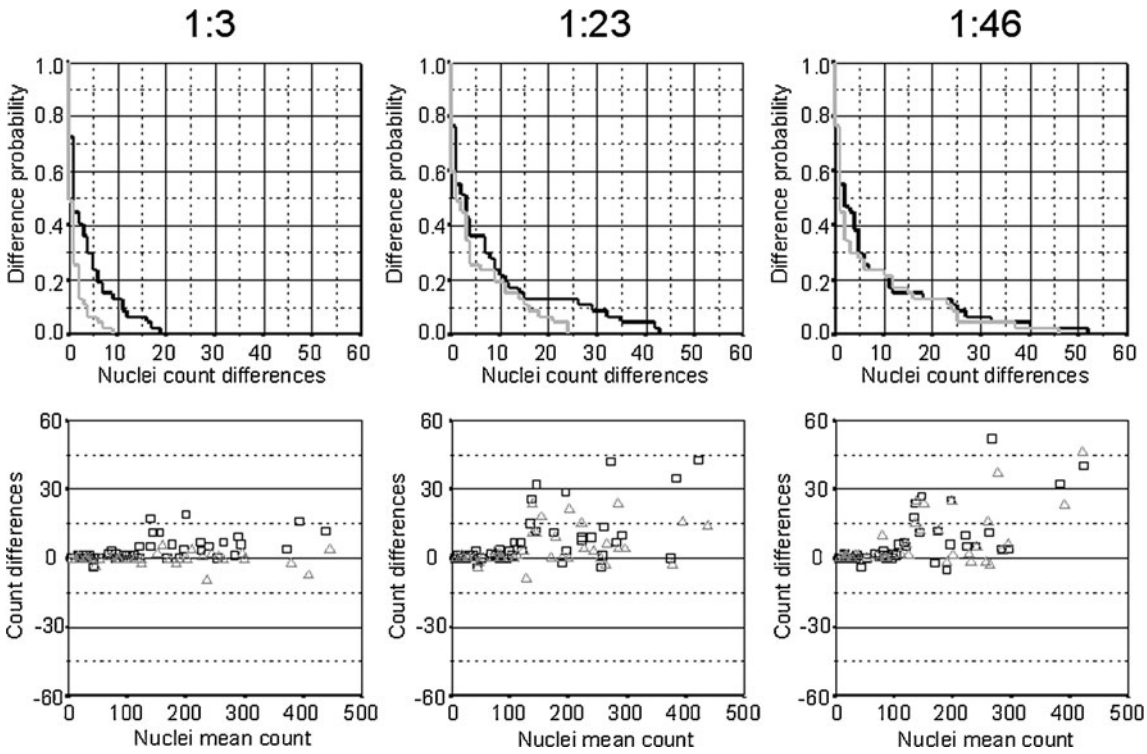

Fig. 1 Overall results obtained by automatic quantification at different compression degrees. Kaplan–Meier curves (*upper row*) compare the probability of difference between TIFF/JPEG (*black*) and TIFF/JPEG2000 compression (*grey*). Bland–Altman graphs (*lower row*) compare count differences between TIFF/JPEG (*black*) and TIFF/JPEG2000 compression (*grey*)

In high-complexity images, the differences in the number of stained nuclei quantified in large-area cluster JPEG2000 images are lower than in corresponding JPEG images (Fig. 5). These differences increase along with the compression level, and at maximum compression the two techniques yield similar count differences. Similar results were obtained from images with more than 100 nuclei, showing that the estimation of the number of stained nuclei in these images is also more accurate in the JPEG2000 format (Fig. 6). However, in all kinds of high-complexity images, maximum level of JPEG2000 compression (1:46) damages the objects so that a similar count variability with JPEG can be observed.

Discussion

For this study, the choice of the two antibodies came from the importance of their accurate immunohistochemical evaluation and quantification. Ki67 is a nuclear marker used for assessing the proliferative index in a neoplastic cell population (all stages in the cell cycle except G_0). The establishment of the growth fraction of neoplasms by quantitatively identifying Ki67-positive cells by immunohistochemistry is useful for the diagnosis (differential or not) of a great number of neoplastic diseases such as lymphoproliferative disorders, breast cancer and other carcinomas [26–31]. The staining pattern of proliferating cells has been also demonstrated to be important for the determination of the nuances and pitfalls that may exist in the interpretation of the Ki67 pattern [26]. The marker of forkhead box protein 3 (FOXP3+) regulatory T cells has been extensively used for research purpose. The presence and the pattern of distribution of these cells, identified by immunohistochemistry, have been demonstrated to be associated with the clinical outcome of patients with different neoplasms. These regulatory T cells were able to reduce tumour-driven immune suppression with clinical benefit in haematological malignancies like follicular and Hodgkin's lymphomas [6, 32–35], whereas in epithelial carcinomas these regulatory T cells correlated inversely with the clinical outcome [36]. Moreover, it has been demonstrated that the presence of these regulatory T cells, as an element of the microenvironment of some lymphomas, predicts these patients' response to the treatment [37].

The choice of an adequate file format in digital image analysis is fundamental in medicine for correct analysis and diagnostic evaluations [19]. The performances of JPEG and JPEG2000 formats have been extensively evaluated in radiological images using subjective and objective metrics. Although some papers mentioned the benefits of JPEG2000 [13, 20, 38–42], others said that the results are indistin-

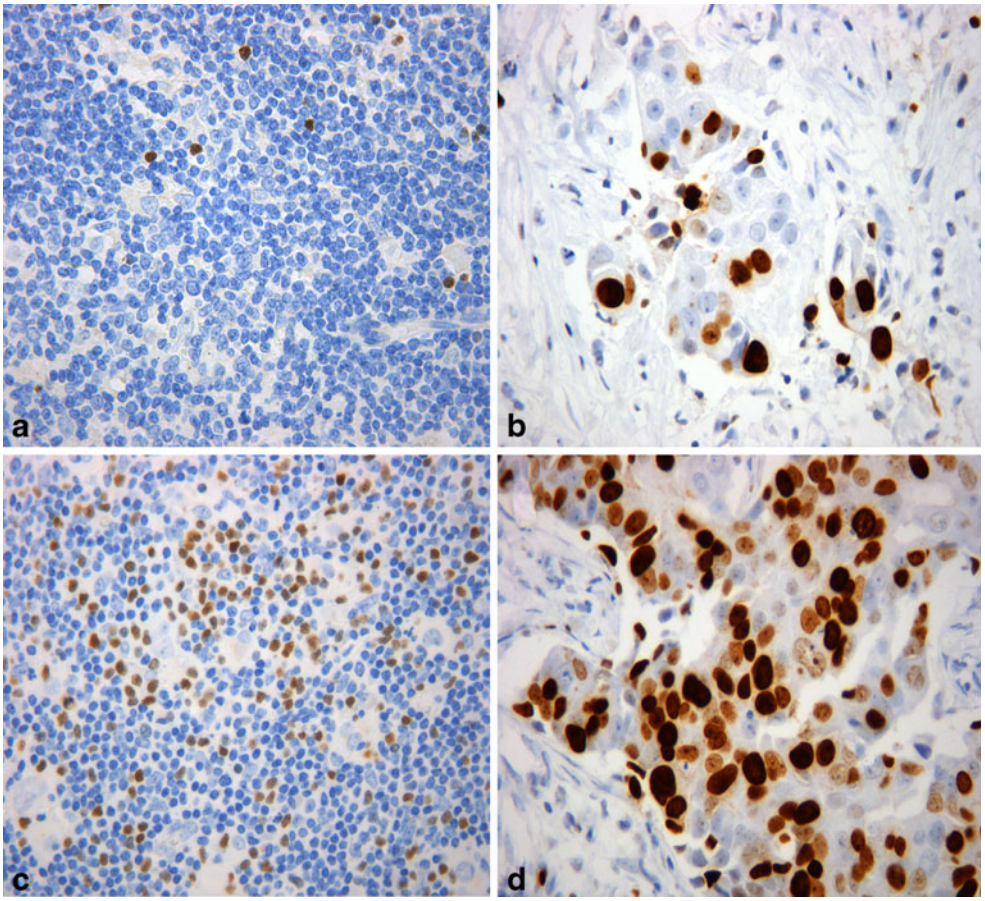

Fig. 2 Representative digital images positively grouped in function of nuclei density complexity. The first column (**a** and **c**) corresponds to FOXP3 marker in lymph node tissues and the second column (**b** and **d**) corresponds to Ki67 marker in breast cancer tissues. **a** Immunostained images classified in the low-complexity group with fewer than 100 nuclei and no clusters. **b** Immunostained images classified in the low-complexity group with fewer than 100 nuclei and small-area clusters of less than 25 μm^2. **c** Immunostained images classified in the high-complexity group with more than 100 nuclei and small-area clusters of less than 25 μm^2. **d** Immunostained images classified in the high-complexity group with more than 100 nuclei and large-area clusters larger than 25 μm^2

guishable [21, 43]. Some papers even reported that JPEG is superior to JPEG2000 for medical images using "mean opinion score", especially in low-compression-ratio areas [18, 44, 45]. Nevertheless, such studies are difficult to compare because different algorithms, image types and evaluation paradigms have been used. In the field of cell quantification in digital pathology, most of the studies use images in an uncompressed TIFF format [10, 22, 46, 47]. This format preserves all photographic information without loss of image quality. Nevertheless, it is clear that the need to reduce the size of files and especially the storage space for these images has stimulated the requirement for different formats of compression. The effects and changes produced by the compression in automated nuclear quantification in digital images have rarely been studied in Feulgen stain [48] or in immunohistochemically stained nuclei [24].

As previously observed, the image complexity and the level of JPEG image compression influenced the automated nuclear quantification results [24, 48] whereby count variability increases as the compression level rises. The present study shows that the JPEG2000 compression method, at low (1:3) and medium (1:23) compression levels, does not disturb the information about immunohistochemically stained nuclei in comparison to the JPEG compression method. Although the JPEG2000 1:3 and JPEG2000 1:23 count differences are less than in JPEG 1:3 and JPEG 1:23, respectively, the variability is similar for both formats at maximum compression. The effectiveness of JPEG2000 compression at minimum and medium compression levels is especially visible in highly complex images. Images with lower complexity could be analysed with uncompressed TIFF or JPEG and JPEG2000 formats without loss of accuracy.

The distortion observed in highly complex images (large-area clusters or more than 100 nuclei) appears to be due to the nearness neighbourhood of the cells and the fact that the boundaries of the cells become blurred during JPEG compression, causing difficulties in cell edge discrimination. Under these conditions, positive pixels that are altered by the compression may fall outside the range of previously selected positive colour values and some negative pixels may fall within the positive range of values [24]. This variability would reduce the efficiency of the segmentation algorithms used in the computer-assisted image analysis procedure, leading to serious and unacceptable inaccuracy in the final nuclear count. The compression gains of JPEG2000 over JPEG are attributed to the use of DWT and a more sophisticated entropy-encoding scheme such as the decomposition of the image into a multiple-

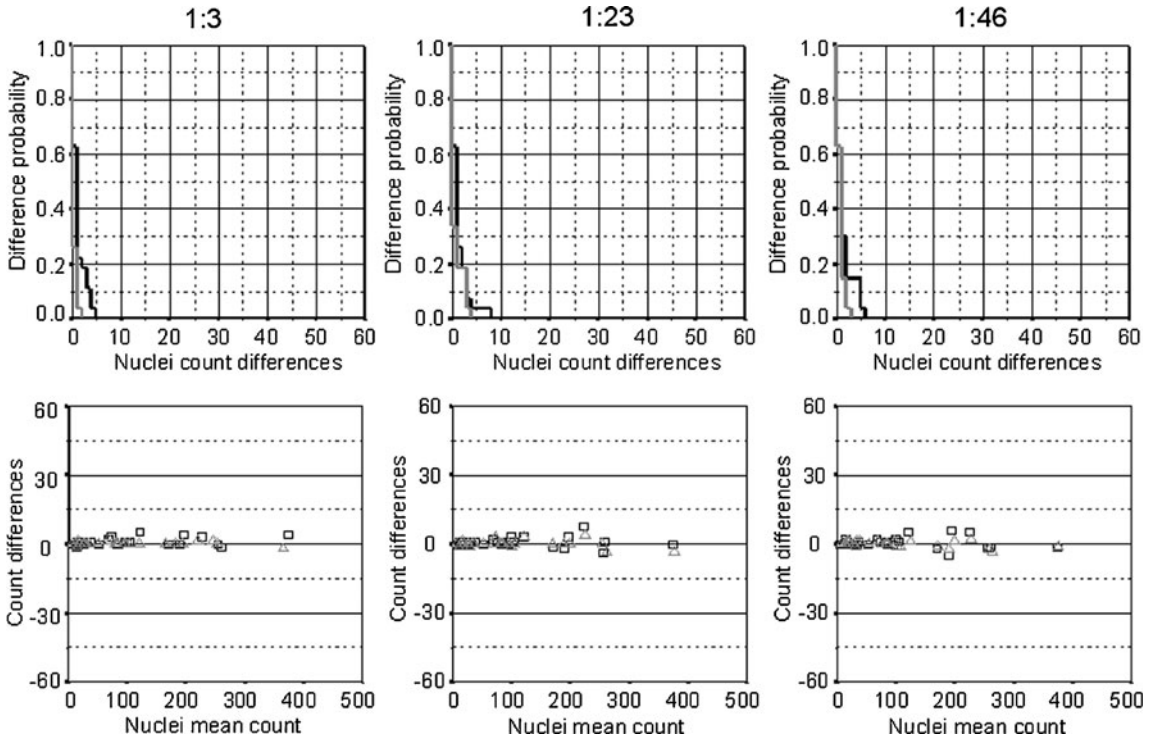

Fig. 3 Results obtained by automatic quantification in images with small-area clusters at different compression levels. Kaplan–Meier curves (*upper row*) compare the probability of difference between TIFF/JPEG (*black*) and TIFF/JPEG2000 compression (*grey*). Bland–Altman graphs (*lower row*) compare count differences between TIFF/JPEG (*black*) and TIFF/JPEG2000 compression (*grey*)

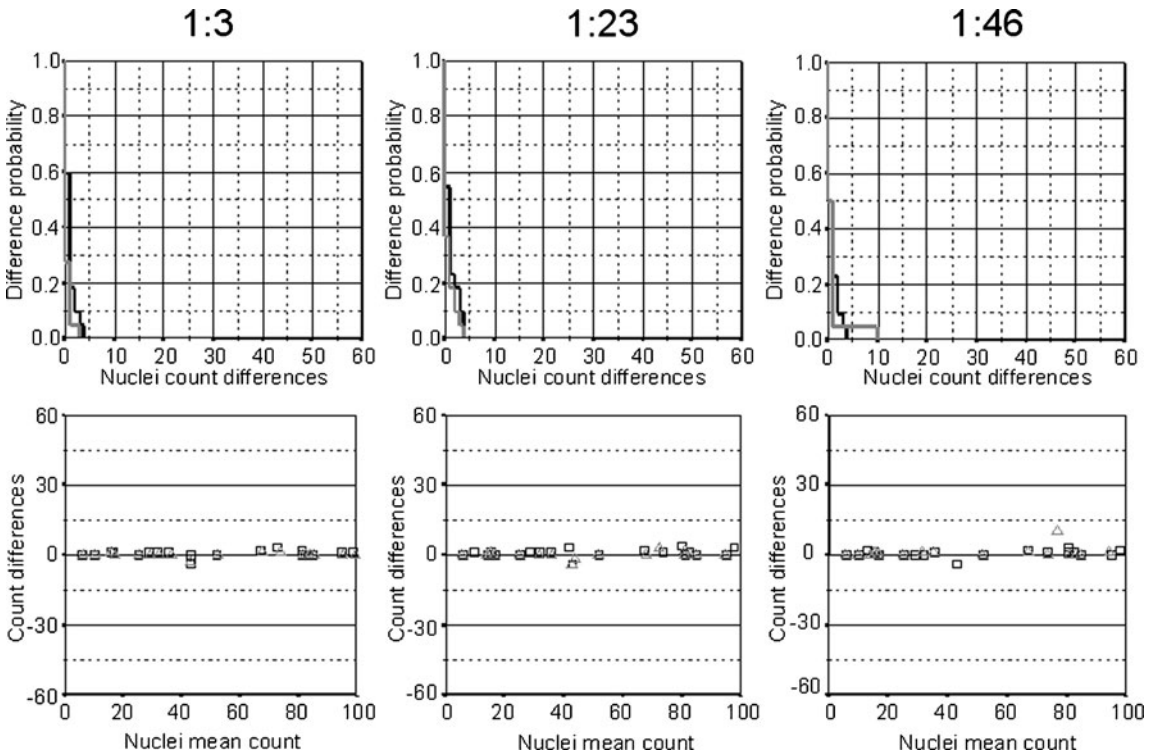

Fig. 4 Results obtained by automatic quantification in images with fewer than 100 nuclei at different compression levels. Kaplan–Meier curves (*upper row*) compare the probability of difference between TIFF/JPEG (*black*) and TIFF/JPEG2000 compression (*grey*). Bland–Altman graphs (*lower row*) compare count differences between TIFF/JPEG (*black*) and TIFF/JPEG2000 compression (*grey*)

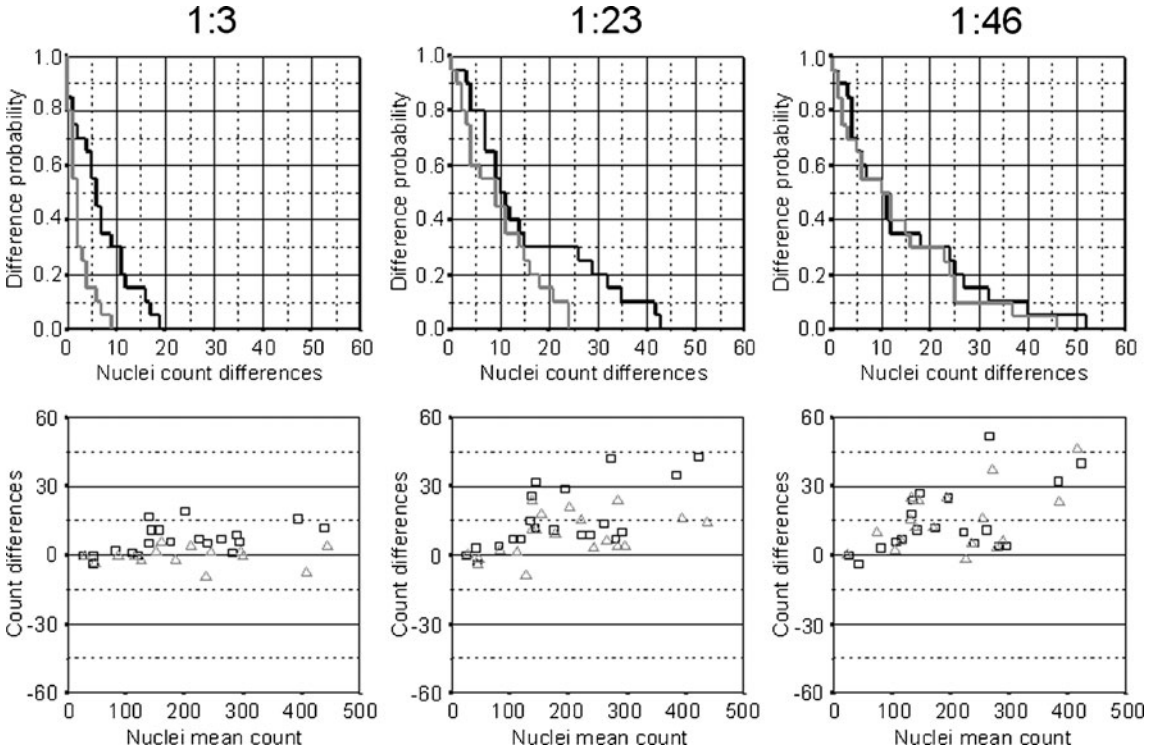

Fig. 5 Results obtained by automatic quantification in images with large-area clusters at different compression levels. Kaplan–Meier curves (*upper row*) compare the probability of difference between TIFF/JPEG (*black*) and TIFF/JPEG2000 compression (*grey*). Bland–Altman graphs (*lower row*) compare count differences between TIFF/JPEG (*black*) and TIFF/JPEG2000 compression (*grey*)

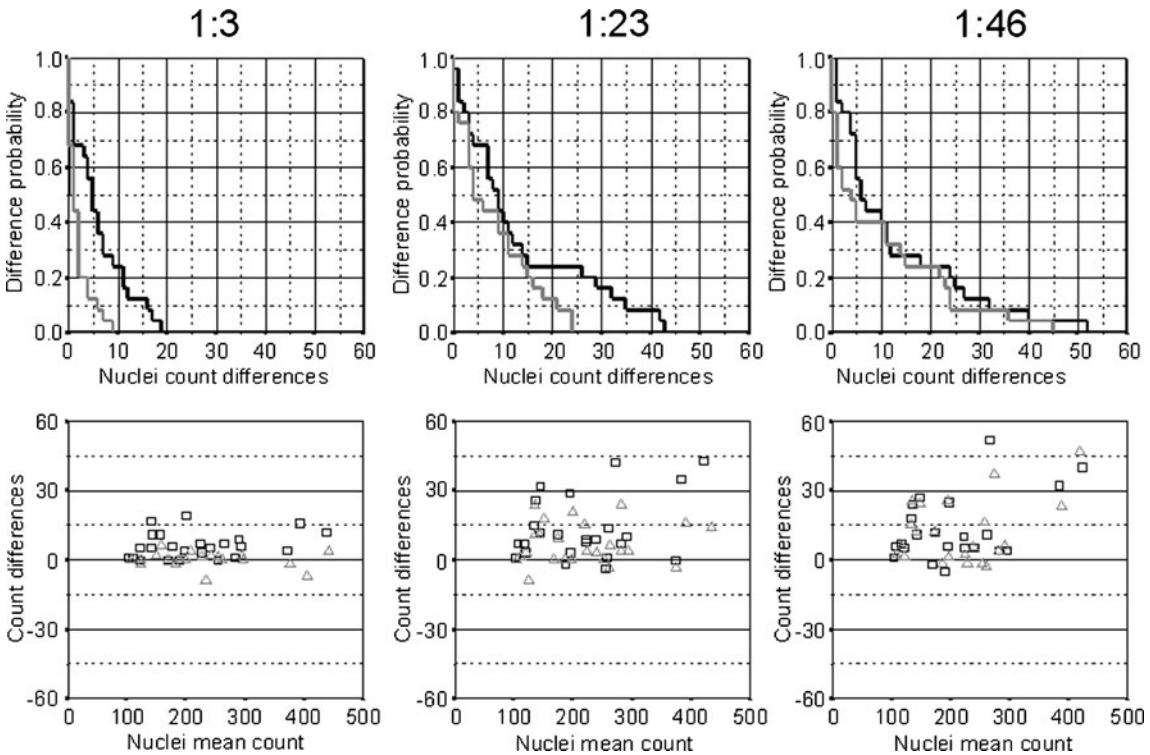

Fig. 6 Results obtained by automatic quantification in images with more than 100 nuclei at different compression levels. Kaplan–Meier curves (*upper row*) compare the probability of difference between TIFF/JPEG (*black*) and TIFF/JPEG2000 compression (*grey*). Bland–Altman graphs (*lower row*) compare count differences between TIFF/JPEG (*black*) and TIFF/JPEG2000 compression (*grey*)

resolution representation during the course of compression. In these circumstances, to reduce the number of bits of a picture below a certain point, it is advisable that the resolution of the input image be reduced with the first JPEG standard (from 4:4:4 to 4:2:2) before encoding it. This is not necessary when using JPEG2000 because this is done automatically through the format's multiresolution decomposition structure. So, at high bit rates, where artefacts become nearly imperceptible, JPEG2000 has a small advantage over JPEG. At lower bit rates, JPEG2000 has a much more significant advantage over certain modes of JPEG in that the artefacts are less visible and there is no blocking. This may explain the greater effectiveness of nuclear quantification in JPEG2000 images when a colour (DAB) and morphological (area and roundness) segmentation model with high complexity is used at minimum and medium compression levels compared with the same images in the corresponding JPEG formats. The variations found in this work are only applicable for this kind of segmentation method based on colour and the morphological parameters cited above. Further studies are required to assess the effects of image compression with various segmentation techniques.

JPEG2000 compression is a better technique than JPEG compression at low and medium levels of compression for highly complex immunohistochemically stained images. Although high-capacity data storage devices are available these days, image compression will continue to be necessary due to the large number of photographs generated in research studies by diagnostic techniques or as a result of the implementation of telepathology in pathology departments. The study of the adequate use of the different compression techniques and their effects on cell quantification could give rise to an efficient means of storage that has no loss of analytical quality and with a reduction in the time required for data transmission.

Acknowledgments This work was supported by grants FIS 08/0796 (Dr. Jaén) from the Ministerio de Ciencia e Innovación (FEDER Fonds, Spain), Fundación Mutua Madrileña (FMM Dr. Bosch 2008, Spain) and the COST Action IC0604 (COST-STSM-IC0604-4046). The authors thank María del Mar Barbera, Bárbara Tomás, Vanesa Gestí, Ainhoa Montserrat, Ana Suñé, Verònica Echevarría and Marc Iniesta for their skilful technical assistance and Anna Carot, Montse Sebastià and Rosa Cabrera for their excellent secretarial work.

Conflicts of interest The authors declare that they have no conflicts of interest.

References

1. Cheretis C, Angelidou E, Dietrich F, Politi E, Kiaris H, Koutselini H (2008) Prognostic value of computer-assisted morphological and morphometrical analysis for detecting the recurrence tendency of basal cell carcinoma. Med Sci Monit 14:MT13–MT19
2. Makarov DV, Marlow C, Epstein JI, Miller MC, Landis P, Partin AW, Carter HB, Veltri RW (2008) Using nuclear morphometry to predict the need for treatment among men with low grade, low stage prostate cancer enrolled in a program of expectant management with curative intent. Prostate 68:183–189
3. Alvaro T, Lejeune M, Garcia JF, Salvado MT, Lopez C, Bosch R, Jaen J, Escriva P, Pons LE (2008) Tumor-infiltrated immune response correlates with alterations in the apoptotic and cell cycle pathways in Hodgkin and Reed–Sternberg cells. Clin Cancer Res 14:685–691
4. Zhang K, Prichard JW, Yoder S, De J, Lin F (2007) Utility of SKP2 and MIB-1 in grading follicular lymphoma using quantitative imaging analysis. Hum Pathol 38:878–882
5. Joshi AS, Sharangpani GM, Porter K, Keyhani S, Morrison C, Basu AS, Gholap GA, Gholap AS, Barsky SH (2007) Semi-automated imaging system to quantitate Her-2/neu membrane receptor immunoreactivity in human breast cancer. Cytom A 71:273–285
6. Alvaro T, Lejeune M, Salvado MT, Lopez C, Jaen J, Bosch R, Pons LE (2006) Immunohistochemical patterns of reactive microenvironment are associated with clinicobiologic behavior in follicular lymphoma patients. J Clin Oncol 24:5350–5357
7. Markiewicz T, Osowski S, Patera J, Kozlowski W (2006) Image processing for accurate cell recognition and count on histologic slides. Anal Quant Cytol Histol 28:281–291
8. Johnsson A, Olsson C, Anderson H, Cavallin-Stahl E (1994) Evaluation of a method for quantitative immunohistochemical analysis of cisplatin–DNA adducts in tissues from nude mice. Cytometry 17:142–150
9. Mosedale DE, Metcalfe JC, Grainger DJ (1996) Optimization of immunofluorescence methods by quantitative image analysis. J Histochem Cytochem 44:1043–1050
10. Johansson AC, Visse E, Widegren B, Sjogren HO, Siesjo P (2001) Computerized image analysis as a tool to quantify infiltrating leukocytes: a comparison between high- and low-magnification images. J Histochem Cytochem 49:1073–1079
11. Lejeune M, Jaen J, Pons L, Lopez C, Salvado MT, Bosch R, Garcia M, Escriva P, Baucells J, Cugat X, Alvaro T (2008) Quantification of diverse subcellular immunohistochemical markers with clinicobiological relevancies: validation of a new computer-assisted image analysis procedure. J Anat 212:868–878
12. Lopez C, Lejeune M, Salvado MT, Escriva P, Bosch R, Pons LE, Alvaro T, Roig J, Cugat X, Baucells J, Jaen J (2008) Automated quantification of nuclear immunohistochemical markers with different complexity. Histochem Cell Biol 129:379–387
13. Shiao YH, Chen TJ, Chuang KS, Lin CH, Chuang CC (2007) Quality of compressed medical images. J Digit Imaging 20:149–159
14. Tuominen VJ, Isola J (2007) The application of JPEG2000 in virtual microscopy. J Digit Imaging 22:250–258
15. Penedo M, Lado MJ, Tahoces PG, Souto M, Vidal JJ (2006) Effects of JPEG2000 data compression on an automated system for detecting clustered microcalcifications in digital mammograms. IEEE Trans Inf Technol Biomed 10:354–361
16. Belair ML, Fansi AK, Descovich D, Leblanc AR, Harasymowycz P (2005) The effect of compression on clinical diagnosis of glaucoma based on non-analyzed confocal scanning laser ophthalmoscopy images. Ophthalmic Surg Lasers Imaging 36:323–326
17. Ohgiya Y, Gokan T, Nobusawa H, Hirose M, Seino N, Fujisawa H, Baba M, Nagai K, Tanno K, Takeyama N, Munechika H (2003) Acute cerebral infarction: effect of JPEG compression on detection at CT. Radiology 227:124–127
18. CM EF, Winkler S (2004) JPEG vs. JPEG2000: an objective comparison of image encoding quality. Proc SPIE Appl Digit Image Proc 5558:300–308

19. Erickson BJ (2002) Irreversible compression of medical images. J Digit Imaging 15:5–14
20. Janhom A, van der Stelt PF, Sanderink GC (2002) A comparison of two compression algorithms and the detection of caries. Dentomaxillofac Radiol 31:257–263
21. Slone RM, Foos DH, Whiting BR, Muka E, Rubin DA, Pilgram TK, Kohm KS, Young SS, Ho P, Hendrickson DD (2000) Assessment of visually lossless irreversible image compression: comparison of three methods by using an image-comparison workstation. Radiology 215:543–553
22. Matkowskyj KA, Cox R, Jensen RT, Benya RV (2003) Quantitative immunohistochemistry by measuring cumulative signal strength accurately measures receptor number. J Histochem Cytochem 51:205–214
23. Sharangpani GM, Joshi AS, Porter K, Deshpande AS, Keyhani S, Naik GA, Gholap AS, Barsky SH (2007) Semi-automated imaging system to quantitate estrogen and progesterone receptor immunoreactivity in human breast cancer. J Microsc 226:244–255
24. Lopez C, Lejeune M, Escria P, Bosch R, Salvadoacute MT, Pons LE, Baucells J, Cugat X, Alvaro T, Jaen J (2008) Effects of image compression on automatic count of immunohistochemically stained nuclei in digital images. J Am Med Inform Assoc 15:794–798
25. Alvaro-Naranjo T, Lejeune M, Salvado-Usach MT, Bosch-Princep R, Reverter-Branchat G, Jaen-Martinez J, Pons-Ferre LE (2005) Tumor-infiltrating cells as a prognostic factor in Hodgkin's lymphoma: a quantitative tissue microarray study in a large retrospective cohort of 267 patients. Leuk Lymphoma 46:1581–1591
26. Bryant RJ, Banks PM, O'Malley DP (2006) Ki67 staining pattern as a diagnostic tool in the evaluation of lymphoproliferative disorders. Histopathology 48:505–515
27. Yerushalmi R, Woods R, Ravdin PM, Hayes MM, Gelmon KA (2010) Ki67 in breast cancer: prognostic and predictive potential. Lancet Oncol 11:174–183
28. Montebugnoli L, Badiali G, Marchetti C, Cervellati F, Farnedi A, Foschini MP (2009) Prognostic value of Ki67 from clinically and histologically 'normal' distant mucosa in patients surgically treated for oral squamous cell carcinoma: a prospective study. Int J Oral Maxillofac Surg 38:1165–1172
29. Ooi SM, Vivian JB, Cohen RJ (2009) The use of the Ki-67 marker in the pathological diagnosis of the epithelioid variant of renal angiomyolipoma. Int Urol Nephrol 41:559–565
30. Aslan DL, Gulbahce HE, Pambuccian SE, Manivel JC, Jessurun J (2005) Ki-67 immunoreactivity in the differential diagnosis of pulmonary neuroendocrine neoplasms in specimens with extensive crush artifact. Am J Clin Pathol 123:874–878
31. Rioux-Leclercq N, Leray E, Patard JJ, Lobel B, Guille F, Jouan F, Bellaud P, Epstein JI (2005) The utility of Ki-67 expression in the differential diagnosis of prostatic intraepithelial neoplasia and ductal adenocarcinoma. Hum Pathol 36:531–535
32. Carreras J, Lopez-Guillermo A, Fox BC, Colomo L, Martinez A, Roncador G, Montserrat E, Campo E, Banham AH (2006) High numbers of tumor-infiltrating FOXP3-positive regulatory T cells are associated with improved overall survival in follicular lymphoma. Blood 108:2957–2964
33. Glas AM, Knoops L, Delahaye L, Kersten MJ, Kibbelaar RE, Wessels LA, van Laar R, van Krieken JH, Baars JW, Raemaekers J, Kluin PM, van't Veer LJ, de Jong D (2007) Gene-expression and immunohistochemical study of specific T-cell subsets and accessory cell types in the transformation and prognosis of follicular lymphoma. J Clin Oncol 25:390–398
34. Lee AM, Clear AJ, Calaminici M, Davies AJ, Jordan S, MacDougall F, Matthews J, Norton AJ, Gribben JG, Lister TA, Goff LK (2006) Number of CD4+ cells and location of forkhead box protein P3-positive cells in diagnostic follicular lymphoma tissue microarrays correlates with outcome. J Clin Oncol 24:5052–5059
35. Alvaro T, Lejeune M, Salvado MT, Bosch R, Garcia JF, Jaen J, Banham AH, Roncador G, Montalban C, Piris MA (2005) Outcome in Hodgkin's lymphoma can be predicted from the presence of accompanying cytotoxic and regulatory T cells. Clin Cancer Res 11:1467–1473
36. Curiel TJ (2007) Tregs and rethinking cancer immunotherapy. J Clin Invest 117:1167–1174
37. de Jong D, Koster A, Hagenbeek A, Raemaekers J, Veldhuizen D, Heisterkamp S, de Boer JP, van Glabbeke M (2009) Impact of the tumor microenvironment on prognosis in follicular lymphoma is dependent on specific treatment protocols. Haematologica 94:70–77
38. Brennecke R, Burgel U, Rippin G, Post F, Rupprecht HJ, Meyer J (2001) Comparison of image compression viability for lossy and lossless JPEG and wavelet data reduction in coronary angiography. Int J Cardiovasc Imaging 17:1–12
39. Eikelboom RH, Yogesan K, Barry CJ, Constable IJ, Tay-Kearney ML, Jitskaia L, House PH (2000) Methods and limits of digital image compression of retinal images for telemedicine. Investig Ophthalmol Vis Sci 41:1916–1924
40. Hui OBR (2002) Medical image compression using JPEG2000 and JPEG: a comparison study. J Mech Med Biol 2:313–328
41. Iyriboz TA, Zukoski MJ, Hopper KD, Stagg PL (1999) A comparison of wavelet and joint photographic experts group lossy compression methods applied to medical images. J Digit Imaging 12:14–17
42. Ricke J, Maass P, Lopez Hanninen E, Liebig T, Amthauer H, Stroszczynski C, Schauer W, Boskamp T, Wolf M (1998) Wavelet versus JPEG (Joint Photographic Expert Group) and fractal compression. Impact on the detection of low-contrast details in computed radiographs. Investig Radiol 33:456–463
43. Li F, Sone S, Takashima S, Kiyono K, Yang ZG, Hasegawa M, Kawakami S, Saito A, Hanamura K, Asakura K (2001) Effects of JPEG and wavelet compression of spiral low-dose CT images on detection of small lung cancers. Acta Radiol 42:156–160
44. Kalyanpur A, Neklesa VP, Taylor CR, Daftary AR, Brink JA (2000) Evaluation of JPEG and wavelet compression of body CT images for direct digital teleradiologic transmission. Radiology 217:772–779
45. Siddiqui KM, Johnson JP, Reiner BI, EL S (2005) Discrete cosine transform JPEG compression vs. 2D JPEG2000 compression: JNDmetrix visual discrimination model image quality analysis. Proc. SPIE 5748:202–207
46. Matkowskyj KA, Schonfeld D, Benya RV (2000) Quantitative immunohistochemistry by measuring cumulative signal strength using commercially available software Photoshop and MATLAB. J Histochem Cytochem 48:303–312
47. Singh SS, Kim D, Mohler JL (2005) Java Web start based software for automated quantitative nuclear analysis of prostate cancer and benign prostate hyperplasia. Biomed Eng Online 4:31
48. Atalag K, Sincan M, Celasun B, Karaagaoglu E (2004) Effects of lossy image compression on quantitative image analysis of cell nuclei. Anal Quant Cytol Histol 26:22–27

Virchows Arch (2011) 458:247–248
DOI 10.1007/s00428-010-1028-z

LETTER TO THE EDITOR

Quality management and accreditation of research tissue banks

Anne Carter · Fotini Betsou · Brian J. Clark

Received: 17 November 2010 / Accepted: 15 December 2010 / Published online: 13 January 2011
© Springer-Verlag 2011

Herpel et al [1] are to be congratulated on achieving accreditation of their tissue bank against ISO 17020:2004 *General criteria for the operation of various types of bodies performing inspection.* However, the appropriateness of the use of this standard can be questioned. This standard is used widely to accredit *inspection bodies* in the engineering, food and asbestos sectors in the UK and in the electrical, gas and pulverisation engineering, food and radiotherapy sectors in France. It is difficult to see the parallels between research tissue banks and inspection bodies. The authors' use of ISO 17020:2004 to accredit some aspects of a research tissue bank's activities, whilst excluding the clinical data associated with the samples, collection and processing of blood and blood derivatives and any testing carried out on these samples, illustrates the difficulty in finding an accreditation standard suitable for human tissue banks set up to support research.

As Herpel et al [1] stated, ISO 9001:2008 is a suitable standard for the certification of the quality management system of all tissue banks' activities, but it does not give assurance of the quality of the technical aspects of a tissue bank's work, the accuracy of any results it produces or the professional competence of its staff. A more specific accreditation would be required to provide assurance to donors, funders, researchers and patients of a tissue bank's technical competence, as well as providing a benchmark for competitors.

There are several publications dealing with the best practices for research tissue banks, as quoted by Herpel et al [1], but these give guidance only, and none are suitable for use as an accreditation standard in their current formats. As a result, in 2007, Betsou and colleagues examined these guidelines and alternative standards for certification and accreditation (ISO 9001:2008 [2], ISO 17025:2005 [3], ISO Guide 34 [4]) and compiled them into a format compatible with an ISO accreditation standard for laboratory testing activities [5]. This proposed new standard has not been taken up by any accreditation bodies yet, and so has not progressed significantly beyond its initial publication.

The only existing national biobank-specific standard is the French standard, NF S 96-900 *Quality of biological resource centres (BRC)–Management system of a BRC and quality of biological resources form human or micro-organism origin,* published in July 2008. Its design was based on ISO9001:2008, and includes some specific technical requirements. It is applicable to the wide activities of research tissue banks and is suitable as a certification, but not as an accreditation standard. Certification against either ISO9001:2008 or NF S 96-900 is requested of research tissue banks by the French research infrastructures funding organisation (IBISA), and so far, 47 organisations have been certified, of which the majority are research tissue banks.

The French standard has not been used outside of France, but its application in France shows that a *specific* standard design for research tissue banks is useful and applicable. A project to develop a European or even better an International (ISO) standard for *accreditation* of research tissue banks is long overdue.

A. Carter (✉) · B. J. Clark
onCore UK,
Devonshire House, Manor Way,
Borehamwood, Herts WD6 1QQ, UK
e-mail: anne.carter@ncri.org.uk

F. Betsou
Integrated Biobank of Luxembourg,
6, rue Ernest Barblé,
1210 Luxembourg, Germany

Conflict of interest statement The authors declare that they have no conflict of interest.

References

1. Herpel E, Rocken C, Manke H, Schirmacher P, Flechtenmacher C (2010) Quality management and accreditation of research tissue banks: experience of the National Centre for Tumor Diseases (NCT) Heidelberg. Virchows Arch 457:741–747. doi:10.1007/s00428-010-0998-1
2. ISO 9001:2008 Quality management system requirements. International Organisation for Standardisation, Geneva
3. ISO 17025:2005 General requirements for the competence of testing and calibration laboratories. International Organisation for Standardisation, Geneva
4. ISO Guide 34 General requirements for the competence of reference material producers. International Organisation for Standardisation, Geneva
5. Betsou F, Luzergues A, Carter A et al (2007) Towards norms for accreditation of biobanks for human health and medical research: compilation of existing guidelines into an ISO certification/accreditation norm-compatible format. Qual Assur J 11:221–294

Virchows Arch (2011) 458:249–250
DOI 10.1007/s00428-010-1029-y

LETTER TO THE EDITOR

Letter to the editor—reply to comments of Carter et al.

Esther Herpel · Christoph Roecken · Heike Manke · Peter Schirmacher · Christa Flechtenmacher

Received: 15 December 2010 / Accepted: 15 December 2010 / Published online: 5 January 2011
© Springer-Verlag 2010

We thank Carter et al. for their contribution, addressing quality standards in research tissue banks and adequate measures to evaluate them (e.g., accreditation or certification).

Accreditation and confirmation of competence of Surgical Pathology Institutions in Germany started many years ago and solely performed on the basis of DIN EN ISO/IEC 17020 and has been carried out successfully for more than 80 institutions (e.g., departments of university hospitals and community hospitals, as well as private institutions). There is no doubt that tissue banks can be accredited also on the basis of DIN EN ISO/IEC 17020. In 2007, the relevant German "Sector Committee of Pathology and Neuropathology" decided that tissue banks can be accredited separately from Departments of Pathology (as was the case for the NCT tissue bank), according to DIN EN ISO/IEC 17020. The NCT tissue bank was the first to successfully make use of this opportunity. However, the precondition of accreditation is the expert evaluation of the tissue by a board certified surgical pathologist. The entry and exit evaluation of the tissue specimens in the NCT tissue bank follows basically the same competence criteria, as applied in diagnostic surgical pathology. Thus, accreditation of the NCT tissue bank according to DIN EN ISO/IEC 17020 states that it has the full competence to evaluate all characteristics, e.g., amount of tumor cells, tumor type according to the WHO-classification, tumor grade, tumor-stage, of the often non-homogeneous tissues. It was our key intention to bring forward, via accreditation, this most relevant aspect of tissue banking, which we consider an invaluable part of good scientific practice. It is true, as mentioned by Betsou et al., that some biobanks do not specifically evaluate material given out for research purposes. We are absolutely convinced that in the case of tissue banking, this is inacceptable, does not comply with minimal criteria of quality management and good scientific practice, and indeed, those "tissue banks" should not be amenable to accreditation. This is actually the main reason, why we believe that tissue banks should be accredited and not certified (possibly in contrast to other biobanks).

However, by referring to ISO guide 34, Carter et al. raised another issue, which is an open international discussion for the very different kinds of biobanks of human and non-human origin, e.g., tissue samples, cell lines, blood, serum, urine, viruses (including plant viruses), bacteria, DNA, RNA etc. Although, this background was not the central part of our publication, we would like to share some general thoughts about accreditation of biobanks in more general, based on discussions about accreditation of reference material producers (RMPs) according to ISO guide 34. In 2004, the General Assembly of International Laboratory

E. Herpel (✉) · P. Schirmacher · C. Flechtenmacher
Institute of Pathology, University Hospital Heidelberg,
INF 220,
69120 Heidelberg, Germany
e-mail: esther.herpel@med.uni-heidelberg.de

E. Herpel
Tissue Bank of the National Center for Tumor Diseases,
University Hospital Heidelberg,
Heidelberg, Germany

C. Roecken
Institute of Pathology, Christian-Albrechts-University,
Kiel, Germany

H. Manke
DAkkS, Deutsche Akkreditierungsstelle GmbH,
Berlin, Germany

Accreditation Cooperation passed a resolution regarding the general approach to be taken by accreditation bodies when assessing and accrediting RMPs: "The General Assembly resolves that accreditation of technically competent bodies producing reference materials with assigned values will be conducted against harmonized criteria based on ISO Guide 34 and ISO/IEC 17025 in combination". This decision was discussed controversially in Europe and in the European co-operation of Accreditation (EA; 2006). Regarding the basis for accreditation, it was discussed whether the competences of RMPs can be accredited when all processes, such as evaluation of stability and homogeneity of the biomaterial, are not performed by the RMP itself. Despite this controversy, the ILAC resolution was generally confirmed by the EA. Simultaneously, the accreditation of biobanks, comparing them with RMPs, was brought into the discussion by the EA as a new field for accreditation already at that time. According to our knowledge, mandatory resolutions were not made until today. In case ISO guide 34 will be established as a basis for tissue bank accreditation, this would require the application in combination with ISO/IEC 17020 and not the ISO/IEC 17025.

Virchows Arch (2011) 458:251–259
DOI 10.1007/s00428-011-1048-3

REVIEW AND PERSPECTIVE

Ductal plates in hepatic ductular reactions. Hypothesis and implications. I. Types of ductular reaction reconsidered

Valeer J. Desmet

Received: 27 November 2010 / Revised: 18 January 2011 / Accepted: 20 January 2011 / Published online: 2 February 2011
© Springer-Verlag 2011

Abstract This article focuses on the observation that most hepatic ductular reactions (DRs) have ductal plate (DP)-like patterns. Considering old and recent data, it hypothesizes that in DR, dedifferentiation of hepatocytes in ductular metaplasia may lead to the de novo development of liver stem/progenitor cells (LPCs). The three recognized types of DR are reconsidered, and an additional fourth type, DR type 2B, is added. In DR type 1 whose pattern differs from DP, the pre-existing cholangiocytes multiply and adjust the ductal structure in response to micro-environmental changes induced by oedema and inflammation. This DR fails to establish new canaliculo-ductular connections. DRs types 2A, 2B and 3 represent progenitor cell-based reactions in DP configuration which establish canaliculo-ductular connections similar to DPs in embryonic and foetal liver development. DR type 2A occurs in periportal areas in chronic cholestatic and inflammatory diseases and is interpreted as a reaction of LPCs, which either pre-exist or derive from dedifferentiated hepatocytes. DR type 2B occurs in centrolobular areas and zones of parenchymal hypoxia, is induced by hypoxia and corresponds to "ductular metaplasia" like type 2A with a presumably similar cellular origin. DR type 3 relates to the well-recognized activation of LPCs that reside in the canals of Hering. All DRs in DP configuration play a role in progression of fibrosis in chronic liver diseases.

V. J. Desmet
Department of Pathology, University Hospital K.U. Leuven,
Campus St. Rafael,
Leuven, Belgium

V. J. Desmet (✉)
Department of Pathology, University Hospital St. Rafael,
Minderbroedersstraat 12,
3000, Leuven, Belgium
e-mail: v.desmet@telenet.be

Keywords Canaliculo-ductular junction · Cholestasis · Differentiation and dedifferentiation · Ductular reaction · Ductal plate · Hypoxia

Introduction

This manuscript describes new histological observations on hepatic ductular reactions (DRs). My interpretations and hypothetical explanations are solely deduced from microscopic findings in human liver specimens and are not based on any experimentally obtained evidence. I report my observations and considerations in the hope that others may confirm, correct or refute part or all of them by adequate investigation.

I noticed during recent years that most hepatic DRs occur in "ductal plate" (DP) configuration. DPs are primitive forms of intrahepatic bile ducts (IHBDs) during embryologic development of the liver, corresponding to a double perforated cylinder of biliary type cells lining a circular slit-like lumen [1] (Fig. 1). A recent review details the molecular changes involved in development of DPs and IHBDs, emphasizing a crucial role for Notch signalling [2]. DP formation is distinct from other types of tube formation in the body [2]; it is the liver-specific mechanism which creates sites of continuity between the canalicular networks of a growing parenchymal mass and the already established parts of the bile draining system in the developing liver.

So-called "ductules" represent the smallest ramifications of the intrahepatic biliary tree, which are entirely lined by cholangiocytes [3]. The actual interface between a ductule and the canalicular network is assured by canals of Hering, lined partly by cholangiocytes and partly by hepatocytes, and also harbouring liver progenitor cells (LPCs). DRs involve both ductules and canals of Hering [3].

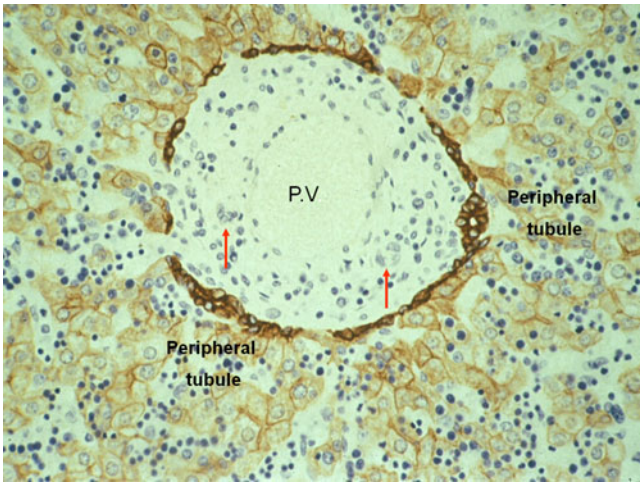

Fig. 1 Remodelling ductal plate in human embryo of 23 weeks. Keratin immunostain (Cam.5.2.). *PV* portal vein. *Red arrows* early appearance of hepatic artery branches in the perivenous mesenchyme

DRs occur in cholestatic diseases [4], in inflammatory diseases with cytokine-induced increase in biliary ductules [5] and in conditions with massive loss of parenchyma, e.g. fulminant hepatitis [6]. Hence, three types of DR are classically recognized: type 1, proliferation of pre-existing ducts and ductules; type 2, ductular metaplasia of hepatocytes and type 3, activation/proliferation of LPCs [7]. I add a fourth not yet explicitly published type of DR induced by hypoxia, indicated as DR type 2B below in "Types of ductular reaction reconsidered" section, which reconsiders the different types of DR.

Ductular reaction in ductal plate configuration

I observed that most DRs occur in the form of small DP patterns or mini-ductal plates (Fig. 2a, b), explaining why DR has been described in primary biliary cirrhosis (PBC) as "Many of these structures are tortuous, contain no discernable lumens, and are seldom cut in cross section" [8] and in biliary atresia as "a complex filigree pattern" [9]. Indeed, predominantly longitudinal profiles and filigree-like patterns are consistent with DP conformation. The mini-ductal plates are composed of a small central blood vessel (altered sinusoid or venule), surrounded by a small amount of mesenchyme derived from the original Disse space, and a (usually) double layer of biliary type epithelial cells lining a circular, nearly virtual luminal cleft between both layers. Often, a tubular dilatation is seen at one or more sites along the luminal perimeter (Fig. 2a, b). This configuration corresponds to the double-layered embryonic DPs in an early remodelling stage, characterized by tubular dilatations at a couple of sites along the perimeter of the DP (compare with Fig. 1). Like DPs during embryonic development, the newly formed mini-ductal plates become remodelled into conduits of tubular shape, explaining why not every section in a liver specimen with DR shows a pattern in DP configuration. DPs are rapidly

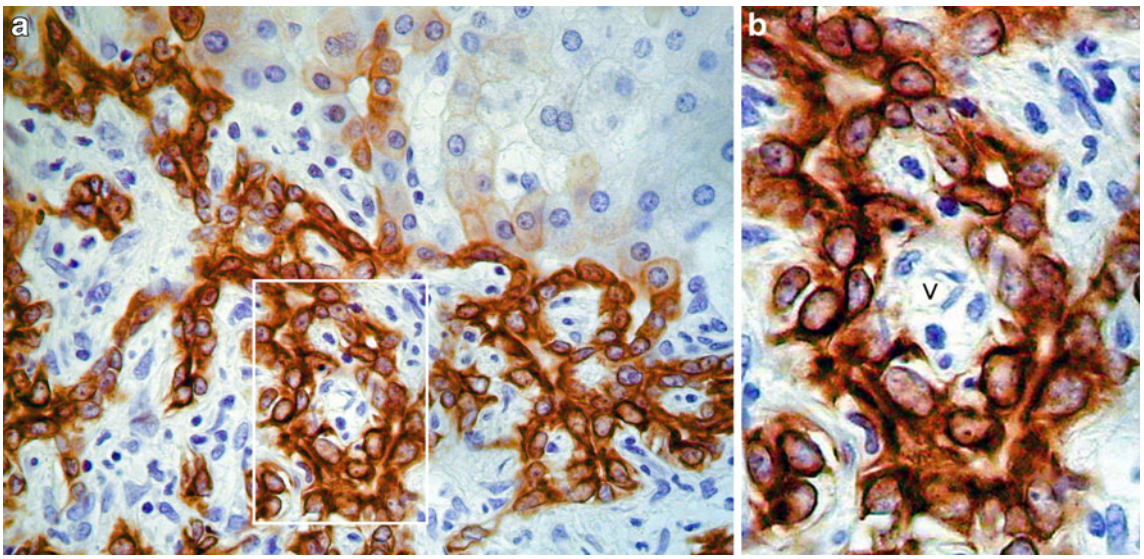

Fig. 2 **a** Ductular reaction (DR) in sclerosing cholangitis. K7 immunostain. DR in DP configuration at the interface between portal tract (*lower left*) and lobular parenchyma (*upper right*). One element of the network (*white box*) is illustrated in **b**. Note the presence of a weaker K7+ cholestatic liver cell rosette at the *central top of the figure*. **b** Enlarged box of **a**. Ductal plate pattern. Note the central vessel (V), corresponding to an altered sinusoid, surrounded by mesenchyme, in turn surrounded by a double layer of small K7+ cholangiocytes delineating a circular cleft in between. At a few sites in the perimeter, "peripheral tubules" are seen in cross-section. This pattern corresponds to that of an embryonic ductal plate in an early stage of remodelling (see text). Compare with Fig. 1

remodelled unless persistence of cholestasis favours a DP configuration for a longer time, facilitating cholehepatic cycling of bile acids [10], because of a larger resorbing cholangiocytic surface in DPs. Hence, the duration of a DP pattern depends on the balance between speed of formation versus speed of remodelling.

DP patterns of DRs were observed in periportal areas in liver biopsies with chronic cholestasis from patients with PBC and primary sclerosing cholangitis (PSC), biliary atresia (BA), idiopathic adulthood ductopenia (IAD), progressive familial intrahepatic cholestasis type 2 (PFIC 2) or bile salt export pump (BSEP) deficiency, in non-alcoholic steatohepatitis (NASH; unpublished observations), and were illustrated in ob/ob mice (Fig. 3b in reference [11]). DP patterns may also be recognized in liver tumours, e.g. in mesenchymal hamartoma of the liver [12], in the "antler-like" pattern of ductules in cholangiolocellular carcinoma [13] and in some mixed hepatocellular–cholangiocellular carcinomas at tumour–stroma interfaces (Fig. 3).

A DP pattern also occurs in parenchymal hypoxic areas: centrolobular in liver lobules or centronodular in cirrhotic nodules, described below as DR type 2B.

Interpretation, hypothesis and supporting components: a remark on terminology as introduction

Recent studies [14, 15] advocate to reserve the term "hepatoblasts" for descendants of human liver stem cells differentiating towards hepatocytes as "precursors with hepatocyte fate". In the present paper as in most studies, "hepatoblasts" refers to liver stem/progenitor cells, whereas the term "intermediate hepatobiliary cells" denotes cell types which express simultaneously both hepatocellular and cholangiocytic characteristics during intermediate stages of their differentiation from progenitor cells to hepatocytes and during dedifferentiation from mature hepatocytes towards more primitive cell types. This nomenclature has the advantage of according with the latest terminology consensus proposals [3] and providing a neutral, morphology-based terminology for intermediate stage cells as well in dedifferentiation as differentiation processes.

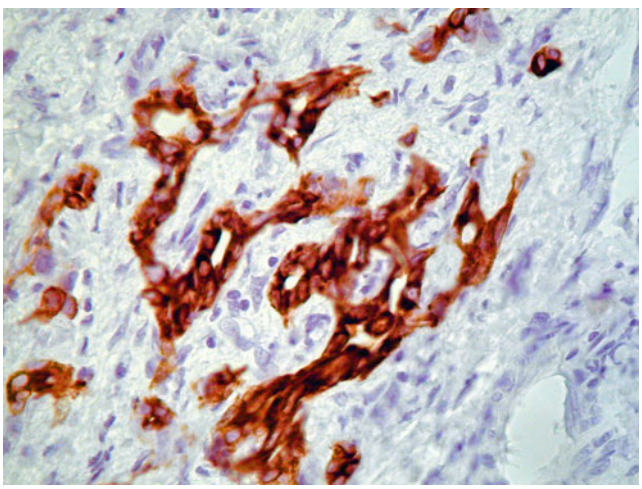

Fig. 3 Immunostain for K7 on section of hepatobiliary liver carcinoma, containing areas of hepatocellular carcinoma and cholangiocarcinoma. The illustrated cholangiomatous structures in vascularized stroma display a distorted ductal plate arrangement. Compare with Fig. 2a

The main components involved in the proposed concept and hypothesis of DRs in DP conformation are first summarized in the following lines.

1. The phenotype of epithelial and mesenchymal cells is influenced by mutual interactions through cell contacts, matrix components and soluble factors. Although several epithelial and mesenchymal cell types co-exist in close proximity in the liver, specific couples of epithelial and mesenchymal cells appear to exert preferential interactions at particular time points or in specific circumstances. Available literature data allow to distinguish the following "couples of preferential partner cells":
   - (A) In embryonic and foetal liver, the involved cell couples comprise the following:
     - (a) Sensitized hepatoblast–hepatic stellate cell (HSC) precursor interactions playing a crucial role during DP formation as part of IHBD development [14–16],
     - (b) Hepatoblast–sinusoidal endothelial cell interaction, involved during differentiation of hepatoblasts towards mature hepatocytes [16].
   - (B) In postnatal liver, one can distinguish as common interactions the following:
     - (a) Hepatocyte–hepatic stellate cell (HSC) interaction, e.g. in vitamin A metabolism [17];
     - (b) Intermediate hepatobiliary cell–activated myofibroblast interaction, whereby the activation into myofibroblasts of HSCs may be induced either by cholestasis [18] or by hypoxia [19], or both together;
     - (c) Interaction between mature cholangiocytes and portal NTPDase2 (nucleoside triphosphate diphosphohydrolase 2) positive portal fibroblasts [20];
     - (d) LPCs interacting with their stem/progenitor cell niche components [3].

In short, all epithelial variants have fitting mesenchymal partners and other accompanying specific "niche" components. This notion of reciprocal cellular determination was recently re-emphasized [21].

2. Cells may change in phenotype by differentiation and dedifferentiation, with mutual impact on the partner cells and other "niche" components. Differentiation of LPCs towards hepatocytes evolves from keratin 19+ (K19+) progenitor cells, over K19+ K7+ intermediate hepatobiliary cells, to K19 negative, K7+ intermediate hepatocytes and finally to K7 negative mature hepatocytes [22]. In contrast, dedifferentiation of mature hepatocytes proceeds from K7 negative hepatocytes, over K7+ intermediate hepatobiliary cells to K7+, K19+ intermediate hepatobiliary cells and finally K19+, K7 negative small cells (Fig. 4). Indeed, so-called cholangiocytic metaplasia of hepatocytes represents a dedifferentiation towards a more primitive cell type [23]. Progression of (de) differentiation depends on mutual cellular interactions, also involving Jagged1/Notch signalling [24], and may eventually result in the hepatic stem cell phenotype and acquisition by the mesenchymal cell of the niche requirements and associated matrix components. The partners may be the physiological ones, or others recruited by cytokine or chemokine signalling, usually in sites of tissue injury [21]. The hypothesis thus invokes the possibility of a maximal degree of hepatocytic dedifferentiation down to the stage of the pluripotent K19+ hepatic progenitor cell. All intermediate stages are accompanied by appropriate mesenchymal and other "niche" components. The maximal dedifferentiation to progenitor cell phenotypes, indicated as in vivo equivalents of "induced pluripotent stem cells" (iPSCs), is based on suggestive evidence from the literature discussed below.
3. All DRs, except type 1, are post-natal equivalents of DP formation during embryonic liver development. This item postulates that during postnatal liver growth and in diseases, a recapitulation takes place of mechanisms at work during embryonic and foetal development.

The second layer of the mini-ductal plate is not easily explained by cholangiocytic metaplasia of hepatocytes alone. The double layer could be generated in three ways: (1) by an activation of LPCs in the canals of Hering as a result of cholestatic or hypoxic changes in the microenvironment (including phenotypic changes of hepatocytes and HSCs); (2) by de novo LPCs generated through maximal dedifferentiation of hepatocytes in the DR itself, or (3) by a combination of both phenomena. In either case, LPCs would be involved. Presumably, the activation of existing LPCs is the only or the prevailing mechanism in a minimal degree of DR like the one postulated during normal liver growth, whereas options 2 and 3 are operating or prevail in pathological conditions with greater or maximal degrees of DR.

The dedifferentiation concept (option 2) is supported by several observations in the literature. Hepatocyte dedifferentiation is a reversible consequence of a specific signalling network triggered by the extracellular matrix [25]. In the

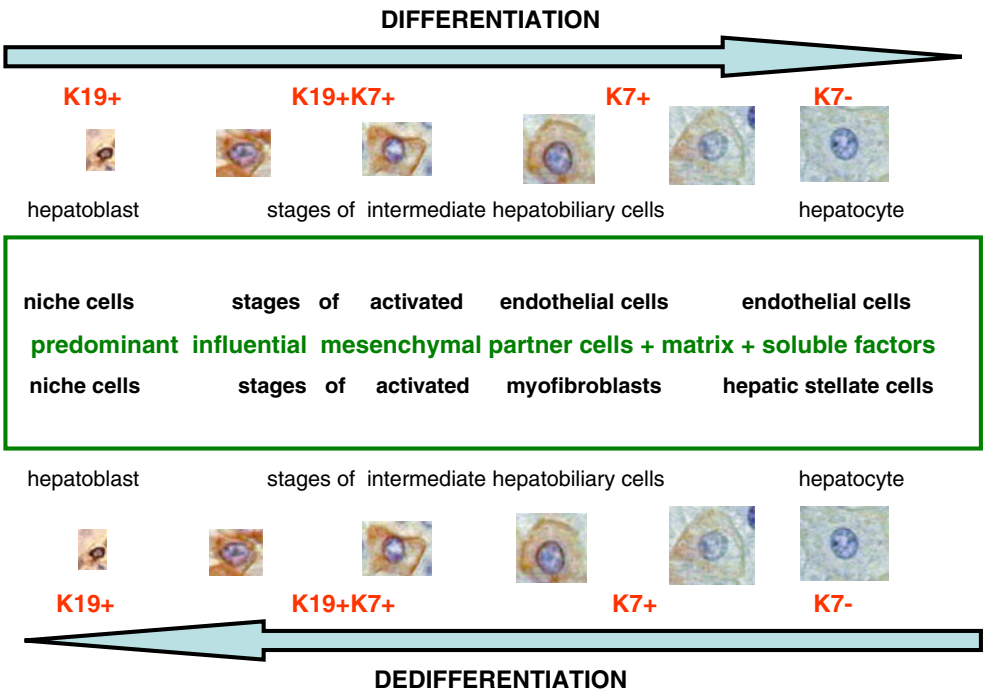

Fig. 4 *Upper and lower parts* schematic overview of hepatocellular differentiation and dedifferentiation through stages of intermediate hepatobiliary cells. *Central part* associated mesenchymal partner cells, with only the predominant ones indicated for differentiation and dedifferentiation, respectively. Intermediate hepatobiliary cells and activated myofibroblasts represent a spectrum of successive stages, which gradually may become better individually identified in the future by use of appropriate markers

choline-deficient, ethionine-supplemented model of LPC proliferation, extracellular matrix deposition and activation of matrix-producing cells occur prior to LPC expansion, in front of the periportally extending LPCs, indicating that LPC activation and proliferation is associated with extracellular matrix remodelling into the equivalent of a "stem cell niche" [26]. Biliary cells in DR express numerous markers of LPCs, including neural cell adhesion molecule (NCAM), bcl2, epithelial cell adhesion molecule (Ep-CAM), polyductin, ATP binding cassette (ABC) transporter proteins MDR1, MRP1 and MRP3; breast cancer resistance protein (BCRP/ABCG2), annexin 3 and claudin 4; and still other markers [27]. Two pluripotent hepatic progenitors, termed hepatic stem cells and hepatoblasts, have been isolated from human livers; the stem cells had characteristics which resemble those of small cholangiocytes in DR and also require paracrine signalling by hepatic stellate cells and/or angioblasts for their survival and proliferation [28]. The gradient in K7 and K19 expression of dedifferentiating hepatocytes reminds the TGFbeta/activin gradient during embryonic bile duct development [2]. Evidence is accumulating on the microenvironment as a critical component in the regulation of a continuum of stem cell phenotypes [29], and experimental studies show that the "mesenchymal niche" of epithelial cells, in the liver represented—at least in part—by the HSCs [30], is crucial in determining hepatocytic phenotype and eventual dedifferentiation [31]. In vitro culture studies of mature hepatocytes revealed their potency to regain a spectrum of progenitor markers, suggesting enormous plasticity and differentiation potential of adult parenchymal cells [32], and under influence of cytokines, mature hepatocytes may become a source of bipotential hepatoblasts [33]. Activation of Notch signalling in postnatal hepatocytes causes them to adopt a biliary fate through a process of reprogramming that recapitulates normal bile duct development [2]. These data support, also for the liver, the suggestion that a transient stem cell state, termed the "stem state", may be assumed by any cell [34]. This hypothesis becomes less far-fetched and more acceptable in the light of recent discoveries of experimentally induced dedifferentiation of mature somatic cells into iPSCs [35] realized by exogeneous induction of a set of transcription factors (Oct4, Sox2, Klf4 and c-Myc) [36].

In the case of hepatocyte-derived iPSCs, their subsequent redifferentiation into hepatic endoderm and functioning hepatocytes could be achieved [37, 38]. These results allow to venture the hypothesis that Nature can perform the same in vivo in the liver, implying that advanced dedifferentiation of hepatocytes may result in stem cell characteristics as suggested above: in vivo equivalents of iPSCs. The origin of LPCs in DR might thus be twofold: a genuine progenitor cell activation or an in vivo iPSC generation.

In short, the presented hypothesis implies that the developmental mechanism of DP formation, operative in the embryonic stage, becomes re-iterated in diverse postnatal hepatic conditions characterized by increased numbers of bile duct structures, like in normal liver growth, and in diseases characterized by DRs such as cholestatic diseases, inflammatory conditions, hypoxic states, and benign and malignant tumours,

Types of ductular reaction reconsidered

DR type 1

DR type 1 is predominant in acute complete bile duct obstruction [39], ANIT (alpha-naphtyl isothiocyanate) intoxication [40] and cytokine (e.g. interleukin 6)-induced ductular increase [5]. It results from proliferation of preexisting cholangiocytes, resulting in elongation, branching and luminal widening of biliary tubes. Type 1 DR represents one of the countless interactions between inflammatory, stromal and bile duct cells [20]. In normal liver, the proliferation of cholangiocytes in portal tracts is kept in check by epithelial–mesenchymal interaction between cholangiocytes and a specific compartment of periductal portal fibroblasts, which inhibit cholangiocyte proliferation via expression of the ecto-nucleotidase NTPDase2 (nucleoside triphosphate diphosphohydrolase 2) which blocks the purinergic ATP (P2Y) receptors on ductal and ductular cells. Bile duct obstruction and interleukin 6 downregulate NTPDase2, thus activating specific PY2 receptors on cholangiocytes, resulting in their proliferation [20]. Simple proliferation occurs without creating new ductular–canalicular connections. Elongation of bile ducts in biliary obstruction increases the total re-absorbing surface area of cholangiocytes, allowing for an increased chole-hepatic cycling of bile acids [10]. Elongation, dilatation and branching of ducts in bile duct obstruction and inflammation adapts the three-dimensional structure of the tubes to the expansion of the portal mesenchyme caused by oedema and inflammation, and is presumed to be involved as well in other structural adjustments, like normal liver growth. In this way, DR type 1 may occur together with other types of DR according to structural needs.

DR type 2

Two types of DR type 2 can be distinguished: type 2A, mostly periportal, and type 2B, mostly centrolobular.

DR 2A has been interpreted as "ductular metaplasia of hepatocytes" [41]; it involves a change in secretory polarity from horizontal (hepatocellular canalicular) to vertical

(cholangiocytic apical-basal) polarity. It is typically observed in periportal areas, most characteristically, though not exclusively, in chronic cholestatic conditions. The newly formed ductules retain the labyrinthic, anastomosing pattern of hepatocellular plates (the muralia system). This pattern was illustrated in three-dimensional reconstruction studies of DR and interpreted as of parenchymal metaplastic origin [42]. Especially incomplete and complete bile duct obstructions of longer duration favour this ductular metaplasia of hepatocytes. It is apparently due to the intracellular accumulation of retained bile acids causing a change in the keratin cytoskeleton [43]. The cells increasingly express K7, starting in the periportal area and extending later towards the centrolobular zone, later followed by K19 expression [23].

This partial cholangiocytic switch in phenotype is accompanied by activation of the hepatocyte–associated HSCs, located in the Disse space and contacting several hepatocytes through tight junctions with their long cytoplasmic extensions [17]. The cholestatic hepatocytes activate HSCs into a myofibroblastic phenotype responsible for increased production of connective tissue matrix, which in turn further modulates the K7+ "intermediate hepatobiliary cell" into a progressively more typical cholangiocytic type of cell [4], which in turn accentuates again the fibrogenic function of the myofibroblast. Cells with cholangiocytic phenotype are activated by taurodeoxycholate and taurocholate [44] and may, through their secretion of chemokines (like monocyte chemotactic protein 1 (MCP-1), attract additional HSCs [45]. Thus, in lasting cholestasis, bile acids induce an increase in cholangiocyte population, contribute to development of pericellular fibrosis and, in this way, promote further bile ductular metaplasia of hepatocytes.

Although debated for a long time, cholangiocytic metaplasia of hepatocytes, especially in cholestasis and in association with fibrosis, has been supported by numerous observations in man [46] and in experimental studies [47]. Also in favour of reactivation of an early developmental mechanism are results in bile duct-ligated rodents revealing a resurrection of the Hedgehog pathway in guiding the remodelling of biliary epithelia and stroma after cholestatic injury [48].

DRs of types 1 and 2A are reversible when the causative trigger is eliminated; excess ductular structures disappear by apoptosis [49], and the associated fibrosis regresses to considerable extent [50]. Such reversibility illustrates the plasticity of tissues and cells, which can be modulated in a finely tuned way according to the needs of the moment.

DR type 2B occurs in parenchymal hypoxic areas: centrolobular in liver lobules and centronodular in cirrhotic nodules, in contrast to a predominantly periportal location of the other types. Although often slower in development, its microscopic pattern is comparable to DR type 2A: ductular metaplasia or dedifferentiation of mature hepatocytes, associated with myofibroblast-induced fibrosis.

The mechanistic pathway is hypoxia-inducible factor 1-alpha (HIF-1α). Longstanding relative ischemia and hypoxia, like in venous outflow block, results in the development of progressive perisinusoidal fibrosis and concomitant reduction in size of hepatocytes in the centrolobular zone. This is due to induction in hypoxic hepatocytes of HIF-1α, which upregulates profibrotic and vasoactive mediators, such as platelet-derived growth factor-A (PDGF-A), PDGF-B and plasminogen activator inhibitor-1 (PAI-1), which in turn activate HSCs into fibrogenetic activity resulting in progressive centrolobular fibrosis [51]. The dedifferentiating hepatocytes start expressing K7, progressing further into a primitive phenotype expressing K19 and finally assume a tubular architecture ("centrolobular ductular metaplasia or DR type 2B"; Fig. 5a–c).

The idea that advanced centrolobular dedifferentiation of hepatocytes may result in acquisition of progenitor cell characteristics is supported by the finding that hypoxia favours the "stem cell niche-quality" of a cellular microenvironment [52]. One might also consider a migration of LPCs from Hering canals into hypoxic centrolobular zones, but such mechanism would not explain the increasing numbers of hepatocytes showing the described progressing changes in a centripetal gradient.

DR type 3 occurs in case of massive loss of parenchymal cells and consists in activation and proliferation of LPCs located in ductules and canals of Hering [3]. As bipotential cells, LPCs can differentiate into hepatocytes and bile duct cells. Differentiation towards hepatocytes occurs as described above ("Interpretation, hypothesis and supporting components: a remark on terminology as introduction" section, item 2 (Fig. 4)). However, in many cases of fulminant liver failure in man characterized by an unfavourable inflammatory microenvironment with progressing fibrosis [53], the dominant accompanying mesenchymal cells are of the myofibroblastic fibrogenic phenotype [54] and hence not favourable for steering the progenitors' differentiation in hepatocellular direction [55].

A personal conclusion from these considerations is that, in contrast to what I agreed with in 2004 [3], ductal plates and ductal plate malformations in embryonic and post-natal normal and pathological liver do belong under the broader umbrella of "ductular reaction".

A recent investigation proposed a new classification of DRs based on immunohistochemical profiles [56]. When comparing this classification based on immunohistochemical features with the one discussed here, which is based on criteria of DP formation, the results can be summarized as follows: the proposed class P (primitive) corresponds to DR

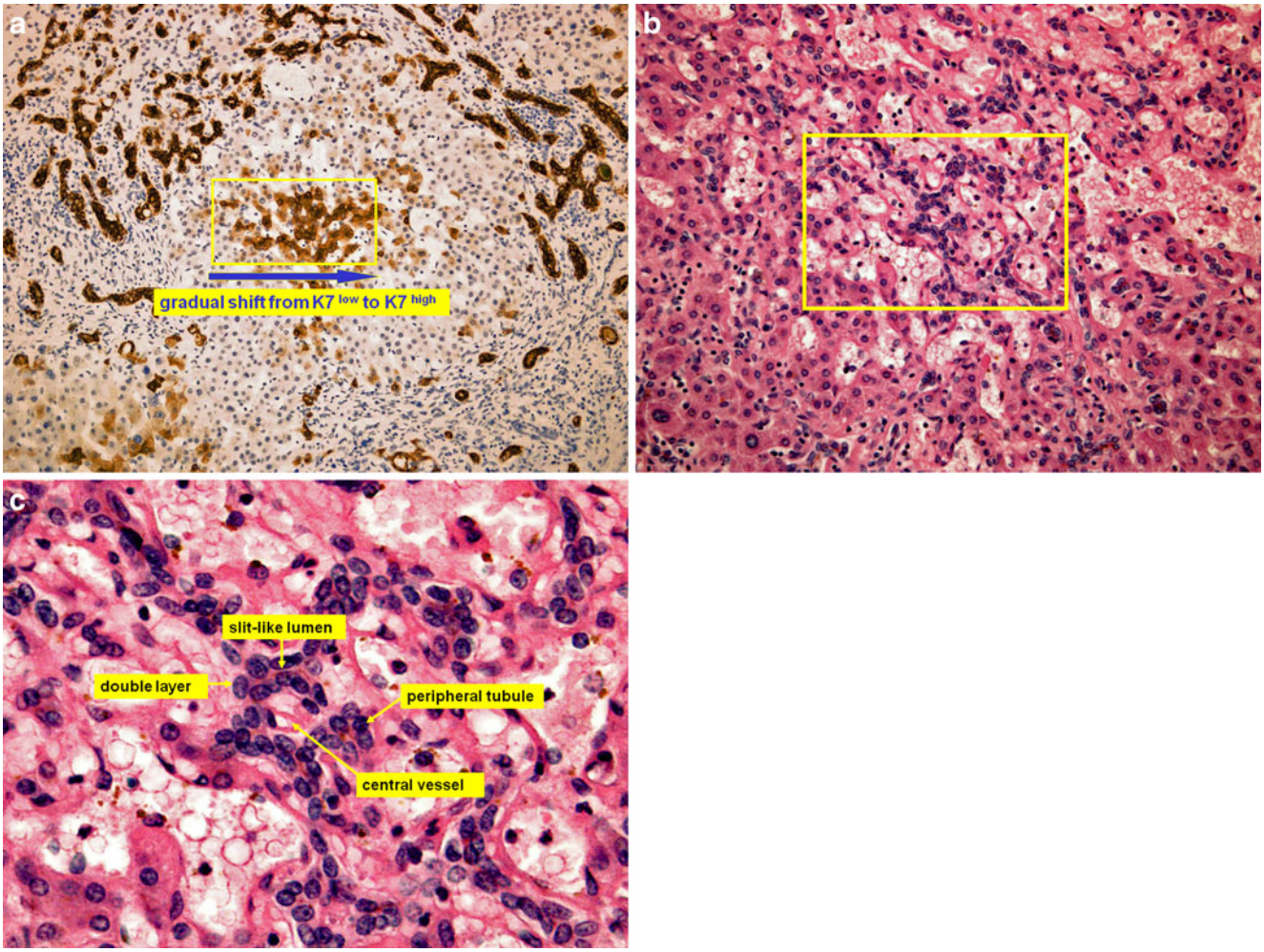

Fig. 5 **a** Liver explant from patient with cystic fibrosis. Cirrhotic nodule with marked perinodular DR (*upper part*), and centronodular parenchymal changes due to hypoxia. Note central area with sinusoidal dilatation and ductular metaplasia of hepatocytes (increasing K7 expression) resulting in areas of DR in DP configuration. K7 immunostain. **b** Section from same liver as **a**. Centronodular area with sinusoidal dilatation, pericellular fibrosis, decreasing hepatocellular size and ductular metaplasia. Haematoxylin–eosin stain. **c** Enlargement of framed area in **b**. Hallmarks of ductal plate configuration: central vessel with surrounding mesenchyme, double layer of small cholangiocyte-like cells lining a slit-like lumen with peripheral tubular dilatation. Haematoxylin–eosin stain. Compare with Figs. 1, 2a, b, and **a**

type 2A, class D (differentiation) to DR type 3 (and 2A in case of failure of hepatocellular differentiation) and O (obstructive) to DR type 1. The DR type 2B caused by hypoxia is not considered [56].

Conclusion

DR type 1 represents multiplication of pre-existing cholangiocytes, playing a role in structural adjustments of bile ducts. DR type 1 develops fast, favouring chole-hepatic cycling of bile acids and assuring an immediate (additional) rescue mechanism against cholestatic parenchymal damage. In contrast, DRs types 2A and 2B represent an activation of LPCs, either pre-existing ones in canals of Hering or LPCs presumed to be de novo induced by cholestasis- or hypoxia-induced dedifferentiation of hepatocytes. DR type 2A develops slowly, creating additional canalicular outlets, and a larger cholangiocytic resorbing surface favouring chole-hepatic cycling in chronic cholestasis. DR type 2B creates ductules in hypoxic areas; this type of DR may be an exaggeration of a mechanism that plays a role in new portal tract induction during liver growth. DR type 3 represents the classical concept of progenitor cell-based parenchymal (re)generation. The concept of DRs in DP shape may explain new lobule formation during postnatal growth, and clarify several features in liver pathology, discussed in a separate paper. All DRs are associated with periductular fibrosis, contributing to cirrhogenic evolution when the causative stimuli persist.

Acknowledgements I thank Tania Roskams for the helpful discussions and for providing the opportunity to keep in touch with progress in hepatopathology after my official retirement in 1996. Rita DeVos and Olivier Govaere deserve my gratitude for the help with the illustrations.

Conflict of interest I declare that I have no conflict of interest.

References

1. Van Eyken P, Sciot R, Callea F, Van der Steen K, Moerman P, Desmet VJ (1988) The development of the intrahepatic bile ducts in man: a keratin-immunohistochemical study. Hepatology 8 (6):1586–1595
2. Zong Y, Panikkar A, Xu J, Antoniou A, Raynaud P, Lemaigre F, Stanger BZ (2009) Notch signaling controls liver development by regulating biliary differentiation. Development 136(10):1727–1739
3. Roskams TA, Theise ND, Balabaud C, Bhagat G, Bhathal PS, Bioulac-Sage P, Brunt EM et al (2004) Nomenclature of the finer branches of the biliary tree: canals, ductules, and ductular reactions in human livers. Hepatology 39(6):1739–1745
4. Desmet VJ (1992) Modulation of the liver in cholestasis. J Gastroenterol Hepatol 7(3):313–323, Review
5. Liu Z, Sakamoto T, Ezure T, Yokomuro S, Murase N, Michalopoulos G, Demetris AJ (1998) Interleukin-6, hepatocyte growth factor, and their receptors in biliary epithelial cells during a type I ductular reaction in mice: interactions between the periductal inflammatory and stromal cells and the biliary epithelium. Hepatology 28(5):1260–1268
6. Roskams TA, Libbrecht L, Desmet VJ (2003) Progenitor cells in diseased human liver. Semin Liver Dis 23(4):385–396
7. Roskams T, Desmet V (1998) Ductular reaction and its diagnostic significance. Sem Diagn Pathol 15(4):259–269, Review
8. Kaplan MM (1993) Primary biliary cirrhosis. In: Schiff L, Schiff ER (eds) Diseases of the liver, 7th edn. Lippincott, Philadelphia, pp 377–410
9. Pacheco MC, Campbell KM, Bove KE (2009) Ductal plate malformation-like arrays in early explants after a Kasai procedure are independent of splenic malformation complex (heterotaxy). Pediatr Dev Pathol 12(5):355–360
10. Yeh H-Z, Schteingart CD, Hagey LR, Ton-Nu H-T, Bolder U, Gavrilkina MA, Steinbach JH, Hofmann AF (1997) Effect of side chain length on biotransformation, hepatic transport, and choleretic properties of chenodeoxycholyl homologues in the rodent: studies with Dinor- (C22), Nor- (C23) and chenodeoxycholic acid (C24). Hepatology 26:374–385
11. Roskams T, Yang SQ, Koteish A, Durnez A, DeVos R, Huang X, Achten R, Verslype C, Diehl AM (2003) Oxidative stress and oval cell accumulation in mice and humans with alcoholic and nonalcoholic fatty liver disease. Am J Pathol 163(4):1301–1311
12. Desmet VJ (1992) Congenital diseases of intrahepatic bile ducts: variations on the theme "ductal plate malformation". Hepatology 16(4):1069–1083, Review
13. Komuta M, Spee B, Vander Borght S, De Vos R, Verslype C, Aerts R, Yano H, Suzuki T, Matsuda M, Fujii H, Desmet VJ, Kojiro M, Roskams T (2008) Clinicopathological study on cholangiolocellular carcinoma suggesting hepatic progenitor cell origin. Hepatology 47(5):1544–1556
14. Zhang L, Theise N, Chua M, Reid LM (2008) The stem cell niche of human livers: symmetry between development and regeneration. Hepatology 48(5):1598–1607
15. Wang Y, Yao HL, Cui CB, Wauthier E, Barbier C, Costello MJ, Moss N, Yamauchi M, Sricholpech M, Gerber D, Loboa EG, Reid LM (2010) Paracrine signals from mesenchymal cell populations govern the expansion and differentiation of human hepatic stem cells to adult liver fates. Hepatology 52(4):1443–1454
16. Sugiyama Y, Koike T, Shiojiri N (2010) Developmental changes of cell adhesion molecule expression in the fetal mouse liver. Anat Rec (Hoboken) 293:1698–1710
17. Geerts A (2001) History, heterogeneity, developmental biology, and functions of quiescent hepatic stellate cells. Semin Liver Dis 21(3):311–335, Review
18. Kinnman N, Goria O, Wendum D, Gendron MC, Rey C, Poupon R, Housset C (2001) Hepatic stellate cell proliferation is an early platelet-derived growth factor-mediated cellular event in rat cholestatic liver injury. Lab Invest 81(12):1709–1716
19. Copple BL, Bai S, Burgoon LD, Moon JO (2011) Hypoxia-inducible factor-1α regulates the expression of genes in hypoxic hepatic stellate cells important for collagen deposition and angiogenesis. Liver Int 31:230–244
20. Dranoff JA, Wells RG (2010) Portal fibroblasts: underappreciated mediators of biliary fibrosis. Hepatology 51(4):1438–1444, Review
21. Theise ND (2010) Stem cell plasticity: recapping the decade, mapping the future. Exp Hematol 38(7):529–539
22. Roskams T, De Vos R, Van Eyken P, Myazaki H, Van Damme B, Desmet V (1998) Hepatic OV-6 expression in human liver disease and rat experiments: evidence for hepatic progenitor cells in man. J Hepatol 29(3):455–463
23. Desmet V, Roskams T, Van Eyken P (1995) Ductular reaction in the liver. Pathol Res Pract 191(6):513–524
24. Hurlbut GD, Kankel MW, Lake RJ, Artavanis-Tsakonas S (2007) Crossing paths with Notch in the hyper-network. Curr Opin Cell Biol 19(2):166–175
25. Godoy P, Hengstler JG, Ilkavets I, Meyer C, Bachmann A, Müller A, Tuschl G, Mueller SO, Dooley S (2009) Extracellular matrix modulates sensitivity of hepatocytes to fibroblastoid dedifferentiation and transforming growth factor beta-induced apoptosis. Hepatology 49(6):2031–2043
26. Van Hul NK, Abarca-Quinones J, Sempoux C, Horsmans Y, Leclercq IA (2009) Relation between liver progenitor cell expansion and extracellular matrix deposition in a CDE-induced murine model of chronic liver injury. Hepatology 49(5):1625–1635
27. Alison MR, Brittan M, Lovell MJ, Wright NA (2006) Markers of adult tissue-based stem cells. Handb Exp Pharmacol 174:185–227
28. Schmelzer E, Zhang L, Bruce A, Wauthier E, Ludlow J, Yao HL, Moss N, Melhem A, McClelland R, Turner W, Kulik M, Sherwood S, Tallheden T, Cheng N, Furth ME, Reid LM (2007) Human hepatic stem cells from fetal and postnatal donors. J Exp Med 204(8):1973–1987
29. Deregibus MC, Tetta C, Camussi G (2010) The dynamic stem cell microenvironment is orchestrated by microvesicle-mediated transfer of genetic information. Histol Histopathol 25(3):397–404, Review
30. Roskams T (2008) Relationships among stellate cell activation, progenitor cells, and hepatic regeneration. Clin Liver Dis 12 (4):853–860, ix. Review
31. Koenig S, Krause P, Drabent B, Schaeffner I, Christ B, Schwartz P, Unthan-Fechner K, Probst I (2006) The expression of mesenchymal, neural and haematopoietic stem cell markers in adult hepatocytes proliferating in vitro. J Hepatol 44(6):1115–1124
32. Taylor RA, Wang H, Wilkinson SE, Richards MG, Britt KL, Vaillant F, Lindeman GJ, Visvader JE, Cunha GR, St John J, Risbridger GP (2009) Lineage enforcement by inductive mesenchyme on adult epithelial stem cells across developmental germ layers. Stem Cells 27(12):3032–3042
33. Block GD, Locker J, Bowen WC, Petersen BE, Katyal S, Strom SC, Riley T, Howard TA, Michalopoulos GK (1996) Population

expansion, clonal growth, and specific differentiation patterns in primary cultures of hepatocytes induced by HGF/SF, EGF and TGF alpha in a chemically defined (HGM) medium. J Cell Biol 132(6):1133–1149
34. Zipori D (2004) The nature of stem cells: state rather than entity. Nat Rev Genet 5(11):873–878
35. Hajkova P (2010) Epigenetic reprogramming—taking a lesson from the embryo. Curr Opin Cell Biol 22(3):342–350
36. Hochedlinger K, Plath K (2009) Epigenetic reprogramming and induced pluripotency. Development 136(4):509–523, Review
37. Si-Tayeb K, Noto FK, Nagaoka M, Li J, Battle MA, Duris C, North PE, Dalton S, Duncan SA (2010) Highly efficient generation of human hepatocyte-like cells from induced pluripotent stem cells. Hepatology 51(1):297–305
38. Sullivan GJ, Hay DC, Park IH, Fletcher J, Hannoun Z, Payne CM, Dalgetty D, Black JR, Ross JA, Samuel K, Wang G, Daley GQ, Lee JH, Church GM, Forbes SJ, Iredale JP, Wilmut I (2010) Generation of functional human hepatic endoderm from human induced pluripotent stem cells. Hepatology 51(1):329–335
39. Slott PA, Liu MH, Tavoloni N (1990) Origin, pattern, and mechanism of bile duct proliferation following biliary obstruction in the rat. Gastroenterology 99(2):466–477
40. Masyuk TV, Ritman EL, LaRusso NF (2001) Quantitative assessment of the rat intrahepatic biliary system by three-dimensional reconstruction. Am J Pathol 158(6):2079–2088
41. Desmet VJ (1986) Current problems in diagnosis of biliary disease and cholestasis. Semin Liver Dis 6(3):233–245, Review
42. Jorgensen M (1973) A stereological study of intrahepatic bile ducts. 2. Bile duct proliferation in some pathological conditions. Acta Pathol Microbiol Scand A 81(5):663–669
43. Desmet VJ (1987) Modulation of biliary epithelium. In: Reutter W, Popper H, Arias IM, Heinrich PC, Keppler D, Landmann L (eds) Modulation of liver cell expression. MTP, Lancaster, pp 195–214
44. Xia X, Francis H, Glaser S, Alpini G, LeSage G (2006) Bile acid interactions with cholangiocytes. World J Gastroenterol 12 (22):3553–3563, Review
45. Clouzeau-Girard H, Guyot C, Combe C, Moronvalle-Halley V, Housset C, Lamireau T, Rosenbaum J, Desmoulière A (2006) Effects of bile acids on biliary epithelial cell proliferation and portal fibroblast activation using rat liver slices. Lab Invest 86 (3):275–285
46. Van Eyken P, Sciot R, Desmet VJ (1989) A cytokeratin immunohistochemical study of cholestatic liver disease: evidence that hepatocytes can express 'bile duct-type' cytokeratins. Histopathology 15(2):125–135
47. Michalopoulos GK, Barua L, Bowen WC (2005) Transdifferentiation of rat hepatocytes into biliary cells after bile duct ligation and toxic biliary injury. Hepatology 41(3):535–544
48. Omenetti A, Yang L, Li YX, McCall SJ, Jung Y, Sicklick JK, Huang J, Choi S, Suzuki A, Diehl AM (2007) Hedgehog-mediated mesenchymal-epithelial interactions modulate hepatic response to bile duct ligation. Lab Invest 87(5):499–514
49. Stähelin BJ, Marti U, Zimmermann H, Reichen J (1999) The interaction of Bcl-2 and Bax regulates apoptosis in biliary epithelial cells of rats with obstructive jaundice. Virchows Arch 434(4):333–339
50. Abdel-Aziz G, Lebeau G, Rescan PY, Clément B, Rissel M, Deugnier Y, Campion JP, Guillouzo A (1990) Reversibility of hepatic fibrosis in experimentally induced cholestasis in rat. Am J Pathol 137(6):1333–1342
51. Copple BL, Bustamante JJ, Welch TP, Kim ND, Moon JO (2009) Hypoxia-inducible factor-dependent production of profibrotic mediators by hypoxic hepatocytes. Liver Int 29(7):1010–1021
52. Lin Q, Lee YJ, Yun Z (2006) Differentiation arrest by hypoxia. J Biol Chem 281(41):30678–30683
53. Pohl JF, Melin-Aldana H, Sabla G, Degen JL, Bezerra JA (2001) Plasminogen deficiency leads to impaired lobular reorganization and matrix accumulation after chronic liver injury. Am J Pathol 159(6):2179–2186
54. Baroni GS, Pastorelli A, Manzin A, Benedetti A, Marucci L, Solforosi L, Di Sario A, Brunelli E, Orlandi F, Clementi M, Macarri G (1999) Hepatic stellate cell activation and liver fibrosis are associated with necroinflammatory injury and Th1-like response in chronic hepatitis C. Liver 19(3):212–219
55. Katoonizadeh A, Nevens F, Verslype C, Pirenne J, Roskams T (2006) Liver regeneration in acute severe liver impairment: a clinicopathological correlation study. Liver Int 26(10):1225–1233
56. Turányi E, Dezsö K, Csomor J, Schaff Z, Paku S, Nagy P (2010) Immunohistochemical classification of ductular reactions in human liver. Histopathology 57(4):607–614

Virchows Arch (2011) 458:261–270
DOI 10.1007/s00428-011-1049-2

REVIEW AND PERSPECTIVE

Ductal plates in hepatic ductular reactions. Hypothesis and implications. II. Ontogenic liver growth in childhood

Valeer J. Desmet

Received: 27 November 2010 / Revised: 18 January 2011 / Accepted: 18 January 2011 / Published online: 5 February 2011
© Springer-Verlag 2011

Abstract This article discusses the processes of bile duct growth and new lobule formation in the liver during childhood in the light of the ductal plate (DP) hypothesis. Unlike in other organs in which tubular elongation and branching ends with the creation of the organ-specific terminal differentiation products, in the liver a steadily enlarging parenchymal mass needs to establish continuity of its canalicular network with the existing bile duct system. The hypothesis suggests that this occurs by DP formation, like in the embryonic liver, and further assumes that pathological ductular reactions (DRs) induced by cholestasis or hypoxia are amplified equivalents of similar mechanisms operating at low level during liver growth. The concept is confronted with data on porcine liver growth, since swine and non-swine liver growth is thought to be comparable. Relative bile acid load may be the driving force for establishment of new canaliculo–ductular connections, supported in zones of relative hypoxia by hypoxia-inducible factor 1 alpha secreted by hepatocytes. The latter mechanism is at the base for induction of appropriate vascular changes in selected sinusoids, resulting in the development of portal inlet venules and additional draining central veins. The process gives rise to the formation of new single lobules by formation of new portal tracts or to the transformation of single lobules in compound lobules by development of new vascular septa. The concept of postnatal DP formation is important in the elucidation of several unexplained findings in adult liver diseases.

Keywords Canaliculo–ductular junction · Choleohepaton · Ductal plate · Ductular reaction · Liver units · Ontogenic liver growth

V. J. Desmet (✉)
Department of Pathology, University Hospital K.U.Leuven,
Campus St Rafael,
Leuven, Belgium
e-mail: v.desmet@telenet.be

V. J. Desmet
Department of Pathology, University Hospital St Rafael,
Minderbroedersstraat 12,
3000 Leuven, Belgium

Introduction

The ductular reaction (DR) types 2A, 2B, and 3 have ductal plate (DP) configuration and are observed in various liver diseases [1]. DRs types 2A (in cholestasis) and 2B (in hypoxia) were proposed to correspond to end stages of cholangiocytic metaplasia or dedifferentiation [1, 2] of hepatocytes resulting in activation of existing liver progenitor cells (LPCs), or in de novo generation of LPCs, or both together. Here the hypothesis is discussed that DRs types 2A and 2B may also play a role during physiological ontogenic liver growth in childhood.

Wondering how intrahepatic bile duct (IHBD) growth occurs in the liver of normal growing children, I searched for studies on mechanisms in epithelial tubulogenesis. Most studies concern tubulogenesis in mammalian organs, including lung, salivary gland, mammary gland, pancreas, and kidney [3] or in the insect tracheal system [4]. In these organs, tubular elongation and branching ends with the creation of the organ-specific terminal differentiation products (alveoli in the lung, glomeruli in the kidney, lobuloalveoli in the mammary gland or terminal cells of the insect trachea) thus creating a single structure at the end, and simultaneously assuring its continuity with the elongating tube (e.g., lung alveoli, pancreatic, and mammary glandular acini) [4].

In the growing liver, however, a steadily enlarging parenchymal mass needs to establish and maintain continuity of its extending canalicular network with the already existing and elongating bile duct system. This is known to occur by DP formation in the embryonic and fetal liver [5–7]. But how do bile ducts form during postnatal liver growth in newly developing portal tracts, and in particular, how do they maintain continuity with new canalicular networks? The problem is that the "exocrine secretory unit" of the liver is not a simple glandular acinus at the end of a tube. It corresponds to a labyrinth of hepatocellular plates (muralia) enclosing a network of bile canaliculi with multiple "exits" at the periphery of a "parenchymal unit" (discussed below). This is entirely different from the functional units composing other epithelial organs and representing one of the characteristics which renders the liver an organ "sui generis." The originality of embryonic bile duct formation was suggested to consist in the fact that, unlike other tubes, bile ducts must retain throughout development connectivity in two planes: hepatocyte canaliculi (*x*-axis) and the ductal tree (*z*-axis) [7]. Below, I propose a hypothesis which hopefully answers at least partially the question of postnatal liver growth.

I postulate that during its postnatal growth the liver re-installs the ontogenetic mechanisms at work during embryonic and fetal stages of IHBD development, i.e., DP formation, since the problem faced is similar: assuring a strictly uninterrupted continuity between expanding canalicular networks with an already present and also growing draining system for bile.

A postnatal DP mechanism may still be concordant with the law in branching morphogenesis, telling that early rounds of branching are controlled genetically in a hardwired fashion in many organs, whereas later, branching is stochastic and responding to environmental cues [4]. A more stochastic pattern of growth, determined by areas of unequally fast postnatal parenchymal growth, might explain the variation in size and shape of the primary and secondary "modules" in the organization of the human liver according to Teutsch [8].

Each newly formed and enlarging parenchymal unit must reach a stage whereby the functional need arises for creating an additional inlet of blood supply, and an additional outlet for drainage of bile in continuity with the biliary tree. The question which parenchymal unit needs to be considered necessitates a choice between the different types of units of the liver which have been proposed over the years—lobule of Kiernan? lobule of Mall? acinus of Rappaport? lobule of Matsumoto? choleohepaton? module of Teutsch? [9]. The most plausible candidate is the choleohepaton [10] since it is the smallest unit comprising all structural and functional characteristics of the whole organ and consistent with the best founded structural organization in human liver, such as the primary and secondary lobule of Matsumoto et al. [11, 12] and basically also compatible (albeit in somewhat different size and shape) with the liver module concept of Teutsch [8].

The additional DP needed to form a bile outlet for a newly formed choleohepaton would be a small structure, a mini-equivalent of the DPs involved in the formation of the larger branches of the IHBDs during embryonic development, since it would have to assure bile drainage of only the smallest subunit of the liver. Instead of surrounding a larger branch of the portal vein, it would surround a representative of the smallest portal vein ramifications, that is: a single sinusoid adapted into an inlet venule. Although small, such mini-ductal plate around a single sinusoid is conceptually equivalent to the DPs observed during embryonic and fetal IHBD development (see below).

It would be difficult to prove the hypothesis in growing livers of normal children. The total number of units in the adult human liver has been estimated at 500,000±100,000 [13], whereas the number of lobules in the neonatal infant liver amount to about 50,000 (see Table 1 in ref 13). This means an increase of about 500,000 units during the years from birth to adulthood. Presumably, the above counted units correspond to classical hexagonal liver lobules of Kiernan, which roughly correspond to secondary lobules according to Matsumoto et al. [11, 12]. The number of choleohepatons per primary or secondary lobule [11, 12] is not known (between 20 and 30?). Anyhow, it would remain a time-consuming task to check histologically in liver biopsies of growing children whether new bile duct-canalicular connections develop in the form of ductal plate equivalents. An average needle biopsy (1/50,000th of the liver volume) would hardly have a chance of hitting a new choleohepaton which happens to be in the process of forming a new canaliculo–ductular connection, also considering that these ductal plates—like those during embryonic development—are rapidly remodeled into normally shaped tubular ducts. Furthermore, such study would meet ethical objections.

It therefore appeared indicated to look for alternatives that may be equivalent, but more informative thanks to a faster progression and higher amplification of the process. The hypothesis considers that "ductular reaction in ductal plate configuration" is the mechanism of new bile duct formation [14], and that such DRs observed in pathological conditions are a grotesquely accelerated and vastly amplified but still instructive equivalent of normal mechanisms during liver growth in childhood. In severe pathological DRs, DP formation may simultaneously occur around virtually every sinusoid, creating a network in the lobular periphery (Fig. 1a), whereas during normal ontogenesis the process should be far less impressive: only selected single sinusoids becoming sequentially involved over a year long-time span from birth to adulthood. The hypothesis further

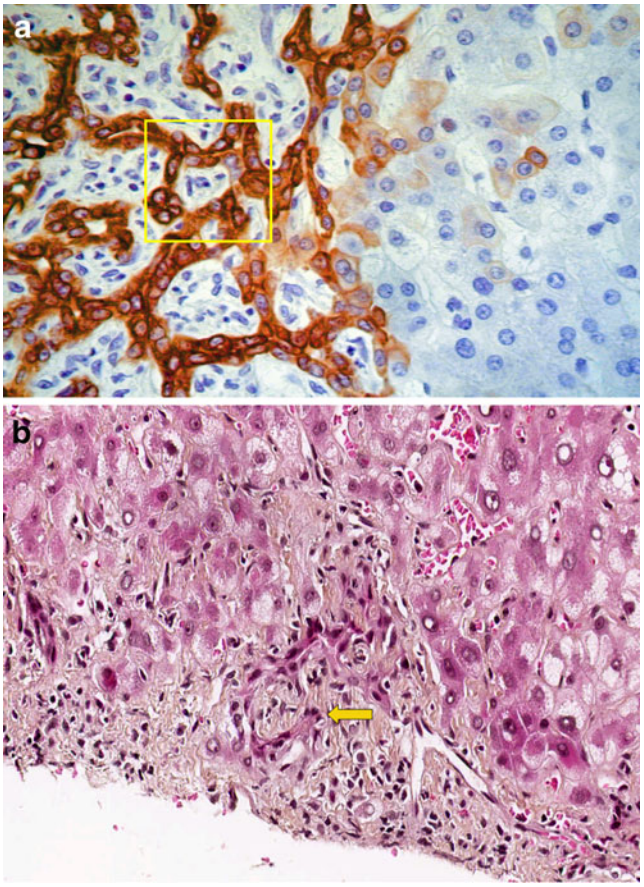

Fig. 1 **a** Ductular reaction in ductal plate configuration, forming a network around several sinusoids. Note the small luminal dilatations (formation of cross-sectioned peripheral tubules) at 1 and 8 o'clock in the framed bi-layered ductal plate. Keratin 7 immunostain, in liver specimen from patient with sclerosing cholangitis. **b** Single focus of ductular reaction in ductal plate configuration (circular structure in lower middle indicated by *arrow*). Cirrhotic stage of liver in biopsy from patient with non-alcoholic steato-hepatitis (NASH). Hematoxylin–eosin stain

relies on established trigger mechanisms for DR, namely relative bile acid overload (cholestasis) and relative lack of tissue oxygenation (hypoxia), and on recent reports on dedifferentiation of hepatocytes and induced pluripotent stem cells (iPSCs) [1].

Ductal plate configuration in ductular reaction

DR occurs in DP configuration in several liver diseases. This observation is described as "mini-ductal plates" and illustrated in a previous communication [1]; it is shortly summarized in the following lines.

The mini-ductal plates in DR (Fig. 1a, b) consist of a small central blood vessel (sinusoid or venule), surrounded by a small or even minimal amount of mesenchymal tissue, and a usually interrupted double layer of epithelial cell segments of biliary phenotype, lining a circular more or less virtual cleft in between both epithelial layers. In many cases, one may observe a tubular dilatation at one or more spots along the perimeter of the cleft. This configuration corresponds to the double-layered embryonic DPs in an early stage of remodeling, characterized by the development of tubular dilatations at a couple of sites along the perimeter of the DP (Fig. 1a, b; see Figs. 1 and 2a, b in ref. 1). Like DPs during embryonic development, these newly formed mini-ductal plates become remodeled into bile draining conduits of tubular shape, unless persistence of cholestasis retards remodeling and retains for a longer time a DP configuration which favors cholehepatic cycling of bile acids [15, 16]. Indeed, a DP pattern favors cholehepatic cycling even more than a type 1 DR because of the larger cholangiocytic surface in ductal plates than in tubular conduits.

The origin of the second layer of the mini-ductal plate is not easily explained by cholangiocytic metaplasia of hepatocytes alone. The most plausible explanation may lie in a doubling of the layer by progenitor cell activation. The origin of the progenitor cells may be that the DR results from activation of existing progenitor cells in the canal of Hering (the classical view), or the progenitor cells derive from the dedifferentiation (identical with ductular metaplasia) [2] of mature hepatocytes giving rise to in vivo equivalents of iPSCs or from both mechanisms together. In either case, a progenitor cell activation would be involved. Although final proof is lacking, a number of literature reports enumerated before are compatible with the hypothesis of newly induced progenitor cells [1]. The activation of existing LPCs may be the only or the prevailing mechanism when only a minimal degree of DR is involved, like the one postulated below during normal liver growth, whereas the options with de novo induced LPCs may be responsible or prevailing in greater degrees of DR occurring in pathological conditions.

The hypothesis thus implies that a hepatic developmental mechanism operative in the embryonic stage becomes re-iterated in diverse pathological conditions characterized by increased numbers of bile duct structures, such as cholestatic diseases, inflammatory conditions, and benign and malignant tumors [1], and that this also occurs in a slower and less obvious way during normal liver growth (this manuscript).

The mesenchyme in areas of DR has been found to be characterized by a high number of capillaries in which electron microscopic investigation allowed to distinguish four types [17]. These can be considered as different transformation stages between sinusoids and small portal venules, compatible with the so-called "portalized sinusoids" according to Ekataksin and Wake [10, 18]. Immunohistochemical studies of the vasculature in DR in human liver have further shown that ductules and vessels react in unison, and that—like in the embryonic period [19]—the ductules precede and induce [20] and also maintain [21] their

escorting arterial vasculature by increased expression of vascular endothelial growth factor (VEGF)-A, thus echoing the sequence of developmental changes during the formation of a portal tract in the embryonic liver [1, 19].

In a similar way, during lobulogenesis in the pig liver, a so-called portalized sinusoid was described to develop into a "portal venous twig, always accompanied by ductular transformation of hepatocellular laminae, which precedes the accompaniment by a hepatic arteriolar twig" [18]. Translated in the language of this paper, this would read: a so-called portalized sinusoid may develop fully into "a small portal vein branch, always accompanied by ductular metaplasia of hepatocytes in ductal plate shape, which precedes the induction of hepatic artery branches by VEGF and angiopoietin in the future portal mesenchyme." The hypothesis of a similar process of ongoing lobule growth and portal tract development in the human liver like in the pig liver, and including DR in mini-ductal plate configuration, is further elaborated in the following section.

Development of new lobules, choleohepatons, and portal tracts

Ontogenic liver growth is characterized by an increase in the number of liver units in man [13], and in the rat [22], hence requiring an ongoing establishment of new parenchymal–ductular connections in the periphery of the new liver units. A few papers have reported an increase in number of liver lobules during growth from neonatal to adult age in the pig [23] and albino rat [24] or after repeated partial hepatectomy in rats [25, 26]. However, there is virtually no published literature on the mechanism of development of new liver units during normal development in man. This is probably due to the lack of a clear mesenchymal anatomic delineation of the units in human liver and to the lasting quest for the structural–functional unit in the human liver as mentioned above [9].

A couple of the animal studies also addressed the mechanism of new lobule formation in the pig [18, 23] and the rat [24]. The latter rat study appears very much in concordance with the former pig study [23]. New lobule development in the piglet liver was described and illustrated in considerable detail in 1919 by Johnson [23] and seven decades later in an even more meticulous study of the porcine liver by Ekataksin and Wake, exploiting the argyrophylic connective tissue skeleton [18]. Although not all details may apply today as in 1919 (replacement of camera lucida drawings by microphotography and use of immunohistochemistry have influenced the interpretation of images in microscopy), and in spite of some difference between the liver of pig and man, the following general scheme for human liver growth can be proposed, largely in analogy with and inspired by the older pig liver study of Johnson [23] and the investigations of Ekataksin and Wake [18]. According to the latter authors, the similarity between the vascular septum in Matsumoto's lobular concept of the human liver [11, 12] and the pre-fibrous septation stages in pig liver imply that lobulation in suine and nonsuine livers is based on essentially identical designs [18]. The similarity with pig liver was confirmed in a later study, which revealed in healthy human livers during the postnatal period interlobular connective tissue septa in a rudimentary form, which regress after early childhood [27]. The following section emphasizes the similarity in the process of new liver unit formation with that of portal tract development during embryonic and fetal development and compares the proposals of the hypothesis with the previously published observations on new lobule formation in the porcine liver.

The details of the anatomical liver unit considered for this discussion do not basically matter, as long as the unit is compatible with a lobular concept (afferent vessels in the periphery and draining vessel(s) in the center and composed of several smaller subunits). One might consider a secondary lobule according to Matsumoto et al. [11, 12], which roughly corresponds to the lobule of Kiernan, classically described as hexagonal with a draining vein in its center, but of which a more recent study pointed out that a pentagonal pattern with five portal tracts in the periphery predominates [18]. For the sake of clarity and ease of explaining the concept, the pentagonal pattern is chosen. Basically, the same reasoning would also be applicable, albeit in a less rigorously geometric pattern, to the modular liver unit of Teutsch [8], which is considered further on. A pentagonal lobule is schematically represented in cross section in Fig. 2. Portal vein branches in the portal tracts represent the "second step" branches of the "parenchymal portion" of the intrahepatic portal vein according to Matsumoto and Kawakami [12]. Their further ramification ("third step"), corresponding to the "terminal portal venules," occurs at regular longitudinal distances and at about right angles, whereby all ramifications come to lack largely or completely connective tissue sheets and their wall structure attenuates, gradually changing over to that of a sinusoid. Yet they are recognizable by their precise interlobular course as well as their larger lumina. They are termed the "septal branches" and form the "vascular septum" spanning the interportal distance and separating adjacent lobules (Fig. 2).

The septal branches tend to run more or less parallel to each other, are interconnected by sinusoidal networks, and form the vascular skeleton of the vascular septum. The latter acts as a watershed between two adjacent lobules, providing blood to the sinusoids of the lobules on both sides. The vascular septum represents the periphery of the liver lobule, and hence, the periphery of its composing

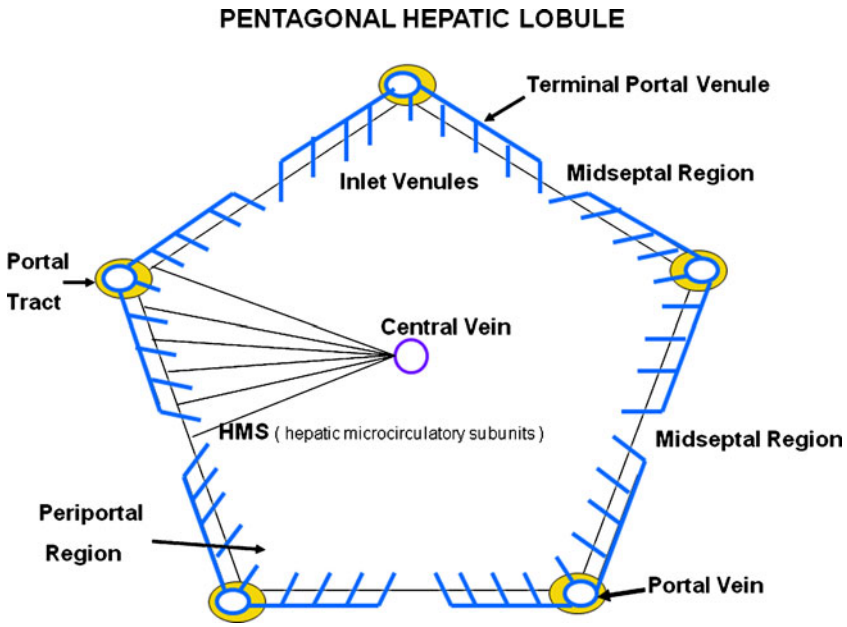

Fig. 2 Schematic representation of a cross section through a pentagonal liver lobule, also illustrating its microcirculatory subunits which equally represent the corresponding choleohepatons. Redrawn with modifications from Ekataksin et al. [46]. With permission from authors and publisher. See text for details and discussion

choleohepatons. A choleohepaton can be viewed as a cone-shaped smaller structure, arranged with its base against the vascular septum and pointing towards the central vein; each choleohepaton has a venule and a ductule running as a couplet together in the vascular septum, adjoined by an arteriolar capillary [18, 27]. It is composed of a pyramidal group of a few liver cell plates and their interposed sinusoids (the "hepatic microcirculatory subunit"; Fig. 2). The bile canalicular network of each choleohepaton is drained by a separate ductule, which connects it with the interlobular bile duct [18].

The peripheral ends of the terminal portal venules arising from two neighboring portal tracts meet each other in the middle of the interportal distance (the "midseptal region"; Fig. 2) [28], which represents the extreme microcirculatory periphery of the portal vein, with lowest perfusion pressure and oxygen content, and with the lowest number of inlet venules into sinusoids [28]. Hence follows that the parenchymal territory of the lobule that is most prone to hypoperfusion and hypoxia (the area with low pO2) [29] corresponds to a roughly star-shaped area comprising the pericentral zone and its radial extensions towards the midseptal region of the vascular septa surrounding the lobule [28].

Longstanding relative ischemia and hypoxia, for instance in partial venous outflow block, results in the development of progressive perisinusoidal fibrosis and concomitant size reduction of hepatocytes in the centrolobular zone. This is due to the induction in hypoxic hepatocytes of hypoxia-inducible factor-1 alpha (HIF-1α), which upregulates profibrotic and vasoactive mediators, such as platelet-derived growth factor-A (PDGF-A), PDGF-B, and plasminogen activator inhibitor-1, which in turn activate hepatic stellate cells (HSCs) into fibrogenetic activity resulting in progressive centrolobular fibrosis [30, 31] (Fig. 3). The dedifferentiating (atrophic looking) hepatocytes start expressing K7 and—with ongoing hypoxia and associated fibrosis—progress further in dedifferentiation into a small, primitive cell phenotype expressing K19 and finally assuming a tubular architecture ("centrolobular ductular metaplasia resulting in DR type 2B"; Fig. 4). The secretion of interleukin 6 and monocyte chemotactic protein-1 by ductular type cells [32, 33] results in attraction of inflammatory cells (neutrophils and monocytes) and additional HSCs [34], thus possibly amplifying the process of fibrogenesis and ductular metaplasia (DR type 2B).

The suggestion that advanced centrolobular ductular metaplasia (representing dedifferentiation) of hepatocytes may result in progenitor/stem cell characteristics and qualities [1] is supported by the finding that hypoxia favors the "stem cell niche—quality" of a cellular micro-environment [35]. One might invoke a migration of LPCs from Hering canals into hypoxic centrolobular zones, but that would not explain the accumulating numbers of hepatocytes with increasing signs of dedifferentiation in terms of steadily decreasing cell size and K7 and subsequent K19 expression in centripetal gradients. If such migration would occur, bile duct induction in hypoxic areas would—according to the hypothesis—comprise a combination of DRs types 2B and 3 (the latter being activation of preexisting progenitors).

DR type 2B occurs in the most hypoxic regions, initially the centrolobular area, gradually extending to midseptal zones and finally to the whole periphery of a growing lobule. The latter areas coincide with the periphery of the growing hepatocyte mass, and thus represent the territories of hepatocytes also first affected by "cholate stasis" (K7

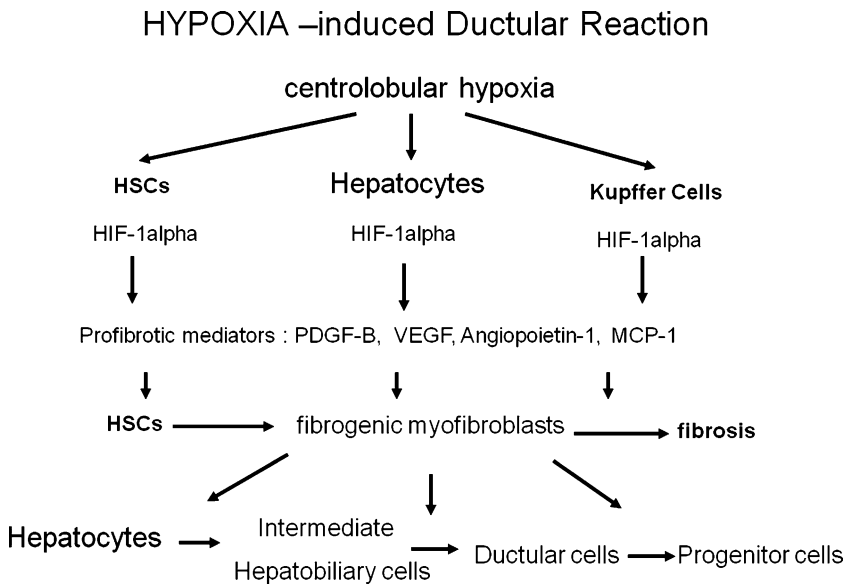

Fig. 3 Scheme illustrating the mechanism of centrolobular hypoxic fibrogenesis and cholangiocytic metaplasia of hepatocytes resulting in ductular reaction type 2B

expression) due to the increasing inadequacy of the available bile duct system. Both mechanisms, relative hypoxia and relative bile acid overload (cholestasis), result in synergistic effects: induction of DR in DP configuration with its associated change in mesenchymal partner cells and increasing fibrogenesis, eventually leading to induction of in vivo equivalents of "iPSCs" [1]. As is suggested for cholestasis-induced DR in cholestatic diseases (DR type 2A), also hypoxia-induced DR type 2B in pathological conditions is a marked amplification of what is supposed to occur during physiological liver growth.

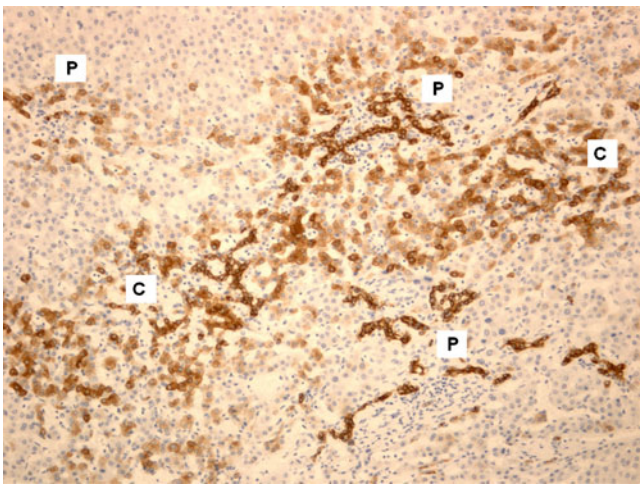

Fig. 4 Centrolobular ductular metaplasia of hepatocytes. Liver specimen from patient with cystic fibrosis, intrahepatic portal vein thromboses, and developing cirrhosis. Area with less cirrhotic change and cholestatic periportal ductular reaction; centrolobular areas are characterized by sinusoidal dilatation and hypoxic cholangiocytic metaplasia progressing into ductular metaplasia in the central part. Keratin 7 immunostain. The centrolobular region showed pericellular fibrosis on Sirius Red staining. *P* portal, *C* central

The DR induced in hypoxia is accompanied by vascular changes as well (Fig. 5). This concept that during normal liver growth the enlargement of a lobule may cause a mild relative hypoxia in the area of low pO2 which plays a role in local vascular change is supported by several observations. It has been shown that exponential hepatocyte proliferation after partial hepatectomy (liver growth) may lead to HIF-1α expression due to relative reduction in sinusoidal space as a cause of relative hypoxia [36]. Reduced oxygen tension induces Vascular Endothelial Growth Factor (VEGF) in the HSCs of hypoxic regions [37–39], resulting in an increased vasculogenesis and angiogenesis in these oxygen poor territories [40]. This may give rise to gradual development of new "second step" portal vein branches along the midseptal regions of the vascular septa by transformation of particular sinusoids into portal venules ("portalized sinusoids "[18], which in the pig liver represent an early change in neo-lobulation (18). These portalized sinusoids initiate the development of new portal tracts, by increase in mesenchymal matrix, DP induction, and formation of hepatic arteriolar branches, a sequence of events similar to those occurring in embryonic development [1, 19]. The newly formed portal tracts in turn initiate the development of new vascular septa between themselves, resulting in division of the original lobule in two parts (see Fig. 6a and b). The midseptal regions correspond to the "nodal points" in the lobular nomenclature of Mall [41], precisely the site of new portal tract development according to the mechanism of lobular development described by Johnson: "the portal veins grow into the nodal points and split them up into additional ones"[23].

Presumably the ductal plates in new portal tracts, which form new conducting bile ducts, develop around and along

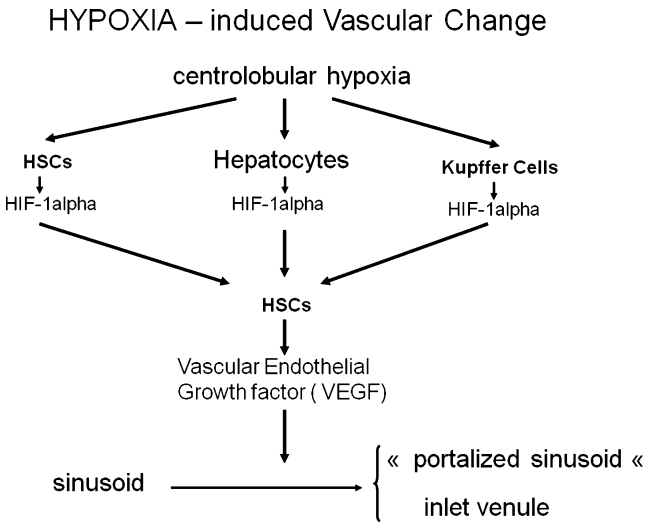

Fig. 5 Scheme illustrating the mechanism of hypoxia-induced vascular change

"portal" sinusoids, that is sinusoids originating directly from step 2 portal vein branches [11, 12] which become transformed into new (additional) step 2 portal veins; whereas ductal plates in new vascular septa, which form terminal ductules and canals of Hering, develop around and along "septal" sinusoids (step 3) [11, 12], and represent new additional step 3 equivalents or terminal branches of the parenchymal portion of the portal vein [11, 12] (Fig. 6b).

The development of a new vascular septum results in a re-location of blood inflow since it functions as a watershed supplying blood towards sinusoids on both its sides. This leads to reorientation of sinusoids, further modulating the afferent vasculature of the liver during growth in childhood, and in this way, adding a new episode in the long and complex saga of the development of the extra-and intra-hepatic segments of the portal vein, which goes on in a multistage manner since the start of embryonic liver development [42]. This re-orientation directs a downstream flow of blood towards particular "preferentially draining" centrolobular sinusoids ["centralized sinusoids" of Ekataksin and Wake 18], resulting in their venular transformation and consequently the development of two new separate branches of the original central vein (Fig. 6a, b). Further progression of this vascular remodeling process ends up with the original central vein becoming an interlobular subhepatic vein draining the two "daughter" lobules, similar to what was described and illustrated by Johnson in growing piglet liver [23].

Like during liver embryogenesis, it is the three-dimensional ramification pattern of the portal vein that determines the angioarchitecture and the direction of blood flow, and hence lobulogenesis, in the growing continuous muralium - network of the hepatic parenchyma [18, 43].

During normal ontogenetic liver growth, the ductal plate formation and vascular change should occur "pianissimo," in a minimal and hardly detectable way, affecting only the single sinusoid in the periphery of the microcirculatory subunit (or choleohepaton) which is located in the zenith of "relative" bile acid overload and hypoxia. In the end, the combined DR and fibro-vascular changes provides each new choleohepaton with a portal inlet venule and a ductular outlet. The end result is the splitting of the enlarged original lobule in two entities while preserving the continuity of the vascular and biliary tube systems (Fig. 6a, b).

In short, the combination of DR and associated vascular changes represents a "dissecting mechanism" that succeeds in subdividing the growing parenchymal mass—by creation of new portal tracts and vascular septa—into an increasing number of functionally workable units, each of them being provided with the necessary equipment of appropriate tubular systems for adequate blood supply and sufficient bile draining capacity.

The mechanism of new lobule development sketched above is a very schematic attempt at conveying some basic principles. Reality is more complex for several reasons.

The length of the portal branches in the vascular septum is certainly not the only factor influencing the intensity of tissue perfusion and creating relative hypoxia in the midseptal zone. Other rheologic determinants may also play a role, including vessel diameter, its wall characteristics (elasticity, contractility), fluid viscosity, and perfusion pressure, possibly causing variability in sizes and shapes of new functional units. Also, considering that the pentagon is a geometrically "idealized" perfection of the real lobular shape, and the observation that growth rates may vary in different diameters [23] further contribute to irregularities in lobular shapes. Irregularity in size and shape of liver units comes closer to the "modular" concept of liver architecture according to Teutsch [8]. The complexity of real shapes in liver units is illustrated in the marked variation in size, in shape, in number of facets, in concavity or convexity of the facets, and also in the number of primary units assembled into secondary modules [8]. However, the mechanism of growth and organization of a secondary module [8] should not basically differ from the preceding schematic description as far as involvement of vasculogenesis, angiogenesis, and ductular reaction are concerned. The concept of the liver module is based on the study of the liver units in the rat [44], and especially on the detailed three-dimensional reconstruction of a secondary module in the liver of a 59-year-old man [8]. This secondary module was composed of 14 primary modules, arranged in three levels, and all drained by a subhepatic vein in the shape of a single ramified hepatic venous tree having its dendritic origins in every one of the composing primary modules. The secondary module was supplied by six portal veins, with three types of branches

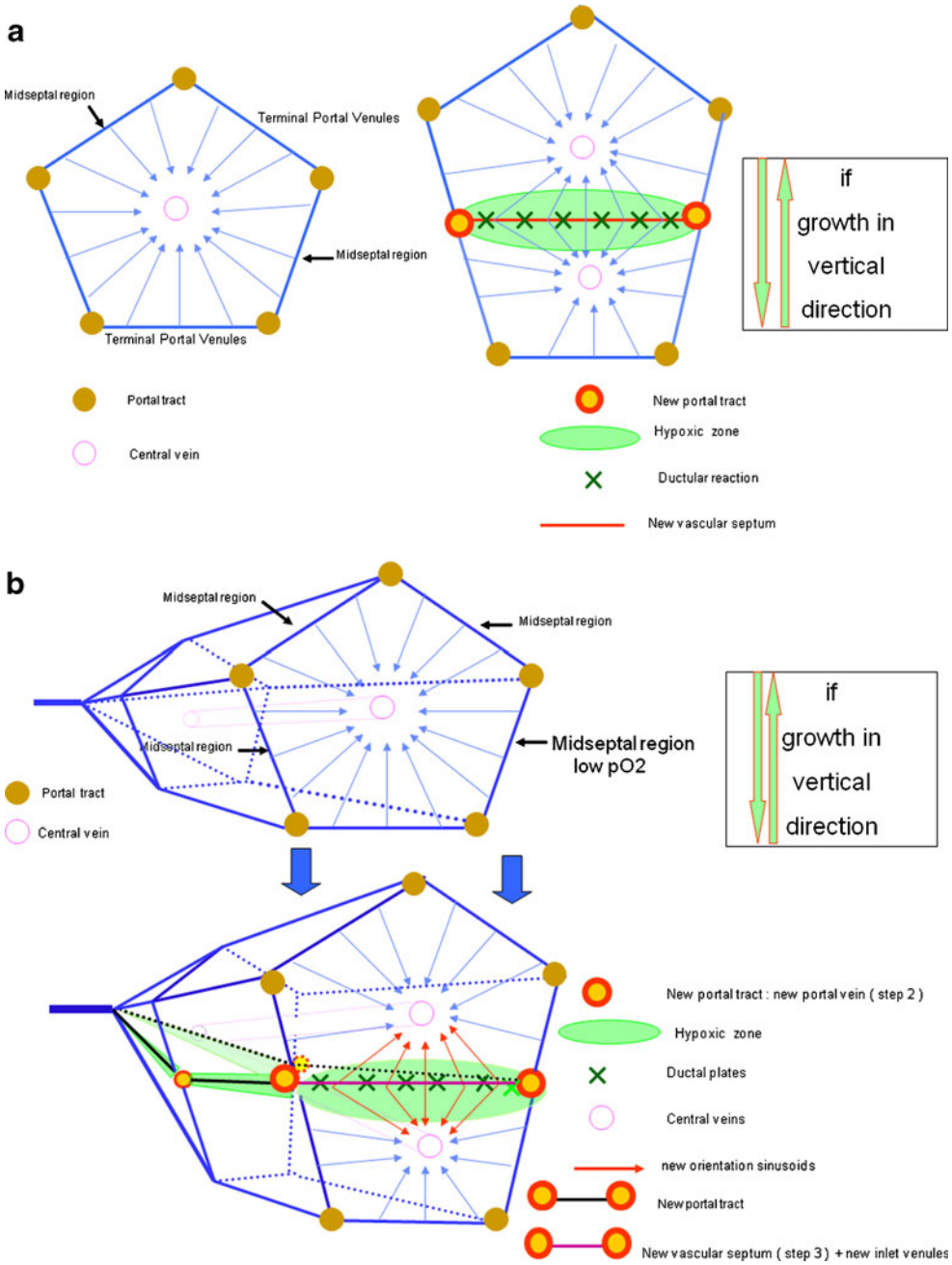

Fig. 6 **a** The purpose of the figure is not to illustrate the still debated exact structure of a standard liver unit, but to convey in a schematic way the general notion of parenchymal–portal tract (and bile duct) relationships. It represents a schematic representation of cross sections of a pentagonal liver lobule. The *right panel* illustrates growth, for simplicity reasons in only vertical direction of the same lobule depicted at the *left*. For discussion, see text. **b** Three-dimensional representation of data from Fig. 6a

(more or less equivalent to the three branching steps of the parenchymal portion of the portal vein described by Matsumoto et al. [11, 12]: two step 1 vessels, eight step 2 vessels, and 24 step 3 branches. However, in spite of this complexity, the structure is compatible with the basic principles of the primary and secondary lobule concept of the human liver according to Matsumoto et al. [11, 12], but differing in the actual mode of implementation of the principles [8]. The modular concept was established from only a single secondary module in the liver of a 59-year-old human male, but at the same time from the most meticulous study available on human liver.

Conclusion

In summary, relative bile acid overload may be an early trigger in ductular metaplasia of hepatocytes, exerting a primary effect on parenchymal cells themselves, which in turn exert an effect on their mesenchymal partner HSCs. On the other hand, relative hypoxia may induce transformation of sinusoids into portal venules (portalized sinusoids) through HIF1-α secreted by hypoxic parenchymal cells and have a fibrogenic effect on centrolobular HSCs, which in turn entails ductular metaplasia or dedifferentiation of hepatocytes. Both mechanisms together are proposed to

play a synergistic role in postnatal ductal plate formation which results in new portal tracts and vascular septa. These ensure the adequate vascularization and biliary drainage of new choleohepatons during enlargement of existing lobules and are the base of ongoing lobulogenesis during liver growth. The proposal that DRs in DP form play a role during normal liver growth in childhood is indirectly supported by several observations in pathological conditions of the liver, including von Meyenburg complexes, Alagille syndrome, and biliary atresia, discussed in a separate paper [45].

The hypothesis thus implies that DRs in DP conformation play a role during all phases of liver development, growth, and disease. The first DP in embryonic development is the first version of a DR resulting in the first formation of IHBDs; a similar mechanism continues at low level and speed during ontogenic liver growth in childhood. It is resuscitated at higher speed and in larger extent in diverse pathological conditions, representing a temporary rescue mechanism for protection of parenchymal integrity [1]. What is presented in this hypothesis as DR type 2A and 2B (of predominantly ductular metaplastic type) may comprise components of LPC activation (DR type 3), thus implying combinations of DR types 2A, 2B, and 3, resulting in the same final phenotype of DR in DP configuration.

Acknowledgment I thank Tania Roskams for the helpful discussions and for providing the opportunity to keep in touch with progress in hepatopathology after my official retirement in 1996. Rita DeVos and Olivier Govaere deserve my gratitude for the help with the illustrations.

Conflict of interest statement I declare that I have no conflict of interest.

References

1. Desmet V (2010) Ductal plates in hepatic ductular reactions. Hypothesis and Implications. I. Types of ductular reaction reconsidered. Virchows Arch. doi:10.1007/s00428-011-1048-3
2. Desmet V, Roskams T, Van Eyken P (1995) Ductular reaction in the liver. Pathol Res Pract 191:513–524
3. Pollack AL, Runyan RB, Mostov KE (1998) Morphogenetic mechanisms of epithelial tubulogenesis: MDCK cell polarity is transiently rearranged without loss of cell-cell contact during scatter factor/hepatocyte growth factor-induced tubulogenesis. Dev Biol 204:64–79
4. Affolter M, Bellusci S, Itoh N, Shilo B, Thiery JP, Werb Z (2003) Tube or not tube: remodeling epithelial tissues by branching morphogenesis. Dev Cell 4:11–18
5. Van Eyken P, Sciot R, Callea F, Van der Steen K, Moerman P, Desmet VJ (1988) The development of the intrahepatic bile ducts in man: a keratin-immunohistochemical study. Hepatology 8:1586–1595
6. Roskams T, Desmet V (2008) Embryology of extra- and intrahepatic bile ducts, the ductal plate. Anat Rec (Hoboken) 291 (6):628–635, Review
7. Zong Y, Panikkar A, Xu J, Antoniou A, Raynaud P, Lemaigre F, Stanger BZ (2009) Notch signaling controls liver development by regulating biliary differentiation. Development 136:1727–1739
8. Teutsch HF (2005) The modular microarchitecture of human liver. Hepatology 42:317–325
9. Desmet VJ (2001) Oganizational principles. In: Arias IM, Boyer JL, Chisari FV, Fausto N, Schachter D, Shafritz DA (eds) The liver. Biology and pathobiology, 4th edn. Lippincott, Williams & Wilkins, Philadelphia, pp 3–15
10. Ekataksin W, Wake K (1997) New concepts in biliary and vascular anatomy of the liver. In: Boyer JL, Ockner RK (eds) Progress in liver diseases, vol XV. Philadelphia, W B Saunders, pp 1–30
11. Matsumoto T, Komori R, Magara T, Ui T, Kawakami M, Tokuda T, Takasaki S, Hayashi S, Jo K, Hano H, Fujino H, Tanaka H (1979) A study on the normal structure of the human liver, with special reference to its angioarchitecture. Jikeikai Med J 26:1–40
12. Matsumoto T, Kawakami M (1982) The unit-concept of hepatic parenchyma. A re-examination based on angioarchitectural studies. Acta Pathol Jpn 32(suppl 2):285–314
13. Landing BH, Wells TR (1991) Considerations of some architectural properties of the biliary tree and liver in childhood. In: Abramowsky CR, Bernstein J, Rosenberg HS (eds) Tranplantation pathology – hepatic morphogenesis. Perspectives Pediatric Pathology vol 14. Karger, Basel, pp 122–142
14. van den Heuvel MC, de Jong KP, van der Horst ML, Poppema S, Slooff MJ, Gouw AS (2004) Impaired regeneration of biliary cells in human chronic liver allograft rejection. Special emphasis on the role of the finest branches of the biliary tree. Liver Transpl 10:28–35
15. Yeh H-Z, Schteingart CD, Hagey LR, Ton-Nu H-T, Bolder U, Gavrilkina MA, Steinbach JH, Hofmann AF (1997) Effect of side chain length on biotransformation, hepatic transport, and choleretic properties of chenodeoxycholyl homologues in the rodent: Studies with Dinor- (C22), Nor- (C23) and Chenodeoxycholic acid (C24). Hepatology 26:374–385
16. Xia X, Francis H, Glaser S, Alpini G, LeSage G (2006) Bile acid interactions with cholangiocytes. World J Gastroenterol 12:3553–3563
17. Carruthers JS, Kalifat SR, Steiner JW (1962) The ductular cell reaction of rat liver in extrahepatic cholestasis. II. The proliferation of connective tissue. Exp Mol Pathol 1:377–396
18. Ekataksin W, Wake K (1991) Liver units in three dimensions. I. Organization of argyrophylic connective tissue skeleton in porcine liver with particular reference to the “compound hepatic lobule”. Am J Anat 191:113–153
19. Fabris L, Cadamuro M, Libbrecht L, Raynaud P, Spirlì C, Fiorotto R, Okolicsanyi L, Lemaigre F, Strazzabosco M, Roskams T (2008) Epithelial expression of angiogenic growth factors modulate arterial vasculogenesis in human liver development. Hepatology 47:719–728
20. van den Heuvel MC, Gouw AS, Boot M, Slooff MJ, Poppema S, de Jong KP (2006) The finest branches of the biliary tree might induce biliary vascularization necessary for biliary regeneration. J Hepatol 44:947–955
21. Gouw ASH, van den Heuvel MC, Boot M, Slooff MJH, Poppema S, de Jong KP (2006) Dynamics of the vascular profile of the finer branches of the biliary tree in normal and diseased human livers. J Hepatol 45:393–400
22. Papp V, Dezsö K, László V, Nagy P, Paku S (2009) Architectural changes during regenerative and ontogenic liver growth in the rat. Liver Transpl 15:177–183
23. Johnson FP (1919) The development of the lobule of the pig’s liver. Am J Anat 25:299–331
24. McKellar M (1949) The postnatal growth and mitotic activity of the liver of the albino rat. Am J Anat 85:263–295

25. Simpson GEC, Finckh ES (1963) The pattern of regeneration of rat liver after repeated partial hepatectomy. J Pathol Bacteriol 86:361–370
26. Yashina IN (1971) Formation of liver lobules in repeatedly regenerating liver. Sov J Dev Biol 2:305–310
27. Dezso K, Paku S, Papp V, Turányi E, Nagy P (2009) Architectural and immunohistochemical characterization of biliary ductules in normal human liver. Stem Cells Dev 8:1417–1422
28. Zou Z, Ekataksin W, Wake K (1998) Zonal and regional differences identified from precision mapping of Vitamin A-storing lipid droplets of the hepatic stellate cells in pig liver: a novel concept addressing the intralobular area of heterogeneity. Hepatology 27:1098–1108
29. Khan Z, Michalopoulos GK, Stolz DB (2006) Peroxisomal localization of hypoxia-inducible factors and hypoxia-inducible factor regulatory hydroxylases in primary rat hepatocytes exposed to hypoxia-reoxygenation. Am J Pathol 169:1251–1269
30. Copple BL, Bustamante JJ, Welch TP, Kim ND, Moon JO (2009) Hypoxia-inducible factor-dependent production of profibrotic mediators by hypoxic hepatocytes. Liver Int 29:1010–1021
31. Moon JO, Welch TP, Gonzalez FJ, Copple BL (2009) Reduced liver fibrosis in hypoxia- inducible factor-1 alpha-deficient mice. Am J Physiol Gastrointest Liver Physiol 296:G582–G592
32. Matsumoto K, Fujii H, Michalopoulos G, Fung JJ, Demetris AJ (1994) Human biliary epithelial cells secrete and respond to cytokines and hepatocyte growth factors in vitro: interleukin-6, hepatocyte growth factor and epidermal growth factor promote DNA synthesis in vitro. Hepatology 20(2):376–382
33. Yasoshima M, Kono N, Sugawara H, Katayanagi K, Harada K, Nakanuma Y (1998) Increased expression of interleukin-6 and tumor necrosis factor-alpha in pathologic biliary epithelial cells: in situ and culture study. Lab Invest 78(1):89–100
34. Ramm GA, Shepherd RW, Hoskins AC, Greco SA, Ney AD, Pereira TN, Bridle KR, Doecke JD, Meikle PJ, Turlin B, Lewindon PJ (2009) Fibrogenesis in pediatric cholestatic liver disease: role of taurocholate and hepatocyte-derived monocyte chemotaxis protein-1 in hepatic stellate cell recruitment. Hepatology 49(2):533–544
35. Lin Q, Lee YJ, Yun Z (2006) Differentiation arrest by hypoxia. J Biol Chem 281:30678–30683
36. Maeno H, Ono T, Dhar D, TS, Yamanoi A, Nagasue N (2005) Expression of hypoxia inducible factor-1alpha during liver regeneration induced by partial hepatectomy in rats. Liver 25:1002–1009
37. Shi YF, Fong CC, Zhang Q, Cheung PY, Tzang CH, Wu RS, Yang M (2007) Hypoxia induces the activation of human hepatic stellate cells LX-2 through TGF-beta signalling pathway. FEBS Lett 581:203–210
38. Siegmund SV, Dooley S, Brenner D (2005) Molecular mechanisms of alcohol- induced hepatic fibrosis. Dig Dis 23:264–274
39. Ankoma-Sey V, Wang Y, Dai Z (2000) Hypoxic stimulation of vascular endothelial growth factor expression in activated rat hepatic stellate cells. Hepatology 31:141–148
40. Corpechot C, Barbu V, Wendum D, Kinnman N, Rey C, Poupon R, Housset C, Rosmorduc O (2002) Hypoxia-induced VEGF and collagen I expressions are associated with angiogenesis and fibrogenesis in experimental cirrhosis. Hepatology 35:1010–1021
41. Mall FP (1906) A study of the structural unit of the liver. Am J Anat 5:227–308
42. Collardeau-Frachon S, Scoazec JY (2008) Vascular development and differentiation during human liver organogenesis. Anat Rec (Hoboken) 291:614–27, Review
43. Desmet VJ (1994) Fibrosis of the liver: a pathologist's view. In: Surrenti C, Casini A, Milani SM, Pinzani M (eds) Fat-storing cells and liver fibrosis. Kluwer Academic Publishers, Dordrecht, pp 257–273
44. Teutsch HF, Schuerfeld D, Groezinger E (1999) Three-dimensional reconstruction of parenchymal units in the liver of the rat. Hepatology 29(2):494–505
45. Desmet V (2010) Ductal plates in hepatic ductular reactions. Hypothesis and Implications. III. Implications for liver pathology. Virchows Arch. doi:10.1007/s00428-011-1050-9
46. Ekataksin W et al (1995) HMS, Hepatic microcirculatory subunits in mammalian species. Intralobular grouping of liver tissue with definition enhanced by dropout sinusoids. In: Wisse E, Knook DL, Wake K (eds) Cells of the Hepatic Sinusoid. Kupffer Cell Foundation, Leiden, The Netherlands, p 247

Virchows Arch (2011) 458:271–279
DOI 10.1007/s00428-011-1050-9

REVIEW AND PERSPECTIVE

Ductal plates in hepatic ductular reactions. Hypothesis and implications. III. Implications for liver pathology

Valeer J. Desmet

Received: 29 November 2010 / Revised: 18 January 2011 / Accepted: 20 January 2011 / Published online: 8 February 2011
© Springer-Verlag 2011

Abstract This article discusses on the basis of the ductal plate hypothesis the implication of the concept for several liver abnormalities. The occurrence of ductal plates (DP) during liver growth in childhood would explain the paraportal and parenchymal localizations of von Meyenburg complexes in postnatally developed parts of the liver, and their higher incidence in adulthood versus childhood. It partly clarifies the lack of postnatal intrahepatic bile duct development in Alagille syndrome and the reduced number of portal tracts in this disease. Ductular reactions (DRs) in DP configuration are the predominant type of progenitor cell reaction in fulminant necro-inflammatory liver disease, when lack of sufficient parenchymal regeneration results in liver failure. The concept of dissecting DRs explains the micronodular pattern of advanced biliary and alcoholic cirrhosis. The concept explains the DP patterns of bile ducts in several cases of biliary atresia, with implications for diagnosis and prognosis. The hypothesis also has an impact on concepts about stem/progenitor cells and their niche.

Keywords Alagille syndrome · Biliary atresia · Cholehepatic cycling · Ductal plate · Ductular reaction · von Meyenburg complex

V. J. Desmet (✉)
Department of Pathology, University Hospital K.U.Leuven,
Campus St Rafael,
Leuven, Belgium
e-mail: v.desmet@telenet.be

V. J. Desmet
Department of Pathology, University Hospital St Rafael,
Minderbroedersstraat 12,
3000 Leuven, Belgium

Introduction

This manuscript completes two papers about ductular reactions (DRs) in the liver, with critical review of current concepts, new observations, and hypothesis [1, 2]. The new observation is that all DRs—except type 1 that corresponds to multiplication of pre-existing cholangiocytes—occur in ductal plate (DP) configuration. The hypothesis posits that postnatal DRs in DP configuration represent a reiteration of tissue-organizing processes during embryonic liver development and correspond to progenitor cell reactions, either activation of resident hepatic progenitor cells in the canals of Hering or de novo generated progenitor cells resulting from advanced dedifferentiation of hepatocytes induced by either cholestasis or hypoxia, or both, giving rise to in vivo equivalents of "induced Pluripotent Stem Cells" (iPSCs) [1]. The first paper discusses the three classical types of DR and adds DR induced by hypoxia as a fourth type [1]. The second paper postulates a role for postnatal DRs in DP configuration during normal liver growth in childhood [2]. The present manuscript considers the implications of the new observation and its interpretation for a number of pathological conditions in the liver, explaining some hitherto less elucidated aspects of several hepatic diseases.

Implications in liver pathology

Implications for the von Meyenburg complex (or bile duct hamartoma)

A von Meyenburg complex (VMC) is composed of a variable number of more or less dilated bile ducts embedded in a fibrous stroma. Serial sections reveal communication between all the lumina of the hamartoma

[3] and continuity with the biliary tree and the canalicular network [4]. Some ductal sections may show polypoid projections in the lumen or a central island of connective tissue covered with epithelium identical to that lining the wall of the dilated duct. Such appearance corresponds to the basic configuration of ductal plate malformation (DPM). The complexes are localized in or close to portal tracts (Fig. 1). In some complexes, the bile duct profiles are involutive and disappear in a hyalinized, scarring stroma [5].

In a study of 2,843 consecutive autopsies, their incidence was 5.6% in adults and 0.9% in children [6]. The histologic appearance of VMCs inspired the hypothesis that they represent partially fibrosing and on occasion slowly involutive remnants of DPM of smaller, more peripheral branches of the intrahepatic biliary tree. This hypothesis invokes a factor arresting or perturbing the remodeling of DPs in later, postnatal phases of intrahepatic bile duct (IHBD) development [5, 7].

A VMC may contain a large number of duct profiles, occasionally appearing like a conglomerate of approximated DP remnants. Therefore, an abnormality in the arborization pattern of the peripheral branches of the portal vein was suspected: a "pollard willow" pattern of ramification, causing a close apposition and even fusion of the corresponding portal tracts [7]. The paraportal localization of most VMCs, when fused to normal-appearing portal tracts, suggested that one of the branches of the pollard willow may give rise to a normal portal tract, whereas the rest of the tuft evolves in hypoplastic vein branches with fusion of adjacent portal tracts and clustering of their ductal plates [7]. An alternative explanation would be that in such VMC the periportal cluster derives from DR in mini-ductal plate configuration in the periphery of the normal appearing portal tract (DR type 2A) [1].

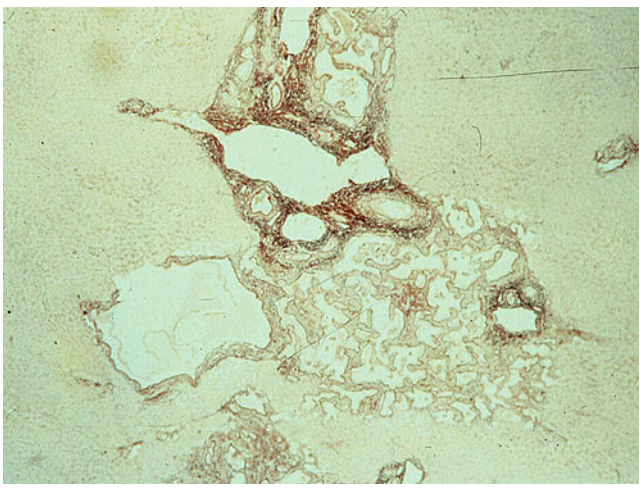

Fig. 1 Von Meyenburg complex in liver of patient with autosomal dominant polycystic kidney disease (ADPKD). Clusters of irregularly shaped ductal structures, one (*left side*) more dilated, close to two portal tracts recognizable by darker stained connective tissue. Orcein stain

If DP formation would be a mechanism restricted to the embryonic and fetal period of liver development, the concept of a VMC being a malformation of a postnatal DP would be hardly tenable. The hypothesis on postnatal bile duct and lobule development [2] explains the morphology of VMCs as a postnatal malformation of DPs, and their general location in the more peripheral areas of liver parenchyma. VMCs in paraportal localization may correspond to malformations of some ductal plates involved in new portal tract development during postnatal life. VMCs with deeper intraparenchymal localization may result from mishaps in mini-ductal plates during formation of new vascular septa. The maldevelopment would consist in the fact that not one sinusoid becomes surrounded by a mini-ductal plate of biliary cells, but a cluster of sinusoids, thus bearing some resemblance—although at smaller scale—to the abnormal "pollard willow" pattern of ramification of the portal vein [7] during embryologic development. The hypothesis equally explains the 6.2 times higher incidence of VMCs in adults than in children [6] in view of their development during postnatal liver growth.

The number of VMCs varies between patients [6], being small in patients with VMCs as incidental findings. In such cases, the VMC may be an incidental local disturbance in development ("a mishap underway", in French—"un accident de parcours") during formation of a particular new portal tract. It has been suggested before that in the absence of autosomal dominant polycystic kidney disease (ADPKD), VMCs are manifestations of a different disease, e.g., secondary to inflammation or ischemia [6]. In patients with ADPKD and with polycystic liver disease (PLD), in whom the VMCs are numerous and at the origin of the liver cysts [5, 7], the origin of the maldevelopments appears of genetic origin.

Implications for Alagille syndrome

Some authors suggested that IHBDs fail in Alagille syndrome (AS) because of lack of elongation and branching of the ducts which are present at the time of birth [8–10]. This was supported by a study of the explant liver of an adult AS patient at the time of liver transplantation [11]. In this specimen, a central area, measuring 8.5×7×5 cm, was sharply delineated from the pale-appearing peripheral part of the organ. The central part was interpreted as corresponding to the patient's liver at the time of birth and the peripheral part as representing the mass increment of the organ attained by postnatal liver growth. This interpretation is supported by case reports of liver imaging in older patients with AS [12, 13] and by the histopathological findings in this case [11]. The central area revealed

mostly normal portal tracts; occasionally, there was discrete damage of the bile ducts and some periportal ductular reaction. A few small portal tracts contained no interlobular bile duct and were also devoid of ductules and canals of Hering, while some surrounding periportal hepatocytes were keratin 7 (K7) positive indicating mild cholestasis. In contrast, specimens from the liver periphery showed periportal fibrosis and some septa; none of the portal tracts here contained an interlobular bile duct. K7 immunostaining revealed marked parenchymal positivity consistent with chronic cholestasis, in total absence of any evidence of past or present DR. The authors concluded: "this indicates that hepatocytes do not have the capacity to transdifferentiate into reactive bile ductules. Conversely, the presence of the biliary tree in the center of the liver made a ductular reaction possible, consistent with the hypothesis that reactive bile ductules arise from progenitor cells in the canals of Hering. However, hepatocytes in the peripheral liver did express the biliary-type K7 as a reaction to the accumulation of bile salts, which can be seen as 'incomplete' ductular metaplasia: hepatocytes can acquire some biliary features but are not capable to transdifferentiate into reactive bile ductules" [11]. The authors further emphasize the difference in bile duct development before and after birth. Fetal bile ducts develop from immature, bipotential cells in the embryonic DP, whereas after birth DPs have completely disappeared, so that new bile ducts can only arise from pre-existing, mature bile ducts by branching and elongation. However, in this reasoning, one wonders how the already existing IHBDs of the neonatal liver further elongate and branch, and especially how the new branches gain or retain continuity with the canalicular networks of the newly developed liver parenchymal units.

In contrast, the hypothesis suggests that the problem in AS lies in a deranged capacity of epithelial–mesenchymal interaction since the cholestatic hepatocytes undergo a partial biliary transformation (K7 expression) under the influence of bile acid overload as recently re-confirmed [14], but further transformation into more primitive cholangiocytes and acquisition of a tubular arrangement fails. This failure is due to insufficiently advanced dedifferentiation of hepatocytes down to the primitive stage of "in vivo equivalents of induced pluripotent stem cells" [1, 2], resulting in lack of formation of ducts, ductules, and canals of Hering, or alternatively, the dedifferentiation is not advanced enough to represent a stimulus for the progenitor cells normally present in the canals of Hering or both mechanisms together [1, 2].

In AS, the failure of mutual stimulation into correct bile duct cell differentiation results from mutation in the (human Jagged-1) JAG-1/Notch proteins, located in adjacent cells and crucial in determining the differentiation fate of these cells [15]. The JAG-1 gene is mutated in the majority of AS patients, whereas the gene of the JAG-1 ligand Notch is mutated in the remaining minority of patients [16]. The precise role of Jag-1 and Notch in determining biliary differentiation is not fully elucidated. It was advised to consider the situation in human liver because of important species differences in Jagged-1/Notch interaction during bile duct development [17]. Anyhow, evidence from multiple studies indicates a role for Notch2 in development and maintenance of bile duct epithelial cells [16–26], and in the induction of tubulogenesis [17, 24–26]. A study in mice indicated a threshold requirement for Notch signaling at multiple steps of IHBD development, including tubulogenesis and maintenance, in order to assure an adequate three-dimensional branching architecture of the peripheral (postnatal) intrahepatic biliary tree [24].

The presence of virtually normal intrahepatic bile ducts in the neonate with AS suggests a normal DP formation, normal remodeling, and normal further duct development during embryonic and fetal stages, in spite of JAG-1 or Notch mutation [11]. This raises the question why the mutation, present before birth as a genetic determinant, has only deleterious effects after birth. One study suggested that the major IHBDs are not as sensitive to levels of Notch signaling [24]. This may be a candidate answer to the problem, at least in experimental models. Another study on Notch receptor expression in human bile duct development and disease [19] reported that during normal embryonic and fetal development, ductal and endothelial cells express JAG-1, whereas Notch3 is expressed in mesenchymal cells. In tissue available from one (single) patient with AS, two types of JAG-1/Notch patterns could be observed. In liver specimens characterized by marked ductular reaction (central liver part?), JAG-1 is expressed on ductular reactive cells, along with marked Notch2 and Notch3 staining. In contrast, in specimens with paucity (liver periphery?), Notch2 and Notch3 are not expressed on remaining biliary cells [19]. Is there a mutual switch of JAG-1 and Notch between mesenchymal and ductular cells, which renders the JAG-1/Notch pathway inefficient after birth? What could be the abrupt trigger which induces inability to form any further bile ducts? Is there a brisk liver change at birth other than the closure of the umbilical circulation and ductus venosus, rendering the portal circulation for the first time the only inflow source of blood [27]? This problem remains unsolved. Also, in the "neonatal" part of the liver, ductless terminal portal tracts are mentioned [11]. Since normally liver growth occurs at the same rate throughout the whole organ [28], this suggests that after birth normal bile duct formation has also failed in the postnatally expanding parts within the original "neonatal" liver.

The absence of postnatal bile duct development demonstrated in the report by Libbrecht et al. [11] does not necessarily prove that ductular metaplasia of hepatocytes

does never occur in general, since the conclusion is based on the study of a single disease (AS), but clearly shows that ductular metaplasia of hepatocytes does not occur *specifically in AS*. Another study revealed that in AS, hepatobiliary cells fail to express hepatocyte nuclear factor 1β (HNF1β), a biliary-specific transcription factor, and thus—in spite of a striking increase in K7+ intermediate hepatocytes—are unable to switch fully into a biliary phenotype and form a DR [26].

The findings in AS suggest that new bile duct development after birth only occurs when it is supported by correct epithelial–mesenchymal cooperation. This places the problem in the broader field of epithelial–mesenchymal interaction and correlates with the fact that the clinical syndrome of AS is not an exclusively hepatic disease but a problem of epithelial–mesenchymal interaction in different organs, causing cardiovascular, renal, ocular, vertebral, and other alterations [29].

The paucity of IHBDs in AS is associated with a concomitant reduction in the number of portal tracts per unit surface of liver sections [30, 31], indicating a deficiency in the development of new portal tracts during postnatal development. The hypothesis on liver growth in childhood [2] explains why the number of portal tracts is reduced: DR types 2A and 2B in DP configuration are an integral component in the splitting of existing lobular units and creating an increase in the number of lobules and portal tracts. DR is the "conditio sine qua non" for normal development of new bile ducts, portal tracts, and liver units [2]. Furthermore, mutations in JAG-1 result in loss of the inhibitory action of normal JAG-1 on hepatocyte growth factor (HGF), resulting in overexpression of HGF and more hepatocyte and less biliary cell production in an off-balanced cell fate determination in AS patients [32].

Implications for biliary atresia

In a number of infants with biliary atresia (BA), histopathological examination of the liver reveals damage and disappearance of interlobular bile ducts which still appear in their primitive DP configuration, corresponding to so-called ductal plate malformation (DPM) [7]. It may be quite difficult to differentiate interlobular ducts from portal and periportal DR in small needle liver biopsies from neonates, possibly causing overdiagnosis of DPM in BA. The hypothesis that DR occurs in a pattern strongly resembling DPs (albeit in smaller caliber) may explain the wide variation of incidence in the reports on this subtype of BA, ranging from 20% to 65% of patients [5]. The diagnostic histopathologist should differentiate antenatal DPM from DR, in order not to overdiagnose this variant of BA, which was termed "early severe biliary atresia" [5, 7] because of advanced fibrosis at a very early age, and which in independent studies was shown to have a worse prognosis [33, 34].

A recent study focused on the occurrence of DPM-like arrays in early liver explants after a Kasai procedure [35]. Having some problem with the definition of authentic DPM, the authors distinguish between "definite" DPM-like arrays (concentric to portal vessels, peripheral in larger portal tracts) and "possible" DPM-like arrays (smaller compact ringlets eccentric to and/or unrelated to portal vessels). They describe florid ductular reaction as "a complex filigree pattern", which in the interpretation of this paper corresponds to DR in more or less remodeled DP configuration (Fig. 1B and E in Ref. [35]). According to the proposed hypothesis, the category of "possible" DPM-like arrays would represent remnants of DRs in DP configuration (mini-ductal plates), in which remodeling did not occur in an appropriate way, possibly due to ongoing cholestasis which favors the DP form as more favorable for chole-hepatic cycling of bile acids [36]. This corresponds to lack of remodeling of the DPs, representing in fact a form of postnatal (mini-) DPM. Since a correlation has been demonstrated between the degree of DR and prognosis in BA [37], an explanation for a worse prognosis of BA with DPM in some reports might be due to the fact that DR in DP conformation was (mis) interpreted as classical (antenatal) DPM.

However, as an alternative, persistence of DP configuration could also result from an intrinsic immaturity of the neonatal cholangiocytes in BA, causing inadequate tissue kinetics for remodeling and hence resulting in persistence of precursor structures. Several studies have suggested an immaturity of cholangiocytes in BA, reflected in a distortion in TGF beta 1 peptide immunolocalization in bile duct cells [38]; in anomalies of cholangiocytic keratin subtypes [39]; in disturbance of the temporal expression pattern of neural cell adhesion molecule (NCAM) [40, 41]; in expression abnormalities of E-cadherin, alpha-catenin, and beta-catenin [42]; and in dysregulation of cholangiocytic apoptosis in DPM structures [43]. Immaturity of cholangiocytes in BA with DPM would explain why in these patients postnatal DPs remain unremodeled and appear as mini-DPMs ("possible" DPM-like arrays [35]), embedded in larger or smaller areas of fibrosis that result from ongoing cholestasis in BA (Fig. 2). This feature of "possible" DPM-like arrays is not (or at least far much less) observed in other cholestatic diseases of childhood and adulthood, suggesting the possibility that the abnormality may represent a prognostic feature since immature bile duct epithelium may lack the required resistance to detergent bile acids characteristic for mature cholangiocytes, resulting in rapid and progressive destruction of IHBDs. The problem posed in the paper of Pacheco et al. [35] comes down to the necessity for differentiating between antenatal and postnatal DPMs. The antenatal DPM corresponds to the "definite" DPM-like arrays [35], whereas the postnatal

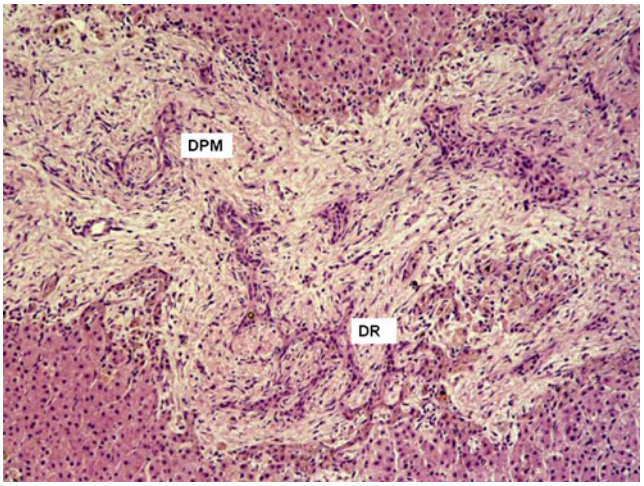

Fig. 2 Liver specimen from child with biliary atresia. Broad fibrous area with bile ducts structures in ductal plate configuration. *DR* area of ductular reaction in ductal plate shape, progressively dissociated by fibrosis. *DPM* postnatal unremodeled ductal plate sequestrated from original DR by progressive cholestasis-induced fibrosis. Hematoxylin–eosin stain

DPM represents the "possible" DPM-like arrays of that study. Adequacy of this differentiation is handicapped by the smaller size of needle biopsy specimens. If the bile duct configuration of postnatal DPM could be confirmed to reflect not only an architectural immaturity of the bile duct structures but also an intrinsic cellular deficit of their lining cholangiocytes, the microscopic abnormality might still characterize a particular subgroup of BA patients.

Implication for acute liver failure

In DR type 3, which occurs in case of massive loss of parenchymal cells and consists in activation and proliferation of liver progenitor cells (LPCs) presumably located in ductules and canals of Hering, the amount of ductular structures may not be very conspicuous as long as differentiation towards fully mature hepatocytes occurs with sufficient speed and in a substantial degree, and hence the LPC intervention is quite successful in restoring parenchymal mass and function. However, in most cases of fulminant liver failure in man with unfavorable inflammatory microenvironment [44] and progressing fibrosis, the accompanying myofibroblastic cells are of the activated fibrogenic phenotype [45, 46] and hence not favorable for steering the progenitors' differentiation in hepatocellular direction [1]; in this case, the LPCs evolve into cholangiocytic differentiation, with insufficient increase in parenchymal mass and more development of ductular structures and accompanying fibrosis. This explains why succumbing patients or those who require liver transplantation have more progenitor cell activation in a ductular pattern than the surviving patients [47]. In this way, liver regeneration in predominantly ductular phenotype indicates a relative failure of progenitor cell-mediated restitution of parenchymal mass since too many progenitor cells evolve into ductules rather than into hepatocytes.

Implications for biliary and alcoholic types of cirrhosis

Chronic cholestasis and chronic liver tissue hypoxia, both instigators of DR [1], result in cirrhosis of micronodular pattern. The latter is explained by the persistence of tissue insults resulting in progressing dissection of parenchymal areas, associated with an inhibiting effect of both cholestasis and hypoxia on the capacity of parenchymal regeneration [48, 49].

In the past, monolobular and multilobular cirrhosis have been used as synonyms for respectively micronodular and macronodular cirrhosis. In micronodular cirrhosis, the nodules are often smaller than a single lobule (pseudolobular), since persistence of cholestasis (in biliary cirrhosis) or persistence of hypoxia (in cirrhosis of alcoholic origin [50]) leads to further dissection of a lobule, resulting in parenchymal remnants of sublobular size with poor regenerative capacity (hyporegenerative type of cirrhosis) (Fig. 3). The lobular subdivision is explained by the presented hypothesis which emphasizes the paramount importance of epithelial–mesenchymal interactions and subdivision of parenchymal territories by DRs associated with vascular change and fibrogenesis.

The proposed sequence of events leading to a subdivision of pre-existing liver units bears resemblance to the sublobulation which occurs in focal nodular hyperplasia

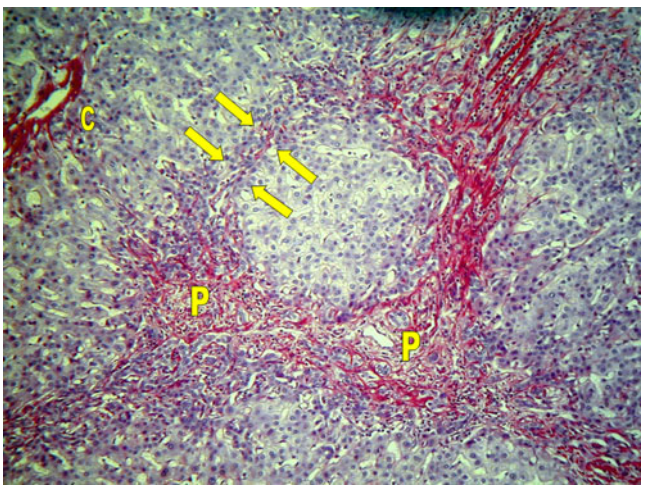

Fig. 3 Liver biopsy from patient with progressive sclerosing cholangitis. The *picture* illustrates developing cirrhotic transformation of the liver architecture. Note the early development of a cross-sectioned thin network of collagen fibers and beginning ductular reaction, which further dissect the parenchyma (between *yellow arrows*). *P* portal tracts, with broad extending fibrous septa and periportal ductular reaction. *C* central vein. Sirius Red stain for collagen

(FNH), in which ductular metaplasia of hepatocytes (DR type 2A) was described to be always accompanied by sinusoidal endothelial cells stained by the endothelial markers BMA 120, M 616, and by an increase in collagen fibers. Ongoing development of this fibrovascular and ductular transformation leads to further subdivision of the involved pseudolobules [51]. FNH may serve as another example of a pathological liver lesion in which normal developmental changes are deranged and amplified.

Implications for the role of DRs in parenchymal protection in cholestatic diseases

DR type 1 is a fast developing mechanism that favors chole-hepatic cycling caused by reabsorption of bile acids through the increased cholangiocytic surface in elongating, tortuous tubes [36, 52]. Chole-hepatic cycling of bile acids takes over the blocked entero-hepatic cycling in case of bile duct obstruction, and thus reduces bile acid-induced hepatocellular damage [53]. It represents a protection mechanism for hepatocytes next to several additional mechanisms, which include development of new canaliculi in the intercellular membranes of hepatocytes [54]; increased expression of basolateral efflux pumps of the hepatocytes which remediate cellular bile acid overload [55]; fibroblast growth factor 19 (FGF19) expression resulting in decreased bile acid synthesis [56]; and increased expression in hepatocellular basolateral membranes of the heteromeric organic solute transporter OSTalpha-OSTbeta [57].

DR type 2A plays a similar role in *chronic* cholestasis. It develops later and at slower speed, but favors chole-hepatic cycling more than DR type 1 due to the still larger surface of cholangiocytes in DPs versus ductular tubules. Further, as a "dissecting mechanism" [2], it creates increasing numbers of biliary outlets for decreasing masses of bile acid overloaded hepatocytes (Fig. 3). This would be an efficient help for a quick return to the (near-) normal state if the causative trigger of the cholestatic disease could be arrested or eliminated. When this succeeds in time, apoptotic deletion of excess bile ductules [58, 59] and regression of fibrosis [60] would allow a return to (near-) normality. Such reversibility illustrates again the plasticity of cells and tissues, which can be modulated in a finely tuned way according to the needs of the moment: the "poise" of Sir Roy Cameron [61].

Possible implications for progenitor cells, stem cells, and the stem cell niche

The hypothesis implies the presence of hepatic stem/progenitor cells in the canals of Hering and also the possibility of in vivo induction of pluripotent stem cells by either relative bile acid overload or relative hypoxia in portions of parenchymal cells [1, 2]. The existence of intraorgan liver progenitor cells is supported by numerous investigations. Canals of Hering constitute the ductal–parenchymal interfaces located at the periphery of the hepatic units throughout the organ and are presumed to harbor resident liver stem cells [62], which are considered to represent remnants of remodeled DPs [63, 64]. This is consistent with the postulate of postnatal occurrence of ductal plates [2]. The increase of the parenchymal mass during liver growth is not exclusively assured by multiplication of pre-existing hepatocytes. Results of recent investigations [65, 66] beautifully reconfirmed the concept of the "streaming liver" [67]; they showed that clusters of hepatocytes migrate from periportal to centrolobular zones in normal liver, suggesting a progenitor cell-fed lineage of parenchymal cells as mechanism of regular cell turnover and indicating the presence of progenitors near the lobular periphery. If life-long maintenance and increase of hepatic epithelial cell populations is assured by periportal liver stem cells, then normal liver growth itself guarantees perpetuated presence of stem cells in the lobular periphery. Accordingly, in the hypothesis participation of activated resident progenitor cells in postnatal ductal plate formation is thought to predominate when DR occurs at very low level, as thought to be the case during development of additional portal tracts and vascular septa during normal ontogenic liver growth in childhood, although a component of newly in vivo induced progenitor cells cannot be excluded [2].

In contrast, an induction of in vivo equivalents of iPSCs is presumed to predominate in pathological conditions characterized by parenchymal cholestasis and hypoxia, in which DRs in DP configuration are vastly amplified, and the parenchymal phenotypic changes simultaneously associated with acquisition of stem cell niche requirements by the equally changing mesenchymal partner cells [1]. In these conditions, progenitor cells derived from dedifferentiation represent an additional resource of progenitors, probably combined with participation of resident progenitors from the canals of Hering [1, 2]. De novo induction is morphologically most convincingly suggested in long-lasting cholestasis (Fig. 3). The option of in vivo equivalents of iPSCs derived from hepatocellular dedifferentiation is compatible with the suggestion that the "stemness" of a cell may vary according to its physiological state (i.e., its current pattern of gene expression) and/or its environment [68]. It further agrees with the suggestion to define stemness not so much as an entity but rather as a state, "which might be a transient and reversible trait that almost any cell can assume given the correct trigger (niche) and that is characterized by having many potential outcomes but no specialization" [69, 70]. If dedifferentiation of

hepatocytes to the stage of early progenitor cells is a reality, it would explain the appearance of progenitor cells in pathological conditions causing centrolobular hypoxia at some distance away from the site of the location of resident precursors in canals of Hering (DR type 2B). Recent studies on iPSCs, mentioned in preceding papers [1, 2], continue to highlight the impressive plasticity of differentiated hepatocytes. Although these studies do not prove the component of "in vivo equivalents of iPSCs" in the proposed hypothesis [1], they render it increasingly more probable. Such probability renders the hypothesis worth considering, surely when one realizes that less than two decades ago, even mentioning hepatic progenitor cells in human liver as equivalents of oval cells in rats was condemned as heresy [71].

In the evaluation of the proposed hypothesis, one also will have to consider the uncertainties which still obscure the field of liver stem cells, including the evidence that also hepatic stellate cells may be hepatic epithelial precursors [72, 73] and the reports on lineage-transgressing transdifferentiations in epithelial–mesenchymal transition (EMT) and in the inverse mesenchymal–epithelial transition (MET) [74, 75].

The observations of DRs in DP configuration allow the idea that different mechanisms of DR (proliferation of existing cholangiocytes, ductular metaplasia of hepatocytes and activation of resident progenitor cells) may occur simultaneously in different combinations, although usually with one of the mechanisms as major contributor [1]. Quite probably, the relative contribution of the different histogenetic procedures vary in the course of time, especially in complex pathological conditions, like human liver diseases characterized by long duration, by progressive changes in mesenchymal micro-environment (fibrosis) and ongoing remodeling of the vasculature, as is the case in cirrhogenesis.

Conclusions

The DP hypothesis posits that, in analogy with embryonic development, also during postnatal liver growth DP formation initiates and guides new portal tract formation resulting in splitting of enlarging liver lobules. In this way, it clarifies some unexplained observations in different hepatic pathological conditions. It explains the localization of VMCs in the peripheral, postnatally developed parts of the liver, their predominant paraportal and occasional intraparenchymal position, and their higher incidence in adults than in children. It is compatible with the absence of postnatal development of IHBDs in AS due to a mutation in the JAG-1/Notch pathway; it explains the reported absence of evidence in AS for past or present DR in postnatally developed liver areas and accounts for the published reduction in number of portal tracts per unit liver mass in AS. The hypothesis is compatible with the higher number of ductular structures in case of fulminant hepatitis with massive hepatic necrosis and insufficient drive for hepatocellular differentiation of the progenitor cells resulting in liver failure. The hypothesis shows the base for the dissecting micronodular pattern of biliary and alcoholic types of cirrhosis. It further warns for overdiagnosis of a more severe variety of BA associated with DPM, by drawing attention to the fact that DR in classical BA may occur in a confusing DP pattern, that may be mistaken for antenatal DPM. Finally, the hypothesis suggests a possible reconsideration of some aspects of liver progenitor cells, in that these also might derive from dedifferentiated mature hepatocytes, especially in pathological conditions, reflecting the plasticity of living matter.

Interactions between hepatic progenitor cells and mesenchymal components of stem cell-niche quality are operative in embryonic liver development, are re-instated during infantile liver growth, and become resuscitated in disease. The liver is similar to other tissues in that regenerative processes in postnatal stages parallel those occurring in development and involve populations of stem cells and progenitor cells [76].

Acknowledgments I thank Tania Roskams for helpful discussions and for providing the opportunity to keep in touch with progress in hepatopathology after my official retirement in 1996. Rita DeVos deserves my gratitude for help with illustrations.

Conflict of interest statement I declare that I have no conflict of interest.

References

1. Desmet V (2011) Ductal plates in hepatic ductular reactions. Hypothesis and implications. I. Types of ductular reaction reconsidered. Virchows Arch (in press)
2. Desmet V (2011) Ductal plates in hepatic ductular reactions. Hypothesis and implications. II. Ontogenic liver growth in childhood. Virchows Arch (in press)
3. Thommesen N (1978) Biliary hamartomas (von Meyenburg complexes) in liver needle biopsies. Acta Pathol Microbiol Scand 86:93–99
4. Ohta W, Ushio H (1984) Histological reconstruction of von Meyenburg's complex on the liver surface. Endoscopy 16:71–74
5. Desmet VJ, Roskams TAD (2007) The cholangiopathies. In: Suchy FJ, Sokol RJ, Balistreri WF (eds) Liver disease in children, 3rd edn. Lippincott Williams & Wilkins, Philadelphia, pp 35–70
6. Redston MS, Wanless IR (1996) The hepatic von Meyenburg complex: prevalence and association with hepatic and renal cysts among 2843 autopsies (corrected). Mod Pathol 9:233–237
7. Desmet VJ (1992) Congenital diseases of intrahepatic bile ducts: variations on the theme "ductal plate malformation". Hepatology 16:1069–1083
8. Treem WR, Krzymowski GA, Cartun RW, Pedersen CA, Hyams JS, Berman (1992) Cytokeratin immunohistochemical examination of liver biopsies in infants with Alagille syndrome and biliary atresia. J Pediatr Gastroenterol Nutr 15:73–80

9. Emerick KM, Rand EB, Goldmuntz E, Krantz ID, Spinnr NB, Piccoli DA (1999) Features of Alagille syndrome in 92 patients: frequency and relation to prognosis. Hepatology 29:822–829
10. Piccoli DA, Spinner NB (2001) Alagille syndrome and the Jagged 1 gene. Semin Liver Dis 21:525–534
11. Libbrecht L, Spinner NB, Moore EC, Cassiman D, Van Damme-Lombaerts R, Roskams T (2005) Peripheral bile duct paucity and cholestasis in the liver of a patient with Alagille syndrome: further evidence supporting a lack of postnatal bile duct branching and elongation. Am J Surg Pathol 29:820–826
12. Aburano T, Yokoyama K, Takayama T, Tonami N, Hisada K (1989) Distinct hepatic retention of Tc-99m IDA in arteriohepatic dysplasia (Alagille syndrome). Clin Nucl Med 14:874–876
13. Jinguji M, Tsuchimochi S, Nakajo M, Hamada H, Kamiyama T, Umanodan T, Tani A, Nakabeppu Y, Kaji T, Takamatsu H, Haga H (2003) Scintigraphic progress of the liver in a patient with Alagille syndrome (arteriohepatic dysplasia). Ann Nucl Med 17:693–697
14. Ernst LM, Spinner NB, Piccoli DA, Mauger J, Russo P (2007) Interlobular bile duct loss in pediatric cholestatic disease is associated with aberrant cytokeratin 7 expression by hepatocytes. Pediatr Dev Pathol 10:383–390
15. Fortini ME (2009) Notch signaling: the core pathway and its posttranslational regulation. Dev Cell 16:633–647
16. McDaniell R, Warthen DM, Sanchez-Lara PA, Pai A, Krantz ID, Piccoli DA, Spinner NB (2006) NOTCH2 mutations cause Alagille syndrome, a heterogeneous disorder of the notch signaling pathway. Am J Hum Genet 79:169–173
17. Kodama Y, Hijikata M, Kageyama R, Shimotohno K, Chiba T (2004) The role of notch signaling in the development of intrahepatic bile ducts. Gastroenterology 127:1775–1786
18. Zong Y, Panikkar A, Xu J, Antoniou A, Raynaud P, Lemaigre F, Stanger BZ (2009) Notch signaling controls liver development by regulating biliary differentiation. Development 136:1727–1739
19. Flynn DM, Nijjar S, Hubscher SG, de Goyet Jde V, Kelly DA, Strain AJ, Crosby HA (2004) The role of Notch receptor expression in bile duct development and disease. J Pathol 204:55–64
20. McCright B, Lozier J, Gridley T (2002) A mouse model of Alagille syndrome: Notch2 as a genetic modifier of Jag1 haploinsufficiency. Development 129:1075–1082
21. Loomes KM, Taichman DB, Glover CL, Williams PT, Markowitz JE, Piccoli DA, Baldwin HS, Oakey RJ (2002) Characterization of Notch receptor expression in the developing mammalian heart and liver. Am J Med Genet 112:181–189
22. Croquelois A, Blindenbacher A, Terracciano L, Wang X, Langer I, Radtke F, Heim MH (2005) Inducible inactivation of Notch1 causes nodular regenerative hyperplasia in mice. Hepatology 41:487–496
23. Geisler F, Nagl F, Mazur PK, Lee M, Zimber-Strobl U, Strobl LJ, Radtke F, Schmid RM, Siveke JT (2008) Liver-specific inactivation of Notch2, but not Notch1, compromises intrahepatic bile duct development in mice. Hepatology 48:607–616
24. Sparks EE, Huppert KA, Brown MA, Washington MK, Huppert SS (2010) Notch signaling regulates formation of the three-dimensional architecture of intrahepatic bile ducts in mice. Hepatology 51:1391–1400
25. Tchorz JS, Kinter J, Müller M, Tornillo L, Heim MH, Bettler B (2009) Notch2 signaling promotes biliary epithelial cell fate specification and tubulogenesis during bile duct development in mice. Hepatology 50:871–879
26. Fabris L, Cadamuro M, Guido M, Spirli C, Fiorotto R, Colledan M, Torre G, Alberti D, Sonzogni A, Okolicsanyi L, Strazzabosco M (2007) Analysis of liver repair mechanisms in Alagille syndrome and biliary atresia reveals a role for notch signaling. Am J Pathol 171:641–653
27. Collardeau-Frachon S, Scoazec JY (2008) Vascular development and differentiation during human liver organogenesis. Anat Rec (Hoboken) 291:614–627, Review
28. Johnson FP (1919) The development of the lobule of the pig's liver. Am J Anat 25:299–331
29. Kamath BM, Spinner NB, Piccoli DA (2007) Alagille syndrome. In: Suchy FJ, Sokol RJ, Balistreri WF (eds) Liver disease in children, 3rd edn. Lippincott Williams & Wilkins, Philadelphia, pp 326–345
30. Hadchouel M, Hugon RN, Gautier M (1978) Reduced ratio of portal tracts to paucity of intrahepatic bile ducts. Arch Pathol Lab Med 102:402–403
31. Hashida Y, Yunis EJ (1988) Syndromatic paucity of interlobular bile ducts: hepatic histopathology of the early and endstage liver. Pediatr Pathol 8:1–15
32. Yuan ZR, Kobayashi N, Kohsaka T (2006) Human Jagged 1 mutants cause liver defect in Alagille syndrome by overexpression of hepatocyte growth factor. J Mol Biol 356:559–569
33. Low Y, Vijayan V, Tan CE (2001) The prognostic value of ductal plate malformation and other histologic parameters in biliary atresia: an immunohistochemical study. J Pediatr 139:320–322
34. Roy P, Chatterjee U, Ganguli M, Banerjee S, Chatterjee SK, Basu AK (2010) A histopathological study of liver and biliary remnants with clinical outcome in cases of extrahepatic biliary atresia. Indian J Pathol Microbiol 53:101–105
35. Pacheco MC, Campbell KM, Bove KE (2009) Ductal plate malformation-like arrays in early explants after a Kasai procedure are independent of splenic malformation complex (heterotaxy). Pediatr Dev Pathol 12:355–360
36. Yeh H-Z, Schteingart CD, Hagey LR, Ton-Nu H-T, Bolder U, Gavrilkina MA, Steinbach JH, Hofmann AF (1997) Effect of side chain length on biotransformation, hepatic transport, and choleretic properties of chenodeoxycholyl homologues in the rodent: studies with Dinor- (C22), Nor- (C23) and Chenodeoxycholic acid (C24). Hepatology 26:374–385
37. Santos JL, Kieling CO, Meurer L, Vieira S, Ferreira CT, Lorentz A, Silveira TR (2009) The extent of biliary proliferation in liver biopsies from patients with biliary atresia at portoenterostomy is associated with the postoperative prognosis. J Pediatr Surg 44:695–701
38. Tan CE, Chan VS, Yong RY, Vijayan V, Tan WL, Fook Chong SM, Ho JM, Cheng HH (1995) Distortion in TGF beta 1 peptide immunolocalization in biliary atresia: comparison with the normal pattern in the developing human intrahepatic bile duct system. Pathol Int 45:815–824
39. Sasaki H, Nio M, Iwami D, Funaki N, Ohi R, Sasano H (2001) Cytokeratin subtypes in biliary atresia: immunohistochemical study. Pathol Int 51:511–518
40. Libbrecht L, Cassiman D, Desmet V, Roskams T (2001) Expression of neural cell adhesion molecule in human liver development and in congenital and acquired liver diseases. Histochem Cell Biol 116:233–239
41. Fabris L, Strazzabosco M, Crosby HA, Ballardini G, Hubscher SG, Kelly DA, Neuberger JM, Strain AJ, Joplin R (2000) Characterization and isolation of ductular cells coexpressing neural cell adhesion molecule and Bcl-2 from primary cholangiopathies and ductal plate malformations. Am J Pathol 156:1599–1612
42. Sasaki H, Nio M, Iwami D, Funaki N, Sano N, Ohi R, Sasano H (2001) E-cadherin, alpha-catenin and beta-catenin in biliary atresia: correlation with apoptosis and cell cycle. Pathol Int 51:923–932
43. Sergi C, Kahl P, Otto HF (2000) Contribution of apoptosis and apoptosis-related proteins to the malformation of the primitive intrahepatic biliary system in Meckel syndrome. Am J Pathol 156:1589–1598

44. Pohl JF, Melin-Aldana H, Sabla G, Degen JL, Bezerra JA (2001) Plaminogen deficiency leads to impaired lobular reorganization and matrix accumulation after chronic liver injury. Am J Pathol 158:921–929
45. Baroni GS, Pastorelli A, Manzin A, Benedetti A, Marucci L, Solforosi L, Di Sario A, Brunelli E, Orlandi F, Clementi M, Macarri G (1999) Hepatic stellate cell activation and liver fibrosis are associated with necroinflammatory injury and Th1-like response in chronic hepatitis C. Liver 19(3):212–219
46. Sato M, Suzuki S, Senoo H (2003) Hepatic stellate cells: unique characteristics in cell biology and phenotype. Cell Struct Funct 28:105–112, Review
47. Katoonizadeh A, Nevens F, Verslype C, Pirenne J, Roskams T (2006) Liver regeneration in acute severe liver impairment: a clinicopathological correlation study. Liver Int 26:1225–1233
48. Yokoyama Y, Nagino M, Nimura Y (2007) Mechanism of impaired hepatic regeneration in cholestatic liver. J Hepatobiliary Pancreat Surg 14:159–166
49. Rosmorduc O, Housset C (2010) Hypoxia: a link between fibrogenesis, angiogenesis, and carcinogenesis in liver disease. Semin Liver Dis 30:258–270
50. Siegmund SV, Dooley S, Brenner DA (2005) Molecular mechanisms of alcohol-induced hepatic fibrosis. Dig Dis 23:264–274, Review
51. Fischer HP, Lankes G (1991) Morphologic correlation between liver epithelium and mesenchyme allows insight into histogenesis of focal nodular hyperplasia (FNH) of the liver. Virchows Arch B Cell Pathol Incl Mol Pathol 60:373–380
52. Xia X, Francis H, Glaser S, Alpini G, LeSage G (2006) Bile acid interactions with cholangiocytes. World J Gastroenterol 12:3553–3563
53. Desmet VJ (1992) Modulation of the liver in cholestasis. J Gastroenterol Hepatol 7:313–323
54. De Vos R, De Wolf-Peeters C, Desmet V, Bianchi L, Rohr HP (1975) Significance of liver canalicular changes after experimental bile duct ligation. Exp Mol Pathol 23(1):12–34
55. Zollner G, Fickert P, Silbert D et al (2003) Adaptive changes in hepatobiliary transporter expression in primary biliary cirrhosis. J Hepatol 38:717–727
56. Schaap FG, van der Gaag NA, Gouma DJ, Jansen PL (2009) High expression of the bile salt-homeostatic hormone fibroblast growth factor 19 in the liver of patients with extrahepatic cholestasis. Hepatology 49:1228–1235
57. Soroka CJ, Ballatori N, Boyer JL (2010) Organic solute transporter, OSTalpha-OSTbeta: its role in bile acid transport and cholestasis. Semin Liver Dis 30(2):178–185
58. Bhathal PS, Gall JAM (1985) Deletion of hyperplastic biliary epithelial cells by apoptosis following removal of the proliferative stimulus. Liver 5:311–325
59. Stähelin BJ, Marti U, Zimmermann H, Reichen J (1999) The interaction of Bcl-2 and Bax regulates apoptosis in biliary epithelial cells of rats with obstructive jaundice. Virchows Arch 434:333–339
60. Abdel-Aziz G, Lebeau G, Rescan PY, Clément B, Rissel M, Deugnier Y, Campion JP, Guillouzo A (1990) Reversibility of hepatic fibrosis in experimentally induced cholestasis in rat. Am J Pathol 137:1333–1342
61. Cameron R (1960) Reversibility and "poise" in liver disease. Arch De Vecchi Anat Patol 31:29–38
62. Saxena R, Theise N (2004) Canals of Hering: recent insights and current knowledge. Semin Liver Dis 24(1):43–48, Review
63. Shah K, Gerber MA (1989) Development of intrahepatic bile ducts in humans. Immunohistochemical study using monoclonal cytokeratin antibodies. Arch Pathol Lab Med 113:1135–1138
64. Shah KD, Gerber MA (1990) Development of intrahepatic bile ducts in humans. Possible role of laminin. Arch Pathol Lab Med 114:597–600
65. Fellous TG, Islam S, Tadrous PJ, Elia G, Kocher HM, Bhattacharya S, Mears L, Turnbull DM, Taylor RW, Greaves LC, Chinnery PF, Taylor G, McDonald SA, Wright NA, Alison MR (2009) Locating the stem cell niche and tracing hepatocyte lineages in human liver. Hepatology 49(5):1655–1663
66. De Alwis N, Hudson G, Burt AD, Day CP, Chinnery PF (2009) Human liver stem cells originate from the canals of Hering. Hepatology 50(3):992–993
67. Zajicek G, Oren R, Weinreb M Jr (1985) The streaming liver. Liver 5(6):293–300
68. Kindler V (2005) Postnatal stem cell survival: does the niche, a rare harbor where to resist the ebb tide of differentiation, also provide lineage-specific instructions? J Leukoc Biol 78:836–844
69. Zipori D (2004) The nature of stem cells: state rather than entity. Nat Rev Genet 5:873–878
70. Zipori D (2005) The stem state: plasticity is essential, whereas self-renewal and hierarchy are optional. Stem Cells 23:719–726
71. Desmet VJ (2009) The amazing universe of hepatic microstructure. Hepatology 50:333–344
72. Yang L, Jung Y, Omenetti A, Witek RP, Choi S, Vandongen HM, Huang J, Alpini GD, Diehl AM (2008) Fate-mapping evidence that hepatic stellate cells are epithelial progenitors in adult mouse livers. Stem Cells 26:2104–2113
73. Kordes C, Sawitza I, Müller-Marbach A, Ale-Agha N, Keitel V, Klonowski-Stumpe H, Häussinger D (2007) CD133+ hepatic stellate cells are progenitor cells. Biochem Biophys Res Commun 352:410–417
74. Choi SS, Omenetti A, Witek RP, Moylan CA, Syn WK, Jung Y, Yang L, Sudan DL, Sicklick JK, Michelotti GA, Rojkind M, Diehl AM (2009) Hedgehog pathway activation and epithelial-to-mesenchymal transitions during myofibroblastic transformation of rat hepatic cells in culture and cirrhosis. Am J Physiol Gastrointest Liver Physiol 297:G1093–G1106
75. Rygiel KA, Robertson H, Marshall HL, Pekalski M, Zhao L, Booth TA, Jones DE, Burt AD, Kirby JA (2008) Epithelial–mesenchymal transition contributes to portal tract fibrogenesis during human chronic liver disease. Lab Invest 88:112–123
76. Zhang L, Theise N, Chua M, Reid LM (2008) The stem cell niche of human livers: symmetry between development and regeneration. Hepatology 48:1598–1607

Virchows Arch (2011) 458:281–290
DOI 10.1007/s00428-010-1023-4

ORIGINAL ARTICLE

The many faces of atypical Ewing's sarcoma. A true entity mimicking sarcomas, carcinomas and lymphomas

Isidro Machado · Rosa Noguera · Eduardo Alcaraz Mateos · Silvia Calabuig-Fariñas · F. Ignacio Aranda López · Antonio Martínez · Samuel Navarro · Antonio Llombart-Bosch

Received: 14 September 2010 / Revised: 3 November 2010 / Accepted: 30 November 2010 / Published online: 23 December 2010
© Springer-Verlag 2010

Abstract Ewing's sarcoma family of tumours (ESFT) comprises a group of small round cell tumours (SRCT) genetically defined by specific chromosomal translocations resulting in a fusion of the *EWSR1* gene with a member of the ETS family of transcription factors. Atypical ESFT are the most challenging of the ESFT subtypes, and the differential diagnosis with other SRCT of bone and soft tissue is difficult since these subtypes can resemble other neoplasms. The present article describes nine cases of genetically confirmed, atypical ESFT, having unusual alterations at morphological and immunohistochemical (IHC) levels associated with atypical clinical presentation mimicking sarcomas, carcinomas and lymphomas. Present results demonstrate that ESFT showing overlapping morphological and immunohistochemical features with other SRCT of soft tissue and bone, or even with carcinomas or lymphoma, can be differentiated using molecular techniques. In SRCT with *EWSR1* translocation demonstrated by FISH, the RT-PCR analysis of specific sarcoma-related gene fusion can offer important clues for the diagnosis of specific entities, especially in tumours with unusual histopathology and/or IHC findings. Thus, we confirm that the integration of clinical, histopathological, IHC and genetic data becomes decisive in the diagnosis of bone and soft tissue sarcomas.

Keywords Atypical ESFT · Differential diagnosis

This study was performed with grants from the European Union (EuroBonet Project, contract no.: 018814) and RD06/0020/0102 Instituto de Salud Carlos III, Madrid.

I. Machado · R. Noguera · S. Calabuig-Fariñas · S. Navarro · A. Llombart-Bosch (✉)
Pathology Department, Medical School, Valencia University, Avda Blasco Ibáñez, 15, Valencia 46010, Spain
e-mail: antonio.llombart@uv.es

E. A. Mateos · F. I. A. López
Pathology Department, General Hospital Alicante, Alicante, Spain

A. Martínez
Pathology Department, General Hospital Torrevieja, Torrevieja, Spain

Introduction

Ewing's sarcoma family of tumours (ESFT) comprises a group of small round cell tumours (SRCT) mainly affecting the bone and soft tissues of children and young adults [12, 16–18, 20, 37]. ESFT are genetically defined by specific chromosomal translocations resulting in a fusion of the *EWSR1* gene with a member of the ETS family of transcription factors: *FLI1* (11q24), *ERG* (21q22), *FEV* (2q33), *ETV1* (7p22) and *ETV4* (17q12). In addition, other, less frequent, gene fusions have been described in ESFT, including *FUS/ERG*, *FUS/FEV*, *EWSR1/POU5F1*, *EWSR1/PATZ1*, *EWSR1/SP3*, *EWSR1/NFATc2*, *BRD4/NUT* and *CIC/DUX4* [3, 7, 20, 24, 32, 35].

The histopathology fluctuates between undifferentiated tumours (Ewing's sarcoma (ES)) and tumours with neuroectodermal differentiation/rosette formation (PNET) [12, 17, 18, 20, 32, 37]. Additionally, several histological varieties of ESFT are considered, including large cell ES, ES with epithelioid cells, clear cells, ES with spindle cells, vascular-like ES with haemangioendothelial features, ES with neuroectodermal features (isolated pseudorosettes), synovial sarcoma-like PNET, sclerosing PNET and adamantinoma-like ES [12, 17, 18, 20, 27, 32, 37]. In order to homogenize these ESFT subtypes, the tumours have been regrouped into three larger categories according

to their predominant morphological criteria: conventional/classical/typical ES, PNET with neuroectodermal features and atypical ES comprising all subtypes distinct from the other two types [12, 20].

Atypical ESFT are the most challenging of this group of tumours, and the differential diagnosis with other SRCT of bone and soft tissue is difficult since these subtypes can resemble other neoplasms [12, 17, 18, 20, 21, 27]. The present article describes nine cases of genetically confirmed, atypical ESFT presenting unusual structural findings at morphological and immunohistochemical (IHC) levels associated with conventional or more uncommon clinical presentations. These characteristics may complicate the differential diagnosis with other sarcomas, carcinomas and lymphomas, thus creating problems in formulating the therapeutic approach.

Clinical data

Age, gender and tumour location, histopathology findings, immunohistochemical, differential diagnosis and genetic results are summarized in Table 1.

Material and methods

The whole tumour specimen was fixed in buffered formalin, embedded in paraffin and processed for pathological investigation. Sections, 4 μm thick, were cut for haematoxylin/eosin (H/E), IHC and fluorescence in situ hybridization (FISH) studies. The antibodies employed, with their source and dilution, are summarized in Table 2. The immunostaining score was classified as non-informative (scant material, artefact and tumour necrosis), negative (mild in <5%), 1+ (mild in 5–10%), 2+ (moderate in 10–50%) and 3+ (intense in >50%). Positive nuclear staining was considered for Fli-1, myogenin and INI1 and cytoplasm/membranous staining was considered for CD99, CAV-1, HNK-1, osteonectin, osteocalcin, LCA, CD20, CD3, CD138, CK (AE1/AE3), CK20, EMA, SMA, desmin, synaptophysin, chromogranin, NB84, TH, HMB-45, Melan-a and CD117. *EWSR1* (22q12) (Vysis) and LSI *SYT* (18q11.2) (Vysis) break apart probes were used for FISH analysis. FISH was performed according to the conventional protocol for paraffin-embedded tumours in whole sections [24, 31, 34]. In normal cells two fused or very close (red-green) signals were observed. In cells with translocations, two types of signals were observed: one fused (red-green) signal, and another signal split into green and red. An average of 200 well-separated nuclei was counted in each case. A positive result was defined as more than 15% of cells with translocation. For RT-PCR analysis, total RNA was extracted using conventional protocols [24, 26]. The primer sets (Table 3) were applied according to the incidence of typical gene fusions for specific SRCT.

Results

Case 1 The histopathology revealed the presence of mature cortical and trabecular bone tissue, as well as soft tissue infiltrated by a malignant neoplasia of small round cells. The cytoplasm was abundant, slightly eosinophilic and occasionally vacuolate. Cells were distributed in strands, nests and small sheets within a richly vascularized, fibrohyaline stroma, and with perivascular deposits of a mantle of fibrillar, hyaline eosinophilic material, interposed among the neoplastic cells corresponding to reactive osteoid formation probably secondary to bone destruction (Fig. 1a, b). IHC study revealed positivity for CD99+++, FLi-1+++, HNK-1++,CAV-1+++, osteonectin+ (Fig. 1c), CK+++, EMA++ and INI1++. The tumour was negative for other markers including S-100, HMB-45, CD45, CD20, SMA and desmin. FISH analysis revealed a positive *EWSR1* break apart, and with RT-PCR an *EWSR1/Fli-1* fusion was demonstrated. The final diagnosis was atypical ESFT mimicking small cell osteosarcoma.

Case 2 Histopathologic studies revealed a proliferation of small round cell cells with scant eosinophilic cytoplasm and ill-defined cell borders, oval to round nuclei and moderate mitotic index. The cells were distributed in nests or strands embedded in a high desmoplastic stroma (Fig. 1d, e). Occasionally, pseudorosette structures were observed. The IHC showed strongly immunoreactive for CD99, Fli-1, CAV-1 (Fig. 1f) and CK (dot-like), moderately positive for HNK-1 and stained weakly for S100. EMA, desmin and SMA were negative. FISH analysis revealed *EWSR1* break apart positive and RT-PCR detected *EWSR1/Fll-1* gene fusion. The final diagnosis was atypical ESFT with desmoplasia, and the differential diagnosis was desmoplastic small round cell tumour (DSRCT).

Case 3 The histopathology showed the presence of a small cell tumour associated with prominent spindle cells proliferation (Fig. 1g, h). The cytoplasm was scant and slightly eosinophilic. Neither rosette formation nor glandular structures were detected. IHC study revealed positivity for CD99+++ (Fig. 1i), Fli-1+++, HNK-1++, CAV-1+++, CK+++ and EMA+. The tumour was negative for other markers including S-100, SMA and desmin. FISH analysis revealed a positive *EWSR1* break apart and negative *SYT*

Table 1 Clinicopathologic and genetic characteristics of the present series

Case	Age	Sex	Tumor location	Histopathology findings	Differential diagnosis	IHC results	FISH / RT-PCR
1	19	M	right Iliac bone	SRCT with reactive osteoid formation	Atypical ESFT vs SCO	CD99+,HNK1+,CAV1+, CK+,EMA+,Ost+	*EWSR1+EWS/Fli-1+*
2	29	M	retroperitoneal area	SRCT with desmoplasic stroma	Atypical ESFT vs DSRCT	CD99+,HNK1+,Fli1+, CAV1+,CK+,EMA-, Desmin-.	*EWSR1+EWS/Fli-1+*
3	15	M	Subscapular soft tissue	SRCT with spindle cells	Atypical ESFT vs Synovial sarcoma	CD99+,HNK1+,Fli1+, CAV1+,CK+,EMA-, Desmin-.	*EWSR1+EWS/ERG+*
4	28	M	Right inguinal area	SRCT with rhabdoid cells	Atypical ESFT vs rhabdomyosarcoma	CD99+,HNK1+,Fli1+, CAV1+,CK+,EMA-, Desmin-. Myogenin-, INI1+	*EWSR1+EWS/Fli-1+*
5	65	F	Right leg, soft tissue location	SRCT with prominent vascular formation	Atypical ESFT vs others soft tissus tumor with hemangioendothelial pattern.	CD99+,HNK1+,Fli1+, CAV1+,CK+,EMA-, Desmin-.Myogenin-,	*EWSR1+EWS/Fli-1+*
6	2	F	Paraverterbral area	SRCT without pseudorosette formation	Atypical ESFT vs neuroblastoma	CD99+,HNK1+,Fli1+, CAV1+,CK+,EMA-, Desmin-,NB84-,TH-.	*EWSR1+MYCN-EWS/Fli-1+*
7	33	F	Back region soft tissue	SRCT with seuglandular formation and desmoplasia	Atypical ESFT adamantinoma-like vs Myoepithelial carcinoma	CD99+,HNK1+,Fli1+, CAV1+,CK-,EMA+, Desmin-,S100-, SMA -.	*EWSR1+EWS/FEV+*
8	38	M	Right arm (superficial location)	SRCT with superficial location	Atypical ESFT vs Merkel carcinoma	CD99+,HNK1+,Fli1+, CAV1+,CK-,CK20-, EMA-,Desmin-,S100-, SMA -.	*EWSR1+EWS/Fli-1+*
9	85	M	Sacral area	SRCT with discohesive cells and previous history of NHL	Atypical ESFT vs NHL	CD99+,HNK1+,Fli1+, CAV1+,CK-,EMA-, Desmin-,S100-, SMA -, CD45-,CD20-,CD138-.	*EWSR1+EWS/Fli-1+*

translocation and the RT-PCR detected *EWSR1/ERG* gene fusion. The final diagnosis was atypical ESFT with spindle cell proliferation mimicking synovial sarcoma.

Case 4 The histopathology revealed the presence of soft tissue infiltrated by a malignant neoplasm of small round cells. The cytoplasm was prominent, eosinophilic with rhabdoid and rhabdomyoblast morphology (Fig. 2a, b). Cells were distributed in large sheets within a richly vascularized stroma. IHC study revealed positivity for CD99+++, Fli-1+++, HNK-1+++, CAV-1+++ (Fig. 2c), CK+++ and INI1++. The tumour was negative for EMA, SMA, desmin and myogenin. FISH analysis revealed a positive *EWSR1* break apart and RT-PCR detected *EWSR1/FLi-1* fusion, although *PAX/FKHR* fusion genes were not demonstrated. The final diagnosis was atypical ESFT with rhabdoid cells resembling adult pleomorphic rhabdomyosarcoma or malignant tumour with rhabdoid phenotype.

Case 5 The neoplasm showed an SRCT morphology, but with prominent vascular formation adopting a haemangioendothelial pattern (Fig. 2d, e). The tumour cell cytoplasm was scant and focal spindle cell morphology was observed. Neither rosette nor pseudorosette formation was detected. IHC study revealed positivity for CD99 (+++) (Fig. 2f), Fli-1 (+++), CAV1 (+++), HNK-1 (+) and CK. EMA, desmin, myogenin, SMA, S100, chromogranin and synaptophysin were negative. FISH analysis revealed positive translocation (break apart) for *EWSR1* gene and negative results for *SYT*. RT-PCR showed the *EWSR1/FEV* fusion transcript. No other gene fusions involved in specific SRCT (synovial sarcoma, extraskeletal myxoid chondrosarcoma, round/myxoid liposarcoma, DSRCT, clear cell sarcoma) were detected. The final diagnosis was atypical vascular ESFT resembling soft tissue tumour with vascular formation.

Table 2 Immunohistochemical study. Antibodies, source and dilution

Antibody	Source	Dilution
CD99	Dako	1:50
Caveolin-1	Santa Cruz	1:200
HNK-1	Valencia	no
Fli1	Santa Cruz	1:50
Osteonectin	Novoc ep	1:50
Osteocalcin	Chemicon	1:50
LCA	Dako	1:50
CD20	Dako	1:100
CD3	Dako	1:100
CD138	Santa Cruz	1:100
CK (AE1/AE3)	Dako	1:50
CK20	Dako	1:50
EMA	Dako	1:200
SMA	Novocastra	1:200
Desmin	Dako	1:100
Myogenin	Santa Cruz	1:50
Synaptophysin	Novoc	1:50
Cromogranin	Dako	1:50
NB84	Novoc	1:100
TH	Novoc ep	1:30
HMB-45	Novoc	1:50
MELAN-A	Dako	1:50
CD117	Dako	1:50
INI-1	BD	1:50

Case 6 Histopathologic studies revealed a proliferation of small round cell with scant cytoplasm and undifferentiated morphology, abundant apoptotic cells were observed and the mitotic index was low (Fig. 2g–i). Occasionally, pseudorosette structures were observed. The IHC showed positivity for CD99 (+++), FLI-1 (+++), CAV-1 (++), HNK-1 (+) and CK (+). EMA, desmin, SMA, NB84, TH, CD45, CD20, chromogranin and synaptophysin were negative. FISH analysis revealed *EWSR1* break apart positive and no *MYCN* gene amplification. RT-PCR detected *EWSR1/Fli-1* gene fusion. The final diagnosis was atypical ESFT (large cells) mimicking undifferentiated neuroblastoma.

Case 7 The neoplasm showed and SRCT morphology. The cytoplasm fluctuated from scant to abundant and clear or eosinophilic appearance was observed. Tumour cells were arranged in several patterns including diffuse SRCT, tubular, cord-like, clear cells, epithelioid and pseudo-glandular. In several areas the tumour cells adopted a palisading architecture, being sustained by a collagen basal-like membrane (Fig. 3a, b). This basement membrane was homogeneous, eosinophilic and PAS positive. IHC study revealed positivity for CD99 (+++) (Fig. 3c), Fli1(+++), CAV1 (+++) and HNK-1 (++). Poor cytoplasmic expression for EMA was observed. CK, desmin, SMA, S100 and myogenin were negative. FISH analysis revealed positive translocation (break apart) for *EWSR1* gene and negative results for *SYT*. RT-PCR showed the *EWSR1/FEV* fusion transcript. No other gene fusions involved in specific SRCT (synovial sarcoma, extraskeletal myxoid chondrosarcoma, round/myxoid liposar-

Table 3 Primers used for RT-PCR

Primers	DNA sequence
EWS7ARF	TCCTACAGCCAAGCTCCAAGTCAATA
EWS8.1RF	GCATGAGTGGCCCTGATAAC
EWS9DRF	CTGGTGGACCCATGGATGAAGGA
EWS10GRF	TGGAGAGCGAGGTGGCTTCAATAA
EWS11RF	TCTGGCAGACTTCTTTAAGCA
FLI6ARR	ATTGCCCCAAGCTCCTCTTCTGAC
FLI5BRR	TCGGTGTGGGAGGTTGTATT
EWS7ARF	TCCTACAGCCAAGCTCCAAGTCAATA
ERG6ERR	CTCCTGGGGGGCTCATATGGTAAAT
ERG9KRR	TGAGGGGTACTTGTACAGA
EWS7ARF	TCCTACAGCCAAGCTCCAAGTCAATA
FEV11	TGTTGGGCTTGCTCTTGCGCTC
FEVF1RR	GCTTGAACTCGCCGTGACCG
EWS7ARF	TCCTACAGCCAAGCTCCAAGTCAATA
ETV6-RF	GCTTACATGAACCACATCATGG
EWS22.3RF	TCCTACAGCCAAGCTCCAAGTC
ATF1-RR1	GAAGTCCCTGTACTCCATCTGTG
EWS22.3RF	TCCTACAGCCAAGCTCCAAGTC
WT1-9RR	GACCAGGAGAACTTTCGCTGAC
WT1-8RR	ACCTTCGTTCACAGTCCTTG
WT1-10RR	GCCACCGACAGCTGAAGGGC
SSX1RR	GGTGCAGTTGTTTCCCATCG
SSX2RR	GGCACAGCTCTTTCCCATCA
SYTRF	CAACAGCAAGATGCATACCA
MGBRF	CTCGCGCTACTCTCTCTTTCT
MGBRR	TGTCGGATTGATGAAACCCAG
EWS12BRF	GCGATGCCACAGTGGCCTATG
CHN2RR	GGACGTCCGGCGAGGCGAAGC
CHN3RR	CCTGGAGGGGAAGGGCTAT
PAX3/7-1	CCGACAGCAGCTCTGCCTAC
PAX3U	CCAAACACAGCATCGACG
PAX7U	TTTGAGAGGACCCACTACCC
FKHR-2	ATGAACTTGCTGTGTAGGGACAG
ETV6-RF	GCTTACATGAACCACATCATGG
NTRK3-RR	GAAGTCGTGCTACAGAGAGG

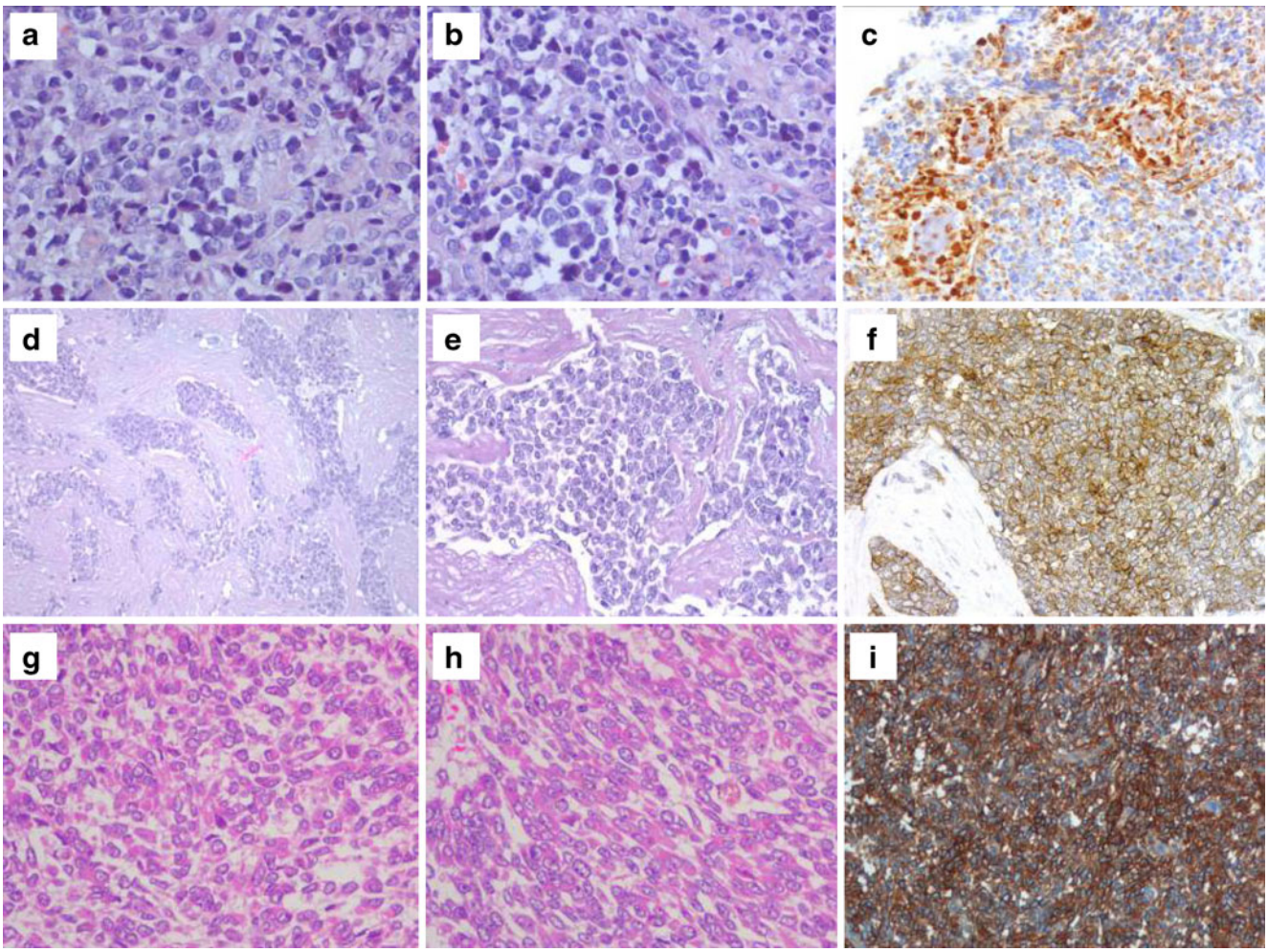

Fig. 1 **a** Case 1, atypical ESFT with hyaline eosinophilic material, interposed among the neoplastic cells [haematoxylin and eosin (H&E ×40)]. **b** Case 1, atypical large cell ESFT (H&E ×40). **c** Case 1, osteonectin cytoplasmic staining (+++) in reactive bone and poor positivity in ESFT neoplastic cells. **d** Case 2, atypical ESFT with extensive desmoplastic stroma (H&E ×20). **e** Case 2, atypical ESFT with cells distributed in nests or strands embedded in a highly desmoplastic stroma (H&E ×40). **f** Case 2, caveolin-1 membranous staining (+++) in neoplastic cells. **g** Case 3, atypical ESFT with small cell tumour showing slightly eosinophilic cytoplasm (H&E ×40), **h** case 3, atypical ESFT associated with prominent spindle cell proliferation (H&E ×40). **i** Case 3, CD99 membranous staining (+++) in tumour cells

coma, DSRCT or clear cell sarcoma) were detected. The final diagnosis was atypical ESFT (adamantinoma-like) resembling soft tissue myoepithelial carcinoma.

Case 8 The round cell neoplasm was restricted to the dermis (Fig. 3d, e). The tumour was composed of sheets and lobules of small- to medium-sized round cells showing scant cytoplasm. Mitotic index was low and neither necrosis nor pseudorosette formation were observed. IHC study revealed positivity for CD99 (+++) (Fig. 3f), Fli1 (++), CAV1 (++) and HNK-1 (+). CK, CK20, EMA, desmin, SMA, S100 and myogenin were negative. FISH analysis revealed positive translocation for *EWSR1* gene and RT-PCR showed the *EWSR1/Fli-1* fusion transcript. No other gene fusions involved in specific SRCT (synovial sarcoma, extraskeletal myxoid chondrosarcoma, round/myxoid liposarcoma, DSRCT or clear cell sarcoma) were detected. The final diagnosis was atypical superficial ESFT mimicking Merkel cell carcinoma.

Case 9 Histopathologic studies revealed a proliferation of small round cell cells with very incohesive cells and no intervening stroma mimicking lymphoma neoplasm (Fig. 3g, h). The cells showed scant cytoplasm and the mitotic index was low. No pseudorosette structures were observed. The IHC showed positivity for CD99, FLI-1, CAV-1 and HNK-1. CK, EMA, desmin, CD45, CD20, CD3 and CD138 were negative. FISH analysis revealed *EWSR1* break apart positivity (Fig. 3i) and RT-

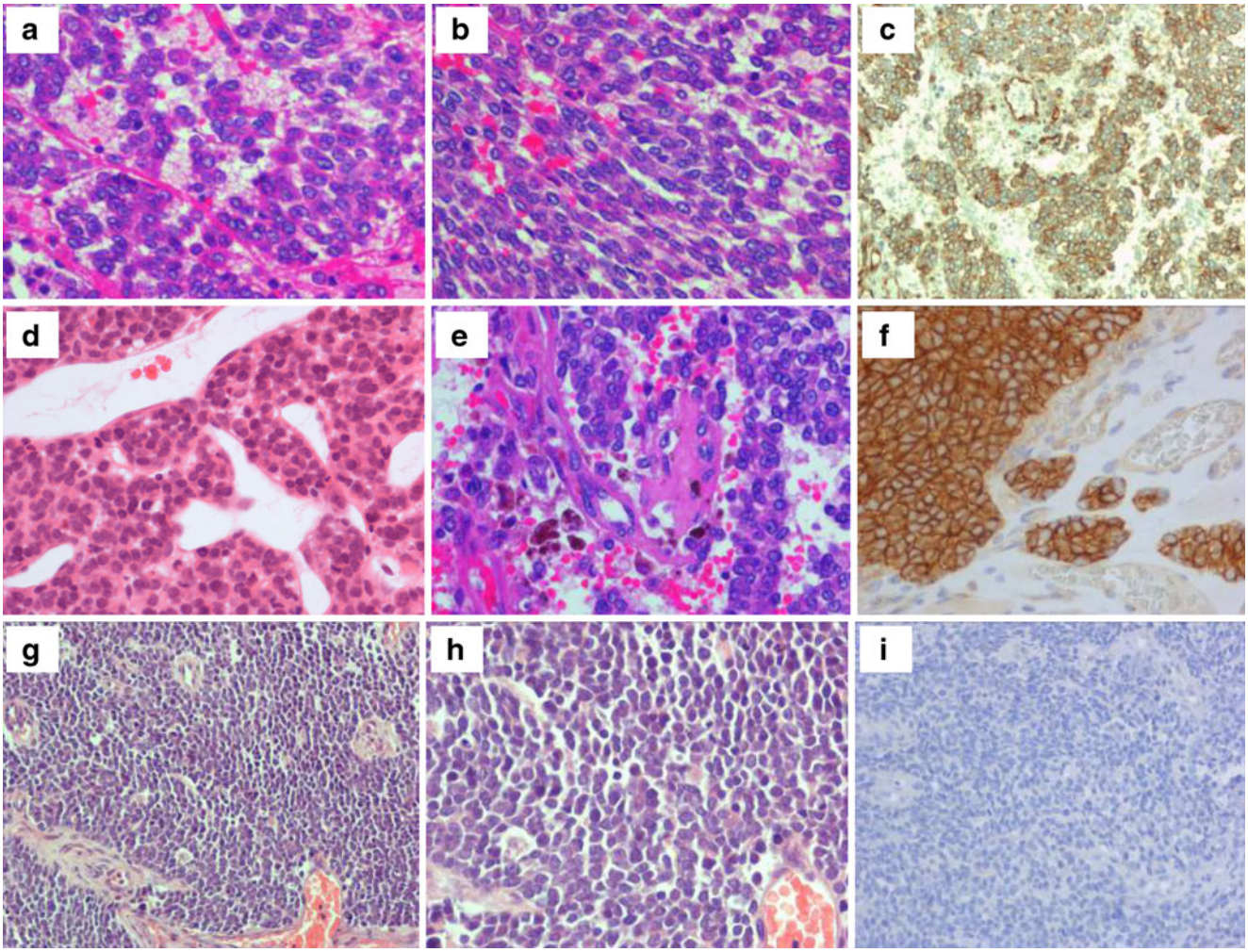

Fig. 2 **a** Case 4, atypical ESFT with prominent eosinophilic cytoplasm (H&E ×40). **b** Case 4, atypical ESFT, the cytoplasm showing rhabdoid and rhabdomyoblast morphology (H&E ×40). **c** Case 4, caveolin-1 cytoplasmic staining (+++) in tumour cells. **d** Case 5, atypical ESFT with prominent vascular formation (H&E ×40). **e** Case 5, atypical ESFT with haemosiderin deposition and vascular formation (H&E ×40). **f** Case 5, CD99 membranous staining (+++). **g** Case 6, atypical ESFT with undifferentiated morphology (H&E ×20). **h** Case 6, atypical ESFT, scant cytoplasm, undifferentiated morphology and vascular formation (H&E ×40). **i** Case 6, atypical ESFT, negative for NB84

PCR detected an *EWSR1/Fli-1* gene fusion. The final diagnosis was atypical ESFT resembling non-Hodgkin lymphoma (patient with previous history of non-Hodgkin lymphoma).

Discussion

Atypical variants of ESFT have been described mostly by Nascimiento et al. [27], Llombart-Bosch et al. [17, 18, 20] and Folpe et al. [12]. The criteria used for these histological subtypes include the high degree of cell heterogeneity, the existence of unusual patterns or the presence of pseudovascular structures [12, 20]. Cell heterogeneity of atypical ESFT is consistent with the presence of large, clear, spindle, epithelioid or rhabdoid cells in wide areas of the tumour [12, 20, 27]. The existence of unusual patterns is characterized by components such as desmoplasia, sclerosis and adamantinoma-like areas [6, 12, 13, 20, 27, 37]. Pseudovascular structures offer in atypical ESFT a vascular-like haemangiomatous appearance [20]. In these cases, the correlation between the clinical data (tumour location, age and sex), morphological, IHC and genetic findings is mandatory [12, 20]. Additionally, epithelial differentiation has been demonstrated in 20% of genetically confirmed ESFT [15]. Particularly, the atypical variant of ESFT frequently shows epithelial differentiation at histological and IHC level, further complicating the differential diagnosis with other SRCT of bone and soft tissue with CK immunoexpression (adamantinoma, synovial sarcoma, rhabdomyosarcoma, epithelioid sarcoma, DSRCT, malignant rhabdoid tumour (MRT) or tumour with rhabdoid

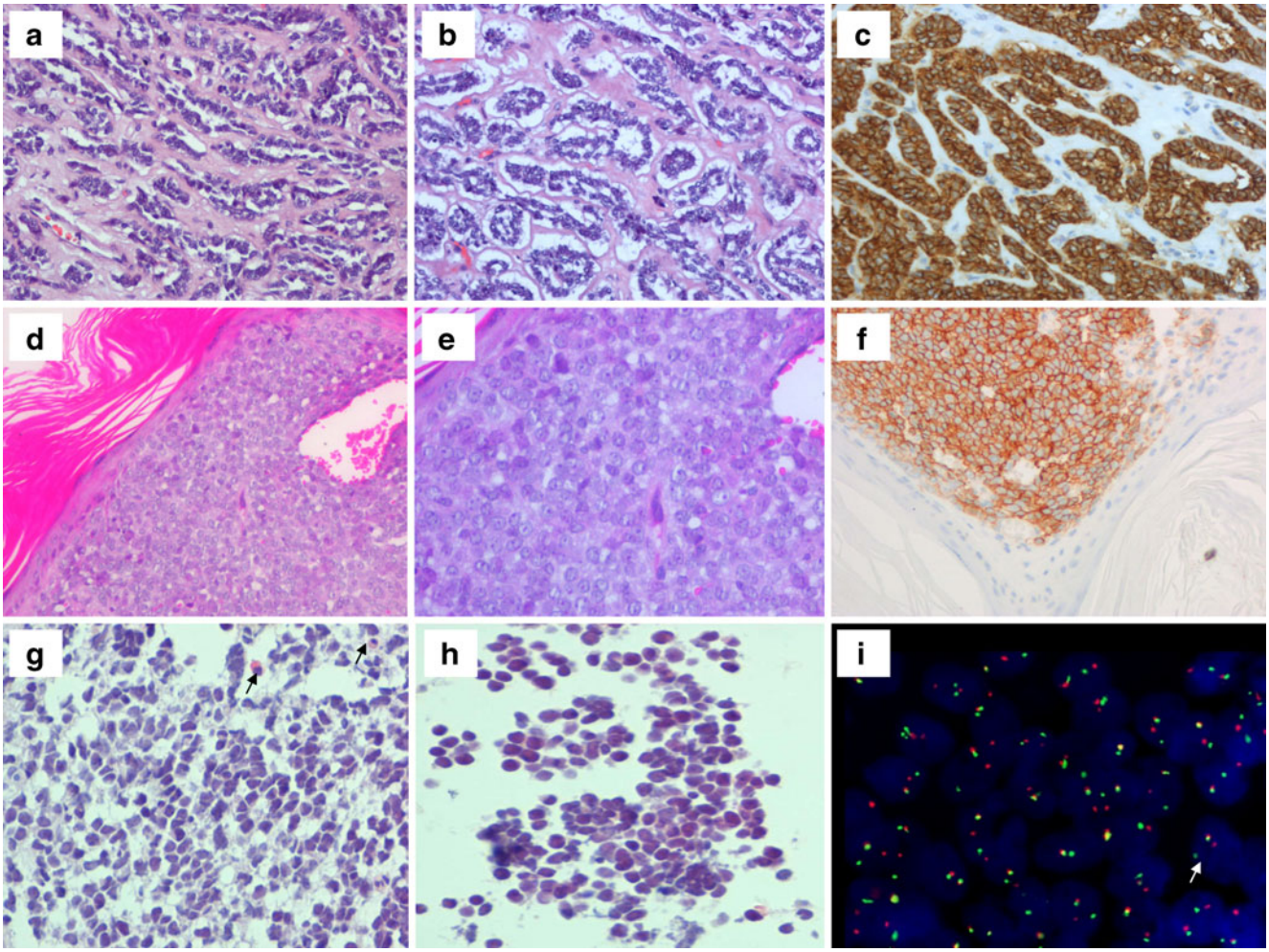

Fig. 3 **a** Case 7, atypical ESFT with adamantinoma-like structures (H&E ×40). **b** Case 7, atypical ESFT, cord-like, clear cells, epithelioid and pseudo-glandular patterns. The tumour cells adopted a palisading architecture, being sustained by a collagen basal-like membrane (H&E ×40). **c** Case 7, CD99 membranous and cytoplasmic staining (+++) in tumour cells. **d** Case 8, atypical cutaneous ESFT with neoplastic cells restricted to the dermis (H&E ×20). **e** Case 8, superficial atypical ESFT (H&E ×40). **f** Case 8, CD99 membranous staining (+++) in tumour cells and negative in cutaneous epithelial structures. **g** Case 9, atypical ESFT with undifferentiated morphology, and scant eosinophilic and plasma cells (*arrow*; H&E ×40). **h** Case 9, atypical ESFT, incohesive cells and undifferentiated morphology mimicking lymphoblastic lymphoma (H&E ×40). **i** Case 9, atypical ESFT, FISH/*EWSR1* with break apart (*arrows*), positive for *EWSR1* translocation

phenotype, myoepithelial carcinoma, neuroendocrine carcinomas and metastatic carcinomas). Furthermore, many of these soft tissue tumours (DSRCT, myoepithelial carcinoma and neuroendocrine carcinoma) can display an *EWSR1* rearrangement by fluorescence in situ hybridization which complicates the differential diagnosis with atypical ESFT [4, 5, 25, 29]. Therefore, the use of RT-PCR analysis to detect specific gene fusions in the latter cases is mandatory.

In the present series, we describe nine cases of SRCT with a genetically confirmed final diagnosis of atypical ESFT, resembling sarcomas, carcinomas and lymphomas due to the presence of unusual cell morphology or atypical patterns. Six cases (1–6) mimic sarcomas with or without osteoid formation. Age and tumour location in (case 1) were concordant with the diagnosis of ESFT; however, osteoid deposition and EMA IHC positivity were unexpected characteristics. The osteoid deposits complicated the differential diagnosis with small cell osteosarcoma (SCO); and the EMA positivity with undifferentiated synovial sarcoma. Molecular studies revealing *EWSR1* translocation and *EWSR1/Fli1* gene fusion, a finding inconsistent with synovial sarcoma, defined the diagnosis of atypical ESFT in case 1. It seems reasonable that in any atypical SRCT with osteoid deposition, CD99 positivity and *EWSR1* rearrangement, the confirmation of the translocation should be carried out by two different molecular methods. On the other hand, ESFT can reveal osteoid deposition and IHC osteonectin positivity due to reactive new bone formation. Moreover, in cases with presumptive diagnosis of ESFT in bone, but negative for the specific translocations or gene

fusions, the possibility of SCO should be excluded and several histopathological sections from the paraffin block are mandatory to exclude malignant osteoid formation [2, 10, 23]. Definitively, despite the morphological link between ESFT and SCO, malignant osteoid formation remains the hallmark of SCO, while the presence of an *EWSR1* translocation with the specific gene fusions are diagnostic of ESFT [23]. Despite the CK and EMA positivity in the present tumour, the diagnosis of synovial sarcoma was excluded since molecular studies did not reveal *SYT* rearrangement. As far as we know, EMA expression has not so far been described in genetically confirmed ESFT, so this finding complicated the differential diagnosis with other SRCT with EMA expression (synovial sarcoma, MRT, epithelioid sarcoma and myoepithelial carcinoma). To our knowledge, loss of INI1 expression has not yet been reported in ESFT; however, this is a frequent event in MRT, and occasionally, epithelioid sarcoma, myoepithelial carcinoma, epithelioid malignant peripheral nerve sheath tumour and synovial sarcoma can reveal loss of INI1 expression.

Findings resembling DSRCT (desmoplastic stroma; case 2) are unusual in ESFT [12, 20, 37]. Nevertheless, an unusual subtype of ESFT with desmoplasia has been described by Folpe et al. [12]. In case 2, the retroperitoneal location, desmin negativity and *EWSR1/Fli1* gene fusion by RT-PCR are more consistent with ESFT than with DSRCT. However, DSRCT with *EWSR1/Fli1* or *EWSR1/ERG* gene fusion have already been described, but with evident IHC desmin expression [28]. Desmin expression is very rare in ESFT, nevertheless sporadic studies have reported this finding in which the tumours were classified as biphenotypic sarcomas with or without *EWSR1* rearrangement [9, 33]. Indeed, in desmin-positive SRCT, the possibility of ESFT remains very unlikely and the possibility of other SRCT with muscular differentiation (rhabdomyosarcoma and SCO) should be exhaustively excluded. Furthermore, in a recent study performed by Llombart-Bosch et al. in more than 500 genetically confirmed ESFT, desmin expression was absent in all tumours (data unpublished). The term 'biphenotypic sarcoma' has been used for tumours with either neural and muscular differentiation, or neural and osteoid production, although the actual existence of these tumours is still under debate. In fact, in the post-molecular era only very sporadic reports regarding biphenotypic sarcoma have been published, and the existence of this particular neoplasm is becoming doubtful.

A sarcoma without osteoid production and with predominant spindle cells expressing CK made the differential diagnosis between atypical ES and undifferentiated synovial sarcoma difficult (case 3). In this case, tumour location and age are suggestive of both tumours; however, EMA negativity and the absence of *SYT* translocation and S*YT/SSX* transcript made the existence of synovial sarcoma improbable [9, 11, 19]. Additionally, the finding of *EWSR1* translocation and *EWSR1/ERG* gene fusion confirms the diagnosis of ESFT, in this case atypical ESFT with spindle cells.

Tumour location (inguinal region), the morphologic characteristics of tumour cells (abundant eosinophilic cytoplasm) made the differential diagnosis between atypical ES and adult rhabdomyosarcoma difficult [11, 19, 30] (case 4). FISH analysis revealed *EWSR1* translocation and the RT-PCR, *EWSR1/Fli1* transcript confirmed the diagnosis of ESFT. In addition, desmin, myogenin and SMA were negative, making the possibility of adult rhabdomyosarcoma unlikely. Despite the age of the patient, the possibility of alveolar rhabdomyosarcoma was excluded since the RT-PCR failed to detect *PAX-FKHR* gene fusion.

In atypical ESFT, vascular-like areas have been reported similar to case 5 in which the tumour cells display a pseudoendothelial pattern forming vascular or lacunar spaces, lined by tumour cells that progressively elongate and cover lacunae filled with erythrocytes and plasma material [12, 18, 20]. Tumour cells, lining the surface of the vessel-like spaces lack basal membrane and are in continuity with the more solid cellular fields [12, 18, 20]. Abundant vascular formation with erythrocyte lysis can generate haemosiderin deposits, misinterpreted clinically as the melanic pigment observed in melanoma or clear cell sarcoma.

Tumour location (paravertebral area), patient age and absence of pseudorosette formation can make the differential diagnosis between neuroblastoma and atypical ESFT difficult (case 6). Children below 5 years of age with SRCT of bone and soft tissue should be carefully evaluated to exclude metastatic neuroblastoma [8, 31]. The present case showed IHC findings suggestive of ESFT instead of neuroblastoma, and additionally the *EWSR1* translocation was demonstrated by FISH and RT-PCR.

Differential diagnosis of atypical ESFT with carcinomas is quite complex in some tumours (cases 7 and 8). The soft tissue tumour location and the trabecular, tubular and pseudo-glandular patterns at histological level made the differential diagnosis with adamantinoma-like EFST and soft tissue myoepithelial carcinoma confusing [5, 14] (case 7). Myoepithelial carcinoma displays epithelial and neural differentiation with CK and S100 expression [5, 14] and both markers were negative in case 7, making the diagnosis of myoepithelial carcinoma improbable. The differential diagnosis has become more complex since Brandal et al. [5] described the *EWSR1* rearrangement in myoepithelial carcinomas with (*EWSR1/ZNF444*) gene fusion. Furthermore, Antonescu et al. [1] described the same finding in a large series of myoepithelial carcinomas. The finding of an *EWSR1/FEV* gene fusion is probably the principal event in this case, and it is unlikely that another gene fusion

involving *EWSR1* would be detected in the same tumour despite *EWSR1* translocation by FISH. On the other hand, due to the partial epithelial nature (EMA positive) of the present tumour, metastatic carcinoma should also be considered in the differential diagnosis, including neuroendocrine carcinoma that may harbour *EWSR1* translocation, as recently described [25]. This patient had no previous history of carcinoma and neuroendocrine markers were negative. Although the morphological features (cord-like, tubular epithelioid and pseudo-glandular patterns) were uncommon for ESFT, case 7 was finally diagnosed as adamantinoma-like ESFT.

The superficial location (dermis) of the tumour and round cell morphology complicated the differential diagnosis between atypical ES and Merkel cell carcinoma [22, 32, 36] (case 8). However, Merkel cell carcinoma usually displays CK20 expression, while the present case was negative for this marker. *EWSR1* translocation (FISH and RT-PCR) confirmed the diagnosis of superficial atypical ESFT. Nevertheless, ESFT can occur as a cutaneous tumour, making the differential diagnosis with Merkel cell tumours complex [22, 32, 36], especially when 20% of ESFT have epithelial differentiation (CK+) and in several cases Merkel cell neoplasms express CD99 [22, 32, 36]. Additionally, CK20 immunoreactivity is consistent with Merkel cell carcinoma, while its expression is absent in ESFT, as confirmed by our working group in more than 500 genetically confirmed ESFT tested with CK20 with lacking expression in all tumours (unpublished data).

Atypical ESFT can be confused with haematological disease [16–18], particularly in patients with a previous history of lymphomas (case 9). Lymphoid markers (CD45, CD20 and CD138) were negative in this case, thus excluding lymphoma/myeloma, and genetic studies revealed *EWSR1* translocation confirming the diagnosis of ESFT.

In conclusion, the cases herein reported represent unusual histological variants of ESFT mimicking sarcomas, carcinomas and lymphomas. These results strongly suggest that tumours showing overlapping morphological and immunohistochemical features with other SRCT of soft tissue and bone can be readily differentiated using complementary molecular techniques. In SRCT with an *EWSR1* translocation demonstrated by FISH, the RT-PCR analysis of specific sarcoma-related gene fusions can offer important clues when diagnosing specific entities, especially in tumours with atypical histopathology and/or IHC findings. However, for the time being the integration of clinical, histopathological, IHC and genetic data remains the corner stone for the diagnosis of bone and soft tissue sarcomas in which genetic rearrangements with reciprocal translocations are present.

Conflict of interest statement We declare that we have no conflict of interest.

References

1. Antonescu CR, Zhang L, Chang NE et al (2010) EWSR1-POU5F1 fusion in soft tissue myoepithelial tumors. A molecular analysis of 66 cases, including soft tissue, bone, and visceral lesions, showing common involvement of the EWSR1 gene. Genes Chromosom Cancer 49:1114–1124
2. Ayala AG, Ro JY, Papadopoulos NK et al (1993) Small cell osteosarcoma. Cancer Treat Res 62:139–149
3. Bovee JV, Hogendoorn PC (2010) Molecular pathology of sarcomas: concepts and clinical implications. Virchows Arch 456:193–199
4. Brandal P, Panagopoulos I, Bjerkehagen B et al (2008) Detection of a t(1;22)(q23;q12) translocation leading to an EWSR1-PBX1 fusion gene in a myoepithelioma. Genes Chromosom Cancer 47:558–564
5. Brandal P, Panagopoulos I, Bjerkehagen B et al (2009) t(19;22)(q13;q12) Translocation leading to the novel fusion gene EWSR1-ZNF444 in soft tissue myoepithelial carcinoma. Genes Chromosom Cancer 48:1051–1056
6. Bridge JA, Fidler ME, Neff JR et al (1999) Adamantinoma-like Ewing's sarcoma: genomic confirmation, phenotypic drift. Am J Surg Pathol 23:159–165
7. Bridge RS, Rajaram V, Dehner LP et al (2006) Molecular diagnosis of Ewing sarcoma/primitive neuroectodermal tumor in routinely processed tissue: a comparison of two FISH strategies and RT-PCR in malignant round cell tumors. Mod Pathol 19:1–8
8. Burgues O, Navarro S, Noguera R et al (2006) Prognostic value of the International Neuroblastoma Pathology Classification in Neuroblastoma (Schwannian stroma-poor) and comparison with other prognostic factors: a study of 182 cases from the Spanish Neuroblastoma Registry. Virchows Arch 449:410–420
9. de Alava E, Lozano MD, Sola I et al (1998) Molecular features in a biphenotypic small cell sarcoma with neuroectodermal and muscle differentiation. Hum Pathol 29:181–184
10. Devaney K, Vinh TN, Sweet DE (1993) Small cell osteosarcoma of bone: an immunohistochemical study with differential diagnostic considerations. Hum Pathol 24:1211–1225
11. Fisher C (2010) Soft tissue sarcomas with non-EWS translocations: molecular genetic features and pathologic and clinical correlations. Virchows Arch 456:153–166
12. Folpe AL, Goldblum JR, Rubin BP et al (2005) Morphologic and immunophenotypic diversity in Ewing family tumors: a study of 66 genetically confirmed cases. Am J Surg Pathol 29:1025–1033
13. Fukunaga M, Ushigome S (1998) Periosteal Ewing-like adamantinoma. Virchows Arch 433:385–389
14. Gleason BC, Fletcher CD (2007) Myoepithelial carcinoma of soft tissue in children: an aggressive neoplasm analyzed in a series of 29 cases. Am J Surg Pathol 31:1813–1824
15. Gu M, Antonescu CR, Guiter G et al (2000) Cytokeratin immunoreactivity in Ewing's sarcoma: prevalence in 50 cases confirmed by molecular diagnostic studies. Am J Surg Pathol 24:410–416
16. Li S, Siegal GP (2010) Small cell tumors of bone. Adv Anat Pathol 17:1–11
17. Llombart-Bosch A (1996) Small round cell tumors of bone and soft tissue. Introduction. Semin Diagn Pathol 13:149–152
18. Llombart-Bosch A, Contesso G, Peydro-Olaya A (1996) Histology, immunohistochemistry, and electron microscopy of small round cell tumors of bone. Semin Diagn Pathol 13:153–170
19. Llombart-Bosch A, Lopez-Guerrero JA, Peydro-Olaya A (2002) Synovial sarcoma (SS): new perspectives supported by modern technology. Arkh Patol 64:39–47

20. Llombart-Bosch A, Machado I, Navarro S et al (2009) Histological heterogeneity of Ewing's sarcoma/PNET: an immunohistochemical analysis of 415 genetically confirmed cases with clinical support. Virchows Arch 455:397–411
21. Llombart-Bosch A, Pellin A, Carda C et al (2000) Soft tissue Ewing sarcoma—peripheral primitive neuroectodermal tumor with atypical clear cell pattern shows a new type of EWS-FEV fusion transcript. Diagn Mol Pathol 9:137–144
22. Llombart B, Monteagudo C, Lopez-Guerrero JA et al (2005) Clinicopathological and immunohistochemical analysis of 20 cases of Merkel cell carcinoma in search of prognostic markers. Histopathology 46:622–634
23. Machado I, Alberghini M, Giner F et al (2010) Histopathological characterization of small cell osteosarcoma with immunohistochemistry and molecular genetic support. A study of 10 cases. Histopathology 57:162–167
24. Machado I, Noguera R, Pellin A et al (2009) Molecular diagnosis of Ewing sarcoma family of tumors: a comparative analysis of 560 cases with FISH and RT-PCR. Diagn Mol Pathol 18:189–199
25. Malone VS, Dobin SM, Jones KA et al (2010) CD99-positive large cell neuroendocrine carcinoma with rearranged EWSR1 gene in an infant: a case of prognostically favorable tumor. Virchows Arch 457:389–395
26. Mangham DC, Williams A, McMullan DJ et al (2006) Ewing's sarcoma of bone: the detection of specific transcripts in a large, consecutive series of formalin-fixed, decalcified, paraffin-embedded tissue samples using the reverse transcriptase-polymerase chain reaction. Histopathology 48:363–376
27. Nascimento AG, Unii KK, Pritchard DJ et al (1980) A clinicopathologic study of 20 cases of large-cell (atypical) Ewing's sarcoma of bone. Am J Surg Pathol 4:29–36
28. Ordi J, de Alava E, Torne A et al (1998) Intraabdominal desmoplastic small round cell tumor with EWS/ERG fusion transcript. Am J Surg Pathol 22:1026–1032
29. Ordonez NG (1998) Desmoplastic small round cell tumor: I: a histopathologic study of 39 cases with emphasis on unusual histological patterns. Am J Surg Pathol 22:1303–1313
30. Parham DM, Ellison DA (2006) Rhabdomyosarcomas in adults and children: an update. Arch Pathol Lab Med 130:1454–1465
31. Piqueras M, Navarro S, Castel V et al (2009) Analysis of biological prognostic factors using tissue microarrays in neuroblastic tumors. Pediatr Blood Cancer 52:209–214
32. Romeo S, Dei Tos AP (2010) Soft tissue tumors associated with EWSR1 translocation. Virchows Arch 456:219–234
33. Sorensen PH, Shimada H, Liu XF et al (1995) Biphenotypic sarcomas with myogenic and neural differentiation express the Ewing's sarcoma EWS/FLI1 fusion gene. Cancer Res 55:1385–1392
34. Subramaniam MM, Noguera R, Piqueras M et al (2007) Evaluation of genetic stability of the SYT gene rearrangement by break-apart FISH in primary and xenotransplanted synovial sarcomas. Cancer Genet Cytogenet 172:23–28
35. Szuhai K, Ijszenga M, de Jong D et al (2009) The NFATc2 gene is involved in a novel cloned translocation in a Ewing sarcoma variant that couples its function in immunology to oncology. Clin Cancer Res 15:2259–2268
36. Terrier-Lacombe MJ, Guillou L, Chibon F et al (2009) Superficial primitive Ewing's sarcoma: a clinicopathologic and molecular cytogenetic analysis of 14 cases. Mod Pathol 22:87–94
37. Ushigome U, Machinami R, Sorensen PH (2002) Ewing sarcoma/Primitive neuroectodermal tumor (PNET). In: Fletcher CDM, Unni K, Mertens F (eds) World health organization classification of tumours. Pathology and genetics of tumours of soft tissue and bone. IARC, Lyon

Virchows Arch (2011) 458:291–300
DOI 10.1007/s00428-010-1039-9

ORIGINAL ARTICLE

Detection of ASPL/TFE3 fusion transcripts and the TFE3 antigen in formalin-fixed, paraffin-embedded tissue in a series of 18 cases of alveolar soft part sarcoma: Useful diagnostic tools in cases with unusual histological features

Ann Williams · Gillian Bartle · Vaiyapuri P. Sumathi · Jeanne M. Meis · D. Chas Mangham · Rob J. Grimer · Lars-Gunnar Kindblom

Received: 12 November 2010 / Accepted: 29 December 2010 / Published online: 29 January 2011
© Springer-Verlag 2011

Abstract Alveolar soft part sarcoma (ASPS) is a rare malignancy; diagnostic problems may occur when cases present as a metastasis or with unusual morphologic features. In this study, a series of 18 cases with follow-up information were analysed with regard to the ASPL/TFE3 fusion transcripts and immuno-detection of TFE3 using archival formalin-fixed, paraffin-embedded tissues. Novel primers to detect ASPL/TFE3 fusion transcripts, type 1 and 2, were designed. The patients, ten female and eight male, ranged in age from 3 to 46 years; 16 involved soft tissues of the extremities (nine, lower; seven, upper), one involved the uterine cervix and one was a primary bone tumour of the foot. Seven ASPS had unusual morphologic features lacking the typical alveolar pattern. Seven had lung metastases at the time of diagnosis, and three developed lung and brain metastases later. Four patients died of disease (after 1–5 years); four are alive with metastases (after 2–15 years), and ten are alive and well (after 1–10 years). Vascular invasion correlated with metastatic disease. All 18 ASPS, four granular cell tumours (one of which was malignant) and one adrenal cortical carcinoma showed TFE3 immuno-positivity. The 18/18 ASPS showed ASPL/TFE3 fusion transcripts (nine, type 1; nine, type 2), four of which had a balanced translocation. ASPL/TFE3 fusion transcripts were not detected in 25 controls. We conclude that immuno-detection of TFE3 and RT-PCR-based identification of ASPL/TFE3 fusion transcripts in formalin-fixed, paraffin-embedded tissues are powerful tools in the diagnosis of ASPS, particularly in cases with unusual morphologic features.

Keywords Alveolar soft part sarcoma · ASPL/TFE3 fusion transcript · Genetics · TFE3 immunohistochemistry

A. Williams · G. Bartle · V. P. Sumathi · D. C. Mangham · R. J. Grimer · L.-G. Kindblom (✉)
Department of Musculoskeletal Pathology and Orthopaedic Oncology, Royal Orthopaedic Hospital NHS Foundation Trust and Division of Cancer Studies, Medical School, University of Birmingham,
Birmingham B15 2TT, UK
e-mail: lars.kindblom@roh.nhs.uk

J. M. Meis
Department of Pathology, The University of Texas, M.D. Anderson Cancer Center,
Houston, TX, USA

Introduction

Alveolar soft part sarcoma (ASPS), first described by Christopherson in 1952 [1], is a rare, high-grade, mesenchymal malignancy with a distinctive histologic and ultrastructural appearance, but still enigmatic in terms of differentiation and origin [2]. It affects mainly adolescents and young adults in the second and third decade, with slight female predominance [2]. In adults, ASPS occurs most commonly in the deep soft tissues of the thigh or buttock whilst, in children and infants, the head and neck regions are often involved [2]. A wide variety of unusual sites have also been reported, including the female genital tract, mediastinum, stomach, breast, bone, and urinary bladder [3–10].

The diagnosis can be problematic due to histologic overlap with other tumours, particularly in small biopsies, as well as when the detection of a metastasis is prior to

identification of a primary, or when presenting at unusual primary sites such as bone. Moreover, there has previously been a lack of specific diagnostic markers. The differential diagnoses include, in particular, paraganglioma, granular cell tumour, metastatic renal cell carcinoma, hepatocellular carcinoma, melanoma, and adrenal cortical carcinoma [2, 11, 12].

Cytogenetically, ASPS is characterised by a specific unbalanced chromosomal translocation, der(17)t(X;17)(p11;q25) [13]. This translocation is present as type 1 and 2 variants involving the fusion of the first seven exons of the ASPL (ASPSCR1) gene to exon 6 (type 1) or 5 (type 2) of the TFE3 transcription factor gene (GenBank NM_006521) [14]. This same fusion transcript occurs as a balanced translocation in a rare subset of renal cell carcinomas predominantly of papillary type, typically seen in children [15]. From a practical standpoint, however, identification of these fusion transcripts by RT-PCR-based techniques offers a valuable tool in the diagnosis of ASPS [13].

Immunohistochemistry is another useful diagnostic tool; anti-TFE3, a commercial polyclonal antibody, recognises the carboxy terminal portion of the TFE3 protein, resulting in strong nuclear staining in tumours characterised by chromosome translocations involving the TFE3 gene [16].

This study aims to investigate the diagnostic usefulness of the RT-PCR technique and immunohistochemistry with the TFE3 antibody in a series of 18 formalin-fixed, paraffin-embedded ASPS within the extremities, uterine cervix, and bone, several of which have unusual morphologic features causing diagnostic problems.

Materials and methods

Clinical material

Eighteen patients with primary ASPS (15 from the Royal Orthopaedic Hospital, Birmingham, UK and three from Sahlgrenska University Hospital, Gothenburg, Sweden) were collected for this study (Table 1). Formalin-fixed, paraffin-embedded (FFPE) material from the primary tumours was available for RT-PCR analysis and immunohistochemistry in all cases. Fresh frozen material was also available in six of the 18 cases. Formalin-fixed, paraffin-embedded tissue blocks from 25 controls were also retrieved from the archives, including other types of sarcoma, metastatic carcinoma, melanoma, paraganglioma, and granular cell tumour (Table 2).

Detection of reciprocal sequences required the use of a renal cell carcinoma containing a balanced ASPL/TFE3 type 1 translocation confirmed by DNA sequencing, as positive control material.

Histopathology review

All tissue blocks were cut and re-examined microscopically, and a representative tissue block was selected for both the RT-PCR and immunohistochemical analyses.

RT-PCR analysis

RNA was extracted from all tissue blocks as previously published with modifications [17], briefly including digestion of tissue in 150 μl proteinase K solution [Tris EDTA buffer pH 8.0 (Sigma-Aldrich, Poole, UK), 1% sodium dodecyl sulphate (Sigma-Aldrich, Poole, UK), 2 mg/ml proteinase K (Applied Biosystems, Warrington, UK)] for 4–24 h at 45°C. This was followed by 600 μl of RNA extraction buffer [4 M guanidine thiocyanate solution (Sigma-Aldrich, Poole, UK), 25 mM sodium citrate (Sigma-Aldrich, Poole, UK), 0.5% lauroyl sarcosine (Sigma-Aldrich, Poole, UK), 0.1 M 2-mercaptoethanol (VWR International, Lutterworth, UK)] [18]. RNA was then extracted with acid phenol/chloroform (Applied Biosystems, Warrington, UK) and precipitated with 2.0 μl linear acrylamide (Applied Biosystems, Warrington, UK) and isopropanol (Sigma-Aldrich, Poole, UK). The resulting pellet was washed in 70% ethanol and dissolved in 20 μl RNA storage solution (Applied Biosystems, Warrington, UK).

RNA was extracted from fresh frozen material in the six corresponding ASPS samples, as previously published, using the RNeasy Mini kit (QIAGEN UK, Crawley, UK) [17].

Novel primers (MWG-Biotech, Ebersberg, Germany) were designed to detect type 1 and type 2 fusions to produce PCR products of 120 and 130 bp, respectively, using Primer3 software (http://frodo.wi.mit.edu). Table 3 shows all primer sequences used, annealing temperatures, PCR cycle numbers, and predicted amplicon size. RT-PCR for both fusion transcripts was performed using QIAGEN OneStep RT-PCR kit (QIAGEN UK, Crawley, UK) on 18 ASPS as well as the 25 controls.

DNA sequencing of all PCR products was performed by the Functional Genomics Laboratory at Birmingham University (http://www.genomics.bham.ac.uk) using a Qiagen 3000 BioRobot (QIAGEN UK, Crawley, UK) and 3700 DNA Analyser (Applied Biosystems, Warrington, UK).

Immunohistochemistry

Immunohistochemistry was carried out on 4-μ paraffin sections of 18 ASPS samples and 25 controls using the P-16 TFE3 goat polyclonal antibody (sc-5958 Santa Cruz Biotechnology, Santa Cruz, USA) diluted 1:200 in 0.05 M TBS pH 7.6. Pretreatment of paraffin sections was carried out in 0.01 M EDTA buffer pH 8.0 overnight at 68°C. Anti-

Table 1 Summary of clinical data in 18 cases of alveolar soft part sarcoma

Case no	Age, years	Sex	Site	Maximum dimension of tumour, cm	Treatment	Mets at diagnosis	Subsequent mets/site, months	Clinical status and follow-up time, months
1	23	F	Buttock	8	Excision+RT	None	Brain/37	AWD 52
2	39	F	Thigh	18	CT+RT	Lung	None	DOD 12
3	16	M	Arm	3	Excision+RT	None	None	ANED 110
4	19	F	Calf	7	Excision+RT	Lung	None	AWD 106
5	13	F	Forearm	2	Excision+RT	None	None	ANED 56
6	31	F	Buttock	11	Excision+RT	None	None	ANED 52
7	46	M	Forearm	15	Excision+RT	None	None	ANED 34
8	10	M	Arm	3	Excision	None	None	ANED 17
9	46	M	Arm	7	Excision+RT	Lung	Brain/32	AWD 24
10	11	M	Thigh	3	CT+Excision	None	None	ANED 16
11	28	M	Thigh	'Very large'	CT	Lung+brain	None	DOD 30
12	3	F	Arm	7	ILPC+Excision	Lung	Multiple sites	DOD 54
13	31	F	Cervix	3	Excision	None	None	ANED 36
14	14	F	Arm	5	Excision+RT	None	None	ANED 12
15	22	F	Thigh	7	Excision+RT	None	lung+brain/7	DOD 57
16	24	M	Foot, cuboid bone	3	Below Knee Amp. + metasteses ectomy	Lung	None	ANED 185
17	24	M	Thigh	4	Excision+RT	None	None	ANED 122
18	35	F	Thigh	8	CT+Excision	Lung	None	AWD 185

RT radiotherapy, *CT* chemotherapy, *Amp* amputation, *AWD* alive with disease, *DOD* died of disease, *ANED* alive with no evidence of disease, *ILPC* isolated limb perfusion chemotherapy

TFE3 was detected with Dako LSAB+streptavidin HRP (Dako UK Ltd, Ely, UK) and visualised with Dako DAB (Dako UK Ltd, Ely, UK) as per manufacturer's instructions.

Nuclear staining was recorded as negative or positive (+ to +++, depending on intensity) and as focal or diffuse.

Results

Data regarding patient age, sex, tumour site and size, treatment and follow-up are summarised in Table 1. RT-PCR analysis and immunohistochemistry data are summarised in Table 4.

Clinical data

Of the 18 patients, ten were female and eight male, and ages ranged from 3 to 46 years (median 23 years). All but one tumour involved the extremities and limb girdles; ten, the lower and seven, the upper extremities. One tumour within the pelvis involved the uterine cervix. One of the extremity tumours was intraosseous involving the cuboid bone of the right foot. The tumours ranged in size from 2 to 18 cm in largest diameter, median 6 cm.

After a diagnostic biopsy, all but two patients received curative surgical resections. One patient (case 12) received preoperative isolated limb perfusion chemotherapy (ILPC). Postoperative radiotherapy was given to ten patients. One patient (case 18) developed a local recurrence 15 years after primary surgery. Four patients received chemotherapy, three of whom had metastatic disease. Seven patients had lung metastases at diagnosis and three developed lung and/or brain metastasis later. At follow-up, four patients were dead of metastatic disease after 1–5 years, four were alive with metastases after 2–15 years, and ten were alive and well after 1–10 years.

Histologic features

Core needle or open surgical biopsies were reviewed in all cases and resection specimens in all but one case. Eleven tumours had the classical appearance of ASPS: large, rounded or polygonal tumour cells with eosinophilic granular or vacuolated cytoplasm and one or more vesicular nuclei forming distinct nests often with central necrosis or loss of cohesion, causing a pseudoalveolar appearance (Fig. 1a–c). Seven tumours had entirely or predominantly divergent histologic features making the diagnosis less obvious. Three tumours had a solid growth pattern lacking the typical alveolar architecture and presented with a

Table 2 Summary of RT-PCR findings and TFE3 immunohistochemistry in 25 non-ASPS controls

Case	Diagnosis	B-2-microglobulin positive control primer pair	Two ASPL/TFE3 type-specific primer pairs	TFE3 immuno
1	Atypical granular cell tumour	Pos.	Neg.	Pos. +++ diffuse
2	Granular cell tumour	Pos.	Neg.	Pos. +++ diffuse
3	Malignant granular cell tumour	Pos.	Neg.	Pos. +++ diffuse
4	Granular cell tumour	Pos.	Neg.	Pos. +++ diffuse
5	Malignant melanoma	Pos.	Neg.	Neg.
6	Malignant melanoma	Pos.	Neg.	Neg.
7	Metastatic renal cell carcinoma	Pos.	Neg.	Neg.
8	Metastatic renal cell carcinoma	Pos.	Neg.	Neg.
9	Metastatic sarcomatoid renal cell carcinoma	Pos.	Neg.	Neg.
10	Ovarian carcinoma	Pos.	Neg.	Neg.
11	Synovial sarcoma	Pos.	Neg.	Neg.
12	Synovial sarcoma	Pos.	Neg.	Neg.
13	Ewing's sarcoma	Pos.	Neg.	Neg.
14	Ewing's sarcoma	Pos.	Neg.	Neg.
15	Ewing's sarcoma	Pos.	Neg.	Neg.
16	Alveolar rhabdomyosarcoma	Pos.	Neg.	Neg.
17	Extraskeletal myxoid chondrosarcoma	Pos.	Neg.	Neg.
18	Extraskeletal myxoid chondrosarcoma	Pos.	Neg.	Neg.
19	Clear cell sarcoma	Pos.	Neg.	Neg.
20	Myxoid liposarcoma	Pos.	Neg.	Neg.
21	Adrenal cortical carcinoma	Pos.	Neg.	Pos. +++ diffuse
22	Hepatocellular carcinoma	Pos.	Neg.	Neg.
23	Hepatocellular carcinoma	Pos.	Neg.	Neg.
24	Paraganglioma	Pos.	Neg.	Neg.
25	Paraganglioma	Pos.	Neg.	Neg.

striking clear cell appearance, closely resembling metastatic clear cell carcinoma, particularly renal cell carcinoma (Fig 1d). Three tumours, also lacking the alveolar pattern, were characterised by tumour cells forming small solid nests and anastomosing cords resembling hepatocellular carcinoma (Fig 1e). Another tumour, also lacking the typical alveolar pattern, showed focally a prominent cytologic pleomorphism, including very large hyperchromatic nuclei (Fig. 1f, g) and multinucleated tumour giant cells, as well as clear cell features. The tumour involving the cuboid bone of the foot was almost entirely intraosseus with only a small area of cortical breakthrough (Fig 1c).

Vascular tumour invasion was a prominent feature in 13 cases. PAS-positive, diastase-resistant rod-shaped cytoplasmic crystals were seen in six of eight cases in which such stains were available. Electron microscopy performed on three cases (cases 11, 12, and 13) identified the typical membrane-bound crystals.

RT-PCR analysis

RNA was successfully extracted from all 18 ASPS and 25 control FFPE tissue samples. In all cases, RT-PCR generated 133 bp amplicons using β-2-microglobulin-specific primers. RNA extracted from all six corresponding ASPS fresh frozen tissue samples generated 652 bp amplicons using β-actin-specific primers.

All 18 ASPS contained a fusion transcript; nine were type 1 and nine were type 2, as determined by RT-PCR and DNA sequencing of the PCR products (Fig 2). Table 4 shows the data relating to transcript variant detection for each case.

Table 3 RT-PCR primer sequences used for FFPE and fresh frozen tissue

P/F	Fusion product	Primers		F/R	Primer Sequence	Amp size	Ann, °C	Cycle no
P	ASPL/TFE3 type 1	ASPL P1	TFE3 P1	F	CCAAGCCAAAGAAGTCCAAG	120/225 (type 1/2)	57	40
				R	CAAGCAGATTCCCTGACACA			
P	ASPL/TFE3 type 2	ASPL P2	TFE3 P2	F	GCCAAAGAAGTCCAAGTCG	130	57	40
				R	GGACTCCAGGCTGATGATCT			
F	ASPL/TFE3	ASPL	TFE3	F	AAAGAAGTCCAAGTCGGGCCA	195/300 (type 1/2)	62	40
				R	CGTTTGATGTTGGGCAGCTCA			
P	TFE3/ASPL type 1	TFE3 P1	ASPL P1	F	ACTGCAGCTCCCCAGCAC	121	59	40
				R	AAAGAACTCATCAGGCAGCTC			
P	TFE3/ASPL type 2	TFE3 P2	ASPL P2	F	GAGAACCCAACGCGCTAC	112	58	40
				R	GCAGCCGCTCCTCCAGGT			
F	TFE3/ASPL type 1	TFE3F1	ASPLR	F	TTGATGATGTCATTGATGAGATC	218	57	40
				R	CACCGTCAGCTCAAAGAACTC			
F	TFE3/ASPL type 2	TFE3F2	ASPLR	F	GCTCAAAAGCCAACCCTTAC	697	57	40
				R	CACCGTCAGCTCAAAGAACTC			
P	β-2-microglobulin	β-2-microglobulin control		F	CTCGCGCTACTCTCTCTTTCT	133	60	40
				R	TGTCGGATTGATGAAACCCAG			
P	β-actin	β-actin control		F	ATCACCATTGGCAATGAGCG	98	53	40
				R	TTGAAGGTAGTTTCGTGGAT			
F	β-actin	β-actin control		F	CACCCACACTGTGCCCATC	652	62	35
				R	CTAGAAGCATTTGCGGTGGAC			

P/F primers for use with paraffin wax embedded or frozen tissue, *F/R* forward or reverse primer, *Amp size* amplicon size in base pairs, *Ann* °*C* annealing temperature, *PCR* cycle no

A reciprocal fusion transcript was detected in four of the type 2 ASPS (cases 3, 6, 15, and 17) using RNA extracted from paraffin tissue; two of these were confirmed by frozen tissue RNA extracts. The sequencing was matched to TFE3 within exon 4/ASPL exon 8 in three out of the four cases [15]. The fourth case lacked a further 15-bp fragment from TFE3 at the breakpoint (Fig 3).

No PCR amplicon was generated with ASPL/TFE type 1 or type 2 specific primers in the 25 FFPE tissue control cases (Table 2), i.e. primer specificity was 100%.

Immunohistochemistry

All 18 ASPS showed strong (+++) nuclear immunostaining, diffusely in 13 cases and focally in five cases (at least 50% of the tumour cells; Table 4; Fig 1h).

Four granular cell tumours, including a malignant case, as well as one metastatic adrenal cortical carcinoma showed strong nuclear staining (Fig 1i); all of these were negative for the fusion transcript. All other tumours tested were negative with anti-TFE3 (Table 2).

Discussion

ASPS is a very rare type of malignancy, estimated to constitute only 0.5% of all soft tissue sarcomas [19]. This corresponds well with our finding of only 15 cases at the Royal Orthopaedic Hospital, Birmingham, in a 15-year period, during which more than 3,500 soft tissue sarcomas were diagnosed and treated. The prominent predilection for the soft tissues of the extremities in our series (16/18) is likely a reflection of the fact that most patients were adults and that we are not involved in the treatment of head and neck tumours, which is the most common site for ASPS in children [2, 19].

The involvement of the uterine cervix, as seen in one of our cases, is unusual, although the uterine cervix is the most common site when ASPS occur in the female genital tract [3]. Our patient had a fairly early detection due to bleeding of a 3-cm tumour and is currently well after 3 years without evidence of disease. Interestingly, most cervical ASPS have been reported to be relatively small and to follow a less aggressive course than extremity and head and neck tumours [3].

Another rare site seen in this series was the primary involvement of the cuboid bone of the foot. Primary ASPS of bone is exceedingly rare; only ten cases have been reported [8, 9, 20–22] of which only one was confirmed by ASPL-TFE3 fusion transcript detection [8]. All previous cases involved the long bones of the lower extremities or the pelvis and mostly occurred in young adults. Of the reported eight cases of ASPS of bone with follow-up, six

Table 4 Summary of RT-PCR analysis, sequencing and immunohistochemistry in 18 ASPS

Case No	FFPE Tissue	Frozen Tissue	Transcript On FFPE	Transcript On Frozen	Reverse Transcript	TFE3 Immuno
1	Y	N	Type 1	N/A	Neg	Pos. +++ diffuse
2	Y	Y	Type 1	Type 1	Neg	Pos. +++ focal
3	Y	Y	Type 2	Type 2	Pos	Pos. +++ focal
4	Y	Y	Type 1	Type 1	Neg	Pos. +++ diffuse
5	Y	N	Type 1	N/A	Neg	Pos +++ diffuse
6	Y	Y	Type 2	Type 2	Pos	Pos +++ focal
7	Y	N	Type 2	N/A	Neg	Pos. +++ diffuse
8	Y	Y	Type 1	Type 1	Neg	Pos. +++ diffuse
9	Y	N	Type 2	N/A	Neg	Pos. +++ diffuse
10	Y	N	Type 1	N/A	Neg	Pos. +++ diffuse
11	Y	N	Type 1	N/A	Neg	Pos. +++ diffuse
12	Y	N	Type 2	N/A	Neg	Pos. +++ focal
13	Y	N	Type 1	N/A	Neg	Pos. +++ diffuse
14	Y	Y	Type 2	Type 2	Neg	Pos. +++ diffuse
15	Y	N	Type 2	N/A	Pos	Pos. +++ focal
16	Y	N	Type 2	N/A	Neg	Pos. +++ diffuse
17	Y	N	Type 2	N/A	Pos	Pos. +++ diffuse
18	Y	N	Type 1	N/A	Neg	Pos. +++ diffuse

Y yes (available), *N* no (not available) *N/A* not applicable (RT-PCR not carried out)

had lung or brain metastases at presentation or developed such after a short period. Our patient presented with two lung metastases, successfully removed, and is alive after 15 years.

The clinical course in our series illustrates the low tendency of ASPS for local recurrence (only 1/16 resected tumours) and high incidence of metastatic disease, particularly to the lungs and brain (9/18 had metastatic spread at diagnosis or subsequently developed metastases). In our series, all cases were diagnosed due to symptoms from the primary tumour, but it is not unusual that metastases are detected prior to the finding of a primary [2].

Poor prognostic factors have been reported to include older patient age and larger tumour size and of course metastatic disease at presentation [2, 19]. In our series, the ten patients who are alive without evidence of disease were somewhat younger than the eight who died of disease or are alive with metastatic disease, and the former group had significantly smaller tumours (8/10 had tumours 5 cm or less compared to 8/8 having tumours of 7 cm or more). Morphologic features seem to have no prognostic significance [2, 19]. For instance, striking pleomorphism has not been associated with a more aggressive behaviour (our patient with a pleomorphic ASPS is alive and well after 4½ years). Interestingly, detection of vascular invasion, a very common finding in ASPS, seems to be associated with metastatic disease in our series. Nine of 13 patients with vascular invasion had metastatic disease as compared with only one of five patients, in whom vascular invasion was not detected.

ASPS has been described as remarkable among soft tissue sarcomas in that its microscopic appearance varies so little from case to case [2]. When presenting in a typical clinical setting and with the classical morphology, the diagnosis is therefore usually uncomplicated despite its rarity. However, when presenting at unusual sites such as in visceral organs or bone, or when presenting as a metastasis prior to the detection of the primary tumour, diagnostic problems may arise. Difficulties are further confounded by the occurrence of rare morphologic variants. In this series, seven of the 18 cases showed predominantly or partly unusual features including solid non-alveolar patterns with clear-cell features, virtually indistinguishable from metastatic renal cell carcinoma, as well as cording and trabecular patterns resembling metastatic hepatocellular carcinoma, adrenal cortical carcinoma and melanoma. Another case, as mentioned above, also lacked the alveolar pattern and showed a striking pleomorphism. Other variants described

Fig 1 **a**, **b** ASPS with the typical organoid and pseudoalveolar arrangement of tumour cells. **c** ASPS primary in the cuboid bones of the foot. **d** ASPS with prominent clear cell features, closely simulating renal cell carcinoma of clear cell type. **e** ASPS showing a cording, trabecular, hepatoid growth pattern. **f**, **g** ASPS showing marked pleomorphism. **h** Nuclear TFE3 immunostaining of ASPS, note vascular invasion. **i** Lymph node metastasis of malignant granular cell tumour with strong nuclear TFE3 positivity

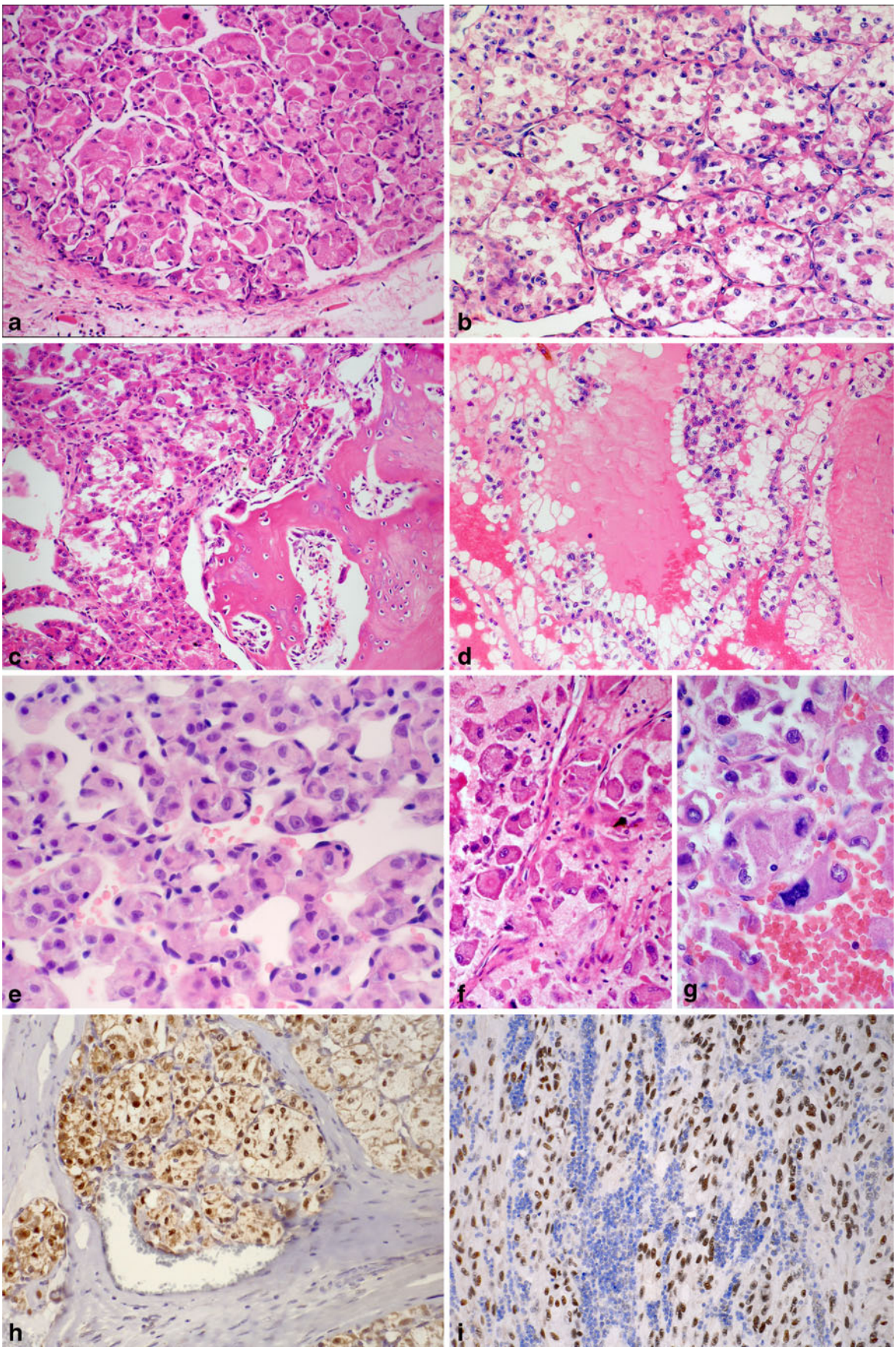
a
b
c
d
e
f
g
h
i

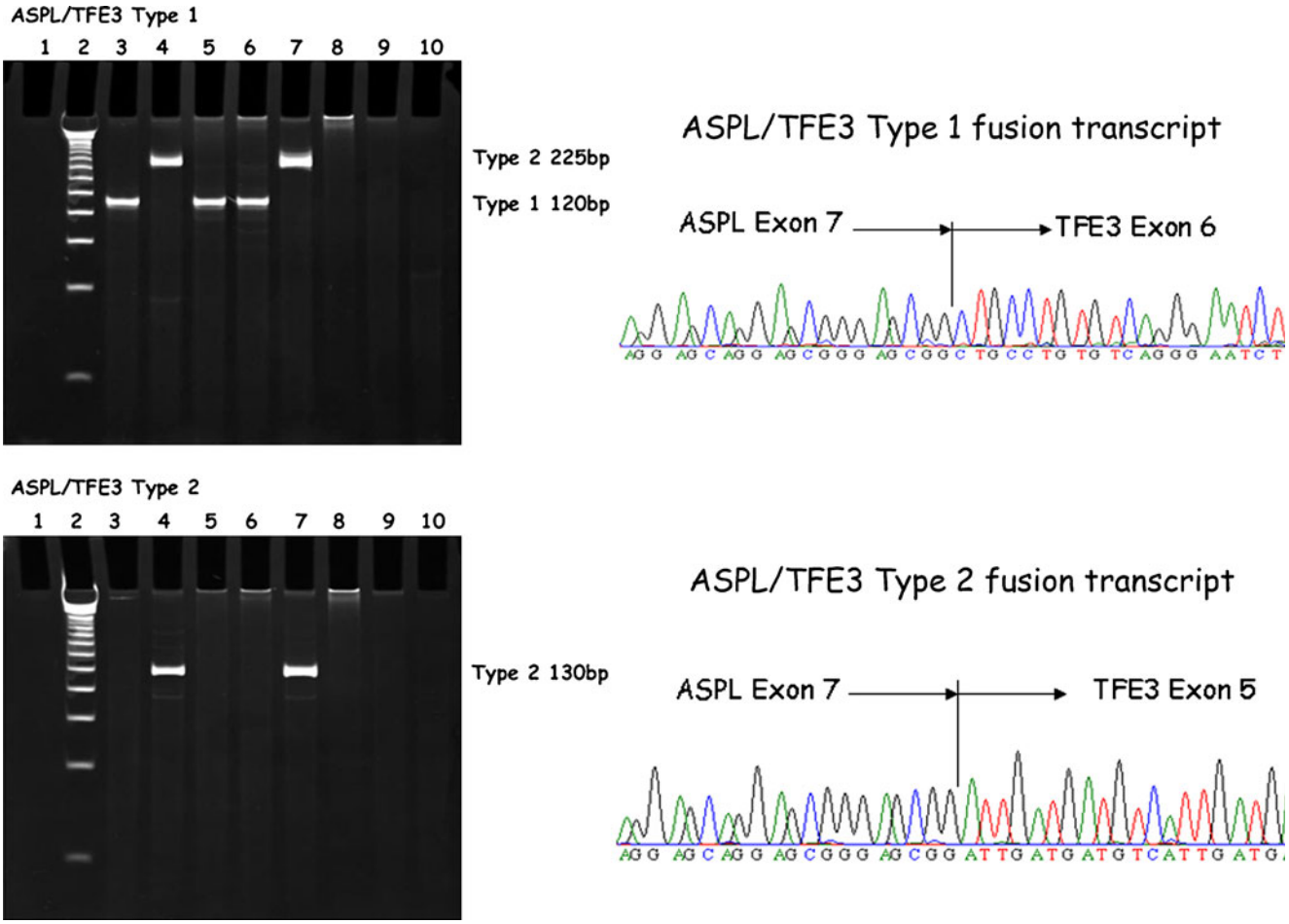

Fig. 2 PCR products using ASPL/TFE3 type 1 and ASPL/TFE3 type 2 primers run on a 10% polyacrylamide gel. *Lane 1*=H_2O negative control, *lane 2*=25 bp marker, *lane 3*=ASPL/TFE3 type 1 sample, *lane 4*=ASPL/TFE3 type 2 sample, *lanes 5* and *6*=ASPL/TFE3 type 1 samples, *lane 7*=ASPL/TFE3 type 2 sample, *lane 8*=granular cell tumour control, *lane 9*=metastatic carcinoma control, *lane 10*=Ewing's sarcoma control. To the *right* of the gels is an example of ASPL/TFE3 type 1 and ASPL/TFE3 type 2 DNA sequences

in the literature include cases with focal myxoid change, extensive cystic and haemorrhagic change, cases with prominent lymphocytic infiltrate and cases with xanthomatous change [2, 6].

With the exception of the characteristic PAS-positive intracytoplasmic crystals seen in many cases, there was previously no unique marker for ASPS. The discovery of an unbalanced X;17 translocation resulting in a fusion of the ASPL gene on chromosome 17 to the TFE3 gene on chromosome X as well as the immunodetection of the C terminus of the TFE3 in ASPS therefore signifies a diagnostic breakthrough [13, 16]. In 2001, Ladanyi et al. [13] and Argani et al. [15] identified the fusion transcripts resulting from the t(X;17)(p11.2;q25) occurring in both ASPS and a subset of paediatric papillary renal carcinomas [23, 24]. Ladanyi et al. [13] reported 12 ASPS, all showing type 1 (nine cases) or type 2 (three cases) fusion transcripts. In a study of 16 ASPS, Pang et al. were only able to detect ASPL/TFE3 fusion transcripts in 11 cases (seven, type 1; four, type 2) [25]. The reason for this is probably the fact that they used the original primers reported by Ladanyi et al., designed for frozen material. Our findings of type 1 and type 2 transcripts in all our 18 cases confirm the

Fig. 3 Reciprocal TFE3-ASPL fusion transcripts detected in four ASPS type 2. One case had 15 fewer bases from TFE3 at the breakpoint

identification of these transcripts as highly sensitive markers of ASPS. Our findings further illustrate a probably equal incidence of the type 1 and 2 variants. Neither previous reports nor our larger series show any differences in terms of clinical setting, morphology or behaviour correlating to the fusion transcript types.

Since we had only frozen tissue available in six cases, we designed new sets of primers for RT-PCR analysis to work on formalin-fixed, paraffin-embedded material, identifying amplicons of 120 and 130 bp for the type 1 and type 2 fusion transcripts, respectively. In the six cases in which we had frozen tissue available, our findings were confirmed by using the primers originally described by Ladanyi et al. [13]. Primers developed by Aulmann et al. [14] for FFPE tissue, having a similar size and position to our own, were published after we had designed our own.

Interestingly, the X;17 translocation in ASPS has been described as an unbalanced chromosomal translocation in contrast to a balanced translocation in the paediatric renal carcinomas [15]. We, however, found that four of the nine ASPS with type 2 transcripts had a reciprocal fusion transcript, and in two of the cases confirmed, also in fresh frozen material. DNA sequencing of the PCR product was matched to TFE3 within exon 4/ASPL exon 8, also described in renal cell carcinoma by Argani et al. [15] in three out of our four cases (the fourth case lacked a further 15-bp fragment from TFE3 at the breakpoint). It is noteworthy that Ladanyi et al. [13] also observed one of their 12 ASPS to have a reciprocal fusion transcript and a further case studied by cytogenetics showed a balanced translocation [26].

The finding of identical fusion genes associated with different tumour types is not unique for ASPS and the subset of paediatric renal cell carcinomas. For instance, expression of the HMGA2-LPP fusion transcript has been identified in lipoma, pulmonary chondroid hamartoma and soft tissue chondroma [27–29]; the ETV6-NTRK3 fusion gene has been found in secretory breast carcinoma, infantile fibrosarcoma, mesoblastic nephroma and acute myeloid leukaemia [30–34]; the FUS-ERG fusion gene has been detected in both acute myeloid leukaemia and Ewing's sarcoma [35, 36] and the EWSR1-ATF1 and EWS-CREB1 fusion genes in clear-cell sarcoma and angiomatoid fibrous histiocytomas [37–40].

In 2003, Argani et al. [16] reported the utility of a polyclonal antibody directed against the C terminus of the TFE3 which, with high sensitivity and specificity, identified tumours with TFE3 gene fusions. Nuclear staining is almost exclusively seen in ASPS and the subset of paediatric renal cell carcinomas characterised by the same fusion transcript. This antibody identifies both fusion variants. Argani et al. [16] studied ten ASPS, all showing strong nuclear staining, while in a huge series of controls only three of eight granular cell tumours and 3/60 adrenal cortical carcinomas showed similar nuclear staining. Our findings of 18/18 ASPS showing strong nuclear staining confirm the very high sensitivity of this marker. Our findings further illustrate that TFE3 immunoreactivity is not entirely specific for ASPS. Thus, one adrenocortical carcinoma metastasis and all four granular cell tumours were positive. The latter finding is of particular importance since especially atypical and malignant granular cell tumours may show overlapping morphological features with ASPS [41].

Antibodies that distinguish ASPL-TFE3 type 1 and type 2 translocations associated protein expression in formalin-fixed, paraffin-embedded tissue have recently been developed but are not yet commercially available [42].

In conclusion, we have demonstrated that immunodetection of TFE3 and RT-PCR-based identification of ASPL/TFE3 fusion transcripts in formalin-fixed, paraffin-embedded tissues are powerful tools in the diagnosis of ASPS, particularly in cases with an unusual clinical setting or morphologic features.

Acknowledgment We thank Hamed Ali for his expert assistance with the figure production.

Conflict of interest statement We declare that we have no conflict of interest.

References

1. Christopherson WM, Foote FW Jr, Stewart FW (1952) Alveolar soft part sarcomas: structurally characteristic tumors of uncertain histogenesis. Cancer 5:100–111
2. Folpe AL, Deyrup AT (2006) Alveolar soft-part sarcoma: a review and update. J Clin Pathol 59:1127–1132
3. Fadare O (2006) Uncommon sarcomas of the uterine cervix: a review of selected entities. Diagn Pathol 1:30
4. Flieder DB, Moran CA, Suster S (1997) Primary alveolar soft-part sarcoma of the mediastinum: a clinicopathological and immunohistochemical study of two cases. Histopathology 31:469–473
5. Yagihashi S, Yagihashi N, Hase Y, Nagai K, Alguacil-Garcia A (1991) Primary alveolar soft-part sarcoma of stomach. Am J Surg Pathol 15(4):399–406
6. Wu J, Brinker DA, Haas M, Montgomery EA, Argani P (2005) Primary alveolar soft part sarcoma (ASPS) of the breast. Int J Surg Pathol 13(1):81–85
7. Liu T-T, Chou Y-H, Lai C-R, Chen C-M, Tsou M-H, Lin H-H, Tiu C-M (1997) Breast mass due to alveolar soft part sarcoma of the pectoris major muscle. Eur J Radiol 24:57–59
8. Aisner SC, Beebe K, Blacksin M, Mirani N, Hameed M (2008) Primary alveolar soft part sarcoma of fibula demonstrating ASPL-TFE3 fusion: a case report and review of the literature. Skeletal Radiol 37:1047–1051
9. Park Y-K, Unni KK, Kim YW et al (1999) Primary alveolar soft part sarcoma of bone. Histopathology 35:411–417
10. Amin MB, Patel RM, Oliveira P et al (2006) Alveolar soft-part sarcoma of the urinary bladder with urethral recurrence: a unique case with emphasis on differential diagnoses and diagnostic utility

of an immunohistochemical panel including TFE3. Am J Surg Pathol 30:1322–1325
11. Weiss SW, Goldblum JR. Enzinger and Weiss's soft tissue tumors fifth edition (2008). Mosby Elsevier 1182-1191
12. Zarrin-Khameh N, Kaye KS (2007) Alveolar soft part sarcoma. Arch Pathol Lab Med 131:488–491
13. Ladanyi M, Lui MY, Antonescu CR et al (2001) The der(17)t (X;17)(p11;q25) of human alveolar soft part sarcoma fuses the TFE3 transcription factor gene to ASPL, a novel gene at 17q25. Oncogene 20:48–57
14. Aulmann S, Longerich T, Schirmacher P, Mechtersheimer G, Penzel R (2007) Detection of the ASPSCR1-TFE3 gene fusion in paraffin-embedded alveolar soft part sarcomas. Histopathology 50:881–886
15. Argani P, Antonescu CR, Illei PB et al (2001) Primary renal neoplasms with the ASPL-TFE3 gene fusion of alveolar soft part sarcoma. A distinctive tumor entity previously included among renal cell carcinomas of children and adolescents. Am J Pathol 159:179–192
16. Argani P, Lal P, Hutchinson B, Lui MY, Reuter VE, Ladanyi M (2003) Aberrant nuclear immunoreactivity for TFE3 in neoplasms with TFE3 gene fusions. A sensitive and specific immunohistochemical assay. Am J Surg Pathol 27(6):750–761
17. Mangham DC, Williams A, McMullan DJ, McClure J, Sumathi VP, Grimer RJ, Davies AM (2006) Ewing's sarcoma of bone: the detection of specific transcripts in a large, consecutive series of formalin-fixed, decalcified, paraffin-embedded tissue samples using the reverse transcriptase-polymerase chain reaction. Histopathology 48:363–376
18. Sorg I, Metzler A (1995) Detection of Borna disease virus RNA in formalin-fixed, paraffin-embedded brain tissues by nested PCR. J Clin Microbiol 33(4):821–823
19. Fletcher CDM, Unni KK, Mertens F (eds) (2002) World Health Organization classification of tumours. Pathology and genetics of tumours of soft tissue and bone, IARC Press
20. Koguchi Y, Yamaguchi T, Yamato M, Osada D, Saotome K (2005) Alveolar soft part sarcoma of bone. J Orthop Sci 10:652–655
21. Durkin RC, Johnston JO (1999) Alveolar soft part sarcoma involving the ilium. Clin Orthop Relat Res 359:197–202
22. Zhu FP, Lu GM, Zhang LJ, Wang JD, An XJ, Dong YC (2009) Primary alveolar soft part sarcoma of vertebra: a case report and literature review. Skeletal Radiol 38(8):825–829
23. Heimann P, Devalck C, Dubusscher C, Sariban E, Vamos E (1998) Alveolar soft-part sarcoma: further evidence by FISH for the involvement of chromosome band 17q25. Genes Chromosom Cancer 23:194–197
24. Hernandez-Marti MJ, Orellana-Alonso C, Badia-Garrabou L, Miralles AV, Paradis-Alos A (1995) Renal adenocarcinoma in an 8-year-old child, with a t(X;17)(p11.2;q25). Cancer Genet Cytogenet 83:82–83
25. Pang LJ, Chang B, Zou H et al (2008) Alveolar soft part sarcoma. A biomarker diagnostic strategy using TFE3 immunoassay and ASPL-TFE3 fusion transcripts in paraffin-embedded tumor tissues. Diagn Mol Pathol 17(4):245–252
26. Uppal S, Aviv H, Patterson F, Cohen S, Benevenia J, Aisner S, Hameed M (2003) Alveolar soft part sarcoma-reciprocal translocation between chromosome 17q25 and Xp11. Report of a case with metastases at presentation and review of the literature. Acta Orthop Belg 69(2):182–187
27. Petit MM, Mols R, Schoenmakers EF, Mandahl N, Van de Ven WJ (1996) LPP, the preferred fusion partner gene of HMGIC in lipomas, is a novel member of the LIM protein gene family. Genomics 36:118–129
28. Rogalla P, Lemke I, Kazmierczak B, Bullerdiek J (2000) An identical HMGIC-LPP fusion transcript is consistently expressed in pulmonary chondroid hamartomas with t(3;12)(q27-28;q14-15). Genes Chromosom Cancer 29:363–366
29. Dahlén A, Mertens F, Rydholm A et al (2003) Fusion, disruption and expression of HMGA2 in bone and soft tissue chondromas. Mod Pathol 16:1132–1140
30. Knezevich SR, Garnett MJ, Pysher TJ, Beckwith JB, Grundy PE, Sorensen PH (1998) ETV6-NTRK3 gene fusions and trisomy 11 establish a histogenetic link between mesoblastic nephroma and congenital fibrosarcoma. Cancer Res 58:5046–5048
31. Knezevich SR, McFadden DE, Tao W, Lim JF, Sorensen PH (1998) A novel ETV6-NTRK3 gene fusion in congenital fibrosarcoma. Nat Genet 18:184–187
32. Rubin BP, Chen CJ, Morgan TW et al (1998) Congenital mesoblastic nephroma t(12;15) is associated with ETV6-NTRK3 gene fusion: cytogenetics and molecular relationship to congenital (infantile) fibrosarcoma. Am J Pathol 153:1451–1458
33. Eguchi M, Eguchi-Ishimae M, Tojo A et al (1999) Fusion of ETV6 to neutrotrophin-3 receptor TRKC in acute myeloid leukemia with t(12;15)(p13;q25). Blood 93:1355–1363
34. Tognon C, Knezevich SR, Huntsman D et al (2002) Expression of the ETV6-NTRK3 gene fusion as a primary event in human secretory breast carcinoma. Cancer Cell 2:367–376
35. Panagopoulos I, Aman P, Fioretos T et al (1994) Fusion of the FUS gene with ERG in acute myeloid leukemia with t(16;21)(p11;q22). Genes Chromosom Cancer 11:256–262
36. Shing DC, McMullan DJ, Roberts P et al (2003) FUS/ERG gene fusions in Ewing's tumors. Cancer Res 63:4568–4576
37. Hallor KH, Mertens F, Jin Y et al (2005) Fusion of the EWSR1 and ATF1 genes without expression of the MITF-M transcript in angiomatoid fibrous histiocytomas. Genes Chromosom Cancer 44:97–102
38. Hallor KH, Micci F, Meis-Kindblom JM et al (2007) Fusion genes in angiomatoid fibrous histiocytoma. Cancer Lett 251:158–163
39. Antonescu CR, Nafa K, Segal NH, Cin PD, Ladanyi M (2006) EWS-CREB1: a recurrent variant fusion in clear cell sarcoma – association with gastrointestinal location and absence of melanocytic differentiation. Clin Cancer Res 12(18):5356–5362
40. Rossi S, Szuhai K, Ijszenga M et al (2007) EWSR1-CREB1 and EWSR1-ATF1 fusion genes in angiomatoid fibrous histiocytoma. Clin Cancer Res 13(24):7322–7328
41. Fanburg-Smith JC, Meis-Kindblom JM, Fante R et al (1999) Malignant granular cell tumor of soft tissue: diagnostic criteria and clinicopathologic correlation. Am J Surg Pathol 23(1):136
42. Vistica DT, Krosky PM, Kenny S, Raffeld M, Shoemaker RH (2008) Immunohistochemical discrimination between the ASPL-TFE3 fusion proteins of alveolar soft part sarcoma. J pediatr hematol/oncol 30:46–52

Virchows Arch (2011) 458:301–312
DOI 10.1007/s00428-010-1017-2

ORIGINAL ARTICLE

Different immunohistochemical and ultrastructural phenotypes of squamous differentiation in bladder cancer

Nadine T. Gaisa · Till Braunschweig · Nina Reimer · Jörg Bornemann · Elke Eltze · Sabine Siegert · Marieta Toma · Luigi Villa · Arndt Hartmann · Ruth Knuechel

Received: 9 October 2010 / Revised: 17 November 2010 / Accepted: 20 November 2010 / Published online: 7 December 2010
© Springer-Verlag 2010

Abstract Besides worse prognosis of bladder cancer with squamous differentiation (pure squamous cell carcinoma (SCC) or mixed urothelial carcinoma (UC/SCC)), high-grade non-keratinising squamous differentiation is difficult to identify in haematoxylin–eosin stainings. This study aims to validate routine immunohistochemical markers for squamous differentiation in a larger cohort of patients. Tissue microarrays of 89 pure SCCs and mixed UC/SCCs, 66 urothelial carcinomas (UC), precursor lesions and normal urothelium were stained for cytokeratin (CK) 5/6, CK 5/14, CK 7, CK 20 and uroplakin III. Electron microscopy was performed to confirm the differentiation. Pure SCCs displayed staining throughout the epithelium for CK 5/6 (76.6% (36/47)) and CK 5/14 (95.8% (46/48)), focal staining for CK 7 (28.9% (13/45)) and no staining for CK 20 and uroplakin III (both 0% (0/48)). UCs exhibited a basal or diffuse staining for CK 5/6 (30.2% (16/53)) and CK 5/14 (57.1% (32/56)), focal positivity for CK 7 (83.6% (46/55)), CK 20 (50.9% (29/57)) and uroplakin III (21.8% (12/55)). Each marker discriminated SCC and UC significantly ($p<0.01$). A third subgroup rarely showed full epithelial staining for CK 5/6 (14.3% (1/7)) and CK 5/14 (28.6% (2/7)), focal staining for CK 7 (85.7% (6/7)) and no staining for CK 20 and uroplakin III (both 0% (0/7)). Electron microscopy could prove both, SCC and UC characteristics, revealing a transient type. A staining pattern with CK 5/6- and CK 5/14-positivity plus CK 20- and uroplakin III-negativity identified squamous differentiation in bladder tumours and revealed a third type of squamous transdifferentiation.

Keywords Squamous cell carcinoma · Bladder · CK 5/6 · CK 5/14 · CK 20 · Uroplakin

N. T. Gaisa · T. Braunschweig · N. Reimer · R. Knuechel (✉)
Institute of Pathology, RWTH Aachen University,
Pauwelsstrasse 30,
52074 Aachen, Germany
e-mail: rknuechel-clarke@ukaachen.de

J. Bornemann
Electron Microscopic Facility, RWTH Aachen University,
Aachen, Germany

E. Eltze
Institute of Pathology Saarbruecken-Rastpfuhl,
Saarbruecken, Germany

S. Siegert
Institute of Pathology LMU Munich,
Munich, Germany

M. Toma
Institute of Pathology, University Dresden,
Dresden, Germany

L. Villa
Division of Nephrology, University Hospital RWTH Aachen,
Aachen, Germany

A. Hartmann
Institute of Pathology, University Hospital Erlangen,
Erlangen, Germany

Introduction

Bladder cancer is the eighth most frequent carcinoma by incidence in men worldwide and the 16th most common cancer in women [1]. In Western countries like Europe, urothelial carcinomas (UC) represent up to 95–97% whereas other histological types are rare (i.e. prevalence of squamous carcinoma <5%) [2]. White Caucasians in the United States display the same distribution (96.2% UC, 0.8% squamous cell carcinomas (SCCs)); African Ameri-

can individuals show a slightly higher prevalence of SCC (90.2% UC, 2.5% SCC). Throughout Africa, UC is still the most frequent type of bladder cancer, but SCC prevalence is enhanced due to the close pathogenetic relation of endemic *Schistosoma haematobium* infection and a course of disease with this type of bladder cancer (Algeria SCC 11.4%, Uganda SCC 6.7%, Zimbabwe SCC 37.8% and Egypt SCC 19.9%). In South Africa, the histology of bladder cancer among white individuals is similar to western countries (2% SCC, 94% UC), whereas in blacks it resembles the overall African prevalence (36% SCC, 41% UCC) [2]. Interestingly, in western countries, up to 50% of poorly differentiated advanced urothelial carcinomas show an additional squamous differentiation component (mixed UC/SCC) [3]. In a study on transurethral resections, this squamous (and/or glandular) differentiation in invasive UCs was associated with advanced tumour stage (>/=pT2 41.2% versus 19.6% pure UC), significantly different recurrence rates (70% versus 42% pure UC), progression rates (35% versus 9.2% pure UC) and mean survival rates (76.5% versus 90.0% pure UC, follow-up period of up to 5 years) [4]. Therefore, a reliable characterisation by histology and immunohistochemistry is important for the further selection of treatment options. However, according to the 2004 World Health Organization classification, the diagnosis of squamous carcinoma is restricted to tumours with complete squamous/keratinous differentiation without any other tumour component including urothelial carcinoma in situ [5]. All tumours with a mixed differentiation are classified as urothelial carcinomas with squamous differentiation (UC/SCC).

Histopathological diagnosis of squamous differentiation is based on the presence of intercellular bridges or keratinisation and can be found in various morphological patterns: (1) nests and cords showing diskeratosis, intercellular bridges and corneous pearls; (2) small foci with intercellular bridges, but no diskeratosis or corneous pearls; (3) additional features suggestive of coilocytosis; (4) occasional intracytoplasmatic lumina in nests of squamous cells and (5) rarely clear cells forming nests of variable size [6]. These features can be recognised easily at haematoxylin–eosin (HE) stains of typically, well- or moderately differentiated SCC with their mainly exophytic or solid appearance, varying necrotic proportions and accompanying squamous epithelial changes (detailed morphological descriptions in [7]). However, for a subset of poor or mixed differentiated tumours, immunohistological verification might be helpful, and antibodies against cytokeratin 14, cytokeratin 19, cytokeratin 10, caveolin 1 or myelomonocytic L1 antigen have been suggested [6]. But so far, no larger evaluation of routinely used immunohistochemical markers for squamous differentiation has been performed. Therefore, the purpose of this study was to evaluate a diagnostically approved immunohistochemical marker panel for squamous differentiation in bladder tumours and to elucidate the different staining patterns in regard to the ultrastructure of the tumours.

Materials and methods

A total of 89 routinely processed formalin-fixed paraffin-embedded (FFPE) cystectomy specimens and transurethral resection biopsies from patients with bladder cancer showing non-schistosoma-associated squamous cell carcinoma (SCC) or urothelial carcinoma with partial squamous differentiation (mixed UC/SCC) were collected in five pathology departments in Germany over the past years. In 39 of the cases, the whole bladder urothelium was sampled for histopathological review, and an absolutely reliable and definite diagnosis of pure squamous differentiation could be performed.

After HE staining and evaluation, tissue microarrays (TMAs) of paraffin-embedded tissue were constructed using Beecher Instruments needles (Beecher Instruments, Sun Prairie, USA) and a self-made positioning system. They include invasive carcinoma (SCC or both parts of mixed carcinomas), normal urothelium, squamous metaplasia and accompanying carcinoma in situ (CIS). Furthermore, TMAs of invasive urothelial carcinomas and corresponding normal urothelium were produced as controls (total patients n=66).

Immunohistochemistry

Immunohistochemistry of TMA slides was performed with DakoAutostainerPlus (Dako, Hamburg, Germany) after heat induced antigen retrieval with low pH citrate buffer (pH 6.0). The following primary antibodies were used: anti-CK 5/6 (D5/16B4, 1:100, Dako), anti-CK 5/14 (XM26/LL002, 1:50, dcs, Hamburg, Germany), anti-CK 7 (OV-TL 2/30, 1:800, Dako) and anti-CK 20 (Ks20.8, 1:200, Dako), all visualized via biotin/streptavidin peroxidase and diaminobenzidine (DAB) method (Dako kit K5001, Dako). Uroplakin III (AU1, 1:10, Progen, Heidelberg, Germany) was detected with Envision polymer and streptavidin peroxidase/DAB (DAKO). Skin/squamous cancers (CK 5/6, CK 5/14), liver/bile ducts (CK7) and normal urothelium (CK 20, uroplakin III) were used as positive controls, respectively. Staining with appropriate isotypic antibodies was used as negative control. Simultaneous cytoplasmatic and membranous staining for all cytokeratins was interpreted as positive. Uroplakin III staining was considered positive only in case of specific membranous staining.

Immunohistochemical stainings were analysed by two independent observers (NTG and MM) according to a

semiquantitative immunoreactive score and the staining patterns shown in Fig. 1 (for CK 5/6 and CK 5/14, Fig. 1) or pattern/judgements according to the literature (CK 7 [8], CK 20 [9], uroplakin III [10]; overview see Table 1). In case of controversial judgements, cores were again reviewed in a two-observer consensus session.

Transmission electron microscopy (TEM)

In six recent cases of unfixed cystectomy specimens (three SCCs and three UCs or mixed UC/SCCs), additional samples of tumour and normal urothelium were fixed in 3% glutaraldehyde (in 0.1 M Soerensen's phosphate buffer [pH 7.4; 13 mM $NaH_2PO_4 \times H_2O$; 87 mM $Na_2HPO_4 \times 2H_2O$]) for 24 h for TEM. For further preparation, they were washed with 0.1 M Soerensen's phosphate buffer overnight, followed by 1 h in 1% OsO_4 (in 17% sucrose buffer [pH 7.4; 88 ml 0.1 M Soerensen's phosphate buffer; 12 ml aqua dest., 17 g sucrose]), rinsed with water and dehydrated with ethanol (30–100%) and propylenoxide (100%). Finally, samples were processed for embedding in Epon, polymerized 8 h at 37°C and 56 h at 60°C, cut into 70–100 nm-thick slices and contrasted with uranyl acetate and lead citrate.

Furthermore, of seven archival FFPE tissues, a paraffin core of the region of interest (identified by comparison of slide and block) was cut out of the block using Beecher Instruments needles. The core was deparaffinized overnight in xylene (100%) and in 3% glutaraldehyde for 24 h. Further processing of samples was identical to fresh tissue (see above).

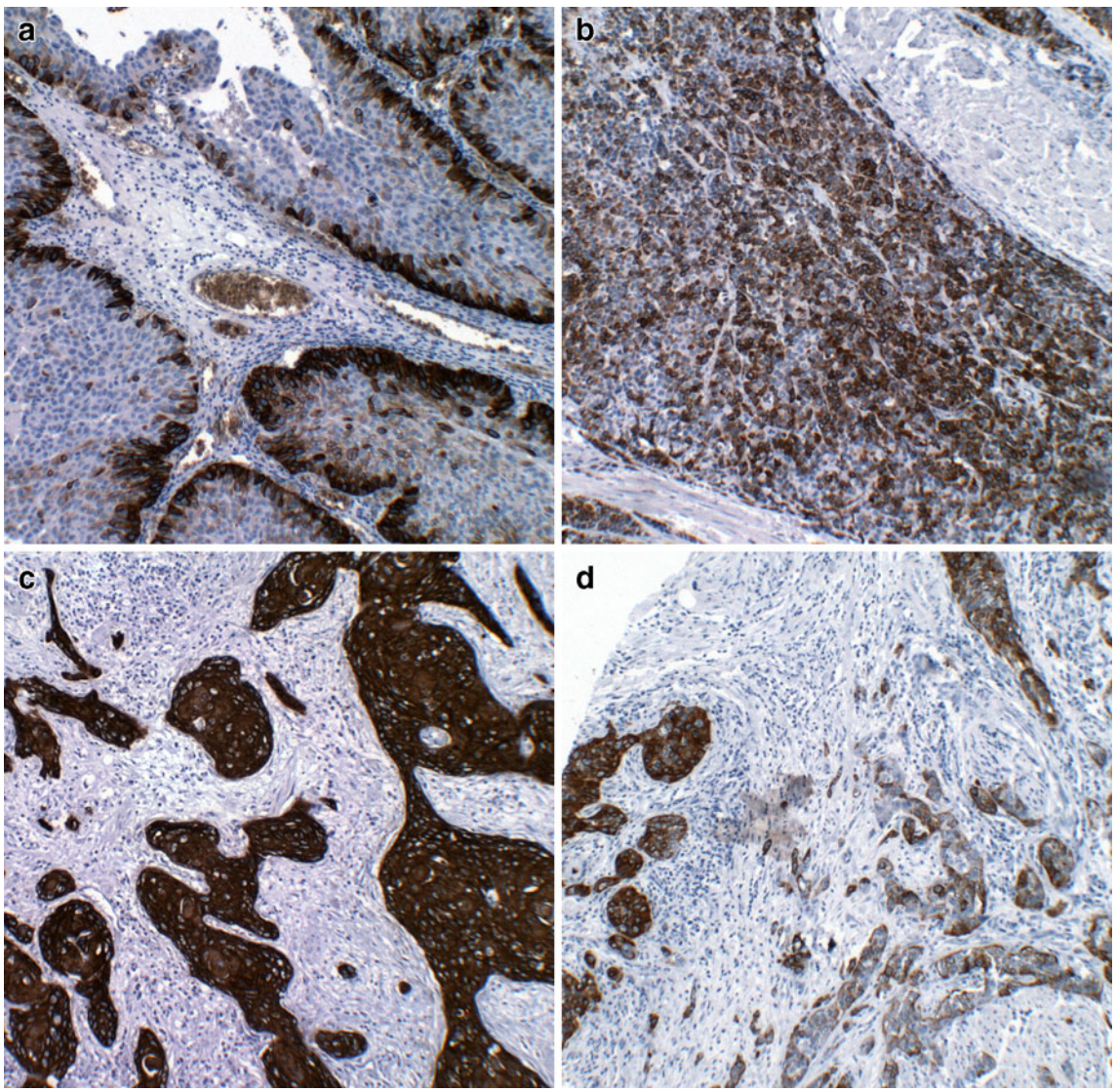

Fig. 1 Staining patterns for CK 5/14; **a** pattern 1=basal staining, **b** pattern 2=diffuse staining, **c** pattern 3=complete/full epithelial thickness staining, **d** typical appearance of mixed tumours with squamous component (*left side*, pattern 3) and urothelial part (right side, pattern 1); original magnifications 100×

Table 1 Definition of the immunohistochemical cutoffs

Staining intensity	% of stained cells	CK 5/6 staining pattern	CK 5/14 staining pattern	CK 7 staining judgement	CK 20 staining judgement	Uroplakin staining judgement
0=negative	0=negative	0=negative	0=negative	0=<5% negative	0=negative	0=negative
1=weak	1=<10%	1=basal	1=basal	1=≥5% positive	1=superficial positive= normal	1=>1% positive
2=medium	2=10–50%	2=diffuse	2=diffuse		2=≤10% weak positive	
3=intense	3=51–80%	3=complete	3=complete		3=>10% positive	
	4=>81%					

Staining intensity, percentage of stained cells and additional pattern (CK 5/6 and CK 5/14) or a staining judgement (CK 7, CK 20 and uroplakin III) were scored for each TMA core and reported as pattern/judgement and product

The samples were analysed with an EM 400 T (Philips, Eindhoven, Netherlands) at 60 kV, and micrographs were taken with a Morada CCD-Camera and analySIS software (both Olympus Soft Imaging Solutions GmbH, Münster, Germany).

Quantitative assessment of desmosomes could be obtained by counting the total number of desmosomes of 10 completely visible cells per case; filaments were assessed semiquantitatively within 10 cells (0=no prominent filaments, 1=single filaments, 2=distinct, prominent filaments).

Statistical analysis

Categorical variables (scores) were expressed as medians± standard deviation (SD), and statistical analysis was performed by non-parametric Kruskal–Wallis test followed by Dunn's multiple comparison post-hoc test. Continuous variables (numbers of desmosomes) were expressed as means±SD, and analysis was performed by ANOVA followed by Bonferroni's post-hoc test. A p value of less than 0.05 was considered as significant and a p value of less than 0.01 as highly significant. SPSS software package (SPSS version 17.0, SPSS Inc., Chicago, IL, USA) and GraphPad Prism version 5 (GraphPad Software Inc.) were used for all analyses.

Results

Immunohistochemistry

After staining procedures TMA slides were read, and only cores with sufficient tissue were counted for statistics (see all results in Table 2).

Immunohistochemistry for CK 5/6 and CK 5/14 revealed a positive staining of the basal cell layer 97.5% and 97.6% of normal urothelium specimens, whereas CK 20 and uroplakin III specifically marked the superficial layers/umbrella cells (75.5% and 86.8% of normal urothelium specimens). CK 7 showed discontinuous patchy staining across the epithelial lining (88.7% of normal urothelium specimens). Squamous metaplasia presented completely positive for CK 5/6 and CK 5/14 (96.8% and 100% of squamous metaplasia specimens, respectively) but was consistently negative for CK 20, uroplakin III and CK 7.

Urothelial carcinoma exhibited either a basal (pattern 1) or a diffuse staining (pattern 2, see Table 1, Fig. 1) for CK 5/6 (pattern 1+2 30.2% of UC specimens) and CK 5/14 (pattern 1+2 57.1% of UC specimens). Staining for CK 7 and CK 20 showed variable positivity (83.6% and 50.9% of UC specimens, respectively). Less frequently, a membranous staining of uroplakin III was observed (21.8% of UC specimens).

Pure SCCs showed a strong positivity of the whole epithelium/tumour for CK 5/6 (76.6% of SCC specimens) and CK 5/14 (95.8% of SCC specimens), as well as a partial, disseminated positivity for CK 7 (28.9% of SCC specimens). Pure SCCs were consistently found negative for CK 20 and uroplakin III.

Mixed differentiated tumours with clearly distinguishable SCC and UC parts presented staining patterns according to the predominant histological phenotype at each core. Squamous or urothelial carcinoma in situ stained correspondent to their invasive counterparts (urothelial CIS only basal cell layer positive for CK 5/6 and CK 5/14, squamous CIS full epithelial positivity for CK 5/6 and CK 5/14). Complete squamous differentiation in invasive carcinoma with concomitant urothelial carcinoma in situ did not show differences in staining compared to pure SCCs (Table 2). A small group of carcinomas with light microscopically and immunohistochemically more urothelial features (rarely staining pattern 3 for CK 5/6 (14.3%) and CK 5/14 (28.6%), 85.7% positivity for CK 7 but negativity for CK 20 as well as uroplakin III (both 0%) (Table 2)) presented a phenotype best fitting to the term "urothelial carcinoma with diffuse squamous transdifferentiation" (third type of squamous differentiation besides

Table 2 Staining results of all antibodies in pattern/judgements for pure UC, normal urothelium, pure SCC, urothelial part of mixed tumours, squamous part of mixed tumours, SCC with urothelial CIS, third group of "urothelial cancers with squamous transdifferentiation", squamous metaplasia, squamous carcinoma in situ and urothelial CIS

	CK 5/6			CK 5/14			CK 20			Uroplakin III			CK 7		
	Pattern	*n*	%	Pattern	*n*	%	Pattern	*n*	%	Pattern	*n*	%	Pattern	*n*	%
UC, *n*=57	0	36		0	20		0	24		0	43		0	9	
	1	14	30.2	1	26	57.1	1	1		1	12	21.8	1	46	83.6
	2	2		2	6		2	3		n.c.	3		n.c.	2	
	3	2		3	4		3	29	50.9						
	n.c.	3		n.c.	1		n.c.	0							
NU, *n*=125	0	2		0	1		0	26		0	15		0	14	
	1	118	97.5	1	120	97.6	1	83	75.5	1	99	86.8	1	110	88.7
	2	0		2	0		2	0		n.c.	11		n.c.	1	
	3	1		3	2		3	1							
	n.c.	4		n.c.	2		n.c.	15							
SCC, *n*=48	0	0		0	0		0	48	100	0	48	100	0	32	
	1	4		1	0		1	0		1	0		1	13	28.9
	2	7		2	2		2	0		n.c.	0		n.c.	3	
	3	36	76.6	3	46	95.8	3	0							
	n.c.	1		n.c.	0		n.c.	0							
UC part of UC/SCC, *n*=24	0	9		0	2		0	19		0	22		0	4	
	1	10	62.5	1	14	86.4	1	0		1	2	8.3	1	6	60
	2	5		2	5		2	3	8.3	n.c.	0		n.c.	14	
	3	0		3	1		3	2							
	n.c.	0		n.c.	2		n.c.	0							
SCC part of UC/SCC, *n*=32	0	0		0	0		0	32	100	0	32	100	0	14	
	1	4		1	2		1	0		1	0		1	6	30
	2	5		2	0		2	0		n.c.	0		n.c.	12	
	3	23	71.9	3	25	92.9	3	0							
	n.c.	0		n.c.	5		n.c.	0							
SCC+Uro CIS, *n*=6	0	0		0	0		0	5	83.3	0	6	100	0	4	
	1	1		1	1		1	0		1	0		1	2	33.3
	2	0		2	0		2	1		n.c.	0		n.c.	0	
	3	5	83.3	3	5	83.3	3	0							
	n.c.	0		n.c.	0		n.c.	0							
UC with diffuse transdiff, *n*=7	0	1		0	0		0	7	100	0	7	100	0	1	
	1	3	71.4	1	3	71.4	1	0		1	0		1	6	85.7
	2	2		2	2		2	0		n.c.	0		n.c.	0	
	3	1		3	2		3	0							
	n.c.	0		n.c.	0		n.c.	0							
Sq-Met, *n*=31	0	0		0	0		0	31	100	0	31	100	0	31	100
	1	0		1	0		1	0		1	0		1	0	
	2	1		2	0		2	0		n.c.	0		n.c.	0	
	3	30	96.8	3	31	100	3	0							
	n.c.	0		n.c.	0		n.c.	0							
Sq CIS, *n*=12	0	0		0	0		0	12	100	0	12	100	0	11	91.7
	1	0		1	0		1	0		1	0		1	1	
	2	1		2	1		2	0		n.c.	0		n.c.	0	
	3	11	91.7	3	11	91.7	3	0							
	n.c.	0		n.c.	0		n.c.	0							

Table 2 (continued)

	CK 5/6			CK 5/14			CK 20			Uroplakin III			CK 7		
	Pattern	*n*	%	Pattern	*n*	%	Pattern	*n*	%	Pattern	*n*	%	Pattern	*n*	%
Uro CIS, *n*=13	0	1		0	0		0	5		0	10		0	2	
	1	10	91.7	1	10	100	1	1		1	3	23.1	1	11	84.6
	2	1		2	1		2	0		n.c.	0		n.c.	0	
	3	0		3	0		3	6	50						
	n.c.	1		n.c.	2		n.c.	1							

Percentage is given only for the presumed typical staining pattern(s) of each entity/differentiation type

UC, pure UC; *NU*, normal urothelium; *SCC*, pure SCC; *UC part of UC/SCC*, urothelial part of mixed tumours; *SCC part of UC/SCC*, squamous part of mixed tumours; *SCC+Uro CIS*, SCC with urothelial CIS; *UC with diffuse transdiff*, third group of "urothelial cancers with squamous transdifferentiation"; *Sq-Met*, squamous metaplasia; *Sq CIS*, squamous carcinoma in situ; *Uro CIS*, urothelial CIS, *n.c.*, not countable cores

pure SCC and mixed tumours with clear UC and SCC parts (UC/SCC), see Fig. 2) and needed further HE and ultrastructural analyses (see "Results" below).

Moreover, we performed a semiquantitative product scoring for CK 5/6 and CK 5/14 (number of stained cells multiplied with score of staining pattern). Both CK 5/6 and CK 5/14 patterns and products significantly ($p<0.01$) discriminated SCC versus UC and UC parts of mixed tumours (UC/SCC). In addition, staining patterns of CK 20, CK 7 and uroplakin III significantly ($p<0.01$) distinguished SCC versus UC (Fig. 3).

Correct SCC classification of CK 5/6 pattern 3 (full epithelial positivity) had a sensitivity/specificity of 76.6%/78.4% whereas pattern 3 for CK 5/14 showed a sensitivity/specificity of 95.8%/72.5%. Correct SCC classification including SCC and SCC as parts of mixed tumours (SCC/UC) showed a sensitivity/specificity of 77.1%/82.8% and 93.8%/80.5% for CK 5/6 and CK 5/14 staining pattern 3, respectively. Sensitivity/specificity calculations for the above-mentioned product scoring showed similar results without enhancement of sensitivity or specificity (numbers not shown).

Electron microscopy

Within the reference set of recent cystectomy specimens (n=2 UCs and n=1 normal urothelium versus n=3 SCCs), SCCs displayed a larger number of desmosomes (SCC mean=16.4±7.7, UC/NU mean=2.3±2.1) and intermediate filaments (SCC median=1±0.5, UC median=0±0.5) (Fig. 4). ANOVA and Kruskal–Wallis tests revealed statistically significant discrimination of SCC versus UC for the numbers of desmosomes and filaments ($p<0.05$). Refixed paraffin samples (n=4) showed slightly enlarged numbers of desmosomes (mean=4.1±4.3) (Fig. 4) and filaments (median=0±0.5), both statistically significant for SCC versus the transdifferentiated subgroup ($p<0.05$) but not for UC versus the transdifferentiated subgroup. In three of the seven primarily refixed cases, no tumour tissue could be obtained after preparation and refixation.

HE evaluation of the transdifferentiated subgroup

All seven carcinomas with "transdifferentiated" immunohistochemical/electronmicroscopical features (see above) were afterwards re-evaluated at complete HE sections. The histological evaluation remained inconclusive, especially in comparison to high-grade urothelial carcinoma (Fig. 5a), and a judgement based on eosinophilic cytoplasm was difficult/not sufficient. The transdifferentiated tumours showed nests or strands of infiltrating tumour cells with large- and medium-sized nuclei, often with nucleolus, and a not clearly separated amphophilic/eosinophilic cytoplasmic background (Fig. 5b, d). However, also typical features of SCC like frequent mitotic figures and single cells with diskeratosis could be found disseminated throughout the tumour (not confined to an area like in UC/SCC). Non-keratinising high-grade SCC (Fig. 5c), in contrast, showed smaller nuclei with dense chromatin, and more separated cells with visible intercellular bridges in high-power magnification as well as clearly defined eosinophilic cytoplasm.

Therefore, HE staining alone is not sufficient for the diagnosis of squamous transdifferentiation in bladder tumours, and additional immunohistochemistry is necessary.

Discussion

The immunohistochemical pattern of full epithelial staining for CK 5/6 and CK 5/14 with parallel negative staining for CK 20 and uroplakin III defined pure squamous carcinoma significantly in this study. Mixed tumours (with clearly distinguishable SCC and UC parts (UC/SCC)) and a third

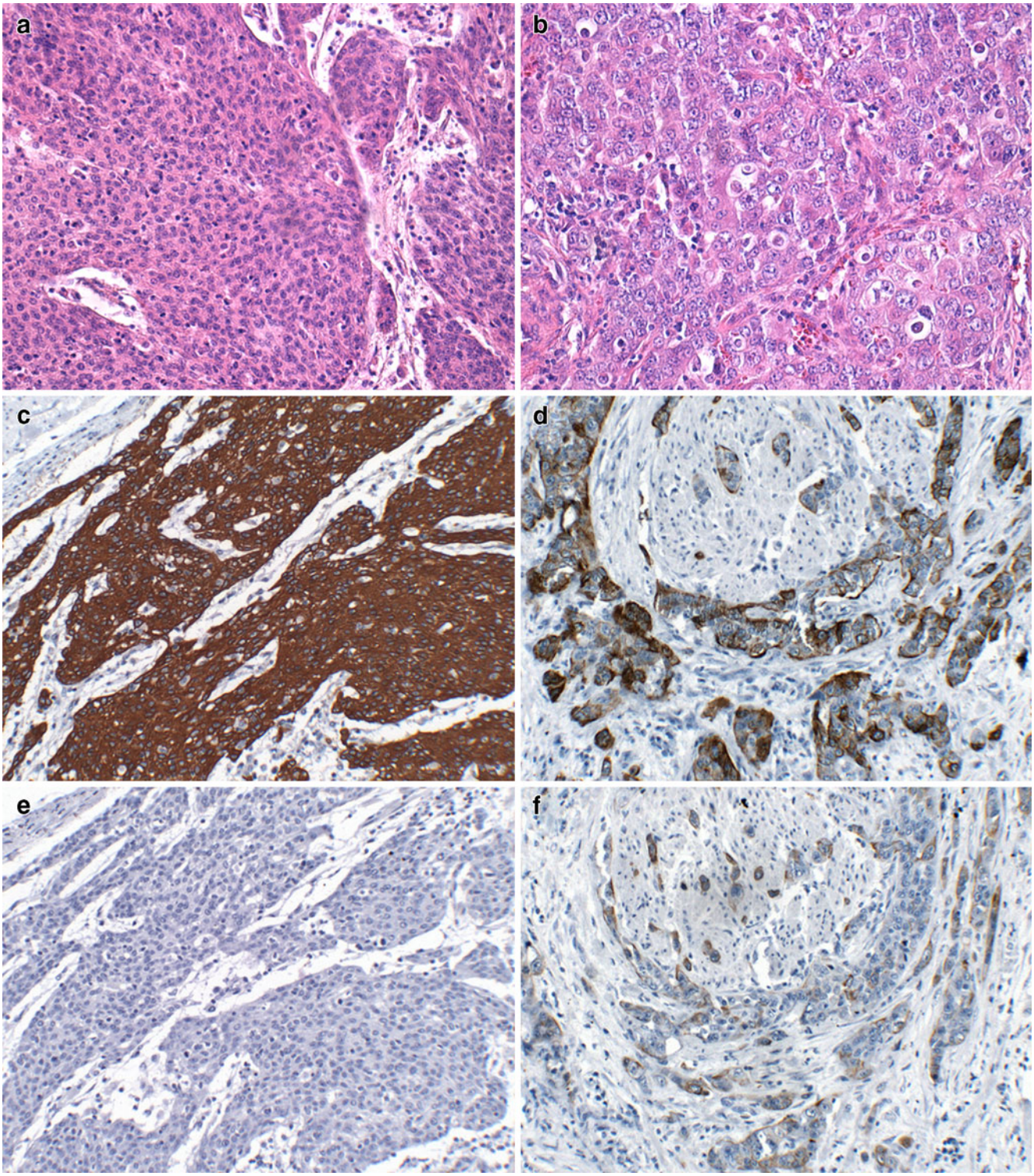

Fig. 2 Staining results for high-grade pure squamous carcinoma (*left column* **a, c, e, g, i**) and urothelial carcinoma with squamous transdifferentiation (*right column* **b, d, f, h, j**). HE stainings of SCC (**a**) and UC with squamous transdifferentiation (**b**), original magnifications 200×. Immunohistochemistry of TMA cores for CK 5/14 (**c**+**d**), CK 7 (**e**+**f**), CK 20 (**g**+**h**) and uroplakin III (**i**+**j**); original magnifications 200×. Staining varies most obviously in the pattern of CK 5/14 (pattern 3=full epithelial height positivity in SCC versus pattern 2=diffuse in UC with diffuse squamous transdifferentiation)

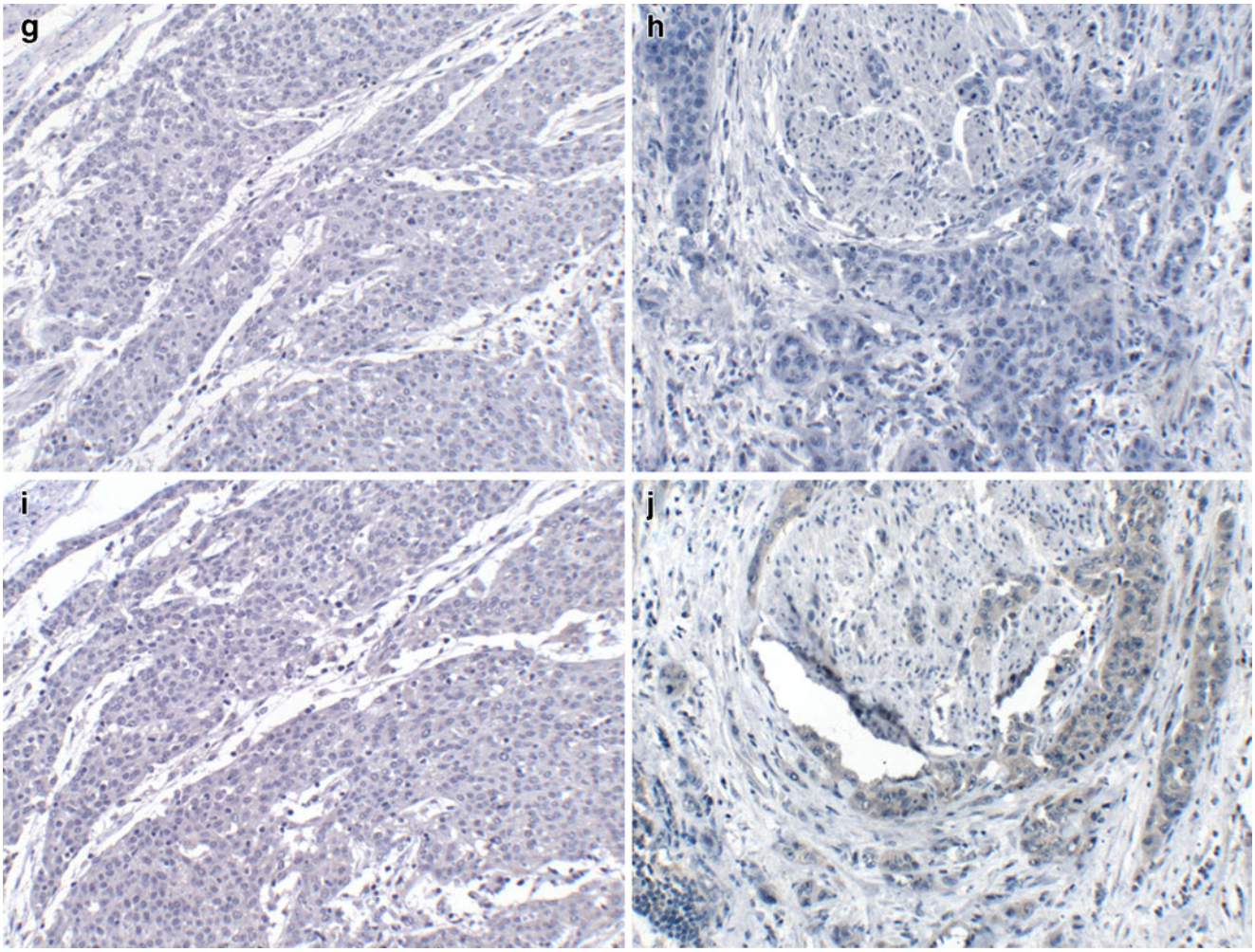

Fig. 2 (continued)

group of tumours with diffuse squamous transdifferentiation could be identified by slightly different immunohistochemical staining patterns and ultrastructural features. Cytokeratin antibodies were selected according to the gel electrophoresis results of normal and malignant urothelium by Moll et al. [11]. CK 10 was not used due to its predominantly staining of suprabasal cells in squamous epithelia and a possible staining failure regarding SCCs with basal cell phenotype. CK 5 and CK 14 are basal type cytokeratins, found in basal layers of multilayered epithelia, myoepithelial cells, Hassall's corpuscles, hair follicles, sebaceous glands and mesothelial cells [12]. CK 14 was also found positive in early stages of squamous differentiation of urothelium [13]. CK 6 is expressed in oral and oesophageal epithelia, hair follicles and occasional glandular cells (other than breast) and epidermis of the palms and soles or hyperplastic areas [12]. CK 7 is not only a widely distributed simple-epithelium type cytokeratin, but expressed as well by normal urothelium and the majority of UCs (88% [8]). CK 20 is a relatively selective marker of superficial cell layers in normal urothelium and positive in more than 75% of urothelial carcinomas [14].

Uroplakins are the most specific markers of terminal differentiation of urothelium because they are part of the asymmetric membrane unit, a special plaque forming plasma membrane complex, stabilizing the apical surface of urothelium during distension of the bladder [15]. The four different uroplakins are membrane proteins localized in all urothelia and are particularly expressed in bladder urothelium (study in cattle, [16]). Uroplakin III clone AU1 is a commercially available monoclonal antibody showing a very high specificity (100%) [17], but due to a high rate of false-negative results in less-differentiated invasive tumours, a low sensitivity (57% [10]) is shown. Therefore, no antibody against uroplakin has been approved for diagnostic purpose so far.

Uroplakin III staining showed less promising results in our study. Only 22% of all UCs showed positive areas, whereas Moll reported up to 53% positive invasive UCs

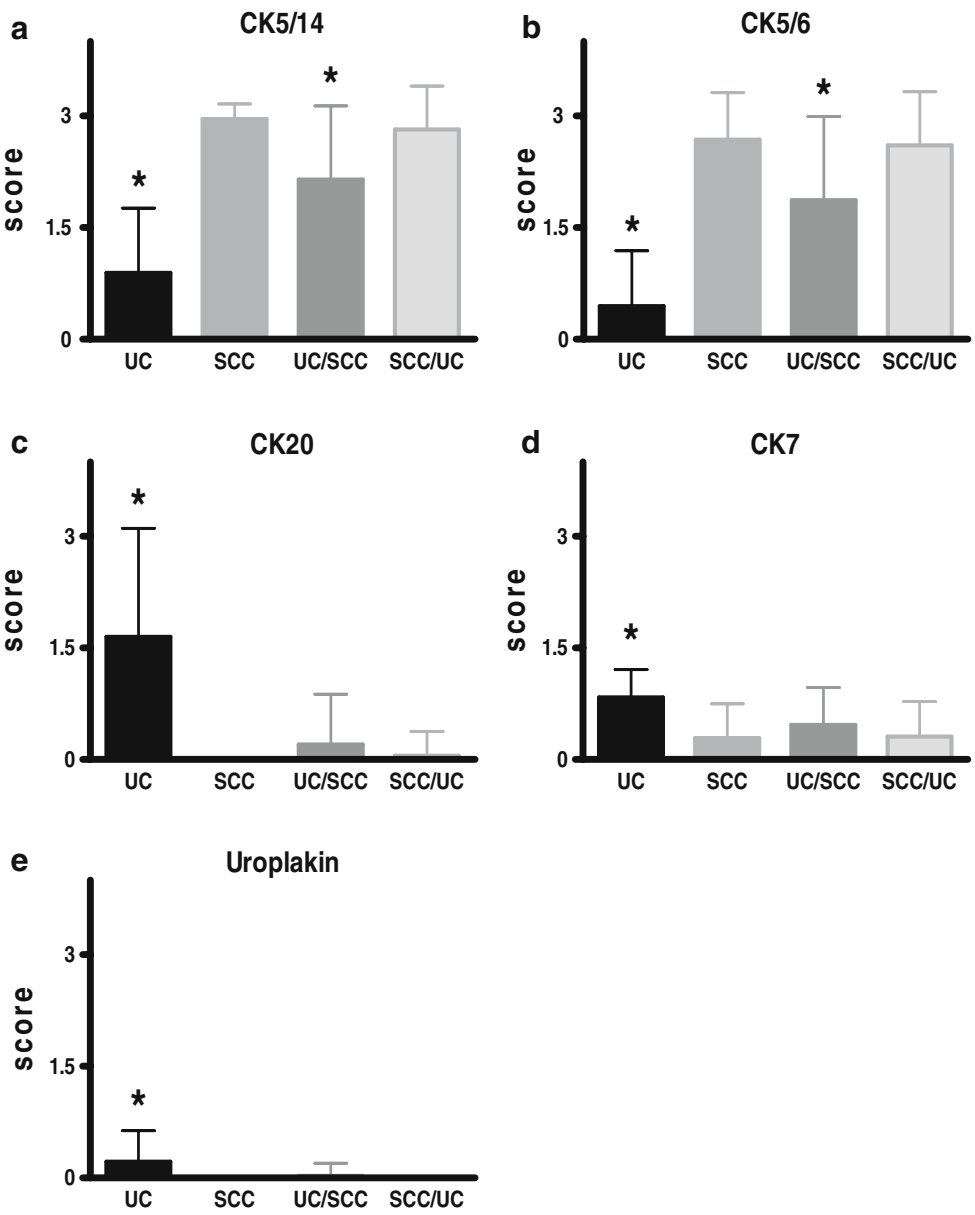

Fig. 3 Graphic view of mean staining patterns of **a** CK 5/14, **b** CK 5/6, **c** CK 20, **d** CK 7 and **e** uroplakin III for UC, SCC, UC part of mixed tumours (named UC/SCC) and SCC part of mixed tumours (named SCC/UC). *Asterisks* point out statistically highly significant ($p<0.01$) differences of entities compared to pure SCC

[17]. All our samples were invasive carcinomas, mainly solid growth without any papillary component. This could explain the lower positivity for uroplakin III in our study. Furthermore, the use of restricted amounts of tissue for microarrays could further reduce the chance to detect a focal positivity for uroplakin III. The loss of uroplakin expression in urothelium is closely linked to the gradual loss of terminal differentiation during experimental carcinogenesis [18]. It was therefore postulated that a complete transformation of UC into SCC or adenocarcinoma has to occur concomitantly with a loss of uroplakin expression [15]. In our study, we observed no staining of uroplakin III in SCCs and in SCC parts of UC/SCCs. These findings confirm the different staining results of bilharzial SCCs and UCs obtained by immunohistochemistry with rabbit antisera against uroplakin II and total uroplakins (mainly uroplakin III/Ib) in 1998 by Wu et al. [19].

In our study, all pure SCCs were strongly positive for CK 5/14 and CK 5/6 while found constantly negative for CK 20. The epithelial staining pattern of CK 5/14 and CK 5/6 showed strong positivity in all cell layers. Therefore, we postulate that complete CK 5/6 and CK 5/14 positivity as well as CK 20 negativity are diagnostic markers for pure squamous differentiation in bladder tumours. This was also reported for CK 14 and CK 20 by Harnden and Southgate [13]. Additionally, they could show that CK 14 detected even clusters of squamous phenotype cells in 47% of tumours without any morphological evidence of squamous

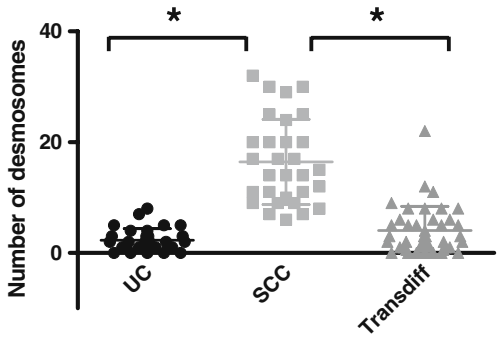

Fig. 4 Boxplots for mean desmosome counts in *UC*, *SCC* and UC with diffuse squamous transdifferentiation (*Transdiff*). *Asterisks* indicate statistically significant ($p<0.05$) differences between SCC and UC as well as SCC and UC with diffuse squamous transdifferentiation

differentiation. They claimed that CK 14 is an early marker of squamous differentiation because CK 14 and its obligatory heterodimer CK 5 are the earliest markers expressed in still non-stratified epidermis in post-gastrulation mouse embryo skin. Due to a partial positivity of CK 14 in UCs, they also proposed the combination of CK 14 positivity and CK 20 negativity for immunohistochemical characterisation of SCCs. The importance of CK 20 negativity in combination with varying expression of other CKs for the diagnosis of squamous carcinomas was further investigated by Suo et al. who found CK 20 negative for all 42 cases of SCC from various locations [20]. Furthermore, two other studies in SCCs and UCs of bladder confirmed the lack of expression of CK 20 in SCCs [14, 21].

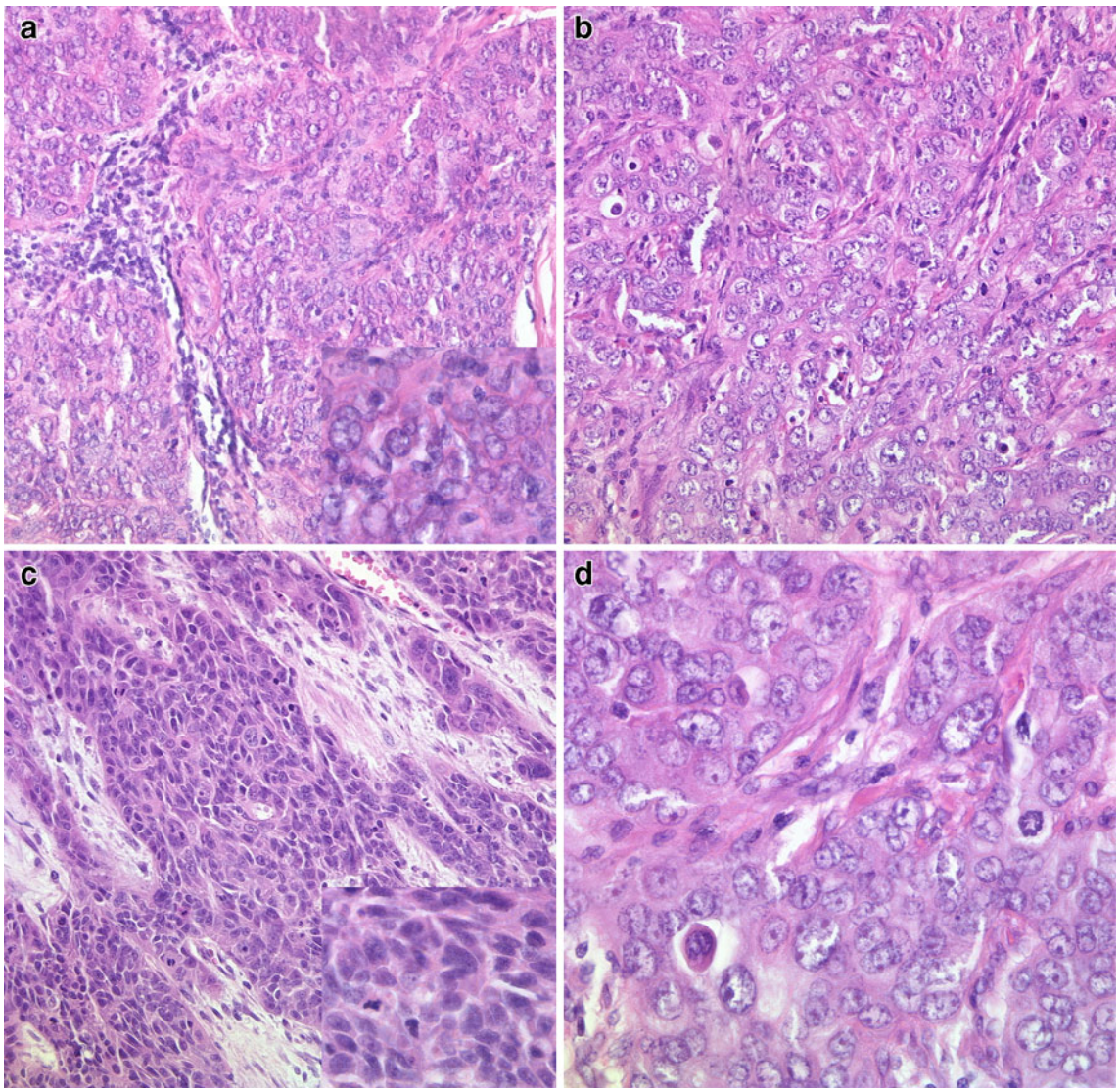

Fig. 5 HE staining of whole tissue sections of high-grade urothelial carcinoma (**a**, original magnification 200×, insert 400×), urothelial carcinoma with squamous transdifferentiation (**b**, original magnification 200×, **d**, original magnification 400×) and high-grade squamous cell carcinoma (**c**, original magnification 200×, insert 400×). The trans-differentiated subgroup mimics both differentiation types with large tumour cells and invisible intercellular bridges (similar to UC) but single signs of diskeratosis and frequent mitotic figures (more SCC phenotype)

Special emphasis in our study was put on the necessity of a positive staining for CK 5/6 and CK 5/14 in all layers of the epithelium (staining pattern 3) for the diagnosis of pure SCC. This is due to the fact that normal urothelium also expresses CK 5/6 (63% [22]) and CK 14 (71% [13]) but mainly restricted to the basal cell layers. None of the previous studies focused on the distribution pattern of cytokeratins to distinguish between pure SCC and UC with squamous differentiation. We observed a basal or rarely diffuse CK 5/6 staining in UCs, which directly reflects the findings of low amounts of cytokeratin 5 also in normal urothelium [23], and a strong uniform expression over all epithelial layers in pure SCCs. In case of partial positivity, some urothelial cells have not undergone squamous differentiation, and according to the WHO classification, these tumours should only be regarded as UC with squamous differentiation (regardless of the extent of squamous areas) [5]. In our study, we could show for the first time that full epithelial height positivity of CK 5/6 and/or CK 5/14 is required in complete squamous differentiation. To confirm this finding, we further investigated a subgroup of tumours with unclear microscopical classification by haematoxylin–eosin stains and a more diffuse staining pattern for CK 5/6 and CK 5/14 than classic UC. We referred them as "UC with diffuse squamous transdifferentiation" and considered these cases as a third distinct group of squamous differentiation in bladder tumours (group 1, pure squamous carcinomas; group 2, UCs with a distinct extent of squamous differentiation and group 3, UCs with diffuse squamous transdifferentiation). This additional type of carcinoma was also described by a mapping study on bladder carcinoma with a squamous phenotype from Sakamoto et al. in 1992 [24]. Besides the different appearances of squamous differentiation in bladder tumours (pure SCC, SCC with urothelial CIS, SCC with pure UC satellite tumours, UC/SCC with lesser extent of UC at the margins, UC/SCC with a big central component of SCC, UC/SCC equally distributed, UC/SCC with only small islands of SCC), they mentioned 10 cases where SCC and UC areas could not be distinguished by light microscopy because of mimicry of each other [24]. In order to evaluate this third type of squamous phenotype and give further proofs on the differences in immunohistochemical staining, we performed TEM. Ultrastructural analysis was done on reference samples of UCs and SCCs as well as refixed pieces of the originally paraffin-embedded material of the samples from group 3. According to Suo et al. [20], squamous differentiation in various carcinomas should display characteristic tonofibrils, tonofilaments and desmosomes. Bundles of tonofibrils, large numbers of desmosomes and wider intercellular spaces with more cytoplasmic projections were associated with well-differentiated SCCs, whereas small quantities of tonofilaments, few desmosomes and aggregates of heterogeneous mitochondria were characteristics of less-differentiated tumours [20].

We could prove with TEM that tumours with diffuse squamous transdifferentiation showed mainly cells with urothelial characteristics and gained only a few more desmosomes. Cells with slightly enhanced numbers of desmosomes were spread throughout the tumour and were not concentrated on a single area. Whether this kind of squamous differentiation is a true phenotype of differentiation or just a transient stage before full squamous transformation is discussed controversial because no cases with longitudinal follow-up were described or available. In our study, this kind of differentiation was observed in large advanced tumours (>3 cm in diameter, ≥pT2) and throughout the whole tumour. Therefore, we favour that it could be an independent subgroup of differentiation. Furthermore, our ultrastructural findings confirmed that pure squamous differentiation requires a complete CK 5/14 and/or CK 5/6 immunohistochemistry staining of all tumour areas and the whole epithelial height.

In conclusion, our study could successfully define a highly significant ($p<0.01$) immunohistochemical marker panel for precise detection of squamous differentiation in bladder cancer specimens (CK 5/6+, CK 5/14+, CK 20−, uroplakin III−). Furthermore, immunohistochemical positivity of all epithelial layers for CK 5/6 and/or CK 5/14 is necessary for the diagnosis of a pure squamous phenotype in bladder cancer. Detailed attention to the staining pattern of CK 5/6 and/or CK 5/14 and ultrastructural analysis revealed three different types of squamous differentiation in bladder tumours (group 1, pure squamous carcinomas; group 2, UC with a distinct extent of squamous differentiation and group 3, UC with diffuse squamous transdifferentiation). A reliable recognition of the subtle squamous transdifferentiation in HE stains is not possible; therefore, immunohistochemistry is recommended for all tumours with mixed appearance or without obvious signs of keratinisation.

Acknowledgement The authors are grateful to Stella Koufou for the sample recruitment and to Marina Molitor as well as Ursula Schneider for the technical support. Furthermore, they like to thank Daniela Smeets, Hiltrud Königs and Rudolf Jung for the excellent sample preparation.

Conflict of interest The authors declare that they have no conflict of interest.

References

1. Ferlay J, Bray F, Pisani P, Parkin DM (2004) GLOBOCAN 2002 cancer incidence, mortality and prevalence worldwide. IARC Cancer Base No 5, version 2.0. IARC, Lyon
2. Parkin DM (2008) The global burden of urinary bladder cancer. Scand J Urol Nephrol 42(Suppl 218):12–20
3. Shanks JH, Iczkowski KA (2009) Divergent differentiation in urothelial carcinoma and other bladder cancer subtypes with selected mimics. Histopathology 54:885–900

4. Erdemir F, Tunc M, Ozcan F, Parlaktas BS, Uluocac N, Kilicaslan I, Gokce O (2007) The effect of squamous and/or glandular differentiation on recurrence, progression and survival in urothelial carcinoma of bladder. Int Urol Nephrol 39:803–807
5. Lopez-Beltran A, Sauter G, Gasser T, Hartmann A, Schmitz-Dräger BJ, Helpap B, Ayala AG, Tamboli P, Knowles MA, Sidransky D, Cordon-Cardo C, Jones PA, Cairns P, Simon R, Amin MB, Tyczynski JE (2004) Infiltrating urothelial carcinoma. In: Eble JN, Sauter G, Epstein JI, Sesterhenn IA (eds) World Health Organization classification of tumors. Pathology and genetics of tumors of the urinary system and male genital organs. IARC press, Lyon, pp 93–109
6. Lopez-Beltran A, Requena MJ, Alvarez-Kindelan J, Quintero A, Blanca A, Montironi R (2007) Squamous differentiation in primary urothelial carcinoma of the urinary tract as seen by MAC387 immunohistochemistry. J Clin Pathol 60:332–335
7. Lagwinski N, Thomas A, Stephenson AJ, Campbell S, Hoschar AP, Eö-Gabry E, Dreicer R, Hansel DE (2007) Squamous cell carcinoma of the bladder: a clinicopathological analysis of 45 cases. Am J Surg Pathol 31(12):1777–1787
8. Chu P, Wu E, Weiss LM (2000) Cytokeratin 7 and cytokeratin 20 expression in epithelial neoplasms: a survey of 435 cases. Mod Pathol 13(9):962–972
9. Harnden P, Mahmood N, Southgate J (1999) Expression of cytokeratin 20 redefines urothelial papillomas of the bladder. Lancet 353:974–977
10. Kaufmann O, Volmerig J, Dietel M (2000) Uroplakin III is a highly specific and moderately sensitive immunohistochemical marker for primary and metastatic urothelial carcinomas. Am J Clin Pathol 113(5):683–687
11. Moll R, Achtstätter T, Becht E, Balcarova-Ständer J, Ittenson M, Franke WW (1988) Cytokeratins in normal and malignant transitional epithelium. Maintenance of expression of urothelial expression features in transitional cell carcinomas and bladder carcinoma cell culture lines. Am J Pathol 132(1):123–144
12. Reis-Filho JS, Simpson PT, Martins A, Preto A, Gärtner F, Schmitt FC (2003) Distribution of p63, cytokeratins 5/6 and cytokeratin 14 in 51 normal and 400 neoplastic human tissue samples using TARP-4 multi-tumor tissue microarray. Virchows Arch 443:122–132
13. Harnden P, Southgate J (1997) Cyokeratin 14 as a marker of squamous differention in transitional cell carcinomas. J Clin Pathol 50:1032–1033
14. Moll R, Löwe A, Laufer J, Franke WW (1992) Cytokeratin 20 in human carcinomas. Am J Pathol 140(2):427–447
15. Ramos-Vara JA, Miller MA, Boucher M, Roudabush A, Johnson GC (2003) Immunohistochemical detection of uroplakin III, cytokeratin 7, and cytokeratin 20 in canine urothelial tumours. Vet Pathol 40:55–62
16. Liang F-X, Bosland MC, Huang H, Romih R, Baptiste S, Deng F-M, Wu X-R, Shapiro E, Sun T-T (2005) Cellular basis of urothelial squamous metaplasia: roles of lineage heterogeneity and cell replacement. JBC 171(5):835–844
17. Moll R, Wu X-R, Lin J-H, Sun T-T (1995) Uroplakins, specific membrane proteins of urothelial umbrella cells, as histological markers of metastatic transitional cell carcinoma. Am J Pathol 147:1383–1397
18. Ogawa K, St John M, Luiza de Oliveira M, Arnold L, Shirai T, Sun TT, Cohen SM (1999) Comparison of uroplakin expression during urothelial carcinogenesis induced by *N*-butyl-*N*-(4-hydroxybutyl)nitrosamine in rats and mice. Toxicol Pathol 27(6):645–651
19. Wu R-L, Osman I, Wu X-R, Lu M-L, Zhang Z-F, Liang F-X, Hamza R, Scher H, Cordon-Cardo C, Sun T-T (1998) Uroplakin II gene is expressed in transitional cell carcinoma but not in bilharzial bladder squamous cell carcinoma: alternative pathways of bladder epithelial differentiation and tumour formation. Cancer Res 58:1291–1297
20. Suo Z, Holm R, Nesland JM (1993) Squamous cell carcinomas. An immunohistochemical study of cytokeratins and involucrin in primary and metastatic tumours. Histopathology 23:45–54
21. Gee JR, Montoya RG, Khaled HM, Sabichi AL, Grossman HB (2003) Cytokeratin 20, AN43, PGDH, and COX-2 expression in transitional and squamous cell carcinoma of the bladder. Urol Oncol 21(4):266–270
22. Chu PG, Weiss LM (2002) Expression of cytokeratin 5/6 in epithelial neoplasma: an immunohistochemical study of 509 cases. Mod Pathol 15(1):6–10
23. Achtstätter T, Moll R, Moore B, Franke WB (1985) Cytokeratin polypeptide patterns of different epithelia of the human male urogenital tract: immunofluorescence and gel electrophoretic studies. J Histochem Cytochem 33(5):415–426
24. Sakamoto N, Tsuneyoshi M, Enjoji M (1992) Urinary bladder carcinoma with a neoplastic squamous component: a mapping study of 31 cases. Histopathology 21:135–141

Virchows Arch (2011) 458:313–322
DOI 10.1007/s00428-010-1030-5

ORIGINAL ARTICLE

Frequent concomitant inactivation of *miR-34a* and *miR-34b/c* by CpG methylation in colorectal, pancreatic, mammary, ovarian, urothelial, and renal cell carcinomas and soft tissue sarcomas

Markus Vogt · Johanna Munding · Martha Grüner · Sven-Thorsten Liffers · Berlinda Verdoodt · Jennifer Hauk · Lars Steinstraesser · Andrea Tannapfel · Heiko Hermeking

Received: 22 July 2010 / Revised: 15 December 2010 / Accepted: 16 December 2010 / Published online: 12 January 2011
© Springer-Verlag 2011

Abstract The microRNA encoding genes *miR-34a* and *miR-34b/c* represent direct p53 target genes and possess tumor suppressive properties as they mediate apoptosis, cell cycle arrest, and senescence. We previously reported that the *miR-34a* gene is subject to epigenetic inactivation by CpG methylation of its promoter region in primary prostate cancer and melanomas, and in 110 different cancer cell lines of diverse origin. Here we analyzed the methylation status of *miR-34a* and *miR-34b/c* in additional primary tumors of divergent sites. We found methylation of *miR-34a* or *miR-34b/c* in formalin-fixed, paraffin-embedded (FFPE) tumor samples from 178 patients with the following frequencies: colorectal cancer (74% *miR-34a*, 99% *miR-34b/c*; $n=114$), pancreatic cancer (64%, 100%; $n=11$), mammary cancer (60%, 90%; $n=10$), ovarian cancer (62%, 69%; $n=13$), urothelial cancer (71%, 57%; $n=7$), and renal cell cancer (58%, 100%; $n=12$). Furthermore, soft tissue sarcomas showed methylation of *miR-34* gene promoters in FFPE samples (64%, 45%; $n=11$), in explanted, cultured cells (53%, 40%; $n=40$), and in frozen tissue samples (75%, 75%, $n=8$). In the colorectal cancer samples a statistically significant correlation of *miR-34a* methylation and the absence of p53 mutation was detected. With the exception of sarcoma cell lines, the inactivation of *miR-34a* and *miR-34b/c* was concomitant in most cases. These results show that *miR-34* inactivation is a common event in tumor formation, and suggest that CpG methylation of *miR-34a* and *miR-34-b/c* may have diagnostic value. The mutual exclusiveness of *miR-34a* methylation and p53 mutation indicates that *miR-34a* inactivation may substitute for loss of p53 function in cancer.

Keywords CpG methylation · p53 · *miR-34a* · *miR-34b/c* · *miR-34* family · Cancer · Epigenetic inactivation

Markus Vogt and Johanna Munding equally contributed to this work

M. Vogt · J. Munding · M. Grüner · S.-T. Liffers · B. Verdoodt · A. Tannapfel · H. Hermeking
Institute of Pathology, Ruhr-University-Bochum,
Bürkle-de-la-Camp-Platz 1,
44789 Bochum, Germany

J. Hauk · L. Steinstraesser
Department of Plastic and Reconstructive Surgery, Department of Hand Surgery, Soft Tissue Tumour Reference Centre, BG University Hospital Bergmannsheil, Ruhr University Bochum,
Buerkle-de-la Camp-Platz 1,
44789 Bochum, Germany

H. Hermeking (✉)
Experimental and Molecular Pathology, Institute of Pathology,
Ludwig-Maximilians-University Munich,
Thalkirchner Str. 36,
80337 Munich, Germany
e-mail: heiko.hermeking@med.uni-muenchen.de

Introduction

In recent years, the important role of microRNAs (miRNAs) in the formation of many types of cancer has become obvious [1, 2]. Although the precise roles they play during carcinogenesis are still being dissected, it is clear that miRNAs can act as tumor suppressors and oncogenes by regulating processes such as proliferation and cell cycle progression, senescence, apoptosis, invasion, and metastasis. miRNAs have been found to be dysregulated in cancer

by DNA copy number changes and epigenetic inactivation, altered processing by the miRNA biogenesis machinery, and transcriptional activation [3]. In particular, the transcription factor and tumor suppressor p53 has been independently shown by several laboratories to directly transactivate the *miR-34a* and *miR-34b/c* genes [4–9]. Ectopic expression of *miR-34* family members induces a G1 arrest, senescence, or apoptosis and inhibits migration and invasion (summarized in [10]). This effect of *miR-34* expression is mediated by down-regulation of numerous important regulatory proteins as, for example, Bcl2, c-MYC, CDK4/6, and c-MET [10]. Therefore, *miR-34* genes may be important mediators of p53 tumor suppressor activity, but may also themselves represent tumor suppressor genes. In fact, *miR-34a* is located on chromosome 1p36, which is frequently deleted in neuroblastoma [11]. *miR-34b* and *miR-34c* are co-transcribed from one transcription unit on chromosome 11q23, which is subject to inactivation by CpG methylation in colorectal cancer (CRC) [12].

Transcriptional silencing by CpG methylation represents an important mechanism for the inactivation of key tumor suppressor genes [13, 14]. Approximately 60% of all genes harbor CpG islands in their promoter region. However, only a portion of these CpG islands display methylation of cytosine at position 5, which is accompanied by inactivation of the surrounding chromatin due to recruitment of histone deacetylases by proteins binding to methylated CpG residues. During development this mechanism is employed to establish and maintain tissue-specific expression patterns. However, during tumor formation aberrant CpG methylation occurs. Similar to genetic mutations, inactivation by CpG methylation is stably inherited to the next cell generation and may therefore allow clonal expansion of a cell population with a selective advantage during tumor progression. Several bona fide tumor suppressor genes are inactivated by CpG methylation [14]. Interestingly, CpG methylation seems to occur early during tumor progression and its detection may therefore be applied to tumor diagnosis and prognosis in the future [15].

We have previously shown that *miR-34a* methylation correlates with down-regulation of *miR-34a* expression in a number of tumor cell lines and primary tumors of different origin [16]. Furthermore, this epigenetic inactivation can be reversed by treatment with 5′-azacytidine and TSA, indicating that it is causally involved in the transcriptional silencing of the *miR-34a* promoter. Interestingly, the CpG-methylation of *miR-34a* was dominant over induction of *miR-34a* by DNA damage, which is mediated by p53 [16]. Therefore, it is conceivable that *miR-34* methylation is an early event in tumor formation that may cancel or at least diminish the p53 response to oncogene-induced DNA damage, which occurs in pre-cancerous lesions [17].

We previously reported that *miR-34a* expression is silenced in 110 cancer cells lines and two different types of primary cancers due to aberrant CpG methylation of its promoter [16]: CpG methylation of the *miR-34a* promoter was detected in breast (6/24, 25%), lung (7/24, 29.1%), colon (3/23, 13%), kidney (3/14, 21.4%), bladder (2/6, 33.3%), and pancreatic (3/19, 15.7%) carcinoma lines, as well as in melanoma cell lines (19/44, 43.2%). Furthermore, 19 out of 24 (79.1%) primary prostate carcinomas displayed CpG methylation of the *miR-34a* promoter and concomitant loss of *miR-34a* expression. Also primary melanoma (20/32 samples, 62.5%) showed methylation of *miR-34a*. To extend these findings to other tumor types and to expand the number of primary tumors analyzed, we used methylation-specific PCR to determine the methylation status of *miR-34a* and *miR-34b/c* in seven primary carcinoma entities and in soft tissue sarcomas. Furthermore, we analyzed whether *miR-34* promoter methylation preferentially occurs in tumors expressing wild-type p53 and correlates with clinical parameters. The results presented here confirm the inactivation of *miR-34* genes as a common hallmark of diverse tumors, which may substitute for p53 inactivation in colorectal cancer and presumably other tumor types.

Material and methods

Isolation of genomic DNA

Formalin-fixed and paraffin-embedded (FFPE) tissues from the Institute of Pathology, BG-University-Hospital Bergmannsheil, Ruhr-University Bochum, Germany, were used to obtain five to 15 sections with 10-μm thickness. Sample collection was performed after approval by an institutional review board. A 3-μm hematoxylin and eosin section was used as a reference. The selected tissue was microdissected with a scalpel. In case of sarcomas the

Table 1 Sequences of the PCR primer sets used for MSP analysis of *mir-34a* and *miR-34b/c*

Primer set	Forward primer	Reverse primer	Fragment size (bp)	Annealing temperature (°C)	References
MSP-34a-m	GGT TTT GGG TAG GCG CGT TTC	TCC TCA TCC CCT TCA CCG CCG	122	65	Lodygin
MSP-34a-u	IIG GTT TTG GGT AGG TGT GTT TT	AAT CCT CAT CCC CTT CAC CAC CA	126	65	et al. [16]
MSP-34b/c-m	TTT AGT TAC GCG TGT TGT GC	ACT ACA ACT CCC GAA CGA TC	169	61	Lujambio
MSP-34b/c-u	TGG TTT AGT TAT GTG TGT TGT GT	CAA CTA CAA CTC CCA AAC AAT CC	174	61	et al. [18]

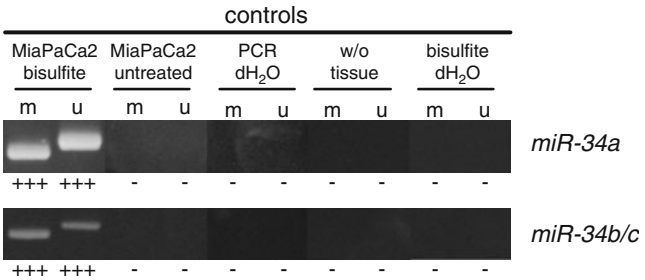

Fig. 1 Methylation-specific PCR controls. *Untreated*: no bisulfite reaction, *PCR dH_2O*: no DNA in PCR, *w/o tissue*: no input of tissue during the gDNA isolation, *bisulfite dH_2O*: no DNA input in bisulfite reaction

genomic DNA (gDNA) was derived from FFPE (Sarc1-11 FFPE), from frozen tissue (Sarc41-48 frozen tissue), or from cells (Sarc1-40 cells) isolated from surgical resection material (Department of Plastic Surgery, Sarcoma Reference Center, BG-University-Hospital Bergmannsheil, Ruhr-University Bochum, Germany).

In all cases the genomic DNA was isolated and purified using a commercially available kit (QIAamp Tissue Kit, Qiagen Hilden, Germany) according to the instructions of the manufacturer.

Bisulfite treatment of gDNA

Three hundred fifty to 2,000 ng gDNA was treated with bisulfite using the EZ DNA methylation kit (Zymo Research). The modified DNA was eluted with a final volume of 16 μl, and 1 to 2 μl were used for the methylation-specific PCR (MSP).

Methylation-specific PCR

The PCR primers used for detection of CpG-methylation of the *miR-34a* promoter are depicted in Table 1 and were previously established [16]. The PCR protocol entailed

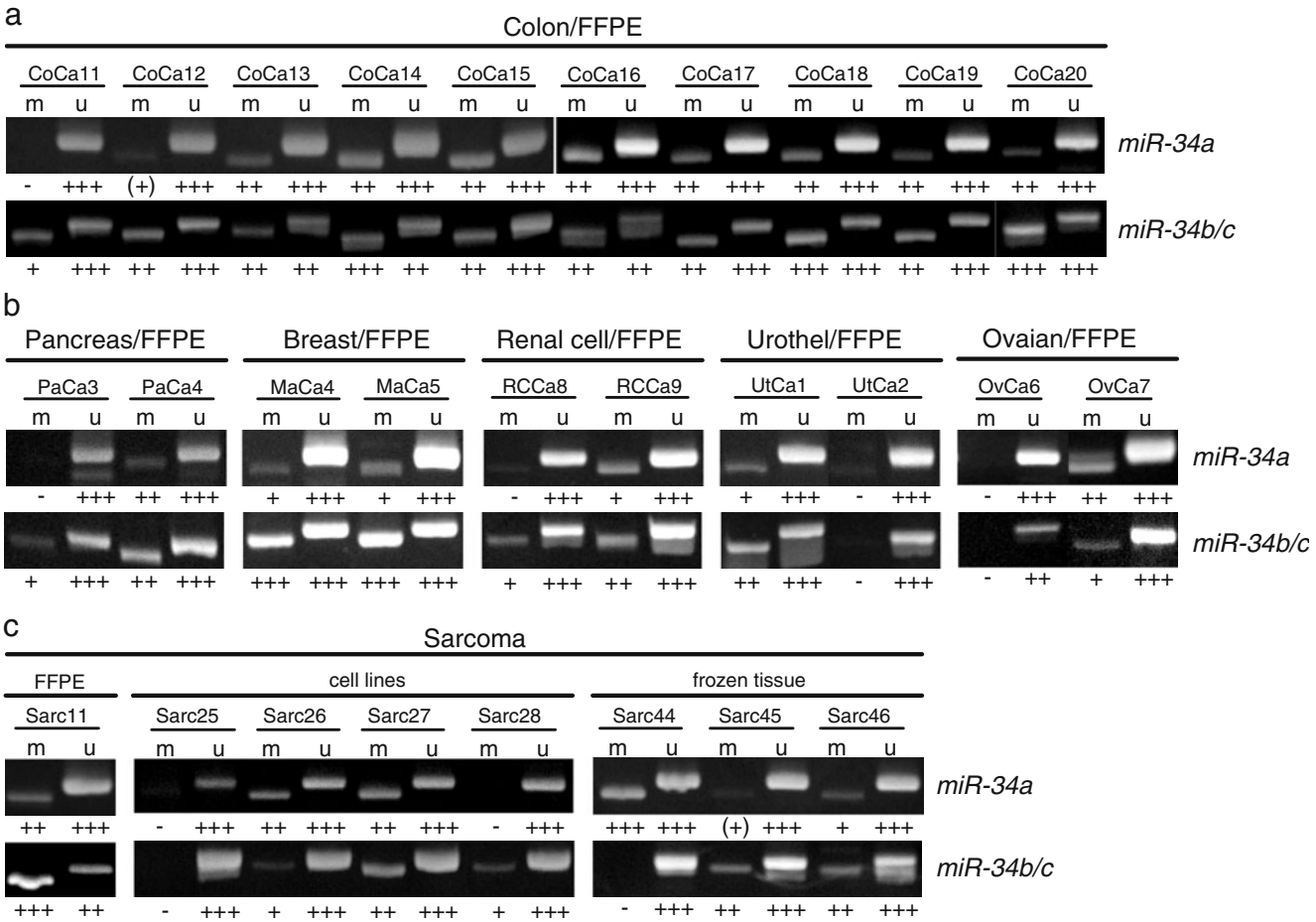

Fig. 2 Methylation-specific PCR analysis for *miR-34a* and *miR-34b/c* in primary human tumors from different tissues. The results from the MSP analysis were visually assigned to five scores: strongly methylated "+++", equal or stronger band intensity than the positive control (MiaPaCa2); medium level methylation "++" slightly weaker than the positive control; weakly methylated "+" clearly weaker than the positive control; very weakly methylated "*(+)*"; whereas samples with extremely weak band intensity and samples with no visible PCR product were regarded as un-methylated "–"

5 min at 95°C; two cycles of 20 s at 95°C, 30 s at 68°C, and 30 s at 72°C; followed by two cycles with 66°C annealing temperature, then 34 cycles with 65°C annealing temperature, and a 4-min final extension at 72°C. For the methylated allele a 122-bp fragment and for the un-methylated allele a 126-bp fragment were obtained. The PCR primers used for detection of CpG-methylation of *miR-34b/c* following primers are also depicted in Table 1 and were described previously [18]. PCR amplifications were carried out for 37 cycles (20 s at 95°C, 30 s at 61°C, and 30 s at 72°C, 4 min final extension). For the methylated allele a 169-bp fragment and for the un-methylated allele a 174-bp fragment were obtained. The PCR protocols are also provided in Table S1. Polymerase chain reaction products were separated by electrophoresis on 8% polyacrylamide gels. The results of the MSP analysis were scored visually.

Immunohistochemistry

For all colorectal cancer samples, 2-μm sections were cut from the paraffin blocks and deparaffinized by routine techniques followed by steaming/microwave treatment for 10 min in EDTA buffer (pH 9.0). After cooling, slides were incubated with monoclonal antibody against p53 (Clone DO-7, DAKO), using an automated staining device (DAKO, Carpinteria, CA, USA) with a dilution of 1:50. Primary antibody was detected by biotinylated secondary antibody followed by avidin–biotin peroxidase complex and 3,3′-diaminobenzidine chromagene. Finally, sections were counterstained by hematoxylin. For statistical analysis a product score consisting of the percentage of the number of positive nuclear staining and the intensity was used.

Statistical analysis

The *miR-34* promoter methylation status in relation to the p53 status and the Union for International Cancer Control (UICC) stage was analyzed by chi-square test. The cut-off for statistical significance was set to $p<0.05$.

Results

In order to analyze the methylation status of *miR-34* genes in primary human cancer, formalin-fixed, paraffin-embedded sections representing several tumor types were subjected to microdissection. In the case of sarcomas, we also analyzed genomic DNA derived from tumor cells passaged in vitro or from frozen tissue. From the collected material, genomic DNA (gDNA) was isolated and treated with bisulfite. This leads to conversion of cytosine in non-methylated CpG-dinucleotides to thymidine residues, whereas cytosine methylated at position 5 is protected from deamination. The converted gDNA was subjected to methylation-specific PCR (MSP) analysis [19] using PCR primers specific for the *miR-34a-* and *miR-34b/c* promoter regions depicted in Table 1. The resulting PCR products discriminate between methylated and un-methylated alleles of *miR-34a* and *miR-34b/c*. In a previous study, we have determined that the *miR-34a*-specific MSP results are comparable to the results obtained by bisulfite sequencing of the *miR-34a* promoter region upstream of the transcription start site encompassing the p53-binding site and can therefore replace the more elaborate analysis by bisulfite sequencing [16]. The conditions for specific MSP analysis of *miR-34b/c* were established by Toyota et al. and Lujambo et al. [12, 18]. Due to the size differences in the PCR products (indicated in Table 1) the signals obtained after polyacrylamide gel electrophoresis could be assigned unambiguously. The PCR conditions and reagents used here were subjected to several control experiments, which demonstrated that the conditions used for the MSP reactions allow to specifically detect methylated and un-methylated *miR-34a* or *miR-34b/c* alleles after bisulfite treatment (Fig. 1): no PCR products were obtained when MiaPaCa2 gDNA not treated with bisulfite or the different reagents used for isolation or treatment were used without addition of a template. However, when MiaPaCa2 gDNA treated with bisulfite was used as a template specific products representing methylated and un-methylated *miR-34a* or *miR-34b/c* alleles were detected (Fig. 1). Next we used these PCR conditions to analyze a larger number of primary tumors derived from diverse sites. For comparative purposes we introduced a score for the intensity of the PCR products representing methylated

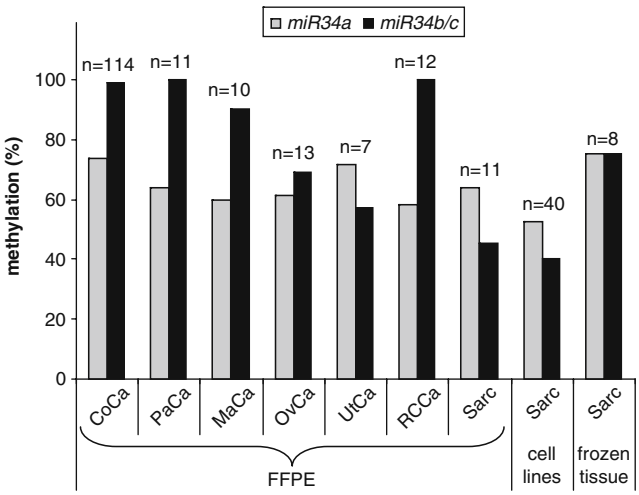

Fig. 3 Summary of the methylation frequencies of *miR-34a* and *miR34-b/c* in several primary tumor types. DNA was derived from formalin-fixed and paraffin-embedded tissue (*FFPE*), cell lines, or frozen tissue as indicated. *CoCa* colon carcinoma, *PaCa* pancreatic carcinoma, *MaCa* mammary carcinoma, *OvCa* ovarial carcinoma, *UtCa* urothelial carcinoma, *RCCa* renal cell carcinoma, *Sarc* sarcoma, *n* number of cases

Table 2 Summary of miR-34 promoter methylation, p53 status, and UICC score in 114 primary colorectal cancers

Case	FFPE	miR34a MSP	mir34b/c MSP	UICC	% p53 nuclear	Intensity	Score
CoCa	1	+	++	IIIb	5	2	2
CoCa	2	+	++	IIIa	<1	1	1
CoCa	3	−	(+)	IIIb	80	3	9
CoCa	4	−	+	IIA	90	3	12
CoCa	5	+	++	I	>95	3	12
CoCa	6	+	+++	IV	75	3	9
CoCa	7	+	+++	I	15	2	4
CoCa	8	+	+++	I	10	1	2
CoCa	9	−	+++	IIA	20	2	4
CoCa	10	+	+++	IIIb	95	3	12
CoCa	11	−	+	IIA	60	2	6
CoCa	12	(+)	++	IIIa	95	3	12
CoCa	13	++	++	IIA	95	3	12
CoCa	14	++	+++	I	<1	2	2
CoCa	15	++	++	I	0	0	0
CoCa	16	++	++	IIIc	70	2	6
CoCa	17	++	++	I	80	3	9
CoCa	18	++	+++	IIB	<5	1	1
CoCa	19	++	++	I	0	0	0
CoCa	20	++	+++	IIA	0	0	0
CoCa	21	++	++	IIA	>95	3	12
CoCa	22	+++	+++	IIB	15	2	4
CoCa	23	+	++	IIIb	80	3	9
CoCa	24	++	++	IIB	0	0	0
CoCa	25	−	+	IIA	95	3	12
CoCa	26	−	++	IIIb	5	2	2
CoCa	27	+	+++	IV	95	2	8
CoCa	28	+	+++	IIIc	80	3	9
CoCa	29	(+)	+++	IIIa	>95	3	12
CoCa	30	−	+++	IIA	10	2	4
CoCa	31	−	++	IIIb	90	3	12
CoCa	32	++	+++	IIIb	n.d.	n.d.	n.d.
CoCa	33	−	++	IV	95	3	12
CoCa	34	−	+++	IIA	75	2	6
CoCa	35	+	+	IIA	10	2	4
CoCa	36	(+)	+	I	95	3	12
CoCa	37	+	++	IIIb	65	2	6
CoCa	38	−	+++	IV	70	2	6
CoCa	39	−	+++	IIIa	75	2	6
CoCa	40	+	+++	IIIb	<1	1	1
CoCa	41	+	+++	IIIb	<1	2	2
CoCa	42	+	++	IIIc	<5	2	2
CoCa	43	+	++	IIA	10	2	4
CoCa	44	−	++	IV	65	3	9
CoCa	45	+	++	IIA	0	0	0
CoCa	46	++	+	IIIb	10	2	4
CoCa	47	−	++	IIIb	70	3	9
CoCa	48	−	+++	IV	10	2	4
CoCa	49	−	+++	IIA	90	3	12
CoCa	50	+	++	I	10	2	4
CoCa	51	+	+++	IV	5	2	2
CoCa	52	+	++	I	45	2	6
CoCa	53	−	++	IIA	90	3	12
CoCa	54	+	++	IIIc	25	2	4
CoCa	55	(+)	−	IIIc	80	3	9
CoCa	56	+	++	I	>95	3	12
CoCa	57	+	++	IIIa	<1	1	1
CoCa	58	+	++	I	<5	1	1
CoCa	59	+	++	IIA	10	2	4
CoCa	60	+	++	IIA	40	2	6
CoCa	61	++	++	IV	80	3	9
CoCa	62	+	++	I	60	3	9
CoCa	63	+	+++	IIIc	90	2	8
CoCa	64	+	+	I	>95	3	12
CoCa	65	+	+++	IIIc	5	2	2
CoCa	66	++	++	IIIc	30	1	2
CoCa	67	(+)	++	IV	15	3	6
CoCa	68	−	++	IIIb	>99	3	12
CoCa	69	−	++	IIIc	>99	3	12
CoCa	70	+	+++	IIIa	10	2	4
CoCa	71	−	++	IIIb	<1	1	1
CoCa	72	+	+++	IV	<5	1	1
CoCa	73	+	+++	I	10	2	4
CoCa	74	−	++	IIIb	90	3	12
CoCa	75	+	+++	IIIb	>95	3	12
CoCa	76	++	+++	I	<5	2	2
CoCa	77	+	+++	I	20	2	4
CoCa	78	+	+++	I	100	3	12
CoCa	79	++	+++	IV	80	3	9
CoCa	80	++	+++	IV	95	3	12
CoCa	81	+	+++	I	5	1	1
CoCa	82	+	+++	IV	5	2	2
CoCa	83	+	+	IIA	25	3	6
CoCa	84	+	++	IV	0	0	0
CoCa	85	+	++	IIA	n.d.	n.d.	n.d.
CoCa	86	−	+++	I	5	2	2
CoCa	87	(+)	++	IV	0	0	0
CoCa	88	+	+++	I	40	3	6
CoCa	89	+	++	IV	75	3	9
CoCa	90	++	+++	IV	>95	3	12
CoCa	91	−	++	IV	50	2	6
CoCa	92	(+)	++	I	0	0	0
CoCa	93	−	++	IIA	5	2	2
CoCa	94	+	++	IIA	60	3	9
CoCa	95	+	++	IV	0	0	0

Table 2 (continued)

Case	FFPE	miR34a MSP	mir34b/c MSP	UICC	% p53 nuclear	Intensity	Score
CoCa	96	++	++	IIA	<5	1	1
CoCa	97	++	+++	IV	90	3	12
CoCa	98	++	++	IIB	100	3	12
CoCa	99	−	++	IIA	35	2	6
CoCa	100	+	++	n.a.	n.d.	n.d.	n.d.
CoCa	101	+	+	n.a.	n.d.	n.d.	n.d.
CoCa	102	+	+	n.a.	n.d.	n.d.	n.d.
CoCa	103	−	++	n.a.	n.d.	n.d.	n.d.
CoCa	104	−	++	IIIb	90	3	12
CoCa	105	+	+++	IIA	10	2	4
CoCa	106	+	++	I	10	2	4
CoCa	107	+	++	IIA	60	3	9
CoCa	108	−	+	IIA	20	2	4
CoCa	109	+	+++	IIA	20	2	4
CoCa	110	−	+++	n.a.	n.d.	n.d.	n.d.
CoCa	111	+	+++	n.a.	n.d.	n.d.	n.d.
CoCa	112	+	++	IV	15	3	6
CoCa	113	−	+++	I	2	2	2
CoCa	114	+	+++	IIA	95	3	12
		73.68% (84/114)	99.12% (113/114)				

The methylation status of *miR-34a* and *miR-34b/c* promoter was determined by MSP of DNA derived from FFPE samples. The relative intensities of the *miR-34a*- and *miR-34b/c*-specific MSP products are indicated with (+), +, ++, +++, and −. The scoring system is explained in the legend of Fig. 2. In parallel the p53 status was determined by immunohistochemistry. The UICC stage is provided as indicator of tumor progression [20]

n.a. not available, *n.d.* not done, *UICC* International Union Against Cancer

miR-34a and *miR-34b/c* promoter fragments (see legend of Fig. 2). Representative MSP results are shown in Fig. 2. All MSP analyses are provided as supplemental Figures S1–S3. A summary of the MSP results is provided in Fig. 3.

The results of the MSP analyses were also compiled as tables to allow the direct comparison of the *miR-34a* and *miR-34b/c* methylation status. The MSP results obtained by analyses of 114 cases of colorectal cancer are listed in Table 2. Of these 114 colon cancer samples, 84 showed *miR-34a* methylation (73.7%) and 113 displayed *miR-34b/c* methylation (99.1%). Table 3 summarizes the results of the MSP analyses of pancreatic, mammary, renal cell, urothelial, and ovarial carcinoma and sarcomas. The gDNA from sarcomas was obtained from different sources: primary tumors (FFPE), explanted tumor cells, and frozen tumor tissue. In pancreatic and renal cancer we detected methylation of *miR-34b/c* in all cases analyzed, whereas *miR-34a* was only methylated in 63.3% of pancreatic and 58% of renal cancer cases. Also in breast and colon cancer the frequency of *miR-34b/c* methylation was higher than *miR-34a* methylation. In the seven cases of urothelial cancers, a strict correlation between methylation of *miR-34a* and *miR-34b/c* was detected.

Immunohistochemical analysis of the colorectal cancer samples showed an overexpression of p53 in 56 of 107 samples (52.3%; Table 1). A product score <6, indicating low expression and therefore lack of mutation, correlated significantly with the methylation of the *miR-34a* promoter ($p=0.0226$), whereas no significant correlation between the *miR34a* methylation and the UICC score was detected (Table 1). For *miR-34b/c*, which showed a promoter methylation in 99.1% of the colorectal cancer samples, no significant correlation with p53 expression/status and UICC stage was found. In addition, we evaluated other clinicopathological parameters, as pTNM stage according to the TNM classification of malignant tumors 2007 as well as infiltration of lymphatic (L) and blood vessels (V) and perineural infiltration [20] for the tumor entities analyzed by MSP, besides sarcomas. However, no significant correlation with promoter methylation of *miR-34a* or *miR-34b/c* was detected for these parameters (Tables S2 and S3)

Discussion

In this study, we found that colorectal, pancreatic, mammary, ovarian, urothelial, and renal cancer display CpG methylation of *miR-34a* and *miR-34b/c* at a relatively high frequency, ranging from 40% to 100%. Compared to our previous analysis of 110 different cell lines [16], the frequencies of CpG methylation were higher in the primary tumors analyzed in the current study. This could be due to a tendency of cell lines to harbor p53 mutations, which may alleviate a requirement for *miR-34a* methylation, or alternatively, loss of CpG-methylation during in vitro passaging. For example, colorectal cancer cell lines displayed *miR-34a* methylation with a frequency of 13% (3/23), whereas the primary CRC showed *miR-34a* methylation in 74% (84/114) of the cases analyzed here. For colorectal cancer, Toyota et al. [12] found a similarly high rate of *miR-34b/c* methylation as detected in this study. Also for mammary carcinoma the frequency of *miR-34a* CpG methylation in the primary tumors was higher than in cell lines (60% (6/10) vs. 25% (6/24)). Similarly, pancreatic cancer cell lines had a low incidence (3/19) of *miR-34a* methylation, whereas the primary pancreatic tumor samples analyzed here showed *miR-34a* methylation in 64% and *miR-34b/c* methylation in all of the 11 cases analyzed here.

As reported recently, *miR-34b/c* promoter methylation correlates with the metastatic potential of tumor cells [18]. However, in our study no correlation of the UICC stage of the colorectal cancers and *miR-34b/c* promoter methylation

Table 3 Summary of the methylation status of *miR-34a* and *miR-34b/c* with patient's UICC score in different human tumors derived from FFPE, primary tissue culture cells, and frozen tissue

FFPE	MSP		UICC
case	*miR-34a*	*miR-34b/c*	
PaCa 1	+	+	IIA
PaCa 2	-	+	IIA
PaCa 3	-	+	IIB
PaCa 4	++	++	IIB
PaCa 5	-	++	IIB
PaCa 6	+	++	IIB
PaCa 7	++	+++	IIA
PaCa 8	+	+++	IV4
PaCa 9	(+)	++	IIB
PaCa 10	-	+++	IIB
PaCa 11	(+)	++	IIB
	63.63% (7/11)	100.00% (11/11)	

FFPE	MSP		UICC
case	*miR-34a*	*miR-34b/c*	
MaCa 1	-	++	IIA
MaCa 2	+	+++	IIIC
MaCa 3	+	+	IIB
MaCa 4	+	+++	IIB
MaCa 5	+	+++	IIA
MaCa 6	+	++	IIIC
MaCa 7	-	+++	IIIC
MaCa 8	-	++	n.a.
MaCa 9	+	++	IIIB
MaCa 10	-	-	IIA
	60.00% (6/10)	90.00% (9/10)	

FFPE	MSP		UICC
case	*miR-34a*	*miR-34b/c*	
RCCa 1	-	+	I
RCCa 2	+	+	IV
RCCa 3	-	+	I
RCCa 4	+	+++	IV
RCCa 5	+	++	I
RCCa 6	-	++	I
RCCa 7	-	+	I
RCCa 8	(+)	+	II
RCCa 9	++	++	I
RCCa 10	+	+++	IV
RCCa 11	+	(+)	III
RCCa 12	-	+	II
	58.33% (7/12)	100.00% (12/12)	

FFPE	MSP		UICC
case	*miR-34a*	*miR-34b/c*	
UtCa 1	+	++	II
UtCa 2	(+)	-	IV
UtCa 3	-	-	IV
UtCa 4	++	++	II
UtCa 5	++	++	III
UtCa 6	++	++	III
UtCa 7	-	-	II
	71.43% (5/7)	57.14% (4/7)	

FFPE	MSP		UICC
case	*miR-34a*	*miR-34b/c*	
OvCa 1	-	-	IIIC
OvCa 2	-	-	IIIa
OvCa 3	(+)	+	IA
OvCa 4	-	+	n.a.
OvCa 5	+	+	IIIC
OvCa 6	-	-	IIA
OvCa 7	++	+	IIIC
OvCa 8	++	(+)	Ic
OvCa 9	++	+	IIIB
OvCa 10	+	+	IIB
OvCa 11	(+)	(+)	IIIC
OvCa 12	-	+	IC
OvCa 13	+	+	IB
	61.54% (8/13)	69.23% (9/13)	

FFPE	MSP	
case	*miR-34a*	*miR-34b/c*
Sarc 1	+	-
Sarc 2	-	+
Sarc 3	++	++
Sarc 4	-	-
Sarc 5	++	+++
Sarc 6	(+)	-
Sarc 7	-	-
Sarc 8	-	-
Sarc 9	(+)	-
Sarc 10	+	+
Sarc 11	++	+++
	63.64% (7/11)	45.45% (5/11)

cells	MSP	
case	*miR-34a*	*miR-34b/c*
Sarc 1	-	+
Sarc 2	+	-
Sarc 3	-	+++
Sarc 4	-	(+)
Sarc 5	-	-
Sarc 6	-	+
Sarc 7	(+)	-
Sarc 8	(+)	-
Sarc 9	++	-
Sarc 10	++	(+)
Sarc 11	+	-
Sarc 12	+	-
Sarc 13	+	-
Sarc 14	-	-
Sarc 15	-	-
Sarc 16	-	-
Sarc 17	+++	-
Sarc 18	-	-
Sarc 19	-	+
Sarc 20	-	+
Sarc 21	+	-
Sarc 22	-	-
Sarc 23	-	-
Sarc 24	(+)	-
Sarc 25	(+)	-
Sarc 26	++	+
Sarc 27	+++	++
Sarc 28	-	+
Sarc 29	+	-
Sarc 30	++	-
Sarc 31	-	+
Sarc 32	++	-
Sarc 33	++	-
Sarc 34	++	+
Sarc 35	++	-
Sarc 36	+	-
Sarc 37	-	+
Sarc 38	-	(+)
Sarc 39	-	(+)
Sarc 40	-	+
	52.5% (21/40)	40.0% (16/40)

frozen tissue	MSP	
case	*miR-34a*	*miR-34b/c*
Sarc 41	-	+
Sarc 42	++	++
Sarc 43	(+)	+++
Sarc 44	+++	-
Sarc 45	(+)	++
Sarc 46	+	++
Sarc 47	-	-
Sarc 48	+	+
	75.00% (6/8)	75.00% (6/8)

The intensity of the presence and absence of *miR-34a*- and *miR-34b/c*-specific MSP products are indicated with (+), +, ++, +++, and −. The scoring system is explained in the legend of Fig. 2. The UICC score of the sarcoma cases was not available

PaCa pancreatic carcinoma, *MaCa* mammary carcinoma, *RCCa* renal cell carcinoma, *UtCa* urothelial carcinoma, *OvCa* ovarial carcinoma, *Sarc* sarcoma, *n.a.* not available, *UICC* International Union Against Cancer

could be shown due to the high methylation rate of 99.1%. Therefore, further analyses especially on the other tumor subtypes analyzed in this study with lower rates of *miR-34b/c* promoter methylation should be performed to clarify this point. Since the receptor tyrosine kinase c-MET is a target of *miR-34b/c* [21], it may be enhanced in expression, when *miR-34* genes are down-regulated by epigenetic silencing. In ovarian cancer, we have recently found that up-regulation of c-MET correlates with down-regulation of *miR-34a* and *miR-34b/c* expression and is required for invasion. Furthermore, ectopic expression of *miR-34* inhibits invasion in gastric and hepatocellular carcinoma, at least in part, by down-regulation of c-MET [22, 23]. Also in prostate cancer cell lines, ectopic expression of *miR-34c* suppresses migration and invasion [24]. It will therefore be interesting to determine whether the additional types of cancer shown to display inactivation of *miR-34* genes in this study also exhibit up-regulation of c-MET and enhanced invasive and metastatic properties, whenever *miR-34* genes are silenced by CpG methylation.

The increased metastatic potential associated with loss of *miR-34a* function may also explain why down-regulation of *miR-34a* correlates with an increased probability of relapse in non-small cell lung carcinoma [25]. In the study by Gallardo et al., down-regulation of *miR-34a* expression emerged as an independent prognostic marker for relapse which correlated with CpG methylation of the *miR-34a* promoter. Therefore, further studies are warranted to determine the prognostic and diagnostic value of *miR-34a* and *miR-34b/c* methylation in the additional types of cancer for which we demonstrated significant frequencies of *miR-34* inactivation by CpG methylation in this report.

Recently, several target mRNAs of *miR-34a* and *miR-34b/c* have been validated [10]. For example, it was shown that *miR-34a* suppresses the growth of brain tumors by targeting Notch [26]. Furthermore, *miR-34a* was shown to be induced during B-RAF-induced senescence in a p53-independent manner and presumably mediates senescence by directly down-regulating c-MYC [27]. The induction of senescence by oncogene activation has been observed in several types of tumors [17]. Since ectopic expression of *miR-34a* has been shown to induce senescence [8, 16, 28], it is possible that *miR-34* inactivation by CpG methylation contributes to the escape from oncogene-induced senescence in the early phase of tumor development. Furthermore, *miR-34c* expression is induced in p53-negative cells after DNA damage via ATM and MAPK kinases and subsequently targets c-MYC, which contributes to a cell cycle arrest [29]. In colorectal cancer, p53 mutation occurs in up to 40-60% of the patients [30–32]. By immunohistochemical analysis we detected similar rates of nuclear accumulation of p53 in the colorectal cancer cases in this study indicating p53 mutations at a similar frequency. The inverse correlation between *miR-34a* promoter methylation and *p53* mutation indicates that the loss of the miR-34a-mediated tumor suppressor function may substitute for loss of the p53 response by *p53* mutations in colorectal cancer. Furthermore, the epigenetic silencing of *miR-34a* may also prevent the induction of *miR-34a* by alternative mechanisms, as for example via ETS transcription factors [27]. Interestingly, ectopic *miR-34a* expression reduces the frequency of tumor-initiating cell in two pancreatic cancer cell lines [33]. It is conceivable that methylation of *miR-34a* may facilitate the emergence of tumor-initiating cells since processes as cell cycle arrest, senescence, or apoptosis will presumably be attenuated in cells with loss of *miR-34a* function.

The inactivation of *miR-34a* by CpG methylation is not restricted to epithelial and mesenchymal tumor types. Recently, it was shown that *miR-34a* is also inactivated by CpG-methylation in non-Hodgkin's lymphoma [34]. Further studies are needed to determine the full spectrum of tumors affected by CpG methylation-mediated inactivation of the *miR-34*a and *miR-34b/c* genes.

Detection of CpG methylation of the *miR-34a* or *miR-34b/c* promoter in tumor DNA released into body fluids may serve as a tumor diagnostic marker, as has been shown for other genes as *GSTP1* [15]. Recently, it was shown that treatment of tumors transplanted into mice using *miR-34a* mimetics leads to complete inhibition of tumor growth without any detectable side effects [35]. Therefore, a combination of *miR-34*-promoter methylation-based diagnostics with a *miR-34*-based therapeutic approach is conceivable. Since *miR-34* defective tumor cells are presumably more susceptible to a re-expression of *miR-34* than the normal, *miR-34* expressing cells this combination seems especially attractive.

Acknowledgments Work in Heiko Hermeking's lab is supported by the Deutsche Krebshilfe, the Deutsche Forschungsgemeinschaft, the Friedrich-Baur-Stiftung, the Rudolf-Bartling-Stiftung, and the German-Israeli-Foundation for Scientific Research and Development (GIF).

Conflict of interest statement We declare that we have no conflict of interest.

Appendix

Supplemental Legends

Table S1 Methylation-specific PCR conditions for the analysis of CpG methylation of the *miR-34a* and *miR-34b/c* promoter. Table S2 Association of methylation status of *miR-34a* and *miR-34b/c* promoter and p53 IHC datas with clinicopathological characteristics of the patients in 114 primary colon cancers. Abbreviations: T: infiltration depth, N: nodal status, M: distant metastasis status, L: lymphatic infiltration, V: infiltration of blood vessels, Pn: perineural infiltration.

Table S3 Association of methylation status of *miR-34a* and *miR-34b/c* with clinicopathological characteristics of the patients in different human tumors derived from FFPE, primary tissue culture cells and frozen tissue. Abbreviations: T: infiltration depth, N: nodal status, M: distant metastasis status, L: lymphatic infiltration, V: infiltration of blood vessels, Pn: perineural infiltration.

Figure S1 Methylation-specific PCR analyses of *mir-34a* and *miR-34b/c* in primary human colorectal cancer containing FFPE samples. a. *miR-34a* MSP of colon carcinomas (CoCa1-114). b. *miR-34b/c* MSP of colon carcinoma (CoCa1-114).

Figure S2 MSP analysis of *miR-34a* and *miR-34b/c* in FFPE tumor samples representing: a. pancreatic carcinoma (PaCa1-11), b. mammary carcinoma (MaCa1-10), c. renal cell carcinoma (RCCa1-12), d. urothelial carcinoma (UtCa1-7), e. ovarian carcinoma (OvCa1-13).

Figure S3 MSP analysis of *miR-34a* and *miR-34b/c* methylation in a. primary sarcoma FFPE (Sarc1-11), b. sarcoma cells cultured in vitro (Sarc1-40), c. frozen sarcoma tissue (Sarc41-48).

References

1. Garzon R, Calin GA, Croce CM (2009) MicroRNAs in Cancer. Annu Rev Med 60:167–179
2. Hermeking H (2007) p53 enters the microRNA world. Cancer Cell 12(5):414–418
3. Croce CM (2009) Causes and consequences of microRNA dysregulation in cancer. Nat Rev Genet 10(10):704–714
4. Tarasov V, Jung P, Verdoodt B, Lodygin D, Epanchintsev A, Menssen A, Meister G, Hermeking H (2007) Differential regulation of microRNAs by p53 revealed by massively parallel sequencing: miR-34a is a p53 target that induces apoptosis and G1-arrest. Cell Cycle 6(13):1586–1593
5. Chang TC, Wentzel EA, Kent OA, Ramachandran K, Mullendore M, Lee KH, Feldmann G, Yamakuchi M, Ferlito M, Lowenstein CJ, Arking DE, Beer MA, Maitra A, Mendell JT (2007) Transactivation of miR-34a by p53 broadly influences gene expression and promotes apoptosis. Mol Cell 26(5):745–752
6. Raver-Shapira N, Marciano E, Meiri E, Spector Y, Rosenfeld N, Moskovits N, Bentwich Z, Oren M (2007) Transcriptional activation of miR-34a contributes to p53-mediated apoptosis. Mol Cell 26 (5):731–743
7. He L, He X, Lim LP, de Stanchina E, Xuan Z, Liang Y, Xue W, Zender L, Magnus J, Ridzon D, Jackson AL, Linsley PS, Chen C, Lowe SW, Cleary MA, Hannon GJ (2007) A microRNA component of the p53 tumour suppressor network. Nature 447 (7148):1130–1134
8. Bommer GT, Gerin I, Feng Y, Kaczorowski AJ, Kuick R, Love RE, Zhai Y, Giordano TJ, Qin ZS, Moore BB, Macdougald OA, Cho KR, Fearon ER (2007) p53-mediated activation of miRNA34 candidate tumor-suppressor genes. Curr Biol 17 (15):1298–1307
9. Corney DC, Flesken-Nikitin A, Godwin AK, Wang W, Nikitin AY (2007) MicroRNA-34b and MicroRNA-34c are targets of p53 and cooperate in control of cell proliferation and adhesion-independent growth. Cancer Res 67(18):8433–8438
10. Hermeking H (2010) The miR-34 family in cancer and apoptosis. Cell Death Differ 17(2):193–199
11. Welch C, Chen Y, Stallings RL (2007) MicroRNA-34a functions as a potential tumor suppressor by inducing apoptosis in neuroblastoma cells. Oncogene 26(34):5017–5022
12. Toyota M, Suzuki H, Sasaki Y, Maruyama R, Imai K, Shinomura Y, Tokino T (2008) Epigenetic silencing of microRNA-34b/c and B-cell translocation gene 4 is associated with CpG island methylation in colorectal cancer. Cancer Res 68(11):4123–4132
13. Jones PA, Baylin SB (2002) The fundamental role of epigenetic events in cancer. Nat Rev Genet 3(6):415–428
14. Jones PA, Baylin SB (2007) The epigenomics of cancer. Cell 128 (4):683–692
15. Laird PW (2003) The power and the promise of DNA methylation markers. Nat Rev Cancer 3(4):253–266
16. Lodygin D, Tarasov V, Epanchintsev A, Berking C, Knyazeva T, Korner H, Knyazev P, Diebold J, Hermeking H (2008) Inactivation of miR-34a by aberrant CpG methylation in multiple types of cancer. Cell Cycle 7(16):2591–2600
17. Halazonetis TD, Gorgoulis VG, Bartek J (2008) An oncogene-induced DNA damage model for cancer development. Science 319(5868):1352–1355
18. Lujambio A, Calin GA, Villanueva A, Ropero S, Sanchez-Cespedes M, Blanco D, Montuenga LM, Rossi S, Nicoloso MS, Faller WJ, Gallagher WM, Eccles SA, Croce CM, Esteller M (2008) A microRNA DNA methylation signature for human cancer metastasis. Proc Natl Acad Sci U S A 105(36):13556–13561
19. Herman JG, Graff JR, Myohanen S, Nelkin BD, Baylin SB (1996) Methylation-specific PCR: a novel PCR assay for methylation status of CpG islands. Proc Natl Acad Sci U S A 93(18):9821–9826
20. Wittekind CM, Bootz F, Meyer HJ (2002) TNM—Klassifikation maligner Tumoren. 6 edn. UICC International Union Against Cancer. Springer, Berlin
21. Corney DC, Hwang CI, Matoso A, Vogt M, Flesken-Nikitin A, Godwin AK, Kamat AA, Sood AK, Ellenson LH, Hermeking H, Nikitin AY (2010) Frequent downregulation of miR-34 family in human ovarian cancers. Clin Cancer Res 16(4):1119–1128
22. Li N, Fu H, Tie Y, Hu Z, Kong W, Wu Y, Zheng X (2009) miR-34a inhibits migration and invasion by down-regulation of c-Met expression in human hepatocellular carcinoma cells. Cancer Lett 275(1):44–53
23. Migliore C, Petrelli A, Ghiso E, Corso S, Capparuccia L, Eramo A, Comoglio PM, Giordano S (2008) MicroRNAs impair MET-mediated invasive growth. Cancer Res 68(24):10128–10136
24. Hagman Z, Larne O, Edsjo A, Bjartell A, Ehrnstrom RA, Ulmert D, Lilja H, Ceder Y (2010) miR-34c is down regulated in prostate cancer and exerts tumor suppressive functions. Int J Cancer 127 (12):2768–2776
25. Gallardo E, Navarro A, Vinolas N, Marrades RM, Diaz T, Gel B, Quera A, Bandres E, Garcia-Foncillas J, Ramirez J, Monzo M (2009) miR-34a as a prognostic marker of relapse in surgically resected non-small-cell lung cancer. Carcinogenesis 30(11):1903–1909
26. Li Y, Guessous F, Zhang Y, Dipierro C, Kefas B, Johnson E, Marcinkiewicz L, Jiang J, Yang Y, Schmittgen TD, Lopes B, Schiff D, Purow B, Abounader R (2009) MicroRNA-34a inhibits glioblastoma growth by targeting multiple oncogenes. Cancer Res 69(19):7569–7576
27. Christoffersen NR, Shalgi R, Frankel LB, Leucci E, Lees M, Klausen M, Pilpel Y, Nielsen FC, Oren M, Lund AH (2010) p53-independent upregulation of miR-34a during oncogene-induced senescence represses MYC. Cell Death Differ 17 (2):236–245
28. Tazawa H, Tsuchiya N, Izumiya M, Nakagama H (2007) Tumor-suppressive miR-34a induces senescence-like growth arrest through modulation of the E2F pathway in human colon cancer cells. Proc Natl Acad Sci U S A 104(39):15472–15477

29. Cannell IG, Kong YW, Johnston SJ, Chen ML, Collins HM, Dobbyn HC, Elia A, Kress TR, Dickens M, Clemens MJ, Heery DM, Gaestel M, Eilers M, Willis AE, Bushell M (2010) p38 MAPK/MK2-mediated induction of miR-34c following DNA damage prevents Myc-dependent DNA replication. Proc Natl Acad Sci U S A 107(12):5375–5380
30. Iacopetta B (2003) TP53 mutation in colorectal cancer. Hum Mutat 21(3):271–276
31. Russo A, Bazan V, Iacopetta B, Kerr D, Soussi T, Gebbia N (2005) The TP53 colorectal cancer international collaborative study on the prognostic and predictive significance of p53 mutation: influence of tumor site, type of mutation, and adjuvant treatment. J Clin Oncol 23(30):7518–7528
32. Hoff PM (2005) Is there a role for routine p53 testing in colorectal cancer. J Clin Oncol 23(30):7395–7396
33. Ji Q, Hao X, Zhang M, Tang W, Yang M, Li L, Xiang D, Desano JT, Bommer GT, Fan D, Fearon ER, Lawrence TS, Xu L (2009) MicroRNA miR-34 inhibits human pancreatic cancer tumor-initiating cells. PLoS ONE 4(8):e6816
34. Chim CS, Wong KY, Qi Y, Loong F, Lam WL, Wong LG, Jin DY, Costello JF, Liang R (2010) Epigenetic inactivation of the miR-34a in hematological malignancies. Carcinogenesis 31(4):745–750
35. Wiggins JF, Ruffino L, Kelnar K, Omotola M, Patrawala L, Brown D, Bader AG (2010) Development of a lung cancer therapeutic based on the tumor suppressor MicroRNA-34. Cancer Res 70(14):5923–5930

Virchows Arch (2011) 458:323–330
DOI 10.1007/s00428-010-1018-1

ORIGINAL ARTICLE

PTOV1 is overexpressed in human high-grade malignant tumors

Sara Fernández · Jose L. Mosquera · Lide Alaña · Alex Sanchez-Pla · Juan Morote · Santiago Ramón y Cajal · Jaume Reventós · Inés de Torres · Rosanna Paciucci

Received: 14 October 2010 / Revised: 22 November 2010 / Accepted: 23 November 2010 / Published online: 23 December 2010
© Springer-Verlag 2010

Abstract The prostate tumor overexpressed-1 (PTOV1) protein was first described overexpressed in prostate cancer but not detected in normal prostate. PTOV1 expression is associated to increased cancer proliferation in vivo and in vitro. In prostate biopsy, PTOV1 detection is helpful in the early diagnosis of cancer. The purpose of this study was to analyze the relevance of PTOV1 expression to identify aggressive tumors derived from 12 different histological tissues. Tissue microarrays (TMAs) containing 182 biopsy samples, including 168 human tumors, were analyzed for PTOV1 and Ki67 expression by immunohistochemistry. Tumors of low and high histological grade were selected from lung, breast, endometrium, pancreas liver, skin, ovary, colon, stomach, kidney, bladder, and cerebral gliomas. One TMA with representative tissues without cancer (14 samples) was used as control. PTOV1 expression was analyzed semiquantitatively for the intensity and percentage of positive cells. Ki67 was evaluated for tumors proliferative index. Results show that PTOV1 was expressed in over 95% of tumors examined. Its expression was significantly associated to high-grade tumors (p=0.014). This association was most significant in urothelial bladder carcinomas (p=0.026). Overall, the expression of Ki67 was associated to high-grade tumors, and it was significant in several tumor types. PTOV1 and Ki67 were significantly co-overexpressed in all tumors (p=0.001), and this association was significant in clear cell renal carcinoma (p=0.005). In conclusion, PTOV1 expression is associated to more aggressive human carcinomas and more significantly to bladder carcinomas suggesting that this protein is a potential new marker of aggressive disease in the latter tumors.

Keywords PTOV1 · Immunohistochemistry · Human tumors · Low and high grade of malignancy · Bladder cancer · Renal carcinoma

Inés de Torres and Rosanna Paciucci equally contributed to the work.

S. Fernández · S. Ramón y Cajal · I. de Torres
Department of Pathology, Vall Hebron Hospital,
Barcelona, Spain

A. Sanchez-Pla
University of Barcelona,
Barcelona, Spain

J. Morote
Department of Urology, Vall Hebron Hospital,
Barcelona, Spain

L. Alaña · J. Reventós
Research Unit in Biomedicine and Translational and Pediatrics Oncology, Vall Hebron Institute of Research,
Colserola building, Pg. Vall d'Hebron 119-129,
Barcelona 08035, Spain

J. L. Mosquera · A. Sanchez-Pla
Unit of Statistic–Bioinformatic, Vall Hebron Institute of Research,
Barcelona, Spain

J. Morote · S. Ramón y Cajal · I. de Torres
Autonoma University,
Barcelona, Spain

R. Paciucci (✉)
Research Unit in Biomedicine and Translational and Pediatrics Oncology, Vall Hebron Institute of Research,
Colserola building, Pg. Vall d'Hebron 119-129,
Barcelona 08035, Spain
e-mail: rpaciucci@ir.vhebron.net

Introduction

Prostate tumor overexpressed-1 (PTOV1) was identified as a novel gene and protein during a differential display

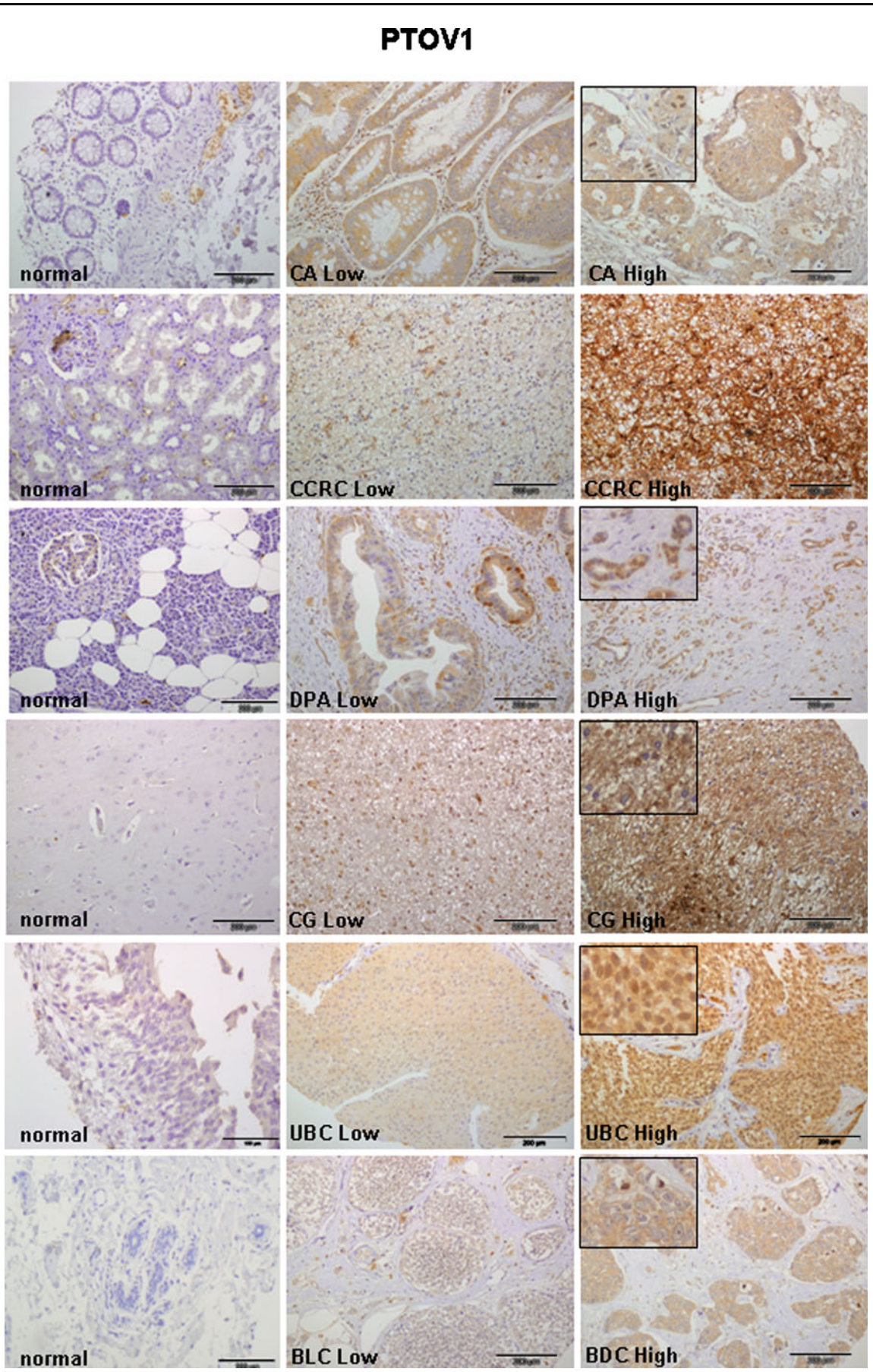
PTOV1
normal
CA Low
CA High
normal
CCRC Low
CCRC High
normal
DPA Low
DPA High
normal
CG Low
CG High
normal
UBC Low
UBC High
normal
BLC Low
BDC High

◀ **Fig. 1** Expression of PTOV1 protein in tumors. Representative images of immunohistochemistry performed with anti PTOV1 antibody. Six histological tumor types of high and low grade were selected together with six representative no cancerous tissues (*normal*). *Insets* are magnifications showing details of PTOV1 protein localization. Faint or absence of staining was observed in no cancerous tissues. Nuclear staining was detected in several tumor types, including ductal pancreatic adenocarcinomas (*DPA*), cerebral gliomas (*CG*), clear cell renal carcinomas (*CCRC*), and urothelial bladder carcinomas (*UBC*). Strong association of PTOV1 with mitotic figures was observed in colon adenocarcinoma (*CA*) and breast ductal carcinomas (*BDC*)

screening for genes overexpressed in prostate cancer [1]. This protein is encoded by a 12-exon gene localized in chromosome 19q13.3. The protein consists of two highly homologous domains of 151 and 147 amino acids arranged in tandem, joined by a short linker peptide. The PTOV1 domain is conserved across distant organisms and does not show significant similarities to known protein motifs [1]. A second gene, PTOV2, later identified as Arc92/MED25/ACID1, was identified in human and other organisms, coding for proteins containing a single PTOV domain [1–3]. PTOV2/Arc92/MED25/ACID1 interacts with retinoic acid receptor (RAR), the histone acetyltransferase CBP, and the mediator complex, suggesting a role for MED25 in chromatin remodeling and pre-initiation complex assembly to recruit activators to the basal transcriptional machinery [3]. PTOV1 is overexpressed in 71% of prostatic carcinomas and 80% of prostate intraepithelial neoplasia but is undetectable or expressed at low levels in normal prostate epithelium [2]. In normal endothelial cells and in neuroendocrine cells, PTOV1 is expressed at high levels [1, 2]. High levels of PTOV1 in prostatic tumors correlated significantly with Ki67 proliferative index and associated with a nuclear localization of the protein, suggesting a functional relationship between PTOV1 overexpression, proliferative status, and nuclear localization [2]. Transient overexpression of a chimeric GFP-PTOV1 protein induced proliferation and forced the entry of cells into the S phase of the cell cycle, suggesting that overexpression of PTOV1 can contribute to the biological behavior of these tumors [4]. PTOV1 interacts with the lipid raft protein flotillin-1, and both proteins colocalize at the plasma membrane and in the nucleus [4]. Depletion of PTOV1 markedly inhibited cell proliferation under basal conditions [4]. Recently, we determined that PTOV1 was significantly overexpressed in HGPIN associated with cancer but not in HGPIN lesions in prostates that do not develop cancer, indicating that PTOV1 is a useful marker to detect cancer in the absence of carcinoma lesions in the biopsy [5].

The proliferative index in human tumors is an important prognostic factor that is frequently evaluated in histological analysis of tumor specimens. The Ki67/MIB-1 antigen is a labile nuclear protein which expression is tightly linked to the cell cycle [6]. It is expressed in proliferating cells during mid-G1, increasing in level through S and G2, and peaking at the end of the M phase. Ki67/MIB-1 is not detected in resting cells [6]. Here we have analyzed the expression of PTOV1 in 12 histological types of human tumors and studied correlation with grade and Ki67 expression. We have found that PTOV1 is significantly overexpressed in the majority of the tumors analyzed, and it may be a new oncogenic factor associated with poor prognosis.

Materials and methods

Specimens One hundred and sixty-nine human tumor specimens were retrieved from the archives of Pathology Department Vall d'Hebron University Hospital. Consent for the use of human tissues was obtained following the rules of the Spanish Biomedical Research Law and approved by the ethical committee of the hospital. Tissue microarrays (TMA) were constructed from formalin-fixed paraffin-embedded blocks of each sample. Histological grade for each tumor was determined on HE-stained slides for the same samples and was classified according to defined criteria [7]. Tumors selected were 27 lung squamous and lung adenocarcinomas (LA), 11 breast ductal, and 10 lobular carcinomas, 10 endometrial adenocarcinomas, 10 ductal pancreatic adenocarcinomas (DPA), 9 hepatocarcinomas, 11 squamous skin carcinomas, 9 malignant melanomas, 8 mucinous (MOC) and 9 serous (SOC) ovarian carcinomas, 10 gastric and 10 colon carcinomas, 11 cerebral gliomas (CG), 13 clear cell renal carcinomas (CCRC), and 11 urothelial bladder carcinomas (UBC). Tumors were classified into two groups according to their histological tumor grade following defined criteria [7]: 87 (51%) tumors were low grade (G1, G2) and 81 (48%) were high grade (G3, G4). Malignant melanomas were classified according to Breslow's definition of staging that considers the area and the depth of invasion of cutaneous melanoma lesions [8]. Low-grade papillary urothelial carcinoma and high-grade papillary urothelial carcinoma were classified as defined [9]. Control tissues not affected by cancer ($n=14$) corresponding to the analyzed histological tissue types were used for one TMA used as reference.

Generation of tissue arrays Ten different tissue arrays were constructed using a semiautomated tissue arrayer (Chemicon International Inc., Billerica, MA, USA), containing the two major histological grades of the 169 tumors under study and one tissue array with normal control tissues. Each tissue array was assembled as a previously described [10]. Briefly, three tissue cylinders of 1.2 mm for each case were punched from morphologically representative tumor areas of each donor tissue paraffin block and brought into one

recipient paraffin block (3×2.5 cm). Representative normal areas without tumoral pathology were included in one TMA. H&E stain for each TMA was performed to verify the histopathological findings.

Immunohistochemistry Four-micron sections were cut from each TMA and transferred to glass slides. Antigen retrieval was carried out by autoclaving for 5 min in citrate buffer. The slides were stained on an automated DAKO stainer (Glostrup, Denmark). Endogenous peroxidase activity was blocked with 0.2% hydrogen peroxidase solution, and non-specific labeling was blocked with serum blocking solution. Sections were incubated in for 2 h at room temperature with PTOV1 antibody. As a negative control, primary antibody was omitted and replaced with phosphate-buffered saline. In addition, non-specific rabbit antibody was used and gave clean negative results in all cases tested (not shown). The reaction was revealed by the avidin–biotin complex peroxidase method (ABC Elite kit, Vector Burlingame, CA, USA) followed by staining with the peroxidase substrate 3.3 diaminobenzidine tetrachloride (Sigma-Aldrich Chemie GmbH., Deisenhofer, Germany). The slides were counterstained with 50% hematoxylin. A case was considered positive when >10% of the cells showed unequivocal staining. Both cytoplasmic and nuclear staining was recorded. A similar procedure was followed for the detection of Ki67 except that incubation with primary antibody was for 30 min at room temperature. Each slide was assessed independently by two pathologists (S.F. and I.d.T.). Discrepancies were resolved by a concurrent reexamination by both investigators using a double-headed microscope. PTOV1 expression was evaluated in a semiquantitative manner whereby the levels of expression are represented as the percentage of positive cells and the intensity of the staining $[\mathrm{H-score} = 1 \times (\%\mathrm{weak}) + 2 \times (\%\mathrm{moderate}) + 3 \times (\%\mathrm{intense})$with a ranking between 0 and 300] [11]. Cases with less than 10% of cells showing positivity were considered negative. To analyze the proliferative index, the proportion of nuclear Ki67 staining over the total number of nuclei per high power field was scored. Four value ranges for Ki67 index were established (negative=0, low=1–5%, moderate=6–25%, and high=>25%).

Statistical analysis Cross-tabulations were used to establish the presence of associations among variables. The Fisher's exact test was used to evaluate associations among variables and the Cramer's V coefficient to measure the strength of relationships [12]. The non-parametric method of Kruskal–Wallis was used to test equality of population medians among groups [13]. A p value <0.05 was considered significant in all analyses. For the multivariate analysis, we used the multiple correspondence analysis (MCA) technique to represent the distances among the categories of the qualitative variables and between the observations [14, 15]. This technique allows to handle large and complex datasets and to represent the pattern of relationships of several categorical dependent variables. MCA can be seen as a generalization of principal component analysis when the variables to be analyzed are categorical instead of quantitative. That is, MCA can be understood as a reduction of the dimensionality of a dataset with a large number of interrelated variables into a smaller number of independent variables (known as new dimensions). First dimension retains as much as possible of the inertia (or variability) present in the data, and similarly each succeeding dimension retains the remaining inertia that it is always less than the previous dimension. Data analyses were performed with the open source R statistical software package [16].

Results

A total of 182 biopsies that included 168 malignant tumors and 14 normal tissues were evaluated for the expression of PTOV1 in a semiquantitative manner. PTOV1 expression, quantified by the H-score value, was absent or very low (less than 10%) in the cytoplasm and nucleus of all normal tissues examined, including lung, breast, endometrium, pancreas, liver, skin, ovary, stomach, colon, kidney, bladder, and brain (Fig. 1). Blood vessels and red blood cells showed positive expression for PTOV1, confirming previous observations [1, 2].

The expression of PTOV1 was detected in 162 of 168 tumors (97%) with a minimum median H-score of 100 and a maximum of 200 (Table 1). The mean H-score of PTOV1 expression in tumors of low grade was 120, ranging between 0 and 240, whereas in high-grade tumors it was 134, with a range between 0 and 300. These data suggested possible differences in the distribution of PTOV1 staining among the tumors analyzed. To confirm this observation, the Kruskal–Wallis test was applied and the results confirmed that the medians of PTOV1 score among tissues are different (p=0.006984). Therefore, in order to compare the levels of PTOV1 expression in the different tumors, the levels of protein detection were defined as follows: No expression was labeled "0", H-score lower or equal to the median for a specific tissue was labeled "low", and H-score greater than the median for a specific tissue was labeled "overexpression". The expression of PTOV1 showed a significant association with tumor grade in UBC (Fisher's exact test p=0.026; Cramer's V coefficient=0.841), where the H-score for PTOV1 expression in the high-grade tumors group is clearly not overlapping with the values encountered in low-grade tumors (Fig. 2). This observation, also

Table 1 PTOV1 H-score values in cancer tissues

Tissue	N	LG	HG	H-score mean	Standard deviation	H-score median	Min	Max
Bladder	11	5	6	154.545	74.346	200	0	230
Breast	21	9	12	124.048	59.258	110	25	205
CNS	11	5	6	147.273	82,23	100	0	280
Colon	10	5	5	132.3	24.658	121	100	180
Endometrium	10	5	5	167.5	46.741	177.5	80	210
Kidney	13	7	6	145.769	79.631	150	10	300
Liver	9	4	5	145	68.829	100	70	250
Lung	27	16	11	88.37	58.664	100	0	190
Ovary	17	8	9	94.412	68.736	110	0	210
Pancreas	10	5	5	126.2	61.001	107.5	40	202
Skin	20	10	10	104.105	61.153	110	10	220
Stomach	10	5	5	84.7	49.022	100	10	140

H-score mean and median indicate the mean and the median values of PTOV1 H-score, respectively

N number of cases analyzed, *LG* number of low-grade tumors, *HG* number of high-grade tumors

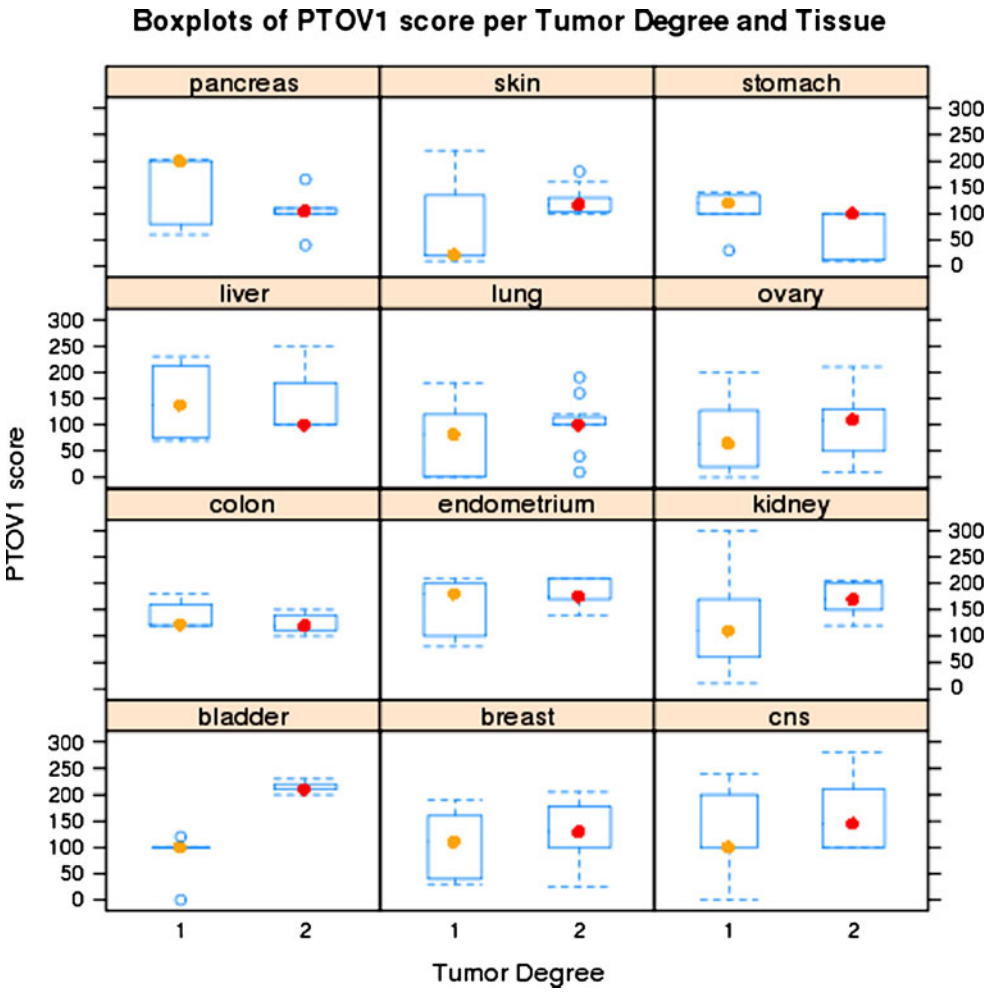

Fig. 2 *Boxplot* of PTOV1 H-score per tumor grade and tissue. *Bar diagrams* and *boxplots* are used to show distributions of protein expression. The *graph* shows the H-score for PTOV1 (*vertical axis*) and the tumor grade (1 for low-grade and 2 for high-grade) for the different histological tumors. *Yellow* and *red dots* show the median values of PTOV1 H-score for each tumor subtype

put into evidence by the high Cramer's coefficient value, suggests that although a low number of cases are included in the group, the detection of PTOV1 is able to distinguish in a significant manner high-grade bladder tumors from low grade. PTOV1 has been previously shown to shift from the cytoplasm to the nucleus [2]. Overexpression of the exogenous PTOV1 is nuclear-localized and promotes cell entry into the S phase of the cell cycle, and in addition, nuclear PTOV1 is significantly associated to higher Ki67 index in prostate tumors [2]. Thus, we have analyzed PTOV1 subcellular localization in relation with tumor grade. PTOV1 nuclear localization was strongly associated with high-grade UBC (p=0.015; Cramer's V coefficient= 0.833) suggesting that its presence in the nucleus is important for the proliferation and progression of this type of cancer (see representative images in Fig. 1).

A significant association with high-grade tumors was also observed considering all tumors (excluding UBC; p= 0.045; Cramer's V coefficient=0.201). The proliferative status of tumors was evaluated by staining for Ki67 (MIB-1). The expression of Ki67 was evaluated considering the proportion of nuclear staining over the total number of nuclei (Ki67 index). Ki67 was absent in 43 (25%) tumors, low in 27 (16%), and high or overexpressed in 96 (56%) tumors. A higher Ki67 index was significantly associated with high-grade tumors in UBC, LA, SOC–MOC, and DPA. Overall, this association was also significant (p= 5.3947e−07), and it was stronger than the one observed with PTOV1 (Cramer's coefficient=0.461).

The association between PTOV1 and Ki67 expression was significant in CCRC (p=0.001; Cramer's V coefficient= 0.557) and considering all tumors (excluding CCRC) (p= 0.004; Cramer's V coefficient=0.268), again suggesting that higher PTOV1 expression levels are associated with more aggressive proliferative tumors, in agreement with previous findings in prostate cancer [2].

Integrating information collected from various sources provides a better interpretation of the underlying biological processes than data from a single source. To get further insight of the biological relevance of our findings and to discover associations among different groups of variables (tissue, tumor grade, Ki67, PTOV1, and nuclear or no-nuclear localization), we performed a multivariate analysis based on a MCA. The results in Fig. 3 show a representation for the first two dimensions: PTOV1 covers quiet well the map representation with the three levels of expression defined. Different groups of tissues are clearly defined and show association with the histological grade of tumors. Tumors overexpressing PTOV1 (labeled PTOV1.2 in Fig. 3) are found in very close proximity with high-grade tumors and UBC (bladder cancer: bladder), confirming our previous results. These parameters are also in close proximity to breast (breast) and pancreas

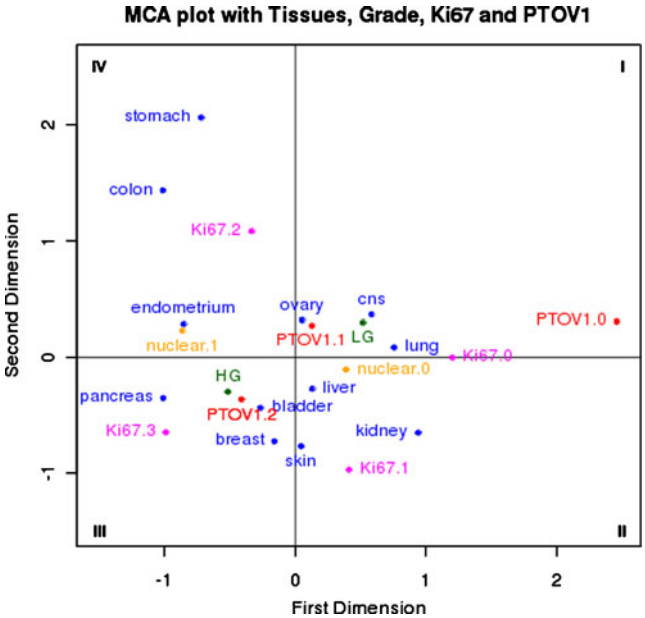

Fig. 3 MCA analysis representation of the variables studied in the first two dimensions. This analysis permits to discover associations among the different groups of variables studied: tissue, tumor grade, Ki67 levels, PTOV1 levels, and PTOV1 nuclear localization. These variables are indicated by *different colors*. *Red* PTOV1 levels, indicated as *PTOV1.2*=overexpression, *PTOV1.1*=low expression (lower or equal to the median for a specific tissue), *PTOV1.0*=no expression. *Yellow* PTOV1 localization, nuclear is indicated by *1* and no-nuclear is indicated by *0*. *Blue* cancer tissues. *Green* tumor grade LG and HG. *Pink* Ki67 levels, indicated by *Ki67.3*=overexpression, *Ki67.2*=moderate, *Ki67.1*=low, *Ki67.0*=no expression. Quadrant III, for example, suggests an association among the variables: high-grade (*HG*) tumors, tumors with overexpression of Ki67, tumors with high levels of PTOV1, as well as bladder, breast, and pancreas tumors

(pancreas) cancer. Lower levels of PTOV1 (PTOV1.1) appear more related to low-grade tumors and specifically to ovary (ovary) and CNS (CNS) cancer. Interestingly, tumors not expressing PTOV1 (PTOV1.0) are quite distant from all the other variables. This unsupervised analysis integrates the five variables studied and confirms our previous observations that higher PTOV1 expression is significantly associated to aggressive bladder carcinomas and high-grade tumors.

Discussion

The PTOV1 protein, first found overexpressed in prostate carcinomas, is involved in the mechanisms leading to the progression of this neoplasia, as reported by previous findings showing that the exogenous overexpression of a recombinant PTOV1 protein activates cell proliferation [1, 2, 4]. To evaluate whether its overexpression is a more general feature associated to neoplastic cells, we have analyzed the expression of PTOV1 in a cohort of 168 malignant tumors of 12 different histological types, each

one comprising low-grade and high-grade tumors. Many types of human neoplasias can be found within a given organ. This heterogeneity and the great variability of oncogenic alterations that have been described to trigger tumor growth are an indication of the numerous regulating circuits and cellular targets that may exist in cancer. It is essential to study several hundreds or several thousands of human tumors to identify critical genetic and biochemical factors associated with the tumor progression and prognosis [10, 17–19]. Our results show that PTOV1 is expressed in 97% of all tumors and, in general, it is overexpressed in more aggressive disease. In our series of 168 tumors, PTOV1 immunoreactivity was cytoplasmic or mixed cytoplasmic nuclear in all primary carcinomas, in contrast with the normal epithelial counterpart lacking significant reactivity. Because the median of expression of PTOV1 was significantly different among the various cancers, the values above the median were taken as "overexpression" levels in each type. This allowed us to compare the levels of the immunoreactive protein in neoplasias of different types. Considering all 168 tumors, those with high grade significantly overexpressed the protein PTOV1. In particular, the association between stronger expression of PTOV1 and high grade of malignancy was very significant in urothelial bladder carcinomas. UBCs are also very significantly associated with nuclear localization of PTOV1, suggesting an action of the protein at this location in promoting UBC cancer progression. These observations would suggest a function for PTOV1 similar to the one described for the related protein PTOV2 in transcription as part of the Mediator complex [3]. PTOV2/MED25 was described to associate with RA-bound RAR and increase RAR/RXR-mediated transcription [20]. The intrinsic transcriptional activity of MED25 was found in its PTOV domain, likely accomplished by direct association with the general activator CBP. In that work, PTOV1 competed with MED25 function, possibly by competition of the co-activator CBP, and blocked RAR response [20].

Several carcinoma types among those studied here showed a higher Ki67 index in association with a high grade of malignancy, in agreement with previous descriptions [21–25]. The proliferative activity of CCRC, measured by Ki67 immunoreactivity, was among the best prognostic tools [21]. However, in our series of CCRC, neither Ki67 index nor PTOV1 expression alone were significantly associated with high-grade tumors. However, when the expression levels of PTOV1 and Ki67 index were considered, a significant association was found, suggesting that assessment of both parameters is useful to indicate tumor aggressiveness. This finding is in part supported by our previous in vitro studies where the exogenous PTOV1 expression induced proliferation of different cell types, including PZHPV7 and PC3 prostate cancer cells and COS7 fibroblasts [2]. In addition, in prostate carcinomas, PTOV1 protein was significantly associated with tumors with higher Ki67 index and increased PSA blood levels [4].

Our previous finding that PTOV1 overexpression is detected in HGPIN lesions specifically associated with cancer but not in HGPIN that are not associated with cancer suggests that high levels of PTOV1 can identify premalignant lesions committed to develop into carcinomas [5]. This observation indicates the implication of PTOV1 in the early changes that lead to full cancer development. Our present findings indicate that the detection of PTOV1 expression might be helpful in the analysis of tumor aggressiveness for UBC and CCRC. Although further studies using a larger number of cases are needed to confirm the usefulness of PTOV1 as a potential therapeutic target in a number of carcinomas from different origin, the results obtained from the present pilot study predict the involvement of this protein in tumor progression, particularly in the bladder.

Acknowledgments This study was supported by the Health Ministry (FIS-PI020764; FIS-PI050818), Science and Education Ministry (SAF05-05848; MTM2008-00642), Science and Innovation Ministry (SAF2008-03936), TV3 Marathon (052610; 052710), and Urologic Research Foundation (01/2004).

Conflict of interest statement The authors declare to have no conflict of interest.

References

1. Benedit P, Paciucci R, Thomson T, Valeri M, Nadal M, Càceres C, de Torres I, Estivill X, Lozano JJ, Morote J, Reventós J (2001) PTOV1, a novel protein overexpressed in prostate cancer containing a new class of protein homology blocks. Oncogene 20:1455–1464
2. Santamaría A, Fernández P, Farré X, Benedit P, Reventós J, Morote J, Paciucci R, Thomson TM (2003) PTOV1, a novel protein overexpressed in prostate cancer, shuttles between the cytoplasm and the nucleus and promotes entry into the S phase of the cell division cycle. Am J Pathol 162:897–905
3. Yang F, DeBeaumont R, Zhou S, Näär AM (2004) The activator-recruited cofactor/Mediator coactivator subunit ARC92 is a functionally important target of the VP16 transcriptional activator. Proc Natl Acad Sci U S A 101(8):2339–2344
4. Santamaría A, Castellanos E, Gómez V, Benedit P, Renau-Piqueras J, Morote J, Reventós J, Thomson TM, Paciucci R (2005) PTOV1 enables the nuclear translocation and mitogenic activity of flotillin-1, a major protein of lipid rafts. Mol Cell Biol 25:1900–1911
5. Morote J, Fernández S, Alaña L, Iglesias C, Planas J, Reventós J, Ramón Y Cajal S, Paciucci R, de Torres IM (2008) PTOV1 expression predicts prostate cancer in men with isolated high-grade prostatic intraepithelial neoplasia in needle biopsy. Clin Cancer Res 14(9):2617–2622
6. Tan PH, Bay BH, Yip G, Selvarajan S, Tan P, Wu J, Lee CH, Li KB (2005) Immunohistochemical detection of Ki67 in breast cancer correlates with transcriptional regulation of genes related to apoptosis and cell death. Mod Pathol 18(3):374–381
7. American Joint Committee on Cancer (2002) AJCC cancer staging manual, 6th edn. Springer, New York

8. Breslow A (1970) Thickness, cross-sectional areas and depth of invasion in the prognosis of cutaneous melanoma. Ann Surg 172:902–908
9. Eble JN, Epstein JI, Sesterhenn I (eds) (2004) World Health Organization classification of tumors. Pathology and genetics of tumors of the urinary system and male genital organs. IARCC, Lyon, p 114
10. Kononen J, Budendorf L, Kallioiemi A, Bärlund M, Schraml P, Leighton S, Torhorst J, Mihatsch MJ, Sauter G, Kallioniemi OP (1998) Tissue microarrays for high-throughput molecular profiling of tumors specimens. Nat Med 4:844–847
11. Detre S, Saclani Jotti G, Dowsett M (1995) A "quickscore" method for immunohistochemical semiquantitation: validation for estrogen receptor in breast carcinomas. J Clin Pathol 48(9):876–878
12. Quinn GP, Keough MJ (2008) Experimental design and data analysis for biologists. Cambridge University Press, Cambridge
13. Sprent P, Smeeton NC (2001) Applied nonparametric statistical methods, 4th edn. Chapman & Hall, Boca Raton
14. Dray S, Dufour AB (2008) The ade4 package: implementing the duality diagram for ecologists. J Stat Software 22(4):1–20
15. Greenacre MJ, Blasius J (2006) Multiple correspondence analysis and related methods. Chapman & Hall, Boca Raton
16. Maindonald J, Braun J (2007) Data analysis and graphics using *R*, 2nd edn. Cambridge University Press, Cambridge
17. Hanahan D, Weinberg RA (2000) The hallmarks of cancer. Cell 100:57–70
18. Bild AH, Yao G, Chang JT et al (2006) Oncogenic pathway signatures in human cancers as a guide to targeted therapies. Nature 439(7074):353–357
19. Lu Y, Yi Y, Liu P, Wen W, James M, Wang D, You M (2007) Common human cancer genes discovered by integrated gene-expression analysis. PLoS ONE 2(11):e1149
20. Lee HK, Park UH, Kim EJ, Um SJ (2007) MED25 is distinct from TRAP220/MED1 in cooperating with CBP for retinoid receptor activation. EMBO J 26:3545–3547
21. Cindolo L, Cantile M, Galasso R, Marsicano M, Napodano G, Altieri V (2001) Not traditional prognostic factors in human conventional renal carcinoma. Minerva Urol Nefrol 53(4):211–219
22. van Diest PJ, van der Wall E, Baak JP (2004) Prognostic value of proliferation in invasive breast cancer: a review. J Clin Pathol 57 (7):675–681
23. Dudderidge TJ, Stoeber K, Loddo M, Atkinson G, Fanshawe T, Griffiths DF, Williams GH (2005) Mcm2, Geminin, and KI67 define proliferative state and are prognostic markers in renal cell carcinoma. Clin Cancer Res 11(7):2510–2517
24. Rindi G, D'Adda T, Froio E, Fellegara G, Bordi C (2007) Prognostic factors in gastrointestinal endocrine tumors. Endocr Pathol 18(3):145–149
25. Ohsie SJ, Sarantopoulos GP, Cochran AJ, Binder SW (2008) Immunohistochemical characteristics of melanoma. J Cutan Pathol 35(5):433–444

Virchows Arch (2011) 458:331–340
DOI 10.1007/s00428-010-1015-4

ORIGINAL ARTICLE

Multiplexed analysis of angiogenesis and lymphangiogenesis factors predicts outcome for non-small cell lung cancer patients

Valsamo K. Anagnostou · Dina G. Tiniakos · Marianthi Fotinou · Apostolos Achimastos · Konstantinos N. Syrigos

Received: 11 August 2010 / Revised: 27 October 2010 / Accepted: 20 November 2010 / Published online: 14 December 2010
© Springer-Verlag 2010

Abstract Angiogenesis and lymphangiogenesis are key components of non-small cell lung cancer (NSCLC) tumor growth and metastatic spread; however, the prognostic and predictive role of angiogenic and lymphangiogenic biomarkers remains controversial for NSCLC patients. We assessed VEGF, VEGFC, VEGFD, VEGFR3 protein expression, tumor microvessel, and lymphatic vessel (LmVD) density by immunohistochemistry in 103 NSCLC; biomarkers were analyzed individually as well as multiplexed with each other. No correlations were identified between VEGF, VEGFC, VEGFD, or LmVD and clinical characteristics. VEGFR3 was correlated with VEGFC (p=0.03), VEGFD (p<0.0001), and intratumor LmVD (p=0.03). Tumors that did not express VEGFR3 had a worse prognosis (log rank p=0.03). VEGF was significantly correlated with survival in adenocarcinomas (log rank p=0.014) but not in squamous cell carcinomas (log rank p=0.5). Multivariate Cox regression analysis confirmed the independent prognostic potential of VEGFR3 (hazard ratio (HR)=0.05; 95% confidence intervals (CI)=0.008–0.32, p=0.002) for all patients and VEGF (HR=8.69, 95% CI=1.4–53.69, p=0.02) for adenocarcinomas. When biomarkers were multiplexed, only stage and VEGFC expression were independent predictors of survival for all patients. Weighted expression of VEGFC, VEGFR3, and stage was used to build a prognostic classifier for stage I–IIIA patients; patients in the low risk group had prolonged survival compared with high risk patients (log rank p=0.02). There was no association between biomarkers and early recurrence or response to treatment. Angiogenic and lymphangiogenic biomarkers studied define subgroups of patients at high risk and may be useful for prognostic stratification of NSCLC patients especially those with early stage disease.

Keywords VEGFC · VEGFR3 · Prognosis · Lung cancer · Early stage

Electronic supplementary material The online version of this article (doi:10.1007/s00428-010-1015-4) contains supplementary material, which is available to authorized users.

V. K. Anagnostou (✉) · K. N. Syrigos
Oncology Unit, Third Department of Medicine,
Sotiria General Hospital,
Athens, Greece
e-mail: valsamo.anagnostou@yale.edu

D. G. Tiniakos
Laboratory of Histology and Embryology, Medical School,
National and Kapodistrian University of Athens,
Athens, Greece

M. Fotinou
Department of Pathology, Sotiria General Hospital,
Athens, Greece

A. Achimastos
Third Department of Medicine, Sotiria General Hospital,
Athens, Greece

Introduction

Angiogenesis is necessary for tumor progression allowing for tumor growth and facilitating local invasion and metastatic spread [1]. Several mechanisms have been

described for tumor angiogenesis involving secretion of angiogenic growth factors that activate tyrosine kinase receptors on surrounding existing endothelial cells as well as contribution of the tumor cells themselves to formation of new vasculature [2]. The major mediators of tumor angiogenesis are members of the vascular endothelial growth factor (VEGF) family and VEGF blockade inhibits angiogenesis and results in tumor suppression in preclinical models including lung cancer [3]. Bevacizumab, a monoclonal antibody that targets VEGF, has shown increased response rate and prolonged time to progression for advanced stage non squamous non-small cell lung cancer (NSCLC) [4]; however, there is no single angiogenesis related biomarker conventionally used as a surrogate marker for response to VEGF targeted therapies.

Angiogenesis in NSCLC is associated with concomitant lymphangiogenesis, and lymphangiogenesis has been shown to play a key role in metastatic tumor growth [5]. The lymphangiogenic growth factors VEGFC and VEGFD acting through their receptor tyrosine kinase VEGFR3 promote formation of tumor lymphatics and metastatic spread of tumor cells to lymph nodes [6–8]. Despite preclinical studies on animal models indicating an association between tumor lymphangiogenesis and metastasis, metastatic spread to lymph nodes has been reported to occur in the absence of tumor lymphangiogenesis (20) suggesting that the role of lymphangiogenesis in metastasis may vary [6].

Expression of angiogenic and lymphangiogenic factors has been found to be associated with both worse [9, 10] and favorable [11] outcomes, whereas the predictive potential of these biomarkers remains largely unstudied. It is now evident that it is the balance between angiogenic and lymphangiogenic factors that regulates tumor progression and metastasis [6]. Here, we studied the differential expression of VEGF, VEGFC, VEGFD, VEGFR3, and their correlation with tumor microvessel (MVD) and lymphatic microvessel (LmVD) density in a cohort of 103 NSCLC patients and assessed their prognostic and predictive impact.

Materials and methods

Cohort description

Formalin-fixed paraffin-embedded (FFPE) primary NSCLC tumors from 103 patients that underwent surgery at Sotiria General Hospital (Athens, Greece) between March 1990 and July 2006 were obtained from the archives of the Pathology Department. The lung cancer cohort consisted of 88 (85.4%) men and 15 (14.6%) women with median age of 60 years (range 34–87, mean 60.41±0.86). According to the World Health Organization classification for NSCLC [12], there were 47 (45.6%) adenocarcinomas (ACs), 50 (48.5%) squamous cell carcinomas (SCCs), three (2.9%) large cell carcinomas (LCC), and three (2.9%) NSCLC not otherwise specified tumors. TNM staging revealed, 23 (22.3%) patients with stage I, 21 (40%) with stage II, 40 (38.8%) with stage III, and 19 (18.4%) patients with stage IV disease. Eight (7.8%) patients were nonsmokers and 92 (89.3%) were smokers; smoking status was not known for three patients. Clinical and pathological characteristics are summarized in Supplementary Table 1.

Treatment and assessment of response

One hundred and one patients were treatment-naïve prior to tumor resection (or acquisition of surgical biopsies for stage IV patients); 17 patients were surgically treated only, 52 patients received adjuvant chemotherapy, 32 patients received first line chemotherapy, and 34 patients received post-recurrence chemotherapy (Supplementary Table 1). Patients were evaluated for response by the Response Evaluation Criteria in Solid Tumors [13] after every three cycles; complete response (CR) was defined as no residual visible tumor, partial response (PR) as >20% of tumor shrinkage, stable disease (SD) as a decrease of <20% or increase of <30% and progressive disease (PD) as an increase of >30% or the emergence of new lesions. Thirteen responders (CR+PR) and 49 nonresponders (SD+PD) were identified. Early recurrence was defined as recurrence within the first year after surgical resection of the tumor and 36 patients were identified. Average follow-up time was 26.05±2.49 months (median 22, range 2–223) and average disease-free survival was 20.29±2.28 months (median 14, range 0–180). The study was approved by the institutional review board.

Immunohistochemistry

Slides were deparaffinized with xylene and rehydrated in graded alcohols and antigen-retrieved for 20 min in 10 mM citrate buffer (pH=6) or 10 mM Tris/1 mM EDTA buffer (pH=9) using a household microwave (800 W). Sections were then immersed in 0.9% hydrogen peroxide (Sigma, St. Louis, MO) in methanol for 30 min in the dark to inactivate endogenous peroxidase followed by an 8-min incubation with normal blocking serum (Biogenex, San Ramon, CA). Slides were then incubated with mouse monoclonal anti-VEGF, anti-VEGFD, anti-CD31, and anti-lymphatic endothelial marker (LEM) and rabbit monoclonal anti-VEGFC and polyclonal anti-VEGFR3 antibodies (Supplementary Table 2) diluted in common antibody diluent (Biogenex, San Ramon, CA) overnight at 4°C followed by a 30-min incubation with a secondary

biotinylated antibody (Biogenex, San Ramon, CA) at room temperature (RT). Detection was performed with the streptavidin–biotin peroxidase complex (Biogenex, San Ramon, CA) applied for 30 min at RT. 3,3′-Diaminobenzidine (Dako, Carpinteria, CA) was used as a chromagen, and slides were counterstained with hematoxylin (Dako, Carpinteria, CA), dehydrated through graded alcohols, cleared in xylene, and coverslipped. FFPE breast cancer, colorectal cancer, placenta, and lymph node specimens were used as positive controls (Supplementary Table 2). Negative control sections in which the primary antibodies were omitted were used for each immunostaining run.

Scoring system for VEGF, VEGFC, VEGFD, and VEGFR3

A semiquantitative scoring system was employed using a 4-point scale for staining intensity (0, no staining; 1+, weak; 2+, moderate; and 3+, strong) and a 3-point scale for percentage area stained (0, 0%; 1, <33%; 2, 33–66%; and 3, >66% positive tumor cells). After careful review of all sections, we observed that tumor specimens showed a homogeneous expression for VEGF, VEGFC, VEGFD, and VEGFR3; as a result, our scoring system was reduced to its four-category intensity equivalent. Patients with biomarker-positive tumors were divided to low (1+), moderate (2+), and high (3+) expressers, accordingly. All cases were scored by two observers at a double-headed microscope blindly to clinical data. Cases with less than 100 tumor cells per section were not scored as for not being representative of the tumor.

Assessment of microvessel density (MVD) and lymphatic microvessel density (LmVD)

The intratumor MVD and LmVD were assessed by CD31 and LEM, respectively, and calculated as follows: three areas of highest CD31/LEM immunoreactivity (hot spots) were identified by scanning the tumor sections at low power (4×), and individual lymphatic microvessel counts were performed at high power (20×) for each "hot spot." The intratumor MVD and LmVD were calculated as the mean microvessel and lymphatic microvessel count per 20× field (area corresponding to 0.385 mm^2), respectively; assessment was carried out by two observers at a double-headed microscope.

Statistical analysis

Spearman's rho correlation coefficient was used to assess associations between angiogenic and lymphangiogenic factors and clinical and pathological variables. The association between angiogenic and lymphangiogenic biomarkers with early recurrence and response to treatment was analyzed by the Wilcoxon rank test. Analysis of variance (ANOVA) was used for comparisons of continuous MVD and LmVD scores among patients with different clinical and pathological characteristics and unpaired t test for comparisons between responders vs. nonresponders to systemic chemotherapy. Survival curves were constructed using the Kaplan–Meier method, and survival differences were analyzed by the log rank test. Cox univariate analysis was used to assess the association between binarized VEGF, VEGFC, VEGFD, and VEGFR3 scores as well as continuous MVD and LmVD scores and disease specific survival. Multivariate Cox proportional hazards regression analysis was used to determine which independent factors jointly had a significant impact on disease specific survival; three LCC and three NSCLC NOS specimens were excluded from multivariate analysis to avoid bias related to small sample size and violation of assumptions of normality. A risk score was calculated for stage I–IIIA patients combining clinical variables and binarized measurements of angiogenic and lymphangiogenic biomarkers significantly correlated with survival in multivariable analysis; each variable was weighted by the regression coefficient resulting into a prognostic score. Patients were stratified into three risk groups using tertiles as cutoff points for risk classification. All p values were based on two-sided testing, and differences were considered significant at $p<0.05$. All statistical analyses were done using the SPSS software program (version 13.0 for Windows, SPSS Inc., Chicago, IL).

Results

Correlation of angiogenic and lymphangiogenic biomarkers with clinical characteristics

VEGF, VEGFC, VEGFD, and VEGFR3 were predominantly expressed in the cytoplasm of NSCLC tumor cells; VEGFR3 immunoreactivity was occasionally observed in endothelial cells in stromal and/or tumor vessels as well as in some stromal macrophages (Fig. 1). Thirty-five (34%), 20 (19.4%), eight (7.8%), and six (5.8%) tumors did not express VEGF, VEGFC, VEGFD, and VEGFR3, respectively, and 35 (34%), 63 (61.2%), 49 (47.6%), and 32 (31.1%) low; six (5.8%), 11 (10.7%), 28 (27.2%), and 28 (41.7%) moderate; and one (1%), 0, 2 (1.9%) and 12 (11.7%) high expressers were identified for VEGF, VEGFC, VEGFD, and VEGFR3, respectively. Tumors were further classified as low (score 0, 1+) and high (score 2+, 3+) VEGF expressers, low (score 0, +1) and high (score 2+) VEGFC expressers, low (0, 1+) and high (2+, 3+) VEGFD expressers and VEGFR3 expressers (score 1+, 2+, 3+) and VEGFR nonexpressers (score 0). Intratumor MVD (Fig. 2) ranged from 7.79 to 246.75 μ vessels per square

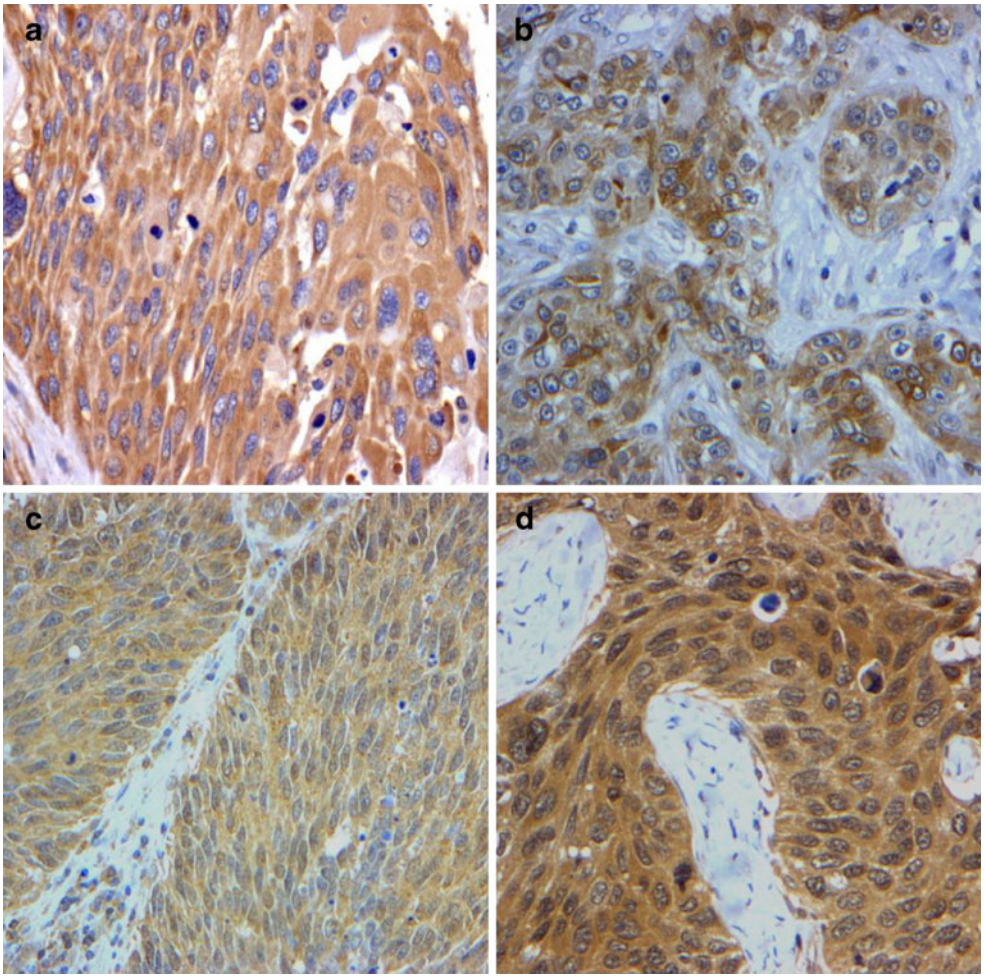

Fig. 1 Immunohistochemical detection of **a** VEGF, **b** VEGFC, **c** VEGFD, and **d** VEGFR3 in primary lung squamous cell carcinomas. VEGF (score 2+, **a**), VEGFC (score 1+, **b**), VEGFD (score 1+, **c**), and VEGFR3 (score 2+, **d**) immunoreactivities were seen in the cytoplasm of NSCLC cells. VEGFR3 immunostaining was also seen in some stromal cells (**d**). Original magnification (**a**–**d**) 20×

millimeter (median 58.87, mean ± standard error (SE) 61.17±3.22) and LmVD (Fig. 2) ranged from 0.87 to 109.9 lymphatic vessels per square millimeter (median 29.87, mean±SE 36.51±2.7). No significant correlations were identified between VEGF, VEGFC, or VEGFD and age, gender, lymph node metastases, stage at diagnosis, histological subtype, differentiation, smoking, and site of first recurrence (Table 1). VEGFR3 expression was significantly correlated with high differentiation, whereas MVD was inversely correlated with age at diagnosis (Spearman's rho=0.36, p=0.001 and rho=−0.22, p=0.03, respectively; Table 1). A trend towards significance was observed for the correlation between high LmVD and squamous cell carcinoma histology (Spearman's rho=0.19, p=0.07).

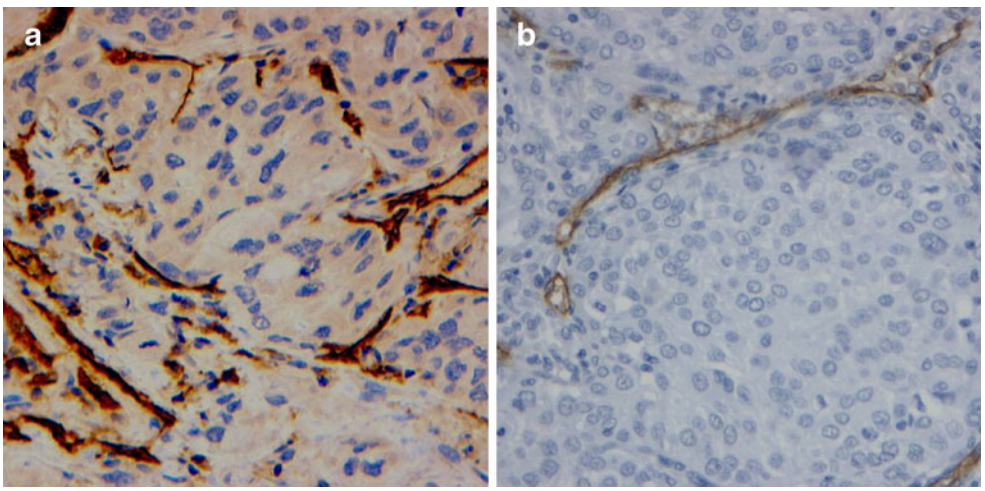

Fig. 2 Detection of **a** CD31-positive intratumor microvessels and **b** LEM-positive intratumor lymphatic vessels, seen in an adenocarcinoma and squamous cell carcinoma, respectively. Original magnification (**a**, **b**) 20×

Table 1 Correlations between biomarkers and tumor and patient characteristics

Biomarker	Stage	Age	Gender	Histology	Differentiation	Smoking	Recurrence (site)
VEGF	0.07 NS	0.06 NS	−0.07 NS	−0.19 NS	0.11 NS	−0.09 NS	0.2 NS
VEGFC	−0.04 NS	0.09 NS	0.05 NS	−0.1 NS	0.02 NS	−0.03 NS	0.006 NS
VEGFD	−0.04 NS	0.1 NS	0.02 NS	−0.05 NS	−0.07 NS	0.04 NS	−0.02 NS
VEGFR3	−0.08 NS	−0.14 NS	−0.09 NS	−0.05 NS	0.36 (***p*=0.001**)	−0.11 NS	0.1 NS
MVD	−0.07 NS	−0.22 (***p*=0.03**)	−0.05 NS	−0.05 NS	−0.12 NS	0.12 NS	−0.22 NS
LVD	0.03 NS	0.008 NS	0,03 NS	0.19 (*p= 0.07*)	−0.03 NS	−0.06 NS	0.19 NS

Spearman's rho coefficient is given for nonparametric correlations between categorical VEGF, VEGFC, VEGFD, VEGFR3, and continuous MVD and LVD scores and patient characteristics. Significant *p* values at a level of 0.05 are shown in bold, trending in italics

VEGF vascular endothelial growth factor, *VEGFC* vascular endothelial growth factor C, *VEGFD* vascular endothelial growth factor D, *VEGFR3* vascular endothelial growth factor receptor 3, *MVD* microvessel density, *LVD* lymphatic vessel density, *NS* nonsignificant

Correlations between angiogenic and lymphangiogenic biomarkers

A strong correlation was identified between VEGFR3 and its ligands VEGFC (rho=0.3, p=0.03) and VEGFD (rho=0.4, p<0.0001; Table 2); VEGFR3 was significantly correlated with intratumor LmVD (rho=0.23, p=0.03). VEGFC was co-expressed with VEGFD (rho=0.27, p=0.01) and marginally with VEGF (rho=0.21, p=0.06). Interestingly a different correlation pattern was observed for ACs compared with SCCs; VEGFR3–VEGFC and VEGFR3–VEGFD correlations were more prominent in the SCC group (rho=0.37, p< 0.001 and rho=0.57, p<0.0001), whereas no correlation was observed between VEGFD and VEGFR3 in ACs.

Univariate analysis for individual angiogenic and lymphangiogenic biomarkers

Survival analysis of individual markers did not reveal any prognostic value for VEGF and VEGFC in all patients (log rank p=0.82 and p=0.79, respectively). A trend towards prolonged survival was observed for patients with high VEGFD expression (median survival 42 months vs. 27 months for the low expressers, log rank p=0.17). Tumors that did not express any VEGFR3 were associated with a shorter median survival compared to VEGFR3 positive tumors (7 vs. 31 months, log rank p=0.03). The prognostic potential of VEGFR3 was more prominent in early stage patients (42 vs. 19 months log rank p=0.01). Cox univariate analysis was used to reveal any association between MVD and LmVD and disease specific survival; both failed to predict survival (hazard ratio (HR)=0.99, 95% confidence intervals (CI)=0.98–1.005, p=0.27 for MVD and HR=0.99, 95% CI=0.98–1.01, p=0.89). We performed subgroup analysis in adenocarcinomas and squamous cell carcinomas; interestingly, VEGF was significantly correlated with survival in the AC group (median survival 42 vs. 7 months for low vs. high expressers, log rank p=0.014) but not in the SCC group (log rank p=0.5).

Assessment of the independent potential of individual angiogenic and lymphangiogenic biomarkers to predict survival

Multivariate Cox proportional hazards regression analysis adjusting for all clinical characteristics and receipt of systemic chemotherapy revealed an independent correlation of VEGFR3 with prolonged disease specific survival for

Table 2 Correlations between among angiogenesis and lymphangiogenesis factors for all patients of the lung cancer cohort

	VEGF	VEGFC	VEGFD	VEGFR3	MVD	LVD
VEGF	1	*p= 0.06*	NS	NS	NS	*p= 0.09*
VEGFC	0.21	1	***p*=0.01**	***p*=0.003**	NS	NS
VEGFD	−0.01	0.27	1	***p*<0.0001**	NS	NS
VEGFR3	0.06	0.3	0.4	1	NS	***p*=0.03**
MVD	−0.04	0.03	0.001	0.09	1	NS
LVD	0.2	0.15	0.06	0.23	−0.01	1

Spearman rho coefficients displayed for nonparametric correlations between semiquantitative VEGF, VEGFC, VEGFD, and VEGFR3 scores and continuous MVD and LVD scores (lower half). Significant *p* values at a level of 0.05 are shown in bold, trending in italics (upper half)

VEGF vascular endothelial factor, *VEGFR* vascular endothelial factor receptor, *MVD* microvessel density, *LVD* lymphatic vessel density, *NS* nonsignificant

stage I–IIIA patients (HR=0.05, 95% CI=0.008–0.32, p=0.002; Table 3). VEGF was significantly associated with survival for AC patients after adjustment for age, gender, stage, smoking, and receipt of chemotherapy (HR=8.69, 95% CI=1.4–53.69, p=0.02; Table 3). No other significant correlations with NSCLC specific survival were observed in multivariable analysis of individual angiogenic and lymphangiogenic biomarkers in all patients as well as stage I–IIIA, adenocarcinomas, and squamous cell carcinomas.

Multiplexed survival analysis of angiogenic and lymphangiogenic factors

Biomarker measurements were multiplexed in a Cox proportional hazards regression model adjusting for clinical characteristics and receipt of systemic chemotherapy; cases with missing values as well as three LCC and three NSCLC NOS specimens were excluded from analysis. Stage and high VEGFC expression were independent predictors of survival (HR=4, 95% CI=1.11–14.27, p=0.03; Table 4); interestingly, when VEGFR3 was multiplexed with other angiogenic and lymphangiogenic markers no association with survival was observed (HR=0.85, 95% CI=0.08–8.46, p=0.88). In a subset analysis of stage I–IIIA patients, VEGFC and VEGFR3 expression significantly contributed to the prognostic value of the model such that patients with high VEGFC expression had a tenfold increase in risk, whereas those with high VEGFR3 expression had a 99% reduction in risk for death of NSCLC (HR=0.01, 95% CI=0–0.34, p=0.01; Table 4).

Table 3 Cox multivariable analysis for VEGFR3 and VEGF in stage I–IIIA and adenocarcinoma patients

Variable	HR (95% CI)	p value
Stage I–IIIA (n=59)		
Gender (Male vs. Female)	0.78 (0.22–2.83)	0.7
Age	1.03 (0.97–1.1)	0.27
Stage I	1.00	**0.028**
Stage II	2.78 (1.01–7.65)	**0.048**
Stage III	4.77 (1.49–15.21)	**0.008**
Smoking (Yes vs. No)	1.5 (0.29–7.77)	0.6
Receipt of Treatment (Yes vs. No)	0.68 (0.27–1.72)	0.4
VEGFR3 (Positive vs. Negative)	0.05 (0.008–0.32)	**0.002**
Adenocarcinomas (n=47)		
Gender (Male vs. Female)	2.58 (0.35–19.1)	0.35
Age	1.02 (1.1–0.52)	0.52
Stage I	1.00	0.28
Stage II	5.2 (0.9–29.2)	**0.06**
Stage III	3.6 (0.69–18.8)	*0.12*
Stage IV	5.4 (0.73–40.4)	**0.09**
Smoking (Yes vs. No)	1.16 (0.06–21.3)	0.9
Receipt of Treatment (Yes vs. No)	0.78 (0.16–3.6)	0.75
VEGF (High vs. Low expression)	8.6 (1.4–53.6)	**0.02**

Statistically significant p values at the 0.05 level in bold; trending p values in italics

Development of a weighted prognostic classifier for stage I–IIIA patients

Weighted expression of the independent prognostic variables in multivariable analysis—VEGFC, VEGFR3, and stage—were used to build a prognostic classifier to stratify early stage patients in high and low risk groups. Based on the Cox regression coefficients (Table 4), we developed a risk scoring system assigning 1 point to stage I, 7.4 points to stage II, 11.86 points to stage III, 1 point to low VEGFC expression, 10.4 points to high VEGFC expression, 1 point to VEGFR3 nonexpressing tumors, and 0.01 points to VEGFR3 expressing tumors. Patients were classified into three groups using tertiles as cutoff points: scores ranged from 0 to 3, 3.01 to 11.41, and >11.42 for the first (n=15), second (n=21), and third (n=20) risk groups, respectively. Patients in the first risk group had a favorable prognosis compared with the second and third risk groups with Kaplan–Meier curves showing a distinct convergence of the top 2 groups (estimated median survival 55 vs. 36 vs. 26 months for the first, second, and third risk groups, respectively, log rank p=0.067; Fig. 3a). On that basis, the second and third risk group were combined and patients were further classified into two risk groups; Kaplan–Meier analysis for the dichotomized scores revealed a statistically significant prolonged disease specific survival for patients in the low risk group (estimated median survival 55 vs. 22 months for the high risk group, log rank p=0.02; Fig. 3b). Interestingly, six stage I NSCLC patients were classified in the high risk group, underlying the weakness of the TNM-based classification to accurately stratify patients by risk.

Assessment of angiogenic and lymphangiogenic factors as predictors of early recurrence

VEGF, VEGFC and VEGFD expression were not associated with early recurrence (Wilcoxon p=0.48, p=0.48, and p=0.23, respectively). Patients that recurred within the first year of diagnosis had lower VEGFR3 expression compared with patients that did not experience an early recurrence; however, this did not reach significance (p=0.14). MVD and LmVD failed to predict early recurrence (p=0.49 and p=0.37, respectively). A trend towards shorter disease-free survival was observed for VEGF expressing tumors (median estimated survival 5 months vs. not reached for the nonexpressers, log rank p=0.065), whereas patients in the VEGFR3 expressing group had prolonged disease-free survival compared with no expressers (12 vs. 6 log rank p=0.06).

Table 4 Multivariate analysis of disease specific survival for angiogenic and lymphangiogenic factors in patients of the lung cancer cohort

Characteristic	All patients (n=97)		Stage I–IIIA patients (n=59)	
	HR (95% CI)	p value	HR (95% CI)	p value
Age	1.03 (0.97–1.09)	0.38	1.05 (0.96–1.13)	0.24
Gender				
Female	1		1	
Male	0.88 (0.21–3.72)	0.86	0.22 (0.03–1.7)	0.15
Stage				
Stage I	1		1	
Stage II	3.64 (1.01–13.3)	**0.05**	7.4 (1.4–38.6)	**0.02**
Stage III	3.9 (1.07–14.3)	**0.04**	11.86 (1.5–89.3)	**0.16**
Stage IV	3.1 (0.62–15.9)	*0.16*		
Histology				
Adenocarcinoma	1		1	
Squamous cell carcinoma	0.77 (0.33–1.8)	0.54	1.8 (0.47–7.1)	0.37
Systemic Treatment				
No	1		1	
Yes	0.58 (0.2–1.7)	0.32	0.46 (0.1–1.92)	0.27
Smoking				
No	1		1	
Yes	3.5 (0.25–51.3)	0.35	4.77 (0.2–20.4)	0.33
VEGF				
High vs. Low expression	1.4 (0.25–7.9)	0.69	0.11 (0.002–5.2)	0.27
VEGFC				
High vs. Low expression	4 (1.11–14.27)	**0.03**	10.6 (4.3–26.5)	**0.004**
VEGFD				
High vs. Low expression	0.61 (0.26–1.42)	0.25	0.75 (0.23–2.4)	0.64
VEGFR3				
Positive vs. Negative	0.85 (0.08–8.46)	0.88	0.01 (0–0.34)	**0.01**
MVD	1 (0.98–1.02)	0.97	1.01 (0.99–1.03)	0.25
LVD	1.01 (0.99–1.03)	0.42	1 (0.97–1.04)	0.9

The p is given for multivariate Cox proportional hazards regression analysis. Statistically significant p values are in boldface; trending p values in italics; MVD and LVD were analyzed as continuous variable

VEGF vascular endothelial growth factor, *VEGFR* vascular endothelial growth factor receptor, *MVD* microvessel density, *LVD* lymphatic vessel density, *HR* hazard ratio, *CI*; confidence interval

Angiogenesis and lymphangiogenesis markers as surrogates for response to chemotherapy

We compared VEGF, VEGFC, VEGFD, and VEGFR3 expression in responders (CR + PR) and nonresponders (SD + PD); however, there was no statistically significant association between biomarker expression and response to chemotherapy (p=0.34, p=0.63, p=0.17, and p=0.2, respectively); no significant association was observed in subgroup analysis of platinum-based or taxane-based

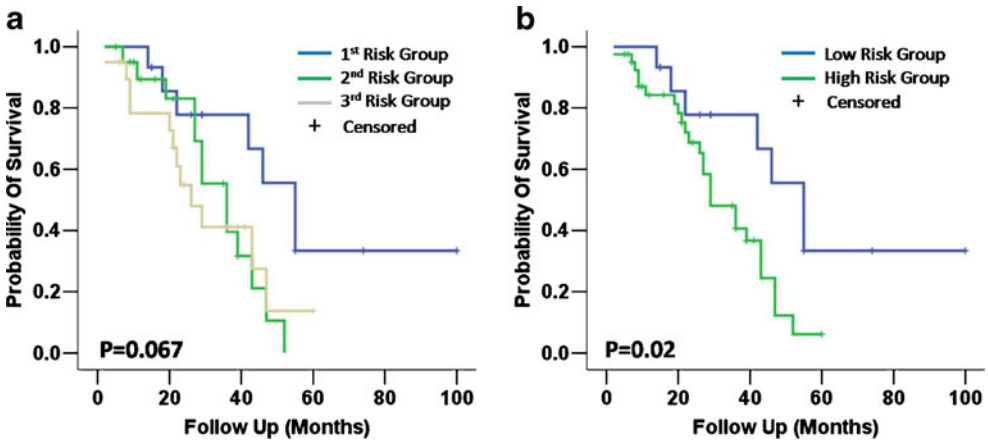

Fig. 3 Disease outcome of stage I–IIIA classified by risk. **a** Survival curves based on cohort division in three risk groups using the tertiles as cutoff points; patients classified in the first risk group show a benefit towards survival (log rank p=0.067). **b** Kaplan–Meier graphical analysis of disease specific survival in patients in the low risk group vs. patients at high risk; patients in the low risk group had a significantly higher median survival (log rank p=0.02)

treated patients. ANOVA revealed no significant differences in MVD or LmVD count among patients with CR, PR, SD, or PD ($p=0.8$ and $p=0.47$ for all comparisons); no significant association was found between responders and non responders ($p=0.43$ and $p=0.61$ for MVD and LmVD, respectively).

Discussion

Members of the vascular endothelial growth factor receptor family have been found to promote tumor growth and metastatic spread and inhibition of the VEGF/VEGFR2 and VEGFC/VEGFD/VEGFR3 axis seems to contribute to tumor regression in animal models including lung cancer [3]. These observations have prompted the development of angiogenic inhibitors [2]; the most robust evidence coming from increased response rates to the vascular endothelial growth factor inhibitor bevacizumab for tumors with adenocarcinoma histology [4]. The potential of angiogenic and lymphangiogenic biomarkers to predict survival for NSCLC patients remains controversial, with different studies demonstrating varying degrees of correlation with outcome [10, 11, 14–17]. The goal of this work was to assess expression of VEGF, VEGFC, VEGFD, and VEGFR3 and their association with intratumor microvessel and lymphatic vessel density in NSCLC to determine their prognostic and predictive value.

In a recent meta-analysis of 51 clinical studies combined hazard ratios suggested that VEGF overexpression had an unfavorable impact on survival of NSCLC patients, especially those with adenocarcinoma histology [10]. The association of VEGFC and VEGFD and their receptor VEGFR3 with disease specific survival is less clear; these biomarkers have been reported to be correlated with poor prognosis [18] or prolonged survival [11, 19], while others failed to demonstrate any prognostic value [10]. VEGFR3 expression in endothelial cells but not tumor cells has been found to be correlated with poor prognosis [20, 21]. We limited our observations to tumor cells and found that only VEGFR3 and VEGF independently predicted outcome when biomarkers were analyzed as individual variables. Microvessel density does not seem to be a prognostic factor in patients with early stage NSCLC in a systematic review of MVD measurements of 3,200 patients [22]; our results are consistent with these findings. Patients with high intratumoral [9] as well as high peritumoral [8, 23] lymphatic vessel density have been shown to have a significantly lower survival; we did not observe any significant association between LmVD and recurrence or NSCLC specific survival.

Early stage NSCLC patients are a heterogeneous group in terms of survival where there is an estimated 33–60% risk of disease-related death within five after "curative" surgical treatment [24]. The current staging system based on tumor characteristics fails to select early stage patients likely to recur and die of their disease after surgery; prognostication of disease outcome would benefit the clinician by categorizing early stage patients by risk and identifying candidates for adjuvant chemotherapy, whereas patients at a low risk could be spared what may be unnecessary treatment. Furthermore, both tumor angiogenesis and lymphangiogenesis are multistep complex processes that require the sequential activation of various receptors by numerous ligands [3]; therefore, analysis of angiogenic and lymphangiogenic factors as single biomarkers is unable to recapitulate the dynamic equilibrium of cancer cells. We developed a weighted classifier using multiplexed VEGFC and VEGFR3 measurements in addition to stage to stratify early stage patients in high and low risk groups; interestingly, our prognostic classification identified six high risk stage I NSCLC patients underlying the weakness of the TNM-based system to accurately predict outcome for those patients.

Gene expression profiling [25] and proteomic [26] studies reveal systematic differences between AC and SCC suggesting that these histological subgroups have distinct biologic and clinical properties. We performed subgroup analysis for ACs and SCCs and found that correlations between VEGFR3–VEGFC and VEGFR3–VEGFD differed significantly between ACs and SCCs. Interestingly, VEGF predicted outcome in the AC group (log rank $p=0.014$) but not in the SCC group (log rank $p=0.5$).

VEGFR3 immunoreactivity has been shown to correlate with lymph node metastases [27, 28]; however, other studies have failed to confirm these findings [19, 29]. VEGFD and VEGFC expression has also been reported to correlate with presence of lymph node metastases [17]; we did not find any significant association between VEGFC, VEGFD, or VEGFR3 and nodal status. The lymphatic microvessel density has been reported to be an independent predictor of lymph node metastasis [8, 14, 30]; our analysis did not confirm these findings.

Given that VEGFC/VEGFR3 pathway inhibition has been shown to inhibit cancer progression one would expect that both high VEGFC and VEGFR3 expression would correlate with unfavorable outcome. While VEGFC induces extensive lymphatic sprouting towards the tumor cells, VEGFD induces lymphangiogenesis and yet, represses angiogenesis and tumor growth highlighting functional differences despite binding VEGFR3 [31]. Signaling through VEGFR3 does not always equate to lymphatic tumor spread [32] and further aspects of VEGFR3 signaling may be complicated by the fact that VEGFR3 can form heterodimers with VEGFR2 localized on lymphatic endothelial cells [33].

Angiogenesis and lymphangiogenesis biomarkers have not been thoroughly studied as predictors of response to chemotherapy. VEGFC serum levels have been shown to decrease after systemic chemotherapy; however, no correlation was found between VEGFC and VEGFD concentrations and the effect of treatment [34]. We did not observe any significant differences in VEGF, VEGFC, VEGFD, or VEGFR3 expression between responders and nonresponders to either platinum-based or taxane-based first line chemotherapy. Furthermore, no significant differences in MVD or LmVD count were found between responders and non responders.

Potential limitations of this study include the retrospective nature of our cohort collection and the heterogeneity of the cohort in terms of treatment. Analysis of archival cohorts, such as this, provides valuable preliminary data for identifying prognostic and predictive biomarkers and could facilitate improving the study design of randomized trials by the inclusion of prospective multiparametric biomarker-based approaches. Further studies in larger cohorts are required to validate our results especially in enriched early stage NSCLC cohorts.

In conclusion, we assessed the prognostic and predictive potential of angiogenic and lymphangiogenic biomarkers in NSCLC patients and found that VEGF and VEGFR3 protein levels are independent prognostic factors for adenocarcinomas and early stage primary NSCLC patients, respectively. We developed a weighted classifier using VEGFC and VEGFR3 measurements and stage to classify early stage patients by risk, and we identified a group of surgically treated early stage patients with a worse prognosis; these patients might be candidates for adjuvant chemotherapy. Our results indicate that none of the biomarkers studied predicts response to conventional chemotherapy. Our multivariable model may be useful for identifying which early stage patients can be treated with surgery alone and which would benefit from adjuvant chemotherapy as well as incorporating angiogenic and lymphangiogenic biomarkers into clinical decisions.

Conflict of interest Authors do not have any conflict of interest.

References

1. Bergers G, Benjamin LE (2003) Tumorigenesis and the angiogenic switch. Nat Rev Cancer 3(6):401–410. doi:10.1038/nrc1093
2. Gasparini G, Longo R, Toi M, Ferrara N (2005) Angiogenic inhibitors: a new therapeutic strategy in oncology. Nat Clin Pract Oncol 2(11):562–577. doi:10.1038/ncponc0342
3. Ferrara N, Gerber HP, LeCouter J (2003) The biology of vegf and its receptors. Nat Med 9(6):669–676. doi:10.1038/nm0603-669
4. Sandler A, Gray R, Perry MC, Brahmer J, Schiller JH, Dowlati A, Lilenbaum R, Johnson DH (2006) Paclitaxel-carboplatin alone or with bevacizumab for non-small-cell lung cancer. N Engl J Med 355(24):2542–2550. doi:10.1056/NEJMoa061884
5. El-Chemaly S, Levine SJ, Moss J (2008) Lymphatics in lung disease. Ann NY Acad Sci 1131:195–202. doi:10.1196/annals.1413.017
6. Achen MG, Stacker SA (2008) Molecular control of lymphatic metastasis. Ann NY Acad Sci 1131:225–234. doi:10.1196/annals.1413.020
7. Stacker SA, Achen MG, Jussila L, Baldwin ME, Alitalo K (2002) Lymphangiogenesis and cancer metastasis. Nat Rev Cancer 2 (8):573–583. doi:10.1038/nrc863
8. Renyi-Vamos F, Tovari J, Fillinger J, Timar J, Paku S, Kenessey I, Ostoros G, Agocs L, Soltesz I, Dome B (2005) Lymphangiogenesis correlates with lymph node metastasis, prognosis, and angiogenic phenotype in human non-small cell lung cancer. Clin Cancer Res 11(20):7344–7353
9. Kadota K, Huang CL, Liu D, Ueno M, Kushida Y, Haba R, Yokomise H (2008) The clinical significance of lymphangiogenesis and angiogenesis in non-small cell lung cancer patients. Eur J Cancer 44(7):1057–1067
10. Zhan P, Wang J, Lv XJ, Wang Q, Qiu LX, Lin XQ, Yu LK, Song Y (2009) Prognostic value of vascular endothelial growth factor expression in patients with lung cancer: a systematic review with meta-analysis. J Thorac Oncol 4(9):1094–1103. doi:10.1097/JTO.0b013e3181a97e31
11. de Santa C, Pau E, Arias FC, Caso Pelaez E, Munoz Molina GM, Sanchez Hernandez I, Muguruza Trueba I, Moreno Balsalobre R, Sacristan Lopez S, Gomez Pinillos A, del Val Toledo Lobo M (2009) Prognostic significance of the expression of vascular endothelial growth factors a, b, c, and d and their receptors r1, r2, and r3 in patients with nonsmall cell lung cancer. Cancer 115(8):1701–1712
12. Travis WD, Brambilla E, Muller-Hermelink HK, Harris CC (2004) World health organization classification of tumors. Pathology and genetics of tumors of the lung, pleura, thymus and heart. IARC Press, Lyon
13. Therasse P, Arbuck SG, Eisenhauer EA, Wanders J, Kaplan RS, Rubinstein L, Verweij J, Van Glabbeke M, van Oosterom AT, Christian MC, Gwyther SG (2000) New guidelines to evaluate the response to treatment in solid tumors. European organization for research and treatment of cancer, national cancer institute of the united states, national cancer institute of canada. J Natl Cancer Inst 92(3):205–216
14. Adachi Y, Nakamura H, Kitamura Y, Taniguchi Y, Araki K, Shomori K, Horie Y, Kurozawa Y, Ito H, Hayashi K (2007) Lymphatic vessel density in pulmonary adenocarcinoma immunohistochemically evaluated with anti-podoplanin or anti-d2-40 antibody is correlated with lymphatic invasion or lymph node metastases. Pathol Int 57(4):171–177
15. Andersen S, Donnem T, Al-Saad S, Al-Shibli K, Busund LT, Bremnes RM (2009) Angiogenic markers show high prognostic impact on survival in marginally operable non-small cell lung cancer patients treated with adjuvant radiotherapy. J Thorac Oncol 4(4):463–471. doi:10.1097/JTO.0b013e3181991d18
16. Arinaga M, Noguchi T, Takeno S, Chujo M, Miura T, Uchida Y (2003) Clinical significance of vascular endothelial growth factor c and vascular endothelial growth factor receptor 3 in patients with nonsmall cell lung carcinoma. Cancer 97(2):457–464. doi:10.1002/cncr.11073
17. Bo C, Xiaopeng D, Chuanliang P, Xiaogang Z (2009) Expression of vascular endothelial growth factors c and d correlates with lymphangiogenesis and lymph node metastasis in lung adenocarcinoma. Thorac Cardiovasc Surg 57(5):291–294. doi:10.1055/s-0029-1185625
18. Saintigny P, Kambouchner M, Ly M, Gomes N, Sainte-Catherine O, Vassy R, Czernichow S, Letoumelin P, Breau JL, Bernaudin JF,

Kraemer M (2007) Vascular endothelial growth factor-c and its receptor vegfr-3 in non-small-cell lung cancer: concurrent expression in cancer cells from primary tumour and metastatic lymph node. Lung cancer (Amsterdam, Netherlands) 58(2):205–213
19. Maekawa S, Iwasaki A, Shirakusa T, Enatsu S, Kawakami T, Kuroki M, Kuroki M (2007) Correlation between lymph node metastasis and the expression of vegf-c, vegf-d and vegfr-3 in t1 lung adenocarcinoma. Anticancer Res 27(6A):3735–3741
20. Kojima H, Shijubo N, Yamada G, Ichimiya S, Abe S, Satoh M, Sato N (2005) Clinical significance of vascular endothelial growth factor-c and vascular endothelial growth factor receptor 3 in patients with t1 lung adenocarcinoma. Cancer 104(8):1668–1677
21. Chen F, Takenaka K, Ogawa E, Yanagihara K, Otake Y, Wada H, Tanaka F (2004) Flt-4-positive endothelial cell density and its clinical significance in non-small cell lung cancer. Clin Cancer Res 10(24):8548–8553
22. Trivella M, Pezzella F, Pastorino U, Harris AL, Altman DG (2007) Microvessel density as a prognostic factor in non-small-cell lung carcinoma: a meta-analysis of individual patient data. Lancet Oncol 8(6):488–499. doi:10.1016/S1470-2045(07)70145-6
23. Sun JG, Wang Y, Chen ZT, Zhuo WL, Zhu B, Liao RX, Zhang SX (2009) Detection of lymphangiogenesis in non-small cell lung cancer and its prognostic value. J Exp Clin Cancer Res 28:21
24. Hoffman PC, Mauer AM, Vokes EE (2000) Lung cancer. Lancet 355(9202):479–485. doi:10.1016/S0140-6736(00)82038-3
25. Weir BA, Woo MS, Getz G, Perner S, Ding L, Beroukhim R, Lin WM, Province MA, Kraja A, Johnson LA, Shah K, Sato M, Thomas RK, Barletta JA, Borecki IB, Broderick S, Chang AC, Chiang DY, Chirieac LR, Cho J, Fujii Y, Gazdar AF, Giordano T, Greulich H, Hanna M, Johnson BE, Kris MG, Lash A, Lin L, Lindeman N, Mardis ER, McPherson JD, Minna JD, Morgan MB, Nadel M, Orringer MB, Osborne JR, Ozenberger B, Ramos AH, Robinson J, Roth JA, Rusch V, Sasaki H, Shepherd F, Sougnez C, Spitz MR, Tsao MS, Twomey D, Verhaak RG, Weinstock GM, Wheeler DA, Winckler W, Yoshizawa A, Yu S, Zakowski MF, Zhang Q, Beer DG, Wistuba II, Watson MA, Garraway LA, Ladanyi M, Travis WD, Pao W, Rubin MA, Gabriel SB, Gibbs RA, Varmus HE, Wilson RK, Lander ES, Meyerson M (2007) Characterizing the cancer genome in lung adenocarcinoma. Nature 450(7171):893–898. doi:10.1038/nature06358
26. Yanagisawa K, Shyr Y, Xu BJ, Massion PP, Larsen PH, White BC, Roberts JR, Edgerton M, Gonzalez A, Nadaf S, Moore JH, Caprioli RM, Carbone DP (2003) Proteomic patterns of tumour subsets in non-small-cell lung cancer. Lancet 362(9382):433–439. doi:10.1016/S0140-6736(03)14068-8
27. Donnem T, Al-Shibli K, Al-Saad S, Delghandi MP, Busund LT, Bremnes RM (2009) Vegf-a and vegfr-3 correlate with nodal status in operable non-small cell lung cancer: Inverse correlation between expression in tumor and stromal cells. Lung cancer (Amsterdam, Netherlands) 63(2):277–283
28. Ko YH, Jung CK, Lee MA, Byun JH, Kang JH, Lee KY, Jo KH, Wang YP, Hong YS (2008) Clinical significance of vascular endothelial growth factors (vegf)-c and -d in resected non-small cell lung cancer. Cancer Res Treat 40(3):133–140
29. Takizawa H, Kondo K, Fujino H, Kenzaki K, Miyoshi T, Sakiyama S, Tangoku A (2006) The balance of vegf-c and vegfr-3 mrna is a predictor of lymph node metastasis in non-small cell lung cancer. Br J Cancer 95(1):75–79
30. Takanami I (2006) Lymphatic microvessel density using d2-40 is associated with nodal metastasis in non-small cell lung cancer. Oncol Rep 15(2):437–442
31. Kopfstein L, Veikkola T, Djonov VG, Baeriswyl V, Schomber T, Strittmatter K, Stacker SA, Achen MG, Alitalo K, Christofori G (2007) Distinct roles of vascular endothelial growth factor-d in lymphangiogenesis and metastasis. Am J Pathol 170(4):1348–1361
32. He Y, Rajantie I, Pajusola K, Jeltsch M, Holopainen T, Yla-Herttuala S, Harding T, Jooss K, Takahashi T, Alitalo K (2005) Vascular endothelial cell growth factor receptor 3-mediated activation of lymphatic endothelium is crucial for tumor cell entry and spread via lymphatic vessels. Cancer Res 65(11):4739–4746. doi:10.1158/0008-5472.CAN-04-4576
33. Dixelius J, Makinen T, Wirzenius M, Karkkainen MJ, Wernstedt C, Alitalo K, Claesson-Welsh L (2003) Ligand-induced vascular endothelial growth factor receptor-3 (vegfr-3) heterodimerization with vegfr-2 in primary lymphatic endothelial cells regulates tyrosine phosphorylation sites. J Biol Chem 278(42):40973–40979. doi:10.1074/jbc.M304499200
34. Naumnik W, Izycki T, Swidzinska E, Ossoliniska M, Chyczewska E (2007) Serum levels of vegf-c, vegf-d, and svegf-r2 in patients with lung cancer during chemotherapy. Oncol Res 16(9):445–451

Virchows Arch (2011) 458:341–348
DOI 10.1007/s00428-010-1026-1

ORIGINAL ARTICLE

Expression pattern of claudins 1 and 3—an auxiliary tool in predicting behavior of mucoepidermoid carcinoma of salivary gland origin

Katri Aro · Luiz Eduardo Blumer Rosa · Ibrahim O. Bello · Ylermi Soini · Antti A. Mäkitie · Tuula Salo · Ilmo Leivo

Received: 14 September 2010 / Revised: 6 November 2010 / Accepted: 5 December 2010 / Published online: 24 December 2010
© Springer-Verlag 2010

Abstract Claudins (CLDNs) are a family of membrane proteins important for permeability of tight junctions. They have also been implicated in carcinogenesis and tumor progression. We analyzed patterns of distribution and intensity of expression of CLDNs 1, 3, 4, and 7 in mucoepidermoid carcinoma (MEC) of salivary gland in 39 patients. Correlations between the expression of CLDNs, tumor grade, and survival were explored. In immunohistochemical analysis, high expression of CLDN 1 was seen in low-grade MEC, and it appeared to be a suitable auxiliary marker of good prognosis. It classified MEC similarly to histological grading in 89.7% of cases (p=0.001). High CLDN 3 expression was seen in intermediate- and high-grade MEC, while it was low in low-grade MEC. CLDN 3 intensity correctly categorized tumors into grades in 71.8% of cases (p= 0.017). However, in multivariate analysis CLDN 1 and CLDN 3 did not achieve significance over tumor grade in predicting patient behavior. We conclude that analysis of staining intensities of CLDN 1 and 3 is useful as an

Katri Aro and Luiz Eduardo Blumer Rosa have equal contribution to this study

K. Aro
Department of Otolaryngology—Head and Neck Surgery,
Helsinki University Central Hospital,
Helsinki, Finland

A. A. Mäkitie
Department of Otolaryngology-Head and Neck Surgery,
University of Helsinki and Helsinki University Central Hospital,
Helsinki, Finland

L. E. B. Rosa · I. O. Bello
Department of Diagnostics and Oral Medicine,
Institute of Dentistry, University of Oulu,
Oulu, Finland

T. Salo
Department of Diagnostics and Oral Medicine,
Institute of Dentistry, University of Oulu
and Oulu University Hospital,
Oulu, Finland

L. E. B. Rosa
Department of Biosciences and Oral Diagnostic, Oral Pathology,
School of Dentistry, UNESP,
São José dos Campos, Brazil

Y. Soini
Department of Clinical Pathology and Forensic Medicine,
University of Eastern Finland and Department of Pathology,
Kuopio University Hospital,
Kuopio, Finland

I. O. Bello
Haartman Institute, Department of Pathology,
University of Helsinki,
Helsinki, Finland

I. Leivo (✉)
Haartman Institute, Department of Pathology,
University of Helsinki and HUSLAB, Helsinki,
and Department of Pathology, University of Turku,
Turku, Finland
e-mail: ilmo.leivo@helsinki.fi
e-mail: ilmo.leivo@utu.fi

auxiliary diagnostic and prognostic tool in patients with salivary gland MEC.

Keywords Claudin · Tight junctions · Mucoepidermoid carcinoma · Immunohistochemistry · Head and neck · Prognostic marker

Introduction

Tight junctions (TJs) are cell organelles that contribute to cellular polarity and paracellular barriers [1]. They control paracellular ion flux and participate in the maintenance of tissue homeostasis [2–7]. Due to their ability to recruit signalling proteins, TJs have been proposed to be involved in the regulation of cell proliferation, differentiation, and other functions [6, 7]. Changes in TJs including loss of cell-to-cell adhesion are seen in tumor cell invasion and at early stages of metastasis [4, 8–13]. The change in the phenotype of TJs leads to increased influx of nutrients and growth factors, and provides an advantageous environment for tumor spread [5].

Claudins (CLDNs) mediate the permeability function of TJs [5]. At present, at least 24 different CLDN proteins are known, and their distributions in various tissues have been disclosed in recent studies [1, 5, 6, 13]. They determine the barrier properties of these cell–cell contacts between plasma membranes of two neighboring cells. CLDN in TJs of epithelial cells may account for observed differences in permeability and electrical resistance between different epithelia [3].

Mucoepidermoid carcinoma (MEC) is subdivided into three categories, low grade (LG), intermediate grade (IMG), and high grade (HG) based on histopathological parameters. HG-MEC is one of the most frequent high-grade carcinomas in salivary glands [14, 15]. Previously, it has been shown that there is a strong association between tumor grade, stage, and prognosis [16, 17]. However, histopathologic grading of MEC has been criticized for problems in reproducibility and its predictive accuracy. In addition, there is a lack of useful prognostic protein markers in MEC. The aim of this study was to investigate the diagnostic and predictive value of different CLDNs in MEC.

Materials and methods

Patients

Between 1976 and 2005, 60 adult patients with MEC of the major salivary glands were diagnosed and treated at the

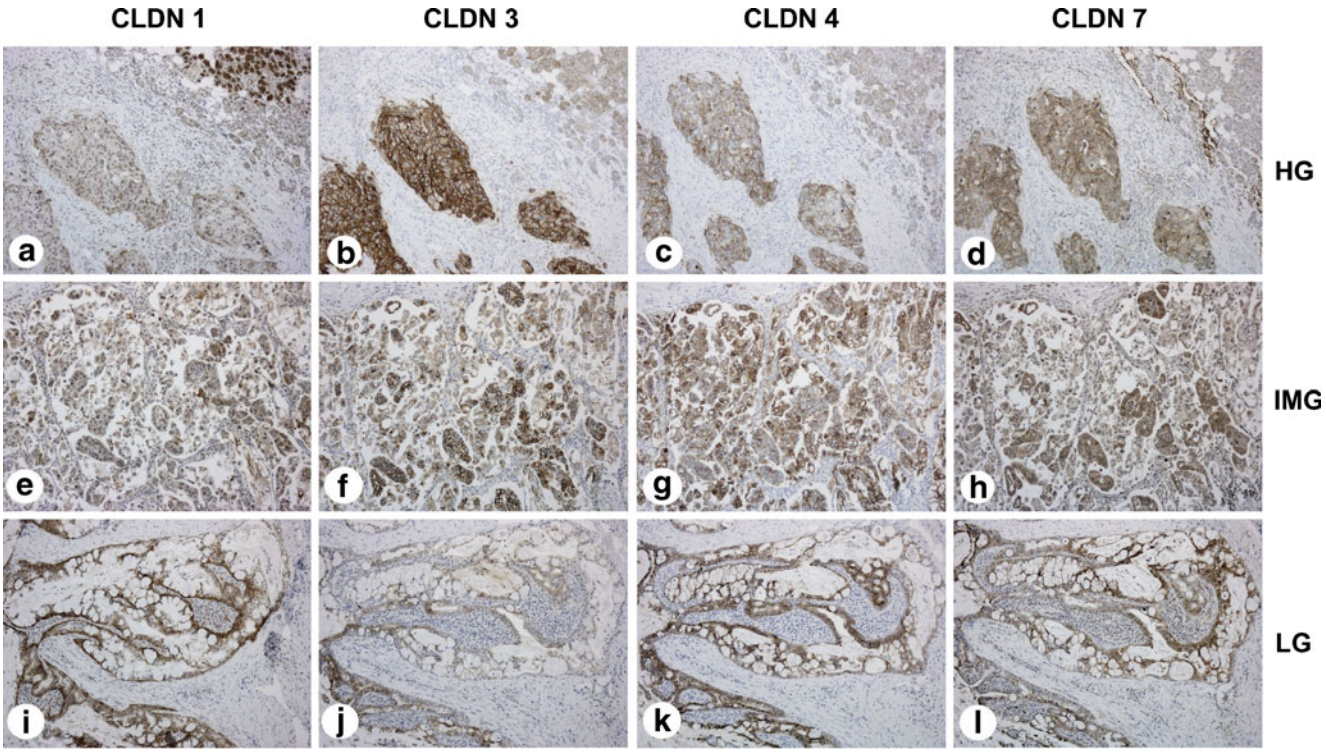

Fig. 1 Tissue distribution of claudins 1 (CLDN 1), -3 (CLDN 3), -4 (CLDN 4), and -7 (CLDN 7) in mucoepidermoid carcinomas (MEC). High-grade (*HG*), intermediate grade (*IMG*), low-grade (*LG*). Normal parotid gland tissue is seen in the *upper right corner* of the photomicrograph (**a**, **e**, **i**). Low intensity of staining for CLDN 1 is seen in HG-MEC (**a**), while epidermoid areas of LG-MEC are strongly stained (**i**). In CLDN 3, HG-MEC is strongly positive (**b**), while there is only weak staining in LG-MEC (**j**). In CLDN 4 (**c**, **g**, **k**) and CLDN 7 (**d**, **h**, **l**), differences in staining intensity between HG-MEC and LG-MEC (**c** to **k**, **d** to **l**) are not pronounced. Magnification ×80

Table 1 Statistical relationship between grade and pattern of CLDN immunostaining. The reference category is HG

	LG $n=17$	IMG $n=6$
CLDN 1 intensity		
P value	0.001[a]	0.557
OR	8.322	1.479
95% CI for OR	2.461–28.147	0.401–5.450
CLDN 3 intensity		
P value	0.017[a]	0.454
OR	0.099	0.660
95% CI for OR	0.015–0.661	0.223–1.956
CLDN 4 intensity		
P value	0.314	0.296
OR	0.601	0.485
95% CI for OR	0.223–1.621	0.125–1.885
CLDN 7 intensity		
P value	0.025[a]	0.518
OR	6.563	1.829
95% CI for OR	1.273–33.832	0.293–11.418
CLDN 1 extent		
P value	0.006[a]	0.312
OR	3.501	1.729
95% CI for OR	1.436–8.534	0.598–5.001
CLDN 3 extent		
P value	0.014[a]	0.192
OR	0.314	0.506
95% CI for OR	0.125–0.793	0.182–1.408
CLDN 4 extent		
P value	0.411	0.120
OR	1.442	0.271
95% CI for OR	0.602–3.454	0.052–1.407
CLDN 7 extent		
P value	0.020[a]	0.224
OR	2.384	1.775
95% CI for OR	1.147–4.955	0.704–4.474

OR odds ratio, logistic regression, *CLDN* claudin, *n* number, *HG* high grade, *IMG* intermediate grade, *LG* low grade

[a] Statistical significance

Department of Otolaryngology—Head and Neck Surgery, Helsinki University Central Hospital, Helsinki, Finland. Of these, 39 patients had sufficient histologic tumor material and clinical data available and were included in this study. There were 15 (38%) males and 24 (62%) females. Mean age was 54 years (range 25 to 84 years). With the exception of one patient, all patients were treated with curative intent.

There were 16 (41%) HG-MECs, 6 (15%) IMG-MECs, and 17 (44%) LG-MECs. Criteria used for diagnosis were those of World Health Organization (2005), and criteria for grading were those recommended by the Armed Forces Institute of Pathology Fascicle (1996).

Immunohistochemistry and analysis of staining

For immunohistochemical analysis, 5-μm-thick sections were cut from the paraffin-embedded blocks that met the above inclusion criteria. The primary antibodies used were all purchased from Zymed Laboratories (South San Francisco, CA, USA) designed to be used in formalin-fixed, paraffin-embedded tissues. They were polyclonal rabbit anti-claudin-1 (clone JAY.8), polyclonal rabbit anti-claudin-3 (clone Z23.JM), monoclonal mouse anti-claudin-4 (clone 3E2C1), and polyclonal rabbit anti-claudin-7 (clone ZDM.241). Before the application of the primary antibodies, all sections were heated in a microwave oven in 10 mmol/L citrate buffer, pH 6.0, for 10 min. After 60 min of incubation with primary antibody (dilution, 1:50 for anti-claudins 1, 3, 4, and 7), a biotinylated secondary antibody and Histostain-SP kit (Zymed Laboratories) were used. For all the immunostaining procedures, the color was developed by diaminobenzidine, after which the sections were slightly counterstained with Harris' hematoxylin and mounted with Eukitt (Kindler, Freiburg, Germany). Negative control staining was carried out by substituting non-immune rabbit or mouse serum and phosphate-buffered saline (PBS) for the primary antibodies. Non-neoplastic kidney, breast, skin, and liver samples were used as positive and negative controls. The study was approved by the Research Ethics Board of the Helsinki University Central Hospital.

The immunostaining intensity of the tumor was compared with the histologically normal-appearing surrounding glandular structures and scored as follows: 0=no immunostaining; 1=less immunostaining intensity; 2=same immunostaining intensity; 3=more immunostaining intensity [13]. Membrane-bounded positivity was considered significant in the evaluation.

Immunostaining was assessed as follows: 0=no immunostaining; percentage of cells immunostained, 1=less than 25%; 2=25–50%; 3=50–75%; 4=more than 75%. To standardize the extent of immunostaining, the following categories were used: 1=low, 2 and 3=medium, and 4=high immunostaining.

The entire areas of the sections were scored. All assessments were made independently by two investigators (I.O.B. and L.E.B.R.). Discrepant cases were reanalyzed for consensus.

Statistical analysis

Thirty-eight out of the 39 patients in the series characterized histologically were included in the statistical analysis. It has been previously shown in our larger patient cohort

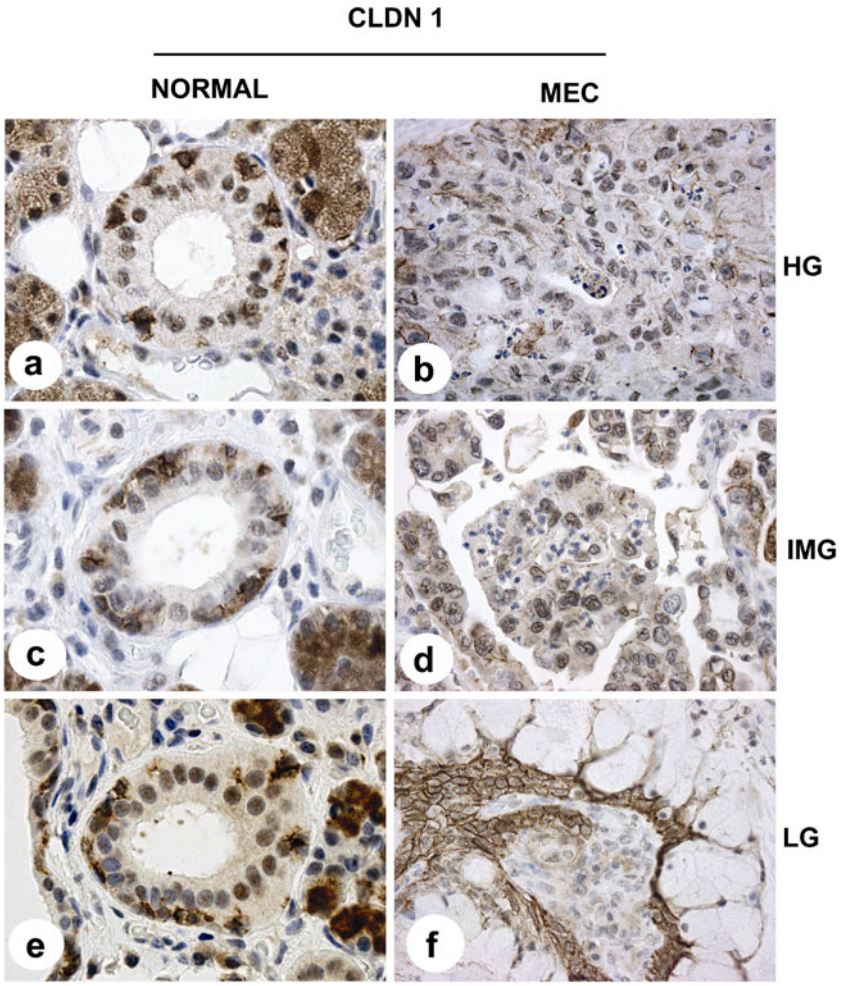

Fig. 2 Intensity and localization of staining for CLDN 1 in MEC and normal salivary gland. In HG- and IMG-MEC (**b**, **d**), only weak and mostly nuclear staining is seen in tumor cells, while in LG-MEC (**f**), stronger and mostly membranous staining is seen in cells with mostly intermediate cell morphology next to mucous tumor cells. For internal control of intensity, staining of tumor tissue was compared to the serous acini of the normal salivary gland of the same sections. Magnification ×250

that IMG-MECs and HG-MECs resemble each other in biologic behavior and patient survival [17]. Therefore, for the purpose of the statistical analysis, IMG-MECs and HG-MECs were combined (n=21), while LG-MECs formed the other group (n=17). Evaluation of the statistical association between results of the immunohistochemical analysis and patient survival was done using Kaplan–Meier survival analysis. Analyses were verified with Cox proportional hazards univariate regression models using the different CLDN intensities and extents. Logistic regression models were used to compare survival plots over the different CLDN staining categories (low, medium, and high).

All statistical analyses were performed using the SPSS statistical software, SPSS for Windows, version 16.0 (SPSS Inc, Chicago, IL, USA), and P values of less than 0.05 were considered statistically significant.

Survival analysis

As previously noted, one patient was excluded from the survival analysis due to less than 3 years of follow-up. Seven subjects were known to have died of salivary gland MEC, two died of other causes, and the cause of death was unknown in one patient. In survival analysis, only patients confirmed to have tumor recurrence or who had died of MEC were regarded as having a terminal event. Cases of death of disease comprised three males and four females. The 3-year overall survival (OS) was 74%, and the 3-year disease-free survival (DFS) was 74% for the whole patient series, and 100%, 50%, and 53% for LG-MECs, IMG-MECs, and HG-MECs, respectively.

Results

Distribution of CLDNs in MEC

Tissue distributions of CLDNs 1, 3, 4, and 7 were studied in 39 cases of MEC, including HG, IMG, and LG tumors. A low intensity of staining for CLDN 1 was seen in all areas of HG-MEC (Fig. 1a), while in LG-MEC, the areas of epidermoid differentiation showed strong positivity (Fig. 1i). In HG- and IMG-MECs, staining for CLDN 1 (Fig. 2b, d) showed only weak and mostly nonspecific nuclear reaction. In LG-MEC, however, a strong and mostly membranous staining was seen

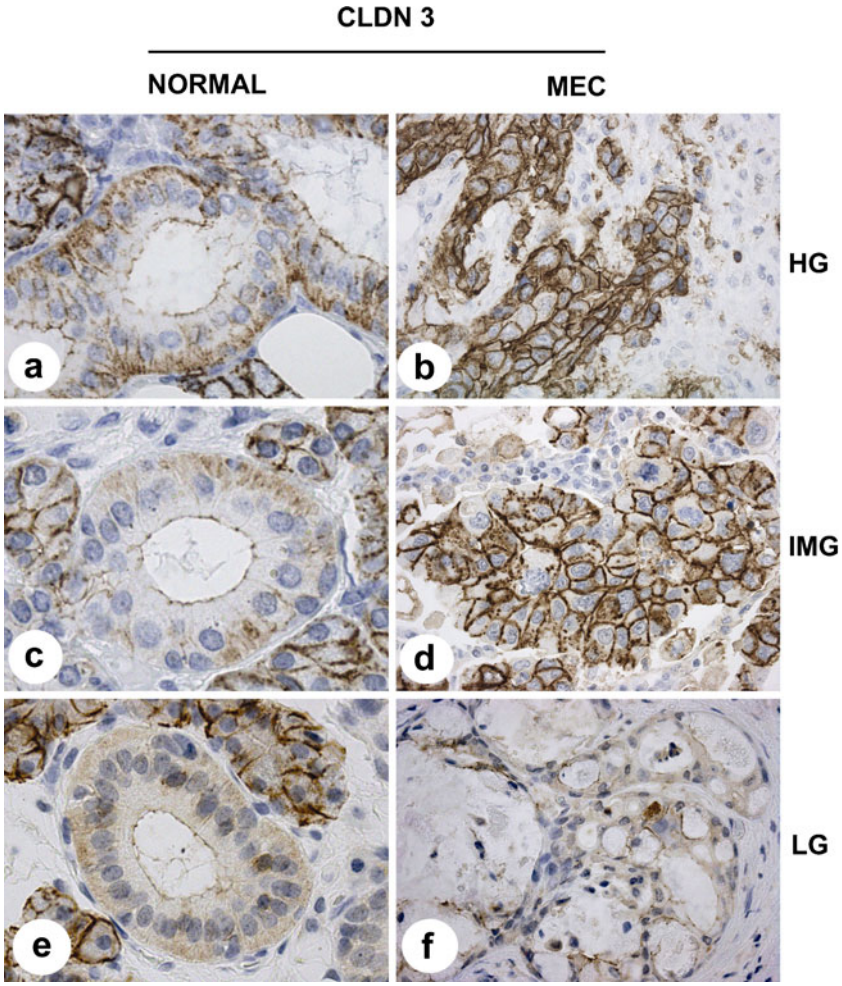

Fig. 3 Intensity and localization of staining for CLDN 3 in MEC and normal salivary gland. In HG- and IMG-MEC (**b**, **d**), strong membranous staining outlines cells with mostly intermediate cell morphology. In LG-MEC (**f**), almost no staining for CLDN 3 is seen. Serous acini of the normal salivary glands were used as internal control. Magnification ×250

in cells with mostly intermediate cell morphology located next to mucous tumor cells (Fig. 2f). In the immunostaining experiments, an internal control for intensity of staining was obtained by comparing the staining of tumor tissue with the staining of areas of normal salivary gland present in the same sections. In all cases, comparisons were made with the serous acini found in the sections.

In contrast to CLDN 1, our cases of HG- and IMG-MEC showed a strong membranous staining for CLDN 3 (Fig. 3b) that outlined cells of mostly intermediate and squamous cell morphology. In LG-MEC, almost no staining for CLDN 3 was seen (Fig. 3f).

In contrast to reactions for CLDN 1 and CLDN 3, the staining reactions for CLDN 4 (Fig. 1c, g, k) and CLDN 7 (Fig. 1d, h, l) showed no clear-cut differences in between HG- and LG-MECs (compare panels c, g, k to panels d, h, l in Fig. 1).

Diagnostic and prognostic significance of CLDNs in MEC

Association between CLDN immunostaining patterns and histopathologic tumor grades is shown in Table 1. In logistic regression model, intensity for CLDN 1 appeared to be better than for CLDN 3, 4, and 7 as a predictive parameter in MEC. It categorized tumors similarly with histopathologic grading (LG vs. IMG and HG) in 89.7% of cases (Table 2). In a hierarchic fitting model, use of the extent of CLDN 1 (p=0.006) did not increase grouping of cases identically with histopathologic grading compared to intensity of CLDN 1 (p=0.001). If a tumor had the highest intensity (score 3) of immunostaining for CLDN 1, it was likely to be LG with no recurrences (Table 2; Fig. 4). When the intensity for CLDN 1 staining differed from 1 to 2 or 3, odds ratio of LG-MEC over HG-MEC was over eightfold (Table 1). Intensity (p=0.017) for CLDN 3 categorized tumors similarly to histopathologic grades in 71.8% of cases, while the extent of CLDN 3 staining gave an almost similar statistical value (p=0.014). If a tumor stained highly for CLDN 3, it was most likely IMG or HG, with a worse prognosis (Fig. 5). Intensity and extent of CLDN 7 staining showed less statistical significance, while intensity and extent for CLDN 4 were not statistically significant (Table 1). In a multivariate analysis, only tumor grade showed statistical significance (not shown).

Table 2 Relationship between clinicopathological features and intensities of CLDNs 1 and 3

	Total n=39	Negative[a] CLDN1 intensity n=23	Positive[b] CLDN1 intensity n=16	Negative[a] CLDN3 intensity n=31	Positive[b] CLDN3 intensity n=8
Tumor grade					
LG	17	3	14	17	0
IMG	6	5	1	5	1
HG	16	15	1	9	7
T status					
T1	17	9	8	16	1
T2	9	3	6	6	3
T3	7	6	1	5	2
T4	6	5	1	4	2
N status					
N0	31	15	16	28	3
N1–3	8	8	0	3	5
Tumor stage					
I	16	8	8	15	1
II	6	0	6	6	0
III	5	4	1	4	1
IV	12	11	1	6	6
Recurrences					
Absent	31	15	16	27	4
Present	8	8	0	4	4

HG high grade, *IMG* intermediate grade, *LG* low grade, *n* number, *CLDN* claudin

[a] Immunostaining intensity 0–2

[b] Immunostaining intensity 3

Discussion

Claudins (CLDNs) are important for the permeability of TJs in normal cells, but they have also been implicated in epithelial carcinogenesis and tumor progression. We have now studied the distribution and intensity of staining for CLDNs 1, 3, 4, and 7 in mucoepidermoid carcinoma (MEC) of salivary gland origin and explored associations between the expression of CLDN proteins, tumor grade, and survival of the patients. High levels of CLDN 1 immunoreactivity were seen in low-grade (LG-) MEC, while the expression of CLDN 3 in LG cases was low. Also, we found that the staining intensities for CLDNs 1 and 3 could be used for classifying MECs into groups. In 89.7% of our 39 cases, CLDN 1 expression, and in 71.8%, CLDN 3 expression defined groups that corresponded to traditional histopathologic grading. However, in multivariate analysis, the expressions of CLDNs 1 and 3 did not achieve significance over tumor grade in predicting tumor

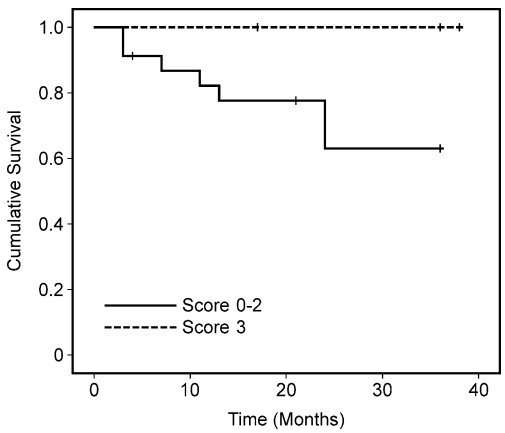

Fig. 4 Three-year disease-free survival (DFS) by CLDN 1 immunostaining intensity, p=0.008. Score 0–2 (n=22)=no immunostaining, less or same immunostaining intensity compared with the histologically normal-appearing glandular structures; score 3 (n=16)=more immunostaining intensity

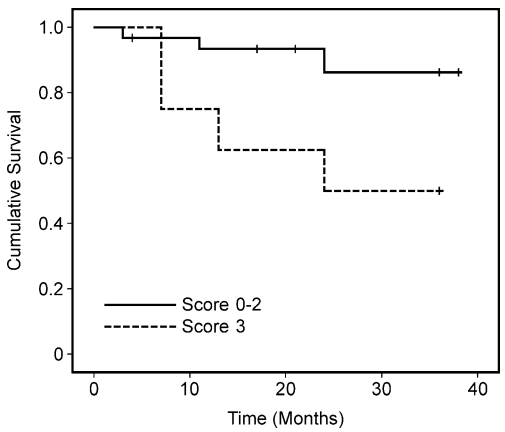

Fig. 5 Three-year DFS by CLDN 3 immunostaining intensity, p=0.015. Score 0–2 (n=30)=no immunostaining, less or same immunostaining intensity compared with the histologically normal-appearing glandular structures; score 3 (n=8)=more immunostaining intensity

behavior. Even CLDNs 4 and 7 did not show prognostic value in this study. We conclude that CLDNs 1 and 3 are useful as auxiliary prognostic markers in a histopathological evaluation of MEC.

Previous studies have shown that CLDNs are mainly expressed in epithelial tumors with site- and type-specific variation [18]. For example, the intestinal type of gastric carcinoma shows a strong expression of different CLDNs, while the diffuse type has a diminished CLDN expression [19]. Similarly, ductal and lobular carcinomas of the breast differ in their expression of CLDNs [20]. Differences in CLDNs also occur between squamous cell carcinomas and adenocarcinomas. In lung and esophageal tumors, squamous cell carcinomas showed a lower expression of CLDN 3 than the adenocarcinomas [21, 22]. Also MECs contain both squamous and adenocarcinomatous elements, but in contrast to the above, the most intense staining for CLDN 3 in MECs was seen in the squamous component.

In prognostic studies, Miyamoto et al. [9] reported that CLDN 1 positive esophageal squamous cell carcinomas had significantly fewer recurrences and that lack of CLDN 1 expression correlated with a poor prognosis. In renal and thyroid papillary carcinomas, CLDN 1 was a marker of favorable prognosis [3, 23]. Furthermore, in lung adenocarcinomas, a low mRNA expression of CLDN 1 was associated with a poor prognosis [24]. In contrast to these results, overexpression of CLDN 1 in oral squamous cell carcinomas and renal clear cell carcinomas was associated with aggressive behavior [10, 24]. Our previous study on oral tongue carcinomas, however, did not confirm the latter results [13]. In breast carcinomas, only CLDN 7 downregulation was associated with histological grade and metastasis [25]. On the other hand, in ovarian cancers, upregulation of CLDNs 3 and 4 led to increased motility, tumor cell survival, and invasion [26, 27]. However, in gastric carcinomas, loss of CLDN 3 was associated with poor prognosis [19]. The above examples indicate that associations of the various CLDNs with tumor prognosis are highly tumor type-specific.

In the present study, the expression of CLDN 1 was associated with good prognosis in MEC, and the expression of CLDN 3 correlated with the histopathological grade of MEC. However, in multivariate analysis neither of them achieved significance over tumor grade in predicting DFS. The present results with MEC suggest that immunohistochemical analysis of CLDNs is useful as an auxiliary prognostic tool in this neoplasia.

Acknowledgements We thank Antti Nevanlinna (MSc) and Professor Seppo Sarna for their expert help in the statistical work. This study was supported by grants from Finnish Cancer Society, Special Government Funding (EVO) of Helsinki, Kuopio and Oulu University Hospitals, Finnish Dental Society Apollonia, Finnish Lung Health Association (Filha), and Maritza and Reino Salonen Foundation.

Disclosure/conflict of interest The authors declare no conflict of interest.

References

1. Lourenco SV, Coutinho-Camillo CM, Buim MEC et al (2007) Human salivary gland branching morphogenesis: morphological localization of claudins and its parallel relation with developmental stages revealed by expression of cytoskeleton and secretion markers. Histochem Cell Biol 128:361–369
2. Morin PJ (2005) Claudin proteins in human cancer: promising new targets for diagnosis and therapy. Cancer Res 65:9603–9606
3. Tzelepi VN, Tsamandas AC, Vlotinou HD et al (2008) Tight junctions in thyroid carcinogenesis: diverse expression of claudin-1, claudin-4, claudin-7 and occludin in thyroid neoplasms. Mod Pathol 21:22–30
4. Michikawa H, Fujita-Yoshigaki J, Sugiya H (2008) Enhancement of barrier function by overexpression of claudin-4 in tight junctions of submandibular gland cells. Cell Tissue Res 334:255–264
5. Tsukita S, Yamazaki Y, Katsuno T et al (2008) Tight junction-based epithelial microenvironment and cell proliferation. Oncogene 27:6930–6938
6. Peppi M, Ghabriel MN (2004) Tissue-specific expression of the tight junction proteins claudins and occludin in the rat salivary glands. J Anat 205:257–266
7. Maria OM, Kim J-WM, Gerstenhaber JA et al (2008) Distribution of tight junction proteins in adult human salivary glands. J Histochem Cytochem 56:1093–1098
8. Singh AB, Sharma A, Dhawan P (2010) Claudin family of proteins and cancer: an overview. J Oncol 2010:541957
9. Miyamoto K, Kusumi T, Kijima H et al (2008) Decreased expression of claudin-1 is correlated with recurrence status in esophageal squamous cell carcinoma. Biomed Res 29:71–76
10. Pintor dos Reis P, Bharadwaj RR, Kamel-Reid S et al (2008) Claudin 1 overexpression increases invasion and is associated with aggressive histological features in oral squamous cell carcinoma. Cancer 113:3169–3180
11. Montgomery E, Mamelak AJ, Berg KD et al (2006) Overexpression of claudin proteins in esophageal adenocarcinoma and its precursor lesions. Appl Immunohistochem Mol Morphol 14:24–30
12. Al Moustafa A, Alaoui-Jamali MA, Foulkes WD et al (2002) Identification of genes associated with head and neck carcinogenesis by cDNA microarray comparison between matched primary normal epithelial and squamous cells. Oncogene 21:2634–2640
13. Bello IO, Vilen ST, Niinimaa A et al (2008) Expression of claudins 1, 4, 5, and 7 and occludin, and relationship with prognosis in squamous cell carcinoma of the tongue. Hum Pathol 39:1212–1220
14. Goode RK, Auclair PL, Ellis GL (1998) Mucoepidermoid carcinoma of the major salivary glands: clinical and histopathologic analysis of 234 cases with evaluation of grading criteria. Cancer 82:1217–1224
15. Luukkaa H, Klemi P, Leivo I et al (2005) Salivary gland cancer in Finland 1991–96: an evaluation of 237 cases. Acta Otolaryngol 125:207–214
16. Brandwein MS, Ivanov K, Mills SE et al (2001) Mucoepidermoid carcinoma: a clinicopathologic study of 80 patients with special reference to histological grading. Am J Surg Pathol 25:835–845
17. Aro K, Leivo I, Mäkitie AA (2008) Management and outcome of patients with mucoepidermoid carcinoma of major salivary gland

origin; a single institution's 30-year experience. Laryngoscope 118:258–262
18. Soini Y (2005) Expression of claudins 1, 2, 3, 4, 5 and 7 in various types of tumours. Histopathology 46:551–560
19. Soini Y, Tommola S, Helin H et al (2006) Claudin 1, 3, 4 and 5 in gastric carcinoma. Loss of claudin expression associates with the diffuse subtype. Virchows Arch 448:52–58
20. Soini Y (2004) Claudins 2, 3, 4 and 5 in Paget's disease and breast carcinoma. Hum Pathol 35:1531–1536
21. Moldway J, Jäckel M, Páska C et al (2007) Distinct claudin expression profile in histologic subtypes of lung cancer. Lung Cancer 57:159–167
22. Takala H, Saarnio J, Wiik H et al (2007) Claudins 1, 3, 4, 5 and 7 in esophageal cancer: loss of claudin 3 and 4 expression is associated with metastatic behavior. APMIS 115:838–847
23. Fritzsche FR, Oelrich B, Johannsen M et al (2008) Claudin-1 protein expression is a prognostic marker of patient survival in renal cell carcinomas. Clin Cancer Res 14:7035–7042
24. Chao YC, Pan SH, Yang SC et al (2009) Claudin-1 is a metastasis suppressor and correlates with clinical outcome in lung adenocarcinoma. Am J Respir Crit Care Med 179:123–133
25. Sauer T, Pedersen MK, Ebeltoft K et al (2005) Reduced expression of claudin-7 in fine needle aspirates from breast carcinomas correlate with grading and metastatic disease. Cytopathology 16:193–198
26. Morin PJ (2007) Claudin proteins in ovarian cancer. Dis Markers 23:453–457
27. Agarwal R, D'Souza T, Morin PJ (2005) Claudin-3 and claudin-4 expression in ovarian epithelial cells enhances invasion and is associated with increased matrix metalloproteinase-2 activity. Cancer Res 65:7378–7385

Virchows Arch (2011) 458:349–356
DOI 10.1007/s00428-010-1024-3

ORIGINAL ARTICLE

Time-specific blockade of PDGFR with Imatinib (Glivec®) causes cataract and disruption of lens fiber cells in neonatal mice

Yin-Pin Zhou · Yang-Tao He · Cheng-Li Chen · Jun Ji · Jian-Qin Niu · Han-Zhi Wang · Shi-Feng Li · Lan Huang · Feng Mei

Received: 19 September 2010 / Revised: 22 November 2010 / Accepted: 27 November 2010 / Published online: 23 December 2010
© Springer-Verlag 2010

Abstract This study aimed at investigating the response of lens epithelial cells in postnatal mice to Imatinib (Glivec®, a potent inhibitor of platelet-derived growth factor receptor (PDGFR)) treatment. Mouse eyes were sampled 10 days after administration of Imatinib (0.5 $mg \cdot g^{-1} \cdot day^{-1}$) for 3 days, at either 7, 14, or 21 days postpartum. Structural changes of lens were revealed by routine H.E. staining. Levels of proliferation and apoptosis were revealed by BrdU incorporation and terminal deoxynucleotidyl transferase dUTP nick end labeling (TUNEL) assay, respectively, and immunofluorescent staining with anti-PDGFRα antibody was carried out on the sections of eyeball. PDGFRα and p-PDGFRαprotein levels were evaluated by Western blot. Our results indicated that administration of Imatinib led to blockade of PDGFR signaling. Formation of cataracts was found only in those mice where treatment started from 7 days postpartum (P7), but was not observed in those samples from P14 nor P21. Fiber cells were disorganized in cataract lens core as observed histologically, and migration of epithelial cells was also inhibited. No apoptosis was detected with the TUNEL method. Our results indicated blockade of PDGFR at the neonatal stage (P7) would lead to cataracts and lens fiber cells disorganization, suggesting that PDGFR signaling plays a time-specific and crucial role in the postnatal development of lens in the mouse, and also may provide a new approach to produce a congenital cataract animal model.

Keywords PDGFR · Cataract · Imatinib · Lens · Congenital · Mouse · Postnatal · Proliferation · Migration

Electronic supplementary material The online version of this article (doi:10.1007/s00428-010-1024-3) contains supplementary material, which is available to authorized users.

Yin-Pin Zhou and Yang-Tao He contributed equally to this work.

Y.-P. Zhou · J. Ji · L. Huang (✉)
Institute of Cardiovascular Disease of PLA, Xinqiao Hospital, Third Military Medical University, Chongqing 400038, China
e-mail:huanglan260@yahoo.com.cn

F. Mei
e-mail:meifeng.mail@163.com

Y.-P. Zhou · Y.-T. He · C.-L. Chen · J.-Q. Niu · H.-Z. Wang · S.-F. Li · F. Mei (✉)
Department of Histology and Embryology, Third Military Medical University, Chongqing 400038, China

Introduction

A congenital cataract is a clouding of the lens, that is present at birth, and this is observed in approximately 0.4% of all births. Vision can be hampered in congenital cataracts that can further cause amblyopia [1]. A number of reasons have been suggested to be involved with the onset of congenital cataracts including inherited tendencies [2], infection [3], metabolic problems [4], diabetes, trauma [5], inflammation or drug reactions, but the underlying mechanisms are complicated and are still not well known.

Lens development is the result of a series of inductive complex processes [6, 7], and growth factors play important regulative roles in lens development. Platelet-derived growth factor (PDGF) is a protein dimer that can consist of two A chains (AA), two B chains (BB), or an A chain and a B chain (AB). All three isoforms of PDGF can bind to the α receptor (PDGFRα), whereas only the AB and the BB isoforms interact with the β receptor (PDGFRβ) [8, 9]. Lens epithelial cells express PDGFR from embryonic stages, and expression persists throughout lifetime in mice

and chickens [10, 11], and PDGF is highly expressed in the iris and ciliary body [12]. PDGFR signaling plays an important role in the control of growth, proliferation, and migration of lens epithelial cells [10, 13–15], and mice with a null mutation in PDGFR die during embryonic stage [16]. However, the effects of PDGFR signaling on the postnatal development of lens in mice are still not fully understood.

Imatinib (Glivec®) is a potent inhibitor of both PDGFR and Kit, a receptor tyrosine kinase, and this drug is used for the treatment of PDGFR-expressing tumors, such as uterine sarcoma and breast cancer [17, 18], or Kit^{+} gastrointestinal stromal tumors in clinical practice [19], in addition, it is also used in treating chronic myelogenous leukemia (CML). In the experiments described herein, Imatinib was used to investigate the PDGFR signaling effects on the postnatal development of lens.

In this paper, we describe the morphologic alterations of lens, and the apoptosis, proliferation, and migration of lens epithelial in response to PDGFR signaling blockade by Imatinib administration in neonatal mice.

Materials and methods

Animals

BALB/C mice were purchased from the Animal Center of the Third Military Medical University (Chongqing, China) and paired to produce offspring. Imatinib mesylate (Glivec®) was purchased from Novartis Pharma AG (Basel, Switzerland). Animals were divided into eight groups (Groups I to VIII). Groups I (n=10), III (n=20), V (n=10), and VII (n=10) were experimental groups in which mice were intragastrically administered Imatinib at a dosage of 0.5 $mg{\cdot}g^{-1}{\cdot}day^{-1}$. Groups II ($n$=5), IV ($n$=5), VI ($n$=5), and VIII ($n$=5) were control groups, in which mice were intragastrically administered glucose (drug vehicle) at the same dosage. All experimental mice were injected intraperitoneally with one dose BrdU (0.1 $mg{\cdot}g^{-1}$) 2 h before the first treatment. Mice at P7 were used in groups I and II, then killed 6 h later, after one administered dose. Mice at stage P7 (groups III and IV), P14 (groups V and VI), or P21 (groups VII and VIII) were treated for 3 days and then sacrificed 10 days later. All experiments were performed in accordance with our University Health Guide for the Care and Use of Laboratory Animals.

Specimen allocation and frozen sections

One eye from each mouse in groups I–VIII was fixed in 4% PFA/PBS and equilibrated in 30% sucrose/PBS, and then put into optimal cutting temperature compound. Fifty continuous sections frozen sections (10-μm thick) were cut with a cryostat from each eyeball (Leica 1850), and ten frozen sections were sampled randomly from each eyeball, and used for either immunofluorescence, BrdU incorporation or terminal deoxynucleotidyl transferase dUTP nick end labeling (TUNEL) assay. The other eye from each mouse in groups I and II, and in groups III–VIII were used for Western blot and H.E staining, respectively.

Immunofluorescence

Frozen sections were incubated with Rat anti-Kit or Goat anti-PDGFRα antibody (Table 1) overnight at 4°C, and then Cy3-conjugated goat anti-rat or Cy3-conjugated donkey anti-goat antibody, respectively (Table 1) for 1 h at room temperature. Sections were counterstained with DAPI (Sigma). The stained results were detected by a 90i fluorescence microscope (Nikon, Japan) with an excitation wavelength appropriate for Cy3 (552 nm). The preparations of mouse small intestine were described in supplemental materials.

Hematoxylin and eosin staining

Eyeballs were fixed in 4% paraformaldehyde and embedded in paraffin according to routine procedures. Paraffin sections were de-paraffinized, hydrated, and then the sections stained with hematoxylin and eosin, dehydrated through a graded alcohol series, then were mounted and coverslipped. Sections were viewed with a 90i microscope (Nikon, Japan), and photomicrographs were taken with a digital camera (Nikon, Japan).

Detection of PDGFR signal blockade by Western blotting

Total protein was extracted from eyeballs using RIPA lysis buffer (50 mM Tris pH 7.4, 150 mM NaCl, 1% Triton X-100, 1% sodium deoxycholate, 0.1% SDS, 1 mM EDTA, 1 mM sodium orthovanadate, 10 mM NaF) containing 10 μg/ml aprotinin, 10 μg/ml leupeptin, and 1 mM phenylmethylsulphonyl fluoride. The protein concentration was measured using a BCA Protein Assay Kit (Beyotime, Hangzhou, China). Total protein (100 μg) was separated on 7.5% SDS-PAGE gel and transferred to a PVDF membrane at 350 mA for 1.5 h by using a semi-dry transfer cell (Bio-Rad). Then the membrane was incubated in blocking buffer consisting of 5% non-fat dry milk for 2 h at room temperature, and then with anti-PDGFRα, anti-p-PDGFRα or anti-β-actin antibody (Table. 1) overnight at 4°C, and HRP-conjugated donkey anti-goat or HRP-conjugated goat anti-mouse antibody (Table 1). Protein-antibody complexes were detected with an ECL Western blotting detection and analysis system (Amersham Biosciences, Buckinghamshire, UK).

Table 1 The antibodies

Antigen	Clone	Supplier	Dilution	Isotype	Conjugated
Kit	ACk2	eBioscience	1:100 IF	Rat IgG	Purified
BrdU	Bu20a	DAKO	1:100 IF	Mouse IgG	Purified
PDGFRα	Polyclone	Santa Cruz	1:100 IF 1:1000 WB	Goat IgG	Purified
p-PDGFRα	Polyclone	Santa Cruz	1:1000 WB	Goat lgG	Purified
β-actin	Polyclone	Santa Cruz	1:1000 WB	Mouse IgG	Purified
Anti-Rat	Polyclone	Zymed	1:100 IF	Goat IgG	Cy3
Anti-Goat	Polyclone	Zymed	1:100 IF	Donkey IgG	Cy3
Anti-Mouse	Polyclone	Zymed	1:100 IF	Goat IgG	FITC
Anti-Mouse	Polyclone	DAKO	1:1000 WB	Goat IgG	HRP
Anti-Goat	Polyclone	DAKO	1:1000 WB	Donkey IgG	HRP

Detection of lens epithelial cell apoptosis

To detect the apoptosis of cells, TUNEL labeling was done using an apoptosis detection Kit (Roche, Switzerland). Frozen sections were fixed with 4% paraformaldehyde for 20 min at 25°C, washed twice with PBS for 30 min and then treated with 0.1% Triton X-100 for 20 min on ice (2–6°C). The sections were incubated with TUNEL reaction buffer containing 45 μL of the labeling solution, and 5 μL of the enzyme solution at 37°C for 1 h in a humidified atmosphere in the dark. Sections were then washed three times for 15 min each with PBS to remove unincorporated fluorescein-dUTP. The specimens were observed with a fluorescence microscope with an excitation wavelength in the range of 450–500 nm.

Detection of epithelial cells proliferation

To identify the migration of lens epithelial cells, BrdU incorporation was detected as follows: frozen sections were additionally fixed in 4% paraformaldehyde in 0.1 MPB at pH 7.2 for 30 min. After rinsing in PBS, the specimens were treated with 2N HCl for 30 min at 37°C for partial denaturation of double-stranded DNA. To reveal BrdU, the specimens were incubated with a mouse monoclonal antibody raised against BrdU (Table 1) overnight at 4°C, and then incubated with a FITC-conjugated goat anti-mouse antibody (Table 1).

Measurements and statistical analysis

After immunofluorescent staining assessment, photomicrographs of $BrdU^+$ cells were taken (×40 magnification, 1.3035 mm^2) per section with a digital camera (Nikon, Japan) mounted on a 90i fluorescence microscope (Nikon, Japan). The numbers of $BrdU^+$ cells were counted with Image-Pro Plus 5.0 (Media Cybernetics, Silver Spring, MD, USA). Data were expressed as means±S.E.M. The *n* value reported in the text refers to the number of animals used. Differences in the data were evaluated by student *t* test, and $P<0.05$ was taken as a statistically significant difference.

Results

PDGF signaling blockade by Imatinib administration

Imatinib can inhibit PDGFR as well as Kit, so we observed the distribution of $PDGFR\alpha^+$ and Kit^+ cells in lens. $PDGFR\alpha^+$ lens epithelial cells were observed, but no Kit^+ cells were detected in lens (Fig. 1a). Kit^+ interstitial cells of Cajal can be observed in mouse small intestine as a positive control (Suppl. Fig. 1). To evaluate the blocking effects of Imatinib on PDGF signal, the Western blot method was applied to assay the alterations of phosphorylated PDGFRα protein (p-PDGFRα) and PDGFRα. The data indicated that the amount of p-PDGFRα was obviously decreased and PDGFR expression was persistent after Imatinib treatment for 6 h (group I and II) (Fig. 1b), demonstrating that Imatinib can inhibit PDGFR signal by hampering the phosphorylation event.

Congenital cataract formation

Ten days after the first drug administration, morphological examination revealed turbid lenses and formation of cataracts only in those mice were treated with Imatinib from P7 for 3 days (group III; Fig. 2a, b) and the incidence rate of cataracts was 70% ($n=20$). In controls, the lenses were transparent (Suppl. Fig. 2), and no cataract was observed in Group V (P14) nor Group VII (P21; data not shown). Subsequent histological examination on paraffin-embedded lenses indicated that those treated with Imatinib from P7 displayed a normal morphology of lens epithelial cells, but a totally disrupted morphology of lens core with

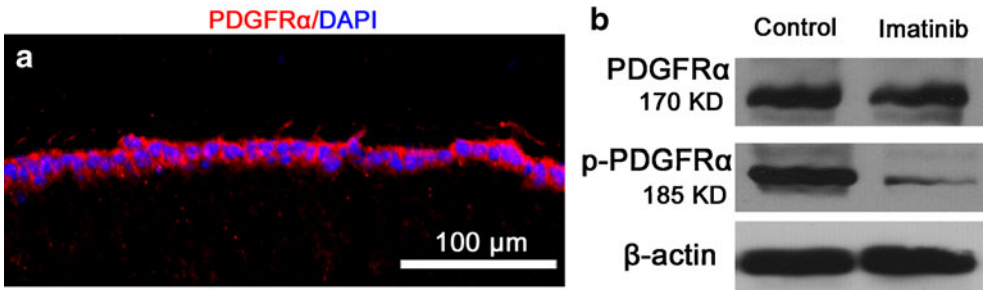

Fig. 1 Photomicrographs showing the expression of PDGFRα in lens (**a**) and Western blotting showing the expression of PDGFRα and p-PDGFRα (**b**). **a** PDGFRα expression (*red*) is restricted to the lens epithelial cells; **b** the p-PDGFRα level is dramatically decreased after Imatinib treatment for 6 h as compared with PDGFRα expression. *Scale bar*=100 μm (**a**)

degenerative fiber cells compared to control (Fig. 3a, b). Around the disrupted lens core, the secondary fiber cells were abnormal in morphology with swelling cytoplasm, and those cells located in the outer cortex of lens were comparably normal, with regular distributed fiber cells seen in control (Fig. 3a', b'). In addition, it should be noted that some secondary fiber cells still have a nucleus (Fig. 3 a") but those cells at the same location in controls have lost their cell nuclei, which may imply a delayed differentiation process after PDGFR blockade (Fig. 3b"). No histological change was observed in those samples where the drug treatment started from either P14 (Groups V and VI) or P21 (Groups VII and VIII), suggesting that cataract induced by the PDGFR signal blockade is time-specific (data not shown).

Proliferation of lens epithelial cells

We used a BrdU incorporation assay to trace the fates of lens epithelial cells. Immunofluorescent staining with anti-BrdU antibody showed BrdU-positive cells appeared in the epithelial cells above the lens equator known as the germinative zone [20], with or without Imatinib treatment at P7 (groups I and II; Fig. 4. a, b). Cell counting indicated that the $BrdU^+$ cell numbers were 21.1±1.2, and 22.1±1.5 per section in the cataract group and control, respectively (n=10, P>0.05) (Fig. 4. a', b'). At P17, 10 days after BrdU injection (groups III and IV), those BrdU-positive cells appeared among the fiber cells of the outer cortex in the Imatinib treatment group (Fig. 4c, c'), and those cells in controls were much closer to the lens core than the cataract group (Fig. 4d, d'). Cell counting showed that those $BrdU^+$ cells were 22.8±1.5 and 23.2±1.9 per section in the cataract group and controls, respectively (n=10, P>0.05), which may suggest that blockade of PDGFR could inhibit the migration of epithelial cells, but not induce the decease of fiber cell numbers.

Detection of apoptosis

To further confirm whether blockade of PDGFR would lead to apoptosis of epithelial cells, apoptosis was detected by the TUNEL method. In a positive control, on a section of mouse small intestine, cells labeled by the TUNEL method were observed in the epithelial cells of small intestine (Suppl. Fig. 3). However, no apoptotic cells were detected in the lens with Imatinib treatment, indicating that blockade of PDGFR may not induce apoptosis of either lens epithelial cells or fiber cells in this case (Fig. 5a–c).

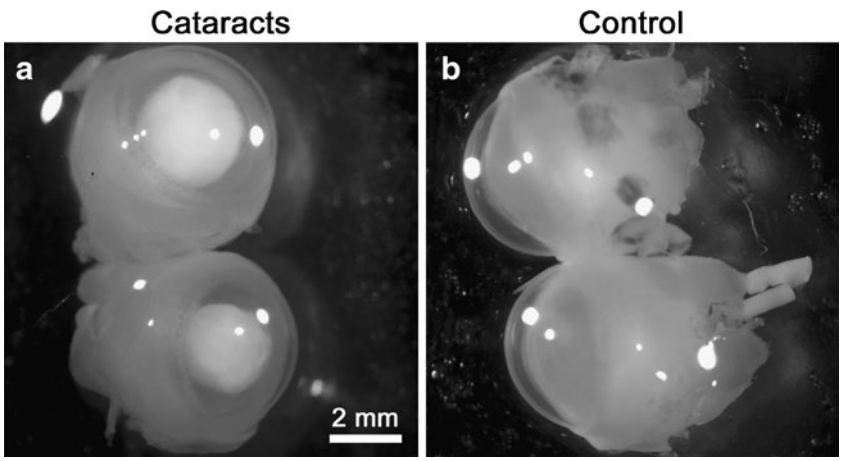

Fig. 2 Under anatomical microscope, note turbid lens of a 17-days old mouse which Imatinib treatment started from P7 for 3 days (**a**) as compared with the control with transparent lens (**b**). *Scale bar* for **a** and **b**=2 mm

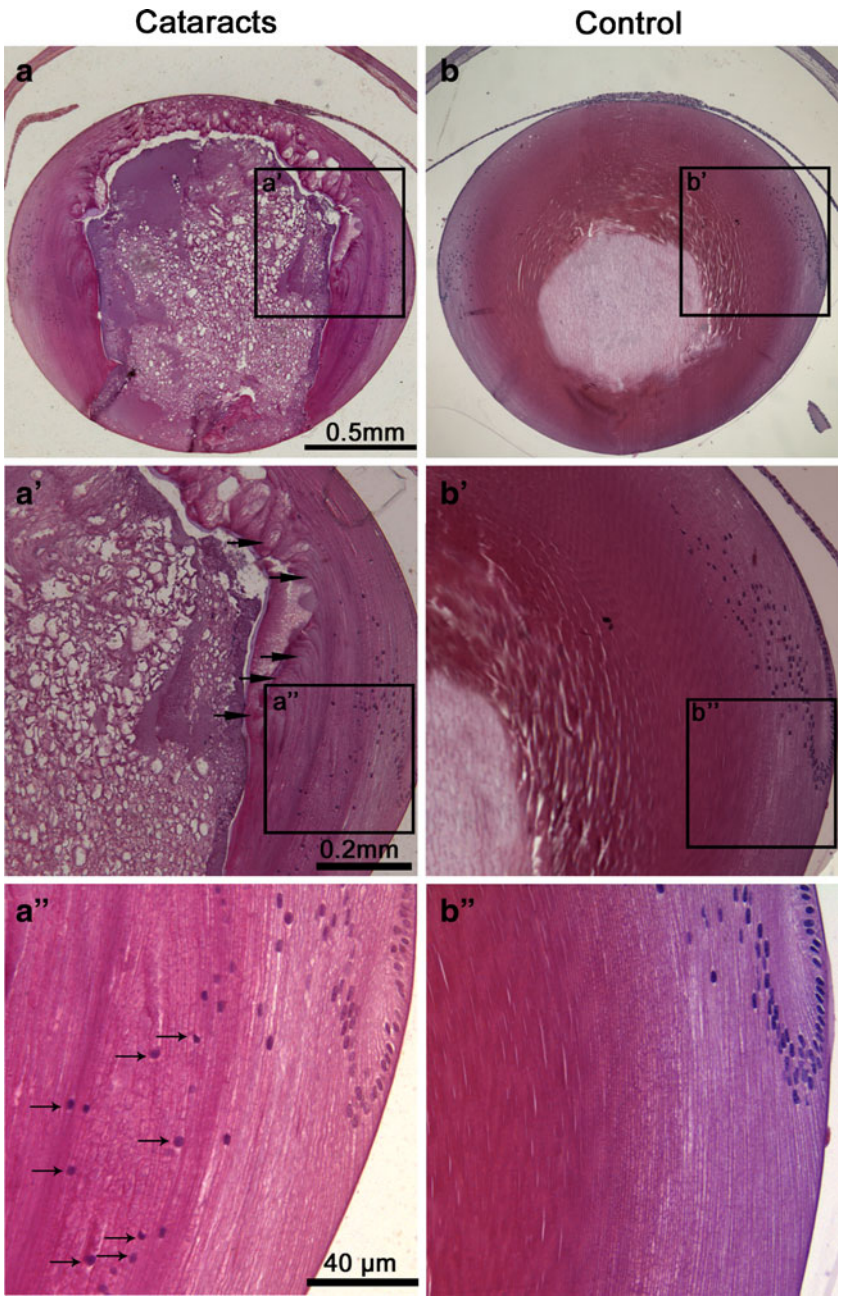

Fig. 3 Photomicrographs showing the histological alterations of cataracts lens on paraffin-embedded H.E. staining sections. A disrupted morphology of lens core with degenerative fiber cells is observed in cataracts lens (**a**) comparing with control (**b**); high magnification of frame in *subpanel* **a** showing a disrupted lens core and swelling secondary fiber cells (*arrows*, **a'**) and regularly distributed fiber cells are seen in control (**b'**) (*frame in subpanel* **b**); It should be noted a number of secondary fibers in lens cortex still contain nuclei (*arrows*, **a"**), while only fiber cells in outer lens cortex still have nuclei under high magnification (**b"**) (*frame in subpanel* **b'**). *Scale bar* for **a** and **b**=0.5 mm, **a'** and **b'**=0.2 mm, **a"** and **b"**=40 μm

Discussion

The present study demonstrates that: (1) time-specific blockade of PDGFR signal with Imatinib (P7) causes congenital cataracts in neonatal mice and this may provide a new approach to produce a mouse model of congenital cataracts; (2) blockade of PDGFR signal leads to a disruption of the morphology and maldevelopment of fiber cells in the lens core; and (3) blockade of the PDGFR signal could inhibit the migration of lens epithelial cells, but does not induce apoptosis.

PDGFR signal blockade

Mice with a null mutation in PDGFR die during embryonic development [16], so administration of PDGFR blocker was used to investigate the PDGFR signal on neonatal development of lens in vivo. Imatinib has been developed as a potent inhibitor of Bcr-Abl tyrosine kinase in CML, PDGFR, and also Kit tyrosine kinase [21]. Our results showed that PDGFRα expression was restricted to lens epithelial cells, and no Kit^{+} cells were detected in lens. Phosphorylation of PDGFR is an

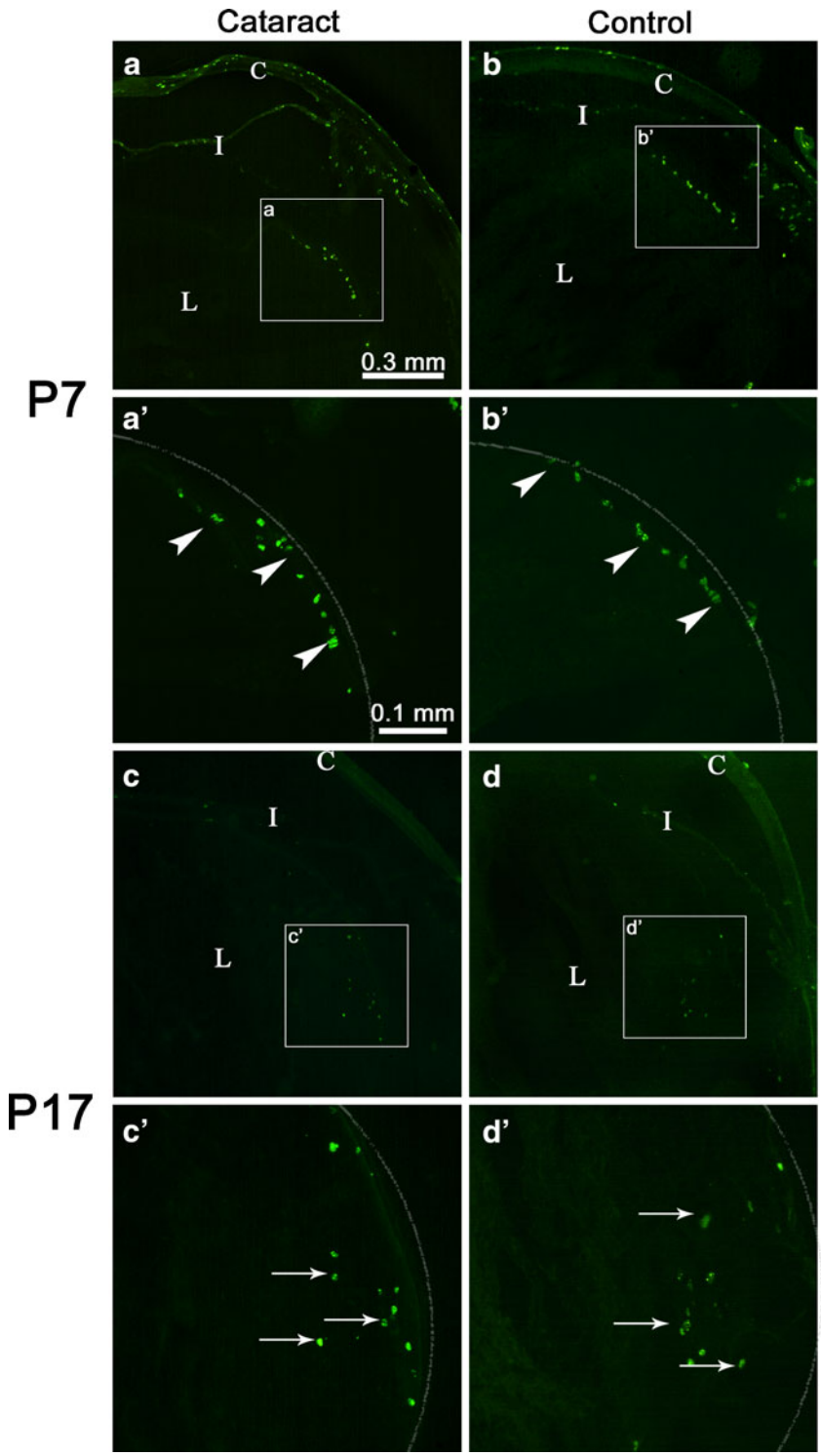

Fig. 4 Photomicrographs showing proliferation and migration of lens epithelial cells by BrdU incorporation methods in Imatinib administration group and control. **a–b** A number of BrdU (*green*) cells are seen in cornea (*C*), iris (*I*), and lens (*L*) at P7 with (**a**) or without (**b**) Imatinib treatment after one dose of BrdU injection. **a'–b'** High magnification (*frames in subpanel* **a** and **b**) showing that those BrdU-positive cells that are distributed in the lens epithelium above the lens equator are similar in location and amount (*arrowheads*). **c–d** The $BrdU^{+}$ cells have migrated from epithelium into lens cortex at P17; **c'–d'** High magnification (*frames in subpanel* **c** and **d**) indicating those cells are much closer to lens core in control as compared with Imatinib treatment group (*arrows*). *Scale bar* for **a–d**= 0.3 mm, **a'–d'**=0.1 mm

essential step for the activation of PDGFR signaling after the binding of PDGFRs with their respective ligands. To further confirm the PDGFR blocking effect by intragastric administration of Imatinib, Western blotting was carried out to assay the level of PDGFRα protein phosphorylation (p-PDGFRα Tyr754), one of the phosphorylation sites of PDGFRα. The results showed that the phosphorylation of PDGFRα was predominantly inhibited by Imatinib administration in vivo, which indicates PDGFR signaling does not proceed.

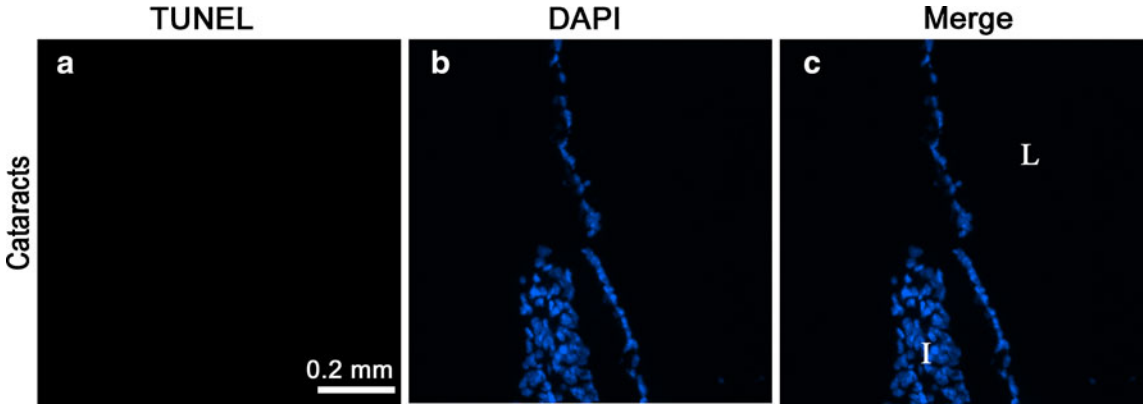

Fig. 5 Photomicrographs showing the apoptosis with TUNEL method in lens. No TUNEL-positive cell is observed in either iris (*I*) or lens (*L*) with Imatinib treatment (**a**–**c**). *Scale bar* for **a**–**c**=0.2 mm

Congenital cataract mouse model

In this research, we investigated the response of lens to PDGFR blockade around the eyes open period (P7, P14, and P21) by using Imatinib. Our results indicated that blockade of PDGFR with Imatinib at P7 for 3 days would cause formation of cataracts and degenerative fiber cells in the lens core, with a disrupted morphology histologically before mice open their eyes. Interestingly, the drug administration if started from either P14 or P21 with the same dosage and duration did not induce abnormal morphologic changes of lens. These results indicate PDGFR signaling is time-specific and crucial for the postnatal development of lens before eyes open in mice, and absence of PDGFR signal would hamper the development of fiber cells that would result in cataracts formation, which also suggests absence of PDGFR signal or exposure to PDGFR blocker during late fetal period might induce congenital cataracts in human. Moreover, a congenital cataract model is a powerful tool to investigate mechanisms underlying the onset of cataracts, and mouse with gene mutation are often used to investigate human hereditary cataracts [2]. A congenital model which results from lens maldevelopment at the late stage is still absent. Our results provide a novel and simple approach to produce a congenital cataract mouse model by blockade of PDGFR signaling.

PDGFR signal and lens development

The development of the lens is under the orchestral control of a series of growth factors, such as fibroblast growth factor (FGF), transforming growth factor, in addition to PDGFs [22–24]. Lens epithelial cells continue to proliferate, differentiating into secondary fiber cells, and migrating in from the equator onto the outer cortex of the lens throughout life [25–29]. Before mice open their eyelids at P14, both the primary and secondary fiber cells have finished their cell nuclei loss during the terminal differentiation process [30], and this process is finished before birth in humans. PDGFR signaling plays a critical role in the regulation of epithelial cell development. It has been shown that transgenic mice with elevated lens-specific expression of PDGF-A would lead to lenticular defects that result in cataracts [12], and PDGF in combination with FGF can potentiate the fiber-differentiating activity of FGF in lens epithelial explant cultures [10]. Our study indicated that blockade of PDGFR signaling inhibit karyorrhexis of fiber cells, and leads to swelling of cytoplasm in neonatal mice that suggest PDGFR signaling plays an important role in regulation of the fiber cells differentiation.

Migration and apoptosis of lens epithelial cells

It has been shown that PDGFR signals normally act as proliferative factors for lens epithelial cells [10, 14, 15, 31], and also can enhance epithelial cells migration by activation of the PI3K/AkT pathway [16]. So we used BrdU incorporation to trace the fates of lens epithelial cells after PDGFR blockade in vivo. Our results also showed the migration of epithelial cells was inhibited to some degree. With respect to the fact that PDGFR signaling is also important for the survival of cells [25], we used the TUNEL assay to detect apoptosis in lens. Apoptotic cells were observed in epithelium of small intestine, the positive control, but not in the lens, suggesting that the blockade of PDGFR would not induce apoptosis in the lens.

In conclusion, our observations may provide a new approach to produce a mouse model of congenital cataracts

in neonatal mice by administration of Imatinib and blockade of PDGFR signaling would lead to maldevelopment of fiber cells and inhibition of lens epithelial cells migration.

Conflict of interest statement We declare that we have no conflict of interest.

References

1. Guercio JR, Martyn LJ (2007) Congenital malformations of the eye and orbit. Otolaryngol Clin North Am 40:113–140
2. Graw J (1999) Cataract mutations and lens development. Prog Retin Eye Res 18:235–67
3. Lim AS (1997) Mass blindness has shifted from infection (onchocerciasis, trachoma, corneal ulcers) to cataract. Ophthalmologica 211:270
4. Esteves JF, Dal Pizzol MM, Sccoco CA (2008) Cataract and type 1 diabetes mellitus. Diabet Res Clin Practic 82:324–8
5. Mitry D, Singh J, Kiire CA (2009) Atopic dermatitis, facial trauma, and cataract surgery. Can J Ophthalmol 44:716
6. Jacobson AG (1996) Inductive processes in embryonic development. Science 152:25–34
7. Grainger RM, Mannion JE, Cook TL (1997) Defining intermediate stages in cell determination: acquisition of a lens-forming bias in head ectoderm during lens determination. Dev Genet 20:246–57
8. Escobedo JA, Navankasatussas S, Cousens LS (1988) A common PDGF receptor is activated by homodimeric A and B forms of PDGF. Science 240:1532–4
9. Hart CE, Forstrom JW, Kelly JD (1988) Two classes of PDGF receptor recognize different isoforms of PDGF. Science 240:1529–31
10. Kok A, Lovicu FJ, Chamberlain CG (2002) Influence of platelet-derived growth factor on lens epithelial cell proliferation and differentiation. Growth Factors 20:27–34
11. Potts JD, Bassnett S, Kornacker S (1994) Expression of platelet-derived growth factor receptors in the developing chicken lens. Invest Ophthalmol Vis Sci 35:3413–21
12. Reneker LW, Overbeek PA (1996) Lens-specific expression of PDGF-A alters lens growth and development. Dev Biol 180:554–65
13. Knorr M, Wunderlich K, Steuhl KP (1993) Lens epithelial cell response to isoforms of platelet-derived growth factor. Graefes Arch Clin Exp Ophthalmol 231:424–8
14. Wunderlich K, Knorr M (1994) Effect of platelet-derived growth factor PDGF on replication of cultivated bovine lens epithelial cells. Ophthalmologe 91:98–102
15. Xiong W, Cheng BH, Jia SB, Tang LS (2010) Involvement of the PI3K/Akt signaling pathway in platelet-derived growth factor-induced migration of human lens epithelial cells. Curr Eye Res 35:389–401
16. Soriano P (1997) The PDGF alpha receptor is required for neural crest cell development and for normal patterning of the somites. Development 124:2691–700
17. Trojan A, Montemurro M, Kamel M (2009) Successful PDGFR-{alpha}/{beta} targeting with imatinib in uterine sarcoma. Ann Oncol 20:1898–9
18. Cristofanilli M, Morandi P, Krishnamurthy S (2008) Imatinib mesylate (Gleevec) in advanced breast cancer-expressing C-Kit or PDGFR-beta: clinical activity and biological correlations. Ann Oncol 19:1713–9
19. Demetri GD (2002) Identification and treatment of chemoresistant inoperable or metastatic GIST: experience with the selective tyrosine kinase inhibitor imatinib mesylate (STI571). Eur J Cancer 38:S52–S59
20. Harding CV, Reddan JR, Unakar NJ, Bagchi M (1971) The control of cell division in the ocular lens. Int Rev Cytol 31:215–300
21. Manley PW, Cowan-Jacob SW, Buchdunger E (2002) Imatinib: a selective tyrosine kinase inhibitor. Eur J Cancer 38:S19–S27
22. Reddan JR, Wilson-Dziedzic D (1983) Insulin growth factor and epidermal growth factor trigger mitosis in lenses cultured in a serum-free medium. Invest Ophthalmol Vis Sci 24:409–16
23. Tripathi BJ, Tripathi RC, Livingston AM (1991) The role of growth factors in the embryogenesis and differentiation of the eye. Am J Anat 192:442–71
24. Lovicu FJ, McAvoy JW (2005) Growth factor regulation of lens development. Dev Biol 280:1–14
25. Cvekl A, Piatigorsky J (1996) Lens development and crystallin gene expression: many roles for Pax-6. BioEssays 18:621–30
26. Graw J (1996) Genetic aspects of embryonic eye development in vertebrates. Dev Genet 18:181–97
27. Oliver G, Gruss P (1997) Current views on eye development. Trends Neurosci 20:415–21
28. McAvoy JW (1978) Cell division, cell elongation and the co-ordination of crystallin gene expression during lens morphogenesis in the rat. J Embryol Exp Morphol 45:271–81
29. McAvoy JW (1978) Cell division, cell elongation and distribution of alpha-, beta- and gamma-crystallins in the rat lens. J Embryol Exp Morphol 44:149–65
30. Vrensen GF, Graw J, De WA (1991) Nuclear breakdown during terminal differentiation of primary lens fibres in mice: a transmission electron microscopic study. Exp Eye Res 52:647–59
31. Knorr M, Wunderlich K, Steuhl KP (1993) Expression of platelet derived growth factor receptors in cultivated lens epithelial cells. Ophthalmologe 90:750–3

Virchows Arch (2011) 458:357–358
DOI 10.1007/s00428-010-1014-5

LETTER TO THE EDITOR

Pathoanatomical museum of Vienna

Roland Sedivy

Received: 16 November 2010 / Accepted: 17 November 2010 / Published online: 1 December 2010
© Springer-Verlag 2010

Dear Sir,

The article by Robin A. Cooke is brilliantly written and gives a fascinating overview about wax models that represent treasures of the history of medicine. However, I am a bit sad that the huge collection of moulages in the Viennese museum of pathological anatomy (PaAM) is not mentioned. Although I understand that lacking space, not all museums could be mentioned, but this very museums is worth to be mentioned!

The Viennese collection comprises more than 50,000 objects, including formalin-fixed human and veterinarian specimens, and moulages mostly made by Henning, who was gratefully mentioned by Robin A Cooke [1]. Karl Portele, the former curator of the museum, described 2,358 specimens and many other facts of the collection of moulages gathered in the PaAM in a journal that is sadly out of print [2]. Thus, I would like to broaden Cooke's article shortly.

Vienna's pathological collection and the associated morgue were founded in 1796 by Johann Peter Frank (1745–1821), director of the General Hospital in Vienna from 1795 onwards. He engaged Aloys Rudolph Vetter (1765–1806), as the first, but unpaid prosector and curator of the pathological–anatomical museum. He was followed by Lorenz Biermayer, who was replaced 2 years later by Johann Wagner (1800–1832). After him, Carl Rokitansky (1804–1878) was the most prominent curator.

The oldest moulage of the museum is that of a man who lost his mandible by trauma. The original head of the injured man has been fixed in alcohol, and a wax replica has been produced. The great anatomist Anton Hyrtl (1810–1894) told about its purchase in an official bulletin, and thus, the specimen seems to originate from the year 1818. The creator of this waxy head, however, is unknown. Two further specimens that display the face of a person with lupus erythematodes were made by Anton Elfinger (1821–1864) who was well known to that time as caricaturist as well. Elfinger also provided some dermatological moulages for Hebra's lectures for students. Nevertheless, the majority of moulages in the collection of the PaAM were built by Karl Henning, and later by his son Theodor. Karl Henning worked at the Department of Dermatology under Moritz Kaposi (1837–1902), and became, in 1897, the head of the "studio moulage". Apart from entities such as lues, variola, and tuberculosis that represent a large group of exhibits, exceptional specimens are nowadays on display (Fig. 1).

R. Sedivy (✉)
Institut für Klinische Pathologie (LK St. Pölten) und Zentrum für Pathologie, Karl Landsteiner Institut, Angewandte Klinische Pathologie, Danube Private University,
3500, Krems an der Donau, Austria
e-mail: roland.sedivy@dp-uni.ac.at

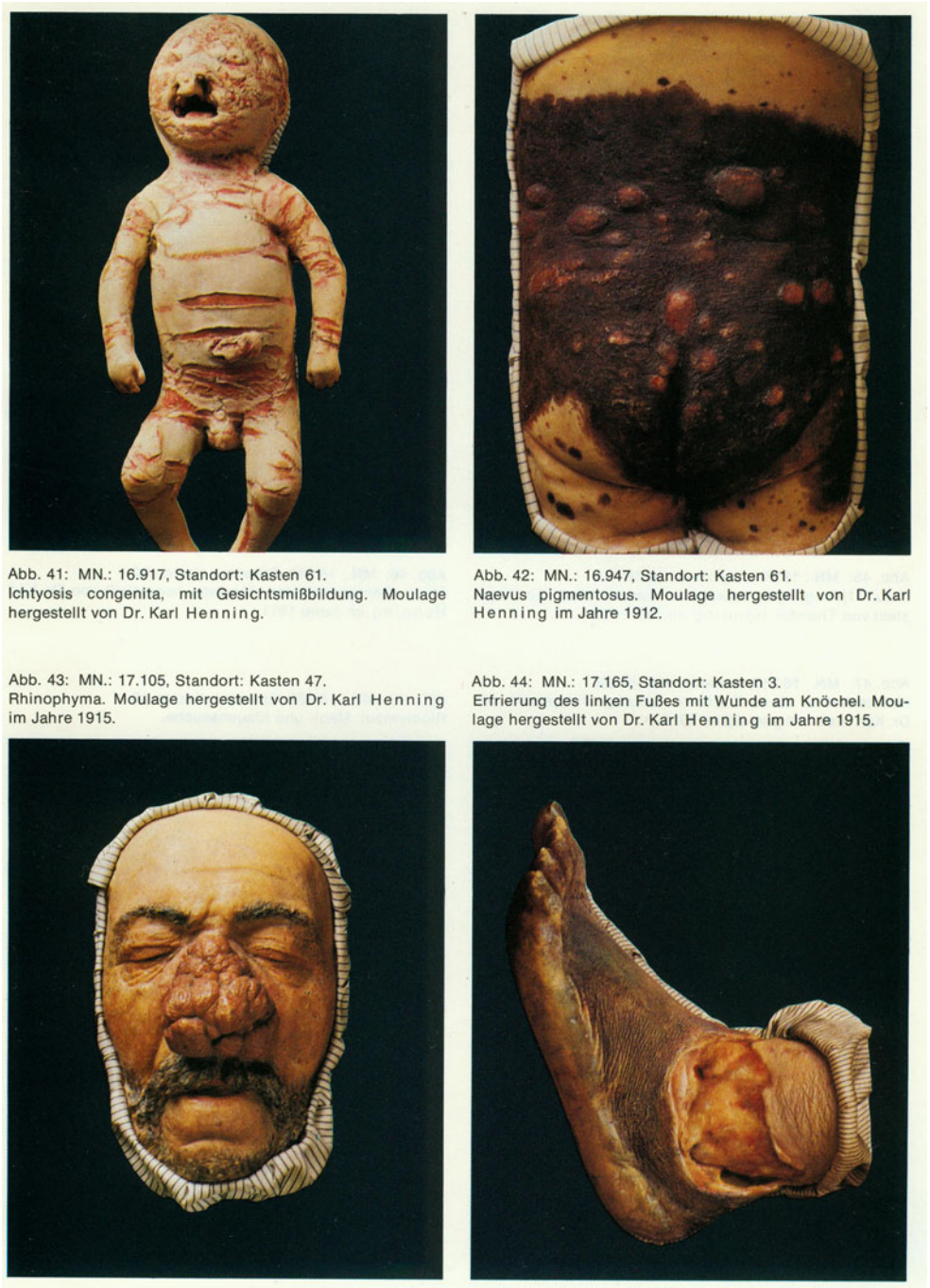

Fig. 1 Some of the moulages of the museum of pathological anatomy in Vienna (Austria). Figure published by KA Portele in Ref. 2 (photo: Sedivy, courtesy of Dir. Dr.Patzak, PaBM)

References

1. Cooke RA (2010) A moulage museum is not just a museum: wax models as teaching instruments. Virchows Arch 457:513–520
2. Portele KA (1977) Die Moulagensammlung des Pathologisch-anatomischen Bundesmuseums. Mitteilungen des Pathologisch-anatomischen Bundesmuseums, Wien

Virchows Arch (2011) 458:359–361
DOI 10.1007/s00428-010-1027-0

LETTER TO THE EDITOR

Melanoma histopathology report: proposal for a standardized terminology

Anna Batistatou · Özay Gököz · Martin G. Cook · Daniela Massi · on behalf of the Dermatopathology Working Group of the European Society of Pathology

Received: 5 December 2010 / Accepted: 7 December 2010 / Published online: 31 December 2010
© Springer-Verlag 2010

Dear Editor,

Pathology diagnosis is the end result of a complicated and highly sophisticated process, which, through interpretation of morphological alterations, generates data required for patient management. It is largely based on the macroscopic and microscopic features, but also considers any other issue, from clinical history and physical examination, through laboratory and radiological findings, to pathobiological and therapeutic implications. However, the correct diagnosis at the microscope is not the final step. Pathologists still need to transfer the final diagnosis to the clinicians and to provide information on the nature of the disease and diagnosis consequences, i.e., to release a final pathology report. Often, the report has the form of a narrative text, which largely reflects the personality and attitudes of the reporting pathologist. Thus, identical or similar cases may be diagnosed with significant variations in the content of their reports. This may generate unwonted diversities in the clinical evaluation and therapy. Another drawback of a free text report is the omission of critical information required for the clinical outcome and research purposes.

Current medical practice is governed by an evidence-based medicine (EBM) approach. The use of standardized pathology reports, based on checklist compilation, is proposed as a major application of EBM to pathology. Such reports provide the basis for consistent reporting.

We have recently surveyed the reporting of melanomas by European pathologists and assessed their current practice and opinions on the information required for the final report, via a web-based questionnaire that was diffused through the members of the Dermatopathology Working Group of the European Society of Pathology. The results of the study indicate that pathology reports for primary cutaneous melanoma vary remarkably among laboratories across Europe [1]. Although the most important prognostic features were reported, some key information which may have an influence on prognosis and treatment were often omitted, while other parameters were inadequately standardized.

The objects of the current letter are to present Europe-wide guidelines for the optimization of the pathology report of skin melanoma and to describe the process that has generated the document through the survey evaluation.

A preliminary draft of the proposed melanoma report presented during the business meeting of the Dermatopathology Working Group, which was held in Florence, in September 2009 (22nd European Congress of Pathology). Debates focused on the need for a clear-cut distinction between essential (mandatory to be reported) and desirable (optional to be reported) information and on the terminol-

A. Batistatou (✉)
Department of Pathology, University of Ioannina,
Medical School,
University Campus, 1186, 45110 Ioannina, Greece
e-mail: abatista@cc.uoi.gr

Ö. Gököz
Department of Pathology, Faculty of Medicine,
Hacettepe University,
Sihhiye,
Ankara, Turkey

M. G. Cook
Department of Histopathology,
Royal Surrey County Hospital and University of Surrey,
Guildford, UK

D. Massi
Division of Pathological Anatomy,
Department of Critical Care Medicine and Surgery,
University of Florence,
Florence, Italy

ogy of reporting features such as regression and ulceration. A working draft was circulated among all members of the Dermatopathology Working Group by e-mail at the end of September 2009. Twenty-one replies with comments and modifications were received. The pathology report was revised according to these comments and criticisms, mainly dictated by the new melanoma staging system [2], thus leading to its final form (Fig. 1). An appendix with explanatory notes was also included (Appendix).

The present proposal is in line with the already existing national guidelines for reporting melanoma [3–5]. The purpose of this work and its final proposal is to offer a novel instrument aimed to harmonize melanoma diagnosis among European pathologists. We believe that the present melanoma report can significantly improve standardization, clinical outcome, and future research in melanoma throughout Europe.

PROPOSED MELANOMA REPORT

CLINICAL DATA

Anatomic site of the lesion……

Other clinical information
duration of lesion……..
previous melanoma Yes □ No □
family history of melanoma Yes □ No □

Specimen type
excisional biopsy □ incisional biopsy □ punch biopsy □
shave □ re-excision □ other □

MACROSCOPIC DESCRIPTION

Dimensions of the specimen …….X……..X……..mm
Dimensions of the lesion …….X…….. mm
Pigmentation of the lesion uniform □ variable □
Outline of the lesion regular □ irregular □
Nodule present □ (…X….X…mm) absent □
Margins of excision (peripheral) distance in mm
Margins of excision (deep) distance in mm

MICROSCOPIC DESCRIPTION

Breslow thickness ……mm
Ulceration present □ (max diameter…..mm) absent □
Mitotic index (VGP only) ……/mm^2
Regression present □ absent □
partial (<75%) □ extensive (>75%) □
Lymphovascular invasion present □ absent □
Microscopic satellites present □ absent □
Margins of excision (peripheral) uninvolved □ involved □
invasive melanoma □ in situ melanoma □
Distance to the nearest peripheral margins …… mm
Margins of excision (deep) uninvolved □ involved □
Distance to the nearest deep margins …… mm
Pathological staging pT_N_M_(edition, year)
SNOMED Code T01000
M87202 (in situ)
M87203 (invasive)

OPTIONAL INFORMATION

Tumor Growth Phase radial (RGP) □ vertical (VGP) □
Clark level I □ II □ III □ VI □ V □
Histological subtype
Superficial spreading melanoma □ Nodular melanoma □
Lentigo maligna melanoma □ Acral lentiginous melanoma □
Desmoplastic melanoma □ Lentiginous melanoma □
Other □
Predominant cell type
Epihelioid □ Spindle □ Small cell □ Pleomorphic □ Other □
Tumor infiltrating lymphocytes (VGP only)
absent □ present, non brisk □ present, brisk □
Perineural invasion present □ absent □
Associated nevus present □ absent □
dysplastic □ common acquired □ congenital □ other □

Fig. 1 Proposed melanoma report

Appendix

Explanatory notes

Breslow thickness (in millimeters)

Breslow thickness is measured from the granular layer of the epidermis (or the base of the ulcer) to the deepest melanoma cell in the dermis (to the nearest 0.1 mm). Melanoma cells forming a sheath around appendages are excluded from measurement. Adventitial dermal invasion is only measured if it is the only site of dermal invasion—from the inner luminal surface of the eccrine or apocrine duct or the inner aspect of the outer root sheath epithelium of the hair follicle.

Ulceration

Ulceration is defined as: (a) full-thickness epidermal defect (including absence of the stratum corneum and basement membrane), (b) evidence of reactive changes (fibrin deposition and neutrophils), (c) thinning, effacement, or reactive hyperplasia of the surrounding epidermis in the absence of trauma or a recent surgical procedure.

Mitotic count

The recommended approach (AJCC 2009, edition 7) [2] is as follows: find the hot spot, count in the hot spot, and then extend to adjacent fields until a 1 mm^2 area is assessed. If mitoses are sparse, then a representative mitosis is chosen, and, beginning with that field, the count is then extended to adjacent fields. When the invasive component is <1 mm^2, the simple presence or absence of mitosis can be designated as at least 1/mm^2 (mitogenic) or 0/mm^2 (nonmitogenic).

Regression

Regression is the segmental replacement of the melanoma by fibrosis, with increased vascularity and melanophages, and a lymphocytic infiltrate of variable density, with or without residual epidermal component. Regression can be defined as partial (involving less than 75% of the lesion) or extensive (involving 75% or more of the lesion).

Microsatellites

Microsatellites are defined as microscopic and discontinuous cutaneous and/or subcutaneous metastases >0.05 mm in diameter found on pathologic examination, adjacent to a primary melanoma (separated from the main invasive component by a distance of at least 0.3 mm).

Tumor growth phase

Radial (RGP) is in situ and microinvasive (individual or small clusters of cells with similar features to those in the epidermis—no nests larger than any epidermal nests, no mitoses).

Vertical (VGP) is (i) the presence in the dermis of a confluent nodule or sheet of cells that is at least 20 cells in width and larger than the largest intraepidermal nest; the cells within this nodule are usually more atypical than any adjacent RGP, or (ii) the presence of any mitoses in the dermis.

Clark level

I. Intraepidermal tumor only.
II. Tumor invades into papillary dermis and/or periadnexal connective tissue sheath.
III. Tumor invades into papillary dermis and expands it.
IV. Tumor invades into reticular dermis.
V. Tumor invades subcutaneous fat.

TIL

Lymphocytes surround and disrupt the tumor cells of the VGP.

Absent means no lymphocytes or lymphocytes are not infiltrating among tumor cells.

Nonbrisk means lymphocytes infiltrate the melanoma patchily.

Brisk means lymphocytes diffusely infiltrate throughout the VGP melanoma (diffuse) or the entire base of the VGP (peripheral).

References

1. Batistatou A, Cook MG, Massi D, ESP Dermatopathology Working Group (2009) Histopathology report of cutaneous melanoma and sentinel lymph node in Europe: a web-based survey by the Dermatopathology Working Group of the European Society of Pathology. Virchows Arch 454:505–511
2. Edge SE, Byrd DR, Carducci MA, Compton CA (2009) AJCC cancer staging manual, 7th edn. Springer, New York
3. Frishberg DP, Balch C, Balzer BL, Crowson AN, Didolkar M, McNiff JM et al (2009) Protocol for the examination of specimens from patients with melanoma of the skin. Arch Pathol Lab Med 133:1560–1567
4. Marsden JR, Newton-Bishop JA, Burrows L, Cook M, Corrie PG, Cox NH et al (2010) Revised U.K. guidelines for the management of cutaneous melanoma 2010. Br J Dermatol 163:238–256
5. Crowson AN, Magro CM, Mihm MC (2006) Prognostications of melanoma, the melanoma report, and the sentinel lymph node. Mod Pathol 19:S71–S87

Virchows Arch (2011) 458:363–369
DOI 10.1007/s00428-010-1034-1

CASE REPORT

An unusual and potentially misleading phenotypic change in a primary gastrointestinal stromal tumour (GIST) under imatinib mesylate therapy

Nikolaos Vassos · Abbas Agaimy · Anne Schlabrakowski · Werner Hohenberger · Regine Schneider-Stock · Roland S. Croner

Received: 21 November 2010 / Revised: 2 December 2010 / Accepted: 17 December 2010 / Published online: 30 December 2010
© Springer-Verlag 2010

Abstract We present a unique case of a 62-year-old female who was diagnosed with a huge gastric gastrointestinal stromal tumour (GIST). Core needle biopsy revealed a cellular spindle cell GIST with diffuse expression of CD117 and CD34. Four mitotic figures were counted in ten available HPFs, indicating a high-risk tumour. Computed tomography scan, performed after 8 months of neoadjuvant imatinib mesylate treatment (Glivec, 400 mg/day), revealed a partial response with reduction of tumour size from 20×15×15 cm to 13.3×8×7.6 cm. The patient underwent complete tumour resection. The tumour revealed extensive cystic changes and hyalinisation in 90% of the tumour mass. Multiple viable tumour clones, measuring up to 1 cm, showed highly anaplastic, large epithelioid cells with vesicular nuclei and prominent, centrally located nucleoli, strikingly mimicking the appearance of proximal-type epithelioid sarcoma, anaplastic carcinoma, melanoma or epithelioid angiosarcoma. These anaplastic tumour cells expressed pankeratin (KL-1) and vimentin, but they were completely negative for CD117, DOG-1, CD34, S100, desmin, α-smooth muscle actin, HMB45, CD30, CD45, CK7, CK20 and 34βE-12. Sufficient tissue for molecular analysis was available from the resected tumour. No mutations were detected in KIT exons 9, 11, 13, 17, PDGFRA exons 12, 14, 18, KRAS and BRAF. The patient was alive with no evidence of recurrence 28 months later. To our knowledge, this represents the first report on this unusual type of trans-differentiation in GIST under imatinib therapy. Awareness of this phenomenon would help to avoid diagnostic confusion when evaluating post-treatment resections from GISTs.

Keywords GIST · Imatinib mesylate · KIT · Wild-type · Neoadjuvant treatment

Introduction

Gastrointestinal stromal tumours (GISTs), previously classified as leiomyoma, leiomyosarcoma or leiomyoblastoma, are currently considered a distinct clinicopathologic and molecular entity, representing the most common mesenchymal tumours of the GI tract [1–3]. GISTs have a wide spectrum of clinical presentation, ranging from small, incidentally detected tumours [4] to those presenting with acute GI bleeding or as huge intra-abdominal masses [5]. Because of their uncertain biological behaviour, different schemes have been suggested for assessment of the malignant potential in GISTs. The two well-established, most widely used risk stratification systems are the National Institute of Health (NIH) consensus criteria [3] and the Armed Forces Institute of Pathology (AFIP) criteria, proposed by Miettinen and Lasota [1]. In addition to the tumour size and mitotic index, the AFIP system has included the anatomic location of the tumour [1].

The discovery of activating mutations in the receptor tyrosine kinases KIT [6] and platelet-derived growth factor

Nikolaos Vassos and Abbas Agaimy have contributed equally to this paper.

N. Vassos · W. Hohenberger · R. S. Croner
Department of Surgery, University Hospital,
Erlangen, Germany

A. Agaimy (✉) · A. Schlabrakowski · R. Schneider-Stock
Institute of Pathology, University Hospital,
Krankenhausstraße 12,
91054 Erlangen, Germany
e-mail: abbas.agaimy@uk-erlangen.de

receptor-α (PDGFRA) [7] resulted in a dramatic change in diagnosis, treatment and prognostication for GISTs. Currently, immunohistochemical expression of the KIT receptor (CD117) and "Discovered-on-GIST-1" (DOG-1) represents the gold standard for the diagnosis of GISTs in the context of typical tumour histology [1, 2]. The tyrosine kinase inhibitor imatinib mesylate (Glivec, Novartis, Basel, Switzerland) has emerged as the treatment of choice for patients with inoperable or metastatic disease [8, 9]. A majority of patients respond to imatinib mesylate or achieve durable tumour growth stabilisation, allowing a R0 resection, but some initially responsive patients experience tumour progress because of secondary drug resistance [10, 11]. Understanding the biologic mechanisms of drug resistance is important, as these patients increasingly represent therapeutic challenges.

Here, we report a unique case of a patient with a huge gastric GIST that underwent unusual phenotypic change, following neoadjuvant imatinib treatment for 8 months.

Case presentation

A 62-year-old woman with no history of relevant diseases was diagnosed with a large upper abdominal mass on clinical evaluation for non-specific symptoms. Laboratory tests including tumour markers (CEA, CA 19-9, CA 72-4 and AFP) were within normal limits. The results of a chest and abdominal radiograph, as well as upper GI panendoscopy and coloscopy, revealed no pathological findings. Ultrasonography showed a non-homogenous hypoechoic mass with cystic areas occupying the upper abdomen. A contrast-enhanced computed tomography (CT) scan confirmed the presence of a voluminous intra-abdominal mass 20×15×15 cm in size with peripheral contrast enhancement. The mass was juxtaposed to the pancreas and the posterior wall of the stomach (Fig. 1a). The bowel was dislocated without signs of intestinal occlusion. It was not possible to define with certainty the origin of the tumour. No liver or lymph node metastases were detected. A percutaneous CT-guided core needle biopsy was performed. According to the size of the tumour and the likely infeasible R0 resection, the patient received neoadjuvant imatinib mesylate therapy (400 mg/day for 8 months). The drug was well tolerated by the patient. A CT scan performed thereafter showed partial response, with a decrease of tumour maximum diameter from 20×15×15 cm to 13.3×8×7.6 cm, without any evidence of metastases (Fig. 1b).

Treatment and follow-up

An explorative laparotomy was performed. The tumour was found adhered to the tail of the pancreas and the posterior wall of the gastric corpus. Notably, no metastases were detected along the gastrointestinal tract and the abdominal cavity during the laparotomic inspection. The tumour mass was removed "en bloc" with a part of the greater omentum, the tail of the pancreas, spleen, the corpus of the stomach and the local lymph nodes. The resection margins were macroscopically free of disease. The post-operative course was uneventful, and the patient was discharged on the 14th post-operative day. Regular follow-up using abdominal ultrasound and CT scan revealed no tumour recurrence or metastasis at last follow-up 28 months later.

Materials and methods

Tumour specimens were fixed in buffered formalin and embedded routinely for histological evaluation. Immunohistochemical stains were performed on 5-μm sections cut from paraffin blocks, using the primary antibodies CD117, CD34, S100, desmin, α-smooth muscle actin and pankeratin

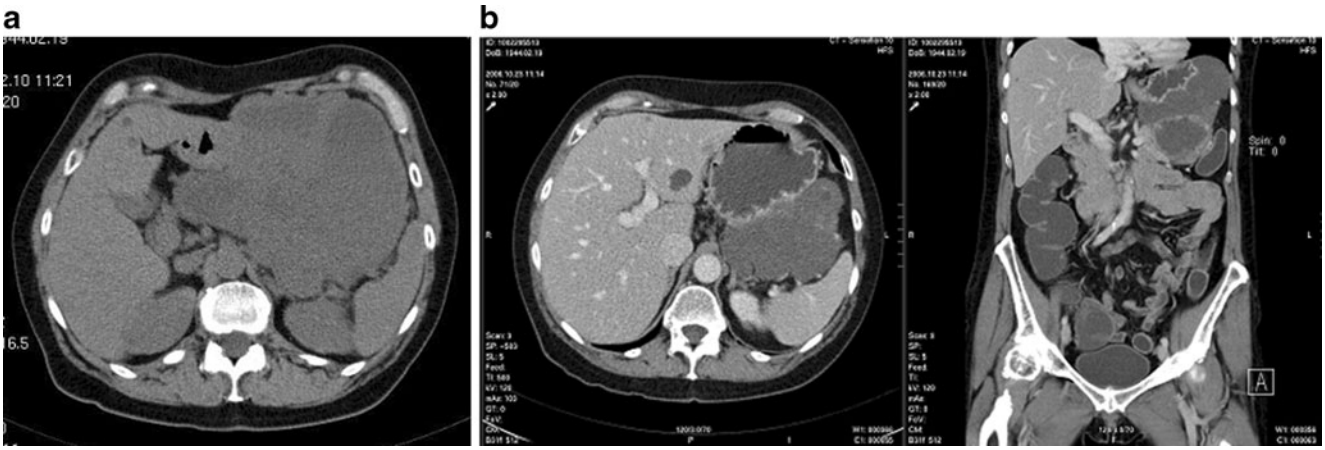

Fig. 1 CT scan of the GIST in the upper abdomen **a** prior to imatinib mesylate therapy and **b** after an 8-month neoadjuvant imatinib mesylate treatment. Note the obvious decrease in size

(KL-1) for the pre-treatment tumour biopsy. The tumour from the resection specimen was, in addition, stained for pankeratin (KL1), CK7, high molecular weight keratins (34βE-12), CK20, DOG-1, PDGFRA, HMB45, melan A, h-caldesmon, CD30, D2-40, factor VIII, FLI-1 and the leucocyte common antigen CD45 on three representative tumour blocks (sources of the antibodies, dilutions and staining protocols are available upon request).

Molecular analysis

For mutational analysis, DNA was extracted from formalin-fixed paraffin-embedded tissue and amplified using primers specific for exons 9, 11, 13 and 17 of the *KIT* gene and exons 12, 14 and 18 of the *PDGFRA* gene, followed by purification of the PCR products and direct bi-directional sequencing. In addition, the tumour was investigated for KRAS and BRAF mutations.

Histopathological findings

The pre-imatinib core biopsy revealed a hypercellular spindle cell tumour with focal areas of stromal edema and a brisk mitotic activity (4 mitoses in 10 available HPFs; 10 HPFs corresponded to an area of 2 mm^2), consistent with a diagnosis of spindle cell gastric GIST (Fig. 2a–b). The immunohistochemistry revealed strong and diffuse expression of CD117 (Fig. 2c) and CD34 (Fig. 2d) in all tumour cells, with limited focal smooth muscle actin reactivity, while desmin and S-100 protein were negative. Retrospectively (for comparison with the resection specimen), the biopsy material was stained with pankeratin antibody (KL-1) and showed a complete lack of staining for this marker. Further slides were not available for other immunostains. Based on the tumour size and mitotic activity, the tumour corresponded to a high-risk GIST in both the NIH and AFIP risk stratification systems [1, 3].

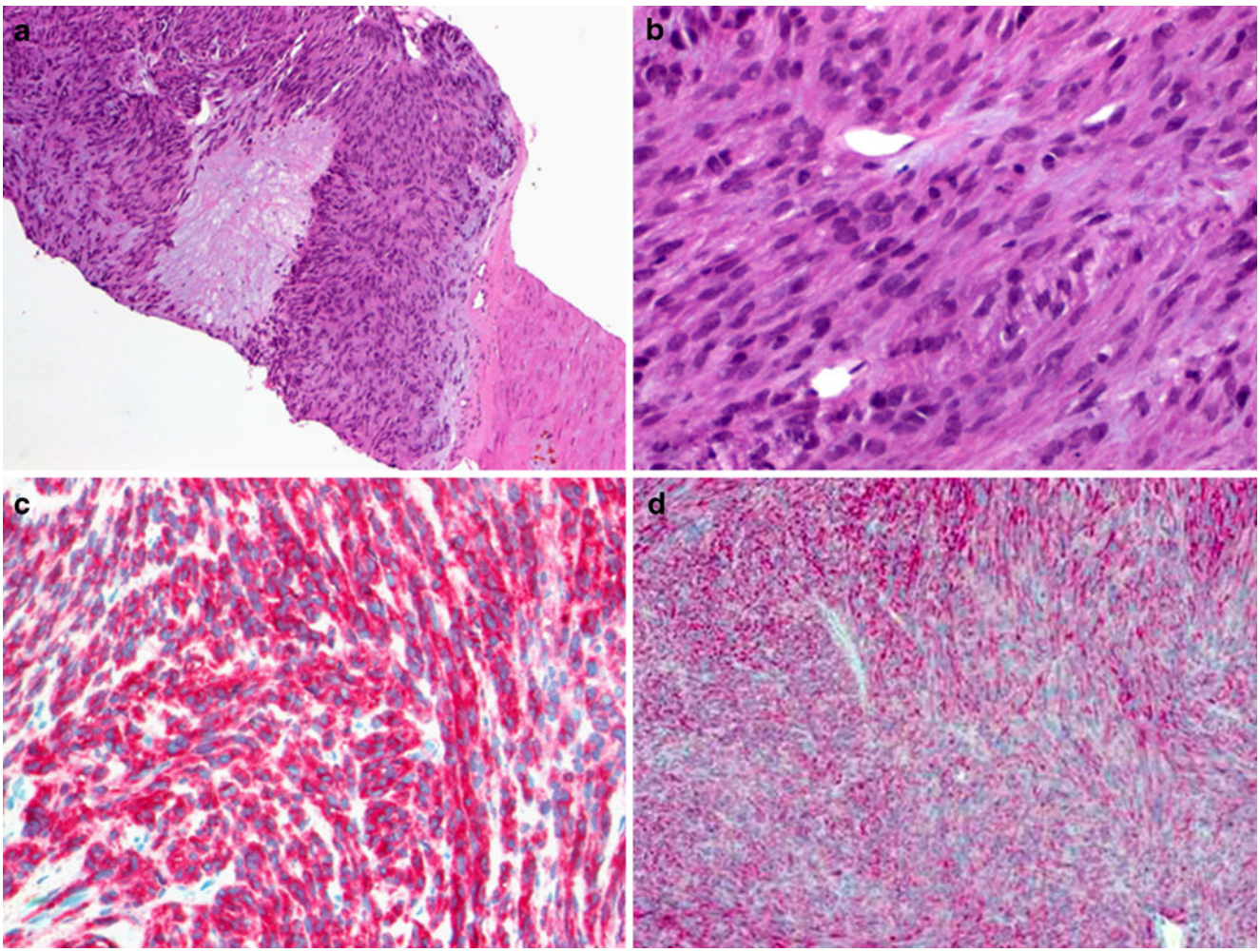

Fig. 2 Findings in the core needle biopsy. **a** Cellular spindle cell neoplasm with focal stromal changes. **b** Spindle cells seen at higher magnification. **c** Strong staining for CD117. **d** CD34 immunostaining

The tumour resection specimen, after neoadjuvant imatinib mesylate treatment, revealed subtotal extensive hyalinisation of tumour tissue with evidence of old haemorrhages associated with focal inflammatory infiltrates affecting >90% of the tumour mass (Fig. 3a). Within this fibrohyaline tissue, there were small fascicles and isolated cells with slender bipolar nuclei. These bland-looking cells strongly expressed CD117 and DOG-1 (Fig. 3b). Around 20% of the cells stained strongly with KL1 (Fig. 3c) and CK7 (Fig. 3d). In addition, multiple well-circumscribed nodules (up to 1 cm) of highly anaplastic, large polygonal epithelioid cells with rhabdoid cytoplasm and vesicular nuclei having centrally located, brightly eosinophilic nucleoli were found (Fig. 4a). Tumour cells were arranged in solid sheets permeated by polymorphonuclear cell-rich inflammatory infiltrates. Bi- and multinucleated tumour cells were common as atypical mitotic figures (Fig. 4b). These highly atypical tumour cells were completely negative for CD117 (Fig. 3c), DOG-1, PDGFRA, CD34, S100, HMB45, melan A, desmin, α-smooth muscle actin, h-caldesmon, CD30, D2-40, factor VIII and leucocyte common antigen (CD45). They expressed strongly and diffusely vimentin and pankeratin marker KL1 (Fig. 4d), but were negative for CK7, high molecular weight keratins (34βE-12) and CK20. A focal, mostly weak and non-specific expression was seen for CD31 and FLI-1 (not shown). Tumour nests were seen permeating small and dilated lymphatic vessels at the periphery of the nodules.

Mutation status

Unfortunately, no sufficient tumour tissue from the pre-operative core needle biopsy was available for mutational analysis. Thus, molecular analysis was performed on tumour DNA gained from the viable tumour clones in the resection

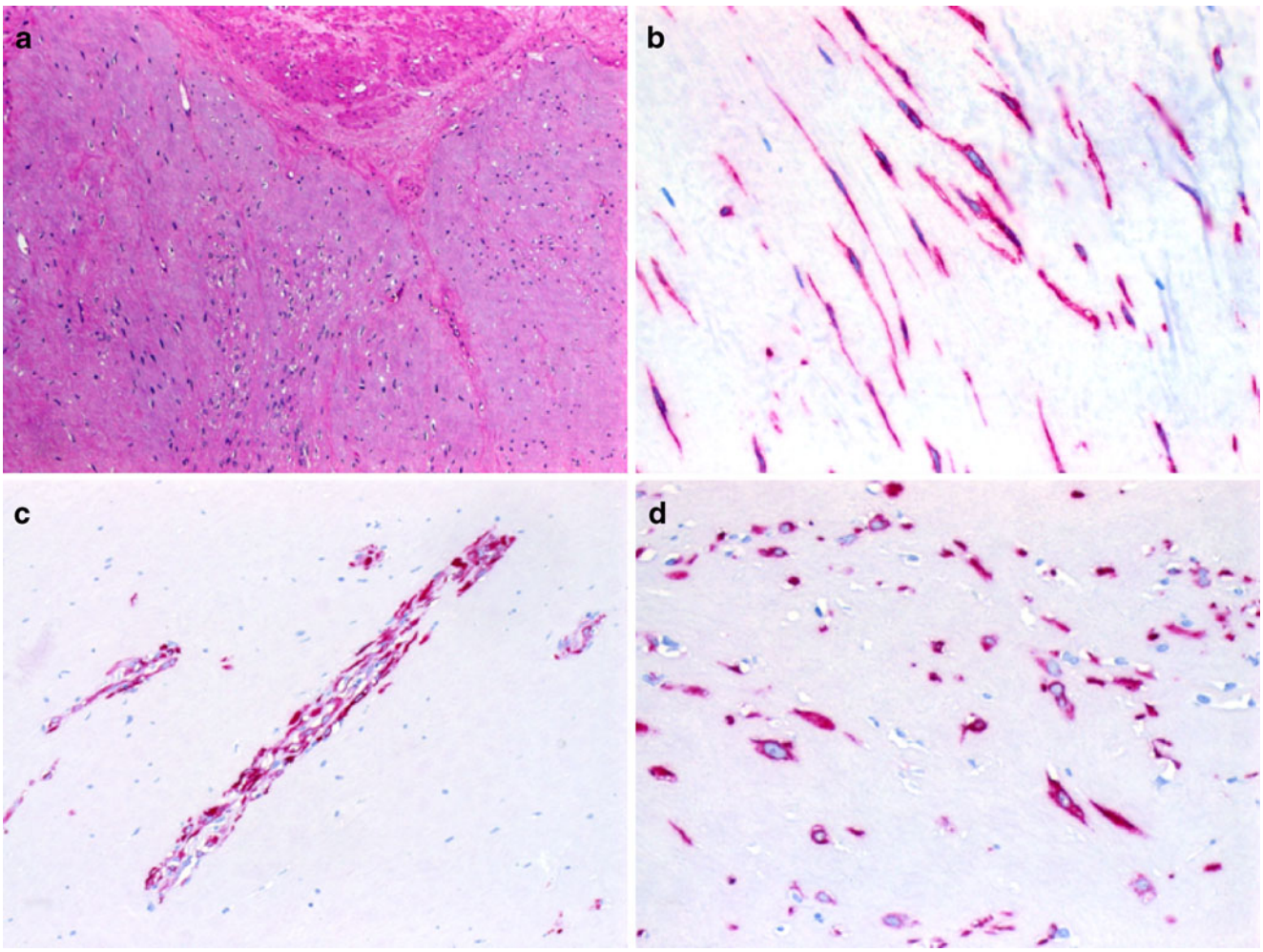

Fig. 3 Phenotypic and immunohistochemical changes in the imatinib-responsive tumor clones. **a** A hyalinized tumor mass contained isolated bland-looking spindle cells (*upper field*, muscle layer of gastric wall). **b** Strong expression of DOG-1 in the spindled cells. **c** Thin fascicles of spindle cells expressed KL-1. **d** Strong expression of CK7 in a subset of the spindled cells

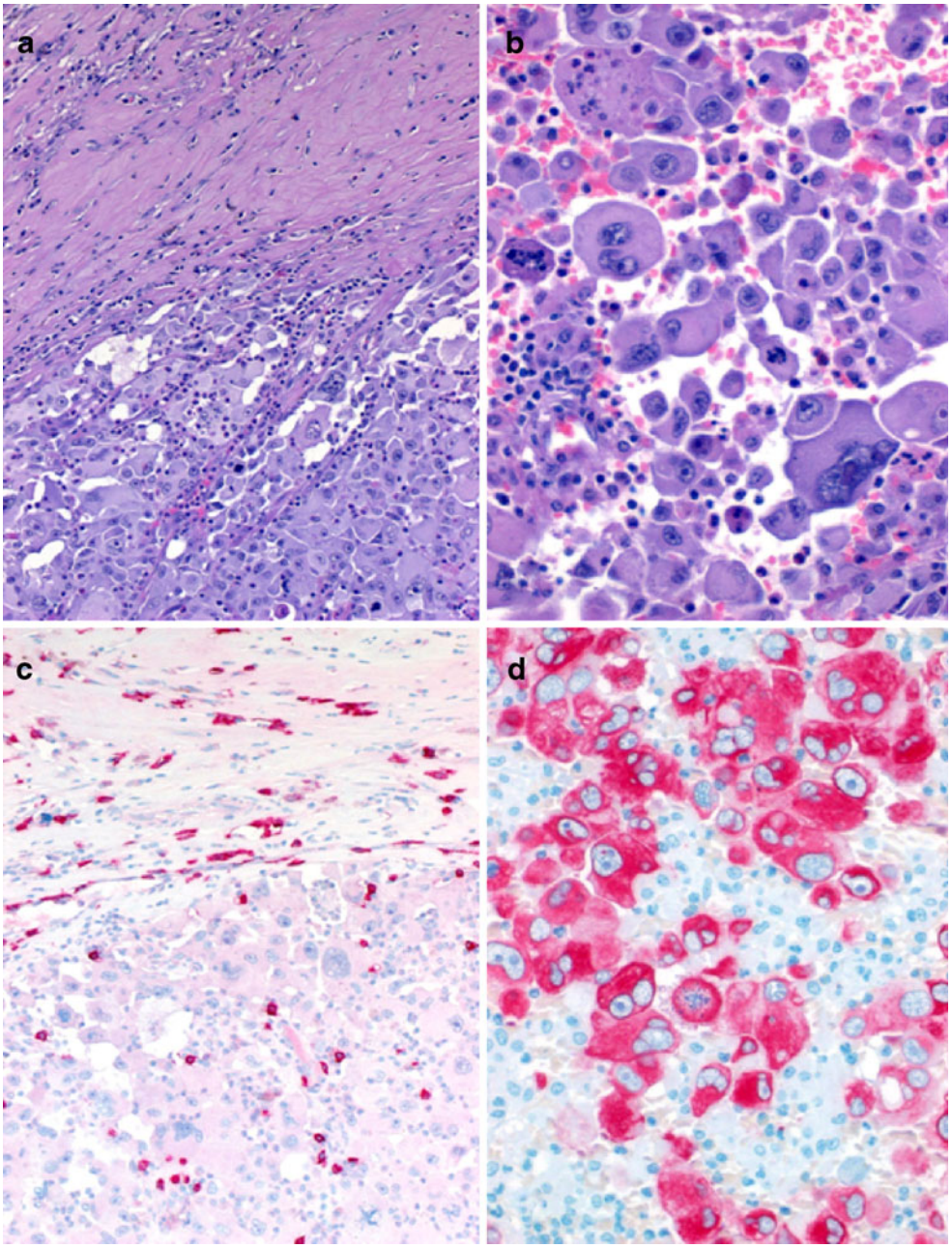

Fig. 4 Phenotypic and immunohistochemical changes in the imatinib-resistant tumour clones. **a** Hyalinized tumour area (*upper*) juxtaposed to a resistant pleomorphic clone (*lower field*). **b** Higher magnification of the resistant clone. Note the remarkable anaplasia with rhabdoid cytomorphology and prominent mixed inflammatory infiltrate. **c** Complete loss of KIT expression in the resistant clone (*lower*). Note the isolated staining spindled cells in the responsive clone (*upper field*) and prominent reactive mast cells (*lower field*). **d** Tumour cells in the resistant clone strongly expressed pankeratin (KL-1)

specimen. This showed a wild type for KIT exons 9, 11, 13, 17, PDGFRA exons 12, 14, 18, KRAS exon 2 and BRAF exon 15.

Discussion

Following the discovery of constitutive KIT activation as the central oncogenic mechanism in the pathogenesis of GIST [5], inhibition of the KIT signalling using diverse tyrosine kinase inhibitors, in particular, imatinib mesylate (Glivec), has emerged as an effective treatment for patients with primary unresectable and metastatic GIST [8, 9]. Furthermore, neoadjuvant imatinib treatment in patients who present with inoperable GISTs might enable a successful and less radical surgery after cytoreduction (down staging) [12]. However, while a majority of patients with tyrosine kinase mutations show an initial response or stable disease, some patients develop resistance to the drug, usually following a period of 12–36 months of treatment [2]. These patients may either show regrowth of an initially responsive primary tumour or development of metastasis under treatment [10, 11]. The mechanisms responsible for secondary imatinib resistance were found to be very heterogeneous [13]; secondary KIT or PDGFRA mutations are found in more than 50% [13], but other mechanisms such as target

gene amplification and activation of other alternative kinases and KIT-independent oncogenic signalling pathways probably play an important role in a subset of the cases [11, 13].

Examination of GIST resection specimens following imatinib treatment has shown variable tumour alterations as evidence of histological response (hyalinisation, necrosis, haemorrhages) [13–15]. Resistant tumour clones may be seen in the primary tumour as well as at metastatic sites. Diverse cytoarchitectural and immunophenotypic changes have been reported in post-imatinib GISTs. In particular, tumours with spindle morphology may show a shift towards pure epithelioid phenotype, with or without immunophenotypic changes [14, 15]. In these circumstances, many tumours show variable to complete loss of KIT expression by immunohistochemistry [13–15]. Less commonly, the primary tumour and/or its metastasis may undergo metaplastic changes, trans-differentiation or heterologous differentiation (dedifferentiation) [13, 15–17].

In the current report, we describe the occurrence of unusual phenotypic and immunohistochemical changes in a huge gastric GIST following neoadjuvant imatinib treatment for 8 months. The tumour showed a shift to a high-grade epithelioid neoplasm, expressing both vimentin and pankeratin that, in conjunction with the tumour morphology, was very reminiscent of the proximal-type epithelioid sarcoma, undifferentiated (anaplastic) carcinoma, melanoma and epithelioid angiosarcoma. Absence of primitive vasoformation by tumour cells, indolent tumour course with absent metastasis for almost 3 years and absent clear-cut expression of the endothelial markers (CD34, factor VIII and D2-40) all argue against true angiosarcomatous trans-differentiation [18].

Liegl et al. [13] described the occurrence of huge epithelioid cells with nuclear atypia and other unusual features in two of four GISTs with secondary clonal imatinib resistance; of these, two were wild-type GISTs similar to our case. One patient (a 67-year-old woman with a primary gastric GIST and KIT exon 11 mutation) revealed a morphology that is somewhat reminiscent of our case. Also, the tumour in their study showed a complete loss of CD117 expression, and no secondary resistant mutation was detected.

Our case revealed a spindle cell phenotype in the pre-imatinib core biopsy with co-expression of CD117 and CD34. The resistant clones showed loss of both markers, combined with a strong aberrant expression of pankeratin. The tumour cells adopted highly anaplastic features with rounded rhabdoid morphology. The expression of low molecular weight keratins have been occasionally observed in GIST (=2%) [1, 2]. The absence of keratin expression in the biopsy and the strong and diffuse expression in the resistant clones indicated a neo-expression related to tumour progression and dedifferentiation. Interestingly, the responsive tumour clone retained the expression of CD117 and DOG-1. However, a variable focal expression of pankeratin and CK7 was seen in these areas, suggesting early aberrant phenotypic changes. In contrast, the most advanced tumour clones have lost CD117, DOG-1 and CK7. Molecular analysis of the resected tumour showed wild-type KIT, PDGFRA, KRAS and BRAF. Unfortunately, there was no sufficient material from the initial biopsy for molecular analysis, but the lack of mutations in the resected specimen indicated absence of a primary mutation in the tumour (wild-type GIST). This is consistent with the tendency of wild-type GISTs to undergo aberrant phenotypic changes following imatinib therapy, as discussed above [11]. Agaram et al. [17] described rhabdomyosarcomatous differentiation in a PDGFRA-mutated GIST following imatinib treatment. The molecular analysis in that case revealed a BRAF mutation (V600E) in the resistant clone, in addition to the initial PDGFRA deletion found in the primary tumour. In our case, no BRAF, KRAS or other resistant kinase mutations were detected. These changes are in line with an acquired imatinib resistance, as a result of yet unknown KIT independent mechanisms. It is remarkable in our case that the highly malignant phenotype seems not to correlate with the aggressiveness of the tumour. Irrespective of a pronounced lymphangioinvasion in the resection specimen, the patient had no evidence of metastatic or recurrent disease at last follow-up, 28 months later.

Trans-differentiation of GIST to a smooth muscle pattern phenotype under imatinib therapy is a well-known phenomenon documented in previous studies. Interestingly, experimental studies have shown that blockage of KIT signalling leads to trans-differentiation of interstitial cells of Cajal to smooth muscle cells [19]. It cannot be excluded that the current case and similar previously reported cases represent a similar phenomenon as a consequence of other mechanisms. Indeed, despite the central role of oncogenic KIT activation in GIST pathogenesis, different and complex intracellular signalling events may be triggered by oncogenic KIT [20, 21]. Also, there is evidence that a specific KIT mutation type can influence specific signal transduction pathways that are activated in that particular subset of GISTs [22], but currently, little is known about these alternative oncogenic mechanisms in GISTs.

In summary, we described an unusual case of GIST showing marked phenotypic and immunohistochemical changes under imatinib. These changes are of great relevance with regard to the histopathologic evaluation of resection specimens of post-imatinib GISTs. Awareness of this phenomenon should prevent diagnostic confusion and false interpretation as “non-GIST” by the unwary or inexperienced pathologist. Furthermore, exploration of the alternative KIT-independent pathways involved in these cases would shed some light on their pathogenetic

mechanisms, with the potential of targeting these alternative resistance mechanisms.

Conflict of interest The authors declare that they have no disclosures.

References

1. Miettinen M, Lasota J (2006) Gastrointestinal stromal tumors: pathology and prognosis at different sites. Semin Diagn Pathol 23:70–83
2. Liegl-Atzwanger B, Fletcher JA, Fletcher CD (2010) Gastrointestinal stromal tumors. Virchows Arch 456:111–127
3. Fletcher CD, Berman JJ, Corless C et al (2002) Diagnosis of gastrointestinal stromal tumors: a consensus approach. Hum Pathol 33:459–465
4. Agaimy A, Wünsch PH, Hofstaedter F et al (2007) Minute gastric sclerosing stromal tumors (GIST tumorlets) are common in adults and frequently show c-KIT mutations. Am J Surg Pathol 31:113–120
5. Scarpa M, Bertin M, Ruffolo C et al (2008) A systematic review on the clinical diagnosis of gastrointestinal stromal tumors. J Surg Oncol 98:384–392
6. Hirota S, Isozaki K, Moriyama Y et al (1998) Gain-of-function mutations of c-kit in human gastrointestinal stromal tumors. Science 279:577–580
7. Lasota J, Miettinen M (2006) KIT and PDGFRA mutations in gastrointestinal stromal tumors (GISTs). Semin Diagn Pathol 23:91–102
8. Joensuu H, Roberts PJ, Sarlomo-Rikala M et al (2001) Effect of the tyrosine kinase inhibitor STI571 in a patient with a metastatic gastrointestinal stromal tumor. N Engl J Med 344:1052–1056
9. Demetri GD, von Mehren M, Blanke CD et al (2002) Efficacy and safety of imatinib mesylate in advanced gastrointestinal stromal tumors. N Engl J Med 347:472–480
10. Heinrich MC, Corless CL, Demetri GD et al (2003) Kinase mutations and imatinib response in patients with metastatic gastrointestinal stromal tumor. J Clin Oncol 21:4342–4349
11. Sciot R, Debiec-Rychter M (2006) GIST under imatinib therapy. Semin Diagn Pathol 23:84–90
12. Casali PG, Jost L, Reichardt P et al (2009) Gastrointestinal stromal tumours: ESMO clinical recommendations for diagnosis, treatment and follow-up. Ann Oncol 20(Suppl 4):64–67
13. Liegl B, Kepten I, Le C et al (2008) Heterogeneity of kinase inhibitor resistance mechanisms in GIST. J Pathol 216:64–74
14. Pauwels P, Debiec-Rychter M, Stul M et al (2005) Changing phenotype of gastrointestinal stromal tumours under imatinib mesylate treatment: a potential diagnostic pitfall. Histopathology 47:41–47
15. Bickenbach K, Wilcox R, Veerapong J et al (2007) A review of resistance patterns and phenotypic changes in gastrointestinal stromal tumors following imatinib mesylate therapy. J Gastrointest Surg 11:758–766
16. Liegl B, Hornick JL, Antonescu CR, Corless CL et al (2009) Rhabdomyosarcomatous differentiation in gastrointestinal stromal tumors after tyrosine kinase inhibitor therapy: a novel form of tumor progression. Am J Surg Pathol 33:218–226
17. Agaram NP, Wong GC, Guo T et al (2008) Novel V600E BRAF mutations in imatinib-naive and imatinib-resistant gastrointestinal stromal tumors. Genes Chromosom Cancer 47:853–859
18. Rossi S, Orvieto E, Furlanetto A et al (2004) Utility of the immunohistochemical detection of FLI-1 expression in round cell and vascular neoplasm using a monoclonal antibody. Mod Pathol 17:547–552
19. Torihashi S, Nishi K, Tokutomi Y et al (1999) Blockade of kit signaling induces transdifferentiation of interstitial cells of cajal to a smooth muscle phenotype. Gastroenterology 117:140–148
20. Janeway KA, Liegl B, Harlow A et al (2007) Pediatric KIT wild-type and platelet-derived growth factor receptor alpha-wild-type gastrointestinal stromal tumors share KIT activation but not mechanisms of genetic progression with adult gastrointestinal stromal tumors. Cancer Res 67:9084–9088
21. Duensing A, Medeiros F, McConarty B et al (2004) Mechanisms of oncogenic KIT signal transduction in primary gastrointestinal stromal tumors (GISTs). Oncogene 23:3999–4006
22. Caruana G, Cambareri AC, Ashman LK (1999) Isoforms of c-KIT differ in activation of signalling pathways and transformation of NIH3T3 fibroblasts. Oncogene 18:5573–5581

Virchows Arch (2011) 458:371–376
DOI 10.1007/s00428-010-1035-0

CASE REPORT

Sudden death of an immunocompetent young adult caused by novel (swine origin) influenza A/H1N1-associated myocarditis

Georg Gdynia · Paul Schnitzler · Eva Brunner · Reinhard Kandolf · Hendrik Bläker · Edith Daum · Philipp Schnabel · Peter Schirmacher · Wilfried Roth

Received: 23 July 2010 / Revised: 3 December 2010 / Accepted: 11 December 2010 / Published online: 14 January 2011
© Springer-Verlag 2011

Abstract The main cause of death from novel (swine origin) influenza A/H1N1 infection is acute respiratory distress syndrome. Most fatal cases are immunocompromised patients or patients with a severe underlying disease. Here, we report a fatal case of acute interstitial myocarditis associated with novel influenza A/H1N1 infection in an immunocompetent young woman. A previously healthy 18-year-old woman experienced malaise, diarrhea, and fever for several days prior to a sudden collapse at home. Autopsy revealed a predominantly lymphocytic myocarditis in the absence of a significant respiratory tract infection. Infection with novel (swine origin) influenza A/H1N1 was confirmed by PCR analysis of blood as well as myocardial tissue. Influenza-caused diarrhea with consecutive hypokalemia potentially contributed to the fatal outcome of the myocarditis, characterized by ventricular fibrillation. In conclusion, sudden death by myocarditis may be a rare complication of novel influenza A/H1N1 infection in otherwise healthy individuals, even in the absence of significant respiratory tract infection.

Keywords Novel influenza A · Swine flu · H1N1 · Myocarditis

G. Gdynia · H. Bläker · P. Schnabel · P. Schirmacher · W. Roth (✉)
Institute of Pathology, University Hospital,
Im Neuenheimer Feld 220/221,
69120 Heidelberg, Germany
e-mail: Wilfried.Roth@med.uni-heidelberg.de

P. Schnitzler · E. Daum
Department of Infectious Diseases, Virology, University Hospital,
Im Neuenheimer Feld 324,
69120 Heidelberg, Germany

E. Brunner · R. Kandolf
Department of Molecular Pathology, University Hospital,
Liebermeisterstraße 8,
72076 Tübingen, Germany

Introduction

The influenza A/H1N1 pandemic of 2009/2010 was mainly characterized by a mild and self-limiting disease. However, a minority of patients exhibited a severe course of the disease, sometimes with a fatal outcome. In contrast to the seasonal influenza, severe and fatal cases occurred frequently in young patients and were characterized by primary viral pneumonia [1], secondary pulmonary bacterial infection, severe diarrhea, acute renal failure, and multiple organ dysfunction [2]. Other persons at increased risk for influenza A/H1N1-caused death included immunocompromised patients after organ transplantation, chemotherapy, or HIV infection, pregnant women, newborns, or chronically ill patients [2, 3].

In respect to seasonal influenza, viral myocarditis is one of the complications associated with a fatal outcome [2]. The main complication of seasonal influenza is extension of the viral infection to the alveoli, often with secondary bacterial infection, resulting in severe pneumonia. In general, complications in extrarespiratory tissues such as encephalopathy, myocarditis, and myopathy occur only occasionally. However, extrarespiratory complications appear to be more common for infections with the avian H5N1 virus than with the human seasonal influenza viruses. The clinical outcome of influenza virus myocarditis depends on the duration of the myocardial

disease: Patients dying acutely of fulminant influenza usually exhibit severe pneumonia with respiratory dysfunction. If the patient dies later, it may be from heart failure. If the patient survives, the resulting myocardial fibrosis may result in heart block due to problems with electrical conduction [4, 5]. Onitsuka et al. [5] reported on influenza-infected patients where cardiac involvement occurred 1 week after the onset of influenza symptoms. Usually, myocarditis occurs mostly in patients with a long-standing disease. However, the clinical features of myocarditis due to novel (swine origin) influenza A/H1N1 infection are unknown.

Clinical history

A previously healthy 18-year-old woman experienced malaise, rhinitis, pharyngitis, minor coughing, diarrhea, and mild fever (38°C) associated with upper respiratory tract infection for 2 days. She had not received vaccination against influenza A/H1N1. The patient did not smoke, abuse alcohol, or use any illicit or other drugs. There was no case of sudden death in the family history. The twin brother of the patient did not suffer from any relevant disease. At physical examination by the general practitioner, the patient presented with normal blood pressure (110/70) and pulse (80 bpm), and no abnormal heart or lung murmurs were detected. She was sent home, but one day later, diarrhea and vomiting occurred, and after a sudden collapse, the patient was admitted to the emergency room. At this time, she was alert and oriented, with no dyspnea or pain. Initially, the laboratory evaluation showed a moderate hypokalemia of 3 mmol/l (normal, 3.5–4.8 mmol/l), leukocytosis of 23.2 leukocytes/nl (normal, 4–10 leukocytes/nl), and C-reactive protein level of 3.78 mg/ml (normal, below 5 mg/ml). Troponin T and CK-MB levels were elevated (5.8 ng/ml and 206 U/l, respectively). An echocardiography was not performed. While still in the emergency room, the patient collapsed again and developed ventricular fibrillation followed by electromechanical dissociation (Fig. 1a). Cardiopulmonary reanimation was immediately started, and a lysis therapy was performed due to suspected acute pulmonary embolism (D-dimers, 1.6 μg/ml). The chest radiograph showed only minimally increased streaking in the right lower lobe and in the middle lobe (Fig. 1b). Despite cardiopulmonary reanimation and percutaneous pacemaker stimulation, the patient died after a prolonged period of resuscitation (200 min).

Materials and methods

Autopsy and histology

Autopsy of the patient was carried out according to standard procedures. During the autopsy, tissue samples from the heart, lung, and other organs were fixed in formalin and embedded in paraffin. Altogether, 25 paraffin-embedded myocardial tissue blocks were generated. Additionally, blood from the ventricles and from the femoral vein was taken and frozen at −20°C. A microscopic examination was performed following standard staining procedures with haematoxylin and eosin. For the diagnosis of myocarditis, 20 microscopic, high-power fields were counted randomly within selected blocks (septum, left and right ventricles), without using a digital camera or a computer. Immunohistochemical staining was performed using a Techmate 500+ automated immunostainer (DakoCytomation, Hamburg, Germany) with an avidin–biotin complex peroxidase detection system. The antibodies specific for CD3 (1:200) and

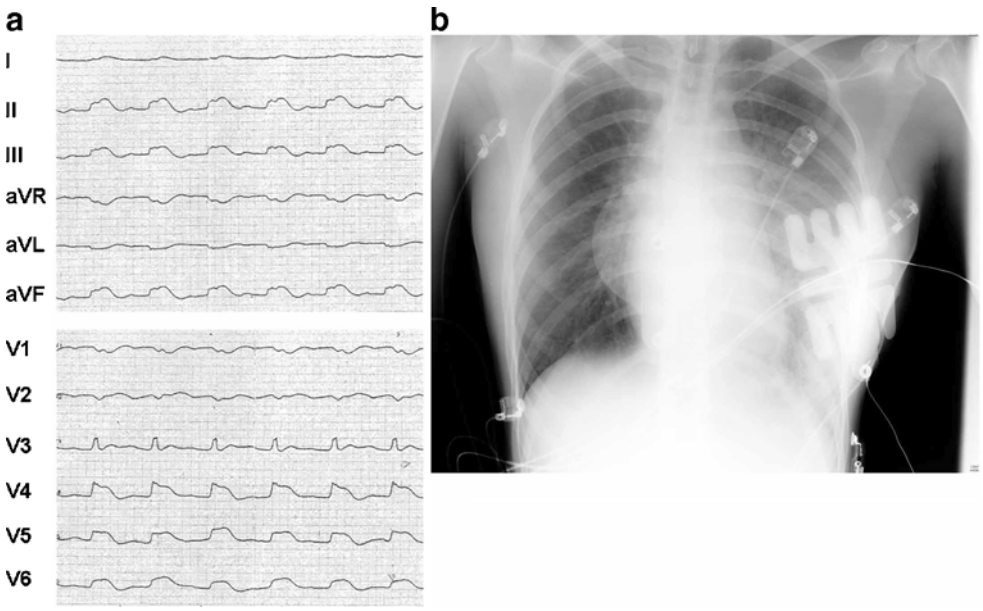

Fig. 1 Electrocardiography and chest x-ray of the patient. **a** Electrocardiography (50 mm/s, 10 mm = 1 mV) showing electromechanical dissociation with broad and plump ventricular complexes with ubiquitary ST elevations. **b** Chest x-ray (anterior–posterior projection) showing a modest streaking in the middle and lower lobes. Note that there is no pneumothorax and that the endotracheal tube is placed correctly

CD68 (1:8,000) were purchased from Labvision (Thermo Fisher Scientific Inc.) and Dako, respectively. Briefly, paraffin-embedded tissue sections were dewaxed and rehydrated using xylene and a series of graded alcohols, followed by heat-induced antigen retrieval using a target retrieval solution (S2023, DakoCytomation) in a pressure cooker for 15 min. The sections were incubated with a primary antibody for 30 min at room temperature and processed according to the manufacturer's instructions for the following kits: ChemMate Detection Kit (K5003, DakoCytomation), ChemMate Buffer Kit (K5003, DakoCytomation), and Avidin/Biotin Blocking Kit (SP-2001, Vector Laboratories).

Real-time RT-PCR analysis

PCR-based detection of influenza A/H1N1 virus was performed by real-time reverse transcription (RT)-PCR, as described before [6]. Total RNA from blood (sampled from the heart ventricles during necropsy), myocardial tissue, lung tissue, and small bowel tissue was isolated with the QIAamp Viral RNA Mini Kit (Qiagen), according to the manufacturer's protocol. Complementary DNA (cDNA) was synthesized from 5.0 μl RNA using reverse transcriptase and random hexamers from the Transcriptor First Strand cDNA Synthesis Kit (Roche). RT-PCR analysis was performed using the LightCycler® 480 Probes Master Mix (Roche) and the LightCycler® 480 System (Roche). The primer pairs were used at a concentration of 10 μM (for sequences, see Table 1). Besides for influenza A/H1N1 virus, a real-time RT-PCR analysis was performed for adenovirus (ADV), human cytomegalovirus (HCMV), enterovirus species (EV, comprising coxsackieviruses and echoviruses), Epstein–Barr virus (EBV), herpes simplex virus types 1 and 2 (HSV1, HSV2), human herpes virus 6 (HHV6), parvovirus B19 (PVB19), and influenza B virus.

Nested PCR

Paraffin-embedded autoptic myocardial tissue sections were dewaxed by xylol and treated with proteinase K, and nucleic acids were isolated by phenol/chloroform extraction. As an endogenous control template for successful RNA extraction, cDNA of the reference housekeeping gene porphobilinogen deaminase was amplified. Detection of influenza A/H1N1 virus RNA (reference, NC_002016 influenza A virus (A/Puerto Rico/8/34(H1N1)) segment 7 matrix protein 2) by nested RT-PCR analysis was performed using OneStep RT-PCR Kit (QIAGEN) and 160 ng RNA as template. Primers were used at a concentration of 15 μM each (for sequences, see Table 1). The RT-PCR-protocol was: first run, 30 min at 50°C, 15 min at 95°C, 30 s at 94°C, 30 s at 55°C, 45 s at 72°C (35 cycles); second run, 30 s at 94°C, 30 s at 55°C, 45 s at 72°C (35 cycles). The specificity of the detection of H1N1 virus is assured by direct sequencing of the amplified positive nested PCR product. In addition, EV, comprising coxsackieviruses and echoviruses, PVB19, ADV, EBV, HHV6, HCMV, HSV1, HSV2, HHV8, influenza B virus, as well as other cardiotropic pathogens, i.e., *Toxoplasma gondii*, *Borrelia burgdorferi*, and *Eubacteria*, were evaluated by nested PCR/RT-PCR as described [7, 8].

Results

At autopsy, the heart showed focal hemorrhage and slight pallor of the myocardial tissue especially in the left ventricle wall and in the septum. The heart weight was 320 g, and the left and right ventricle walls were 14 mm and 3 mm in thickness, respectively; the circumferences of the valves were 10 cm, 6 cm, 11 cm, and 6 cm for the mitral, aortic, tricuspid, and pulmonary valves, respectively. Signs of pericarditis were not detected. The coronary

Table 1 Primer and probe sequences

Real-time RT-PCR analysis of H1N1, segment 4	
Target gene	Primer sequence
Nucleotides 380–404	5′-CATTTGAAAGGTTTGAGATATTCCC-3′ (forward)
Nucleotides 457–437	5′-ATGCTGCCGTTACACCTTTGT-3′ (reverse)
Hybridization probe	5′-FAM (6-carboxyfluorescein)-ACAAGTTCATGGCCCAAT CATGACTCG-BBQ (BlackBerry™ Quencher 650)-3′
Nested RT-PCR analysis of H1N1 segment 7 matrix protein 2	
Target gene	Primer sequence
First run: nucleotides 76–94	5′-AGGCCCCCTCAAAGCCGAG-3′ (forward)
First run: nucleotides 252–273	5′-GCATTYTGGACAAAGCGTCTAC-3′ (reverse)
Second run: nucleotides 110–135	5′-GAAGATGTCTTTGCAGGGAAGAACAC-3′ (forward)
Second run: nucleotides 224–242	5′-CTCGCTCACTGGGCACGGT-3′ (reverse)

arteries were normal. The kidneys exhibited a pale renal cortex, and blood pooling was observed both in the renal medulla and in the basal lung lobes. Macroscopically, the bowel did not show abnormalities, except very prominent Peyer plaques. Histological examination of the heart tissue (from the left ventricle, right ventricle, septum, papillary muscle, and myocardium close to the aortic and mitral valves) revealed interstitial edema and a mainly lympho-monocytic inflammatory infiltrate with focal necrosis of cardiomyocytes (Fig. 2a–d). In 1 mm^2, 16 (mean) CD3-

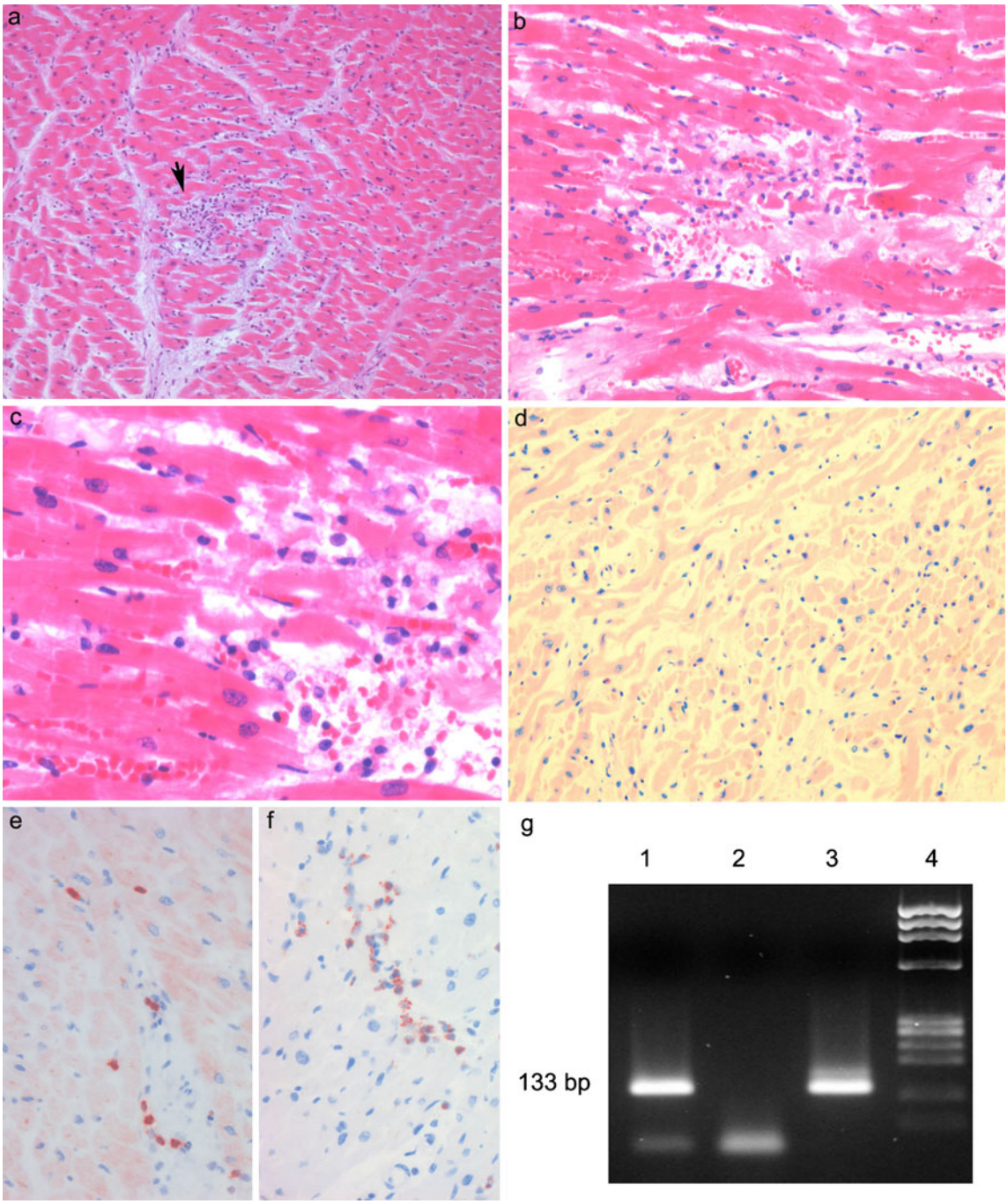

Fig. 2 Histological findings in H1N1-associated myocarditis. **a** Myocardial tissue from the septum (H&E, ×100). The *arrow* indicates the interstitial inflammatory infiltrate. **b**, **c** Immune-mediated destruction of cardiomyocytes in the septum (H&E; b, ×200; c, ×400). **d** Myocardial tissue from the septum (Giemsa, ×100). **e** Immunohistochemical detection of CD3-positive T lymphocytes in the right ventricle (×200, CD3 staining). **f** Myocardium with CD68-positive macrophages (×200). **g** Detection of influenza A/H1N1 virus RNA in paraffin-embedded heart tissue (right ventricle centered between the heart valve level and apex) by nested RT-PCR (2×35 cycles) (lane *1*, patient, H1N1 segment 7 matrix protein 2, product size 133 bp; lane *2*, negative control, water; lane *3*, positive control, plasmid, insert influenza A/H5N2; lane *4*, marker)

positive T lymphocytes (Fig. 2e) and CD68-positive macrophages (Fig. 2f) were counted. In the right ventricle, dense lymphocytic infiltrates with single cell necrosis of cardiomyocytes, destruction of heart muscle fibers, and focal fibrosis of the interstitium were observed. Moreover, focal accumulation of neutrophil granulocytes was detected, presumably representing a reaction to the prolonged resuscitation (not shown). The mitral and aortic valves did not exhibit any abnormalities macroscopically or histologically. The lung parenchyma did not show significant inflammatory changes or intraalveolar edema. No viral inclusion bodies were observed. There were no significantly abnormal findings in the other organs. Additionally, we tested the paraffin-embedded heart tissue for the presence of viral RNA from known cardiotropic viruses and the H1N1 virus. Reverse transcriptase nested PCR provided evidence for influenza A/H1N1-specific RNA sequences of the viral segment 7 matrix protein 2 (Fig. 2g). The 133-bp amplification product showed a 98% identity with influenza A virus subtype H1N1 (reference NC_002016), as confirmed by automatic DNA sequencing. In contrast, the nested PCR analysis yielded negative results for common cardiotropic viruses, i.e., EV, comprising coxsackieviruses and echoviruses, PVB19, HHV6, EBV, ADV, HCMV, HSV1, HSV2, HHV8, influenza B virus, as well as other cardiotropic pathogens, i.e., *Toxoplasma gondii*, *Borrelia burgdorferi*, and *Eubacteria*. Moreover, in blood samples taken during the autopsy as well as in lung tissue from the middle lobe, swine flu H1N1 hemagglutinin RNA was detected by real-time RT-PCR (data not shown), whereas RNA of other common cardiotropic pathogens (see above) was not detected. The PCR analysis of bowel tissue (terminal ileum) was negative for H1N1.

Discussion

Myocarditis has been described as a potentially fatal complication of seasonal influenza during the past pandemics [9, 10]. The histological findings in influenza-associated myocarditis are characterized by cardiomyocyte necrosis and infiltration of predominantly mononuclear inflammatory cells [11]. Necrosis and consecutive inflammation in the myocardium might result from a combination of the direct cytolytic effect of the viral infection and the host immune response [2]. In some cases, the influenza A virus could be detected in the myocardium using in situ RT-PCR hybridization [9, 12]. However, the cardiac host cells of the influenza virus have not been clearly identified. Viral RNA could be detected in the lymphocytes and macrophages of the myocardial interstitium [12] and in whole myocardial tissue [9]. In our study, the influenza A/H1N1 virus RNA was detected both in the myocardial tissue and blood. Our attempt to spatially allocate virus particles in the myocardial tissue by electron microscopy was not successful (data not shown). Thus, it still remains an open question whether the H1N1 virus can primarily infect cardiomyocytes, such as in the case of genuine cardiotropic viruses. It cannot be excluded that lymphocytes or macrophages are the primary target cells for the H1N1 virus in myocardial tissue. Future studies are required to address this question in more detail.

In contrast to the seasonal influenza, severe and fatal cases of the H1N1 pandemic were observed more frequently in young patients with comorbidities [1]. Our observation of the sudden death of an immunocompetent 18-year-old adolescent points to a possible novel feature of the H1N1 pandemic, which is fatal myocarditis as a rare complication of H1N1 infection. Fatal outcomes associated with fulminant myocarditis have already been described in children with H1N1 infections [13]. However, to our knowledge, this is the first reported case of an immunocompetent adult dying from a primary H1N1-associated myocarditis without significant concomitant pulmonary symptoms. Similarly, a most recent report describes H1N1 infection in a previously healthy young adult leading to myocarditis and subsequent myocardial dysfunction [14]. In contrast to our case, this patient received antiviral therapy and was discharged home after 2 weeks.

The sudden fatal course of the disease in the young woman described in our study might have been promoted by hypokalemia due to an episode of diarrhea before the collapse. Thus, the combination of H1N1-mediated damage to the myocardium and the pro-arrythmogenic effects of hypokalemia could have been decisive in triggering fatal ventricular fibrillation.

Importantly, our patient did not receive vaccination against the new swine origin influenza. Inevitably, there will be epidemics of influenza during the next winters, probably with the new influenza A/H1N1 virus dominating [15]. However, the mild and self-limiting course in the last pandemic elicited an on-going discussion on the necessity and usefulness of H1N1 immunization [13, 15, 16]. The knowledge of the rare, but potentially lethal, cases of myocarditis associated with influenza A/H1N1 infection affecting even healthy, immunocompetent young people without any comorbidities should be integrated into the discussion about the vaccination against influenza A/H1N1.

Acknowledgment We thank Roland Penzel for the extraction of nucleic acids from paraffin-embedded tissue.

Conflict of interest The authors declare that they have no conflict of interest.

References

1. Perez-Padilla R, de la Rosa-Zamboni D, Ponce de Leon S, Hernandez M, Quinones-Falconi F, Bautista E, Ramirez-Venegas A, Rojas-Serrano J, Ormsby CE, Corrales A, Higuera A, Mondragon E, Cordova-Villalobos JA (2009) Pneumonia and respiratory failure from swine-origin influenza A (H1N1) in Mexico. N Engl J Med 361 (7):680–689. doi:10.1056/NEJMoa0904252
2. Kuiken T, Taubenberger JK (2008) Pathology of human influenza revisited. Vaccine 26(Suppl 4):D59–D66
3. Echevarria-Zuno S, Mejia-Arangure JM, Mar-Obeso AJ, Grajales-Muniz C, Robles-Perez E, Gonzalez-Leon M, Ortega-Alvarez MC, Gonzalez-Bonilla C, Rascon-Pacheco RA, Borja-Aburto VH (2009) Infection and death from influenza A H1N1 virus in Mexico: a retrospective analysis. Lancet 374(9707):2072–2079. doi:10.1016/S0140-6736(09)61638-X
4. McGovern PC, Chambers S, Blumberg EA, Acker MA, Tiwari S, Taubenberger JK, Carboni A, Twomey C, Loh E (2002) Successful explantation of a ventricular assist device following fulminant influenza type A-associated myocarditis. J Heart Lung Transplant 21(2):290–293. doi:S1053249801003369
5. Onitsuka H, Imamura T, Miyamoto N, Shibata Y, Kashiwagi T, Ayabe T, Kawagoe J, Matsuda J, Ishikawa T, Unoki T, Takenaga M, Fukunaga T, Nakagawa S, Koiwaya Y, Eto T (2001) Clinical manifestations of influenza A myocarditis during the influenza epidemic of winter 1998-1999. J Cardiol 37(6):315–323
6. Panning M, Eickmann M, Landt O, Monazahian M, Olschlager S, Baumgarte S, Reischl U, Wenzel JJ, Niller HH, Gunther S, Hollmann B, Huzly D, Drexler JF, Helmer A, Becker S, Matz B, Eis-Hubinger A, Drosten C (2009) Detection of influenza A (H1N1)v virus by real-time RT-PCR. Euro Surveill 14 (36)
7. Kindermann I, Kindermann M, Kandolf R, Klingel K, Bultmann B, Muller T, Lindinger A, Bohm M (2008) Predictors of outcome in patients with suspected myocarditis. Circulation 118(6):639–648. doi:10.1161/CIRCULATIONAHA.108.769489
8. Bultmann BD, Klingel K, Sotlar K, Bock CT, Baba HA, Sauter M, Kandolf R (2003) Fatal parvovirus B19-associated myocarditis clinically mimicking ischemic heart disease: an endothelial cell-mediated disease. Hum Pathol 34(1):92–95. doi:10.1053/hupa.2003.48S0046817703000030
9. Ray CG, Icenogle TB, Minnich LL, Copeland JG, Grogan TM (1989) The use of intravenous ribavirin to treat influenza virus-associated acute myocarditis. J Infect Dis 159(5):829–836
10. Nolte KB, Alakija P, Oty G, Shaw MW, Subbarao K, Guarner J, Shieh WJ, Dawson JE, Morken T, Cox NJ, Zaki SR (2000) Influenza A virus infection complicated by fatal myocarditis. Am J Forensic Med Pathol 21(4):375–379
11. Oseasohn R, Adelson L, Kaji M (1959) Clinicopathologic study of thirty-three fatal cases of Asian influenza. N Engl J Med 260 (11):509–518
12. Cioc AM, Nuovo GJ (2002) Histologic and in situ viral findings in the myocardium in cases of sudden, unexpected death. Mod Pathol 15(9):914–922. doi:10.1097/01.MP.0000024291.37651.CD
13. Bratincsak A, El-Said HG, Bradley JS, Shayan K, Grossfeld PD, Cannavino CR (2010) Fulminant myocarditis associated with pandemic H1N1 influenza A virus in children. J Am Coll Cardiol 55(9):928–929. doi:10.1016/j.jacc.2010.01.004
14. Haessler S, Paez A, Rothberg M, Higgins T (2010) 2009 pandemic H1N1-associated myocarditis in a previously healthy adult. Clin Microbiol Infect. doi:10.1111/j.1469-0691.2010.03315.x
15. Nokleby H, Nicoll A (2010) Risk groups and other target groups–preliminary ECDC guidance for developing influenza vaccination recommendations for the season 2010-11. Euro Surveill 15 (12)
16. Seale H, Heywood AE, McLaws ML, Ward KF, Lowbridge CP, Van D, MacIntyre CR (2010) Why do i need it? I am not at risk! Public perceptions towards the pandemic (H1N1) 2009 vaccine. BMC Infect Dis 10:99. doi:10.1186/1471-2334-10-99

Virchows Arch (2011) 458:377–392
DOI 10.1007/s00428-011-1057-2

REVIEW AND PERSPECTIVE

What is expected from the pathologist in the diagnosis of viral hepatitis?

Helmut Denk

Received: 31 January 2011 / Accepted: 3 February 2011 / Published online: 26 February 2011
© Springer-Verlag 2011

Abstract The clinician expects from the pathologist a clinically relevant diagnosis on the basis of liver biopsy interpretation. Today, a liver biopsy, as invasive procedure, is only justified when a significant benefit for the patient can be expected particularly with respect to the clinical management. Consequently, liver biopsy is usually not required in uncomplicated acute viral hepatitis. It is, however, an important diagnostic tool in chronic hepatitis and in transplanted liver to confirm the clinical diagnosis and to assess stage and grade of necroinflammation, treatment efficiency, and concurrent diseases. The diagnosis of liver disease is based on teamwork between clinician and pathologist. Evaluation of the biopsy in the clinical context requires clinical information and appropriate size and handling of the biopsy specimen. Aim of this review is the discussion of morphologic features of acute and chronic viral hepatitis with regard to their clinical relevance.

Keywords Viral hepatitis · Liver biopsy · Clinical relevance · Review

Introduction

The answer to the question raised in the title could be rather short: the clinician expects from the pathologist a precise and clinically relevant diagnosis. If this is impossible, differential diagnostic considerations have to be provided and discussed. It is imperative for the pathologist to analyze the morphologic features of the liver biopsy carefully and open-mindedly in the light of the present state of the art in clinical medicine and in consideration of the scientific progress. Single morphologic features per se are often not diagnostically specific and only their integrated assessment in the context of clinical information reveals a diagnostically, prognostically, and therapeutically relevant picture. Therefore, in hepatopathology, like in other areas of histopathology, an adequate diagnosis with optimum benefit for the patient requires close collaboration between clinician and pathologist. The invasive diagnostic procedure of the liver biopsy, which still bears the risk of unfavorable side effects [1], is only justified when it can be expected to change the clinical management. To extract clinically useful information "buried" in the biopsy, the specimen has to be appropriate regarding size and preservation and it has to be processed and evaluated in the clinical context. Although many modern analytical techniques can now be applied to processed tissue, for specific needs deviations from conventional processing of the biopsy material (e.g., frozen sections, special fixations, etc.) may be necessary [1, 2].

In view of the presently available non-invasive diagnostic procedures, a liver biopsy is not, or at least only rarely, needed in uncomplicated acute viral hepatitis. However, the morphologic analysis of liver tissue provides the (admittedly imperfect) "gold standard" for validation of non-invasive diagnostic procedures [3–7]. Particularly in chronic hepatitis, the liver biopsy is indispensible to confirm diagnosis, assess stage and grade of severity, detect concurrent diseases, obtain evidence of neoplastic or pre-neoplastic conditions, and correlate morphology with clinical manifestations and treatment efficiency.

H. Denk (✉)
Institute of Pathology, Medical University of Graz,
Auenbruggerplatz 25,
8036 Graz, Austria
e-mail: helmut.denk@medunigraz.at

Aim of the present review is to discuss light microscopic and immunohistochemical features of acute and chronic viral hepatitis in the light of their clinical relevance.

Basic morphologic features of acute viral hepatitis

Morphologic characteristics of acute viral hepatitis are hepatocellular damage and regeneration, portal and lobular inflammation, cholestasis, and macrophage activation (Fig. 1), depending in degree and relative proportion on viral factors, duration of the infection and host response [8]. Worldwide, hepatitis B virus (HBV) is the most common and hepatitis A virus (HAV) the second most common viral cause.

Hepatocellular damage is spotty (disseminated) or confluent. Affected hepatocytes may be swollen, rounded and (in H&E stained sections) pale staining (ballooned) with enlarged and occasionally multiple nuclei and prominent nucleoli. Ballooning degeneration can progress to lytic necrosis. The pathogenesis of cell swelling is multifactorial: excess influx or retention of electrolytes and water due to failure of membrane transport pumps are major causes [9]. Leaky membranes account for the elevation of serum aminotransferases. Acidophilic degeneration of hepatocytes is regarded as precursor of apoptotic cell death. Apoptosis is characterized by shrinkage and fragmentation resulting in "apoptotic bodies" with or without nuclear remnants (acidophilic bodies, Councilman bodies) extruded into the sinusoids. Hepatocyte loss and regeneration (mitotic figures) cause irregularities of liver cell plates. Cholestasis with deposition of bile plugs in canaliculi is common; it may be morphologically and clinically prominent (cholestatic hepatitis). The term "confluent necrosis" denotes the dropout of hepatocytes in a larger area (involving at least

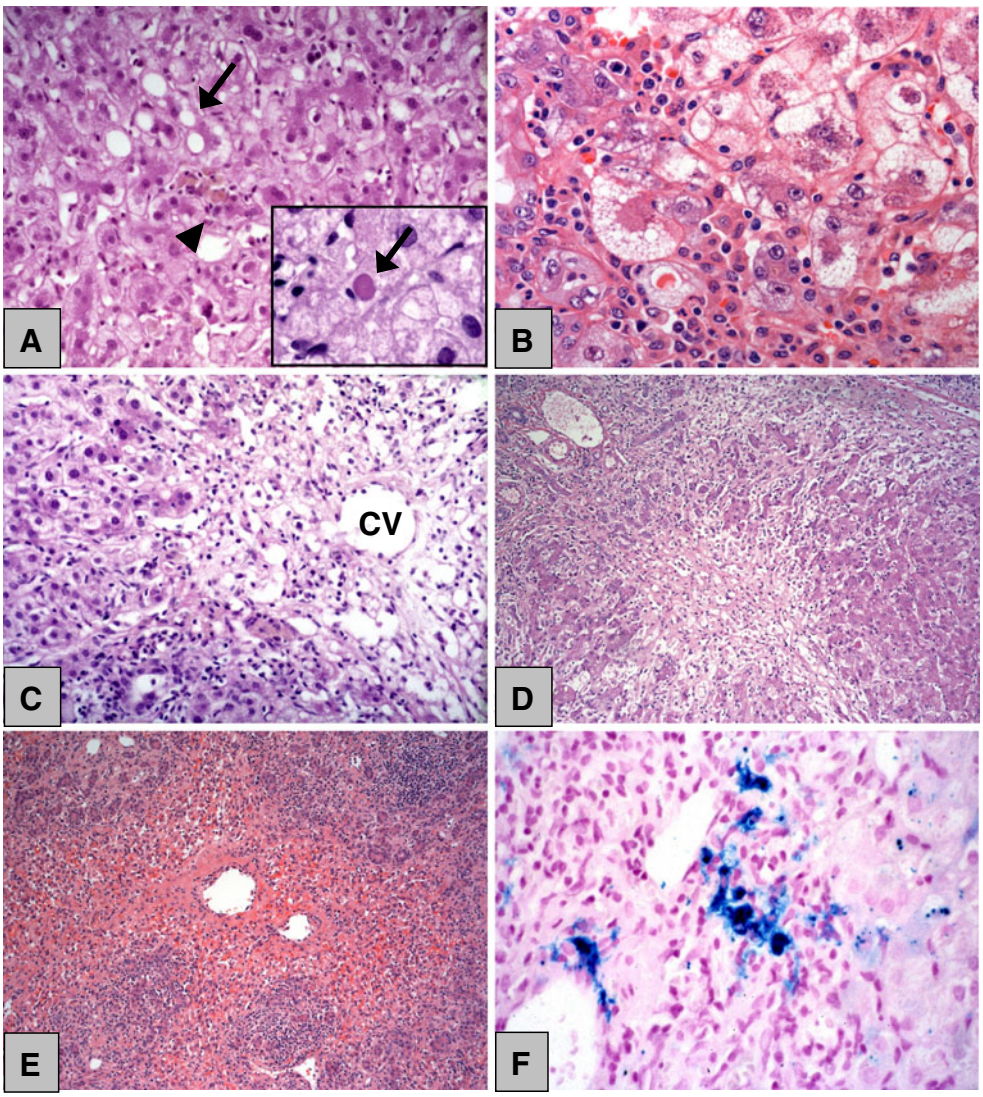

Fig. 1 Acute viral hepatitis. **a** Diffuse lobular infiltration by mononuclear cells and Kupffer cell activation (containing brown pigment; *arrow head*), some hepatocytes exhibit macrovesicular steatosis (*arrow*). The *inset* shows apoptotic liver cell (acidophilic body; *arrow*). **b** Ballooned hepatocytes in fulminant hepatitis. **c** Confluent necrosis around central vein (cv). **d** Extensive confluent and bridging hepatic necrosis. **e** Fulminant hepatitis with panacinar necrosis. **f** Siderin-containing macrophages in a portal tract. **a–d** Hematoxylin–eosin; **e** Prussian blue stain

ten neighboring hepatocytes), preferentially in the perivenular zone (zone 3 of Rappaport). If necrosis links perivenular zones with portal tracts or portal tracts with neighboring portal tracts, the lesion is termed bridging (central–portal and portal–portal, respectively) necrosis; central–portal bridges carry a more adverse prognosis due to early distortion of liver architecture with related hemodynamic consequences. Necrosis may be followed by collapse or condensation of the extracellular matrix, best demonstrated with the reticulin stain, and appearance of passive septa which are paucicellular and sharply delineated from the surrounding surviving parenchyma. Necrosis may also involve entire or almost entire lobules/acini, multiple lobules/acini, or even larger parenchymal areas (panacinar/panlobular, multiacinar/multilobular, submassive, massive necrosis) as morphologic equivalent of clinical fulminant hepatitis [8, 10]. In submassive necrosis, the perivenular parenchymal zone is eradicated, and only the periportal parenchyma survives [8]. Ductular reaction with abundance of neutrophils associated with confluent necrosis may even mimic bile duct obstruction. Boyer and Klatskin [11] correlated the clinical course of acute viral hepatitis with spotty necrosis with that associated with bridging necrosis and found that the disease with bridging necrosis is prone to hepatic failure or liver cirrhosis. However, since necrosis may be patchy, presence or absence of necrosis in the biopsy cannot be regarded as definitive parameter of clinical severity, and thus, morphologic evaluation can lead to over- but also underestimation of liver damage and related functional consequences [8, 12].

Lobular inflammation dominated by lymphocytes (cytotoxic T lymphocytes prevail over B lymphocytes), most pronounced in the perivenular area, predominates the morphologic picture in acute hepatitis [8, 12]. Monocytes, neutrophils, and eosinophils may also be present in various proportions. Enlarged Kupffer cells accumulate, often forming small nodules together with lymphocytes, in later stages often containing brownish ceroid pigment, siderin, and bile. *Portal inflammation* is variable in intensity and usually more pronounced in smaller portal tracts. It may be diffuse or focally accentuated. Inflamed portal tracts may be normal in size or expanded. Lymphoid aggregates and even lymph follicles are occasionally seen, particularly in hepatitis C, but not pathognomonic for this etiology. The limiting plate is usually blurred due to periportal extension (spill over) of the inflammatory infiltrate, closely resembling interface hepatitis of chronic hepatitis, from which it has to be distinguished on the basis of clinical information and careful histologic evaluation.

Small interlobular bile ducts may be irregular and occasionally show vacuolated, multilayered, or disrupted epithelia. Bile duct lesions can be seen in about 15% of acute hepatitides, predominantly in hepatitis C. Their frequency in acute hepatitis B varies from 1% to 10%; they are very rare in hepatitis A [13].

How can morphology contribute to the recognition of etiologically different types of acute viral hepatitis?

Acute viral hepatitides of different etiology share basic morphologic features. Therefore, the pathologist is unable to identify the cause of the hepatitis on the basis of morphology alone. However, certain morphologic patterns are more common in one type than in another and, therefore, at least suggest a specific viral etiology.

Hepatitis A In addition to classical morphology of acute hepatitis, a distinct variant with prominent perivenular cholestasis but mild liver cell damage and inflammation, and another variant with prominent periportal necroinflammation often with abundant plasma cells but little or even absent perivenular necrosis may occur separately or in combination [8, 14]. In severe cases, hepatocyte swelling and microvesiculation can be observed. Confluent/multilobular necrosis with the clinical manifestation of acute liver failure is rare. It more likely occurs in the elderly but carries a better prognosis (in comparison to hepatitis B) with about 55% survival without transplantation [10].

Hepatitis B The morphologic features of HBV infection resemble the basic pattern of acute hepatitis, but extensive necrosis (i.e., confluent and bridging necrosis) is more common [8, 12]. Hepatitis B is responsible for about 7% of cases with acute liver failure which carry a poor prognosis (26% survival without transplantation) [10].

Hepatitis C Acute hepatitis C virus (HCV) infection resembles morphologically acute hepatitis due to other viruses (but also toxins) [8, 12, 15, 16]. Steatosis and bile duct alterations may be present (Fig. 2) [13, 17]. Only in severe cases do perivenular confluent necrosis and very rarely bridging necrosis occur [17].

Hepatitis D Acute hepatitis D virus (HDV) infections morphologically resemble usual acute viral hepatitis with the same range of necroinflammatory lesions [8, 12, 18]. HDV can cause fulminant hepatitis and finally cirrhosis in HBV-positive hosts. Occasionally, the liver biopsy shows signs of severe cytopathic damage with vesicular steatosis, vacuolization of hepatocytes, abundant macrophages, and few parenchymal inflammatory cells morphologically resembling the epidemic HDV hepatitis in Venezuelan Indians [19].

Hepatitis E Hepatitis E virus (HEV) is the most common cause of feco-orally transmitted acute hepatitis [8, 12] worldwide. Epidemics have mostly been reported from Asia. In western countries, most of the infections are seen in travellers arriving from endemic areas. Liver morphology resembles classical or cholestatic types of acute hepatitis. In some patients, it equals hepatitis A with conspicuous cholestasis and predominantly portal and periportal inflammation. The cholestatic form displays rosette-like arrangement of hepatocytes and canalicular cholestasis with less prominent parenchymal damage. Rarely, fulminant forms have been reported. HEV-associated acute liver failure is more frequent in pregnant women [20, 21]. HEV does not usually lead to chronic disease but may cause decompensation of preexisting chronic liver disease. However, in some situations, chronic progression of HEV infection has been reported [10, 22].

Common morphologic features of chronic viral hepatitis

Chronic hepatitis is a clinical-pathologic syndrome rather than an etiologically uniform disease. Its classification, therefore, relies on a combination of clinical, histological, and serological features [5, 7, 8, 12, 23, 24]. Etiology is the major determinant of disease course, prognosis, and therapy. Chronic hepatitis may be due to infections with hepatotropic viruses (HBV, HCV, HDV; a chronic course of HAV and HEV infections does not exist or is extremely rare), autoimmune reactions, drugs, or metabolic disturbances. Moreover, primary biliary cirrhosis and primary sclerosing cholangitis can mimic chronic hepatitis or overlap with autoimmune or viral hepatitis.

Etiologically different forms of chronic hepatitis share common morphologic features (Fig. 2), but in certain cases, the viral etiology can be recognized on the basis of light microscopy or immunohistochemistry.

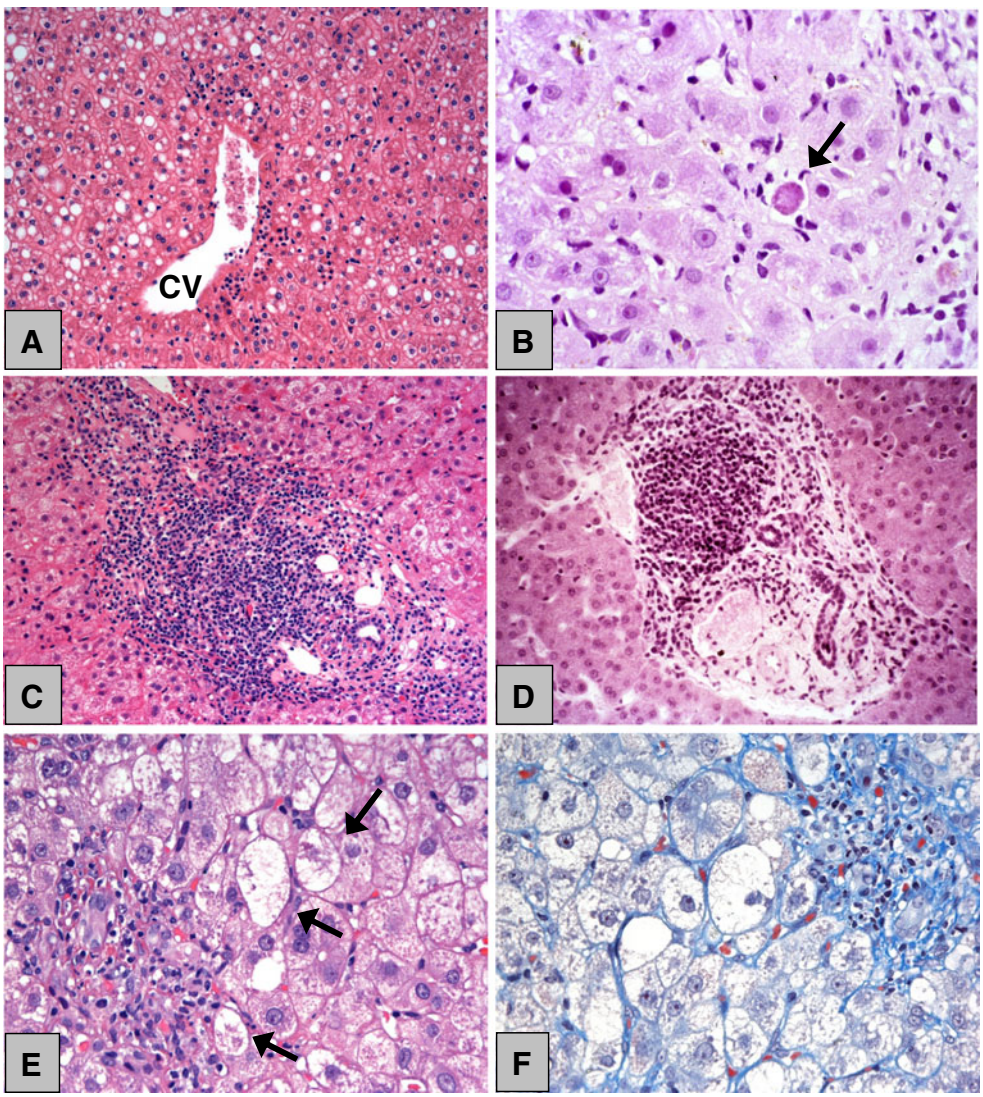

Fig. 2 Acute (**a**, **b**) and chronic (**c–f**) hepatitis C. **a** Lobular mononuclear inflammation with concentration in the perivenular area (*cv*, central vein). The liver parenchyma displays moderate macrovesicular steatosis. An apoptotic body is shown in **b** (*arrow*). Portal inflammation with different degrees of interface activity (**c**, **d**). The inflammatory cell are arranged in a follicular pattern (**d**). Hepatitis C may be associated with morphologic features of steatohepatitis (**e**, **f**), like ballooning of hepatocytes, Mallory–Denk bodies (*arrows* in **e**) and pericellular fibrosis. **a–e** Hematoxylin–eosin; **f** chromotrope aniline blue

Portal inflammation with lymphocyte predominance is the most characteristic lesion in chronic hepatitis. The inflammatory infiltrate, predominantly consisting of T lymphocytes with admixed plasma cells, histiocytes and macrophages, may involve all or only some portal tracts [7, 9]. In less active disease, inflammation is largely restricted to normal-sized or expanded portal tracts (i.e., portal hepatitis), but with increasing activity, the necroinflammatory process attacks the periportal (periseptal) hepatocytes of the limiting plate. This interface hepatitis (originally called lymphocytic piece meal necrosis) is diagnostically important.

Hepatitis-associated bile duct lesions have been classified in three types [13]: (1) Type 1 is mostly associated with severe hepatitis. The affected ducts measure 40–120 μm in diameter and are surrounded by collagen fibers. The epithelium shows vacuolization, pseudostratification, and lymphocytic infiltration. (2) Ducts with type 2 lesions are smaller, usually 15–40 μm in diameter, and surrounded by scarce collagen fibers. The lesions are segmental, damage is more conspicuous, but the basement membrane is preserved. The cholangiocytes are frequently enlarged with more abundant eosinophilic cytoplasm. The abnormal ducts are embedded in a dense lymphocytic infiltrate and often in proximity to lymph follicles with germinal centers. Type 2 seems to prevail in chronic hepatitis C. (3) The type 3 lesion resembles an irregular diverticulum in continuity with small bile ducts consisting of biliary hepatocyte-like cells and intermediate cell types with severe epithelial alterations. Three-dimensional reconstruction revealed that diverticuli budd from small slightly ectatic bile ducts [12–25 μm in diameter) which are partly surrounded by a basement membrane and embedded in a dense inflammatory infiltrate associated with pronounced interface hepatitis. They probably represent Hering ducts and groups of periportal liver cells which have escaped necrosis. Serial sections may reveal shifts from one type to another. No definitive conclusion can be drawn regarding prognostic significance. In acute hepatitis C, bile duct lesions have been found to correlate with a chronic or relapsing course but do not seem to predict progression to cirrhosis. Moreover, they are not pathognomonic for classical viral hepatitis but have, although rarely, also been found in Epstein–Barr virus, CMV and HIV infections, autoimmune, drug-induced, and unclassified hepatitis. Their pathogenesis is unclear. The close association with lymphoid aggregates and lymph follicles suggests an immunologic process directed against biliary epithelium. Moreover, hepatitis viruses (HBV, HCV) may infect cholangiocytes making them targets for direct viral as well as immune-mediated attack [7, 13].

Intralobular necroinflammatory activity varies with severity of the disease and resembles that of acute hepatitis. Disseminated lytic and apoptotic liver cell dropout is associated with macrophages containing PAS-positive diastase-resistant cell debris. Severe cases show confluent, bridging, panlobular, or even multilobular necrosis. Steatosis may be present. Parenchymal extinction following bridging necrosis is followed by collapse of the reticulin meshwork and the appearance of passive collagenous (mostly type I collagen) septa without pronounced inflammatory infiltrate. In contrast, active septa developing in the course of interface hepatitis are rich in inflammatory cells and expand the portal tracts by progressively replacing zone 1 parenchyma. Liver cell regeneration and fibrosis contribute to distortion of the liver architecture finally leading to cirrhosis. In later stages, ductular reaction at the mesenchymal/parenchymal interface results from activation of the progenitor cell compartment [25]. More pronounced lobular activity can occur during exacerbation or relapse of the necroinflammatory process [7, 26]. Morphologic characteristics are ballooning (often most severe in zone 3), cholestasis, spotty, and eventually confluent, bridging or multiacinar necrosis followed by fibrosis, superimposed on the morphologic features of chronic hepatitis.

Morbidity and mortality of chronic hepatitis is largely determined by fibrosis and its progression to cirrhosis with its consequences [27]. Assessment of fibrosis is, therefore, a major goal of liver biopsy interpretation [27, 28]. In hepatitis C, progressive fibrosis occurs mainly in patients aged over 50 years [29]. Significant fibrosis and inflammation was found in 37% of patients with persistently normal ALT in chronic hepatitis B. Although prominent fibrosis is readily detectable in conventionally stained sections, special stains (e.g., Masson's trichrome stain and its modifications, reticulin stain, Sirius red stain) are essential for assessment of discrete and early fibrosis. Elastic fibers are present in older fibrous septa and scars [8]. Because of sampling variation, the diagnostic accuracy is impaired with decreasing biopsy size, in a biopsy in 1.5 cm in length the diagnosis of cirrhosis may be missed in up to 40% of cases [30]. However, the diagnostic accuracy of a biopsy is still better than that of most non-invasive tests.

Individual types of chronic viral hepatitis: how can morphology contribute to etiologic classification?

The liver has a limited repertoire of morphologically detectable reaction mechanisms. Consequently, all types of viral hepatitis share common morphologic features [7, 8, 12]. In most instances, it is not possible for the pathologist to make an etiologic diagnosis on the basis of morphology alone. However, some features at least suggest a specific etiology.

Chronic hepatitis B

In chronic HBV infection, the appearance of ground glass cells is a distinctive morphologic feature. Ground

glass cells are characterized by finely granular eosinophilic cytoplasmic change surrounded by a peripheral clear rim (Fig. 3). Classical ground glass cells contain HBsAg in association with the smooth endoplasmic reticulum (SER). Morphologically, similar changes can result from enzyme induction and hyperplasia of the SER, cyanamide treatment, myoclonus epilepsy (Lafora bodies), fibrinogen storage or type IV glycogenosis [31]. Nuclear accumulation of HBcAg leads to finely granular inclusions in nuclei ("sanded nuclei") of hepatocytes [7, 8, 12].

HBV type and severity of liver damage are related since viral characteristics play an important role in the pathogenesis of liver damage due to modification of virus–host interactions

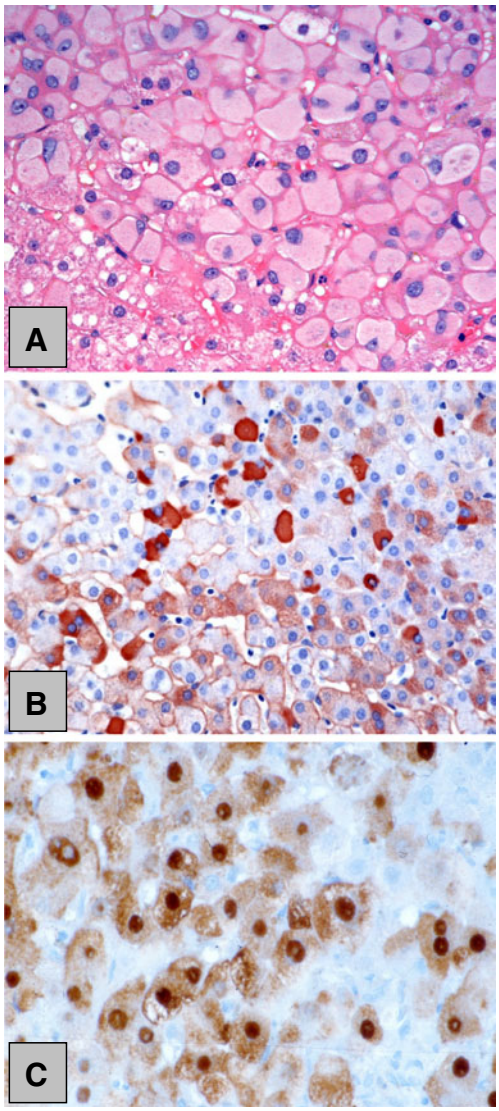

Fig. 3 Ground glass cells (**a**). HBs and HBc antigens can be immunohistochemically demonstrated in hepatocytes. HBs antigen is located in the cytoplasm and in a membraneous position (*red* in **b**). The HBc antigen is present in nuclear but also in cytoplasmic position (*brown* in **c**). **a** Hematoxylin–eosin; **b**, **c** immunohistochemistry

[31, 33, 34]. HBV mutations can affect several viral genes, particularly those encoding for envelope and nucleocapsid proteins [34, 35]. In addition to precore and core gene mutations, Pre-S1/Pre-S2/S gene mutations have also been observed [34, 35]. Patients infected with precore mutant virus express nuclear/cytoplasmic HBcAg and HBeAg, show high viral DNA serum levels and "active" chronic hepatitis, whereas in patients infected with a mixture of wild type and mutant viruses, low activity was observed with weaker expression of nuclear HBcAg, no cytoplasmic HBcAg or HBeAg, and low viremia [34, 36]. The point mutation at position 1896 (G to A substitution) of the precore region creates a stop codon inhibiting the translation of HBeAg [9, 32, 34, 36]. Since translation from the second start codon in the core region is still possible, HBcAg can arise and virus replication is maintained. Originally, it was believed that this mutation was consistently associated with severe liver damage, but can also be found in patients without hepatic necroinflammation [34, 36].

The degree of liver damage induced by HBV mutants, particularly the 1896 HBV variant, is related to a variety of factors (level of virus replication, modified T cell reactions due to different composition of presented viral antigens, differences in antibody-dependent cytotoxicity or cytokine release, altered intracellular transport and packing of core particles with increased cytoplasmic and membraneous expression). Moreover, newly emerging HBV strains may have direct cytopathic effects. HBeAg positivity, older age, and elevated ALT levels play a role for development of cirrhosis [37]. Regarding prognosis of bridging hepatic necrosis (BHN) in chronic hepatitis B, it has been shown that BHN can heal even more rapidly than intralobular spotty necrosis; however, the risk of progression to cirrhosis was found to be about four times higher in the BHN than in the spotty necrosis group [36, 37]. Portal–portal and portal–central bridging necrosis differed in their clinical significance; 29% of patients with portal–central bridging developed cirrhosis in contrast to 10% of patients with portal–portal bridging [38, 39]. Exacerbation or relapse of necroinflammation in chronic hepatitis B may occur spontaneously, upon interferon therapy, withdrawal of immunosuppresive therapy or HAV, HDV, or HIV superinfection [7, 9, 26]. Exacerbation in chronic hepatitis B is characterized by lobular hepatitis, eventually with BHN combined with signs of chronicity [40].

Some morphologic features, although not pathognomonic, may suggest the HCV etiology (Fig. 2). They include parenchymal steatosis, prominent portal lymphoid aggregates or lymph follicles, and bile duct injury [7]. In chronic hepatitis C, plasma cells are generally rare but may be abundant in one subtype characterized by autoimmune features [7]. Occasionally, granulomas may be present [7, 41]. They may predict favourable response

to interferon-α-therapy. Distinct genotypes of HCV are associated with distinct morphology [26]. For example, moderate to severe steatosis and bile duct lesions more often accompany HCV type 3 infection [42, 43]. Mild steatosis, particularly in non-3 genotype infections, points to the presence of the metabolic syndrome and insulin resistance [44–46]. Even morphologic features of steatohepatitis may be present (Fig. 2) [45, 47]. Moderate to severe steatosis, typically found in patients with HCV genotype 3 infection, is most probably virally induced [43, 44, 46–48]. It has been shown in transgenic mice that the expression of HCV core protein and other viral proteins causes steatosis via mitochondrial toxicity and production of reactive oxygen species [48, 49]. Steatosis is an important cofactor of liver damage leading to increased necroinflammatory activity and fibrosis [42, 50, 51]. Moreover, steatosis is also a risk factor for the development of HCC [52], together with male sex and older age [53]. HCV core protein plays a chief role in tumor development [54, 55]. Cirrhotic patients infected with HCV type 1b carry a significantly higher risk of developing HCC than those with other types. Stainable iron can be found in Kupffer cells, hepatocytes, and portal tracts without clear-cut relationship to histologic activity index or fibrosis score [56]. Hepatic iron has been found to be significantly higher in patients with HCV genotype 1b infection than in those with genotype 2a and 2b; a significant correlation was found between hepatic iron content and plasma HCV-RNA levels. Hepatic iron content may also serve as predictor of response to interferon therapy. Non-responders stored more iron, whereas absence or low amounts of stainable iron were frequently associated with sustained response. Iron removal can delay progression of liver injury and also seems to be beneficial, at least in conjunction with higher doses of interferon [57]. The mechanism by which HCV interferes with iron metabolism is poorly understood. HCV-induced oxidative stress suppresses hepcidin expression, a key regulator of iron availability, through increased histone deacetylase activity and inactivation of transcription factors [58]. Bile duct injury is usually mild with vacuolization, stratification, and crowding of cholangiocytes [13]. Rarely, bile duct loss mimicking primary biliary cirrhosis is observed.

What can histology and immunohistochemistry tell us about the pathogenesis of viral hepatitis?

In acute hepatitis B, viral antigens are usually not demonstrable immunohistochemically [9]. Presence of HBsAg confirms chronic HBV infection (Fig. 3). Immunohistochemical staining patterns of HBsAg and HBcAg vary during the course of the disease [59–62]. Three phases can be distinguished: (1) In the replicative phase (high HBV-DNA serum levels) abundant nuclear and cytoplasmic HBeAg and HBcAg can be seen. Histologic alterations are mild or even absent. Since viral replication and HBcAg expression may vary in different regions of the liver, sampling variation is possible. HBsAg is found in the cytoplasm and membrane of hepatocytes. Membraneous HBsAg staining correlates with serum HBV-DNA and can therefore be regarded as marker of active HBV replication but is not responsible for histologic activity. (2) The low replicative (virus clearance) phase is associated with prominent necroinflammation, activity, and elimination of virus-infected hepatocytes. Immunostaining reveals nuclear, cytoplasmic, and membranous HBcAg expression. Cytoplasmic HBcAg correlates with liver damage indicating that cytoplasmic HBcAg is the target for immune-mediated cytolysis of hepatocytes. HBsAg can be demonstrated within the cytoplasm and in membranous position. This phase is associated with sero-conversion to the anti-HBc status. (3) In the non-replicative phase with anti-HBe positivity and without liver disease, HBcAg is generally not demonstrable in liver tissue, whereas cytoplasmic HBsAg persists and is frequently detected in clusters of hepatocytes containing HBV-DNA integrated into the host genome. Since active HBV replication in the liver is minimal, hepatocytes are not efficiently attacked by immune cells. If liver cirrhosis is already present at this point, the process will slowly progress, whereas in the absence of cirrhosis, an inactive state will remain.

In immuno-compromised subjects with recurrent HBV infection, nuclear HBcAg staining is usually most conspicuous in association with the rapidly progressive fibrosing cholestatic hepatitis [63, 64].

During the course of the disease, mutations of the viral genome, particularly in the precore promoter region, can alter the replication efficiency and/or subcellular localization of HBV antigens [34, 37]. Naoumov et al [34] distinguished two groups of patients harbouring precore mutant and wild type species: group A predominantly infected with precore mutant virus showed active hepatitis and displayed nuclear and cytoplasmic HBcAg and HBeAg and high viral DNA serum levels; group B infected with a mixture of wild type and mutant viruses showed inactive hepatitis with weaker expression of nuclear HBcAg without cytoplasmic HBcAg or HBeAg. A higher prevalence of [1896] precore mutant viruses was found in anti-HBeAg carriers with chronic liver disease [34]. It has been shown that these mutations are associated with increased replicative efficiency and changes in the nuclear to cytoplasmic expression of HBcAg in hepatocytes [36, 37, 65]. Predominant cytoplasmic HBcAg expression is the major pattern in precore mutant cases

and might be involved in severe liver injury. For example, a mutant strain with enhanced replication competence was described in patients with fulminant hepatitis. A recently described replacement mutation also showed higher replication efficiency than the wild type and excess HBcAg expression in the cytoplasm of hepatocytes [66].

In hepatitis C, HCV can be detected immunohistochemically in short-term formaldehyde-fixed liver tissue; the sensitivity decreases slightly with intermediate length fixation, and HCV is undetectable after prolonged fixation. Shiha et al. [67] using a HCV monoclonal antibody (TOR DJI-22) reported positive immunohistochemical staining in 91% of HCV-RNA positive cases. Hepatocyte staining was cytoplasmic (with an occasional nuclear hue), which was either diffuse or membranous (pattern A), patchy (pattern B) or paranuclear (pattern C).

HCV-RNA can be detected with high sensitivity in formaldehyde-fixed paraffin-embedded biopsy material [67]. Storage of formaldehyde-fixed paraffin-embedded tissue does not impair the sensitivity of HCV (RNA) detection [68].

In hepatitis D, viral antigen is demonstrated immunohistochemically in hepatocyte nuclei (Fig. 4). Sometimes, cytoplasmic and membrane-associated staining is present [7–9, 12, 69].

Coinfection by multiple hepatotropic viruses and HIV

No specific morphologic picture can be assigned to coinfections by several hepatotropic viruses. Superinfection/coinfection of chronic hepatitis B with other hepatotropic and nonhepatotropic viruses often leads to modification of morphology and clinical course. Coinfection with HAV aggravates chronic hepatitis B. In HBV/HCV coinfection, HCV interferes with HBV replication with the consequence of partial or even complete suppression of antigen expression [7, 9, 70]. Chronic HBV/HCV coinfection can stimulate progression and bears a higher risk of HCC development than HBV infection alone [37]. HBV/HDV coinfection results in more severe acute hepatitis than HBV infection alone but rarely results in chronicity. In chronic hepatitis B with HDV coinfection, necrosis is more pronounced. HDV superinfection of a HBV carrier may be followed by clinical and morphologic manifestations of acute hepatitis with severe hepatocellular damage, vacuolar liver cell degeneration, mild inflammation, and almost always results in persistence of both viruses [8, 36, 69]. These patients develop cirrhosis, liver failure, and eventually HCC in a higher percentage [37]. In chronic hepatitis B patients with HIV infection, mostly milder histologic activity is observed, and chronicity is more common. [7, 37]. In HCV/HIV coinfected immunosuppressed patients, chronic hepatitis C is more severe and fibrosis is more pronounced than in HCV monoinfection, suggesting an HIV-associated fibrogenic effect [71]. Coinfection with CMV is often followed by fatal outcome [8, 12].

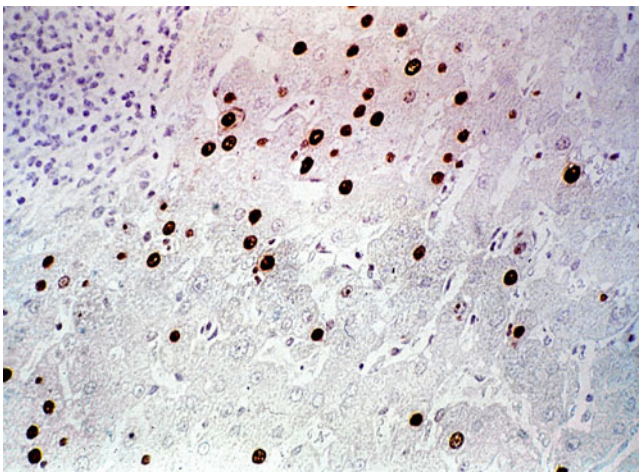

Fig. 4 Immunohistochemical demonstration of HDV antigen in hepatocyte nuclei

Accuracy and reproducibility of liver biopsy interpretation: size matters

Since lesions may be unevenly distributed in the liver, the size of the liver biopsy is decisive for the accuracy of the morphologic diagnosis [1, 8, 72–78]. Colloredo et al. [74] examined the effect of biopsy size on grading and staging in chronic hepatitis B and C using the Ishak scoring system [79]. They showed that reducing length and width of the specimen led to underscoring due to low number of portal tracts. According to Bedossa et al. [80, 81], the variability in the assessment of fibrosis decreases with increasing length of the biopsy specimen with little further improvement beyond 40 mm. These authors also correlated the results of image analysis with the semiquantitative METAVIR scoring system and concluded that the minimum specimen length acceptable for staging was 25 mm. The German Society of Pathology [82] recommends a biopsy of at least 15 mm in length and 1.2–1.8 mm in width which should guarantee the presence of ten intact portal tracts. The thickness of the section also influences the judgement of the intensity of the portal inflammatory infiltrate.

We thus agree with the statement of P. Scheuer "*Bigger is Better*", although even biopsies containing less than ten portal tracts might eventually be adequate for grading and staging of chronic hepatitis [77].

Histologic grading and staging of chronic hepatitis

At least in the eyes of clinicians, the conventional morphologic diagnosis has the disadvantage of providing descriptive and qualitative rather than quantitative information with a subjective touch. Numerical scoring is expected by the clinician particularly in the context of clinical trials. Morphometric quantification by computer-assisted image analysis is time-consuming, largely restricted to research, and not necessary in every day practice [30, 83]. Semi-quantitative scoring systems assessing the degree of necroinflammatory activity ("grading") and stage of disease, e.g., degree of fibrosis, ("staging") can supplement the verbal diagnosis [5, 23, 30, 79, 84, 85]. Necroinflammatory activity and fibrosis are indicators of severity and progression of the pathologic process, and thus prognostically important [3, 4, 16, 26, 28, 86]. Numerical scores can be assigned to grade and stage, providing the possibility of statistical evaluation and better comparison of results between different centers. However, these scores are flawed by inter- and intraobserver variation. Grading and staging in a single biopsy have several limitations. Sampling variability is an inherent problem in biopsy diagnosis. It can be minimized by adequate size and quality of the specimen [75, 82]. A minimum of ten complete portal tracts is regarded necessary for accurate grading and staging. Particularly in fibrosis or cirrhosis, cutting needles are superior to suction devices to produce adequate material. Scores represent categories rather than continuous variables in contrast to real measurements, and this has to be accounted for in the statistical evaluation [1, 5, 7, 23, 79, 84]. In addition, overall scores may be clinically and prognostically less relevant than individual components of the necroinflammatory process; for example, Hübscher [23] clearly demonstrated that different patterns of activity can lead to an identical final score.

Currently used scoring systems

In addition to the Knodell system [87], other scoring systems are presently used; all have advantages and disadvantages. In the Knodell system, four main histologic features (periportal/ bridging necrosis, intralobular degeneration and focal necrosis, portal inflammation, fibrosis) are scored together resulting in a histology activity index (HAI). However, since fibrosis and associated structural distortion are consequences of liver cell damage, they should be scored separately. Indeed, the authors allowed for that by stating that the overall HAI score could be "broken into individual components of necrosis, inflammation, and fibrosis to yield additional information not provided by conventional composite scales for grading necroinflammatory liver disease". According to Ishak et al [79] the different features are scored as a continuous scale, and necroinflammation and fibrosis are separated. Confluent necrosis and interface hepatitis are also separated. In the Scheuer system, portal/ periportal activity, lobular activity, and fibrosis are separately scored on a scale of 0–4 [6, 23, 84]. The METAVIR system [81, 88] focuses on focal lobular necrosis, portal inflammation, piecemeal necrosis, and bridging necrosis. Piecemeal necrosis (interface hepatitis) and lobular necrosis are combined in an algorithm to yield a histologic activity index under the assumption that chronic hepatitis progresses through bouts of lobular necrosis. Fibrosis is scored separately.

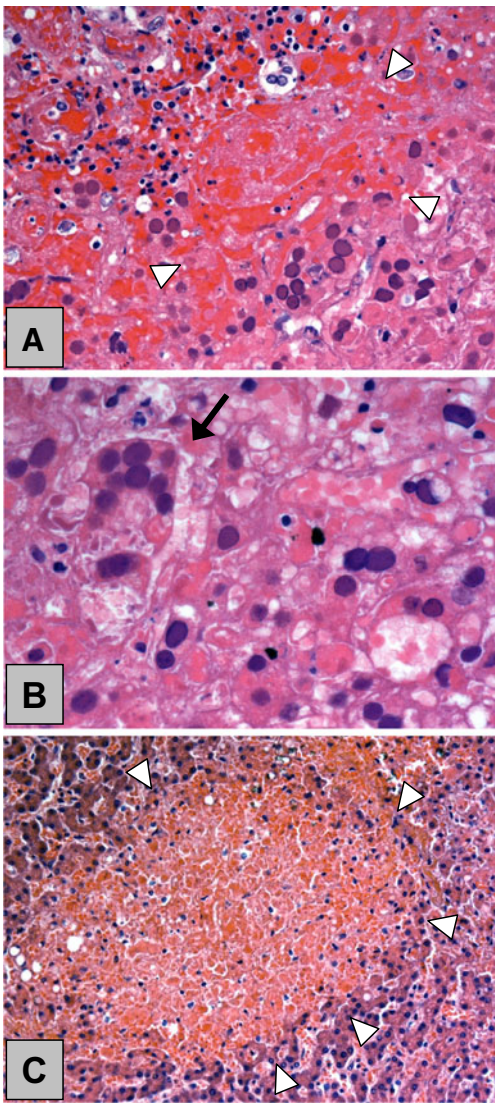

Fig. 5 Hepatitis associated with herpes simplex virus (HSV type 2; **a**, **b**) and herpes zoster virus (**c**) infection. Note parenchymal necrosis (*arrow heads* in **a** and **c**). Surrounding surviving hepatocytes show darkly stained nuclei (nuclear viral inclusions) in **a** and **b**. In addition, multinucleated hepatocytes are also observed (*arrow* in **b**). Hematoxylin–eosin

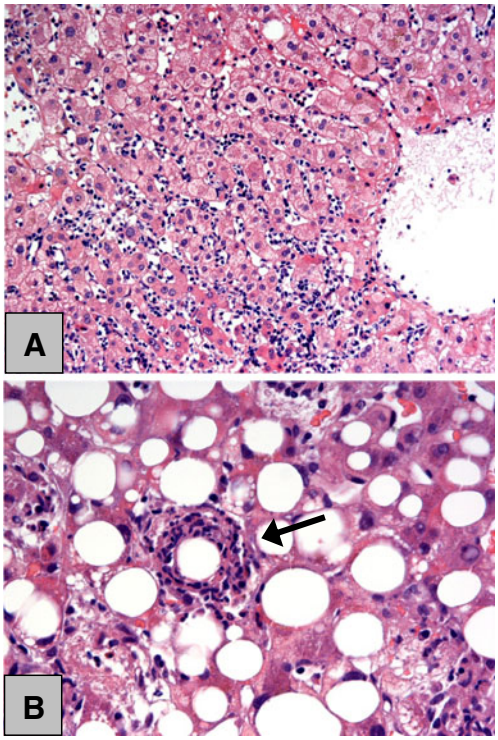

Fig. 6 Epstein–Barr-virus (EBV)-associated hepatitis. **a**, **b** Lobular inflammation is characterized by dense mononuclear infiltration of sinusoids (**a**). Note fibrin ring granuloma in an area of steatosis (*arrow* in **b**). Hematoxylin–eosin

Taken together, for practical purposes, a scoring system should be simple, reproducible and clinically relevant. Usually, a compromise between the complexity of the morphologic features and reproducibility has to be found [1]. Clear-cut definition of the parameters to be assessed (like "tuning the instruments" before starting a musical performance; V. Desmet, personal communication) is imperative. Because of sampling error and the variable natural history, particularly of chronic hepatitis C, a precise assessment of prognosis for an individual patient on the basis of the biopsy finding alone is impossible. For clinical trials, it may be necessary to tailor and adapt scoring according to the need and expectations of the clinicians for optimal benefit for the patient [1].

Other viral liver diseases in differential diagnosis to classical viral hepatitis

Due to its central position in the blood stream, the liver is the primary target of many infections.

Members of the herpes virus group (herpes simplex virus, herpes zoster virus, cytomegalovirus, Epstein–Barr virus) may directly affect the liver [8, 12]. Herpes simplex virus (HSV) infection may lead to coagulative necrosis with little inflammation, particularly in immuno-compromised patients (i.e., transplant recipients, patients treated for hematologic malignancies, HIV infection; Fig. 5). Moreover, pregnancy is also a risk factor for life-threatening HSV (type 1 or 2) hepatitis. Surviving hepatocytes, some of them multinucleate, in the peri-necrotic area, contain eosinophilic nuclear inclusions [89, 90]. In severe herpes zoster infections, similar morphologic features may be seen. In Epstein–Barr virus (EBV)-caused infectious mononucleosis, the biopsy shows a diffuse sinusoidal mononuclear infiltrate consisting of B lymphocytes, T lymphocytes, and natural killer cells accompanied by apoptotic hepatocytes. Non-caseating sarcoid-like granulomas and fibrin ring granulomas may also be found (Fig. 6). In immuno-compromised patients, EBV infection

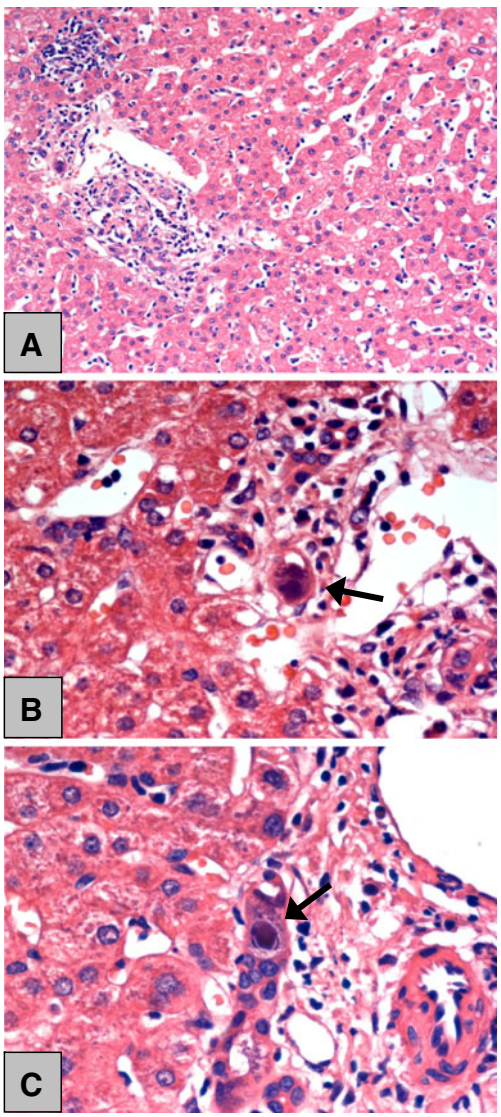

Fig. 7 Cytomegalovirus (CMV)-associated hepatitis with portal and lobular inflammation (**a**). CMV lesions with nuclear inclusions are found in endothelial cells (**b**, *arrow*) and ductular epithelium (**c**, *arrow*). Hematoxylin–eosin

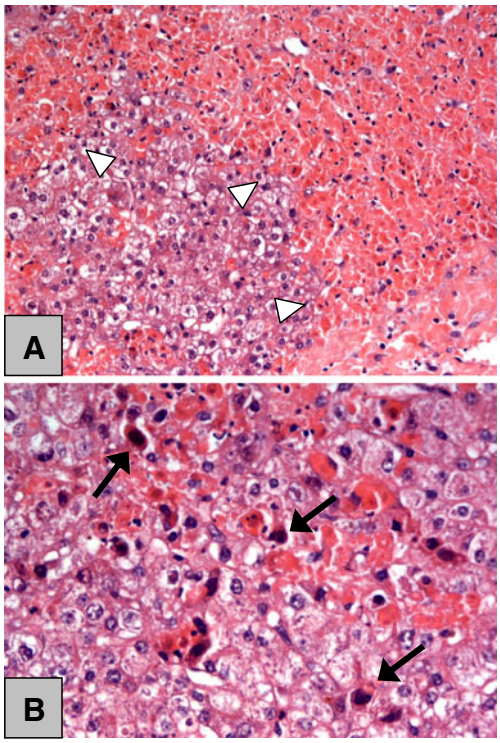

Fig. 8 Adenovirus-associated liver lesion. Note extensive parenchymal necrosis (*arrow heads* in **a**). Surrounding surviving hepatocytes contain darkly stained nuclei (*arrows in* **b**). Hematoxylin–eosin

may lead to more extensive parenchymal necrosis [91]. Cytomegalovirus (CMV) mainly affects newborns and immuno-compromised patients. CMV hepatitis is characterized by scattered aggregates of neutrophils, microgranulomas, occasionally lobular inflammation, portal inflammation, Kupffer cell enlargement, and mild hepatocellular alterations with increased mitotic activity. In immuno-competent individuals, the liver shows a mononucleosis-like picture with focal hepatocyte damage and sinusoidal lymphocytic infiltration. Characteristic are enlarged endothelial and other sinusoidal lining cells, hepatocytes, or cholangiocytes with enlarged nuclei containing amphophilic inclusions. Basophilic viral material is also present in the cytoplasm (Fig. 7). In immuno-compromised individuals, CMV inclusions are often seen without associated necroinflammation. In neonates, the virus may be responsible for giant cell hepatitis and cholestasis. Immunohistochemistry for CMV antigens is a sensitive technique to confirm the diagnosis even in the absence of inclusions [8, 12, 92–94].

Adenovirus may cause severe liver damage in children and immunosuppressed adults. Morphologically, the lesions closely resemble herpes simplex infection with liver cell necrosis and dark nuclear viral inclusions in surviving hepatocytes (Fig. 8) [95].

Flavivirus (Dengue fever) and Hantavirus infections can lead to hepatic necrosis [96]. In yellow fever, apoptotic (acidophil) bodies are abundant and are known as the classical Councilman bodies [97].

Viral hepatitis and liver transplantation

With improved long-term survival after transplantation, secondary complications, such as disease recurrence and opportunistic infections, are observed with increased frequency. Recurrent disease may be confused with transplantation-related alterations, e.g., acute cellular rejection, or modifications of recurrent disease manifestation by immunosuppression.

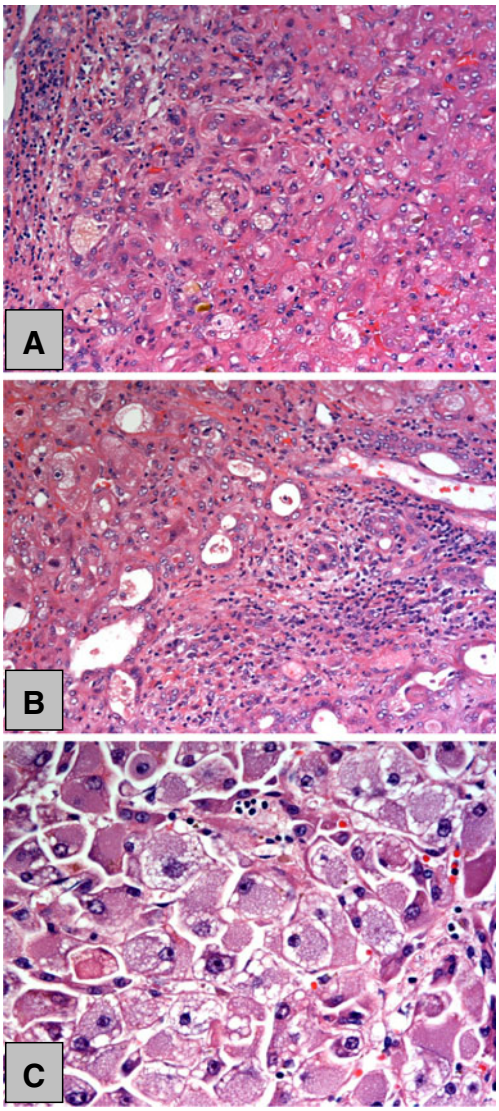

Fig. 9 Fibrosing cholestatic hepatitis B in the liver transplant. Note cholestasis, fibrosis, and ductular reaction (**a**, **b**). Hepatocyte enlargement and ground glass cells are demonstrated at higher magnification in **c**. Hematoxylin–eosin

Recurrence of HBV infection

In the initial phase of HBV reinfection (within 3 months post transplant), focal nuclear and cytoplasmic HBeAg and HBcAg immunoreactivity appears in an otherwise normal biopsy. Later (1–6 months post transplant) features of mild lobular hepatitis and portal inflammation can be seen which increase in severity resembling chronic hepatitis B in non-transplanted liver. Within 8 to 70 months cirrhosis may result [98]. Fibrosing cholestatic hepatitis is morphologically characterized by hepatocyte ballooning, steatosis, cholestasis, ductular reaction, minimal inflammation, portal/periportal fibrosis extending into the lobule, and pronounced cytoplasmic and nuclear HBcAg and variable HBsAg immunostaining, suggesting extensive viral replication and direct cytopathic hepatocyte injury (Fig. 9); [64, 98, 99]. The pronounced ductular reaction could be due to interference of the virus with hepatocyte regeneration. Antiviral drug therapy improves the previously usually fatal condition [98]. Precore or core promoter variants have no impact on pre- and post-orthotopic liver transplantation outcomes in hepatitis B patients [100]. Immunostaining of liver allograft biopsies from patients with HBV recurrence revealed predominance of CD4+T lymphocytes and close correlation between the number of IFN-γ producing cells in the graft, IFN-γ serum levels, and necroinflammatory activity [64].

Recurrence of HCV infection

Graft reinfection is an almost constant feature in patients with chronic HCV infection [17, 101, 102]. Recurrent HCV infection mostly displays the morphologic features of hepatitis C. Immunohistochemically and by in situ PCR, HCV can be detected already a few days after transplantation. In the early stage of graft reinfection (0–2 months after transplantation), morphologic alterations are minor and non-specific and cannot be distinguished from those associated with acute rejection or preservation/reperfusion injury. Histologic features in early post transplant biopsies predicting a more aggressive course include increased severity of necroinflammation, macrovesicular steatosis, and prominent

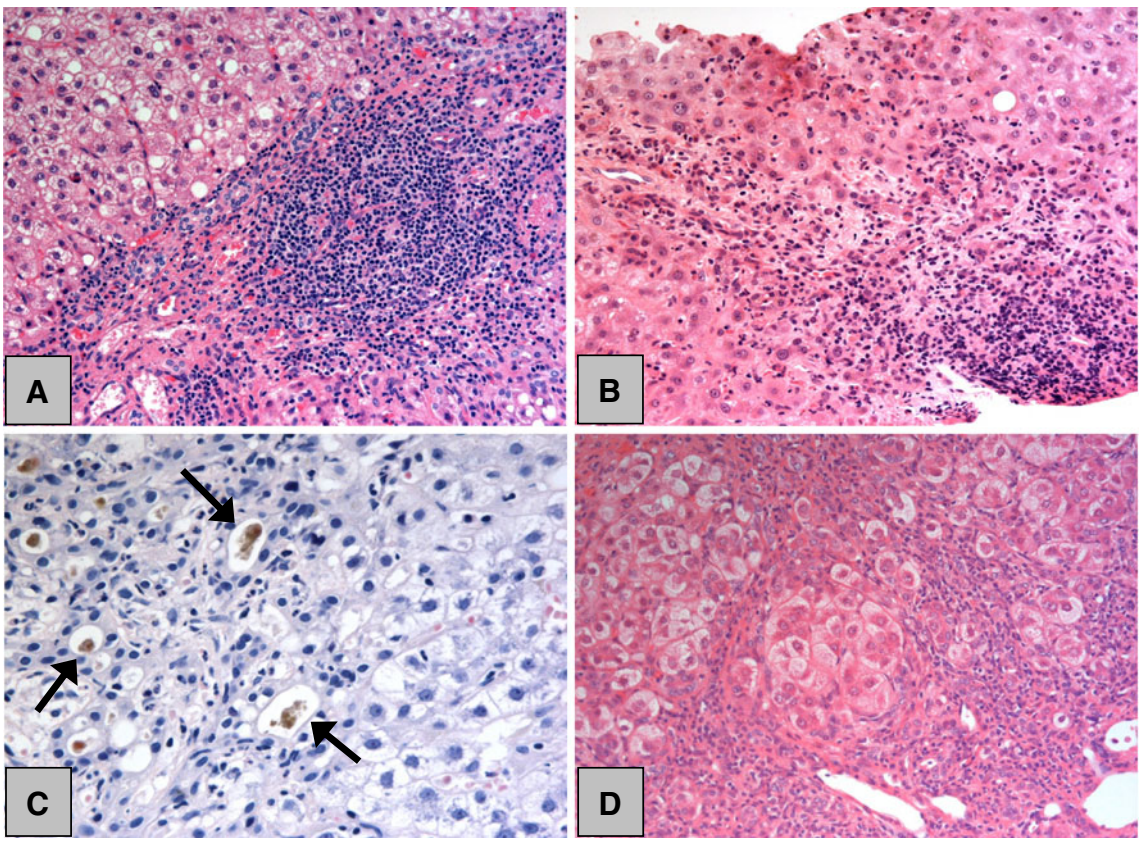

Fig. 10 Recurrent hepatitis C and fibrosing cholestatic hepatitis C in the transplanted liver. **a**, **b** Morphology of recurrent hepatitis C in the transplant resembles that in the native liver. In the fibrosing cholestatic variant (**c**, **d**) note enlarged hepatocytes and moderate inflammation, ductular reaction, and cholestasis (*arrows* in **c**), the process may rapidly lead to cirrhosis (**d**). **a**, **b**, **d** Hematoxylin–eosin; **c** chromotrope aniline blue

hepatocyte ballooning and/or cholestasis [101, 103–105]. In HCV genotype 3, severe steatosis may be the initial histologic manifestation of recurrent hepatitis [17]. Morphology resembles mild acute lobular hepatitis with varying degrees of portal inflammation 2–4 months after transplantation. About 6 months after transplantation, morphology of chronic hepatitis is present. Bile duct damage is difficult to discriminate from that of acute cellular rejection. In some cases, HCV infection has a more aggressive course in transplanted patients and even confluent and bridging necrosis, only very rarely present in immuno-competent individuals, may occur. Rapid progression to fibrosis and cirrhosis follows, even within 1–2 years after transplantation, and at 10 years after transplantation, cirrhosis is present in about 50% of the patients. More atypical morphologic manifestations of recurrent HCV infection resemble fibrosing cholestatic B hepatitis (Fig. 10). Hepatocyte ballooning and cholestasis may be related to cytopathic effects of HCV, particularly since they are associated with high virus load. Most cases, however, display inflammation in contrast to recurrent hepatitis B in which inflammation is minimal or absent. Portal tract expansion and ductular reaction have to be discriminated from alterations associated with bile duct obstruction and drug-induced cholestasis [106].

The differential diagnosis between recurrent HCV infection and acute cellular rejection is a major challenge to the pathologist and sometimes even impossible since morphologic features are similar. Careful evaluation, particularly in view of the time course of the liver alterations in correlation with the clinical history, is required. Whereas the majority of acute rejection episodes occur within the first month after transplantation, HCV-related alterations are usually absent during this early period. On the other hand, acute rejection with mixed portal inflammation is rare at 12 months after transplantation, whereas at the same time, HCV-related portal inflammation is conspicuous. Bile duct damage is usually mild in HCV infection but prominent in acute rejection leading to loss of bile ducts in later stages. Endotheliitis is a feature of acute rejection but absent or mild in hepatitis C [105]. Recurrent HCV infection seems to increase the incidence of chronic (ductopenic) rejection. HBV-positive patients coinfected with HCV have less severe disease than patients with HBV infection alone which may be due to HCV-induced inhibition of HBV replication. Moreover, HBV-infected patients with HDV coinfection are at lower risk of recurrent HBV infection than those infected with HBV alone, although also fulminant courses have been reported. HDV reinfection in the absence of HBV infection has been reported, but sensitive detection techniques (PCR) for HBV and HDV revealed low levels of HBV viremia in these cases. Risk of progression to cirrhosis in HBV/HDV infection is lower and fibrosing cholestatic hepatitis is very uncommon [105, 107].

Molecular pathologic techniques applied to the liver biopsy in support of conventional histology

At present, clinical decisions are often guided by the results of histopathological examination of the liver biopsy. However, the inclusion of molecular techniques can provide additional clinically relevant information [108]. It can be expected that microarray studies with the identification of genes associated with increased risk of progression or resistance to therapy will improve and extend the predictive value of the liver biopsy [108, 109].

What is expected from the pathologist in the future?

In order to improve its diagnostic and predictive value, liver biopsy interpretation cannot be static but has to evolve together with the progress of knowledge and methodology of basic and clinical science. Detailed analysis of the inflammatory infiltrate, assessment of virus characteristics, evaluation of cytokines, gene expression studies, and other molecular approaches in correlation with clinical information will serve that purpose.

Conflict of interest statement I declare that I have no conflict of interest.

References

1. Desmet VJ (2003) Liver tissue examination. J Hepatol 39:543–549
2. Rockey DC, Caldwell SH, Goodman ZD et al (2009) Liver biopsy. Hepatology 49:1017–1044
3. Dienstag JL (2002) The role of liver biopsy in chronic hepatitis C. Hepatology 36:152–160
4. Lefkowitch JH (2007) Liver biopsy assessment in chronic hepatitis. Arch Med Res 38:634–643
5. Gebo KA, Herlong F, Torbenson MS et al (2002) Role of liver biopsy in management of chronic hepatitis C: a systematic review. Hepatology 36:161–172
6. Brunt EM (2000) Grading and staging the histopathological lesions of chronic hepatitis: the Knodell histology activity index and beyond. Hepatology 31:241–246
7. Ishak KG (2000) Pathologic features of chronic hepatitis. A review and update. Am J Clin Pathol 113:40–55
8. Scheuer PJ, Lefkowitch JH (2005) Liver biopsy interpretation, 7th edn. WB Saunders, New York
9. Huang SN, Chen TC, Tsai SL et al (1997) Histopathology and pathobiology of hepatotropic virus-induced liver injury. J Gastroenterol Hepatol 12(Suppl):195–217
10. Ichai P, Samuel D (2008) Etiology and prognosis of fulminant hepatitis in adults. Liver Transplant 14:67–79
11. Boyer JL, Klatskin G (1970) Pattern of necrosis in acute viral hepatitis. N Engl J Med 283:1063–1071
12. Theise ND, Bodenheiner HC Jr, Ferrell LD (2007) Acute and chronic viral hepatitis. In: Burt AD, Portmann BC, Ferrell LD (eds)

MacSween's pathology of the liver, 5th edn. Churchill Livingstone, Philadelphia, pp 399–441
13. Vyberg M (1993) The hepatitis-associated bile duct lesion. Liver 13:289–301
14. Kobayashi K, Hashimoto E, Ludwig J (1993) Liver biopsy features of acute hepatitis C compared with hepatitis A, B, and non-A, non-B, non-C. Liver 13:69–73
15. Hoofnagle JH (2002) Course and outcome of hepatitis C. Hepatology 36:21–29
16. Missiha SB, Ostrowski M, Heathcote EJ (2008) Disease progression in chronic hepatitis C: modifiable and nonmodifiable factors. Gastroenterology 134:1699–1714
17. Gordon FD, Pomfret EA, Pomposelli JJ et al (2004) Severe steatosis as the initial histologic manifestation of recurrent hepatitis C genotype 3. Hum Pathol 35:636–63848
18. Karayiannis P (1998) Hepatitis D virus. Rev Med Virol 8:13–24
19. Lefkowitch JH, Goldstein H, Yatto R et al (1987) Cytopathic liver injury in acute delta virus hepatitis. Gastroenterology 92:1262–1266
20. Benjaminov FS, Heathcote J (2004) Liver disease in pregnancy. Am J Gastroenterol 99:2479–2488
21. Navaneethan U, Mohajer MA, Shata MT (2008) Hepatitis E and pregnancy: understanding the pathogenesis. Liver Int 28:1190–1199
22. Kamar N, Selves J, Mansury JM et al (2008) Hepatitis E: does it cause chronic hepatitis? Hepatology 48:1328–1330
23. Hübscher SG (1998) Histological grading and staging in chronic hepatitis: clinical applications and problems. J Hepatol 29:1015–1022
24. Dries V, Odenthal M, Schirmacher P et al (2001) Liver biopsy in chronic hepatitis C. Histopathology, molecular diagnostic analysis, and implications for therapeutic management. Patholoe 22:362–368
25. Roskams T, Libbrecht L, Desmet VJ (2003) Progenitor cells in diseased human liver. Semin Liver Dis 23:385–396
26. Liaw YF, Yang SS, Chen TJ et al (1985) Acute exacerbation in hepatitis B e antigen positive chronic type B hepatitis. J Hepatol 1:227–233
27. Koukoulis GK (2001) Chronic hepatitis C: grading, staging, and searching for reliable predictors of outcome. Hum Pathol 32:899–903
28. Thein HH, Yi Q, Dore GJ et al (2008) Estimation of stage-specific fibrosis progression rates in chronic hepatitis C virus infection: a meta-analysis and meta-regression. Hepatology 48:418–431
29. Poynard T, Ratziu V, Charlotte F et al (2001) Rates and risk factors of liver fibrosis progression in patients with chronic hepatitis C. J Hepatol 34:730–739
30. Goodman ZD (2007) Grading and staging systems for inflammation and fibrosis in chronic liver diseases. J Hepatol 47:598–607
31. Alonso-Marti C, Moreno A, Barat A et al (1990) Co-existence of hepatocyte ground-glass inclusions from several causes. Histopathol 16:304–307
32. Naoumov NV, Eddleston AL (1994) Host immune response and variations in the virus genome: pathogenesis of liver damage caused by hepatitis B virus. Gut 35:1013–1017
33. Baumert TF, Thimme R, von Weizsäcker F (2007) Pathogenesis of hepatitis B virus infection. World J Gastroenterol 13:82–90
34. Naoumov NV, Schneider R, Grötzinger T et al (1992) Precore mutant hepatitis B virus infection and liver disease. Gastroenterology 102:538–543
35. Blum HE, Moradpour D, Weizsäcker F et al (1997) Hepatitis-B-Virusmutanten—Klinische Bedeutung. Z Gastroenterol 35:347–355
36. Park YN, Han KH, Kim KS et al (1999) Cytoplasmic expression of hepatitis B core antigen in chronic hepatitis B virus infection: role of precore stop mutants. Liver 19:199–205
37. Lok ASF, McMahon BJ (2001) Chronic hepatitis B. Hepatology 34:1225–1241
38. Chen TJ, Liaw YF (1988) The prognostic significance of bridging hepatic necrosis in chronic type B hepatitis: a histopathologic study. Liver 8:10–16
39. Cooksley WGE, Bradbear RA, Robinson W et al (1986) The prognosis of chronic active hepatitis without cirrhosis in relation to bridging necrosis. Hepatology 6:345–348
40. Villari D, Raimondo G, Brancatelli S et al (1991) Histological features in liver biopsy specimens of patients with acute reactivation of chronic type B hepatitis. Histopathol 18:73–77
41. Harada K, Mihato H, Hiramatsu K et al (1998) Epithelioid cell granulomas in chronic hepatitis C: immunohistochemical character and histologic marker of favourable response to interferon-α therapy. Histopathol 33:216–221
42. Mihm S, Fayyazi A, Hartmann H et al (1997) Analysis of histopathological manifestations of chronic hepatitis C virus infection with respect to virus genotype. Hepatology 25:735–739
43. Rubbia-Brandt L, Leandro G, Spahr L (2001) Liver steatosis in chronic hepatitis C: a morphological sign suggesting infection with HCV genotype 3. Histopathology 39:119–124
44. Younossi ZM, McCullough AJ (2009) Metabolic syndrome, non-alcoholic fatty liver disease and hepatitis C virus: impact on disease progression and treatment response. Liver Int 29:3–12
45. Bedossa P, Moucari R, Chelbi E et al (2007) Evidence for a role of nonalcoholic steatohepatitis in hepatitis C: a prospective study. Hepatology 46:380–387
46. Serfaty L, Capeau J (2009) Hepatitis C, insulin resistance and diabetes: clinical and pathogenic data. Liver Int 29:13–25
47. Negro F, Sanyal AJ (2009) Hepatitis C virus, steatosis and lipid abnormalities: clinical and pathogenic data. Liver Int 29:26–37
48. Kumar D, Farrell GC, Fung C et al (2002) Hepatitis C virus genotype 3 is cytopathic to hepatocytes: reversal of hepatic steatosis after sustained therapeutic response. Hepatology 36:1266–1272
49. Korenaga M, Wang T, Li Y et al (2005) Hepatitis C virus core protein inhibits mitochondrial electron transport and increases reactive oxygen species (ROS) production. J Biol Chem 280:37481–37488
50. Sanyal AJ (2005) Review article: non-alcoholic fatty liver disease and hepatitis C—risk factors and clinical implications. Aliment Pharmacol Ther 22(Suppl 2):48–51
51. Fartoux L, Charzouillères O, Wendum D et al (2005) Impact of steatosis on progression of fibrosis in patients with mild hepatitis C. Hepatology 41:82–87
52. Ohata K, Hamasaki K, Toriyama K et al (2003) Hepatic steatosis is a risk factor for hepatocellular carcinoma in patients with chronic hepatitis C virus infection. Cancer 97:3036–3043
53. Bruno S, Silini E, Crosignani A et al (1997) Hepatitis C virus genotypes and risk of hepatocellular carcinoma in cirrhosis: a prospective study. Hepatology 25:754–758
54. Moriya K, Fujie H, Shintani Y et al (1998) The core protein of hepatitis C virus induces hepatocellular carcinoma in transgenic mice. Nat Med 4(9):1065–1067
55. Lai MM (2002) Hepatitis C virus proteins: direct link to hepatic oxidative stress, steatosis, carcinogenesis and more. Gastroenterology 122(2):568–571
56. Haque S, Chandra B, Gerber MA et al (1996) Iron overload in patients with chronic hepatitis C: a clinicopathologic study. Hum Pathol 27:1277–1281
57. Desai TK, Jamil LH, Balasubramaniam M et al (2008) Phlebotomy improves therapeutic response to interferon in patients with chronic hepatitis C: a metaanalysis of six prospective randomized controlled trials. Dig Dis Sci 53:815–822
58. Miura K, Taura K, Kodama Y et al (2008) Hepatitis C virus-induced oxidative stress suppresses hepcidin expression through increased histone deacetylase activity. Hepatology 48:1420–1429

59. Chen DS (1993) Natural history of chronic hepatitis B virus infection: new light on an old story. J Gastroenterol Hepatol 8:470–475
60. Naoumov NV, Portmann BC, Tedder RS et al (1990) Detection of hepatitis B virus antigens in liver tissue. A relation to viral replication and histology in chronic hepatitis B infection. Gastroenterology 99(4):1248–1253
61. Chu CM, Liaw YF (1995) Membrane staining for hepatitis B surface antigen on hepatocytes: a sensitive and specific marker of active viral replication in hepatitis B. J Clin Pathol 48:470–473
62. Chu CM, Liaw YF (1987) Intrahepatic distribution of hepatitis B surface and core antigens in chronic hepatitis B virus infection. Gastroenterology 92:220–225
63. Davies SE, Portmann BC, O'Grady JG et al (1991) Hepatic histological findings after transplantation for chronic hepatitis B virus infection, including a unique pattern of fibrosing cholestatic hepatitis. Hepatology 13:150–157
64. Marinos G, Rossol S, Carucci P et al (2000) Immunopathogenesis of hepatitis B recurrence after liver transplantation. Transplantation 69(4):559–568
65. Kawai K, Horiike N, Michitaka K et al (2003) The effects of hepatitis B virus core promoter mutations on hepatitis B core antigen distribution in hepatocytes as detected by laser-assisted microdissection. J Hepatol 38:635–641
66. Fujiwara K, Tanaka Y, Paulon E et al (2005) Novel type of hepatitis B virus mutation: replacement mutation involving a hepatocyte nuclear factor 1 binding site tandem repeat in chronic hepatitis B virus genotype E. J Virol 79:14404–14410
67. Shiha GE, Khaled RZ, Abdulla AF et al (2005) Immunohistochemical identification of HCV target antigen in paraffin-embedded liver tissue: reproducibility and staining patterns. Liver Internat 25:254–260
68. Guerrero RB, Batts KP, Brandhagen DJ et al (1997) Effects of formalin fixation and prolonged block storage on detection of hepatitis C virus RNA in liver tissue. Diagn Mol Pathol 6:277–28149
69. Bean P (2002) Latest discoveries on the infection and coinfection with heptatitis D virus. Am Clin Lab 21:25–27
70. Guido M, Swan NT, Fattovich G et al (1999) Intrahepatic expression of hepatitis B virus antigens: effect of hepatitis C virus infection. Mod Pathol 12:599–603
71. Blackard JT, Sherman KE (2008) HCV/HIV co-infection: time to re-evaluate the role of HIV in the liver. J Viral Hepat 15:323–330
72. Regev A, Berho M, Jeffers LJ et al (2002) Sampling error and intraobserver variation in liver biopsy in patients with chronic HCV infection. Am J Gastroenterol 97:2614–2618
73. Demetris AJ, Ruppert K (2003) Pathologist's perspective on liver needle biopsy size. J Hepatol 39:275–277
74. Colloredo G, Guido M, Sonzogni A et al (2003) Impact of liver biopsy size on histological evaluation of chronic viral hepatitis: the smaller the sample, the milder the disease. J Hepatol 39:275–277
75. Shiano TD, Azeem S, Bodia CA et al (2005) Importance of specimen size in accurate needle liver biopsy evaluation of patients with chronic hepatitis C. Clin Gastroenterol Hepatol 3:930–935
76. Skripenova S, Trainer T, Krawitt E et al (2007) Variability of grade and stage in simultaneous paired liver biopsies in hepatitis C. J Clin Pathol 60:321–324
77. Scheuer PJ (2003) Liver biopsy size matters in chronic hepatitis: bigger is better. Hepatology 38:1356–1358
78. Shiano TD, Azeem S, Bodian CA et al (2005) Importance of specimen size in accurate needle liver biopsy evaluation of patients with chronic hepatitis C. Clin Gastroenterol Hepatol 3:930–935
79. Ishak K, Baptista A, Bianchi L et al (1995) Histological grading and staging of chronic hepatitis. J Hepatol 22:696–699
80. Bedossa P, Dargere D, Paradis V (2003) Sampling variability of liver fibrosis in chronic hepatitis C. Hepatology 38:1449–1457
81. Bedossa P, and The METAVIR cooperative study group (1996) An algorithm for the grading of activity in chronic hepatitis. Hepatology 24:289–293
82. Schirmacher P, Fleig WE, Tannapfel A et al (2004) Bioptische Diagnostik der chronischen Hepatitis. Pathologe 25:338–348
83. Goodman ZD, Becker RL, Pockros PJ et al (2007) Progression of fibrosis in chronic hepatitis C: evaluation by morphometric image analysis. Hepatology 45:886–894
84. Scheuer P (1997) Chronic hepatitis: what is activity and how should it be assessed. Histopathol 30:103–105
85. Batts KP, Ludwig J (1995) Chronic hepatitis. An update on terminology and reporting. Am J Surg Pathol 19:1409–1417
86. Zhu R, Huang H, Zhang H et al (2006) Prognostic analysis in chronic hepatitis B patients: a retrospective study of 216 cases about Scheuer scores, in situ expression of viral antigens and tissue hepatitis B virus DNA levels. Liver Int 26:82–89
87. Knodell RG, Ishak KG, Black WC et al (1981) Formulation and application of a numerical scoring system for assessing histological activity in asymptomatic chronic active hepatitis. Hepatology 1:431–435
88. METAVIR cooperative group (1994) Inter- and intra-observer variation in the assessment of liver biopsy of chronic hepatitis C. Hepatology 20:15–20
89. Goodman ZD, Ishak KG, Sesterhenn IA (1986) Herpes simplex hepatitis in apparently immunocompetent adults. Am J Clin 85:694–699
90. Jaques SM, Qureshi F (1992) Herpes simplex virus hepatitis in pregnancy: a clinicopathologic study of three cases. Hum Pathol 23:183–187
91. Markin RS (1994) Manifestations of Epstein–Barr-virus in inflammatory diseases of the liver and liver allografts: an in situ hybridization study. Hepatology 20:899–907
92. Seehofer D, Rayes N, Tullius SG et al (2002) CMV hepatitis after liver transplantation: incidence, clinical course, and long-term follow up. Liver Transplant 8:1138–1146
93. MacDonald GA, Greenson JK, DelBuono EA et al (1997) Mini-microabscess syndrome in liver transplant patients. Hepatology 26:192–197
94. Theise ND, Conn M, Thung SN (1993) Localization of cytomegalovirus antigens in liver allografts over time. Hum Pathol 24:103–108
95. Carmichael GP Jr, Zahradnik JM, Moyer GH et al (1979) Adenovirus hepatitis in an immunosuppressed adult patient. Am J Clin Pathol 71:352–355
96. Huerre MR, Lan NT, Marianneau P et al (2001) Liver histopathology and biological correlates in five cases of fatal dengue fever in Vietnamese children. Virchow's Arch 438:107–114
97. Vieira WT, Gayotto LC, de Lima CP et al (1983) Histopathology of the human liver in yellow fever with special emphasis on the diagnostic role of the Councilman body. Histopathology 7:195–208
98. Harrison RF, Davies MH, Goldin RD et al (1993) Recurrent hepatitis B in liver allografts: a distinctive form of rapidly developing cirrhosis. Histopathology 23:21–28
99. Lau JY, Bain VG, Davies SE et al (1992) High-level expression of hepatitis B viral antigens in fibrosing cholestatic hepatitis. Gastroenterology 102:956–962
100. Gaglio P, Singh S, Degertekin B et al (2008) Impact of the hepatitis B virus genotype on pre- and post-liver transplantation outcomes. Liver Transplant 14:1420–1427
101. Demetris AJ, Eghtesad B, Marcos A et al (2009) Evolution of hepatitis C virus in liver allografts. Liver Transplant 15:35–41

102. Guerrero RB, Batts KB, Burgart LJ et al (2000) Early detection of hepatitis C allograft reinfection after orthotopic liver transplantation: a molecular and histologic study. Mod Pathol 13:229–237
103. Saxena R, Crawford JM, Navarro VJ et al (2002) Utilization of acidophil bodies in the diagnosis of recurrent hepatitis C infection after orthotopic liver transplantation. Mod Pathol 15:897–903
104. Ercolani G, Grazi GL, Ravaioli M et al (2006) Histological recurrent hepatitis C after liver transplantation: outcome and role of retransplantation. Liver Transplant 12:1104–1111
105. Hübscher SG, Portmann BC (2007) Transplantation pathology. In: Burt AD, Portmann BC, Ferrell LD (eds) MacSween's pathology of the liver, 5th edn. Churchill Livingstone, Philadelphia, pp 815–879
106. Schluger LK, Sheiner PA, Thung SN et al (1996) Severe recurrent cholestatic hepatitis C following orthotopic liver transplantation. Hepatology 23:971–976
107. David E, Rahier J, Pucci A et al (1993) Recurrence of hepatitis D (delta) in liver transplants: histopathological aspects. Gastroenterology 104:1122–1128
108. Libbrecht L, Roskams T (2006) Molecular diagnostic approach to liver tissue as an ancillary tool for liver histopathology. Semin Liver Dis 26:328–336
109. Geller SA, Pitman MB, Nichols WS (2007) Cellular and molecular diagnostic techniques. In: Burt AD, Portmann BC, Ferrell LD (eds) MacSween's pathology of the liver, 5th edn. Churchill Livingstone, Philadelphia, pp 119–146

Virchows Arch (2011) 458:393–402
DOI 10.1007/s00428-011-1060-7

REVIEW AND PERSPECTIVE

The pathological diagnosis of neuroendocrine tumors: common questions and tentative answers

Marco Volante · Luisella Righi · Alfredo Berruti · Guido Rindi · Mauro Papotti

Received: 10 December 2010 / Revised: 11 February 2011 / Accepted: 13 February 2011 / Published online: 23 February 2011
© Springer-Verlag 2011

Abstract Neuroendocrine neoplasms (NEN) develop in many organs, and although they share some pathological and clinical features, significant differences do exist among different tumor types and locations. The correct classification of NENs is based on the recently published WHO classification according to the various locations, and is relevant for the appropriate treatment in each group. The apparently easy diagnostic categorization in well-differentiated NENs, called neuroendocrine tumors, and poorly differentiated NENs, called neuroendocrine carcinomas, is complicated by the existence, among others, of different terminologies, morphological criteria of malignancy, combined exocrine–endocrine tumors, as well as of heterogeneous diagnostic, prognostic, and predictive markers. The present paper is an overview of the most frequently asked questions and an attempt to provide practical answers related to NEN diagnosis in the daily pathology work.

M. Volante · L. Righi · M. Papotti
Divisions of Pathology, University of Turin at San Luigi Hospital, Orbassano, Torino, Italy

A. Berruti
Division of Medical Oncology,
University of Turin at San Luigi Hospital,
Orbassano, Torino, Italy

G. Rindi
Università Cattolica del Sacro Cuore (UCSC) at Policlinico Gemelli,
Rome, Italy

M. Papotti (✉)
Department of Clinical and Biological Sciences,
University of Turin,
Regione Gonzole 10,
10043 Orbassano, Turin, Italy
e-mail: mauro.papotti@unito.it

Keywords Neuroendocrine tumor · Carcinoid · Small cell carcinoma · Ki-67 · Mixed exocrine–endocrine carcinoma · Classification

Introduction

A "carcinoid is a carcinoid", universally means an easy diagnosis and easy clinical management. However, not necessarily recent but compelling evidences changed this easy-going "carcinoid" attitude, and life for both pathologists and clinicians is no longer that easy as it used to be. "Carcinoids", now more appropriately defined as neuroendocrine tumors (NETs) belong indeed to a family of rare neoplasms more often encountered in gastroenteric, pancreatic, and pulmonary tissues, but virtually present in any organ of the body. Different epidemiological, clinical, biological, and pathological features are described for different types, including different response to available therapeutic options [1–4].

The correct classification of different neuroendocrine neoplasm (NEN) is increasingly relevant for the purpose of selecting the appropriate treatment by homogeneous groups of tumors. It is well known that the pathological recognition of a classical neuroendocrine neoplasm is generally easy, if supported by a high index of suspicion (i.e., in expert hands), especially when looking at a lesion of organs typically hosting such neoplasms.

It is, however, also known that an apparently easy diagnosis is complicated by the different terminology, morphological criteria of malignancy, diagnostic and prognostic markers developed, and of proven diagnostic utility in different organs [5]. Additional issues are the classification of NENs in non-endocrine organs and the definition of mixed or combined exocrine and endocrine carcinomas.

High quality pathology reports are uncommon in some centers [6, 7] and a need for a minimal standard of pathology reporting has been recognized [2, 7, 8]. Most issues related to pathological reporting of NETs found a consensus among clinicians and pathologists in a recent study. Of note, all participants to this study are experts in NET pathology; nonetheless, disagreement persisted as for classification systems and other relatively minor issues [8].

This article reflects our common diagnostic practice in the field of neuroendocrine tumors and addresses the most frequently asked questions (FAQ) regarding their pathological characterization (Table 1 and Fig. 1). FAQs are usually raised by clinicians in order to select the most appropriate therapeutic option or by pathologists not familiar with current diagnostic and classification criteria. All definitions used here refer to the current WHO classifications [9–11].

FAQ 1: can terms such as "carcinoid" and NET be used interchangeably?

Answer: NO. The terminology used to identify NETs is heterogeneous and has undergone major changes in recent years, with the result that similar tumors from different organs are labeled with different terms, according to the respective WHO classification schemes. Organ-specific tumors, such as pheochromocytoma, paraganglioma, medullary thyroid carcinoma, parathyroid and pituitary adenomas, and carcinomas maintain their original label, and the malignant potential is defined by the use of the term "carcinoma" for the latter or by entering "malignant" before the diagnosis of pheochromocytoma and paraganglioma (according to more or less well-defined morphological criteria).

By contrast, in the gastroenteropancreatic (GEP) and bronchopulmonary systems NETs are to be classified in a

Table 1 Frequently asked questions on NET pathological characterization

Question	Context	Relevance	Criticism
FAQ 1: terminology of NETs (GEP system)	Carcinoid vs. (neuro) endocrine tumor/ carcinoma terms	Terminology reflects classification and prognosis	Not accepted worldwide
FAQ 2: criteria to define malignant potential in NETs	Combination of clinical (presence of metastases) and morphological parameters	Determine the classification (and prognosis) of a NET	Change according to the tumor site; some equivocal/difficult to assess
FAQ 3: nomenclature for functioning versus non functioning tumors	Terms such as insulinoma, gastrinoma, etc. and the concept of functioning tumors	Functioning tumors are defined by the presence of clinical symptoms related to hormone production	Terminology reflects clinical picture rather than pathological features; no link with malignancy
FAQ 4: classification of extra-pulmonary poorly differentiated NE carcinomas	Existence of extra-pulmonary small and large cell carcinomas	Aggressive as the pulmonary counterpart	Difficult to be distinguished from those of the lung (ambiguous phenotype); pitfalls in the differential diagnosis with other "small cell" NETs
FAQ 5: grading and staging of NETs	Necessity to apply novel grading and staging systems	NET stage (ENETS and AJCC) and grade (ENETS) are of prognostic value	Recent, to be validated prospectively, sometimes confusing and discordant
FAQ 6: pathological diagnosis of NETs in biopsy/cytology material	The type of information that may be determined in preoperative material from NETs	In inoperable cases, biopsy/cytology material may be the only tissue sample available	Classification criteria not applicable; immunoprofile (included Ki-67) affected by sampling error
FAQ 7: the role of Ki-67 in NETs	Diagnostic vs. prognostic vs. predictive role of Ki-67 determination in NETs	Most relevant marker in NETs (upon NE differentiation is established)	Still poorly reproducible; diagnostic vs. prognostic vs. predictive uses often erroneously interpreted
FAQ 8: precursor lesions of NETs	Prevalence and classification of NET precursor lesions	Potentially useful to understand pathogenesis of NETs	Poorly defined, their clinical meaning poorly recognized
FAQ 9: classification of mixed exocrine-endocrine carcinomas	Definition of diagnostic criteria in different organs	Imply pathogenetic aspects; clinical and biological behavior may be different	Classification criteria ambiguous; overlap with the concept of NE differentiation in conventional non-NE carcinomas of various locations
FAQ 10&11: prognostic and predictive factors in NETs	Molecular and immunohistochemical markers of prognostic and predictive value	Correct classification and proliferative index are is the only prognostic and predictive features of relevance, to date	Several molecules proposed, none turned to be useful in clinical application

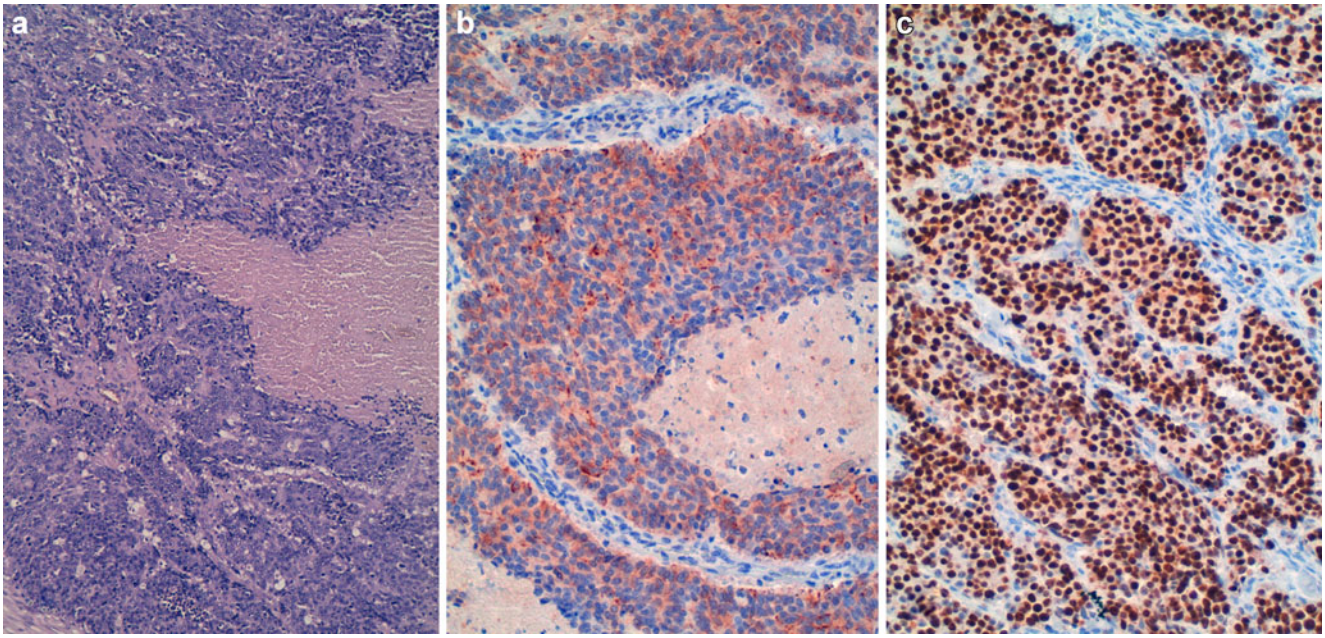

Fig. 1 Rectal NEC, large cell type, with solid/diffuse growth, cytological atypia, and extensive necrosis (**a**), diffusely positive for chromogranin A (**b**), and showing a very high proliferative index (G3) (**c**); all original magnifications, ×200

three or four tier system, respectively. In the GEP area, the year 2000 WHO classification of endocrine tumors [9] proposed to label endocrine tumors according to their malignant potential as: (1) well-differentiated (neuro) endocrine (NE) tumor (including the two groups of "benign behavior" and "uncertain behavior"); (2) well-differentiated NE carcinoma; (3) poorly differentiated NE carcinoma (of the small or large cell type). Such a general scheme, based on the recognition of clinical and pathological characteristics, was maintained irrespective of the tumor location, although the rules for classification change according to the different sites, and has been incorporated in the year 2004 WHO Classification of Tumors of Endocrine Organs as to concern pancreatic endocrine tumors [12]. However, the novel 2010 WHO classification of gastrointestinal tumors [11] has introduced substantial changes in the first two subtypes, which are now labeled NET G1 and NET G2, and restricted the term carcinoma to high-grade poorly differentiated large cell or small cell NE carcinomas. Both grading and site-specific TNM staging (with defined relevant clinical-pathological variables) were thus required for the definition of malignant potential. In the GEP area, terms such as carcinoid, malignant carcinoid, neuroendocrine carcinoma, apudoma, etc., are, as such, incomplete descriptors of a NEN are strongly discouraged and should be accurately avoided. Even the embryological derivation (foregut, midgut, hindgut "carcinoids") is not a useful criterion to classify benign and malignant tumors. In fact, these terms fail to convey information related to malignancy, in the absence of specific details within each single location.

In bronchopulmonary NENs, similar tumor groups as described above are recognized. However, their terminology, i.e., typical carcinoid, atypical carcinoid, large cell NEC, and small cell NEC, still differs from that of the GEP-NENs [3, 10]. The distinction is based on specific morphological criteria and is highly relevant for clinical purposes, since a significantly different prognosis is associated to each tumor type (with the possible exception of the two latter categories of poorly differentiated large or small cell cancers) [13–15].

FAQ 2: can the malignant potential be defined in NETs (G1 and G2)?

Answer: YES, applying a site-specific TNM staging. Local invasion and/or lymph node or distant metastases are the only diagnostic criteria of malignant potential in the most well-differentiated NETs (including those in the GEP area, paragangliomas/pheochromocytomas, parathyroid tumors). In the GEP area, cyto-morphological features of aggressive behavior, such as cellular atypia, increased mitotic index, vascular invasion, etc., do not qualify a tumor as malignant per se, and the terminology "well-differentiated neuroendocrine tumor, uncertain behavior" had been proposed in prior classifications of these cases, in the absence of local or distant dissemination [9]. According to the novel 2010 WHO classification of GI NETs, no case could be defined benign per se and stratification of malignancy-related risk groups is based on grading—mitotic count and Ki-67 index—and TNM staging [11]. Poorly differentiated NENs, now

called NECs, are graded G3 and are recognized by a solid/non-cohesive growth pattern, extensive necrosis, and high mitotic index (>20×10 high-power fields—HPF), usually associated to extensive vascular and local invasion and metastatic dissemination at diagnosis.

Similarly, in the lung, local invasion and metastases are not considered criteria for classification which is rather based on necrosis and mitotic index in all NET categories, except for small cell carcinoma. Therefore "typical carcinoids" are distinguished from "atypical carcinoids" by the presence of necrotic foci or mitotic count exceeding 2×10 HPF, sharing both tumor types either the "organoid" growth pattern classically characterizing well-differentiated NETs, and the metastatic potential (higher in atypical carcinoids, but also present in typical ones).

FAQ 3: is any immunohistochemically detected hormone production sufficient to label a GEP NET with the suffix "oma" following the hormone? [In other words, are insulin-positive tumors insulinomas, are gastrin-positive tumors gastrinomas, etc.?]

Answer: NO. The immunohistochemical demonstration of a specific hormone production (insulin, gastrin, glucagon, etc.) in tumor cells does not qualify the tumor itself as a "hormone-oma" (insulinoma, gastrinoma, glucagonoma, etc.). This terminology is restricted to those tumors associated to a clinical syndrome sustained by the excess production of that specific hormone. Pathologists should therefore avoid using terms such as insulinoma, gastrinoma, glucagonoma, etc., unless specific information were provided in the patient's clinical history and the corresponding hormone has been identified in tumor cells. The definition of the hormonal immunophenotype is not necessarily part of the diagnostic algorithm of GEP NETs, but once tumor type, grade, and stage have been defined, the hormonal characterization can be performed and the hormone(s) detected in tumor cells can be listed in the final report.

FAQ 4: do extra-pulmonary small and large cell carcinomas exist?

Answer: YES. The past terminology in the GEP area was "poorly differentiated (neuro)endocrine carcinoma (PDEC)", and the novel 2010 WHO classification of digestive system tumors proposed to label these neoplasms as NE carcinomas (large cell or small cell type) [11]. As a matter of fact, these tumors are examples of either small cell or large cell NE carcinomas, as originally described in the lung or even of a combination of the two (combined small and large cell NE carcinoma). Apart from the GEP area, such tumors are also rarely observed in non-endocrine organs, including the urinary bladder, prostate, kidney, breast, larynx, parotid, gallbladder, in which the pulmonary terminology is applied for pure forms of small cell or large cell NE carcinoma. The morphological appearance and diagnostic criteria are generally similar to those currently applied for their pulmonary counterpart, and correspond to malignant neoplasms composed of small or large-to-intermediate cells with high-grade features (marked nuclear atypia, multifocal necrosis, and high mitotic index) and diffuse growth sometimes with organoid architecture. Indeed, before a primary small or large cell NE carcinoma is diagnosed in any of the above organs, an accurate clinical history and radiological investigation is required to exclude the possibility of the dissemination from an occult primary pulmonary neoplasia. In this respect, the expression of a marker considered as of tissue origin such as TTF-1, may generate confusion due to its expression in extra-pulmonary tumors, too [16]. As reported in the lung, small and large cell NE carcinomas may also develop in association with conventional urothelial carcinomas or adenocarcinomas of individual organs, and the prognosis is generally driven by the small or large cell NE component. It is worth noticing that "small cell" cytology is not a unique feature of small cell carcinoma, since both in the lung and in extra-pulmonary sites, well-differentiated NETs/carcinoids may be composed of small cells in an otherwise organoid structure. If a distinction may be easily achieved in surgical samples, this diagnosis may be less straightforward in small biopsy samples: additional diagnostic tools, such as proliferation markers, are useful in this respect (see also below FAQ 6).

FAQ 5: are tumor grading and staging necessary?

Answer: YES. In recent years, the value of a grading system has been recognized in GEP NETs [17, 18] and both grading and staging were incorporated in the NET diagnostic algorithm of the new 2010 WHO classification of digestive system tumors [11]. Three grades of differentiation have been proposed in GEP tumors (G1, G2, G3) based on the mitotic count (cut offs 2 and 20 per 2 mm^2) and the Ki-67 proliferation index (cut offs 3% and 20%). Poorly differentiated NE carcinomas are grade 3 by default and thus correctly defined as "high grade". The mitotic or Ki-67 index counts are generally done in areas of highest labeling density (in the so called "hot spots"), although this practice has been recently challenged by a study showing that, at least in lung carcinoids, the mitotic count is more reliable combining figures obtained in hot spots with those of a random count [19]. In lung NETs, a well-defined grading system, although advocated, is still missing.

A staging system has been proposed for GEP and lung NETs [10, 17, 18, 20], modifying or accepting the TNM of corresponding carcinomas at the same locations. In the

gastrointestinal tract, few confounding factors exist, which include (a) the difference between the ENETS and AJCC staging systems for the stomach, pancreas and, more significantly, for the appendix [21] and (b) the absence of a specific rule for mixed carcinoma, in some instances being equivocal the stage definition (if for the exocrine or neuroendocrine component).

The above-described grading and staging systems perform rather well for segregating statistically different survival groups of patients with GEP NETs and broncho-pulmonary carcinoids [22, 23]. Minor changes were also recently proposed in the TNM staging of pancreatic NET [24], since extra-pancreatic infiltration and tumor size over 4 cm were found to have the best prognostic significance in non-metastatic NETs. Therefore, any surgically resected tumor specimen from the lung or GEP areas should be diagnosed according to a checklist including information related to tumor grade (for GEP NETs only) and tumor stage, in order to stratify prognostically relevant groups of patients. By contrast, grading of a NET in biopsy material may not be reliable, though information on proliferation and mitotic count might be relevant for clinicians and should be included in the final pathological report of biopsies, as well.

FAQ 6: is the diagnosis of neuroendocrine tumors possible in small biopsy or cytology material?

Answer: YES, although classification is limited to some cases. The recognition of a NET is largely based on structural (organoid versus diffuse growth) and cytological (cell size, chromatin, atypias, mitoses, etc.) features. These may not be readily apparent in some small pathological specimens, and especially in cytological preparations. The demonstration of a minimum set of NE markers [7] is essential to drive the diagnosis. The minimal requirements for a diagnosis of a NET in preoperative biopsies or cytological materials include the recognition of an organoid pattern or diffuse growth (e.g., in a biopsy or in a cell block from cytology) in a neoplasm composed of round, homogeneous, small (oat), or large cells, with variable nuclear atypia, associated with neuroendocrine marker expression. In this context, the diagnosis of a NET is possible and the definition of its malignant potential feasible, especially in samples obtained from proven metastatic deposits (e.g., lymph nodes or liver) or in the presence of poorly differentiated small or large cell carcinoma features [9], since in this latter case, the architecture, high mitotic count, and proliferative index generally allow to meet the minimal diagnostic requirements. By contrast, the risk of malignancy in low-grade, well-differentiated tumors cannot be accurately defined as such on biopsy material, due to the lack of relevant diagnostic criteria. In bronchial biopsies or trans-thoracic fine needle aspirates, a generic diagnosis of "carcinoid" is advised in the absence of necrosis and a mitotic count <2 per 2 mm^2. In abdominal masses (e.g., pancreatic), a generic diagnosis of NET is advised for those tumors displaying a well-differentiated organoid growth. Moreover, in our experience, well-differentiated tumors made of small cells may occur, and in the absence of an architectural evaluation of the tumor and unless on the same material, an immunoprofiling is possible (NE markers expression and Ki-67 proliferative index), the identification of small tumor cells should not automatically lead to a diagnosis of (poorly differentiated) NE carcinoma/small cell carcinoma but rather to a descriptive diagnosis of a "small cell neoplastic proliferation".

Since primary NET of the liver are extremely rare (if ever exist), a NET in a liver biopsy can be reliably labeled as metastatic NET or NE carcinoma In these cases, a Ki-67 immunostaining may provide a superficial indication of the growth fraction within the small tissue fragments of the biopsy and assist in the distinction between NET and (poorly differentiated) NE carcinoma, with a proven acceptable concordance as compared to the primary tumor [25].

An additional issue is related to the recognition of the primary origin in the case of metastatic NETs of unknown origin in biopsy or cytological material. To address such issue, markers such as TTF-1 (for lung tumors) [26], CDX-2 (for EC-cell intestinal tumors) [27], and Isl-1 (for pancreatic tumors) [28] may be relevant and often informative enough.

FAQ 7: is Ki-67 to be determined in all NETs?

Answer: YES. Although the only official diagnostic application of Ki-67 immunostaining in the classification of a NET is restricted to pancreatic well-differentiated tumors [9], there are several good reasons for having the Ki-67 index evaluated in all cases. With regard to the diagnostic criterion, the new 2010 WHO classification of gastrointestinal tumors followed the ENETS proposal for a role of Ki-67 immunostaining in GEP NETs grading, with cut-off levels set at </=2%, 3–20%, and >20% positive nuclei. In addition, the Ki-67 labeling index was found to bear prognostic significance (see review of Jamali & Chetty [29]) in pancreatic [30] and in gastrointestinal NETs, especially when homogeneous tumor groups were analyzed [31], being high Ki-67 index associated to a worse prognosis. Finally, several clinical papers have proposed therapeutic algorithms for the management of patients affected by progressing NETs of any type (not only in the GEP area) and the Ki-67 index was one of the parameters considered in the decision tree [32]. Using different Ki-67

cut-offs (generally between 10% and 25%), the indication for biotherapy versus chemotherapy was variably modulated in individual patients undergoing tumor progression [33–36].

An accurate and reproducible procedure to assess Ki-67 index is mandatory. The issue is largely controversial, and it is suggested to use MIB1 monoclonal antibody and count at least 2,000 nuclei in areas of highest labeling density in all surgically resected tumors as indicated for grading purposes [11]. In biopsy or cytology material, the number of tumor nuclei may be lower than 2,000 and the observed proliferative fraction may not reflect that of the whole tumor. However, although caution is advisable in such cases, it has to be kept in mind that the Ki-67 determination in biopsy or cytological material may well be the only available proliferation data for clinical/therapeutic decisions in inoperable cases.

A final "question in the question" is whether Ki-67 is the gold prognostic/predictive parameter? The answer is no, although it is the best that we have. As a prognostic parameter, the hindrances are that the subgroup of patients with Ki-67 between 2% and 20% may be too heterogeneous, and in addition, the clinicians would prefer two prognostic groups rather than three. Moreover, the prognostic groups were arbitrarily defined, so a better cut-off can be identified by a careful examination of the relationship between changes in Ki-67 index (considered as a continuous variable) and hazard ratio of recurrence or death. As a predictive parameter, Ki-67 can roughly take tumors potentially sensitive to chemotherapy apart from those that do not, but it cannot predict the efficacy of the molecular target therapies increasingly used in the management of G1-G2 NETs.

FAQ 8: do precursor lesions of interest or significance exist?

Answer: YES, at least in the stomach and lung. A large body of evidence has been accumulated in the stomach, since atrophic corpus gastritis may associate with hyperplastic conditions of the NE cell compartment, as a result of a hypergastrinemic status. Atrophic glands may contain excess number of NE cells, a finding which has to be confirmed (indeed often recognized) by means of chromogranin A immunostaining. NE cells may be increased diffusely in the glands and crypts or as a single-chain layer occupying the majority of the gland or as small nodules in the mucosal chorion. This is generally referred to as diffuse, linear, or nodular NE cell hyperplasia and is considered a background condition of gastric "carcinoids", being such hyperplasia often detected in the peri-tumoral mucosa of type I gastric carcinoids. Patients affected by atrophic gastritis usually undergo regular endoscopic controls and the presence, type, and extent of NE cell hyperplasia on gastric biopsies is part of the follow up program for these patients.

NE cell hyperplastic or dysplastic conditions in other organs are less well known nor is the pre-neoplastic potential well established, except for gastrin and somatostatin cell hyperplasia of the duodenal mucosa in the setting of MEN1 syndrome; in the pancreas, a peculiar condition of unknown pre-neoplastic potential is nesidioblastosis, a rare functional disorder of the beta cells that causes persistent hyperinsulinemic hypoglycemia associated to beta-cell hypertrophy, islet hyperplasia, and an increase in the beta-cell mass [37].

A possible exception is represented by the bronchial tree, in which NE cell proliferations include NE cell hyperplasia, tumorlets, and the rare lesion called DIPNECH (diffuse idiopathic pulmonary NE cell hyperplasia). NE cell hyperplasia occurs as isolated cells or linear growth in small bronchi, while tumorlets are well-differentiated NE cell growth not exceeding 5 mm in size located in the bronchial or bronchiolar walls. Their structure is not different from that of typical bronchial carcinoids, and they are occasionally encountered in the peri-tumoral lung parenchyma of carcinoid-bearing patients. They should be incorporated in the pathology report, although their pre-neoplastic potential is not well established. DIPNECH is also found in association with carcinoid tumors and is considered a pre-invasive form of NET. Since it may occur in association to interstitial lung disease, it may be observed in lung biopsies taken for diagnostic purposes in association with a fibrotic area and should be documented with NE markers and become part of the pathology report.

FAQ 9: do diagnostic criteria exist for mixed exocrine-endocrine carcinomas?

Answer: YES, depending on tumor site. The original definition of mixed endocrine–exocrine carcinoma (MEEC) was incorporated in the WHO classification of GEP endocrine tumors since 2000 [9], stating that a MEEC was a tumor having two different populations of cells, each represented by at least one third of the tumor area. This definition included also goblet cell carcinoids, an extremely rare entity of the appendix but also moderately aggressive and representing a diagnostic challenge [38, 39]. The new WHO classification of digestive system tumors [11], proposed the term mixed adeno-neuroendocrine carcinoma (MANEC) to classify these tumors, with similar criteria. Besides the GEP area, malignant tumors with combined exocrine and neuroendocrine features are found in most organs and apparatuses, although specific diagnostic criteria are often missing. In the lung [10], the term "combined" replaces "mixed" with a similar significance, except that a minimal percent of each component is not indicated as a required diagnostic criterion. Such combined carcinomas are indeed accepted by the WHO classification as variants of either small cell or large cell neuroendocrine carcinomas,

only (ICD-0 codes 8045/3 and 8013/3, respectively). Morphologically, a squamous cell carcinoma, a large cell carcinoma or alternatively an adenocarcinoma component may be admixed with the neuroendocrine small or large cell population. In the breast, a neuroendocrine carcinoma variant has been included in the last WHO classification [40], being defined as a "special group of primary breast carcinomas exhibiting morphological features similar to those of GEP and lung NETs and expressing NE markers in >50% of tumor cells". These tumors may show different morphological patterns (solid, small/oat cell, and large cell variants) [41]. According to this definition, it seems that the remaining percentage of tumor is one of the conventional breast cancer subtypes, and in addition, the NE component has to be defined by means of NE marker expression in such tumors. In these locations, the diagnostic criteria are therefore different (in terms of extension of the NE component and methods to assess it) from those of the digestive system tumors (MANEC).

A controversial issue is the presence of NE differentiation in conventional non-NE carcinomas as determined by the expression of NE immunohistochemical markers, in the absence of a corresponding recognizable NE morphology [42]. In several organs, such as prostate, lung, colon–rectum, and stomach, there are no specific definitions for adenocarcinomas having a fraction of NE-differentiated cells. Indeed, this event is relatively common in the above listed locations, although it is of limited clinical significance, at least to our current knowledge, with the possible exception of the prostate gland. In this latter, NE-differentiated tumors are generally identified by means of chromogranin A immunostaining, which defines a more or less represented NE cell population admixed with exocrine (PSA positive) cells in neoplastic acini or cords. The event is more common in high Gleason grade and high-stage tumors and has been associated to a worse prognosis [43]. Recent data indicate that the presence of a NE-differentiated component in treatment-naive prostate cancer patients is predictive of a poor response to androgen-deprivation therapy (rather than prognostic) [44], thus highlighting the possible importance of determining the presence of NE-differentiated tumor clones in prostate cancer for therapeutic purposes. In practical terms, we generally investigate chromogranin A expression in both needle biopsy or surgical specimens in the presence of adenocarcinomas having a Gleason grade 8 or higher (an exception being those cases associated to high serum levels of chromogranin A, as reported by the clinicians, for whom NE differentiation is analyzed in all cases). However, the clinical usefulness of this determination and a standardized categorization of relevant cut-offs for chromogranin A positivity need to be further evaluated prospectively. Previous observations [43, 45, 46] that 1neuroendocrine differentiation is not a stable phenotype being destined to increase in the natural history of the disease as a consequence of systemic treatments (androgen deprivation in particular) add difficulties in the interpretation of the clinical significance of this phenomenon.

To summarize, a mixed exocrine and endocrine carcinoma is identified in GEP tumors in the presence of at least 30% for each tumor component, identified by morphology and supported by an appropriate immunoprofiling [9, 11]. In other organs, the diagnostic criteria are different and merge with the concept of divergent NE differentiation in morphologically non-NE carcinomas.

FAQ 10: are prognostic factors other than Ki-67 to be assessed in all NETs?

Answer: NO (or not yet). This is a tentative answer and does not take into account Ki-67 determination, which has already been dealt with above. With regard to other markers having prognostic significance, none has entered in the routine practice, yet. Nevertheless, for some of them a positive or negative association with prognosis has been demonstrated in NETs from different organs. One of the last entries of the list is Pax8, which was found predominantly expressed by benign well-differentiated 1pancreatic NETs (as opposed to ileal NETs which are negative, thus serving as a diagnostic marker, as well). In addition, Pax8 was shown to bear prognostic implications, being significantly reduced in "uncertain behavior" and in malignant well-differentiated pancreatic NETs and NE carcinomas [47]. Earlier reports associated various other markers (CK19, CD99, p27, cyclin E, GLUT-1, TSC2, angiopoietin-2, etc.) to an unfavorable prognosis of GEP and/or lung NETs, but their use is still far from entering the daily practice.

To summarize, to date, there are no single markers bearing relevant prognostic implications and the most accurate prognostic stratification derives from clinicopathological data [48] including gross and microscopic evaluations (tumor type, grading, staging), according to the ENETS guidelines [7].

FAQ 11: is the analysis of predictive markers of response to therapy always required?

Answer: NO, only upon request by the clinicians. Whenever chemotherapy or biotherapies are to be administrated, some predictive markers of response may be determined in the tumor tissue, assessing the expression levels of target molecules of specific drugs. In our view, the pathologist must be guided by the clinician in this specific area, and the search for predictive markers

has to be selective and performed by highly experienced laboratories, according to the specific targets. In the field of NETs, biotherapy with somatostatin analogs may take advantage from a combined morpho-functional pre-treatment investigation, resulting from octreotide scintigraphy (which provides functional data on the somatostatin receptors expressed by tumor cells) and tissue determination of the various somatostatin receptor subtypes by means of immunohistochemistry or gene expression analysis. These latter options provide a map of which receptor subtype is expressed by each single tumor that is correlated with in vivo imaging and response to somatostatin analogs treatment [49], thus possibly helping in the selection of patients to be addressed to the most appropriate somatostatin analog-based treatment.

Recent data indicate that intracellular signaling pathways are variably active in NETs, such as those involving mTOR, and these can be targeted by specific inhibitors of different molecules implicated in the intracellular cascade [50]. The expression profile of activated forms of mTOR and of the downstream molecules associated to its activation has been investigated in pancreatic [51] and pulmonary [52] NETs, and their expression levels seem to be associated to response to mTOR inhibition, at least in the lung [50].

In the case of aggressive and/or rapidly progressing NETs, chemotherapy protocols are required and some target enzymes or genes are known to be associated to specific drugs (e.g., ERCC1 for platinum, topoisomerase IIα for etoposide, thymidilate synthase for antifolates, etc.). In both GEP and lung NETs, low levels of thymidilate synthase were detected in well-differentiated NETs, only (as opposed to high grade carcinomas) and the expression levels were associated to patients' response to 5-FU [53]. From a practical point of view, the pathologist must be aware of the existence of predictive markers of response also in the field of NETs, but their determination is not performed on a routine basis, requires specifically equipped laboratories, and is to be requested and guided by the clinicians.

Practical conclusion

From the above summarized FAQs and tentative answers, a final surgical pathology report of a NET will therefore necessarily have to encompass all the following information:

Diagnosis: site-specific WHO classification terminology (state which)

Relevant pathological features: depth of invasion, size, mitotic count, vascular/nerve invasion, capsular penetration (if applicable), necrosis, associated precursor lesions, other associated diseases/features

Tumor grade: ENETS, AJCC, WHO

Tumor stage: ENETS, AJCC, WHO (use all systems, when different)

Immunoprofile: NE marker panel (mandatory), Ki-67 (mandatory), hormonal production (optional), prognostic and predictive markers of response to therapy (upon request)

Molecular markers: germline mutations screening (if appropriate), molecular markers predictive of response to therapy (upon request)

Acknowledgments Supported by grants from the Italian Ministry of University (Rome), and the University of Turin (to MV and MP), and UCSC (to GR).

Conflict of interests The authors have no conflicts of interest to declare with regard to the topics covered in this paper.

References

1. Yao JC, Hassan M, Phan A et al (2008) One hundred years after "carcinoid": epidemiology of and prognostic factors for neuroendocrine tumors in 35, 825 cases in the United States. J Clin Oncol 26(18):3063–3072
2. Modlin IM, Moss SF, Chung DC, Jensen RT, Snyderwine E (2008) Priorities for improving the management of gastroenteropancreatic neuroendocrine tumors. J Natl Cancer Inst 100 (18):1282–1289
3. Righi L, Volante M, Rapa I, Scagliotti GV, Papotti M (2007) Neuroendocrine tumours of the lung. A review of relevant pathological and molecular data. Virchows Arch 451(Suppl 1):S51–S59
4. Modlin IM, Oberg K, Chung DC et al (2008) Gastroenteropancreatic neuroendocrine tumours. Lancet Oncol 9(1):61–72
5. Klimstra DS, Modlin IR, Coppola D, Lloyd RV, Suster S (2010) The pathologic classification of neuroendocrine tumors: a review of nomenclature, grading, and staging systems. Pancreas 39 (6):707–712
6. Ploeckinger U, Kloeppel G, Wiedenmann B, Lohmann R (2009) The German NET-registry: an audit on the diagnosis and therapy of neuroendocrine tumors. Neuroendocrinology 90(4):349–363
7. Kloppel G, Couvelard A, Perren A et al (2009) ENETS Consensus Guidelines for the Standards of Care in Neuroendocrine Tumors: towards a standardized approach to the diagnosis of gastroenteropancreatic neuroendocrine tumors and their prognostic stratification. Neuroendocrinology 90(2):162–166
8. Klimstra DS, Modlin IR, Adsay NV et al (2010) Pathology reporting of neuroendocrine tumors: application of the Delphic consensus process to the development of a minimum pathology data set. Am J Surg Pathol 34(3):300–313
9. Solcia E, Kloppel G, Sobin L (2000) Histological typing of endocrine tumors. World Health Organization International Histological Classification of Tumors. Springer, Berlin
10. Travis WD, Brambilla E, Muller-Hermelink HK, Harris CC (2004) Tumours of the lung, pleura, thymus and heart. World Health Organization Classification Tumours. Pathology and genetics. IARC Press, Lyon
11. Bosman FT, Carneiro F, Hruban RH, Theise ND (2010) Tumors of the digestive system. World Health Organization Classification of Tumours. Pathology and genetics. IARC Press, Lyon
12. DeLellis RA, Lloyd RV, Heitz PU (2004) Tumors of endocrine organs. World Health Organization Classification of Tumors. Pathology and genetics. IARC Press, Lyon

13. Asamura H, Kameya T, Matsuno Y et al (2006) Neuroendocrine neoplasms of the lung: a prognostic spectrum. J Clin Oncol 24 (1):70–76
14. Righi L, Volante M, Tavaglione V et al (2010) Somatostatin receptor tissue distribution in lung neuroendocrine tumours: a clinicopathologic and immunohistochemical study of 218 'clinically aggressive' cases. Ann Oncol 21(3):548–555
15. Skov BG, Krasnik M, Lantuejoul S, Skov T, Brambilla E (2008) Reclassification of neuroendocrine tumors improves the separation of carcinoids and the prediction of survival. J Thorac Oncol 3 (12):1410–1415
16. Cheuk W, Chan JK (2001) Thyroid transcription factor-1 is of limited value in practical distinction between pulmonary and extrapulmonary small cell carcinomas. Am J Surg Pathol 25(4):545–546
17. Rindi G, Kloppel G, Alhman H et al (2006) TNM staging of foregut (neuro)endocrine tumors: a consensus proposal including a grading system. Virchows Arch 449(4):395–401
18. Rindi G, Kloppel G, Couvelard A et al (2007) TNM staging of midgut and hindgut (neuro) endocrine tumors: a consensus proposal including a grading system. Virchows Arch 451(4):757–762
19. Tsuta K, Raso MG, Kalhor N, Liu DD, Wistuba II, Moran CA (2011) Histologic features of low- and intermediate-grade neuroendocrine carcinoma (typical and atypical carcinoid tumors) of the lung. Lung Cancer 71(1):34–41
20. Rami-Porta R, Ball D, Crowley J et al (2007) The IASLC Lung Cancer Staging Project: proposals for the revision of the T descriptors in the forthcoming (seventh) edition of the TNM classification for lung cancer. J Thorac Oncol 2(7):593–602
21. Klöppel G, Rindi G, Perren A, Komminoth P, Klimstra DS (2010) The ENETS and AJCC/UICC TNM classifications of the neuroendocrine tumors of the gastrointestinal tract and the pancreas: a statement. Virchows Arch 456(6):595–597
22. Pape UF, Jann H, Muller-Nordhorn J et al (2008) Prognostic relevance of a novel TNM classification system for upper gastroenteropancreatic neuroendocrine tumors. Cancer 113 (2):256–265
23. Travis WD, Giroux DJ, Chansky K et al (2008) The IASLC lung cancer staging project: proposals for the inclusion of bronchopulmonary carcinoid tumors in the forthcoming (seventh) edition of the TNM classification for lung cancer. J Thorac Oncol 3(11):1213–1223
24. Scarpa A, Mantovani W, Capelli P et al (2010) Pancreatic endocrine tumors: improved TNM staging and histopathological grading permit a clinically efficient prognostic stratification of patients. Mod Pathol 23(6):824–833
25. Couvelard A, Deschamps L, Ravaud P et al (2009) Heterogeneity of tumor prognostic markers: a reproducibility study applied to liver metastases of pancreatic endocrine tumors. Mod Pathol 22 (2):273–281
26. Srivastava A, Hornick JL (2009) Immunohistochemical staining for CDX-2, PDX-1, NESP-55, and TTF-1 can help distinguish gastrointestinal carcinoid tumors from pancreatic endocrine and pulmonary carcinoid tumors. Am J Surg Pathol 33(4):626–632
27. La Rosa S, Rigoli E, Uccella S, Chiaravalli AM, Capella C (2004) CDX2 as a marker of intestinal EC-cells and related well-differentiated endocrine tumors. Virchows Arch 445(3):248–254
28. Schmitt AM, Riniker F, Anlauf M et al (2008) Islet 1 (Isl1) expression is a reliable marker for pancreatic endocrine tumors and their metastases. Am J Surg Pathol 32(3):420–425
29. Jamali M, Chetty R (2008) Predicting prognosis in gastroenteropancreatic neuroendocrine tumors: an overview and the value of Ki-67 immunostaining. Endocr Pathol 19(4):282–288
30. Ekeblad S, Skogseid B, Dunder K, Oberg K, Eriksson B (2008) Prognostic factors and survival in 324 patients with pancreatic endocrine tumor treated at a single institution. Clin Cancer Res 14 (23):7798–7803
31. Brizzi MP, Berruti A, Ferrero A et al (2009) Continuous 5-fluorouracil infusion plus long acting octreotide in advanced well-differentiated neuroendocrine carcinomas. A phase II trial of the Piemonte oncology network. BMC Cancer 9:388
32. Oberg K, Akerstrom G, Rindi G, Jelic S (2010) Neuroendocrine gastroenteropancreatic tumours: ESMO clinical practice guidelines for diagnosis, treatment and follow-up. Ann Oncol 21(Suppl 5):v223–v227
33. Oberg K, Astrup L, Eriksson B et al (2004) Guidelines for the management of gastroenteropancreatic neuroendocrine tumours (including bronchopulmonary and thymic neoplasms). Part I-general overview. Acta Oncol 43(7):617–625
34. Kaltsas GA, Besser GM, Grossman AB (2004) The diagnosis and medical management of advanced neuroendocrine tumors. Endocr Rev 25(3):458–511
35. Vilar E, Salazar R, Perez-Garcia J, Cortes J, Oberg K, Tabernero J (2007) Chemotherapy and role of the proliferation marker Ki-67 in digestive neuroendocrine tumors. Endocr Relat Cancer 14 (2):221–232
36. O'Toole D, Couvelard A, Rebours V et al (2010) Molecular markers associated with response to chemotherapy in gastro-enteropancreatic neuroendocrine tumors (GEP). Endocr Relat Cancer 17 (4):847–856
37. Klöppel G, Anlauf M, Raffel A, Perren A, Knoefel WT (2008) Adult diffuse nesidioblastosis: genetically or environmentally induced? Hum Pathol 39(1):3–8
38. Tang LH, Shia J, Soslow RA et al (2008) Pathologic classification and clinical behavior of the spectrum of goblet cell carcinoid tumors of the appendix. Am J Surg Pathol 32(10):1429–1443
39. Volante M, Righi L, Asioli S, Bussolati G, Papotti M (2007) Goblet cell carcinoids and other mixed neuroendocrine/nonneuroendocrine neoplasms. Virchows Arch 451(Suppl 1):S61–S69
40. Tavassoli FA, Devilee P (2003) Tumours of the breast and female genital organs. World Health Organization Classification of Tumours. Pathology and genetics. IARC Press, Lyon
41. Righi L, Sapino A, Marchio C, Papotti M, Bussolati G (2010) Neuroendocrine differentiation in breast cancer: established facts and unresolved problems. Semin Diagn Pathol 27(1):69–76
42. Volante M, Rindi G, Papotti M (2006) The grey zone between pure (neuro)endocrine and non-(neuro)endocrine tumours: a comment on concepts and classification of mixed exocrine-endocrine neoplasms. Virchows Arch 449(5):499–506
43. Berruti A, Mosca A, Porpiglia F et al (2007) Chromogranin A expression in patients with hormone naive prostate cancer predicts the development of hormone refractory disease. J Urol 178(3 Pt 1):838–843
44. Berruti A, Bollito E, Cracco CM et al (2010) The prognostic role of immunohistochemical chromogranin a expression in prostate cancer patients is significantly modified by androgen-deprivation therapy. Prostate 70(7):718–726
45. Sciarra A, Monti S, Gentile V et al (2003) Variation in chromogranin A serum levels during intermittent versus continuous androgen deprivation therapy for prostate adenocarcinoma. Prostate 55(3):168–179
46. Yuan TC, Veeramani S, Lin MF (2007) Neuroendocrine-like prostate cancer cells: neuroendocrine transdifferentiation of prostate adenocarcinoma cells. Endocr Relat Cancer 14(3):531–547
47. Long KB, Srivastava A, Hirsch MS, Hornick JL (2010) PAX8 Expression in well-differentiated pancreatic endocrine tumors: correlation with clinicopathologic features and comparison with gastrointestinal and pulmonary carcinoid tumors. Am J Surg Pathol 34(5):723–729
48. Durante C, Boukheris H, Dromain C et al (2009) Prognostic factors influencing survival from metastatic (stage IV) gastroenteropancreatic well-differentiated endocrine carcinoma. Endocr Relat Cancer 16(2):585–597

49. Volante M, Brizzi MP, Faggiano A et al (2007) Somatostatin receptor type 2A immunohistochemistry in neuroendocrine tumors: a proposal of scoring system correlated with somatostatin receptor scintigraphy. Mod Pathol 20(11):1172–1182
50. Yao JC, Phan AT, Chang DZ et al (2008) Efficacy of RAD001 (everolimus) and octreotide LAR in advanced low- to intermediate-grade neuroendocrine tumors: results of a phase II study. J Clin Oncol 26(26):4311–4318
51. Missiaglia E, Dalai I, Barbi S et al (2010) Pancreatic endocrine tumors: expression profiling evidences a role for AKT-mTOR pathway. J Clin Oncol 28(2):245–255
52. Righi L, Volante M, Rapa I et al (2010) Mammalian target of rapamycin signaling activation patterns in neuroendocrine tumors of the lung. Endocr Relat Cancer 17(4):977–987
53. Ceppi P, Volante M, Ferrero A et al (2008) Thymidylate synthase expression in gastroenteropancreatic and pulmonary neuroendocrine tumors. Clin Cancer Res 14(4):1059–1064

Virchows Arch (2011) 458:403–411
DOI 10.1007/s00428-011-1058-1

ORIGINAL ARTICLE

Inflammation in gastric adenocarcinoma of the cardia: how do EBV infection, Her2 amplification and cancer progression influence tumor-infiltrating lymphocytes?

Matthias Haas · Maike Büttner · Tilman T. Rau · Rainer Fietkau · Gerhard G. Grabenbauer · Luitpold V. Distel

Received: 28 September 2010 / Revised: 11 January 2011 / Accepted: 10 February 2011 / Published online: 26 February 2011
© Springer-Verlag 2011

Abstract Tumor-infiltrating lymphocytes (TILs) in gastric adenocarcinoma show a strong compartmentalization with high numbers of lymphocytes in the stroma and low intraepithelial lymphocyte counts. Our previous study has shown stromal regulatory T cells (Treg) to be associated with a beneficial outcome in intestinal type cancer of the cardia. We undertook the present study to further evaluate the immunogenic and inflammatory environment in intestinal-type gastric adenocarcinoma of the cardia. We assessed CXCR3 expression, Epstein–Barr virus (EBV) status, Her2/ERBB2 status and overexpression/amplification using tissue microarrays (immunohistochemistry and in situ hybridization) of 52 patients. The data were correlated to different TIL subset counts (CD3, CD8, GranzymeB, FoxP3 and CD20) and to infiltrating histiocytes (CD68) both in the tumor and the surrounding stromal tissue that were reported earlier. Her2/ERBB2 overexpression/amplification showed no correlation to tumor stage. Moreover, for the first time, we show here that Her2/ERBB2 overexpression/amplification has no correlation to overall or subset-specific TIL infiltration. EBV infection was seen in four cases and showed a strong association with intratumoral $CD8^+$ T cell infiltration as well as a moderate correlation to stromal $CD8^+$ T cell accumulation. Intratumoral $CD8^+$ T cell infiltration was significantly correlated to intratumoral $FoxP3^+$ Treg infiltration, and to a lesser extent, to stromal $FoxP3^+$ Treg counts. Stromal $CXCR3^+$ T cell infiltration showed an inverse correlation to T category. This highlights the importance of stromal immune processes for cancer growth and suggests a subversion of Th1 immunoresponse in cancer progression and underlines the important role of inflammation for early carcinogenesis

Keywords Gastric cancer · Cardia · EBV · CXCR3 · Regulatory T cells · Tumor-infiltrating lymphocytes

Matthias Haas and Maike Büttner contributed equally to this work.

M. Haas · R. Fietkau · G. G. Grabenbauer · L. V. Distel (✉)
Department of Radiation Oncology,
University Hospital Friedrich-Alexander-University
of Erlangen-Nuremberg,
Universitätsstr. 27,
91054 Erlangen, Germany
e-mail: Luitpold.Distel@uk-erlangen.de

M. Büttner · T. T. Rau
Institute for Pathology, University Hospital
Friedrich-Alexander-University of Erlangen-Nuremberg,
Universitätsstr. 22,
91054 Erlangen, Germany

Introduction

An important step in cancerogenesis is immunoevasion of malignant cells [1]. Recent research has focused on tumor-infiltrating lymphocytes (TILs) in different types of cancer to investigate the interplay between immune response and cancer development. TILs are considered as manifestations of host anti-tumor immunity. However, prognostic implications of TIL infiltration showed to be complex. While cytotoxic T cells (CTL) proved to be prognostically beneficial, e.g., in colorectal [2], esophageal [3] and gastric cancers [4], opposite effects were observed in nasopharyngeal carcinoma [5] and Hodgkin's lymphoma [6]. The subtype of $CD4^+/CD25^+$ regulatory T cells (Treg) can inhibit effector T cells by direct cell–cell contact or through cytokine secretion [7] and therefore has the potential to hamper host anti-tumor immunity [8]. The most specific Treg marker identified to date is the transcription factor

FoxP3 [9]. It is important to assess the different subtypes of TILs in human cancer to better understand the interaction of different inflammatory cells in the tumor milieu.

In a previous study of gastric adenocarcinoma of the cardia [10], we showed the importance of TIL in the stromal compartment and a beneficial effect of abundant stromal Treg for no evidence of disease (NED) survival. The results indicated a possible involvement of Tregs in the regulation of preneoplastic inflammation, which may be tumorigenic, and highlighted the complex immunological interactions in cancer development. The stroma surrounding gastric tumors has come into focus both in cancerogenesis and cancer progression. Modulation of the amount of stromal collagen had an impact on TIL infiltration, with increased stromal collagen impeding $CD8^+$ T cell infiltration and possibly promoting tumor escape [11].

CXCR3 is a chemokine receptor selectively expressed by T helper 1 (Th1) cells [12, 13]. Th1 cells are needed to promote the antitumoral immunoresponse of CTL. In lymphocyte-rich gastric carcinomas, a strong helper type 1-shifted immune response was recently shown [14]. These carcinomas show abundant TIL infiltration [15]. Moreover, they have a better prognosis than conventional gastric carcinomas [16, 17].

It is well established that 2–16% of gastric cancers worldwide are Epstein–Barr virus (EBV)-associated [18]. Studies for prognosis in EBV-positive gastric carcinomas showed conflicting results [19–21]. We assessed EBV status of the tumor by in situ hybridization for the EBV-encoded small RNAs (EBERs). We tried to investigate the influence of the EBV status on the surrounding immune processes. Our rationale was that the presence of viral EBV antigens might have implications for the immune reaction in the tumor environment. Moreover, a Th1-shifted immune response is considered favorable for anti-tumor immunity by promoting the CTL reaction. Therefore, we investigated the $CXCR3^+$ T cell infiltration in comparison with the CTL marker CD8 and the CTL activation marker Granzyme B.

Recently, the human epidermal growth factor receptor 2 (Her2) status of gastric carcinoma has come into focus. Some studies suggested that Her2-positive status was associated with aggressive disease and poor outcome [22, 23], yet reports yield conflicting results. The role of Her2 status for applicability of Trastuzumab-based therapy is rapidly evolving [24]. To further characterize our set of patients with regard to Her2 expression and amplification, we tested the Her2 status by means of immunohistochemistry and chromogenic in situ hybridization (CISH) following recent guidelines [25]. In vitro studies showed the immunogenicity of Her2-derived peptides in gastric cancer-specific cytotoxic T lymphocytes [26]. Moreover, in the context of CTL response, the overexpression of Her2 might be relevant, as Her2 induces anti-apoptotic pathways which mediate the cytotoxicity of CTL [27]. Therefore, an overexpression of Her2 might counteract the tumoricidal potential of CTL.

In the present study, we wanted to further investigate the interplay of immunological and pathophysiological factors in both the stromal and epithelial compartments of gastric adenocarcinoma of the cardia in a set of 52 patients we characterized previously [10]. Therefore, we tested this set of patients for $CXRC3^+$ TIL counts, EBV status and Her2 overexpression/amplification.

Material and methods

Patient selection

Between 1993 and 2004, a total of 135 patients with gastric adenocarcinoma of the cardia were admitted for primary surgical treatment at the Erlangen University Hospital. For this study, a subgroup of 52 patients was selected according to the criteria shown in Fig. 1. There were no lymphocyte-rich carcinomas included. No patient received (neo)adjuvant radiotherapy or chemotherapy. Patients with esophageal Barrett's adenocarcinoma were excluded. All cases were adenocarcinoma of the esophagogastreal junction (AEG) II and II tumors according to the classification of cancers of the gastroesophageal junction [28]. Staging was recorded according to the International Union against Cancer system (UICC 2002). Minimum follow-up was 36 months; mean follow-up was 71.2 months (median, 61.0 months; 95% CI, 54.7–57.8 months). The use of the tissue sections and the patients' survival data following patient consent was approved by the Friedrich-Alexander University Erlangen-Nuremberg ethics committee.

Tissue microarray

Paraffin-embedded tumor samples obtained from the 52 patients with gastric adenocarcinoma of the cardia were processed into a tissue microarray (TMA) using a manual tissue arrayer (MTA-1, Beecher Instruments Inc., Sun Prairie,

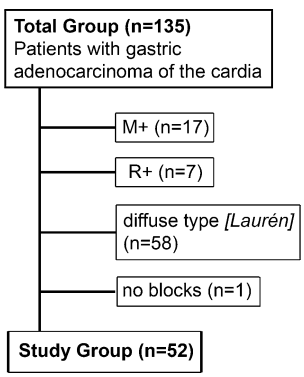

Fig. 1 Flowchart showing patient selection criteria

WI, USA). From the tumor site blocks, a total of six 1.0-mm cores from two representative areas (three cores each) were collected and arrayed in a recipient paraffin block (Fig. 2a).

Immunohistochemistry

Dewaxed paraffin sections of the TMA were rehydrated. For antigen retrieval, slides were cooked in a steam cooker (Biocarta Europe, Hamburg, Germany) at 120°C for 1 min using 0.1 M citrate buffer, pH 6.0. The method of the immunohistochemical stainings of CD3, CD8, CD20, CD68, FoxP3 and Granzyme B that have already been published has been described previously [10]. The stainings for the present study were performed with appropriately diluted primary antibodies specific for CXCR3 (CXCR3, abcam, Cambridge, UK, dilution 1:200), EBV-encoded latent membrane protein 1 (LMP1, clone CS1–4, Dako Cytomation, Hamburg, Germany, dilution 1:30), and Her2 (Her2neu, clone c-erbB2. Dako Cytomation, Hamburg, Germany, dilution 1:200) by adding the antibodies at room temperature overnight. Subsequently, an alkaline phosphatase-labeled polymer was added according to the manufacturer's instructions (Zytochem-Plus AP-Polymer Kit, Zytomed Systems, Berlin, Germany). Fast Red was

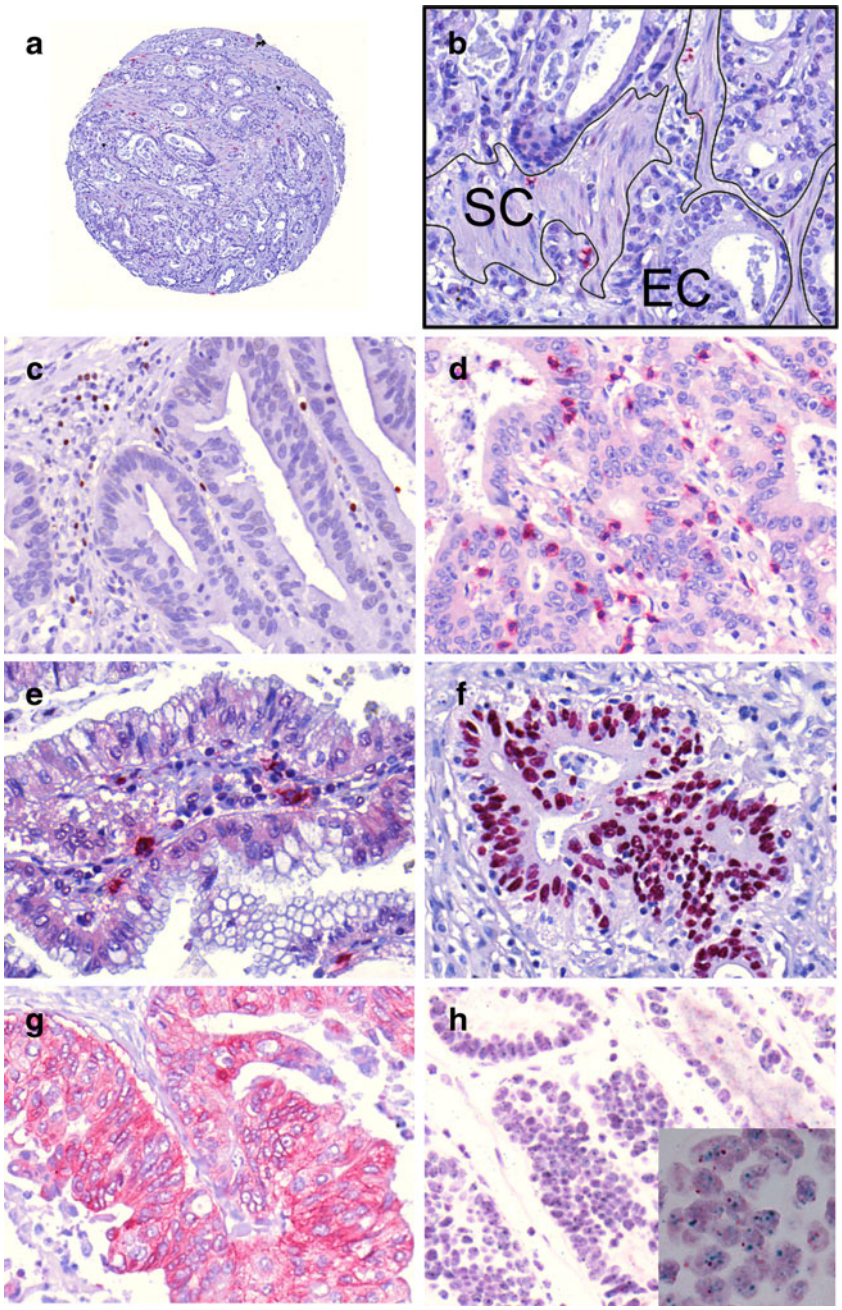

Fig. 2 Gastric cancer specimens were processed into tissue microarrays using a 1-mm needle core (**a**). The count of positively stained cells was set into relation to the surface area of the epithelial compartment (*EC*) and the stromal compartment (*SC*), respectively (**b**) using a semi-automatic image processing software (Biomas, Erlangen, Germany). Immunohistochemistry for FoxP3$^+$ (**c**), CD8$^+$ cells (**d**), and CXCR3$^+$ cells (**e**). In situ hybridization was used to detect EBER (**f**). Immunohistochemistry for Her2neu, showing Her2 3+ overexpression with strong membranous labeling (**g**). Her2neu chromogenic in situ hybridization showing a HER2/CEP17 (centromeric probe 17) ratio of ≥2 (**h**, for details, see "Materials and methods" Section)

used as a chromogen (Sigma-Aldrich, Deisenhof, Germany). Sections were counterstained with Mayer's hemalaun solution (Merck, Darmstadt, Germany).

In situ hybridization for EBER

EBV positivity was tested using in situ hybridization for the EBV-encoded small RNAs (EBER). Digoxigenin-labeled RNA probes were used. Briefly, sections were dewaxed and rehydrated, incubated in 0.2 N HCL for 20 min, rinsed with DEPC water, incubated in 0.5 mg/ml pronase per 1× PBS for 10 min, fixed in 4% paraformaldehyde for 20 min, rinsed with PBS, dehydrated in 70% ethanol and 96% ethanol, 3 min each and air-dried. The hybridization cocktail consisted of 50% formamide, 10% 20× SSC, 20% dextran sulfate, 1% yeast tRNA and the EBER probes. Hybridization was done overnight at 50°C. Sections were then washed in 50% formamide/1× SSC at 52°C for 2 h, 2× SSC at 37°C for 30 min, 20 μg/ml RNase/2× SSC at 37°C for 30 min and 2× SSC at room temperature for 10 min. The digoxigenin-labeled probes were visualized using an anti-digoxigenin monoclonal antibody (Roche, Mannheim, Germany) and an alkaline phosphatase-labeled polymer (Zytochem-Plus AP-Polymer Kit, Zytomed Systems, Berlin, Germany). Fast Red was used as a chromogen (Sigma-Aldrich, Deisenhof, Germany).

Chromogenic in situ hybridization for ERBB2

The Her2 protein is encoded by the ERBB2 gene. ERBB2 amplification was evaluated using a kit for Her2neu chromogenic in situ hybridization (CISH) (Zytovision, ZytoDot HER2/CEN17, Dual Color Probe Kit) according to the manufacturer's instructions. Because of intratumoral Her2 heterogeneity in gastric carcinomas, we assessed the areas which were also used for TIL evaluation. Thus, our results represent Her2 status in vicinity of TIL response. For scoring, we used the recommendations for a standardized testing suggested by Rüschoff et al. [24, 25]. Accordingly, only positive Her2 staining of cell clusters was regarded as Her2 overexpression. For CISH assessments, a HER2/centromeric probe 17 (CEP17) ratio of ≥2 was defined as positive for HER2 amplification; chromosome 17 polysomy was defined as ≥3 CEP17 signals on average per cell. Here, according to the guidelines mentioned above, we evaluated 20 cohesive tumor cells showing the highest gene count.

Quantification of TILs

Quantification of TILs was performed using a standard light microscope at a magnification of ×200, a CCD camera and a semi-automatic image processing software (Biomas, Erlangen, Germany). The surface areas of the epithelial and the stromal compartments were manually marked and calculated with the Biomas software. For scoring, positively stained cells were manually labeled and counted with the software. For every case, we evaluated two tumor areas from which we had retrieved three TMA cores each.

Validation of TMA method

To show the validity of our methodical approach, we tested both the cell count correlation in between the cores and between the cores and whole sections. For the former, we compared the cell counts we found in the TMA cores of the two different tumor areas. For ten cases, we evaluated whole sections of the tumor. We compared the cell counts in three different whole-section areas with the TMA core cell counts (Fig. 3).

Statistical methods

Correlation analysis was performed using Pearson's correlation coefficient (SPSS, Chicago, IL, USA). NED survival was calculated according to Kaplan–Meier. Survival curves were compared using the log-rank test. For all immunohistochemical markers, cutoff for definition of subgroups was the median value. NED survival was defined with appearance of local, nodal or distant recurrence as end points.

Results

Study group

The patients' clinical and histological characteristics are depicted in Table 1 as they were published before [10].

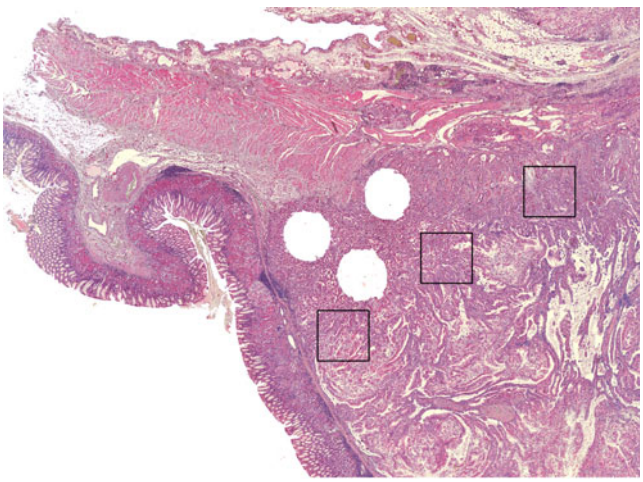

Fig. 3 Whole section of tumor with holes from TMA core-punching. The three marked areas of the tumor were evaluated for CXCR3 cell counts to assess the validity of the TMA method

Table 1 Patient characteristics (as published previously [10])

		N (%)
Factor	All patients	52 (100)
Gender	Male	40 (76.9)
	Female	12 (23.1)
TNM stage (UICC 2002)	I	20 (39.2)
	II	19 (36.5)
	III	10 (19.2)
	IV	3 (5.8)
Grading	G 1	1 (2)
	G 2	29 (56)
	G 3	21 (40)
	G 4	1 (2)
T category	T 1	12 (23)
	T 2	32 (62)
	T 3	5 (10)
	T 4	3 (6)
N category	N 0	24 (46.2)
	N +	28 (53.8)
	N 1	22 (42.3)
	N 2	6 (11.5)

Overall survival and NED survival of the study group were 53.7% and 63.7% at 5 years, respectively. Median overall survival and NED survival time for all patients were 50 months (range, 46.4–70.8) and 41.5 months (range, 43.1–68.3 months), respectively.

Validation of TMA method

The CXCR3 cell counts in the two tumor areas evaluated by TMA cores showed a high and significant correlation for both the tumoral and the stromal compartments (Pearson's correlation coefficient 0.434, p=0.001 and 0.837, p<0.0005, respectively). Furthermore, the CXCR3 cell counts in the ten representative whole sections showed a high and significant correlation to the cell counts in the TMA cores (tumoral compartment: Pearson's correlation coefficient 0.846, p=0.002, stromal compartment: Pearson's correlation coefficient 0.793, p=0.006). Thus, the TMA technique is valid for assessing the local tumor immunoenvironment.

EBV association and Her2 expression in the tumors

In situ hybridization for EBER identified four patients with EBV-associated gastric carcinomas equaling 7.7% in our study population of 52 individuals. In the EBV-positive carcinomas, all tumor cells stained positive for EBER (Fig. 2f). Staining for LMP1 was negative in all EBER-positive cases (not shown). ERBB2 overexpression (2+ and 3+) and amplification (ratio ERBB2/CEP17 ≥2) were found in seven cases (13.4%; Fig. 2g, h, Table 2). Five (9.6%) cases were 3+ and two (3.8%) 2+ with an ERBB2/CEP17 ratio of >2. Eight patients (15.4%) were 1+, and 37 (71.2%) patients scored as negative (0). No correlation of ERBB2 amplification/overexpression to tumor stage could be found. Furthermore, no correlation of Her2 status and ERBB2 amplification/overexpression to overall TIL infiltration or subset-specific infiltration could be found.

Distribution pattern of lymphocytes and implications for the tumor progression and prognosis

All TIL subsets, including $CXCR3^+$ cells, and macrophages showed higher cell counts in the stromal compartment and lower counts in the epithelial compartment (Tables 3 and 4) [10]. Stromal $FoxP3^+$ cell counts showed a significant inverse correlation to T category (Pearson's correlation coefficient −0.524, p<0.0005), thus, Treg infiltration decreased with cancer progression.

Cell counts for CXCR3 staining (Fig. 2e) are shown in Tables 3 and 4. NED survival rates in relation to stromal $CXCR3^+$ T cell invasion (high versus low) calculated by the Kaplan–Meier method did not differ significantly between these groups (not shown). There was a significant inverse correlation of the number of stromal $CXCR3^+$ cells and T category (Pearson's correlation coefficient −0.363, p=0.008; Fig. 4a). Similar to Treg, the number of $CXCR3^+$ cells decreased with cancer progression. The number of stromal $CXCR3^+$ T cells correlated significantly with $CXCR3^+$ T cell invasion in the tumor epithelium (Pearson's correlation coefficient 0.532, p<0.0005).

EBER positivity is associated with increased intratumoral and stromal CTL infiltration

EBER-positive tumors were strongly associated with an intratumoral accumulation of $CD8^+$ T cells (Pearson's correlation coefficient 0.817, p<0.0005; Fig. 4b). Additionally, these EBER-positive tumors showed a significant

Table 2 Her2 expression in tumors

ERBB2 status	Number of cases	Percentage
ERBB2 overexpression/amplification	7	13.4%
3+	5	9.6%
2+ with ERBB2/CEP17 ratio >2	2	3.8%
1+	8	15.3%
Negative	37	71.2%
Total	52	100%

Table 3 Descriptive statistics for CXCR3 cell counts per TMA core

CXCR3: total number of cells counted per core	Mean	95% confidence interval of the mean
Tumor	3.1	1.7–4.5
Stroma	96.1	68.3–126.5
Mean tumoral surface area evaluated per case (mm²)	2.2	1.86–2.57
Mean stromal surface area evaluated per case (mm²)	2.4	2.08–2.68
Ratio tumoral/stromal surface area (mean)	0.9	

correlation with stromal $CD8^+$ T cells (Pearson's correlation coefficient 0.360, $p<0.009$). No association of EBV status and intratumoral $CXCR3^+$, $CD3^+$, $CD20^+$, $CD68^+$, Granzyme B^+ or $FoxP3^+$ cells was detected.

In EBV-positive cases, intratumoral $CD8^+$ CTL correlated both with high intratumoral and stromal FoxP3 cell counts (Pearson's correlation coefficient 0.506, $p<0.0005$ and 0.312, $p=0.024$, respectively). Stromal Granzyme B^+ cells correlated with stromal $CD8^+$ cells (Pearson's correlation coefficient 0.372, $p=0.007$). Numbers of epithelial Granzyme B^+ cells did not correlate with epithelial $CD8^+$ cells (Pearson's correlation coefficient 0.068, $p=0.633$) The Granzyme $B^+/CD8^+$ ratio, as estimated for the activated CTL within the entirety of CTL, was 2.6% and 9.4% in the epithelial and the stromal compartments, respectively. In neither compartment, the Granzyme $B^+/CD8^+$ ratio differed significantly between EBER-positive and EBER-negative tumors.

Discussion

In the past it has become obvious that inflammatory cells infiltrating malignant tumors can influence the clinical outcome of the patients [2–6]. In the present study, we show a significant inverse correlation between stromal $CXCR3^+$ T cell infiltration and T stage. As CXCR3 is regarded as a Th1 marker [12, 13], it suggests a reduction of the Th1 response in the process of tumor progression. Therefore, one could argue that during progression, the tumor acquires the ability to hamper the Th1 response. The Th1 cells promote cytotoxic T cell development and macrophage activation by production of IL-2, IFNγ and other cytokines and have been implicated as mediators of the anti-tumor immunity [29]. Thus, a downregulation of the Th1 response in tumors might be one mechanism of immunoevasion used by the tumor that may be associated with an advantage for tumor growth.

Additionally, we found that the increasing T category of adenocarcinomas of the cardia is accompanied by a reduction of Treg counts. This goes in line with our previous observation that higher Treg counts are associated with a beneficial prognosis [10]. There, we argued that the presence of numerous Tregs in the context of chronic inflammation might inhibit carcinogenesis because of its capacity to decrease the production of inflammatory mediators with oncogenic potential secreted by effector lymphocytes. In distal gastric cancer inflammatory processes like *Helicobacter pylori* infection or atrophic gastritis have been implicated in the tumorigenesis. However, the role of these inflammatory stimuli in proximal gastric cancer has been questioned [30–32]. The incidence of cancer of the gastric cardia remains stable despite an overall decline in gastric cancers in developed countries [33]. This is attributed to a different risk profile for cancer of the cardia: environmental factors or chemical carcinogens (e.g., smoking and alcohol) seem to have a stronger association with cardiac carcinomas compared with more distal carcinomas [34, 35] as these yet poorly defined environmental factors probably provoke inflammation. Taken together, Treg might play an important role by modulating immunoediting and premalignant progression in the gastric cardia and thereby slowing down the tumor progression. However, additional mechanisms appear to evolve during tumor progression, which cause a failure to maintain the Treg-mediated regulation of inflammation.

Table 4 Descriptive statistics for TILs (cells per mm², data for CD3, CD8, CD20, CD68, FoxP3, Granzyme B published previously [10] and listed here for comparative reasons)

Cells per mm²	Mean		95% confidence interval of the mean		Median	
	Epithelial	Stromal	Epithelial	Stromal	Epithelial	Stromal
CD3	122.8	895.7	71.2–174.5	714.6–1076.8	40.9	752.1
CD8	114.5	424.4	51.1–178.0	299.6–549.2	21.6	212.7
CD20	18.9	438.7	0 (−0.1)–37.9	249.7–627.7	0	146.7
CD68	18.7	482.7	12.5–24.9	407.6–557.7	11.5	480.9
FoxP3	14.3	187.5	6.5–22.2	142.0–233.0	3.6	125.9
Gran. B	3.0	39.8	0.6–5.4	28.3–51.2	0	26.7
CXCR3	1.5	45.2	0.8–2.2	29.4–60.9	0.5	27.4

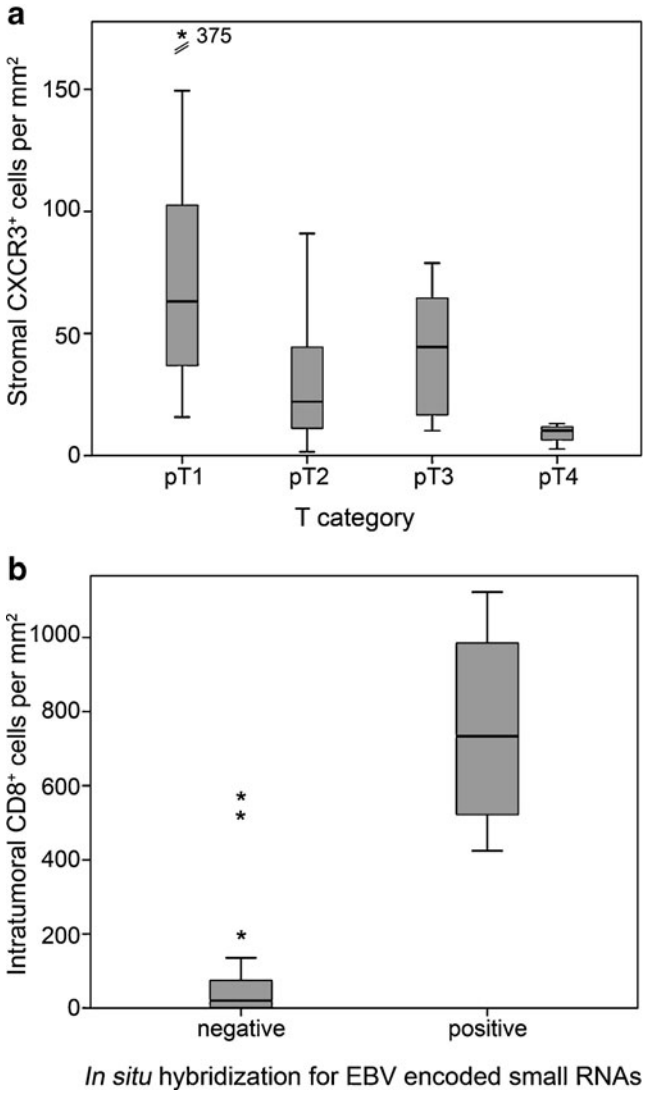

Fig. 4 Box–whisker plots showing the correlation between stromal CXCR3 count and T category (**a**) and between EBER status of the tumor and intratumoral $CD8^+$ cytotoxic T cells (**b**)

It is important to note that the here described association between Treg and $CXCR3^+$ Th1 cells has been found for stromal TIL infiltration only. The significance of the stromal localization pattern of Tregs in gastric cancer has been described previously: Mizukami et al. found tumors with pronounced diffuse stromal FoxP3 infiltration as compared to a predominantly peritumoral infiltration to be associated with a poor survival [36]. Our study emphasizes this significance of the tumor-surrounding stroma. In lymphocyte-rich gastric carcinomas the stroma has even been termed a "tertiary lymphoid tissue" [15, 37]. In these cancers, a strong Th1-shifted immune response was noted [14], which might account for their better prognosis as compared to conventional cancers [16]. Therefore, the fact that in early disease more $CXCR3^+$ Th1 cells were found in our study might implicate an inhibition of tumor progression by a Th1-dominated response. A validation of our findings in a larger cohort will be necessary.

The immunologic cross talk between epithelial and stromal compartment depends on the tumor growth pattern [11, 36]. We investigated a uniform set of intestinal-type cancers growing in glandular complexes. These differ from diffuse-type gastric carcinomas which lose their intercellular adhesions by mutations in E-cadherin [38]. The growing evidence for the importance of Her2 overexpression in intestinal type gastric cancers [22] brought us to investigate Her2 status in conjunction with TILs. Hypothetically, Her2 upregulation might be a mechanism to evade CTL-induced apoptosis in the tumor [27]. Our study shows no prognostic significance of Her2 status. To our knowledge, for the first time we investigated Her2 status in conjunction with TIL infiltration. We did not find any correlation of Her2 status to overall or subset-specific TIL infiltration.

Here, we further show an association between tumor EBV status and intratumoral accumulation of CTL. This accumulation of CTL might, for example, be caused by the presence of viral antigens as potential CTL targets. It is thought that some EBV-induced proteins might be involved in a strong T cell response, yet this response is not an effective way of killing EBV-infected cells [18]. However, in EBV-associated B cell post-transplantation disorders, $CD8^+$ cells and Granzyme B^+ T cells are able to mediate regression [39]. In our study, we could not show the presence of the EBV-encoded latent antigen, LMP1, which was representatively investigated. The accumulation of $CD8^+$ CTL in EBV^+ cases was not accompanied by high Granzyme B^+-activated CTL counts. At the same time, high numbers of intratumoral $CD8^+$ cells correlated with high intratumoral $FoxP3^+$ cell counts. This might be an indicator of a successful immunoevasion of EBV^+ tumors via the inhibition of CTL activation by an increased regulatory activity of numerous Tregs. We found a percentage of 7.7% EBV-associated gastric carcinomas in our study, which goes in line with earlier epidemiological findings that 2–16% of gastric cancers are EBV-positive [40]. However, the very low absolute number of EBV^+ carcinomas in our study makes further investigations with larger numbers of EBV-associated gastric carcinomas necessary, in order to verify our findings. In conclusion, while playing potentially an important role in carcinogenic inflammatory processes, Treg might be of lower prognostic significance in advanced stages of gastric cancer. Along with the subversion of Th1 response in cancer progression, this underlines the importance of inflammation for early carcinogenesis.

Acknowledgments We thank Birgit Meyer for excellent technical assistance.

Conflict of interest None.

References

1. Dunn GP, Old LJ, Schreiber RD (2004) The immunobiology of cancer immunosurveillance and immunoediting. Immunity 21 (2):137–148. doi:10.1016/j.immuni.2004.07.017
2. Menon AG, Janssen-van Rhijn CM, Morreau H, Putter H, Tollenaar RA, van de Velde CJ, Fleuren GJ, Kuppen PJ (2004) Immune system and prognosis in colorectal cancer: a detailed immunohistochemical analysis. Lab Invest 84(4):493–501. doi:10.1038/labinvest.37000553700055
3. Schumacher K, Haensch W, Roefzaad C, Schlag PM (2001) Prognostic significance of activated CD8(+) T cell infiltrations within esophageal carcinomas. Cancer Res 61(10):3932–3936
4. Solcia E, Klersy C, Mastracci L, Alberizzi P, Candusso ME, Diegoli M, Tava F, Riboni R, Manca R, Luinetti O (2009) A combined histologic and molecular approach identifies three groups of gastric cancer with different prognosis. Virchows Arch 455(3):197–211. doi:10.1007/s00428-009-0813-z
5. Oudejans JJ, Harijadi H, Kummer JA, Tan IB, Bloemena E, Middeldorp JM, Bladergroen B, Dukers DF, Vos W, Meijer CJ (2002) High numbers of granzyme B/CD8-positive tumour-infiltrating lymphocytes in nasopharyngeal carcinoma biopsies predict rapid fatal outcome in patients treated with curative intent. J Pathol 198(4):468–475. doi:10.1002/path.1236
6. Oudejans JJ, Jiwa NM, Kummer JA, Ossenkoppele GJ, van Heerde P, Baars JW, Kluin PM, Kluin-Nelemans JC, van Diest PJ, Middeldorp JM, Meijer CJ (1997) Activated cytotoxic T cells as prognostic marker in Hodgkin's disease. Blood 89(4):1376–1382
7. Piccirillo CA, Thornton AM (2004) Cornerstone of peripheral tolerance: naturally occurring CD4+CD25+ regulatory T cells. Trends Immunol 25(7):374–380. doi:10.1016/j.it.2004.04.009
8. Sakaguchi S, Sakaguchi N, Shimizu J, Yamazaki S, Sakihama T, Itoh M, Kuniyasu Y, Nomura T, Toda M, Takahashi T (2001) Immunologic tolerance maintained by CD25+ CD4+ regulatory T cells: their common role in controlling autoimmunity, tumor immunity, and transplantation tolerance. Immunol Rev 182:18–32. doi:1820102
9. Hori S, Nomura T, Sakaguchi S (2003) Control of regulatory T cell development by the transcription factor Foxp3. Science 299 (5609):1057–1061. doi:10.1126/science.1079490
10. Haas M, Dimmler A, Hohenberger W, Grabenbauer GG, Niedobitek G, Distel LV (2009) Stromal regulatory T-cells are associated with a favourable prognosis in gastric cancer of the cardia. BMC Gastroenterol 9:65. doi:1471-230X-9-65
11. Ohno S, Tachibana M, Fujii T, Ueda S, Kubota H, Nagasue N (2002) Role of stromal collagen in immunomodulation and prognosis of advanced gastric carcinoma. Int J Cancer 97(6):770–774. doi:10.1002/ijc.10144
12. Krieg C, Boyman O (2009) The role of chemokines in cancer immune surveillance by the adaptive immune system. Semin Cancer Biol 19(2):76–83. doi:10.1016/j.semcancer.2008.10.011
13. Syrbe U, Siveke J, Hamann A (1999) Th1/Th2 subsets: distinct differences in homing and chemokine receptor expression? Springer Semin Immunopathol 21(3):263–285
14. Ohtani H, Yoshie O (2010) Morphometric analysis of the balance between CXCR3+ T cells and FOXP3+ regulatory T cells in lymphocyte-rich and conventional gastric cancers. Virchows Arch 456(6):615–623. doi:10.1007/s00428-010-0921-9
15. Ohtani H, Jin Z, Takegawa S, Nakayama T, Yoshie O (2009) Abundant expression of CXCL9 (MIG) by stromal cells that include dendritic cells and accumulation of CXCR3+ T cells in lymphocyte-rich gastric carcinoma. J Pathol 217(1):21–31. doi:10.1002/path.2448
16. Watanabe H, Enjoji M, Imai T (1976) Gastric carcinoma with lymphoid stroma. Its morphologic characteristics and prognostic correlations. Cancer 38(1):232–243
17. Minamoto T, Mai M, Watanabe K, Ooi A, Kitamura T, Takahashi Y, Ueda H, Ogino T, Nakanishi I (1990) Medullary carcinoma with lymphocytic infiltration of the stomach. Clinicopathologic study of 27 cases and immunohistochemical analysis of the subpopulations of infiltrating lymphocytes in the tumor. Cancer 66 (5):945–952
18. Takada K (2000) Epstein–Barr virus and gastric carcinoma. Mol Pathol 53(5):255–261
19. van Beek J, zur Hausen A, Klein Kranenbarg E, van de Velde CJ, Middeldorp JM, van den Brule AJ, Meijer CJ, Bloemena E (2004) EBV-positive gastric adenocarcinomas: a distinct clinicopathologic entity with a low frequency of lymph node involvement. J Clin Oncol 22(4):664–670. doi:10.1200/JCO.2004.08.061
20. Lee JH, Kim SH, Han SH, An JS, Lee ES, Kim YS (2009) Clinicopathological and molecular characteristics of Epstein–Barr virus-associated gastric carcinoma: a meta-analysis. J Gastroenterol Hepatol 24(3):354–365. doi:10.1111/j.1440-1746.2009.05775.x
21. Song HJ, Srivastava A, Lee J, Kim YS, Kim KM, Ki Kang W, Kim M, Kim S, Park CK (2010) Host inflammatory response predicts survival of patients with Epstein–Barr virus-associated gastric carcinoma. Gastroenterology 139(1):84–92.e82. doi:10.1053/j.gastro.2010.04.002
22. Gravalos C, Jimeno A (2008) HER2 in gastric cancer: a new prognostic factor and a novel therapeutic target. Ann Oncol 19 (9):1523–1529. doi:10.1093/annonc/mdn169
23. Tanner M, Hollmen M, Junttila TT, Kapanen AI, Tommola S, Soini Y, Helin H, Salo J, Joensuu H, Sihvo E, Elenius K, Isola J (2005) Amplification of HER-2 in gastric carcinoma: association with Topoisomerase IIalpha gene amplification, intestinal type, poor prognosis and sensitivity to trastuzumab. Ann Oncol 16 (2):273–278. doi:10.1093/annonc/mdi064
24. Bang YJ, Van Cutsem E, Feyereislova A, Chung HC, Shen L, Sawaki A, Lordick F, Ohtsu A, Omuro Y, Satoh T, Aprile G, Kulikov E, Hill J, Lehle M, Ruschoff J, Kang YK (2010) Trastuzumab in combination with chemotherapy versus chemotherapy alone for treatment of HER2-positive advanced gastric or gastro-oesophageal junction cancer (ToGA): a phase 3, open-label, randomised controlled trial. Lancet 376(9742):687–697. doi:10.1016/S0140-6736(10)61121-X
25. Ruschoff J, Dietel M, Baretton G, Arbogast S, Walch A, Monges G, Chenard MP, Penault-Llorca F, Nagelmeier I, Schlake W, Hofler H, Kreipe HH (2010) HER2 diagnostics in gastric cancer—guideline validation and development of standardized immunohistochemical testing. Virchows Arch 457(3):299–307. doi:10.1007/s00428-010-0952-2
26. Kono K, Rongcun Y, Charo J, Ichihara F, Celis E, Sette A, Appella E, Sekikawa T, Matsumoto Y, Kiessling R (1998) Identification of HER2/neu-derived peptide epitopes recognized by gastric cancer-specific cytotoxic T lymphocytes. Int J Cancer 78(2):202–208. doi:10.1002/(SICI)1097-0215(19981005)78:2<202::AID-IJC14>3.0.CO;2-C
27. Kiessling R, Wei WZ, Herrmann F, Lindencrona JA, Choudhury A, Kono K, Seliger B (2002) Cellular immunity to the Her-2/neu protooncogene. Adv Cancer Res 85:101–144
28. Stein HJ, Feith M, Siewert JR (2000) Cancer of the esophagogastric junction. Surg Oncol 9(1):35–41. doi:S0960-7404(00)00021-9
29. Pellegrini P, Berghella AM, Del Beato T, Cicia S, Adorno D, Casciani CU (1996) Disregulation in TH1 and TH2 subsets of CD4+ T cells in peripheral blood of colorectal cancer patients and involvement in cancer establishment and progression. Cancer Immunol Immunother 42(1):1–8
30. Hansen S, Vollset SE, Derakhshan MH, Fyfe V, Melby KK, Aase S, Jellum E, McColl KE (2007) Two distinct aetiologies of cardia cancer; evidence from premorbid serological markers of gastric atrophy and *Helicobacter pylori* status. Gut 56(7):918–925. doi:10.1136/gut.2006.114504

31. Siman JH, Engstrand L, Berglund G, Forsgren A, Floren CH (2007) *Helicobacter pylori* and CagA seropositivity and its association with gastric and oesophageal carcinoma. Scand J Gastroenterol 42(8):933–940. doi:10.1080/00365520601173863
32. Tajima Y, Nakanishi Y, Yoshino T, Kokawa A, Kusano M, Shimoda T (2001) Clinicopathological study of early adenocarcinoma of the gastric cardia: comparison with early adenocarcinoma of the distal stomach and esophagus. Oncology 61(1):1–9. doi:ocl61001
33. Powell J, McConkey CC (1990) Increasing incidence of adenocarcinoma of the gastric cardia and adjacent sites. Br J Cancer 62 (3):440–443
34. Sarbia M, Becker KF, Hofler H (2004) Pathology of upper gastrointestinal malignancies. Semin Oncol 31(4):465–475. doi: S0093775404002416
35. Kalish RJ, Clancy PE, Orringer MB, Appelman HD (1984) Clinical, epidemiologic, and morphologic comparison between adenocarcinomas arising in Barrett's esophageal mucosa and in the gastric cardia. Gastroenterology 86(3):461–467. doi:S0016508584000615
36. Mizukami Y, Kono K, Kawaguchi Y, Akaike H, Kamimura K, Sugai H, Fujii H (2008) Localisation pattern of Foxp3+ regulatory T cells is associated with clinical behaviour in gastric cancer. Br J Cancer 98(1):148–153. doi:10.1038/sj.bjc.6604149
37. Aloisi F, Pujol-Borrell R (2006) Lymphoid neogenesis in chronic inflammatory diseases. Nat Rev Immunol 6(3):205–217. doi:10.1038/nri1786
38. Becker KF, Atkinson MJ, Reich U, Becker I, Nekarda H, Siewert JR, Hofler H (1994) E-cadherin gene mutations provide clues to diffuse type gastric carcinomas. Cancer Res 54(14):3845–3852
39. Krenauer A, Moll A, Ponisch W, Schmitz N, Niedobitek G, Niederwieser D, Aigner T (2010) EBV-associated post-transplantation B-cell lymphoproliferative disorder following allogenic stem cell transplantation for acute lymphoblastic leukaemia: tumor regression after reduction of immunosuppression—a case report. Diagn Pathol 5:21. doi:10.1186/1746-1596-5-21
40. Sugiura M, Imai S, Tokunaga M, Koizumi S, Uchizawa M, Okamoto K, Osato T (1996) Transcriptional analysis of Epstein–Barr virus gene expression in EBV-positive gastric carcinoma: unique viral latency in the tumour cells. Br J Cancer 74(4):625–631

Virchows Arch (2011) 458:413–419
DOI 10.1007/s00428-011-1046-5

ORIGINAL ARTICLE

PDCD4 nuclear loss inversely correlates with miR-21 levels in colon carcinogenesis

Matteo Fassan · Marco Pizzi · Luciano Giacomelli · Claudia Mescoli · Kathrin Ludwig · Salvatore Pucciarelli · Massimo Rugge

Received: 1 December 2010 / Revised: 8 January 2011 / Accepted: 11 January 2011 / Published online: 29 January 2011
© Springer-Verlag 2011

Abstract Programmed cell death 4 (*PDCD4*) has recently been demonstrated to be a new tumor suppressor gene involved in colon carcinogenesis. PDCD4 immunohistochemical expression was assessed in 300 polypoid lesions of the colon mucosa (50 hyperplastic polyps [HP], 50 serrated adenomas [SA], 50 tubular adenomas with low-grade-intraepithelial neoplasia [LG-IEN], 50 tubular adenomas with high-grade-IEN [HG-IEN]), and in 50 colon adenocarcinomas (CRC). As normal controls, we considered 50 biopsy samples obtained from patients with irritable bowel syndrome (N). We further investigated *PDCD4* messenger RNA (mRNA) levels by quantitative real-time polymerase chain reaction (PCR) in a different series of N, LG-IEN, HG-IEN, and CRC biopsy samples. *miR-21* expression (an important *PDCD4*-expression regulator) was also determined by quantitative real-time PCR and in situ hybridization. Normal colocytes and HP featured strong PDCD4 nuclear immunostaining whereas a significantly lower PDCD4 nuclear expression was observed in dysplasia (low- and high-grade adenomas and SA) and invasive CRC. PDCD4 immunostaining and mRNA levels decreased significantly as the phenotypic changes occurring during colon carcinogenesis progressively increased ($p<0.001$). As expected, *miR-21* expression was significantly upregulated in preneoplastic/neoplastic samples, consistent with *PDCD4* downregulation. These results consistently support the use of nuclear PDCD4 immunohistochemical downregulation as a novel biomarker for the diagnosis of dysplastic/neoplastic lesions in colon biopsy samples.

Keywords *PDCD4* · *miR-21* · Tumor suppressor gene · Colon biopsy · Colon cancer

M. Fassan · M. Pizzi · C. Mescoli · K. Ludwig · M. Rugge (✉)
Department of Medical Diagnostic Sciences & Special Therapies, Surgical Pathology & Cytopathology Unit,
University of Padua-Italy,
Padua, Italy
e-mail: massimo.rugge@unipd.it

L. Giacomelli · M. Rugge
Surgical Pathology & Cytopathology Unit,
Azienda Ospedaliera di Padova,
Padua, Italy

S. Pucciarelli
Department of Oncological and Surgical Sciences, Clinica Chirurgica II, University of Padua-Italy,
Padua, Italy

M. Rugge
Surgical Pathology Unit, Istituto Oncologico Veneto–IOV-IRCCS,
Via Aristide Gabelli, 61,
Padua 35121, Italy

Introduction

Colorectal cancer (CRC) is one of the most common malignancies of the industrialized world [1–3]. Colorectal oncogenesis is a multistep process that passes through various grades of glandular dedifferentiation (dysplastic stage) and eventually progresses to invasive adenocarcinoma [3–7]. In the adenoma–carcinoma sequence, the stepwise phenotypic shift is determined by a concurrent stepwise accumulation of genetic alterations [4].

Programmed cell death 4 (*PDCD4*) has recently been characterized as a new tumor suppressor gene involved in the apoptotic machinery, suppressing cell transformation and invasion by interacting with translation initiation factors eIF4A and eIF4G [8–18]. Molecules regulated by *PDCD4* include p21, Cdk4, ornithine decarboxylase, carbonic anhydrase II, and JNK/c-Jun/AP-1 [18]. *PDCD4*

expression is consistently downregulated in several human cancers and cancer cell lines [17, 19–26].

Different mechanisms have been implicated in *PDCD4* dysregulation. Among others, the oncogenic microRNA *miR-21* (*hsa-miR-21*) has been shown to specifically target the *PDCD4* 3′ untranslated region (3′ UTR), which negatively regulates *PDCD4* expression [19, 23].

In their seminal work, Mudduluru and colleagues demonstrated a significant *PDCD4* downregulation in both colonic adenomas and CRC [17], and we have recently added evidence that *PDCD4* is more frequently downregulated in metastases than in their corresponding primary CRCs [23]. *PDCD4* expression has also been shown to be an independent prognostic factor in CRC patients [17].

Few translational studies have explored the use of *PDCD4* expression to support routine biopsy findings in colon precancerous/cancerous lesions [18]. To investigate the diagnostic usefulness of PDCD4 immunostaining in the colorectal cancer setting, the protein's expression was assessed in a series of biopsy samples representing the whole phenotypic spectrum of colon oncogenesis. We also examined *miR-21* expression levels in dysplastic/neoplastic biopsy samples by quantitative real-time PCR (qRT-PCR) and in situ hybridization (ISH).

Materials and methods

cDNA microarray analysis

The Oncomine database and gene microarray analysis tool, a repository for published cDNA microarray data (http://www.oncomine.org) [27, 28], was explored (on 03 January 2011) for *PDCD4* messenger RNA (mRNA) expression in non-neoplastic colonic tissues, colon adenomatous lesions, and primary CRC. Oncomine algorithms were used to perform a statistical analysis of the differences in *PDCD4* expression because it allows for multiple comparisons between different studies [27–29]. Only studies with analytical results with a $p<0.005$ were considered.

Patients

The cases considered in the present study were retrospectively collected from the files of the Surgical Pathology & Cytopathology Unit at the University of Padua. The institute's ethical regulations on research conducted on human tissues were followed.

In all, 360 endoscopic biopsy samples were obtained from patients with different types of sporadic colonic polyps, i.e., 50 hyperplastic polyps (HP), 50 serrated adenomas (SA), 65 tubular adenomas with low-grade intraepithelial neoplasia (LG-IEN), and 65 tubular adenomas with high-grade IEN (HG-IEN), and from 65 patients with CRC, all of them well-differentiated (G1) tumors. Another 65 normal colonic mucosa biopsy samples (N) were obtained from patients who underwent colonoscopy for irritable bowel syndrome (Clinica Chirurgica II–University of Padua). No samples were obtained from cases of familial adenomatous polyposis syndrome.

Histology and immunohistochemistry

All biopsy specimens were immediately fixed in 10% buffered formalin and embedded in paraffin. Serial histological sections 4–6 μm thick were obtained from each paraffin block selected. The histological sections were stained with hematoxylin and eosin. The original diagnosis was confirmed by histologically re-evaluating all cases. Immunohistochemical staining was done automatically (Ventana Benchmark XT system; Touchstone, AZ) [19, 25, 30] for PDCD4 (catalog #HPA001032; Atlas Antibodies, Stockholm, Sweden; 1:100) according to the manufacturer's instructions. Sections were lightly counterstained with hematoxylin. Appropriate positive and negative controls were run concurrently. In cancer samples, the presence of positive stromal and inflammatory cells served as an internal control. PDCD4 nuclear expression was jointly scored by two pathologists (MF and CM) unaware of the patients' clinical history. As described previously [17, 19], nuclear PDCD4 staining was scored on a four-tiered scale (score 0, no nuclear staining; score 1, ≥1 ≤30% positive nuclear staining; score 2, >30%≤70% positive nuclear staining; score 3, ≥71% positive nuclear staining. A total of 50 N, 50 HP, 50 SA, 50 LG-IEN, 50 HG-IEN, and 50 CRC biopsy samples were considered.

Quantitative real-time polymerase chain reaction

Formalin-fixed paraffin-embedded biopsy samples were deparaffinized with xylene at 50°C for 3 min. Total RNA extraction was done using the RecoverAll kit (Ambion Inc, Austin, TX) according to the manufacturer's instructions. qRT-PCR analysis was performed using the GeneAmp PCR 9700 thermocycler (Applied Biosystems, Foster City, CA), and gene expression levels were quantified using the ABI Prism 7900HT Sequence Detection System (Applied Biosystems), as previously described [31]. Primers' sequences for *PDCD4* were: forward 5′-ggcctccaaggagtaagacc-3′; reverse 5′-aggggtctacatggcaactg-3′. *GAPDH* was used as the internal control gene (forward 5′-aagggaaggttgctggatagg-3′; reverse 5′-cacatccacctcctccacatc-3′). The NCodeTM miRNA qRT-PCR method (Invitrogen, Carlsbad, CA) was used to detect and quantify mature *miR-21* (primer sequence: 5′-CGGTAGCTTATCAGACTGATGTTGA-3′) according to the manufacturer's instructions. Normalization

was done with the small nuclear RNA *U6B* (*RNU6B*; Invitrogen). PCR reactions were run in triplicate, including no-template controls. The data were analyzed using the comparative CT method. Biopsy samples of 10 N, 10 LG-IEN, 10 HG-IEN, and 10 CRC were considered for the qRT-PCR study.

In situ hybridization

In situ hybridization was performed using the GenPoint™ Catalyzed Signal Amplification System (DakoCytomation) according to the manufacturer's protocol. Briefly, slides were incubated at 60°C for 30 min and deparaffinized as described in [24, 32]. Sections were treated with Proteinase K (DakoCytomation) for 30 min at room temperature, rinsed several times with dH_2O, and immersed in 95% ethanol for 10 s before air-drying. The slides were pre-hybridized at 49–56°C for 1 h with mRNA ISH buffer (Ambion) before incubation overnight at 49–56°C in buffer containing the 5′-biotin-labeled *miR-21* miRCURY™ LNA detection probe (Exiqon, Woburn, MA) or the scrambled negative control probe (U6, Exiqon) at a final concentration of 200 nM. The slides were washed in both Tris-buffered saline with Tween (TBST) and GenPoint™ stringent wash solution (54°C for 30 min), then exposed to H_2O_2 blocking solution (DakoCytomation) for 20 min, and then further blocked in a blocking buffer (DakoCytomation) for 30 min before they were exposed to primary streptavidin–horseradish peroxidase (HRP) antibody, biotinyl tyramide, secondary streptavidin–HRP antibody, and DAB chromogen solutions, following the manufacturer's protocol. The slides were then briefly counterstained in hematoxylin and rinsed with TBST and water before mounting. Biopsy samples of five N, five LG-IEN, five HG-IEN, and five CRC were considered for the ISH study.

Statistical analysis

Differences and correlations between groups were tested by applying the modified Kruskal–Wallis nonparametric test for trend, Pearson's correlation, and the *t* test. *P* values <0.05 were considered significant. All statistical assessments were performed with STATA software (Stata Corporation, College Station, Texas, USA).

Results

The PDCD4 gene is downregulated in colon adenomas and CRC

PDCD4 gene expression was analyzed by checking different publicly available colon microarray studies using the Oncomine database and gene microarray data analysis tools [27, 28]. The analysis considered the mRNA expression levels for each of the studies involved. Two studies showed a significant downregulation of *PDCD4* mRNA expression levels in adenomas by comparison with normal colonic mucosa (Fig. 1a; Sabates-Bellver et al. [33], *t* test p=1.48E−16, fold change=−2.524, 32 normal and 25

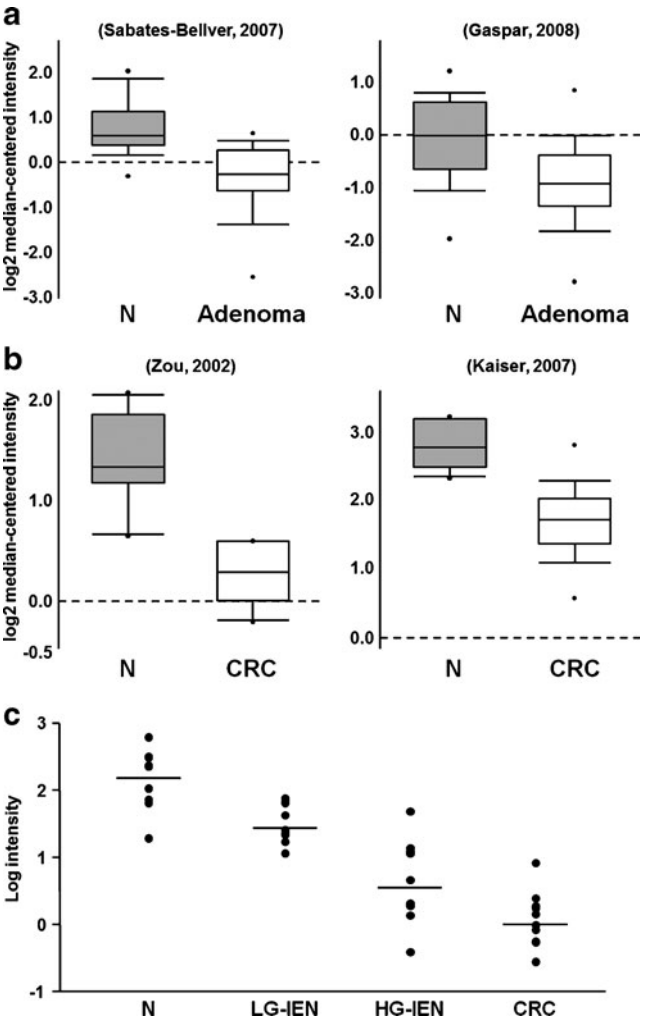

Fig. 1 *PDCD4* downregulation during colon carcinogenesis. **a–b** *PDCD4* expression (mRNA) array results of four microarray data sets [33–36] are considered; statistical significance is calculated using the Oncomine website (www.oncomine.org). **a** Box plots show differences in mRNA expression in normal colonic mucosa (*gray*) versus adenoma (*white*). Class analysis: Sabates-Bellver 2007 (*t* test p=1.48E−16, fold change=−2.524, 32 normal and 25 adenomas) [33]; Gaspar 2008 (*t* test p=2.49E−4, fold change=−1.709, 22 normal and 56 adenomas) [34]. **b** Box plots show differences in mRNA expression in normal colonic mucosa (*gray*) versus adenocarcinoma (*white*). Class analysis: Zou 2002 (*t* test p=1.91E−5; fold change=−2.230; eight normal and nine CRC) [35]; Kaiser 2007 (*t* test p=1.67E−6; fold change=−2.617; 5 normal and 89 CRC) [36]. **c** *PDCD4* mRNA levels in the present series of polypoid lesions of the colon mucosa by qRT-PCR analysis. *PDCD4* is significantly downregulated in IEN and CRC (*filled circles* represent individual samples; *horizontal lines* indicate the mean)

adenomas; Gaspar et al. [34], *t* test p=2.49E−4, fold change=−1.709, 22 normal and 56 adenomas). In two other independent data sets, a significant decrease in *PDCD4* mRNA expression levels was apparent in CRC samples (Fig. 1b; Zou el al. [35], *t* test p=1.91E−5; fold change=−2.230; eight normal and nine CRC; Kaiser et al. [36], *t* test p=1.67E−6; fold change=−2.617; 5 normal and 89 CRC). To further support these data, we investigated *PDCD4* mRNA levels in a series of dysplastic/neoplastic polypoid lesions of the colon mucosa by qRT-PCR analysis. A significant *PDCD4* downregulation was found in samples of LG-IEN (with a 0.7-fold decrease; *t* test p=0.043), HG-IEN (with a 1.5-fold decrease; *t* test p=0.001), and CRC (with a 2.1-fold decrease; *t* test p<0.001; Fig. 1c).

Nuclear PDCD4 expression is downregulated during colon carcinogenesis and in serrated adenomas

Normal colonic mucosa biopsy samples consistently featured a strong PDCD4 expression in the nucleus coexisting with a moderate–strong cytoplasmic PDCD4 expression (Fig. 2a–c). In normal and cancer tissue samples, non-cancerous and non-epithelial cells (fibroblasts, lymphocytes, smooth muscle cells, and endothelia) always featured PDCD4 nuclear expression (considered as a positive internal control; not considered for immunohistochemistry (IHC) scoring) [17, 19, 25, 26, 37].

Hyperplastic polyps retained a PDCD4 expression that was strong in the nuclei and moderate in the cytoplasm (Fig. 2d). Nuclear PDCD4 loss was consistently observed

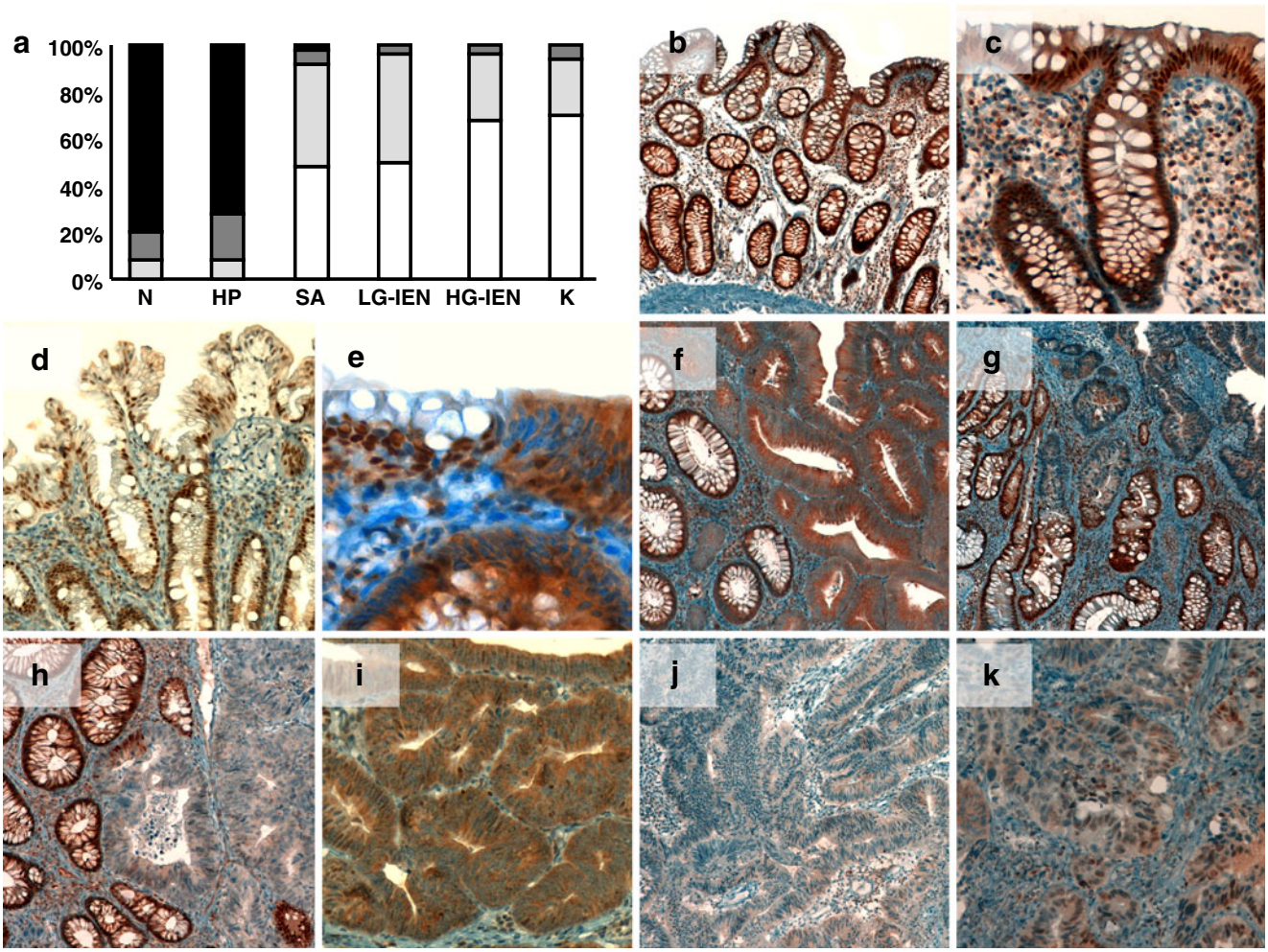

Fig. 2 Representative PDCD4 immunostaining of non-cancerous colonic tissues and preneoplastic/neoplastic lesions of carcinogenic cascade. **a** Immunohistochemical scores of nuclear PDCD4 in the different histological lesions (*white* score 0, *light gray* score 1, *dark gray* score 2; *black* score 3). Nuclear PDCD4 staining was significantly lower in preneoplastic/neoplastic lesions (i.e., SA, LG-IEN, HG-IEN, and K) than in normal tissues or hyperplastic polyps (p<0.001). **b–c** In native colonic mucosa, colocytes featured strong nuclear and moderate–strong cytoplasmic staining. **d** HP maintain strong nuclear and weak cytoplasmic immunostaining. Note the presence in SA (**e**), LG-IEN (**f–g**), and HG-IEN (**h**) samples of residual normal colocytes with PDCD4-positive nuclei. **i–j** Little or no cytoplasmic immunostaining was associated to HG-IEN. **k** CRC showing scattered PDCD4-positive nuclei (original magnifications, ×20 and ×40)

in dysplastic (LG-IEN and HG-IEN) and neoplastic samples (Kruskal–Wallis, $p<0.001$; Fig. 2). In particular, samples of LG-IEN showed moderate–strong cytoplasmic staining coexisting with a significant nuclear PDCD4 downregulation; HG-IEN and CRC biopsy samples showed little or no cytoplasmic protein expression (Fig. 2f–k). In SA, the dysplastic component of the polypoid lesions featured much the same PDCD4 expression as in LG-IEN (Fig. 2e).

Overall, PDCD4 nuclear downregulation (i.e., scores 0 and 1) consistently discriminates dysplastic/neoplastic (scores 0–1, $n=188$; scores 2–3, $n=12$) versus non-dysplastic/neoplastic (scores 0–1, $n=8$; scores 2–3, $n=92$) samples (sensibility=94%; specificity=92%).

miR-21 is overexpressed in preneoplastic and neoplastic polypoid lesions of the colon mucosa

The oncomiR *miR-21* directly regulates *PDCD4* by binding to its 3′ UTR target sequence with a 100% match sequence at nt228–249 [19]. We investigated *miR-21* expression in dysplastic and neoplastic polypoid lesions of the colon mucosa by qRT-PCR analysis. A significant *miR-21* upregulation was found in samples of LG-IEN (with a 1.5-fold increase; *t* test $p=0.007$), HG-IEN (with a 2.2-fold increase; *t* test $p=0.001$), and CRC (with a 4.8-fold increase; *t* test $p<0.001$; Fig. 3a). To further confirm these data, we investigated *miR-21* expression by ISH, which confirmed a consistently significant overexpression in IEN and CRC samples (Fig. 3b). miR-21 expression was identifiable as a granular brown cytoplasmic staining consistently expressed by cancerous epithelia.

As expected, an inverse correlation ($r=-0.3611$) between the expression of *miR-21* and *PDCD4* was observed among the 40 biopsy samples analyzed by qRT-PCR (Fig. 3c).

Discussion

PDCD4 has been characterized as a new tumor suppressor gene that is downregulated in several human malignancies, including CRC [18]. In their seminal study, Göke and colleagues reported loss of nuclear PDCD4 staining in six of seven CRC specimens [26]. Following this preliminary observation, Mudduluru and colleagues investigated the usefulness of PDCD4 as a diagnostic marker in the adenoma/carcinoma sequence [17]. They did not consider the grade of the dysplastic lesions examined, but they found a significant downregulation in PDCD4 expression in adenoma and CRC samples, and they suggested that PDCD4 has promise as a marker of progression in the process of colon mucosa transformation. In a series of 71 CRC patients, they also found loss of total or nuclear PDCD4, an independent predictor of disease-specific and overall survival [17]. Taken together, the available information points to a role for *PDCD4* as a key colonic mucosa regulatory gene.

We explored the immunohistochemical expression of PDCD4 in a series of sporadic colonic polypoid lesions and CRC biopsy samples. As expected, we found that PDCD4 nuclear expression decreased significantly as the lesions became dedifferentiated. In fact, normal colonic mucosa

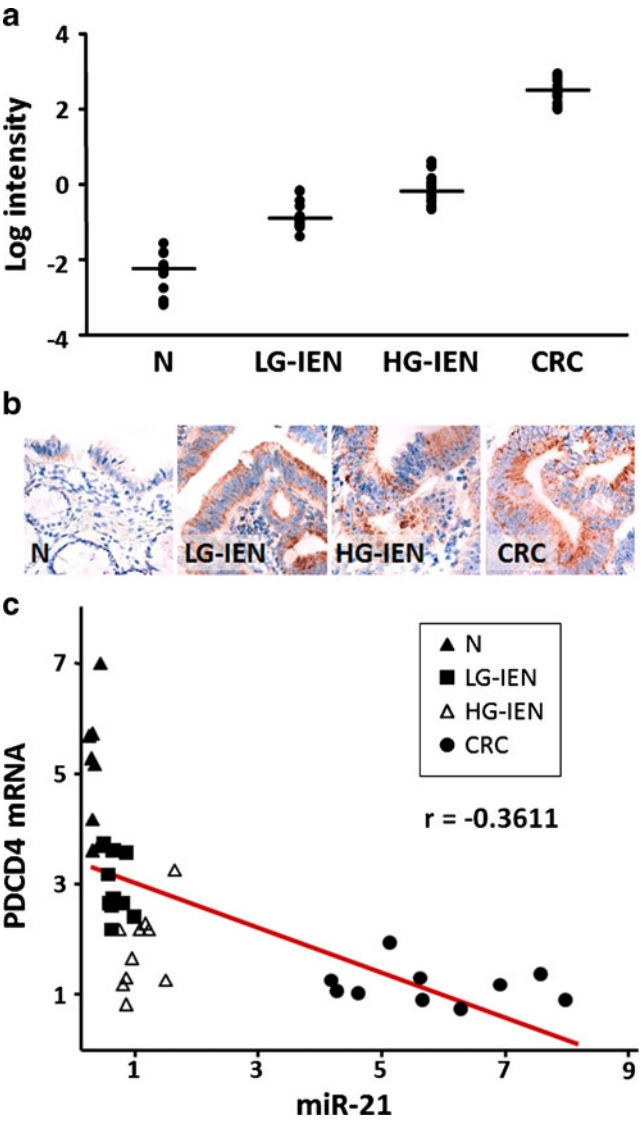

Fig. 3 *miR-21* is overexpressed in dysplastic and neoplastic polypoid lesions of the colonic mucosa. **a** Different *miR-21* expressions between different biopsy samples by qRT-PCR analysis. *miR-21* was significantly upregulated in IEN lesions and CRC. Each *filled circle* represents an individual sample; *horizontal lines* indicate the mean. **b** Representative examples of *miR-21* expression in normal colonic epithelium and polypoid lesions by ISH analysis. The presence of *miR-21* is revealed by a granular brown stain. (original magnifications, ×20 and ×40). **c** Inverse correlation between the expression of *miR-21* and *PDCD4* among the 40 biopsy samples analyzed by qRT-PCR. (*symbols* represent individual samples)

and HP biopsy samples consistently featured a strong nuclear and moderate–strong cytoplasmic PDCD4 expression (Fig. 2a–d) whereas LG-IEN and HG-IEN lesions showed a weak–moderate cytoplasmic immunostaining. A similar nuclear-to-cytoplasmic shift was documented by Mudduluru and colleagues in the adenoma–carcinoma sequence [17]. We found this shift in the Barrett's esophagus setting too, with a significant and consistent decrease in nuclear PDCD4 in both dysplastic and neoplastic samples [19]. The reasons behind this particular subcellular reallocation are only partially understood. In vitro studies have shown that, under normal growth conditions, PDCD4 is located mainly in the nucleus, while it moves to the cytoplasm on serum withdrawal [8]. The nuclear-to-cytoplasmic shift documented in preneoplastic/neoplastic lesions could thus theoretically result from epigenetic (and/or genetic) mutations.

Serrated adenomas show characteristic molecular changes not commonly seen in traditional colorectal adenomas, and they probably progress to colorectal cancer via a different pathway (the so-called serrated neoplasia pathway) [38], so we decided to study the "serrated" dysplastic component in terms of PDCD4 expression. The similar nuclear loss observed in SA and IEN lesions would suggest that PDCD4 is associated with a major tumor suppressor function that is soon lost in different pathways of carcinogenesis.

Colonoscopy has acquired a central role in CRC detection and prevention, thanks to its impact on the adenoma–carcinoma sequences (the "traditional" and the "serrated"). Observational data support a role for colonoscopy and polypectomy in reducing the incidence of CRC and the related mortality [7, 39]. Dysplasia (particularly high-grade dysplasia) is still the fundamental element in cancer prediction for most preneoplastic GI conditions, and it is an independent marker of cancer risk [40]. The histological evidence of dysplasia may be very subtle and difficult to diagnose, however, even in the presence of well-established diagnostic criteria, because of the intrinsic characteristics of biopsy samples (i.e., shrinkage, fragmentation, and "burning"). Pathologists must therefore strive to reduce the uncertainties in the diagnosis of dysplastic lesions and to improve the management of CRC-prone asymptomatic patients. From the practical standpoint, PDCD4 immunohistochemical analysis could be valuable in discriminating between dysplastic and non-dysplastic lesions, and between SA and HP. PDCD4 (and its nuclear staining) may therefore be associated with more traditional IHC markers in the routine histological assessment of colonic biopsy samples.

miR-21 has been described as being upregulated in CRC and an important regulator of *PDCD4* expression [16]. Unlike most mRNAs, moreover, miRNAs are long-lived in vivo and very stable in vitro, a feature that might be crucial in a clinical setting and enables the analysis of formalin-fixed, paraffin-embedded samples. Confirming these data, we found *miR-21* significantly upregulated in IEN and CRC biopsy samples, pointing to a potential diagnostic role for this miR in discriminating neoplastic from non-neoplastic lesions.

In conclusion, our findings further support the primary role of *PDCD4* as a tumor suppressor gene of the colonic mucosa and consistently point to *PDCD4* being a promising additional diagnostic tool for discriminating normal colonic tissues from benign adenomas and CRC in biopsy samples. Further studies on larger series should investigate the prognostic role of PDCD4 nuclear staining in stratifying dysplastic lesions into appropriate categories of CRC evolution.

Acknowledgements This work has been partly supported by an AIRC Regional grant 2009 (assigned to M.R.). The authors are grateful to Vincenza Guzzardo, Mariangela Balistreri, Vanni Lazzarin, and Cristiano Lanza for their technical assistance.

Conflict of interest The authors declare that they have no conflict of interest.

References

1. Jemal A, Siegel R, Ward E et al (2009) Cancer statistics, 2009. CA Cancer J Clin 59:225–249
2. Cunningham D, Atkin W, Lenz HJ et al (2010) Colorectal cancer. Lancet 375:1030–1047
3. Lieberman D (2010) Progress and challenges in colorectal cancer screening and surveillance. Gastroenterology 138:2115–2126
4. Vogelstein B, Fearon ER, Hamilton SR et al (1988) Genetic alterations during colorectal tumor development. N Engl J Med 319:525–532
5. Renehan AG, O'Dwyer ST, Haboubi NJ et al (2002) Early cellular events in colorectal carcinogenesis. Colorectal Dis 4:76–89
6. Cappell MS (2008) Reducing the incidence and mortality of colon cancer: mass screening and colonoscopic polypectomy. Gastroenterol Clin North Am 37:129–160
7. Hewett DG, Kahi CJ, Rex DK (2010) Does colonoscopy work? J Natl Compr Canc Netw 8:67–76, quiz 77
8. Bohm M, Sawicka K, Siebrasse JP et al (2003) The transformation suppressor protein Pdcd4 shuttles between nucleus and cytoplasm and binds RNA. Oncogene 22:4905–4910
9. Yang HS, Cho MH, Zakowicz H et al (2004) A novel function of the MA-3 domains in transformation and translation suppressor Pdcd4 is essential for its binding to eukaryotic translation initiation factor 4A. Mol Cell Biol 24:3894–3906
10. Afonja O, Juste D, Das S et al (2004) Induction of PDCD4 tumor suppressor gene expression by RAR agonists, antiestrogen and HER-2/neu antagonist in breast cancer cells. Evidence for a role in apoptosis. Oncogene 23:8135–8145
11. Bitomsky N, Bohm M, Klempnauer KH (2004) Transformation suppressor protein Pdcd4 interferes with JNK-mediated phosphorylation of c-Jun and recruitment of the coactivator p300 by c-Jun. Oncogene 23:7484–7493
12. Zakowicz H, Yang HS, Stark C et al (2005) Mutational analysis of the DEAD-box RNA helicase eIF4AII characterizes its interaction with transformation suppressor Pdcd4 and eIF4GI. RNA 11:261–274

13. Jansen AP, Camalier CE, Colburn NH (2005) Epidermal expression of the translation inhibitor programmed cell death 4 suppresses tumorigenesis. Cancer Res 65:6034–6041
14. Dorrello NV, Peschiaroli A, Guardavaccaro D et al (2006) S6K1- and betaTRCP-mediated degradation of PDCD4 promotes protein translation and cell growth. Science 314:467–471
15. Bitomsky N, Wethkamp N, Marikkannu R et al (2008) siRNA-mediated knockdown of Pdcd4 expression causes upregulation of p21(Waf1/Cip1) expression. Oncogene 27:4820–4829
16. Carayol N, Katsoulidis E, Sassano A et al (2008) Suppression of programmed cell death 4 (PDCD4) protein expression by BCR-ABL-regulated engagement of the mTOR/p70 S6 kinase pathway. J Biol Chem 283:8601–8610
17. Mudduluru G, Medved F, Grobholz R et al (2007) Loss of programmed cell death 4 expression marks adenoma–carcinoma transition, correlates inversely with phosphorylated protein kinase B, and is an independent prognostic factor in resected colorectal cancer. Cancer 110:1697–1707
18. Allgayer H (2010) Pdcd4, a colon cancer prognostic that is regulated by a microRNA. Crit Rev Oncol Hematol 73:185–191
19. Fassan M, Pizzi M, Battaglia G et al (2010) Programmed cell death 4 (PDCD4) expression during multistep Barrett's carcinogenesis. J Clin Pathol 63:692–696
20. Chen Y, Knosel T, Kristiansen G et al (2003) Loss of PDCD4 expression in human lung cancer correlates with tumour progression and prognosis. J Pathol 200:640–646
21. Zhang H, Ozaki I, Mizuta T et al (2006) Involvement of programmed cell death 4 in transforming growth factor-beta1-induced apoptosis in human hepatocellular carcinoma. Oncogene 25:6101–6112
22. Wang Q, Sun Z, Yang HS (2008) Downregulation of tumor suppressor Pdcd4 promotes invasion and activates both beta-catenin/Tcf and AP-1-dependent transcription in colon carcinoma cells. Oncogene 27:1527–1535
23. Baffa R, Fassan M, Volinia S et al (2009) MicroRNA expression profiling of human metastatic cancers identifies cancer gene targets. J Pathol 219:214–221
24. Yamamichi N, Shimomura R, Inada K et al (2009) Locked nucleic acid in situ hybridization analysis of miR-21 expression during colorectal cancer development. Clin Cancer Res 15:4009–4016
25. Fassan M, Cagol M, Pennelli G et al (2010) Programmed cell death 4 (PDCD4) protein in esophageal cancer. Oncol Rep 24:135–139
26. Goke R, Barth P, Schmidt A et al (2004) Programmed cell death protein 4 suppresses CDK1/cdc2 via induction of p21(Waf1/Cip1). Am J Physiol Cell Physiol 287:C1541–C1546
27. Rhodes DR, Yu J, Shanker K et al (2004) ONCOMINE: a cancer microarray database and integrated data-mining platform. Neoplasia 6:1–6
28. Rhodes DR, Yu J, Shanker K et al (2004) Large-scale metaanalysis of cancer microarray data identifies common transcriptional profiles of neoplastic transformation and progression. Proc Natl Acad Sci USA 101:9309–9314
29. Xin W, Rhodes DR, Ingold C et al (2003) Dysregulation of the annexin family protein family is associated with prostate cancer progression. Am J Pathol 162:255–261
30. Rugge M, Fassan M, Clemente R et al (2008) Bronchopulmonary carcinoid: phenotype and long-term outcome in a single-institution series of Italian patients. Clin Cancer Res 14:149–154
31. Reis PP, Tomenson M, Cervigne NK et al (2010) Programmed cell death 4 loss increases tumor cell invasion and is regulated by miR-21 in oral squamous cell carcinoma. Mol Cancer 9:238
32. Fassan M, Volinia S, Palatini J et al (2011) MicroRNA expression profiling in human Barrett's carcinogenesis. Int J Cancer (in press)
33. Sabates-Bellver J, Van der Flier LG, de Palo M et al (2007) Transcriptome profile of human colorectal adenomas. Mol Cancer Res 5:1263–1275
34. Gaspar C, Cardoso J, Franken P et al (2008) Cross-species comparison of human and mouse intestinal polyps reveals conserved mechanisms in adenomatous polyposis coli (APC)-driven tumorigenesis. Am J Pathol 172:1363–1380
35. Zou TT, Selaru FM, Xu Y et al (2002) Application of cDNA microarrays to generate a molecular taxonomy capable of distinguishing between colon cancer and normal colon. Oncogene 21:4855–4862
36. Kaiser S, Park YK, Franklin JL et al (2007) Transcriptional recapitulation and subversion of embryonic colon development by mouse colon tumor models and human colon cancer. Genome Biol 8:R131
37. Yoshinaga H, Matsuhashi S, Fujiyama C et al (1999) Novel human PDCD4 (H731) gene expressed in proliferative cells is expressed in the small duct epithelial cells of the breast as revealed by an anti-H731 antibody. Pathol Int 49:1067–1077
38. Leggett B, Whitehall V (2010) Role of the serrated pathway in colorectal cancer pathogenesis. Gastroenterology 138:2088–2100
39. Smith RA, Cokkinides V, Brooks D et al (2010) Cancer screening in the United States, 2010: a review of current American Cancer Society guidelines and issues in cancer screening. CA Cancer J Clin 60:99–119
40. Jankowski JA, Odze RD (2009) Biomarkers in gastroenterology: between hope and hype comes histopathology. Am J Gastroenterol 104:1093–1096

Virchows Arch (2011) 458:421–430
DOI 10.1007/s00428-011-1053-6

ORIGINAL ARTICLE

Analysis of select members of the E26 (ETS) transcription factors family in colorectal cancer

Candida Deves · Daiana Renck · Bernardo Garicochea · Vinicius Duval da Silva · Tiago Giulianni Lopes · Henrique Fillman · Lucio Fillman · Silvana Lunardini · Luis Augusto Basso · Diogenes Santiago Santos · Eraldo L. Batista Jr.

Received: 29 June 2010 / Revised: 25 January 2011 / Accepted: 28 January 2011 / Published online: 12 February 2011
© Springer-Verlag 2011

Abstract The E-twenty-six (ETS) family of transcription factors is known to act as positive or negative regulators of the expression of genes that are involved in diverse biological processes, including those that control cellular proliferation, differentiation, hematopoiesis, apoptosis, metastasis, tissue remodeling, and angiogenesis. Identification of target gene promoters of normal and oncogenic transcription factors provides new insights into the regulation of genes that are involved in the control of normal cell growth and differentiation. The aim of the present investigation was to analyze the differential expression of 11 ETS (ELF-3, ESE3, ETS1, ETV3, ETV4, ETV6, NERF, PDEF, PU1, Spi-B, and Spi-C) as potential markers for prognostic of colorectal cancer. A series of paired tissue biopsies consisting of a tumor and a non-affected control sample were harvested from 28 individuals suffering from diagnosed colorectal lesions. Total RNA was isolated from the samples, and after reverse transcription, differential expression of the select ETS was carried out through real-time polymerase chain reaction. Tumor staging as determined by histopathology was carried out to correlate the degree of tumor invasiveness with the expression of the ETS genes. The results demonstrated a different quantitative profile of expression in tumors and normal tissues. ETV4 was significantly upregulated with further increase in the event of lymph node involvement. PDEF and Spi-B presented down-regulation, which was more significant when lymph node involvement was present. These findings were supported by immunohistochemistry of tumoral tissues. The results suggest that select ETS may serve as potential markers of colorectal cancer invasiveness and metastasis.

C. Deves · D. Renck · L. A. Basso · D. S. Santos · E. L. Batista Jr.
Center for Research on Molecular
and Functional Biology (CP-BMF),
Pontificia Universidade Catolica do Rio Grande do Sul (PUCRS),
Av. Ipiranga 6681 Bld. 92A,
Porto Alegre, RS, Brazil

B. Garicochea · H. Fillman · L. Fillman · S. Lunardini
Department of Internal Medicine,
School of Medicine, Hospital São Lucas,
Pontificia Universidade Catolica do Rio Grande do Sul (PUCRS),
Av. Ipiranga, 6690,
90610-000, Porto Alegre, RS, Brazil

V. D. da Silva · T. Giulianni Lopes
Department of Pathology, School of Medicine,
Hospital São Lucas,
Pontificia Universidade Catolica do Rio Grande do Sul (PUCRS),
Av. Ipiranga, 6690,
90610-000, Porto Alegre RS, Brazil

C. Deves · D. Renck · L. A. Basso · D. S. Santos · E. L. Batista Jr.
Graduate Program in Cellular and Molecular Biology,
Faculdade de Biociencias,
Pontificia Universidade Catolica do Rio Grande do Sul (PUCRS),
Av. Ipiranga 6681 Bld. 12,
Porto Alegre, RS, Brazil

E. L. Batista Jr.
School of Dental Medicine,
Pontificia Universidade Catolica do Rio Grande do Sul (PUCRS),
Av. Ipiranga 6681 Bld. 06,
Porto Alegre, RS, Brazil

D. S. Santos (✉) · E. L. Batista Jr. (✉)
Centro de Pesquisas em Biologia
Molecular e Funcional—CPBMF/Tecnopuc,
Pontifícia Universidade Católica do Rio Grande do Sul - PUCRS,
Av. Ipiranga 6681 Bld. 92A,
90619-900, Porto Alegre, RS, Brazil
e-mail: diogenes@pucrs.br
e-mail: eraldo.junior@pucrs.br

Keywords ETS transcription factors · Colorectal cancer · Markers of tumor progression · Quantitative expression of biomarkers

Introduction

ETS proteins comprise a family of transcription factors that share a unique DNA binding domain, the ETS domain [1, 2]. All ETS members have a highly conserved amino acid sequence over a region of 84 to 90 residues referred to as the ETS domain [3]. This amino acid region forms the winged helix-turn-helix DNA binding domain composed of three alpha helices and four-stranded, beta sheet that recognizes a core GGAA/T sequence (ETS binding site (EBS)) [4–9]. The ETS domain family of eukaryotic transcription factors is currently composed of more than 30 members from metazoan organisms as diverse as sponges and humans [4].

ETS factors are known to act as positive or negative regulators of the expression of genes that are involved in various biological processes, including control of cellular proliferation, differentiation, hematopoiesis, apoptosis, metastasis, tissue remodeling, and angiogenesis [7–11]. Several lines of evidence have established that protein–protein interactions between the ETS proteins and other cellular patterns modulate gene expression [7].The regulation of either the expression or function of the ETS domain transcription factors and fusion with other proteins may contribute to the development of particular types of cancer [5, 12]. The ETS family of transcription factors typically activates the transcription of genes associated with pathogens and tumor defense, but several members also demonstrate ability to repress transcription. As a consequence, most ETS factors have oncogenic potential. Understanding the molecular mechanisms of transcription factors actions in cancer will provide new insights for earlier detection, diagnosis, and staging of the disease.

In the present study, we analyzed the differential expression of 11 ETS members (ESE3, ETV3, ETV4, ETV6, ETS1, PDEF, SPI-B, SPI-C, PU1, NERF, and ELF-3) as potential markers for prognostic of colorectal cancer. The choice of the aforementioned ETS genes took into account their potential roles in tumor progression as well as processes related to cells or systems associated with tumor development as previously reported [9, 13, 14]. We investigated the differential expression of the aforementioned ETS members in 28 colorectal tumors and adjacent normal tissues by FRET-based differential gene expression technology. In parallel, tumor staging as determined by histopathology was carried out to associate the degree of tumor invasiveness with the variation in the expression of the select ETS genes. Our results showed that most ETS genes analyzed are subject to changes in the neoplasic tissues. Nevertheless, only select ETS members underwent significant changes that could make them potential markers of disease invasiveness.

Materials and methods

Study population and tissue samples

Twenty-eight specimens of colorectal tumor and normal adjacent tissues consecutively harvested were obtained from patients who underwent surgical treatment at the São Lucas Hospital, Pontifical Catholic University of Rio Grande do Sul (PUCRS). The surgical protocol and research proposal were approved by the Human Studies and Ethics Committee of the Pontifical Catholic University of Rio Grande do Sul and the National Commission of Research Ethics (CONEP) under protocol number 07/03601. Subjects received a detailed description of the purpose of the study and signed an informed consent before entering the trial.

Sample processing and RNA purification

Tissue samples were harvested, cut into halves, and immediately processed either for histopathology and immunohistochemistry (4% buffered formalin), or total RNA isolation. Fixed samples were processed according to standard procedures for paraffin embedding, cutting, HE staining, and optical microscopy analysis. For total RNA isolation, the specimens were immediately stored in RNA stabilization reagent (RNA later™, RNA Stabilization Reagent, Ambion, Austin, TX, USA) after the surgical procedure and kept at −20°C. Total RNA was isolated from approximately 30 mg of non-tumor and tumor tissues using affinity chromatography and on-column DNase I treatment according to the manufacturer's protocol (RNasy® Protect Qiagen, Valencia, CA, USA). RNA concentrations were spectrophotometrically determined at 260 nm (1 OD= 40 μg/ml), as well as sample purity determined by the 260/280 ratio. Only samples whose 260/280 ratio was higher than 1.7 were included. The purified RNA was stored at −80°C. The quality of RNA was assessed by separation in 1% formaldehyde denaturing gels stained with SYBRGold™ (Invitrogen™, Molecular Probes, Carlsbad, CA, USA). Sharp 28- and 18-s ribosomal RNA bands without smearing were obtained for all samples enabling their use for reverse transcription.

Reverse transcription and real-time PCR

cDNA was synthesized from 500 ng of total RNA, primed with random hexamers in a reaction mixture containing

10 mM of each dNTP, 2 mM $MgCl_2$, and 1 U of the Murine Leukemia Virus Reverse Transcriptase (MultiScribe™ Reverse Transcriptase, TaqMan® Reverse Transcription Reagents, Roche Molecular) in 20-μl reaction mixtures (final concentration of approximately 25 ng/μl of cDNA). Reaction mixtures were subjected to 25°C for 10 min, 48°C for 30 min, and 95°C for 5 min in a thermal cycler (Techne™ TC-412, Duxford, Cambridge, UK). Real-time RT-polymerase chain reaction (PCR) was performed using primers and TaqMan probes labeled with FAM-MGB dye (Applied Biosystems, Assay-on-Demand, Foster, CA, USA) for the chosen ETS family genes, i.e., ESE3, ETV3, ETV4, ETV6, ETS1, PDEF, Spi-B, Spi-C, PU1, NERF, and ELF-3. Furthermore, genes that are known to be regulated by the differentially expressed ETS were also assessed, i.e., COX-2, MMP-7, and MMP-9. Reverse transcription products were prepared in 25-μl duplicates, and GAPDH (Human Endogenous Controls, Applied Biosystems, Foster, CA, USA), which was amplified in parallel with the genes of interest, was used for normalization of the RT reactions. GAPDH was chosen because of its low variability in colon tissues [15]. Before starting the amplification assays, the efficiency of the system was checked for every gene of interest according to previously established guidelines [16]. Briefly, approximately 500 ng of a randomly selected tumor cDNA was subjected to a tenfold serial dilution (500 to 0.5 ng and non-template control) for every target including the housekeeping gene. R^2 values ranged between 0.9789 and 0.9976 for all the selected ETS including GADPH. Relative expression was calculated according to a previously described method ($2^{\Delta\Delta Ct}$), having the control tissue as the calibrator or reference variable [16].

Histopathology and lesion staging

Samples fixed in 4% buffered formalin were processed according to standard procedures for HE staining. The histopathological features of the specimens were classified according to the TNM classification system [17]. After staging, information regarding patient demographical profiling was also gathered and added to the analysis. Locations of the tumors were divided into proximal colon (cecum, ascending, and transverse colon) and distal colon (descending, sigmoid colon, and rectum).

Immunohistochemistry

Serial sections were mounted over sialinized slides, deparaffinized, and incubated with diluted monoclonal antibodies (Santa Cruz Biotechnology, Santa Cruz, CA, USA) against human Spi-B (goat, 1:200), ETV4 (rabbit, 1:100), and PDEF (goat, 1:200). Detection of the primary antibodies was carried out with HRP conjugated secondary antibodies and DAB (Picture Max®, Zymed, Invitrogen, Carlsbad, CA, USA). Negative controls included sections incubated with non-immunized serum of the respective sources where the primary antibodies have been raised.

Statistical analysis

Expression was assessed using the ΔΔCt method, which delivered the variation of the target genes in tumors relative to a calibrator, i.e., the normal control tissue, which was assigned a value that equals "1." The data was analyzed using the Kruskal–Wallis non-parametric test; when significant differences were found ($P<0.05$), the Dunn's post hoc test was used to assess differences between groups. The Pearson correlation and linear regression were used to quantify the degree to which the genes (transcription factor × target gene) were related. A statistical pack (Prism 4 for Mac, GraphPad Software, La Jolla, CA, USA) was used for that purpose.

Results

mRNA-based expression of ETS genes in colorectal lesions

The changes in the expression of the ETS genes were calculated using relative expression; in this system, the fold-change in the expression of the target gene observed in the tumor tissue is presented relative to the normal tissue, which is herein represented as "1." The demographic and staging distribution of the lesions and participating subjects is presented in Table 1. Differential expression of ELF-3, ESE-3, ETS1, ETV3, ETV4, ETV6, NERF, PDEF, SPI1/PU.1, Spi-B, and Spi-C ETS genes was determined in 28 colorectal tumor tissues compared with adjacent normal mucosa. Lymph node involvement as determined by the TNM staging system was used as a grouping variable for association with expression changes. Eighteen out of the 28 individuals without lymph node involvement composed the first subgroup of analysis, and their tumor tissues fell into the I, IIA, or IIB TNM classification [17]. The second group was composed of ten patients with lymph node involvement whose tumor tissues corresponded to IIIB, IIIC, or IV.

Figures 1, 2, and 3 show the expression of ETS genes considering the adopted criteria; the results demonstrated an overall different quantitative profile of expression in tumors and normal tissues. Noteworthy, a closer analysis of lymph node involvement showed variable results among different ETS. ETV4, PDEF, and Spi-B presented the most significant changes on colorectal cancer: ETV4 mRNA was significantly upregulated ($P<0.01$), a 10.02-fold increase

Table 1 TNM distribution of the lesions

	n	Percent
Gender		
Male	16	60
Female	12	40
Tumor location		
Cecum	2	5
Sigmoid	5	20
Rectum	19	70
Lower rectum	2	5
TNM stage		
I	3	10
IIA	13	50
IIB	2	10
IIIB	3	5
IIIC	6	20
IV	1	5
Cancer grade		
Adenocarcinoma	26	92.85
Differentiated moderate adenocarcinoma	2	7.15

Age: median, 69.05±9.91 years; range, 45–84 years

without lymph node involvement, and a 19.46-fold increase when lymph node involvement was detected in comparison with normal mucosa (Fig. 1, upper panel). The involvement of lymph nodes was associated with an almost twofold increase in the expression of ETV4 compared to tumors whose staging was N_0 ($P<0.05$). Differently from ETV4, PDEF analysis showed a completely different outcome; in neoplasic tissues without lymph node involvement, PDEF showed little if any variation relative to the control non-affected tissues (Fig. 1, central panel). Nevertheless, involvement of the lymph nodes was associated with a threefold decrease in the expression of PDEF ($P<0.05$). Another relevant finding among the analyzed ETS was related to Spi-B, whose expression underwent a striking decrease in colorectal cancer tissues regardless of the association with lymph node involvement (Fig. 1, lower panel). A closer analysis showed there was a 14-fold decrease (0.07; $P<0.01$) and a 50-fold decrease (0.02; $P<0.01$) for Spi-B compared to non-neoplasic tissues in the absence and in the presence of lymph node involvement, respectively. Importantly, lymph node involvement was associated with a further downregulation of Spi-B that was significantly lower compared to samples N_0 ($P<0.05$).

The remaining ETS analyzed, ELF-3, ESE-3, ETS1, ETV2, ETV3, ETV6, NERF, SPI1/PU.1, and Spi-C, presented different expression patterns compared with normal tissues, but no significant variation relative to lymph node involvement was observed (Fig. 2). ELF-3, ESE-3, ETV3, and Spi-C showed an increase in the mRNA levels in the event of lymph node involvement, and ETS1, ETV2, ETV6, and Spi1/PU.1 presented a slight down-regulation; these variations, however, were not significant. NERF, on the other hand, presented unaltered gene expression regardless of the presence of lymph node involvement. Figure 3 shows the data for individual samples with the variations for each of the 28 cases analyzed; samples 19 to 28 were harvested from lymph node + subjects, which showed a more evident variation compared to lymph node − samples. The correlation between the three differentially expressed ETS is showed in Fig. 4; it revealed an inverse correlation between ETV4 and Spi-B and PDEF (Pearson coefficient=−0.6758 and −0.8776, respectively), whereas PDEF and Spi-B were positively correlated (Pearson coefficient=0.5336).

Expression of COX-2, MMP-7, and MMP-9 was assessed to validate the changes observed in the differentially expressed ETS genes. Figure 5 shows that COX-2 and MMP-7, known to be regulated by ETV4, were also upregulated in tumors. Accordingly, MMP-9, which is repressed by PDEF expression, was upregulated in tumors. Expression of the target genes was markedly affected by the presence of lymph node involvement.

Immunohistochemistry

Expression of ETV4, PDEF, and Spi-B in colorectal tumors and control tissues, as depicted by detection with antibodies, revealed a pattern that resembled gene expression analysis. ETV4 showed an intense nuclear and cytosolic staining pattern (Fig. 6a) as opposed by control tissue. PDEF (Fig. 6b) and Spi-B (Fig. 6c), on the other hand, were upregulated in control tissues and presented decreased immunodetection in tumor samples.

Discussion

The ETS transcription factor family has gained increased attention due to its regulatory function over genes that are key to cancer development and progression. Along with its potential use as target ETS in cancer therapy, ETS factors could be also useful markers of cancer progression and disease prognosis. In this study, we demonstrated the quantitative variable expression of ETS transcription factors in tumors and normal tissues and the expression correlated with involvement of lymph nodes, an important step in tumor metastasis. Among the findings herein reported, three ETS members showed marked variation; ETV4 mRNA levels were significantly higher in colorectal tumors compared to normal tissues, while PDEF and Spi-B were downregulated. Our results showed a 10.02-fold increase in

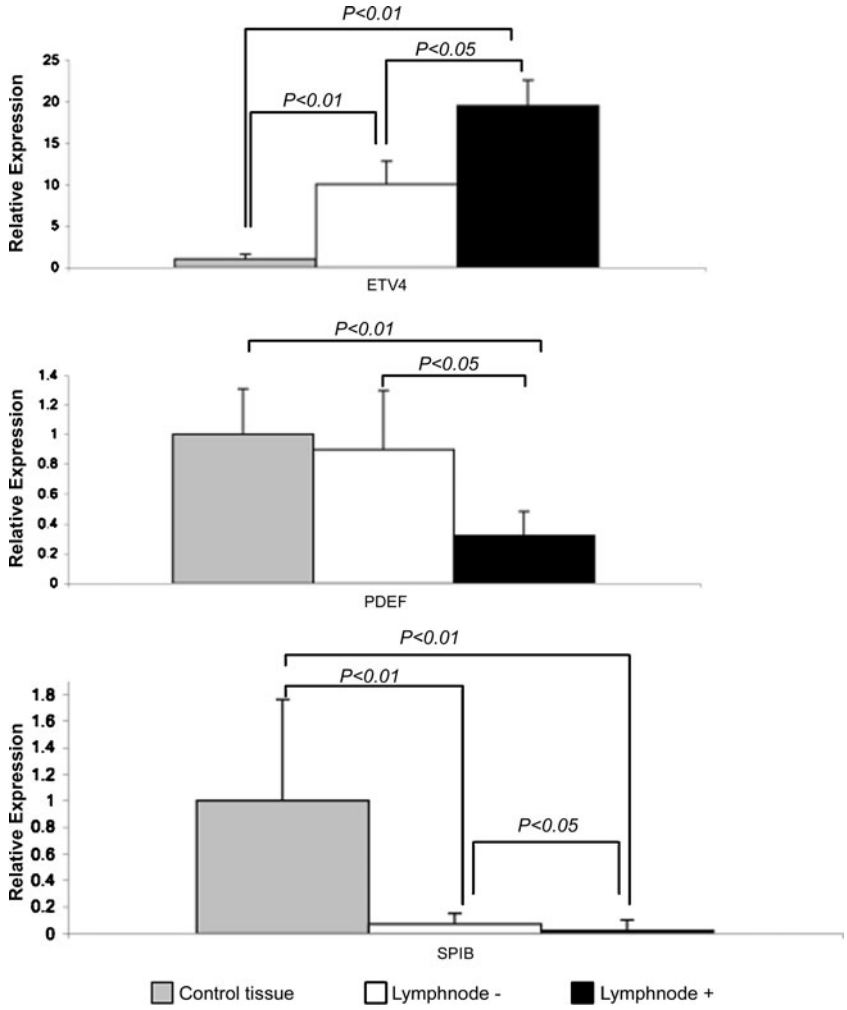

Fig. 1 Expression of select ETS relative to control non-neoplasic tissues. ETV4 (*upper panel*) presented a significant increase (tenfold) in colorectal cancer tissues, which underwent a nearly twofold increase when lymph nodes were involved. There were no major changes in PDEF expression in the absence of lymph node involvement (*central panel*), but a threefold decrease was observed when the analysis was restricted to patients with lymph node involvement. Spi-B (*lower panel*) also presented a significant decrease in colorectal cancer relative to normal tissues (14-fold). Noteworthy, involvement of lymph nodes was associated with a decrease in the levels of Spi-B, which reached a 50-fold downregulation. *Bars* and *error bars* stand for means and SD, respectively; significance was set at 5%

mRNA levels of ETV4 in cases without lymph node involvement. This finding seems to corroborate previous studies that showed that ETV4 mRNA is overexpressed in colorectal cancer tissues compared to normal colorectal tissue [18, 19]. Boedefeld et al. [18] evaluated the expression of ETV4 in colorectal tumor tissues and reported a 17-fold increase in the mRNA level. Moss et al. found a 14-fold increase in the mRNA level in colorectal

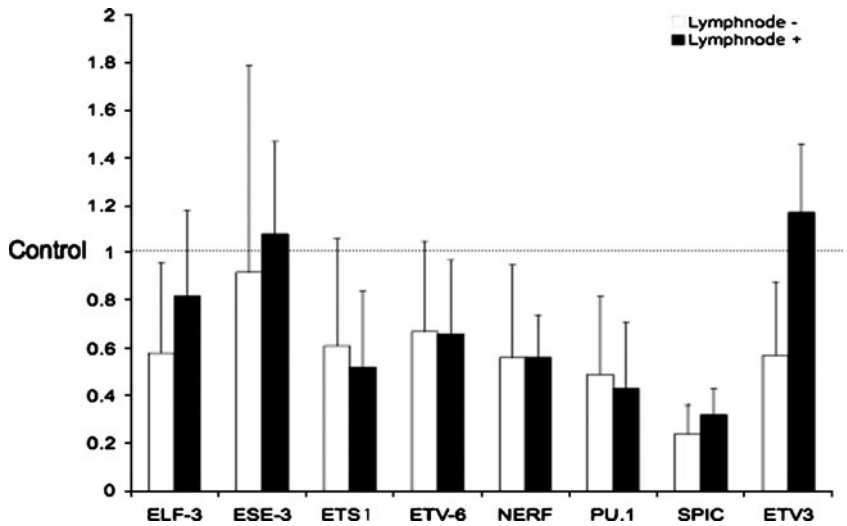

Fig. 2 Overview of remaining ETS relative expression. Changes (means and SD of the mean) for the remaining ETS are presented relative to normal tissues ("1"), which is depicted by the *horizontal dotted line*; no significant variations in the expression were observed for any of the analyzed ETS, although a clear variation is depicted for select target genes ($P>0.05$)

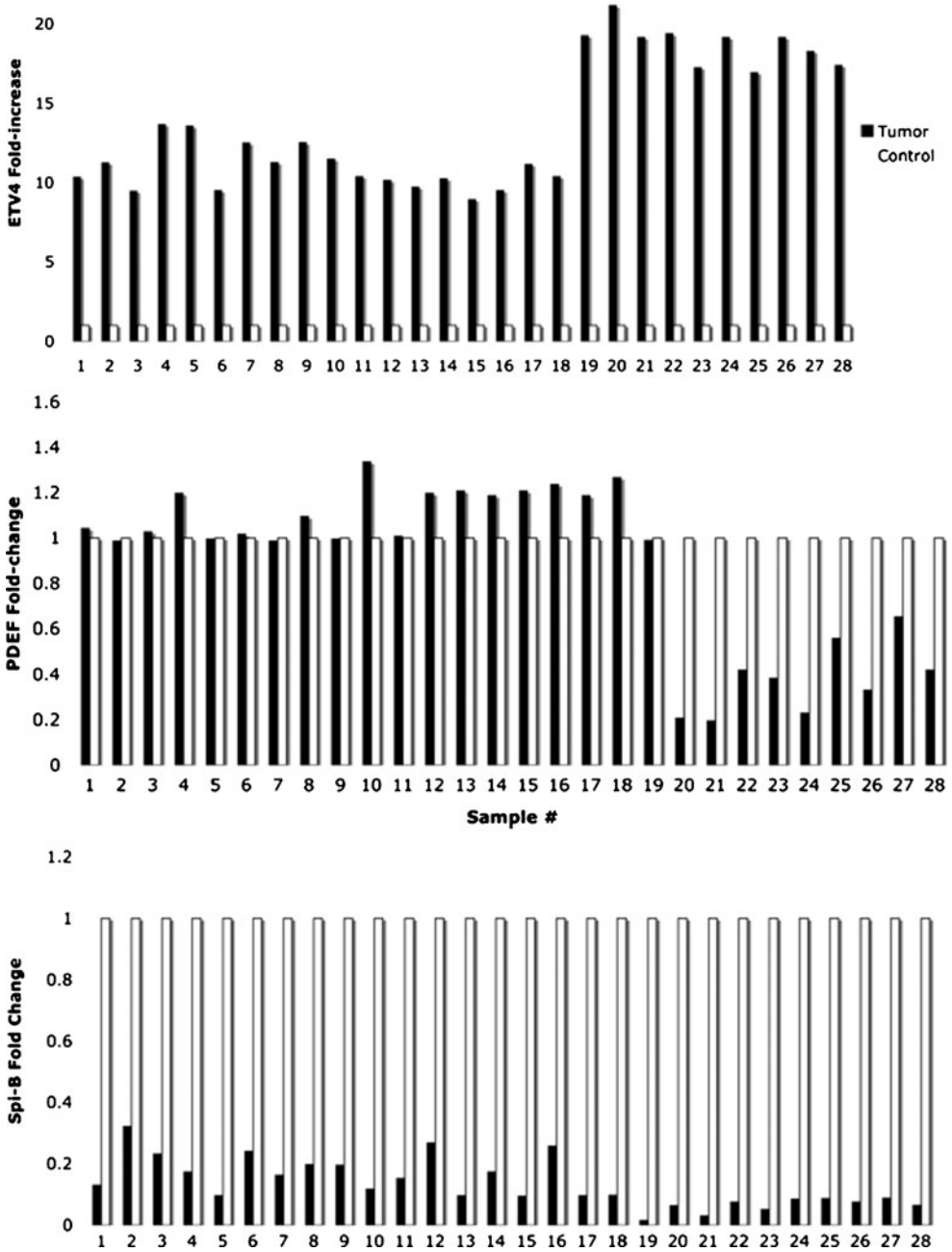

Fig. 3 Expression data for individual samples depicting changes among subjects (n=28). Samples 19 to 28 are from individuals with lymph node involvement, whereas the remaining samples were harvested from lymph node− patients

carcinomas compared with adjacent normal mucosa [19]. Our results further support the aforementioned findings in colorectal lesions but in a different population, in this case, South-American patients. Importantly, and differently from the previous reports, here we show that increase in ETV4 expression may be further associated with lymph node involvement, an important event in the metastatic process. We observed a 19.46-fold increase when lymph node involvement was present compared with adjacent normal mucosa, a twofold increase relative to lesions without lymph node involvement. This finding points out ETV4 as a potential marker of severity and invasiveness of colorectal tumors. The ETV4 transcription factor, an ETS family gene, is also known as E1A enhancer binding protein (E1A-F), a homolog of the murine PEA-3 [8]. Among the genes regulated by ETV4 are metalloproteinases (MMPs) [1, 20, 21] and cyclooxygenase-2 (COX-2) [22], whose upregulation has been associated with the invasion potential of tumor cells. Degradation of the extracellular matrix mediated by MMPs is an important mechanism of invasiveness, progression, and metastasis of tumors [23]. Moreover, nitric oxide (NO) generated by iNOS stimulates an increase of COX-2 expression in colorectal cancer resulting in tumor angiogenesis due to VEGF upregulation [24]. ETS2, ETV4, and ELF-3, also known as ESE-1, subfamilies of ETS are overexpressed in ductal carcinoma

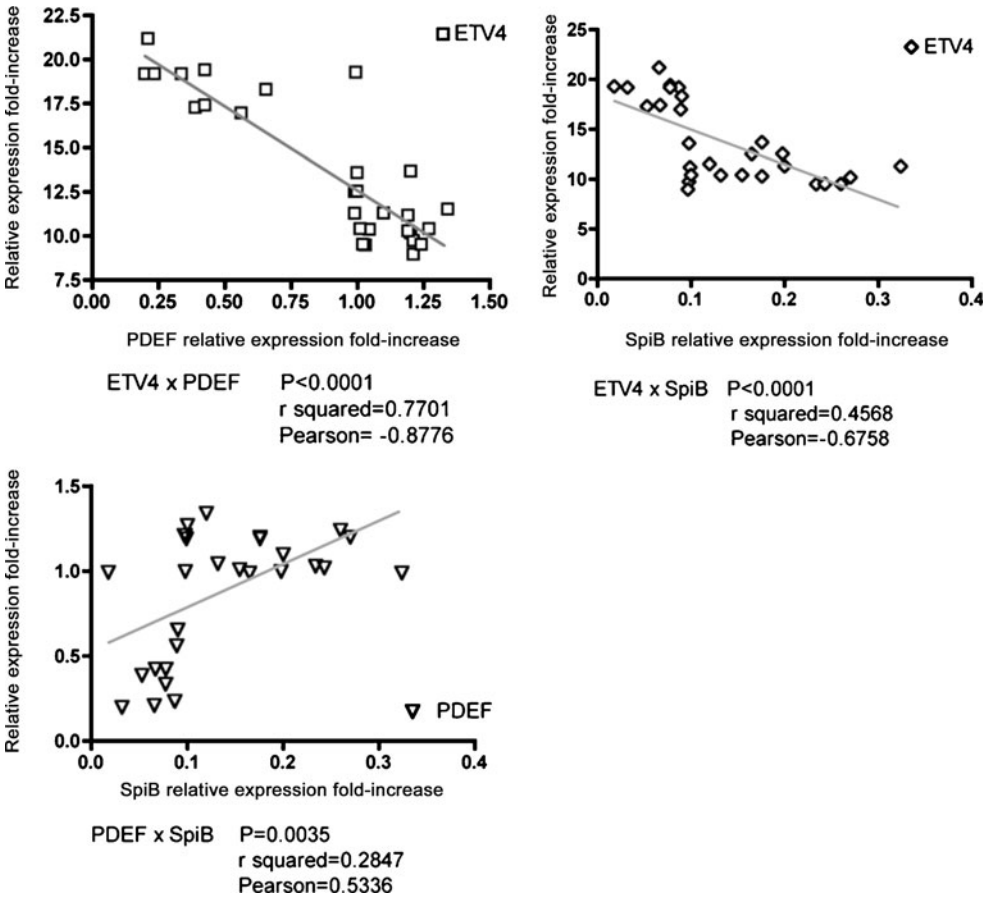

Fig. 4 Correlation among expressed ETS. Analysis revealed that ETV4 mRNA levels were inversely correlated with PDEF and Spi-B (Pearson=−0.8778 and −0.6758), suggesting a reciprocal pattern of regulation. On the other hand, PDEF and Spi-B were positively correlated (Pearson=0.5336)

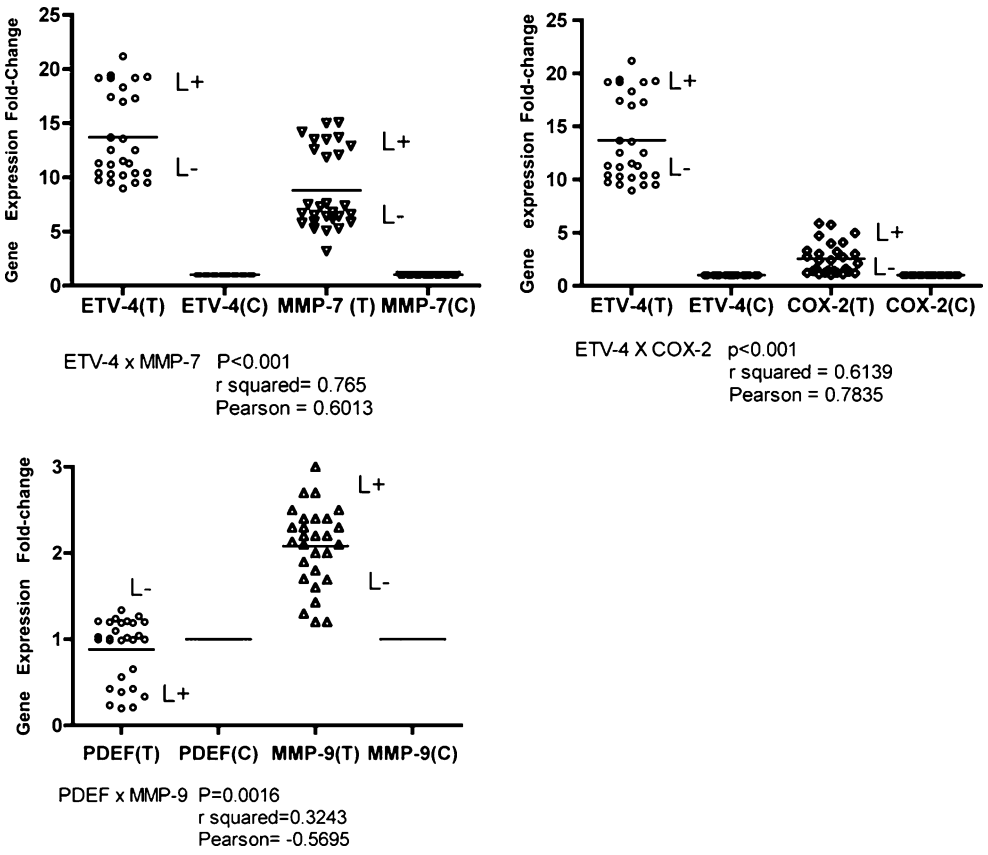

Fig. 5 Expression of ETS-regulated genes in control (C) and tumor (T) samples. Genes regulated by ETV4 (MMP-7 and COX-2, *upper panels*) and PDEF (MMP-9) were assessed as described in "Materials and methods" section. COX-2 and MMP-7 were upregulated in tumor samples, following the same pattern observed for ETV4. COX-2 variation was not marked as for MMP-7, but still reached significance. Corroborating PDEF as a tumor repressor, MMP-9 (*lower panel*) was upregulated in tumor samples where PDEF was downregulated. For all genes assessed, lymph node involvement (L+) had a role in the observed variations of gene expression

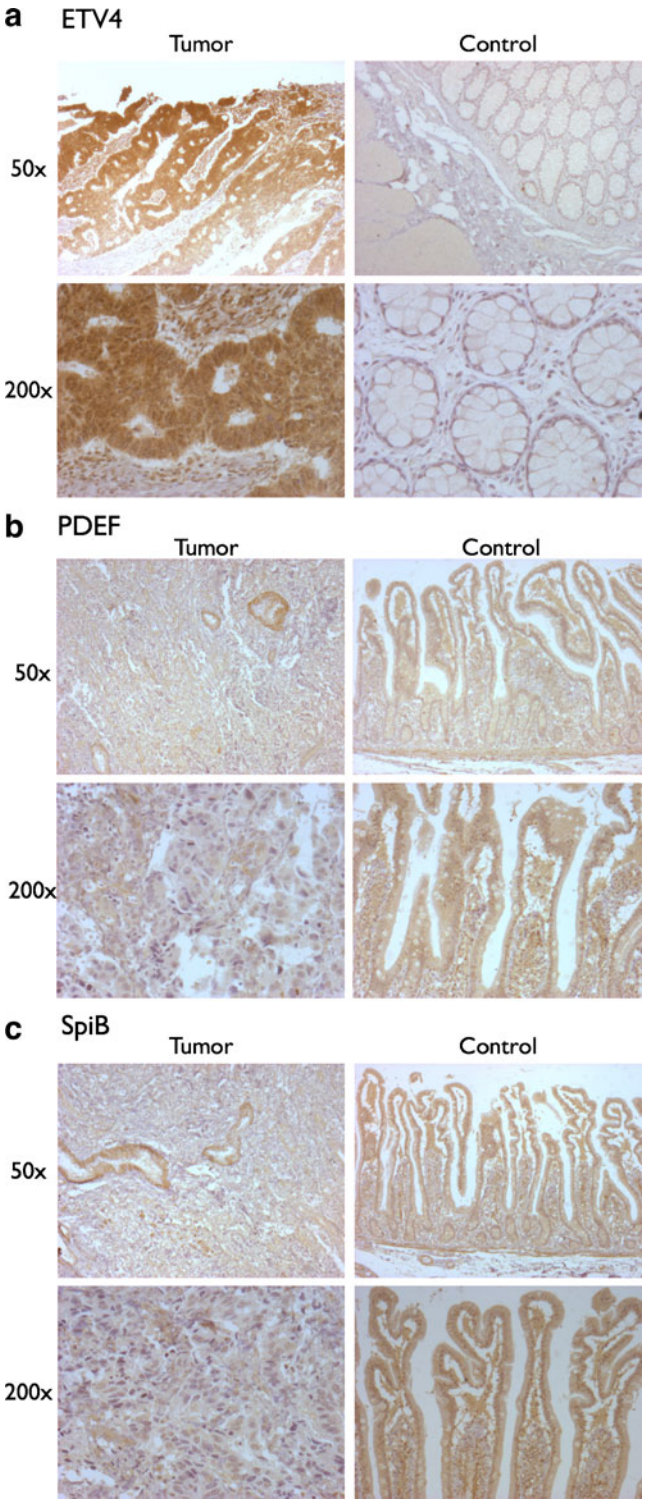

Fig. 6 Immunohistochemical localization of ETV4, PDEF, and Spi-B. A dense staining for ETV4 is depicted in tumor cells as opposed to control tissue (**a**). PDEF (**b**) and Spi-B (**c**) demonstrated a pale cytoplasmic staining in tumor samples as opposed to control tissues, where more intense immunostaining can be observed. Noteworthy, a marked staining can be observed in the cells of normal glands within neoplasic tissue. These findings corroborated those of gene expression. Hematoxylin counterstaining

in situ and invasive carcinoma and appear to act as oncogenes [25, 26]. The significant upregulation observed in colorectal samples of lymph node-involved individuals could reflect an increase in the metastatic activity of the lesions due to downstream upregulation of the aforementioned genes, along with others that have yet to be characterized. In support of this premise, we found that MMP-7 and COX-2, two ETV4 regulated genes that have been linked to tumor progression [18, 27], were also upregulated in the analyzed samples. Importantly, the expression for both, COX-2 and MMP-7, was higher in patients were lymph node involvement was diagnosed even though COX-2 did not variate as much as MMP-7 in ETV4 upregulated tumors.

PDEF was originally identified as a prostate-derived ETS factor, present in normal prostate luminal cells and in ovary, mammary, and salivary glands [9, 28]. Reports have indicated that PDEF expression is reduced in invasive breast cancer [28], and no detectable expression was observed in prostate cancer [29], suggesting that it works as a tumor suppressor. Furthermore, expression of PDEF in invasive cancer cells inhibits their ability to invade and migrate [28], and loss of PDEF is associated with aggressive prostate cancer. In our study, we observed a slight, albeit not significant, decrease in PDEF mRNA levels in colorectal carcinomas in the absence lymph node involvement. Nevertheless, PDEF underwent a threefold decreased when lymph node involvement was diagnosed, which corroborates previous studies that point out PDEF as a cancer suppressor. As a matter of fact, a recently published investigation showed that activation of PDEF downregulates MMP-9 in prostate cancer [30]. Supporting this finding, our results showed that MMP-9 was significantly upregulated in tumors where PDEF expression was reduced; noteworthy, lymph node involvement was associated with both, decreased PDEF and increased MMP-9, suggesting that malignancy has an impact in the reciprocal expression pattern observed. Further studies are warranted to investigate the expression of PDEF mRNA in a larger collection of tumors to display the important role this gene might have in the progression of colorectal cancer. Likewise, a better understanding of the genes that are regulated by PDEF may provide invaluable information about tumor progression and treatment.

Another important finding was related to Spi-B expression, which presented a 50-fold and 14-fold downregulation in lymph node+ and lymph node− cases, respectively. Previous studies have associated Spi-B with the early stages of development of T-cells [31] and immunity [32], and only few links with tumor progression in humans have been directly made. Spi-B has been implicated in signaling pathways downstream of the B cell receptor and is essential for germinal center formation and maintenance [33]. Hence,

children suffering from acute lymphoblastic leukemia present a decrease in the expression of Spi-B [34], and a recent report shows that Spi-B may be a predictor of the chemosensitivity to therapy in this type of leukemia [35]. Moreover, loss of Spi-B can be detected in plasma leukemia cells as opposed to normal plasma cells [36]. We could not assess the expression of genes potentially regulated by Spi-B since previous investigations with this ETS have primarily focused on human immune cell development. No Spi-B-related target genes associated with cancer progression have been consistently characterized thus far, and prospection of genes regulated by Spi-B is beyond the scope of the present study. Nevertheless, our results indicate that Spi-B is a potential target to be further investigated in the progression and response to therapy in colorectal cancer.

We showed the differential expression profile of select members of the ETS family in colorectal cancer compared with normal colorectal tissue. While some of the ETS genes demonstrated a significant variation in the levels of mRNA, others showed only a modest change. Our results seem to point out that the genes regulated by ETV4, PDEF, and Spi-B deserve further attention, which may pave the way for a better understanding of the progression and development of colorectal cancer. Likewise, and according to the findings presented herein, ETV4 and Spi-B might be potential biological markers of progression and invasiveness of colorectal cancer. Additional studies are warranted to investigate the actual roles of each ETS gene in the progression and development of cancer, which make them likely markers for earlier detection, diagnosis, staging of disease, and targets for development of anticancer drugs.

Acknowledgments This work was supported by Hewlett-Packard grant HP47 and by CNPq 400790/2005-0 (Brasilia, DF, Brazil) awarded to DSS.

Conflicts of interest The authors declare no conflict of interest.

References

1. Sharrocks AD, Brown AL, Ling Y, Yates PR (1997) The ETS-domain transcription factor family. Int J Biochem Cell Biol 29 (12):1371–1387
2. Shindoh M, Higashino F, Kaya M, Yasuda M, Funaoka K, Hanzawa M, Hida K, Kohgo T, Amemiya A, Yoshida K, Fujinaga K (1996) Correlated expression of matrix metalloproteinases and ETS family transcription factor e1a-f in invasive oral squamous-cell-carcinoma-derived cell lines. Am J Pathol 148(3):693–700
3. Graves BJ, Petersen JM (1998) Specificity within the ETS family of transcription factors. Adv Cancer Res 75:1–55
4. Degnan BM, Degnan SM, Naganuma T, Morse DE (1993) The ETS multigene family is conserved throughout the metazoa. Nucleic Acids Res 21(15):3479–3484
5. Dittmer J (2003) The biology of the ETS1 proto-oncogene. Mol Cancer 2:29
6. Hollenhorst PC, Jones DA, Graves BJ (2004) Expression profiles frame the promoter specificity dilemma of the ETS family of transcription factors. Nucleic Acids Res 32(18):5693–5702
7. Li R, Pei H, Watson DK (2000) Regulation of ETS function by protein–protein interactions. Oncogene 19(55):6514–6523
8. Sementchenko VI, Watson DK (2000) ETS target genes: past, present and future. Oncogene 19(55):6533–6548
9. Seth A, Watson DK (2005) ETS transcription factors and their emerging roles in human cancer. Eur J Cancer 41(16):2462–2478
10. Hsu T, Trojanowska M, Watson DK (2004) ETS proteins in biological control and cancer. J Cell Biochem 91(5):896–903
11. Oikawa T, Yamada T (2003) Molecular biology of the ETS family of transcription factors. Gene 303:11–34
12. Sharrocks AD (2001) The ETS-domain transcription factor family. Nat Rev Mol Cell Biol 2(11):827–837
13. Jedlicka P, Gutierrez-Hartmann A (2008) ETS transcription factors in intestinal morphogenesis, homeostasis and disease. Histol Histopathol 23(11):1417–1424
14. Turner DP, Findlay VJ, Moussa O, Watson DK (2007) Defining ETS transcription regulatory networks and their contribution to breast cancer progression. J Cell Biochem 102(3):549–559
15. Andersen CL, Jensen JL, Orntoft TF (2004) Normalization of real-time quantitative reverse transcription-PCR data: a model-based variance estimation approach to identify genes suited for normalization, applied to bladder and colon cancer data sETS. Cancer Res 64(15):5245–5250
16. Livak KJ, Schmittgen TD (2001) Analysis of relative gene expression data using real-time quantitative PCR and the 2(-delta delta c(t)) method. Methods 25(4):402–408
17. Sobin LH, Wittekind C (2002) TNM classification of malignant tumors, 6th edn. Wiley, Washington
18. Boedefeld WM 2nd, Soong R, Weiss H, Diasio RB, Urist MM, Bland KI, Heslin MJ (2005) E1a-f is overexpressed early in human colorectal neoplasia and associated with cyclooxygenase-2 and matrix metalloproteinase-7. Mol Carcinog 43(1):13–17
19. Moss AC, Lawlor G, Murray D, Tighe D, Madden SF, Mulligan AM, Keane CO, Brady HR, Doran PP, MacMathuna P (2006) Etv4 and Myeov knockdown impairs colon cancer cell line proliferation and invasion. Biochem Biophys Res Commun 345 (1):216–221
20. Adachi Y, Yamamoto H, Itoh F, Arimura Y, Nishi M, Endo T, Imai K (2001) Clinicopathologic and prognostic significance of matrilysin expression at the invasive front in human colorectal cancers. Int J Cancer 95(5):290–294
21. Horiuchi S, Yamamoto H, Min Y, Adachi Y, Itoh F, Imai K (2003) Association of ETS-related transcriptional factor e1af expression with tumour progression and overexpression of MMP-1 and matrilysin in human colorectal cancer. J Pathol 200(5):568–576
22. Howe LR, Crawford HC, Subbaramaiah K, Hassell JA, Dannenberg AJ, Brown AM (2001) Pea3 is up-regulated in response to wnt1 and activates the expression of cyclooxygenase-2. J Biol Chem 276 (23):20108–20115
23. Chambers AF, Matrisian LM (1997) Changing views of the role of matrix metalloproteinases in metastasis. J Natl Cancer Inst 89 (17):1260–1270
24. Nosho K, Yoshida M, Yamamoto H, Taniguchi H, Adachi Y, Mikami M, Hinoda Y, Imai K (2005) Association of ETS-related transcriptional factor e1af expression with overexpression of matrix metalloproteinases, COX-2 and INOS in the early stage of colorectal carcinogenesis. Carcinogenesis 26(5):892–899
25. Chang CH, Scott GK, Kuo WL, Xiong X, Suzdaltseva Y, Park JW, Sayre P, Erny K, Collins C, Gray JW, Benz CC (1997) Esx: a structurally unique ETS overexpressed early during human breast tumorigenesis. Oncogene 14(13):1617–1622
26. Sapi E, Flick MB, Rodov S, Kacinski BM (1998) ETS-2 transdominant mutant abolishes anchorage-independent growth

and macrophage colony-stimulating factor-stimulated invasion by bt20 breast carcinoma cells. Cancer Res 58(5):1027–1033
27. Maruta S, Sakai H, Kanda S, Hayashi T, Kanetake H, Miyata Y (2009) E1af expression is associated with extra-prostatic growth and matrix metalloproteinase-7 expression in prostate cancer. APMIS 117(11):791–796
28. Feldman RJ, Sementchenko VI, Gayed M, Fraig MM, Watson DK (2003) PDEF expression in human breast cancer is correlated with invasive potential and altered gene expression. Cancer Res 63 (15):4626–4631
29. Nozawa M, Yomogida K, Kanno N, Nonomura N, Miki T, Okuyama A, Nishimune Y, Nozaki M (2000) Prostate-specific transcription factor hPSE is translated only in normal prostate epithelial cells. Cancer Res 60(5):1348–1352
30. Johnson TR, Koul S, Kumar B, Khandrika L, Venezia S, Maroni PD, Meacham RB, Koul HK (2010) Loss of PDEF, a prostate-derived ETS factor is associated with aggressive phenotype of prostate cancer: regulation of MMP 9 by PDEF. Mol Cancer 9:148
31. Anderson MK, Hernandez-Hoyos G, Diamond RA, Rothenberg EV (1999) Precise developmental regulation of ETS family transcription factors during specification and commitment to the T cell lineage. Development 126(14):3131–3148
32. Gallant S, Gilkeson G (2006) ETS transcription factors and regulation of immunity. Arch Immunol Ther Exp Warsz 54 (3):149–163
33. Bartholdy B, Du Roure C, Bordon A, Emslie D, Corcoran LM, Matthias P (2006) The ETS factor Spi-b is a direct critical target of the coactivator OBF-1. Proc Natl Acad Sci USA 103 (31):11665–11670
34. Niini T, Vettenranta K, Hollmen J, Larramendy ML, Aalto Y, Wikman H, Nagy B, Seppanen JK, Ferrer Salvador A, Mannila H, Saarinen-Pihkala UM, Knuutila S (2002) Expression of myeloid-specific genes in childhood acute lymphoblastic leukemia—a cDNA array study. Leukemia 16(11):2213–2221
35. Talby L, Chambost H, Roubaud MC, N'Guyen C, Milili M, Loriod B, Fossat C, Picard C, Gabert J, Chiappetta P, Michel G, Schiff C (2006) The chemosensitivity to therapy of childhood early B acute lymphoblastic leukemia could be determined by the combined expression of CD34, Spi-b and BCR genes. Leuk Res 30(6):665–676
36. Nagy M, Chapuis B, Matthes T (2002) Expression of transcription factors pu.1, Spi-b, Blimp-1, BSAP and oct-2 in normal human plasma cells and in multiple myeloma cells. Br J Haematol 116 (2):429–435

Virchows Arch (2011) 458:431–438
DOI 10.1007/s00428-011-1059-0

ORIGINAL ARTICLE

Expression of p21^{WAF1} in Astler–Coller stage B2 colorectal cancer is associated with survival benefit from 5FU-based adjuvant chemotherapy

Violetta Sulzyc-Bielicka · Pawel Domagala · Elzbieta Urasinska · Dariusz Bielicki · Krzysztof Safranow · Wenancjusz Domagala

Received: 7 December 2010 / Revised: 7 February 2011 / Accepted: 10 February 2011 / Published online: 3 March 2011
© The Author(s) 2011. This article is published with open access at Springerlink.com

Abstract In several, but not all, previous studies, positive p21^{WAF1} expression has been suggested as an indicator of a good prognosis in patients with stage III/IV colorectal cancer. However, it is not known whether the same is true for stage B2 patients. The purpose of this study is to assess the influence of p21^{WAF1} expression in tumor cells on disease-free survival (DFS) and overall survival (OS) of Astler–Coller stage B2 and C patients with colorectal cancer who underwent 5-fluorouracil-based adjuvant chemotherapy. Nuclear p21^{WAF1} was detected by immunohistochemistry in tissue microarrays from 275 colorectal cancers. The expression of p21^{WAF1} was associated with DFS (p=0.025) and OS (p=0.008) in the subgroup of stage B2 patients that was treated with adjuvant chemotherapy. In multivariate analysis, it remained the only independent prognostic parameter in relation to DFS and OS (p=0.035 and p=0.02, respectively). In the subgroup of 72 stage B2 patients with positive p21^{WAF1} expression but not in the subgroup of 61 stage B2 patients with negative p21^{WAF1} expression, adjuvant chemotherapy was associated with better DFS (85% 5-year survival versus 65% without chemotherapy, p=0.03) and OS (96% versus 82%, p=0.014). In the combined stage B2 and C group of patients treated with adjuvant chemotherapy, positive p21^{WAF1} expression was also associated with better DFS and OS (p=0.03, p=0.002, respectively). Expression of p21^{WAF1} in colorectal tumor cells identifies a subgroup of Astler–Coller stage B2 patients who could benefit significantly from 5FU-based chemotherapy and may improve the selection of patients for adjuvant chemotherapy.

Keywords Colorectal cancer · Survival · Chemotherapy · 5-fluorouracil · p21^{WAF1}

V. Sulzyc-Bielicka
Department of Clinical Oncology,
Pomeranian Medical University,
Powstancow Wielkopolskich 72,
70–111 Szczecin, Poland

P. Domagala
Department of Genetics and Pathology,
Pomeranian Medical University,
Polabska 4,
70–115 Szczecin, Poland

E. Urasinska · W. Domagala (✉)
Department of Pathology, Pomeranian Medical University,
Unii Lubelskiej 1,
71–252 Szczecin, Poland
e-mail: sekrpato@ams.edu.pl

D. Bielicki
Department of Gastroenterology and Internal Medicine,
Pomeranian Medical University,
Unii Lubelskiej 1,
71–252 Szczecin, Poland

K. Safranow
Department of Biochemistry and Medical Chemistry,
Pomeranian Medical University,
Powstancow Wielkopolskich 72,
70–111 Szczecin, Poland

Introduction

The efficacy of 5-fluorouracil (5FU)-based adjuvant chemotherapy and the associated survival benefit have been firmly established for patients with stage III colorectal cancer (CRC) [1]. However, the use of adjuvant therapy for stage II colon cancer patients remains controversial [2]. Typically, only high-risk stage II CRCs are treated. Hence,

there is a need for predictive factors to support treatment decisions in this group of patients, the majority of whom will be cured by surgery alone [3]. This is especially important because a wider implementation of prophylactic programs in recent years has resulted in an increased number of patients with stage B2 tumors.

5-Fluorouracil has been used to treat colorectal cancer patients for a long time [4]. The target enzyme for 5FU is thymidylate synthase (TS). This enzyme catalyzes the conversion of deoxyuridine-5′monophosphate to deoxythymidine-5′-monophosphate and is therefore essential for DNA synthesis and repair. Resistance to 5FU-based treatment might depend both on the level of expression of TS and other enzymes involved in the metabolism of 5FU and on mechanisms involved in cell growth or apoptosis. $p21^{WAF1}$ is a multifunctional cell cycle-related protein that inhibits cyclin-dependent kinases (CDKs), which results in cell cycle arrest in the G1 phase [5]. $p21^{WAF1}$ expression is known to be inversely related to cell proliferation and directly related to terminal differentiation [6]. Recently, it has been shown that TS expression was upregulated in $p21^{WAF1}$-/- human colorectal cancer HCT116 cells, and TS promoter activity was downregulated by ectopic p21 expression [7]. Furthermore, a CDK inhibitor reduced expression of TS in a dose-dependent manner, and the reduction resulted in enhancement of sensitivity to 5FU in cultured human colon cancer cells [8]. Taken together with other reports [9], this suggests a great importance of $p21^{WAF1}$ for in vitro response to chemotherapeutic agents and that the CDK inhibitor $p21^{WAF1}$ regulates thymineless stress-induced DNA damage. Hence, $p21^{WAF1}$ expression might have a predictive significance in 5FU-treated CRC patients. In several [10–19] but not all [20–24] previous studies, positive $p21^{WAF1}$ expression has been suggested as an indicator of good prognosis in patients with stage III/IV CRC. However, it is not known whether the same is true for stage B2 patients. Therefore, our purpose was to assess the influence of $p21^{WAF1}$ expression on disease-free survival (DFS) and overall survival (OS) of Astler–Coller stage B2 patients with CRC who either were or were not treated with 5FU-based adjuvant chemotherapy, and of stage C patients treated with adjuvant chemotherapy.

Materials and methods

Patients This retrospective study was based on tumor tissue from 275 unselected patients who underwent potentially curative colorectal resection for sporadic CRC (defined as an absence of relevant family history at the time of admission to the hospital). Distant metastases at the time of operation were excluded by preoperative liver ultrasonography, chest x-ray, and intraoperative exploration. Table 1 lists the clinico-pathological details of the 275 tumors and patients. Astler–Coller staging of CRC based on the extent of local invasion and the status of lymph nodes was used [25]. In this system, stage B2 denotes the tumor penetrating through the muscularis propria and uninvolved nodes, stage C—tumors extending into the muscularis propria or penetrating through it with lymph node metastases. The mean age of the patients was 61.1±10.8 years (range, 33–83; median, 62). The splenic flexure was regarded as the border between the proximal and distal colon. The Research Ethics Committee of Pomeranian Medical University approved this study.

Tumors were resected between July 1997 and April 2004 in the Departments of Surgery of the teaching hospitals of Pomeranian Medical University in Szczecin and the Regional Oncological Center in Szczecin, Poland. The operations consisted of either a resection with lymphadenectomy or a total mesorectal excision for rectal carcinomas. A total of 203 (74%) patients (83 high-risk stage B2 and 120 stage C) were treated with adjuvant chemotherapy (six 5-day courses of bolus infusion of 5FU (425 mg/m^2) every 4 weeks combined with leucovorin, 20 mg/m^2). A

Table 1 Relations between $p21^{WAF1}$ expression and clinico-pathological parameters

Parameter	$p21^{WAF1}$ Expression		
	n	*n* (%)	*p*
Age (years)			
<62	138	87 (63)	0.39
>62	137	79 (58)	
Sex			
Females	120	75 (63)	0.54
Males	155	91 (59)	
Grade			
G1+G2	156	91 (58)	0.46
G3[a]	119	75 (63)	
Astler–Coller			
B2	133	72 (54)	*0.049*
C	142	94 (66)	
Site			
Proximal	53	37 (70)	0.16
Distal	222	129 (58)	
Site			
Rectum	138	81 (59)	0.62
Colon	137	85 (62)	
Radiotherapy (rectal tumors)			
Preoperative	43	26 (61)	0.85
Postoperative RT and no RT[b]	93	53 (57)	

[a] Including mucinous carcinoma

[b] Radiotherapy status unknown in two cases

total of 72 patients (22 stage C patients) did not receive adjuvant chemotherapy due to internist contraindications.

A total of 41 patients with rectal cancer received postoperative radiotherapy (50.4 Gy), and 43 patients, preoperative radiotherapy (5×5 Gy). Of the 133 Astler–Coller stage B2 tumors, there were 65 rectal tumors, and of these, 24 (18%) received preoperative and 11 (8.3%) received postoperative radiotherapy. Radiotherapy did not influence DFS (p=0.61) nor OS (p=0.83) of patients with rectal tumors. Since we did not find a statistically significant difference in $p21^{WAF1}$ expression between the group of patients subjected to preoperative radiotherapy and the remaining 93 rectal tumors not treated with preoperative radiotherapy (Table 1), the former was included in the study.

Time from the surgery until the time of death due to cancer or to last known follow-up was regarded as OS, and the time until the first appearance of metastasis or local recurrence was regarded as DFS. The median follow-up was 54 months (mean, 57.3±30.5 months; range, 5–143 months). During the follow-up, 66 of the 275 (24%) patients died of their disease, and 165 (60%) were alive without symptoms from the disease. Recurrences were found in 106 patients. Four patients died of non-cancer-related causes, and they were treated as censored observations.

Tissue microarray (TMA) construction Tumor areas with the highest mitotic activity at the outer invasive zone of the cancer were chosen for tissue microarrays which were constructed as previously described [26].

Immunohistochemistry Slides with tissue microarrays were deparaffinized, rehydrated, and had the endogenous peroxidase activity blocked. Slides were immersed in pH 9.0 buffer, and heat-induced antigen retrieval was performed in a pressure cooker (Pascal, Dako, Glostrup, Denmark). Monoclonal $p21^{WAF1}$ antibody (Dako) was used (dilution, 1:25; incubation time, 30 min), and the slides were immunostained using a Dako EnVision+ kit according to the manufacturer's instructions. We used the sensitive EnVision+ visualization system because the detection system used is regarded as a critically important variable in immunohistochemical analysis, and detection methods using signal amplification with HRP-labeled polymers have been shown to be more sensitive than methods without such a layer of amplification [27]. The reaction was developed with diaminobenzidine substrate–chromogen solution, and the slides were counterstained with hematoxylin. Positive controls included colorectal adenocarcinoma previously shown to have a high level of $p21^{WAF1}$ expression. Negative controls omitted the primary antibody. The immunohistochemical procedure for all tissue microarrays from 275 tumors was performed at the same time in identical conditions because, instead of 275 histological slides of whole tissue sections, only four slides containing tissue cores from all 275 tumors were processed.

Scoring Immunohistochemical staining for each tumor core was independently assessed by two observers (PD and WD) who were blinded to the clinical and pathological data. In cases of disagreement, the result was reached by consensus. The percentage of tumor cell nuclei with unequivocal staining was recorded for each core. $P21^{WAF1}$ expression in tumors was variable, and so, tumors were classified as negative (<1% of positive tumor cells) or positive (if ≥1% of tumor cells showed nuclear immunoreactivity).

Statistical analysis Associations between the presence of $p21^{WAF1}$ expression in tumors and other categorical variables were analyzed with the Fisher exact test. The Kaplan–Meier method was used for the univariate survival analysis, and the differences between compared groups were assessed by the log-rank test. A Cox proportional hazards model was used for univariate and multivariate analyses of factors associated with OS and DFS. The independent variables included in the model were: age, gender, tumor site, Astler–Coller stage, histological grade, 5FU-based adjuvant chemotherapy, and presence of $p21^{WAF1}$ expression. A $p<0.05$ was considered statistically significant. STATISTICA version 9.1 (StatSoft Inc., Tulsa, USA) was used for the statistical analysis.

Results

Expression of $p21^{WAF1}$ (Fig. 1a–d) was found in the nuclei of 60.4% (166/275) of all cases, in 54.1% (72/133) of stage B2 cancers, and in 66.2% (94/142) of stage C tumors. Of all the parameters examined, only Astler–Coller stage was associated with $p21^{WAF1}$ expression (Table 1).

Group B2 No association was found between $p21^{WAF1}$ expression and DFS or OS in the whole B2 group, neither in univariate or multivariate analysis (data not shown). However, 83 patients in this group were treated with 5FU-based adjuvant chemotherapy, and 50 patients were not. Further analysis of the association of $p21^{WAF1}$ expression with DFS and OS in these subgroups showed that expression of $p21^{WAF1}$ was associated with DFS (p=0.025) and OS (p=0.0079) only in the subgroup of stage B2 patients that were treated with adjuvant chemotherapy (Fig. 2a). Moreover, $p21^{WAF1}$ expression remained in this subgroup as the only independent prognostic parameter in the multivariate analysis in relation to DFS and OS (p=0.035 and p=0.02, respectively; Table 2). In the stage B2 subgroup of patients not treated with chemotherapy, none

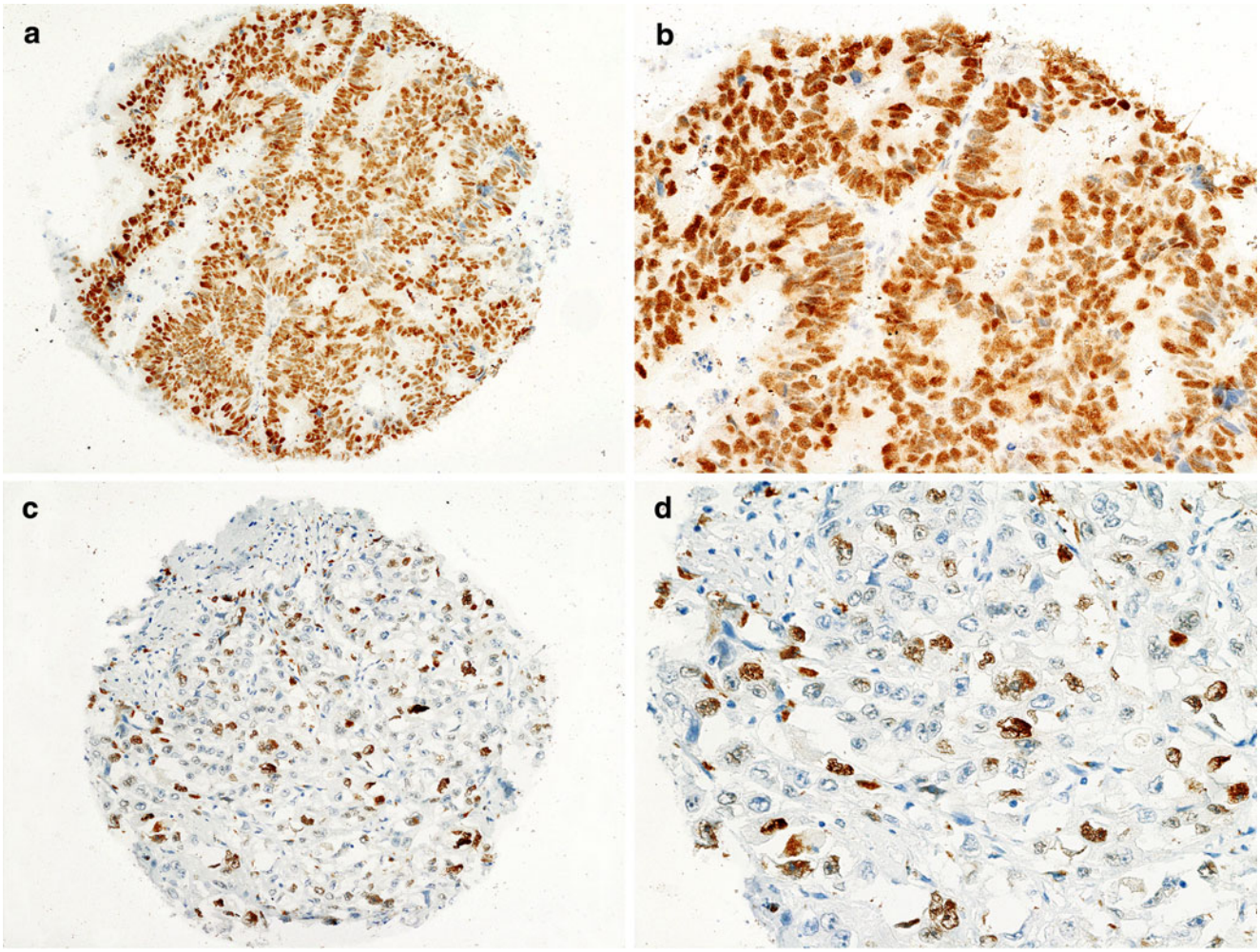

Fig. 1 Expression of $p21^{WAF1}$ in representative cores of CRC. **a**, **b** High expression of $p21^{WAF1}$ in the nuclei of tumor cells. **c**, **d** Low expression of $p21^{WAF1}$ in the nuclei of cancer cells. **b**, **d** Fragments of the cores from a and c, respectively, at high magnification

of the parameters studied were associated with DFS or OS (data not shown).

In the subgroup of 72 stage B2 patients with $p21^{WAF1}$ expression, adjuvant chemotherapy was associated with better DFS (85% 5-year survival versus 65% without chemotherapy, $p=0.03$; Fig. 2b) and OS (96% 5-year survival versus 82% without chemotherapy, $p=0.014$; Fig. 2b). In the subgroup of 61 stage B2 patients with negative $p21^{WAF1}$ expression, a trend for the association of chemotherapy with worse survival (both DFS and OS) was observed, but the differences were not statistically significant (data not shown).

Group C The expression of $p21^{WAF1}$ in tumors of patients treated with adjuvant chemotherapy was associated with DFS in a univariate analysis (HR=0.58, 95% CI=0.34–0.99, $p=0.047$) and was on the verge of statistical significance in the multivariate analysis ($p=0.07$) (Table 2). In terms of OS, there was a statistically significant association with $p21^{WAF1}$ expression in both the univariate (HR=0.41, 95% CI=0.21–0.80, $p=0.008$) and multivariate ($p=0.03$) (Table 2) analyses. Kaplan–Meier survival curves of patients with $p21^{WAF1}$ expression in the nuclei of cancer cells indicate better DFS ($p=0.055$) and significantly better OS (72% versus 45% 5-year survival of patients with negative $p21^{WAF1}$ expression, $p=0.0079$; Fig. 2c).

Stage B2+C patients treated with adjuvant chemotherapy Expression of $p21^{WAF1}$ was associated with DFS and OS ($p=0.03$ and $p=0.002$, respectively) in a univariate analysis. The Astler–Coller stage and $p21^{WAF1}$ expression were found to be independent prognostic factors for DFS and OS (Table 3). In multivariate analysis, there was no statistically significant association between site of CRC

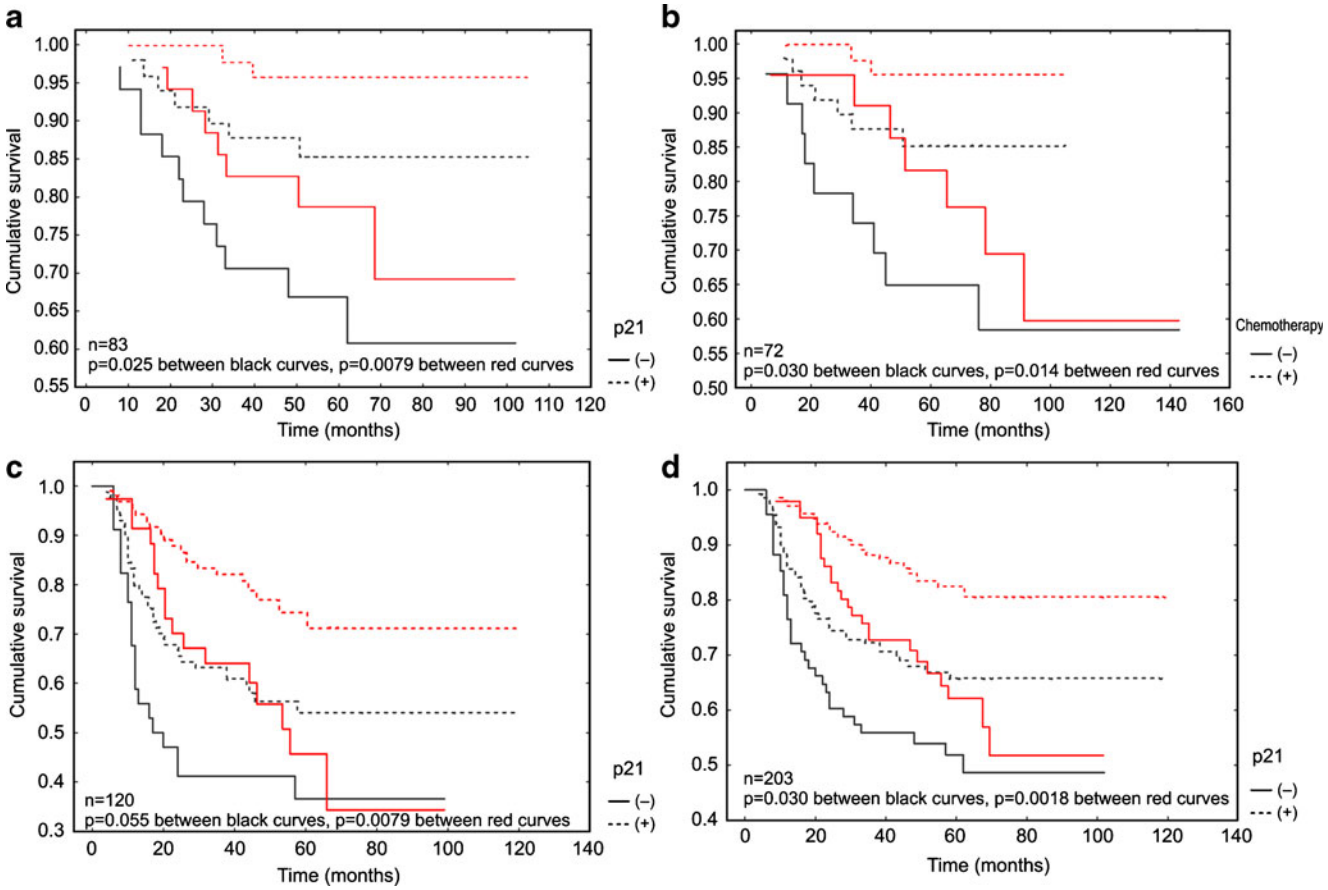

Fig. 2 DFS (*black curves*) and OS (*red curves*) of stage B2 patients treated with adjuvant chemotherapy categorized according to the p21 expression (n=83) (**a**) and of stage B2 patients with p21-positive tumors categorized according to adjuvant chemotherapy (n=72) (**b**). DFS (*black curves*) and OS (*red curves*) of stage C patients (n=120) (**c**) and of stage B2+C patients (n=203) (**d**) treated with adjuvant chemotherapy categorized according to p21 expression

(neither rectum versus colon nor proximal versus distal as defined by the splenic flexure) and DFS (p=0.77, p=0.28, respectively) or OS (p=0.77, p=0.28, respectively). Kaplan–Meier survival curves showed significantly better DFS and OS of patients with tumors showing $p21^{WAF1}$ expression as compared to those negative for $p21^{WAF1}$ (p=0.03 and p=0.0018, respectively; Fig. 2d).

Discussion

We found $p21^{WAF1}$ nuclear expression in 60.4% CRCs which is comparable to the literature data (16–87%) [11, 13–15, 28, 29]. The majority of reports (but not all) concerning the prognostic role of $p21^{WAF1}$ expression in CRCs indicate better OS and/or DFS for patients with

Table 2 Multivariate analysis of disease-free and overall survival of stage B2 and C patients treated with adjuvant chemotherapy

Category	B2 (n=83)				C (n=120)			
	Disease-free survival		Overall survival		Disease-free survival		Overall survival	
	Hazard ratio (95% CI)	p	Hazard ratio (95% CI)	p	Hazard ratio (95% CI)	p	Hazard ratio (95% CI)	p
Sex	0.97 (0.37–2.53)	0.95	0.99 (0.24–4.04)	0.99	1.21 (0.71–2.08)	0.49	1.50 (0.73–3.05)	0.27
Age	0.99 (0.95–1.03)	0.63	1.00 (0.94–1.07)	0.99	1.02 (0.99–1.05)	0.12	1.02 (0.99–1.05)	0.29
Grade	0.56 (0.20–1.57)	0.27	0.39 (0.08–1.86)	0.24	1.93 (1.12–3.33)	*0.018*	2.87 (1.37–6.01)	*0.005*
Tumor site	0.99 (0.29–3.47)	0.10	2.55 (0.64–10.15)	0.19	0.57 (0.27–1.17)	0.13	0.35 (0.10–1.15)	0.08
$P21^{WAF1}$	0.36 (0.14–0.93)	*0.035*	0.16 (0.03–0.76)	*0.02*	0.60 (0.35–1.04)	0.07	0.48 (0.24–0.93)	*0.03*

Table 3 Multivariate analysis of disease-free and overall survival of patients treated with adjuvant chemotherapy (group B2+C, *n*=203)

Category	Disease-free survival		Overall survival	
	Hazard ratio (95% Cl)	*p*	Hazard ratio (95% Cl)	*p*
Sex	1.20 (0.75–1.90)	0.44	1.42 (0.77–2.65)	0.27
Age	1.01 (0.99–1.03)	0.32	1.01 (0.98–1.04)	0.58
Astler–Coller	3.16 (1.86–5.36)	*<0.0001*	3.60 (1.77–7.33)	*0.0004*
Grade	1.48 (0.94–2.32)	0.09	1.95 (1.07–3.56)	*0.03*
Tumor site	0.64 (0.34–1.20)	0.17	0.62 (0.26–1.49)	0.28
$P21^{WAF1}$	0.52 (0.33–0.83)	*0.0062*	0.36 (0.20–0.66)	*0.0009*

tumors showing $p21^{WAF1}$ expression (Table 4). In some of these reports, $p21^{WAF1}$ expression was an independent prognostic factor for OS and/or DFS (Table 4). However, in those reports, patients with various stages of the disease who were subjected to different treatment protocols (surgery alone, surgery and adjuvant chemotherapy, radiochemotherapy) were often grouped together for the analysis, or no information on the mode of therapy is given. Thus, it is difficult to infer whether stage II patients with $p21^{WAF1}$-positive tumors may receive any benefit from adjuvant chemotherapy.

The benefit of adjuvant 5FU-based chemotherapy has been firmly established for patients with stage III CRC. However, in the stage B2 group, it is not known whether the survival benefit from chemotherapy is sufficient to outweigh the toxicity and cost of the treatment [2]. Only one study [20] has addressed the issue of the influence of 5FU-based adjuvant chemotherapy on the survival of patients with stage B2 CRC in relation to $p21^{WAF1}$ expression. In that study, pretreatment levels of $p21^{WAF1}$ were not related to survival of patients with stage II (and III) CRC treated with adjuvant chemotherapy. However, increased levels of $p21^{WAF1}$ were associ-

Table 4 Major reports on $p21^{WAF1}$ expression and survival of patients with CRCs

Source	Study group	Stage of CRC and type of treatment	Results
Cheng J.D., et al. [10]	*n*=39	Metastatic CRC 5FU CHTH	5FU responders had greater p21 expression
Ropponen K.M, et al. [11]	*n*=162	0–D incl. 62–B majority: surgery only; 22–CHTH	Better OS and RFS for patients with p21+ tumors; p21: independent prognostic parameter for OS and RFS (MA)
Viale G., et al. [12]	*n*=191	I–IV CHTH?	↓p21→poor OS and DFS (UA)
Bukholm I.K., et al. [13]	*n*=61	B–D CHTH?	Low p21→increased risk of metastases and death
Zirbes T.K., et al. [14]	*n*=294	I–IV incl. 90–II. surgery CHTH?	Better OS for patients with p21+ tumors; p21 independent prognostic parameter (MA)
Holland T.A., et al. [15]	*n*=126	A–D RCHTH?	Better OS for patients with high p21 expression
Pasz-Walczak G., et al. [16]	*n*=122	I–IV CHTH?	Better OS for patients with p21+ tumors (UA)
Watanabe T., et al. [20]	*n*=460	II (B)–105 III (C)–355, 5FU CHTH	No association of p21 expression with survival in all and in stage B tumors
Hoss A., et al. [21]	*n*=100	T2–3, N0 rectum, surgery only	No association of p21 expression with survival
Schwandner O., et al. [17]	*n*=160	I–III rectum, surgery, *n*=69 surgery+CHTH+RT, *n*=91	Better RFS but not OS for patients with p21+ tumors; p21 independent prognostic parameter for RFS but not OS (MA)
Rau B., et al. [22]	*n*=66	T3–4, N0–2, M0–1 rectum, RCHTH	No prognostic significance of pretreatment p21 expression. Post-treatment increase of p21: shorter DFS
Prall F., et al. [18]	*n*=184	I–IV incl. 55-III, III: *n*=32 -5FU, *n*=23-5FU+RT	Better OS for patients with p21+tumors (MA)
Mitomi H., et al. [19]	*n*=211	B–D incl. 83-B CHTH for C–D	Better OS for patients with high p21 expression; p21 independent prognostic parameter (MA)
Ioachim E., et al. [23]	*n*=97	Dukes B, C, surgery, CHTH?	No association of p21 expression with OS and DFS
Noske A., et al. [24]	*n*=116	II–III RCHTH	Better RFS and OS for patients with p21- tumors

↓ down regulation, *UA* univariate analysis, *MA* multivariate analysis, *OS* overall survival, *DFS* disease-free survival, *RFS* relapse-free survival, *RT* radiotherapy, *CHTH* chemotherapy, *RCHTH* radiochemotherapy, *?* not known

ated with the sensitivity of metastatic CRC to 5FU-based chemotherapy [10].

Our results indicate for the first time that $p21^{WAF1}$ expression in CRC tumor cells is an independent factor that is associated with favorable DFS and OS in patients with stage B2 tumors treated with 5FU-based adjuvant chemotherapy. Striking survival benefits were seen for stage B2 patients who received adjuvant chemotherapy compared with those who did not. Conversely, chemotherapy did not significantly influence DFS or OS of stage B2 patients with $p21^{WAF1}$-negative tumors. Rather, a statistically non-significant trend towards worse survival was observed for stage B2 patients with $p21^{WAF1}$-negative tumors treated with chemotherapy. The differences between our results and those of Watanabe et al. [20] may be attributed to the different scoring systems and different cutoff points used for the interpretation of immunohistochemical staining, as well as to differences in immunohistochemical methods. The major advantage of tissue microarrays is that tens of cases can be processed in identical laboratory conditions which greatly improves the reproducibility of the immunohistochemical method. Prall et al. [18] used tissue microarrays (n=184) and found better OS for combined group of stage I–IV patients with $p21^{WAF1}$-positive tumors. Our results (from the whole group) are well in accord with this report and give further support for the association of $p21^{WAF1}$ expression and longer survival of patients with stage C/III CRCs treated with adjuvant 5FU-based chemotherapy as has been reported previously (Table 4). One limitation of TMA technology is that "punched" cores from donor tissues may not always be representative of the entire tumor. In this report, we applied one core from carefully identified, histologically relatively homogenous area with the highest mitotic activity in the outer invasive zone of each CRC. Using this approach, we found 60.4% of $p21^{WAF1}$-positive CRCs which is within the range reported in the literature. Hoos et al. [30] reported that correlations between phenotypes and clinical outcome were not significantly different between full sections and triplicate 0.6-mm core tissue microarrays. However, on the other hand, they were not significantly different when only one 0.6-mm core tissue microarray was used [31]. The authors of the latter report conclude that tissue microarray "with a single core per specimen ensures full biological representativeness to identify the associations between biomarkers and clinicopathological parameters, with no significant associated sampling bias." So, careful sampling of the representative region of the tumor is regarded as the key step in the construction of tissue microarrays.

TS, the target enzyme for 5FU, is essential for DNA synthesis [32], and it may function as an oncogene [33]. Inhibition of TS induces apoptosis and cytotoxicity in human colorectal cancer cells [7]. The importance of $p21^{WAF1}$ in the response of CRC to chemotherapeutic agents is supported by in vitro studies [7–9]. It has been reported that $p21^{WAF1}$ (a CDK inhibitor) regulates thymineless stress-induced cytotoxicity of human colon carcinoma cell lines [7]. Also, TS expression is mediated through the inhibition of CDK: TS expression was upregulated by the knockout of the $p21^{WAF1}$ gene in a CRC cell line [8]. In addition, reduction of TS expression results in enhancement of the sensitivity to 5FU in human CRC cell lines [8]. Our results are in line with other reports that show that $p21^{WAF1}$ is a critical mediator of the cytotoxic action of TS inhibitors in cultured human colorectal cancer cells [7] and that CDK inhibitor enhances the sensitivity to 5FU in colorectal cancer cell lines [8]. In fact, $p21^{WAF1}$ is required for maximal cytotoxicity induced by thymineless stress in colorectal cancer cells in culture [7]. Poor survival of patients with $p21^{WAF1}$-negative tumors treated with adjuvant 5FU-based chemotherapy may perhaps be attributed to inherent resistance to 5FU. It has been shown that development of resistance to 5FU by colon cancer cell lines is associated with downregulation of the *CDKN1A* gene, along with other genes engaged in DNA damage response/repair pathway [34].

In summary, we found that $p21^{WAF1}$ expression in CRC tumor cells identifies a subgroup of Astler–Coller stage B patients who would benefit significantly from 5FU-based chemotherapy and may therefore allow for better selection of patients for adjuvant chemotherapy. We believe that, in order to maximize the benefit of 5FU-based adjuvant therapy and to spare patients from unnecessary toxicity, stage B2 patients should be stratified according to $p21^{WAF1}$ status. However, because this is a retrospective study, our results should be confirmed by further prospective randomized investigations.

Acknowledgments This work was supported by the grant KBN 2P05B 174 28 from the Committee for Scientific Research.

Conflict of interest We declare that we have no conflict of interest.

Open Access This article is distributed under the terms of the Creative Commons Attribution Noncommercial License which permits any noncommercial use, distribution, and reproduction in any medium, provided the original author(s) and source are credited.

References

1. Wolpin BM, Meyerhardt JA, Mamon HJ, Mayer RJ (2007) Adjuvant treatment of colorectal cancer. CA Cancer J Clin 57:168–185
2. Wolpin BM, Mayer RJ (2008) Systemic treatment of colorectal cancer. Gastroenterology 134:1296–1310
3. Segal NH, Saltz LB (2008) Is adjuvant therapy for stage II colon cancer worthwhile, and for whom? Nat Clin Pract Gastroenterol Hepatol 5:422–423

4. Pinedo HM, Peters GF (1988) Fluorouracil: biochemistry and pharmacology. J Clin Oncol 6:1653–1664
5. Dotto GP (2000) p21(WAF1/Cip1): more than a break to the cell cycle? Biochim Biophys Acta 1471:M43–56
6. Doglioni C, Pelosio P, Laurino L, Macri E, Meggiolaro E, Favretti F, Barbareschi M (1996) p21/WAF1/CIP1 expression in normal mucosa and in adenomas and adenocarcinomas of the colon: its relationship with differentiation. J Pathol 179:248–253
7. Geller JI, Szekely-Szucs K, Petak I, Doyle B, Houghton JA (2004) P21Cip1 is a critical mediator of the cytotoxic action of thymidylate synthase inhibitors in colorectal carcinoma cells. Cancer Res 64:6296–6303
8. Takagi K, Sowa Y, Cevik OM, Nakanishi R, Sakai T (2008) CDK inhibitor enhances the sensitivity to 5-fluorouracil in colorectal cancer cells. Int J Oncol 32:1105–1110
9. O'Connor PM, Jackman J, Bae I, Myers TG, Fan S, Mutoh M, Scudiero DA, Monks A, Sausville EA, Weinstein JN, Friend S, Fornace AJ Jr, Kohn KW (1997) Characterization of the p53 tumor suppressor pathway in cell lines of the National Cancer Institute anticancer drug screen and correlations with the growth-inhibitory potency of 123 anticancer agents. Cancer Res 57:4285–4300
10. Cheng JD, Werness BA, Babb JS, Meropol NJ (1999) Paradoxical correlations of cyclin-dependent kinase inhibitors p21waf1/cip1 and p27kip1 in metastatic colorectal carcinoma. Clin Cancer Res 5:1057–1062
11. Ropponen KM, Kellokoski JK, Lipponen PK, Pietilainen T, Eskelinen MJ, Alhava EM, Kosma VM (1999) p22/WAF1 expression in human colorectal carcinoma: association with p53, transcription factor AP-2 and prognosis. Br J Cancer 81:133–140
12. Viale G, Pellegrini C, Mazzarol G, Maisonneuve P, Silverman ML, Bosari S (1999) p21WAF1/CIP1 expression in colorectal carcinoma correlates with advanced disease stage and p53 mutations. J Pathol 187:302–307
13. Bukholm IK, Nesland JM (2000) Protein expression of p53, p21 (WAF1/CIP1), bcl-2, Bax, cyclin D1 and pRb in human colon carcinomas. Virchows Arch 436:224–228
14. Zirbes TK, Baldus SE, Moenig SP, Nolden S, Kunze D, Shafizadeh ST, Schneider PM, Thiele J, Hoelscher AH, Dienes HP (2000) Prognostic impact of p21/waf1/cip1 in colorectal cancer. Int J Cancer 89:14–18
15. Holland TA, Elder J, McCloud JM, Hall C, Deakin M, Fryer AA, Elder JB, Hoban PR (2001) Subcellular localisation of cyclin D1 protein in colorectal tumours is associated with p21(WAF1/CIP1) expression and correlates with patient survival. Int J Cancer 95:302–306
16. Pasz-Walczak G, Kordek R, Faflik M (2001) P21 (WAF1) expression in colorectal cancer: correlation with P53 and cyclin D1 expression, clinicopathological parameters and prognosis. Pathol Res Pract 197:683–689
17. Schwandner O, Bruch HP, Broll R (2002) p21, p27, cyclin D1, and p53 in rectal cancer: immunohistology with prognostic significance? Int J Colorectal Dis 17:11–19
18. Prall F, Ostwald C, Nizze H, Barten M (2004) Expression profiling of colorectal carcinomas using tissue microarrays: cell cycle regulatory proteins p21, p27, and p53 as immunohistochemical prognostic markers in univariate and multivariate analysis. Appl Immunohistochem Mol Morphol 12:111–121
19. Mitomi H, Ohkura Y, Fukui N, Kanazawa H, Kishimoto I, Nakamura T, Yokoyama K, Sada M, Kobayashi K, Tanabe S, Saigenji K (2007) P21WAF1/CIP1 expression in colorectal carcinomas is related to Kras mutations and prognosis. Eur J Gastroenterol Hepatol 19:883–889
20. Watanabe T, Wu TT, Catalano PJ, Ueki T, Satriano R, Haller DG, Benson AB 3rd, Hamilton SR (2001) Molecular predictors of survival after adjuvant chemotherapy for colon cancer. N Engl J Med 344:1196–1206
21. Hoos A, Nissan A, Stojadinovic A, Shia J, Hedvat CV, Leung DH, Paty PB, Klimstra D, Cordon-Cardo C, Wong WD (2002) Tissue microarray molecular profiling of early, node-negative adenocarcinoma of the rectum: a comprehensive analysis. Clin Cancer Res 8:3841–3849
22. Rau B, Sturm I, Lage H, Berger S, Schneider U, Hauptmann S, Wust P, Riess H, Schlag PM, Dorken B, Daniel PT (2003) Dynamic expression profile of p21WAF1/CIP1 and Ki-67 predicts survival in rectal carcinoma treated with preoperative radiochemotherapy. J Clin Oncol 21:3391–3401
23. Ioachim E (2008) Expression patterns of cyclins D1, E and cyclin-dependent kinase inhibitors p21waf1/cip1, p27kip1 in colorectal carcinoma: correlation with other cell cycle regulators (pRb, p53 and Ki-67 and PCNA) and clinicopathological features. Int J Clin Pract 62:1736–1743
24. Noske A, Lipka S, Budczies J, Muller K, Loddenkemper C, Buhr HJ, Kruschewski M (2009) Combination of p53 expression and p21 loss has an independent prognostic impact on sporadic colorectal cancer. Oncol Rep 22:3–9
25. Astler VB, Coller FA (1954) The prognostic significance of direct extension of carcinoma of the colon and rectum. Ann Surg 139:846–852
26. Sulzyc-Bielicka V, Domagala P, Majdanik E, Chosia M, Bielicki D, Kladny J, Kaczmarczyk M, Safranow K, Domagala W (2009) Nuclear thymidylate synthase expression in sporadic colorectal cancer depends on the site of the tumor. Virchows Arch 454:695–702
27. Chung GG, Kielhorn EP, Rimm DL (2002) Subjective differences in outcome are seen as a function of the immunohistochemical method used on a colorectal cancer tissue microarray. Clin Colorectal Cancer 1:237–242
28. Sinicrope FA, Roddey G, Lemoine M, Ruan S, Stephens LC, Frazier ML, Shen Y, Zhang W (1998) Loss of p21WAF1/Cip1 protein expression accompanies progression of sporadic colorectal neoplasms but not hereditary nonpolyposis colorectal cancers. Clin Cancer Res 4:1251–1261
29. Valassiadou KE, Stefanaki K, Tzardi M, Datseris G, Georgoulias V, Melissas J, Tsiftsis DD, Delides G, Kanavaros P (1997) Immunohistochemical expression of p53, bcl-2, mdm2 and waf1/p21 proteins in colorectal adenocarcinomas. Anticancer Res 17:2571–2576
30. Hoos A, Urist MJ, Stojadinovic A, Mastorides S, Dudas ME, Leung DH, Kuo D, Brennan MF, Lewis JJ, Cordon-Cardo C (2001) Validation of tissue microarrays for immunohistochemical profiling of cancer specimens using the example of human fibroblastic tumors. Am J Pathol 158:1245–1251
31. Zhang D, Salto-Tellez M, Putti TC, Do E, Koay ES (2003) Reliability of tissue microarrays in detecting protein expression and gene amplification in breast cancer. Mod Pathol 16:79–84
32. Longley DB, Harkin DP, Johnston PG (2003) 5-Fluorouracil: mechanisms of action and clinical strategies. Nat Rev Cancer 3:330–338
33. Rahman L, Voeller D, Rahman M, Lipkowitz S, Allegra C, Barrett JC, Kaye FJ, Zajac-Kaye M (2004) Thymidylate synthase as an oncogene: a novel role for an essential DNA synthesis enzyme. Cancer Cell 5:341–351
34. De Angelis PM, Svendsrud DH, Kravik KL, Stokke T (2006) Cellular response to 5-fluorouracil (5-FU) in 5-FU-resistant colon cancer cell lines during treatment and recovery. Mol Cancer 5:20

Virchows Arch (2011) 458:439–451
DOI 10.1007/s00428-011-1056-3

ORIGINAL ARTICLE

Precursor lesions of early onset pancreatic cancer

Łukasz Liszka · Jacek Pająk · Sławomir Mrowiec · Ewa Zielińska-Pająk · Dariusz Gołka · Paweł Lampe

Received: 18 October 2010 / Revised: 3 February 2011 / Accepted: 7 February 2011 / Published online: 3 March 2011
© The Author(s) 2011. This article is published with open access at Springerlink.com

Abstract Early onset pancreatic cancer (EOPC) constitutes less than 5% of all newly diagnosed cases of pancreatic cancer (PC). Although histopathological characteristics of EOPC have been described, no detailed reports on precursor lesions of EOPC are available. In the present study, we aimed to describe histopathological picture of extratumoral parenchyma in 23 cases of EOPCs (definition based on the threshold value of 45 years of age) with particular emphasis on two types of precursor lesions of PC: pancreatic intraepithelial neoplasia (PanIN) and intraductal papillary mucinous neoplasms (IPMNs). The types, grades, and densities of precursor lesions of PC were compared in patients with EOPCs, in young patients with neuroendocrine neoplasms (NENs), and in older (at the age of 46 or more) patients with PC. PanINs were found in 95.6% of cases of EOPCs. PanINs-3 were found in 39.1% of EOPC cases. Densities of all PanIN grades in EOPC cases were larger than in young patients with NENs. Density of PanINs-1A in EOPC cases was larger than in older patients with PC, but densities of PanINs of other grades were comparable. IPMN was found only in a single patient with EOPC but in 20% of older patients with PC. PanINs are the most prevalent precursor lesions of EOPC. IPMNs are rarely precursor lesions of EOPC. Relatively high density of low-grade PanINs-1 in extratumoral parenchyma of patients with EOPC may result from unknown multifocal genetic alterations in pancreatic tissue in patients with EOPCs.

Keywords Pancreas · Pancreatic neoplasms · Pancreatic ductal carcinoma · Pancreatic ducts · Intraepithelial carcinoma

Ł. Liszka (✉) · J. Pająk · E. Zielińska-Pająk · D. Gołka
Department of Histopathology, Medical University of Silesia,
Medyków 18,
40–754 Katowice, Poland
e-mail: lliszka@mp.pl

S. Mrowiec · P. Lampe
Department of Gastrointestinal Surgery,
Medical University of Silesia,
Katowice, Poland

D. Gołka
Department of Pathology, Victoria Hospital,
Blackpool, UK

Introduction

Pancreatic cancer (PC) is one of the most frequent and most deadly abdominal cancers [1]. The mean age of patients diagnosed with PC of ductal origin (i.e., ductal adenocarcinoma) in the USA is 70.2 years (Surveillance, Epidemiology, and End Results database, 1988–2003) [2]. PC is a rare diagnosis in young patients. Early onset PC (EOPC, definition based on the threshold of 40, 45, or 50 years of age [3–9]) constitutes less than 5% of all newly diagnosed cases of PC [4, 6, 9]. Nowadays, it is clear that cancers in young patients need a specific management since they often differ in molecular, epidemiological, and therapeutic aspects from cancers in older population [10, 11]. Several groups of investigators studied the issue of EOPC [3, 4, 6–9, 12]. Inherited predisposition and smoking are believed to be the major EOPC risk factors [6]. Younger age of an individual patient at the PC onset may be a hallmark of so-called familial PC [13]. However, the mean age of patients with familial PC is less than 5 years younger than the mean age of patients with sporadic PC [13]. That is why only a small portion of patients with familial PC are diagnosed as EOPC [4]. Unfortunately, there are no sensitive nor specific clinical, histopathological, genomic, or proteomic features which could clearly distinguish EOPC from PC in older patients [3, 9].

Pancreatic intraepithelial neoplasia (PanIN) is a well-recognized and extensively studied precursor lesion of PC of ductal lineage [14–23]. PanINs may present as flat, micropapillary, or papillary noninvasive intraductal lesions, which usually develop within small pancreatic ducts (less than 5 mm [18–20] or less than 10 mm in diameter [15]). PanINs are divided into four categories based on grade of dysplasia (1A, 1B, 2, and 3) [15–18, 20, 21, 23]. Low-grade PanINs (PanINs-1A, PanINs-1B, PanINs-2) may be found in pancreata of 16–80% of individuals without any clinically detectable pancreatic disease. In contrast, PanINs-3 are very rarely seen in pancreata of individuals without PC [reviewed in Refs. 16, 17]. In a proportion of cases, PanINs (particularly low-grade ones) may be associated with obstruction of branch pancreatic ducts. This may lead to localized atrophy of pancreatic lobule [focal lobular atrophy (FLA)] drained by the affected duct and subsequent focal fibrosis of the pancreatic parenchyma [24]. Atrophy and fibrosis within areas of FLA are frequently associated with acinar–ductal metaplasia and formation of so-called tubular complexes. Tubular complexes may develop within atrophic lobules with or without associated PanIN within a draining duct. At the advanced stage of this process, mucinous metaplasia within ductules of tubular complexes may develop (mucinous tubular complexes) [25, 26]. It should be distinguished from PanIN (i.e., mucinous change within pre-existing duct) [27].

PanINs and FLAs are more frequent in older individuals, and therefore, they are believed to represent an age-related phenomenon [24, 28, 29]. However, PanIN–FLA complexes are particularly frequent in pancreata of individuals with a strong family history of PC [19, 26, 30]. This may be very useful for screening of persons with high risk of developing PC, since FLAs may be visualized by endoscopic ultrasonography [19, 26, 30–34].

Up to 20% of ductal PC (both sporadic and familial) are derived from other type of PC precursor lesions–intraductal papillary mucinous neoplasms (IPMNs) [19].

Rare reports on histopathological characteristics of EOPCs are available [3, 9]. In contrast, we are not aware of any detailed reports on precursor lesions of EOPC. Therefore, in the present study, we aimed to provide a histopathological description of extratumoral pancreatic parenchyma (EPP) in patients with EOPCs. We particularly emphasized morphological types of EOPC precursor lesions and their density in EPP.

Materials and methods

The study was performed in concordance with the Helsinki Declaration.

Study design and selection of cases

We reviewed retrospectively all cases of pancreatic resections received and diagnosed in our institution between January 1985 and December 2010. In all cases, available clinical data, gross pathology reports, as well as microscopic slides, were reexamined by two of the authors (LL and JP). Histopathological diagnoses were based on the criteria published in the U.S. Armed Forces Institute of Pathology Fascicle [35] and the recent World Health Organization reference book [36]. A minority (less than 10%) of cases were not available for rereview, and these cases were excluded from the study.

The main study group (EOPC cases)

The main study group included patients with pancreatic ductal adenocarcinoma diagnosed at the age of 45 and younger between 1985 and 2010. These patients were diagnosed as EOPCs. The age cut-off value we implemented here (45 years) was selected based on the largest so far study of patients with EOPC performed by Dr. Duffy and associates at Memorial Sloan Kettering Cancer Center, New York [4]. Patients with neoplasms of non-ductal origin [e.g., acinar cell carcinomas, neuroendocrine neoplasms (NENs), solid pseudopapillary neoplasms] were carefully excluded from the main study group. Cases of invasive carcinomas associated with mucinous cystic neoplasms were also excluded since their pathogenesis, demographic characteristics, and clinical presentation differ in significant extent from those of PCs [35, 36].

Control groups

For comparative purposes, we distinguished two control groups.

Control group 1 included cases of primary pancreatic NENs diagnosed in patients at the age of 45 or less between 1985 and 2010. That control group was established since it is highly probable that the prevalence of PC precursor lesions in patients with NENs represent their "baseline" prevalence in the general population. It was showed previously that the prevalence of PC precursor lesions in patients with NENs is primarily related to the patients' age and/or presence of chronic pancreatitis [37, 38]. Moreover, there is no convincing evidence that NENs are related pathogenetically to PanINs/IPMNs [35].

Control group 2 included patients with pancreatic ductal adenocarcinoma diagnosed at the age of 46 or older in 2009 and 2010. That control group was established since we aimed to examine whether types and density of PC precursor lesions in patients with EOPC differ from PC precursor lesions in older patients. This could potentially indicate that PCs in younger and older patients differ in some aspects of their pathogenesis.

Data collection and histopathological examination

All available slides of cases of EOPCs and control groups were examined for the presence of EPP. Since in the present study we aimed to describe the characteristics of PC precursor lesions, we selected a subgroups of cases of EOPCs, NENs in young patients, and PCs in older patients in which at least 2 cm^2 of EPP was found. In some specimens, smaller portions of EPP were available for review. In those cases, EPP was frequently localized in a very close proximity to the tumor border, and it showed usually changes compatible with mass-related atrophy and/or inflammation.

The main lesions which EPP was searched for were PanINs and IPMNs [15, 16]. In cases when the particular precursor lesion was less than 0.5 cm in diameter, it was classified as PanIN. When it was larger than 0.5 cm but smaller than 1 cm, it was called "incipient IPMN." Larger lesions were named as IPMNs. These diagnostic categories were based on the previous study [19]. The grade of dysplasia within PanINs was assessed using internationally accepted criteria [18]. In cases of IPMNs/incipient IPMNs, grade of dysplasia (low grade, moderate grade, or high grade) as well as histopathological variant (gastric foveolar, intestinal, pancreatobiliary, oncocytic) was described [35, 39]. PanINs-3 and incipient IPMNs with high-grade dysplasia were classified as high-grade PC precursor lesions [19]. Reactive atypical epithelium, transitional/squamous cell metaplasia, as well as cancerization of ducts, were taken into account in differential diagnosis of PanINs/IPMNs and carefully excluded before establishing the PanINs/IPMNs diagnosis, based on previously proposed criteria [17, 18]. In particular, abrupt transition from highly dysplastic epithelium to the "normal" epithelium, continuity of dysplastic intraductal foci with invasive carcinoma, as well as flat rather than (micro) papillary configuration of the lesion, were considered as hallmarks of secondary colonization of pre-existing ducts by invasive carcinoma rather than the presence of primary non-invasive high-grade lesion, PanIN-3 [17, 18].

EPP was also searched for foci of FLA related to PanINs [24]. Acinar cell atrophy, islet aggregation, tubular complexes, small intralobular retention cysts, fatty change, as well intralobular fibrosis, are frequently seen in FLAs [19, 24–26, 28, 30, 40–42]. Additionally, a subcategory of FLA associated with mucinous tubular complexes was separately distinguished.

EPP areas were additionally studied for other lesions of ductal origin (squamous cell metaplasia, goblet cell metaplasia, oncocytic metaplasia, mucinous nonneoplastic cysts), acinar origin (acinar cell nodules), endocrine origin (endocrine-ductular/ductuloinsular lesions, NENs), and centroacinar/intercalated origin (squamoid cysts, centroacinar cell hyperplasia, microscopic serous cystic, or solid neoplasms) [27, 35, 42, 43]. Intensity of fibrosis was described semiquantitatively as mild, moderate, or marked. Moreover, histopathological features suggestive of acute pancreatitis were documented if present [44].

Data analysis and statistics

In each case, duct profiles containing PC precursor lesions were counted. The EPP surface was measured directly on microscopical slides with the area rounded up to nearest 0.25 cm^2. The densities of PC precursor lesions were calculated as a number of lesions per square centimeter of EPP (PanIN-1A density, PanIN-1B density, PanIN-2 density, PanIN-3 density, overall PanIN density, low-grade incipient IPMN density, moderate-grade incipient IPMN density, high-grade incipient IPMN density, overall incipient IPMN density, overall PC precursor density, overall high-grade PC precursor density) [19]. PanINs and IPMNs visualized in the main pancreatic duct were documented but not included in the above counts.

Additionally, in each case, the proportion of PanINs associated with FLAs among all PanIN lesions (FLA to PanIN rate) and the proportion of PanINs associated with FLAs with mucinous tubular complexes among all PanIN lesions (rate of mucinous tubular complexes to PanINs) were calculated.

Medians of densities of PC precursor lesions, FLA-related rates, and patients' age were compared between the main study group and control groups using Mann–Whitney *U* tests. Proportions were compared between study groups using Fisher's exact tests. The statistical relationship between patients' age and PanINs' densities was assessed using the Spearman's rank correlation coefficient. All statistical tests were two-tailed. Significance was set up at $p \leq 0.05$.

Results

Basic clinical and histopathological characteristics of EOPCs and control cases

We selected only these resected cases of EOPCs, NENs in young patients, and PCs in older patients, in which adequate EPP area (at least 2 cm^2) could be examined. Therefore, the study included 23 out of 26 EOPC cases, 13 out of 22 NEN cases in young patients (the two additional enucleated tumors not taken into account), and 41 out of 44 PCs in older patients.

Two cases of PCs in older patients were then excluded since they were associated with intraductal tubulopapillary neoplasms [36]. At the moment, it is not clear whether intraductal tubulopapillary neoplasms represent a morphological variant of IPMNs or rather separate intraductal pancreatic lesions of separate origin and/or differentiation.

Basic clinical and histopathological characteristics of cases included in the present study were presented in Table 1. A single EOPC case was diagnosed as familial PC—the two first-degree relatives of that patient were affected with PC. Another EOPC patient had a family history of a single case of PC. Another EOPC patient had a family history of multiple cancers of different types and locations. There was no family history of PC in young patients with NENs. Two patients with PC older than 45 years had a first-degree relative with PC. Another two patients with PCs at the age above 45 years had a family history of several PC cases, but no case was diagnosed in first-degree relatives. No family history of three patients with PC at the age above 45 years was available. None of the patients or their family kindred in the main study group and in the control groups was diagnosed with hereditary syndromes associated in an increased risk of developing PC.

The median value of age of patients with EOPC was 6.0 years higher than the median value of age of young patients with NENs (Mann–Whitney U test, $p=0.087$, Table 1). Lack of (statistical) significance concerning that comparison might result from relatively small numbers of patients included, but we believe that difference was of no "clinical" significance. Previously reported PanIN prevalence rates in individuals in their 30s and 40s seemed to be comparable [23, 29]. It is not known, however, whether densities of PC precursor lesions in individuals in their 30s and 40s are the same.

Only 1 out of 23 EOPC cases (4.4%) was derived from IPMN. That was colloid carcinoma [45] associated with intestinal type IPMN with moderate and focally high-grade dysplasia present within the main pancreatic duct and additionally in a branch duct. In contrast, 8 out of 39 (20.5%) studied cases of PC in older patients were associated with IPMNs. That difference was of no statistical (Fisher's exact test, $p=0.136$) but possibly of clinical significance. Among older patients with PCs, two cases of colloid carcinomas were associated with intestinal type IPMNs, three cases of tubular carcinomas were associated with pancreaticobiliary-type IPMNs (one with focal oncocytic differentiation), two cases of tubular carcinomas were associated with gastric foveolar-type IPMNs and a single case of tubular carcinoma was associated with IPMN of mixed differentiation. All cases were present in main pancreatic ducts and in some proportion of branch ducts. The detailed data on clinical–pathological characteristics of all EOPC cases are to be described in a separate manuscript (in preparation).

EPP in patients with EOPCs (main study group)

Among 23 studied patients, PanINs (Fig. 1a–b) were found in 22 (95.6%) of them. PanINs-3 were found in nine (39.1%) cases. The overall PanIN density ranged from 0.0 to 2.00 lesions cm^{-2} of EPP. The PanIN-3 density ranged from 0.0 to 0.60 lesions cm^{-2} of EPP. As mentioned earlier, a single PC developed from IPMN (Fig. 2a–b). IPMNs or incipient IPMNs were not found in any other EOPC cases. FLAs (Fig. 3a–f) were present in 13 cases (from one to five lesions per case); in seven of them, they showed features of mucinous tubular complexes. The FLA to PanIN rate ranged

Table 1 Basic clinical and histopathological characteristics of patients with EOPCs and patients in control groups 1–2

Variable	Main study group: EOPCs ($n=23$)	Control group 1: NENs of the pancreas in young patients ($n=13$)	Control group 2: Ductal pancreatic adenocarcinomas in older patients ($n=39$)
Gender (male/female)	13:10	7:6	23:16
Age (median, interquartile range)	42.0 (40.0–44.0)[a]	36.0 (35.0–44.0)[a]	60.0 (55.0–66.0)
Localization (head/body/tail/more than 1 segment/not known)	18:0:2:3:0	5:1:6:0:1	37:0:1:1:0
Tumor characteristics	21 cases of conventional ductal adenocarcinoma, a single case of undifferentiated carcinoma, a single case of invasive carcinoma associated with IPMN (colloid carcinoma)	12 cases of neuroendocrine tumors G1/G2, a single case of (poorly differentiated) neuroendocrine carcinoma	30 cases of conventional ductal adenocarcinoma, a single case of undifferentiated carcinoma, eight cases of invasive carcinoma associated with IPMN (six of tubular differentiation and two of colloid differentiation)

EOPC Early onset pancreatic cancer; *NEN* neuroendocrine neoplasm; *IPMN* intraductal papillary mucinous neoplasm

[a] Median age of patients with EOPCs versus median age of young patients with NENs, Mann–Whitney U test, $p=0.087$

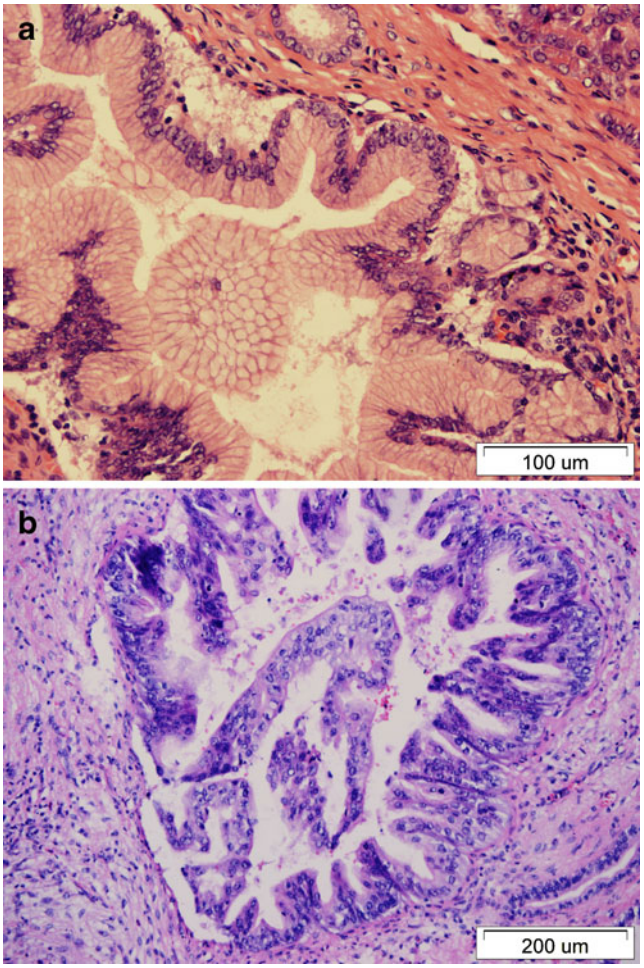

Fig. 1 **a–b** PanIN in patients with EOPCs. **a** PanIN-1B. **b** PanIN-3 (micropapillary pattern)

from 0.0 to 0.66, whereas the rate of mucinous tubular complexes to PanINs ranged from 0.0 to 0.33. Two patients showed features of moderate to marked chronic obstructive pancreatitis. Fat necrosis was seen focally in six cases. Amyloid deposits in islets, small oligocystic serous adenoma, PanIN-1A within the main pancreatic duct (not included in the above counts) were present in one case each. In one patient, there was a neuroendocrine tumor G1 coexistent with PC. In EPP of a single case, diffuse centroacinar cell hyperplasia (Fig. 4), but no PanINs were found. The significance of this finding remained unknown. In several cases, invasive carcinoma secondarily involved pre-existing ducts (Fig. 5a–b).

EPP in young patients with NENs (control group 1)

Among the 13 NENs studied, PanINs were found in eight cases. PanIN-1A lesions in the main pancreatic ducts were found in two additional cases. In a single patient, ductules with PanINs-1A were entrapped within tumor mass (so-called ductuloinsular neuroendocrine tumor). Incipient IPMNs and high-grade PC precursor lesions were absent. FLAs associated with PanINs were present in seven cases. In four of these cases, mucinous tubular complexes were found. In one patient, mucinous nonneoplastic cyst, amyloid islet depositions as well as islet microadenomatosis were found. In another patient, a small squamoid cyst was found. Focus of fat necrosis and focal squamous cell metaplasia of branch pancreatic duct were found in one case each. Features of moderate chronic pancreatitis were present in two cases. A single patient showed histopathological features of groove (paraduodenal) pancreatitis with duodenal intramural cyst.

EPP in older patients with PC (control group 2)

PanINs were found in all 39 cases studied. PanINs-3 were visualized in 30 (76.9%) out of 39 cases. The figures concerning PanIN prevalence in older patients obviously cannot be compared to the parallel values in EOPC group since the studied EPP areas in both groups did evidently differ. The overall PanIN density ranged from 0.21 to

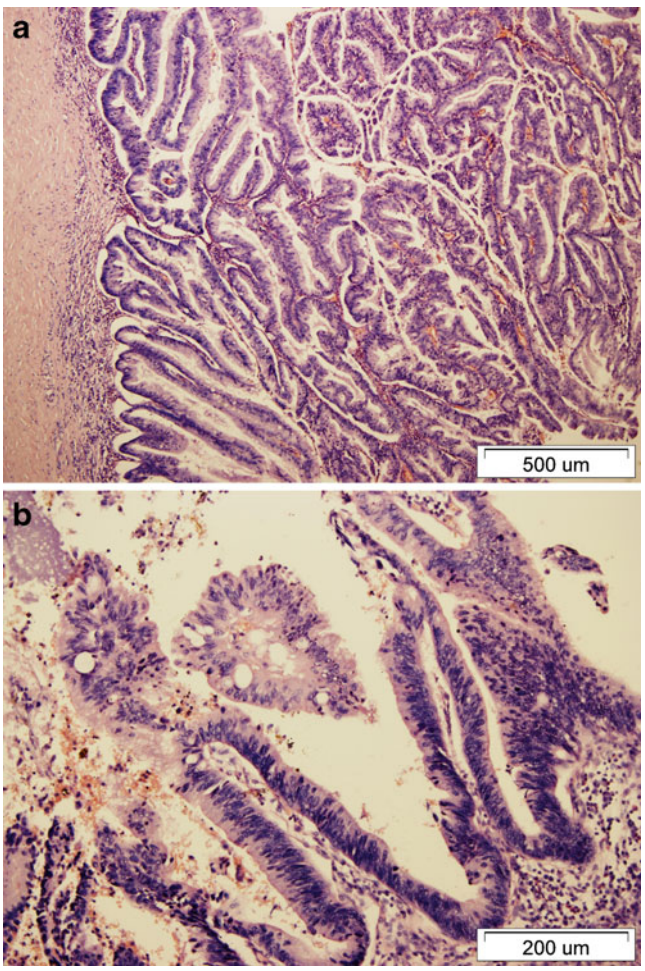

Fig. 2 **a–b** IPMN in patient with EOPC. That was intestinal type neoplasm within the main pancreatic duct and branch ducts which progressed to colloid (mucinous noncystic) carcinoma (not shown)

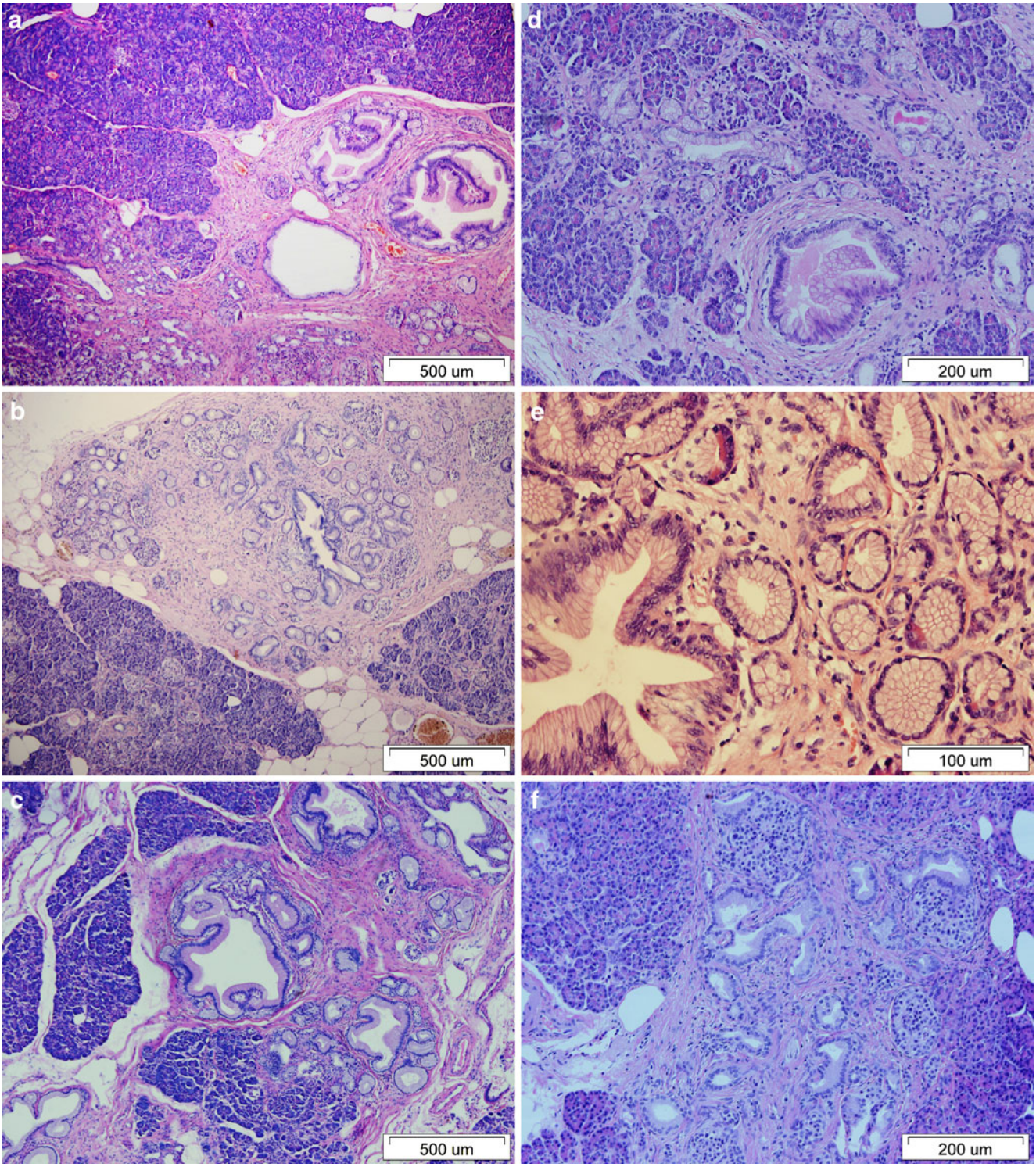

Fig. 3 **a–f** FLA related to low-grade PanIN in patients with EOPCs. Intralobular fibrosis, acinar dropout, "naked" islets, ductules with mucinous metaplasia (mucinous tubular complexes). In some tubular complexes, residual acinar cells intermixed with mucin-rich metaplastic cells (**d**, **e**). Mucinous tubular complexes in close proximity to residual islets (**f**)

1.89 lesions cm^{-2} of EPP. The PanIN-3 density ranged from 0.0 to 0.44 lesions cm^{-2} of EPP. As mentioned earlier, eight cases were associated with IPMNs. Incipient IPMNs were found in branch ducts of all of these eight patients, but they presented different grades of dysplasia, morphological types, and extent of EPP involvement. A single incipient IPMN of low-grade dysplasia and gastric foveolar differentiation was found in the EPP area peripheral to the

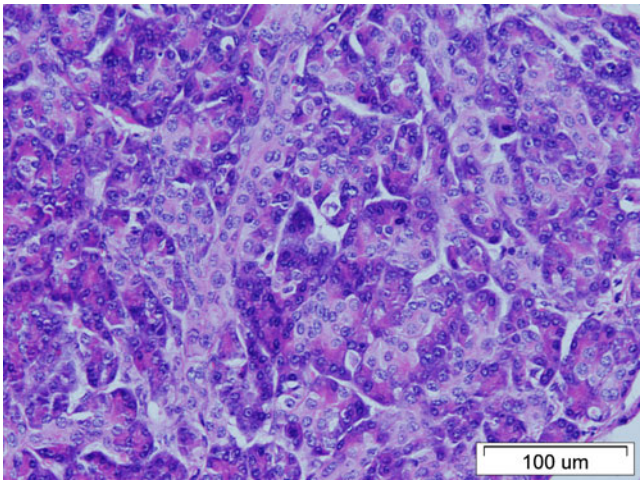

Fig. 4 Centroacinar cell hyperplasia

invasive lesion in a single case of conventional PC related to the PanIN-3. The FLA to PanIN rate in older patients with PCs ranged from 0.0 to 0.79, whereas the rate of mucinous tubular complexes to PanINs ranged from 0.0 to 0.64. Twelve patients showed features of moderate to marked chronic obstructive pancreatitis. Fat necrosis was seen focally in seven cases. Pseudocysts were found in two cases. Squamous cell metaplasia of pancreatic dusts was seen in 11 cases; in two of them, it was extensively distributed in EPP. Neuroendocrine microadenomas were noticed in four patients (in one of them, two lesions were visualized). Squamoid cyst was found in a single patient. In another single patient, well-developed epithelioid granulomas with Langhans cells but without necrosis were found in EPP and in several peripancreatic lymph nodes. PanINs-1A, PanINs-1B, PanINs-2, and PanINs-3 in main pancreatic duct were found in 1, 3, 1, and 1 patient, respectively.

Comparison of densities of PC precursor lesions in patients with EOPCs and in young patients with NENs

Densities of PanINs of all grades were significantly larger in EPP of patients with EOPCs as compared to EPP of young patients with NENs (Table 2). However, there were no differences concerning the rate of FLAs to PanINs and the rate of mucinous tubular complexes to PanINs between those groups of patients.

Comparison of densities of PC precursor lesions in patients with EOPCs and in older patients with PCs

Densities of PanINs-1B, PanINs-2, and PanINs-3 in EPP of patients with EOPCs and older patients with PCs were comparable (Table 2). In contrast, density of PanINs-1A was twofold larger in cases of EOPC than in older PC cases. This fact contributed to statistically significant difference of overall PanIN density between the main study group and control group 2. In contrast, rate of FLAs to PanINs and the rate of mucinous tubular complexes to PanINs were higher in older patients with PCs in comparison with patients with EOPCs. Since more cases of PC in older patients with PCs than cases of EOPC were related to IPMNs, it was not surprising that the densities of incipient IPMNs (except those of moderate grade) were higher in the former group. Overall density of PC precursor lesions was larger patients with EOPCs, but overall density of high-grade PC precursor lesions was higher in older patients with PCs.

Correlation between patients' age and PanINs' densities

We did not find significant correlations between patients' age and overall PanIN density in EOPC patients and in young

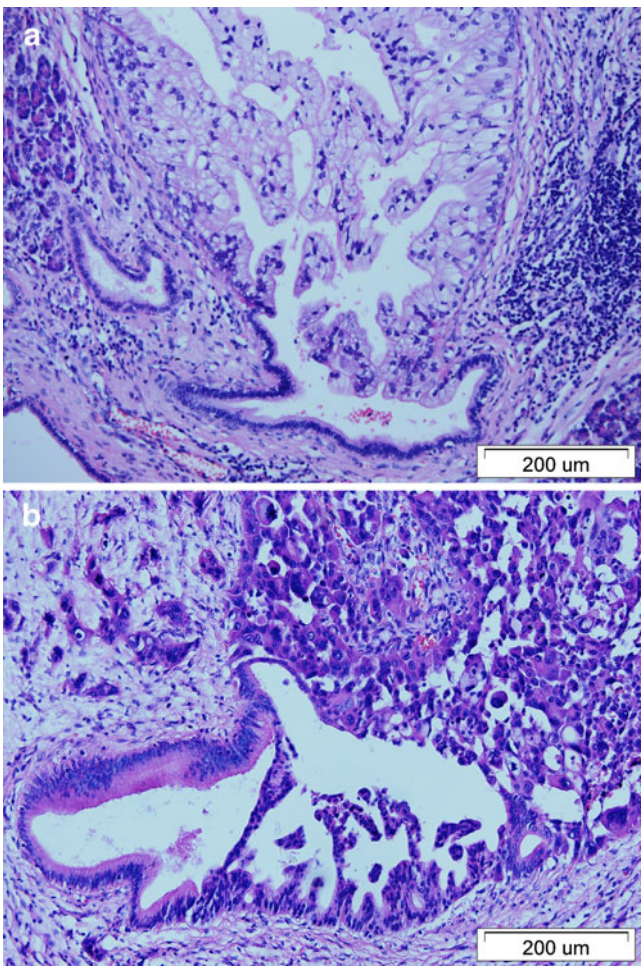

Fig. 5 **a–b** Secondary cancerization of pre-existing ducts by invasive carcinoma. Conventional ductal adenocarcinoma with abundant intracellular mucin involving normal branch duct (**a**) and undifferentiated carcinoma (**b**) involving branch duct with PanIN-1A (all figures in hematoxylin and eosin)

Table 2 PC precursor lesions in extratumoral parenchyma of patients with EOPCs and patients in control groups 1–2

Variable	Main study group: EOPCs (n=23)	Control group 1: NENs of the pancreas in young patients (n=13)	Control group 2: ductal pancreatic adenocarcinomas in older patients (n=39)
Studied area of EPP (cm^2, median, IQR)	6.0 (4.0–7.0)	6.0 (4.0–9.5)	19.0 (15.5–33.0)
Prevalence of PanINs-1A	22/23	7/13	39/39
Density of PanINs-1A (no. of lesions cm^{-2}, median, IQR)	0.40 (0.24–0.77)	0.11 (0.0–0.21), **p=0.0001**[a]	0.19 (0.12–0.27), **p=0.0002**[b]
Prevalence of PanINs-1B	21/23	7/13	39/39
Density of PanINs-1B (no. of lesions cm^{-2}, median, IQR)	0.34 (0.17–0.50)	0.07 (0.0–0.21), **p=0.006**[a]	0.26 (0.16–0.42), p=0.536[b]
Prevalence of PanINs-2	15/23	0/13	37/39
Density of PanINs-2 (no. of lesions cm^{-2}, median, IQR)	0.17 (0.0–0.25)	0.0 (0.0–0.0), **p=0.0003**[a]	0.12 (0.06–0.16), p=0.683[b]
Prevalence of PanINs-3	9/23	0/13	30/39
Density of PanINs-3 (no. of lesions cm^{-2}, median, IQR)	0.0 (0.0–0.17)	0.0 (0.0–0.0), **p=0.012**[a]	0.07 (0.02–0.12), p=0.069[b]
Overall prevalence of PanINs	22/23	8/13	39/39
Overall density of PanINs (no. of lesions cm^{-2}, median, IQR)	1.20 (0.75–1.33)	0.17 (0.0–0.42), **p=0.0001**[a]	0.71 (0.47–1.04), **p=0.003**[b]
Prevalence of FLA	13/23	7/13	38/39
Rate of FLA to PanINs (median, IQR)	0.17 (0.0–0.33)	0.32 (0.21–1.0), **p=0.077**[a]	0.29 (0.19–0.52), **p=0.018**[b]
Prevalence of mucinous tubular complexes	7/23	4/13	28/39
Rate of mucinous tubular complexes to PanINs (median, IQR)	0.0 (0.0–0.13)	0.1 (0.0–0.58), **p=0.135**[a]	0.17 (0.0–0.28), **p=0.002**[b]
Prevalence of low-grade incipient IPMNs	0/23	0/13	7/39
Density of low-grade incipient IPMNs (no. of lesions cm^{-2}, median, IQR)	0.0 (0.0–0.0)	0.0 (0.0–0.0), NA	0.0 (0.0–0.0), **p=0.034**[b]
Prevalence of moderate-grade incipient IPMNs	1/23	0/13	7/39
Density of moderate-grade incipient IPMNs (no. of lesions cm^{-2}, median, IQR)	0.0 (0.0–0.0)	0.0 (0.0–0.0), p=0.488	0.0 (0.0–0.0), p=0.154[b]
Prevalence of high-grade incipient IPMNs	0/23	0/13	8/39
Density of high-grade incipient IPMNs (no. of lesions cm^{-2}, median, IQR)	0.0 (0.0–0.0)	0.0 (0.0–0.0), NA	0.0 (0.0–0.0), **p=0.022**[b]
Overall prevalence of incipient IPMNs	1/23	0/13	9/39
Overall density of incipient IPMNs (no. of lesions cm^{-2}, median, IQR)	0.0 (0.0–0.0)	0.0 (0.0–0.0), p=0.488	0.0 (0.0–0.0), **p=0.059**[b]
Overall prevalence of precursor lesions of PC	22/23	8/13	39/39
Overall density of precursor lesions of PC (no. of lesions cm^{-2}, median, IQR)	1.20 (0.87–1.33)	0.17 (0.0–0.42), **p=0.0001**[a]	0.75 (0.48–1.08), **p=0.008**[b]
Overall prevalence of high-grade precursor lesions of PC	9/23	0/13	32/39
Overall density of high-grade precursor lesions of PC (no. of lesions cm^{-2}, median, IQR)	0.0 (0.0–0.17)	0.0 (0.0–0.0), **p=0.012**[a]	0.09 (0.05–0.18), **p=0.024**[b]

EOPC Early onset pancreatic cancer, *NEN* neuroendocrine neoplasm, *EPP* extratumoral pancreatic parenchyma, *IQR* interquartile range, *PanIN* pancreatic intraepithelial neoplasia, *FLA* focal lobular atrophy, *IPMN* intraductal papillary mucinous neoplasm, *NA* not available (cannot be calculated), *PC* pancreatic cancer

[a] Median values of studied variables in patients with EOPCs versus median values in young patients with NENs, Mann–Whitney *U* tests, statistically significant results are in bold

[b] Median values of studied variables in patients with EOPCs versus median values in older patients with ductal pancreatic adenocarcinomas, Mann–Whitney *U* tests, statistically significant results are in bold

patients with NENs (Spearman's rank correlation coefficients, p=0.992 and p=0.725, respectively). In contrast, overall PanIN density was rather weakly but significantly positively correlated with age of older patients with PC (r=0.330, p=0.040). Similar levels of correlation were found between age of older patients with PCs and their overall PC precursor density and overall high-grade PC precursor density, but not incipient IPMN density (specific data not shown).

Discussion

Pathogenesis and histopathology of EOPC

Due to its rarity, there is relatively small amount of data concerning epidemiology, symptomatology, optimal treatments options, as well as long-term prognosis in EOPC [3, 4, 6, 9]. Bergmann et al. [3] and Lüttges et al. [9] presented data on histopathology and molecular characteristics of EOPC. The pathogenesis of EOPC is poorly understood. Some PC cases including EOPC ones may be associated with individual genetic predisposition [46]. Noteworthy, the percentage of EOPC patients with positive family history of PC (10.3%) [4] is similar to the percentage in overall population of patients with PC (8.5%) [47]. Our data were in concordance with those observations. Interestingly, none of 136 EOPC cases in the study of Duffy et al. [4] and none of EOPC cases in the present study were associated with inherited syndromes associated with elevated risk of developing PC. Only a single patient with EOPC in the present study was diagnosed with familial PC. The issue of familial PC was extensively reviewed previously [33, 46, 48].

PanINs prevalence and densities

Several groups of investigators studied the prevalence of PC precursor lesions in patients without clinically detectable pancreatic diseases and/or patients with different types of tumors of non-ductal origin [21, 23, 29, 37, 38, 49–51].

PanINs are very frequent in adult pancreata (up to 80% of cases studied), but the prevalence rates of PanIN of different grades of dysplasia differ significantly [16, 21, 23, 29, 49, 50]. PanINs-1A lesions are more prevalent (19–68.2% [21, 49–51]) as compared to PanINs-1B (12–20% [23, 49–51]) and PanINs-2 lesions (0–13.6% [49–51]). PanINs-3 lesions are very rare [37] or nonexistent in patients without PC [21, 23, 49–51]. In our opinion, the differences between studies concerning PanIN prevalence rates in patients without PC may be caused by a number of methodological causes, e.g., different criteria of inclusion of patients across the studies, extensiveness of EPP sampling, or technique of statistical reporting.

Concerning the issue of PanIN prevalence in individuals without detectable pancreatic diseases, PanINs are more prevalent in older persons in comparison to younger ones (reviewed in Refs. [16, 17]). However, it is not definitely clear if the grade of PanINs found in asymptomatic individuals increases with their age, since results of different studies are discrepant [21, 29, 37, 49, 50]. Even if such a correlation exists, it is rather weak [37]. There is no significant difference between genders in the prevalence of PanINs [21, 23, 29, 50]. The PanIN prevalence is not associated with history of tobacco smoking [19, 23] or alcohol abuse [23]. Is it not definitely clear whether PanIN prevalence is higher in the pancreatic head in comparison to other segments [16], since results of studies on that issue were inconsistent [21, 23, 26, 29].

In the present study, we assumed that prevalence of PanINs in patients with NENs may be an indicator of their prevalence in individuals without pancreatic diseases. That was acknowledged by Stelow et al. [37] and, very recently, by Recavarren et al. [38]. However, the average age of patients with NENs included in those reports was above 45 years; that is, they were in significant proportion older than patients with NENs included in the present study. This may explain why we did not see PanINs-2 and PanINs-3 in patients with NENs despite they were seen (albeit rarely) in patients with NENs described in those reports [37, 38].

It is clear that PanIN-2 and PanIN-3 lesions are not supposed to be found in young patients without PCs (vide control group 1 in the present study), but they exist in patients with PCs (both younger and older ones). The PanINs-3 prevalence in patients with EOPCs in the present study was 39.1%. It was much lower than the PanINs-3 prevalence in older patients (76.9%, high-grade incipient IPMNs not included). That was obviously caused by differences in the studied EPP areas between those groups; therefore, it was of no significance.

Recently, it was proposed that not only prevalence of PanINs of different grades but also their density in EPP may be of clinical significance [19]. The issue of densities of PC precursor lesions was also raised in earlier studies [21, 23]. It is not known whether PanIN densities differ in young and older patients with or without PCs and whether PanIN density may change in a particular individual during his/her lifetime. Lüttges et al. [21] did not find any differences in numbers of intraductal lesions (compatible with present-day PanINs and squamous cell metaplasias) in systematically sampled pancreata of autopsied patients aged 6–92 who died of nonpancreatic diseases. This may indicate that PanIN density is relatively constant during lifetime in individuals who did not develop PC.

There is more data on PanIN density in patients with PCs. Shi et al. [19] showed that EPP in patients with familial PCs contained 2.75 times more PanINs than EPP in patients with sporadic PCs (PanIN densities of 1.51 and 0.55 lesions cm^{-2} of EPP, respectively). The densities of all grades of PanINs were higher in familial PCs than in sporadic cases. Incipient IPMNs were detected in EPP in one third of familial PC cases, and their density was 11.8 times higher in familial PC cases than in sporadic ones [19]. The densities on PanINs in older patients with PCs reported in the present study (control group 2) were comparable, but

slightly higher to those reported by Shi et al. [19] in their sporadic PC cases.

The median overall PanIN density in EOPC cases examined in the present study (1.20 lesions cm^{-2}) was significantly higher than PanIN density in older patients with PCs (0.75 lesions cm^{-2}) and slightly lower than previously mentioned PanIN density in familial PC cases in the study of Shi et al. [19]. This finding was quite intriguing since only one patient with EOPC in the present study was diagnosed with familial PC. However, it should be noticed that significant differences in PanIN densities between particular patients with PCs may exist. Shi et al. [19] showed that overall PanIN densities in patients with familial PCs and sporadic PCs may range from 0 to 3.8 and from 0 to 2.01 lesions cm^{-2} of EPP, respectively. We also noticed differences in overall PanIN density ranging from 0 up to 2 lesions cm^{-2} in both young and older patients with PCs. However, in any of the studied patients the overall PanIN density was not as high as 3.8 lesions cm^{-2} of EPP.

We did not observe statistically significant differences concerning densities of PanINs-1B, PanINs-2, and PanINs-3 between patients with EOPCs and older patients with PCs. In contrast, the PanIN-1A density in patients with EOPCs was significantly higher than in older patients with PCs. We are not aware on any other studies on the relationship between PanIN-1A density and age of patients with PCs. It is possible that some PanIN-1A lesions may progress to PanINs-1B, and therefore, their density in older patients with PCs may decline. However, as mentioned earlier, we did not see any increase of PanIN-1B density in older patients with PCs as compared to younger ones. PanIN-1B density in older patients with PCs was even paradoxically lower than in patients with EOPCs, but that difference was not statistically significant. Lüttges et al. [21] showed that prevalence of mucinous cell hypertrophy (present-day PanINs-1A) but not ductal papillary hyperplasia (present-day PanINs-1B and PanINs-2) increased with age of individuals without PCs.

In the present study, we also showed that densities of PanIN of all grades (including low-grade ones) were significantly higher in patients with EOPCs than in young patients with NENs.

Higher PanINs-1A density in patients with EOPCs as compared to young patients with NENs and older patients with PCs may indicate that in at least some EOPC patients, there is a tendency to develop multifocal low-grade PanINs. Although a great majority of these low-grade lesions did not progress to high-grade ones and invasive carcinomas (we did not observe any multifocal cancers in any of the studied cases), their relatively high density might reflect an alteration of some "gatekeeper" genes similarly as it was postulated by Shi et al. [19] in familial PC.

IPMNs prevalence

In the present study, only one EOPC (4.3%) was associated with IPMN. In contrast, as many as 20% of cases of PCs in older patients were associated with IPMNs. That percentage was higher than the prevalence of invasive carcinomas associated with IPMNs among resected ductal PCs reported in the large series presented by Poultsides et al. [52] (132/1260, 10.5%). At present, IPMNs do not seem to be particularly frequent PC precursor lesion among patients with EOPCs, but further studies related to this issue are needed.

Focal lobular atrophy

Detlefsen et al. [24] and Kloppel et al. [28] showed that FLAs are frequent feature of pancreata of persons without clinically detectable pancreatic disorders. Interestingly, it may be often but not always associated with intraductal lesions mainly PanIN-1B. That seemed to be age-related phenomenon [24, 28]. Adenomatous hyperplasia of pancreatic ducts [21, 29], which probably equals to mucinous tubular complexes [25], was reported in 40% of "normal" pancreata and 26.9% of cases of normal pancreata with "ductal hyperplasia" [21, 29]. Changes compatible with FLA may be found in approximately one third of normal pancreata with ductal hyperplasia [29]. Meckler et al. [53] described in detail parenchymal changes in members of the family with many cases of PCs. They found FLAs with cystic transformation and "mucinous metaplasia" of the intralobular ductules, PanINs of all grades, interstitial endocrine cell hyperplasia, numerous endocrine cells within ductal epithelial lining, and nuclear atypia in some endocrine cells and rarely mild inflammatory infiltrate, squamous cell metaplasia [53]. Later Brune at al. [26] showed that similar lesions but of high density may be found in patients without clinically detectable PC but with strong family history of PC. These patients presented multiple foci of PanINs of all grades as well as IPMNs with low-grade dysplasia [26]. FLAs were related to almost all PanIN lesions including PanINs-1A [26]. Brune et al. [26] also documented less frequent FLAs associated with PanINs (including PanIN-1A) in patients without PCs. Moreover, PanIN-1B lesions may undergo "cystic transformation" to gastric foveolar IPMN [16]. FLA related to PC precursor lesions may be actually focal or multifocal response to pancreatic duct obstruction, since it closely resembles obstructive chronic pancreatitis [28]. It is possible to detect lobular fibrosis which is caused by obstruction of lobular duct by intraductal lesion using endoscopic ultrasonography [26, 30–34, 54]. In rare cases, multicentric PanINs with associated lobular atrophy and fibrosis involving the entire pancreas may develop in patients with negative family history of PC [55]. PanINs and IPMNs lesions with or

without associated FLAs were also documented in patients from families with familial PCs submitted to prospective screening programs [30, 32, 33].

Related issue is the rate of FLAs to PanINs in patients with and without PCs. Detlefsen et al. [24] found FLA in one of four autopsied patients with PanIN-1B lesions under the age of 60 years without clinical or grossly detectable pancreatic disease. In patients at the age of 60 or older, PanIN-1B–FLA complexes were found in 25/31 (80.6%) of cases [24]. Shi et al. [19] showed that the prevalence rates of FLAs in both familial and sporadic PC cases is related to the frequency of PC precursor lesions and they were 86% and 53%, respectively. The fact that the prevalence of PanIN-1B–FLA complexes in autopsied persons without evident pancreatic diseases at the age of 60 or older in the study of Detlefsen et al. [24] was higher than the prevalence of FLA in patients with sporadic PCs in the study of Shi et al. [19] is quite intriguing. It indicates that some not yet known factors may influence results of studies on FLAs. The parenchymal changes compatible with FLA diagnosis may be of different stage [26] and extent and the FLA prevalence may be related to the "threshold" of features, which are identified as sufficient for the diagnosis of FLA. The FLA prevalence may be also related to extensiveness of EPP sampling. We found FLAs in as many as 38/39 (97.4%) of older patients with PCs. However, EPP was very extensively sampled, and we saw a correlation between EPP area and the number of FLAs in EPP of those patients (specific data not shown). FLA changes are also similar in pathogenesis and histopathology to obstructive pancreatitis [24, 28]. Such changes are more prevalent in the portion of pancreas distal to the tumor, which obstruct the duct. In the present study, we examined a low number of tumors (PCs and NENs) localized in the body or tail of the pancreas and therefore were not able to assess whether the localization of tumor influenced the prevalence of FLA.

In the present study, the rate of FLA to PanINs and the rate of FLA with mucinous tubular complexes to PanINs in patients with EOPCs did not differ from those in young patients with NENs, but they were significantly lower than in older patients with PCs. This may indicate that the increase of these rates represent an age-related phenomenon in patients with PCs, similarly to patients without PCs [24]. We observed statistically significant correlations between the rate of FLA to PanINs (r=0.368, p=0.003) and the rate of FLA with mucinous tubular complexes to PanINs (r=0.509, p=0.0001) versus age in all studied patients with PCs.

Other lesions in pancreatic parenchyma of EOPC and control cases

Lesions other than PanINs/IPMNs/FLAs found in EPP of cases studied in the present study did not seem to be related to the development of PC. Their prevalence rates were too low to be reliably compared between the study groups. Interestingly, we did not observe any cases of microscopic hyperplasia of endocrine component or exocrine-to-endocrine metaplasia, which may be related to the obstruction of pancreatic ducts and may represent a field effect in both ductal and endocrine component in patients at high risk of PC development or patients with familial PCs [31, 41, 53]. In one single patient with EOPC, a separate NEN was found, but the significance of that finding was unclear. The EPP in that patient did not show any features of endocrine cell hyperplasia or microadenomatosis.

Study limitations

The limitation of the study resulted from the fact that not all EPP present in the specimen was submitted to histopathological examination. Majority of EOPCs were sampled and diagnosed before we introduced protocols of very extensive sampling of pancreatectomy specimens [56]. This may explain why PanIN-3 density was (albeit not significantly) lower in patients with EOPCs in comparison with older patients with PCs. In some cases of EOPCs, the studied EPP area might be not large enough to detect PanINs-3.

Another limitation may be related to the presence of features of chronic pancreatitis in the studied cases since it may influence the prevalence of PC precursor lesions [23]. Moderate or marked features of chronic pancreatitis were present in a small proportion of patients with EOPCs and young patients with NENs but in 30% of older patients with PCs.

Surgical resection is possible only in a minority of patients with PCs. Since all EOPC cases described in the present study were resected, we cannot exclude that very aggressive cases of EOPCs (which are less likely to be resectable) show different types or extent of histopathological alterations in EPP.

Conclusion

PanINs is the most prevalent precursor lesion of EOPCs. PanINs of all grades are frequent but not the universal finding in EPP in patients with EOPCs. The density of all grades of PanINs in EPP is significantly higher in patients with EOPCs than in young patients with NENs. Density of PanINs-1A is higher in patients with EOPCs than in older patients with PCs, but densities of PanINs of other grades are comparable. Some of PanINs are related to FLAs with or without formation of mucinous tubular complexes. EOPCs less frequently than PCs in older patients are derived from IPMNs. Relatively high density of low-grade PanINs in EPP of patients with EOPCs as compared to

young patients with NENs and older patients with PCs may result from unknown multifocal genetic alterations in pancreatic tissue of EOPC patients.

Conflicts of interest None.

Open Access This article is distributed under the terms of the Creative Commons Attribution Noncommercial License which permits any noncommercial use, distribution, and reproduction in any medium, provided the original author(s) and source are credited.

References

1. Jemal A, Siegel R, Ward E, Hao Y, Xu J, Thun MJ (2009) Cancer statistics, 2009. CA: A Cancer Journal for Clinicians 59:225–249
2. Wisnoski NC, Townsend CM Jr, Nealon WH, Freeman JL, Riall TS (2008) 672 patients with acinar cell carcinoma of the pancreas: a population-based comparison to pancreatic adenocarcinoma. Surgery 144:141–148
3. Bergmann F, Aulmann S, Wente MN, Penzel R, Esposito I, Kleeff J, Friess H, Schirmacher P (2006) Molecular characterization of pancreatic ductal adenocarcinoma in patients under 40. J Clin Pathol 59:580–584
4. Duffy A, Capanu M, Allen P, Kurtz R, Olson SH, Ludwig E, Klimstra DS, O'Reilly EM (2009) Pancreatic adenocarcinoma in a young patient population–12-year experience at Memorial Sloan Kettering Cancer Center. J Surg Oncol 100:8–12
5. Baxter NN, Whitson BA, Tuttle TM (2007) Trends in the treatment and outcome of pancreatic cancer in the United States. Ann Surg Oncol 14:1320–1326
6. Raimondi S, Maisonneuve P, Lohr JM, Lowenfels AB (2007) Early onset pancreatic cancer: evidence of a major role of smoking and genetic factors. Canc Epidemiol Biomarkers Prev 16:1894–1897
7. Brune KA, Lau B, Palmisano E, Canto M, Goggins MG, Hruban RH, Klein AP (2010) Importance of age of onset in pancreatic cancer kindreds. J Natl Cancer Inst 102:119–126
8. Soliman AS, El-Ghawalby N, Ezzat F, Bondy ML, Soultan A, Abdel-Wahab M, Fathy O, Ebidi G, Bassiouni N, El-Ghawalbi A, Levin B, Abbruzzese JL (2002) Unusually high rate of young-onset pancreatic cancer in the East Nile Delta region of Egypt. Int J Gastrointest Cancer 32:143–151
9. Lüttges J, Stigge C, Pacena M, Klöppel G (2004) Rare ductal adenocarcinoma of the pancreas in patients younger than age 40 years. Cancer 100:173–182
10. Bleyer A (2007) Young adult oncology: the patients and their survival challenges. CA: A Cancer Journal for Clinicians 57:242–255
11. Bleyer A, Barr R, Hayes-Lattin B, Thomas D, Ellis C, Anderson B (2008) Biology and clinical trials subgroups of the US National Cancer Institute progress review group in adolescent and young adult oncology. The distinctive biology of cancer in adolescents and young adults. Nat Rev Canc 8:288–298
12. Zogopoulos G, Rothenmund H, Eppel A, Ash C, Akbari MR, Hedley D, Narod SA, Gallinger S (2007) The P239S palladin variant does not account for a significant fraction of hereditary or early onset pancreas cancer. Hum Genet 121:635–637
13. James TA, Sheldon DG, Rajput A, Kuvshinoff BW, Javle MM, Nava HR, Smith JL, Gibbs JF (2004) Risk factors associated with earlier age of onset in familial pancreatic carcinoma. Cancer 101:2722–2726
14. Hruban RH, Fukushima N (2007) Pancreatic adenocarcinoma: update on the surgical pathology of carcinomas of ductal origin and PanINs. Mod Pathol 20:S61–S70
15. Singh M, Maitra A (2007) Precursor lesions of pancreatic cancer: molecular pathology and clinical implications. Pancreatology 7:9–19
16. Sipos B, Frank S, Gress T, Hahn S, Kloppel G (2009) Pancreatic intraepithelial neoplasia revisited and updated. Pancreatology 9:45–54
17. Andea AA, Basturk O, Adsay NV (2005) Pancreatic intra-epithelial neoplasia: current clinicopathological and molecular considerations. Curr Diagn Pathol 11:80–94
18. Hruban RH, Takaori K, Klimstra DS, Adsay NV, Albores-Saavedra A, Biankin AV, Biankin SA, Compton CC, Fukushima N, Furukawa T, Goggins M, Kato Y, Kloppel G, Longnecker DS, Luttges J, Maitra A, Offerhaus GJA, Shimizu M, Yonezawa S (2004) An illustrated consensus on the classification of pancreatic intraepithelial neoplasia and intraductal papillary mucinous neoplasms. Am J Surg Pathol 28:977–987
19. Shi C, Klein AP, Goggins M, Maitra A, Canto M, Ali S, Schulick R, Palmisano E, Hruban RH (2009) Increased prevalence of precursor lesions in familial pancreatic cancer patients. Clin Cancer Res 15:7737–7743
20. Ottenhof NA, Milne AN, Morsink FH, Drillenburg P, Ten Kate FJ, Maitra A, Offerhaus GJ (2009) Pancreatic intraepithelial neoplasia and pancreatic tumorigenesis: of mice and men. Arch Pathol Lab Med 133:375–381
21. Lüttges J, Reinecke-Lüthge A, Möllmann B, Menke MA, Clemens A, Klimpfinger M, Sipos B, Klöppel G (1999) Duct changes and K-ras mutations in the disease-free pancreas: analysis of type, age relation and spatial distribution. Virchows Arch 435:461–468
22. Shi C, Hong SM, Lim P, Kamiyama H, Khan M, Anders RA, Goggins M, Hruban RH, Eshleman JR (2009) KRAS2 mutations in human pancreatic acinar–ductal metaplastic lesions are limited to those with PanIN: implications for the human pancreatic cancer cell of origin. Mol Cancer Res 7:230–236
23. Andea A, Sarkar F, Adsay VN (2003) Clinicopathological correlates of pancreatic intraepithelial neoplasia: a comparative analysis of 82 cases with and 152 cases without pancreatic ductal adenocarcinoma. Mod Pathol 16:996–1006
24. Detlefsen S, Sipos B, Feyerabend B, Kloppel G (2005) Pancreatic fibrosis associated with age and ductal papillary hyperplasia. Virchows Arch 447:800–805
25. Esposito I, Seiler C, Bergmann F, Kleeff J, Friess H, Schirmacher P (2007) Hypothetical progression model of pancreatic cancer with origin in the centroacinar–acinar compartment. Pancreas 35:212–217
26. Brune K, Abe T, Canto M, O'Malley L, Klein AP, Maitra A, Volkan Adsay N, Fishman EK, Cameron JL, Yeo CJ, Kern SE, Goggins M, Hruban RH (2006) Multifocal neoplastic precursor lesions associated with lobular atrophy of the pancreas in patients having a strong family history of pancreatic cancer. Am J Surg Pathol 30:1067–1076
27. Hruban RH, Adsay NV, Albores-Saavedra J, Anver MR, Biankin AV, Boivin GP, Furth EE, Furukawa T, Klein A, Klimstra DS, Kloppel G, Lauwers GY, Longnecker DS, Luttges J, Maitra A, Offerhaus GJ, Pérez-Gallego L, Redston M, Tuveson DA (2006) Pathology of genetically engineered mouse models of pancreatic exocrine cancer: consensus report and recommendations. Cancer Res 66:95–106
28. Kloppel G, Detlefsen S, Feyerabend B (2004) Fibrosis of the pancreas: the initial tissue damage and the resulting pattern. Virchow Arch 445:1–8
29. Kozuka S, Sassa R, Taki T, Masamoto K, Nagasawa S, Saga S, Hasegawa K, Takeuchi M (1979) Relation of pancreatic duct hyperplasia to carcinoma. Cancer 43:1418–1428

30. Langer P, Kann PH, Fendrich V, Habbe N, Schneider M, Sina M, Slater EP, Heverhagen JT, Gress TM, Rothmund M, Bartsch DK (2009) Five years of prospective screening of high-risk individuals from families with familial pancreatic cancer. Gut 58:1410–1418
31. Steinberg WM, Barkin JS, Bradley EL III, DiMagno E, Layer P, Canto MI, Levy MJ (2009) Should patients with a strong family history of pancreatic cancer be screened on a periodic basis for cancer of the pancreas? Pancreas 38:e137–e150
32. Poley JW, Kluijt I, Gouma DJ, Harinck F, Wagner A, Aalfs C, van Eijck CH, Cats A, Kuipers EJ, Nio Y, Fockens P, Bruno MJ (2009) The yield of first-time endoscopic ultrasonography in screening individuals at a high risk of developing pancreatic cancer. Am J Gastroenterol 104:2175–2181
33. Larghi A, Verna EC, Lecca PG, Costamagna G (2009) Screening for pancreatic cancer in high-risk individuals: a call for endoscopic ultrasound. Clin Cancer Res 15:1907–1914
34. Canto MI, Goggins M, Hruban RH, Petersen GM, Giardiello FM, Yeo C, Fishman EK, Brune K, Axilbund J, Griffin C, Ali S, Richman J, Jagannath S, Kantsevoy SV, Kalloo AN (2006) Screening for early pancreatic neoplasia in high-risk individuals: a prospective controlled study. Clin Gastroenterol Hepatol 4:766–781
35. Hruban RH, Pitman MB, Klimstra DS (2007) AFIP atlas of tumor pathology. Fourth series. Fascicle 6. Tumors of the pancreas. American Registry of Pathology–AFIP, Washington
36. Bosman FT, Carneiro F, Hruban RH, Theise ND (eds) (2010) WHO classification of tumours of the digestive system. International Agency for Research on Cancer, Lyon
37. Stelow EB, Adams RB, Moskaluk CA (2006) The prevalence of pancreatic intraepithelial neoplasia in pancreata with uncommon types of primary neoplasms. Am J Surg Pathol 30:36–41
38. Recavarren C, Labow DM, Liang J, Zhang L, Wong M, Zhu H, Wang J, Francis F, Xu R (2011) Histologic characteristics of pancreatic intraepithelial neoplasia associated with different pancreatic lesions. Human Pathol 42:18–24
39. Furukawa T, Kloppel G, Adsay NV, Albores-Saavedra J, Fukushima N, Horii A, Hruban RH, Kato Y, Klimstra DS, Longnecker DS, Lüttges J, Offerhaus GJ, Shimizu M, Sunamura M, Suriawinata A, Takaori K, Yonezawa S (2005) Classification of types of intraductal papillary-mucinous neoplasm of the pancreas: a consensus study. Virchows Arch 447:794–799
40. Kloppel G (2004) Chronic pancreatitis of alcoholic and nonalcoholic origin. Semin Diagn Pathol 21:227–236
41. Lardon J, Bouwens L (2005) Metaplasia in the pancreas. Differentiation 73:278–286
42. Oertel JE (1989) The pancreas. Nonneoplastic alterations. Am J Surg Pathol 13(Suppl 1):50–65
43. Othman M, Basturk O, Groisman G, Krasinskas A, Adsay NV (2007) Squamoid cyst of pancreatic ducts: a distinct type of cystic lesion in the pancreas. Am J Surg Pathol 31:291–297
44. Kloppel G (2004) Acute pancreatitis. Semin Diagn Pathol 21:221–226
45. Liszka L, Pająk J, Zielińska-Pająk E, Gołka D (2008) Colloid carcinoma of the pancreas: review of selected pathological and clinical aspects. Pathology 40:655–663
46. Jorgensen MT, Mortensen MB, Gerdes AM, De Muckadell OB (2008) Familial pancreatic cancer. Scand J Gastroenterol 43:387–397
47. Hassan MM, Bondy ML, Wolff RA, Abbruzzese JL, Vauthey JN, Pisters PW, Evans DB, Khan R, Chou TH, Lenzi R, Jiao L, Li D (2007) Risk factors for pancreatic cancer: case–control study. Am J Gastroenterol 102:2696–2707
48. Shi C, Hruban RH, Klein AP (2009) Familial pancreatic cancer. Arch Pathol Lab Med 133:365–374
49. Rosty C, Geradts J, Sato N, Wilentz RE, Roberts H, Sohn T, Cameron JL, Yeo CJ, Hruban RH, Goggins M (2003) p16 inactivation in pancreatic intraepithelial neoplasias (PanINs) arising in patients with chronic pancreatitis. Am J Surg Pathol 27:1495–1501
50. Ito R, Kondo F, Yamaguchi T, Kato K, Sakai Y, Saisho H, Yamazaki K (2008) Pancreatic intraepithelial neoplasms in the normal appearing pancreas: on their relationship with age. Hepatogastroenterology 55:1103–1106
51. Cubilla AL, Fitzgerald PJ (1976) Morphological lesions associated with human primary invasive nonendocrine pancreas cancer. Cancer Res 36:2690–2698
52. Poultsides GA, Reddy S, Cameron JL, Hruban RH, Pawlik TM, Ahuja N, Jain A, Edil BH, Iacobuzio-Donahue CA, Schulick RD, Wolfgang CL (2010) Histopathologic basis for the favorable survival after resection of intraductal papillary mucinous neoplasm-associated invasive adenocarcinoma of the pancreas. Ann Surg 251:470–476
53. Meckler KA, Brentnall TA, Haggitt RC, Crispin D, Byrd DR, Kimmey MB, Bronner MP (2001) Familial fibrocystic pancreatic atrophy with endocrine cell hyperplasia and pancreatic carcinoma. Am J Surg Pathol 25:1047–1053
54. Takaori K, Matsusue S, Fujikawa T, Kobashi Y, Ito T, Matsuo Y, Oishi H, Takeda H (1998) Carcinoma in situ of the pancreas associated with localized fibrosis: a clue to early detection of neoplastic lesions arising from pancreatic ducts. Pancreas 17:102–105
55. Aimoto T, Uchida E, Nakamura Y, Matsushita A, Katsuno A, Chou K, Kawamoto M, Naito Z, Tajiri T (2008) Multicentric pancreatic intraepithelial neoplasias (PanINs) presenting with the clinical features of chronic pancreatitis. J Hepatobiliary Pancreat Surg 15:549–553
56. Liszka L, Pajak J, Zielinska-Pajak E, Golka D, Mrowiec S, Lampe P (2010) Different approaches to assessment of lymph nodes and surgical margin status in patients with ductal adenocarcinoma of the pancreas treated with pancreaticoduodenectomy. Pathology 42:138–146

Virchows Arch (2011) 458:453–465
DOI 10.1007/s00428-011-1043-8

ORIGINAL ARTICLE

Gene expression profiling of human hepatoblastoma using archived formalin-fixed and paraffin-embedded tissues

Eun Shin · Kyoung-Bun Lee · Soo-Young Park · Soo-Hee Kim · Han-Suk Ryu · Young-Nyun Park · Eunsil Yu · Ja-June Jang

Received: 23 August 2010 / Revised: 7 December 2010 / Accepted: 9 January 2011 / Published online: 3 March 2011
© Springer-Verlag 2011

Abstract We elucidated the genetic profile of hepatoblastomas (HBLs) to identify diagnostic and prognostic markers. RNA was extracted from 32 formalin-fixed, paraffin-embedded HBLs and corresponding nonneoplastic liver (NNL) tissues, and cDNA-mediated annealing, selection, extension, and ligation (DASL) chip assays were performed. Immunohistochemistry was performed to confirm the expression of Yin Yang 1 (*YY1*) protein in HBL. Twenty-four genes that were associated with signal transduction, cell–cell adhesion, cell cycle regulation, and apoptosis were differentially expressed in HBL and NNL tissues. Two apoptosis-associated genes, *MYCN* and *BIRC5*, were highly upregulated in HBL. Eight genes, including *YY1* and *IGF1*, were upregulated in HBL cases that had a poor prognosis. Thirty-eight genes, including *YY1*, were differentially expressed according to histologic differentiation of HBL, and the immunohistochemical expression of *YY1* was correlated with poor HBL differentiation. Thus, using DASL chip assays, we report the gene expression profiles of HBL, which suggest new candidate prognostic and diagnostic genetic markers and putative therapeutic targets for HBL.

E. Shin · K.-B. Lee · S.-Y. Park · S.-H. Kim · H.-S. Ryu · J.-J. Jang (✉)
Department of Pathology,
Seoul National University College of Medicine,
#28 Yongon-dong, Jongro-gu,
Seoul 110-799, South Korea
e-mail: tripj@snu.ac.kr

Y.-N. Park
Department of Pathology, Yonsei University College of Medicine,
Seoul, South Korea

E. Yu
Department of Pathology, Seoul Asan Medical Center,
Seoul, South Korea

Keywords Hepatoblastoma · DASL chip assay · YY1 · Prognosis

Introduction

Hepatoblastoma (HBL) is the most common malignant liver tumor in children, accounting for 40% of all pediatric hepatic tumors and 50–62% of all pediatric hepatic malignancies. Although HBL has been reported in adolescents and adults, it usually affects infants and young children between the ages of 6 months and 3 years. HBL cells are derived from pluripotent hepatic stem cells and resemble immature hepatocytes during development. There are two HBL subtypes, an epithelial type and a mixed type that contains tissues of both epithelial and mesenchymal origin. Epithelial components are classified as fetal, embryonal, and small-cell type. Stage I pure fetal HBL can be treated successfully with surgery alone, whereas small-cell undifferentiated histology is associated with an unfavorable outcome regardless of resectability [1]. Due to advances in surgical techniques and the use of chemotherapy, the prognosis of patients with HBL has improved, and the 5-year survival rate is now over 70%. However, large tumors, multifocal tumors, and metastatic spread are associated with poor prognosis [2]. Nonrandom chromosomal imbalances involving 1q, 2q, 8q, 4q, and 20q [3, 4] and alterations in the *wnt* signaling pathway [5, 6] or the insulin-like growth factor (IGF) axis are considered to contribute to the development of HBL [7, 8], but the molecular mechanisms responsible for the pathogenesis and progression of HBL are largely unknown.

DNA microarrays have many possible applications in the field of human cancer research, especially when high throughput is required. For example, microarrays have

been used to analyze genetic profiles of tumors, identify genes that are differentially expressed at different clinical statuses [9, 10], identify biomarkers that predict treatment responsiveness or prognosis, and identify pharmacological targets [11, 12]. A small number of DNA chip studies have been performed on HBLs. Nagata et al. identified genes that were differentially expressed between normal liver and HBL [13]. Luo et al. compared genetic expression profiles between hepatocellular carcinoma and HBL [14]. Yamada et al. suggested that overexpression of the PLK1 oncogene indicates a poorer prognosis [15].

Although DNA chip technology is widely applicable, its application to clinical specimens is limited because it requires frozen tissue. For over a century, almost all surgical and biopsy specimens have been preserved as formalin-fixed, paraffin-embedded (FFPE) tissues. Accordingly, retrospective clinical studies are almost invariably conducted using FFPE tissues. When combined with the potential of genomics, these tissues become an invaluable resource for elucidating disease mechanisms and searching for novel therapeutic targets or prognostic indicators.

The cDNA-mediated annealing, selection, extension, and ligation (DASL) assay was recently developed and applied to genome-wide gene expression profiling of FFPE tissues [16], and its reproducibility and accuracy have been shown to be satisfactory [17]. In our current study, we performed DASL chip assays on tumor and corresponding normal liver tissues from 32 HBL cases and recorded HBL gene expression changes compared to the paired normal tissues. Furthermore, we identified gene expression patterns according to clinical outcomes and histological characteristics.

Materials and methods

Case selection for DASL

For this retrospective study, 32 HBL samples and 32 samples of corresponding nonneoplastic liver (NNL) tissues from the same patient were analyzed. HBL samples represented 24 cases from Seoul National University Hospital and 8 cases from Asan Medical Center (Seoul), and all were taken from 1991 to 2007.

Collection of pathologic and clinical data

Histologic subtypes and HBL grades were determined by reviewing hematoxylin and eosin-stained slides. Histologic subtypes were classified according to the WHO classification system. HBL grades were classified as well or poorly differentiated. If the major histologic subtype of the epithelial component was fetal, the tumor histologic type was defined as well differentiated (W/D); if the major component of the epithelial portion was of the embryonal or small-cell type, histologic type was defined as poorly differentiated (P/D). Numbers of lesions and tumor sizes were obtained from pathology reports. Cases were also divided into good and poor prognosis groups. The poor prognosis group was composed of cases that demonstrated local recurrence or metastasis within 2 years of surgery. Clinicopathologic features of HBL are listed in Table 1, and detailed histologic types of HBL samples are shown in Table 2.

Isolation of RNA

To isolate total RNA from FFPE tissues, paraffin blocks that contained a sufficient amount of tumor were selected. Where possible, paraffin blocks containing pure epithelial HBL were chosen. Four paraffin blocks contained mesenchymal components, and macrodissection was performed to avoid contamination with normal tissues and mesenchymal components. Three 10-μm-thick sections were cut from each tissue block and placed in a 2.0-ml tube. A High Pure RNA paraffin kit (Roche, Mannheim, Germany) was used for RNA extraction. Samples were digested with proteinase K for 12 h. All purification steps, DNase treatment, and

Table 1 Clinicopathological features of HBL samples used in the DASL assay

Age (months)	
Median	67
Range	2–204
Sex	
Female	12 (37.5%)
Male	20 (62.5%)
Histologic type	
Well differentiated	18 (56.2%)
Poorly differentiated	14 (43.8%)
Tumor size (cm)	
Median	7.7
Range	1.6–25
Preoperative chemotherapy	
Yes	23 (71.9%)
No	8 (2%5)
Not available	1 (3.1%)
Resection margin state	
Not involved	28 (87.5%)
Involved	0 (0%)
Not available	4 (12.5%)
Clinical course	
Good	19 (59.3%)
Poor	10 (31.%3)
Not available	3 (9.4%)

Table 2 Histologic composition of HBL samples

Type	
Well differentiated	18 (56.25%)
Pure fetal	13
Mixed, fetal dominant	4
Fetal and embryonal, fetal dominant	1
Poorly differentiated	14 (43.75%)
Pure embryonal	3
Mixed, embryonal dominant	6
Fetal and embryonal, embryonal dominant	4
Small cell	1

other steps were performed according to manufacturer's instructions. To increase RNA quantities, five tubes were pooled per case after the initial proteinase K digestion step. Isolated total RNA samples were stored at −80°C until required. RNA concentrations and purities were determined using a spectrophotometer (Ultrospec 2100 pro, Amersham Pharmacia Biotech, Little Chalfont, UK). The ratio of absorbance at 260 and 280 nm (OD_{260}/OD_{280}) was used as an indicator of contamination of RNA preparations with protein. OD_{260}/OD_{280} ratios ranged from 1.23 to 1.90.

Quantitative reverse-transcriptase polymerase chain reaction

To determine the amount of cDNA produced, quantitative reverse-transcriptase polymerase chain reaction (qRT-PCR) was performed for the highly expressed RPL13a ribosomal protein gene using a protocol developed by Illumina (San Diego, CA, USA). cDNA was produced by a Single-Use cDNA Synthesis Kit (Illumina) and 200 ng total RNA as input. Real-time PCR was performed in 10-μl reactions containing 5 μl SYBR Green PCR Master Mix, 1 μl cDNA product, and 250 nM each forward and reverse primer. Forty amplification cycles of 95°C for 5 s and 60°C for 30 s were carried out in an ABI Prism 7900HT Sequence Detection apparatus (Applied Biosystems, CA, USA). The primer sequences were 5′-GTACGCTGTGAAGGCAT CAA-3′ (forward) and 5′-GTTGGTGTTCATCCGCTTG-3′ (reverse). Amplification of β-actin served as an internal control. Gene expression was quantified using the comparative Ct method. Mean RPL13a Ct values ranged from 20.48 to 32.11.

Monitoring of gene expression

Gene expression was monitored using the DASL assay with Illumina's standard DASL Human Cancer Panel, which contains 1,536 sequence targets and 512 cancer-related genes. cDNA synthesis, the DASL process, array image processing, and signal extraction were performed as described [18]. Total RNA was converted to cDNA in a 20-μl RT-PCR reaction (MMC; Illumina) containing biotinylated random hexamers, oligo$(dT)_{18}$, and total RNA. The mixture was incubated at room temperature for 10 min and then at 42°C for 1 h. Pooled assay oligos were annealed to their sequence-specific targets on the cDNA using a controlled hybridization program. Assay oligo probes were designed to interrogate specific target sites on the cDNA as described [18, 19]. The first oligo consisted of the gene-specific sequence and a universal PCR primer sequence (P1, 5′-ACTTCGTCAGTAACGGAC-3′) at the 5′ end. The second oligo consisted of a gene-specific sequence, a unique address sequence complementary to one of the 1,520 capture sequences on the array, and a universal PCR primer sequence (P2, 5′-GTCTGCCTATAGTGAGTC-3′) at the 3′ end. The address sequence uniquely associates with a single target site and allows the PCR-amplified products to hybridize to universal microarray elements bearing complementary sequences. The cDNA was immobilized on paramagnetic beads and washed to remove any excess or mishybridized oligos. Hybridized oligos were then extended and ligated to generate amplifiable templates using reagents and conditions established by the manufacturer (BeadStation User's Manual, Illumina). PCR was performed using Cy3-labeled universal PCR primers. Single-stranded PCR products were prepared by denaturation and then hybridized to Sentrix arrays using a temperature-gradient program. The platform (Sentrix Universal-16 Beadchip, Illumina) was comprised of 16 bundles in which approximately 50,000 optical fibers were hexagonally packed and assembled into an 8×12 matrix. Arrays were imaged using a BeadArray Reader (Illumina), and intensity data were extracted. All above procedures were performed at Macrogen, Inc. (Seoul, Republic of Korea).

Statistical analysis of DASL chip data

Acquired data were $\log_2$-transformed and used for analysis. Genes with signal detection p values of <0.05 in more than 50% of the 64 samples were included in the analysis. To eliminate systematic variance, data were normalized using the quantile normalization method developed for Affymetrix probe set arrays. Normalized data were clustered using the hierarchical clustering method. A paired t test was used to compare gene expression differences between tumor and NNL samples. A two fold cutoff was applied for expression changes.

Comparison of gene expression profiles between clinicopathological subgroups of tumor samples was performed. Tumor expression values were normalized to corresponding NNL values using log-transformed tumor-to-NNL signal ratios ($\log_2$ HBL/NNL). Analysis was performed using an

unpaired *t* test in GenePlex 3.0 software (Istech Corp., Seoul, Republic of Korea) at a 1.5-fold cutoff level. Filtering and normalization were conducted as described above.

Differentially expressed genes were functionally annotated using two web-based intelligent systems (PANTHER 6.1, http://www.pantherdb.org/ and DAVID version 6.7, http://david.abcc.ncifcrf.gov/).

Case selection for tissue microarray assay

A total of 69 HBL cases were selected for the immunohistochemical (IHC) study (47 from the Department of Pathology, Seoul National University Hospital; 14 from Asan Medical Center, Seoul; and 8 from Yonsei University Hospital, Seoul). Twenty-nine of these cases were also used for the DASL chip assay. An additional 29 cases with other primary pediatric hepatic tumors (9 hepatocellular carcinomas, 2 embryonal sarcomas, 2 focal nodular hyperplasias, 6 infantile hemangioendotheliomas, 1 liver cell adenoma, 5 mesenchymal hamartomas, 1 malignant lymphoma, 2 inflammatory myofibroblastic tumors, and 1 rhabdomyosarcoma) and 2 cases with metastatic tumors (1 pancreatoblastoma and 1 metastatic neuroblastoma) were also selected for IHC. All patients had been treated between 1991 and 2008. As controls, 19 normal pediatric hepatic tissue samples and 6 samples of fetal hepatic tissues were selected. Normal hepatic tissues were obtained from normal components of liver tissues surgically resected because of a primary hepatic tumor. To collect clinicopathological data, hematoxylin and eosin-stained slides and pathology reports were reviewed. Among the 69 HBL patients, surgical resection margins were involved by tumor in three cases. Forty-seven patients with HBL (68%) received treatment for cancer before surgery. Data about preoperative chemotherapy were not available in three cases.

All tissues were evaluated using tissue array methods. Core tissue biopsies (2 mm in diameter) were taken from

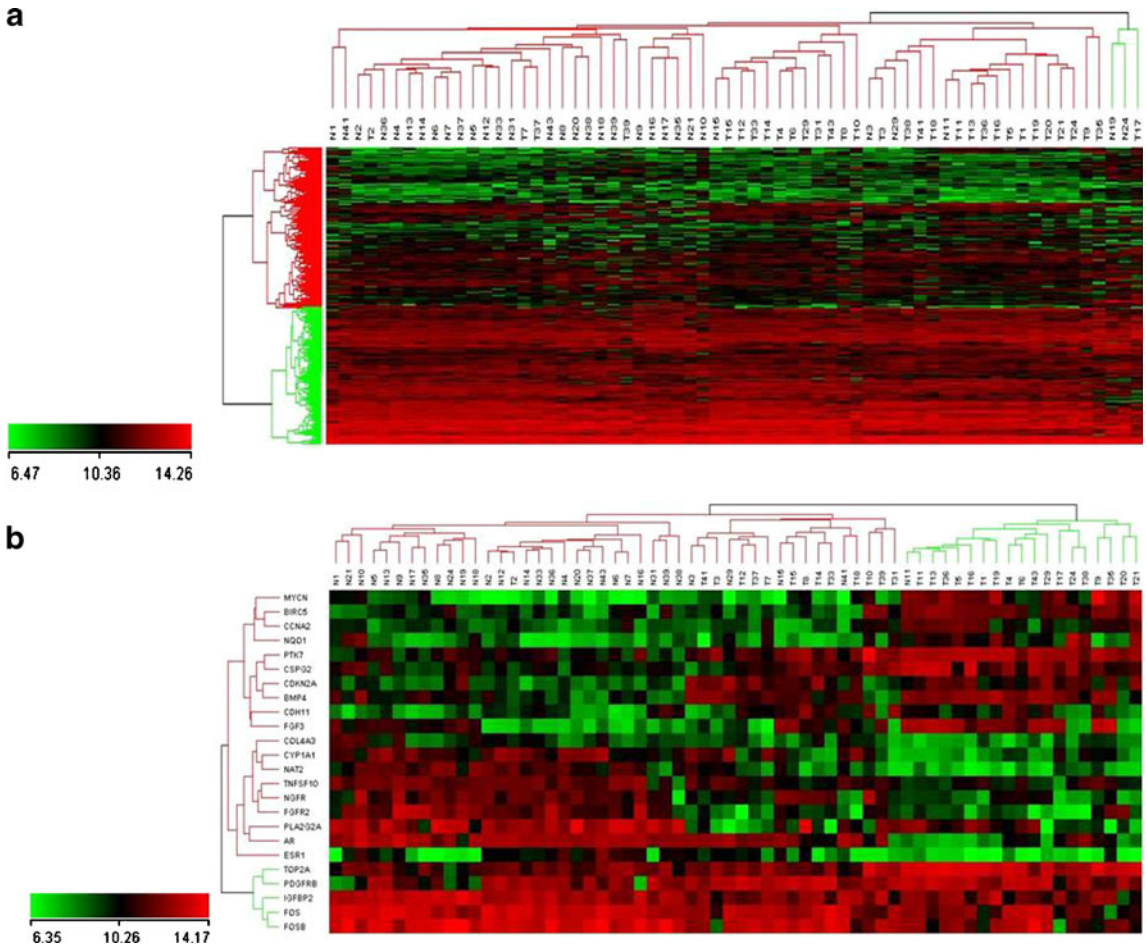

Fig. 1 Two-dimensional hierarchical clustering of genes reveals differences between HBL and corresponding NNL. The *horizontal axis* of the dendrogram indicates similarities across 32 HBL and 32 corresponding normal hepatic tissues, whereas the *vertical axis* reveals similarities across genes. **a** Clustering of HBL and NNL using the total gene set. **b** Clustering of HBL and NNL using 24 differentially expressed genes

individual paraffin-embedded tissues and arranged in a new recipient paraffin block (tissue array block) using a trephine apparatus (Superbiochips Laboratories, Seoul, Republic of Korea). An acceptable case was defined as one with a tumor occupying more than 10% of the core area.

Immunohistochemical staining

Immunohistochemistry was performed on Bond Max Autostainer (Leica Microsystems, Bannockburn, IL, USA) according to manufacturer's protocol. Briefly, 4-μm-thick sections from tissue array blocks were deparaffinized and hydrated using an ethanol-deionized water series. The sections were then washed, and antigens were retrieved using Bond Epitomic Retrieval Solution2 (Leica Microsystems2) for 20 min at 100°C. Endogenous peroxidase activity was blocked using 0.3% H_2O_2 in methanol for 5 min. Then, the sections were incubated with a mouse monoclonal antibody for YY1 (1:1,000 dilution; Abnova, Taipei, Taiwan) for 15 min. Antibody detection was performed using the Bond Polymer Detection Kit (Leica Microsystems). Slides were then counterstained with hematoxylin.

Immunostaining intensities were graded as no staining, faint staining, weak to moderate staining, or strong staining. At least, weak to moderate staining in more than 10% of neoplastic cells was considered to indicate positivity.

Statistical analysis of immunohistochemistry results

A chi-square test was used to compare YY1 expression in HBL, other childhood hepatic tumors, and normal liver tissue. An unpaired *t* test was used to identify differences in clinicopathological parameters between YY1-negative and YY1-positive HBL samples. Kaplan–Meier survival and Cox regression analyses were used to compare survival curves. Statistical significance was accepted for p values of <0.05. All statistical analyses were conducted using SPSS version 10.0 (SPSS, Chicago, IL, USA).

Table 3 Genes that are differentially expressed between HBL and NNL

Accession[a]	Symbol	Definition	Mean HBL	Mean NNL	Fold change (HBL/NNL)[b]	No. of cases (%)
NM_005378.3	MYCN	v-myc myelocytomatosis viral related oncogene	10.26	7.94	5.01	24 (75.0)
NM_002821.3	PTK7	PTK7 protein tyrosine kinase 7	12.32	10.39	3.82	26 (81.3)
NM_001168.1	BIRC5	Baculoviral IAP repeat-containing 5 (survivin)	10.89	9.35	2.90	19 (59.4)
NM_058196.1	CDKN2A	Cyclin-dependent kinase inhibitor 2A	10.94	9.41	2.89	22 (68.8)
NM_001067.2	TOP2A	Topoisomerase (DNA) IIα 170 kDa (TOP2A)	12.73	11.49	2.36	17 (53.1)
NM_004385.2	CSPG2	Chondroitin sulfate proteoglycan 2 (versican)	11.54	10.30	2.36	18 (56.3)
NM_001797.2	CDH11	Cadherin 11, type 2, OB-cadherin (osteoblast)	10.06	8.90	2.23	19 (59.4)
NM_000903.1	NQO1	NAD(P)H dehydrogenase, quinone 1	9.61	8.49	2.17	17 (53.1)
NM_002609.2	PDGFRB	Platelet-derived growth factor receptor, β	12.62	11.52	2.15	15 (37.5)
NM_005247.2	FGF3	Fibroblast growth factor 3	10.49	9.40	2.13	18 (56.3)
NM_001202.2	BMP4	Bone morphogenetic protein 4	11.27	10.20	2.09	18 (56.3)
NM_001237.2	CCNA2	Cyclin A2	10.13	9.09	2.05	15 (46.9)
NM_000597.1	IGFBP2	Insulin-like growth factor binding protein 2	11.80	12.81	−2.02	14 (43.8)
NM_031366.1	COL4A3	Collagen, type IV, α3 (Goodpasture antigen)	8.59	9.61	−2.03	19 (59.4)
NM_003810.2	TNFSF10	Tumor necrosis factor (ligand) superfamily, member 10	10.39	11.47	−2.11	26 (81.3)
NM_005252.2	FOS	v-fos FBJ murine osteosarcoma viral oncogene homolog	12.02	13.13	−2.16	13 (40.6)
NM_002507.1	NGFR	Nerve growth factor receptor (TNFR superfamily, member 16)	9.79	11.06	−2.40	18 (56.3)
NM_006732.1	FOSB	FBJ murine osteosarcoma viral oncogene homolog B	12.03	13.39	−2.56	16 (50.0)
NM_000125.1	ESR1	Estrogen receptor 1	7.73	9.42	−3.22	20 (62.5)
NM_000499.2	CYP1A1	Cytochrome P450, family 1, subfamily A, polypeptide 1	9.24	11.16	−3.79	23 (71.9)
NM_000300.2	PLA2G2A	Phospholipase A2, group IIA (platelets, synovial fluid)	9.96	12.20	−4.75	23 (71.9)
NM_022973.1	FGFR2	Fibroblast growth factor receptor 2	9.03	11.28	−4.76	26 (81.3)
NM_000044.2	AR	Androgen receptor	10.15	12.40	−4.77	20 (62.5)
NM_000015.1	NAT2	*N*-Acetyltransferase 2 (arylamine *N*-acetyltransferase)	8.31	10.87	−5.90	28 (87.5)

[a] GenBank accession number

[b] Ratio of $\log_2$-transformed mean values (HBL vs. NNL)

Results

Statistical comparison of overall gene expression patterns

The expression profiles of 512 genes were analyzed for 32 HBL and 32 corresponding NNL panels using a paired *t* test. Genes with fold changes of >2.0 were defined as being differentially expressed, and genes with signal detection *p* values of <0.05 in more than 50% of all samples were included in the analysis.

After filtering, the 463 remaining probes were compared in HBL and corresponding NNL tissues, and 24 genes were found to be differentially expressed. Gene expression patterns of HBL and NNL samples are shown as a dendrogram in Fig. 1, and differentially expressed genes are listed in Table 3. Using the PANTHER classification, these genes were classified into 17 biological process categories (Table 4). Upregulated genes in HBL were associated with apoptosis (*MYCN, BIRC5*), cell–cell adhesion (*CDH11*), cell cycle (*TOP2A, CCNA2*), cell proliferation and differentiation (*CSPG2, FGF3*), and signal transduction (*PDGFRB*). Downregulated genes in HBL were related to apoptosis (*TNFSF10, NGFR*), developmental processes (*ESR1, FOSB, FOS*), lipid metabolism (*CYP1A1, PLA2G2A*), and signal transduction (*AR, IGFBP2*).

Table 4 Biological process categories of genes differentially expressed between HBL and NNL

Category	Gene symbol	HBL	Category	Gene symbol	HBL
Apoptosis	MYCN	Up	Lipid, fatty acid, and steroid metabolism	CYP1A1	Down
	BIRC5	Up		PLA2G2A	Down
	TNFSF10	Down	Neuronal processes	ESR1	Down
	NGFR	Down		AR	Down
Cell adhesion	CDH11	Up	Nucleoside, nucleotide, and nucleic acid metabolism	TOP2A	Up
Cell cycle	TOP2A	Up		MYCN	Up
	MYCN	Up		AR	Down
	CCNA2	Up		ESR1	Down
	FGF3	Down		FOS	Down
	ESR1	Down		FOSB	Down
	FOS	Down	Oncogenesis	PDGFRB	Up
	FOSB	Down		CCNA2	Up
Cell proliferation and differentiation	CSPG2	Up		FGF3	Up
	FGF3	Up		MYCN	Up
	PDGFRB	Up		AR	Down
	ESR1	Down		FOS	Down
	FOS	Down	Other metabolism	NAT2	Down
Cell structure and motility	PTK7	Up	Protein metabolism and modification	PTK7	Up
	PDGFRB	Up		PDGFRB	Up
	CSPG2	Up	Signal transduction	PTK7	Up
	ESR1	Down		FGF3	Up
Developmental processes	PDGFRB	Up		CSPG2	Up
	BMP4	Up		CDH11	Up
	PTK7	Up		PDGFRB	Up
	CDH11	Up		MYCN	Up
	NGFR	Down		NGFR	Down
	ESR1	Down		TNFSF10	Down
	FOSB	Down		ESR1	Down
	FOS	Down		AR	Down
Electron transport	CYP1A1	Down		IGFBP2	Down
Homeostasis	IGFBP2	Down	Unclassified	CDKN2A	Up
Immunity and defense	PDGFRB	Up		NQO1	Up
	FOS	Down		COL4AE	Down
	TNFSF10	Down			

Pathway analysis of the differentially expressed genes suggested deregulation of the *MAPK* pathway in HBL. Two genes associated with the *MAPK* pathway (*FGF3* and *PDGFRB*) were upregulated, and three (*FGFR2*, *PLA2G2A*, and *FOS)* were downregulated.

Comparison of HBL gene expression patterns in poor and good prognosis groups

When metastasis or recurrence occurred within 2 years postoperatively, cases were considered to have a poor prognosis. Of the 32 cases, 10 were classified as having a poor prognosis, 19 were classified as good, and clinical data were unavailable for 3 cases.

An unpaired *t* test showed that 8 genes were upregulated and 15 were downregulated in the poor prognosis HBL group (Table 5). Two of the upregulated genes in this group were associated with cell proliferation (*IGF1, NEO1*), and two (*HCK, NEO1*) were associated with cell migration. Three genes were associated with organ development (*HCK, YY1, NRAS*), and one (*RIPK1*) was associated with apoptosis. An unpaired *t* test was also performed to find upregulated and downregulated genes in the poor prognosis HBL group that received chemotherapy before surgical resection. *YY1, NEO1, RIPK1,* and *NRAS* were upregulated in this group of patients (Table 6).

Downregulated genes in HBLs with poor prognosis included four DNA repair genes (*MSH2, LIG3, DDB2, WRN*) and three apoptosis-associated genes (*E2F1, PML, ING1*). One gene (*RBBP1*) with growth arrest activity and one (*CYP1A1*) with metabolic function were downregulated in HBLs with poor prognosis (Table 5).

Comparison of gene expression patterns with respect to HBL differentiation

An unpaired *t* test showed that 38 genes were differentially expressed between 18 W/D HBL and 14 P/D HBL (Table 7). Of these, eight genes were upregulated in the P/D HBL group, and 30 genes were upregulated in the W/D HBL group. Genes overexpressed in P/D HBL were mainly found to be involved in organ development and cell proliferation.

Table 5 Genes that are differentially expressed between poor and good prognosis groups of HBL

Accession[a]	Symbol	Definition	Fold change (poor vs. good)[b]	*p* value
NM_002110.2	HCK	Hemopoietic cell kinase	8.213554	0.00
NM_003804.2	RIPK1	Receptor (TNFRSF)-interacting serine-threonine kinase 1	5.664403	0.01
NM_000618.2	IGF1	Insulin-like growth factor 1 (somatomedin C)	3.095069	0.04
NM_003403.3	YY1	YY1 transcription factor	3.040470	0.02
NM_002499.1	NEO1	Neogenin homolog 1	2.697968	0.04
NM_130804.1	MEN1	Multiple endocrine neoplasia I	2.641837	0.04
NM_002524.2	NRAS	Neuroblastoma RAS viral (v-ras) oncogene homolog	2.562960	0.04
NM_001071.1	TYMS	Thymidylate synthetase	2.125266	0.05
NM_023001.1	RBBP1	AT-rich interactive domain 4A	0.522375	0.03
NM_003633.1	ENC1	Ectodermal-neural cortex (with BTB-like domain)	0.354223	0.00
NM_005225.1	E2F1	E2F transcription factor 1	0.130524	0.03
NM_000251.1	MSH2	mutS homolog 2, colon cancer, nonpolyposis type 1 (i)	0.119834	0.04
NM_173844.1	MALT1	Mucosa-associated lymphoid tissue lymphoma translocation gene 1	0.048121	0.04
NM_005962.2	MXI1	MAX interacting protein 1	0.046807	0.01
NM_007313.1	ABL1	v-abl Abelson murine leukemia viral oncogene homolog 1	−0.03561	0.04
NM_002311.2	LIG3	Ligase III, DNA, ATP-dependent	−0.12192	0.02
NM_000499.2	CYP1A1	Cytochrome P450, family 1, subfamily A, polypeptide 1	−0.25303	0.04
NM_033240.1	PML	Promyelocytic leukemia	−0.36173	0.01
NM_014210.1	EVI2A	Ecotropic viral integration site 2A	−0.74539	0.01
NM_000107.1	DDB2	Damage-specific DNA-binding protein 2,48 kDa	−0.95372	0.01
NM_006060.2	ZNFN1A1	Zinc finger protein, subfamily 1A,I (Ikaros)	−1.14447	0.04
NM_005537.3	ING1	Inhibitor of growth family, member 1	−2.9374	0.02
NM_000553.2	WRN	Werner syndrome	−2.94875	0.01

[a] GenBank accession number

[b] Ratio of $\log_2$-transformed mean expression values (HBL with poor vs. good prognosis)

Table 6 Genes that are differentially expressed between poor and good prognosis groups of HBL patients that received preoperative chemotherapy

Accession[a]	Symbol	Definition	Fold change (poor vs. good)[b]	*p* value
NM_000499.2	CYP1A1	Cytochrome P450, family 1, subfamily A, polypeptide 1	6.84842	0.00
NM_000015.1	NAT2	*N*-Acetyltransferase 2	4.65267	0.03
NM_003403.3	YY1	YY1 transcription factor	3.30504	0.04
NM_003810.2	TNFSF10	Tumor necrosis factor (ligand) superfamily, member 10	2.66402	0.02
NM_000553.2	WRN	Werner syndrome	2.24022	0.04
NM_002035.1	FVT1	Follicular lymphoma variant translocation 1	2.21335	0.01
NM_002499.1	NEO1	Neogenin homolog 1	2.07469	0.05
NM_000107.1	DDB2	Damage-specific DNA-binding protein 2, 48 kDa	2.05888	0.01
NM_005901.2	MADH2	Mothers against decapentaplegic (MAD) homolog 2	2.00142	0.03
NM_003804.2	RIPK1	Receptor (TNFRSF)-interacting serine-threonine kinase 1	1.94858	0.01
NM_023001.1	RBBP1	AT-rich interactive domain 4A (RBP1-like), transcript variant 3	1.83411	0.03
NM_002524.2	NRAS	Neuroblastoma RAS viral (v-ras) oncogene homolog	1.79923	0.03
NM_005962.2	MXI1	MAX interacting protein 1, transcript variant 1	1.63536	0.03
NM_000546.2	TP53	Tumor protein p53	1.58960	0.04
NM_004323.2	BAG1	BCL2-associated athanogene	1.51434	0.02
NM_173844.1	MALT1	Mucosa-associated lymphoid tissue lymphoma translocation gene 1	0.66484	0.04
NM_005356.2	LCK	Lymphocyte-specific protein tyrosine kinase	0.61849	0.03
NM_001759.2	CCND2	Cyclin D2	0.61203	0.03
NM_002110.2	HCK	Hemopoietic cell kinase	0.59385	0.03
NM_033240.1	PML	Promyelocytic leukemia	0.51227	0.03
NM_003392.2	WNT5A	Wingless-type MMTV integration site family, member 5A	0.49805	0.00
NM_005225.1	E2F1	E2F transcription factor 1	0.46065	0.03
NM_001657.2	AREG	Amphiregulin (schwannoma-derived growth factor)	0.26774	0.03
NM_001244.2	TNFSF8	Tumor necrosis factor (ligand) superfamily, member 8	0.23817	0.01
NM_001797.2	CDH11	Cadherin 11, type 2, OB-cadherin (osteoblast)	0.23161	0.02

[a] GenBank accession number

[b] Ratio of $\log_2$-transformed mean expression values (HBL with poor vs. good prognosis)

YY1 expression in HBL

YY1, which was upregulated in the poor prognosis group, was chosen for IHC to verify its protein expression in HBLs. Of 69 HBL cases, 13 (19.1%) were positive for *YY1* by IHC. HBL showed strong, diffuse nuclear staining for *YY*1 (Fig. 2). In contrast, none of the 19 normal hepatic tissues or 6 fetal liver tissues was positive for *YY1* (p= 0.017). Of the other childhood hepatic tumors, only two cases of infantile hemangioendothelioma showed weak to moderate positivity for *YY1*.

In the comparative analysis between *YY1* gene expression value in DASL chip study and protein expression by immunohistochemistry, the mean signal intensity for *YY1* of *YY1*-immunopositive HBLS was higher than that of *YY1*-immunonegative HBLs with marginal significance (mean ± SD, positive vs. negative, 9,624.78±3,257.07 vs. 6,684.44 ±3,062.76, p=0.057). The distribution of signal intensities for *YY1* is shown in Fig. 3.

P/D HBLs were more frequently positive for *YY1* than W/D HBLs (34.6% vs. 9.5%, P=0.023), but other clinicopathologic parameters including tumor metastasis and recurrence were not related to *YY1* expression.

Kaplan–Meier analysis showed that HBL tumors that expressed *YY1* protein tended to recur more rapidly, and Cox regression analysis also showed a tendency for rapid progression in the *YY1*-immunopositive HBL group, but these results could not fulfill the statistical significance due to small number of cases (p=0.327 in log-rank test and p= 0.599 in Cox regression analysis; Fig. 4a, b).

Discussion

Hoshida et al. used the DASL chip assay to analyze 307 FFPE hepatocellular carcinoma tissues and demonstrated its feasibility for genome-wide expression profiling [17]. In our current study, we used the DASL chip assay to profile

Table 7 Genes that are differentially expressed between poorly differentiated and well-differentiated HBL

Accession[a]	Symbol	Definition	Fold change (P/D vs. W/D)[b]	*p* value
NM_139355.1	MATK	Megakaryocyte-associated tyrosine kinase	12.05143	0.02
NM_001909.3	CTSD	Cathepsin D (lysosomal aspartyl protease)	5.159696	0.00
NM_000044.2	AR	Androgen receptor	3.597843	0.01
NM_000963.1	PTGS2	Prostaglandin-endoperoxide synthase 2	3.239847	0.01
NM_003403.3	YY1	YY1 transcription factor	2.924429	0.02
NM_007111.3	TFDP1	Transcription factor Dp-1	2.858537	0.01
NM_130804.1	MEN1	Multiple endocrine neoplasia I (MEN1)	2.673531	0.00
NM_004985.3	KRAS2	v-Ki-ras2 Kirsten rat sarcoma 2 viral oncogene homolog	1.641395	0.00
NM_003177.3	SYK	Spleen tyrosine kinase	0.650559	0.01
NM_004449.2	ERG	v-ets erythroblastosis virus E26 oncogene like	0.464515	0.04
NM_024767.2	DLC1	Deleted in liver cancer 1	0.442596	0.02
NM_000362.3	TIMP3	Tissue inhibitor of metalloproteinase 3 (pseudoinflammatory) (TIMP3), mRNA	0.192861	0.04
NM_001983.1	ERCC1	Excision repair cross-complementing rodent repair deficiency, complementation group 1	0.14861	0.04
NM_005253.2	FOSL2	FOS-like antigen 2	0.080652	0.03
NM_000657.1	BCL2	B-cell CLL/lymphoma 2	0.060524	0.00
NM_004995.2	MMP14	Matrix metalloproteinase 14	0.04335	0.01
NM_000168.2	GLI3	GLI-Kruppel family member GLI3	0.013116	0.01
NM_173844.1	MALT1	Mucosa-associated lymphoid tissue lymphoma translocation gene 1	0.002804	0.05
NM_015832.2	MBD2	Methyl-CpG-binding domain protein 2	−0.02143	0.03
NM_001951.2	E2F5	E2F transcription factor 5	−0.02648	0.00
NM_002467.2	MYC	v-myc myelocytomatosis viral oncogene homolog	−0.16704	0.02
NM_000061.1	BTK	Bruton agammaglobulinemia tyrosine kinase	−0.24961	0.00
NM_033240.1	PML	Promyelocytic leukemia	−0.32251	0.00
NM_001799.2	CDK7	Cyclin-dependent kinase 7	−0.38012	0.05
NM_000799.1	EPO	Erythropoietin	−0.44451	0.00
NM_003390.2	WEE1	WEE1 homolog (*Schizosaccharomyces pombe*)	−0.45203	0.02
NM_022443.2	MLF1	Myeloid leukemia factor 1	−0.51295	0.01
NM_000534.2	PMS1	PMS1 postmeiotic segregation increased 1	−0.52106	0.01
NM_182649.1	PCNA	Proliferating cell nuclear antigen	−0.53203	0.02
NM_022406.1	XRCC4	X-ray repair complementing defective repair in Chinese hamster cells 4	−0.55105	0.04
NM_006060.2	ZNFN1A1	Zinc finger protein, subfamily 1A	−0.65323	0.01
NM_033016.1	PDGFB	Platelet-derived growth factor β-polypeptide	−0.7487	0.04
NM_003023.2	SH3BP2	SH3-domain binding protein 2	−1.29947	0.03
NM_002585.1	PBX1	Pre-B-cell leukemia transcription factor 1	−1.38161	0.02
NM_002875.2	RAD51	RAD51 homolog	−2.65553	0.03
NM_016724.1	FOLR1	Folate receptor 1	−2.79683	0.00
NM_002229.1	JUNB	jun B proto-oncogene	−8.22171	0.02
NM_001067.2	TOP2A	Topoisomerase (DNA) IIα	−9.47598	0.02

[a] GenBank accession number

[b] Ratio of $\log_2$-transformed mean expression values (poorly differentiated to well differentiated)

HBL gene expression. The assay detected a unique gene expression pattern in HBL, which allowed us to identify candidate genes for prognostic markers.

We found 24 differentially expressed genes in HBL tissues compared to paired NNL tissues. Among them, 12 genes were upregulated in HBL, and these were associated with apoptosis, cell adhesion, cell cycle, cell proliferation, cell structure, development, oncogenesis, and signal transduction. Few of these genes were identified in a previous gene expression profile study on HBL and NNL [13, 15]. This discordance may have arisen from differences in control samples, statistical analysis methods, and/or probe

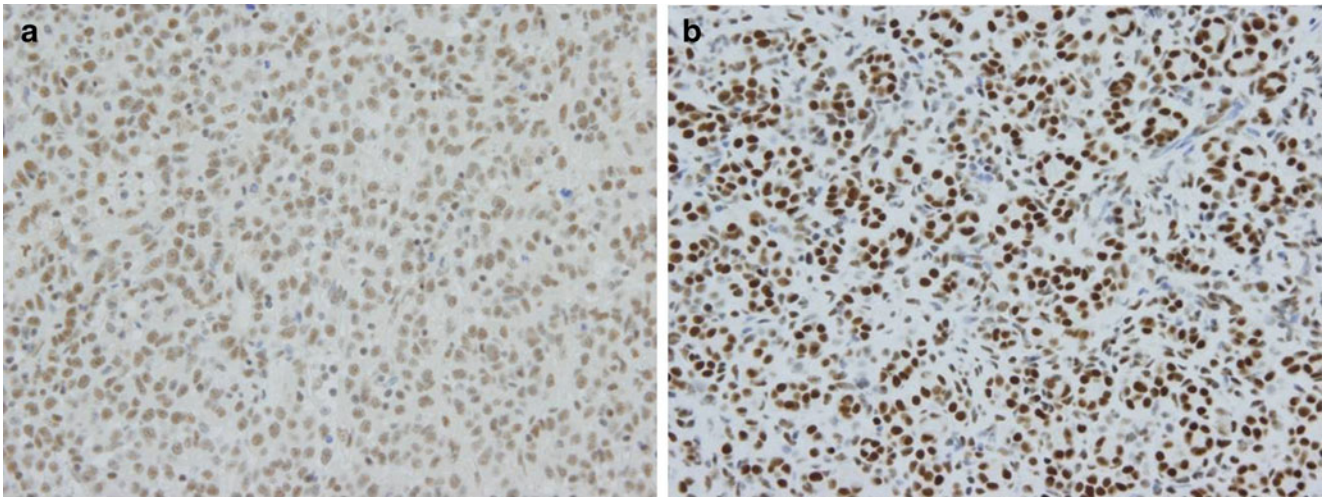

Fig. 2 Immunohistochemistry using a monoclonal antibody against *YY1*. **a** Weak to moderate staining for *YY1* in hepatoblastoma (×200). **b** Strong staining for *YY1* in hepatoblastoma (×200)

sets. We used paired control tissues and a paired *t* test to reflect the baseline amount of mRNA in normal tissues. The probe sets used in our genetic profiling study included cancer-related genes, whereas other genetic profiling studies used other probe sets. In particular, Yamada et al. used a gene set extracted from a cDNA library produced from HBL tissue [15].

MYCN, the most highly upregulated gene in HBL, is a member of the *MYC* family of oncogenes, which encode nuclear transcription factors. The protein products of *MYC* genes have been reported to participate in human and animal cancers by deregulating cellular proliferation and cell death [20]. In particular, *MYCN* is known to be upregulated in neuroblastomas and is considered an indicator for poor prognosis [21]. Deregulation of *MYCN* has also been observed in rhabdomyosarcoma, another common solid tumor in children [22]. Therefore, *MYCN* deregulation is considered a potential target for therapy in these two childhood tumor types [21, 22]. In the case of HBL, *MYCN* gene amplification was not observed in previous studies [23, 24]. Other mechanisms inducing an increase in *MYCN* transcription may be involved in the overexpression of *MYCN* mRNA found in our current study. This possibility requires further study. *BIRC5*

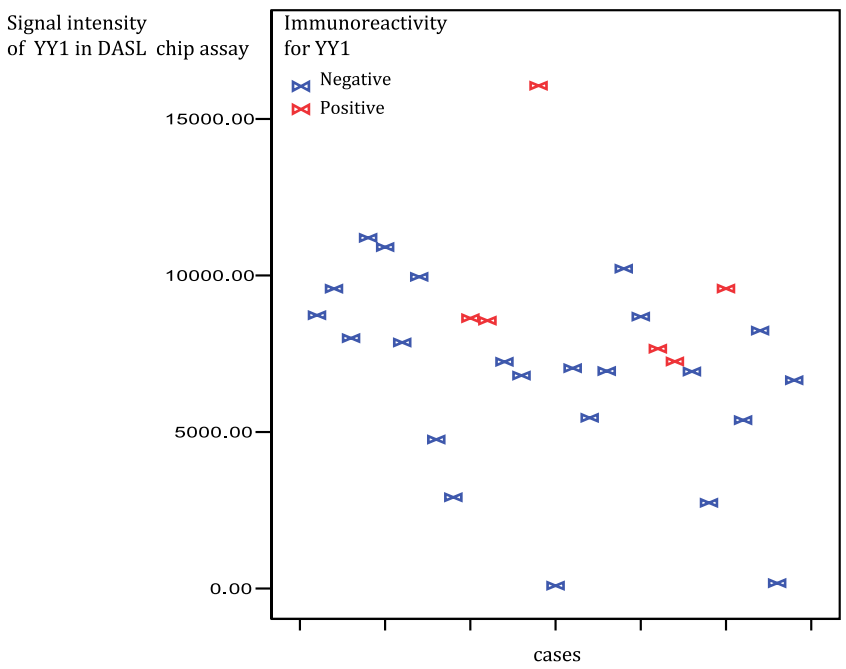

Fig. 3 Distribution of signal intensity of *YY1* immunoreactivity

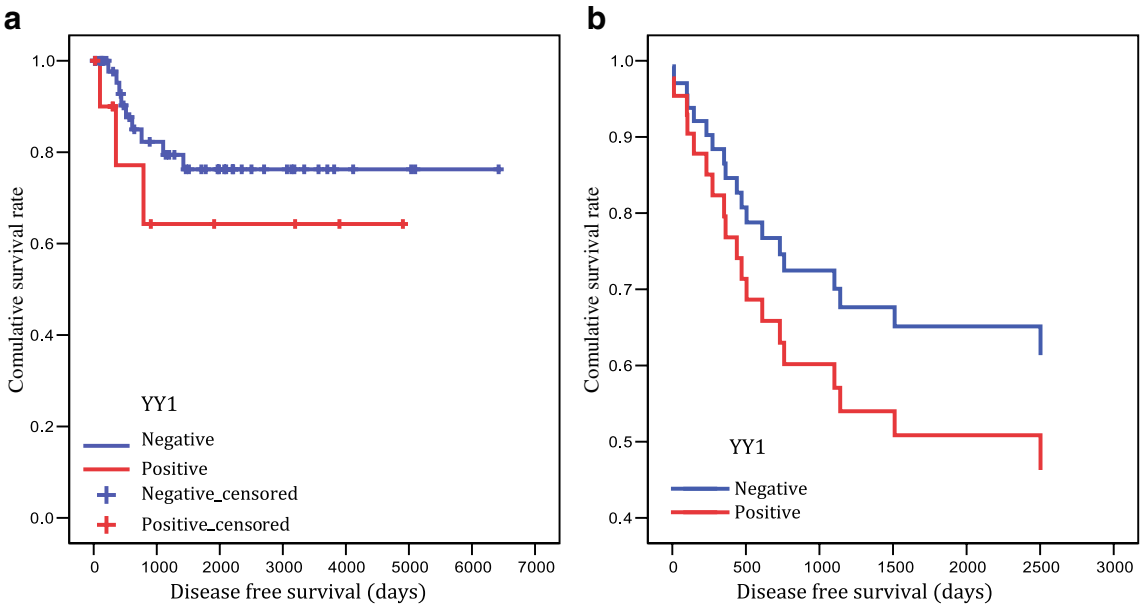

Fig. 4 **a** Kaplan–Meier disease-free survival curve for patients with HBL according to *YY1* expression. **b** Cox regression disease-free survival curve for patients with HBL according to *YY1* expression

(survivin), an inhibitor of apoptosis, is also highly expressed in neuroblastomas, and therapeutic targeting of this protein has been investigated [25]. Several studies have revealed that *BIRC5* may be induced via functional cooperation with *MYCN* [26]. Interestingly, the signal intensities of the mRNA for these two genes were correlated in our DASL chip assay (correlation coefficient =0.718, $p<0.001$). Our findings suggest that these two apoptosis-associated genes may be therapeutic targets in HBL, and we suggest that their protein expression should be confirmed in future studies.

The other 12 genes identified in our current study were downregulated, and these were more often involved in metabolism than the upregulated genes, which is consistent with the findings of previous studies [13, 15]. *IGF* plays a key role in mammalian growth and fetal cell division, and its expression is frequently altered in cancers and overgrowth disorders, presumably because of its proliferative and antiapoptotic effects. Members of the *IGF*-binding protein (*IGFBP*) family bind *IGF* 1/2 and modulate many aspects of the *IGF* axis. We observed significant decrease of *IGFBP2* and marginal decrease of *IGFBP3* (fold change −1.58). Gray et al. reported downregulation of *IGFBP2* in HBL versus normal liver tissues [8], which is consistent with our findings. By binding *IGF, IGFBPs* form biologically inactive complexes and thus prevent *IGFs* from binding to their receptors. Therefore, downregulation of *IGFBP2/3* mRNA may increase the biological activity of *IGFs* and potentiate their proliferative effect in HBLs. In our current study, *CYP1A1*, a member of the cytochrome P450 family, was also downregulated in HBL. Consistent with this result, Yamada et al. reported the downregulation of several metabolism-associated genes in HBL, including lipid metabolism-associated genes [15], and Nagata et al. found that several cytochrome P450 family members are downregulated in HBL [15].

Pathway analysis of the differentially expressed genes revealed deregulation of the *MAPK* pathway in HBL. Two *MAPK* pathway genes (*FGF3* and *PDGFRB*) were upregulated, and three (*FGFR2, PLA2G2A,* and *FOS*) were downregulated. Until recently, only a few cases of HBL were reported in patients with an activated *RAS/MAPK* pathway, and most of these were associated with a congenital syndrome [27]. In our current genetic profiling study, the *MAPK* signaling pathway was deregulated in HBL samples compared to NNL. Adekule et al. also reported altered expression of genes involved in the *MAPK* signaling pathway in aggressive HBL with a small-cell component [28]. *MAPK* signaling pathways play critical roles in cell proliferation, differentiation, and survival or death, and have thus been implicated in pathogenesis of many human diseases including cancer. The *MAPK* pathway is indirectly connected to the *wnt* signaling pathway, which is also related to development of HBL. Therefore, wider deregulation of signaling pathways, including the *MAPK* and *wnt* signaling pathways, may be involved in the pathogenesis of HBL.

In another comparison, we identified 8 genes that were upregulated and 15 that were downregulated in the poor prognosis group relative to the good prognosis group, and found that *IGF1* was upregulated in the rapid metastasis and recurrence group. Although current evidence demonstrates

that *IGFs* play important roles in the development of several cancers including breast, prostate, colon, and lung cancer [8, 29], the association between *IGF1* expression and prognosis has only been demonstrated for gastrointestinal stromal tumors [30]. The relationship between *IGF1* mRNA expression and prognosis in HBL found in our current study is worth examining further.

The transcription factor *YY1* plays a fundamental role in normal biological processes such as embryogenesis, differentiation, replication, and cellular proliferation. Furthermore, *YY1* overexpression is believed to be associated with unchecked cellular proliferation, resistance to apoptotic stimuli, tumorigenesis, and metastatic potential in several tumor types such as hematopoietic tumors, epithelial-based tumors, endocrine organ malignancies, hepatocellular carcinoma, and retinoblastoma. Thus, *YY1* may be a suitable target for antitumor chemotherapy or immunotherapy [31]. In our current study, we found that *YY1* mRNA was upregulated in the HBL group with poor prognosis and in the HBL group that received preoperative chemotherapy. In addition, both *YY1* mRNA upregulation and *YY1* protein expression were associated with high histological grade in HBL. Although survival analysis failed to show a relationship between *YY1* expression and prognosis, early recurrence was associated with *YY1* expression. These results suggest the need for verification of the prognostic implications of *YY1* expression in HBL with a larger-scale study.

In summary, we used the DASL chip assay to investigate gene expression in HBL. We confirm expression changes in *IGFBP2* and *CYP1A1* that have already been reported in HBL, and we report for the first time the altered expression of 22 other genes in HBL. In particular, two apoptosis-associated genes, *MYCN* and *BIRC5*, were found to be highly overexpressed in HBL, and thus may be considered as candidates for therapeutic targets. Furthermore, we found that upregulation of *IGF1* and *YY1* mRNA in HBL was associated with poor prognosis, and that *YY1* mRNA and protein expression were both correlated with poor differentiation in HBL. The gene expression profiles reported here suggest candidate prognostic and diagnostic markers and potential therapeutic targets in HBL.

Acknowledgments This study was supported by grant 0420090660 from the Clinical Institute of Seoul National University Hospital, Seoul, Republic of Korea.

Conflict of interest The authors declare no conflicts of interest.

References

1. Roebuck DJ, Perilongo G (2006) Hepatoblastoma: an oncological review. Pediatr Radiol 36:183–186
2. Schnater JM, Kohler SE, Lamers WH, von Schweinitz D, Aronson DC (2003) Where do we stand with hepatoblastoma? A review. Cancer 98:668–678
3. Hu J, Wills M, Baker BA, Perlman EJ (2000) Comparative genomic hybridization analysis of hepatoblastomas. Genes Chromosom Cancer 27:196–201
4. Weber RG, Pietsch T, von Schweinitz D, Lichter P (2000) Characterization of genomic alterations in hepatoblastomas. A role for gains on chromosomes 8q and 20 as predictors of poor outcome. Am J Pathol 157:571–578
5. Curia MC, Zuckermann M, De Lellis L, Catalano T, Lattanzio R, Aceto G, Veschi S, Cama A, Otte JB, Piantelli M, Mariani-Costantini R, Cetta F, Battista P (2008) Sporadic childhood hepatoblastomas show activation of beta-catenin, mismatch repair defects and p53 mutations. Mod Pathol 21:7–14
6. Jeng YM, Wu MZ, Mao TL, Chang MH, Hsu HC (2000) Somatic mutations of beta-catenin play a crucial role in the tumorigenesis of sporadic hepatoblastoma. Cancer Lett 152:45–51
7. Akmal SN, Yun K, MacLay J, Higami Y, Ikeda T (1995) Insulin-like growth factor 2 and insulin-like growth factor binding protein 2 expression in hepatoblastoma. Hum Pathol 26:846–851
8. Gray SG, Eriksson T, Ekstrom C, Holm S, von Schweinitz D, Kogner P, Sandstedt B, Pietsch T, Ekstrom TJ (2000) Altered expression of members of the IGF-axis in hepatoblastomas. Br J Cancer 82:1561–1567
9. Golub TR, Slonim DK, Tamayo P, Huard C, Gaasenbeek M, Mesirov JP, Coller H, Loh ML, Downing JR, Caligiuri MA, Bloomfield CD, Lander ES (1999) Molecular classification of cancer: class discovery and class prediction by gene expression monitoring. Science 286:531–537
10. Perou CM, Sorlie T, Eisen MB, van de Rijn M, Jeffrey SS, Rees CA, Pollack JR, Ross DT, Johnsen H, Akslen LA, Fluge O, Pergamenschikov A, Williams C, Zhu SX, Lonning PE, Borresen-Dale AL, Brown PO, Botstein D (2000) Molecular portraits of human breast tumours. Nature 406:747–752
11. Boyer J, Allen WL, McLean EG, Wilson PM, McCulla A, Moore S, Longley DB, Caldas C, Johnston PG (2006) Pharmacogenomic identification of novel determinants of response to chemotherapy in colon cancer. Cancer Res 66:2765–2777
12. Dhanasekaran SM, Barrette TR, Ghosh D, Shah R, Varambally S, Kurachi K, Pienta KJ, Rubin MA, Chinnaiyan AM (2001) Delineation of prognostic biomarkers in prostate cancer. Nature 412:822–826
13. Nagata T, Takahashi Y, Ishii Y, Asai S, Nishida Y, Murata A, Koshinaga T, Fukuzawa M, Hamazaki M, Asami K, Ito E, Ikeda H, Takamatsu H, Koike K, Kikuta A, Kuroiwa M, Watanabe A, Kosaka Y, Fujita H, Miyake M, Mugishima H (2003) Transcriptional profiling in hepatoblastomas using high-density oligonucleotide DNA array. Cancer Genet Cytogenet 145:152–160
14. Luo JH, Ren B, Keryanov S, Tseng GC, Rao UN, Monga SP, Strom S, Demetris AJ, Nalesnik M, Yu YP, Ranganathan S, Michalopoulos GK (2006) Transcriptomic and genomic analysis of human hepatocellular carcinomas and hepatoblastomas. Hepatology 44:1012–1024
15. Yamada S, Ohira M, Horie H, Ando K, Takayasu H, Suzuki Y, Sugano S, Hirata T, Goto T, Matsunaga T, Hiyama E, Hayashi Y, Ando H, Suita S, Kaneko M, Sasaki F, Hashizume K, Ohnuma N, Nakagawara A (2004) Expression profiling and differential screening between hepatoblastomas and the corresponding normal livers: identification of high expression of the PLK1 oncogene as a poor-prognostic indicator of hepatoblastomas. Oncogene 23:5901–5911
16. Bibikova M, Talantov D, Chudin E, Yeakley JM, Chen J, Doucet D, Wickham E, Atkins D, Barker D, Chee M, Wang Y, Fan JB (2004) Quantitative gene expression profiling in formalin-fixed,

paraffin-embedded tissues using universal bead arrays. Am J Pathol 165:1799–1807
17. Hoshida Y, Villanueva A, Kobayashi M, Peix J, Chiang DY, Camargo A, Gupta S, Moore J, Wrobel MJ, Lerner J, Reich M, Chan JA, Glickman JN, Ikeda K, Hashimoto M, Watanabe G, Daidone MG, Roayaie S, Schwartz M, Thung S, Salvesen HB, Gabriel S, Mazzaferro V, Bruix J, Friedman SL, Kumada H, Llovet JM, Golub TR (2008) Gene expression in fixed tissues and outcome in hepatocellular carcinoma. N Engl J Med 359:1995–2004
18. Fan JB, Yeakley JM, Bibikova M, Chudin E, Wickham E, Chen J, Doucet D, Rigault P, Zhang B, Shen R, McBride C, Li HR, Fu XD, Oliphant A, Barker DL, Chee MS (2004) A versatile assay for high-throughput gene expression profiling on universal array matrices. Genome Res 14:878–885
19. Fan JB, Oliphant A, Shen R, Kermani BG, Garcia F, Gunderson KL, Hansen M, Steemers F, Butler SL, Deloukas P, Galver L, Hunt S, McBride C, Bibikova M, Rubano T, Chen J, Wickham E, Doucet D, Chang W, Campbell D, Zhang B, Kruglyak S, Bentley D, Haas J, Rigault P, Zhou L, Stuelpnagel J, Chee MS (2003) Highly parallel SNP genotyping. Cold Spring Harb Symp Quant Biol 68:69–78
20. Schwab M (2004) MYCN in neuronal tumours. Cancer Lett 204:179–187
21. Mertens F, Mandahl N, Mitelman F, Heim S (1994) Cytogenetic analysis in the examination of solid tumors in children. Pediatr Hematol Oncol 11:361–377
22. Morgenstern DA, Anderson J (2006) MYCN deregulation as a potential target for novel therapies in rhabdomyosarcoma. Expert Rev Anticancer Ther 6:217–224
23. Tsuda H, Shimosato Y, Upton MP, Yokota J, Terada M, Ohira M, Sugimura T, Hirohashi S (1988) Retrospective study on amplification of N-myc and c-myc genes in pediatric solid tumors and its association with prognosis and tumor differentiation. Lab Invest 59:321–327
24. Mares J, Polanska V, Gorgens H, Sedlacek Z, Marikova T, Bocek P, Kodet R, Schackert J, Goetz P (1998) Oncogene amplification and expression in pediatric solid tumors. Neoplasma 45:123–127
25. Fest S, Huebener N, Bleeke M, Durmus T, Stermann A, Woehler A, Baykan B, Zenclussen AC, Michalsky E, Jaeger IS, Preissner R, Hohn O, Weixler S, Gaedicke G, Lode HN (2009) Survivin minigene DNA vaccination is effective against neuroblastoma. Int J Cancer 125:104–114
26. Eckerle I, Muth D, Batzler J, Henrich KO, Lutz W, Fischer M, Witt O, Schwab M, Westermann F (2009) Regulation of BIRC5 and its isoform BIRC5-2B in neuroblastoma. Cancer Lett 285:99–107
27. Yoshida R, Ogata T, Masawa N, Nagai T (2008) Hepatoblastoma in a Noonan syndrome patient with a PTPN11 mutation. Pediatr Blood Cancer 50:1274–1276
28. Adesina AM, Lopez-Terrada D, Wong KK, Gunaratne P, Nguyen Y, Pulliam J, Margolin J, Finegold MJ (2009) Gene expression profiling reveals signatures characterizing histologic subtypes of hepatoblastoma and global deregulation in cell growth and survival pathways. Hum Pathol 40:843–853
29. LeRoith D, Roberts CT Jr (2003) The insulin-like growth factor system and cancer. Cancer Lett 195:127–137
30. Braconi C, Bracci R, Bearzi I, Bianchi F, Sabato S, Mandolesi A, Belvederesi L, Cascinu S, Valeri N, Cellerino R (2008) Insulin-like growth factor (IGF) 1 and 2 help to predict disease outcome in GIST patients. Ann Oncol 19:1293–1298
31. Gordon S, Akopyan G, Garban H, Bonavida B (2006) Transcription factor YY1: structure, function, and therapeutic implications in cancer biology. Oncogene 25:1125–1142

Virchows Arch (2011) 458:467–476
DOI 10.1007/s00428-011-1047-4

ORIGINAL ARTICLE

Differentially expressed genes in giant cell tumor of bone

Erica Babeto · André Luis Giacometti Conceição · Marina Curado Valsechi · Paulo Peitl Junior · Débora Aparecida Pires de Campos Zuccari · Luiz Guilherme Cernaglia Aureliano de Lima · Jane Lopes Bonilha · Marília de Freitas Calmon · José Antônio Cordeiro · Paula Rahal

Received: 11 May 2010 / Revised: 19 January 2011 / Accepted: 20 January 2011 / Published online: 9 February 2011
© Springer-Verlag 2011

Abstract Giant cells tumors of bone (GCTB) are benign in nature but cause osteolytic destruction with a number of particular characteristics. These tumors can have uncertain biological behavior often contain a significant proportion of highly multinucleated cells, and may show aggressive behavior. We have studied differential gene expression in GCTB that may give a better understanding of their physiopathology, and might be helpful in prognosis and treatment. Rapid subtractive hybridization (*RaSH*) was used to identify and measure novel genes that appear to be differentially expressed, including *KTN1*, *NEB*, *ROCK1*, and *ZAK* using quantitative real-time polymerase chain reaction (qRT-PCR) and immunohistochemistry in the samples of GCTBs compared to normal bone tissue. Normal bone was used in the methodology RaSH for comparison with the GCTB in identification of differentially expressed genes. Functional annotation indicated that these genes are involved in cellular processes related to their tumor phenotype. The differential expression of *KTN1*, *ROCK1*, and *ZAK* was independently confirmed by qRT-PCR and immunohistochemistry. The expression of the *KTN1* and *ROCK1* genes were increased in samples by qRT-PCR and immunohistochemistry, and *ZAK* had reduced expression. Since *ZAK* have CpG islands in their promoter region and low expression in tumor tissue, their methylation pattern was analyzed by MSP-PCR. The genes identified *KTN1*, *ROCK1*, and *ZAK* may be responsible for loss of cellular homeostasis in GCTB since they are responsible for various functions related to tumorigenesis such as cell migration, cytoskeletal organization, apoptosis, and cell cycle control and thus may contribute at some stage in the process of formation and development of GCTB.

Keywords Giant cell tumor of bone · RaSH · Gene expression · Methylation · Quantitative real-time polymerase chain reaction (qRT-PCR) · Immunohistochemical

E. Babeto · A. L. G. Conceição · M. C. Valsechi · P. Peitl Junior · M. de Freitas Calmon · P. Rahal
Laboratory of Genomics Studies,
São Paulo State University - UNESP,
Cristóvão Colombo, 2265,
15054-000 São José do Rio Preto, SP, Brazil

D. A. P. de Campos Zuccari
Center for the Study of Cancer Prognosis - CEPC,
College of Medicine - FAMERP,
Brigadeiro Faria Lima, 5416,
15090-000 São José do Rio Preto, SP, Brazil

L. G. C. A. de Lima · J. L. Bonilha
Department of Pathology, College of Medicine - FAMERP,
Brigadeiro Faria Lima, 5416,
15090-000 São José do Rio Preto, SP, Brazil

J. A. Cordeiro
Department of Epidemiology and Collective Health,
College of Medicine - FAMERP,
Brigadeiro Faria Lima, 5416,
15090-000 São José do Rio Preto, SP, Brazil

P. Rahal (✉)
Department of Biology, Instituto de Biociências,
Letras e Ciências Exatas - IBILCE/UNESP,
Cristóvão Colombo, 2265,
15054-000 São José do Rio Preto, SP, Brazil
e-mail: rahalp@yahoo.com.br

Introduction

Giant cell tumor of bone (GCTB) is a rare benign lesion that comprises ~5% of primary bone tumors [1, 2]. They can be locally aggressive and destructive with rapid growth

leading to thinning and rupture of the cortical bone with invasion of adjacent soft tissues, but without invading and ulcerating the skin and subcutaneous tissue [3, 4]. Generally, GCTBs most frequently occur in young adults between 20 and 40 years of age, with a slight predominance in females. They affect mainly the ends of long bones, and frequently occur in the distal end of the femur and the proximal end of the tibia [5–8].

GCTB is characterized by the presence of numerous osteoclast-like giant cells, and a mononuclear component that includes proliferating mononuclear stromal cells and infiltrating macrophages [9–11]. The mononuclear stromal cell represents the neoplastic component of the tumor, whereas monocytes represent a minor component of the mononuclear cell population [10, 12]. There is consensus among most authors regarding the true histogenesis of these lesions, with the evidence favoring a mesenchymal and mononuclear cells as stem cells of GCTB [13].

Despite its benign histological appearance, GCTB has an unpredictable clinical course [14]. The rate of local recurrence following surgical curettage is relatively high at 18–60%, and some occasionally undergo malignant transformation [15]. Metastasis occurs most commonly to the lung, variously reported in 1–9% of cases [16]. The outcome cannot be predicted on the basis of histological or radiographical criteria. In the absence of a clear histogenetic origin, GCTB is currently classified among lesions with an uncertain derivation and named after its peculiar morphologic appearance [14].

A better understanding of the mechanisms underlying the complex physiopathology of GCTBs, including a characterization of the gene expression profile and the functions of the genes involved in this phenomenon, and the molecular environment that might typify the tumor. We have investigated the molecular biology characteristics of GCTB to determine whether a more directed targeted clinical intervention can be adopted in the future.

The rapid subtraction hybridization approach (*RaSH*) [17] has been used to identify genes involved in tumorigenesis and the development of GCTBs. Subtraction hybridization methods are designed to identify the expression of complementary DNAs (cDNAs) in one of the two analyzed groups, thereby detecting differentially expressed messenger RNAs (mRNAs).

Tumorigenesis is a process of accumulation of genetic and epigenetic abnormalities that lead to cellular dysfunction and malignant transformation. Epigenetic mechanisms involving DNA methylation, histone modifications, and non-coding RNAs regulate and maintain gene expression states. Similar to genetic mutations, alterations in epigenetic regulation can lead to uncontrolled cell division, tumor initiation and growth, and invasiveness and metastasis [18].

The role of DNA methylation in cancer has received much attention; it is accepted that the methylation of the promoter region of many genes is associated with gene silencing [19]. The DNA methylation is the addition of a methyl group for the carbon atom 5′cytosine, present in the dinucleotide CpG, resulting in the formation of a 5-methylcytosine [20]. The methyl groups found mainly on the islands of CpGs promoter regions of genes can influence the changes between the molecule of DNA and proteins, reducing the binding affinity between the promoter regions and transcription factors through mechanisms involving changes in chromatin structure or levels of histone acetylation [21].

Thus, our aim has been to identify and characterize differentially expressed genes in GCTBs compared to normal bone tissue that may be involved in the molecular biology and development of the disease, generating insight for the new prognosis, and treatment and understanding of this tumor.

Materials and methods

Patients and tissues

GCTB tissue samples were obtained from the tumor bank at The Pio XII Foundation/IBILCE-UNESP, São Paulo, Brazil. The use of all patient-derived material was approved by institution's research ethics board, The Pio XII Foundation—Cancer Hospital Barretos, and informed consent was obtained individually from the patients. The diagnosis of GCTB was established by biopsy prior to surgical excision by pathologists. Tissues were obtained at surgery from patients undergoing tumor resection. Microdissection was performed to collect samples.

Fifty-six samples were collected from primary GCTB, 23 fresh frozen samples of GCBT, 24 paraffin-embedded samples of GCTB, and 9 fresh histologically normal medullar bone tissue evaluated by a pathologist for confirmation of any morphological alteration. (Table 1 gives the clinicopathologic features of these tumors).

The study population included 43 patients. Twenty-one (48%) were male and 22 (52%) female, and the minimum and maximum ages were 13 and 74 years, respectively, mean 35.6 years±14.9. Main localizations of the GCTBs were femur (26%), tibia (21%), and radius (14%). Eight patients (17%) had recurrence between 11 and 42 months after surgery and six patients (12, 7%) had metastases between 1 and 65 months after surgery.

RNA extraction and RT-PCR

Total RNA was isolated from GCTB tissue and normal tissue using the TRIzol reagent (solution for extraction of RNA, Life Technologies, Grand Island, NY) according to the

Table 1 Epidemiological, clinical, and pathological characteristics of 23 fresh samples of GCTB and 24 paraffin-embedded samples of GCTB

Sample	Age (years)	Sex	Anatomic location	Recurrence (date)	Metastasis (date)
1F	37	M	Proximal tibia L	No	19 months
2F	41	F	Distal radius R	No	No
3F	24	M	Proximal femur L	No	No
4F/P	52	F	Distal femur L	No	No
5F	17	M	Scapula L	No	No
6F	32	F	Olecranon R	11 months	No
7F/P	52	M	Distal femur L	11 months	No
8F/P	74	F	Distal femur L	19 months	No
9F	35	M	Distal femur L	No	No
10F	33	M	Proximal tibia R	20 months	No
11F	21	F	Proximal tibia R	No	No
12F	37	F	Proximal tibia L	No	No
13F	13	F	[a]	No	41 months
14F/P	28	F	Distal femur R	19 months	No
15F	19	F	Sacrum	No	No
16F	22	F	Distal fibula R	No	No
17F	16	F	Ischium R	No	No
18F	22	M	Distal fibula L	No	20 months
19F	27	M	Proximal humerus L	No	No
20F	69	F	Occipital	No	No
21F	24	M	Proximal tibia R	22 months	No
22F	46	F	Distal radius L	No	No
23F	58	F	Hemipelvis R	No	No
24P	55	M	Proximal tíbia L	No	No
25P	22	F	Ischium R	No	65 months
26P	57	M	Proximal tíbia L	42 months	No
27P	34	M	Proximal tíbia R	No	No
28P	24	M	Distal radius L	No	No
29P	27	M	Distal femur L	No	No
30P	51	F	Scapula L	Yes[a]	07 months
31P	31	M	Wrist R	No	No
32P	22	F	Distal radius R	No	No
33P	41	M	Distal femur L	No	01 months
34P	24	F	Wrist L	No	No
35P	41	M	Distal femur R	No	No
36P	55	M	Distal radius L	No	No
37P	41	F	Distal radius L	No	No
38P	35	M	Thumb L	No	No
39P	39	M	Proximal fíbula L	No	No
40P	53	M	Proximal tibia R	No	No
41P	38	F	Distal femur L	No	No
42P	19	F	Distal fêmur L	No	No
43P	23	F	Forefinger R	No	No

F fresh tumor, *P* paraffin-embedded tumor, *F* female, *M* male, *R* right, *L* left,

[a] No information was obtained

manufacturer's instructions. RNA integrity post-purification was checked using the Agilent 2100-Bioanalyser, giving a minimal RIN value of 5.5.

For quantitative real-time PCR (qRT-PCR), ~5 μg of total RNA from each sample were used to synthesize cDNA with a high-capacity cDNA Archive Kit (Applied Biosystems), according to the manufacturer's instructions. The quality of the cDNA was checked by PCR of the housekeeping gene, *β-ACTIN*. The primer sets were 5′ to 3′ GGCATCGTGATG GACTCCG and GCTGGAAGGTGGACAGCG. The PCR

products were analyzed by electrophoresis on 1% agarose gel and stained with ethidium bromide.

Rapid subtractive hybridization

For this methodology, paired samples of the same patient (2F) were used, a sample of GCTB and a sample of histologically normal bone tissue. RaSH cDNA libraries were performed as described previously [17] with modifications. From the 25 μg total RNA pool, cDNAs were synthesized and digested with MboI (Invitrogen Life Technologies) at 37°C for 1 h and extracted with phenol–chloroform followed by ethanol precipitation. The digested cDNAs were mixed with 20 mmol/L of primers XDPN-14 (50CTGATCACTCGAGA30) and XDPN-12 (50GATCTCTCGAGT30) in 30 μL of 1X T4 DNA Ligase Buffer (Invitrogen Life Technologies), heated at 55°C for 1 min, and cooled to 14°C within 1 h. Ligation was carried out overnight at 14°C After adding 9 units of T4 DNA ligase to the mixtures individually.

The mixtures were diluted to 100 μL and >40 mL of the mixtures were used for PCR amplification with primer XDPN-18 (5′CTGATCACTCGAGAGATC′3). Portions (10 μg) of the tester PCR products (CGT or normal tissue) were digested with 20 units of XhoI and purified with phenol–chloroform extraction and ethanol precipitation. The fragments were inserted into XhoI-digested pZERO plasmid (1 μg/μl) at 16°C for 3 h. The constructs were introduced into the TOP10 competent cells. Two RaSH cDNA libraries were prepared, one using cDNA from the CGT as tester with the normal bone as driver, and the other using cDNA from the normal bone as tester with cDNA from the CGT as driver.

All bacterial colonies were analyzed by PCR with use of the M13 forward and M13 reverse primers to verify those with an insert. The sequences of these clones were determined with DNA sequencer (ABI PRISM 377, Applied Biosystems) and DYEnamic ET dye terminator sequencing kit (Amersham Biosciences). The sequences were analyzed using an annotation pipeline that had 4 steps: (1) quality checking, phred base-calling, cutoff 0.05; (2) vector trimming and removal of undesirable sequences, such as bacterial, mitochondrial, and rRNA sequences; (3) masking of repetitive elements and screening of low-complexity regions by Repeat Masker, using the default settings; and (4) annotation against existing databases, using BLASTN with default parameters. Significant hits were determined by using an *E* value threshold of 10–15 for searches against nucleotide sequence databases [22].

Validation by quantitative real time

The qRT-PCR was used to assess the expression of genes found by the RaSH method in all fresh samples of CGTB individually. For analysis, we used 23 fresh samples of CGTBs and a pool of total RNA from a subset of nine fresh tissue of normal bone, defined as normal reference. Gene-specific primers for qRT-PCR were designed for optimal hybridization kinetics, using the Primer 3.0 program (provided by the Whitehead/MIT Center for Genome Research, Cambridge, MA).

Quantitative real-time PCR was performed using an ABI prism 7300 sequencer detector system and Sybr Green PCR Core Reagent (Applied Biosystems), following the manufacturer's protocol. In brief, the reaction mixture (20 μl total volume) contained 25 ng of cDNA, gene-specific forward and reverse primers for each gene, and 10 μL of 2× quantitative Sybr Green PCR Master Mix. Relative quantification is given by the CT values, determined for triplicate reactions for GCTB samples and reference sample from each gene, and for the endogenous control (glyceraldehyde 3-phosphate dehydrogenase; *GAPDH*). The primer sequences are given in Table 2.

Thus, the relative expression of each specific gene was calculated by using the formula: $R = (E\ \text{target})^{\Delta \text{Ct target(control}-\text{sample)}} / (E\ \text{endogenous})^{\Delta \text{Ct endogenous(control}-\text{sample)}}$, as previously described [23].

DNA extraction

DNA samples of fresh tissue were isolated using TRIzol Reagent (Life Technologies). For the extraction of DNA from

Table 2 Primer sets used for validation by qRT-PCR amplification

Gene	Primers 5′–3′:	Primers concentration (μM)	Base pair
GAPDH	5′ ACCCACTCCTCCACCTTTGA 5′CTGTTGCTGTAGCCAAATTCGT	0.4 μM	79 pb
KTN1	5′GTTTCCCCAGAAACGGAGTC 5′TGTGAGCTGTTGGTTTACCG	0.5 μM	150 pb
NEB	5′GAAGTGGCCAAGAAGCAAAG 5′TGTGGCCTTCTTGATGTCTG	0.5 μM	102 pb
ROCK1	5′CTGGTTTTGTTCGTGCTTCC 5′GTAGCATCCCACACGATTCC	0.5 μM	142 pb
ZAK	5′TATGGAGGCTCCTGTCAAGG 5′TCCAACCAAGGACATGTGTG	0.5 μM	139 pb

paraffin, samples were first deparaffinized with xylene, and the tissue samples digested in a buffer (100 mmol/L NaCl, 10 mmol/L Tris-HCl pH 8.0, 25 mmol/L ethylenediamine tetraacetic acid [EDTA], and 1% sodium dodecyl sulfate) containing 20 mg/mL proteinase K at 50°C for 3 days. Total DNA was isolated by phenol–chloroform extraction and ethanol precipitation. The DNA pellets were suspended with 20 mL TE buffer (10 mmol/L Tris-HCl, 1 mmol/L EDTA, pH 8.0) and stored at −20°C until PCR amplification.

Methylation-specific PCR

Genomic DNA from both tumoral and normal tissues was treated with sodium bisulfite to modify unmethylated cytosine to uracil [24]. After the DNA conversion, hypermethylation in CGTs was determined by the MSP method [25], to analyze the methylation pattern of the *ZAK* gene. The primers used for PCR reaction were specific for methylated and unmethylated DNA (Table 3). PCR was individually performed in 25-μL reaction volumes, containing 1 × Platinum Taq buffer, 1.5 mmol/L $MgCl_2$, 0.2 mmol/L of each dNTP, 0.4 μmol/L of each primer set, 1 U of Platinum Taq DNA Polymerase (Invitrogen), and 1 μL of treated DNA. In vitro methylated DNA (IVD) was used as a positive control, and DNA from lymphocytes of healthy donors were used as negative controls. PCR products were separated on silver-staining 8% non-denaturing polyacrylamide gels. PCR amplification conditions are available on request.

Statistical analysis of quantitative real-time PCR data

Statistical analysis was performed using the Minitab Student 14 software, and the significance level was set at $p \leq 0.05$. Relative expression levels detected by qRT-PCR for the four genes in CGTs samples were transformed into natural logarithms. The Wilcoxon Signed Ranks Test was applied to compare the gene expression levels in tumor tissue and normal bone tissue.

Immunohistochemical staining

Immunohistochemistry was used to assess the expression of proteins found by the RaSH method in paraffin-embedded samples of CGTB individually. For analysis, we used 22 paraffin-embedded samples of CGTBs.

Immunohistochemical staining was performed on 4-μm sections obtained from formalin-fixed, paraffin-embedded blocks. Endogenous peroxidase activity was blocked with 3% hydrogen peroxide for 30 min. Antigen retrieval was carried out in citrate buffer (10 mM, pH 6) for 30 min at 95°C in a Pan Steam. Polyclonal antibodies used were rabbit anti-human KTN1, rabbit anti-human ROCK1, and polyclonal rabbit anti-human ZAK (Sigma, St. Louis, MO, USA) antibodies at 1:100 were applied incubated at 4°C overnight. Afterward, sections were incubated with a biotinylated secondary antibody and then exposed to a streptavidin complex (HRP ready-to-use, DakoCytomation, Carpinteria, CA). Positive reactions were visualized with 3,3′ diaminobenzidine tetrahydrochloride (DAB, Signet® Laboratories, Dedham, MA, USA), followed by counter-staining with hematoxylin.

Normal testicle was used as a positive control for KTN1 and normal liver were used as the positive control to ROCK1 and ZAK. Sections treated without primary antibodies were used as negative controls. Immunoreactivity was evaluated blindly by two observers, who independently assessed the immunostainings with a semi-quantitative grading system (− no staining; + weak staining in 10–30% of cells; ++ moderate staining in 31–65% of cells; +++ strong staining of more than 66% of cells) [15].

Results

The RaSH approach was adopted to identify differentially expressed genes in GCTBs compared with the normal bone tissue. A total of 619 cDNA clones were sequenced, 169 clones were obtained from the reverse library (down-regulated genes) and 450 clones were obtained from the upregulated genes library. To analyze the sequences, phred and phrap software were used to select the best quality sequences according to the following pattern: phred cutoff of 0.09, minmatch 10, and minscore 20; sequences with >100 base pairs of quality were accepted. The best quality sequences were submitted to the BLAST alignment

Table 3 Primer set used for methylation-specific polymerase chain reaction

Gene	Primer sequence		T (°C)	Size of product M
	Methylated sequence (5′-3′)	Unmethylated sequence (5′-3′)		
ZAK Primer 1	F: GGGTCGTTGTCGTTTTAATTTTCGTC R: CGAAACGTAAACAACAACCGAAAAACG	F: GTTGTGTGGGTTGTTGTTGTTTTAATTTTTGTTG R: TCCCAAACAAAACATAAACAACAACCAAAAACA	67	76 pb
ZAK Primer 2	F: GAGGGCGGTTTAGTCGTTTC R: TCCGCCTCTCTACACGACG	F: GGGAGGGTGGTTTAGTTGTTTTG R: TTAAAAATTAAACATTCCACCTCTCTACACAACA	64	86 pb

T annealing temperature (°C), *U* unmethylated sequence, *M* methylated sequence

program [26]. After alignment with the RefSeq database, the sequences that presented >90% of the target sequence length at alignment were selected. These included *KTN1*, *NEB*, *ROCK1*, and *ZAK*.

We compared the relative expression levels of four genes by qRT-PCR, using triple determination and normalization based on the GAPDH level. In the validation of the target genes, GCTBs samples were used and normal bone tissue as reference (group control).

KTN1 and *ROCK1* were significantly upregulated in 100% tumor tissues compared to normal bone tissue ($p<0.000$). *ZAK* was significantly downregulated in 100% tumor tissues compared to normal bone tissue ($p<0.001$). *NEB* gene was not differentially expressed in GCTBs compared with normal bone tissue ($p=0.964$). Relative gene expression data are presented in Fig. 1.

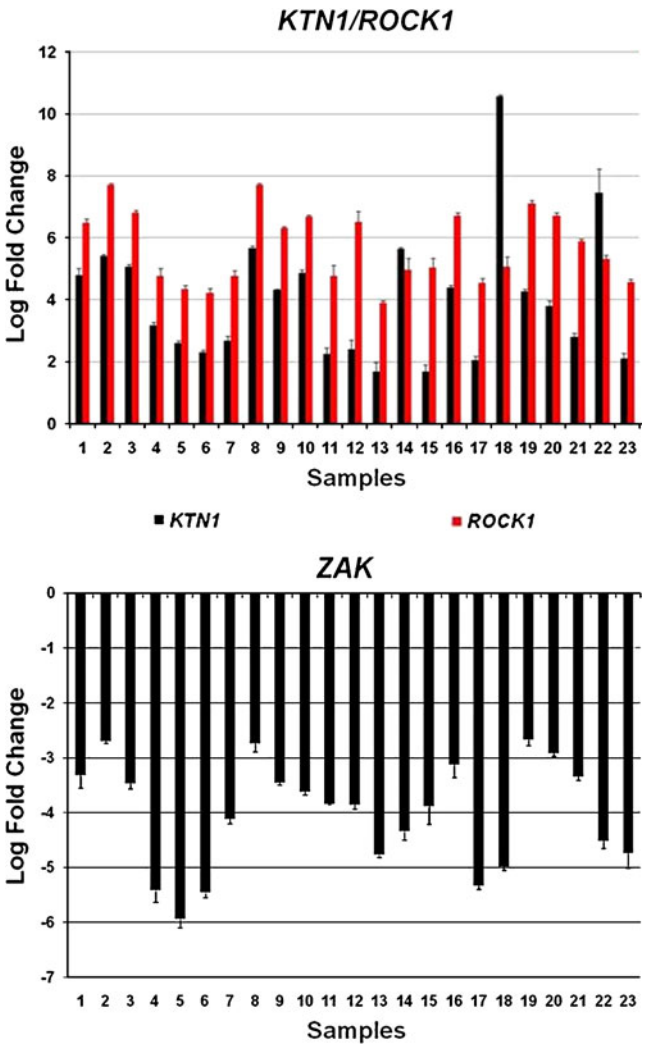

Fig. 1 Relative expression values of the selected genes for validation by qRT-PCR. Expression of gene *ZAK* was significantly lower in GCTB compared to normal reference (normal tissue bone). *ROCK1 and KTN1* are overexpressed in GCTB. The samples used correspond to the samples 1F–23F Table 1

The methylation pattern of the promoter region of *ZAK* by MSP-PCR was investigated after gene expression analysis. Two pairs of primers for the gene *ZAK* were designed. *ZAK* hypermethylation was detected in 18.2% (4/22) ($p=0.82$) of the samples with the P1 primers and none ($p=1.000$) of the samples when the P2 primer was used (Fig. 2). The sets of primers for the gene *ZAK* did not indicate hypermethylation in the lymphocytes analyzed. The methylation pattern data are presented in Table 4.

We used immunohistochemistry to evaluate protein expression of genes found by RaSH in different cell types due to the heterogeneity of histological CGTBs. Immunohistochemical staining of GCTB samples confirmed the presence of KTN1 and ROCK1 in the GCTB microenvironment. KTN1 immunostaining revealed cellular strong staining in 90% (20/22) of GCTB tissue samples, localized mainly in the multinucleated giant cells and stromal cells and occasionally monocytic cell (Fig. 3a). ROCK1 staining was strongly positive in 59% (13/22) of the samples in the cytoplasm of multinucleated giant cells, stromal cells, and monocytic cells (Fig. 3b). In contrast, the expression of ZAK was weakly localized mainly in 82% (18/22) of the samples in the cytoplasm of the multinucleated giant cells and stromal cells, and occasionally in some of the monocytic cells (Fig. 3b). In normal bone tissue, there

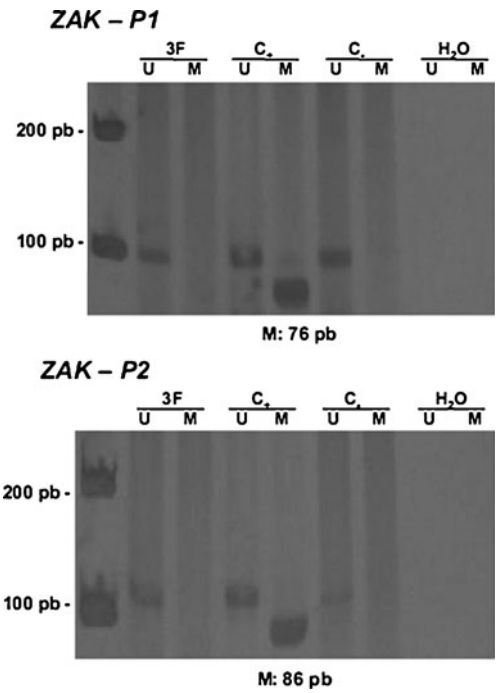

Fig. 2 Representative examples of MSP reaction for gene *ZAK* P1 and *ZAK* P2. Tumor (3F) of a GCTB patient. *Lanes U* and *M* correspond to unmethylated and methylated reactions, respectively. In each case, *C−* indicates DNA from lymphocyte, *C+* indicates IVD, H_2O indicates negative PCR control. On the *left*: molecular weight marker; and *below*: the size of methylated PCR product

Table 4 Methylation pattern of *ZAK* in 27 tumor samples of GCTB

Sample	*ZAK* (P1)	*ZAK* (P2)
3F	○	○
4F	X	○
7F	●	○
8F	○	○
9F	●	○
10F	○	○
11F	○	○
12F	○	○
13F	○	○
14F	○	○
15F	●	X
18F	○	○
19F	○	○
23F	○	○
24P	X	X
25P	○	○
28P	X	X
29P	○	○
30P	○	○
35P	X	X
37P	○	○
38P	X	X
39P	○	○
40P	○	○
41P	○	○
42P	●	○
43P	○	○

Solid circles methylated genes, *hollow circles* unmethylated genes, *x* not amplified

was no immunohistochemical staining in different cell types for the three genes analyzed.

The results showed that genes *ROCK1* and *KTN1* were upregulated in GCTB, confirmed by qRT-PCR and immunohistochemistry, *ZAK* was significantly lower, by qRT-PCR and immunohistochemistry, in the GCTB samples, and that the *NEB* gene was not differentially expressed by qRT-PCR.

Discussion

GCTB does not fit well into a strictly defined category. Therefore, it has been approached in the context of its morphological definition of reactive rounded mononuclear cells, reactive osteoclastic giant cells, and neoplastic mononuclear spindle-shaped cells. It is clinically defined as a benign bone tumor, but it has a tendency to recur and can behave aggressively in a local manner, occasionally metastasizing to the lungs. Although both morphologic and radiologic examination can lead to the correct diagnosis in most cases, diagnosis of GCTB can often be difficult, with no clear diagnostic marker currently being available.

RaSH in allowing us to analyze genes that are expressed differentially in two samples, including genes that have not previously been characterized and rare transcripts, led to the identification of specific genes and signaling pathways involved in the regulation of the disease process. This method has simpler hybridization and subtraction steps than other subtractive hybridization methods.

Three potential biomarkers of giant cell tumor of bone were identified, validated by qRT-PCR and immunohistochemistry, and proved to have distinct differences in expression between tumor and non-neoplastic samples. The markers were genes *KTN1, ROCK1*, and *ZAK,* the first two being significantly upregulated and the last down-regulated. The expression of genes *ROCK1* and *KTN1* were significantly high in GCTBs than in normal bone tissue and *ZAK* was significantly lower in tumor tissues than in the non-tumor adjacent tissue.

ROCK1 located in 18q11.1, encodes a protein associated with Rho kinase and belongs to a family of serine/threonine kinases activated via interaction with Rho GTPases. *ROCK* is involved in a wide range of fundamental cellular functions such as regulation the reorganization of the actin cytoskeleton, formation of the focal adhesion, smooth muscle contraction, cell migration, gene expression, and apoptosis [27, 28]. Rho-associated serine-threonine protein kinase, *ROCK*, one of the best characterized downstream effectors of Rho, is activated when it selectively binds to the active GTP-bound form of Rho. Activated *ROCK* interacts with the actin cytoskeleton to promote stress fiber formation and assembly of focal contacts [29]. There is considerable evidence to suggest that Rho–ROCK signalling is deregulated in cancer, and thereby contributes to invasive and metastatic behavior [30].

Upregulation of Rho–ROCK signaling in tumors is well-known to be linked to increased invasion and metastatic potential, which may occur as a result of increased *RhoA, RhoC*, or *ROCK1* expression [30]. Cell migration is pivotal in metastasis, and rearrangements in the actin cytoskeleton are certainly involved. Overexpression of Rho has been linked to progression of human cancers, and therefore the Rho/ROCK pathway is a major player in cancer progression through its regulation of actin cytoskeleton reorganization; indeed, a specific ROCK inhibitor can suppress the tumor growth and metastasis [29], and therefore could be a prime molecular target for the prevention of cancer invasion and metastasis [30].

Rho kinase (ROCK) through its regulating of cytoskeletal events increases with the degree of malignancy, and is

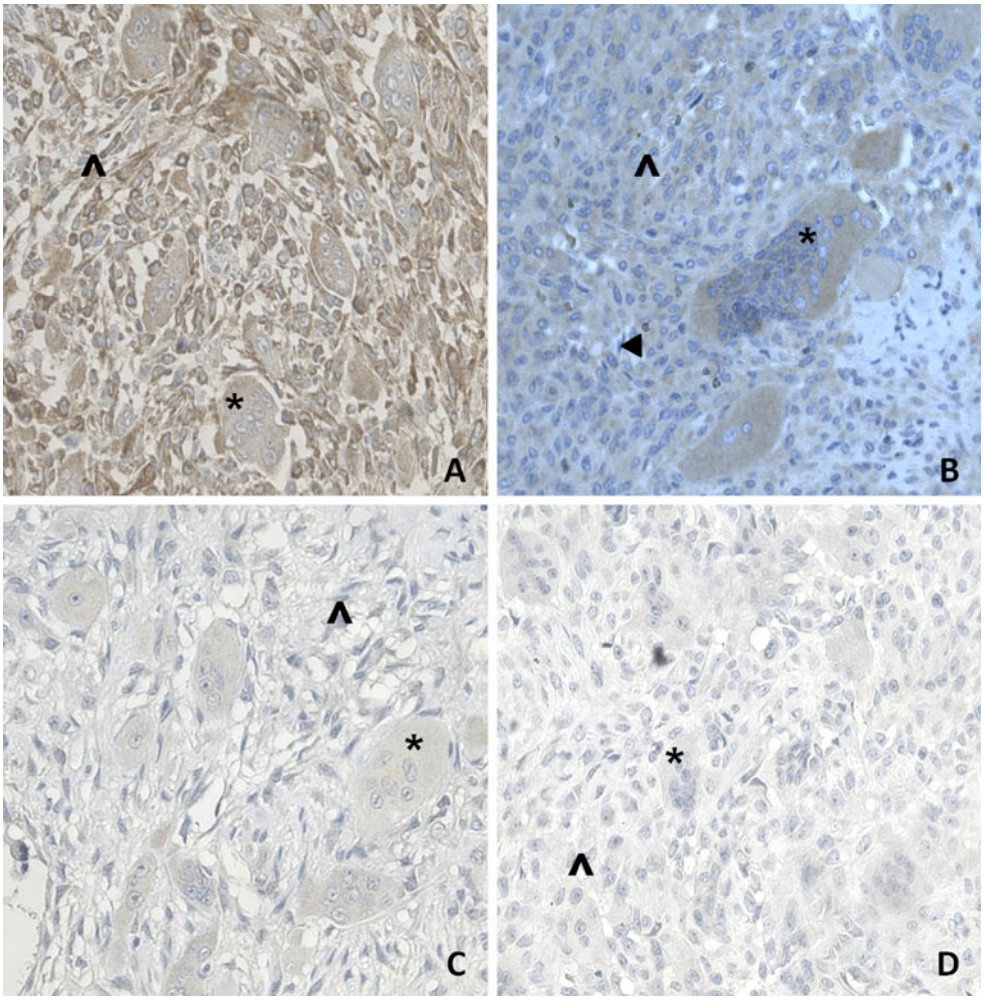

Fig. 3 Immunolocalization of KTN1, ROCK1, and ZAK in human specimens of primary GCTB samples. **a** KTN1; **b** ROCK1; **c** ZAK; **d** negative control (original magnification 400×). These are representative figures from 22 GCTB patient tissue samples. The staining patterns for KTN1, ROCK1, and ZAK were generally consistent among all the patient samples. The presence of multinucleated giant cells is marked with *stars*, mesenchymal stromal cells with *caret*, and monocytes cell with *arrow*. Positive stainings of the corresponding antigens show *brownish color* in various degrees, in contrast to the *bluish color* in negative stainings

known to contribute to the invasion of hepatocellular carcinoma [31], bladder cancer [29], melanoma [30], and to be upregulated in anaplastic astrocytomas and glioblastomas [32]. Since ROCK1 was upregulated in multinucleated giant cells, stromal cells, and monocytic cells of GCTBs, we believe that overexpression in these tumors may contribute to their occasional invasion, metastasis, and increased malignancy.

KTN1 gene is located in the region 14q22.1 and encodes the full kinectin, membrane receptor for kinesin that is found in the endoplasmic reticulum and is responsible for the transport of vesicles along microtubules. It is expressed in the brain, liver, ovarian, and hematopoietic cells [33, 34]. The kinectin has an important role in vesicle transport as a receptor for kinesin and dynein, thereby aiding the movement of motor proteins within the cell. However, the exact mechanism by which cells control the transport of vesicles remains unclear [35]. According to Santama et al. [36], kinectin was demonstrated in vivo by overexpression and RNA interference assay, and is selectively involved in the transport of specific types of organelles.

Besides interacting with the kinesin, the kinectin also interacts with other proteins, such as Rho protein, which forms the complex Rho-kinectin responsible for transport of microtubules between the actin filaments and the elongation factor of translation-1δ [37, 38]. The latter plays an important role in regulating the synthesis of proteins that participate in the elongation phase of mRNA translation.

The exact function of *KTN1* and its role in tumor progression remain unclear. There are no reports in the literature about the relationship of *KTN1* gene in tumors, but this gene was highly expressed in all GCTBs.

ZAK gene is located in the region 2q24.2 and belongs to the family of mixed lineage kinase, which comprises a group of serine/threonine kinases that works with *MAP3K* [39, 40]. It is expressed in most tissues and is regulated by environmental stresses [39]. The expression of *ZAK* arrests cells in G2, due to the effect that its protein somehow decreases the expression of cyclin E [41].

In addition to this important function for example, overexpression can induce apoptosis in hepatocyte cell line [39. The gene *NF-κB* belongs to a gene family of

transcription factors regulating the transcription of several genes related to immune response, cell proliferation, apoptosis, and the progression and maintenance of the status factor [42, 43]. *NF-κB* super can regulate the expression of proteins that interfere with the receptor via apoptosis, and induce the expression of apoptosis inhibitors and some family members of anti-apoptotic Bcl-2 [44]. Another way of induction of apoptosis by *ZAK* gene is via the JNK/SAPK, which belongs to the MAPK family and is activated by many types of cellular stresses or extracellular signals. The activation of this pathway is associated with regulation of cell proliferation, survival, apoptosis, and immune response by regulating the gene expression of cytokines. Furthermore, this protein is associated with the regulation of mRNA stabilization, cell migration, and integrity of the cytoskeleton [44, 45].

The low expression of the *ZAK* gene can therefore lead to poorer inhibition of cell proliferation by cycle arrest in tumor cells and more sustained growth of the cells of CGTBs.

Regarding the methylation pattern of gene *ZAK* presenting island CpGs in their promoter region, we found that this gene was downregulated in GCTBs, although no methylation occurred in the promoter region. Other mechanisms of gene silencing might be eliminating their activities, such as microRNAs and RNA interference.

In conclusion, differentially expressed genes in the CGTBs include those whose deregulation is potentially associated with disease progression. Methylation of the promoter region is not responsible for the downregulation of gene *ZAK*. These findings will contribute to the understanding of the molecular basis of GCTB, thus helping to improve diagnosis, treatment, and patient outcome. Further studies are required to evaluate whether the identified genes are specifically altered in GCTB or might also be deregulated in other tumors.

Acknowledgments The authors thank the State of São Paulo Research (FAPESP), The National Council for Scientific and Technological Development (CNPq), and Coordination for the Improvement of Higher Education Personnel (CAPES) for their financial support.

We are also grateful to Sandra Morini MD, Valter Penna MD, and André Stellet MD for their collaboration in this work.

Conflict of interest The authors declare that they have no conflict of interest with the organization that sponsored the research.

References

1. Mendenhall WM, Zlotecki RA, Scarborough MT, Gibbs CP, Mendenhall NP (2006) Giant cell tumor of bone. Am J Clin Oncol 29(1):96–99. doi:10.1097/01.coc.0000195089.11620.b7
2. Luther N, Bilsky MH, Härtl R (2008) Giant cell tumor of the spine. Neurosurg Clin N Am 19(1):49–55. doi:10.1016/j.nec.2007.09.009
3. De Camargo O, Croci AT, De Oliveira CRGC AM, Caiero MT, Giannotti CM (2001) Giant cells tumor—diagnosis and treatment history evolution in Instituto de Ortopedia eTraumatologia from FMUSP. Acta Ortop Bras 9(4):46–52. doi:10.1590/S1413-78522001000400006
4. Lee CH, Espinosa I, Jensen KC, Subramanian S, Zhu SX, Varma S, Montgomery KD, Nielsen TO, van de Rijn M, West RB (2008) Gene expression profiling identifies p63 as a diagnostic marker for giant cell tumor of the bone. Mod Pathol 21(5):531–539. doi:10.1038/modpathol.3801023
5. Khalil ESA, Younis A, AziZ SA, Shahawy ME (2004) Surgical management for giant cell tumor of bones. J Egypt Natl Canc Inst 16(3):145–152. doi:10.1038/modpathol.3801023
6. Turcotte RE (2006) Giant cell tumor of bone. Orthop Clin North Am 35(1):35–51. doi:10.1016/j.ocl.2005.08.005
7. Haque AU, Moatasim A (2008) Giant cell tumor of bone: a neoplasm or a reactive condition? Int J Clin Exp Pathol 1:489–501
8. Bassiony AA, Abdelrahman M, Abdelhady A, Assal MK (2009) Resection arthrodesis for the management of aggressive giant cell tumor of the distal femur. Indian J Orthop 43(1):67–71. doi:10.4103/0019-5413.44432
9. Wülling M, Engels C, Jesse N, Werner M, Delling G, Kaiser E (2001) The nature of giant cell tumor of bone. J Cancer Res Clin Oncol 127(8):467–474. doi:10.1007/s004320100234
10. Morgan T, Atkins GJ, Trivett MK, Johnson SA, Kansara M, Schlicht SL, Slavin JL, Simmons P, Dickinson I, Powell G, Choong PF, Holloway AJ, Thomas DM (2005) Molecular profiling of giant cell tumor of bone and the osteoclastic localization of ligand for receptor activator of nuclear factor kappaB. Am J Pathol 167(1):117–128
11. Alberghini M, Kliskey K, Krenacs T, Picci P, Kindblom L, Forsyth R, Athanasou NA (2010) Morphological and immunophenotypic features of primary and metastatic giant cell tumour of bone. Virchows Arch 456(1):97–103. doi:10.1007/s00428-009-0863-2
12. Goldring SR, Roelke MS, Petrison KK, Bhan AK (1987) Human giant cell tumors of bone identification and characterization of cell types. J Clin Invest 79(2):483–491. doi:10.1172/JCI112838
13. Salerno M, Avnet S, Alberghini M, Giunti A, Baldini N (2008) Histogenetic characterization of giant cell tumor of bone. Clin Orthop Relat Res 466(9):2081–2091. doi:10.1007/s11999-008-0327-z
14. Mak IW, Cowan RW, Popovic S, Colterjohn N, Singh G, Ghert M (2009) Upregulation of MMP-13 via Runx2 in the stromal cell of giant cell tumor of bone. Bone 45(2):377–386. doi:10.1016/j.bone.2009.04.253
15. Viswanathan S, Jambhekar NA (2010) Metastatic giant cell tumor of bone: are there associated factors and best treatment modalities? Clin Orthop Relat Res 468(3):827–833. doi:10.1007/s11999-009-0966-8
16. Jiang H, Kang DC, Alexandre D, Fisher PB (2000) RaSH, a rapid subtraction hybridization approach for identifying and cloning differentially expressed genes. Proc Natl Acad Sci USA 97 (23):12684–12689
17. Fouse SD, Costello JF (2009) Epigenetics of neurological cancers. Future Oncol 5(10):1615–1629. doi:10.2217/fon.09.132
18. Fourkala EO, Hauser-Kronberger C, Apostolidou S, Burnell M, Jones A, Grall J, Reitsamer R, Fiegl H, Jacobs I, Menon U, Widschwendter M (2009) DNA methylation of polycomb group target genes in cores taken from breast cancer centre and periphery. Breast Cancer Res Treat 120(2):345–355. doi:10.1007/s10549-009-0384-3
19. Van der Auwera I, Elst HJ, Van Laere SJ, Maes H, Huget P, van Dam P, Van Marck EA, Vermeulen PB, Dirix LY (2009) The presence of circulating total DNA and methylated genes is associated with circulating tumour cells in blood from breast cancer patients. Br J Cancer 100(8):1277–1286. doi:10.1038/sj.bjc.6605013

20. Lopez-Serra L, Esteller M (2008) Proteins that bind methylated DNA and human cancer: reading the wrong words. Br J Cancer 98 (12):1881–1885. doi:10.1038/sj.bjc.6604374
21. Calmon MF, Rodrigues RV, Kaneto CM, Moura RP, Silva SD, Mota LD, Pinheiro DG, Torres C, de Carvalho AF, Cury PM, Nunes FD, Nishimoto IN, Soares FA, da Silva AM, Kowalski LP, Brentani H, Zanelli CF, Silva WA Jr, Rahal P, Tajara EH, Carraro DM, Camargo AA, Valentini SR (2009) Epigenetic silencing of CRABP2 and MX1 in head and neck tumors. Neoplasia 11 (12):1329–1339. doi:10.1593/neo.91110
22. Pfaffl MW (2001) A new mathematical model for relative quantification in real-time RT-PCR. Nucleic Acids Res 29(9):2002–2007
23. Calmon MF, Colombo J, Carvalho F, Souza FP, Filho JF, Fukuyama EE, Camargo AA, Caballero OL, Tajara EH, Cordeiro JA, Rahal P (2007) Methylation profile of genes CDKN2A (p14 and p16), DAPK1, CDH1, and ADAM23 in head and neck cancer. Cancer Genet Cytogenet 173(1):31–37. doi:10.1016/j.cancergencyto.2006.09.008
24. Herman JG, Graff JR, Myöhänen S, Nelkin BD, Baylin SB (1996) Methylation-specific PCR: a novel PCR assay for methylation status of CpG islands. Proc Natl Acad Sci USA 93(18):9821–9826
25. Meola J, Rosa E, Silva JC, Dentillo DB, da Silva WA, Jr Veiga-Castelli LC, de Souza Bernardes LA, Ferriani RA, Paro de Paz CC, Giuliatti S, Martelli L (2009) Differentially expressed genes in eutopic and ectopic endometrium of women with endometriosis. Fertil Steril 93(6):1750–1773. doi:10.1016/j.fertnstert.2008.12.058
26. Shi J, Wei L (2007) Rho kinase in the regulation of cell death and survival. Arch Immunol Ther Exp (Warsz) 55(2):61–75. doi:10.1007/s00005-007-0009-7
27. Noma K, Rikitake Y, Oyama N, Yan G, Alcaide P, Liu PY, Wang H, Ahl D, Sawada N, Okamoto R, Hiroi Y, Shimizu K, Luscinskas FW, Sun J, Liao JK (2008) ROCK1 mediates leukocyte recruitment and neointima formation following vascular injury. J Clin Invest 118(5):1632–1644. doi:10.1172/JCI29226
28. Kamai T, Tsujii T, Arai K, Takagi K, Asami H, Ito Y, Oshima H (2003) Significant association of Rho/ROCK pathway with invasion and metastasis of bladder cancer. Clin Cancer Res 9(7):2632–2641
29. Pinner S, Sahai E (2008) PDK1 regulates cancer cell motility by antagonising inhibition of ROCK1 by RhoE. Nat Cell Biol 10 (2):127–137. doi:10.1038/ncb1675
30. Man K, Ng KT, Xu A, Cheng Q, Lo CM, Xiao JW, Sun BS, Lim ZX, Cheung JS, Wu EX, Sun CK, Poon RT, Fan ST (2010) Suppression of liver tumor growth and metastasis by adiponectin in nude mice through inhibition of tumor angiogenesis and downregulation of Rho kinase/IFN-inducible protein 10/matrix metalloproteinase 9 signaling. Clin Cancer Res 16(3):967–977. doi:10.1158/1078-0432
31. Oellers P, Schröer U, Senner V, Paulus W, Thanos S (2009) ROCKs are expressed in brain tumors and are required for glioma-cell migration on myelinated axons. Glia 57(5):499–509. doi:10.1002/glia.20777
32. Hirano N, Butler MO, Guinan EC, Nadler LM, Kojima S (2005) Presence of anti-kinectin and anti-PMS1 antibodies in Japanese aplastic anaemia patients. Br J Haematol 128(2):221–223. doi:10.1111/j.1365-2141.2004.05317.x
33. Bai JZ, Mon Y, Krissansen GW (2006) Kinectin participates in microtubule-dependent hormone secretion in pancreatic islet beta-cells. Cell Biol Int 30(11):885–894
34. Tran H, Pankov R, Tran SD, Hampton B, Burgess WH, Yamada KM (2002) Integrin clustering induces kinectin accumulation. J Cell Sci 115:2031–2040
35. Santama N, Connie PNE, Lee-Lee O, Hanry Y (2004) Distribution and functions of kinectin isoforms. J Cell Sci 117(19):4537–4549
36. Hotta K, Tanaka K, Mino A, Kohno H, Takai Y (1996) Interaction of the Rho family small G proteins with kinectin, an anchoring protein of kinesin motor. Biochem Biophys Res Commun 225 (1):69–74. doi:10.1006/bbrc.1996.1132
37. Ong LL, Lin PC, Zhang X, Chia SM, Yu H (2006) Kinectin-dependent assembly of translation elongation factor-1 complex on endoplasmic reticulum regulates protein synthesis. J Biol Chem 281(44):33621–33634. doi:10.1074/jbc.M607555200
38. Liu TC, Huang CJ, Chu YC, Wei CC, Chou CC, Chou MY, Chou CK, Yang JJ (2000) Cloning and expression of ZAK, a mixed lineage kinase-like protein containing a leucine-zipper and a sterile-alpha motif. Biochem Biophys Res Commun 274(3):811–816. doi:10.1006/bbrc.2000.3236
39. Huang CY, Kuo WW, Chueh PJ, Tseng CT, Chou MY, Yang JJ (2004) Transforming growth factor-beta induces the expression of ANF and hypertrophic growth in cultured cardiomyoblast cells through ZAK. Biochem Biophys Res Commun 324(1):424–431. doi:10.1016/j.bbrc.2004.09.067
40. Yang JJ (2003) A novel zinc finger protein, ZZaPK, interacts with ZAK and stimulates the ZAK-expressing cells re-entering the cell cycle. Biochem Biophys Res Commun 301(1):71–77. doi:10.1016/S0006-291X(02)02980-7
41. Tergaonkar V (2006) NFKB pathway: a good signaling paradigm and therapeutic target. Int J Biochem Cell Biol 38:1647–1653. doi:10.1016/j.biocel.2006.03.023
42. Dolcet X, Llobet D, Pallares J, Matias-Guiu X (2005) NF-kB in development and progression of human cancer. Virchows Arch 446(5):475–482. doi:10.1007/s00428-005-1264-9
43. Wang TH, Wang HS, Soong YK (2000) Regulation and functions of c-Jun N-terminal kinase/stress-activated protein kinase. Chang Gung Med J 23(2):57–72
44. Nishina H, Nakagawa K, Azuma N, Katada T (2003) Activation mechanism and physiological roles of stress-activated protein kinase/c-Jun NH2-terminal kinase in mammalian cells. J Biol Regul Homeost Agents 17(4):295–302

Virchows Arch (2011) 458:477–486
DOI 10.1007/s00428-011-1051-8

ORIGINAL ARTICLE

Kidney histologic alterations in α-Galactosidase-deficient mice

Carmen Valbuena · João Paulo Oliveira · Fátima Carneiro · Sandra Relvas · Mariana Ganhão · M. Clara Sá-Miranda · Lorena G. Rodrigues

Received: 25 August 2010 / Revised: 18 January 2011 / Accepted: 22 January 2011 / Published online: 16 February 2011
© Springer-Verlag 2011

Abstract Fabry disease is a rare X-linked disorder caused by mutations in the α-galactosidase gene (*GLA*), the resultant deficiency of lysosomal α-galactosidase enzyme activity leading to systemic accumulation of globotriaosylceramide and other glycosphingolipids. *GLA* knockout mice ("Fabry mice") were generated as an animal model for Fabry disease but, as they do not manifest progressive chronic kidney disease (CKD), their relevance as a model for human Fabry nephropathy is uncertain. We evaluated the histological alterations in the kidneys of Fabry mice at different ages, as contrasted to those observed in wild-type mice. Furthermore, we compared the renal histological alterations of Fabry mice to the kidney pathology reported in patients with Fabry disease at comparable age ranges and across different CKD stages, using a scoring system that has been developed for Fabry nephropathy. Fabry mice are phenotypically different from wild-type mice, displaying progressive age-related accumulation of glycosphingolipids in all types of renal cells. There were no statistically significant differences between Fabry mice and Fabry patients in the prevalence of glycosphingolipid storage per renal cell type with the exceptions of mesangial (higher in humans) and proximal tubular cells (higher in mice). However, Fabry mice lack the nonspecific histological glomerulosclerotic and interstitial fibrotic renal lesions that best correlate with progressive CKD in Fabry patients, and do not develop large podocyte inclusions. We postulate that the elucidation of the mechanisms underlying these species differences, may contribute important clues to a better understanding of the pathogenesis of Fabry nephropathy.

Keywords Fabry disease · α-Galactosidase-deficient mice · Histology · Kidney · Glycosphingolipids · Score

F. Carneiro · S. Relvas · M. Ganhão
Department of Pathology,
Faculty of Medicine and Hospital São João,
Porto, Portugal

J. P. Oliveira
Department of Nephrology, Hospital São João,
Porto, Portugal

J. P. Oliveira
Unit of Research and Development in Nephrology
and Department of Genetics, Faculty of Medicine,
Porto, Portugal

F. Carneiro
Department of Pathology, Institute of Molecular Pathology
and Immunology of the University of Porto (IPATIMUP),
Porto, Portugal

M. C. Sá-Miranda · L. G. Rodrigues
Lysosome and Peroxisome Biology Unit (UniLiPe),
Instituto de Biologia Molecular e Celular (IBMC),
Porto, Portugal

C. Valbuena (✉)
Serviço de Anatomia Patológica, Faculdade de Medicina da
Universidade do Porto (FMUP) e Hospital São João,
Al. Hernani Monteiro, 4200-319 Porto, Portugal
e-mail: valbuena@med.up.pt

Introduction

Fabry disease [OMIM #301500] is an X-linked inborn error of glycosphingolipid (GSL) catabolism, caused by mutations in the α-Gal gene (*GLA*) [1]. Deficient or absent activity of the lysosomal enzyme α-galactosidase (α-Gal) [2, 3] leads to systemic accumulation of neutral GSL with terminal α-D-galactosyl residues, predominantly globotriaosylceramide (Gb3), within a variety of cell types and organic fluids [4]. Classically affected patients often present

in childhood with acroparesthesias due to small-fibre peripheral neuropathy and angiokeratomas [4, 5]. Complications arising during adulthood include progressive renal failure, cardiac disease, and cerebrovascular disease [4, 5].

In humans, the Fabry nephropathy is characterized by initial (micro) albuminuria and development of proteinuria between the second to third decades of life. Glomerular filtration rate gradually declines and classically affected males progress to end-stage renal disease before their fifth decade [4–7]. A spectrum of histological lesions can be observed in the kidneys, even in cases with normal glomerular filtration rate and minimal proteinuria [8–15]. These lesions may include intracellular GSL deposits and nonspecific chronic glomerular, vascular, and tubulo-interstitial fibro-sclerotic lesions.

A range of kidney biopsy studies have been undertaken to gain a better understanding of the natural history of Fabry nephropathy [8, 12–15] and to evaluate the response to enzyme replacement therapy (ERT) [16–18]. Fogo et al. aimed to standardize the reading of kidney biopsies and quantification of the histological alterations [15]. Kidney biopsies from 59 adult Fabry patients, both males and females, were assessed using a validated scoring system. The investigators concluded that important information is provided by kidney biopsy in Fabry nephropathy that is not available from routine assessment of kidney function and proteinuria.

An appropriate animal model of Fabry disease would be invaluable to foster the study of the pathophysiology of Fabry disease, and to assess the efficacy of ERT and other therapeutic strategies. Ohshima et al. generated a *GLA*-deficient ("Fabry") mouse by gene targeting a mutated allele [19]. Marked Gb3 accumulations have been observed in plasma and lysosomes of the kidneys, liver, spleen, heart, and skin of these knockout mice, whereas Gb3 was present only in small amounts in wild-type mice [20–23]. The knockout mice have been reported to accumulate ±25% of Gb3 in kidney tissue as compared to the level measured in a single male patient [20]. Data on progression of Gb3 accumulation in the kidneys of Fabry mice have been inconclusive one group having reported stabilization between age 20 and 40 weeks [20], whereas others found significant increases between the ages of 24 and 48 weeks [23].

Fabry mice accumulate Gb3 in vascular endothelial and smooth muscle cells and in plasma membranes of endothelial cells. Gb3 storage at these sites correlates with the development of a complex vasculopathy, including thrombosis, atherogenesis, and endothelial dysfunction [20, 24–28]. Nevertheless, these mice have no clinical phenotype of Fabry disease [20].

Our study aimed to characterize the kidney pathology of this *GLA*-deficient mouse using a standardized histological scoring method that has been developed for Fabry nephropathy in humans [14, 15]. The results were compared with observations in wild-type mice, and with similar data of previously published series in human Fabry patients.

Subjects, materials, and methods

Fabry knockout and wild-type mice

Alpha-Gal$^{(-)}$ males and α-Gal$^{(-/-)}$ females were provided by the National Institutes of Health (Bethesda, MD, USA), and a colony was maintained at "Instituto de Biologia Celular e Molecular" (IBMC), University of Porto (Porto, Portugal). Given the genetic background of this Fabry mice colony, C57BL/6 wild-type mice were used as controls. The genotype of each mouse was confirmed by polymerase chain reaction (PCR) analysis of genomic DNA extracted from tail biopsies using a standard method [29]. PCR amplification was done according to previously described protocols [23]. Mice were kept in group cages with woodchip bedding under 12/12 h light–dark cycle (lights on at 08:00). Food and water were provided *ad libitum*. Mice were bred under standard conditions established by the Institute Committee on the Use and Care of Animals. Euthanasia was done by cervical dislocation followed by decapitation, at ages 12, 24, and 48 weeks. Tissue samples of all sacrificed animals were collected and processed for microscopy according to published procedures [20].

This project was approved by the Portuguese Veterinary Authority–"Direcção-Geral de Veterinária"—under the name of "Estudo de patofisiologia da doença de Fabry", DGV 2005-03-09 003758.

Processing of kidney parenchyma for microscopy

Immediately following euthanasia, the kidneys were dissected from the involving tissues, immersion fixed in 2% paraformaldehyde/2% glutaraldehyde in 0.1-M cacodylate buffer for 1 h, and preserved in the refrigerator at 4°C until histological processing.

One whole kidney of each animal was collected for this study with the exception of two Fabry and one wild-type mice, of which there was only one-half kidney available. Each kidney or half kidney was equally divided in two parts: one half was preserved for later studies, while the other was divided in two fragments: one was embedded in paraffin, and the other was processed for semi-thin sectioning. Thick serial sections (3 μm) were cut from each paraffin block and stained with hematoxylin and eosin (HE), periodic acid Schiff (PAS), and modified trichrome (MT). The fragment selected for the preparation of semi-thin sections was further cut into a minimum of five 1×1 mm pieces, which

were post-fixed in 1% osmium tetroxide and embedded in epoxy resin (Epon™). Semi-thin sections (1 μm) were obtained from each of these Epon-embedded kidney tissue samples and stained with methylene blue (MB) and toluidine blue (TB).

Reading and scoring of kidney samples

A single nephropathologist (CV), experienced in evaluating and scoring kidney biopsies of Fabry patients, assessed and scored all the histological sections, blinded as to the genotype, gender, and age of the mice. The slides were evaluated according to standard methods of kidney pathology reading and to scoring methods recently used for Fabry nephropathy [14, 15]. In short, disease-specific GSL storage-related, as well as nonspecific histological features of Fabry nephropathy, including glomerular sclerosis, interstitial fibrosis, and vascular abnormalities, were assessed and semi-quantified.

The involvement of the various types of renal cells was estimated in each of the TB- and MB-stained semi-thin cuts and scored according to the percentage of cells of each particular type containing any visible deposits of GSL: a storage score of "1+" was given to a cell type when less than 1/3 of all cells of that type had cytoplasmic GSL inclusions; a score of "2+" was given when between 1/3 to 2/3 of those cells were involved; and the score of "3+" was given when GSL inclusions were present in more than 2/3 of the cells. A final intermediate storage scoring could be assigned to a specific cell type when the scores assigned to that cell in the different semi-thin cuts were not entirely concordant. As a surrogate for the degree of GSL accumulation in the kidney parenchyma, a combined GSL storage score was calculated for each mouse, by averaging the storage scores assigned to the various renal cell types. The prevalence of involvement of the different renal cell types in each mouse cohort or sub-cohort was estimated as the percentage of mice in that specific series that were

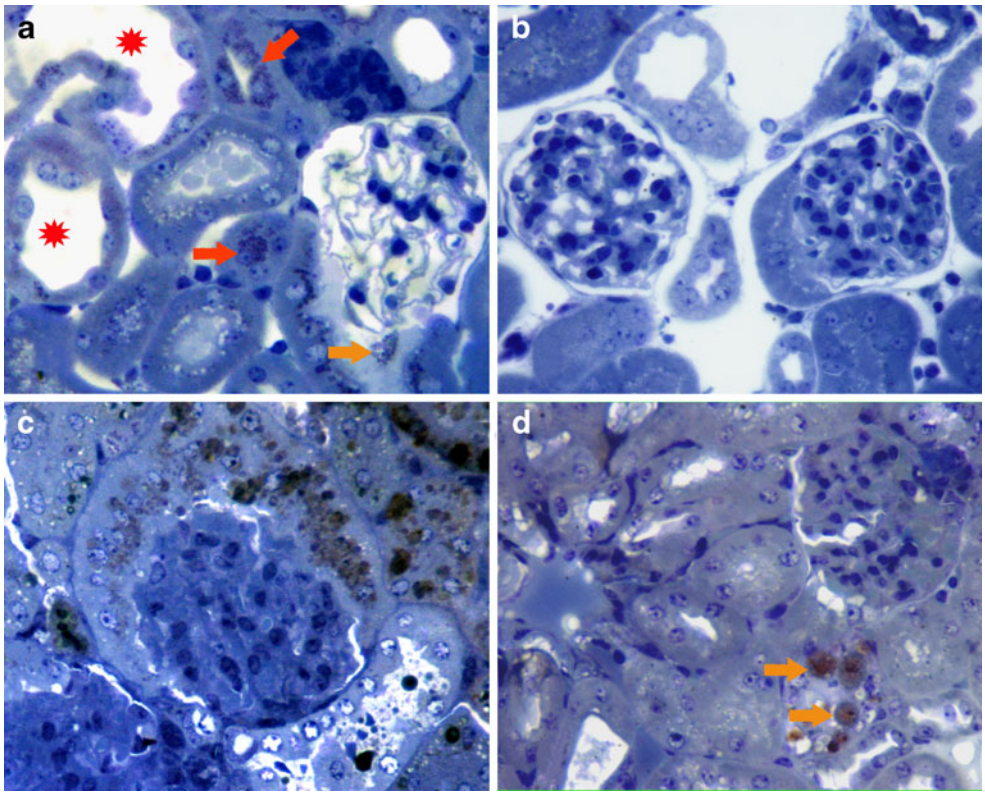

Fig. 1 Representative photomicrographs of cross sections of kidney tissue stained with toluidine blue. **a** Female Fabry mouse aged 24 weeks. —Glomerulus opening in a proximal tubule, showing osmiophilic inclusions in epithelial tubular cells; a podocyte contains small and dark-stained osmiophilic inclusions (*orange arrow*). Some tubuli show all epithelial cells with small and dark-stained deposits (*red arrows*), and others show all epithelial cells with light-stained deposits (*red stars*). **b** Female wild-type mouse aged 24 weeks. —Two glomeruli, both with squamous parietal epithelium, without any visible osmiophilic inclusions. No osmiophilic inclusions were visible in any of the renal cells of this mouse. **c** Male Fabry mouse aged 48 weeks. —Glomerulus limited by prominent cuboidal parietal epithelium containing osmiophilic inclusions. Tubular cells are also filled with large and dark-stained osmiophilic deposits. **d** Female wild-type mouse aged 48 weeks. —Glomerulus with squamous parietal epithelium without any visible osmiophilic inclusions. Some tubular cells contain osmiophilic inclusions (*orange arrows*). Sections stained with toluidine blue. Magnification ×600

assigned a storage scoring of at least "1+" for the particular cell type.

The presence of nonspecific histological features was assessed in TB-and MB-stained semi-thin sections and in HE-, PAS-, and MT-stained paraffin sections. The degree of interstitial fibrosis was reported as the estimated percentage of affected cut section, at ×200 magnification.

An atlas of the microanatomy and histology of the mouse available online was used for histological guidance on evaluation of the murine renal parenchyma [30].

Statistical analyses

The Fisher exact, Mann–Whitney *U*, and Kruskal–Wallis tests were used as appropriate for statistical comparisons of the prevalence and scoring of renal histological features in wild-type and Fabry mice of both genders across different age groups, and to compare the prevalence of GSL inclusions in the various renal cell types between Fabry mice and Fabry patients. All statistical calculations were carried out with the software PASW® (Predictive Analytics SoftWare; SPSS Inc., Chicago, IL, USA), version 18.0. *P* values<0.05 were reported as statistically significant.

Results

Characterization of GSL deposits

GSL deposits were seen as grey to black osmiophilic inclusions in semi-thin cuts. Three different types of osmiophilic inclusions were present in all Fabry mice: (1) small, diffuse, finely granular ("sand-like"), and light-stained; (2) small, punctiform, and dark-stained; (3) round, large, and dark-stained. These three kinds of inclusions were found in Fabry mice of all age groups,

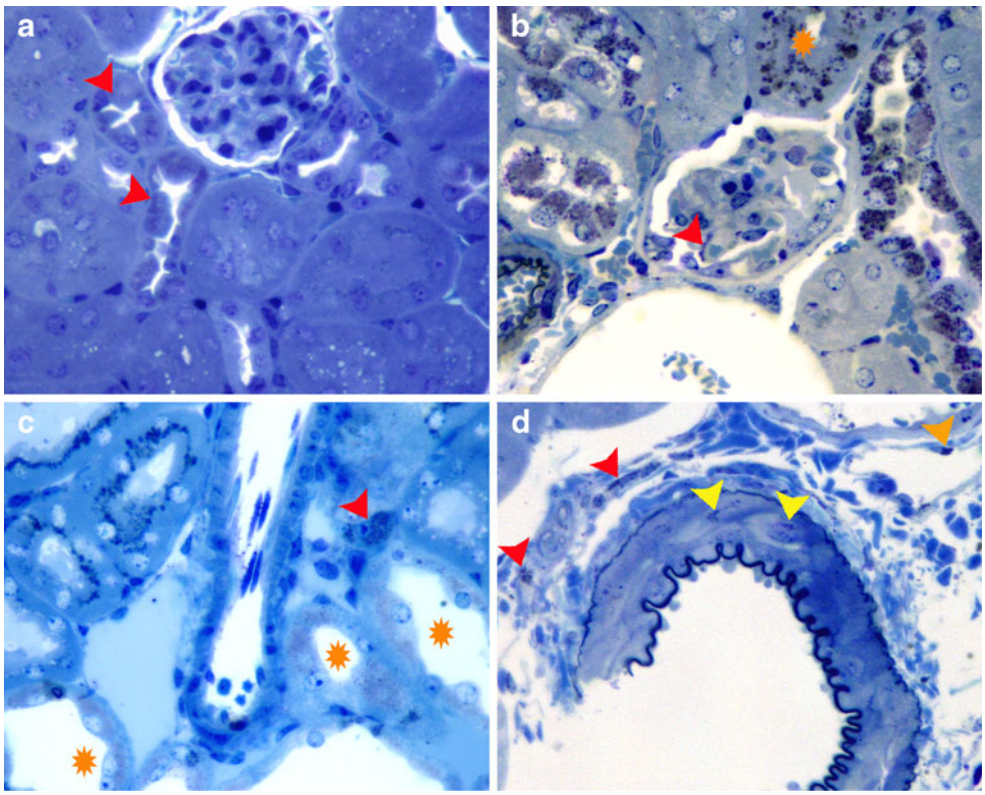

Fig. 2 Glycosphingolipid deposits in different renal cell types in Fabry mice. **a** Glomerulus with squamous parietal epithelial cells, without any visible osmiophilic inclusions. All the epithelial cells of two adjacent distal tubules are filled with finely granular ("sand-like") osmiophilic deposits (*red arrows*). **b** Glomerulus with squamous parietal epithelial cells containing small intracytoplasmic osmiophilic inclusions and one podocyte with small and inconspicuous osmiophilic inclusions (*red arrow*). The tubular epithelial cells are filled with small dark-stained osmiophilic inclusions and/or large and dark-stained osmiophilic inclusions (*orange star*). **c** Tubulo-interstitial area with small dark-stained osmiophilic inclusions in proximal tubular epithelial cells and finely granular ("sand-like") osmiophilic deposits in distal tubular epithelial cells (*orange stars*). Interstitial cell with intracytoplasmic osmiophilic inclusions (*red arrow*). Arteriolar vessel with prominent and reactive endothelial cells containing osmiophilic inclusions. **d** Perivascular interstitial area with osmiophilic inclusions visible in interstitial cells (*red arrows*) and in capillary endothelial cells (*orange arrow*); inclusions are also visible in vascular smooth muscle cells of an arteriolar vessel (*yellow arrows*). Sections stained with toluidine blue (**a, d, c**) or methylene blue (**b**). Magnification ×600

Table 1 Distribution of osmiophilic inclusions per renal cell type in male and female Fabry and wild-type mice

Age (weeks)	Strain	Osmiophilic inclusions in renal cells	
		Males	Females
12	Control	Absent	DT
12	Control	PT, DT	Absent
12	Fabry	G, PT, DT, I, PTC	G, PT, DT, PTC,V
12	Fabry	G, PT, DT	G, PT, DT, I, PTC, V
24	Control	Absent	PT
24	Control		Absent
24	Fabry	G, PT, DT, V	G, PT, DT, I, V
24	Fabry	G, PT, DT, I, PTC, V	G, PT, DT, I, PTC, V
24	Fabry	G, PT, DT, PTC, V	
48	Control	DT	Absent
48	Control	Absent	Absent
48	Fabry	G, PT, DT, I, PTC, V	G, PT, DT, I, PTC, V
48	Fabry	G, PT, DT, V	G, PT, DT, I, PTC, V

G glomerular; *PT* proximal tubular; *DT* distal tubular; *I* interstitial; *PTC* peritubular capillary; *V* vascular arterial/arteriolar

but the first type was more frequent in the 12-week-old mice and the third type in the older age group, suggesting that the size of inclusions may increase with age (Figs. 1 and 2).

Tables 1 and 2 and Figs. 1 and 2 summarize the histological findings in the various mice sub-cohorts evaluated in this study.

Evaluation of the glomerular compartment

No osmiophilic inclusions were found in the glomerular cells of wild-type mice (Table 1, Fig. 1). All Fabry mice showed GSL inclusions in some of the glomerular cells (Table 1, Figs. 1 and 2). Parietal epithelial cells showed the highest prevalence and amount of cytoplasmic inclusions,

Table 2 Semi-quantification of osmiophilic deposits per renal cell type in the semi-thin cuts of Fabry mice

Age (weeks)	Gender	Glomerular cells				Tubular cells		Interstitial cells	PTC cells	Arterial / arteriolar vascular cells	
		Podocytes	Mesangial	Endothelial	Parietal	Proximal	Distal			Endothelial	Smooth muscle
12	♂	+	−	+	++	+	++	+	+	−	−
12	♂	+	−	−	−	+	+/++	−	−	−	−
12	♀	+	−	−	+	+	++	−	+	−	+
12	♀	+	−	−	++	++	++	++	+	+	+
24	♂	−	−	−	+	+	++	−	−	−	+
24	♂	+	+	−	+	+	++	+	++	−	+
24	♂	+	−	−	+	+	++	−	+	−	+
24	♀	+	+	−	+	++	+	+	−	+	+
24	♀	+	+	+	+	+	++/+++	+	++	+	++
48	♂	+	+	−	+/++	+	++/+++	++	++	++	−
48	♂	+	−	−	++	+	++	−	−	−	+
48	♀	+	−	−	+	+	++	++	++	+	+/++
48	♀	−	−	−	+	+/++	++	+	+	−	+/++

PTC peritubular capillary cells

The involvement of the different renal cell types was semi-quantitatively scored ("−" through "+++"). There were no statistically significant differences between gender and age groups in the prevalence and storage score per cell type

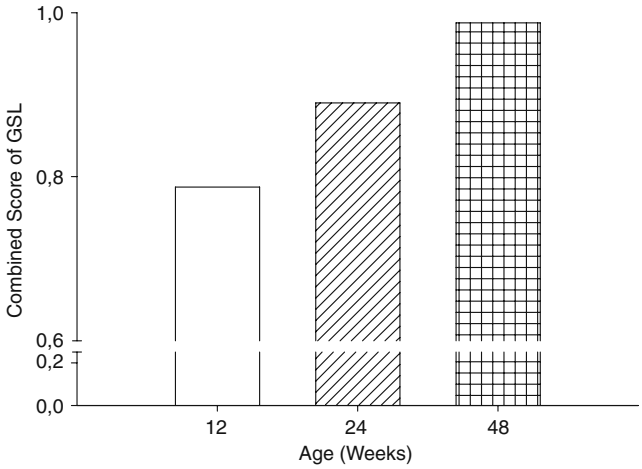

Fig. 3 Combined glycosphingolipids storage score in Fabry mice. There is an increase of the combined semi-quantification scoring of osmiophilic inclusions related to age

followed by podocytes, mesangial, and endothelial cells (Table 2). In all 11 mice showing podocyte involvement, the podocyte inclusions were small and inconspicuous (Fig. 2). There were no statistically significant differences between gender and age groups in the prevalence and semi-quantification of osmiophilic inclusions per glomerular cell type (Table 2).

Evaluation of tubular compartment

Four out of 11 wild-type mice presented scattered punctiform osmiophilic inclusions in some tubular epithelial cells (Table 1). These osmiophilic bodies were visible only at ×400 or ×600 magnification under light microscopy (Fig. 1). Semi-quantification showed very low amounts of this type of inclusions in wild-type mice. All Fabry mice had osmiophilic inclusions in proximal and distal tubular epithelial cells, visible even at ×40 magnification in mice aged more than 12 weeks, and at ×200 magnification in 12-week-old mice (Tables 1 and 2, Figs. 1 and 2). Indeed, these tubular cells were the renal cell types with the highest prevalence and amount of cytoplasmic inclusions, showing an age-related tendency to increase in distal tubular cells and to decrease in proximal tubular cells. There were no statistically significant differences between gender and age groups of Fabry mice in the prevalence and semi-quantification of osmiophilic inclusions per tubular cell type (Table 2).

Evaluation of interstitial compartment

No osmiophilic inclusions were found in interstitial cells of wild-type mice (Table 1). Eight out of 13 Fabry mice showed accumulation of osmiophilic inclusions in these cells (Tables 1 and 2, Fig. 2). There were no statistically significant differences between gender and age groups in the prevalence and semi-quantification of osmiophilic inclusions in interstitial cells (Table 2), although the semi-quantification of osmiophilic inclusions in these cells showed a trend to increasing from the ages 24 to 48 weeks.

Evaluation of vascular compartment

No osmiophilic inclusions were found in vascular cells of wild-type mice (Table 1). Twelve out of 13 Fabry mice contained osmiophilic inclusions in some of the vascular cells—peritubular capillary cells (PTC), endothelial cells of arterial or arteriolar vessels, and/or smooth muscle vascular cell (Tables 1 and 2, Figs. 1 and 2). Vascular endothelial (glomerular capillary, PTC, and/or arterial/arteriolar) and/or arterial or arteriolar smooth muscle cells inclusions were

Table 3 Presence of GSL inclusions in each renal cell type: comparison between Fabry mice and Fabry patients

	Glomerular cells				Tubular cells		Interstitial cells	PTC cells	Arterial / arteriolar vascular cells	
	Podocytes	Mesangial	Endothelial	Parietal	Proximal	Distal			Endothelial	Smooth muscle
Gubler et al., 1978 (n=12) [8]	91.7%	NA	16.7%	91.7%	33.3%	91.7%	91.7%	NA	83.3%	91.7%
Tøndel et al., 2008 (n=9) [13]	100%	88.9%	77.8%	NA	NA	100%	NA	NA	NA	NA
Valbuena et al., 2008 (n=4) [14]	100%	75%	50%	100%	50%	100%	25%	75%	75%	100%
Fogo et al., 2010 (n=59) [15]	98.3%	NA	NA	NA	36.4%	75%	NA	58.9%	50%	65.8%
Human cases, combined	97.6%	92.3%	44%	93.3%	36.6%	81.5%	81.3%	60%	59.2%	74.1%
Fabry mice (n=13)	84.6%	30.8%	15.4%	92.3%	100%	100%	61.5%	69.2%	46.2%	76.9%
P value	0.09	0.004	0.15	1.0	0.0001	0.12	0.38	0.75	0.53	1.0

NA data not available

Data are presented as the percentages of Fabry mice or Fabry patients with GSL deposits in each specific renal cell type. P values are for the statistical comparison of the prevalence of GSL deposits per cell type in Fabry patients and in Fabry mice

found in ten cases (76.9%). Eight Fabry mice showed inclusions in both vascular cell types (Table 2). There were no statistically significant differences between gender and age groups in the prevalence and semi-quantification of osmiophilic inclusions per vascular cell type, although the semi-quantification of osmiophilic inclusions in endothelial vascular cells showed a trend to increase with age (Table 2).

Comparison of the prevalence, semi-quantification, and histological characteristics of GSL deposits in Fabry mice versus wild-type mice and their evolution with age

In all types of renal cells, the semi-quantification of osmiophilic inclusions was significantly different between the Fabry mice and wild-type mice ($p<0.0001$).

Although none had deposits in other renal cell types, 36.4% of the wild-type mice showed osmiophilic inclusions in tubular cells (Table 1). These tubular inclusions were inconspicuous, scant, lightly stained and visible only at a minimum magnification of ×400.

All Fabry mice showed osmiophilic inclusions in tubular and glomerular cells, 92.3% had deposits in PTC and/or arterial or arteriolar cells, and 61.5% had inclusions in interstitial cells (Table 1). The combined semi-quantification scoring of osmiophilic inclusions in Fabry mice increased with age (Fig. 3). In all Fabry mice, different proportions of the three types of osmiophilic inclusions were found in tubular cells. Tubular inclusions were seen at a minimum ×200 magnification at 12 weeks of age and at minimum ×40 magnification at 24 and 48 weeks of age. Deposits in the other renal cells were almost always small and dark stained.

Comparison of renal GSL deposits in Fabry mice and Fabry human patients

Table 3 shows the prevalence of GSL deposits in the different renal cells in Fabry patients and in Fabry mice. The prevalence of GSL deposits in proximal tubular cells in Fabry mice was significantly higher as compared to human patients, whereas the reverse was true for mesangial cells. In all other renal cell types, the prevalence of GSL deposits was similar in both Fabry mice and Fabry patients.

Nonspecific histological alterations in the kidney parenchyma

Table 4 and Fig. 4 summarize the nonspecific renal histological alterations observed in the two mice cohorts. Twelve Fabry mice out of 13 (92.3%) and 10 wild-type mice out of 11 (90.9%) had some morphologic nonspecific alterations in the kidney parenchyma, including hypertrophy of arteriolar vascular wall, venous dilatation, interstitial

Table 4 Nonspecific histological alterations in the kidney parenchyma of male and female Fabry and wild-type mice

Age (weeks)	Strain	Males					Females				
		Glomerular alterations	Tubular alterations	Inflammatory cells	Interstitial fibrosis	Vascular alterations	Glomerular alterations	Tubular alterations	Inflammatory cells	Interstitial fibrosis	Vascular alterations
12	Control	–	–	–	<1%	VD	–	–	–	–	–
12	Control	–	UC	+	–	VD	–	–	–	–	VD
12	Fabry	–	–	–	–	VD	–	TC	+	–	VD
12	Fabry	–	–	–	–	–	–	–	+	<1%	VD
24	Control	–	TC	+	–	VD	–	DTL	–	–	–
24	Control						–	TC	–	–	–
24	Fabry	–	TC	+	–	VD	–	TC, DTL	+	–	VD
24	Fabry	–	TC	–	<1%	VD	–	–	+	–	VD
24	Fabry	–	TC	–	–	VD					
48	Control	–	TC	+	<1%	–	–	UC	–	–	–
48	Control	–	TC	+	–	VD	–	UC	–	–	VD
48	Fabry	–	–	+	<1%	VD	–	–	–	–	VD
48	Fabry	–	TC	+	–	–	–	UC	+	<1%	HVAA

–/+ feature absent/present; *DTL* dilated tubular lumen; *HVAA* hypertrophy of arteriolar vascular wall; *TC* tubular casts; *UC* urinary cyst; *VD* vein dilatation

Interstitial fibrosis reported as the percentage of affected cut section, as estimated at ×200 magnification

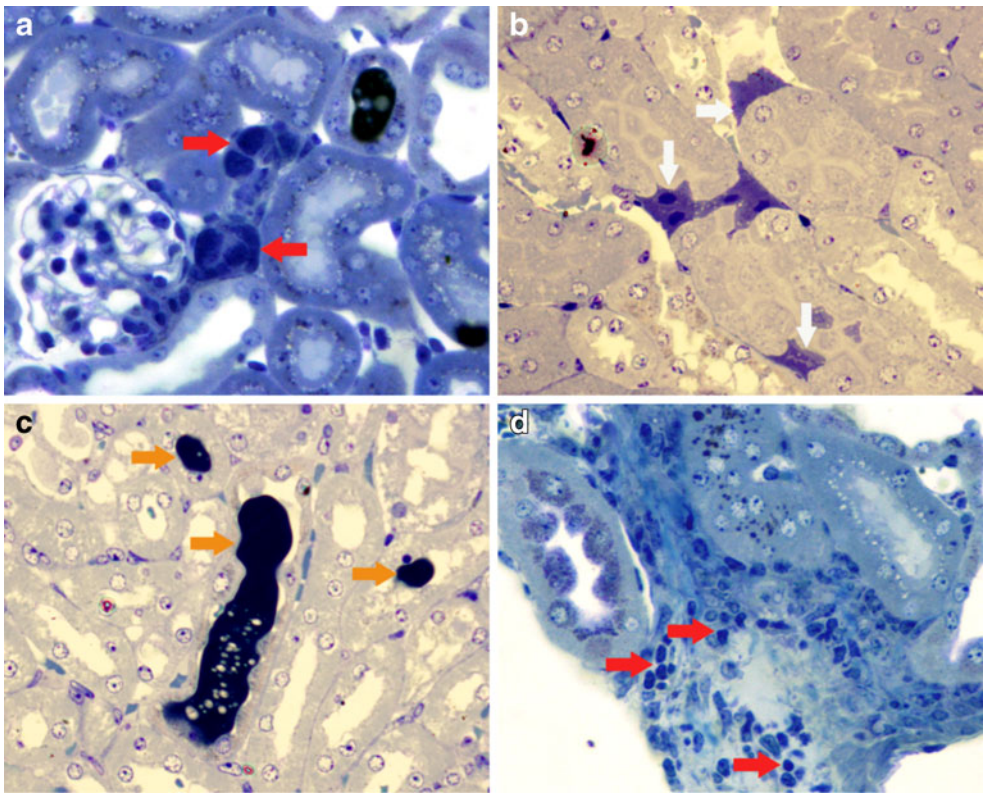

Fig. 4 Nonspecific lesions found in Fabry mice. **a** Cluster of amorphous, undifferentiated cells (*red arrows*) in the glomerular vascular pole and in periglomerular location. Dark osmiophilic cast within the tubular lumen. **b** Prominent stellate interstitial cells visible in the tubulo-interstitial area (*white arrows*). **c** Dark casts within tubular lumina (*orange arrows*). **d** Inflammatory cells (*red arrows*) in perivascular and peritubular interstitial location. Sections stained with toluidine blue (**a**) or methylene blue (**b–d**). Magnification ×600 (**a**, **d**) and ×560 (**b, c**)

fibrosis, presence of inflammatory cells in the tubulo-interstitial area, tubular dilatation, tubular casts, and urinary cysts. There were no statistically significant differences between the Fabry and the wild-type mice regarding the prevalence of any of these features.

Discussion

We describe the renal histological phenotype of α-Gal-deficient mice and compare these findings with observations in wild-type mice and reported biopsy data from Fabry patients.

The histological phenotypes of GSL accumulation in the kidneys of Fabry mice and wild-type mice were clearly distinct. Inconspicuous, finely granular osmiophilic inclusions, possibly composed of intrinsically expressed GSL or of other lipid-related deposits [20, 23], were observed in tubular cells of some wild-type mice. In the Fabry mice, osmiophilic inclusions were more abundant, larger, and more darkly stained as compared to the wild-type mice. Small inclusions were observed in all types of renal cells, and both small and large inclusions were seen in tubular and cuboidal parietal epithelial glomerular cells (Fig. 1). Diversity of size of GSL deposits in renal cell types has also been observed in kidney biopsies from Fabry patients, the largest inclusions being present in epithelial tubular cells and podocytes [8]. However, despite the sexual dimorphism of murine glomerular parietal cells, with cuboidal cells more prevalent in males and squamous cells more prevalent in females [30], there were no statistically significant gender differences in the prevalence of GSL deposits per renal cell type.

The patterns of distribution of GSL deposits in the different types of renal cells in the Fabry mice and in male and female patients of comparable age ranges were not statistically different, except in proximal tubular and mesangial cells. Fabry mice had a significantly higher prevalence of inclusions in proximal tubular cells as compared to Fabry patients, whereas mesangial cell inclusions were more prevalent in Fabry patients. Notably, large GSL podocyte inclusions, which are a distinctive feature of the human Fabry nephropathy, were not present in the Fabry mice.

The combined GSL storage score increased with age. The size and staining intensity of the osmiophilic inclusions

were, in general, more prominent in 48-week-old mice as compared to 12-week-old mice. Although this finding lacked statistical significance, it may suggest that accumulation of GSL in the kidneys of Fabry mice is progressive over time. This is in agreement with an earlier report describing a significant increase of GSL concentration in extracts of kidney tissue in 48-week-old Fabry mice as compared to 24-week-old mice [23]. It has been postulated that the Fabry nephropathy in humans results from progressive accumulation of GSL in the kidney parenchyma [31]. However, we are not aware of any biopsy studies in Fabry patients demonstrating an age-related increase in the size of deposits in renal cells, as we have observed in Fabry mice.

Glomerular sclerosis and tubulo-interstitial fibrosis are the histological features that best correlate with the progression of Fabry nephropathy in humans [14, 15, 31]. In our study, such nonspecific lesions were virtually absent in both the Fabry and wild-type mice in all three age groups studied. This represents a major difference between the kidney pathology of Fabry mice and human Fabry disease, and may correlate with the lack of clinical kidney disease in the Fabry mice [20].

Ischaemic damage resulting from microvascular endothelial disease and/or necrosis of vascular smooth muscle cells and/or pericyte injury is the major theory for the pathogenesis of the classical phenotype of Fabry disease [4, 8, 10, 32]. However, we found a largely comparable prevalence of GSL deposits in the vascular and endothelial cells in Fabry mice and patients. These findings do not support a major role of ischaemic injury in the initiation of Fabry nephropathy, and is in agreement with observation by Valbuena et al. who concluded that vascular damage did not seem to have a major role in the early pathogenesis of Fabry nephropathy in females [14].

The prevalence of histological involvement of podocytes in Fabry mice and in Fabry patients was similar. However, the size of GSL deposits was smaller in Fabry mice than is typically seen in humans with Fabry nephropathy. Therefore, progressive increase of lysosomal GSL deposits in podocytes, ultimately causing irreversible cell injury [10, 14], may be a critical mechanism in the pathogenesis of human Fabry nephropathy.

We found a relatively low prevalence of GSL accumulation in mesangial cells of Fabry mice as compared to Fabry patients. Additional studies will have to be performed to investigate a possible role of mesangial cell necrosis in the pathogenesis of glomerular sclerosis and deterioration of renal function in humans with Fabry disease [8].

In conclusion, Fabry mice show a distinct phenotype with regard to the accumulation of GSL in the kidney parenchyma, if compared to wild-type mice. The pattern of involvement of the different renal cell types is mostly similar to that observed in Fabry patients but the amount of accumulated GSL is smaller. The absence of nonspecific sclerotic and fibrotic kidney lesions represents a major difference between the kidney pathology of Fabry mice and human Fabry disease, and explains the lack of clinical kidney disease in the Fabry mice. This may be related to genetic background of the Fabry mice, since C57BL/6 mice are particularly resistant to all types of kidney disease [33]. However, as human tissues from Fabry patients are limitedly available and experimental interventions are constrained by ethical and legal issues, this Fabry knockout mouse model remains valid and useful for new lines of specific research into the mechanisms underlying the species differences and factors driving development of the Fabry nephropathy.

Acknowledgments The authors would like to acknowledge Dr. Isabel Carvalho, Fátima Martins, and Isabel Duarte for helpful assistance in the maintenance of the mice colony at the IBMC. We thank David Warnock, M.D. for critically reviewing and commenting the manuscript and Hans Ebels, M.D. for the valuable assistance in the text editing. This work was supported by Fundação para a Ciência e Tecnologia (FCT) of Portugal (PTDC/SAU-NEU/66740/2006) and co-funded by FEDER. Carmen Valbuena was a recipient of a non-restricted research grant from Genzyme Portugal, and Lorena G. Rodrigues was supported by a personal grant from FCT (SFRH/BPD/25333/2005).

References

1. Bishop DF, Kornreich R, Desnick RJ (1988) Structural organization of the human alpha-galactosidase A gene: further evidence for the absence of a 3' untranslated region. Proc Natl Acad Sci USA 85:3903–3907
2. Brady RO, Gal AE, Bradley RM, Martensson E, Warshaw AL, Laster L (1967) Enzymatic defect in Fabry's disease. Ceramide-trihexosidase deficiency. N Engl J Med 276:1163–1167
3. Kint JA (1970) Fabry's disease: alpha-galactosidase deficiency. Science 167:1268–1269
4. Desnick RJ, Ioannou YA, Eng CM (2001) Alpha-Galactosidase A deficiency: Fabry disease. In: Scriver C, Beaudet A, Sly W, Valle D (eds) The metabolic bases of inherited disease, 8th edn. McGraw-Hill, New York, pp 3733–3774
5. Desnick RJ, Brady R, Barranger J, Collins AJ, Germain DP, Goldman M, Grabowski G, Packman S, Wilcox WR (2003) Fabry disease, an under-recognized multisystemic disorder: expert recommendations for diagnosis, management, and enzyme replacement therapy. Ann Intern Med 138:338–346
6. Branton MH, Schiffmann R, Sabnis SG, Murray GJ, Quirk JM, Altarescu G, Goldfarb L, Brady RO, Balow JE, Austin Iii HA, Kopp JB (2002) Natural history of Fabry renal disease: influence of alpha-galactosidase A activity and genetic mutations on clinical course. Medicine 81:122–138
7. Schiffmann R, Warnock DG, Banikazemi M, Bultas J, Linthorst GE, Packman S, Sorensen SA, Wilcox WR, Desnick RJ (2009) Fabry disease: progression of nephropathy, and prevalence of cardiac and cerebrovascular events before enzyme replacement therapy. Nephrol Dial Transplant 24:2102–2111
8. Gubler MC, Lenoir G, Grunfeld JP, Ulmann A, Droz D, Habib R (1978) Early renal changes in hemizygous and heterozygous patients with Fabry's disease. Kidney Int 13:223–235
9. Sessa A, Meroni M, Battini G, Maglio A, Brambilla PL, Bertella M, Nebuloni M, Pallotti F, Giordano F, Bertagnolio B, Tosoni A

(2001) Renal pathological changes in Fabry disease. J Inherit Metab Dis 24:66–70
10. Alroy J, Sabnis S, Kopp JB (2002) Renal pathology in Fabry disease. J Am Soc Nephrol 13:S134–S138
11. Sessa A, Toson A, Nebuloni M, Pallotti F, Giordano F, Battini G, Maglio A, Meroni M, Calconi G, Bertolone G, Gatti P (2002) Renal ultrastructural findings in Anderson-Fabry disease. J Nephrol 15:109–112
12. Fischer EG, Moore MJ, Lager DJ (2006) Fabry disease: a morphologic study of 11 cases. Mod Pathol 19:1295–1301
13. Tøndel C, Bostad L, Hirth A, Svarstad E (2008) Renal biopsy findings in children and adolescents with Fabry disease and minimal albuminuria. Am J Kidney Dis 51:767–776
14. Valbuena C, Carvalho E, Bustorff M, Ganhao M, Relvas S, Nogueira R, Carneiro F, Oliveira JP (2008) Kidney biopsy findings in heterozygous Fabry disease females with early nephropathy. Virchows Arch 453:329–338
15. Fogo AB, Bostad L, Svarstad E, Cook WJ, Moll S, Barbey F, Geldenhuys L, West M, Ferluga D, Vujkovac B, Howie AJ, Burns A, Reeve R, Waldek S, Noel LH, Grunfeld JP, Valbuena C, Oliveira JP, Muller J, Breunig F, Zhang X, Warnock DG (2010) Scoring system for renal pathology in Fabry disease: report of the International Study Group of Fabry Nephropathy (ISGFN). Nephrol Dial Transplant 25:2168–2177
16. Eng CM, Guffon N, Wilcox WR, Germain DP, Lee P, Waldek S, Caplan L, Linthorst GE, Desnick RJ (2001) Safety and efficacy of recombinant human alpha-galactosidase A—replacement therapy in Fabry's disease. N Engl J Med 345:9–16
17. Schiffmann R, Kopp JB, Austin HA 3rd, Sabnis S, Moore DF, Weibel T, Balow JE, Brady RO (2001) Enzyme replacement therapy in Fabry disease: a randomized controlled trial. J Am Med Assoc 285:2743–2749
18. Thurberg BL, Rennke H, Colvin RB, Dikman S, Gordon RE, Collins AB, Desnick RJ, O'Callaghan M (2002) Globotriaosylceramide accumulation in the Fabry kidney is cleared from multiple cell types after enzyme replacement therapy. Kidney Int 62:1933–1946
19. Ohshima T, Murray GJ, Swaim WD, Longenecker G, Quirk JM, Cardarelli CO, Sugimoto Y, Pastan I, Gottesman MM, Brady RO, Kulkarni AB (1997) alpha-Galactosidase A deficient mice: a model of Fabry disease. Proc Natl Acad Sci USA 94:2540–2544
20. Ohshima T, Schiffmann R, Murray GJ, Kopp J, Quirk JM, Stahl S, Chan CC, Zerfas P, Tao-Cheng JH, Ward JM, Brady RO, Kulkarni AB (1999) Aging accentuates and bone marrow transplantation ameliorates metabolic defects in Fabry disease mice. Proc Natl Acad Sci USA 96:6423–6427
21. Ioannou YA, Zeidner KM, Gordon RE, Desnick RJ (2001) Fabry disease: preclinical studies demonstrate the effectiveness of alpha-galactosidase A replacement in enzyme-deficient mice. Am J Hum Genet 68:14–25
22. Aerts JM, Groener JE, Kuiper S, Donker-Koopman WE, Strijland A, Ottenhoff R, van Roomen C, Mirzaian M, Wijburg FA, Linthorst GE, Vedder AC, Rombach SM, Cox-Brinkman J, Somerharju P, Boot RG, Hollak CE, Brady RO, Poorthuis BJ (2008) Elevated globotriaosylsphingosine is a hallmark of Fabry disease. Proc Natl Acad Sci USA 105:2812–2817
23. Rodrigues LG, Ferraz MJ, Rodrigues D, Pais-Vieira M, Lima D, Brady RO, Sousa MM, Sa-Miranda MC (2009) Neurophysiological, behavioral and morphological abnormalities in the Fabry knockout mice. Neurobiol Dis 33:48–56
24. Eitzman DT, Bodary PF, Shen Y, Khairallah CG, Wild SR, Abe A, Shaffer-Hartman J, Shayman JA (2003) Fabry disease in mice is associated with age-dependent susceptibility to vascular thrombosis. J Am Soc Nephrol 14:298–302
25. Shu L, Shayman JA (2007) Caveolin-associated accumulation of globotriaosylceramide in the vascular endothelium of alpha-galactosidase A null mice. J Biol Chem 282:20960–20967
26. Park JL, Whitesall SE, D'Alecy LG, Shu L, Shayman JA (2008) Vascular dysfunction in the alpha-galactosidase A-knockout mouse is an endothelial cell-, plasma membrane-based defect. Clin Exp Pharmacol Physiol 35:1156–1163
27. Park JL, Shu L, Shayman JA (2009) Differential involvement of COX1 and COX2 in the vasculopathy associated with the alpha-galactosidase A-knockout mouse. Am J Physiol 296:H1133–H1140
28. Shu L, Park JL, Byun J, Pennathur S, Kollmeyer J, Shayman JA (2009) Decreased nitric oxide bioavailability in a mouse model of Fabry disease. J Am Soc Nephrol 20:1975–1985
29. Miller SA, Dykes DD, Polesky HF (1988) A simple salting out procedure for extracting DNA from human nucleated cells. Nucleic Acids Res 16:1215
30. Conti CJ, Gimenez-Conti IB, Benavides F, Frijhoff AFW, Conti MA (reviewed by) Ward JM (2004) Atlas of Laboratory Mouse Histology. Texas Histopages, Inc. http://ctrgenpath.net/static/atlas/mousehistology. Accessed 2 January 2010
31. Warnock DG, Valbuena C, West M, Oliveira JP (2010) Renal manifestations of Fabry disease. In: Elstein D, Altarescu G, Beck M (eds) Fabry disease, 1st edn. Springer, Dordrecht, pp 211–244
32. Meehan SM, Junsanto T, Rydel JJ, Desnick RJ (2004) Fabry disease: renal involvement limited to podocyte pathology and proteinuria in a septuagenarian cardiac variant. Pathologic and therapeutic implications. Am J Kidney Dis 43:164–171
33. Brosius FC (2010) Susceptible mice: identifying a diabetic nephropathy disease locus using a murine model. Kidney Int 78:431–432

Virchows Arch (2011) 458:487–496
DOI 10.1007/s00428-011-1052-7

ORIGINAL ARTICLE

A subset of metzincins and related genes constitutes a marker of human solid organ fibrosis

Silke Rödder · Andreas Scherer · Meike Körner · Hans-Peter Marti

Received: 7 December 2010 / Revised: 20 January 2011 / Accepted: 23 January 2011 / Published online: 20 February 2011
© Springer-Verlag 2011

Abstract Metzincins and functionally related genes play important roles in extracellular matrix remodeling both in healthy and fibrotic conditions. We recently presented a transcriptomic classifier consisting of 19 metzincins and related genes (MARGS) discriminating biopsies from renal transplant patients with or without interstitial fibrosis/tubular atrophy (IF/TA) by virtue of gene expression measurement (Roedder et al., Am J Transplant 9:517–526, 2009). Here we demonstrate that the same algorithm has diagnostic value in non-transplant solid organ fibrosis. We used publically available microarray datasets of 325 human heart, liver, lung, kidney cortex, and pancreas microarray samples (265 with fibrosis, 60 healthy controls). Expression of nine commonly differentially expressed genes was confirmed by TaqMan low-density arrays (Applied Biosystems, USA) in 50 independent archival tissue specimens with matched histological diagnoses to microarray patients. In separate and in combined, integrated microarray data analyses of five datasets with 325 samples, the previously published MARGS classifier for renal post-transplant IF/TA had a mean AUC of 87% and 82%, respectively. These data demonstrate that the MARGS gene panel classifier not only discriminates IF/TA from normal renal transplant tissue, but also classifies solid organ fibrotic conditions of human pancreas, liver, heart, kidney, and lung tissue samples with high specificity and accuracy, suggesting that the MARGS classifier is a cross-platform, cross-organ classifier of fibrotic conditions of different etiologies when compared to normal tissue.

Keywords Fibrosis · Microarray · Classifier · Metzincins and related genes (MARGS)

Electronic supplementary material The online version of this article (doi:10.1007/s00428-011-1052-7) contains supplementary material, which is available to authorized users.

S. Rödder · H.-P. Marti (✉)
Department of Nephrology and Hypertension, Inselspital, University of Bern,
Freiburgstrasse 15,
3010 Bern, Switzerland
e-mail: Hans-Peter.Marti@insel.ch

A. Scherer
Spheromics,
Kontiolahti, Finland

M. Körner
Institute of Pathology, University of Bern,
Bern, Switzerland

Introduction

Fibrosis is a tissue-repair response to chronic and severe tissue injury, including chronic exposure to pathogens or toxins like cigarette smoke, asbestos, and alcohol. A major cause of long-term organ failure, fibrosis is currently irreversible and is hence subject to extensive research efforts. Tissue repair is a delicately balanced process of sequential interplay of secretion of growth factors, chemokines, the deposition and degradation of extracellular matrix (ECM), angiogenesis, apoptosis, and eventually either resolution of the injury through regeneration, or healing accompanied by scar formation. Disruption or deregulation of any of those processes, or persistent tissue injury, leads to abnormal tissue repair, termed fibrosis, which consequently results in sclerosis. The role of inflammation as a trigger of normal and abnormal tissue repair cascades is still under debate [2, 3].

A common denominator of fibrotic wound repair is excessive deposition, reorganization, and remodeling of extracellular matrix (ECM). ECM remodeling is mediated by a number of genes and pathways, among others by the superfamily metzincins, which are zinc-dependent metal-

loproteases. Metzincins can be subdivided into groups of proteins with a disintegrin and metalloprotease domain (ADAM), ADAM with thrombospondin motif (ADAMTS), serralysins, papalysins, and matrix metalloproteases (MMP). All have been shown to play roles during fibrogenesis [4, 5]. As we have previously reported, we have extended the group of metzincins and generated a gene set termed MARGS (metzincins and related genes). We included transcription factors, activators, inhibitors and substrates, and cell-surface and cytoplasmic proteins which regulate the functions of metzincins [1]. The list of 191 MARGS includes genes with roles in epithelial cell damage (e.g., fibrin, fibronectin, collagens), fibroblast proliferation (e.g., TGF, TNF, SERPINE), basement membrane remodeling (e.g., MMP2, MMP9), fibroblast foci formation (e.g., TIMP1, TIMP2), as well as angiogenesis (e.g., VEGF) and impaired re-epithelialization (e.g., MMPs/TIMPs) (Supplementary Table TS1). Thus, MARGS are representative of important phases of normal and fibrotic tissue repair.

Timely diagnosis of fibrosis through molecular markers and classical clinical parameters may be an invaluable indication for treatment adjustment prior to the development of irreversible sclerosis.

We have previously demonstrated that gene expression of MARGS correlates at large with progression of human interstitial fibrosis/tubular atrophy (IF/TA) in renal allograft biopsies [1]. We also showed in three independent microarray datasets that a gene panel consisting of 19 MARGS could be used to classify human renal biopsies with and without IF/TA.

Here we extend those findings and test the performance of the IF/TA gene expression classifier in human fibrosis of various etiologies in five different organs. Using publically available microarray datasets, we demonstrate first that MARGS indeed are differentially expressed under conditions of fibrosis in aging kidney, heart failure, liver cirrhosis, idiopathic pulmonary fibrosis, and pancreatitis. We confirm these data by TaqMan quantitative RT–PCR in independent etiology-matched patient samples, and finally show in support of our hypothesis good diagnostic value of the MARGS-panel classifier in the microarray datasets.

Materials and methods

Datasets

An overview of the microarray datasets is shown in Table 1. The expression data for the kidney dataset was downloaded from http://genome-www5.stanford.edu [6]. Gene expression datasets for heart and lung were downloaded from Gene Expression Omnibus, http://www.ncbi.nlm.nih.gov/geo, Heart: GSE5406 [7], Lung: GSE10667 [1]. Liver and pancreas data were provided by the authors [9, 10].

Microarray analysis

Gene expression analysis was performed in Partek Genomics Suite 6.5 (http://www.Partek.com) and R (http://www.bioconductor.org). Where non-processed data were available, datasets were quantile normalized with RMA background correction and median polish. The manuscript is based on the assumption that genes are appropriately matched to common identifiers across platforms to achieve comparability of data. We used Entrez Gene IDs for this purpose, as they appear to be relatively stable over time (J.S. Marron, personal observation). Expression signal intensities for features mapping to the same Entrez GeneID were averaged. Pseudogenes and all features on the platforms without Entrez Gene ID were excluded.

Expression filters were applied to all datasets, except those with ratio measures. Only genes with signal intensity measurements of at least 6.5 in $\log_2$ scale in a number of samples corresponding to 75% in the smallest analysis group were considered further. Differentially expressed genes were identified by ANOVA after application of a gene list filter. No expression filter was applied for testing the MARGS classifier. Receiver operator characteristic (ROC) curves and calculation of the AUC was done with the R package ROCR [11].

Classifier algorithm was linear discriminant analysis (LDA) with leave-one-out cross-validation.

Patients for confirmation analyses

For confirmation of microarray results, we utilized archival formalin fixed paraffin embedded (FFPE) pancreas, lung, liver, kidney, and heart tissue from the Institute of Pathology, University of Berne, Switzerland. Fibrotic and non-fibrotic tissue specimens from a total of 50 patients were utilized (Table 2). Great care was taken to select the cases with best match to the histological diagnosis of cases used for microarray data analyses [6–10]. All patients remained anonymized except for age and gender, and all studies were approved by the local ethics commission.

Preparation of tissue

Sections 8–10 μm thick were cut from each FFPE tissue block of healthy and fibrotic kidneys, hearts, livers, lungs, and pancreas (n=5 per case). Sections were deparaffinized in xylene three times for 5 min with gentle inversion. A maximum of 150 mm^2 of tissue was scraped off using a

Table 1 Documentation of gene expression microarray datasets used analysis (all datasets are publically available)

Data			Array type		Samples			
Organ	Reference	Source	Name	# Features	# Fibrosis	# Control	Fibrosis	Control
Kidney	Rodwell GEJ et al., PLoS Biology 2004;2:e427	http://genomewww5.stanford.edu/	Affymetrix HG-U133A and B	44,928	11	16	IF/TA 3	IF/TA 0–1
Heart	Hannenhalli S et al., Circulation, 2006;114:1269–1276	GEO GSE5406	Affymetrix HG-U133A	22,283	194	16	Systolic heart failure	Non-failing
Liver	Utsunomiya T et al., World J Gastroenterol, 2007;13:383–390	Authors	Agilent Human 1A	22,153	15	8	MFI adj>10	MFI adj=0
Lung	Konishi K et al., Am J Respir Crit Care Med, 2009;180:167–175	GEO GSE10667	Agilent 4×4 4k Whole Human Genome	43,376	31	15	IPF; IPF+Aex	Normal
Pancreas	Binkley CE et al., Pancreas 2004;29:254–263	Authors	Affymetrix HuGeneFL	7,129	15	5	Adenocarc., pancreatitis	Normal

sterile scalpel and stencil and transferred into a 1.5-mL microcentrifuge tube. For tissue digestion, 150 μL Proteinase K mix (20 μg/μL; Arcturus Bucher Biotec, Basel, Switzerland) were added, and tissue was incubated in a thermoshaker at 37°C and 300 rpm for 20 h. All procedures were carried out under RNase-free conditions.

Isolation of total RNA and TaqMan® custom array microfluidic cards

Total RNA was isolated in a final volume of 12 μL using the Paradise Plus WT RT Reagent System (Arcturus, Bucher Biotec) according to the manufacturer's protocol. Total RNA was quantified using NanoDrop (Thermo Scientific NanoDrop, USA), and quality was controlled applying the BioAgilent, USA Nanochip (Agilent, USA). Finally, 200 ng total RNA was reverse transcribed into cDNA, and 50 μL Universal PCR master mix and nuclease-free water were added up to a final volume of 100 μL. This sample was subsequently loaded onto TaqMan custom arrays consisting of 384-well microfluidic cards and run on ABI PRISM 7900HT (total of 40 cycles) (Applied Biosystems). Gene expression assays came pre-pipetted and lyophilized in the wells. Selection of gene expression assays for the LDA based on short amplicon size (<100 bp) and proximity to the 3′ prime end. The following assays were used: THBS2 Hs01568063_m, HYOU1 Hs00197328_m, MMP7 Hs01042795_m, MMP2 Hs00234422_m, PXN Hs00236064_m, COL1A2 Hs01028970_m, TIMP1 Hs00171558_m, COL3A1 Hs00943809_m, and HNRNPU Hs00244919_m. qRT–PCR results were analyzed by SDS V2.01 (Applied Biosystems) and Partek Genomics Suite. Triplicate TaqMan qRT–PCR Ct values were normalized by geometric averaging of multiple internal control genes [12].

Table 2 Information on samples used for TaqMan qRT–PCR confirmation analysis (samples were selected to match the setting of the samples used for the microarray studies as close as possible)

Organ	Group	Tissue specification	Diagnosis	#	Age (years)	% Male
Kidney	Control	Tumor unaffected kidney cortex of nephrectomy	Wilms tumor	5	5 +7/−3	60
	Fibrosis		Renal carcinoma	5	77 +7/−6	80
Heart	Control	Time point zero biopsy	Healthy	5	46 +17/−26	80
	Fibrosis	Explant	Terminal cardiac failure	5	56 +9/−7	100
Liver	Control	Tumor unaffected region of hepatectomy	Cancer metastasis	5	60 +16/−21	80
	Fibrosis	Hepatectomy	Liver cirrhosis	5	53 +8/−6	60
Lung	Control	Tumor unaffected region of resectomy	Primary lung cancer; cancer metastasis	3	62 +16/−13	40
	Fibrosis	Resectomy	Usual interstitial pneumonia	5	74 +12/−11	60
Pancreas	Control	Tumor unaffected region of pancreatectomy	Pancreatic carcinoma: pseudomyxoma peritonei	4	58 +12/−14	60
	Fibrosis	Pancreatectomy	Chronic pancreatitis	5	57 +24/−17	60

Results

Data pre-processing

We have previously shown that MARGS are differentially expressed in conditions of renal transplant interstitial fibrosis and tubular atrophy (IF/TA) [1]. In addition, a panel of 19 MARGS genes in conjunction with the decision algorithm Linear Discriminant Analysis had been identified as molecular marker of IF/TA in renal allografts. To investigate the relevance of MARGS in fibrotic, non-transplant conditions of various etiologies, we turned to publically available microarray datasets and compared cases of healthy controls and fibrosis (Table 1). In the kidney cortex dataset [6], we grouped samples with IF/TA grade 0–1, so that mild fibrosis was included in the control group. Those were compared to samples with severe IF/TA (grade 3). For the heart analysis, we used microarray data from 194 samples from advanced systolic heart failure and from 16 non-failing hearts [7]. Heart failure patients suffered either from ischemic (n=86) or idiopathic dilated (n=108) cardiomyopathy. This difference was neglected in the present analysis. The lung analysis comprised samples from 23 patients with interstitial pulmonary fibrosis (IPF) and eight with acute exacerbation of IPF (IPF-AEx) [8]. For the purpose of our study, these two groups were combined to one and compared to 16 samples from patients with normal lung histology. Samples for the liver analysis were selected from the healthy control group and from those patients with an adjusted morphologic fibrosis index (MFI) score ≥10 (average F-score for this group is 3.4). The adjusted MFI is the mean MFI determined from nine section images, adjusted by a factor of 1.13, which corrects for a mean MFI of 1.13 in samples of healthy control patients [9]. The majority of the fibrosis samples originated from patients with hepatocellular carcinoma, most of which were positive for hepatitis C virus (HCV) antibody. Finally, the pancreas dataset consisted of samples from patients with chronic pancreatitis (n=5), pancreatic adenocarcinoma (n=10), and five normal pancreas samples [10]. Chronic pancreatitis and adenocarcinoma samples were grouped into one.

Due to the different platforms and population of features on the arrays, different numbers of MARGS are represented on the platforms. For instance, the kidney cortex dataset with HG-U133A and B included 175 MARGS, while 100 MARGS were represented on the platform of the pancreas dataset. This has implications for the comparison of differentially expressed MARGS, as we do not have information on the expression of many MARGS on some of the platforms (see below).

The initial analytical steps had to be adjusted to each dataset. The kidney cortex data where distributed on HG-U133A and HG-U133B arrays. We used only array pairs which had been generated from the same patient RNA. As 99 probesets are shared between both array types, data were merged into one matrix by mean adjustment of the expression values of those probesets. The signal intensities of the pancreas dataset were floored to a minimum value of 10 and $\log_2$ transformed. The liver dataset had been Lowess normalized. As the samples had been split into training and test set by the authors, we treated the technical effect by mean adjustment. Sample A47, adjusted morphologic fibrosis index (MFI) 17.43, was excluded in the further analysis due outlier-like behavior which could not be explained with the data at hand.

Differentially expressed MARGS

Figure 1 shows principal component analysis (PCA) of differentially expressed MARGS which pass the expression filter (see "Materials and methods") and had a false discovery rate q-value qFDR <0.01 in each dataset separately. The number of MARGS with differential expression naturally is dependent on the significance of biological/clinical differences between the sample groups, but also influenced by the platform design, i.e., how many MARGS are represented on the platforms. In kidney cortex, 59 of overall 175 MARGS on the platform pass our filter criteria and only four of a total of 179 MARGS in liver.

It is obvious that differentially expressed MARGS are sufficient in the kidney cortex, liver, and pancreas dataset to separate fibrosis samples from control samples. The PCA of the heart samples showed some overlap between normal and fibrotic samples due to the inclusion of samples with mild to very mild grades of fibrosis. In lung, there are three samples of the control group, GSM269754, GSM269762, and GSM269757, which display extreme behavior with respect to MARGS expression and tend to be placed close to the fibrosis group. Technical or biological/clinical reasons not known to us may account for this.

Five-way Venn diagram

Uniformly deregulated genes in kidney cortex, heart, liver, lung, and pancreas fibrosis were identified by Venn analyses, comparing all deregulated MARGS in each organ fibrosis dataset having a qFDR <0.1 (Fibrosis vs. Control) after expression filter. In this analysis, we chose a larger qFDR threshold to compensate for the—in relation to the other datasets—larger qFDR values in the liver dataset. We had also noticed that the set of MARGS with smallest qFDR in liver are different from the set of MARGS with smallest qFDR in the other datasets. To recruit a sufficient number of MARGS as candidates for qRT–PCR confirma-

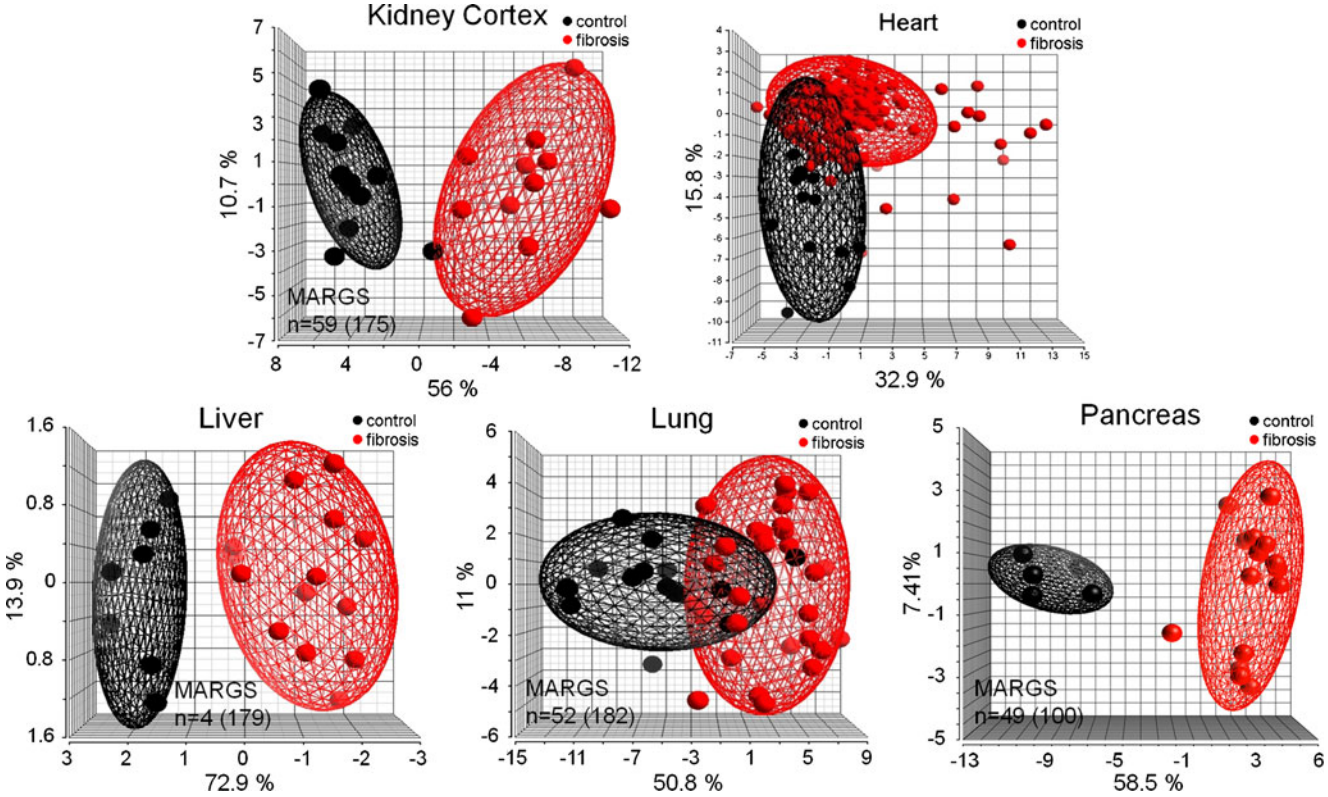

Fig. 1 Principal component analysis (PCA) of samples with or without fibrosis from published datasets. Differentially expressed MARGS are sufficient to separate fibrotic samples from healthy [or mild fibrosis (kidney)] in kidney, heart, liver, lung, and pancreas. Each sphere represents one sample. For visualization purposes, ellipsoids which encompass 95% of the samples per group were added. Criterion for differential expression is a qFDR <0.01 after expression filter (see "Materials and methods"). *Number before bracket* is the number of MARGS genes with qFDR <0.01, the *number inside the bracket* is the number of MARGS represented on the array platform

tion from this analysis, we applied a more permissive qFDR cutoff.

Eighty-five MARGS in kidney cortex were compared to 40 MARGS in heart fibrosis, 48 MARGS in liver fibrosis, 110 MARGS in lung fibrosis, and 78 MARGS in pancreas fibrosis (Fig. 2a). The set union formed by all five datasets consisted of tissue inhibitor of metalloproteinase 1 (TIMP1) and hypoxia upregulated protein 1 (HYOU1). The analyses revealed that 14 MARGS were only deregulated in kidney fibrosis, whereas 25 genes were identified to be solely deregulated in lung fibrosis, two genes in heart fibrosis, seven genes in liver fibrosis, and 11 in pancreas fibrosis (Fig. 2b). Nine genes were differentially expressed in kidney cortex, liver, lung, heart, and pancreas, but not in liver. These genes were collagen, type I, alpha 1 (COL1A1), collagen type I, alpha 2 (COL1A2), collagen type III, alpha 1 (COL3A1), matrix metallopeptidase 2 (MMP2), secreted protein, acidic, cysteine-rich (SPARC), thrombospondin 2 (THBS2), thrombospondin 3 (THBS3), TIMP metallopeptidase inhibitor 3 (TIMP3), and vascular endothelial growth factor C (VEGFC). Genes belonging to the family of thrombospondins (THBS) were deregulated in each organ. THBS2, previously identified as IF/TA marker in kidney allograft biopsies (1), was deregulated in fibrosis of all organs but liver. Here, the family member THBS1 was deregulated. MMP7, besides THBS2, another candidate as IF/TA marker, showed deregulation in kidney, pancreas, and lung fibrosis but not in liver and heart (Fig. 2b).

Cross-organ deregulated MARGS are confirmed in independent patient samples

From the list of 11 MARGS which were differentially expressed in all organs or all organs but liver, and from results of our previous studies [1], we selected seven MARGS for confirmation analyses: THBS2, TIMP1, COL1A2, COL3A1, HYOU1, MMP2, and MMP7. As control genes served two genes which had a coefficient of variation less than 7.5 % in each dataset, heterogeneous nuclear ribonucleoprotein U (HNRNPU) and paxillin (PXN). Archival biopsy specimens of patients with

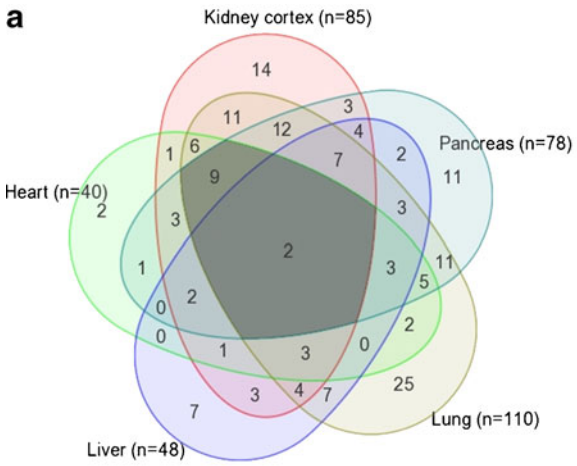

b

set-union	all but liver	Kidney only	Heart only	Liver only	Lung only	Pancreas only
HYOU1	COL1A1	EMILIN3	HIF3A	ADAMTS18	ADAM12	ADAM8
TIMP1	COL1A2	RELT	MMP17	MMP26	ADAM20	CD44
	COL3A1	ADAM29		NFKB2	ADAM23	COL2A1
	MMP2	ADAMTS10		THSD1	ADAM28	FAS
	SPARC	ADAMTS12		TNFRSF10D	ADAMDEC1	ITGB1
	THBS2	ADAMTS13		TNFSF14	ADAMTS14	LAMB3
	THBS3	FBN3		TNFSF9	ADAMTS19	LAMC2
	TIMP3	MMP24			ADAMTS3	MEP1B
	VEGFC	NFKB1			ADAMTS6	MMP8
		PRG3			ADAMTS8	TGFB2
		TNFRSF10A			ADAMTSL2	TNF
		TNFRSF13B			COL4A6	
		TNFRSF25			EMILIN1	
		TNFSF13			EMILIN2	
					MMP21	
					MMP3	
					RSPO3	
					TLL2	
					TNFRSF11B	
					TNFRSF19	
					TNFRSF6B	
					TNSFS11	
					TNSRSF10C	
					TNSRSF18	
					YBX1	

Fig. 2 Differentially expressed MARGS in fibrosis datasets. **a** Five-way Venn diagram identifies two MARGS genes which are differentially expressed in all five datasets. Nine additional MARGS are differentially expressed in all datasets but liver (*shaded fields*). Criterion for differential expression is a qFDR <0.1 and passing an expression filter (see "Materials and methods"). **b** Gene lists from Venn diagram. Genes which were selected for confirmation analyses are *underlined*. In addition, MMP7 was selected based on previous findings (see main text). MMP7 was differentially expressed in kidney, lung, and pancreas microarray datasets (not shown)

matched histological diagnosis to microarrays served as RNA source (Table 2, "Materials and methods").

Of 28 confirmation tests in kidney cortex, heart, lung, and pancreas, 25 (89%) confirmed the direction of expression changes observed in the microarray datasets (Fig. 3a). Of the three which could not be confirmed, MMP7 was expressed at low levels in the heart microarray dataset and had not passed the qFDR filter. The other two tests which failed were COL3A1 in kidney cortex and TIMP1 in pancreas.

THBS2 and MMP2 were upregulated in fibrosis of all organs. HYOU1 showed increased expression in fibrosis of kidney, liver, and lung, and showed decreased expression in heart and pancreas fibrosis. TIMP1 was upregulated in all organs except heart (Fig. 3a). The same pattern was observed for MMP7 with decreased expression only in heart fibrosis. Highest expression values in heart fibrosis were observed for COL3A1 and COL1A2 (fc vs. Normal 0.73 and 0.61, $\log_2$ scale, respectively). All candidate MARGS showed increased expression in pancreas, liver, and lung fibrosis; only in heart and kidney fibrosis decreased expression was identified for certain selected MARGS when compared to healthy tissue (Fig. 3a). As shown in Fig. 3b, TaqMan qRT–PCR data lead to cluster formation of in-house samples according to diagnosis in a PCA in all five tissues.

Interestingly, out of seven liver tests, only two could be confirmed, MMP7 and MMP2, where MMP2 had a small fold change in the microarray dataset (0.03, $\log_2$ scale). All candidate MARGS were upregulated in liver fibrosis in the in-house samples, while five of seven were downregulated in the microarray dataset.

Classifier analysis

We have previously shown in an in-house gene expression microarray dataset as well as other published datasets that a classifier model consisting of 19 MARGS in combination with Linear Discriminant Analysis decision algorithm can discriminate human renal allograft biopsies with interstitial fibrosis and tubular atrophy (IF/TA) from those without [1]. To test our hypothesis, that the same classifier panel could discriminate fibrosis of different etiology from non-fibrosis in non-transplant setting, we applied the published classifier to the microarray datasets, including internal leave-one-out cross-validation.

Without expression filter, the MARGS classifier list was applied to the datasets, along with the algorithm Linear Discriminant Analysis and full leave-one-out internal cross-validation. As not all MARGS of the classifier panel were represented on each platform, gene subsets of the classifier had to be used in some instances (Table 3). In kidney cortex, 18 of the 19 classifier MARGS could be used, in heart 15, in lung and liver all 19, and in pancreas 10 (Supplementary Table TS2). As can be seen in Table 3, the performance estimate "area under the ROC curve" (AUC) for the binary prediction of "fibrotic" or "healthy" exceeded 0.78 in each dataset. The mean AUC was 0.872. The mean accuracy was 88%. The best classification rate was achieved in kidney cortex, where all samples were correctly classified; the lowest performance was measured with the liver dataset where the correct classification rate was 72.7% (AUC=0.786). The significance of the AUC was estimated by bootstrapping (seed=100,000). A lower limit of the 95th

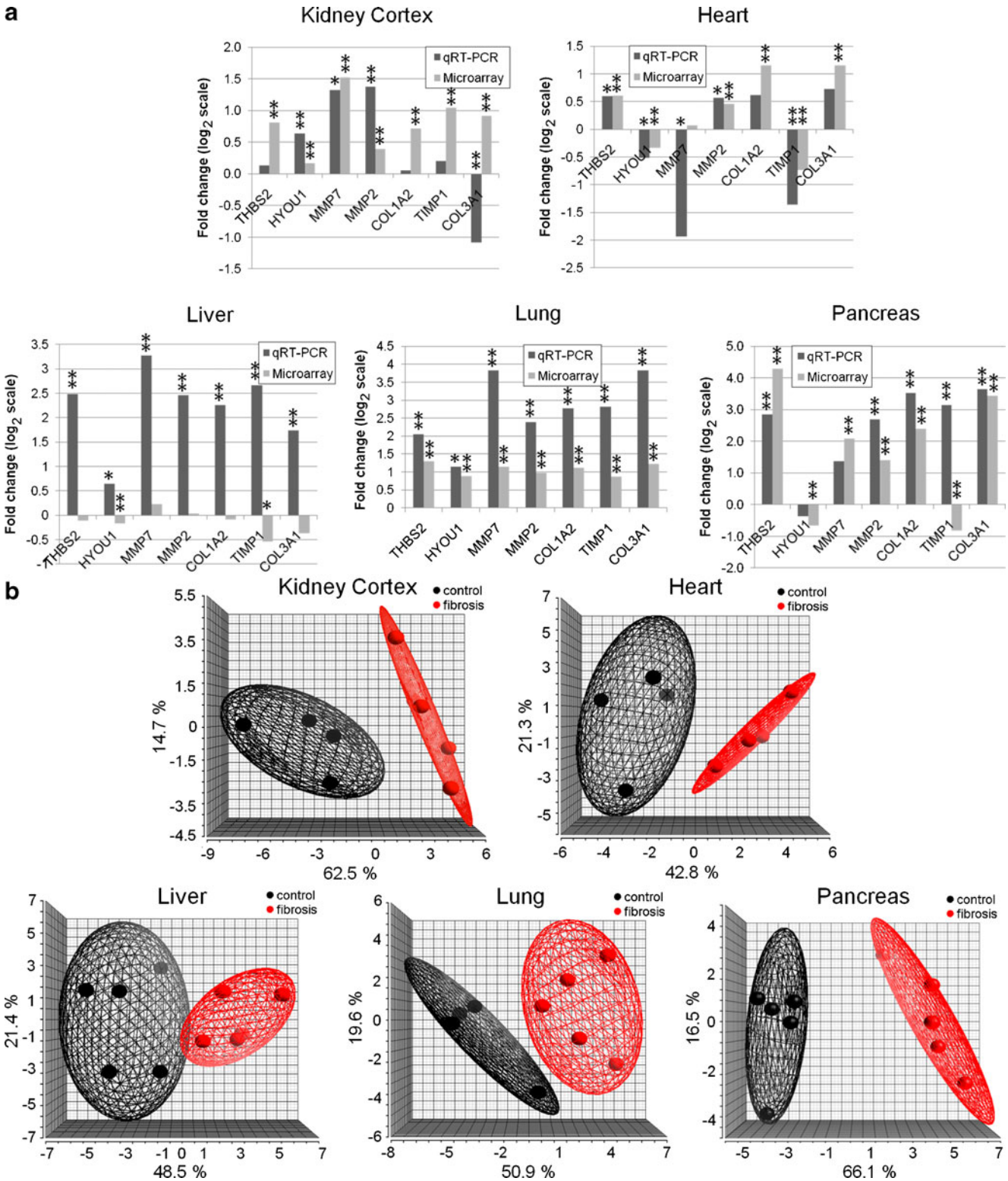

Fig. 3 TaqMan RT–PCR confirmation of microarray data in independent sample sets. **a** TaqMan qRT–PCR confirmation of seven MARGS genes in five tissues. In kidney, heart, lung, and pancreas, 89% of the tests successfully confirmed the direction of expression changes. In liver, only two of seven tests were successful. TaqMan qRT–PCR: *$p<0.1$, **$p<0.05$; microarray: *qFDR value<0.1, qFDR value<0.05. **b** Principal component analysis of normalized TaqMan qRT–PCR values of seven MARGS. In an unsupervised analysis, the expression values of the genes separate the tissue samples in each comparison by diagnosis. Each sphere represents one sample. For visualization purposes, ellipsoids which encompass 95% of the samples per group were added

Table 3 IF/TA classifier performance in microarray studies

Organ	Number of samples (total/fibrosis/control)	Fibrosis correct classification	Control correct classification	Number of variables	Sensitivity (%)	Specificity (%)	ACC	AUC	AUC 95% CI	Chi square	Chi-square *p* value
(a) Individual performance estimation of the classifier in each dataset separately											
Kidney cortex	27/11/11	11 (of 11)	16 (of 16)	18	100	100	1.00	1.00	1.00–1.00	27	2.04E−07
Heart	210/194/16	186 (of 194)	13 (of 16)	15	96	81	0.95	0.89	0.77–0.98	97.7	4.90E−23
Liver	22/14/8	8 (of 14)	8 (of 8)	19	57	100	0.73	0.79	0.67–0.92	7.2	7.00E−23
Lung	46/31/15	26 (of 31)	12 (of 15)	19	84	80	0.83	0.82	0.70–0.94	17.7	2.00E−05
Pancreas	20/15/5	14 (of 15)	4 (of 5)	10	93	80	0.90	0.87	0.63–1.00	10.8	1.00E−03
Mean					86	88	0.88	0.87			
(b) Cross-organ, cross-platform performance estimation of the classifier in the merged dataset											
Cross-platform, cross-organ, integrated	325/265/60	241 (of 265)	44 (of 60)	10	91	73	0.88	0.82	0.76–0.88	122.2	2.12E−28

ACC accuracy, *AUC* area under the ROC curve

percentile confidence interval larger than 0.5 indicates that the model performance is significantly better than random. This is the case in all analyses. A chi-square p value <0.5 indicates a significant dependence of the actual and the predicted values. In all tests, the chi-square p value is smaller than 0.5.

Next we integrated all five datasets across tissue and platform to obtain a set with 265 fibrosis samples and 65 control samples (Table 3). Due to the integration of the pancreas dataset, only 10 MARGS genes could be used in this approach: CD44, THBS2, VEGFA, PLG, TNFAIP3, LAMB1, TNFSF10, COL3A1, THBS1, and MGP. Despite these limitations, the classifier performance reached a significant AUC of 0.82 and an accuracy of 88%.

Discussion

Genes comprising the MARGS gene set are known to be involved in remodeling of ECM under healthy and disease conditions [13–16]. It is therefore conceivable that they play important roles in fibrotic/sclerotic conditions in organs, which may result in response to tissue injury, or as progression of age. Along those lines, differential expression of hypoxia-regulated genes, such as HYOU1 (hypoxia up-regulated 1), HIF1-target gene TIMP1 in all datasets, and THBS2, MMPs and collagens I and III in all but the liver microarray dataset are in correspondence with earlier findings which showed an involvement of hypoxia in fibrosis (kidney [17, 18], pancreas [19], lung [20, 21], heart [22–24], liver [25–27]).

We were able to validate the gene expression trends we saw in kidney, heart, lung, and pancreas in 89% (25 of 28 tests) of the TaqMan qRT–PCR tests using archival tissue specimens, which is an exceptionally high rate considering that all sample sets were completely independent. Confirmation results were unsatisfactory for the liver microarray data (Fig. 3a), where five of seven tests failed to validate the microarray data, although the TaqMan data themselves were significantly different between healthy and fibrotic samples (Fig. 3a, b). Compared to the datasets of the other organs, only few MARGS in the liver dataset had qFDR values <0.01 (Fig. 1). In our own analysis of the liver microarray data, we observed similar trends of gene expression changes as the Utsunomiya group and confirm the importance of inflammatory genes in that dataset (not shown). We found that most MARGS were in fact underrepresented in the fibrosis group (not shown), while proinflammatory genes were largely overrepresented and correlated with the adjusted MFI fibrosis grade, as published [9]. Recently, the group of Takahara has shown in gene expression studies of fibrosis in HCV patients that ECM modulatory genes in general positively correlate with

the METAVIR F-score 1 through 4, and some genes had peak expression changes in fibrosis score 2 and 3 [28]. In accordance with these data, we observe similar trends in expression changes with MARGS ECM genes when we use the categorical average METAVIR F-score instead of the continuous adjusted MFI; however, the qFDR values for the individual genes increase (not shown). We do not obtain a better correlation of TaqMan qRT–PCR and microarray data in terms of trends of "over- and under-representation" when we use the METAVIR F-score annotation of the microarray data. We believe that the differences between the microarray data of Utsunomiya's group and the Inselspital TaqMan qRT–PCR data may reveal differences in etiology or be of other clinical or biological origin which was impossible to capture from the annotations at hand despite our efforts to match our patient groups as much as possible with the published samples. The increases in, e.g., MMP2 and collagens type I and III that we observe in TaqMan qRT–PCR data match well with published findings (see [29] for review). Separately, the two analyses revealed significant differences for MARGS between liver fibrosis and healthy groups, leading to a separation of the sample groups in PCA of the microarray data and of the TaqMan qRT–PCR data (Figs. 1 and 3, respectively).

Let us consider two major valid methods of identifying molecular markers, e.g., gene expression panels in combination with a decision algorithm. One method, let us use the term "gene-to-biology-method", essentially employs testing of all features on a technology platform (such as microarrays) and then, once the feature panel has been identified, links to the biology and pathways underlying the studied disease. While in theory it is not given that genes, or generally speaking, features, of a classifier which has been identified in an unbiased way are involved in the disease biology, in practice many researchers and clinicians feel much more comfortable with the classifier panel if they do, as it is intuitively plausible [30]. In our studies, we have employed another method, a "biology-to-gene-method". We first considered the biology of the diseases or complications we were interested in, used literature searches and knowledge to assemble a list of genes which play important roles in that biology, and asked whether those genes could serve as the starting gene list to generate a classifier panel. Hence, we easily linked the biology of fibrosis, post-transplant or in other etiologies, with molecular markers (the MARGS).

We previously showed that a subset of MARGS can be used to discriminate human renal allograft biopsy samples with IF/TA from non-IF/TA samples [1]. In the present study, we demonstrate that the IF/TA MARGS transcriptomics classifier panel also classifies solid organ fibrotic conditions of human aging kidney, cardiac failure, hepatic cirrhosis, pulmonary fibrosis, and pancreatitis tissue samples with high accuracy, AUC, specificity, and sensitivity (the sensitivity for the liver dataset was exceptionally low and the reason remains uncertain). Our studies suggest that the MARGS classifier is a valid candidate for a cross-platform, cross-organ classifier of normal tissue vs. fibrotic conditions of different etiologies. Obvious next steps are the application of the classifier to blood sample gene expression data, to see whether a minimally invasive, easily applicable gene expression marker could accompany or outperform other minimally and non-invasive methods [31–34]. Given that, e.g., plasma levels of TIMP1 protein have been found elevated in diastolic dysfunction [35], transfer of our data to, for instance, peripheral blood appears promising. From a clinical perspective, the MARGS classifier may be used to detect fibrosis prior to the development of irreversible tissue sclerosis, and thus enhance organ preservation through treatment adjustment. The classifier should be tested for its ability to diagnose fibrosis at a very early time point, ideally before fibrosis is visible on tissue sections and therapy is still most effective. In this respect, it will be interesting to test the classifier for its ability to be utilized to monitor drug effects. Future work will tell if some of the genes present in the MARGS panel represent therapeutic targets.

Acknowledgments This work was supported by Grant No. 32003B-114054 to Hans-Peter Marti from the Swiss National Science Foundation (SNSF).

We are grateful to Dr. Simeone and Dr. Logsdon for providing the pancreas dataset, and Dr. Utsunomiya and Dr. Mori for providing the liver dataset.

Conflict of interest statement We declare that we have no conflict of interest

Funding Grant Nr. 32003B-114054 to Hans-Peter Marti from the Swiss National Science Foundation (SNSF)

References

1. Roedder S, Scherer A, Raulf F, Berthier CC, Hertig A, Couzi L, Durrbach A, Rondeau E, Marti HP (2009) Renal allografts with IF/TA display distinct expression profiles of metzincins and related genes. Am J Transplant 9:517–526
2. Meneghin A, Hogaboam CM (2007) Infectious disease, the innate immune response, and fibrosis. J Clin Invest 117:530–538
3. Selman M, King TE, Pardo A (2001) Idiopathic pulmonary fibrosis: prevailing and evolving hypotheses about its pathogenesis and implications for therapy. Ann Intern Med 134:136–151
4. Nagase H, Woessner JF Jr (1999) Matrix metalloproteinases. J Biol Chem 274:21491–21494
5. Woessner JF Jr, Gunja-Smith Z (1991) Role of metalloproteinases in human osteoarthritis. J Rheumatol Suppl 27:99–101
6. Rodwell GE, Sonu R, Zahn JM, Lund J, Wilhelmy J, Wang L, Xiao W, Mindrinos M, Crane E, Segal E, Myers BD, Brooks JD, Davis RW, Higgins J, Owen AB, Kim SK (2004) A

transcriptional profile of aging in the human kidney. PLoS Biol 2:e427
7. Hannenhalli S, Putt ME, Gilmore JM, Wang J, Parmacek MS, Epstein JA, Morrisey EE, Margulies KB, Cappola TP (2006) Transcriptional genomics associates FOX transcription factors with human heart failure. Circulation 114:1269–1276
8. Konishi K, Gibson KF, Lindell KO, Richards TJ, Zhang Y, Dhir R, Bisceglia M, Gilbert S, Yousem SA, Song JW, Kim DS, Kaminski N (2009) Gene expression profiles of acute exacerbations of idiopathic pulmonary fibrosis. Am J Respir Crit Care Med 180:167–175
9. Utsunomiya T, Okamoto M, Wakiyama S, Hashimoto M, Fukuzawa K, Ezaki T, Aishima S, Yoshikawa Y, Hanai T, Inoue H, Barnard GF, Mori M (2007) A specific gene-expression signature quantifies the degree of hepatic fibrosis in patients with chronic liver disease. World J Gastroenterol 13:383–390
10. Binkley CE, Zhang L, Greenson JK, Giordano TJ, Kuick R, Misek D, Hanash S, Logsdon CD, Simeone DM (2004) The molecular basis of pancreatic fibrosis: common stromal gene expression in chronic pancreatitis and pancreatic adenocarcinoma. Pancreas 29:254–263
11. Sing T, Sander O, Beerenwinkel N, Lengauer T (2005) ROCR: visualizing classifier performance in R. Bioinformatics 21:3940–3941
12. Vandesompele J, De PK, Pattyn F, Poppe B, Van RN, De PA, Speleman F (2002) Accurate normalization of real-time quantitative RT–PCR data by geometric averaging of multiple internal control genes. Genome Biol 3:RESEARCH0034
13. Zaoui P, Cantin JF, Alimardani-Bessette M, Monier F, Halimi S, Morel F, Cordonnier D (2000) Role of metalloproteases and inhibitors in the occurrence and progression of diabetic renal lesions. Diabetes Metab 26(Suppl 4):25–29
14. Klein T, Bischoff R (2010) Physiology and pathophysiology of matrix metalloproteases. Amino Acids. doi:10.1007/s00726-010-0689-x
15. Klein T, Geurink P, Overkleeft S, Kauffman K, Bischoff R (2009) Functional proteomics on zinc-dependent metalloproteinases using inhibitor probes. ChemMedChem 4:164–170
16. Berthier CC, Pally C, Weckbecker G, Raulf F, Rehrauer H, Wagner U, Le HM, Marti HP (2009) Experimental heart transplantation: effect of cyclosporine on expression and activity of metzincins. Swiss Med Wkly 139:233–240
17. Tanaka T, Kato H, Kojima I, Ohse T, Son D, Tawakami T, Yatagawa T, Inagi R, Fujita T, Nangaku M (2006) Hypoxia and expression of hypoxia-inducible factor in the aging kidney. J Gerontol A Biol Sci Med Sci 61:795–805
18. Fine LG, Norman JT (2008) Chronic hypoxia as a mechanism of progression of chronic kidney diseases: from hypothesis to novel therapeutics. Kidney Int 74:867–872
19. Leung PS (2007) The physiology of a local renin–angiotensin system in the pancreas. J Physiol 580:31–37
20. Corte TJ, Wort SJ, Wells AU (2009) Pulmonary hypertension in idiopathic pulmonary fibrosis: a review. Sarcoidosis Vasc Diffuse Lung Dis 26:7–19
21. Zhou G, Dada LA, Wu M, Kelly A, Trejo H, Zhou Q, Varga J, Sznajder JI (2009) Hypoxia-induced alveolar epithelial–mesenchymal transition requires mitochondrial ROS and hypoxia-inducible factor 1. Am J Physiol Lung Cell Mol Physiol 297: L1120–L1130
22. Tamamori M, Ito H, Hiroe M, Marumo F, Hata RI (1997) Stimulation of collagen synthesis in rat cardiac fibroblasts by exposure to hypoxic culture conditions and suppression of the effect by natriuretic peptides. Cell Biol Int 21:175–180
23. de Boer RA, Pinto YM, van Veldhuisen DJ (2003) The imbalance between oxygen demand and supply as a potential mechanism in the pathophysiology of heart failure: the role of microvascular growth and abnormalities. Microcirculation 10:113–126
24. Gramley F, Lorenzen J, Jedamzik B, Gatter K, Koellensperger E, Munzel T, Pezzella F (2010) Atrial fibrillation is associated with cardiac hypoxia. Cardiovasc Pathol 19:102–111
25. Rosmorduc O, Housset C (2010) Hypoxia: a link between fibrogenesis, angiogenesis, and carcinogenesis in liver disease. Semin Liver Dis 30:258–270
26. Copple BL, Bai S, Moon JO (2010) Hypoxia-inducible factor-dependent production of profibrotic mediators by hypoxic Kupffer cells. Hepatol Res 40:530–539
27. Corpechot C, Barbu V, Wendum D, Kinnman N, Rey C, Poupon R, Housset C, Rosmorduc O (2002) Hypoxia-induced VEGF and collagen I expressions are associated with angiogenesis and fibrogenesis in experimental cirrhosis. Hepatology 35:1010–1021
28. Takahara Y, Takahashi M, Zhang QW, Wagatsuma H, Mori M, Tamori A, Shiomi S, Nishiguchi S (2008) Serial changes in expression of functionally clustered genes in progression of liver fibrosis in hepatitis C patients. World J Gastroenterol 14:2010–2022
29. Hui AY, Friedman SL (2003) Molecular basis of hepatic fibrosis. Expert Rev Mol Med 5:1–23
30. Halloran PF, Reeve J, Kaplan B (2006) Lies, damn lies, and statistics: the perils of the P value. Am J Transplant 6:10–11
31. Korosoglou G, Humpert PM (2007) Non-invasive diagnostic imaging techniques as a window into the diabetic heart: a review of experimental and clinical data. Exp Clin Endocrinol Diabetes 115:211–220
32. Tatsumi C, Kudo M, Ueshima K, Kitai S, Ishikawa E, Yada N, Hagiwara S, Inoue T, Minami Y, Chung H, Maekawa K, Fujimoto K, Kato M, Tonomura A, Mitake T, Shiina T (2010) Non-invasive evaluation of hepatic fibrosis for type C chronic hepatitis. Intervirology 53:76–81
33. Tham RT, Heyerman HG, Falke TH, Zwinderman AH, Bloem JL, Bakker W, Lamers CB (1991) Cystic fibrosis: MR imaging of the pancreas. Radiology 179:183–186
34. van den Blink B, Wijsenbeek MS, Hoogsteden HC (2010) Serum biomarkers in idiopathic pulmonary fibrosis. Pulm Pharmacol Ther 23:515–520
35. Ahmed SH, Clark LL, Pennington WR, Webb CS, Bonnema DD, Leonardi AH, McClure CD, Spinale FG, Zile MR (2006) Matrix metalloproteinases/tissue inhibitors of metalloproteinases: relationship between changes in proteolytic determinants of matrix composition and structural, functional, and clinical manifestations of hypertensive heart disease. Circulation 113:2089–2096

Virchows Arch (2011) 458:497–503
DOI 10.1007/s00428-010-1011-8

CASE REPORT

Combined small-cell carcinoma of the lung with quadripartite differentiation of epithelial, neuroendocrine, skeletal muscle, and myofibroblastic type

Giuseppe Pelosi · Angelica Sonzogni · Domenico Galetta · Federica Perrone · Paola Braidotti · Michela Manzotti · Alessandra Fabbri · Lorenzo Spaggiari · Giulia Veronesi · Giuseppe Viale

Received: 16 October 2010 / Revised: 7 November 2010 / Accepted: 8 November 2010 / Published online: 6 January 2011
© Springer-Verlag 2010

Abstract The combined variant of small-cell lung carcinoma (SCLC) refers to the variable admixture of small cell and non-small cell carcinoma, whereas the association with sarcoma or sarcoma-like elements is exceedingly rare. A 76-year-old Caucasian man underwent right upper lobectomy with regional lymphadenectomy because of a symptomatic 7 cm-sized tumor mass. Formalin fixed-paraffin embedded material was used to highlight several differentiation cell lineages by means of immunohistochemistry, electron microscopy, and mutational assay. The tumor was discovered as being IIB stage (pT2b $pN1_{1/51}$ pM0) and featured biphasic appearance with close intermingling of SCLC (40%) and collagen-rich spindle cell sarcoma (60%). Epithelial (cytokeratins, TTF-1), neural (neurofilaments, GFAP), endocrine (chromogranin, synaptophysin, CD56), and skeletal muscle (desmin, sarcomeric actin, myogenin) markers were variably co-expressed by SCLC elements, whereas mesenchymal (vimentin), smooth muscle (actin, myosin, H-caldesmon, calponin), fibroblastic (CD10), and, more focally, skeletal muscle (desmin, sarcomeric actin and myogenin) markers were highlighted in the spindle cell sarcoma elements. *TP53* codon V274F mutation in exon 8 was shared by either cell component. After undergoing adjuvant chemotherapy, the patient is currently alive and well at the 40-month follow-up. To the best of our knowledge, this is the first report of combined SCLC with quadripartite differentiation of epithelial, neuroendocrine, skeletal muscle, and myofibroblastic type, somewhere at the level of the same individual tumor cells. This tumor had probably derived for clonal evolution of a *p53*-mutated common ancestor lesion.

Keywords SCLC · Sarcoma · Immunohistochemistry · Mutation · Electron microscopy

G. Pelosi · A. Sonzogni · M. Manzotti · G. Viale
Division of Pathology and Laboratory Medicine,
European Institute of Oncology,
Milan, Italy

G. Pelosi · P. Braidotti · L. Spaggiari · G. Viale
Department of Medicine, Surgery and Dentistry,
San Paolo Hospital, University of Milan School of Medicine,
Milan, Italy

D. Galetta · L. Spaggiari · G. Veronesi
Division of Thoracic Surgery, European Institute of Oncology,
Milan, Italy

G. Pelosi · F. Perrone · A. Fabbri
Department of Pathology and Laboratory Medicine,
Fondazione IRCCS National Cancer Institute,
Milan, Italy

P. Braidotti
Fondazione IRCCS Policlinico, Mangiagalli and Regina Elena,
Milan, Italy

G. Pelosi (✉)
Dipartimento di Patologia Diagnostica e Laboratorio,
Fondazione IRCCS Istituto Nazionale Tumori,
Via G. Venezian, 1,
20133, Milan, Italy
e-mail: giuseppe.pelosi@istitutotumori.mi.it

Introduction

As many as one third of small cell lung carcinomas (SCLC) are associated with non-small cell lung carcinoma (NSCLC) elements, mainly featuring large cell neuroendocrine carcinoma (LCNEC), adenocarcinoma or squamous cell carcinoma in that order [1]. This association solidifies

the so-called combined variant of SCLC under WHO-2004 classification criteria on lung cancer [2]. In this frame of mind, the combination with sarcoma or sarcoma-like elements is deemed to be exceedingly rare, probably reflecting the inherent rareness of pulmonary sarcomatoid carcinomas, which account for by far less than 5% of all NSCLC [3]. While diverse variations on the theme of combined small cell carcinoma with sarcoma or sarcoma-like elements have been described in the English literature [4–11], quadripartite differentiation clustering epithelial, neuroendocrine, skeletal muscle, and smooth muscle/myofibroblastic features has not thus far been reported in the lung, to the best of our knowledge.

Clinical history

A 76-year-old Caucasian man, former smoker since 30 years after consuming 30 cigarettes per day for 20 years, underwent left upper lobectomy for Aspergillus-related fungus ball in 1980. Clinical history also included diabetes mellitus, urolithiasis, polyps of the vocal cords, cataract, subphrenic abscess after spontaneous right pneumothorax and anal fissures. In 2003, the patient complained of hemoptysis for granulomatous inflammation of the left main bronchus (likely due to the previous surgery), which was treated conservatively with LASER cauterization. In 2007, he suffered again from hemoptysis with thoracic pain and a chest X ray examination showed a huge tumor mass in the right upper lobe. A chest CT scan confirmed a 67×48×50-mm-sized tumor mass, which was close to both pleural layers and azygos vein. Pleural effusion was lacking. As PET scan with radio-labeled [^{18}F]-2-fluoro-2-deoxy-D-glucose (FDG) denied distant metastases, a right upper lobectomy along with complete hilar-mediastinal lymphadenectomy was performed: the final tumor stage was pT2b pN$1_{1/51}$ pM0 (IIB) according to the seventh edition of TNM system. The patient underwent adjuvant chemotherapy with cisplatin and etoposide. At the 40-month follow-up, he is alive and well with no signs of local recurrences or distant metastases.

Material and methods

The investigation was carried out upon formalin-fixed, paraffin-embedded material by using the antibodies listed in Table 1 according to previously refined immunohistochemical methods. Moreover, an electron microscopic study was accomplished upon formalin-fixed tissue fragments, which were washed in phosphate buffer, post-fixed in 2.5% glutaraldehyde solution (0.13 M, pH 7.3), reacted with 1% buffered osmium tetroxide, dehydrated through graded alcohols and propylen oxide, embedded in epoxy resin, counterstained with uranyl acetate and lead citrate and then examined with a Jeol JEM 1010 (Jeol, Tokyo, Japan) transmission electron microscope.

Results

The tumor measured 7 cm in its greatest dimension, did not attain the pleura layers and azygos vein and featured biphasic epithelial/sarcomatous appearance with intimate intermingling of small cell carcinoma (40%) and spindle cell sarcoma (60%) components. Small cells had a variable amount of eosinophilic to fairly clear cytoplasm, ill-defined cell borders and finely granular and even chromatin with inconspicuous nucleoli (Fig. 1). Less than 10% tumor cells showed vesicular chromatin and more evident nucleoli. Small cells were round or oval to spindle, somewhere also arranged in neuroendocrine rosettes, and clustered into nests, trabeculae or solid aggregates with peripheral palisading and nuclear molding. The predominant sarcoma component comprised spindle to pleomorphic or multinucleated cells with abundant collagen deposition. Plentiful were mitotic figures, as well as abundant the tumor necrosis with geographic configuration (Fig. 1). Immunohistochemical results are detailed in Table 1 and depicted in Fig. 2. The small cell carcinoma component exhibited positivity for cytokeratins with dot-like quality (both AE1-AE3 clone and cytocheratin 7), synaptophysin, CD56, TTF-1, and, focally, chromogranin B, S-100 protein, GFAP, neurofilaments, sarcomeric actin and desmin, whereas immunoreactivity for vimentin, smooth-muscle actin and myosin, CD10, calponin, H-caldesmon, desmin, myogenin and CD56 was found to variable extent in the spindle cell sarcoma component, which focally resembled rhabdomyoblasts (Fig. 2). Completely negative were cytokeratin 5/6, CD34 and chromogranin A immunolabeling in both tumor components. Remarkably, cytokeratins (AE1-AE3 and 7) and myogenin co-localized in the same aggregates of small cell carcinoma, with minor contribution of desmin and sarcomeric actin that was only seen in scattered tumor cells inside these aggregates. Proliferative activity evaluated by Ki-67 immunoreactivity showed 80–90% labeling index in small cell carcinoma and 40–50% in spindle cell sarcoma. Finally, p53 staining was detected in almost all tumors cells of both components as a strong nuclear decoration. Electron microscopy study indicated that the spindle cell sarcoma exhibited myofibroblastic differentiation with cytoplasmic processes and huge collagen fiber deposition, whereas small cell carcinoma showed paranuclear cytokeratin filaments, abnormal rough endoplasmic reticulum, dense-core neuroendocrine granules and, less frequently, abortive Z bands reminiscent of rhabdomyoblastic differentiation

Table 1 Antibody panel used in the current study and results of immunostaining in either tumor cell component

Antibodies	Clone	Source	Dilution	Pretreatment	Small cell carcinoma	Spindle cell sarcoma
Acidic and basic cytokeratins	AE1-AE3	Novocastra Laboratories, Newcastle upon Tyne, UK	1:50	MWO-CB	+++ (dot-like)	−
Calponin	CALP	DAKO, Glostrup, Denmark	1:400	MWO-EDTA	−	++
CD10	56C5	Novocastra Laboratories, Newcastle upon Tyne, UK	1:10	MWO-EDTA	−	+
CD34	QBEnd/10	Novocastra Laboratories, Newcastle upon Tyne, UK	1:400	MWO-CB	−	−
CD56	123C3.D5	NeoMarkers, Fremont, CA	1:400	MWO-EDTA	+++	+++
Chromogranin A	LK2H10	DAKO, Glostrup, Denmark	1:40	with and without MWO-CB	−	−
Chromogranin B	polyclonal	Santa Cruz Biotechnology, Santa Cruz, CA	1:2,000	MWO-CB	+	−
Cytokeratin 7	OV-TL 12/30	DAKO, Glostrup, Denmark	1:400	pepsin	++ (dot-like)	−
Cytokeratins 5/6	D5/16 B4	Chemicon International, Temecula, CA	1:400	MWO-EDTA	−	−
Desmin	D-33	DAKO, Glostrup, Denmark	1:50	MWO-CB	+	+
GFAP	polyclonal	DAKO, Glostrup, Denmark	1:400	none	+	−
H-caldesmon	h-CD	DAKO, Glostrup, Denmark	1:200	MWO-EDTA	−	++
Ki-67 antigen	MIB-1	DAKO, Glostrup, Denmark	1:200	MWO-EDTA	+++	++
Myogenin	F5D	DAKO, Glostrup, Denmark	1:800	MWO-EDTA	+++	+
Neurofilaments	NF68.04	NeoMarkers, Fremont, CA	1:100	MWO-CB	+	−
P53 protein	D07	Novocastra Laboratories, Newcastle upon Tyne, UK	1:400	MWO-EDTA	+++	+++
S-100 protein	polyclonal	DAKO, Glostrup, Denmark	1:1,600	none	+	−
Sarcomeric actin	5C5	Sigma-Aldrich, Saint Louis, MI	1:2,000	MWO-CB	+	+
Smooth muscle actin	1A4	DAKO, Glostrup, Denmark	1:200	none	−	+++
Smooth muscle myosin	SMMS-1	DAKO, Glostrup, Denmark	1:50	MWO-CB	−	+
Synaptophysin	SY38	DAKO, Glostrup, Denmark	1:20	MWO-EDTA	+++	−
TTF-1	8G7G3/1	NeoMarkers, Fremont, CA	1:1,000	MWO-EDTA	+++	−
Vimentin	V9	DAKO, Glostrup, Denmark	1:50	MWO-CB	−	+++

Pepsin digestion with 5% pepsin solution for 5 min;

MWO-CB: microwave oven at 750W for 30 min in citrate buffer pH6

MWO-EDTA: microwave oven at 750W for 30 min in EDTA buffer pH8

- : negative; + : < 10% postive tumor cell; ++ : 11-50% positive tumor cells; +++ : >50% positive tumor cells

(Fig. 3). Mutation analysis showed V274F substitution in exon 8 in both small cell carcinoma and spindle cell sarcoma components, after accurate microdissection under microscopic control (Fig. 4).

Discussion

The case described deals with a high-grade malignant tumor with quadripartite differentiation clustering epithelial (cytokeratins, TTF-1), neuro/endocrine (synaptophysin, chromogranin, CD56, GFAP, neurofilaments), skeletal muscle (desmin, myogenin, sarcomeric actin), and mesenchymal/myofibroblastic/smooth muscle (vimentin, smooth muscle actin and myosin, CD10, desmin, calponin, H-caldesmon) cell lineages. The final diagnosis was thus a descriptive one on the theme of SCLC, combined type, with skeletal muscle differentation and spindle cell sarcoma of myofibroblastic type. Worth mention was the widespread reactivity for CD56 (a sensitive but not specific marker of neuroendocrine differentiation) in the spindle cell sarcoma component, a feature which could be somewhat related to the reported distribution of the molecule in mesoderm during fetal life, rhabdomyosarcoma [12], leiomyosarcoma [13], sarcomatoid mesothelioma [14], or other biphasic tumors [15]. Combinations of small cell carcinoma with spindle cell [9, 11] or giant cell carcinoma [4, 8], small cell carcinoma plus adenocarcinoma and spindle-shaped cell tumor [7], small cell carcinoma plus squamous cell carcinoma and spindle cell carcinoma [6], or small cell carcinoma plus sarcomatoid carcinoma with either spindle cell or giant cell carcinoma [5] are exceedingly rare but

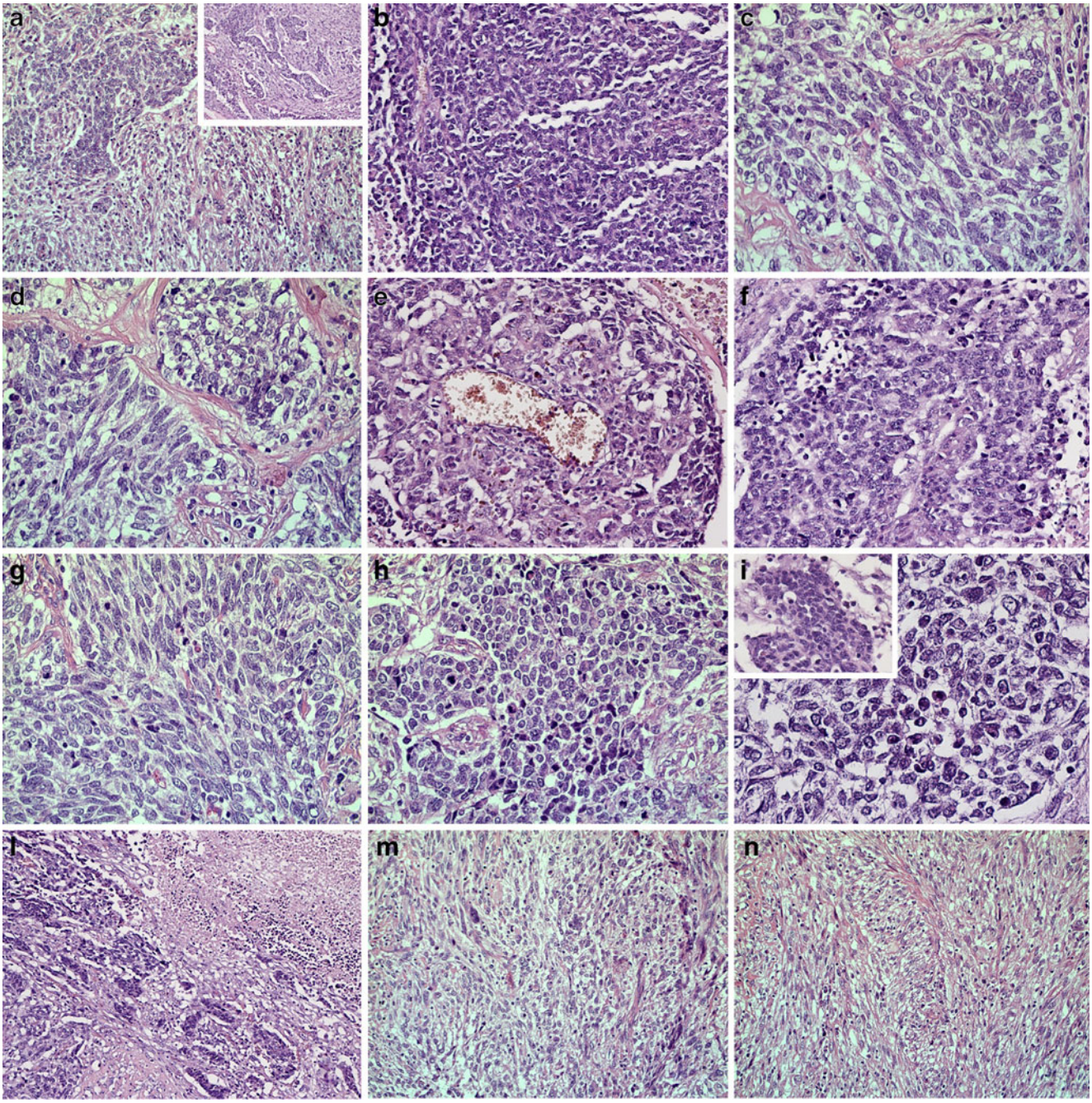

Fig. 1 **a**–**n** The tumor was biphasic (**a**), with intimate intermingling of both components (**a**, *inset*), and comprised small cells with scant cytoplasm (**b**), ill-defined cell borders (**c**), finely granular chromatin with inconspicuous nucleoli (**d**), which only in <10% tumor cells was vesicular with prominent nucleoli (**e**), round-oval shape with neuroendocrine rosettes (**f**, in the *center*) or spindled appearance (**g**), plentiful mitoses (**h**), and evident nuclear molding (**i**), and geographic necrosis (**l**). The spindle cell sarcoma component showed pleomorphic cells (**m**) and abundant collagen deposition (**n**)

well-known occurrences among combined variants of SCLC, as well as associations of atypical carcinoid plus rhabdomyosarcoma [10], carcinoid plus hamartoma [16, 17], carcinoid plus adenocarcinoma [18, 19], or incidental small neuroendocrine lesions resembling tumorlets in intrathoracic lymph nodes of patients with primary lung adenocarcinoma [20]. Intimate intermingling of small cell carcinoma and rhabdomyoblasts in the larynx [21], skin, nasal cavity, urinary bladder [22], and anorectal junction [23], as well as tripartite differentation in individual cells carcinomas with concurrent epidermoid, glandular, and neuroendocrine features in lung [24] or esophagus [25] or dipartite differentiation with rhabdomyogenous and cytokeratin expression within the same mesenchymal tumor

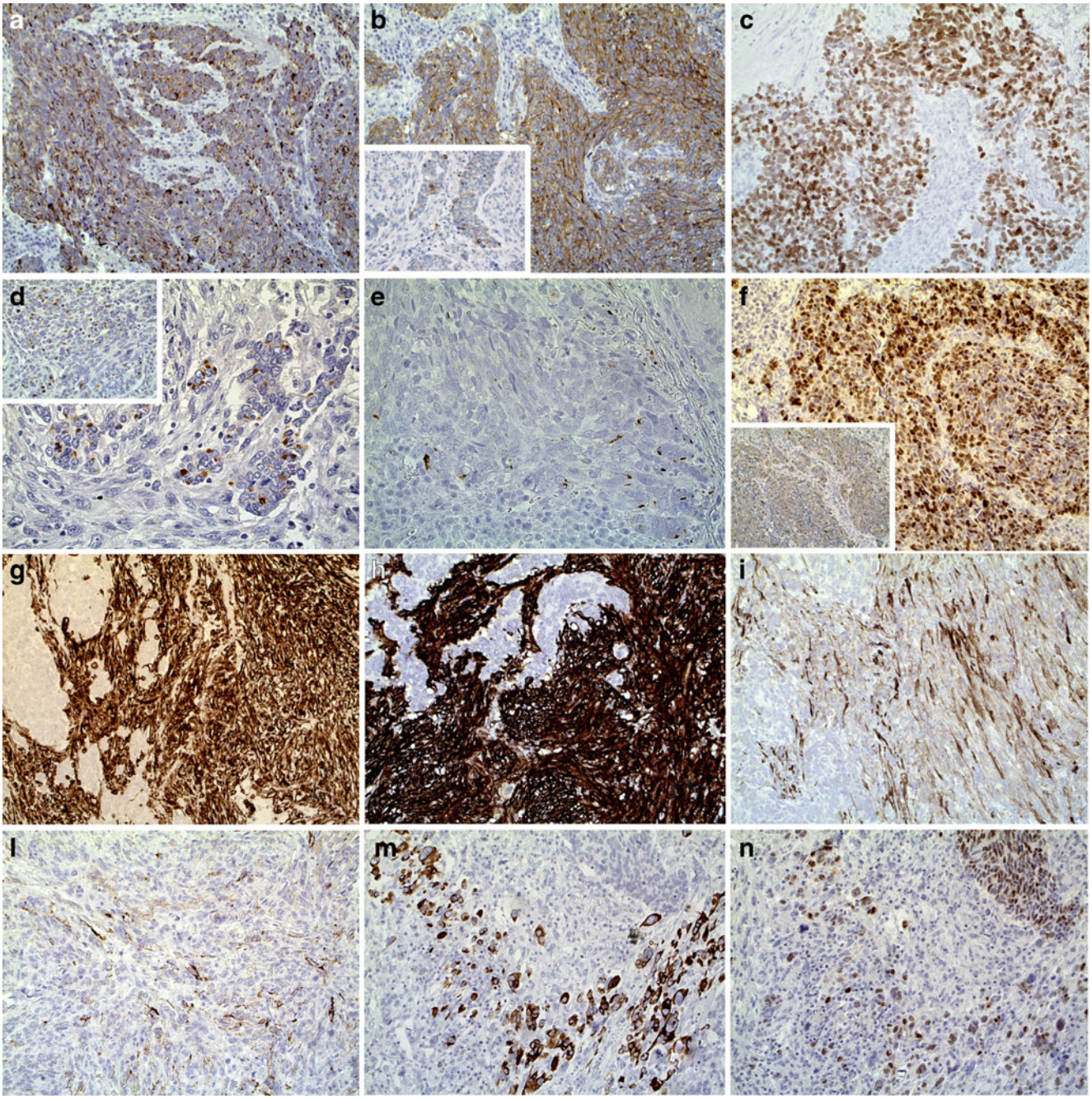

Fig. 2 **a**–**n** The small cell carcinoma component showed immunoreactivity for cytokeratins (**a**, clone AE1-AE3 with dot-like pattern), synaptophysin (**b**) and focally chromogranin B (**b**, *inset*), TTF-1 (**c**), GFAP (**d**), and neurofilaments (**d**, *inset*), desmin (**e**), and myogenin (**f**), the latter co-localized with cytokeratins in the same cell clusters (F, *inset*). The spindle cell sarcoma was immunolabeled for vimentin (**g**), smooth muscle actin (**h**), calponin (**i**), H-caldesmon (**l**), and, focally, featured rhabdomyoblasts highlighted by desmin (**m**) and myogenin (**n**)

cells in pulmonary carcinosarcomas [26] are likely to be further variants on the theme of multidirectional differentiation of common tumor ancestors.

The current case report, the first to highlight quadripartite differentiation inside a combined variant of SCLC, focused on epithelial, neuroendocrine and skeletal muscle cell lineages even at the level of individual cells, for the concurrent expression of these markers in the same tumor cells. Once excluded a collision tumor due to the close admixture of either type of components, the existence of different cell lineages was probably the result of the plasticity of a common proto-epithelial stem cell. This assumption was further supported by the strong p53 protein accumulation in SCLC and spindle cell sarcoma, as well as the same amino acidic substitution (V274F) in exon 8 of TP53 gene in either tumor component. These findings are

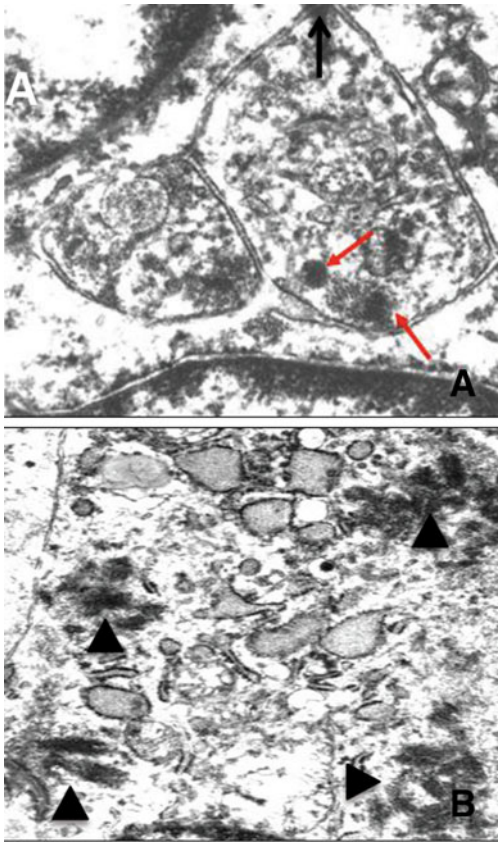

Fig. 3 **a**, **b** Electron microscopic features of epithelial tumor cells showing desmosomes (*black arrow*), dense-core granules of neuroendocrine type (*red arrows*) (**a**) and abortive Z bands reminiscent of rhabdomyoblastic differentiation (**b**, *black arrowheads*)

in keeping with the view that sarcomatous or sarcoma elements of pulmonary sarcomatoid carcinomas derive from carcinoma elements according to a process of sarcomatous metaplasia (conversion paradigm) during tumor progression rather than to be collision tumors [27–29]. In our case, the complete lack of epithelial differentiation in the spindle cell sarcoma component, which only focally retained rhabdomyoblastic features, made us hypothesize an almost complete myofibroblastic/smooth muscle transdifferentiation of carcinomatous cells rather than early divergence of the same ancestor lesion.

The differential diagnosis of this tumor included pleomorphic carcinoma because of its biphasic appearance, carcinosarcoma for the presence of heterologous elements, pulmonary metastasis of mixed mullerian malignant tumors with neuroendocrine differentiation for the immunoreactivity for CD10 and smooth muscle markers in spindle cell sarcoma [30] and the exceedingly rare primary pulmonary rhabdomyosarcoma in adults [31]. It is worth bearing in mind that the occurrence of neuroendocrine components in the form of SCLC and/or LCNEC in pulmonary carcinomas harboring sarcoma or sarcomatous components should be handled by regarding them as combined variants of either tumor with associated sarcoma or sarcoma-like elements rather than classifying them as pulmonary sarcomatoid carcinomas exhibiting small-cell and/or large cell neuroendocrine components [3]. The term carcinosarcoma should be discouraged despite the presence of a heterologous population, whether a high-grade neuroendocrine carcinoma of any amount is

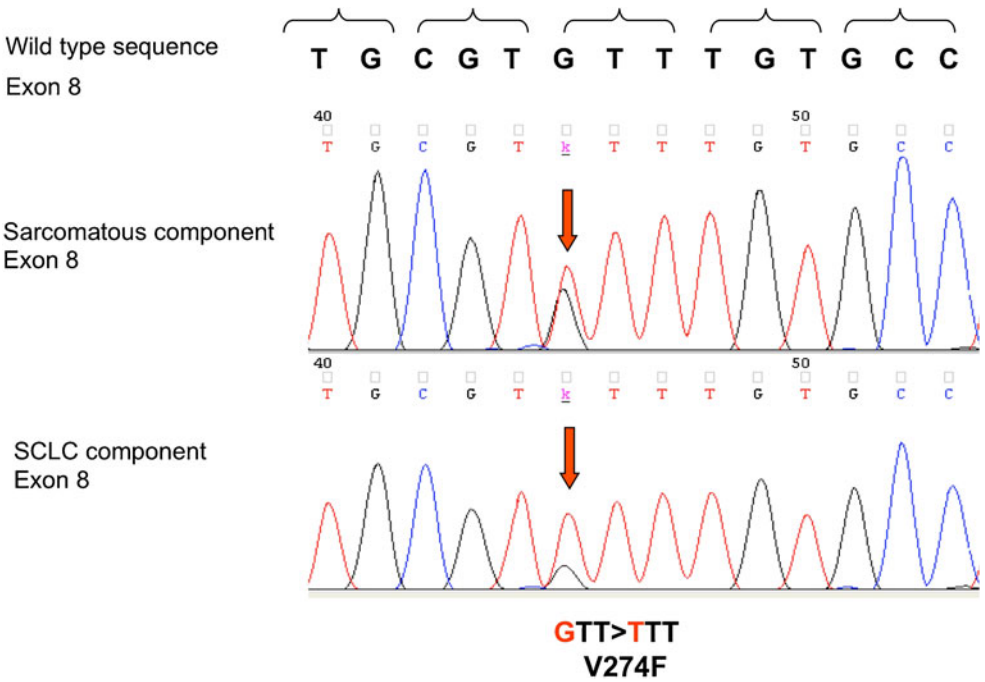

Fig. 4 Direct sequencing of PCR-amplified DNA of *TP53* exon 8 extracted from the SCLC and sarcomatous components after accurate microdissection: the same mutation (GTT>TTT, V274F) supports the tumor origin from a common ancestor lesion

recognizable [3]. Albeit more uncommonly, even LCNEC may bear a sarcomatoid component in the form of spindle cell carcinoma [32]: remarkably, however, the association with sarcoma featuring rhabdomyosarcoma is mainly limited to SCLC-containing tumors at least in the lung [33]. Adult primary pulmonary rhabdomyosarcoma are referred as negative for epithelial and neuroendocrine markers [31].

Acknowledgments This work is dedicated to the memory of Carlotta, an extraordinarily lively girl who untimely died of cancer in the prime of life.

Conflict of interest statement The authors declare that they have no conflicts of interest.

References

1. Nicholson SA, Beasley MB, Brambilla E, Hasleton PS, Colby TV, Sheppard MN, Falk R, Travis WD (2002) Small cell lung carcinoma (SCLC): a clinicopathologic study of 100 cases with surgical specimens. Am J Surg Pathol 26:1184–1197
2. Travis W, Brambilla E, Muller-Hermelink H, Harris C (2004) Tumours of the lung, pleura, thymus and heart. IARC, Lyon
3. Pelosi G, Sonzogni A, De Pas T, Galetta D, Veronesi G, Spaggiari L, Manzotti M, Fumagalli C, Bresaola E, Nappi O, Viale G, Rosai J (2010) Review article: pulmonary sarcomatoid carcinomas: a practical overview. Int J Surg Pathol 18:103–120
4. Bégin P, Sahai S, Wang N (1983) Giant cell formation in small cell carcinoma of the lung. Cancer 52:1875–1879
5. Fishback N, Travis W, Moran C, Guinee D, McCarty W, Koss M (1994) Pleomorphic (spindle/giant cell) carcinoma of the lung. A clinicopathologic correlation of 78 cases. Cancer 73:2936–2945
6. Gotoh M, Yamamoto Y, Huang C, Yokomise H (2004) A combined small cell carcinoma of the lung containing three components: small cell, spindle cell and squamous cell carcinoma. Eur J Cardiothorac Surg 26:1047–1049
7. Hsiao H, Tsai H, Liu Y, Tseng Y, Tseng S, Chai C, Lin S (2006) A rare case of combined small-cell lung cancer with unusual soft tissue metastasis. Kaohsiung J Med Sci 22:352–356
8. Müller K, Fisseler-Eckhoff A (1991) Small cell bronchial cancer–pathologic anatomy. Langenbecks Arch Chir Suppl Kongressbd: 534–43.
9. Niho S, Yokose T, Nagai K, Nishiwaki Y, Kodama T, Mukai K (1999) A case of synchronous double primary lung cancer with neuroendocrine features. Jpn J Clin Oncol 29:219–225
10. Rainosek D, Ro J, Ordonez N, Kulaga A, Ayala A (1994) Sarcomatoid carcinoma of the lung. A case with atypical carcinoid and rhabdomyosarcomatous components. Am J Clin Pathol 102:360–364
11. Tsubota Y, Kawaguchi T, Hoso T, Nishino E, Travis W (1992) A combined small cell and spindle cell carcinoma of the lung. Report of a unique case with immunohistochemical and ultrastructural studies. Am J Surg Pathol 16:1108–1115
12. Bahrami A, Gown AM, Baird GS, Hicks MJ, Folpe AL (2008) Aberrant expression of epithelial and neuroendocrine markers in alveolar rhabdomyosarcoma: a potentially serious diagnostic pitfall. Mod Pathol 21:795–806
13. Miettinen M, Cupo W (1993) Neural cell adhesion molecule distribution in soft tissue tumors. Hum Pathol 24:62–66
14. Lantuejoul S, Laverriere MH, Sturm N, Moro D, Frey G, Brambilla C, Brambilla E (2000) NCAM (neural cell adhesion molecules) expression in malignant mesotheliomas. Hum Pathol 31:415–421
15. Kourea HP, Adonakis G, Androutsopoulos G, Zyli P, Kourounis G, Decavalas G (2008) Fallopian tube malignant mixed mullerian tumor (carcinosarcoma): a case report with immunohistochemical profiling. Eur J Gynaecol Oncol 29:538–542
16. Cavazza A, Paci M, Rossi G (2006) Pulmonary hamartoma associated with typical carcinoid/tumorlet. Virchows Arch 449:392–393
17. Guerrero ML, Lazcano FF, Manzuco JM (1975) Carcinoid bronchial adenoma and pulmonary hamartoma. Rev Clín Esp 137:87–90
18. Cavazza A, Toffanetti R, Ferrari G, Piana S, Putrino I, Gardini G (2001) Combined neoplasia of the lung: description of a case of adenocarcinoma mixed with typical carcinoid. Pathologica 93:216–220
19. Sen F, Borczuk AC (1998) Combined carcinoid tumor of the lung: a combination of carcinoid and adenocarcinoma. Lung Cancer 21:53–58
20. Li F, Wang X, Xu H, Roggli VL (2010) Small neuroendocrine lesions in intrathoracic lymph nodes of patients with primary lung adenocarcinoma: real metastasis? Am J Surg Pathol 34:1701–1707
21. Doglioni C, Ferlito A, Chiamenti C, Viale G, Rosai J (1990) Laryngeal carcinoma showing multidirectional epithelial neuroendocrine and sarcomatous differentiation. ORL J Otorhinolaryngol Relat Spec 52:316–326
22. Eusebi V, Damiani S, Pasquinelli G, Lorenzini P, Reuter V, Rosai J (2000) Small cell neuroendocrine carcinoma with skeletal muscle differentiation: report of three cases. Am J Surg Pathol 24:223–230
23. Roncaroli F, Montironi R, Feliciotti F, Losi L, Eusebi V (1995) Sarcomatoid carcinoma of the anorectal junction with neuroendocrine and rhabdomyoblastic features. Am J Surg Pathol 19:217–223
24. McDowell EM, Trump BF (1981) Pulmonary smell cell carcinoma showing tripartite differentiation in individual cells. Hum Pathol 12:286–294
25. Nishimaki T, Nakagawa S, Aizawa K, Suzuki T, Hatakeyama K, Watanabe H (1997) Composite tumor of the esophagus with tripartite differentiation. Dig Dis Sci 42:1041–1046
26. Wick MR, Ritter JH, Humphrey PA (1997) Sarcomatoid carcinomas of the lung: a clinicopathologic review. Am J Clin Pathol 108:40–53
27. Pelosi G, Scarpa A, Manzotti M, Veronesi G, Spaggiari L, Fraggetta F, Nappi O, Benini E, Pasini F, Antonello D, Iannucci A, Maisonneuve P, Viale G (2004) K-ras gene mutational analysis supports a monoclonal origin of biphasic pleomorphic carcinoma of the lung. Mod Pathol 17:538–546
28. Blaukovitsch M, Halbwedl I, Kothmaier H, Gogg-Kammerer M, Popper HH (2006) Sarcomatoid carcinomas of the lung–are these histogenetically heterogeneous tumors? Virchows Arch 449:455–461
29. Dacic S, Finkelstein S, Sasatomi E, Swalsky P, Yousem S (2002) Molecular pathogenesis of pulmonary carcinosarcoma as determined by microdissection-based allelotyping. Am J Surg Pathol 26:510–516
30. Cokelaere K, Michielsen P, De Vos R, Sciot R (2001) Primary mesenteric malignant mixed mesodermal (mullerian) tumor with neuroendocrine differentiation. Mod Pathol 14:515–520
31. Przygodzki RM, Moran CA, Suster S, Koss MN (1995) Primary pulmonary rhabdomyosarcomas: a clinicopathologic and immunohistochemical study of three cases. Mod Pathol 8:658–661
32. Khalifa M, Hruby G, Ehrlich L, Danjoux C, Perez-Ordonez B (2001) Combined large cell neuroendocrine carcinoma and spindle cell carcinoma of the lung. Ann Diagn Pathol 5:240–245
33. Ueo T, Kaku N, Kashima K, Daa T, Kondo Y, Yoshida K, Suzuki M, Yokoyama S (2005) Carcinosarcoma of the parotid gland: an unusual case with large-cell neuroendocrine carcinoma and rhabdomyosarcoma. APMIS 113:456–464

Virchows Arch (2011) 458:505–509
DOI 10.1007/s00428-011-1055-4

LETTER TO THE EDITOR

Diffuse lymphangiomatous hyperplasia of the spleen with hyaline bodies. A pseudotumoral proliferation arising from the lymphatic vessels of the periarteriolar lymphatic sheath

Dimas Suárez-Vilela · Francisco Miguel Izquierdo · Jose Ramón Méndez · Juliana Escobar · Gerardo Urdiales · Pilar Junco

Received: 31 January 2011 / Accepted: 1 February 2011 / Published online: 20 February 2011
© Springer-Verlag 2011

Sir:

Diffuse lymphangiomatosis (DL) is a very uncommon condition that involves bone, soft tissue or viscera in a diffuse fashion [1, 2]. The spleen is affected in 10% of cases [2], but isolated splenic lymphangiomatosis (ISL), without other visceral location, is extremely rare, with very few cases described [3, 4]. We report the case of a rare splenic lymphangiomatous proliferation in a patient with DL in peripancreatic fibro-fatty tissue. The splenic lesion consisted in a multicentric growth in white pulp, and showed numerous hyaline inclusions in the endothelial cells.

Our case corresponded to a 22-year-old female with frequent episodes of abdominal pain since her adolescence. The different radiologic studies of the abdomen did not display remarkable findings. In January 2010, she was sent to our hospital with hypovolemic shock without previous trauma. At the surgical procedure, a massive hemoperitoneum with diffuse bleeding from the peripancreatic and porta hepatis area was found. The great vessels were well preserved without either rupture or aneurysms. Despite the surgical treatment (splenectomy and partial pancreatectomy) and numerous blood transfusions, the patient died shortly afterwards because of intractable abdominal haemorrhage and disseminated intravascular coagulation. Autopsy was not performed.

The spleen weighted 106 g and on cut section showed a congestive pulp and small isolated bad delimited microcysts. The fragment of pancreas weighted 30 g and did not present remarkable findings. Microscopically, the red pulp was normal whereas numerous solid and cystic structures, measuring between 0.5 and 2 mm in size, were found in the white pulp. These lesions displayed irregular, scalloped outlines and showed clefts and papillae lined by flat or hobnail cells, arranged in one or several layers (Fig. 1a). Within the cyst lumina, abundant histiocytes and cells detached from the lining were found. Many of the luminal cells contained cytoplasmic hyaline globules that filled the cytoplasm and rejected the nuclei. They stained with periodic acid-Schiff stain and were red in colour using the Masson trichrome stain (Fig. 1b). The underlying stroma of the clefts and papillae was dense with round and spindle cells and numerous arterioles similar to those included inside the periarteriolar lymphatic sheath (PALS). Patchy lymphoid aggregates were present in the subendothelial stroma.

The pancreas did not show histologic changes but the fibro-fatty peripancreatic tissue displayed a thin-walled irregular vascular proliferation. These vessels did not contain red blood cells. The wall of some of them presented a thin muscle layer. They infiltrated focally inside the pancreas, along the interacinar interstitium (Fig. 1c). In the endothelium of this peripancreatic vascular proliferation, hyaline bodies were not present.

On the immunohistochemical study, the luminal cells of the splenic lesions were positive for vimentin, CD31 and

D. Suárez-Vilela · F. M. Izquierdo (✉) · J. R. Méndez · J. Escobar · P. Junco
Department of Anatomía Patológica,
Hospital Valle del Nalón,
Polígono de Riaño, S/N,
33920 Riaño (Langreo) Asturias, Spain
e-mail: fizquierdog@saludcastillayleon.es

G. Urdiales
Department of Surgery, Hospital Valle del Nalón,
Polígono de Riaño, S/N,
33920 Riaño (Langreo) Asturias, Spain

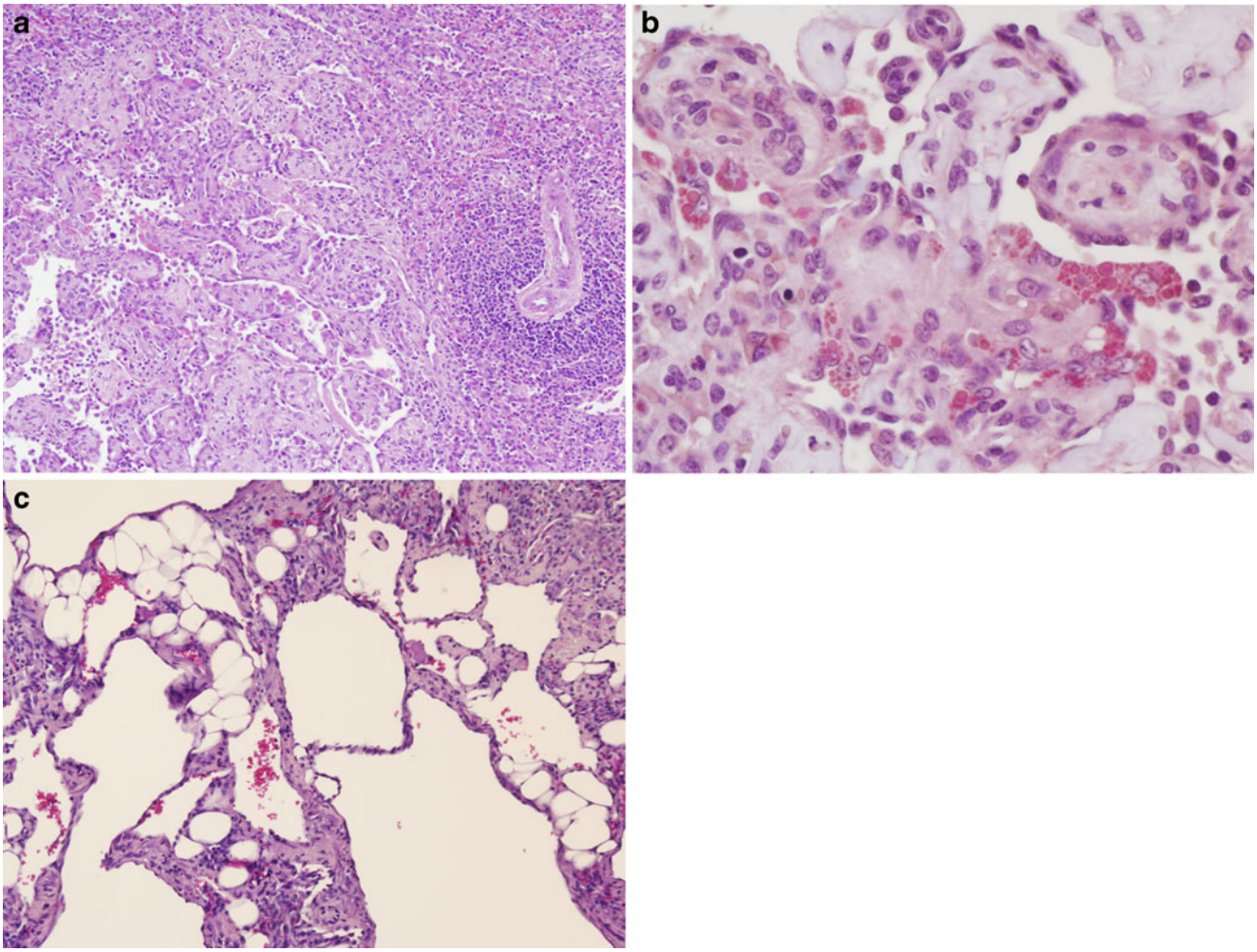

Fig. 1 **a** Cystic lesion adjacent to a lymphoid follicle. Inside the lumen, there are numerous papillae and clefts lined by flat cells. Some cytoplasmic globules are present. **b** Endothelial hyaline bodies are stained red in colour with Masson trichrome stain. **c** Proliferation of irregular vessels in the fibro-fatty tissue around the pancreas

D2-40 (Fig. 2a), being negative for CD34, cytokeratin AE1-AE3 and cytokeratinratin 18. The cells with cytoplasmic inclusions showed the same immunophenotype. In the subendothelial layer, there were abundant round and spindle cells which were stained for CD34. These cells were in continuum with the periadventitial layer of the arterioles of the wall of the cysts (Fig. 2b). In this location, other fusiform cells stained with smooth muscle actin antibody (Fig. 2c). All the subendothelial cells resulted negative for CD31 and D2-40. Incipient microcystic lesions, localized in the PALS and in the marginal area of the follicles, were demonstrated with CD31, CD34, smooth muscle actin and D2-40 (Fig. 2d). The lymphoid component that surrounded the wall of the cysts was composed of B lymphocytes (CD20 positive) and T lymphocytes (CD3 positive). CD8 antibody stained the sinusoids of the red pulp but was negative on both the luminal cells and the cells of the wall of the cysts (Fig. 2e). The hyaline globules were positive for α-1-antitrypsin and stained for light chains at the periphery (Fig. 2f). The endothelial cells of peripancreatic vascular proliferation presented immunostains similar to those of the luminal cells of the splenic cysts and some vessels disclosed additional stain with smooth muscle actin and caldesmon on the cells of the wall. HMB-45 and s-100 antibodies displayed negative results in both splenic and peripancreatic lesions.

The case that we report corresponds to an unusual vascular splenic lesion in a patient with DL in fibro-fatty peripancreatic tissue. Both vascular proliferations disclosed an endothelial lining of probably lymphatic origin, being positive for CD31 and D2-40 and negative for CD34 [5, 6]. In systemic DL, the spleen is involved in 10% of cases [2], whereas ISL is a more uncommon form with less than ten cases reported [3, 4]. Whatever the type of these entities, the spleen is usually enlarged and multicystic, with cysts that vary from a few millimetres to 2 or 3 cm in diameter [1–4].

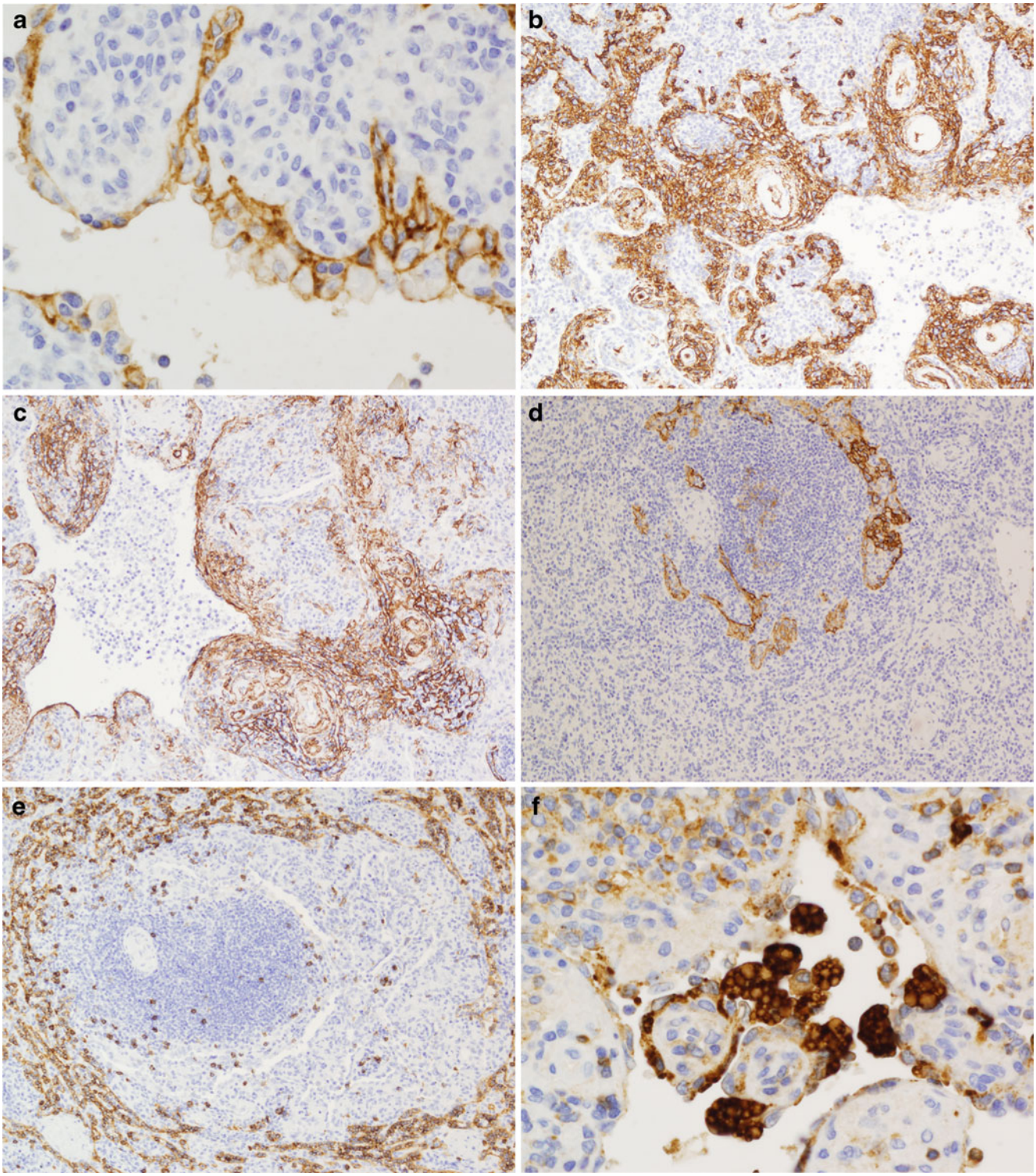

Fig. 2 **a** Stain of superficial cells for D2-40. Some of them show cytoplasmic globules. **b** CD34 on subendothelial cells. Abundant arterioles are enmeshed with the cells positive for CD34. **c** Smooth muscle actin on the spindle cells that surround the cysts. These cells are in continuum with the PALS. **d** Incipient lymphangiomatous proliferation made up by elongated and tortuous vessels which are included inside the PALS and surround it. It involves the marginal area of the lymphoid follicle as well. (D2-40 immunohistochemical stain). **e** With the stain for CD8, a lymphangiomatous lesion close to a lymphoid follicle, is well remarked. **f** Peripheral stain of the endothelial hyaline globules with antilambda light chain antibody

In our case, the splenic weight was normal and on cut section the lesions were almost undistinguishable. Microscopically, the lymphangiomatous proliferation was multicentric and localized inside the white pulp or around it. On the immunohistochemical study, these lesions showed a very characteristic luminal-parietal immunophenotype. In the human spleen, the marginal area of the lymphoid follicles and the PALS are limited by myofibroblastic cells positive with smooth muscle actin, whereas the arterioles included inside the PALS are surrounded by several layers of perivascular cells positive for CD34 [7]. In the PALS, there are in addition small lymphatic vessels localized very close to the arterioles [8, 9]. In present case, both the close location of the lesions to the white pulp and the "subendothelial scaffold" composed of numerous arterioles and several layers of cells positive for CD34 and smooth muscle actin, are very similar to the arrangement of the deep efferent lymphatic vessels of the spleen in relation with the arterioles included inside the PALS and its support of perivascular cells and myofibroblasts [8, 9]. On the immunohistochemical study, we find slit-like lymphatic vessels within the PALS, which lining was stained with D2-40 and CD31 antibodies. Likewise, incipient lesions of lymphangiomatosis were present in the area of PALS and around the secondary lymphoid follicles (Fig. 2d).

The aggregates of B and T lymphocytes found in the splenic lesions can correspond to the lymphoid population of the white pulp [10] and as in the normal human spleen, these aggregates of B and T lymphocytes are intricately interdigitated [10]. The stain with CD8 antibody showed an expansive growth of the lymphangiomatous proliferation from the white pulp. This proliferation was sharply delimited from the sinusoids of the red pulp (Fig. 2e).

The histologic findings of the present case have not been described in detail in any case of splenic involvement in DL or ISL [1–4]. Ramani et al [1] have reported a case of DL with microscopic features in the spleen very similar to present case. However, these authors did not determine either the exact location of the lesions in the spleen, or the immunoprofile of the subendothelial cells.

Our case presented hyaline inclusions in endothelial cells. Hyaline globules or thanatosomes have been observed in a large variety of unrelated categories of tumours and benign tissues [11]. In vascular tumours, these hyaline bodies have been described in both neoplasms of supposed origin from lymphatic endothelium, as Kaposi's sarcoma or kaposiform haemangioendothelioma are [5, 12, 13], and in tumours of blood vessel endothelium as glomeruloid haemangioma, papillary haemangioma or other vascular tumours [14, 15]. The pathogenesis of these inclusions is not clear. Some authors believe that the globules are related to apoptotic cell death [11], whereas for other authors, they are related to dysfunction of the autophagic-lysosomal pathway [15]. In our knowledge, these intracytoplasmic globular structures have not been described in ISL or DL [1–4].

The massive haemorrhage suffered by this patient is an uncommon event that may occur in DL [16, 17]. The aetiology of the haemorrhage in these cases is not well-known but it can be related with the infiltrative proliferation of lymph vessels or with coagulation problems as disseminated intravascular coagulation [16, 17].

We believe that our case corresponds more to a splenic diffuse lymphangiomatous hyperplasia in a patient with DL than to a SL, inasmuch as at the histological and immunohistochemical studies the lesions present a multicentric, progressive and tidy growth from the white pulp. This lymphangiomatous hyperplasia could arise from the deep efferent lymph vessels of the PALS, and shows a prominent subendothelial expansion of other elements of the PALS.

Conflict of interest The authors declare that they have no conflict of interest.

References

1. Ramani P, Shah A (1993) Lymphangiomatosis. Histologic and immunohistochemical analysis of four cases. Am J Surg Pathol 17:329–335
2. Barbagallo M, Incorpora G, Magro G, DÀmico S, Pavone V (2009) Splenic lymphangiomatosis associated with skeletal involvement (Gorham`s disease): a new case and review of literature. Minerva Pediatr 61:231–236
3. Schmid C, Beham A, Uranüs S et al (1991) Non-systemic diffuse lymphangiomatosis of spleen and liver. Histopathology 18:478–480
4. Patti R, Iannitto E, Di Vita G (2010) Splenic lymphangiomatosis showing rapid growth during lactation: a case report. World J Gastroenterol 16:1155–1157
5. Kahn HJ, Bailey D, Marks A (2002) Monoclonal antibody D2-40, a new marker of lymphatic endothelium, reacts with Kaposi`s sarcoma and a subset of angiosarcomas. Mod Pathol 15:434–440
6. Evangelou E, Kyzas PA, Trikalinos TA (2005) Comparison of the diagnostic accuracy of lymphatic endothelium markers: Bayesian approach. Mod Pathol 18:1490–1497
7. Steineger B, Barth P, Hellinger A (2001) The perifollicular and marginal zones of the human splenic with pulp: do fibroblasts guide lymphocyte immigration? Am J Pathol 159:501–512
8. Saitoh K, Kamiyama R, Hatakeyama S (1982) A scanning microscopic study of the boundary zone of the human spleen. Cell Tissue Res 222:655–665
9. Hokazono K, Miyoshi M (1984) Scanning-and transmission electron-microscopic study of lymphatic vessels in the splenic white pulp of the macaque monkey. Cell Tissue Res 237:1–6
10. Steineger B, Rüttinger L, Barth PJ (2003) The three-dimensional structure of human splenic with pulp compartments. J Histochem Cytochem 51:655–663
11. Papadimitriou JC, Drachenberg CB, Brenner DS, Newkirk C, Trump BF, Silverberg SG (2000) "Thanatosomes": a unifying morphogenetic concept for tumour hyaline globules related to apoptosis. Hum Pathol 31:1455–1465

12. Lyons LL, North PE, Mac-Moune Lai F, Stoler MH, Folpe AL, Weiss SW (2004) Kaposiform hemangioendothelioma: a study of 33 cases emphasizing its pathologic, immunophenotypic, and biologic uniqueness from juvenile hemangioma. Am J Surg Pathol 28:559–568
13. Debelenko LV, Perez-Atayde AR, Mulliken JB, Liang MG, Archibald TH, Kozakewich HPW (2005) D2-40 immunohistochemical analysis of pediatric vascular tumors reveals positivity in kaposiform hemangioendothelioma. Mod Pathol 18:1454–1460
14. Chan JKC, Fletcher CDM, Hicklin GA, Rosai J (1990) Glomeruloid hemangioma. A distinctive cutaneous lesion of multicentric Castleman`s disease associated with POEMS syndrome. Am J Surg Pathol 14:1036–1046
15. Suurmeijer AJH, Fletcher CDM (2007) Papillary haemangioma. A distinctive cutaneous haemangioma of the head and neck area containing eosinophilic hyaline globules. Histopathology 51:638–648
16. Iwabuchi A, Otaka M, Okuyama A et al (1997) Disseminated intra-abdominal cystic lymphangiomatosis with severe intestinal bleeding. A case report. J Clin Gastroenterol 25:383–386
17. Tamay Z, Saribeyoglu E, Ones U et al (2005) Diffuse thoracic lymphangiomatosis with disseminated intravascular coagulation in a child. J Pediatr Oncol 27:685–687

Virchows Arch (2011) 458:511–523
DOI 10.1007/s00428-011-1066-1

REVIEW AND PERSPECTIVE

Histopathological diagnosis of non-alcoholic and alcoholic fatty liver disease

Andrea Tannapfel · Helmut Denk · Hans-Peter Dienes · Cord Langner · Peter Schirmacher · Michael Trauner · Berenike Flott-Rahmel

Received: 7 October 2010 / Revised: 2 March 2011 / Accepted: 8 March 2011 / Published online: 26 March 2011
© Springer-Verlag 2011

Abstract The diagnostic procedures in patients with suspected fatty liver disease—with or without known alcohol consumption—should be standardized and generally accepted. We therefore present a guideline, summarizing the current concepts of etiology, diagnostic as well as differential diagnostic of patients with fatty liver disease. Alcoholic as well as and non-alcoholic fatty liver are characterised by lipid deposition in hepatocytes. The diagnosis of steatosis is made when lipid deposition exceeds 5% of hepatocytes, while involvement of more than 50% is called "fatty liver". An additional inflammatory reaction leads to alcoholic (ASH) or non-alcoholic steatohepatitis (NASH). Steatohepatitis is present when both inflammatory infiltrates of mixed cells in the small liver lobules as well as liver cell injury in terms of ballooning can be detected. Liver biopsy represents the "golden standard" for confirming diagnosis and determining inflammatory activity and potential fibrosis of fatty liver disease. The differential diagnosis of ASH vs. NASH cannot be made on the basis of histological criteria alone. Steatosis, inflammatory changes and hepatocytic injury can be semiquantified as a "Brunt Score" or "NAS" (NAFLD activity score), providing the basis on which to decide whether or not steatohepatitis is present. People at increased risk of developing a fatty liver possess an increased risk of developing chemotherapy-associated steatohepatitis. Histologically, pediatric NASH differs from adult NASH and is often only clinically manifest through a mild if persistent elevation in transaminases.

Keywords Non-alcoholic steatohepatitis · Alcoholic steatohepatitis · Chemotherapy · NASH in children · Ballooning · Fibrosis · Cirrhosis · Differential diagnosis · Scoring · Liver biopsy

A. Tannapfel (✉) · B. Flott-Rahmel
Institut für Pathologie, Ruhr-Universität Bochum,
Bürkle-de-la-Camp Platz 1,
44789 Bochum, Germany
e-mail: Andrea.Tannapfel@rub.de

H. Denk · C. Langner
Institut für Pathologie, Medizinische Universität Graz,
Auenbruggerplatz 25,
8036 Graz, Austria

H.-P. Dienes
Institut für Pathologie, Universität zu Köln,
Kerpener Str. 62,
50924 Köln, Germany

P. Schirmacher
Pathologisches Institut, Universitätsklinikum Heidelberg,
Im Neuenheimer Feld 220/221,
69120 Heidelberg, Germany

M. Trauner
Klinische Abteilung für Gastroenterologie und Hepatologie,
Medizinische Universität Graz,
Auenbruggerplatz 15,
8036 Graz, Austria

Introduction

It has long been known that the typical manifestations of alcoholic liver damage (including cirrhosis of the liver) can also be found in patients who consume no alcohol. For such persons, the incorrect diagnosis of "alcohol-related liver disease" on the basis of the histopathological findings can have grave social, legal, and insurance implications.

The term "non-alcoholic steatohepatitis" (NASH) was coined by Ludwig et al. [1] in 1980; the definition of the entity was later expanded [2]. Patients who manifested the typical histomorphological picture of alcoholic steatohepatitis

(ASH), but without immoderate alcohol consumption, were described [3].

Diagnosis by means of biopsy is the gold standard for differentiation between reversible steatosis and progressive steatohepatitis. There are numerous publications on this topic with the aim of developing uniform standards for biopsy diagnosis or identifying reliable non-invasive or only slightly invasive alternatives to biopsy, particularly driven by the increasing prominence of alcoholic and non-alcoholic steatohepatitis.

The publications on predisposition to ASH or NASH, however, cannot be uniformly interpreted because of ethnic or physiological differences among the populations analysed.

It is therefore important to evaluate the situation in Germany, Austria, as well as Switzerland (and, where applicable, the rest of Europe) objectively and work towards reasonable diagnostic procedures that serve the needs of these patients.

The goal of this guideline is thus to delineate the current state of knowledge with regard to the pathohistological diagnosis of ASH and NASH and to provide expert assessment of the non-invasive alternatives.

Definitions and diagnostic criteria

Definitions

An alcoholic (AFL) and a non-alcoholic fatty liver (NAFL) are characterised by variable deposition of lipids (principally triglycerides) in the hepatocytes. Involvement of more than 5% of hepatocytes is termed "fatty degeneration"; if more than 50% are affected, the patient has a "fatty liver". A subsequent inflammatory reaction with ballooning of the hepatocytes results in ASH or NASH. ASH or NASH may lead to fibrosis or cirrhosis.

Light microscopically detectable deposition of lipid droplets in the cytoplasm of hepatocytes is termed steatosis. Microvesicular and macrovesicular steatosis can be distinguished; mixed forms occur [4].

The accumulation of fat in the liver essentially results from four pathogenetic processes: (1) increased uptake of free fatty acids (from food or body fat) via the portal vein; (2) increased synthesis of free fatty acids in the liver (from glucose or acetate); (3) decreased β-oxidation of free fatty acids (above all in the mitochondria); (4) decreased synthesis or secretion of lipoproteins (very low density lipoproteins, VLDL), the principal route for elimination of lipids from the liver [4].

In the past, alcohol abuse—leading to AFL—was usually suspected as the cause of steatosis. Today, however, one frequently observes steatosis in (abdominal, visceral) adiposity, diabetes mellitus type II, and hyperlipidaemia—components of the so-called metabolic syndrome. Moreover, other factors such as medications, toxins or (rarely) congenital metabolic disorders (e.g., a-beta-lipoproteinaemia/hypobetalipoproteinaemia) or hormonal imbalances, as in polycystic ovary syndrome, may cause steatosis—NAFL. In some cases, the cause of steatosis remains unresolved [5–7].

The morphological spectrum of the non-alcoholic fatty liver diseases (NAFLD) stretches—like that of alcoholic fatty liver disease—from simple steatosis over steatohepatitis to liver fibrosis and cirrhosis, and thus ultimately to hepatocellular carcinoma. Pure steatosis, unaccompanied by inflammation or fibrosis, is in principle reversible and generally displays an indolent, non-progressive course. Steatohepatitis is—from the hepatological viewpoint—the progressive lesion in this spectrum.

The diagnosis of NAFLD thus emerges from a combination of clinical (exclusion of significant alcohol consumption) and histopathological (demonstration of steatosis or steatohepatitis) findings. What constitutes immoderate (significant) alcohol consumption is controversial. Nowadays, an upper limit of 20 g of alcohol per day is accepted, in men up to 40 g/day [8, 9]. NAFLD is thought to be the most frequent liver disease in the western industrial nations and thus the commonest cause of elevated transaminases.

The *prevalence* of NAFL in the western industrial nations is assumed to be 20–30%, that of NASH, 2–3% [6, 10, 11]. There is a direct relationship with body weight; in obesity (BMI >30) the prevalence of sonographically detectable steatosis is 76–89%, compared with 46–50% in alcoholics [12]. NAFLD is increasingly being diagnosed in childhood, again predominantly in association with obesity, but occasionally with suprasellar tumours [13].

The *natural course* of NAFLD in the individual case cannot be predicted. Only a small proportion of those affected show progression of their liver disease. The assumption is that simple steatosis will progress to NASH in around 10–20% of patients, and that of these, less than 5% will develop cirrhosis [11, 14, 15]. Nevertheless, NAFL and NASH are currently believed to be the most important cause of so-called cryptogenic cirrhosis of the liver [7, 16].

The *pathogenesis* of NASH remains unclear, however, with many aspects unresolved. In Day and James's "two-hit" hypothesis, simple steatosis, with an accumulation of free fatty acids and triglycerides in the liver, represents the first hit, rendering the organ more vulnerable to a second hit that leads to steatohepatitis and ultimately, in the event of persisting or recurring damage, to fibrosis and cirrhosis [17, 18]. A central part is played by insulin resistance, which can be demonstrated in virtually all patients [19]. Elevated peripheral lipolysis and decreased glucose uptake by the musculature form the basis for increased uptake of free fatty acids from the bloodstream and thus a rise in hepatic

triglyceride synthesis and simultaneous inhibition of triglyceride secretion in the form of VLDL as a result of decreased apoprotein synthesis. The increase in the hepatic pool of free fatty acids leads to a rise mitochondrial and peroxisomal β-oxidation with formation of free oxygen radicals (reactive oxygen species) and development of oxidative stress and increased lipid peroxidation. Facilitated by the action of proinflammatory cytokines (via activation of NFκB, release of TNF-α), steatohepatitis develops. Via Kupffer cell activation, liver fibrosis or cirrhosis arises [7, 9, 10, 14, 15, 20–22].

The possible direct or indirect (increased insulin resistance) role of the adipocyte hormones (leptin and adiponectin) in the pathogenesis of NASH remains largely unclear, as does the recently discussed influence of bacterial overgrowth in the small intestine with endogenous production of ethanol and possible direct cytokine activation [6, 21, 23].

Diagnostic criteria

In clinical practice, it is impossible to differentiate reliably between simple steatosis and steatohepatitis solely on the basis of non-invasive (e.g., laboratory chemical) diagnostic tests. The diagnosis "steatosis" should be assigned when more than 5% of the hepatocytes display fat deposits. Steatohepatitis is present when steatosis is accompanied by mixed-cell inflammatory infiltrates in the hepatic lobes and damage (ballooning) of the hepatocytes.

Clinically, most patients with NAFLD exhibit no liver symptoms. The disease is often suspected merely on grounds of (mildly) raised transaminase levels and/or gamma-glutamyltranspeptidase. An ASAT to ALAT ratio of >1 points to an alcoholic aetiology. Patients with NASH often suffer from illnesses that go hand in hand with insulin resistance. However, the presence of a metabolic syndrome does not exclude alcoholic hepatopathy [24]. In clinical practice, there is so far no means of differentiating reliably between simple steatosis and steatohepatitis solely on the basis of non-invasive (e.g., laboratory chemical) diagnostic tests, i.e., without liver biopsy [7, 12, 25]. Moreover, histological demonstration of long-standing liver cell damage is believed to be the best available marker for evaluation of disease progression [26]. The question of whether transaminase levels correlate with the histological findings, particularly with necroinflammatory activity and the degree of fibrosis, has still not been answered definitively [27]. It was reported that determination of the hepatic apoptotic activity in serum (activated caspase 3, keratin-18 fragment analysis) may have clinical value as a non-invasive diagnostic criterion for NASH [28]. Furthermore, there have been isolated reports of non-invasive scoring systems for fibrosis, but their potential (diagnostic or prognostic) role in routine clinical practice remains unclear [7, 29].

The *morphological sign* of non-alcoholic *steatosis* is a predominantly macrovesicular accumulation of lipids (mainly triglycerides) in the cytoplasm of hepatocytes, usually beginning at a perivenular site in the centre of a lobe. The lower limit has been set at fatty degeneration of 5% of the surface of the liver parenchyma [9, 30], but this does not seem to be adequately justified [10, 31]. Mild steatosis affects <33% of the parenchymal surface, moderate steatosis involves 33–66%, and severe steatosis covers >66% [4, 8, 31–37].

In *NASH*, the variable degree of steatosis is accompanied by (usually only slight) mixed-cell (neutrophilic, granulocytic, and lymphocytic) inflammatory infiltrate in the hepatic lobes. A further morphological criterion is the demonstration of liver cell damage in the form of swelling (ballooning), usually in the vicinity of fat-laden hepatocytes and thus also typically in the centre of a lobe. Other typical, albeit not diagnostically decisive, parameters are lipogranulomas and the demonstration of periportal glycogen containing nuclei. Mallory-Denk bodies (MDB)—usually small, poorly developed cytoplasmic inclusions—can be demonstrated in the swollen cells. The fibrosis also begins in the centre of the affected lobe, in perivenular and perisinusoidal locations; pericellular fibrosis (of the "chicken wire" type) is sometimes found. As the disease progresses, there is portal fibrosis with formation of bridging (portoportal and portocentral) septa. No single one of these parameters is diagnostic per se for NASH; even the combination of steatosis and (slight) lobular hepatitis should not be used as a so-called minimal criterion without the simultaneous demonstration of liver cell damage in the form of swelling (ballooning) [4, 8, 9, 31–36].

On prognostic grounds, the Cleveland group suggested classification of NAFLD into the following types: type 1, simple steatosis; type 2, steatosis and inflammation; type 3, steatosis and cell swelling (ballooning); type 4, steatosis, cell swelling (ballooning), and MDB or fibrosis. Progression to cirrhosis is found predominantly in types 3 and 4, both of which correspond to the typical histopathological picture of NASH [8, 9, 31–36, 38, 39]. For the morphological manifestations of paediatric NASH, see "Special form: paediatric fatty liver disease".

Finally, it should be pointed out that the structural diagnostic criteria for NAFLD may be unevenly distributed in the liver, so that histological diagnosis on the basis of biopsy samples may be associated with no inconsiderable sampling error [40]. This affects not only the diagnostic differentiation between steatosis and steatohepatitis but also estimation of the extent of fibrosis (staging); see also "Harvesting and processing of biopsy material/histomorphological evaluation/scoring system".

Indications for biopsy

Liver biopsy is the gold standard for confirmation of the diagnosis and for determination of the inflammatory activity and possible presence of fibrosis in fatty liver disease. In deciding whether biopsy is indicated, one should weigh the potential information gain and its consequences against the resources invested and the complication rate, i.e. consider the clinical context. No blanket recommendation for liver biopsy in either suspected or confirmed fatty liver disease can currently be given.

The indication for biopsy in assumed fatty liver disease depends on the clinical context. Decisive is the likelihood that the biopsy findings will have consequences for the patient's behaviour or for therapy. These possible consequences include:

- Confirmation of fatty liver disease, in particular steatohepatitis, and its treatability; exclusion of steatohepatitis as cause of unexplained elevation of transaminases; exclusion or confirmation of comorbidities; ascertainment of status quo [9, 35, 41, 42]
- Deciding the appropriate treatment approach (e.g. bariatric surgery, suitability for transplantation; treatment of any comorbidity)
- Motivation for behavioural modification or ascertainment of its effect (e.g. weight reduction, physical activity)
- Participation in clinical studies or protocol biopsies
- Special indications (e.g. assessment of explanted livers)

In this context, liver biopsy must clarify the following points:

- Confirmation of possible or assumed fatty liver; clarification of steatohepatitis; confirmation or exclusion of liver disease other than fatty liver disease (typing)
- Extent of inflammatory activity (grading)
- Degree of fibrosis and any destruction of hepatic architecture (staging)

Liver biopsy is the current "gold standard" for analysis of these issues and cannot be replaced by any non-invasive procedure [35, 43–47]. It is advisable to discuss the implications of liver biopsy with the patient during the course of diagnostic clarification of possible or probable fatty liver disease. While a pronounced case of fatty liver can be diagnosed with some certainty from the findings of clinical examination and imaging procedures, particularly the extent of the fatty degeneration and the presence or absence of the many possible accompanying liver diseases cannot be determined with any certainty by non-invasive means. There are no serological tests for diagnosis or quantification of fatty degeneration of the liver parenchyma. Comparative investigations have shown that elevation of serum transaminase concentrations can point to impairment of the hepatic parenchyma, but an absence of serum transaminase elevation in fatty liver disease does not exclude inflammatory activity in liver tissue [42]. While in principle, fatty liver disease is thought to be swiftly reversible and unlikely to progress, steatohepatitis entails a significant risk of progression to severe fibrosis or cirrhosis, so that the determination of inflammatory activity has considerable prognostic relevance [39, 41, 46–48].

Numerous non-invasive procedures for diagnosis of liver fibrosis have been and are being developed. Serological tests are based on algorithms, some of which are independent of fibrosis while others integrate parameters associated with hepatic fibrogenesis [49]. Currently, these tests can support the diagnosis of advanced liver fibrosis, but alone, particularly in the presence of only slight to moderate changes, they can neither confirm nor exclude fibrosis with sufficient certainty; therefore, they are unsuitable for staging. Elastography is a method for determining the stiffness of the liver, which correlates with extent of fibrosis, at least during follow-up. Particularly the presence or absence of severe fibrosis/cirrhosis can be assessed with high accuracy [50]. The advantages of this method are its repeatability, its low inter- and intra-observer variability and its lack of side effects; its disadvantages are inadequate detection of slight and moderate fibrosis, lack of grading ability, significant interference by other liver changes (fatty degeneration, inflammatory activity, cholestasis, congestion) and by extrahepatic factors (morbid obesity, ascites) [51]. For these reasons the diagnostic potential of elastography in fatty liver disease has been evaluated in only a few studies to date, so the method has not yet been adequately validated. In particular, its role in the monitoring of the course of fatty liver disease should be further investigated. None of the tests mentioned above is suitable for assessment of destruction of hepatic architecture. Other procedures, e.g. magnetic resonance elastography for measurement of fibrosis [52], are currently inadequately validated or not validated at all, and therefore cannot be recommended.

Although liver biopsy is superior to all other investigations with regard to the number of relevant parameters assessed and predictive power, it cannot always be recommended as diagnostic method in possible or sufficiently confirmed fatty liver disease. Several factors affect the decision whether or not to perform biopsy:

- Because biopsy is an invasive technique, the information it can be expected to yield must be balanced against the resources invested and the—albeit low—complication rate. The rate of fatal complications of liver biopsy is generally reported as 0.01%. Major intervention—or

hospitalisation-related complications such as intraperitoneal haemorrhage occur in about 0.3% of cases, while more minor complications, e.g. transient pain, are observed in 20–30% of patients [53].

- The issue of clinical consequences: The current treatment options for fatty liver disease are limited. Biopsy sampling of liver tissue for examination may be particularly useful, however, before invasive treatment measures such as bariatric surgery or liver transplantation [54]. In the medium term novel treatments, including medicinal approaches, can be expected, entailing reassessment of the value and necessity of liver biopsy. To what extent knowledge of the findings of liver biopsy influences the patient's behaviour (weight reduction, physical activity) has to be considered on an individual basis.
- Donor livers with <30% fatty degeneration can be transplanted with no danger of primary transplant failure [55].

Harvesting and processing of biopsy material/ histomorphological evaluation/scoring system

Harvesting and processing of the biopsy cylinder should observe the standard recommendations for liver biopsy. Differentiation between ASH and NASH is generally not possible on histological criteria alone. Nevertheless, information may be yielded that may make differential diagnosis easier. Fatty degeneration, inflammatory changes and signs of damage to hepatocytes can be semiquantitatively pooled to yield the Brunt score or NAS (NAFLD activity score), offering a basis to decide whether steatohepatitis is present or not. The staging should also be evaluated according to the degree of fibrosis. Numerical scores alone should not replace histological diagnosis.

Harvesting and processing of the biopsy sample observe the standard recommendations for liver biopsy. The cylinder should contain representative tissues, be about 25 mm long and/or contain 15 portal fields [56]. Fixation and processing are routine (4% neutral buffered formalin, embedding in paraffin with the usual dehydration and preparation of routine stains such as haematoxylin and eosin, Berlin blue for demonstration of iron, PAS-diastase stain and reticulin and connective tissue staining). Sirius red staining is recommended for morphometric assessment. Immunohistological staining is not routinely required. An immunohistochemical reaction with antibodies to keratin 7 or 19 can be carried out to facilitate demonstration of gall duct lesions. Sensitive depiction of any MDB that may be present can be achieved with ubiquitin antibodies. With regard to ballooning of hepatocytes, which is included in the scoring system, demonstration of the intermediate filament cytoskeleton with antibodies against keratin 8 or 18 may be helpful, as this cytoskeletal system is reduced in cell ballooning [57]. The staging of fibrosis is shown in Table 1.

The following histological criteria should be considered when interpreting and diagnosing non-alcoholic steatohepatitis: micro- or macrovesicular fatty degeneration, fibrosis, lobular inflammation—typically comprising polymorphonuclear granulocytes, lymphocytes and activated Kupffer cells—lipogranulomas, hepatocyte ballooning, acidophilic bodies, ceroid-containing macrophages and megamitochondria. Additional changes are MDB and glycogen-contaning nuclei.

Fatty degeneration, inflammatory changes and signs of damage to hepatocytes are often semiquantitatively pooled to yield the so-called Brunt score [58] (Table 2).

The NAS (NAFLD activity score; Table 3) is a refinement of the Brunt score, derived by separate semiquantification of each of the three components—steatosis, hepatocyte ballooning and lobular inflammation—and addition to form a total score.

Evaluation and semiquantitative analysis for grading [58]:

Grade of fatty degeneration:	
<5%	= grade 0
5–33%	= grade 1
34–66%	= grade 2
More than 66%	= grade 3
Grade of lobular inflammation:	
Absent	= grade 0
Up to two foci per field of view (×200 magnification)	= grade 1
Two to four foci per field of view	= grade 2
More than four foci per field of view	= grade 3
Lipogranulomas are included in the category of inflammation	
Ballooning:	
Absent	= grade 0
Few ballooned hepatocytes	= grade 1
Many ballooned hepatocytes	= grade 2

Table 1 Degree of fibrosis (staging)

Stage	Histological findings
0	No fibrosis
1a	Zone 3, perisinusoidal fibrosis, special staining (i.e. EvG) required for identification
1b	Zone 3, perisinusoidal fibrosis, can be detected with H & E
1c	Only periportal/portal fibrosis
2	Zone 3, plus portal/periportal fibrosis
3	As above, but with bridging fibrosis
4	Cirrhosis

EvG Elastica-van-Gieson

Table 2 NASH activity grading

Activity	Steatosis	Ballooning	Inflammation
Mild: grade 1	1–2 (up to 66%)	Minimal	Lobular: 1–2 Portal: none to mild
Moderate: grade 2	2–3 (>33%, occasionally >66%)	Clear	Lobular: 2 Portal: mild to moderate
Severe: grade 3	3 (≥66%)	Marked	Lobular: 3 Portal: mild to moderate

Steatosis: grade 1, ≤33%; grade 2, >33%, <66%; grade 3, ≥66%

This scoring system is readily reproducible and can provide the basis for deciding whether steatohepatitis should be diagnosed or not: 0–2, definitely no steatohepatitis; 3–4, questionable; 5 or more, definite steatohepatitis. The scoring can also be applied to paediatric cases [59, 60].

The staging according to grade of fibrosis (Table 1, after Kleiner et al. [30]) should also be evaluated:

Stage 1 is divided into 1a with slight central fibrosis and 1b with dense perisinusoidal fibrosis accompanied by central vein sclerosis and adjacent perisinusoidal fibrous extension. Stage 1c is used only for portal fibrosis, which may certainly occur at an early stage. Stage 2 is portal and central fibrosis. In analogy with the staging of chronic hepatitis, stage 3 is bridging fibrosis and stage 4 corresponds to cirrhosis. The presence of MDB should also be recorded [61].

The proposed scoring systems have not yet been generally accepted. Numerical scores alone should not replace histological diagnosis (Figs. 1, 2, 3, 4, 5, 6, 7 and 8).

Diagnosis and differential diagnosis

The criteria for differentiation of NASH or ASH from hepatitis C virus infection are firstly the characteristic portal inflammatory infiltration pattern of HCV infection, and

Table 3 NAFLD activity score (grading)

NAS	Steatosis (% fat deposition in hepatocytes)	Ballooning hepatocytes	Lobular inflammation
0	<5% (0)	None (0)	None (0)
3	5–33% (1)	Few (1)	1–2 foci per ×200 field (1)
6	34–66% (2)	Many (2)	2–4 foci per ×200 field (2)
8	>66% (3)	Many (2)	>4 foci per ×200 field (3)

The numbers in parentheses give the NAS for each histological criterion

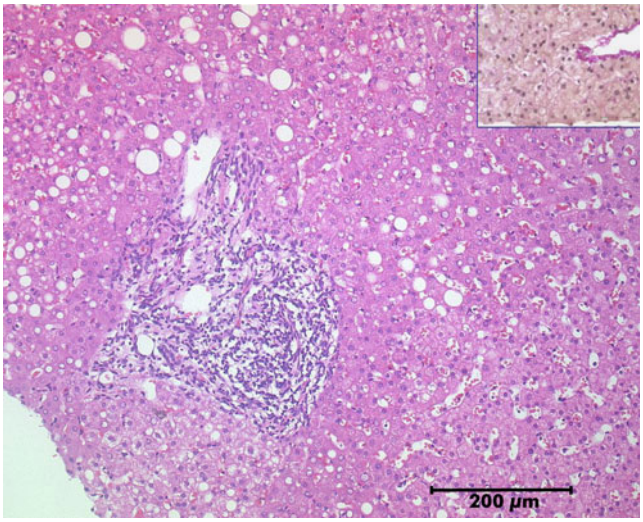

Fig. 1 NASH and chronic hepatitis C virus infection. Steatosis grade 2, fibrosis grade 1a (*inset*, Elastica-van-Gieson (EvG))

secondly the lack of typical hepatocyte ballooning and the intra-acinar granulocytic inflammation.

Differential diagnoses

It is important to differentiate between ASH and NASH and also to differentiate both of them from viral hepatitides and chemotoxicity-related steatohepatitides. The histopathological peculiarities of fatty liver diseases in the paediatric age group must also be borne in mind.

The criteria used for the morphological definition of steatohepatitis are *fatty degeneration of liver cells (steatosis)*, predominant in zone 3, *lobular and/or portal field-dominant inflammatory reaction (inflammation)*, direct liver cell damage in the form of *ballooned hepatocytes*, possibly MDB, *fibrosis* and possibly accumulation of iron.

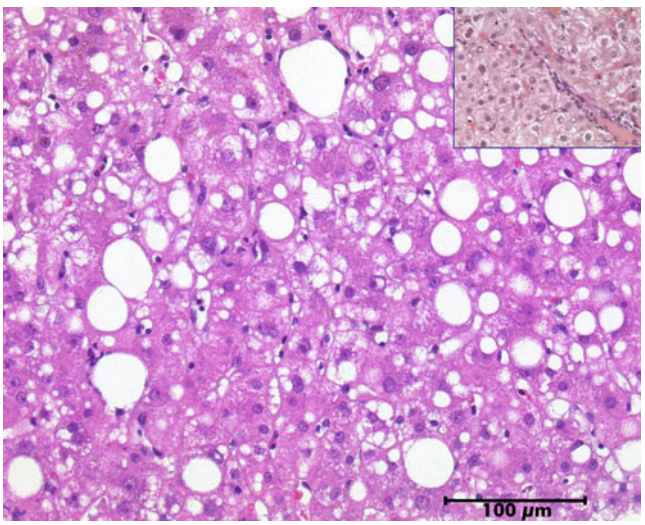

Fig. 2 NASH. Steatosis grade 3, fibrosis grade 1c (*inset*, EvG)

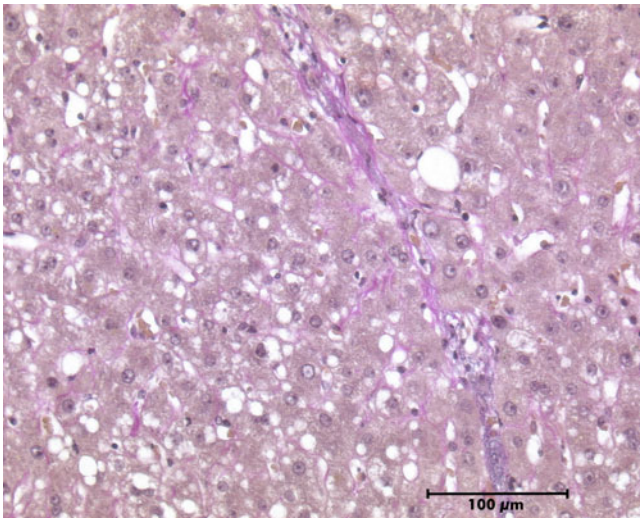

Fig. 3 NASH. Steatosis grade 3, fibrosis grade 2

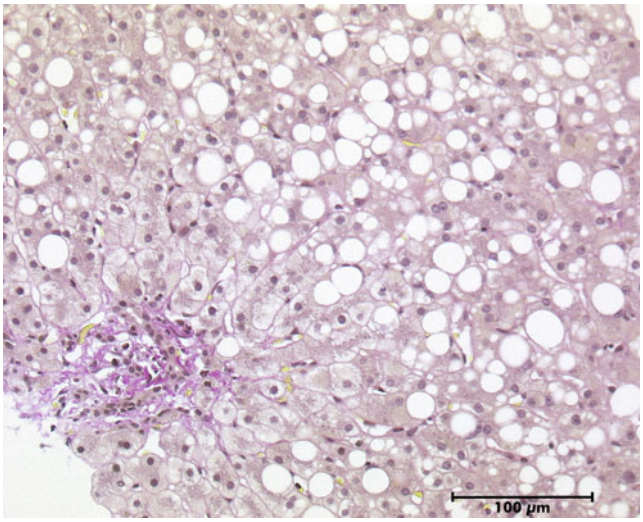

Fig. 5 NASH. Steatosis grade 3, fibrosis grade 1c

– Steatosis

  Fatty degeneration of liver cells is documented in virtually all existing studies on ASH and NASH [4]. Macrovesicular steatosis results from the discrepancy between synthesis of lipids and their export from the hepatocytes. Microvesicular steatosis, a possible precursor of macrovesicular steatosis, is thought to be a consequence of severe hepatocytic damage as a result of defective β-oxidation of fatty acids. The toxic effects of some medicinal drugs can also lead to microvesicular steatosis. In the course of ASH or NASH, there may be complete loss of fat; thus, for example, cryptogenic cirrhosis with only slight fatty degeneration of liver cells is not infrequently ascribable to NASH [16, 62].
– Lobular and/or portal inflammation and hepatocyte ballooning

  ASH and NASH are characterised by a lobular inflammatory cell infiltrate with a variable number of leucocytes. Not infrequently, the inflammatory cells are found to enclose ballooned hepatocytes. So-called lipogranulomas, i.e. inflammatory cells (including Kupffer cells and eosinophilic granulocytes) enclosing a fat-laden hepatocyte, may be seen but are not considered pathognomonic for NASH or ASH [16, 63]. The direct hepatocyte damage is shown by the aforementioned ballooning, which may progress to necrosis or apoptosis. Hepatocytes of zone 3 are affected most frequently [4, 9, 31, 37]. MDB do not contribute to differentiation between ASH and NASH.
– Fibrosis

  The characteristic fibrosis pattern in ASH and NASH is pericellular fibrogenesis. Collagen is found in the Disse spaces. In both ASH and NASH, zone 3 is

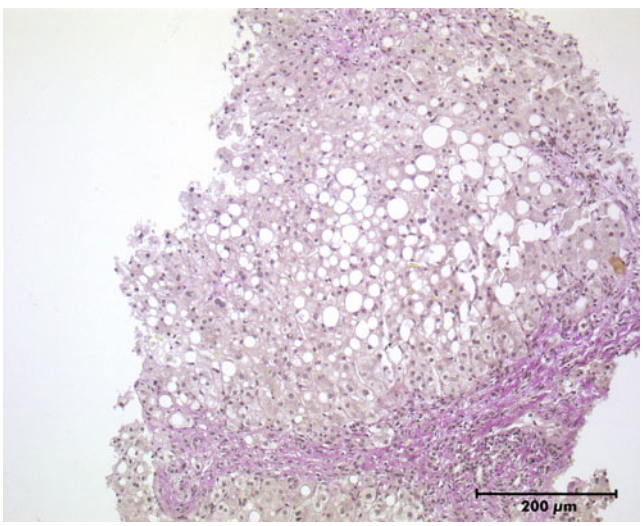

Fig. 4 NASH. Steatosis grade 3, fibrosis grade 4

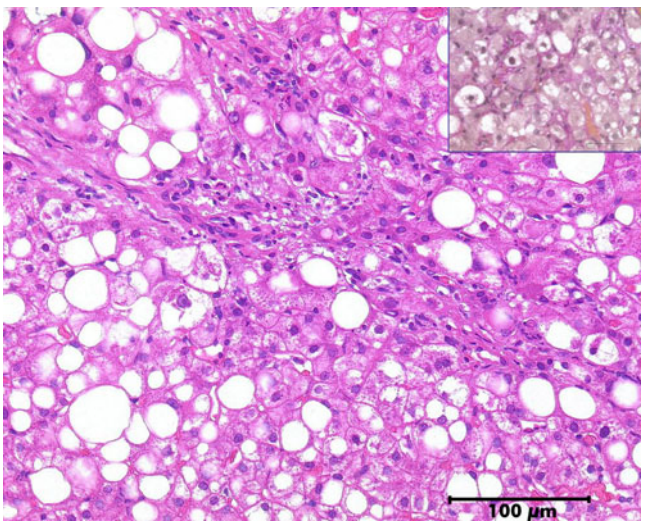

Fig. 6 ASH. Steatosis grade 2, fibrosis grade 2 (*inset*, EvG)

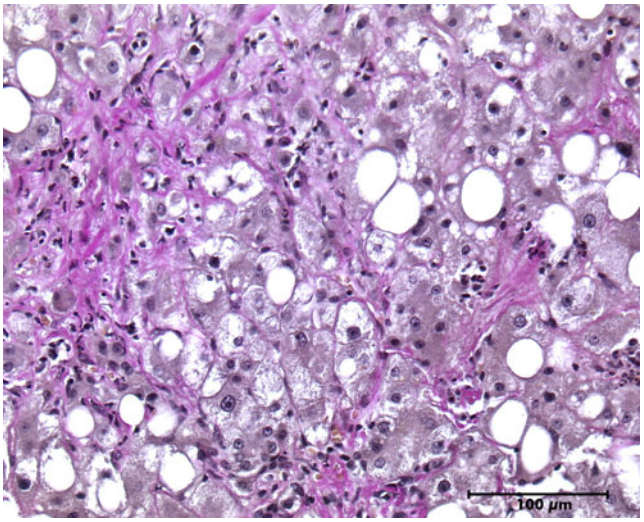

Fig. 7 ASH. Steatosis grad 3, fibrosis grad 3

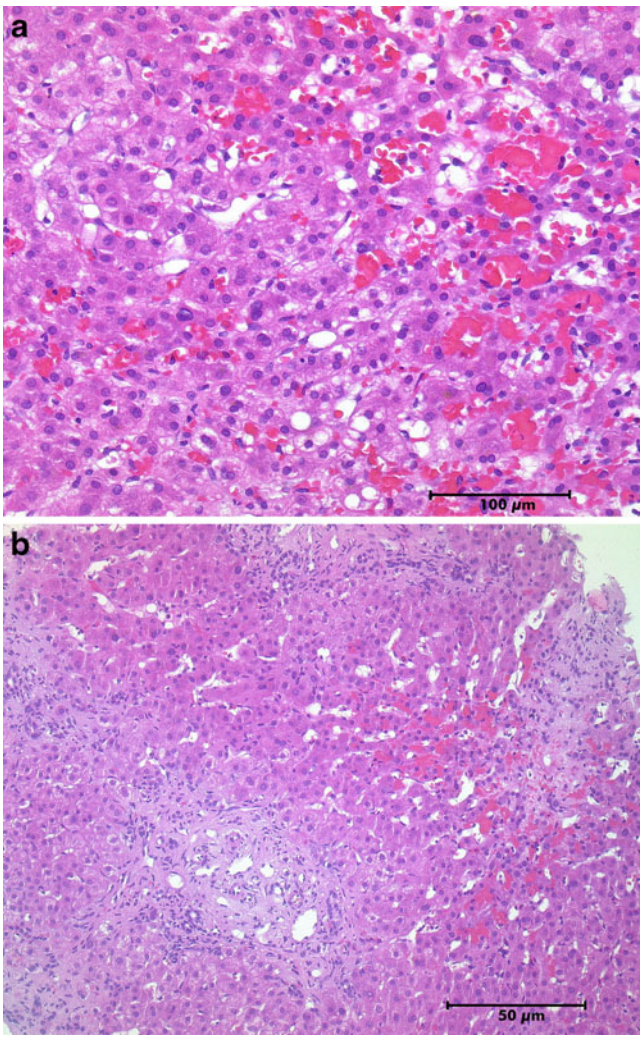

Fig. 8 CASH. Early (**a**) and late stage (**b**), with diffuse haemorrhage

affected first, with periportal fibrosis not infrequently observed in the liver of patients with diabetes mellitus type 1 (NASH patients). It seems that portal field fibrosis tends to predominate in ASH. Taken alone, however, this pattern of fibrosis is not a criterion for differentiation between ASH and NASH.

Differential diagnosis of alcoholic and non-alcoholic steatohepatitis

In general, histological criteria alone do not permit confident differentiation between ASH and NASH [63]. Nevertheless, some findings may be helpful in differential diagnosis [33, 59], although to date there is no published evidence:

- Fat

  Microvesicular steatosis and "foamy" degeneration of the liver seem to indicate incipient hepatic decompensation in patients with ASH and are less common in NASH.

  Patients with NASH usually exhibit more advanced fatty degeneration of liver cells than those with ASH. The affected hepatocytes, concentrated at periportal sites, more frequently display intranuclear vacuoles. In addition to the nuclear vacuoles, patients with diabetes mellitus show fibrosis usually starting in zone 1, where MDB may also be found. Patients with NAFL who display pronounced weight increase or a jejunoileal bypass tend to exhibit portal inflammation with only slight portal fibrosis. Only in decompensated ASH may any appreciable cholestasis occur, usually intracanalicular and sometimes with a secondary phenomenon such as pancreatitis or haemolysis as a contributory cause.

- Inflammation

  As a general rule, the inflammatory infiltrate in NASH is somewhat less pronounced than in ASH. MDB are more frequent and more distinctive in ASH than they are in NASH. So-called satellitosis, granulocytic demarcation of a hepatocyte with MDB, is more frequent in ASH than in NASH.

- Fibrosis

  Indicative, though not specific, for ASH are the so-called sclerosing hyaline necroses, usually in combination with obliterating vascular lesions. The latter are also considered to be responsible for the non-cirrhotic portal hypertension in patients with ASH. Sclerosing hyaline necroses are thought to represent a combination of liver cell necrosis and loss (predominantly in zone 3) and dense perivenular and perisinusoidal fibrosis to the point of venous obliteration (with or without MDB).

Venous or perivenular fibrosis, phlebosclerosis and (less commonly) lymphocytic phlebitis occur more frequently in ASH than in NASH. Phlebosclerosis is a frequent sign of alcohol-associated cirrhosis of the liver. Cholestasis is found in around a third of all livers with ASH, less often in patients with NASH. Ductular proliferates are encountered more frequently in ASH than in NASH.

Criteria for differentiation of ASH and NASH can be seen in Table 4.

Differential diagnosis of ASH, NASH/hepatitis/ drug-induced hepatitis

Differentiation among ASH/NASH, hepatitis C virus infection and liver damage by toxic effects of medications ("drug-induced hepatitis") is possible. In patients exhibiting signs of more than one of these diseases, discussion embracing the clinical parameters is necessary to identify the essential contributory factors.

The characteristic portal inflammatory infiltration pattern of HCV infection permits differentiation from ASH or NASH [64]. Combined manifestations occasionally have to be discussed in the light of the clinical data. Chronic HCV infection can also lead to macrovesicular steatosis. In particular, patients infected with HCV genotype 3 usually show more advanced fatty degeneration. However, the hepatocyte ballooning and intralobular granulocytic inflammation typical of ASH and NASH are absent.

Drug-induced hepatitis is characterised by portal and particularly intra-acinar inflammation that consists principally of neutrophilic and eosinophilic granulocytes. Cholestasis is found, and in severe cases liver cell necrosis. Steatosis does not necessarily occur in drug-induced hepatitis (exceptions include tamoxifen and amiodarone), but is often found in patients who evince certain risk factors (high BMI, diabetes mellitus).

Table 4 Criteria for differentiation of ASH and NASH

Finding	ASH	NASH
Steatosis	+	++
Ballooning	++	++
Lobular inflammation	++	+/++
Portal granulocytic inflammation	++	−−/+
Mallory-Denk bodies (MDB	+++	+
Satellitosis	+++	−−
Acute cholestasis	+	−−
Perisinusoidal fibrosis	+	+
Sclerosing hyaline necrosis	++	−−
Veno-occlusive disease (VOD)	++	−−

Selected drugs that may lead to steatosis are listed in Table 5.

Special form: chemotherapy-associated steatohepatitis

Persons at increased risk of developing fatty liver are in greater danger of developing chemotherapy-associated steatohepatitis (CASH). Close monitoring of liver function before hepatic resection is recommended in these patients. Possible causes of elevation of liver enzymes before initiation of chemotherapy include malignant involvement of the liver and other chronic hepatic diseases as well as fatty liver disease. Liver biopsy may be necessary for differential diagnosis.

Chemotherapy and liver damage

Severe liver changes have been observed following chemotherapy administered in the context of liver resection, particularly extirpation of colorectal metastases. These adverse effects of chemotherapy on the liver tissue around a tumour can lead to postoperative impairment of liver function. The described changes resemble the histological findings after conditioning chemotherapy and subsequent allogenic stem cell transplantation in the liver. The liver damage after chemotherapy depends decisively on the degree of previous liver impairment. Neoadjuvant chemotherapy may be followed not only by sinusoidal obstruction syndrome [65] (SOS), but also by slight steatosis, steatohepatitis or even combined steatohepatitis and SOS [66]. In principal, any of the cell populations in the liver can be affected by drug-induced damage. Cholangiocytes are considered to be relatively inert. Hepatocytes, followed by vascular endothelia, are the primary cell systems in which damage may also be visible on light microscopy. The changes may extend as far as fibrosis, accompanied by vascular wall damage and parenchymal bleeding.

– Fatty degeneration of liver cells

  Fatty degeneration after chemotherapy with 5-fluorouracil (5-FU) is generally considered to be reversible after discontinuation of the treatment. Particularly in the case of pre-existing fatty liver, however, the rate of complications after liver resection is higher. Chemotherapy-induced fatty

Table 5 Selected drugs that may lead to steatosis

Acetylsalicylic acid
Amiodarone
Didanosine, stavudine
MDMA (amphetamines)
Tetracyclines
Valproic acid

degeneration of liver cells can lead to functional impairment after liver resection.

– Steatohepatitis (fatty liver hepatitis)

  It is known that, for example, 5-FU, taxanes or platinum-containing chemotherapeutics exert oxidative stress not only on tumour cells but also on non-neoplastic parenchymal and stromal cells [67]. This prompted the proposal to adopt the term "chemotherapy-associated steatohepatitis" (CASH) [68, 69]. The metabolic pathway of some drugs is known in detail. Thus, the topoisomerase-I inhibitor irinotecan (CPT11) is thought to trigger CASH even in a previously intact liver. The damage is assumed to be predominantly hepatocytic because of the glucuronidation of hepatocytes. Sublethal liver damage may be manifested by hepatocyte ballooning, microvesicular steatosis and finally inflammation with subsequent fibrosis. Like ballooning, hepatocellular cholestasis is considered to be a sign of direct cell damage. In the treatment of colorectal carcinoma irinotecan is almost always used in combination with 5-FU, so the hepatotoxic effects may be additive.

Vascular endothelial damage

The endothelial cells can also be damaged by oxidative stress. Histologically, the vessels are occluded by connective tissue [69–72], with coexisting inflammation, fibrosis and embolic occlusion of small and larger downstream vessels. Damage of these cells in the terminal hepatic venules and sublobular veins causes on the one hand activation of the coagulation cascade (thrombosis) and on the other, hyperfibrinolysis (bleeding). These disseminated intravasal coagulations in the liver result in inflammation and subsequent fibrosis to the point of vascular occlusion. Macroscopically, the affected liver is rich in blood, spongy and livid ("blue liver"); its elasticity is diminished. Here too, the effects of various substances may be additive. Platinum-containing chemotherapeutics (particularly oxaliplatin) also possess high hepatotoxic potential (endothelial damage, sinusoidal lesions, SOS). Resected liver tissue from patients treated with a combination of 5-FU and oxaliplatin reveal, besides sinusoidal lesions with bleeding, vascular thrombosis and vascular fibrosis, signs of CASH, with hepatocytic necrosis, fatty degeneration of liver cells and cholestasis. These changes may be visible as early as 20 days after inception of therapy. The histological changes after administration of site-specific treatments, e.g. monoclonal antibodies against the EGF receptor or VEGF, have not yet been the subject of controlled studies.

– Classification system for staging

  The precise relationship between fatty degeneration of liver cells and SOS has not yet been clearly defined. A further open question is the dose–effect relationship. Moreover, it remains unclear whether the histological changes are reversible. There seems to be no linear correlation between liver damage and elevated liver enzymes in peripheral blood. To date there is neither a clinical nor a histological classification or graduation system that would allow "staging" of the change, much less prediction of the outcome. Therefore, it can merely be recommended that liver function be closely monitored before liver resection in patients at risk of developing fatty liver (e.g. high BMI, metabolic syndrome, diabetes mellitus) [70, 73]. If the liver enzymes are elevated before initiation of chemotherapy and the cause is not tumour involvement, a full battery of laboratory tests may need to be accompanied by liver biopsy to establish the exact extent of fatty degeneration, ballooning or fibrosis. In particular, special attention should be paid to histological processing of the tissue surrounding the metastasis in specimens resected from patients who have undergone chemotherapy.

Special form: paediatric fatty liver disease

Paediatric NASH exhibits histological differences from adult NASH; the sole clinical manifestation is usually a persistent slight elevation in transaminases. Before liver biopsy is considered, other chronic liver diseases should be ruled out and, when indicated, moderate weight reduction achieved. If still required, liver biopsy should then be performed for definitive confirmation of the diagnosis.

The term non-alcoholic fatty liver (NAFL) is not restricted to adults but also used to describe the same condition in children and adolescents [74]. Accordingly, the term non-alcoholic steatohepatitis (NASH) is used in the paediatric age group for the more aggressive form of hepatocellular degeneration accompanied by fibrosis [75, 76].

In about 80% of the affected children and adolescents, the NAFL is discovered incidentally in overweight or obese individuals. The remainder display normal weight but the majority are diabetics.

For assignment of the diagnosis of NAFLD in childhood or adolescence, fat has to make up at least 5–10% of the liver by weight. In analogy to the classification of fatty liver disease in adults, the steatosis is categorised as mild (less than a third of hepatocytes affected), moderate (up to two thirds of hepatocytes affected) or severe (more than two thirds of hepatocytes affected) [77]. Since some 4–8% of Germans in the paediatric age group, i.e. 500,000 to 1 million children and adolescents, are obese [77, 78], around 400,000 are likely to have NAFLD. Among adults with

NAFLD, 1–3% go on to develop cirrhosis of the liver. If this is true for the paediatric age group, then around 4,000 children and adolescents in Germany are at increased risk of early progressive liver fibrosis or cirrhosis. As in adult NAFLD, the only clinical manifestation is usually a persistent slight (one- to twofold) elevation in transaminases. The question of liver biopsy is controversial; nevertheless, there is consensus that, particularly in the event of repeated elevation of liver enzymes, chronic liver diseases such as hepatitis B and C, Wilson's disease and autoimmune hepatitides should first be ruled out. Weight reduction should be attempted. In patients who lose a moderate amount of weight over a period of 6 months but do not achieve normalisation of liver function, liver biopsy should be performed for definitive confirmation of the diagnosis and assessment of the prognosis. If at any time during this period evidence emerges of another disease or a competing or concurrent liver ailment (demonstration of autoantibodies, caeruloplasmin decrease), diagnosis should not be postponed until after weight reduction but ascertained immediately, with liver biopsy if necessary.

Differences between paediatric and adult NAFLD: To date there have been no studies on the prognosis of NAFLD. It also remains unclear what influence puberty and growth have on the time course of the disease. Adult NASH patients have a 25% risk of developing advanced liver fibrosis within 5 years and a 15% risk of cirrhosis in the same period [9]. The significance of ethnicity is hotly debated. Children of Hispanic and Asiatic origin are at greater risk. In contrast to the situation in adults with non-alcoholic liver disease, males are predominantly affected in the paediatric age group [65, 79].

The first study on the histopathology of paediatric NAFLD and hepatitis found that they largely resemble the picture in adult disease, but display differing morphological aspects. With regard to inflammation and fibrosis, two subtypes can be distinguished [60]. In general, the livers of children and adolescents with NASH reveal less lobular and more portal inflammation, and the fibrosis tends to be more portal rather than perisinusoidal [75, 79, 80]. This distinctive histological feature could explain the early progression of the NAFLD score in children and adolescents compared with adults. Biopsy samples exhibit more marked fatty degeneration than in adult NASH. The characteristic ballooning of hepatocytes in adults is also absent, as is the pronounced lobular inflammation with perisinusoidal fibrosis. Only in 12% of cases is paediatric NAFLD histologically comparable to the adult disease [60, 81]. The differential diagnoses include Wilson's disease, other disorders of hepatic metabolism (including rare diseases) and chronic inflammatory bowel diseases, which may manifest as diarrhoea with weight loss. Differentiation from hepatitis is particularly important.

Perspective

At the moment, the question of genetic prevalence of NAFLD and NASH is under investigation and is obviously higher than estimated previously [82]. Recently, several genetic factors such as patatin-like phospholipase 3 or apolipoprotein C3 have been characterised in NAFLD [83, 84].

Even genome-wide association studies of liver histology in patients with non-alcoholic fatty liver disease have been performed to estimate genetic susceptibility to NASH [85]. However, these findings have to be validated especially for the German/European population.

The consensus guideline is an S2-consensus guideline (AWMF S2k) and will be updated by the end of 2013, including all new data concerning genetic variability. When updated and adopted by all participating societies, genetic susceptibility will be included into the revised manuscript.

The question if NASH may be virus-associated, up to now, has been poorly addressed. The authors will include latest findings in the guideline update.

Conflict of interest statement We declare that we have no conflict of interest.

References

1. Ludwig J, Viggiano TR, McGill DB et al (1980) Nonalcoholic steatohepatitis: Mayo Clinic experiences with a hitherto unnamed disease. Mayo Clin Proc 55:434–438
2. Bacon BR, Farahvash MJ, Janney CG et al (1994) Nonalcoholic steatohepatitis: an expanded clinical entity. Gastroenterology 107:1103–1109
3. Ludwig J, McGill DB, Lindor KD (1997) Review: nonalcoholic steatohepatitis. J Gastroenterol Hepatol 12:398–403
4. Burt AD, Mutton A, Day CP (1998) Diagnosis and interpretation of steatosis and steatohepatitis. Semin Diagn Pathol 15:246–258
5. Church TS, Kuk JL, Ross R et al (2006) Association of cardiorespiratory fitness, body mass index, and waist circumference to nonalcoholic fatty liver disease. Gastroenterology 130:2023–2030
6. Dancygier H (2006) Pathogenese und Therapie der nichtalkoholischen Fettlebererkrankungen. Dtsch Ärzteblatt 103:A1301–A1307
7. Farrell GC, Larter CZ (2006) Nonalcoholic fatty liver disease: from steatosis to cirrhosis. Hepatology 43:S99–S112
8. Brunt EM (2001) Nonalcoholic steatohepatitis: definition and pathology. Semin Liver Dis 21:3–16
9. Neuschwander-Tetri BA, Caldwell SH (2003) Nonalcoholic steatohepatitis: summary of an AASLD single topic conference. Hepatology 37:1202–1219
10. Cortez-Pinto H, de Moura MC, Day CP (2006) Non-alcoholic steatohepatitis: from cell biology to clinical practice. J Hepatol 44:197–208
11. Day CP (2006) Non-alcoholic fatty liver disease: current concepts and management strategies. Clin Med 6:19–25

12. Bellentani S, Bedogni G, Miglioli L et al (2004) The epidemiology of fatty liver. Eur J Gastroenterol Hepatol 16:1087–1093
13. Alfire ME, Treem WR (2006) Nonalcoholic fatty liver disease. Pediatr Ann 35:290–299
14. Kacerovsky M, Roden M (2007) Nichtalkoholische Fettleber. Diabetologe 3:176–183
15. Mendez-Sanchez N, Arrese M, Zamora-Valdes D et al (2007) Current concepts in the pathogenesis of nonalcoholic fatty liver disease. Liver Int 27:423–433
16. Caldwell SH, Oelsner DH, Iezzoni JC et al (1999) Cryptogenic cirrhosis: clinical characterization and risk factors for underlying disease. Hepatology 29:664–669
17. Day CP, James OF (1998) Steatohepatitis: a tale of two "hits"? Gastroenterology 114:842–845
18. Day CP (2002) Pathogenesis of steatohepatitis. Best Pract Res Clin Gastroenterol 16:663–678
19. Chitturi S, Abeygunasekera S, Farrell GC et al (2002) NASH and insulin resistance: insulin hypersecretion and specific association with the insulin resistance syndrome. Hepatology 35:373–379
20. Duvnjak M, Lerotic I, Barsic N et al (2007) Pathogenesis and management issues for non-alcoholic fatty liver disease. World J Gastroenterol 13:4539–4550
21. Edmison J, McCullough AJ (2007) Pathogenesis of non-alcoholic steatohepatitis: human data. Clin Liver Dis 11:75–104
22. Medina J, Fernandez-Salazar LI, Garcia-Buey L et al (2004) Approach to the pathogenesis and treatment of nonalcoholic steatohepatitis. Diabetes Care 27:2057–2066
23. Targher G, Bertolini L, Rodella S et al (2006) Associations between plasma adiponectin concentrations and liver histology in patients with nonalcoholic fatty liver disease. Clin Endocrinol (Oxf) 64:679–683
24. Dufour JF, Oneta CM (2004) Alcoholic and non-alcoholic steatohepatitis. Ther Umsch 61:505–512
25. AGA (2002) American Gastroenterological Association medical position statement: nonalcoholic fatty liver disease. Gastroenterology 123:1702–1704
26. Gramlich T, Kleiner DE, McCullough AJ et al (2004) Pathologic features associated with fibrosis in nonalcoholic fatty liver disease. Hum Pathol 35:196–199
27. Sonsuz A, Basaranoglu M, Ozbay G (2000) Relationship between aminotransferase levels and histopathological findings in patients with nonalcoholic steatohepatitis. Am J Gastroenterol 95:1370–1371
28. Wieckowska A, Zein NN, Yerian LM et al (2006) In vivo assessment of liver cell apoptosis as a novel biomarker of disease severity in nonalcoholic fatty liver disease. Hepatology 44:27–33
29. Angulo P, Hui JM, Marchesini G et al (2007) The NAFLD fibrosis score: a noninvasive system that identifies liver fibrosis in patients with NAFLD. Hepatology 45:846–854
30. Kleiner DE, Brunt EM, Van NM et al (2005) Design and validation of a histological scoring system for nonalcoholic fatty liver disease. Hepatology 41:1313–1321
31. Brunt EM, Tiniakos DG (2005) Pathological features of NASH. Front Biosci 10:1475–1484
32. Brunt EM, Tiniakos DG (2002) Pathology of steatohepatitis. Best Pract Res Clin Gastroenterol 16:691–707
33. Brunt EM (2002) Alcoholic and nonalcoholic steatohepatitis. Clin Liver Dis 6:399–420
34. Brunt EM, Ramrakhiani S, Cordes BG et al (2003) Concurrence of histologic features of steatohepatitis with other forms of chronic liver disease. Mod Pathol 16:49–56
35. Brunt EM, Neuschwander-Tetri BA, Oliver D et al (2004) Nonalcoholic steatohepatitis: histologic features and clinical correlations with 30 blinded biopsy specimens. Hum Pathol 35:1070–1082
36. Brunt EM (2005) Pathology of nonalcoholic steatohepatitis. Hepatol Res 33:68–71
37. Brunt EM (2005) Nonalcoholic steatohepatitis: pathologic features and differential diagnosis. Semin Diagn Pathol 22:330–338
38. Falck-Ytter Y, Younossi ZM, Marchesini G et al (2001) Clinical features and natural history of nonalcoholic steatosis syndromes. Semin Liver Dis 21:17–26
39. Matteoni CA, Younossi ZM, Gramlich T et al (1999) Nonalcoholic fatty liver disease: a spectrum of clinical and pathological severity. Gastroenterology 116:1413–1419
40. Ratziu V, Charlotte F, Heurtier A et al (2005) Sampling variability of liver biopsy in nonalcoholic fatty liver disease. Gastroenterology 128:1898–1906
41. Teli MR, James OF, Burt AD et al (1995) The natural history of nonalcoholic fatty liver: a follow-up study. Hepatology 22:1714–1719
42. Mofrad P, Contos MJ, Haque M et al (2003) Clinical and histologic spectrum of nonalcoholic fatty liver disease associated with normal ALT values. Hepatology 37:1286–1292
43. Angulo P, Lindor KD (2002) Non-alcoholic fatty liver disease. J Gastroenterol Hepatol 17(Suppl):S186–S190
44. Neuschwander-Tetri BA (2002) Evolving pathophysiologic concepts in nonalcoholic steatohepatitis. Curr Gastroenterol Rep 4:31–36
45. Joy D, Thava VR, Scott BB (2003) Diagnosis of fatty liver disease: is biopsy necessary? Eur J Gastroenterol Hepatol 15:539–543
46. Adams LA, Talwalkar JA (2006) Diagnostic evaluation of nonalcoholic fatty liver disease. J Clin Gastroenterol 40:S34–S38
47. Wieckowska A, McCullough AJ, Feldstein AE (2007) Noninvasive diagnosis and monitoring of nonalcoholic steatohepatitis: present and future. Hepatology 46:582–589
48. Harrison SA, Torgerson S, Hayashi PH (2003) The natural history of nonalcoholic fatty liver disease: a clinical histopathological study. Am J Gastroenterol 98:2042–2047
49. Younossi ZM, Jarrar M, Nugent C et al (2008) A novel diagnostic biomarker panel for obesity-related nonalcoholic steatohepatitis (NASH). Obes Surg 18(11):1430–1437
50. Castera L, Forns X, Alberti A (2008) Non-invasive evaluation of liver fibrosis using transient elastography. J Hepatol 48:835–847
51. Friedrich-Rust M, Ong MF, Martens S et al (2008) Performance of transient elastography for the staging of liver fibrosis: a meta-analysis. Gastroenterology 134:960–974
52. Bonekamp S, Kamel I, Solga S et al (2009) Can imaging modalities diagnose and stage hepatic fibrosis and cirrhosis accurately? J Hepatol 50:17–35
53. Strassburg CP, Manns MP (2006) Approaches to liver biopsy techniques—revisited. Semin Liver Dis 26:318–327
54. Tannapfel A, Reinacher-Schick A (2008) Chemotherapy associated hepatotoxicity in the treatment of advanced colorectal cancer (CRC). Z Gastroenterol 46:435–440
55. Nocito A, El-Badry AM, Clavien PA (2006) When is steatosis too much for transplantation? J Hepatol 45:494–499
56. Rousselet MC, Michalak S, Dupre F et al (2005) Sources of variability in histological scoring of chronic viral hepatitis. Hepatology 41:257–264
57. Lackner C, Gogg-Kamerer M, Zatloukal K et al (2008) Ballooned hepatocytes in steatohepatitis: the value of keratin immunohistochemistry for diagnosis. J Hepatol 48:821–828
58. Brunt EM, Janney CG, Di Bisceglie AM et al (1999) Nonalcoholic steatohepatitis: a proposal for grading and staging the histological lesions. Am J Gastroenterol 94:2467–2474
59. Brunt EM (2007) Pathology of fatty liver disease. Mod Pathol 20 (Suppl 1):S40–S48

60. Schwimmer JB, Behling C, Newbury R et al (2005) Histopathology of pediatric nonalcoholic fatty liver disease. Hepatology 42:641–649
61. Mendler MH, Kanel G, Govindarajan S (2005) Proposal for a histological scoring and grading system for non-alcoholic fatty liver disease. Liver Int 25:294–304
62. Oneta CM, Dufour JF (2003) Diagnostik, Prognose und therapeutische Möglichkeiten der nicht-alkoholischen Fettlebererkrankung. Schweiz Med Forum 37:862–868
63. Reid AE (2001) Nonalcoholic steatohepatitis. Gastroenterology 121:710–723
64. Sanyal AJ, Banas C, Sargeant C et al (2006) Similarities and differences in outcomes of cirrhosis due to nonalcoholic steatohepatitis and hepatitis C. Hepatology 43:682–689
65. DeLeve LD, Shulman HM, McDonald GB (2002) Toxic injury to hepatic sinusoids: sinusoidal obstruction syndrome (veno-occlusive disease). Semin Liver Dis 22:27–42
66. Karoui M, Penna C, min-Hashem M et al (2006) Influence of preoperative chemotherapy on the risk of major hepatectomy for colorectal liver metastases. Ann Surg 243:1–7
67. Tannapfel A, Geissler F, Witzigmann H et al (2001) Analysis of liver allograft rejection related genes using cDNA-microarrays in liver allograft specimen. Transplant Proc 33:3283–3284
68. Gentilucci UV, Santini D, Vincenzi B et al (2006) Chemotherapy-induced steatohepatitis in colorectal cancer patients. J Clin Oncol 24:5467–5468
69. Zivkovic AM, German JB, Sanyal AJ (2007) Comparative review of diets for the metabolic syndrome: implications for nonalcoholic fatty liver disease. Am J Clin Nutr 86:285–300
70. Aloia T, Sebagh M, Plasse M et al (2006) Liver histology and surgical outcomes after preoperative chemotherapy with fluorouracil plus oxaliplatin in colorectal cancer liver metastases. J Clin Oncol 24:4983–4990
71. Vauthey JN, Pawlik TM, Ribero D et al (2006) Chemotherapy regimen predicts steatohepatitis and an increase in 90-day mortality after surgery for hepatic colorectal metastases. J Clin Oncol 24:2065–2072
72. Nordlinger B, Van CE, Rougier P et al (2007) Does chemotherapy prior to liver resection increase the potential for cure in patients with metastatic colorectal cancer? A report from the European Colorectal Metastases Treatment Group. Eur J Cancer 43:2037–2045
73. Nakano H, Oussoultzoglou E, Rosso E et al (2008) Sinusoidal injury increases morbidity after major hepatectomy in patients with colorectal liver metastases receiving preoperative chemotherapy. Ann Surg 247:118–124
74. Baumann U (2005) Die kindliche Fettlebererkrankung. Dtsch Ärzteblatt 102:A2634–A2639
75. Rashid M, Roberts EA (2000) Nonalcoholic steatohepatitis in children. J Pediatr Gastroenterol Nutr 30:48–53
76. Roberts EA (2002) Steatohepatitis in children. Best Pract Res Clin Gastroenterol 16:749–765
77. Hubscher SG (2004) Role of liver biopsy in the assessment of non-alcoholic fatty liver disease. Eur J Gastroenterol Hepatol 16:1107–1115
78. Moss A, Wabitsch M, Kromeyer-Hauschild K et al (2007) Prevalence of overweight and adiposity in German school children. Bundesgesundheitsblatt Gesundheitsforschung Gesundheitsschutz 50:1424–1431
79. Roberts EA (2007) Non-alcoholic steatohepatitis in children. Clin Liver Dis 11:155–172
80. Papandreou D, Rousso I, Mavromichalis I (2007) Update on non-alcoholic fatty liver disease in children. Clin Nutr 26:409–415
81. Schwimmer JB (2007) Definitive diagnosis and assessment of risk for nonalcoholic fatty liver disease in children and adolescents. Semin Liver Dis 27:312–318
82. Williams CD, Stengel J, Asike MI et al (2011) Prevalence of nonalcoholic fatty liver disease and nonalcoholic steatohepatitis among a largely middle-aged population utilizing ultrasound and liver biopsy: a prospective study. Gastroenterology 140:124–131
83. Valenti L, Alisi A, Galmozzi E et al (2010) I148M patatin-like phospholipase domain-containing 3 gene variant and severity of pediatric nonalcoholic fatty liver disease. Hepatology 52:1274–1280
84. Petersen KF, Dufour S, Hariri A et al (2010) Apolipoprotein C3 gene variants in nonalcoholic fatty liver disease. N Engl J Med 362:1082–1089
85. Chalasani N, Guo X, Loomba R et al (2010) Genome-wide association study identifies variants associated with histologic features of nonalcoholic Fatty liver disease. Gastroenterology 139:1567–1576

Virchows Arch (2011) 458:525–536
DOI 10.1007/s00428-011-1069-y

ORIGINAL ARTICLE

Involvement of HER-2/*neu* and metastasis-related proteins in the development of ileal neuroendocrine tumors

Cinzia Azzoni · Lorena Bottarelli · Stefano Cecchini · Costanza Lagrasta · Silvia Pizzi · Tiziana D'Adda · Elisa Tamburini · Guido Rindi · Cesare Bordi

Received: 7 December 2010 / Revised: 14 March 2011 / Accepted: 17 March 2011 / Published online: 29 March 2011
© Springer-Verlag 2011

Abstract HER-2/neu overexpression and/or gene amplification occurs in several human malignancies, frequently correlates with tumor aggressiveness, and provides the basis for treatment with trastuzumab. Among neuroendocrine neoplasms (NEN) of the gastroenteropancreatic (GEP) tract, ileal neuroendocrine tumors show peculiar features of malignancy with frequent metastases at the diagnosis. We investigated the overexpression and/or amplification of HER-2/*neu* and the involvement of the metastasis-related proteins c-Met, MTA-1, and VEGF in 24 primary ileal NEN by immunohistochemistry and fluorescence in situ hybridization (FISH). Data were compared with those of 43 GEP endocrine tumors of other sites. All primary ileal NEN showed an intense membranous and cytoplasmic immunostaining for HER-2/*neu*. According to the breast cancer scoring system, 17% of ileal carcinoids showed a score of 3+ and 71% with a score of 2+ with a significant difference respect the non-ileal GEP endocrine tumors ($p<0.0000$). FISH analysis revealed chromosome 17 polysomy in 33% of 2+/3+ ileal tumors but not HER-2/*neu* gene amplification. The c-Met and MTA-1 but not VEGF were overexpressed in almost all ileal NEN, whereas VEGF presented more frequently a normal staining. The comparisons with the other GEP NEN demonstrated significant differences for all the three proteins ($p<0.0000$, $p<0.0002$, and $p<0.001$, respectively). These findings suggest that in ileal NEN, HER-2/*neu* overexpression plays a role in the carcinogenetic process and by triggering the altered expression of c-Met and MTA-1, may activate the molecular pathway(s) promoting tumor progression and metastasis development. Ileal HER-2/*neu* overexpressing neuroendrocrine tumors may constitute potential candidates for target therapy with specific humanized monoclonal antibodies.

Keywords HER2/*neu* · c-Met · MTA-1 · VEGF · Ileal neuroendocrine tumors · Polysomy

C. Azzoni · L. Bottarelli · C. Lagrasta · S. Pizzi · T. D'Adda · E. Tamburini · C. Bordi
Department of Pathology, Section of Anatomic Pathology, University of Parma, Parma, Italy

S. Cecchini
Department of Surgery, Institute of General Surgery, School of Medicine, Parma, Italy

G. Rindi
Università Cattolica del Sacro Cuore, Institute of Anatomic Pathology, Roma, Italy

C. Azzoni (✉)
Dipartimento di Patologia e Medicina di Laboratorio, Sezione di Anatomia e Istologia Patologica, Università di Parma, Via Gramsci 14, 43123 Parma, Italy
e-mail: cinzia.azzoni@unipr.it

Introduction

Gastroenteropancreatic (GEP) neuroendocrine neoplasms (NEN) encompass a broad category of tumors composed of cells showing a phenotype similar to that of normal neuroendocrine cells of the gastrointestinal (GI) tract and pancreas. In spite of this, the development of NEN in different GEP locations was found to involve different genes that are associated with distinct abnormalities [1–3].

Among GEP NEN, those arising in the ileum are characterized by pronounced tendency to metastatic spread

mostly to lymph node and liver in contrast with the low levels of cell proliferation shown by the Ki67 index. In these tumors, no proven etiologic factors have been demonstrated and the genetic mechanisms involved in the tumorigenesis are still poorly understood [2, 4]. Using comparative genomic hybridisation in sporadic GEP NEN, Tonnies et al. [1] found that in midgut carcinoids gains (67.2% of aberrations) were more frequent than losses (32.8%) with the higher frequency of gain in chromosomes 17q and 19p (57%).

The region q21 of chromosome 17 harbors the HER-2/neu proto-oncogene (also called c-*erb*B-2) encoding a M_r 185,000 transmembrane glycoprotein ($p185^{HER2/neu}$) with tyrosine kinase activity [5, 6]. This oncogene is a member of the epidermal growth factor receptor family and is overexpressed in many different types of human cancers, including breast, ovarian, oral, gastric, and lung [6–10]. In breast tumors HER-2/*neu* overexpression has been associated with malignancy, metastatic phenotypes, and overall poor survival [5].

The overexpression of HER-2/*neu* is crosslinked with other growth factor-signalling pathways such as IGF-IR [11], which activates the c-Met signalling pathway [12], in turn, linked to the VEGF activation [13]. In this regard, HER-2/neu was found to form heterodimers with IGF-IR, activating c-Met [14]. This is of importance as Met and HER-2/neu have been shown to synergize in promoting cellular invasion, suggesting that tumors expressing both receptors may be more aggressive [15]. Moreover, using stable MDCK cell lines, the Met/HGF receptor has been found to convert an epithelial morphogenic program induced by activated HER-2/neu to cell invasion [16]. In addition, the HER-2/*neu* induces expression of the metastasis-associated protein 1 [metastasis tumor antigen-1 (MTA-1)], a member of a protein family highly conserved through evolution with nuclear regulatory function interacting with specific genes involved in cell regulation, invasion, and progression [17, 18]. In malignant breast epithelial cells and in immortalized human keratinocyte, MTA-1 expression is induced by activation of the heregulin/HER2 pathway [17, 19]. Finally, in NIH 3T3 fibroblasts transfected to overexpress HER-2/neu, VEGF production was found to be increased, an increase blocked by a specific monoclonal antibody directed against HER-2/neu [20].

The present study on a series of ileal NEN was designed to examine: (a) the occurrence of overexpression and/or amplification of HER-2/neu, and (b) the possible involvement of the metastasis-related proteins Met, MTA-1, and VEGF. The results obtained in ileal tumors were compared with those of a series of GEP NEN of different anatomical origin.

Materials and methods

Patients and tissue specimens

The study was performed on 24 cases of malignant primary ileal NEN and in six corresponding metastases. All tumors proved to be composed of EC cells by either serotonin immunostaining and/or Masson–Fontana argentaffin reaction (Table 1). For comparison, 43 malignant NEN from other regions of the GEP tract were also investigated (Table 2). Both series of cases were classified according to the WHO 2010 criteria [21] and ENETS grading and staging [22]. Ethical approval for the study was obtained from the Human Ethics Committee of the University of Parma.

Immunohistochemical staining

All specimens were formalin-fixed and paraffin-embedded. Five-μm sections were stained with hematoxylin and eosin for histological diagnosis and with the following primary monoclonal antibodies: HER-2/neu protein (Dakocytomation, Denmark, working dilution 1:50); Met protein (clone Sc-161, Santa Cruz, Biotechology, USA, working dilution: 1:50); MTA-1 protein (clone Sc-17773, Santa Cruz, Biotechology, USA, working dilution: 1:50), and VEGF protein (clone Sc-7269, Santa Cruz, Biotechology, USA, working dilution: 1:100).

For antigen retrieval, sections were treated with 10-mM citrate at pH 6.0, in a 750-W microwave oven for three 5-min cycles for HER-2/neu protein and with EDTA pH 9.0 using a water bath at 95°C for 40 min for the other three antibodies. The sections were immunostained with the streptavidin–biotin kit (LSAB2, Dako) in accordance with the manufacturer's specifications and counterstained with hematoxylin. Moreover, HER-2/*neu* positive GEP neuroendocrine neoplasms were also tested with the FDA-approved HercepTest (Dakocytomation, Denmark) on adjacent paraffin tissue sections for validation. Positive control tests for HER-2/*neu*, c-Met, and VEGF were conducted on samples of sections from invasive breast carcinomas and for MTA-1 on a malignant glioma samples [23–25]. Negative control tests consisted of either omission of the primary antibody or use of non-immune serum.

Semiquantitative analysis

For HER-2/neu protein in all cases, the degree (weak, moderate or strong) of immunoreactivity (either cytoplasmic or membranous), the pattern (incomplete or complete) of membrane labeling and the rough semiquantitative percentage of immunoreactive neoplastic cells were assessed using the staining intensity of normal mucosa for

Table 1 Clinicopathological data of 24 patients affected by EC cell ileal neuroendocrine tumors

Case	Age	Sex	Size (cm)	WHO 2010 class[a]	Grading[a]	Staging[b]	FU (months)	Analyzed tissues
1	59	M	1.1	NET	G2	IIA	NOD (55)	P
2	65	M	2.5	NET	G1	IIA	NOD (53)	P
3	69	M	1.5	NET	G1	IIA	NOD (64)	P
4	75	M	1	NET	G1	IIA	NOD (71)	P
5	73	F	2	NET	G2	IIA	nd	P
6	75	F	1.7	NET	G1	IIIA	TU (36)	P
7	55	M	1.5	NET	G1	IIIB	NOD (51)	P
8	72	M	5	NET	G1	IIIB	TUD (61)	P
9	66	M	3	NET	G1	IIIB	NOD (74)	P
10	70	M	ns	NET	G1	IIIB	nd	P
11	67	M	4	NET	G1	IIIB	NOD (140)	P
12	75	F	1.5	NET	G1	IIIB	NOD (72)	P, MtLn
13	53	M	3	NET	G2	IIIB	TU (100)	P
14	86	M	5	NET	G1	IIIB	TD (0)	P
15	39	F	1.2	NET	G1	IIIB	nd	P
16	42	F	2.2	NET	G1	IV	AWD (52)	P
17	53	F	3.5	NET	G1	IV	nd	P, MtLn
18	60	F	1.8	NET	G1	IV	AWD (96)	P, MtLn
19	68	F	3	NET	G1	IV	AWD (100)	P
20	53	M	1	NET	G1	IV	AWD (135)	P
21	69	F	1.9	NET	G1	IV	AWD (134)	P, MtLn
22	49	F	ns	NET	G1	IV	NOD (96)	P, MtLn
23	49	F	1.4	NET	G2	IV	NOD (72)	P, MtL
24	61	F	2	NET	G2	IV	AWD (172)	P

[a] According to WHO 2010 [21]

[b] According to WHO 2010 [21] and ENETS 2007 [22, 73]

NET neuroendocrine tumor, *F* female, *M* male, *P* primary tumor, *MtLn* lymph node metastasis, *MtL* liver metastasis, *ns* not specified, *FU* follow-up status, *AWD* alive with disease, *NOD* no evidence of disease, *TD* tumor-related death, *TUD* tumor-unrelated death

reference (control). The tumors were classified using two different systems: (a) the crude percentage of immunoreactive tumor cells (i.e., the sum of cells with either cytoplasmic and/or membranous immunostaining);(b) the FDA-approved (0 to 3+) scoring system for breast carcinoma based on membranous pattern [26]: undetectable staining or staining in <10% of the tumor cells, score 0; faint staining in >10% of the tumor cells, score 1+; weak to moderate complete staining in >10% of the tumor cells, score 2+; and moderate to strong complete staining in >10% of the tumor cells, score 3+.

For the analysis of MTA-1, c-Met and VEGF a four-point scale for nuclear, cytoplasmic, or membranous staining, respectively, was used as follows: (0) no staining, (1) mild staining, (2) moderate staining, and (3) intense staining. In specific, for the Met and MTA-1 immunohistochemistry, the scores 2–3 (H) were considered as altered expression and score 1 (L) and 0 as normal [25, 27, 28]. For VEGF, cases with score 3 were categorized as (H), whereas cases with scores 0–2 were defined as (L) [24].

Fluorescence in situ hybridization

FISH was performed on all ileal tumors as well as on GEP tumors positive at HER-2/*neu* immunohistochemistry. A commercially available dual color FISH kit (PathVision, Vysis, Downers Grove, IL) for simultaneous evaluation of HER-2/*neu* gene and chromosome 17 copy number was used according to the manufacturer's instructions. The slides were counterstained using 4,6-diamino-2-phenylindole and processed with an Olympus BX60 fluorescence microscope equipped with a 100-W mercury lamp. Separate band pass filters were used for the detection of CEP LSI HER-2 orange spectrum and CEP 17 green spectrum probe signals. The slides were examined independently by two expert observers (LC and CA) who were blinded to both the clinical and immunohistochemical data. At least 100 cells of the tumor component were evaluated. In each positive case, polysomy was confirmed in two separate slides. According to the FDA-scoring guidelines [26], specimens with LSI HER-2/neu and CEP 17 signal ratio

Table 2 Clinicopathological data of 43 patients affected by gastroenteropancreatic neuroendocrine neoplasms of non-ileal origin

Case	Age	Sex	Site	Size (cm)	WHO 2010 class[a]	Grading[a]	Staging[b]	FU (months)
1	50	F	Stomach	0.5	NET	G1	I	NOD (120)
2	61	M	Stomach	1.2	NET	G1	IIA	NOD (120)
3	58	M	Stomach	7.0	NET	G2	IIIB	TD (18)
4	40	M	Stomach	3.0	NET	G3	IIIB	TD (24)
5	66	M	Stomach	8.0	NET	G3	IIIB	TD (13)
6	83	F	Stomach	2.5	NEC	G3	IIIB	TD (2)
7	55	M	Stomach	3.0	NEC	G3	IIIB	TD (8.5)
8	76	M	Stomach	7.0	NEC	G3	IIIB	TUD (5)
9	63	M	Stomach	0.4	NEC	G3	IIIB	NOD (54)
10	60	M	Stomach	3.0	NET	G3	IV	TD (15)
11	44	F	Stomach	6.0	NET	G2	IV	TD (84)
12	29	M	Stomach	16.0	NET	G1	IV	TD (12)
13	43	M	Stomach	2.8	NET	G1	IV	NOD (101)
14	55	M	Stomach	3.0	NEC	G3	IV	TD (1)
15	73	M	Stomach	10.0	NEC	G3	IV	nd
16	44	M	Stomach	1.0	NEC	G3	IV	TD (6)
17	62	M	Duodenum	1.5	NET	G2	IIIB	TD (96)
18	47	F	Duodenum	1.2	NET	G1	IV	AWD (113)
19	59	M	Duodenum	0.7	NET	G1	IV	TD (10)
20	87	F	Pancreas	1.8	NET	G2	I	TUD (63)
21	53	F	Pancreas	0.7	NET	G1	I	NOD (84)
22	68	M	Pancreas	3.0	NET	G1	IIA	TUD (19)
23	54	F	Pancreas	4.0	NET	G2	IIIB	nd
24	67	M	Pancreas	3.0	NET	G1	IIIB	TD (133)
25	63	F	Pancreas	4.0	NET	G2	IIIB	AWD (76)
26	51	F	Pancreas	6.0	NET	G2	IV	TD (18)
27	23	F	Appendix	0.5	NET	G1	I	AWD (216)
28	22	F	Appendix	0.8	NET	G1	I	NOD (161)
29	34	F	Appendix	1.0	NET	G1	I	NOD (147)
30	28	F	Appendix	0.6	NET	G1	I	NOD (137)
31	41	M	Appendix	1.1	NET	G1	IIA	NOD (214)
32	13	M	Appendix	1.7	NET	G2	IIA	NOD (226)
33	23	F	Appendix	0.9	NET	G1	IIA	NOD (234)
34	32	F	Appendix	1.4	NET	G2	IIA	NOD (137)
35	71	M	Appendix	0.6	NET	G1	IIA	NOD (67)
36	74	F	Appendix	1	NET	G1	IIIB	NOD (101)
37	77	M	Colon	7.0	NET	G3	IIIB	TD (1)
38	63	F	Colon	4.0	NET	G3	IIIB	NOD (137)
39	81	F	Colon	ns	NET	G3	IV	TD (0.5)
40	68	F	Rectum	0.9	NET	G1	IA	NOD (149)
41	56	M	Rectum	1.0	NET	G1	IB	NOD (134)
42	62	M	Rectum	2.0	NET	G1	IB	NOD (115)
43	67	M	Rectum	ns	NET	G2	IIIB	NOD (19)

[a] According to WHO 2010 [21]

[b] According to WHO 2010 [21] and ENETS 2007 [22, 73]

NEC neuroendocrine carcinoma, *NET* neuroendocrine tumor, *F* female, *M* male, *ns* not specified, *FU* follow-up status, *AWD* alive with disease, *NOD* no evidence of disease, *TD* tumor-related death, *TUD* tumor-unrelated death

greater than or equal to 2.0 were considered amplified; normal specimens showed a ratio less than 2.0. The occurrence of more than two signals for both HER-2/neu and chromosome 17 probes, with a ratio ranging from 1.0 to 2.0 in the majority (>70%) of tumor cells were indicative of polysomy.

Statistical analysis

Data were compared using the chi-square or Fisher exact test corrected for multiple testing. Two-sided p values less than 0.05 were considered statistically significant. These analyses were performed using the SPSS 11.5 statistical software package (SPSS, Inc., Chicago, IL).

Results

The clinical and pathological data on the 24 cases of ileal and 43 cases of non-ileal NEN are represented in Tables 3 and 4. According to the WHO 2010 classification, all ileal neoplasms were defined as NET, whereas NEN of non-ileal origin included both NET and NEC. All ileal tumors proved to be composed of enterochromaffin cells (EC)

Table 3 Immunohistochemical expression and FISH of HER-2/*neu* and immunostaining of the metastasis-related proteins in 24 ileal endocrine tumors and in six metastases

	HER-2/*neu*			Metastasis-related proteins			
Case	Positive cells (%) (type of immunoreactivity)	Degree of intensity	Breast score	FISH	c-MET	MTA-1	VEGF
1	100 (C, M)	Moderate	2+	POL	nd	H	L
2	100 (C, M)	Moderate	2+	Nor	H	H	L
3	100 (C)	Weak	1+	Nor	H	L	L
4	100 (C, M)	Moderate	2+	Nor	nd	H	L
5	100 (C, M)	Strong	2+	Nor	H	nd	L
6	100 (C, M)	Strong	2+	POL	H	H	L
7	100 (C, M)	Moderate	2+	Nor	nd	H	L
8	100 (C, M)	Strong	2+	POL	nd	H	nd
9	100 (M)	Moderate	3+	POL	H	H	L
10	100 (C, M)	Moderate	2+	Nor	H	H	L
10 Mt	100 (C, M)	Strong	3+	Nor	H	H	L
11	100 (M)	Strong	3+	POL	H	H	L
11 Mt	100 (M)	Strong	3+	POL	H	H	L
12	100 (C, M)	Moderate	2+	Nor	H	nd	L
13	70 (C, M)	Strong	2+	POL	H	H	H
14	100 (C, M)	Moderate	2+	Nor	nd	H	L
15	70 (C, M)	Moderate	2+	Nor	H	H	L
15 Mt	80 (C, M)	Moderate	2+	Nor	H	H	L
16	100 (M)	Strong	3+	POL	H	H	nd
17	80 (C, M)	Moderate	2+	Nor	H	H	L
17 Mt	100 (C, M)	Strong	3+	POL	H	H	L
18	100 (C, M)	Moderate	2+	Nor	H	H	L
18 Mt	100 (C, M)	Moderate	2+	Nor	H	H	L
19	100 (M)	Strong	3+	POL	H	H	H
19 Mt	100 (M)	Strong	3+	POL	H	H	H
20	100 (C)	Weak	1+	Nor	H	nd	nd
21	100 (C, M)	Moderate	2+	Nor	H	L	L
22	100 (C, M)	Moderate	2+	Nor	nd	H	nd
23	100 (C, M)	Moderate	2+	Nor	H	nd	L
24	80 (C)	Weak	1+	Nor	nd	H	nd

FISH fluorescence in situ hybridization, *VEGF* vascular endothelial growth factor, *C* cytoplasmic staining, *M* membranous staining, *nor* normal pattern, *POL* polysomy, *H* high expression, *L* normal expression, *nd* not done

Table 4 Immunohistochemical expression and FISH of HER-2/*neu* and immunonostaining of the metastasisis-related proteins in 43 non-ileal gastroenteropancreatic endocrine tumors

	HER-2/*neu*			Metastasis-related proteins			
Case	Positive cells (%)	Degree of intensity	Breast score	FISH	c-MET	MTA-1	VEGF
1	Neg				H	L	H
2	<10% (M, C)	Weak	0	POL	L	nd	L
3	Neg				L	H	L
4	Neg				L	L	nd
5	Neg				L	nd	H
6	Neg				H	L	L
7	Neg				nd	nd	nd
8	20% (M, C)	Moderate	1+	Nor	L	H	nd
9	20% (M, C)	Weak	1+	Nor	L	L	H
10	Neg				L	H	H
11	Neg				nd	nd	nd
12	Neg				nd	nd	nd
13	Neg				L	L	L
14	Neg				L	H	L
15	<10% (C)	Weak	0	Nor	L	H	H
16	30% (M,C)	Moderate	1+	Nor	L	H	H
17	Neg				H	L	L
18	Neg				nd	nd	nd
19	Neg				L	H	H
20	Neg				L	H	H
21	Neg				H	L	H
22	Neg				L	L	H
23	Neg				nd	nd	nd
24	Neg				H	H	H
25	Neg				L	L	L
26	60% (M, C)	Moderate	2+	POL	L	L	L
27	Neg				H	nd	L
28	80% (M, C)	Moderate	2+	POL	H	nd	nd
29	Neg				nd	nd	nd
30	Neg				nd	nd	nd
31	1%	Weak	0	Nor	nd	L	L
32	Neg				nd	L	nd
33	80% (C, M)	Moderate	1+	Nor	nd	L	nd
34	50% (C, M)	Moderate	1+	Nor	nd	L	nd
35	100% (M, C)	Moderate	2+	POL	L	L	H
36	Neg				L	L	nd
37	Neg				nd	L	nd
38	Neg				nd	H	H
39	Neg				L	H	nd
40	Neg				H	H	nd
41	Neg				H	nd	L
42	Neg				nd	L	H
43	Neg				nd	L	H

FISH fluorescence in situ hybridization, *VEGF* vascular endothelial growth factor, *C* cytoplasmic staining, *M* membranous staining, *nor* normal pattern, *POL* polysomy, *H* high expression, *L* normal expression, *nd* not done

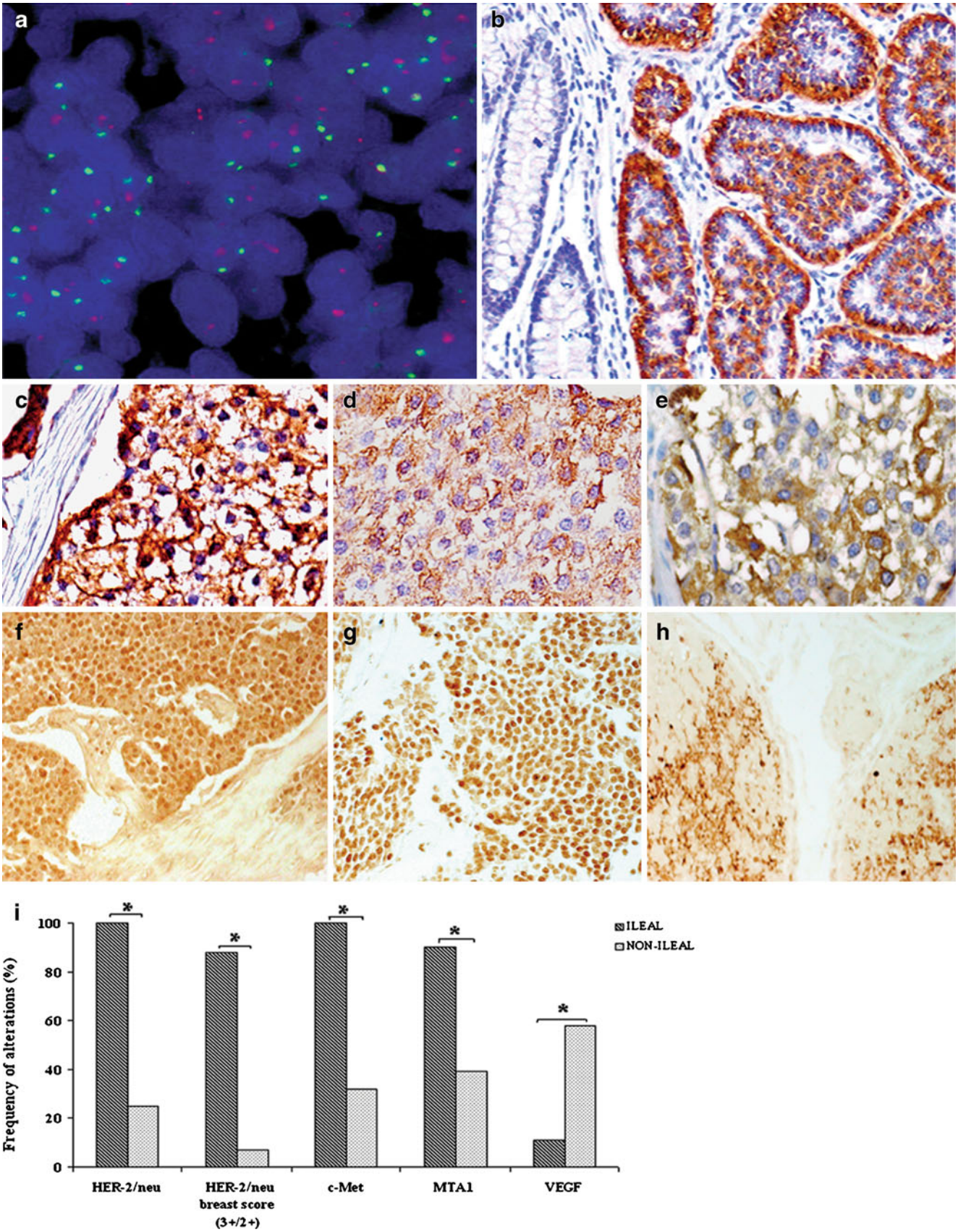
a
b
c
d
e
f
g
h
i
Frequency of alterations (%)
100
80
60
40
20
0
*
ILEAL
NON-ILEAL
HER-2/neu
HER-2/neu breast score (3+/2+)
c-Met
MTA1
VEGF

◀ **Fig. 1** Ileal neuroendocrine tumor with polysomy of chromosome 17 and strong immunohistochemical expression of HER-2/*neu*, c-Met, and MTA-1 proteins. **a** FISH analysis **b** immunohistochemical demonstration of the abnormal expression of HER-2/*neu* in tumor cell clusters with lack of expression in adjacent mucosal glands. **c**–**e** Representative figures for HER-2/*neu* immunohistochemical scores: 3+ (*C*), 2+ (*D*), and 1+ (*E*). **f**–**h** Expression of metastasis-related proteins in tumor cells: c-Met (*F*), MTA-1 (*G*), and VEGF (*H*). **i** Distribution of the alterated expression of HER-2/*neu*, c-Met, MTA-1, and VEGF in ileal and non-ileal GEP neuroendocrine neoplasms. *Showed statistically significant differences between ileal and non-ileal endocrine tumors

cells by either Masson's argentaffin reaction or serotonin immunocytochemistry.

HER-2/neu immunohistochemistry

All 24 ileal NETs showed HER-2/*neu* expression (see Fig. 1b, c, d, e), the crude percentage of immunoreactive tumor cells (i.e., including both cytoplasmic and membranous patterns) being 100% in 20 cases and 70% to 80% in the remaining four cases. In the 43 GEP tumors from other sites, HER-2/*neu* immunoreactivity was present only in 11 cases (25%), five from the stomach, five appendixes, and one from the pancreas. With the exception of one pancreatic and four appendiceal tumors, the crude percentage of immunoreactive cells in non-ileal tumors was low (Table 4, Fig. 1i).

Using FDA breast scoring system [26] based on HER-2/*neu* membranous staining, ileal NET presented score a of 3+ in four cases (17%) (Fig. 1b), score 2+ in 17 cases (71%), and score 1+ in three cases (12%). In non-ileal GEP tumors, a score of 2+ was observed in three cases (7%; one from the pancreas, and two from the appendix) and score 1+ in five cases (11%; three from the stomach and two from the appendix), the remaining 33 cases (75%) being negative (Fig. 1i). These results showed no relation with the tumor grade, whereas it should be noted that no score 3+ cases were present in stage II tumors and no score 1+ cases were present in stage IV tumors. With both score systems, the difference between ileal and non-ileal neoplasms was statistically significant ($p<0.0000$).

The analysis of primary and metastatic tumors in six patients with ileal NET revealed identical results in all cases with the exception of one case of ileal tumor (#22) with increased HER-2/*neu* expression in metastasis (Table 3).

Comparison of results with the rabbit polyclonal antiserum to HER-2/*neu* and the FDA-approved HercepTest in adjacent tumor sections revealed no differences in the percentage of immunoreactive tumor cells, intensity and pattern of staining, and related scoring in all 35 cases analyzed. The normal mucosa adjacent of the tumoral tissue was consistently unreactive for HER-2/*neu* in all cases (Fig. 1b).

HER-2/*neu* FISH

FISH analysis for HER-2/*neu* status was performed in all 24 ileal and in the 11 non-ileal tumors positive for HER-2/*neu* immunohistochemistry.

Chromosome 17 polysomy (3 CEP 17 signals) was detected in 8 of 24 primary ileal tumors (33%), all showing 2+ ($n=4$) or 3+ ($n=4$) scores of membrane labeling (see Fig. 1a). The case with increased HER-2/*neu* expression in the metastasis (#22), displayed polysomy in metastasis only. Among 11 non-ileal tumors, chromosome 17 polysomy was found in four (one each from the stomach and pancreas and two from the appendix) neoplasms. HER-2/*neu* amplification was never observed (Table 4).

c-Met, MTA-1, and VEGF immunohistochemistry

c-Met immunoreactivity was investigated in 17 ileal tumors and in 28 non-ileal endocrine tumors with both cytoplasmic and membranous patterns (Fig. 1f). The immunohistochemical results are summarized in Fig. 1i. The c-Met score H was observed in all 17 ileal NETs (high expressors) and in nine of non-ileal GEP neuroendocrine neoplasms (32%, $p<0.0000$).

MTA-1 protein expression was mainly localized in the nucleus and was assessed in 20 ileal NETs and in 31 non-ileal GEP NEN. Score H immunostaining was found in 18 (90%) of the ileal tumors and in 12 (39%) of the non-ileal neoplams, ($p<0.0002$). The representative immunohistochemical results are shown in Table 3 and Fig. 1g.

Score H cytoplasmic staining of VEGF was found in 2/19 (11%) of ileal tumors and in 15/26 (58%) of non-ileal GEP tumors ($p<0.001$; Fig. 1h). Metastases of ileal NETs showed c-Met, MTA-1, and VEGF expression identical to the corresponding primaries (Table 3).

Results in neuroendocrine tumors of the appendix

All 11 appendiceal tumors proved to be composed of EC cells. Five of them showed extra-appendiceal extension with invasion of the mesoappendix. HER-2/*neu* positivity was concentrated in the latter group comprising the two cases with chromosome 17 polysomy and breast score 2+, one case with score 1+ and one with 80% cytoplasmic immunostaining. No evidence of HER-2/*neu* amplification was found in the intraappendiceal neoplasm and in a single case with extensive mesoappendix and vascular invasion.

Discussion

HER-2/*neu* shares extensive sequence homology with the epidermal growth factor receptor family gene and its

tyrosine kinase activity, following ligand–receptor interaction, triggers intracellular signalling events which are crucial for cell growth, differentiation, and survival [29]. In experimental studies, the overexpression of the HER-2/neu protein has been shown to be an important determinant of malignant transformation, development of metastatic disease, and increased cell proliferation [5, 6]. Additionally, HER-2/*neu* expression is used as a predictive marker, to select candidate patients for anti-HER-2/*neu* monoclonal antibody (trastuzumab) immunotherapy [30].

In this study, Her-2/*neu* status and protein expression were evaluated by IHC and FISH in a series of 24 ileal NETs and compared with that of 43 NEN arising from other GEP regions.

Our results demonstrated that Her-2/*neu* immunoreactivity is markedly expressed in all primary ileal NETs with a statistically significant difference as compared to non-ileal NEN ($p<0.0000$) which were mostly unreactive. Previous studies have shown immunoreactivity for HER-2/*neu* in 30% of 20 midgut NETs of which only six from the ileum [31] as well as in nine intestinal NETs but not in three gastric NETs [32]. However, the limited number of patients included in these studies did not permit to draw any conclusion about the frequency and preferential regional distribution of HER-2/*neu* expression in GEP NEN. Our study performed in a larger number of patients supports a role of HER-2/*neu* in the carcinogenetic process of ileal endocrine tumors.

All ileal NET showed a diffuse and intense positivity of tumoral cells considering both the cytoplasmatic and the membranous immunostaining. The significance of cytoplasmic staining of Her-2/neu protein in view of the membranous location of the Her-2/*neu* receptor has been questioned. Xia et al. [33] suggested that the cytoplasmic staining may be a consequence of the fact that the members of the EGFR family not only function as membrane-associated receptors but are also capable of performing other unknown functions inside or even outside the cell [33]. Cytoplasmic staining of HER-2/neu protein was found to be as an independent prognostic indicator of poor outcome in endometrial cancer [34] and to correlate with gene amplification in breast cancer [35].

Considering only the membranous overexpression, evaluated according the FDA-approved score for breast tumors [26], ileal NET showed score 3+ and 2+ in the 88% of cases. A marked Her-2/*neu* membranous overexpression was already found in other endocrine tumors including papillary thyroid [36], pheochromocytomas [37], and small cell lung carcinomas [38] as well as in nonendocrine tumors including those of esophagus [8], stomach [8, 39], breast [40], head and neck [41], colon [8, 42], and ovary [43]. In all these studies, HER-2/*neu* overexpression inversely correlates with survival and directly with increased invasiveness and aggressive growth, representing an important prognostic factor for many human tumors.

The FISH assay showed chromosome 17 polysomy as the genetic alteration underlying HER-2/*neu* overexpression in eight (33%) ileal NET, whereas no gene amplification was recorded. These findings are similar to those observed in other endocrine tumors, such as in pituitary [44] and thyroid cancer [45], showing concomitant protein overexpression and lack of HER-2/*neu* gene amplification.

HER-2/neu protein overexpression without gene amplification has been found in various nonendocrine tumors such as non-small cell lung cancer [46, 47], prostate [48], and urinary bladder cancer [49]. In breast cancer, most studies have linked chromosome 17 polysomy with greater HER-2 protein overexpression [50–52]. In particular, polysomy of chromosome 17 was found in less extent in advanced bladder [53] and in endometrial carcinomas [54]. In breast cancer, Salido et al. [50] found a statistical association between polysomy 17 and nodal involvement with a trend towards worse prognosis. Similar results were reported in invasive bladder cancer [53] and in endometrial [54] carcinoma.

The chromosome 17 polysomy vs HER-2/*neu* amplification is an important issue in terms of tumor treatment. Established treatment guidelines considered trastuzumab as an effective agent, either single or in combination with chemotherapy, in tumors with Her-2/neu amplification [55, 56]. More recently, however, Hofmann et al. showed response to trastuzumab monotherapy also in patients with 17 polysomy alone [57]. Beyond trastuzumab therapy, a "second wave" of monoclonal antibodies and tyrosine kinase inhibitors has emerged including pertuzumab, inhibiting the dimerization of HER2 with other HER receptors and ertumaxomab, a trifunctional bispecific antibody targeting HER-2 on tumor cells and CD3 on T cells [58, 59]. In particular, in preclinical studies, pertuzumab has inhibitory functions to breast, prostate, and non-small cell lung cancer cell lines, both over- and non-expressing HER-2/*neu* [60].

To further characterize the pathogenetic mechanism of HER-2/*neu* alterations in NEN, we have investigated the expression of the metastasis-related proteins Met, MTA-1, and VEGF whose activation is triggered by the overexpression of HER-2/*neu* and may explain the worst prognosis of the HER-2/*neu* overexpressor tumors [23].

The proto-oncogene c-Met codifies the hepatocyte growth factor receptor that plays an important role in physiological processes such as embryological development, wound healing, tissue regeneration, and morphogenic differentiation, as well as in pathological processes such as angiogenesis, scattering, cellular motility, growth, invasion, differentiation, and migration [61]. The overexpression of c-Met was found to relate with metastasis development and worse prognosis in several types of human cancers [62, 63]. In our study, the high expression of c-Met in ileal HER-2/

neu-overexpressing NET of the ileum is in agreement with a HER-2/*neu*-activating mechanism and may be involved in the frequent metastatic behavior of these tumors.

The nuclear regulatory protein MTA-1 is part of the nucleosome remodeling and deacetylation complex that is involved in transcriptional silencing machinery of mammalian cells repression [18, 64]. The expression of MTA-1 has been found to be associated with several metastatic human cancers and experimental overexpression of MTA-1 in human cell lines promotes cellular migration and invasion, supporting the possible role of MTA-1 in tumor progression and the development of metastasis [18, 65–71]. The overexpression of MTA-1 protein found in 90% of ileal NET may also reflect an activating interaction with HER-2/*neu* and may contribute to metastatic spread of the tumors. Our data are in agreement with the findings of Kidd et al. [72] that found increased expression level of MTA-1 protein in tumor and metastatic tissues of small intestinal EC cell-derived NET and suggested the utility of this marker for identifying metastatic gastrointestinal tumor tissues.

In contrast, the overall unfrequent expression of VEGF in ileal NET as compared to non-ileal NEN does not support a role for such protein in ileal tumors.

The results in NET of the appendix that shared with the ileal one the composition of EC cells were of interest. In this location, the evidence for HER-2/*neu* overexpression was concentrated in the five tumors out of 11 that showed extra-appendiceal extension. Although the data warrant confirmation in additional cases, these results suggest a preferential association of the gene protein overexpression with EC cells and with invasive features.

In summary, HER-2/*neu* overexpression secondary to chromosomal 17 polysomy may play a role in the carcinogenetic process of ileal NET. Such overexpression may trigger the altered expression of metastasis-related proteins Met and MTA-1, potential factors influencing the aggressive behavior of these neoplasms. Finally, the ileal endocrine tumors overexpressing HER-2/*neu* may constitute potential candidates for target therapy involving humanized monoclonal antibodies. Further studies are warranted to assess usefulness of polysomy 17 as a target for therapy in this type of tumors.

Acknowledgment This study was partly supported by a grant from the "Associazione Chiara Tassoni", Parma, Italy.

Conflicts of interest The authors declare no conflicts of interest.

References

1. Tonnies H, Toliat MR, Ramel C et al (2001) Analysis of sporadic neuroendocrine tumours of the enteropancreatic system by comparative genomic hybridisation. Gut 48:536–541
2. Leotlela PD, Jauch A, Holtgreve-Grez H, Thakker RV (2003) Genetics of neuroendocrine and carcinoid tumours. Endocr Relat Cancer 10:437–450
3. Modlin IM, Kidd M, Latich I et al (2005) Current status of gastrointestinal carcinoids. Gastroenterology 128:1717–1751
4. Oberg K (2002) Carcinoid tumors: molecular genetics, tumor biology, and update of diagnosis and treatment. Curr Opin Oncol 14:38–45
5. Hung MC, Lau YK (1999) Basic science of HER-2/neu: a review. Semin Oncol 26:51–59
6. Kaptain S, Tan LK, Chen B (2001) Her-2/neu and breast cancer. Diagn Mol Pathol 10:139–152
7. Tapia C, Glatz K, Novotny H et al (2007) Close association between HER-2 amplification and overexpression in human tumors of non-breast origin. Mod Pathol 20:192–198
8. Ross JS, McKenna B (2001) The HER-2/neu oncogene in tumors of the gastrointestinal tract. Cancer Investig 19:554–568
9. Slamon DJ, Clark GM, Wong SG et al (1987) Human breast cancer: correlation of relapse and survival with amplification of the HER-2/neu oncogene. Science 235:177–182
10. Zhau HE, Wan DS, Zhou J, Miller GJ, von Eschenbach AC (1992) Expression of c-erb B-2/neu proto-oncogene in human prostatic cancer tissues and cell lines. Mol Carcinog 5:320–327
11. Balañá ME, Labriola L, Salatino M et al (2001) Activation of ErbB-2 via a hierarchical interaction between ErbB-2 and type I insulin-like growth factor receptor in mammary tumor cells. Oncogene 20:34–47
12. Tolgay OI, Dolled-Filhart M, D'Aquila TG, Camp RL, Rimm DL (2003) Tissue microarray-based studies of patients with lymph node negative breast carcinoma show that met expression is associated with worse outcome but is not correlated with epidermal growth factor family receptors. Cancer 97:1841–1848
13. Laughner E, Taghavi P, Chiles K, Mahon PC, Semenza GL (2001) HER2 (neu) signaling increases the rate of hypoxia-inducible factor 1alpha (HIF-1alpha) synthesis: novel mechanism for HIF-1-mediated vascular endothelial growth factor expression. Mol Cell Biol 21:3995–4004
14. Katoh R (2003) Angiogenesis in endocrine glands: special reference to the expression of vascular endothelial growth factor. Microsc Res Tech 60:181–185
15. Shattuck DL, Miller JK, Carraway KL 3rd, Sweeney C (2008) Met receptor contributes to trastuzumab resistance of Her2-overexpressing breast cancer cells. Cancer Res 68:1471–1477
16. Khoury H, Naujokas MA, Zuo D et al (2005) HGF converts ErbB2/Neu epithelial morphogenesis to cell invasion. Mol Biol Cell 16:550–561
17. Mazumdar A, Wang RA, Mishra SK et al (2001) Transcriptional repression of oestrogen receptor by metastasis-associated protein 1 corepressor. Nat Cell Biol 3:30–37
18. Toh Y, Pencil SD, Nicolson GL (1994) A novel candidate metastasis-associated gene, mta1, differentially expressed in highly metastatic mammary adenocarcinoma cell lines. cDNA cloning, expression, and protein analyses. J Biol Chem 269:22958–22963
19. Mahoney MG, Simpson A, Jost M et al (2002) Metastasis-associated protein (MTA)1 enhances migration, invasion, and anchorage-independent survival of immortalized human keratinocytes. Oncogene 21:2161–2170
20. Petit AM, Rak J, Hung MC et al (1997) Neutralizing antibodies against epidermal growth factor and ErbB-2/neu receptor tyrosine kinases down-regulate vascular endothelial growth factor production by tumor cells in vitro and in vivo: angiogenic implications for signal transduction therapy of solid tumors. Am J Pathol 151 (6):1523–1530
21. Bosman F, Carneiro F, Hruban R, Theise N (2010) WHO classification of tumours of the digestive system. IARC, Lyon

22. Rindi G, Klöppel G, Couvelard A et al (2007) TNM staging of midgut and hindgut (neuro) endocrine tumors: a consensus proposal including a grading system. Virchows Arch 451:757–762
23. Kim R, Arihiro K, Emi M, Tanabe K, Osaki A (2006) Potential role of HER-2; in primary breast tumor with bone metastasis. Oncol Rep 15:1477–1484
24. Duncan TJ, Al-Attar A, Rolland P et al (2008) Vascular endothelial growth factor expression in ovarian cancer: a model for targeted use of novel therapies? Clin Cancer Res 14:3030–3035
25. Balasenthil S, Broaddus RR, Kumar R (2006) Expression of metastasis-associated protein 1 (MTA1) in benign endometrium and endometrial adenocarcinomas. Hum Pathol 37:656–661
26. Birner P, Oberhuber G, Stani J et al (2001) Evaluation of the United States Food and Drug Administration-approved scoring and test system of HER-2 protein expression in breast cancer. Clin Cancer Res 7:1669–1675
27. Seiwert TY, Jagadeeswaran R, Faoro L et al (2009) The MET receptor tyrosine kinase is a potential novel therapeutic target for head and neck squamous cell carcinoma. Cancer Res 69:3021–3031
28. Li SH, Wang Z, Liu XY (2009) Metastasis-associated protein 1 (MTA1) overexpression is closely associated with shorter disease-free interval after complete resection of histologically node-negative esophageal cancer. World J Surg 33:1876–1881
29. Akiyama T, Sudo C, Ogawara H, Toyoshima K, Yamamoto T (1986) The product of the human c-erbB-2 gene: a 185-kilodalton glycoprotein with tyrosine kinase activity. Science 232:1644–1646
30. Aasland R, Lillehaug JR, Male R et al (1988) Expression of oncogenes in thyroid tumours: coexpression of c-erbB2/neu and c-erbB. Br J Cancer 57:358–363
31. Wang DG, Johnston CF, Buchanan KD (1997) Oncogene expression in gastroenteropancreatic neuroendocrine tumors: implications for pathogenesis. Cancer 80:668–675
32. Yamaguchi M, Hirose K, Hirai N (2007) HER2 expression in gastrointestinal carcinoid tumors: high in intestinal but not in gastric tumors. Surg Today 37:270–271
33. Xia W, Lau YK, Zhang HZ et al (1999) Combination of EGFR, HER-2/neu, and HER-3 is a stronger predictor for the outcome of oral squamous cell carcinoma than any individual family members. Clin Cancer Res 5:4164–4174
34. Lambropoulou M, Stefanou D, Alexiadis G et al (2007) Cytoplasmic expression of c-erb-B2 in endometrial carcinomas. Onkologie 30:495–500
35. Gusterson BA, Gullick WJ, Venter DJ et al (1987) Immunohistochemical localization of c-erbB-2 in human breast carcinomas. Mol Cell Probes 1:383–391
36. Soda G, Antonaci A, Bosco D, Nardoni S, Melis M (1999) Expression of bcl-2, c-erbB-2, p53, and p21 (waf1-cip1) protein in thyroid carcinomas. J Exp Clin Cancer Res 18:363–367
37. de Krijger RR, van der Harst E, van der Ham F et al (1999) Prognostic value of p53, bcl-2, and c-erbB-2 protein expression in phaeochromocytomas. J Pathol 188:51–55
38. Potti A, Willardson J, Forseen C et al (2002) Predictive role of HER-2/neu overexpression and clinical features at initial presentation in patients with extensive stage small cell lung carcinoma. Lung Cancer 36:257–261
39. Park DI, Yun JW, Park JH et al (2006) HER-2/neu amplification is an independent prognostic factor in gastric cancer. Dig Dis Sci 51:1371–1379
40. Koeppen HK, Wright BD, Burt AD et al (2001) Overexpression of HER2/neu in solid tumours: an immunohistochemical survey. Histopathology 38:96–104
41. Cavalot A, Martone T, Roggero N et al (2007) Prognostic impact of HER-2/neu expression on squamous head and neck carcinomas. Head Neck 29:655–664
42. Park DI, Kang MS, Oh SJ et al (2007) HER-2/neu overexpression is an independent prognostic factor in colorectal cancer. Int J Colorectal Dis 22:491–497
43. Verri E, Guglielmini P, Puntoni M et al (2005) HER2/neu oncoprotein overexpression in epithelial ovarian cancer: evaluation of its prevalence and prognostic significance. Clin Study Oncol 68:154–161
44. Ezzat S, Zheng L, Smyth HS, Asa SL (1997) The c-erbB-2/neu proto-oncogene in human pituitary tumours. Clin Endocrinol (Oxf) 46:599–606
45. Bieche I, Franc B, Vidaud D, Vidaud M, Lidereau R (2001) Analyses of MYC. ERBB2, and CCND1 genes in benign and malignant thyroid follicular cell tumors by real-time polymerase chain reaction. Thyroid 11:147–152
46. Schneider PM, Hung MC, Chiocca SM et al (1989) Differential expression of the c-erbB-2 gene in human small cell and non-small cell lung cancer. Cancer Res 49:4968–4971
47. Pelosi G, Del Curto B, Dell'Orto P et al (2005) Lack of prognostic implications of HER-2/neu abnormalities in 345 stage I non-small cell carcinomas (NSCLC) and 207 stage I-III neuroendocrine tumours (NET) of the lung. Int J Cancer 113:101–108
48. Kuhn EJ, Kurnot RA, Sesterhenn IA, Chang EH, Moul JW (1993) Expression of the c-erbB-2 (HER-2/neu) oncoprotein in human prostatic carcinoma. J Urol 150:1427–1433
49. Mellon JK, Lunec J, Wright C et al (1996) C-erbb-2 in bladder cancer: molecular biology, correlation with epidermal growth factor receptors and prognostic value. J Urol 155:321–326
50. Salido M, Tusquets I, Corominas JM et al (2005) Polysomy of chromosome 17 in breast cancer tumors showing an over-expression of ERBB2: a study of 175 cases using fluorescence in situ hybridization and immunohistochemistry. Breast Cancer Res 7:R267–R273
51. Downs-Kelly E, Yoder BJ, Stoler M et al (2005) The influence of polysomy 17 on HER2 gene and protein expression in adenocarcinoma of the breast: a fluorescent in situ hybridization, immunohistochemical, and isotopic mRNA in situ hybridization study. Am J Surg Pathol 29:1221–1227
52. Hyun CL, Lee HE, Kim KS et al. (2007) The effect of chromosome 17 polysomy on HER-2/neu status in breast cancer. J Clin Pathol
53. Latif Z, Watters AD, Dunn I et al (2004) HER2/neu gene amplification and protein overexpression in G3 pT2 transitional cell carcinoma of the bladder: a role for anti-HER2 therapy? Eur J Cancer 40:56–63
54. Cianciulli AM, Guadagni F, Marzano R et al (2003) HER-2/neu oncogene amplification and chromosome 17 aneusomy in endometrial carcinoma: correlation with oncoprotein expression and conventional pathological parameters. J Exp Clin Cancer Res 22:265–271
55. Nahtaa R, Estevaa FJ (2006) Herceptin: mechanisms of action and resistance. Cancer Lett 232:123–138
56. Wolff AC, Hammond ME, Schwartz JN et al (2007) Guideline recommendations for human epidermal growth factor receptor 2 testing in breast cancer. J Clin Oncol 25:118–145
57. Hofmann M, Stoss O, Gaiser T et al (2008) Central HER2 IHC and FISH analysis in a trastuzumab (Herceptin(R)) phase II monotherapy study: assessment of test sensitivity and impact of chromosome 17 polysomy. J Clin Pathol 61:89–94
58. Kiewe P, Hasmuller S, Kahlert S et al (2006) Phase I trial of the trifunctional anti-HER2 x anti-CD3 antibody ertumaxomab in metastatic breast cancer. Clin Cancer Res 12:3085–3091
59. Kiewe P, Thiel E (2008) Ertumaxomab: a trifunctional antibody for breast cancer treatment. Expert Opin Investig Drugs 17:1553–1558
60. Bianco AR (2004) Targeting c-erbB2 and other receptors of the c-erbB family: rationale and clinical applications. J Chemother 16:52–54

61. Birchmeier C, Birchmeier W, Gherardi E, Vande Woude GF (2003) Met, metastasis, motility and more. Nat Rev Mol Cell Biol 4:915–925
62. Di Renzo MF, Olivero M, Giacomini A et al (1995) Overexpression and amplification of the met/HGF receptor gene during the progression of colorectal cancer. Clin Cancer Res 1:147–154
63. Takeuchi H, Bilchik A, Saha S et al (2003) c-MET expression level in primary colon cancer: a predictor of tumor invasion and lymph node metastases. Clin Cancer Res 9:1480–1488
64. Xue Y, Wong J, Moreno GT et al (1998) NURD, a novel complex with both ATP-dependent chromatin-remodeling and histone deacetylase activities. Mol Cell 2:851–861
65. Toh Y, Oki E, Oda S et al (1997) Overexpression of the MTA1 gene in gastrointestinal carcinomas: correlation with invasion and metastasis. Int J Cancer 74:459–463
66. Toh Y, Kuwano H, Mori M, Nicolson GL, Sugimachi K (1999) Overexpression of metastasis-associated MTA1 mRNA in invasive oesophageal carcinomas. Br J Cancer 79:1723–1726
67. Nawa A, Nishimori K, Lin P et al (2000) Tumor metastasis-associated human MTA1 gene: its deduced protein sequence, localization, and association with breast cancer cell proliferation using antisense phosphorothioate oligonucleotides. J Cell Biochem 79:202–212
68. Iguchi H, Imura G, Toh Y, Ogata Y (2000) Expression of MTA1, a metastasis-associated gene with histone deacetylase activity in pancreatic cancer. Int J Oncol 16:1211–1214
69. Sasaki H, Moriyama S, Nakashima Y et al (2002) Expression of the MTA1 mRNA in advanced lung cancer. Lung Cancer 35:149–154
70. Sasaki H, Yukiue H, Kobayashi Y et al (2001) Expression of the MTA1 mRNA in thymoma patients. Cancer Lett 174:159–163
71. Hofer MD, Chang MC, Hirko KA, Rubin MA, Nosé V (2009) Immunohistochemical and clinicopathological correlation of the metastasis-associated gene 1 (MTA1) expression in benign and malignant pancreatic endocrine tumors. Mod Pathol 22:933–939
72. Kidd M, Modlin IM, Mane SM et al (2006) The role of genetic markers—NAP1L1, MAGE-D2, and MTA1—in defining small-intestinal carcinoid neoplasia. Ann Surg Oncol 13:253–262
73. Rindi G, Klöppel G, Alhman H et al (2006) TNM staging of foregut (neuro)endocrine tumors: a consensus proposal including a grading system. Virchows Arch 449:395–401

Virchows Arch (2011) 458:537–546
DOI 10.1007/s00428-011-1067-0

ORIGINAL ARTICLE

Primary neuroendocrine tumors of the main pancreatic duct: a rare entity

Thomas Walter · Valérie Hervieu · Mustapha Adham · Rodica Gincul · Gilles Poncet · Frank Pilleul · Jean-Alain Chayvialle · Christian Partensky · Catherine Lombard-Bohas · Jean-Yves Scoazec

Received: 28 December 2010 / Revised: 5 March 2011 / Accepted: 8 March 2011 / Published online: 23 March 2011
© Springer-Verlag 2011

Abstract Very few cases of primary neuroendocrine tumors of the main pancreatic duct have been reported. This paucity has hampered an accurate description of the distinctive clinical and pathological features of these tumors and the correct evaluation of the diagnostic and therapeutic problems which they may raise. We report here five additional cases in order to underline the clinical, histological, and immunohistochemical features of this tumor entity. There were three male and two female, aged 43–72 years; in all patients, but one, who presented with epigastric pain, the diagnosis was made after the incidental discovery of a dilatation of the main pancreatic duct. The preoperative diagnosis was ductal adenocarcinoma in one case, IPMN in one case and neoplastic stenosis of unknown etiology in four cases. Surgical resection was performed in all cases. The diagnosis of neuroendocrine tumor was made at histological examination. All lesions were small, ranging from 5 to 15 mm. They had a predominantly intramural growth. The growth pattern was nodular in three cases, circumferential in two; there was no intra-luminal component. All cases were well-differentiated neuroendocrine neoplasms of low histological grade (G1); four cases expressed serotonin. One case was associated with regional lymph node metastases. All cases were cured by surgery alone; no recurrence was observed at the end of the follow-up period. In conclusion, despite their rarity, primary neuroendocrine tumors of the main pancreatic duct deserve recognition and must be considered in the etiological diagnosis of ductal stenosis.

Keywords Gastroenteropancreatic neuroendocrine tumors · Main pancreatic duct · Serotonin · Carcinoid tumors

T. Walter · M. Adham · R. Gincul · G. Poncet · J.-A. Chayvialle · C. Partensky · C. Lombard-Bohas
Hospices Civils de Lyon, Hôpital Edouard Herriot,
Fédération des Spécialités Digestives,
Lyon, France

T. Walter · V. Hervieu · G. Poncet · J.-Y. Scoazec
INSERM, UMR S865, IFR62, Faculté Laennec,
Lyon, France

T. Walter · V. Hervieu · M. Adham · F. Pilleul · J.-A. Chayvialle · C. Partensky · J.-Y. Scoazec
Université de Lyon, Université Lyon 1,
Villeurbanne, France

V. Hervieu · J.-Y. Scoazec
Hospices Civils de Lyon, Hôpital Edouard Herriot,
Service Central d'Anatomie et Cytologie Pathologiques,
Lyon, France

F. Pilleul
Hospices Civils de Lyon, Hôpital Edouard Herriot, Service de Radiologie Digestive,
Lyon, France

J.-Y. Scoazec (✉)
Anatomie Pathologique, Hôpital Edouard Herriot,
69437 Lyon, France
e-mail: jean-yves.scoazec@chu-lyon.fr

Introduction

Pancreatic neuroendocrine tumors are rare and heterogeneous tumors with a large spectrum of clinical, biological, and pathological characteristics. Most of them are well-differentiated neuroendocrine neoplasms made of neoplastic cells resembling normal islet endocrine cells [1–4]. They may be either functional (with eutopic or ectopic hormonal secretions, which may be responsible for a clinical syndrome due to excessive hormone production) or nonfunctional. Their course ranges from benign to malignant; malignancy is frequent, with about 50% of cases associated with regional or distant metastases at diagnosis; moreover, the rate of progression of malignant tumors is highly variable, from slow to aggressive. Whereas pancreatic neuroendocrine tumors may be diagnosed because of functional clinical symptoms or because of a tumor mass syndrome, they are now often incidentally diagnosed at imaging studies performed for an unrelated indication. The vast majority of pancreatic neuroendocrine tumors have a predominant intra-parenchymal pattern of growth and rarely involve the pancreatic ducts; however, some large tumors may be responsible for an extrinsic compression or an invasion by contiguity of an adjacent duct: these cases are usually associated with symptomatic complications, such as acute or chronic pancreatitis [5].

A few cases of pancreatic neuroendocrine tumors present with distinctive features, which suggest an origin directly from the pancreatic ducts. They present as minute or small lesions characterized by a predominantly intramural pattern of growth along the main or the secondary pancreatic ducts, with no or minimal limited invasion of the adjacent pancreatic parenchyma and no intra-ductal component. A handful of such tumors have been reported in the literature [6–10]. The paucity of observations and their publication as isolated case reports have so far hampered the recognition of the salient features distinguishing this tumor entity.

We were therefore prompted to report the results of a retrospective study of five cases of neuroendocrine tumors deriving from the main pancreatic duct, all diagnosed in our institution, in order: (a) to underline their characteristic clinical and morphological features, (b) to discuss the possible histogenesis of this tumor entity, and (c) to point out to the diagnostic and therapeutic problems raised by these rare tumors

Material and methods

Inclusion criteria

The files of the Departments of Pathology and Surgery, Hôpital Edouard Herriot, Lyon, were reviewed in order to find all cases fulfilling the following criteria: (a) patients diagnosed and treated in our institution between 1990 and 2010; (b) pancreatic neuroendocrine tumor having its main development in the wall of the main pancreatic duct or of secondary ducts and showing only limited invasion of the adjacent parenchyma; (c) clinical charts, initial pathological reports, archival tissue material, and complete follow-up available.

Study group

The study group consisted of five patients retrieved from the files of the Departments of Pathology and Surgery, Hôpital Edouard Herriot, Lyon, and referred to our institution between 1990 and 2009. During the same period, 225 cases of pancreatic neuroendocrine tumors were referred to our institution for diagnosis and/or treatment.

Clinical charts and laboratory data were analyzed. The original pathological reports, and all the available histological material were reviewed; additional immunohistochemical studies were performed when necessary. Complete follow-up was obtained for all patients; the end of follow-up period was December 1, 2010.

Clinical and laboratory data

The following information were recorded: sex, age at diagnosis, circumstances of diagnosis, results of imaging studies, evidence of regional and distant metastases, treatment, duration of follow-up, status at the end of follow-up period. Among the laboratory data, the serum levels of amylase, lipase, and of the following tumor markers: carcinoembryonic antigen, CA 19–9, and chromogranin A, were recorded when available.

Pathological data

The following macroscopical data were extracted from the original reports: location within the pancreas, maximal tumor size, associated lesions. All the available histological material was reviewed by two experienced pathologists (JYS and VH) in order to evaluate the following parameters: degree of morphological differentiation, extent of local invasion, evidence of angioinvasion, and/or perineural invasion.

Immunohistochemical studies were performed in all cases to detect the following markers: chromogranin A (clone DAK-A3, Dako, Glostrup, Denmark), synaptophysin (clone 27 G12, Novocastra, Newcastle upon Tyne, UK), NCAM (clone C56-504, Novocastra), CDX2 (clone CDX2-88, Biogenex, San Ramon, CA, USA), Islet1 (polyclonal antibody, Abcam, Cambridge, UK), somatostatin receptor type 2A (BioTrend, Cologne, Germany), and to evaluate

the expression of the following hormones: serotonin (clone 5HT-H209, Dako), somatostatin (polyclonal, INSERM U45, Lyon, France), gastrin (polyclonal, INSERM U45), insulin (clone 2D11-H5, Novocastra), glucagon (clone K79bB10, Sigma, St Louis, MI, USA), pancreatic polypeptide (polyclonal, INSERM U45), ghrelin (clone Ab57222, Abcam), calcitonin (polyclonal, Dako). The mitotic index and the Ki67 index were determined according to the current recommendations [11].

Tumors were classified according to the WHO classifications of 2000 [12] and 2010 [13] for gastroenteropancreatic neuroendocrine tumors. They were graded according to ENETS proposals [11]. For TNM classification, various schemes were tested and compared: ENETS proposals for the TNM classification of pancreatic endocrine tumors [11], UICC criteria for the TNM classification of pancreatic tumors, which includes endocrine tumors and tumors of the pancreatic ducts [14].

Results

Clinical, biological, and imaging features

There were three male and two female patients, aged from 43 to 72 years (Table 1). Only one patient (patient #2) was symptomatic and presented with epigastric pain. The four other patients were asymptomatic; their pancreatic lesion was diagnosed incidentally at imaging studies performed for an unrelated indication: exploration of peripheral arterial ischemia (patient #4) or rectal hemangioma (patient #1), workout of abnormal liver tests (patient #3), follow-up of prostate cancer (patient #5). There was no evidence of functional hormonal syndrome in any patient. There was no familial history of neuroendocrine tumor in any patient. Serum levels of amylase and lipase, as well as serum levels of tumor markers (including carcinoembryogenic antigen and CA 19–9 in all patients and chromogranin A in patients #1, #2, and #4) were within the normal range.

Abdominal imaging studies included abdominal CT scan associated with abdominal MRI in four cases and endoscopic ultrasound examination in four patients. In all cases, a segmental dilation of the main pancreatic duct was present; it was located in the head of the pancreas in two cases (patients #3 and #4), in the body in one case (patient #1), and in the tail in two cases (patients #2 and #5). In addition, in four patients, it was possible to demonstrate the existence of a localized stricture of the main pancreatic duct located just at the tip of the dilated segment; this stricture was interpreted as secondary to a mass located within the duct wall and protruding within the lumen. The radiological diagnosis was ductal adenocarcinoma in one case (patient #3), IPMN in one case (patient #1), and neoplastic stenosis of unknown etiology in the four remaining cases.

In three patients (cases #3, 4, and 5), endoscopic ultrasonography was performed. It showed an interruption of the main pancreatic duct by a stenosing, ill-defined, isoechoic mass. Brushing cytology and biopsies were attempted in one case (patient #3), but they were non-contributive to the diagnosis because of insufficient material.

Pathological features

Macroscopical features

In all cases, macroscopical examination confirmed the presence of a localized stenosis of the main pancreatic duct, measuring 5–15 mm in length (Table 1). In three cases (patients #1, 2, and 3), the narrowing of the lumen of the main pancreatic duct was due to a small tumor mass, measuring 5–15 mm, nodular, yellowish, well-demarcated, developed within the wall of the duct, and focally extending within the adjacent pancreatic parenchyma. In the two other cases (patients #4 and 5), the stenosis was secondary to a dense circumferential fibrosis of the duct wall, without clearly identifiable tumor tissue. In all cases, the distal part of the duct was mildly or moderately dilated. Lesions of chronic obstructive pancreatitis, including fibrosis and loss of parenchymal tissue, were present; their distribution was focal in two cases (patients #3 and 4) and lobular in the three other cases.

Histological features

Histological examination confirmed the existence of two different patterns of growth. In three cases (patients #1, 2, and 3), the tumor formed a well-demarcated mass, originating from the wall of the main pancreatic duct and extending within the adjacent pancreatic parenchyma (Fig. 1a). The tumor invaded a variable portion of the circumference of the duct and protruded within its lumen. The abluminal part of the tumor nodule was sometimes demarcated by a fibrous capsule (patient #3), but was usually ill-limited, with direct but limited invasion of the adjacent glandular tissue.

In the two other cases (patients #4 and 5), the pattern of growth was mainly intramural. Tumor cells grew in a circumferential manner along the main pancreatic duct, which was markedly thickened by a dense fibrosis (Fig. 1b); focally, the thickening of the duct wall was so marked as to result in a near complete obstruction of the lumen (Fig. 1c); in one patient (patient #5), tumor cells spread along the adjacent collateral ducts in the same circumferential manner (Fig. 2a).

Table 1 Clinical and pathological features of the five patients included in the present study

	Patient 1	Patient 2	Patient 3	Patient 4	Patient 5
Gender	Male	Female	Female	Male	Male
Age at diagnosis (years)	57	53	53	43	72
Presenting symptoms	None	Epigastric pain	None	None	None
Type of surgery	Median pancreatectomy	Splenopancreatectomy	PDPP	PDPP	Splenopancreatectomy
Size of the tumor (mm)	11	15	5	8	10
Growth pattern	Nodular	Nodular	Nodular	Circumferential	Circumferential
Angioinvasion	–	–	–	–	–
Perineural invasion	–	–	–	–	+
Surgical resection	R0	R0	R0	R0	R0
LN+/LN	0/1	0/5	0/3	1/7	0/6
Mitotic index	<1	<1	<1	<1	<1
Ki67 index	<2%	<2%	<2%	<2%	<2%
Hormonal profile	Serotonin, somatostatin, insulin, glucagon	Serotonin	Serotonin	Serotonin	Serotonin
WHO classification (2000)	Well-differentiated endocrine tumor, benign behavior	Well-differentiated endocrine tumor, benign behavior	Well-differentiated endocrine tumor, benign behavior	Well-differentiated endocrine carcinoma	Well-differentiated endocrine tumor, uncertain behavior
WHO classification (2010)	Neuroendocrine neoplasm, G1	Neuroendocrine neoplasm, G1	Neuroendocrine neoplasm, G1	Neuroendocrine neoplasm, G1	Neuroendocrine neoplasm, G1
TNM (ENETs)	T1N0M0	T1N0M0	T1N0M0	T1N1M0	T1N0M0
TNM (UICC)	T1N0M0	T1N0M0	T1N0M0	T1N1M0	T1N0M0
Status	Alive	Deceased	Alive	Alive	Alive
Follow-up (months)	76	12	126	30	13

PDPP pancreaticoduodenectomy with pylorus preservation, *LN+/LN* lymph node involvement among total lymph node resected, *NA* nonapplicable, *R0* surgical margins with free of tumor

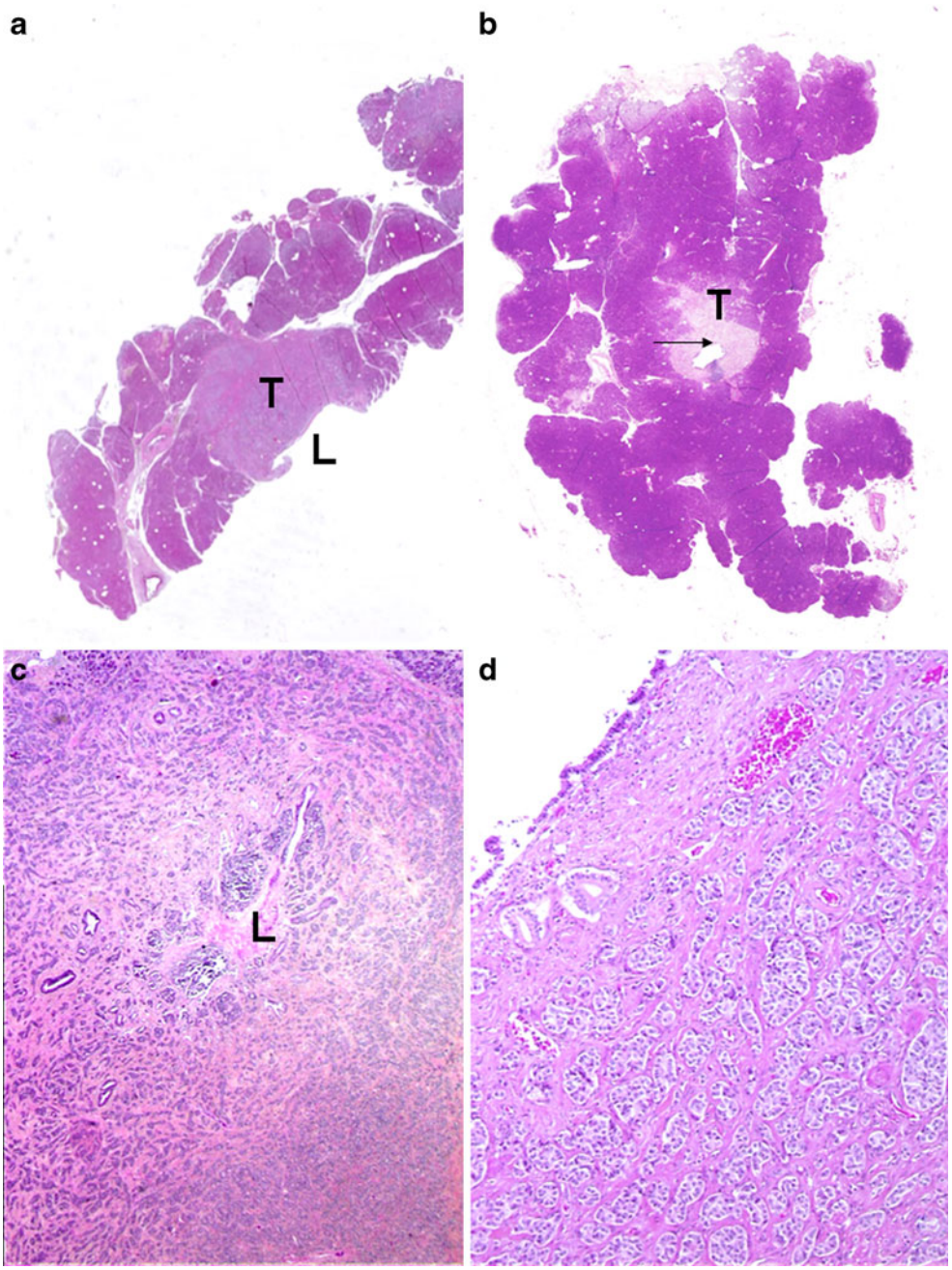

Fig. 1 Histological features. At low magnification (**a** and **b**), the two patterns of growth are well-recognizable. In the first pattern (**a**, whole mount of a hemi-section of the surgical specimen open longitudinally along the main pancreatic duct), the endocrine tumor (*T*) forms a nodular mass bulging from the duct wall (*L*, lumen) within the adjacent pancreatic parenchyma (patient #3). The other growth pattern observed in our study (**b**, whole mount of a transversal section of the surgical specimen) is circumferential; the tumor tissue (*T*) induces a major thickening of the duct wall, inducing a stenosis of the lumen (*arrow*); there is only a minimal invasion of the adjacent parenchyma (patient #5). At higher magnification (**c**), tumor cell nests present within the coarse fibrous tissue thickening the duct wall is readily visible; the lumen (*L*) is almost completely obliterated (patient #5). At an even higher magnification (**d**), the typical architectural pattern of this tumor is well-visible: tumor cells form nests and plates scattered within a dense extracellular matrix (patient #1). Hematoxylin-eosin-saffron; original magnifications: **a**, ×25; **b**, ×25; **c**, ×70; **d**, ×310

At a higher magnification, irrespectively of their growth pattern, all tumors displayed the same overall appearance, typical of a well-differentiated endocrine neoplasm. Tumor cells were arranged in thick plates or in small nests, separated by large fibrous septa, containing small capillary vessels (Fig. 1d). They were small to medium-sized, with an abundant eosinophilic cytoplasm, well-defined cytoplasmic limits and a central nucleus containing a "salt and pepper" chromatin. Mitoses were rare; the mitotic index ranged from 0 to 1. In three cases (patients #1, 4, and 5), endocrine tumor nests were present within the surface epithelium of the duct (Fig. 2b). No evidence of angio-invasion was found in any case. Perineural invasion was found in one case (patient #5). Regional lymph node metastases were detected in one case (patient #4). In all cases, the surgical resection was complete.

In three patients (patients # 1, 3, and 5), numerous endocrine cells were readily visible within the epithelium lining of the main pancreatic duct (Fig. 2d); they remained either isolated or formed linear aggregates or small nests along the basement membrane.

Immunohistochemical features

The neuroendocrine nature of tumor cells was confirmed in all cases by their expression of chromogranin A (Fig. 2a) and

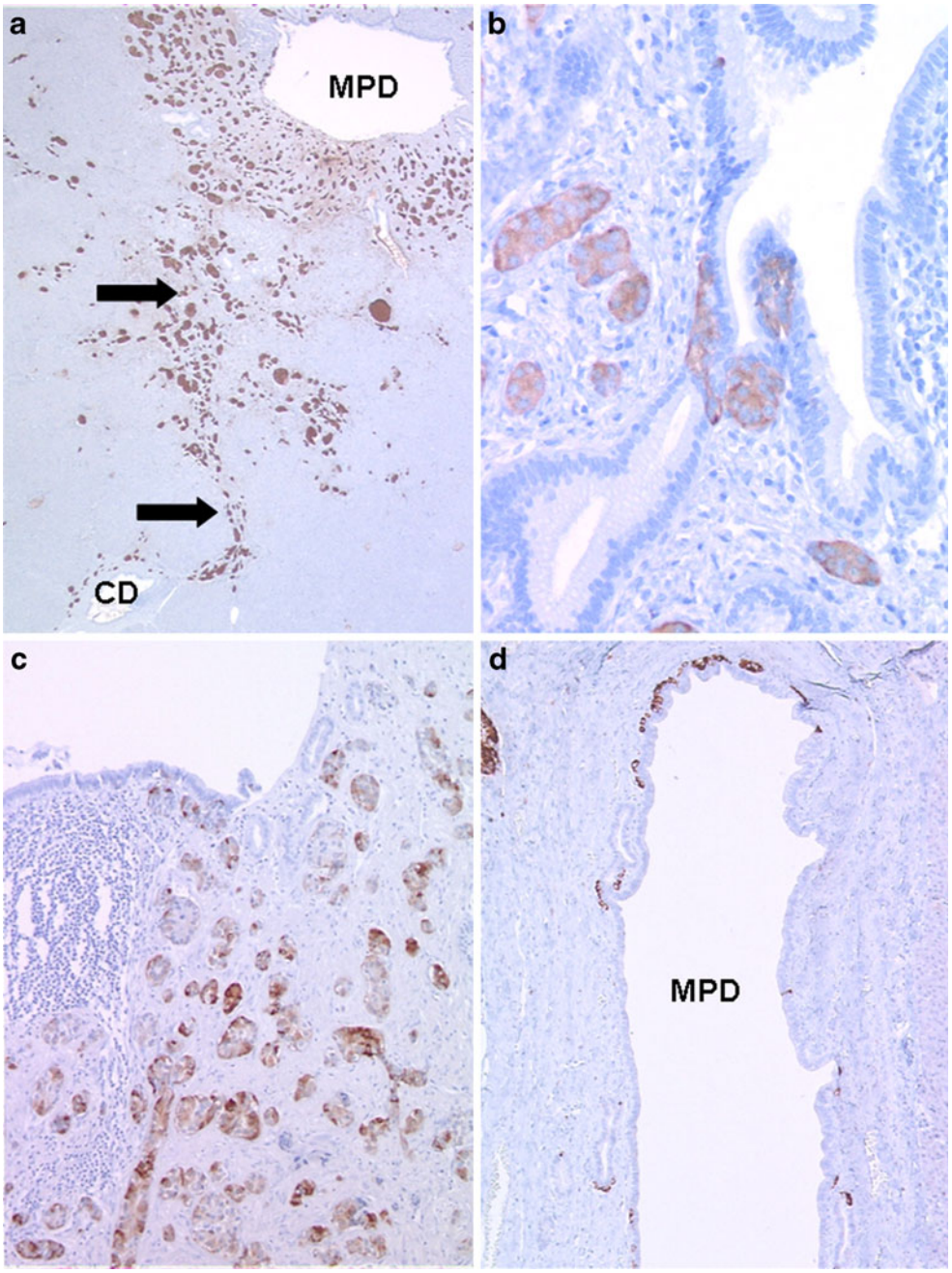

Fig. 2 Immunohistochemical features. The neuroendocrine nature of the tumor is confirmed by the strong expression of chromogranin A (**a**) by neoplastic cells; in this picture taken at very low magnification, the growth pattern of the tumor is well-visible: the tumor involves the wall of the main pancreatic duct (*MPD*) in a circumferential manner and spreads along collateral ducts (*CD*) (*arrows*) (patient #5). In **b**, nests of neoplastic endocrine cells positive for synpatophysin are visible within the epithelial lining of the main pancreatic duct. In **c**, serotonin expression in the majority of endocrine tumor cells is readily visible (patient #2). In **d**, low magnification of a segment of the main pancreatic duct (*MPD*) adjacent to the tumor shows the presence of numerous endocrine cells isolated or grouped in small contiguous nests within the lining epithelium (patient #1). Immunoperoxidase with nuclear counterstaining by Mayer's hematoxylin; original magnifications: **a**, ×40; **b**, ×380; **c**, ×210; **d**, ×110

synaptophysin (Fig. 2b). No expression of cytokeratins 7 and 20 was detectable. Among the hormones tested, serotonin was detected in the majority of tumor cells in four cases (Fig. 2c). In one case (patient #1), serotonin was detected in about 10% of cells, in addition to a few cells positive for somatostatin, insulin, and glucagon (patient #1). Four cases presented immunoreactivity for somatostatin receptor type 2A. CDX2 and Islet1 were undetectable in all cases. Ki67 index was <2% in all cases.

Endocrine cells visible in large numbers along the pancreatic excretory ducts contained various cell populations, expressing serotonin, glucagon, pancreatic polypeptide and, occasionally, gastrin.

Classification, grading, and staging

All tumors were well-differentiated neuroendocrine neoplasms of low histological grade (G1 according to ENETS criteria [11]). By analogy with the 2000 WHO classification of pancreatic endocrine tumors [12], three cases (patients #1, 2, and 3) could be classified as well-differentiated endocrine tumors of benign behavior, one case (patient #5)

was classified as well-differentiated endocrine tumor of uncertain behavior because of the presence of perineural invasion, and the remaining case (patient #4) was classified as well-differentiated endocrine carcinoma because of the presence of regional lymph node metastases. According to the 2010 WHO classification of gastroenteropancreatic neuroendocrine tumors [13], all tumors were classified as neuroendocrine tumors, grade 1.

Various systems for TNM classification were compared. According to the ENETS proposals for the TNM classification of pancreatic neuroendocrine tumors [11], all tumors would have been T1N0M0 (stage I), except one (patient #4), which would have been T1N1M0 (stage IIIb). According to the UICC criteria classification for pancreatic tumors, identical for both neuroendocrine tumors and tumors of the pancreatic ducts [14], four cases would have been classified as T1N0M0 and 1 as T1N1M0.

Treatment and clinical course

All patients underwent surgery. The type of surgical resection depended on the location of the pancreatic lesion (Table 1). Pancreaticoduodenectomy with pylorus preservation was performed in two cases (patients #3 and #4), median pancreatectomy in one case (patient #1), and splenopancreatectomy in two cases (patients #2 and #5). There were no early or late post-operative complications in any case. No adjuvant therapy was performed. Octreotide scintigraphy was performed after surgical treatment in two cases; no residual disease was detected.

The duration of follow-up ranged from 12 to 126 months. At the date of the end of the follow-up period, all patients were alive, without evidence of disease; there were no evidence of local recurrence or of regional or distant metastasis.

Discussion

We report here a series of five cases of primary neuroendocrine tumors of the main pancreatic duct, characterized by their main development within the wall of the pancreatic ducts, with limited invasion of the adjacent parenchymal tissue and no evidence of intra-ductal involvement. Their growth pattern, as well as their clinical presentation and histological features, are different from those of the majority of pancreatic neuroendocrine tumors, often referred in the older literature as to “islet cell tumors”.

Primary neuroendocrine tumors of the pancreatic ducts seem to be exceedingly rare. In our institution, they accounted for less than 2% of all neuroendocrine tumors of the pancreas. An extensive search of the English literature has produced only six cases described in sufficient detail to be identified as representative of the same entity [6–10]: their characteristics are summarized in Table 2. Some other cases reported in the literature [15–17] may also belong to the same entity, but the information provided does not allow an unequivocal distinction between a primary endocrine tumor originating from a pancreatic duct and an intra-parenchymal tumor with secondary infiltration of a pancreatic duct.

Based on the previously published cases and on our own series of five patients, the salient features of the primary neuroendocrine tumors of the main pancreatic duct may be summarized as follows: (a) these tumors always are minute or small, ranging from 5 to 15 mm in diameter; (b) they result in a localized stricture and/or stenosis of the main pancreatic duct, which, in turn, is responsible for an upstream dilatation of the excretory ducts and of lesions of chronic obstructive pancreatitis, clinically asymptomatic; (c) they present as well-differentiated neuroendocrine neoplasms of low histological grade; (d) their architecture recalls that of the so-called *carcinoids* of the distal ileum and the appendix and is characterized by the presence of tumor nests or plates separated by large fibrous septa; in addition, tumor cells express frequently, but not constantly, serotonin, as in four of our cases and in several previously reported cases [7, 9, 10]; (e) these tumors are localized, follow a benign course and are curable by surgery alone.

The involvement of pancreatic ducts by a primary intramural neuroendocrine tumor must be distinguished from the other types of excretory duct involvement by pancreatic endocrine tumors. The most frequent situation is the secondary infiltration or the indirect compression of an excretory duct by an otherwise typical neuroendocrine tumor of parenchymal origin [5, 18–21]. In this situation, the clinical presentation and the pathological features are usually very different from those associated with our cases: (a) the clinical picture is usually severe, with symptomatic acute or chronic pancreatitis; (b) the endocrine tumor is usually large; (c) its histological and morphological characteristics lie within the spectrum of conventional pancreatic neuroendocrine tumors; (d) direct infiltration of the excretory duct by tumor cells is not constant; when it occurs, it clearly results from the entrapment of the excretory duct by a primarily intra-parenchymal tumor [5]; (e) most of these tumors behave as malignant tumors and present with lymph node and/or distant metastases at diagnosis [21]. The second situation is represented by the rare cases of pancreatic endocrine tumors with intra-ductal growth [22–32], defined by the presence of a large intra-luminal tumor mass, obliterating the lumen of an excretory duct, which may be isolated or, more commonly, connected to an adjacent intra-parenchymal mass. Any of our cases was associated with an intra-luminal component.

Table 2 Main characteristics of the previously published cases of primary neuroendocrine tumors of the main pancreatic duct

Reference	Sex	Age at diagnosis	Circumstances of diagnosis	Location	Imaging features	Tumor size (cm)	Tumor architecture	Hormonal pattern	Type of surgery	Stage at diagnosis
Sarles et al. (1988) [6]	F	58	Epigastric pain	Body	Dilatation of MPD	1	"Carcinoid"-like	Insulin, glucagon and somatostatin	Distal P	N0M0
Nagai et al. (1992) [7]	M	66	Incidental discovery	Body	Dilatation of MPD	ND	"Carcinoid"-like	Serotonin	Distal P	N0M0
Dei Tos et al. (1993) [8]	M	49	Abdominal pain	Head	Dilatation of MPD	1	"Carcinoid"-like	PP, gastrin and calcitonin	PD	N0M0
Kim et al. (2005) [9]	M	50	Epigastric pain	Body	Dilatation of MPD	1	"Carcinoid"-like	Serotonin	PD	N0M0
Hamada et al. (2009) [10]	1 F	48	Incidental discovery	Body	Dilatation of MPD	0.7	"Carcinoid"-like	Serotonin	PD	N0M0
	2 F	69	Epigastric pain	Body	Dilatation of MPD	0.8	"Carcinoid"-like	Serotonin	Distal P	N0M0

M male, *F* female, *MPD* main pancreatic duct, *PP* pancreatic polypeptide, *P* pancreatectomy, *PD* pancreaticoduodenectomy, *N* node metastasis, *M* distant metastasis

Primary neuroendocrine tumors of the pancreatic duct have many features in common with the slightly less rare primary neuroendocrine tumors of the extra-hepatic bile ducts [33–37]. Like their pancreatic counterparts, biliary tumors usually are minute or small lesions lying within the wall of the excretory duct and show an overall architecture recalling that of ileal "carcinoids"; again like their pancreatic counterparts, biliary tumors usually express serotonin; finally, like their pancreatic counterparts, biliary tumors usually follow an indolent course, even in the presence of signs of local invasion or of regional lymph node dissemination. It is likely that neuroendocrine tumors of both pancreatic and biliary ducts derive from the endocrine cells normally associated with the pancreato-biliary epithelium. This hypothesis is supported by the frequent expression of serotonin observed in these neuroendocrine neoplasms, which is in agreement with the fact that serotonin-producing enterochromaffin cells are the predominant endocrine population found in the normal pancreato-biliary epithelium [38]. However, it must be recalled that rare pancreatic neuroendocrine tumors without any obvious connection with pancreatic ducts and presenting as typical "islet cell tumors" may also express serotonin [39–41]. Interestingly, in some of our cases, we observed unusually large numbers of normal endocrine cells within the epithelial lining of the pancreatic ducts adjacent to the neuroendocrine tumor: this suggests the possible existence of a degree of peritumoral endocrine hyperplasia, which, however, remains difficult to demonstrate in the absence of precise quantitative data about the normal density of endocrine cells along pancreatic ducts.

Primary neuroendocrine tumors of the main pancreatic duct raise some diagnostic and therapeutic problems. Their diagnosis is usually post-operative, at histological examination of a surgical specimen. In our series, as in the cases reported so far [10], the pre-operative diagnosis suggested by imaging and endoscopic studies was adenocarcinoma involving the main pancreatic duct when stenosis was predominant or intraductal papillary and mucinous neoplasm, when duct dilatation was the prominent radiological sign. However, a correct pre-operative diagnosis may be obtained by endoscopically guided brushing or biopsy, as shown in one of the previously reported cases [8]; unfortunately, the rate of false-negative results is high, as shown by our own experience, in agreement with previous literature data [6]. Obtaining a correct pre-operative diagnosis would be of major importance in deciding the surgical strategy. In view of the highly localized character of the tumor and of its benign course, parenchyma-sparing pancreatic resections, including median pancreatectomy, can be successfully used and may be preferred to larger resections. No adjuvant therapy is required.

In conclusion, we report here the distinctive clinical and pathological features of the primary neuroendocrine tumors of the main pancreatic duct, which, despite their extreme rarity, deserve recognition and must be included in the differential diagnosis of pancreatic duct stenosis.

Conflict of interest statement We declare that we have no conflict of interest.

References

1. Modlin IM, Oberg K, Chung DC, Jensen RT, de Herder WW, Thakker RV, Caplin M, Delle Fave G, Kaltsas GA, Krenning EP, Moss SF, Nilsson O, Rindi G, Salazar R, Ruszniewski P, Sundin A (2008) Gastroenteropancreatic neuroendocrine tumours. Lancet Oncol 9:61–72
2. Davies K, Conlon KC (2009) Neuroendocrine tumors of the pancreas. Curr Gastroenterol Rep 11:119–127
3. Capelli P, Martignoni G, Pedica F, Falconi M, Antonello D, Malpeli G, Scarpa A (2009) Endocrine neoplasms of the pancreas: pathologic and genetic features. Arch Pathol Lab Med 133:350–364
4. Falconi M, Plockinger U, Kwekkeboom DJ, Manfredi R, Korner M, Kvols L, Pape UF, Ricke J, Goretzki PE, Wildi S, Steinmuller T, Oberg K, Scoazec JY (2010) Well-differentiated pancreatic nonfunctioning tumors/carcinoma. Neuroendocrinology 84:196–211
5. Obara T, Shudo R, Fujii T, Tanno S, Mizukami Y, Izawa T, Saitoh Y, Satou S, Kohgo Y (2000) Pancreatic duct obstruction caused by malignant islet cell tumors of the pancreas. Gastrointest Endosc 51:604–607
6. Sarles H, Cambon P, Choux R, Payan MJ, Odaira S, Laugier R, Sahel J (1988) Chronic obstructive pancreatitis due to tiny (0.6 to 8 mm) benign tumors obstructing pancreatic ducts: report of three cases. Pancreas 3:232–237
7. Nagai E, Yamaguchi K, Hashimoto H, Sakurai T (1992) Carcinoid tumor of the pancreas with obstructive pancreatitis. Am J Gastroenterol 87:361–364
8. Dei Tos AP, Laurino L, De Boni M, Doglioni C (1993) Preoperative cytodiagnosis of primitive carcinoid tumor of the Wirsung duct: a case report with immunocytochemical study. Diagn Cytopathol 9:471–474
9. Kim HC, Park SI, Park SJ, Shin HC, Oh MH, Kim CH, Kim TY, Kim HH, Bae WK, Kim IY (2005) Pancreatic carcinoid tumor with obstructive pancreatitis: multislice helical CT appearance: case report. Abdom Imaging 30:601–604
10. Hamada Y, Nakayama Y, Maeshiro K, Ikeda T, Hayashi H, Iwasaki H (2009) Two cases of primary carcinoid tumor of the pancreas associated with marked stenosis of the main pancreatic duct. Pancreas 38:834–835
11. Rindi G, Kloppel G, Alhman H, Caplin M, Couvelard A, de Herder WW, Erikssson B, Falchetti A, Falconi M, Komminoth P, Korner M, Lopes JM, McNicol AM, Nilsson O, Perren A, Scarpa A, Scoazec JY, Wiedenmann B (2006) TNM staging of foregut (neuro)endocrine tumors: a consensus proposal including a grading system. Virchows Arch 449:395–401
12. Solcia E, Klöppel G, Sobin L (2000) Histological typing of endocrine tumours, 2nd edn. Springer, New York
13. Rindi G, Klimstra DS, Arnold R, Klöppel G, Bosman FT, Komminoth P, Capella C, Solcia E (2010) Nomenclature and classification of neuroendocrine neoplasms of the digestive system. In: Bosman FT, Carneiro F, Hruban RH, Theise ND (eds) WHO classification of tumours of the digestive system. IARC, Lyon, pp 13–14
14. Sobin LH, Gospodarowicz MK, Wittekind C (2009) TNM classification of malignant tumors, 7th edn. Wiley, New York
15. Odaira C, Choux R, Payan MJ, Bockman DE, Sarles H (1987) Chronic obstructive pancreatitis, nesidioblastosis, and small endocrine pancreatic tumor. Dig Dis Sci 32:770–774
16. Jukemura J, Montagnini AL, Perini MV, de Almeida JL, Rodrigues JJ, da Cunha JE (2006) Acute pancreatitis associated with neuroendocrine tumor of the pancreas. JOP 7:56–61
17. Uemura K, Murakami Y, Hayashidani Y, Sudo T, Hashimoto Y, Ohge H, Sasaki T, Arihiro K, Sueda T (2009) Main pancreatic duct obstruction due to a small nonfunctioning endocrine tumor of the pancreas. Hiroshima J Med Sci 58:45–48
18. Simpson WF, Adams DB, Metcalf JS, Anderson MC (1988) Nonfunctioning pancreatic neuroendocrine tumors presenting as pancreatitis: report of four cases. Pancreas 3:223–231
19. Pech O, Lingenfelser T, Wunsch P (2000) Pancreatic glucagonoma as a rare cause of chronic obstructive pancreatitis. Gastrointest Endosc 52:562–564
20. Ramsay D, Gibson P, Edmunds S, Mendelson R (2001) Pancreatic islet cell tumours presenting as recurrent acute pancreatitis: imaging features in three cases. Australas Radiol 45:520–523
21. Azumi Y, Isaji S, Kato H, Kuriyama N, Kishiwada M, Hamada T, Mizuno S, Usui M, Sakurai H, Tabata M, Inoue H, Katsurahara M, Takei Y, Uchida K, Shiraishi T (2009) A case of a tiny (1.2 cm) non-functioning pancreatic endocrine tumor invading the main pancreatic duct successfully treated by laparoscopy-assisted distal pancreatectomy with splenectomy. Suizo 24:717–725
22. Shimizu K, Shiratori K, Toki F, Suzuki M, Imaizumi T, Takasaki K, Kobayashi M, Hayashi N (1999) Nonfunctioning islet cell tumor with a unique pattern of tumor growth. Dig Dis Sci 44:547–551
23. Kitami CE, Shimizu T, Sato O, Kurosaki I, Mori S, Yanagisawa Y, Ajioka Y, Hatakeyama K (2000) Malignant islet cell tumor projecting into the main pancreatic duct. J Hepatobiliary Pancreat Surg 7:529–533
24. Terada T, Kawaguchi M, Furukawa K, Sekido Y, Osamura Y (2002) Minute mixed ductal-endocrine carcinoma of the pancreas with predominant intraductal growth. Pathol Int 52:740–746
25. Akatsu T, Wakabayashi G, Aiura K, Suganuma K, Takigawa Y, Wada M, Kawachi S, Tanabe M, Ueda M, Shimazu M, Sakamoto M, Kitajima M (2004) Intraductal growth of a nonfunctioning endocrine tumor of the pancreas. J Gastroenterol 39:584–588
26. Kawakami H, Kuwatani M, Hirano S, Kondo S, Nakanishi Y, Itoh T, Asaka M (2007) Pancreatic endocrine tumors with intraductal growth into the main pancreatic duct and tumor thrombus within the portal vein: a case report and review of the literature. Intern Med 46:273–277
27. Inagaki M, Watanabe K, Yoshikawa D, Suzuki S, Ishizaki A, Matsumoto K, Haneda M, Tokusashi Y, Miyokawa N, Sato S, Kasai S (2007) A malignant nonfunctioning pancreatic endocrine tumor with a unique pattern of intraductal growth. J Hepatobiliary Pancreat Surg 14:318–323
28. Eto K, Kawakami H, Kuwatani M, Haba S, Hirano S, Kondo S, Kubota K, Matuno Y, Hirayama A, Gotouda Y, Asaka M (2009) A malignant pancreatic neuro-endocrine tumor with intraductal growth within the main pancreatic duct and tumor thrombus within the splenic vein. Suizo 24:537–547
29. Fassan M, Pizzi S, Pasquali C, Parenti AR (2009) Pancreatic endocrine tumor in multiple endocrine neoplasia type 1 syndrome with intraductal growth into the main pancreatic duct. Pancreas 38:341–342
30. Itoh T, Nakayama N, Kikuyama M, Kajiwara T, Yoshizawa A, Manabe T (2009) Endocrine tumor of the pancreas with intraductal spreading. Suizo 24:527–531
31. Chetty R, El-Shinnawy I (2009) Intraductal pancreatic neuroendocrine tumor. Endocr Pathol 20:262–266

32. Kobayashi S, Asakura T, Ohike N, Enomoto T, Sakurai J, Koizumi S, Watanabe T, Nakano H, Otsubo T (2010) Mixed acinar-endocrine carcinoma of the pancreas with intraductal growth into the main pancreatic duct: report of a case. Surg Today 40:380–384
33. Maitra A, Krueger JE, Tascilar M, Offerhaus GJ, Angeles-Angeles A, Klimstra DS, Hruban RH, Albores-Saavedra J (2000) Carcinoid tumors of the extrahepatic bile ducts: a study of seven cases. Am J Surg Pathol 24:1501–1510
34. Hubert C, Sempoux C, Berquin A, Deprez P, Jamar F, Gigot JF (2005) Bile duct carcinoid tumors: an uncommon disease but with a good prognosis? Hepatogastroenterology 52:1042–1047
35. Modlin IM, Shapiro MD, Kidd M (2005) An analysis of rare carcinoid tumors: clarifying these clinical conundrums. World J Surg 29:92–101
36. Nesi G, Lombardi A, Batignani G, Ficari F, Rubio CA, Tonelli F (2006) Well-differentiated endocrine tumor of the distal common bile duct: a case study and literature review. Virchows Arch 449:104–111
37. Albores-Saavedra J, Batich K, Hossain S, Henson DE, Schwartz AM (2009) Carcinoid tumors and small-cell carcinomas of the gallbladder and extrahepatic bile ducts: a comparative study based on 221 cases from the surveillance, epidemiology, and end results program. Ann Diagn Pathol 13:378–383
38. Carlei F, Barsotti P, Crescenzi A, Bologna M, Muzi P, Schietroma M, Lomanto D, LeZoche E, Simi M, Speranza MS (1993) Neuroendocrine epithelial cells of the main pancreatic ducts and ampulla. Ital J Gastroenterol 25:171–173
39. Maurer CA, Baer HU, Dyong TH, Mueller-Garamvoelgyi E, Friess H, Ruchti C, Reubi JC, Büchler MW (1996) Carcinoid of the pancreas: clinical characteristics and morphological features. Eur J Cancer 32A:1109–1116
40. Mao C, el Attar A, Domenico DR, Kim K, Howard JM (1998) Carcinoid tumors of the pancreas. Status report based on two cases and review of the world's literature. Int J Pancreatol 23:153–164
41. Soga J (2005) Carcinoids of the pancreas: an analysis of 156 cases. Cancer 104:1180–1187

Virchows Arch (2011) 458:547–559
DOI 10.1007/s00428-011-1065-2

ORIGINAL ARTICLE

Measurement of human epidermal growth factor receptor type-2 extracellular domain and cancer antigen 15–3 levels in needle washout fluid: a potential adjunct to the cytological diagnosis of breast cancer

Shu Ichihara · Suzuko Moritani · Masaki Hasegawa · Misaki Shiraiwa · Mikinao Oiwa · Tokiko Endo · Aya Kato · Takako Hayashi · Yasuyuki Sato · Akiko Saito

Received: 28 October 2010 / Revised: 10 February 2011 / Accepted: 14 February 2011 / Published online: 25 March 2011
© Springer-Verlag 2011

Abstract To determine whether the measurement of biomarkers in the needle washout fluid after fine needle aspiration cytology could strengthen cytological diagnosis, 29 benign lesions, 26 ductal carcinomas in situ (DCIS), and 95 invasive carcinomas of the breast were analyzed. Immediately after the aspiration samples were expelled onto glass slides, the needle was rinsed out with 2 ml of saline. Human epidermal growth factor receptor two extracellular domain (HER2-ECD) and cancer antigen 15–3 (CA 15–3) in the washout fluid were measured using chemiluminescence. The measuring limit for HER2-ECD (0.5 ng/ml) and that for CA 15–3 (4 U/ml) were used as the cutoff values, respectively. The proportion of patients with positive HER2-ECD values was 6.9% in cases of benign lesions, 26.9% in DCIS, and 10.5% in invasive carcinomas. The proportion of patients with positive CA 15–3 values was 6.9% in cases of benign lesions, 42.3% in DCIS, and 10.5% in invasive carcinomas. The proportion of patients with any biomarker elevation was 6.9% in cases of benign lesions, 46.2% in DCIS, and 15.8% in invasive carcinomas. Thus, biomarker elevation was most frequent in cases of DCIS, followed by invasive carcinomas ($P<0.01$). HER2-ECD values over 6 ng/ml or CA 15–3 values over 25 U/ml were seen exclusively in cases of DCIS or invasive ductal carcinomas with an extensive intraductal component. If the biomarker status is included, 5 of 12 cases of DCIS with equivocal cytology categories would be upgraded. Further clinicopathological validation is necessary before applying this new approach to the clinical setting.

Keywords Ductal carcinoma in situ · Biomarker · Chemiluminescence · Cytology · Cystic hypersecretory carcinoma · Extensive intraductal component

S. Ichihara (✉) · S. Moritani · M. Hasegawa
Department of Pathology,
National Hospital Organization Nagoya Medical Center,
Aichi 460-0001, Japan
e-mail: shu-kkr@umin.ac.jp

M. Shiraiwa · M. Oiwa · T. Endo
Department of Radiology,
National Hospital Organization Nagoya Medical Center,
Aichi 460-0001, Japan

A. Kato · T. Hayashi · Y. Sato
Department of Surgery,
National Hospital Organization Nagoya Medical Center,
Aichi 460-0001, Japan

A. Saito
Laboratory of Clinical, Epidemiological and Health Services Research, Clinical Research Center,
National Hospital Organization Nagoya Medical Center,
Aichi 460-0001, Japan

Abbreviations

FNAC	Fine needle aspiration cytology
DCIS	Ductal carcinoma in situ
HER2-ECD	The human epidermal growth factor receptor 2 extracellular domain
CA 15–3	Cancer antigen 15–3
NAF	Nipple aspiration fluid
BI-RAD	Breast Imaging Reporting and Data System
MUC 1	Mucin 1 (CA 15–3 antigen)

Introduction

Cytopathological diagnostic approaches focus on the cells rather than on the extracellular substances. Therefore, after

the aspiration samples are expelled onto glass slides for cytology or ancillary techniques, the needles are usually discarded. However, previous reports have indicated that the measurement of biomarkers in the needle washout fluid may provide information regarding the extracellular substances. For example, thyroglobulin detection in fine needle aspiration cytology (FNAC) washout fluid from cervical lymph nodes in which metastatic papillary carcinoma is suspected strengthens the cytological interpretation [1–13]. Another example is assaying for calcitonin in FNAC washout fluid from a mass suggestive of medullary carcinoma of the thyroid [14–16]. Although no study has been performed to measure biomarker levels in FNAC washout fluid from the breast, Inaji et al. analyzed nipple discharge from women with and without breast carcinoma and found that discharge from patients with ductal carcinoma in situ (DCIS) contained high levels (>1,000 ng/ml) of human epidermal growth factor receptor 2 (HER2) protein [17]. This suggests that biomarkers accumulate in the basement membrane-bound space of intraductal carcinoma until the continuity of the basement membrane is lost during stromal invasion. De Roos et al. noted that DCIS of the breast is almost exclusively positive for MUC1 (CA 15–3 antigen) [18]. Therefore, measurements of the HER2 extracellular domain (HER2-ECD) and cancer antigen 15–3 (CA 15–3) concentrations in FNAC washout fluid were studied to determine whether these biomarker levels could serve as an adjunct to cytological diagnosis. To the best of our knowledge, this is the first study to measure biomarker concentrations in breast FNAC washout fluid in the context of early diagnosis of breast cancer [19, 20].

Materials and methods

Samples

At the breast unit of Nagoya Medical Center, FNAC is used as the first-line diagnostic modality for most breast lesions visualized by ultrasonography [21]. Core biopsy with or without vacuum assistance is used when the FNAC results have been inadequate or are discordant with the radiology. During a 15-month period, a total of 378 ultrasound-guided FNAC samples were taken preoperatively from 292 patients with breast lesions. The median age of the patients was 49 years (range, 15–94 years).

Using the Breast Imaging Reporting and Data System assessment categories, the ultrasound images were categorized as category 0, additional imaging evaluation needed; category 1, negative; category 2, benign findings; category 3, probably benign findings, short interval follow-up suggested; category 4, suspicious abnormality—biopsy should be considered; category 5, highly suggestive of malignancy—appropriate action should be taken (almost certainly malignant); and category 6, known biopsy—proven malignancy—appropriate action should be taken [22].

Based on the UK National Health Service Breast Screening Program guidelines, the smears were classified into the following five categories: C1, inadequate or unsatisfactory smear; C2, benign cells present; C3, mild atypia within some cells but probably benign; C4, suspicious of malignancy; and C5, malignant cells present [23]. To avoid false positivity, a cytological diagnosis of malignancy (C5) was issued only when the samples contained cells characteristics of carcinoma from which the pathologist could make a confident diagnosis of malignancy. Among the cytological criteria for malignancy, we especially relied on the following features: nuclear pleomorphism, absence of naked bipolar cells, high cellularity, and discohesion (dissociated cells with cytoplasm and clusters of cells with three-dimensional arrangements) [24].

Based on clinical imaging and cytological diagnosis with or without core biopsy diagnosis, mastectomies (75 cases), wide local excision (56 cases), and biopsies (19 cases) were performed (Table 1). The final histopathological diagnoses of 150 breast lesions were 29 benign lesions (seven fibroadenomas, four phyllodes tumors, eight papillomas,

Table 1 Pathological group characteristics

Pathological group	No. of cases	Median age in years [range]	Treatment		
	n (%)		Mastectomy *n* (%)	Wide local excision *n* (%)	Biopsy *n* (%)
Benign lesions	29 (19.3)	47 [15–86]	1 (3.5)	14 (48.3)	14 (48.3)
DCIS	26 (17.3)	57 [38–85]	13 (50.0)	10 (38.5)	3 (11.5)
Invasive carcinoma	95 (63.3)	56 [30–85]	61 (64.2)	32 (33.7)	2 (2.1)
Total	150	55 [15–86]	75 (50.0)	56 (37.3)	19 (12.7)

One mastectomy for benign lesion was performed for a phyllodes tumor measuring 70 mm in length

DCIS ductal carcinoma in situ

five fibrocystic change, and five radial scar/others), 26 pure DCIS (Van Nuys classification: nine low grade, five intermediate grade, and 12 high grade), and 95 invasive carcinomas (modified Broom Richardson Grading by Elston and Ellis: 19 grade 1, 49 grade 2, and 27 grade 3). Invasive carcinomas consisted of 81 invasive ductal carcinomas (not otherwise specified) and 14 rare types (seven invasive lobular carcinomas, four invasive micropapillary carcinomas, one mucinous carcinomas, one pleomorphic carcinoma, and one solid papillary carcinoma).

The primary diagnosis and immunostaining of paraffin sections using antibodies shown in Table 2 were performed following the surgical excision or biopsy of the primary tumor. Tumors were considered HER2-positive if they were scored as 3+ or 2+ with amplification tested by fluorescence in situ hybridization. Estrogen receptors (ER) and progesterone receptors were considered positive if staining was detected in ≥1% of nuclei [25]. Based on tissue immunohistochemistry, DCIS and invasive carcinomas were characterized as ER+/HER2−, ER+/HER2+, ER−/HER2+ (HER2 overexpressing) or ER−/HER2− (triple negative). A similar classification has been shown to be a reliable surrogate for molecular classification as categorized by gene expression profiling studies [26]. The 150 breast lesions were examined to determine whether the biomarker assays of FNAC needle washout fluid could provide information that is useful to the cytological interpretation.

Chemiluminescence assay

Immediately after the aspiration samples were expelled onto glass slides for cytology, the needle (22-gauge, 70 mm long) was rinsed out with 2 ml of saline into centrifuged tubes. The sample was then centrifuged at 3,500 rpm for 5 min, and the supernatant was stored at −80°C until biochemical analysis. The HER2-ECD concentrations in needle washout fluid and serum samples were measured using the ADVIA Centaur immunoassay system (Siemens Healthcare Diagnostics, Deerfield, IL, USA) as previously described and validated [27]. In brief, the HER2 assay is a two-site sandwich immunoassay that uses two monoclonal antibodies specific for unique epitopes on the extracellular domain of HER2 and direct chemiluminescence technology. The measured chemiluminescence is directly proportional to the quantity of HER2-ECD antigen in the sample. Washout fluid and serum samples were also tested for CA 15–3 concentrations using the ADVIA Centaur immunoassay system according to the manufacturer's instructions.

The volume of the material (cells and extracellular substance) that remained within the needle was estimated to be 0.07 ml from the gain of the weight after the needle procedure with normal saline measured by precision weighing balance (PB153-S, Mettler Toledo International Inc., Greifensee, Switzerland). This indicates that the washout fluid diluted the original biomarkers by 3.5%.

The serum cutoff values are 15.2 ng/ml for HER2-ECD and 27 U/ml for CA 15–3. However, the cutoff values in the FNAC washout fluid for these markers are not known because no previous study on this subject has been performed. The number of cases analyzed in the present study is not large enough to clarify the cutoff values in the washout fluid using a receiver operating characteristic curve. If the cutoff values in the serum were applied to those in the washout fluid, they would be 0.53 ng/ml for HER2-ECD and 0.95 U/ml for CA 15–3 because the biomarkers are diluted by 3.5% in the washout fluid. The measuring limit for HER2-ECD of the system (0.5 ng/ml) is almost the same as the assumed cutoff value (0.53 ng/ml) and that for CA 15–3 (4 U/ml) is over the assumed cutoff value (0.95 U/ml). This implies that all values in the washout fluid measured in this study are over the cutoff values extrapolated from those in the serum. Although the cutoff values in the FNAC washout fluid for HER2-ECD and CA 15–3 should be determined, they were set at 0.5 ng/ml for HER2-ECD and 4 U/ml for CA 15–3 due to the sensitivity of the system in this preliminary study.

Statistical analysis

For statistical evaluation, contingency table analysis using the chi-square test, Fisher exact test, and Cochran–Armitage trend test were conducted. No statistical adjustment was made for performing multiple tests, but P values >0.01 were interpreted with care. P values were calculated from two-sided tests. The protocol of this research was approved by the institutional review board, and all subjects gave written informed consent to participate.

Table 2 Sources of primary antibodies used in this study

Antibody specificity	Clone	Dilution	Vendor
HER2	4B5	Prediluted	Roche
ER	SP1	Prediluted	Roche
PgR	IE2	Prediluted	Roche
CA 15–3	DF3	Prediluted	Fujirebio Diagnostics, Inc.

HER2 human epidermal growth factor receptor 2, *ER* estrogen receptor, *PgR* progesterone receptor, *CA 15–3* cancer antigen 15–3

Results

The proportion of patients with positive HER2-ECD values, defined as HER2-ECD concentrations over 0.5 ng/ml, is 2 of 29 (6.9%) in cases of benign lesions, 7 of 26 (26.9%) in DCIS, and 10 of 95 (10.5%) in invasive carcinomas (Fig. 1). The proportion of patients with positive CA 15–3 values, defined as CA 15–3 concentrations over 4 U/ml, is 2 of 29 (6.9%) in cases of benign lesions, 11 of 26 (42.3%) in DCIS, and 10 of 95 (10.5%) in invasive carcinomas (Fig. 2). The proportion of patients with any biomarker concentration elevation is 2 of 29 (6.9%) in cases of benign lesions, 12 of 26 (46.2%) in DCIS, and 15 of 95 (15.8%) in invasive carcinomas. Thus, the proportion of patients with a positive biomarker elevation was the highest in cases of DCIS, followed by invasive carcinomas. This trend was linear (Cochran–Armitage trend test, $P<0.01$; Table 3).

Using tissue-based immunohistochemistry, 21 cases of breast carcinomas (8 DCIS and 13 invasive carcinomas) with HER2 overexpression were identified (Fig. 1). The proportion of patients with HER2-ECD values over 6 ng/ml was three of eight (37.5%) in DCIS with HER2 overexpression and 1 of 13 (8.3%) in invasive carcinomas with HER2 overexpression. HER2-ECD values over 6 ng/ml were not observed in carcinomas without HER2 overexpression and in benign lesions.

CA 15–3 concentrations over 25 U/ml occurred exclusively in breast carcinomas, including seven DCIS of various grades (two high, two intermediate, and three low grade) and four invasive ductal carcinomas with an extensive intraductal component (two G3 and two G1; Fig. 2). Of two benign lesions that showed slightly elevated CA 15–3 concentrations (24.8 and 12 U/ml) in washout fluid, one was a cyst and the other was a benign phyllodes tumor.

The relationship between cytological category and washout fluid biomarker status is shown in Table 4. Of 29 cases of benign lesions, six cases were categorized as C2 (benign), 22 cases were categorized as C3 (benign with atypia), and one case was categorized as C4 (suspicious) by cytology. Five of eight papillomas (including one infarcted papilloma) were categorized as C3 because of the presence of clusters of epithelial cells with mildly atypical nuclei in the cytological specimen. In cases of DCIS, biomarker level elevation occurred in 7 of 12 (58.3%) cases with equivocal categories (C3 and C4) and 5 of 14 (35.7%) cases categorized as C5. In cases of invasive carcinomas, biomarker level elevation occurred in 6 of 44 (13.6%) cases with equivocal categories (C3 and C4) and 9 of 51 (17.6%) cases categorized as C5.

Biomarker status from different puncture sites of the ipsilateral breast in six cases of DCIS was well correlated

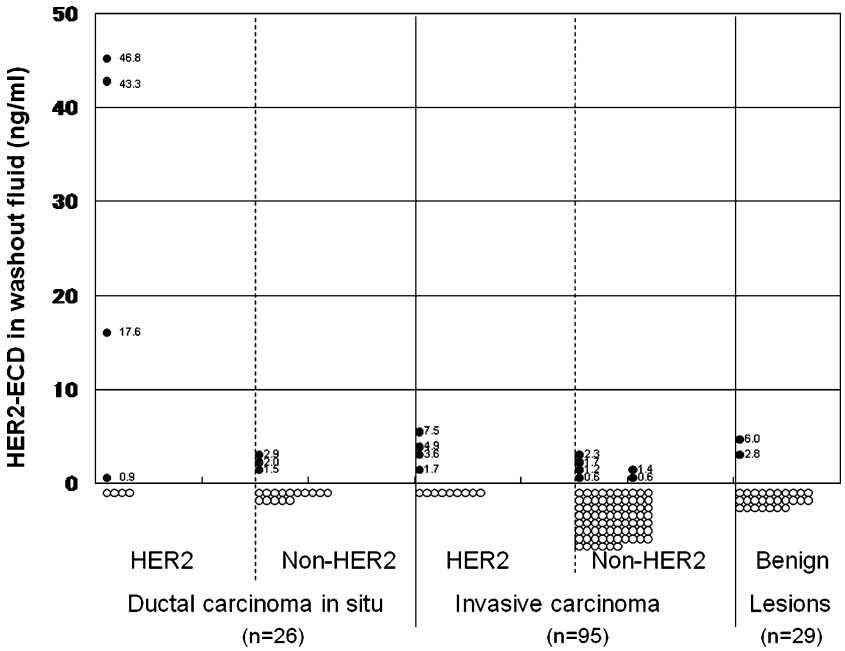

Fig. 1 The HER2-ECD assay in washout fluid from benign lesions ($n=29$), DCIS ($n=26$), and invasive carcinomas ($n=95$). The proportion of patients with positive HER2-ECD values, defined as HER2-ECD values over 0.5 ng/ml, is 2 of 29 (6.9%) in benign lesions, 7 of 26 (26.9%) in DCIS, and 10 of 95 (10.5%) in invasive carcinomas. The cases of DCIS were divided into DCIS with HER2 overexpression (HER2, $n=8$) and DCIS without HER2 overexpression (non-HER2, $n=18$). Cases of invasive carcinomas were divided into those with HER2 overexpression (HER2, $n=13$) and those without HER2 overexpression (non-HER2, $n=82$). Note that prominent elevation of HER2-ECD values occurred only in cases of DCIS with HER2 overexpression

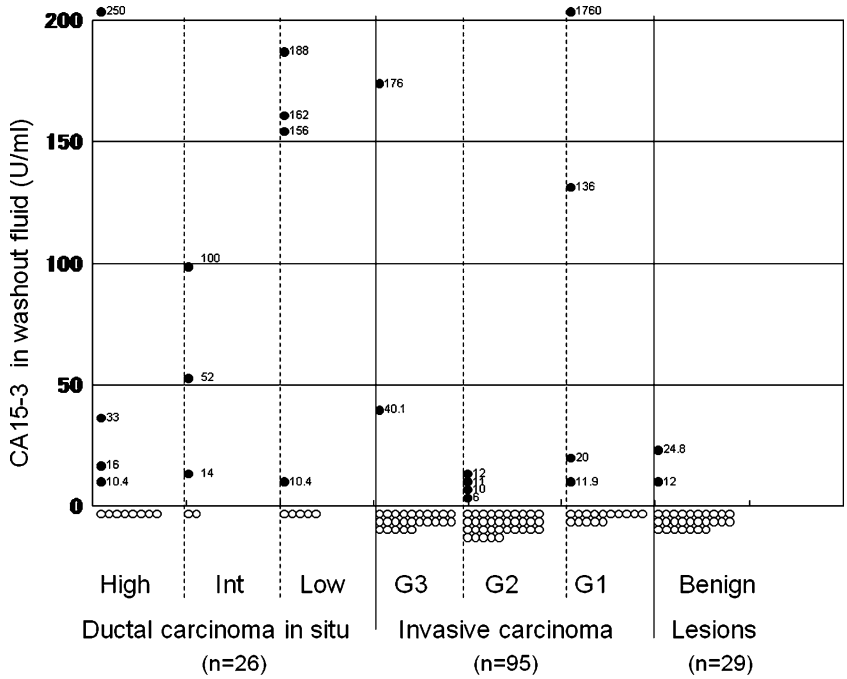

Fig. 2 The CA 15–3 assay in washout fluid from benign lesions (n=29), ductal carcinoma in situ (n=26), and invasive carcinomas (n=95). In one case of high-grade DCIS and one case of invasive ductal carcinoma (G1), the initial CA 15–3 values exceeded 200 U/ml, the measuring upper limit of the system. By measuring the samples again after they were diluted 1:10 with saline, the concentrations proved to be 250 and 1,760 U/ml, respectively

with the disease extent determined by histopathological examination (Table 5 cases no. 8, 11, and 12; Figs. 3, 4, 5, and 6). In one case of intermediate-grade DCIS of (Table 5 case 8; Figs. 3 and 4), the washout fluid obtained from two different sites at the same time showed almost the same levels of CA 15–3 (48 and 52 U/ml), although the serum CA 15–3 concentration (10.6 U/ml) was within the normal range. In one case of high-grade DCIS with HER2 overexpression (Table 5, case 11), the washout fluid obtained from three different FNAC sites showed high HER2-ECD concentrations (38.0, 40.8, and 43.3 ng/ml), whereas the serum HER2-ECD concentration (9.4 ng/ml) was within the normal range. In the other case of high-grade DCIS with HER2 overexpression (Table 5, case 12; Figs. 5 and 6), the washout fluid was taken twice within a 6-month interval. The first CA 15–3 value was 250 U/ml and the first HER2-ECD value was 46.8 ng/ml; the later CA 15–3 value was 93 U/ml and the later HER2-ECD value was 14.3 ng/ml. The preoperative serum concentrations of CA 15–3 (8.9 U/ml) and HER2-ECD (7.1 ng/ml) were within their normal ranges. In cases with biomarker level elevation in the FNAC washout fluid, the serum concentrations of CA 15–3 and HER2-ECD were within their normal ranges except in one case of DCIS with

Table 3 Biomarker status in FNAC washout fluid from DCIS (n=26), invasive carcinomas (n=95), and benign lesions (n=29)

Biomarker status in FNAC washout fluid		DCIS	Invasive carcinomas	Benign lesions	P value		
		n (%)	n (%)	n (%)	Chi-square test	Fisher exact test	Cochran–Armitage trend test[a]
HER2-ECD	Positive	7 (26.9)	10 (10.5)	2 (6.9)	0.048	0.071	0.0003
	Negative	19 (73.1)	85 (89.5)	27 (93.1)			
CA 15–3	Positive	11 (42.3)	10 (10.5)	2 (6.9)	0.0001	0.0005	0.0004
	Negative	15 (57.7)	85 (89.5)	27 (93.1)			
HER2-ECD or CA 15–3	Positive	12 (46.2)	15 (15.8)	2 (6.9)	0.0004	0.0008	0.0003
	Negative	14 (53.8)	80 (84.2)	27 (93.1)			

Among three pathological groups, the number of patients with a positive biomarker was highest in DCIS, followed by invasive carcinomas. This trend was linear (Cochran–Armitage trend test, $P<0.01$)

FNAC fine needle aspiration cytology, *DCIS* ductal carcinoma in situ, *HER2-ECD* human epidermal growth factor receptor 2-extracellular domain, *CA 15–3* cancer antigen 15–3

[a] The Cochran–Armitage trend test, named for William Cochran and Peter Armitage, is used in categorical data analysis to assess the presence of an association between a variable with two categories and a variable with k categories. It is a modified chi-square test that incorporates a suspected ordering in the effects of the k categories of the second variable

Table 4 Cytology category and FNAC washout fluid biomarker status (n=150)

Histopathological diagnosis		*Cytology category*				
		C1	C2	C3	C4	C5
Benign lesions (n=29)	Fibroadenoma (n=7)		○	○○○○○	○	
	Phyllodes tumor (n=4)			①○○○		
	Papilloma (n=8)		○○○	○○○○○		
	Fibrocystic change (n=5)		○	②○○○		
	Radia scar/others (n=5)		○	○○○○		
DCIS (n=26)	Low grade (n=9)			④⑤⑥○	③○○○	○
	Intermediate grade (n=5)				⑧	⑦⑨○○
	High grade (n=12)			⑩○	⑫	⑪⑬⑭○○ ○○○○
Invasive carcinomas (n=95)	Grade 1 (n=19)			⑮⑯⑱○○ ○○○○○	⑰○○○○ ○○	○○
	Grade 2 (n=49)			○○○○○ ○○	㉑○○○○ ○○○○○ ○○○○○	⑲⑳㉒㉓○ ○○○○○ ○○○○○ ○○○○○ ○○○○○ ○○
	Grade 3 (n=27)			○○	㉙○○	㉔㉕㉖㉗㉘ ○○○○○ ○○○○○ ○○○○○ ○○

○ case without biomarker elevation, ⓝ case with biomarker elevation (the numbers corresponds to the case numbers shown in Table 5), *C1* unremarkable, *C2* benign, *C3* benign with atypia, *C4* suspicious, *C5* malignant, *FNAC* fine needle aspiration cytology, *DCIS* ductal carcinoma in situ

HER2 overexpression (Table 5, case 13). This case showed slightly elevated HER2-ECD concentration (0.9 ng/ml) in the washout fluid whereas the serum HER2-ECD concentration was 67.9 ng/ml.

Discussion

Using chemiluminescence technology, this study revealed that FNA washout fluid from cases of breast cancer frequently contains high levels of HER2-ECD or CA 15–3 even when the serum concentrations of the markers are within their normal ranges. Significantly, biomarker level elevation was most frequent in cases of DCIS, followed by invasive carcinomas (P<0.01). The majority of invasive carcinomas with biomarker level elevation had extensive intraductal components. Furthermore, HER2-ECD values over 6 ng/ml or CA 15–3 values over 25 U/ml were seen exclusively in cases of DCIS or invasive carcinoma with extensive intraductal components. These results are consistent with the hypothesis that biomarkers accumulate in the duct involved in DCIS.

Although there is no previous study on biomarker measurement of FNAC washout fluid from breast lesions, our data are comparable to those in reports on HER2 levels in the nipple discharge or the nipple aspiration fluid (NAF) from cases of breast cancer. According to Inaji et al., marked elevation of HER2 protein levels (>1,000 ng/ml) in nipple discharge were observed in two of nine patients with breast cancer and nipple discharge [17]. Histologically, these cases were comedo- or solid-type intraductal carcinomas with HER2 overexpression. Two cases of DCIS with HER2 overexpression in the present study showed high levels of HER2-ECD in the washout fluid—43.3 ng/ml (Table 5, case 11) and 46.8 ng/ml (Table 5, case 12; Figs. 5 and 6). Because the biomarkers contained in the space of a fine needle (about 0.07 ml) were diluted by 2 ml saline in the present study, the undiluted concentrations of HER2-ECD in cases 11 and 12 were estimated to be 1,237.1 and 1,337.1 ng/ml, respectively. These values are consistent with the nipple discharge HER2-

Table 5 Breast lesions with FNAC washout fluid biomarker elevation over measuring limits

Case no.	age (y)	Histological diagnosis (grade)	Subtype by tissue-based immunohistochemistry	EIC	BI-RAD US category	First puncture			Second puncture			Third puncture			Serum	
						Category	HER2-ECD	CA 15–3	Category	HER2-ECD	CA 15–3	Category	HER2-ECD	CA 15–3	HER2-ECD	CA 15–3
1	57	Cyst			4	C3	5.9	24.8	C3	5.6	24	C3	6	24	ND	ND
2	41	PT (benign)			4	C3	2.8	12							ND	6.5
3	58	DCIS (low)	ER+/HER2−		4	C4	2.9	**156**	C4	0	8				10.0	19
4	63	DCIS (low)	ER+/HER2−		3	C3	0	**162**							ND	7.7
5	85	DCIS (low)	ER+/HER2−		3	C3	0	**188**							ND	16.3
6	38	DCIS (low)	ER+/HER2−		4	C3	0	10.4							ND	13.1
7	40	DCIS (Int)	ER+/HER2−		4	C5	0	**100**	C5	0	0	C5	0	0	ND	5.1
8	67	DCIS (Int)	ER+/HER2−		4	C4	2	**48**	C4	0	**52**				ND	10.6
9	82	DCIS (Int)	ER+/HER2−		5	C5	0	14							ND	5.7
10	85	DCIS (high)	ER−/HER2−		4	C3	0	0	C3	1.5	16				ND	7.2
11	49	DCIS (high)	ER−/HER2+		4	C5	**38**	9.8	C5	**40.8**	10.3	C5	**43.3**	10.4	9.4	7.4
12	54	DCIS (high)	ER−/HER2+		4	C4	**46.8**	**250**	C4	**14.3**	**93**				7.1	8.9
13	46	DCIS (high)	ER−/HER2+		4	C5	0.9	0							9.7	**67.9**
14	55	DCIS (high)	ER−/HER2+		4	C5	**17.6**	**33**							ND	9.8
15	38	IDC (G1)	ER+/HER2−	−	4	C3	1.2	20							ND	ND
16	48	IDC (G1)	ER+/HER2−	+	5	C3	1.7	**136**							ND	14.8
17	50	IDC (G1)	ER+/HER2−	−	5	C4	0	11.9							ND	17.0
18	40	IDC (G1)	ER−/HER2+	+	4	C3	4.9	**1,760**							ND	22.6
19	73	IDC (G2)	ER+/HER2−	+	5	C5	0	6.0							ND	14.3
20	51	IDC (G2)	ER+/HER2−	+	5	C5	0	11							ND	8.0
21	39	IDC (G2)	ER+/HER2−	+	5	C4	2.3	0							ND	10.9
22	61	IDC (G2)	ER+/HER2−	+	4	C5	1.4	10							ND	5.3
23	37	IDC (G2)	ER+/HER2−	+	5	C5	0	12							ND	7.1
24	61	IDC (G3)	ER+/HER2+	−	5	C5	0.6	0							ND	ND
25	60	IDC (G3)	ER+/HER2−	+	5	C5	0	**176**							ND	14.9
26	35	IMPC (G3)	ER−/HER2+	+	5	C5	1.7	0							ND	ND
27	52	IDC (G3)	ER−/HER2+	+	5	C5	**7.5**	0							8.4	8.0
28	48	PLM (G3)	ER−/HER2+	−	4	C5	3.6	0							ND	8.6
29	64	IDC (G3)	ER−/HER2−	+	4	C4	0.6	**40.1**							ND	7.6

The cutoff value in the washout fluid is 0.5 ng/ml for HER2-ECD and 4 U/ml for CA 15–3. The HER2-ECD values over 6 ng/ml and CA 15–3 values over 25 U/ml are indicated by boldface. The cutoff value in the serum was 15.2 ng/ml for HER2-ECD and 27 U/ml for CA 15–3. Most cases of invasive carcinomas with elevated biomarkers were cases of invasive ductal carcinoma, not otherwise specified (NOS). The exceptions were a case of invasive micropapillary carcinoma (case no. 26) and a case of pleomorphic carcinoma (case no. 28). Both were of HER2 overexpressing subtype (ER−/HER2+) and showed slight elevation of HER2-ECD concentration in the washout fluid

FNAC fine needle aspiration cytology, *PT* phyllodes tumor, *DCIS* ductal carcinoma in situ, *low* low grade, *Int* intermediate grade, *high* high grade, *IDC* invasive ductal carcinoma, *IMPC* invasive micropapillary carcinoma, *PLM* pleomorphic carcinoma, *G1* grade 1, *G2* grade 2, *G3* grade 3, *C1* unremarkable, *C2* benign, *C3* benign with atypia, *C4* suspicious, *C5* malignant, *EIC* extensive intraductal component (defined as the presence of DCIS within an invasive carcinoma that occupies 25% or more of the overall tumor mass and that extends beyond the confined of that main mass), *BI-RADS* Breast Imaging Reporting and Data System, *ND* not done

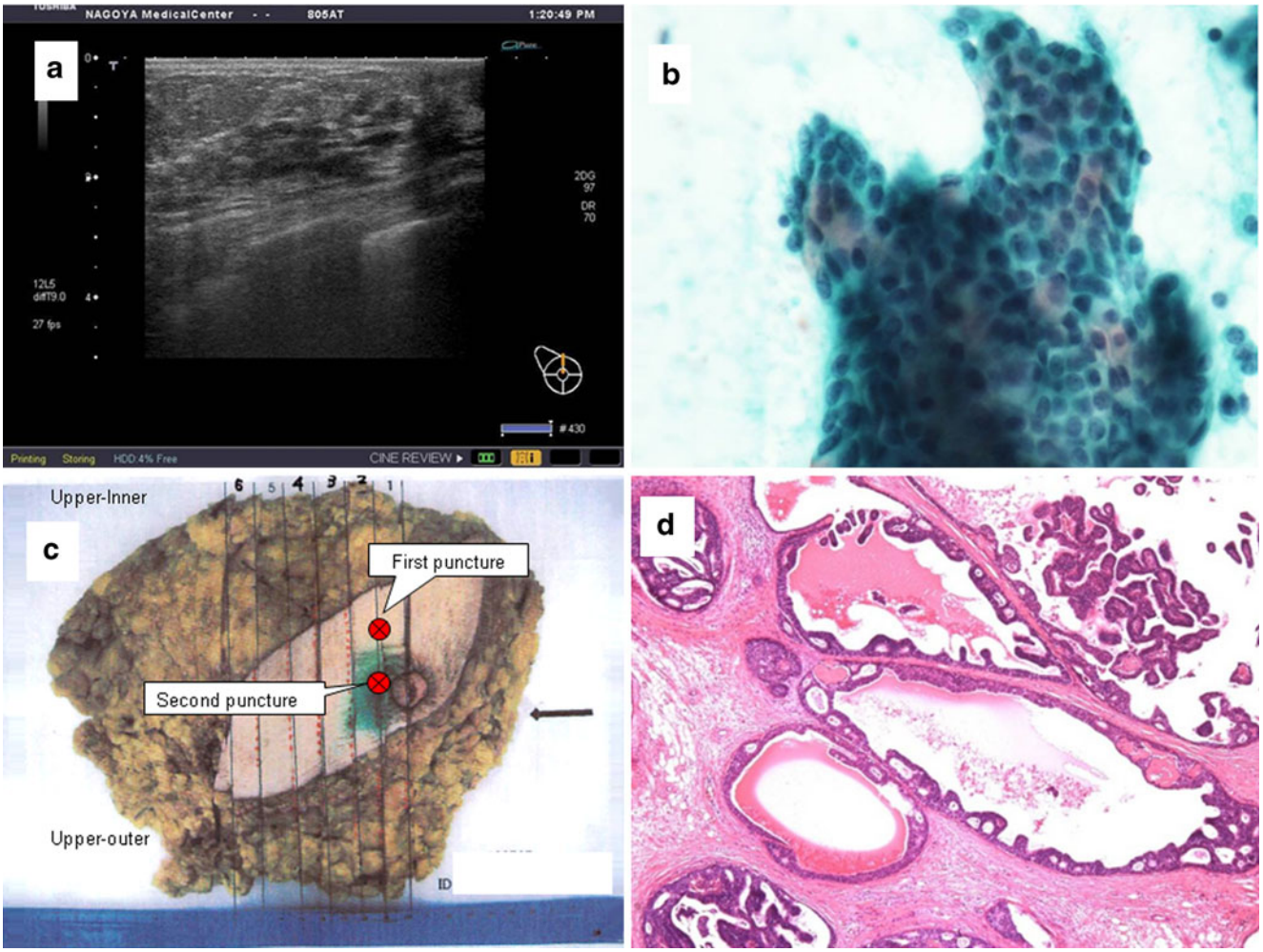

Fig. 3 A case of intermediate-grade DCIS with marked elevation of CA 15–3 in washout fluid (case 8 in Table 5). **a** Ultrasonography showed multiple irregular hypoechoic masses in the mammary parenchyma, categorized as BI-RADS 4. Aspiration cytology was performed on the hypervascular area guided by power Doppler ultrasound. **b** Cytology showed a cohesive cluster of monomorphic cells in the background of many foamy macrophages. The cytology was reported as C4 (suspicious). **c** Fine needle aspiration cytology sites shown in a mastectomy specimen. The *red dotted line* shows DCIS confirmed by microscopic examination. **d** Histological images of a mastectomy specimen. On microscopy, the lesion was multicystic. The cysts were filled with eosinophilic secretions. The epithelium of the cysts grew as micropapillary intraductal carcinoma with Roman arch or flat patterns. This particular case is consistent with cystic hypersecretory DCIS described by Rosen et al. [29, 30]

ECD levels of >1,000 ng/ml from cases of DCIS with HER2 overexpression reported by Inaji et al.

In contrast to DCIS, marked elevation of HER2-ECD levels was not observed in washout fluid from 13 cases of invasive carcinomas with HER2 overexpression (Fig. 1; Table 5). The HER2-ECD concentration was less than 6 ng/ml in 12 cases and was slightly over 6 ng/ml in one case (Fig. 1; Table 5, cases 18, 26, 27, and 28). The undiluted concentrations of HER2-ECD of cases 18, 26, 27, and 28 were estimated to be 140, 48.6, 214.3, and 102.9 ng/ml, respectively. These values were comparable to those in NAF from 12 patients with invasive carcinomas with HER2 overexpression reported by Kuerer et al. [28], although it is not apparent whether these cases had extensive intraductal components. According to Kuerer et al., there was a clear difference in NAF HER2 levels between the healthy and affected breasts from the same patient, with the affected breast having a significantly elevated HER2 level (653.6 vs. 101.7 ng/ml, P=0.016).

This study was conducted to determine whether measurement of HER2-ECD protein and CA 15–3 in the needle washout fluid could contribute to the non-operative diagnosis of breast carcinoma. When the cutoff values in the washout fluid are set at 0.5 ng/ml for HER2-ECD and 4 U/ml for CA 15–3 (measuring limits), 29 of 121 carcinomas (24.0%) showed elevated concentration of a biomarker, indicating that the overall sensitivity of the biomarker assay for the detection of

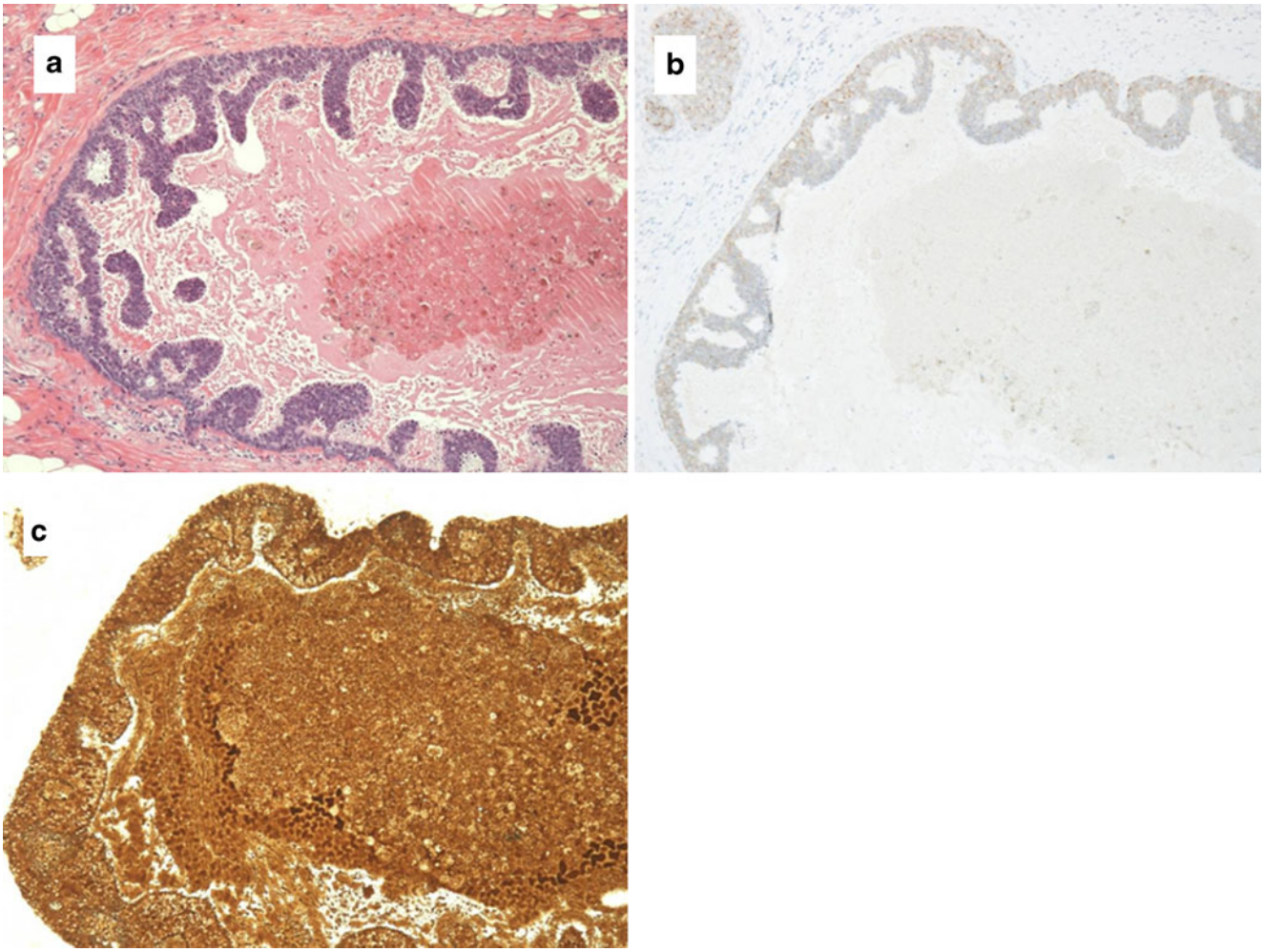

Fig. 4 Immunohistochemical study of a case of intermediate-grade DCIS with marked elevation of CA 15–3 concentration (case 8 in Table 5). **a** Intraductal carcinoma with Roman arch or flat patterns. **b** HER2 immunostain. No immunoreactivity for HER2 was seen. **c** CA 15–3 immunostaining demonstrated positive reactions in the tumor cells and intracystic secretory material

breast cancer was not high. However, the sensitivity for the detection of DCIS was 46.2% (12 of 26) and the specificity for malignancy was 93.1% (27 of 29). Among 12 cases of DCIS categorized as equivocal (C4 or C3) by cytology, five cases of DCIS showed CA 15–3 values over 50 U/ml in FNAC needle washout fluid (Tables 4 and 5). If biomarker status is taken into account in the final cytological diagnosis, 5 of 12 (41.7%) cases of DCIS with equivocal cytology categories could be upgraded and additional core biopsies could be omitted. The present data indicate that washout fluid biomarker elevation is more frequent in cases of DCIS than invasive carcinoma. This is important because the proportion of equivocal cytological diagnoses was larger in cases of DCIS than in cases of invasive carcinomas in a series of primary breast cancer samples (n=102, 58.8% vs. 33.8%, P<0.05) [21]. Although recent advancements in breast imaging have increased the number of breast lesions that FNAC alone does not reliably distinguish as malignant from benign, the findings of this preliminary study suggest that FNAC may improve the diagnostic accuracy if biomarker concentrations in needle washout fluid are measured at the same time.

The mechanism for marked elevation of HER2-ECD and CA 15–3 levels in FNAC washout fluid from cases of DCIS is noteworthy. In a healthy breast, MUC 1 (CA 15–3 antigen) is expressed in the ducts and acini, from where it is released into the milk in a soluble form or bound to milk fat globules [19]. De Roos et al. noted that cases of DCIS are almost exclusively MUC1-positive, and they classified the immunoreactivity patterns as membranous, apical, focal cytoplasmic, and diffuse cytoplasmic [18]. They found that membranous and apical patterns reflect a pathologically and biologically less aggressive profile, whereas focal and diffuse cytoplasmic patterns are related to a more aggressive profile. They suggested that DCIS is associated with disruption of cell polarization and tissue architecture and

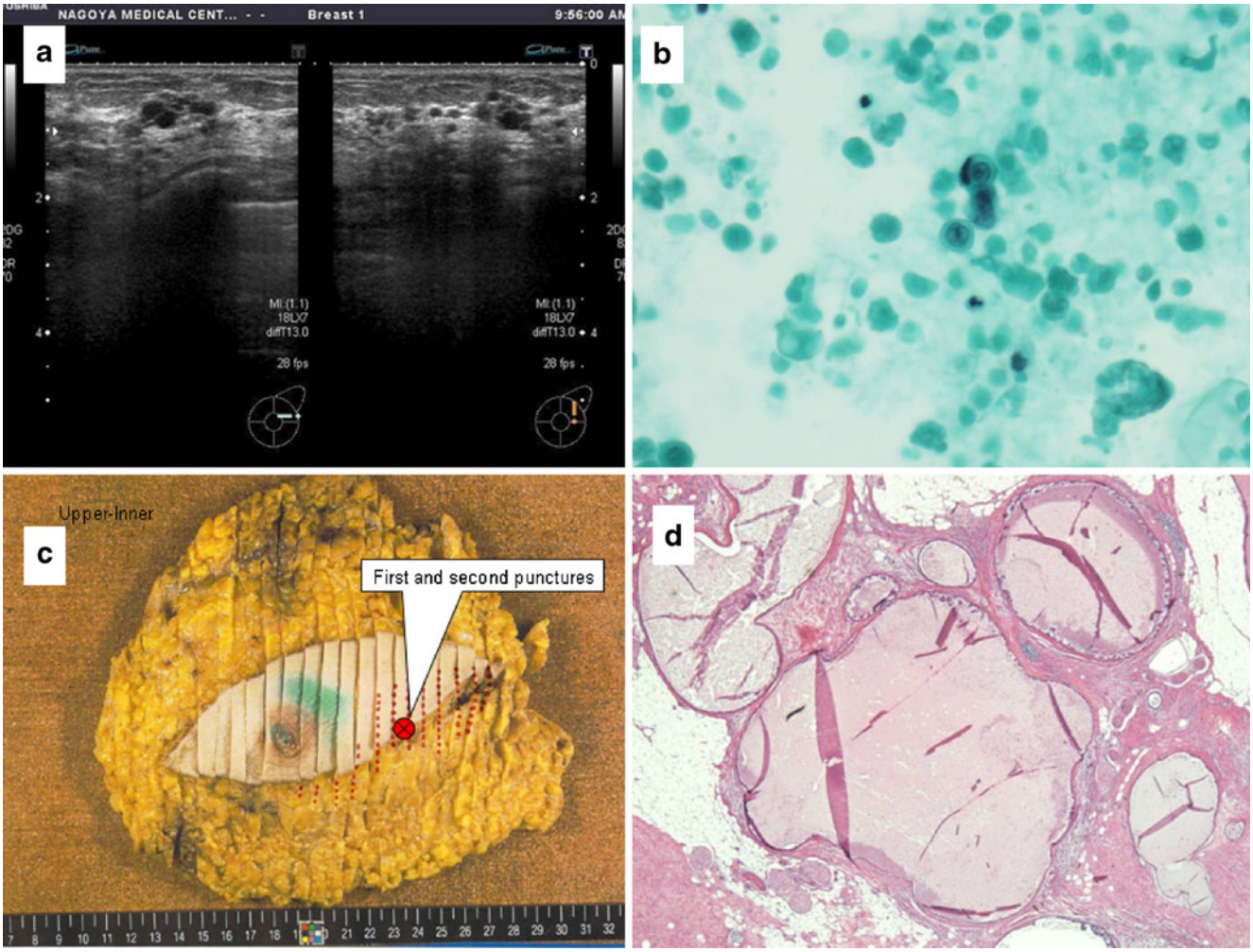

Fig. 5 A case of high-grade DCIS with marked elevation of both CA 15–3 and HER2-ECD concentrations in washout fluid (case 12 in Table 5). **a** Ultrasonography showed clustered microcysts in the mammary parenchyma, categorized by ultrasound as BI-RADS 4A. **b** Cytology showed a few atypical cell clusters with hyperchromatic and molded nuclei in the background of numerous ghost cells. **c** Fine needle aspiration cytology sites shown in a mastectomy specimen. The *red dotted line* shows DCIS confirmed by microscopic examination. **d** Histologically, the mastectomy specimen showed widespread multicysts filled with necrotic material. Each cyst is lined with flat layers or micropapillary structures of large atypical tumor cells

leads to aberrant expression of CA 15–3 in cytoplasm. The present study showed that such aberrantly expressed tumor-associated antigens are concentrated in cases of DCIS but not in cases of invasive carcinomas.

This study was designed based on the hypothesis that biomarkers accumulate in the duct involved with DCIS as long as carcinoma cells and their products are confined to the basement membrane-bound space. The basis of this hypothesis is as follows: By definition, the basement membrane and a layer of myoepithelial cells serve to demarcate DCIS from the surrounding stroma. This barrier may work to prevent secretory and necrotic materials originating from the cancer cells from diffusing into the stroma in the same manner as it prevents the milk from diffusing into the stroma during lactation. When this barrier is disrupted and destroyed during invasion, the biomarkers rapidly spread and diffuse into the connective tissue stroma, resulting in the elevation of biomarker levels in the serum.

Our hypothesis is not only supported by the chemiluminescence measurement of FNAC washout fluid but also by the microscopic observation of the DCIS with elevated biomarker levels in washout fluid. As shown in Figs. 3, 4, 5, and 6, the terminal duct lobular units and ducts were distended and filled with secretory or necrotic materials. The case shown in Figs. 3 and 4 (case 8 in Table 5) is consistent with cystic hypersecretory DCIS, a rare form of micropapillary DCIS, described by Rosen et al. [29, 30] because it showed homogenous eosinophilic secretion resembling thyroid colloid. Although some DCIS cases with elevated biomarker levels in FNAC washout fluid resembled cystic hypersecretory DCIS in part, the nature of the cyst content was not necessarily homogeneous eosinophilic secretion, a

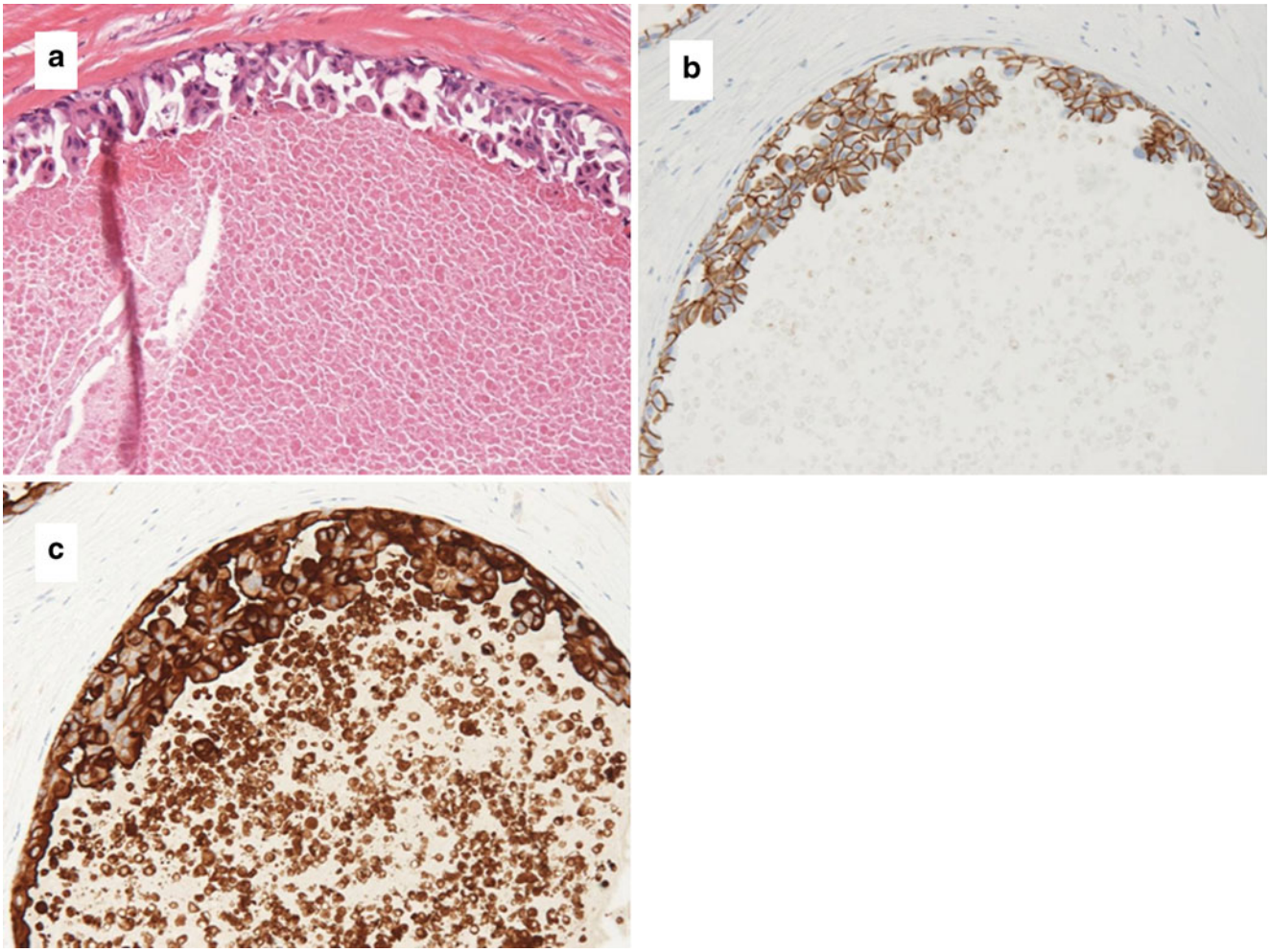

Fig. 6 Immunohistochemical study of high-grade DCIS with marked elevation of both HER2-ECD and CA 15–3 concentrations (case 12 in Table 5). **a** High-grade DCIS with comedo necrosis and a micropapillary pattern. **b** HER2 immunostain demonstrated a positive reaction on the cell membrane of the tumor cells. **c** CA 15–3 immunostaining demonstrated positive reactions in the tumor cells and necrotic material

prerequisite for the diagnosis. For example, the cyst content of the DCIS shown in Figs. 5 and 6 was ghost cells and necrotic granular debris rather than homogenous secretion. Despite this, it is important to note that assaying the biomarker levels in washout fluid may be a useful adjunct to the cytological diagnosis of cystic hypersecretory DCIS of the breast, sometimes a source of diagnostic confusion.

In contrast to serum prostate-specific antigen concentration, serum breast tumor marker concentrations are not recommended as a screening tool for breast cancer [31]. Serum CA 15–3 and HER2-ECD concentrations are of limited value in the detection of early-stage breast cancer because of their low sensitivity and specificity [31–33, 19, 34, 35]. The mechanism for the low sensitivity of blood-based markers for the early detection of localized breast cancer has remained poorly understood. Although it is suggested that the serum values of breast tumor markers reflect tumor burden, invasive carcinoma does not necessarily surpass DCIS in volume because what discriminates invasive carcinoma from DCIS is not the tumor volume but the presence of invasive growth beyond the basement membrane. Our hypothesis explains why remarkable elevation of tumor markers levels in the serum does not occur in most cases of breast DCIS but occurs in advanced or metastatic disease.

Conclusion

Chemiluminescence measurement of the needle washout fluid after FNAC revealed that 46.2% of DCIS cases and 15.8% of invasive carcinoma cases showed elevation of HER2-ECD and/or CA 15–3 concentrations even if the marker concentrations were within their normal ranges in the serum. It is suggested that these tumor antigens accumulate in the duct involved with DCIS until the basement membrane is disrupted and broken during

invasion. Biomarker assays of needle washout fluid after FNAC may improve diagnostic accuracy of the cytological diagnosis of breast cancer.

Acknowledgments This study was supported in part by the National Hospital Organization Research Fund. The authors thank Miss Megumi Yokoyama for her excellent data management and Prof. Tsuguhiro Kaneda for his critical review of the manuscript.

Competing interest The authors received funding from Siemens Healthcare Diagnostics K.K. (Tokyo, Japan) to conduct HER2-ECD and CA 15–3 assays. However, study investigators acted independently in generating research hypotheses, achieving results, interpreting the data, and deciding to submit the paper for publication.

References

1. Pacini F, Fugazzola L, Lippi F, Ceccarelli C, Centoni R, Miccoli P, Elisei R, Pinchera A (1992) Detection of thyroglobulin in fine needle aspirates of nonthyroidal neck masses: a clue to the diagnosis of metastatic differentiated thyroid cancer. J Clin Endocrinol Metab 74:1401–1404
2. Frasoldati A, Toschi E, Zini M, Flora M, Caroggio A, Dotti C, Valcavi R (1999) Role of thyroglobulin measurement in fine-needle aspiration biopsies of cervical lymph nodes in patients with differentiated thyroid cancer. Thyroid 9:105–111
3. Baskin HJ (2004) Detection of recurrent papillary thyroid carcinoma by thyroglobulin assessment in the needle washout after fine-needle aspiration of suspicious lymph nodes. Thyroid 14:959–963
4. Uruno T, Miyauchi A, Shimizu K, Tomoda C, Takamura Y, Ito Y, Miya A, Kobayashi K, Matsuzuka F, Amino N, Kuma K (2005) Usefulness of thyroglobulin measurement in fine-needle aspiration biopsy specimens for diagnosing cervical lymph node metastasis in patients with papillary thyroid cancer. World J Surg 29:483–485
5. Mikosinski S, Pomorski L, Oszukowska L, Makarewicz J, Adamczewski Z, Sporny S, Lewinski A (2006) The diagnostic value of thyroglobulin concentration in fine-needle aspiration of the cervical lymph nodes in patients with differentiated thyroid cancer. Endokrynol Pol 57:392–395
6. Boi F, Baghino G, Atzeni F, Lai ML, Faa G, Mariotti S (2006) The diagnostic value for differentiated thyroid carcinoma metastases of thyroglobulin (Tg) measurement in washout fluid from fine-needle aspiration biopsy of neck lymph nodes is maintained in the presence of circulating anti-Tg antibodies. J Clin Endocrinol Metab 91:1364–1369
7. Sigstad E, Heilo A, Paus E, Holgersen K, Groholt KK, Jorgensen LH, Bogsrud TV, Berner A, Bjoro T (2007) The usefulness of detecting thyroglobulin in fine-needle aspirates from patients with neck lesions using a sensitive thyroglobulin assay. Diagn Cytopathol 35:761–767
8. Cunha N, Rodrigues F, Curado F, Ilheu O, Cruz C, Naidenov P, Rascao MJ, Ganho J, Gomes I, Pereira H, Real O, Figueiredo P, Campos B, Valido F (2007) Thyroglobulin detection in fine-needle aspirates of cervical lymph nodes: a technique for the diagnosis of metastatic differentiated thyroid cancer. Eur J Endocrinol 157:101–107
9. Snozek CL, Chambers EP, Reading CC, Sebo TJ, Sistrunk JW, Singh RJ, Grebe SK (2007) Serum thyroglobulin, high-resolution ultrasound, and lymph node thyroglobulin in diagnosis of differentiated thyroid carcinoma nodal metastases. J Clin Endocrinol Metab 92:4278–4281
10. Baloch ZW, Barroeta JE, Walsh J, Gupta PK, Livolsi VA, Langer JE, Mandel SJ (2008) Utility of thyroglobulin measurement in fine-needle aspiration biopsy specimens of lymph nodes in the diagnosis of recurrent thyroid carcinoma. Cytojournal 5:1
11. Giovanella L, Ceriani L, Suriano S, Crippa S (2009) Thyroglobulin measurement on fine-needle washout fluids: influence of sample collection methods. Diagn Cytopathol 37:42–44
12. Kim MJ, Kim EK, Kim BM, Kwak JY, Lee EJ, Park CS, Cheong WY, Nam KH (2009) Thyroglobulin measurement in fine-needle aspirate washouts: the criteria for neck node dissection for patients with thyroid cancer. Clin Endocrinol (Oxf) 70:145–151
13. Jeon SJ, Kim E, Park JS, Son KR, Baek JH, Kim YS, Park do J, Cho BY, Na DG (2009) Diagnostic benefit of thyroglobulin measurement in fine-needle aspiration for diagnosing metastatic cervical lymph nodes from papillary thyroid cancer: correlations with US features. Korean J Radiol 10:106–111
14. Kudo T, Miyauchi A, Ito Y, Takamura Y, Amino N, Hirokawa M (2007) Diagnosis of medullary thyroid carcinoma by calcitonin measurement in fine-needle aspiration biopsy specimens. Thyroid 17:635–638
15. Boi F, Maurelli I, Pinna G, Atzeni F, Piga M, Lai ML, Mariotti S (2007) Calcitonin measurement in wash-out fluid from fine needle aspiration of neck masses in patients with primary and metastatic medullary thyroid carcinoma. J Clin Endocrinol Metab 92:2115–2118
16. Siqueira D, Rocha AP, Punales MK, Maia AL (2009) Identification of occult metastases of medullary thyroid carcinoma by calcitonin measurement in washout fluid from fine needle aspiration of cervical lymph node. Arq Bras Endocrinol Metabol 53:479–481
17. Inaji H, Koyama H, Motomura K, Noguchi S, Mori Y, Kimura Y, Sugano K, Ohkura H (1993) ErbB-2 protein levels in nipple discharge: role in diagnosis of early breast cancer. Tumour Biol 14:271–278
18. de Roos MA, van der Vegt B, Peterse JL, Patriarca C, de Vries J, de Bock GH, Wesseling J (2007) The expression pattern of MUC1 (EMA) is related to tumour characteristics and clinical outcome in 'pure' ductal carcinoma in situ of the breast. Histopathology 51:227–238
19. Seregni E, Coli A, Mazzucca N (2004) Circulating tumour markers in breast cancer. Eur J Nucl Med Mol Imaging 31(Suppl 1):S15–S22
20. Krishnamurthy S (2007) Applications of molecular techniques to fine-needle aspiration biopsy. Cancer 111:106–122
21. Oiwa M, Yoshikawa K, Sato Y, Hayashi T, Ichihara S, Moritani S, Hasegawa M, Ogashiwa H, Yamashita M, Endo T (2010) Ultrasound-guided fine-needle aspiration cytology in the mammographic screening era. J Jpn Soc Clin Cytol 49:142–151
22. ACR (2003) BI-RADS®—ultrasound, 1st edn. http://www.acr.org/SecondaryMainMenuCategories/quality_safety/BIRADSAtlas/BIRADSAtlasexcerptedtext/BIRADSUltrasoundFirstEdition.aspx?css=print. Accessed 23 Jan 2011
23. Wells CA, Perera R, White FE, Domizio P (1999) Fine needle aspiration cytology in the UK breast screening programme: a national audit of results. Breast 8:261–266
24. Koshikawa T, Tokoro Y, Suzuki M, Kobayashi M, Sasaki E, Hosoda K, Kitamura A, Yatabe Y, Iwata K, Ichihara S (2010) A useful scoring system for breast cytology diagnosis corresponding to the development of imaging modalities. J Jpn Soc Clin Cytol 49:134–141
25. Hammond ME, Hayes DF, Dowsett M, Allred DC, Hagerty KL, Badve S, Fitzgibbons PL, Francis G, Goldstein NS, Hayes M, Hicks DG, Lester S, Love R, Mangu PB, McShane L, Miller K, Osborne CK, Paik S, Perlmutter J, Rhodes A, Sasano H, Schwartz JN, Sweep FC, Taube S, Torlakovic EE, Valenstein P, Viale G, Visscher D, Wheeler T, Williams RB, Wittliff JL, Wolff AC,

American Society of Clinical Oncology/College Of American (2010) Pathologists guideline recommendations for immunohistochemical testing of estrogen and progesterone receptors in breast cancer. J Clin Oncol 28:2784–2795
26. Tamimi RM, Baer HJ, Marotti J, Galan M, Galaburda L, Fu Y, Deitz AC, Connolly JL, Schnitt SJ, Colditz GA, Collins LC (2008) Comparison of molecular phenotypes of ductal carcinoma in situ and invasive breast cancer. Breast Cancer Res 10:R67
27. Luftner D, Henschke P, Flath B, Akrivakis C, Schnabel S, Prinz B, Geppert R, Wernecke KD, Possinger K (2004) Serum HER-2/neu as a prediction and monitoring parameter in a phase II study with weekly paclitaxel in metastatic breast cancer. Anticancer Res 24:895–906
28. Kuerer HM, Thompson PA, Krishnamurthy S, Fritsche HA, Marcy SM, Babiera GV, Singletary SE, Cristofanilli M, Sneige N, Hunt KK (2003) High and differential expression of HER-2/neu extracellular domain in bilateral ductal fluids from women with unilateral invasive breast cancer. Clin Cancer Res 9:601–605
29. Rosen PP, Scott M (1984) Cystic hypersecretory duct carcinoma of the breast. Am J Surg Pathol 8:31–41
30. Guerry P, Erlandson RA, Rosen PP (1988) Cystic hypersecretory hyperplasia and cystic hypersecretory duct carcinoma of the breast. Pathology, therapy, and follow-up of 39 patients. Cancer 61:1611–1620
31. Harris L, Fritsche H, Mennel R, Norton L, Ravdin P, Taube S, Somerfield MR, Hayes DF, Bast RC Jr (2007) American Society of Clinical Oncology 2007 update of recommendations for the use of tumor markers in breast cancer. J Clin Oncol 25:5287–5312
32. Stearns V, Yamauchi H, Hayes DF (1998) Circulating tumor markers in breast cancer: accepted utilities and novel prospects. Breast Cancer Res Treat 52:239–259
33. Brooks M (2009) Breast cancer screening and biomarkers. Methods Mol Biol 472:307–321
34. Kong SY, Kang JH, Kwon Y, Kang HS, Chung KW, Kang SH, Lee DH, Ro J, Lee ES (2006) Serum HER-2 concentration in patients with primary breast cancer. J Clin Pathol 59:373–376
35. Ichihara S, Aoyama H (1994) Intraductal carcinoma of the breast associated with high levels of circulating tumor-associated antigens (CA 15-3 and NCC-ST-439). Cancer 73:2181–2185

Virchows Arch (2011) 458:561–569
DOI 10.1007/s00428-011-1042-9

ORIGINAL ARTICLE

Frequent loss of heterozygosity on chromosome 12q in non-small-cell lung carcinomas

Xiao-Jie Ding · Min-Xia Liu · Lei Ao · Yi-Rong Liang · Yi Cao

Received: 3 May 2010 / Revised: 4 December 2010 / Accepted: 6 January 2011 / Published online: 29 January 2011
© Springer-Verlag 2011

Abstract Chromosomal aberrations in non-small-cell lung carcinomas (NSCLCs) are common events. In our study, the lung cancer cell lines (NCI-H446 and SPC-A-1) displayed numerous numerical and structural alterations in their chromosomes by G-banded karyotypic analysis, and abnormalities of chromosome 12 by fluorescence in situ hybridization. Sequentially, we used 14 microsatellite markers within 12q to analyze loss of heterozygosity (LOH) in lung cancer cell lines and NSCLCs. Possible LOH on 12q were statistically inferred to occur in five lung cell lines. Importantly, 17 out of 25 NSCLCs (68%) showed LOH at chromosome 12q. Frequencies of LOH for individual markers ranged from 18% to 44%. Several deletions which were marked with D12S1301, D12S2196, D12S398, D12S90, D12S1056, D12S1713, D12S375, D12S1040, D12S326, and D12S106 were newly detected. Allelic loss on 12q15–q21 detected with D12S1040 occurred at the later stages of NSCLC progression ($p<0.05$, Fisher's exact test). LOH on 12q marked with D12S2196, D12S398, D12S326, and D12S106 were frequently found in NSCLCs from the patients without smoking history ($p<0.05$, Fisher's exact test). These findings indicated that allelic loss on 12q is commonly involved in NSCLCs, and new tumor suppressor genes may occur within 12q.

X.-J. Ding · M.-X. Liu · L. Ao · Y.-R. Liang · Y. Cao (✉)
Key Laboratory of Animal Models and Human Disease Mechanisms of CAS and Yunnan Province,
Kunming Institute of Zoology,
Chinese Academy of Sciences,
32 Jiaochang Donglu,
Kunming, Yunnan 650223, China
e-mail: caoy@mail.kiz.ac.cn

M.-X. Liu
Graduate University of the Chinese Academy of Sciences,
Beijing 100049, China

Keywords Non-small-cell lung carcinoma (NSCLC) · Chromosome · Karyotype · 12q · Loss of heterozygosity

Introduction

Lung cancer is the number one cause of cancer death in the world, and the incidence of lung cancer has rapidly increased in many countries [1]. The tumor suppressor genes or oncogenes are involved in the development and progression of lung cancer. Chromosomal aberrations associated with mutations in tumor suppressor genes or gene amplifications of dominant oncogenes are well-known genetic abnormalities in tumors including lung cancer [2]. Analysis of chromosomal abnormalities in tumors has proven helpful to search new tumor suppressor genes or oncogenes. Losses of 3p, 6q, 8p, 9p, 9q, 13q, 17p, 18q, 19p, 21q, and 22q as well as gains of 1p, 1q, 3q, 5p, 7p, 7q, 11q, and 12q are common in lung cancers [3]. In these regions there may be tumor suppressor genes or oncogenes and their changes may be necessary for conversion of normal bronchial epithelium to lung cancer. Loss of heterozygosity (LOH) or genomic instability in human neoplasms indicates the occurrence of tumor suppressor genes in the chromosomal regions. Microsatellites (single tandem repeat-STR loci) which are small nucleotide repeats are used as markers to study LOH or genomic instability. In this research, karyotypic and LOH analyses were introduced to study alterations of chromosomes in lung cancers. At first, we performed G-banded karyotypic analysis and chromosome painting by using fluorescence in situ hybridization (FISH) to characterize chromosomal aberrations in lung cancer cell lines. The chromosomal aberrations were drastic and complex. Abnormalities of chromosome 12 were observed in two cell lines. Several studies demon-

strated that the abnormalities of chromosome 12q were a frequent event in lung cancer [4–7]. Interestingly, a chromosomal breakpoint at 12q14 was found on two lung cancer cell lines in a most recent study [8]. Based on these observations, thereafter we performed LOH analyses using 14 microsatellite markers within 12q on five lung cancer cell lines and 25 cases of non-small-cell lung carcinoma (NSCLC), which accounts for approximately 80% of all lung carcinomas, in order to further study chromosomal deletions in lung cancers.

Materials and methods

Cell lines and cell culture

Five human lung cancer cell lines, SPC-A-1 (adenocarcinoma), NCI-H446 (small cell lung cancer), GLC-82 (adenocarcinoma), EPLC-32M1 (squamous carcinoma), and 801-D (large cell lung cancer), were employed. The five cell lines were cultured in Petri dishes containing RPMI1640 supplemented with 10% fetal bovine serum.

G-banding analysis and fluorescence in situ hybridization

Cytogenetic study was performed on the SPC-A-1 and NCI-H446 at three to four passages after thawing. Absolute numbers of the passage are not available. Cell metaphase preparation and G-banding were performed following conventional procedures as described previously [9]. The painting probe of HSA chromosome 12 is provided by Cell Bank, Kunming Institute of Zoology, Chinese Academy of Sciences. Chromosome painting in the two lung cancer cell lines with HSA 12 paints followed the procedures described previously [10]. For single-color detection, biotin-labeled probes were visualized by Cy3-avidin (1 μg/ml; Amersham). Thereafter, slides were mounted with Antifade AF1 (Citifluor Ltd) containing 0.08 mg/ml DAPI (4′6-diamidino-2-phenylindole) and covered with 22×32 mm^2 coverslips. Images were captured using the Genus System (Applied Imaging) with a CCD camera mounted on a Zeiss Axioplan 2 microscope. Hybridization signals were assigned to specific chromosomes or chromosome regions defined by enhanced DAPI-banding or pre-captured G-banding patterns [10].

Tissue specimens

Twenty-five cases of lung cancer and adjacent nontumorous lung tissues were obtained from patients undergoing resection. Patients included 19 males and six females; the mean age was 55.28 years (range, 32 to 75 years). There were 17 cases of adenocarcinoma (ACA) and eight cases of squamous cell carcinoma (SCC). The pathological diagnosis was done with hematoxylin–eosin-stained sections according to the WHO classification [11]. Tumors were staged according to TNM criteria published by International Union Against Cancer in 1997 [12]. Smoking status means that the smokers had at least 10 years of smoking history and smoked 20 cigarettes or more a day. Clinic and pathologic characteristics of the patients are given in Table 1. The samples were fully encoded to protect patient confidentiality and were approved by the local research ethics committees at all participating sites.

Loss of heterozygosity assays

Fourteen microsatellite markers within 12q were selected from the National Center for Biotechnology Information (http://www.ncbi.nlm.nih.gov/genome/sts/), the codes of the markers and the primers are list below (Table 2). The markers have an average separation of about 3 Mb.

DNA of the cultured cells was isolated by detergent lysis and proteinase K digestion followed by phenol extraction. All DNA samples were subjected to touchdown PCR amplification. PCR reactions were performed in 15-μl total volumes containing 0.5 μl prepared genomic DNA, 0.75 U of Jump Start Taq DNA Polymerase (SIGMA), and appropriate primers at a final concentration of 0.2 μmol/L. Reactions were performed in the following buffer conditions: 10 mmol/L Tris–HCl (pH 8.3), 50 mmol/L KCl, 1.5 mmol/L $MgCl_2$, 0.001% (*w*/*v*) gelatin, and 0.2 mmol/L dNTP mix. The PCR run conditions were as follows: initial denaturation at 95°C for 5 min, followed by 20 cycles consisting of 1 min at 94°C, 1 min at 64°C and lowering 0.5°C every cycle, 1 min at 72°C, then 20 cycles consisting of 1 min at 94°C, 1 min at 54°C, 1 min at 72°C, and a final extension at 72°C for 7 min. The PCR products were denatured by incubation with formamide buffer (95% formamide, 20 mM EDTA, 0.05% bromophenol blue, 0.05% xylenecyanole) at 95°C for 5 min and immediately iced for 1 min, then loaded on denaturing polyacrylamide gel electrophoresis and followed by silver staining. The intensity of the silver staining was measured using software Bandscan 5.0 (Glyko Inc., Novato, CA, USA) after scanning. Normal cells obtained from a healthy person's blood cells were used as control. Homozygous deletions in lung cancer cell lines were determined as described previously [13]. Briefly, they were assessed by statistical analysis of: (a) intramarker homozygosity, i.e., the deviation from the expected frequency of heterozygosity for each locus in the cell lines using Fisher's exact test; and (b) intermarker homozygosity within individual cell lines exhibiting extensive regions of contiguous homozygous loci. For the latter, the probability of observing contiguously homozygous loci is given by F_{Hom} at locus A × F_{Hom}

Table 1 Clinical and pathologic data of 25 NSCLC patients

Case no.	Gender	Age	Histologic type	TNM stage	Differentiation	Smoking
1	F	62	ACA	I	Well	N
2	M	34	ACA	I	Well moderately	Y
3	F	52	ACA	I	Well	N
4	M	58	SCC	I	Poorly	Y
5	F	54	ACA	I	Well	N
6	M	39	ACA	I	Moderately	Y
7	M	38	ACA	I	Moderately	Y
8	F	72	ACA	I	Moderately	N
9	F	52	ACA	II	Well	N
10	M	63	SCC	I	Well moderately	Y
11	M	75	ACA	II	Well	N
12	M	58	ACA	II	Moderately	Y
13	M	62	ACA	III	Poorly	Y
14	M	57	ACA	II	Well moderately	Y
15	M	71	ACA	III	Moderately	Y
16	F	52	ACA	III	Well moderately	N
17	M	32	SCC	IV	Well moderately	Y
18	M	69	ACA	IV	Moderately	Y
19	M	35	SCC	III	Moderately	Y
20	M	57	SCC	II	Poorly	Y
21	M	61	SCC	III	Poorly	Y
22	M	73	SCC	I	Well moderately	Y
23	M	35	SCC	III	Poorly	Y
24	M	63	ACA	I	Poorly	Y
25	M	58	ACA	II	Moderately	Y

F female, *M* male, *ACA* denocarcinoma, *SCC* squamous cell carcinoma, *well* well differentiated, *moderately* moderately differentiated, *poorly* poorly differentiated, *N* no, *Y* yes

at locus B ×..... × F_{Hom} at locus *N*, where F_{Hom} is the expected frequency of homozygotes for a given locus calculated by $(1-P)$, where P is the population of heterozygotes among the 25 normal lung DNAs, and N is the total number of contiguously homozygous loci.

Twenty-five cases of lung cancer and matched non-tumorous lung tissues adjacent to the tumors were immediately frozen and stored in liquid nitrogen. Both kinds of tissue specimens from each patient were micro-dissected in order to enrich the appropriate cell population

Table 2 Primers sequences of STS markers used for LOH analysis

Regions	STS	Forward primer (5–3)′	Reverse primer (5–3)
12q12	D12S1301	ACACAGATGTGCATCTATCTCG	TATTGGACAGTAAAGAAACCTGC
12q12–q13.13	D12S1713	GCTATTTGGGAGGCCAGTTG	TCCCTCTGGGTAGAATGTTTTTG
12q12–q13.13	D12S1997	AAGAAATGATTGAATAAAATGAGGG	TATCTTTGCCTCCTTGACAGC
12q12–q13.13	D12S2196	ATGAGGCAAAATCCTGGTCT	CCCAAGGATCTGGAATTTTT
12q13.11–q13.12	D12S1401	CAGCATTATCACAATGTAAAGAACC	TAAATGACTCTTATTACCACAACCC
12q11.2–q14	D12S398	GGTGGATGGATGGATGAATA	AGTGTTTGGACTGTCATTTGC
12q13.2–13.3	D12S1927	GAGTGGAACTTATGACTTGGGC	AGAGAGAGGGTAGGTTGCAGC
12q14.1	D12S90	AGCAGCAGCAGCCATATTGT	AGTCAGGCCCACCCAATTTA
12q14.1	D12S1056	GGGAAAGAGTTGGGGATTAA	TCCTTGGGTGTGATTAGCAT
12q14.3	D12S1511	AAAATAGCTGGTATGGTGGC	GTAATCAACCATTCCCCTGA
12q14.1–q23.1	D12S375	TTGTTGAGGGTCTTTCTCCA	TCTTCTTATTTGGAAAAGTAACCC
12q15–q21	D12S1040	TATGACAGGATGAACAAAAACG	AAATTGAATTTGATTTCTTCATAGC
12q13.2–q24.1	D12S326	CCCAGCAGTGCTAGTGTTGA	GGGCTAGGGTGGAGAATCAA
12q21.31	D12S106	CATAATTTCTGCCGAAGTCA	GATTAATGGTAAAATGTTTTGCATA

for subsequent DNA extraction. Microdissection was done on cryosections with 10–12 μm thickness according to hematoxylin–eosin staining. Tumor purity was judged to be at least 70%. Genomic DNA was extracted from microdissected tissues for LOH analysis as previously described [14]. LOH analysis was performed as described above. Tumor was determined to have undergone LOH at particular locus only if the predominant band associated with one allele showed a complete loss or a decrease of 50% intensity in the tumor relative to the adjacent nontumorous tissue [15]. All losses were confirmed in an independent PCR assay and triple time PCR was performed with each pair of primers.

Statistical analysis

The statistical SPSS software package (SPSS Inc., Chicago, IL, USA) was used to analyze data. Statistical analysis was performed using the Fisher's exact test (two-tailed) to compare the LOH status of chromosome 12q with the clinical and pathologic characteristics of the patients and to examine intramarker differences between the observed and the expected heterozygosity for each locus in the cell lines. The probability value of $p<0.05$ or $p<0.01$ was assumed to be significant or extreme significant, respectively.

Results

Chromosomal abnormalities detected by G banding

The G-banded karyotypes of NCI-H446 and SPC-A1 are shown in Fig. 1. The karyotype of SPC-A-1 has a triploid number ($3n$) of 67. There were about 40 normal chromosomes and about 27 derived chromosomes to be identified in the karyotype. The approximate number of chromosome of NCI-H446 was 80, around 46 normal chromosomes and around 34 derived chromosomes. Some derived chromosomes and many rearrangement were present that were too complex to identify using the technique of G-banding and light microscopy.

Abnormalities of chromosome 12 detected by FISH

HSA chromosome 12-specific painting probe was hybridized onto metaphase of the two lung cancer cell lines, respectively. The probe of HSA 12 delineated five homologous chromosome or chromosomal region in the genomes of lung cancer cell line SPC-A-1 (Fig. 2a) and four in NCI-H446 (Fig. 2b).

Loss of heterozygosity analysis on 12q region in the cell lines

Fourteen microsatellite markers on 12q were selected for LOH analysis in five lung cancer cell lines. We found significant intramarker differences between the observed and the expected heterozygosity for D12S1301, D12S2196, D12S398, D12S90, D12S 1056, D12S1713, D12S375, D12S1040, and D12S2196 (Table 3). Representative examples of LOH analysis for various loci using lung cancer cell lines along with normal human controls were shown in Fig. 3a and b. All of the cell lines showed contiguous intermarker homozygosity (Table 4). Among these cell lines, NCI-H446, SPC-A-1, and GLC-32 had a common region of the homozygous deletion that was located between D12S1301 and D12S1713 loci.

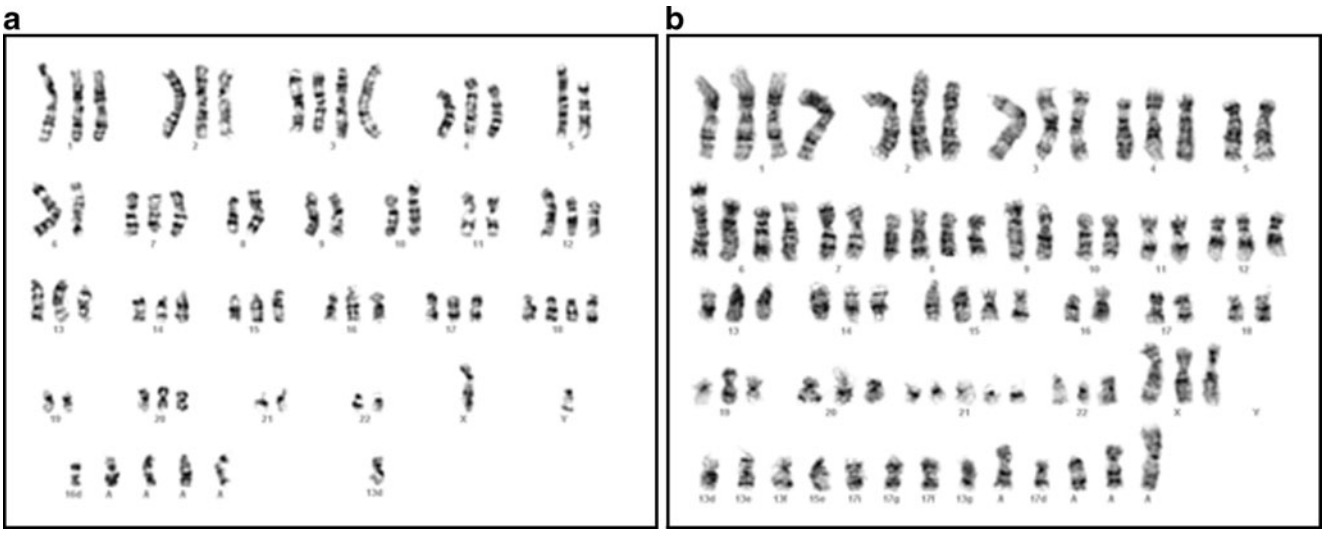

Fig. 1 The composite karyotype for SPC-A-1 and NCI-H446 analysis by metaphase. **a** The karyotype for SPC-A-1. **b** The karyotype for NCI-H446

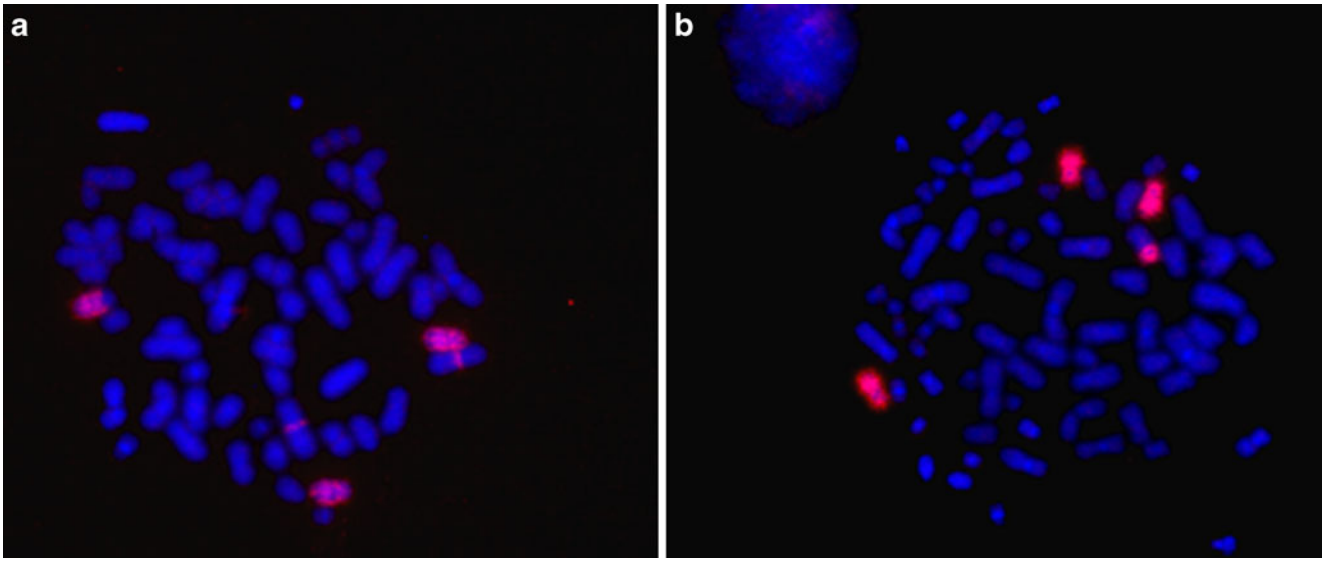

Fig. 2 In situ hybridization with HSA 12 chromosome-specific painting probe on SPC-A-1 (**a**) and NCI-H446 (**b**)

Loss of heterozygosity analysis on 12q region in the tissues

Thirteen microsatellite markers on chromosome 12q12–q15 and a microsatellite marker (D12S106) on 12q21.31 were used for LOH analysis to characterize the losses of chromosome 12q in NSCLCs. Representative examples of LOH analysis for various loci using tumor samples along with their corresponding matching adjacent nontumorous tissues were shown in Fig. 3c–e. The microsatellite markers located in this region and the results of LOH analysis were present in Fig. 4. Totally, 68% (17 of 25) of NSCLC cases displayed LOH at chromosome 12q with at least one microsatellite marker. Frequencies of LOH for individual markers ranged from 12% to 44%. The most frequent loss occurred in 44% (11 of 25) at the region marked with D12S1301. The following frequency (40%, 10 of 25) of LOH was observed for D12S375. The losses of the regions marked with D12S2196, D12S1056, and D12S1713 were present in 32% (eight of 25). Frequency of LOH detected with D12S90 and D12S326 was 28% (seven of 25). The rates of LOH for D12S1040, D12S398, and D12S106 were 24% (six of 25), 20% (five of 25), and 12% (three of 25), respectively.

Relationship of LOH presence to pathologic parameters of NSCLC

The relation between presence of LOH and pathologic parameters was summarized in Table 5. Statistical analysis (Fisher's exact test) revealed that the LOH at chromosome

Table 3 Homozygosity mapping of chromosome 12q loci in human five lung cancer cell lines

Loci	NCI-H446	SPC-A-1	GLC-82	EPLC-32M1	801-D	P
D12S1301	−	−	−	−	−	–*
D12S1997	−	−	−	−	−	NS
D12S2196	−	−	−	−	+	–*
D12S1401	−	−	−	−	−	NS
D12S 398	−	−	−	+	−	–*
D12S1927	−	−	−	−	−	NS
D12S 90	−	−	−	−	−	–**
D12S1056	−	−	−	−	−	–*
D12S1713	−	−	−	−	−	–*
D12S1511	+	+	+	+	+	NS
D12S 375	−	−	−	−	−	–**
D12S1040	−	−	−	−	−	–*
D12S 326	+	+	+	+	+	NS
D12S 106	−	−	−	+	−	NS

Discrepancies in the expected number of heterozygotes for a given locus were calculated using Fisher's exact test

− homozygote, + heterozygote, *NS* no significance

*$P<0.05$; **$P<0.01$

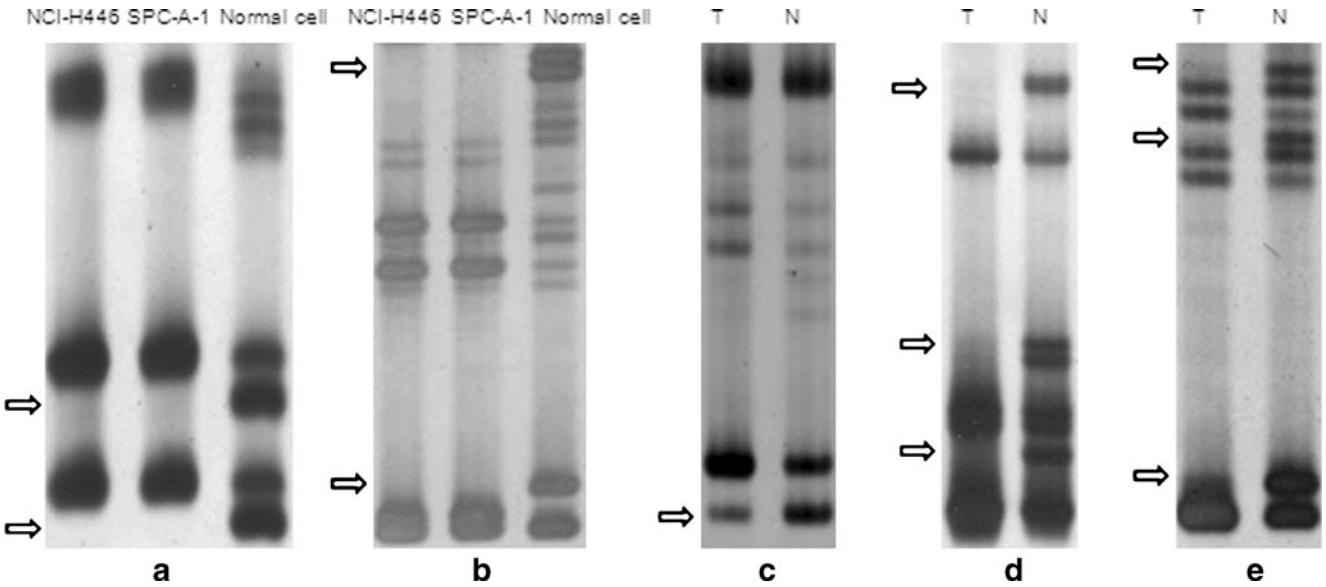

Fig. 3 Representative gel pictures of LOH analysis within the region of 12q in the cell lines and the tissues of non-small-cell lung carcinoma. Normal cells were obtained from a healthy person's blood cells. *T* and *N* denote the tumors and the nontumorous lung tissues adjacent to the tumors. *Hollow arrows* mean loss of heterozygosity. **a** D12S1713 for NCI-H446, SPC-A-1, and the normal cell; **b** D12S2196 for NCI-H446, SPC-A-1, and the normal cell; **c** D12S375 for no. 7 case; **d** D12S326 for no. 9 case; **e** D12S2196 for no. 10 case

12q21 marked with D12S106 was correlated significantly with histological types of NSCLC (p=0.02). The NSCLCs with higher TNM stages displayed more frequency of the LOH for D12S1040 (p=0.03). The LOH at chromosome 12q detected with D12S1301, D12S2196, D12S398, D12S90, D12S1056, D12S1713, D12S375, and D12S326 was not correlated significantly with histological types, TNM stages, and differentiated status of NSCLC.

Correlation of LOH presence with gender and smoking histories of the patients

We compared gender and smoking histories of the patients with the presence of LOH at each of the loci in the NSCLCs (Table 5). The LOH for D12S2196 (p=0.006), D12S398 (p=0.014), D12S1040 (p=0.03), and D12S106 (p=0.009) markers had significant relations with gender of patients. The status of LOH at chromosome 12q marked with D12S2196 (p=0.017), D12S398 (p=0.014), D12S326 (p=0.007), and D12S106 (p=0.015) was found to be significantly different between patients with and without smoking histories. The female patients and the patients without smoking habits exhibited more frequent allelic loss at chromosome 12q. The similar statistical results of both the gender and smoking status may be due to the phenomena that almost all female patients had no smoking histories. No significant correlation between the LOH for D12S1301, D12S90, D12S1056, D12S1713, and D12S375 as well as gender and smoking histories of the patients had been observed.

Table 4 Regions of significant intermarker homozygosity in human five lung cancer cell lines

Cell line	Region of homozygosity[a]	Probability[b]
NCI-H446/SPC-A-1/ GLC-82	D12S1301-D12S1713	1.95×10^{-3}
EPLC-32M1	D12S1917-D12S1713	4.65×10^{-2}
801-D	D12S1401-D12S1713	2.33×10^{-2}

[a] Marker loci that define the boundaries of the regions exhibiting continuous homozygosity

[b] Probability of contiguous loci exhibiting homozygosity by chance alone (see Materials and methods)

Discussion

Cancer is a genetic disease caused by accumulation of chromosomal and genetic changes. Over the past decade chromosomes and genes have been found to undergo drastic changes in lung cancer [3]. However, only a small fraction of the chromosomes and genes has been analyzed so far, and the number and type of alterations responsible for the development and progression of lung cancer are unknown. Thus, more comprehensive analysis of chromosomal and genetic changes in lung cancer is required. Karyotypic and LOH analyses are routine methods for studying chromosome aberrations. In the study, we use cytogenetic techniques to investigate chromosome aberrations in two lung cancer cell lines. The karyotypes of the

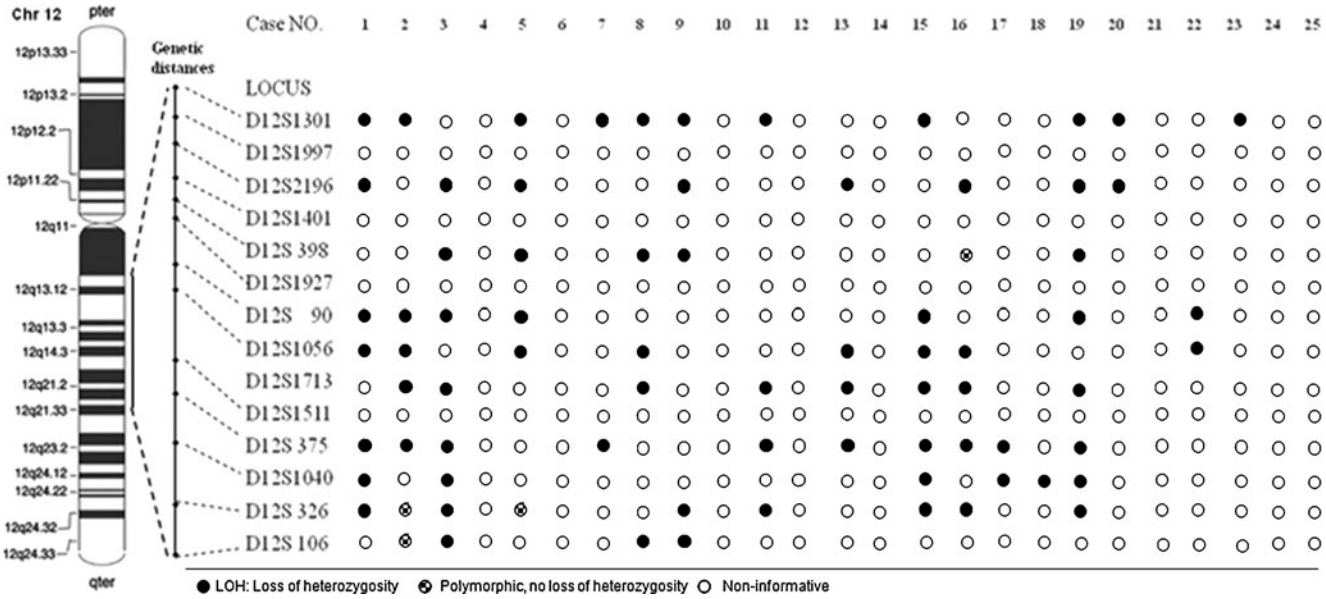

Fig. 4 The results of LOH analysis in the 25 NSCLCs and 14 microsatellite markers on chromosome 12q used in the study. The microsatellite markers used are listed on the *left*, in order from pter (*top*) to qter (*bottom*). Genetic distances are obtained from National Center for Biotechnology Information, Sequence Map: HuRef (http://www.ncbi.nlm.nih.gov/genome/sts/). The *black circles* indicate deleted loci

two lung cancer cell lines (NCI-H446 and SPC-A-1) were well documented. Both cell lines exhibited numerous numerical and structural alterations in their chromosomes. We also found that aberrations of chromosome 12 were involved in the two cell lines. The abnormalities of chromosome 12q have been observed in lung cancers by comparative genomic hybridization [4–7]. In a very current study, a new chromosomal breakpoint at the 12q13–14 region was found in two lung cancer cell lines, A549 and GLC-82 [8]. However, little is known of occurrence of

Table 5 Comparison of clinical and pathologic characteristics to LOH status of chromosome 12q

Clinical and pathologic characteristics	LOH of different regions				
	D12S2196	D12S398	D12S1040	D12S326	D12S106
Gender					
Male	3/19 (16%)[1]**	1/19 (5%)[2]**	3/19 (16%)[3]*	4/19 (21%)	0/19 (0%)[4]**
Female	5/6 (83%)[1]**	4/6 (7%)[2]**	4/6 (67%)[3]*	3/6 (50%)	3/6 (50%)[4]**
Histologic type					
ACA	6/17 (35%)	4/17 (24%)	4/17 (24%)	6/17 (35%)	0/17 (0%)[5]*
SCC	2/8 (25%)	1/8 (13%)	2/8 (25%)	1/8 (13%)	3/8 (38%)[5]*
TNM stage					
I+II	5/18 (28%)	4/18 (22%)	2/18 (11%)[6]*	4/18 (22%)	3/18 (17%)
III+IV	3/7 (43%)	1/7 (43%)	4/7 (57%)[6]*	3/7 (43%)	0/7 (0%)
Differentiation					
Poor	2/6 (33%)	0/6 (0%)	0/6 (0%)	0/6 (0%)	0/6 (0%)
Well or moderate	6/19 (32%)	5/19 (26%)	6/19 (32%)	7/19 (37%)	3/19 (16%)
Smoking					
No	5/7 (71%)[7]*	5/7 (71%)[8]*	2/7 (29%)	5/7 (71%)[9]**	3/7 (43%)[10]*
Yes	3/18 (17%)[7]*	1/18 (6%)[8]*	4/18 (22%)	2/18 (11%)[9]**	0/18 (0%)[10]*

Values are number of cases applicable/total number of cases examined (with percent in parentheses)

ACA adenocarcinoma, *SCC* squamous cell carcinoma

*$P<0.05$; **$P<0.01$

[1–10] The statistical differences were compared using the Fisher's exact test (two-tailed)

LOH at 12q in NSCLCs. Thus, we investigated LOH at this region in lung cancer cell lines and tissues of NSCLC.

LOH analysis is a common technique to investigate chromosomal deletions and rearrangements within a region, and has been largely carried out in NSCLCs. The most of previous studies dealt with chromosomes 1, 2, 3, 5, 8, 9, 11, 13, 17, 18, 21, 22 [16–26]. In our study, 13 microsatellite markers on chromosome 12q12–q15 and a microsatellite marker (D12S106) on 12q21.31 were used to analyze LOH in the lung cancer cell lines and the tissues of NSCLC. To our knowledge, this is a first report on LOH at 12q in NSCLCs. LOH analysis in the cell lines showed significant intramarker differences between the observed and the expected heterozygosity, and contiguous intermarker homozygosity. These implied deletions on chromosome 12q involving in lung cancer. Furthermore, the data obtained from the tissues of NSCLC demonstrated that rate of overall LOH on 12q was 68%, suggesting that abnormal alterations of 12q were frequent incidents in NSCLCs. Several deletions were newly detected. These losses on chromosome 12 were marked with D12S1301, D12S2196, D12S398, D12S90, D12S1056, D12S1713, D12S375, D12S1040, D12S326, and D12S106. Frequencies of LOH for individual markers ranged from 12% to 44%. At the region marked with D12S1301, the rate of the LOH was even to 44%. Several studies reported that there are gains on 12q in NSCLCs [4–6]. The studies on chromosomal mechanisms causing LOH revealed that the majority of LOH were partial chromosome LOH caused by structural chromosomal alterations, and unbalanced translocation which is the most frequent alteration accounted for 30% of all LOH [16]. We guessed that structural alterations of chromosome 12q may be involved in gains, LOH, and unbalanced translocation at the region. Gains, LOH, and unbalanced translocation could be simultaneously present at one aberrant region of chromosome. Besides NSCLCs in which the LOH at chromosome 12q13–15 was found in this study, LOH on 12q13 also has been observed in adenoid cystic carcinoma [27] and salivary gland pleomorphic adenomas [28]. LOH observed in an identified region indicates that there are fragments of deletion around the region. An almost universal loss of genetic material from an identified region in cancer cells foretells that one or more tumor suppressor genes may reside in this region. The region of 12q13–15 contains a lot of genes that are associated with regulating cell cycle, cytokinesis, or signal transduction. Some genes located in the region [for example, CDK2 (12q13), ESPLI (12q13), ACVR1B (12q13), ATF7 (12q13), NR4A1 (12q13), and GRASP (12q13)] involved in carcinogenesis have been observed [29–31]. Although in the task we have not found that one or more tumor suppressor genes within the 12q13 were deleted in lung cancers, the present results opened up a new insight into aberrations of chromosomes during carcinogenesis of NSCLC, and they emerged as a starting point for tumor suppressor gene discovery. This will, however, be addressed in further studies.

We have also noted that LOH at chromosome 12q marked with D12S106 was present on squamous cell carcinomas in higher frequency, but absent on adenocarcinomas. More importantly, allelic loss on 12q15–q21 detected with D12S1040 occurred at the later stages of NSCLC progression. It is tempting to speculate that the allelic losses on 12q15–q21 might be associated with progression of NSCLC. Here it must be categorized as a pilot study. More works are certainly needed.

We would like to emphasize an interesting observation that the presence of LOH at 12q in NSCLCs was significantly related to gender and smoking histories of patients. We thought that both gender and smoking status of the patients displayed the similar statistical results of LOH because almost all female patients had no smoking histories. In previous studies, LOH at 2q and 12p in histologically normal-appearing bronchial epithelium was significantly associated with long-term smoking [32], and LOH at 3p and 9p was detected in precancerous lesions and in normal epithelium of heavy smokers [33]. By comparison of presence of the LOH in tobacco smoke-exposed bronchial epithelial cells and NSCLCs, LOH at 8p, 9p, 11p, and 13p could be early events during the carcinogenesis induced with smoking, and LOH at 1p, 3p, 5q, 17p, and 18q could occur at the later stages of smoking-related NSCLC [34]. In contrast, allelic losses on 12q marked with D12S2196, D12S398, D12S326, and D12S106 were frequently found in NSCLCs from the patients without smoking history here. Besides smoking, other factors (for example, indoor or/and outdoor air pollution) are also important causes for the development of lung cancer, particularly in China nowadays. Thus, pathophysiologic roles and etiologic significances of the allelic losses on 12q deserve further investigation in the future.

In summary, the lung cancer cell lines (NCI-H446 and SPC-A-1) display numerous numerical and structural alterations in their chromosomes. Allelic losses on 12q are common events in NSCLCs. Our findings provide a road map for further research on new tumor suppressor genes located within 12q.

Acknowledgment We thank the colleagues from the Department of Surgery of Yunnan First People Hospital for providing surgical specimens. Supported by Hundred Talents Program (Grant Cao) and West Light Foundation (Grant Liang) of Chinese Academy of Sciences.

Conflict of interest statement We declare that we have no conflict of interest.

References

1. Parkin DM, Bray F, Ferlay J et al (2005) Global cancer statistics. CA Cancer J Clin 55:74–108
2. Gazdar AF, Bader S, Hung J et al (1994) Molecular genetic changes found in human lung cancer and its precursor lesions. Cold Spring Harb Symp Quant Biol 59:565–572
3. Mitsuuchi Y, Testa JR (2002) Cytogenetics and molecular genetics of lung cancer. Am J Med Genet 115:183–188
4. Tonon G, Brennan C, Protopopov A et al (2005) Common and contrasting genomic profiles among the major human lung cancer subtypes. Cold Spring Harb Symp Quant Biol 70:11–24
5. Shen H, Gao W, Wu YJ et al (2009) Multicolor fluorescence in situ hybridization and comparative genomic hybridization reveal molecular events in lung adenocarcinomas and squamous cell lung carcinomas. Biomed Pharmacother 63:396–403
6. Sy SM, Wong N, Lee TW et al (2004) Distinct patterns of genetic alterations in adenocarcinoma and squamous cell carcinoma of the lung. Eur J Cancer 40:1082–1094
7. Berrieman HK, Ashman JN, Cowen ME et al (2004) Chromosomal analysis of non-small-cell lung cancer by multicolour fluorescent in situ hybridization. Br J Cancer 90:900–905
8. Peng KJ, Wang JH, Su WT et al (2010) Characterization of two human lung adenocarcinoma cell lines by reciprocal chromosome painting. Dongwuxue Yanjiu 31:113–121
9. Seabright M (1971) A rapid staining technique for human chromosomes. Lancet 2:971–972
10. Yang F, Fu B, O'Brien PCM et al (2004) Refined genome-wide comparative map of the domestic horse, donkey and human based on cross-species chromosome painting: insight into the occasional fertility of mules. Chromosome Res 12:65–76
11. Brambilla E, Travis WD, Colby TV et al (2001) The new World Health Organization classification of lung tumours. Eur Respir J 18:1059–1068
12. Sobin LH, Wittekind C (1997) In: Sobin LH, Wittekind C (eds) International Union Against Cancer [UICC], TNM Classification of Malignant Tumours, 5th edn. Wiley-Liss, Baltimore, pp 93–97
13. Takei K, Kohno T, Hamada K et al (1998) A novel tumor suppressor locus on chromosome 18q involved in the development of human lung cancer. Cancer Res 58:3700–3705
14. Moskaluk CA, Kern SE (1997) Microdissection and polymerase chain reaction amplification of genomic DNA from histological tissue section. Am J Pathol 150:1547–1552
15. Emmer-buck MR, Lubensky IA, Dong Q et al (1997) Localization of multiple endocrine neoplasia type I (MEN1) gene based on tumor loss of heterozygosity analysis. Cancer Res 57:1855–1858
16. Ogiwara H, Kohno T, Nakanishi H et al (2008) Unbalanced translocation, a major chromosome alteration causing loss of heterozygosity in human lung cancer. Oncogene 14(27):4788–4797
17. Woenckhaus M, Grepmeier U, Wild PJ et al (2005) Multitarget FISH and LOH analyses at chromosome 3p in non-small cell lung cancer and adjacent bronchial epithelium. Am J Clin Pathol 123:752–761
18. Powell CA, Bueno R, Borczuk AC et al (2003) Patterns of allelic loss differ in lung adenocarcinomas of smokers and nonsmokers. Lung Cancer 39:23–29
19. Carpagnano GE, Spanevello A, Carpagnano F et al (2009) Prognostic value of exhaled microsatellite alterations at 3p in NSCLC patients. Lung Cancer 64:334–340
20. Yamada H, Yanagisawa K, Tokumaru S et al (2008) Detailed characterization of a homozygously deleted region corresponding to a candidate tumor suppressor locus at 21q11-21 in human lung cancer. Genes Chromosom Cancer 47:810–818
21. Ninomiya H, Nomura K, Satoh Y et al (2006) Genetic instability in lung cancer: concurrent analysis of chromosomal, mini- and microsatellite instability and loss of heterozygosity. Br J Cancer 94:1485–1491
22. Tai AL, Mak W, Ng PK et al (2006) High-throughput loss-of-heterozygosity study of chromosome 3p in lung cancer using single-nucleotide polymorphism markers. Cancer Res 66:4133–4138
23. Tseng RC, Chang JW, Hsien FJ et al (2005) Genomewide loss of heterozygosity and its clinical associations in non small cell lung cancer. Int J Cancer 117:241–247
24. Chmara M, Wozniak A, Ochman K et al (2004) Loss of heterozygosity at chromosomes 3p and 17p in primary non-small cell lung cancer. Anticancer Res 24:4259–4263
25. Sasatomi E, Finkelstein SD, Woods JD et al (2002) Comparison of accumulated allele loss between primary tumor and lymph node metastasis in stage II non-small cell lung carcinoma: implications for the timing of lymph node metastasis and prognostic value. Cancer Res 62:2681–2689
26. Woenckhaus M, Stoehr R, Dietmaier W et al (2003) Microsatellite instability at chromosome 8p in non-small cell lung cancer is associated with lymph node metastasis and squamous differentiation. Int J Oncol 23:1357–1363
27. Rutherford S, Hampton GM, Frierson HF et al (2005) Mapping of candidate tumor suppressor genes on chromosome 12 in adenoid cystic carcinoma. Lab Invest 85:1076–1085
28. El-Naggar AK, Callender D, Coombes MM et al (2000) Molecular genetic alterations in carcinoma ex-pleomorphic adenoma: a putative progression model? Genes Chromosom Cancer 27:162–168
29. White DT, McShea KM, Attar MA et al (2010) GRASP and IPCEF promote ARF-to-Rac signaling and cell migration by coordinating the association of ARNO/cytohesin 2 with Dock180. Mol Biol Cell 21:562–571
30. Su GH, Bansal R, Murphy KM et al (2001) ACVR1B (ALK4, activin receptor type 1B) gene mutations in pancreatic carcinoma. Proc Natl Acad Sci U S A 98:3254–3257
31. Dobashi Y, Shoji M, Jiang SX et al (1998) Active cyclin A-CDK2 complex, a possible critical factor for cell proliferation in human primary lung carcinomas. Am J Pathol 153:963–972
32. Grepmeier U, Dietmaier W, Merk J et al (2005) Deletions at chromosome 2q and 12p are early and frequent molecular alterations in bronchial epithelium and NSCLC of long-term smokers. Int J Oncol 27:481–488
33. Capkova L, Kalinova M, Krskova L et al (2007) Loss of heterozygosity and human telomerase reverse transcriptase (hTERT) expression in bronchial mucosa of heavy smokers. Cancer 109:2299–2307
34. Pan H, Califano J, Ponte JF et al (2005) Loss of heterozygosity patterns provide fingerprints for genetic heterogeneity in multistep cancer progression of tobacco smoke-induced non-small cell lung cancer. Cancer Res 65:1664–1669

Virchows Arch (2011) 458:571–581
DOI 10.1007/s00428-011-1062-5

ORIGINAL ARTICLE

EGFR/erB-1, HER2/erB-2, CK7, LP34, Ki67 and P53 expression in preneoplastic lesions of bronchial epithelium: an immunohistochemical and genetic study

Vítor Sousa · Joana Espírito Santo · Maria Silva · Teresa Cabral · Ana Maria Alarcão · Ana Gomes · Patrícia Couceiro · Lina Carvalho

Received: 14 September 2010 / Revised: 20 January 2011 / Accepted: 16 February 2011 / Published online: 22 March 2011
© Springer-Verlag 2011

Abstract A prognostic interpretation of preneoplastic lesions would have impact in bronchial carcinoma early diagnosis and through the study of Erb-B family receptors as they have an important role in lung carcinogenesis. The existence of drugs as tyrosine kinase inhibitors stressed the importance of studying gene alterations for selected chemoprevention schemes and characterization of carcinogenesis. Bronchial preneoplastic lesions were characterized by immunohistochemistry using the antibodies LP34 (high weigh molecular cytokeratin), CK7, chromogranin A, Ki67, p53, C-erbB-2 and EGFR. *HER2* and *EGFR* gene copy number was also evaluated by fluorescent in situ hybridization in those lesions. The expected results defined the origin cell for basal cell hyperplasia and squamous metaplasia as adaptative lesions and dysplasia. By known experiences and published data, beyond the stem cell, the spectral evolution of bronchial preneoplastic lesions was demonstrated by characterizing basal cells (LP34) and their neoplastic potentiality. Dysplasias showed a higher expression of EGFR, Ki67 and p53 with a stepwise increase with the gravity of the respective grading. C-erbB-2 immunohistochemical overexpression was a rare event in preneoplastic lesions. Polysomy was the main mechanism for *EGFR* and *HER2/neu* higher gene copy number and together with increased proliferation index (Ki67) will account to preview bronchial carcinogenesis.

Keywords Bronchial squamous metaplasia · EGFR, HER2/c-erB-2 · CK7 · LP34

Sources of support CIMAGO-Centro de Investigação em Meio Ambiente, Genética e Oncobiologia; ROCHE PHARMACEUTICALS

V. Sousa · J. E. Santo · M. Silva · T. Cabral · A. M. Alarcão · A. Gomes · P. Couceiro · L. Carvalho (✉)
IAP-FMUC-Institute of Pathology, Faculty of Medicine, University of Coimbra,
3000–054 Coimbra, Portugal
e-mail: lcarvalho@huc.min-saude.pt

V. Sousa · L. Carvalho
Pathology Institute, Coimbra University Hospital, Coimbra, Portugal

Introduction

Lung cancer is the leading cause of death by malignancy in developed countries and throughout the world. Environmental and occupational exposures, such as polyaromatic hydrocarbons, radon, asbestos, nickel, arsenic and chromium, are important determinants of lung cancer risk, but cigarette smoking is the main risk factor, accounting for about 90% of the cases in men, 70% of the cases in women and within today ex-smokers comprising nearly 50% of all new lung cancer cases [1–5].

The overall 5-year survival rate for lung cancer patients remains less than 15% [6], and the death rate for lung cancer exceeds the combined total for breast, prostate and colon cancer in developed countries [5]. The major reasons for the poor prognosis for lung cancer are the lack of effective screening and early diagnosis procedures, the propensity for early metastasis and the inability of systemic therapies to cure patients with widely metastatic disease [7]. Lung cancer is the result of a multi-step accumulation of genetic and/or epigenetic alterations; therefore, a better understanding of the molecular mechanism, by which these alterations affect lung cancer pathogenesis, would provide new and more effective strategies for chemoprevention,

early diagnosis and targeted treatment [8]. The existence of novel drugs against specific molecular targets like EGFR and HER2/neu genes leads to the importance of defining their expression as biomarkers in preneoplastic lesions.

The 1999/2004 WHO lung tumour classification recognizes three types of preinvasive lesions: squamous dysplasia and carcinoma in situ (CIS); atypical adenomatous hyperplasia and diffuse idiopathic pulmonary neuroendocrine cell hyperplasia [9]. Respiratory epithelium adaptative lesions include basal cell hyperplasia, squamous metaplasia, followed by dysplasia and CIS, which precede or accompany microinvasive or invasive carcinoma. Hyperplasia and squamous metaplasia are considered reversible lesions, while dysplasia and CIS are not [10–15].

Squamous metaplasia as a common adaptative lesion of the bronchial mucosae, especially in smokers, represents a precursor step in the development of invasive squamous cell carcinoma, deserving an accurate study to define its evolutionary potential to lung cancer, in order to be determined in bronchial biopsies [10, 14, 16, 17].

Several molecular and genetic abnormalities have been described in lung carcinogenesis, including activation of proto-oncogenes and loss of tumour suppressor genes and DNA repair genes. Proto-oncogenes can be activated by point mutations, amplification, chromosomal rearrangement and expression of a high gene copy number. [18–20]. Those genomic and molecular abnormalities are early events in lung carcinogenesis and can persist in bronchial lesions for months or years and their persistence or regression have been correlated with lesions' evolution [15, 21–30]. Molecular changes are recognized not only in lung cancer, but also in bronchial epithelium and parenchyma of current and former smokers without the development of lung cancer [31, 32].

Epidermal growth factor receptor (EGFR; *ErbB-1* gene) and ErbB-2 (*HER2/neu*) belong to ErbB family, a family of tyrosine kinase receptor proteins that includes also ErbB-3 (*HER-3*) and ErbB-4 (*HER-4*). The ErbB receptors are composed of three major domains: an extracellular ligand binding; a transmembranar segment and a cytoplasmic with tyrosine kinase activity. ErbB receptor function begins upon ligand binding and is followed by receptor homo (e.g. Erb-1/Erb-1) or heterodimerization (e.g. Erb-1/Erb-2), activating the tyrosine kinase domain of the receptor, which becomes phosphorylated and acts as a docking site for downstream signalling molecules and cytoplasmic messenger proteins that then trigger a cascade of cytoplasmic and nuclear pathways [15].

It has been suggested and supported by experimental data that aberrant activation of the kinase activity of ErbB receptors plays an important role in the neoplastic transformation and progression, prognosis, survival and resistance to cytotoxic therapies [6, 7, 15, 33–38]. EGFR's high expression is an early event in preneoplastic lesions, with an increasing expression from normal mucosae to hyperplasia, metaplasia and dysplasia [6, 38–42]. EGFR is overexpressed in 84% of squamous cell carcinoma, 65% of adenocarcinomas and 68% of large cell lung carcinomas [41]. As it seems, that ErbB2 is also highly expressed in bronchial preneoplastic lesions and its overexpression is less common in carcinomas (less than 35% of non-small cell lung carcinomas (NSCLC), mainly adenocarcinomas) [18, 41, 43]. The heterodimer EGFR/HER2-neu has been shown to have a stronger proliferative effect than the corresponding homodimers [38, 44–46]. Amplification and polysomy of EGFR and HER2-neu and overexpressed proteins have been related to survival in patients with NSCLC (non- small cell lung cancer), but contradictory results have been published [47–51]. New therapies have also been developed recently directed to these two molecular targets, some of them being applied in chemoprevention trials, stressing the necessity to understand their expression in adaptative and preneoplastic lesions [5, 52–56]. This study concerned bronchial preneoplastic lesions observed in biopsies as basal cell hyperplasia, squamous metaplasia and dysplasia. Using immunohistochemistry, those lesions were characterized by antibodies applied against LP34, CK7, chromogranin A, Ki67, p53, C-erbB-2 and EGFR. *HER2* and *EGFR* gene copy number was also evaluated by fluorescent in situ hybridization (FISH), using normal controls. The aim of the present study is to achieve a better understanding of the spectral evolution of bronchial adaptative and preneoplastic lesions, by recognizing the expression of *EGFR* and *HER2-neu* as potential biomarkers for lung cancer risk assessment. This knowledge would help to provide new and more effective strategies for chemoprevention, early diagnosis and targeted treatment.

Materials and methods

Material

A number of 67 bronchial biopsies were included in this study, comprising 89 preneoplastic lesions, selected from recent data base, by considering the preservation, number and dimension of the small fragments obtained by bronchial fibroscopy and represented 16 basal cell hyperplasia, 40 squamous metaplasia and 33 epidermoid dysplasia (7 mild dysplasia, 7 moderate dysplasia, 4 severe dysplasia and 15 CIS) (Fig. 1a, b, c, d, e); in 22 cases there was concomitancy of the lesions. The population consisted of 57 men and 10 women, with 66.3 years as mean age (range 38–92).

Hyperplasia was defined when more than four basal cell layers were observed. Squamous metaplasia was considered when there was replacement of ciliated columnar epithelium by pavimentous epithelium without atypia. Dysplasia

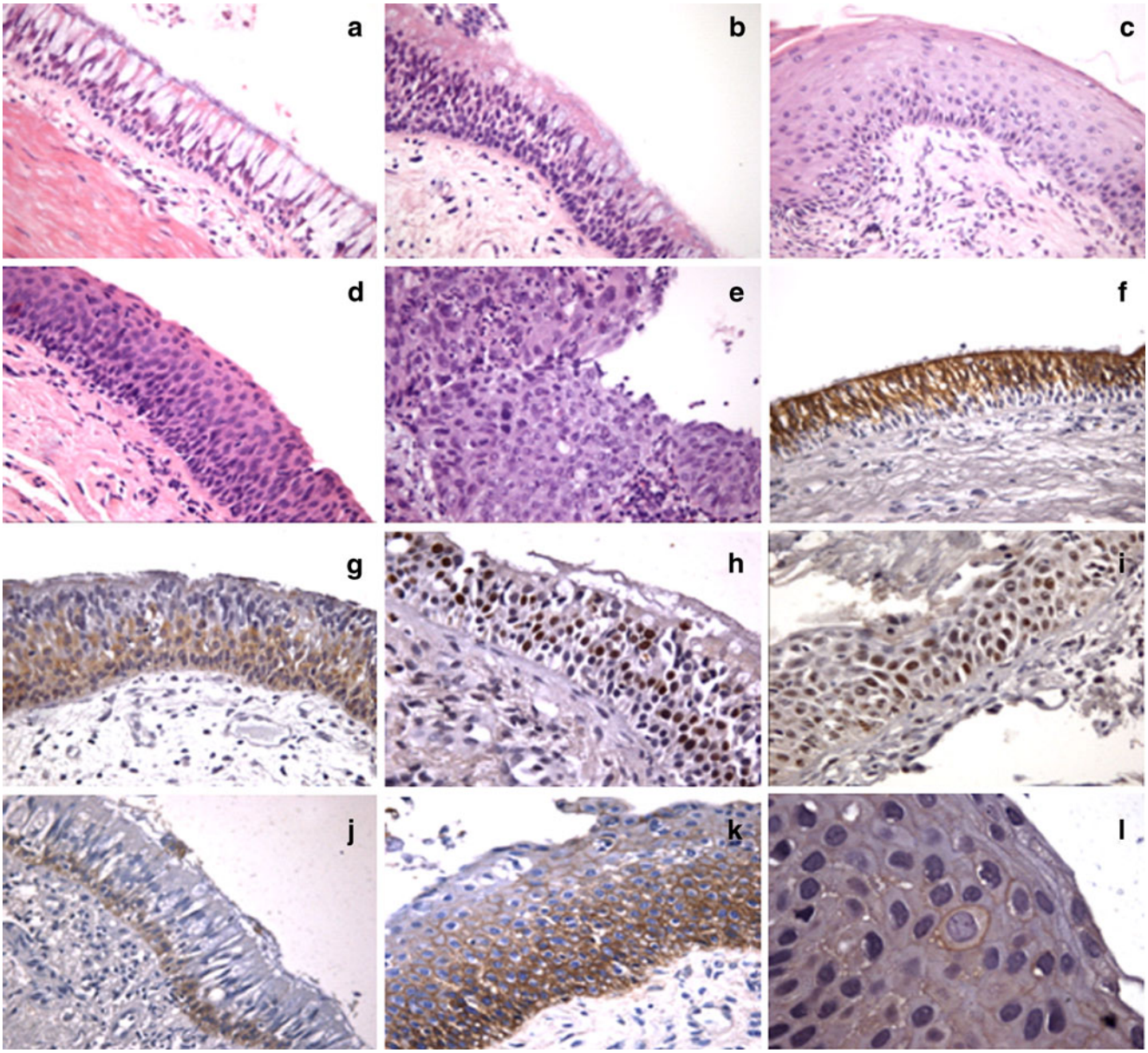

Fig. 1 Morphology and immunostaining: **a** Normal bronchial epithelium, H&E, ×400. **b** Basal cell hyperplasia, H&E, ×400. **c** Squamous metaplasia, H&E, ×400. **d** Moderate dysplasia, H&E, ×400. **e** In situ carcinoma, H&E, ×400. **f** CK7 expression, normal bronchial epithelium, ×400. **g** Basal cell hyperplasia, LP34, ×400. **h** Ki67 3+/70%, ×400. **i** P53 2+/50%, ×400. **j** EGFR negative, normal epithelium, ×400 **k** EGFR, 3+/60%, ×400. **l** C-erbB-2, 2+, ×1,000

was graded as mild, moderate and severe/CIS according to the levels of atypia.

Biopsy products were routinely fixed in 4% neutral buffered formalin immediately after bronchial fibroscopy. They were processed and embedded in paraffin. One paraffin block was chosen from each case, containing several representative fragments. From each paraffin block, several cuts 5-μm thick sections were made and put on glass slides then stained with haematoxylin–eosin and reviewed by two pathologists in order to ensure the optical criteria for preneoplastic bronchial lesions according to the 1999/2004 histological WHO/IASLC classification of preinvasive squamous lesions of the bronchi.

Methods

Immunohistochemistry

The imunnohistochemical analysis included seven different antibodies: CK7 (Monoclonal Mouse Anti-human, OV-TL 12/30, Dako); LP34 (Monoclonal Mouse Anti-human, Clone LP34, Dako); chromogranin A (Monoclonal Mouse

Anti-human, Clone DAK-A3, Dako); Ki67 (Monoclonal Mouse Anti-human, Clone MIB-1, Dako); p53 (Monoclonal Mouse Anti-human, Clone DO-7, Dako); C-erbB-2 (Policlonal Mouse Anti-human, Dako) and EGFR (Monoclonal Mouse Anti-human, Clone 31G7, Zymed Laboratories Inc.). The procedure was performed according to a standard avidin-biotin-peroxidase complex. Three-micrometer tissue sections were placed on coated slides and allowed to dry overnight. After deparaffinization and rehydration, antigen unmasking was performed using Module PT (Lab Vision®) for citrate buffer for 25 min at pH 6, 98°C for chromogranin A, p53, Ki67 and c-erbB-2 antibodies. Antigen unmasking was performed with Pronase E, for 10 min at room temperature for CK7, LP34 and EGFR antibodies. Endogenous peroxidase activity was quenched using 15 min incubation in 3% diluted hydrogen peroxide (H_2O_2). For blocking nonspecific binding, Ultra V Block (Ultra Vision Kit®; TP-015-HL) was applied to the sections and then they were incubated at room temperature, with primary antibodies against CK7 at a dilution of 1/50 for 30 min, LP34 at a dilution of 1/100 for 60 min, chromogranin A at a dilution of 1/300 for 30 min, p53 at a dilution of 1/40 for 30 min, Ki67 at a dilution of 1/50 for 30 min, c-erbB-2 at a dilution of 1/40 for 60 min and EGFR at a dilution of 1/20 for 30 min. After washing with phosphate-buffered saline, slides were incubated with biotin-labelled secondary antibody (Lab Vision®) for 15 min. Primary antibody binding was localized in tissues using peroxidase-conjugated streptavidin (Lab Vision®) and 3,3-diaminobenzidine tetrahydrochloride was used as the chromogen according to manufacturer's instructions. The slides were counterstained with hematoxylin, dehydrated and mounted.

For each biopsy, external and the intrinsic positive control were considered: basal cells for LP34 and columnar ciliated cells for CK7 in normal bronchial epithelium; carcinoid tumour sections for chromogranin A; sections of a colonic tubulo-villous adenoma for p53; female breast ductal carcinoma in situ for C-erbB-2 and sections of lung adenocarcinoma with intense EGFR IHC positivity. Ki67 was validated by a small cell lung carcinoma.

LP34, CK7 and chromogranin A expression were classified as negative if there was no expression or mild focal expression or positive when there was moderate or intense and diffuse expression. The cut off to classify a lesion as positive for proliferative marker Ki67 was 10% in at least two layers of positive nuclei above the epithelial basal membrane, since it is normal to observe some proliferative activity mainly in the basal cell layer.

A score established by other authors was applied to Ki67, p53 and EGFR protein expression: 0-negative; 1-focal positivity; 2-mild positivity; 3-moderate positivity; 4-intense positivity. The intensity was multiplied by the percentage of positive cells, thus defining a 0–200% score as negative or low expression, 201–300% score as intermediate expression and a 301–400% score as high expression [19].

The expression of C-erbB-2 was validated by membrane staining and an identical score to the one used in breast cancer was applied with some alterations because of the limited number of cells observed. Each specimen was scored semi-quantitatively according to the intensity of membrane immunostaining in a 4-point scale: 0/negative - absence of staining; + - weak staining and/or no homogeneous staining; ++ - moderate homogeneous membrane staining; +++ - intense homogeneous membrane staining. For the ++ and +++, we registered the number/percentage of stained cells. Cytoplasmic staining was not considered when present.

Fluorescence in situ hybridization (FISH)

Sections of formalin-fixed paraffin-embedded specimens, 4-μm thick, were incubated at 65°C for 24 h, deparaffinized in two xylene washes for 10 min and dehydrated in ethanol. The slides were then incubated at 120°C for 4 min with 10 mM citrate buffer (ph 6.0), followed by saline sodium citrate buffer (2×SCC pH 7.0) washes. Sections were digested with proteinase K (0.25 mg/ml in 2×SCC, Sigma, pH 7.0) for 5 min at 37°C, followed by new 2×SCC wash and post-fixation with 1% formalin for 10 min at room temperature. The slides were later on dehydrated in ethanol series (70–90–100%) for 2 min. Dual-colour FISH assays for HER2 were performed by using Qbiogene HER2/neu (17q21)/Alphasatellite 17 dual colour probe, and for EGFR, the Vysis, Inc. USA LSI EGFR Spectrum Orange/CEP 7 Spectrum Green probe was used. Ten-microliter probe set was applied to the selected area of the slides and the hybridization areas were covered with a glass cover slip and sealed with rubber cement. The slides were incubated at 90°C for 6 min for co-denaturation and at 37°C for 12–18 h for hybridization in a humidified chamber. Post-hybridization washes were performed with 50% formamide/2×SCC (pH 7.0) at 46°C for 5 min, followed by 2×SSC at 46°C for 2 min. After dehydratation in ethanol series, 4′, 6′-diamidino-2-phenylindole (DAPI; 0.15 mg/ml in Vectashield mounting medium, Vector Laboratories, Bulingame, CA, USA) was applied for chromatin counterstaining.

Microscopic analysis was performed on a Nikon Eclipse 80i bright field and epifluorescent microscope equipped with LUCIA cytogenetics software. Fluorescence signals were scored using single-band filters for DAPI, FITC, Texas Red and triple-band pass filter (DAPI, FITC and Texas Red). Images were recorded with a Nikon digital DMX 1200 F camera in monochromatic layers, which were subsequently merged by Nikon ACT-1 capture software.

The reference slide (stained with haematoxylin–eosin) usually contained normal bronchial epithelium adjacent to the adaptative and preneoplastic lesions and at least 100 non-

overlaping interphase nuclei were scored in each fragment for both *HER2* and chromosome17 centromer signals and for *EGFR* and chromosome7 centromer signals, following scoring guidelines and constant adjustments of microscope focus when signals were located at different levels.

Two independent observers performed analysis in a blinded study and scored results, restricted to the selected lesions and bronchial epithelium in each case, with reproducible results.

Six major FISH patterns were identified: disomy (≤2 gene copies per nucleus in >90% of cells); low trisomy (≤2 gene copies per nucleus in ≥40% of cells, 3 gene copies in 10–40% of cells, ≥4 gene copies in <10% of cells); high trisomy (≤2 gene copies per nucleus in ≥40% of cells, 3 gene copies in ≥40% of cells, ≥4 gene copies in <10% of cells); low polysomy (≥4 gene copies per nucleus in 10–40% of cells); high polysomy (≥4 gene copies per nucleus in ≥40% of cells) and gene amplification (defined by presence of tight *EGFR* gene clusters and a ratio of *EGFR* gene to chromosome of ≥2 or ≥15 copies of *EGFR* per cell in ≥10% of analysed cells), according to a FISH scoring System defined by Cappuzzo et al. [57]. Amplification and high polysomy were considered as FISH-positive results.

Statistical analysis

Comparisons were performed using bilateral chi-squared tests or Fisher exact test when needed, because of the small number of lesions in some categories. Anova test was applied to compare the markers expression's percentage.

Results

Differentiation markers

Basal cell hyperplasia positive LP34 cells in the lower cell layers revealed clear cut to squamous metaplasia staining up to the top cell layer, by loss of CK7 expression (Table 1, Fig. 1f, g). Accordingly, dysplasias showed always LP34 positivity and CK7 negativity.

Chromogranin A expression was negative in all the cases (Table 1).

Caliciform cell hyperplasia, when present, was negative for LP34 (only the basal cell layer remained positive) and maintained the expression for CK7.

Proliferation (Ki67) and apoptotic (p53) markers

Significant differences of Ki67 expression were found between basal cell hyperplasia and squamous metaplasia group and dysplasia group cases ($p=0.001$). Ki67 expression was higher in dysplasia ($p=0.0007$). There was also found a stepwise increment of expression from basal cell hyperplasias, to squamous metaplasia and dysplasia ($p<0.0001$). The intense expression of Ki67 (intense positive cases) was shown to have a statistical significant increase from basal cell hyperplasia, to squamous metaplasia and dysplasia ($p=0.0002$). (Tables 2 and 3, Fig. 1h). Intense positive cases were observed in 19 (57.6%) dysplasias, 9 (22.5%) metaplasias and one basal cell hyperplasia (6.25%). There were no significant differences between the three grades of dysplasia. Despite the intense positive cases observed, moderate expression of Ki67 was the second predominant type of expression in dysplasia (11 cases, 33.3%). Weak expression of Ki67 was mainly observed for basal cell hyperplasia (8 cases, 50%) and squamous metaplasia (13 cases, 32.5%).

An increasing expression for p53 in all the three types of lesions was observed ($p<0.0001$). P53 expression was significantly higher in dysplasia when compared with basal cell hyperplasias and metaplasias ($p=0.0007$). Intense positive cases were also more frequent in dysplasia ($p=0.0001$). In 10 basal cell hyperplasias (62.5%) and 22 squamous metaplasias (55%), it was possible to observe a weak p53 expression. An intense expression of p53 was observed in 20 cases (60.6%) of dysplasia (Tables 2 and 3, Fig. 1i).

EGFR and C-erbB-2/HER2 protein and gene expression

EGFR immunohistochemical expression was significantly higher in dysplasias when compared with other preneo-

Table 1 LP34, CK7 and chromogranin A expression in preneoplastic lesions

	LP34		CK7		Chromogranin A	
	Positive	Negative	Positive	Negative	Positive	Negative
Basal cell hyperplasia $n=16$	16	0	0	16	0	16
	100%	0%	0%	100%	0%	100%
Squamous Metaplasia $n=40$	40	0	0	40	0	40
	100%	0%	0%	100%	0%	100%
Dysplasia $n=33$	33	0	0	33	0	33
	100%	0%	0%	100%	0%	100%

Table 2 Ki67, p53, C-erbB-2 and EGFR intensity of expression in preneoplastic lesions

		Ki 67		p53		C-ErbB-2		EGFR	
		No. (%)		No. (%)		No. (%)		No. (%)	
Basal cell hyperplasia (n=16)	Negative	1	6.25	1	6.25	15	93.75	5	31.25
	+	9	56.25	10	62.5	1	6.25	9	43.75
	++	5	31.25	5	31.25	0	0	1	6.25
	+++	1	6.25	0	0	0	0	1	6.25
Squamous metaplasia (n=40)	Negative	8	20	5	12.5	39	97.5	6	15
	+	18	45	22	55	0	0	13	32.5
	++	9	22.5	12	30	1	2.5	14	35
	+++	5	12.5	1	2.5	0	0	7	17.5
Dysplasia (n=33)	Negative	0	0	1	3	27	81.8	4	12.1
	+	3	9.1	8	24.2	5	15.2	7	21.3
	++	17	55.5	9	27.3	1	3	15	45.5
	+++	13	39.4	15	45.5	0	0	4	12.1

plastic lesions (p=0.009) (Tables 2 and 3, Fig. 1j, k, Fig. 2). EGFR IHC expression increased between the three groups of lesions (p=0.0005). The intensity of the expression was higher in the group of dysplasia followed by squamous metaplasia, with 18 (54.5%) dysplasias showing moderate expression and 3 cases (9.1%) intense expression, while 14 (35%) squamous metaplasia presented moderate expression and 1 (2.5%) intense expression (p=0.005). Basal cell hyperplasia showed mainly a low EGFR expression, counting ten (62.5%) cases. Statistical differences between the different grades of dysplasia were not found (Fig. 2). C-erbB-2 protein overexpression was clearly observed in only one severe dysplasia (Tables 2 and 3, Fig. 1l), without statistical differences between the three groups of lesions or according to the severity of the dysplasia (p=0.14). C-erbB-2 protein expression was less frequent than EGFR.

EGFR and *HER2* gene increased copy number was more often due to polysomy than to amplification. Among the four cases with intense EGFR protein expression, three had high polysomy and one showed disomy.

The number of FISH EGFR positive cases were higher in the group of dysplasia (p=0.0002) (Fig. 3). Statistical significant correlation between EGFR IHC expression and FISH *EGFR* results was determined when the intensity of IHQ expression (positive intense vs. non-intense positive cases) was considered (p=0.0092) (Fig. 4).

HER2 FISH positive cases (n=4) were due to high polysomy. In one case (n=1), high trisomy was observed. All high polysomy cases were identified in CIS cases, and the high trisomy case was identified in a basal cell hyperplasia. These cases were IHC negative. The IHC-positive C-erbB-2 case showed low trisomy and was considered FISH *HER2* negative (Fig. 5a, b, c).

Table 3 Ki67, p53, c-erbB-2 and EGFR expression in preneoplastic lesions considering intensity and percentage of cells with expression

		Ki 67		p53		C-ErbB-2		EGFR	
		No. (%)		No. (%)		No. (%)		No. (%)	
Basal cell hyperplasia (n=16)	Neg	2	12.5	1	6.25	15	93.75	5	31.25
	Low pos	8	50	10	62.5	1	6.25	10	62.5
	Mod pos	5	31.25	2	12.5	0	0	1	6.25
	Pos int	1	6.25	3	18.75	0	0	0	0
Squamous metaplasia (n=40)	Neg	13	32.5	5	12.5	39	97.5	6	15
	Low pos	13	32.5	22	55	0	0	19	47.5
	Mod pos	5	12.5	4	10	1	2.5	14	35
	Pos int	9	22.5	9	22.5	0	0	1	2.5
Dysplasia (n=33)	Neg	0	0	1	3	27	81.8	4	12.2
	Low pos	3	9.1	8	24.2	5	15.2	8	24.2
	Mod pos	11	33.3	4	12.2	1	3	18	54.5
	Pos int	19	57.6	20	60.6	0	0	3	9.1

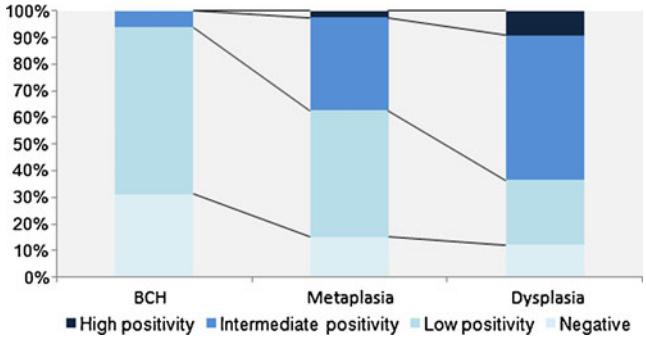

Fig. 2 (MS Excell) Immunohistochemical EGFR expression between the preneoplastic lesions

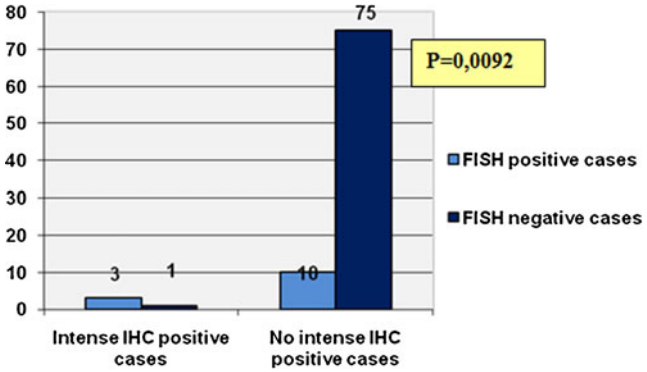

Fig. 4 (MS Excell) Correlation between immunohistochemical EGFR expression and FISH results

Discussion

As lung carcinogenesis is a multistep process, preneoplastic or preinvasive bronchial lesions' evolution to bronchial carcinoma depends upon the molecular and genetic abnormalities accumulated in time. Those abnormalities increase from the normal bronchial epithelium through basal cell hyperplasia, squamous metaplasia and low-grade to high-grade dysplasia. Certain proteins and genes play key roles in lung carcinogenesis and their aberrant expression in that process makes them as potential biomarkers susceptible to discriminate a subpopulation of patients with particularly active mutagenesis, progressive cancerization process and at very high risk to develop lung cancer [58].

LP34, CK7, chromogranin A, Ki67, p53, EGFR and C-erbB2 were the seven biomarkers chosen for this study as their abnormal expression is related with the oncogenic process. The first three were used successfully as differentiation markers of the preneoplastic lesions.

A basal cell origin for basal hyperplasia, squamous metaplasia and dysplasia was clearly defined, based on LP34 and CK7 expression. Immunohistochemical differentiation markers like LP34, CK7 and chromogranin A demonstrated useful to discriminate preneoplastic lesions from other proliferative lesions like caliciform cell hyperplasia or neuroendocrine cell hyperplasia. As expected, basal cell hyperplasia and squamous metaplasia are always LP34-positive and CK7 and chromogranin A-negative, indicating basal cell origin and conditioning squamous cell carcinoma as a basal cell carcinoma. In contrast, caliciform cell hyperplasia maintains cytoplasmic CK7 positivity cells and inconstant LP34 membrane positivity, reflecting an origin in cylindrical cells of the upper cell layer of the respiratory epithelium in bronchial adenocarcinoma carcinogenesis. Chromogranin A, a neuroendocrine marker, was constantly negative in this study, emphasizing that neuroendocrine cell hyperplasia has a different cell commitment.

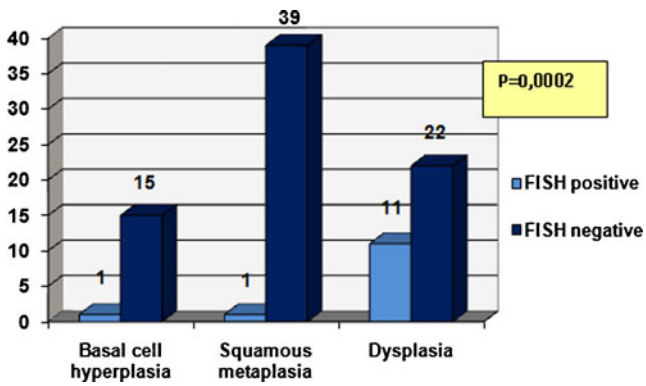

Fig. 3 (MS Excell) *EGFR* FISH results according to preneoplastic lesions

Ki67 expression stepwise increment reflects the increasing proliferative index observed in the spectrum of preneoplastic lesions. The statistical higher expression observed in dysplasia group compared to basal cell hyperplasia and squamous metaplasia defines two groups of lesions according to their proliferative index. As other authors observed, the intensity of Ki67 expression is also higher in dysplasia. This way, we reinforce the utility of Ki67 as a biomarker, namely for dysplasia, as it appears as a group characterized by high proliferative index, subscribing the literature and other authors' study of preneoplastic lesions [22–26, 59].

P53, the "guardian" maintaining the integrity of the genome by participating in the DNA damage checkpoints in the cell cycle, regulating cellular proliferation and apoptosis [20], has been detected in preneoplastic lesions of the lung, suggesting that it occurs early during lung carcinogenesis [14, 18, 20] as the obtained results confirmed. P53 expression was significantly higher in dysplasia when compared with hyperplasia and metaplasia, and the intensity of expression was also higher in the dysplasia group, supporting p53 accumulation involvement in the development of squamous cell lung cancer and fixing p53 as a remarkable biomarker in lung carcinogenesis.

There are many studies concerning EGFR, C-erbB-2, Ki67 and p53 expression in lung cancer. However, there are

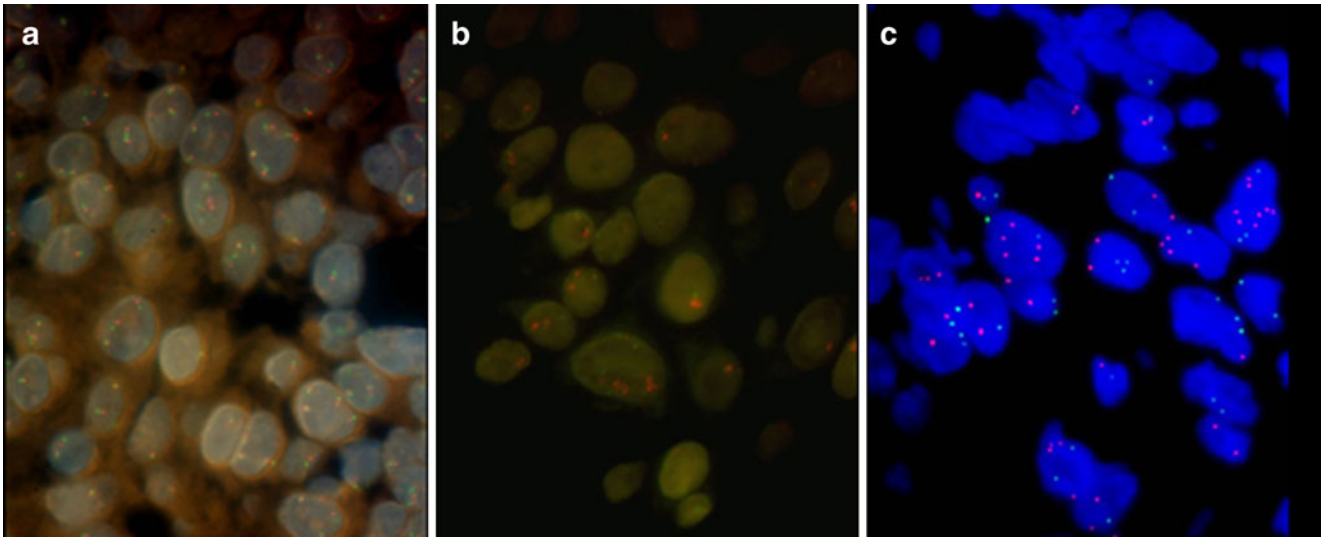

Fig. 5 **a** Dual-colour FISH assay with EGFR (*red*) and chromosome 7 (*green*), balanced polysomy, ×1,000. **b** Dual-colour FISH assay with EGFR (*red*) and chromosome 7 (*green*), amplification, ×1,000. **c** Dual-colour FISH assay with HER2neu (*red*) and chromosome 17 (*green*), amplification, ×1,000

fewer results validating these markers in preneoplastic lesions and most of them used only immunochemistry techniques. By analysing the expression of those biomarkers, using not only immunohistochemistry but also feasible molecular techniques, such as FISH and correlating the results obtained by the two different techniques, bronchial preneoplastic lesions achieve prognostic significance.

EGFR immunohistochemical increased expression in preneoplastic lesions, increasing from basal cell hyperplasia to dysplasia, had been demonstrated [6, 7, 21, 38–42, 55, 60]. Meert et al. [21] also demonstrated not only an increasing EGFR rate from normal bronchial epithelium to CIS and microinvasive tumours, but also a statistically significant cut off between mild dysplasia and severe dysplasia. Although the greater expression has been seen in dysplasia, statistical differences between the different grades of dysplasia were not demonstrated (probably because the number of cases of dysplasia was limited).

EGFR high gene copy number was due more frequently to polysomy than to amplification. FISH-positive *EGFR* cases are present in all types of preneoplastic lesions and were higher in dysplasia group. Polysomy appears as an early event in the sequence of hyperplasia–metaplasia–dysplasia. The higher frequency of polysomy in preneoplastic lesions is reflected in the high frequency of this event in squamous cell carcinomas, constituting the earliest molecular event in lung carcinogenesis [17, 22, 41].

EGFR protein was overexpressed in all lesions with an increased gene copy number. There was statistical significant correlation between EGFR immunohistochemical expression and FISH *EGFR* results, when considering the intensity of IHC expression [17]. Therefore, it was demonstrated that protein expression does reflect high gene copy number, like polysomy and amplification. Although *EGFR* gene amplification is implicated as one mechanism for EGFR overexpression, it does not seem to be the main one [61].

Despite an increasing expression of EGFR and Ki67 along the spectrum of preneoplastic lesions, no correlation between the two markers was found. Meert et al. recently described that low-grade lesions showed no EGFR or Ki67 expression contrasting with high-grade lesions. EGFR overexpression is associated with cell proliferation, making EGFR an early marker of malignant transformation in lung carcinogenesis [21, 38, 59].

C-erbB-2 immunohistochemical overexpression is less frequent than EGFR overexpression, supporting the minor role of C-erbB-2 in squamous cell carcinogenesis when compared with EGFR [17, 62]. In our study, only one case of severe dysplasia showed C-erbB-2-positive immunohistochemical expression and polysomy was observed in 70% of the cells. *C-erB-2* FISH-positive cases were due to high polysomy, showing that amplification is less frequent as a high gene copy number event. No statistical significant correlation was obtained between *C-erbB-2* gene and protein expression.

C-erB-2 does not seem to be involved in the first steps of lung carcinogenesis [16]. For Piyathilake et al., the expression of C-erbB-2 was significantly higher in squamous cell carcinoma and associated precancerous lesions than in normal epithelium and hyperplastic lesions, but no stepwise expression of C-erbB-2 was observed, suggesting its lack of importance in the squamous cell lung carcinogenesis [38]. *HER2/neu* increased copy number is observed in approximately 35% of adenocarcinomas and slightly less

frequently in squamous cell carcinomas [18], assuming more importance in the development of lung adenocarcinomas. The increased copy number of *HER2/neu* in NSCLC is most often attributable to chromosome duplication and polysomy [50], rather than amplification [18].

Although EGFR and Ki67 expression increases from normal epithelium to preinvasive lesions together, this was not seen for C-erbB-2. Therefore, any correlation between EGFR and Ki67 expressions and C-erbB-2 expression was established, like other studies also registered [21, 41, 63–66]. Interestingly, other studies revealed that EGFR/HER2/neu heterodimerization expression is capable to induce a stronger and more sustained proliferative signal than EGFR homodimers [60, 62].

The need to accurate detection of the *EGFR* and *HER2/neu* gene copy number and protein overexpression, reflecting their importance as biomarkers in squamous cell pathogenesis, has become even more important because despite recent advances in lung cancer treatments, improvement in survival has only been modest, showing that effective therapeutic and early detection approaches are still lacking [38]. Selection of patients with preneoplastic lesions expressing selected biomarkers is the way to provide new and more effective strategies for early diagnosis, a posterior closer follow-up and eventually chemoprevention and targeted treatment with better safety profiles. A variety of new approaches that target selected biomarkers in lung carcinogenesis are in clinical development or have already been approved for second and third line lung cancer treatment [5, 52–56, 67].

Our comparison between gene copy number and protein expression contributes to define which are the most reliable methods to be used in patient selection. Since our study includes a large number of preneoplastic lesions in a different population analysed by two different techniques (IHC and FISH), the results obtained reinforce other results published before, some of them centred only in one molecular marker and/or have used a single technique, which measures either the protein level or the gene expression. By identifying dysplasia as a group of preneoplastic lesions, chemoprevention targeted schemes can be delineated to select individual patients, considering protein expression, gene copy number and gene mutational status with repercussions in drug sensitivity.

Conclusions

We conclude that squamous cell carcinoma preneoplastic lesions studied have a basal cell origin, as demonstrated by the unbalance between LP34 and CK7. The differentiation markers, LP34, CK7 and chromogranin A, successfully discriminate preneoplastic lesions origin.

Dysplasias showed a higher expression of EGFR, Ki67 and p53 with a stepwise expression with the gravity of the preneoplastic lesions, reflecting their importance as potential biomarkers of preinvasive lesions of the bronchial epithelium and may be used to identify patients with a higher risk of developing squamous cell lung carcinoma. C-erbB-2 immunohistochemical overexpression is a rare event in bronchial preneoplastic lesions, emphasizing the minor role of C-erbB-2 as a biomarker in squamous cell carcinogenesis.

EGFR and *HER2/neu* high gene copy number was present in preneoplastic lesions, with a higher EGFR gene copy number in dysplasias. *EGFR* and *HER2/neu* high gene copy number was due to polysomy more often than to amplification, reinforcing that amplification is not the main mechanism for protein overexpression. Although *HER2/neu* does not seem to be involved in the early steps of squamous cell lung carcinogenesis, *HER2/neu* gene copy number is important because this gene is a HER family member and an important heterodimerizarion partner for EGFR.

Biological/genetic markers associated with several molecular and genetic abnormalities, such as Ki67, p53, EGFR and HER2/neu, need to be validated as potential and useful preneoplastic bronchial lesion biomarkers. Risk assessment should be based not only on smoking consumption and on histopathology of bronchial lesions, but also on the basis of in situ molecular biomarkers [58]. Therefore, in the future, the recognition of those biomarkers will allow a targeted screening and a posterior closer follow-up to select patients for chemoprevention schemes and will have a positive impact on survival.

Acknowledgements The authors would like to thank Isabel Carreira and Paula António.

Conflicts of interest We declare that we have no conflict of interest.

References

1. Doll R, Peto R (1981) The causes of cancer: quantitative estimates of avoidable risks of cancer in the United States today. J Natl Cancer Inst 66:1191–1308
2. Shopland DR (1995) Tobacco use and its contribution to early cancer mortality with a special emphasis on cigarette smoking. Environ Health Perspect 103(Suppl 8):131–142
3. Devereux TR, Taylor JA, Barrett JC (1996) Molecular mechanisms of lung cancer. Interaction of environmental and genetic factors. Giles F. Filley Lecture. Chest 109:14S–19S
4. Jemal A, Murray T, Samuels A, Ghafoor A, Ward E, Thun MJ (2003) Cancer statistics, 2003. CA Cancer J Clin 53:5–26
5. Winterhalder RC, Hirsch FR, Kotantoulas GK, Franklin WA, Bunn PA Jr (2004) Chemoprevention of lung cancer—from biology to clinical reality. Ann Oncol 15:185–196
6. Meert AP, Martin B, Delmotte P, Berghmans T, Lafitte JJ, Mascaux C et al (2002) The role of EGF-R expression on patient survival in lung cancer: a systematic review with meta-analysis. Eur Respir J 20:975–981

7. Herbst RS, Bunn PA Jr (2003) Targeting the epidermal growth factor receptor in non-small cell lung cancer. Clin Cancer Res 9:5813–5824
8. Shigematsu H, Lin L, Takahashi T, Nomura M, Suzuki M, Wistuba II et al (2005) Clinical and biological features associated with epidermal growth factor receptor gene mutations in lung cancers. J Natl Cancer Inst 97:339–346
9. Travis WD (1999) Histological Classification of Lung and Pleural Tumors. International Histological Classification of Tumors, Berlin, PA
10. Auerbach O, Forman JB, Gere JB, Kassouny DY, Muehsam GE, Petrick TG et al (1957) Changes in the bronchial epithelium in relation to smoking and cancer of the lung; a report of progress. N Engl J Med 256:97–104
11. Colby TV (1999) Precursor lesions to pulmonary neoplasia. In: Brambilla C, Brambilla E (eds) Lung Tumours. Fundamental Biology and Clinical Management (pp. 61–87). Marcel Dekker Inc, New York, PA
12. Wistuba II, Behrens C, Milchgrub S, Bryant D, Hung J, Minna JD et al (1999) Sequential molecular abnormalities are involved in the multistage development of squamous cell lung carcinoma. Oncogene 18:643–650
13. Franklin WA (2000) Pathology of lung cancer. J Thorac Imaging 15:3–12
14. Piyathilake CJ, Frost AR, Manne U, Weiss H, Heimburger DC, Grizzle WE (2003) Nuclear accumulation of p53 is a potential marker for the development of squamous cell lung cancer in smokers. Chest 123:181–186
15. Rowinsky EK (2003) Signal events: cell signal transduction and its inhibition in cancer. Oncologist 8(Suppl 3):5–17
16. Peters EJ, Morice R, Benner SE, Lippman S, Lukeman J, Lee JS et al (1993) Squamous metaplasia of the bronchial mucosa and its relationship to smoking. Chest 103:1429–1432
17. Hirsch FR, Varella-Garcia M, Bunn PA Jr, Di Maria MV, Veve R, Bremmes RM et al (2003) Epidermal growth factor receptor in non-small-cell lung carcinomas: correlation between gene copy number and protein expression and impact on prognosis. J Clin Oncol 21:3798–3807
18. Giaccone G (1996) Oncogenes and antioncogenes in lung tumorigenesis. Chest 109:130S–134S
19. Fong KM, Sekido Y, Minna JD (1999) Molecular pathogenesis of lung cancer. J Thorac Cardiovasc Surg 118:1136–1152
20. Kohno T, Yokota J (1999) How many tumor suppressor genes are involved in human lung carcinogenesis? Carcinogenesis 20:1403–1410
21. Meert AP, Verdebout JM, Martin B, Ninane V, Feoli F, Sculier JP (2003) Epidermal growth factor receptor expression in pre-invasive and early invasive bronchial lesions. Eur Respir J 21:611–615
22. Hirano T, Franzen B, Kato H, Ebihara Y, Auer G (1994) Genesis of squamous cell lung carcinoma. Sequential changes of proliferation, DNA ploidy, and p53 expression. Am J Pathol 144:296–302
23. Li ZH, Zheng J, Weiss LM, Shibata D (1994) c-k-ras and p53 mutations occur very early in adenocarcinoma of the lung. Am J Pathol 144:303–309
24. Betticher DC, Heighway J, Thatcher N, Hasleton PS (1997) Abnormal expression of CCND1 and RB1 in resection margin epithelia of lung cancer patients. Br J Cancer 75:1761–1768
25. Satoh Y, Ishikawa Y, Nakagawa K, Hirano T, Tsuchiya E (1997) A follow-up study of progression from dysplasia to squamous cell carcinoma with immunohistochemical examination of p53 protein overexpression in the bronchi of ex-chromate workers. Br J Cancer 75:678–683
26. Brambilla E, Gazzeri S, Lantuejoul S, Coll JL, Moro D, Negoescu A et al (1998) p53 mutant immunophenotype and deregulation of p53 transcription pathway (Bcl2, Bax, and Waf1) in precursor bronchial lesions of lung cancer. Clin Cancer Res 4:1609–1618
27. Sugio K, Kishimoto Y, Virmani AK, Hung JY, Gazdar AF (1994) K-ras mutations are a relatively late event in the pathogenesis of lung carcinomas. Cancer Res 54:5811–5815
28. Hung J, Kishimoto Y, Sugio K, Virmani A, McIntire DD, Minna JD et al (1995) Allele-specific chromosome 3p deletions occur at an early stage in the pathogenesis of lung carcinoma. JAMA 273:1908
29. Kishimoto Y, Sugio K, Hung JY, Virmani AK, McIntire DD, Minna JD et al (1995) Allele-specific loss in chromosome 9p loci in preneoplastic lesions accompanying non-small-cell lung cancers. J Natl Cancer Inst 87:1224–1229
30. Wistuba II, Behrens C, Virmani AK, Milchgrub S, Syed S, Lam S et al (1999) Allelic losses at chromosome 8p21-23 are early and frequent events in the pathogenesis of lung cancer. Cancer Res 59:1973–1979
31. Wistuba II, Lam S, Behrens C, Virmani AK, Fong KM, LeRiche J et al (1997) Molecular damage in the bronchial epithelium of current and former smokers. J Natl Cancer Inst 89:1366–1373
32. Franklin WA, Wistuba II, Geisinger K, Lam S, Hirsh FR (2004) Squamous dysplasia and carcinoma in situ. In Travis WD, Brambilla E, Müller-Hermelink HK, & Harris CK (Eds.) Tumours of the lung, pleura, thymus and heart. Pathology and genetics. pp. 68–72. Lyon, PA: IARC Press
33. Stoscheck CM, King LE Jr (1986) Role of epidermal growth factor in carcinogenesis. Cancer Res 46:1030–1037
34. Berger MS, Gullick WJ, Greenfield C, Evans S, Addis BJ, Waterfield MD (1987) Epidermal growth factor receptors in lung tumours. J Pathol 152:297–307
35. Sobol RE, Astarita RW, Hofeditz C, Masui H, Fairshter R, Royston I et al (1987) Epidermal growth factor receptor expression in human lung carcinomas defined by a monoclonal antibody. J Natl Cancer Inst 79:403–407
36. Prenzel N, Fischer OM, Streit S, Hart S, Ullrich A (2001) The epidermal growth factor receptor family as a central element for cellular signal transduction and diversification. Endocr Relat Cancer 8:11–31
37. Yarden Y, Sliwkowski MX (2001) Untangling the ErbB signalling network. Nat Rev Mol Cell Biol 2:127–137
38. Piyathilake CJ, Frost AR, Manne U, Weiss H, Bell WC, Heimburger DC et al (2002) Differential expression of growth factors in squamous cell carcinoma and precancerous lesions of the lung. Clin Cancer Res 8:734–744
39. Rusch V, Baselga J, Cordon-Cardo C, Orazem ZM, Hoda S et al (1993) Differential expression of the epidermal growth factor receptor and its ligands in primary non-small cell lung cancers and adjacent benign lung. Cancer Res 53:2379–2385
40. Kurie JM, Shin HJ, Lee JS, Morice RC, Ro JY, Lippman SM et al (1996) Increased epidermal growth factor receptor expression in metaplastic bronchial epithelium. Clin Cancer Res 2:1787–1793
41. Franklin WA, Veve R, Hirsch FR, Helfrich BA, Bunn PA Jr (2002) Epidermal growth factor receptor family in lung cancer and premalignancy. Semin Oncol 29:3–14
42. Lonardo F, Dragnev KH, Freemantle SJ, Ma Y, Memoli N, Sekula D et al (2002) Evidence for the epidermal growth factor receptor as a target for lung cancer prevention. Clin Cancer Res 8:54–60
43. Hirsch FR, Franklin WA, Veve R, Varella-Garcia M, Bunn PA Jr (2002) HER2/neu expression in malignant lung tumors. Semin Oncol 29:51–58
44. Beerli RR, Hynes NE (1996) Epidermal growth factor-related peptides activate distinct subsets of ErbB receptors and differ in their biological activities. J Biol Chem 271:6071–6076
45. Pinkas-Kramarski R, Soussan L, Waterman H, Levkowitz G, Alroy I, Klapper L et al (1996) Diversification of Neu differentiation factor and epidermal growth factor signaling by combinatorial receptor interactions. EMBO J 15:2452–2467
46. Graus-Porta D, Beerli RR, Daly JM, Hynes NE (1997) ErbB-2, the preferred heterodimerization partner of all ErbB receptors, is a mediator of lateral signaling. EMBO J 16:1647–1655

47. Bongiorno PF, Whyte RI, Lesser EJ, Moore JH, Orringer MB, Beer DG (1994) Alterations of K-ras, p53, and erbB-2/neu in human lung adenocarcinomas. J Thorac Cardiovasc Surg 107:590–595
48. Tateishi M, Ishida T, Kohdono S, Hamatake M, Fukuyama Y, Sugimachi K (1994) Prognostic influence of the co-expression of epidermal growth factor receptor and c-erbB-2 protein in human lung adenocarcinoma. Surg Oncol 3:109–113
49. Brabender J, Danenberg KD, Metzger R, Schneider PM, Park J, Salonga D et al (2001) Epidermal growth factor receptor and HER2-neu mRNA expression in non-small cell lung cancer Is correlated with survival. Clin Cancer Res 7:1850–1855
50. Bunn PA Jr, Helfrich B, Soriano AF, Franklin WA, Varella-Garcia M, Hirsch FR et al (2001) Expression of Her-2/neu in human lung cancer cell lines by immunohistochemistry and fluorescence in situ hybridization and its relationship to in vitro cytotoxicity by trastuzumab and chemotherapeutic agents. Clin Cancer Res 7:3239–3250
51. Lai WW, Chen FF, Wu MH, Chow NH, Su WC, Ma MC et al (2001) Immunohistochemical analysis of epidermal growth factor receptor family members in stage I non-small cell lung cancer. Ann Thorac Surg 72:1868–1876
52. Khuri FR (2003) Primary and secondary prevention of non-small-cell lung cancer: the SPORE Trials of Lung Cancer Prevention. Clin Lung Cancer 5(Suppl 1):S36–S40
53. Khuri FR, Cohen V (2004) Molecularly targeted approaches to the chemoprevention of lung cancer. Clin Cancer Res 10:4249s–4253s
54. Hirsch FR, Lippman SM (2005) Advances in the biology of lung cancer chemoprevention. J Clin Oncol 23:3186–3197
55. Meert AP, Martin B, Verdebout JM, Ninane V, Sculier JP (2005) Does c-erbB-2 play a role in the first steps of lung carcinogenesis? Anticancer Res 25:2005–2008
56. Saba NF, Khuri FR (2005) Chemoprevention strategies for patients with lung cancer in the context of screening. Clin Lung Cancer 7:92–99
57. Cappuzzo F, Hirsch FR, Rossi E, Bartolini S, Ceresoli GL, Bemis L et al (2005) Epidermal growth factor receptor gene and protein and gefitinib sensitivity in non-small-cell lung cancer. J Natl Cancer Inst 97:643–655
58. Jeanmart M, Lantuejoul S, Fievet F, Moro D, Sturm N, Brambilla C et al (2003) Value of immunohistochemical markers in preinvasive bronchial lesions in risk assessment of lung cancer. Clin Cancer Res 9:2195–2203
59. Meert AP, Martin B, Verdebout JM, Feoli F, Mascaux C, Ninane V et al (2006) EGFR, c-erbB-2 and ki-67 in NSCLC and preneoplastic bronchial lesions. Anticancer Res 26:135–138
60. Scagliotti GV, Selvaggi G, Novello S, Hirsch FR (2004) The biology of epidermal growth factor receptor in lung cancer. Clin Cancer Res 10:4227s–4232s
61. Atkins D, ReiffenKA TCL, Winther H, Bonato MS, Storkel S (2004) Immunohistochemical detection of EGFR in paraffin-embedded tumor tissues: variation in staining intensity due to choice of fixative and storage time of tissue sections. J Histochem Cytochem 52:893–901
62. Onn A, Correa AM, Gilcrease M, Isobe T, Massarelli E, Bucana CD et al (2004) Synchronous overexpression of epidermal growth factor receptor and HER2-neu protein is a predictor of poor outcome in patients with stage I non-small cell lung cancer. Clin Cancer Res 10:136–143
63. Giatromanolaki A, Koukourakis MI, O'Byrne K, Kaklamanis L, Dicoglou C, Trichia E et al (1996) Non-small cell lung cancer: c-erbB-2 overexpression correlates with low angiogenesis and poor prognosis. Anticancer Res 16:3819–3825
64. Reinmuth N, Brandt B, Kunze WP, Junker K, Thomas M, Achatzy R et al (2000) Ploidy, expression of erbB1, erbB2, P53 and amplification of erbB1, erbB2 and erbB3 in non-small cell lung cancer. Eur Respir J 16:991–996
65. Kanematsu T, Yano S, Uehara H, Bando Y, Sone S (2003) Phosphorylation, but not overexpression, of epidermal growth factor receptor is associated with poor prognosis of non-small cell lung cancer patients. Oncol Res 13:289–298
66. Meert AP, Feoli F, Martin B, Verdebout JM, Mascaux C, Verhest A et al (2004) Ki67 expression in bronchial preneoplastic lesions and carcinoma in situ defined according to the new 1999 WHO/IASLC criteria: a preliminary study. Histopathology 44:47–53
67. Hirsch FR, Scagliotti GV, Langer CJ, Varella-Garcia M, Franklin WA (2003) Epidermal growth factor family of receptors in preneoplasia and lung cancer: perspectives for targeted therapies. Lung Cancer 41(Suppl 1):S29–S42

Virchows Arch (2011) 458:583–592
DOI 10.1007/s00428-011-1063-4

ORIGINAL ARTICLE

Aberrant PLAG1 expression in pleomorphic adenomas of the salivary gland: a molecular genetic and immunohistochemical study

Atsuji Matsuyama · Masanori Hisaoka · Yuichi Nagao · Hiroshi Hashimoto

Received: 2 December 2010 / Revised: 8 February 2011 / Accepted: 22 February 2011 / Published online: 11 March 2011
© Springer-Verlag 2011

Abstract The morphologic distinction of pleomorphic adenoma from other benign or low-grade salivary gland tumors is sometimes difficult and problematic because of their potentially overlapping histological patterns. A subset of pleomorphic adenoma harbors specific gene alterations involving *PLAG1* or *HMGA2*, and the detection of these fusion genes and their products using formalin-fixed, paraffin-embedded (FFPE) tumor specimens may be a useful diagnostic adjunct. In the present study, gene fusions involving *PLAG1* or *HMGA2* were examined by reverse transcription-polymerase chain reaction (RT-PCR) analysis, with FFPE tumor tissues and immunohistochemical expression of PLAG1 in 45 pleomorphic adenomas, using a commercially available antibody. RT-PCR analyses identified the CTNNB1-PLAG1, LIFR-PLAG1, CHCHD7-PLAG1, and HMGA2-WIF1 fusion transcripts in eight, two, one, and one case, respectively. The TCEA1-PLAG1, HMGA2-FHIT, and HMGA2-NFIB fusion transcripts were not detected. Immunohistochemically, tumor cells in all 45 pleomorphic adenomas were positive for PLAG1, irrespective of PLAG1 rearrangements, even in the case with the HMGA2-WIF1 fusion transcript. Tumor cells displaying myoepithelial or cartilaginous differentiation were almost constantly positive for PLAG1, whereas a limited expression was observed in glandular or keratinizing cells. Among the 46 tumors other than pleomorphic adenoma, 4 carcinomatous components of carcinomas ex pleomorphic adenoma were positive for PLAG1, the other 39 were negative for PLAG1, and the remaining 3 were only faintly and/or focally stained, indicating that the immunohistochemical detection of PLAG1 is diagnostically useful. The present results also suggest that overexpression of PLAG1 is essential for the tumorigenesis of pleomorphic adenomas, although the mechanisms mediating PLAG1 overexpression seem to be variable.

Keywords Pleomorphic adenoma · PLAG1 · HMGA2 · Immunohistochemistry · RT-PCR

A. Matsuyama (✉) · M. Hisaoka · Y. Nagao · H. Hashimoto
Department of Pathology and Oncology, School of Medicine,
University of Occupational and Environmental Health,
1–1 Iseigaoka, Yahatanishi-ku,
Kitakyushu 807–8555, Japan
e-mail: amatsu@med.uoeh-u.ac.jp

H. Hashimoto
e-mail: hiroshi@med.uoeh-u.ac.jp

Introduction

The classification of salivary gland tumors includes a wide variety of tumor entities that show a pronounced morphological complexity and diversity with often overlapping histological patterns [1]. The morphologic distinction of pleomorphic adenoma, the most common tumor of the salivary gland, accounting for 60% of all the tumors arising in this organ [1], from other benign or low-grade tumors is sometimes difficult and problematic. Pleomorphic adenoma has been cytogenetically demonstrated to harbor specific chromosomal aberrations, most of which result in fusion genes involving *PLAG1* on 8q12 [2–8] or *HMGA2* on 12q13-15 [7–11]. Several fusion partners including *CTNNB1* [4, 5], *CHCHD7* [2], *LIFR* [6], and *TCEA1* [2, 3] fused to *PLAG1*, and *FHIT* [10], *NFIB* [9], and *WIF1* [11] fused to *HMGA2* have been identified by reverse transcription-polymerase chain reaction (RT-PCR), fluorescence in situ hybridization (FISH), or chromogenic in situ hybridization (CISH) by using fresh tumor tissue specimens. Although the fusion patterns are variable, detection

of these fusion genes, particularly by using formalin-fixed, paraffin-embedded (FFPE) tumor specimens, may be a useful adjunct in the diagnosis of pleomorphic adenomas. RT-PCR using FFPE tumor tissues may also be applicable to the detection of gene alterations involving *PLAG1* or *HMGA2* in pleomorphic adenomas, because such a molecular assay has been carried out to identify fusion genes in a variety of tumors [12–16].

Certain tumor-specific genetic alterations, which are usually chromosomal translocations, can also be identified using an immunohistochemical technique, and the proteins translated from the fusion gene transcripts such as FLI1 expressed in Ewing sarcoma carrying EWS-FLI1 [17], WT1 in desmoplastic small round cell tumor with EWS-WT1 [18], TFE3 expressed in alveolar soft part sarcoma and renal cell carcinoma with ASPL-TFE3 [19], and ALK expressed in anaplastic large cell lymphoma and inflammatory myofibroblastic tumor [15, 20] can be detected. The PLAG1 protein is a nuclear oncoprotein that functions as a DNA-binding transcription factor, and the transcriptional upregulation of *PLAG1* results in a high level of protein expression in pleomorphic adenomas with *PLAG1* rearrangements [4, 6]. The antibody against the PLAG1 protein is commercially available and can be used to complement the histological diagnosis of pleomorphic adenoma by using FFPE specimens.

In the present study, we analyzed gene fusions involving *PLAG1* or *HMGA2* by RT-PCR using FFPE tumor tissues derived from a series of pleomorphic adenomas of the salivary gland. In addition, the immunohistochemical expression of PLAG1 in pleomorphic adenomas and other types of salivary gland tumors was also examined to evaluate the correlation between PLAG1 protein expression and genetic alterations.

Materials and methods

Forty-seven tumors diagnosed as pleomorphic adenomas between 2004 and 2008 were retrieved from the files of the Department of Pathology, University of Occupational and Environmental Health Hospital, Kitakyushu, Japan, and the corresponding clinicopathologic findings and hematoxylin and eosin-stained slides were critically reviewed. Two of the 47 cases were reclassified as basal cell adenoma and were included in the study as negative controls. All 45 pleomorphic adenomas were examined using molecular genetic and immunohistochemical methods. The negative controls consisted of 46 other types of major and minor salivary gland tumors including 11 Warthin's tumors, 7 adenoid cystic carcinomas, 7 mucoepidermoid carcinomas, 4 carcinomatous components of carcinomas ex pleomorphic adenoma (CPAs), which displayed features of adenocarcinoma not otherwise specified (NOS) in two cases, salivary duct carcinoma in one or malignant myoepithelioma in one, three acinic cell carcinomas, three salivary duct carcinomas, two basal cell adenomas, two polymorphous low-grade adenocarcinomas, one adenocarcinoma NOS, one basal cell adenocarcinoma, one clear cell carcinoma NOS, one cystadenocarcinoma, one epithelial–myoepithelial carcinoma, one malignant myoepithelioma, and one squamous cell carcinoma, which were also immunohistochemically examined. RT-PCR analyses were also carried out in 12 of the controls (4 carcinomatous components of CPAs, 2 adenoid cystic carcinomas, 2 mucoepidermoid carcinomas, 2 basal cell adenomas, 1 basal cell adenocarcinoma, and 1 Warthin's tumor).

RT-PCR

The extraction of RNA from FFPE tumor tissue was performed as described previously [12, 13]. Briefly, 5-μm FFPE tumor sections of each sample were collected in a sterile microtube, deparaffinized with xylene and ethanol, and minced in 200 μL of lysis buffer (20 mmol/L tris–HCl, pH 8.0; 20 mmol/L ethylenediaminetetraacetic acid; and 2% sodium dodecyl sulfate), and then, 10 μL of proteinase K (100 mg/mL) was added to each sample. After incubation at 55°C overnight, 1.0 mL of Trizol reagent (Invitrogen, San Diego, CA, USA) was added to the sample, followed by 200 μL of chloroform. After vortexing and centrifugation, the aqueous phase was carefully transferred to a 2.0-mL sterile microtube and precipitated with 0.75 mL of 2-propanol. The RNA pellet was resuspended in 11 μL DNase- and RNase-free water. RNA extracts were treated with DNase I (Invitrogen) for 15 min at 37°C. For the analysis of CPAs, RNA was extracted from FFPE tumor tissues containing both benign and malignant tumor components, because the adenoma components were too small to enable the molecular genetic evaluation of benign and malignant components separately.

A total of 11 μL of the extracted RNA solution was reverse transcribed into complementary DNA (cDNA) using 1 μL of random primers (Invitrogen) and 200 U of reverse transcriptase (SuperScript III, Invitrogen). The cDNA was then incubated with 60 U RNase H (Takara, Ohtsu, Japan) for 20 min at 37°C. To assess the quality and integrity of the mRNA, RT-PCR for phosphoglycerate kinase (PGK) and porphobilinogen deaminase (PBGD) was performed as described previously [12, 14]. PCR was performed using 2.5 U of Taq DNA polymerase (AmpliTaq Gold, Perkin Elmer, Norwalk, CT, USA), 1.5 mmol/L $MgCl_2$, PCR buffer (Perkin Elmer), 200 μmol/L deoxynucleotide triphosphates, and 0.2 μmol/L of each of the forward and reverse primers. CHCHD7, CTNNB1, LIFR, and TCEA1 forward and PLAG1 reverse primers for

PLAG1-associated fusion transcripts, and HMGA2 forward and FHIT, NFIB, and WIF1 reverse primers for HMGA2-associated fusion transcripts were designed to specifically amplify the junctional regions of each fusion gene previously reported (Table 1, Fig. 1) [2–4]. PCR amplification consisted of 40 cycles of denaturation at 94°C for 30 s, annealing at 59°C for 30 s, and elongation at 72°C for 30 s, followed by a final extension at 72°C for 10 min. A negative control containing distilled water instead of cDNA template was included in each PCR procedure.

To confirm the sequences of the amplified fusion gene transcripts, the PCR products were cloned into a pCR2.1 vector by using a TA cloning kit (Invitrogen). After transfection into DH-5α (Toyobo, Osaka, Japan) and incubation at 37°C overnight on Luria-Bertani medium plates, white colonies were collected from the plates and distributed into microtubes containing PCR buffer. PCR was performed to confirm the presence of inserts. Sequence analysis was performed using the ALF express automated DNA sequencing system (Pharmacia Biotech, Uppsala, Sweden).

Immunohistochemistry

For immunohistochemical analysis, specimens were incubated with a polyclonal anti-PLAG1 antibody (1:500; Sigma–Aldrich Co., St. Louis, MO, USA) for 24 h after the heat-mediated antigen retrieval in 10 mM citrate buffer (pH 6.0). After rinsing in 10 mM phosphate-buffered saline, the antigenic sites were linked using the universal immunoenzyme amino acid polymer method (Histofine Simple Stain MAX PO; Nichirei, Tokyo, Japan). The reaction products were visualized by immersing sections in 0.2 mg/mL diaminobenzidine in 0.05 mol/L tris–HCl buffer (pH 7.6) containing 0.003% hydrogen peroxide.

Results

The patients consisted of 27 women and 18 men, with ages from 28 to 78 years (mean, 50.3 years). Twenty-eight tumors were located in the parotid glands; ten in the submandibular glands; four in the hard palates, and one each in the upper lip, nasal cavity, and parapharyngeal space. Histologically, the tumors were composed of a proliferation of myoepithelial tumor cells and glandular, keratinizing, cartilaginous components with a chondromyxoid or hyalinized stroma. Twelve tumors contained areas of plasmacytoid cells; 11 had bundles or fascicles of spindle cells; 6 showed a lipomatous component; 2 had mucous glands, and 2 contained an epithelial component with sebaceous differentiation.

The results of the molecular and immunohistochemical analyses are summarized in Table 2. RT-PCR using FFPE tumor tissue successfully amplified the PGK and PBGD transcripts in all 45 pleomorphic adenomas of the salivary

Table 1 Primers for PCR

Designation of primer	Sequence (5′→3′)	Size of PCR product (bp)
Primers for PLAG1-associated fusion		
Reverse primers		
PLAG1-exon2R	gaccgtcacagaatgaagca	
PLAG1-exon3R	gccagtcccattgactcttc	
Forward primers		
CHCHD7-exon1F	gtgagccattgacgtgtttg	124 (with exon2R), 123 & 228 (with exon3R)
CTNNB1-exon1F	gaggaaggtctgaggagcag	159 (with exon2R), 158 & 263 (with exon3R)
LIFR-exon1F	agctcagaaagggagcctct	105 (with exon2R), 104 & 209 (with exon3R)
TCEA1-exon1F	gctttgccaagaagatggac	106 (with exon2R), 105 & 210 (with exon3R)
Primers for HMGA2-associated fusion		
Forward primers		
HMGA2-exon2F[a]	cctaagagacccaggggaag	
HMGA2-exon3F	agcagaagccactggagaaa	
Reverse primers		
FHIT-exon9R1	ctgatctccaagaggcagga	196 (with exon2F), 95 & 128 (with exon3F)
FHIT-exon9R2	tgaaagtagacccgcagagc	242 (with exon2F), 141 & 174 (with exon3F)
NFIB-exon9R	ccggtaagatgggtgtccta	212 (with exon2F), 111 & 144 (with exon3F)
WIF1-exon3R	ggacattgacggttggatct	193 (with exon2F)
WIF1-exon4R	aaatgctgccaccccatc	170 (with exon2F)
WIF1-exon9R	attggcatttgttgggttca	177 (with exon2F)
WIF1-exon10R	ttaagtgaaggcgtgtgctg	190 (with exon2F)

[a] Identical primer sequence as used in reference 19

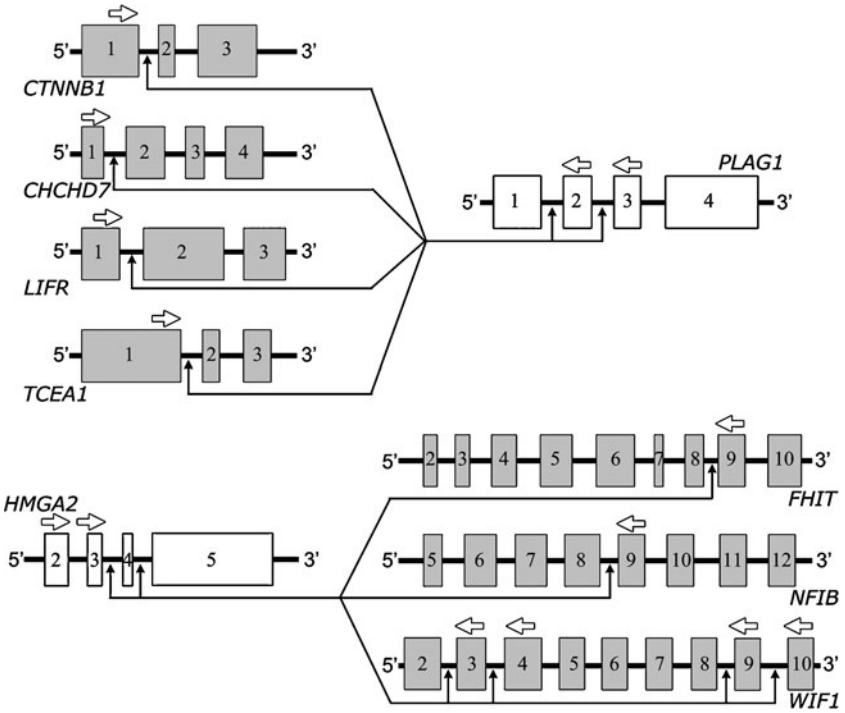

Fig. 1 A schematic representation of portions of *PLAG1*, *CTNNB1*, *CHCHD7*, *LIFR*, and *TCEA1* breakpoints in fusion genes involving *PLAG1*, and *HMGA2*, *FHIT*, *NFIB*, and *WIF1* breakpoints in fusion genes involving *HMGA2*. *Open arrows* represent the primers used

glands. RT-PCR analyses amplified the CTNNB1-PLAG1, LIFR-PLAG1, CHCHD7-PLAG1, and HMGA2-WIF1 fusion transcripts in eight (18%), 2 (4.4%), one (2.2%), and one (2.2%) tumor case, respectively (Fig. 2). In all the eight cases with detectable CTNNB1-PLAG1 fusion transcripts, PCR using the CTNNB1-exon1F forward and PLAG1-exon2R reverse primer combination amplified a 159-bp fragment of the fusion gene transcript. Nucleotide sequence analysis revealed that the PCR products were composed of exon 1 of *CTNNB1* and exon 2 of *PLAG1*. PCR amplification using the CTNNB1-exon1F forward and PLAG1-exon3R reverse primer combination generated PCR products of 158 bp in all eight cases and of 263 bp in four cases. The 158-bp PCR products consisted of exon 1 of *CTNNB1* and exon 3 of *PLAG1*, whereas the 263-bp products consisted of exon 1 of *CTNNB1* and exons 2 and 3 of *PLAG1*. The LIFR-exon1F and PLAG1-exon3R primer combination produced a 104-bp product, consistent with fusion transcripts composed of exon 1 of *LIFR* and exon 3 of *PLAG1*. No fusion transcript was identified by the LIFR-exon1F and PLAG1-exon2R primer combination. In CHCHD7-PLAG1 fusion transcripts, PCR products of 123 bp and 228 bp were amplified by the CHCHD7-exon1F forward and PLAG1-exon3R reverse primer combination, and a 124-bp product was amplified by the CHCHD7-exon1F forward and PLAG1-exon2R reverse primer combination. Nucleotide sequence analysis showed that these fusion transcripts contained exon 1 of *CHCHD7*

Table 2 Summary of the results

	PA (n=45)	Salivary gland tumors other than PA	
		Carcinoma component of CPA (n=4)	Other tumors (n=42)
RT-PCR			
CTNNB1-PLAG1	8/45 (18%)	0/4 (0%)	0/8 (0%)
LIFR-PLAG1	2/45 (4.4%)	0/4 (0%)	0/8 (0%)
CHCHD7-PLAG1	1/45 (2.2%)	0/4 (0%)	0/8 (0%)
TCEA1-PLAG1	0/45 (0%)	0/4 (0%)	0/8 (0%)
HMGA2-WIF1	1/45 (2.2%)	0/4 (0%)	0/8 (0%)
HMGA2-FHIT	0/45 (0%)	0/4 (0%)	0/8 (0%)
HMGA2-NFIB	0/45 (0%)	0/4 (0%)	0/8 (0%)
IHC for PLAG1	45/45 (100%)	4/4 (100%)	3/42 (focal, 7.1%)

PA pleomorphic adenoma, *CPA* carcinoma ex pleomorphic adenoma, *IHC* immunohistochemistry

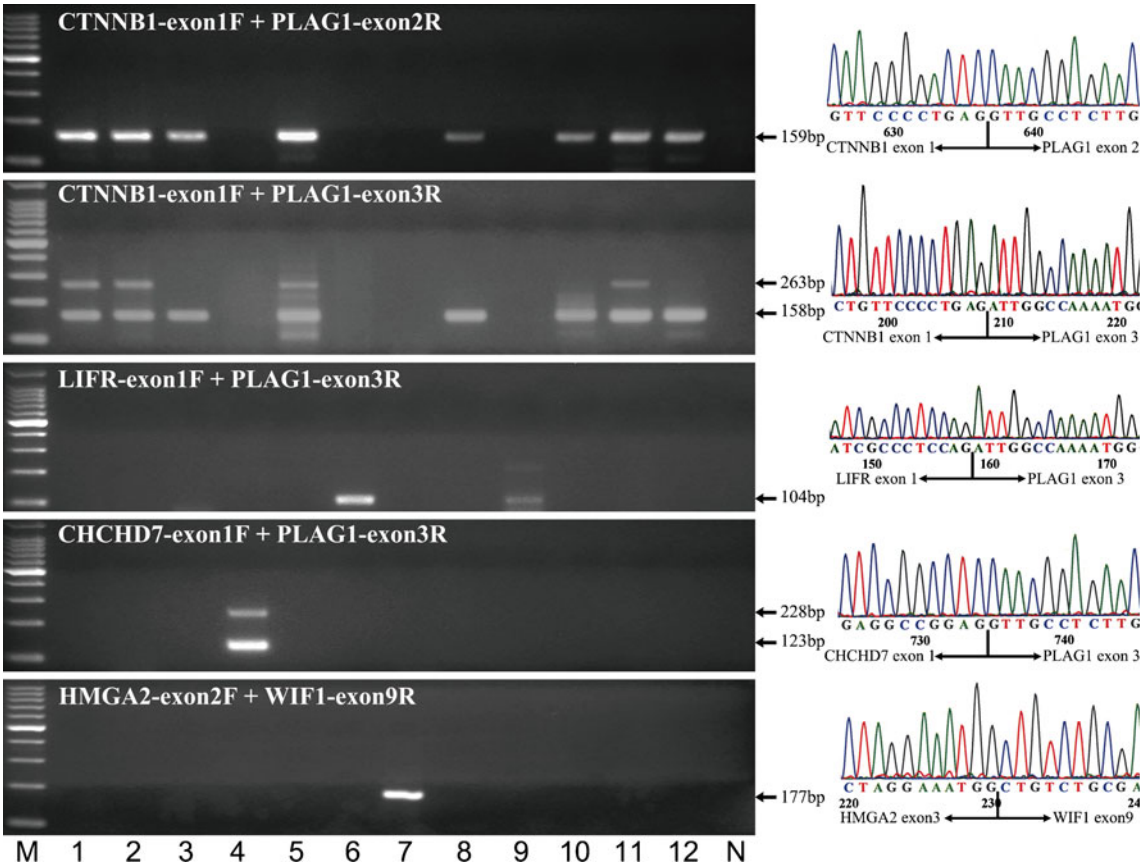

Fig. 2 Identification of the CTNBB-PLAG1, LIFR-PLAG1, CHCHD7-PLAG1, and HMGA2-WIF1 fusion transcripts in 12 fusion-positive pleomorphic adenomas by RT-PCR (*left*), and partial nucleotide sequences containing junctions of the fusion transcripts in the representative cases (*right*). The primer combinations used are indicated. *M* 100-bp DNA ladder, *N* negative controls, lanes *1–12* case numbers of pleomorphic adenomas

fused to exon 3 or exons 2 and 3 of *PLAG1*. By using the HMGA2-exon2F and WIF1-exon9R primer combination, a 177-bp PCR product was identified in 1 case, and sequence analysis confirmed that exon 3 of HMGA2 was fused with exon 9 of WIF1 in the HMGA2-WIF1-positive case. No fusion transcripts were identified by PCR using the primers for the TCEA1-PLAG1, HMGA2-FHIT, or HMGA2-NFIB fusion transcripts in any of the cases. None of the 4 CPAs demonstrated to harbor any fusion transcript. No fusion transcripts were identified by PCR using any primer combinations in 8 tumors other than pleomorphic adenoma or CPA including the 3 tumors with focal and/or faint immunoreaction to PLAG1 (described below).

Immunohistochemical evaluation was performed in 91 salivary gland tumors consisting of 45 pleomorphic adenomas and 46 tumors other than pleomorphic adenoma. Many tumor cells in the 45 pleomorphic adenomas examined showed a positive reaction to PLAG1 (Fig. 3) that was unrelated to the presence or absence of PLAG1 rearrangements or to the presence of the HMGA2-WIF1 fusion transcript (Fig. 4). Among the heterogeneously differentiated components, tumor cells displaying myoepithelial differentiation, including those showing spindle (Fig. 3a, b), stellate (Fig. 3c, d), and plasmacytoid (Fig. 3e, f) appearances in cellular areas or embedded in hyalinized or myxoid matrices, were almost constantly positive for PLAG1. Most tumor cells with cartilaginous differentiation were also positive for PLAG1 (Fig. 3g, h), whereas the lipomatous components observed in 6 cases were not stained (Fig. 3i, j). Among the epithelial components, a glandular component was focally positive for PLAG1, but its expression was limited to less than 10% of cells in most cases (Fig. 3k, l). The keratinizing tumor cells were also essentially negative for PLAG1 (Fig. 3m, n), whereas cells exhibiting sebaceous differentiation were consistently positive for PLAG1 (Fig. 3o, p). Mucous epithelium was also focally positive for PLAG1. Among the 46 tumors other than pleomorphic adenoma, 4 carcinomatous components of CPAs were variably positive for PLAG1 (Fig. 5) as well as their benign tumor components. Components of 1 of the 2 adenocarcinomas NOS, salivary duct carcinoma, and myoepithelial carcinoma in CPAs were intensely positive for PLAG1 in >75% of areas, whereas the other adenocarcinoma NOS component was only

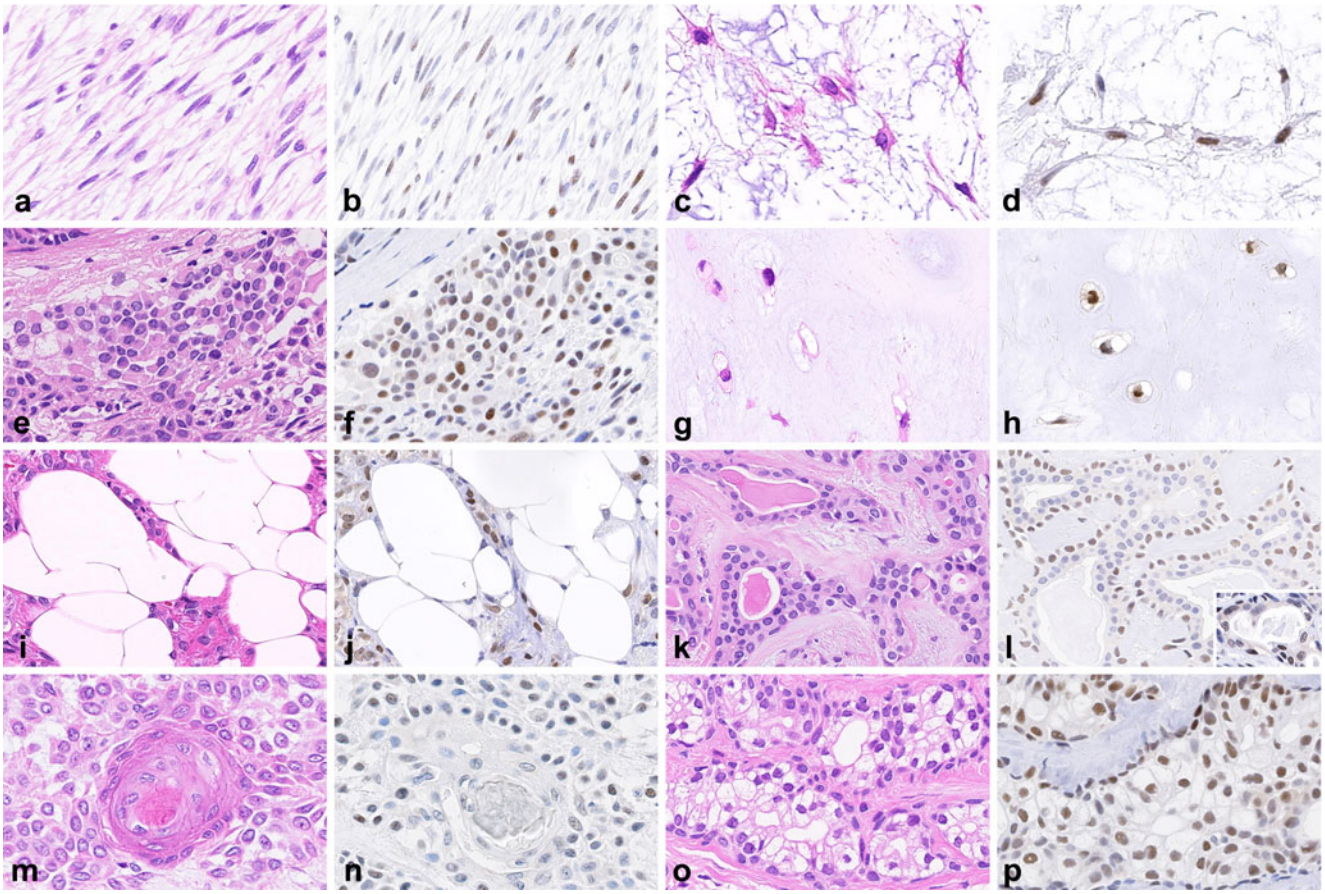

Fig. 3 Hematoxylin and eosin staining (**a**, **c**, **e**, **g**, **i**, **k**, **m**, and **o**) and immunohistochemical staining for PLAG1 (**b**, **d**, **f**, **h**, **j**, **l**, **n**, and **p**) of tumor cells in each component of pleomorphic adenomas. Spindle (**a** and **b**), stellate (**c** and **d**), plasmacytoid (**e** and **f**), and chondroid (**g** and **h**) cells are constantly positive for PLAG1, whereas cells with adipocytic differentiation are negative (**i** and **j**). Among epithelial components, tumor cells with glandular (**k** and **l**) and squamous (**m** and **n**) differentiation are negative for PLAG1, whereas cells with sebaceous differentiation are positive (**o** and **p**)

focally stained. Other 39 tumors were negative for PLAG1. Among the remaining three tumors, one case of adenoid cystic carcinoma displayed a positive immunoreaction to PLAG1 in <1% of the tumor cells, and the remaining two cases of mucoepidermoid carcinoma and acinic cell carcinoma revealed focally and faintly stained (Fig. 6).

Discussion

Recent cytogenetic and molecular tumor analyses identified several tumor-specific chromosomal alterations and their molecular consequences in many types of malignancies including not only hematopoietic or mesenchymal neoplasms but also epithelial tumors such as pulmonary adenocarcinoma [21], prostatic adenocarcinoma [22], and salivary gland mucoepidermoid carcinoma [16]. Approximately 50–80% of pleomorphic adenomas were also shown to carry clonal chromosomal abnormalities, according to cytogenetic studies [7, 8, 23]. Alterations involving 8q12, the chromosome region where the *PLAG1* gene is located, are the most common abnormalities that account for 25% of pleomorphic adenomas [7], and 40% of them are characterized by a specific t(3;8)(p21;q12) translocation that results in *CTNNB1-PLAG1* gene fusion [5]. *LIFR-PLAG1* fusion, which is derived from t(5;8)(p13;q12) translocation, has also been identified in some cases of pleomorphic adenomas [6]. Another group of fusions that has been associated with 12q14-15 rearrangements targeting *HMGA2* (also called *HMGI-C*) was found to harbor *HMGA2-NFIB* [9], *HMGA2-FHIT* [10], or *HMGA2-WIF1* fusions [11]. The remaining tumors, which account for more than 50% of pleomorphic adenomas, are characterized by sporadic cytogenetic changes not involving 8q12, 12q13-15, or a normal karyotype [7, 8, 23]. However, cytogenetic analysis is not sufficient to evaluate gene alterations in pleomorphic adenomas. Because the *CHCHD7* and *TCEA1* genes are located only approximately 500 bp and 2 Mb apart from the *PLAG1* gene in 8q, respectively, *CHCHD7-PLAG1* and *TCEA1-PLAG1* may not be detectable by G-banding or

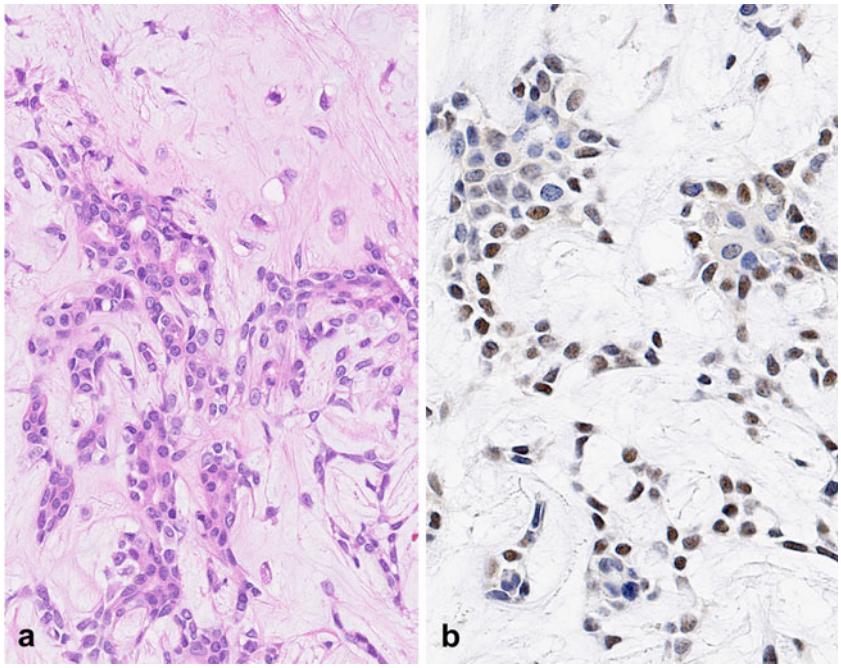

Fig. 4 A pleomorphic adenoma with the HMGA2-WIF1 fusion transcript (case 7 in Fig. 2). **a** Hematoxylin and eosin staining. **b** A positive immunoreaction to PLAG1

even by the spectral karyotype analysis method [2, 3], suggesting that these cryptic fusions may have been overlooked in most cytogenetic studies addressing gene rearrangements in pleomorphic adenomas [7, 8, 24]. In addition, cytogenetic assays require fresh tumor tissue materials, which are not always available. Although chromosomal translocations have also been examined also by FISH or CISH using fresh-frozen or FFPE tissue specimens in some studies [2, 4, 24, 25], these methods fail to show detailed fusion patterns or are unable to detect the known cryptic fusions. In the present study, RT-PCR analysis was used to detect the previously reported pleomorphic adenoma-associated fusion transcripts, including the CTNNB1-PLAG1, CHCHD7-PLAG1, LIFR-PLAG1, TCEA1-PLAG1, HMGA2-FHIT, HMGA2-NFIB, and HMGA2-WIF1 fusion transcripts, using FFPE tumor tissue specimens. The CTNNB1-PLAG1, CHCHD7-PLAG1, LIFR-PLAG1, and HMGA2-WIF1 fusion transcripts were specifically detected in a subset of pleomorphic adenoma using FFPE tumor samples, suggesting the validity of our RT-PCR assays for the detection of these fusion transcripts. A nucleotide sequence analysis of the PCR products confirmed that exon 1 of *CTNNB1* or exon 1 of *CHCHD7* was fused with both exons 2 and 3 of *PLAG1*, exon 1 of *LIFR* was fused with exon 3 of *PLAG1*, and exon 3 of *HMGA2* was fused with exon 9 of *WIF1*, in an in-frame manner, as shown

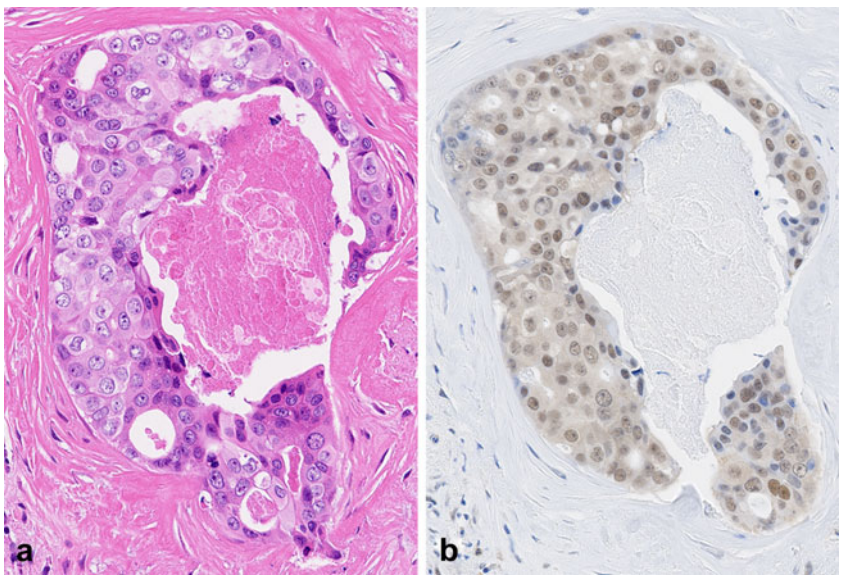

Fig. 5 A carcinoma ex pleomorphic adenoma with features of salivary duct carcinoma. **a** Hematoxylin and eosin staining. **b** A positive immunoreaction to PLAG1

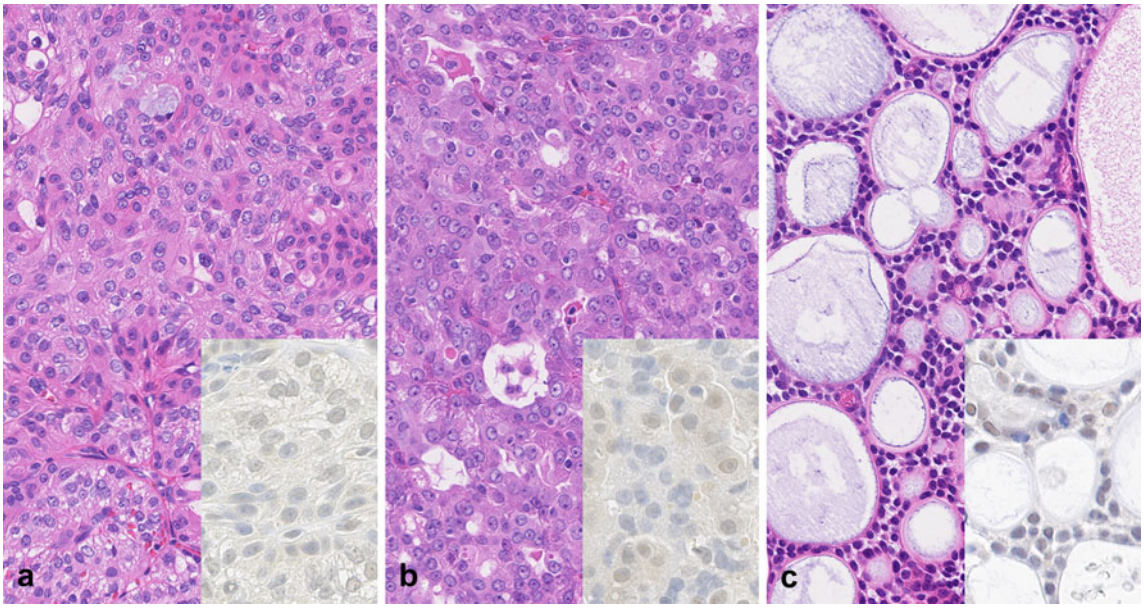

Fig. 6 Exceptional tumors other than pleomorphic adenoma that are faintly and focally positive for PLAG1, including mucoepidermoid carcinoma (**a**), acinic cell carcinoma (**b**), and adenoid cystic carcinoma (**c**). *Insets*: immunohistochemistry for PLAG1

in previous studies [2, 5, 11]. Pleomorphic adenoma-associated translocations are characterized by an almost constant and alternatively spliced fusion transcript. Further retrospective investigations using large series of tumors and the present assay will provide detailed clinicopathologic and molecular findings regarding this type of tumor. However, the TCEA1-PLAG1, HMGA2-FHIT, and HMGA2-NFIB fusion transcripts were not detected in any of the cases examined. This could be attributable to primer design or PCR amplification profiles that are not adequate for the detection of these fusion transcripts. However, assessment of the PCR procedures and primers used in the current study is difficult because positive control samples with these rare gene fusion variants could not be obtained. Fresh-frozen tumor materials for cytogenetic or other analyses to examine these fusion genes were not available.

Immunohistochemical detection of PLAG1 in pleomorphic adenomas by using a commercially available anti-PLAG1 antibody has not been fully examined. In the present study, the immunohistochemical expression of PLAG1 was examined in 45 pleomorphic adenomas and in 46 other types of benign and malignant salivary gland tumors. The results showed that PLAG1 was variably expressed in all of the 45 pleomorphic adenomas tested, including not only tumors with a PLAG1-associated fusion transcript detected by our RT-PCR assay but also a tumor possessing the HMGA2-WIF1 fusion. These findings are in line with the results of the study by Aström et al., who identified PLAG1 overexpression in pleomorphic adenomas with 12q13-15 rearrangements by northern blot analysis [3]. Although the mechanism mediating the overexpression in these cases remains unclear, a subset of pleomorphic adenomas were shown to possess amplification/gain of both HMGA2 and PLAG1 in a previous study [11]. In contrast, the study by Debic-Rychter et al. detected only weak PLAG1 immunoreactivity in 10% of pleomorphic adenoma cells with t(3;12) or t(X;2) [26]. This discrepancy might be explained by methodological differences, because Debic-Rychter et al. used an immunofluorescence cytochemistry technique with primary cultured tumor cells. Our results and those of other studies suggest that overexpression of the PLAG1 protein is essential for the tumorigenesis of pleomorphic adenomas, including cases with the HMGA2-associated fusion, and that its mechanisms of action in pleomorphic adenomas were variable. All of the 4 carcinomatous components in CPAs also variably expressed PLAG1, consistent with the results of previous studies that detected PLAG1 translocation in CPAs [3, 4, 11]. However, RT-PCR analyses of CPAs that included the extraction of RNA from FFPE tumor tissues containing both benign and malignant components did not detect fusion transcripts, suggesting that such fusion gene transcripts were absent even in pleomorphic adenoma components. On the other hand, negative or only focal and/or faint PLAG1 staining was observed in all the salivary gland tumors other than the pleomorphic adenoma and CPA we examined. Two lesions that were previously diagnosed as pleomorphic adenoma but re-diagnosed as basal cell adenoma according to the histological review were also negative for PLAG1. These results suggest that PLAG1 is a specific and reliable immunohistochemical marker for the diagnosis of pleomorphic adenoma.

Basal cell adenoma is a benign salivary gland tumor characterized by basaloid appearance of tumor cells with immunohistochemical and ultrastructural profiles suggestive of both ductal and myoepithelial differentiation, and this characteristic overlaps with that of pleomorphic adenoma. Rare cases of cellular pleomorphic adenoma with a minimal amount of chondromyxoid tissue can mimic the features of basal cell adenoma [1], suggesting that these 2 tumors are closely related to each other. However, the two basal cell adenomas we examined were negative for PLAG1 and lacked a PLAG1- or HMGA2-translocation, indicating that basal cell adenoma and pleomorphic adenoma are two distinct tumor entities with probably different molecular mechanisms. On the other hand, PLAG1 expression was not examined in myoepithelioma, a rare benign salivary gland tumor composed entirely of myoepithelial tumor cells without a ductal or chondroid component, because such a sample could not be obtained in the present study. Myoepithelioma and pleomorphic adenoma also share biological characteristics, and the distinction between these two tumors is often arbitrary [1]. Although cytogenetic or molecular genetic studies of salivary gland myoepithelioma are not readily available, one case of myoepithelioma arising in the parotid gland was cytogenetically shown to have a 12q alteration, similar to the observation in a subset of pleomorphic adenomas [27]. These findings suggest that myoepithelioma only represents one end of a single histological spectrum of pleomorphic adenomas with common genetic backgrounds. Additional genetic and immunohistochemical studies of myoepithelioma, including immunohistochemistry for PLAG1 and RT-PCR analysis of PLAG1 or HMGA2 alterations by using FFPE specimens, are required to address these hypotheses.

Immunohistochemical detection of the target proteins of fusion genes resulting from characteristic balanced chromosomal translocations has played an important role in the diagnosis of many translocation-associated tumors [15, 17–20]. Immunohistochemical staining of a target protein is usually observed in almost all tumor cells, whereas PLAG1 expression in the pleomorphic adenomas we examined was not detected frequently, and certain tumor components were not immunoreactive. This phenomenon may be characteristic of pleomorphic adenoma and seems to be related to the heterogeneous differentiation of tumor cells. PLAG1-negative cells do not necessarily correspond to non-neoplastic cells.

In conclusion, PLAG1- or HMGA2-associated fusion transcripts were successfully detected in 12 of the 45 pleomorphic adenomas by RT-PCR by using FFPE tumor tissue specimens. In addition, all the pleomorphic adenomas examined showed constant and specific immunohistochemical expression of PLAG1 irrespective of detectable gene rearrangements, suggesting that the immunohistochemistry for PLAG1 is diagnostically useful, and that overexpression of the PLAG1 protein occurs by a variable mechanism.

Acknowledgments The authors thank Kazumi Tanaka for her technical assistance.

Conflict of interest We declare that we have no conflict of interest.

References

1. Barnes L, Eveson JW, Reichart PA, Sidransky D (eds) (2005) World Health Organization classification of tumours. Pathology and genetics of head and neck tumours. IARC Press, Lyon
2. Asp J, Persson F, Kost-Alimova M, Stenman G (2006) CHCHD7-PLAG1 and TCEA1-PLAG1 gene fusions resulting from cryptic, intrachromosomal 8q rearrangements in pleomorphic salivary gland adenomas. Genes Chromosom Cancer 45:820–828
3. Aström AK, Voz ML, Kas K, Röijer E, Wedell B, Mandahl N, Van de Ven W, Mark J, Stenman G (1999) Conserved mechanism of PLAG1 activation in salivary gland tumors with and without chromosome 8q12 abnormalities: identification of SII as a new fusion partner gene. Cancer Res 59:918–923
4. Martins C, Fonseca I, Roque L, Pereira T, Ribeiro C, Bullerdiek J, Soares J (2005) PLAG1 gene alterations in salivary gland pleomorphic adenoma and carcinoma ex-pleomorphic adenoma: a combined study using chromosome banding, in situ hybridization and immunocytochemistry. Mod Pathol 18:1048–1055
5. Kas K, Voz ML, Röijer E, Aström AK, Meyen E, Stenman G, Van de Ven WJ (1997) Promoter swapping between the genes for a novel zinc finger protein and beta-catenin in pleiomorphic adenomas with t (3;8)(p21;q12) translocations. Nat Genet 15:170–174
6. Voz ML, Aström AK, Kas K, Mark J, Stenman G, Van de Ven WJ (1998) The recurrent translocation t(5;8)(p13;q12) in pleomorphic adenomas results in upregulation of PLAG1 gene expression under control of the LIFR promoter. Oncogene 16:1409–1416
7. Bullerdiek J, Wobst G, Meyer-Bolte K, Chilla R, Haubrich J, Thode B, Bartnitzke S (1993) Cytogenetic subtyping of 220 salivary gland pleomorphic adenomas: correlation to occurrence, histological subtype, and in vitro cellular behavior. Cancer Genet Cytogenet 65:27–31
8. Mark J, Dahlenfors R, Wedell B (1997) Impact of the in vitro technique used on the cytogenetic patterns in pleomorphic adenomas. Cancer Genet Cytogenet 95:9–15
9. Geurts JM, Schoenmakers EF, Röijer E, Aström AK, Stenman G, van de Ven WJ (1998) Identification of NFIB as recurrent translocation partner gene of HMGIC in pleomorphic adenomas. Oncogene 16:865–872
10. Geurts JM, Schoenmakers EF, Röijer E, Stenman G, Van de Ven WJ (1997) Expression of reciprocal hybrid transcripts of HMGIC and FHIT in a pleomorphic adenoma of the parotid gland. Cancer Res 57:13–17
11. Persson F, Andrén Y, Winnes M, Wedell B, Nordkvist A, Gudnadottir G, Dahlenfors R, Sjögren H, Mark J, Stenman G (2009) High-resolution genomic profiling of adenomas and carcinomas of the salivary glands reveals amplification, rearrangement, and fusion of HMGA2. Genes Chromosom Cancer 48:69–82
12. Hisaoka M, Tsuji S, Morimitsu Y, Hashimoto H, Shimajiri S, Komiya S, Ushijima M (1998) Detection of TLS/FUS-CHOP

fusion transcripts in myxoid and round cell liposarcomas by nested reverse transcription-polymerase chain reaction using archival paraffin-embedded tissues. Diagn Mol Pathol 7:96–101
13. Tsuji S, Hisaoka M, Morimitsu Y, Hashimoto H, Shimajiri S, Komiya S, Ushijima M, Nakamura T (1998) Detection of SYT-SSX fusion transcripts in synovial sarcoma by reverse transcription-polymerase chain reaction using archival paraffin-embedded tissues. Am J Pathol 153:1807–1812
14. Argani P, Zakowski MF, Klimstra DS, Rosai J, Ladanyi M (1998) Detection of the SYT-SSX chimeric RNA of synovial sarcoma in paraffin-embedded tissue and its application in problematic cases. Mod Pathol 11:65–71
15. Li XQ, Hisaoka M, Shi DR, Zhu XZ, Hashimoto H (2004) Expression of anaplastic lymphoma kinase in soft tissue tumors: an immunohistochemical and molecular study of 249 cases. Hum Pathol 35:711–721
16. Okabe M, Miyabe S, Nagatsuka H, Terada A, Hanai N, Yokoi M, Shimozato K, Eimoto T, Nakamura S, Nagai N, Hasegawa Y, Inagaki H (2006) MECT1-MAML2 fusion transcript defines a favorable subset of mucoepidermoid carcinoma. Clin Cancer Res 12:3902–3907
17. Llombart-Bosch A, Machado I, Navarro S, Bertoni F, Bacchini P, Alberghini M, Karzeladze A, Savelov N, Petrov S, Alvarado-Cabrero I, Mihaila D, Terrier P, Lopez-Guerrero JA, Picci P (2009) Histological heterogeneity of Ewing's sarcoma/PNET: an immunohistochemical analysis of 415 genetically confirmed cases with clinical support. Virchows Arch 455:397–411
18. Barnoud R, Sabourin JC, Pasquier D, Ranchère D, Bailly C, Terrier-Lacombe MJ, Pasquier B (2000) Immunohistochemical expression of WT1 by desmoplastic small round cell tumor: a comparative study with other small round cell tumors. Am J Surg Pathol 24:830–836
19. Argani P, Lal P, Hutchinson B, Lui MY, Reuter VE, Ladanyi M (2003) Aberrant nuclear immunoreactivity for TFE3 in neoplasms with TFE3 gene fusions: a sensitive and specific immunohistochemical assay. Am J Surg Pathol 27:750–761
20. Nakamura S, Shiota M, Nakagawa A, Yatabe Y, Kojima M, Motoori T, Suzuki R, Kagami Y, Ogura M, Morishima Y, Mizoguchi Y, Okamoto M, Seto M, Koshikawa T, Mori S, Suchi T (1997) Anaplastic large cell lymphoma: a distinct molecular pathologic entity: a reappraisal with special reference to p80(NPM/ALK) expression. Am J Surg Pathol 21:1420–1432
21. Takeuchi K, Choi YL, Soda M, Inamura K, Togashi Y, Hatano S, Enomoto M, Takada S, Yamashita Y, Satoh Y, Okumura S, Nakagawa K, Ishikawa Y, Mano H (2008) Multiplex reverse transcription-PCR screening for EML4-ALK fusion transcripts. Clin Cancer Res 14:6618–6624
22. Tomlins SA, Rhodes DR, Perner S, Dhanasekaran SM, Mehra R, Sun XW, Varambally S, Cao X, Tchinda J, Kuefer R, Lee C, Montie JE, Shah RB, Pienta KJ, Rubin MA, Chinnaiyan AM (2005) Recurrent fusion of TMPRSS2 and ETS transcription factor genes in prostate cancer. Science 310:644–648
23. Sandros J, Stenman G, Mark J (1990) Cytogenetic and molecular observations in human and experimental salivary gland tumors. Cancer Genet Cytogenet 44:153–167
24. Rohen C, Rogalla P, Meyer-Bolte K, Bartnitzke S, Chilla R, Bullerdiek J (1999) Pleomorphic adenomas of the salivary glands: absence of HMGIY rearrangements. Cancer Genet Cytogenet 111:178–181
25. Jin C, Martins C, Jin Y, Wiegant J, Wennerberg J, Dictor M, Gisselsson D, Strömbeck B, Fonseca I, Mitelman F, Tanke HJ, Höglund M, Mertens F (2001) Characterization of chromosome aberrations in salivary gland tumors by FISH, including multicolor COBRA-FISH. Genes Chromosom Cancer 30:161–167
26. Debiec-Rychter M, Van Valckenborgh I, Van den Broeck C, Hagemeijer A, Van deVen WJ, Kas K, Van Damme B, Voz ML (2001) Histologic localization of PLAG1 (pleomorphic adenoma gene 1) in pleomorphic adenoma of the salivary gland: cytogenetic evidence of common origin of phenotypically diverse cells. Lab Invest 81:1289–1297
27. el-Naggar AK, Lovell M, Callender DL, Ordonez NG, Killary AM (1999) Cytogenetic analysis of a primary salivary gland myoepithelioma. Cancer Genet Cytogenet 113:49–53

Virchows Arch (2011) 458:593–602
DOI 10.1007/s00428-011-1054-5

ORIGINAL ARTICLE

Adenomatoid tumors of the female and male genital tract. A comparative clinicopathologic and immunohistochemical analysis of 47 cases emphasizing their site-specific morphologic diversity

David L. Wachter · Peter H. Wünsch · Arndt Hartmann · Abbas Agaimy

Received: 21 December 2010 / Revised: 31 January 2011 / Accepted: 1 February 2011 / Published online: 20 February 2011
© Springer-Verlag 2011

Abstract Adenomatoid tumors (ATs) are uncommon benign mesothelial tumors with a predilection for the genital tract. We reviewed 47 ATs diagnosed at our institutions during 10-year period. Thirty tumors (64%) originated in the female (21 uterine, 8 tubal, and 1 ovarian) and 17 (36%) in the male (9 epididymal and 8 testicular) genital tract. The median age for females and males was 47.5 and 51 years, respectively. While 83% of tumors in females were incidental findings in resections for unrelated diseases, 94% of male lesions presented as clinical masses leading to surgery. The median size was 2, 1, and 0.5 cm for uterine, epididymo-testicular, and tubo-ovarian lesions, respectively. Architecturally, the microcystic/angiomatoid pattern was the most frequent (32/47; 68%), followed by combined microcystic/trabecular (26/47; 55%) and retiform/adenoid (15/47; 32%) pattern. The trabecular/solid (6%) and macrocystic (4%) patterns were uncommon. However, 57% of cases revealed ≥2 growth patterns. Taken by anatomic site, 20 of 21 uterine cases were at least focally microcystic but none was retiform. In contrast, the retiform pattern dominated in male genital tract tumors (12/17; 71%). Immunohistochemistry showed expression of calretinin (36/36) and D2-40 (30/30) and lack of CD34 (0/30) and PAX8 (0/32). GLUT-1 was expressed in 11/11 male genital tract tumors but in none of the microcystic uterine lesions. Estrogen and progesterone receptor expression was weak and focal (two and three uterine cases, respectively). None stained for the androgen receptor. Our study illustrates the great site-specific morphological diversity of ATs emphasizing their wide site-dependant differential diagnosis.

Keywords Adenomatoid tumor · Genital tract · D2-40 · PAX8 · GLUT-1

D. L. Wachter · A. Hartmann · A. Agaimy (✉)
Institute of Pathology, University Hospital Erlangen,
Krankenhausstr. 12,
91054 Erlangen, Germany
e-mail: abbas.agaimy@uk-erlangen.de

P. H. Wünsch
Institute of Pathology, Nuremberg Clinic Center,
Nuremberg, Germany

Introduction

Adenomatoid tumors (ATs) are rare benign tumors, which predominantly arise in the male and female genital tract organs. First described by Sakaguchi in 1916 as adenomyomata [1], later studies by Masson (in 1942) and Evans (in 1943) pointed to a mesothelial differentiation of these uncommon tumors [2, 3]. Because of the initial uncertainty regarding their cell of origin, Golden and Ash coined the descriptive term *adenomatoid* tumor [4], which is still in use to date. The histogenesis of ATs was an issue of controversy for several decades. Derivation from differentiated mesothelial cells, for example by inclusion [5] or embolization [6] has been postulated. Others suggested an origin from pluripotent Müllerian mesenchymal stem cells [7]. Of note, both differentiated mesothelium and Müllerian mesenchymal stem cells develop from the same origin, the coelomic epithelium [8]. Currently, the mesothelial derivation of ATs is widely accepted.

Besides the male and female genital tract, ATs have been recognized at extragenital sites, particularly in the vicinity of serosal membranes (pleura, peritoneum, and pericardium), the adrenal gland, and other visceral organs [5, 8–16]. Previously described growth patterns of ATs include

plexiform, tubular, and canalicular [17], as well as adenomatoid, angiomatoid, solid, and cystic patterns [18]. However, increasing recognition of these uncommon tumors suggested a greater morphological diversity than initially appreciated. The aim of this study was to review the clinicopathological and immunohistochemical features of a large series of ATs from the female and male genital tract in order to compare their possible site-specific morphological and immunohistochemical heterogeneity.

Materials and methods

ATs diagnosed between 1999 and 2010 at the Institute of Pathology of the University Hospital of Erlangen-Nuremberg and the Institute of Pathology, Nuremberg Clinic Center were retrieved from routine surgical pathology files by a computer search irrespective of tumor site. All available slides were reviewed by two pathologists (D. L.W and A.A) to verify diagnosis. Fifty-three cases of ATs could be retrieved. In two cases, diagnosis was revised to calcifying fibrous tumor of the epididymis and hyperplastic rete ovarii. Two further cases proved to represent extensions from mesothelioma of the spermatic cord and the peritoneum. Another two cases of verified AT were excluded due to extragenital site of origin (one from the subserosa of the stomach and one from the adrenal gland, both in male patients). The adrenal tumor has been reported in detail previously [19]. Thus, a total of 47 genital tract ATs were included in this study. In brief, all tumors met both histological and immunohistochemical diagnostic criteria including (1) proliferation of large polygonal commonly vacuolated cells forming gland-like cystic spaces, tubules, cords or trabeculae, (2) presence of thread-like bridging strands resulting from prominent vacuolization of the tumor cells; sometimes imparting a signet-ring or double barrel appearance to lesional cells, (3) luminal hyaluronic acid secretion with characteristic bluish tinge, (4) detached luminal cells occasionally displaying a histiocytoid appearance, (5) focal stromal lymphocytic aggregates in several cases, and (6) strong expression of the mesothelial markers. All or most of these features were variably present in combination in almost all cases. Five different architectural growth patterns were recognized and recorded in every case: microcystic, combined microcystic/trabecular, trabecular/solid, retiform/adenoid, and gross cystic. Of note, the only case that presented with a papillary architecture was the AT of the adrenal gland, which is not included in this clinicopathological analysis. Thus, the papillary pattern was not included in further analysis in this study. Paraffin blocks were available for 30 cases. From the remaining 17 cases, at least hematoxylin and eosin-stained slides were available, in addition to immunohistochemical stains in most of the cases. In the cases with available paraffin blocks, additional immunohistochemical stains were performed on newly cut 5 μm sections using a polymer kit from Zytomed Systems Ltd., Berlin, Germany according to the manufacturer's protocol and the following antibodies: calretinin (polyclonal rabbit anti-Calretinin, 1:2, Zytomed), D2-40 (clone M2A, 1:40, Novocastra), CD31 (clone JC70A, 1:20, DakoCytomation), CD34 (clone QBEnd10, 1:200, Immunotech), estrogen receptor (ER) (clone 6F11, 1:200, Novocastra), progesterone receptor (PR) (clone 16, 1:200, Novocastra), androgen receptor (AR) (clone AR441, 1:2000, Labvision), PAX8 (polyclonal rabbit anti-PAX-8, 1:50, Cell Marque), glucose transporter-1 (GLUT-1, polyclonal rabbit anti-GLUT-1, 1:200, Thermo Fisher Scientific), and Ki-67 (clone Mib1, 1:100, DakoCytomation). Furthermore, we classified the intensity of lymphoid aggregates semi-quantitatively into absent/mild (none or focal scattered or perivascular aggregates, but no follicle formation) or prominent (well-formed lymphoid follicles with or without germinal centers).

Results

ATs of the female genital tract

Clinicopathologic features of uterine ATs

The median age of the 21 patients with uterine ATs was 44 years. The majority of uterine ATs represented incidental findings in resection specimens for unrelated diseases. These associated diseases included one or more of the following conditions: endometriosis (three cases), adenomyosis uteri interna (eight cases), leiomyomata of the myometrium (nine cases), endometrial hyperplasia (two cases), endocervical polyp (one case), cervical intraepithelial neoplasia (CIN) III (one case), corpus luteum cyst (one case), and paraovarian cyst (one case). Only 19% of uterine ATs represented the indication for surgery. The clinical diagnosis in the latter was always “uterus myomatosus” (Table 1).

Gross features of uterine ATs

Uterine ATs had a median size of 2.0 cm (range, 0.8–3.5 cm). Almost all tumors presented grossly as circumscribed but non-encapsulated firm nodular masses. Their cut-surface was gray-whitish and whorled similar to leiomyoma, but with less sharply demarcated periphery that blended with the surrounding myometrium in a manner very reminiscent of adenomyosis/adenomyoma (Fig. 1a). Two uterine tumors showed a grossly visible cystic cut-surface. The tumors were almost invariably located beneath

Table 1 Clinicopathological features of adenomatoid tumors of female and male genital tract (n=47)

Site	Number of cases	Age range (years) (median)	Size range (cm) (median)	AT as operative indication (%)
Uterus	21	30–63 (44)	0.8–3.5 (2.0)	19.1
Fallopian tube	8	48–75 (56)	0.1–2.4 (0.5)	12.5
Ovary	1	78	0.5	0
Epididymis	9	38–63 (52)	0.6–1.4 (1.0)	88.9
Testis	8	20–57 (47.5)	0.5–7.5 (1.1)	100
Female total	30	30–78 (47.5)	0.1–3.5 (1.0)	16.7
Male total	17	20–63 (51)	0.6–7.5 (1.0)	94.1
Total	47	20–78 (51)	0.1–14.0 (1.0)	44.7

AT indicates adenomatoid tumor

the serosal surface without grossly discernible surface involvement.

Histological features of uterine ATs

The microcystic growth pattern (previously described as angiomatoid pattern [18]) was the predominant pattern in uterine ATs (20/21; 95%). It is characterized by slightly dilated gland-like structures, very reminiscent of lymphatic spaces, lined by one layer of flattened cells but occasionally lined by cells with hobnail or even epithelioid appearance. These cystic structures typically showed circular outlines and were separated by abundant smooth muscle bundles that occasionally entrapped small nerve twigs. Some uterine lesions of this type were composed of only a few scattered microcystic spaces in a background of prominent smooth muscle component so that their nature could be easily overlooked (Fig. 1b). The combined microcystic/trabecular growth pattern (also called adenoid pattern in previous studies [18]) was the second most frequent pattern in uterine ATs in our study (variably seen in 13/21; 62%). It is characterized by smaller, crowded or confluent microcyst-like structures, often arranged in trabeculae, lined by cells with variable but usually pronounced cytoplasmic vacuolization and many thread-like bridging strands (Fig. 1c). The macrocystic growth pattern was seen in 2/21 (10%) uterine tumors and is characterized by large, grossly visible cysts, lined by a single layer of flattened mesothelial cells admixed with a few microcystic spaces (Fig. 1d). However, the majority of uterine ATs (12/21; 57%) revealed a mixture of two or more of the above-described growth patterns (Fig. 1e). A pure trabecular (also called solid [18]) pattern was seen in a single case of uterine AT and is characterized by solid/ trabecular proliferations of epithelioid mesothelial cells (Fig. 1f). No uterine ATs with papillary or retiform patterns were seen. Of 21 cases, 18 (85.7%) revealed absent/mild and 3 cases (14.3%) revealed prominent lymphoid aggregates, usually localized at the tumor periphery (Table 2).

Immunohistological features of uterine ATs

All uterine ATs exhibited cytoplasmic/nuclear calretinin and apical membranous D2-40 expression. All were negative for CD31, CD34, PAX-8, and the AR. PAX-8 invariably stained nuclei of lymphocytes. Only two cases (10%) showed weak nuclear staining for ER and three cases stained weakly for PR (14%). GLUT-1 was positive in 9/17 cases (53%). The areas with microcystic growth pattern were invariably negative, whereas growth patterns with more epithelioid tumor cells showed mild (7/17) to moderate (2/17) cytoplasmic staining. The proliferative index (Ki-67) of the tumor cells was invariably ≤10%.

Clinicopathologic features of tubo-ovarian ATs

The median age of the eight patients with tubal ATs was 56 years and the median tumor size was 0.5 cm (range, 0.1–2.4 cm). The majority of these tumors (7/8; 88%) were incidental findings in resection specimens for one or more of the following conditions: adenomyosis uteri (one case), leiomyomata of the myometrium (four cases), complex endometrial hyperplasia with atypia (one case), endocervical polyp (one case), ovarian corpus luteum/follicle cyst (one case), paraovarian cyst (one case), endometrial polyp (one case), and ovarian fibroma (two cases). Thus, only 13% of tubal ATs represented the indication for surgery. The ovarian AT was an incidental finding in a hysterectomy-salpingo-oophorectomy specimen for poorly differentiated squamous cell carcinoma of the cervix uteri. The patient was 78 years old, and the AT measured 0.5 cm (Table 1).

Gross features of tubo-ovarian ATs

The tubal ATs formed small nodular subserosal masses usually associated with eccentric displacement of the lumen of the Fallopian tube. Their cut-surface was firm and whitish. The single ovarian AT was an incidental histological finding and was not appreciated on gross examination.

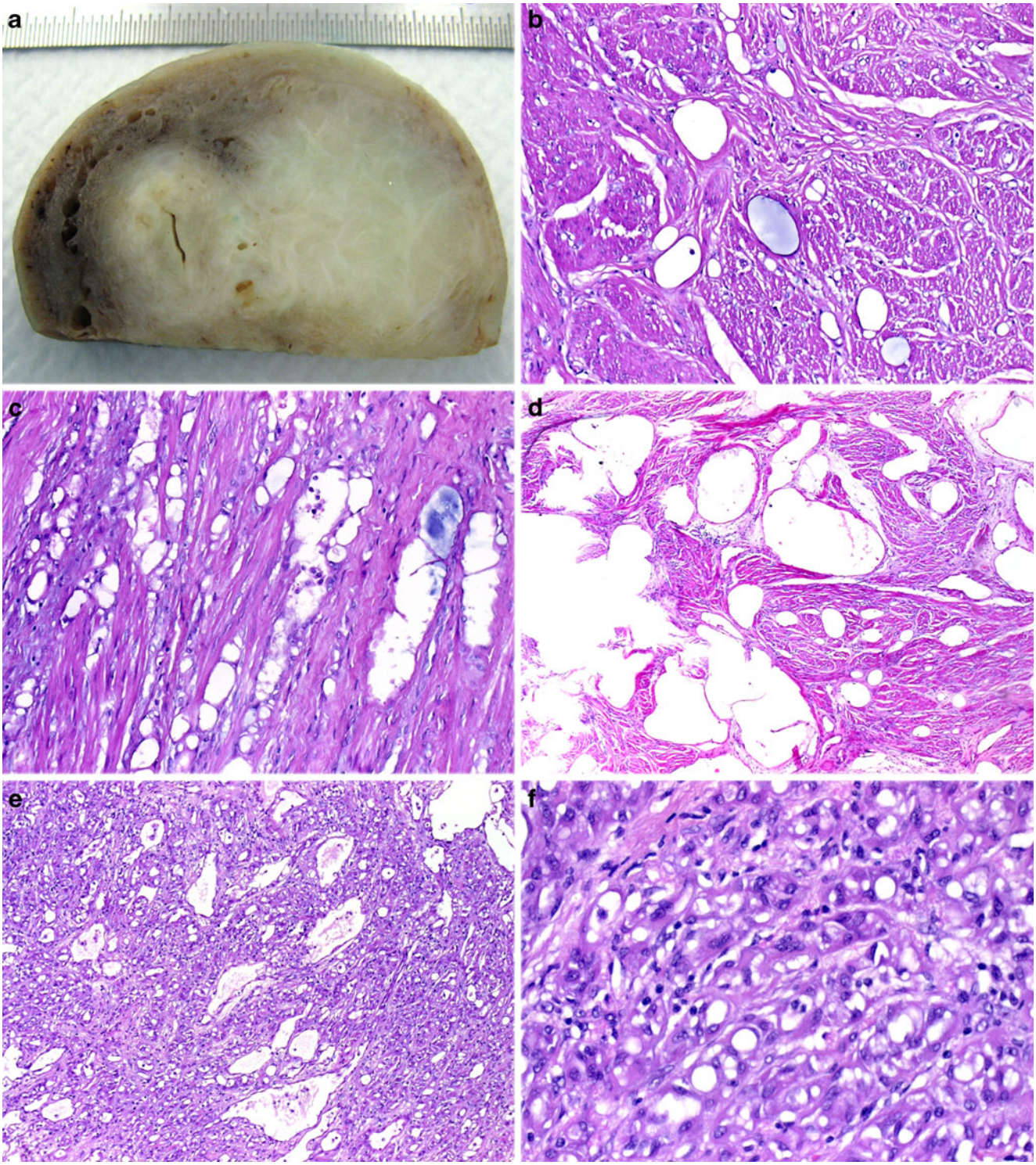

Fig. 1 Pathological features of uterine ATs. **a** A large AT showed gray-whitish whorled appearance with ill-defined margins mimicking adenomyosis. **b** Microcystic AT showed a few small cystic spaces amid smooth muscle bundles, some spaces contained bluish secretion. **c** Cystic spaces were occasionally smaller and crowded into a trabecular pattern. **d** Gross cystic spaces were seen in two tumors. **e** Mixed microcystic/trabecular pattern showed isolated microcysts within hypercellular trabecular background. **f** Trabecular/solid areas may closely mimic poorly differentiated adenocarcinoma (note prominent vacuoles and low to absent atypia)

Table 2 Histological growth pattern of adenomatoid tumors from different genital organs (n=47)

Site	Growth pattern			Prominent lymphoid infiltrates
	Pure microcystic	Mixed microcystic/trabecular	Retiform pattern present	
Female genital tract	7/30 (23%)	18/30 (60%)	3/30 (10%)	11/30 (36.7%)
Male genital tract	0/17 (0%)	7/17 (41%)	12/17 (71%)	15/17 (88.2%)
Total	7/47 (15%)	25/47 (53%)	15/47 (32%)	26/47 (55.3%)

Histological features of tubo-ovarian ATs

Tubal ATs predominantly exhibited a combined microcystic/trabecular pattern (6/8; 75%). The retiform growth pattern which was subsumed under the adenoid pattern in a previous study [18] was seen in 3/8 (38%) cases. This pattern is characterized by irregular microcystic or duct-like structures lying in a predominantly fibrous stroma. Importantly, these structures show prominent branching, thus forming communicating networks lined by flattened and occasionally large epithelioid cells (Fig. 2a–d). Interestingly, this pattern was particularly prominent in the periphery of the tumors. No tumors with trabecular, papillary, or macrocystic pattern were seen. All (8/8) of the tubal ATs showed prominent lymphoid infiltrates. The ovarian AT exhibited a mixture of microcystic and combined microcystic/trabecular pattern in a fibrous stroma with focally prominent lymphoid infiltrates (Table 2).

Immunohistological features of tubo-ovarian ATs

All tubal ATs with available paraffin blocks exhibited cytoplasmic/nuclear calretinin (Fig. 2c) and apical membraneous D2-40 expression (Fig. 2d) (4/4 and 3/3, respectively). One case exhibited mild nuclear expression of PR whereas ER and AR were negative in all cases. All cases were negative for CD31, CD34, and PAX8. Cytoplasmic GLUT-1 expression was found in 3/4 cases, each with moderate staining intensity (Fig. 2b). Lymphocytes and peg cells of tubal epithelium revealed intense nuclear positivity for PAX-8, thereby negatively highlighting the non-staining ATs. No paraffin-embedded formalin fixed tissue was available for the ovarian case. The proliferative index (Ki-67) of the tumor cells was invariably ≤10%.

Adenomatoid tumors of the male genital tract

Clinicopathologic features of epididymo-testicular ATs

The median age of the nine patients with ATs of the epididymis and testis was 51 years. All but one AT represented the indication for surgical intervention (16/17; 94%). One case of epididymal AT was found incidentally in an orchiectomy specimen removed for mature teratoma of the testis (Table 1).

Gross features of epididymo-testicular ATs

ATs had a median size of 1.0 cm (range, 0.5–7.5 cm). All tumors presented as well circumscribed mass lesions lacking a fibrous capsule. The cut-surface of the tumors was usually homogenous and tan (seldom whorled), reminiscent of ATs of the Fallopian tube (Fig. 3a). The tumors were typically located beneath the serosal surface.

Histological features of epididymal-testicular ATs

In contrast to their female genital tract lesions, the microcystic and combined microcystic/trabecular (Fig. 3b) patterns were less common (each 6/17; 35%). However, ATs of the epididymis and testis predominantly exhibited a retiform pattern (12/17; 71%). In this pattern, the tumor cells were embedded in a predominantly fibrous stroma with only sparse interspersed smooth muscle cells (Fig. 3c, d). As noted in the tubal ATs, this pattern was particularly prominent in the periphery of the tumor, occasionally showing prominent cystic dilatation (Fig. 3e, f). Similar to their uterine counterparts, the pure trabecular pattern was uncommon (seen in two cases; 12%). No tumors with papillary or macrocystic pattern were seen. Two of 17 (11.8%) tumors exhibited absent/mild and 15/17 (88.2%) tumors displayed prominent lymphoid infiltrates (Fig. 3f) (Table 2).

Immunohistological features of epididymo-testicular ATs

All ATs of the epididymis and testis exhibited cytoplasmic/nuclear calretinin and apical membraneous D2-40 expression (12/12 and 10/10, respectively). In 3/10 cases, weak cytoplasmic positivity for CD31 was noted. Of note, detached luminal cells occasionally revealed prominent CD31 positivity. All cases were negative for CD34 (0/10), PAX-8 (0/11), ER, PR, and AR (0/10). All examined tumors (11/11) revealed cytoplasmic GLUT-1 expression; 6/11 tumors with mild and 5/11 tumors with moderate staining intensity. Epithelial cells of rete testis and ducts of

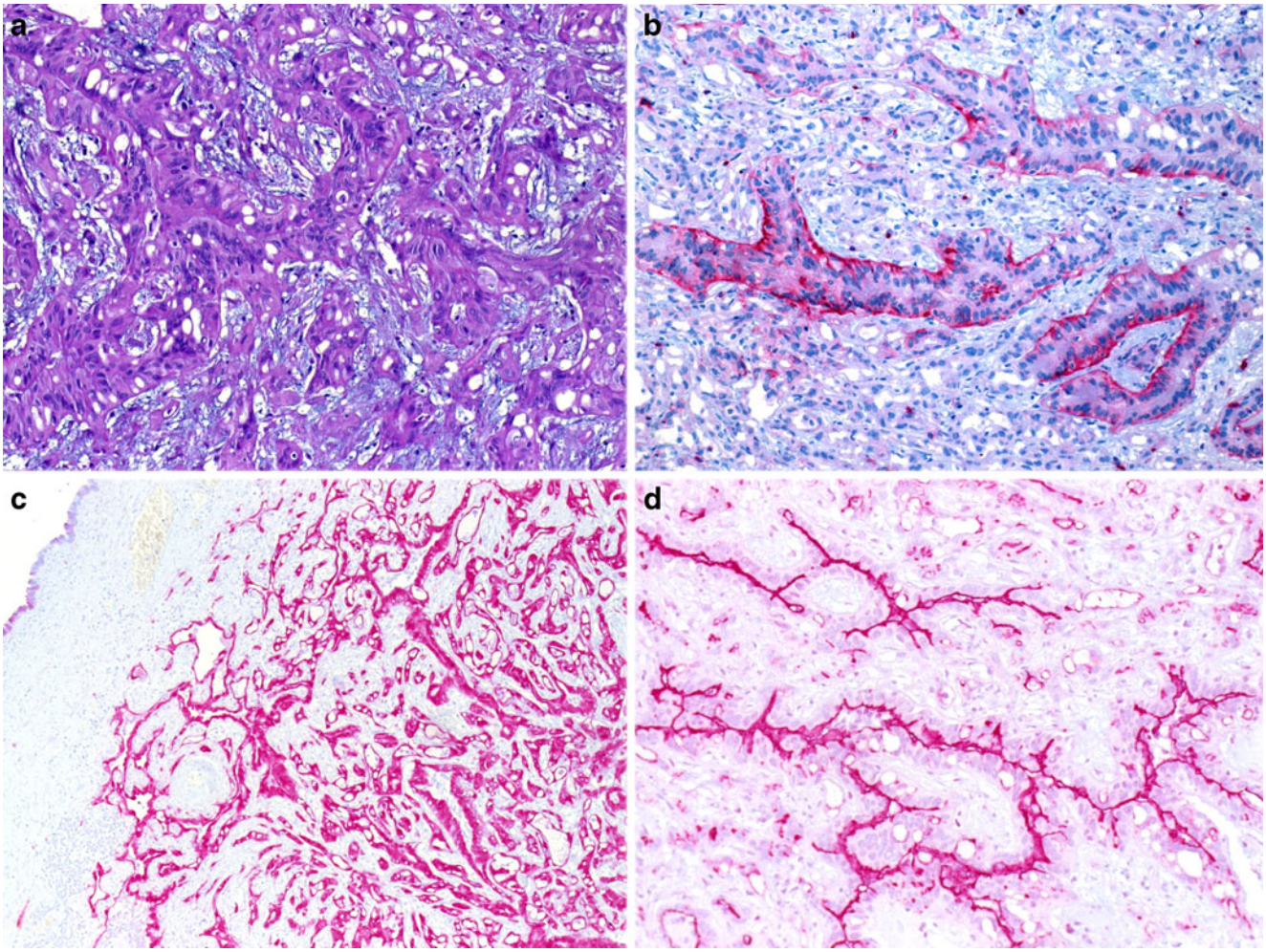

Fig. 2 Pathological features of tubal ATs. **a** Some lesions showed unusual communicating narrow tubules with columnar cells. **b** Strong expression of GLUT-1 in a subnuclear pattern. **c** Strong expression of calretinin revealed a mixed growth pattern with the retiform pattern being well appreciated at the periphery of the tumor (tubal epithelium at *upper left*). **d** Strong luminal D2-40 expression highlighting the retiform pattern

the epididymis (Fig. 3d) as well as lymphocytes (Fig. 3f) invariably revealed intense nuclear positivity for PAX-8. The proliferative index (Ki-67) of the tumor cells was invariably ≤10%.

Discussion

Given their relative rarity, ATs have been mainly described in single case reports and small case series with only two recently published larger studies [20, 21]. Most ATs represent incidental findings in resection specimens for unrelated diseases. Rare ATs of the female genital tract have been associated with tubal pregnancy and menorrhagia and one lesion presented in endometrial curettage specimen [22–24]. Tiltman found uterine and tubal ATs in 1% and 0.3% of 1,000 thoroughly examined hysterectomy specimens, respectively [25]. Given that more than 7,000 hysterectomy specimens were examined at our departments during the same study period, one would expect some ~70 uterine lesions for this study. However, only 21 uterine ATs have been diagnosed at our departments during the 10-year period. Thus, we strongly suspect that ATs are significantly under-diagnosed, probably due to lacking familiarity with these uncommon tumors and their usually bland histology. The majority of ATs occur as small solitary lesions, but some may present as large tumors [12] and up to 10–20% of the uterine ATs were reportedly multifocal [25, 26]. On the other hand, most of ATs of the male genital tract (~90%) present as clinical masses that prompt surgical intervention. Accordingly, pathologists are increasingly confronted with these lesions at the time of frozen section. Thus, awareness of their wide morphological spectrum and their site-specific differential diagnoses is essential for proper diagnosis and to avoid over-treatment of these invariably benign lesions.

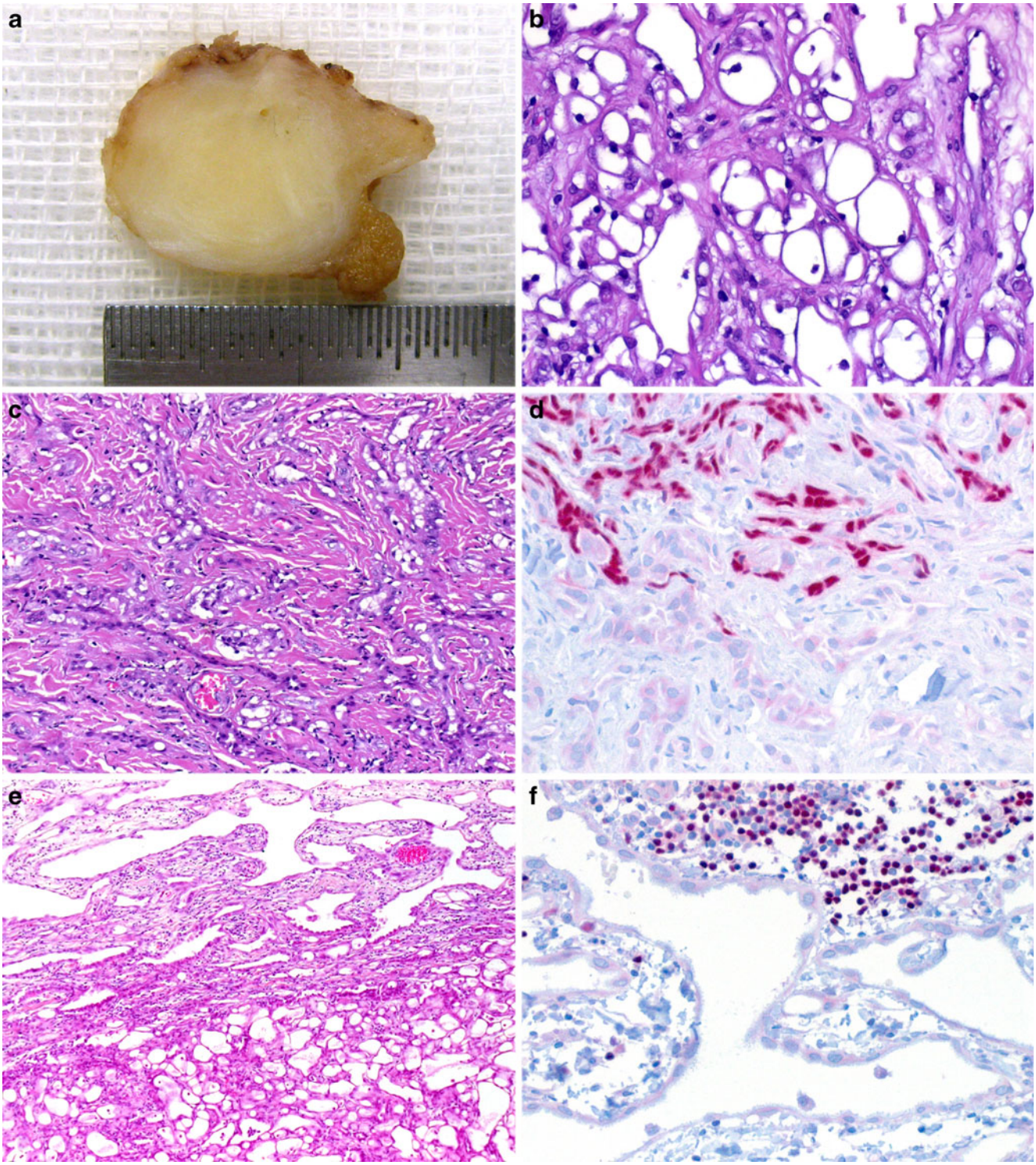

Fig. 3 Pathological features of ATs in the male genital tract. **a** Grossly, testicular ATs were well circumscribed with a tan-yellow non-whorled cut-surface. **b** Crowded microcystic/trabecular pattern was seen in the center of most lesions. **c** A retiform pattern with prominent fibrous stroma. **d** Prominent nuclear expression of PAX8 in the rete testis system (*upper*) but not in the tumor (*lower*). **e** Some ATs showed abrupt transition from microcystic (*lower*) to a dilated retiform (*upper*) pattern. **f** Absent PAX8 in the dilated retiform component confirmed tumor tissue and excluded dilated rete testis (note nuclear PAX8 expression in peripheral lymphoid aggregates)

Although no detailed follow-up data were available for most of our patients (probably due to the benign nature of the disease), there were no recorded histologically verified disease recurrences at the hospitals where the patients have been initially operated. This is consistent with the reported uniformly benign course of ATs.

In this study, we addressed the site-specific morphological diversity of ATs. All but one of the uterine tumors showed, at least focally, a microcystic pattern, occasionally admixed with trabecular growth. Only a single uterine case showed a uniformly trabecular pattern. On the other hand, a prominent retiform pattern was seen in the majority of ATs of the male genital tract and in tubo-ovarian tumors but was absent in the uterine tumors. The cause of this site-dependant diversity might be the result of local stromal environment (presence of smooth muscle bundles in the uterus and absence of this in the epididymis, testis, ovary, and Fallopian tube) or the consequence of site-dependant different proliferative dynamics of the lesional cells. Interestingly, some of the previously reported ATs showed hybrid features of benign papillary mesothelioma or multilocular peritoneal inclusion cysts/multicystic mesothelioma in addition to a typical AT component [27–29]. Chan suggested that this phenomenon might indicate lesions of the same process and that differences of their architecture may result from either intramural versus superficial localization of the lesion [29].

The site-dependant different growth patterns of ATs lead to differential diagnostic considerations embracing a wide and heterogeneous group of benign and malignant conditions including in particular leiomyoma, malignant mesothelioma, and adenocarcinoma. Some paucicellular microcystic uterine lesions were predominated by smooth muscle and can easily be mistaken for leiomyoma [30], a fact probably leading to under-diagnosis of small ATs in hysterectomy specimens. Some authors have suggested the term *leiomyo-adenomatoid tumor* for this variant [31]. However, the smooth muscle component in these lesions obviously represents hyperplastic original smooth muscle tissue of the myometrium as evidenced by entrapment of small nerve fibers within the muscle. One may argue that the architectural similarity of *leiomyo-adenomatoid tumor* to the common endometrioid adenomyoma might suggest *mesothelial adenomyoma* as an alternative term. However, we recommend using the well-established diagnostic term *adenomatoid tumor* until further studies are done to clarify the histogenesis and possible differences, if any, between *leiomyo-adenomatoid tumor* and conventional ATs.

Compared to malignant mesothelioma, ATs usually represent small lesions and they exhibit bland nuclei and a circumscribed growth pattern [14]. Nevertheless, AT may occasionally show a diffuse growth within the involved organ [25] associated with adjacent peritoneal surface involvement, raising concern about extension from malignant peritoneal mesothelioma. Furthermore, malignant mesothelioma may contain bland looking AT-like areas. These observations underline the need for cautious interpretation, particularly in larger lesions and in lesions with surface involvement. It is noteworthy that two cases of malignant mesothelioma extending into the testis and ovary have been initially misdiagnosed as ATs at our departments. Importantly, these two cases revealed at least focally a papillary pattern, a feature not seen in any of the ATs of the genital tract in our cohort. Mesothelial markers are not useful in differentiating malignant mesothelioma and ATs. In this study, we investigated for the first time expression of PAX8 in ATs. The results showed uniform absence of PAX8 similar to a previous study on malignant mesothelioma. Thus, the value of PAX8 is limited to distinguishing AT and malignant mesothelioma from serous carcinoma that they may closely mimic [32]. The strong nuclear expression of PAX8 in the epididymal ducts and the rete testis/ovarii was very helpful in highlighting the lesional cells and separating them from hyperplastic rete testis/ovarii that can be intimately intermixed with or mimic AT [21]. Another new finding in this study is the systematic study of GLUT-1 expression in ATs. We detected a weak to moderate cytoplasmic reactivity for GLUT-1 in 71% of ATs. However, a strong linear membranous staining compared to that reported in malignant mesothelioma [33] was not detected, indicating a potential value of this marker in distinguishing AT from malignant mesothelioma, but more studies that analyze in particular AT-like areas in malignant mesothelioma are needed to definitely clarify this issue. Interestingly, GLUT-1 expression was completely absent in the microcystic component of ATs. The tumor cells of the ATs in our study invariably showed a proliferative index of ≤10%. A previous study reported a mean Ki-67 labeling index of 24.6% (range, 1–66%) in malignant mesothelioma compared to a value of 6.2% (range, 0–25%) for benign reactive mesothelial lesions [34]. These overlapping findings in malignant mesothelioma and benign mesothelial lesions indicate a limited sensitivity and specificity of this parameter as a distinguishing feature between the two entities.

ATs with trabecular or microcystic/trabecular pattern can be confused with infiltrating adenocarcinoma, particularly at the time of frozen section [8]. However, adenocarcinoma usually displays frankly malignant cytological and architectural features and lacks the diffuse expression of mesothelial markers seen in ATs.

Other rare differential diagnostic considerations include epithelioid hemangioendothelioma [16], lymphangioma [35], multilocular peritoneal inclusion cyst/multicystic mesothelioma, benign papillary mesothelioma, yolk sac tumor [36], “ovarian tumor of probable wolffian origin” [37], Sertoli cell tumor, and sclerosing lipogranuloma [38]. Detection of typical growth patterns of ATs and adjunct

immunohistochemical studies using endothelial and mesothelial markers are helpful in excluding epithelioid vascular tumors. Previous studies showed limited specificity of CD34 as an endothelial cell marker as it also labels fibroblasts, some vascular smooth muscle cells, and various mesenchymal tumors [39]. On the other hand, factor VIII related antigen is greatly limited by common background staining and a lower sensitivity. CD31 was considered most useful for detection of endothelial differentiation in routinely fixed tissues, but it also may react with platelets, megakaryocytes, and histiocytes [39]. Care should be taken not to interpret a positive D2-40 staining in AT as indicative of lymphatic endothelial differentiation [35].

Cystic ATs can be mistaken for multilocular peritoneal inclusion cysts. However, the latter is located on the serosal surface and does not represent a solid circumscribed mass [37]. Benign papillary mesothelioma usually presents as small polypoid peritoneal lesions that lack other features of AT.

While the architectural pattern of yolk sac tumors may closely mimic AT, they usually exhibit other varied but more typical diagnostic patterns and their primitive appearing nuclei contrast to the bland nuclei of ATs [37]. The tubules of Sertoli cell tumors are lined by large columnar cells with abundant pale cytoplasm. Sclerosing lipogranuloma may occasionally mimic the morphology of AT with small spaces lined by flattened macrophages but typically reveals foreign body giant cells and dense fibrosis [38]. In the case of "ovarian tumors of probable wolffian origin", the adenomatoid-like foci usually are small, and other more typical areas of these tumors are present [37]. Additionally, rare and potentially misleading variants of ATs have been reported. Phillips et al described an oxyphilic AT presenting as an ovarian tumor and discussed differential diagnoses of this challenging variant [40]. Curiously, a recent report described a skin adnexal tumor with AT-like morphology that lacked immunohistochemical evidence of mesothelial differentiation [41].

In summary, we reviewed the clinicopathological features of a large series of ATs from the female and male genital tract emphasizing their site-dependant morphological diversity, weak to absent sex steroid hormone expression, varied GLUT-1 reactivity, and complete lack of PAX8 positivity. Our findings stress the wide site-dependant differential diagnostic spectrum of ATs.

Conflict of interest statement We declare that we have no conflict of interest.

References

1. Sakaguchi Y (1916) Über das Adenomyom des Nebenhodens Ztschr. Path 18:379–387
2. Masson P, Riopelle JL, Simard LC (1942) Le mésothéliome bénin de la sphere génitale. Rev can biol 1:720–751
3. Evans N (1943) Mesotheliomas of the uterine and tubal serosa and the tunica vaginalis testis: report of four cases. Am J Pathol 19:461–471
4. Golden A, Ash JE (1945) Adenomatoid tumors of the genital tract. Am J Pathol 21:63–79
5. Simpson PR (1990) Adenomatoid tumor of the adrenal gland. Arch Pathol Lab Med 114:725–727
6. Isotalo PA, Veinot JP, Jabi M (2000) Hyperplastic mesothelial cells in mediastinal lymph node sinuses with extranodal lymphatic involvement. Arch Pathol Lab Med 124:609–613
7. Jackson JR (1958) The histogenesis of the adenomatoid tumor of the genital tract. Cancer 11:337–350
8. Isotalo PA, Nascimento AG, Trastek VF, Wold LE, Cheville JC (2003) Extragenital adenomatoid tumor of a mediastinal lymph node. Mayo Clin Proc 78:350–354
9. Benisch BM (1973) A retroperitoneal mesonephric cystadenoma with features of the adenomatoid tumor of the genital tract. J Urol 110:44–46
10. Craig JR, Hart WR (1979) Extragenital adenomatoid tumor: evidence for the mesothelial theory of origin. Cancer 43:1678–1681
11. Glatz K, Wegmann W (2000) Papillary adenomatoid tumour of the adrenal gland. Histopathology 37:376–377
12. Hanada S, Okumura Y, Kaida K (2003) Multicentric adenomatoid tumors involving uterus, ovary, and appendix. J Obstet Gynaecol Res 29:234–238
13. Hayes SJ, Clark P, Mathias R, Formela L, Vickers J, Armstrong GR (2007) Multiple adenomatoid tumours in the liver and peritoneum. J Clin Pathol 60:722–724
14. Kaplan MA, Tazelaar HD, Hayashi T, Schroer KR, Travis WD (1996) Adenomatoid tumors of the pleura. Am J Surg Pathol 20:1219–1223
15. Natarajan S, Luthringer DJ, Fishbein MC (1997) Adenomatoid tumor of the heart: report of a case. Am J Surg Pathol 21:1378–1380
16. Plaza JA, Dominguez F, Suster S (2004) Cystic adenomatoid tumor of the mediastinum. Am J Surg Pathol 28:132–138
17. Lee MJ Jr, Dockerty MB, Thompson GJ, Waugh JM (1950) Benign mesotheliomas (adenomatoid tumors) of the genital tract. Surg Gynecol Obstet 91:221–231
18. Quigley JC, Hart WR (1981) Adenomatoid tumors of the uterus. Am J Clin Pathol 76:627–635
19. Hoffmann M, Yedibela S, Dimmler A, Hohenberger W, Meyer T (2008) Adenomatoid tumor of the adrenal gland mimicking an *Echinococcus* cyst of the liver—a case report. Int J Surg 6:485–487
20. Nogales FF, Isaac MA, Hardisson D, Bosincu L, Palacios J, Ordi J, Mendoza E, Manzarbeitia F, Olivera H, O'Valle F, Krasevic M, Marquez M (2002) Adenomatoid tumors of the uterus: an analysis of 60 cases. Int J Gynecol Pathol 21:34–40
21. Sangoi AR, McKenney JK, Schwartz EJ, Rouse RV, Longacre TA (2009) Adenomatoid tumors of the female and male genital tracts: a clinicopathological and immunohistochemical study of 44 cases. Mod Pathol 22:1228–1235
22. Carlier MT, Dardick I, Lagace AF, Sreeram V (1986) Adenomatoid tumor of uterus: presentation in endometrial curettings. Int J Gynecol Pathol 5:69–74
23. Inoue T, Nabeshima K, Shimao Y, Akiyama Y, Ohtsuka T, Koono M (2001) Tubal ectopic pregnancy associated with an adenomatoid tumor. Pathol Int 51:211–214
24. Honore LH, Korn GW (1976) Coexistance of tubal ectopic pregnancy and adenomatoid tumor. J Reprod Med 17:342–344
25. Tiltman AJ (1980) Adenomatoid tumours of the uterus. Histopathology 4:437–443

26. Huang CC, Chang DY, Chen CK, Chou YY, Huang SC (1995) Adenomatoid tumor of the female genital tract. Int J Gynaecol Obstet 50:275–280
27. Hanrahan JB (1963) A combined papillary mesothelioma and adenomatoid tumor of the omentum; report of a case. Cancer 16:1497–1500
28. Livingston EG, Guis MS, Pearl ML, Stern JL, Brescia RJ (1992) Diffuse adenomatoid tumor of the uterus with a serosal papillary cystic component. Int J Gynecol Pathol 11:288–292
29. Chan JK, Fong MH (1996) Composite multicystic mesothelioma and adenomatoid tumour of the uterus: different morphological manifestations of the same process? Histopathology 29:375–377
30. Wood C, Bouchelle WH (1978) Benign mesothelioma simulating a uterine leiomyoma. Am J Obstet Gynecol 132:225–226
31. Kausch I, Galle J, Buttner H, Bohle A, Jocham D (2002) Leiomyo-adenomatoid tumor of the epididymis. J Urol 168:636
32. Laury AR, Hornick JL, Perets R, Krane JF, Corson J, Drapkin R, Hirsch MS (2010) PAX8 reliably distinguishes ovarian serous tumors from malignant mesothelioma. Am J Surg Pathol 34:627–635
33. Kato Y, Tsuta K, Seki K, Maeshima AM, Watanabe S, Suzuki K, Asamura H, Tsuchiya R, Matsuno Y (2007) Immunohistochemical detection of GLUT-1 can discriminate between reactive mesothelium and malignant mesothelioma. Mod Pathol 20:215–220
34. Taheri ZM, Mehrafza M, Mohammadi F, Khoddami M, Bahadori M, Masjedi MR (2008) The diagnostic value of Ki-67 and repp86 in distinguishing between benign and malignant mesothelial proliferations. Arch Pathol Lab Med 132:694–697
35. Kuroda N, Toi M, Hiroi M, Lee GH (2007) Diagnostic pitfall of D2-40 in adenomatosid tumour. Histopathology 51:719–721
36. Huntington RW Jr, Morgenstern NL, Sargent JA, Giem RN, Richards A, Hanford KC (1963) Germinal tumors exhibiting the endodermal sinus pattern of Teilum in young children. Cancer 16:34–47
37. Young RH, Silva EG, Scully RE (1991) Ovarian and juxtaovarian adenomatoid tumors: a report of six cases. Int J Gynecol Pathol 10:364–371
38. Banks ER, Mills SE (1990) Histiocytoid (epithelioid) hemangioma of the testis. The so-called vascular variant of "adenomatoid tumor". Am J Surg Pathol 14:584–589
39. Miettinen M, Lindenmayer AE, Chaubal A (1994) Endothelial cell markers CD31, CD34, and BNH9 antibody to H- and Y-antigens—evaluation of their specificity and sensitivity in the diagnosis of vascular tumors and comparison with von Willebrand factor. Mod Pathol 7:82–90
40. Phillips V, McCluggage WG, Young RH (2007) Oxyphilic adenomatoid tumor of the ovary: a case report with discussion of the differential diagnosis of ovarian tumors with vacuoles and related spaces. Int J Gynecol Pathol 26:16–20
41. Crippa S, Di Bella C, Faravelli A (2006) Skin adnexal neoplasm closely resembling adenomatoid tumor: a unique occurrence. Int J Surg Pathol 14:177–178

Virchows Arch (2011) 458:603–613
DOI 10.1007/s00428-011-1045-6

ORIGINAL ARTICLE

Altered expression of UPIa, UPIb, UPII, and UPIIIa during urothelial carcinogenesis induced by N-butyl-N-(4-hydroxybutyl)nitrosamine in rats

Daša Zupančič · Zdenka Ovčak · Gaj Vidmar · Rok Romih

Received: 24 October 2010 / Revised: 21 December 2010 / Accepted: 10 January 2011 / Published online: 8 February 2011
© Springer-Verlag 2011

Abstract In normal urothelium, superficial umbrella cells express four major integral membrane proteins, uroplakins UPIa, UPIb, UPII, and UPIIIa, which compose urothelial plaques. In the apical plasma membrane, urothelial plaques form microridges. During neoplastic changes, microridges are replaced by microvilli, while uroplakin expression is retained. We correlated individual uroplakin expression with apical plasma membrane structure, cytokeratin 20 expression, and urothelial cell proliferation (Ki-67). Male Wistar rats were treated with 0.05% N-butyl-N-(4-hydroxybutyl)nitrosamine (BBN) in drinking water, which caused flat hyperplasia with mild dysplasia, low-grade papillary urothelial carcinoma, invasive low- and high-grade papillary urothelial carcinoma and invasive squamous cell carcinoma with extensive keratinization, grade 2. During urothelial carcinogenesis, UPII expression was the most decreased in all urothelial lesions, while UPIa, UPIb, and UPIIIa expression was differently altered in different types of lesions. Superficial cells were covered with microvilli and ropy ridges, while microridges were disappearing. The expression of cytokeratin 20 was decreased and limited to superficial urothelial cells. Proliferation indices were increased, except for invasive squamous cell carcinoma with extensive keratinization. Our results indicate that during urothelial carcinogenesis the expression of UPII is diminished, suggesting that UPIb/UPIIIa heterodimer can still be formed, while heterodimer UPIa/UPII formation is disrupted. Correlation between decreased level of UPII expression and changed apical plasma membrane structure suggests that diminished expression of UPII hinders the urothelial plaque formation.

Keywords Urothelium · Uroplakins · Carcinogenesis · Plasma membrane · CK 20 · Ki-67

Introduction

The epithelium of the urinary bladder, known as urothelium, acts as a constant permeability barrier and protects the blood from toxic urinary substances [1]. The apical surface of normal urothelium is covered by large, highly differentiated, superficial umbrella cells [2]. Umbrella cells elaborate membrane specialization called the urothelial plaque that contribute to functional blood-urine barrier [3, 4]. Urothelial plaques are rigid-looking, concave-shaped biomembrane structures that occupy almost complete urothelial apical surface, interrupted by narrow "hinge" regions [5]. On cross-sections, the plaques (0.3–1 μm in diameter) exhibit outer membrane leaflets twice as thick as the inner ones, hence the name asymmetric unit membrane (AUM) [3]. This unique apical plasma membrane of umbrella cells form microridges observed by scanning electron microscopy [6, 7]. Each microridge corresponds to hinge region encircling one urothelial plaque [8].

Electronic supplementary material The online version of this article (doi:10.1007/s00428-011-1045-6) contains supplementary material, which is available to authorized users.

D. Zupančič (✉) · R. Romih
Institute of Cell Biology, Faculty of Medicine,
Lipičeva 2,
1000 Ljubljana, Slovenia
e-mail: dasa.zupancic@mf.uni-lj.si

Z. Ovčak
Institute of Pathology, Faculty of Medicine,
Korytkova 2,
1000 Ljubljana, Slovenia

G. Vidmar
University Rehabilitation Institute,
Linhartova 51,
1000 Ljubljana, Slovenia

Urothelial plaques consist of two-dimensional, hexagonally packed 16-nm protein particles [5, 9] that contain four major proteins uroplakins UPIa (27 kDa), UPIb (28 kDa), UPII (15 kDa) and UPIIIa (47 kDa) [10, 11]. Among uroplakins, UPIa and UPIb belong to a tetraspanin family of integral membrane proteins [12], while UPII and UPIIIa both have a single transmembrane domain [13, 14]. Within the plaques, these four major uroplakins form two heterodimers consisting of UPIa/UPII and UPIb/UPIIIa, as demonstrated by chemical cross-linking [15] and protein isolation [16]. In addition, transfection experiments showed that when individual uroplakins are expressed in 239 T cells, only UPIb can exit from the endoplasmic reticulum (ER) and move to the plasma membrane, whereas UPII and UPIIIa reach the plasma membrane only when they form heterodimeric complexes with UPIa and UPIb, respectively [17].

The assembly of 16-nm particles and urothelial plaques are interesting and still unresolved issues. Ablation of genes encoding UPII or UPIIIa inhibited the formation of UPIa/UPII and UPIb/UPIIIa pairs, respectively [18, 19]. UPIIIa knockout yielded small plaques and UPII knockout abolished plaque formation, indicating that both uroplakin heterodimers are required for normal plaque formation [19].

The fact that uroplakins are the major differentiation products of urothelium implies that they would be significantly downregulated during urothelial dedifferentiation, transformation, and carcinogenesis. This was proven to be the case in cultured normal urothelial cells and human bladder cancer cell lines [20, 21]. Surprisingly, however, this idea is not supported by data from urothelial carcinomas. For example, Ogawa et al. showed that in N-butyl-N-(4-hydroxybutyl)nitrosamine (BBN)-induced urothelial carcinogenesis of rats, the expression of total uroplakins in superficial cells is decreased but the expression in some intermediate cells is increased [22]. Their results, combined with data of human, mouse, canine, and cow carcinogenesis [22–25], suggest that uroplakin downregulation does not strictly parallel urothelial tumorigenesis and progression. All of the existing studies were limited to the use of antibodies that mainly recognize UPIIIa, i.e., anti-AUM or anti-UPIIIa antibody [22–25].

Besides altered uroplakin expression, bladder carcinogenesis is accompanied by other characteristics, such as: (1) the appearance of microvilli on the urothelial apical surface [26, 27], (2) the disappearance of AUM [28] and microridges [29, 30], (3) altered expression pattern of cytokeratin 20 (CK 20) [31, 32] and (4) increased urothelial cell proliferation, as determined by Ki-67 antigen [33, 34].

In the present study, the expression patterns of individual uroplakin were investigated during urothelial carcinogenesis induced by BBN in rats. Since uroplakins on urothelial apical surface form microridges, we correlated their expression with apical plasma membrane structure. For additional bladder carcinogenesis characterization, CK 20 and Ki-67 expression was evaluated to determine differentiation state and proliferation activity of urothelial cells, respectively.

Materials and methods

Animals and treatment

Eighteen adult male Wistar rats were used in this study in accordance with European guidelines and Slovenian legislation. Rats were divided into six groups by simple random sampling. They were housed in plastic cages at 23±2°C and 50–60% relative humidity. Basal diet was available ad libitum.

The BBN was obtained from Tokyo Chemical Industry Co., Ltd. (Tokyo, Japan) and diluted to 0.05% with tap water. This mixture was then provided as drinking water (ad libitum) for 5 weeks (group BBN 5 weeks), 10 weeks (group BBN 10 weeks), 15 weeks (group BBN 15 weeks) or 20 weeks (groups BBN 20 weeks and BBN 20+15 week). For the BBN 20+15-week group, animals drank tap water for 15 weeks after withdrawal of BBN administration. Control group (C) of animals had tap water available ad libitum (for 5, 10, and 15 weeks, one animal under each condition). At specified time-points, the rats were euthanized by CO_2 inhalation. Urinary bladder of each animal was cut sagittaly into three parts, designated for paraffin embedding, scanning electron microscopy, and western blot analysis.

Paraffin embedding, histological examination, and classification of urothelial lesions

The urinary bladder samples were fixed in 4% paraformaldehyde overnight and embedded in paraffin. All paraffin blocks were cut into serial sections and every tenth section was stained with hematoxylin and eosin and examined by a uropathologist. Histological changes were classified according to WHO classification of tumors of the urinary tract [35].

Immunohistochemical detection of Ki-67, CK 20, UPIa, UPIb, UPII, and UPIIIa

Paraffin sections were deparaffinized and hydrated, the endogenous peroxidase activity was blocked with 3% H_2O_2 in methanol. For detection of Ki-67, UPIa, UPIb, UPII, and UPIIIa sections were microwave heated and for detection of CK 20, they were treated with 0.1% trypsin (Sigma, Taufkirchen, Germany). Non-specific labeling was blocked

by 5% fetal calf serum and 1% bovine serum albumin. Sections were incubated overnight at 4°C with the following primary antibodies: monoclonal anti-Ki-67 (clone MIB-5, Dako, Glostrup, Denmark; diluted 1:50), monoclonal anti-CK 20 (Dako, Glostrup, Denmark; diluted 1:20), polyclonal anti-UPIa (diluted 1:1,000), polyclonal anti-UPIb (diluted 1:2,000), polyclonal anti-UPII (diluted 1:2,000), or monoclonal anti-UPIIIa (diluted 1:20; all four uroplakin antibodies were a kind gift from Prof. T.T. Sun, Department of Dermatology, New York University Medical School, New York, NY 10016). Uroplakin labeling was done on sequential serial sections. For negative controls, the incubation with primary antibody was omitted or the specific primary antibody was replaced by a non-relevant antibody. For secondary antibodies, biotinylated rabbit anti-mouse (Dako, Glostrup, Denmark; diluted 1:100) or swine anti-rabbit immunoglobulins (Dako, Glostrup, Denmark; diluted 1:400) were applied for 1 h at room temperature, followed by ABC/HRP complex (Vector Laboratories, Burlingame, CA) incubation. After the standard DAB (Sigma, Taufkirchen, Germany) development procedure, sections were counterstained with hematoxylin, examined with a Nikon Eclipse TE300 (Nikon Corporation, Tokyo, Japan) and classified by a uropathologist.

To determine optimal dilutions for all anti-uroplakin antibodies, immunohistochemical reactions described above were performed with dilution series for each antibody. Dilutions 1:20, 1:200, 1:1,000, 1:2,000, and 1:20,000 were tested on control normal urothelium and on urothelial carcinomas.

Scanning electron microscopy

The urinary bladder samples were cut transversally into three parts (each with apical area approximately 4 mm^2) and fixed in 4.5% paraformaldehyde and 2% glutaraldehyde for 3 h. The samples were postfixed in osmium tetroxide and critical-point dried. After sputter-coating with gold, they were examined at 15 kV with a Jeol JSM 840 A scanning electron microscope (Jeol Ltd., Tokyo, Japan).

Quantitative analysis

Quantitative analysis was performed on all samples from all animals in each group. Changes of the apical plasma membrane structure were analyzed by scanning electron microscopy. On three bladder samples (each with apical area approximately 4 mm^2) of each animal, the presence of microvilli, ropy ridges, and microridges was evaluated by four-point scale (1=none, 2=weak, 3=moderate, 4=strong presence).

To estimate proliferative activity, cells with a positive immunohistochemical reaction against Ki-67 were used for scoring of proliferation indices. All urothelial cells per tissue section were counted on two paraffin sections per animal and the indices for each tissue section were defined as a percentage ratio of labeled urothelial cells to the total number of counted cells.

To evaluate differentiation state and uroplakin expression in urothelial cells, results of CK 20, UPIa, UPIb, UPII, and UPIIIa staining were evaluated on two paraffin sections per animal. The intensity of staining in superficial, in intermediate and in basal urothelial cells was rated on a four-point scale (1=none, 2=weak, 3=moderate, 4=strong staining) [36].

Statistical analysis

Data from scanning electron microscopy were analyzed using one-way analysis of variance with Scheffe post-hoc comparisons as a compromise between simplicity (since all three bladder samples from each animal were used as independent data because the samples were too small for multilevel modeling) and power (since parametric analysis was chosen despite discrete limited-range data). It should be noted that other multiple comparisons methods, as well as nonparametric analyses, lead to equivalent conclusions. Controls were pooled into a single group because all values were equal between animals.

For Ki-67, proliferation index was compared between the BBN and the control group using exact Mann–Whitney test at each of the three time-points for which the controls were available. Association between lesion severity and proliferation index was tested using exact Kruskal–Wallis test.

For CK 20, the mean of the two sections was calculated for superficial and intermediate cells and analyzed the same way as data from scanning electron microscopy.

Analyses of uroplakins immunohistochemistry data were first performed for each uroplakin separately for superficial and intermediate cells in the same way as for the data from scanning electron microscopy, including using the two sections from each animal as independent and pooling the controls into a single group. Then, the four uroplakins were compared within each stage of tumor evolution using repeated-measures analysis of variance with simple contrasts.

Association of uroplakin expression with proliferation index and CK 20 expression in BBN-treated animals was assessed using Spearman rank-correlation (Rho) taking animal as the unit of analysis, i.e., after calculating the median across sections and sections for each animal.

All statistical analyses were performed using SPSS for Windows 15.0 (SPSS Inc., Chicago, IL, 2007).

Western blot

Urothelial cells were scrubbed from urinary bladders and homogenized in ice-cold buffer (0.8 M Tris-HCl, 7.5%

SDS, 1 mM phenylmethylsulfonyl fluoride). The lysate was centrifuged and the protein concentration in the supernatant was determined by using a BCA™ protein assay kit (Pierce, Rockford, IL). Sample proteins (50 μg/lane) were size fractionated on 12% or 15% SDS-polyacrylamide gels and then transferred to Hybond ECL nitrocellulose membranes (Amersham Biosciences, Buckinghamshire, UK) by electroblotting. After blocking overnight at 4°C in 5% skim milk in PBS-Tween, membranes were incubated for 2 h at room temperature with the polyclonal anti-UPIa (diluted 1:2,000), polyclonal anti-UPIb (diluted 1:3,000), polyclonal anti-UPII (diluted 1:3,000), or monoclonal anti-UPIIIa (diluted 1:1,000). After washing in PBS-Tween, membranes were incubated for 1 h with adequate secondary antibodies horseradish peroxidase-conjugated goat anti-mouse (Dako, Glostrup, Denmark; diluted 1:1,000), or goat anti-rabbit (Sigma, Taufkirchen, Germany; diluted 1:1,000). Membranes were finally probed with enhanced chemoluminescence reagent (ECL; Amersham Biosciences, Buckinghamshire, UK) and exposed to X-ray films. To confirm equal protein loading, the blots were striped with Restore Western Blot Stripping Buffer (Pierce, Rockford, IL) and reprobed with anti-actin antibody (Sigma, Taufkirchen, Germany; diluted 1:2000).

Results

The urothelial apical surface changes after BBN administration

In the control urothelium, scanning electron microscopy showed large polygonal superficial cells, covered with microridges (Fig. 1a). Administration of BBN for 5, 10, and 15 weeks resulted in strong presence of ropy ridges and moderate presence of microvilli, while the presence of microridges was weak (Fig. 1b and Online Resource 1). At 20 weeks of BBN administration, the presence of microvilli and ropy ridges was strong, while the presence of microridges was still weak (Online Resource 1). At 20 weeks of BBN followed by 15 weeks of tap water administration resulted in strong presence of microvilli (Fig. 1c) and moderate presence of ropy ridges, while microridges were not observed (Online Resource 1). In all samples, cells with microvilli and ropy ridges were smaller than those covered with microridges (Fig. 1).

BBN induces various urothelial lesions

In control group of rats, urothelium showed normal histology, consisting of three cell layers (Fig. 2a, 3a–d). Administration of BBN to rats for 5 and 10 weeks resulted in flat hyperplasia accompanied by mild dysplasia in 2/3 animals. In 1/3 animals, low-grade papillary urothelial carcinoma was noted. At 15 weeks of BBN administration, flat hyperplasia with mild dysplasia were observed in 2/3 animals, against a background of low-grade papillary urothelial carcinoma in 3/3 animals. At 20 weeks of BBN administration, low-grade papillary urothelial carcinoma developed in all three animals sacrificed at this time point. At 20 weeks of BBN followed by 15 weeks of tap water administration, low-grade papillary urothelial carcinoma was noted in 1/3 animals. Lamina propria invasion was observed in 1/3 animals with low-grade papillary urothelial carcinoma and in 2/3 animals with high-grade papillary urothelial carcinoma. Furthermore, at this stage, squamous cell carcinoma with extensive keratinization and lamina propria invasion, grade 2 were noted in 2/3 animals. The results are summarized in Table 1 and representative carcinomas are shown in Fig. 2b–c and 3e–p.

BBN increases proliferation indices in urothelium

In control urothelium, Ki-67 positive cells were extremely rare and exclusively limited to the basal cell layer, with proliferation indices below 1% (Online Resource 2A, 3, 4). After BBN administration, substantial elevation of proliferation indices (Online Resource 2B, 2C, 3, 4) was observed, whereby proliferation indices were significantly higher after BBN administration than in the control group ($p<0.001$ at 5, 10, and 15 weeks). Proliferation index was statistically significantly associated with lesion severity ($p<0.001$) in a curvilinear way (Online Resource 4): mean proliferation index (across animals, pooled over sections within each animal) of flat hyperplasia with mild dysplasia was 12.9%, in low-grade papillary urothelial carcinoma it was 20.5%, the highest proliferation index was observed in invasive low- and high-grade papillary urothelial carcinoma (mean 29.7% and 28.7%, respectively), while the mean proliferation index of invasive squamouse cell carcinoma with extensive keratinization, grade 2, was 5.0%. In all urothelial lesions, a Ki-67 reaction positive signal was observed not only in the nuclei of basal cells, but also in the nuclei of intermediate and superficial cells (Online Resource 2B, 2C).

CK 20 expression in urothelial cells decreases after BBN administration

CK 20 positive staining was observed in all superficial urothelial cells of control urothelium, while intermediate and basal cells were completely negative (Fig. 2a). After BBN administration, CK 20 labeling was statistically significantly decreased in superficial cells ($p<0.001$) and kept decreasing until the end of the experiment (Online Resource 5). In intermediate cells, statistically significant

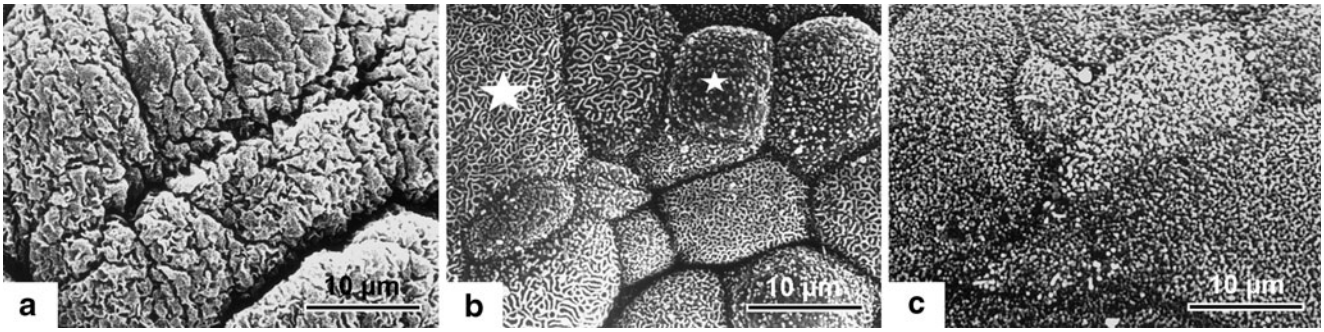

Fig. 1 Scanning electron microscopy. **a** Large polygonal superficial cell covered with microridges in control urothelium. **b** Small superficial cells with ropy ridges (*large star*) and microvili (*small star*) at 10 weeks of BBN administration. **c** Small superficial cells with microvili at 20 weeks of BBN followed by 15 weeks of tap water administration

increase in CK 20 labeling was also observed (p=0.001), but the values rose only at 10 weeks of BBN administration and return to baseline at the end of the experiment (Online Resource 5).

Intensity of staining was statistically significantly associated with lesion severity for superficial (p<0.001) as well as intermediate cells (p=0.020).Flat hyperplasia with mild dysplasia and low-grade papillary urothelial carcinoma exhibited CK 20-positive staining only in some individual superficial urothelial cells and rare intermediate cells (Fig. 2b and Online Resource 5). All three carcinomas with lamina propria invasion showed mainly negative labeling in all cell layers (Fig. 2c and Online Resource 5).

Uroplakins expression is altered after BBN administration

Highest specific staining for each anti-uroplakin antibody was obtained by dilution series. They were 1:1,000 for anti-UPIa, 1:2,000 for anti-UPIb, 1:2,000 for anti-UPII (Online Resource 6) and 1:20 for anti-UPIIIa. These optimal dilutions were further used to estimate expression of individual uroplakin.

The typical pattern for all four individual uroplakins in control rat urothelium was limited to staining of superficial cells (Fig. 3a–d, Table 2, and Online Resource 7). In the flat hyperplasia with mild dysplasia almost all superficial cells showed strong UPIa, UPIb, and UPIIIa staining, while UPII staining was weak to moderate (Fig. 3e–h and Table 2). Considerable staining of UPIa, UPIb, and UPIIIa was also observed in intermediate cells, whereas UPII staining of intermediate cells was weak (Fig. 3e–h and Table 2). Similar pattern of uroplakins staining appeared in low-grade papillary urothelial carcinoma. In superficial cells, UPIa staining was strong, UPIb and UPIIIa staining was moderate and UPII staining was weak or absent (Fig. 3i–l and Table 2). In intermediate cells, UPIa and UPIb staining was moderate, while UPII and UPIIIa staining was weak or negative (Fig. 3i–l and Table 2). All invasive carcinomas showed decreased expression of all uroplakins. In superficial cells of invasive low-grade papillary urothelial carcinoma, UPIa and UPIb staining was weak or absent, whereas staining of UPII and UPIIIa was completely negative (Table 2). In intermediate cells, UPII and UPIIIa staining was com-

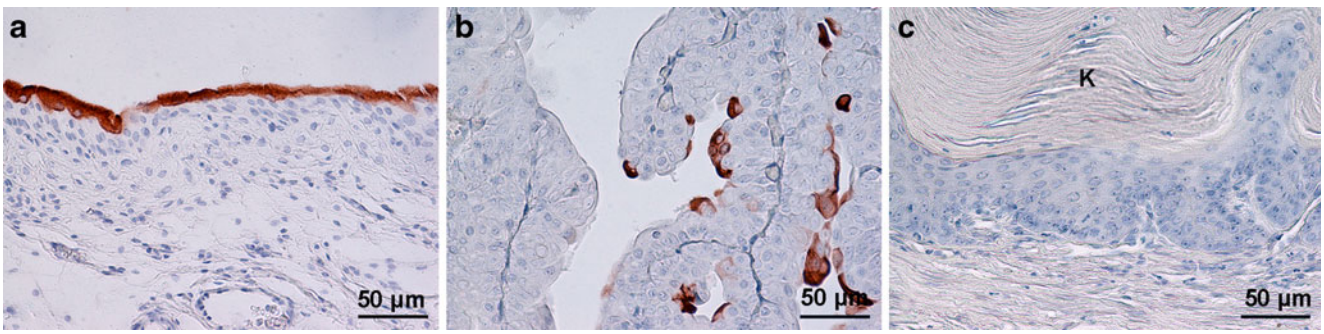

Fig. 2 CK 20 immunohistochemistry. **a** All superficial urothelial cells of control urothelium are CK 20 positive. **b** Some superficial cells are CK 20 positive in the low-grade papillary urothelial carcinoma (at 20 weeks of BBN administration). **c** Negative CK 20 staining of the invasive squamous cell carcinoma with extensive keratinization (*K*), grade 2, (at 20 weeks of BBN followed by 15 weeks of tap water administration)

Table 1 Urothelial lesions during carcinogenesis induced by BBN administration

Weeks of BBN	Urothelial lesion
5	flat hyperplasia with mild dysplasia (2/3)
	papillary urothelial carcinoma, low grade (pTa) (1/3)
10	flat hyperplasia with mild dysplasia (2/3)
	papillary urothelial carcinoma, low grade (pTa) (1/3)
15	flat hyperplasia with mild dysplasia (2/3)
	papillary urothelial carcinoma, low grade (pTa) (3/3)
20	papillary urothelial carcinoma, low grade (pTa) (3/3)
20 + 15	papillary urothelial carcinoma, low grade (pTa) (1/3)
	papillary urothelial carcinoma, low grade, with lamina propria invasion (pT1) (1/3)
	papillary urothelial carcinoma, high grade, with lamina propria invasion (pT1) (2/3)
	squamous cell carcinoma with extensive keratinization, grade 2, with lamina propria invasion (pT1) (2/3)

Darker shading indicates more severe lesions

pletely negative, while UPIa and UPIb staining was weak in some intermediate cells (Table 2). In BBN-induced invasive high-grade papillary urothelial carcinoma, some superficial cells were stained with anti-UPIa and anti-UPIb antibody, rare superficial cells were stained with anti-UPIIIa antibody, while UPII staining was negative (Fig. 3m–p and Table 2). Rare intermediate cells of invasive high-grade papillary urothelial carcinoma were UPIa and UPIb positive, while UPII and UPIIIa staining was negative (Fig. 3m–p and Table 2). In invasive squamous cell carcinoma with extensive keratinization, grade 2, all uroplakins staining was negative in all cells (Table 2).

Statistically significantly differences in immunohistochemistry of all uroplakins between control normal samples and the samples with different duration of BBN administration were observed in superficial and intermediate cells (Online Resource 7). Simultaneously with longer BBN administration, the intensity of staining of all uroplakins was decreased, with UPII staining being the most diminished (Online Resource 7). Results were confirmed by Western blot analysis of urothelial protein samples obtained from control animals and at 5, 10, 15, 20 weeks of BBN administration and at 20 weeks of BBN followed by 15 weeks of tap water administration (Fig. 4). At the same time, staining intensity of all uroplakins was significantly associated with lesion severity for both superficial and intermediate cells (Table 2). In both superficial and intermediate cells, staining of UPII was less intense than that of UPIa, UPIb, and UPIIIa within each lesion type, except within squamous cell carcinoma with extensive keratinization (where there was no staining of any uroplakin) and within invasive high-grade papillary urothelial carcinoma in intermediate cells (Table 2).

Correlations between uroplakins, CK 20, and proliferation indices

Among BBN-treated animals, expression of different uroplakins was highly positively correlated within superficial cells, within intermediate cells and between superficial and intermediate cells. Expression of all uroplakins in superficial and intermediate cells was highly positively correlated with expression of CK 20 in superficial cells, while there could be no association with CK 20 expression in intermediate cells since the median value of the later was 1 (i.e., no expression) in all animals. Expression of all uroplakins in superficial and intermediate cells tended to be negatively correlated with Ki-67 proliferation index, though not statistically significantly. There was also a weak negative association between Ki-67 proliferation index and CK 20 expression in superficial cells. The correlations are summarized in Online Resource 8.

Discussion

In our study, we demonstrate alterations in individual uroplakin expression during carcinogenesis in rat bladder urothelium. BBN-induced carcinogenesis model was used as it mimics the morphological, biological, and molecular features of human bladder cancer [37–40]. Flat hyperplasia with mild dysplasia and low-grade papillary urothelial carcinomas develop at 5, 10, and 15 weeks of BBN administration. At 20 weeks, low-grade papillary urothelial carcinomas occur in all animals. Invasive tumors appear at 20 weeks of BBN followed by 15 weeks tap water administration and they are either low- or high-grade papillary urothelial carcinomas or squamous cell carcinoma with extensive keratinization. Taking together, prevailing

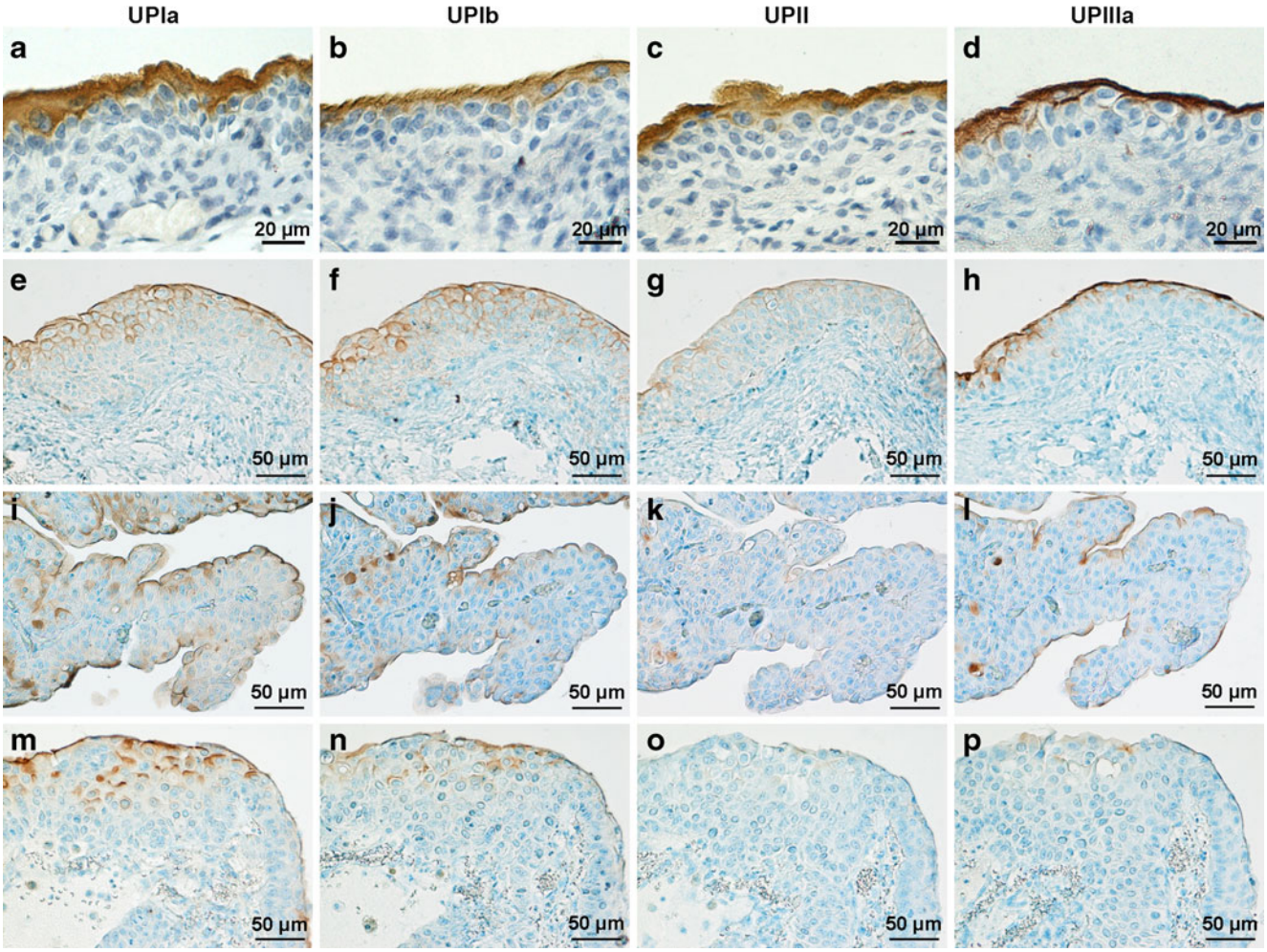

Fig. 3 Uroplakins immunohistochemistry on sequential serial sections of normal control urothelium (**a**–**d**), of flat hyperplasia with mild dysplasia (5 weeks of BBN administration) (**e**–**h**), of low-grade papillary urothelial carcinoma (20 weeks of BBN administration) (**i**–**l**) and of invasive high-grade papillary urothelial carcinoma (20 weeks of BBN followed by 15 weeks of tap water administration) (**m**–**p**). In normal control urothelium, UPIa (**a**), UPIb (**b**), UPII (**c**), and UPIIIa (**d**) staining of all superficial cells is strong. In flat hyperplasia with mild dysplasia, UPIa (**e**), UPIb (**f**), and UPIIIa (**h**) staining of almost all superficial cells and some intermediate cells is strong, while UPII (**g**) staining is weak. In low-grade papillary urothelial carcinoma, UPIa (**i**) staining is strong to moderate in superficial cells and moderate in some intermediate cells. UPIb (**j**) and UPIIIa (**l**) staining is moderate in some superficial cells and weak to moderate in some intermediate cells; UPII (**k**) staining is weak or negative in superficial and intermediate cells. In invasive high-grade papillary urothelial carcinoma, some superficial and intermediate cells are UPIa (**m**) and UPIb (**n**) positive; rare superficial and none intermediate cells are UPIIIa (**p**) positive; UPII (**o**) staining is completely negative

types of cancers are papillary carcinomas and invasiveness appears at the end of the experiment, which is consistent with previously published data.

Since identification of uroplakins as the major differentiation products of normal urothelium [11], several studies have been made to determine whether these proteins are expressed in urothelial carcinomas [22–25]. Most of the published studies have evaluated the expression of total uroplakins [22, 23, 25]. Our findings suggest that during progression from hyperplasia to invasive carcinomas, UPII is the most diminished of all uroplakins in superficial urothelial cells and the least present in intermediate urothelial cells. UPII is the only uroplakin synthesized as a precursor (pro-UPII), which presumably undergo furin-mediated removal of the prosequence before oligomerization of heterotetramers (UPIa/UPII and UPIb/UPIII) and formation of 16-nm protein particles could occur [41]. The lack of mature UPII in BBN-induced urothelial lesions can hamper the assembly of urothelial plaques. This is consistent with the fact that after BBN administration, microridges are almost completely replaced by microvilli and ropy ridges. Similarly, in UPII knockout mouse urothelial plaque formation is completely abolished and apical surface is smooth [19]. Moreover, cultured urothelial cells, which fail to form properly glycosylated pro-UPII, are unable to assemble uroplakins into particles and plaques

Table 2 Statistics for uroplakins immunohistochemistry data by lesion severity

Mean (range)	UP	Normal control urothelium (C)	Flat hyperplasia with mild dysplasia (f)	Papillary urothelial carcinoma, low-grade q(p)	Papillary urothelial carcinoma, low grade, with lamina propria invasion (l)	Papillary urothelial carcinoma, high grade, with lamina propria invasion (h)	Squamous cell carcinoma with extensive keratinization, grade 2, with lamina propria invasion (e)	*P* for difference between groups	Homogeneous subsets
Superficial cells	UPIa	3.9 (3–4)	3.7 (2–4)	3.2 (1–4)	1.5 (1–2)	1.3 (1–3)	1.0 (1–1)	<0.001	e, h, l < p, f < C
	UPIb	3.7 (3–4)	3.0 (2–4)	2.7 (1–4)	1.6 (1–3)	1.3 (1–3)	1.0 (1–1)	<0.001	e, h, l < p, f < C
	UPII	3.9 (3–4)	2.2 (1–3)	1.7 (1–3)	1.0 (1–1)	1.0 (1–1)	1.0 (1–1)	<0.001	e, h, l < p, f < C
	UPIII	3.9 (3–4)	3.0 (1–4)	2.4 (1–4)	1.0 (1–1)	1.1 (1–2)	1.0 (1–1)	<0.001	e, l, h < p < f < C
P for difference between UPs		0.703	<0.001	<0.001	0.003	0.064	NA		
Homogenous subsets		all UPs equal	II < III, Ib < Ia	II < III < Ib < Ia	II, III < Ia, Ib	II, III < Ia, Ib	all UPs equal		
Intermediate cells	UPIa	1.3 (1–2)	2.8 (1–4)	2.6 (1–4)	1.0 (1–1)	1.1 (1–2)	1.0 (1–1)	<0.001	e, l, h, C < p, f
	UPIb	1.2 (1–2)	2.2 (1–3)	2.1 (1–3)	1.3 (1–2)	1.1 (1–2)	1.0 (1–1)	<0.001	e, h, C, l < p, f
	UPII	1.2 (1–2)	1.6 (1–2)	1.2 (1–2)	1.0 (1–1)	1.0 (1–1)	1.0 (1–1)	<0.001	e, h, l, p, C < f
	UPIII	1.2 (1–2)	1.9 (1–3)	1.6 (1–3)	1.0 (1–1)	1.0 (1–1)	1.0 (1–1)	<0.001	e, h, l < C < p, f
P for difference between UPs		0.144	<0.001	<0.001	0.020	0.400	NA		
Homogenous subsets		all UPs equal	II < III < Ib < Ia	II < III < Ib < Ia	Ia, II, III < Ib	all UPs equal	all UPs equal		

Post-hoc comparisons are summarized using homogeneous subsets, which are separated by the < (less than) symbol, whereby ordering within homogeneous subsets corresponds to observed means across groups

NA not applicable

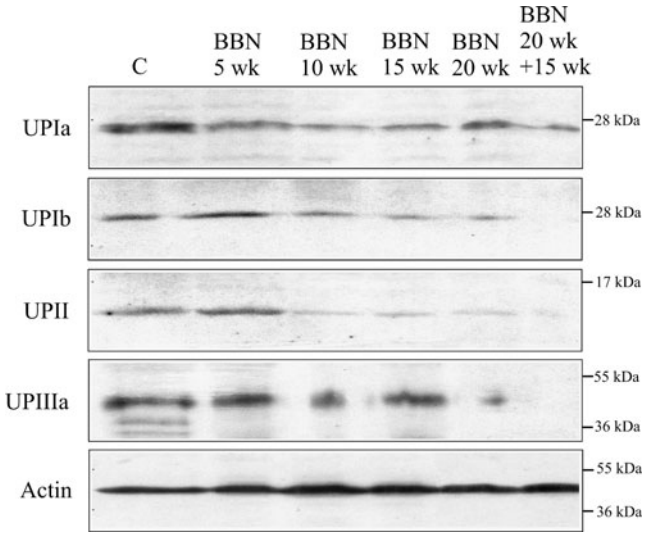

Fig. 4 Western blot analysis of UPIa, UPIb, UPII, UPIIIa, and actin in control normal urothelium and at 5, 10, 15, 20 weeks of BBN administration and at 20 weeks of BBN followed by 15 weeks of tap water administration. *Bands* correspond to expected molecular weights (27, 28, 15, 47, and 43 kDa for UPIa, UPIb, UPII, UPIIIa, and actin, respectively), that confirm specificity of used antibodies. All four uroplakins are detected in control normal urothelium. After BBN administration, the intensity of all bands decrease, with UPII bands being the most diminished. Western blot experiments were performed twice with similar results. Molecular weight standards are shown on the *right*

[41] and do not exhibit microridges [42–44]. Furthermore, expression of CK 20 is also decreased. As both, microridges and CK20 are markers of terminally differentiated umbrella cells [7, 45], negative CK 20 staining and the appearance of microvilli and ropy ridges indicate low differentiation state of superficial urothelial cells in urothelial lesions. Ki-67 immunohistochemistry show that proliferation indices are increasing, except for invasive squamous cell carcinoma with extensive keratinization, which is similar as in human bladder carcinogenesis [46–48]. These data show that BBN-induced carcinogenesis is accompanied by increased proliferation and altered differentiation of urothelial cells. Furthermore, decreased expression of UPII during urothelial carcinogenesis results in diminished urothelial plaque formation and changed apical plasma membrane structure.

In BBN-induced flat hyperplasia with mild dysplasia expression of UPIIIa is similar to that of UPIa and UPIb. This indicates: (1) persistent strong expression of UPIa, UPIb, and UPIIIa in superficial cells; and (2) the appearance of many intermediate cells that express UPIa and UPIb and some of those that express UPIIIa. Changes in expression of UPIIIa, UPIa, and UPIb are in accordance with previously published data obtained by anti-AUM antibody, which reacts strongly with UPIIIa and moderately with UPIa and UPIb [22]. Expression of uroplakins in intermediate cells is in contrast to the fact that uroplakins are synthesized primarily in the umbrella cells of the normal urothelium and may reflect aborted attempts at terminal differentiation during carcinogenesis [22].

In low-grade papillary urothelial carcinomas, the mostly expressed uroplakin in superficial and intermediate cells is UPIa, closely followed by UPIb and UPIIIa. In contrast to UPII-deficient urothelium, where UPIa is entrapped in ER [19], in BBN-induced urothelial carcinogenesis UPIa despite the lack of UPII can reach the urothelial surface (Fig. 3m, o).

In invasive low- and high-grade papillary urothelial carcinomas, the expression of UPIa and UPIb in superficial and intermediate cells is very low, while UPII and UPIIIa are not expressed. It seems that, despite the lack of their partners, UPIa and UPIb can reach the urothelial surface (Fig. 3m, n). This is not unexpected for UPIb, as it is the only uroplakin that, when expressed alone in 293 T cells, can exit from the ER to reach the cell surface [17]. Similar to noninvasive low-grade papillary urothelial carcinomas, UPIa immunohistochemistry again indicates that UPIa could reach the urothelial surface without its partner UPII. These data indicate that the assembly of uroplakins and their transport to apical plasma membrane is altered in cancer urothelial cells.

Invasive squamous cell carcinoma with extensive keratinization exhibits no uroplakin expression. This is not surprising as squamous cell carcinomas closely resemble epidermal keratinocytes both in morphology and in protein expression profiles [49, 50]. Obviously, the neoplastic transformation of the urothelium leading to squamous cell carcinoma is so severe that uroplakin expression is completely lost.

An important finding of this study is that during urothelial carcinogenesis UPII expression is the most diminished in all urothelial lesions, while the expression of UPIa, UPIb, and UPIIIa is differently altered in different types of lesions. We assume that decreased level of UPII expression hinders the urothelial plaque formation and therefore changes apical plasma membrane structure. While BBN model of urothelial carcinogenesis has morphological, biological, and molecular parallels to human bladder cancer, our results about individual uroplakin expression and apical plasma membrane structure could be valuable for further human bladder cancer research.

Acknowledgment We are grateful to Prof. T.T. Sun for careful reading of the manuscript and valuable suggestions. We thank Nada Pavlica, Sabina Železnik, Sanja Čabraja, and Linda Štrus for their technical assistance. This study was supported by a grand from Ministry of Higher Education, Science and Technology, Republic of Slovenia (P3-0108).

Conflict of interests The authors declare that they have no conflict of interest.

References

1. Negrete HO, Lavelle JP, Berg J, Lewis SA, Zeidel ML (1996) Permeability properties of the intact mammalian bladder epithelium. Am J Physiol 271:F886–F894
2. Staehelin LA, Chlapowski FJ, Bonneville MA (1972) Lumenal plasma membrane of the urinary bladder. I. Three-dimensional reconstruction from freeze-etch images. J Cell Biol 53:73–91
3. Koss LG (1969) The asymmetric unit membranes of the epithelium of the urinary bladder of the rat. An electron microscopic study of a mechanism of epithelial maturation and function. Lab Invest 21:154–168
4. Min G, Zhou G, Schapira M, Sun TT, Kong XP (2003) Structural basis of urothelial permeability barrier function as revealed by Cryo-EM studies of the 16 nm uroplakin particle. J Cell Sci 116:4087–4094
5. Kachar B, Liang F, Lins U, Ding M, Wu XR, Stoffler D, Aebi U, Sun TT (1999) Three-dimensional analysis of the 16 nm urothelial plaque particle: luminal surface exposure, preferential head-to-head interaction, and hinge formation. J Mol Biol 285:595–608
6. Romih R, Jezernik K (1996) Reorganization of the urothelial luminal plasma membrane in the cyclophosphamide treated rats. Pflugers Arch Suppl 431:R241–R242
7. Romih R, Veranic P, Jezernik K (2002) Appraisal of differentiation markers in urothelial cells. Appl Immunohistochem Mol Morphol 10:339–343
8. Kreplak L, Wang H, Aebi U, Kong XP (2007) Atomic force microscopy of mammalian urothelial surface. J Mol Biol 374:365–373
9. Hicks RM, Ketterer B (1969) Hexagonal lattice of subunits in the thick luminal membrane of the rat urinary bladder. Nature 224:1304–1305
10. Wu XR, Manabe M, Yu J, Sun TT (1990) Large scale purification and immunolocalisation of bovine uroplakins I, II, and III. Molecular markers of urothelial differentiation. J Biol Chem 265:1775–1784
11. Wu XR, Lin JH, Walz T, Häner M, Yu J, Aebi U, Sun TT (1994) Mammalian uroplakins. A group of highly conserved urothelial differention-related membrane proteins. J Biol Chem 269:13716–13724
12. Yu J, Lin JH, Wu XR, Sun TT (1994) Uroplakins Ia and Ib, two major differention products of bladder epithelium, belong to a family of four transmembrane domain (4TM) proteins. J Cell Biol 125:171–182
13. Wu XR, Sun TT (1993) Molecular cloning of a 47 kDa tissue-specific and differentiation-dependent urothelial cell glycoprotein. J Cell Sci 106:31–43
14. Lin JH, Wu XR, Kreibich G, Sun TT (1994) Precursor sequence, processing, and urothelium specific expression of a major 15-kDa protein subunit of asymmetric unit membrane. J Biol Chem 269:1775–1784
15. Wu XR, Medina JJ, Sun TT (1995) Selective interactions of UPIa and UPIb, two members of the transmembrane 4 superfamily, with distinct single transmembrane-domained proteins in differentiated urothelial cells. J Biol Chem 270:29752–29759
16. Liang FX, Riedel I, Deng FM, Zhou G, Xu C, Wu XR, Kong XP, Moll R, Sun TT (2001) Organisation of uroplakin subunits: transmembrane topology, pair formation and plaque composition. Biochem J 355:13–18
17. Tu L, Sun TT, Kreibich G (2002) Specific heterodimer formation is a prerequisite for uroplakins to exit from the endoplasmic reticulum. Mol Biol Cell 13:4221–4230
18. Hu P, Deng FM, Liang FX, Hu CM, Auerbach A, Shapiro E, Wu XR, Kachar B, Sun TT (2000) Ablation of uroplakin III gene results in small urothelial plaques, urothelial leakage, and vesicoureteral reflux. J Cell Biol 151:961–972
19. Kong XT, Deng FM, Hu P, Liang FX, Zhou G, Auerbach AB, Genieser N, Nelson PK, Robbins ES, Shapiro E, Kachar B, Sun TT (2004) Roles of uroplakins in plaque formation, umbrella cell enlargement, and urinary tract diseases. J Cell Biol 167:1195–1204
20. Sun TT (2006) Altered phenotype of cultured urothelial and other stratified epithelial cells: implications for wound healing. Am J Physiol Ren Physiol 291:F9–F21
21. Kreft ME, Romih R, Kreft M, Jezernik K (2009) Endocytotic activity of bladder superficial urothelial cells is inversely related to their differentiation stage. Differentiation 77:48–59
22. Ogawa K, St John M, Luiza de Oliveira M, Arnold L, Shirai T, Sun TT, Cohen SM (1999) Comparison of uroplakin expression during urothelial carcinogenesis induced by N-butyl-N-(4-hydroxybutyl)nitrosamine in rats and mice. Toxicol Pathol 27:645–651
23. Huang HY, Shariat SF, Sun TT, Lepor H, Shapiro E, Hsieh JT, Ashfaq R, Lotan Y, Wu XR (2007) Persistent uroplakin expressin in advanced urothelial carcinomas: implications in urothelial tumors progression and clinical outcome. Hum Pathol 38:1703–1713
24. Ramos-Vara JA, Miller MA, Boucher M, Roudabush A, Johnson GC (2003) Immunohistochemical detection of uroplakin III, cytokeratin 7, and cytokeratin 20 in canine urothelial tumors. Vet Pathol 40:55–62
25. Ambrosio V, Borzacchiello G, Bruno F, Galati P, Roperto F (2001) Uroplakin expression in the urothelial tumors of cows. Vet Pathol 38:657–660
26. Jacobs JB, Arai M, Cohen SM, Friedell GH (1977) A long-term study of reversibile and progressive urinary bladder cancer lesions in rats fed N-[4-(5-nitro-2-furyl)-2-thiazolyl]formamide. Cancer Res 37:2817–2821
27. Fukushima S, Cohen SM (1980) Saccharin-induced hyperplasia of the rat urinary bladder. Cancer Res 40:734–736
28. Pauli BU, Alroy J, Weinstein RS (1983) The ultrastructure and pathobiology of urinary bladder cancer. In: Bryan GT, Cohen SM (eds) The pathology of bladder cancer, vol 2. CRC Press, Boca Raton, FL, pp 41–140
29. Arai M, Kani T, Sugihara S, Matsumura K, Miyata Y, Shinohara Y, Ito N (1974) Scanning and transmission electron microscopy of changes in the urinary bladder in rats treated with N-butyl-N-(4-hydroxy-butyl)nitrosamine. Gann 65:529–540
30. Jacobs JB, Arai M, Cohen SM, Friedell GH (1976) Early lesions in experimental bladder cancer: scanning electron microscopy of cell surface markers. Cancer Res 36:2512–2517
31. Moll R, Löwe A, Laufer J, Franke WW (1992) Cytokeratin 20 in human carcinomas. Am J Pathol 140:427–447
32. Parker DC, Folpe AL, Bell J, Oliva E, Young RH, Cohen C, Amin MB (2003) Potential utility of uroplakin III, thrombomodulin, high molecular weight cytokeratin, and cytokeratin 20 in noninvasive, invasive, and metastatic urothelial (transitional cell) carcinomas. Am J Surg Pathol 27:1–10
33. Stavropoulos NE, Ioackim-Velogianni E, Hastazeris K, Kitsiou E, Stefanaki S, Agnantis N (1993) Growth fractions in bladder cancer defined by Ki67: association with cancer grade, category and recurrence rate of superficial lesions. Br J Urol 72:736–739
34. Margulis V, Lotan Y, Karakiewicz PI, Fradet Y, Ashfaq R, Capitanio U, Montorsi F, Bastian PJ, Nielsen ME, Müller SC, Rigaud J, Heukamp LC, Netto G, Lerner SP, Sagalowsky AI, Shariat SF (2009) Multi-institutional validation of the predictive value if Ki-67 labeling index in patients with urinary bladder cancer. J Natl Cancer Inst 101:114–119
35. Eble JN, Sauter G, Epstein J, Sesterhenn IA (2004) World Health Organization Classification of Tumours: Tumours of the Urinary System and Male Genital Organs. IARC Press, Lyon, France

36. Zupančič D, Jezernik K, Vidmar G (2008) Effect of melatonin on apoptosis, proliferation and differentiation of urothelial cells after cyclophosphamide treatment. J Pineal Res 44:299–306
37. Ito N (1976) Early changes caused by N-butyl-N-(4-hydroxybutyl) nitrosamine in the bladder epithelium of different animal species. Cancer Res 36:2528–2531
38. Gofrit ON, Birman T, Dinaburg A, Ayesh S, Ohana P, Hochberg A (2006) Chemically induced bladder cancer—a sonographic and morphological description. Urology 68:231–235
39. Kunze E, Schauer A (1977) Morphology classification, and histogenesis of N-butyl-N-(4-hydroxybutyl)nitrosamine in rats. Z Krebsforsch Klin Onkol Cancer Res 88:273–289
40. Ariel I, Ayesh S, Gofrit O, Ayesh B, Abdul-Ghani R, Pizov G, Smith Y, Sidi AA, Birman T, Schneider T, de Groot N, Hochberg A (2004) Gene expression in the bladder carcinoma rat model. Mol Carcinog 41:69–76
41. Hu CC, Liang FX, Zhou G, Tu L, Tang CH, Zhou J, Kreibich G, Sun TT (2005) Assembly of urothelial plaques: tetraspanin function in membrane protein trafficking. Mol Biol Cell 16:3937–3950
42. Surya B, Yu J, Manabe M, Sun TT (1990) Assessing the differentiation state of cultured bovine urothelial cells: elevated synthesis of stratification-related K5 and K6 keratins and persistent expression of uroplakin I. J Cell Sci 97:419–432
43. Kreft ME, Sterle M, Veranic P, Jezernik K (2005) Urothelial injuries and the early wound healing response: tight junctions and urothelial cytodifferentiation. Histochem Cell Biol 123:529–539
44. Kreft ME, Sterle M, Jezernik K (2006) Distribution of junction- and differentiation-related proteins in urothelial cells at the leading edge of primary explant outgrowths. Histochem Cell Biol 125:475–485
45. Veranic P, Romih R, Jezernik K (2004) What determines differentiation of urothelial umbrella cells? Eur J Cell Biol 83:27–34
46. Yin H, Leong AS (2004) Histologic grading of noninvasive papillary urothelial tumors: validation of the 1998 WHO/ISUP system by immunophenotyping and follow-up. Am J Clin Pathol 121:679–687
47. Serio G (1994) PCNA/cyclin expression in transitional cell carcinomas of the human bladder: its correlation with Ki-67 and epidermal growth factor receptor immunostainings. Pathologica 86:161–166
48. Mallofré C, Castillo M, Morente V, Solé M (2003) Immunohistochemical expression of CK20, p53, and Ki-67 as objective markers of urothelial dysplasia. Mod Pathol 16:187–191
49. Friedell GH, Nagy GK, Cohen SM (1983) Pathology of human bladder cancer and related lesions. In: Bryan GT, Cohen SM (eds) The pathology of bladder cancer, vol 2. CRC Press, Boca Raton, FL, pp 11–42
50. Celis JE, Rasmussen HH, Vorum H, Madsen P, Honoré B, Wolf H, Orntoft TF (1996) Bladder squamous cell carcinomas express psoriasin and externalize it to the urine. J Urol 155:2105–2112

Virchows Arch (2011) 458:615–620
DOI 10.1007/s00428-011-1041-x

ORIGINAL ARTICLE

MUC1 expression in thymic epithelial tumors: MUC1 may be useful marker as differential diagnosis between type B3 thymoma and thymic carcinoma

Kyoichi Kaira · Haruyasu Murakami · Masakuni Serizawa · Yasuhiro Koh · Masato Abe · Yasuhisa Ohde · Toshiaki Takahashi · Haruhiko Kondo · Takashi Nakajima · Nobuyuki Yamamoto

Received: 10 October 2010 / Revised: 21 November 2010 / Accepted: 31 December 2010 / Published online: 21 January 2011
© Springer-Verlag 2011

Abstract MUC1 is a transmembrane mucin that has been related to tumor progression and outcome in various malignancies. However, the clinical significance in thymic epithelial tumors remains unknown. We investigated the clinical significance of MUC1 expression in thymic epithelial tumors. Fifty-five patients with thymic epithelial tumors were included in this study. Tumors sections were stained by immunohistochemistry for MUC1, vascular endothelial growth factor (VEGF), microvessel density (MVD) determined by CD34, and p53. MUC1 were expressed in 29%. The expression of MUC1 was significantly correlated with the grade of malignancy in thymic epithelial tumors. MUC1 was closely associated with VEGF, p53 and MVD, and the overexpression of MUC1 was a prognostic marker for predicting poor outcome in univariate analysis. A positive rate of MUC1 expression was 94% (16/17) in thymic carcinomas and 0% (0/5) in type B3 thymomas, demonstrating a significant difference ($p<0.0001$). The expression of MUC1 was closely related to the grade of malignancy in thymic epithelial tumors. A positive expression of MUC1 was significantly associated with poor outcome in this disease. MUC1 may be useful marker for differentiating thymic carcinoma from type B3 thymoma.

Keywords MUC1 · Thymic epithelial tumor · Prognosis · Thymic carcinoma · Type B3 thymoma

K. Kaira (✉) · H. Murakami · M. Serizawa · Y. Koh · M. Abe · Y. Ohde · T. Takahashi · H. Kondo · T. Nakajima · N. Yamamoto
Division of Thoracic Oncology, Shizuoka Cancer Center,
1007 Shimonagakubo Nagaizumi-cho, Sunto-gun,
Shizuoka 411-8777, Japan
e-mail: kkaira1970@yahoo.co.jp

M. Serizawa · Y. Koh
Division of Drug Discovery and Development,
Shizuoka Cancer Center Research Institute,
1007 Shimonagakubo Nagaizumi-cho, Sunto-gun,
Shizuoka 411-8777, Japan

M. Abe · T. Nakajima
Division of Pathology, Shizuoka Cancer Center,
1007 Shimonagakubo Nagaizumi-cho, Sunto-gun,
Shizuoka 411-8777, Japan

Y. Ohde · H. Kondo
Division of Thoracic Surgery, Shizuoka Cancer Center,
1007 Shimonagakubo Nagaizumi-cho, Sunto-gun,
Shizuoka 411-8777, Japan

Introduction

Thymic epithelial tumors are broadly classified into thymoma and thymic carcinoma. Thymic tumors represent 0.2–1.5% of all malignancies; overall, it is an uncommon malignancy with an incidence of 0.15 cases per 100,000 populations [1]. Tumors of the thymus are a heterogenous group of tumors, ranging from relatively benign thymomas to high aggressive carcinomas. The World Health Organization (WHO) published a new histological classification of thymic epithelial tumors into three subgroups: low-risk thymomas (types A, AB, and B1), high-risk thymomas (types B2 and B3), and thymic carcinomas [2, 3]. Complete surgical resection of the tumor offers the best chance of a favorable outcome in patients with thymic epithelial tumor. However, thymic carcinomas, and less frequently, thymo-

mas display an aggressive behavior requiring systemic chemotherapy. Development of new agents and identification of biomarker are important in thymic malignancies but are hampered by the rarity of this disease.

MUC1 is a transmembrane mucin consisting of a heavily *O*-glycosylated excellilar domain, a transmembrane domain and a cytoplasmic tail of 72 amino acids [4]. Recent reports described that MUC1 oncoprotein is aberrantly expressed at high levels in most human neoplasms, and MUC1 plays important roles in development and progression of malignant tumors [5–7]. Moreover, MUC1 has emerged as a target molecule in immunotherapy for various cancers. As the mechanism of a target for cancer treatment, unmasked epitopes of MUC1 core protein expressed on tumor cells have been described to be able to elicit a strong antitumor immunity [7]. The overexpression of MUC1 has been also reported to be closely associated with poor outcome in various malignant tumors [6, 8]. However, the precise expression profiles of MUC1 have not been yet determinate in thymic tumor cell.

To elucidate the role of MUC1 expression in thymic epithelial tumors, we conducted an immunohistochemical examination of MUC1in primary site. In addition, these markers were correlated with vascular endothelial growth factor (VEGF), microvessel density (MVD), and cell cycle control (p53). In vitro studies were also performed to investigate the expression of MUC1 expression in thymic epithelial tumors.

Material and methods

Patients

Between October 2002 and February 2010, 63 consecutive patients with thymic epithelial tumors were analyzed in the study. Of these patients, eight patients were excluded for further studies because the tissue specimens were not available. Thus, a total of 55 patients (27 men, 28 women) were eligible in the study. The study protocol was approved by the institutional review board.

The age of the patients ranged from 29 to 80 years (median age, 61 years). Thirty-eight of the 55 patients underwent surgical resection, and the remaining 17 underwent only percutaneous needle-core biopsy. All tumors were staged according to Masaoka's classification [9]. In patients with surgical excision, the stage was determined by operative and pathological findings. In patients with biopsy only, the stage was determined by diagnostic imaging including computed tomography and 2-[^{18}F]-fluoro-2-deoxy-D-glucose positron emission tomography (^{18}F-FDG PET). All surgical specimens were reviewed and classified according to the WHO classification [2, 3] by an experienced lung pathologist (T. N) who was unaware of clinical or imaging findings. According to Masaoka classification, 14 were in stage I, 15 in stage II, 9 in stage III, and 17 in stage IV (7 in stage IVa and 10 in stage IVb). For patients without surgery, the histological classification was determined by specimens obtained through needle-core biopsy. As the initial treatment, 37 patients were treated with surgery, 14 chemotherapy and 4 thoracic irradiation. The tumor size of primary tumors ranged from 15 to 140 mm (median, 63 mm). All tumors were regrouped into three subgroups: low-risk thymomas (types A, AB, and B1), high-risk thymomas (types B2 and B3), and thymic carcinomas. According to the WHO classification, the tumors included 27 low-risk thymomas (5 type A, 17 type AB, and 5 type B1), 11 high-risk thymomas (6 type B2 and 5 type B3), and 17 thymic carcinomas. The histological subtype of thymic carcinoma was as follows; eight squamous cell carcinoma, two undifferentiated carcinoma, four large cell carcinoma, one basaloid carcinoma, and two others.

Immunohistochemical staining

Immunohistochemical staining was performed according to the procedure described in the previous reports [10]. The following antibodies were used: a rabbit monoclonal antibody against MUC1 (Ma 552; Novocastra; 1:100 dilution); a monoclonal antibody against VEGF (Immuno-Biological Laboratories Co.,Ltd., Japan, 1:100 dilution); a mouse monoclonal antibody against CD34 (Nichirei, Tokyo, Japan,1:800 dilution); a mouse monoclonal antibody against p53 (D07; DAKO, 1:50 dilution).

The expression of MUC1 was considered if membrane or cytoplasm staining was present. For MUC1, a semi-quantitative scoring method was used: 0=0%, 1=<5%, 2=<10%, 3=10–25%, 4=>25% of cells positive. The tumors in which stained tumor cells made up more than 10% of the tumor were graded as positive.

The expression of VEGF was quantitatively assessed according to the percentage of immunoreactive cells in a total of 1,000 neoplastic cells. The number of CD34-positive vessels was counted in four selected hot spots in a X 400 field (0.26 mm^2 field area). MVD was defined as the mean count of microvessels per 0.26 mm^2 field area [10].

For p53, microscopic examination for the nuclear reaction product was performed and scored. According to previous report [10], p53 expression in more than 10% of tumor cells was defined as high expression. The assessment of MUC1, VEGF, CD34, and p53 was performed in a blinded fashion by at least two of the authors, using a light microscopic. To test interobserver variability, each section was reassessed by the same investigators after completion of the first assessment. The time interval between the first and second assessments was at least 4 weeks. Intraobserver variability was also determined by comparing the values of the first measurements of two investigators.

Statistical analysis

Probability values of <0.05 indicated a statistically significant difference. Fisher's exact test was used to examine the association of two categorical variables. Correlation of different variables was analyzed using the nonparametric Spearman's rank test. The Kaplan–Meier method was used to estimate survival as a function of time, and survival difference were analyzed by the log-rank test. Multivariate analyses were performed using stepwise Cox proportional hazards model to identify independent prognostic factors. Statistical analysis was performed using JMP 8 (SAS, Institute Inc., Cary, NC, USA) for Windows.

Results

Immunohistochemical analysis

Each protein revealed a profile pattern of the unique expression. The immunohistochemical staining of MUC1, VEGF, CD34, and p53 was evaluated for the 55 primary lesions (Fig. 1).

MUC1 was overexpressed in 29% (16/55) of thymic epithelial tumors. A positive rate of MUC1 was recognized in 0% (0/27) of low-risk thymomas, 0% (0/11) of high-risk thymomas, and 94% (16/17) of thymic carcinomas. The histological type of MUC1-negative thymic carcinoma was found in squamous cell carcinoma. According to WHO classification, the mean scoring of MUC1 was 0.14 in low-risk thymomas, 1.0 in high-risk thymomas, and 3.0 in thymic carcinomas, demonstrating a significant difference among the three groups (Fig. 2). Significant correlation was found between the mean scoring of MUC1 (γ=0.8492, p<0.0001) and the risk groups by suggested by the WHO classification, and between the mean scoring of MUC1 (γ=0.8076, p=0.0007) and the grading of Masaoka classification.

The median rate of VEGF positivity was 12% (range, 0–82%), and the value of 12 was chosen as a cutoff point. High expression was recognized in 47% (26/55). The median numbers of CD34 was 26 (range, 8–45), and the values of cutoff point was 26. High expression of CD34 was seen in 45% (25/55). High expression of p53 was recognized in 38% (21/55).

Demographics of patients according to MUC1

The demographic result of the patients according to MUC1 is listed in Table 1. Gender, tumor size, histology, Masaoka staging, VEGF, MVD, and p53 yielded a statistically significant positive correlation.

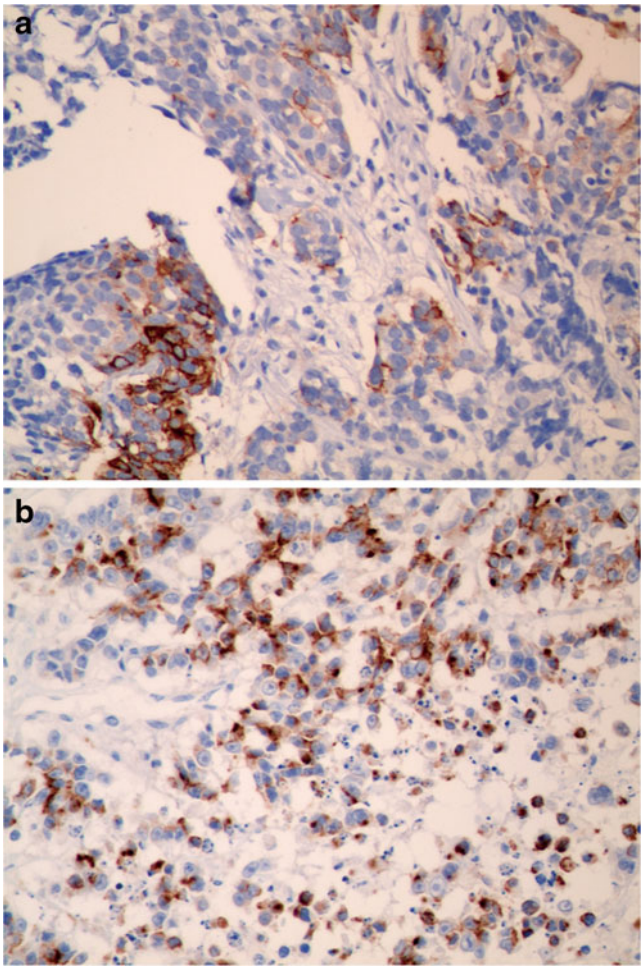

Fig. 1 Immunohistochemical staining of MUC1 in thymic carcinoma. **a** MUC1 in the biopsy specimens obtained throughout core needle biopsy is stained in cytoplasm and membrane (score 3). **b** MUC1 in resected primary site is stained in cytoplasm and membrane (score 3)

Univariate and multivariate survival analysis in thymic epithelial tumors

Median follow-up time for all patients was 34.5 months (range, 8.0–92.0 months). The 5-year survival rate was 70.2%, and the

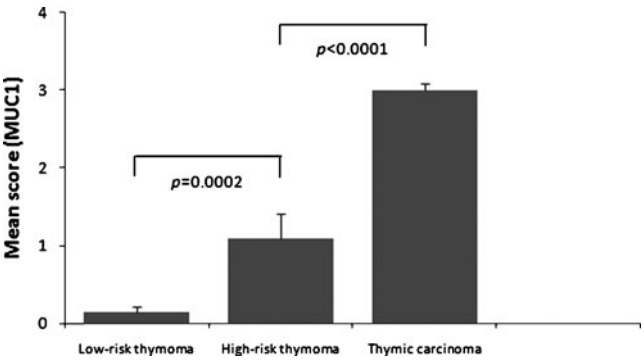

Fig. 2 **a** Mean scoring of MUC1 was 0.14 in low-risk thymomas, 1.00 in high-risk thymomas, and 3.00 in thymic carcinomas, demonstrating significant differences among the three groups

Table 1 Patient's characteristics according to MUC1

Parameter	MUC1		
	Positive (n=16)	Negative (n=39)	p value
Age (≤65/>65 year)	10/6	27/12	0.76
Gender (male/female)	12/4	15/24	0.01
Tumor size (≤63/>63 mm)	3/13	27/12	<0.01
Histology (thymoma/thymic carcinoma)	0/16	38/1	<0.01
Masaoka classification (I–II/III–IV)	0/16	29/10	<0.01
VEGF (positive/negative)	15/1	11/28	<0.01
MVD (CD34) (positive/negative)	11/5	14/25	0.03
*P*53 (positive/negative)	13/3	8/31	<0.01

median survival time was not reached. In thymic epithelial tumors (n=55), the 5-year survival rates of the MUC1-positive and MUC1-negative patients were 28.9 and 94.6 %, respectively, (p<0.0001). Univariate and multivariate analysis of factors, which affected the overall survival, was performed (Table 2;Fig. 3). Univariate analysis demonstrated that a statistically significant difference in the overall survival was observed in tumor size, histology, MUC1, VEGF, MVD, and p53. Multivariate analysis revealed that thymic carcinoma was an independent and significant factor to predict a poor prognosis.

Comparison between type B3 thymoma and thymic carcinoma

The comparison between type B3 thymoma and thymic carcinoma is listed in Table 3. A positive rate of MUC1 expression was 94% (16/17) in thymic carcinomas and 0% (0/5) in type B3 thymomas, demonstrating a significant difference (p<0.0001). No statistically significant difference was observed in the other parameters (Fig. 4) The mean scoring of MUC1 was 1.66 in type B3 thymomas and 3.00 in thymic carcinomas, demonstrating a significant difference (p<0.0001).

Discussion

This is the first study to evaluate the clinicopathological significance of MUC1 expression in thymic epithelial tumors. The expression of MUC1 was significantly associated with the grade of malignancy in thymic epithelial tumors. MUC1 was closely associated with angiogenesis and p53, and the overexpression of MUC1 was a prognostic marker for predicting poor outcome in this disease. Moreover, the expression of MUC1 was significantly higher in thymic carcinoma (94%) than in type B3 thymoma (0%). The results of our series suggest that MUC1 is a useful marker as differential diagnosis between type B3 thymoma and thymic carcinoma.

Recently, several researchers have described that overexpression of MUC1 may be a useful marker of tumor progression and poor outcome in a variety of malignant tumors, including breast, gastric, pancreatic, thyroid, bileduct, gallbladder, ovarian, uterus endometrial, prostate, colorectal, and lung cancers [6, 11–18]. The result of the present study indicated that a positive expression of MUC1 plays an important role on tumor progression and prognosis in thymic epithelial tumors. Kojika et al. have reported an immunohistochemical study using 49 antibodies for differentiating thymic carcinomas from type B3 thymomas [19]. In their study, all of 27 patients with thymomas had a negative MUC1 expression, and 4 (33%) of 12 patients with thymic carcinomas a positive MUC1 expression. They described that MUC1 might be suitable for differentiating thymic carcinomas from type B3 thymomas; however, the low sensitivity of 33% may not be suitable for use in small biopsy specimens. In our series, a negative expression of

Table 2 Univariate and multivariate survival analysis

Parameter	Univariate analysis p value	Multivariate analysis p value
Age (≤65/>65 year)	0.8994	
Gender (male/female)	0.1667	
Tumor size (≤63/>63 mm)	0.0045	0.2782
Histology (thymoma/thymic carcinoma)	<0.0001	0.0294
Masaoka classification (I–II/III–IV)	<0.0001	0.1695
MUC1 (positive/negative)	<0.0001	0.1991
VEGF (positive/negative)	0.0003	0.8497
MVD (CD34) (positive/negative)	0.0032	0.5819
*P*53 (positive/negative)	0.0001	0.7520

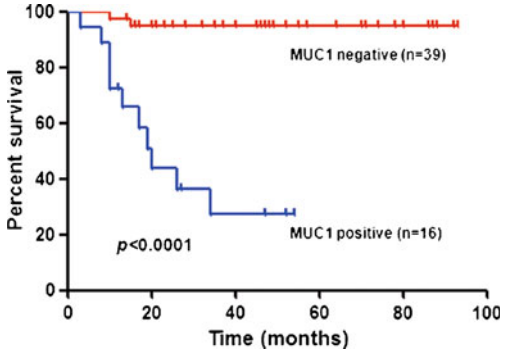

Fig. 3 Overall survival curve of all patients (n=55) according to MUC1

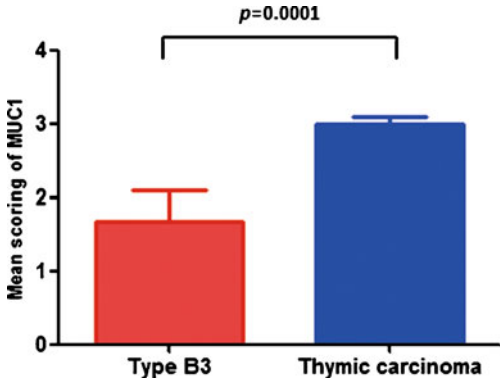

Fig. 4 Mean scoring of MUC1 showing significantly higher in thymic carcinoma than type B3 thymoma (p<0.0001)

MUC1 was also observed in all of 38 patients with thymomas. But 16 (94%) of 17 patients with thymic carcinoma had a positive MUC1 expression. Although Fig. 1a shows the immunohistochemical staining of MUC1 in the biopsy specimens, 13 of 16 patients with a positive MUC1 expression were diagnosed by core needle biopsy. Our results suggest that MUC1 expression could be immunohistochemically investigated in the small biopsy specimens. However, the sensitivity of MUC1 expression in thymic carcinomas was markedly different between our series (94%) and their report (33%). This discrepancy may be due to the difference in the clone of MUC1 antibody or the technique of immunohistochemical staining.

In the present study, overexpression of MUC1 is closely associated with poor outcome in univariate analysis, but multivariate analysis demonstrated that MUC1 expression was not an independent prognostic factor for predicting poor outcome. But, all of 16 patients with a positive MUC expression had histology of thymic carcinoma, and one patient with thymic carcinoma alone had a negative MUC1 expression. The outcome of patients with a positive MUC1 expression was considered to be almost similar to that of thymic carcinoma. Considering the results of our series, MUC1 may be an important marker for predicting poor survival in patients with thymic epithelial tumors.

It is sometimes difficult to make the differential diagnosis between type B3 thymoma and thymic carcinoma, if small biopsy specimens. Glucose transporter 1 (Glut1), carbonic anhydrase IX (CA-IX), c-kit (CD117), CD5, MUC1, CEA, and cytokeratin 18 (CK18) had been described to be significantly higher in the thymic carcinomas than in the type B3 thymomas [19]. Of these biomarkers, Glut1 has been reported to be the best marker for thymic carcinoma because of a highest sensitivity (91%) and specificity. In our series, VEGF, CD34, and p53 were not suitable for differentiating thymic carcinomas from type B3 thymomas. Additionally, our recent report demonstrated that Glut1 is overexpressed in thymic carcinomas as compared to thymomas, but the expression of Glut1 was not significantly higher in thymic carcinoma than in type B3 thymoma [10]. Therefore, Glut1 may be not a best marker for thymic carcinoma. In the present study, the sensitivity of MUC1 expression was 94%, and MUC1 may be useful marker for differentiating thymic carcinoma from type B3 thymoma. However, a large-scale study is warranted to evaluate the usefulness of MUC1 expression in thymic carcinoma.

In unresectable/metastatic thymic epithelial tumors, systemic chemotherapy plays a very important role in the treatment of this disease. Especially, the outcome of inoperable thymic carcinomas remains unsatisfactory. Nowadays, the development of immunotherapy is important as new option for cancer therapy. MUC1 core protein may be a useful target molecule for immunotherapy in breast cancer, lung cancer, and other malignancies expressing MUC1 [20, 21]. Most patients with thymic carcinoma had a

Table 3 Comparison of type B3 thymoma and thymic carcinoma

Parameter	Type B3 thymoma (n=5)	Thymic carcinoma (n=17)	p value
Age (≤65/> 65 year)	4/1	10/7	0.61
Gender (male/female)	2/3	13/5	0.29
Tumor size (≤63/>63 mm)	3/2	13/4	0.58
Masaoka classification (I–II/III–IV)	1/4	0/17	0.22
MUC1 (positive/negative)	0/5	16/1	<0.01
VEGF (positive/negative)	5/0	16/1	1.00
MVD (CD34) (positive/negative)	5/1	12/5	1.00
*P*53 (positive/negative)	4/1	14/3	1.00

positive expression of MUC1; therefore, a MUC1-targeted immunotherapy may be appropriate for thymic carcinomas showing MUC1 expression. In a further study, it is necessary to investigate the relationship between MUC1 expression and the efficacy of a MUC1-targeted immunotherapy in thymic carcinoma.

The present study has several limitations. One of the limitations is that our sample size was small, including a heterogenous group of tumors. Thymic epithelial tumors are rare neoplasms, thus, a larger multicenter cohort study is warranted. Another limitation is that the present study includes specimens obtained though core needle biopsy. However, only patients with an adequate specimen for immunohistochemical examination were included. A further limitation is that the follow-up period was not long enough for thymic epithelial tumors.

In conclusion, a positive expression of MUC1 was significantly associated with poor outcome in thymic epithelial tumors. The expression of MUC1 tended to increase from low-grade to high-grade thymic epithelial tumors. MUC1 may be a useful marker for differentiating thymic carcinoma from type B3 thymoma.

Acknowledgments This work was supported in part by Grant 21790793 (K. K) from the Ministry of Education, Culture, Sports, Science, and Technology, Japan, and National Hospital Organization Policy Based Medical Services.

We thank all the staff of the Department of Pathology in Shizuoka Cancer Center for their technical assistance of immunohistochemical analysis.

Conflicts of interest statement We, all authors, have no financial or personal relationships with other people or organizations that could inappropriately influence our work.

References

1. Engels EA, Pfeiffer RW (2003) Malignant thymoma in the United States: demographic patterns in incidence and associations with subsequent malignancies. Int J Cancer 105:546–551
2. Rosai J, Sobin LH (1999) Histological typing of tumours of the thymus, International histological classification of tumours, 2nd edn. Springer, New York, pp 1–59
3. Travis WD, Brambillia E, Muller-Hermelink HK (2004) WHO classification of tumors. Pathology and genetics of tumors of the lung, pleura, thymus and heart. IARC Press, Lyon
4. Gendler SJ, Lancaster CA, Taylor-Papadimitriou J et al (1990) Molecular cloning and expression of human tumor-associated polymorphic epithelial mucin. J Biol Chem 265:15286–15293
5. Schroeder JA, Masril AA, Adriance MC et al (2004) MUC1 overexpression results in mammary gland tumorigenesis and prolonged alveolar differentiation. Oncogene 23:5739–5747
6. Nagai S, Takenaka K, Sonobe M et al (2006) A novel classification of MUC1 expression is correlated with tumor differentiation and postoperative prognosis in non-small cell lung cancer. J Thorac Oncol 1:46–51
7. Broadbent R, Thynne G, McKenzie IFC (1997) Antibody and T cell responses of patients with adenocarcinoma immunized with mannan-MUC1 fusion protein. J Clin Invest 100:2783–2792
8. Woenckhaus M, Merk J, Stoehr R et al (2008) Prognostic value of FHIT, CTNNB1, and MUC1 expression in non-small cell lung cancer. Hum Pathol 39:126–136
9. Masaoka A, Monden Y, Nakahara K et al (1981) Follow-up study of thymomas with special reference to their clinical stages. Cancer 48:2485–2492
10. Kaira K, Endo M, Abe M et al (2010) Biologic correlation of 2-[^{18}F]-fluoro-2-deoxy-D-glucose uptake on positron emission tomography in thymic epithelial tumors. J Clin Oncol 28:3746–3753
11. Utsunomiya T, Yonezawa S, Sakamoto H et al (1998) Expression of MUC1 and MUC2 mucins in gastric carcinomas: its relationship with the prognosis of the patients. Clin Cancer Res 4:2605–2614
12. Hinoda Y, Ikematsu Y, Horinouchi M et al (2003) Increased expression of MUC1 in advanced pancreatic cancer. J Gastroenterol 38:1162–1166
13. Tamada S, Goto M, Nomoto M et al (2002) Expression of MUC1 and MUC2 mucins in extrahepatic bile duct carcinomas: its relationship with tumor progression and prognosis. Pathol Int 52:713–723
14. Kawamoto T, Shoda J, Miyahara N et al (2004) Expression of MUC1 recognized by a monoclonal antibody MY.1E12 is a useful biomarker for tumor aggressiveness of carcinoma of the gallbladder. Clin Exp Metastasis 21:353–362
15. Feng H, Ghazizadeh M, Konishi H et al (2002) Expression of MUC1 and MUC2 mucin gene products in human ovarian carcinomas. Jpn J Clin Oncol 32:525–529
16. Sivridis E, Giatromanolaki A, Koukourakis MI et al (2002) Patterns of episialin/MUC1 expression in endometrial carcinomas and prognostic relevance. Histopathology 40:92–100
17. Baldus SE, Monig SP, Huxel S et al (2004) MUC1 and nuclear beta-catenin are coexpressed at the invasion front of colorectal carcinomas and are both correlated with tumor prognosis. Clin Cancer Res 10:2790–2796
18. Kirschenbaum A, Itzkowitz SH, Wang JP et al (1999) MUC1 expression in prostate carcinoma: correlation with grade and stage. Mol Urol 3:163–168
19. Kojika M, Ishii G, Yoshida J et al (2010) Immunohistochemical differential diagnosis between thymic carcinoma and type B3 thymoma: diagnostic utility of hypoxic marker, GLUT1, in thymic epithelial neoplasms. Modern Pathol 22:1341–1350
20. Kontani K, Taguchi O, Ozaki Y et al (2003) Dendritic cell vaccine immunotherapy of cancer targeting MUC1 mucins. Int J Mol Med 12:493–502
21. Kufe DW (2009) Functional targeting of the MUC1 oncogene in human cancers. Cancer Biol Ther 8:1197–1203

Virchows Arch (2011) 458:621–630
DOI 10.1007/s00428-011-1044-7

ORIGINAL ARTICLE

Stromal expression of vascular endothelial growth factor C is relevant to predict sentinel lymph node status in melanomas

Elena Gallego · Luis Vicioso · Martina Álvarez · Isabel Hierro · Lidia Pérez-Villa · Alfredo Blanes · Alfredo Matilla

Received: 13 September 2010 / Revised: 9 January 2011 / Accepted: 10 January 2011 / Published online: 29 January 2011
© Springer-Verlag 2011

Abstract The dissemination of tumour cells to the lymph nodes is a complex process involving the formation of new lymph vessels, or lymphangiogenesis, produced by the tumour itself. The main growth factor involved in lymphangiogenesis is vascular endothelial growth factor C (VEGF-C), which is secreted by several different malignant tumours, including melanoma. Not only has VEGF-C expression been found in tumour cells, it has also been detected in tumour stromal cells like macrophages and fibroblasts. This study aimed to determine whether the expression of VEGF-C in tumour and stromal cells in cutaneous melanoma determines lymphangiogenesis and neoplastic dissemination to lymph nodes. We examined cases from 50 patients with melanoma who underwent selective biopsy of the sentinel lymph node. Immunohistochemical study was done with D2-40 to label lymph vessels, and the expression of VEGF-C was evaluated in tumour and stromal cells. Lymph vessel density was greater in sentinel lymph node-positive than in sentinel lymph node-negative cases, though the difference was not significant (P=0.075). A significant correlation was seen between lymph vessel density and tumour thickness and the presence of ulceration. The main finding was that the expression of VEGF-C in fibroblasts was highly associated with the presence of metastasis in the sentinel node and with the Clark level. However, VEGF-C expression showed no relation in either tumour cells or macrophages with node status or other prognostic factors, such as the Breslow index or Clark level. Our results highlight the relevance of the stroma in tumour progression in cutaneous melanoma and its role in the spread to lymph nodes.

Keywords Melanoma · Lymphangiogenesis · VEGF-C · Sentinel lymph node · Tumour stroma · Immunohistochemistry

E. Gallego · L. Vicioso (✉) · I. Hierro · L. Pérez-Villa · A. Blanes · A. Matilla
Department of Pathology, Virgen de la Victoria University Hospital, Campus Universitario de Teatinos s/n, 29010, Malaga, Spain
e-mail: vicioso@uma.es

M. Álvarez
Department of Pathology, Faculty of Medicine, Malaga, Spain

Introduction

The regional lymph node status is the most important prognostic factor in patients with melanoma. The state of lymph node involvement can be determined by selective sentinel lymph node biopsy. This node is considered to be the first node in the lymph chain into which lymph from an organ or body region drains. Since 1992, when Morton et al. [1] undertook the first sentinel node study in melanoma patients, this technique has proven of great use for the surgical treatment of these patients, avoiding unnecessary lymphadenectomies with the resulting effect on morbidity.

Tumours induce the formation of new blood vessels from already existing vessels that permit their growth in the primary site by a process known as angiogenesis [2]. These newly formed vessels also seem to play an important role in the production of distant metastasis [3]. In addition, the tumour can also induce the growth of new lymph vessels, a phenomenon called lymphangiogenesis [4].

The clinical importance of tumour lymphangiogenesis has recently been noted [5]. A relation exists between lymph vessel density (LVD) and the presence of lymph

node metastasis in carcinomas of various sites, including the stomach [6], head and neck [7], breast [8], prostate [9] and colon [10]. However, research so far in malignant skin melanoma has provided contradictory findings. Whereas some authors found that lymphangiogenesis in primary melanoma was significantly increased in metastatic melanomas and that it could predict the status of the sentinel node [11–13], others reported that an increase in LVD was related with fewer lymph node metastases and a better prognosis [14, 15].

The vascular endothelial growth factors (VEGFs) comprise a family of five key factors (A, B, C, D and E) involved in the process of vascular growth. Of these, VEGF-C and VEGF-D have been directly implicated in the promotion of lymphangiogenesis, via their binding to the receptor VEGFR-3 that is present in the lymph vessel endothelium [16]. In cutaneous melanoma, VEGF-C expression in tumour cells has been related with the stage of progression [17], and some data suggest that VEGF-C expression in primary skin melanoma may be predictive of lymph node metastasis dissemination [18, 19]. However, VEGF-C is not only expressed in tumour cells; it is also expressed in tumour stroma cells, like macrophages and fibroblasts. The importance of the stroma in the development and progression of malignant neoplasia, via epithelial–mesenchymal interactions, is a concept that is acquiring greater scientific support [20].

The aim of this study was to determine whether VEGF-C expression is correlated with lymphangiogenesis in a group of patients with cutaneous melanoma and to assess whether this factor is determinant in the neoplastic dissemination to lymph nodes. We studied the immunohistochemical expression of VEGF-C in tumour cells and in macrophages and fibroblasts, comparing the results with the tumour-related LVD and the presence of sentinel lymph node metastasis.

Materials and methods

The study involved 50 cases of cutaneous melanoma collected retrospectively from the records of the Pathology Service of the Virgen de la Victoria University Hospital in Malaga, Spain, diagnosed between 2001 and 2004. All the patients gave informed consent, and the sentinel lymph node technique was performed in all. The node was resected and fully embedded in paraffin. In each tissue block, two consecutive sections were made each 40 μm until the tissue was consumed and stained with haematoxylin–eosin and immunohistochemically with HMB-45 antibody. Of the 50 cases in the study, the sentinel lymph node was negative (SLN negative) in 40 and positive (SLN positive) in 10.

The clinical records of the patients were used to collect data on age, sex and location of the lesion. The histological slides were reviewed to confirm the diagnosis and establish the following parameters: histological type, tumour thickness or Breslow index, Clark level, presence of ulceration, signs of histological regression, vascular invasion and inflammatory infiltrate. The tumour thickness was divided into two ranges, ≤1.5 and >1.5 mm. The inflammatory infiltrate was evaluated as absent, moderate, or intense. Table 1 summarises the clinical and pathological characteristics of the series. The mean age was 49.68 years (range, 14–78 years); most of the patients were older than 35 years

Table 1 Clinical and pathological characteristics of the melanomas

Characteristic	SLN-negative (n=40)	SLN-positive (n=10)
Age		
≤35 years	15	3
36–55 years	17	3
>55 years	8	4
Sex		
Male	15	3
Female	25	7
Location		
Head and neck	3	1
Trunk	18	4
Extremities	19	5
Histological type		
SSM	31	4
NM	6	6
ALM	2	0
Others	1	0
Tumour thickness		
≤1.5 mm	22	3
>1.5 mm	18	7
Clark level		
II	6	0
III	17	4
IV	15	4
V	2	2
Ulceration		
Yes	7	4
No	36	3
Regression		
Yes	5	0
No	35	10
Inflammatory infiltrate		
Absent	14	5
Moderate	21	4
Intense	5	1

SSM superficial spreading melanoma, *ALM* acral lentiginous melanoma, *NM* nodular melanoma

of age. The location of the lesions was mainly on the trunk and extremities, both in SLN-negative and in SLN-positive cases. In both groups, there were more women. The most common histological type in the SLN-negative cases was superficial spreading (77.5%), whereas in the SLN-positive cases, it was nodular melanoma (60%).

Immunohistochemical study

The immunohistochemical study was done with the most representative paraffin block of tumour tissue from the primary lesion and included both superficial and deep areas. Consecutive sections (5 μm in thickness) of paraffin-embedded cancer tissue were cut, mounted on xylan-coated slides, deparaffinised in xylene and rehydrated in a graded series of ethanol. Heat-induced epitope retrieval was done with the pressure cooker method in 0.1 mol/L sodium citrate buffer (pH 6). Endogenous peroxidase activity was blocked by incubation in 1% hydrogen peroxide in methanol for 30 min. Slides were incubated with primary antibody and stained according to the standard LSAB+, Dako REAL™ (K5005) method using an automatic immunostainer (TechMate, Dako, Copenhagen, Denmark). The chromogen used was a ready-to-use biotinylated link antibody and a ready-to-use streptavidin conjugated with alkaline phosphatase (Dako K5005) and slides were counterstained with haematoxylin. Sections of tumour tissue known to express the investigated antigens were used as positive controls. Negative controls were routinely carried out by substituting the primary antibody by non-specific IgG. The control sections were treated in parallel with the samples in the same run.

The mouse monoclonal antibody D2-40 (clone D2-40) (Signet Laboratories, Dedham, MA, USA) was used as a marker of lymphatic vessels. Incubation with the antibody was carried out for 20 min at a 1/200 dilution at room temperature. LVD was defined as the number of vessels per square millimetre. To determine LVD, we reviewed sections stained with D2-40 at low power (20×) seeking the areas of greater vessel density (hot spots) of the tumour. In each case, four hot spots, two intratumoral and two peritumoral, were selected. The quantification of the lymph vessels was done from digitalised images of 800×600 pixels obtained with a Polaroid I DMC camera and a Nikon Eclipse E400 microscope, with a magnification of ×100. The resulting image occupied an area of 0.68 mm^2. The digitalised images were analysed with Visilog 6.3 software (Noesis, France), which provides the automatic quantification of the objects indicated. Isolated cells with no vascular lumen were not considered. The vessels in each previously selected hot spot were counted, and the number of vessels in each area was summed to obtain the total number of vessels per square millimetre.

For VEGF-C immunohistochemical detection, a rabbit antibody (from Zymed Laboratories, South San Francisco, CA, USA) was used with incubation overnight at 4°C in a humidified chamber at a 1/300 dilution. VEGF-C expression was evaluated in the tumour cells, macrophages and stromal cells according to the overall staining intensity as: 1, negative (low or absent expression); 2, (moderate staining); or 3 (strong staining). Stromal cells were identified as cells with fine elongated nuclei, with elongated cytoplasms, generally situated among collagen bundles, in the tumour periphery, surrounding tumour nests (Fig. 1).

Statistical analysis

The statistical study was done with SPSS (version 17.0) for Windows. The study variables were first submitted to a basic descriptive analysis. The continuous variables were evaluated by their real numerical value, taking as representative values the arithmetic mean, range and standard deviation. The qualitative nominal variables, distributed in two or more categories depending on the case, were evaluated by studying the counts and corresponding frequencies. The Student's t and ANOVA tests were used to examine the association of lymphatic vessel parameters with vascular vessel and clinicopathological parameters. Intratumoral and peritumoral lymphangiogenesis parameters were compared by means of the Spearman rho test. Associations between immunohistochemical parameters in tumour and stromal cells and clinicopathological parameters were assessed by the χ^2 test. A $P<0.05$ was considered significant.

Results

D2-40 immunostaining

D2-40 stained endothelial cells of the lymph vessels but not of the blood vessels. The vessels had thin walls, covered by a single layer of poorly prominent endothelial cells. Occasional lymph vessels could be seen among the cell nests of the tumour mass, generally small, dispersed and with a collapsed lumen. The lymph vessels in the peritumoral areas were more frequent, larger and with dilated and tortuous lumina. The mean number of intratumoral and peritumoral lymph vessels in the whole series was 9.84 and 16.98/mm^2, respectively. The great majority of cases had more lymph vessels in the periphery than in the intratumoral area ($P<0.001$).

Although no significant association was seen between the LVD and sentinel node status, the mean LVD was greater in the SLN-positive cases than the SLN-negative cases in both intratumoral and peritumoral locations, with the corrected P for peritumoral location almost reaching

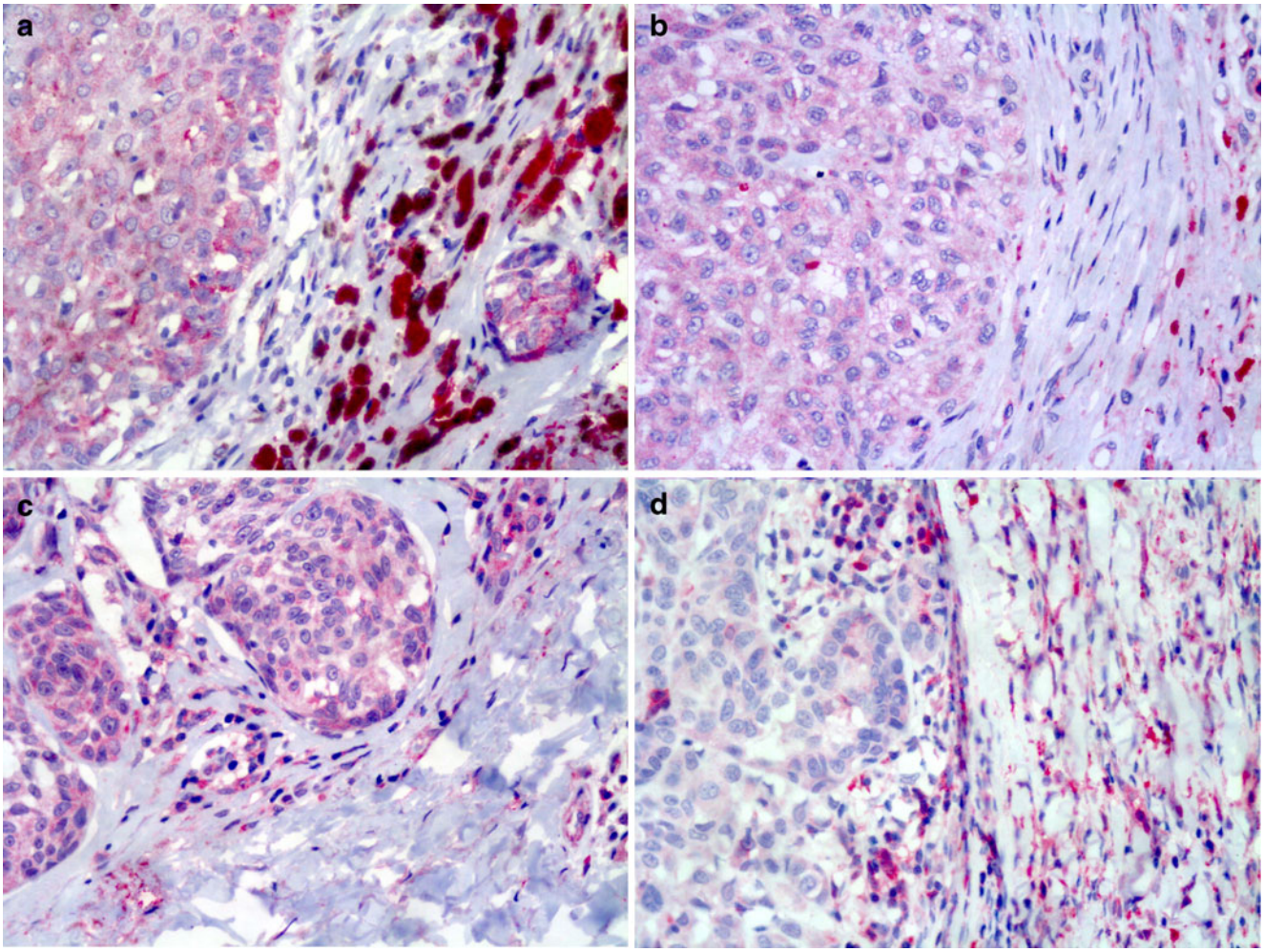

Fig. 1 Immunohistochemical expression of VEGF-C in the peritumoral stroma: **a** stromal cells with very scant staining, valued as 1, the surrounding macrophages show a strong stain; **b** slight staining in some fibrocytes, also valued as 1; **c** moderate staining intensity, valued as 2; **d** VEGF-C negative melanoma with positive stroma, valued as 3

significance (P=0.075). A significant correlation was seen between LVD and tumour thickness (P=0.003). Melanomas with a Breslow index of <1.5 mm had a lower intratumoral LVD than the melanomas with Breslow of >1.5 mm. Likewise, the presence of ulceration was significantly associated with an increase in intratumoral lymph vessels (P=0.019), but not peritumoral vessels. The histological type and the intensity of the inflammatory infiltrate showed no relation with the number of lymph vessels within or around melanomas. The presence of regression phenomena, however, was associated with a lower LVD (P=0.026) (Table 2).

VEGF-C immunostaining

VEGF-C immunostaining was studied in three cell types: melanoma cells, macrophages and fibroblastic stromal cells (Table 3). The VEGF-C staining was diffuse in the tumour cells from most cases, though a certain degree of heterogeneity was seen in the cell to cell staining intensity, and some cases even showed a clear difference in the staining intensity in a few tumour areas. The macrophages, both intratumoral and in the tumour periphery, generally stained stronger than in the melanoma cells. In fact, some melanoma-negative cases also showed strong staining in macrophages. In the tumour periphery, and occasionally among the tumour nests, fibroblastic stromal cells could be seen among the collagen bundles, generally with a concentric arrangement around the tumour, which also stained positively. As expected, VEGF-C expression in fibroblasts was almost absent in Clark II melanomas, in which the presence of fibroblasts around the tumour cells was minimal. The fibroblastic reaction was more evident in melanomas with levels of deeper infiltration into the dermis or the subcutaneous adipose tissue, though the fibroblast density was similar, independently of the level of invasion and the presence of lymph node involvement.

VEGF-C immunostaining of tumour cells was considered moderate or high in 29 cases and absent or low in 21 cases.

Table 2 Relation between intratumoral and peritumoral LVD and histopathological parameters

Parameter	Intratumoral LVD, mean (SD)	*P* value	Peritumoral LVD, mean (SD)	*P* value
Tumour thickness		0.003		NS
≤1.5 mm	6.28 (7.09)		16.56 (10.27)	
>1.5 mm	13.40 (9.09)		17.40 (9.44)	
Clark level		NS		NS
II	4.33 (8.73)		15.50 (10.48)	
III	10.47 (7.61)		15.19 (7.36)	
IV	11.27 (10.39)		19.16 (11.87)	
V	10.00 (7.52)		14.00 (5.35)	
SLN		NS		0.075
Positive	13.10 (8.03)		21.90 (12.24)	
Negative	9.02 (8.93)		15.75 (8.82)	
Ulceration		0.019		NS
No	8.30 (7.95)		18.36 (7.10)	
Yes	15.27 (10.02)		16.58 (10.45)	
Regression		0.026		NS
Yes	1.6 (2.07)		9.80 (7.15)	
No	10.75 (8.82)		17.77 (9.76)	
Inflammatory infiltrate		NS		NS
Absent	6.5 (5.6)		16.83 (10.57)	
Sparse	9.05 (8.61)		16.83 (10.91)	
Intense	11.32 (9.71)		17.28 (9.30)	

Macrophages showed moderate or high staining in 33 cases and stromal cells in 16 cases. VEGF-C expression in tumour cells was of a similar intensity in the SLN-positive cases as in the SLN-negative cases. No significant differences were seen between metastatic and non-metastatic melanomas regarding macrophage staining. VEGF-C expression in the stroma, however, was clearly greater in those cases with a positive sentinel lymph node than those with a negative sentinel lymph node ($P<0.001$). Nine SLN-positive cases (90%) showed moderate or high staining, whereas in 82.5% of the SLN-negative cases, the staining was null or slight in the stromal cells. In addition, stromal VEGF-C expression was also related with the Clark level of invasion ($P=0.05$), mainly because most of the level V melanomas had a high expression of the marker, whereas all the level II cases were negative. No other significant differences were seen in VEGF-C expression in the tumour cells, macrophages, or stromal cells regarding histological type, thickness, inflammatory infiltrate, or regression signs. VEGF-C expression in the melanoma cells, the macrophages and the stroma showed no correlation with the intratumoral or peritumoral LVD.

Discussion

In most human cancers, including malignant cutaneous melanoma, the lymph vessels constitute the pathway of dissemination to the lymph nodes. In cutaneous melanoma, the first metastases to be detected affect the regional lymph nodes in at least 50% of patients [21]. In this case, the first lymph node in the lymph node drainage chain, known as the sentinel lymph node, is the first to be affected, and its status can predict that of the other lymph nodes [22]. Thus, the study of the sentinel lymph node provides important information on staging and prognosis, which in turn aid in treatment decisions [23]. Nonetheless, the sentinel lymph node procedure is not free from postoperative complications such as wound infection, seroma, haematoma, or lymphoedema [24].

Malignant tumours have recently been shown to induce the formation of new lymph vessels, a process known as lymphangiogenesis. Various clinicopathological studies have found a strong association between tumour lymphangiogenesis and metastatic involvement of the lymph nodes [6–9, 25–28].

Lymph vessel proliferation in malignant cutaneous melanoma exists not only in the periphery of the tumour but also within the tumour. Although the relevance of intratumoral versus peritumoral lymphatic vessels for cancer metastasis in lymph nodes remains unclear, some data suggest that the latter play a more active role. Whereas the intratumoral vessels are generally collapsed, the peritumoral vessels show wider, more dilated lumina, and tumour emboli within lymphatics are more common within the peritumoral vessels [13, 29]. As we found in our series, the density of lymphatic

Table 3 Relation between intensity of immunohistochemical VEGF-C staining and sentinel lymph node (SLN) status and other pathological characteristics

VEGF-C	SLN		P value	Histological type				P value	Tumour thickness		P value	Clark level				P value	Ulceration		P value	Regression		P value	Inflammatory infiltrate			P value
	+	−		SSM	NM	ALM	Other		≤1.5 mm	>1.5 mm		II	III	IV	V		Yes	No		Yes	No		Absent	Moderate	Intense	
Tumour cells																										
Absent/low	4	17	NS	14	6	1	0	NS	10	11	NS	3	8	9	1	NS	4	17	NS	3	18	NS	6	12	3	NS
Moderate	3	16	NS	16	2	1	1		12	7		3	7	8	1		5	14		2	17		8	9	2	
High	3	7		5	4	0	0		3	7		0	6	2	2		2	8		0	10		5	4	1	
Macrophages																										
Absent/low	5	12	NS	9	6	2	1	NS	6	11	NS	1	7	8	1	NS	7	10	NS	1	16	NS	5	10	2	NS
Moderate	4	15		14	5	0	0		10	9		3	6	9	1		2	17		3	16		8	9	2	
High	1	13		12	1	0	0		9	5		2	8	2	2		2	12		1	13		6	6	2	
Stromal cells																										
Absent/low	1	33	<0.001	25	7	0	0	NS	17	17	NS	6	15	11	2	NS	7	27	NS	4	30	NS	11	20	3	NS
Moderate	4	5		6	2	1	1		5	4		0	2	7	0		1	8		0	9		5	2	2	
High	5	2		4	3	1	0		3	4		0	4	1	2		3	4		1	6		3	3	1	

SSM superficial spreading melanoma, *ALM* acral lentiginous melanoma, *NM* nodular melanoma

vessels is usually greater at the periphery than in the intratumoral location. This finding is similar to that of most studies on lymphangiogenesis in human cutaneous melanomas [11, 13, 29], though exceptions exist, with no significant differences being found [30]. However, the presence (as opposed to the absence) of intratumoral lymphatic vessels has been correlated with poor disease-free survival [11].

Comparison of LVD in SLN-positive versus SLN-negative cases showed a slightly increased number of lymphatic vessels in both intratumoral and peritumoral locations (intratumoral LVD, 9.02±1.4 in SLN-negative and 13.10±2.5 in SLN-positive cases; peritumoral LVD, 15.75±1.4 in SLN-negative and 21.90±3.9 in SLN-positive cases). However, the differences were not statistically significant, although peritumoral LVD reached levels close to significance (P=0.075). Several authors have investigated the correlation between the degree of development of tumour lymphangiogenesis in cutaneous melanoma and the presence of metastases in the sentinel node, with conflicting results**.** Massi et al. [13], in a series of 15 melanomas with 30 matched controls, using immunochemistry for D2-40 and computer assisted morphometric analysis, found that the number and area of peritumoral and intratumoral lymphatic vessels were significantly higher in melanomas with SLN metastasis than in non-metastatic melanomas. Dadras et al. [11] reported that the number of peritumoral lymphatics and the average lymphatic vessel size were significantly increased in melanomas with early lymph node metastasis compared with non-metastatic melanomas. In this latter work, immunofluorescence staining for LYVE-1 on paraffin sections was used to recognise lymphatic vessels and computer-assisted morphometric analysis to obtain vessel density and size. These findings were subsequently validated in a prospective series [12] of 45 cutaneous melanomas with SLN biopsy, using similar methods. The results showed that the lymphatic vascular area was a highly sensitive and specific prognostic marker of sentinel node metastases, even more accurately than tumour thickness. Sahni et al. [30], on the other hand, found no significant difference in lymphatic counts between SLN-positive and SLN-negative cases using LYVE-1 and Chalkley point counting in 36 cases of cutaneous melanoma. Straume et al. [14] reported similar findings, but their series only included nodular melanoma, with LYVE-1 as a lymphatic marker. Surprisingly, in another report [15], lymphatic capillary density as assessed by immunohistochemical staining of VEGFR-3 showed an inverse correlation with SLN metastasis.

Methodological variability, particularly the antibody used as a marker of lymphatic vessels, may be the cause, at least in part, of disagreement in the results. In our study, we used D2-40, a specific marker of lymphatic vessels that recognises podoplanin, a mucin-type transmembrane glycoprotein [31].

Lyve-1 and D2-40 (podoplanin) are markers of lymphatic vessels commonly used to assess LVD in melanoma, and both have proved to be specific for lymphatic endothelial cells. However, in a comparative study on the usefulness of various immunohistochemical markers (Lyve-1, D2-40 and Prox-1) to identify lymphatic vessels in breast cancer, D2-40 proved to be the most sensitive marker [32]. In the "First international consensus on the methodology of lymphangiogenesis quantification in solid human tumors", podoplanin, which is recognised by D2-40 antibody, was considered the most reliable marker of lymphatic vessels at present [33]. However, the consensus also recommended using a combination of markers that could vary depending on the type of tissue. It is necessary to standardise the methodology of lymphangiogenesis quantification in melanoma to determine its true prognostic significance.

The presence of ulceration could affect lymphangiogenesis. Our results show that intratumoral lymphatic vessels are significantly more numerous in ulcerated melanomas, whilst the density of peritumoral lymphatic vessels is similar in ulcerated and non-ulcerated lesions. Sahni et al. [30] found a significant difference when peritumoral and intratumoral lymphatic areas combined were considered but not when only intratumoral areas were taken into account. In the study of Massi et al. [13], the parameter associated with ulcerated melanoma was the average vessel area both in intratumoral and peritumoral locations. These results may be conflicting, but all agree that lymphangiogenesis is dependent on ulceration. The inflammation usually associated with ulceration may be one of the causes of the increase in lymph vessels. Both the inflammatory cells themselves as well as the proinflammatory cytokines secreted in this context have been implicated in the regulation of lymph vessel growth [34, 35]. We, too, found that tumour thickness was associated with significantly higher intratumoral LVD. However, ulceration and Breslow index are characteristics that are frequently associated as ulceration is more commonly present in thicker melanomas, as was the case in our series. Release of VEGFs mediated by hypoxia is proposed by Massi et al. [13] as the reason for the enlargement of lymphatic vessels in ulcerated melanomas. Likewise, primary melanomas in the vertical growth phase were reported to express more VEGF-C than those in the horizontal growth phase [17]. However, in our experience, VEGF-C is not increased in ulcerated melanomas nor is it associated with the Breslow index.

These findings, as well as the absence of a correlation between VEGF-C expression of the tumour or stromal cells and LVD, may be explained because lymphangiogenesis, just like angiogenesis, is a complex process in which multiple growth factors are involved, all inter-related. Factors other than VEGF-C, such as VEGF-A, hepatocyte growth factor, fibroblast growth factor-2, platelet-derived growth factors and insulin-like growth factors, may also contribute to promoting lymphangiogenesis during growth of the melanoma [36, 37]. In a large series of 175 melanomas, Straume et al. found no association between LVD and the immunohistochemical expression VEGF-C or other factors related with lymphangiogenesis [14].

Earlier data suggested that VEGF-C might be involved in the localisation of melanoma metastasis to the lymph nodes [18, 38]. In order to determine whether VEGF-C secreted by melanoma cells correlates with SLN involvement, we studied the immunohistochemical expression of VEGF-C in tumour cells from SLN-positive and SLN-negative patients. Of the 50 cases, 29 presented a moderate or intense stain, 23 (77%) of the SLN-negative and six (60%) of the SLN-positive cases. Thus, no significant association was seen between tumour VEGF-C and SLN involvement. These results agree with observations of both Dadras et al. [11] and Massi et al. [13], who reported that VEGF-C expression by tumour cells was detected in both metastatic and non-metastatic melanomas, with no correlation with lymph node status. Dadras et al. [12], on the other hand, detected moderate to high levels of cytoplasmatic VEGF-C in the majority of SLN-positive melanomas but in a minority of the SLN-negative melanomas (88.2% vs. 40.0%), and they found that tumour cell expression of VEGF-C may be useful to predict metastasis to the SLN. In addition, Bonne et al. [19], in a study of 113 cases, found that high VEGF-C expression in melanoma cells was positively associated with the presence of a positive SLN. These discordant results highlight the need for yet more research in this field to determine the usefulness of VEGF-C expression in tumour cells from cutaneous melanoma as a predictive factor of node status in the clinical setting.

This study focussed on VEGF-C secretion not only in tumour cells but also in stromal cells accompanying the cutaneous melanoma. The contribution of stromal cells to the formation of new lymphatic vessels or the appearance of lymph node metastasis is poorly understood. A great deal of evidence, both experimental and clinical, shows that the stroma and extracellular matrix play an important role in the development of human tumours [39]. The stromal cells around a tumour are mainly fibroblasts and inflammatory cells, like macrophages. The relevance of macrophages in angiogenesis has been determined in tumours from several different tumour locations [40, 41]. Macrophages are a source of antigenic factors, including VEGF-C and VEGF-D, that have also been associated with lymphangiogenesis, in both inflammatory and tumoral processes [42, 43].

Positive VEGF-C staining in cutaneous melanoma is usually more frequent in macrophages than in melanoma cells [12, 19]. Bonne et al. [19] observed that VEGF-C expression in tumour-associated macrophages (TAMs) was strongly associated with the sentinel lymph node status, just

like VEGF-C expression in melanoma cells. This finding was not corroborated in our study, in which the SLN-negative and the SLN-positive cases showed a high level of positivity for VEGF-C in macrophages. However, like Bonne et al., we too failed to find an association with the pathological characteristics of the primary tumour, such as Breslow thickness, Clark level, inflammatory infiltrate, regression signs or ulceration.

In addition to macrophages, fibroblasts from the tumour stroma, also termed tumour-associated fibroblasts or carcinoma-associated fibroblasts (CAFs), play a relevant role in the development and progression of tumours. In vivo experiments mixing fibroblasts and epithelial cells from tumorigenic cell lines accelerated the growth and shortened the latency period of human epithelial tumours in athymic mice [44]. This protumorigenic action can be more clearly seen when CAFs are used in the models to study tumour stroma interaction, with the authors concluding that CAFs can direct tumour progression of initiated epithelial cells [45]. CAFs are able to secrete growth factors that contribute to the creation of a favourable microenvironment for tumour growth, promoting angiogenesis**,** migration and spread of tumour cells [46]. Fibroblasts can secrete VEGF, among other growth factors, and, together with inflammatory cells, are the principal source of host-derived VEGF in a tumour [47]. Interestingly, Koyama et al. [48], in an experimental study in breast carcinoma, also showed secretion of VEGF-D and VEGF-C by fibroblasts using immunohistochemistry and real-time quantitative RT-PCR. The authors conclude that lymphangiogenesis is probably also controlled by interaction between the tumour cells and the components of the stroma and that the stromal cells may serve as important inducers of tumour lymphangiogenesis in a suitable microenvironment.

Previous studies in cutaneous melanoma have shown VEGF-C expression in peritumoral dermal fibroblasts [11, 13]. However, a relation with the presence of metastasis in regional lymph nodes has not previously been reported. Surprisingly, in our study, the expression of VEGF-C in the fibroblasts was significantly associated with SLN status, more so than that of the epithelial cells or macrophages. Marked staining was seen in the vast majority of melanomas with lymphatic vessel metastasis, whereas in the SLN-negative cases, the VEGF-C staining was generally scarce or absent. Thus, evaluation of VEGF-C expression in the fibroblasts that are mainly found at the base of the tumour, around tumour nests of melanoma cells, may be useful as a predictive factor of SLN involvement.

The localisation of the fibroblasts in the periphery of the melanoma is coincident with that of the functionally active lymph vessels, which are mainly responsible for the dissemination to lymph nodes [49]. Thus, VEGF-C secreted by fibroblasts can act directly on local lymph vessels, creating a favourable microenvironment for metastatic dissemination. Although experimental studies have shown that overexpression of VEGF-C by tumour cells induces tumour-associated lymph vessel growth [50], a direct relation between a high immunohistochemical VEGF-C expression and a high LVD has not always been found in cutaneous melanomas [14]. This observation suggests the additional existence of a qualitative action of VEGF-C on lymph vessels, promoting tumour metastasis. This qualitative action may be exerted by facilitating the entry of tumour cells via the formation of intercellular gaps [51] or promoting the dilation of collecting lymph vessels, which would then cause an increase in the flow of lymph and the transport and dissemination of tumour cells [52]. Additionally, the lymphangiogenic factors secreted by the tumour may also act at a distance, provoking the appearance of areas of lymph vessel proliferation in draining lymph nodes and thus contributing to the settling and survival of tumour cells via the induction of a specific tumour microenvironment or “lymphvascular niche” [53].

Our findings underline the importance of tumour-associated stroma in the promotion of intratumoral lymphangiogenesis and show that it may also be a target for antineoplastic therapy. Given the results of this study, we consider that VEGF-C secretion by tumour-associated fibroblasts should be considered in future studies about prognostic factors in cutaneous melanoma.

Acknowledgements This study was supported by the Consejería de Salud de la Junta de Andalucía, Spain (grant number PI-0322/2007). We are very grateful to María José Lozano, from the Malaga University Pathology Department laboratory, for her technical collaboration in this study.

Conflict of interest statement The authors declare that they have no conflict of interest.

References

1. Morton DL, Wen DR, Wong JH, Economou JS, Cagle LA, Storm FK, Foshag LJ, Cochran AJ (1992) Technical details of intraoperative lymphatic mapping for early stage melanoma. Arch Surg 127:392–399
2. Folkman J (1971) Tumor angiogenesis: therapeutic implications. N Engl J Med 285:1182–1186
3. Folkman J (1995) Clinical applications of research on angiogenesis. N Engl J Med 333:1757–1762
4. Karpanen T, Egeblad M, Karkkainen MJ, Kubo H, Ylä-Herttuala S, Jäättelä M, Alitalo K (2001) Vascular endothelial growth factor C promotes tumor lymphangiogenesis and intralymphatic tumor growth. Cancer Res 61:1786–1790
5. Schacht V, Dadras SS, Johnson LA, Jackson DG, Hong YK, Detmar M (2005) Up-regulation of the lymphatic marker podoplanin, a mucin-type transmembrane glycoprotein, in human squamous cell carcinomas and germ cell tumors. Am J Pathol 3:913–921

6. Kitadai Y, Kodama M, Cho S et al (2005) Quantitative analysis of lymphangiogenic markers for predicting metastasis of human gastric carcinoma to lymph nodes. Int J Cancer 115:388–392
7. Franchi A, Gallo O, Massi D, Baroni G, Santucci M (2004) Tumor lymphangiogenesis in head and neck squamous cell carcinoma. A morphometric study with clinical correlations. Cancer 5:973–978
8. Nakamura Y, Yasuoka H, Tsujimoto M, Imabun S, Nakahara M, Nakao K, Nakamura M, Mori I, Kakudo K (2005) Lymph vessel density correlates with nodal status, VEGF-C expression, and prognosis in breast cancer. Breast Cancer Res Treat 91:125–132
9. Zeng Y, Opeskin K, Horvath LG, Sutherland RL, Williams ED (2005) Lymphatic vessel density and lymph node metastasis in prostate cancer. Prostate 9999:1–9
10. Yan G, Zhou XY, Cai SJ, Zhang GH, Peng JJ, Du X (2008) Lymphangiogenic and angiogenic microvessel density in human primary sporadic colorectal carcinoma. World J Gastroenterol 14:101–107
11. Dadras SS, Paul T, Bertoncini J, Brown LF, Muzikansky A, Jackson DG, Ellwanger U, Garbe C, Mihm MC, Detmar M (2003) Tumor lymphangiogenesis. A novel prognostic indicador for cutaneous melanoma metastasis and survival. Am J Pathol 162:1951–1960
12. Dadras SS, Lange-Asschenfeldt B, Velasco P, Nguyen L, Vora A, Muzikansky A, Jahnke K, Hauschild A, Hirakawa S, Mihm MC, Detmar M (2005) Tumor lymphangiogenesis predicts melanoma metastasis to sentinel lymph node. Mod Pathol 18:1232–1242
13. Massi D, Puig S, Franchi A, Malvehy J, Vidal-Sicart S, González-Cao M, Baroni G, Ketabchi S, Palou J, Santucci M (2006) Tumour lymphangiogenesis is a possible predictor of sentinel lymph node status in cutaneous melanoma: a case–control study. J Clin Pathol 59:166–173
14. Straume O, Jackson DG, Akslen LA (2003) Independent prognostic impact of lymphatic vessel density and presence of low-grade lymphangiogenesis in cutaneous melanoma. Clin Cancer Res 9:250–256
15. Wobser M, Siedel C, Schrama D, Bröcker EB, Becker JC, Vetter-Kauczok CS (2006) Expression pattern of the lymphatic and vascular markers VEGFR-3 and CD31 does not predict regional lymph node metastasis in cutaneous melanoma. Arch Dermatol Res 297:352–357
16. Joukov V, Pajusola K, Kaipainen A, Chilov D, Lahtinen I, Kukk E, Saksela O, Kalkkinen N, Alitalo K (1996) A novel vascular endothelial growth factor, VEGF-C, is a ligand for the Flt4 (VEGFR-3) and KDR (VEGFR-2) receptor tyrosine kinases. EMBO J 15:1751
17. JS Goydos, Gorski DH (2003) Vascular endothelial growth factor-C mRNA expression correlates with stage of progression in patients with melanoma. Clin Cancer Res 9:5962–5967
18. Schietroma C, Cianfarani F, Lacal PM, Odorisio T, Orecchia A, Kanitakis J, D'Atri S, Failla CM, Zambruno G (2003) Vascular endothelial growth factor-C correlates with lymph node localization of human melanoma metastases. Cancer 98:789–797
19. Boone B, Blokx W, De Bacquer D, Lambert J, Ruiter D, Brochez L (2008) The role of VEGF-C staining in predicting regional metastasis in melanoma. Virchows Arch 453:257–265
20. Shekhar MP, Pauley R, Heppner G (2003) Host microenvironment in breast cancer development: extracellular matrix-stromal cell contribution to neoplastic phenotype of epithelial cells in the breast. Breast Cancer Res 5:130–135
21. Meier F, Will S, Ellwanger U, Schlagenhauff B, Schittek B, Rassner G, Garbe C (2002) Metastatic pathways and time courses in the orderly progression of cutaneous melanoma. Br J Dermatol 147:62–70
22. Reintgen D, Cruse CW, Wells K et al (1994) The orderly progression of melanoma nodal metastases. Ann Surg 220:759–767
23. Morton DL, Thompson JF, Cochran AJ, Mozzillo N, Elashoff R, Essner R, Nieweg OE, Roses DF, Hoekstra HJ, Karakousis CP, Reintgen DS, Coventry BJ, Glass EC, Wang HJ (2006) Sentinel-node biopsy or nodal observation in melanoma. N Engl J Med 355:1307–1317
24. Kretschmer L, Thoms KM, Peeters S, Haenssle H, Bertsch HP, Emmert S (2008) Postoperative morbidity of lymph node excision for cutaneous melanoma-sentinel lymphonodectomy versus complete regional lymph node dissection. Melanoma Res 18:16–21
25. Sleeman JP, Thiele W (2009) Tumor metastasis and the lymphatic vasculature. Int J Cancer 125:2747–2756
26. Tobler NE, Detmar M (2006) Tumor and lymph node lymphangiogenesis—impact on cancer metastasis. J Leukoc Biol 80:691–696
27. Choi WW, Lewis MM, Lawson D, Yin-Goen Q, Birdsong GG, Cotsonis GA, Cohen C, Young AN (2005) Angiogenic and lymphangiogenic microvessel density in breast carcinoma: correlation with clinicopathologic parameters and VEGF-family gene expression. Mod Pathol 18:143–152
28. Ueda M, Hung YC, Terai Y, Kanda K, Kanemura M, Futakuchi H, Yamaguchi H, Akise D, Yasuda M, Ueki M (2005) Vascular endothelial growth factor-C expression and invasive phenotype in ovarian carcinomas. Clin Cancer Res 11:3225–3232
29. Skobe M, Hamberg LM, Hawighorst T, Schirner M, Wolf GL, Alitalo K, Detmar M (2001) Concurrent induction of lymphagiogenesis, angiogénesis and macrophage recruitment by vascular endothelial growth factor-C in melanoma. Am J Pathol 159:893–903
30. Sahni D, Robson A, Orchard G, Szydlo R, Evans AV, Russell-Jones R (2005) The use of LYVE-1 antibody for detecting lymphatic involvement in patients with malignant melanoma of known sentinel node status. J Clin Pathol 58:715–721
31. Breiteneder-Geleff S, Soleiman A, Kowalski H, Horvat R, Amann G, Kriehuber E, Diem K, Weninger W, Tschachler E, Alitalo K, Kerjaschki D (1999) Angiosarcomas express mixed endothelial phenotypes of blood and lymphatic capillaries: podoplanin as a specific marker for lymphatic endothelium. Am J Pathol 154:385–394
32. Van der Auwera I, Van den Eynden GG, Colpaert CG, Van Laere SJ, van Dam P, Van Marck EA, Dirix LY, Vermeulen PB (2005) Tumor lymphangiogenesis in inflammatory breast carcinoma: a histomorphometric study. Clin Cancer Res 11:7637–7642
33. Van der Auwera I, Cao Y, Tille JC, Pepper MS, Jackson DG, Fox SB, Harris AL, Dirix LY, Vermeulen PB (2006) First international consensus on the methodology of lymphangiogenesis quantification in solid human tumours. Br J Cancer 95:1611–1625
34. Cursiefen C, Chen L, Borges LP, Jackson D, Cao J, Radziejewski C, D'Amore PA, Dana MR, Wiegand SJ, Streilein JW (2004) VEGF-A stimulates lymphangiogenesis and hemangiogenesis in inflammatory neovascularization via macrophage recruitment. J Clin Invest 113:1040–1050
35. Ristimaki A, Narko K, Enholm B, Joukov V, Alitalo K (1998) Proinflammatory cytokines regulate expression of the lymphatic endothelial mitogen vascular endothelial growth factor-C. J Biol Chem 273:8413–8418
36. Rinderknecht M, Detmar M (2008) Tumor lymphangiogenesis and melanoma metastasis. J Cell Physiol 216:347–354
37. Alitalo K, Tammela T, Petrova TV (2005) Lymphangiogenesis in development and human disease. Nature 438:946–953
38. Vihinen PP, Hilli J, Vuoristo MS, Syrjänen KJ, Kähäri VM, Pyrhönen SO (2007) Serum VEGF-C is associated with metastatic site in patients with malignant melanoma. Acta Oncol 46:678–684
39. Angeli F, Koumakis G, Chen MC, Kumar S, Delinassios JG (2009) Role of stromal fibroblasts in cancer: promoting or impeding? Tumour Biol 30:109–120
40. Vicioso L, Gonzalez FJ, Alvarez M, Ribelles N, Molina M, Marquez A, Perez L, Matilla A, Alba E (2006) Elevated serum

levels of vascular endothelial growth factor are associated with tumor-associated macrophages in primary breast cancer. Am J Clin Pathol 125:111–118
41. Coffelt SB, Hughes R, Lewis CE (2009) Tumor-associated macrophages: effectors of angiogenesis and tumor progression. Biochim Biophys Acta 1796:11–18
42. Yamashita M, Iwama N, Date F, Shibata N, Miki H, Yamauchi K, Sawai T, Sato S, Takahashi T, Ono M (2009) Macrophages participate in lymphangiogenesis in idiopathic diffuse alveolar damage through CCL19-CCR7 signal. Hum Pathol 40:1553–1563
43. Schoppmann SF, Birner P, Stöckl J, Kalt R, Ullrich R, Caucig C, Kriehuber E, Nagy K, Alitalo K, Kerjaschki D (2002) Tumor-associated macrophages express lymphatic endothelial growth factors and are related to peritumoral lymphangiogenesis. Am J Pathol 161:947–956
44. Camps JL, Chang SM, Hsu TC, Freeman MR, Hong SJ, Zhau HE, von Eschenbach AC, Chung LW (1990) Fibroblast-mediated acceleration of human epithelial tumor growth in vivo. Proc Natl Acad Sci USA 87:75–79
45. Olumi AF, Grossfeld GD, Hayward SW, Carroll PR, Tlsty TD, Cunha GR (1999) Carcinoma-associated fibroblasts direct tumor progression of initiated human prostatic epithelium. Cancer Res 59:5002–5011
46. Kalluri R, Zeisberg M (2006) Fibroblasts in cancer. Nat Rev Cancer 6:392–401
47. Fukumura D, Xavier R, Sugiura T, Chen Y, Park EC, Lu N, Selig M, Nielsen G, Taksir T, Jain RK, Seed B (1998) Tumor induction of VEGF promoter activity in stromal cells. Cell 94:715–725
48. Koyama H, Kobayashi N, Harada M, Takeoka M, Kawai Y, Sano K, Fujimori M, Amano J, Ohhashi T, Kannagi R, Kimata K, Taniguchi S, Itano N (2008) Significance of tumor-associated stroma in promotion of intratumoral lymphangiogenesis: pivotal role of a hyaluronan-rich tumor microenvironment. Am J Pathol 172:179–193
49. Tammela T, Alitalo K (2010) Lymphangiogenesis: molecular mechanisms and future promise. Cell 140:460–476
50. Skobe M, Hawighorst T, Jackson DG, Prevo R, Janes L, Velasco P, Riccardi L, Alitalo K, Claffey K, Detmar M (2001) Induction of tumor lymphangiogenesis by VEGF-C promotes breast cancer metastasis. Nat Med 7:192–198
51. Tammela T, Saaristo A, Holopainen T, Lyytikka J, Kotronen A, Pitkonen M, Abo-Ramadan U, Yla-Herttuala S, Petrova TV, Alitalo K (2007) Therapeutic differentiation and maturation of lymphatic vessels after lymph node dissection and transplantation. Nat Med 13:1458–1466
52. He Y et al (2005) Vascular endothelial cell growth factor receptor 3-mediated activation of lymphatic endothelium is crucial for tumor cell entry and spread via lymphatic vessels. Cancer Res 65:4739–4746
53. Hirakawa S (2009) From tumor lymphangiogenesis to lymphvascular niche. Cancer Sci 100:983–989

Virchows Arch (2011) 458:631–636
DOI 10.1007/s00428-011-1064-3

CASE REPORT

Iatrogenic EBV-positive lymphoproliferative disorder with features of EBV+ mucocutaneous ulcer: evidence for concomitant TCRγ/IGH rearrangements in the Hodgkin-like neoplastic cells

Arianna Di Napoli · Maria Giubettini · Enrico Duranti · Antonella Ferrari · Cesare Guglielmi · Stefania Uccini · Luigi Ruco

Received: 1 February 2011 / Revised: 21 February 2011 / Accepted: 24 February 2011 / Published online: 12 March 2011
© Springer-Verlag 2011

in which various numbers of atypical large B cells with Hodgkin/Reed-Sternberg-like (H/RS-like) morphology are embedded. The atypical B cells are EBER+/CD30+/CD15+/PAX5+/MUM-1+. IGH clonality was detected in 7 of 18 cases (39%); TCR clonality in 6 of 16 cases (38%); moreover, a monoclonal IGH rearrangement associated with restricted/clonal T cell responses was observed in 3 of 16 cases. In the present report, we describe a case of a malignant lymphoproliferative disorder of the large intestine with features of Epstein–Barr virus (EBV)+ mucocutaneous ulcer; the novel contribution provided by our study is the demonstration of concomitant clonal IGH and TCRγ rearrangements in the neoplastic B cells with H/RS-like morphology.

Introduction

Iatrogenic immunodeficiency-associated lymphoproliferative disorders are a heterogeneous group of rare diseases related to therapy with immunosuppressive drugs for conditions other than the transplant setting [1]. The first description concerned patients who developed Hodgkin's disease or Hodgkin-like lymphoproliferations after long-term, low-dose methotrexate therapy [2–4]. Very recently, in a multicenter study, 26 cases of a distinct clinicopathologic entity, the EBV+ mucocutaneous ulcer, were described [5]. The disease affects immunosuppressed and/or elderly patients, and consists of isolated, sharply circumscribed ulcers involving oropharyngeal mucosa, skin or gastrointestinal tract. Lesions are characterized by the presence of a polymorphous inflammatory-like infiltrate,

A. Di Napoli · M. Giubettini · E. Duranti · S. Uccini · L. Ruco
UOC Anatomia Patologica,
Dipartimento di Medicina Clinica e Molecolare, Ospedale Sant'Andrea,
II Facoltà di Medicina e Chirurgia, Università "Sapienza",
Rome, Italy

A. Ferrari · C. Guglielmi
UOC Ematologia, Dipartimento di Medicina Clinica e Molecolare,
Ospedale Sant'Andrea, II Facoltà di Medicina e Chirurgia,
Università "Sapienza",
Rome, Italy

A. Di Napoli (✉)
UOC Anatomia Patologica, Dipartimento di Medicina Clinica e Molecolare, II Facolta' di Medicina e Chirurgia,
Università degli Studi di Roma "Sapienza",
Ospedale Sant'Andrea, Via di Grottarossa 1035–1039,
00189 Rome, Italy
e-mail: arianna.dinapoli@uniroma1.it

Clinical history

An 81-year-old female patient was admitted at the emergency room of the Sant'Andrea Hospital of Rome because of abdominal pain due to intestinal perforation assumed to be related to diverticulosis. In the clinical history, the patient had diabetes, vascular hypertension, ischemic cardiopathy, a previous cerebral infarction, and an autoimmune thrombocytopenia since 2006; this latter was treated with steroids and azathioprine for 1 year with no response; more recently, the patient received romiplostim obtaining a complete response. The patient underwent an intervention of left colectomy; the sigmoid colon (length 9.3 cm) was involved by multiple diverticula and by a shallow mucosal ulceration in continuity with transmural fissures resulting in intestinal perforation. Seven mesenteric lymph nodes (diameter of the largest 0.5 cm) were detected on gross inspection.

During the post-operative period, the patient suffered of progressive and severe liver dysfunction, and died 1 month later; an autopsy was performed. The ultimate cause of death was liver failure due to diffuse involvement of the organ by the lymphoproliferative disease; moreover, multiple nodular areas of liver infarction were noted. Some mesenteric and aortic lymph nodes were involved by the lymphoproliferative disease; the bone marrow was not involved.

Materials and methods

Immunohistochemistry and in situ hybridization Paraffin sections were immunostained for CD30 (UCS Diagnostics, Italy), CD3, CD4, CD8, CD20, CD34, CD10 (Novocastra, UK); CD5, CD79a, CD15, BCL-6, MUM-1, LMP-1, CD68, CD117, BCL-2 (DAKO, Denmark), CD45, PAX5 (Thermo Scientific,USA), CD56 (Neomarkers, USA). The immune reaction product was developed using LSAB-2 plus (DAKO, Denmark). In situ hybridization for EBV-encoded RNA (EBER) was performed on paraffin sections using EBV (EBER) PNA Probe/Fluorescein, and FITC/HRP (DAKO, Denmark).

Polymerase chain reaction (PCR) for immunoglobulin (IGH) and T-cell receptor (TCR) gene rearrangements PCR clonal analysis was performed on three different paraffin blocks (two from the intestinal lesion and one from an involved regional lymph node). Total DNA was extracted from paraffin tissue sections with a lysis buffer containing proteinase K. Molecular evaluation of T cell receptor gamma (TCRγ) gene rearrangement was performed by PCR amplification of DNA fragments corresponding to the VJ segment of hyper-variable region of the TCR range. For the amplification reaction, a kit for molecular diagnosis analysis of clonal rearrangements of TCRγ (Master Diagnostica, Spain) was used. Molecular evaluation of immunoglobulin heavy chain (IGH) gene rearrangements was performed by PCR amplification of DNA fragment corresponding to the VD-JH segment of hyper-variable region of the IGH. Results of TCRγ and IGH gene rearrangements were analysed according to the BIOMED-2 report [6] with 3,100 Genetic Analyzer (Applied Biosystem).

Laser capture microdissection Laser capture microdissection was performed using the microdissection laser system SL CUT (NIKON Instruments, Italy). Atypical H/RS-like cells were isolated on haematoxylin and eosin-stained sections based on morphology, collecting approximately 200 cells. Three different microdissections were performed on sections of the involved lymph nodes. Moreover, about 300 morphologically typical lymphocytes were picked from the same tissue section. DNA extraction was performed using the PicoPure Isolation Kit (ARCTURUS, Bioscience Inc., Mountain View, CA, USA).

Results

EBV+ mucosal ulcer of the large intestine

The sigmoid colon was involved by multiple diverticula and by a shallow mucosal ulceration resulting in intestinal perforation. Seven enlarged mesenteric lymph nodes were detected. The mucosal ulceration and some of the intestinal diverticula were associated with a prominent inflammatory-

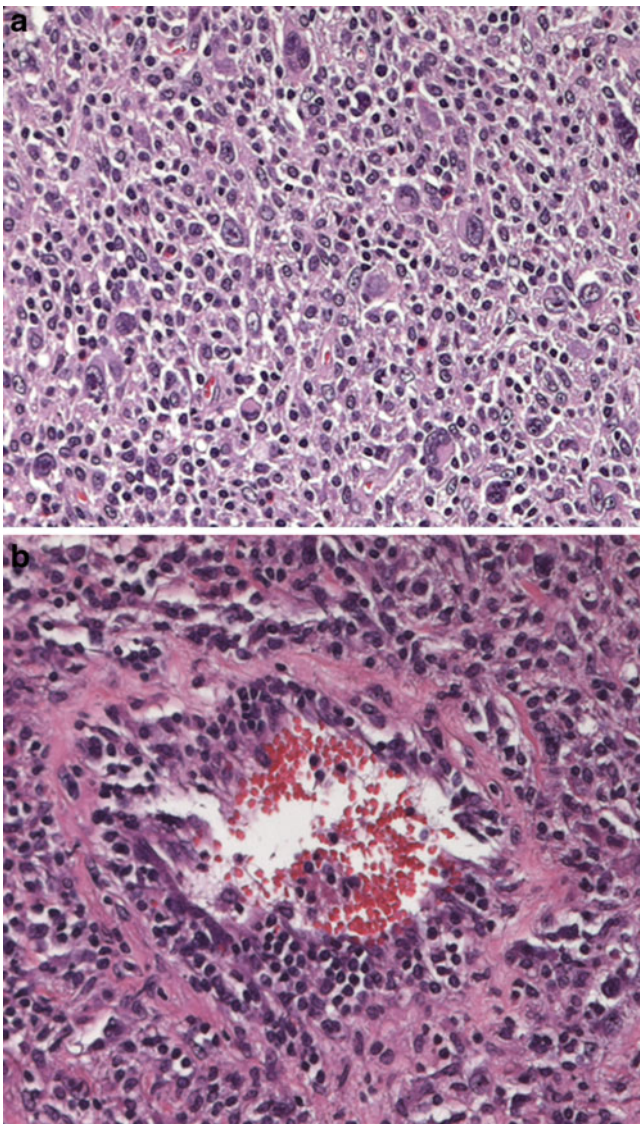

Fig. 1 The lymphoproliferative disease was characterized by an inflammatory-like background in which atypical cells with Hodgkin/Reed–Sternberg-like morphology were embedded (**a**). The wall of a medium-size artery is infiltrated by numerous lymphoid cells (**b**). (H&E, original magnification **a**, **b** ×200)

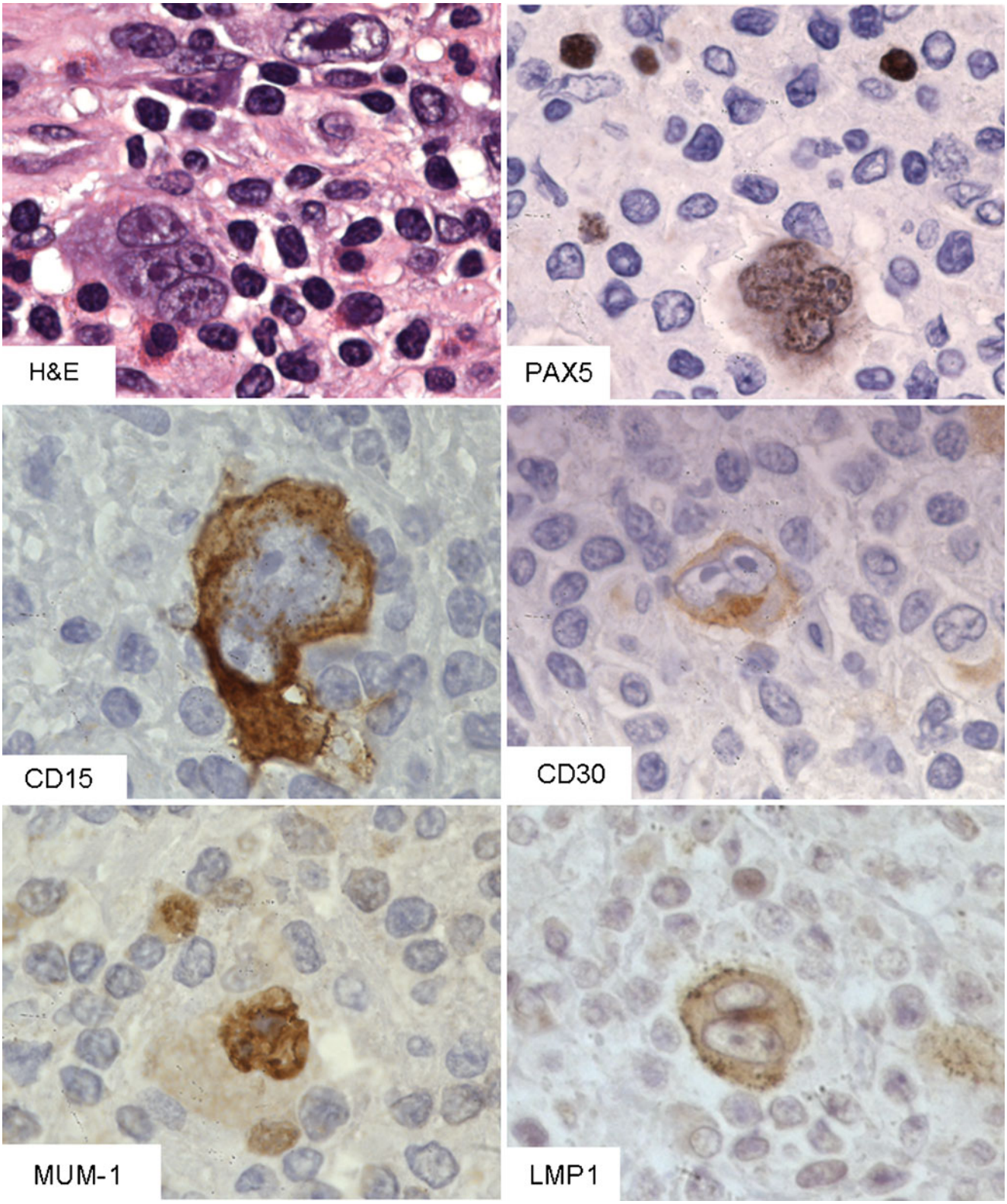

Fig. 2 Hodgkin/Reed–Senberg-like cells exhibited nuclear staining for PAX5 and MUM1, had a paranuclear dot of reactivity for CD30, were intensely CD15+ and were EBV-infected as indicated by cytoplasmic staining for LMP-1. (ABC-immunoperoxidase, counterstained with haematoxylin, original magnification for all panels ×1,000)

like reaction. The cellular infiltrate was polymorphous, and was composed mainly of mature CD3+ T lymphocytes (CD4/CD8 ratio about 3:1), and CD68+ macrophages (Fig. 1a). Occasional CD20+/CD79a+ B cell nodules were sparsely present. Lymphocyte infiltration of blood vessels resulting in angiocentric lesions was occasionally observed (Fig. 1b). The inflammatory background was associated with scattered large pleomorphic cells, reminiscent of H/RS cells; these latter were CD30+/PAX5+/MUM-1+, were intensely CD15+ (Fig. 2), were negative for CD3, CD4, CD8, CD20, CD79a, CD10, bcl-2, bcl-6, CD45, CD34, CD68 and CD117, and were infected by EBV as suggested by positive staining for EBER and LMP-1. The seven regional lymph nodes were completely effaced by a lymphoproliferative disease with a similar histological picture.

IGH and TCRγ clonality

PCR analysis of DNA extracted from two different paraffin blocks of the intestinal lesion and from one lymph node revealed the concomitant presence of a monoclonal IGH rearrangement and of a monoclonal TCRγ rearrangement (Fig. 3a–b). The H/RS-like cells were easily recognizable by morphology, and could be singly collected with laser capture microdissection. PCR analysis of DNA obtained from about 200 microdissected H/RS-like cells revealed the presence of a clonal TCRγ rearrangement undistinguishable from that observed in the whole tissue section (Fig. 3b); as expected, in the pherogram of the microdissected H/RS-like cells the polyclonal T cell background was no longer present. Moreover, DNA extracted from about 300 microdissected surrounding lymphocytes did not show the presence of a clonal peak of TCRγ rearrangement.

Discussion

EBV is associated with numerous malignant haematological diseases, including drug-induced immunosuppression-associated lymphoproliferative disorders [1] and diffuse large

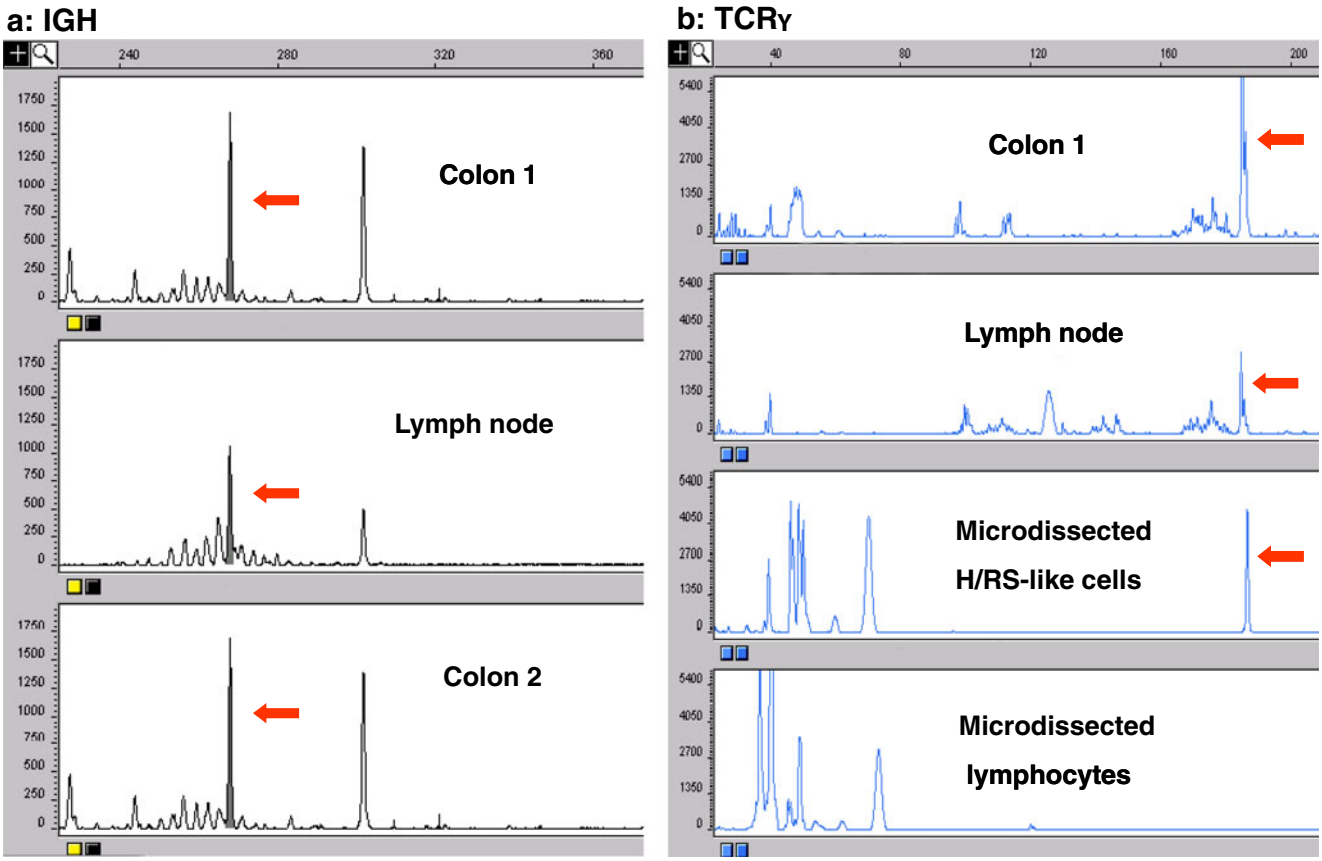

Fig. 3 Molecular evaluation of IGH clonal analysis performed on DNA extracted from three different paraffin blocks (two from the intestinal lesion and one from an involved regional lymph node) revealed the presence of a similar peak of clonality in the three samples (**a**). Molecular evaluation of TCRγ rearrangement in DNA extracted from the intestinal lesion and from an involved lymph node revealed the presence of a similar peak of clonality. When DNA was extracted from 200 H/RS-like cells isolated with laser capture microdissection, a TCRγ clonal rearrangement undistinguishable from those present in the whole tissue sections was detected; as expected, in microdissected H/RS-like cells the polyclonal T cell background was no longer present. Moreover, DNA extracted from microdissected surrounding lymphocytes did not show the presence of clonal TCRγ rearrangement (**b**)

B cell lymphoma of the eldery (aEBVLPD) [7]. The clinical and pathological features observed in our case were closely similar to those recently described in an immunodeficiency-associated EBV+ lymphoproliferative disorder termed "EBV+ mucocutaneous ulcer" [5]. In fact, the patient had an advanced age and was previously treated with an immunosuppressive agent for autoimmune thrombocytopenia; the shallow intestinal ulceration was associated with a local irritative spine, i.e. intestinal diverticulosis; the histology of the lesion was highly reminiscent of Hodgkin's disease except for strong expression of CD15 by H/RS-like cells, for the presence of angiocentric lesions leading to ischemic necrosis in intestine and liver, and for concomitant IGH and TCRγ clonal gene rearrangements. A major difference with the previously reported cases [5] is that the disease spread with a metastatic pattern from the large intestine to mesenteric and aortic lymph nodes, and to the liver, ultimately causing death because of hepatic failure. Indeed, all cases reported by Dojcinov et al. [5] exhibited a benign clinical course consisting in either spontaneous regression, or in complete and persistent remission after chemotherapy or radiotherapy; no disease-related deaths were reported after an overall follow-up of 22 months. Thus, it seems reasonable to postulate that "EBV+ mucocutaneous ulcer" covers a spectrum of differently aggressive diseases, perhaps as a consequence of the immunocompetence status of the host.

The advanced age of the patient prompt us to consider also a diagnosis of age-related EBV-associated lymphoproliferative disorder (aEBVLPD) [7–9]. This entity is an EBV-associated large B cell lymphoma in the elderly without predisposing immunodeficiency. In about one third of cases, aEBVLPD occurs as a polymorphous subtype with reactive cell-rich components, bearing a morphologic similarity to classic Hodgkin's lymphoma. Unlike our case, in a series of 96 cases of aEBVLPD, H/RS-like cells were consistently positive for the B cell markers CD20/CD79a and lacked CD15 expression [8, 9]. Thus, a diagnosis of immunodeficiency-associated EBV+ lymphoproliferative disorder similar to EBV+ mucocutaneous ulcer appeared to us to be more appropriate. An alternative diagnosis to take in consideration could be that of EBV+ lymphomatoid granulomatosis; indeed this possibility was supported by the extranodal localization of the EBV-related disease, and mainly, by the presence of angiocentric/angiodestructive lesions; however, the demonstration of numerous CD30+/CD15+ H/RS-like cells within the lesion was strongly against lymphomatoid granulomatosis.

To explain the pathogenesis of EBV+ mucocutaneous ulcer, Dojcinov et al. [5] suggested that minor localized mucosal irritations, or mucocutaneous injury due to microtraumatisms, created a point of lowered resistance for localized proliferation of EBV-infected cells. In our case, we noted a close spatial association between EBV+ mucocutaneous ulcer and intestinal diverticulosis; thus, it can be speculated that intestinal diverticulosis may be added to the possible triggering events favouring the local development of the disease.

Dojcinov et al. [5] investigated IGH and TCR rearrangements in 18 cases of EBV+ mucocutaneous ulcer. IGH clonality was detected in 7 of 18 cases (39%); TCR clonality in 6 of 16 cases (38%); monoclonal IGH rearrangements associated with restricted T cell responses were detected in three cases. The authors interpreted the monoclonal IGH rearrangements as indicative of the clonality of the EBV-driven B cell proliferation, and the monoclonal or oligoclonal TCR gene rearrangements as indicative of a "restricted" T cell response, perhaps driven by EBV-infected cells. It was speculated that elderly subjects are markedly restricted and deficient in their epitope specific T cell repertoire, rendering the host at increased risk of infection and favouring the development of oligoclonal T cell responses.

Thanks to laser capture micro-dissection, we provide evidence that the TCRγ clonal rearrangement was present in neoplastic B cells with H/RS-like morphology lacking expression of CD79a/CD20/CD3/CD4/CD8. Thus, our findings raise the possibility of an alternative interpretation. In fact, it could be speculated that a still unrecognized transforming event might cause deregulation/impairment of the recombination-activating gene enzyme system and hence might induce TCR rearrangements in B cells which have already undergone IGH rearrangements. A similar pathogenetic mechanism has already been proposed to explain the presence of concomitant IGH and TCR rearrangements in a consistent number of cases of precursor-B-ALL [10].

Acknowledgements This work has been supported by funding from Università degli Studi di Roma "Sapienza".

Conflict of interest We declare that we have no conflict of interest.

References

1. Gaulard P, Swerdlow SH, Harris NL, Jaffe ES, Sundström C (2008) Other iatrogenic immunodeficiency-associated lymphoproliferative disorders. In: Swerdlow SH, Campo E, Harris NL, Jaffe ES, Pileri SA, Stein H, Thiele J, Vardiman JW (eds) WHO Classification of Tumours of Haematopoietic and Lymphoid tissues, 4th edn. International Agency for Research on Cancer, Lyon, PA, pp 350–351
2. Kamel OW, van de Rijn M, Weiss LM et al (1993) Brief report: reversible lymphomas associated with Epstein–Barr virus occurring during methotrexate therapy for rheumatoid arthritis and dermatomyositis. N Engl J Med 328:1317–1321
3. Ferraccioli GF, Casatta L, Bartoli E et al (1995) Epstein-Barr virus-associated Hodgkin's lymphoma in a rheumatoid arthritis patient treated with methotrexate and cyclosporin A. Arthritis Rheum 38:867–868

4. Kamel OW, Weiss LM, van de Rijn M, Colby TV, Kingma DW, Jaffe ES (1996) Hodgkin's disease and lymphoproliferations resembling Hodgkin's disease in patients receiving long-term low-dose methotrexate therapy. Am J Surg Pathol 20:1279–1287
5. Dojcinov SD, Venkataraman G, Raffeld M, Pittaluga S, Jaffe ES (2010) EBV positive mucocutaneous ulcer—a study of 26 cases associated with various sources of immunosuppression. Am J Surg Pathol 34:405–417
6. van Dongen JJ, Langerak AW, Brüggemann M et al (2003) Design and standardization of PCR primers and protocols for detection of clonal immunoglobulin and T-cell receptor gene recombinations in suspect lymphoproliferations: report of the BIOMED-2 Concerted Action BMH4-CT98-3936. Leukemia 17:2257–2317
7. Nakamura S, Jaffe ES, Swerdlow SH (2008) EBV positive diffuse large B cell lymphoma of the eldery. In: Swerdlow SH, Campo E, Harris NL, Jaffe ES, Pileri SA, Stein H, Thiele J, Vardiman JW (eds) WHO Classification of Tumours of Haematopoietic and Lymphoid tissues, 4th edn. International Agency for Research on Cancer, Lyon PA, pp 243–244
8. Oyama T, Ichimura K, Suzuki R et al (2003) Senile EBV+ B-cell lymphoproliferative disorders: a clinicopathologic study of 22 patients. Am J Surg Pathol 27:16–26
9. Asano N, Yamamoto K, Tamaru J et al (2009) Age-related Epstein-Barr virus (EBV)-associated B-cell lymphoproliferative disorders: comparison with EBV-positive classic Hodgkin lymphoma in elderly patients. Blood 113:2629–2636
10. Szczepański T, Beishuizen A, Pongers-Willemse MJ et al (1999) Cross-lineage T cell receptor gene rearrangements occur in more than ninety percent of childhood precursor-B acute lymphoblastic leukemias: alternative PCR targets for detection of minimal residual disease. Leukemia 13:196–205

Virchows Arch (2011) 458:637–648
DOI 10.1007/s00428-011-1083-0

REVIEW AND PERSPECTIVE

Classifications of lymphoma; reflections of time and technology

Clive R. Taylor · Robert J. Hartsock

Received: 15 March 2011 / Accepted: 3 April 2011 / Published online: 19 April 2011
© Springer-Verlag 2011

Abstract

'Nowhere in pathology has a chaos of names so clouded clear concepts as in the subject lymphoid tumors'. R.A. Willis.

In 1858, Rudolf Virchow, with a primitive microscope and limited experiential base, recognized *'at least three different conditions here, hyperinosis, leucocytosis and leukemia….'*. One hundred and fifty years later, the World Health Organization (WHO 2008), with a much more extensive armamentarium of tools, and a wealth of diverse experience, promulgated criteria distinguishing more than 100 types of '*Tumors of the Hematopoietic and Lymphoid Tissues*'. From three to one hundred and three; this is progress! And this is history! Our goal is to examine the course and causes of this history; how we moved from three entities to a hundred and three, what we have learned from it, and how we may use the insights that we have gained to anticipate 'future histories' in this marvelously dynamic area of biology and disease.

Keywords WHO classification of hematopoietic neoplasms · Malignant lymphoma · Non-Hodgkin lymphoma · Hodkgin lymphoma · Classification · Immunohistochemistry · Phenotyping · Monoclonal antibodies · B and T lymphocytes

C. R. Taylor (✉)
Department of Pathology, Keck School of Medicine,
Los Angeles, CA, USA
e-mail: cltaylor@usc.edu

R. J. Hartsock
Allegheny Valley Hospital,
Natrona Heights, PA, USA
e-mail: randmhartsock@comcast.net

I have no objection to your giving names any signification which you please, if you will only tell me what you mean by them.

Plato. Charmides.

Once upon a time

Pluralitas non est ponenda sine necessitate.

William of Occam, 1491. (his 'razor')

From the very beginning, scientists have evinced an irresistible urge to define and classify all of the natural world, and all of its aberrations. Give a natural scientist two of anything, she or he will observe, describe, name, and classify them, employing whatever techniques are available at the time; Plantae–Animalia; maximus–minimus; the more the merrier; but they won't always agree about it. Aristotle (384–322 BC) did it first, in a formal sense; his use of the terms '*genera*' and '*species*', although broad in connotation, endured for two millennia. Carl (Carolus) Linnaeus (Karl von Linné) (1707–1778) did it while studying therapeutic plants at medical school. He was a peripatetic student, moving from Lund to Uppsala, to Harjwick, to Leiden, subjected to diverse influences. An initial 11-page paper, *Systema Naturae* (1735) [1], expanded over three decades to 12 editions and two volumes (Fig. 1), including also animals and then diseases (*Genera Morborum*, 1763). Linnaeus is credited with setting forth principles of meticulous observation that provided impetus for much of the scientific renaissance that was to follow. A century later, Alfred Russell Wallace (1823–1913) and Charles Darwin (1809–1882), by these same methods of meticulous observation, assembled the tangible basis for their theory of evolution, but not without

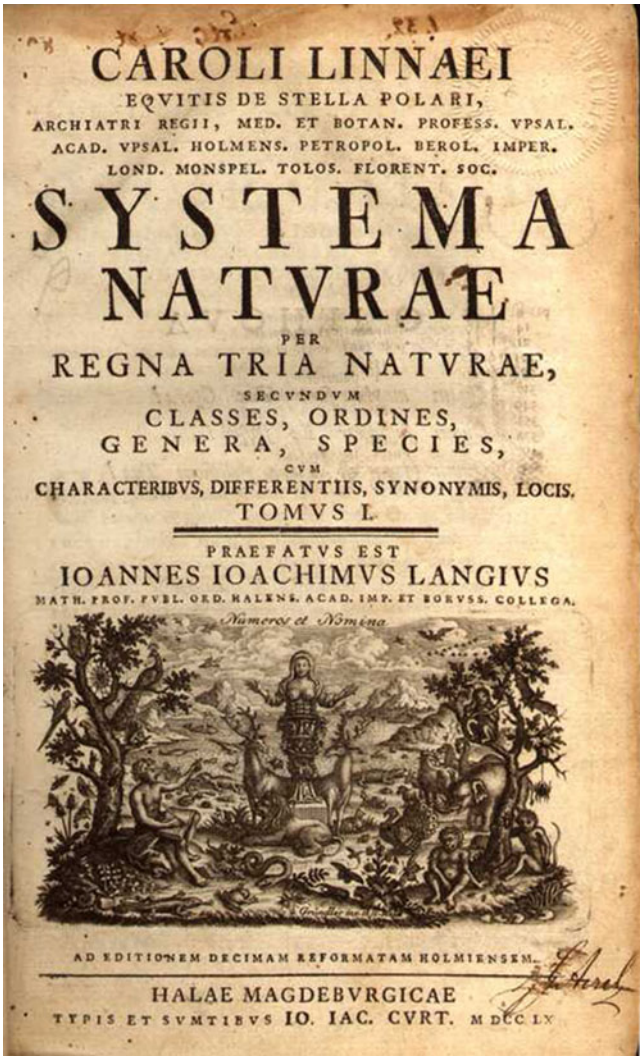

Fig. 1 Cover of *Systema Naturae* by Caroli Linnaei (Carl Linnaeus) 10th edition (reprint by Halae, Germany). The 10th edition existed in multiple copies in libraries and is that generally used as the basis for subsequent classification schemes

controversy. Wallace forwarded his "Ternate Essay" *'On the Tendency of Varieties to Depart Indefinitely From the Original Type'* directly to Darwin in February of 1858. It was received by Darwin in June and presented to the Linnean Society of London, on July 1st 1858, together with two papers from Darwin [2]. In its collective wisdom, the Society '*decided to give credit to Wallace's brilliance, but simultaneously established Darwin's priority*'. In his autobiography Darwin's recollection was of a 'non-event'—*"our joint productions excited very little attention"* [3]. Darwin's *'Origin of the Species'* appeared in November 1859.

Pathologists are not immune to this primal urge, displaying startling creativity and nosological zeal beyond parallel in the nomenclature and classification of malignant lymphomas. In 1858, Virchow (1821–1902), with a primitive microscope and limited experiential base, recognized *'at least three different conditions here, hyperinosis, leucocytosis and leukemia … which are not infrequently combined' [4: p 170]. One hundred and fifty years later, the World Health Organization (WHO), with a much more extensive armamentarium of tools, and a wealth of diverse experience, promulgated criteria distinguishing more than 100 types of 'Tumors of the Hematopoietic and Lymphoid Tissues' [5].*

From three to one hundred and three; this is progress! But how did it happen? It was not an orderly progression; not uniform, certainly not planned, but rather characterized by spontaneity, by fits and starts. It was never smooth and rarely collaborative, but instead individualistic, opinionated, and often contentious. A goal of this history is to examine how the process occurred; how we moved from three entities to a hundred and three. It was a prodigious effort, driven by the fervor and imagination of generations of pathologists, fueled by technical advances that facilitated the testing of new hypotheses as they appeared; comets of the intellect, to flare briefly, and then mostly disappear into oblivion.

The impact of technology—the microscope

The year was 1800. In the 'Old World', France and Britain were at war, again, while in the 'New World' classifiers were rampant, renaming whole countries. Medicine, a reflection of the times, had not stood still. Following the anatomical dissections of the John and William Hunter (1725–1793 and 1718–1783), their nephew Matthew Baillie (1761–1823) and others, diseases were described and named according to some combination of clinical manifestations and findings at autopsy [see this series—6]. Diagnosis was made absolute at the autopsy table, the realm of the early pathologist. Such was the prevailing practice in 1832 when Dr. Samuel Lee delivered to the Chirurgical Society of London a paper by Thomas Hodgkin , entitled *'Some Morbid Appearances of the Absorbent Glands and Spleen'* [7], based upon autopsy findings. The import of this work was that it recognized for the first time *'a primitive affection of those bodies, rather than the result of an irritation propagated to them—'*; widely credited as the 'first lymphoma'. Some 30 years later, Baronet Sir Samuel Wilks (1824–1911), also at Guys Hospital, encountered 15 similar cases and unearthed Hodgkin's original description. Wilks was perfectly altruistic in bestowing the title 'Hodgkin's Disease'; *'Although my own observations were at the time original, I had been forestalled by Dr. Hodgkin—'* [8].

The mid-part of the nineteenth century witnessed remarkable technical improvements in the quality of microscopes. Tissue sectioning techniques and new biolog-

ical stains developed 'pari passu'. The impact on biological sciences and Medicine was to be enormous, exemplified by the founding of the Royal Microscopical Society (1839), the first course in histology at a medical school (Edinburgh—John Hughes Bennett, 1842), and descriptions of diseases that now we recognize as leukemias and lymphomas. It is no coincidence that Virchow's 'Cellularpathologie' appeared at this time (1858) [4], along with terminologies for diseases that may or may not have been similar—'lymphadenoma' (Cornil, 1855, Wunderlich, 1856); 'lymphosarcoma' (Virchow 1864); 'pseudo-leukemia' (Cohnheim 1865); 'malignant lymphoma' (Billroth 1871) [9]. The debate over nomenclature of tumors of the lymphoid system, and their classification, had begun.

From 1860 onward, there was an early fascination with the microscopic features of Hodgkin's disease and the giant cells intrinsic to the process. First noted by Billroth in 1858, then Virchow in 1864, these giant cells were described in great detail by W.S. Greenfield, at the Pathological Society in London on March 19th, 1878 [10]. The later descriptions of Ludwig Sternberg (1898) and Dorothy Reed (1902) are better known, in effect immortalizing both the cell and those who described it. While the nature and derivation of these giant cells, and of Hodgkin's disease, would provoke fierce debate for another century [reviews, 11, 12], other diseases of lymph glands were quietly being described. Inevitably, from this growing constellation of diseases, there emerged the first attempts to organize them into orderly classification schemes.

The principles and the 'players'

Just as the development of new laboratory techniques led to the identification of new 'types' of tumors, so these same methods gave rise to new perceptions of the normal cells from which the tumors were derived. In short, classification was in reality driven by technology, permitting both formulation of new hypotheses and their testing. Over the succeeding decades, driven by the curiosity of remarkable men and women, several principles emerged that serve us still today. The authors enjoyed the privilege and fortune to rub shoulders with some of the (more recent) players in this classification saga, who are given emphasis as the story unfolds.

Reticulosis and reticulosarcoma; from Aschoff and Maximow to Robb-Smith

Early attempts at classification of lympho-reticular tumors followed naturally upon definition of the reticulo-endothelial system, and subsequent concepts of the reticulum cell, as some sort of shadowy ancestral hematopoietic cell.

The idea of the 'reticulo-endothelial system' evolved over the course of several years, a product of the vital staining studies of Aschoff (1866–1942) (Fig. 2) and colleagues, published formally in 1924 [13]. Derivative classifications soon appeared but gained little traction due to the fact that the reticulo-endothelial system was a 'functional' concept that encompassed several cell types, and therefore did not lend itself to histologic classification.

By way of contrast, Maximow's (1874–1928) (Fig. 3) vision of undifferentiated mesenchymal stem cells was based upon detailed histologic description (1927) [14]. He postulated that, when stimulated, reticulum cells displayed extensive cytoplasm and a large vesicular nucleus with prominent nucleolus and had the potential to differentiate along hemic, lymphocytic, or histiocytic lines. With considerable prescience, Maximow anticipated the discovery of the hematopoietic stem cell as early as 1909 [15]; he believed that the small lymphocyte was a form of 'haemocytoblast' that could revert to the large cell from which it was derived. Maximow expressed the view that under pathologic conditions this same reticulum cell gave rise to the 'mirror image' Reed–Sternberg cell, by abortive cell division.

Adami (1913) added another intellectual twist, purporting to distinguish a category of diffuse new growth ('hyperblastosis'), from true neoplasia: '*every transition is observable in this series between the development of overgrowths of fully differentiated tissue, non-malignant grades of anaplasia and diffuse malignant infiltrative growths*' [16]. Letterer (1924) linked this idea to Maximow's

Fig. 2 Ludwig Aschoff, 1866–1942. Entered to public domain by Jürgen Aschoff

Fig. 3 Alexander A. Maximov at the University of Chicago, following his departure from Russia, across frozen Lake Lagoda to Finland and then Sweden in 1922. From the Scientific Papers and Drawings of Alexander Maximow. Box III, Folder 10. Department of Special Collections, The University of Chicago Library. *IN SEARCH OF ALEXANDER A. MAXIMOW: THE MAN BEHIND THE UNITARIAN THEORY OF HEMATOPOIESIS IGOR E. KONSTANTINOV Perspectives in Biology and Medicine, 43, 2 • 2000–269*

reticulum cell theory, introducing the term 'reticulosis' for the 'not quite malignant' proliferation of reticulum cells in Letterer–Siwe disease [17]. 'Reticulosis' acquired broad usage for an ill-defined group of diseases that appeared neither to be simple hyperplasias nor true malignant neoplasms, but something in between. Oberling (1928) completed the chain of thought and proposed use of the term 'reticulosarcoma' for malignant tumors of lymphoreticular tissues [18].

In 1928, James Ewing (1866–1943) wrote as follows: *'The discussion of lymphoma in general, necessarily includes the consideration of several processes, some of which are chiefly inflammatory, some neoplastic and others intermediate in position'* [19]. He recognized lymphoma, leukemia, pseudo-leukemia, Hodgkin's disease, and lymphosarcoma. George Callender (1934) at the American Lymph Node Registry, followed a similar theme, with differing terminology, identifying specific cell types within different generic forms of proliferation: Reactive; Leukemic; Aleukemic; and Malignant [20].

The ultimate iteration of this concept is to be found in *'Reticulosis and Reticulo-sarcoma: a histological classification'* [21] by Alistair Hamish Tearlock Robb-Smith (1908–2000), whose doctoral thesis at the University of London, titled *'Hyperplasia and Neoplasia of the Lymphoreticular Tissue'* was hailed as a pioneering work in the field. Robb-Smith *'offered clear histologic distinctions between reactive conditions, reticuloses (progressive lymphoproliferative conditions) and reticulosarcomas (frank malignancies)'*. In 1979 (Fig. 4), reflecting back upon his classification, Robb-Smith wrote—"*the general reaction to the classification in Europe was that it was interesting*". With wry Scot's humor, he went on to quote two notable names in the field: *"Bodley Scott said (1951): ... 'it avoids ... the fallacy of oversimplification', while Willis (1960) wrote: 'Complicated histopathologic subdivision, like that of Robb-Smith, which praiseworthy though it may be as an attempt to clarify a confused subject, obscures the essential unity ... what is wanted is not more but less complexity....'"* [9: Appendix 1].

There were two notable publications in 1947; Robb-Smith's review of 1,000 cases in the Oxford Registry [22] and Jackson and Parker's monograph from Oxford University Press, *'Hodgkin's Disease and Allied Disorders'* [23]. While the main focus of the latter was Hodgkin's disease, the 'Allied Disorders' included giant follicle lymphoma and reticulum sarcoma. Notably, Jackson and Parker deplored the use of the term malignant lymphoma; *'This we believe to be a mistake (we ourselves have so erred), for these terms connote to some a specific disease while to others they are vague and meaningless.'* Jackson and Parker found the term reticulum cell to be *'unfortunate'* and considered it to be *'identical with the histiocyte, clasmatocyte, macrophage.... Tumors arising from this cell ... constitute a distinct cell type in no way related to neoplasms arising from cells of the lymphoid series'* [23, p. 114]. In this they erred once more.

In the face of such ambivalence the reticulosis–reticulosarcoma concept proved durable in Europe: as late as 1967 Lennert wrote: *'we differentiate according to Robb-Smith*

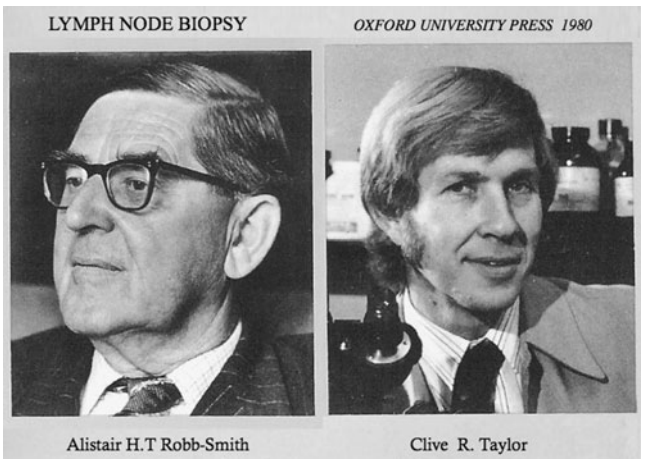

Fig. 4 Alistair HT Robb-Smith at Oxford in 1979, from cover sheet of Lymph Node Biopsy, Oxford University Press, 1980 [9], with one of the authors (CRT) (personal collection)

and in analogy to Ewing, three categories of lymphadenopathy (1) reactive hyperplasia, (2) sarcomas of the lymphoreticular tissue and (3) a group of diseases lying between' [24]. However, it found few takers in the New World, where the term 'malignant lymphoma', first used almost a century earlier by Theodor Billroth (1829–1894), slowly gained currency, over the protestations of Jackson, Parker, and others.

The fluid lymphoma school; from Mallory to Custer

Underlying these disparate opinions was a fundamental problem, a divergence of evolution. Adherence to Maximow's unitarian concept of lymphoreticular neoplasia constituted the *'fluid lymphoma'* school. Standing in opposition were those pathologists exemplified by Jackson and Parker (vide supra), who subscribed to the view that the different tumors of lymph glands were separate, constant, and immutable—the *'fixed entity hypothesis'*.

In 1914, Frank Burr Mallory (1862–1941) wrote in his '*Principles of Pathological Histology'* [25]; *'Tumors are classified like normal tissues, on a histologic basis. ... The type of cell is the one important element in every tumor. From it the tumor should be named'* [25, p. 275]. Few would disagree with the principle. Logic dictated that if Maximow's reticulum cells could 'transmute', then so might any derivative neoplasms, providing the basis for the notion that lymphosarcoma, lymphatic leukemia, and Hodgkin's disease were all variants of one tumor, 'malignant lymphoblastoma'. Initially, the concept found little support, until revived by Aldred Warthin in 1931, *'Hodgkin's disease is a neoplasm and related genetically to the lymphoblastomas .... Transition forms exist between all of these groups, and one type may be transformed into another'* [26]. Pullinger (1932) also embraced the pluripotentiality of the reticulum cell, when she wrote: *'it seems probable that a group of diseases of reticulum exist in which proliferation is followed by differentiation into one or several of the possible cell progeny'* [27].

In 1942, Gall and Mallory [28] had a different view: reporting a series of 600 cases they used the term reticulum cell sarcoma, for tumors of either stem cell or histiocytic origin, without subscribing to the 'reticulum cell theory'; stating that '*it has been shown by multiple examinations at significant time intervals that the cytologic type is remarkably constant*'.

Custer and Bernhard (1948) reported findings that were directly contradictory—*'Analysis of 1300 lymphatic tumors ... showed a striking fluidity of histologic pattern with transitions and combinations ... a single neoplastic entity having a number of variants'* [29, p. 641]. Custer's view [30, 31] (Figs. 5 and 6) provided the ultimate expression of the fluid lymphoma theory: *'They are all mesenchymal tumors which vary only in degree and type of differentiation'* [29, p. 625].

Thus, for 20 years, classifications rose and classifications fell. While many reflected this concept of the reticulum cell as the mother lode of the lymphoid tissues, it was all a matter of opinion.

Willis—a view from the outside

Rupert A. Willis (1898–1980), initially of the University of Melbourne (1930–1945), then Professor of Human and Comparative Anatomy at the Royal College of Surgeons in London, is known especially for two major published works, *Pathology of Tumours (1948)* [32] and *The Borderlands of Embryology and Pathology (1958)* [33].

Willis brought something different to the debate over the nature and nomenclature of lymphomas, namely an outside view. His '*Pathology of Tumours*' contains a chapter on comparative pathology and includes illustrations of animal as well as human tumors. As an 'outsider', he brought some objectivity to the field, perhaps best illustrated in his own words: *'There occur tumors corresponding to almost all kinds of normal tissues, and clearly a classification of tumors will run parallel with the classification of normal tissues'* [32]. This principle followed the basic tenet set forth by Mallory 40 years earlier (vide supra) [14]. However, Willis, while stressing the importance of nomenclature, made the critical observation that nomenclature also constrained constructive thought; *'Perhaps pathology more than most branches of biological sciences suffers from this "tyranny of names"'* [32].

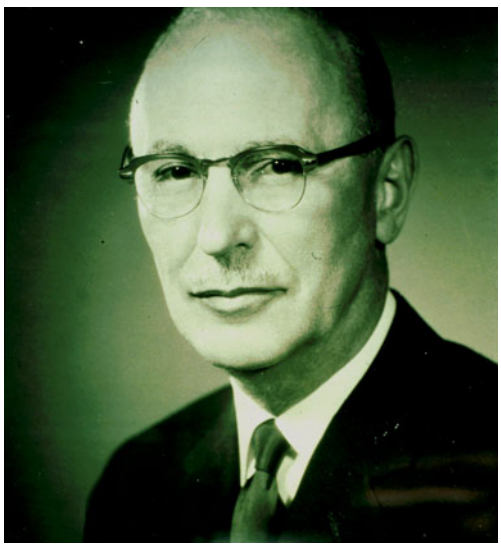

Fig. 5 R. Philip Custer from the author's (RJH) collection

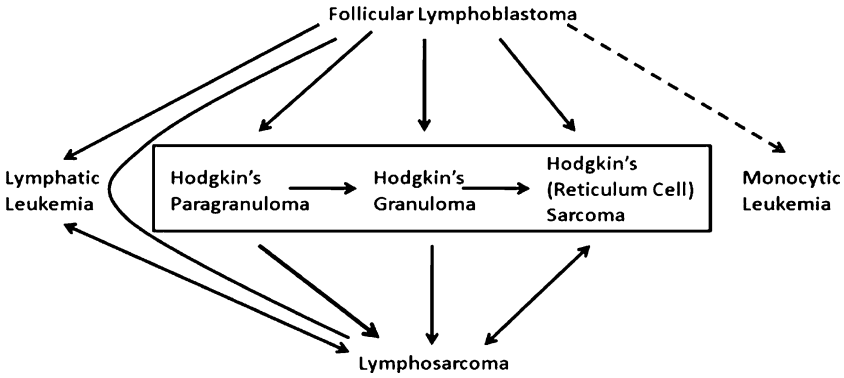

Fig. 6 Custer's 'fluid lymphoma' diagram (redrawn from Custer RP, Borderlands Dim in Malignant Disease, 1953 [30]; a more complex evolution appeared in Custer, 1960 [31])

His chapter on 'Tumours of Lymphoid Tissue' [32, Ch. 49] opens with the words: '*Nowhere in pathology has a chaos of names so clouded clear concepts as in the subject lymphoid tumors*'. Willis's own views come across clearly. As already noted, he found Robb-Smith's classification *'praiseworthy'* but guilty of clouding the *'essential unity of lymphoid neoplasms'*. Willis recognized just four groups: follicular lymphoma, lymphosarcoma, Hodgkin's disease, and reticulum cell sarcoma, stating that *'combinations and transitions will cause us perplexity only if we allow the names of our four main groups to assume the status of distinct species'* [32].

From Rappaport to Lennert, Lukes, and Collins

Although, in the final analysis, mistaken in his major premises, Henry Rappaport (1913–2003) had a major impact. In 1956, Rappaport and colleagues [34] reported a series of 253 cases of 'follicular lymphoma' from the Armed Forces Institute of Pathology (AFIP), emphasizing the use of precise morphologic criteria. They recognized 'lymphocytic and reticulum cell types', with an intermediate 'mixed' category, and clearly separated Hodgkin's disease. A flurry of other classifications occurred around this time (from Lumb 1954, Harrison 1956, Marshall 1956, Custer 1960, and Gall 1962) [9], but all were eclipsed by the final iteration of the Rappaport proposal that appeared in the 1966 AFIP Fascicle [35] (Fig. 7), albeit with significant modification, notably abandoning the reticulum cell. This publication heralded a major shift of opinion and had unforeseen consequences; it sounded the death knell of the reticulum cell, it usurped by the histiocyte, and it portended the eclipse of the fluid lymphoma school. Lymphomas came to be regarded as fixed immutable entities, distinct and distinguishable from one another, and of lymphocytic, histiocytic or 'mixed cell' derivation. Furthermore, Hodgkin's disease was effectively divorced from other lymphomas, giving rise to the unnatural term 'Non-Hodgkin lymphoma', an unfortunate separation that hampered progressive thinking for decades [12]; but that is the theme of another history (Poppema—in preparation—this series).

Rappaport's classification found favor among pathologists for its relative simplicity and ease of application. However, even as it became established in the minds of clinicians and pathologists, new discoveries in the field of cellular immunology revealed major flaws in its basic premises; the morphologic features of lymphocytes are not fixed and immutable; the large cells are not histiocytes; lymphomas are 'monoclonal' and not of 'mixed cell' origin; and, the ultimate paradox, Hodgkin's disease is a neoplasm of lymphocytes and is therefore a 'non-Hodgkin lymphoma' [12].

Immunologic concepts

The B cell emerged by one of science's favored modes of discovery; 'fortuitous accident coupled with astute observation'. In 1956, Bruce Glick was exploring the function of the bursa described in 1621 by Heironymus Fabricius (1533–1619), one of William Harvey's mentors, when a fellow graduate student, Timothy Chang, had need of

Diffuse	Nodular (follicular)
1. Lymphocytic type, well-differentiated	
2. Lymphocytic type, poorly differentiated	
3. Mixed type (lymphocyte and reticulum cell)	
4. Reticulum-cell type	
5. Hodgkin's type	

Fig. 7 Classification from Rappaport, Winter, and Hicks, 1956 [34]. In its 1966 iteration in the AFIP Fascicle [35] 'Reticulum-cell type' was usurped by 'Histiocytic and Undifferentiated types', and Hodgkin's type was divided in to paragranuloma, granuloma, and sarcoma. This classification scheme marked a watershed, the last of the purely morphology-based classification schemes

chicks in an experiment testing for antibody production after inoculation with Salmonella. By happenstance, the only chickens immediately available were the bursectomized survivors of Glick's studies; the astute observation was that these chicks failed to produce antibody [36, 37]. This seminal work failed to gain the recognition it deserved [38]. It was confirmed and extended by Max Cooper, Robert Good, and others to include also observations of the effect of thymectomy [39]. Thus, B cells (Bursa derived) and T cells (thymus derived) entered the lexicon (Fig. 8), joining the menagerie of normal cells within the lymph node from which neoplasms might be expected to derive; the advent of B and T cell lymphomas was but a matter of time.

A salvo of papers from Yoffey and colleagues at Bristol, introduced the dramatic observation that PHA (phytohemagglutinin) induced *'proliferation and transformation'* of small lymphocytes, culminating in the *'development of blast-like cells'* [40], igniting renewed speculation as to the *'Identity of the Haemopoietic Stem Cell'* [41]. These nascent cellular immunologists operated in a parallel non-connecting universe. Yet their discoveries were eventually to change the face of malignant lymphoma, radically and forever: it just took a while. The morphology of the lymphocyte was not fixed and immutable, cells changed form, but not family; the large activated cells of lymphoid tissue were not histiocytes, they were not even the reticulum cells of yore, they were 'transformed' lymphocytes. This notion was embraced by William Dameshek (1900–1969), in a brief but elegant editorial in Blood in 1963, in which he coined the term 'immunoblast' as a functional designation (Fig. 9)*: "It is recognized that such an attempt at functional nomenclature may be premature, but … After all what is language, but symbolic shorthand"* [42]*?* The impact of these observations upon strict morphologists and their serried ranks of 'classifiers' was slow to dawn, but inevitable.

Germinocytes and germinoblasts; cleaved and non-cleaved cells

Morphologists continued to do what they had always done, organize by histologic and cytologic detail, but now they began to look into the microscope through the eyes of the cellular immunologists. The tissue section was perceived as but a single frame in a moving picture that histopathologists were seeing as for the first time. There was a new cellular hierarchy to accommodate, namely immunoblasts, that were curiously plastic, appearing both to derive from, and give rise to, lymphocytes. Also, there were new functional pigeonholes, B and T types, into which the next generation of aspiring taxonomists contrived to fit lymphocytes and their neoplasms.

An intriguing retrospective of Robert Good's earlier observation (1954) [43], that patients with Bruton's agammaglobulinemia [44] lacked both germinal centers and plasma cells, set the stage for a new enlightened interest in germinal centers, their function and their neoplasms. In the proceedings of a symposium, '*Germinal Centers in Immune Responses*', held in Bern in 1966, Good and colleagues formally launched a revolution with a paper titled *'Lymphomagenesis in Relation to Germinal Centers*

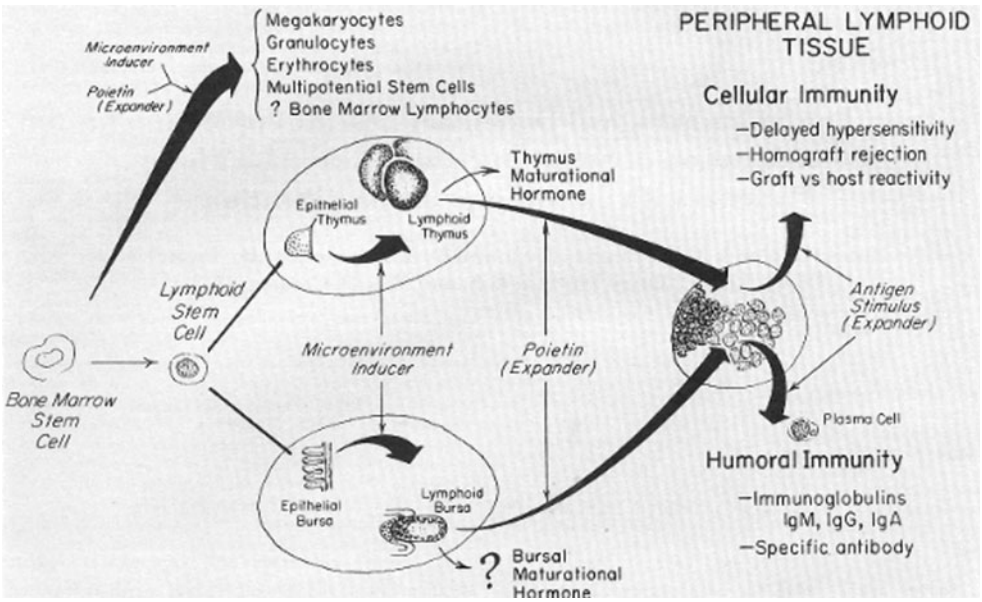

Fig. 8 Schematic defining differentiation of the bone marrow stem cell. Modified from Good RA. Immunologic Deficiency Diseases in Man. Birth Defect Series, p18, Vol. IV 1968 (variant appeared in Lymph Node Biopsy p. 16 [9])

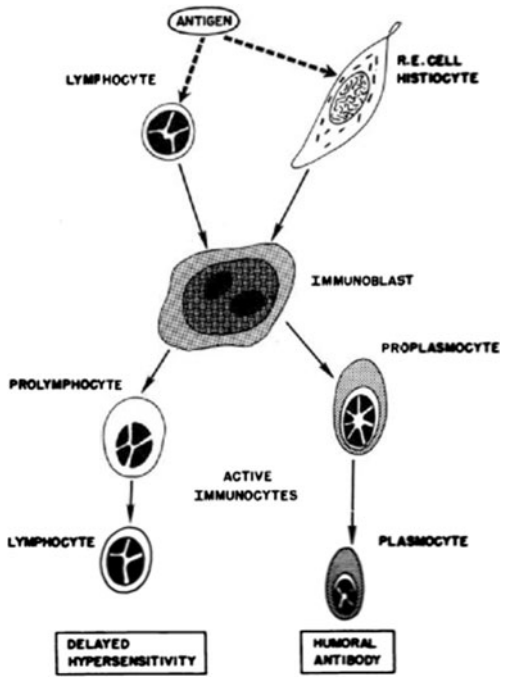

Fig. 9 Dameshek's depiction of the 'immunoblast'. Note that the R.E. (reticulo-endothelial) cell/histiocyte as 'progenitor' had yet to die a decent death, reflecting the final years of the reticulum cell sarcoma and histiocytic lymphoma nomenclature (from 'Immunoblasts and Immunocytes', 1963 [42])

Fig. 10 Walther Flemming, initially of the University of Prague, and then at Kiel

and the Bursa of Fabricius' [45]. Karl Lennert presented on the electron microscopic features of the germinal center at the same conference and came under the spell of the immunologists.

Walther Flemming's (1843–1905) (Fig. 10) book, *Zellsubstanz, Kern und Zelltheilung* (1882) [46] was in some respects the first cytogenetics text. Flemming coined the words 'chromatin' and 'mitosis' (Gr thread) to describe the separation of fine threadlike structures in dividing cells, stained red with 'new' synthetic aniline dyes. Flemming also described 'germinal centers', anticipating with remarkable prescience the generative nature of the cells therein (*"omnis nucleus e nucleo"*, paraphrasing Virchow's *"omnis cellula e cellula"*). Karl Lennert, fittingly also at Kiel, added hauntingly beautiful drawings of the component cells of the germinal centers, and by 1968 he and others were beginning to speculate anew as to their role and function.

The time was ripe for *'new thinking on old thoughts'* [47], at first sporadic, then a trickle, soon becoming a torrent that culminated in a deluge of 'new classifications'; these still were primarily morphologic, but at the same time attempted to incorporate immunologic criteria. Debate was fierce, and not always bloodless. By the end of a decade of *'nosologic frenzy'* [48], from among more than a dozen offerings, *'only two classification schemes had survived even this brief test of time'* [49]. These were the Kiel Classification [50], embracing the *'centrocytes and centroblasts'* of Lennert, and the Lukes–Collins classification with its *'cleaved and non-cleaved'* follicular center cells [51].

The impact of technology—combining immunology and morphology

Subsequent studies by Karl Lennert and his group in Kiel [52], and Robert Lukes (1922–1994), with John Parker and others [53] at the University of Southern California in Los Angeles examined the relative merits of 'multiparameter' approaches (Figs. 11 and 12). Eventually, the principal parties (Fig. 13) agreed formally that the major classifications were 'more alike than different' [54]. Increasingly morphologic opinion was shaped, even replaced, by scientific evidence, as immunologic methods of cell identification began to find application in the diagnostic arena. The technology advanced rapidly. Sheep red cells (T cells) and surface immunoglobulin (B cells) had their day, but were soon supplanted by several interrelated advances that continue to the present. In Robb-Smith's department in Oxford, one of the authors (CRT) with Ian Burns, shortly to be joined by David York Mason (1941–2008), adapted the immunoperoxidase technique for use on formalin paraffin sections [55], for the first time permitting direct correlation of traditional morphologic features with immunologic criteria for recognition of cells. The method was immediately applied to lymphomas, using Robb-Smith's Oxford

Fig. 11 The Multiparameter Approach. New Approaches to the Evaluation of Lymphoproliferative Diseases; The 8th Course 1982, faculty; *left* to *right*: Stebbins B. Chandor, John W. Parker, Robert D. Collins, Robert J. Hartsock, Alexandra Levine, Robert J. Lukes, A. Bowdler, Clive R. Taylor (author, CRT, personal collection)

series [56], and transferred to Los Angeles was incorporated into the multiparameter approach of Lukes and colleagues [53]. The method was limited at first to the few antibodies (antisera) that were effective in fixed tissues. The discovery of the hybridoma method [Georges Köhler (1946–1995) and César Milstein (1927–2002)] [57] soon solved that problem, facilitating the production of monoclonal antibodies, literally in their thousands. Today, with antigen retrieval, developed by Shan-Rong Shi and colleagues in the early 1990s [reviews; 58, 59] and improved detection systems, a hundred or so of these antibodies are in use for phenotyping leucocytes in formalin paraffin sections. Many of these same antibodies also find application for leucocyte phenotype studies by 'flow cytometry', a field that advanced enormously in capability and sophistication, and also contributed to the 'reshaping' of morphologic classifications.

One key consequence of this rapid expansion of immunologic techniques, and their diversity, was that no one pathologist, however expert, could maintain currency

Fig. 12 Early variants of the Lennert (Kiel) and Lukes and Collins classification, as compared by Hansen JA and Good RA in Human Pathology in 1974 (taken from Robb-Smith and Taylor, 1980 [9]). These two classifications continue to form the basis of the current consensus WHO classification [5]

Lennert	Lukes and Collins
I. Undefined (not B or T) stem cell, (?) precursor cell (?)	
II. B-cell (lymphocytic) types	
1. Chronic lymphatic leukemia	1. Small lymphocytic type chronic lymphatic leukemia
2. Lymphoplasmacytoid immunocytoma	2. Plasmacytoid lymphocytic
3. Germinal center cell tumors	3. Follicle center cell tumors (follicular, diffuse, sclerotic)
a. Diffuse germinocytoma b. Germinoblastoma (follicular, diffuse, sclerotic)	a. Cleaved follicle center cell tumors
c. Germinoblastic sarcoma d. Paraleukoblastic (B-lymphoblastic) sarcoma including Burkitt's lymphoma	b. Noncleaved follicle center cell tumors 1. Small (Burkitt) 2. Large
4. Immunoblastic (reticulo-) sarcoma, B-cell type	4. Immunoblastic (reticulum cell) sarcoma, B-cell type
III. T-cell (lymphocytic) types	
1. Sézary syndrome	1. Sézary syndrome
2. ? Lymphoblastic sarcoma (acute lymphoblastic leukemia), T-cell type	2. Convoluted lymphocytic (acute lymphoblastic leukaemia), T-cell type
3. Chronic lymphatic leukemia, T-cell type	3. Small lymphocytic type (chronic lymphatic leukemia), T-cell type
IV. Reticulohistiocytic, M-cell types	
1. Reticulosarcoma, M-cell type	1. Histiocytic
V. Unclassifiable	

Fig. 13 'An Exaltation of Experts' [67]; collaborative efforts. The 1979 NIH Pathology Panel for the Working Formulation of Non-Hodgkin Lymphoma, Stanford University. *Left* to *right*: Koji Nanba, Gerhard Krueger, Ronald Dorfman, Gregory O'Conor, Karl Lennert, Alistair HT Robb-Smith, Henry Rappaport, Martin Sacks, Kristin Henry, Robert J. Lukes, Robert J. Hartsock, Costan Berard (author, RJH, personal collection)

in all. Conferences became more productive of collaboration; individualistic classifications ceased to be born, and 'working groups' (Fig. 13) developed consensus documents that evolved in a collegial fashion [60]. From these efforts there emanated a series of evolving classifications. Most importantly from the International Lymphoma Study Group in 1994 came the Revised European-American Lymphoma Classification (REAL classification) [60, 61] providing the basis for the WHO 2001 version [62], which in turn became WHO 2008 [5] being the most recent iteration and the classification used worldwide today, without significant challenge. The essence of this recent history has been well summarized elsewhere [60–62] and will not here be repeated.

Back to the future. The continuing impact of technology—molecular morphology

> "History is the essence of innumerable biographies."
> (Thomas Carlyle, 1795–1881).

So what is there to learn from this history as we return to this twenty-first century? That remarkable pathologists, men and women, have made a difference, but it has been the relentless advance of technology that has given effect to their creativity.

Just as the microscope, 150 years past, transformed medical research from the study of whole bodies and organs to a new microscopic level of tissues and cells, so modern molecular methods are forcing another transformation, down to the sub-cellular level of genes and molecules. The classification of lymphomas began in the age of microscopy, but it will go forward into the age of 'molecular morphology'. The seeds of tomorrow already may be seen. Each 'entity' in the WHO monograph is identified first by morphology, but then further qualified by immunologic phenotype, and in some instances by gene signature (genotype).

This approach was in fact not new; the use of 'genetic information' for classification of hematopoietic neoplasms may be traced back to 1960, to a simple one page paper in which Nowell and Hungerford described a certain 'minute chromosome in human granulocytic leukemia' [63]. Further discoveries awaited the advent of an enabling technology. Again this came from a parallel largely unconnected universe, this time a *'small oncogenic virus SV40, (that) contains double-stranded covalently-closed circular DNA'* [64]. In this 1971 paper, Dan Nathans and his graduate student, Kathleen Danna, used *'a bacterial restriction endonuclease … to produce specific fragments of SV40 DNA'*, thereby forging the first link in an unlikely chain that waited a further decade before 'fortuitous accident and astute observation' once more propelled science forward. Kary Mullis, in his own words: *"Sometimes a good idea comes to you when you are not looking for it. Through an improbable combination of coincidences, naivete and lucky mistakes, such a revelation came to me one Friday night in April 1983, as I gripped the steering wheel of my car and snaked along a moonlit mountain road into northern California's redwood country. That was how I stumbled across … the polymerase chain reaction (PCR)"* [65].

This was new machinery. Molecular genetics, 'genomics', was born. Technical progress has been exponential and astonishing. On the one hand, the human genome has been mapped almost in its entirety; on the other, it has been dissected to the level of single nucleotide pairs (SNPs). 'Genomics', in 2010, already is part of our daily lexicon, extending beyond the compass of mere 'classifiers of lymphoma' to 'Time' magazine, the popular press and the universe of the 'internet'. Inevitably molecular methods have been applied to the lymphomas and related entities, generating a wealth of new information that must await future histories for full address. Chips for performance of mRNA expression arrays are widely available (at a price) and are in regular use for research in lymphoma. Already we know that many lymphomas show characteristic genetic changes, exemplified by the translocations present in B cell lymphomas, readily demonstrable by FISH and chips (fluorescent in situ hybridization and expression arrays). In the WHO monograph [5], many lymphomas characterized first by morphology, then by phenotype and, or, genetic data. Molecular Morphology is not perfect, but it is here.

Phenotype is a portrait of protein expression, falling under the general rubric of proteomics. Some 30,000 genes are mapped in the human genome, but may yield an astonishing 1,000,000 or so proteins. While the genome determines which proteins will be expressed, it is the actual expression of proteins that is the precise measure of the cell and its function. Phenotypic studies with monoclonal antibodies already contribute to lymphoma diagnosis in important, perhaps essential ways, but only 100 or so proteins are 'routinely' open to examination by IHC or 'flow cytometry'. New methods such as mass spectrometry and reverse phase protein arrays (RPPA) applied to extracts of formalin fixed paraffin-embedded tissues already have the capability of identifying hundreds to thousands of proteins in a single tissue, and are beginning to correlate those findings back to cells as 'liquid morphology' [66].

If we have learned anything from the past, it is the certainty that the full flowering of genomics and proteomics will identify cells and tumors with a degree of discrimination and accuracy far beyond anything we can envisage today, just as our present methods are far removed beyond the imagination of the early microscopists. Once more, an exaltation of experts [67] gathers in the wings, latter-day taxonomists, disciples of the molecule and of the gene, gleefully whetting the edge of Occam's razor. But that is another history for another day.

Acknowledgments The authors would like to thank the Editorial Board of Virchows Archiv for the opportunity to develop this history, in particular Fred Bosman, M.D. and Jan Van den Tweel, M.D. for encouragement and review.

We declare that we have no conflict of interest.

References

1. Linnaeus C (1756) Systema Naturae, 9th edn. Theodor Haak, Leiden (Lugdunum Batavorum)
2. Darwin CR, Wallace AR (1858) On the tendency of species to form varieties; and on the perpetuation of varieties and species by natural means of selection. Journal of the Proceedings of the Linnean Society of London Zoology 3:46–50 [Read 1st. July, 1858]
3. Barlow N (1958) The autobiography of Charles Darwin 1809–1882. Collins, London, p 122
4. Virchow R (1858) Die Cellularpathologie in ihrer Begrundung auf physiologische und pathologische Gewebelehre. Berlin. Verlag von August Hirschwald, Berlin (English translation). Chance F (1860) Cellular Pathology. John Churchill, London. Reissued; Classics of Medicine Library, Birmingham. Alabama, 1979, pp 170–171
5. Swerdlow SH, Campo E, Harris NL et al (2008) WHO classification of tumors of the haematopoietic and lymphoid tissues. IARC. WHO, Geneva
6. Taylor CR (2010) From anatomy to surgery to pathology: eighteenth century London and the Hunterian schools. Virchows Arch 247:405–414
7. Hodgkin T (1832) On some morbid appearances of the absorbent glands and spleen. Med-Chir Trans 17:68–114
8. Wilks SS (1865) Cases of enlargement of the lymphatic glands and spleen (or Hodgkin's Disease) with remarks. Guy's Hosp Rep 11:56–67
9. Robb-Smith AHT, Taylor CR (1980) Lymph node biopsy. Oxford University Press, Oxford
10. Greenfield WS (1878) Specimens illustrative of the pathology of lymphadenoma and leucocythemia. Trans Path Soc Lond 29:272–304
11. Taylor CR (1978) A history of the Reed–Sternberg cell. Biomedicine 28:196–203
12. Taylor CR (2005) Hodgkin's disease is a non-Hodgkin lymphoma. Hum Pathol 36:1–4
13. Aschoff L (1924) Das reticulo-endotheliale system. Ergebn inn Med Kinderheilkd 26:1–118
14. Maximow AA (1927) In: von Mollendorf W (ed) Handbuch der Mikrosp Anat des Menschen, II. Springer, Berlin, p 359
15. Maximow AA (1909) Der Lymphozyt als gemeinsame Stammzelle der verschiedenen Blutelemente in der embryonalen Entwicklung und im postfetalen Leben der Säugetiere. (Demonstrationsvortrag, gehalten in der ausserordentlichen Sitzung der Berliner Hämatologischen Gesellschaft am 1. Juni, 1909). Folia Haematol 8:125–134
16. Adami JG (1913) On the relationship between tumours proper (blastomas) and hyperblastosis. Communicated to the Pathological Section of the 17th International Medical Congress, London, August 1913. Can Med Assoc J III:953–961. Available at http://www.ncbi.nlm.nih.gov. Accessed June 2010
17. Letterer E (1924) Aleukamische Retikulose: Ein Beitrag zu den proliferativen Erkrankungen des Retikuloendothelialapparates. Frankf Z Pathol 30:377–394
18. Oberling C (1928) Les reticulosarcomes et les reticulo-endothelialsarcomes de la moelle osseuse (sarcomes D'Ewing). Bull Cancer (Paris) 17:259
19. Ewing J (1928) The classification and treatment of bone sarcoma. Report of the International Conference on Cancer 17th to 20th of July 1928, 3rd ed. John Wright and Sons Ltd, Bristol. Simkin Marshall Ltd, London, p 365
20. Callender GR (1934) Tumors and tumor-like conditions of the lymphocyte, the myelocyte, the erythrocyte and the reticulum cell. Am J Pathol 10:443–466

21. Robb-Smith AHT (1938) Reticulosis and reticulosarcoma: a histological classification. J Path XLVII:457–480
22. Robb-Smith AHT (1947) In: Dyke SC (ed) Recent advances in clinical pathology. Churchill, London, p 350
23. Jackson H, Parker F (1947) Hodgkin's disease and allied disorders. Oxford University Press, New York
24. Lennert K (1967) In: Ruttiman AG (ed) Progress in lymphology. Thieme, Stuttgart, p 103
25. Mallory FB (1914) The principles of pathological histology. Saunders, Philadelphia
26. Warthin AS (1931) The genetic neoplastic relationships of Hodgkin's disease. Ann Surg 93:153–161
27. Pullinger BD (1932) In: Gordon MH (ed) Rose research on lymphadenoma. Wright, Bristol, p 117
28. Gall EA, Mallory FB (1942) Malignant lymphoma. A clinicopathological survey of 618 cases. Am J Pathol 18:381–429
29. Custer RP, Bernhard WG (1948) The interrelationship of Hodgkin's disease and other lymphatic tumors. Am J Med Sci 216:625–642
30. Custer RP (1953) Borderlands dim in malignant disease. Radiology 61:764–770
31. Custer RP (1960) The changing patterns of lymphocytic malignancies. In: Rebuck JW (ed) The lymphocyte and lymphocytic tissues. International Academy of Pathology Monograph. Hoeber, New York, pp 181–193
32. Willis RA (1960) Pathology of tumours, 1st edn. Butterworths, London, 1948
33. Willis RA (1958) The borderland of embryology and pathology. Butterworths, London
34. Rappaport H, Winter WJ, Hicks EB (1956) Follicular lymphoma. A re-evaluation of its position in the scheme of malignant lymphomas based on a survey of 253 cases. Cancer 9:792–821
35. Rappaport H (1966) Tumors of the hematopoietic system (atlas of tumor pathology, section 3, fasc. 8). Armed Forces Institute of Pathology, Washington
36. Chang TS, Glick B, Winter AR (1955) The significance of the bursa of Fabricius of chickens in antibody production. Poultry Sci 34:1187
37. Glick B (1955) Growth and function of the bursa of Fabricius in the domestic fowl. Ph.D. thesis, Ohio State University
38. Sternberg SS (2003) Bottoms up to a Nobel-worthy chicken's bottom. Am J Surg Pathol 27:1471–1472
39. Cooper MD, Peterson RDA, Good RA (1965) Delineation of the thymic and bursal lymphoid systems in chickens. Nature (Lond) 205:143–146
40. Yoffey JM, Winter GCB, Osmond DG et al (1965) Morphological studies in the culture of human leucocytes with phytohaemagglutinin. Brit J Haematol 11:488–497
41. Moffatt DJ, Rosse C, Yoffey JM (1965) Hypothesis. Identity of the haematopoietic stem cell. Lancet 290:547–548
42. Dameshek W (1963) Editorial: "immunoblasts" and "immunocytes"—an attempt at a functional nomenclature. Blood 21:243–245
43. Good RA (1954) Agammaglobulinemia: an experimental study. Am J Dis Child 88:625–626
44. Bruton OC (1952) Agammaglobulinemia. Pediatrics 9:722–728
45. Peterson RDA, Burmester BR, Cooper MD, Good RA (1967) Lymphomagenesis in relation to germinal centers and the bursa of Fabricius. In: Germinal center in immune responses. Springer, New York, pp 443–446
46. Flemming W (1882) Zellsubstanz, Kern und Zelltheilung. Vogel, Liepzig
47. Taylor CR (1978) Classification of lymphomas: 'new thinking' on old thoughts. Arch Pathol Lab Med 102:549–554
48. Taylor CR (1982) Pathobiology of lymphocyte transformation. In: Ioachim HL (ed) Lecture, Leukemia Research Fund Symposium, Royal College of Physicians, London, April, 1981. Pathobiology Annual 1982. Raven, New York, pp 65–83
49. Taylor CR (1980) Changing concepts in classification of lymphoma. In: Bosman F, van den Tweel J, Taylor CR (eds) Malignant lymphomas, the pathophysiology of the lymphocyte and its neoplasms. Leiden University Press, Leiden, pp 175–184
50. Gerard Marchant R, Hamlin I, Lennert K et al (1974) Classification of non-Hodgkin's lymphomas. Lancet II:405–408
51. Lukes RJ, Collins RD (1974) A functional approach to the classification of the lymphomata. Rec Res Cancer Res 46:18–30
52. Musshoff K, Schmidt-Vollmer H, Lennert K, Sandritter W (1976) Preliminary clinical findings on the Kiel classification of malignant lymphomas. Z Krebsforsch 87:229–238
53. Lukes RJ, Parker JW, Taylor CR et al (1978) Immunologic approach to non-Hodgkin's lymphomas and related leukemias. An analysis of the results of multiparameter studies of 425 cases. Semin Hematol 15:322–351
54. Lennert K, Collins RD, Lukes RJ (1983) Concordance of the Kiel and Lukes–Collins classifications of non-Hodgkin's lymphomas. Histopathology. Intersciences.Wiley.com
55. Taylor CR, Burns J (1974) The demonstration of plasma cells and other immunoglobulin-containing cells in formalin-fixed, paraffin-embedded tissues using peroxidase-labelled antibody. J Clin Pathol 27:14–20
56. Taylor CR (1974) The nature of Reed–Sternberg cells and other malignant reticulum cells. Lancet II:802–807
57. Kohler G, Milstein C (1975) Continuous cultures of fused cells secreting antibody of predefined specificity. Nature 256:495–497
58. Shi S-R, Cote RJ, Taylor CR (2001) Antigen retrieval immunohistochemistry and molecular morphology in the year 2001. Appl Immunohistol Mol Morphol 9:107–116
59. Shi SR, Taylor CR (eds) (2010) Immunohistochemistry and antigen retrieval based research and diagnosis. Wiley, Hoboken
60. Harris NL, Jaffe ES, Diebold J et al (2000) Lymphoma classification—from controversy to consensus: the R.E.A.L. and WHO Classification of lymphoid neoplasms. Ann Oncol S 1:3–10
61. Harris NL et al (1994) A revised European-American classification of lymphoid neoplasms: a proposal from the International Lymphoma Study Group. Blood 84:1361–1392
62. Jaffe ES, Harris NL, Stein H, Vardiman JW (eds) (2001) World Health Organization classification of tumours. Pathology and genetics of tumours of haematopoietic and lymphoid tissues. IARC, Lyon
63. Nowell PC, Hungerford DA (1960) A minute chromosome in human chronic granulocytic leukemia. Science 132:147
64. Danna K, Nathans D (1971) Specific cleavage of simian virus 40 DNA by restriction endonuclease of *Hemophilus influenzae*. Proc Nat Acad Sci 68:2913–2917
65. Mullis KB (1990) The unusual origin of the polymerase chain reaction. Scientific American, April, pp 56–65
66. Taylor CR, Becker KF (2011) Liquid morphology: immunochemical analysis of proteins extracted from formalin fixed paraffin embedded tissues: combining proteomics with immunohistochemistry. Appl Immunohistochem Mol Morphol 19:1–9
67. Taylor CR (1994) Viewpoint: an exaltation of experts: concerted efforts in the standardization of immunohistochemistry. Appl Immunohistochem 1:232–243, Reproduced in Hum Pathol 25:2–11, 1994

Virchows Arch (2011) 458:649–657
DOI 10.1007/s00428-011-1075-0

REVIEW AND PERSPECTIVE

The Kaiser's cancer revisited: was Virchow totally wrong?

Antonio Cardesa · Nina Zidar · Llucia Alos · Alfons Nadal · Nina Gale · Günter Klöppel

Received: 28 March 2011 / Accepted: 30 March 2011 / Published online: 15 April 2011
© Springer-Verlag 2011

Abstract On 15 June 1888, the German Emperor, Kaiser Friedrich III, died of laryngeal cancer. Three biopsies of his laryngeal lesion had been taken by the British laryngologist, Morel Mackenzie, in 1887 and diagnosed by Rudolf Virchow as "pachydermia verrucosa laryngis", confirming Mackenzie's assessment that the Kaiser's disease was benign. A fourth specimen coughed up by the patient was considered by Virchow to be nondiagnostic. A further specimen expectorated by the patient 3 months before his death was diagnosed as carcinoma by Wilhelm Waldeyer. The autopsy revealed squamous carcinoma in the larynx with a cervical lymph node metastasis. The discrepancies between the initial diagnoses and the final outcome of the Kaiser's disease gave rise to a never-ending medical controversy. Our investigations on this historical case were limited to the official German documents and publications and their English translations and to subsequent literature sources of the time, after having received confirmation that the histological slides and Virchow's original reports had been lost. Based on current surgical pathology knowledge, we propose that the tumour that challenged the diagnostic skills of the founder of pathology was hybrid verrucous carcinoma (HVC), an extremely rare, metastasizing variant of verrucous carcinoma (VC) composed of pure VC mixed with clusters of conventional squamous cell carcinoma. As we see it now, Virchow was therefore not totally wrong. Our retrospective evaluation suggests that Virchow's detailed description of the Kaiser's cancer preceded the paper that contributed to the full understanding of HVC of the larynx by 110 years.

Keywords Kaiser's cancer · Larynx · Hybrid verrucous carcinoma · Mixed verrucous and squamous cell carcinoma

Dedication This article is dedicated in memory of Mario A. Luna, a distinguished member of the Head and Neck Working Group of the European Society of Pathology and one of the great pathologists who initially contributed to the knowledge of hybrid verrucous carcinoma.

A. Cardesa (✉) · L. Alos · A. Nadal
Anatomia Patologica, Facultat de Medicina, Hospital Clinic, Universitat de Barcelona, Institut D'Investigacions Biomediques August Pi i Sunyer (IDIBAPS),
Villarroel 170,
08036 Barcelona, Spain
e-mail: acardesa@clinic.ub.es

L. Alos
e-mail: lalos@clinic.ub.es

A. Nadal
e-mail: anadal@clinic.ub.es

N. Zidar · N. Gale
Institute of Pathology, Faculty of Medicine,
University of Ljubljana,
Korytkova 2,
1000 Ljubljana, Slovenia

N. Zidar
e-mail: nina.zidar@mf.uni-lj.si

N. Gale
e-mail: nina.gale@mf.uni-lj.si

G. Klöppel
Department of Pathology, Consultation Center of Pancreatic and Endocrine Tumors, Technical University of München,
Ismaningerstr. 22,
81675 Munich, Germany
e-mail: guenter.kloeppel@alumni.uni-kiel.de

Historical perspective

On 15 June 1888, the German Emperor, Kaiser Friedrich III, died of laryngeal cancer at the New Palace in Potsdam. He was 57 years old and had reigned for only 99 days. While still Crown Prince Friedrich Wilhelm, he had been treated by Morel Mackenzie, Britain's leading laryngologist, who

Fig. 1 Crown Prince Friedrich Wilhelm chatting with Virchow who is dressed in red robe and others during a court ball in 1878. Painting by Werner

maintained for a long time, contrary to the opinion of German laryngologists that the disease was a benign wart and not a cancer [1–7]. Three biopsies of the Crown Prince's laryngeal lesion were taken by Mackenzie in 1887 and diagnosed by Rudolf Virchow, the founder of "cellular pathology" and the world's foremost pathologist of the time, as a benign lesion, "pachydermia verrucosa laryngis" [3, 8, 9]. A fourth specimen coughed up by the patient was considered by Virchow to be nondiagnostic [10]. A further specimen, spontaneously expectorated by the patient on 4 March 1888, 3 months before his death, was diagnosed as carcinoma by Wilhelm Waldeyer [3], known for his description of "Waldeyer's ring" and his work on the development of carcinomas [11]. The autopsy was performed by Virchow himself, assisted by Wilhelm Waldeyer and Paul Langerhans, who first described the pancreatic islets and the specialized dendritic cells of the skin that both bear his name. It revealed squamous carcinoma in the larynx and a metastasis in one cervical lymph node [12]. The early death of Kaiser Friedrich III generated enduring political controversies, as it was considered to have dramatically influenced the course of the subsequent political development in Europe [5, 6], a topic that was lucidly discussed and accurately put into perspective by Ober [7]. Furthermore, the seeming discrepancies between the initial clinical and pathological diagnoses and the final outcome of the August patient (Figs. 1, 2) were not understood at that time. They gave rise to a bitter and continuous medical controversy, which has never been brought to a satisfactory close [13]. In this paper, we present a novel interpretation of the difficulties and potential diagnostic pitfalls that may have been lurking behind the case of the Kaiser's cancer and provide new insights based on current surgical pathology knowledge [14, 15].

Information regarding the histological slides containing the biopsy and autopsy specimens and the original reports written by Virchow in German was requested from Professor Manfred Dietel, director of the Department of Pathology of the Charité in Berlin, Germany. He answered as follows: "Unfortunately, the histological sections and the autopsy protocol of the Kaiser's cancer were lost during the war". This statement was confirmed by the director of the "Berliner Medizinhistorisches Museum" of the Charité, Professor Thomas Schnalke. This unfortunate fate presumably occurred during the last days of the Second World War, when Virchow's Institute was almost entirely destroyed.

Therefore, our sources of information were limited to the German publications and the translations of Virchow's original reports into English and to the additional documents available in the English medical literature on the subject. These were fortunately abundant, because Friedrich III was married to Crown Princess Victoria, the oldest daughter of Queen Victoria of England. According to Lin

Fig. 2 Photograph of Kaiser Friedrich III, probably at the beginning of his 99-days reign

[16], all of Virchow's pathological reports were translated into English and recorded in Mackenzie's book [3] or published in the *British Medical Journal* or the *Lancet*. Moreover, we correlated all of this documentation with the histopathological descriptions of the various types of laryngeal carcinomas and their distinctive biological behaviours according to the latest (2005) WHO classification of head and neck tumours [14].

Among the English translations of the official German documents of the time [2, 8–10, 12] and of contemporary or subsequent historical literature sources [3–7, 13, 17], we selected as leading reference for our approach the review written by William B. Ober in 1970 [7]. In this comprehensive and historically well-documented article, the medical records and the histopathological descriptions of the Kaiser's laryngeal cancer are presented as case report in such a straightforward manner that it most adequately suits our purposes:

> The patient, a 56-year-old man, pipe smoker [18], previously in good health, contracted an upper respiratory infection in the autumn of 1886. It lingered unduly and was followed by mild hoarseness in January 1887. He was treated by his Physician-in-Ordinary (Dr. Wegner) with gargles and inhalations. Hoarseness persisted, and laryngoscopy by a consulting physician (Prof. Gebhardt) on March 6, 1887, revealed a sessile nodule 4×2 mm on the left vocal cord. Both vocal cords moved freely. Attempted removal by snare, then by ring-knife, failed because the nodule was flat, smooth and hard. Under cocaine for local anesthesia, galvanocautery was applied 3 times between March 8 and March 21, but re-examination showed it had increased in size. Between March 29 and April 7, galvanocautery was applied daily (10 times). Following this treatment, the patient was sent to a spa for convalescence; inhalations and douches were prescribed. It was noted that the surface of the lesion did not heal, and the suspicion of carcinoma was first voiced at this time.
>
> Reexamination by a clinical consultant, Professor von Bergman, on May 16 revealed "a growth that cannot be got at from inside the throat, as it may also exist under the larynx in a fold, where it cannot be reached." Because the possibility of carcinoma was strongly entertained, laryngofissure was recommended.
>
> Prince Bismark intervened, and the proposed operation was deferred pending on consultation. A panel of consultants, including Professor Tobold, the senior laryngologist in Berlin, examined Friedrich on May 18. Tobold's opinion was that the lesion "could be considered a cancer without any other diagnosis." …

After some discussion among the attending physicians Morel Mackenzie was selected to perform the operation, and he was summoned from London (via the Crown Princess to Queen Victoria by Sir James Reid, the Queen's resident physician).

On May 20 Mackenzie consulted for the first time with the German physicians, and then examined the patient. There was no pain, no difficulty in swallowing, and no obstruction to breathing. Laryngoscopy revealed "a growth about the size of a split pea at the posterior part of the left vocal cord . . . pale pink, slightly rough on the surface, but not lobulated . . . a portion of the growth disappeared from view . . . it was partly attached to the under-surface as well as the side of the vocal cord . . . partly subglottic in situation. There was no trace of ulceration . . . to the naked eye it bore the look of a simple wart or papilloma."

Mackenzie suggested surgery be deferred until the nature of the process was established by transoral biopsy. On May 21 using an unfamiliar instrument, his own being in London, he succeeded in removing a small fragment of superficial tissue. Microscopic examination by Virchow, reported two days later, revealed a "very superficial piece of mucous membrane . . . to which at one spot only a somewhat shred of deeper tissue adhered. In a few spaces, nests of epithelial cells had originated. Thus nothing was found that contradicted a simple irritative process".

Rebiopsy was scheduled for May 25, Mackenzie's own instruments having arrived, but was not carried out because of local congestion and edema. The second biopsy was performed on June 8, and Mackenzie succeeded in removing more than half the growth from the vocal cord. Virchow's examination described two fragments of tissue, the larger 3× 2.5 mm, the smaller 2 mm in diameter. Microscopic examination showed thickening of the squamous epithelium with papillae formation, but there was no invasion of the underlying connective tissue by epithelial nests. The submucosa was richly vascular and congested. Virchow's diagnosis was pachydermia verrucosa and he concluded his report with a favourable prognosis, but cautioned whether such an opinion would be justified with respect to the entire disease or could be certain from the two portions removed. He added that there was nothing in the biopsy likely to arouse suspicion of more widespread or more serious disease.

Virchow lectured on "pachydermia laryngis" to the Berlin Medical Society on June 27, letting it be understood that the Crown Prince's illness was his

point of departure. In the mean time, following the second biopsy, the Crown Prince's symptoms had improved, and he was able to attend in London Queen Victoria's Golden Jubilee on June 21. During this period, he continued under treatment by Mackenzie. Dr. Wegner, his Physician-in-Ordinary was also in attendance.

On June 28, the patient's symptoms were much relieved; laryngoscopy showed that local congestion and oedema had subsided. Accordingly, using his own instruments, in his own office, in the presence of Wegner, Mackenzie performed a third biopsy which was sent to Berlin for pathologic examination. It was an apparently adequate biopsy, and Virchow's report was translated and published in England [9]. It merits extensive quotation: "The object was in absolute alcohol, in one piece, and though somewhat shrivelled, was well preserved. It had a flat base of longish oval form, 5 mm long and 3 mm broad, upon which was a small semi-spherical granular surface about 2 mm high… Further examination showed that the flattened base consisted of club-shaped, rounded papillary outgrowths lying in juxtaposition… Microscopic examination showed still more decisively than the previous occasion that the surface of the excised portion was almost wholly occupied by papillary outgrowths of various size. Only in the immediate neighbourhood of the surface of excision was there found a small zone of perfectly smooth, superficial, tissue. Within the papillae, the large and hard epithelial cells, in layers and flattened towards the outer parts, represented by far the chief portion of the new formation; the connective tissue framework was thin, soft and vascular. No peculiar cell-formation was observed … No alveolar structure, or deposition, or penetration of epithelial cell masses could anywhere be perceived in this tissue … Nowhere did this proliferation reach the character of an independent centre or formation. Thus, this excised portion, in a still higher degree than was the case with the portions obtained in previous operations, has shown itself to be a hard, warty growth, that has started from a moderately irritated and thickened surface, and the examination of its base has not afforded the least support for the idea of a new formation penetrating inwards".

This report was reassuring and the Crown Prince's symptoms remained silent. He continued his visit to England until September 3, when on Mackenzie's advice, he avoided returning to Berlin and went to the milder climate of the Tyrol. … From there Friedrich went to Venice, then Lake Maggiore, and finally to San Remo where he arrived, accompanied by Mark Howell, Mackenzie's assistant, on November 3, 1887. From this point Friedrich's condition began to deteriorate:

On November 4 Howell noticed increased subglottic swelling and summoned Mackenzie. Laryngoscopy on November 6 revealed the left arythenoid swollen and bright pink. There was a subglottic tumour half an inch below the left vocal cord and a smaller one behind the right vocal cord.

The patient was informed that "a very unfavourable change had taken place". He asked: "Is it cancer?" Mackenzie replied: "I am sorry to say, sir, it looks very much like it, but it is impossible to be certain". Mackenzie requested immediate consultation with von Schrötter, who arrived on November 9. At the request of the patient's son, Dr. Moritz Schmidt of Frankfurt, a prominent laryngologist, was also called in consultation. Professors Gebhardt and von Bergman came from Berlin. The question of syphilis was raised, and potassium iodide medication was suggested, even given, but on November 10 von Schrötter delivered the combined opinion to the patient and his family that the disease was malignant. Alternative methods of management were discussed. The patient declined laryngectomy but agreed to submit to tracheotomy should that become necessary. A bulletin signed by Mackenzie, von Schrötter and other physicians in attendance was issued on November 13 stating: "On examining His Imperial and Royal Highness the Crown Prince's larynx, the assembled physicians have been able to establish the fact that the disease is due to a malignant new growth." In January1888 a fever developed with productive cough. The patient coughed up several pieces of slough, which were sent to Virchow for examination. Virchow reported that the majority of the tissue was necrotic; a few viable tissue fragments were present but they revealed no cancer [10]. Tracheotomy proved necessary and was done on January 8, 1888 at San Remo. A fragment of tissue spontaneously expectorated by the patient on March 4 was diagnosed by Wilhelm Waldeyer as carcinoma [3].

Kaiser Wilhelm I died on March 9, and Friedrich acceded to reign for only 99 days before he died on June 15, 1888. An autopsy, limited to the cervical and thoracic organs was performed by Virchow, assisted by Waldeyer and Langerhans. The larynx, except for the epiglottis, had been destroyed and was a large gangrenous ulcer. A nodule at the base of the epiglottis contained nests of carcinoma, and a lymph

node from the left cervical region was extensively replaced by metastatic squamous carcinoma. The immediate cause of death was septic bronchopneumonia without abscess formation. There were no pulmonary metastases; the carcinoma had not extended below the clavicles. In all probability bronchopneumonia was due to aspiration.

Even today, over 120 years after the death of Kaiser Friedrich III, the reasons for Virchow's presumed failure to diagnose the Kaiser's cancer early enough, continue to be an enigma and to intrigue historians and oncologists in general, as well as surgical pathologists specialising in head and neck, and laryngologists in particular, making this case the most controversial laryngeal cancer in the history of medicine.

In the second half of the nineteenth century, laryngology and pathology were in their inception. In 1854, the Spanish singing teacher Manuel Garcia first viewed his own vocal cords by means of a laryngeal mirror, thus initiating the use of indirect laryngoscopy for educating the voice, and shortly thereafter as a diagnostic and therapeutic procedure [19]. Although rudimentary, this instrument allowed one polypoid nodule to be removed as early as 1860 [6]. Already in 1871, Morel Mackenzie published a book advocating the use of the laryngoscope and reporting on 100 laryngeal biopsies of his own and 89 by other colleagues [20]. The first total laryngectomy for cancer was performed by Theodor Billroth in 1873; samples from that tumour were studied microscopically and a diagnosis of epidermoid carcinoma was rendered [21].

Histology began under Schleiden and Schwann in 1847 [22], and by 1863, Virchow had postulated the principle of “omnis cellula e cellula” [23]. The use of microscopy in medicine expanded after that, as Gerlach demonstrated that tissues could be stained with natural dyes [24]. Shortly thereafter, aniline dyes further improved the quality of tissue staining. By 1889, Cajal had established the individuality of the nerve cells in bird embryos while working in Barcelona [25]. This discovery supplied the last needed evidence for the validity of the cellular doctrine in all tissues, providing full support for its universal application in pathology at a crucial moment at which its use for clinical diagnosis and prognosis was being brought into question. Our retrospective interpretation is that at such an early stage of scientific medicine the reasons for the discrepancies between the initial clinical and pathological diagnoses and the fatal outcome of Kaiser Friedrich III could not be understood, because the natural history and the histopathology of the very unusual type of carcinoma afflicting him were not perceived by pathologists and laryngologists in their full significance until 110 years later.

Head and neck cancer in general and laryngeal carcinoma in particular are common cancers today all over the world, with high incidences in European countries. More than 90% of these tumours are squamous cell carcinomas (SCC) [26]. Among the nine different types of SCC of the larynx recognized by the 2005 WHO classification of head and neck tumours [14], the hybrid subtype of verrucous carcinoma (VC) [27] is the one that in our view fits Virchow's reports of the Kaiser's cancer very well. Hybrid verrucous carcinoma (HVC) is a very unusual cancer, accounting for about 0.17% of all laryngeal SCCs [28].

VC is a very well-differentiated SCC [29], occurring predominantly in men in the sixth and seventh decades of life [30]. Its aetiology has been related in 95% of the cases to the use of tobacco and alcohol [31]. Human papilloma virus genotypes 16 and 18, and also 6 and 11, have been identified in some VC [32, 33]. Approximately 90% of all head and neck VC arise in two main sites: the oral cavity (55%) and the larynx (35%) [34]. In the larynx, 85% of VC arise in the glottis, extending from there to the epiglottis, subglottis or both in about 17% of cases [28]. VC of the larynx accounts for 1–3.4% of all SCCs [35, 36] with an average of 1.7% [28]. The glottis is the single most commonly affected site, accounting for about 30% of all the head and neck cases, being followed by the gums (11.5%) and the buccal mucosa (10%) [34].

Clinically, hoarseness is the main presenting symptom of laryngeal VC [28]. Grossly, VC of the larynx usually presents as a broad-based exophytic tumour with a white keratotic and warty surface. On cut surface, it is firm to hard, tan to white, and may show keratin-filled surface clefts. It can be large by the time of diagnosis and involve contiguous structures, measuring up to 5–7 cm [28]. Microscopically (Fig. 3), VC consists of thickened club-shaped papillae and blunt intrastromal invaginations of very well-differentiated squamous epithelium with marked surface keratinization and thin fibrovascular cores [28]. The deceivingly bland appearance of the squamous epithelium and its lack of atypia prototypically belay malignancy [37]. The cells in VC are larger than those seen in common SCCs [38] and express TGFβ-R [39]. Mitoses are rare and are only observed in the suprabasal layer; there are no abnormal mitoses. VC invades the subjacent stroma with well-defined pushing rather than infiltrative borders. A lymphoplasmacytic inflammatory response is common in the stroma. VC pursues a slow and locally invasive growth, causing extensive destruction if inadequately treated. Bona fide and unperturbed VC do not metastasize [28, 30, 36, 40]. VC therefore bears an excellent prognosis and the survival rate for patients with pure VC ranges from 85% to 95%. Although surgery appears to be a more effective treatment for VC, radiotherapy seems an alternative option for patients who are not good candidates for surgery [28, 34]. Early

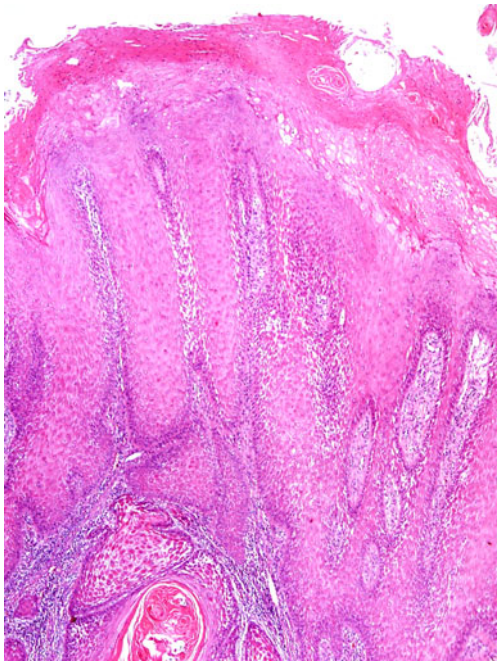

Fig. 3 Panoramic view of verrucous carcinoma showing marked surface keratinisation, very well-differentiated squamous epithelium with blunt intrastromal invaginations and thin fibrovascular cores. The *upper part* of this type of lesion is what Virchow presumably saw in the second biopsy performed on June 8, 1887. H&E

reports suggested anaplastic transformation of VC following radiotherapy; however, more recent studies do not support this notion [28, 40].

VC is characterised by a high frequency of initial misdiagnosis. In a recent series of 53 VC of the larynx, 16 of 31 patients (52%) had received an incorrect diagnosis of a benign lesion before referral to the consultation centre [28], underlining the need for better knowledge of this entity even today. VC has been controversial since its beginning. As described by Ackerman: "The biopsy material from this neoplasm is often confusing. Superficial biopsies are often taken and a positive diagnosis of carcinoma cannot be made. Even with deep biopsies, which are recommended, diagnosis may be difficult (Fig. 4a) because of the intact basement membrane and the well-differentiated nature of the growth." [29]. According to Fechner [41], Ackerman's paper was a paradigm of the failure to diagnose a tumour microscopically without knowing its true clinical nature. Ackerman himself delighted in recounting the events leading to the correct diagnosis. He had received multiple biopsy specimens from a lesion of the oral cavity that he had repeatedly called papilloma. The surgeon insisted that Ackerman see the patient, who had a tumour extending from the buccal mucosa into the skin of the cheek. The surgeon asked pointedly: "Now what do you think of *THAT* papilloma, doctor"? Ackerman replied: "Well,

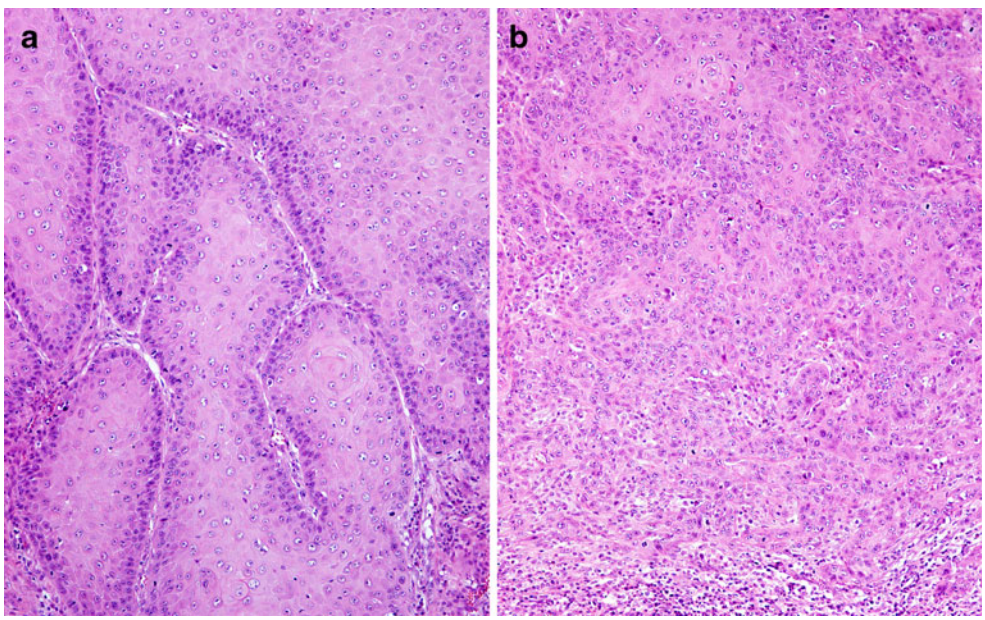

Fig. 4 **a** Deep part of a verrucous carcinoma composed of blunt intrastromal invaginations of very well-differentiated squamous epithelium with large cells and thin fibrovascular cores, invading with well-defined pushing borders. The preserved basement membrane, the bland appearance of the squamous epithelium and its lack of atypia do not reveal the malignancy of the tumour. This type of lesion is what Virchow presumably saw at the bottom of the third biopsy removed on June 28, 1887. H&E. **b** Hybrid verrucous carcinoma. In the *upper part* of the picture, there are residual components of verrucous carcinoma which merge with abundant less-differentiated conventional SCC structures that are particularly seen in the deeper parts of the picture. Here, the tumour invades with poorly defined infiltrating borders. H&E

Table 1 Comparison between terms used to report, Kaiser's third biopsy and to describe verrucous carcinoma

Kaiser's third biopsy[a]	Verrucous carcinoma[b]
Hard warty growth	Wart-like tumour
Papillary surface of various sizes	Club-shaped-to-filiform surface papillae
Club-shaped flattened base with outgrowths in juxtaposition	Blunt down-growing bulbous invaginations
Connective tissue thin, soft, vascular	Thin fibrovascular connective tissue cores
Large epithelial cells flattened towards outer part	Large intermediate keratinocytes
No penetration inwards	Expansive pushing margins
No new formation	Bland appearance belies malignancy

[a] References [7–9]

[b] References [27–29, 37]

doctor, it still looks like a papilloma, but I must say it is the *BAD* kind of papilloma".

Does this enlightened conversation not remind us of the pioneering difficulties faced by Virchow in 1887 in his report on the third biopsy from the Kaiser's tumour, whose passages fit like a jigsaw puzzle with Ackerman's description of "verrucous carcinoma" in 1948 [29]? In our view, what in Virchow's time was sarcastically regarded as a wrong diagnosis should nowadays be considered a masterpiece on how to report an unknown tumour that was first recognized as a distinct clinicopathologic entity 61 years later (Table 1). A similar view was previously held by Lin [16]. However, this is only the first part of the riddle.

The solution to the second part of this conundrum lies behind the differential diagnosis of VC and the report of the Kaiser's autopsy. The differential diagnosis of VC includes exophytic SCC, hybrid VC, papillary SCC, verruca vulgaris, keratinizing squamous cell papilloma and verrucous hyperplasia [27]. VC lacks cytological atypia, and this distinguishes it from exophytic SCC, hybrid VC and papillary SCC; the latter tumour distinctly shows more prominent branching of the papillae than the former two. The pushing margins of VC are smooth in distinction to the irregular-shaped invasive islands of SCC. Papillomas have thin, well-formed papillary fronds with limited keratinization, as compared to the markedly keratinized papillae of VC. Verruca vulgaris of the larynx contains layers of parakeratotic squamous cells with large keratohyaline granules identical to their counterpart in the skin [42]. Invasion below the level of the basal cell layer of the neighbouring normal squamous epithelium distinguishes VC from verrucous hyperplasia [43]; this latter term is similar to the "pachydermia verrucosa laryngis" of Virchow's terminology. Whether this feature adequately discriminates between VC and verrucous hyperplasia is debatable, as verrucous hyperplasia could be an initial form of VC as well [40, 44, 45].

The autopsy report that ultimately disclosed the whole spectrum of the malignant new growth that the Kaiser suffered from revealed not only carcinoma at the base of the epiglottis, but also metastatic squamous carcinoma that involved one cervical lymph node ipsilateral to the primary tumour. This latter finding precludes VC as the final diagnosis for the Kaiser's cancer, because by definition it never metastasizes to lymph nodes [36]. Nevertheless, this lymph node metastasis provides the final additional piece of the jigsaw puzzle. It is what makes the Kaiser's cancer fit the complex and subtle entity we know nowadays as "hybrid verrucous carcinoma", which was initially reported in the larynx by Batsakis et al. in 1982 [40], and thereafter in the oral cavity by Medina et al. in 1984 [46] and by Luna and Tortoledo in 1988 [45]. In 1998 Orvidas et al. [28] expanded our knowledge of this variant of VC of the larynx, documenting for the first time three patients with metastases to regional lymph nodes (Table 2).

HVC is an aggressive variant of VC, composed of "pure" VC mixed with nests of conventional SCC, usually sitting in the deeper parts of the tumour (Fig. 4b). These less-differentiated nests enable HVC to recur more fre-

Table 2 Comparison of the course of Kaiser's cancer with that of verrucous carcinomas of larynx metastasizing to regional lymph nodes

Cases	Initial diagnosis	Recurrence in months	Recurrence	Diagnosis after recurrence	Follow-up	Dead months
Kaiser's cancer [7]	Pachydermia verrucosa laryngis	4	Local + regional lymph nodes	Squamous cell carcinoma	Dead of disease	12
Orvidas et al., Mayo Clinic [28]	Verrucous carcinoma	14	Regional lymph nodes	Squamous cell carcinoma	Dead of other cause	128
Orvidas et al., Mayo Clinic [28]	Verrucous carcinoma	4	Local + regional lymph nodes	Squamous cell carcinoma	Dead of disease	16
Orvidas et al., Mayo Clinic [28]	Hybrid verrucous carcinoma	3	Local + regional lymph nodes	Squamous cell carcinoma	Dead of disease	4

quently than VC and to metastasize into the regional lymph nodes. An adequate, full-thickness biopsy specimen must be taken when a clinician suspects HVC. Moreover, multiple biopsies and serial sectioning of the entire specimen may be needed to rule out a conventional SCC component in any VC [28]. Very recently, analysis of desmosomal proteins has proven to be of assistance in problematic cases of VC, as the expression of desmocollin 3 is retained in pure VC but lost in the SCC nests of HVC [47]. If the diagnosis of HVC is confirmed, the patients must be treated as if they had conventional SCC [28, 46]. It appears that some of the reported cases of transformation of VC to SCC after radiotherapy were examples of HVC [28, 40, 46].

In its early stages, HVC goes unrecognized as just another verruciform growth. Different from pure VC, which evolves as a persistent and progressive lesion with a clinical phase that last several years, HVC may arise suddenly, or a period of slow growth may be followed by rapid enlargement [40]. HVC has a higher tendency to recur locally than pure VC [28]. Recurrence of HVC can be either in the form of a hybrid pattern or as conventional SCC [28]. The report by Batsakis et al. consisted of three HVC out of seven verrucous malignant tumours of the larynx [40]. The one by Medina et al. documented 20% HVC out of a series of 104 VC of the oral cavity; none of these HVC was found to metastasize [46]. In the series of 53 VC of the larynx reported by Orvidas et al., there were six (10%) HVC observed de novo [28]; four additional patients with an initial diagnosis of pure VC recurred in the form of conventional SCC, and were considered cases of HVC that were not apparent at the initial diagnosis. Eventually, three of these ten aggressive cases metastasized to the regional lymph nodes as typical SCC. Their initial diagnosis was pure VC in two patients and a hybrid VC in one [28].

To conclude this review on the fatal cancer afflicting Friedrich III, we propose for the first time that it was HVC, a very rare, metastasizing variant of VC composed of pure VC mixed with nests of “conventional” SCC that is difficult to diagnose even today which challenged the diagnostic skills of the founder of pathology. Was Virchow totally wrong? Not in our view which differs from what was contended in Virchow's time. We rather believe, based on our retrospective evaluation of pathology reports and clinical records in comparison with our current knowledge of larynx cancer, that in the case of the Kaiser's cancer, Virchow's reports described in detail the microscopic features and the loco-regional dissemination of a very complex and extremely rare neoplastic entity. Assuming that our hypothesis is correct, these thorough descriptions anticipated the first paper on VC [29] by 61 years and preceded the paper that contributed to the full understanding of HVC of the larynx [28] and its subsequent worldwide recognition [14, 27] by 110 years.

Acknowledgements The authors would like to thank Professor Manfred Dietel and Professor Thomas Schnalke for the information they provided concerning the fate of the histological slides and of Virchow's original reports on the case. They are also grateful to Mrs. Katherine Dege for language editing.

References

1. von Bergman E, Gebhardt C, Schrötter L et al (1888) Die Krankheit von Friedrich des Dritten dargestellt nach amtlichen Quellen den im Königlichen Hausministerium niedergelegten Berichten der Ärzte. Kaiserl Reichsdruckerei, Berlin
2. von Bergman E, Gebhardt C, Schrötter L et al. (1888) The Illness of the Emperor Frederick the Third, an authentic record derived from official sources and founded upon the reports deposited in the archives of the Royal House of Prussia. Berlin, R. v. Decker
3. Mackenzie M (1888) The fatal illness of Frederick the Noble. Sampson Low, Marston Searle & Rivington, London
4. Schweig H (1888) The case of the Emperor Frederick III: full official reports by the German physicians and by Sir Morel Mackenzie. Edgar S. Werner, New York
5. Pack GT, Campbell R (1940) Historical case records of cancer; laryngeal cancer of Frederick III of Germany. Ann Med Hist 2:151–170, 3d Series
6. Stevenson RS, Morel Mackenzie (1946) The story of a Victorian tragedy. William Heinemann, London
7. Ober WB (1970) The case of the Kaiser's cancer. Pathol Annu 5:207–216
8. Virchow R (1887) The Crown Prince of Germany: nature of the laryngeal growth. Lancet 129:1302
9. Virchow R (1887) Professor Virchow's report on the portion of the growth removed from the larynx of H.I.H. the Crown Prince of Germany by Dr. M. Mackenzie on June 28th. BMJ 2:199
10. Virchow R (1888) Report of the examination of the slough from larynx of His Imperial Highness The Crown Prince of Germany. Lancet 130:340
11. Waldeyer W (1867) Die Entwicklung der Carcinome. Arch Path Anat 41:470–523
12. Virchow R, Mackenzie M, Hovell TM et al (1888) Medical protocol concerning the examination of the body of His Majesty the late Emperor and King Frederic the Third. Br Med J 2:141
13. Folz BJ, Ferlito A, Weir N, Pratt LW et al (2007) A historical review of head and neck cancer in celebrities. J Laryngol Otol 121:511–520
14. Barnes L, Eveson JW, Reichart P, Sidransky D (eds) (2005) Pathology and genetics of tumours of the head and neck. WHO Classification of Tumours. IARC, Lyon, pp 107–162
15. Gale N, Zidar N (2006) Benign and potentially malignant lesions of the squamous epithelium and squamous cell carcinoma. In: Cardesa A, Slootweg PJ (eds) Pathology of the head and neck. Springer, Berlin, pp 1–38
16. Lin JI (1984) Virchow's pathological reports on Frederich's III cancer. N Engl J Med 311:1261–1264
17. Krietsch P, Dietel M (1996) Pathologisch-Antonisches Cabinet. Vom Virchow-Museum zum Berliner Medizinhistorischen Museum in der Charité. Blackwell, Oxford, pp 100–101
18. Laurenson RD (1995) The Emperor who smoked a pipe. J Laryngol Otol 109:1–4
19. Pratt LW (1993) Historical perspective. In: Ferlito (ed) Neoplasms of the larynx. Churchill Livingstone, Edingurgh, pp 1–25
20. Mackenzie M (1871) Essay on growths in the larynx: with reports, and an analysis of one hundred consecutive cases treated by the author. Lindsay & Blakiston, Philadelphia

21. Gussenbauer C (1874) Ueber die erste durch Th Billroth am Menschen ausgeführte Kehlkopf-Exstirpation und die Anwendung eines künstlichen Kehlkopfes. Arch Klin Chir 17:343–356
22. Schwann T, Schleiden MJ (1847) Microscopic investigations on the accordance in the structure and growth of plants and animals. London, pp 1–265
23. Virchow R (1863) Die Cellularpathologie in ihrer Begründung auf physiologische und pathologische Gewebelehre. August Hirschwald, Berlin
24. von Gerlach L (1851) Über das Hautathmen. Arch Anat Physiol 102:419–425
25. Ramon Y, Cajal S (1889) On the morphology and the connections of elements of the retina of birds. Anat Anzeiger 4:111–121, in French
26. Parkin DM, Bray F, Ferlay J, Pisani P (2001) Estimating the world cancer burden. Globocan: 2000. Int J Cancer 94:153–156
27. Cardesa A, Zidar N (2005) Verrucous Carcinoma. In: Barnes L, Eveson JW, Reichart PA, Sidransky D (eds) Larynx, hypopharynx and trachea, pathology and genetics of tumours of the head and neck. WHO Classification of Head and Neck Tumours. IARC, Lyon, pp 122–123
28. Orvidas LJ, Kerry DK, Lewis JE, Suman VJ (1998) Verrucous carcinoma of the larynx. Head Neck 20:197–203
29. Ackerman LV (1948) Verrucous carcinoma of the oral cavity. Surgery 23:670–678
30. McCaffrey TV, White M, Ferguson MT (1998) Verrucous carcinoma of the larynx. Ann Otol Rhinol Laryngol 107:391–395
31. Kolbusz RV, Goldberg LH (1994) Verrucous carcinoma of the oral cavity. Int J Dermatol 33:618–622
32. Kasperbauer JL, O'Halloran GL, Espy MJ et al (1993) Polymerase chain reaction (PCR) identification of human papillomavirus (HPV) DNA in verrucous carcinoma of the larynx. Laryngoscope 103:416–420
33. Fliss DM, Noble-Topham SE, McLachin CM, Freeman JL et al (1994) Laryngeal verrucous carcinoma: a clinicopathologic study and detection of human papillomavirus using polymerase chain reaction. Laryngoscope 104:146–152
34. Koch BB, Trask DK, Hoffman HT, Karnell LH et al (2001) National survey of head and neck verrucous carcinoma. Patterns of presentation, care, and outcome. Cancer 92:110–120
35. van Nostrand AWP, Olofson J (1972) Verrucous carcinoma of the larynx: a clinicopathologic study of 10 cases. Cancer 30:691–702
36. Ferlito A, Recher G (1980) Ackerman's tumor (verrucous carcinoma) of the larynx: a clinicopathologic study of 77 cases. Cancer 46:1617–1630
37. Shanmugaratnan K, Barnes L, Cardesa A, Ferlito A et al (1991) WHO histological typing of tumours of the upper respiratory tract and ear. Springer, Berlin, pp 29–30
38. Cooper JR, Hellquist H, Michaels L (1992) Image analysis in the discrimination of verrucous carcinoma and squamous papilloma. J Pathol 166:383–387
39. Muro-Cacho CA, Anderson M, Cordero J, Munoz-Antonia T (1999) Expression of transforming growth factor β type II receptors in head and neck squamous cell carcinoma. Clin Cancer Res 5:1234–1248
40. Batsakis JG, Hybels R, Crissman JD et al (1982) The pathology of head and neck tumors: verrucous carcinoma. Head Neck Surg 5:29–38
41. Fechner RE (2002) A brief history of head and neck pathology. Mod Pathol 15:221–228
42. Fechner RE, Mills SE (1997) Verruca vulgaris of the larynx a distinctive lesion of probable viral origin confused with verrucous carcinoma. Am J Surg Pathol 6:357–362
43. Shear M, Pindborg JJ (1980) Verrucous hyperplasia of the oral mucosa. Cancer 46:1855–1862
44. Slootweg PJ, Muller H (1983) Verrucous hyperplasia or verrucous carcinoma. An analysis of 27 patients. J Maxillofac Surg 11:13–19
45. Luna MA, Tortoledo ME (1988) Verrucous carcinoma. In: Gnepp DR (ed) Pathology of the head and neck. Churchill Livingstone Inc, London, pp 497–515
46. Medina JE, Dichtel W, Luna MA (1984) Verrucous-Squamous carcinomas of the oral cavity. A clinicopathologic study of 104 cases. Arch Otolaryngol 110:437–440
47. Zidar N, Gale N, Odar K et al. (2010) Desmosomes in squamous cell carcinoma of the head and neck. Advances in Pathology. 42J Plečnik Memorial Meeting, Medical Faculty, Ljubljana, pp 31–35 (in Slovenian)

Virchows Arch (2011) 458:659–664
DOI 10.1007/s00428-011-1072-3

ORIGINAL ARTICLE

Histologic grading of urothelial papillary neoplasms: impact of combined grading (two-numbered grading system) on reproducibility

Burçin Tuna · Kutsal Yörükoglu · Ender Düzcan · Sait Şen · Nalan Nese · Banu Sarsık · Aysegul Akder · Sehnaz Sayhan · Uğur Mungan · Ziya Kirkali

Received: 10 January 2011 / Revised: 1 March 2011 / Accepted: 13 March 2011 / Published online: 12 April 2011
© Springer-Verlag 2011

Abstract The clinical management of tumor patients is often strongly infuenced by the tumor grade. The presence of heterogeneity is well recognized in a variety of tumors. Overall grade is based on highest grade area identified within a tumor. Urothelial carcinoma often contains different histological grades within the same tumor. This study investigates the impact of a combined grading system on the reproducibility of papillary urothelial neoplasms. A set prepared for an earlier study consisting of ten cases of each category (papillary urothelial neoplasm of low malignant potential (PUNLMP), LGPUC, and HGPUC) was used. Agreement between pairs of pathologists was evaluated using κ statistics for the combined scoring system. Interobserver agreement was fair to substantial as reflected by κ values ranging from 0.24 to 0.74 (mean κ=0.43). The combined scores of 2 and 3 which included PUNLMP showed the lowest degree of agreement and when this category was excluded from the analysis, interobserver agreement increased significantly (mean κ=0.65; ranging from 0.43 to 0.92) in terms of combined scores of 4, 5, and 6. PUNLMP has been shown to be the least reproducible component of a combined scoring system even among experienced observers. Exclusion of PUNLMP from grading scheme seems to improve interobserver variability.

Keywords Bladder neoplasms · Grading · Reproducibility

B. Tuna (✉) · K. Yörükoglu
Department of Pathology, School of Medicine,
Dokuz Eylul University,
Izmir, Turkey
e-mail: burcin.tuna@deu.edu.tr

E. Düzcan
Department of Pathology, School of Medicine,
Pamukkale University,
Denizli, Turkey

S. Şen · B. Sarsık
Department of Pathology, School of Medicine,
Ege University,
Izmir, Turkey

N. Nese
Department of Pathology, School of Medicine,
Celal Bayar University,
Manisa, Turkey

A. Akder · S. Sayhan
Department of Pathology,
Izmir Ataturk Education and Research Hospital,
Izmir, Turkey

U. Mungan · Z. Kirkali
Department of Urology, School of Medicine,
Dokuz Eylul University,
Izmir, Turkey

Introduction

Determining tumor grade is an essential part of pathologic diagnosis because of its prognostic and therapeutic implications. Ideally, a grading system has to be practical, reproducible, and clinically relevant, with clear prognostic power. Several histopathological grading systems have been developed for different tumors as well as papillary urothelial neoplasms. The 1973 World Health Organization (WHO) grading system is currently the most widely used system worldwide for papillary urothelial neoplasms [1]. The main problem with this grading system has been the lack of defined cutoff points among the three grades of differentiation, giving rise to high intra- and interobserver variability. Several efforts have been made to improve

existing ones or to develop new grading systems. Thus, the International Society of Urologic Pathology (WHO/ISUP) consensus classification was introduced in 1998 [2] and adopted in 2004 in the most recent WHO classification and grading system. An important aim of the 2004 WHO classification was to improve reproducibility in diagnosis and grading among different pathologists by providing detailed histological criteria for each diagnostic category. In this classification system, non-invasive papillary neoplasms were categorized as papilloma, papillary urothelial neoplasm of low malignant potential (PUNLMP), low- (LGPUC), and high-grade (HGPUC) papillary urothelial carcinoma [3].

In general, overall grade is based on a highest grade area identified within a tumor. The presence of heterogeneity is well recognized in a variety of tumors but has not been fully investigated in bladder cancer. However, urothelial carcinoma often contains areas with different histological grades. The influence of tumor heterogeneity on outcome was first questioned by Cheng et al. who evaluated the primary (most common) and secondary (second most common) patterns of tumor growth by using the 2004 WHO grading system in Ta bladder tumors [4]. In their study, prognostic accuracy was increased when combined primary and secondary grades were applied, and they recommended the use of combined grading of urothelial carcinoma.

We aimed to investigate the impact of combined grading system on the reproducibility of papillary urothelial neoplasms.

Materials and methods

A set prepared for an earlier study consisting ten cases of each category (PUNLMP, LGPUC, and HGPUC) was used. A written guideline was prepared from the original references [4,5] and attached to the set (Table 1; Figs. 1, 2, and 3). Eight uropathologists participated in the study. All of the authors interpreted the set, gave a combined grade, and returned the set. All cases were re-coded and re-sent to the authors for the second round. The time interval between the two interpretations was at least 6 weeks. Data were analyzed using Scientific Package for Social Sciences software. Agreement between pairs of pathologists was evaluated using κ statistics for the combined scoring system. Statistical comparisons in agreement between classifications were made using a paired t test of differences in κ statistics. For positive κ values, the following interpretations are generally accepted: slight agreement, κ=0.00–0.20; fair agreement, κ=0.21–0.40; moderate agreement, κ=0.41–0.60; substantial agreement, κ=κ0.61–0.80; and almost perfect agreement, κ=0.81–1.00 [6–8].

Table 1 Histological features of urothelial papillary tumors

Primary grade	Secondary grade	Combined scores
PUNLMP	PUNLMP	2
PUNLMP	LGPUC	3
LGPUC	PUNLMP	3
LGPUC	LGPUC	4
LGPUC	HGPUC	5
HGPUC	LGPUC	5
HGPUC	HGPUC	6

Combined scores based on primary and secondary grades of non-invasive papillary urothelial tumors. Histologic grading according to 2004 WHO grading system. Scores of 1, 2, and 3 are assigned to PUNLMP, LGPUC, and HGPUC, respectively. The primary (most common) and secondary (second most common, if at least 5% of the cancer) grades are evaluated for each tumor, and combined scores were derived from summation of primary and secondary grades

PUNLMP papillary urothelial neoplasm of low malignant potential (orderly arrangement of cells within papillae, minimal to slight nuclear enlargement, normal or slightly distorted architecture, rare or absent mitotic figures), *LGPUC* low-grade papillary urothelial carcinoma (greater nuclear pleomorphism than PUNLMP, coarsely clumped nuclear chromatin, disruption of the normal architecture, infrequent mitotic figures), *HGPUC* high-grade papillary urothelial carcinoma (loss of normal architecture and cell polarity, increased cellularity and nuclear crowding, variation in nuclear shape and chromatin pattern, increased number of mitotic figures)

All pathologists involved in this study had at least 4 years experience of urologic pathology and each gained their specialization at different institutes. Five of the participants were using the 2004 WHO classification system and three were using both the modified Bergkvist grading and 2004 WHO classification in their daily routine practice.

Results

Intra- and interobserver variation

The intraobserver agreement for combined scoring ranged from 26.6% to 96.6% (κ 0.38 to 0.91). Mean observer reproducibility was 70.5% (mean κ=0.66; Table 2). The number of duplicates was between 8 and 29. Interobserver agreement among eight pathologists was fair to substantial as reflected by κ values ranging from 0.24 to 0.74 (mean κ=0.43; Table 3). The agreement rates of the eight pathologists were 33.3% for a combined score of 2 (LMP plus LMP), 38.1% for a combined score of 3 (LMP plus LGPC or LGPC plus LMP), 55.1% for a combined score of 4 (LGPC plus LGPC), 65.1% for a combined score of 5 (LGPC plus HGPC or HGPC plus LGPC), and 74.3% for a combined score of 6 (HGPC plus HGPC; Table 4).

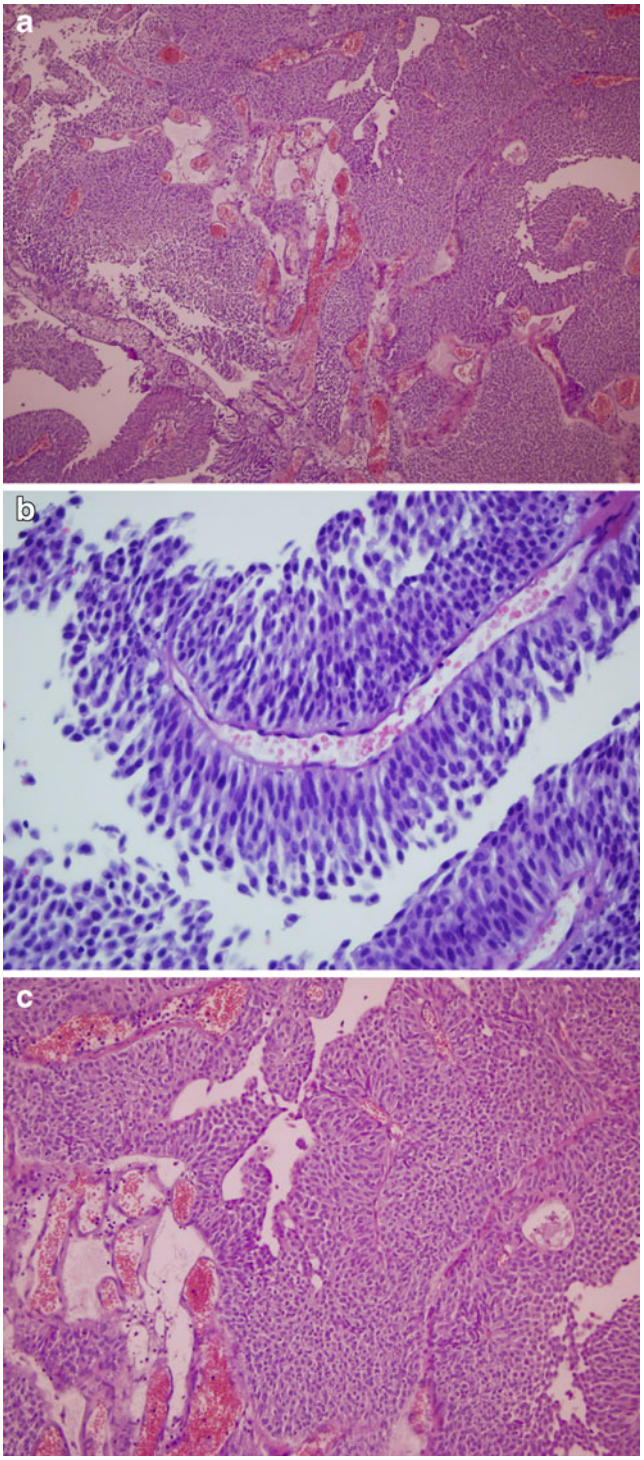

Fig. 1 Papillary urothelial tumor containing both papillary urothelial neoplasm of low malignant potential and low-grade papillary urothelial carcinoma (**a**). PUNLMP (**b**) and low-grade (**c**) areas are represented in high power

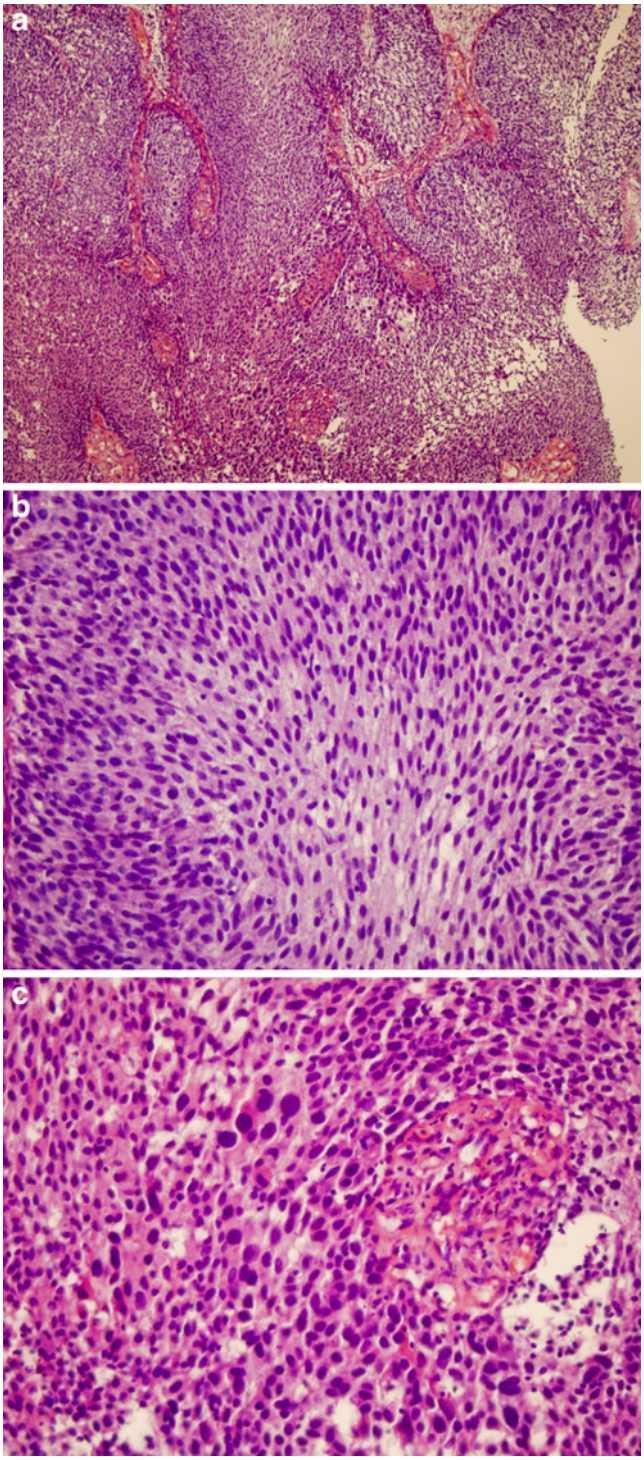

Fig. 2 Papillary urothelial tumor containing both low- and high-grade areas (**a**). Low- (**b**) and high-grade (**c**) areas are represented in high power

The combined scores of 2 and 3 which included PUNLMP showed the lowest degree of agreement, and when this category was excluded from the analysis, interobserver agreement increased significantly (mean κ= 0.657; ranged from 0.43 to 0.92) in terms of the combined scores of 4, 5, and 6. The agreement rates of eight pathologists were 90% for the combined score of 4 (LGPC plus LGPC), 70.4% for the combined score of 5 (LGPC

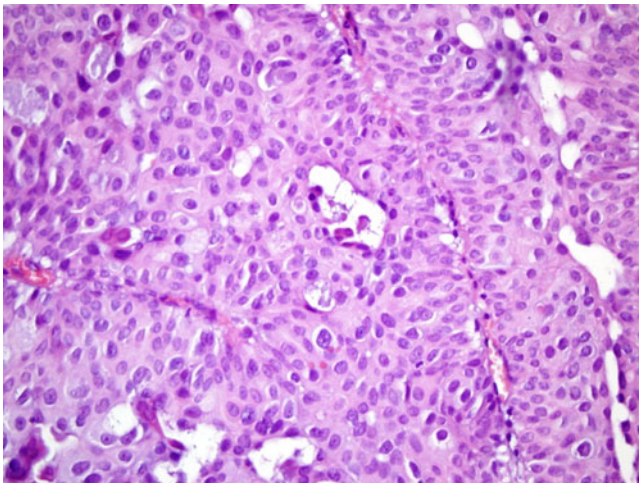

Fig. 3 Tumor with grading discrepancies

plus HGPC or HGPC plus LGPC), and 74.3% for the combined score of 6 (HGPC plus HGPC).

Discussion

Like other tumors, urothelial tumors are known to be both biologically and morphologically heterogeneous. Consequently, all grading systems have an inherent degree of subjectivity, which gives rise to both intra- and interobserver variability. In general, reproducibility levels of grading systems are fair to moderate and grading of low-grade tumors is more difficult than of high-grade tumors for pathologists. The reproducibility of these grading systems among pathologists has been analyzed in several studies [7–10].

Heterogeneity in tumor grade is another reason which contributes to interobserver variability. Overall grade is based on the highest grade but different grades are often found within the same tumor. Although there is no uniformity in how to grade these cases, the 5% cutoff is identical to that used in Gleason grading [4]. However, some pathologists assign the highest grade as their final diagnosis regardless of the percentage area. Whereas, other pathologists assign a high tumor grade only when the high-grade area comprises more than 5%.

Table 2 Intraobserver reproducibility in duplicate classification of non-invasive urothelial neoplasms according to combined scoring

Observer	No. of duplicates	Rate of agreement	Kappa
A	29	96.6	0.914
B	27	90.0	0.868
C	8	26.6	0.380
D	18	60.0	0.489
E	28	93.3	0.911
F	26	86.6	0.808
G	19	63.3	0.522
H	18	60	0.442
Total	127	70.5	0. 663

The morphologic heterogeneity of transitional cell carcinoma (TCC) is influenced by molecular events involved in carcinogenesis. The current bladder cancer classification of urothelial neoplasms was based on an attempt to reconcile molecular genetic and pathologic findings. Most of the World Health Organization 2004 categories have been successfully validated by expression and genome profiling and by identification of distinctive genetic alterations. Mutations in the *FGFR3* and *TP53* genes define two independent and distinct pathways in superficial papillary and invasive/flat urothelial carcinomas. *FGFR3* mutations are usually present in low-grade papillary carcinomas with limited genetic instability, whereas high-grade urothelial carcinomas are characterized by *TP53* mutation. *TP53* mutations have been found to be almost always mutually exclusive of *FGFR3* mutations, a fact that could potentially be exploited as a tool for the molecular grading of TCC [11,12].

The influence of tumor heterogeneity on the outcome was first questioned by Cheng et al. who evaluated the primary (most common) and secondary (second most common) patterns of tumor growth by the WHO/ISUP grading system in non-invasive papillary (Ta) bladder tumors [4]. In their study, they noted that over one third of Ta bladder tumors contained different histological grades within the same tumor. They applied the primary and secondary grades to all of the tumors. They also applied the 5% rule to define the second most common tumor pattern. Scores of 1, 2, and 3 were assigned to PUNLMP, LGPUC, and HGPUC, respectively. Each tumor was evaluated by the combined scoring system on a scale of 2–6. In their study, they found that 7-year progression-free survival rates for patients with LMP, LGPUC, and HGPUC were 93%, 82%, and 61%, respectively. Whereas, for patients with combined scores of 2, 3, 4, 5, and 6, the survival rates were 93%, 80%, 82%, 68%, and 40%, respectively. They stated that the difference between patients with combined scores of 5 and 6 was statistically significant in terms of survival rates. Despite some limitations of their study, they concluded that the combined system improved the accuracy of prognosis and the 2004 WHO system stratified patients into prognostically different groups [4].

Although, the influence of tumor heterogeneity on outcome was first questioned by Cheng et al., to the best of our knowledge there is no data available at this moment about whether the combined scoring system has a higher rate of agreement among pathologists than other grading systems of papillary urothelial neoplasms.

Table 3 Interobserver reproducibility (Kappa) according to combined scoring

Observer	Observer						
	B	C	D	E	F	G	H
A	0.742	0.384	0.243	0.392	0.478	0.541	0.478
B		0.413	0.331	0.254	0.547	0.267	0.402
C			0.244	0.245	0.527	0.305	0.245
D				0.240	0.247	0.280	0.475
E					0.333	0.474	0.242
F						0.393	0.252
G							0.258

In a previous study, we showed that the reproducibility was lower in low-grade tumors for both classification systems (1973 WHO and 2004 WHO). Mean rates of agreement for PUNLMP, LGPUC, and HGPUC were 48%, 72.7%, and 92%, respectively [10]. To date, a significant improvement in intra–interobserver variability compared with the 1973 WHO system has not been reported [7,10,13–17].

In this study, we found lowest rates of agreement with the combined scores of 2 and 3 (LMP plus LMP and LMP plus LGPC or LGPC plus LMP; 33.3% and 38.1%, respectively) whereas, agreement was higher significantly for combined the scores of 4, 5, and 6 (55.1%, 65.1%, and 74.3%, respectively). Although, overall agreement rates in the combined grading system was moderate (κ=0.428, ranged from 0.24 to 0.74). We also found lowest degree of agreement for combined scores 2 and 3 including PUNLMP, and if PUNLMP was excluded from the analysis, interobserver agreement increased significantly (κ=0.574; ranged from 0.43 to 0.92) in terms of the combined scores of 4, 5, and 6.

These results may largely be attributed to the difficulties of histological distinction between PUNLMP and LGPUC, even for experienced pathologists. Keeping in mind that the difference between PUNLMP and LGPUC remains somewhat subjective, it is not surprising that these two categories appear to result in fair interobserver variability.

Table 4 Distribution of interobserver agreement rates according to combined score

Primary grade	Secondary grade	Combined scores	Interobserver agreement (%)
PUNLMP	PUNLMP	2	33.3
PUNLMP	LGPUC	3	38.1
LGPUC	PUNLMP	3	38.1
LGPUC	LGPUC	4	55.1
LGPUC	HGPUC	5	65.1
HGPUC	LGPUC	5	65.1
HGPUC	HGPUC	6	74.3

In this way, it should be questioned whether a distinction between PUNLMP and LGPUC is of any prognostic and clinical use. In several studies, PUNLMPs have been reported to recur in up to 60% and to progress to invasive carcinoma in up to 8% of the cases while LGPUC recurred in up to 77% and progressed in up to 13% of the cases [2,17–23]. On the other hand, Oosterhuis et al. found no difference between PUNLMP and LGPUC in terms of recurrence-free and progression-free survival, and they concluded that no distinction is needed between these two categories [24]. Consequently, the clinical management of patients with PUNLMP or LGPUC is currently similar, if not identical [24,25]. Moreover, Holmang et al. significantly observed more recurrences (71%) and lower disease-free survival rate (25%) in LGPUC compared with PUNLMP which showed a recurrence rate of 35% and disease-free survival of 62% after 5 years of follow-up, and the authors stated that these rates should not be ignored [21].

These conflicting results mentioned above show that the 1998 WHO/ISUP classification and its new category of PUNLMP has not yet been verified by the majority of both the pathologists' and the clinicians' aspects.

The main reasons to propose a new classification system were (1) to separate indolent and relatively benign non-invasive papillary urothelial tumors from aggressive ones and not to call them carcinoma, (2) the lack of clear definitions of the 1973 WHO grading system, and (3) the high percentage of cases diagnosed as grade 2 in the 1973 WHO system, thus creating the PUNLMP category. However, the most important problem with the 2004 WHO classification system is the difficulty in the diagnosis of PUNLMP. The low incidence of PUNLMP cases in a recent study shows the difficulty in the diagnosis of PUNLMP and the cases overlap in the LGPUC category, as in the 1973 WHO system [26]. Also, the recurrence and progression rates of PUNLMP in the 2004 WHO classification system are conflicting and we still do not know the biological behavior of PUNLMP [25,27].

Similarly, our study clearly showed the problems especially concerning the diagnosis of PUNLMP and its separation from LGPUC.

In conclusion, PUNLMP has been shown to be the least reproducible component of combined scoring system even among experienced observers. Exclusion of PUNLMP from grading scheme seems to improve interobserver variability.

Conflict of interest We declare that we have no conflict of interest.

References

1. Montironi R, Mazzucchelli R, Colanzi P, Streccioni M, Scarpelli M, Thompson D, Bartels PH (2002) Improving inter-observer agreement and certainty level in diagnosing and grading papillary urothelial neoplasms: usefulness of a Bayesian belief network. Eur Urol 41:449–457
2. Samaratunga H, Makarov DV, Epstein JI (2002) Comparison of WHO/ISUP and WHO classification of noninvasive papillary urothelial neoplasms for risk of progression. Urology 60:315–319
3. Epstein JI (2003) The new World Health Organization/International Society of Urological Pathology (WHO/ISUP) classification for Ta, T1 bladder tumors: is it an improvement? Crit Rev Oncol Hematol 47:83–89
4. Cheng L, Neumann RM, Nehra A, Spotts BE, Weaver AL, Bostwick DG (2000) Cancer heterogeneity and its biologic implications in the grading of urothelial carcinoma. Cancer 88:1663–1670
5. Epstein JI, Amin MB, Reuter VR, Mostofi FK (1998) The World Health Organization/International Society of Urological Pathology consensus classification of urothelial (transitional cell) neoplasms of the urinary bladder. Bladder Consensus Conference Committee. Am J Surg Pathol 22:1435–1448
6. Wells WA, Carney PA, Eliassen MS, Grove MR, Tosteson ANA (2000) Pathologists' agreement with experts and reproducibility of breast ductal carcinoma-in-situ classification schemes. Am J Surg Pathol 24:651–659
7. Gönül II, Poyraz A, Ünsal C, Acar C, Alkibay T (2007) Comparison of 1998 WHO/ISUP and 1973 WHO classifications for interobserver variability in grading of papillary urothelial neoplasms of the bladder. Pathological evaluation of 258 Cases. Urol Int 78:338–344
8. Bircan S, Candir O, Serel TA (2004) Comparison of WHO 1973, WHO/ISUP 1998, WHO 1999 grade and combined scoring systems in evaluation of bladder carcinoma. Urol Int 73:201–208
9. Murphy WM, Takezawa K, Maruniak NA (2002) Interobserver discrepancy using the 1998 World Health Organization/International Society of Urologic Pathology classification of urothelial neoplasms: practical choices for patient care. J Urol 168:968–972
10. Yorukoglu K, Tuna B, Dikicioglu E, Duzcan E, Isisag A, Sen S, Mungan U, Kirkali Z (2003) Reproducibility of the 1998 World Health Organization/International Society of Urologic Pathology classification of papillary urothelial neoplasms of the urinary bladder. Virchows Arch 443:734–740
11. Shariat SF, Ashfaq R, Sagalowsky AI, Lotan Y (2007) Predictive value of cell cycle biomarkers in nonmuscle invasive bladder transitional cell carcinoma. J Urol 177:481–487
12. van Rhijn BW, van der Kwast TH, Vis AN, Kirkels WJ, Boevé ER, Jöbsis AC, Zwarthoff EC (2004) FGFR3 and P53 characterize alternative genetic pathways in the pathogenesis of urothelial cell carcinoma. Cancer Res 64:1911–1914
13. Ooms EC, Anderson WA, Alons CL, Boon ME, Veldhuizen RW (1983) Analysis of the performance of pathologists in the grading of bladder tumors. Hum Pathol 14:140–143
14. Abel PD, Henderson D, Bennett MK, Hall RR, Williams G (1998) Differing interpretations by pathologists of the pT category and grade of transitional cell cancer of the bladder. Br J Urol 62:339–342
15. Robertson AJ, Beck JS, Burnett RA, Howatson SR, Lee FD, Lessells AM, Mclaren KM, Moss SM, Simpson JG, Smith GD (1990) Observer variability in histopathological reporting of transitional cell carcinoma and epithelial dysplasia in bladders. J Clin Pathol 43:17–21
16. Tosoni I, Wagner U, Sauter G, EgloV M, Knonagel H, Alund G, Bannwart F, Mihatsch MJ, Gasser TC, Maurer R (2000) Clinical significance of interobserver differences in the staging and grading of superficial bladder cancer. BJU Int 85:48–53
17. Campbell PA, Conrad RJ, Campbell CM, Nicol DL, MacTaggart P (2004) Papillary urothelial neoplasm of low malignant potential: reliability of diagnosis and outcome. BJU Int 93:1228–1231
18. MacLennan GT, Kirkali Z, Cheng L (2007) Histologic grading of noninvasive papillary urothelial neoplasms. Eur Urol 51:889–897
19. Cheng L, Neumann RM, Bostwick DG (1999) Papillary urothelial neoplasms of low malignant potential. Clinical and biologic implications. Cancer 86:2102–2108
20. Holmang S, Andius P, Hedelin H, Wester K, Busch C, Johansson SL (2001) Stage progression in Ta papillary urothelial tumors: relationship to grade, immunohistochemical expression of tumor markers, mitotic frequency and DNA ploidy. J Urol 165:1124–1128
21. Holmang S, Hedelin H, Anderstrom C, Holmberg E, Busch C, Johansson SL (1999) Recurrence and progression in low grade papillary urothelial tumors. J Urol 162:702–707
22. Pich A, Chiusa L, Formiconi A, Galliano D, Bortolin P, Comino A, Navone R (2002) Proliferative activity is the most significant predictor of recurrence in noninvasive papillary urothelial neoplasms of low malignant potential and grade 1 papillary carcinomas of the bladder. Cancer 95:784–790
23. Fujii Y, Kawakami S, Koga F, Nemoto T, Kihara K (2003) Long term outcome of bladder papillary urothelial neoplasms of low malignant potential. BJU Int 92:559–562
24. Oosterhuis JW, Schapers RF, Janssen-Heijnen ML, Pauwels RP, Newling DW, ten Kate F (2002) Histological grading of papillary urothelial carcinoma of the bladder: prognostic value of the 1998 WHO/ISUP classification system and comparison with conventional grading systems. J Clin Pathol 55:900–905
25. Jones TD, Cheng L (2006) Papillary urothelial neoplasm of low malignant potential: evolving terminology and concepts. J Urol 175:1995–2003
26. May M, Brookman-Amissah S, Roigas J, Hartmann A, Störkel S, Kristiansen G, Gilfrich C, Borchardt R, Hoschke B, Kaufmann O, Gunia S (2010) Prognostic accuracy of individual uropathologists in noninvasive urinary bladder carcinoma: a multicentre study comparing the 1973 and 2004 World Health Organization classifications. Eur Urol 57:850–858
27. van Rhijn BW, van Leenders GJ, Ooms BC, Kirkels WJ, Zlotta AR, Boevé ER, Jöbsis AC, van der Kwast TH (2010) The pathologist's mean grade is constant and individualizes the prognostic value of bladder cancer grading. Eur Urol 57:1052–1057

Virchows Arch (2011) 458:665–670
DOI 10.1007/s00428-011-1076-z

ORIGINAL ARTICLE

Detection of smoothelin expression in the urinary bladder is strongly dependent on pretreatment conditions: a critical analysis with possible consequences for cancer staging

Claes Lindh · Robert Nilsson · Marie Louise Lindstrom · Lilian Lundin · Goran Elmberger

Received: 18 October 2010 / Revised: 24 February 2011 / Accepted: 31 March 2011 / Published online: 15 April 2011
© Springer-Verlag 2011

Abstract Distinguishing urinary bladder muscularis propria (MP) from muscularis mucosae (MM) is crucial in bladder cancer staging. Immunohistochemical staining for the smooth muscle-specific protein smoothelin has been reported to be a robust marker for MP. The aim of this study was to investigate how smoothelin immunostaining in the bladder varies with pretreatment techniques and if it can be used to discriminate between MM and MP. Immunohistochemistry (IHC) for smoothelin was performed on non-tumoral sections from 18 cystectomy specimens using three different pretreatment protocols. The immunoreactivity of MM, MP and blood vessels was scored semiquantitatively. Staining intensity depended strongly on the different pretreatment protocols used. Heat-induced epitope retrieval (HIER) in alkaline buffer resulted in the strongest staining with a moderate or strong immunostaining of the MP in 18/18 (100%) of cases, but in 11/18 (61%), the MM was moderately or strongly stained. HIER in acidic buffer resulted in a suboptimal staining of the MP. Enzymatic pretreatment resulted in absent or weak staining. In conclusion, smoothelin IHC is strongly dependent on epitope retrieval, and smoothelin staining did not discriminate reliably between MP and MM with any of the tested pretreatment protocols.

Keywords Smoothelin · Urothelial carcinoma · Urinary bladder · Muscularis mucosae · Muscularis propria

C. Lindh (✉) · R. Nilsson · M. L. Lindstrom · L. Lundin · G. Elmberger
Department of Clinical Pathology and Cytology,
Karolinska University Hospital,
171 76 Stockholm, Sweden
e-mail: claes.lindh@karolinska.se

Introduction

Urinary bladder cancer is a significant cause of morbidity and mortality in the world with an estimated 357,000 cases and 145,000 deaths in 2002 [1]. It is estimated that worldwide, at any point in time, 2.7 million people have a history of urinary bladder cancer and that the incidence will increase strongly in developing countries [2].

The most important prognostic factor in urothelial carcinoma is pathological staging which includes depth of invasion [3]. Carcinoma limited to the lamina propria is staged as a pT1 disease and is usually treated conservatively, whereas carcinoma involving the bladder muscularis propria (MP) is staged as at least a pT2 disease, typically leading to radical surgical cystectomy. Correct staging on bladder biopsy or transurethral resection of bladder tumour (TURBT) specimens is therefore crucial for correct treatment of the patient.

The existence of muscularis mucosae (MM) in the human urinary bladder was first described by Dixon in 1983 [4]. The MM is usually made up of thin, wispy and often discontinuous smooth muscle fibres that are closely associated with blood vessels of the lamina propria. MM is usually easily distinguishable from the thick muscle bundles of the MP in cystectomy specimens [5, 6], but discrimination can be challenging in TURBT specimens and bladder biopsies. Factors making proper staging on these specimens difficult include fragmentation, poor orientation, thermal artefacts, inflammatory response and infiltrative tumour cells splaying the muscle bundles. Another well-known pitfall is MM hyperplasia which can resemble muscle bundles of the MP [7].

Smoothelin is a cytoskeletal smooth muscle-specific protein reported to be almost exclusively expressed in

terminally differentiated smooth muscle [8–12]. Recently, attempts have been made to use immunohistochemistry (IHC) for smoothelin to differentiate between MM and MP in the bladder [10, 11, 13–15]. These studies have reported strong expression of smoothelin in the MP contrasted to absent or weak expression in the MM. Smoothelin has therefore been suggested as a marker for MP to be used in bladder cancer staging. However, in a study by Miyamoto et al. [13], smoothelin expression in a series of TURBT cases was investigated, and an approximately 25% staining overlap between MM and MP was found. In this study, we investigated how smoothelin immunostaining in the bladder is dependent on pretreatment techniques and if it can be used to discriminate between MM and MP.

Materials and methods

Tissue samples

Archival formalin-fixed, paraffin-embedded tissue blocks from 18 cystectomy specimens resected at the Karolinska University Hospital for invasive bladder cancer were reviewed. From each specimen, a representative nontumoral bladder wall section was selected. No sections from the trigone area, ureteral ostia or bladder neck were included in the study because of the more superficial MP in these regions [9, 10].

Immunohistochemistry

Immunostaining on 3-μm-thick tissue sections was performed with mouse monoclonal anti-human smoothelin (clone R4A) antibody (Biocare Medical, Concord, CA) using a Bond Max automated immunostainer (Leica, Bannockburn, IL). The tissue sections were baked at 60°C overnight before loading on autostainers. Standard IHC protocol was applied to all slides. Following deparaffinization and rehydration, antigen retrieval was performed on all slides using three different protocols: Bond Enzyme Pretreatment Kit for 5 min, heat-induced epitope retrieval (HIER) in Bond Epitope Retrieval Solution 1 (pH 6.0) and HIER in Bond Epitope Retrieval Solution 2 (pH 9.0) for 20 min. Peroxidase block for 5 min was performed followed by incubation of the primary antibody (dilution, 1:100) at room temperature for 30 min. The slides were then incubated with post primary reagent for 15 min at room temperature. The reaction was developed using BOND Polymer Refine Detection followed by colour development using 3,3′-diaminobenzidine tetrahydrochloride as a chromogen. The slides were then counterstained with hematoxylin and coverslipped. Before the study, several different concentrations of the primary antibody were evaluated. The dilution 1:100 was chosen because it gave the best signal intensity and lowest background staining.

The interpretation of immunoreactivity was done in a semiquantitative manner by analysing, and separately scoring, the intensity of positive immunostaining in the MM, MP and smooth muscle in blood vessels (SMBV). Staining intensity was scored as absent (0), weak (1+), moderate (2+) or strong (3+).

Results

Staining intensity of the MP, MM and SMBV depended strongly on the different pretreatment protocols used (Fig. 1a–d). The strongest staining was achieved using HIER in alkaline buffer as pretreatment. HIER in acidic buffer resulted in weaker staining. In the specimens that received enzymatic pretreatment, staining was absent or weak while staining without pretreatment resulted in weak staining of smooth muscle in the blood vessels.

In sections pre-treated with HIER in alkaline buffer, there was a moderate or strong smoothelin immunoreactivity in the MP in 18/18 (100%) of the cases. Using this pretreatment, the staining results for the MM were: absent in 1/18 (6%), weakly positive in 6/18 (33%), moderately positive in 7/18 (39%) and strongly positive in 4/18 (22%) (Table 1, Fig. 1d, Fig. 2a–d).

In contrast to the alkaline buffer, HIER in acidic buffer as pretreatment resulted in a suboptimal staining of the MP. MP staining was absent in 1/18 (5.5%), weak in 19/18 (56%), moderate in 7/18 (33%) and strong in 1/18 (5.5%) of cases. Labelling of the MM was also weaker with a moderate staining in only 1/18 (5%) while the rest of the cases had absent or weak staining (Table 1, Fig. 1b).

Enzymatic pretreatment resulted in weak staining of the MM in 1/18 (6%) cases and absence of staining in the rest of the cases. MP staining was absent in 14/18 (78%) and weak in 4/18 (22%) of cases using this pretreatment (Table 1, Fig. 1c).

In general, with all the pretreatment protocols used, the staining intensity of MP was stronger than the staining intensity of MM. Throughout the study, the staining intensity of the SMBV correlated well with the staining intensity of the MM.

In addition to the main study, where nontumoral tissue was used, we also stained for smoothelin in a number of specimens with MP-invasive urothelial carcinoma. In these specimens, we found that splayed MP fibres, engulfed in tumour masses, tended to show weaker staining for smoothelin than uninvolved MP (Fig. 3). Furthermore, smoothelin did not stain the myofibroblasts in the tumoral

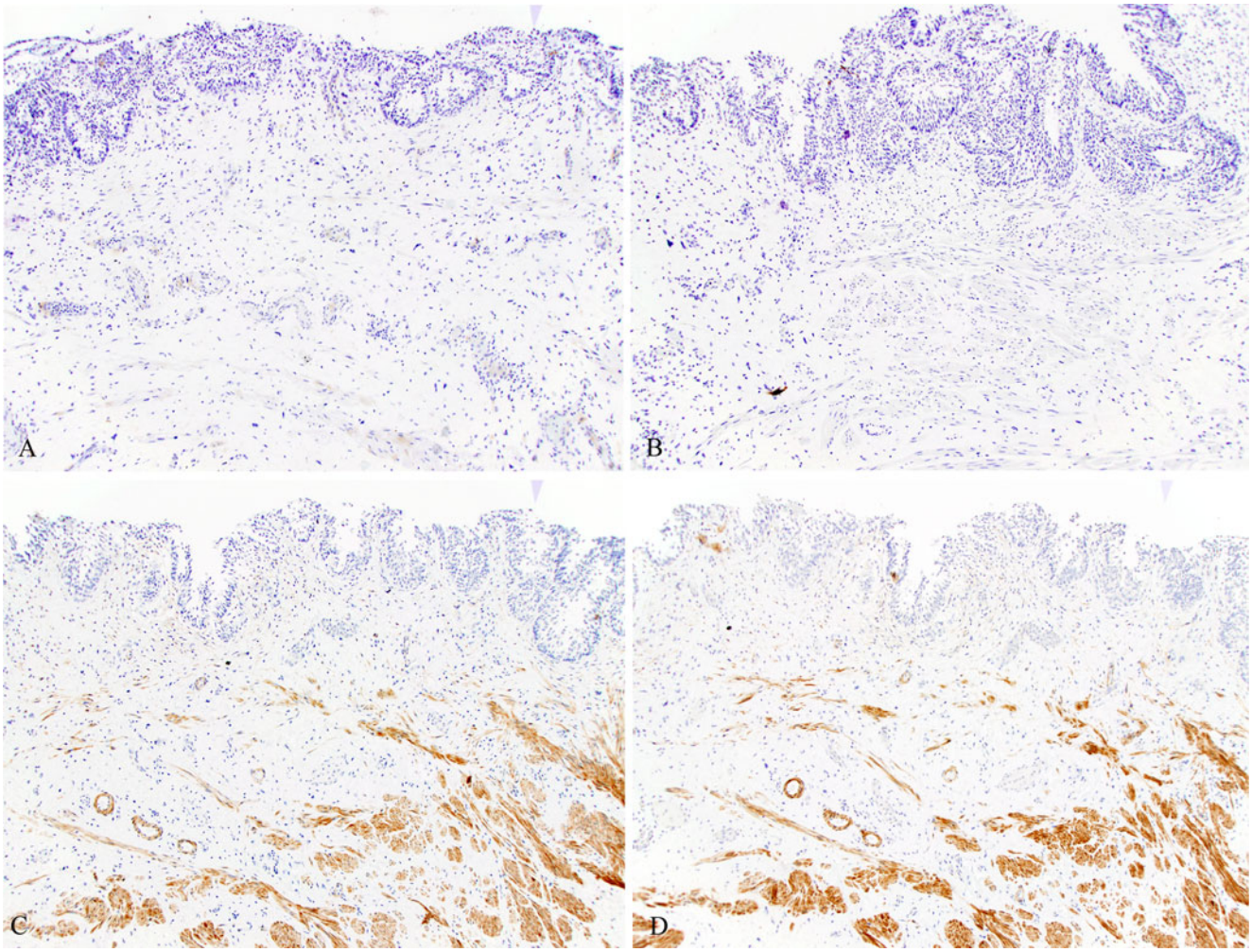

Fig. 1 Staining intensity of the muscularis mucosae, muscularis propria and smooth muscle in blood vessels depended strongly on pretreatment conditions. Staining without pretreatment resulted in weak staining of smooth muscle in the blood vessels (**a**) while staining was virtually absent when using enzymatic pretreatment (**b**). HIER in acidic buffer resulted in weak–moderate staining (**c**), but the strongest staining was achieved using HIER in alkaline buffer as pretreatment (**d**) (a–d lens magnification ×10)

Table 1 Intensity of smoothelin IHC staining depending on pretreatment conditions

Intensity		Muscularis mucosae (%)	Muscularis propria (%)
Enzymatic pretreatment			
Negative	0	17/18 (94)	14/18 (78)
Weak	2+	1/18 (6)	4/18 (22)
	3+	0/18 (0)	0/18 (0)
Strong	4+	0/18 (0)	0/18 (0)
HIER in acidic buffer			
Negative	0	10/18 (56)	1/18 (5.5)
Weak	1+	7/18 (39)	10/18 (56)
	2+	1/18 (5)	6/18 (33)
Strong	3+	0/18 (0)	1/18 (5.5)
HIER in alkaline buffer			
Negative	0	1/18 (6)	0/18 (0)
Weak	1+	6/18 (33)	0/18 (0)
	2+	7/18 (39)	1/18 (6)
Strong	3+	4/18 (22)	17/18 (94)

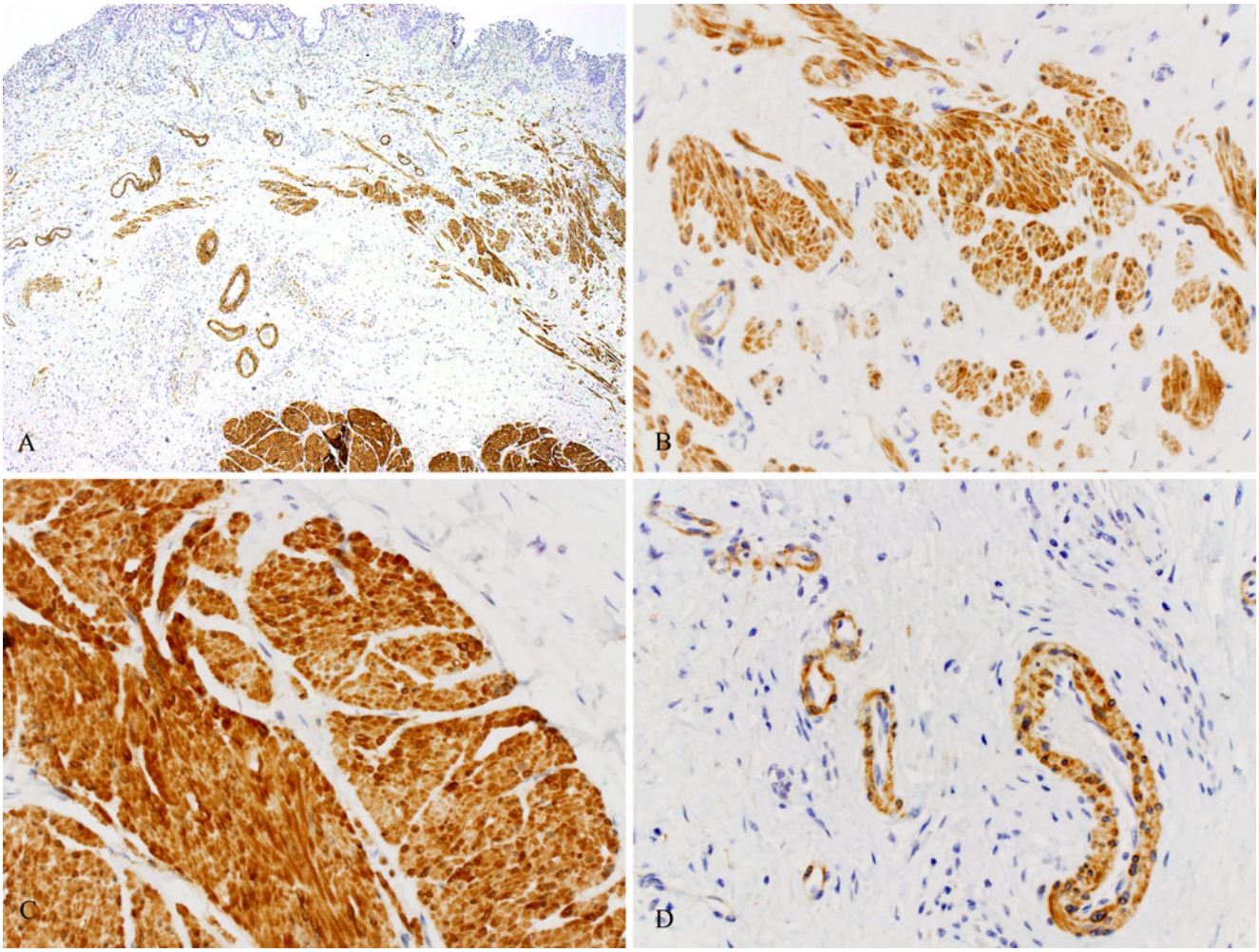

Fig. 2 Representative smoothelin stained bladder wall section pretreated with HIER in alkaline buffer. Strong staining of muscularis mucosae, muscularis propria and smooth muscle in blood vessels (**a**) (lens magnification ×4). Smoothelin staining of hyperplastic muscularis mucosae (**b**), muscularis propria (**c**) and smooth muscle in blood vessels (**d**) (b–d lens magnification ×40)

desmoplastic response irrespective of pretreatment protocols used.

Discussion

Bladder cancer diagnosis and staging is done on bladder biopsy or TURBT specimens. Because of the fragmentated nature of these specimens, difficulties sometimes arise in determinating whether smooth muscle invaded by carcinoma represents MP or MM. In bladder cancer staging, it is crucial to separate MP-invasive carcinoma (pT2) and carcinoma confined to the lamina propria (pT1) because pT2 disease usually leads to radical surgical cystectomy. Thus, cancer overstaging leads to unnecessary surgical cystectomies while understaging leads to proper surgical treatment being withheld from patients. Therefore, identifying a robust immunohistochemical marker for bladder MP would be a welcome addition to the diagnostic armamentarium. Paner et al. [10] and Council et al. [11] have reported promising results with a strong immunostaining for smoothelin of the MP in 86% (36/42) and 100% (15/15) of the cases, respectively. In both these studies, the staining of the MM was reported to be absent or weak in virtually all the cases. The authors consequently hypothesised that even though immunoreactivity for smoothelin was not specific for the MP, the quantitative difference in staining intensity between the MP and MM could be used as a diagnostic tool in discriminating MP from MM. To increase specificity and sensitivity in discrimination between MP and MM, the combination of smoothelin and vimentin IHC was also suggested by Council et al. [11]. In a recent study by Paner et al. [14], investigating 70 TURB cases, smoothelin had a sensitivity, specificity, positive predictive value and negative predictive value of 98%, 95%,

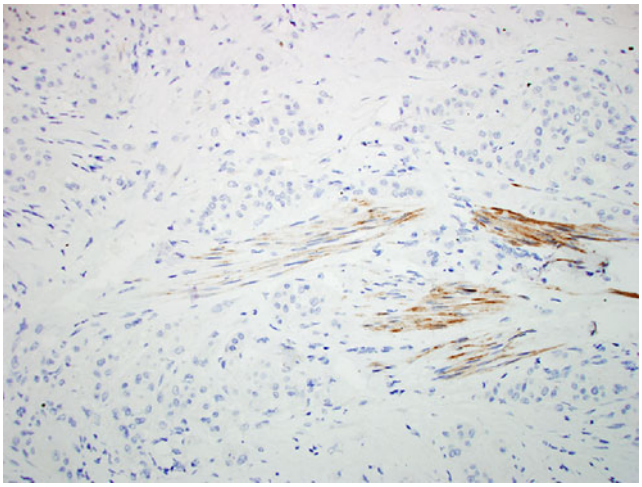

Fig. 3 Smoothelin stained section with tumour-involved muscularis propria. The thin, splayed MP fibres engulfed in tumour masses exhibit only weak immunohistochemical staining for smoothelin. Histomorphologically distinguishing these muscle fibres from MM is difficult, and smoothelin staining, with the staining overlap between MM and MP in mind, does not help in the discrimination (lens magnification ×20)

98% and 95% when setting a 3+ or 2+ staining of MP as threshold. Miyamoto et al. [13] investigated smoothelin staining in TURBT specimens where it was difficult to distinguish MM from MP invasion and found a generally stronger staining of MP as compared to MM, but there was a staining overlap in approximately 25% of cases.

In our study, we investigated how different IHC pretreatment protocols affect staining for smoothelin in the bladder and if smoothelin expression, under any of these pretreatment conditions, could be used as a reliable discriminant between MP and MM.

Staining results were shown to depend strongly on the different IHC pretreatment protocols used. HIER in alkaline buffer resulted in the strongest staining of the MP but with a moderate or strong staining of the MM in more than 60% of cases. On the other hand, HIER in acidic buffer caused a suboptimal staining of the MP (strong staining in 39%). Such a weak MP staining would disqualify it as a robust marker for MP. Enzymatic pretreatment resulted in weak staining of both the MM and the MP. Thus, our pretreatment protocols either resulted in a staining overlap between MM and MP, which could lead to cancer overstaging, or a suboptimal staining of MP, which could lead to understaging.

Our results differ from the results published earlier [10, 11, 13–15]. In all published articles, the same smoothelin antibody clone has been used (R4A) but from different manufacturers. Primary antibody dilution varies from 1:100 to 1:400 in the different studies. Increasing the dilution could possibly reduce the MM staining. Another factor that could influence the results of staining is the choice of IHC platform. We used the Bond Max platform (Leica, Bannockburn, IL) while the other groups all used Ventana Benchmark System (Ventana Medical Systems, Tuscon, AZ). Furthermore, we tested three different pretreatment protocols and found that HIER in alkaline buffer gave the strongest MP staining. Both Paner [10] and Council [11] used HIER in acidic buffer for epitope retrieval while Miyamoto et al. performed antigen retrieval in mild CC1 buffer (high pH). Technical aspects of the immunohistochemical studies done by the above-mentioned groups are summarised in Table 2.

We stained for smoothelin in a number of cases with MP-invasive urothelial carcinoma and found that tumour-involved MP tended to show weaker staining for smoothelin than uninvolved MP (Fig. 3). This weakening of the immunostaining in tumour-involved MP is in accordance with earlier published findings [13]. The thin, wispy appearance of splayed MP fibres makes it difficult to distinguish them from muscle fibres of the MM. Taking into account the staining overlap between MM and MP that we have shown, this reduction of immunoreactivity would make smoothelin even less suitable as a marker for distinguishing MM from MP in histomorphologically challenging cases.

The results of our study highlight the importance of validating and optimizing antibodies at the local clinic before usage in routine diagnostics. IHC is a multistep procedure where numerous factors influence the end result. This inherent instability is especially important when using an IHC staining that relies on differences in staining intensity rather than being specific.

In conclusion, in our study, smoothelin IHC is strongly dependent on epitope retrieval techniques, and smoothelin staining did not discriminate reliably between MP and MM with any of the tested pretreatment protocols. With these

Table 2 Summary of IHC protocols used by different groups

	Antibody	Dilution	HIER	Platform
Paner et al.	R4A (Abcam Inc.)	1:150	Citrate buffer (acidic, pH 6.0)	Ventana Benchmark System
Council et al.	R4A (Chemicon International)	1:400	Citrate buffer (acidic)	Ventana Benchmark System
Miyamoto et al.	R4A (Abcam Inc.)	1:200	Mild CC1 buffer (high pH)	Ventana Benchmark System
Lindh et al.	R4A (Biocare Medical)	1:100	EDTA (alkaline, pH 9.0)	Bond Max

results, we conclude that smoothelin IHC should be used with caution because it can, if used overconfidently in bladder cancer staging, potentially lead to misstaging if not properly validated and optimized. With the conflicting results regarding the utility of smoothelin staining to differentiate between MM and MP in mind, confirmative and larger studies investigating how smoothelin staining is influenced by varying pretreatment protocols should be performed. The possible influence of different antibody dilutions and the utilization of different commercial automated immunostainers could also be worth further investigations.

Conflict of interest We declare that we have no conflict of interest.

References

1. Parkin DM (2008) The global burden of urinary bladder cancer. Scand J Urol Nephrol Suppl 218:12–20
2. Ploeg M, Aben KK, Kiemeney LA (2009) The present and future burden of urinary bladder cancer in the world. World J Urol 27:289–293
3. Greene FLPD, Fleming ID et al (2002) AJCC Cancer Staging Manual. Springer, New York, 2002
4. Dixon JS, Gosling JA (1983) Histology and fine structure of the muscularis mucosae of the human urinary bladder. J Anat 136:265–271
5. Aydin A, Ucak R, Karakok M, Guldur ME, Kocer NE (2002) Vascular plexus is a differentation criterion for muscularis mucosa from muscularis propria in small biopsies and transurethral resection materials of urinary bladder? Int Urol Nephrol 34:315–319
6. Ro JY, Ayala AG, el-Naggar A (1987) Muscularis mucosa of urinary bladder. Importance for staging and treatment. Am J Surg Pathol 11:668–673
7. Vakar-Lopez F, Shen SS, Zhang S, Tamboli P, Ayala AG, Ro JY (2007) Muscularis mucosae of the urinary bladder revisited with emphasis on its hyperplastic patterns: a study of a large series of cystectomy specimens. Ann Diagn Pathol 11:395–401
8. Kuijpers KA, Heesakkers JP, Jansen CF, Schalken JA (2007) Cadherin-11 is expressed in detrusor smooth muscle cells and myofibroblasts of normal human bladder. Eur Urol 52:1213–1221
9. Paner GP, Ro JY, Wojcik EM, Venkataraman G, Datta MW, Amin MB (2007) Further characterization of the muscle layers and lamina propria of the urinary bladder by systematic histologic mapping: implications for pathologic staging of invasive urothelial carcinoma. Am J Surg Pathol 31:1420–1429
10. Paner GP, Shen SS, Lapetino S, Venkataraman G, Barkan GA, Quek ML, Ro JY, Amin MB (2009) Diagnostic utility of antibody to smoothelin in the distinction of muscularis propria from muscularis mucosae of the urinary bladder: a potential ancillary tool in the pathologic staging of invasive urothelial carcinoma. Am J Surg Pathol 33:91–98
11. Council L, Hameed O (2009) Differential expression of immunohistochemical markers in bladder smooth muscle and myofibroblasts, and the potential utility of desmin, smoothelin, and vimentin in staging of bladder carcinoma. Mod Pathol 22:639–650
12. van der Loop FT, Schaart G, Timmer ED, Ramaekers FC, van Eys GJ (1996) Smoothelin, a novel cytoskeletal protein specific for smooth muscle cells. J Cell Biol 134:401–411
13. Miyamoto H, Sharma RB, Illei PB, Epstein JI (2010) Pitfalls in the use of smoothelin to identify muscularis propria invasion by urothelial carcinoma. Am J Surg Pathol 34:418–422
14. Paner GP, Brown JG, Lapetino S, Nese N, Gupta R, Shen SS, Hansel DE, Amin MB (2010) Diagnostic use of antibody to smoothelin in the recognition of muscularis propria in transurethral resection of urinary bladder tumor (TURBT) specimens. Am J Surg Pathol 34:792–799
15. Bovio IM, Al-Quran SZ, Rosser CJ, Algood CB, Drew PA, Allan RW (2010) Smoothelin immunohistochemistry is a useful adjunct for assessing muscularis propria invasion in bladder carcinoma. Histopathology 56:951–956

Virchows Arch (2011) 458:671–678
DOI 10.1007/s00428-010-1003-8

ORIGINAL ARTICLE

Cardiac sarcoidosis and sudden death. The heart may look normal or mimic other cardiomyopathies

Izhar N. Bagwan · Lucy V. B. Hooper · Mary N. Sheppard

Received: 24 August 2010 / Revised: 8 October 2010 / Accepted: 14 October 2010 / Published online: 5 February 2011
© Springer-Verlag 2011

Abstract Cardiac sarcoidosis has been known to give rise to heart failure, arrhythmias and sudden cardiac death. We have a large database of sudden cardiac death cases at the CRY Centre for Cardiac Pathology at Imperial College, London, UK in which we found 17 of 1,720 cases with a diagnosis of cardiac sarcoid. Macroscopic examination showed a variety of findings including left ventricular hypertrophy, a dilated thin-walled left ventricle ,areas of fibrosis, changes resembling arrhythmogenic right ventricular cardiomyopathy and in some cases, no gross abnormalities. Histological examination revealed large areas of fibrosis and focal lymphocytic inflammation mimicking infarction/myocarditis. Careful search had to be made for non-necrotizing granulomata, since the lymphocytic foci, fibrosis and granulation tissue often predominated throughout the heart. The conduction tissue is often not sampled at autopsy despite the history of heart block. The heterogeneous nature of the macroscopic appearance and histological findings means that widespread sampling of the heart and the conduction system is essential in cases of sudden death in order that a diagnosis of myocardial sarcoidosis is not missed.

I. N. Bagwan · L. V. B. Hooper · M. N. Sheppard (✉)
CRY Centre for Cardiac Pathology, Imperial College,
London SW3 6NP, UK
e-mail: m.sheppard@rbht.nhs.uk

M. N. Sheppard
The Royal Brompton Hospital,
London, UK

I. N. Bagwan
The Royal Surrey County Hospital,
Guildford, Surrey, UK

Keywords Sarcoidosis · Heart · Sudden cardiac death

Introduction

Sarcoidosis is multisystemic disorder of unknown aetiology characterised by non-caseating granulomatous inflammation [1]. It was first described in 1869 by Hutchinson in a patient with characteristic skin lesions. In 1929, Bernstein identified cardiac involvement for the first time [2]. The incidence of cardiac sarcoidosis has been reported as 3–17% in clinical series and 20–30% in pathology series [3]. Cardiac involvement may manifest as heart failure, bradycardia or atrial/ventricular tachycardias [4]. Sudden cardiac death is a recognised mode of death in patient with cardiac sarcoidosis [5, 6]. The present study describes 17 cases with sudden cardiac death where sarcoid involvement of heart was the predominant pathology, and the diagnosis was not established during life and in which the macroscopic appearance suggested cardiomyopathy or was normal, prompting the pathologist to send it for a second opinion.

Materials and methods

The present study included 17 cases of cardiac sarcoidosis referred to the CRY (Cardiac Risk in the Young) Centre for Cardiac Pathology, Imperial College, over a period of 15 years (from 1994 to 2008). In all these cases, the presentation was sudden cardiac death with full coroner's autopsy at referring centres. Cases were sent as partially dissected whole heart (n=4) or as blocks/slides (n=13) for

Table 1 Study of cardiac sarcoidosis and sudden death

Age	Sex	History	ECG	Macro	HT wt(g)	Coronaries	Scar RV macro	Scar LV macro	LV micro gran	RV micro gran	Other organs gran
67	M	af	af	arvc	nk	Mild atheroma	Yes outflow	No	Yes	Yes	Liver
54	F	nil	nk	lvh, floppy mv	460	Normal	No	No	Yes	Yes	nk
38	M	Palpitations	arvc	lvh,arvc	609	Normal	Yes outflow ivs	ivs posterobasal	Yes	Yes	nk
56	F	nil	nk	bivent scar	nk	Normal	Yes patchy	Yes patchy	Yes	No	Spleen, liver
46	M	Palpitations	wpw	bivent scar	474	Normal	Yes patchy	ivs and free wall	Yes	No	nk
55	M	nil	nk	Normal	349	Normal	No	No	Yes	No	nk
89	F	ccf	nk	lvh	532	Mild atheroma	No	Yes patchy	Yes	No	nk
50	M	Palpitations	Irregular hr	arvc	nk	Normal	Yes patchy	ivs only	Yes	Yes	Lung
38	M	nil	nk	lvh	540	Normal	Yes patchy	lv patchy	Yes	Yes	Spleen
49	M	Syncope	af with hb	dcm	564	Normal	No	Yes circum	Yes	Yes	nk
52	M	nil	nk	Normal	nk	Normal	No	No	Yes	Yes	Lung, ln
41	M	nil	nk	dcm	452	Normal	Yes patchy	Yes patchy	Yes	Yes	nk
70	M	ihd ccf	nk	ihd	460	Diffuse atheroma	Yes patchy	Yes ivs	Yes	Yes	ln, liver
57	M	ccf	nk	dcm	625	Normal	No	Yes circum	Yes	No	Spleen, lung, pituitary
39	F	Palpitations	nk	arvc	335	Normal	rv outflow	Yes ant wall	Yes	Yes	Lung
68	M	ihd ccf	nk	ihd	nk	Diffuse atheroma	No	Yes free wall lv	Yes	No	Lung, liver, spleen
36	M	ccf hb	Complete hb	dcm	nk	Normal	No	Yes patchy	Yes	Yes	ln, spleen

af atrial fibrillation, *ant* anterior, *arvc* arrhythmogenic right ventricular cardiomyopathy, *bivent* biventricular, *ccf* congestive cardiac failure, *dcm* dilated cardiomyopathy, *gran* granuloma, *hb* heart block, *hr* heart rate, *ihd* ischaemic heart disease, *ivs* interventricular septum, *ln* lymph node, *lv* left ventricle, *lvh* left ventricular hypertrophy, *macro* macroscopically, *mv* mitral valve, *nk* not known, *rv* right ventricle, *wpw* Wolff Parkinson Whyte

specialist examination. The clinical data and the postmortem examination findings were obtained from the information provided by the referring pathologists.

Macroscopic description and sections for histological examination from post mortem hearts were taken from specific areas that included anterior, lateral and posterior walls of right and left ventricles, anterior and posterior portions of interventricular septum, left and right atria, ascending aorta and heart valves, respectively. However, in only one case referred, were we able to examine the full conduction system. The tissue was embedded in paraffin, and 4 μm sections were examined following staining with haematoxylin and eosin stain (H&E) and elastic Van Gieson to demonstrate collagen. The H&E slides were examined microscopically for the presence and location of non-caseating epithelioid cell granulomata, lymphocytic foci and areas of fibrosis. Cardiac sarcoidosis was diagnosed using the following criteria [7]:

1. Well-formed non-necrotising granulomata noted in the myocardium.
2. Granulomata in pericardium.
3. Granulomata in other organs including lung, spleen, liver and lymph nodes.
4. Stains for acid fast bacilli and fungi were negative.

Not all cases fulfilled all the criteria. The major criterion was well-formed granulomas in the myocardium with

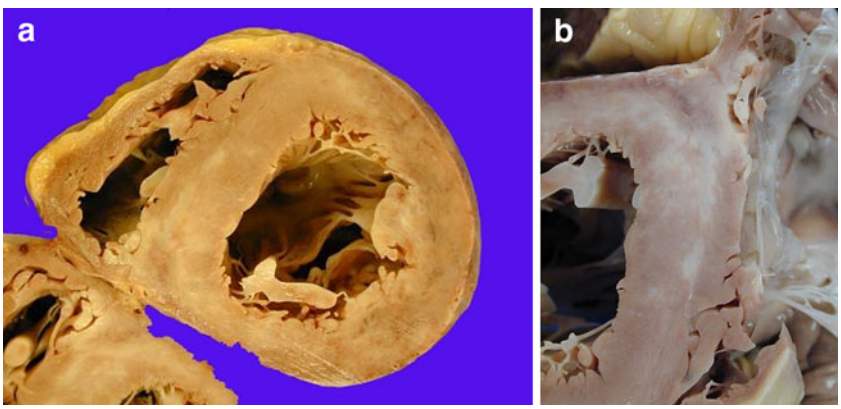

Fig. 1 **a** The transverse section or short axis of the right and left ventricle which emphasises the scarring in the interventricular septum and the posterobasal wall of the left ventricle with hypertrophy of the free wall and the interventricular septum. **b** The interventricular septal scarring and posterobasal scarring

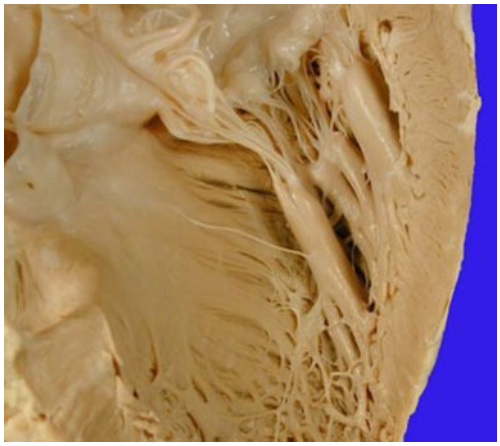

Fig. 2 A long axis view of the left ventricle noting thinning of the wall

negative stains for acid fast bacilli and fungi, while other criteria such as granulomas in the pericardium and other organs, were not documented in all cases.

Results

Clinical data

The total number of sudden cardiac death cases referred to our centre from 1994 to 2008 was 1,720, of which 17 were diagnosed to have cardiac sarcoidosis (incidence, 0.1%). The clinical features of these 17 cases are summarised in Table 1. The cases comprised 13 men and 4 women, ranging in age from 36 to 89 years with maximum number of patients in third to fifth decades. The mean age in this study was 52.4 years (Table 1).

With available clinical information in 11 cases, there was a history of palpitations (4), ischaemic heart disease with cardiac failure (2), cardiac failure (2), cardiac failure with heart block (1), atrial fibrillation (1) and syncope(1). Previous electrocardiographic (ECG) findings were unknown in 11 of the 17 cases, indicating how pathologist often may not have access to this, or there were no ECGs prior to the sudden death. In the six cases with ECG findings, there was irregular heart beat (1), atrial fibrillation (1), atrial fibrillation and variable heart block (1), Wolf Parkinson White syndrome (1), and changes suspicious for arrhythmogenic right ventricular cardiomyopathy (1) with T wave inversion in V1–V3, premature ventricular complexes of left bundle branch block morphology and epsilon waves and complete heart block (1). Echocardiography performed during life in three cases revealed one with mitral regurgitation, one with mitral and tricuspid regurgitation; the latter also had complete heart block. One case showed anteroseptal hypokinesis. None had a specific diagnosis made prior to death.

Macroscopic examination-

We relied on the macroscopic description of the referring pathologist in most cases with only one heart referred intact in which detailed examination of the ventricles atria and conduction system could be carried out. The heart weight was available in 11 of 17 cases and ranged from 335 to 625 g with a mean of 490.9 g (Table 1). Left ventricular hypertrophy was described in four of the 17 cases (Fig. 1a, b). Ventricular dilatation with wall thinning resembling dilated cardiomyopathy was noted in five cases (Fig. 2a, b). Four cases resembled arrhythmogenic right ventricular cardiomyopathy (one with left ventricular hypertrophy also), with fatty infiltration, thinning and scarring in the right ventricle particularly in the outflow tract and anterior wall (Fig. 3a, b), two were presumed ischaemic heart disease with scarring in the left ventricle associated with significant diffuse coronary artery disease, two had right/left ventricular scarring and two cases looked normal. The coronary arterial system was normal in 13 of 17 cases with mild atheroma in two cases and significant diffuse atheroma in all three vessels in the two cases who had a history of ischaemic heart disease clinically.

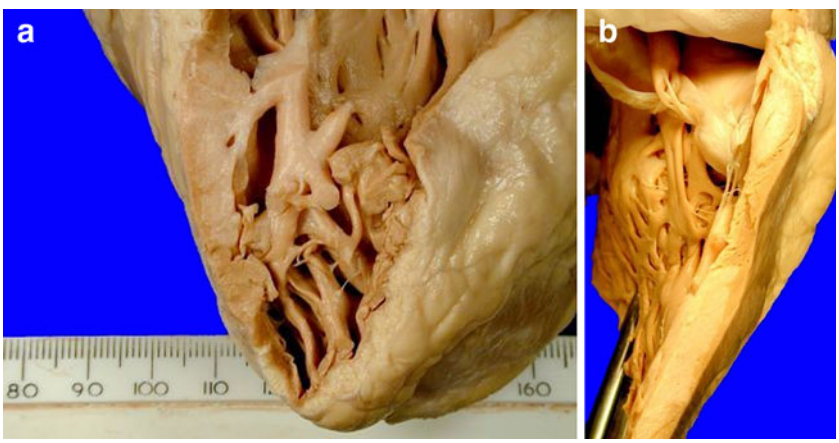

Fig. 3 **a** The right ventricle with what appears to be focal fatty infiltration of the anterior wall with thinning and pale areas extending onto the trabeculae. **b** Long axis view of right ventricle showing the scarred areas which look like fatty infiltration of the right ventricular outflow tract

Focal pale areas of presumed scarring involving both the right and left ventricles and the interventricular septum was observed in eight of the 17 cases as irregular pale patchy areas affecting both the left and right ventricles and the interventricular septum particularly involving the posterobasal zone of the left ventricle (Fig. 1a, b). There was right predominance in one case and left predominance in five cases while one LVH case had no scarring and two appeared normal. In only one intact case, could we observe the fibrosis involved the triangle of Koch outlined from the right atrioventricular aspect of the heart by the coronary sinus and the septal leaflet of the tricuspid valve, within which lies the membranous septum and atrioventricular (AV) node (Fig. 4).

Microscopic examination

Histological examination of the heart revealed widespread dense fibrosis in 15 of 17 cases (85%) (Fig. 5), while the remaining two showed patchy fibrosis despite being macroscopically normal. These areas of fibrosis predominantly affected the free wall of the left ventricle (100%) and extended to involve the interventricular septum (93.7%). Right ventricular fibrosis was noted in 75% of cases. Fibrous involvement of papillary muscles on both sides was seen in 70% of cases. These areas of fibrosis were admixed with aggregates of lymphocytes (Fig. 6). In the areas of widespread fibrosis, these focal lymphocytic aggregates extended into the myocardium with myocyte degeneration which could have been interpreted as myocarditis if further sampling had not shown granulomas elsewhere. These extensive areas of lymphocytic inflammation devoid of giant cells were noted in all cases. Other areas showed admixed giant cells with lymphocytes and myocyte necrosis resembling giant cell myocarditis (Fig. 7). The presence of scattered epithelioid cell clusters in all cases pointed to possibility of granulomatous inflammation (Fig. 8a, b), and these were found after careful review in all cases throughout the heart. The granulomata varied considerably in appearance from well-defined non-necrotizing epithelioid cell clusters with multinucleate giant cells and surrounding lymphocytic foci (Fig. 9) to scattered giant cells with or without surrounding lymphocytes (Fig. 10). The distribution of the granulomata was as follows: left ventricle, 17/17 (100%); interventricular septum, 16/17 (93.7%); right ventricle, 12/17 (75%). Only in one case which we sampled of left atrium and right atrium showed granulomatous inflammation in these chambers. The presence of granulomas was patchy and scattered with decrease in number in areas of dense fibrosis. Granulomas were noted within the epicardium and the pericardium in 11 of the 17 cases (68.7%) (Fig. 11). Perivascular and interstitial location of granulomata was seen in all 17 cases (Fig. 12), with direct involvement of small intramural vessels in two cases (Fig. 13), while one case showed lymphocytic inflammation of veins (Fig. 14). The AV node and AV conduction bundles sampled in one case showed extensive

Fig. 4 The right ventricle and right atrium with tricuspid valve in between. There is a rectangular pale area of thickening in the septomarginal trabeculation beneath the septal leaflet of the tricuspid valve

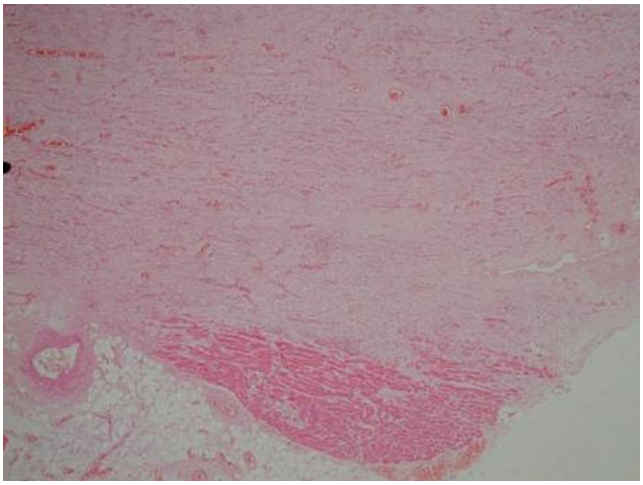

Fig. 5 The left ventricle showing replacement of the wall by dense fibrous tissue. Haematoxylin and eosin section, ×150

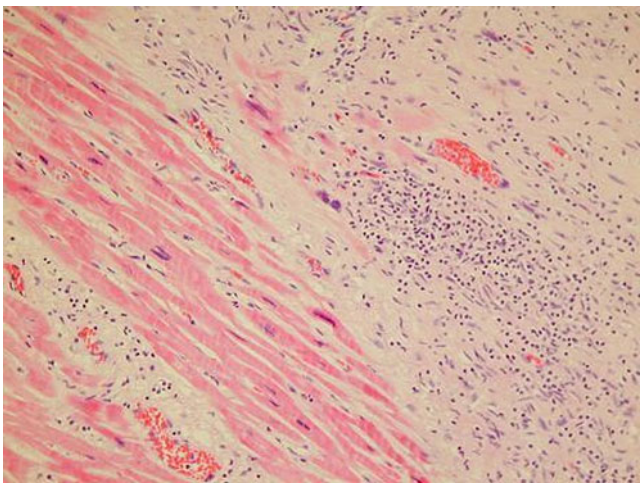

Fig. 6 Myocardium mixed with inflamed fibrous tissue with degeneration of myocytes giving impression of myocarditis. Haematoxylin and eosin section, ×300

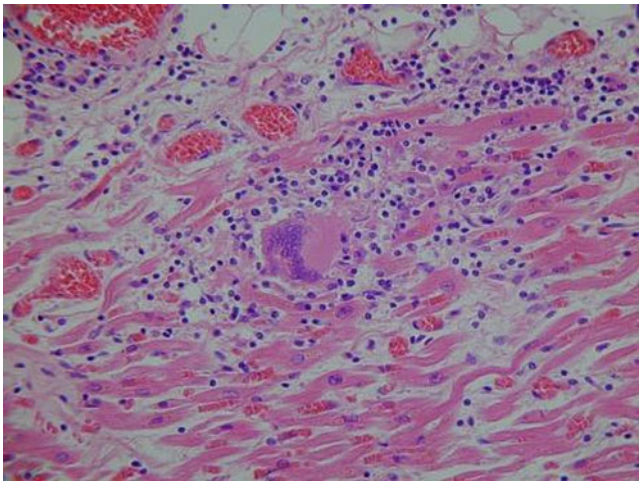

Fig. 7 Section of ventricle showing giant cells with surrounding lymphocytes in the myocardium with myocyte necrosis resembling giant cell myocarditis. Haematoxylin and eosin section, ×400

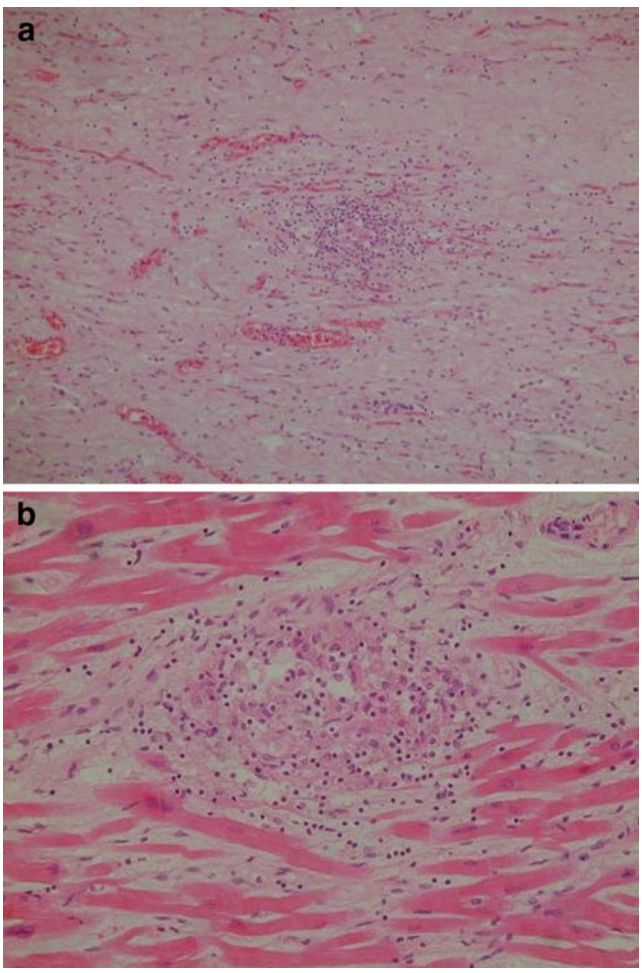

Fig. 8 **a** Inflamed fibrous tissue in which a collection of epithelioid cells is noted with surrounding lymphocytes. Haematoxylin and eosin, ×200. **b** A section of ventricle showing a collection of epithelioid cells in the interstitium with surrounding myocytes. Haematoxylin and eosin section, ×350

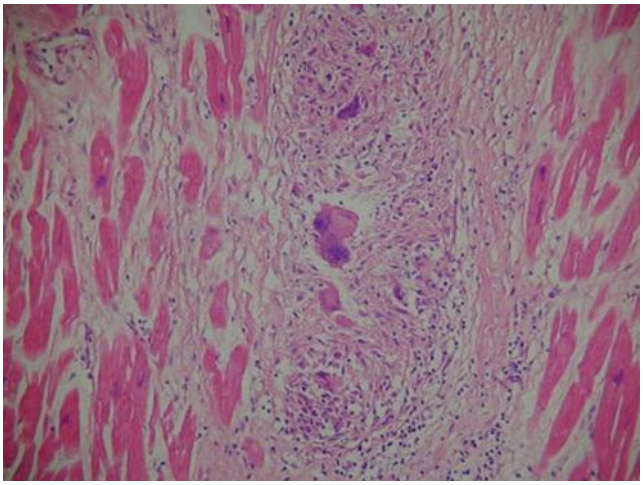

Fig. 9 A well-formed interstitial granuloma with epithelioid cells and multinucleated giant cells mixed with myocardium. Haematoxylin and eosin section, ×350

replacement of the node itself, bundle of His and left bundle branch by granulomatous inflammation including giant cells, epithelioid cells and lymphocytes as well as fibrosis.

Information regarding involvement of other organs was available in ten of the 17 cases. The organs that showed non-necrotizing granulomata in addition to the heart included spleen (5), lung (5), lymph nodes (3) and liver (4), and in one case, pituitary gland as well. Special stains like Ziel Nielson, PAS and Grocott stains were negative in all cases.

Discussion

Isolated/predominantly cardiac involvement with sarcoidosis is rare and can be difficult to diagnose [8]. Cardiac sarcoidosis can have a variety of manifestations including

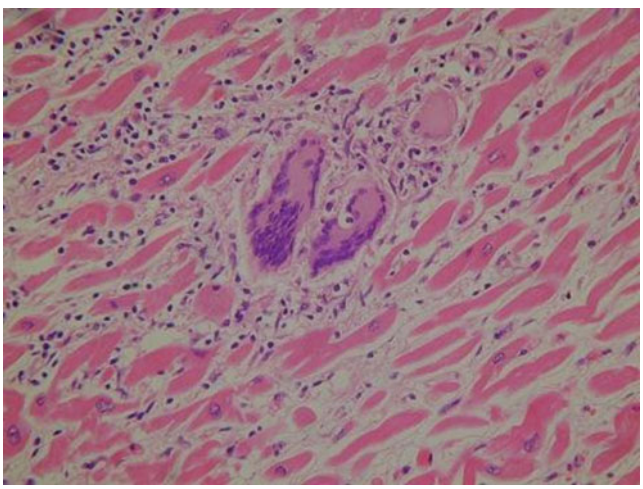

Fig. 10 A section showing giant cells with scattered lymphocytes. Haematoxylin and eosin section, ×500

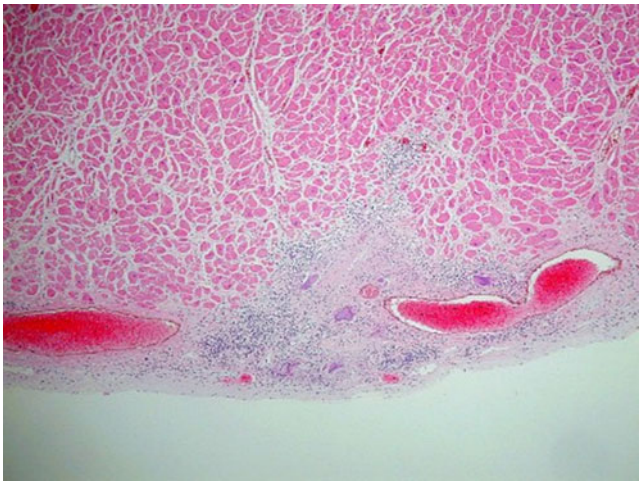

Fig. 11 The myocardium with overlying pericardium in which there is granulomatous inflammation present with multiple giant cells extending into the underlying myocardium. Haematoxylin and eosin section, ×200

conduction disease, congestive heart failure, valvular heart disease, pericardial effusions, tamponade, ventricular arrhythmias and sudden cardiac death. In patients with sarcoidosis, the reported incidence of cardiac involvement ranges from 20% in US autopsy studies to nearly 60% in Japan, where it accounts for the majority of deaths as a result of sarcoidosis. Recent evidence suggests that gadolinium-enhanced magnetic resonance imaging can potentially offer high sensitivity and specificity for both disease presence and activity [2]. Here, we describe in detail, the post mortem pathological features encountered in the hearts of patients dying suddenly without a diagnosis of sarcoidosis antemortem, which can present a diagnostic challenge to the pathologist. This was despite the history of

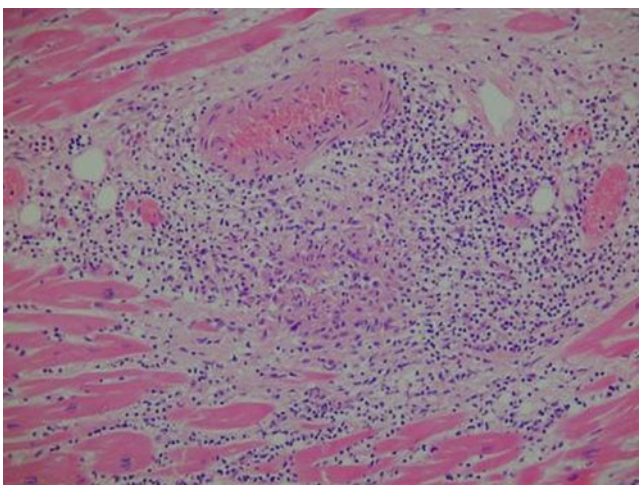

Fig. 12 The interstitium with accompanying blood vessel in which epithelioid cells with surrounding lymphocytic inflammation is noted and extending into the myocardium. Haematoxylin and eosin section, ×350

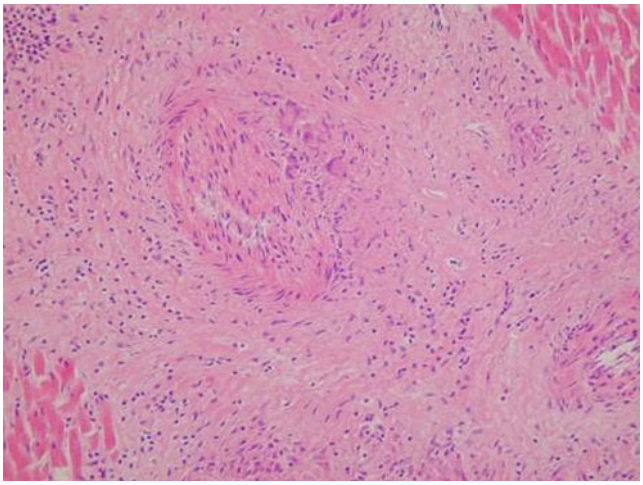

Fig. 13 An intramural arteriole in which giant cells are infiltrating the wall. Haematoxylin and eosin section, ×200

heart block in two cases which points to this possibility. While heart block has many causes, clinicians must include cardiac sarcoid in the differential diagnosis. The clinical history is interesting in that the history of palpitations, supraventricular tachycardia with WPW syndrome, irregular heart rate as well as heart block and also an ECG suggestive of ARVC all can be found in sarcoid heart disease [9, 10].

Macroscopically, the heart can have a variable appearance with left ventricular hypertrophy and dilated cardiomyopathy-like picture as well as arrhythmogenic right ventricular cardiomyopathy if there is right-sided predominance which occurred in four of our cases. There have been reports of right-sided predominant sarcoid mimicking ARVC [11, 12]. The patchy nature of the pale scarring in the right ventricle may resemble fatty infiltration and makes the pathologist think of this entity as occurred in our cases. Most studies emphasise left ventricular involvement, but right ventricular predomi-

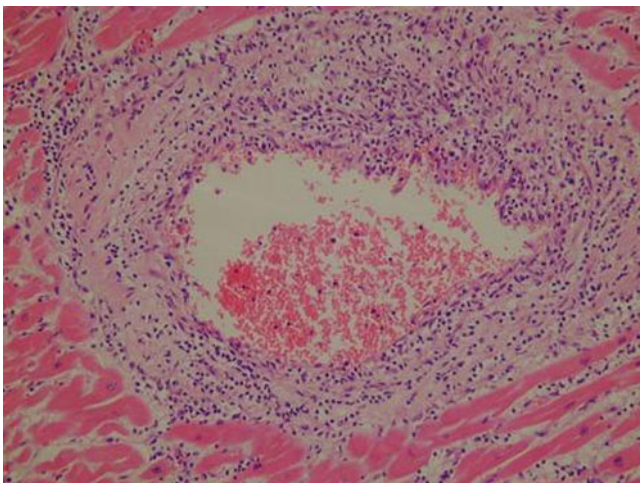

Fig. 14 A section of intramural vein showing lymphocytes infiltrating the wall and extending into surrounding myocytes. Haematoxylin and eosin section, ×400

nance has not been highlighted before and needs emphasis. In the left ventricle, posterobasal involvement may hint at sarcoid, but posterobasal predominant scarring is also seen in dilated cardiomyopathy particularly those associated with muscular dystrophies [13]. The heart may also appear normal as two of our cases demonstrate. Thus, changes may be subtle and can be missed. Cases in which the heart is macroscopically normal with only conduction system involvement by granulomatous inflammation have been reported [14]. A recent review [15] emphasises the epidemiology and histology with differential diagnosis but did not dwell on the macroscopic appearance. The fact that pathologists can see ventricular hypertrophy, left ventricular dilatation and scarring resembling fatty infiltration in the right ventricle and presume a specific cardiomyopathy is important to remember. This study emphasises that pathologists need to take extensive histology from both ventricles and also the atria (when there is a history of atrial fibrillation or supraventricular tachycardia) in routine investigation of the heart in sudden death and also take the conduction system with or without a history of heart block or arrhythmias. The variable appearances of the histology ranging from bland fibrosis, through chronically inflamed fibrous tissue through to areas resembling giant cell myocarditis to epithelioid cells and well-formed granulomas is also highlighted and again emphasises that extensive sampling is required to come to a specific diagnosis of cardiac sarcoid.

The histology of cardiac sarcoid is well known [15], but the spectrum of histology needs reemphasising. The spectrum can vary from dense fibrosis to fibrosis mixed with chronic inflammation mimicking myocarditis to the fully blown granulomatous inflammation which may mimic giant cell myocarditis [16]. If the pathologist takes only one block of tissue when the heart is sampled at routine autopsy or no tissue as sometimes occurs in coronial autopsies, the diagnosis will be missed. In our study, the highest frequency of granulomata were noted in the left ventricle followed by the interventricular septum, and this was in accordance with previous autopsy studies of sarcoidosis in the literature [17]. The granulomas noted in the pericardium and epicardium in 11 of 17 cases helps to differentiate from giant cell myocarditis in which multinucleate giant cells are not seen in the pericardium. Also, increased number of eosinophils with associated abscesses and extensive necrosis are noted in giant cell myocarditis [18]. The study also highlights the extensive fibrosis throughout the heart in both ventricles, indicating that it is possible for patients to have extensive disease and be asymptomatic until presentation with sudden death.

Two of our cases had significant coronary atheroma, and usually, scarring would be considered ischaemic with no histology taken so the diagnosis could be missed in these cases, and yet most cardiac sarcoid occurs in older patients. Therefore, cases may be underreported in sudden death series. Obviously, scarring can be attributed to ischaemic damage in these cases, but the presence of granulomas within the fibrotic areas point to inflammation playing a prominent role in the evolution of the scarring. Sudden death in cardiac sarcoidosis is likely to be the result of ventricular arrhythmias or complete heart block. Ventricular tachycardia has been reported in 23–50% of patients with myocardial sarcoidosis [19].

From examining post mortem reports in our published cardiac sudden death study [20], there is marked variation in the quality of autopsies, and in particular, the way the cardiovascular system is examined [21]. Note that the conduction system was only examined in one case which emphasises that pathologists do not routinely take it at autopsy. This is despite published guidelines for pathologists investigating sudden death [22].

In summary, cardiac sarcoid can be missed both clinically and pathologically. This study emphasises the widespread variation in macroscopic appearance mimicking cardiomyopathies in sarcoid heart disease and also in the microscopic findings at autopsy. The taking of multiple samples from all chambers of even normal looking heart is required in sudden cardiac death and the conduction system should also be taken.

Acknowledgements We are grateful to CRY (Cardiac Risk in the Young) for a grant enabling us to carry out this research cry@c-r-y.org.uk.

Conflict of interest statement We declare that we have no conflict of interest.

References

1. Vladimirova EB, Romanov VV, Shmelev EI (2006) Systemic manifestations of sarcoidosis. Probl Tuberk Bolezn Legk (10):36–39
2. Habersberger J, Manins V, Taylor AJ (2008) Cardiac sarcoidosis. Intern Med J 38:270–277
3. Nunes H, Freynet O, Naggara N, Soussan M, Weinman P, Diebold B, Brillet PY, Valeyre D (2010) Cardiac sarcoidosis. Semin Respir Crit Care Med 31:428–441
4. Chapelon-Abric C (2004) Epidemiology of sarcoidosis and its genetic and environmental risk factors. Rev Méd Interne 25:494–500
5. Kollermann J, Roos G, Helpap B (2001) Sudden cardiac death from unrecognized cardiac sarcoidosis. Pathologe 22:141–144
6. Veinot JP, Johnston B (1998) Cardiac sarcoidosis—an occult cause of sudden death: a case report and literature review. J Forensic Sci 43:715–717
7. Chapelon-Abric C (2001) Cardiac sarcoidosis. Ann Méd Interne 152:125–133 (Paris)
8. Milman N, Andersen CB, Mortensen SA (2006) Cardiac sarcoidosis—a difficult diagnosis. A report of eight consecutive patients with arrhythmias and cardiomyopathy. Ugeskr Laeger 168:3822–3824
9. Greif M, Petrakopoulou P, Weiss M, Reithmann C, Reichart B, Nabauer M, Steinbeck G (2008) Cardiac sarcoidosis concealed by arrhythmogenic right ventricular dysplasia/cardiomyopathy. Nat Clin Pract Cardiovasc Med 5:231–236
10. Ladyjanskaia GA, Basso C, Hobbelink MG, Kirkels JH, Lahpor JR, Cramer MJ, Thiene G, Hauer RN, Oosterhout MFV (2009)

Sarcoid myocarditis with ventricular tachycardia mimicking ARVD/C. J Cardiovasc Electrophysiol 21:94–98
11. Halushka MK, Yuh DD, Russell SD (2006) Right ventricle-dominant cardiac sarcoidosis with sparing of the left ventricle. J Heart Lung Transplant 25:479–482
12. Jain R, Dalal D, Daly A, Tichnell C, James C, Evenson A, Jain R, Abraham T, Tan BY, Tandri H, Russell SD, Judge D, Calkins H (2009) Electrocardiographic features of arrhythmogenic right ventricular dysplasia. Circulation 120:477–487
13. Finsterer J, Stollberger C (2000) Cardiac involvement in primary myopathies. Cardiology 94:1–11
14. Abeler V (1979) Sarcoidosis of the cardiac conducting system. Am Heart J 97:701–707
15. Lagana SM, Parwani AV, Nichols LC (2010) Cardiac sarcoidosis: a pathology-focused review. Arch Pathol Lab Med 134:1039–1046
16. Imai M, Takeishi M, Toyoda C, Kaneda Y (1975) Myocardial sarcoidosis—pathological studies on seven autopsy cases with particular reference to histological variations. Acta Pathol Jpn 25:477–497
17. Roberts WC, McAllister HA Jr, Ferrans VJ (1977) Sarcoidosis of the heart. A clinicopathologic study of 35 necropsy patients (group 1) and review of 78 previously described necropsy patients (group 11). Am J Med 63:86–108
18. Rosenstein ED, Zucker MJ, Kramer N (2000) Giant cell myocarditis: most fatal of autoimmune diseases. Semin Arthritis Rheum 30:1–16
19. Silverman KJ, Hutchins GM, Bulkley BH (1978) Cardiac sarcoid: a clinicopathologic study of 84 unselected patients with systemic sarcoidosis. Circulation 58:1204–1211
20. Bowker TJ, Wood DA, Davies MJ, Sheppard MN, Cary NR, Burton JD, Chambers DR, Dawling S, Hobson HL, Pyke SD, Riemersma RA, Thompson SG (2003) Sudden, unexpected cardiac or unexplained death in England: a national survey. QJM 96:269–279
21. Ranson D (2007) Coroners' autopsies: quality concerns in the United Kingdom. J Law Med 14:315–318
22. Sheppard MN (2003) Sudden adult death and the heart. Kirkham N, Shepherd N. [6], 185–202. 2003. London, Greenwich Medical Media. Progress in Pathology. 1-1-2003.

Virchows Arch (2011) 458:679–688
DOI 10.1007/s00428-011-1077-y

ORIGINAL ARTICLE

Claudins and tricellulin in fibrolamellar hepatocellular carcinoma

Attila Patonai · Boglárka Erdélyi-Belle · Anna Korompay · Áron Somorácz · Beate K. Straub · Peter Schirmacher · Ilona Kovalszky · Gábor Lotz · András Kiss · Zsuzsa Schaff

Received: 9 February 2011 / Revised: 29 March 2011 / Accepted: 31 March 2011 / Published online: 19 April 2011
© Springer-Verlag 2011

Abstract Fibrolamellar hepatocellular carcinoma is a subtype of hepatocellular carcinoma occurring in non-cirrhotic liver at a younger age. The tumor expresses both hepatocellular and cholangiocellular markers. Previously, our group described overexpression of tight junction protein claudin 4 in cholangiocellular carcinoma in contrast to hepatocellular carcinoma. In the present study, tight junction protein expressions were studied to possibly clarify bipotential lineage of fibrolamellar hepatocellular carcinoma. Eleven fibrolamellar hepatocellular carcinomas were compared with seven "conventional" hepatocellular carcinomas, seven cholangiocellular carcinomas, and five normal liver samples. By immunohistochemistry, all fibrolamellar hepatocellular carcinomas were positive for Hep-Par1 and cytokeratins 7, 8, and 18, but negative for cytokeratin 19. Glypican-3 gave weak staining in two cases. Expression of claudin 1 was lower, while that of claudin 2 was higher in fibrolamellar hepatocellular carcinomas than in other tumors. Claudins 3, 4, and 7 were not detectable in fibrolamellar hepatocellular carcinomas as in the majority of "conventional" hepatocellular carcinomas, contrary to high expression observed in cholangiocellular carcinomas. Focal or diffuse claudin 5 expression was detected in nine of 11 fibrolamellar hepatocellular carcinomas contrary to other tumors. Tricellulin was significantly downregulated in all tumors compared with normal liver. Our findings showed claudins to exhibit specific expression patterns in fibrolamellar hepatocellular carcinomas not observed in other primary liver tumors, with unique claudin 5 expression and pattern features similar to common hepatocellular carcinoma, but different from cholangiocellular carcinoma. This is the first report describing the loss of tricellulin expression in human hepatic tumors.

Keywords Fibrolamellar hepatocellular carcinoma · Tight junction proteins · Claudins · Hepatocellular carcinoma · Cholangiocellular carcinoma · Tricellulin

András Kiss and Zsuzsa Schaff equally contributed to this work.

A. Patonai · B. Erdélyi-Belle · A. Korompay · Á. Somorácz · G. Lotz · A. Kiss · Z. Schaff (✉)
2nd Department of Pathology, Semmelweis University,
Üllői út 93,
1091 Budapest, Hungary
e-mail: schaff@korb2.sote.hu

B. K. Straub · P. Schirmacher
Institute of Pathology, University Clinic Heidelberg,
Ruprecht-Karls University,
Im Neuenheimer Feld 220,
69120 Heidelberg, Germany

I. Kovalszky
First Institute of Pathology and Experimental Cancer Research,
Semmelweis University,
Üllői út 26,
1085 Budapest, Hungary

Introduction

Fibrolamellar hepatocellular carcinoma (FLC) is a distinct variant of primary hepatocellular carcinoma (HCC) with unique clinical and pathological features [1–6]. FLC occurs in younger individuals, even in children in non-cirrhotic liver. Incidence varies by geographical regions between 1% and 5%, with the rate reported to be 1–2% of total HCC cases in the USA [7, 8] and much higher in Mexico [9] and Poland [10].

The etiology of FLC is still unknown. In contrast to the "conventional" types of HCC (cHCC), no viral infection, toxic effect, metabolic alterations, or previous chronic liver diseases, including cirrhosis, were detected in patients with

FLC [4, 5]. Few reports described hepatitis B viral proteins (HBV) or DNA in FLC tumor tissue [11, 12], but the association seems accidental and not found by others [13].

The histopathology of FLC, including its immunohistochemical characteristics, is well defined [5]; however, differential diagnosis with cHCC with fibrous stroma presents a challenge even for the experts [14]. Both the molecular background and pathogenesis of FLC are obscure and limited, possibly owing to the relatively low number of cases studied by individual groups. FLC expresses features typical for cHCC, such as hepatocyte specific antigen (HSA, HepPar1) and cytokeratins (CK) 8 and 18, but alpha fetoprotein (AFP) is not expressed, and cytokeratin 7 (CK7), a cholangiocellular marker, is highly positive in FLC. Data suggest that there are subtypes of HCC which might arise from bipotential hepatic progenitor cells that can differentiate into both hepatocytes and cholangiocytes, whereas the majority of HCCs derive from hepatocytes [15].

Several novel emerging tumor markers are available in the diagnostics of HCC with varying value and prognostic significance [1, 3, 16–18]. Previously, we described for the first time that cholangiocellular carcinoma (CCC) is characterized by high expression of tight junction (TJ) protein claudin (CLDN) 4 in contrast to cHCC [19], which was later confirmed by others [20, 21]. CLDN 4 also serves as the receptor for *Clostridium perfringens* enterotoxin and may even be a target for future therapy [22–25]. CLDNs 1, 6, and 9 are entry co-factors for hepatitis C virus (HCV) [26, 27], and aberrant expression of CLDN 1 was detected in diverse forms of carcinomas, including HCC [28]. A dynamic model of TJs has been proposed [29], and data suggest that TJs undergo a continuous cycle of rapid association and dissociation (for review, see Steed et al., Ref. [30]). Several evidences of changes in the molecular composition of TJs are noticeable in a number of pathological conditions, particularly during tumorigenesis, and aberrations in expression are associated with tissue of origin, type of cancer, and even invasiveness and survival [23, 31–35].

The aim of the present study was to evaluate the expression of TJ proteins in FLC in order to define the changes in protein composition of intercellular connections of tumor cells and to compare the characteristic pattern of TJ composition with the pattern in cHCC and CCC.

Material and methods

Patients' tissue specimens

Eleven cases of FLC were studied with the permission of the Regional Ethical Committee of the Semmelweis University (#192). The patients were between 11 and 66 years of age (mean, 20.81 years), and the male/female ratio was 5/6 (Tables 1, 2, and 3). The cases were from the archives of the 1st and 2nd Departments of Pathology of the Semmelweis University, Budapest, Hungary (six cases), from other parts of Hungary (three cases), and from the University of Heidelberg, Germany (two cases). Out of the 11 cases, eight were surgically removed resection specimens, while liver core needle biopsy samples were available in three cases. None of the cases were associated with viral infection (Tables 1, 2, and 3). Surrounding non-tumorous liver samples were available in the five surgically removed resection specimens. For comparisons, five "normal" liver samples obtained from surrounding normal liver tissue of patients with focal nodular hyperplasia (two cases), one liver sample from an autopsy case (tissue samples taken within 12 h of a sudden death due to car accident) and two surrounding non-tumorous liver tissue samples from FLC cases were used. Seven "conventional" (not fibrolamellar, trabecular-acinar type) HCC cases (cHCC) of grades II–III and seven intrahepatic CCC cases

Table 1 Patients with fibrolamellar carcinoma

Patient	Gender	Age (years)	Cirrhosis	Viral infection	Tumor size (mm)	Metastasis
1	F	11	No	No	80×80×35	No
2	M	15	No	No	66×96×66	Lymph node
3	F	14	No	No	100×80×80	No
4	F	21	No	No	100×60×90	Lymph node, lung
5	M	19	No	No	110×70×100	Lymph node, lung, liver
6	M	16	No	No	30×40	No
7	F	16	No	No	110×90×80	No
8	F	18	No	No	60×36	Retroperitoneal lymph node
9	F	18	No	No	110×104×94	Metastasis (peritoneal carcinosis)
10	M	66	No	No	Multifocal	Metastasis (peritoneal carcinosis)
11	M	15	No	No	100×80×70	No

Table 2 Patients with "conventional" hepatocellular carcinoma

Patient	Gender	Age (years)	Cirrhosis	Viral infection	Tumor size (mm)	Metastasis
1	F	82	Yes	No	50×60	No
2	M	78	No	No	65×55	No
3	M	70	Yes	No	90×75	No
4	M	60	Yes	HCV, EBV	55×50	Multiplex
5	M	75	No	No	33×30	No
6	M	67	No	No	42×30	No
7	M	30	No	CMV	80×100	No

of grades II–III were selected from the archives for comparison. There was no possibility, however, for matching age because the cHCC and CCC cases involved a much higher age group (average 66 and 60 years, respectively) than the FLC cases (Tables 1, 2, and 3). Three cases of cHCCs developed on cirrhotic background, while in four other cases, no cirrhotic architectural changes were notable. The clinical diagnosis of FLC was established on the basis of imaging techniques (ultrasound, computer tomography, and magnetic resonance imaging).

Histology

Tissue samples were fixed immediately after removal in 10% neutral buffered formalin (in PBS, pH 7.0) at room temperature for 24 h, dehydrated in graded ethanol and xylene, and embedded in paraffin (FFPE). The 3–4-μm-thick sections were routinely stained with hematoxylin and eosin (H&E) and picrosirius red for detection of fibrous tissue.

Immunohistochemistry

FFPE sections, 3–5 μm thick, were cut. Primary antibodies and dilutions used are listed in Table 4. Primary antibodies were obtained from the following manufacturers; Dako Cytomation (Glostrup, Denmark), Vision Biosystems/ Novocastra (Newcastle upon Tyne, UK), Zytomed Systems (Berlin, Germany), Zymed (South San Francisco, CA, USA), Invitrogen (Carlsbad, CA, USA), BD Biosciences (Mississauga, ON, Canada), and Ventana Medical Systems (Tucson, AZ, USA). Reactions were carried out using Ventana Benchmark XT automated immunohistochemical staining system (Ventana) with HRP multimer-based, biotin-free detection technique. Reagents and secondary antibodies were obtained from Ventana, and reactions were visualized by UltraView TM Universal DAB Detection Kit (Ventana).

Morphometric analysis

CLDN 1, 2, 4, and 5 and tricellulin immunoreactions were evaluated by digital morphometrical analysis. All slides were digitalized by scanning with Mirax Panoramic MIDI and Mirax Panoramic SCAN digital slide scanners (3D Histotech Ltd., Budapest, Hungary). Fifteen non-overlapping fields of vision were selected from each slide at 40× virtual objective magnification. The extension of immunostained area was measured by Leica QWin Software (Leica Microsystems Imagine Solutions, Cambridge, UK). To compensate for discrepancies among samples in background noises, staining intensity, and prevalence of nonspecific reactions, minor adjustments in the color threshold levels of positive immunostaining were made.

Real-time RT-PCR

RNA extraction

Total RNA was isolated from eight to ten 3–5 μm sections of FFPE tissues using RNeasy FFPE Kit according to manufacturer instructions (QIAGEN, Hilden, Germany). To avoid the

Table 3 Patients with cholangiocellular carcinoma

Patient	Gender	Age (years)	Cirrhosis	Viral infection	Tumor size (mm)	Metastasis
1	F	78	No	No	6×25	Lymph node
2	F	49	Yes	No	85×70	Lymph node
3	M	65	No	No	40×8	Lymph node
4	F	61	No	No	50×30	No
5	F	36	No	No	35×22	No
6	F	74	No	No	50×30	No
7	M	57	Fibrosis	No	5×25	Lymph node

Table 4 Primary antibodies used in the study

Primary antibodies	Dilution	Species/clonality	Positive control	Manufacturer
CK7	1:1,000	Monoclonal Mouse	Urinary bladder transitional cc	Dako
CK8	1:80	Monoclonal Mouse	Normal liver	Dako
CK18	1:400	Monoclonal Mouse	Normal skin	Vision/Novocastra
CK19	1:100	Monoclonal Mouse	Normal skin	Dako
AFP	1:2,000	Monoclonal Mouse	Human placenta	Vision/Novocastra
HepPar1 (HSA)	1:50	Monoclonal Mouse	Normal adult liver	Vision/Novocastra
Glypican-3	1:100	Monoclonal Mouse	Hepatocellular carcinoma	Zytomed
Claudin-1	1:100	Polyclonal Rabbit	Normal skin	Invitrogen
Claudin-2	1:20	Monoclonal Mouse	Normal colon	Invitrogen
Claudin-3	1:80	Polyclonal Rabbit	Normal colon	Invitrogen
Claudin-4	1:200	Polyclonal Rabbit	Normal colon	Invitrogen
Claudin-5	1:200	Polyclonal Rabbit	Normal colon	Invitrogen
Claudin-7	1:100	Polyclonal Rabbit	Normal breast	Invitrogen
Tricellulin (C-term)	1:50	Polyclonal Rabbit	Normal duodenum	Invitrogen
CD-31 (PECAM-1)	1:80	Monoclonal Mouse	Epithelial angiosarcoma	Dako
CD-34 (Class II)	1:500	Monoclonal Mouse	Normal skin, tonsilla	Dako

amplification of genomic DNA, Turbo DNA-free™ Kit (Applied Biosystems Life Technologies, Carlsbad, CA, USA) was applied before transcription. cDNA samples were prepared from 1 μg of total RNA using High Capacity RNA-to-cDNA Kit (Applied Biosystems Life Technologies, Carlsbad, CA, USA) as specified by the manufacturer.

Primer design

Gene-specific primers were designed by AlleleID 6.01 (Premier Biosoft International, Palo Alto, CA, USA) primer design software. The used primers related to CLDN-1 and TRIC genes were designed to exon–exon borders to avoid the amplification of genomic DNA. The genes of CLDNs 3, 4, and 5 have only one exon. Isoform specificity and size of primers were checked by BioEdit biological sequence alignment editor software 7.01 (Tom Hall Ibis Therapeutics, Carlsbad, CA, USA). Primer specificity was checked by BiSearch software (Institute of Enzymology, Budapest, Hungary). Primer sequences used are listed in Table 5.

Real-time RT-PCR

Real-time reverse-transcriptase PCR (RT-PCR) analysis was performed by SYBR Green technology on ABI Prism 7000 Sequence Detection System (Applied Biosystems), according to manufacturer's instructions. As internal control gene 36b4 was used. Primer specific amplification was controlled by gel electrophoresis as well as melting temperature analysis. Primer concentrations were optimized for 60°C annealing temperature. The final 20 μl reaction mixture contained 10 μl Power SYBR Green PCR Master Mix (Applied Biosystems), 0.4 μl of 25 μM forward and reverse primers, 8.2 μl water, and 1 μl template cDNA. Cycling was performed using the following amplification conditions: incubation at 95°C for 10 min followed by 45 cycles at 95°C for 15 s, 60°C for 60 s, and 72°C for 15 s with subsequent melting analysis:

Table 5 Primers used for RT-PCR

Gene name	Primer sequences (5′-3′)	Amplicon sizes (bp)
ABL	ACGAGTCTGGTTGATGCTGTG (sense) GGCGGACTGTGGCTTTGG (antisense)	105
TRIC	TGGAACAACAGGAGATAAATGAGC (sense) GTCTCTTTGTCTGTCACCACTG (antisense)	86
CLDN-1	GTGCGATATTTCTTCTTGCAGGTC (sense) TTCGTACCTGGCATTGACTGG (antisense)	113
CLDN-3	CTGCTCTGCTGCTCGTGTCC (sense) TTAGACGTAGTCCT GCGGTCGTAG (antisense)	129
CLDN-4	GGCTGCTTTGCTGCAACTGTC (sense) GAGCCGTGGCACCTTACACG (antisense)	108
CLDN-5	TTCCTGAAGTGGTGTCACCTGAAC (sense) TGGCAGCTCTCAATCTTCACAG (antisense)	97

heating to 95°C for 20 s, cooling to 45°C for 10 s, and reheating to 95°C at a rate of 0.11°C per second.

Statistical analysis

Statistical analysis was carried out using STATISTICA software version 8.0 (Tulsa, OK, USA). The non-parametric Kruskal–Wallis test was used to analyze the differences. P values <0.05 were considered statistically significant.

Results

Macroscopy of FLC

The eight resected cases diagnosed as FLC showed typical gross appearance. The removed surgical specimens presented small central or eccentric scars, and the cut surface had a yellow-white color and was soft to firm (Fig. 1a). The average tumor sizes were 86×73×76 mm in diameter (Tables 1, 2, and 3). The surrounding livers were not cirrhotic, and the architecture was normal.

Histology

All 11 FLC cases showed typical histopathology. The tumors consisted of large, polygonal tumor cells with granular eosinophilic cytoplasm, arranged in columns and nests or forming glandular structures. The tumor cells contained intracytoplasmic pale bodies, intranuclear pseudoinclusions, and large prominent nucleoli, and cholestasis was occasionally seen. The groups of tumor cells were separated by lamellar fibrotic bands (Fig. 1b). Small calcifications were noticeable in two cases. No so called "clear cell variant" of FLC [5] was observable among the

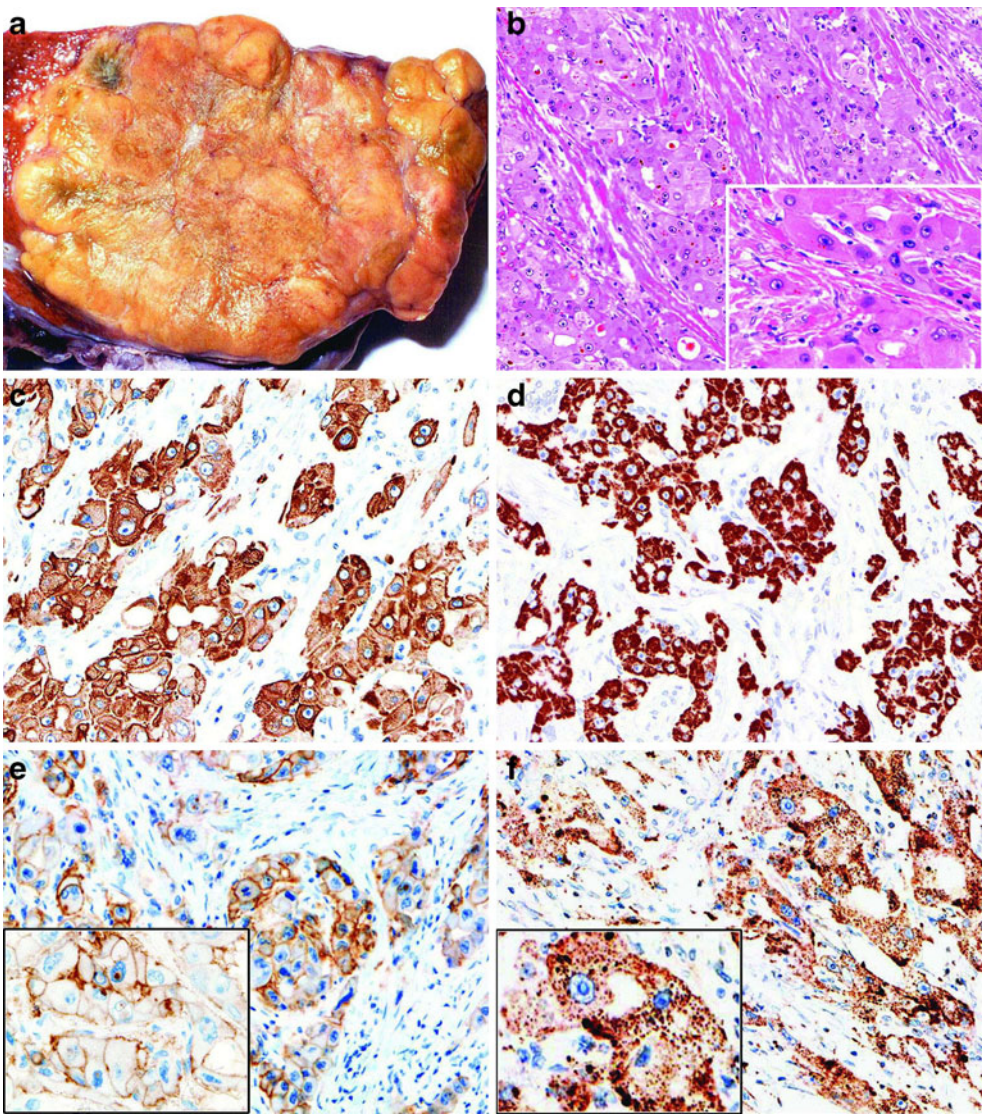

Fig. 1 Gross and histological appearance and immunohistochemical reactions in FLC. **a** Surgical specimen of FLC (case 1) with small eccentric scar, thin septa, and nodular structure. **b** FLC tumor cells with prominent nucleoli separated by variable width lamellar fibrotic bands (H&E, ×200, *inset* ×400). **c** Intensive CK7 and **d** HSA (HepPar1) positivity by immunohistochemistry in FLC. (×200). **e** Positive CLDN 1 membranous immunohistochemical reaction showing "honeycomb" pattern in FLC. Nuclear positivity is demonstrated in the inset (×200, inset ×600). **f** CLDN 2 shows a granular cytoplasmic and submembranous immunohistochemical localization in FLC (×200, inset ×600)

cases studied. The surrounding liver tissues available in five cases were normal, with mild nonspecific portal inflammation detectable in a few areas.

Immunohistochemistry, mRNA expression

Immunohistochemistry showed the typical features of FLC. HSA (HepPar1), CK7, 8, and 18 were positive (Figs. 1c, d), whereas AFP and CK19 were negative in all FLC cases studied. Glypican-3 was also negative in the majority of FLCs, and only weak focal cytoplasmic reaction was noted in two cases.

CLDNs 1 and 2 showed similar staining pattern in all three groups of tumors studied. Reaction with anti-CLDN 1 antibody was intense and membranous, completely surrounding the tumor cells in a honeycomb pattern (Fig. 1e). Significantly higher expression of CLDN 1 was observed in CCCs than in control livers, followed by cHCCs and FLCs (Fig. 2). Low percentage (0.5%) of nuclear staining was detected in four of the 11 FLCs (Fig. 1e, inset) and four of the cHCCs, while no staining was observed in any of the CCC cases and non-tumorous tissues. CLDN 1 mRNA was higher in cHCC and normal liver than in FLC; however, the differences were not significant (Fig. 3; $p>0.05$).

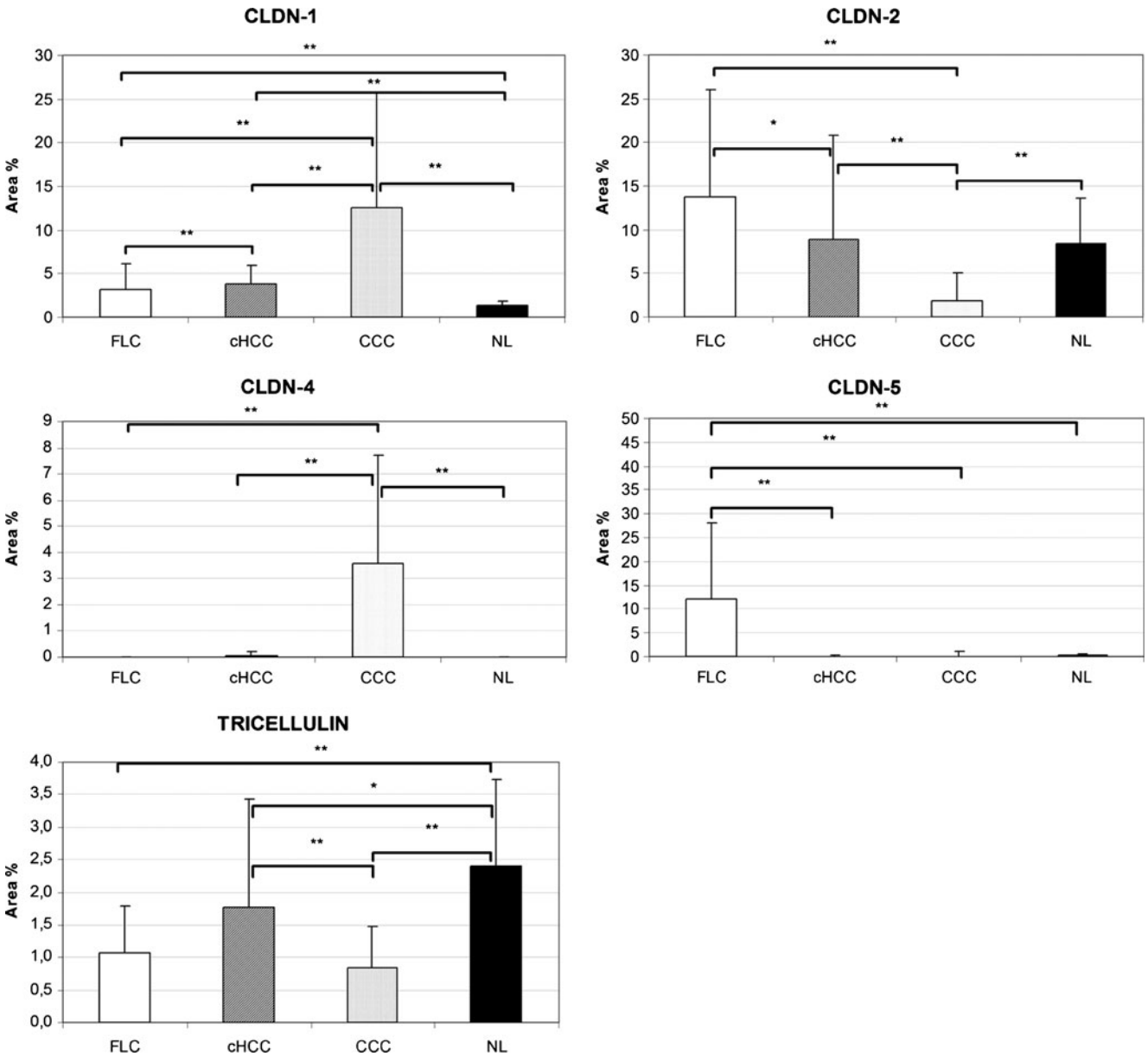

Fig. 2 Morphometric analysis of immunohistochemical reactions. Significant correlations: *$p<0.05$; **$p<0.001$. *FLC* fibrolamellar hepatocellular carcinoma, *cHCC* "conventional" hepatocellular carcinoma, *CCC* cholangiocellular carcinoma, *NL* normal liver, *CLDN* claudin

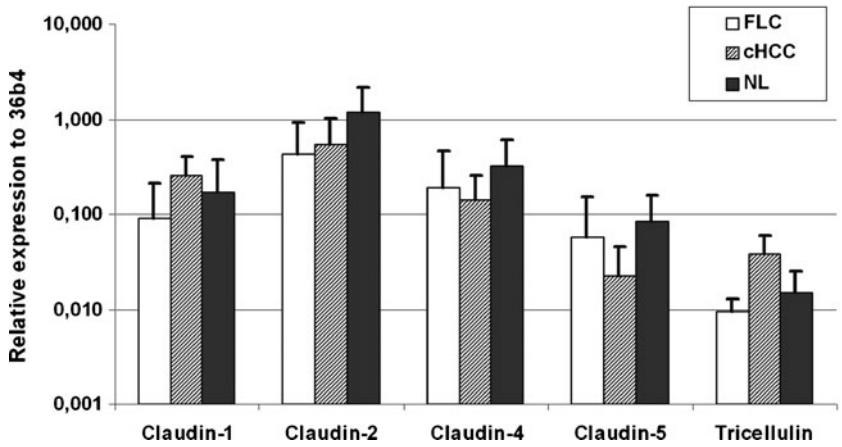

Fig. 3 mRNA expression detected by RT-PCR reaction. *FLC* fibrolamellar hepatocellular carcinoma, *cHCC* "conventional" hepatocellular carcinoma, *CCC* cholangiocellular carcinoma

CLDN 2 gave strong granular cytoplasmic/submembranous immunoreactivity (Fig. 1f), with the highest expression in FLCs; however, the difference to normal liver was not significant (Fig. 2). The tumor groups, however, significantly differed from each other in protein expression (Fig. 2), but no difference in mRNA expression was detected (Fig. 3). CLDN 3 was seen as scattered, weak membranous staining on normal hepatocytes, and weak staining was detected in HCC and FLC cells with no significant differences (not shown). No CLDN 4 and CLDN 7 were found by immunohistochemistry in HCCs and FLCs, in contrast to CCCs which showed intense significantly increased membranous positivity for CLDN 4 (Fig. 2). The mRNA, however, did not differ significantly between the FLC, cHCC, and control groups (Fig. 3).

CLDN 5 was positive in the tumor cells in nine out of 11 FLC cases with varying intensity (Fig. 4a), in contrast to cHCCs and CCCs which were negative. The reaction was mainly membranous; a weak cytoplasmic reaction was noted in three cases in addition to the membranous staining. Diffuse distribution of CLDN 5 staining with focally increased intensity was detected in five surgically resected cases; the needle biopsy samples showed intense positive staining. The endothelial cells in control livers and tumor samples were positive for CLDN 5 as well as for CD31 (Fig. 4b). Anti-CD34 antibody stained the vascular endothelial cells in all tumor groups with "typical" linear staining (Fig. 4c). CLDN 5 mRNA did not differ significantly in the FLC, cHCC, and non-tumorous control groups (Fig. 3).

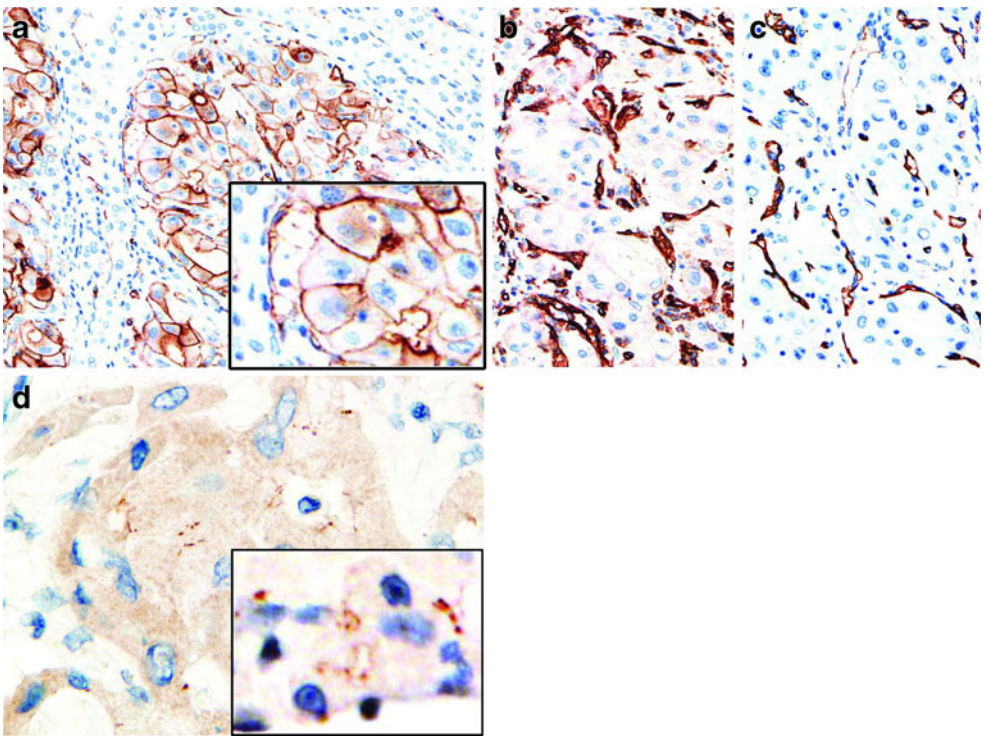

Fig. 4 Immunohistochemical reactions in FLC. **a** CLDN 5 membranous immunostaining with varying density in the FLC tumor cells. (×200, *inset* ×600). **b** CD34 and **c** CD31 immunostainings. The blood vessels are intensively positive, but the FLC tumor cells are negative. (×200). **d** Tricellulin immunostaining in FLC. The dot-like reaction follows the pseudoglandular structures or is located along the trabecules formed by the tumor cells. (×600, *inset* ×1200)

Tricellulin was seen mainly as linear or spotty focal membranous staining decorating the gland-like (pseudoglandular) structures, or was observable along the trabecules formed by the tumor cells in all tumors (Fig. 4d). Expression was higher in the well-differentiated tumor areas along the trabecular and pseudoglandular formations while being almost absent in the anaplastic, solid areas. The pattern and intensity of staining was similar to the surrounding liver; however, the percentage of positive tumor cells was significantly lower in tumors than in normal liver samples (Fig. 2). Tricellulin mRNA was not significantly different when comparing the FLC, cHCC, and control samples (Fig. 3).

Statistical analysis

By statistical analysis, based on the above presented data, FLC significantly differed from the normal liver in CLDN 5 and tricellulin protein expression (Fig. 2). FLC expressed significantly lower CLDN 1 (p=0.0007) and higher CLDN 2 (p=0.003) and CLDN 5 (p=0.0001) proteins than cHCC by immunohistochemistry. CLDN 4 was significantly higher in CCCs than in every other sample studied, which were all negative. The differences, however, at mRNA level were not significant.

Discussion

FLC is a variant of HCC, with unknown etiology and pathogenesis. Besides clinical characteristics, the expression or lack of expression of several markers differentiates FLC from cHCC, CCC, and hepatoblastomas [2]. The cytokeratin profile of FLCs presents both hepatocytic (CK8, 18) and biliary features (CK7) as found in our study and by others [1, 6]. Recent data proved expression of glypican-3 in FLCs with variable percentage [1, 6]. Glypican-3 was positive in two out of 11 FLC cases studied by us, with only weak staining reaction [21].

Our study is the first to demonstrate that the expression pattern of CLDNs in FLCs is altered and is more similar to cHCCs than to CCCs; however, FLCs differ from both in quantitative and qualitative tight junction protein characteristics.

CLDNs are the main transmembrane proteins of TJs; they exhibit important barrier function and are responsible for the polarization of hepatocytes separating the sinusoidal (basolateral) and bile canalicular (apical) plasma membrane domains [25, 36, 37]. Recent data suggested that TJs participate in signal transduction as well, influencing cell proliferation and differentiation [22, 32, 36], and are also expressed in a tissue-specific manner (for review, see Förster, Ref. [31]). Most epithelial cells express multiple CLDNs which interact with each other and other TJ proteins to form homo- and heterodimers [25]. Up to now, 24 members of the integral transmembrane claudin family have been described in mammals with differential distribution and functional characteristics. Regulation of TJ function is fundamental to several physiological processes and alterations influencing paracellular permeability [38].

In our study, FLCs showed lower CLDN 1 and higher CLDN 2 protein expression than cHCCs and CCCs, and expression of both claudins was significantly higher than in non-tumorous normal liver. CLDN 1 is usually highly expressed in epithelia, which exhibit barrier function and maintain cellular polarity. Dysregulation may be associated with alterations of the molecular pathways leading to development of squamous cell carcinomas and aggressive behavior of tumors [39–42]. In contrast, reduced expression was noted in several tumors of glandular origin such as breast cancer [43], type 1 endometrial cancer [44], colorectal cancer [45], and several other malignancies [25, 32, 33, 41, 46, 47]. Data about the role of CLDN 1 in hepatocarcinogenesis are controversial. Loss of CLDN 1 expression correlated with malignancy of HCC [28]; however, it was also demonstrated in vitro that CLDN 1 plays a critical role in HCC cell invasion [35]. According to our findings, cHCCs and CCCs significantly overexpressed CLDN 1 as compared with the normal liver, supporting its role in the invasive behavior of human liver cells.

CLDN 2, which showed higher expression in FLCs than in cHCCs and CCCs, is associated with higher paracellular ion permeability by pore formation and reduced transepithelial electric resistance (TER) [48]. Up- or downregulations were noted in several tumors [44, 49].

CLDN 4 was not detected by immunohistochemistry in FLCs similarly to cHCCs. Our group previously detected high expression of CLDN 4 in CCCs as compared with HCCs [19], and this protein was found to be differentially expressed in various parts of the normal and neoplastic biliary tract [20]. The observation that CLDN 4 is not expressed by the tumor cells of FLC, even in gland-forming areas, further supports the hepatocytic rather than cholangiocytic differentiation of the tumor despite its CK7 expression and lack of AFP production.

An interesting finding was the expression of CLDN 5 in FLCs, considered earlier as an endothelium-specific TJ protein. Several groups, however, identified CLDN 5 in normal epithelial cells [50], during development of the retinal epithelium [51], in normal lung cylindrical cells and pneumocytes [41]. CLDN 5 expression was observed in tumors as well [47], in Paget's disease of the breast [46] and lung adenocarcinoma [41]. Furthermore, CLDN 5 was detected in canine hepatoid glands, adenomas, and even in poorly differentiated carcinomas [52]. Comper et al. [53] detected CLDN 5 together with CLDN 2 cytoplasmic

staining in human solid pseudopapillary neoplasms in contrast to other pancreatic tumors and suggested that this finding might be associated with the specific morphology of the tumors. None of the cHCCs or CCCs in our study expressed CLDN 5 in the tumor cells except in the neovascular endothelium. CD34, another vascular marker, was detected in the endothelial cells only, with no expression noted in the tumor cells of FLCs and no differences notable between cHCCs and FLCs, as previously observed [1]. At the moment, there are no explanations to our finding that CLDN 5 was expressed in FLCs in contrast to cHCCs and CCCs; however, it suggests that these tumors differ in their molecular biological background. More recently, CLDN 5 was found to be a novel estrogen target in vascular endothelium, thus our finding of the expression of CLDN 5 in FLC might even be important for pathogenesis or future therapy [54].

We detected for the first time the presence of tricellulin, a novel TJ transmembrane protein in human hepatic tumors. A significant decrease of tricellulin was noted in all cancer groups as compared with the normal control liver. No differences were detected, however, between FLCs and cHCCs. Tricellulin, which is essential for barrier formation, is enriched in tricellular TJs, where three cells meet, but is also identified in bicellular TJs [55, 56]. It was recently demonstrated that at low tricellulin expression level, the tricellulin-containing TJ central tube forms a pathway for macromolecules [57]. In contrast to other TJ proteins, mainly claudins, overexpressions of which are known in several tumors [44], increased expression of tricellulin has not been described so far.

Our study contributes to the specific characteristics of FLC. Several differences have been shown to exist between FLC and cHCC in protein composition of TJs; however, the CLDN pattern is more similar to cHCCs than CCCs. A unique characteristic of FLC is the expression of the CLDN 5 protein, which differs from all other primary malignant epithelial tumors of the liver; therefore, it can be used as another differential diagnostic marker and may add further information in regard to the pathogenesis of this distinct entity.

Acknowledgments This work was supported by grants ETT-089/2009 by the Hungarian Ministry of Health and OTKA T 75468 by the Hungarian National Scientific Research Fund.

Conflict of interest The authors have no financial relationship with the organizations that sponsored the research. The authors declare that they have no conflict of interest.

References

1. Abdul-Al HM, Wang G, Makhlouf HR, Goodman ZD (2010) Fibrolamellar hepatocellular carcinoma: an immunohistochemical comparison with conventional hepatocellular carcinoma. Int J Surg Pathol 18:313–318
2. Ishak KG, Goodman ZD, Stocker JT (2001) Tumors of the Liver and Intrahepatic Bile Ducts. Atlas of Tumor Pathology, Third Series, Fascicle 31. Armed Forces Institute of Pathology, Washington, DC
3. Kannangai R, Vivekanandan P, Martinez-Murillo F, Choti M, Torbenson M (2007) Fibrolamellar carcinomas show overexpression of genes in the RAS, MAPK, PIK3, and xenobiotic degradation pathways. Hum Pathol 38:639–644
4. Liu S, Chan KW, Wang B, Qiao L (2009) Fibrolamellar hepatocellular carcinoma. Am J Gastroenterol 104:2617–2624
5. Torbenson M (2007) Review of the clinicopathologic features of fibrolamellar carcinoma. Adv Anat Pathol 14:217–223
6. Ward SC, Huang J, Tickoo SK, Thung SN, Ladanyi M, Klimstra DS (2010) Fibrolamellar carcinoma of the liver exhibits immunohistochemical evidence of both hepatocyte and bile duct differentiation. Mod Pathol 23:1180–1190
7. Craig JR, Peters RL, Edmondson HA, Omata M (1980) Fibrolamellar carcinoma of the liver: a tumor of adolescents and young adults with distinctive clinico-pathologic features. Cancer 46:372–379
8. El-Serag HB, Davila JA (2004) Is fibrolamellar carcinoma different from hepatocellular carcinoma? A US population-based study. Hepatology 39:798–803
9. Arista-Nasr J, Gutierrez-Villalobos L, Nuncio J, Maldonaldo H, Bornstein-Quevedo L (2002) Fibrolamellar hepatocellular carcinoma in Mexican patients. Pathol Oncol Res 8:133–137
10. Górnicka B, Ziarkiewicz-Wróblewska B, Wróblewski T, Wilczynski GM, Koperski L, Krawczyk M, Wasiutynski A (2005) Carcinoma, a fibrolamellar variant—immunohistochemical analysis of 4 cases. Hepatogastroenterology 52:519–523
11. Chang YC, Dai YC, Chow NH (2003) Fibrolamellar hepatocellular carcinoma with a recurrence of classic hepatocellular carcinoma: a case report and review of Oriental cases. Hepatogastroenterology 50:1637–1640
12. Davison FD, Fagan EA, Portmann B, Williams R (1990) HBV-DNA sequences in tumor and nontumor tissue in a patient with the fibrolamellar variant of hepatocellular carcinoma. Hepatology 12:676–679
13. Lapis K, Zs S, Kopper L, Karácsonyi S, Ormos J (1990) Fibrolamellar carcinomas of the liver. Zentralbl Allg Pathol Pathol Anat 136:135–149
14. Malouf G, Falissard B, Azoulay D, Callea F, Ferrell LD, Goodman ZD, Hayashi Y, Hsu HC, Hubscher SG, Kojiro M, Ng IO, Paterson AC, Reynes M, Zafrani ES, Emile JF (2009) Is histological diagnosis of primary liver carcinomas with fibrous stroma reproducible among experts? J Clin Pathol 62:519–524
15. Lee J-S, Heo J, Libbrecht L, Chu IS, Kaposi-Novak P, Calvisi DF, Mikaelyan A, Roberts LR, Demetris AJ, Sun Z, Nevens F, Roskams T, Thorgeirsson SS (2006) A novel prognostic subtype of human hepatocellular carcinoma derived from hepatic progenitor cells. Nat Med 12:410–416
16. Kakar S, Chen X, Ho C, Burgart LJ, Sahai V, Dachrut S, Yabes A, Jain D, Ferrell LD (2009) Chromosomal changes in fibrolamellar hepatocellular carcinoma detected by array comparative genomic hybridization. Hum Pathol 22:134–141
17. International Consensus Group for Hepatocellular Neoplasia (2009) Pathologic diagnosis of early hepatocellular carcinoma: a report of the International Consensus Group for Hepatocellular Neoplasia. Hepatology 49:658–664
18. Libbrecht L, Severi T, Cassiman D, Vander Borght S, Pirenne J, Nevens F, Verslype C, van Pelt J, Roskams T (2006) Glypican-3 expression distinguishes small hepatocellular carcinomas from cirrhosis, dysplastic nodules, and focal nodular hyperplasia-like nodules. Am J Surg Pathol 30:1405–1411

19. Cs L, Szabó E, Holczbauer Á, Batmunkh E, Szíjártó A, Kupcsulik P, Kovalszky I, Paku S, Illyés G, Kiss A, Schaff Z (2006) Claudin-4 differentiates biliary tract cancers from hepatocellular carcinomas. Mod Pathol 19:460–469
20. Zs N, Szász AM, Tátrai P, Németh J, Gyorffy H, Somorácz A, Szíjártó A, Kupcsulik P, Kiss A, Schaff Z (2009) Claudin-1, -2, -3, -4, -7, -8, and -10 protein expression in biliary tract cancers. J Histochem Cytochem 57:113–121
21. Nishino R, Honda M, Yamashita T, Takatori H, Minato H, Zen Y, Sasaki M, Takamura H, Horimoto K, Ohta T, Nakanuma Y, Kaneko S (2008) Identification of novel candidate tumour marker genes for intrahepatic cholangiocarcinoma. J Hepatol 49:207–216
22. Balda MS, Matter K (2008) Tight junctions and the regulation of gene expression. Biochim Biophys Acta 1788:761–767
23. Lal-Nag M, Morin PJ (2009) The claudins. Genome Biol 10:235
24. Saeki R, Kondoh M, Kakutani H (2009) A novel tumor-targeted therapy using a claudin-4-targeting molecule. Mol Pharmacol 76:918–926
25. Tsukita S, Yamazaki Y, Katsuno T, Tamura A, Tsukita S (2008) Tight junction-based epithelial microenvironment and cell proliferation. Oncogene 27:6930–6938
26. Evans MJ, von Hahn T, Tscherne DM, Syder AJ, Panis M, Wölk B, Hatziioannou T, McKeating JA, Bieniasz PD, Rice CM (2007) Claudin-1 is a hepatitis C virus co-receptor required for a late step in entry. Nature 446:801–805
27. Meertens L, Bertaux C, Cukierman L, Cormier E, Lavillette D, Cosset FL, Dragic T (2008) The tight junction proteins claudin-1, -6, and -9 are entry cofactors for hepatitis C virus. J Virol 82:3555–3560
28. Higashi Y, Suzuki S, Sakaguchi T, Nakamura T, Baba S, Reinecker HC, Nakamura S, Konno H (2007) Loss of claudin-1 expression correlates with malignancy of hepatocellular carcinoma. J Surg Res 139:68–76
29. Shen L, Weber CR, Turner JR (2008) The tight junction protein complex undergoes rapid and continuous molecular remodeling at steady state. J Cell Biol 181:683–695
30. Steed E, Balda MS, Matter K (2010) Dynamics and functions of tight junctions. Trends Cell Biol 20:142–149
31. Förster C (2008) Tight junctions and the modulation of barrier function in disease. Histochem Cell Biol 130:55–70
32. Martin TA, Jiang WG (2009) Loss of tight junction barrier function and its role in cancer metastasis. Biochim Biophys Acta 1788:872–891
33. Ouban A, Ahmed AA (2010) Claudins in human cancer: a review. Histol Histopathol 25:83–90
34. Sawada N, Murata M, Kikuchi K, Osanai M, Tobioka H, Kojima T, Chiba H (2003) Tight junctions and human diseases. Med Electron Microsc 36:147–156
35. Yoon CH, Kim MJ, Park MJ, Park IC, Hwang SG, An S, Choi YH, Yoon G, Lee SJ (2010) Claudin-1 acts through c-Abl-protein kinase Cdelta (PKCdelta) signaling and has a causal role in the acquisition of invasive capacity in human liver cells. J Biol Chem 285:226–233
36. Kojima T, Murata M, Yamamoto T, Lan M, Imamura M, Son S, Takano K, Yamaguchi H, Ito T, Tanaka S, Chiba H, Hirata K, Sawada N (2009) Tight junction proteins and signal transduction pathways in hepatocytes. Histol Histopathol 24:1463–1472
37. Rahner C, Mitic LL, Anderson JM (2001) Heterogeneity in expression and Subcellular localization of claudins 2, 3, 4, and 5 in the rat liver, pancreas and gut. Gastroenterology 120:411–422
38. Ikari A, Atomi K, Takiguchi A, Yamazaki Y, Miwa M, Sugatani J (2009) Epidermal growth factor increases claudin-4 expression mediated by Sp1 elevation in MDCK cells. Biochem Biophys Res Commun 384:306–310
39. Bello IO, Vilen S-T, Niinimaa A, Kantola S, Soini Y, Salo T (2008) Expression of claudins 1, 4, 5, and 7 and occludin, and relationship with prognosis in squamous cell carcinoma of the tongue. Hum Pathol 39:1212–1220
40. Dos Reis PP, Bharadwaj RR, Machado J, Macmillan C, Pintilie M, Sukhai MA, Perez-Ordonez B, Gullane P, Irish J, Kamel-Reid S (2008) Claudin 1 overexpression increases invasion and is associated with aggressive histological features in oral squamous cell carcinoma. Cancer 113:3169–3180
41. Paschoud S, Bongiovanni M, Pache J-C, Citi S (2007) Claudin-1 and claudin-5 expression patterns differentiate lung squamous cell carcinomas from adenocarcinomas. Mod Pathol 20:947–954
42. Sobel G, Cs P, Szabó I, Kiss A, Kádár A, Schaff Z (2005) Increased expression of claudins in cervical squamous intraepithelial neoplasia and invasive carcinoma. Hum Pathol 36:162–169
43. Tőkés AM, Kulka J, Paku S, Szik A, Páska C, Novák PK, Szilák L, Kiss A, Bögi K, Schaff Z (2005) Claudin −1, -3 and -4 proteins and mRNA expression in benign and malignant breast lesions: a research study. Breast Cancer Res 7:R296–R305
44. Szabó I, Kiss A, Zs S, Sobel G (2009) Claudins as diagnostic and prognostic markers in gynecological cancer. Histol Histopathol 24:1607–1615
45. Resnick MB, Konkin T, Routhier J, Sabo E, Pricolo VE (2005) Claudin-1 is a strong prognostic indicator in stage II colonic cancer: a tissue microarray study. Mod Pathol 18:511–518
46. Soini Y (2004) Claudins 2, 3, 4, and 5 in Paget's disease and breast carcinoma. Hum Pathol 35:1531–1536
47. Soini Y (2005) Expression of claudins 1, 2, 3, 4, 5 and 7 in various types of tumours. Histopathology 46:551–560
48. Van Itallie CM, Holmes J, Bridges A, Anderson JM (2009) Claudin-2-dependent changes in noncharged solute flux are mediated by the extracellular domains and require attachment to the PDZ-scaffold. Ann NY Acad Sci 1165:82–87
49. Sobel G, Németh J, Kiss A, Lotz G, Szabó I, Udvarhelyi N, Schaff Z, Páska C (2006) Claudin 1 differentiates endometrioid and serous papillary endometrial adenocarcinoma. Gynecol Oncol 103:591–598
50. Amasheh S, Schmidt T, Mahn M, Florian P, Mankertz J, Tavalali S, Gitter AH, Schulzke JD, Fromm M (2005) Expression of claudin-5 contributes to barrier properties in tight junctions of epithelial cells. Cell Tissue Res 321:89–96
51. Kojima S, Rahner C, Peng S, Rizzolo LJ (2002) Claudin 5 is transiently expressed during the development of the retinal pigment epithelium. J Membr Biol 186:81–88
52. Jakab C, Rusvai M, Gálfi P, Mándoki M, Demeter Z, Szabó Z, Kulka J (2009) Expression of claudin-5 in hepatoid gland biopsies. Vet Dermatol 21:276–281
53. Comper F, Antonello D, Beghelli S, Gobbo S, Montagna L, Pederzoli P, Chilosi M, Scarpa A (2009) Expression pattern of claudins 5 and 7 distinguishes solid-pseudopapillary from pancreatoblastoma, acinar cell and endocrine tumors of the pancreas. Am J Surg Pathol 33:768–774
54. Burek M, Arias-Loza PA, Roewer N, Förster CY (2010) Claudin-5 as a novel estrogen target in vascular endothelium. Arterioscler Thromb Vasc Biol 30:298–304
55. Ikenouchi J, Furuse M, Furuse K, Sasaki H, Tsukita S, Tsukita S (2005) Tricellulin constitutes a novel barrier at tricellular contacts of epithelial cells. J Cell Biol 171:939–945
56. Westphal JK, Dörfel MJ, Krug SM, Cording JD, Piontek J, Blasig IE, Tauber R, Fromm M, Huber O (2010) Tricellulin forms homomeric and heteromeric tight junctional complexes. Cell Mol Life Sci 67:2057–2068
57. Krug SM, Amasheh S, Richter JF, Milatz S, Günzel D, Westphal JK, Huber O, Schulzke JD, Fromm M (2009) Tricellulin forms a barrier to macromolecules in tricellular tight junctions without affecting ion permeability. Mol Biol 20:3713–3724

Virchows Arch (2011) 458:689–696
DOI 10.1007/s00428-011-1071-4

ORIGINAL ARTICLE

Nicotinamide inhibits hepatic fibrosis by suppressing DNA synthesis and enhancing apoptosis of hepatic stellate cells

Jing Jin · Kyong Bun Lee · Soo Young Park · Ja-June Jang

Received: 29 December 2010 / Revised: 22 February 2011 / Accepted: 21 March 2011 / Published online: 9 April 2011
© Springer-Verlag 2011

Abstract Liver fibrosis and its end-stage disease, cirrhosis, are major worldwide healthcare burdens. In this study, we evaluated the inhibitory effects of nicotinamide (NA) on rat hepatic fibrogenesis and investigated its underlying mechanism. We examined the inhibitory effects of NA in vivo by using F344 rats in a thioacetamide (TAA)-induced fibrogenesis model and assessed the inhibitory effects in vitro by using the rat hepatic stellate cell line THSC-Cl6. In vivo, NA significantly attenuated liver fibrosis in TAA-treated rats as assessed by histological analysis using hematoxylin-eosin and Masson's trichrome staining. In vitro, NA inhibited viability of THSC-Cl6 cells in a dose- and time-dependent manner, suppressed DNA synthesis, and induced apoptosis. Transcription of collagen mRNA and expression of alpha smooth muscle actin (the hallmark of activated hepatic stellate cells) were reduced by NA. Expression of the cell cycle-related proteins cyclin E, cyclin D1, and cyclin-dependent kinase (cdk)4, was reduced by NA treatment, but expression of cyclin A and cdk2 was not. Expression of the cdk inhibitors p16 and p21 was decreased by NA treatment, whereas expression of p27 was increased. It appears that NA inhibits rat hepatic fibrogenesis by suppressing DNA synthesis and enhancing apoptosis of hepatic stellate cells.

Keywords Hepatic stellate cells · Nicotinamide · Apoptosis · Cell proliferation · Cell cycle

J. Jin · K. B. Lee · S. Y. Park · J.-J. Jang (✉)
Department of Pathology,
Seoul National University College of Medicine,
28 Yongon-Dong, Chongno-Gu,
Seoul 110-799, South Korea
e-mail: tripj@snu.ac.kr

Abbreviations

NA	Nicotinamide
TAA	Thioacetamide
α-SMA	Alpha smooth muscle actin
cdk	Cyclin-dependent kinase
ECM	Extracellular matrix
H&E	Hematoxylin-eosin
PCR	Polymerase chain reaction

Introduction

Liver fibrosis is a common consequence of chronic liver injury with a variety of causative factors and results in liver cirrhosis [1]. This progressive pathological process is characterized by the accumulation of extracellular matrix (ECM) proteins. Activation of hepatic stellate cells plays a critical role in the excessive production and secretion of ECM proteins, resulting in the deposition of fibrous tissue and scar formation [2].

Nicotinamide (NA), also known as nicotinic acid amide, is the amide of nicotinic acid (vitamin B3/niacin). NA is a water-soluble vitamin and is part of the vitamin B group. NA exerts anti-inflammatory actions that may be of benefit to patients with inflammatory skin diseases [3]. Over the years, NA has been used to treat various diseases such as pellagra, psoriasis, schizophrenia, and type I diabetes [4, 5]. Although NA at doses above 3 g/day can produce liver toxicity [4], at doses below this, side effects are rare. Thus, it is generally considered safe as a food additive and as a component of cosmetics and medicines [6]. NA is sometimes used in combination with intravenous vitamin C therapy for cancer patients [7].

In recent years, several lines of evidence have suggested that NA is a potential antifibrotic agent. Treatment with NA was found to attenuate collagen accumulation and lung fibrosis in a bleomycin hamster model [8, 9]. In vitro, NA can induce apoptosis of hepatic stellate cells and reduce the expression of collagen I and proinflammatory cytokines [10]. However, a more in-depth understanding of the apoptosis mechanism is required. Moreover, in vivo studies on the effects of NA on liver fibrosis have not been published.

The purpose of the present study was to investigate the impact of NA on liver fibrosis in vivo and in vitro through evaluation of the effects of NA on the proliferation, apoptosis, and collagen expression of hepatic stellate cells.

Materials and methods

Reagents

NA was purchased from Sigma (St. Louis, MO, USA). For the in vivo study, NA was dissolved in saline to obtain a final concentration of 1%; for the in vitro study, NA was dissolved in the culture medium and stored at 4°C until assay.

Animals

Fifty-two male F344 rats (6 weeks old) were obtained from Orient Bio. (Korea). Throughout the experimental period, all rats were handled following the guidelines for the care and use of laboratory animals and fed an AIN-76 diet and were randomly divided into four groups of 13 rats each (Fig. 1). To induce liver cirrhosis, group-A and group-B rats were given intraperitoneal injections of thioacetamide (TAA; diluted with 0.15 M NaCl) at a dose of 200 mg kg^{-1} body weight. The injections were given three times per week over a 7-week period. In the case of groups B and C, 1% NA was added in the AIN-76 diet for 7 weeks. Group D was the control group, and neither NA nor TAA was injected. All animals were euthanized at week 7 under ether anesthesia. Blood and livers were collected, and the liver samples were fixed in formalin for histopathological examination.

Histological analysis

Livers were fixed in 4% paraformaldehyde, embedded in paraffin, and sectioned. The sections were used for hematoxylin and eosin (H&E) and Masson's trichrome collagen staining. The degree of fibrosis was evaluated according to the METAVIR scoring system on the basis of histological examination of slides (F0, no portal fibrosis; F1, portal fibrosis without septum formation; F2, portal fibrosis with few septum formation; F3, portal fibrosis with many septum formation but no cirrhosis; and F4, cirrhosis). The areas with fibrosis were evaluated using Aperio Image scope program.

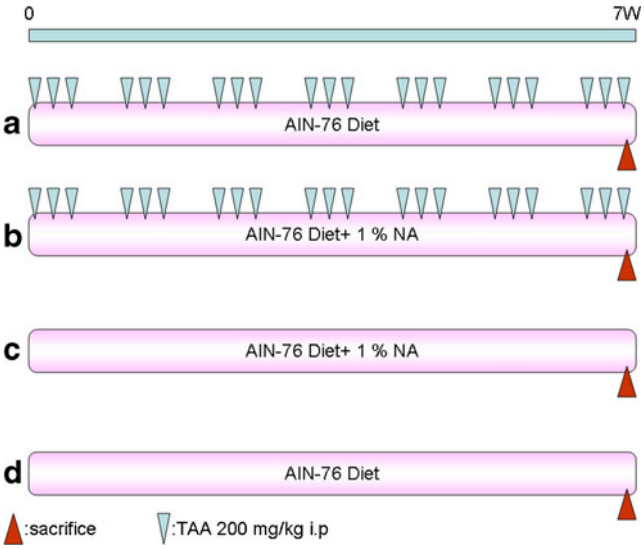

Fig. 1 Experimental protocol for animal study. To induce liver cirrhosis, rats in group **a** and **b** were given intraperitoneal injections of thioacetamide at a dose of 200 mg kg^{-1} body weight. The rats in group **b** and **c** were given 1% nicotinamide in drinking water for 7 weeks. Group **d** was given neither NA nor TAA. All animals were sacrificed at week 7

Cell culture and treatment

THSC-Cl6 cells were maintained in William's E medium (Sigma, MD, USA), supplemented with 10% (*v/v*) fetal bovine serum (GIBCO-BRL, NY, USA), 1% penicillin–streptomycin (10,000 units mL^{-1} of penicillin and 10,000 μg mL^{-1} of streptomycin; GIBCO-BRL, NY, USA), and $NaHCO_3$ (2.2 gL^{-1} of medium) [11]. The cells were detached from the monolayer by incubation in phosphate-buffered saline (Sigma, MD, USA) containing 0.5% trypsin (1:250). The cells were then incubated in a humidified incubator at 37°C under a 5% CO_2 atmosphere and passaged every second day.

Cell proliferation analysis

THSC-Cl6 cells were seeded in a 96-well plate, with 200 μL (1×10^2 cells mL^{-1}) per well. After incubation for 18 h, the cells were preincubated with NA (0, 10, 15, and 20 mM) and assayed at 0, 12, 24, 36, and 48 h. Cell viability was evaluated using a PreMix WST-1 Cell Proliferation Assay System (TaKaRa Bio Inc., Japan). Results are presented as mean (SD) absorbances of triplicate assays.

DNA synthesis assay

DNA synthesis was detected using an ELISA BrdU colorimetric kit (Roche, Mannheim, Germany), according to the manufacturer's instructions. THSC-Cl6 cells were seeded in a 96-well plate, with 200 μL (1×10^2 cells mL^{-1}) per well. After incubation for 18 h, the cells were preincubated with NA (0, 10, 15, and 20 mM) for 48 h. Results are presented as mean (SD) absorbances of triplicate assays.

Annexin V-FITC staining and FACS analysis

An MBL MEBCYTO Apoptosis Kit (Medical & Biological Laboratories Co., Nagoya, Japan) was used to determine NA-induced apoptosis. After incubation with NA (0, 10, 15, and 20 mM) for 48 h, the cells were trypsinized and resuspended in 300 μL of binding buffer. Thereafter, 5 μL of Annexin V-FITC and 2.5 μL of propidium iodine were added to the 300 μL of cell suspension. The samples were kept in the dark for 15 min and analyzed using a BD FACS Caliber Flow Cytometer (BD Biosciences, MA, USA).

DNA ladder of the cell apoptosis test

The cells were treated with 0, 10, 15, or 20 mM NA for 48 h, and DNA was extracted using an Apoptotic DNA Ladder Kit (Roche, Mannheim, Germany). Electrophoresis using 1.5% agarose gel was performed for 4 h at a constant voltage of 50 V and the gel observed with a Gel Doc™ XR+System (BIO-RAD, Milan, Italy).

Protein extraction and Western blot analysis

THSC-Cl6 cells were incubated with NA (0, 10, 15, or 20 mM) for 48 h, and whole proteins were extracted by T-PER (Pierce, Rockford, IL, USA) with cocktail protease inhibitors (Roche, Mannheim, Germany). Protein concentrations were measured by BCA™ (Pierce, Rockford, IL, USA). The samples were boiled at 100°C for 8 min, and 30–100 μg of proteins was loaded onto a 10%, 15%, or 20% SDS gel. After electrophoresis, the gel was electro-transferred onto PVDF membranes (Millipore Corporation, Bedford, MA, USA) or nitrocellulose membranes (BIO-RAD, Hercules, CA, USA). After 30 min of blocking with 5% skim milk in TBS-T, the membranes were incubated with appropriate primary and HRP-conjugated secondary antibodies (Zymed, CA, USA) for the required times. An enhanced chemiluminescent ECL assay kit (Pierce, Rockford, IL, USA) was used to incubate the membranes, with the chemiluminescence detected by BioMax XAR film (Kodak, NY, USA).

Quantitative real-time polymerase chain reaction

THSC-Cl6 cells, incubated with or without NA for 48 hours, were used. Total RNA was separately isolated using trizol (Invitrogen, CA, USA), chloroform (Sigma, St. Louis, MO, USA), isopropyl alcohol (Sigma, St. Louis, MO, USA), and 70% cold ethanol. The RNA pellets were briefly air-dried and dissolved in ultrapure water. First-strand cDNA was generated with M-MLV reverse transcriptase (ELPIS, Taejon, Korea), using random primers (Promega, WI, USA) and 3 μg of total intracellular RNA. A mixture containing dNTP (2.5 mM; Applied Biosystems, Foster City, CA, USA), 40 units of RNasin (Promega, Madison, WI, USA), 200 units of reverse transcriptase (ELPIS, Taejon, Korea), and RT buffer was mixed with the previous RNA primer mixture and incubated at 37°C for 2 hours. For the SDS 7000 system reactions, SYBR Premix Ex Taq (TaKaRa Bio Inc., Japan) was prepared with 20-pM primers and 1 μL cDNA as polymerase chain reaction (PCR) template. Relative quantitative real-time PCR on 96-well optical plates was performed using the above reagents, and the products were analyzed on an ABI Prism 7000 Sequence Detection System (Perkin-Elmer Applied Biosystems, CA, USA). The level of expression of the target gene was normalized to internal SDR-GAPDH and represented as a relative expression. The PCR primer and probe sets used in the real-time PCR investigation are listed in Table 1.

Statistical analysis

Data are presented as means (SD). The statistical analysis was performed by the Mann–Whitney *U* test, using SPSS 17.0. Results were considered statistically significant at $p<0.05$.

Results

Effect of NA on liver fibrosis in rats

We used a series of experimental approaches to evaluate whether NA inhibited hepatic fibrosis. In the Masson's

Table 1 Primers used for reverse transcriptase PCR and quantitative real-time PCR

Gene	Primer	Sequence
SDR-Collagen	Forward	CCTCAAGGGCTCCAACGAG
	Reverse	TCAATCACTGTCTTGCCCC
SDR-GAPDH	Forward	GGCAAATTCAACGGCACAGT
	Reverse	AGATGGTGATGGGCTTCCC

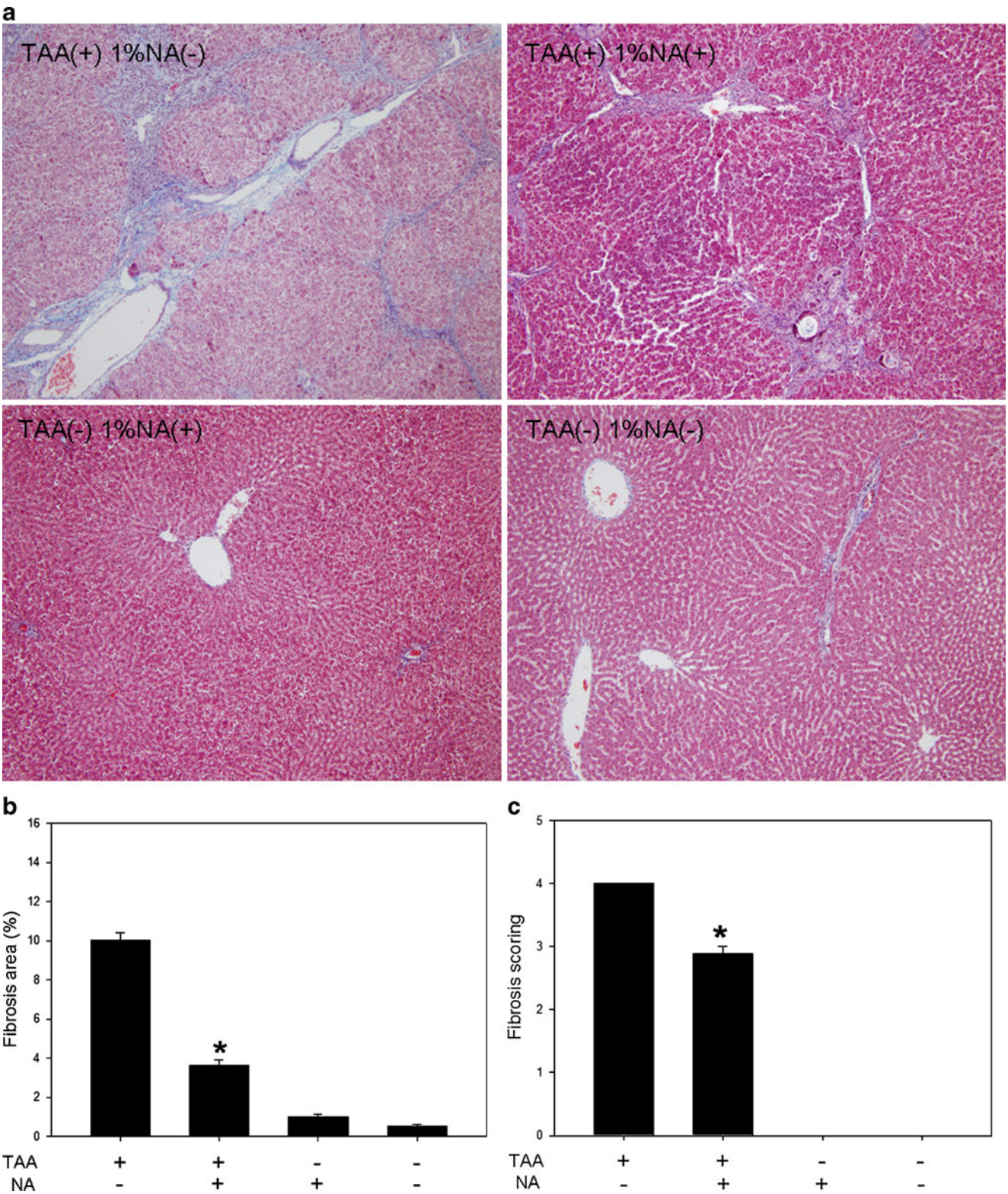

Fig. 2 Attenuation of liver fibrosis in NA-treated rats. NA attenuated in TAA-induced hepatic fibrosis in rats. **a** Photographs of Masson's trichome staining (×40). **b** Fibrosis area analysis using morphometry. **c** The degree of fibrosis by METAVIR scoring system. *$p<0.05$ compared with the TAA-only-treated group

trichome-stained sections, histological evaluation of the liver tissues of rats that had undergone TAA treatment showed severe fibrosis leading to cirrhosis (Fig. 2a), and the NA-treated group showed significant reduction of fibrosis area than untreated group (Fig. 2b). In the NA-treated TAA group, the incidence of cirrhosis was significantly decreased and the fibrosis grade was 2 (periportal) to 3 (septal) compared with grade 4 for the TAA-only-treated group (Fig. 2c). The rat livers that received NA alone showed no histological abnormalities.

Inhibition of THSC-Cl6 cell proliferation

Treatment with NA significantly reduced the cell viability of THSC-Cl6 cells in a dose- and time-dependent manner (Fig. 3). The inhibitory effect of NA was most significant at 48 h. Thus, the 48-h time point was used to calculate the half maximal inhibitory concentration (IC50), of 17 mM. The four different NA treatment groups (0, 10, 15, and 20 mM) were then subjected to a series of experimental approaches.

Reduction in collagen mRNA and alpha smooth muscle actin protein expression

Treatment with NA markedly decreased the collagen mRNA levels of THSC-Cl6 cells in dose-dependent manner (Fig. 4a). The protein expression of alpha smooth muscle actin (α-SMA) was also reduced in a dose-dependent fashion (Fig. 4b).

Induction of apoptosis of THSC-Cl6 cells

We measured apoptosis of THSC-Cl6 cells on the cell morphology, a DNA fragmentation assay, flow cytometric analysis, and proteolytic cleavage of caspase 3. NA-treated THSC-Cl6 cells produced a DNA ladder, indicating prominent apoptosis (Fig. 5). Treatment with NA at doses 15 and 20 mM for 48 h significantly increased apoptotic cell populations (Fig 6a). NA also increased cleaved caspase 3 and decreased p21 expression in a dose-dependent manner (Fig. 6b).

Inhibition of DNA synthesis and modulation of cell cycle regulatory proteins

NA significantly inhibited DNA synthesis at the highest concentration used (20 mM; Fig. 7a). NA also reduced cyclin D1, cyclin-dependent kinase (cdk)4, and cyclin E protein expression in THSC-Cl6 cells (Fig. 7b). By contrast, the level of p27 was increased. The levels of p16, cdk2, and cyclin A were not influenced by NA treatment.

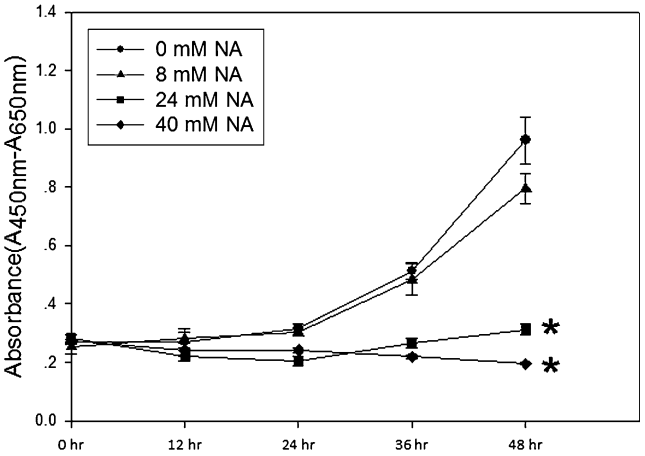

Fig. 3 Inhibition of THSC-Cl6 cell proliferation. NA inhibited THSC-Cl6 cell proliferation dose-dependently. *$p<0.05$ compared with the NA untreated group

Discussion

It is believed that liver fibrosis can be reversed through the apoptosis of activated hepatic stellate cells and the degradation of ECM proteins [12]. Recently, a study indicated that NA prevented fatty liver and fibrosis in glycine *N*-methyltransferase knockout mice [13]. Also, Gurujeyalakshmi et al. [9] showed that combined treatment

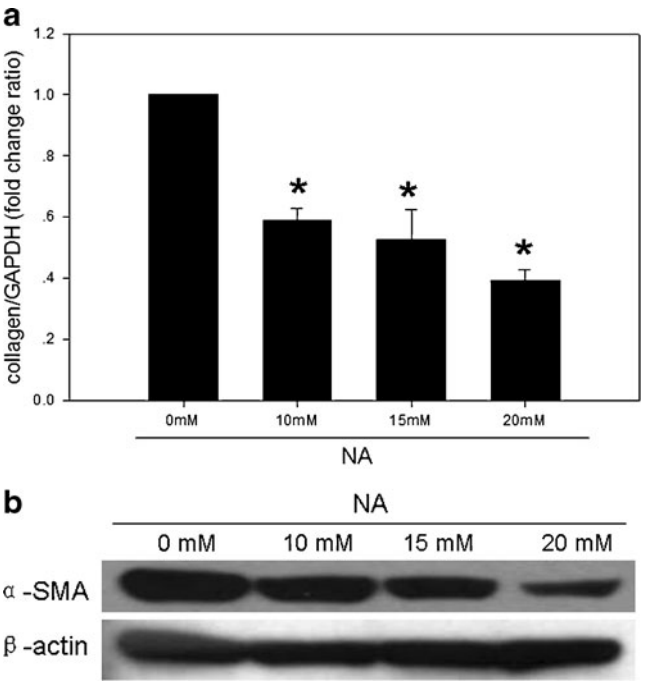

Fig. 4 Reduction in collagen mRNA expression and α-SMA protein expression in THSC-C16 cells. **a** NA reduced collagen mRNA in dose-dependent manner detected by real-time polymerase chain reaction. **b** NA reduced α-SMA expression detected by Western blot analysis. *$p<0.05$ compared with the NA untreated group

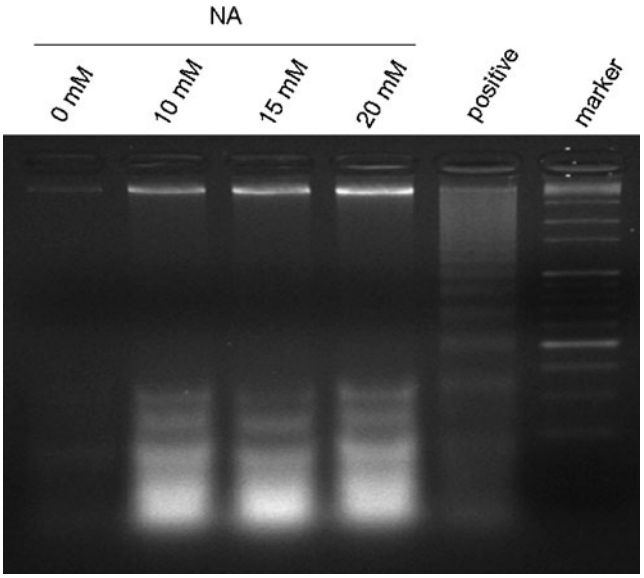

Fig. 5 Induction of DNA fragmentation in THSC-Cl6 cells. NA induced DNA fragmentation in THSC-Cl6 cells

with taurine and niacin (a precursor of NA) attenuated bleomycin-induced lung fibrosis in hamsters via inhibition of TGF-β1 mRNA expression. Traister et al. [10] investigated the effect of NA on HSC-T6 rat hepatic stellate cells, using TGF-β1 for activation of the cell line. They found that NA treatment resulted in cell apoptosis and reduction of collagen I and also in the expression of proinflammatory cytokines. In present study, we used the activated rat hepatic stellate cell line THSC-Cl6. We confirmed that NA is capable of inhibiting proliferation of THSC-Cl6 cells in a dose- and time-dependent manner, with an IC50 of 17 mM at 48 h. The IC50 in Traister et al.'s study was 16 mM, and the differences in the results may reflect the use of different cells and different treatment periods.

Cellular proliferation can be suppressed either by cell apoptosis or by interruption of the cell cycle. Traister et al. [10] showed that HSC-T6 cells undergo apoptosis when treated with NA, by staining cells with only propidium iodine. In our study, we showed the presence of apoptosis in three ways. First, the apoptosis of cells was observed by Annexin V-FITC and propidium iodine double-staining.

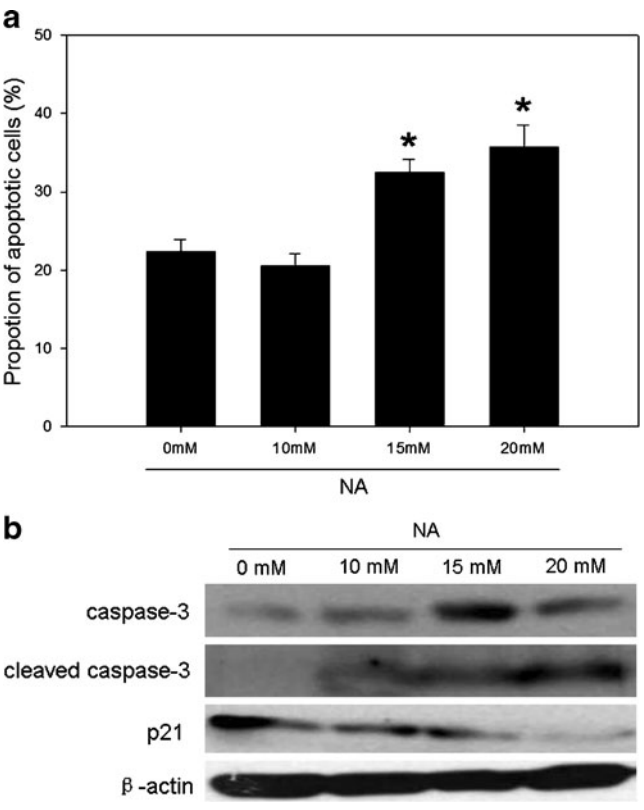

Fig. 6 Increase in apoptotic cell fraction and cleaved caspase 3, accompanied by a decrease in p21 expression. **a** NA increased apoptotic cell fraction in high-dose groups. *$p<0.05$ compared with the NA untreated group. **b** NA induced caspase-3 cleavage and decreased p21 expression

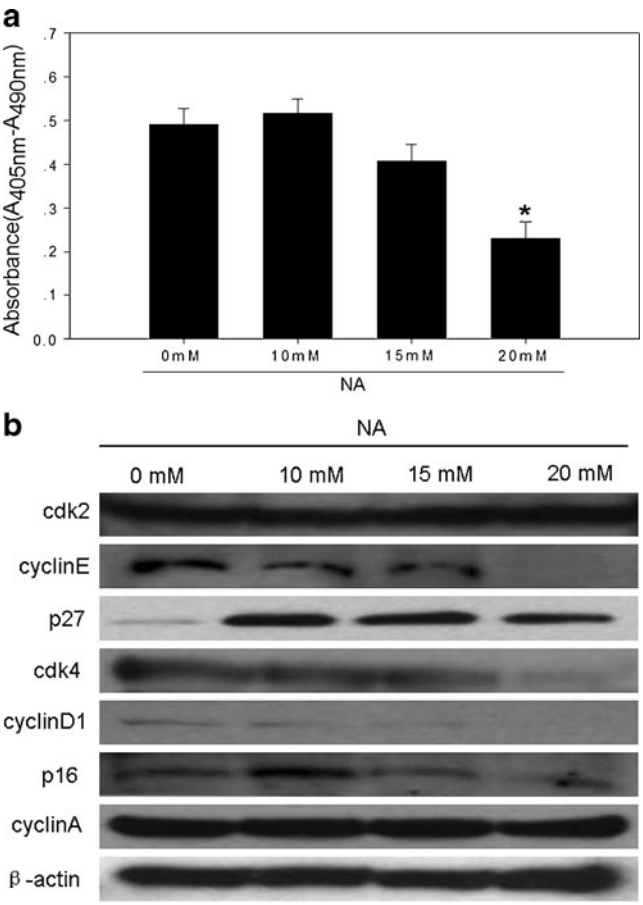

Fig. 7 Inhibition of DNA synthesis and modulation of cell cycle-related proteins. **a** NA inhibited BrdU incorporation in high-dose group. *$p<0.05$ compared with the NA untreated group. **b** NA reduced cyclin E, cdk4, cyclin D1, and increased p27 expressions

Treatment with 10 mM NA did not influence the apoptosis. By contrast, treatment with 15 and 20 mM NA induced cell apoptosis in a dose-dependent manner. Second, the apoptosis was presented by DNA fragmentation into fragments smaller than 500 bp. Caspases themselves are activated by cleavage of aspartate residues; certain caspases are called effector or downstream caspases because they cleave key substrates and eventually lead to apoptotic cell death [14–16]. In the present study, NA increased the active form of caspase-3 and reduced p21 in THSC-Cl6 cells in a dose-dependent manner. This confirms the finding by Alexandra that NA is able to decrease pro-caspase in a dose-dependent manner. A recent study showed that p21, which is believed to be a tumor suppressor, exerts oncogenic activity by blocking the processing of pro-caspase-3 into its active form [17]. In the present study, it appears that NA-treated THSC-Cl6 cells entered the apoptotic process via cleavage of caspase-3, with concomitant p21 reduction.

Finally, we investigated several cell cycle-related proteins. Cdks are the enzymatic subunits of cyclins and must form complexes with their respective cyclins for activity. Cdk2 requires either cyclin A or cyclin E for activation. Cyclin E regulates progression through the restriction point R at the end of the G1 phase to allow cells to enter the S phase [18]. Ink4 and Cip/Kip are the two gene families that act as cdk inhibitors [17]. Furthermore, p16 is encoded by the *Ink4* gene, which binds to cdk4 and cdk6 and inhibits their kinase activities by interfering with their association with cyclin Ds [19]; p27 is a member of Cip/Kip family and can bind to both cyclin and cdk subunits as well as modulate the activities of cyclin D–, cyclin E–,cyclin A–, and cyclin B–cdk complexes [19]. The inhibitory effect of p27 on cyclin E–cdk2 activity has been shown by Vidal et al. [20]. In the present study, NA treatment of THSC-Cl6 cells resulted in an increase in the p27 level, which inhibited the cyclin E–cdk2 complex in a dose-dependent manner. Alexandra et al. showed that cyclin D1 was not influenced by NA treatment for 24 h. However, we observed a significant reduction in cdk4 and cyclin D1 expression after NA treatment. The different results may reflect the use of different treatment periods. Moreover, in our study, the decrease in cdk4 and cyclin D1 was not accompanied by a change in p16. This suggests that the down-regulation of cdk4–cyclin D1 may be caused by other inhibitors, such as p15. In addition, the fact that DNA synthesis was down-regulated following treatment with a 20-mM dose of NA may further explain the inhibitory effect of NA on THSC-Cl6 cells.

During liver injury, quiescent hepatic stellate cells undergo activation to myofibroblasts, characterized by expression of activation markers, such as α-SMA, and enhanced expression of extracellular matrix proteins. In our study, NA decreased the activation of hepatic stellate cells, as assessed by decreased expression of the activation marker α-SMA in THSC-Cl6 cells. This confirms the findings of Traister et al. [10]. Recently, Gurujeyalakshmi et al. showed that gene expression of procollagens I and III in bleomycin-induced lung fibrosis in hamsters is down-regulated by combined treatment with taurine and niacin [8]. Similarly, our experiments show that NA reduces collagen mRNA expression in THSC-Cl6 cells in a dose-dependent manner in vitro and also in vivo. In rats with TAA-induced liver fibrosis, NA significantly lowered the fibrosis scoring when compared with TAA-only-treated rats, indicating that NA exhibits in vivo antifibrotic effects that alleviate liver fibrogenesis. These results suggest that NA is a potential antifibrotic agent for liver injury.

In conclusion, NA inhibited liver fibrosis in rats and induced apoptosis and reduced DNA synthesis by modulating the expression of cell cycle-related proteins. These results suggest that NA plays a beneficial role in attenuating liver fibrogenesis.

Conflict of interest statement We declare that we have no conflict of interest.

References

1. Friedman SL (2008) Mechanisms of hepatic fibrogenesis. Gastroenterology 134(6):1655–1669
2. Parola M, Marra F, Pinzani M (2008) Myofibroblast-like cells and liver fibrogenesis: emerging concepts in a rapidly moving scenario. Mol Aspects Med 29(1–2):58–66
3. Niren NM (2006) Pharmacologic doses of nicotinamide in the treatment of inflammatory skin conditions: a review. Cutis 77(1 Suppl):11–16
4. Knip M, Douek IF, Moore WPT, Gillmor HA, McLean AEM, Bingley PJ, Gale EAM (2000) Safety of high-dose nicotinamide: a review. Diabetologia 43(11):1337–1345. doi:10.1007/s001250051536
5. Marcus R CA (2001) Water-soluble vitamins. The vitamin B complex and ascorbic acid. The pharmacological basis of therapeutics
6. Cosmetic Ingredient Review Expert Panel (2005) Final report of the safety assessment of niacinamide and niacin. Int J Toxicol 24 (Suppl 5):1–31
7. Padayatty SJ, Riordan HD, Hewitt SM, Katz A, Hoffer LJ, Levine M (2006) Intravenously administered vitamin C as cancer therapy: three cases. CMAJ 174(7):937–942
8. Gurujeyalakshmi G, Iyer SN, Hollinger MA, Giri SN (1996) Procollagen gene expression is down-regulated by taurine and niacin at the transcriptional level in the bleomycin hamster model of lung fibrosis. J Pharmacol Exp Ther 277(2):1152–1157
9. Gurujeyalakshmi G, Hollinger MA, Giri SN (1998) Regulation of transforming growth factor-beta1 mRNA expression by taurine and niacin in the bleomycin hamster model of lung fibrosis. Am J Respir Cell Mol Biol 18(3):334–342
10. Traister A, Breitman I, Bar-Lev E, Zvibel I, Harel A, Halpern Z, Oren R (2005) Nicotinamide induces apoptosis and reduces

collagen I and pro-inflammatory cytokines expression in rat hepatic stellate cells. Scand J Gastroenterol 40(10):1226–1234
11. Kim JY, Kim KM, Nan JX, Zhao YZ, Park PH, Lee SJ, Sohn DH (2003) Induction of apoptosis by tanshinone I via cytochrome c release in activated hepatic stellate cells. Pharmacol Toxicol 92 (4):195–200
12. Elsharkawy AM, Oakley F, Mann DA (2005) The role and regulation of hepatic stellate cell apoptosis in reversal of liver fibrosis. Apoptosis 10(5):927–939. doi:10.1007/s10495-005-1055-4
13. Varela-Rey M, Martinez-Lopez N, Fernandez-Ramos D, Embade N, Calvisi DF, Woodhoo A, Rodriguez J, Fraga MF, Julve J, Rodriguez-Millan E, Frades I, Torres L, Luka Z, Wagner C, Esteller M, Lu SC, Martinez-Chantar ML, Mato JM (2010) Fatty liver and fibrosis in glycine *N*-methyltransferase knockout mice is prevented by nicotinamide. Hepatology 52(1):105–114
14. Goldin RD, Hunt NC, Clark J, Wickramasinghe SN (1993) Apoptotic bodies in a murine model of alcoholic liver disease: reversibility of ethanol-induced changes. J Pathol 171(1):73–76
15. Adams JM, Cory S (1998) The Bcl-2 protein family: arbiters of cell survival. Science 281(5381):1322–1326
16. French SW, Nash J, Shitabata P, Kachi K, Hara C, Chedid A, Mendenhall CL (1993) Pathology of alcoholic liver disease. VA Cooperative Study Group 119. Semin Liver Dis 13(2):154–169
17. Besson A, Dowdy SF, Roberts JM (2008) CDK inhibitors: cell cycle regulators and beyond. Dev Cell 14(2):159–169
18. Moroy T, Geisen C (2004) Cyclin E. Int J Biochem Cell Biol 36 (8):1424–1439
19. Sherr CJ, Roberts JM (1999) CDK inhibitors: positive and negative regulators of G1-phase progression. Genes Dev 13(12):1501–1512
20. Vidal A, Koff A (2000) Cell-cycle inhibitors: three families united by a common cause. Gene 247(1–2):1–15

Virchows Arch (2011) 458:697–708
DOI 10.1007/s00428-011-1070-5

ORIGINAL ARTICLE

The homeobox gene HLXB9 is upregulated in a morphological subset of poorly differentiated hepatocellular carcinoma

Ludwig Wilkens · Rolf Jaggi · Caroline Hammer · Daniel Inderbitzin · Olivier Giger · Nils von Neuhoff

Received: 8 October 2010 / Revised: 9 February 2011 / Accepted: 21 March 2011 / Published online: 12 April 2011
© Springer-Verlag 2011

Abstract The prognostic outcome for hepatocellular carcinoma (HCC) remains poor. Disease progression is accompanied by dedifferentiation of the carcinoma, a process that is not well understood. The aim of this study was to get more insight into the molecular characteristics of dedifferentiated carcinomas using high throughput techniques. Microarray-based global gene expression analysis was performed on five poorly differentiated HCC cell lines compared with non-neoplastic hepatic controls and a set of three cholangiolar carcinoma (CC) cell lines. The gene with the highest upregulation was HLXB9. HLXB9 is a gene of the homeobox genfamily important for the development of the pancreas. RT-PCR confirmed the upregulation of HLXB9 in surgical specimens of carcinoma tissue, suggesting its biological significance. Interestingly, HLXB9 upregulation was primary observed in poorly differentiated HCC with a pseudoglandular pattern compared with a solid pattern HCC or in moderate or well-differentiated HCC. Additional the expression of translated HLXB9, the protein HB9 (NCBI: NP_001158727), was analyzed by western blotting. Expression of HB9 was only detected in the cytoplasm but not in the nuclei of the HCC cells. For validation CC were also investigated. Again, we found an upregulation of HLXB9 in CC cells accompanied by an expression of HB9 in the cytoplasms of these tumor cells, respectively. In conclusion, homeobox HLXB9 is upregulated in poorly differentiated HCC with a pseudoglandular pattern. The translated HB9 protein is found in the cytoplasm of these HCC and CC. We therefore assume HLXB9 as a possible link in the understanding of the development of HCC and CC, respectively.

Keywords Hepatocellular carcinoma · Cholangiocellular carcinoma · HLXB9 · Histological differentiation

L. Wilkens · C. Hammer · O. Giger
Institute of Pathology, University of Bern,
Murtenstr. 10,
3010 Bern, Switzerland

L. Wilkens (✉)
Institute of Pathology, Hospitals of the Region Hannover,
Haltenhoffstr. 41,
30167 Hannover, Germany
e-mail: ludwig.wilkens@krh.eu

R. Jaggi
Department of Clinical Research, University of Bern,
Murtenstr. 35,
3010 Bern, Switzerland

D. Inderbitzin
Department of Visceral and Transplantation Surgery,
Inselspital Bern,
3010 Bern, Switzerland

N. von Neuhoff
Institute of Cell and Molecular Pathology,
Medical School Hannover,
30625 Hannover, Germany

Introduction

Hepatocellular carcinoma (HCC) is the fifth most common malignant tumor, with more than one million patients affected worldwide each year and a generally very poor prognosis [1, 2]. Large-scale gene expression profiling has provided important insights into the biology of HCC in recent years, and there have been advances in terms of HCC etiology, survival prediction, and the identification of signaling pathways that could serve as therapeutic targets [3–7]. Mutations in several genes (e.g., P53, IGF2R, P16, PTEN) have been associated with the development of HCC [8].

Morphological diagnosis of HCC is guided by criteria defined in early studies still accepted as the standard for pathologists [9, 10]. Over time, HCC tends to dedifferentiate

morphologically. In more than half of all patients, dedifferentiation occurs within 7–34 months of diagnosis [11, 12]. Dedifferentiation is accompanied by increasing chromosomal instability [13]. Dedifferentiation is also accompanied by the occurrence of chromosomal imbalances, such as loss of 13q, associated with loss of genes involved in cell cycle regulation and proliferation [14]. Even more dedifferentiated HCC are often difficult to separate from its cholangiocellular counterpart, i.e., cholangiocarcinoma (CC).

Because morphological dedifferentiation of HCC is associated with decreased survival time [15, 16], it is important to elucidate the processes that lead to dedifferentiation. Towards this end, we analyzed poorly differentiated cell lines derived from HCC and CC, respectively, to search for candidate genes involved in dedifferentiation. Surgical specimens were included to determine whether these in vitro findings had biological relevance. Microarray-based global mRNA expression analysis was performed at first. Additional gene expression analysis, transfection- and RNA-silencing assays were done to verify the results.

Using this approach, we identified the homeobox gene HLXB9 as a gene that is likely to be involved in morphological dedifferentiation in a subset of HCC.

Methods

Cell lines

The HCC cell lines HLE, HLF, Huh7, HepG2, and Hep3b were kindly provided by Stefan Kubicka (Department of Gastroenterology, Hannover Medical School, Germany). The control cell lines were HHep (Provitro, Berlin, Germany), and an immortalized hepatocytic cell line (HImo, kindly provided by Prof. Dr. Didier Trono, Ecole Polytechnique Federale de Lausanne, Switzerland). Since cryopreservation can influence gene expression status [17], experiments were performed both in freshly harvested cells and in cells that had been cryopreserved. Additionally, three CC cell lines were analyzed (EGI-1, MzCha1, TFK-1) kindly provided by Nisar Malek (Department of Gastroenterology, Hannover Medical School, Germany).

The hepatocellular origin of all HCC cell lines was confirmed by immunohistochemistry (IHC) using antibodies specific for CK8 and CK18, which are typically expressed in hepatocytic cells. CK7 and CK19 were used to exclude cholangiocellular differentiation. Ki67 was used for determination of proliferative activity (all antibodies supplied by DAKO, Hamburg, Germany). IHC was performed on histological sections of cells after formalin fixation and paraffin embedding using the cell block technique (BBCBiochemicals, Seattle, WA, USA). All HCC cell lines with the exception of Hep3b were positive for CK8 and CK18 and negative for CK7 and CK19. Hep3b showed a positive staining for CK19. The proliferation marker Ki67 was positive in 54–88% of the nuclei of cells in all HCC cell lines. Overall, proliferative activity and pleomorphism of nuclei indicated a low differentiation (data not shown).

This was comparable for the CC cell lines. Here, antibodies for CK7 and CK 19 were giving a positive staining indicating cholangiocellular differentiation. Of the nuclei, 45–55% were positive for Ki67 also indicating a high proliferative activity.

Cell culture

Cell line HImo was maintained in DMEM plus 10% fetal calf serum supplemented with glutamine and penicillin/streptomycin at 37°C in a 5% CO_2 atmosphere using 25 cm^2 tissue culture flasks (TPP 90025, Oxoid, Prattelen, Switzerland). Cell line HHep was cultured in hepatocyte maintenance medium (Provitro, Berlin, Germany). Control cell lines were maintained as recommended by the supplier.

Tumor cell lines were incubated in DMEM with 10% fetal calf serum supplemented with glutamine and penicillin/streptomycin at 37°C in a 5% CO_2 atmosphere.

Mycoplasma infections were excluded using the Lookout Mycoplasma PCR Detection Kit (Sigma, Germany). Growth dynamics were determined by counting cells over a period of at least 7 days. Cells were harvested in the ascending part of the growth curve.

Surgical specimens

Twenty eight tumor tissues were obtained from 27 patients as surgical specimens taken for diagnostic purposes (permitted by the Ethics Committee of the University of Bern). Tissues were paraffin-embedded after 24-h fixation in 4% formaldehyde. Histological grading of tumors was performed according to the WHO criteria [18].

For comparison of results obtained in these specimens, we included also 10 samples of CC and five samples of hepatocellular adenoma (HCA). As a control five non-neoplastic tissues samples were chosen of livers ruptured due to trauma.

mRNA isolation

For mRNA expression analyses of the cell lines, total RNA was isolated using a commercially available system (Ambion, Cambridge, UK). Transcription to cDNA was performed using the High Capacity cDNA Reverse Transcription Kit (#4374966, Applied Biosystems, Rotkreuz, Switzerland).

Five 10-μm sections were used for total RNA isolation from formalin-fixed paraffin-embedded (FFPE) tissues. RNA was isolated exactly as described previously [19]. One section was

Table 1 Primers for qRT-PCR amplification using reagent concentrations and amplification conditions as specified by Applied Biosystems

Gene symbol	Assay ID	Ref. Seq	Amplicon length (bp)
PXDN	Hs00395488_m1	NM_012293.1	99
HLXB9	Hs00232128_m1	NM_005515.3	71

cut for H&E staining before sectioning material for mRNA isolation, and one was cut just after sectioning. This ensured the closest proximity and greatest homogeneity of tissues used for experiments. The quality and quantity of total RNA was determined photometrically (NanoDrop Technologies, Wilmington, Germany).

Microarray analysis

A whole human genome oligonucleotide microarray kit was used for global mRNA expression analysis (array G4112F, Agilent, Waldbronn, Germany). This kit allows detection of more than 41,000 unique human transcripts. After one-color mRNA labeling and hybridization according to the supplier's instructions, microarray images were acquired (Agilent Scanner System 2605, Waldbronn, Germany). Hybridization spots were normalized using the feature extraction software (version 9.5.3.1.) and processed as described below.

mRNA microarray data from all four cell lines and the control cell lines were further normalized and processed using GeneSpring GX software version 9.0 (Agilent, Waldbronn, Germany). GeneSpring software computes a

Table 2 Genes found to be significantly ($p<0.01$) up- ($n=54$) or downregulated ($n=125$) in hepatocellular carcinoma compared to non-neoplastic cell lines using the unpaired *t* test (asymptotic) corrected for multiple testing (Benjamini–Hochberg correction)

Gene symbol	Accession no.	Fold change	Corrected *p* value
Upregulated genes			
MNX1	NM_005515	364	0.00074790
LIN28B	NM_001004317	43	0.00859069
TERT	NM_198253	30	0.00976756
ELOVL7	NM_024930	18	0.00971980
PCDHB2	NM_018936	15	0.00051022
FAM184A	NM_024581	11	0.00974849
PRKAA2	NM_006252	7	0.00051022
PCDHB11	NM_018931	6	0.00882593
ZCCHC2	BC006340	5	0.00406914
PCDHB13	NM_018933	5	0.00216112
SPRED2	NM_181784	4	0.00676678
DBNDD1	NM_001042610	4	0.00678942
MCM9	NM_153255	4	0.00582031
AGPAT9	NM_032717	4	0.00500372
DNMT3B	NM_175850	4	0.004270845
Downregulated genes			
PXDN	NM_012293	2,199	0.00051022
COL1A1	Z74615	587	0.00971980
RAC2	NM_002872	559	0.00032802
GREM1	NM_013372	540	0.00009805
LZTS1	NM_021020	486	0.00026493
TOX2	NM_032883	376	0.00067963
CHST2	NM_004267	308	0.00223079
BNC1	NM_001717	266	0.00047324
RNF135	NM_032322	237	0.00047324
KRT7	NM_005556	202	0.00052403
PDLIM4	NM_003687	133	0.00018231
TMTC1	NM_175861	120	0.00089063
IL7R	NM_002185	113	0.00042864
CDCP1	NM_022842	110	0.00348664
AR	NM_000044	93	0.00029425

The 15 genes with the highest fold changes for up- or downregulation, respectively, are listed here

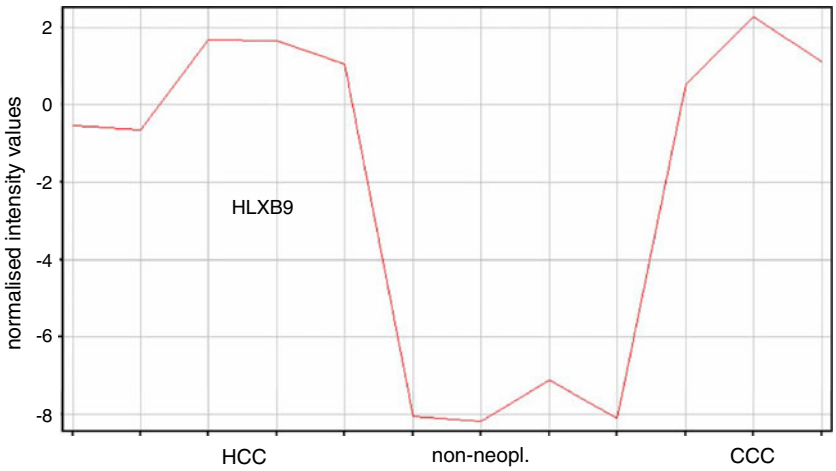

Fig. 1 Graphical illustration of intensity values obtained for HLXB9 by microarray-based expression analysis in HCC and CC cell lines. Comparison was done to non-neoplastic cell lines. Dysregulation of HLXB9 is similar in both, HCC and CC cell lines

unique value for each miRNA and mRNA by taking the average of replicates spotted on the microarrays. Specimens were normalized using median normalization. HCC cell lines were taken together as one group and non-neoplastic hepatocytic cell lines as a second group. The mRNAs with a positive or negative fold change >1.5 between these two groups were further analyzed for significantly different expression using an unpaired *t* test and the Benjamini–Hochberg calculation for multiple test controls to reduce false positive results. The level of significance was set at $p<0.01$.

qRT-PCR

Quantitative reverse transcription-polymerase chain reaction (qRT-PCR) using mRNA obtained from cell lines was performed using the TaqMan® Universal PCR Master Mix AmpErase® (#4324018, Applied Biosystems, Rotkreuz, Switzerland) and the primers listed in Table 1. The cycling conditions were set as instructed by the supplier. A real-time PCR system (7500, Applied Biosystems, Rotkreuz, Switzerland) was used for quantification.

mRNA from FFPE samples was measured using a SuperScript™ III Platinum® One-Step qRT-PCR Kit following the instructions of the supplier (#11732020, Invitrogen, Basel, Switzerland). A 7500 Fast System (Applied Biosystems, Rotkreuz, Switzerland) was used for quantification.

siRNA-based knock down of gene expression

HLXB9 was selectively suppressed by siRNA experiments using a commercially available system (On-TARGETplus SMARTpool system, Dharmacon, Chicago, IL, USA) with a specific siRNA (Human HLXB9, DHARMACON). As a negative control from the same supplier, we used the "On-TARGETplus siCONTROL Non-targeting POOL" reagents. mRNA of the manipulated cells was isolated as described above.

Transfection experiments

Immortalized hepatocytic cell line was transfected with the pCMV5-HLXB9 expression vector using the TurboFectin 8.0 reagent (Origene, Rockville, MD, USA). The media and transfection components were used exactly as specified by the supplier. The pCMV5 vector without the HLXB9 was transfected as a negative control.

Separation of subcellular compartment proteins

The Qproteome cell compartment kit (Qiagen, Hilden, Germany) was used to separate proteins in the following cellular compartments: cytosol, membranes, and nucleus. About 1×10^7 cells were harvested and lysed in accordance with the Qiagen protocol. All buffers were supplemented

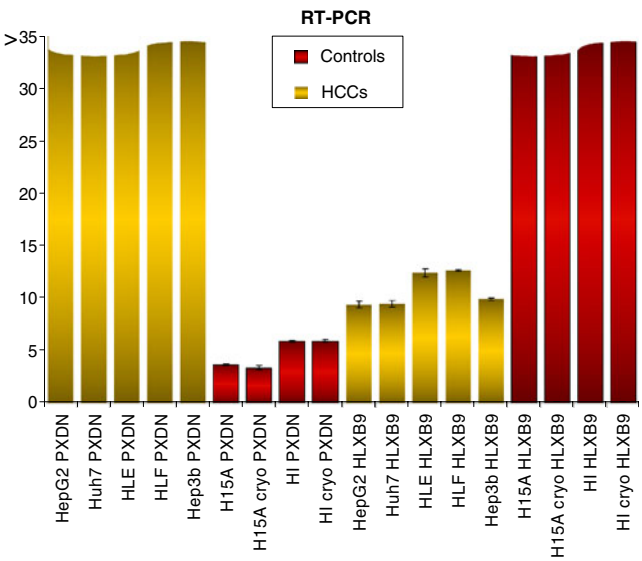

Fig. 2 qRT-PCR confirmed the results of microarray-based expression analysis. RT-PCR analysis was conducted on the two genes with the highest fold changes in hepatocellular carcinoma (HCC) cell lines: PXDN, which was downregulated, and HLXB9, which was upregulated

with protease inhibitors (as per the protocol) and 1 mM $NaVO_3$ as a phosphatase inhibitor. The resulting proteins from each subcellular compartment were concentrated and desalted by acetone precipitation. The pellets were then resuspended in the appropriate buffer, which depended on the analysis. Protein concentration was measured photometrically (Biophotometer, Eppendorf, Hamburg, Germany). Protein concentration in each sample was measured directly by Bradford assay before SDS-PAGE (sodium dodecyl sulfate polyacrylamide gel electrophoresis).

Immunoblot analysis

Proteins were separated by SDS-PAGE on 10% gels. A prestained PageRuler protein ladder (#SM0671, Fermentas, Germany) was included on each gel to standardize the molecular weights of proteins in the samples. Following protein transfer to nitrocellulose membranes (Amersham Bioscience GmbH, Freiburg, Germany), the blots were incubated with a monoclonal antibody against HB9 (ab79541, ABCAM, Germany). To verify that proteins in subcellular compartments had been separated efficiently, antibodies against marker proteins for the compartments were used: anti-GAPDH (Santa Cruz Biotechnology, Santa Cruz, CA, USA) for the cytosolic compartment and anti-actin (#69100, MP Biomedicals, Ohio) for the nuclear compartment. HLXB9 (48 kDa) and actin (42 kDa) are similar in size; therefore the actin antibody was incubated subsequent to the HB9 antibody. Following incubation with a peroxidase-conjugated secondary antibody (Amersham, Germany), the blots were developed using an electrochemiluminescence detection kit (Perkin Elmer, Boston, MA, USA). Blot results were scanned using a standard scanning device HP5470c (Boeblingen, Germany). The digitized intensities were subse-

Table 3 Genes found to be significantly ($p<0.01$) up- ($n=986$) or downregulated ($n=191$) in hepatocellular carcinoma compared to cholangiocarcinoma cell lines using the parameter as described above

Gene symbol	Accession no.	Fold change	Corrected p value
Upregulated genes			
KLK10	NM_002776	2,944	0.00087690
TACSTD2	NM_002353	2,527	0.00455577
SPINT2	NM_021102	2,219	0.00058975
MALL	NM_005434	1,913	0.00648792
GPR110	NM_153840	820	0.00485874
RAB25	NM_020387	688	0.00030306
ALDH1A3	NM_000693	653	0.00166345
RAC2	NM_002872	630	0.00224070
C19orf33	NM_033520	468	0.00284474
CDCP1	NM_022842	415	0.00305156
RNF135	NM_032322	415	0.00052486
BACE2	NM_012105	382	0.00168082
KLK10	NM_002776	360	0.00287167
GJB3	NM_024009	347	0.00061644
FXYD3	NM_005971	343	0.00966693
Downregulated genes			
SDC2	NM_002998	1,620	0.00127171
GPC6	NM_005708	1,056	0.00281812
ACSS3	NM_024560	596	0.00348787
CDH2	NM_001792	399	0.00394804
LIN28B	NM_001004317	387	0.00058975
EFHA2	NM_181723	376	0.00101820
MPDZ	NM_003829	229	0.00052486
NID1	NM_002508	205	0.00168082
CBS	NM_000071	180	0.00505487
ZIK1	NM_001010879	175	0.00140458
CBS	NM_000071	131	0.00291453
DCDC2	NM_016356	127	0.00459634
LIN28B	NM_001004317	118	0.00147870
ELOVL2	NM_017770	109	0.00532469
MYEF2	NM_016132	91	0.00201893

The 15 genes with the highest fold changes for up- or downregulation, respectively, are again listed here

quently analyzed and quantified using the ImageJ 1.36b software (http://rsb.info.nih.gov/ij).

Results

Microarray-based mRNA analysis

Global mRNA expression analysis results were compared at first in HCC tumor cell lines and non-neoplastic hepatocytic cell lines (all raw data can be obtained as additional files from the authors). After use of the unpaired *t* test corrected for multiple testing (Benjamini–Hochberg) for all genes with a fold change >2, we identified 54 genes that were significantly up-and 125 genes that were significantly downregulated ($p<0.01$) in tumor cell lines (Table 2). The highest fold changes were seen for MNX1 (also known as HLXB9) mRNA, which was upregulated 364-fold, and for PXDN mRNA, which was downregulated 2,199-fold (Fig. 1). qRT-PCR was used to confirm these results (Fig. 2).

We then looked for differential expression of HCC cell lines compared to CC cell lines. Using the same criteria as described above, 986 genes were up- and 191 genes were downregulated, respectively (Table 3).

Comparing CC cell lines with non-neoplastic cell lines led to the detection of 623 upregulated genes and 388 downregulated genes (Table 4). Again MNX1 (HLXB9) was found upregulated with a high fold change of 572. In contrast PXDN was not dysregulated significantly.

Table 4 Comparing CC cell lines with non-neoplastic cell lines revealed 623 genes upregulated and 388 genes downregulated

Gene	Accession no.	Fold change	Corrected *p* value
Upregulated genes			
KLK10	NM_002776	1,258	0.0050223
OVOL1	NM_004561	592	0.00310259
MNX1	NM_005515	572	0.001556501
RAB25	NM_020387	482	0.001031751
ANO1	NM_018043	402	0.005484599
EPN3	NM_017957	307	0.001031751
TMEM125	NM_144626	291	0.007592963
KLK10	NM_002776	225	0.008101207
GJB2	NM_004004	189	0.004909608
FUT3	NM_000149	176	0.008854575
TNS4	NM_032865	162	0.002774253
GRHL2	NM_024915	155	0.004259103
ATP2C2	NM_014861	148	0.005392212
LOC645249	BC033117	143	0.006074598
TMC5	NM_024780	138	0.005551621
Downregulated genes			
EFEMP1	NM_004105	17,326	0.00017120
CNN1	NM_001299	2,612	0.00007205
GJA1	NM_000165	2,105	0.00015593
PDGFRB	NM_002609	2,051	0.00290483
SPARC	NM_003118	1,693	0.00442776
COL5A1	NM_000093	1,298	0.00523753
SDC2	NM_002998	1,247	0.00145708
GPC6	NM_005708	1,221	0.00885457
ODZ2	NM_001122679	1,180	0.00140017
LAYN	NM_178834	1,146	0.00442776
GREM1	NM_013372	955	0.00097044
PNMAL1	NM_018215	944	0.00030502
SNURF	NM_022804	916	0.00144029
ADAMTS1	NM_006988	904	0.00011429
SNRPN	NM_022807	840	0.00030502

Within the group of 15 genes with the highest fold changes HLXB9 is again found

HLXB9 expression in cell lines

Since HLXB9 is a known homeobox gene involved in the development of the pancreas and, most likely, cholangiocytes [20], and was found upregulated in both HCC cell lines and CC cell lines, further analysis was focused onto this gene. For confirmation of the microarray based results, we selectively knocked down expression of HLXB9 in HCC cell lines by RNA interference using a known specific RNA primer. This led to the most significant decrease of HLXB9 when using a concentration of 200 mM for 24 h of incubation. HLXB9 was downregulated then to 12–29% in HCC cell lines and to 18–43% in CC cell lines, respectively (Fig. 3). We next transfected the immortalized hepatocytic cell line with a pCMV5-HLXB9 vector. Microarray-based mRNA analysis detected a 2,383-fold increase in HLXB9

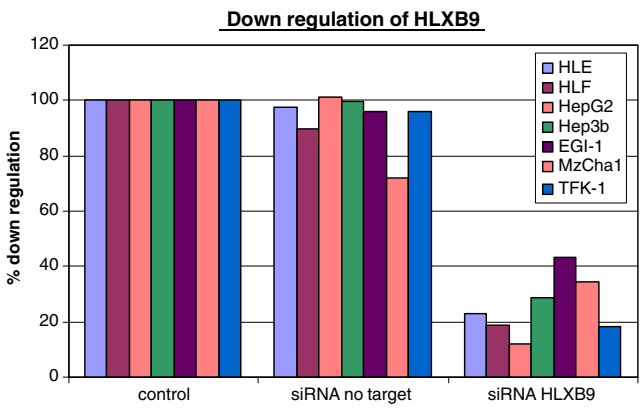

Fig. 3 siRNA-based knock down of HLXB9 in hepatocellular carcinoma (HCC) cell lines. Using specific siRNAs, HLXB9 was knocked down by 12–29% compared to controls defined as 100%. The greatest inhibition of HLXB9 was observed after 12 h with 200 mM siRNA. In CC cell lines, downregulation was in the range of 19–42%

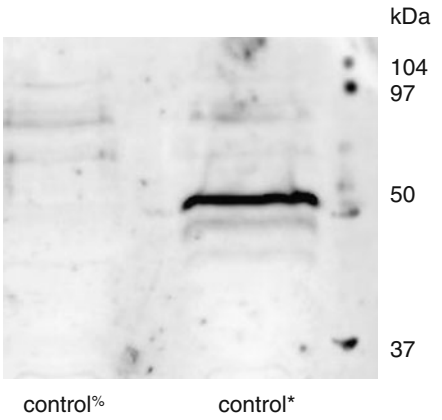

Fig. 4 Transfection of cell line HImo with the pCMV5-HLXB9 expression vector resulted in HB9 expression. The immunoblot shows non-transfected and pCMV5-HLXB9-transfected cells

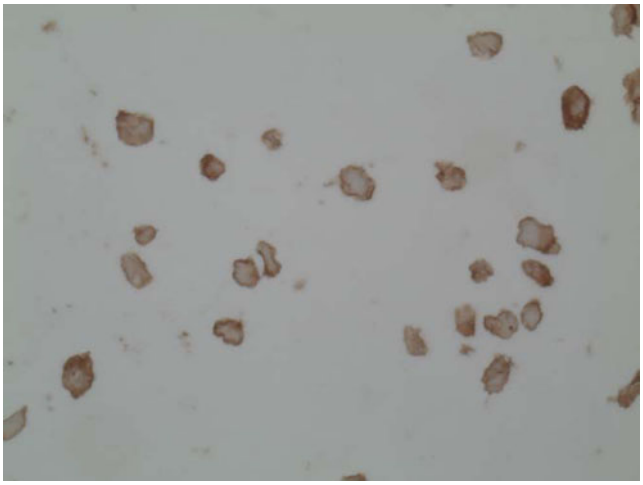

Fig. 6 Immunohistochemical detection of HB9 in Hep3b cells. HB9 was detected in the cytoplasm but not in the nuclei

mRNA in the transfected cells. Immunoblot analysis for HB9 revealed a clear band at 48 kDa; this band was not seen in non-transfected cells (Fig. 4). Applying the pCMV5 vector only was giving negative results. We assumed HLXB9 as identified correctly by these experiments.

Consistent with the results on mRNA expression level, HCC and CC cell lines were also positive on the protein level for HB9; HB9 was detected in the cytoplasmic and cell membrane fractions, but not in the nuclear fraction (Fig. 5). This was confirmed by immunohistochemical analysis of HB9. HB9 staining was observed in the cytoplasm but not in the nuclei (Fig. 6).

HLXB9 and HB9 in surgical HCC specimens

Based on our findings, we surmised that HLXB9 was stably upregulated in HCC and CC cell lines. We next examined HLXB9/HB9 expression in surgical HCC specimens that had not been cultured by analyzing 29 surgical HCC specimens from 28 patients as well as non-neoplastic liver tissue from the same patients.

None of the 17 moderately or well-differentiated HCC tissues expressed HLXB9 mRNA, nor did the corresponding non-neoplastic tissues (Table 5). In contrast, 5/12 samples with low histological differentiation (Edmondson grade III or IV) [10] demonstrated HLXB9 mRNA upregulation. The ΔΔct values were generally ~22. An exception was case B07-2284. Two samples were analyzed: one showed no upregulation of HLXB9 mRNA; the other specimen showed an upregulation compared to the non-neoplastic tissue. Interestingly, the B07-2284 tumor without upregulation had a solid growth pattern, whereas the tumor with upregulation had a pseudoglandular pattern (Fig. 7).

We reevaluated all other poorly differentiated HCC and found that poorly differentiated HCC that lacked HLXB9 upregulation grew in a solid pattern. Two of these HCC

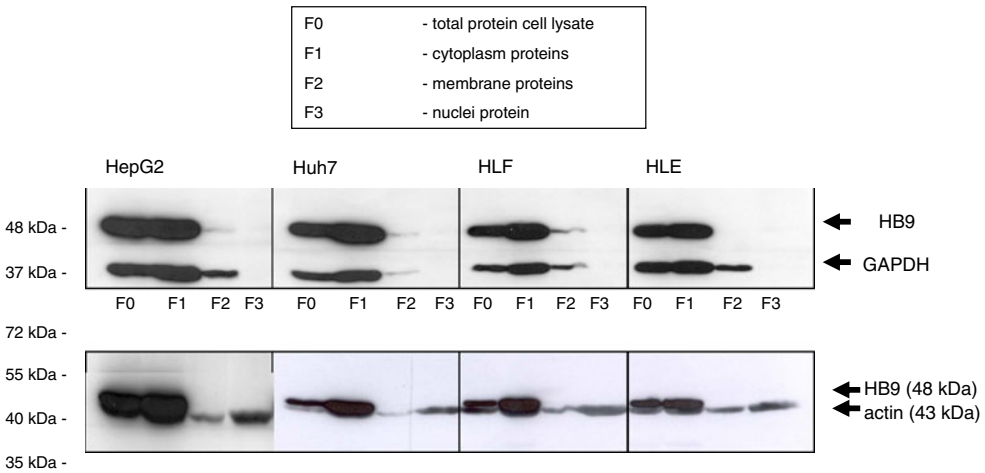

Fig. 5 HB9 immunoblot analysis of four hepatocellular carcinoma (HCC) cell lines after separation of proteins in the sub-cellular compartments (*Tot* total cell lysate, *Cyt* cytoplasm, *M* membranes, *N* nuclei). HB9 was only detected in cytoplasmic and membrane fractions but not in the nuclei of carcinoma cells. As an internal control GAPDH was used. Since this gene is not expressed in nuclei actin was used as an additional control for this compartment

Table 5 Expression of HLXB9 in HCC surgical specimens

Case	HLXB9 ΔΔ-ct values	Histological grade
B08-4628	n.u.	2
B07-24021	n.u.	2
B04-17547	n.u.	1
B06-28291	n.u.	2
B08-3896	n.u.	2
B06-24377	n.u.	2
B05-9393	n.u.	2
B04-24966	n.u.	2
B04-1095	n.u.	2
B04-1420	n.u.	2
B03-15870	n.u.	2
B03-15602	n.u.	2
B05-25757	n.u.	2
B03-12301	n.u.	2
B03-15870	n.u.	2
B03-10403	n.u.	2/3
B03-20246	n.u.	2
B06-26164	n.u.	3
B05-24806	n.u.	3
B04-10840	n.u.	3
B05-24972	n.u.	3
B03-22359	n.u.	3
B07-2284 I	n.u.	3
B07-23968	23.0	3
B07-2284 II	22.3	3
B08-4419	23.7	3
B06-11514	24.9	3
B08-2087	23.9	3

n.u. Not upregulated. ΔΔct values >35 in both, tumor and non-neoplastic tissues

(B04-10840 and B05-24972) demonstrated remarkable pleomorphic nuclei. In turn, poorly differentiated HCC with upregulated HLXB9 mRNA demonstrated a pseudo glandular pattern of growth. Indeed, two of these HCC were difficult to differentiate from CC (B07-23968 and B08-4419). Therefore, IHC for CK7 and CK19, respectively, was done for these cases to exclude CC and probably find progenitor cell derived subtype as described by Lee et al. [21]. These stainings were giving variable results with B08-4419 negative for CK7 and positive for CK19 and B07-23968 positive for both markers as given in Table 6 and demonstrated in Fig. 8. Variable findings occurred also for the other three HCC analyzed as listed in that Table.

In a very recently published paper of Wildenhain et al. analyzing HLXB9-TEL positive acute myeloid leukemia in children EDIL, ITGAV, KDR, SIGLEC6, CNTNAP%, ANGPT1, DSG, and ITGA9, respectively, were detected as upregulated. Since these genes are active in cell–cell contact, we reevaluated our data for these genes. Indeed we found EDIL, ITGAV, KDR, CNTNAP5, ANGPT1, ITGA as upregulated in HCC and/or CCC, too. Detailed data are given in Table 7.

HLXB9 in surgical CC, HCA, and non-neoplastic specimens

Upregulation of mRNA encoding HLXB9 was found in 1/10 CC sample as listed in Table 8. In this sample, a clearly glandular pattern of growth with moderately to low differentiated tumor cells were seen. Two other CC with glandular pattern were well or moderately differentiated. Six CC revealed a solid growth pattern. No upregulation of HLXB9 was found in HCA and non-neoplastic liver samples.

Discussion

The morphological characteristics of HCC have been well-established since Edmondson and Steiner published their basic grading system in 1954 [9]. Most HCC demonstrate moderate differentiation at the time of surgical intervention. Well-differentiated HCC are rare, making up fewer than 10% of all HCC cases. In contrast, dedifferentiated HCC are seen more frequently as the disease progresses [11, 12]. Since dedifferentiation is accompanied by decreased survival time [15, 16], we wished to gain insights into the mechanisms underlying dedifferentiation.

Molecular analysis of HCC biopsies is hampered by the accompanying non-neoplastic cells and by the variable morphological differentiation of the carcinomas. To avoid these issues, we began our investigation with HCC cell lines. All of these HCC cell lines were highly proliferative, which we assumed as an indicator of dedifferentiation beside the pleomorphism of these cells.

Microarray-based mRNA expression analysis of these cell lines identified a set of 54 upregulated and 125 downregulated genes in HCC. The HLXB9 gene was the most upregulated and had the highest fold increase of any gene. HLXB9 is an evolutionarily highly conserved homeobox gene that belongs to the MNX gene class [22]. It is involved in differentiation of beta cells [20] and motor neurons [23, 24]. During mouse embryonic development, HLXB9 is expressed at somite day 8 in the notochord, the dorsal gut endoderm, and the ventral endoderm at the prospective pancreatic anlage [25]. Despite PDX1 mutations that prevent pancreas development, the initial stadium of the pancreas anlage is still developing when HLXB9 is functionally expressed. HLXB9 is detected in a dorsal–ventral gradient during embrogenesis of mice [26]. This is in concordance with the observation that mice lacking HLXB9 are missing dorsal pancreas rudiments. HLXB9

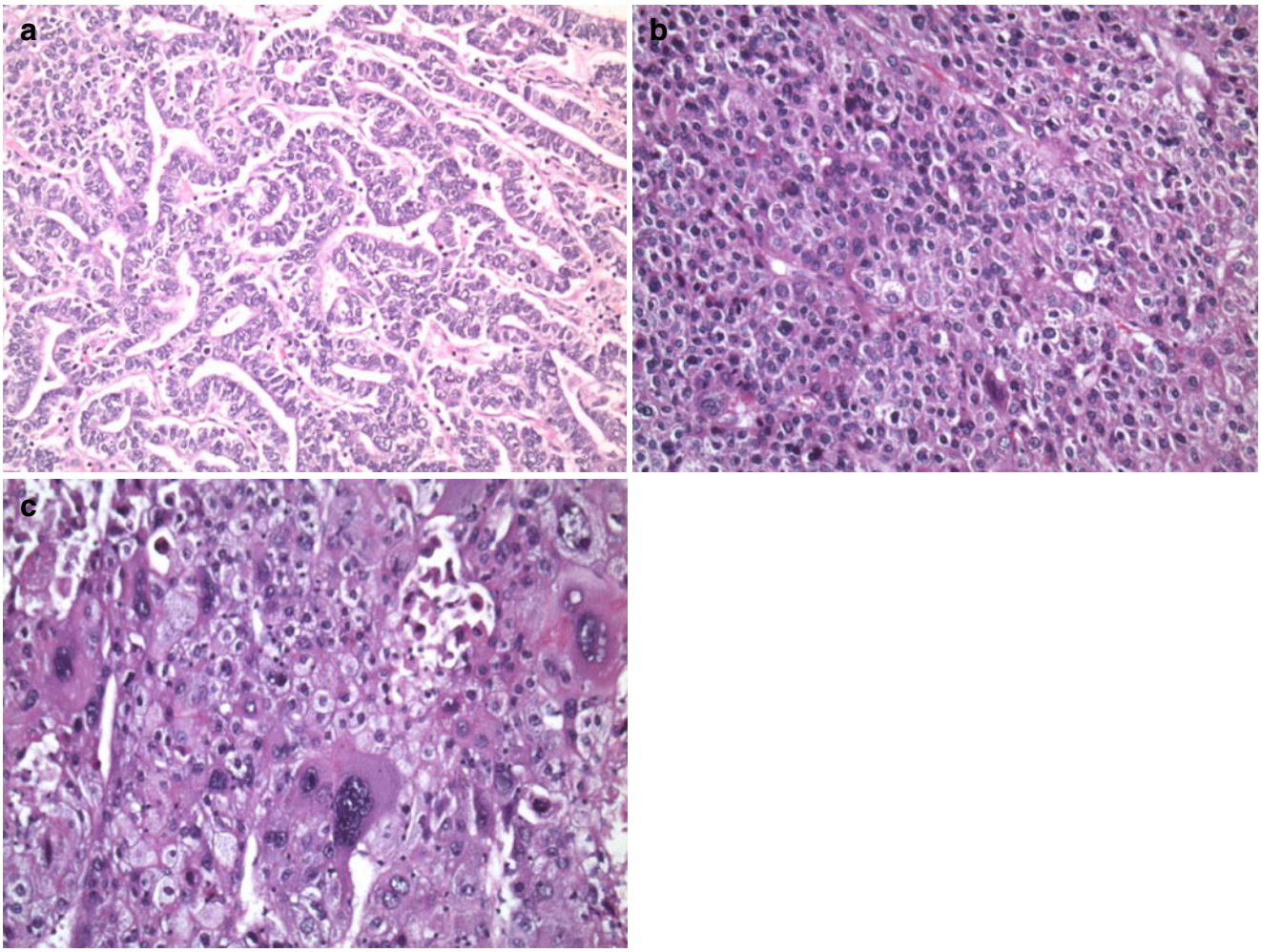

Fig. 7 Morphology of poorly differentiated HCC (**a**–**c**). In **a**, a pseudoglandular pattern is found; in **b**, a solid pattern is shown; in **c**, solid pattern with highly irregular nuclei of HCC is demonstrated. In cases of pseudoglandular pattern upregulation of HLXB9 was detectable

Table 6 Immunohistochemical stainings for CK7 and CK19 in HCC samples found upregulated for HLXB9

Case	Detectable staining for	
	CK7	CK19
B07-23968	Yes	Yes
B07-2284 II	No	Patchy
B08-4419	No	Yes
B06-11514	Patchy	No
B08-2087	No	No

Staining pattern was variable. Beside cases with positive staining in all cells and cases without any positive cells there were tumor samples with variable expression of cytokeratins as named "patchy" here and demonstrated in Fig. 8

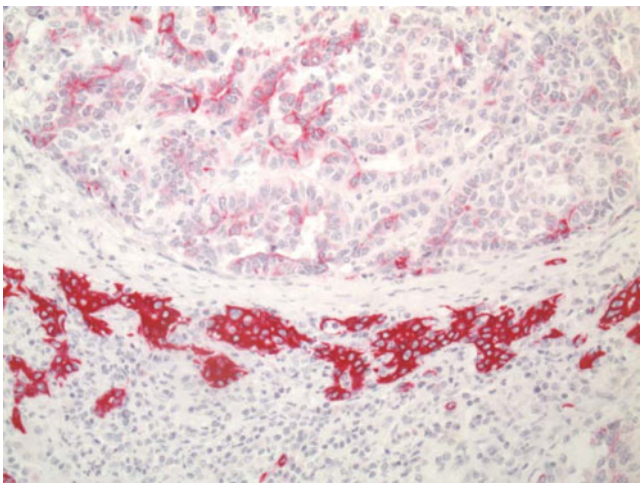

Fig. 8 Immunohistochemical staining of case 2294–07 for CK7. Ductular reactions serve as an internal positive control. Tumor cells are giving a variable "patchy" pattern

Table 7 Wildenhain et al. reported eight genes upregulated in HLXB9/TEL translocated childhood AML

Gene	Cell lines	
	HCC	CCC
EDIL3	10	27
ITGAV	2.4	<2
KDR	4.5	5.3
CNTNAP5	<2	2.2
ANGPT1	<2	31
ITGA9	<2	2.7

These genes are acting in cell–cell contact. Six of these genes were also found upregulated in HCC and/or CCC cell lines in our study with the fold changes given below. EDIL3 war remarkable highly expressed in CCC as discussed in the text

mutations are rare and cause Currarino syndrome, an autosomal dominant congenital malformation that causes anorectal malformations and sacral agenesis [27].

In malignant transformed cells such as Hodgkin lymphoma cell lines, HLXB9 activates IL6 and is regulated by PI3K signaling that involves E2F3 [28]. van Bergh et al. reported a high incidence of t(7;12)(q36;p13) in infant AML with a poor outcome and ectopic expression of HLXB9. HLXB9 upregulation is mirrored by an intracellular shift away from the periphery (cytoplasm) to a more central position in the nucleus [29]. It is of high interest, that activation of IL6 together with NF-κB and dysregulation of miRNAs Lin28, and Let-7 can lead to an epigenetic shift involved in the development of a neoplastic growth of tumor cells [30]. Although we did not find direct evidence of upregulation of IL6 in the cell lines analyzed here, we assume this as an important point to consider for further research purposes.

We confirmed upregulation of HLXB9 in surgical HCC specimens in a subgroup of poorly differentiated HCC with a pseudoglandular pattern of growth. Indeed, in two samples, it was not easy to differentiate HCC from CC. We therefore looked also for expression of CK7 and CK19, since these intermediar filaments are expressed in CC and also in a subset of HCC with impaired clinical outcome [21]. Interestingly, those samples revealing upregulation of HLXB9 in our study expressed at least one of these cytokeratins in a uniform or patchy pattern. As demonstrated in the study mentioned above, this subset of HCC reveals gene expression patterns of hepatoblasts. Differentiation of hepatocytes and cholangiocytes is not finished at this time which is in concordance with the assumption that tumors cells of this particular group of HCC derive from a progenitor cell. Unfortunately in the article mentioned above, photographs of immunostainings are not given for direct comparison. Nevertheless, we assume this as an important aspect worth spending further efforts on. In contrast, to HCC with pseudo glandular pattern, HCC revealing solid growth were not associated with increased expression of HLXB9, nor were moderate- or well-differentiated HCC. By these findings, we speculate that poorly differentiated HCC with a pseudoglandular

Table 8 Expression of HLXB9 in samples of CC, HCA, and non-neoplastic liver specimens

Case	Histological diagnosis	Histological pattern	Grade	HLXB9 ΔΔ-ct values
B04-17723	CC	Solid	G3	n.u.
B05-11029	CC	Glandular	G1	n.u.
B05-32694	CC	Solid/trabecular	G2	n.u.
B06-1266	CC	Solid/trabecular	G2	n.u.
B06-6539	CC	Solid/trabecular	G2	n.u.
B06-11307	CC	Glandular	G2	n.u.
B06-14496	CC	Solid/trabecular	G2	n.u.
B07-4482	CC	Solid/trabecular	G2	n.u.
B07-5154	CC	Glandular	G2-3	11,7
B07-13723	CC	Solid/trabecular	G2	n.u.
B09-14730	HCA			n.u.
B07-13618	HCA			n.u.
B06-15259	HCA			n.u.
B01-19096	HCA			n.u.
B04-30498	HCA			n.u.
B03-29375	Non-neoplastic[a]			n.u.
B05-12945	Non-neoplastic			n.u.
B05-29110	Non-neoplastic			n.u.
B09-19946	Non-neoplastic			n.u.
B09-31593	Non-neoplastic			n.u.

n.u. Not upregulated. ΔΔct values >35 in both, tumor and non-neoplastic tissues

[a] Obtained from livers ruptured due to trauma

pattern could reflect an mRNA expression pattern that is related to a cholangiolar expression pattern. This would be in concordance with the finding of upregulation of HLXB9 in the CC cell lines examined here since growth of both carcinoma types in one tumor has been reported repeatedly, HLXB9 could be a link [10]. Further, hepatocytes and cholangiocytes are assumed to be derived from hepatoblast/oval cells, since the same progenitor cells localize to the ductal plate area [31].

Interestingly, all HCC cell lines, but only half of the surgical specimens of poorly differentiated HCC demonstrated HLXB9 upregulation. This raises the question of whether there is a bias in terms of the morphological subtype of the HCC cell line. This may be related to the observation that HCC tumor cells are difficult to establish in vitro. It seems likely that a particular subtype of HCC cell is needed for successful growth in vitro. Since the cell lines analyzed here were grown as suspensions, we cannot address this question at this time.

Very recently Wildenhain et al. [32] reported the expression of cell–cell interacting genes upregulated in childhood acute myeloid leukemia bearing a HLXB9-TEL translocation and HB9 overexpression. They found an upregulation of eight genes, six of them upregulated at least twofold in HCC and/or CCC cell lines in our study, too. EGF-like repeats and discoidin I-like domains 3 (EDIL3) was found upregulated highest in both tumor types. This gene encodes the protein of an integrin ligand. It is important in mediating angiogenesis and probably plays a role in vessel wall remodeling and development (as describe in RefSeq). Interestingly, EDIL3 is correlated to a shorter survival of HCC patients as reported by Sun et al. [33]. As HCC and CCC of low differentiation are correlated to a shorter survival of patients and also express HLXB9 in a number of such tumors as shown here, it may be speculated that there could be a link. Unfortunately, Sun et al. did not provide their data in regard to the grading of the tumors analyzed.

In conclusion, HLXB9 is significantly upregulated in HCC and CCC cell lines and in poorly differentiated HCC with a pseudoglandular pattern. The protein encoded by HLXB9, HB9, is found only in the membrane and cytoplasm of these tumor cells. This observation may provide insights into the mechanism(s) underlying development of malignancy and dedifferentiation in hepatocellular and cholangiolar cells.

Conflict of interest The authors declare that they have no conflict of interests.

Funding This work was supported by the Schweizerischer Nationalfonds (SNF, grant 31003A-118065).

References

1. Schirmacher P, Dienes HP (1999) Hepatocellular carcinoma. In: Kurzrock R, Talpaz M (eds) Molecular biology in cancer medicine. Dunitz, London, pp 355–366
2. El-Serag HB (2002) Hepatocellular carcinoma: an epidemiologic view. J Clin Gastroenterol 35(5 Suppl 2):72–78
3. Wu CG, Salvay DM, Forgues M, Valerie K, Farnsworth J, Markin RS, Wang XW (2001) Distinctive gene expression profiles associated with hepatitis B virus × protein. Oncogene 20:3674–3682
4. Smith MW, Yue ZN, Geiss GK, Sadovnikova NY, Carter VS, Boix L, Lazaro CA, Rosenberg GB, Bumgarner RE, Fausto N, Bruix J, Katze MG (2003) Identification of novel tumor markers in hepatitis C virus-associated hepatocellular carcinoma. Cancer Res 63:859–864
5. Okabe H, Satoh S, Kato T, Kitahara O, Yanagawa R, Yamaoka Y, Tsunoda T, Furukawa Y, Nakamura Y (2001) Genome-wide analysis of gene expression in human hepatocellular carcinomas using cDNA microarray: identification of genes involved in viral carcinogenesis and tumor progression. Cancer Res 61:2129–2137
6. Iizuka N, Oka M, Yamada-Okabe H, Hamada K, Nakayama H, Mori N, Tamesa T, Okada T, Takemoto N, Matoba K, Takashima M, Sakamoto K, Tangoku A, Miyamoto T, Uchimura S, Hamamoto Y (2004) Molecular signature in three types of hepatocellular carcinoma with different viral origin by oligonucleotide microarray. Int J Oncol 24:565–574
7. Neo SY, Leow CK, Vega VB, Long PM, Islam AF, Lai PB, Liu ET, Ren EC (2004) Identification of discriminators of hepatoma by gene expression profiling using a minimal dataset approach. Hepatology 39:944–953
8. Thorgeirsson SS, Grisham JW (2002) Molecular pathogenesis of human hepatocellular carcinoma. Nat Genet 31:339–346
9. Edmondson HA, Steiner PE (1954) Primary carcinoma of the liver: a study of 100 cases among 48,900 necropsies. Cancer 7:462–503
10. Ishak KG, Goodman ZD, Stocker JT (2001) Tumors of the liver and intrahepatic bile ducts, vol. 31, 3rd edn. Armed Forces Institute of Pathology, Washington
11. Kenmochi K, Sugihara S, Kojiro M (1987) Relationship of histologic grade of hepatocellular carcinoma (HCC) to tumor size, and demonstration of tumor cells of multiple different grades in single small HCC. Liver 7:18–26
12. Sugihara S, Nakashima O, Kojiro M, Majima Y, Tanaka M, Tanikawa K (1992) The morphologic transition in hepatocellular carcinoma. A comparison of the individual histologic features disclosed by ultrasound-guided fine-needle biopsy with those of autopsy. Cancer 70:1488–1492
13. Wilkens L, Flemming P, Gebel M, Bleck J, Terkamp C, Kreipe H, Schlegelberger B (2004) Induction of aneuploidy by increasing chromosomal instability during dedifferentiation of hepatocellular carcinoma. Proc Natl Acad Sci USA 101:1309–1314
14. Skawran B, Steinemann D, Weigmann A, Becker T, Flik J, Kreipe H, Schlegelberger B, Wilkens L (2008) Gene expression profiling in hepatocelluar carcinoma: coordinated up-regulation of genes localised in amplified chromosome regions. Mod Pathol 21:505–516
15. Nzeako UC, Goodman ZD, Ishak KG (1995) Comparison of tumor pathology with duration of survival of North American patients with hepatocellular carcinoma. Cancer 76:579–588
16. Lauwers GY, Terris B, Balis UJ, Batts KP, Regimbeau JM, Chang Y, Graeme-Cook F, Yamabe H, Ikai I, Cleary KR, Fujita S, Flejou JF, Zukerberg LR, Nagorney DM, Belghiti J, Yamaoka Y, Vauthey JN (2002) Prognostic histologic indicators of curatively resected hepatocellular carcinomas: a multi-institutional analysis of 425 patients with definition of a histologic prognostic index. Am J Surg Pathol 26:25–34
17. Alexandre E, Viollon-Abadie C, David P, Gandillet A, Coassolo P, Heyd B, Mantion G, Wolf P, Bachellier P, Jaeck D, Richert L

(2002) Cryopreservation of adult human hepatocytes obtained from resected liver biopsies. Cryobiology 44:103–113
18. Ishak KG, Anthony PP, Sobin LH (1994) WHO: histological typing of tumours of the liver, 2 edn
19. Oberli A, Popovici V, Delorenzi M, Baltzer A, Antonov J, Matthey S, Aebi S, Altermatt HJ, Jaggi R (2008) Expression profiling with RNA from formalin-fixed, paraffin-embedded material. BMC Med Genomics 1:9
20. Harrison KA, Thaler J, Pfaff SL, Gu H, Kehrl JH (1999) Pancreas dorsal lobe agenesis and abnormal islets of Langerhans in Hlxb9-deficient mice. Nat Genet 23:71–75
21. Lee JS, Heo J, Libbrecht L, Chu IS, Kaposi-Novak P, Calvisi DF, Mikaelyan A, Roberts LR, Demetris AJ, Sun Z, Nevens F, Roskams T, Thorgeirsson SS (2006) A novel prognostic subtype of human hepatocellular carcinoma derived from hepatic progenitor cells. Nat Med 12:410–416
22. Ross AJ, Ruiz-Perez V, Wang Y, Hagan DM, Scherer S, Lynch SA, Lindsay S, Custard E, Belloni E, Wilson DI, Wadey R, Goodmann F, Orstavik KH, Monclair T, Robson S, Reardon W, Burn J, Scambler P, Strachan T (1998) A homoebox gene, HLXB9, is the major locus ofr dominantly inherited sacral agenesis. Nat Genet 20:358–361
23. Saha MS, Miles RR, Grainger RM (1997) Dorsal-ventral patterning during neural induction in *Xenopus*: assessment of spinal cord regionalization with xHB9, a marker for the motor neuron region. Dev Biol 187:209–223
24. Hagan DM, Ross AJ, Strachan T, Lynch SA, Ruiz-Perez V, Wang YM, Scambler P, Custard E, Reardon W, Hassan S, Nixon P, Papapetrou C, Winter RM, Edwards Y, Morrison K, Barrow M, Cordier-Alex MP, Correia P, Galvin-Parton PA, Gaskill S, Gaskin KJ, Garcia-Minaur S, Gereige R, Hayward R, Homfray T (2000) Mutation analysis and embryonic expression of the HLXB9 Currarino syndrome gene. Am J Hum Genet 66:1504–1515
25. Li H, Arber S, Jessell TM, Edlund H (1999) Selective agenesis of the dorsal pancreas in mice lacking homeobox gene Hlxb9. Nat Genet 23:67–70
26. Sherwood RI, Chen TY, Melton DA (2009) Transcriptional dynamics of endodermal organ formation. Dev Dyn 238:29–42
27. Currarino G, Coln D, Votteler T (1981) Triad of anorectal, sacral, and pre sacral anomalies. Am J Roentgenol 137:395–398
28. Nagel S, Scherr M, Quentmeier H, Kaufmann M, Zaborski M, Drexler HG, MacLeod RA (2005) HLXB9 activates IL6 in Hodgkin lymphoma cell lines and is regulated by PI3K signalling involving E2F3. Leukemia 19:841–846
29. Ballabio E, Cantarella CD, Federico C, Di MP, Hall G, Harbott J, Hughes J, Saccone S, Tosi S (2009) Ectopic expression of the HLXB9 gene is associated with an altered nuclear position in t (7;12) leukaemias. Leukemia 23:1179–1182
30. Iliopoulos D, Hirsch HA, Struhl K (2009) An epigenetic switch involving NF-kappaB, Lin28, Let-7 MicroRNA, and IL6 links inflammation to cell transformation. Cell 139:693–706
31. Roskams T, Desmet V, Verslype C (2007) Development, structure and function of the liver. In: Burt A, Portmann B, Ferrell L (eds) MacSween's pathology of the liver. Churchill Livingstone Elsevier, Philadelphia, pp 1–74
32. Wildenhain S, Ruckert C, Rottgers S, Harbott J, Ludwig WD, Schuster FR, Beldjord K, Binder V, Slany R, Hauer J, Borkhardt A (2010) Expression of cell–cell interacting genes distinguishes HLXB9/TEL from MLL-positive childhood acute myeloid leukemia. Leukemia 24:1657–1660
33. Sun JC, Liang XT, Pan K, Wang H, Zhao JJ, Li JJ, Ma HQ, Chen YB, Xia JC (2010) High expression level of EDIL3 in HCC predicts poor prognosis of HCC patients. World J Gastroenterol 16:4611–4615

Virchows Arch (2011) 458:709–716
DOI 10.1007/s00428-011-1087-9

ORIGINAL ARTICLE

Pathology of flupirtine-induced liver injury:

a histological and clinical study of six cases

Florian Puls · Clemens Agne · Fritz Klein · Martin Koch · Kinan Rifai · Michael P. Manns · Jürgen Borlak · Hans H. Kreipe

Received: 8 March 2011 / Revised: 16 April 2011 / Accepted: 21 April 2011 / Published online: 18 May 2011
© Springer-Verlag 2011

Abstract Drug-induced liver injury may cause impairment of liver function and is a leading cause of acute liver failure. Identification of the causative substance in patients receiving several drugs is often difficult in clinical practice. Evaluation of liver biopsies in suspected drug-induced injury is a challenging task that requires close clinicopathological correlation. Recognizing a characteristic morphological pattern of liver injury may contribute to identification of the causative drug. Flupirtine, a non-opioid analgesic, has been reported to cause liver injury of idiosyncratic type in rare instances. We wished to characterize the histopathological features of flupirtine-induced liver injury, which have not been reported so far. Liver biopsies of five patients with severe liver injury and one explanted liver of a patient with flupirtine-induced acute liver failure that required transplantation were assessed. In addition clinical presentation and course were reviewed and clinical follow up was performed. Extensive perivenular necrosis with associated ceroid pigment-laden macrophages and a mild to moderate lymphocytic infiltrate was a common feature in all cases. Histological extent of liver necrosis corresponded well to serum amino-transferase levels. Accidental reexposure of one patient resulted in a plasma cell rich hepatitis with perivenular necrosis. This study provides evidence that flupirtine can cause substantial liver injury of hepatocellular type. Liver damage is associated with a characteristic morphological picture, the recognition of which will aid in causality assessment of drug-induced liver injury. Clinical and histological features raise the possibility of an immune-mediated toxicity.

Keywords Drug-induced liver injury · Flupirtine · Liver failure · Liver biopsy

Florian Puls and Clemens Agne contributed equally to this work.

Electronic supplementary material The online version of this article (doi:10.1007/s00428-011-1087-9) contains supplementary material, which is available to authorized users.

F. Puls (✉) · H. H. Kreipe
Department of Pathology, Hannover Medical School,
Carl-Neuberg-Str.1,
30625 Hannover, Germany
e-mail: Puls.Florian@mh-hannover.de

C. Agne · K. Rifai · M. P. Manns
Department of Gastroenterology, Hepatology and Endocrinology,
Hannover Medical School,
Carl-Neuberg-Str.1,
30625 Hannover, Germany

F. Klein
Department of General, Visceral, and Transplantation Surgery,
Charité,
Augustenburger Platz 1,
13353 Berlin, Germany

M. Koch
Department of Pathology, Charité,
Charitéplatz 1,
10117 Berlin, Germany

J. Borlak
Fraunhofer Institute of Toxicology and Experimental Medicine,
Centre for Drug Research and Medical Biotechnology,
Nicolai-Fuchs-Strasse 1,
30625 Hannover, Germany

Introduction

Drug-induced liver injury (DILI) is an important cause of liver injury that can severely impair liver function and lead to acute liver failure. DILI is the most common cause for drug withdrawal from the market [1]. It is estimated to account for one-third to one-half of cases of acute liver

failure in the United States [2]. The exact incidence of DILI is uncertain due to a lack of a standard definition, stringent reporting practice and difficulty in assignment of causality [3]. Retrospective analysis found DILI in 6.6% of outpatients in a hepatology clinic and in 8.1% of patients with parenchymal liver dysfunction [4, 5]. The spectrum of clinical manifestations of DILI is broad and separation from potentially coexisting primary liver disease therefore difficult. In daily clinical practice, DILI is a commonly entertained differential diagnosis in patients receiving several medications. DILI is divided into predictable/dose-dependent and unpredictable/idiosyncratic types [6]. Idiosyncratic reactions are rare, independent of dose and occur after a variable latency period after initiation of medication. Methods to quantify the probability of DILI by a specific drug on clinical grounds have been developed to aid the diagnosis of DILI [7]. The most commonly used is the Roussel Uclaf Causality Assessment Method (RUCAM score) [8]. Moreover liver biopsies are sometimes obtained in the diagnostic workup of suspected DILI. In such clinical setting morphological assessment can contribute valuable diagnostic and prognostic information about the causative drug and any additional primary liver disease. Drug-induced injury patterns can be classified into several morphological patterns or categories [9]. Since most drugs produce a limited morphological spectrum of injury, the number of causative drugs can be narrowed down by morphological assessment of the injury pattern [10]. Liver pathologists rely on compiled lists of drugs and associated injury patterns derived from reviews of small case series and case reports [6, 11]. Because idiosyncratic DILI cannot be determined in preclinical safety studies experimentally, these observational studies of small case series provide the main body of evidence that permits identification of a causative drug in DILI by its morphological pattern. In addition histological review of DILI case series provides clues to the mechanism of hepatocellular injury and has contributed to understanding its mechanisms, e.g. in Tienilic-acid induced liver injury [12, 13].

The morphological pattern of liver injury associated with the widely used non-opioid analgesic flupirtine has not been described so far. Flupirtine is licensed in several European countries, Russia and China for treatment of acute and chronic musculosketelal pain, tension-type headache, pain in metastatic malignancies, dysmenorrhea as well as postoperative pain [14–16]. In 2008, 26 million daily defined doses were prescribed in Germany [17]. The increase of 16.1% in comparison to 2007 highlights its increasing importance in pain management.

The analgesic effects of flupirtine are believed to be mediated through activation of G-protein-regulated inwardly rectifying potassium channels, which results in stabilization of the membrane resting potential in neurons. This also accounts for its relaxing effects on muscle tone [18]. Flupirtine has recently gained renewed interest due to its antioxidant and anti-apoptotic properties, that may convey therapeutic benefits in neurodegenerative and neuroinflammatory diseases [1].

A comprehensive understanding of its metabolism is still lacking, but it is known that hepatic metabolism plays an important part and yields several metabolites by acetylation and glucuronidation of flupirtine. Glucuronidated metabolites are excreted in the urine, which can take on a green tint [19, 20].

Well-known side effects of flupirtine are vertigo, nausea, diarrhea, heart burn and urticaria [18, 21]. Frequent and mild elevation of liver enzymes, which subsided after discontinuation of flupirtine intake, is well documented [22]. Aggravation of preexisting liver disease during flupirtine intake has been described and flupirtine is therefore not recommended in patients with co-existing liver disease [23, 24]. Until September 2007, 151 cases of DILI associated with flupirtin intake have been reported within the voluntary German reporting system for adverse drug reactions. Liver failure was reported in seven cases, four of which were fatal [24]. Here, we report the clinical manifestations and morphological features of liver damage associated with flupirtine intake in six patients.

Materials and methods

Case selection

A full text search of the Hannover University Hospital Department of Histopathology's database for "flupirtine" was performed. Three cases recently noticed by the authors were added, one of which has recently been published in a case report [25].

Clinical review

Clinical notes and laboratory findings were retrieved and causality assessment according to the Roussel Uclaf Causality Assessment Method (RUCAM) was performed [8]. Patient follow up was conducted by patients' general practitioners and/or in outpatient clinics of Hannover and Charite University Hospitals. Latest medications and laboratory findings were reviewed.

Histological review

Sections from formalin-fixed, paraffin-embedded material of the liver biopsies and of one representative block of the explanted liver were stained with haematoxylin/eosin, periodic acid-Schiff, reticulin silver, Elastica van Gieson

and Perl's iron. Location and extend of necrosis as percentage of total depicted area was recorded. The presence of portal and lobular inflammation, interface hepatitis, ductular reaction, lobular disarray (defined as the disruption of trabecular arrangement of liver cell plates), plasma cells, ceroid-laden macrophages and fibrosis was recorded and graded semiquantitatively. Acidophil bodies and eosinophils were counted in three 40× objective fields in the area of highest density, and an average number per 40× objective field (high power field) was calculated. One 40× objective field covered an area of 0.238 mm^2 (Olympus microscope, 40× objective, ×10 eyepiece, field number 22).

Results

Clinical findings

Six cases of flupirtine associated liver injury with clinical details and histological material were available. The four female and two male patients were 48 to 78 years old (mean, 56 years, median 53 years). All patients were Caucasian. One patient, who received flupirtine monotherapy presented with jaundice, hepatic encephalopathy and coagulopathy. Liver function declined further after discontinuation of flupirtine necessitating orthotopic liver transplantation for acute liver failure after 3 days. Three patients presented with jaundice and mild coagulopathy, but without encephalopathy, one of whom also complained of pruritus and fatigue. Two patients did not have any symptoms, but had elevated serum aminotransferase levels observed on routine controls. All patients were hospitalized. After discontinuation of flupirtine as well as other medications serum amino-transferase, alkaline phosphatase and bilirubin levels fell rapidly and normalized after several weeks. Serum alanine aminotransferase was the last parameter to normalize in patients 1–5 (Fig. 1). Two patients (patients 1 and 2) were initially treated with a reducing dose regime of prednisone. None of the patients had preexisting liver disease. Five patients did not drink alcohol. Moderate alcohol consumption on rare occasions was reported by one patient. Medical conditions and medications are summarized in Table 1. Ultrasonography did not detect signs of obstructive cholestasis. One of the patients (patient 4) was accidentally exposed to flupirtine a second time after 4 years. Three weeks after beginning of the second exposure elevated serum aminotransferase levels were noted on routine controls. Detailed description of presentation and clinical course of all patients is available in the supplementary material.

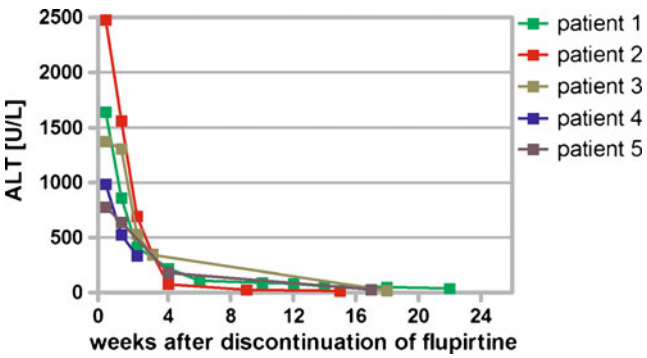

Fig. 1 Levels of serum alanine aminotransferase of patients 1–5 after discontinuation of flupirtine

Causality assessment

Liver injury in all patients was of hepatocellular type according to the standardized nomenclature: the ratio of serum alanine aminotransferase (ALT) to alkaline phosphatase (AP) with respect to their upper limits of normal (ULN), the *R* ratio (ALT/ULN)/(AP/ULN) was above 5 [7]. All except one patient were taking additional medication other than flupirtine. Flupirtine was the only common medication in all cases. The likelihood of flupirtine as the cause of liver injury was "probable" (7–8 points) in four cases and "highly probable" (9 and 13 points) in two cases when RUCAM criteria were applied [8].

Laboratory data

Time to clinical presentation after initiation of flupirtine medication ranged from less than 1 to 24 months (median 4 months). In patient 2, who by far had the longest duration of flupirtine exposure, it remained uncertain if flupirtine had been continuously taken during the 24-month period since initial prescription. Patients 1, 2, 3 and 6, who presented with jaundice and had received flupirtine for 7, 24, 3 and 3 months, respectively, had highest bilirubin levels (168, 555, 218 and 597 μmol/l, respectively). These four patients also had elevated international normalized ratio (INR) (Table 2). ALT/AST ratios ranged from 0.85 to 3.0. Maximum aminotransferase levels did not correlate with cumulative dose or time of treatment. One patient (patient 6) presented with hepatic encephalopathy and showed rapid decline in liver function necessitating orthotopic liver transplantation. All other patients showed a rapid decrease of ALT levels (Fig. 1) after discontinuation of flupirtine medication, although time to normalization of alanine aminotransferase levels was more than 4 weeks in some patients. An accidental rechallenge occurred in one patient 4 years after the initial event causing an ALT peak of 1,216 U/l after 3 weeks of reexposure (patient 4). In all patients there was no serological or clinical evidence of infection by hepatotrophic viruses (see Supplementary Table 1). Although borderline anti-nuclear antibodies

Table 1 Clinical details and medication of flupirtine-associated liver injury

Patient	1	2	3	4, First exposure	4, Second exposure	5	6
Sex (M/F)	F	F	F	F	F	M	M
Age (y)	55	51	57	75	78	49	48
Medical conditions	Post herpes zoster pain	Osteo-arthritis, hypertension	Chronic low back pain	Chronic low back pain		Vertebral disc prolaps	Vertebral disc prolaps
Time to presentation	7 months	24 months	3 months	1 month	3 weeks	4 months	3 months
Presenting complaint	Jaundice ~4 weeks	Jaundice ~3 days, nausea, fatigue, pruritus	Jaundice, fatigue, right upper quadrant pain	Abdominal pain, fatigue, weight loss	Asymptomatic, elevation of serum aminotransferases	Asymptomatic, elevation of serum aminotransferases	Jaundice, hepatic encephalopathy
Prescribed medication at time of presentation	Flupirtine, pregabalin	Flupirtine, simvastatin, carvedilol	Flupirtine, ibuprofene, tramadol	Flupirtine, isosorbide dinitrate, aspirine		Flupirine, hydromorphone, frusemide, ramipril, bisoprolol, domperidone, pantoprazole, insulin lispro	Flupirtine
Flupirtine dose/day	3×100 mg	2–3×100 mg	1×100 mg	1×400 mg		3×100 mg	1×400 mg
RUCAM score for flupirtine	7 “probable”	7 “probable”	9 “highly probable”	9 “highly probable”	13 “highly probable”	7 “probable”	8 “probable”
Medication at follow-up	Prednisone 5 mg/day (tapered off)	Omeprazole, tramadol, ramipril, mirtazapine, carvedilol, thyroxine	Hydro-morphone		Isosorbide dinitrate, aspirine	Furosemid, ramipril, bisoprolol, domperidone, pantoprazole, insulin lispro	Tacrolimus
Time to normalisation of ALT levels	22 weeks	9 weeks	Less than 17 weeks	Not traceable	8 weeks	Less than 17 weeks	Not applicable

Table 2 Laboratory findings of six cases of flupirtine associated liver injury on admission

Patient	1	2	3	4, First exposure	4, Second exposure	5	6
ALT (<35 IU/l)	1,399	2,476	1,371	986	1,216	775	2,902
AST (<32 IU/l)	1,643	2,059	1,181	330	759	630	2,089
AP (40–129 IU/l)	303	173	138	123	177	143	165
GGT (<39 IU/l)	503	680	182	228	223	282	140
ALT/AP (*R* ratio)	18.6	52.8	36.6	29.5	23.7	20.0	64.8
Prothrombin time INR (0.9–1.25)	1.81	1.53	1.7	1.16	1.13	1.1	3.65
Total bilirubin (<17 μmol/l)	168	555	218	48	70	26	597
Leukocyte count (<11.3×10^9/l)	10.8	6,8	4.3	4.2	4.3	4.2	4.7
ANA (<1:40)	1:80	Negative	1:160	Negative	Negative	1:80	Negative
SMA (<1:40)	1:80	Negative	1:80	n/a	n/a	1:40	Negative

ALT serum alanine aminotransferase, *AST* aspartate aminotransferase, *AP* alkaline phosphatase, *GGT* gamma-glutamyl transpeptidase, *INR* international normalized ratio, *ANA* anti-nuclear antibodies, *SMA* smooth muscle actin antibodies, *n/a* not assessed. *R* ratio = (ALT/ULN)/(AP/ULN); *ULN* upper limit of normal [7]

(ANA) titers were found in two patients, there was no further serological or clinical evidence to support a diagnosis of autoimmune hepatitis.

Histopathology of liver biopsies

One patient was biopsied a second time after an accidental reexposure to flupirtine, another patient received a liver transplant without a previous biopsy resulting in six biopsies and one explanted liver for histological review. Liver biopsies from all patients were adequate containing at least ten portal tracts. All biopsies showed a necroinflammatory picture. Necrosis exhibited a strict zonal character with perivenular (zone 3) hepatocellular dropout and red blood cell congestion within dilated sinusoids. Abundant ceroid-laden macrophages were present in all cases. At the edge of the necrotic zone there was swelling of single hepatocytes, acidophil bodies as well as occasional mitotic figures illustrating injury, apoptosis and ongoing regeneration, respectively. In four cases, that showed severe injury, there was central–central and also central–portal bridging necrosis illustrated by a collapsed reticulin network. When bridging necrosis extended to the portal areas, it was associated with a mild to marked ductular reaction (patients 1, 2, 3 and 6). Patient 6 showed almost complete collapse of reticulin network with only scattered surviving areas of liver parenchyma and formation of periportal neoductuli indicative of regenerative activity. The inflammatory infiltrate comprised mainly lymphocytes and a variable proportion of plasma cells and eosinophils. The density of the infiltrate was variable as was the presence of portal inflammation and interface hepatitis. There was no correlation with borderline ANA titers that were present in two patients. Steatosis was not observed. Based on

Table 3 Histological features of six patients with flupirtine-associated liver injury

Patient	1	2	3	4, First exposure	4, Second exposure	5	6
Lobular disarray	++	+++	++	+++	+++	++	
Necrosis, location	c–c; c–p	c–c; c–p	c–c; c–p	c–c	c–c	c–c	c–c; c–p
Necrosis, % of depicted area	25%	25%	30%	10%	10%	20%	95%
Lobular inflammation	+	+++	+	+	+++	+	++
Portal inflammation	+	+++	++	−	+++	+	++
Plasma cells	−	++	+	+	+++	−	++
Eosinophils	+	++	+	+	+++	+	−
Ceroid-macrophages	+++	++	+++	+++	−	++	+++
Interface hepatitis	+	++	++	−	+++	−	++
Ductular reaction	++	+	++	−	−	−	+++
Acidophil bodies	+	++	+++	+	+++	+	++
Fibrosis	−	+	+	−	−	−	−
Canalicular cholestasis	+	−	−	−	−	−	−

c–c central–central, *c–p* central–portal; + mild, ++ moderate, +++ marked, − absent

In acidophil bodies: + 1–3/average high power field (avhpf), ++ 4–6/avhpf, +++ >6/avhpf

In interface activity: + focal, ++ <50% portal circumference, +++ >50% portal circumference

In eosinophils: + 1–3/avhpf, ++ 4–6/avhpf, +++ >6/avhpf

the morphological appearance the differential diagnosis of an autoimmune hepatitis with a predominately perivenular activity was entertained in one case. The extent of necrosis (in percentage of depicted area as well as the occurrence of central–portal bridging necrosis) was largest in patients presenting with hyperbilirubinaemia and elevated INR (patients 1, 2, 3 and 6). Deposition of delicate collagenous fibers within the necrotic areas was noted in two patients. Canalicular cholestasis was noted in one focus in the biopsy from patient 1. In patient 4 a second liver biopsy after reexposure to flupirtine showed a striking infiltration by plasma cells and eosinophils and no prominent ceroid macrophages when compared to the first biopsy (Table 3). Salient histological features are depicted in Fig. 2 and additional histological pictures from each patient are available in the supplementary material.

Outcome

The average follow up was 16 months (range, 5–55 months; median, 9 months). ALT and AST levels, INR, platelets and bilirubin were within normal limits in all patients. None of the patients developed signs of other underlying liver disease. Patient 6, who underwent liver transplantation, is alive without evidence of transplant dysfunction. Except for flupirtine patients continued to take at least part of their previous medication (see Table 2).

Discussion

Our aim was to investigate the clinical and histological findings of flupirtine-associated liver injury in order to identify a pattern that would aid in prompt recognition of

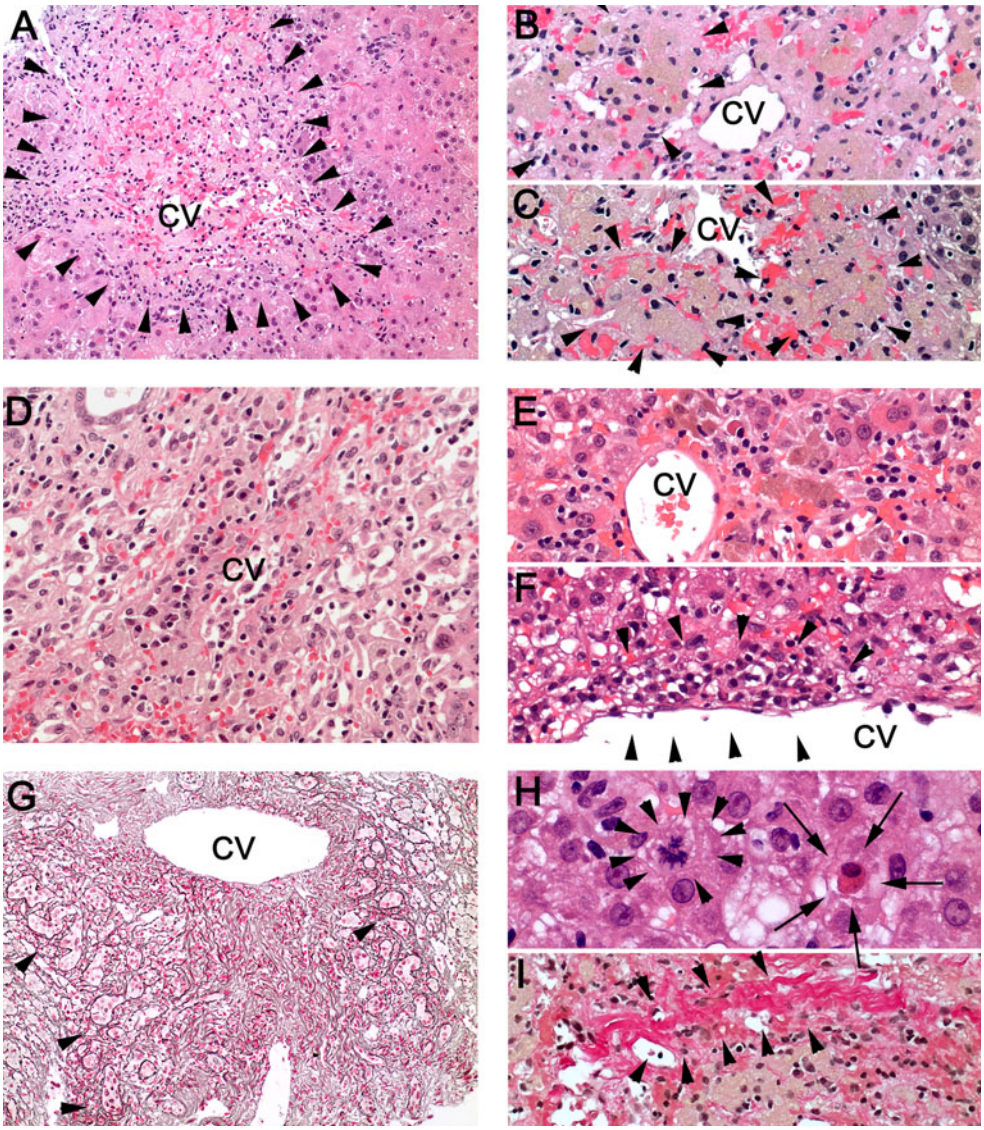

Fig. 2 Histopathology of flupirtine-associated liver injury. **a** Confluent zone 3 necrosis around the central vein (CV) with abundant ceroid-laden macrophages, patient 3 (*arrowheads*: necrotic zone, haematoxylin and eosin (H/E), ×100). **b** and **c** Collections of ceroid macrophages with tan/greenish cytoplasm in necrotic zone, patients 1 and 3, respectively (*arrowheads*: ceroid macrophages, H/E, ×200). **d** Panlobular necrosis with ceroid laden macrophages, patient 6 (H/E, ×200). **e** and **f** Zone 3 necrosis in patient 4 at first and second exposure, respectively (*arrowheads*: collections of plasma cells, H/E, ×200). **g** Collapse of reticulin network in central–portal bridging necrosis with ductular reaction, patient 1 (*arrowheads*: ductular reaction, reticulin silver (*RS*), ×100). **h** Hepatocytes and apoptotic (*arrows*) and mitotic (*arrowheads*) activity, patient 2 (H/E, ×400). **i** Deposition of collagen fibers within zone 3 necrosis, patient 3 (Elastica van Gieson, ×200)

future cases. Analysis of drug-induced hepatic injury depends on the reliability of identifying the correct causative agent in the studied series. Five out of six patients took prescribed drugs other than flupirtine at the time of presentation. Flupirtine was the only common drug in all patients. All five patients who recovered shared characteristic histological features on liver biopsies and identical clinical courses after discontinuation of flupirtine. The patient who required liver transplantation showed similar features, only that necrosis was far more pronounced. Using the international consensus score (RUCAM) flupirtine causality was "probable" in four cases and "highly probable" in two cases. In one case, ultimate proof of flupirtine causality was provided by accidental reexposure. Patients continued to take most of the other medication after the event without any evidence of liver injury. Therefore flupirtine has to be regarded as the causative drug in our series.

Morphological features shared by all initial biopsies were centrolobular necrosis with prominent ceroid (or "pigment-laden") macrophages. Zone 3 necrosis is commonly seen with many intrinsic and idiopathic hepatotoxins [6]. The presence of ceroid-laden macrophages is a common feature in liver injury related to halogenated hydrocarbons or dihydralazine [10, 11, 26–28]. Except for the latter prominent collections of macrophages can be encountered in NSAID-associated liver injury, but were a less constant feature in a larger series [29]. NSAID-associated liver injury is usually associated with pronounced hepatocellular swelling and a dense inflammatory infiltrate creating a chronic hepatitis-like picture [29, 30]. An additional lymphocytic infiltrate was seen in several of our patients. It remains unclear, if these were reactive or a major mediator of hepatocellular necrosis. However the plasma cell rich hepatitis after reexposure in one patient suggests that an immune-mediated mechanism may contribute to hepatocellular damage. There was no evidence of autoimmune hepatitis in any of our patients. None of the patients showed signs of congestive heart failure, a recognized cause of zone 3 necrosis that may have entered the differential diagnosis. Clinical signs of systemic hypersensitivity as observed in halothane-hepatitis were not present in our series. The presence of apoptotic as well as regenerative activity and ductular reaction at the edge of the necrotic zones with cellular debris suggests incessant liver damage prior to clinical presentation. The clinical course of patient 6 that necessitated liver transplantation differs from the remainder of the series. It remains unclear if this was due to non-symptomatic liver damage before clinical presentation or if this reflects different kinetics of hepatocellular injury in this patient. The presence of regenerative features illustrated by the ductular reaction suggests liver damage prior to the onset of symptoms.

Flupirtine associated liver injury appears to be rare given its widespread use. Until September 2007, 151 cases of flupirtine associated liver injury including 70 cases of hepatitis have been reported and the need for surveillance of liver function tests after initiation of treatment has been postulated [24]. During a clinical trial of 100 patients receiving flupirtine for 5–7 days, elevated liver enzymes and bilirubin levels were observed in three patients [22]. Our patients became symptomatic after a longer time of exposure and showed more advanced injury. The median latency (time to admission after drug initiation) in our series was 4 months (3 weeks to 24 months), which is long in comparison to hepatotoxicity caused by other drugs. Therefore a dose-dependent mechanism is unlikely and flupirtine-mediated liver injury has to be classified as idiosyncratic or type B reaction [31].

Our patients illustrate the difficulty in assessing cause-and-effect relationship in DILI. Drugs often show a consistent pattern of clinical, laboratory and histological features when causing idiosyncratic hepatotoxic reactions, also referred to as "drug's signature" [32]. Although the mechanism of flupirtine-induced liver injury remains to be elucidated, this study has identified some common morphological and clinical features of flupirtine associated hepatotoxicity that may assist in recognition of future cases. Flupirtine should therefore be included in the list of drugs capable of causing severe liver injury in rare instances. The monitoring of liver function in patients taking flupirtine is warranted.

Conflicts of interest The authors have no conflicts to declare.

References

1. Hoofnagle JH (2004) Drug-induced liver injury network (DILIN). Hepatology 40(4):773. doi:10.1002/hep.20445
2. Kaplowitz N (2007) Drug-induced liver disease. In: Kaplowitz N, DeLeve LD (eds) Drug-induced liver disease, 2nd edn. Informa Healthcare, New York, pp 1–13
3. Bell L, Chalasani N (2009) Epidemiology of idiosyncratic drug-induced liver injury. Semin Liver Dis 29(04):337–347. doi:10.1055/s-0029-1240002
4. De Valle MB, Av Klinteberg V, Alem N, Olsson R, Bjornsson E (2006) Drug-induced liver injury in a Swedish University hospital out-patient hepatology clinic. Aliment Pharmacol Ther 24 (8):1187–1195. doi:10.1111/j.1365-2036.2006.03117.x
5. Hussaini SH, O'Brien CS, Despott EJ, Dalton HR (2007) Antibiotic therapy: a major cause of drug-induced jaundice in southwest England. Eur J Gastroenterol Hepatol 19(1):15–20. doi:10.1097/01.meg.0000250581.77865.68
6. Kanel GC (2007) Histopathology of drug-induced liver disease. In: Kaplowitz N, DeLeve LD (eds) Drug-induced liver disease, 2nd edn. Informa Healthcare, New York, pp 237–290
7. Fontana RJ, Seeff LB, Andrade RJ, Bjornsson E, Day CP, Serrano J, Hoofnagle JH (2010) Standardization of nomenclature and causality

assessment in drug-induced liver injury: summary of a clinical research workshop. Hepatology 52(2):730–742. doi:10.1002/hep.23696
8. Danan G, Benichou C (1993) Causality assessment of adverse reactions to drugs—I. A novel method based on the conclusions of international consensus meetings: application to drug-induced liver injuries. J Clin Epidemiol 46(11):1323–1330
9. Kleiner DE (2009) The pathology of drug-induced liver injury. Semin Liver Dis 29(4):364–372. doi:10.1055/s-0029-1240005
10. Ramachandran R, Kakar S (2009) Histological patterns in drug-induced liver disease. J Clin Pathol 62(6):481–492. doi:10.1136/jcp.2008.058248
11. MacSween RNM, Burt AD, Portmann BC, Ferrell LD (2007) MacSween's pathology of the liver, 5th edn. Elsevier, Churchill Livingstone, Philadelphia
12. Zimmerman HJ, Lewis JH, Ishak KG, Maddrey WC (1984) Ticrynafen-associated hepatic injury: analysis of 340 cases. Hepatology 4(2):315–323
13. Neuberger J, Williams R (1989) Immune mechanisms in tienilic acid associated hepatotoxicity. Gut 30(4):515–519
14. Pothmann R, Lobisch M (2000) Acute treatment of episodic childhood tension-type headache with flupirtine and paracetamol — a double-blind crossover-study. Schmerz 14(1):1–4. doi:10.1007/s004820000058
15. Muller-Schwefe GH, Uberall MA (2007) Analgesic and muscle tonus normalizing effect of flupirtine retard in chronic back pain. MMW Fortschr Med 149(43):47
16. Goodchild CS, Nelson J, Cooke I, Ashby M, Jackson K (2008) Combination therapy with flupirtine and opioid: open-label case series in the treatment of neuropathic pain associated with cancer. Pain Med 9(7):939–949. doi:10.1111/j.1526-4637.2008.00512.x
17. Schwabe U, Paffrath D (2009) Arzneiverordnungs—Report 2009: Aktuelle Daten, Kosten. Trends und Kommentare, Springer, Berlin
18. Klawe C, Maschke M (2009) Flupirtine: pharmacology and clinical applications of a nonopioid analgesic and potentially neuroprotective compound. Expert Opin Pharmacother 10 (9):1495–1500. doi:10.1517/14656560902988528
19. Hufschmidt A, Krisch A, Peschen I (2009) A girl with headache, confusion and green urine. J Neurol 256(7):1169–1170. doi:10.1007/s00415-009-5061-2
20. Hlavica P, Niebch G (1985) Pharmacokinetics and biotransformation of the analgesic flupirtine in humans. Arzneimittelforschung 35(1):67–74
21. Friedel HA, Fitton A (1993) Flupirtine. A review of its pharmacological properties, and therapeutic efficacy in pain states. Drugs 45(4):548–569
22. Li C, Ni J, Wang Z, Li M, Gasparic M, Terhaag B, Uberall MA (2008) Analgesic efficacy and tolerability of flupirtine vs. tramadol in patients with subacute low back pain: a double-blind multicentre trial. Curr Med Res Opin 24(12):3523–3530. doi:10.1185/03007990802579769
23. Powell-Jackson P, Williams R (1985) Use of flupirtine maleate as an analgesic in patients with liver disease. Br J Clin Pract 39 (2):63–66
24. Arzneimittelkommission der deutschen Ärzteschaft (2007) Mitteilungen: "Aus der UAW-Datenbank" Leberschäden unter Flupirtin. http://www.aerzteblatt.de/v4/archiv/artikel.asp?src=heft&id=57646. Accessed 11.04.2011
25. Klein F, Glanemann M, Rudolph B, Seehofer D, Neuhaus P (2011) Flupirtine induced hepatic failure requiring orthotopic liver transplantation. Experimental and Clinical Transplantation, in press
26. Wills EJ, Walton B (1978) A morphologic study of unexplained hepatitis following halothane anesthesia. Am J Pathol 91(1):11–32
27. Klion FM, Schaffner F, Popper H (1969) Hepatitis after exposure to halothane. Ann Intern Med 71(3):467–477
28. Benjamin SB, Goodman ZD, Ishak KG, Zimmerman HJ, Irey NS (1985) The morphologic spectrum of halothane-induced hepatic injury: analysis of 77 cases. Hepatology 5(6):1163–1171
29. Banks AT, Zimmerman HJ, Ishak KG, Harter JG (1995) Diclofenac-associated hepatotoxicity: analysis of 180 cases reported to the Food and Drug Administration as adverse reactions. Hepatology 22(3):820–827
30. Scully LJ, Clarke D, Barr RJ (1993) Diclofenac induced hepatitis. 3 cases with features of autoimmune chronic active hepatitis. Dig Dis Sci 38(4):744–751
31. Pirmohamed M, Breckenridge AM, Kitteringham NR, Park BK (1998) Adverse drug reactions. BMJ 316(7140):1295–1298
32. Navarro VJ, Senior JR (2006) Drug-related hepatotoxicity. N Engl J Med 354(7):731–739. doi:10.1056/NEJMra052270

Virchows Arch (2011) 458:717–724
DOI 10.1007/s00428-011-1086-x

ORIGINAL ARTICLE

Aberrant activation-induced cytidine deaminase expression is associated with mucosal intestinalization in the early stage of gastric cancer

Ayako Goto · Minako Hirahashi · Mikako Osada · Kazuhiko Nakamura · Takashi Yao · Masazumi Tsuneyoshi · Ryoichi Takayanagi · Yoshinao Oda

Received: 7 March 2011 / Revised: 13 April 2011 / Accepted: 14 April 2011 / Published online: 3 May 2011
© Springer-Verlag 2011

Abstract Although *Helicobacter pylori* is a risk factor for gastric cancer (GC), its detailed carcinogenesis remains unclear. Recently, aberrant expression of activation-induced cytidine deaminase (AID) was demonstrated in gastric epithelium with *H. pylori* infection and seems to cause the accumulation of mutation. This investigation aims to elucidate whether or not AID expression plays an important role in the carcinogenesis of early GC. We examined the correlation between immunohistochemical AID expression and histological characteristics, including pre-existing chronic gastritis and cellular mucin phenotype in 138 cases of intramucosal GC. Furthermore, we investigated the relationship between AID, p53 protein, and β-catenin. The low degree of polymorphonuclear neutrophil activity, and the high degree of glandular atrophy and intestinal metaplasia were significantly correlated with the high levels of AID expression in non-neoplastic mucosa (P=0.007, P≤0.001, and P=0.003). With regard to mucin phenotype of carcinoma, the intestinal phenotype tended to have the higher AID expression levels (P=0.052). AID showed close correlations with Cdx2 and nuclear staining of β-catenin (P=0.003, P=0.034). As for p53 protein, no correlation was found with AID expression. Our findings suggest that aberrant AID expression is correlated with persistent inflammatory condition induced by *H. pylori* infection and may contribute to the development of GC through an inflammatory condition and intestinalization.

Keywords Intramucosal gastric adenocarcinoma · Activation-induced cytidine deaminase · Cdx2 · *Helicobacter pylori*

A. Goto · M. Hirahashi (✉) · M. Osada · M. Tsuneyoshi · Y. Oda
Department of Anatomic Pathology, Pathological Sciences,
Graduate School of Medical Sciences, Kyushu University,
Maidashi 3-1-1, Higashi-ku,
Fukuoka 812-8582, Japan
e-mail: mi-hira@surgpath.med.kyushu-u.ac.jp

Y. Oda
e-mail: oda@surgpath.med.kyushu-u.ac.jp

A. Goto · M. Osada · K. Nakamura · R. Takayanagi
Department of Medicine and Bioregulatory Sciences,
Graduate School of Medical Sciences, Kyushu University,
Fukuoka, Japan

T. Yao
Department of Human Pathology,
Juntendo University School of Medicine,
Tokyo, Japan

Introduction

The histological classification of gastric adenocarcinoma is based on gland formation, such as the "intestinal" and "diffuse" types described by Lauren [1], that are generally similar to well- and poorly differentiated adenocarcinoma, respectively, according to the Japanese classification of gastric carcinoma [2]. Well-differentiated adenocarcinoma, which is associated with *Helicobacter pylori* infection, was considered to develop through sequential stages—such as chronic gastritis, atrophy, intestinal metaplasia, and dysplasia [3–7]. As for the carcinogenesis of early gastric cancer (GC), p53 mutation has been detected in 25–34% of early GC [6, 8], and the occurrence of p53 mutation has been found more in well-differentiated adenocarcinoma [9]. Furthermore, intestinal mucin phenotypic GC demonstrated more frequent p53 overexpression than the gastric mucin phenotypic GC [10].

Activation-induced cytidine deaminase (AID) is an enzyme that resides in a member of the apolipoprotein B

mRNA-editing catalytic polypeptide (APOBEC) family. AID has been reported to be essential for immunoglobulin gene diversification, which is caused by somatic hypermutation and class-switch recombination (CSR) [11]. Furthermore, aberrant AID expression has been reported to induce mutations in fibroblasts and cause not only malignant lymphomas but also of human malignancy [12, 13]. Although it remains controversial as to whether AID acts on RNA or DNA, the currently proposed hypothesis is the RNA-editing theory that AID converts cytosine nucleotides to uracils in mRNA and converted mRNA encodes an endonuclease which generates DNA cleavage [14]. The nucleotide alterations induced by AID activation were distributed across the entire transcribed regions of the TP53 gene, and some alterations that emerged in the TP53 coding region resulted in amino acid substitutions with potential functional consequences [15]. Persistent inappropriate AID expression is considered to be a genotoxic factor under an inflammatory condition [15–17]. Some investigators have revealed that cag pathogenicity island (cagPAI)-positive *H. pylori* infection triggers aberrant expression of AID in gastric epithelium and that this expression leads to the accumulation of nucleotide alterations in *p53*, *K-ras*, and *β-catenin* genes [18–20]. However, no clinicopathological studies have assessed the relationship between histological background and aberrant AID expression in GC.

The current study aims to clarify the correlation between clinicopathological findings and aberrant AID expression in early-phase GC and in the non-neoplastic gastric mucosa by immunohistochemistry. We also assess the relationship between AID expression and histological or mucin phenotype, as well as the background conditions of gastric mucosa.

Materials and methods

Materials and histological evaluation

We selected 138 cases of sporadic and primary intramucosal gastric cancer (GC) surgically resected at Kyushu University and its affiliated hospitals between 1999 and 2007. These included 66 males and 72 females, ranging in age from 24 to 86 years (median, 64 years). None of the patients had received chemotherapy or radiation therapy before surgery. In addition, our cases included no autoimmune gastritis, chemical reactive gastritis, and postoperative gastritis, and none had received eradication therapy. Histological classification was carried out according to the Japanese Research Society for Gastric Cancer [2]. GC consisted of 53 pure well-differentiated adenocarcinomas (well-differentiated type), 66 pure poorly differentiated and signet-ring cell carcinomas (poorly differentiated type), and 19 well-differentiated adenocarcinomas with a poorly differentiated adenocarcinoma component (mixed type). There were 14 elevated and 124 depressed lesions. The tumors ranged from 2 to 9.2 cm in size (median, 2 cm). Two of the carcinomas were in the upper third, 76 in the middle third, and 60 in the lower third of the stomach. There was one lymphatic permeation and no venous invasion. Four patients had lymph node metastasis, and the frequency of lymph node metastasis was equal to that in the epidemiological analysis of Japanese intramucosal gastric cancer [21], although five other cases were lost to follow-up. The resected tissue specimens were fixed in 10% buffered formalin and embedded in paraffin. This study was approved by the institutional ethics committee of Kyushu University.

Evaluation of the chronic gastritis in the non-neoplastic mucosa

We analyzed the non-neoplastic mucosa around the cancer as the background gastric mucosa [22]. We then evaluated five histological factors—(1) *H. pylori* density, (2) polymorphonuclear neutrophil activity, (3) degree of chronic inflammation, (4) degree of glandular atrophy, and (5) degree of intestinal metaplasia—according to the updated Sydney system (1994) [23]. *H. pylori* infection was detected by immunohistochemical staining (anti-*H. pylori*, B0471; dilution 1/200; Dako, Carpinteria, CA, USA). The above five factors ware divided into two groups according to score: low group (scores 0 and 1) and high group (scores 2 and 3).

Immunohistochemical staining of AID, cellular mucin phenotype, CDX2, p53, and β-catenin

Immunohistochemical staining was carried out using monoclonal antibodies to AID (ZA001; dilution 1/100; Zymed Laboratories, San Francisco, CA, USA), MUC5AC, MUC6, MUC2 (CLH2, CLH5, Ccp58; dilution 1/200; Novocastra, Newcastle, UK), Cdx2 (CDX2-88; dilution 1/100; Biogenex, San Ramon, CA, USA), p53 (Pab1801; dilution 1/500; Oncogene Research Products, Cambridge, MA, USA), and β-catenin (14; dilution 1/200; Transduction Laboratories, Lexington, KY, USA). Sections were cut to a thickness of 4 μm, deparaffinized in xylene, and dehydrated in descending dilutions of ethanol. Antigen retrieval was performed by using a pressure cooker at 120°C (Decloaking Chamber; Biocare Medical, Walnut Creek, CA, USA) in a BORG Decloaker (Biocare Medical) for 5 min (AID), and by using a microwave heating in citrate buffer (pH 6.0) for 20 (CDX2, p53, and β-catenin) or 30 min (MUC2, MUC5AC, and MUC6). Endogenous peroxidase activity was blocked by 30 min of incubation with 0.3% hydrogen peroxidase in absolute methanol. Background staining was minimized by incubation with 1% normal rabbit serum for 10 min. Sections were incubated for 120 min at room air temperature with a primary antibody and 3% nonfat milk (AID) or overnight at

4°C with a primary antibody (MUC2, MUC5AC, MUC6, CDX2, p53, and β-catenin), followed by reacting with a streptavidin–biotin–peroxidase kit (Nichirei, Tokyo, Japan). Diaminobenzidine tetrahydrochloride was used as the chromogen. Finally, sections were counterstained with Mayer's hematoxylin.

We estimated cellular mucin phenotype, Cdx2, and β-catenin of GC. We examined AID in both GC and the non-neoplastic mucosa.

As for AID, tonsil and lymph nodes were used as positive controls, and negative controls were performed by omitting the primary antibody. Others have reported that AID protein was a nucleocytoplasmic shuttling protein with NLA and NES in its N and C termini, respectively, but located mainly in the cytoplasm [18, 24]. Immunoreactivity was scored according to the summation of the number of stained elements (0=no staining; 1=up to 5% stained cells; 2=>5% to 10% stained cells; 3=>10% to 25% stained cells; 4=>25% to 50% stained cells; 5=>50% stained cells) and cytoplasmic staining intensity (0=no expression; 1+=weak expression; 2+=strong expression) in the gastric cancer and the non-neoplastic mucosa around the cancer, respectively. We used some lymphocytes of germinal centers in lymphoid follicles as internal positive controls because they were mostly activated B cells and were strongly stained throughout the specimens. We defined 2+ as when the cytoplasm was stained the same or more than germinal centers. The immunohistochemical expression levels of AID were classified as low expression (score is ≦4) and high expression (score was ≧5).

The expression levels of Cdx2 and p53 were interpreted as positive when nuclear staining was observed in more than 10% of the carcinoma cells [25].

The results of cytoplasmic staining of MUC5AC, MUC6, and MUC2 were interpreted as positive when more than 10% of the carcinoma cells were stained [22, 25, 26]. These phenotypes were classified into four categories according to the combination of the expression of MUC5AC, MUC6, and MUC2. The gastric phenotype was positive for MUC5AC or MUC6 and negative for MUC2. In contrast, the intestinal phenotype exhibited expression of MUC2 but not of MUC5AC or MUC6. The mixed phenotype exhibited expression of MUC5AC or MUC6, and additionally MUC2. The unclassified phenotype exhibited no expression of any antibodies [25, 27].

Membranous expression of β-catenin was designated as preserved (3+) when >60% of tumor cells were stained, similar to the case in normal gastric mucosa; moderately reduced (2+) when 20–60% of tumor cells were positive; highly reduced (1+) when 5–20% of tumor cells were stained; and no or very weak dotted staining (−) when <5% of all tumor cells were stained [28]. Nuclear expression of β-catenin defined brown staining of the nucleus as positive, regardless of membranous or cytoplasmic staining.

Statistical analysis

Statistical analyses were performed using Fisher's exact test, the χ^2 test, analysis of variance, and the Mann–Whitney test using JMP Statistical Discovery software (version 7.0; SAS Inc., Cary, NC, USA). A P value <0.05 was considered statistically significant.

Results

Relationship between AID expression and the degree of the chronic gastritis in the non-neoplastic mucosa

AID expression was rarely seen in the gastric mucosa without chronic active inflammation, glandular atrophy, and intestinal metaplasia. AID expression occasionally expressed in the gastric proper glands within the inflamed gastric mucosa without atrophy and intestinal metaplasia. On the other hand, AID was strongly expressed mainly in the deep portion of atrophic gastric mucosa with intestinal metaplasia (Fig. 1). The cause of this phenomenon is unclear, but AID expression may be localized in the proliferative zone.

Table 1 summarized the correlations between the chronic gastritis and AID expression levels in the non-neoplastic gastric mucosa. The histological incidence of *H. pylori* infection was 63.0% (87/138 cases), and the AID expression levels were not correlated with the presence or absence of *H. pylori* infection (P=0.619). The low degree of polymorphonuclear neutrophil activity, and the high degree of glandular atrophy and intestinal metaplasia were significantly correlated with the high AID expression levels (P=0.007, P≤0.001, and P=0.003). The degree of *H. pylori* density and chronic inflammation had no significant difference between AID expression percentages (P=0.365 and P=0.128).

Relationship between AID expression in gastric cancer and clinicopathological findings

The clinicopathological findings in GC are summarized in Table 2. The immunohistochemical AID expression levels of GC were higher in the depressed type (P=0.039). Although lymph node metastasis was very rare, all four cases with nodal metastasis had higher AID expression percentages of GC (P=0.036). When we classified gastritis status into normal (*H. pylori*-negative cases), active *H. pylori*-gastritis (*H. pylori*-positive cases with prominent neutrophilic infiltration, such as the high degree of polymorphonuclear neutrophil activity and the low degree of glandular atrophy and intestinal metaplasia), and atrophic *H. pylori*-gastritis (*H. pylori*-positive cases with prominent atrophic change and intestinal metaplasia, such

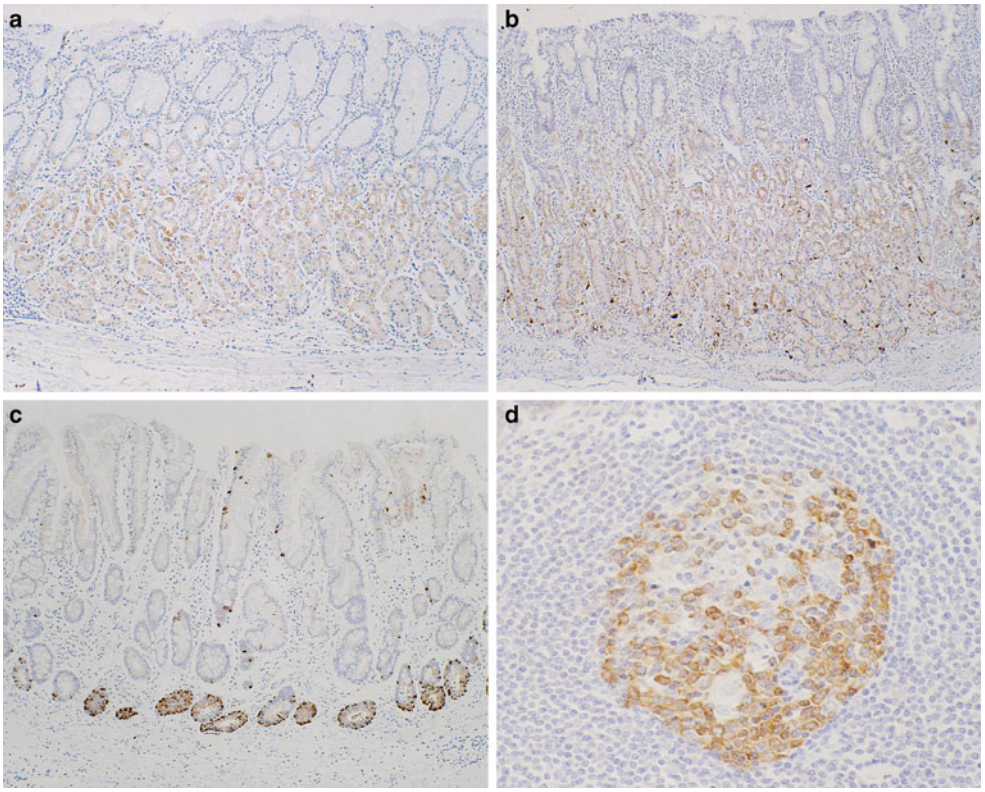

Fig. 1 Representative histological features of the non-neoplastic gastric mucosa by AID immunostaining. In gastric normal mucosa without inflammation (**a**), AID-positive cells are scattered throughout the fundic glands with inflammation (**b**). In severely atrophic mucosa with intestinal metaplasia, immunoreactivity of AID is prominent in the deep portion of glands (**c**). AID immunostaining of a germinal center in lymphoid follicles (**d**). (original magnification—**a**, **b**, and **c**, ×40; **d**, ×400)

as the low degree of polymorphonuclear neutrophil activity and the high degree of glandular atrophy and intestinal metaplasia), AID expression levels in GC showed no significant difference in gastritis status (P=0.340). There was no significant relationship between AID expression and other clinicopathological findings, including age, gender, tumor size, tumor location, or histological differentiation (Table 2). One case with lymphatic permeation showed a high AID expression.

Table 1 Relationship between AID expression and the degree of chronic gastritis in the non-neoplastic gastric mucosa

Factors	AID expression		*P* value
	Low (n=118)	High (n=20)	
Helicobacter pylori density			0.365
Low (n=112)	94	18	
High (n=26)	24	2	
Polymorphonuclear neutrophil activity			0.007
Low (n=70)	54	16	
High (n=68)	64	4	
Chronic inflammation			0.128
Low (n=47)	37	10	
High (n=91)	81	10	
Glandular atrophy			<0.001
Low (n=73)	70	3	
High (n=65)	48	17	
Intestinal metaplasia			0.003
Low (n=56)	54	2	
High (n=82)	64	18	

Relationship between AID expression and mucin phenotype, expression of Cdx2, p53, and β-catenin in gastric cancer

The correlation between AID status and mucin phenotype or cancer-associated protein is summarized in Table 3. With regard to mucin phenotype of GC, the intestinal and mixed phenotype, which were positive for MUC2, had higher AID expression levels, compared with the gastric phenotype, which was negative for MUC2 (P=0.052). Moreover, Cdx2 expression was significantly correlated with the high AID expression levels of GC (P=0.003) (Fig. 2). There was no significant relationship between AID and p53 expression of GC (P=0.275). Membranous expression of β-catenin was relatively preserved regardless of AID expression levels (P=0.894). In contrast, there was a significant relationship between AID expression percentage and nuclear staining of β-catenin (P=0.034).

Discussion

We investigated whether and how AID is expressed in the early stage of GC. The current study revealed that AID was

Table 2 Relationship between AID expression in gastric cancer and clinicopathological findings

Factors	AID expression		*P* value
	Low (*n*=107)	High (*n*=31)	
Age (years)			0.839
<64 (*n*=67)	51	16	
≥64 (*n*=70)	55	15	
Gender			0.839
Male (*n*=72)	55	17	
Female (*n*=66)	52	14	
Tumor size			0.878
<2.0 cm (*n*=64)	50	14	
≥2.0 cm (*n*=74)	57	17	
Tumor location			0.717
Upper third (*n*=2)	2	0	
Middle third (*n*=76)	58	18	
Lower third (*n*=60)	47	13	
Microscopic type			0.039
Elevated type (*n*=14)	14	0	
Depressed type (*n*=124)	93	31	
Histological differentiation			0.404
Well-differentiated type (*n*=53)	38	15	
Mixed type (*n*=19)	16	3	
Poorly differentiated type (*n*=66)	53	13	
Lymph node metastasis[a]			0.036
− (*n*=129)	102	27	
+ (*n*=4)	1	3	
Gastritis status[b]			0.340
Normal (*n*=51)	43	8	
Active *H. pylori* gastritis (*n*=39)	29	10	
Atrophic *H. pylori* gastritis (*n*=48)	35	13	

[a] Five cases were lost to follow-up

[b] Normal: [*H. pylori* (−)], active *H. pylori* gastritis: [*H. pylori* (+) with prominent neutrophilic infiltration], atrophic *H. pylori* gastritis: [*H. pylori* (+) with prominent atrophic change and intestinal metaplasia]

expressed not only in GC but also in the non-neoplastic mucosa with atrophy and intestinal metaplasia. We also detected a strong correlation between AID expression percentages and Cdx2 or nuclear β-catenin expression of GC. In the non-neoplastic gastric mucosa, we demonstrated that the high AID expression levels were frequently associated with the low degree of polymorphonuclear neutrophil activity, and the high degree of glandular atrophy and intestinal metaplasia. We failed to reveal the relationship between AID expression levels and the histological grade of *H. pylori* density or chronic inflammation. The gastric mucosa infected by *H. pylori* has been to be marked by severe atrophic

Table 3 Relationship between AID expression and mucin phenotype, expression of Cdx2, p53, and β-catenin

Factors	AID expression		*P-value*
	Low (n=103)	High (n=31)	
Phenotypic classification			0.052*
Gastric phenotype (n=50)	43	7	
Intestinal phenotype (n=20)	13	7	*
Mixed phenotype (n=60)	44	16	
Unclassified phenotype (n=8)	7	1	
Cdx2 expression			0.003
Negative (n=90)	77	13	
Positive (n=48)	30	18	
p53 expression			0.275
Negative (n=94)	70	24	
Positive (n=44)	37	7	
Nuclear expression of β-catenin			0.034
Negative (n=105)	86	19	
Positive (n=33)	21	12	

*The gastric phenotype vs. the intestinal and mixed phenotype, which were positive for MUC2

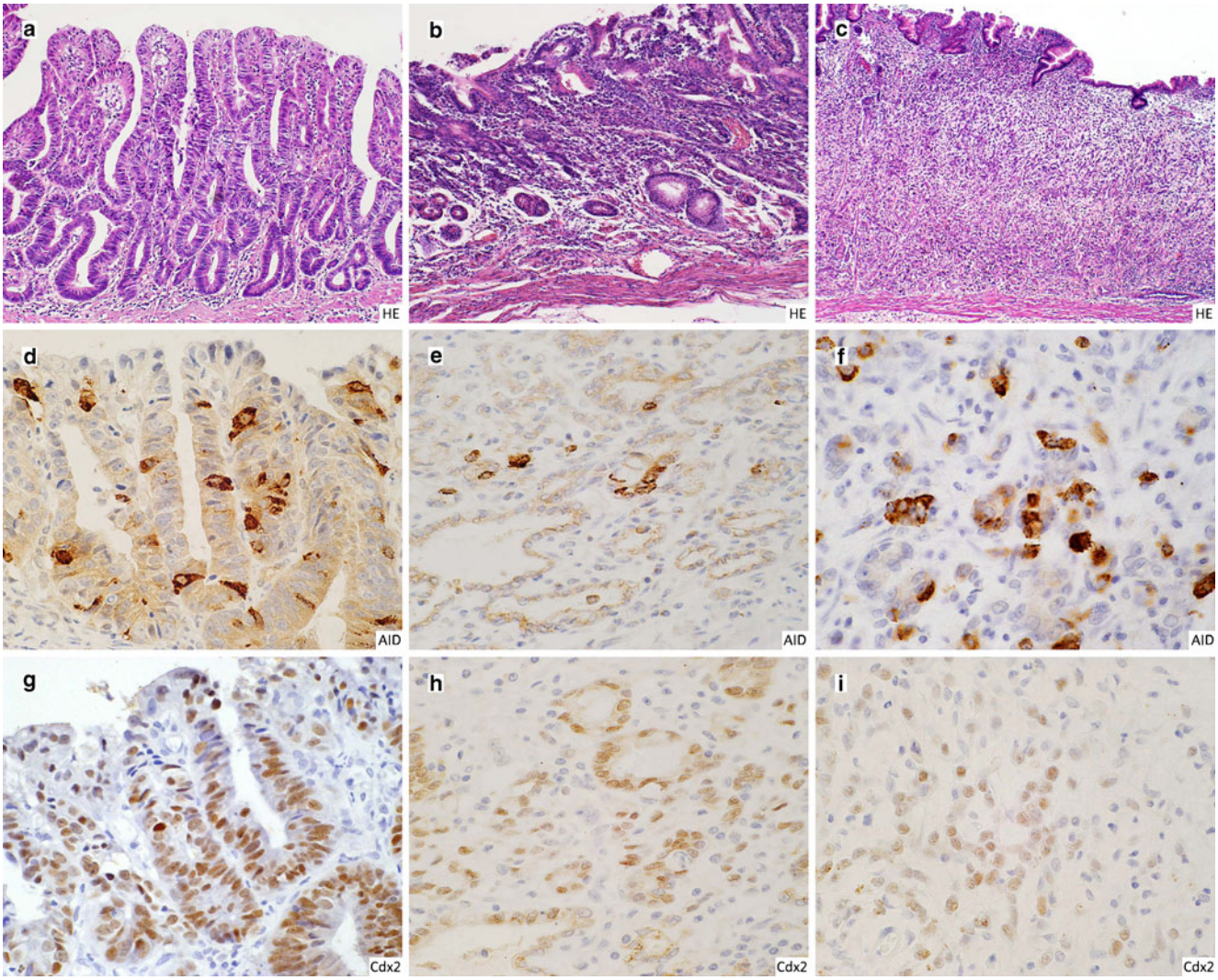

Fig. 2 Significant correlation between Cdx2 and AID expression in early gastric cancer. Hematoxylin and eosin staining (**a**, **b**, **c**) and positive staining for AID (**d**, **e**, **f**) and Cdx2 (**g**, **h**, **i**) immunostaining. Well-differentiated adenocarcinoma (**a**, **d**, **g**). Well-differentiated adenocarcinoma with poorly differentiated adenocarcinoma component/mixed type (**b**, **e**, **h**). Poorly differentiated adenocarcinoma (**c**, **f**, **i**)

changes with intestinal metaplasia. However, *H. pylori* cannot survive in the metaplastic mucosa, so, some cases, which show no *H. pylori* infection but have atrophy and intestinal metaplasia in pathological findings, have a possibility to be the *H. pylori* false-negative cases [5, 28, 29]. The degree of atrophy and intestinal metaplasia, regarded as precancerous condition [7], is a reliable parameter of a persistent inflammatory condition induced by *H. pylori* infection. So, aberrant AID expression in non-neoplastic gastric mucosa may have a genotoxic effect linking a persistent inflammatory condition, as well as in the case of hepatocellular carcinoma, cholangiocarcinoma, and colitis-associated colorectal cancer [18–20].

The present study showed no significant relationship between the nuclear p53 expression and the AID expression percentages of GC. The p53 tumor suppressor gene plays a role in control of cell proliferation, and the loss of its function has been found in various human malignancies, including primary human gastric cancer [6, 8–10]. Even if p53 nuclear accumulation is negative by immunohistochemistry, *p53* mutation is present in gastric intestinal metaplasia (25–37.5%) [9, 30, 31]. We found that aberrant AID-positive cells exist in the mainly inferior layer of intestinal metaplasia of the non-neoplastic mucosa as well as carcinoma, and these findings raise the possibility that aberrant AID expression induces genetic alterations of the *p53* gene in non-neoplastic mucosa, especially the intestinal metaplasia.

In the present study, the high AID expression levels were significantly correlated with Cdx2 expression. The homeoprotein Cdx2 is important for the early differentiation and maintenance of intestinal epithelial cells, and ectopic Cdx2 expression induces intestinal metaplasia in esophageal and

gastric epithelial cells [32, 33]. Additionally, Cdx2 activates the expression of the MUC2 mucin gene [32], an intestinal phenotype marker, and Cdx2 expression indicates intestinalization. Therefore, we considered that AID expression is related to mucosal intestinalization.

As for carcinogenesis, Cdx2 inhibits cell proliferation and plays a role as a tumor suppressor in colorectal and pancreas cells [34, 35]. In some reports, Cdx2-positive cases showed an improved survival rate in gastric cancer [25]. Meanwhile, other authors have reported that all Cdx2-transgenic mice have gastric polyps developing from long-term intestinal metaplasia, and these polyps contain well-differentiated adenocarcinoma, which reveals *APC* gene mutations, as well as nuclear staining of β-catenin [36, 37]. Furthermore, one investigator revealed that human well-differentiated adenocarcinoma with intestinal phenotype shows the nuclear expression of β-catenin and an association with APC promoter hypermethylation [26]. In the current study, the high AID expression levels were frequently positive for both Cdx2 and β-catenin within the nuclei. Our results also suggest that the high AID expression levels had the potential to cause the development of adenocarcinoma with the intestinal phenotype through the Cdx2 pathway.

In conclusion, we found that aberrant AID expression has a relationship with a persistent inflammatory condition induced by *H. pylori* infection in the background gastric mucosa, and that AID may play an important role in intestinalization of gastric mucosa and cancer. Furthermore, AID-positive cells may play some role in carcinogenesis under a persistent inflammatory condition or through the Cdx2 pathway.

Acknowledgments The authors thank Ms. Y. Kamitani for her technical assistance. The English used in the manuscript was revised by Miss K. Miller (Royal English Language Centre, Fukuoka, Japan).

Conflict of interest statement We declare that we have no conflict of interest.

References

1. Lauren P (1965) The two histological main types of gastric carcinoma: diffuse and so-called intestinal-type carcinoma. Acta Pathol Microbiol Immunol Scand 64:31–49
2. Japanese Research Society of Gastric Cancer (2010) Japanese classification of gastric carcinoma, 14th edn. Kanehara, Tokyo, p 8
3. Correa P (1992) Human gastric carcinogenesis: a multistep and multifactorial process—First American Cancer Society Award Lecture on cancer epidemiology and prevention. Cancer Res 52:6735–6740
4. IARC monographs on the evaluation of carcinogenic risks to humans (1994) Schistosomes, liver flukes and *Helicobacter pylori*. WHO Lyon 61:1–241
5. Uemura N, Okamoto S, Yamamoto S et al (2001) *Helicobacter pylori* infection and the development of gastric cancer. New Engl J Med 345:784–789
6. Tajima Y, Yamazaki K, Makino R et al (2006) Gastric and intestinal phenotypic marker expression in early differentiated type tumors of the stomach: clinicopathologic significance and genetic background. Clin Cancer Res 12:6469–6479
7. Sugiyama T (2004) Development of gastric cancer associated with *Helicobacter pylori* infection. Cancer Chemother Pharmacol 54 (1):S12–S20
8. Maeda K, Onoda N, Ogawa M et al (1998) Expression of p53 and vascular endothelial growth factor associated with tumor angiogenesis and prognosis in gastric cancer. Oncology 55:594–599
9. Fenoglio-Preiser CM, Wang J, Stemmermann GN et al (2003) TP53 and gastric carcinoma: a review. Hum Mutat 21:258–270
10. Sasaki I, Yao T, Nawata H et al (1999) Minute gastric carcinoma of differentiated type with special reference to the significance of intestinal metaplasia, proliferative zone, and p53 protein during tumor development. Cancer 85:1719–1729
11. Muramatsu M, Sankaranand VS, Anant S et al (1999) Specific expression of activation-induced cytidine deaminase (AID), a novel member of the RNA-editing deaminase family in germinal center B cells. J Biol Chem 274:18470–18476
12. Okazaki I, Hiai H, Kakazu N et al (2003) Constitutive expression of AID leads to tumorigenesis. J Exp Med 2:1173–1181
13. Kinoshita K, Nonaka T (2006) The dark side of activation-induced cytidine deaminase: relationship with leukemia and beyond. Int J Hematol 83:201–207
14. Shivarov V, Shinkura R, Doi T et al (2009) Molecular mechanism for generation of antibody memory. Phil Trans R Soc B 364:569–575
15. Endo Y, Marusawa H, Kou T, Nakase H et al (2008) Activation-induced cytidine deaminase between inflammation and the development of colitis-associated colorectal cancers. Gastroenterology 135:889–898
16. Endo Y, Marusawa H, Kinoshita K, Morisawa T et al (2007) Expression of activation-induced cytidine deaminase in human hepatocytes via NF-κB signaling. Oncogene 26:5587–5595
17. Komori J, Marusawa H, Machimoto T et al (2008) Activation-induced cytidine deaminase links bile duct inflammation to human cholangiocarcinoma. Hepatology 47:888–896
18. Matsumoto Y, Marusawa H, Kinoshita K et al (2007) *Helicobacter pylori* infection triggers aberrant expression of activation-induced cytidine deaminase in gastric epithelium. Nat Med 13:470–476
19. Morisawa T, Marusawa H, Ueda Y et al (2008) Organ-specific profiles of genetic changes in cancers caused by activation-induced cytidine deaminase expression. Int J Cancer 123:2735–2740
20. Kim C, Song J, Cho Y et al (2007) Activation-induced cytidine deaminase expression in gastric cancer. Tumor Biol 339:333
21. Nakajima T, Yamaguchi T (eds) (2006) Gannkenn Igan Database 1946–2004 (Cancer Institute Hospital Gastric Cancer Database, 1946–2004) (in Japanese). Kanehara, Tokyo, 37
22. Kabashima A, Yao T, Sugimachi K et al (2000) Gastric or intestinal phenotypic expression in the carcinomas and background mucosa of multiple early gastric carcinomas. Histopathology 37:513–522
23. Dixon MF, Genta RM, Yardley JH et al (1996) The participants in the international workshop on the histopathology of gastritis, Houston 1994. Classification and grading of gastritis: the updated Sydney system. Am J Surg Pathol 20:1161–1181
24. Ito S, Nagaoka H, Shinkura R et al (2004) Activation-induced cytidine deaminase shuttles between nucleus and cytoplasm like apolipoprotein B mRNA editing catalytic polypeptide 1. PNAS 101:1975–1980
25. Kumashiro Y, Yao T, Aishima S et al (2007) Hepatoid adenocarcinoma of the stomach: histogenesis and progression in association with intestinal phenotype. Hum Pathol 38:857–863
26. Son HL, Hyun JK, Dong-Hun S et al (2009) Expression of beta-catenin and its mechanism of delocalization in intestinal-type early gastric cancer based on mucin expression. Histol Histopathol 24:831–838

27. Yao T, Akira K, Toshio K et al (1999) The phenotypes of the gastric carcinoma—evaluation by a new immunohistochemical method. Stomach Intestine 34:477–485
28. Grabsch H, Takeno S, Noguchi T et al (2001) Different patterns of b-catenin expression in gastric carcinomas: relationship with clinicopathological parameters and prognostic outcome. Histopathology 39:141–149
29. Kato S, Matsukura N, Tsukada K et al (2007) *Helicobacter pylori* infection-negative gastric cancer in Japanese hospital patients: incidence and pathological characteristics. Cancer Sci 98:790–794
30. Siano Y, Rugge M, Correa P et al (1994) p53 Alteration in gastric precancerous lesions. Am J Pathol 144:511–517
31. Ochiai A, Yamaguchi Y, Hirohasu S (1996) p53 Mutation in the non-neoplastic mucosa of the human stomach showing intestinal metaplasia. Int J Cancer 69:28–33
32. Mesquita P, Jonckheere N, Almeida R et al (2003) Human MUC2 mucin gene is transcriptionally regulated by Cdx homeodomain proteins in gastrointestinal carcinoma cell lines. J Biol Chem 278:51549–51556
33. Philip R, Debruyne, Matthew W et al (2006) Bile acids induce ectopic expression of intestinal guanylyl cyclase C through nuclear factor-kB and Cdx2 in human esophageal cells. Gastroenterology 130:1191–1206
34. Bai YQ, Miyake S, Iwai T et al (2003) CDX2, a homeobox transcription factor, upregulates transcription of the p21/WAF1/CIP1 gene. Oncogene 22:5998–6005
35. Takahashi K, Hirano F, Matsumoto K et al (2009) Homeobox gene CDX2 inhibits human pancreatic cancer cell proliferation by down-regulating cyclin D1 transcriptional activity. Pancreas 38:49–57
36. Kim HS, Lee JS, Freund JN et al (2006) CDX-2 homeobox gene expression in human gastric carcinoma and precursor lesions. J Gastroenterol Hepatol 21:438–442
37. Mutoh H, Sakurai S, Satoh K et al (2004) Development of gastric carcinoma from intestinal metaplasia in Cdx2-transgenic mice. Cancer Res 64:7740–7747

Virchows Arch (2011) 458:725–731
DOI 10.1007/s00428-011-1085-y

ORIGINAL ARTICLE

Differential expression of MYC in *H. pylori*-related intestinal and diffuse gastric tumors

Isabelle Joyce de Lima Silva-Fernandes · Markênia Kélia Santos Alves · Valeska Portela Lima · Marcos Antônio Pereira de Lima · Marcos Aurélio Pessoa Barros · Márcia Valéria Pitombeira Ferreira · Silvia Helena Barem Rabenhorst

Received: 3 February 2011 / Revised: 10 April 2011 / Accepted: 11 April 2011 / Published online: 3 May 2011
© Springer-Verlag 2011

Abstract Evidence suggests that the carcinogenic process guided by *Helicobacter pylori* is related to the expression of cell cycle and apoptosis proteins as BCL-2, BAX, and MYC. However, the literature is conflicting regarding the expression frequency in the histological subtypes and did not consider *cag*A gene presence. To investigate the expression of these proteins considering the histological subtypes of gastric cancer associated with *H. pylori* (*cag*A), a total of 89 cases were used. *H. pylori* infection and *cag*A status were determined by PCR. Immunodetection was performed for MYC, BCL-2, and BAX proteins. *H. pylori* was found in 95.5% of the patients, among them, 65.8% were *cag*A(+). Nuclear MYC was detected in 36.4%, BAX in 55.7%, while BCl-2 in just 5%. Nuclear MYC staining was significantly lower in the intestinal than diffuse subtype ($p=0.008$) and was related with the presence of *H. pylori* *cag*A(+). Additionally, most of the few cases cytoplasmic MYC positive were in the intestinal subtype. In diffuse tumors, although most nuclear MYC positive cases were *cag*A(+), it was not significant. No difference was observed between BCL-2 or BAX expression considering the presence of *cag*A gene in the histological subtypes. It seems that MYC could be relevant for the diffuse tumorigenic pathway associated with *H. pylori* and possibly influenced by the presence of *cag*A gene, while in intestinal tumors, the tumorigenic pathway does not occur through the MYC expression.

Keywords Gastric cancer · *H. pylori* · *cag*A · MYC

I. J. L. Silva-Fernandes (✉) · M. K. S. Alves · V. P. Lima · M. A. P. de Lima · M. V. P. Ferreira · S. H. B. Rabenhorst
Department of Pathology and Forensic Medicine, Microbiology and Pathologic Section, Federal University of Ceará State, 60183-630, Fortaleza, Brazil
e-mail: isabellejoyce@gmail.com

M. A. P. Barros
Santa Casa de Misericórdia Hospital Fortaleza, Fortaleza, Brazil

Introduction

Gastric carcinoma is the fourth most common cancer worldwide, and in Brazil, it is a relevant cause of cancer mortality [1, 2]. Adenocarcinomas, the most frequent gastric tumors, are classified by Laurén [3] into intestinal and diffuse subtypes, which differ regarding their epidemiological and prognostic features [4] and develop through distinct genetic pathways [5, 6].

Gastric cancer has a multifactorial etiology [7] and *Helicobacter pylori* is the major etiologic risk [8]. Evidence suggests that the presence of virulence factors could be responsible for the organism's ability to cause different diseases. In fact, only 1–2% of the population infected with *H. pylori* will develop gastric cancer [9]. This bacterium has a great genetic diversity, and strains carrying the *cag*A gene are strongly associated with the development of gastric cancer [10]. However, despite some advances, the pathway associated with *H. pylori* in gastric pathogenesis remains poorly understood. For a better understanding of this process, several studies have investigated specific patterns in the expression of apoptosis or cell cycle-related proteins such as BCL-2, BAX, and MYC, associated with the carcinogenic process guided by *H. pylori.*

BCL-2 and BAX are members of the BCL-2 family. BAX is a cytosolic monomer in viable cells, but during apoptosis it changes its conformation, integrates into the outer mitochondrial membrane, and oligomerizes. In contrast, antiapoptotic BCL-2 prevents BAX activation/oligomerization

and consequently inhibits mitochondrial proapoptotic events [11, 12].

Overexpression of BCL-2 suppresses cell proliferative activity in human gastric carcinomas and is correlated with less aggressive biological behavior [13]. The difference in BCL-2 protein expression in the Lauren subtypes is controversial. Xu et al. demonstrated that BCL-2 expression was higher in the diffuse subtype [14], but Liu et al. showed that it was higher in the intestinal subtype [15]. As for BCL-2, there is no consensus on the relevance of BAX expression in any of the Lauren histological [12]. Besides, Ashktorab et al. observed that BAX is translocated from the cytoplasm to the mitochondria, triggering apoptosis in cells infected with *H. pylori* [11]. However, the relationship of these proteins and *H. pylori* infection in gastric cancer is still controversial, and the majority of reports have not considered the bacterial genotype.

MYC plays a key role in the regulation of cell cycle progression and apoptosis. The *MYC* gene, located on human chromosome 8q24, encodes a transcriptional factor involved in proliferation, growth, and apoptosis [16, 17]. It is tightly regulated in normal cells and is only expressed during embryogenesis and in tissue compartments that possess high proliferative capacity, while having a short half-life. In human tumors, its expression is frequently enhanced. Deregulated expression of MYC occurs in a broad range of human cancers, indicating a key role in tumor progression [18, 19]. Several studies have demonstrated *MYC* gene amplification and increased protein expression in precancerous gastric lesions and in gastric cancer [17, 20]. The increase in MYC expression has also been associated with *H. pylori* infection in adenocarcinomas [5].

Therefore, the aim of this study was to investigate whether there are differences in the expression of BCL-2, BAX, and MYC proteins in adenocarcinomas in association with the *cagA* genotype of *H. pylori*, also considering the histological subtypes. The identification of a characteristic genetic pattern in gastric tumors may help predict prognosis and may be helpful in therapeutic research.

Materials and methods

Patients and specimens

This study was approved by the ethics committee of the Federal University of Ceará. A total of 89 surgically resected adenocarcinoma specimens were obtained from two hospitals in Fortaleza, Ceará State, Brazil: Walter Cantideo Hospital at Federal University of Ceará and Santa Casa de Misericórdia Hospital. Fragments of tumor were collected during the gastrectomies and frozen at −80°C. Representative formalin-fixed tumor specimens were selected and histological sections (5 μm) were made for immunohistochemical assays. The histological diagnoses and tumor classification were based on Lauren's criteria.

DNA extraction, *H. pylori* urease C and *cag*A gene detection

Genomic DNA was extracted from frozen tumor tissue samples consisting mainly (>80%) of tumor cells using the cetyltrimethyl ammonium bromide method adapted from Foster and Twell [21]. *H. pylori* infection was detected by amplification of the *urease*C gene using specific primers and conditions, as previously described by Lage et al. [22]. The *cag*A gene was identified using the primers described by Domingo et al. [23]. Negative (water) and positive (case *H. pylori/cag*A positive) controls were assayed in each run. PCR products were separated on 6% polyacrylamide electrophoretic gels, silver stained, and considered *H. pylori*(+) and *cag*A(+) when fragments of 294 and 297 bp, respectively, were present.

Immunohistochemistry

MYC protein expression was determined in all 85 cases while expression of BCL-2 and BAX was analyzed in only 70 cases due to the unavailability of material for such analysis. Immunostaining was performed according to the protocol previously described by Lima et al. using the following primary antibodies: Bcl-2 clone 124, mouse, dilution 1:80; Bax, polyclonal, rabbit, dilution 1:400 (both from DakoCytomation); and MYC, clone 9E10, mouse, dilution 1:80, from Labvision [24]. The reaction was developed with the LSAB + system (DakoCytomation) according to the manufacturer's recommendation.

Histopathological and immunostaining analysis

The histological classification was obtained from the medical reports and was confirmed by a pathologist on our team. The cases with mixed pattern were re-evaluated and the prevalent tumor pattern was considered. The slides were independently evaluated by three experienced technicians using light microscopy at ×400 magnification. Specimens were considered positive for related proteins if they demonstrated ≥5% stained tumor cells.

Statistical analysis

All statistical analyses were conducted using the SPSS® 15.0 version statistical software program (SPSS, Chicago, IL, USA) using the χ^2 and Fisher's exact tests. Correlations were analyzed using Spearman's correlation coefficient and considered statistically significant at $p<0.05$.

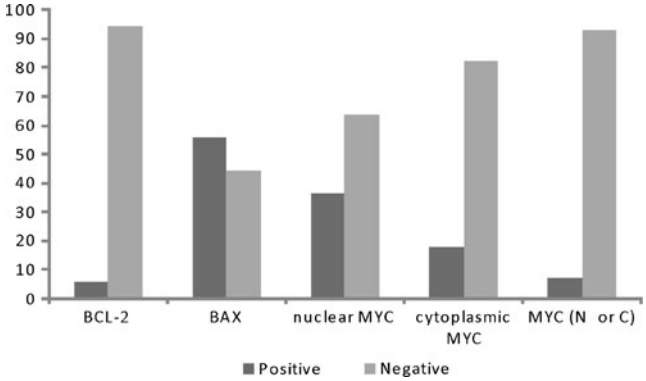

Fig. 1 Frequency of immunostaining of MYC, BCL-2, and BAX in gastric adenocarcinomas. (*N*) nuclear MYC; (*C*) cytoplasmic MYC

Results

Of the 89 tumor samples analyzed, 61 (71%) were from males and 24 (28%) from females. The average age was 56.5 years (range 23–90 years old). *H. pylori* was found in 95.5% (85/89) of the patients. Among them, 65.8% (56/85) were *cag*A(+). *H. pylori*-negative tumors were not considered for the *H. pylori* association because this was not the subject of this study and also because of the small number of cases. Of the *H. pylori* positive cases, the intestinal subtype was more frequent (63.5%, 54/85) than the diffuse (36.4%, 31/85). Most of the cases (60%) were in advanced grade (III–IV). BAX protein was detected in 55.7% of the cases (39/70), while BCL-2 was detected in just 5.7% (4/70) (Fig. 1). MYC staining was observed in the nucleus (36.4%; 31/85) or in the cytoplasm (17.6%; 15/85) and co-localization occurred in 7% (6/85) of the cases with a total of 47% (40/85) of MYC staining.

No correlation was found between BCL-2, BAX, and MYC in the total samples. However, considering each histological subtype, there was a negative correlation in the diffuse tumors between nuclear MYC and BAX positivity ($r=-0.395$; $p=0.038$). Conversely, despite the few cases that were BCL-2 positive, a probable association between BCL-2 and cytoplasmic MYC was demonstrated by a significant positive correlation between them ($r=0.801$; $p=0.000$). No significant correlation was observed in the intestinal subtype.

Table 1 shows the frequencies of positive cases for BCL-2, BAX, and MYC distributed according to histological subtype. There was a difference between these tumors only with respect to nuclear MYC immunostaining, where a significantly lower detection ($p=0.008$) was observed in the intestinal subtype (74%, 40/54) than the diffuse subtype (45%, 14/31). When the positivity of MYC was considered independent of the stain location (cytoplasmic/nuclear), no statistically significant difference was found.

To verify if the frequency of BCL-2, BAX, and MYC protein expression is influenced by the presence of *H. pylori cag*A(+), we distributed the data considering this aspect. Table 2 shows that most cases infected with *H. pylori* cagA(+) were negative for nuclear MYC (83%, 31/37) in the intestinal subtype, contrasting with a substantial nuclear MYC positivity (63%) in the diffuse tumors (Fig. 2a, b). Indeed, among the intestinal tumors, there were significantly fewer cases of *H. pylori cag*A(+) with nuclear MYC immunoreactivity ($p=0.023$) than cases of *H. pylori cag*A(−). This difference was not observed in the diffuse tumors.

Considering only the cases of *H. pylori cag*A(+), regarding to MYC expression (Fig. 3, Table 3), a significant difference between the intestinal and diffuse tumors seen before (shown in Table 2) was confirmed ($p\leq0.001$), and also the absence of either MYC cytoplasmic or nuclear MYC expression remained associated with the intestinal tumors ($p=0.028$). Positivity was similar in both histological subtypes regardless of the pattern of MYC staining (C + N), and no difference was observed when only the cytoplasm staining was analyzed (intestinal $p=0.876$; diffuse $p=0.672$). However, the few cases (15) with only MYC cytoplasmic staining, most of them (12/15; 80%) were in the intestinal subtype as seen in Table 1.

Table 1 Frequency of positive cases of markers in histological subtypes

		Intestinal *n* (%)	Diffuse *n* (%)	Total *n* (%)	*p* Value
MYC (N)	+	14/54 (26)	17/31 (55)	31/85 (36.4)	0.008*
	−	40/54 (74)	14/31 (45)	54/85 (63)	
MYC (C)	+	12/54 (22.2)	03/31 (9.6)	15/85 (17.6)	0.144
	−	42/54 (77)	28/31 (90)	70/85 (82)	
MYC (N and C)	+	22/54 (40.7)	18/31 (58)	40/85 (47)	0.123
	−	32/54 (59.2)	13/31 (42)	45/85 (53)	
BCL-2	+	01/41 (2.4)	03/29 (10)	4/70 (5.7)	0.160
	−	40/41 (97)	26/29 (89)	66/70 (94)	
BAX	+	21/41 (51)	18/29 (62)	39/70 (55.7)	0.368
	−	20/41 (48)	11/29 (37)	31/70 (44)	

N nuclear staining, *C* cytoplasmic staining

* $p<0.05$

Table 2 Frequency of detection of markers between the histological subtypes

		Intestinal				Diffuse			
		*cag*A+*n* (%)	*cag*A−*n* (%)	Total *n* (%)	*p* Value	*cag*A+*n* (%)	*cag*A−*n* (%)	Total *n* (%)	*p* Value
MYC (*N*)	+	6/37 (16)	8/17 (47)	14/54 (25)	0.023*	12/19 (63)	05/12 (41)	17/31 (54)	0.242
	−	31/37 (83)	9/17 (52)	40/54 (74)		07/19 (36)	07/12 (58)	14/31 (45)	
MYC (*C*)	+	08/37 (21)	04/17 (23)	12/54 (22)	0.876	02/19 (10)	01/12 (8.3)	03/31 (9)	0.672
	−	29/37 (78)	13/17 (76)	42/54 (77)		17/19 (89)	11/12 (91)	28/31 (90)	
BCL-2	+	1/27 (3)	0/14 (0)	1/41 (2)	0.659	02/17 (11)	01/12 (8.3)	03/29 (10)	0.633
	−	26/27 (96)	14/14 (100)	40/41 (97)		15/17 (88)	11/12 (91)	26/29 (89)	
BAX	+	13/27 (48)	8/14 (57)	21/41 (51)	0.585	09/17 (52)	09/12 (75)	18/29 (62)	0.208
	−	14/27 (51)	06/14 (42)	20/41 (4)		08/17 (47)	03/12 (25)	11/29 (37)	

N nuclear staining, *C* cytoplasmic staining

* $p<0.05$

Discussion

In this work, almost all (95.5%, 85/89) of the cases were from *H. pylori*-infected patients. This high incidence is in agreement with other studies of gastric cancer either using PCR, in which *H. pylori* was detected in 95% [25] and 100% [26] of cases, or using serology [27] where *H. pylori* was identified in 94% of specimens.

Currently, a research challenge is to identify the pathways by which *H. pylori* can contribute to gastric carcinogenesis. Several studies have focused on markers related to cell proliferation control and apoptosis. In fact, there are consistent data regarding an association between the presence of the bacterium and *TP53* mutation and a decrease in p27 protein expression influenced by *H. pylori* genotype [28–31]. However, the data are controversial regarding the influence of *H. pylori* or its genotype on the expression of key regulatory genes of apoptosis, such as BAX and BCL-2.

Konturek et al. showed that *H. pylori* infection is associated with increased BAX and decreased BCL-2 protein expression in duodenal ulcer patients [32]. Conversely, another study by the same author in gastric cancer patients demonstrated an increased protein expression of BCL-2 and decreased expression of BAX with no association with *H. pylori* infection [33]. In a cell culture study, Yang et al. observed that the presence of *H. pylori* has suppressed the BCL-2 protein expression [34]. Considering the presence of *cag*A(+), Cabral et al. showed that the infection caused by *H. pylori cag*A(+) was related to the increased expression of BAX in patients with *H. pylori*-related gastritis [35]. However, Zhu et al. using cultured cells, showed that *H. pylori cag*A(+) did not alter BCL-2 or BAX expression [36].

In the present study, few cases were BCL-2 positive. As all the cases were *H. pylori*(+), this low frequency agrees with the findings of Yang et al. in which *H. pylori* downregulates BCL-2 [34]. Additionally, the cases in the present study were mainly represented by more malignant tumors, and according to Xu et al. the peak of BCL-2 expression occurs in the early stages and lowers in progressive gastric cancer [14]. However, in our study we intended to evaluate the importance of genotype comparing the difference with strains carrying the *cag*A gene, since this gene is associated with more aggressive lesions and risk for gastric cancer development [37]. Therefore, we classified the data according to the presence of *H. pylori*

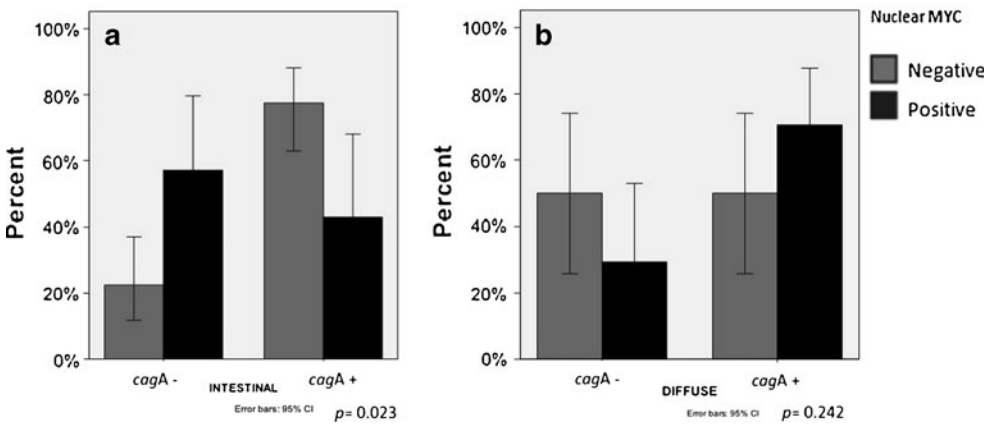

Fig. 2 Nuclear MYC immunostaining in intestinal and diffuse subtypes, considering the presence of the *H. pylori* cagA gene. *$p<0.05$

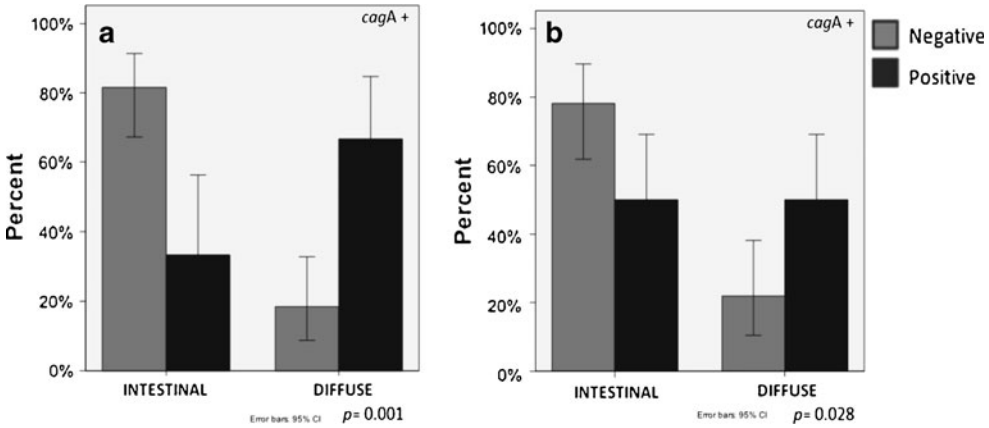

Fig. 3 Analysis of the difference in detection of MYC in cases *H. pylori cag*A (+) strains. **a** Nuclear staining; **b** nuclear and cytoplasmic staining. *$p<0.05$; **$p<0.01$

*cag*A. From this analysis, we did not detect any significant difference between BCL-2 and BAX expression according to *H. pylori cag*A status, which is in agreement with the findings of Zhu et al. [36].

Few papers have analyzed BCL-2 and BAX protein expression patterns considering the histological subtypes. As in this study, van der Woude et al. and Lee et al. did not observe any difference in BCL-2 or BAX immunostaining between intestinal and diffuse subtypes [12, 13]. Alternatively, Xu et al. found that BCL-2 positivity was higher in diffuse tumors [14]. Although none of these studies considered *H. pylori* infection, in our study, we found no association between *cag*A status and BAX or BCL-2 positivity according to the histological subtype. Thus, divergence in BCL-2 and BAX protein expression does not depend on the presence of the *cag*A gene and is not specific for a histological subtype.

Yang et al. in a cell culture study suggested the involvement of *H. pylori*-induced apoptosis by increasing BAX and MYC expression and decreasing BCL-2 expression [34]. However, in diffuse tumors, we observed a significant negative association between nuclear MYC and BAX and a positive correlation between BCL-2 and cytoplasmic MYC. Considering these results, it seems that the MYC protein expression in diffuse tumors is not influenced by *cag*A presence.

Recently, the expression of MYC has been regarded as an important alteration in gastric tumorigenesis, also, Kim et al. showed that the combined expression of MYC with EGFR and FGFR2 could predict overall survival and time to progression of chemotherapy-treated gastric cancer patients [38]. However, the exact role of MYC in gastric cancer is not well-established. Our study agree with Calcagno et al. and Zhang et al. that showed that MYC expression was higher in *H. pylori*-associated cases of gastric cancer than without infection [17, 20]. Additionally, our findings showed that the lack of MYC detection was associated with the presence of the *cag*A gene. This finding is in agreement with that of Bach et al. whose study in AGS cells showed that *MYC* was downregulated when coincubated with *cag*A(+) and upregulated by up to 6.8-fold when coincubated with mutant *cagA*(−) [39].

There is still controversy regarding the histological type that prevails in the expression of MYC. In the present study, we found a significantly higher number of negative cases more associated with intestinal tumors than with diffuse tumors. This result is in contrast to the findings of Xu et al., where MYC levels were higher in the intestinal than in the diffuse subtype [14], and of Calcagno et al. where MYC protein was present in both subtypes with all intestinal tumors showing nuclear MYC staining [17]. However, only seven cases were analyzed in the latter

Table 3 MYC, BCL-2 and BAX immunostaining frequencies in both histological subtypes considering the presence of the *cag*A gene

		*cag*A+strains			
		Intestinal *n* (%)	Diffuse *n* (%)	Total *n* (%)	*p* Value
MYC (N)	+	06/37 (16)	12/19 (63)	18/56 (32)	0.001*
	−	31/37 (83)	7/19 (36)	38/56 (67)	
MYC (C)	+	8/37 (21)	2/19 (10)	10/56 (17)	0.262
	−	29/37 (78)	17/19 (89)	46/56 (82)	
BCL-2	+	01/27 (3)	02/17 (11)	3/44 (6)	0.329
	−	26/27 (96)	15/17 (88)	41/44 (93)	
BAX	+	13/27 (48)	09/17 (52)	22/44 (50)	0.757
	−	14/27 (51)	08/17 (47)	22/44 (50)	

N nuclear staining, *C* cytoplasmic staining

*$p<0.05$

study. Although these studies indicated that the deregulation of MYC expression is a characteristic of intestinal tumors, the discrepancy can be explained by the fact that they did not consider the presence of *H. pylori* or *cag*A or differentiate between nuclear and cytoplasmic MYC staining.

In fact, in the *cag*A + cases, nuclear positivity of MYC was more associated with the diffuse subtype (63%), although with no statistical difference, while the negativity was significantly associated with the intestinal subtype (83%). Previously, our research group showed the relevance of MYC in diffuse type tumors where it was associated with p27 negativity [6]. Since the histological subtypes act through different carcinogenic pathways, our findings indicate that in a relevant number of cases of the intestinal tumors, the carcinogenesis process *H. pylori*-related does not occur through the MYC protein expression. Interestingly, the observation that most of the few cytoplasmic MYC positive cases were in the intestinal subtype and were associated with the presence of *cag*A + (8/12, 66.7%), suggest that in these few tumors there is a blockage in the transport of MYC protein through the nuclear membrane. Additional studies of the molecular events (transcriptional or post-transcriptional level) are required to better understand this and other molecular markers involved in the gastric cancer carcinogenesis process considering the *H. pylori* and *cag*A gene.

In this report, we emphasize the difference between intestinal and diffuse tumors. The data indicate that in diffuse tumors, the *H. pylori*-associated tumorigenic pathway occurs preferentially through the MYC protein but not in the intestinal tumors. Also, nuclear and cytoplasmic MYC detection was categorized, since MYC protein plays a role as a transcription factor only in the nucleus. Thus, the expression of MYC related to a specific subtype of gastric tumor may help to elucidate the distinct carcinogenic pathways of these tumors and could work as therapeutic target.

Conflicts of interest The authors declare that they have no conflicts of interest.

References

1. Costa-Raiol L, Figueira-Silva E, Mendes-da-Fonseca D, Leal M, Guimarães A, Calcagno D, Khayat A, Assumpção P, Smith M, Burbano R (2008) Interrelationship between MYC gene numerical aberrations and protein expression in individuals from northern Brazil with early gastric adenocarcinoma. Cancer Genet Cytogenet 181:31–35
2. Hatakeyama M (2009) *Helicobacter pylori* and gastric carcinogenesis. J Gastroenterol 44:239–248
3. Lauren P (1965) The two histological main types of gastric carcinoma: diffuse and so-called intestinal-type carcinoma. Acta Pathol Microbiol Scand 64:31–49
4. Kountouras J, Zavos C, Chatzopoulos D, Katsinelos P (2008) New aspects of *Helicobacter pylori* infection involvement in gastric oncogenesis. J Surg Res 146:149–158
5. Calcagno D, Leal M, Assumpcao P, Smith M, Burbano R (2008) MYC and gastric adenocarcinoma carcinogenesis. World J Gastroenterol 14:5962–5968
6. Alves M, Lima V, André A, Ferreira M, Barros M, Rabenhorst S (2010) p27(KIP1) expression in gastric cancer: differential pathways in the histological subtypes associated with *Helicobacter pylori* infection. Scand J Gastroenterol 45:409–420
7. Bir F, Calli-Dermikan N, Tufan-Akbulut A, Satiroglu-Tufan N (2007) Apoptotic cell death and its relationship to gastric carcinogenesis. World J Gastroenterol 13:3183–3188
8. Wang C, Yuan Y, Hunt R (2007) The association between *Helicobacter pylori* infection and early gastric cancer: a meta-analysis. Am J Gastroenterol 102:1789–1798
9. Wen S, Moss S (2009) *Helicobacter pylori* virulence factors in gastric carcinogenesis. Cancer Lett 282:1–8
10. Atherton J, Cao P, Peek R, Tummuru M, Blaser M, Cover T (1995) Mosaicism in vacuolating cytotoxin alleles of *Helicobacter pylori*. Association of specific vacA types with cytotoxin production and peptic ulceration. J Biol Chem 270:17771–17777
11. Ashktorab H, Frank S, Khaled R, Durum S, Kifle B, Smoot D (2004) Bax translocation and mitochondrial fragmentation induced by *Helicobacter pylori*. Gut 53:805–813
12. van der Woude C, Kleibeuker J, Tiebosch A, Homan M, Beuving A, Jansen P, Moshage M (2003) Diffuse and intestinal type gastric carcinomas differ in their espression of apoptosis related proteins. J Clin Pathol 56:699–702
13. Lee H, Lee H, Yang H, Kim W, Lee K, Choe K, Kim J (2003) Prognostic significance of Bcl-2 and p53 expression in gastric cancer. Int J Coloretal Dis 18:518–525
14. Xu A, Li S, Liu J, Gan A (2001) Function of apoptosis and expression of the proteins Bcl-2, p53 and C-myc in the development of gastric cancer. World J Gastroenterol 7:403–406
15. Liu H, Liu W, Fang D, Men R (1998) Expression of bcl-2 protein in gastric carcinoma and its significance. World J Gastroenterol 4:228–230
16. Pelengaris S, Khan M, Evan G (2002) c-MYC: more than just a matter of life and death. Nat Rev Cancer 2:764–776
17. Calcagno D, Leal M, Seabra A, Khayat A, Chen E, Demachki S, Assumpção P, Faria M, Rabenhorst S, Ferreira M, Smith M, Burbano R (2006) Interrelationship between chromosome 8 aneuploidy, C-MYC amplification and increased espression in individuals from northern Brazil with gastric adenocarcinoma. World J Gastroenterol 12:6207–6211
18. Pelengaris S, Khan M (2003) The many faces of c-MYC. Arch Biochem Biophys 416:129–136
19. Faria M, Patrocínio R, Moraes-Filho M, Rabenhorst S (2006) Expressão das proteínas BCL-2 e BAX em tumores astrocíticos humanos. Jornal Brasileiro de Patologia e Medicina Laboratorial 4:271–278
20. Zhang G, Gu Y, Zhao Z, Xu S, Zhang H, Wang H, Hao B (2004) Coordinate increase of telomerase activity and c-Myc expression in *Helicobacter pylori*-associated gastric diseases. World J Gastroenterol 10:1759–1762
21. Foster G, Twell D (eds) (1996) Plant gene isolation: principles and practice. Wiley, New York
22. Lage A, Godfroid E, Fauconnier A, Burette A, Butzler J, Bollen A, Glupczynski Y (1995) Diagnosis of *Helicobacter pylori* infection by PCR: comparison with other invasive techniques and detection of *cag*A gene in gastric biopsy specimens. J Clin Microbiol 33:2752–2756
23. Domingo D, Alarcon T, Prieto N, Sanchez I, Lopez-Brea M (1999) cagA and vacA status of Spanish *Helicobacter pylori* clinical isolates. J Clin Microbiol 37:2113–2114

24. Lima V, Lima M, André A, Ferreira M, Barros M, Rabenhorst S (2008) *H pylori* (Cag A) and Epstein-Barr vírus infection in gastric carcinomas: correlation with p53 mutation and c-Myc, Bcl-2 and Bax expression. World J Gastroenterol 14:884–891
25. Thomazini C, Pinheiro N, Pardini M, Naresse L, Rodrigues M (2006) *Helicobacter pylori* and gastric cancer: distribution of cagA and vacA genotypes in patients with gastric carcinoma. J Bras Patol Med Lab 42:25–30
26. Saribasak H, Salih B, Yamaoka Y, Sander E (2004) Analysis of *Helicobacter pylori* genotypes and correlation with clinical outcome in Turkey. J Clin Microbiol 42:1648–1651
27. Nomura A, Stemmermann G, Chyou P, Kato I, Perez-Perez G, Blaser M (1991) *Helicobacter pylori* infection and gastric carcinoma among Japanese Americans in Hawaii. N Engl J Med 325:1132–1136
28. Yu J, Leung W, Ng E, To K, EbertM Go M, Chan W, Chan F, Chung S, Malfertheiner P, Sung J (2001) Effect of *Helicobacter pylori* eradication on expression of cyclin D2 and p27 in gastric intestinal metaplasia. Aliment Pharmacol Ther 15:1505–1511
29. Eguchi H, Herschenhous N, Kuzushita N, Moss S (2003) *Helicobacter pylori* increases proteasome-mediated degradation of p27kip1 in gastric epithelial cells. Cancer Res 63:4739–4746
30. Kim S, Meitner P, Konkin T, Cho Y, Resnick M, Moss S (2006) Altered expression of Skp2, c-Myc and p27 proteins but not mRNA after H. pylori eradication in chronic gastritis. Mod Pathol 19:49–58
31. André A, Ferreira M, Mota R, Ferrasi A, Pardini M, Rabenhorst S (2010) Gastric adenocarcinoma and *Helicobacter pylori*: correlation with p53 mutation and p27 immunoexpression. Cancer Epidemiol 34:618–625
32. Konturek P, Pierzchalski P, Konturek S, Meixner H, Faller G, Kirchner T, Hahn E (1999) *Helicobacter pylori* induces apoptosis in gastric mucosa through an upregulation of Bax expression in humans. Scand J Gastroenterol 34:375–383
33. Konturek P, Konturek S, Sulekova Z, Meixner H, Bielanski W, Starzynska T, Karczewska E, Marlicz K, Stachura J, Hahn E (2001) Expression of hepatocyte growth factor, transforming growth factor alpha, apoptosis related proteins Bax and Bcl-2, and gastrin in human gastric cancer. Aliment Pharmacol Ther 15:989–999
34. Yang Y, Deng C, Peng J, Wong B, Lam S, Xia H (2003) Effect of *Helicobacter pylori* on apoptosis and apoptosis related genes in gastric cancer cells. Mol Pathol 56:19–24
35. Cabral M, Mendes C, Castro L, Cartelle C, Guerra J, Queiroz D, Nogueira A (2006) Apoptosis in *Helicobacter pylori* gastritis is related to cagA status. Helicobacter 11:469–476
36. Zhu Y, Wang C, Huang J, Ge Z, Dong Q, Zhong X, Su Y, Zheng S (2007) The *Helicobacter pylori* virulence factor CagA promotes Erk1/2-mediated Bad phosphorylation in lymphocytes: a mechanism of CagA-inhibited lymphocyte apoptosis. Cell Microbiol 9:952–961
37. Ding S, O'Hara A, Denning T, Dirden-Kramer B, Mifflin R, Reyes V, Ryan K, Elliott S, Izumi T, Boldogh I, Mitra S, Ernst P, Crowe S (2004) *Helicobacter pylori* and H_2O_2 increase AP endonuclease-1/redox factor-1 in human gastric epithelial cells. Gastroenterology 127:845–858
38. Kim HK, Choi IJ, Kim CG, Kim HS, Oshima A, Yamada Y, Arao T, Nishio K, Michalowski A, Green JE (2010) Three-gene predictor of clinical outcome for gastric cancer patients treated with chemotherapy. Pharmacogenomics J. doi:10.1038/tpj.2010.87
39. Bach S, Makristathis A, Rotter M, Hirschl A (2002) Gene expression profiling in AGS cells stimulated with *Helicobacter pylori* isogenic strains (*cagA* positive or *cagA* negative). Infect Immun 70:988–992

Virchows Arch (2011) 458:733–739
DOI 10.1007/s00428-011-1078-x

ORIGINAL ARTICLE

Qualitative and quantitative alterations in the parietal cell domain in chronic gastritis

Carlos A. Rubio · Gabriella Nesi

Received: 11 January 2011 / Revised: 22 March 2011 / Accepted: 31 March 2011 / Published online: 15 April 2011
© Springer-Verlag 2011

Abstract Hematoxylin and eosin (H&E) is not an optimal stain to discriminate between parietal and chief cells in gastric biopsies; modified Giemsa (G) and toluidine blue (TB) were found more suitable stains to characterize these two cell phenotypes. Sixty-eight well-oriented sections from the fundic mucosa were stained with H&E, and with G or TB. With G or TB the normal fundic mucosa clearly displayed a parietal cell domain (PCD) and a chief-cell domain (CCD). The continuity of these two cell domains was assessed in the entire section at ×4 magnification and the thickness of the PCD. The total mucosal thickness (TMT) was measured in three different HPF at ×20 magnifications. Qualitative observations indicated that the PCD and CCD were (a) continuous in normal fundic mucosa or having slight chronic gastritis, (b) fragmented in moderate chronic gastritis, in focal glandular atrophy or focal IM or (c) absent in severe chronic gastritis, including autoimmune gastritis and extensive IM. Quantitative measurements showed that the thickness of the PCD in chronic gastritis could be (a) normal, (b) reduced by partial destruction of the parietal cell population by chronic inflammation, or (c) absent, in extensive IM or total glandular atrophy ($p<0.05$). Toluidine blue gave a better contrast between the two cell phenotypes than modified Giemsa stain. Future studies might elucidate whether qualitative and quantitative studies of toluidine blue-stained sections of the fundic mucosa are useful in monitoring the results of therapy in individual patients with chronic gastritis.

Keywords Gastric biopsies · Parietal cell domain · Chronic gastritis

C. A. Rubio (✉)
Gastrointestinal and Liver Pathology Research Laboratory,
Department of Pathology,
Karolinska Institute and University Hospital,
Building P1/03/057,
17176 Stockholm, Sweden
e-mail: Carlos.Rubio@ki.se

G. Nesi
Department of Human Pathology and Oncology,
University of Florence,
Viale G.B. Morgagni 85,
50134 Florence, Italy
e-mail: gabriella.nesi@unifi.i

Introduction

The gastric mucosa is classically subdivided into three different histological zones: the cardia, a 0–9-mm-long mucosal segment between the esophagus and the stomach; the fundus, built with oxyntic glands; and the antrum with antro-pyloric glands [1]. In recent years, several authors have questioned the identity of the cardia mucosa claiming that it is not a natural mucosal phenotype but rather a metaplastic transformation resulting from protracted acid reflux into the esophageal mucosa [2]. The latter notion was recently substantiated by studies carried out in nonhuman primates [3].

The fundic or oxyntic mucosa is assembled with mucus-secreting foveolar cells, hydrochloric acid–intrinsic factor-producing parietal cells, pepsin-secreting chief cells and endocrine cells, predominantly ECL cells and few EC and X cells [1].

Sections from the normal fundic mucosa stained with hematoxylin and eosin (H&E) show parietal cells mainly in the upper part of the glands and chief cells in the lower part. Parietal cells are triangular in shape with eosinophilic cytoplasm and a centrally located nucleus and chief cells,

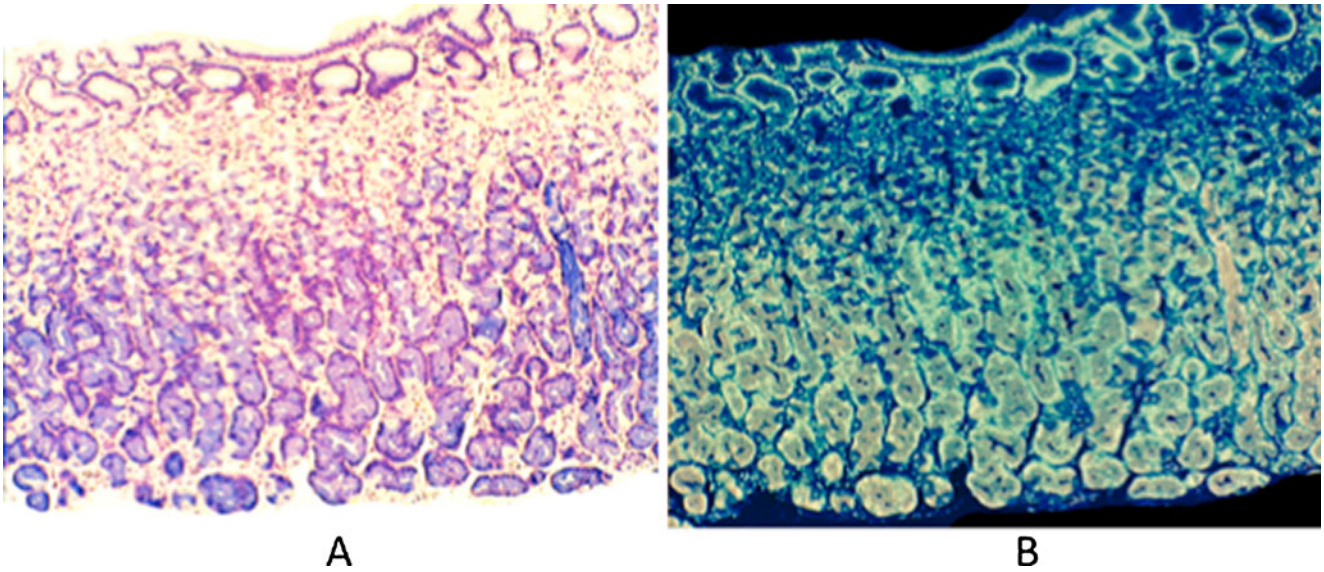

Fig. 1 **a** Normal fundic mucosa (toluidine blue, ×10) **b** Same picture using the INVERT function of a Photoshop program (Ps Adobe Photoshop CS3 extended, ×10)

cuboidal with a pale blue–gray (amphophilic) cytoplasm and a basally located nucleus [1]. Despite differences in topographical location and characteristic cytological features, the discrimination between chief cells and parietal cells is, however, not always straightforward in H&E sections, as disclosed in histological trials with the participation of male and female pathologists [4].

Searching for *Helicobacter pylori* in sections from the fundic mucosa stained with Giemsa stain [4] and more recently with toluidine blue [5], it became apparent that parietal cells and chief cells could easily be discriminated by the aid of these two dyes.

In the present work, qualitative observations and quantitative measurements were carried out in a cohort of sections stained with these two dyes, in order to study the parietal cell domain in gastric biopsies.

Material and methods

Sections from 110 consecutive gastric biopsies were stained with H&E and with modified Giemsa or toluidine blue stains. Good mucosal orientation was a prerequisite for including cases. Only 68 biopsy cases fulfilled these

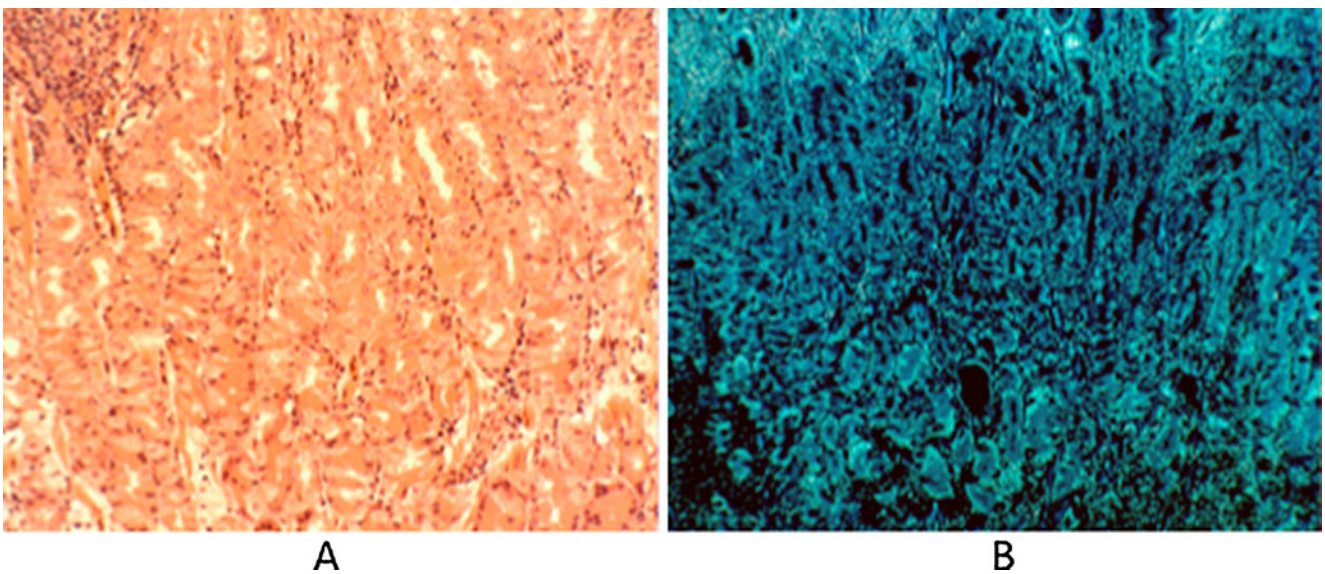

Fig. 2 **a** Normal fundic mucosa (H&E, ×20). Compare with Fig. 1a. **b** Same picture using the INVERT function of a Photoshop program (Ps Adobe Photoshop CS3 extended, ×20). Compare with Fig. 1b

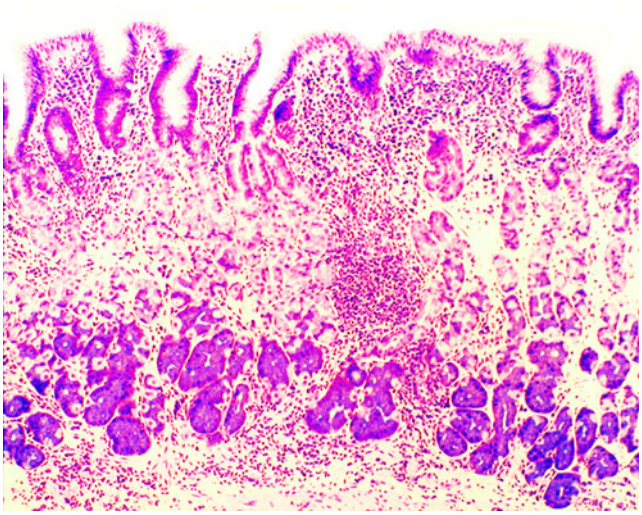

Fig. 3 Fundic gastritis showing fragmentation of the parietal cell and chief cell domains (toluidine blue, ×20)

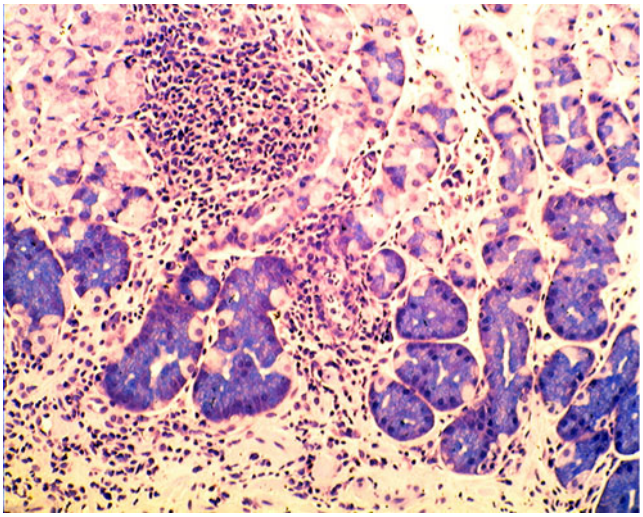

Fig. 5 Detail of fundic gastritis showing fragmentation of the chief cell domain (toluidine blue, ×20)

requirements; the remaining 42 cases were rejected because of poor mucosa orientation. H&E was available in all 68 cases, modified Giemsa in 20 and toluidine blue in 48.

In Giemsa or toluidine blue-stained sections, the normal fundic mucosa displayed at low-power (×4) examination, two apparently distinct zones: a parietal cell domain (PCD), defined as a continuous, side-to-side zone of parietal cells intercalated between the fovelar epithelium on top and chief glands underneath, and a chief-cell domain (CCD), as a continuous, side-to-side zone of chief cells intercalated between the parietal cell domain on top and the muscularis mucosae underneath (Fig. 1). Figure 2 shows normal fundic mucosa stained with H&E, for comparison.

The continuity of these two domains was estimated in the entire section at ×4 magnification. The thickness of the PCD as well as the total mucosal thickness (TMT) was measured in three different HPF at ×20 magnification, using a calibrated ocular microscale. The ratio PCD/TMT was then calculated.

Occasional parietal cells were found outside the PCD, amidst the CCD. These parietal cells were disregarded

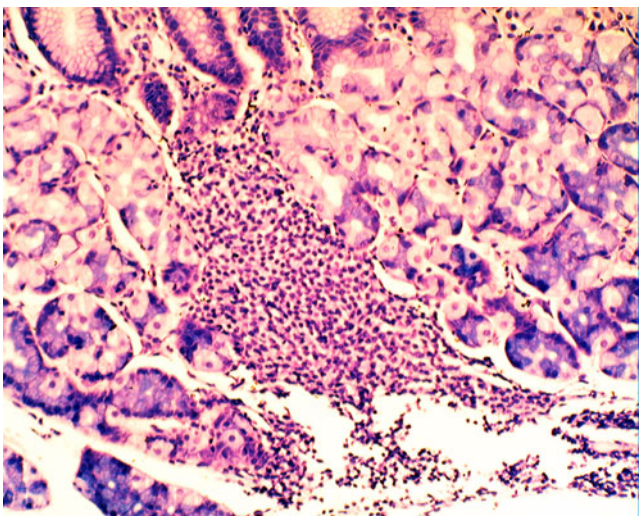

Fig. 4 Another case with fundic gastritis showing fragmentation of the parietal cell domain (toluidine blue, ×20)

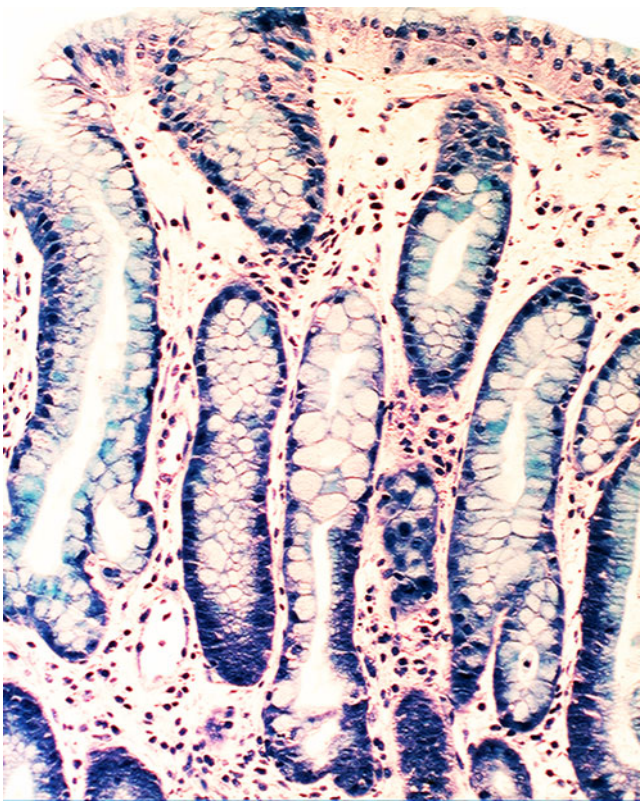

Fig. 6 Fundic mucosa with extensive intestinal metaplasia (toluidine blue, ×20)

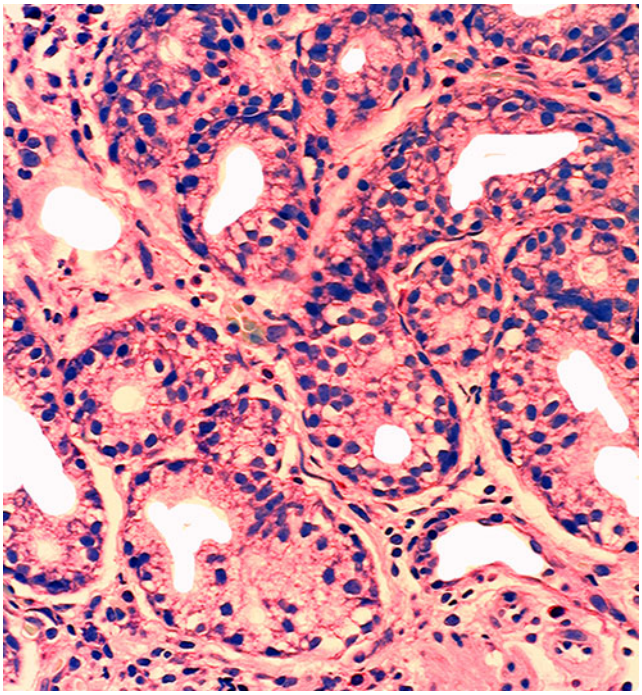

Fig. 7 Fundic mucosa with pseudopyloric metaplasia (toluidine blue, ×40)

when calculating the thickness in both the PCD and the TMT.

Statistical analysis The Mann–Whitney test was used to compare difference between groups. Statistical significance was defined as $p<0.05$. The Regional Ethical Committee approved the study.

Results

1. Qualitative studies of fundic biopsies

   Using low-power examination, the normal fundic mucosa or with slight chronic gastritis showed a distinct, continuous side-to-side PCD and CCD (Fig. 1). On the other hand, sections with moderate chronic gastritis, with focal glandular atrophy or with focal intestinal metaplasia (IM) reaching the muscularis mucosae displayed PCD and CCD fragmentation at one or more spots (Figs. 3, 4, and 5). Severe chronic gastritis including advanced autoimmune gastritis and extensive IM showed absence of PCD and CCD in the entire section (Figs. 6 and 7). The glands in these domains were replaced by hyperplastic neck cells (pseudopyloric metaplasia, PPM) and/or by IM glands.
2. Quantitative studies of fundic biopsies

   The results of micrometric measurements are shown in Tables 1 and 2. In the normal fundic mucosa (Table 1), the PCD mean thickness was 164.8 μm (range 102.6–248.4 μm); the mean TMT, 792.0 μm

Table 1 The thickness (in micrometer) of the parietal cell domain (PCD) and of the total mucosal thickness (TMT) in 41 normal fundic biopsies stained with modified Giemsa or toluidine blue

PCD (mean in μm)	TMT (mean in μm)	PCD/TMT ratio
189.9	937.0	0.20
116.4	700.6	0.16
203.8	751.2	0.27
248.4	938.4	0.26
243.8	869.4	0.28
151.8	703.8	0.22
155.2	835.2	0.19
136.2	703.8	0.19
134.8	874.0	0.15
138.0	983.2	0.14
110.4	801.8	0.14
122.8	812.8	0.15
138.0	640.8	0.22
179.4	659.2	0.27
180.8	739.2	0.24
170.2	792.6	0.21
155.0	849.6	0.18
99.8	751.2	0.13
211.6	792.1	0.27
224.0	958.2	0.23
191.8	823.4	0.24
208.4	886.4	0.24
184.0	832.6	0.22
122.8	764.9	0.16
205.6	676.2	0.30
194.6	749.8	0.26
168.8	741.9	0.23
207.0	837.2	0.25
176.2	952.2	0.19
193.2	907.6	0.21
182.6	805.0	0.23
122.8	668.4	0.18
113.2	754.4	0.15
122.8	703.8	0.17
102.6	579.6	0.18
104.4	662.4	0.16
138.0	760.4	0.18
136.6	740.6	0.18
176.2	854.2	0.21
216.2	874.0	0.21
179.4	803.6	0.22
Mean, 164.8	Mean, 792.0	Mean, 0.21
Range, 102.6–248.4	Range, 579.6–983.2	Range, 0.13–0.30

The PCD/TMT ratio is also shown

Table 2 The thickness (in micrometer) of parietal cell domain (PCD), of total mucosal thickness (TMT) and the PCD/TT ratio in 27 fundic biopsies having chronic gastritis with or without sequels, stained with modified Giemsa or toluidine blue

PCD (mean in μm)	TMT (mean in μm)	PCD/TMT ratio	Diagnosis
0	896.4	0.00	CAG HP−, IM, PPM
134.8	745.2	0.18	CG HP+
0	795.8	0.00	CAG HP+, atrophy, IM
0	1012.0	0.00	CAG HP+, chief cell expansion
188.2	828.0	0.23	CG HP+
0	1029.0	0.00	CG HP+, chief cell expansion
125.6	1027.8	0.12	CG HP+
102.6	868.0	0.12	CG HP−
122.8	879.9	0.14	CAG HP+
102.6	933.8	0.11	CG IM, HP-
101.2	757.6	0.13	CG HP+
0	969.2	0.00	CAG HP−, atrophy, IM
0	950.8	0.00	CG HP+, chief cell expansion
226.8	915.4	0.25	CG HP+
241.9	952.2	0.25	CG HP+
88.8	840.2	0.11	CG HP+
248.4	979.8	0.25	CG HP−
0	879.9	0.00	CAG, atrophy, IM
155.2	723.8	0.21	CG HP+
237.8	907.6	0.26	CG HP+
0	815.6	0.00	CAG HP−, atrophy, IM
0	791.2	0.00	CAG HP−, atrophy, IM
0	846.4	0.00	KAG, atrophy, IM
184.0	832.6	0.22	CG HP+
122.8	764.9	0.16	CG HP+
201.2	868.2	0.23	CG HP+
Mean, 101.6	Mean, 875.1	Mean, 0.12	
Range, 0–248.4	Range, 723.8–1,029.0	Range, 0–0.23	

(range 579.6–983.2 μm); the mean PCD/TMT ratio, being 0.21 (range 0.13–0.30).

In chronic fundic gastritis (Table 2) showing either severe glandular atrophy with or without PPM, or extensive IM, the mean PCD thickness was 101.6 μm (range 0–248.4 μm); the mean TMT, 875.1 μm (range 723.8–1.029.0 μm); the mean PCD/TMT ratio being, 0.12 (range 0–0.26).

The difference in thickness of the PCD and of the ratio PCD/TMT between normal mucosa and chronic gastritis and its sequels was significant ($p<0.05$). On the other hand, the difference in TMT between the normal fundic and chronic fundic gastritis with or without sequels was non-significant ($p<0.6$).

In three cases with chronic gastritis, the chief cells were found even in the parietal cell compartment. This phenomenon called chief cell expansion was defined as the presence of chief cells admixed with parietal cells high up in the mucosa, near or juxtaposing neck cells (Figs. 8 and 9). In these three cases, the PCD was recorded as 0 (Table 2).

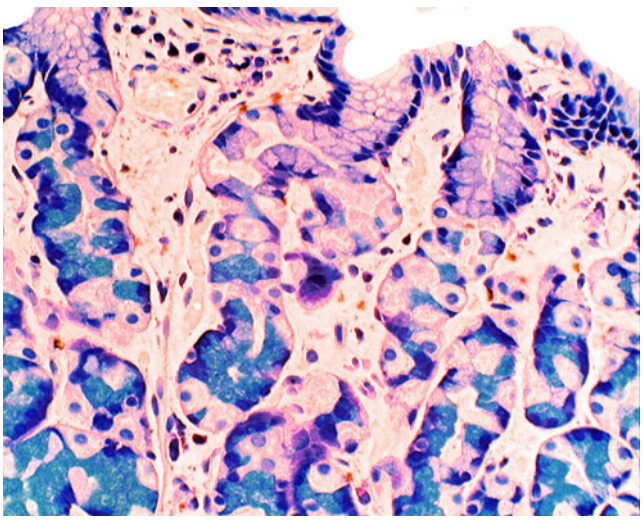

Fig. 8 Fundic gastritis demonstrating chief cell expansion into parietal cell domain (toluidine blue, ×10)

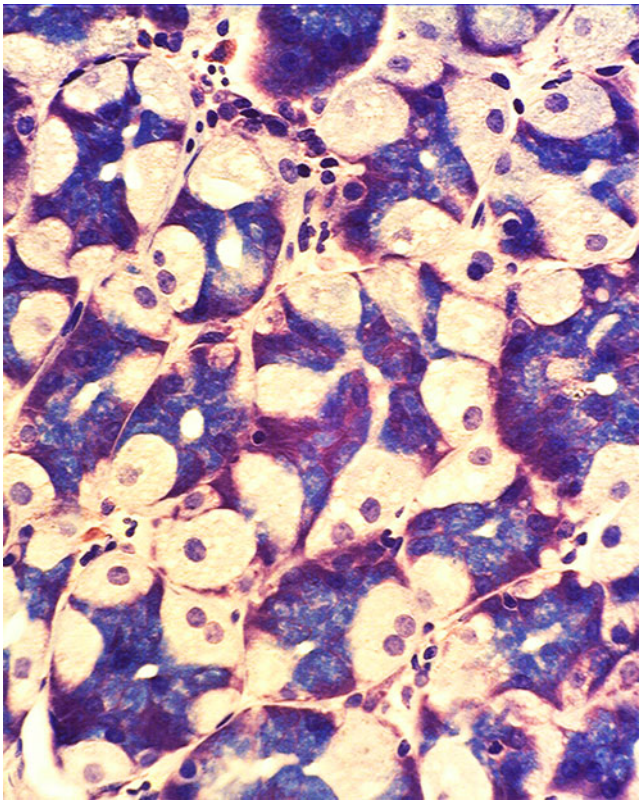

Fig. 9 Detail of fundic gastritis with chief cell expansion into parietal cell domain (toluidine blue, ×40)

Discussion

In a previous test, three male pathologists gathered around a multi-headed microscope, in order to identify all parietal cells present in H&E-stained sections from the normal fundic mucosa [4]. The test showed that these male pathologists could recognize only few parietal cells. Although the cause for this snare remained unclear, it appeared unrelated to the fact that 10% of male pathologists suffer from Daltonism [6]. This was so since the same difficulty arose when a female and a male pathologist tried to recognize parietal cells in H&E-stained sections from the stomach in a knock-out mouse model [7, 8]. Based on this experience, five sections with normal fundic mucosa stained with H&E were subsequently reviewed at this laboratory by two female pathologists and by one of us (CAR). Using a multi-headed microscope, the two female pathologists—unaware of the purpose of the microscopic séance—were asked to identify all parietal cells. Here again, only few parietal cells could be recognized with certainty. In contrast, the three pathologists were able to identify with confidence parietal and chief cells in sections from the same cases stained with modified Giemsa or with toluidine blue (unpublished trial). Hence, the gender of the observer does not seem to be the main reason for the failure in recognizing many parietal cells in H&E-stained sections.

The limitation in discriminating parietal and chief cells with H&E lead Gherardi et al. [9] to test other staining procedures in the stomach of rats. Four different methods were used: a modification of the H&E method proposed by Drysdale and Marks [10], haematoxylin–eosin–saffron fluorochrome stain, haematoxylin–azophloxin–saffron fluorochrome stain, and May–Grünwald–Giemsa stain on thin sections from plastic-embedded specimens. Results showed that May–Grünwald–Giemsa stain using plastic-embedded specimens provided the best results for discriminating parietal cell in rat stomachs [9]. Other methods have been used to identify gastric parietal cells: WGA and HPA-L lectins in guinea pig stomachs [11], flow cytometry in mouse and guinea pig stomachs [12, 13] and in human gastric biopsies [14], huntingtin interacting protein 1 in mice stomachs [15], parietal-specific H+K+-ATPase antibody in mice stomachs [16, 17], as well as prostaglandin E2 [18], and transmission electron microscopy in stomachs of laboratory animals [19, 20]. These laborious methods are, however, costly, time consuming, and to date, none of them has been used to differentiate parietal cells from other cells in human gastric biopsies in health and disease.

Few morphometric studies have been done to assess the thickness of the parietal cell population. Using point count morphometry, Sipponen et al. [21] found in AB-PAS-stained sections that the chief cell/parietal cell (C/P) ratio was higher after partial gastrectomy for duodenal ulcer, suggesting a proportional loss of parietal cells than chief cells after operation. In non-operated control patients, the C/P ratio decreased with increasing degree of gastritis, suggesting that in the general population the chief cells are more sensitive than parietal cells to those factors that lead to age-dependent progression of gastritis. The possible occurrence of glandular fragmentation or absence of a parietal cell zone in patients with chronic gastritis is not explored by Sipponen et al. [21].

Farinati et al. [22] used morphometry to study the influence of age on the normal parietal cell mass of the mucosa of the antrum. These authors found that the number of parietal cells in the antrum increased with increasing age. The mucosa of the fundus was not investigated.

In this work, sections from the gastric fundus stained with modified Giemsa or with toluidine blue stains were used to evaluate the continuity of the fundic mucosa and to quantitatively assess the thickness of the PCD in relationship to the TMT. When using these two stains, qualitative observations at low-power examination permitted to discriminate two distinct zones, a PCD and a CCD. These cellular domains were found to be (a) continuous, in the normal fundic mucosa or in the fundic mucosa with slight chronic gastritis; (b) fragmented; in moderate chronic

fundic gastritis having focal glandular atrophy or focal IM; or (c) absent, in biopsies with extensive sequels of chronic gastritis or autoimmune gastritis. In three cases of chronic fundic gastritis, many chief cells were found within the parietal cell compartment. The possibility that this phenomenon was the result of a chief cell expansion in response to the loss of parietal cells in cases of chronic superficial gastritis appears unlikely. The cause(s) for this phenomenon, clearly evidenced in toluidine-stained sections, remains elusive; it deserves to be further investigated.

Quantitative studies at higher power examination indicated that in chronic gastritis, the thickness of the PCD could be (a) normal, (b) reduced, or (c) absent. The reduction of the PCD was apparently conveyed by the partial destruction of the parietal cell population by the chronic inflammation, and its absence by extensive IM or total glandular atrophy, as in autoimmune gastritis.

Toluidine blue gave a better contrast between a light-stained PCD and a dark-stained CCD than modified Giemsa stain. Toluidine blue stain has several other advantages: it is cheap and available at most pathology laboratories, the staining procedure takes only 30 s—instead for 30 min with modified Giemsa, and the interpretation of the three qualitative PCD groups at low-power examination, which is glandular continuity, glandular fragmentation, or absence of glands, is unsophisticated. Moreover, toluidine blue stain improves the detection of *H. pylori* (unpublished trial) and permit male pathologists with Daltonism [6] to easily recognize parietal cells by their light cytoplasm shade and not by the red color of the cytoplasm in H&E-stained sections or in color illustrations. Black and white illustrations of toluidine blue stains clearly discriminate between light-shaded parietal cells and dark-shaded chief cells, even by pathologists with Daltonism.

Future studies might elucidate whether qualitative and quantitative studies of toluidine blue stain sections of the fundic mucosa are useful in monitoring the results of therapy in individual patients with chronic gastritis.

Conflict of interest statement We declare that we have no conflict of interest.

References

1. Owen DA (1997) Stomach. In: Stenrberg SS (ed) Histology for pathologists, chapter 20, 2nd edn. Lippincott , Philadelphia, pp 481–493
2. Chandrasoma P (2007) Four directed biopsies are better than eight random biopsies to find intestinal metaplasia in columnar lined esophagus. Am J Gastroenterol 102:2352–2353
3. Rubio CA, Dick EJ, Schlabritz-Loutsevitch NE, Orrego A, Hubbard GB (2009) The columnar-lined mucosa at the gastro-esophageal junction in non-human primates. Int J Clin Exp Pathol 2:481–488
4. Rubio CA (2010) An easy method to identify parietal cells in gastric biopsies. In Vivo 24:599–602
5. Rubio CA (2011) An easy method to highlight chief cells in gastric biopsies. Vivo 25(1):137–140
6. Bogman MJ (1992) Colour blindness and pathologists. Lancet 339:185–186
7. Judd LM, Andringa A, Rubio CA, Spicer Z, Shull GE, Miller ML (2005) Gastric achlorhydria in H/K-ATPase-deficient (Atp4a(−/−)) mice causes severe hyperplasia, mucocystic metaplasia and upregulation of growth factors. J Gastroenterol Hepatol 20:1266–1278
8. Rubio CA, Miller M (2009) Fundic gland cysts in Atp4a−/− mice mimic fundic gland polyps in humans. In Vivo 23:979–98
9. Gherardi G, Del Tacca M, Paparelli A, Bernardini C, Polloni A (1987) Staining methods for morphometric studies of parietal and gastrin cells in the rat stomach. Int J Tissue React 9:499–508
10. Drysdale K, Marks I (1957) A modification of Zimmermann's method for differential staining of gastric mucosa. Stain Technol 32:48–49
11. Lueth M, Sturegård E, Sjunnesson H, Wadström T, Schumacher U (2005) Lectin histochemistry of the gastric mucosa in normal and Helicobacter pylori infected guinea-pigs. J Mol Histol 36:51–58
12. Zavros Y, van Antwerp M, Merchant J (2000) Use of flow cytometry to quantify mouse gastric epithelial cell populations. Dig Dis Scien 45:1192–1199
13. Giebel J, Arends H, Fanghänel J, Cetin Y, Thiedemann KU, Schwenk M (1995) Suitability of different staining methods for the identification of isolated and cultured cells from guinea pig (Cavia aperea porcellus) stomach. Eur J Morphol 33:359–372
14. Biernacka D, Tomaszewska A, Muszynski J, Moskalewski S (1996) Concomitant staining of mast and parietal cells in human gastric mucosa. Biotech Histochem 71:234–236
15. Legendre-Guillemin V, Metzler M, Lemaire JF, Philie J, Gan L, Hayden MR, McPherson PS (2005) Huntingtin interacting protein 1 (HIP1) regulates cla thrin assembly through direct binding to the regulatory region of the clathrin light chain. J Biol Chem 280:6101–608
16. Spicer Z, Miller ML, Andringa A, Riddle TM, Duffy JJ, Doetschman T, Shull GE (2002) Stomachs of mice lacking the gastric H, K-ATPase alpha-subunit have achlorhydria, abnormal parietal cells, and ciliated metaplasia. Cell Tissue Res 309:369–380
17. D'Elios MM, Bergman MP, Azzurri A, Amedei A, Benagiano M, De Pont JJ, Cianchi F, Vandenbroucke-Grauls CM, Romagnani S, Appelmelk BJ, Del Prete G (2001) H(+), K(+)-atpase (proton pump) is the target autoantigen of Th1-type cytotoxic T cells in autoimmune gastritis. Gastroenterology 120:377–386
18. Ota S, Razandi M, Krause W, Terano A, Hiraishi H, Ivey KJ (1993) Prostaglandin E2 output by isolated rat gastric parietal cells and non-parietal epithelial cells. Eur J Cell Biol 60:76–87
19. Sato A, Spicer SS, Tashian RE (1980) Ultrastructural localization of carbonic anhydrase in gastric parietal cells with the immunoglobulin-enzyme bridge method. Histochem J 12:651–659
20. Bal HS, Ghoshal NG (1992) Electron microscopy of the oxynticopeptic cells of the gastric glands and the intestinal glands of the caecum of the guineapig. Lab Anim 26:47–52
21. Sipponen P, Saukkonen M, Varis K, Siurala M (1979) Morphometric analysis of the loss of chief and parietal cells after partial gastrectomy for duodenal ulcer. Acta Hepatogastroent 26:493–498
22. Farinati F, Formentini S, Della Libera G, Valiante F, Fanton MC, Di Mario F, Vianello F, Pilotto A, Naccarato R (1993) Changes in parietal and mucous cell mass in the gastric mucosa of normal subjects with age: a morphometric study. Gerontology 39:146–151

Virchows Arch (2011) 458:741–748
DOI 10.1007/s00428-011-1084-z

ORIGINAL ARTICLE

High CD10 expression in lymph node metastases from surgically treated prostate cancer independently predicts early death

Achim Fleischmann · Carla Rocha · Nikolina Saxer-Sekulic · Inti Zlobec · Guido Sauter · George N. Thalmann

Received: 21 December 2010 / Revised: 24 March 2011 / Accepted: 10 April 2011 / Published online: 3 May 2011
© Springer-Verlag 2011

Abstract Patients with nodal positive prostate cancers are an important cohort with poorly defined risk factors. CD10 is a cell surface metallopeptidase that has been suggested to play a role in prostate cancer progression. CD10 expression was evaluated in 119 nodal positive prostate cancer patients using tissue microarrays constructed from primary tumors and lymph node metastases. All patients underwent radical prostatectomy and standardized extended lymphadenectomy. They had no neoadjuvant therapy and received deferred androgen deprivation. In the primary tumor, high CD10 expression was significantly associated with earlier death from disease when compared with low CD10 expression (5-year survival 73.7% vs. 91.8%; $p=0.043$). In the metastases, a high CD10 expression was significantly associated with larger total size of metastases (median 11.4 vs. 6.5 mm; $p=0.015$), earlier death of disease (5-year survival 71.5% vs. 87.3%; $p=0.017$), and death of any cause (5-year survival 70.0% vs. 87.2%; $p=0.001$) when compared with low CD10 expression. CD10 expression in the metastases added independent prognostic information for overall survival ($p=0.029$) after adjustment for Gleason score of the primary tumor, nodal tumor burden, and resection margins. In conclusion, a high CD10 expression in prostate cancer predicts early death. This information is inherent in the primary tumors and in the lymph node metastases and might help to personalize patient management.

Keywords CD10 · Prostate cancer · Metastases · Prognosis · Tissue microarray

A. Fleischmann (✉) · C. Rocha · N. Saxer-Sekulic · I. Zlobec
Institute of Pathology, University of Bern,
CH-3010 Bern, Switzerland
e-mail: achim.fleischmann@pathology.unibe.ch

G. Sauter
Department of Pathology, University Medical Center
Hamburg-Eppendorf,
Hamburg, Germany

G. N. Thalmann
Department of Urology, University of Bern,
Bern, Switzerland

Introduction

Prostate cancer is the second most frequently diagnosed cancer and the sixth leading cause of cancer death in males worldwide [1]. Surgically treated lymph node positive prostate cancer patients are an important subpopulation having a similar incidence in the US like men with esophageal, gastric, or testicular cancer [2] and showing a considerable clinical, morphological, and biological heterogeneity of disease [3]. For these men, risk factors predicting fatal outcome are poorly defined.

CD10, also known as neutral endopeptidase, might be a molecular biomarker with the ability to predict death in prostate cancer. CD10 is a zinc-dependent cell surface metallopeptidase which is widely expressed in epithelial cells of various sites including kidney, breast, lung, intestine, and prostate [4]. CD10 contains a large extracellular domain known to process a variety of more than 20 neuropeptides by enzymatic cleavage [4] thus modifying the pericellular concentration of specific peptides available for receptor binding. There is evidence that peptide-mediated cell growth can be suppressed or promoted by CD10 expression [5]. More recently, the effects of CD10 on growth and migration of cells have been reported which are

independent from its enzymatic property [6]; however, the entire biological significance of CD10 is still largely unknown. The potential of CD 10 expression in prostate cancer to predict prostate-specific antigen (PSA) recurrence has been evaluated in few cohorts with conflicting results [7–11]. Importantly, survival data obtained from our cohort of 2,385 hormone naive prostate cancer patients treated by radical prostatectomy indicate early PSA failure for patients with CD10 expression [11]. This contrasts with the tumor-suppressing functions of CD10 in prostate cancer observed in functional studies [6]. Here, we tested the potential of CD10 to predict death in another well-defined cohort of surgically treated patients with lymph node positive prostate cancers.

Materials and methods

Patients

One hundred and nineteen consecutive prostate cancer patients without clinical evidence of metastases (physical examination, abdominal/pelvic computerized tomography, bone scan, and chest X-ray) but with nodal metastases upon histological examination of the lymphadenectomy specimens were studied. All patients underwent a standardized bilateral extended pelvic lymphadenectomy and radical prostatectomy as a single procedure between February 1989 and December 2006 at the Department of Urology, University of Bern. They received no neoadjuvant therapy and were followed prospectively. No adjuvant therapy, androgen deprivation in particular, was recommended until symptomatic disease progression had occurred.

Surgical technique of lymphadenectomy

Bilateral pelvic lymphadenectomy was performed in all patients as previously described [12]. Briefly, lymph node dissection was performed along the external iliac vein down to the deep circumflex iliac vein and femoral canal with the bifurcation of the common iliac artery as proximal limit of the surgical field. Next, the obturator fossa was cleared of all tissues except the nerve and vessels. Lastly, the lymphatic tissue along the medial and lateral aspect of the internal iliac artery and vein was removed. The three tissue samples from each side were submitted separately for examination.

Pathology

All prostatectomy and lymphadenectomy specimens were processed at the Institute of Pathology, University of Bern as previously described [3, 13]. For this study, all slides were re-evaluated by experienced genitourinary pathologists (AF, CR, and NS). All Gleason patterns present in the primary tumors and lymph node metastases were tightly encircled for subsequent tissue microarray (TMA) construction.

The prostates were totally embedded. The following microscopic tumor characteristics were noted: type, Gleason score, and tumor stage. Tumor volume was estimated by multiplying the percentage of the specimen involved by cancer by the prostate volume [3, 13]. The diameter of each lymph node metastasis was measured. The seventh edition of the TNM classification [14] was used for staging.

TMA

The TMA [15] was constructed with tissue cores of 0.6 mm in diameter. Each Gleason pattern present in every primary tumor and in the matched lymph node metastases as well as non-neoplastic prostate tissue (peripheral zone) is represented by one tissue core. This TMA contains 403 punch biopsy specimens from prostates (mean per patient, 3.3; range, 2–4) and 167 from lymph node metastases (mean per patient, 1.4; range, 1–3). The distribution of these samples in the prostates is as follows: normal prostate tissue (n=119), Gleason pattern 3 (n=101), Gleason pattern 4 (n=112), and Gleason pattern 5 (n=71). The distribution of these samples in the metastases is as follows: Gleason pattern 3 (n=35), Gleason pattern 4 (n=103), and Gleason pattern 5 (n=29).

Immunohistochemistry

Freshly cut TMA sections were analyzed in 1 day in one experiment. High-temperature pretreatment of slides was done in steam with target retrieval solution, pH 9 (Dako, Glostrup, Denmark). CD10 expression was assessed using the monoclonal antibody CD10 (clon 56C6; Novocastra, Newcastle-upon-Tyne, UK). Optimal staining was achieved at 1:50 antibody dilution. Bound primary antibodies were visualized using the Envision Plus system (Dako, Glostrup, Denmark). CD10 expression was observed on the cell membrane and in the cytoplasm (Fig. 1). Tumors could be heterogeneous in subcellular CD10 expression between different spots. Therefore, only the percentage of positive tumor cells per patient in the primary tumor and the lymph node metastases was determined. The percentage of CD10 positive tumor cells was determined for each Gleason pattern averaged over all primary tumors and nodal metastases, respectively.

Statistical analysis

CD10 expression in normal prostate, primary cancer, and metastases was compared using Kruskal–Wallis test.

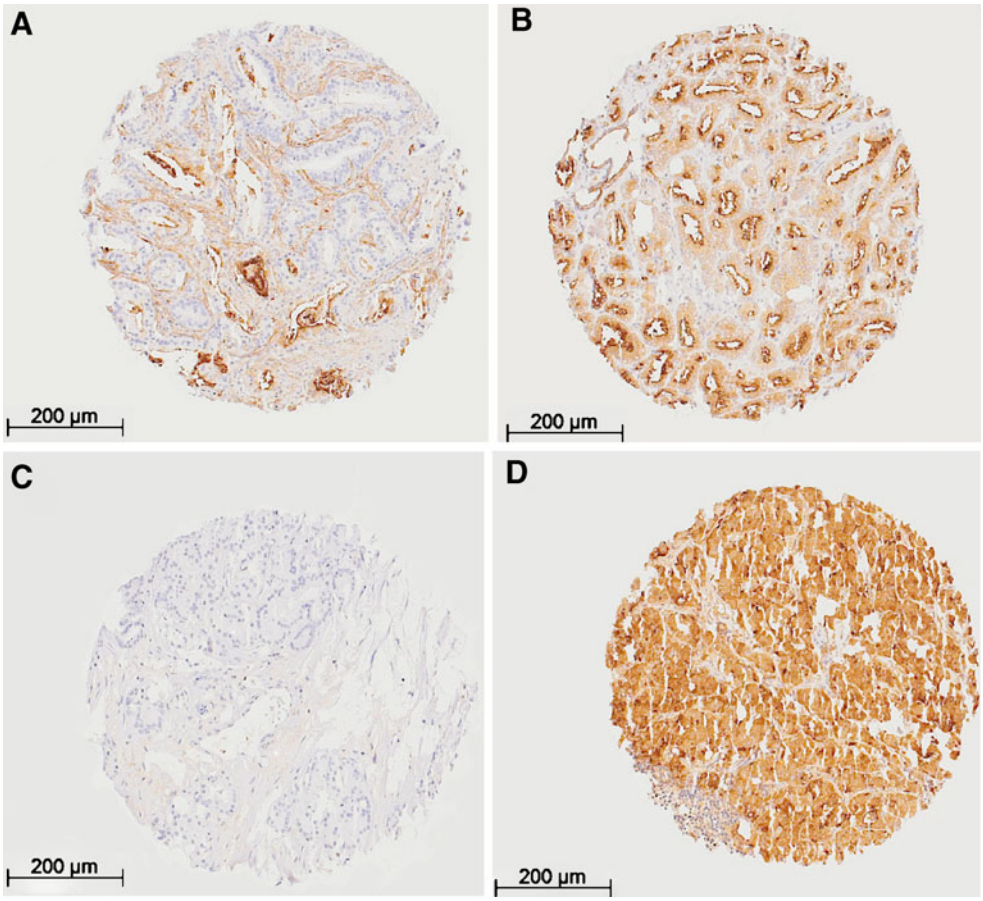

Fig. 1 CD10 expression in primary prostate cancer (**a**, **b**) and in lymph node metastases (**c**, **d**). **a** Few neoplastic cells with CD10 expression at the apical membrane and in the cytoplasm and immunoreactivity in the stroma. **b** Virtually all neoplastic cells with membranous and cytoplasmic CD10 expression. **c** No CD10 expression in the neoplastic cells. **d** Strong cytoplasmic CD10 expression in the neoplastic cells

Friedman Test was used to evaluate differences between Gleason patterns 3, 4, and 5 within primary tumors and lymph node metastases, the Wilcoxon two-sample test compared expression in primary tumors and metastases stratified by the Gleason patterns. CD10 expression was correlated with (a) quantitative tumor features using the *t* test (age) or Wilcoxon test (tumor volume, total size, and number of metastases) and (b) categorical tumor features using Fisher's exact test. Receiver-operating characteristic curves [16] were used to determine the optimal cut-off values for high (greater than 40% positive cells) and low (40% positive cells or less) CD10 expression in both the primary tumors and lymph node metastases. Outcome was analyzed for biochemical recurrence-free, disease-specific (DSS), and overall (OS) survival defined as the intervals from surgery to the date of biochemical recurrence (PSA failure defined as values >0.2 ng/ml), death from prostate carcinoma, and death from any cause, respectively. Patients without event for the respective endpoints were censored at the date of last follow-up. The above time-to-events were compared between groups using log-rank test. *P* values less than 0.05 were considered significant for all tests. After verification of the proportional hazards assumption, multiple Cox regression analysis was used for all three endpoints to determine the prognostic impact of CD10 expression in primary tumors and metastases controlling for independent risk factors determined previously in a subset of this cohort [3, 13]: Gleason score of the primary tumor (6/7/8 vs. 9/10 grouped according to similar survival curves between the clustered subsets) and lymph node tumor burden reflected by the total diameter of all nodal metastases (median value, 7.5 mm, was used as cut-off).

Results

Characteristics of patients, prostatectomy specimens, lymphadenectomy specimens, and lymph node metastases

Baseline data of the cohort are given in Table 1.

Expression of CD10 in normal prostate, primary tumors, and lymph node metastases considering the Gleason patterns

CD10 expression was lost in primary tumors (63.3%) and lymph node metastases (46.9%) when compared with normal prostate glands (90.1%; $p<0.001$). No significant difference was detected between the different Gleason patterns (GP) in the primary tumors (GP3, 60.1%; GP4,

Table 1 Characteristics of 119 surgically treated prostate cancer patients with pelvic lymph node metastases

Patient data (n=119)	
Age (median, range) at surgery (years)	65 (45–75)
Follow-up (median, range) (years)	5.9 (1–15.2)
Patients with biochemical failure at last follow-up (n)	103
Patients dead of disease at last follow-up (n)	33
Patients dead at last follow-up (n)	40
Prostatectomy data	
Stage	
pT2 (n)	14
pT3a (n)	55
pT3b (n)	50
Prostate carcinoma volume (median, range) (cm^3)	12.6 (0.66-127)
Gleason score	
6 (n)	12
7 (3+4; 4+3) (n)	63 (33; 30)
8 (n)	21
9 (n)	23
Positive resection margins (n)	84
Lymphadenectomy data	
Total number of evaluated nodes (n)	2,794
Total number of evaluated lymph node metastases (n)	382
Evaluated nodes per patient (median, range) (n)	22 (9–68)
Positive nodes per patient (median, range) (n)	2 (1–24)
Total diameter of metastases per patient (median, range) (mm)	7.5 (0.3–204)

61.0%; GP5, 68.8%; p=0.198) and in the metastases (GP3, 65.3%; GP4, 38.2%; GP5, 53.7%; p=0.058).

Correlations of CD10 expression in primary tumors and metastases with clinicopathological tumor characteristics

In the primary tumors, there was no trend for the association of CD10 with Gleason score, tumor stage, or tumor volume. In the metastases, high CD10 expression was significantly associated with larger total size of metastases (median 11.4 vs. 6.5 mm; p=0.015) but not with the median number of positive nodes (2.5 vs. 2.0; p=0.169) or lymph node Gleason score.

Univariate survival analysis according to CD10 expression

In primary prostate cancer, high CD10 expression (average percentage of CD10 positive cancer cells, 74%) significantly predicted early death of disease (p=0.043; Fig. 2) with a 5-year DSS rate of 73.7%, while patients with low CD10 expression (average percentage of CD10 positive cancer cells, 20%) had a 5-year DSS rate of 91.8%. In the metastases, high CD10 expression (average percentage of CD10 positive cancer cells, 76%) was a significant adverse risk factor for DSS (p=0.017) and OS (p=0.001) compared with low CD10 expression (average percentage of CD10 positive cancer cells, 11%; 5-year DSS, 71.5% vs. 87.3%; 5-year OS, 70.0% vs. 87.2%; Fig. 2). The difference in PSA recurrence-free survival between patients with high and low CD10 expression was not significant (Fig. 2).

Multivariate analysis

Two separate multivariate analyses tested the prognostic impact of CD10 expression in the primary tumors and in the metastases, respectively, after adjusting for the prognostic effects of size of metastases and Gleason score of the primary tumor (Table 2). Patients with high CD10 expression in the metastases had a nearly tripled mortality (hazard ratio 2.81) compared with patients with low CD10 expression. This difference added an independent prognostic information (p=0.029). The strongest prognostic factor for all endpoints was nodal tumor burden reflected by the total diameter of all metastases.

Discussion

Functional studies in single prostate cancer cell lines suggested a tumor suppressor function of CD10 [6]. However, when prostate cancer tissues were evaluated,

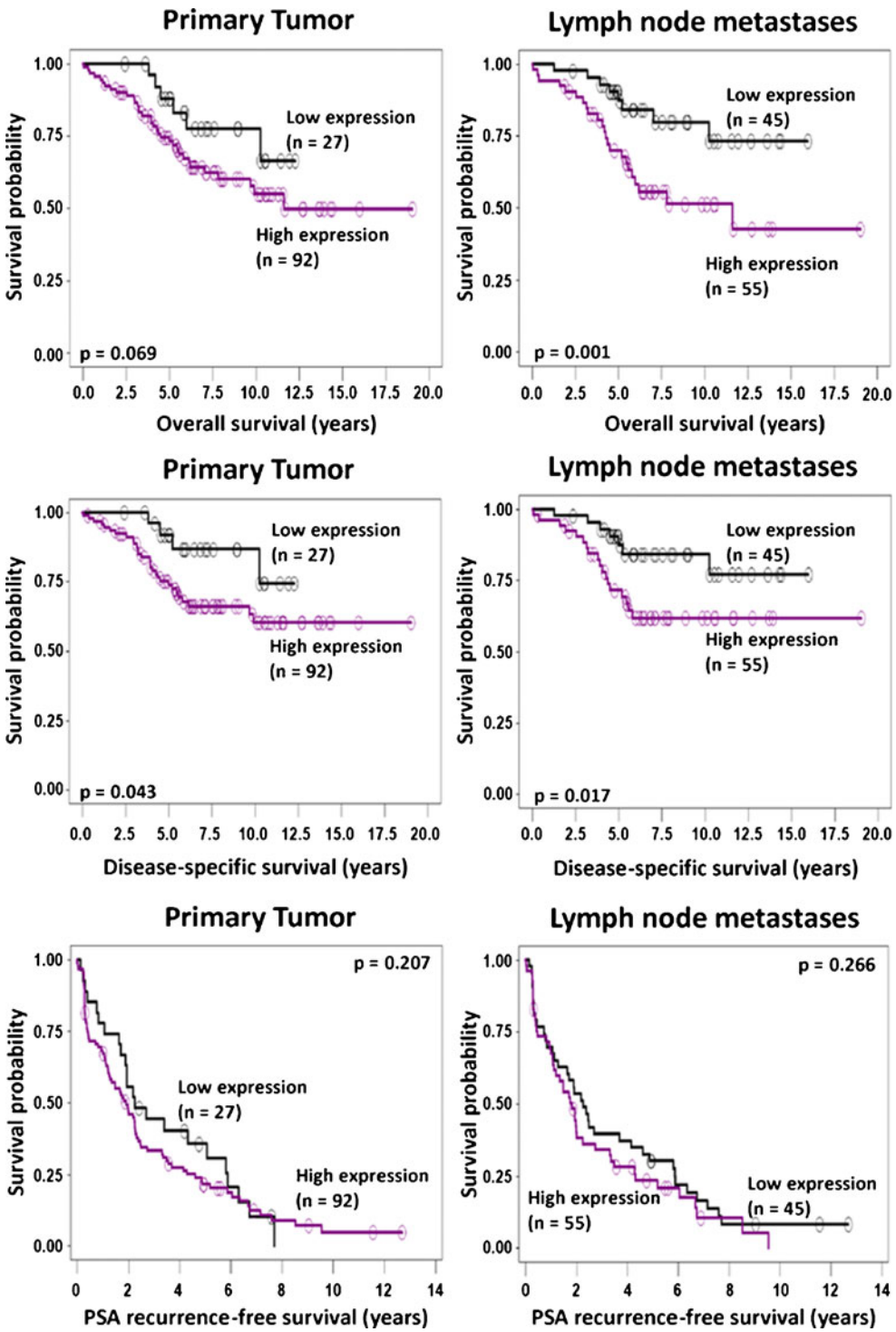

Fig. 2 Survival analysis according to CD10 expression in primary prostate cancer (*left*) and lymph node metastases (*right*). Overall (*first row*) and disease-specific (*second row*) survivals are significantly better in patients with low CD10 expression in primary tumors or metastases when compared to patients with high expression in these tumor components

results were conflicting. Depending on the cohort, CD10 expression was considered as unfavorable [7, 11], favorable [9], or no risk factor [8, 10] for PSA recurrence after therapy. The comparability of these results, however, is limited due to large differences between the evaluated cohorts. The better outcome for CD10 positive patients reported by Osman et al. [9] was detected in a cohort of mainly African–American men with significant race-dependent differences in CD10 expression potentially impacting on results. Zellweger et al. [10] evaluated a cohort of heterogeneously treated patients including patients with hormonal therapy, which is known to suppress CD10 expression in prostate cancer via androgen responsive elements [17]. Recent data showing CD10 expression as an independent adverse risk factor for PSA recurrence-free survival in a surgically treated, hormone naive

Table 2 Separate multivariate analyses for the prognostic impact of CD10 expression in primary prostate cancer (*upper half*) and lymph node metastases (*lower half*), respectively, after adjustment for total size of metastases, Gleason score of primary tumor, and resection margin

Parameter	Cut-off	Overall survival		Disease-specific survival		Recurrence-free survival	
		HR (95%CI)	*P*	HR (95%CI)	*P*	HR (95%CI)	*P*
CD10 in primary tumor	Low	1.0	0.425	1.0	0.296	1.0	0.996
	High	1.43 (0.6–3.5)		1.76 (0.6–5.1)		1.0 (0.6–1.6)	
Total diameter of metastases	<7.5 mm	1.0	<0.001	1.0	0.006	1.0	0.016
	≥7.5 mm	3.76 (1.7–8.2)		3.45 (1.4–8.3)		1.7 (1.1–2.6)	
Gleason score	6 to 8	1.0	0.292	1.0	0.069	1.0	0.488
	9 to 10	1.49 (0.7–3.1)		2.05 (1.0–4.4)		1.2 (0.7–2.0)	
Resection margin	Negative	1.0	0.468	1.0	0.724	1.0	0.289
	Positive	1.34 (0.6–3.0)		1.17 (0.5–2.7)		1.29 (0.8–2.1)	
CD10 in metastases	Low	1.0	0.029	1.0	0.227	1.0	0.865
	High	2.81 (1.1–7.1)		1.92 (0.7–5.5)		1.04 (0.7–1.7)	
Total diameter of metastases	<7.5 mm	1.0	0.003	1.0	0.007	1.0	0.061
	≥7.5 mm	5.18 (1.7–15.3)		7.66 (1.7–34.0)		1.59 (1.0–2.6)	
Gleason score	6 to 8	1.0	0.532	1.0	0.075	1.0	0.789
	9 to 10	1.31 (0.6–3.1)		2.33 (0.9–5.9)		1.08 (0.6–1.9)	
Resection margin	Negative	1.0	0.462	1.0	0.825	1.0	0.133
	Positive	1.45 (0.5–3.9)		1.14 (0.4–3.5)		1.5 (0.9–2.5)	

HR hazard ratio, *CI* confidence interval

population of 2,385 prostate cancer patients [11] were in accordance with findings reported by Dall'Era et al. [7].

In this study, we extended the analysis of CD10 in prostate cancer in two respects: first, we tested the potential of CD10 to predict fatal outcome; second, the prognostic relevance was determined in a particular cohort of hormone naive, surgically treated patients with lymph node metastases. Importantly, patients with high CD10 expression, no matter if in the primary prostate cancer or in the metastasis, experience early death. High CD10 expression in the lymph node metastases added independent prognostic information and was associated with a nearly tripled risk of dying compared with patients with low CD10 expression. This is of considerable clinical interest because (a) prognostic factors are only poorly defined in surgically treated lymph node positive prostate cancer what is an important disease with a similar incidence in US American men as esophageal, gastric, or testicular cancer [2]; and (b) death is a more robust endpoint than PSA recurrence. The clinical course following PSA recurrence after radical prostatectomy is extremely variable with rapid progression in some men and an indolent course in others [18]. By contrast, death is an outcome measure of the "true" clinical course. Therefore, our data suggest that the natural history of disease in surgically treated lymph node positive prostate cancer can be accurately predicted by CD10 expression.

The prognostic potential of biomarker expression in the different tumor components of lymph node positive cancer has been compared in only few tumors [19–21] including prostate cancers [22–25]. In case of successful survival stratification, the metastasizing tumor component but not the primary tumor [19, 20, 22] or both tumor components [21, 23, 25] may harbor the prognostic information. In prostate cancer, CD10 expression in both tumor components, the primary cancers and the nodal metastases, predicts survival significantly. This is clinically relevant for lymph node positive patients treated by surgery because their clinical course can be predicted more precisely and adjuvant therapies might be scheduled accordingly. Moreover, risk assessment in patients with metastasized prostate cancers not qualifying for local therapies with curative intent might be improved by CD10 determination in core needle biopsies of the primary tumor. Important risk factors in this population like metastatic tumor burden and Gleason score of the primary tumor [3] can only be imprecisely determined and, therefore, the prognostic information by CD10 expression might even be superior. In this context, it is noteworthy that the tumor amount analyzed on TMAs is highly comparable to the one in the core needle biopsies so that prognostic markers identified in prostate cancer TMAs may also be relevant in the biopsy setting.

CD10 expression in lymph node metastases of prostate cancer is positively correlated with nodal tumor burden. The pathophysiological link, however, is obscure. Conceivably, CD10 in prostate cancer metastases inactivates antiproliferative peptides thus promoting tumor growth what would be in line with the well-known enzymatic property of CD10. Alternatively, the enzymatic activity of CD10 could promote tumor growth by conversion of a propeptide into a biologically active, stimulatory form. These basic mechanisms have been suggested for ectopeptidases in general [26] and might also apply to CD10 function in prostate cancer in vivo. CD10 function depends on tissue type [7] indicated by specific tumor cell lines promoted [5] or suppressed [27] by CD10. Accordingly, CD10 expression can be a favorable [28] or an unfavorable [29] prognostic factor dependent on the cancer type.

Finally, CD10 expression in prostate cancer might also be therapeutically relevant. Newly developed CD10 inhibitors [30] may complement established therapies to counteract the unfavorable effects of CD10 on survival. Alternatively, peptide prodrugs might be applied which are enzymatically activated by CD10 expression on tumor cells. This antitumor effect has been applied successfully in a xenograft model using a CD10-overexpressing prostate cancer cell line [31].

In conclusion, CD10 expression in nodal positive prostate cancer predicts early death. This information may help to better predict survival individually and to personalize adjuvant therapies, thus improving patient management.

Acknowledgment This project received funding from the Bernische Krebsliga by Grant 34–904 (AF).

Conflicts of interest The authors declare that they have no conflicts of interest.

References

1. Jemal A, Bray F, Center MM, Ferlay J, Ward E, Forman D (2011) Global cancer statistics. CA Cancer J Clin 61:69–90
2. Swanson GP, Thompson IM, Basler J (2006) Current status of lymph node-positive prostate cancer: incidence and predictors of outcome. Cancer 107:439–450
3. Fleischmann A, Schobinger S, Schumacher M, Thalmann GN, Studer UE (2009) Survival in surgically treated, nodal positive prostate cancer patients is predicted by histopathological characteristics of the primary tumor and its lymph node metastases. Prostate 69:352–362
4. Erdos EG, Skidgel RA (1989) Neutral endopeptidase 24.11 (enkephalinase) and related regulators of peptide hormones. FASEB J 3:145–151
5. Carl-McGrath S, Lendeckel U, Ebert M, Rocken C (2006) Ectopeptidases in tumour biology: a review. Histol Histopathol 21:1339–1353
6. Sumitomo M, Shen R, Nanus DM (2005) Involvement of neutral endopeptidase in neoplastic progression. Biochim Biophys Acta 1751:52–59
7. Dall'Era MA, True LD, Siegel AF, Porter MP, Sherertz TM, Liu AY (2007) Differential expression of CD10 in prostate cancer and its clinical implication. BMC Urol 7:3
8. Freedland SJ, Seligson DB, Liu AY et al (2003) Loss of CD10 (neutral endopeptidase) is a frequent and early event in human prostate cancer. Prostate 55:71–80
9. Osman I, Yee H, Taneja SS et al (2004) Neutral endopeptidase protein expression and prognosis in localized prostate cancer. Clin Cancer Res 10:4096–4100
10. Zellweger T, Ninck C, Mirlacher M et al (2003) Tissue microarray analysis reveals prognostic significance of syndecan-1 expression in prostate cancer. Prostate 55:20–29
11. Fleischmann A, Schlomm T, Huland H et al (2008) Distinct subcellular expression patterns of neutral endopeptidase (CD10) in prostate cancer predict diverging clinical courses in surgically treated patients. Clin Cancer Res 14:7838–7842
12. Bader P, Burkhard FC, Markwalder R, Studer UE (2003) Disease progression and survival of patients with positive lymph nodes after radical prostatectomy. Is there a chance of cure? J Urol 169:849–854
13. Fleischmann A, Schobinger S, Markwalder R et al (2008) Prognostic factors in lymph node metastases of prostatic cancer patients: the size of the metastases but not extranodal extension independently predicts survival. Histopathology 53:468–475
14. Sobin LH, Gospodarowicz MK, Wittekind C (eds) (2009) TNM classification of malignant tumours, 7th edn. Wiley, New York
15. Kononen J, Bubendorf L, Kallioniemi A et al (1998) Tissue microarrays for high-throughput molecular profiling of tumor specimens. Nat Med 4:844–847
16. Soreide K (2009) Receiver-operating characteristic curve analysis in diagnostic, prognostic and predictive biomarker research. J Clin Pathol 62:1–5
17. Zheng R, Shen R, Goodman OB Jr, Nanus DM (2006) Multiple androgen response elements cooperate in androgen regulated activity of the type 1 neutral endopeptidase promoter. Mol Cell Endocrinol 259:10–21
18. Freedland SJ, Humphreys EB, Mangold LA et al (2005) Risk of prostate cancer-specific mortality following biochemical recurrence after radical prostatectomy. JAMA 294:433–439
19. Cabanillas R, Rodrigo JP, Astudillo A, Dominguez F, Suarez C, Chiara MD (2007) P53 expression in squamous cell carcinomas of the supraglottic larynx and its lymph node metastases: new results for an old question. Cancer 109:1791–1798
20. Harigopal M, Berger AJ, Camp RL, Rimm DL, Kluger HM (2005) Automated quantitative analysis of E-cadherin expression in lymph node metastases is predictive of survival in invasive ductal breast cancer. Clin Cancer Res 11:4083–4089
21. Wang YF, Chen JY, Chang SY et al (2008) Nm23-H1 expression of metastatic tumors in the lymph nodes is a prognostic indicator of oral squamous cell carcinoma. Int J Cancer 122:377–386
22. Cheng L, Leibovich BC, Bergstralh EJ et al (1999) p53 alteration in regional lymph node metastases from prostate carcinoma: a marker for progression? Cancer 85:2455–2459
23. Masuda M, Takano Y, Iki M et al (1998) Prognostic significance of Ki-67, p53, and Bcl-2 expression in prostate cancer patients with lymph node metastases: a retrospective immunohistochemical analysis. Pathol Int 48:41–46
24. Bostwick DG, Qian J, Pacelli A et al (2002) Neuroendocrine expression in node positive prostate cancer: correlation with systemic progression and patient survival. J Urol 168:1204–1211
25. Quek ML, Daneshmand S, Rodrigo S et al (2006) Prognostic significance of neuroendocrine expression in lymph node-positive prostate cancer. Urology 67:1247–1252
26. Nanus DM (2003) Of peptides and peptidases: the role of cell surface peptidases in cancer. Clin Cancer Res 9:6307–6309

27. Erhuma M, Kobel M, Mustafa T et al (2007) Expression of neutral endopeptidase (NEP/CD10) on pancreatic tumor cell lines, pancreatitis and pancreatic tumor tissues. Int J Cancer 120:2393–2400
28. Mondada D, Bosman FT, Fontolliet C, Seelentag WK (2006) Elevated hepatocyte paraffin 1 and neprilysin expression in hepatocellular carcinoma are correlated with longer survival. Virchows Arch 448:35–45
29. Tajima Y, Yamazaki K, Nishino N et al (2004) Gastric and intestinal phenotypic marker expression in gastric carcinomas and recurrence pattern after surgery-immunohistochemical analysis of 213 lesions. Br J Cancer 91:1342–1348
30. Battistini B, Daull P, Jeng AY (2005) CGS 35601, a triple inhibitor of angiotensin converting enzyme, neutral endopeptidase and endothelin converting enzyme. Cardiovasc Drug Rev 23:317–330
31. Pan C, Cardarelli PM, Nieder MH et al (2003) CD10 is a key enzyme involved in the activation of tumor-activated peptide prodrug CPI-0004Na and novel analogues: implications for the design of novel peptide prodrugs for the therapy of CD10+ tumors. Cancer Res 63:5526–5531

Virchows Arch (2011) 458:749–759
DOI 10.1007/s00428-011-1074-1

ORIGINAL ARTICLE

Expression of pERK and pAKT in human astrocytomas: correlation with IDH1-R132H presence, vascular endothelial growth factor, microvascular characteristics and clinical outcome

Angelica A. Saetta · Georgia Levidou · Elias A. El-Habr · Ioannis Panayotidis · Vassilis Samaras · Irene Thymara · Stratigoula Sakellariou · Efstathios Boviatsis · Efstratios Patsouris · Penelope Korkolopoulou

Received: 14 November 2010 / Revised: 25 March 2011 / Accepted: 30 March 2011 / Published online: 15 April 2011
© Springer-Verlag 2011

Abstract Although pERK and pAKT are reportedly activated in various neoplasms, little information is available about their significance in astrocytomas. Paraffin-embedded tissue from 82 patients with diffuse infiltrating astrocytomas (grades II to IV) was investigated for the association of pERK and pAKT activation with clinicopathological features, vascular endothelial growth factor (VEGF), isocitrate dehydrogenase 1 and microvascular parameters. Nuclear pERK labelling index (LI) increased with increasing cytoplasmic pERK LI and nuclear and cytoplasmic pAKT LI (p=0.0019, p=0.0260 and p=0.0012, respectively). Accordingly, cytoplasmic pERK increased with increasing levels of nuclear (p=0.0001) and marginally with cytoplasmic pAKT LI (p=0.0526). Nuclear and cytoplasmic pERK LI and nuclear pAKT LI were positively correlated with tumour histological grade (p=0.0040, p=0.0238 for pERK and p=0.0004 for pAKT, respectively). VEGF expression was correlated with nuclear pERK (p=0.0099) and nuclear pAKT LI (p=0.0002). Interestingly, pERK cytoplasmic LI increased with microvessel calibre (p=0.0287), whereas pAKT nuclear LI was marginally related to microvessel density (p=0.0685). The presence of IDH1-R132H was related only to histological grade and lower microvessel calibre. Multivariate survival analysis in the entire cohort selected cytoplasmic pAKT LI (p=0.045), histological grade, microvessel calibre (p=0.028), patients' age, gender and surgical excision as independent predictors of survival. Moreover, in glioblastomas, pERK nuclear LI emerged as a favourable prognosticator in the presence of IDH1-R132H. pERK and pAKT in astrocytomas are interrelated and associated with tumour grade and angiogenesis. Moreover, the importance of cytoplasmic pAKT immunoexpression in patients' prognosis and nuclear pERK immunoexpression in glioblastomas is confirmed.

Keywords pERK · pAKT · IDH1-R132H · Angiogenesis · Survival · Astrocytomas

Angelica A. Saetta, Georgia Levidou and Elias A. El-Habr equally contributed to this manuscript.

A. A. Saetta (✉) · G. Levidou · E. A. El-Habr · V. Samaras · I. Thymara · S. Sakellariou · E. Patsouris · P. Korkolopoulou
First Department of Pathology, Laiko Hospital,
National and Kapodistrian University of Athens, Medical School,
75 Mikras Asias Street,
11527 Athens, Greece
e-mail: asaetta@med.uoa.gr

I. Panayotidis
Second Department of Pathology, Attikon Hospital,
National and Kapodistrian University of Athens, Medical School,
Athens, Greece

E. Boviatsis
Department of Neurosurgery, Medical School,
National and Kapodistrian University of Athens, Evangelismos Hospital,
Athens, Greece

Introduction

Diffuse infiltrating gliomas of astrocytic origin are the most common type of primary intracranial malignant neoplasm in adults. Significant differences exist in patient survival among the various histological grades of diffuse astrocytic tumours. The malignant transformation of precursor cells as well as the progression of diffuse astrocytoma to glioblastoma entails the sequential acquisition of genetic alter-

ations. Among these genetic lesions, p53, epidermal growth factor receptor (EGFR) and phosphatase and tensin homologue (PTEN) alterations discriminate between the two pathways during the evolution of glioblastomas, i.e. primary vs. secondary [1]. In the same context, IDH1-R132H mutations have been recently established as molecular markers to distinguish primary and secondary glioblastomas as they are considered to be highly selective markers of secondary ones [2]. On the contrary, EGFR and PTEN mutations are more frequent in primary glioblastomas and result in the constitutive activation of downstream signalling pathways such as mitogen-activated protein kinase (MAPK) and phosphatidylinositol-3 kinase/AKT (PI3K/AKT), which contribute not only to the suppression of apoptosis but also to the promotion of cell survival and resistance to radiation, which characterise these tumours [3].

MAP kinases are major components of transduction pathways controlling embryogenesis, cell differentiation, cell cycle progression and cell death. They are activated in response to various extracellular mitogenic ligands [4–7]. The pathway is organised as a cascade containing at least three protein kinases sequentially activated that culminate in the activation of a multifunctional MAP kinase. The first component of this pathway, RAS, recruits to the cell membrane Raf, which in turn activates mitogen-activated protein kinase/ERK kinase 1/2 and ultimately the effector MAP kinases extracellular signal-regulated kinase 1/2 (ERK1/2) [8]. ERKs target a vast array of substrates with different functions, such as membrane, cytoplasmic, cytoskeletal, ribosomal, and nuclear proteins (transcription factors) and therefore can influence cell fate [6, 9, 10]. In this context, it is not surprising that ERK1/2 are ubiquitously expressed in mammalian cells and constitutively activated in several human cancers and cell lines, e.g. breast, colon, melanoma, thyroid cancer as well as melanoma [8, 11].

AKT, or protein kinase B, is a serine/threonine protein kinase which mediates growth factor-associated cell survival. All three AKT isoforms (AKT 1, 2, 3) are ubiquitously expressed in normal cells, although the levels of expression among tissues vary. EGFR (as well as other growth factor receptors) recruits PI3K to the cell membrane, which then is able to convert phosphatidyloinositol 4,5-biphosphate (PIP2) to PIP3. The latter activates downstream effector molecules such as AKT. Following activation, AKT translocates to the nucleus in order to phosphorylate its cytosolic as well as nuclear substrates. Full activity is achieved by phosphorylation at both $Thr^{308/309}$ in the kinase activation loop and $Ser^{473/474}$ in the COOH-terminal tail [12].

In the current investigation, we first compared the protein levels of pERK and pAKT and examined their relationship with histological grade, morphometric characteristics of the microvascular network and vascular endothelial growth factor (VEGF) expression in a large series of diffuse infiltrating astrocytic tumours. Given recently published data regarding the prognostic importance of mutant isocitrate dehydrogenase 1 (*IDH1*) in diffuse infiltrating astrocytic tumours [13], we also included in our immunohistochemical analysis the IDH1-R132H antibody which is a surrogate marker of mutant *IDH1* in a subset of our cases in order to examine any possible relationships with pERK and pAKT. We then evaluated the relative clinical importance of the expression levels of pERK and pAKT in order to delineate their role as prognostic factors in astrocytic neoplasms.

Methods

Patients

This is a study of 82 patients with diffuse infiltrating astrocytomas diagnosed in the Departments of Pathology of Laiko Hospital and Asklepeion Hospital in Athens between 1999 and 2006 for whom archival tumour material was available. During this period, 120 patients with diffuse infiltrating astrocytomas had been diagnosed, but 38 patients had to be excluded because of the insufficient tumour tissue provided by stereotactic biopsy. The demographic data and pathological features of these patients were not significantly different from those of the remaining 82 patients. The study was approved by the Ethical Committee of the University of Athens Medical School, and informed consent was obtained from each patient before their enrollment in the study. The mean age of the patients was 57.11±14.76, ranging from 19 to 84 years, whereas the male-to-female ratio was 48:34. All cases were reviewed by two experienced pathologists and assigned a histological grade according to the principles laid down in the latest World Health Organization Classification [1]: There were 20 grade II, 14 grade III and 48 grade IV tumours.

During the observation period, 51 disease-specific deaths were recorded, whereas the remaining 31 patients had been followed up for 5–104 months (median 13 months). Treatment consisted of surgery [partial (38 patients) or complete (44 patients) resection] and postoperative radiation (52 patients, 48 grade IV and 4 partially resected grade III astrocytomas).

Immunohistochemical staining

Paraffin-embedded sections of tumour tissue fixed in 10% buffered formalin were used for immunohistochemistry. Serial sections (4 μm) were cut on Superfrost plus glass slides and left to dry overnight at 37°C. After deparaffini-

zation, immunostaining was performed using the standard avidin–biotin complex (Ultra Vision Polymer, Lab Vision) and visualised with diaminobenzidine tetrahydrochloride. The following primary antibodies were used: mouse monoclonal anti-pERK1/2 antibody (sc-7383; Santa Cruz Biotechnology, Sta. Cruz, CA, USA), diluted 1:350 [14], and rabbit polyclonal anti-pAKT1/2/3 antibody (sc-16646; Santa Cruz Biotechnology), diluted 1:250 [15]. Both antibodies were incubated overnight at 4°C. For detection, antigen unmasking with microwaving for 15 min, at 750 W, in citrate buffer (pH 6.0) was required. Known positive controls (i.e. breast carcinoma for pERK and mouse kidney for pAKT) as well as negative controls [sections in which pERK and pAKT primary antibodies were pre-absorbed with an equal amount of their corresponding peptides (sc-7383P and sc-16646P, respectively, Santa Cruz Biotechnology, as provided on the data sheet of the used primary antibodies anti-pERK1/2 and anti-pAKT1/2/3 by the manufacturer)] (Fig. 1b, d) were also stained in each run. Immunoreactivity data for pAKT were available in 72 of 82 cases. Moreover, 39 of our cases (12 grade II, 5 grade III and 22 grade IV astrocytomas) were stained for IDH1-R132H with the mouse monoclonal antibody H09 (DIA H09, Dianova, Hamburg, Germany) as described previously [2].

Light microscopic evaluation of pERK and pAKT was performed independently by three (PK, IP, GL) experienced pathologists without previous knowledge of the clinical information. If a discrepancy occurred between the three assessments, the slides were reassessed jointly. In each case, 1,000–1,500 neoplastic cells throughout the section were counted at high-power magnification. Nuclear and cytoplasmic pERK and pAKT expression was recorded separately. The percentage of neoplastic cells with nuclear or cytoplasmic immunoreactivity for pERK and pAKT out of the total number of neoplastic cells counted was estimated (labelling index, LI).

In addition, results regarding VEGF expression and microvessel counts on CD34-stained slides were available in 69 and 68 cases, respectively, from our previous investigation [16]. Evaluation of microvascular parameters was performed as detailed in an earlier study of our group [17]. Briefly, immunostained slides for CD34 were examined field per field at ×40 (Zeiss Axiolab microscope) to identify the area showing the vascular "hot spot" which was then photographed at ×100 (with an Olympus EVOLT E-510 Digital SLR Camera), printed on high-quality photographic paper and stored as bmp files (1,480× 1,070 pixels, 16.7 million colours, 24-bit). Quantification of digital images was performed using the Sigma Scan software (Jandel Scientific, Erkrath, Germany) on a Pentium III P/C. For each countable microvessel, the outline was manually identified and the following morphometric parameters were automatically estimated: major axis length (the distance between the two most remote points along the vessel periphery) and minor axis length, perimeter (the largest axis perpendicular to major axis formed by two points across the vessel), area (luminal plus endothelial cell area), Feret diameter ($\sqrt{4\text{area}/\pi}$), shape factor ($4\pi\text{area}/\text{perimeter}^2$), microvessel density (MVD) and total vascular area (TVA). Data regarding pERK, pAKT, VEGF and CD34 were available in 60 cases (13 grade II, 10 grade III and 37 grade IV astrocytomas). IDH1-R132H immunostaining was evaluated as positive or negative according to Hartmann et al. and Capper et al. [2, 13].

Statistical methods

In the basic statistical analysis, pERK and pAKT expressions (nuclear and cytoplasmic) were treated as continuous variables. Correlations of pERK and pAKT nuclear and cytoplasmic expression were tested with Spearman's correlation coefficient. Associations of pERK and pAKT nuclear and cytoplasmic expression with VEGF, IDH1-R132H, microvascular characteristics, grade and other clinicopathological parameters were tested using nonparametric tests (Kruskal–Wallis ANOVA, Mann–Whitney *U* test and Spearman's rank correlation coefficient as appropriate).

The set of microvascular parameters was subjected to factor analysis using the principal component extraction method. Three factors were extracted. Each of the nine microvascular parameters was assigned to the factor with which it had the closest correlation. The first factor represented microvessel calibre (area, perimeter, Feret diameter, and major and minor axis lengths). The second factor represented microvessel shape (shape factor and compactness), whereas the third factor represented the extent of microvascular network (TVA and MVD). In order to reduce the number of variables to be introduced into the model, the estimated factor scores were used in multivariate survival analysis instead of the original microvascular parameters.

Survival analysis was performed using death by disease as endpoint. The effect of various parameters (age, sex, tumour location, radiotherapy, histological grade, extent of surgical resection, pERK and pAKT nuclear and cytoplasmic LI, IDH1-R132H expression) on clinical outcome was assessed by plotting survival curves according to the Kaplan–Meier method and comparing groups using the log-rank test, as appropriate. Numerical variables were categorised on the basis of the median value, except for age which was categorised on the basis of the 10th percentile value. Multivariate analysis was performed using Cox's model forward selection in order to evaluate the predictive power of each power independently of others. Numerical variables were introduced in continuous form. Apart from

the parameters examined in univariate analysis, VEGF and the estimated angiogenesis factor scores as well as IDH1-R132H (expression status) were introduced into Cox's model. Statistical calculations were performed using the Statistical package STATA 9.0 for Windows. All results with a two-sided p level ≤0.05 were considered statistically significant.

Results

pERK, pAKT and IDH1-R132H immunoreactivity in human astrocytomas

The immunostaining pattern of pERK and pAKT and the interrelationships between protein expressions have been previously described in a smaller series from our group (Fig. 1a, c) [18]. In accordance with these results, in the present study, the staining pattern was both nuclear and cytoplasmic. Both staining patterns were abolished in negative control sections. All cases displayed nuclear immunoreactivity for pERK, whereas cytoplasmic immunoreactivity was found in 74.39% of cases (61/82). Nuclear pAKT immunoreactivity was seen in 93.05% of cases (67 in 72), whereas cytoplasmic immunoreactivity was seen in 43 cases (59.72%). Normal brain tissue displayed no immunoreactivity for pERK or pAKT. Non-neoplastic elements, such as endothelial cells, were positively stained in both cases and served as internal positive controls.

The presence of IDH1-R132H was observed in 15 of the examined cases (38.46%) and was cytoplasmic, as previously described [2]. In particular, 6 of 12 diffuse astrocytomas, 4 of 5 anaplastic astrocytomas and 5 of 22 glioblastomas were positive for IDH1-R132H.

Nuclear pERK LI increased with increasing levels of cytoplasmic immunopositivity (Spearman's rank correlation coefficient: R=0.3384, p=0.0019 and R=0.2624, p=0.0260). Accordingly, pAKT nuclear LI was positively correlated with pAKT cytoplasmic LI (R=0.2495, p=0.0345).

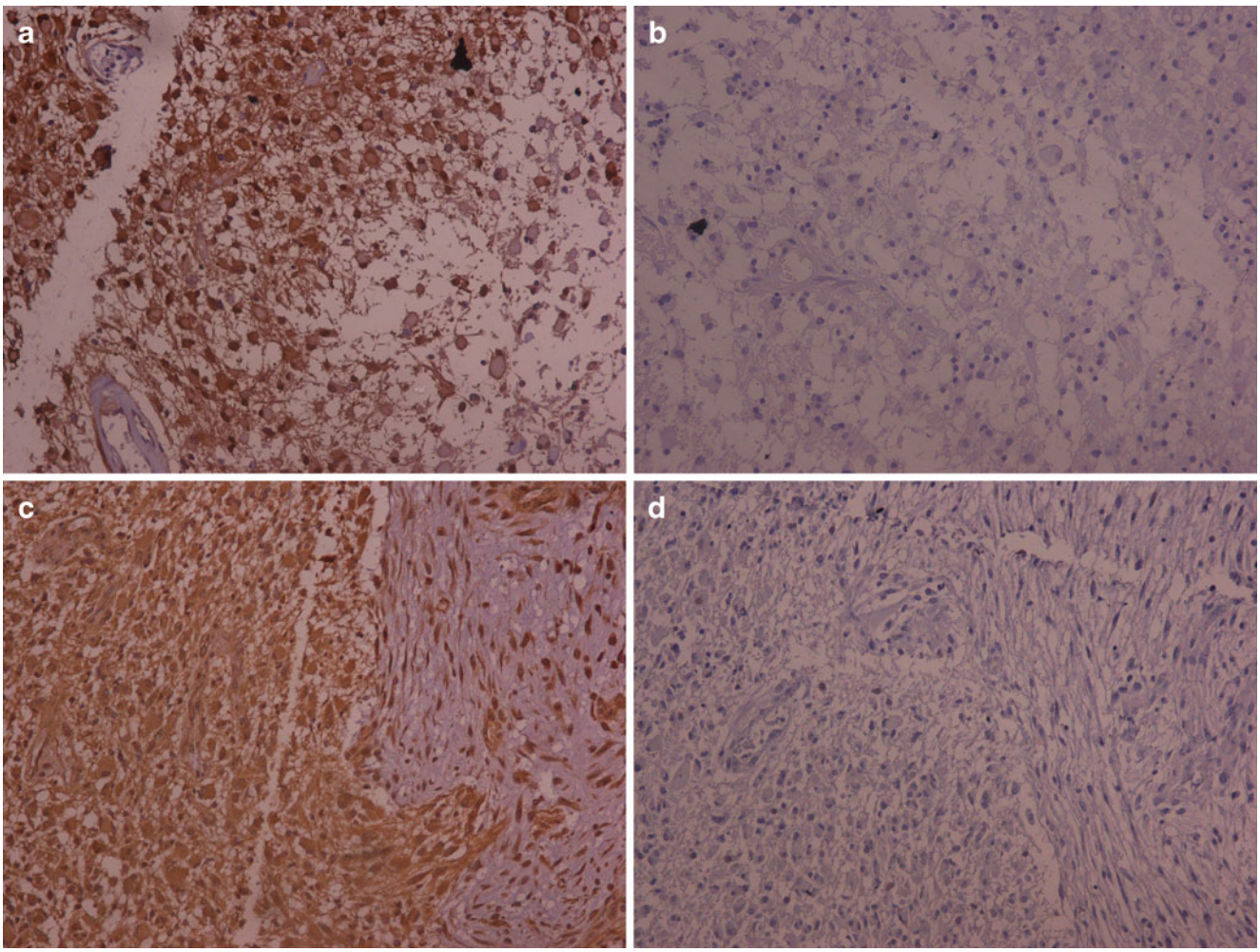

Fig. 1 Nuclear and cytoplasmic expression of pERK (**a**) and pAKT (**c**) in astrocytic tumours. The same cases following absorption with the corresponding pERK (**b**) and pAKT (**d**) peptides in which no staining is seen

Nuclear immunoreactivity of pERK increased with increasing levels of cytoplasmic immunoreactivity as well as pAKT nuclear and cytoplasmic immunoreactivity levels (Spearman's rank correlation coefficient: R=0.3384, p=0.0019; R=0.2624, p=0.0260; and R=0.3738, p=0.0012, respectively). When we adjusted these relationships for grade in a multivariate model, the respective relationship between nuclear pERK and cytoplasmic pAKT remained significant (p=0.040). Importantly, pERK cytoplasmic immunoreactivity positively correlated with nuclear and cytoplasmic pAKT immunoreactivity, although the relationship between cytoplasmic pERK and cytoplasmic pAKT immunoreactivity was of marginal significance (Spearman's rank correlation coefficient: R=0.4348, p=0.0001 and R=0.2293, p=0.0526, respectively). On the other hand, IDH1-R132H expression status was unrelated to nuclear and cytoplasmic pERK or pAKT expression (p>0.10).

Associations between nuclear and cytoplasmic pERK or pAKT expression as well as IDH1-R132H expression status and clinicopathologic features

Data representing the distribution of pERK nuclear and cytoplasmic expression per histological grade are shown in Table 1. The pERK nuclear and cytoplasmic LI were related to histological grade (p=0.0040 and p=0.0238, respectively; Fig. 2). pERK nuclear immunoreactivity was also related to patients' age (Spearman's rank correlation coefficient: R=0.2293, p value=0.0421), but was unrelated to patients' gender and tumour location (p>0.10). Cytoplasmic pERK immunoreactivity was not significantly correlated with the aforementioned parameters.

Data representing the distribution of pAKT nuclear and cytoplasmic immunoreactivity levels per histological grade are shown in Table 1. pAKT nuclear and cytoplasmic expression were positively correlated with tumour grade (Mann–Whitney: grade II/III vs. IV, p=0.0004 and p=0.0822, respectively; Fig. 3), although the latter relationship was of marginal significance. Moreover, pAKT cytoplasmic LI was correlated with patients' age (Spearman's rank correlation coefficient: R=0.2878, p=0.0165), but was unrelated to patients' gender and tumour location (p>0.10). Nuclear pAKT expression was not significantly correlated with the aforementioned parameters (p>0.10).

The frequency of IDH1-R132H immunopositivity increased with increasing histological grade (Fischer's exact test: II/III vs. IV, p=0.045). However, it was unrelated to patients' age and gender as well as tumour location (p>0.10).

Correlations between pERK or pAKT LI and IDH1-R132H expression status with VEGF and vascularity

The associations of VEGF and microvascular parameters with clinicopathologic characteristics in astrocytic tumours have been examined in detail previously [16, 17, 19] and will not be mentioned. Cytoplasmic VEGF expression was seen in 88.4% of cases (61/69).

VEGF expression significantly correlated with the levels of pERK nuclear immunoreactivity (Spearman's rank correlation coefficient: R=0.3084, p=0.0099) and marginally with pERK cytoplasmic immunoreactivity (Spearman's rank correlation coefficient: R=0.2160, p=0746; Fig. 4a). Furthermore, it was positively correlated with pAKT nuclear expression (Spearman's rank correlation coefficient:

Table 1 Distribution (median, range) of pERK, pAKT, VEGF expression and microvascular parameters per histological grade in patients with astrocytomas

Variable	Grade II	Grade III	Grade IV	Total
pERK nuclear	8 (1–80)	22.5 (2–90)	40 (1–95)	30 (1–95)
pERK cytoplasmic	5 (0–70)	5 (0–90)	17.5 (0–95)	10 (0–95)
pAKT nuclear	5 (0–90)	5 (0–80)	45 (0–90)	25 (0–90)
pAKT cytoplasmic	0 (0–45)	5 (0–60)	8.5 (0–90)	5 (0–90)
VEGF	25 (0–90)	15 (0–40)	70 (0–95)	50 (0–95)
MVD	14.5 (6–128)	15 (11–140)	23 (3–169)	20 (3–169)
TVA (μm^2)	7,112.5 (1,958–46,434)	17,204 (3,229.2–100,110)	13,250.3 (3,104–133,626)	13,148.3 (1,958–133,626)
Shape factor	0.61 (0.39–0.77)	0.628 (0.33–0.72)	0.65 (0.39–0.81)	0.635 (0.33–0.81)
Compactness	22.165 (15.64–36.8)	27.755 (18.2–49.44)	18.71 (15.46–27.55)	19.75 (15.46–49.44)
Feret diameter (μm)	26.8 (17.3–45.46)	25.11 (20.94–43.8)	29.28 (14.3–89.8)	27.63 (14.3–89.8)
Major axis length (μm)	43.215 (24.07–91.2)	40.39 (28.3–86.8)	38.26 (17.2–120.06)	40.455 (17.2–120.06)
Minor axis length (μm)	17.6 (9.2–37.18)	18.8 (13.2–38.2)	18.52 (4.2–75.66)	18.6 (4.2–75.66)
Perimeter (μm)	114.895 (52.4–231.9)	111.19 (76.09–219.4)	103.41 (32.1–332.41)	109.635 (32.1–332.41)
Area (μm^2)	563.9 (244.7–2,852.5)	537.6 (248.4–3,056.7)	513.23 (112.2–7,032.95)	525.4 (112.2–7,032.95)

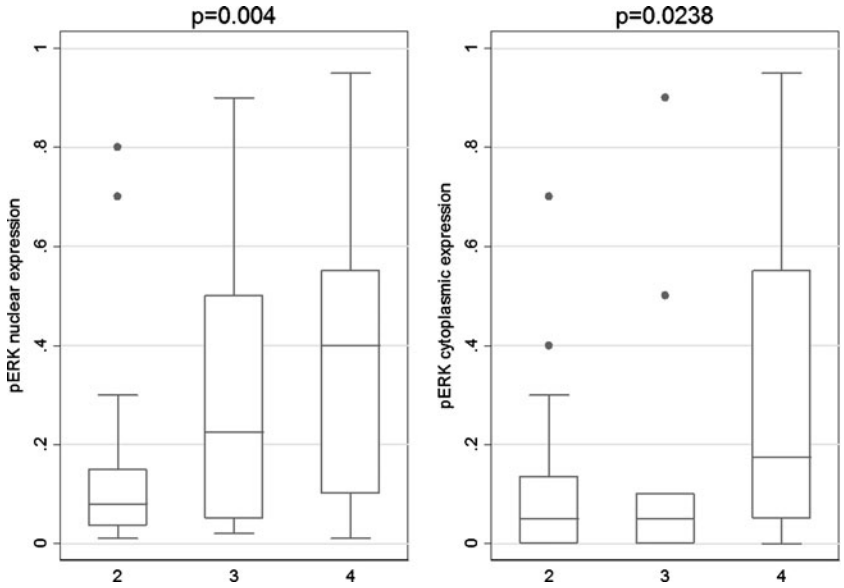

Fig. 2 Schematic representation of the association of pERK nuclear and cytoplasmic expression with tumour histological grade

R=0.4492, p=0.0002; Fig. 4b), but was not correlated with pAKT cytoplasmic expression or the presence of IDH1-R132 expression (p>0.10).

As far as morphometric microvascular characteristics are concerned, pERK cytoplasmic LI was positively correlated with minor axis length (0.0287) and Feret diameter (p=0.0287) and marginally with vascular area (p=0.0824). Nuclear pAKT LI was marginally higher in cases with MVD higher than the median (i.e. 20 microvessels; Mann–Whitney U test: p=0.0685). Nuclear pERK and cytoplasmic pAKT immunoreactivity were not correlated with any of the microvascular characteristics (p>0.10).

In addition, IDH1-R132H expression status was associated with four of the examined microvascular parameters (Mann–Whitney U test: area, p=0.0593; TVA, p=0.0271; major axis length, p=0.0367; perimeter, p=0.0492), the former relationship being of marginal significance. Thus, tumours negative for IDH1-R132H tended to display higher values of these parameters.

Survival analysis

Given that results for VEGF and morphometric microvascular characteristics were not available in many cases and their influence on prognosis has been investigated previously [16, 17, 19], we excluded them from univariate analysis. The parameters adversely affecting survival in the entire cohort were high histological grade, female sex, advanced age and the absence of postoperative administration of radiotherapy. Neither pAKT nor pERK expression

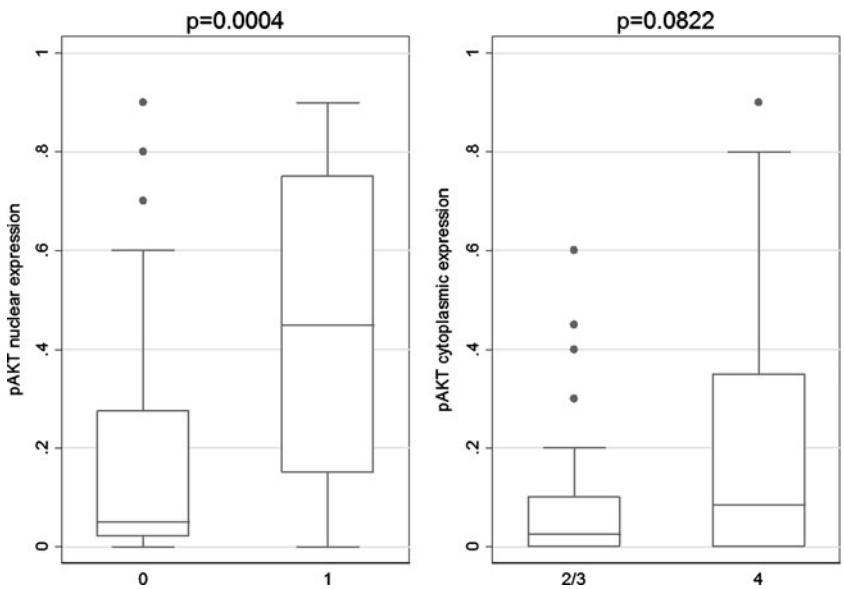

Fig. 3 Schematic representation of the association of pAKT nuclear and cytoplasmic expression with tumour histological grade

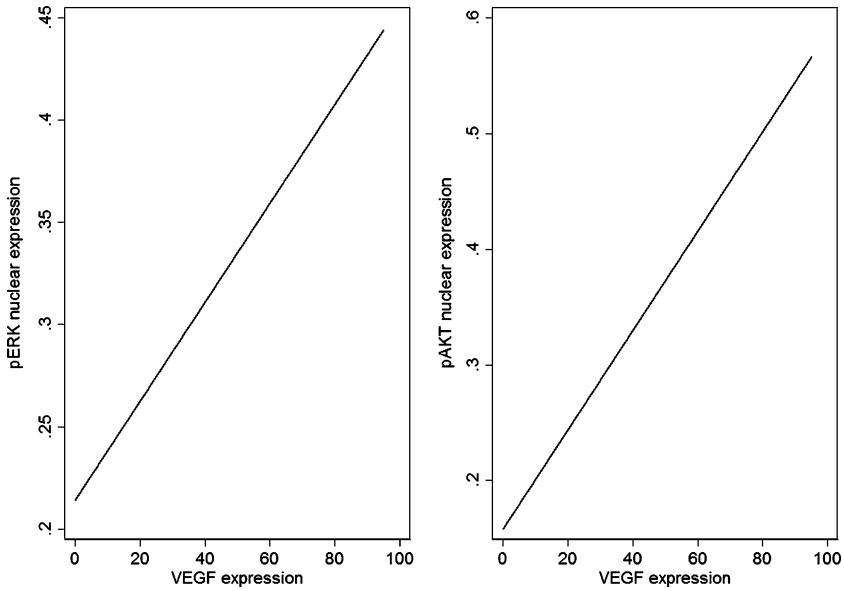

Fig. 4 Schematic representation of the association between pERK nuclear and pAKT nuclear expression with VEGF immunoreactivity

was found to be statistically significant in this regard. In addition, IDH1-R132H immunopositivity was not correlated with patients' survival in the entire cohort (p=0.2997). However, when analysis was restricted to glioblastomas, tumours positive for IDH1-R132H tended to have a more favourable prognosis, although this relationship failed to attain statistical significance (p=0.1028), possibly due to the small number of the examined cases.

Multivariate survival analysis results including all parameters for the 82 patients, for whom pERK staining results were available, are presented in Table 2. pERK nuclear expression along with tumour grade, patients' age and gender, as well as surgical excision, were proven to independently affect survival. We performed a separate multivariate analysis introducing into the model (which included 72 patients, Table 2) pAKT immunoexpression in order to examine its prognostic value in the presence of all clinicopathological parameters and pERK expression. pERK nuclear and pAKT cytoplasmic expression, along with tumour grade, patients' age and gender, as well as surgical excision, emerged as independent predictors of survival. Importantly, both nuclear pERK and cytoplasmic pAKT implied a higher survival probability in all multivariate models. Finally, we adjusted the prognostic significance of the aforementioned parameters for VEGF expression and microvascular parameters. The final model included 60 patients. VEGF and pERK expressions (nuclear and cytoplasmic) were removed, whereas pAKT

Table 2 Cox's proportional hazard estimations in grades, a model including only pERK immunostaining results (model A) and a model including both pERK and pAKT (model B) staining results

	Variable	HR	SE	p value	95% CI
A	pERK nuclear expression (%)	0.318	0.179	0.041	0.106–0.956
	pERK cytoplasmic expression (%)	2.255	1.259	0.145	0.755–6.734
	Grade (II vs. III vs. IV)	2.982	0.823	<0.001	1.737–5.122
	Age (years)	1.028	0.013	0.027	1.003–1.053
	Gender 1:male 2:female	2.977	0.954	0.001	1.589–5.577
	Radiotherapy 0: absence 1:presence	0.875	0.302	0.699	0.445–1.720
	Surgery 0: absence 1:presence	0.270	0.113	0.002	0.118–0.615
B	pERK nuclear expression (%)	0.245	0.168	0.041	0.064–0.941
	pERK cytoplasmic expression (%)	2.768	1.981	0.155	0.681–11.254
	pAKT nuclear expression (%)	1.597	0.916	0.415	0.519–4.915
	pAKT cytoplasmic expression (%)	0.139	0.112	0.014	0.029–0.675
	Grade (II vs. III vs. IV)	3.703	1.226	<0.001	1.936–7.084
	Age (years)	1.056	0.018	0.001	1.021–1.093
	Gender 1:male 2:female	4.243	1.680	<0.001	1.953–9.217
	Radiotherapy 0: absence 1:presence	0.912	0.344	0.807	0.435–1.912
	Surgery 0: absence 1:presence	0.180	0.096	0.001	0.063–0.511

cytoplasmic expression along with factor 1 of microvascular characteristics (corresponding to microvessel calibre), patients' age and gender and surgical excision emerged as independent predictors of survival (Table 3).

Finally, since IDH1-R132H expression status was marginally related with survival in glioblastomas in univariate analysis, we adjusted a multivariate model for this subset of grade IV tumours including IDH1-R132H expression status. In this model, pERK nuclear immunoreactivity retained its statistical significance (p=0.044) and was proven to be an independent prognostic factor of favourable prognosis (HR=0.005, 95% CI=0.0015–0.874).

Discussion

To date, research in astroglial tumours focuses on the prediction of tumour aggressiveness and disease recurrence as well as on the development of more effective treatment strategies. However, the determination of those astrocytic tumours, which are prone to progress, remains still a matter of debate. *IDH1* mutations have recently been identified as frequent and early genetic alterations in astrocytomas, oligodendrogliomas, oligoastrocytomas and secondary glioblastomas, conferring a favourable prognosis and providing information with regard to time to progression in anaplastic astrocytomas [20] and survival time in glioblastomas [13].

Accumulating evidence suggests that deregulation of the MAPK signalling cascade is often involved in oncogenic transformation of various human cancers, such as prostate, breast, colorectal and ovarian [21–23]. More importantly, it has been postulated that protein kinases represent a group of molecular targets characterised by a cancer-specific potential, allowing the development of a new generation of chemotherapy agents acting as kinase inhibitors. Regarding astrocytic tumours, there are few reports looking separately into the significance of pERK and AKT or pAKT as factors involved in the progression and aggressive behaviour of these neoplasms, most of them focusing on glioblastomas [3, 24–27]. However, none of these studies has examined the relationship between these two molecules or their involvement into the angiogenic process. More importantly, no discrimination is made between the nuclear and cytoplasmic localisation of these molecules. The importance of the subcellular localisation of the above activated molecules should be highlighted since recent research has indicated that signalling could be differentially shaped in a spatially restricted way. It is now acknowledged that ERK signalling, for example, is under strict space-related regulation and that the localisation defines its site-specific activities [28].

In our cohort, all cases displayed nuclear pERK immunoreactivity, whereas 74% of them showed also cytoplasmic immunostaining. This figure is broadly in line with observations reported previously in gliomas by us [18] and other investigators [24, 29], as well as in other tumours [30–33]. Interestingly, nuclear and cytoplasmic pERK expressions were positively correlated and associated with tumour grade, strengthening the findings of previous investigations [18, 24, 28, 32] and bringing forward the dual role of pERK as a regulator of gene expression, targetting proteins localised in both the cytoplasm and the nucleus. Taking into account that normal brain tissues were devoid of pERK immunoreactivity, our results implicate pERK in both the development of astrocytic tumours as well as the acquisition of a more aggressive phenotype. Along this line, it has been postulated that constitutively activated ERK is capable of affecting gene expression, thus being able to influence many of the hallmarks of tumourigenesis [6].

Table 3 Results of stepwise Cox's proportional hazard model in the entire cohort for 60 patients with astrocytic tumours (all the available parameters were included during modelling)

Variable	HR	SE	p value	95% CI
pERK nuclear expression (%)	0.271	0.220	0.108	0.055–1.334
pERK cytoplasmic expression (%)	2.745	2.395	0.247	0.496–15.177
pAKT nuclear expression (%)	2.158	1.501	0.269	0.552–8.436
pAKT cytoplasmic expression (%)	0.149	0.141	0.045	0.023–0.955
Grade III vs. II	43.274	42.419	<0.001	6.336–295.539
Grade IV vs. II	27.247	25.840	<0.001	4.247–174.817
Age (years)	1.065	0.022	0.002	1.023–1.109
Gender 1: male 2: female	3.636	1.678	0.005	1.472–8.985
Radiotherapy 0: absence 1: presence	1.645	0.738	0.267	0.683–3.965
Surgery 0: absence 1: presence	0.116	0.087	0.004	0.027–0.505
VEGF (%)	1.007	0.008	0.403	0.991–1.023
Microvascular factor 2	0.883	0.199	0.580	0.568–1.023
Microvascular factor 3	1.082	0.336	0.799	0.589–1.988
Microvascular factor 1	1.715	0.421	0.028	1.059–2.775

Accordingly, most of the cases in our study showed nuclear (93%) and/or cytoplasmic (60%) immunolocalisation of pAKT, in keeping with previous investigations in gliomas [34–36] and in other neoplasms [23, 37–39]. The adjacent normal brain tissue displayed essentially no immunoreactivity for pAKT, supporting that AKT activation may be essential for malignant transformation. Hlobilkova et al. [27], however, concluded that pAKT activation is an early event in astrocytoma genesis since no difference in pAKT expression was seen among low- and high-grade cases. Both nuclear and cytoplasmic pAKT immunoreactivities increased in parallel with tumour grade, although the relationship between cytoplasmic pAKT and grade attained marginal significance. Similar findings have been reported by other investigators, suggesting that AKT activation may also participate in the progression of astrocytic tumours [34, 35]. This observation is of importance since nuclear translocation of AKT is considered to be a crucial step for AKT-mediated anti-apoptosis and proliferation.

As previously reported by our group in a smaller series [18], pAKT is strongly related to pERK1/2 expression in gliomas, a correlation which appeared to be independent of the association of both pERK1/2 and pAKT with grade since it remained significant after adjustment for histological grade in a multivariate regression model. This relation could be attributed to the simultaneous stimulation of these parallel pathways by common upstream receptor tyrosine kinases (e.g. EGFR). In this context, the reported correlation of the activation of both molecules with EGFR gene amplification and progression from anaplastic astrocytomas to glioblastoma [24] lends support to this explanation. More direct proof of a possible functional cooperation that could promote gliomagenesis and progression comes from in vitro data documenting the induction of high-grade gliomas in mouse models [40] by the combined activation of these two pathways. Interestingly, it has been observed that increased expression of EGFR truncated mutant (EGFR-vIII) in glioblastoma cell lines shifts signalling from the MAPK pathway towards the PI3K cascade [41].

An important finding emerging from the present study is that VEGF expression parallels nuclear pERK as well as cytoplasmic pAKT immunopositivities. The close liaison between pERK or pAKT and VEGF is illustrated in the similar distribution of the three in perinecrotic areas of glioblastomas—a finding bringing out hypoxia as the common pathogenetic event of the induction of pAKT, pERK and VEGF. These observed correlations are to be expected since it is a common belief that VEGF initiates several intracellular signalling pathways including the MAP kinase/ERK and PI-3 kinase/AKT signal transduction cascades [42]. Moreover, the activation of AKT, which is downstream of PI3K, has been shown to increase VEGF expression in vitro via HIF-1- or alternatively via Sp1- or HIF-1-independent mechanism [43].

Given the aforementioned association of pERK and pAKT with VEGF, the correlations of the two molecules under study with microvascular characteristics are somewhat expected. It is of note that increased pERK cytoplasmic expression is related with larger vessel calibre, in agreement with the initial observation of Mandell et al. [29] who found that elevated pERK nuclear expression is correlated with hyperplastic tumour vasculature. The correlation between nuclear pAKT expression and vascularity was elicited only with MVD, a parameter representing the degree of vascularity. Taken together, these observations implicate pERK and pAKT as key components of the angiogenic cascade in astrocytic gliomas.

IDH1-R132H immunoreactivity prevailed in grade II and grade III astrocytomas and was cytoplasmic, in keeping with previous investigations [2]. Glioblastomas positive for IDH1-R132H tended to display a less aggressive behaviour than those without IDH1-R132H, although this relationship failed to attain statistical significance because of the small number of examined cases. In the 39 cases analysed for IDH1-R132H, the latter was not related to pERK, pAKT or to VEGF expression, but its absence was associated with higher values of microvessel calibre. We have previously reported that the adverse prognostic significance of increased microvessel calibre may express a normal sequence of events as rapidly growing neoplasms soon lead their environment to hypoxia, which will trigger the production of angiogenic factors and result in an increase of vessel number and calibre [17]. Given the adverse prognostic significance of increased microvessel calibre in astrocytic tumours, this finding may, to some extent, explain the worse clinical behaviour of IDH1-R132H negative cases.

At present, investigations dealing with the prognostic significance of ERK and AKT activation in human carcinogenesis have produced contradictory results, with some studies supporting the role of elevated pERK and pAKT expressions as a favourable prognostic factor for ovarian, lung, endometrial and breast cancer, on the one hand [21, 32, 37, 38, 44], and others documenting the relation of pERK expression with metastasis and poor prognosis for prostate, lung, pancreatic and colon cancer, on the other hand [23, 33, 45, 46]. It could be hypothesised that activation of the MAPK cascade may initiate different cellular processes due to the complex signal transduction network ERKs involved, which could result in either favourable or worse clinical outcome. It has been suggested that opposing effects such as proliferation or differentiation could be provoked, depending on transient or sustained activation of ERKs [47].

In our study, in univariate survival analysis, pERK and pAKT immunoexpressions did not reach statistical significance, whereas in multivariate survival analysis for the entire cohort, decreased nuclear pERK and decreased cytoplasmic pAKT expressions emerged as adverse independent prognosticators along with high tumour grade, advanced patients' age, female gender and the absence of total surgical excision. Cytoplasmic pERK or nuclear pAKT expression did not seem to convey any important prognostic information in this regard. These results concerning pAKT immunoreactivity are in line with recent observations in lung and ovarian cancers [37, 38]. However, published information regarding the prognostic utility of AKT or pAKT in astrocytic tumours is controversial, in some studies emerging as an adverse prognostic factor in grade II [25] and malignant astrocytomas [24, 35] whereas in others failing to attain statistical significance in glioblastomas [3]. On the contrary, the favourable affect of pERK expression on survival is in discordance with the results reported by Mawrin et al. [25] in glioblastomas. The fact that pERK and pAKT expression attained statistical significance only in multivariate analysis adjusted for tumour grade is obviously attributed to their relationship with tumour grade masking their intrinsic favourable prognostic effect. Interestingly, pERK nuclear expression lost its statistical significance when VEGF and microvascular factors were introduced in multivariate analysis, implying that the prognostic information provided by pERK largely lies in its correlation with angiogenesis. The prognostic significance of microvessel calibre established in the present series conforms to previously published results from our group [17]. However, pERK nuclear expression retained its independent prognostic significance in glioblastomas in which IDH1-R132H staining was available.

The results of survival analysis recapitulate most of the parameters that have been advanced as important determinants of clinical outcome in patients with astrocytic tumours, namely, the age of the patient and tumour grade, denoting that our cohort was representative and that survival analysis is valid. An issue that remains to be addressed is the fact that our patients were not uniformly treated. However, treatment-related variables were accounted for in multivariate analysis.

In summary, we present evidence that nuclear pERK1/2 and cytoplasmic pAKT expressions in diffuse astrocytic tumours parallel histological grade as well as VEGF expression and microvascular characteristics, which implicates them in the acquisition of a more aggressive and angiogenic phenotype. Moreover, pERK was correlated with pAKT expression, further supporting a functional cooperation between these molecules. Finally, in multivariate analysis, although both nuclear pERK and cytoplasmic pAKT implied a better survival probability, cytoplasmic pAKT remained significant in the presence of VEGF and microvascular parameters, whereas nuclear pERK remained significant in glioblastomas in the presence of IDH1-R132H. These data stand in favour of the role of activated ERK and AKT as promising molecular markers for the treatment of tumours of astroglial origin and delineate the necessity of testing the effectiveness of various currently available inhibitors targetting the MAPK and PI3K/AKT signalling pathways in astrocytoma patients, as performed in other tumours [48]. Prospective investigations are warranted to validate the role of pERK and pAKT as prognostic factors and as therapeutic targets in astrocytic tumours.

Conflict of interest statement We declare that we have no conflict of interest.

References

1. Louis DN, Ohgaki H, Wiestler OD et al (2007) The 2007 WHO classification of tumours of the central nervous system. Acta Neuropathol 114:97–109
2. Capper D, Weissert S, Balss J et al (2010) Characterization of R132H mutation-specific IDH1 antibody binding in brain tumors. Brain Pathol 20:245–254
3. Pelloski CE, Lin E, Zhang L et al (2006) Prognostic associations of activated mitogen-activated protein kinase and Akt pathways in glioblastoma. Clin Cancer Res 12:3935–3941
4. Robinson MJ, Cobb MH (1997) Mitogen-activated protein kinase pathways. Curr Opin Cell Biol 9:180–186
5. Schaeffer HJ, Weber MJ (1999) Mitogen-activated protein kinases: specific messages from ubiquitous messengers. Mol Cell Biol 19:2435–2444
6. Pearson G, Robinson F, Beers Gibson T et al (2001) Mitogen-activated protein (MAP) kinase pathways: regulation and physiological functions. Endocr Rev 22:153–183
7. Torii S, Yamamoto T, Tsuchiya Y et al (2006) ERK MAP kinase in G cell cycle progression and cancer. Cancer Sci 97:697–702
8. Hoshino R, Chatani Y, Yamori T et al (1999) Constitutive activation of the 41-/43-kDa mitogen-activated protein kinase signaling pathway in human tumors. Oncogene 18:813–822
9. Mercer K, Chiloeches A, Hüser M et al (2002) ERK signalling and oncogene transformation are not impaired in cells lacking A-Raf. Oncogene 21:347–355
10. Yoon S, Seger R (2006) The extracellular signal-regulated kinase: multiple substrates regulate diverse cellular functions. Growth Factors 24:21–44
11. Davies H, Bignell GR, Cox C et al (2002) Mutations of the BRAF gene in human cancer. Nature 417:949–954
12. Carnero A (2010) The PKB/AKT pathway in cancer. Curr Pharm Des 16:34–44
13. Hartmann C, Hentschel B, Wick W et al (2010) Patients with IDH1 wild type anaplastic astrocytomas exhibit worse prognosis than IDH1-mutated glioblastomas, and IDH1 mutation status accounts for the unfavorable prognostic effect of higher age:

implications for classification of gliomas. Acta Neuropathol 120:707–718
14. Rajput A, Koterba AP, Kreisberg JI et al (2007) A novel mechanism of resistance to epidermal growth factor receptor antagonism in vivo. Cancer Res 67:665–673
15. Renken C, Fischer DC, Kundt G et al (2011) Inhibition of mTOR with sirolimus does not attenuate progression of liver and kidney disease in PCK rats. Nephrol Dial Transplant 26:92–100
16. Korkolopoulou P, Perdiki M, Thymara I et al (2007) Expression of hypoxia-related tissue factors in astrocytic gliomas. A multivariate survival study with emphasis upon carbonic anhydrase IX. Hum Pathol 38:629–638
17. Korkolopoulou P, Patsouris E, Kavantzas N et al (2002) Prognostic implications of microvessel morphometry in diffuse astrocytic neoplasms. Neuropathol Appl Neurobiol 28:57–66
18. El-Habr EA, Tsiorva P, Theodorou M et al (2010) Analysis of PIK3CA and B-RAF gene mutations in human astrocytomas: association with activation of ERK and AKT. Clin Neuropathol 29:239–245
19. Perdiki M, Korkolopoulou P, Thymara I et al (2007) Cyclooxygenase-2 expression in astrocytomas. Relationship with microvascular parameters, angiogenic factors expression and survival. Mol Cell Biochem 295:75–83
20. Takano S, Tian W, Matsuda M et al. (2011) Detection of IDH1 mutation in human gliomas: comparison of immunohistochemistry and sequencing. Brain Tumor Pathol (in press)
21. Givant-Horwitz V, Davidson B, Lazarovici P et al (2003) Mitogen-activated protein kinases (MAPK) as predictors of clinical outcome in serous ovarian carcinoma in effusions. Gynecol Oncol 91:160–172
22. McCubrey JA, Steelman LS, Chappell WH et al (2007) Roles of the Raf/MEK/ERK pathway in cell growth, malignant transformation and drug resistance. Biochim Biophys Acta 1773:1263–1284
23. Schmitz KJ, Wohlschlaeger J, Alakus H et al (2007) Activation of extracellular regulated kinases (ERK1/2) but not AKT predicts poor prognosis in colorectal carcinoma and is associated with k-ras mutations. Virchows Arch 450:151–159
24. Mizoguchi M, Betensky RA, Batchelor TT et al (2006) Activation of STAT3, MAPK, and AKT in malignant astrocytic gliomas: correlation with EGFR status, tumour grade, and survival. J Neuropathol Exp Neurol 65:1181–1188
25. Mawrin C, Diete S, Treuheit T et al (2003) Prognostic relevance of MAPK expression in glioblastoma multiforme. Int J Oncol 23:641–648
26. Matsutani T, Nagai Y, Mine S et al (2009) Akt/protein kinase B overexpression as an accurate prognostic marker in adult diffuse astrocytoma. Acta Neurochir Wien 151:263–268
27. Hlobilkova A, Ehrmann J, Sedlakova E et al (2007) Could changes in the regulation of the PI3K/PKB/Akt signaling pathway and cell cycle be involved in astrocytic tumor pathogenesis and progression? Neoplasma 54:334–341
28. Calvo F, Agudo-Ibáñez L, Crespo P (2010) The Ras-ERK pathway: understanding site-specific signaling provides hope of new anti-tumor therapies. Bioessays 32:412–421
29. Mandell JW, Hussaini IM, Zecevic M et al (1998) In situ visualization of intratumour growth factor signaling: immunohistochemical localization of activated ERK/MAP kinase in glial neoplasms. Am J Pathol 153:1411–1423
30. Albanell J, Codony-Servat J, Rojo F et al (2001) Activated extracellular signal-regulated kinases: association with epidermal growth factor receptor/transforming growth factor alpha expression in head and neck squamous carcinoma and inhibition by anti-epidermal growth factor receptor treatments. Cancer Res 61:6500–6510
31. Jørgensen K, Holm R, Maelandsmo GM et al (2003) Expression of activated extracellular signal-regulated kinases 1/2 in malignant melanomas: relationship with clinical outcome. Clin Cancer Res 9:5325–5331
32. Mizumoto Y, Kyo S, Mori N et al (2007) Activation of ERK1/2 occurs independently of KRAS or BRAF status in endometrial cancer and is associated with favorable prognosis. Cancer Sci 98:652–658
33. Vicent S, López-Picazo JM, Toledo G et al (2004) ERK1/2 is activated in non-small-cell lung cancer and associated with advanced tumours. Br J Cancer 90:1047–1052
34. Wang H, Wang H, Zhang W et al (2004) Analysis of the activation status of AKT, NFkappaB, and Stat3 in human diffuse gliomas. Lab Invest 84:941–951
35. Chakravarti A, Zhai G, Suzuki Y et al (2004) The prognostic significance of phosphatidylinositol 3-kinase pathway activation in human gliomas. J Clin Oncol 22:1926–1933
36. Suzuki Y, Shirai K, Oka K et al (2010) Higher pAkt expression predicts a significant worse prognosis in glioblastomas. J Radiat Res Tokyo 51:343–348
37. Woenckhaus J, Steger K, Sturm K et al (2007) Prognostic value of PIK3CA and phosphorylated AKT expression in ovarian cancer. Virchows Arch 450:387–395
38. Shah A, Swain WA, Richardson D et al (2005) Phospho-akt expression is associated with a favorable outcome in non-small cell lung cancer. Clin Cancer Res 11:2930–2936
39. Le Page C, Koumakpayi IH, Alam-Fahmy M et al (2006) Expression and localisation of AKT-1, AKT-2 and AKT-3 correlate with clinical outcome of prostate cancer patients. Br J Cancer 94:1906–1912
40. Holland EC (2000) A mouse model for glioma: biology, pathology, and therapeutic opportunities. Toxicol Pathol 28:171–177
41. Kolch W, Pitt A (2010) Functional proteomics to dissect tyrosine kinase signalling pathways in cancer. Nat Rev Cancer 10:618–629
42. Li B, Xu W, Luo C et al (2003) VEGF-induced activation of the PI3-K/AKT pathway reduces mutant SOD1-mediated motor neuron cell death. Brain Res Mol Brain Res 111:155–164
43. Pore N, Liu S, Shu HK et al (2004) Sp1 is involved in AKT-mediated induction of VEGF expression through an HIF-1-independent mechanism. Mol Biol Cell 15:4841–4853
44. Milde-Langosch K, Bamberger AM, Rieck G et al (2005) Expression and prognostic relevance of activated extracellular-regulated kinases (ERK1/2) in breast cancer. Br J Cancer 92:2206–2215
45. Adeyinka A, Nui Y, Cherlet T et al (2002) Activated mitogen-activated protein kinase expression during human breast tumorigenesis and breast cancer progression. Clin Cancer Res 8:1747–1753
46. Chadha KS, Khoury T, Yu J et al (2006) Activated AKT and Erk expression and survival after surgery in pancreatic carcinoma. Ann Surg Oncol 13:933–939
47. Marshall CJ (1995) Specificity of receptor tyrosine kinase signaling: transient versus sustained extracellular signal-regulated kinase activation. Cell 80:179–185
48. Myers AP, Cantley LC (2010) Targeting a common collaborator in cancer development. Sci Transl Med 2:48ps45

Virchows Arch (2011) 458:761–765
DOI 10.1007/s00428-011-1073-2

CASE REPORT

IgG4-associated cholangitis with cholangiocarcinoma

Beate K. Straub · Irene Esposito · Daniel Gotthardt · Boris Radeleff · Dalibor Antolovic · Christa Flechtenmacher · Peter Schirmacher

Received: 8 October 2010 / Revised: 8 March 2011 / Accepted: 30 March 2011 / Published online: 12 April 2011
© Springer-Verlag 2011

Abbreviations

AIP	Autoimmune pancreatitis
AIPC	Autoimmune pancreatocholangitis
ANA	Antinuclear antibodies
IAC	IgG4-associated cholangitis
CC	Cholangiocarcinoma
HPF	High-power field
MRCP	Magnetic resonance cholangiopancreatography
PSC	Primary sclerosing cholangitis

B. K. Straub (✉) · C. Flechtenmacher · P. Schirmacher
Institute of Pathology, University Hospital,
Im Neuenheimer Feld 220/221,
69120 Heidelberg, Germany
e-mail: beate.straub@med.uni-heidelberg.de

I. Esposito
Institute of Pathology, Technische Universität München,
Ismaningerstr. 22,
81675 Munich, Germany

I. Esposito
Institute of Pathology, Helmholtz Zentrum München,
Ingolstädter Landstraße 1,
85764 Neuherberg, Germany

D. Gotthardt
Department of Internal Medicine IV, University Hospital,
Im Neuenheimer Feld 410,
69120 Heidelberg, Germany

B. Radeleff
Department of Diagnostic and Interventional Radiology,
University Hospital,
Im Neuenheimer Feld 110,
69120 Heidelberg, Germany

D. Antolovic
Department of Surgery, University Hospital,
Im Neuenheimer Feld 110,
69120 Heidelberg, Germany

Introduction

Autoimmune pancreatitis (AIP) was first described by Sarles and coauthors [1] as a primary inflammatory sclerosis of the pancreas and is currently subclassified into two clinical entities named type 1 and type 2 AIP [2]. Clinical features of type 1 AIP include elevated IgG4-levels in the serum and excellent response to steroids, whereas in type 2 AIP, IgG4 levels are not elevated. Histologic criteria for type 1 AIP include periductal lymphoplasmacytic infiltrate, storiform fibrosis, and obliterative venulitis, whereas the hallmark of type 2 AIP is the presence of epithelial granulocytic lesions. Extrapancreatic disease occurs in more than 45% of patients with AIP, and especially intra- and extrahepatic biliary tree involvement has been described as a peculiar form of sclerosing cholangitis [3–5]. Less frequently, the disease may only involve the intra- and/or extrahepatic bile ducts, then termed IgG4-associated cholangitis (IAC) [6]. Currently, IAC and AIP are seen as manifestations of a systemic IgG4-disease [6], often occurring together as autoimmune pancreatocholangitis (AIPC) [7]. While in primary sclerosing cholangitis (PSC), an association with malignancy, i.e., cholangiocarcinoma (CC), is well established with an incidence rate of 1.5% per year [8], an association of IAC/AIPC with invasive carcinoma of the biliary tree has not been demonstrated so far. Only recently, a case of biliary intraepithelial neoplasia in the common bile duct in the presence of bile duct affection of AIPC has been described [9]. Here, we demonstrate the first case of co-occurrence with a potentially correlated malignancy, i.e., intrahepatic CC.

Clinical history

A 75-year-old male patient with coronary heart disease, high blood pressure, and hypercholesterolemia, but no

known preexistent disease of the pancreas or of the liver, presented with a tumor in the left lobe of the liver. CEA and CA19-9 levels in the serum were not or only slightly elevated (CEA 2.3 μg/l, CA19-9 40.8 U/ml). The liver enzyme levels were moderately elevated (AP 96 U/l, AST 65 U/l, ALT 41 U/l, GGT 496 U/l), lipase levels were normal. While the level of IgG4 in the serum was normal (0.84 g/l), ANA titer was positive (1:1,280). There was no known preexisting chronic inflammatory bowel disease. In magnetic resonance cholangiopancreatography, the left lobe of the liver (segment 4b) presented with a subcapsular tumor characteristic of cholangiocarcinoma and accompanying cholestasis/cholangitis which was interpreted as being secondary to the tumor (Fig. 1). The pancreas did not show any abnormalities. By CT-guided liver biopsy, the diagnosis of adenocarcinoma of the pancreatobiliary system was made and left hemihepatectomy was performed. After surgery, cholestasis disappeared rapidly, the patient was not treated with steroids. More than 2 years after hemihepatectomy, the patient is well, CT scan of thorax and abdomen show no relapse, osseous, or pulmonary metastases; CA19-9-levels in serum are normal.

Results

At gross examination of the hemihepatectomy specimen, liver segment 4b presented with a whitish and compact subcapsular tumor with bilobated aspect measuring 4.5 cm in diameter, in continuity with the bile ducts (Fig. 2). In addition, some larger intra- and extrahepatic bile ducts were surrounded by whitish tissue with tumorlike appearance. The liver parenchyma was not cirrhotic.

At microscopic examination, the larger intrahepatic bile ducts showed chronic cholangitis with marked storiform fibrosis and periductal lymphoplasmacellular infiltrates with few eosinophilic granulocytes. Part of the bilobated tumorous lesion in segment 4b resembled inflammatory pseudotumor (Fig. 3) but actually represented a tumorous manifestation of the cholangitis. The ductal epithelium appeared intact; no biliary intraepithelial neoplasia was detected. Additionally, the lymphoplasmacellular infiltrate surrounded veins and arteries as well as nerves. Lymph follicles were present in the periphery. No granulocytic epithelial lesions were present, nor were stigmata of PSC such as onion-skin-like periductal fibrosis, ductopenia, or degenerative changes of the bile duct epithelium. In conclusion, due to its typical histomorphology, the cholangitis was classified as IAC. Immunohistochemistry was performed to identify IgG4-positive plasma cells. More than 10 IgG4-positive cells/high-power field were detected in the inflammatory infiltrate surrounding intrahepatic bile ducts as well as vessels and nerves (Fig. 3) with little regional heterogeneity, further confirming the diagnosis of IgG4-associated cholangitis. The second, subcapsular part of the bilobated tumor situated in direct continuity to the pseudotumorous manifestation of IAC represented an intrahepatic cholangiocarcinoma, peripheral type, with tubular growth pattern, without angioinvasion (pT1, pN0, pMx, and G2; Fig. 3). No biliary intraepithelial neoplasia was detected in proximity of the cholangiocarcinoma. In the surrounding liver parenchyma, marked hepatocellular siderosis (siderosis index 3/4) was detected suggesting iron storage disease without cirrhosis. Bidirectional sequencing of exons 2 and 4 of the *HFE* gene showed no mutations in codon 63 and codon 282, excluding HFE-related hereditary

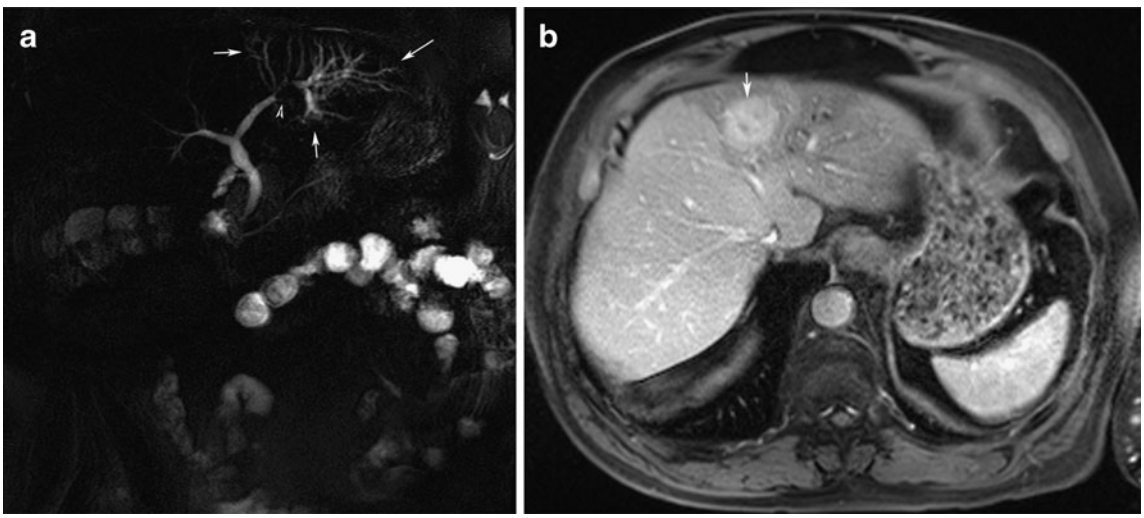

Fig. 1 Preoperative magnetic resonance cholangiopancreatography (MRCP) images. **a** MRCP showing cholestasis/cholangitis (*arrows*) and infiltration by an intrahepatic cholangiocarcinoma (*arrowheads*). **b** Transversal sections of MRCP in portal-venous, contrast medium-enhanced phase, showing an intrahepatic cholangiocarcinoma in the left lobe of the liver (*arrow*)

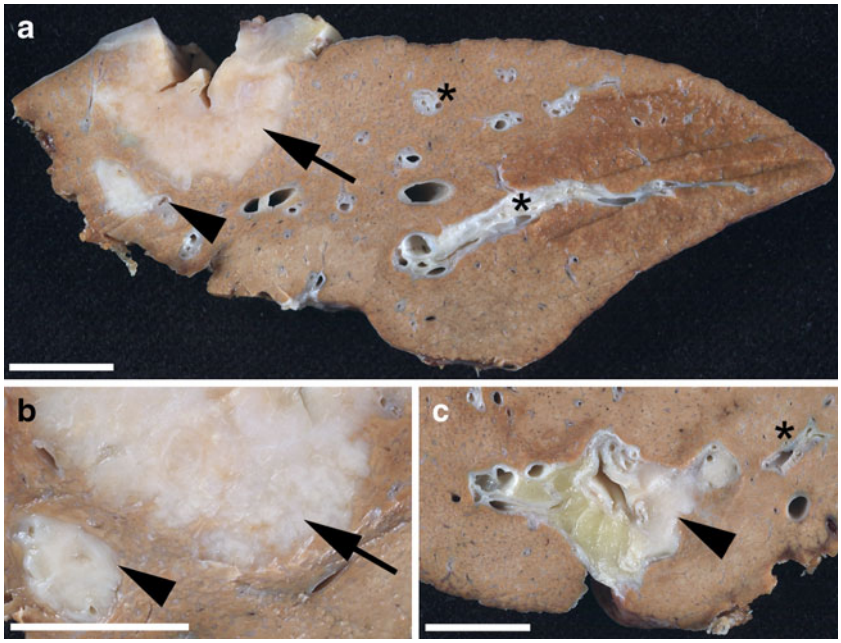

Fig. 2 Gross findings in the hemihepatectomy specimen. **a** Hemihepatectomy specimen showing 4.5-cm subcapsular cholangiocarcinoma (*arrow*) and neighbouring whitish bile ducts with tumorlike manifestation of IAC (*arrowhead*). **b** Enlarged image of cholangiocarcinoma and IAC. Note rounded enlarged whitish portal tracts in **a** and **c** (*asterisks*). Bars, each 2 cm

hemochromatosis; the cause of the significant siderosis could not be defined further.

Discussion

IgG4-associated cholangitis is a recently described steroid-responsive disease comprising chronic inflammation and storiform fibrosis of the intra- and extrahepatic bile ducts. It is often associated with AIP and involvement of pancreas and bile ducts is termed AIPC [3, 4]. In patients with primary sclerosing cholangitis, the development of intrahepatic cholangiocarcinoma is a known consequence [8]. While IAC or AIPC or AIP may present as a tumor mass mimicking cholangiocarcinoma or ductal adenocarcinoma of the pancreas [10] by imaging techniques, these diseases have not been demonstrated to be associated with an increased risk of developing cancers of the liver or pancreas so far.

To date only a few cases of synchronous autoimmune pancreatitis and infiltrating pancreatic ductal adenocarcinoma have been reported [11, 12] as well as one case of a patient with salivary duct carcinoma arising in IgG4-related autoimmune disease of the parotid gland [13]. Additionally, one report describes epithelial atypia in the common bile duct (suggestive of biliary intraepithelial neoplasia) in the presence of bile duct affection of AIPC [9].

The cholangitic lesion was classified as IAC type 1 due to the presence of several classical histological features: typical duct lesion with storiform periductal fibrosis but intact ductal epithelium, lymphoplasmacytic infiltrate with sufficient content of IgG4 positive plasma cells, simultaneous vascular and nerval affections, and focal inflammatory myofibroblastic tumorlike manifestation. Besides IAC, the hemihepatectomy specimen also showed significant siderosis. Iron storage disease in general carries an increased risk of hepatic malignancy, with HCC by far outscoring intrahepatic CC [14]. A contribution of increased iron storage to the genesis of CC has to be considered in principle, but it is certainly not the predominant cause of CC in our case, since hepatic malignancy in iron storage disease almost exclusively occurs at stage 4 (cirrhosis).

The rarity of IgG4 disease and the fact that IAC and AIPC have been described only recently may have obscured a potential causal relationship between these chronic inflammatory processes and tumor development in the affected organs. It is also possible that previous cases of IAC/AIPC (with CC) may have been diagnosed as PSC, which may share overlapping morphological characteristics with IAC [15].

Affection of the same target structure and close topographical correlation of CC and maximal (tumorlike) manifestation of IAC in the absence of other known relevant causes fuels the suspicion that IAC may have contributed to CC development in our case. Of course an inverse relationship, i.e., that intrahepatic CC may have triggered IAC cannot be ruled out. Nevertheless, as the tumor was localized in the subcapsular periphery of the liver and as the larger and hilar bile ducts were affected, IgG4-associated cholangitis in our case is unlikely a secondary cause of physical blockage or recurrent cholangitis. Yet, further observation and investigation are required to establish or rule out a possible relation between IAC/AIPC and the development of CC.

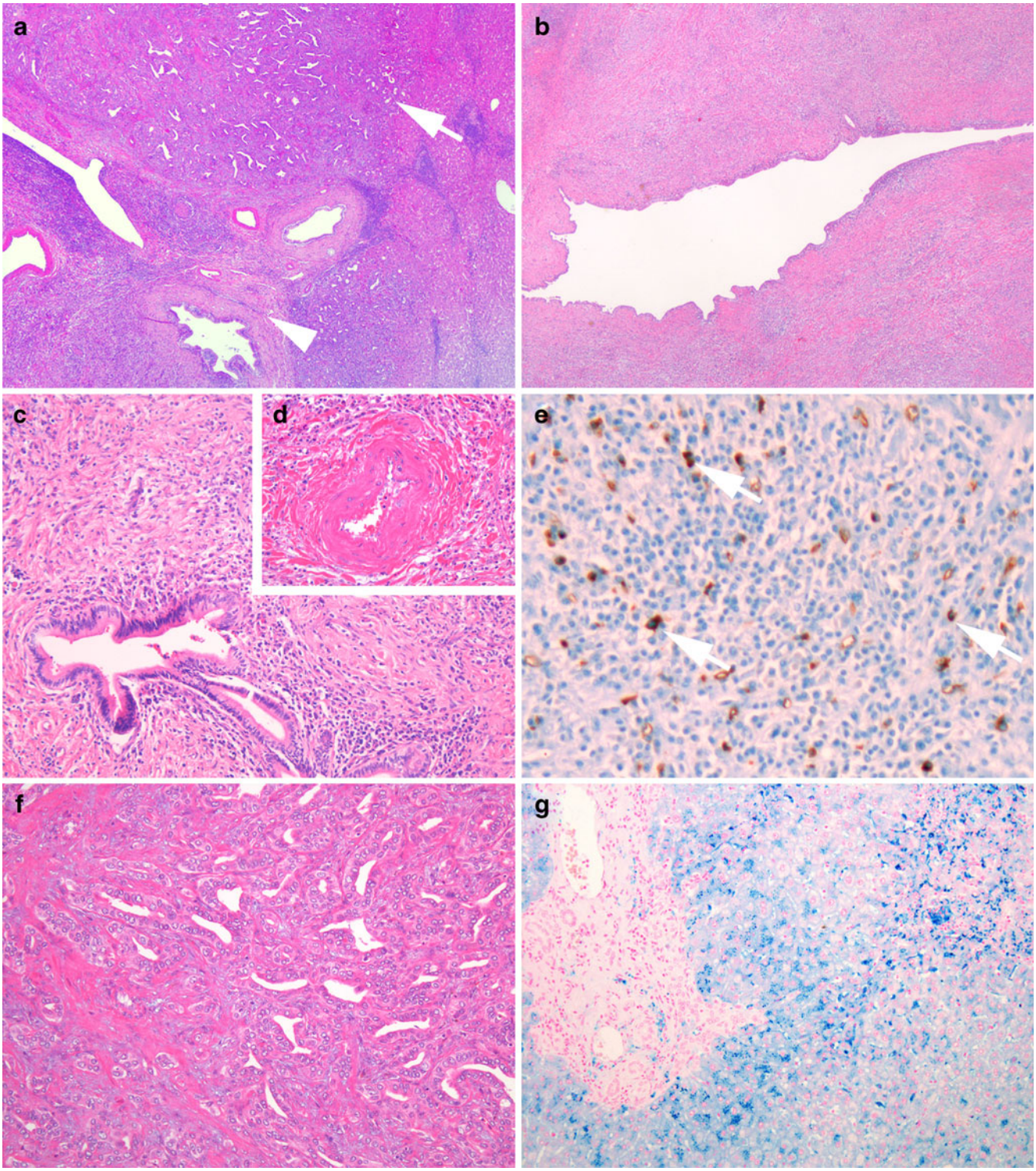

Fig. 3 Microscopic images of the intrahepatic cholangiocarcinoma and of the tumorlike manifestation of IAC. **a** Overview over the intrahepatic cholangiocarcinoma (*arrow*) and IAC (*arrowhead*). **b** Large bile duct in the centre with surrounding inflammatory cells, **c** smaller bile ducts with periductal lymphoplasmacytic infiltration with lack of duct destruction, and excessive storiform fibrosis with **d** encasement of a small artery. **e** Immunohistology for IgG4 demonstrated significantly elevated number of IgG4-positive plasma cells (>10/HPF). **f** Moderately differentiated intrahepatic cholangiocarcinoma. **g** The surrounding liver parenchyma with grade 3 siderosis. Magnification: ×12.5 (**a**), ×40 (**b**), ×200 (**c**, **d**, and **f**), ×400 (**e**), and ×100 (**g**)

Acknowledgment BKS was supported by a stipend of the Olympia-Morata program of the Medical Faculty of Heidelberg University.

Disclosure statement The authors declare that no financial or other conflict of interest exists in relation to the content of the article.

References

1. Sarles H, Sarles JC, Muratore R, Guien C (1961) Chronic inflammatory sclerosis of the pancreas—an autonomous pancreatic disease? Am J Dig Dis 6:688–698
2. Sah RP, Chari ST, Pannala R, Sugumar A, Clain JE, Levy MJ et al (2010) Differences in clinical profile and relapse rate of type 1 vs type 2 autoimmune pancreatitis. Gastroenterology 139:140–148
3. Esposito I, Born D, Bergmann F, Longerich T, Welsch T, Giese NA et al (2008) Autoimmune pancreatocholangitis, non-autoimmune pancreatitis and primary sclerosing cholangitis: a comparative morphological and immunological analysis. PLoS One 3:e2539
4. Ghazale A, Chari ST, Zhang L, Smyrk TC, Takahashi N, Levy MJ et al (2008) Immunoglobulin G4-associated cholangitis: clinical profile and response to therapy. Gastroenterology 134:706–715
5. Webster GJ, Pereira SP, Chapman RW (2009) Autoimmune pancreatitis/IgG4-associated cholangitis and primary sclerosing cholangitis-overlapping or separate diseases? J Hepatol 51:398–402
6. Alderlieste YA, Van den Elzen BD, Rauws EA, Beuers U (2009) Immunoglobulin G4-associated cholangitis: one variant of immunoglobulin G4-related systemic disease. Digestion 79:220–228
7. Umemura T, Zen Y, Hamano H, Kawa S, Nakanuma Y, Kiyosawa K (2007) Immunoglobin G4-hepatopathy: association of immunoglobin G4-bearing plasma cells in liver with autoimmune pancreatitis. Hepatology 46:463–471
8. Bergquist A, Ekbom A, Olsson R, Kornfeldt D, Lööf L, Danielsson A et al (2002) Hepatic and extrahepatic malignancies in primary sclerosing cholangitis. J Hepatol 36:321–327
9. Oh HC, Kim JG, Kim JW, Lee KS, Kim MK, Chi KC et al (2008) Early bile duct cancer in a background of sclerosing cholangitis and autoimmune pancreatitis. Intern Med 47:2025–2028
10. Cheung MT, Lo IL (2008) IgG4-related sclerosing lymphoplasmacytic pancreatitis and cholangitis mimicking carcinoma of pancreas and Klatskin tumour. ANZ J Surg 78:252–256
11. Inoue H, Miyatani H, Sawada Y, Yoshida Y (2006) A case of pancreas cancer with autoimmune pancreatitis. Pancreas 33:208–209
12. Witkiewicz AK, Kennedy EP, Kennyon L, Yeo CJ, Hruban RH (2008) Synchronous autoimmune pancreatitis and infiltrating pancreatic ductal adenocarcinoma: case report and review of the literature. Hum Pathol 39:1548–1551
13. Gill J, Angelo N, Yeong ML, McIvor N (2009) Salivary duct carcinoma arising in IgG4-related autoimmune disease of the parotid gland. Hum Pathol 40:881–886
14. Hsing AW, McLaughlin JK, Olsen JH, Mellemkjar L, Wacholder S, Fraumeni JF Jr (1995) Cancer risk following primary hemochromatosis: a population-based cohort study in Denmark. Int J Cancer 60:160–162
15. Zhang L, Lewis JT, Abraham SC, Smyrk TC, Leung S, Chari ST et al (2010) IgG4+ plasma cell infiltrates in liver explants with primary sclerosing cholangitis. Am J Surg Pathol 34:88–94